

ISBN: 978-4-909106032 C3051

# SEE BANGKOK 2019

## Proceedings



EDITED BY

Zakaria Hossain  
Suksun Horpibulsuk  
Jim Shiau

November 11 – 13, 2019

Swissotel Le Concorde, Bangkok, Thailand

SEE 2019, BANGKOK, THAILAND  
SCIENCE, ENGINEERING AND ENVIRONMENT



PROCEEDINGS OF FIFTH INTERNATIONAL CONFERENCE – SEE 2019  
SCIENCE, ENGINEERING & ENVIRONMENT BANGKOK, THAILAND  
11-13 NOVEMBER, 2019

# Science, Engineering and Environment

*Edited by*

**Prof. Zakaria Hossain**

*Graduate School of Bioresources  
Mie University, Japan*

**Prof. Suksun Horpibulsuk**

*Center of Excellence in Innovation for Sustainable Infrastructure Development  
School of Civil Engineering Suranaree University of Technology, Thailand*

**Dr. Jim Shiau**

*School of Civil Engineering and Surveying  
University of Southern Queensland, Australia*



THE GEOMATE INTERNATIONAL SOCIETY

Copyright © 2019 by The GEOMATE International Society

All rights reserved. In principle, no part of this publication or the information contained herein may be reproduced in any form or by any means, translated in any language, stored in any data base or retrieval system, or transmitted in any form or by any means without prior permission in writing from the publisher.

Disclaimer: The editors and the publisher have tried their best effort to ensure the integrity and the quality of this publication and information herein. However, they give no warranty of any kind, expressed or implied with regard to the material contained in this book, and will not be liable in any event for the consequences of its use.

Published by:  
The GEOMATE International Society  
Tsu city, Mie, Japan  
E-mail: [society@geomate.org](mailto:society@geomate.org)  
<http://www.geomate.org/>

ISBN Number: 978-4-909106032 C3051

## Table of Contents

|           |  |           |
|-----------|--|-----------|
|           | Preface  | xii       |
|           | Organization   | xiii      |
| <b>ID</b> | <b>Keynote Papers</b>  | <b>1</b>  |
| 1k        | A CONCRETE WALL ELEMENT TEST TO EVALUATE COM-PRESSIVE FRACTURE ENERGY<br>Tetsuya Ohmura, Kyouhei Iwasaki and Hiroaki Matsufuji   | 2         |
| 2k        | LANDSLIDES: BEHAVIOR AND MITIGATION APPROACH<br>Avirut Chinkulkijniwat, Somjai Yubonchit   | 8         |
|           |  | 21        |
|           | <b>Technical Papers</b>  |           |
| <b>ID</b> | <b>Science</b>   | <b>22</b> |
| 5508      | DIFFERENT RATIOS OF OKRA JUICE AND PANDAN LEAF JUICE ON SPORT DRINK<br>Wattana Wirivutthikorn  | 23        |
| 5513      | ESTIMATING PEOPLE'S TRAVEL BEHAVIOR TOWARDS TRANSIT-ORIENTED DEVELOPMENT IN<br>DUKUH ATAS, DKI JAKARTA PROVINCE<br>Gemala Pritha Ryzki Rynjani, Chotib   | 29        |
| 5533      | ABOUT KARST (CHEMICAL) DENUDATION IN ZEMO IMERETI PLATEAU. GEORGIA,<br>CAUCASUS<br>Zaza Lezhava, Lasha Asanidze, Kukuri Tsikarishvili, Nino Chikhradze, Lela Gadrani   | 35        |
| 5536      | RESEARCH AND DEVELOPMENT OF PILLOW FOR HEALTH IN THAI PEOPLE: A PILOT STUDY<br>Panida Chaiming, and Wichai Eungpinichpong  | 41        |
| 5540      | THE IMPACT OF URBANIZATION ON THE WATER QUALITY OF UTTARA LAKE, DHAKA – CASE<br>STUDY.<br>Shama Emy Haque and Farhana Aktar  | 47        |
| 5542      | THE EFFECTS OF COMBINED ELECTRICAL STIMULATION WITH SHORT FOOT EXERCISE ON<br>MEDIAL LONGITUDINAL ARCH AND INTRINSIC FOOT MUSCLE SIZE: A PILOT STUDY<br>Juntip Namsawang, Ratana Vichiansiri, Wichai Eungpinichpong, and Somchai Rattanathongkom | 53        |
| 5543      | EFFECT OF LAND MANAGEMENT OF HORTICULTURAL TO SOIL ERODIBILITY AT THE<br>UPSTREAM OF SUMANI WATERSHED<br>Aprisal, Bambang Istijono and Indradwipa  | 58        |
| 5544      | A NEW REPORT OF ARGULUS INDICUS (CRUSTACEA: BRANCHIURA) INFESTATION IN RED TILAPIA<br>(OREOCHROMIS NILOTICUS X OREOCHROMIS MOSSAMBICUS) IN THAILAND<br>Supamas Sriwongpuk  | 64        |
| 5545      | IMMEDIATE EFFECTS OF ARM SWING EXERCISE THERAPY ON THE RANGE OF SHOULDER<br>MOTION AND STAND POSTURE: A PILOT STUDY IN YOUNG ADULTS<br>Zhen Xiao, Wichai Eungpinichpong, Xingze Wang, and Uraiwan Chatchawan                                     | 70        |

|      |   |     |
|------|---|-----|
| 5559 | COMPARISON OF INTRAOCULAR PRESSURE CHANGES AFTER VIEWING LAPTOP COMPUTER AND TABLET COMPUTER: A PILOT STUDY<br>Pattawan Pattaranit, Tanapat Ratanapakorn, Rungthip Puntumetakul, Orawan Buranruk, and Wichai Eungpinichpong   | 76  |
| 5562 | THE CRUDE TANNIN EXTRACTION FROM WOOD SCRAP WASTES FOR PROLONGING THE SHELF LIFE OF LITCHI FRUITS<br>Pornanan Boonkorn, Angkhana Chuajedton and Weeranuch Karuehanon  | 81  |
| 5566 | EXTRACTION OF PECTIN FROM PEANUT SHELL WASTE WITH HEATING IN COMBINATION WITH ULTRASONIC-ASSISTED EXTRACTION<br>Chuajedton, A., Karuehanon W. and Boonkorn, P.  | 87  |
| 5567 | EFFECT OF COMBINATION MICROWAVE AND OVEN DRYING ON THE CHEMICAL PROPERTIES OF CRUDE PALM OIL OBTAINED FROM DIFFERENT OIL PALM FRUIT RIPENESS<br>Mallika Tapanwong, Rayakorn Nokkaew and Vittaya Punsuvon  | 93  |
| 5602 | EFFECTS OF CHLORINE DIOXIDE DIPPING ON PERICARP BROWNING REDUCTION OF LONGAN FRUIT<br>Suttinee Likhitragulrung, Tanachai Pankasemsuk, Kanda Whangchai, Wittaya Apai and Wanwarang Patanapoh   | 98  |
| 5612 | SPATIAL DISTRIBUTION OF RESTAURANT POPULARITY INDEX BASED ON CONSUMER REVIEW WEBSITE IN JAKARTA<br>Dewi Susiloningtyas, Alexander Tio, Supriatna and Sidiq, IPA   | 104 |
| 5618 | EFFECT OF ELECTROLYZED REDUCING WATER ON CARBENDAZIM SOLUTION AND RESIDUES DEGRADATION OF CHERRY TOMATO ( <i>Solanum lycopersicum</i> L. var. <i>cerasiforme</i> )<br>Wanwarang Pattanapo, Kanda Whangchai, Jamnong Uthaibutra, Tanachai Pankasemsuk and Usawdee Chanasut | 110 |
| 5619 | EFFECT OF FRUIT BAGGING ON QUALITIES OF PUMMELO CV. KAO NAM PHEUNG AND KAO YAI<br>Yaowarat Wongsrisakulkaew, Chanpen Chaimongkol and Niyom Buaban   | 116 |
| 5624 | EFFECT OF ELECTROLYZED OXIDIZING WATER AND ULTRASONICATION ON PATHOGENIC CONTROL OF FRESH TURMERIC ( <i>Curcuma longa</i> L.)<br>Santirote Keatsirirote, Angkhana Chuajedton, Jamnong Uthaibutra and Kanda Whangchai  | 120 |
| 5629 | EXTRACTED OF THE ANTHOCYANINS FROM <i>Clitoria ternatea</i> FOR STAINED PROTOZOA AND ANTIAMOEBIAC ACTIVITY<br>Chanyapat Sangsuwon   | 126 |
| 5636 | EFFECT OF TRADITIONAL THAI MASSAGE ON MUSCLE OXYGEN SATURATION IN LOW BACK PAIN PATIENTS: A PRELIMINARY STUDY<br>Ketsarakon Oatyimprai, Wichai Eungpinichpong, Orawan Buranruk and Kurusart Konharn   | 131 |
| 5640 | PROBIOTICS ENCAPSULATED FRUIT JUICE PEARLS AS FUNCTIONAL FOOD PRODUCT<br>Palida Tanganurat, Intira Lichanporn, Nunchanok Nanthachai and Charoen Charoenchai   | 138 |
| 5642 | EFFECT OF ENVIRONMENTAL FLUCTUATIONS ON INCIDENCE OF MYCOFLORA<br>H. N. P. Singh, Sunita Kumarii and M.M. Prasad  | 144 |
| 5654 | EFFECT OF KNEADING AND FERMENTATION TIME ON CHEMICAL QUALITY OF HERBAL TEA FROM MANGO PEEL<br>Nunchanok Nanthachai, Intira Lichanporn, Palida Tanganurat and Pradit Kumnongphai   | 148 |
| 5656 | FORMULATION, ANTIOXIDANT AND ANTIBACTERIA ACTIVITIES OF PEEL-OFF GEL MASK, ENRICHED WITH BIDARA LEAF ( <i>ZIZIPHUS SPINA-CHRISTI</i> L.) EXTRACT<br>Hendrawati, Aziza, La Ode Sumarlin, Yulyani Nur Azizah  | 155 |
| 5659 | A STUDY ON ELECTRICAL IMPEDANCE IN RIPENING AMBON-BANANAS ( <i>MUSA PARADISIACA</i> VAR. <i>SAPIENTUM</i> ) PROCESSES STIMULATED BY ETHREL (2-CHLOROETHYL PHOSPHONIC ACID)<br>Chomsin S Widodo, Didik Rahadi Santosa, Wahyu Sugianto, Arinto Yudi P Wardoyo               | 162 |
| 5660 | DNA EXTRACTION METHODS FOR FIN OF MACKERELS IN THAILAND<br>Walaiporn Makkapan, Patcharaporn Narkthewan and Kaewalee Viboonkit   | 168 |



|           |  |            |
|-----------|--|------------|
| 5678      | ANGIOTENSION CONVERTING ENZYME (ACE) INHIBITORY ACTIVITY OF PROTEIN EXTRACT OF MUNG BEANS ( <i>Vigna radiata</i> L.) TEMPEH FERMENTED BY <i>Rhizopus</i> sp.<br>Sri Yadiyal Chalid, Siti Nurbayti, Zeldi Zein Zunaedi  | 173        |
| 5679      | ESTIMATION OF PROPENSITY SCORE USING LOGISTIC REGRESSION (CASE STUDY: BREASTFEEDING DATA IN SELOPURO SUB-DISTRICT BLITAR REGENCY)<br>Hilwin Nisa', Maria Bernadetha Theresia Mitakda, and Suci Astutik   | 179        |
| 5680      | THE MORPHOLOGY AND PHENOLOGY OF YELLOW COMMON BEAN (F7) AS OFFSPRING OF INTRODUCED AND LOCAL VARIETY CROSSING<br>Fathiyah, Sumeru Ashari and Andy Soegianto  | 183        |
| 5690      | FORWARD MODELING FOR SUBSURFACE SYNTHETIC SEISMOGRAM<br>Wasis Wasis, Adi Susilo, Musthofa Nuh  | 187        |
| 5693      | THE PERFORMANCE OF INDONESIAN AGRICULTURAL EXTENSION WORKER<br>Siti Rochaeli, Muchlis R. Luddin, Mansyur Ramly, and Dewi Susita  | 191        |
| 5695      | DETERMINATION OF HISTAMINE-FORMING BACTERIA, TOTAL COLIFORM AND <i>ESCHERICHIA COLI</i> IN FERMENTED FOODS<br>Patcharaporn Narkthewan and Walaiporn Makkapan   | 196        |
| 5696      | VITAMIN AND MINERAL CONTENT OF SIX NATIVE VARIETIES OF RICE IN THAILAND<br>Intira Lichanporn, Nanchanok Nantachai, Palida Tunganurat, Unchalin Singkhum, Nowapor Lapsongphon, Anchalee Sawatthum, Ratchata Tonwitawat, Tongmee Mosom and Purin Akkarakultron | 201        |
| 5710      | AFM VISUALIZATION OF PHYTOPLASMA DNA IMMOBILIZATION AND HYBRIDIZATION EVENT ON CHITOSAN MODIFIED SPCE SURFACE<br>Porntip Wongkaew, Buddhapala Wongkaew   | 205        |
| 5716      | IMPROVEMENT THE PROPERTIES OF POLY(L-LACTIDE) FILMS WITH CELLULOSE FIBER FROM RICE STRAW WASTE IN AGRICULTURAL PRODUCTS<br>Chutima Banthao, Patcharin Kumpolsan, Yodthong Baimark, Sujitra Wongkasemjit, and Kansiri Pakkethati                              | 211        |
| 5727      | SUSTAINABLE AQUACULTURE MANAGEMENT OF VANAMEI SHRIMP ( <i>Litopenaeus vannamei</i> ) IN BATUKARAS VILLAGE, PANGANDARAN, INDONESIA<br>Andrian Achmad, Dewi Susiloningtyas and Tuty Handayani  | 217        |
| 5749      | EVALUATION OF THE TOXIC EFFECTS OF SMOKELESS TOBACCO CHEWING MIXTURES BASED ON BIOLUMINESCENCE TESTING USING THE EXAMPLE OF NASWAR<br>Dianna B. Kosyan, Olga V. Kvan, Elena A. Rusakova, Inara E. Larjushina, Elena V. Kiyeva, Galimzhan K. Duskaev          | 222        |
| 5780      | THE MODIFIED DECOMPOSITION METHOD FOR SOLVING VOLTERRA FREDHOLM INTEGRO-DIFFERENTIAL EQUATIONS USING MAPLE<br>Dalal Adnan Maturi   | 229        |
| 5785      | STUDY OF ELECTRON FLUXES IN IONOSPHERE-PLASMASPHERE COUPLING FROM WHISTLERS OBSERVED AT LOW LATITUDE GROUND STATION JAMMU $L= 1.17$<br>M. Altaf  | 233        |
| 5789      | METAL PLASTICITY AND PERIODIC TABLE<br>Lev B. Zuev, Svetlana A. Barannikova and Albina M. Zharmukhambetova   | 240        |
| <b>ID</b> | <b>Engineering</b>   | <b>246</b> |
| 5506      | ECONOMICAL ANALYSIS OF THE GEOGRID REINFORCED RAILWAY TRACK<br>ASaad Farhan Ibrahim, Ali Jabbar Kadhim and Harith Basim Khalaf   | 247        |
| 5507      | A STOCHASTIC MODEL OF THE MRO SPARE PARTS PROCUREMENT PLANNING PROBLEM FOR AIRCRAFT MAINTENANCE SERVICE PROVIDER<br>Yichen QIN, Felix T.S. CHAN, S.H. CHUNG and T. QU  | 252        |

|      |  |     |
|------|--|-----|
| 5510 | COMPUTING PROGRAM FOR EVALUATING RESSUREMETER TEST RESULTS OF CLAY<br>Radhi Alzubaidi and Athra Al-Kanim   | 256 |
| 5516 | ANALYSIS OF PROBLEMS AND SOLUTIONS IN THE HEAT INSULATING GLASS MANUFACTURING<br>INDUSTRY USING FMEA<br>Natsuda Paiboon, Nipalai Inplaeng, Wisitsree Wiyaratn and Anucha Watanapa          | 261 |
| 5519 | APPLICATION OF DEAGGREGATION OF SPATIAL PROBABILISTIC SEISMIC HAZARD TO DISASTER<br>PREPAREDNESS<br>Takayuki Hayashi and Harumi Yashiro  | 267 |
| 5521 | A CONCRETE WALL ELEMENT TEST TO EVALUATE COM-PRESSIVE FRACTURE ENERGY<br>Tetsuya Ohmura, Kyouhei Iwasaki and Hiroaki Matsufuji   | 273 |
| 5525 | THE EFFECTS OF BATANG KANDIS RIVER FLOOD CONTROL IN PADANG CITY-PALAPA<br>METROPOLITAN AREA<br>Benny Hidayat, Bambang Istijono, Irwan Irwan, Taufika Ophiyandri and Akhmad Junaidi         | 279 |
| 5527 | FATIGUE STRENGTH OF HEADED STUDS WELDED WITH IMPROVED FERRULE IN CONCRETE UNDER<br>UNIDIRECTIONAL CYCLIC LOADING<br>Hiroshi Higashiyama, Kenji Yoshida, Satoshi Banba and Shigeyuki Matsui | 285 |
| 5528 | DESIGN AND ANALYSIS OF FORMULA SPACE FRAME CHASSIS<br>WITH SIDE IMPACT<br>Boonthum Wongchai  | 291 |
| 5529 | PUBLIC TRANSPORT INITIATIVES IN WEST AFRICA, A CASE STUDY OF ABIDJAN<br>Leonard Johnstone and Vatanavongs Ratanavaraha   | 297 |
| 5530 | PRELIMINARY RESULTS OF SITE-SPECIFIC GROUND RESPONSE ANALYSIS<br>Bambang Setiawan, Taufiq Saidi and Mark B. Jaksa  | 305 |
| 5531 | STUDY OF SEEPAGE THROUGH AN EARTH DAM CASE STUDY (AJDABIYA RESERVOIR)<br>Prof. Salem Al- Sanusi, Mervat J. M. Alarosh  | 311 |
| 5532 | ANALYSIS OF SLOPE STABILITY (AJDABIYA RESERVOIR)<br>Prof. Salem Al- Sanusi, Abier J. M. Alarosh  | 315 |
| 5534 | PREDICTION OF FLEXURAL STRESS IN UNBONDED POST-TENSIONED STEEL AT DIFFERENT LOADING<br>STAGES<br>Nazar Oukaili and Iqbal Peera   | 320 |
| 5539 | THE DURABILITY OF LIME STABILIZED EXPANSIVE SOIL<br>Yulvi Zaika, Eko Andi Suryo  | 326 |
| 5541 | DURABILITY OF CONCRETE CONTAINING RECYCLED ASPHALTIC CONCRETE AGGREGATE AND HIGH<br>CALCIUM FLY ASH<br>Prinya Chindaprasirt, Pornnapa Kasemsiri, Sompron Leekongbub3 and Patcharapol Posi  | 332 |
| 5549 | WALKING AUTHENTICATION BASED ON POWER SPECTRUM DENSITY OF ACCELERATION AT LUMBER<br>PART<br>Masahiro Yoneda  | 339 |
| 5553 | EFFECT OF SALT CONTENTS ON COMPRESSIVE STRENGTH OF DMM IN SALINITY CLAY SOFT SOILS<br>FOUNDATION IN VIETNAM<br>Tran Thi Nguyen Hao, Tran Thi Thanh and Vo Phan                             | 344 |
| 5554 | CORRELATION BETWEEN VIBRATION SIGNALS AND SOUND SIGNALS OF A PERSONAL CAR WITH<br>GASOLINE ENGINE<br>Suphattharachai Chomphan, Boonthum Wongchai   | 349 |
| 5558 | STRESS ANALYSIS OF EMBANKMENT DUE TO DIFFERENT IN CONSTRUCTION CONDITIONS<br>Shin-ichi Kanazawa and Satoe Suzuki   | 355 |

|      |   |     |
|------|---|-----|
| 5560 | INVESTIGATION OF OPTIMAL CONTACT TYPE ULTRASONIC COLLECTING DEVICE FOR MEASURING ROUGHNESS USING AERIAL ULTRASONIC SENSOR<br>Seiya Nagaoka, Kenji Okajima, Mohammad Raihanul Islam, Ryoei Ito and Ken Watanabe          | 361 |
| 5561 | Experimental Investigation of Multi-axial Mechanical Behavior of Rubber Materials for Base-Isolated Bridges<br>Hiromichi Narita, Junji Yoshida, and Kouichi Takeya  | 367 |
| 5563 | HIGHLY ACCURATE ESTIMATION OF DAILY SUSPENDED SEDIMENT LOAD USING MULTIVARIATE HYDROLOGICAL<br>Phakawat Lamchuan, Adichai Pornprommin, Jiramate Changklom   | 372 |
| 5569 | FATIGUE STRENGTH OF HEADED STUDS UNDER ROTATIONAL SHEAR LOADING FOCUSING ON WEIGHT REDUCTION OF STEEL-CONCRETE COMPOSITE BRIDGE DECK<br>Kenji Yoshida, Hiroshi Higashiyama, Hideki Ogomori and Shigeyuki Matsui         | 378 |
| 5582 | LABORATORY EXPERIMENT OF CHANNEL HEAD BIFURCATION BY RADIAL OVERLAND FLOW<br>Adichai Pornprommin, Ravicha Thaisiam and Wandee Thaisiam  | 384 |
| 5583 | IDENTIFICATION OF DRAINAGE SYSTEMS CAPACITY USING EPA-SWMM 5.1 VERSION MODELING IN GUNUNG PANGILUN OF PADANG CITY-PALAPA METROPOLITAN AREA<br>Taufika Ophiyandri, Bambang Istijono, Milania, Benny Hidayat, and Aprisal | 390 |
| 5584 | SIMULATION OF THE COLLAPSE PROCESS OF INFRASTRUCTURE USING GENERAL-PURPOSE PHYSICS ENGINE<br>Yoshihiro Kabeyama, Sunao Fujimura and Shinichiro Okazaki  | 396 |
| 5587 | MOTORCYCLE-RELATED DEATHS AND HELMET USAGE SITUATION IN THAILAND<br>Jetsada Kumphong, Thaned Satiennam and Wichuda Satiennam  | 402 |
| 5589 | STUDY ON SEISMIC LOAD ON BUILDINGS CONSIDERING RESIDUAL RISK<br>Sei'ichiro Fukushima, Takayuki Hayashi and Mitsuo Tsuzuki   | 408 |
| 5593 | CONSTRUCTION OF DAMAGE FUNCTION FOR AN ANALYSIS OF THE ECONOMIC DAMAGE BY EARTHQUAKES WITH A FOCUS ON THE RECONSTRUCTION OF SHARED HOUSING<br>Norikazu Sakaba, Yashiro Harumi   | 414 |
| 5594 | GROUND SURVEY BASED ON THE DISTRIBUTION OF SURFACE WAVE VELOCITY AND ELECTRICAL RESISTIBILITY<br>Katsuyuki Kawai, Ryosuke Hamada and Koji Nakashima   | 420 |
| 5604 | BASIC STUDY ON BRIDGE WEIGH-IN-MOTION USING OPTICAL FLOW ANALYSIS<br>Kouichi Takeya, Junji Yoshida  | 426 |
| 5609 | EFFECT OF REINFORCEMENT STIFFNESS ARRANGEMENT ON SEISMIC PERFORMCANCE OF GEOGRID REINFORCED SOIL WALLS<br>Albano Acacio Ajuda, Jiro Kuwano and Kosuke Hoshina   | 432 |
| 5611 | THE IMPACT AGGREGATE QUALITY MATERIAL AS A LINEAR REGRESSION STUDY ON MIXTURE CONCRETE<br>Ranti Hidayawanti, Dicki Dian Purnama , Tommy Iduwin, Supriadi Legino and Fahdun Ibnu Wachid                                  | 439 |
| 5616 | DEVELOPMENT OF A MICROBIAL-BASED GROUTING MATERIAL WITH CALCIUM CARBONATE PRECIPITATES<br>Yoko Sakakihara, Yoshihiro Kabeyama and Shinichiro Okazaki  | 446 |
| 5620 | EVALUATION OF LARGE DIAMETER JET GROUTING TECHNIQUE USED FOR TUNNEL CONSTRUCTION IN BANGKOK<br>Kuo Chieh Chao, Ph.D., P.E., Sasirada Seepim, Ricky K. N. Wong, Takeshi Iwakubo, and Morris Wang                         | 452 |
| 5623 | STRUCTURAL BEHAVIOR OF NON-DUCTILE REINFORCED CONCRETE COLUMNS<br>Ari Wibowo, Rizki Amalia Tri Cahyani  | 458 |
| 5628 | STATISTICAL ANALYSIS OF THE INFLUENCE OF TRAFFIC AND ENVIRONMENTAL DISTURBANCES ON DAMPING IN A BRIDGE<br>Koharu Ota, Kouichi Takeya, Junji Yoshida   | 465 |

|      |  |     |
|------|--|-----|
| 5631 | REDUCTION IN BEARING CAPACITY OF GYPSEOUS SOILS WITH CAVITIES<br>Ahmed A. Al-Obaidi and Reem S. Najim  | 471 |
| 5634 | A STUDY OF THE EFFECTS OF THE FLOOD IN 2554 ON AGRICULTURAL MACHINERY USE IN RICE<br>PADDY FIELDS IN PATHUMTHANI PROVINCE<br>Dowroong Watcharinrat   | 478 |
| 5637 | DESIGN AND IMPLEMENT A MONITORING SYSTEM OF TRAFFIC SIGNAL USING MICROCONTROLLER<br>DEVICES<br>Aleksander Purba, Rahayu Sulistyorini, Agung Ilhami and Ageng Sadnowo Repelianto  | 484 |
| 5645 | ENHANCING THE ROLE OF BENT-UP BARS IN SHEAR BEYOND THE CODE REQUIREMENTS BY USING<br>PLANE-CRACK INTERCEPTOR-CROSS DIAGONAL FORM<br>Ms. Naim Asha  | 490 |
| 5650 | EFFECT OF EXCESS PORE WATER PRESSURE IN SATURATED SANDY SOIL FOR EVALUATING<br>LIQUEFACTION POTENTIAL DURING EARTHQUAKE DURATION<br>Hua Thanh Than, Nguyen Ngoc Phuc and Tran Thi Thanh  | 497 |
| 5653 | PREDICTION OF GROUNDWATER LEVEL USING A DISCRETE SPACE-STATE MODEL AS AN<br>ALTERNATIVE TO PHYSICALLY BASED GROUNDWATER MODELLING<br>Dilip Kumar Roy, Sujit Kumar Biswas and Khandakar Faisal Ibn Murad  | 506 |
| 5661 | EXPERIMENTAL INVESTIGATION OF RESPONSE OF SEGMENT LINING DUE TO ADJACENT PILE UNDER<br>LOADING<br>Pattanasak Chaipanna, Kisada Trakoonjannak and Pornkasem Jongpradist   | 512 |
| 5663 | THE STUDY ON EFFECT OF LIGHTWEIGHT CONCRETE BLOCK BY WATER HYACINTH ADDING<br>Prang Subpa-Asa, Laemthong Laokongthavorn, Shigeyuki Date  | 516 |
| 5669 | STUDY ON THE PROPERTIES OF CEMENT MILK ADDED WITH BAKING SODA -COMPRESSION<br>STRENGTH ESTIMATION FROM BLEEDING REDUCTION AND INITIAL ELECTRICAL RESISTIVITY<br>Yasuhide Mochida, Joshua O. Ogunbiyi ,Makoto Minemoto,and Keisuke Funato             | 523 |
| 5761 | SHEAR STRENGTH AND PERMEABILITY ANALYSIS OF GEOTEXTILE FROM PINEAPPLE LEAVES AND<br>LUFFA<br>INZ Baharuddin, Hairin Taha, RC Omar, R.Roslan and S.Nadirah  | 529 |
| 5673 | APPLICATION OF WASTE WATER AND GREEN ALGAE<br>TO STRENGTHEN SOIL<br>R.Roslan, RC Omar, INZ Baharuddin, Hairin Taha and M.Syafiq  | 535 |
| 5674 | QUANTITATIVE INTERPRETATION OF LANDSLIDE OCCURRENCE SITE BY AI TECHNOLOGY OF IMAGE<br>CLASSIFICATION AND TOPOGRAPHICAL ANALYSIS MAP CREATED BY AERIAL LASER DATA<br>Koki Sakita, Satoshi Nishiyama, Teruyuki Kikuchi, Junsheng Song and Yuzo Ohnishi | 541 |
| 5681 | LIQUEFACTION MAPPING PROCEDURE DEVELOPMENT: DENSITY AND MEAN GRAIN SIZE<br>FORMULATIONS<br>Abdul Hakam, Bayu Martanto Adji and Junaidi   | 547 |
| 5682 | COMPARISON STUDY ON DAMAGE PATTERN OF TWO STORIES BUILDING: SIMULATION VS<br>FIELD RECORD<br>Febrin Anas Ismail, Abdul Hakam, Hendri Gusti Putra, M Maisaquddus Hape, M Sofian<br>Asmirza  | 553 |
| 5700 | LIQUEFACTION POTENTIAL MAPPING OF THE CITY OF VALENZUELA, PHILIPPINES<br>Angelo S. Enoria, Jr., Sophia Joy Q. San Juan, Hiyasmin F. Ubaldo   | 558 |
| 5702 | THE PROPERTIES OF POROUS CONCRETE PAVING BLOCKS<br>Nurul Rezuana Buyung and Abdul Naser Abdul Ghani  | 562 |
| 5703 | CONSTRUCTING AN ARTIFICIAL INTELLIGENCE MODEL FOR WATER ENVIRONMENT EVALUATION<br>Shengping Zhang and Jie Qi   | 568 |



|      |   |     |
|------|---|-----|
| 5705 | INFLUENCE OF ERRORS THAT RESULT FROM CONSIDERATION OF WATER IN-FLOW DIMENSION DIFFERENCES BASED ON OBSERVATION METHOD FOR MOUNTAIN TUNNEL CONSTRUCTION<br>Yasuyuki Kubota, Moritada Mori, Toru Yasuda, Satoshi Nishiyama                            | 575 |
| 5706 | THE USE OF SAWDUST WASTE ON PHYSICAL PROPERTIES AND THERMAL CONDUCTIVITY OF FIRED CLAY BRICK PRODUCTION<br>Nonthaphong Phonphuak, Anuwat Srisuwan, Must Srila, Siriwan Artbumrung and Panuwat Ruenruangrit  | 581 |
| 5707 | THE VERIFICATION OF DIFFERENCE ANALYSIS IN THE HIGH PRECISION INSPECTION TECHNOLOGY FOR SLOPE SURFACE, USING MOBILE MAPPING SYSTEM<br>Naoto Samori, Satoshi Nishiyama, Koki Sakita, Michinari Fuziki, Naoya Ono and Junsheng Song                   | 587 |
| 5709 | LESSON LEARNED IN MAINTAINING THE PRECAST CONCRETE BUILDINGS<br>Zul-Atfi Ismail   | 593 |
| 5720 | ON THE SEASONAL COLORS AND SMELLS ANALYZING SOCIAL NETWORKING SERVICE<br>Tatsuya Matsuura, Momoko Tanaka, Hayate Deguchi and Kazunari Tanaka  | 599 |
| 5724 | PROPOSED ANGAT RIVER WATER IMPOUNDING AND FLOOD MITIGATION PROJECT<br>Bon Ryan P. Aniban, Roniel C. Naungayan, Sheina R. Pallega  | 602 |
| 5728 | A RISK ASSESSMENT FRAMEWORK FOR HIGH-RISE SCHOOL BUILDING PROJECT IN METRO MANILA, PHILIPPINES<br>Michael V. Almeida and Andres Winston C. Oreta  | 608 |
| 5732 | ASSESSMENT OF DEBRIS FLOW VELOCITY USING A SIMPLE LUMPED MASS MODEL FOR DEBRIS FLOW MOBILIZATION<br>Thapthai Chaithong  | 616 |
| 5739 | DYNAMIC ANALYSIS OF NAILED SLOPE<br>Srinivas Ch, Padmavathi M and Sanjeeva P  | 621 |
| 5741 | SETTLEMENT OF SILTY SOIL UNDER SATURATION USING MICRO SYNTHETIC FIBERS<br>Padmavathi, V. and Rao, P. N.   | 627 |
| 5743 | GROUND IMPROVEMENT USING GEOSYNTHETICS ~ A LITERATURE REVIEW<br>Mohamed Eltaher, Zakaria Hossain, Jim Shiau, and Hajime Takami  | 632 |
| 5745 | STATIC MODEL OF THE PIEZOELECTRIC SELF-ADJUSTING GYROSCOPE-ACCELEROMETER<br>Arif Pashayev, Anvar Hazarkhanov, Toghrul Karimli, Vasif Neymatov   | 640 |
| 5757 | PROPORTION AND PROPERTY SPECIFICATIONS AND STRENGTH BEHAVIOR OF MORTAR USING WOOD ASH AS PARTIAL REPLACEMENT OF LIME<br>Robert Michael Tampus, Janine R. Lardizabal, Dennise Linoel M. Acena, Michaela Angelica M. Uy, and Kenneth Vance R. Arcenal | 647 |
| 5758 | IMPACTS OF WEATHER VARIABLES ON URBAN WATER DEMAND AT MULTIPLE TEMPORAL SCALES<br>Chinnapan Makpiboon, Adichai Pornprommin and Surachai Lipiwattanakarn   | 653 |
| 5760 | GROUNDWATER LEVEL RISE IN MUSCAT AIRPORT AREA AND WAYS OF MANAGING THE ISSUE<br>Luminda Gunawardhana, Mahad Baawain and Ahmed Sana  | 659 |
| 5767 | LIGHTWEIGHT FOAMED CONCRETE INTERLOCKING BLOCK UTILISING UNGROUND OIL PALM ASH<br>Hanizam Awang, Mohammed Zuhair Al-Mulali and Wenny Arminda  | 665 |
| 5768 | FINANCIAL AND INSTITUTIONAL ASPECT FOR APPLICATION OF A CENTRALIZED DOMESTIC WASTEWATER MANAGEMENT SYSTEM IN SUKOLILO DISTRICT, SURABAYA, INDONESIA<br>Dwi Agustiang Ningsih, Eddy Setiadi Soedjono and Nurina Fitriani                             | 671 |
| 5772 | ANALYSIS OF CHANGES IN SHEAR STRENGTH AND STIFFNESS OF HO CHI MINH CITY' SOFT SOIL UNDER THE UNLOADING STRESS PATHS FOR DEEP EXCAVATIONS CALCULATION<br>Trung Ngo Duc, Phan Vo and Thanh Tran Thi   | 677 |

|           |  |            |
|-----------|--|------------|
| 5773      | SELF-SUPPORT SHELTER AS AN ALTERNATIVE SOLUTION IN THE TSUNAMI-PRONE AREA<br>Anas Febrin Ismail, Taufika Ophiyandri, Abdul Hakam, Afdilla Yofianda, Dicky Kurnia Adha, Tria Yuli Anggraini                 | 683        |
| 5774      | GREEN CONCRETE HOLLOW BLOCKS UTILIZING<br>BASIC OXYGEN FURNACE STEEL SLAG<br>Santiago, Karen Joyce B. and Juan, Jose Arnel P.  | 689        |
| 5776      | RESPONSE OF A SINGLE PILE LOCATED ON SLOPING GROUND UNDER DYNAMIC LOADING<br>Deendayal Rathod, D. Nigitha and Krishnanunni K T   | 695        |
| 5777      | BIM-BASED SIMPLIFIED APPROACH TO AUTOMATICALLY ESTIMATE BUILDING COSTS FOR PROJECTS<br>IN THAILAND<br>Suon Tokla, and Kumpon Subsomboon  | 701        |
| 5779      | EMOTIONAL QUOTIENT ASSESSMENT PROGRAM FOR STUDENTS<br>Nualsawat Hiransakolwong   | 707        |
| 5781      | ELECTROMAGNETIC SWITCHING TRANSIENTS IN TRANSMISSION LINE COOPERATING WITH<br>THE LOCAL SUBSYSTEM<br>Pawel Sowa, Daria Macha   | 714        |
| 5784      | SAFETY, CONNECTIVITY, AND COMFORTABILITY AS INDICATORS TO IMPROVE WALKABILITY TO THE<br>BUS STOPS IN PENANG ISLAND<br>Nur Sabahiah Abdul Sukor and Siti Fadhlin Muhammad Fisal                             | 720        |
| 5787      | APPLICATION OF CONDITIONAL CULTURE ALGORITHM AND SIMULATION FOR OPTIMAL RESERVOIR<br>RULE CURVES PROJECTS<br>Anujit Phumiphan and Anongrit Kangrang  | 729        |
| 5791      | A STUDY OF FLOOD FORECASTING AND MAPPING FOR THE ATTANAGALU OYA<br>W.C.P. Wickramarachchi, N.K. Gunasekara, W.C.D.K. Fernando and S.S. Wickramasuriya  | 735        |
| 5793      | LAO KHAM'S VARISCITE PROPERTIES AND APPLICATION IN CHEMICALLY BONDED PHOSPHATE<br>CEMENT<br>Watcharagon Wongkamjan and Thanawat Jumeapaeng   | 741        |
| 5794      | PERFORMANCE EVALUATION OF CONCRETE WITH RECYCLED WASTE POLYPROPYLENE<br>N. Haque, M.J Islam, A. Tahsin & T. Mehdi  | 746        |
| 5809      | LIFE CYCLE COST ANALYSIS FOR REINFORCED GEOGRID RAILWAY TRACK<br>Saad Farhan Ibrahim Alabdullah, Ali Jabbar Kadhim and Harith Basim Khalaf   | 751        |
| 5810      | CHARACTERIZATION OF NEW TYPES OF GEOSYNTHETICS EMBEDDED IN SOIL USING CALIFORNIA<br>BEARING RATIO TEST<br>Mohamed Eltaher, Zakaria Hossain, Jim Shiao, and Hajime Takami                                   | 756        |
| <b>ID</b> | <b><i>Environment</i></b>  | <b>763</b> |
| 5514      | A STUDY ON HUMAN DAMAGE IN EVACUATION FROM TSUNAMICONSIDERING STREET-BLOCKADES<br>CAUSED BY DESTROY OF BUILDINGS<br>Ken-ichi Fujita, Harumi Yashiro  | 764        |
| 5518      | DEVELOPING AGE-FRIENDLY CITY: CASE STUDY FROM DEPOK<br>Fatmah Fatmah   | 770        |
| 5537      | BIOMONITORING OF WATER POLLUTION IN LAKE CHEBARKUL BY THE CONTENT OF HEAVY METALS<br>IN MACROPHYTE ORGANS, RUSSIA<br>I.V. Mashkova, A.M. Kostryukova , E.E. Schelkanova, V.V. Trofimenko and A.I. Slavnaya | 781        |
| 5538      | GROUND REACTION FORCE OF STEP MARCHING: A PILOT STUDY<br>Pairaya Sitthiracha, Wichai Eungpinichpong  | 787        |

|      |  |     |
|------|--|-----|
| 5546 | THE EFFECTS OF WATERING RATES USING THE DRIP IRRIGATION METHOD ON THE ROOT MASS GROWTH OF BIRD'S NEST FERNS<br>Sawat Pimsuwan and Dowroong Watcharinrat  | 791 |
| 5548 | THE INFLUENCES OF HEAVY METALS AND MAJOR IONS IN STREAM WATERS, RUNNING IN SERPENTINE, LIMESTONE, AND CLOSED-MINE AREAS, ON MACROINVERTEBRATE COMMUNITIES, KINKI AND CHUGOKU, JAPAN<br>Akio Nishida and Hiroyuki Ii        | 796 |
| 5551 | LANDSCAPE OPPORTUNITIES AND PREFERENCES FOR CHOOSING RECREATIONAL PLACES OF MEGALOPOLIS RESIDENTS (ON EXAMPLE OF ST. PETERSBURG)<br>Pogodina V., Matveevskaya A., Filippova I., Evseeva L. and Evseev V.                   | 802 |
| 5557 | ANALYSING THE INFLUENCE OF COGNITIVE, AFFECTIVE, CONATIVE AND MOTIVATION ASPECTS ON TRAIN PASSENGER'S DEVIANT BEHAVIOUR: COMMUTER LINE, INDONESIA<br>Ahmad Zubair, Chotib  | 809 |
| 5565 | IMMEDIATE EFFECTS OF THAI MASSAGE ON GAIT SPEEDS AND BALANCE PARAMETERS IN ELDERLY<br>Nutthanun Tatchananusorn, and Wichai Eungpinichpong  | 815 |
| 5570 | A COMPARISON STUDY BETWEEN CHEMICAL COAGULATION AND ELECTRO-COAGULATION PROCESSES FOR THE TREATMENT OF WASTEWATER CONTAINING REACTIVE BLUE DYE<br>Nidaa Adil Jasim, Tamara Kawther Hussein                                 | 821 |
| 5572 | INDOOR PLANT SPECIES SURVIVAL UNDER DIFFERENT ENVIRONMENT IN INDOOR VERTICAL GARDEN<br>Sukanya Chaipong  | 827 |
| 5573 | THE CONSIDERATIONS FOR URBAN DESIGN REGARDING THE PRESENCE OF ONLINE TAXI BIKE<br>Heidy Octaviani Rachman, Chotib and Kemas Ridwan Kurniawan   | 831 |
| 5575 | SERVICE QUALITY GAP ANALYSIS OF WATER SUPPLY IN URBAN AREAS: WATER SUPPLY COMPANY, KABUPATEN BOGOR<br>Armeinita Octavia and Chotib   | 837 |
| 5576 | ISOLATION OF HEAVY METAL DEGRADABLE HALOPHILIC BACTERIA FROM SOIL IN SAMUT SAKHON PROVINCE, THAILAND<br>Jaruwan Chutrtong and Waradoon Chutrtong   | 847 |
| 5579 | FACTORS AFFECTING COMMUNITY PERCEPTION AROUND BETAWI CULTURE TOURISM ACTIVITIES SETU BABAKAN JAKARTA SELATAN<br>Dwinanto and Chotib  | 852 |
| 5591 | QUALITY OF VERICOMPOST BY Pheretima peguana On Different Organic Wastes<br>Pornpailin Boonna, Nipapun Kungskulniti, Rochana Tangkoonboribun, Naowarut Charoenca  | 858 |
| 5592 | EVALUATION OF METHANE AND CARBON DIOXIDE EMISSIONS FROM LIVESTOCK WASTE, COMPOST, AND BIOGAS SLUDGE<br>Ambar Pertiwinigrum, Margaretha Arnita Wuri, Dina Setiyana, Benito Heru Purwanto, Andang Widi Harto and Misri Gozan | 863 |
| 5597 | STUDY ON ELUTION REDUCTION OF HEXAVALENT CHROMIUM FROM RECYCLED BASE COURSE MATERIAL USING WASTE SYRUP<br>Keiichiro Shibata, Hidenori Yoshida, Hiroki Yokoyama, Shinichiro Okazaki and Matsumoto Naomichi                  | 868 |
| 5599 | GEOINFORMATICS OF TUBERCULOSIS (TB) DISEASE IN JAKARTA CITY YEAR 2017<br>Titin Siswantining, NPC Purwandani, MHD Susilowati, and Adi Wibowo  | 874 |
| 5610 | SPATIAL AND TEMPORAL PATTERN OF SOIL CONSERVATION IN MOUNTAIN ECOSYSTEM: CASE STUDY OF PATUHA MOUNTAIN, WEST JAVA – INDONESIA<br>Satia Nisa Firdhauzi, Astrid Damayanti, Jarot Mulyo Semedi, Muhammad Dimyati              | 879 |

|      |  |     |
|------|--|-----|
| 5621 | SPATIO-TEMPORAL RICE PHENOLOGY USING UAV IN PARAKAN SALAK, SUKABUMI REGENCY, INDONESIA<br>Rokhmatuloh, Supriatna, Adi Wibowo and Iqbal Putut Ash Shidiq  | 885 |
| 5622 | RICE PRODUCTIVITY ESTIMATION BY SENTINEL-2A IMAGERY IN KARAWANG REGENCY, WEST JAVA, INDONESIA<br>Suprianta, Rokhmatuloh, Adi ibowo and Iqbal Putut Ash Shidiq                                      | 889 |
| 5625 | EFFECTS OF OZONE SPARGING ON GROUNDWATER PHYSICALCHEMICAL PARAMETERS DURING IN SITU REMEDIATION OF A SITE CONTAMINATED WITH CHLORIDES<br>Erica Kotani Caram and Maria Eugênia Gimenez Boscov       | 893 |
| 5641 | DAIRY WASTEWATER TREATMENT BY VERMI-BIOFILTRATION<br>Rabee Rustum, Shebin Akbar K and Adebayo J. Adeloye   | 899 |
| 5643 | System Dynamic Modelling for Sword and White Pomfret Fish Resources at Depok Coast, Bantul Regency<br>Dewi Susiloningtyas, Hengki Tasman, Tuty Handayani and Arti Aulia                            | 904 |
| 5651 | FRESH PROPERTIES PERFORMANCE OF ALKALINE ACTIVATED PALM OIL PASTE<br>Aidan N, Nuradila Izzaty H, Muhd Norhasri M.S, Sharifah A   | 909 |
| 5652 | ANALYSIS OF THE PERFORMANCE AND ELEMENTAL ANALYSIS ON LIME ACTIVATOR POFA<br>Nuradila Izzaty H, Aidan N, Muhd Norhasri M.S, Sharifah A   | 914 |
| 5658 | PHYSICAL AND CHEMICAL PROPERTIES OF WATER: CASE OF TAAL LAKE, PHILIPPINES<br>Merlita C. Medallon, Ed.D. & Enrico Garcia  | 918 |
| 5672 | DURABILITY STUDY OF MALAYSIA ROCK MASS FOR TUNNELLING CONSTRUCTION<br>RC Omar, R.Roslan, INZ Baharuddin, Hairin Taha and Vigneswaran V   | 926 |
| 5675 | H2 PRODUCTION FROM LACTIC ACID RICH MEDIUM AND CASSAVA STARCH WASTEWATER BY Klebsiella pneumoniae subsp. Pneumonia<br>Piyawadee Saraphirom, Napapach Chainamom, Piyarat Namsena                    | 931 |
| 5676 | OPTIMIZATION OF PARAQUAT DEGRADATION WITH MICROBIAL CONSORTIUM FROM CONTAMINATED SOIL USING STATISTIC METHOD<br>Mullika Teerakun Alissara Reungsang Monrodee Chaowarat and Piyawadee Saraphirom    | 937 |
| 5683 | CRAFTING A THEORETICAL FRAMEWORK ON WASTE MANAGEMENT: A CASE FOR SUSTAINABLE CITIES<br>Jennie Lagman-Bautista  | 943 |
| 5689 | HUMAN BEHAVIOUR AND WORKPLACE SAFETYOF READY-MADE GARMENT FACTORIES IN DHAKA DURING FIRE: A CURRENT SCENARIO<br>A S M Fahad Hossain, Ishraq Tasnim Hossain and Prof. Dr. Mehedi Ahmed Ansary       | 948 |
| 5698 | ULTRAFINE PARTICLE FILTER DESIGN FOR MOTORCYCLE EMISSION EXHAUST SYSTEM: A HIGH VOLTAGE ELECTROSTATIC-BASED SYSTEM<br>Arinto Y. P. Wardoyo, Hari A. Dharmawan, Muhammad Nurhuda, and Arif Budianto | 954 |
| 5711 | EXPERIMENTAL STUDY ON SOIL IMPROVEMENT OF COHESIVE SOIL FOR CONSTRUCTION FIELD<br>Shoji Kamao  | 960 |
| 5721 | ANALYSIS OF HABITAT AREA FOR ENDANGERED SPECIES USING MAXENT BY ROAD CONSTRUCTION AND HOUSING LAND DEVELOPMENT IN CHIBA, JAPAN<br>Hideyuki Ito, Koji Hayakawa, Makoto Ooba and Takahiro Fujii      | 964 |



|      |  |      |
|------|--|------|
| 5726 | SOLID WASTE GENERATION IN THE PHILIPPINES: A CORRELATIONAL ANALYSIS ON ECONOMIC AND SOCIAL METRICS<br>Jennie Lagman-Bautista   | 970  |
| 5742 | ANALYSIS ON SPATIAL USE AND LAND USE IN NORTH JAKARTA ADMINISTRATIVE CITY<br>Galih Jati Utomo, Hafid Setiadi, Rudy P. Tambunan and Komara Djaja  | 976  |
| 5744 | THE PATHWAY TO THE ORGANIZATION SUSTAINABILITY THROUGH THE LAND FOOTPRINT METHOD<br>Karin Kandananond  | 986  |
| 5748 | DESIGN AND ASSESSMENT OF A BATTERY OPERATED ROTARY TYPE LOW COST WEEDER FOR NON-CHEMICAL UP-LAND CROP MANAGEMENT<br>Mohammad Ashrafuzzaman Gulandaz, Dr. Md. Israil Hossain, Dr. Md. Ayub Hossain                | 990  |
| 5761 | SHEAR STRENGTH AND PERMEABILITY ANALYSIS OF GEOTEXTILE FROM PINEAPPLE LEAVES AND LUFFA<br>INZ Baharuddin, Hairin Taha, RC Omar, R.Roslan and S.Nadirah   | 998  |
| 5762 | PARTICIPATION IN WASTE MANAGEMENT BY UNDERGRADUATE STUDENTS OF RAJAMANGALA UNIVERSITY OF TECHNOLOGY THANYABURI<br>Korntouch Kosidphokin  | 1004 |
| 5763 | ENVIRONMENTAL MANAGEMENT FOR GREEN UNIVERSITY BASED ON THE UI GREEN METRIC OF UNIVERSITY SUCCEED<br>Korntouch Kosidphokin  | 1008 |
| 5764 | INVESTIGATING OZONE LEVELS IN MUSCAT AREA, OMAN BY USING ARTIFICIAL NEURAL NETWORKS<br>Mahad Baawain, Hasina Al-Hinai and Abdullah Almamun   | 1014 |
| 5769 | STUDY ON MUSRENBANG MECHANISM IN INDONESIA TO PROMOTE SANITATION<br>Eddy Soedjono , Wahyu Wijaya and Nurina Fitriani   | 1019 |
| 5770 | THE IMPACT OF EXPOSURE TO AEROSOL MOSQUITOES REPELLENT RELATED TO FREE RADICALS ON THE ORGANS OF MALE RATS<br>Unggul P. Juswono, Arinto Y. P. Wardoyo, Chomsin S. Widodo, Johan A. E. Noor, and Didik R. Santoso | 1024 |
| 5782 | VARIATIONS IN WATER QUALITY ALONG ACIDIC RIVERS IN VOLCANIC AREAS OF EASTERN JAPAN<br>Takeshi Saito and Naoki Watanabe   | 1030 |
| 5792 | WATER FOOTPRINT OF RICE IN MYAUNGMYA TOWNSHIP, MYANMAR<br>May Myo Han  | 1035 |
| 5797 | THE EFFECT OF INSIDE CIRCUMSTANCE OF THE HAZARDOUS WASTE LANDFILL ON THE LEACHING BEHAVIOR OF HARMFUL HEAVY METALS<br>Yasumasa Tojo, Taira Ikeda, Takayuki Matsuo and Toshihiko Matsuto                          | 1040 |
| 5798 | COSTS AND BENEFITS OF USING PARABOLIC GREENHOUSE SOLAR DRYERS FOR DRIED HERB PRODUCTS IN THAILAND<br>Samatcha Krungkaew, Kanokwan Kingphadung, Suphaphat Kwonpongsagoon, Busarakorn Mahayothee                   | 1045 |
| 5804 | AIR POLLUTION CONCENTRATION AND COST FOR THE DIFFERENT ROAD CORRIDORS<br>LasminiAmbarwati, Amelia K. Indriastuti   | 1051 |
| 5805 | MICROBIOLOGICAL AND CHEMICAL PROPERTIES OF THE CHI RIVER, MAHA SARAKHAM PROVINCE, THAILAND<br>Yuwadee Insumran, Jackaphan Sriwongsa, Panuwat Ruenruangrit and Supattra Chinakool                                 | 1057 |

|      |   |                    |
|------|---|--------------------|
| 5807 | EFFECTS OF CLIMATE CHANGE ON MILK YIELD AND MILK COMPOSITION IN THAI CROSSBRED HOLSTEIN COWS<br>Doungnapa Promket, Wootichai Kenchaiwong, and Khanitta Ruangwittayanusorn | <b>1062</b>        |
| 5671 | STEADY STATE GROUNDWATER FLOW MODEL OF WADI SAMAIL CATCHMENT<br>Sharifa AL-Hashmi, Luminda Hewawasam, Ahmed Sana and Mahad Baawain  | <b><u>1067</u></b> |

## Preface

On behalf of the SEE 2019 Organizing Committee, it is our great pleasure to welcome you to the Fifth International Conference on Science, Engineering & Environment (SEE2019) will be held in Bangkok on Nov. 11-13, 2019, Thailand in conjunction with Suranaree University of Technology, Mie University Research Center for Environmental Load Reduction, The GEOMATE International Society, Useful Plant Spread Society, Glorious International, AOI Engineering, HOJUN, JCK, CosmoWinds and Beppu Construction, Japan..

The conference covers three major themes with many specific themes including:

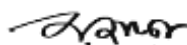
| Engineering  | Science   | Environment  |
|--|---|--|
| <ul style="list-style-type: none"> <li>· Environmental Engineering</li> <li>· Chemical Engineering</li> <li>· Civil and Structural Engineering</li> <li>· Computer Software Web Engineering</li> <li>· Electrical and Electronic Engineering</li> <li>· Energy and Thermal Engineering</li> <li>· Aerospace Engineering</li> <li>· Agricultural Engineering</li> <li>· Biological Engineering and Sciences</li> <li>· Biological Systems Engineering</li> <li>· Biomedical and Genetic Engineering</li> <li>· Bioprocess and Food Engineering</li> <li>· Geotechnical Engineering</li> <li>· Industrial and Process Engineering</li> <li>· Manufacturing Engineering</li> <li>· Mechanical and Vehicle Engineering</li> <li>· Materials and Nano Engineering</li> <li>· Nuclear Engineering</li> <li>· Petroleum and Power Engineering</li> <li>· Forest Industry Engineering</li> </ul> | <ul style="list-style-type: none"> <li>· Environmental Sciences</li> <li>· Chemistry and Chemical Sciences</li> <li>· Fisheries and Aquaculture Sciences</li> <li>· Astronomy and Space Sciences</li> <li>· Atmospheric Sciences</li> <li>· Botany and Biological Sciences</li> <li>· Genetics and Bacteriology</li> <li>· Forestry Sciences</li> <li>· Geological Sciences</li> <li>· Materials Science and Mineralogy</li> <li>· Statistics and Mathematics</li> <li>· Microbiology and Medical Sciences</li> <li>· Meteorology and Palaeo Ecology</li> <li>· Pharmacology</li> <li>· Physics and Physical Sciences</li> <li>· Plant Sciences and Systems Biology</li> <li>· Psychology and Systems Biology</li> <li>· Zoology and Veterinary Sciences</li> </ul> | <ul style="list-style-type: none"> <li>· Environmental Technology</li> <li>· Recycle Solid Wastes</li> <li>· Environmental dynamics</li> <li>· Meteorology and Hydrology</li> <li>· Atmospheric and Geophysics</li> <li>· Physical oceanography</li> <li>· Bio-engineering</li> <li>· Environmental sustainability</li> <li>· Resource management</li> <li>· Modelling and decision support tools</li> <li>· Institutional development</li> <li>· Suspended and biological processes</li> <li>· Anaerobic and Process modelling</li> <li>· Modelling and numerical prediction</li> <li>· Interaction between pollutants</li> <li>· Water treatment residuals</li> <li>· Quality of drinking water</li> <li>· Distribution systems on potable water</li> <li>· Reuse of reclaimed waters</li> </ul> |

As expected, this year we have received many submissions from different countries all over the world. The technical papers were selected from the vast number of contributions submitted after a review of the abstracts. The final papers in the proceedings have been peer reviewed rigorously and revised as necessary by the authors. It relies on the solid cooperation of numerous people to organize a conference of this size. Hence, we appreciate everyone who support as well as participate in the joint conferences.

Last but not least, we would like to express our gratitude to all the authors, session chairs, reviewers, participants, institutions and companies for their contribution to SEE 2019. We hope you enjoy the conference and find this experience inspiring and helpful in your professional field. We look forward to seeing you at our upcoming conference next year.

Best regards,


Prof. Dr. Zakaria Hossain, Chairman



Prof. Dr. Suksun Horpibulsuk, Conference Chairman



Dr. Jim Shiau, USQ, Australia (Assistant to Chairman)



## **Organization**

### *Scientific Committees:*

Honorary Chairman: Dr. Sohji Inoue, E/Prof. Mie University, Japan  
Dr. Suksun Horpibulsuk, Prof. Suranaree University of Tech., Thailand (Program)  
Dr. Zakaria Hossain, Prof. Mie University, Japan (General)  
Assistant to Chairman Dr. Jim Shiau, University of Southern Queensland, Australia

### *Conference Organizing Committee:*

Dr. Suksun Horpibulsuk, Prof. Suranaree Uni of Tech (Chair)  
Dr. Zakaria Hossain, Prof. Mie University, Japan (Chair)  
Dr. Jim Shiau, USQ, Australia (Assistant to Chairman)  
Dr. Satoshi Kaneco, Prof., Mie University, Japan (Co-Chair)  
Dr. Sohji Inoue, E/Prof. Mie University, Japan (Co-Chair)  
Dr. Toshinori Sakai, Prof. Mie University, Japan (Co-Chair)  
Dr. Takamitsu Kajisa, Prof. Mie University, Japan (Co-Chair)  
Dr. Masaaki Kondo, A/Prof. Mie University, Japan (Co-Chair)

### *National & International Advisory Committee:*

Dr. Fumio Tatsuoka, Prof., Tokyo University of Science, Japan Dr.  
Junichiro Takeuchi, Prof., Kyoto University, Japan  
Dr. Kingshuk Roy, Prof., Nihon University, Japan  
Dr. Nakib Dad Khan, A/Prof. Mie University, Japan  
Dr. Sai Vanapalli, Prof., University of Ottawa, Canada  
Dr. Musharraf Zaman, Prof. Univ. of Oklahoma, USA  
Dr. Rafiqul Tarefder, Prof. University of New Mexico, USA  
Dr. M. Bouassida, Prof., National Sch. of Engg. of Tunis  
Dr. L.R. Austriaco, Prof., Angeles Univ. Found., Philippines  
Dr. A.S.M. Abdul Awal, Prof., Univ. Technology Malaysia  
Dr. M. Ibn Ibrahimy, Prof., Int. Islamic Univ., Malaysia  
Dr. Mohammad Shariful Islam, Prof., BUET, Bangladesh.  
Dr. Bujang B.K. Huat, Prof., Univ. Putra Malaysia  
Dr. Nemy Banthia, Prof., UBC, Canada  
Dr. Ian Jefferson, Prof., Univ. of Birmingham, UK  
Dr. John Bolander, Prof., Univ. of California, USA  
Dr. Shamsul Chowdhury, Prof., Roosevelt Univ., USA  
Dr. Isabel Pinto, Prof., University of Coimbra, Portugal  
Dr. Mark Jaksa, Prof., University of Adelaide, Australia  
Dr. Hj. Ramli Bin Hj. Nazir, A/Prof., UTM, Malaysia  
Dr. M.S. Hossain, Prof., International Islamic Univ. Bangladesh  
Dr. Md. Ariful Islam, A/Prof. Dhaka University, Bangladesh  
Dr. Md. Nurul Amin, Prof. Dhaka University, Bangladesh



*International Technical Program Committee:*

Prof. Adolf Heinrich Horn, Geological Institute - Federa University of Minas Gerais, Brazil  
Prof. Bang-Fuh Chen, National Sun Yat-sen University, Taiwan  
Prof. Bindeshwar Singh, Kamla Nehru Institute of Technology, India  
Prof. Catherine Mulligan, Concordia Institute of Water, Energy and Sustainable Systems, Canada  
Prof. Chi-Min Liu Chienkuo Technology University, Taiwan  
Prof. Daffalla Rabih, Kenana Sugar Company, Sudan  
Prof. Essaid Bilal, Ecole Nationale Supérieure Des Mines De Saint Etienne, France  
Prof. Hakan Caliskan, Usak University, Faculty of Engineering, Turkey  
Prof. Ibrahim Maiyza, National Institute of Oceanography & Fisheries, Egypt  
Prof. Loc Nguyen, Sunflower Soft Company, Vietnam  
Prof. Marilia Hagen, Indiana University, United States  
Prof. Md Najib bin Ibrahim, Universiti Teknologi MARA, Malaysia  
Prof. Md. Abdul Baset Mia, BSMR Agri. Univ., Bangladesh  
Prof. Mihaela Popescu, University of Craiova, Romania  
Prof. Mohamed Abdou, Faculty of Education Department of Mathematics, Egypt  
Prof. Mohamed Tahiri, Présidence de l'Université Hassan II de Casablanca, Morocco  
Prof. Nazar Oukaili, University of Baghdad, Iraq  
Prof. Radim Cajka, Technical University Ostrava, Faculty of Civil Engineering, Czech Republic  
Prof. Rajaraman Jambunathan, AMET University, India  
Prof. Saad Farhan Ibrahim Alabdullah, University of Almustansiriyah, Iraq  
Prof. Salem Alsanusi, Benghazi, Libya  
Prof. Sudhir Kumar Das, Retired Senior Project Manager of Indian Railways, India  
Prof. Zachary Senwo, Alabama A&M University, United States  
Prof. Imed Jabri, University of Tunis, Tunisia  
A/Prof. Bindeshwar Singh Kamla Nehru Institute of Technology, India  
A/Prof. Hasi Rani Barai, Yeungnam University, South Korea  
A/Prof. Jamaluddin Mahmud, Universiti Teknologi MARA, Malaysia  
A/Prof. Mohamed Ramadan, University of Hail, Saudi Arabia  
A/Prof. Najam Hasan, Dhofar University, Oman  
A/Prof. Nosina Krishna Chaitanya, Jawaharlal Nehru Technological University, India  
A/Prof. Nurbek Saparkhojayev, Almaty Management University, Kazakhstan  
A/Prof. Pandian Vasant, Universiti Teknologi Petronas, Malaysia  
A/Prof. Teodor Lucian Grigorie, University of Craiova, Romania  
A/Prof. Zawawi Daud, Universiti Tun Hussein Onn Malaysia  
A/Prof. Abdull Halim Abdul, Oil and Gas department, Malaysia  
A/Prof. Baoping Cai, China University of Petroleum, China  
A/Prof. Dariusz Jakóbczak, Koszalin University of Technology, Poland  
A/Prof. Edgar Allan Mendoza, University of the Philippines  
A/Prof. Lakhveer Singh, Universiti Malaysia Pahang (UMP) Malaysia, Malaysia  
A/Prof. Lidia Sas Paszt, Research Institute of Pomology, Poland  
A/Prof. Mahmood Barbooti, University of Technology, Iraq  
A/Prof. Majid Mirzaei, Universiti Tunku Abdul Rahman, Malaysia  
A/Prof. Najeh Lakhroua, University of Carthage, Tunisia  
A/Prof. Ryan Joseph Calinao, Lyceum of the Philippines University-Laguna  
A/Prof. Sarawut Thepanondh, Mahidol University, Thailand  
A/Prof. Yasir Al Hussein, Jerash University, Faculty of Engineering, Jordan  
A/Prof. Grigorie Teodor Lucian, University of Craiova, Romania  
A/Prof. Hêriş Golpîra, Islamic Azad University, Sanandaj, Iran  
A/Prof. Muhammad Aslam, King Abdulaziz University, Saudi Arabia  
A/Prof. Tomasz Plech, Medical University of Lublin, Poland  
A/Prof. Fellah Mamoun, Abbes laghrour University, Algeria  
A/Prof. R. S. Ajin, GeoVin Solutions Pvt. Ltd., India  
A/Prof. Roman Szewczyk, Industrial Research Institute for Automation and Measurements, Poland

Dr. Abolghasem Akbari, University Malaysia Pahang, Malaysia  
 Dr. Ahmad Safuan A Rashid, Universiti Teknologi Malaysia, Malaysia  
 Dr. Akinola Johnson Olarewaju, Federal Polytechnic Ilaro, Ogun State, Nigeria  
 Dr. Alexandre Costa, Federal University of the valleys of Jequitinhonha and Mucuri, Brazil  
 Dr. Angelo Gallone, Scotland's Rural College (SRUC), United Kingdom  
 Dr. Azizul Azhar Ramli, Universiti Tun Hussein Onn Malaysia  
 Dr. Bashir Dar, University of kashmir Delina Baramulla J&K India, India  
 Dr. Bassam Abdellatif, National Authority for Remote Sensing and Space Sciences, Egypt  
 Dr. Binh Phu Nguyen, National University of Singapore, Singapore  
 Dr. Cazacu Gabriela, S.C. Geotech Dobrogea, Romania  
 Dr. Chengen Yang, Intel Corporation, United States  
 Dr. Dayang Norulfairuz Abang Zaidel, Universiti Teknologi Malaysia  
 Dr. Evgeni Starikov, KIT, Karlsruhe, Germany; Chalmers, Gothenburg Sweden, Germany  
 Dr. Fatma Khanchel, University of Tunis El Manar, Tunisia  
 Dr. Hamidreza Khataee, Griffith University, Australia  
 Dr. Hêriş Golpîra, Islamic Azad University, Iran  
 Dr. Iskhaq Iskandar, Dept. Physics, University of Sriwijaya, Indonesia  
 Dr. Jingwei Zhao, University of Wollongong, Australia  
 Dr. Jitendra Agrawal, Rajiv Gandhi Proudhyogiki Vishwavidyalaya, India  
 Dr. Liza Patacsil, Malayan Colleges Laguna, Philippines  
 Dr. Mohamed Amine, Ferrag Guelma University, Algeria  
 Dr. Mohd Afendi Rojan, Universiti Malaysia Perlis, Malaysia  
 Dr. Mohd Altaf, University of kashmir Delina Baramulla J&K India, India  
 Dr. Mohd Hairy Ibrahim, Sultan Idris Education University, Malaysia  
 Dr. Mostafa Khater, Egypt - El sharqia - Zagazig, Egypt  
 Dr. Najam Hasan, Dhofar University, Oman  
 Dr. Namir Alkawaaz, University of Almustansiriyah, Iraq  
 Dr. Nashrul Fazli Mohd Nasir, Universiti Malaysia Perlis, Malaysia  
 Dr. Naufal Mansor Kampus Umiciti Alam, Universiti Malaysia Perlis (UniMAP), Malaysia  
 Dr. Obed Majeed Ali, Northern Technical University, Iraq  
 Dr. Piyapong Janmaimool, King Mongkhut' University of Technology, Thailand  
 Dr. Po-Sheng Chiu, National Cheng Kung University, Taiwan  
 Dr. Prabu Mohandas, Adhiyamaan College of Engineering, India  
 Dr. Raman Kumar, D A V Institute of Engineering and Technology, India  
 Dr. Riccardo Colella, University of Salento, Italy  
 Dr. Rolando Javellonar, Romblon State University, Philippines  
 Dr. Shikha Agrawal, Rajeev Gandhi Technical University, India  
 Dr. Stefania Tomasiello CORISA, University of Salerno, Italy  
 Dr. Sumiyyah Sabar, Universiti Sains Malaysia, Malaysia  
 Dr. Suphaphat Kwonpongsagoon, Mahidol University, Thailand  
 Dr. Wei Hong Tan, Universiti Malaysia Perlis, Malaysia  
 Dr. Yoshiro Fujii, Shin Kobe Dental Clinic, Japan  
 Dr. Yuk Feng Huang, Universiti Tunku Abdul Rahman (UTAR), Malaysia  
 Dr. Zongyan Zhou, Monash University, Australia  
 Dr. Purnanand Savoikar, Goa Engineering College, India  
 Dr. Ahmed Toaha Mobashsher, University of Queensland, Australia  
 Dr. Chupong Pakpum, Maejo University  
 Dr. Emanuele Quaranta, Politecnico di Torino, Italy  
 Dr. Jiangling Yin, Apple Inc., Cupertino, CA, United States  
 Dr. Khor Shing Fhan, Universiti Malaysia Perlis, Malaysia  
 Dr. Mario Chauca, Ricardo Palma University, Peru  
 Dr. Santosh Gaikwad, Model College, Ghansawangi, India  
 Dr. Tse Guan Tan, Universiti Malaysia Kelantan  
 Dr. Vikas Panthi, National Institute of Technology, India  
 Dr. Watoo Phrompittayarat, Naresuan University, Thailand

Dr. Hamidreza Namazi, Nanyang Technological University, Singapore  
Dr. Parichat Phumkhachorn, Ubon Ratchathani University, Thailand  
Dr. Subhasis Roy, University of Calcutta, India

*Conference Correspondence:*

Prof. Dr. Zakaria Hossain (Director)  
Dept. of Environmental Science and Technology, Mie University, Japan  
E-mail: conference@geomate.org  
Tel & Fax: +81-59-231-9578

*Editorial and Executive Committee:*

Prof. Dr. Zakaria Hossain  
Dr. Jim Shiau  
Engr. Jamie Ovia  
Engr. Mohamed Mahmoud Ahmed Eltaher

## ***Keynote Papers***

## A CONCRETE WALL ELEMENT TEST TO EVALUATE COMPRESSIVE FRACTURE ENERGY

Tetsuya Ohmura<sup>1</sup>, Kyouhei Iwasaki<sup>1</sup> and Hiroaki Matsufuji<sup>1</sup>

<sup>1</sup>Faculty of Architecture, Tokyo City University, Japan;

### ABSTRACT

Concrete walls are significantly effective seismic elements to resist lateral force due to an earthquake, because they have much stiffness and strength. A building with a number of concrete walls would be generally designed for just the strength. On the other hand, a building with a few of concrete walls would be designed for not only the strength but also the ductility. In other words, the ductility of a concrete wall is the key thing considering the survey reports of concrete walls damaged by an earthquake. Generally speaking, the ductility of a concrete building depends on the ductility of the concrete with rebar. According to some previous studies, the fracture energy was focused to evaluate the ductility. However, their test specimen were cylindrical columns, not to target for a concrete wall. In this paper, the ductility of a concrete wall is focused and test the specimen of a concrete wall element. The fracture energy of a concrete wall element was examined, the thickness of a wall and the amount of their rebar were evaluated.

*Keywords: Concrete wall, Ductility, Element test, Concrete strain*

### INTRODUCTION

Lateral strength and ductility significantly depend on the property of the concrete strain softening. It is well-known that the stress decreasing is controlled even in the post peak in the confined concrete with rebar. The column well-confined by rebar has great ductility and hardly collapsed even after a maximum considered earthquake (MCE). The strength of the girder well-confined by rebar is not decreased as well. Those are based on a number of technical reports, and the amount of the rebar is estimated due to the Japanese code.

The depth of the concrete wall is much larger than one of the concrete column. Therefore, the concrete strain at the end of the compressive area at the peak is significantly large, and the compressive area would be developed at the post peak.

The accurate concrete model considered the strain softening is needed to estimate the lateral strength and the ductility of a concrete wall, and the way to estimate the rest of the lateral and axial strength after MCE is expected.

FE analysis is often used to simulate the lateral strength, damage and ductility under an earthquake loading, and to easily have the data that is hard to measure at the test. In addition, parametric analyses could be performed after being verified.

Not to mention, the concrete model is consequence in a FE analysis and sufficient verification must be needed for the material property with compressive fracture energy

For example, Drucker Prager fracture criterion and Mohr-Coulomb fracture criterion were well-known to estimate their maximum compressive stress.

Rots <sup>[1]</sup> defined the effective band width with integrated point of 4 was two times of root of the element area.

Nishiyama and Watanabe et al. <sup>[2]</sup> examined the relationship between stress and strain of the axial and transverse for the concrete cylinder with 135mm of diameter in the concrete strength of 25 to 83 N/mm<sup>2</sup>.

Priestley and Park <sup>[3]</sup> suggested the model with strain softening for a concrete cylinder and a cuboid with enough transverse rebar under one-way cyclic loading.

Higai and Nakamura <sup>[4]</sup> suggested the compressive fracture energy was 8.8 times of concretes strength and the compressive fracture zone length of 1,300 divided by the root of the concrete strength based on the test data of cylinder with no transverse rebar, concrete strength of 11 to 52 N/mm<sup>2</sup> and the diameter of 100 to 150mm and height of 100 to 600mm.

Niwa et al. <sup>[5]</sup> suggested the equation of the fracture zone length and compressive fracture energy based on the test data of cylinder with no transverse rebar, concrete strength of 26 to 48N/mm<sup>2</sup> and the diameter of 100mm, the height of 200 to 800mm.

Koshikawa et al. <sup>[6]</sup> suggested compressive zone length and compressive fracture energy based on the test data of cylinder with no transverse rebar, concrete strength of 29 to 36N/mm<sup>2</sup> and diameter of 100 to 200mm, height of 200 to 600mm.

Their specimen shape mentioned above were cylinder and cuboid for making not a wall but a column concrete model. The fracture energy and fracture zone length of wall in former studies haven't been referred and they are not obvious.

Moreover, the confined effect of the transverse rebar in their cylinders might be definitely different from the one of the vertical and horizontal rebar in a wall.

In this paper, several wall element tests were performed for a concrete wall. The concrete strain softening property was examined and the fracture energy was focused for a wall element with vertical and horizontal rebar.

## TEST

## Specimen

Specimen are shown in Table 1. The number of all of specimen was four. The common factors are concrete material, the width and depth. The parameters are the wall thickness and the rebar ratio ( $p_w$ ). The wall thickness is 150 or 180mm. The rebar is located single or double.  $p_w$  is 0.24 to 1.11 percent. The diameter of rebar is #3 to #5.

Specimen geometrics are shown in Fig. 1. The wall consists of the confined area (Focused area), the extra area and stub. The concrete was cast from top.

Table 1 Specimen

| # | Name       | t (mm) | $f'_c$<br>(N/mm <sup>2</sup> ) | $P_w$ (%) | Rebar         |
|---|------------|--------|--------------------------------|-----------|---------------|
| 1 | 150-21-024 | 150    | 20.7                           | 0.24      | #3(D10)@200-S |
| 2 | 180-21-039 | 180    |                                | 0.39      | #3(D10)@200-D |
| 3 | 180-21-071 |        |                                | 0.71      | #4(D13)@200-D |
| 4 | 180-21-111 |        |                                | 1.11      | #5(D16)@200-D |

Note: S and D indicate single and double rebar respectively. t: Thickness

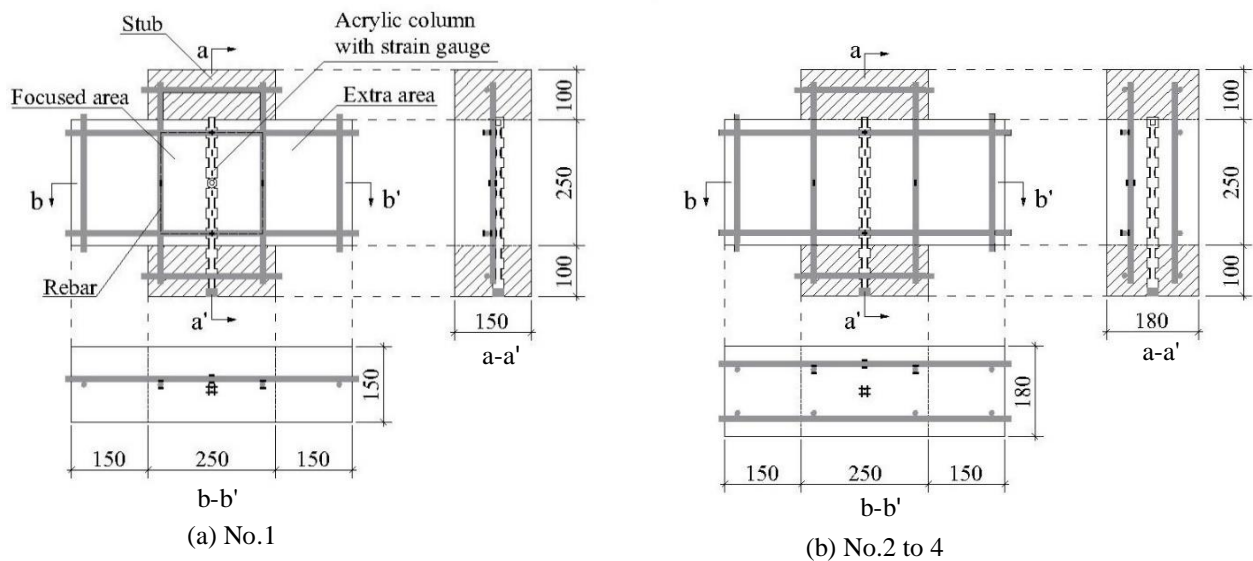


Fig. 1 Specimen geometrics

Table 2 The material property

| a) Concrete |                                |                         |  | b) Rebar |                                      |                     |  |  |
|-------------|--------------------------------|-------------------------|--|----------|--------------------------------------|---------------------|--|--|
|             | $f'_c$<br>(N/mm <sup>2</sup> ) | Strain at $f'_c$<br>(%) | Young modulus<br>(kN/mm <sup>2</sup> ) | Rebar    | Yield stress<br>(N/mm <sup>2</sup> ) | Yield strain<br>(%) | Young modulus<br>(kN/mm <sup>2</sup> ) | Tensile strength<br>(N/mm <sup>2</sup> ) |
| Wall        | 20.7                           | 0.1955                  | 20.9                                   | #3 (D10) | 362                                  | 0.2123              | 170                                    | 495                                      |
| Stub        | 43.4                           | 0.1982                  | 29.4                                   | #4 (D13) | 352                                  | 0.1998              | 176                                    | 481                                      |
|             |                                |                         |  | #5 (D16) | 351                                  | 0.2056              | 171                                    | 501                                      |

## Material property

The material property of concrete and rebar is shown in Table 2. The compressive strength of the cylinder with 100mm of the diameter and 200mm of the height ( $f'_c$ ) was 20.7 N/mm<sup>2</sup> for the wall and 43.4N/mm<sup>2</sup> for the stub.

## Loading

Repeated compressive load was applied via the rigid body of the top and bottom of the specimen by 2,000kN amsler testing machine.

Loading plan is shown in Fig. 2. The repeated compressive load was unloaded at the one-third and two-third of the  $f'_c$  on the material test. Next, it was unloaded at every 10% decreased load after the maximum load.

## Measurement

The measurement plan is shown in Fig. 3. The compressive load ( $P$ ) and the vertical displacement at the center of the specimen were measured by the load

cell and the displacement gage, respectively. The acrylic column with the strain gages was located at the center of the specimen. The strain gages were measured via a data logger as the same strain of the concrete, because of the ruggedness shape of the acrylic column.

## TEST RESULTS

### Load and displacement

The enveloped curve of the relationship between the compressive load and the displacement are shown in Fig. 4. The compressive displacement ( $\delta$ ) of the specimen was defined as the two time of the displacement at the center without the elastic displacement of the rigid body.

The comparison of the enveloped curve between No.1 and 2 are shown in Fig. 4(a). The displacement at the maximum load ( $P_{max}$ ) of No.1 with 150mm thickness and single rebar was larger than one of No.2 with 180mm thickness and double rebar.

For No.1, the displacement of 2.1mm was meas-

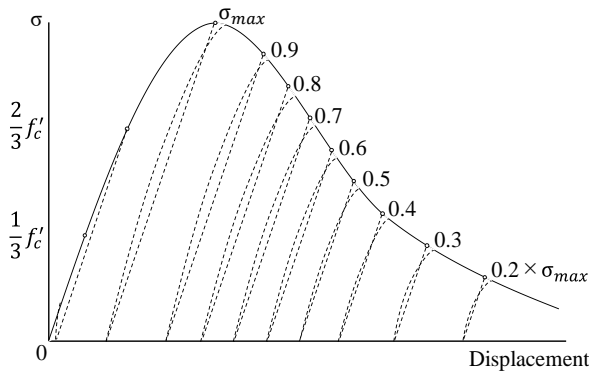


Fig. 2 Loading plan

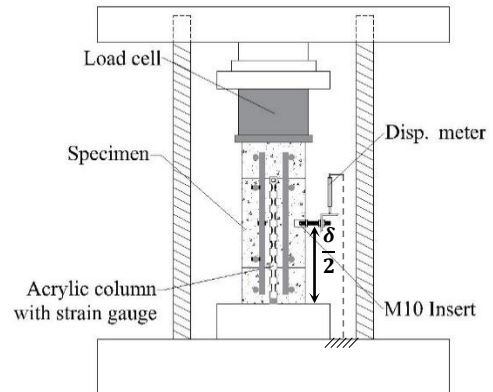
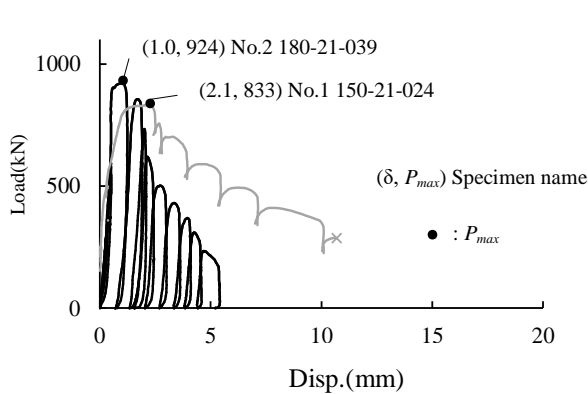
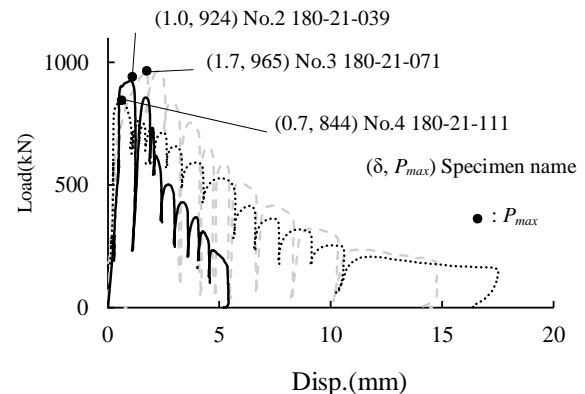


Fig. 3 The measurement



(a) No.1, 2



(b) No.2 to 4

Fig. 4 The enveloped curve of the relationship between the compressive load and the displacement

ured at the  $P_{max}$  of 833kN and the crack width developed and the eccentricity of damage was observed at the displacement of 10.7 and load of 286kN, and then the test was stopped.

For No.2, the displacement of 1.0mm was measured at the  $P_{max}$  of 924kN and the significant damage was observed with 82 % of the decreased load, and then the test was stopped. The eccentricity of damage as well as No.1 was not observed and stable compared with No.1.

The enveloped curves of No2 to 4 are shown in Fig. 4(b). Their wall thickness was 180mm with double rebar of the  $p_w$  of 0.39 to 1.11%.

For No.3 and 4, the displacement of 1.7 and 0.7 mm at the  $P_{max}$  of 965 and 844kN were observed, respectively. The eccentricity of damage was not observed as well as No.2.

The enveloped curve of the load of the concrete resisted ( $cP$ ) and  $\delta$  is shown in Fig. 5.  $cP$  was defined as the  $P$  without the load of rebar resisted ( $sP$ ). And then the relative load was defined as  $cP$  divided by  $cP_{max}$ .

The strain of the vertical and horizontal rebar showed approximately yield at around  $cP_{max}$  in all specimens.

The displacement at the yield was defined as the

minimum displacement at the  $cP_{max}$  or 0.01 time of the elastic stiffness.

The same tendency was shown in Fig. 4 and 5, and the concrete confined effect was not observed even in the specimen with the rebar ratio of 0.71%.

### Damage and Cracking

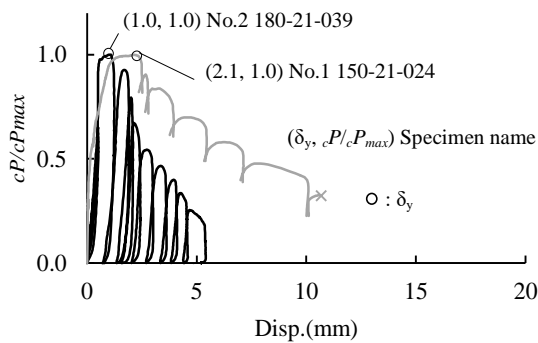
The final crack behavior was shown in Fig. 6. For all specimen, about 0.2mm of the crack width was observed before  $P_{max}$ , the crack was developed and the crack width was increased following increase of the displacement.

Crack was hardly observed in the extra area and stub.

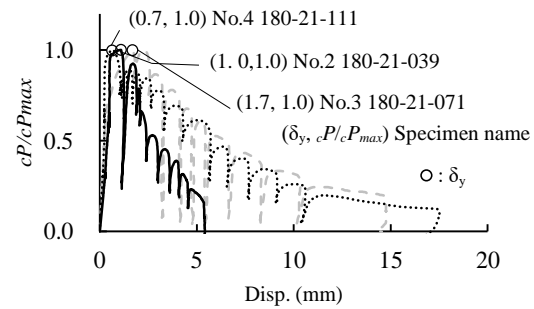
For No.1 with the wall thickness 150mm and single rebar, the crack width surrounded by dashed ellipse shown in Fig. 6(a) was significantly developed and the eccentricity of the rebar strain and crack damage were observed, then the fragile behavior was shown.

For No.2 to 4 with the wall thickness 180mm and double rebar, the difference of the crack behavior was not observed independent of the rebar ratio.

### Concrete Strain Distribution

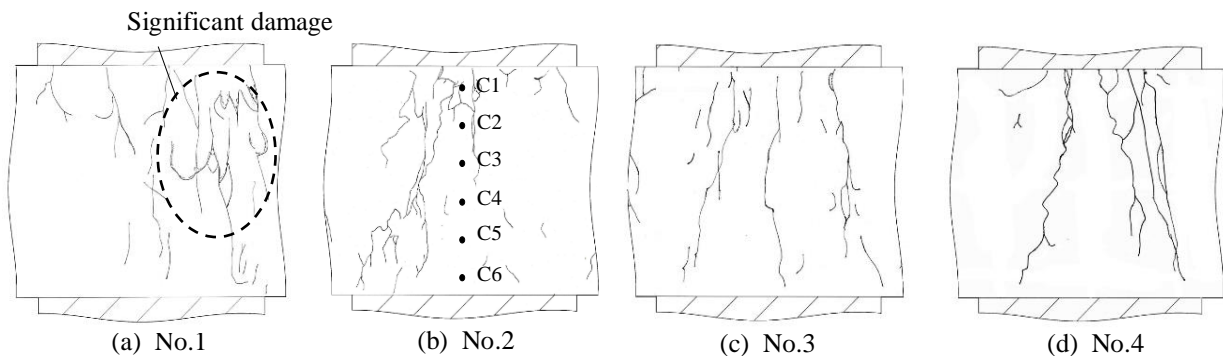


(a) No.1, 2



(b) No.2 to 4

Fig. 5 The enveloped curve of the relationship between the compressive relative load and the displacement



Note: C1 to C6 indicate the gauge location.

Fig. 6 The final crack behavior



The concrete strain distribution was shown in Fig. 7. The strain gages location number of C1 to C6 were indicated the location in Fig. 6(b). For all specimen, it was assessed that up to 2 % of the concrete strain

was appropriate. The amount of over 2% of the stain was estimated as 2% over.

The concrete strain at the center of the wall was

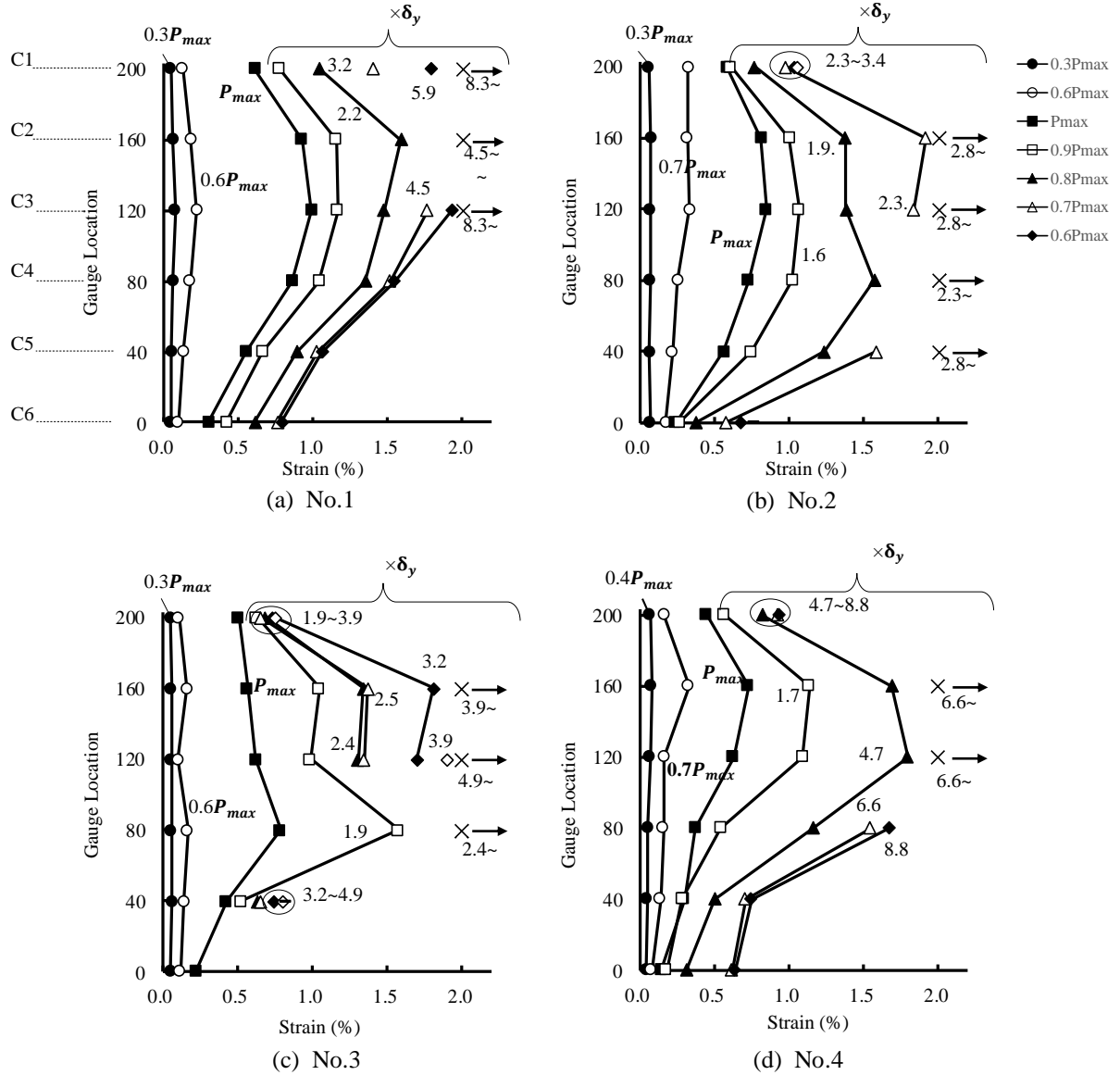


Fig. 7 The concrete strain distribution

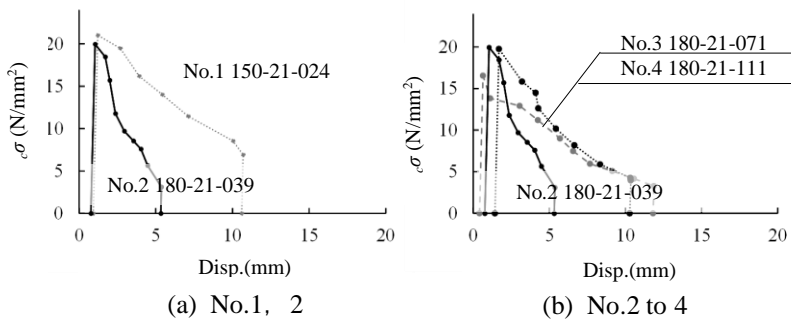


Fig. 8 The envelopment curve between the stress and the displacement

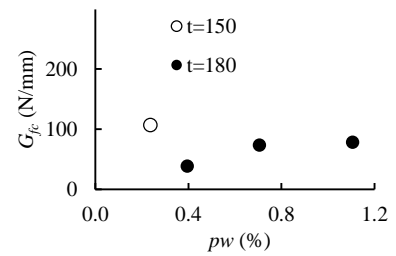


Fig. 9 The relationship between  $G_{fc}$ , wall thickness, and  $p_w$

larger than one of the top and bottom due to the concrete confined effect by rebar.

### Compressive Fracture Zone Length

As mention above, the eccentricity of the concrete strain distribution was not shown along the wall height due to concrete confined effect by the wall rebar. In addition, the all concrete strain in all specimens was the strain at the  $f'_c$  or more at the  $P_{max}$ , therefore the compressive fracture zone length in this paper was defined as 200mm.

### Compressive Fracture Energy

The envelopment curve between the concrete stress and the displacement is shown in Fig. 8. The concrete stress was the  $cP$  divided by the wall thickness and 250mm. The compressive fracture energy ( $G_{fc}$ )<sup>[6]</sup> was estimated as the area.

The relationship between  $G_{fc}$ , wall thickness, and  $p_w$  is shown in Fig. 9.

The displacement for  $G_{fc}$  ( $\delta_{conf}$ ) was calculated as the displacement of the focused area i.e. confined area as below.

$$\delta_{conf} = \frac{h_{conf}}{h} \cdot \delta$$

Where  $h$  is the wall height 200mm,  $h_{conf}$  is focused area i.e. confined area 200mm.

For the specimen with the wall thickness of 180mm and double rebar in No.2 to 4,  $G_{fc}$  was increased following increasing of the  $p_w$  and the confined effect.

However, for the specimen with the  $p_w$  of 0.71% more in No.4,  $G_{fc}$  was slightly increased, because the concrete strain was gradually increased.

For the specimen with the wall thickness of 150mm and single rebar in No.1, the  $G_{fc}$  of No.1 was largest. It should be examined in our future study.

### Equivalent Compressive Fracture Zone Width

The test result is shown in Table 3. The equivalent compressive fracture zone width ( $e b_p$ ) was defined as  $P_{max}$  divided by the wall thickness and  $f'_c$ .

$cP$  was decreased following increasing of  $p_w$ , because the  $sP$  was increased.

In other word,  $e b_p$  was decreased following increasing of  $p_w$ .

### CONCLUSION

Basic concrete walls with rebar test was performed applying compressive stress to estimate their compressive fracture energy for a concrete wall element model with rebar.

We reached several conclusions as below.

1) For the specimen with the wall thickness of 150mm and single rebar, the eccentricity of the rebar

Table 3 The test result

| #    | $P_{max}$<br>(kN) | $cP_{max}$<br>(kN) | $\delta$ at $cP_{max}$<br>(mm) | $\delta_y$<br>(mm) | $A'$<br>(cm <sup>2</sup> ) | $e b_p$<br>(mm) |
|------|-------------------|--------------------|--------------------------------|--------------------|----------------------------|-----------------|
| No.1 | 833               | 807                | 2.1                            | 1.2                | 389                        | 260             |
| No.2 | 924               | 898                | 1.0                            |                    | 433                        | 241             |
| No.3 | 965               | 889                | 1.7                            |                    | 429                        | 238             |
| No.4 | 844               | 747                | 0.7                            | 0.6                | 361                        | 200             |

Note:  $P_{max}$  : Maximum load

$cP_{max}$  : Maximum load of concrete

$\delta$  : Displacement

$\delta_y$  : Displacement at Minimum ( $P_{max}$  or  $0.01 \cdot K_0$ )

$A'$  :  $cP_{max}$  divided by  $f'_c$

$e b_p$  :  $A'$  divided by thickness

strain and crack damage were observed, then the fragile behavior was shown. For specimen with the wall thickness 180mm and double rebar, the difference of the crack behavior was not observed independent of the rebar ratio.

2) The concrete strain at the center of the wall was larger than one of the top and bottom due to the concrete confined effect by rebar.

3) For all test specimens the compressive fracture zone length was defined as 200mm.

4) For the specimen with the  $p_w$  of 0.71% more in No.4,  $G_{fc}$  was slightly increased, because the concrete strain was gradually increased.

5)  $e b_p$  was decreased following increasing of  $p_w$ .

### REFERENCES

- [1] ROTS, J. G.: Computational Modeling of Concrete Fracture, PhD thesis, Delft University of Technology, 1988.
- [2] Naoki Takamori, Benny Benni Assa, Minehiro Nishiyama, Fumio Watanabe : Confined Stress concrete - Strain Relationship formulation Fundamental Study, Proceedings of the Japan Concrete Institute, Vol.18, No.3, pp.395-400, 1996.
- [3] J. B. Mander, M. J. N. Priestley, R. Park, Fellow, ASCE : Theoretical Stress-strain Model for Confined Concrete, J. Struct. Eng., Vol.114, Issue.8, pp 1804-1826, Sep.1998.
- [4] Hikaru Nakamura, Takeshi Higai : Compressive Fracture Energy and Fracture Zone Length of Concrete - JCI-C51E Seminar on Post-Peak Behavior of RC Structures Subjected to Seismic Loads, Vol.2, pp.259-272, 1999.10.
- [5] Ken Watanabe, Junichiro Niwa, Hiroshi Yokota, Mitsuyasu Iwanami : Formulation of Stress-strain Relationship of Concrete Considering The Localized Compressive Failure Zone, Journal of JSCE, Vol.58, No.725, pp 197-211, 2003.2.
- [6] Shinya Muramatsu, Koshikawa Takeaki, Takanori Saito, Takuya Hasegawa : Quantitative Evaluation of Strain Softening Characteristics of Concrete Subjected to Uniaxial Compression, Architectural Institute of Japan Hokkaido Branch research report, No.83, pp.81-84, 2010.

## LANDSLIDES: BEHAVIOR AND MITIGATION APPROACH

Avirut Chinkulkijniwat<sup>1</sup>, Somjai Yubonchit<sup>2</sup>

<sup>1</sup>Suranaree University of Technology, Thailand

<sup>2</sup>Rajamangala University of Technology Isan, Thailand

### ABSTRACT

Assessment of rainfall-induced shallow slope failures is very important to reduce damages of infrastructures and lives of people living close to hazardous areas. Understanding the hydrological and physical responses of shallow slopes, subject to rainfall events is vital for the efficiency of a warning system setup. A series of experiments were undertaken to evaluate the hydrological responses of shallow slopes of varying steepness and when subjected to varying intensities, periods, and inter- storm periods of rainfall. The hydrological and physical responses were characterized to infiltration and saturation phases. During the infiltration phase, the maximum magnitude of water content was found behind the wetting front, termed as the water content behind the wetting front ( $\theta_w$ ). For a certain soil type, the magnitude of  $\theta_w$  was found to be dependent on the magnitude of rainfall intensity, regardless of the slope gradient and initial water content. This knowledge was further extended to characterize the stability of shallow landslides. Numerical experiments were also conducted to perform parametric study on the most common used tool for land sliding mitigation: the rainfall intensity-duration thresholds (ID threshold). It was found that the slope angle and antecedent rainfall play role on instability of the shallow slope. They control the initial stability of slope, which results in the different linear relationship of ID thresholds. In addition, the slope angle might accelerate the rate of rain water infiltration, and hence it reflects the slope of the ID thresholds.

*Keywords: Rainfall-induced landslides; Physically-based warning system; ID thresholds; Rainfall infiltration*

### INTRODUCTION

Rainfall-induced shallow landslides frequently result in natural disasters in many countries. One of the worst natural disasters in Thailand due to failure of slope was in 1988. Extremely rainfall in the southern part of Thailand in 1988 resulted in widespread slope failures and caused more than 240 deaths, as well as the destruction of 1560 bridges and 5694 km of roads (Oh et al., 2008). Another great tragedy in Thailand was due to a slope failure on 10 August 2001 in Phetchabun province when a rainfall intensity of 100 mm/day induced hundreds of slope failure and sequential mudflows resulting in 136 deaths as well as economic damages of more than 15 million USD (Yumuang, 2006).

An early warning system represents effective tool widely used to manage rainfall-induced disasters, including landslides, floods, and debris flows (Brand et al., 1984; Keefer et al., 1987; Wilson et al., 1993; Sirangelo and Braca, 2004). In Thailand, 1,052 early warning stations has been established by the Department of Water Resources since in 2004, which covers all 3,207 hazardous villages in Thailand. Monitoring devices including automatic thermometer, rain gauge and soil moisture sensor have been installed at warning stations to collect real-time temperature, rainfall and soil water content. The real-time rainfall data are typically evaluated through the risk thresholds to interpret the disaster risk. The risk thresholds are usually critical rainfall

triggering the initiation of rainfall-induced landslides, in which it has been empirically recognized as the cumulative rainfall of 100-300 mm in a day (the Department of Mineral Resources, 2004). The real-time rainfall data of 50-65%, 65-80%, and >80% of the critical rainfall are considered as immunity, caution and evacuation levels of the disaster risk, respectively.

The advantage of using critical rainfall thresholds as a part of early warning is its ease for fast assessment of rainfall-induced landslides. However, the rainfall thresholds have been empirically obtained by analyzing historical data of the landslides. Several factors such as soil's hydraulic properties (Pradel and Raad, 1993; Rahimi et al., 2010; Ma et al., 2011; Li et al., 2013), slope geometries (Rahardjo et al., 2007; Cho, 2009; Ali et al., 2014a) and antecedent rainfall conditions (Rahardjo et al., 2001; Rahimi et al., 2011; Cuomo and Della Sala, 2013) that affect hydro-mechanical interactions and hence landslide characteristics are neglected. Previous literatures also reveal that other instrumentations (i.e., moisture sensor, tensiometers and inclinometer) can be effectively used in warning system (e.g., Tohari et al., 2007; Gallage and Uchimura, 2010; Greco et al. 2010), in which warning levels can be directly interpreted via real-time responses from those devices. Nevertheless, prior to install those devices, a suitable location for monitoring of rainfall-induced landslides needs to be examined.

This paper presents recent research regarding to both empirical and physical landslides warning systems. Efforts had been devoted to examine the factors influencing landslide characteristics and the critical rainfall thresholds which will provide comprehensive understanding of rainfall-induced shallow landslide mechanisms and subsequently a guideline for building up powerful warning system based on monitoring device installations.

## PHYSICAL-BASED WARNING APPROACH

Previous studies (Tohari et al., 2007; Gallage and Uchimura, 2010; Greco et al., 2010; Eichenberger et al., 2013) revealed that the physically-based prediction can be used to build up an early warning system, interestingly. In the method, the warning levels are evaluated via the real-time hydraulic responses read from a set of monitoring devices. The common monitoring devices are moisture sensors, piezometers and tensiometers. Location of instrumentation is vital for early warning systems to be effective. Few attempts have been made to date on the study of suitable instrumentation locations for effective early warning systems. This part of research is systematically divided into two parts: 1) laboratory experiments and 2) stability analysis of the slope. A physical slope model was constructed to evaluate the hydrological responses on various steepness of soil slopes when subject to various rainfall intensities and periods. Subsequently, a series of infinite slope analysis was conducted to develop a fundamental understanding of the characteristics of failure planes in shallow slopes when subjected to varying rainfall conditions.

## Moisture Responses During Rainfall Infiltration

- Physical slope model and experimental program

To investigate moisture responses during rainfall, a local sandy soil was used in this study to prepare the homogeneous soil slope. The soil was classified as poorly-graded sand (SP) according to Unified Soil Classification System. A schematic diagram of the physical model is shown in Fig. 1. The model consists of four components including the rainfall simulator, the experiment box, the box supports, and the chain pulley system. The box supports are pin and roller type supports such that the experiment box can be raised one side to a prescribed inclined angle by the chain pulley.

Fig. 2 shows details of the experiment box. The dimensions of this box are 1550 mm length, 1000 mm high, and 200 mm width. The sides and bottom base of the box were made from impervious acrylic plates of 15 mm thick. Five of 5 mm diameter holes were vertically drilled at mid of the side boundary to insert the moisture sensor probes (Decagon 5TE, Decagon Devices Inc. (2007-2010)). Three of 9 mm diameter holes were drilled at bottom of the experiment box at distances of 375 mm (downslope), 750 mm (middle slope), and 1125 mm (upslope). These holes were used to insert the piezometers. To reduce entrapped air that might be affecting to measurement of the volumetric moisture content ( $\theta_w$ ), three other holes were drilled nearby the piezometer holes to install the opening valves. At downslope, permeable porous concrete overlaid by geotextile was placed to allow free water outflow at nearly saturated state, and to prevent the clogged soil in porous concrete.

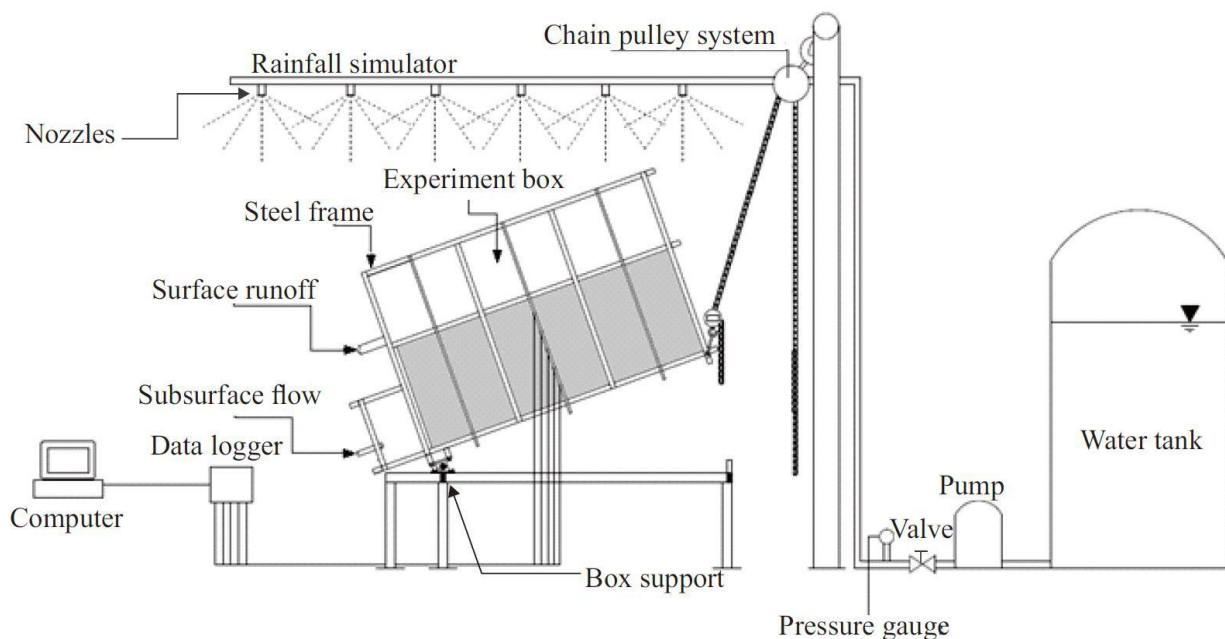


Fig. 1. Schematic diagram of the physical slope model

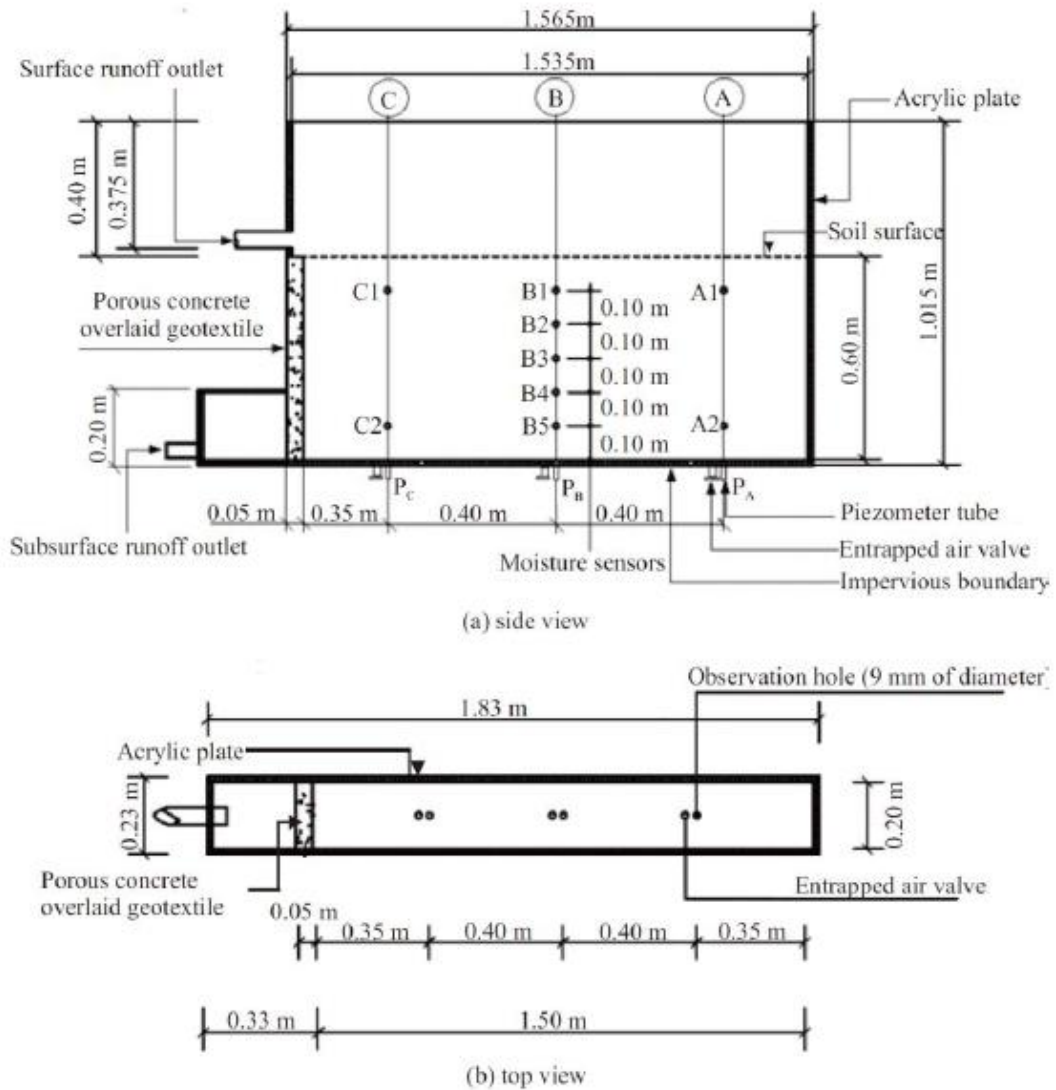


Fig.2 Details of the experiment box (a) side view (b) top view

Three set of laboratory experiments were conducted as shown in Table 1. In total, 13 tests were carried out. Each test, rainfall was continuously applied until the arrival of the steady state which is indicated by the rate of water outflow at slope toe equals to the rainfall intensity. The magnitudes of rainfall intensity assigned to each test were lower than the soil' saturated permeability ( $= 1.54 \times 10^{-4} \text{ m/sec} = 554.4 \text{ mm/hr}$ ). Monitored data were recorded during the test until the steady state (end of each test) was achieved. s k

The variation of rainfall intensity was conducted in test series I. The rainfall intensities of 45, 70, 100, 130, 160 mm/hr were applied to the model at slope angle ( $\beta$ ) of  $20^\circ$ . The variation of slope angle was conducted in the test series II. The slope angles ( $\beta$ ) of  $5^\circ$ ,  $10^\circ$ ,  $20^\circ$  and  $30^\circ$  were assigned to the model subjected to rainfall intensity of 100 mm/hr. The inter-storm rainfall period was assigned to the model

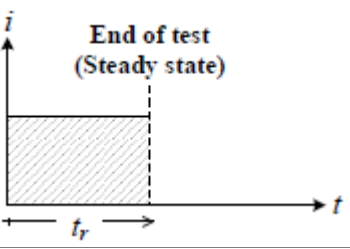
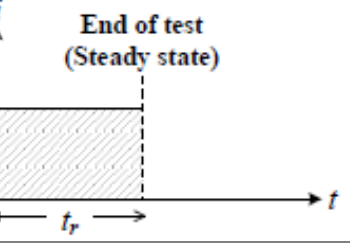
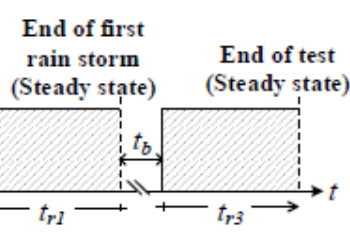
in the test series III. This test is to study the effect of antecedent water content from the previous rainfall, which might affect the hydrological responses. The two rainfall events of 100 mm/hr each were applied to the model at slope angle ( $\beta$ ) of  $20^\circ$  with the inter-storm period of 4, 7 and 14 days

#### • Tested results

The volumetric water contents ( $\theta_w$ ) read from the moisture sensors B1, B2, B3, B4, and B5, located at a vertical distance from the impervious surface of 100 mm, 200 mm, 300 mm, 400 mm, and 500 mm, respectively (see Fig. 2a).

Fig. 3, 4 and 5 present developments of  $\theta_w$  profile in the soil subjected to rainfall experiment series I, II, and III, respectively. The developments of  $\theta_w$  profile of all experimental series look similar to

Table 1 Experimental programs conducted in this study

| Series rainfall intensity, $i$ (mm/hr) | Slope angle $\beta$ (deg) | Rainfall sequence  | Inter-storm rainfall period $t_b$ (day) |
|--|---------------------------|--|---|
| I                                      | 20                        |    | -                                       |
| II                                     | 5<br>10<br>20<br>30       |    | -                                       |
| III                                    | 20                        |  | 4<br>7<br>14<br>-                       |

each other. The general characters of  $\theta_w$  profile development were determined as follows:

1) The development of  $\theta_w$  profile begins since the rainwater starts infiltrating into the soil. During the rainwater infiltration process termed as the infiltration phase, the volumetric water content increases from its initial value ( $\theta_{wi}$ ) to a volumetric moisture content of  $\theta_{wb}$ , named the volumetric water content behind the wetting front. The  $\theta_{wb}$  presents a possible maximum magnitude  $\theta_w$  of taking place during the infiltration phase.

2) After reaching the impervious boundary of the wetting front, an upward movement of water table begins. This process is called saturation phase. At this phase,  $\theta_w$  increases from the  $\theta_{wb}$  to the magnitude of  $\theta_w$  that closes to  $\theta_{sat}$ .

The characters of  $\theta_w$  development summarized above are in accordance with those reported by previous studies (Tohari et al., 2007; Huang et al., 2008; Huang and Yuin, 2010; Sharma and Nakagawa, 2010; Phi et al., 2013).

Fig. 3(a) – (e) present the variation of volumetric

water content in shallow slope of the experimental series I for rainfall intensity of 45, 70, 100, 130 and 160 mm/hr, respectively. The results show that the  $\theta_w$  profile development in the infiltration phase clearly depends on the magnitudes of rainfall intensity. The higher rainfall intensity results in the faster move of wetting front, and hence the deeper development of a wetting front. In addition, the results show that the magnitude of  $\theta_{wb}$  increases with the magnitude of rainfall intensity. These findings are similar to those reported by Lee et al., 2011.

The rainfall intensity also affects the  $\theta_w$  profile development in the saturation phase. In the plots, the rise of water table is indicated at the magnitude where  $\theta_w$  reaches  $\theta_{sat}$ . The level of water table is indicated by the point where the  $\theta_w$  profile in the saturation phase deviates from  $\theta_{sat}$ . It is found that the greater rainfall intensity causes the faster rise of water table. In addition, the final level of water table at the steady state also depend on the rainfall intensity and the greater rainfall intensity yields the higher level of water table at steady state.



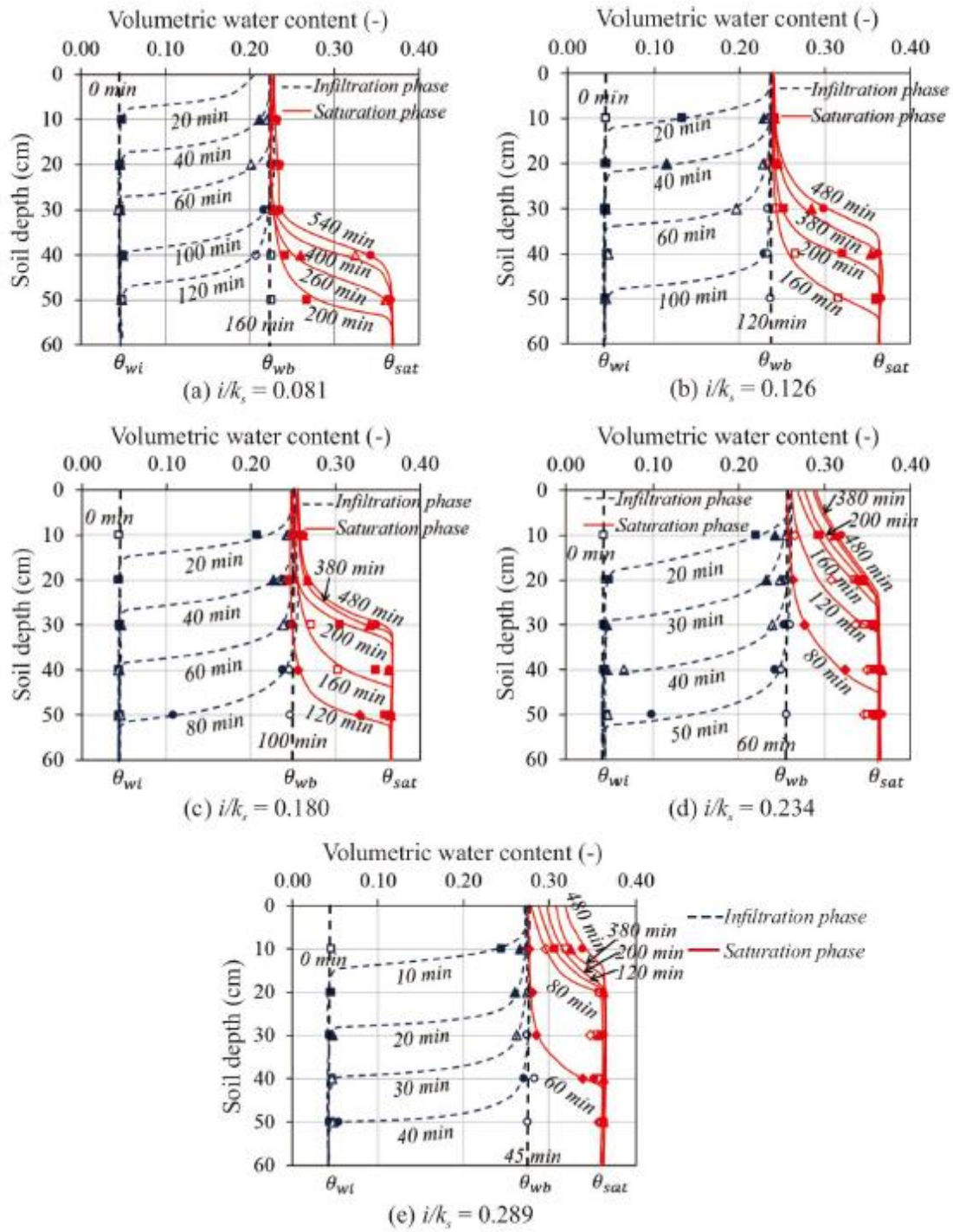


Fig. 3. Volumetric water content profiles for the test series I: (a)  $i/k_s = 0.081$ , (b)  $i/k_s = 0.126$ , (c)  $i/k_s = 0.180$ , (d)  $i/k_s = 0.234$ , and (e)  $i/k_s = 0.289$

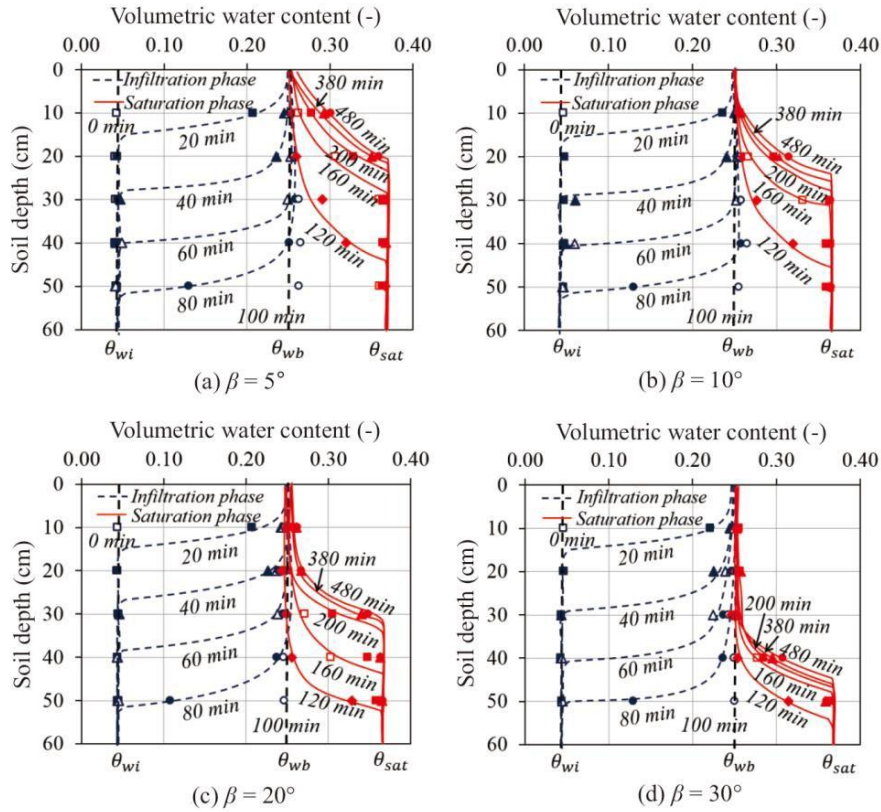


Fig. 4. Volumetric water content profiles for the test series II: (a)  $\beta = 5^\circ$ , (b)  $\beta = 10^\circ$ , (c)  $\beta = 20^\circ$ , and (d)  $\beta = 30^\circ$

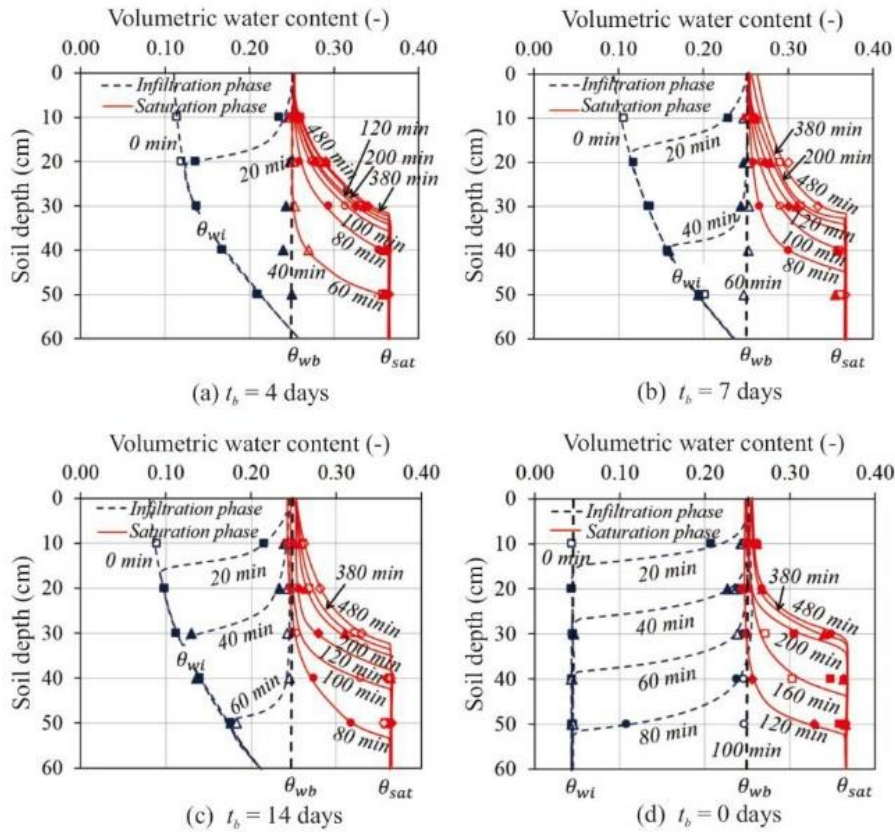


Fig. 5 Volumetric water content profiles for the test series III: (a)  $t_b = 4$  days, (b)  $t_b = 7$  days, (c)  $t_b = 14$  days and (d) continuous storm  $t_b = 0$  days



Fig. 4(a)-(d) present variation of volumetric water content in shallow slope of the experimental series II for the slope angle ( $\beta$ ) of  $5^\circ$ ,  $10^\circ$ ,  $20^\circ$  and  $30^\circ$ , respectively. The  $\theta_w$  development and the magnitude of  $\theta_{wb}$  in the infiltration phase are not dependent on the slope angle. In other words, within the  $\beta$  range conducted in this study, the magnitude of slope angle  $\beta$  do not affect the hydrological response. It is due to the vertical seepage flow plays important role to the hydrological responses in isotropic shallow slope soil during rainwater infiltration process. This finding is similar to that

found by Lee et al., 2011 who conducted two sets of laboratory seepage flow tests: one-dimensional soil column and  $18^\circ$  tilted slope model. The slope angle, however, affects the  $\theta_w$  profile development in the saturation phase. Figures 4 (a)-(d) clearly show that the rise of water table depends on the slope angle, the faster water table development is found at mild slope angle. This results may naturally be attributed to a dominant role of lateral flow along the impervious layer at the soil saturated state. The higher slope angle provides the higher hydraulic gradient and the faster lateral flow, and thus the less accumulated rain water at the impervious boundary.

Fig. 5 presents variation of volumetric water content in shallow slope of the experimental series III for a continuous storm, and for the different inter-storm period ( $t_b$ ) of 4, 7, 14 days, respectively. The  $\theta_w$  development in the infiltration phase depends on the magnitude of  $t_b$  as it affects the magnitude of an initial  $\theta_w$  of the subsequent rainfall ( $\theta_{wi}$ ); the shorter  $t_b$  results in the higher magnitude of  $\theta_{wi}$ . The speed of the wetting front advancement is more rapid for the shorter  $t_b$ . Although the variation of  $t_b$  significantly affects the wetting front development, it does not affect the magnitude of the volumetric moisture content behind the wetting front ( $\theta_{wb}$ ). In the other word, the magnitude of  $\theta_{wb}$  is independent of the magnitude of  $t_b$ .

### Analysis of Failure Plane

Location where failure plane takes place is vital for assessment of the slope failure. In this study, an infinite slope analysis was used to assess the failure plane based on the moisture responses characterized by physical slope model test. For the shallow slope failure taken place during the saturation phase, the failure plane always takes place at the interfacial between the soil and the impervious layers. However, the location of failure plane taken place during the infiltration phase might vary from the depth to depth depending on many factors. Fig. 6 presents the relationships between the normalized critical depth ( $Z_{wf}/Z_t$ ) and the infiltration index ( $i/k_s$ ) for various

magnitudes of stability index ( $\tan\phi'/\tan\beta$ ) for this demonstrated case. The vertical distance measured from the slope surface to the failure plane is called the critical depth ( $Z_{wf}$ ), while the thickness of the shallow slope is denoted as  $Z_t$ . For a certain soil, the critical depth decreases with an increasing rainfall intensity. In the other words, the shallower depth of failure plane is encountered in the slope subjected to the greater magnitude of rainfall intensity.

Fig. 6 shows that the depth of failure plane is very sensitive to the change of rainfall intensity for the stability index ranged from 0.9 to 1.0. The depth of failure plane can occur at any depth depending on the magnitudes of the infiltration and stability indices. However, the depth of failure plane is inert to the change of rainfall intensity for the stability index of lower than 0.9. In addition, in this case the depth of failure plane might take place at very shallow depth ( $Z_{wf}/Z_t < 0.2$ ).

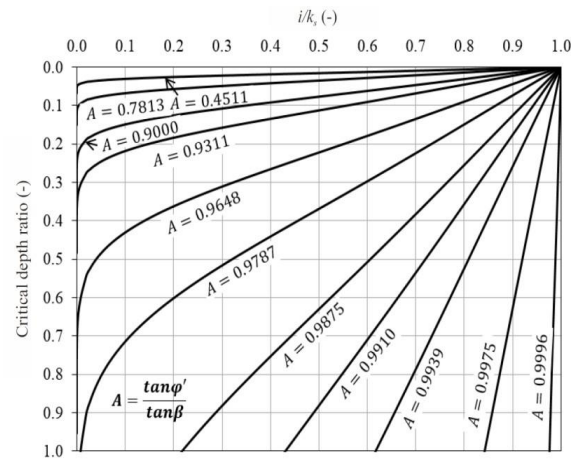


Fig.6. Critical depth chart

### Categorization of the Slope Failures

Once the critical depth chart is available, the threshold value can be assigned to the slope based on personal judgment. The threshold is the stability number at which the critical depth is slightly sensitive to rainfall intensity, i.e. the threshold value used in the illustrated case is 0.9 which is the stability index at which an infiltration index ( $i/k$ ) to a normalized critical depth ( $Z_{wf}/Z_t$ ) ratio is no greater than 0.2.

Based on the relative depth of the failure plane, possible modes of slope failure are: 1) along the impervious layer mode, 2) shallow depth mode which occurs very close to the slope surface, and 3) transitional mode which occurs at any depth from the impervious layer to the slope surface. These modes are governed by the stability index ( $\tan\phi'/\tan\beta$ ) as depicted in Fig. 7 and summarized below:

1. For the mild slope ( $\tan\phi'/\tan\beta \geq 1.0$ ), the failure mode is the along the impervious layer mode

which is triggered by an increment of positive pore water pressure taking place during the saturation phase.

2. For the steep slope ( $\tan\phi'/\tan\beta < 1.0$ ), the failure is triggered by the loss of matric suction during the infiltration phase. With the assistance of the critical depth chart, the failure mode is characterized according to the magnitude of  $\tan\phi'/\tan\beta$  ratio.

- If the slope's stability number ( $\tan\phi'/\tan\beta$ ) is lower than the threshold (for the illustrated case, the  $\tan\phi'/\tan\beta$  ratio is lower than 0.9), the failure mode is the shallow depth mode which occurs closed to the slope surface.
- If the slope angle is within a small range between the soil frictional angle and an angle of slightly greater than the soil frictional angle (for the illustrated case shown in the study, the  $\tan\phi'/\tan\beta$  ratio ranges from 0.90 to 1.0), the failure mode is the transitional model. The depth of the failure plane can occur at any depth in the soil layer depending on the magnitude of infiltration index. A greater  $\tan\phi'/\tan\beta$  ratio results in a more sensitive depth of failure plane relative to the infiltration index.

According to the failure modes shown in Fig. 7, instrumentations on a specific slope can be characterized by its stability index. In the mild slope ( $\tan\phi'/\tan\beta \geq 1.0$ ), slope failure will be triggered during the saturation phase. The end of infiltration phase, which is notified by the arrival of  $\theta_{wb}$  at near interface layer, may be set as the first warning point. For the very steep slope ( $\tan\phi'/\tan\beta \leq \text{threshold}$ ), the mode of failure is a shallow depth slope failure. Time to reach the failure might occur shortly after a rainfall event. Warning systems might not be suitable for this type of slope. The area and the vicinities should be classified as a sensitive area, in which human activities are prohibited. For an intermediate steep slope ( $1.0 > \tan\phi'/\tan\beta > \text{threshold}$ ), the failure plane can occur at various depths depending on the stability and infiltration indices. Intensive instrumentation to monitor the rainfall intensity and the development of wetting front must be assigned to this area.

### RAINFALL INTENSITY-DURATION THRESHOLDS (ID THRESHOLDS)

The rainfall intensity-duration thresholds for initiation of slope failure (ID thresholds) which is a relationship between the rainfall intensity ( $I_f$ ) and rainfall period ( $T_{rf}$ ) to trigger slope failure is widely used to simply assess the stability of shallow slope (Caine, 1980; Calcaterra et al., 2000; Corominas, 2000; Crosta and Frattini, 2001; Aleotti, 2004; Cannon and Gartner, 2005; Chien et al., 2005; Guzzetti et al., 2007). Fig. 8 shows a set of ID

thresholds developed from the above mentioned literatures. From these thresholds, a mathematic expression for ID thresholds can be expressed as:

$$I_f = a + cT_{rf}^m \quad (1)$$

where  $a$ ,  $c$  and  $m$  are the ID thresholds parameters which represent the curvature, intercept and gradient of ID thresholds, respectively.

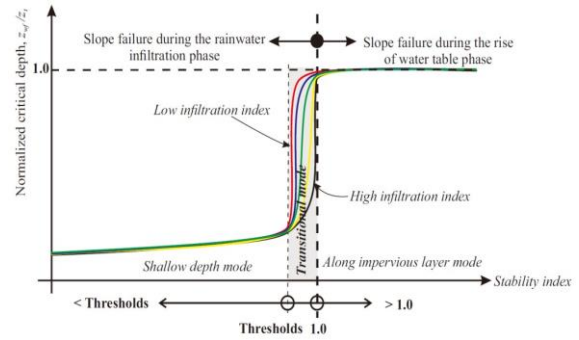


Fig. 7 Modes of failure in shallow slope classified by the stability number

### Numerical Modelling

Slope geometry, boundary conditions and fixity used in this study are shown in Figure 9. The slope model is divided into two layers. The bedrock is overlaid by a uniform shallow soil layer with thickness of 3 meters ( $d = 3$  m.), which gives the ratio of slope length ( $L$ ) to soil depth ( $d$ ) of about 31, 29 and 26 for the slope angle of  $20^\circ$ ,  $30^\circ$  and  $40^\circ$ , respectively. These  $L/d$  ratios are greater than 20 which is far enough to avoid boundary effects in calculation of safety factor (Griffiths et al., 2011; Tiwari et al., 2014).

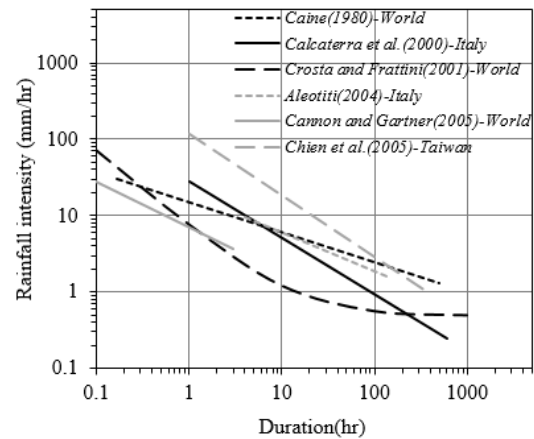


Fig. 8 ID thresholds for initiation of shallow slope failures proposed by previous researchers

Standard fixities were prescribed to allow only vertical movement along the boundary sides, while

lateral and vertical movements were fixed at bottom boundary. 15-node triangular finite element mesh is assigned in the problem. The finer elements were generated at the soil layer, and the finest mesh was generated along the soil slope where the failure tends to occur.

A prescribed flux, which relates to the desired intensity of rainfall, was assigned along the slope surface BC. Along the slope surface BC, a range of pore water pressure between -0.05 m and 0.05 m was prescribed. By this maximum pore water pressure of 0.05 m, the ponding water due to the excess of rainfall intensity over the infiltration capacity at soil saturation state could be developed up to 5 cm. over the slope surface. While the minimum pore water pressure of -0.05 m was used to represent a depth of negative flux due to evaporation. The boundaries AB and CD were assigned as no flux boundaries, while the boundaries AHG, DEF and GF were prescribed as impervious boundaries. The initial conditions were prescribed by variation of initial pore water pressure ( $u_{wi}$ ) ranges from -50 kPa to -80 kPa from soil-bedrock interface to soil surface to represent ground conditions prior to rainfall season. The volumetric water content at field capacity ( $\theta_{fc}$ ) and the residual water content ( $\theta_{res}$ ) were used as references to prescribe the range of  $\theta_i$ , and hence  $u_{wi}$ . The  $\theta_{fc}$  is known as the content of water, on a mass or volume basis, remaining in a soil 2 or 3 days after having been wetted with water and after free drainage is negligible (Soil Science Glossary Terms Committee, 2008; Meyer and Gee, 1999). It corresponds to the pore water pressure of -34 kPa (Dingman, 2002) for any soil type. If no addition water added into the soil for 2-3 days after rainfall, the water content might further decrease due to evaporation and plant root uptake. As such, a range of  $\theta_i$  might possibly be between  $\theta_{fc}$  and  $\theta_{res}$ . According to the soil water characteristic assigned to the model the variation of pore water pressure range from -80 kPa to -50 kPa is presented by the variation of volumetric water content of 20% to 22% as shown in Fig. 9.

Table 2 summarizes the material properties categorized into three categories; strength parameters, hydraulic related parameters, and deformation parameters. Mohr-Coulomb model was used to explain the mechanical behavior of soil and bedrock layers. Van Genuchten and van Genuchten-Mualem models were used to explain the hydraulic behavior of the soil layer, while the bedrock layer was assumed as an impermeable non-porous material.

## Experimental Program

Three series called series I, series II and series III were conducted in this study to evaluate stability and time to failures of the shallow slope under various conditions of the influence factors, including rainfall intensity; slope angle; and antecedent rainfall. As shown in Table 3, the numerical experiment includes 156 cases of the simulation run. The simulations include 78 cases of rainfall period of 24 hours and 78 cases of continuous rainfall until the arrival of slope failure.

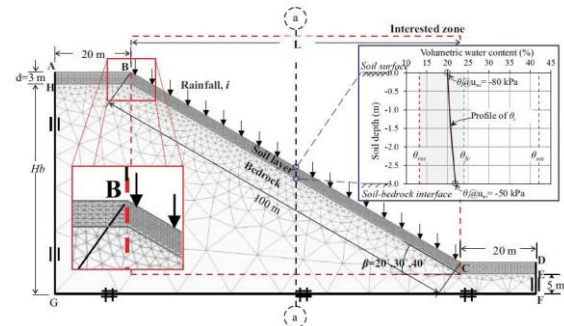


Fig.9 Slope geometry and boundary conditions

For series I, 21 cases of continuous rainfall until the arrival of slope failure were conducted. For each soil type, a constant rainfall intensity was assigned in a range from 0.36 to 360 mm/hr depending on the saturated permeability of each soil type. In addition, an extreme rainfall condition (EXT) is assigned to every soil types. This condition may occur once the rainfall intensity is much higher than the drainage capacity of soil at saturation ( $i \geq k_{sat}$ ) and the infiltration excess might exist since the start of rainfall. In this study, the extreme rainfall condition is assumed to generate a ponding rain water height of 5 cm for a whole period of the simulation. In PLAXIS, this condition can be simulated by a prescribed maximum pressure head ( $\Psi_{max}$ ) of 5 cm.

The effect of slope angle on the stability and time to failure were evaluated in series II. 39 cases of simulation run were conducted by varying the slope angle from 20° to 40°. Three types of soil with three or four rainfall intensities were assigned to each slope angle in this series.

Finally, 18 cases of simulation run were conducted in series III to evaluate the effect of antecedent rainfall. The antecedent rainfall imitates the periodical rainfall in real field. The previous rainfall affects the initial conditions of the soil subjected to the sequential rainfall, and hence the initial stability of the slope. The simulation started with an antecedence rainfall of certain rainfall intensity for 24 hours. Subsequently, the rainfall was terminated for a certain period (antecedent condition) prior to an arrival of another rainfall event. In series III, two antecedent conditions of rainfall of 48 and 168 hours (2 days and 7 days) were prescribed to the simulations.

Table 2 Soil parameters required for Mohr-Coulomb model

| Parameter                       | Symbol                  | Soil layer         |                    |                    | Bedrock layer    | Unit                 |
|---------------------------------|-------------------------|--------------------|--------------------|--------------------|------------------|----------------------|
| Material models                 |                         |                    |                    |                    |                  |                      |
| Mechanical model                | Model                   | Mohr-Coulomb       |                    |                    | Mohr-Coulomb     | -                    |
| Type of material behavior       | Type                    | Undrained A        |                    |                    | Non-porous       | -                    |
| Cohesion                        | $c'$                    | 6.74               |                    |                    | 25 <sup>a*</sup> | kPa                  |
| Friction angle                  | $\varphi'$              | 33.62              |                    |                    | 50 <sup>a*</sup> | deg                  |
| Hydraulic model                 | Model                   | Van Genuchten      |                    |                    | -                | -                    |
| Soil type                       | -                       | A                  | B                  | C                  | -                | -                    |
| Saturated permeability of soil  | $k_{sat,x} = k_{sat,y}$ | 1x10 <sup>-6</sup> | 1x10 <sup>-5</sup> | 1x10 <sup>-4</sup> | -                | m/sec                |
| $n$                             | $n$                     |                    | 1.564              |                    | -                | -                    |
| $\alpha$                        | $\alpha$                |                    | 0.162              |                    | -                | kPa <sup>-1</sup>    |
| Deformation parameters          |                         |                    |                    |                    |                  |                      |
| Effective modulus of elasticity | $E'{}^{a*}$             |                    | 50000              |                    | 100000           | kPa                  |
| Effective Poisson´s ratio       | $\nu'{}^{a*}$           |                    | 0.33               |                    | 0.2              | -                    |
| Dry unit weight                 | $\gamma_{unsat}$        |                    | 17.36              |                    | 23 <sup>a*</sup> | kN/m                 |
| Total unit weight               | $\gamma_{sat}$          |                    | 17.36              |                    | 23 <sup>a*</sup> | <sup>3</sup><br>kN/m |

<sup>a\*</sup> is assumed values.

The magnitudes of rainfall intensity, rainfall duration, and period of the antecedent condition used in this case series are summarized Table 3. For sake of simplicity, the effects of evaporation is neglected in this study. The slope instability triggered rainfall is typically taken place during rainfall period having high relative humidity, and hence evaporation is negligible.

## Numerical Results

Fig. 10 shows the ID thresholds for various type of soils (in term of their saturated permeability) with the slope angle of 30°. The coordinates ( $I_f$ ,  $T_{rf}$ ) lay on a single linear line on log-log scale regardless of the magnitude of saturated permeability. The  $T_{rf}$  decreases with increasing the rainfall intensity. However, the  $T_{rf}$  does not decrease if rainfall intensity increases beyond the infiltration capacity at saturated state of the corresponding soils (shown as black star symbols for the rainfall intensity of greater than the infiltration capacity at soil saturated state and as vertical dashed line for the extreme rainfall condition). According to the Green and Ampt model (Green and Ampt, 1911), if rainfall intensity is greater than the infiltration capacity of the soil at

saturation, the final rate of infiltrated rainwater is equal to the infiltration capacity at the soil saturation state. And the infiltration excess of rainwater is formed as the surface runoff. In the other words, the  $T_{rf}$  decreases with increasing the rainfall intensity if the rainfall intensity is not greater than the infiltration capacity of the soil at saturation. Therefore, the maximum rainfall intensity, which the relationship between  $I_f$  and  $T_{rf}$  obeys the ID thresholds, is governed by soil types in term of their saturated permeability.

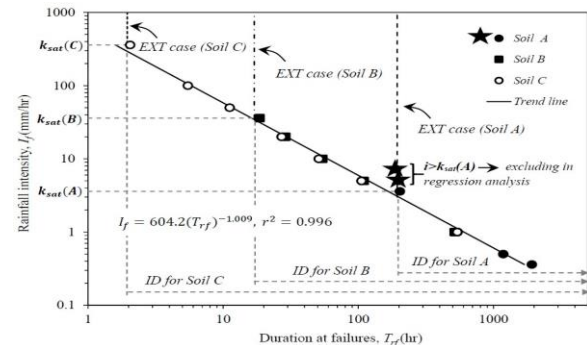


Fig. 10 ID thresholds based on Soil A, B, C with varying rainfall intensities,  $\beta=30^\circ$ , non-stop rainfall.



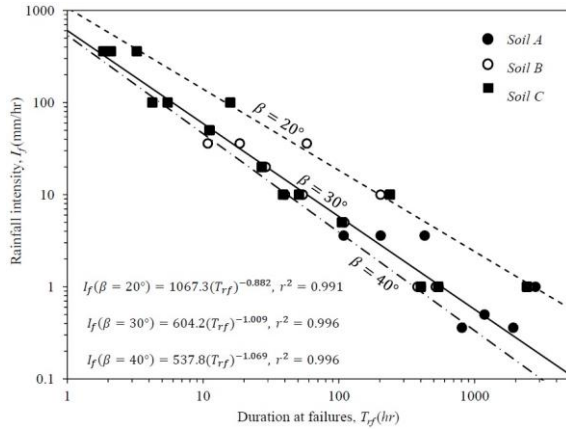


Fig.11. ID thresholds based on slope angle 20, 30 and 40° with varying rainfall intensities, Soil A, B, C, non-stop rainfall.

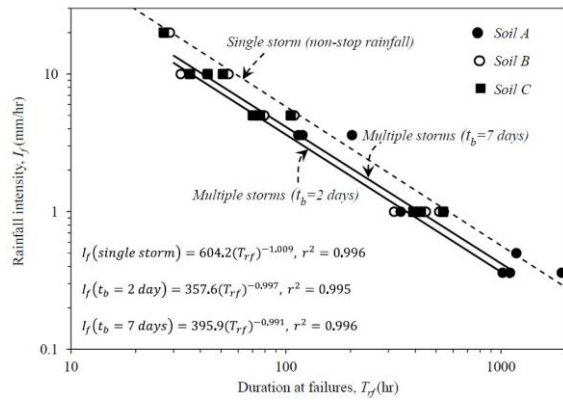


Fig. 12. ID thresholds based on 2 types of antecedent rainfall ( $t_b=2$  and 7 days) with varying rainfall intensities,  $\beta=30^\circ$ , Soil A, B and C

Fig. 11 presents the effect of slope angle on the time-intensity of rainfall at the failures state. The absolute value of ID thresholds parameter  $m$  slightly increases with increasing slope angle. In the other word, the steepness of the ID thresholds increases with increasing slope angle. Moreover, the ID threshold parameter,  $c$ , which represents the rainfall intensity required to trigger the slope failure at a unit time of rainfall, clearly decreases with increasing slope angle. The drop of the ID threshold parameter  $c$  with increasing slope angle is due to the lower initial FS for the greater slope angle. The increment of the ID threshold parameter  $m$  with increasing slope angle implies that the time to failure is faster for the steeper slope. Chinkulkijniwat et al., 2016 investigated the depth of failure plane in cohesionless soil slope subjected to continuous rainfall. For the soil slope of greater than the soil frictional angle itself, they found that the greater slope angle results in the shallower depth of failure plane, and hence the faster the time to failure. In total, the time to slope failure is accelerated by the slope angle. Under a specific rainfall intensity, the higher slope angle results in the shorter  $T_{rf}$ .

Fig. 12 presents the effect of antecedent rainfall on the ID thresholds. Prior to the continuous rainfall R3, the slope is subjected to 24 hours of the rainfall R1 followed by between-storm period  $t_b$  of 2 days or 7 days. The ID thresholds parameter  $m$  remains almost constant regardless the magnitude of  $t_b$ , but the parameter  $c$  increases with increasing the magnitude of  $t_b$ . The drop of the ID threshold parameter  $c$  with decreasing  $t_b$  is due to the lower of initial FS for the shorter  $t_b$ . As shown in Figure 4.9 that the shorter  $t_b$  results in the lower initial FS prior to the subsequent rainfall. Under the same rainfall intensity, the  $T_{rf}$  decreases with decreasing  $t_b$  from that of 7 days to that of 2 days. In the other word, the faster slope failure is found for the slope subjected to the shorter between-storm period  $t_b$ .

## CONCLUSIONS

This paper presents two main parts. First part is to obtain comprehensive understanding of hydro-mechanical responses within shallow slope leading to primary framework for quantifying critical locations, which is useful for early warning system based on monitoring device installations. A series of experiments were undertaken in this part to evaluate the hydrological responses of shallow slopes of varying steepness and when subjected to varying intensities, periods, and inter-storm periods of rainfall. A series of analysis of infinite slopes was also undertaken to develop a fundamental understanding of rainfall-induced shallow landslide characteristics. Thereafter, factors influencing rainfall-induced shallow landslides and the critical rainfall thresholds (ID thresholds) were investigated through a series of numerical experiment. The conclusions can be deduced as following:

### Physically-based Warning Approach

The experimental results showed that the hydrological and physical responses within shallow slope subjected to rainfall were characterized in the infiltration and saturation phases. During the infiltration phase, the maximum magnitude of water content was found behind the wetting front, termed as the water content behind the wetting front ( $\theta_{wb}$ ). For a certain soil type, the magnitude of  $\theta_{wb}$  was found to be dependent on the magnitude of rainfall intensity, regardless of the slope gradient and initial water content. Based on the relative depth of the failure plane, the failure can be categorized by three prime modes: 1) along the impervious layer mode, 2) shallow depth mode, and 3) transitional mode. These modes can be characterized by the magnitude of a stability index termed as  $\tan\phi'/\tan\beta$  ratio. An infiltration index, termed as  $i/k_s$  ratio, was found to play a role in the depth of failure plane only for the transitional mode.

### Rainfall Intensity-duration Thresholds approach

The critical rainfall thresholds (ID thresholds) were examined via finite element method. The numerical results showed that the rate of reduction in safety factor ( $FS$ ) increases with an increasing the intensity of rainfall, only in a range of lower than the infiltration capacity at soil saturated state. As such the saturated permeability of the soil, which is equal to the infiltration capacity at soil saturated state, plays an important role in the shallow slope failure. The saturated permeability was found also to govern a range of applicability of ID thresholds. If the rainfall intensity is not greater than the infiltration capacity at soil saturated state, the rainfall duration to failure ( $T_{rf}$ ) can be read from the ID thresholds. Slope angle and antecedent rainfall were found to play significant roles on instability of shallow slopes, as they control the initial stability of slope, which results in the different linear relationship of ID thresholds. In addition, the slope angle might accelerate the rate of rain water infiltration, and hence it reflects the slope of the ID thresholds.

### ACKNOWLEDGEMENTS

This work was supported by the Thailand Research Fund under the TRF Senior Research Scholar program grant No. RTA5680002, Suranaree University of Technology, and the Office of Higher Education Commission under NRU project of Thailand.

### REFERENCES

- [1] Aleotti P. 2004. A warning system for rainfall-induced shallow failures. *Engineering Geology* 73(3-4):247-265.
- [2] Ali A, Huang J, Lyamin AV, Sloan SW, and Cassidy MJ. 2014a. Boundary effects of rainfall-induced landslides. *Computers and Geotechnics* 61: 341-354.
- [3] Brand EW, Premchitt J, and Phillipson HB. 1984. Relationship between Rainfall and Landslides in Hong Kong. In *Proceedings of the 4th International Symposium on Landslides*, Toronto, Canada 1: 377 - 384.
- [4] Caine N. 1980. The rainfall intensity-duration control of shallow landslides and debris flows. *Geografiska Annaler Series A-physical Geography*: 62:23-27.
- [5] Calcaterra D, Parise M, Palma B, and Pelella L. 2000. The influence of meteoric events in triggering shallow landslides in pyroclastic deposits of Campania. *Proc. 8th Int. Symp. on Landslides*, (Bromhead E, Dixon N, Ibsen ML, eds) Cardiff: AA Balkema 1:209-214.
- [6] Cannon SH, and Gartner JE. 2005. Wildfire-related debris flow from a hazards perspective. In: *Debris flow Hazards and Related Phenomena* (Jakob M, Hungr O, eds). Springer Berlin Heidelberg, 363-385.
- [7] Chien YC, Tien CC, Fan CY, Wen CY, and Chun CT. 2005. Rainfall duration and debrisflow initiated studies for real-time monitoring. *Environmental Geology*:47, 715-724.
- [8] Chinkulkijniwat A, Yubonchit S, Horpibulsuk S, Jothityangkoon C, Jeebtaku C, and Arulrajah A. 2016. Hydrological responses and stability analysis of shallow slopes with cohesionless soil subjected to continuous rainfall. *Canadian Geotechnical Journal*, <http://dx.doi.org/10.1139/cgj-2016-0143>.
- [9] Corominas J. 2000. Landslides and climate. Keynote lecture- In: *Proc. 8th Int. Symp. on Landslides*, (Bromhead E, Dixon N, Ibsen ML, eds) Cardiff: AA Balkema, 4:1-33.
- [10] Crosta GB, and Frattini P. 2001. Rainfall thresholds for triggering soil slips and debris flow. In: *Proc. 2nd EGS Plinius Conference on Mediterranean Storms* (Mugnai A, Guzzetti F, Roth G, eds) Siena, 463-487.
- [11] Cho SE. 2009. Infiltration analysis to evaluate the surficial stability of two-layered slopes considering rainfall characteristics. *Engineering Geology* 105: 32-43.
- [12] Cuomo S, and Della Sala M. 2013. Rainfall-induced infiltration, runoff and failure in steep unsaturated shallow soil deposits. *Engineering Geology* 162: 118-127.
- [13] Dingman SL. 2002. *Physical Hydrology*. Prentice Hall, NJ, USA.
- [14] DMR (Department of Mineral Resource), Thailand. 2004. *Landslide risk map of Thailand*.
- [15] Lichtenberger J, Ferrari A, and Laloui L. 2013. Early warning thresholds for partially saturated slopes in volcanic ashes. *Computers and Geotechnics* 49: 79-89.
- [16] Gallage C, and Uchimura T. 2010. Investigation on parameters used in warning systems for rain-induced embankment instability. In: *Proceedings from the 63rd Canadian Geotechnical Conference (GEO2010)*, 12 - 16 September 2010, Calgary, Alberta.
- [17] Green WH, and Ampt CA. 1911. Studies on soil physics: flow of air and water through soils. *Journal of Agricultural Sciences*, 4, 1-24.
- [18] Griffiths DV, Huang J, and de Wolfe GF. 2011. Numerical and analytical observations on long and infinite slopes. *International Journal for Numerical and Analytical Methods in Geomechanics* 35:569-585.
- [19] Greco R., Guida A, Damiano E, and Olivares L. 2010. Soil water content and suction monitoring

- in model slopes for shallow flowslides early warning applications. *Physics and Chemistry of the Earth* 35(3-5): 127-136.
- [20] Guzzetti F, Peruccacci S, Rossi M, and Stark CP. 2007. Rainfall thresholds for the initiation of landslides in central and southern Europe. *Meteorology and Atmospheric Physics* 98: 239-267.
- [21] Huang C-C, Lo C-L, Jang J-S, and Hwu L-K. 2008. Internal soil moisture response to rainfall-induced slope failures and debris discharge. *Engineering Geology* 101(3-4):134-145.
- [22] Huang C-C, and Yuin S-C. 2010. Experimental investigation of rainfall criteria for shallow slope failures. *Geomorphology* 120(3- 4):326-338.
- [23] Keefer DK., Wilson RC, Mark RK, Brabb EE, Brown III WM, Ellen SD, Harp EL, Wiczorek GF, Alger CS and Zatzkin RS. 1987. Real-time landslide warning during heavy rainfall. *Science* 238: 921–925.
- [24] Lee LM, Kassim A, and Gofar N. 2011. Performances of two instrumented laboratory models for the study of rainfall infiltration into unsaturated soils. *Engineering Geology* 117(1-2):78-89.
- [25] Li WC, Lee LM, Cai H, Li HJ, Dai FC, and Wang ML. 2013. Combined roles of saturated permeability and rainfall characteristics on surficial failure of homogeneous soil slope. *Engineering Geology* 153: 105-113.
- [26] Ma K-C, Tan Y-C, and Chen C-H. 2011. The influence of water retention curve hysteresis on the stability of unsaturated soil slopes. *Hydrological Processes* 25: 3563-3574.
- [27] Meyer PD, and Gee GW. 1999. Flux-based estimation of field capacity. *Journal of Geotechnical and Geoenvironmental Engineering* 125(7):595-599.
- [28] Oh H-J, Lee S, Chotikasathien W, Kim CH, and Kwon JH. 2008. Predictive landslide susceptibility mapping using spatial information in the Pechabun area of Thailand. *Environmental Geology* 57(3):641-651.
- [29] Phi S, Clarke W, and Li L. 2013. Laboratory and numerical investigations of hillslope soil saturation development and runoff generation over rainfall events. *Journal of Hydrology* 493:1-15.
- [30] Pradel D, and Raad G. 1993. Effect of permeability on surficial stability of homogeneous slope. *Journal of Geotechnical Engineering* 119: 315-332.
- [31] Rahardjo H, Nio AS, Leong EC, Song NY. 2010. Effects of groundwater table position and soil properties on stability of slope during rainfall. *Journal of Geotechnical and Geoenvironmental Engineering* 136: 1555-1564.
- [32] Rahardjo H, Rezaur RB, Leong EC. 2007. Factors controlling instability of homogenous soil slopes under rainfall. *Journal of Geotechnical and Geoenvironmental Engineering* 133: 1532.
- [33] Rahimi A, Rahardjo H, Leong E-C. 2010. Effect of hydraulic properties of soil on rainfall-induced slope failure. *Engineering Geology* 114: 135-143.
- [34] Rahimi A, Rahardjo H, and Leong E-C. 2011. Effect of Antecedent Rainfall Patterns on Rainfall-Induced Slope Failure. *Journal of Geotechnical and Geoenvironmental Engineering*, 137(5): 483-491.
- [35] Sharma RH, and Nakagawa H. 2010. Numerical model and flume experiments of single- and two-layered hillslope flow related to slope failure. *Landslides* 7(4):425-432.
- [36] Sirangelo B, Braca G. 2004. Identification of hazard conditions for mudflow occurrence by hydrological model. Application of FLAIR model to Sarno warning system. *Engineering Geology* 73: 267–276.
- [37] Soil Science Glossary Terms Committee. 2008. *Glossary of Soil Science Terms 2008*. Madison: SSSA, pp. 92.
- [38] Tiwari RC, Bhandary NP, and Yatabe R. 2014. Spectral element analysis to evaluate the stability of long and steep slopes. *Acta Geotechnica* 9:753–770.
- [39] Tohari A, Nishigaki M, and Komatsu M. 2007. Laboratory rainfall-induced slope failure with moisture content measurement. *Journal of Geotechnical and Geoenvironmental Engineering* 133(5): 575-587.
- [40] Wilson RC, Mark RK, Barbato G. 1993. Operation of a real-time warning system for debris flows in the San Francisco Bay area, California. In: *Conference Hydraulics Division, ASCE*, vol. 2, pp. 1908-1913.
- [41] Yumuang S. 2006. 2001 debris flow and debris flood in Nam Ko area, Phetchabun province, central Thailand. *Environmental Geology* 51(4):545-564.

## *Technical Papers*



## *Science*

## DIFFERENT RATIOS OF OKRA JUICE AND PANDAN LEAF JUICE ON SPORT DRINK

Wattana Wirivutthikorn<sup>1</sup>

<sup>1</sup>Faculty of Agricultural Technology, Rajamangala University of Technology Thanyaburi (RMUTT)  
2 Phaholyothin 87 Soi 2 Phaholyothin Road Thanyaburi Pathum Thani 12130 Thailand

### ABSTRACT

The major advantage is that there are good bioactive ingredients and antioxidants that are beneficial to the body are possible when used as a sport drink. There were possibility to produce sport drink by using Thai herb as raw materials. The objective of this research was to study the optimum ratios of okra juice and pandan leaf juice with vitamin C supplementation of mixed juice. Four ratios of okra juice and pandan leaf juice were performed into 4 experiments. Experiment 1: (control formula) okra juice 100 ratio, Experiment 2: blended okra juice and pandan leaf 70:30 ratio, Experiment 3: blended okra juice and pandan leaf 60:40 ratio and Experiment 4: blended okra juice and pandan leaf 50:50 ratio were obtained. The results from physical measurement (L, -a\*, b\* and percent of transmittance) were significantly different ( $P \leq 0.05$ ). The study chemical of measurements, i.e. pH, percentage of acidity and total soluble solid were performed. The results showed that Experiment 4 had the lowest pH and gave the highest percentage of acidity values of 3.15 and 0.28, respectively. The microbiological properties revealed that amount of microorganism in each treatment was not found. The sensory evaluation on overall acceptability by using 9-point hedonic scale revealed that panelists accepted with the highest scores of 7.13 on okra juice (control). From the information obtained, the formulation of sport drink produced from Thai herbs can be developed to be accepted by consumers, which has increased steadily and expanded in the large future level in beverage industry.

*Keywords: Okra, Pandan leaf, Juice, Sport, Drink*

### INTRODUCTION

At present, Thai society has seen the importance and pay attention to exercise more sports. In order to have a healthy, healthy body without disease, athletes must pay attention to their health care. Health supplement products have become more actives. Especially the use of vitamins and minerals to enhance health and fitness [1]. Sport drinks, called electrolyte drinks, refer to beverages that contain minerals as the main ingredients. Includes dry mineral drinks as well is a liquid replacement drink that is lost during exercise or sport. The lost fluid is the loss of sweat. The sweat contains as much as 99 percent water and contains 1 percent more minerals. Drinking of sodium-containing solutions during exercise and recovery may help maintain the condition and normalize the amount of blood and also help maintain the water in the space between cells. But still have thirst, while drinking clean water will help suppress appetite [2]. The major components of sport drink according to the FDA requirements are that they should contain sodium chloride minerals and magnesium in quantities not exceeding 25 g / l. If the concentration of minerals and sugar is high, will slow down the absorption, so drinking mineral drinks or other beverages need to be diluted before. To allow the absorption of water to replace sweat quickly. Sport drink are a specific control food. It must have

quality or standards as announced by the Thai Ministry of Public Health. Especially minerals controlled in 1 liter sport drink containing these minerals: sodium not less than 20 meq, glucose not less than 2 percent of weight or sucrose not less than 4 percent of weight, potassium not more than 5 meq (if any) and bicarbonate or citrate not more than 15 meq. In addition to previous components may use minerals other than 3 and 4 or other sugars to be approved by the Food and Drug Administration [3]. Chloride is one of the minerals that is controlled in sport drinks. The reason for having to control the amount of salt in food or chloride in sport drinks, if there is too much salt, it may be a major cause of high blood pressure. Chloride is the most important negative ion in the body. Most of the body gets it in the form of sodium salt. Chloride acts to balance the pH of the body and a component of hydrochloric acid in the stomach. If the body is absent, will vomit. In general, the body gets chloride along together with sodium [4]. The utilization possibility of okra to be processed into sport drinks for those who lack nutrients and exercise Because, it is rich in nutrients that are nutritious, such as carbohydrates as fiber, protein, folate, calcium, phosphorus, potassium, magnesium, iron, vitamin A, vitamin B1, vitamin B2 and vitamin C in sufficient quantities. Because okra is highly nutritious, in addition to food and the drink also has properties for the treatment of diseases such as fresh okra with high amounts of ginseng and

pectin. Several compounds such as gum and pectin in high amounts cause mucus, which will help reduce the symptoms of gastroenteritis, prevent atherosclerosis, maintaining normal blood pressure, nourishing the brain and also being a good laxative [5]. Pandan leaf has a fragrant aroma of essential oils. The aroma of pandan leaf is very much from the chemical called 2-acetyl-1-pyrroline, which is the same smell that can be found in jasmine rice, white bread and flowers. Pandan leaf contains proteins, carbohydrates, fiber, calcium, phosphorus, iron, essential oils (containing linalil acetate, benzyl acetate, linoleol and ethyl vanillin, geranium, and kumarin fragrance). It contains chlorophyll pigment, making it green with  $\beta$ -carotene, which is the essence that is beneficial to the body, helps in excretion and can resist cancer as well [6]. There is research related to comparison of chloride determination in 10 commercially available sport drinks by using titration method and sedimentation method for silver chloride analysis. The results showed that the values obtained in both methods are highly correlated ( $r^2 = 0.9582$ ) and when analyzing results were tested with t-test. It was found that both methods were not statistically different. When calculating the cost of chemicals used, it was found that the method of precipitation in silver chloride required a cost of 1.3 times higher than the titration method. The cost of chemicals is 7.1455 and 5.5424 baht, respectively. In addition to, the titration method took 15 minutes per sample, whereas the settling silver chloride method took approximately 9 hours per sample [7]. But there was no information about the formulation of okra mixed with pandan leaf. For this reason, of okra and pandan leaf benefits, the researchers mentioned the importance of producing water-based okra and pandan leaf with the healthy sport drink by studying appropriate amounts of okra and pandan leaf ratios on the physical, chemistry quality and sensory acceptance of the consumer towards the product in order to obtain the taste that is acceptable to the consumer, which help with the quenching of thirst and help relax or make the body. The data obtained from this research was an alternative to apply by making sport drink containing both of okra and pandan leaf as raw materials to improve the nutritional quality and good health. Sport drink that has benefits and suitable for people who love to exercise, love health and also solve the problems of bringing agricultural products that are processed with higher values.

## METHODOLOGY

The research was carried out at the Division of Food Science and Technology, Faculty of Agricultural Technology, Rajamangala University of Technology Thanyaburi. (RMUTT) Pathum Thani Province Thailand. The samples used in this study

were purchased from Rangsit Market which located in Pathum Thani Province Thailand.

### Dried Okra Preparation

The okra was washed and cut into thin small pieces. Then 5 kg of dried okra was dried at 75°C for 3 hrs. Stored products that were packed in plastic zipper bags with desiccants [8].

### Pandan Leaf Preparation

The pandan leaf was washed and cut into thin small pieces. Then 100 g of broken pandan leaf was dried at 75°C for 2 hrs. Stored products that were packed in plastic zipper bags with desiccants adapted from [8].

### Production of Blended Dried Okra Juice and Pandan Leaf Juice with Vitamin C Supplementation

#### Okra Juice Preparation

Weigh 50 g of dried okra was placed in a stainless steel pot containing 1,000 ml of water and heated to 100°C. Then, put pandan leaf to reduce the green odor of okra. The aliquot was filtered through a cloth until there was no sediment and then stored its in the refrigerator [8].

#### Pandan Leaf Preparation

Weigh 10 g of dried pandan leaf was placed in a stainless steel pot containing 1,000 ml of water and heated to 100°C. Then, put pandan leaf to reduce the green odor of okra. The aliquot was filtered through a cloth until there was no sediment and then stored its in the refrigerator adapted from [8].

#### Blended Okra Juice and Pandan Leaf Juice Preparation

This research was performed as four experiments (three replications): 1) okra juice (control); 2) blended okra juice and pandan leaf juice 70:30; 3) blended okra juice and pandan leaf juice 60:40 and 4) blended okra juice and pandan leaf juice 50:50. Bring the okra juice mixed with pandan leaf juice to be homogeneous and add other ingredients as shown in Table 1.

#### Production of Blended Okra Juice and Pandan Leaf Juice with Vitamin C Supplementation

Weigh 50 g of dried okra was placed in a stainless steel pot containing 1,000 ml of water and

heated to 100°C for 5 minutes. The aliquot was filtered through a cloth until there was no sediment. Bring okra juice blended with pandan leaf juice. Addition of some detailed ingredients as shown (Table 1). (65 g of sucrose, 1.2 g of citric acid, 8g of sodium chloride and 0.5 g of vitamin C), then cooling and heated to 70°C for 15 minutes. The blended aliquots were placed in 250 ml of sterilize colored glass bottles by means of cooling immediately and storage at 4°C adapted from [9].

### Recording of Data

Collect and record numerical data from experiments (three replications) and calculate data and statistical analysis. The Experimental design for physical and chemical quality analysis were evaluated by using a completely randomized design (CRD). A randomized complete block design (RCBD) for sensory evaluation was used with analysis of variance. Analysis of the mean differences of experiments was performed using Duncan's new multiple range test [10].

### Physical Measurement

#### Observation by eyes

Observation of the external appearance of mineral drink products, okra juice, mixed with pandan leaf juice, vitamin C supplementation in all 4 experiments [11].

#### Measurement by using instrument

Color brightness ( $L^*$ ), color as green ( $-a^*$ ) and yellow ( $+b^*$ ) were measured by using Minolta CR-10 and recorded as values adapted from [11]. The sedimentation was detected by using Visible Spectrophotometer Metertech Model SP830 and the sedimentation value was recorded as values adapted from were recorded as percent of transmittance values (% T) adapted from [11].

### Chemical Measurement

The pH, total soluble solid (TSS) and percentage of total acidity (calculated as citric acid) were measured by using pH meter OHAUS ST3100-F, using hand refractometer (measured as °Brix and titration with 0.1N sodium hydroxide (phenolphthalein as indicator as values), respectively adapted from [12].

### Microbiological Measurement

The total microbiology was measured as total plate count by using plate count agar adapted from

[12].

### Sensory Evaluation

The sensory evaluation was carried out by 30 untrained panelists in Rajamangala University of Technology Thanyaburi (RMUTT), Thailand. Panelists were asked to analyze their level of preference for each treatment by using a 9-point hedonic scale test based on the attributes of color, odor, taste, clarify and overall acceptability. A randomized complete block design was used with analysis of variance. Analysis of the mean differences of experiments was performed using Duncan's new multiple range test [13].

## RESULTS AND DISCUSSION

### Physical appearances of okra juice and passion leaf

Figure 1, The characteristics of sport drink products, okra juice was mixed with pandan leaf juice and vitamin C supplementation. When considering the appearance, it was found that the Experiment 1 and 2 had a lot of suspended sediments of okra. The Experiment 3 showed that there was a little suspended okra and Experiment 4 was found that there was no sediment of okra. When considering the color, it was found that the Experiment 1 had a light brown color, but the Experiment 2 had an orange-brown color, whereas the Experiment 3 was yellowish brown, the last the Experiment 4 had a clear yellow color. The results revealed that the Experiment 1, 2 and 3 were brown in color from the okra juice in a ratio greater than pandan leaf [14]. Possible reason was that okra contains a soluble fiber pigment such as pectin and mucilage caused by acetylated acidic polysaccharide compounds and galactulonic acid. The Experiment 4 had a clear yellow color due to the ratio of okra juice and pandan leaf juice in the same ratio. When considering the smell, it was found that the smell varies according to the amount of okra juice that was reduced and the amount of pandan leaf juice was increased. Compared to the control sample, when considering the taste, it revealed that all experiments had a slightly sour, sweet, salty taste due to flavoring with sucrose at the equal amount of sodium chloride and citric acid in all experiments [15].

### Physical measurement

Table 2, The results revealed that all of ( $L^*$ ), ( $a^*$ ), ( $b^*$ ) and percent of transmittance values and physical appearance depending on different ratios of okra juice and pandan leaf juice. The results showed that all values were different ( $P \leq 0.05$ ). The physical characteristics of blended okra juice and pandan

leaf juice products with vitamin C supplementation, comparing the differences between the experiments of color values ( $L^*$ ), ( $-a^*$ ), ( $b^*$ ) and percent of transmittance. The results revealed that the brightness value ( $L^*$ ) were of 27.61, 28.48, 29.78 and 29.58, respectively. The color values ( $-a^*$ ) and ( $b^*$ ) were -3.00, -2.67, -6.35 and -10.08, 10.59, 12.13, 12.51 and 13.55, respectively. The percentage of transmittance from all treatments with value of 77.09, 74.02, 83.63 and 87.50, respectively [15]. This may be caused by the ratios between okra juice and pandan leaf juice with different amounts due to each experiment to have different values. The experiment with a large amount of pandan leaf ratio had a darker color and more brightness than the experiment with ratio of the less amount of okra juice. One possible reason was both okra and pandan leaf have a chlorophyll (as green pigment), but increasing the amount of pandan leaf juice results in an increasing trend of all values [16],[17].

### Chemical Measurement

Table 3, The results indicated that the pH, total soluble solid and percentage of total acidity in okra juice products with pandan leaf juice, depended on the different ratios (Table 3) [18]. The result was found that the measured values were statistically significant differences ( $P \leq 0.05$ ), while total soluble solid was not statistically different. This value depends on the increasing okra juice and pandan leaf juice ratio, resulting in lower pH values (more acidity). The results indicated a tendency for the percent of total acidity did not decrease low values in comparison with the control samples. The values analyzed were consistent with the percentage of total acid content in the form of citric acid that was higher with the increase in vitamin C. The total soluble solid was not significantly different ( $p > 0.05$ ) due to the amount of solid ingredients added in all experiments [19],[20].

### Microbiological Measurement

Based on the analysis of total microbial counts by using the total plate count method in blended okra juice, and pandan leaf juice with vitamin C supplementation. The results showed that microorganisms were not found in all experiments. One reason possibility was due to the pasteurization process of sport drink before packaging. This processing is a thermal processing method with the main purpose to destroy pathogenic microorganisms, including microorganisms and related enzymes that cause food degradation [21].

### Sensory Evaluation

Table 4, The sensory characteristics It was found

that the sensory scores on color, smell, taste, texture from comparison of differences between experimental items were not statistically significant difference ( $p > 0.05$ ) in which each experiment had not different on preference scores [22],[23],[24]. The experiment with the highest liking scores was the Experiment 1. For one possible reason was the ratios of okra juice and pandan leaf juice were not significantly different, resulting in the consumer's acceptability for color, odor, taste and clarity [25]. The other reason, may be amount of vitamin C that was added to each experiment may be too little, therefore almost panelists could not to clearly distinguished in each experiment. For overall acceptability, panelists preferred the Experiment 1 than compared to the other experiments, since there was only okra juice. From the results of this research, it indicated that increasing the proportion of pandan leaf juice was likely to cause consumers to dislike it, possibly due to the pandan leaf smell that is too strong [26],[27].



E1 E2 E3 E4

E1: Okra juice )Control)

E2: Blended okra juice and pandan leaf juice  
70:30

E3: Blended okra juice and pandan leaf juice  
60:40

E4: Blended okra juice and pandan leaf juice  
50:50

Table 1 Different ratios of blended okra juice and pandan leaf with vitamin C supplementation

| Ingredient          | Experiment |     |     |     |
|---------------------|------------|-----|-----|-----|
|                     | 1          | 2   | 3   | 4   |
| okra juice )ml(     | 1000       | 700 | 600 | 500 |
| pandan leaf )ml(    | 0          | 300 | 400 | 500 |
| sucrose )g(         | 65         | 65  | 65  | 65  |
| citric acid )g(     | 1.2        | 1.2 | 1.2 | 1.2 |
| sodium chloride )g( | 8          | 8   | 8   | 8   |

|               |     |     |     |     |
|---------------|-----|-----|-----|-----|
| vitamin C )g( | 0.5 | 0.5 | 0.5 | 0.5 |
|---------------|-----|-----|-----|-----|

Table 2 Physical measurement of blended okra juice and pandan leaf juice products with vitamin C supplementation

| Experiment | physical values*   |                     |                     |                    |
|------------|--------------------|---------------------|---------------------|--------------------|
|            | L*                 | -a*                 | b*                  | % T                |
| 1          | 27.61 <sup>b</sup> | -3.00 <sup>a</sup>  | 10.59 <sup>c</sup>  | 77.09 <sup>c</sup> |
| 2          | 28.48 <sup>b</sup> | -2.67 <sup>a</sup>  | 12.13 <sup>b</sup>  | 74.02 <sup>d</sup> |
| 3          | 29.78 <sup>a</sup> | -6.35 <sup>b</sup>  | 12.51 <sup>ab</sup> | 83.63 <sup>b</sup> |
| 4          | 29.58 <sup>a</sup> | -10.08 <sup>c</sup> | 13.55 <sup>a</sup>  | 87.50 <sup>a</sup> |

Note: \*a-d The different letters in the same column mean significant difference ( $P \leq 0.05$ )

Table 3 Chemical measurement of blended okra juice and pandan leaf juice products with vitamin C

| Experiment | chemical values   |                           |                   |
|------------|-------------------|---------------------------|-------------------|
|            | pH*               | TSS (°Brix) <sup>ns</sup> | % total acidity*  |
| 1          | 4.01 <sup>b</sup> | 9.00                      | 0.13 <sup>b</sup> |
| 2          | 4.08 <sup>a</sup> | 9.10                      | 0.21 <sup>a</sup> |
| 3          | 3.65 <sup>d</sup> | 9.08                      | 0.23 <sup>a</sup> |
| 4          | 3.71 <sup>c</sup> | 9.07                      | 0.14 <sup>b</sup> |

Note: \*a-d The different letters in the same column mean significant difference ( $P \leq 0.05$ ) and ns non significant difference ( $P > 0.05$ )

Table 4 Mean score of preference for sensory properties of blended okra juice and pandan leaf juice products with vitamin C supplementation

| Experiment t | scores              |                    |                     |                       |                       |
|--------------|---------------------|--------------------|---------------------|-----------------------|-----------------------|
|              | color <sup>ns</sup> | odor <sup>ns</sup> | taste <sup>ns</sup> | clarify <sup>ns</sup> | overall acceptability |
| 1            | 7.03                | 6.77               | 6.63                | 6.83                  | 7.13 <sup>a</sup>     |
| 2            | 7.30                | 6.57               | 5.91                | 6.57                  | 6.77 <sup>ab</sup>    |
| 3            | 7.13                | 6.37               | 5.80                | 6.31                  | 6.57 <sup>b</sup>     |
| 4            | 6.77                | 6.30               | 6.17                | 6.42                  | 6.63 <sup>b</sup>     |

Note: \*a-d The different letters in the same column mean significant difference ( $P \leq 0.05$ ) and ns non significant difference ( $P > 0.05$ )

## CONCLUSION

1. The uses of different ratios of raw material preparation had effects on the quality of mixed okra juice and pandan leaf juice.

2. The results of the physical properties analysis showed that all values were statistically significant differences ( $P \leq 0.05$ ).

3. The results of the chemical analysis showed that percent of total acidity (except pH and total soluble solid) were significantly different ( $P \leq 0.05$ ).

4. Blended okra juice (control) gave the most overall acceptability of 7.13 values from the panelists.

5. The results of total plate count indicated that no microorganism in each experiment was not found.

6.. Based on this research, researchers will be able to launch new sport drink products in the future by selecting the appropriate Thai local vegetables and fruits that are beneficial for antioxidants, an option for health-conscious consumers.

## ACKNOWLEDGMENTS

The researchers would like to thank the 4 the grade students and officials of the Division of Food Science and Technology, the Faculty of Agricultural Technology Rajamangala University of Technology Thanyaburi (RMUTT), Pathum Thani Thailand that contributed some parts in the research. The Faculty of Agricultural Technology provided support facilities and budgets for the research.

## REFERENCES

- [1] Nguyen, T. H. and Gizaw, A., Factors that influence consumer purchasing decisions of Private Label Food Products, School of Business, Society and Engineering Bachelor thesis in Business Administration, 2014, 92 p.
- [2] Wiriyajaree, P., Role of beverage industry. Department of Food Science and Technology, Faculty of Agriculture, Chiang Mai University, Chiang Mai; 1992.
- [3] Ministry of Public Health, Notification of the Ministry of Public Health (No. 195) (2000). Electrolyte Drinks [Internet]2000 [cited 2017 Januray 25]. Available from: [http://food.fda.moph.go.th/law/data/announ\\_moph/P195.pdf](http://food.fda.moph.go.th/law/data/announ_moph/P195.pdf).
- [4] Zoroddu, M.A., et al., The essential metals for humans: a brief overview. Journal of Inorganic Biochemistry, Vol 195, 2019, pp. 120–129.
- [5] Singh, P., et al., An overview on okra (*Abelmoschus esculentus*) and its importance as a nutritive vegetable in the world, International Journal of Pharmacy and Biological Sciences, Vol. 4, 2014, pp. 227-233.
- [6] Aini, R. and Mardiyansih, A., Pandan leaves extract (*Pandanus amaryllifolius* Roxb) as a food preservative. Indonesian Journal of Medicine and Health, Vol 7, 2016, pp. 166-173
- [7] Phiomkraipak, C., Comparison of the determination of chloride content in electrolyte drinks by titration and sedimentation. Research report, Phetchaburi Rajabhat University; 1997.
- [8] Mak, S. and Engwongtrakoon, A., The optimum temperature on dried okra for phenolic compound of green tea mixed with okra by tray drying, B.Sc. Senior Project, Division of Food Science and Technology Faculty of Agricultural Technology Rajamangala University of Technology Thanyaburi. Thailand, 2013, 97 pp.
- [9] Rapeesak, S., Effect of Pasteurization storage and food additive on capable of antioxidant in

- tangerine Juice, Faculty of Agricultural Technology, King Mongkut's Institute of Technology Ladkrabang, 2004.
- [10] Damnum, A., Statistical analysis and data analysis, Kasetsart University Press. Bangkok, 2006.
- [11] Lozano, J.E., Fruit manufacturing: Scientific: basis, engineering properties, and deteriorative reactions of technological importance, Springer Science & Business Media, LLC.. USA, 2006.
- [12] AOAC, Official Method of analysis. Verginia: The Association of official Analytical Chemists, 2000.
- [13] Anprung, P., Principle of food analysis by sensory evaluation, Bangkok.: Chulalongkorn University Press.
- [14] Wirivutthikorn, W. and Jenkunawatt, S., Preference colors of gac fruit blended with pineapple juice, Tien-Rein LEE (Editor –in-Chief), The 2nd Conference of Asia Color Association URBAN COLOR FOR LIFE 4-7 September 2014, Taipei, Taiwan, 2014, pp.304-307.
- [15] Wirivutthikorn, W., Effect of lemongrass and pandan leaf ratios on production of mixed juice with lycopene supplementation, International Conference of Agriculture and Natural Resources 26-28 April 2018, Proceedings ANRES 2018, Bangkok., pp. 378-381.
- [16] Wirivutthikorn, W. and Jenkunawatt, S., Factors affecting on drying of okra and gac fruit in okra blended with gac fruit powdered beverage production, Research Report. Faculty of Agricultural Technology, Rajamangala University of Technology Thanyaburi, 2017, pp. 1-44.
- [17] Wirivutthikorn, W., Effect of ratio of okra gac fruit and passion fruit on color and preferences of mixed juice, International Journal of Food Engineering, Vol 4, 2018, pp. 212-215.
- [18] Kinchampa, A and Anothaiwattana, A., Study of physical and sensory properties on the consumer of carrot juice products with passion fruit juice. Bachelor of Science degree Science and Food Technology, Faculty of Agricultural Technology, Rajamangala University of Technology Thanyaburi, Pathum Thani; 2009.
- [19] Rebecca, L. J., et al., Extraction and purification of carotenoids from vegetables, Journal of Chemical and Pharmaceutical Research, Vol. 6, 2014, pp. 594-598.
- [20] Wirivutthikorn, W., Effect of passion fruit Juice and sugarcane juice ratios on blended passion fruit juice and sugarcane juice production, Agricultural Sci. J. 49, No.3 (Suppl), 2018: pp. 229-235.
- [21] Ciuffreda, E. et al., *Alicyclobacillus* spp.: New insights on ecology and preserving food quality through new approaches, Microorganisms, Vol 3, 2015, pp. 625–640.
- [22] Obasi, B.C., Whong C.M.Z. and Ameh, J.B., Nutritional and sensory qualities of commercially and laboratory prepared orange juice, African Journal of Food Science, Vol. 11, 2017, pp. 189-199.
- [23] Wirivutthikorn, W., Effects of types and quantities of sweeteners on development of blended lotus root juice and goji berry product In: Proc. the 6th Academic Science and Technology Conference 2018 6 June 2018. p. AS176-AS180.
- [24] Intakul, N., Product development of passion fruit product. Research report. Division of Food Science and Technology, Faculty of Science and Technology, Chiang Rai Institute. Chiang Rai; 2001.
- [25] Figueiredo, L.P. et al., Influence of process parameters on the color and texture of passion fruit albedo preserved in syrup. J Food Sci Technol Campinas, 2013, Vol 33(1), pp. 116-121.
- [26] Wirivutthikorn W., Appropriate ratios of producing riceberry blended with gac fruit and roselle beverage. In Proc 3rd National and International Research Conference 2019 : NIRC III 2019 “Challenges of Higher Education in Production of Graduate Students in the 21st Century” 1st February 2019. Buriram Rajabhat University, Buriram, Thailand: 2019, pp. 2117-2126.
- [27] Wirivutthikorn W., Effect of okra and tangerine ratios on production of mixed juice with lycopene supplementation. In: proceedings of the 4th Int. Conf. on Science, Engineering & Environment (SEE), November 12-14, 2018; Nagoya, Japan; 2018, pp.15-19.

## ESTIMATING PEOPLE'S TRAVEL BEHAVIOR TOWARDS TRANSIT-ORIENTED DEVELOPMENT IN DUKUH ATAS, DKI JAKARTA PROVINCE

Gemala Pritha Ryzki Rynjani<sup>1</sup>, Chotib<sup>2</sup>

<sup>1</sup>Faculty of Economics and Business, Universitas Indonesia, Indonesia; <sup>2</sup>Faculty of Economics and Business, Universitas Indonesia, Indonesia

### ABSTRACT

Increasing resident activity in Jabodetabek has highlighted that increased traffic flow and transportation needs could cause congestion and environmental problems. To address these possible transportation problems, a transit-oriented development (TOD) policy is soon to be implemented in Dukuh Atas, Jakarta. Therefore, the research objective was to examine resident travel behavior based on socioeconomic characteristics and land use based on the TOD policy in Dukuh Atas. A model was developed to more closely examine the travel behavior influencing factors in the Dukuh Atas TOD area. Questionnaires were distributed to 300 respondents (150 inhabitants near the transit station and 150 commuters), and the data analyzed using structural equation modeling (SEM). It was found that the travel behavior in Dukuh Atas TOD was more influenced by socioeconomic status than land use in the TOD area. In general, the income, transportation costs, and educational background variables were found to be the most influential socioeconomic variables. Moreover, respondent travel behavior was not found to be unduly influenced by transit area facilities.

*Keywords: Travel Behavior, Transit-Oriented Development, Structural Equation Modeling*

### INTRODUCTION

As cities drive economic growth and development, urbanization has been seen as a policy tool to drive city development and improve the quality of life of the residents. According to the World Bank (2007), by 2025, approximately 67.5% of Indonesia's population are expected to be living in urban areas. In recent years, due to an increase in infrastructure facilities and qualified jobs, Jakarta has been growing rapidly, with an estimated increase in population of 269 people a day. Until 2017, the population density in Jakarta was 15,234 people / km<sup>2</sup>.

According to Statistics Indonesia, the average population growth rate in Jakarta was 1.09 since 2000. However, after 2010, the number of migrants to Jakarta city started to decline, with many migrants preferring to move to the Jakarta hinterland to Bogor, Depok, Tangerang, and Bekasi (JABODETABEK) possibly because the land prices were lower than in Jakarta.

JABODETABEK commuter survey in 2014 found out that the 28 million JABODETABEK residents, 13% or  $\pm$  3.5 million people were commuter residents. Data from the JABODETABEK Transportation Management Agency (BPTJ) also found that the volume of vehicles per day in Jakarta was 940,000, the toll road load per day for four-wheeled vehicles heading to Jakarta was 31% or 423,000 vehicles per day from Tangerang and South Tangerang, 31% or

426,000 vehicles per day from Depok and Bogor, and 38% or 571,000 vehicles per day from Bekasi.

The increase in population density has begun to affect the urban transportation facilities in Jakarta. Because of the urban sprawl, the government is expected to implement technical instruments and planning regulations, especially for the transportation sector.

Jakarta's urban problems are a government concern as it is the government's responsibility to provide quality urban infrastructure facilities that are capable of accommodating large numbers of commuters. With the rising commuter loads from BODETABEK, multimodal transport systems and networks and convenient public transport services are needed. Therefore, the government needs to "force" people to switch to public transportation rather than using private transport.

Transit-oriented development (TOD) is a concept that supports smart growth, increases economic growth, is able to change market demand and lifestyle preferences (Cervero, 2004), also minimizes human and vehicle movements. Therefore, the TOD concept could be the answer to ensuring sustainable economic, social and environmental urban development. TOD concentrates urban activities in one transit point through mixed land use (mixed-use) and compact development (Calthrope et al., 2004). Which means, placing commercial centers, housing, offices, parks and public facilities within walking distance of transit stops. To support the



transportation system development, the government through the Minister of ATR / BPN in Indonesia is responsible for developing policies for TOD. Basically, the regulation reviews the basis and purpose for TOD areas to support urban transportation systems that are pro-commuter and are aligned with the socioeconomic carrying capacity of the community in the TOD area as well as the residents living in the transit area vicinity.

Because the policy has now been drafted, it is expected that there will be several TOD areas announced for Jakarta. These areas need to be able to accommodate at least two modes of public transportation, one of which should be rail-based and located downtown; therefore, the Jakarta TOD is to be centralized in the Dukuh Atas area. Several rules for the Jakarta TOD have been made to comply with Governor Regulation No. 44 of 2017 concerning the Development of Oriented Development Areas. The existing conditions in Dukuh Atas are basically in accordance with the requirements for TOD areas. Data from the PT MRT Jakarta (2018) show that Dukuh Atas is already an intermodal mass transportation area with connections to Sudirman KRL Station, the Airport Train Station, Jakarta MRT Station, Dukuh Atas LRT Station and the Transjakarta Bus Stop. Dukuh Atas also has many commercial and residential activities such as offices, retail stores, hotels, and apartments. Therefore, developing this area as the key transportation node and the center of economic development in Jakarta has many challenges because of the current inadequate environmental, social and economic quality, flood risks, urban congestion problems, and poorly functioning pedestrian (pedestrian) and bicycle road network. For this reason, this development requires the implementation of regional principles that are focused on land use with mixed functions that allow for high density development and ensure increased connectivity, an improved quality of life, social justice, environmental sustainability, infrastructure resilience, and economic regeneration.

As well as the aim to streamline public transport services in TOD areas, the TOD can also increase social capital by improving the kinship between the local communities or neighbors (Nallari, Griffith, & Yusuf, 2012), which could overcome the main problems associated with urbanization; the lack of strong social bonds. However, TOD have been found to increase the social capital for people living closer to the station. TOD research in China in Beijing and Shenzhen, found that accommodating the development of multimodal transportation was able to improve ecological, economic and social sustainability in these rapidly growing cities (Xie, 2017). Although TOD implementation development indicators have shown that it can be successfully applied, each city has varying

development needs. Therefore, this paper examines travel behavior around the Transit-Oriented Development in Dukuh Atas in terms of the socioeconomic characteristics and land use development policy and develops a model that explains the influencing factors for travel behavior in the Dukuh Atas TOD area.

## METHODS

This research was conducted in the transit-oriented area Dukuh Atas located on Jalan Juana, Jalan Kendal, to Jalan Blora, Kelurahan Menteng, Kecamatan Menteng, City of Central Jakarta. In the DKI Jakarta Provincial Spatial Plan for 2012 - 2030 and the DKI Jakarta Province Spatial Detail Plan for 2014 –2019, the Dukuh Atas area was identified as a priority area for the primary TOD activity. Dukuh Atas is a large scale, high density residential, commercial and business area in the Sudirman-Thamrin area and has significant potential as a central transit-oriented area. The focus of the research was the TOD area and the surrounding areas that would be affected by the TOD. The buffer Map (Figure 1) shows the 800 meters transit point area that is to be affected by the TOD.

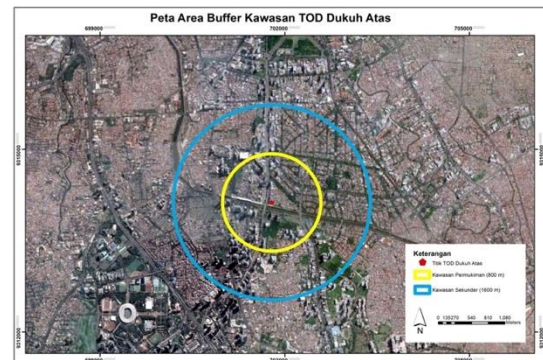


Fig. 1 Buffer Area for the Dukuh Atas TOD

The research took a stratified random sampling approach, which is considered suitable for proportional and heterogeneous populations (Margono, 2004; Sugiyono, 2001; Meng, 2013). Stratified random sampling was also used because the sampling could be done in all survey locations and because the estimates have been found to be more accurate for each section of the population. Sample collection was conducted on people in the area around the TOD Dukuh Atas. The determination of the number of respondents to be approached in this study was according to Joreskog & Sorbom (1996) based on the number of research variables. In this research, as there were 22 variables, the sample was determined based on the following formula:

$$\text{Sample minimum} = \frac{\kappa(\kappa + 1)}{2} \quad (1)$$

k = number of variables

The estimation of the minimum study population using the Joreskog & Sorbom's (1996) formula was 210 local residents and commuters; because of a possible sampling error of 5%, the research sample was rounded to 300 respondents; 150 resident respondents and 150 commuter respondents. The commuters were identified as people who were travelling across districts and cities to carry out their daily activities and the residents were people who had been living within a radius of  $\pm 800$  meters around the Dukuh Atas TOD area transit point for at least 6 months or not up to 6 months but with the intention to stay. The occupant data was obtained using a questionnaire that required the respondent to systematically answer the study questions. The household questionnaire was designed to capture the characteristics of the housing environment and socioeconomic characteristics of the household (e.g., car ownership and household income) (Van Acker, Witlox, & Van Wee, 2007).

The resident and commuter travel behavior model in the TOD area was developed using the structural equation modeling (SEM) approach, which is a multivariate analysis technique used to build and test a statistical model and develop a causal model (Golob, 2001; Hairulsyah, 2013). SEM is a hybrid statistical modeling technique that includes confirmatory aspects from the factor, path, and regression analyses, and has cross-sectional, linear and general properties. The SEM analysis in this study was processed using SmartPLS software, which is used for structural equation modeling and includes formative indicators to make predictions through relationship testing between each variable construct (Soo, 2016).

This research examined government policies on the development of the TOD area regarding the behavior of public transportation users in the Dukuh Atas TOD area and the population around Dukuh Atas.

The analysis included three latent variables. The latent construct predictor variable was socioeconomic (X1), the observation variables were gender (X11), age (X12), occupation (X13), education (X14), income (X15), and transportation costs (X16), and the mediator variables were the TOD (X2) simultaneous variables; walkability predictor variables (X21), walking distance (X22), walking time (X23), alternative mode (X24), cycle (X25), cycling access (X26), connect (X27), signage (X28), pedestrian access (X29), one-stop center (X210), parking (X211), park and ride

(X212), and livability (X213). The latent travel behavior construct (Y) was explained using the following observation variables; distance (Y1), choice of public transportation mode (Y2), trip (Y3), and time (Y4). The results of the model are shown in Figure 2.

## RESULTS AND DISCUSSION

To identify the characteristics of each of the inhabitant and commuter respondents, a questionnaire was distributed to 150 residents in the vicinity of the Dukuh Atas TOD area and 150 commuter respondents. The respondents' socioeconomic quantitative data is shown in Table 1.

Table 1 Respondent Characteristics

| Social<br>Economics                            | Frequency (%) |           |
|--|---------------|-----------|
|  | Inhabitants   | Commuters |
| <b>Gender</b>                                  |               |           |
| Male   | 58%           | 52,7%     |
| Female   | 42%           | 47,3%     |
| <b>Age</b>                                     |               |           |
| 15–25  | 32.0%         | 38.7%     |
| 26–35  | 28.7%         | 34.0%     |
| 36–45  | 20.7%         | 16.7%     |
| 46–55  | 8.7%          | 10.7%     |
| 56–65  | 4.0%          | 0.0%      |
| 66–80  | 6.0%          | 0.0%      |
| <b>Job</b>                                     |               |           |
| Employee                                       | 32%           | 60.7%     |
| Entrepreneurship                               | 12,7%         | 21.3%     |
| Merchant                                       | 7.3%          | 1,3%      |
| Housewife & Student                            | 39.3%         | 14.7%     |
| Others   | 8.7%          | 2%        |
| <b>Education</b>                               |               |           |
| Not Graduated                                  | 0.7%          | 0.0%      |
| Graduated from elementary school               | 2.0%          | 4.0%      |
| Graduated from junior high school / equivalent | 9.3%          | 4.7%      |
| Graduated from high school / equivalent        | 59.3%         | 26.0%     |
| Graduated from Diploma                         | 10.7%         | 23.3%     |

| Social Economics    | Frequency (%) |           |
|---------------------|---------------|-----------|
|                     | Inhabitants   | Commuters |
| Graduated (S1)      | 18.0%         | 40.0%     |
| Graduated (S2)      | 0.0%          | 2.0%      |
| <b>Income/month</b> |               |           |
| <=3,5 million       | 36%           | 34%       |
| 3,51 - 5 million    | 41.3%         | 34%       |
| >= 5,1 million      | 22.7%         | 32%       |

Source: Primary Data, processed with SPSS, 2018

The Jakarta urban sprawl has had an impact on the many daily commuters to Jakarta. As shown in Table I, the majority of people commute for employment purposes, with the others attending school or involved in activities around the Dukuh Atas transit area. The survey revealed that 60.7% of commuters came to Jakarta for work, and 39.3% of local residents were either housewives or students. Around 40% of commuters had graduated from college (40%), but the majority of local residents had only graduated from high school (59.3%). In terms of income, however, 41.3% of residents earned 3.51–5 million and 36% earned up to 3.5 million, whereas 34% of commuters earned below 3.5 million, 34% earned between 3.51 to 5 million, and 32% earned more than 5.1 million, which means that one-third of commuters were in the upper middle category based on the World Bank calculations. Previous studies have found that populations around transit areas are generally low-income households without cars (Cervero, 2004), which was also found in this study.

Table 2 Travel Behavior Characteristics

| Social Economics     | Frequency (%) |           |
|----------------------|---------------|-----------|
|                      | Inhabitants   | Commuters |
| <b>Distance (km)</b> |               |           |
| 00 - 0.4 km          | 70.0%         | 76.7%     |
| 0.41 - 1 km          | 26.7%         | 13.3%     |
| 1.1 - 4 km           | 2.7%          | 9.3%      |
| 4.1 - 7 km           | 0.7%          | 0.7%      |
| <b>Time (min)</b>    |               |           |
| <= 0 - 2 minutes     | 68.0%         | 73.3%     |
| 2.1 - 7 minutes      | 2.0%          | 5.3%      |
| 7.1 - 15 minutes     | 26.0%         | 18.0%     |
| 15 - 30 minutes      | 4.0%          | 3.3%      |
| <b>Trip</b>          |               |           |
| Walking              | 6.0%          | 1.3%      |

| Social Economics  | Frequency (%) |           |
|---|---------------|-----------|
|   | Inhabitants   | Commuters |
| 1 time  | 60.7%         | 46%       |
| 2 times   | 18.0%         | 46%       |
| More than 3 times   | 15.3%         | 6.7%      |
| <b>Public Transport Usage</b>   |               |           |
| Never   | 15.3%         | 8.0%      |
| Sometimes (<5 times a week)   | 50.0%         | 43.3%     |
| Often (5–10 times a week)   | 21.3%         | 14.0%     |
| Yes, always (> 10 times a week)                                       | 13.3%         | 34.7%     |
| <b>Mode Choice</b>  |               |           |
| Not Using Public Transport  | 20%           | 17.3%     |
| KRL / Commuter line   | 38%           | 49.3%     |
| Transjakarta bus  | 30.7%         | 32.7%     |
| Public vehicles with routes (Metromini, Kopaja, Mayasari Bakti, etc.) | 8.7%          | 0.7%      |
| Busway Integrated Border Transportation (APTB)                        | 2.0%          | 0%        |
| Pick-up public transportation   | 0.7%          | 0%        |
| <b>Future Mode Choice</b>   |               |           |
| MRT   | 81.3%         | 79.3%     |
| LRT   | 6.0%          | 18.7%     |
| Airport Train   | 7.3%          | 0.7%      |
| Others  | 4.0%          | 1.3%      |

Source: Primary Data, processed with SPSS, 2018

In terms of the land use in the TOD area, the rail and non-rail mass public transportation, the pedestrian and bicycle lane transit functions are very important. Moreover, to reduce the use of personal vehicles, walking or cycling provisions are needed. Table 2 shows the resident and commuter travel behavior, from which it can be seen that most residents (70%) and commuters (76.7%) travelled 00 - 0.4 km from the transit point from their place of residence to the place of their activities. More local residents (26.75) walked 0.41 - 1 km to their place of activity than commuters (13.3%), but more commuters (9.3%) walked 1- 4 km to their place of

activity than local residents (2.7%). However, very few commuters or residents walked 4.1 - 7 km (0.7%).

To improve the quality of Jakarta's development, the government plans to operate sustainable transportation; the Mass Rapid Transit (MRT) and Light Rapid Transit (LRT). The rail-based Mass Public Transport System (SAUM) was put into operation to complement the integration of the intermodal transportation in Dukuh Atas, following the opening of the airport fast train, Transjakarta, and the Busway Integrated Border Transportation (APTB). If it were already operating, most respondents claimed that they would switch to the MRT; 81.3% of residents and 79.3% of commuters. However, the propose used of the LRT mode was much lower at only 18.75 of commuters and 6% of residents.

### Analysis of Structural Equation Modeling

The travel behavior resident and commuter TOD area model was then analyzed using a SEM approach.

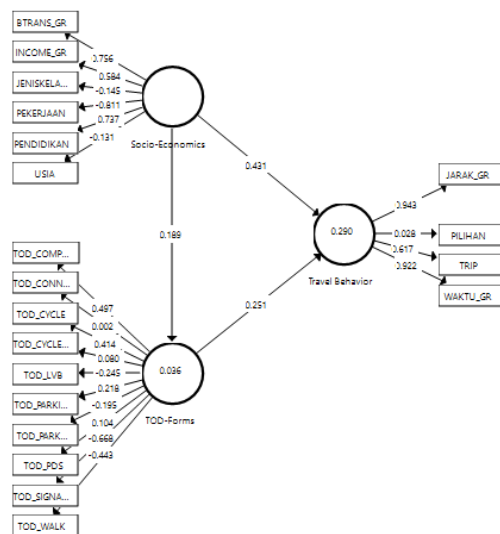


Fig. 2 SEM Result

Source: Primary Data, processed with SmartPLS, 2018

The SEM model analysis in Figure 3 revealed that the model fit was in accordance with previous research. The model test obtained a Chi-Square of 586.122.

Table 3 Model Fit

|            | Saturated Model | Threshold      | Evaluation |
|------------|-----------------|----------------|------------|
| SRMR       | 0.092           | <0.08          | -          |
| Chi-Square | 586.122         | Small          | -          |
| NFI        | 0.533           | Between 0 to 1 | -          |
| Prob.      | 0.000           | >0.05          | Good       |

Source: Primary Data, processed with SmartPLS, 2018

SEM research proposes that a normed fit index (NFI) be the first measurement after the calculation of the Chi-Square value (Bentler & Bonett, 1980). NFI values are between 0 and 1; the closer to the value is to 1 or when it is above 0.90, the model is seen to have acceptable compatibility. The NFI value in Table 3 was found to be 0.533, and as this value was between 0 and 1, the model was judged to be of average acceptability. The standardized root mean square residual (SRMR) value is used as a measure of goodness of fit to avoid misspecification in the model (Dijkstra & Henseler, 2015). From the SRMR value of 0.092 or <0.08 shown in Table III, it was concluded that there was no model misspecification. From Table III, it can also be seen that the model form was not good enough because the indicator variables in the model were not significant to each other.

Table 4 Average Variance Extracted (AVE)

|                 | Original Sample (O) | Sample Mean (M) | Standard Deviation (STDEV) | T Statistics ( O/STD EV ) | P Values |
|-----------------|---------------------|-----------------|----------------------------|---------------------------|----------|
| Socioeconomics  | 0.359               | 0.358           | 0.017                      | 21.135                    | 0.000    |
| TOD Forms       | 0.123               | 0.131           | 0.014                      | 9.044                     | 0.000    |
| Travel Behavior | 0.530               | 0.532           | 0.015                      | 34.528                    | 0.000    |

Source: Primary Data, processed with SmartPLS, 2018

Hypotheses test are used to assess the probability value of each variable if the value of  $P < 0.05$ . When the value of  $P > 0.05$ , this indicates that there is no correlation between the variables. As shown in Table IV, the AVE was found to have a correlation with all formative indicators <0.05, with all socioeconomic variables, TOD forms, and travel behavior being 0.000, clearly indicating that there was a significant effect between the independent variables and the dependent variables. As the t-statistic value for the formative indicator had a value higher than 1.96, the null hypothesis was rejected, which meant that all the formative indicators were in accordance with the study hypotheses.

Therefore, it was found that the travel behavior of Dukuh Atas TOD users was influenced more by socioeconomic status (0.431) than TOD land use (0.251). In general, income, transportation costs, and educational background had the most influence on the socioeconomic of the respondents. The choice of the place of residence was also influenced by the social status of the respondent, which indirectly affected travel behavior (Van Acker et al., 2007). That is, indirectly, the respondents who had higher transportation costs and travelled further for a longer time used several modes of transport to get

to their place of activity before transiting in the Dukuh Atas TOD area.

The behavior related to the respondents' travel was not found to be influenced by the transit area facilities, which was in disagreement with research in San Diego, in which it was found that this type of land use greatly influenced travel behavior (Boarnet & Crane, 2001). The difference between these findings was possible because of the marked differences between the socioeconomic status of the respondents and the urban facilities in Jakarta and those in San Diego.

The model analysis indicated that even though respondents were not satisfied with the service facilities in the transit area, the highly educated and high incomes respondents used public transportation because they lived quite far away and the travel time was quite long; however, socioeconomic status was not found to affect respondent activities in Dukuh Atas (0.189). Although in general the respondents were not satisfied with the infrastructure services at Dukuh Atas, the travel behavior was more influenced by social status, with respondents having a higher social status travelling longer distances for a longer time and taking more trips per day. Travel behavior was found to be less complex in respondents who had fewer household responsibilities and those living in urban environments.

## CONCLUSION

Based on the analysis results, the following conclusions were made.

The commuter and resident trip behavior around the transit area were somewhat similar. Most respondents did not see public transportation as the main means for their daily activities. In addition, both the commuters and residents were less willing if they had to walk and/or use bicycles to conduct their activities in the transit area.

The income, transportation costs, and educational background variables were found to be the most influential socioeconomic variables, and the respondent travel behavior was not found to be influenced by the transit area facilities. Respondents' socioeconomic backgrounds were found to have a greater influence on travel behavior than the land use in the TOD area. In contrast to many previous studies, in which it was found that compact land use significantly affected walking and public transportation use travel behavior, this was not found in this study, possibly because most respondents expressed a degree of dissatisfaction with the Dukuh Atas land use infrastructure quality.

## ACKNOWLEDGEMENT

The authors wish to acknowledge that this research was supported by Publications Grant for Thesis and Dissertation of Universitas Indonesia (PITTA UI Grant).

## REFERENCES

- [1] Bentler, P. M., & Bonett, D. G. (1980). Significance tests and goodness-of-fit in the analysis of covariance structures. *Psychological Bulletin*, 88, 588–600. doi:10.1037/0033-2909.88.3.588
- [2] Boarnet, M.G., & Crane, R. (2001). *Travel by Design*. Oxford, UK: Oxford University Press.
- [3] Calthrope, Peter. (1993). *The Next American Metropolis—Ecology, Community, and The American Dream*. Canada: Princeton Architectural Press.
- [4] Cervero, R. (2004). *Transit-oriented development in the United States: Experiences, Challenges, and Prospects*. Washington: Transit Cooperative Research Program.
- [5] Dijkstra, T. K., & Henseler, J. (2015). Consistent and Asymptotically Normal PLS Estimators for Linear Structural Equations, *Computational Statistics & Data Analysis*. 81(1): 10–23.
- [6] Golob, T. F. (2001). *Structural equation modeling for travel behavior research*. California: Institute of Transportation Studies.
- [7] Hairulsyah. (2013). *The influence of public participation on sustainable transportation and regional development in Medan*. Medan: UGM.
- [8] Nallari, R., Griffith, B., & Yusuf, S. (2012). *Geography of growth: Spatial economics and competitiveness*. Washington, DC: The World Bank.
- [9] Soo, Kim Gye. (2016). *Partial Least Squares Equation Modeling (PLS-SEM) an Application in Customer Satisfaction Research*, *International Journal of Service, Science and Tech*. <http://dx.doi.org/10.14257/ijunesst.2016.9.4.07>
- [10] Van Acker, V., Witlox, F., & Van Wee, B. (2007). The effects of the land use system on travel behavior: A structural equation modeling approach. *Transportation Planning and Technology*, 30(4), 331–353, DOI: 10.1080/03081060701461675
- [11] Xie, Jing. (2017). *Transit Oriented Development (TOD) for Urban Sustainability: A Comparative Case Study of Beijing and Shenzhen, China*. Canada: University of Waterloo

## ABOUT KARST (CHEMICAL) DENUDATION IN ZEMO IMERETI PLATEAU. GEORGIA, CAUCASUS

Zaza Lezhava<sup>1</sup>, Lasha Asanidze<sup>1</sup>, Kukuri Tsikarishvili<sup>1</sup>, Nino Chikhradze<sup>2</sup>, Lela Gadrani<sup>1</sup>

<sup>1</sup>Vakhushti Bagrationi Institute of Geography, TSU. Tbilisi, Georgia

<sup>2</sup>School of Natural Sciences and Engineering, Ilia State University. Tbilisi, Georgia

### ABSTRACT

One of the discussion issues of karstological studies is the identification of karst denudation intensity; it means the quantitative evaluation of the intensity of this process, which, in turn, allows to predict the karst development. The problem of karst denudation is developed insufficiently today, which can be explained by the complexity of the issue and at the same time, the methods used to assess the intensity of denudation are not yet refined. The intensity of denudation and its general regularities in the Zemo Imereti Plateau can be judged based on the materials available at our disposal today, which were obtained based on field, experimental and laboratory multi-year studies. Based on the materials obtained by comprehensive research conducted by us, we have studied and calculated the intensity of karst denudation in the Zemo Imereti Plateau. Studies have identified that the karst denudation intensity (surface - 64.2-190.6 m<sup>3</sup>/km<sup>2</sup>; underground - 1.5-117 m<sup>3</sup>/km<sup>2</sup> a year) in the Zemo Imereti Plateau significantly exceeds the similar indices of Apkhazeti (values of surface and underground karst denudation in high karst strip is equal to 75-108 and 30-45 m<sup>3</sup>/km<sup>2</sup> a year respectively, and in the foothills - 38-58 and 5-12 m<sup>3</sup>/km<sup>2</sup> a year respectively) and Askhi karst massifs (59 m<sup>3</sup>/km<sup>2</sup> a year), which is a result of impact of technogenic factor.

*Keywords: Karst, Plateau, Massif, Technogenic factor, Denudation intensity*

### INTRODUCTION

Definition of karst denudation intensity that allows predicting karst development is one of the discussing problems of karstological studies.

Karst denudation problem is weakly developed in general, which can be explained by the problem complexity. Modern methods to assess denudation intensity are not finally developed so far. For this purpose, it is necessary to identify the rivers' topographic and underground basins areas true boundaries, as well as indices of rainfall amount, runoff and evaporation, to take into account the mineralogical and chemical features of karstified rocks, etc. In addition, it is difficult to get a full picture of the real indicators of the denudation with single or episodic observations. Such conclusions on the karst rivers and karst sources should be based on seasonal observations if not on annual ones.

The intensity of denudation in the Zemo Imereti Plateau and their general regularities can be judged based on the materials available at our disposal today, which have been obtained on the basis of multi-annual field, experimental and laboratory studies.

The amount of ion runoff determines the rock destruction and distribution of rock destruction product:

$$Ru=31.54 \cdot QC \quad (1),$$

where:  $Ru$  – is the ion runoff, t/year;  $Q$  – stream discharge, m<sup>3</sup>/sec; and  $C$  – is the concentration of ions, mg/l.

Different modifications of this (1) formula are used in assessing chemical denunciation in karstology. Mostly they are based on the amount of runoff and the calcium content in it. The intensity of karst denudation in the study area has been calculated by us according to the formulas of A. Kruber [1], Zh. Korbel [2] and M. Pulina [3].

A. Kruber (2) was one of the first who calculated karst denudation. The mentioned author and Zh. Korbel [2] identify the amount of chemical denunciation by the amount of dissolved calcium carbonate. Their formulas have the following look:

$$Q=31.54 \cdot 10^3 \cdot n \cdot a \quad (2),$$

where  $Q$  – is a leaked CaCO<sub>3</sub> mass in kg/year;  $n$  – discharge, l/s; and  $a$  – CaCO<sub>3</sub> content, gr/l.

$$X = \frac{4ET}{100} \quad (3),$$

where  $x$  – is karst denudation value, m<sup>3</sup>/km<sup>2</sup> per year or mm/millennium;  $E$  – the height of runoff layer, dm;  $T$  – content of calcium carbonate in water, mg/l;

$$\frac{4}{100}$$

– is the coefficient of transfer of the weight units into the volume units.

Somewhat different formula is offered by M. Pulina (4). It has the following look:



$$D=0.0126 \cdot V \cdot \Delta T \quad (4)$$

where:  $D$  – is the speed of karst denudation in  $\text{m}^3/\text{km}^2$  per year or  $\text{mm}/\text{millennium}$ ,  $\Delta T$ – the mineralization of karst waters ( $\Delta T = T_1 - T_a$ , where  $T_1$ – is the karst waters mineralization,  $T_a$  – atmospheric precipitations mineralization), and  $V$  – runoff module from  $1/\text{sec.km}^2$ .

From the results obtained from the abovementioned three methods, we believe that to this actual situation is most fitted the results obtained by the karst- hydrometeorological method offered by M. Pulina, as it considers the mineralization of atmospheric precipitations, ignoring of which gives 8-12% of error. It is also calculated not only the number of ions in water but also the overall mineralization ( $\text{mg/l}$ ). Therefore, during the analysis, we mainly depend on the results obtained by the formula of M. Pulina [3]. A number of papers were dedicated to karst denudation in Georgia [4]-[10]. In this respect, there is no such investigation has been conducted in the karst region of Zemo Imereti.

## STUDY AREA

Zemo Imereti Plateau includes the easternmost part of western Georgia's limestone strip, characterized by its peculiar natural conditions (relief, tectonics, climate, surface and underground waters) and is the only region of the platform karst in Georgia [11]-[14].

The main morphological peculiarity of the study area is determined by geological structure. The boundary of the Zemo Imereti Plateau's karst region coincides with the surface of the surface contact of the Cretaceous limestones with the older formations (Bajocian porphyritic suite in the north and east and the Middle Paleozoic granitoids in the south and west), which is the geological substrate of the karst. The existence of a solid Hercynian platform stipulated the character of layout of the Meso-Cenozoic suites (subhorizontal or slightly inclined), which is represented mainly by the Valanginian-Hauterivian, Barremian and Turonian-Danian limestones, Tertiary clays and sandstones. Platform construction of the plateau has played an important role in the genesis and development of surface and underground karst forms and underground karst streams developed here (Fig. 1, 2).

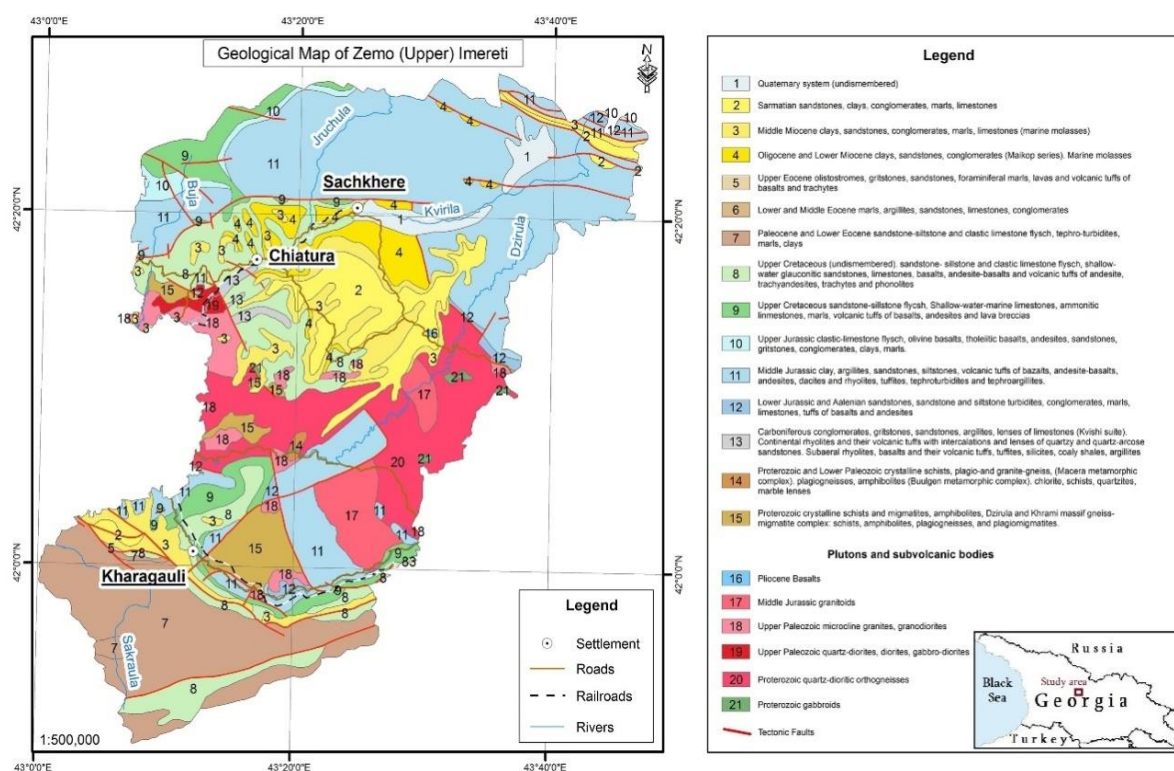


Fig. 1 Geological map of the Zemo Imereti Plateau [15].

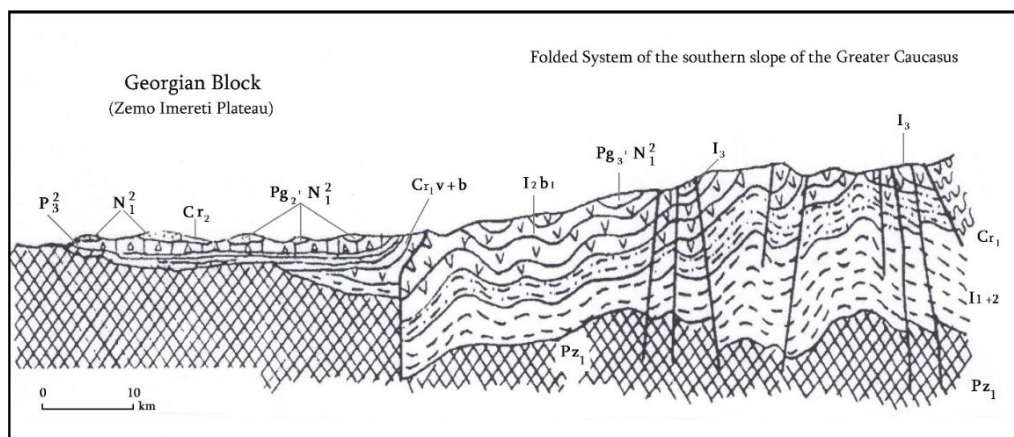


Fig. 2 Geological sections of the folded system of the southern slope of the Greater Caucasus and the Georgian block [16].

As it is known, the intensity of the karst processes greatly depends on the physical-geographic and geological conditions of the region. The amount of atmospheric precipitations and a runoff module along increase according with the increase in altitude of the karst massifs of Georgia that stipulate activation of karst processes. Korbel [2] and later M. Pulina's [3] observations confirmed this opinion by the case study of the karst regions of the moderate and subtropical regions of the Eurasian continent. Indeed, with the increase in precipitation and runoff by altitude, the speed of karst denudation increases gradually. Namely, intensity of karst denudation increases up to 4 m<sup>3</sup>/km<sup>2</sup> in foothills and up to 8 m<sup>3</sup>/km<sup>2</sup> – in high karst per year when the amount of annual precipitations increases by 100 mm [3].

What is the situation on the Zemo Imereti (Chiatura) Plateau? Based on the comparison of amount of atmospheric precipitations and the evaporability data, it may be noted that the balance of the annual runoff is everywhere positive within the karst strip of the study area [17], [18], which leads to the activity of karst processes throughout the year, especially in the cold period of the year. Apparently, in the abovementioned trend, there may be made corrections by technogenic factors and play stimulating role in the activation of karst processes that are confirmed by our studies.

## RESEARCH METHODS

Field, experimental and laboratory research methods were used in the study. Cartographic methods were used for determination of surface water catchment basins, and the method of painted water tracing with special paints (indicators) to determine the boundaries of underground basins.

The available climatic and hydrological data and the results of our long-term observations have been used to determine the amount of atmospheric precipitation, runoff and evaporation indicators.

The chemical composition and hydro-chemical regime of karst waters (namely, surface streams, karst sources and cave streams) were determined by stationary observations and laboratory investigations.

## RESULTS

Based on the materials obtained by our researches, first time was studied (calculated) the intensity of karst denudation on the Zemo Imereti Plateau, the results of which are given in the Table 1. The obtained data is partially based on episodic observations, though the chemical analysis of vaucluse sources and surface streams have been carried out once again several times in the different seasons of the year. In addition, detailed hydrochemical studies of karst waters were carried out, as well as regime observations on karst sources. Laboratory and experimental methods have identified the true boundaries of the areas of topographic and underground riverbasins. At the same time, for solution of a number of issues (substances migration, formation of composition of underground karst waters is formed, and etc.) the chemical (namely, macro and micro elements of surface streams, karst springs and cave streams) composition and hydrodynamic regime have been identified by stationary observations and laboratory studies [19], [11].

As it is known, the feature of the atmospheric precipitation, the fissureness of karstified rocks, the lithology and others have a considerable impact on the intensity of karst denudation. Based on the results obtained by us, we can discuss some of the trends that is characteristic of the karst massif of Zemo Imereti Plateau. In particular, there is a close relation between runoff and karst denudation, which means that karst denudation increases with the increase of runoff (Table 1).



Table 1 Karst denudation intensity in the Zemo Imereti Plateau.

| The source or river name  | Water catchment basin area, km <sup>2</sup> | Water discharge, l/sec | Run off module, l/sec km <sup>2</sup> | Common Mineralization, mg/l | Composition of CaCO <sub>3</sub> , m/l | Dissolved CaCO <sub>3</sub> amount, kg/day | Dissolved substance general amount (ion runoff), kg/day | Dissolved substance general amount (ion runoff), kg/year | Karst denudation, m <sup>3</sup> /km <sup>2</sup> per year |           |           |
|---------------------------|---|------------------------|---------------------------------------|-----------------------------|--|--|---|--|--|-----------|-----------|
|                           |   |                        |                                       |                             |  |  |   |  | By Kruber  | By Korbel | By Pulina |
| Ekvtimeskide (cave)       | 0.7   | 1.0                    | 1.4                                   | 409                         | 139.5                                  | 12.0                                       | 18  | 6570   | 1.5  | 2.2       | 5.6       |
| Namdzeviskide (cave)      | 0.5   | 1.0                    | 0.5                                   | 318                         | 116.2                                  | 10.0                                       | 10.5  | 3650   | 1.2  | 0.5       | 1.5       |
| Kidekari (cave)           | 3.8   | 45.0                   | 11.8                                  | 531                         | 210.0                                  | 34.0                                       | 1287  | 468755   | 102.0  | 30.5      | 60.8      |
| Nekrisa (cave)            | 12.9  | 260.0                  | 20.2                                  | 959                         | 268.8                                  | 251.7                                      | 16850   | 6150250  | 762.0  | 67.7      | 190.6     |
| Ormoebi (cave)            | 0.5   | 0.5                    | 1.0                                   | 1932                        | 213.1                                  | 0.3  | 75  | 27375  | 1.1  | 25.5      | 19.1      |
| Shvilobisa (cave)         | 1.1   | 7.5                    | 6.8                                   | 368                         | 115.0                                  | 3.1  | 109   | 39785  | 9.0  | 9.6       | 24.0      |
| Jruchula (cave)           | 2.5   | 5.0                    | 2.0                                   | 469                         | 245.0                                  | 4.4  | 116   | 42340  | 13.1   | 5.9       | 9.0       |
| Karianikide (cave)        | 4.8   | 250.0                  | 52.0                                  | 240                         | 125.0                                  | 112.5                                      | 3024  | 1103760  | 327.3  | 82.0      | 117       |
| Shekiladzeebiskide (cave) | 0.6   | 16.0                   | 26.6                                  | 349                         | 183.0                                  | 10.5                                       | 206   | 75190  | 31.4   | 60.8      | 84.0      |
| Rganisghele (river)       | 13.0  | 320.0                  | 24.6                                  | 276                         | 126.0                                  | 145.1                                      | 2101  | 766865   | 452.7  | 39.0      | 64.2      |

Distribution of karst denudation by heights is also interesting. In particular, in the study area, the increase of karst denudation intensity is observed with the increase of absolute height. For example, in the underground stream (570 m above sea level) basin of the Namdzeviskide Cave, the karst denudation value is 1.5 m<sup>3</sup>/km<sup>2</sup> per year, in the underground stream of the Shvilobisa Cave (612 m above sea level) – 24 m<sup>3</sup>/km<sup>2</sup> per year, in the underground stream of the Shekiladzeebi cave (860 m above sea level) – 84 m<sup>3</sup>/km<sup>2</sup> per year, and in the underground stream basin of the Karianikide Cave (1300 m above sea level) – 117 m<sup>3</sup>/km<sup>2</sup> per year.

The intensity of karst denudation is different for the different limestone stratigraphic horizons. Relatively low rate of denudation (1.5-5.6 m<sup>3</sup>/km<sup>2</sup>) was observed in the areas built by Middle Miocene limestones and marls, the average values (9.0-60.8 m<sup>3</sup>/km<sup>2</sup>) – in the areas built by Upper Cretaceous limestones, and the highest rates (84-117 m<sup>3</sup>/km<sup>2</sup>) in the areas built with by Barremian limestones.

It means that the intensity of karst denudation increases more, the more pure the limestones are. Surface streams are also distinguished by high intensity of denudation (Nekrisa River - 190.6 m<sup>3</sup>/km<sup>2</sup> per year, Rganisghele River – 64.2 m<sup>3</sup>/km<sup>2</sup> per year).

As hydrochemical studies of karst waters have been identified, the mineralization of underground karst waters of the research area is 1.5-3 times higher than the analog indicators of neighboring karst regions. The reason for this is not only the complex lithological-stratigraphic structure of the region but also the wide distribution of open pits of manganese ore (Fig. 3). In open pit areas (especially during rainfalls) intensive washing of substances from loose rocks take place [20], [21].



Fig. 3 Karst relief of the Zemo Imereti Plateau transformed under the anthropogenic impact.

Due to the above reason, mineralization of karst waters in the areas of distribution of open quarries on the Zemo Imereti Plateau varies between 500-712  $\text{mg.l}^{-1}$  and occasionally reaches the anomalous high values ( $\Sigma_i$  1052-2290  $\text{mg.l}^{-1}$ ) [19], [11].

The sharp increase in the overall mineralization of sources also leads to increased intensity of karst denudation. That is why a number of deviations are observed in the above mentioned trend. For example, the underground water discharge of the Ormoebi Cave is the lowest among the streams we have studied, but with the karst denudation rate (19.1  $\text{m}^3/\text{km}^2$  per year) it exceeds the sources with excess discharge that can be explained with a high rate of total mineralization of the underground stream of the Ormoebi Cave ( $\Sigma_i = 1932 \text{ mg/l}$ ) (Table 1). By the same reason is explained the high karst denudation rate (190.6  $\text{m}^3/\text{km}^2$  per year) of the Nekrisa River, which is fed with high mineralization karst springs and cave streams ( $\Sigma_i$  1052-2290  $\text{mg.l}^{-1}$  accordingly). Such high rates of mineralization are mainly because of the widespread of manganese open pits in the underground karst waters feeding basins. The influence of high mineralization is noticeable in the distribution of karst denudation according to the height above sea level.

## CONCLUSION

Based on the research material available at our disposal, it is possible to note that the Zemo Imereti Plateau exceeds the Apkhazeti (in the high karst strip the surface and underground karst denudation values are correspondingly 75 - 108 and 30 - 45, and in the foothills – 38-58 and 5-12  $\text{m}^3/\text{km}^2$  per year) and Askhi (59  $\text{m}^3/\text{km}^2$  per year) karst massifs with the indices of karst denudation (surface – 64.2-190.6; underground - 1.5-117.0  $\text{m}^3/\text{km}^2$ ) [7], [4]. In our opinion, the higher indicators of chemical denunciation intensity in the Zemo Imereti karst region are related to the technogenic factors (especially the open mining of manganese): the overall increase of water aggression, the high mineralization (mineralization of karst waters of the manganese areas is 1.5-3 times higher than the same indices of the karst regions of Georgia) and intensive washting of substances.

In order to avoid adverse consequences during agricultural use of karst massifs of the study area, we consider it necessary to consider and predict karst denudation.

## ACKNOWLEDGEMENTS

This work was supported by Shota Rustaveli National Science Foundation of Georgia (SRNSFG), grant number: №YS-18-096.

## REFERENCES

- [1] Kruber A.A. Karst region of the mountain Crimea. 1915.
- [2] Korbel J. Annales de geographie. № 336. 1959. LXIII, Mars-Avril.
- [3] Pulina M. Geogr. Polon. №14. 1968.
- [4] Jishkariani V. M. On karst denudation in the basin of the r. Tsachkhuri (Askhi massif, western Georgia). Bulletin of the Academy of Sciences of Georgia, 60, №2. 1970. Tb.
- [5] Abashidze E. M. Intensity of leaching of rocks of the thicket of the Shaori reservoir. Collection "Caves of Georgia". 1973. T. U, Tb.
- [6] Gabechava D. Sh. Ion current and denudative action of the karst waters of western Georgia. In the book "Problems of hydrogeology and engineer-geology of mountainous-folded area", № 8. 1978.Tb.
- [7] Kiknadze T. Z. Geology, hydrogeology and limestone karst activity (case study of Abkhazia). 1979. Tb.
- [8] Kochetov N. I. K. On comparative assessment of the intensity of karst denudation of some limestone massifs of the Western Caucasus. Geomorphology, №2. 1983.
- [9] Tintilozov Z. K. Karst caves of Georgia (morphological analysis). 1976. Tb.
- [10] Tintilozov Z. The karst and cave of Bzipi massive. Metsniereba. 1988. Tbilisi.
- [11] Lezhava Z. The Karst of Zemo Imereti Plateau and Its Surrounding Areas. Publishing House Universali, Tbilisi. 2015. (In Georgian)
- [12] Lezhava Z., Bolashvili N., Tsikarishvili K., Asanidze L., Chikhradze N. Hydrological and Hydrogeological Characteristics of the Platform Karst (Zemo Imereti Plateau, Georgia). 14th Multidisciplinary Conference on Sinkholes and the Engineering and Environmental Impacts of Karst. pp. 93-100. 2015. Rochester, USA.
- [13] Asanidze L., Chikhradze N., Lezhava Z., Tsikarishvili K., Polk J., Chartolani G. Sedimentological Study of Caves in the Zemo Imereti Plateau, Georgia, Caucasus Region. Open Journal of Geology. Scientific Research. 7. 2017a. p. 465-477.
- [14] Asanidze L., Lezhava Z., Tsikarishvili K., Chikhradze N., Polk J. Karst morphological processes and evolution of the limestone massif of Georgia from depositional, sedimentary, and structural investigations in Muradi Cave. Proceedings of 17th international congress of speleology. 2017b. Sydney, Australia.
- [15] Gudjabidze GE. Geological map of Georgia, Scale 1:500 000. (Editor: Gamkrelidze et al.). Georgian State Department of Geology and National Oil Company Saqnavtobi. Tbilisi, Georgia. 2003. (in Georgian).
- [16] Gamkredidze PD. The structure and development of the western part of the southern slope of the Greater Caucasus and the Georgian block. Geotectonics, № 4. Tbilisi. 1969. (in Russian).
- [17] Kordzakhia M. Climate of Georgia. 1961. Tbilisi.
- [18] Kordzakhia M. Javakhishvilisi Sh. Evaporability in the territory of Georgia. Works of the Vakhushti Institute of Geography, vol. 17. 1962. Tbilisi.
- [19] Supatashvili G. D., Lezhava Z. I., Tintilozov Z. K., Shioshvili L. Sh. Hydrochemical characteristics of the karst regions of Zemo Imereti. Bulletin of the Academy of Sciences of Georgia. 1990. 140, pp. 345-348.
- [20] Lezhava Z., Tsikarishvili K., Asanidze L., Bolashvili N., Chikhradze N., Chartolani G. Ecological Investigation of karst water in the central part of Georgia. Lap Lambert Academic Publishing. Saarbrucken. 2017. ISBN: 978-620-2-02210-1.
- [21] Lezhava Z., Tintilozov Z., Jamrlishvili A. Technogenic factor and karst genesis on Chiatura structural plateau. Vakhushti Bagrationi Institute of Geography, Summary Session. 1991. Tbilisi.

# RESEARCH AND DEVELOPMENT OF PILLOW FOR HEALTH IN THAI PEOPLE: A PILOT STUDY

Panida Chaiming<sup>1</sup>, and Wichai Eungpinichpong<sup>2\*</sup>

<sup>1</sup>Ph.D candidate, Exercise and Sport Science, Faculty of Graduated School, Khon Kaen University, Thailand

<sup>2</sup>BNOJPH Research Center, Faculty of Associated Medical Sciences, Khon Kaen University, Thailand

\*Corresponding author, E-mail: [wiceun@yahoo.com](mailto:wiceun@yahoo.com)

## ABSTRACT

Proper size of pillow is an important factor in promoting quality and quantity of sleep. However, the most of pillows available in the market are built according to the curve of the cervical spine of the people in the west which may not be suitable for Thai people. We preliminarily determine the proper pillow size by verifying the effect of 8 cm, 10 cm, and 12 cm based on the perception of comfort, the ability to produce force of the wrist flexor muscles, electromyography (EMG) signals of the upper trapezius muscle and wrist flexor muscle, and skin temperature of neck. In addition, we studied on the correlation between the body height and the preferred pillow size. Thirty healthy individuals aged 20-80 years participated. The participants underwent baseline tests. After 5 minutes, the participants performed the post-tests and rated on perception of comfort as they rested in the supine position with their heads supported on three different heights of an adjustable pillow. Descriptive analysis and Spearman rank test were used to evaluate for pillow size preference. Most of the participants preferred the 8 cm. pillow heights. However, most of the force and EMG of the wrist flexor muscle were greatest when they rested on the 10 cm, and 12 cm of pillow heights. EMG of the upper trapezius muscle and the temperature of the neck were not statically significant among resting on the three of pillows. There was no correlation between the body height and the preferred pillow size. The three pillow heights could be suitable for sleeping in Thai people.

**Keywords:** Pillow, Healthy, Comfortable, Thai people

## INTRODUCTION

In daily life, people need to sleep for at least 8 hours, which is one third in daily life. Having good sleep results in a better immune system of the body [1]. After a good sleep, people can work efficiently during the day. On the other hand, insomnia or insufficient sleep can lead to negative effects on the body and mind such as colds, stress, other infections, metabolic syndrome, reduced performance of work, and wrong decision [7].

To have a good sleep, proper pillow size and shape is essential for supporting the head and neck. Prolonged use of improper pillow size and shape may lead to neck strain, headache, and chronic cervical spine disorders. The optimal pillow size and shape require that the sleeper feels comfortable, relax the neck muscles, reduce core temperature of the body, and allow the cervical spine being in neutral position during sleep. Previous studies reported that, reducing of the core temperature could decrease resting heart rate, provide deep sleep, and increase sleep quality [2,4,5,6]

Many materials, such as polyester, foam, feather, and latex, have been used to make pillows since they could restrain the head and neck during sleep. Proper pillows made from latex have been found to reduce

neck pain, stiff neck, headache, scapula and arm pain. They could provide the feeling of comfortable sleep, and better sleep quality when compared to pillows made from polyester, foam, and feather [2,3,4,]. It was possible that when people were lying on the side on the pillows made from latex, the curvature of the cervical spine did not change much [4]. This may be due to the properties of the latex with moderate tensile strength, high elasticity, and good tear resistance.

In addition to the type of material used to make the pillows, it is important to sleep on a proper dimension of the pillow. The size, height and length of the pillows according to the cervical spine are also important for sleeping. If the pillows are not suitable for head support while sleeping, it can make the sleeper feel unwell, and neck pain. This could reflexly result in the inhibition of arm muscle function [11]. Therefore, pillows with proper height, and fully support the cervical spine could help increase arm muscle strength [12].

Commonly used pillows by Thai people currently have a variety of forms such as squares, spherical discs, and wedge-shaped pillows. To prevent neck pain or help the cervical spine to be in a natural alignment, a pillow that has a convex section fitted to the curvature of the cervical spine and fully support the head is needed. Most of the pillows available in



the markets are replicated from the Western countries where the curves of the cervical spine of people are different from of the Thai or Asian people with similar physical structure. Therefore, the researchers are interested in developing proper pillows to suit Thai or Asian people where physical stature, social and cultural context is different from those in the Western countries. Specifically, purpose of this study was to evaluate the three levels pillow height on the feeling of comfort, electromyography of upper trapezius and the wrist flexor muscles of dominant limb, skin temperature of neck while lying on the pillow, and hand grip strength. We also verify the relationship between anthropometry of the body and the pillow height that provide the most comfortable sleep.

## METHOD

### Participants

This preliminary underwent on 30 participants. They were healthy Thai people, aged between 20 -80 years old, and were randomly allocated in three different age groups of 10 20-35 years, 36-60 years, and 61- 80 years respectively. The participants were excluded if they had a cervicothoracic spine injury or accident within 6 months, the dominant upper limb injury within 6 months, cervical vertigo, and muscle weakness of the dominant upper limb.

### Experimental Procedure

The study was approved by the Institutional Review Board of the Khon Kaen University Ethics Committee in Human Research (HE592390). All participants were received informed consent. This study was a cross sectional study. All participants were asked to test the anthropometry, comfort level of each pillow height, and the electromyography of upper Trapezius muscle and the wrist flexor muscle of the dominant upper limb, hand grip strength and skin temperature, respectively.

### Measurements

#### *The anthropometry*

The anthropometry of the neck in this study included neck length, neck thickness, and the occiput-wall distance (OWD). The neck measurements were tested the participant's neck position in the neutral while standing erectly. Neck length was measured from the external occipital protuberance to the seventh cervical spinous process. Neck thickness was measured while the participant standing erectly against the wall, by measuring the length from the

apex of the cervical lordosis curve to the wall. The occiput-wall distance (OWD) was measured from the seventh cervical spinous process to the wall (Fig. 1).



Fig.1 The occiput-wall distance (OWD) test.

#### *The comfortable*

Comfortable was measured by using the Visual analog scale. Visual analog scale is a straight line of 10 cm. The left end of the scale represents the value 0, or the most comfort. The right end of the scale represents the value of 10, or the less comfortable. All participants were asked to rest on supine lying position on a pillow with three height levels including 8 cm., 10 cm., and 12 cm. for 5 minutes, and marked on this line to show comfort and values was recorded in centimeters with 2 decimals from 0-10 (Fig.2).

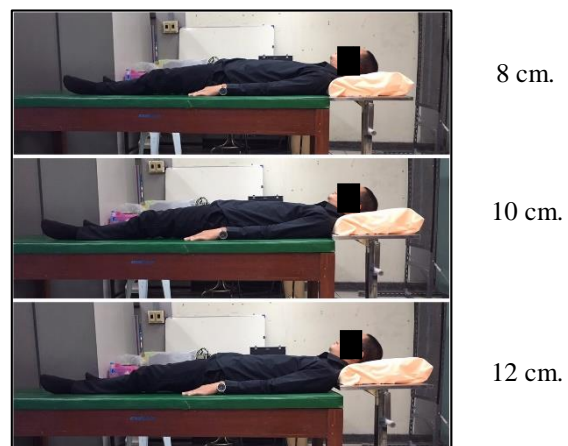


Fig. 2 A pillow, three height levels as 8 cm., 10 cm., and 12 cm.

#### *The Electromyography (EMG)*

A researcher attached electrodes to both sides of upper trapezius muscles, and the wrist flexor muscles of the dominant upper limb. The participants were asked to rest in the supine lying on the pillows with three height levels for 5 minutes/level. The EMG test was repeated three times with 1-minute rest intervals between the trials. Cometa Wave Plus Device (Cometa®, Bareggio, Italy) was used as surfaced EMG in this study. The mean value of the three trials

was used (Fig. 3).



Fig. 3 Electrodes on the upper trapezius muscles both sides, and the wrist flexor muscles of the dominant upper limb

#### *The hand grip strength*

All participants were asked to rest on the supine lying on the pillows with three level heights and measured the hand grip strength for three times with 1-minute rest intervals between the trials. The mean value of three repetitions was used (Fig. 4).



Fig. 4 The hand grip strength test

#### *The skin temperature*

The distribution of skin temperature was measured every 2 minutes with the Thermograph at pillow after rest supine lying on three pillows. The mean value was recorded.

#### **Statistical Analysis**

Descriptive statistics were used to determine the clinical characteristics and anthropometric data of the participants. The one-way repeated measures analysis of variance (ANOVA) statistics was used to determine the effects of pillow height on the anthropometry, comfortable, EMG, hand grip strength, and skin thermometer with mean, standard deviation or percentage data. The Spearman Rank Correlation Coefficient statistics were used to analyze

the relationship between the anthropometry and the height of the pillow that was most comfortable. The statistically significant level is  $p < 0.05$ . SPSS version 17 was used to analyze data in this study.

#### **RESULT**

Thirty individuals participated in the study. Demographic and clinical characteristics of the participants are presented in Table 1.

Table 1 Demographics and anthropometric measurements of the participants.

|                          | 20-35 (y) | 36-60 (y) | 61-80 (y) |
|--------------------------|-----------|-----------|-----------|
| Age (y)                  | 26±3.7    | 45±7.9    | 69.9±5.3  |
| Sex (M/F)                | 3:7       | 3:7       | 0:10      |
| Body length (m)          | 1.6±0.1   | 1.6±0.1   | 1.5±0.1   |
| Body weight (kg)         | 65.1±18.1 | 66.2±11.2 | 56.09±5.5 |
| BMI (kg/m <sup>2</sup> ) | 24.3±5.1  | 25.7±2.9  | 23.5±2.6  |
| Neck length (cm)         | 10.8±1.3  | 10.6±1.6  | 8.9±1.1   |
| Neck thickness (cm)      | 6.6±1.3   | 7.2±1.1   | 6.9±1.4   |
| OWD (cm)                 | 5.2±1.5   | 5.4±1.8   | 5.3±1.5   |

Data are presented as n or mean ± standard deviation. BMI = body mass index; F = female; M = male.

The occiput-wall distance = OWD

#### **The Effectiveness of Health Pillows for Thai People Aged 20-80 Years**

##### *Age 20-35 years group*

The comfortable, the EMG of the upper trapezius muscle and the wrist flexor muscle of the dominant upper limb, the hand grip strength, and the skin temperature were not significantly different between the three-pillows ( $p > 0.05$ ) in Table 2.

##### *Age 36-60 years group*

The pillow height at 8 cm. was the most comfortable ( $p < 0.05$ ). On the other hand, the EMG of the upper trapezius muscle and the wrist flexor muscle of the dominant upper limb, the hand grip strength, and the skin temperature were not

Table 2 The Effectiveness of Health Pillows for Thai People Aged 20-80 Years.

| Age (y)                            | 20-35 group     |                |                 | 36-60 group    |                |                | 61-80 group    |                |                |
|------------------------------------|-----------------|----------------|-----------------|----------------|----------------|----------------|----------------|----------------|----------------|
| The pillow height (cm)             | 8               | 10             | 12              | 8              | 10             | 12             | 8              | 10             | 12             |
| Comfortable (cm)                   | 2.27<br>±1.35   | 2.19<br>±2.05  | 2.56<br>±1.84   | 1.59<br>±1.66* | 2.56<br>±2.41  | 3.74<br>±2.41  | 2.39<br>±1.71  | 2.4<br>±1.63   | 2.55<br>±2.06  |
| EMG of Rt. upper trapezius m. (μV) | 2.2<br>±0.63    | 2.2<br>±0.42   | 2.2<br>±0.63    | 2.1<br>±0.31   | 2.4<br>±0.70   | 2<br>±0.00     | 2.2<br>±0.42   | 2.3<br>±0.48   | 2.3<br>±0.68   |
| EMG of Lt. upper trapezius m. (μV) | 3<br>±0.67      | 3<br>±0.67     | 2.9<br>±0.99    | 3.2<br>±1.48   | 3.8<br>±1.03   | 3.5<br>±0.71   | 3.5<br>±1.65   | 3.8<br>±1.03   | 3.5<br>±1.72   |
| EMG of wrist flexor m. (μV)        | 74.6<br>±30.02  | 68.3<br>±20.87 | 73.8<br>±30.20  | 63.7<br>±20.02 | 67.9<br>±16.31 | 63.7<br>±18.67 | 69.2<br>±26.14 | 66.3<br>±26.12 | 62.7<br>±20.48 |
| Forces of wrist flexor m. (kg)     | 26.05<br>±10.45 | 24.99<br>±8.01 | 25.42<br>±11.17 | 27.91<br>±8.76 | 28.77<br>±8.37 | 26.34<br>±9.67 | 20.72<br>±3.46 | 21.18<br>±4.09 | 20.88<br>±3.96 |
| Skin temp.(°c)                     | 35.11<br>±0.97  | 34.94<br>±0.88 | 35.19<br>±0.70  | 34.92<br>±0.87 | 34.84<br>±0.84 | 34.82<br>±0.80 | 33.82<br>±1.24 | 34.4<br>±1.10  | 34.56<br>±1.03 |

Data are presented as n or mean ± standard deviation.

\* between group sig.  $p < 0.05$

significantly different between the three-pillows ( $p > 0.05$ ) in Table 2.

#### Age 61-80 years group

The comfortable, the EMG of the upper trapezius muscle and the wrist flexor muscle of the dominant upper limb, the hand grip strength, and the skin temperature were not significantly different between the three-pillows ( $p > 0.05$ ) in Table 2.

#### The Relationship Between the Anthropometry and The Height of The Pillow That the Most Comfortable

There is no relationship between the anthropometry (neck length, neck thickness, and occipital to the wall) and the height of the pillow that was most comfortable of the three age groups ( $p > 0.05$ ).

#### DISCUSSION

This research aimed to study and develop health pillows for Thai people with a physical structure and Thai social and cultural context. The objectives were to test the health pillows for three level heights on the comfortable, EMG, hand grip strength, skin temperature, and the relationship between the anthropometry and the pillow height that the most comfortable.

#### The Pillow Heights on The Comfortable

The height level of pillows that the participants feel the most comfortable was 8 centimeters, which was consistent with Wang JC et al [12]. They conducted by asking participants to rest in the supine lying on 11 pillows of different height, and then choose the pillow that feels the most comfortable. They found a pillow height at 8 cm. was the most comfortable. Inconsistent with Sacco IC et al [9], studied the participants by lying on three pillow height 5 cm. 10 cm. and 14 cm. They measured the comfortable while lying on the pillow for 5 min/pillow height. They found the participants lying



on a pillow height 10 cm. feel the most comfortable when comparing the height of other two pillows. The length of the cervical spine of the participants tended to decrease by their. The pillows with a height of 8 cm. were the height that could be recommended for Thai people to sleep for health.

### **The Pillow Heights On EMG**

The EMG of the upper trapezius muscle, and the wrist flexor muscle of the dominant upper limb were not significantly different between the three pillows which is consistent with Sacco IC et al [9]. They studied the EMG signal of the sternocleidomastoid muscle, and upper trapezius muscle; the EMG was not significantly different between lying on the three pillows. However, Sacco IC et al [9] found that the EMG of the middle trapezius muscle was reduced when lying on the pillow with the height that feels most comfortable. On the other hand, Wang JC, et al [12] found that the pillows that the most comfortable had the highest EMG signal in wrist extensor muscle. However, EMG signal of the wrist flexor muscle also tended to increase in the pillow height level that the most comfortable in participants age 61-80 years group of this study had.

### **The Pillow Heights on The Hand Grip Strength**

The pillow height could affect the cervical spine causing uncomfortable sleep and resulting reflex-type muscle inhibition of the upper extremity. Inhibition has been frequently in muscles that cross the joints owing to joint pathology [8]. However, previous studies demonstrated that muscle inhibition due to spinal dysfunction can occur in muscle groups that are not directly connected to the spine. Suboptimal cervical alignment due to an uncomfortable pillow may produce sensory inputs and therefore affect the normal function to the muscles of the upper extremity [10,11]. In this study, muscle forces of the hand grip strength were not different between the pillow heights. Inconsistent with Wang JC, et al [12] found that the pillows that the most comfortable effected to the highest forces in wrist extensor muscle. Due to the small sample size of this study, the results may be observed with only some degree of difference of wrist flexor muscle forces between the pillow heights.

### **The Pillow Heights on The Skin Temperature**

The skin temperature of the three-pillow height was not different which is not consistent with Jeon et al. [6]. Jeon et al. found that proper pillow must be reduced the temperature of the head or body core temperature and causing the heart rate to slow down and sleep deeper. Due to this study asked the participants to lying 5 minutes/pillow height, it might be that experimental period was not long enough for

inducing relaxation and the heart rate to slow down. Therefore, it did not affect the temperature reduction of the head while lying on the most comfortable pillow.

### **The Relationship Between the Anthropometry and The Pillow Height That the Most Comfortable**

The three age groups had no relationship between the anthropometry (neck length, neck thickness, and occipital to the wall) and the height of the pillow that was most comfortable. It corresponded to Wang JC, et al [12], which allowed the participants to rest on 11 pillows of various heights and chose the pillows that the most comfortable. They found that the anthropometry had the relationship with the most comfortable pillow. However, this study found that the anthropometry was not related to the pillow that feels comfortable.

### **CONCLUSIONS**

The three pillow heights could be suitable for sleeping in Thai or Asian people who have similar physical stature. Study in the future should be done on a larger sample size to get a clearer answer.

### **ACKNOWLEDGMENTS**

This work was supported by the Research Fund for Supporting Lecturer to Admit High Potential Student to Study and Research on His Expert Program Year 2017, graduate school of Khon Kaen University, THAILAND.

### **REFERENCES**

- [1] Faraut Brice., Boudjeltia Karim Zouaou., Vanhamme Luc., Kerkhofs Myriam., Immune, inflammatory and cardiovascular consequences of sleep restriction and recovery, *Sleep Medicine Reviews*, Vol. 16, Issue 2, 2012, pp. 137-149.
- [2] Gordon Susan J., Grimmer-Somers Karen., Trott Patricia., Pillow use: The behaviour of cervical pain, sleep quality and pillow comfort in side sleepers. *Manual Therapy*, Vol. 14, Issue 6, 2009, pp. 671-678.
- [3] Gordon Susan J., Karen A Grimmer-Somers., Patricia H Trott., Pillow use: the behavior of cervical stiffness, headache and scapular/arm pain. *Journal of Pain Research*. Vol. 3, 2010, pp. 137-145.
- [4] Gordon. Susan J., Karen A Grimmer-Somers., Patricia H Trott., A randomized, comparative trial: does pillow type alter cervicothoracic spinal posture when side lying?. *Journal of*

- Multidisciplinary Healthcare, Vol. 4, 2011, pp. 321–327.
- [5] Gordon, Susan J., Grimmer-Somers, K., Your Pillow May Not Guarantee a Good Night's Sleep or Symptom-Free Waking. *PHYSIOTHERAPY CANADA*; SPR, Vol. 63, Issue 2, 2011, pp. 183-190.
- [6] Jeon, MY., Jeong, H., Lee, SW., Choi, W., Park, JH., Tak, SJ., Choi, DH., Yim, J., Improving the Quality of Sleep with an Optimal Pillow: A Randomized, Comparative Study. *TOHOKU JOURNAL OF EXPERIMENTAL MEDICINE*, Vol. 233, Issue 3, 2014, pp. 183-188.
- [7] Kyle, Simon D., Morgan, Kevin., Espie, Colin A., Insomnia and health-related quality of life. *Sleep Medicine Reviews*, Vol. 14, Issue 1, 2010, pp. 69-82.
- [8] Rice DA., McNair PJ., Quadriceps arthrogenic muscle inhibition: neural mechanisms and treatment perspectives. *Seminars in Arthritis and Rheumatism*, Vol. 40, Issue 3, 2010, pp. 250-266.
- [9] Sacco Ic., Pereira Il., Dinato Rc., Silva Vc., Friso B., Viterbo Sf., The Effect of Pillow Height on Muscle Activity of The Neck And Mid-Upper Back and Patient Perception of Comfort. *Journal of Manipulative & Physiological Therapeutics*. Vol. 38, Issue 6, 2015, pp. 375-381.
- [10] Suter E., Lindsay D., Back muscle fatigability is associated with knee extensor inhibition in subjects with low back pain. *Spine*, Vol. 26, Issue 16, 2001, pp. 361-366.
- [11] Suter, E., McMorland, G., Decrease in elbow flexor inhibition after cervical spine manipulation in patients with chronic neck pain. *CLINICAL BIOMECHANICS*, Vol. 17, Issue 7, 2002, pp. 541-544.
- [12] Wang, Jia-Chi., Chan, Rai-Chi., Wu, Han-Lin., Lai, Chih-Jou., Effect of pillow size preference on extensor digitorum communis muscle strength and electromyographic activity during maximal contraction in healthy individuals: A pilot study. *Journal of the Chinese Medical Association*, Vol. 78, Issue 3, 2015, pp. 182-187.

## THE IMPACT OF URBANIZATION ON THE WATER QUALITY OF UTTARA LAKE, DHAKA – CASE STUDY.

\*Shama Emy Haque<sup>1</sup> and Farhana Aktar<sup>2</sup>

<sup>1</sup>Associate professor, North South University, Bangladesh;

<sup>2</sup>North South University, Bangladesh

### ABSTRACT

This study evaluates the water quality of Uttara Lake in Dhaka to understand the impacts of urban environment in a developing country. In recent years, the lake has suffered episodes of fish kills, which have been described by the local media and residents as cases of intentional poisoning of the water body. To evaluate Uttara Lake's water quality, a series of water samples were collected and analyzed for various water quality parameters (e.g., temperature, pH, conductivity, alkalinity, turbidity, total dissolved solids, dissolved oxygen, chemical oxygen demand and biochemical oxygen demand, concentrations of dissolved phosphate and nitrate). The results indicate that the majority of the water samples exceed the Bangladesh Environment Conservation Rules (1997) standards for various water quality parameters. Here, the water quality data are presented to determine the possible mechanisms responsible for the reported fish kills and determine whether the water quality is suitable for its intended uses.

*Keywords: Urbanization, Lake, Surface Water, Water Quality, Eutrophication*

### INTRODUCTION

The total population of Bangladesh is estimated at 159 million and its population is growing annually at 1.37% [1]. A large portion of the population is migrating to Dhaka, the capital of Bangladesh for better employment and investment opportunities [2]. The trend towards urbanization along with encroachment of water bodies, rapid industrial expansion, overloaded infrastructure and ineffective enforcement of environmental regulations have all taken their toll on the water quality of the city's hydrographic network [3]-[4]. Nine industrial areas (Tongi, Tejgaon, Hazaribagh, Tarabo, Narayanganj, Savar, Ghorashal, Gazipur, and Dhaka export processing zone) neighboring the city have been identified to be the primary contributors to river pollution [5]. Locally, 10% of the industries discharge treated effluent whereas the remainder of the industries discharges effluent into the water bodies without any treatment or with minimal treatment [6]. Due to insufficient sewage treatment facilities 72% of sewage generated along with storms-drainage is discharged to the environment and make their way into the Dhaka's surface water bodies untreated and eventually leach into the groundwater system [7]-[9].

In the past few decades, the surface water-body areas in and around Dhaka has significantly reduced and has also been polluted due to rapid urbanization [10]-[12]. Well documented cases of pollution of surface water bodies by domestic, industrial and agricultural effluent are reported from various parts of the city [13]-[17].

This contribution focuses on the water quality

of Uttara Lake, which is located in Uttara Model Town, a northern sub-administrative district and a suburb of Dhaka (Fig. 1). Uttara Lake is one of the main lakes in the City. Until the 1990s, Uttara Model Town was considered a generally quiet neighborhood. However, in recent years, it has been transformed into a densely populated neighborhood to accommodate the increasing influx of people moving in from the city. Currently, the neighborhood accommodates high-rise apartment buildings along with hospitals, shopping complexes, garment factories, and educational institution [18].

Over the years, fish farming or pisciculture has continued in Uttara Lake at various capacities. Initially, the local Ministry of Fisheries permitted fish farming in the lake water; however after the recent fish kill episodes, the permission was revoked. In recent years, episode of fish kills have been reported by local residents and also through the local media [19]-[21]. The term 'fish kill' refers to any sudden and unexpected mass mortality of wild or cultured fish over a short period of time [22]. The most recent fish kill episode has been explained by the local media and residents as alleged 'poisoning' of the lake water resulting from dispute related to lease of the lake for fish cultivation. During field investigation, it was noted that numerous effluent channels drain into the lake carrying contaminated water. Based on observation and discussion with local fishermen, it is our understanding that illegal fish farming still continues throughout the lake.

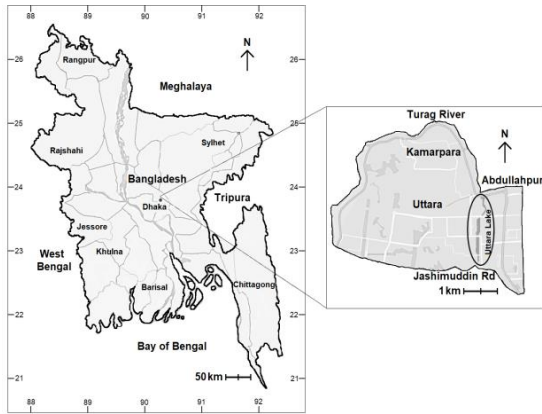


Fig. 1 Map of Bangladesh showing location of Dhaka (modified from [4] and Google Maps).

In the past, the Department of Environment (DoE), Dhaka measured the dissolved oxygen (DO) and biochemical oxygen demand (BOD) values of Uttara Lake water, which were reported to be 0.6 mg/L and 15.07 mg/L, respectively [21]. To the best of our knowledge there is no further information available about the lake's hydro-geochemistry and the lake's residence time.

The study aims to investigate, examine and evaluate the water quality of the lake and determine the possible circumstances for fish kill. To achieve the goal, a series of surface water samples were collected and analyzed for various water quality parameters such as temperature, pH, conductivity, alkalinity, turbidity, total dissolved solids (TDS), DO, chemical oxygen demand (COD) and BOD<sub>5</sub> along with concentrations of dissolved phosphate (PO<sub>4</sub>) and nitrate (NO<sub>3</sub>). Measurements of these water quality parameters are expected to determine whether the quality of the water is suitable for the health of the natural environment and the uses for which the water is required [23]. The results of the study are expected to provide the foundation for further research on the water quality of the lake. The results are expected to serve as a reference to assist relevant agencies to take positive steps to improve the lake's water quality and to restore the environment.

## STUDY AREA

Uttara Model Town is a planned square grid residential suburb, geographically elevated from southern Dhaka and is divided into several 'sectors'. The suburb is planned by Rajdhani Unnayan Karttripakkha (RAJUK), which is the Capital Development Authority of the Government of Bangladesh, and divided into 14 sectors (sector 1 to sector 14). The peripheral areas of the lake are sectors 3, 5, 7, 9, 11 and 13 (Fig. 2). At the southern and northern ends, the lake is bordered by

Jasimuddin Avenue and by Ashulia, a suburban area, respectively (Fig. 2). The length and average width of the lake is 2.35 km and 62 m, respectively, and the mean depth of the lake is 4.1 m [21]. Originally, the lake was designed to prevent water logging of the area during the wet months of the year. However, over the years, encroachers have filled up a portion of lake near the southeastern part near Sector-3.

The first water sample was collected from sampling location 1, which is located 0.25 km north from Jasimuddin Avenue (Fig. 2). Seven additional water samples were collected from the lake in a general northerly direction towards the Turag River. Specifically, sampling locations, 2, 3, 4, 5, 6, 7 and 8 are located at ~0.53 km, 0.82 km, 1.13 km, 1.36 km, 1.55 km, 1.77 km and 1.90 km, respectively, northwards commencing from Jasimuddin Avenue (Fig. 2). Following sampling location 8, the lake curves and turns towards the west. Two additional samples were collected from sampling locations 9 and 10 that are located in the westerly portion of the lake at 2.13 km and 2.31 km, respectively from Jasimuddin Avenue (Fig. 2).

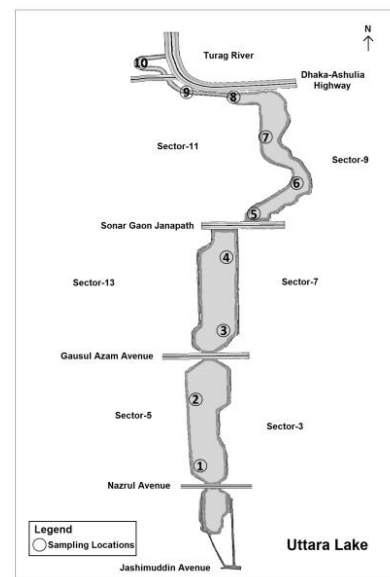


Fig. 2 Uttara Lake water sampling locations (modified from RAJUK and Google Maps).

## SAMPLING TECHNIQUES

The sampling event took place in February of 2018, which falls during the dry months of the year (November to May). During the wet season, influx of rainwater into the lake causes dilution of water. Thus, sampling was done during the dry season that is the yearly period of low rainfall. Ten water samples were collected from midstream and few centimeters below the surface using clean 1 L polyethylene bottles. For each sample, the bottle

was rinsed three times with lake water. After rinsing, the bottle was submerged below the water level to allow it to fill completely to the top with minimum disturbance. All sample bottles were stored in the dark and 'on ice' at  $\sim 4^{\circ}\text{C}$  [24]-[25], and were transferred to the DoE Laboratory for immediate chemical analysis.

## ANALYTICAL TECHNIQUES

A HACH HQ40D portable multi-meter was used to determine temperature, pH, EC and TDS. The Winkler test method was employed to determine the DO levels. To determine the turbidity a Hanna HI 83414 turbidity meter was employed. Biochemical oxygen demand and COD were measured using a Lovibond incubator (incubation at  $20^{\circ}\text{C}$ ) and a HACH DRB200 COD reactor, respectively. Dissolved  $\text{PO}_4$  and  $\text{NO}_3$  levels were determined using a HACH DR 2700 portable spectrophotometer. Analytical instruments were calibrated in accordance with the manufacturer instructions prior to sample analysis.

## RESULTS AND DISCUSSION

The temperatures of the water samples range between  $21.7$  and  $22.1^{\circ}\text{C}$ , with a mean value of  $21.9^{\circ}\text{C}$ . The variations in water temperature were relatively small from one site to another. It is well established that the water temperature influences the amount of DO present; less  $\text{O}_2$  dissolves in warm water than cold water. Water temperature is an important parameter of water quality (especially for DO) for the survival of aquatic organisms especially fish are sensitive to temperature changes in the water.

The sampled waters are near-neutral, with pH values ranging from 6.58 to 7.20 (Table 1), with a mean value of 6.93. More specifically, pH exhibits an initial increase from 7.14 to 7.20 in the first 0.53 km, before decreasing to  $\text{pH} < 6.58$  at 2.13 km. The pH values fall within the Environment Conservation Rules (ECR, 1997) of Bangladesh standards for pH range of 6.5 to 8.5 for inland surface water.

Electrical conductivity values range from 465 to 698  $\mu\text{S}/\text{cm}$  (Table 1), with a mean value of 587  $\mu\text{S}/\text{cm}$ . The EC values of all water samples are well below the Bangladesh standard (800-1000  $\mu\text{S}/\text{cm}$ ) for pisciculture [27]. Note that EC of most natural water generally ranges from about 50 to 1500  $\mu\text{S}/\text{cm}$  [28].

In almost all natural waters, alkalinity is due to the presence of certain ions: carbonates, bicarbonates, and hydroxides in water. Alkalinity is important for aquatic life as it protects them against rapid changes in pH. Alkalinity values range from 204 to 348  $\text{mg}/\text{L}$  expressed as  $\text{CaCO}_3$

in  $\text{mg}/\text{L}$  (Table 1), with a mean value of 276  $\text{mg}/\text{L}$ . The mean alkalinity value of the lake water samples are below the Bangladesh (1997) guidelines of 50-300  $\text{mg}/\text{L}$  for fisheries.

Table 1 Uttara Lake's water quality data: pH, Conductivity (Cond), Alkalinity (Alk; expressed as  $\text{CaCO}_3$  in  $\text{mg}/\text{L}$ ), Turbidity (Turb), Total Dissolved Solids (TDS).

| Sample | pH   | Cond<br>$\mu\text{S}/\text{cm}$ | Alk<br>$\text{mg}/\text{L}$ | Turb<br>NTU | TDS<br>$\text{mg}/\text{L}$ |
|--------|------|---------------------------------|-----------------------------|-------------|-----------------------------|
| 1      | 7.14 | 497                             | 206                         | 23.1        | 258                         |
| 2      | 7.20 | 490                             | 216                         | 18.2        | 253                         |
| 3      | 7.02 | 465                             | 204                         | 18.2        | 240                         |
| 4      | 7.20 | 465                             | 208                         | 22.1        | 240                         |
| 5      | 6.92 | 575                             | 264                         | 29.2        | 299                         |
| 6      | 6.60 | 698                             | 330                         | 118         | 364                         |
| 7      | 6.98 | 680                             | 348                         | 48.0        | 354                         |
| 8      | 7.06 | 670                             | 312                         | 34.0        | 349                         |
| 9      | 6.58 | 658                             | 338                         | 73.4        | 342                         |
| 10     | 6.61 | 673                             | 332                         | 84.5        | 349                         |

The turbidity values range from 18.2 to 118 NTU, with a mean value of 46.6 NTU. The ECR 1997 does not list a turbidity standard for inland waters for fish farming. However, others have suggested that turbidity should be  $< 50$  NTU for lakes for aquatic life [27]. The water sample collected at location 6 is characterized with the lowest pH value of 6.60 and highest turbidity value of 118 NTU (Table 1). Here, domestic waste water is directly discharged into the lake water through a drainage pipe and field observation indicates visible algal bloom. Increased growth in algae can cause an increase in the turbidity of water and can create odors problems [29], both of which were observed in the collected samples.

The TDS values range from 240 to 364  $\text{mg}/\text{L}$ , with a mean of 305  $\text{mg}/\text{L}$ . There is no ECR (1997) standard available for TDS for fisheries [26], however according to WHO (1996; [30]), the acceptable range for TDS for fisheries is 0-1000  $\text{mg}/\text{L}$ . In general, The TDS values appear to increase after sampling location 5 and towards to Turag River. At location 6, the TDS value is at maximum. Here, the direct discharge of domestic waste water into the lake likely plays a key role in the increase in TDS values. Total dissolved solid values have strong positive correlation with EC ( $r = 0.99$ ) and turbidity ( $r = 0.78$ ).

Oxygen parameters were determined to assess the biological and industrial pollution of Uttara Lake. The DO values range from 0.00 to 7.10  $\text{mg}/\text{L}$ , with mean value of 2.98  $\text{mg}/\text{L}$ . Dissolved oxygen levels were below detection at locations 6

and 10 (Table 2), which is indicative of an excessive demand on the DO in the water. At location 2, the measured DO value is 7.1 mg/L, which is significantly higher than that of at the other locations (Table 2). Note that compared to the remainder of the sampling locations, this portion of the lake water appeared to relatively clear and garbage free. The ECR (1997) standards of DO for inland surface water bodies suggest a minimum DO requirement of 5 mg/l for different purposes including fish farming [26]. As mentioned earlier, in recent years, the lake has suffered from episodes of fish kills. In over-enriched lakes ‘algal blooms’ can occur, which are surface accumulations of free-floating or attached eukaryotic algae or cyanobacteria [31]. As the masses of algae decay, they can disturb the DO regime of the lake water. As algae carry out photosynthesis they consume CO<sub>2</sub> and release O<sub>2</sub> to the water body. During night, however, the algae respire and consume DO and the DO levels may become low enough to cause fish mortality. The reduced DO values are likely to have negative influence on the aquatic life of the lake.

The COD values of the lake water range from 44.0 and 439 mg/L. There is no ERC (1997) COD standard for fisheries but the ECR (1997) COD standard for waste from industrial units is 200 mg/L [26], which is lower than the mean BOD value of 207.9 mg/L, which gives an indication of the levels of organic pollution. The results show positive correlation parameters between COD and BOD<sub>5</sub> values ( $r = 0.66$ ), and COD and turbidity values ( $r = 0.86$ ). The maximum COD value of 439 mg/L was measured at location 10 (Table 2).

Table 2 Uttara Lake water quality data: Values of oxygen parameters and dissolved PO<sub>4</sub> and NO<sub>3</sub>.

| Sample | DO<br>mg/L | COD<br>mg/L | BOD <sub>5</sub><br>mg/L | PO <sub>4</sub><br>mg/L | NO <sub>3</sub><br>mg/L |
|--------|------------|-------------|--------------------------|-------------------------|-------------------------|
| 1      | 2.30       | 130         | 30.0                     | 29.1                    | 4.00                    |
| 2      | 7.10       | 44.0        | 27.0                     | 30.8                    | 7.10                    |
| 3      | 6.80       | 191         | 23.0                     | 30.7                    | 5.50                    |
| 4      | 6.30       | 108         | 56.0                     | 43.8                    | 2.90                    |
| 5      | 0.70       | 152         | 38.0                     | 43.1                    | 4.70                    |
| 6      | 0.00       | 351         | 65.0                     | 48.2                    | 8.20                    |
| 7      | 0.30       | 206         | 24.0                     | 44.0                    | 8.10                    |
| 8      | 6.10       | 196         | 54.0                     | 48.1                    | 6.80                    |
| 9      | 0.20       | 262         | 68.0                     | 44.8                    | 7.90                    |
| 10     | 0.00       | 439         | 67.0                     | 54.4                    | 8.70                    |

The residents of slums located between sampling locations 8 and 9 dispose of their household waste along with human wastes into these water. Note that this study is part of a bigger

project that aims to determine the water and sanitation condition of Uttara Lake slum. In the bigger project, analysis of total and fecal coliform bacteria (i.e., the primary indicator of potability of water) is currently being carried out. Near location 9, a hospital dumps medical waste into the lake. Moreover, there are numerous hidden drainage pipes that are illegally discharging untreated waste water into the lake [21]. At location 10, waste water is directly discharged into the lake through a domestic sewage pipe and the lake water appeared to be black with a denser consistency.

The BOD<sub>5</sub> values range from 23 mg/L to 68 mg/L (Table 1), with mean of 45.2 mg/L. The BOD<sub>5</sub> values of all water samples are significantly higher than the Bangladesh standard for pisciculture (<6 mg/L) and recreation (3 mg/L; [26]. In general, the lake water is characterized by relatively low DO levels and elevated levels of BOD<sub>5</sub>, which indicate significant organic pollution. A negative correlated parameter was found between BOD<sub>5</sub> and DO values ( $r = -0.38$ ).

The BOD<sub>5</sub> value is the highest at location 9 and the DO values are low in these waters (Table 2). The waste disposal activities of slum dwellers are likely a major factor dictating the observed trend in these water quality parameters. The consequences of elevated levels of BOD are the same as those for low DO: aquatic organisms become stressed, suffocate, and eventually die [28]. The sampled water from locations 1, 5 and 7 have relatively low DO values against relatively low BOD values. Currently, there is no physical evidence available for this observation.

Concentrations of PO<sub>4</sub> range from 29.1 to 54.4 mg/L (Table 2), with a mean value of 41.7 mg/L. The highest PO<sub>4</sub> level was found in water sample collected from location 10. The source of PO<sub>4</sub> in surface water can be natural or anthropogenic depending on the activities occurring in the neighboring area [32]. In nature, phosphorus (P) occurs in rocks and mineral deposits and during the natural weathering processes the rocks release the P as PO<sub>4</sub> ions. Dissolved PO<sub>4</sub> can also be introduced into water bodies due to usage of PO<sub>4</sub> based detergents, septic tank failure, fertilizer runoff and improperly treated waste-water. The ECR (1997) does not list a standard for PO<sub>4</sub> in inland surface water [26], however others have indicated that a value of >10 µg/l of PO<sub>4</sub>-P is indicative of eutrophication [33] and the PO<sub>4</sub> levels of Uttara Lake are well above this level. Elevated PO<sub>4</sub> levels in surface water have been linked to accelerated rates of plant growth, changes in species composition and proliferation of planktonic, epiphytic and epibenthic algae [34]-

[35]. The bacteria responsible for decomposition of the dead algal mass can use up and deplete DO to such levels that it can result in fish kills [32].

The levels of  $\text{NO}_3$  range from 2.90 to 8.70 mg/L, with a mean value of 6.39 mg/L. Numerous past studies have indicated that in surface waters, the  $\text{NO}_3$  levels remain generally low, ranging from 0 to 18 mg/L [36]-[37]. Note that  $\text{NO}_3\text{-N}$  levels  $>1.5$  mg/L indicate a hyper-eutrophic condition [32], [38]. The mean value of  $\text{NO}_3$  is of 6.39 mg/L indicates that the lake waters are hyper-eutrophic, which suggests that due to excessive nutrients, the water body is able to support an abundance of aquatic plants or algae. Dissolved  $\text{NO}_3$  levels can be elevated due to runoff of agrochemicals, sewage leak, refuse dump runoff, runoff from animal manure storage areas [32], [37]. There are several nurseries located along the lake that uses inorganic and organic fertilizers along with agrochemicals.

Data analyses indicate that dissolved  $\text{PO}_4$  was more concentrated than  $\text{NO}_3$  (Table 2). A possible explanation underlying the concentration differential is likely the unique behavior of P in shallow waters. In general, lakes have relatively long retention times and store large amounts of P in their bottom sediments. When a lake becomes eutrophic, the waters at the lake bottom are more likely to become anoxic during the growing season. In turn this process tends to rapidly regenerate the soluble  $\text{PO}_4$  from the bottom sediments and this dissolved P is then released to the surface waters in shallow lakes [39].

## CONCLUSION

The analyzed water quality data indicate that Uttara Lake is hyper-eutrophic and the water is not suitable for pisciculture. The results suggest that the majority of the samples exceed the Bangladesh ECR (1997) standards for various water quality parameters. The results indicate that unplanned urbanization and improper disposal of untreated waste from various sources is contributing to the degradation of the water quality of lake's water.

## ACKNOWLEDGMENTS

We acknowledge Mr. Md. Enamul Quadir, Project Manager of Uttara Lake Development Project, for his support. The authors thank Mr. MD. Raisul Mondal for assistance with sample analyses. The authors sincerely appreciate Mr. Mahbub Haque for his valuable guidance. The authors thank Mr Ashrful Alam for his help with editing.

## REFERENCES

- [1] BBS (Bureau of Statistics), and SID (Statistics and Informatics Division (SID)), Bangladesh Statistics 2017, Ministry of Planning.
- [2] BBS, Population Distribution and Internal Migration in Bangladesh. Population Monograph, Ministry of Planning, Dhaka, Vol 6, 2015, pp. 1-131.
- [3] Bodrud-Doza M., Islam A.R.M.T., Ahmed F., Das S., Saha, N., and Rahman M.S., Characterization of groundwater quality using water evaluation indices, multivariate statistics and geostatistics in central Bangladesh. *Water Sci*, Vol. 30, Issue 1, 2016, pp. 19-40.
- [4] Haque S.E., An Overview of Groundwater in Bangladesh, Mukherjee, A. (ed) *Groundwater of South Asia*, Springer Publishing Company, Singapore, 2018, pp. 202-232.
- [5] Kibria M.G., Kadir M.N., and Alam S., Buriganga River Pollution: Its causes and impacts, International conference on recent innovation in civil engineering for sustainable development. DUET-Gazipur, Bangladesh, 2015, pp. 323-328.
- [6] Satter M.A., and Islam M.S. Quality assessment of river water around Dhaka City. Bangladesh. *J Environ Sci*, Vol. 10, 2005, pp. 326-329.
- [7] Naziruzzaman M., Performance of the existing sewerage system of Dhaka City and Pagla sewage treatment plant. Master's thesis, Bangladesh University of Engineering and Technology, 1999, pp. 1-88.
- [8] DOE (Department of Environment), and LGED (Local Government Engineering Department, Dhaka Environment and Water Project, Executive Summary, 2010, Dhaka.
- [9] Islam M.S., Shahabuddin A.K.M., Kamal M.M., and Ahmed R., Wetlands of Dhaka City: its past and present scenario. *J Life Earth Sci*, Vol. 7, 2012, pp. 83-90.
- [10] Kamal M.M., and Midorikawa S., GIS-based geo-morphological mapping using remote sensing data and supplementary geo information: A case study of the Dhaka city area, Bangladesh. *Intern J Appl Earth Observ Geoinform*, Vol 6, 2004, pp. 111-125.
- [11] Dewan A.M., and Nishigaki K.T.M., Flood hazard delineation in greater Dhaka, Bangladesh using an Integrated GIS and remote sensing approach. *Geo-carto Intern*, Vol. 21, 2006, pp. 33-38.
- [12] Islam M.R., Sarkar M.K.I., Afrin T., and Khaleque A., A study on the total dissolved solids and hardness level of drinking mineral water in Bangladesh. *American J Appl Chem*, Vol.4, Issue 5, 2016, pp. 164-169.
- [13] Ahmed M., Water Quality and Pollution Sources of Gulshan Lake. *Intern J Inform*



- Tech Bus Manage, Vol. 16, Issue 1, 2013, pp. 78-82.
- [14] Mokaddes M.A.A., Nahar B.S., and Baten M.A., Status of Heavy Metal Contaminations of Lake Water of Dhaka Metropolitan City. *J Environ Sci Nat Res*, Vol. 6, Issue 1, 2013, pp. 345-348.
- [15] Razzak N.R.B., Siddik A.Z., and Ahmeduzzaman M., Evaluation of water quality of Ramna and Gulshan lakes. *Intern J Environ Monitor Analysis*, Vol. 1, Issue 6, 2013, pp. 273-278.
- [16] Roy S., Banna L.N., Hossain M., and Rahman H., Water quality of Narai canal and Balu River of Dhaka City: An impact of industrialization. *J Bangladesh Agri Uni*, Vol. 12, Issue 2, 2014, pp. 285-290.
- [17] Jan-E-Alam M., Reza P., Hossain S., and Hossain Z.M., Water quality assessment of Dhanmondi Lake in Dhaka city. *Multidis J European Uni Bangladesh*, 2017, pp. 1-6.
- [18] Ahmed S. Mohuya A.F., Growth and development of Dhaka North: 1971-2011. *J Asiatic Soc Bangladesh (Hum.)* Vol. 58, Issue 2, 2013, pp. 303-334.
- [19] Islam R., Killing fish with poison at Uttara Lake. Retrieved on 4 Jun 2018, from <http://en.prothomalo.com/bangladesh/news/166203/Killing-fish-with-poison-at-Uttara-lake>.
- [20] The Daily Star, Poisoning of Uttara Lake a devilish propensity, Retrieved on 5 Jun 2018, from <https://www.thedailystar.net/editorial/poisoning-uttara-lake-devilish-propensity-1490680>.
- [21] Interview with E. Quadir, RAJUK, personal communication, 20 January 2018
- [22] Lugg J., Fish kills in New South Wales. NSW Department of Primary Industries, Cronulla, New South Wales, 2000, pp. 1-22.
- [23] Postolache O., Giro P.S., and Pereira J.M.D., Water quality monitoring and associated distributed measurement systems: an overview. *Intech Open*, 2012, pp. 26-64.
- [24] Haque S., and Johannesson K., Arsenic concentrations and speciation along a groundwater flow path: The Carrizo Sand aquifer. Texas, USA. *Chem Geol*, Vol. 228 2006a, pp. 57-71.
- [25] Haque S., and Johannesson K., Concentrations and speciation of arsenic along a groundwater flow-path in the Upper Floridan aquifer, Florida. USA. *Environ Geol* Vol. 50, 2006b, pp. 219-228.
- [26] ECR (Environmental Conservation Rules), Ministry of Environment and Forest, Government of Bangladesh, Bangladesh, 1997.
- [27] Rahman M.S, Islam M.N., Hoque M.M., and Roy S., Assessment for treated wastewater comes from decentralized wastewater treatment system at Rakibnagar slum, tangail, Bangladesh. *Bangladesh J Environ Sci*, Vol. 27, 2014, pp.106-109.
- [28] Uddin M.N., Alam M.S., Mobin M.N., and Miah M.A. An assessment of the river water quality parameters: A case of Jamuna River. *J Environ Sci Nat Res*, Vol. 7, Issue 1, 2014. Pp. 249-256.
- [29] Sanseverino I., Conduto D., Pozzoli L., Dobrici S., and Lettier T., Algal bloom and its economic impact. *JRC Technical Reports*, EUR 27905 EN, 2016.
- [30] WHO (World Health Organization), Guidelines for drinking water quality, health criteria, and other supporting information. Geneva, 1996.
- [31] WHO, Monitoring bathing waters – a practical guide to the design and implementation of assessments and monitoring programmes. Bartram, J., Rees, G (eds.), 2000, ISBN 0-419-24390-1.
- [32] Fadiran A.O., Dlamini S.C., and Mavuso A., A comparative study of the phosphate levels in some surface and groundwater bodies of Swaziland. *Bull ChemSoc Ethiopia* Vol. 22, Issue 2, 2008, pp. 197-206.
- [33] Sengupta M., and Dalwani R., Proceedings of Taal: The 12th World Lake Conference xiii – xxii, India, 2007, pp. 209-216.
- [34] Mainstone C.P., and Parr W., Phosphorus in rivers – ecology and management. *Sci Tot Environ*, Vol. 282, 2002, pp. 25-47.
- [35] Carpenter S.R., Eutrophication of aquatic ecosystems: Biostability and soil phosphorus. *PNAS* Vol. 102, Issue 29, 2005, pp. 1-4.
- [36] Davies O.A., Ugwumba A.A.A., and Abolude D.S., Phytoplankton of the lower reaches of Okpoka creek, Port Harcourt, Nigeria. *J Fish Intern* Vol. 3, Issue 3, 2008, pp. 70-77.
- [37] Adesuyi A.A., Nnodu V.C., Njoku K.L., Jolaosos A., Nitrate and Phosphate Pollution in Surface Water of Nwaja Creek, Port Harcourt, Niger Delta, Nigeria, *Intern J Geol, Agri Environ Sci* Vol. 3, 2015, pp. 14-20.
- [38] US EPA (United States Environment Protection Agency, Nutrient Criteria Technical Guidance Manual Lakes and Reservoirs (First edition), USA, 2000.
- [39] Hutchinson G.E., A Treatise on Limnology, Wiley, New York, NY, Vol. 1, 1957.

## THE EFFECTS OF COMBINED ELECTRICAL STIMULATION WITH SHORT FOOT EXERCISE ON MEDIAL LONGITUDINAL ARCH AND INTRINSIC FOOT MUSCLE SIZE: A PILOT STUDY

Juntip Namsawang<sup>1</sup>, Ratana Vichiansiri<sup>2</sup>, Wichai Eungpinichpong<sup>3</sup>, and Somchai Rattanathongkom<sup>1</sup>

<sup>1</sup>Faculty of associated medical sciences, KhonKaen University, Thailand;

<sup>2</sup> Faculty of medicine, KhonKaen University, Thailand;

<sup>3</sup> BNOJPH Research Center, Faculty of associated medical sciences, KhonKaen University, Thailand

### ABSTRACT

The important function of the intrinsic foot muscles is the dynamic stabilization of the medial longitudinal arch (MLA). Several studies have reported that implementing strengthening exercises amid the intrinsic foot muscles may increase MLA height. Functional electrical stimulation may also enhance muscle strength. Nevertheless, the effect of electrical stimulation (ES) in combination with short foot exercise (SFE) as an exercise method amid intrinsic foot strengthening has to date, not been shown. Hence, the aim of this study was to compare the effects of combined ES and SFE versus SFE alone on navicular drop (ND), in addition to the cross-sectional area (CSA) of the abductor hallucis (AbdH) muscle. Ten healthy female subjects were randomly assigned to undergo combined ES with SFE (n=5) or SFE with sham ES (n=5). Both groups performed 30 repetitions of SFE followed by 20 minutes of ES per day, 3 days a week, for 4 weeks. ND and the CSA of the AbdH muscle were assessed before and after intervention. The results showed that combined ES with the SFE group significantly decreased in ND after training ( $p<0.05$ ). However, there were no significant differences between the two groups. The CSA of the AbdH muscle in both groups was increased (ES with SFE=10.93 mm<sup>2</sup> and SFE=7.44 mm<sup>2</sup>;  $p<0.05$ ) but without significant differences between the groups. These results demonstrated that ES with SFE and SFE alone could improve intrinsic foot muscle size. Nevertheless, combined ES with SFE tended to increase MLA more than SFE alone. Hence, ES in combination with SFE may be used as an alternative treatment to increase MLA and intrinsic foot muscle size.

*Keywords: electrical stimulation, short foot exercise, medial longitudinal arch, intrinsic foot muscles*

### INTRODUCTION

The foot is an importantly complex structure which serves as the propulsive organ and supporting pedestal during weight bearing throughout locomotion [1]. Foot function efficiency depends on the integrity of the medial longitudinal arch (MLA) [2].

The MLA is the primary structure responsible for stability and resiliency of the foot load [3]. Arch configuration can be maintained via passive and active support. The most significant static contributors are the plantar fascia, the long and short plantar ligaments, and the spring ligament. Whereas, the intrinsic and extrinsic foot muscles play a role in dynamic contributors [4]. However, recent evidence has suggested that the intrinsic foot muscles (IFM) play a crucial role in supporting MLA [5]-[6]. What's more, it is believed that the intrinsic foot muscles have their origins and insertions within the foot. These muscles act as local stabilizers, and thus, they serve primarily to stabilize the arch [6].

Previous studies have confirmed the function of the IFM. A study by Fiolkowski et al. [7] and Headlee et al. [8] demonstrated the inhibition of the tibial nerve amid the IFM in addition to exercise until IFM fatigue increased significantly enough to render a

navicular drop (ND). The height of the navicular bone serves as the key to the MLA. Moreover, previous studies demonstrated that muscle strength had significant correlation with cross-sectional area (CSA) [9]. IFM weakness and atrophy commonly result in several conditions such as plantar fasciitis [10], hallux valgus, and pes planus [11]. Pes planus, in particular, is associated with heel eversion and forefoot abduction. In the long term, these changes may be a cause of overuse injuries [12], functional limitation, and disability [13]. Therefore, the rehabilitation and prevention of these problems are resultant of necessarily reinforcing IFM strength aimed at improving MLA.

Several studies have reported the beneficial effects of IFM training, especially short foot exercise (SFE) on navicular drop [10] and the cross-sectional area of the abductor hallucis muscle (AbdH) [12]. Jung et al. reported that SFE can improve IFM activity and prevent the fall of MLA [14].

Today, functional electrical stimulation is an alternative method for the rehabilitation of a paralyzed muscle as well as strength promotion [15] because this treatment has the ability to isolate contraction of the desired muscle group [16]. A study by Fourchet et al. [17] found that neuromuscular electrical stimulation of the abductor hallucis (AbdH)

muscle decreased ND post training. Moreover, electrical stimulation (ES) significantly increased CSA of the vastus lateralis, vastus medialis, and vastus intermedius muscles post training [18].

Conversely, some evidence suggests that combined ES in addition to exercise training is more effective for strengthening the muscles than exercise alone [19]-[21]. Nevertheless, the short-term effect of ES in combination with SFE as an intrinsic foot strengthening exercise method has to date not been discussed. Therefore, the purpose of this study was to compare the effects of combined ES and SFE versus SFE alone on ND and CSA of the AbdH muscle.

## METHOD

### Design and setting

A double-blinded randomized controlled trial was used in this study. Subjects were recruited from Muang district, Chonburi province, Thailand. This present study was approved by the Khon Kaen University Ethics Committee in Human Research. All subjects were randomly assigned to undergo combined ES with the SFE group (experimental group) or SFE with sham ES group (control group). Numbered lots (1, control; 2, experimental) were placed in sealed opaque envelopes by physiotherapist 1. The subjects were then allocated and assigned for intervention by physiotherapist 2. The investigators in this study were blinded.

### Participants

Ten healthy females between 18 and 40 years of age volunteered to participate. All subjects reported good health, no contraindication of ES, and no history of lower extremity orthopedic or neurologic disorders within the previous 6 months.

### Outcome measures

The measurements of outcome in this study were assessed at the site of both feet prior to and 4 weeks succeeding training intervention by the same investigators.

#### *Navicular drop*

The differences in distances between navicular tuberosity and the floor while sitting and standing are defined as the navicular drop. Subjects sat on a chair with the hips, knees, and ankles at a 90 degree angle. Each subject was marked for their navicular tuberosity using a permanent marker. The investigator measured navicular tuberosity height utilizing a digital vernier caliper (CD-20AX, Mitutoyo, Kawasaki, Japan). Then, subjects were instructed to stand with their weight equally

distributed between both legs. The knees were extended and feet relaxed. Navicular tuberosity height was then measured again. The test was performed three times with the mean value of three measurements calculated. Consequently, navicular drop was calculated by subtracting navicular height standing measurement from the sitting measurement.

#### *Cross-sectional area of abductor hallucis*

An ultrasound machine (M5 series, Shenzhen Mindray Bio-Medical Electronics Co., China) with 7.5 MHz linear array probe was applied to render an image of the AbdH muscle. Subjects lie down in the supine position with a 15 degree knee flexion with the ankle in the neutral position. An ultrasound probe with a sufficient amount of gel was placed perpendicularly to the AbdH muscle. The anterior margin of the ultrasound probe should be positioned 1cm posteriorly to the navicular tuberosity. The image of the AbdH muscle was taken with only minimal pressure applied to the ultrasound probe. CSA mean was calculated from three separate images using software Image J version 1.52b (NIH, Bethesda, MD, USA). The CSA measures the desired area by tracing the muscle border [22].

### Procedure

Subjects in the experimental group received ES with SFE, whereas the control group received SFE with sham ES.

ES training was performed using an electrical stimulator (Endomed 482, Enraf-Nonius Co., Netherlands) with two electrodes. The passive electrode was placed behind the head of the first metatarsal bone. Meanwhile, the active electrode was placed over the motor point of the AbdH muscle. Each individual was trained at 85 Hz frequency, 5 seconds pulse duration, and 6 seconds pause duration for 20 minutes each session, once daily covering 3 sessions weekly for a period of 4 weeks. Intensity was adjusted to each subject's maximum tolerance without pain and discomfort. Subjects in the control group were administered with sham ES according to the same location, using the same ES device and training protocol, but without the releasing of intensity.

Subjects in both groups received SFE post ES performed in the sitting position. Subjects were asked to place their feet on the ground. Then, they attempted to pull the head of metatarsal bones toward the heel without flexing the toes, nor lifting the forefoot and heel from the ground. Exercise training was performed for 30 repetitions per day, 3 days per week, for 4 weeks. Each repetition required a contraction of 5 seconds. Throughout the 4 weeks, subjects were not allowed to participate in any other exercise.

## DATA ANALYSIS

All data were analyzed using SPSS version 19. Descriptive data was expressed as mean with standard deviation. The student t-test was implemented to compare demographic characteristics. Changes to ND and CSA in the AbdH muscle between the two groups at baseline and 4 weeks post-intervention were compared utilizing the student t-test. A p-value of less than 0.05 was considered statistically significant. All data are presented as mean  $\pm$  standard deviation.

## RESULTS

### Demographic Characteristics

Subjects' demographic and clinical characteristics are shown in Table 1. There were no significant

differences between groups in terms of baseline and clinical (navicular drop, ND and cross-sectional area, CSA) characteristics.

### Navicular drop and cross-sectional area

After 4 weeks, the results showed a significant decrease in navicular drop (ND) in ES amid the SFE group subsequent to training, whereas the SFE group alone revealed no statistically significant decrease in ND from baseline. However, there were no significant differences between groups (Table 2).

The cross-sectional area (CSA) of the AbdH muscle in both groups was increased (ES with SFE=10.93 mm<sup>2</sup> and SFE=7.44 mm<sup>2</sup>;  $p<0.05$ ) but without significant differences between groups.

Table 1 Baseline characteristics of each subject group.

| Characteristic                       | ES with SFE<br>(n=5) | SFE<br>(n=5)       | P    |
|--------------------------------------|----------------------|--------------------|------|
| Age (years)                          | 20.60 $\pm$ 0.89     | 20.40 $\pm$ 0.55   | 0.22 |
| Height (cm)                          | 158.40 $\pm$ 7.30    | 158.20 $\pm$ 6.42  | 0.98 |
| Weight (kg)                          | 50.40 $\pm$ 6.89     | 53.50 $\pm$ 4.72   | 0.20 |
| Body mass index (kg/m <sup>2</sup> ) | 19.80 $\pm$ 1.56     | 21.59 $\pm$ 1.13   | 0.40 |
| ND (mm)                              | 6.28 $\pm$ 1.50      | 7.47 $\pm$ 2.31    | 0.36 |
| CSA (mm <sup>2</sup> )               | 191.25 $\pm$ 35.43   | 190.24 $\pm$ 25.33 | 0.96 |

Table 2 ND and CSA comparison of AbdH muscle between both groups.

| Parameter              | ES with SFE (n=5)  |                    | P     | SFE (n=5)          |                    | P    | P<br>(between groups) |
|------------------------|--------------------|--------------------|-------|--------------------|--------------------|------|-----------------------|
|                        | Baseline           | 4 weeks            |       | Baseline           | 4 weeks            |      |                       |
| ND (mm)                | 6.28 $\pm$ 1.50    | 4.77 $\pm$ 1.50    | 0.03  | 7.47 $\pm$ 2.31    | 6.45 $\pm$ 1.07    | 0.40 | 0.08                  |
| CSA (mm <sup>2</sup> ) | 191.25 $\pm$ 35.43 | 202.18 $\pm$ 38.05 | 0.003 | 190.24 $\pm$ 25.33 | 197.68 $\pm$ 21.19 | 0.04 | 0.82                  |

## DISCUSSION

The purpose of the current study was to compare the effects of combined ES and SFE versus SFE alone on ND and CSA amid the AbdH muscle. Hence, our results demonstrate that 4 weeks of ES with SFE tend to increase MLA height more than SFE alone. More recently, a study conducted by Kaur et al. [22] showed the use of ES in flexible flatfoot significantly decreased navicular drop after 3 weeks of therapy. This is consistent with a study by Fourchet et al. [17] which revealed that stimulation of the AbdH muscles in healthy young adults significantly caused navicular drop to decrease after 3 weeks of training.

The possible mechanism was the ES involved in the reverse motor unit recruitment in the skeletal muscles. Large fibers have a lower threshold for stimulation, thus large type II fibers are recruited preferentially, resulting in a greater potential for muscle force production [23]. Therefore, ES can facilitate muscle strength to gain more rapidly than

exercise alone [24].

Moreover, the results in this study incorporated measured muscle size measurement which is considered to be one of the preminent determinants of muscle strength [11]. A previous study reported that the cases of IFM weakness presented a significant reduction in CSA [11],[25]. Recent studies on the uses of SFE or ES to treat flatfoot suggest that both methods tend to improve plantar intrinsic foot muscle strength [26].

In a similar way, the results of this study support a previous finding in that ES with SFE and SFE tends to increase muscle size. Furthermore, the present study demonstrates that the increase to CSA changed more rapidly than in the previous study. CSA was significantly increased after 4 weeks of intervention. In addition, the previous study demonstrated that CSA may increase after 5 to 12 weeks of strength training [27]. Gondin et al. [18] found the CSA of the quadricep muscles increased after 8 weeks of electro-stimulation. Jung et al. [12] demonstrated that AbdH muscle CSA significantly increased after 8 weeks of

SFE. On the other hand, a recent study incorporating 8 weeks of plantar intrinsic foot muscles strength training in a small group of healthy subjects revealed no significant difference in CSA among an NMES group [28].

The finding in terms of increased CSA of the AbdH muscle CSA may be described by the proper intensity and duration of strength training. An increase in muscle size using NMES with exercise and exercise alone rendered the enlargement of muscle fibers due to the resistance training mechanism [29]. ES with SFE and SFE is effective in producing hypertrophy of type I and II muscle fibers by increasing protein synthesis within muscle fibers, resulting in an increase in the physiologic cross-sectional area of the whole [3].

This pilot study has some limitations. Firstly, the sample size was small. Secondly, subjects were young. Thus, the result cannot be generalized to fit the general population. Lastly, we selected subjects without muscle weakness. In the future, the study will be conducted among participants with intrinsic foot muscle weakness in order to examine the effects of SFE or ES with SFE after training.

## CONCLUSION

These results demonstrate that ES with SFE and SFE alone, can improve intrinsic foot muscle size. An increase in AbdH muscle size is one factor relating to IFM strength. Hence, combined ES with SFE tended to increase MLA over SFE alone. Consequently, ES in combination with SFE may be recommended as an alternative treatment to increase MLA.

## REFERENCES

- [1] Altchek D.W., DiGiovanni C.W., Dines J.S., and Positano R.G., *Foot and ankle sports medicine*. Lippincott Williams & Wilkins, 2013, pp. 11.
- [2] Robbins S.E. and Hanna A.M., *Running-related injury prevention through barefoot adaption*, *Medicine and Science in Sports and Exercise*, Vol. 19, Issue 2, 1987, pp. 148-156.
- [3] Neumann D.A., *Kinesiology of the musculoskeletal system: foundations for rehabilitation*, 2nd ed. Mosby Elsevier, 2010, pp. 593-594.
- [4] Sammarco G.J. and Hockenbury R.T., *For Chapter in a Book, Biomechanics of the foot and ankle*, 3rd ed. Lippincott Williams & Wilkins, 2001, pp 235-238.
- [5] Kirby K.A., *Longitudinal arch load-sharing system of the foot*, *Revista Española de Podología*, Vol. 28, Issue 1, 2017, pp. e18-e26.
- [6] McKeon P.O., Hertel J., Bramble D., and Davis I., *The foot core system: a new paradigm for understanding intrinsic foot muscle function*. *British Journal of Sports Medicine*, Vol. 49, Issue 5, 2015, pp. 290.
- [7] Fiolkowski P., Burnt D., Bishop M., Woo R., and Horodyski M., *Intrinsic pedal musculature support of the medial longitudinal arch: an electromyography study*, *The Journal of Foot and Ankle Surgery*, Vol. 42, Issue 6, 2003, pp. 327-333.
- [8] Headlee D.L., Leonard J.L., Hart J.M., Ingersoll C.D., and Hertel J., *Fatigue of the plantar intrinsic foot muscles increases navicular drop*, *Journal of Electromyography and Kinesiology*, Vol. 18, 2008, pp. 420-425.
- [9] Young A., Stokes M., Round J.M., Edwards R.H., *The effect of high-resistance training on the strength and cross-sectional area of the human quadriceps*, *European Journal of Clinical Investigation*, Vol. 13, 1983, pp. 411-417.
- [10] Mulligan E.P. and Cook P.G., *Effect of plantar intrinsic foot muscle training on medial longitudinal arch morphology and dynamic function*, *Manual Therapy*, Vol. 18, Issue 5, 2013, pp. 425-430.
- [11] Stewart S., Ellis R., Heath M., and Rome K., *Ultrasonic evaluation of the abductor hallucis muscle in hallux valgus: A cross-sectional observation study*, *BMC Musculoskeletal Disorders*, Vol. 14, 2013, pp. 45.
- [12] Jung D.Y., Koh E.K., and Kwon O.Y., *Effects of foot orthoses and short-foot exercise on the cross-sectional area of the abductor hallucis muscle in subjects with pes planus: a randomized controlled trial*, *Journal of Back and Musculoskeletal Rehabilitation*, Vol. 24, Issue 4, 2011, pp. 225-231.
- [13] Pita-Fernandez S., Gonzalez-Martin C., Alonso-Tajes F., Seoane-Pillado T., Pertega-Diaz S., Perez-Garcia S., Seijo-Bestilleiro R., and Balboa-Barreiro V., *Flat foot in a random population and its impact on quality of life and functionality*, *Journal of Clinical and Diagnostic Research for doctors*, Vol. 11, Issue 4, 2017, pp. 22-27.
- [14] Jung D.Y., Kim M.H., Koh E.K., Kwon O.Y., Cynn H.S., and Lee W.H., *A comparison in the muscle activity of the abductor hallucis and the medial longitudinal arch angle during toe curl and short foot exercise*, *Physical Therapy in Sport*, Vol. 12, Issue 1, 2011, pp. 30-35.
- [15] Takeda K., Tanino G., and Miyasaka H., *Review of devices used in neuromuscular electrical stimulation for stroke rehabilitation*, *Medical Devices Evidence and Research*, Vol. 10, 2017, pp. 207-213.
- [16] Hainaut K. and Duchateau J., *Neuromuscular electrical stimulation and voluntary exercise*, *Sport Medicine*, Vol. 14, Issue 2, 1992, pp. 100-113.
- [17] Fourchet F., Kuitunen M., Loepelt H., and Millet G.P., *Plantar muscles electro-stimulation and navicular drop*, *Science & Sports*, Vol. 24, 2009,

- pp. 262-264.
- [18] Gondin J., Guette M., Ballay Y., and Martin A., Electromyostimulation training effects on neural drive and muscle architecture, *Medicine & Science in Sports & Exercise*, Vol. 37, Issue 80, 2005, pp. 1291-1299.
  - [19] Alon G., McCombe S.A., Koutsantonis S., Stumphauser L.J., Burgwin K.C., Parent M.M., and Bosworth R.A., Comparison of the effects of electrical stimulation and exercise on abdominal musculature, *Journal of Orthopaedic & Sport Physical Therapy*, Vol. 8, 1987, pp. 567-573.
  - [20] Alon G. and Taylor D.J., Electrically elicited minimal visible tetanic contraction and its effect on abdominal muscles strength and endurance, *European Journal of Physical and Rehabilitation Medicine*, Vol. 7, 1997, pp. 2-6.
  - [21] Kim K.M., Croy T., Hertel J., and Saliba S., Effects of neuromuscular electrical stimulation after anterior cruciate ligament reconstruction on quadriceps strength, function, and patient-oriented outcomes: a systematic review, *Journal of Orthopaedic & Sport Physical Therapy*, Vol. 40, Issue 7, 2010, pp. 383-391.
  - [22] Kaur V., Kaur P., and Kaushal K., Effect of faradic foot bath on flexible flat foot, *International Journal of Science and Research*, Vol 7, Issue 7, 2016, pp. 556-558.
  - [23] Lake D.A., Neuromuscular electrical stimulation. An overview and its application in the treatment of sports injuries, *Sports Medicine*, Vol. 13, Issue 5, 1992, pp. 320-336.
  - [24] Stevens J.E., Mizner R.L., and Snyder-Mackler L., Neuromuscular electrical stimulation for quadriceps muscle strengthening after bilateral total knee arthroplasty: A case series, *Journal of Orthopaedic & Sports Physical Therapy*, Vol. 34, Issue 1, 2004, pp. 21-29.
  - [25] Angin S., Crofts G., Mickle K.J., and Nester C.J., Ultrasound evaluation of foot muscles and plantar fascia in pes planus, *Gait & Posture*, Vol. 40, Issue 1, 2014, pp. 48-52.
  - [26] Fourchet F. and Gojanovic B., Foot core strengthening: relevance in injury prevention and rehabilitation for runners, *Swiss Sports & Exercise Medicine*, Vol. 64, Issue 1, 2016, pp. 26-30.
  - [27] Kawakami Y., The effects of strength training on muscle architecture in humans, *International Journal of Sport and Health Science*, Vol. 3, 2005, pp. 208-217.
  - [28] Ebrecht F. and Sichtung F., Does neuromuscular electrostimulation have the potential to increase intrinsic foot muscle strength?, *Foot*, Vol. 35, 2018, pp. 56-62.
  - [29] Aagaard P., Andersen J.L., Dyhre-Poulsen P., Leffers A.M., Wagner A., Magnusson S.P., Halkjaer-Kristensen J., and Simonsen E.B., Mechanism for increased contractile strength of human pennate muscle in response to strength training: changes in muscle architecture, *The Journal of Physiology*, Vol. 15, 2001, pp. 613-623.

## EFFECT OF LAND MANAGEMENT OF HORTICULTURAL TO SOIL ERODIBILITY AT THE UPSTREAM OF SUMANI WATERSHED

\*Aprisal, Bambang Istijono and Indradwipa  
Andalas University, Padang Indonesia

### ABSTRACT

Upstream watersheds (DAS) in Sumani, is a large horticultural farming area widely cultivated by vegetables, such as cabbage, onions, potatoes etc. Due to intensive farming business activities, which tend to have an impact on the level of erodibility inherent soils, a large portion of land is destroyed by rain leading to erosion. The purpose of this study therefore is to determine the erosion level and determining erodibility factor on farm lands on the upstream of Sumani Watershed. The research method adopted, is the purposive random sampling. Furthermore, soil samples were taken in order to analyze its physical properties (texture, organic matter, structure, permeability) at a depth of 0-20 cm. The samples were analyzed in the soil Department laboratory at Faculty of Agriculture Andalas University. Data analysis was processed using the soil erodibility equation and to determine the factors, the principal component analysis (PCA) was utilized. The results of the analysis showed the value of soil erodibility against rainfall which was determined by using its organic matter, structure and permeability. The soil was also prepared by applying the conservation method. The resh organic material of the harvest is capable of improving its durability damaged by rainfall.

*Keyword; watersheds soil, horticultural, erodibility, rainfall*

### INTRODUCTION

The use of various poor farming management activities leads to land damage. Agricultural ventures, which fail to implement the conservation rule, tend to make the land susceptible by rainfall thereby, leading to erosion. Furthermore, this is influenced by several factors which is dependent on the soil's characteristics, precipitation, land management, and its cover vegetation.

To determine the erodibility factor and predict the misplaced land, the researcher used the USLE method, therefore, the lost soil's erodibility factor was analyzed. According to some researchers, erosion is sometimes in the form of land resistance owing to heavy rainfall. The K factor is an integrated effect from rainfall precipitation and land resistance to the detachment particle and transportation. This process is influenced by soil characteristics such as particle size distribution, structural stability, organic material content, land chemistry, loam mineralogy, and water transmission characteristic. Therefore, erodibility is a combined influence of land attributes with very powerful conditions used to arrange the power which can refuse the debris potency from rainfall erosivity [1].

To appraise and decide the land misplaced across the globe, the researcher used soil erodibility. [2] The research proved that there is a strong relation between the soil erodibility value and proved-lost land. [3] Furthermore, it consists of several land characteristics

which includes physique, chemical, biology, and mineralogy capable of influencing the land. [4] This is also related to the combination actions from rainfall, run-off, and land infiltration. K factor is the effect of land and its profile reduction features. [5] Nowadays, it has been considered as erosion indicator due to its detachment sensitivity and particle transportation [6].

Land erosion has become a reduction problem at farming soil regions, especially at sulfur regions such as the upstream watersheds in Sumani (DAS). Furthermore, this research aims to review the land erodibility value of horticulture farming.

### MATERIALS AND METHOD

#### The Research Setting

The research is located in the upstream watersheds Sumani (DAS). *Andisol* and *Inseptisol* are dominant materials found in volcanic ash. The rainfall precipitation in this area is 2.333 mm/year. The research is agriculturally grouped into A, B, C and D. Group A cultivates radish, potato, and tomato, B consists of chili, radish, and tomato, while C comprises of onion, chili, and potato, and group D (chili, radish, and tomato). Therefore, it is the center of horticulture production.

#### The Derivation of Rainfall Precipitation Data

The rainfall precipitation data is taken from suppressor station in Alahan Panjang, to determine



soil erosivity. This was calculated using the Lenvain 1989 formula as follows;  $R = 2,21 P^{1,36}$  in which R represents rain erosivity and P the monthly average rainfall precipitation in the research setting [7].

### Management Area

The land is cultivated by hacking it twice in each agriculture season conventionally. The hacking location is made different in line with its gradient. Furthermore, the land surface is refined and clear from organic material residue. Afterwards, group B returned the harvest residue and used it in cultivating the land.

### The Taking of Soil Sample

A total of 12 sample points were randomly taken by the researcher using the purposive technique in the horticulture area (Figure 1). These are indicated in chart 1 at four agriculture groups. Group A was at points 1, 2, and 3, B at 4, 5, and 6, C at 7, 8, and 9, while D was at points 10, 11, and 12. The researcher took the land sample at depth of 0-20 cm, with the agitated land sample for four fractions of texture analysis, and organic materials. While the unagitated land is examined by permeability analysis and soil structure. To determine the land sample and analysis, the Soil Department, Faculty of Agriculture, Andalas University's laboratory was utilized



Figure 1. location of research area

### Deciding the Land Erodibility Value

Furthermore, the researcher also made use of the nomograph formula to decide the land erodibility value using factors such as texture, structure, organic substance, and land permeability [8]. The equation is as follows:

$$100 K = 1,292 [2,1 M^{1,14} (10^{-4}) (12-a)] + 3,25 (b-2) + 2,5 (c-3)$$

that:

K = soil erodibility

M = the percentage of the very fine sand and silt (diameter 0,1 – 0,05 and 0,05 – 0,02 mm) x (100 – % cay)

- a = organic matter content (% c x 1,724)
- b = soil structure
- c = soil permeability

To determine the land susceptibility, its erodibility value is obtained comparing the formula with the criteria in table 1.

Table 1. The criteria of land erodibility value

| No | Class         | Criteria    |
|----|---------------|-------------|
| 1  | Very slow     | 0,00 – 0,10 |
| 2  | Slow          | 0,11 – 0,20 |
| 3  | Average       | 0,21 – 0,32 |
| 4  | Slightly high | 0,33 – 0,43 |
| 5  | High          | 0,44 – 0,55 |
| 6  | Very high     | 0,56 – 0,64 |

### The Main Component Analysis of Land Characteristic to the Erodibility

The Principal Component Analysis (PCA), is used to ascertain the land's deteriorating ability as a result of heavy rainfall. The researcher also uses this method to decide the main factor which influences its value using a PC with an eigen value  $\geq 1$  as its independent variable. Therefore, it consists of the highest correlated independent value in PC, [9]. The researcher also uses Minitab 17 to analyze.

## RESULT AND DISCUSSION

### Rainfall Erosivity

Approximately 2333 mm/year of rainfall data was obtained for ten years from Kembar lake climate. From these numbers of precipitations, the erosivity energy capable of running the structure became fragmented, thereby, leading to smooth particles which later floated off the surface. The calculation using the Lenvain formula results in rainfall erosivity energy of 1535, 99. Its energy is big huge enough to destroy the land structure on surface area. Furthermore, it causes erosion velocity on the horticulture region to often open when cultivated.

### Land Erodibility Value at Upstream of Sumani Watersheds (DAS)

The erodibility land result taken at 12 sample points in the horticulture region ranges from low to high, with the highest value at 0,33. Furthermore, this is drawn from the susceptible and precipitation of erosivity, with a higher value. Some factors like texture, structure, organic material, and soil permeability influences its value. However, these these factors are also influenced by land management. In the horticulture region, the cultivation management and plant types have a high impact on soil erosivity precipitation. The plants which cover the land surface, also reduces the rain erosivity. According to

Santos et al. 2003, vegetation or plant has the ability to push rain energy and increase the infiltration rate into the land.

The land surface closure by plants tend to reduce rainfall kinetic energy and in turn, it the land can be pushed, thereby lowering its erodibility. The

percentage increase in content, improves the infiltration rate while decreasing its flow rate [10]. Therefore, the loamy fraction content helps to reduce the particle thereby, lowering its erodibility value.

Table 1. The land erodibility value in research setting.

| Sample | Pasir halus | debu | liat | a   | b   | c   | M      | K    |
|--------|-------------|------|------|-----|-----|-----|--------|------|
| 1      | 8.3         | 29.0 | 29.5 | 6.9 | 3.0 | 5.0 | 2630.7 | 0.21 |
| 2      | 10.1        | 16.4 | 33.3 | 8.6 | 3.0 | 5.0 | 1767.5 | 0.16 |
| 3      | 9.8         | 28.9 | 22.0 | 6.9 | 2.0 | 6.0 | 3017.8 | 0.18 |
| 4      | 1.0         | 24.5 | 70.6 | 8.1 | 2.0 | 5.0 | 750.4  | 0.13 |
| 5      | 0.8         | 81.4 | 14.4 | 2.2 | 2.0 | 6.0 | 7039.7 | 0.30 |
| 6      | 6.4         | 60.9 | 7.1  | 3.4 | 2.0 | 5.0 | 6253.9 | 0.26 |
| 7      | 11.8        | 40.8 | 0.3  | 1.7 | 3.0 | 3.0 | 5245.1 | 0.32 |
| 8      | 6.3         | 13.7 | 54.9 | 2.9 | 3.0 | 5.0 | 899.5  | 0.31 |
| 9      | 8.6         | 43.8 | 13.4 | 6.9 | 3.0 | 6.0 | 4539.2 | 0.22 |
| 10     | 10.6        | 42.7 | 4.1  | 3.4 | 3.0 | 6.0 | 5116.0 | 0.31 |
| 11     | 11.8        | 36.9 | 4.3  | 3.4 | 3.0 | 3.0 | 4658.5 | 0.27 |
| 12     | 10.5        | 21.4 | 25.9 | 2.9 | 3.0 | 6.0 | 2367.1 | 0.33 |

Note; a = organic material, b = structure, c = permeability, M = the percentage of the very fine sand and silt (diameter 0,1 – 0,05 and 0,05 – 0,02 mm) x (100 – loam percentage), K = soil erodibility

#### The Analysis of Main Component (PCA) Erodibility Value in Horticulture Area.

The dominant factors influencing the erodibility value, is determined by analyzing the principal component (PCA). The analysis result on table 2

shows that in eigen value the two PCA pools have scores above 1 which is the most influencing land erodibility value. The biggest value in PCA1 are smooth sand variable and dust.

Table 2. The land variable analysis result with PCA

|                |        |        |        |        |        |        |
|----------------|--------|--------|--------|--------|--------|--------|
| Eigenvalue     | 2.7829 | 2.0248 | 0.9003 | 0.2743 | 0.0176 | 0      |
| Proportion     | 0.464  | 0.337  | 0.15   | 0.046  | 0.003  | 0      |
| Cumulative     | 0.464  | 0.801  | 0.951  | 0.997  | 1      | 1      |
| Variable       | PC1    | PC2    | PC3    | PC4    | PC5    | PC6    |
| K              | 0.54   | 0.04   | 0.443  | 0.02   | 0.714  | 0      |
| Very Fine sand | 0.288  | -0.542 | -0.371 | 0.433  | 0.031  | -0.545 |
| Silt           | 0.261  | 0.575  | -0.317 | -0.431 | -0.021 | -0.561 |
| Clay           | -0.487 | -0.044 | 0.611  | 0.009  | -0.009 | -0.622 |
| a              | -0.518 | -0.185 | -0.412 | -0.289 | 0.666  | 0      |
| b              | 0.229  | -0.581 | 0.149  | -0.737 | -0.212 | 0      |

The land erodibility (table 1) is also has the highest value found in sand content and dust which plays an essential role in determining the land erodibility value.

#### The Texture Relation with Land Erodibility

The land texture is very relevant with its erodibility. For instance, in Figure 2, there is polynomial relation between its texture using a coefficient value of  $R^2 = 0.92$ . It means that in each loam improvement, about 1 % value land erodibility reduction value of 0,005 at 0,34 with a credibility of 91 % is obtained. .

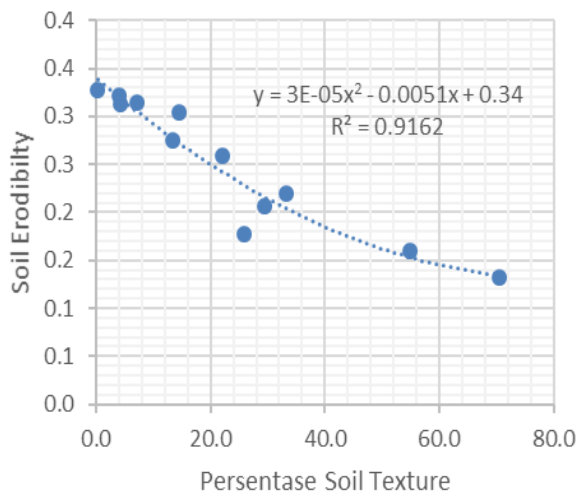


Figure 2. The relation of loamy fraction with the land erodibility.

In addition, the relationship between silt and land erodibility also has a negative relation with determination  $R^2$  having a value of 0,89. Figure 3 shows that the improvement of 1% leads to a reduction of about 0.003 and a credibility level of 89% at 0.37.

The land fraction or texture is an important characteristic owing to its ability to retain water movement rate through the land matric. Furthermore, the land texture influences the soil fertility and the cultivation rate. While the relation of silt fraction with land erodibility is linear in relation with  $R^2 = 0.89$ . This means, that each dust improves by 1% with a reduction rate of 0.003 while the soil erodibility value 0,37 has a credibility level of 0,92%.

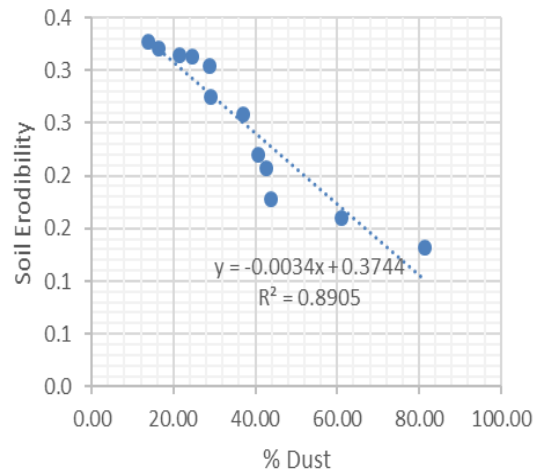


Figure 3. The relation of silt fraction with the land erodibility.

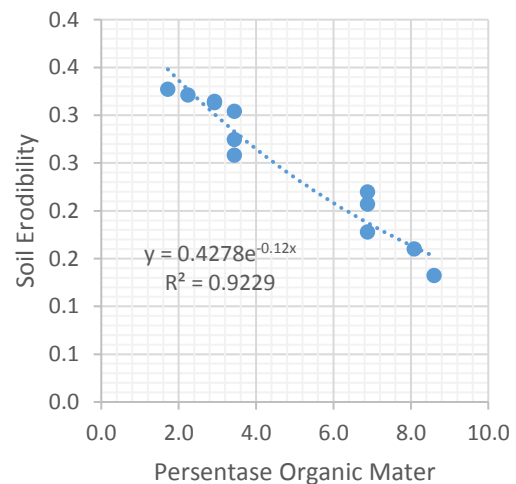


Figure 4. The organic matter relation with the land erodibility

Dust is a smooth fraction with no capacity and incapable of making ligament without adhesive content therefore, it will be easy for erosion to occur on the surface flow [11]. In addition, the loamy fraction has capacity and capable of creating a ligament. Therefore, this fraction will be hard difficult to undergo erosion compared to the dusty fraction. The land which is dominant by loamy fraction will be very cohesive and hard to get ruined. The Organic Substance relation with erodibility

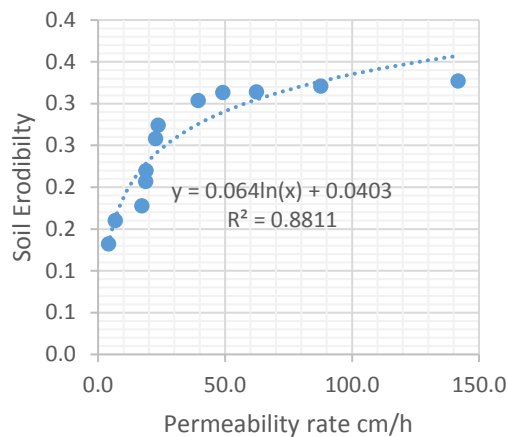


Figure 5. Permeability relation with soil erodibility

The organic substance seems to influence the land erodibility (figure 4) with power relation between it and the organic substance using a coefficient  $R^2$  value of 0,92. This means that each improvement in accordance to the organic material degree of 1% influences the land erodibility by 0,43 with credibility level of 92%. According to [12], the positive effect of organic carbon is for aggregate stabilization and the land structure, while [13] stated that organic material functions as layer and loamy fraction in increasing the land aggregate stability, thereby reducing its degradation. Previously [14], people argue that aggregation improves land endurance towards the rainfall boundary, thereby, reducing its fall

#### The Relation of Permeability with Erodibility

The land erodibility has a logarithm relation (figure 5) with determinant  $R^2$  of about 0,88. It means that each land permeability increases by 1 cm/hour which reduces the land erodibility reduction by 0,06 cm/hour an erodibility of 0,04, and a credibility level of 88%.

Its permeability lead to the drop of rainfall in the land surface therefore it is capable of reducing stagnant water. According to [15], the soil permeability rate is influenced by the total amount of land pore with macro pore being the primary factor. According to [16] the soil which has a high infiltration and percolation rate, has low relative value.

## CONCLUSION

From the result, the following conclusions were made as follows:

1. The land erodibility at the flow of Sumani river hilt is highest with average criteria.
2. Based on the PCA analysis, the dusty fraction content and smooth sand are the main factors which improve the value in this region.
3. In addition, there are other factors that indicates the relationship between the land erodibility with loamy content, organic matter and soil permeability which also influences it.
4. The other environmental factor which influences this value is horticulture management enterprise by the farmer..

## ACKNOWLEDGMENTS

The researcher is wishes to express his profound gratitude to the rector of Andalas University for the support and providing all the facilities needed to carry out this study. Furthermore, the researcher is also grateful to all students who participated in the field and laboratory activities. Hopefully, this paper will enhance students literation.

## REFERENCES

- [1] Lal, R., research method of 1994 erosion. Land. 3rd edition. Land and Water Conservation Society (Aukeny), & St. Lucie Press (Delray Beach), United States, 352 p.
- [2] Zhang ZG, Fan BE, Bai WJ, Jiao JY, J. Tanah. Air. Conserv. 5 (2007) 7-13.
- [3] Tejada M., Gonzalez JL, Tanah. Sampai. Res. 91 (2006) 186-198.
- [4] Veihe A., Geoderma. 106 (2002) 101-120.
- [6] Manyiwa T., Dikinya O., Afr. J. Agric. Res. 8 (2013) 4170-4178.
- [7] Asdak, Chay. 2010. Hydrology and river basin management. Yogyakarta: Gadjah Mada University Press.
- [8] Wischmeier, W., Johnson, C., Cross, B., 1971. Sebuah tanah erodibilitas nomograph untuk lahan pertanian dan konstruksi situs. Jurnal Konservasi Tanah dan Air 26 (3): 189-193
- [9] Andrews, SS, Carroll, CR, 2001. Merancang alat penilaian kualitas tanah untuk manajemen agro-ekosistem yang berkelanjutan. *Aplikasi ekologi* 11 (6): 1573-1585.
- [10] Santos, FL, Reis, JL, Martins, OC, Castanheira, NL, Serralheiro, RP 2003 penilaian Perbandingan infiltrasi, limpasan dan erosi sprinkler irigasi tanah. *Biosystem Teknik* 86 (3): 355-364.
- [11] Dariah, A., F. Agus, S. Aryad, Sudarsono, and Maswar. 2003. The relationship between soil

- characteristics and erosion rate of coffee based farming area in Sumberjaya, West Lampung. Journal of Land and Climate No. 21/2003, soil Research Hall. Bogor. 78-86 things.
- [12] Emami, H., Astaraei, AR, 2012. Pengaruh amandemen organik dan anorganik pada parameter dari kurva retensi air, bulk density dan diameter agregat dari tanah salin-sodik. Jurnal Ilmu Pertanian dan Teknologi 14: 1625-1636.
- [13] Kodešová, R., Rohošková, M., Žigová, A. 2009. Perbandingan stabilitas agregat dalam waktu enam profil tanah di bawah pengolahan tanah konvensional menggunakan berbagai tes laboratorium. Biologia 64 (3): 550-554.
- [14] Baldock, JA, Skjemstad, JO, 2000. Peran matriks tanah dan mineral dalam melindungi bahan organik alami terhadap serangan biologis. Organik Geokimia 31 (7-8): 697-710.
- [15] Aprisal, Rusman. B. Dwipa. I., Refdinal. Erlina, R., Fajriwandi 2016. The dynamics of some of the physical properties of soil under conservation farming. On the critical land of Arian in DTA Singkarak. Journal of Land Suboptimal: 5 (2) 137-144.
- [16] Irma. F., Saka., Arief. 2008. Agricultural land Erosion analysis and economic parameters using nail (net agricultural income loss) method based on geographic information system in Hulu Das Jeneberang.

## A NEW REPORT OF ARGULUS INDICUS (CRUSTACEA: BRANCHIURA) INFESTATION IN RED TILAPIA (OREOCHROMIS NILOTICUS X OREOCHROMIS MOSSAMBICUS) IN THAILAND

Supamas Sriwongpuk<sup>1</sup>

<sup>1</sup>Faculty of Agricultural Technology, Rajamangala University of Technology Thanyaburi, Thailand

### ABSTRACT

*Argulus indicus* (Crustacea: Branchiura), or the fish louse, is an external parasite in Phylum Arthropoda found on the skin, fin or gills of freshwater fish species. It is very flat with an oval or rounded carapace, two compound eyes, sucking mouthparts with a piercing stylet, and two suction cups it uses to attach to its host. Clinical signs in infected fishes include scratching on aquarium walls, erratic swimming and poor growth. It causes pathological changes due to direct tissue damage and secondary infections. In the present study, red tilapia (*Oreochromis niloticus* x *Oreochromis mossambicus*), with symptoms such as abnormal swimming or scratches on their skin, were collected from a cage culture at Klong Rapee-Phat, Nong-Seau District, Pathum-Thani Province in Thailand. The parasites collected from the skin and fins of infected red tilapia were identified as *Argulus indicus*. This is the first report of infection with *A. indicus* of red tilapia (*O. niloticus* x *O. mossambicus*) in Thailand.

**Keywords:** *Argulus indicus*, Fish louse, Red tilapia, *Oreochromis niloticus* x *Oreochromis mosambicus*, Thailand

### INTRODUCTION

Among crustaceans, more than 1,500 species of copepods are parasitic on fishes. *Argulus* Müller, 1785 is one genera belonging to the class Branchiura, most commonly known as fish lice or fish louse, a class of crustacean arthropods [1] that are members of a large group of branchiuran parasites related to crabs, lobsters and shrimp [2]. The genus *Argulus* (Crustacea: Branchiura), or fish louse, is a common parasite of freshwater fishes [3]. Nearly 15 species are found in freshwater fishes and several of the species are parasitic on marine fishes [4]. Fish louse belonging to the Argulidae family are skin parasites. About one hundred known species have worldwide distribution [5] and cause damage to skin epithelium by their feeding activity. The wounds bleed slowly and become the sites of secondary infections by pathogens [6]. The injury to tissue manifests as inflammation and secondary infections by microbes. If the infection is high, these parasites can cause great damage to populations of fishes in pond culture and cage culture systems [7].

Parasitic crustaceans are among the most harmful pests for fishes. Certain species cause mass infestation and mortality in fish cultures, sometimes even in nature, resulting in considerable economic losses. Fish cultures now include raising fishes not only in man-made ponds and tanks, but also in cages and pens built or suspended in large bodies of water such as reservoirs, lakes, and even marine coastal areas [8]. Fishes serve as a potential source of animal protein for humans [9]. About 40% of the protein diet of 2/3 of the entire global population comes from fishes [10]. The majority of fishes serve as an

intermediate host for many parasites which can cause mass mortality thereby reducing the food value of fishes [11]. Tilapia species are freshwater fishes belonging to the family of Cichlidae which are considered to be more resistant as compared to other species of cultured fishes [12]. Crustaceans constitute one of the four recent subphyla of phylum Arthropoda which includes 1,242,040 species [13].

Tilapia is a freshwater fish belonging to the family Cichlidae. It is native to Africa, but was introduced into many tropical, subtropical and temperate regions of the world during the second half of the 20th century [14]. Tilapia is a worldwide fish of great commercial importance and it is recognized as one of the most important aquaculture species of the 21<sup>st</sup> century. Tilapia is currently ranked second only to carp in global production [15]. The world's total tilapia production in 2012 was 4.2 million tonnes. Tilapia aquaculture is rapidly expanding with a global production of about 2.8 million metric tonnes in 2008 [16] and estimated to increase to 8.89 million metric tonnes by the year 2020 [17]. The red tilapia (*Oreochromis* hybrids or *O. niloticus* x *O. mossambicus*) developed from crosses of the main *Oreochromis* culture species has also become popular in recent years [18].

The parasites use the fish for their shelter and food and destruct more or less each and every organ resulting in pathogenic effects [19]. Crustacean is an important disease producing parasites of freshwater fishes. *Argulus* is one of a serious pathogen of fish in natural and intensive fish cultures. Many problems associated with argulid infections are a reduced rate of growth and impact on the aesthetic value of the fish host which results in economic losses in fisheries



[20]. This is the first report of infection with *A. indicus* of red tilapia (*O. niloticus* x *O. mossambicus*) in Thailand. As such, the present study aims to make a survey to elucidate the morphological characteristics of *A. indicus*.

## MATERIALS AND METHODS

In March 2017, thirty red tilapias were collected using gill nets from a cage culture at Klong Rapee-Phat, Nong-Seau District, Pathum-Thani Province in Thailand. These fishes were examined for ectoparasites. Twenty four fishes were found to be infected with copepod parasites. *Argulus* were found attached to the bodies on scales and fins. The parasites were carefully removed with the help of a needle and a soft brush. The specimens of *Argulus* collected from the body surface of the red tilapias were preserved in 70% ethyl-alcohol and then transferred to 2% formalin for detailed study. Using a compound light microscope at x10 and x40 magnifications, the fishes were dissected and examined. The *Argulus* parasites were fixed in 70% ethyl-alcohol and then transferred to the laboratory. The identification of the morphometric characteristics of this parasite was carried out as described previously [5, 21, 22, 23 and 24].

## RESULTS AND DISCUSSION

Specimens of fish louse were collected in March 2017 of the body surfaces (scales, skin and fins) of red tilapias in a cage culture at Klong Rapee-Phat, together with the number of infestation values are given in table 1.

Table 1 Infestation values of *Argulus indicus* on Red Tilapia caught from Klong Rapee-Phat

| Infestation values                     | Number |
|--|--------|
| Number of fish investigated            | 30     |
| Number of fish infested                | 24     |
| Prevalence (%)                         | 80     |
| Number on 1 fish                       | 1-28   |
| Total number of <i>Argulus indicus</i> | 736    |

Twenty four red tilapias were found to be heavily infested with *A. indicus*. Acute haemorrhagic septicemia inflamed skin wounds, an increased production of mucosal material, loss of scales and corrosion of fins were observed in these red tilapias. Fish louse causes damage to the skin epithelium by their feeding activity. The wounds bleed slowly and become the site of secondary infection by pathogens [6]. The small lesions and collagen of the dermis were secondarily infected by bacteria and fungi leading to further degeneration of the epidermal layer and disruption of the basal membrane [25].

The systematic position of the genus *Argulus* is as follows:

Class: Crustacea  
 Subclass: Branchiuran  
 Order: Arguloidea  
 Family: Argulidae  
 Genus: *Argulus*  
*Argulus indicus* Weber, 1892

The morphological description of *Argulus indicus* can be expressed as follows (Figure 1 to 3); a wide, oval body, dorso-ventrally flattened and 2 complex faceted eyes. The cephalothorax is covered with a wide convex scutum and its posterior margin is indented. First maxillae are usually modified as powerful suctorial organs, which are clearly visible at the ventral surface. The second maxilla or suction cup, posterior to the sucker, has 5 segments. Four pairs of thoracic legs are modified for swimming. Each thoracic segment bears a single pair of biramous swimming legs (thoracopods), the first 2 pairs of which in both sexes have a backwardly projecting process or flabellum. The urosome with rounded lobes is covered marginally with small spines. The anterior end of the cephalothorax forms a broad protrusion and is delimited laterally by shallow grooves. The posterior incisures of the urosome do not reach into the center.



Fig.1 Ventral view of *A. indicus* (female) (scale = 1 mm), where 1=1<sup>st</sup> antenna, 2=2<sup>nd</sup> antenna, 3=eye, 4=1<sup>st</sup> maxilla or suction cup, 5=respiratory area, 6=thorax, 7=thoracic appendage, 8=spermathecal, 9=abdomen (urosome or caudal fin)



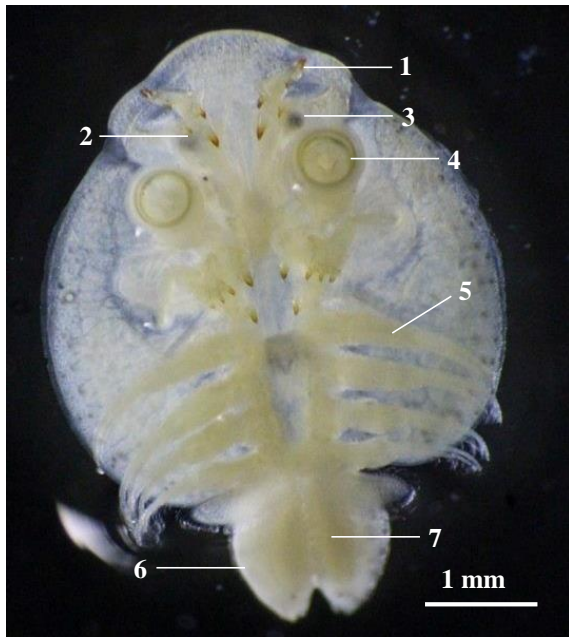


Fig.2 Ventral view of *A. indicus* (male) (scale = 1 mm), where 1=1<sup>st</sup> antenna, 2=2<sup>nd</sup> antenna, 3=eye, 4=1<sup>st</sup> maxilla or suction cup, 5= thoracic appendage, 6= abdomen (urosome or caudal fin), 7=testes

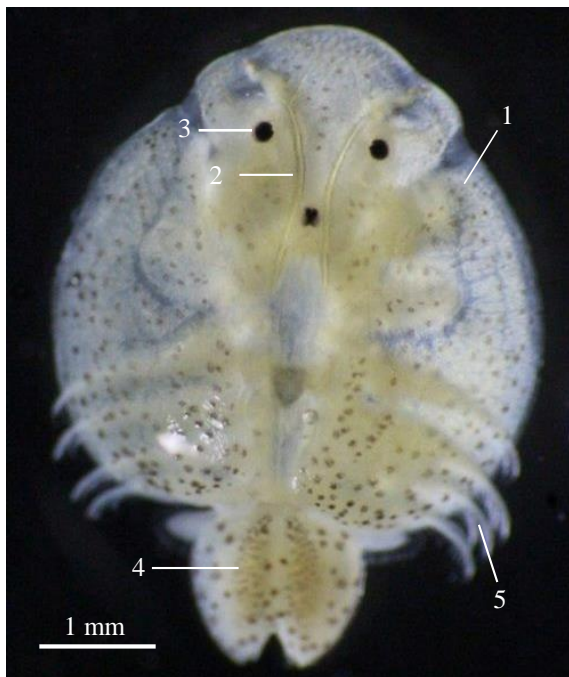


Figure 3 Dorsal view of *A. indicus* (Male) (scale = 1 mm), where 1= carapace, 2=ridges, 3=eye, 4=testes, 5=swimming leg

The carapace is almost as broad as it is long with a deep posterior sinus. The lateral lobes of the carapace convex overlap all the swimming legs. The dorsal paired ridges of the carapace curve outward beyond the paired eyes anteriorly and discontinue posteriorly with the posterior straight pieces ending near the posterior transverse groove of the cephalic region (Figure 3).

The minute anterior respiratory area just anterior to the very large and oblong posterior one (Figure 1 and Figure 4); the ribs of the suction cup with 3 rods and not of the imbricate plates (Figure 5); the second maxilla slender, basal plate with three large teeth.

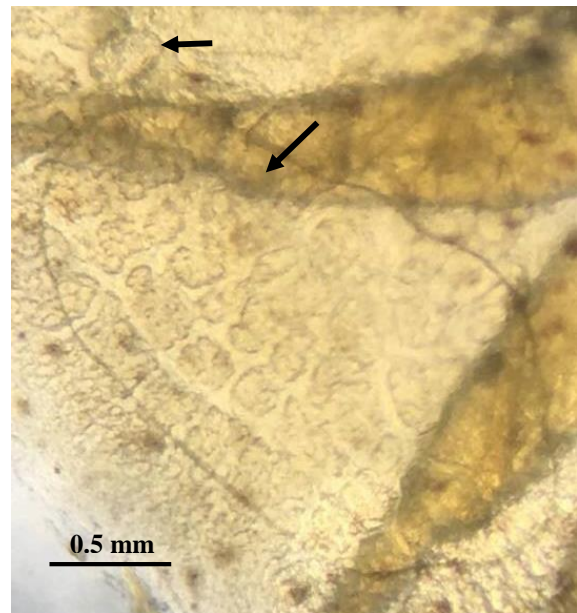


Figure 4 The respiratory area of *A. indicus* (arrow) (scale = 0.5 mm)

The species of the fish louse *Argulus* (Crustacea: Branchiura) are found distributed throughout the world and 143 species in the genus have been described, although it is likely that many of these are synonymous [6]. Species of *Argulus* are characterized by a depressed ovoid and broad body. The head is fused with the thoracic segment forming a cephalothorax covered by a dorsal, broad, flat shield (carapace) with posterolateral lobes. Two pair of maxillae are present, the first maxillae in the genus *Argulus* is highly modified to form cup-like suckers with strongly reinforced walls [26].

This genus is distributed worldwide in both marine and freshwater habitats [5]. The genus *Argulus* causes problems in many types of aquatic systems throughout the world. Although there is a considerable literature available on the group of parasites, most is concerned with the taxonomy,

morphology and development of the parasite, about which aspects are fairly well understood. There is much less reliable information available on other aspects of the biology of *Argulus*; in particular there is a need for quantitative and experimentally based studies. *A. indicus* was found on *Ophiocephalus punctatus* from West Bengal [27], *Ophiocephalus micropeltes* from Tasik Temengor, Parak from Malaysia [28] and on Major carps from Hyderabad from Pakistan [29]. There are four species of *Argulus* reported in Thailand such as *A. foliaceus*, *A. indicus*, *A. siamensis* and *A. alosae* [21]. *A. indicus* was found on the skin of Siam fighting fish (*Betta splendens* Regan, 1910) from Bangkok, Thailand [30]. If it is physically possible the best control method for *Argulus*-infected waters is to empty them of fish and allow a fallow period before re-stocking. This would have to be long enough to allow for the hatching of eggs and the death of resulting parasites. Alternatively lakes could be drained and left empty for sufficient time for eggs to be killed by desiccation or frost [31].

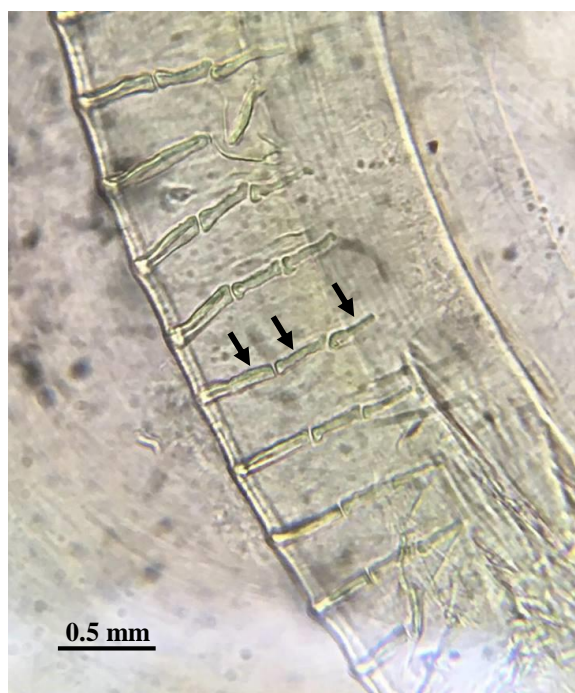


Figure 5 Ribs of the suction cup with 3 rods (arrow) (scale = 0.5 mm)

## CONCLUSIONS

This research has identified and characterized the parasites residing in the red tilapia (*O. niloticus* x *O. mossambicus*) from Klong Rapee-Phat, Nong-Seau District, Pathum-Thani Province in Thailand. This is

valuable information given the widespread local consumption of the fish and its significance as the main source of protein. In the study, a total of thirty red tilapia fish samples were examined and the findings revealed the existence of fish louse or *A. indicus* (Crustacea: Branchiura). The external copepod parasitic species were found on the scales, skin and fins with the highest prevalence of parasitic infection (80%) (Table 1) with the characteristic of the anterior respiratory area minute just anterior to the very large and oblong posterior one; ribs of suction cup with three rods and not of imbricate plates. All of parasites from this study were fish louse in genus *Argulus* and were identified as *A. indicus*. This is the first report of infection with *A. indicus* of red tilapia (*O. niloticus* x *O. mossambicus*) in Thailand.

## ACKNOWLEDGMENTS

The author would like to express sincere appreciation to the Faculty of Agricultural Technology and the Institute of Research and Development, Rajamangala University of Technology Thanyaburi (RMUTT), for their financial support.

## REFERENCES

- [1] Piasecki W. and Avenant-Oldewage A., Diseases caused by Crustacea. In Eiras J.C., Segner H., Wahli T. and Kapoor B.G. (Eds) Fish Diseases. Enfield (N.H.): Science Publishers, 2008, pp. 1115-1200.
- [2] Natalie S. and Roy P.E.Y., *Argulus* (Fish Louse) Injections in Fish, The Institute of Food and Agricultural Science (IFAS), University of Florida., 2012, p.1.
- [3] Mirzaei M. and Khovand H., Prevalence of *Argulus foliaceus* in Ornamental Fishes [Goldfish (*Carassius auratus*) and Koi (*Cyprinus carpio*)] in Kerman, Southeast of Iran, J. Parasit. Dis., Vol. 39, Issue 4, 2015, pp.780-782.
- [4] Noaman V., Chelongar Y. and Shahmoradi A.H., The First Record of *Argulus foliaceus* (Crustacea: Branchiura) Infestation on Lionhead Goldfish (*Carassius auratus*) in Iran, Iranian J. Parasitol., Vol. 5, No.2, 2010, pp.71-76.
- [5] Kabata Z., Parasites and Disease of Fish Cultured in Tropics. Tylor and Francis, London, 1985, pp. 1-317.
- [6] Kabata, Z. Diseases of Fishes, Book.1: Crustacea as Enemies of Fishes, T.F.H. Publication, New Jersey, 1970, pp. 1-171.
- [7] Yambot A.V. and Lopez E.A., Gill Parasite *Lamproglana monodi* Capart, Infecting the Nile Tilapia, *Oreochromis niloticus* L. Cultured in Phillipines. In Diseases in Asian Aquaculture III

- (Flagel T.W. and Mac Rae I.H. eds.), As. Fish. Soc. Manila, 1997, pp. 175-177.
- [8] Lopez N.C., Helminth and Arthropod Parasites of Some Freshwater Fishes from Laguna Lake and Vicinities. In Fish Health Problems in Laguna de Bay and Environs. PCARRD Book Series, No. 49, Los Baños, Laguna, 1988, pp.7-14.
- [9] Abdel-Gaber R., Abdel-Ghaffar F., Bashtar A.R., Morsy K. and Saleh R., Interaction between the Intestinal Cestode *Polyonchobothrium clarias* (Cestode: Ptychobothriidae) from the African Sharptooth Catfish *Clarias gariepinus* and Heavy Metal Pollutants in an Aquatic Environment in Egypt, J. Helminthol., Vol 90, Issue 6, 2016, pp. 742-752.
- [10] Abdel-Ghaffar F., Abdel-Gaber R., Bashtar A.R., Morsy K., Al Quraishy S., Saleh R. and Mehlhorn H., Molecular Characterization and NewG record of *Lecithochirium priacanthi* (Digenea: Hemiuiridae) Infecting the Moontail Bullseye Fish *Priacanthus hamrur* (Perciformes: Priacanthidae) from the Red Sea, Egypt, Parasitol. Res., Vol. 114, Issue 12, 2015, pp. 4471-4477.
- [11] Bunkley-Williams L, Williams E.H. and Bashirullah A.K.M., Isopods (Isopoda: Aegidae, Cymothoidae, Gnathiidae) Associated with Venezuelan Marine Fishes (Elasmobranchii, Actinopterygii), Rev. Biol. Trop., Vol. 54 (Suppl. 3), 2006, pp. 175-188.
- [12] Akoll P., Konecny R., Mwanja W.W., Nattabi J.K., Agoe C. and Schiemer F, Parasite Fauna of Farmed Nile Tilapia (*Oreochromis niloticus*) and African Catfish (*Clarias gariepinus*) in Uganda, Parasitol. Res., Vol. 110, Issue 1, 2012, pp. 315-323.
- [13] Zhang Z.Q., Animal Biodiversity: an Outline of Higher-Level Classification and Survey of Taxonomic Richness, Zootaxa, Vol. 3148, 2011, pp. 1-237.
- [14] Pillay T.V.R., Aquaculture: Principle and Practices, Fishing Book News, London, 1990, pp. 1-575.
- [15] Ridha M.T., Comparative Study of Growth Performance of Three Strains of Nile Tilapia, (*Oreochromis niloticus* L.) at Two Stocking Densities, Aquaculture Research, Vol. 37, Issue 2, 2005, pp. 172-179.
- [16] FAO, FAOSTAT. Food and Agriculture Organization of the United Nations, 2010.
- [17] Tacon, A.G.J. and Metian, M., Global Overview on the Use of Fish Meal and Fish Oil in Industrially Compounded Aquafeeds: Trends and Future Prospects, Aquaculture, Vol. 285, No. 1-4, 2008, pp. 146-158.
- [18] Teichert-Coddington, D.R., Green B., Boyd C.E., Harvin J.L., Rodriguez R., Martinez D., and Ramirez E., Effect of Diet Protein on Food Conversion and Nitrogen Discharge During Semi-Intensive Production of *Penaeus vannamei* During the Wet Season. In Burke D., Goetze B., Clair D. and Egna H. (Editors), Fourteenth Annual Technical Report, Pond Dynamics/Aquaculture CRSP, Office of International Research and Development, Oregon State University, Corvallis, Oregon, 1997, pp. 71-77.
- [19] Lilley, J.H., Philips, M.J. and Thongutai, K., A Review of Epizootic Ulcerative Syndrome (EUS) in Asia. Publ. Aquatic Animal Health Research Institute and Network of Aquaculture Center in Asia-Pacific, Bangkok, Thailand, 1992, pp.1-73.
- [20] Taylor N.G.H., Sommerville C. and Wootten R., The Epidemiology of *Argulus* spp. (Crustacea: Branchiura) Infections in Stillwater Trout Fisheries, Journal of Fish Diseases, Vol. 29, Issue 4, 2006, pp 193-200.
- [21] Sirikanchana P., Parasites of Aquatic Animal, Sky Word Advertising Partnership Ltd., Bangkok, 2003, pp. 1-270.
- [22] Bykhoskaya-pavlovskaya I.E., Gusev A.V., Dubinina M.N., Izvumova N.A., Smimova T.S., Sokolo-vskava I.L., Shietin G.A., Shulman S.S. and Epstein V.M., Key to Parasites of Freshwater Fish of USSR, Israeli Program for Scientific Translation, Jerusalem, 1964, pp. 1-694.
- [23] Hoffman G.L., *Argulus*, a Branchiuran Parasite of Freshwater Fishes, U.S. Fish and Wildlife Service. Fish Disease Leaflet 49, 1977, pp. 1-9.
- [24] Thomas M.M. and Devaraj M., Two New Species of *Argulus* Müller (Crustacea: Branchiura) from River Cauvery with a Key to Indian Species, Central Marine Fisheries Research Inst., Regional Centre, Mandapam Camp (India), 1977, pp 215-220.
- [25] Bauer O.N., Musselius V.A. and Strelkov Y.A., Disease of Pond Fishes, Israel Program for Scientific Translations, Jerusalem, 1973, pp 152.
- [26] Richard H., Other Ectoparasites Infesting Fish; Copepods, Branchiurans, Isopods, Mites and Bivalves, Aquaculture Magazine November/December, 2003, pp. 1-7.
- [27] Ramakrishna G., Note on the Indian Species of the Genus *Argulus* Müller (Crustacea, Copepoda) Parasitic on Fishes, Indian Museum Calcutta Records, Vol. 49, Issue 2, 1951, pp. 207-215.
- [28] Seng L.T., Two Ectoparasitic Crustaceans Belonging to the Family Argulidae (Crustacea: Branchiura) in Malaysian Freshwater Fishes, Malayan Nature Journal, Vol. 39, 1986, pp. 157-164.
- [29] Jafri S.I.H. and Ahmed S.S., A New Record of Ectoparasitic Crustaceans (Branchiura: Argulidae) from Major Carps in Sindh, Pakistan, Pakistan Journal of Zoology, Vol.17, Issue 1, 1991, pp. 11-13.
- [30] Wilson C.B., A Copepod (*Argulus indicus*) Parasitic on the Fighting-Fish in Siam, Journal of the Siam Society, Natural History Supplement,

Vol. 7, Issue 1, 1972, pp. 1-3.  
[31] Tonguthai K., Control of Freshwater Fish  
Parasites: a Southeast Asian Perspective,

International Journal of Parasitology, Vol. 27,  
Issue 10, 1997, pp. 1185-1191.

## IMMEDIATE EFFECTS OF ARM SWING EXERCISE THERAPY ON THE RANGE OF SHOULDER MOTION AND STAND POSTURE: A PILOT STUDY IN YOUNG ADULTS

Zhen Xiao<sup>1,3</sup>, Wichai Eungpinichpong<sup>1,2,3\*</sup>, Xingze Wang<sup>4</sup>, and Uraiwan Chatchawan<sup>2,3</sup>

<sup>1</sup> Division of Physical Therapy, Faculty of Associated Medical Sciences, Khon Kaen University, Thailand;

<sup>2</sup> Back, Neck and Other Joints Pain and Human Performance (BNOJPH), Thailand;

<sup>3</sup> Research and Training Center for Enhancing Quality of Life of Working-Age People, Thailand;

<sup>4</sup> School of Physical Education and Training, Shanghai University of Sport, Shanghai, China

### ABSTRACT

People who work in offices for a long time tend to have poor posture and a decreased range of motion throughout the body. This could lead to chronic neck and shoulder pain if not corrected. Shuai Shou Gong, a version of Arm Swing Exercise (ASE), has been developed and practiced by some Chinese people for over one thousand years to maintain physical well-being. Its beneficial effects on posture and range of motion have not yet been verified. Thus, the purpose of this study was to preliminarily examine the immediate effects of ASE on shoulder range of motion (ROM) and occiput-wall distance (OWD) in young adults. The before-after study design was used in fifteen healthy office workers (6 males, 9 females), aged 20-40 years, who participated in the study. The shoulder ROM and OWD of the participants were measured before and immediately after a 10-minute session of supervised ASE. A paired-sample t-test was used to estimate the mean changes in the outcome. Results in this study revealed that shoulder ROM was increased in all directions ( $P < 0.05$ ) while the OWD was decreased ( $P < 0.05$ ) after the 10-minute session. However, a postural assessment method using a mobile application (PostureScreen) could not demonstrate a significant improvement. In conclusion, ASE may provide immediate improvements on shoulder ROM and forward head posture as indicated by a decreased OWD. Further research using a randomized controlled trial is needed.

*Keywords: Arm Swing Exercise, Shoulder Range of Motion, Occiput-wall Distance, Posture*

### INTRODUCTION

Arm Swing Exercise (ASE) is a type of traditional Chinese QiGong which has been practiced by Chinese people for ages to maintain both physical and mental wellbeing. ASE first appeared in the book of Dharma Yi Jin Jing more than a thousand years ago [1]. The performance of ASE consists of a series of rhythmic arm swinging and body swaying back-and-forth plus on the fifth swing, the participants slightly bent their knees and dipped down twice. ASE normally lasts for 5-15 minutes depending upon the health conditions of the performers. It has been classified as a low-intensity exercise, based on approximately 23% of the maximum  $\text{VO}_2$  and 45% of the maximum HR (HR Max) during the exercise [2]. Based on traditional Chinese medicine, ASE may facilitate the circulation of Qi, the internal energy [3], throughout the whole body, since Qi nourishes the internal organs and helps recovery from illnesses and provide positive effects for health [4].

Performing ASE training quickly and repeatedly stimulates the muscles, improves the transmission rate of nerve transmissions across synapses, improves tonic reflexes that causes the muscle to contract and increases muscular activity [5]. ASE is beneficial for increasing muscle strength and balance stability [6]. Since rapid vibration stimulates the receptors in the

joints, muscles, ligaments, activation reflection, and proprioception circuit, improves the sensory function of upper limbs and promotes neuromuscular recovery [7], ASE is conducive to the accurate coordination of space and time between sensory center and muscle proprioception [8] then it may facilitate having good standing posture.

Theoretically, repeatedly swinging the arms may stimulate the nerves, tendons and muscles surrounding the shoulder joint [9]. When the arms are swinging, the latissimus dorsi muscle and the gluteus maximus that are connected by the superficial layer of the lumbar fascia, can transfer the forces and rotate the torso [9]. In previous studies, ASE training has shown a protective effect on vascular complications by improving blood glucose control and improving oxidative stress through exercise [11]. Exercise capacity and oxygen consumption in overweight and normal weight sedentary young adults are improved through ASE [11]. ASE was also found to improve the pulmonary functions in type 2 diabetes mellitus (T2DM) patients [12].

Nowadays, there is an increase in the number of people who work in offices for an extended time. This can lead to poor posture and a decreased range of motion throughout the body because of tiredness and muscle tightness resulting in chronic neck and shoulder pain. Since the effects of ASE on improving the



shoulder range of motion and standing posture has not been verified, this study aims to preliminarily examine the immediate effects of ASE on shoulder range of motion (ROM) and occiput-wall distance (OWD) in these office-working people.

## METHODOLOGY

### Study design and participants

This pilot study employed a before-after research design. Healthy people aged between 20-40 years who met the inclusion criteria were recruited. Exclusion criteria was based on reviewing past medical records. Participants with a pre-existing medical condition with contra-indication to exercise were excluded. Before and immediately after the experimental intervention, the evaluation parameters of the young adults were investigated to explore an immediate effect of ASE on posture and on active range of motion of the shoulder joints. The whole process of the study is presented in the following flowchart (Figure 1).

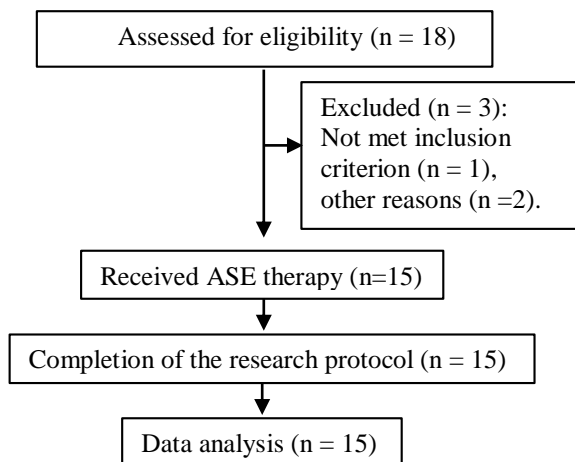


Fig. 1 Flowchart of study process (n=15)

### Arm Swing Exercise Intervention

The ASE training was performed in a research room with proper light and ventilation where the room temperature was set at 25°C. Participants were told to wear suitable cotton T-shirt and shorts. The ASE protocol consisted of a 3-minute period of warm-up and active stretching of the main muscle groups of the body. Then the participants performed a 10-minute session of ASE as guided by a pre-recorded video tape. Finally, the session ended with a 3-minute cool-down. All of the procedures of ASE were guided by an exercise coach using a metronome to control the rhythm.

### Arm Swing Exercise protocol

The participants stood with their feet apart about shoulder width. The arms were actively raised to shoulder-height with comfortably straightened fingers. While their trunk and neck were kept upright, their arms swung back and forth, naturally following the preset tempo of the metronome. Breathing through their nose, they breathed in during the up-swing and breathed out on the down swing. Each set of ASE consisted of five arm-swings, where the action from 1 to 4 was the same. However, on the fifth swing, the participants slightly bent their knees and dipped down twice (Figure 2). The participants were encouraged to swing their arms rhythmically in a relaxed manner [4].

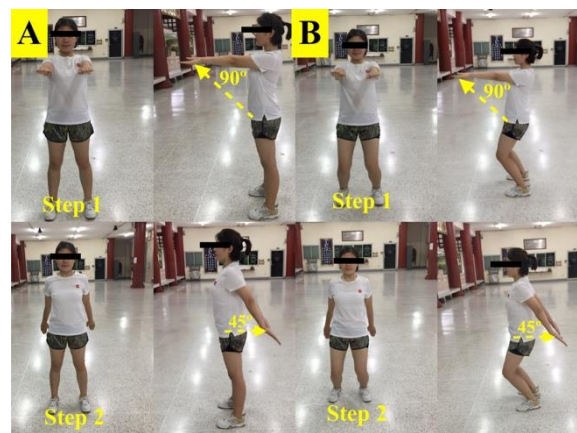


Fig. 2 Single set of ASE performance. Consisted of the first four swings (A) with knees extended and the fifth swing (B) with slightly bent knees.

## OUTCOME MEASURES

### Shoulder Range of Motion (ROM)

Active shoulder ROM is defined as the range of motion where participants could move their shoulders to the end of each of the cardinal plane while maintaining a neutral thorax (no compensatory movement of the trunk) [13]. A standard goniometry of shoulder joint ROM was measured by a licensed physical therapist (the examiner). The examiner asked the participants to lay supine on a massage bed to measure ROM in order to minimize the compensatory movement of the thorax during the measurement [14]. Movements in shoulder flexion, abduction, medial (internal) rotation, lateral (external) rotation and extension were measured bilaterally [15]. The first four directions were measured in the supine lying position. Only the shoulder extension was measured when the participants were in the prone lying position. Three consecutive measurements were made on each direction, after which the average was used.

### Occiput-Wall Distance (OWD)

The distance between occiput and wall (OWD) in standing position was measured by the examiner. OWD has been used to determine the amount of kyphosis [16]. The flexed posture defined by OWD is also associated with increased posterior chest convexity [16]. OWD has been widely used in epidemiological studies, although it cannot replace the clinical measures of highly accurate kyphosis deformity such as Cobb's Angle [17]. However, it could be used as screening tool for early detection of forward neck posture and possible weakness of posterior neck muscles in non-disabled elderly people [18]. The examiner used a ruler to measure the distance between the protuberance of the 7th cervical spinous process and the wall as the participants stood up erect where the heels, sacrum, and upper back were positioned against the wall [19].

### Posture

The posture can be defined as the rotation and straight position of adjacent body segments and its direction relative to gravity [20]. The proper alignment of the body's segments so that the least amount of energy is required to maintain a desired position is the ideal posture. The examiner used the PostureScreen Mobile APP to take the participants' photos in front view, right side view, back view, and left side view [21]. Through the taken photos of the standing body, the average of lateral postural displacements was determined. Previous studies have shown that this mobile APP has high reliability and validity. Inter-rater reliability was good to excellent for all translations and a range of 0.71 to 0.99 for the intra-rater reliability [18].

### Heart Rate

HR was measured to monitor the exercise intensity of the participants while doing the ASE. The examiner used the Jumper JPD-500A pulse oximeter to measure the heart rate of participants. The heart rate was measured: before exercise, during exercise (at 5-minute mark), and immediately after exercise.

### Data collection

The trained examiner measured all before and after exercise data in the laboratory where the intervention occurred in the same sequence. Data from shoulder ROM, OWD and posture were collected twice, whereas heart rate was collected three times.

### Data Analysis

SPSS 20.0 was used to process and analyze all data. Paired-sample T test was used to compare the means of before and after the intervention. The level of significance was set at  $p < 0.05$ .

## RESULT

Fifteen participants (6 males, 9 females), aged  $28.8 \pm 7.03$  years, were included. Their mean height, weight, and BMI (Body Mass Index) were  $162.62 \pm 7.08$ cm,  $65.95 \pm 14.72$  kg,  $25.07 \pm 4.52$  kg/m<sup>2</sup>, respectively.

### Shoulder ROM

Shoulder ROM was increased in all directions when participants finished 10-minutes of ASE. Based on changes from baseline to intervention, the significant improvement was shown in shoulder flexion, abduction, medial rotation, lateral rotation and extension measurements in all participants ( $P < 0.05$ ) (Table 1).

Table 1. Pre-ASE and Post-ASE values of the shoulder range of motion

| Parameters                   | Pre-ASE      | Post-ASE     | p-value |
|------------------------------|--------------|--------------|---------|
| Shoulder range of motion (°) |              |              |         |
| <b>Left side</b>             |              |              |         |
| Shoulder Flexion             | 173.86± 4.67 | 186.33± 6.44 | .001    |
| Shoulder Abduction           | 184.33±13.97 | 191.13±16.75 | .012    |
| Shoulder Medial Rotation     | 80.06±8.49   | 96.73±13.29  | .001    |
| Shoulder Lateral Rotation    | 82.33±8.47   | 95.20±10.11  | .001    |
| Shoulder Extension           | 38.40± 15.22 | 57.86±19.85  | .001    |
| <b>Right side</b>            |              |              |         |
| Shoulder Flexion             | 173.40±10.83 | 182.40±7.02  | .005    |
| Shoulder Abduction           | 181.70±12.63 | 195.93±14.93 | .001    |
| Shoulder Medial Rotation     | 80.00±7.66   | 92.46±12.19  | .001    |
| Shoulder Lateral Rotation    | 86.06±11.77  | 96.86±8.91   | .001    |
| Shoulder Extension           | 35.80±15.22  | 53.40±18.78  | .001    |

Note: Values are means ± standard deviation, P value (2-tailed); Pre-ASE means pre-Arm Swing Exercise; Post-ASE means post-Arm Swing Exercise.

Figures 3, 4 are shoulder flexion, abduction measurements presented in box plot format. The results showed the positively skewed distribution. According to the results, there was significant improvement in shoulder range of motion after ASE. When the arm is swinging back and forth, the arm swings forward to 90 degrees and backward swing to 45 degrees. Increased shoulder range of motion can be achieved by repeatedly stimulating shoulder muscles and joints [33].



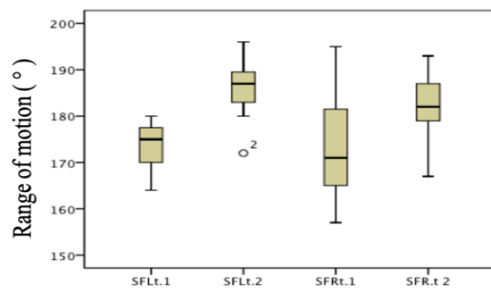


Figure. 3 Shoulder flexion

Note: SFLt.1 means Shoulder flexion before exercise (left); SFLt.2 means Shoulder flexion after exercise (left); SFRt.1 means Shoulder flexion before exercise (right); SFRt.2 means Shoulder flexion after exercise (right)

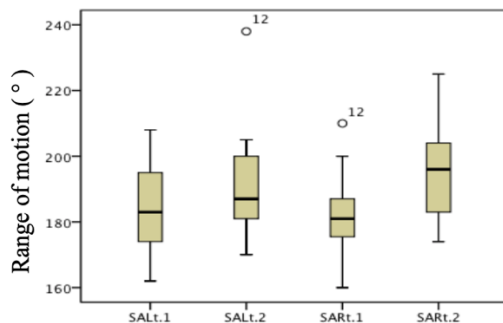


Fig. 4 Shoulder abduction

Note: SALT.1 means Shoulder abduction before exercise(left); SALT.2 means Shoulder abduction after exercise (left); SART.1 means Shoulder abduction before exercise (right); SART.2 means Shoulder abduction after exercise (right)

### Occiput-wall distance (OWD)

The median measurement of OWD before the ASE was 4.93cm and after the ASE median measurement was 3.63cm (Figure 5). OWD was decreased by 1.3cm after the ASE ( $P < 0.05$ ). This decreased in OWD indicated that the kyphotic posture of the participants has been decreased.

### Heart Rate (HR)

Before ASE the mean HR was 79 bpm (beats per minute), during exercise (at 5-minute mark) the mean HR was 93 bpm and after ASE, the mean HR was 103 bpm. ASE is a low-intensity traditional Chinese QiGong [19]. The result from the HR monitoring has confirmed that the intensity of this observed ASE was low.

### Posture

This study used the PostureScreen mobile application to take participants photos: front view, right

side view, back view, left view. Through Posture-Screen

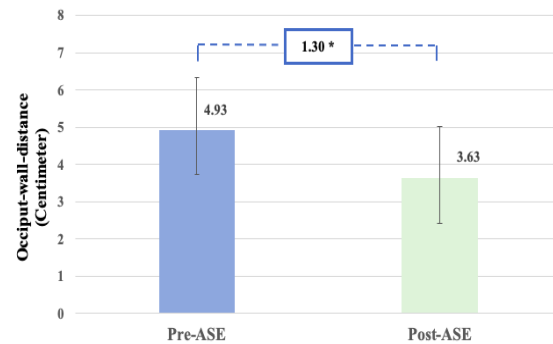


Fig 5 Occiput-wall distance between Pre-ASE and Post-ASE

analysis, average lateral postural displacements of participants were measured. The results showed no significant improvement in average lateral postural displacements of participants ( $P > 0.05$ ), however, the results of this study may be due to the short time of intervention of ASE, the usual training period being eight weeks or more to improve posture significantly.

### DISCUSSION

This study was to preliminarily examine the immediate effects of ASE on shoulder range of motion (ROM): after 10 minutes of ASE, shoulder ROM was increased in all directions. Based on changes from baseline to intervention, all participants showed improvement in shoulder flexion, abduction, medial rotation, lateral rotation and extension measurements. Short-term exercise can effectively increase the shoulder range of motion. These results are in line with other previous studies using different types of exercise. One study reported that regular exercise is an important factor in maintaining the shoulder range of motion of older women. Women between the ages of 50 and 71 who participate in regular exercise (twice a week) can improve and/or maintain a shoulder range of motion [24]. Pilates exercises are effective in improving shoulder abduction and external rotation ROM [25]. Traditional Chinese Qigong training among breast cancer patients effectively increased shoulder muscle strength, shoulder range of motion and was associated with better functional wellbeing [26].

In this study, however, after one session of practicing traditional Chinese ASE training, the range of motion of shoulders was significantly improved. Probably the manner of ASE directly affects the muscles around the shoulder joints. Clinical observations have shown that posterior shoulder tightness leads to

a variety of kinematic changes, such as decreased shoulder rotation, horizontal adduction, abduction, flexion, and increased external rotation. During ASE, the posterior shoulder, acromioclavicular joints, biceps, trapezius and deltoid were fully mobilized [33]. This may be one reason to increase the range of shoulder movement.

The results of this study also demonstrate that ASE therapy may provide immediate improvements on OWD in young adults as indicated by a significant decrease OWD after ASE. OWD is a quick and simple method for the evaluation of kyphosis and also an effective way to assess posture [28]. Long-term ASE training in the future may improve OWD more effectively and decrease kyphotic posture.

During ASE the body was in a straight line; head and shoulders move back, chest moved forward, feet shoulder-width apart, which allows the entire core muscles to be activated. If ASE is done correctly, it can improve the participant's core muscle control, effectively promoting the participant's core strength, core endurance, and it can mobilize the spinal joint [29]. Therefore, it provides benefits to the participant's posture (decrease in OWD). It may help activate many major core and limb muscles, for example, splenius capitis and splenius cervicis, deltoids, triceps, brachialis, biceps and core muscles, such as erector spinae, multifidus, gluteus maximus and rectus femoris [30].

A 10-minute training did not significantly improve participants' standing posture as detected by the Postural Screen application program. Probably the changes in whole-body posture have been compensated by many axial joints and core muscles. It may require long-term and regular ASE training to affect the improvement in posture. In addition, the participants in this pilot study were healthy young adults having no significant posture problems such that no changes could be observed after a single session of ASE.

A targeted exercise program (10-week trial) was found to improve posture adjustments associated with forward head posture. [30] The formation of human posture is a long-term development, so correcting a person's established posture or posture may also require a long process [32], [33]. In order to detect a significantly change in posture, a randomized controlled trial on the effect of ASE on posture is needed in future studies.

We acknowledge that our research design has some limitations. Firstly, the physiological mechanism of ASE in this study cannot be fully explained, nor did it fully explain the physiological mechanism of ASE on the shoulder ROM, OWD and Posture. Secondly, the power of statistical analysis of this study was limited due to the small sample size yet there was no control group for comparison. In the future, an improved randomized controlled trial will be more appropriate.

## CONCLUSIONS

ASE may provide immediate improvements on shoulder ROM and forward head posture as indicated by a decreased OWD. A 10-minute training did not significantly improve participants' standing posture. Long-term and regular ASE training is required to maximize its benefits including improvement in posture. Further research using a randomized controlled trial is needed.

## ACKNOWLEDGMENTS

We would like to thank the Faculty of Associated Medical Sciences, the research center in Back Neck and Other Joint Pain Research Group, Research and Training Center for Enhancing Quality of Life of Working-Age People and the Khon Kaen University for financially supporting this project.

## REFERENCES

- [1] C. Kejin, Dharma Yi Jin Jing. 3rd ed. Vol. 3, Chengdu times press, Chengdu, China, 2014, pp.127-131
- [2] Leelayuwat, N., 2013. Beneficial effects of alternative exercise in patients with diabetes type II. In Type 2 Diabetes. InTech.
- [3] Y. Minghui, [online] 2004 [ cited 2019 Mar 9] Traditional Chinese medicine: Energy, Available from: Energy <https://baike.baidu.com/item/气/10603498> 2004
- [4] M. Y. Popular, [online] 2008 [cited 2019 Mar 9]. Available from: [http://www.meimen.org/health\\_effort\\_01.php#WzBfASptDA](http://www.meimen.org/health_effort_01.php#WzBfASptDA)
- [5] G. Zhengwei, 3 rd, Physical education teaching theory, 3 ed. Vol. 3, SongLi, Ed. Beijing sports university press: Beijing, China, 2004; pp. 223-229
- [6] Fleg, J.L., Aerobic exercise in the elderly: a key to successful aging. Discovery medicine, Vol. 13, Issue 70, 2012. pp. 223-228.
- [7] Gertenbach, H.J., The influence of proprioceptive training on the functional balance of older adults (Doctoral dissertation, Stellenbosch: University of Stellenbosch). 2002.
- [8] Z. kai., Effects of whole-body vibration training on muscle strength and balance ability of lower limbs in the elderly. Jilin university, Vol. 35 Issue 4, 2015, pp. 79-86.
- [9] Pool-Goudzwaard, A., van Dijke, G.H., van Gurp, M., Mulder, P., Snijders, C. and Stoeckart, R., Contribution of pelvic floor muscles to stiffness of the pelvic ring. Clinical Biomechanics, Vol 19, Issue 6, 2004. pp.564-571.
- [10] Jwing-Ming Y. Swinging the Arms or Bai Bi [online] 2012 [cited 2018 June 23]. Available from: [http://dactrung.net/Bai-tr4058dat\\_Ma\\_](http://dactrung.net/Bai-tr4058dat_Ma_)

- Dich\_Can\_Kinh.aspx
- [11] N. Leelayuwat et al., An alternative exercise and its beneficial effects on glycaemic control and oxidative stress in subjects with type 2 diabetes. *Diabetes Res. Clin. Pract.*, Vol. 82, Issue 2, 2008, pp. 168-171.
  - [12] Gleeson, M., Nieman, D. C., & Pedersen, B. K. Exercise, nutrition and immune function. *Journal of sports sciences*, Vol. 22, Issue 1, 2004, pp. 115-125.
  - [13] Namdari, S., Yagnik, G., Ebaugh, D. D., Nagda, S., Ramsey, M. L., Williams Jr, G. R., & Mehta, S., Defining functional shoulder range of motion for activities of daily living. *Journal of shoulder and elbow surgery*, Vol.21, Issue 9, 2012, pp 1177-1183.
  - [14] I. E. Eriks-Hoogland, S. De Groot, M. W. M. Post, and L. H. V. Van Der Woude., Correlation of shoulder range of motion limitations at discharge with limitations in activities and participation one year later in persons with spinal cord injury. *J. Rehabil. Med*, Vol. 43, Issue 3, 2011, pp. 210-215.
  - [15] S. W. Muir, C. L. Corea, and L. Beaupre., Evaluating change in clinical status: reliability and measures of agreement for the assessment of glenohumeral range of motion. *N Am J Sport. Phys Ther*, Vol. 5, Issue 3, 2010, pp. 98-110.
  - [16] Antonelli-Incalzi, R., Pedone, C., Cesari, M., Di Iorio, A., Bandinelli, S. and Ferrucci, L., Relationship between the occiput-wall distance and physical performance in the elderly: a cross sectional study. *Aging clinical and experimental research*, Vol. 19, Issue 3, 2007, pp. 207-212.
  - [17] Graham, J.E., Middleton, A., Roberts, P., Mallinson, T. and Prvu-Bettger, J., Health services research in rehabilitation and disability—the time is now. *Archives of physical medicine and rehabilitation*, Vol.99, Issue 1, 2018, pp. 198-203.
  - [18] Szucs, K.A. and Brown, E.V.D., Rater reliability and construct validity of a mobile application for posture analysis. *Journal of physical therapy science*, Vol. 30, Issue 1, 2018, pp. 31-36.
  - [19] Lyles, K.W., Gold, D.T., Shipp, K.M., Pieper, C.F., Martinez, S. and Mulhausen, P.L., Association of osteoporotic vertebral compression fractures with impaired functional status. *The American journal of medicine*, Vol. 94, Issue 6, 1993, pp. 595-601.
  - [20] Danis, C.G., Krebs, D.E., Gill-Body, K.M. and Sahrman, S., Relationship between standing posture and stability. *Physical Therapy*, Vol.78, Issue 5, 1998, pp. 502-517.
  - [21] Boland, D.M., Neufeld, E.V., Ruddell, J., Dolezal, B.A. and Cooper, C.B., Inter-and intra-rater agreement of static posture analysis using a mobile application. *Journal of physical therapy science*, Vol. 28, Issue 12, 2016, pp. 3398-3402.
  - [22] de Groot, M.H., van der Jagt-Willems, H.C., van Campen, J.P., Lems, W.F., Beijnen, J.H. and Lamoth, C.J., A flexed posture in elderly patients is associated with impairments in postural control during walking. *Gait & posture*, Vol. 39, Issue 2, 2014, pp. 767-772.
  - [23] Ma, J.S. and Kim, H.J., The effect of arm swing exercise on gait and balance in stroke patients. *American Journal of Clinical and Experimental Medicine*, Vol 2, Issue 6, 2014, pp.151-155.
  - [24] Misner, J. E., Massey, B. H., Bembien, M., Going, S., & Patrick, J., Long-term effects of exercise on the range of motion of aging women. *Journal of Orthopaedic & Sports Physical Therapy*, Vol. 16, Issue 1, 1992, pp 37-42.
  - [25] Keays, K. S., Harris, S. R., Lucyshyn, J. M., & MacIntyre, D. L., Effects of Pilates exercises on shoulder range of motion, pain, mood, and upper-extremity function in women living with breast cancer: a pilot study. *Physical Therapy*, Vol. 88, Issue 4, 2008, pp. 494-510.
  - [26] Fong, S. S., Ng, S. S., Luk, W. S., Chung, J. W., Chung, L. M., Tsang, W. W., & Chow, L. P., Shoulder mobility, muscular strength, and quality of life in breast cancer survivors with and without Tai Chi Qigong training. *Evidence-based complementary and alternative medicine*, 2013.
  - [27] American College of Sports Medicine. 8 th, ACSM's guidelines for exercise testing and prescription. 9th ed. Lippincott Williams & Wilkins Ed. 2013, pp. 208-209.
  - [28] Antonelli-Incalzi, R., Pedone, C., Cesari, M., Di Iorio, A., Bandinelli, S., & Ferrucci, L., Relationship between the occiput-wall distance and physical performance in the elderly: a cross sectional study. *Aging clinical and experimental research*, Vol. 19, Issue 3, 2007, pp. 207-212.
  - [29] Akuthota, V., & Nadler, S. F., Core strengthening. *Archives of physical medicine and rehabilitation*, Vol. 8, Issue 5, 2004, pp 86-92.
  - [30] Janda., Vladimír., *Muscle function testing*. Elsevier, Vol.7, Issue 3, 2013, pp. 137-139.
  - [31] Harman, K., Hubley-Kozey, C. L., & Butler, H., Effectiveness of an exercise program to improve forward head posture in normal adults: a randomized, controlled 10-week trial. *Journal of Manual & Manipulative Therapy*, Vol. 13, Issue 3, 2005, pp.163-176.
  - [32] Tje rnström, F., Fransson, P. A., Hafström, A., & Magnusson, M., Adaptation of postural control to perturbations—a process that initiates long-term motor memory. *Gait & posture*, Vol. 15, Issue 1, 2002, pp. 75-82.
  - [33] Burkhart, S.S., Morgan, C.D. and Kibler, W.B., The disabled throwing shoulder: spectrum of pathology Part I: pathoanatomy and biomechanics. *Arthroscopy: The Journal of Arthroscopic & Related Surgery*, Vol. 19, Issue 4, 2003, pp. 404-420

## COMPARISON OF INTRAOCULAR PRESSURE CHANGES AFTER VIEWING LAPTOP COMPUTER AND TABLET COMPUTER: A PILOT STUDY

Pattrawan Pattaranit<sup>1</sup>, Tanapat Ratanapakorn<sup>2</sup>, Rungthip Puntumetakul<sup>3</sup>, Orawan Buranruk<sup>3</sup>, and  
\* Wichai Eungpinichpong<sup>3</sup>

<sup>1</sup>Faculty of associated medical sciences, Khon Kaen University, Thailand;

<sup>2</sup>Faculty of medicine, Khon Kaen University, Thailand;

<sup>3</sup>Research and Training Center for Enhancing Quality of Life of Working Age People, Khon Kaen University,  
Thailand

### ABSTRACT

Prolonged computer use has been reported to be associated with elevated intraocular pressure and an increased risk of Computer Vision Syndrome. However, this issue has been one of controversy. The aim of this study was to preliminarily investigate the effect of using a laptop computer and tablet computer in terms of changes to intraocular pressure (IOP) in healthy young participants. Ten healthy participants (aged 29±6.36 years; male: female = 3:7) participated and were randomly allocated into one of the two groups (laptop computer users and tablet computer users). Each subject was requested to work on either a laptop or tablet for 60 minutes. IOP was subsequently measured via a non-contact tonometer in both eyes at 15, 30, 45, and 60 minute intervals. Pre-intervention IOP and IOP changes were compared within and between groups. The results showed that the mean IOP at each time point was not significantly different when compared among pre-intervention at different time points in both eyes. Mean IOP in the laptop computer group was slightly higher than that of the tablet computer group, yet there was no significant difference. The results of this study demonstrate that laptop and tablet usage for 60 minutes may have no effect on IOP levels in healthy volunteers. Hence, further research involving a larger sample size and longer exposure time to computer screens is needed.

*Keywords: Intraocular pressure, Laptop computer, Tablet computer, Computer vision syndrome*

### INTRODUCTION

Nowadays, computers have a great deal of impact in almost every aspect of our daily lives. Moreover, they have been developed to be easily carried in the form of portable computers including laptop computers, tablet computers and smartphones [1]. These devices are employed worldwide due to their convenience and efficiency with regards to accessing information, writing articles, communicating with others, and watching videos [2]. Consequently, many individuals spend a significant amount of time utilizing digital devices. With the rapid growth of digital device usage, there has been an increase in the development of numerous computer-related visual symptoms. Symptoms reported include headaches, eye strain, blurred vision, and eye irritation with symptom severity rising with the number of hours spent on devices [3]-[5]. Collectively, these disorders are known as computer vision syndrome (CVS) [6]. Many studies have recently suggested that long exposure to computer screens can cause elevated

intraocular pressure (IOP) [7], [8]. Elevated IOP is one of the major risk factors in relation to degenerative eye disease and glaucoma: one of the leading causes of preventable blindness worldwide [9]-[12]. This ocular disease, if untreated, may lead to optic nerve degeneration and possibly result in visual impairment and blindness [13]. IOP is considered to be normal between the ranges of 9 and 21 mmHg [14], [15]. The risk of developing glaucoma may increase if IOP rises above 21 mmHg [15]. There is a significant increase in the risk of developing visual field loss (even with only a small increase in IOP), especially once IOP rises above 26 mmHg to 30 mmHg [16], [17]. Therefore, almost all current treatment options for glaucoma are aimed at lowering or preventing a rise in IOP [18]. Body posture is believed to be one factor which influences IOP fluctuation [19]. A previous study found that there was a significant increase in IOP during neck flexion when measured in a sitting position among healthy participants [21]. Furthermore, due to the portability of and ability to carry computer devices, many individuals tend to spend several hours a day

using a laptop or tablet computer in a poor and damaging posture. A prolonged poor-posture coupled with staring at a computer screen for long periods may cause more severe elevation of IOP, and subsequently appear to put users at an increased risk of developing glaucoma. One study demonstrated that the use of smartphones rendered a greater head flexion when compared to utilizing desktop computers [20].

As noted previously, some studies have reported that the range of head flexion among users is related to different types of computer tasks and computer devices [20], [22]. Another study highlighted that visual fatigue and discomfort were significantly induced by tablet computer screen viewing, [23] and another recent study was focused on using smartphones in daylight and low-light conditions in terms of alterations to IOP.

To date, no definite conclusion has been mentioned in terms of the effects of prolonged usage of portable computers incorporating different degrees of head flexion on IOP in healthy participants. Hence, this study aimed to preliminarily explore the effect of two different head positions while viewing a computer screen. The study also compared IOP values between laptop and computer users, and tablet computer users at difference time points.

## METHOD

### Participants

The participants in this study were students and employees of Khon Kaen University, Thailand aged 20-40 years. This study followed the Declaration of Helsinki and was approved by the Khon Kaen University Ethics Committee for Human Research. All participants were given details of experimental procedures before the study, and they gave their consent to participate. They were then requested to complete a questionnaire on computer usage amid their daily lives. Participants who spent more than 4 hours a day viewing a computer or tablet were selected to participate. Moreover, participants were included if they presented no signs or symptoms of glaucoma, crossed eyes, narrow angles, corneal infection or ulcer, corneal scarring, uveitis, retinal tear or detachment. The IOP of each of the recruited participants was less than or equal to 22 mmHg in the sitting position with refractive error at between -4.00 and +2.00 diopters. Participants were excluded if 1. They had received  $\beta$ -blockers or steroids prior to the IOP measurements, and 2. They were unable to maintain the head in the neck flexion or neck extension position for at least 15 minutes. In order to avoid IOP disturbance, participants were asked not to drink caffeinated products or alcohol 12 hours

prior, and they were requested to sleep for at least 6-8 hours the night before determination of IOP.

### Materials and Procedures

In this preliminary study, participants were randomly divided into two groups of 5 (10 eyes/group). They were grouped as follows:

Group 1 (laptop computer user group): firstly, participants were seated quietly in an examination chair with an adjusted backrest angle of 90° for 5 minutes. Subsequent to resting, participants were assessed for IOP as a pre-intervention value. Then, they were asked to watch a laptop computer screen (LENOVO™ Ideapad 310, Lenovo Group Ltd., China, 14-inch screen, 141 PPI) with brightness set at 188 cd/m<sup>2</sup>. Viewing distance was approximately 50 cm. IOPs were subsequently, measured at 15, 30, 45 and 60 minutes after exposure to the laptop screen.

Group 2 (tablet computer user group): in this group, tablet computer (iPad® Pro 3rd Generation, Apple Inc., California, USA, 12.9-inch screen, 264 PPI) with brightness set at 600 cd/m<sup>2</sup> was employed. After a resting period of 5 minutes, a tablet was placed on a participant's lap at a distance of 30-40 cm from the eyes. IOPs were measured before viewing and at 15, 30, 45, 60 minutes post viewing. Each participant was requested to maintain a head posture with the neck at a 40°-60° flexion while viewing the tablet for 15 minutes. IOP was then evaluated in the upright position. All IOP measurements were taken within 30 seconds in a 90° upright sitting posture with the right eye always measured first. Three consecutive IOP readings were obtained with the same non-contact tonometer (NCT; Nidek Co., Ltd., Aichi, Japan) and the means of readings were recorded for further statistical analysis. During laptop computer and tablet computer usage, participants were requested to continuously maintain the same head posture and distance from the screen.

Data was collected in the research laboratory which was set up and located in the Faculty of Associated Medical Sciences, Khon Kaen University, Thailand. The experiments were performed in an experimental room incorporating an illumination level of 300 lux and a room temperature of 25°C. To avoid possible diurnal IOP variation, all measurements were scheduled between 08:00-10:00 in the morning.

### Statistical Analysis

Statistical analysis was done using SPSS software version 23.0 for Windows (SPSS Inc., Chicago, IL). All values were presented as mean  $\pm$  standard deviation. Comparison of mean values between pre-intervention and different time points

within each group was analyzed by applying a paired-sample t-test, while the independent-sample t-test was used to compare between groups. For all tests, P-values less than 0.05 were considered statistically significant.

## RESULTS

A total of 10 healthy participants (20 eyes) were included (7 female and 3 male) into this preliminary study with a mean age of  $29 \pm 6.36$  (range 23-39) years. Five of the 10 individuals were assigned to watch a laptop computer screen while the remaining participants were assigned to watch a tablet computer screen. Participants' demographic data are summarized in Table 1.

Table 2 shows the IOP measurements obtained in both the right and left eyes of both the laptop computer user group and the tablet computer user

group. IOP values at 4 check-out points (15, 30, 45 and 60 minutes) were compared to pre-intervention IOP values. Accordingly, it was discovered that there was no significant difference in IOP at different time points. The mean IOP value at pre-intervention in the right eye among laptop users was slightly lower than IOP at 60 minutes, yet this difference was not statistically significant.

Table 3 shows mean IOP between both laptop computer user and tablet computer user groups. When comparing IOP values between the 2 groups, the mean value of eyes in the laptop group was higher than in the tablet user group at every time check-point. However, no significant difference in their IOP value was observed between the groups in the right eye as well as in all left eye IOP measurements.

Table 1 Participant demographic data.

| Group        | N | Age (years)      | Gender (male/female) |
|--------------|---|------------------|----------------------|
| Laptop users | 5 | $29.80 \pm 7.98$ | 2/3                  |
| Tablet users | 5 | $28.2 \pm 5.07$  | 1/4                  |

Table 2 Within-group comparison of IOP value (mmHg) changes among study participants.

| Group                | Side     | Pre-intervention | 15 min           | 30 min           | 45 min           | 60 min           |
|----------------------|----------|------------------|------------------|------------------|------------------|------------------|
| Laptop computer user | Right    | $14.52 \pm 1.91$ | $15.12 \pm 2.01$ | $14.94 \pm 4.39$ | $15.14 \pm 2.51$ | $15.32 \pm 2.15$ |
|                      | P-value* |                  | 0.325            | 0.787            | 0.176            | 0.203            |
|                      | Left     | $14.00 \pm 2.41$ | $14.74 \pm 2.05$ | $14.32 \pm 2.80$ | $14.14 \pm 2.37$ | $13.20 \pm 1.62$ |
|                      | P-value  |                  | 0.191            | 0.716            | 0.828            | 0.465            |
| Tablet computer user | Right    | $13.14 \pm 1.66$ | $13.52 \pm 1.91$ | $12.38 \pm 1.98$ | $12.86 \pm 2.32$ | $12.92 \pm 1.77$ |
|                      | P-value  |                  | 0.696            | 0.473            | 0.757            | 0.808            |
|                      | Left     | $12.46 \pm 1.86$ | $12.72 \pm 1.86$ | $12.26 \pm 2.18$ | $12.46 \pm 2.32$ | $12.26 \pm 1.96$ |
|                      | P-value  |                  | 0.834            | 0.717            | 1.000            | 0.618            |

Table 3 Between-group comparison of IOP value (mmHg) changes at different checkout points among laptop computer and tablet computer user groups.

| Group Side  | Pre-intervention |                  | 15 min           |                  | 30 min           |                  | 45 min           |                  | 60 min           |                  |
|-------------|------------------|------------------|------------------|------------------|------------------|------------------|------------------|------------------|------------------|------------------|
|             | Right            | Left             | Right            | Left             | Right            | Left             | Right            | Left             | Right            | Left             |
| Laptop user | 14.52            | 14.00            | 15.12            | 14.74            | 14.94            | 14.32            | 15.14            | 14.14            | 15.32            | 13.20            |
|             | $\pm 1.91$       | $\pm 2.42$       | $\pm 2.01$       | $\pm 2.06$       | $\pm 4.39$       | $\pm 2.80$       | $\pm 2.51$       | $\pm 2.37$       | $\pm 2.15$       | $\pm 1.62$       |
| Tablet user | $13.14 \pm 1.66$ | $12.46 \pm 1.86$ | $13.52 \pm 1.91$ | $12.72 \pm 1.86$ | $12.38 \pm 1.98$ | $12.26 \pm 2.18$ | $12.86 \pm 2.32$ | $12.46 \pm 2.32$ | $12.92 \pm 1.77$ | $12.26 \pm 1.96$ |
|             |                  |                  |                  |                  |                  |                  |                  |                  |                  |                  |
| P-value*    | 0.26             | 0.29             | 0.23             | 0.14             | 0.27             | 0.23             | 0.17             | 0.29             | 0.09             | 0.43             |

## DISCUSSION

Prolonged viewing of a computer screen can cause IOP elevation which is a major risk in relation to developing glaucoma [8], [25]. The underlying mechanism of ocular dynamics in regards these IOP changes during prolonged work in front of a computer screen is not yet fully

understood. Available evidence has suggested that IOP alterations are supposed to be involved during the occurrence of accommodation and convergence when the eyes attempt to focus on images in close proximity.

Moreover, the researchers assume further studies are needed to confirm that dry eyes and neck flexion posture due to extended periods of

electronic display usage can cause IOP elevation. In addition, psychophysiological stress is reportedly associated with fluctuations in IOP [8]. In this study, we examined the changes to IOP at different time junctures using 2 types of computer screen in different head flexion angles.

Studies in normal participants have revealed that numerous factors affect IOP. IOP measurements were taken when sitting with the neck in the neutral position. Whereas, all other head positions including flexion, extension and supine body positions result in IOP elevation. [21]. Additionally, a study revealed that participants maintained a head flexion of 33°-45° from vertical when using a smartphone [20]. Similarly, another study showed that head and neck flexion angles during tablet use were higher than when utilizing desktop and notebook computers [22]. Ha [8] reported that IOP was significantly increased immediately after 5 minutes and continued to be elevated throughout 25 minutes post smartphone use under lowlight conditions. Another research showed that 4 hours of computer work resulted in significant IOP elevation among healthy young participants [7]. Based on the aforementioned information, it would be reasonable to suggest that a forward head and neck flexion posture when using a mobile computer may cause IOP fluctuation.

To the best of our knowledge, the current study is the first research to investigate IOP changes induced by viewing both laptop and tablet screens. Nonetheless, our findings did not support any of the earlier findings because the results did not show any significant changes to IOP amid pre-intervention compared with different check-time points in both groups. In addition, IOP among participants who used a laptop computer for a prolonged duration did not demonstrate statistical significant difference when compared with participants who used a tablet computer at any time point.

This preliminary study has several limitations that require consideration. First, the present study was limited in terms of the small number of participants. Thus, further studies are needed to be carried out among larger populations. Another limitation is that IOP value was collected for only a short time. Hence, a study employing a longer duration of computer usage will be considered. Lastly, IOP measurement utilizing a reliable method is necessary. Goldmann applanation tonometry (GAT) is regarded as the gold standard and thus ought to be applied amid further studies.

## CONCLUSION

The study results suggest that laptop and tablet usage for 60 minutes may have no effect on IOP in

healthy participants. However, further studies are needed in order to clarify whether or not postural changes associated with prolonged use of laptop computers or tablet computers cause IOP fluctuation.

## ACKNOWLEDGEMENTS

This study was granted by the Research and Training Center for Enhancing Quality of Life of Working Age People, Khon Kaen University, Thailand.

## REFERENCES

- [1] McWay D.C., *Today's Health Information Management: An Integrated Approach*, 2nd ed, Clifton Park, New York, 2014, pp 284.
- [2] Reddy S., Low C.K., Lim Y.P., Low L.L., Mardina F., and Nursaleha M.P., Computer vision syndrome: a study of knowledge and practices in university students Nepalese, *Journal of Ophthalmology*, Vol. 5, Issue 10, 2013, pp. 161-168.
- [3] Mashige K.P., Computer-related symptoms in the workplace: causes and preventive strategies, *Occupational Health Southern Africa*, Vol. 20, Issue 3, 2014, pp. 13-17.
- [4] Portello J.K., Rosenfield M., Bababekova Y., Estrada J.M., and Leon A., Computer-related visual symptoms in office workers, *Ophthalmic and Physiological Optics*, Vol. 32, 2012, pp. 375-382.
- [5] Sheppard A.L. and Wolffsohn J.S., Digital eye strain: prevalence, measurement and amelioration, *BMJ Open Ophthalmology*, Vol. 3, 2018, pp.1-10.
- [6] Rosenfield M., Computer vision syndrome: a review of ocular causes and potential treatments, *Ophthalmic and Physiological Optics*, Vol. 31, 2011, pp. 502-515.
- [7] Sanam M.Q., Farisa K., Aftab A.K., Mohammed A.A., Mohammed A.H.H., Fareen S., et al., Study of intraocular pressure among individuals working on computer screens for long hours, *Annals of Medical Physiology*, Vol. 1, Issue 1, 2017, pp. 22-25.
- [8] Ha A., Kim Y.K., Park Y.J., Jeoung J.W., and Park KH, Intraocular pressure change during reading or writing on smartphone, *PLoS ONE*, Vol. 13, Issue 10, 2018, pp. 1-12.
- [9] Killer H.E. and Pircher A., Normal tension glaucoma: review of current understanding and mechanisms of the pathogenesis, *Eye*, Vol. 32, Issue 5, 2018, pp. 924-930.
- [10] Jasien J.V., Jonas J.B., de Moraes C.G., and Ritch R., Intraocular Pressure Rise in Subjects with and without Glaucoma during Four Common Yoga Positions, *PLoS ONE*,



- Vol. 10, Issue 12, 2015, pp. 1-16.
- [11] Na R.K., Ji H. K., and Chan Y. K., Effect of Korean Red Ginseng Supplementation on Ocular Blood Flow in Patients with Glaucoma, *Journal of Ginseng Research*, Vol. 34, Issue 3, 2010, pp. 237-245.
  - [12] Seth R.F., Rupert R.A.B., Serge R., Peter A., Tasanee B., Maria V.C., et al., Global causes of blindness and distance vision impairment 1990-2020: a systematic review and meta-analysis, *Lancet Glob Health*, Vol. 5, 2017, pp. 1221-1234.
  - [13] Huihui C., Kin S.C., Khanh T.H.V., Ching H.S., Mandeep K., Guochun C., et al., Commensal microflora-induced T cell responses mediate progressive neurodegeneration in glaucoma, *Nature Communications*, Vol. 9, 2018, pp. 3209.
  - [14] Wang Y.X., Xu L., Wei W.B., and Jonas J.B., Intraocular pressure and its normal range adjusted for ocular and systemic parameters, *The Beijing Eye Study*, *PLoS ONE*, Vol. 13, Issue 5, 2018, pp. 1-16.
  - [15] Wolfs R.C., Klaver C.C., Ramrattan R.S., van Duijn C.M., Hofman A., and de Jong P.T., Genetic risk of primary open-angle glaucoma. Population-based familial aggregation study, *Archives of Ophthalmology*, Vol. 116, Issue 12, 1998, pp. 1640-1645.
  - [16] Prum B.E., Rosenberg L.F., Gedde S.J., Mansberger S.L., Stein J.D., Moroi S.E., et al., Primary Open-Angle Glaucoma Preferred Practice Pattern(®) Guidelines, *Ophthalmology*, Vol. 123, Issue 1, 2016, pp. 41-111.
  - [17] Dielemans I., Vingerling J.R., Wolfs R.C., Hofman A., Grobbee D.E., and de Jong P.T., The prevalence of primary open-angle glaucoma in a population-based study in The Netherlands. The Rotterdam Study, *Ophthalmology*, Vol. 101, Issue 11, pp. 1851-1855.
  - [18] Yanlin G., Bing W., Peiyu L., Yan Z., and Xin T., Short-term reproducibility of intraocular pressure and ocular perfusion pressure measurements in Chinese volunteers and glaucoma patients, *BMC Ophthalmology*, Vol. 16, 2016, pp. 145.
  - [19] Liu J.H., Sit A.J., and Weinreb R.N., Variation of 24-hour intraocular pressure in healthy individuals: right eye versus left eye, *Ophthalmology*, Vol. 112, Issue 10, 2005, pp. 1670-1675.
  - [20] Sojeong L., Hwayeong K., and Gwanseob S., Head flexion angle while using a smartphone, *Ergonomics*, Vol. 58, Issue 2, 2015, pp. 220-226.
  - [21] Malihi M. and Sit A.J., Effect of head and body position on intraocular pressure, *Ophthalmology*, Vol. 119, 2012, pp. 987-991.
  - [22] Justin G.Y., Matthieu T., Dan O., Kim M., and Jack T.D., Touch-screen tablet user configurations and case-supported tilt affect head and neck flexion angles, *Work*, Vol. 41, 2012, pp. 81-91.
  - [23] Dong J.K., Chi Y.L., Namyi G., and Choul Y.P., Visual Fatigue Induced by Viewing a Tablet Computer with a High resolution Display, *The Korean Ophthalmological Society*, Vol. 31, Issue 5, 2017, pp. 388-393.
  - [24] Ha A., Kim Y.K., Park Y.J., Jeoung J.W., and Park K.H., Intraocular pressure change during reading or writing on smartphone, *PLoS ONE*, Vol. 13, Issue 10, 2018, pp. 1-12.
  - [25] Kim J.H. and Caprioli J., Intraocular pressure fluctuation: Is it important?, *Journal of ophthalmic and vision research*, Vol. 13, 2018, pp. 170-174.

## THE CRUDE TANNIN EXTRACTION FROM WOOD SCRAP WASTES FOR PROLONGING THE SHELF LIFE OF LITCHI FRUITS

Pornanan Boonkorn, Angkhana Chuajedton and Weeranuch Karuehanon  
Science Faculty, Lampang Rajabhat University, Lampang, Thailand

### ABSTRACT

Waste from wood scrap is an important problem in areas of wood handicraft performed. The purposes of this research was to study the optimum condition for crude tannin extraction from those wastes and usage them for prolonging shelf life of litchi fruits. Various chemicals used for the extraction included distilled water, 95% ethanol, 8% sodium carbonate and their combinations. The proportion between wood scrap per solvent were 1:10 or 1:20 g.mL<sup>-1</sup> and extraction temperature were 70, 80 or 90°C. The basic chemical characteristics of the extracted tannin were tested. Quantification of tannin was performed by spectrophotometry. The results found that optimum solvent was 95% ethanol with proportion at 1:10 g.mL<sup>-1</sup> and 80°C extracted temperature, which gave the maximum amount of tannin (12.34 mg.g<sup>-1</sup> dry weight). Then, crude tannin was tested for the *in vitro* fungicidal effect to pathogenic fungi isolated from litchi fruits. The PDA medium containing crude tannin at different concentrations including; 0, 0.1, 0.2 and 0.4 % were tested in comparing to 0.1 % benomyl fungicide. The result was found that PDA containing 0.2 and 0.4 % of extracted tannin significantly ( $P \leq 0.05$ ) inhibited growth of fungal mycelium better than 0 and 0.1 % but still lower than benomyl fungicide. The *in vivo* test with litchi fruits by soaking the fruits in various concentrations of crude tannin; 0, 0.1, 0.2 and 0.4%, compared to 0.1% benomyl fungicide was found that 0.2% tannin could extend the shelf life of litchi fruits better than other concentrations but its efficiency was still lower than benomyl fungicide.

**Keywords:** Tannin, Wood scrap, Shelf life, Litchi

### INTRODUCTION

Tannins are polyphenolic compounds found in almost plants. The compounds are widely used in tanning leather industries, clarifying wine and beer, or used as mordant in dyeing and astringents in medicine. Mangrove is well known as tannin resources [1]. The increasing demand for the raw material in extracting natural tannin along with the conservation of mangrove as a coastal protection and cultivated area for various marine lives, new resources of tannin are needed. Wooden handicraft, such as carvings, mortars and mobiles, is one of an important products of Northern Thailand. Wastes from wood scrap is a problem in the area. Villagers re-use them as mushroom cultivation medium and charcoal briquette. Tannin extracted from these wood scraps is one of an interesting way in reducing wooden waste. There are several studies on antimicrobial effects of tannin extracts from various plants such as rain tree pods [2], coconut mesocarp [3], guava leaves [4] or chestnut and quabacho [5]. A number of tannin extraction solvents and conditions have also been tested and reported.

Litchi (*Litchi chinensis* Sonn. cv. Hong Huay) is an economically important fruit of Thailand. Postharvest loss of the fruit is a big problem for both domestic and foreign markets. Postharvest deterioration of the fruit is mainly due to fungal

decay. The high incidence of postharvest disease in litchi is primarily caused by green mold, *P. digitatum*. The fungus preferentially penetrate through wounds that occur during harvesting and postharvest handling. Fungicide is widely used to reduce pathogenic fungi and extend shelf life of litchi fruits. However it is becoming less effective because of pathogenic resistance, along with consumer concerns about possible risk associated with the use of chemicals. Among a number of new strategies being investigated to control postharvest decay, natural plant extract may be an alternative to traditional postharvest fungicide practices. The purposes of this research was to study the optimum condition for crude tannin extraction from wood scrap wastes and usage them as an antifungal agent for prolonging shelf life of litchi fruits.

### MATERIALS AND METHODS

Wood scrap waste was collected from Look village, Lampang province, Thailand in May, 2018. It was dried, cut into small pieces and milled to a fined powder. Tannin extraction was conducted with various solvents included distilled water, 95% ethanol, 8% sodium carbonate, 95% ethanol : distilled water (1:1 v/v) and 8% sodium carbonate : distilled water (1:1 v/v). The proportion between wood scrap per solvent were 1:10 or 1:20 g.mL<sup>-1</sup> and extraction

temperature were 70, 80 or 90°C. Each experiment was performed in triplicate.

Wood scrap and solvent at the tested ratio were added into a 1000-ml flask and then incubated in a water bath at the tested temperature with the shaking speed of 100 rpm for 2 hours. Crude extracted tannin from all treatments were then evaporated to dryness in hot air oven at 50°C to constant weight. Quantification of tannin was performed by spectrophotometry at 700 nm, serial dilutions of standard tannic acid were used to obtain the calibration curve [2]. The basic chemical characteristics of the extracted tannin were tested comparing to standard tannic acid by the interaction with ferric chloride (1%  $\text{FeCl}_3$ ), 1% gelatin, and lead acetate (1%  $\text{Pb}(\text{C}_2\text{H}_3\text{O}_2)_2$ ) followed the methods of Moosophon et al. [6] and Elgailani and Ishak [7].

### In vitro and in vivo antifungal activity screening test

A 7-day-old of *Penicillium digitatum* on potato dextrose agar (PDA) plate, obtained from the Department of Biology, Faculty of Science, Lampang Rajabhat University, Lampang, Thailand, was used for the study.

For the *in vitro* test, crude extracted tannin with the optimum extraction condition from the previous experiment was used. The crude extract was suspended in a newly prepared PDA medium, before the agar hardened, to make a concentration of 0, 0.1, 0.2 and 0.4 percent. Positive control was 0.1% benomyl. Mycelium discs of *P. digitatum* were cut with a sterile cork-borer (0.4 cm diameter) and each one was placed on the surface of a treatment PDA plate, 5 plates per treatment. All the dishes were then incubated at 25°C. Mycelium diameter was measured after 72 hours of the incubation

For the *in vivo* test, 'Hong Huay' litchi fruits that grown under standard cultural practices were harvested at commercial maturity stage from an orchard in Amphoe Mae-rim, Chiang Mai, Thailand

in May, 2018. Before any commercial postharvest treatment was applied, the fruits were selected by hand and transported to the laboratory at Lampang Rajabhat University within 5 hours. The uniform and non-damage fruits were selected. The pedicels of the fruit were cut, 0.5 mm left intact on fruit, and divided into 5 groups. Crude extracted tannin was suspended in distilled water to make a concentration of 0, 0.1, 0.2 and 0.4 percent. Positive control was 0.1% benomyl fungicide. All the fruits were then soaked in the prepared tannin treatment suspensions or fungicide suspension for 20 minutes with softly shaking fruits in the suspensions every 2 minutes. After soaking, fruits were dried at 25°C for 1 hour and then kept in foam tray, 10 fruits per tray, and wrapped with polyvinylchloride plastic. All treatments were stored at  $15 \pm 1^\circ\text{C}$ , samples were taken every 2 days. Fruit samples in each treatment, three replicates of ten fruits, were inspected for disease incidence. Fruits showing white mycelium on the peels were considered as infected fruits. Disease incidence was expressed as percentage of infected fruits from three replicates of ten fruits. Shelf life of the fruits were considered acceptable only if disease incidence was less than 50%.

### Statistical analysis

All analyses were run in triplicate or more. Data analysis was done by One-Way ANOVA and mean differences were analyzed by least significant differences at  $P \leq 0.05$ .

## RESULTS

Wood scrap waste sample of rain tree (*Samanea saman* (Jacq.) Merr.), from mortars handicraft, was collected from Look village, Lampang province, Thailand in May, 2018 as shown in Fig. 1. Woods of rain tree were left outdoor until making mortars and left a lot of wood scrap waste under the machine.



Fig. 1 Woods of rain tree and their scrap waste from mortars handicraft

Maceration method was used for tannin extraction in this study. It is a simple extraction method, done by immersing plant sample in an organic solvent. Organic solvents will penetrate the cell wall into the cavity of the cell that contains the active substances so the active substances will dissolve [4]. In this study, the appropriate condition in extracting tannin from wood waste was 95% ethanol with a proportion of wood scrap per solvent at 1:10 or 1:20 g.mL<sup>-1</sup>, 80 or 90°C extracted temperature, which gave the maximum amount of tannin (Table 1). The color of all crude extracts were present in Fig.2 which shown that the color of the extract were not accordance to tannin content. Various researchers tried to find an appropriate solvents in extracting tannin from plants. Various results of that were found, such as acetone for *Galium tunetanum* extraction [8], acetone-water mixtures for grape skin extraction [9], 8% sodium carbonate for *Pinus oocarpa* extraction [10], mixture of water and 95% ethanol for mangosteen peel extraction [6] and n-hexane for pods of rain tree extraction [2]. These different results may come from the different in plant species, part of the plants or conditions and methods of the extraction. In this study, we found that extraction ratio of wood scrap per solvent at 1:10 or 1:20 and extraction temperature at 80°C or 90°C gave the similar content of crude tannin (not statistically difference at  $P \leq 0.05$ ). So, for an economically reason, the low solvent and temperature usage would be an ideal extraction procedure for feasible usage. As a reason, the ratio at 1:10 and temperature at 80 °C were suitable in tannin extraction in this study. Dried brownish crude extract from the optimum extraction condition was shown in Fig. 3.

Tannin extracted from wood scrap of rain tree with 95% ethanol at 80°C extraction temperature and 1:10 g.mL<sup>-1</sup> proportion of wood scrap per solvents was then tested for antifungal effect against mycelium disc of *Penicillium digitatum*, which is an important pathogenic fungi of litchi fruits after harvest, and the ability for prolonged the storage life of litchi fruits at  $15 \pm 1^\circ\text{C}$ . The basic chemical characteristics of the crude tannin extract in comparison with standard tannin was shown in Table 2. The ability to interact with metal ions such as FeCl<sub>3</sub> and Pb(C<sub>2</sub>H<sub>3</sub>O<sub>2</sub>)<sub>2</sub> and the ability to precipitate protein such as gelatin in comparison to standard tannin indicated the presence of tannin in the crude extract as described by Moosophin et al. [6] and Elgailani and Ishak [7].

with various conditions

| Solvents                              | Extraction ratio (g.mL <sup>-1</sup> ) | Extraction temperature (°C) | Tannin content (mg. g <sup>-1</sup> ) |
|---------------------------------------|--|-----------------------------|---------------------------------------|
| Distilled water                       | 1:10                                   | 70                          | 2.05 <sup>c</sup>                     |
|                                       |  | 80                          | 2.46 <sup>c</sup>                     |
|                                       |  | 90                          | 2.54 <sup>c</sup>                     |
|                                       | 1:20                                   | 70                          | 2.18 <sup>c</sup>                     |
|                                       |  | 80                          | 2.62 <sup>c</sup>                     |
|                                       |  | 90                          | 2.76 <sup>c</sup>                     |
| 95% ethanol                           | 1:10                                   | 70                          | 7.26 <sup>b</sup>                     |
|                                       |  | 80                          | 12.34 <sup>a</sup>                    |
|                                       |  | 90                          | 12.55 <sup>a</sup>                    |
|                                       | 1:20                                   | 70                          | 7.65 <sup>b</sup>                     |
|                                       |  | 80                          | 12.12 <sup>a</sup>                    |
|                                       |  | 90                          | 12.47 <sup>a</sup>                    |
| 8% sodium carbonate                   | 1:10                                   | 70                          | 4.06 <sup>b</sup>                     |
|                                       |  | 80                          | 5.11 <sup>b</sup>                     |
|                                       |  | 90                          | 6.03 <sup>b</sup>                     |
|                                       | 1:20                                   | 70                          | 4.51 <sup>b</sup>                     |
|                                       |  | 80                          | 6.14 <sup>b</sup>                     |
|                                       |  | 90                          | 7.03 <sup>b</sup>                     |
| 95% ethanol : distilled water         | 1:10                                   | 70                          | 5.11 <sup>b</sup>                     |
|                                       |  | 80                          | 6.10 <sup>b</sup>                     |
|                                       |  | 90                          | 6.55 <sup>b</sup>                     |
|                                       | 1:20                                   | 70                          | 6.02 <sup>b</sup>                     |
|                                       |  | 80                          | 6.54 <sup>b</sup>                     |
|                                       |  | 90                          | 7.11 <sup>b</sup>                     |
| 8% sodium carbonate : distilled water | 1:10                                   | 70                          | 2.06 <sup>c</sup>                     |
|                                       |  | 80                          | 2.63 <sup>c</sup>                     |
|                                       |  | 90                          | 2.65 <sup>c</sup>                     |
|                                       | 1:20                                   | 70                          | 2.42 <sup>c</sup>                     |
|                                       |  | 80                          | 2.47 <sup>c</sup>                     |
|                                       |  | 90                          | 2.83 <sup>c</sup>                     |

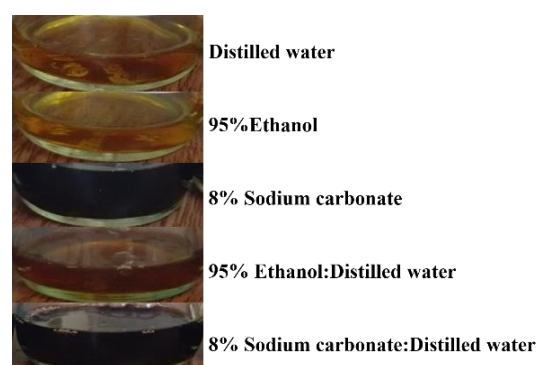


Fig. 2 Color of the crude extract after extraction with various solvents

Table 1 Tannin content from wood scrap extracted



Fig. 3 Crude extract of tannin extracted with 95% ethanol, 80°C at 1:10 g.mL<sup>-1</sup> proportion

Table 2 Test of basic chemical characteristics of the extracted tannin from wood scrap in comparison with standard tannin

| Tannin type          | Chemical tests             |                   |   |     |
|----------------------|----------------------------|-------------------|---|-----|
|                      | 1% FeCl <sub>3</sub>       | 1% gelatin        | 1% Pb(C <sub>2</sub> H <sub>3</sub> O <sub>2</sub> ) <sub>2</sub> |     |
| Standard tannic acid | Black precipitate          | White precipitate | Dark precipitate  | red |
| Extracted tannin*    | Greenish black precipitate | White precipitate | Dark precipitate  | red |

Note: \*Tannin was extracted with an optimum extraction condition (95% ethanol, 80°C and 1:10 g.mL<sup>-1</sup> proportion)

Tannin treatment *in vitro* resulted in significantly reduced mycelium disc diameter of *P. digitatum* when compared to control (Table 3 and Fig.4). The mycelium growth inhibition was numerically but not significantly ( $P \leq 0.05$ ) enhanced with increasing tannin concentration from 0.1 to 0.4 percent. The mycelium diameter after growth on PDA with tannin at concentrations 0, 0.1, 0.2 and 0.4% for 72 hours were 9.00, 3.18, 2.68 and 2.66 cm, respectively. The results confirm with the findings of Mailoa et al. [4] who found a significant inhibition of five different pathogen microbial growth after treated with tannin extracted from guava leaves with 30% ethanol. They estimated that tannin in an extract can inhibit the synthesis of 1,3  $\beta$ -glucan, the main component of the fungal cell wall, by inhibiting the enzyme responsible for building that polymer. Although tannin treatment could obviously suppressed the mycelium growth when compared to the control, but the efficacy was less than 0.1% benomyl fungicide. Hoque et al. [5] also found that Chestnut tannin and Quabracho tannin did not show satisfactory inhibition of mycelium growth of six fungal pathogens when compared to fungicides.

The incidence of disease from *in vivo* test on litchi fruit peels first appeared on the 8th day of storage at 15±1°C in all groups, except for the 0.2% tannin and 0.1% benomyl treatment (data not shown). Symptoms of fungal attack first appeared with white mycelium on fruit peel (which was judged as infected fruit). Severity increased with storage time

with the development of mass white mycelia and powdery masses of olive green spores. The disease incidence increased to 100, 100, 73.33, 100 and 46.66% in 0, 0.1, 0.2 and 0.4% tannin or 0.1% benomyl, respectively after 14 days of storage at 15±1°C (Table 4 and Fig. 5).

The 0.1% benomyl and 0.2% tannin treatments could delay the disease incidence after storage. Interestingly that litchi fruits in 0.4% tannin treatment had more severely disease incidence than the 0.2% treated fruits. The fruit peel damage from acidic suspension of 0.4% tannin may be the reason for this situation, because pH of the 0.4% tannin suspension were 3.21 (data not shown) which may destroy litchi fruit peel compared to the 0.2% tannin treatment which had higher pH value (4.56). Damage on fruit peel led the fungal easily penetrated through wounds and growth rapidly.

Although 0.2% tannin and fungicide treatment could delay disease incidence on litchi fruits, however, it should be noted that the treatments did not totally control the fruit decay at the end of storage period. The inability of tannin and fungicide to control final incidence of mold may be attributed to the growth of survival fungal spores after treatments or fungal spores in ambient air penetrated into natural micro-cracking on the fruit peel tissues as described by Underhill and Critchley [11].

Table 3 Mycelium disc diameter of *P. digitatum* after placed on PDA plate with various concentrations of tannin or 0.1% benomyl fungicide for 72 hours

| Treatment    | Diameter (cm)      |
|--------------|--------------------|
| Control      | 9.00 <sup>a</sup>  |
| 0.1% tannin  | 3.18 <sup>b</sup>  |
| 0.2% tannin  | 2.68 <sup>b</sup>  |
| 0.4% tannin  | 2.66 <sup>b</sup>  |
| 0.1% benomyl | 0.00* <sup>c</sup> |

Note: \*The fungal was died after 48 hours of the incubation in PDA with benomyl fungicide

Table 4 Percent of disease incidence of litchi fruits after soaked in various concentrations of tannin or 0.1% benomyl fungicide and then kept at 15±1°C for 14 days

| Treatment    | Percent of disease incidence (%) |
|--------------|----------------------------------|
| Control      | 100.00 <sup>a</sup>              |
| 0.1% tannin  | 100.00 <sup>a</sup>              |
| 0.2% tannin  | 73.33 <sup>b</sup>               |
| 0.4% tannin  | 100.00 <sup>a</sup>              |
| 0.1% benomyl | 46.66 <sup>c</sup>               |



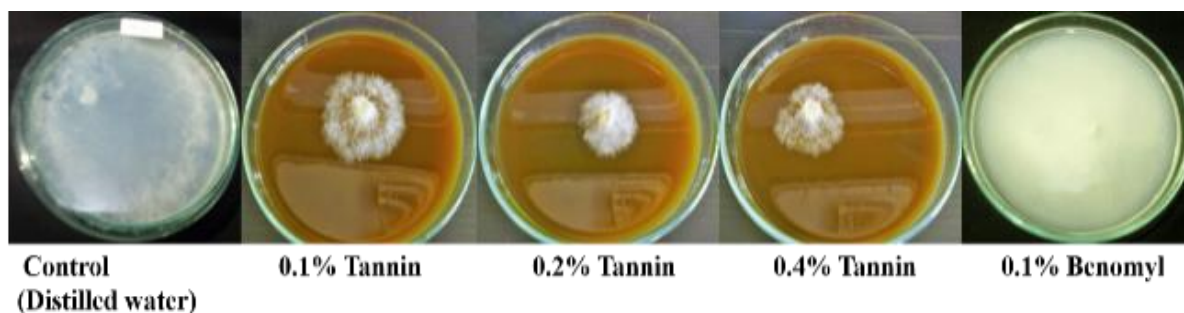


Fig. 4 Mycelium diameter of *P. digitatum* after placed on PDA plate with various concentrations of tannin or 0.1% benomyl fungicide for 72 hours

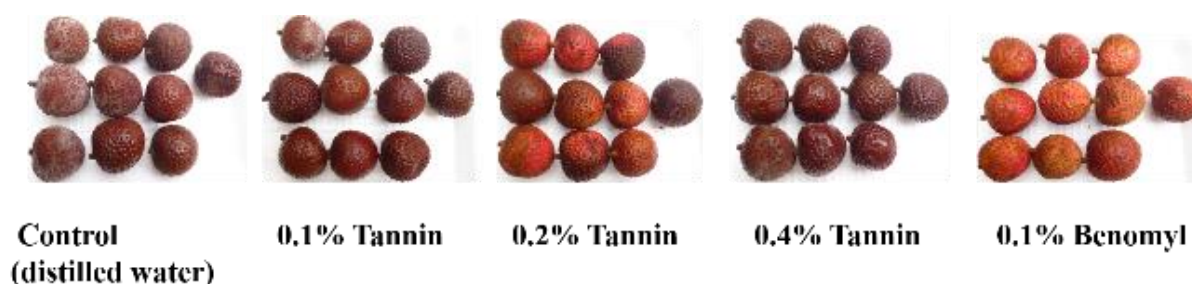


Fig. 5 Disease incidence of litchi fruits after soaked in various concentrations of tannin or 0.1% benomyl fungicide and then kept at  $15 \pm 1^\circ\text{C}$  for 14 days

## CONCLUSIONS

1. The optimum solvent to obtain tannin extract of wood scrap waste of rain tree was 95% ethanol with proportion of samples per solvent at  $1:10 \text{ g.mL}^{-1}$  and  $80^\circ\text{C}$  extracted temperature, which gave the maximum amount of tannin at  $12.34 \text{ mg.g}^{-1}$  dry weight
2. Tannin extract from wood scrap waste of rain tree had antifungal activity against *Penicillium digitatum* (*in vitro*) and could prolonged the storage life of litchi fruits

## ACKNOWLEDGMENTS

I would like to thank the Faculty of Sciences, Lampang Rajabhat University, Lampang, Thailand, for supporting grant of the study. And I would like to thanks all villagers in Look village, Lampang province, Thailand for supporting wood scrap wastes for this study.

## REFERENCES

[1] Hardoko, Sasmito, B.B., and Puspitasari, Y.E., Antidiabetic and Antioxidant Activities of Tannin Extract of *Rhizophora mucronata* leaves. Journal of Chemical and Pharmaceutical Research, Vol.8, Issue 3, 2016, pp. 143-148.

[2] Ukoha, P.O., Cemaluk, E.A.C., Nnamdi, O.L., and Madus, E.P., Tannins and Other Phytochemical of The *Samanea saman* Pods and Their Antimicrobial Activities. African Journal of Pure and Applied Chemistry, Vol.5, Issue 8, 2011, pp. 237-244.

[3] Ramirez, M.G.L., Ruiz, H.G.O., Arzate, F.N., Gallegos, M.A.C., and Enriques, S.G., Evaluation of Fungi Toxic Activity of Tannins and a Tannin-copper Complex From the Mesocarp of *Cocos nucifera* Linn. Wood and Fiber Science, Vol.44, Issue 4, 2012, pp. 357-364.

[4] Mailoa, M.N., Mahendradatta, M., Laga, A., and Djide, N., Antimicrobial Activities of Tannins Extract from Guava Leaves (*Psidium guajava* L.) on Pathogens Microbial. International Journal of Scientific and Technology Research, Vol. 3, Issue 1, 2014, pp. 236-241.

[5] Hoque, M.Z., Akanda, A.M., Miah, M.I.H., Bhuiyan, M.K.A., Miah, M.G., and Begum, F., *In vitro* Screening of Fungicides and Tannins Against Fungal Pathogens of Jujube Fruits. Progressive Agriculture, Vol. 27, Issue 2, 2016, pp.154-161.

[6] Moosophon, K., Wetthaisong, T., Seeratchakot, L., and Kokluecha, W., Tannin Extraction from Mangosteen Peel for Protein Precipitation in Wine. Khon Kaen University Research Journal, Vol. 15, Issue 5, 2010, pp. 337-385.

[7] Elgailani, I.E.H., and Ishak, C.Y., Methods for Extraction and Characterization of Tannins from

- some Acacia Species of Sudan. Pakistan Journal of Analytical and Environmental Chemistry, Vol.17, Issue 1, 2016, pp. 43-49.
- [8] Gaamoune, S., Harzallah, D., Kada, S., and Dahamna, S., The Comparison of Two Tannin Extraction Methods from *Galium tunetanus* Poiret and Their Antioxidant Capacities. Der Pharmacia Lettre, Vol. 6, Issue 1, 2014, pp. 114-119.
- [9] Downey, M.O., and Hanlin, R.L., Comparison of Ethanol and Acetone Mixtures for Extraction of Condensed Tannin from Grape Skin. South African Journal for Enology and Viticulture, Vol. 31, Issue 2, 2010, pp. 154-159.
- [10] Vieira, M.C., Lelis, R.C.C., da Silva, B.C., and Oliveira, G.L., Tannin Extraction from the Bark of *Pinus oocarpa* var. *oocarpa* with Sodium Carbonate and Sodium Bisulfite. Floresta e Ambiente Vol. 18, Issue 1, 2011, pp. 1-8.
- [11] Underhill, S.J.R., and Critchley, C., Physiological Biochemical and Anatomical Changes in Lychee (*Litchi chinensis* Sonn.) Pericarp during Storage. Journal of Horticultural Science, Vol. 68, Issue 3, 1993, pp. 327-335.



## EXTRACTION OF PECTIN FROM PEANUT SHELL WASTE WITH HEATING IN COMBINATION WITH ULTRASONIC-ASSISTED EXTRACTION

Chua Jedton, A.<sup>1</sup>, Karuehanon W.<sup>2</sup> and Boonkorn, P.<sup>1</sup>

<sup>1</sup>Department of Biology, Faculty of Science, Lampang Rajabhat University, Thailand

<sup>2</sup>Department of Chemistry, Faculty of Science, Lampang Rajabhat University, Thailand

### ABSTRACT

The extraction of pectin from peanut shell waste with heating in combination with ultrasonic-assisted extraction (UAE) was studied. Powder of peanut shell was extracted at a temperature of 70, 80 and 90 °C for 2 hr. It was shown that the pectin extraction at 80 °C had the highest amount of pectin at 1.56±0.07 %, compared to other treatments and the chemical characteristics of the extracted pectin were similar to commercial pectin. Then, the pectin extraction condition at 80 °C for 2 hr was combined with UAE at 40kHz/1500W for 10, 20, and 30 min. Results shown that pectin extraction at 80 °C for 2 hr in combination with UAE at 40kHz/1500W for 10 min had the highest amount of extracted pectin at 1.61±0.04 % with 88.64± 2.69 % degree of esterification, 52.12±1.46 % galacturonic acid, 9.40 % moisture and 13.50 % ash which were the most similar properties to commercial pectin compared to other treatments. Therefore, pectin extraction with heating in combination with UAE method appeared to be an increasing pectin extraction when compared to the conventional method.

*Keywords: extraction, peanut shell, pectin, ultrasonic*

### INTRODUCTION

Peanut (*Arachis hypogaea* L.) is an important oil and protein crop in the world. It belongs to Leguminosae. Peanut crops used for oil production, roasted peanut and snack product, etc. [1] However, the amount of waste is generated in the process of harvest or oil extraction which is only a few wastes of peanut is used as animal feed and treated as a fertilizer. It regarded as agriculture waste. Peanut shell waste derived from the harvested groundnut such as the kernels is used to roasted snack peanuts and peanut oil, which generated a shelled peanut kernel. Sobolev and Cole [2] reported that a little peanut shell makes the cattle feed or extract of phenolic compounds. So, the more efficient utilization of peanut shell as a renewable raw material can provide for the extraction of compounds.

Pectin is a polysaccharide in the primary cell walls and middle lamellae of many plants and fruits and associated with cellulose, hemicellulose, and lignin structures [3]. Pectin forms the most complex of polysaccharides, which pectin backbone composed of (1 → 4)- α -D-galacturonic acid molecules [4], [5]. For example, plants of *Lupinus* genus had pectin contents around 1.5%–7% or peach (*Persica vulgaris* L.) had pectin contents up to 10%. [6]. As well as from the agricultural and food industries to obtain pectin contents with over 15% on dry basis by-products [7]. The extraction method for pectin is a new trend for the revalorization of

agricultural residues. Pectin is one of the most important and widely used in the food industry. It is used as a gelling, stabilizing, encapsulating agents, and a thickening agent such as jellies and jams [8]. The pectin content has resulted in different extraction methods. It depended on the raw material, the extraction methods, and further chemical purification treatments. The conventional extraction technique was a regular solvent extraction based on stirring and heating. It was extracted by acidic solvent at high temperature [6]., microwave-assisted extraction (MAE), ultrasound-assisted extraction (UAE), and enzymatic extraction. Moreover, the extracted pectin investigated the combination of two or more techniques.

UAE is a process that highly efficient in terms of acoustic energy and solvents to extract compounds from various plant matrices. It can be relatively short times and obtain the yield quantity and high purity [9]. The mechanism of UAE based on the interaction of the ultrasonic waves and molecules of the solvent allowing cavitation and cell disruption by ultrasonic waves may enhance the mass transfer across the cell membranes [6]. The increasing extraction yield is fragmentation mechanisms that result in reducing particle size and increasing the surface area of the mass transfer [10]. The standard frequencies of ultrasonic waves comprised between 20 kHz and 100 kHz.

Furthermore, the high ultrasonic power induces the greater shorten that results in the fragmentation of material [11]. High efficiencies recently reported

for the UAE of pectin from several agricultural wastes, such as pomegranate peel [12], passion fruit peel [13] and *Opuntia ficus indica* cladodes [14]. However, this study about the peanut shell waste for a renewable raw material can provide for the extraction of pectin. Thus, this research was to determine the extraction of pectin from peanut shell waste with heating in combination with ultrasonic-assisted extraction (UAE).

## MATERIALS AND METHODS

### The plant materials

Peanut shell (*Arachis hypogaea* L.) collected from peanut farm in Mae-Tha, Lampang Province, Thailand and transported to the Laboratory at Lampang Rajabhat University. The peanut shell was immersed in hot air oven at 55°C for 24 hr and then dried peanut shell were ground until obtaining a fine powder using a grinding machine and stored at room temperature until use.

### Determination of heating for pectin extraction

The extraction process was performed using the following condition by Pagan [15]. The powder of peanut shell 33 g added to 100 ml of distilled water after that, pH of solution was adjusted to 2.0 using 0.25 M HCl. The extraction by using the thermostatic bath at three different temperatures (70, 80, and 90°C) for 120 minutes and stir every 30 minutes. After heating, each treatment filtered with a white cloth, and then the solution was precipitated using 95% ethanol (solution/ethanol ratio 1:3). And then, the precipitate was filtered using vacuum filtration. The precipitate was later rinsed three times using 70% ethanol. Subsequently, it was dried at 40°C using an oven until constant weight. The extraction yield was calculated as follows:

$$\text{Extraction yield (\%)} = \frac{\text{Pectin weight (g)}}{\text{Sample weight (g)}} \times 100$$

### Determination of heating in combination with ultrasonic-assisted extraction for pectin extraction

The powders of peanut shells were extracted with the optimal condition determined from conventional heating. The powder of peanut shell 33 g was added to 100 ml of distilled water and pH 2.0 (0.25 M HCl). The pectin extraction condition at 80 °C for 2 hr was combined with UAE [14] at the frequency of 40 kHz and the power of intensity of 1500 W for 10, 20 and 30 min. After the time extraction, each treatment was cooled at room

temperature for 120 minutes and adjusted to 2.0 using 0.25 M HCl. Then, the solution was filtered with a white cloth, and then the solution was precipitated using 95% ethanol (solution/ethanol ratio 1:3). And then, the precipitate was filtered using vacuum filtration. The precipitate was later rinsed three times using 70% ethanol. Subsequently, it was dried at 40°C using an oven until constant weight. The extraction yield was calculated

### Physiochemical analyses of the extracted pectin

#### Degree of esterification

The degree of esterification (DE) of pectin was determined by Rangana [16]. A dried sample of pectin (0.5 g) was solubilized in 100 ml of water without CO<sub>2</sub> with 2 ml of ethanol. After the sample completely dissolved, five drops of phenolphthalein were added. The solution was titrated with 0.5 NaOH, and the volume of NaOH dissolved was recorded as the initial titer. Then, 10 ml of 0.5 NaOH was added and allowed to stand for 15 minutes. And then, 10 ml of 0.5 HCl was added, and the sample was shaken until the pink color disappeared. Five phenolphthalein was added and titrated with 0.5 NaOH to pink color, and the volume of NaOH dissolved was recorded as the final titer. The DE was calculated from the following equation:

$$\text{DE\%} = \frac{\text{final titer}}{\text{initial titer} + \text{final titer}} \times 100$$

#### Galacturonic acid

Galacturonic acid (GA) was determined by Rangana [16]. A dried sample of pectin (0.01 g) was solubilized in 100 ml of 0.05 N NaOH and allowed stand for 25 minutes. The sample 2 ml was diluted with 100 ml of distilled water and then sampling 2 ml immersed into the test tube with 1 ml of 0.1% carbazole. Then, 12 ml of 98% H<sub>2</sub>SO<sub>4</sub> was added and allowed stand for 25 minutes, and absorbance was measured at 525 nm with UV-VIS spectrophotometer. The GA content was expressed as GA% (w/w), obtained from a calibration curve of galacturonic acid standard solutions (Fig. 1).

#### Determination of moisture content and ash content

The moisture content and ash content were determined by the standard test method (ASTM D3173-95). For moisture content, a dried sample of pectin (1 g) was immersed into the crucible, close with a cover and inserted into the furnace chamber which maintained the temperature at 150 for 3 hr until constant weight. The moisture content was calculated as follows:

$$\text{Moisture (\% wb)} = \frac{A-B}{A} \times 100$$

where: A = weight of sample used (g)  
B = weight of sample after heating (g)

For ash content, a dried sample of pectin (1 g) was immersed into the crucible, close with a cover and inserted into the furnace chamber which maintained the temperature at 650 for 3 hr until constant weight. The ash content was calculated as follows:

$$\text{Ash (\% wb)} = \frac{\text{weight of sample used (g)}}{\text{weight of sample after heating (g)}} \times 100$$

### Statistical analysis

All experiments were replicated three times and evaluated with the regression procedure using SPSS version 17. Differences among treatments performed using Duncan's Multiple Range test ( $P \leq 0.05$ ).

## RESULTS AND DISCUSSION

### Determination of heating for pectin extraction

The yield of pectin extraction revealed in Fig. 2. The result showed that the amount of pectin extracted significantly obtained the highest yield at 80°C of 1.56 yield% (w/w). Meanwhile, the temperature at 70°C and 90°C had a yield of 1.19 and 0.72 yield% (w/w), respectively. The high extraction yields were obtained at high temperatures and low pH values due to the separating of pectin, and other cell wall materials. As well as Oliveira [17] reported that the extraction of banana fruit had been considered an excellent source of pectin which was used to determine the effect of pH 2.0–4.5 and the temperature between 70–90 °C for 120–240 minutes under stirring at 150 rpm. In the same way, Korish [18] reported that *Citrullus lanatus* var. Colocynthoides watermelon obtained the optimum yield (16.7%) with acidic water solution (HCl, pH 2.0) at 85 °C for 60 min. In the other agricultural residues, peels of yellow passion fruit and dragon fruit gave pectin yield of 14.2% and 12.6% at pH 2.4 and the extraction times for 58 and 65 min, respectively [19]. Physiochemical analysis of heating for the extracted pectin as represented in Table 1. The result showed that DE and GA content of pectin extraction had non-significant when compared to commercial pectin. DE content at 80°C obtained the highest amount of DE of 70.41 %, which the degree of methyl-esterification containing up to 50% was pectin with high DM. It was used as a gelling component in heat-resistant bakery jams,

fruit preservatives and juices and jellies [20]. While GA content of all treatments was similar to commercial pectin, which is related to the characteristic of the ability of pectin to form gels. Moisture contents were similar to all treatments and ash content had significantly, and at 80°C had the highest when compared to all treatments.

### Determination of heating in combination with ultrasonic-assisted extraction for pectin extraction

Pectin extraction with heating in combination with UAE represented Fig. 3 and Fig. 4. The yield of pectin extraction showed the highest yield at 80°C in combination with UAE for 10 minutes of 1.67 yield% (w/w) while, UAE for 20 minutes UAE for 30 minutes had the yield of 1.37 and 1.21 yield% (w/w), respectively. Xu [21] found that the longer time of extraction occurred the yield slightly decreased. The extraction with heating in combination with UAE could result in the enhanced ability of pectin extraction. Wang [9] reported that the pectin extraction of grapefruit peel obtained the optimum time was 29.95 minutes at the power intensity of 12.56W and the temperature at 66.71°C, as well as Moorthy [12], found that the maximum extraction yields of pomegranate peel were determined at 61.9 °C for 28.3 minutes resulting in yield extraction of 24.2%. The extraction temperature and sonication time are essential for UAE. In the other hand, the extraction conditions of sisal fibers showed the optimal extraction condition was 61 W for 26 min and temperature at 50 °C resulting in pectin yield of 29.3% [22]. Therefore, UAE destructed the cell wall by allowing cavitation and enhance the mass transfer across the cell membranes [6]. The characteristic of pectin as represented in Table 2. The result showed that the amount of DE and GA significantly obtained the highest DE% at UAE 10 minutes gave the amount of DE of 88.64 %, which was high DM. And GA% in UAE 30 minutes was similar to UAE 10 and 20 minutes. Moisture contents were similar to all treatments and ash content had significantly, and UAE 20 minutes had the highest when compared to all treatments.

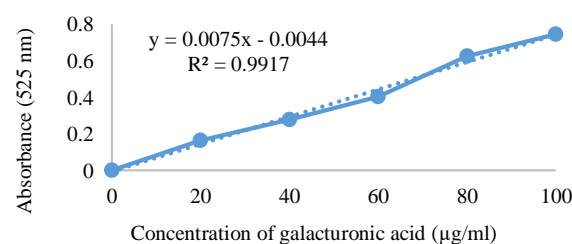


Fig. 1 Standard curve of galacturonic acid

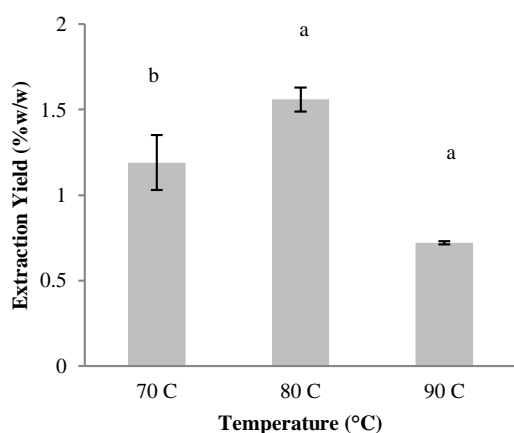


Fig. 2 Yield of pectin extracted at different temperatures. The result followed by error bar represented standard deviations. Values with the same letter on the same color bars represented no significance differences (\* $P \leq 0.05$ )

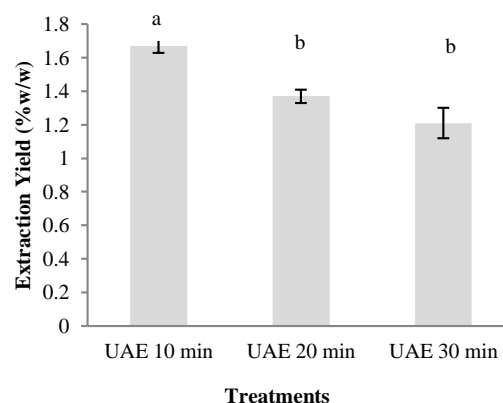


Fig. 3 Yield of pectin extracted with heating at 80°C and UAE. The result followed by error bar represented standard deviations. Values with the same letter on the same color bars represented no significance differences (\* $P \leq 0.05$ )

Table 1 Characteristics of pectin extracted at different temperatures.

| Characteristics | Commercial pectin       | 70 °C                   | 80 °C                   | 90 °C                    |
|-----------------|-------------------------|-------------------------|-------------------------|--------------------------|
| DE%             | 83.10±4.63 <sup>a</sup> | 29.35±4.82 <sup>b</sup> | 70.41±9.23 <sup>a</sup> | 66.37±10.15 <sup>a</sup> |
| GA (% w/w)      | 30.36±8.33 <sup>a</sup> | 24.85±0.54 <sup>a</sup> | 24.18±0.38 <sup>a</sup> | 24.18±0.69 <sup>a</sup>  |
| Moisture (% wb) | 9.10 ±0.55 <sup>a</sup> | 7.00±0.32 <sup>a</sup>  | 8.00±0.87 <sup>a</sup>  | 8.30±0.52 <sup>a</sup>   |
| Ash (% wb)      | 8.70±0.19 <sup>a</sup>  | 13.00±0.72 <sup>a</sup> | 28.20±0.13 <sup>c</sup> | 20.10±0.46 <sup>b</sup>  |

\*mean value followed by different superscript in the same row differs significantly by Duncan's new multiple range test ( $P \leq 0.05$ ).

Table 2 Characteristics of pectin extracted with heating at 80°C and UAE at different times.

| Characteristics | Commercial pectin       | UAE 10 min              | UAE 20 min              | UAE 30 min              |
|-----------------|-------------------------|-------------------------|-------------------------|-------------------------|
| DE%             | 83.10±4.63 <sup>a</sup> | 88.64±2.69 <sup>a</sup> | 62.25±5.82 <sup>b</sup> | 79.35±5.21 <sup>a</sup> |
| GA(% w/w)       | 30.36±8.33 <sup>b</sup> | 57.12±1.46 <sup>a</sup> | 56.96±4.14 <sup>a</sup> | 58.58±0.87 <sup>a</sup> |
| Moisture(% wb)  | 9.10±0.03 <sup>a</sup>  | 9.40±0.11 <sup>a</sup>  | 9.30±0.12 <sup>a</sup>  | 12.70±0.55 <sup>a</sup> |
| Ash(% wb)       | 8.70±0.32 <sup>a</sup>  | 13.50±0.72 <sup>a</sup> | 27.80±0.13 <sup>b</sup> | 24.10±0.55 <sup>b</sup> |

\*mean value followed by different superscript in the same row differs significantly by Duncan's new multiple range test ( $P \leq 0.05$ ).

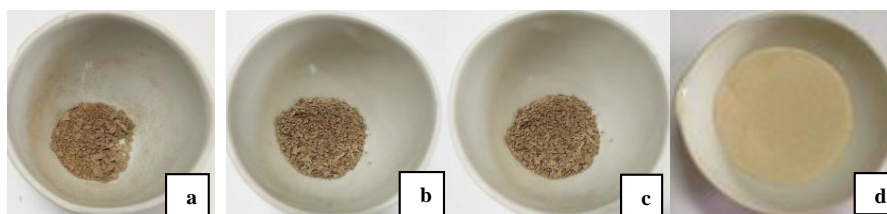


Fig. 4 Pectin extracted from peanut shell waste with heating at 80°C and UAE at different times (a) UAE 10 min (b) UAE 10 min (c) UAE 10 min (d) commercial pectin.

## CONCLUSIONS

The extraction of pectin from peanut shell waste with heating in combination with ultrasonic-assisted extraction (UAE) appeared to be an increasing pectin extraction. The pectin extraction at 80 °C had optimal condition and the pectin extraction condition at 80 °C for 2 hr was combined with UAE at 40kHz/1500W for 10 min had the amount of extracted pectin, degree of esterification, galacturonic acid, moisture and ash content which were the most similar properties to commercial pectin compared to other treatments.

## ACKNOWLEDGMENTS

This work has been supported by Department of Biology, Faculty of Science, Lampang Rajabhat University.

## REFERENCES

- [1] Rustom I. Y. S., Lopez-Leiva M. H. and Nair B. M. Nutritional, Sensory and Physiochemical Properties of Peanut Beverage Sterilized under Two Different UHT Condition. *Food Chemistry*, Vol. 56, 1996, pp. 45-53.
- [2] Sobolev V. S. and Cole R. J. Note on Utilization of Peanut Seed Test. *J. Sci. Food. Agric*, Vol 84, 2003, pp. 4295-4302.
- [3] Anuradha K., Padma P.N., Venkateshwar S. and Reddy G. Fungal Isolates from Natural Pectic Substrates for Polygalacturonase and Multienzyme Production. *Indian J. Microbiol.*, Vol. 50, 2010, pp. 339-344.
- [4] Pedrolli D.B., Monteiro A.C., Gomes E. and Carmona E.C. Pectin and Pectinases: Production, Characterization and Industrial Application of Microbial Pectinolytic Enzymes. *Open Biotechnol. J.*, Vol. 3, 2009, pp.9-18.
- [5] Caffall K.H. and Mohnen D. The Structure, Function, and Biosynthesis of Plant Cell Wall Pectic Polysaccharides. *Carbohydr. Res.* Vol. 344, 2009, pp. 1879-1900.
- [6] Ovodov Y.S. Current Views on Pectin Substances. *Russ. J. Bioorg. Chem.*, Vol. 35, 2009, pp. 269-284.
- [7] Giovanetti M.H., Nogueira A., de Oliveira, C.L. and Wosiacki G. Chromatography—The Most Versatile Method of Chemical Analysis InTech: Rijeka, Croatia, 2012.
- [8] Thakur B. R. and Handa A. K. Chemistry and Use of Pectin- a Review. *Critical Reviews in Food Science and Nutrition*, Vol. 37, Issue 1, 199, pp. 47-73.
- [9] Wang W., Ma X., Xu Y., Cao Y., Jiang Z., Ding T., Ye X. and Liu, D. Ultrasound-Assisted Heating Extraction of Pectin from Grapefruit peel: Optimization and Comparison with the Conventional Method. *Food Chem.*, Vol, 178, 2015, pp. 106-114.
- [10] Chamet F., Huma Z. and Khan M. K. Application of Ultrasound in Food Technology : Processing Preservation and Extraction, *Ultrasonics Sonochemistry*, Vol. 18. Issue 4, 2011, pp. 813-835.
- [11] Bermudez D. A., Mobbs T. and Barbosa C. G. Ultrasound Application in Food Processing. In H. Feng G., Barbosa C. and Weiss J. (Eds.) *Ultrasound Technologies for Food and Bioprocessing*, New York Springer, 2011, pp. 65-105.
- [12] Moorthy I. G., Maran J. P., Surya S. M., Naganyashree S. and Shivamathi C. S. Response Surface Optimization of Ultrasound Assisted Extraction of Pectin from Pomegranate Peel. *Int. J. Biol. Macromol.* Vol. 72, 2015, pp. 1323-1328.
- [13] Cibele F. O., Giordani D. Lutckemeier R. Gurak P. D. Olivera F. C. and Markczak L. D .F. Extraction of Pectin from Passion Fruit Peel Assisted by Ultrasound. *LWT- Food Science and Technology*, Vol. 71, 2016, pp. 110-115.
- [14] Bayar N., Bouallegue T. Achour M. Kriaa M. and Bougatef A. Ultrasonic Extraction of Pectin from *Opuntia ficus indica* Cladodes after Mucilage removal: Optimization of Experimental Condition and Evaluation of Chemical and Functional Properties. *Food Chemistry*, Vol. 235, 2017, pp. 275-282.
- [15] Pagan J., IbarzA., Lorca M., Pagan A. and Barboza-Canovas G. V. Extraction and Characterization of Pectin for stored peach pomace. *Food Research International*, Vol. 24, 2001, pp.605-612.
- [16] Rangana S. *Manual of Analysis of Fruit and Vegetable Products*. Tata Mc. Graw Hill - Publishing Company Limited. 1977.
- [17] Oliveira T. Í. S., Rosa M. F., Cavalcante F. L., Pereira P. H. F., Moates G. K., Wellner N., Mazzetto S. E., Waldron K.W. and Azeredo H. M. C. Optimization of Pectin Extraction from Banana Peels with Citric acid by Using Response Surface Methodology. *Food Chem.* 2015, in press.
- [18] Korish M. Potential Utilization of *Citrullus lanatus* var. *Colocynthis* Waste as a Novel Source of Pectin. *J. Food Sci. Technol.* Vol. 52, 2015, pp. 2401-2407.
- [19] Liew S. Q., Chin N. L.; Yusof Y. A. and Cheok C. Y. Citric acid Extraction of Pectin from Tropical Fruit Peels of Passion fruit, Dragon fruit and Soursop. *J. Food Agric. Environ.* Vol. 13, 2015, pp. 45-51.
- [20] Valdes A. Burgos N. Jimenez A. and Garriagos M. C. Naurak Pectin Polysaccharides as Edible Coatings. *Coating*,

- Vol. 5, 2015, pp. 865-886.
- [21] Xu Y. Zhang L. Bailina Y., Ge Z. and Ye T.  
Effect of Ultrasound and/or heating on the  
Extraction of Pectin from Grapefruit Peel.
- Journal of Food Engineering, Vol. 126, 2014,  
pp. 72-81.
- [22] Maran J. P. and Priya B. Ultrasound-assisted  
Extraction of Pectin from Sisal Waste.  
Carbohyd. Polym. Vol. 115, 2015, pp. 732–738.

## EFFECT OF COMBINATION MICROWAVE AND OVEN DRYING ON THE CHEMICAL PROPERTIES OF CRUDE PALM OIL OBTAINED FROM DIFFERENT OIL PALM FRUIT RIPENESS

Mallika Tapanwong<sup>1</sup>, Rayakorn Nokkaew<sup>2</sup> and Vittaya Punsuvon<sup>1,2</sup>

<sup>1</sup>Faculty of Science, Kasetsart University, Thailand; <sup>2</sup>Center of Excellence-Oil Palm  
Kasetsart University, Thailand

### ABSTRACT

Small crude palm oil mill in Thailand produced the low quality of crude palm oil by using oven drying to dry palm fruits for 14-16 hours. So, the aim of this study is to replace oven drying by using the combined microwave and oven drying to dry palm fruits at different ripeness for 3-4 hours. The effects of combined methods on the chemical properties of crude palm oil are evaluated and compared the properties with premium crude palm oil. The experiments of study follow this details. The raw materials were 18, 20, 22 and 24% of oil content consisted in oil palm bunch. In experiment, 1 kg of each sample was heated at 750 watt for 10 minutes in microwave followed oven drying for 3 hours. Heated palm fruits were further separated the mesocarp from kernel seed. The mesocarp was further pressed by hydraulic presser to obtain crude palm oil. The oil was analyzed the chemical properties in term of free fatty acid (FFA), deterioration of bleaching (DOBI), carotene content, vitamin E content, fatty acid composition, iodine value (IV) and peroxide value (PV). The results showed that all of oil palm fruits ripeness can produce a grade A crude palm oil with low free fatty acid content and high DOBI value.

*Keywords: Microwave, Oven, Oil palm fruit, Ripeness*

### INTRODUCTION

At the present, large and medium scale palm oil mills in Thailand were used a steam sterilization process which has pressurized the palm bunches of 15-45 psi for 90 min at a temperature more than 100 °C. Palm oil from this process has a good quality. Nevertheless, effective steam sterilization process has produce many waste water because of the large amount water used in the process. Thus, the high cost of discharge treatment was necessary to rigorous environmental standard [1]. Most small scale mills in Thailand do not have more ability to generate steam for sterilization. Therefore, non-steam sterilization of the bunch such as drying by hot air is alternative process. But the disadvantage of this process is getting lower quality of crude palm oil due to excessive temperature and drying time of operation.

Microwave is electromagnetic waves with wavelengths ranging from 1 nm to 1 m, or frequencies between 0.3 GHz to 300 GHz. Industry utilizes microwave energy as a source of energy for heating and sterilization [2]. The mechanism of heat generation in the palm oil fruit at a microscopic level is due to the re-orientation of water molecules in the palm fruit to follow electric field direction and interact among themselves which creates friction and heat. The temperature rises of oil palm fruit that exceed 47 °C enhance reduction or inhibition of lipase enzyme activity [3]. Several studies reported the utilization of microwave to heat and sterilize oil palm

fruit follow these details. Cheng [4] found that the quality of the crude palm oil produced by microwave pretreatment followed with solvent extraction was superior compared to that produced by using conventional means in terms of lower acidity, lower moisture content, higher carotene content and higher vitamin E content. Tan [5] studied the combined process of microwave pretreatment and solvent extraction in the laboratory scale and found that this process gave high yield of palm oil, low free fatty acid content, low peroxide value, low anisidine value and high carotene content of the obtained palm oil. Chow [6] studied the detachment of palm fruits from whole bunches and spikelets using microwave heating. The result showed that microwave heating had high sufficiently detached the palm fruits from both whole bunches and spikelets in the easy way by using a slight push of the finger. Sarah [2] studied the effect of sterilization time and temperature on fatty acids composition, carotene and vitamin E content of oil extracted from palm fruit that irradiated by microwave energy. The results showed that fatty acids composition and vitamin E content were not influenced by time and temperature increment but carotene content greatly influenced by temperature increment.

Our studied replaced the drying palm fruit by hot air into microwave for sterilization of palm fruit and we found that microwave drying can inactivated the lipase enzyme activity that result in decreasing of the free fatty acid in crude palm oil. In addition, the



deterioration of bleachability index (DOBI) value, carotene content in crude palm oil can increase after microwave drying of palm fruit, too. However, the drying by microwave is not enough to decrease the moisture content in palm fruit to less than 10 % w/w that is suitable for screw pressing. Thus, the palm fruit obtained after microwave drying need to decrease the moisture content by drying again with hot air in oven drying for a few hour.

The aim of this research is to determine the effect of palm fruit maturity on the quality that obtained after drying by microwave combined with oven drying. Quality in term of chemical properties measured were free fatty acid content (FFA), DOBI, peroxide value (PV), Iodine value (IV), carotene content and tocopherol content. All of these term are compared significant differences or similarity between different ripeness of palm fruit bunches using statistical analysis.

## MATERIAL AND METHOD

### Material

Fresh palm fruit bunch at the different ripeness of 18, 20, 22 and 24% based on oil content of bunch were collected from local oil palm plantation in Pangnga province, Thailand. Fresh fruit bunches were chopped into fruit spikelets and 1 kg of each piece was weighed for microwave drying.

### Microwave and Oven Drying Experiments

1 kg of fruit spikelet was weighed before undergoing microwave drying (microwave oven sharp model with maximum power output of 850 W at 2,450 MHz) for 10 minute intervals time until 100% stripping reach. The fruit at the spikelets were detached with a slight push of a finger until the fruits were completely detached from the spikelet. The detached palm fruit were kept at room temperature for one night after that they were dried in oven at 70-75 °C for 3 hours. After the drying process, the mesocarp of the fruit was peeled and the seeds were removed. The peeled mesocarp was pressed using hydraulic presser to extract the oil and the oil was collected for its chemical analysis

### Chemical Analysis

#### *Determination of free fatty acid content (FFA)*

The FFA content of the oil sample was measure by dissolving oil in 95% ethanol and titrated with 0.1 N sodium hydroxide solution using a phenolphthalein indicator. A blank determination was also made with the sample procedure without the oil sample. The percentage of FFA content was calculated using this Eq. (1)

$$\text{FFA (\%)} = \frac{(S - B) \times N \times 25.6}{W} \quad (1)$$

Where, S is the volume of sodium hydroxide used for oil titration, B is the volume of sodium hydroxide used for blank titration, N is the concentration of sodium hydroxide, W is the weight of oil.

#### *Determination of peroxide value (PV)*

A 5 g oil sample was dissolved in a 30 ml mixture of acetic acid and chloroform which was further reacted with 0.5 ml of saturated potassium iodine solution. After one minute of shaking, 30 ml of water were added and the contents were shaken vigorously to liberate iodine from the organic to aqueous layer. Iodine was titrated with a 0.1 N sodium thiosulphate solution using a starch indicator. A blank determination was made using the same procedure without the oil sample. PV was calculated using the Eq. (2) (AOCS official method cd 8-53, 1997)

$$\text{PV} = \frac{(S - B) \times N \times 1000}{W} \quad (2)$$

Where, S is the volume of sodium thiosulphate used to titrate with oil sample, B is the volume of sodium thiosulphate used to titrate with blank, N is the concentration of sodium thiosulphate, W is the weight of oil.

#### *Determination of iodine value (IV)*

IV was determined followed AOCS official method cd 1-25. Briefly explained, 0.2 g of oil sample was weight into 250 ml of iodine flask. Then, 10 ml of chloroform and 25 ml of wijs reagent was added to into a flak, respectively. The analytical flask was shaken vigorously and stored in a dark place for 2 hours. After that, the flask was added with 20 ml of potassium iodide followed with 15 ml of distilled water. The sample solution was titrated immediately with 0.1 N sodium thiosulphate until yellow color almost disappears. A starch indicator was added into sample and titrated continuously until the blue starch-iodine color disappeared. In addition, a blank was made in the same manner. The IV value is calculated followed Eq. (3)

$$\text{IV} = \frac{(B - S) \times N \times 12.69}{W} \quad (3)$$

Where, B is the volume of sodium thiosulphate used to titrate with blank, S is the volume of sodium thiosulphate used to titrate with oil sample, N is the concentration of sodium thiosulphate, W is the weight of oil.

#### *Determination of carotene content*

Carotene content were carried using MPOB test method (2004). Briefly explained, 0.1 g of oil sample was dissolved in n-hexane in a 25 ml volumetric flask. The absorbance reading of the solution at 446 nm was taken using UV-VIS spectrophotometer. The carotene content is calculated as Eq. (4).

$$\text{Total carotene content (ppm)} = \frac{383(A)(V)}{100(W)} \quad (4)$$

Where, A is the absorbance at 446 nm, V is the volume of oil solution (25 ml) and W is the weight in gram of oil sample.

#### *Determination of deterioration of bleachability index (DOBI)*

DOBI was determined followed MPOB test method (2004). DOBI is defines as the ratio of the spectrometric absorbance at 446 nm to 269 nm. Briefly explained, 0.1 g of oil sample was weighed into 25 ml of volumetric flask and dissolved with n-hexane. The sample solution was measured absorbance at 269 and 446 nm using UV-VIS spectrophotometer. The value of DOBI is calculated followed Eq. (5)

$$\text{DOBI} = \frac{\text{Absorbance at 446 nm}}{\text{Absorbance at 269 nm}} \quad (5)$$

#### *Determination of $\alpha$ -tocopherol and $\gamma$ -tocotrienol by HPLC*

A 20  $\mu$ l of oil sample (obtained by solubilizing 250 mg of oil in 25 ml of n-hexane) was directly injected to a HPLC column 15cm x 4.6 mm ID (Unison UK-Silica UK505, Intakt, USA) at a flow rate of 1 ml/min and 292 nm of wavelength. The HPLC system for  $\alpha$ -tocopherol and  $\gamma$ -tocotrienol content analysis consisted of Yonglin-HPLC equipped UV detector. Standard solution of  $\alpha$ -tocopherol and  $\gamma$ -tocotrienol were used at 0-150 pm concentration for quantification. The mobile phase was 99.5% n-hexane and 0.5% isopropanol which was HPLC grade.

#### **Statistical Analysis**

All independent parameter were carried out in triplicated and the result were expressed as the mean value. Data were statistically analyzed by analysis of variance (ANOVA) followed by Duncan test. The significant level of difference between chemical properties from different ripeness of oil palm bunch were accessed. The level of significance is  $p < 0.05$ .

## **RESULTS AND DISCUSSION**

### **Effect of Drying Process on FFA Content**

A FFA content of each sample is shown in Table 1.

Table 1 The relationship of FFA on the ripeness of oil palm fruit at different condition of experiment

| Ripeness based on %oil content | Average FFA (%w/w) |                   |                   |                   |
|--------------------------------|--------------------|-------------------|-------------------|-------------------|
|                                | Raw material       | MW*               | Left for 1 night  | After oven drying |
| 18                             | 28.80 <sup>a</sup> | 4.69 <sup>b</sup> | 2.21 <sup>b</sup> | 1.08 <sup>b</sup> |
| 20                             | 28.41 <sup>a</sup> | 3.26 <sup>b</sup> | 1.25 <sup>b</sup> | 1.28 <sup>b</sup> |
| 22                             | 30.76 <sup>a</sup> | 4.17 <sup>b</sup> | 1.69 <sup>b</sup> | 1.63 <sup>b</sup> |
| 24                             | 28.43 <sup>a</sup> | 2.87 <sup>b</sup> | 1.64 <sup>b</sup> | 1.65 <sup>b</sup> |

\*MW means after microwave drying

<sup>a-b</sup> Denotes statistically significant in a same row ( $P < 0.05$ )

It indicates that the microwave drying can reduce the FFA content of all ripeness. Due to the lipase enzyme which induces the hydrolysis reaction of triglyceride to generate the FFA is inactivated by microwave. The results showed that the drying process affected to reduce the FFA content while the different ripeness at the same drying step was not affected. The statistical analysis showed that the FFA content was not significant difference in all experiment. In addition, the FFA content after oven drying was 1.08-1.65 %w/w in all ripeness of palm fruit.

### **Effect of Drying Process on Carotene Content and DOBI**

The total carotene content is shown in Table 2. The result showed that the carotene content increase after microwave drying. The carotene content was slightly decreased after left for one night and after oven drying. The obtained carotene content in all ripeness of palm fruit was 554.7-731.5 ppm.

Table 2 The relationship of total carotene content on the ripeness of oil palm fruit at different condition of experiment

| Ripeness based on %oil content | Average total carotene content (ppm) |       |                  |                   |
|--------------------------------|--------------------------------------|-------|------------------|-------------------|
|                                | Raw material                         | MW*   | Left for 1 night | After oven drying |
| 18                             | 396.2                                | 610.2 | 598.4            | 554.7             |
| 20                             | 411.8                                | 682.3 | 755.3            | 639.2             |
| 22                             | 599.0                                | 689.4 | 714.8            | 646.0             |
| 24                             | 699.7                                | 742.7 | 704.0            | 731.5             |

\*MW means after microwave drying

The statistical analysis showed that the carotene content was not significant different in all experiment

of different ripeness of oil palm fruit.

Table 3 The relationship of DOBI on the ripeness of oil palm fruit at different condition of experiment

| Ripeness based on %oil content | Average DOBI      |                   |                   |                   |
|--------------------------------|-------------------|-------------------|-------------------|-------------------|
|                                | Raw material      | MW*               | Left for 1 night  | After oven drying |
| 18                             | 1.05 <sup>b</sup> | 4.07 <sup>a</sup> | 4.10 <sup>a</sup> | 3.89 <sup>a</sup> |
| 20                             | 1.74 <sup>b</sup> | 4.49 <sup>a</sup> | 4.83 <sup>a</sup> | 4.61 <sup>a</sup> |
| 22                             | 2.05 <sup>b</sup> | 4.75 <sup>a</sup> | 4.78 <sup>a</sup> | 4.18 <sup>a</sup> |
| 24                             | 2.17 <sup>b</sup> | 4.31 <sup>a</sup> | 4.29 <sup>a</sup> | 4.00 <sup>a</sup> |

\*MW means after microwave drying

<sup>a-b</sup> Denotes statistically significant in a same row (P<0.05)

In addition, The DOBI of oil after treatment was affected by drying process (Table 3). The results indicated that DOBI value of all maturity increased when the sample was treated by microwave and kept constant though left for one night or oven drying. The statistical analysis showed that DOBI value was not significant different in all experiment of different ripeness of oil palm fruit. The obtained DOBI after oven drying was 3.89-4.61.

#### Effect of Drying Process on Peroxide Value

The peroxide value which represents the first oxidation reaction is shown in Table 4.

Table 4 The relationship of peroxide value on the ripeness of oil palm fruit at different condition of experiment

| Ripeness based on %oil content | Average peroxide value (meq O <sub>2</sub> /kg oil) |                  |                  |                     |
|--------------------------------|---|------------------|------------------|---------------------|
|                                | Raw material  | MW*              | Left for 1 night | After oven drying   |
| 18                             | 5.5 <sup>a</sup>                                    | 1.5 <sup>b</sup> | 1.7 <sup>b</sup> | 0.4 <sup>b,C</sup>  |
| 20                             | 0.2 <sup>b</sup>                                    | 0.7 <sup>a</sup> | 0.6 <sup>a</sup> | 0.8 <sup>a,BC</sup> |
| 22                             | 1.2   | 0.9              | 1.8              | 1.4 <sup>B</sup>    |
| 24                             | 3.8   | 2.3              | 2.7              | 2.5 <sup>A</sup>    |

\*MW means after microwave drying

<sup>a-b</sup> Denotes statistically significant in a same row (P<0.05)

<sup>A-C</sup> Denotes statistically significant in a same column (P<0.05)

In comparison of drying process, the statistical analysis investigated that the microwave drying had affected on peroxide value at 18 and 20% of oil content while the other was not. The peroxide value of palm oil after microwave treatment was decreased from raw material at 18% of oil content. In 20% of oil content, the result was contrast with 18% of oil

content. The peroxide value increased when the sample was treated by microwave. Due to the microwave can induce the peroxide species on unsaturated fatty acid molecule in palm oil. In oven drying, the peroxide value increased when the ripeness was increased.

#### Effect of Drying Process on Iodine Value

The iodine value represents the number of unsaturated species. Table 5 indicated that the drying process wasn't affected on iodine value for all ripeness.

Table 5 The relationship of iodine value on the ripeness of oil palm fruit at different condition of experiment

| Ripeness based on %oil content | Average iodine value (g I <sub>2</sub> /100 g oil) |      |                  |                   |
|--------------------------------|--|------|------------------|-------------------|
|                                | Raw material                                       | MW*  | Left for 1 night | After oven drying |
| 18                             | 53.5   | 54.0 | 54.0             | 52.0 <sup>B</sup> |
| 20                             | 56.9   | 56.2 | 56.8             | 55.9 <sup>A</sup> |
| 22                             | 53.5   | 54.5 | 53.7             | 52.8 <sup>B</sup> |
| 24                             | 54.0   | 54.2 | 53.8             | 53.3 <sup>B</sup> |

\*MW means after microwave drying

<sup>A-B</sup> Denotes statistically significant in a same column (P<0.05)

However, the statistical analysis showed significant difference of iodine value on different ripeness. For palm oil after oven drying, the highest iodine value was 20% of oil content because of high originated amount. The obtained iodine value after oven drying was 52.0-55.9.

#### Effect of Drying Process on $\alpha$ -tocopherol content

Crude palm oil is the one of vitamin E resources which contained about 600-1000 ppm. A vitamin E in palm oil consists of both tocopherol (21.3%) and tocotrienol (78.7%) [7]. A beneficial of vitamin E is antioxidant characterization that prevents the oxidation reaction of oil. In this study, the vitamin E in form of  $\alpha$ -tocopherol was study and shown in Table 6. The  $\alpha$ -tocopherol content of sample after drying process indicated that the microwave had affected to reduce the amount of  $\alpha$ -tocopherol content. In the ripeness comparison, the 18% of oil content gave the highest  $\alpha$ -tocopherol content and decreased when the oil content was increased. For  $\gamma$ -tocotrienol, the result gave the same trend of  $\alpha$ -tocopherol (Table 7). The  $\gamma$ -tocotrienol decreased when the sample was treated by microwave but the ripeness was insignificant difference.

Table 6 The relationship of  $\alpha$ -tocopherol content on the ripeness of oil palm fruit at different

condition of experiment

| Ripeness based on %oil content | Average $\alpha$ -tocopherol content (ppm) |                    |                    |                    |
|--------------------------------|--|--------------------|--------------------|--------------------|
|                                | Raw material                               | MW*                | Left for 1 night   | After oven drying  |
| 18                             | 1,248 <sup>a,A</sup>                       | 920 <sup>b,A</sup> | 967 <sup>b,A</sup> | 911 <sup>b,A</sup> |
| 20                             | 933 <sup>a,B</sup>                         | 781 <sup>b,B</sup> | 784 <sup>b,B</sup> | 798 <sup>b,B</sup> |
| 22                             | 811 <sup>B</sup>                           | 744 <sup>B</sup>   | 739 <sup>B</sup>   | 715 <sup>BC</sup>  |
| 24                             | 803 <sup>B</sup>                           | 722 <sup>B</sup>   | 737 <sup>B</sup>   | 740 <sup>C</sup>   |

\*MW means after microwave drying

<sup>a-b</sup> Denotes statistically significant in a same row (P<0.05)<sup>A-C</sup> Denotes statistically significant in a same column (P<0.05)Table 7 The relationship of  $\gamma$ -tocotrienol content on the ripeness of oil palm fruit at different condition of experiment

| Ripeness based on %oil content | Average $\gamma$ -tocotrienol content (ppm) |                 |                   |                   |
|--------------------------------|---|-----------------|-------------------|-------------------|
|                                | Raw material                                | MW*             | Left for 1 night  | After oven drying |
| 18                             | 719 <sup>a</sup>                            | 64 <sup>b</sup> | 27 <sup>b</sup>   | -                 |
| 20                             | 474 <sup>a</sup>                            | 32 <sup>b</sup> | 24 <sup>b,c</sup> | 13 <sup>c</sup>   |
| 22                             | 727 <sup>a</sup>                            | 41 <sup>b</sup> | 8 <sup>b</sup>    | 20 <sup>b</sup>   |
| 24                             | 809 <sup>a</sup>                            | 17 <sup>b</sup> | 12 <sup>b</sup>   | 19 <sup>b</sup>   |

\*MW means after microwave drying

<sup>a-b</sup> Denotes statistically significant in a same row (P<0.05)

However,  $\gamma$ -tocotrienol was more decreased by drying treatment than  $\alpha$ -tocopherol. The almost 90% of  $\gamma$ -tocotrienol was destructed by microwave whereas  $\alpha$ -tocopherol was lost about 15-30% in this process. The reason might be molecular structural difference between both forms. The structure of both vitamin E forms have the same chromanol ring but it differ at the position of the side chain. The unsaturated side chain of  $\gamma$ -tocotrienol is more sensitive to microwave heating than  $\alpha$ -tocopherol consisting saturated side chain. Thus,  $\gamma$ -tocotrienol are easily destroy.

## CONCLUSIONS

Microwave is one of several technique to improve the quality of crude palm oil but this technique consumes the high production cost. Thus, the combination between microwave and oven drying are the better choice for crude palm oil production. The studied shows that the combined microwave and oven drying can reduce the FFA content to less than 3% and increase DOBI value to excess 3.5 which is the standard of premium crude palm oil. This process is

beneficial for small palm oil mill to produce the premium crude palm oil using the oil palm fruit ripeness from 18-24% as raw materials.

## ACKNOWLEDGMENTS

This research was supported by Tech Enterprise Service Network (TESNet), Center of Excellence-Oil Palm, Kasetsart University and Department of Chemistry, Faculty of Science, Kasetsart University.

## REFERENCES

- [1] Umudee I., Chongcheawchamnan M., Kaitweerasakul M. and Tongurai C., Sterilization of Oil Palm Fresh Fruit Using Microwave Technique, International Journal of Chemical Engineering and Applications, Vol. 4, Issue 3, 2013, pp.111-113.
- [2] Sarah M., Ramadhan M.R. and Zahra A., Effect of Sterilization Time and Temperature on Fatty Acids, Carotenoids and Vitamin E of Oil Extracted from Palm Fruit Irradiated by Microwave Energy, Proceedings of the 4th International Symposium on Applied Chemistry, 2018, pp.020068-1 – 020068-8.
- [3] Sarah M., Widyastuti S. and Ningsih D., Red Palm Oil Production by Microwave Irradiation, IOP Conference Series: Materials Science and Engineering, Vol. 309, 2018, pp.1-5.
- [4] Cheng S.F., Mohd N.L. and Chuah C.H., Microwave Pretreatment: A Clean and Dry Method for Palm Oil Production, Industrial Crops and Products, Vol. 34, 2011, pp.967-971.
- [5] Tan J. CX., Chuah C.H. and Cheng S.F., A Combined Microwave Pretreatment/Solvent Extraction Process for the Production of Oil from Palm Fruit: Optimisation, Oil Quality and Effect of Prolonged Exposure. Journal of the Science of Food and Agriculture, Vol. 97, 2017, pp.1784-1789.
- [6] Chow M.C. and Ma A.N., Processing of Fresh Palm Fruits Using Microwaves, Journal of Microwave Power and Electromagnetic Energy, Vol. 40, Issue 3, 2007, pp.165-173.
- [7] Kua Y.L., Gan S., Morris A. and Ng H.K., Optimization of Simultaneous Carotenes and Vitamin E (Tocols) Extraction from Crude Palm Olein Using Response Surface Methodology, Chemical Engineering Communications, Vol. 205, Issue 5, 2018, pp.596-609.
- [8] Erkan, N., Ayranci G. and Ayranci, E., A Kinetic Study of Oxidation Development in Sunflower Oil under Microwave Heating: Effect of Natural Antioxidant, Food Research International, Vol. 42, Issue 5, 2009, pp. 1171-1177.

## EFFECTS OF CHLORINE DIOXIDE DIPPING ON PERICARP BROWNING REDUCTION OF LONGAN FRUIT

Suttinee Likhitrarung<sup>1,6</sup> Tanachai Pankasemsuk<sup>2,3,4</sup> Kanda Whangchai<sup>4,5</sup>

Wittaya Apai<sup>6</sup> and Wanwarang Patanapoh<sup>1</sup>

<sup>1</sup>Postharvest Technology Research Center, Faculty of Agriculture, Chiang Mai University,  
Chiang Mai 50200, Thailand

<sup>2</sup>Department of Plant and Soil Sciences, Faculty of Agriculture, Chiang Mai University,  
Chiang Mai 50200, Thailand;

<sup>3</sup>International College of Digital Innovation, Faculty of Agriculture, Chiang Mai University,  
Chiang Mai 50200, Thailand

<sup>4</sup>Postharvest Technology Innovation Center, Office of the Higher Education Commission,  
Bangkok 10400, Thailand

<sup>5</sup>Department of Biology, Faculty of Science, Chiang Mai University,  
Chiang Mai 50200, Thailand

<sup>6</sup>Office of Agricultural Research and Development region 1, Chiang Mai 50100, Thailand

### ABSTRACT

Pericarp browning is the main factor to reduce the storage life and marketability of longan fruit. In the present study evaluated chlorine dioxide (ClO<sub>2</sub>) dipping on reducing pericarp browning. Fresh longan fruit was dipped in 1%, 1.25% and 1.5% ClO<sub>2</sub> for 5 min and stored at 5±2 °C, 85±5% RH for 42 days, investigated every 7 days. Evaluation by browning index (BI) as pericarp browning, outer pericarp color by a chromameter expressed as L\* and b\* value and hue angle, disease incidence, ClO<sub>2</sub> residue and sensory acceptance was determined. The result showed that dipping in 1%, 1.25% and 1.5% ClO<sub>2</sub> could reduce pericarp browning (lower BI, higher L\* and b\* value and hue angle). However, they showed no significant differences with commercial SO<sub>2</sub> fumigation but they were significant differences with untreated fruit. ClO<sub>2</sub> treatments could reduce disease incidence and low ClO<sub>2</sub> residue in flesh. The sensory acceptance such as outer pericarp color, flesh and flavor treated with 1.5% ClO<sub>2</sub> had shown great potential. The results suggested that 1.5% ClO<sub>2</sub> dipping could reduce pericarp browning of longan fruit as same as the commercial SO<sub>2</sub> fumigation.

*Keywords: Longan fruit, Chlorine dioxide, Pericarp browning, and Sulfur dioxide*

### INTRODUCTION

Longan (*Dimocarpus longan* Lour.) is non-climacteric fruit, widely cultivated in many countries especially in China, Vietnam and Thailand. In Thailand cv. Daw is an important economic exported fruit. It was very short postharvest life for 3-4 days under ambient temperatures. The main factors reduce storage life and marketability of longan fruit are pericarp browning, fungal and microbial decay [1], [2]. Sulfur dioxide (SO<sub>2</sub>) fumigation is commercially to extend shelf life of fresh longan at least 45 days at low temperature [3]. It is the most popular commercial means for prevention of fruit decay and browning because it was effective and inexpensive [1]. However, SO<sub>2</sub> fumigation leaves SO<sub>2</sub> residues and toxic ingredients that may have adverse effects on human health. Therefore, a replacement of SO<sub>2</sub> or improve process with the safer for consumer are required.

Acidified sodium chlorite (ASC) is a sanitizing agent approved by Food and Drug Administration

(FDA) for dip or spray treatment of food items, including fresh and fresh-cut fruits and vegetables, and has shown a strong ability to control pathogen [4]. ASC is mixture of sodium chlorite (SC) and an acid. Sodium chlorite, the major component of ASC, also had strong anti-microbial ability against human pathogenic bacteria. SC was strongly inhibited enzymatic browning on fresh-cut apples. Because of its dual role in browning inhibition and pathogen inactivation, the anti-browning property of SC could be attributed to two modes of action, i.e., direct inactivation of polyphenol oxidase (PPO) activity and oxidative degradation of the phenolic substrates [5]. It could be combined with a substance for improving better good quality that hydrochloric acid (HCl) mixed with SC produced chlorine dioxide (ClO<sub>2</sub>). It is one of the disinfectants has been used to control microbial contamination. ClO<sub>2</sub> solution offers several advantages for food sanitizing, especially for processing vegetables and fruits. The used of ClO<sub>2</sub> to reduce microorganism have been reported in apple, carrot, lettuce, cabbage, tomato

and blueberries [6]-[8]. In addition to the studies of  $\text{ClO}_2$  has been used to reduce enzymatic and maintain quality such as fresh-cut lotus roots, flesh-cut asparagus lettuce and litchi fruit [9]-[11]. In longan, the use of gaseous  $\text{ClO}_2$  concentration 10 mg/L for 10 min. was effective to reduce pericarp browning during storage at 25 °C for 7 days [12]. Although gaseous form has greater penetration ability and leave behind less residue [13] but the aqueous  $\text{ClO}_2$  form to reduce pericarp browning in longan had still lack enough data. Therefore the objective of this study was the effects of fruit dipping in various concentration of  $\text{ClO}_2$  solution on pericarp browning control and fruit quality of longan fruit during cold storage.

## MATERIAL AND METHOD

### Plant Material and $\text{ClO}_2$ Treatment

Mature longan fruits (Daw) for export were transported from packing house in Lamphun province, Thailand. They were placed in 11.5 kg commercial perforated plastic basket, 15 baskets (9 baskets for  $\text{ClO}_2$  treated, 3 baskets  $\text{SO}_2$  fumigated and 3 baskets not treated) were transferred to laboratory 1 day before testing and stored overnight at 5°C with 80-90% relative humidity (RH). Next day, longan fruits were selected with uniformity shape, color size and without disease or insect infected and divided into 3 treatments for dipping in  $\text{ClO}_2$  solution. Before treating each basket were cleaned with tap water, after that each treatment (3 basket/treatment) were dipped in  $\text{ClO}_2$  solutions at different concentration of 1%, 1.25% and 1.5% for 5 min which tested in only a fume hood for safer and allowed to air dry for 2 h and then stored at 5°C with 80-90% (RH) for 42 days. The samples were taken every 7 days for quality evaluation as browning index, pericarp color, disease incidence, sensory evaluation and  $\text{ClO}_2$  residue and storage life until day 42.

### Fruit Quality Evaluation

#### *Browning index*

Browning index was assessed visually the total of brown area on fruit surface by following scale: 1= no browning, 2= slight browning, 3= less than 25% browning of the total surface, 4= 25-50% browning and 5= >50% browning. The browning index was calculated by  $\Sigma(\text{browning scale} \times \text{percentage of fruit in each scale})$ . A browning index scale over 3.0 was considered as unacceptable marketability [14].

#### *Pericarp color*

Pericarp color was measured by chromameter (Model CR400, Minolta Japan). The results were expressed as  $L^*$ ,  $b^*$  value and hue angle.  $L^*$  value indicated lightness of color wheel, ranged from black = 0 to white = 100,  $b^*$  value = (-) blue to yellow (+) and hue angle was true color. Two spots on opposite sides of the fruit were measured and the mean of the two measurements considered as one reading. The results were expressed as a mean value from three replications of the 5 measured samples.

#### *Flesh discoloration*

The following scale was used: 1 = normal (excellent quality); 2 = slight flesh discolored; 3 = less than 25% discolored of the total surface; 4 = 25-50% discolored; and 5 = 50% discolored (poor quality). A flesh discoloration index was calculated using the following formula:  $\sum (\text{discolor scale} \times \text{number of fruit in each class}) / \text{Total fruit}$ . Fruits flesh having a discolor score above 3.0 were rated as unacceptable.

#### *Disease incidence (DI) and sensory evaluation*

Disease incidence was visually assessed by counting the fruits that showed lesions of mycelium or rot on the fruit surface. Sensory evaluation was evaluated during cold storage every 7 days. The in-house trained panel consisting of 10 members assessed the samples. The acceptability of pericarp color, flesh quality, taste and overall quality using a five-point hedonic scale where 5 = like extremely, 3 = neither like nor dislike and 1 = dislike extremely.

#### *Chlorine dioxide residues and storage life*

$\text{ClO}_2$  residues was evaluated by using DPD method [15]. The samples (100 g) of whole fruit ( $\text{ClO}_2$  residue on pericarp) and just a flesh ( $\text{ClO}_2$  residue on flesh) were rinsed with 100 ml distilled water shaken at 160 rpm for 10 min. Ten milliliters of rinsed water were collected for analyze  $\text{ClO}_2$  residues [12]. The  $\text{ClO}_2$  residue in fruits was expressed as mg/kg. Storage life was determined from 3 parameters as browning index below 3.0 (score) Jiang and Li, 2001, disease incidence (%) below 25% and sensory evaluation above 5.0 [16], [17]. Analysis of variance (ANOVA) and the test of mean comparison according to least significant difference (LSD) were applied with a significance level of 0.05.

## RESULT AND DISCUSSION

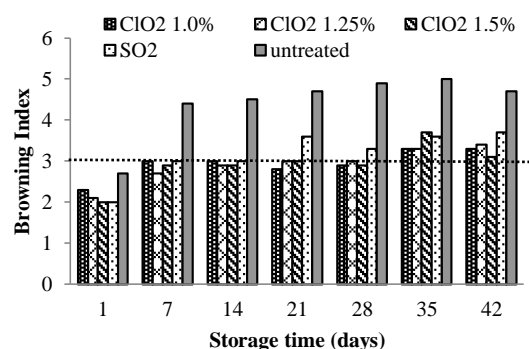
### Pericarp Browning, Pericarp Color and Flesh discoloration

In preliminary test was studied the effect of different ASC ( $\text{HCl} + \text{NaClO}_2$ ) concentration on longan pericarp browning and extended shelf life. It was found that fruits were dipped in  $\text{HCl}$  or  $\text{NaClO}_2$  alone did not reduced pericarp browning, the used of  $\text{HCl}$  9% combined with  $\text{NaClO}_2$  7.5% could produced  $\text{ClO}_2$  2% (maximum concentration) was the effective treatment to reduce pericarp browning and had storage life for 35 day at  $5^\circ\text{C}$ . In this study was investigated in the effect of difference concentration of  $\text{ClO}_2$  (1.0%, 1.25% and 1.5%) on reducing pericarp browning. Pericarp browning was shown as browning index (BI) and pericarp color. Fruits dipping in all  $\text{ClO}_2$  concentration at 1.0%, 1.25% and 1.5% for 5 min could prevent pericarp browning for 28 day (BI below 3.0) at  $5^\circ\text{C}$  (Fig. 1). Whereas untreated fruit, pericarp became browning by 7 days at  $5^\circ\text{C}$  which indicated by BI above 3.0 due to chilling injury occurrence. For flesh discoloration, all treatment was increased with storage time increased but scores showed less than limit of acceptance (less than 3.0) throughout period of time (Fig.2). BI was corresponded with pericarp color as shown in  $L^*$ ,  $b^*$  value and hue angle, all treatment of  $\text{ClO}_2$  were higher than the control after treated and were maintained color for during 42 day storage (Fig. 3a-c). This study was found that high  $\text{ClO}_2$  concentration from 1 to 1.5% increased high bleaching effects in controlling pericarp browning which was contrasted that of Wu et al.[8] who found that litchi were dipped in  $\text{ClO}_2$  at low concentration of 120 mg/l was significantly lower BI than the control after 5 day of harvest and the same as Saengnil et al.[12] who use 10 and 25 mg/l  $\text{ClO}_2$  fumigation on longan fruit found that they were maintained marketing quality of fruit at room temperature for 5 day and delayed the decrease in  $L^*$  and  $b^*$  value and hue angle. This could be explained that pericarp browning of longan fruit is primarily attributed to oxidation of phenolic compounds by PPO and POD [12],[18],[19] and possible that  $\text{ClO}_2$  might discolor longan pericarp by oxidation of lignin as lignin oxidation in pulp bleaching [20].  $\text{ClO}_2$  treatment significantly delayed the decrease in total phenolic content which was accompanied with a decrease in activity of PPO and POD, leading to a lower BI of longan pericarp [12].

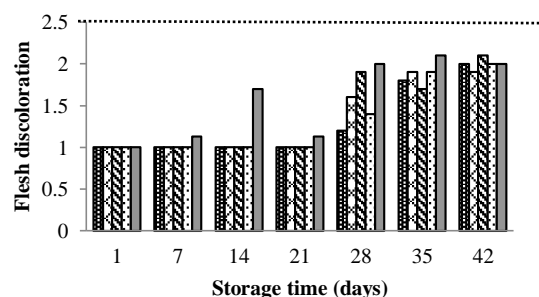
### Disease Incidence (%)

In this study found that the treated treatment with 1.25% and 1.5% of  $\text{ClO}_2$  showed no sign of disease developed during 42 day storage as same as  $\text{SO}_2$  treatment but  $\text{ClO}_2$  1.0% treated found disease

incidence (DI) at 6.7% at 42 day. Whereas the untreated fruit had DI over than 25% in 28 days of storage at  $5^\circ\text{C}$  (Fig. 4) due to fruit rotting from many diseases. The result found that high  $\text{ClO}_2$  concentration more than 1.25% increased high efficiency in preventing DI because  $\text{ClO}_2$  act as oxidizing agent could kill many pathogens. This result was likely of Wu et al.[11] who observed dipped litchi in  $\text{ClO}_2$  solution concentration at 80 mg/l and 120 mg/l were significantly to reduce postharvest disease. On the other  $\text{ClO}_2$  treatment were reduced microflora in mulberry fruit [21]. Saengnil et al.[12] was fumigated longan with 10 and 25 mg/l  $\text{ClO}_2$  could delay and reduced disease. Due to  $\text{ClO}_2$  is the strong oxidizing and sanitizing agents [simpson2005] possible to kill endospores, virus, algae, fungi and some common bacillus [22]. Furthermore the various observations indicated that the increase BI is associated with DI development [11],[23] and also susceptible to various pathogen [2].



**Fig.1** Effect of  $\text{ClO}_2$  dipping on browning index of longan pericarp during store at  $5^\circ\text{C}$  for 42 days (Dot line represents limit of acceptance).



**Fig.2** Effect of  $\text{ClO}_2$  dipping on flesh discoloration of longan during store at  $5^\circ\text{C}$  for 42 days (Dot line represents limit of acceptance).



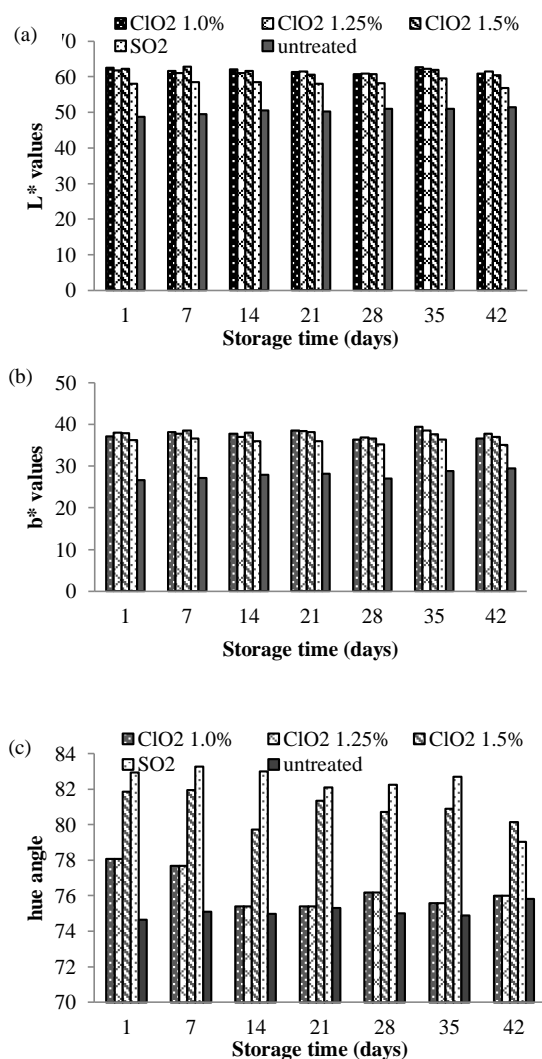


Fig.3 Effect of ClO<sub>2</sub> dipping on L\*(a), b\*(b) value and hue angle (c) of longan pericarp during store at 5°C for 42 days.

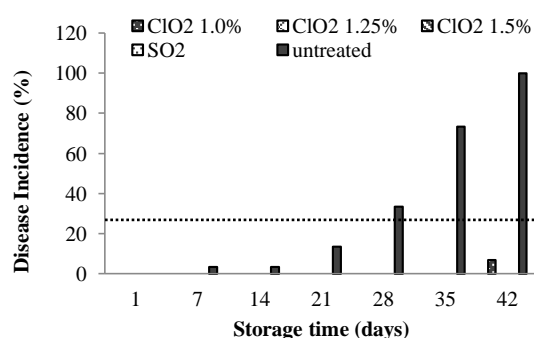


Fig.4 Effect of ClO<sub>2</sub> dipping on disease incidence (%) of longan during store at 5°C for 42 days (Dot line represents limit of acceptance).

## Sensory Evaluation

Pericarp color acceptance of longan fruit were treated with 1.0%, 1.25% and 1.5% ClO<sub>2</sub> were acceptable for 42 days during storage. Whereas untreated fruit was accepted for 1 day (Fig. 5a). Flesh color and tasty acceptance, treated with ClO<sub>2</sub> were accepted for 35 days showed no significant difference with SO<sub>2</sub>, but untreated fruit was accepted at 21 days and 35 days, respectively (fig. 5b,c). The overall acceptance, dipped in 1.0%, 1.25%, 1.5% ClO<sub>2</sub> and SO<sub>2</sub> fumigation were high acceptance as compared with untreated fruit at 42 day, whereas untreated fruit acceptable at 28 day (fig. 5c). The result of this study are relate with Saengnil et al. [12] which longan fruit treated with 2.5-10 mg/l ClO<sub>2</sub> 10 min maintained higher sensory quality scores than those of the control. Furthermore sensory quality evaluation just likely an overall visual quality (OVQ) of Du et al. [9] study found that 100 mg/l ClO<sub>2</sub> treatment 10 min generated high OVQ values during storage time.

## Chlorine Dioxide Residues

ClO<sub>2</sub> can participate in series of oxidation reactions and subsequently degrade to chlorite, chlorate and chloride, they are the principal residues from chlorine dioxide gas interaction with food [6], [15]. The Environmental Protection Agency (EPA) and The National Institute for occupational Safety and Health have established residual acceptance levels as 0.8 mg/L for chlorine dioxide and 1.0 mg/L for chlorite in drinking water [24]. Although it is well known that a major benefit of ClO<sub>2</sub> for disinfecting drinking water is the lack of organo-chlorine compounds, the residues from the direct treatment of fruits and vegetables have not been well established [15]. In this study ClO<sub>2</sub> residues on longan pericarp was detected every 7 days during storage time after treated with 1.0%, 1.25% and 1.5% ClO<sub>2</sub> solution, the levels of ClO<sub>2</sub> residues was in ranking 0-0.12 mg/Kg, 0.07-0.22 mg/Kg and 0.04-0.17 mg/Kg, respectively. Furthermore, ClO<sub>2</sub> residues on fruit flesh was evaluated as pericarp, there were 0-0.02 mg/Kg, 0-0.02 mg/Kg and 0-0.03 mg/Kg, respectively (data not shown). The levels of ClO<sub>2</sub> residues on pericarp and flesh of all treatment were very low. The results are consistent with Saengnil [12] who reported that ClO<sub>2</sub> residues on longan fruit were less than 0.014 mg/kg and not detected in flesh. For this study is indicating that the physiological of pericarp is different, ClO<sub>2</sub> solution can absorbed into flesh easily, but ClO<sub>2</sub> residues level on flesh was very low and less than 3 mg/kg that limitation imposed by the FDA [FDA1998].

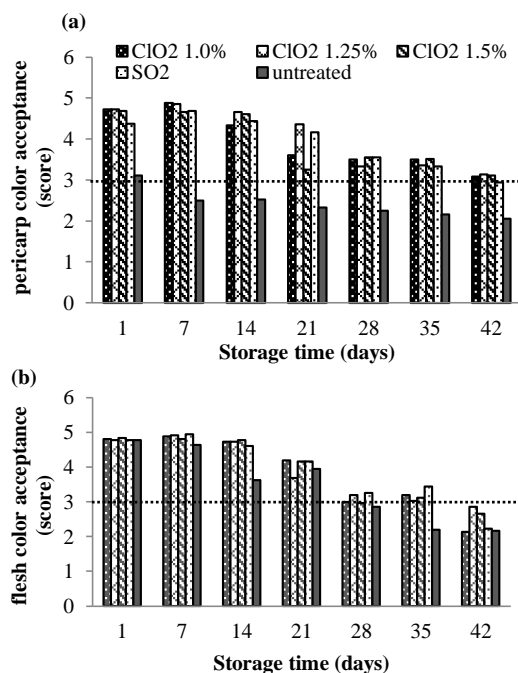


Fig.5 Effect of  $\text{ClO}_2$  dipping on sensory evaluation (a) pericarp color, (b) flesh color of longan pericarp during store at 5°C for 42 days (Dot line represents limit of acceptance).

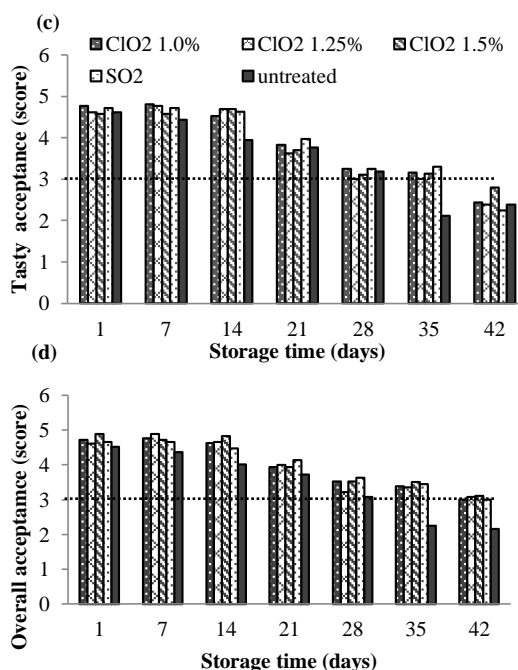


Fig.5 Effect of  $\text{ClO}_2$  dipping on sensory evaluation (c) tasty and (d) overall quality acceptance of longan pericarp during store at 5°C for 42 days (Dot line represents limit of acceptance).

## CONCLUSION

The results showed that dipping in 1.0%, 1.25% and 1.5%  $\text{ClO}_2$  for 5 min were effective to reduce pericarp browning, postharvest decay and extended storage time for 42 days at 5°C. Therefore, dipping in 1.5%  $\text{ClO}_2$  solution could be used to reduce pericarp browning and further study more. It will be one of alternative to replace  $\text{SO}_2$  in the future.

## ACKNOWLEDGMENTS

This work was funded in part by grants from the Agricultural Research Development Agency, Thailand through Postharvest Technology Research Center, Faculty of Agriculture, Chiang Mai University. The authors wish to thank all the staff of researchers in the Laboratory of OARD1, Department of Agriculture.

## REFERENCES

- [1] Jiang, Y.M., Q.Z. Zhang, C.D. Joyce and Ketsa, S., Postharvest biology and handling of longan fruit (*Dimocarpus longan* Lour.). Postharvest Biology and Technology, 26, 2002, pp. 241–252.
- [2] Apai, W., Effects of fruit dipping in hydrochloric acid then rinsing in water on fruit decay and browning of longan fruit. Crop Prot, 29, 2010, pp. 1184–1189.
- [3] Tongdee, S.C., “Sulfur dioxide fumigation in postharvest handling of fresh longan and lychee for export”. In: ACIAR Proceedings, an International Conference Postharvest Handling of Tropical Fruit. Chiang Mai, Thailand, vol. 50, 1994, pp. 186–195.
- [4] FDA., Acidified Sodium Chlorite Solutions. 21 CFR 173.325. Office of the Federal Register, U.S. Government Printing Office, Washington DC, USA, 2000.
- [5] He, Q., Y. Luo and Chen, P., Elucidation of the mechanism of enzymatic browning inhibition by sodium chlorite. Food Chemistry, 110, 2008, pp. 847–851.
- [6] Gomez-Lopez, V.M., Rajkovic, A., Ragaert, P., Smigic, N. and Devlieghere, F., Chlorine dioxide for minimally processed produce preservation: a review. Trends Food Sci. Technol, 20, 2009, pp.17–26.
- [7] Lee, S. Y., Dancer, G.I., Chang, S., Rhee, M.S. and Kang, D.H., Efficacy of chlorine dioxide gas against *Alicyclobacillus acidoterrestris* spores on apple surfaces. Int. J. Food Microbiol., 108, 2006, pp. 364–368.
- [8] Wu, V.C.H. and Kim, B., Effect of a simple chlorine dioxide method for controlling five

- foodborne pathogens, yeasts and molds on blueberries. *Food Microbial*, 24, 2007, pp. 794-800.
- [9] Du, J., Fu, Y., Wang, N., Effects of aqueous chlorine dioxide treatment on browning of fresh-cut lotus root. *LWT-Food Science and Technology*, 42, 2009, pp. 654-659.
- [10] Chen, Z., Zhu, C., Zhang, Y., Niu, D. and Du, J., Effects of aqueous chlorine dioxide treatment on enzymatic browning and shelf-life of fresh-cut asparagus lettuce (*Lactuca sativa* L.). *Postharvest Biol. Technol*, 58, 2010, pp. 232-238.
- [11] Wu, B., P.X. Li, G.H. Hu, Y.A. Liu and Chen, X.W., Effect of chlorine dioxide on the control of postharvest diseases and quality of litchi fruit. *African Journal of Biotechnology*, 10, 2011, pp. 6030-6039.
- [12] Saengnil, K., A. Chumyama, B. Faiyuec and Uthaibutra, J., Use of chlorine dioxide fumigation to alleviate enzymatic browning of harvested 'Daw' longan pericarp during storage under ambient conditions. *Postharvest Biology and Technology*, 91, 2014, pp. 49-56.
- [13] Knapp, J. and Battisti, D., Chlorine dioxide. In: Block S, editor. *Disinfection, sterilization and preservation*. Philadelphia: Lippincott, Williams & Wilkins, 2001, pp. 215-228.
- [14] Jiang, Y.M. and Li, Y.B., Effects of chitosan coating on postharvest life and quality of longan fruit. *Food chem*, 73, 2001, pp. 139-143.
- [15] Trinetta, V., N. Vaidya, R. Linton and M. Morgan., Evaluation of chlorine dioxide gas residues on selected food produce. *Journal of Food Science*, 76, 2011, pp. T11-T15.
- [16] Lawless, H.T. and Heymann, H., *Sensory Evaluation of Food: Principles and Practices*. Chapman and Hall. New York, 1998, pp. 848.
- [17] Apai, W., Klongdee, H., Sukhvibul, N., Noppakoonwong, U., Lim, S.S., Luk, C.S., Tan, S.C.A., Neo, S.Y., Hoon, K.G., Lee, C.A., Amareok, S., Rattanakam, S. and Sardud, V., Study on the Feasibility of Use of Hydrochloric Acid as an Alternative to Sulphur Dioxide for Preserving Longan. *Food and Applied Bioscience Journal* 3, 2015, pp 193-205.
- [18] Khunpon, B., J. Uthaibutra, B. Faiyue and K. Saengnil. Reduction of enzymatic browning of harvested 'Daw' longan exocarp by sodium chlorite. *Science Asia*. 37, 2011, pp. 234-239.
- [19] Chomkititichai, W., Faiyue, B., Rachtanapun, P., Uthaibutra, J., Saengnil, K., Enhancement of the antioxidant defense system of post-harvested 'Daw' longan fruit by chlorine dioxide fumigation. *J. of Scientia Horticulture*, 178, 2014 pp. 138-144.
- [20] Tarvo, V., Modeling chlorine dioxide bleaching of chemical pulp. (Ph.D. Thesis in Chemical Engineering). School of Science and Technology, Aalto University. 2010.
- [21] Chen, Z., Zhu, C. and Han, Z., Effects of aqueous chlorine dioxide treatment on nutritional components and shelf-life of mulberry fruit (*Morus alba* L.). *J. Biosci. Bioeng*, 111, 2011, pp 675-681.
- [22] Du, J.H., Fu, M.R., Li, M.M. and Xia, W., Effects of chlorine dioxide gas on postharvest physiology and storage quality of green bell pepper (*Capsicum frutescens* L. var. Longrum). *Agric. Sci. China* 6, 2007, pp. 214-219.
- [23] Li, X., Liu, A.Y. and Chen, W., Studies on development and control of anthracnose of lychee fruit before and after harvest. *Acta Horti*, 665, 2005, pp. 409-413.
- [24] EPA, Environmental Protection Agency, IRIS., Information on chlorine dioxide. <http://www.epa.gov/iris/subt/0496.htm>. 2003.
- [25] FDA. Secondary Direct Food Additives Permitted in Food for Human Consumption. 21 CFR, Part 173.300 chlorine dioxide. Office of the Federal Register, U.S. Government Printing Office, Washington DC, USA. 1998.

# SPATIAL DISTRIBUTION OF RESTAURANT POPULARITY INDEX BASED ON CONSUMER REVIEW WEBSITE IN JAKARTA

Dewi Susiloningtyas<sup>1</sup>, Alexander Tio<sup>2</sup>, Supriatna<sup>3</sup> and Sidiq, IPA<sup>4</sup>

Department of Geography, Faculty of Mathematics and Natural Sciences, Universitas Indonesia, Indonesia

## ABSTRACT

Nowdays there has been a remarkable surge in the usage of social media specially in urban area in choosing restaurant that they want to visit. This surge becoming new phenomenon that change people lifestyle and behavior in urban area and that is include how people receive information from word of mouth (WoM) recommendation for restaurant and becoming electronic-word of mouth information. Consumer review websites (CRW) are e-word of mouth (e-WoM) information that using people information as main database for restaurant recommendation. Zomato are one of the CRW that have around 4032 database for DKI Jakarta and that include popularity index. Each restaurant divided by 3 classification of popularity group: high popularity, middle popularity, and low popularity. First by using Nearest Neighbor Analysis (NNA) and second Kernel Dencity Analysis (KDA) that each clasification have different spatial distribution and high popularity group are cluster and high dencity with 59 restaurant/km<sup>2</sup> in Center and South Jakarta, middle popularity with cluster and mid dencity (29 restaurant/km<sup>2</sup>) in Center, South, and North Jakarta and low popularity are cluster too but with very low dencity up to 4 restaurant/km<sup>2</sup> in East and South Jakarta. Factor that effect for each classification popularity are shopping mall, hotel 4 & 5 star and Central Bussines Distric (CBD) then by using proximity for each classification that high popularity restaurant group are close to urban functional unit and CBD. Low popularity are more likely place in outside of town and have far distance from urban fungtional unit.

*Keywords: Spatial distribution, Consumer review website, Popularity index, Zomato*

## INTRODUCTION

Rising of social media users have a lot of impact in surge of Electronic word of mouth or E-WoM. This becoming valuable infromation in moderen era for helping someone to buy from internet [1]. This information from social media users have become E-WoM that can be affect others people decition whether or not they have to buy or use that service [1]. Consumer review website or CRW are platform for consumers in catering and tourism industry that use social media users as participant in giving their opinion on service or product [2]. This platform gave easy access for consumers connected to each other and give rating or review for product or service based on their experience [3]. People in urban district using more and more consumer review website as their reliable information for choosing what restaurant they want to eat because people behavior for service or product depend on other online review [4].

Zomato is one of consumer review websites that have restaurant database for Jakarta based on people rating and review. Zomato also have foodie index or popularity index for each restaurant in their database. Rating system is process of subjectif scoring from consumer based on restaurant food, service, price, location and environment [5]. This scoring become popualrity index for each restaurant and based on this research that use zomato as main database, score for each restaurant vary from 1 to 5. Popularity index can

be visualized based on their rating and geographic information [6].

## VARIABEL

### Popularity Index

Zomato have foodie index that become popularity index in this research. Each restaurant have their own rating and this rating from user will be calculated based on Zomato algorythma and become popularity index. This popularity index then classified to 3 different group based on their rating which is high popularity, mid popularity and low popularity

Table 1 Classification group for popularity index

| Group<br>Restaurant  | Rating<br>Restaurant | Total<br>Restaurant |
|----------------------|----------------------|---------------------|
| High<br>Popularity   | 4.0 – 5.0            | 1494                |
| Middle<br>Popularity | 3.0 – 3.9            | 1970                |
| Low<br>Popularity    | 1.0 – 2.9            | 568                 |

\*Rating is based on zomato scoring for restaurant

### Urban Functional Unit

Urban functional unit are all unit that support all the activity in city [7] this unit typically consist of grocery store, hospital, mall, bank, office, school etc. Restaurants that close to urban functional unit are more likely have higher popularity and restaurants that far from urban functional are more likely have low popularity [6].

#### Shopping Mall

Shopping mall have impact on popularity index based on their distance with restaurant [6]. this research include 90 mall from all Jakarta.

#### Hotel

Beside shopping mall, hotel also one of urban functional unit that have impact on popularity index [6]. This research include 150 hotel across all region in Jakarta .

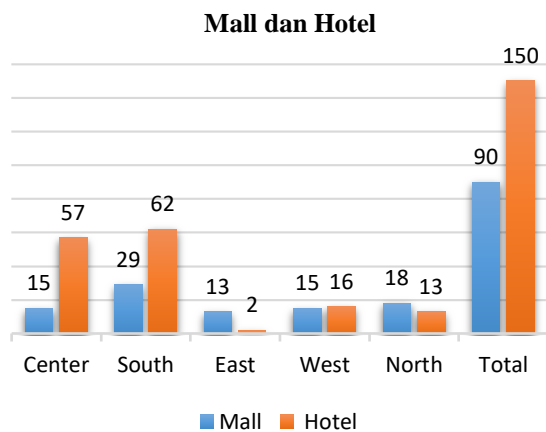


Fig. 1 Shopping mall and hotel in Jakarta

#### Central Bussines District (CBD)

Central bussines distric or CBD is one of the focal point that have economic impact in city. Jakarta has 6 main roads that include in CBD: Thamrin, Rasuna Said, Mega Kuningan, Gatot Subroto, and Satrio.

#### Accessibility

Accessibility in this research were using 2 type of road based on closest distance to each restaurant which is arterial and collector

#### Land Use (LU)

Land use or LU were using in this research to see every type of LU that effect index popularity in each restaurant. Land use that include in this research: business, settlement, religion, social-cultural, and other.

## METHOD

### Study Area

Jakarta is the capital city of the Republic of Indonesia that located on the northwest coast Java. Jakarta has an area of 662 km<sup>2</sup> and total population of 10 million people as of 2014. Jakarta also the growth center fo economic, cultural, and social in Indonesia. Jakarta divided by 5 adminitration region which is West, Center, South, East, and North. Jakarta becoming growth center for food industry and tourism and also Zomato have the most data for popularity index in Jakarta.



Fig. 2 Jakarta the Capital City of the Republic of Indonesia

### Spatial Distribution

Spatial distribution for each restaurant in Jakarta based on popularity index was analyzed using two method: Nearest neighbor analysis (NNA) and Kernel dencity analysis (KDA). Using NNA we can see how distribution each restaurant in Jakarta based on its popularity whether its cluster, random or spread in all region across Jakarta.

Then by using KDA we can confirm NNA anlysis and see how each class have different dencity that affect each class spatial distributin across all region in Jakarta. This two method will strengthen spatial distributin analysis in each class and see what region that have each classification restaurant based on their popularity index. KDA and NNA in Spatial distribution analysis using Arc-GIS software.

## Statistical Analysis

Before using statistical method, popularity group was divide to 5 group this is done to see how popularity group for high and low have significant interval rating number:

Table 2 Popularity group divided to 5 group

| Popularity Group | H-Test Popularity Group | Rating    |
|------------------|-------------------------|-----------|
|                  |                         |           |
| High             | Very High               | 4,5 – 5,0 |
|                  | High                    | 4,0 – 4,4 |
| Middle           | Middle                  | 3,0 – 3,9 |
| Low              | Low                     | 2,6 – 2,9 |
|                  | Very Low                | 1,0 – 2,5 |

\*Rating is based on zomato scoring for restaurant

Statistical analysis that this research used was kruskall-wallis test or H-test based on each restaurant distance to 3 urban functional unit; mall, hotel and CBD. H-test was conduct on 3 classification group; high, mid, and low in SPSS program [8]. Then using distance for each restaurant to analyzed accessibility and land use for each class by using proximity distance in Arc-GIS.

## RESULTS AND DISCUSSIONS

### Restaurant Distribution

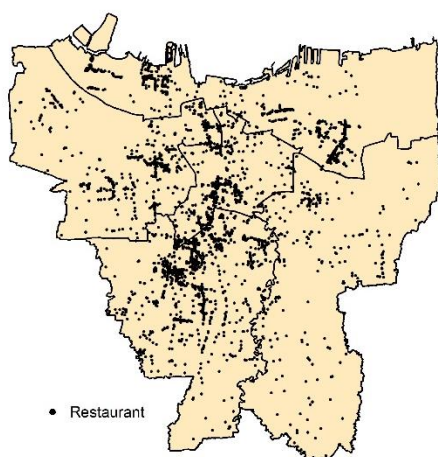


Fig. 3 Location of 4032 restaurant in Jakarta

Distribution for 4032 restaurant in Jakarta based on Zomato as seen in figure 3 and 4 that most restaurant was located in south, north, and central

Jakarta.

### Restaurant Distribution In Jakarta

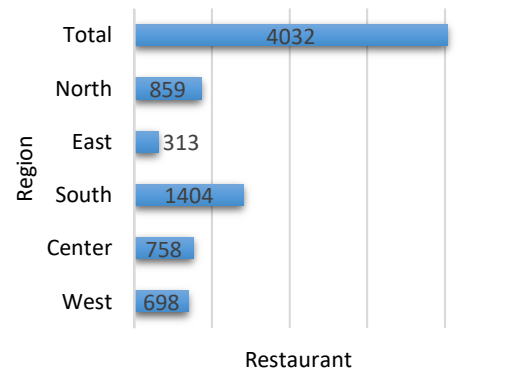


Fig. 4 Distribution for 4032 restaurant in Jakarta

### Popularity Distribution

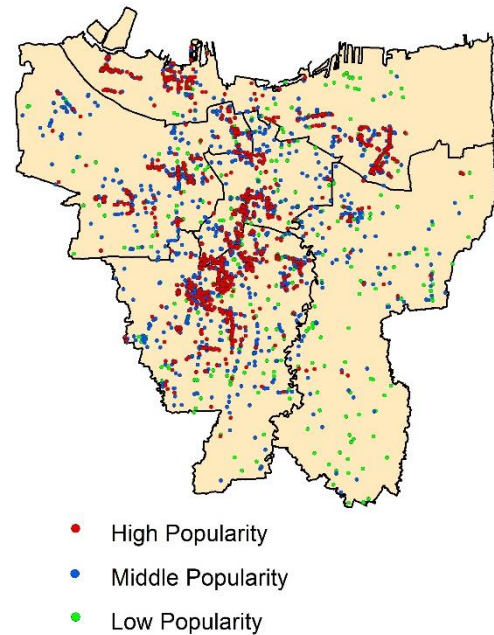


Fig. 5 Popularity group of restaurant in Jakarta

#### 4.2.1 High Popularity

High restaurant was located in center and south of Jakarta as seen in fig. 5. Using NNA as seen in figure 6 NNA that classify cluster this mean that restaurant with high popularity is cluster in Jakarta.

With KDA result as seen in fig. 7 we can see that dencity of high popularity group were between 0 to high as 59 restaurant/km<sup>2</sup>. Based on this analysis most of high popularity group were located in central and south with few in north and west Jakarta.

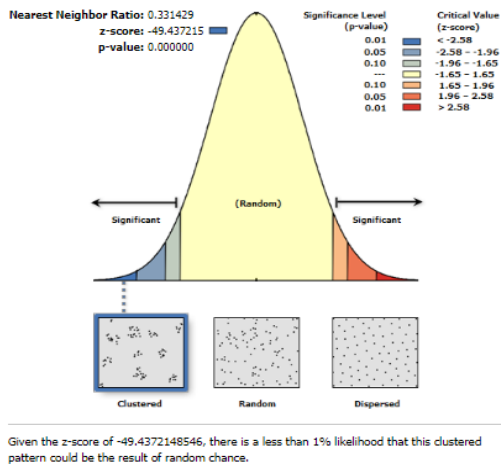


Fig. 6 NNA result for high popularity group in Jakarta

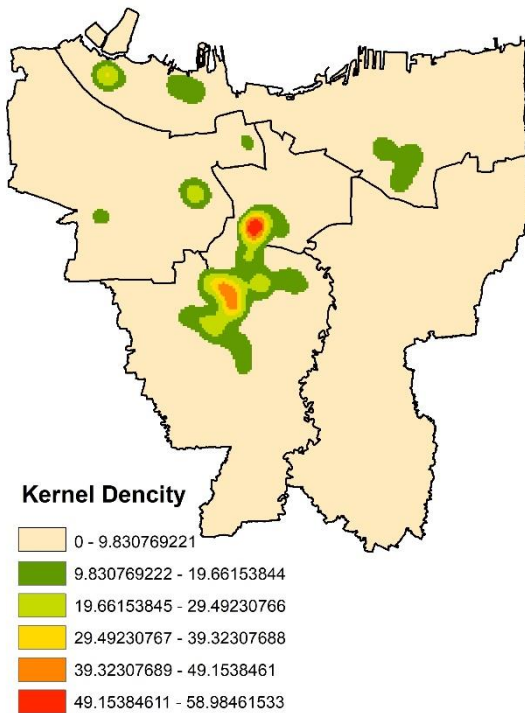


Fig. 7 KDA result for high popularity group in Jakarta

#### Middle Popularity

Mid popularity was located in center, south, north, west and very few in east Jakarta. Based on NNA result in fig 8 we can see that like high popularity group, mid popularity also had cluster classification. This mean that mid popularity restoran was cluster in Jakarta.

Based on NNA, that mid popularity group was cluster in Jakarta to see which region it was clustered then using KDA result in fig 9 we can see that density for mid popalrity was cluster in south, center, and

west with 0 to 28 restaurant/km<sup>2</sup>. North region also have density around 0 to 19 restaurant/km<sup>2</sup> and east region have the lowest density with 0 to 14 restaurant/km<sup>2</sup>.

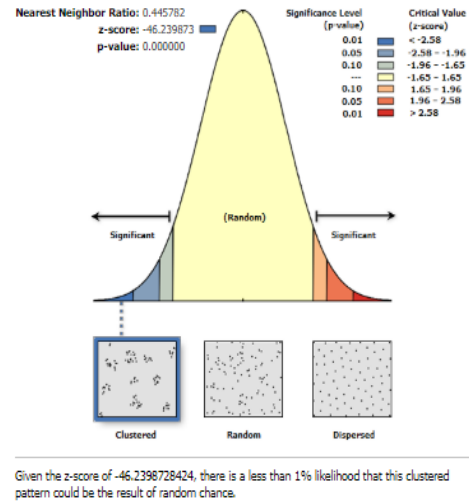


Fig. 8 NNA result for middle popularity group in Jakarta

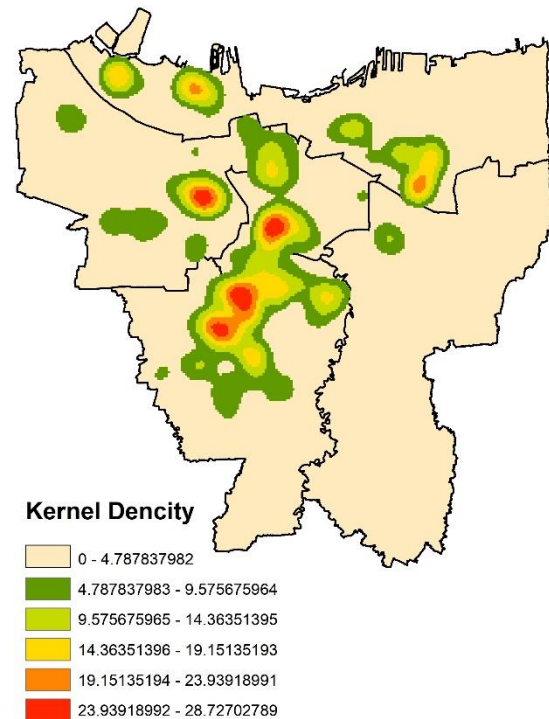


Fig. 9 KDA result for middle popularity group in Jakarta

#### Low Popularity

Low popularity restaurant was located spread across region in Jakarta. Based on NNA result in fig 10 we can see that low popularity restaurant also cluster in Jakarta but to analyzed this more deep by



using KDA as seen in fig 11 and the result was density for restaurant with low popularity group were 0 to 4 restaurant/km<sup>2</sup>. Although NNA result were cluster but with KDA results were very low density.

This means that low popularity group actually spread across all region in Jakarta and NNA result were to sensitive with how large the area.

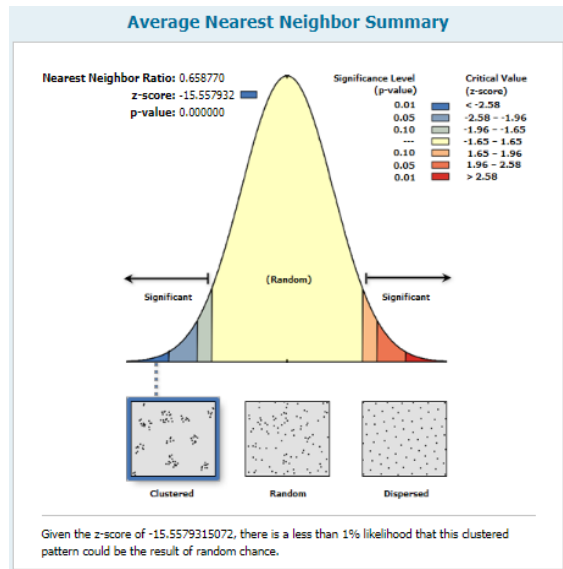


Fig. 10 NNA result for low popularity group in Jakarta

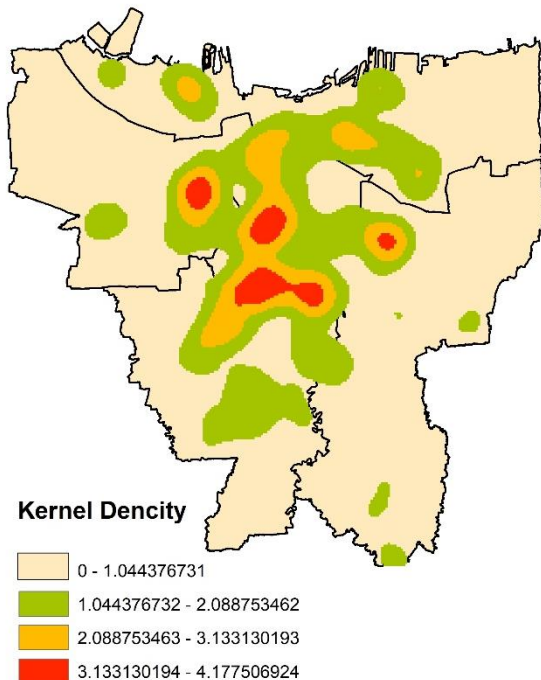


Fig. 11 KDA result for low popularity group in Jakarta

### Popularity Index Factor

Factor that affect popularity index; urban

functional unit, accessibility, and land use. Urban functional unit include shopping mall, hotel and CBD. Using statistical analysis, H-test or kruskal-wallis test in table 3 using spss software we can see that between 5 group popularity that distance for each restaurant to 3 urban functional unit was not the same or there is connection/relations between popularity group with their distance to urban functional unit.

Table 3 H-Test or Kruskal-Wallis test between popularity group with urban functional unit

| Hypothesis Test Summary |   |   |      |                             |
|-------------------------|---|---|------|-----------------------------|
|                         | Null Hypothesis   | Test                                    | Sig. | Decision                    |
| 1                       | The distribution of Mall is the same across categories of Popularitas.    | Independent-Samples Kruskal-Wallis Test | .000 | Reject the null hypothesis. |
| 2                       | The distribution of Hotel is the same across categories of Popularitas.   | Independent-Samples Kruskal-Wallis Test | .000 | Reject the null hypothesis. |
| 3                       | The distribution of CBDline is the same across categories of Popularitas. | Independent-Samples Kruskal-Wallis Test | .000 | Reject the null hypothesis. |

Asymptotic significances are displayed. The significance level is .05.

Connection between this variable were restaurant that closer to urban functional have more high popularity and the more far away from urban functional unit is more likely to have low popularity as seen in table 4. Interval 2 group that has been divided show that there is significant different but only in high popularity group.

Table 4 Rank H-Test based on their distance (meter)

### Kruskal-Wallis Test

| Ranks   |             |      |           |
|---------|-------------|------|-----------|
|         | Popularitas | N    | Mean Rank |
| Mall    | Very High   | 212  | 1637.96   |
|         | High        | 1282 | 1794.43   |
|         | Middle      | 1970 | 2123.73   |
|         | Low         | 514  | 2295.09   |
|         | Very Low    | 54   | 2211.19   |
|         | Total       | 4032 |           |
| Hotel   | Very High   | 212  | 1377.39   |
|         | High        | 1282 | 1752.63   |
|         | Middle      | 1970 | 2115.33   |
|         | Low         | 514  | 2507.58   |
|         | Very Low    | 54   | 2510.23   |
|         | Total       | 4032 |           |
| CBDline | Very High   | 212  | 1533.45   |
|         | High        | 1282 | 1854.42   |
|         | Middle      | 1970 | 2083.55   |
|         | Low         | 514  | 2333.29   |
|         | Very Low    | 54   | 2299.49   |
|         | Total       | 4032 |           |

Accessibility for each restaurant can have and impact on how popular that restaurant. By using arterial and collector road to see how distance

between 2 road with popularity for each restaurant we can see that affect the road to restaurant popularity.

Table 5 Accessibility for popularity group

| Popularity | Arterial | Collector | Mean<br>Distance<br>to<br>Arterial | Mean<br>Distance<br>to<br>Collector |
|------------|----------|-----------|------------------------------------|-------------------------------------|
| High       | 909      | 585       | 178.82<br>Meter                    | 471.71<br>Meter                     |
| Middle     | 982      | 988       | 505.08<br>Meter                    | 413.87<br>Meter                     |
| Low        | 283      | 285       | 583.95<br>Meter                    | 413.67<br>Meter                     |

Based on table 5 that high popularity are mostly close to arterial and low popularity closer to collector road. The last factor that affect popularity index was land use.

Table 6 Land use for popularity group

| Popularity | Business | Settlement | Religion | Social<br>Cultural | Other |
|------------|----------|------------|----------|--------------------|-------|
| High       | 1237     | 209        | 5        | 21                 | 22    |
| Mid        | 1456     | 349        | 5        | 41                 | 51    |
| Low        | 394      | 140        | 2        | 11                 | 21    |

Based on table 6 that 75% restaurant regarding their popularity were in business, and few were in settlement.

## CONCLUSIONS

Spatial distribution for popularity index restaurant in Jakarta for high popularity were cluster in center and south with high density up to 59 restaurant/km<sup>2</sup> and 28 restaurant/km<sup>2</sup> for mid in center, south and west. Low popularity restaurant were spread across all region in Jakarta with low density up to 4 restaurant/km<sup>2</sup>. Factor that affect popularity index are urban functional unit, accessibility and land use for business. The closer restaurant to this factor making

it have high chance to have high popularity and getting further it from this factor are more likely having low popularity restaurant.

## ACKNOWLEDGEMENTS

We would like to thank to Hibah PITTA 2019 (NKB-0626/UN2.R3.1/HKP.05.00/2019) have supported in funding of this research.

## REFERENCES

- [1] Su Jung Kim, Ewa Maslowska & Edward C. Malthouse. 2017. Understanding The Effects Of Different Review Features On Purchase Probability. *International Journal of Advertising*. Vol. 37, Issue 1, 29-53.
- [2] Liu, C., Su, C., Gan, B., & Chou, S. 2014. Effective Restaurant Rating Scale Development And A Mystery Shopper Evaluation Approach. *International Journal of Hospitality Management*. 43
- [3] Laurell, C., & Sandström, C. 2013. Value Creation And Appropriation In Social Media - The Case Of Fashion Bloggers In Sweden. In *Int. J. of Technology Management* (Vol. 61)
- [4] Chevalier, J. A., & Mayzlin, D. 2006. The Effect of Word of Mouth on Sales: Online Book Reviews. *Journal of Marketing Research*, 43(3), 345-354
- [5] Zhang, Z., Zhang, Z., & Law, R. (2014). Positive And Negative Word Of Mouth About Restaurants: Exploring The Asymmetric Impact Of The Performance Of Attributes. *Asia Pacific Journal of Tourism Research*, 19, 162-180
- [6] Zhai, Shixiao. Xu, Xiaolin. Yang, Lanrong. Zhou, Min. Zhang, Lu. 2015. Mapping The Popularity of Urban Restaurants Using Social Media Data. *Applied geography*, 63, 113-120
- [7] Myint, S. W. 2008. An Exploration of Spatial Dispersion, Pattern, And Association of Socio Economic Functional Units In An Urban System. *Applied Geography*, 28, 168-188
- [8] Silverman, B. W. 1998. *Density Estimation For Statistics and Data Analysis* (p. 48). London: Chapman & Hall/CRC

## EFFECT OF ELECTROLYZED REDUCING WATER ON CARBENDAZIM SOLUTION AND RESIDUES DEGRADATION OF CHERRY TOMATO (*Solanum lycopersicum* L. var. *cerasiforme*)

Wanwarang Pattanapo<sup>1,2</sup> Kanda Whangchai<sup>1,2,3</sup> Jamnong Uthaibutra<sup>1,2,3</sup> Tanachai Pankasemsuk<sup>1,2,4,5</sup>  
and Usawdee Chanasut<sup>1,2,3</sup>

<sup>1</sup>Postharvest Technology Research Center, Faculty of Agriculture, Chiang Mai University,  
Chiang Mai 50200, Thailand

<sup>2</sup>Postharvest Technology Innovation Center, Office of the Higher Education Commission,  
Bangkok 10400, Thailand

<sup>3</sup>Department of Biology, Faculty of Science, Chiang Mai University,  
Chiang Mai 50200, Thailand

<sup>4</sup>Department of Plant and Soil Sciences, Faculty of Agriculture, Chiang Mai University,  
Chiang Mai 50200, Thailand;

<sup>5</sup>International College of Digital Innovation, Faculty of Agriculture, Chiang Mai University,  
Chiang Mai 50200, Thailand

### ABSTRACT

The effect of electrolyzed reducing water (ER) on a degradation of carbendazim residues degradation of cherry tomato (*Solanum lycopersicum* L. var. *cerasiforme*) was investigated. Electrolyzed water was generated by electrolysis from 5% NaCl solution. The cherry tomato samples were washed in ER water at different concentrations (100, 250, 500 and 1000 mg/L) and in distilled water (control). The standard carbendazim solution (5 mg/L) was treated with the previous concentrations of ER. Reduction of residual carbendazim was determined by high performance liquid chromatography (HPLC) while liquid chromatography-quadrupole-time-of-flight mass spectrometer (Agilent, LC-6545 Q-TOF/MS) was used to determine the concentration of anions as major degradation products. It was found that all concentration of ER water significantly reduced carbendazim solution, compared to control. The ER water at 250 mg/L could effectively remove carbendazim residues from cherry tomato, most of the degradation occurred within 30 min. Residue of carbendazim on cherry tomato were reduced by 60.36%, 80.49%, 67.32%, and 64.68% after 30 min washing in ER 100 mg/L, 250 mg/L, 500 mg/L, and 1000 mg/L, respectively.

**Keywords:** *Electrolyzed reducing water, Carbendazim degradation and Cherry tomato*

### INTRODUCTION

Cherry tomato (*Solanum lycopersicum* L. var. *cerasiforme*) is one of the popular tomato varieties in Thailand which is locally consumed and exported. It is a small tomato with high nutritional value and can be consumed as fresh or processed tomato. The cherry tomato growers usually apply fungicides and insecticides many times until the fruit were harvested. As a result, there are excessive amounts of various of pesticides left on the fruits. The pesticide residue is an important problem and becomes seriously related to human health problems and hazardous to the environment. One of the serious problems of harvested tomato is pesticide residue over the Maximum Residues Limits (MRLs). Thai Pesticide Alert Network [1] also reported that 11.11% of tomato samples in Bangkok, Chiang Mai and Ubon Ratchathani province were contaminated with the pesticide residues over the MRLs. It was shown that pesticide residue mostly found in tomato was carbendazim. Carbendazim is a very active systemic broad spectrum fungicide. It is very cheap and

effective, so it is used extensively in each harvesting season to control fungal diseases. For example, it is used to prevent *Sclerotinia* stem rot (caused by *Sclerotinia sclerotiorum*) in various fruits, vegetables, and other plants [2]-[4]. Carbendazim is classed as a possible human carcinogen [5], [6]. It is persistent and very toxic and has been banned in Australia, USA and most European Union countries [7,8]. The MRLs for carbendazim in tomato is 0.5 mg/kg. The carbendazim residues in vegetables affects on the health of customers and causes huge downside for Thai clients and exporters. The residue problem comes from the inefficient processes of planting and cleaning raw materials. The most common practice for reducing contamination is using a sanitizer. Finding the appropriate process to eliminate chemical contaminant which has the least impact on human health and environment would be an ideal requirement. In the past, the researchers applied different techniques to reduce the pesticide residues such as washing with tap water or strong oxidizing agent e.g. ozone and chlorine dioxide.

Nowadays, the advanced oxidation processes (AOPs) have been proposed for removing pesticide residues from fruits and vegetables such as electrolyzed water. Various studies on the application of AOPs for the pesticide residue reduction have been reported electrolyzed water is a chlorine based solution produced by electrolyzing a diluted salt (usually NaCl) solution in an electrolytic chamber with anode and cathode. ER water is generated from the cathode side. It may also be able to reduce the residues through alkaline hydrolysis. Moreover, it was found that electrolyzed water is an effective treatment to degrade the insecticide residues on agricultural products. For example, Qi [9] suggested that ER water was effective in degrading phosmet and the longer treatment time resulted in the higher reductions of diazinon, cyprodinil, and phosmet. Jianxiong *et al.* [10] also found that using ER water in fresh spinach for 30 mins reduced acephate by 86%, omethoate by 75% and DDVP by 46%. In addition, Tamjapo *et al.* [11] indicated that chlopyrifos residues in yard long bean could be degraded using ER water for 30 min. Furthermore, Al-taher *et al.* [12] reported the effect of various washing treatments with a combination of the ultrasonication on acephate, malathion, carbaryl, bifenthrin, cypermethrin, permethrin, cyhalothrin, chlorothalonil, and imidacloprid removal from tomatoes. They found that removing of pesticides from tomato surface depended on the washing treatments e.g. washed with water, sodium hypochlorite, peroxyacetic acid, or Tween 20 with and without sonication.

Therefore, this study focused on the effect of ER water on the carbendazim fungicide removal from cherry tomato fruit.

## MATERIALS AND METHODS

### Plant Material

Organic cherry tomato fruit at a commercial harvesting stage was obtained from a local market, Chiang Mai Province, Thailand and was transported to the Postharvest Technology Research Center, Faculty of Agriculture, Chiang Mai University. It was carefully selected for uniformity in shape, color and size, and insect bites, blemished or diseased fruit was discarded.

### Chemicals Preparation

Standard carbendazim fungicide was purchased from Ehrenstorfer™ with 99.0% purity. Stock solution (1000 mg/L) for the residue analysis was prepared in acetone. The solution was diluted with distilled water to appropriate working concentration (5 mg/L).

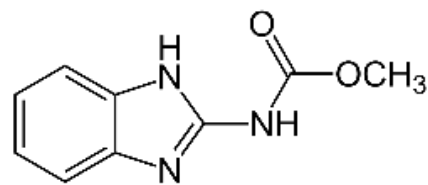


Fig. 1 Structure of carbendazim

### Electrolyzed Water Preparation

The ER water was generated by electrolyzing 5% NaCl solution by mixing 500 g NaCl in 10 liters of distilled water in an electrolytic chamber with anode and cathode. The electrodes were then subjected to a direct current of 8 A and 8 V using DC power source for 1 hour. The ER water was in the cathode side. The pH and Oxidation Reduction Potential (ORP) were measured using pH/ion meter. The properties of ER water were determined immediately after preparation. The physical and chemical parameters of ER water were pH 11.5, ORP 260 mV. The concentrations of ER water used in this study, were 100, 250, 500 and 1000 mg/L. Ten milliliters of standard carbendazim solution (5 mg/L) was added to 20 mL of ER water at the concentrations previously mentioned and distilled water (control). The removal percentages of each standard carbendazim fungicide sample were determined by high performance liquid chromatography (HPLC).

### Washing Treatments

One kilogram of cherry tomato was divided into 5 groups of 200 g each group were spiked with 5 mg/L carbendazim and 1% tween20 then air dried at room temperature. After that, the fruits were left to soak in different concentrations of ER water (100, 250, 500 and 1000 mg/L) and distilled water (control) for 30 min (without shaking). After treatment, all samples were air dried at room temperature for 1 hour before fungicide extraction.

### Analytical Method

The carbendazim residue in cherry tomato was extracted with the QuEChERS extraction kit (Agilent Quick, USA.) and homogenized according to Anastassiades *et al.* [13]. Tomato sample (15 g) was cut into small pieces and extracted with 15 mL acetonitrile in a 50 mL Teflon centrifuge tube. The Q-sep QuEChERS Extraction Salt was added, immediately shaken on a vortex mixer for 2 min. Then centrifuged at 4,000 rpm for 5 min.

Additionally, a clean-up step was conducted in the optimization procedure. After centrifugation step, the supernatant (about 5 ml) was transferred into a QuEChERS Dispersive SPE 15 mL. After shaking for

2 min and centrifugation at 8,000 rpm for 12 min, 1 mL of the supernatant was taken, filtered through a 0.45 µm nylon filter and injected into the LC-MS/MS system. The samples were analyzed with LC-6545 Q-TOF/MS, each analysis was done with 5 replicates.

For the LC analysis, an Agilent 1260 infinity II with a Poroshell 120 EC-C18 analytical column of 2.1 mm x 100 mm and 2.7 µm particle size was used. The mobile phases, A and B, were H<sub>2</sub>O + 5 mM NH<sub>4</sub> formate + 0.1% formic acid and MeOH + 5 mM NH<sub>4</sub> formate + 0.1% formic acid, respectively. The gradient program started with 95% of A for 1.5 min, changed to 5% (10 min) then followed by a return to the initial conditions within 5 min.

A liquid chromatography-quadrupole-time-of-flight mass spectrometer (Agilent, LC-6545 Q-TOF/MS) was used to analyze the mass spectrometry. The electrospray ionization (ESI) source was operated in positive ionization mode and its parameters were as follows: temperature: 150°C, gas flow of 10 L/min, nebulizer gas: 45 psig, capillary voltage: 3500 V. Nitrogen was served as the nebulizer and collision gas. The multiple reaction monitoring (MRM) was used, with a delta time of 1.0 min for each analyte.

### Statistical Analysis

The data were analyzed by SPSS 16.0, Significant difference was considered at  $p < 0.05$ .

## RESULTS AND DISCUSSION

It was found that the removal percentage of standard carbendazim was significantly increased at all concentration of ER applied, compared to control. ER water at 250 mg/L was the most effective concentration for removing carbendazim residues, the removal was 52.80%. Washing cherry tomato with ER water was more effective than washing with distilled water. Residue of carbendazim on cherry tomato were reduced by 60.36%, 80.49%, 67.32%, and 64.68% after 30 min washing in ER 100 mg/L, 250 mg/L, 500 mg/L, and 1000 mg/L, respectively (Fig. 2). Similarly, Tamjapo *et al.* [11] reported that treatment of yard long bean with ER water 250 mg/L for 30 min could degrade chlorpyrifos residues. It was also found that the ER water could be used as a cleaning solution to reduce pesticide residues in fruits and vegetables; for example, cabbage, leek [10], beans, grapes [14], and cowpea [15].

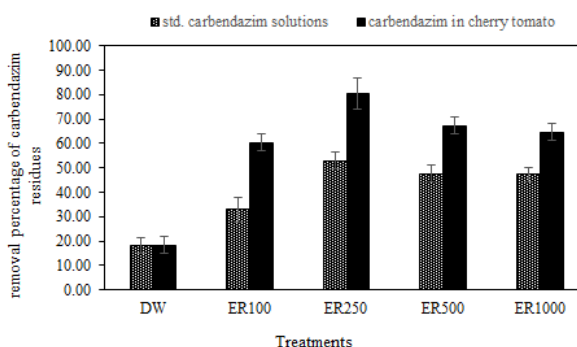
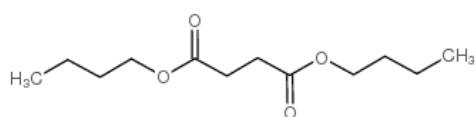


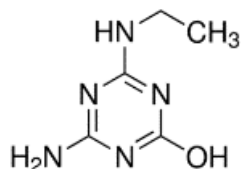
Fig. 2 Removal percentage of standard carbendazim solution and carbendazim in cherry tomato after ER water treatment at different concentrations

Table 1 Degradation product of Standard carbendazim after treatment of ER water

| Treatments      | Compound name                  | measured mass (m/z) |
|-----------------|--------------------------------|---------------------|
| DW<br>(control) | dibutyl succinate              | 253                 |
| ER100           | dibutyl succinate              | 253                 |
| ER250           | -                              | -                   |
| ER500           | atrazine-<br>desisopropyl-2-OH | 173                 |
|                 | dibutyl succinate              | 253                 |
| ER1000          | atrazine-<br>desisopropyl-2-OH | 173                 |



(a)



(b)

Fig.3 Structure of dibutyl succinate (a) and atrazine-desisopropyl-2-OH (b)

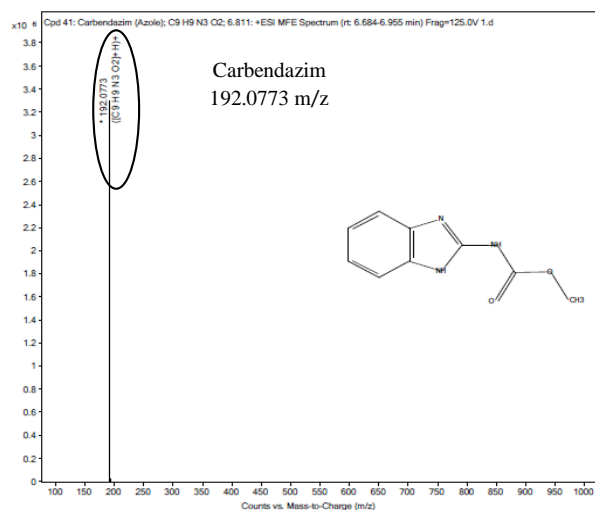


Fig.4 Mass spectrum of carbendazim

The degradation products that found in each treatment of standard carbendazim were dibutyl succinate and atrazine-desisopropyl-2-OH (Table 1 and Fig.3). The fragment ion at  $m/z$  192 was from molecular ions of carbendazim (Fig.4). After treatment with the various concentrations of ER water, the fragment ion at  $m/z$  192 was loss. It found dibutyl succinate after washing in distilled water, ER 100 mg/L and ER 500 mg/L, but it could not found in ER 1000 mg/L. However, after washing in ER 1000 mg/L and ER 500 mg/L found atrazine-desisopropyl-2-OH. Anywise, in ER 100 mg/L could not found the degradation product. The fragment ion from the 2 degradation product are shown in Table 1 and Figs.5-8. In Michale *et al.* [16] studied in skin of tomato that wash with methanol for remove the white powder, found the ion trap MS/MS analysis in carbendazim was  $m/z$  192 as in these studied. They mentioned that

the ion trap MS/MS analysis of the  $m/z$  192 resulted in a  $m/z$  160 ion with a loss of methanol. This loss is consistent with the structure of carbendazim and which the accurate mass neutral loss from  $m/z$  192 to 160. There are carbendazim-methanol (160  $m/z$ ), buprofezin (306  $m/z$ ), buprofezin fragment ion (201  $m/z$ ), thiophanate methyl (343  $m/z$ ), thiophanate methyl minus methanol (311  $m/z$ ) and basic thiophanate fragmentation (151  $m/z$ ). But in this study, there found dibutyl succinate (253  $m/z$ ), atrazine-desisopropyl-2-OH (173  $m/z$ ) and butopyronoxyl (244  $m/z$ ) were detected.

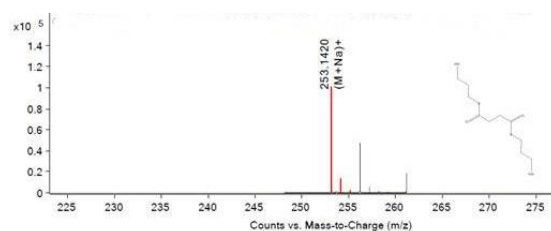


Fig.5 Mass spectrum of dibutyl succinate after treatment of carbendazim with distilled water (DW)

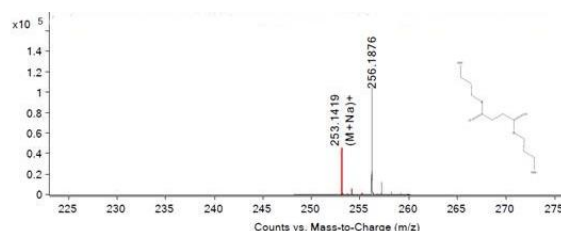
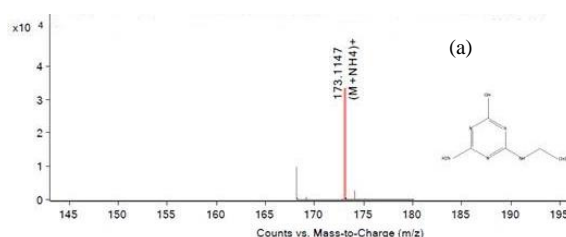
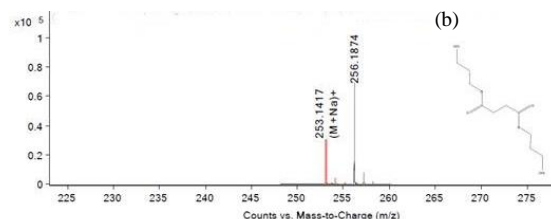


Fig.6 Mass spectrum of dibutyl succinate after treatment of carbendazim with ER water 100 mg/L (ER100)



(a)



(b)

Fig.7 Mass spectrum of atrazine-desisopropyl-2-OH (a) and dibutyl succinate (b) after treatment of carbendazim with ER water 500 mg/L (ER500)

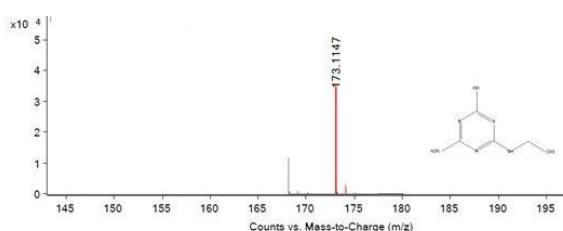


Fig.8 Mass spectrum of atrazine-desisopropyl-2-OH after treatment of carbendazim with distilled water, ER water 100 mg/L, 250 mg/L, 500 mg/L and 1000 mg/L (ER1000)

## CONCLUSIONS

ER water at 250 mg/L could effectively remove carbendazim residues from cherry tomato, most of the degradation occurred within 30 min. This study demonstrated the ER water could be used to reduced cabendazim residues on tomato and have a positive impact on ensuring safety of tomatoes for consumption. Further studies are also needed to investigate the degradation mechanism and possible disinfection of by-products after ER washing.

## ACKNOWLEDGMENTS

We would like to thank the Postharvest Technology Research Center and Department of Plant and Soil Sciences, Faculty of Agriculture, Chiang Mai University; Department of Biology, Faculty of Science, Chiang Mai University and The Graduate School Chiang Mai University, Chiang Mai, Thailand for providing research facilities; Postharvest Technology Innovation Center, Office of the Higher Education Commission, Bangkok, Thailand for a research fund.

## REFERENCES

- [1] Thai Pesticide Alert Network. 2016. Surveillance of pesticide residues in fruits and vegetables on 2016. [Online]. Available: [http://www.thaipan.org/sites/default/files/file/pesticide\\_doc24\\_press\\_4\\_5\\_2559.pdf](http://www.thaipan.org/sites/default/files/file/pesticide_doc24_press_4_5_2559.pdf) (15 May 2018).
- [2] Ma, H. X., Yu, C., Wang, J. X., Yu, W. Y., Tang, Z. H., Chen, C. J. Activity of carbendazim, dimethachlon, iprodione, procymidone and boscalid against sclerotinia stem rot in jiangsu province of China. *Phytoparasitica*, Vol. 37(5), 2009, pp.421-429.
- [3] Tortella, G. R., Mella-Herrera, R. A., Sousa, D. Z., Rubilar, O., Briceno, G., Parra, L. Carbendazim dissipation in the biomixture of on-farm biopurification systems and its effect on microbial communities. *Chemosphere*, Vol. 93(6), 2013, pp.1084-1093
- [4] Devi, P. A., Paramasivam, M., and Prakasam, V. Degradation pattern and risk assessment of carbendazim and mancozeb in mango fruits. *Environmental Monitoring and Assessment*, Vol. 187, 2015, pp. 1-6.
- [5] Goodson, W. H., Lowe, L., Carpenter, D. O., Gilbertson, M., Ali, A. M., de Cerain Salsamendi, A. L. Assessing the carcinogenic potential of low-dose exposures to chemical mixtures in the environment: The challenge ahead. *Carcinogenesis*, Vol. 36(1), 2015, pp. 254-296
- [6] Selmanoglu, G., Barlas, N., Songür, S., and Koçkaya, E. A. Carbendazim-induced haematological, biochemical and histopathological changes to the liver and kidney of male rats. *Human and Experimental Toxicology*, Vol. 20(12), 2001, pp. 625.
- [7] Huan, Z., Luo, J., Xu, Z., & Xie, D. Acute toxicity and genotoxicity of carbendazim, main impurities and metabolite to earthworms (*eisenia foetida*). *Bulletin of Environmental Contamination and Toxicology*, Vol. 96(1), 2016, pp. 62-69.
- [8] Zhang, X., Huang, Y., Harvey, P. R., Li, H., Ren, Y., Li, J., Wang, J. and Hetong Y. Isolation and characterization of carbendazim-degrading *Rhodococcus erythropolis* djl-11. *PLoS One*, Vol. 8(10), 2013, pp. e74810.
- [9] Qi, H. Efficacy of electrolyzed water in degrading and removing pesticide residues on fresh produce. M.S. Thesis. Faculty of the University of Georgia, Georgia, 2015, 122 pp.
- [10] Jianxiong H., Wuyundalai, H. Liu, T. Chen, Y. Zhou, Y. Su, and Lite L. reduction of pesticide residues on fresh vegetables with electrolyzed water treatment. *Journal of Food Science* Vol. 76, Nr. 4, 2011, C520- C524.
- [11] Tamjapo, A., J. Uthaibutra, and K. Whangchai. Effect of electrolyzed oxidizing and reducing water on the reduction of pesticide residue and microbial contamination in yardlong bean. *Agricultural Science Journal*, Vol.47 (3) (Suppl), 2016, pp. 39-42.
- [12] Al-taher, F., C. Yang, W. Philip and C. Jack. Reduction of pesticide residues in tomatoes and other produce. *Journal of Food Protection*, Vol. 76(3), 2013, pp. 510-515.
- [13] Anastassiades, M., S.J. Lehotay, D. Stajnbaher and F.J Schenck. Fast and easy multiresidue method employing acetonitrile extraction/partitioning and “dispersive solid-phase extraction for determination of pesticide residue in produce. *Journal of AOAC International*, Vol. 86(2), 2003, pp. 412-431.
- [14] Qi, H., Q. Huang, and Hung Y.C. Effectiveness of electrolyzed oxidizing water treatment in removing pesticide residues and its effect on produce quality, *Food Chemistry*, Vol. 239, 2018, 561–568.
- [15] Han, Y., L. Song, Q. An, and Pan C. Removal of



- six pesticide residues in cowpea with alkaline electrolyzed water, *Journal of the Science of Food and Agriculture*, Vol. 97, 2017, pp. 2333–2338.
- [16] Michael E. T, I. Ferrer, Amadeo R. F. Matching unknown empirical formulas to chemical structure using LC/MS TOF accurate mass and database searching: example of unknown pesticides on tomato skins, *Journal of Chromatography A*, Vol. 1067, 2005, pp.127-134

## EFFECT OF FRUIT BAGGING ON QUALITIES OF PUMMELO CV. KAO NAM PHEUNG AND KAO YAI

Yaowarat Wongsrisakulkaew, Chanpen Chaimongkol and Niyom Buaban  
Faculty of Agricultural Technology, Rajamangala University of Technology Thanyaburi, Thailand

### ABSTRACT

The effect of fruit bagging on qualities of pummelo cv. Kao Nam Pheung and Kao Yai. The aim of this work was to study fresh weight, circumference of fruit, peel thickness, the color value ( $L^*$ ,  $a^*$ ,  $b^*$ ) of peel and internal qualities. The experimental design was CRD (Completely Randomized Design) with 5 treatments and 4 replications include newspaper bags, commercial bags, nylon bags and plastic bags compared with non-bagging treatment. This experiment was conducted in farmer's orchard at Sam Phran, Nakhon Pathom province and Amphawa, Samut Songkhram province, Thailand. The results showed that the bagging in both cultivar had no effect on color value of peel at harvesting stage. The bagging in pummelo cv. Kao Nam Pheung had effect on the total soluble solids (TSS). Also, there was not difference on fresh weight, circumference and peel thickness. The bagging could be improved the peel quality of pummelo fruit for export.

*Keywords: Pummelo, Bagging, Fruit Quality, Kao Nam Pheung, Kao Yai*

### INTRODUCTION

Pummelo (*Citrus maxima* L. Osbeck) is referred to a type of giant citrus fruit and parent of many citrus fruits such as grapefruits and tangelos and belongs to the family Rutaceae [1]. It is native of southern Asia and Malaysia [2] although, [3] reported that pummelo is a native of Asia especially in China (primary centre of origin), southern Japan, Vietnam, Malaysia, Indonesia and Thailand (secondary centre)[3],[4]. Pummelo has been regarded as one of the ancestral species as well as important commercial fruit tree under the genus *Citrus* [5]. Pummelo is one of the favorite fruits of the many people because of its delicious taste and high nutritional value. The fruit is a good source of vitamins C, B1, B2 and B12 and protein as well as an excellent source of water, fat, carbohydrates, vitamin A, and niacin [6]-[8]. It is also excellent source of antioxidant flavonoids, potassium, phosphorus, folic acid, citric acid, etc. [9],[10]. Many of the outstanding cultivars from Thailand have been introduced to other countries, commonly with the terms "Siamese" and "Bangkok" attached to their names. Some common cultivars are the 'Tongdee' (brilliant gold pomelo), 'Kao Nam Pueng' (white honey pomelo) [11]. 'Khao Paen', 'Khao Phuang', 'Khao Yai', 'Khao Taengkwa', and 'Tha Khoi' [12]. It has good market potential and of low perishability allowing for distant transport to overseas consumers.

The problem of pummelo fruit is not only assimilate requirement for fruit growth but also the fruit external and internal quality. The most important of external quality improvement is fruit appearance. One of the technique to improve the fruit appearance is bagging. Bagging could reduced pests attack and improved fruit quality on guava [13]. Grapefruit

bagged by black paper could change the peel color and had influence on TSS/TTA ratio [14].

### OBJECTIVE

The aims of this research were to evaluate effect of fruit bagging and their relationship on quality of pummelo fruit for export.

### METHODOLOGY

The 5 years old of pummelo cv. Kao Nam Pheung and Kao Yai tree grown at Sam Phran, Nakhon Pathom province and Amphawa, Samut Songkhram province, Thailand was used for the experiment. Laboratory analysis has been conducted at the Division of Crop Production, Faculty of Agricultural Technology, Rajamangala University of Technology Thanyaburi.

### Time of Bagging

Bagging was done during the 3<sup>rd</sup> months of fruit pummelo.

### Experimental Design

This study used a Completely Randomized Design with 5 treatments and 4 replications include newspaper bags, commercial bags, nylon bags and plastic bags compared with non-bagging treatment. The experimental data were analyzed using analysis of variance at level  $\alpha = 5\%$ , followed by Duncan Multiple Range Test (DMRT) at level  $\alpha = 5\%$

monitoring was regularly done on weekly basis. Observation on the occurrence of other insect pests was also undertaken.

### Harvesting and Evaluation

Fruits were harvested at 160-170 days from fruit set. The following were recorded and evaluated:

- 1) The quality of fruit: fruit weight, circumference, diameter, peel thickness and total soluble solids (TSS)
- 2) Pigments and color of fruit peel

## RESULTS AND DISCUSSION

### Kao Nam Pheung Pummelo

Observations on pummelo fruit in the field showed that the bagging in pummelo cv. Kao Nam Pheung was not difference on circumference and peel thickness and the total soluble solids (TSS)(Table 1). The bagging in pummelo cv. Kao Nam Pheung had effect on diameter and fruit weight (Table 2). Fruit peel color indicated by the lightness (L) and color value of peel. The bagging in pummelo cv. Kao Nam Pheung had no effect on color value of peel at harvesting stage (Table 3). However, comparison of the lightness among five treatments found that the maximum average of the lightness was the bagging commercial bags.

Table 1 The quality of pummelo fruit cv. Kao Nam Pheung.

| Treatment       | Fruit weight (kg) | Circumference (cm) | Peel thickness (cm) |
|-----------------|-------------------|--------------------|---------------------|
| Control         | 1.32 ab           | 46.93              | 1.53                |
| Newspaper bags  | 1.23 b            | 47.50              | 1.53                |
| Plastic bags    | 1.30 ab           | 48.20              | 1.70                |
| Commercial bags | 1.63 a            | 52.03              | 1.88                |
| Nylon bags      | 1.30 ab           | 47.85              | 1.88                |
| F-test          | **                | ns                 | ns                  |
| CV (%)          | 11.34             | 4.65               | 21.85               |

Means followed by the same letter at the same column were not significantly different at the 5% level by DMRT.

\*\* = significant different at  $P < 0.01$

ns = not significantly

Table 2 The quality of pummelo fruit cv. Kao Nam Pheung.

| Treatment       | Diameter (cm) | TSS (°Brix) |
|-----------------|---------------|-------------|
| Control         | 14.35 b       | 12.70       |
| Newspaper bags  | 15.25 ab      | 12.00       |
| Plastic bags    | 15.10 ab      | 12.80       |
| Commercial bags | 16.68 a       | 12.63       |
| Nylon bags      | 15.38 a       | 13.40       |
| F-test          | **            | ns          |
| CV (%)          | 5.44          | 10.26       |

Means followed by the same letter at the same column were not significantly different at the 5% level by DMRT.

\*\* = significant different at  $P < 0.01$

ns = not significantly

Table 3 The color value (L, a, b) of fruit peel

| Treatment       | L     | a      | b     |
|-----------------|-------|--------|-------|
| Control         | 54.26 | -9.67  | 67.20 |
| Newspaper bags  | 52.96 | -10.12 | 59.90 |
| Plastic bags    | 53.84 | -8.95  | 60.59 |
| Commercial bags | 56.73 | -9.33  | 59.08 |
| Nylon bags      | 56.72 | -7.02  | 58.37 |
| F-test          | ns    | ns     | ns    |
| CV (%)          | 8.58  | 29.22  | 12.49 |



Control plastic bags commercial bags newspaper bags nylon bags

Fig. 1 The peel quality of pummelo fruit cv. Kao Nam Pheung.

### Kao Yai Pheung Pummelo

Fruit quality consist of the external and internal quality. External quality fruit include fruit weight, circumference, peel thickness and diameter. Internal quality include juice content and TSS. The bagging in pummelo cv. Kao Yai was not difference on fruit

weight, circumference and peel thickness (Table 4). Sweetness of fruit indicated by TSS, it was not affected by the bagging there was not difference on diameter and TSS (Table 5). The results showed that the bagging in both cultivar had no effect on color value of peel at harvesting stage (Table 6). The bagging could be improved the peel quality of pummelo fruit cv. Kao Yai (Fig 2).

Table 4 The quality of pummelo fruit cv. Kao Yai

| Treatment       | Fruit weight (kg) | Circumference (cm) | Peel thickness (cm) |
|-----------------|-------------------|--------------------|---------------------|
| Control         | 1.71              | 54.20              | 1.86                |
| Newspaper bags  | 1.43              | 48.80              | 1.58                |
| Plastic bags    | 1.61              | 50.80              | 1.68                |
| Commercial bags | 1.74              | 51.60              | 1.60                |
| Nylon bags      | 1.47              | 49.60              | 1.70                |
| F-test          | ns                | ns                 | ns                  |
| CV (%)          | 16.82             | 5.97               | 17.25               |

Table 5 The quality of pummelo fruit cv. Kao Yai

| Treatment       | Diameter (cm) | TSS (°Brix) |
|-----------------|---------------|-------------|
| Control         | 16.34         | 12.26       |
| Newspaper bags  | 15.44         | 11.36       |
| Plastic bags    | 16.04         | 12.40       |
| Commercial bags | 14.46         | 12.24       |
| Nylon bags      | 15.38         | 11.94       |
| F-test          | ns            | ns          |
| CV (%)          | 12.96         | 8.90        |

Table 6 The color value (L, a, b) of fruit peel

| Treatment       | L     | a      | b     |
|-----------------|-------|--------|-------|
| Control         | 54.08 | -11.77 | 59.67 |
| Newspaper bags  | 55.72 | -8.68  | 54.72 |
| Plastic bags    | 55.08 | -9.53  | 56.00 |
| Commercial bags | 55.30 | -8.81  | 48.58 |
| Nylon bags      | 51.31 | -8.82  | 54.63 |
| F-test          | ns    | ns     | ns    |
| CV (%)          | 6.43  | 18.88  | 14.64 |



Fig. 2 The peel quality of pummelo fruit cv. Kao Yai.

Fruit peel color indicated by the lightness (L) and color value of peel. (Table 3 and 6). The color value of peel showed the reflection color of fruit peel. The bagging bag treatment have no significant effect on the lightness of the peel (L) but effect on the color value of peel. Interaction between L a and b was significantly affected by carotenoid content and peel color. Insect pests were also observed in control fruits (without bagging treatment) (Figure 1 and 2). Scale insect infestation was observed in all bagged treatments. Fruitfly infestation was not observed on fruits bagged with newspaper, commercial bag and plastic bag. Mealybug infested the fruits bagged with nylon bag. Bagging could reduced pests attack and improved fruit quality similar result was reported on guava [13].

## CONCLUSIONS

Bagging could be improved the peel quality of pummelo fruit cv. Kao Nam Pheung and Kao Yai for export. Insect pests can be controlled by bagging at pre-bloom stage because it is in this stage that the said pest starts infestation. It is recommended to bag pummelo fruits to prevent or minimize the use of pesticides for the control of insect pests infestation thereby enhances production of good quality and pesticide-free pummelo fruits at reduced cost. Pesticide free fruits also can command premium price. However, the use of bagging material is limited to a smaller scale of pummelo plantings.

## ACKNOWLEDGMENTS

The author would like express thanks to RMUTT for providing the research fund.

## REFERENCES

- [1] Scora R.W. 1975. On the history and origin of citrus. Bull. Torrey Bot. Club. 102: 369-375.
- [2] Purseglove J.W. 1968. Tropical Crops. Dicotyledons. 502 p.

- [3] Burana-osota J., Soonthornchareonnonb N., Chaidegumjorna A., Hosoyamac S., Toidac T. 2010. Determination of galacturonic acid from pomelo pectin in term of galactose by HPAEC with fluorescence detection. *Carbo. Poly.* 81: 461-465.
- [4] Min Y.Y. 1997. Study on the diverse centre of origin of pummelo germplasms. *China Citrus.* 26(1): 3-5.
- [5] Verdi A. 1988. Application of recent taxonomical approaches and new techniques to citrus breeding, Balaban Publishers.
- [6] Rahman M.M., Rabbani M.G., Khan A.S.M.M.R., Ara N., Rahman M.O. 2003. Study on physio- morphological characteristics of different local pummelo accessions. *Pakistan J. Bio. Sci.* 6(16): 1430- 1434.
- [7] Xu G., Liu D., Chen J., Ye X., Ma Y., Shi J. 2008. Juice components and antioxidant capacity of citrus varieties cultivated in China. *Food Chem.* 106: 545-551.
- [8] Gopalan C.B., Sastri B.V.R., Balasubramaniam S.C. 2000. Nutritional value of Indian food. National Institute of Nutrition, Indian Council of Medical Research, Hyderabad, India.
- [9] Tsai H.L., Chang S.K.C., Chang S.J. 2007. Antioxidant content and free radical scavenging ability of fresh red pummelo (*Citrus grandis* (L.) Osbeck) juice and freeze-dried products. *J. Agri. Food Chem.* 55: 2867-2872.
- [10] Igual M., Martinez E.G., Camacho M.M., Navarrete N.M. 2010. Effect of Thermal Treatment and Storage on the Stability of Organic acids and the Functional value of Grapefruit juice. *Food Chem.* 118: 291-299
- [11] Tongdee, S.C. n.d. Impact on farming practices of producing pummelos under the Nakornchaisri geographical indication. Retrieved October 26, 2010 from <http://www.foodquality-origin.org/documents/Nakhonchaisri.pdf>.
- [12] Chomchalow, N., Somsri, S. and P.N. Songkhla. n.d. Market trends and export of Thai fruits. Retrieved October 26, 2010 from <http://www.itfnet.org/gfruit/Slides/Session%201/Market%20Trends%20and%20Export%20of%20Thai%20Fruits.pdf>
- [13] Harach, S. and K. Wanichkul, 2006. Influences of bagging methods on fruit quality of guava (*Psidium guajava* L.) cv. Yen Song. *Kamphaengsaen Acad. J.*, 4: 41-47.
- [14] Hwang, A.S., K.L. Huang and S.H. Hsu, 2004. Effect of bagging with black paper on coloration and fruit quality of Ruby grapefruit. *J. Agric. Res. China*, 53: 229-238.

## EFFECT OF ELECTROLYZED OXIDIZING WATER AND ULTRASONICATION ON PATHOGENIC CONTROL OF FRESH TURMERIC (*Curcuma longa* L.)

Santirote Keatsirirote<sup>1,2</sup> Angkhana Chuajedton<sup>4</sup> Jamnong Uthaibutra<sup>1,2,3</sup> and Kanda Whangchai<sup>1,2,3</sup>

<sup>1</sup>Postharvest Technology Research Center, Faculty of Agriculture,  
Chiang Mai University, Chiang Mai 50200, Thailand

<sup>2</sup>Postharvest Technology Innovation Center, Office of the Higher Education Commission,  
Bangkok 10400, Thailand

<sup>3</sup>Department of Biology, Faculty of Science, Chiang Mai University, Chiang Mai 50200, Thailand

<sup>4</sup>Department of Biology, Faculty of Science, Lampang Rajabhat University, Lampang 52100, Thailand

### ABSTRACT

Effect of electrolyzed oxidizing water (EO) and ultrasonic (US) waves on a pathogenic control of fresh turmeric (*Curcuma longa* L.) were studied. Electrolyzed water was generated by electrolysis from 5% NaCl solution, which produced the EO water. The fresh turmeric samples were washed with EO solution at different concentrations (0, 100, 200, 300 and 400 mg/L residual chlorine) and ultrasonic waves (43 and 1000 kHz.). The percentage of redact of total bacteria, yeast and mold and *Escherichia coli* was counted with the determined by compact dry plate. It was found that pathogenic control of fresh turmeric increased with EO all concentrations and ultrasonication.

**Keywords:** *Electrolyzed oxidizing water, Pathogenic control, Turmeric and ultrasonic wave*

### INTRODUCTION

Turmeric (*Curcuma longa* L.) is an edible and medicinal plant is the family Zingiberaceae, known as Indian saffron. Turmeric rhizome when dry and ground provides a yellow and flavorful powder, used for natural coloring agent in food, cosmetic and textile. Also flavoring compounds as insect repellent and medicine. Recently, it has been valued worldwide as a functional food, due to its health promoting properties. Turmeric has been used as antioxidant, digestive, anti-microbial, anti-inflammatory and anti-carcinogen [1].

Thailand is one of the turmeric major exporter country. [2,3]. However, the major problem of fresh turmeric is the microbial contamination during harvest [4]. Naruemon and Dariwan [5] reported that the contamination of turmeric was due to mold 40.45% and *Escherichia coli* 62.34%. Postharvest disease control can be done with many methods, such as chemical disinfection, hot water treatment or washing with clean water. Washing fresh turmeric with hot water is recommended in many countries, such as India [6]. In Thailand, the harvested turmeric distributed in markets are washed with clean water only. Normally, fungi and bacteria present in the packing-house and in the field after harvest. Moreira [7] reported that the symptoms of rot ginger (*Zingiber officinale* Roscoe) rhizomes in Brazil was caused from *Fusarium oxysporum* 74% . Recently, electrolyzed water (EO) has been reported to have strong anti-bacterial effects on most

pathogenic bacteria [8]. Electrolyzed water is powerful bactericidal effects and is applied in a wide range of fields, including aquaculture, agriculture and food industry [9,10]. Buck [11] reported that electrolyzed water used to treat 22 fungal species significantly reduced growth of the thin-walled species (e.g., *Botrytis* and *Monilinia*) within 30 seconds. Additionally, it significantly reduces growth of the thicker-walled, pigmented fungi, *Curvularia* and *Helminthosporium* within 2 minutes or less. In addition, Deza [12] found that tomato peel treated with electrolyzed water resulted in a decline of bacteria such as *Escherichia coli* 0157:H7, *Salmonella enteritidis* and *Listeria monocytogenes*, without any effect on the environment. Hung [13] reported that electrolyzed water treatment on strawberries and broccoli significantly reduced *E. coli* 0157:H7. Paola [14] found that washing lettuce with electrolyzed water for 5 minutes significantly inhibited the growth of *L. monocytogenes*. Guentzel [15] also found that spraying electrolyzed water at the surfaces of food service areas on spinach and lettuce reduced the growth of microbial. Whangchai [16] found that electrolyzed water treatment on tangerine cv. Sai Nam Pung at a free chlorine concentration of 215 ppm for 120 and 240 seconds completely inhibited the growth and development of *Penicillium digitatum*. In addition, Whangchai [17] found that washing orange with electrolyzed water and exposure to ozone gas for 2 hours per day significantly controlled *P. digitatum*. Ultrasonic

(US) waves have been used in postharvest treatment to reduce decay incidence and maintain the quality of fruits and vegetables. The high power ultrasound wash water decontamination process in the fruits and vegetable industry is effective to decrease of foodborne outbreaks [18]. Ultrasound treatment has been reported to be effective in food processing and preservation, such as cleans surfaces, inactivation of microorganisms and enzymes, disruption of cells [19]. Thus, the objective of this research was to determine the effect of electrolyzed oxidizing water with ultrasonication on pathogenic control of fresh turmeric.

## MATERIALS AND METHODS

### The plant materials

Fresh turmeric (*Curcuma Longa* L.) was collected from a commercial turmeric farm in Mae-Tang, Chiang Mai Province, Thailand and transported to the Postharvest Physiology Research Laboratory at Chiang Mai University within 3 hrs. Fresh turmeric rhizomes (50 gram) were sampled for each replicates. All experiments were designed as a Completely Randomized Design (CRD) and each treatment was done in triplicate.

### Preparation of electrolyzed water

Electrolyzed water (EO) generated by electrolysis in a cell with positively and negatively charged titanium electrodes separated by a polypropylene membrane. The electrodes were subjected to a direct current of 8 volts. A 5% NaCl solution was added into the above system (Fig. 1). The pH of EO water was recorded with pH/ion meter. Free-chlorine concentration was determined by using N,N-diethyl-P-phenylene diamine (DPD) test and oxidation-reduction potential (ORP) was measured by pH/ ORP meter.

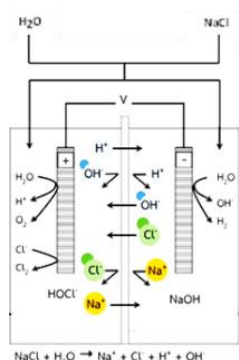


Fig. 1 Schematics of electrolyzed water generator. (Huang [20] )

### Preparation of ultrasonication

Ultrasonic wave (US) devices with the input power of 3 watts and 2 frequencies of 43 and 1000 kHz, (Honda Electronics Company, Toyohashi, Aichi, Japan) were utilized for 3 replications. A polyethylene cylinder reactor, 10 cm in diameter, equipped with a transducer at the lower part was used.

### Effect of electrolyzed water on microbial growth inhibition

The fresh turmeric (50g of each replication) was immersed into 450 ml of electrolyzed water at different concentrations (0, 100, 200, 300 and 400 mg/L residual chlorine) for 10 minutes and then the samples were subjected to microbiologically analyzed by putting 25g fresh turmeric into 225ml sterile 0.1% peptone and homogenizing in a stomacher blender for 2 min and 30 second for gravitation. Serial ten-fold dilution of the homogenate was down in 0.1% peptone. One milliliter of each dilution was dropped onto compact dry plate (R-Biopharm AG Company, Darmstadt, Germany) All the plates were incubated at 37°C for 24 hr for total plate counts, and *E. coli* and incubated at room temperature 28±2°C for 72 hr for yeast and mold.

### Effect of electrolyzed water and ultrasonic wave on microbial growth inhibition

The fresh turmeric (50g) was immersed into 450 ml of electrolyzed water at different concentrations (0, 100 and 200 mg/L residual chlorine) combined with ultrasonic wave 43 and 1000 kHz for 10 minutes the samples were microbiologically analyzed fresh turmeric. 25g from each treatment was put into 225ml sterile 0.1% peptone and homogenized in a stomacher blender for 2 min. and 30 second for gravitation. Serial ten-fold dilution of the homogenate was down in 0.1% peptone. One milliliter of each dilution was dropped onto compact dry plate (R-Biopharm AG Company, Darmstadt, Germany) which incubated at 37°C for 24 hr for total plate counts, and *E. coli* and incubated at room temperature 28±2°C for 72 hr for yeast and mold.

### Statistical analysis

All the experiments were replicated three times and evaluated with regression procedure using SPSS version 17. Differences among treatments were performed using Duncan's Multiple Range test ( $P > 0.05$ ).



## RESULTS AND DISCUSSION

### Effect of electrolyzed water on microbial growth inhibition

The reduction in microbial cells is shown in Fig. 2. EO water significantly inhibited the cell growth at 100 mg/L and EO water at 300 and 400 mg/L obtained the best result in the reduction of *E. coli* by 1.80 and 1.84 log CFU/g, respectively (Fig. 3). The total plate count, also showed that EO water at 300 mg/L significantly inhibited the cell growth by 1.47 log CFU/g when compared with the control. EO water was effective against bacteria. Tomás-Callejas [21] reported that washing fresh-cut baby mizuna leaves with EO water showed an inhibitory effect on natural microflora. In the another report, Issa-Zacharia [22] demonstrated that EO water treatment significantly reduced the total aerobic mesophilic bacteria from Chinese celery, lettuce and daikon sprouts by  $\geq 2.5$  log CFU/g. *E.coli* and *Salmonella* spp. were also significantly reduced by  $\geq 2.7$  log CFU/g and  $\geq 2.9$  log CFU/g, respectively. EO water has a strong oxidation potential and bactericidal effect that can be used as a disinfectant. Electrolyzed oxidizing water (pH < 2.7, ORP > 1100 mV) and the presence of hypochlorous acid were produced at the anode side. This solution has a strong oxidation potential in which oxidation-reduction potential (ORP) was measured for the oxidation reaction of all treatments at EO water as represented in Table 1. The highest value of ORP occurred in EO treatment at 400 mg/L. The ORP showed more oxidation efficiency which promoted the rising of oxidation efficiency by the concentrations. Suslow [18] reported that an ORP had the activity to eliminate the pathogens that promoted the rising of ORP. An ORP at 650-700 mV reduced the sterilization time of *Escherichia coli*, *Salmonella* sp. and *Listeria* sp. when comparatively with the ORP lower than 485 mV.

### Effect of electrolyzed water and ultrasonic wave on microbial growth inhibition

Combination of electrolyzed water and ultrasonic wave inhibited the bacterial growth which all treatments were presented the value of log reduction. The high value of log reduction occurred in EO 300+US 43 kHz, EO 300 +US 1000 kHz, EO 400+US 43 kHz and EO 400 +US 1000 kHz (data not shown). Combination of electrolyzed water and ultrasonic wave significantly inhibited bacterial growth a Fig. 4. Treatments showed of log reduction of *E. coli* after treated with EO 0 +US 43 kHz, EO 100 +US 43 kHz and EO 200 +US 43 kHz by 1.19, 1.15 and 1.00 log CFU/g, respectively (Fig. 5) meanwhile EO 200 +US 1000 kHz, EO 100 +US

1000 kHz and EO 200 +US 1000 kHz could inhibit the growth at 0.93, 0.35 and 0.63 log CFU/g, respectively. The combined treatment was able to inhibit the growth of *E. coli*. Hung [13] reported that a combination of EO water and US wave resulted in a greater reduction of the bacterial contamination of broccoli. For total plate count, EO 100 + US 43 kHz gave the best result in log reduction by 2.14 log CFU/g. For Yeast & Mold, EO 200 + US 43 kHz obtained the best result in log reduction by 1.27 log CFU/g. The efficiency of EO and US combined showed a significant enhanced control of microbial cells. US wave destroyed microorganism by the physical forces of cavitation which is the mechanical effect responsible for the destruction of fungal cells [23]. In the same way, Cao [24] used ultrasound treatment on strawberries at 0, 25, 28, 40 or 59 kHz at 20°C for 10 min, and then stored at 5°C for 8 days. Hypochlorous acid damages the microbial cell by oxidizing nucleic acids and proteins, causing lethal damage [25]. Scouten and Beuchat [26] reported that combined treatments of chemical, heat, and ultrasound were effective at killing *Salmonella* and *E. coli* O157:H7 on alfalfa seeds. The result of this research also suggested that the application of EO water combined with US wave could pathogenic control of fresh turmeric.

Table 1 Effect of Electrolyzed water on pH, and ORP (mV)

| Treatments           | Parameters |          |
|----------------------|------------|----------|
|                      | pH         | ORP (mV) |
| No washed (NW)       |            |          |
| Distilled water (DW) |            |          |
| EO 100 mg/L          | 2.64       | 224      |
| EO 200 mg/L          | 2.51       | 238      |
| EO 300 mg/L          | 2.50       | 246      |
| EO 400 mg/L          | 2.39       | 250      |

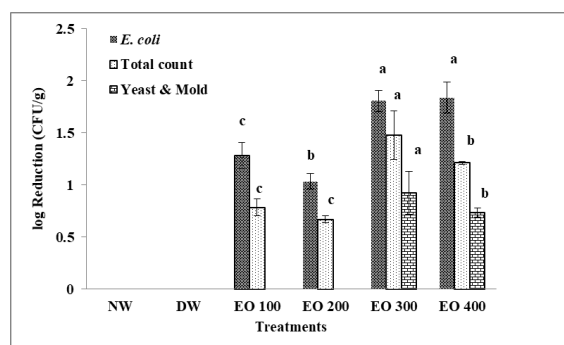


Fig. 2 Effect of electrolyzed water on microbial growth inhibition after incubated at 37 °C for 24 h. \*Error bar represented standard deviations. Values with the same letter on the same color bars represented no significant differences (\*P>0.05)

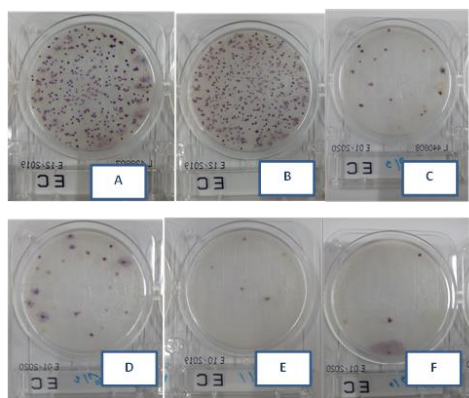


Fig. 3 Effect of electrolyzed water (A) control (no washed: NW) (B) distilled water: DW (C) EO 100 ppm (D) EO 200 ppm (E) EO 300 ppm (F) EO 400 ppm on growth inhibition of *E. coli* after incubation at 37 °C for 24 hr.

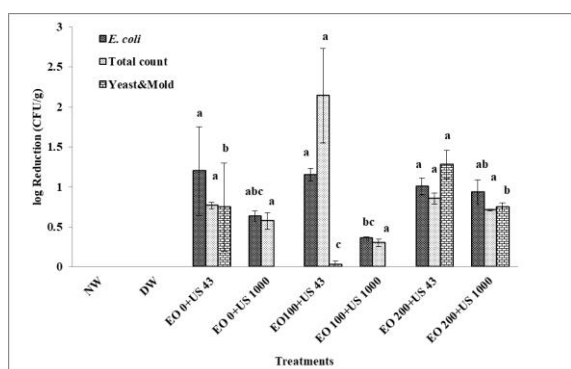


Fig. 4 Effect of electrolyzed water and ultrasonic wave on microbial growth inhibition after incubation at 37 °C for 24 h. \*Error bar represented standard deviations. Values with the same letter on the same color bars represented no significant differences (\*P>0.05)

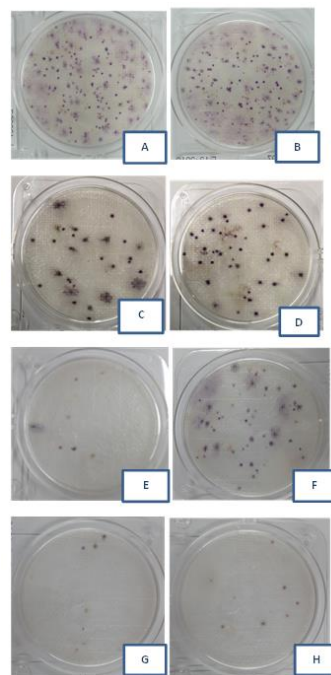


Fig. 5 Effect of electrolyzed water and ultrasonic wave (A) control (no washed: NW) (B) distilled water: DW (C) EO 0+US 43 kHz (D) EO 0+US 1000 kHz (E) EO 100+US 43 kHz (F) EO 100+US 1000 kHz (G) EO 200+US 43 kHz (H) EO 200+US 1000 kHz on growth inhibition of *E. coli* after incubation at 37 °C for 24 hr.

## CONCLUSIONS

EO water significantly inhibited the cell growth and the application of EO water combined with US wave gave the best inhibition of microbial cells (*E. coli*, total plate count and yeast and mold). Therefore, EO water and US wave could enhance pathogenic control of fresh turmeric.

## ACKNOWLEDGMENTS

This work was supported by Postharvest Technology Research Center, Faculty of Agriculture, Chiang Mai University, Chiang Mai and Postharvest technology Innovation Center, Commission on Higher Education, Bangkok, Thailand.

## REFERENCES

- [1] Bambirra, M. L. A., Junqueira, R. G. and Gloria, B. A. 2002. Influence of postharvest processing conditions on yield and quality of ground turmeric (*Curcuma longa* L.). Brazilian Archives of Biology and technology 45(4):

- 423-429.
- [2] TNAU Agritech Portal. 2015. Tumeric (Online) Available:  
<http://agritech.tnau.ac.in/banking/PDF/Tumeric.pdf> (April.17.2019).
  - [3] Selvan. S. 2016. Pre & postharvest processing of turmeric. (Online) Available:  
<https://www.slideshare.net/senthamizhselvan1481/turmeric-processing.html> (April.17.2019).
  - [4] Monton, C. 2016. Microbial contamination of turmeric capsules produced at a secondary government hospital in the northeastern Thailand. Thai Journal of Pharmaceutical Science 40 (Supplement Issue): 143-145.
  - [5] Naruemon, C. and Dariwan, S. 2014. Microorganism contamination and standard of supplement products consumed in household case study: Municipal of Thapra, Muang District, Khon Kean Province. KKU Research Journal 14(3): 81-91.
  - [6] FAO. 2004. Turmeric post-harvest operation. Food and Agriculture Organization of the United Nation (FAO.), AGST. 20 pp.
  - [7] Moreira, S. I., Dutra, D.C., Rodrigues, A.C., Oliveira, J.R., Dhingra, O.D. and Pereira, O.L. 2013. Fungi and bacteria associated with post-harvest rot of ginger rhizomes in Espírito Santo, Brazil. Tropical Plant Pathology, 38(3): 218-226.
  - [8] Al – Haq, M. I., Seo, Y., Oshita, S. and Oshita, Y. 2002. Disinfection effects of electrolyzed oxidizing water on suppressing fruit rot of pear caused by *Botryosphaeria berengeriana*. Food Research International 35: 657–664.
  - [9] Whangchai, N., Nomura, N. and Matsumura, M. 2003. Factors affecting phytoplankton removal by electro-oxidation of artificial seawater. Chiangmai Journal of Science 30: 255 – 259.
  - [10] Kim, C., Hung, Y.C. and Brackett, R.E. 2000. Efficacy of electrolyzed oxidizing (EO) and chemically modified water on different types of foodborne pathogens. International Journal of Food Microbiology 61: 199–207.
  - [11] Buck, J.W., Van Iersel, M.W., Oetting, R.D. and Hung, C.Y. 2002. In vitro fungicidal activity of acidic electrolyzed oxidizing water. Plant Disease 86: 278-281.
  - [12] Deza, M.A., Araujo, M. and Garido, J. M. 2003. Inactivation of *Escherichia coli* O157:H7, *Salmonella enteritidis* and *Listeria monocytogenes* on the surface of tomatoes by neutral electrolyzed water. The Society for Applied Microbiology 37:482-487.
  - [13] Hung, Y. C., Tilly, P. and Kim, C. 2010. Efficacy of electrolyzed oxidizing (EO) water and chlorinated water for inactivation of *Escherichia coli* O157:H7 on strawberries and broccoli. Journal of Food Quality 33: 559-577.
  - [14] Paola, C. L., Vivian, R. C., Mercado, M., Deaz M. and Carrascal A. K. 2005. Effectiveness of electrolyzed oxidizing water for inactivating *Listeria monocytogenes* in lettuce. Universitas Scientiarum 10: 97-108.
  - [15] Guentzel, J. L., Liang, L. K., Callan, M. A., Emmons, S. A. and Dunham, V. L. 2008. Reduction of bacteria on spinach, lettuce, and surfaces in food service areas using neutral electrolyzed oxidizing water. Food Microbiology 25(1): 36-41.
  - [16] Whangchai, K., Saengnil, K., Singkamanee, C. and Uthaibutra, J. 2009. Use of Electrolyzed oxidizing water to control postharvest disease during storage of tangerine cv. Sai Nam Pung. Acta Horticulturae 837: 211-215.
  - [17] Whangchai, K., Saengnil, K., Singkamanee, C. and Uthaibutra, J. 2010. Effect of electrolyzed oxidizing water and continuous ozone exposure on the control of *Penicillium digitatum* on tangerine cv. Sai Nam Pung during storage. Crop Protection 29: 386-389.
  - [18] Suslow, T. V. 2004. Oxidation-reduction potential (ORP) for water disinfection monitoring, control, and documentation. University of California. Division of Agriculture and Natural Resources. Publication 8149.
  - [19] Knorr, D., Zenker, M., Heinz, V. and Lee, D.U. 2004. Applications and potential of ultrasonic in food processing. Trends in Food Science and Technology 15: 261–266.
  - [20] Huang, Y.R., Hung, Y.C., Hsu, S.Y., Huang, Y.W. and Hwang, D.F. 2007. Application of electrolyzed water in the food industry. Food Control 19: 329–345.
  - [21] Tomás-Callejas, A., Martínez-Hernández, G.B., Artés, F., Artés-Hernández, F. and Trevor, V.S. 2011. Neutral and acidic electrolyzed water as emergent sanitizers for fresh-cut mizuna baby leaves. Postharvest Biology and Technology 55: 114 -120.
  - [22] Issa-Zacharia, A., Kamitani, Y., Miwa, N., Muhimbula, H. and Iwasaki, K. 2010. Application of slightly acidic electrolyzed water as a potential non-thermal food sanitizer for decontamination of fresh ready-to-eat vegetables and sprouts. Food Control 22: 601-607.
  - [23] Piyasena, P., Mohareb, E. and McKellar, R. C. 2003. Inactivation of microbes using ultrasound: a review. International Journal Food Microbiology 87(3): 207-216.
  - [24] Cao, S., Hu, Z. and Pang, B. 2010a. Optimization of postharvest ultrasonic treatment of strawberry fruit. Postharvest Biology and Technology 55: 150 – 153.
  - [25] Acher, A., Fisher, E., Turnheim, R. and Manor,

- Y. 1997. Ecologically friendly wastewater disinfection techniques. *Water Research* 31: 1398–1404.
- [26] Scouten, A.J. and Beuchat, L.R. 2002. Combined effects of chemical, heat and ultrasound treatments to kill *Salmonella* and *Escherichia coli* O157:H7 on alfalfa seeds. *Journal of Applied Microbiology* 92: 668–674.

## EXTRACTED OF THE ANTHOCYANINS FROM *Clitoria ternatea* FOR STAINED PROTOZOA AND ANTIAMOEBC ACTIVITY

Chanyapat Sangsuwon

Department of Science and Technology, Suan Sunandha Rajabhat University, Bangkok, Thailand

### ABSTRACT

*Clitoria ternatea* L. (CT) is family Fabaceae, commonly known as Butterfly pea and a popularly plant consumed for blue color. A wide range of medicinal compounds are including triterpenoids, flavonol glycosides, anthocyanins and steroids has been isolated from CT. Dried flowers were 30g extracted individually with water, water: ethanol in ratio 1:1 and 1:2 gave F1, F2 and F3 respectively. The maceration gave F1(1.8g), F2(2.2g) and F3(3.5g), respectively. F1-F3 were monitoring with Thin layer chromatography (TLC) were showed anthocyanins(ATN) components. TLC showed clearly of the anthocyanins chemical constituents in F2. *Acanthamoeba keratitis* (AK) is pathogens of human eyes which the causative by *Acanthamoeba* protozoa. It is the free living protozoa in the environment which are opportunistic diseases. Antiamoebic therapy by chemical drug of biguanides chlorhexidine (BCH) or polyhexamethylene biguanide (PHMB) which were not effective enough to kill *Acanthamoeba* cysts. CT plant has bioactivities in anti-inflammatory and analgesic properties. Which were interesting of studied CT for antiamoebic by anthocyanins which has vivid blue color. Extracted of F2 has Anthocyanin which stained *Acanthamoeba* cysts cells and damaged morphological and changed structural of *Acanthamoeba* cysts, detected by anthocyanins staining are shown under the light microscope. Anthocyanins of F2 in concentration (250, 125, 62.5, and 31.25 µg/ml) showed dead of cysts by 50% were antiamoebic effect for 24, 48 and 72h were 140.4, 113.3 and 90µg/ml, respectively.

**Keywords:** *Acanthamoeba*, Antiamoebic, *Clitoria ternatea*, Extracted, Stained.

### INTRODUCTION

*Clitoria ternatea* L. (CT) (Family: Fabaceae) commonly known as Butterfly pea, a traditional Ayurvedic medicine, has been used for centuries as a memory enhancer, antistress, anxiolytic, antidepressant, anticonvulsant[1], root, seed and flower of CT have long been widely used as a brain tonic and is believed to promote memory and intelligence[2]. CT flowers are used for cosmetics as ATN was smear on brows for black and shiny. The anthocyanins is deep violet which was the natural dye for cotton and enhanced by Ultrasonic assistance [4]. The phenolic and ATN compounds of the flowers suggest that they may have antioxidant activity [5]. The common ATN based on delphinidin and derivatives (Fig1)[6].

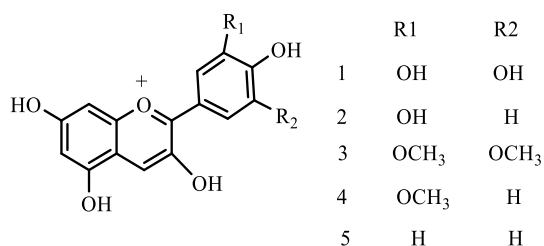


Fig.1 The most common ATN distributed in the plants. Delphinidin(1), Cyanidin(2), Malvidin(3), Peonidin(4) and Pelargonidin(5).

Ternatins are blue anthocyanins aglycone which soluble in water gave vivid blue and found in the petals of CT [7].

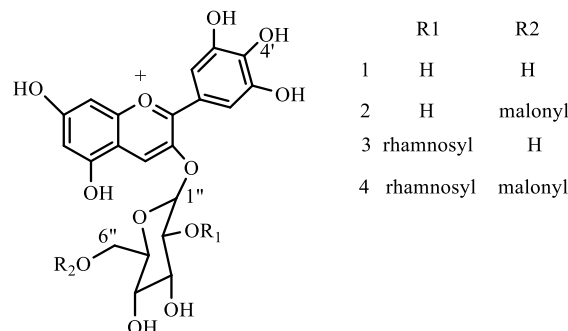


Fig. 2 Anthocyanin aglycone of (1) and their derivatives (2-4) isolated from *C. ternatea*

The flowers of CT was isolated the chemical constituents are flavonoids such as kaempferol and kaempferol glycosides kaempferol 3-neo hesperidoside, kaempferol 3-rutinoside, kaempferol 3-glucoside, quercetin, quercetin glycoside. The phenolic compounds of the flowers suggest that they may have antioxidant activity (Fig3) [8]. ATN is the polar components which can dissolves in the water and deep blue color which absorbed by UV spectrometer at 275 nm and 520 nm, respectively [9].

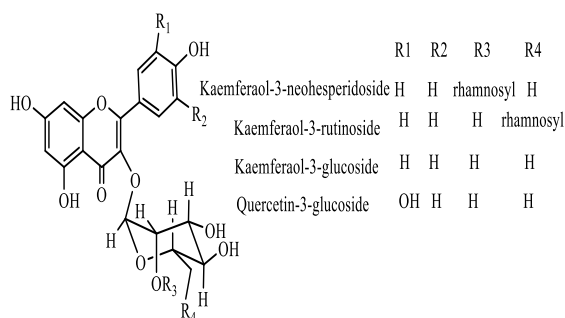


Fig. 3 Quercetin aglycone and their derivatives isolated from CT.

*Acanthamoeba* spp. is protozoa and found in virtually every environment. The life cycle was trophozoite and cyst [10]. Trophozoites feed on bacteria and other microorganism that retained viable bacteria. Unfavorable conditions become cyst form capable of surviving up to many year, is resistant to high temperature and in acid or base condition. *Acanthamoeba*-resistant are known to be reservoirs of bacterial pathogens such as *Ligionella pneumophila*, *Mycobacterium avium*. This disease is known as granulomatous amoebic encephalitis (GAE) [11]. Further, *Acanthamoeba* is the causative agents of AK, a painful eye infection mainly associated with contact lens use [12]. The chemical drugs for therapy of AK included biocides such as biguanide chlorhexidine and polyhexamethylene biguanides (PHMB) were not effective enough to kill cysts [13]. Recently, the anti-amoebic drug was on the way of improvement. The disinfecting solution used included Povidone-Iodine and Virkon® which damaged *Acanthamoeba* cyst [14]. The alternative use of medicinal plants is another interest as plants can have low toxicity than chemicals. *P. pellucida* was studied the ability to kill *Acanthamoeba* cyst *in vitro*. *P. pellucida* is a plant in the family of Piperaceae [15]. Reported, CT was extracted with water by ultrasonic and were used ultrafilter for sterilized anthocyanin for antibacterial ingredient in eye drop drug [16].

## METHODOLOGY

### Plant Material

CT flowers bought at Rajchaburi province, Thailand in February 2018. The dried flower plant of CT was powdered in a blender and then 30g, it extracted individually with water (200 ml), water: ethanol in ratio 1:1 (100:100) and 1:2 (70:130 ml) gave F1, F2, and F3 respectively. The solvents were removed by rotary evaporate at 120°C.

### Phytochemical screening by TLC

F1- F3 fractions are monitored the chemical constituent by Si gel TLC Kieselgel 60F<sub>254</sub> (Merck). The solvent system was used n-butanol: acetic acid: H<sub>2</sub>O (4: 2: 2), TLC screening was examined the

anthocyanin by 10% H<sub>2</sub>SO<sub>4</sub>-ethanol spray reagent and flavonoids intense fluorescence is produced in UV365 nm by NP/PEG (NP=diphenylboryloxyethyl amine, PEG: polyethylene glycol-4000), authentic standard were anthocyanin and quercetin. Concentrations of anthocyanin measurement by UV spectrometer by preparing standard curve of 1-100 µg/ml of anthocyanin at λ<sub>max</sub> 530 nm. F1-F3 were prepared in concentration 1mg/1 ml for measurement quantitative of ATN.

### DPPH Radical Assay

Determination of antioxidant activity using 2, 2-diphenyl-1-picrylhydrazyl (DPPH) radical scavenging method by prepared 0.2 mM of DPPH in MeOH. F1 was crude extracted by ether of CT flowers was prepared of serial concentration as 10, 20, 30, 40, 50, 100, 250, 500 and 1000 ppm. Pipettes 1ml each of concentration of sample and added 1ml of DPPH to each well. Mixtures were variously shaken and left for 30 min in the dark. Absorbance was measured at 515 nm using MeOH as blank. Percentage of radical scavenging was calculated using the equation: S(%) =  $(A_0 - A_s) / A_0 \times 100$ , which  $A_0$  is the absorbance of the control (0.2mM of DPPH, 2 ml), and  $A_s$  is the absorbance of the tested sample. The half maximal inhibitory concentration (IC<sub>50</sub>) value represented the concentration of the samples which have the antioxidant activity. Results were compared with of L-ascorbic acid. The results were expressed in percentage of inhibition as mean of three replicates. Repeated were testing with the crudes fraction F2-F3.

### Antiamoebic Test

*Acanthamoeba* cysts were isolated from an immune suppressed patient at Siriraj Hospital was designated. *Acanthamoeba* were cultured in normal saline solution seeded with *E. coli* heat-killed (NNA-*E.coli*) in 24 well plate incubated at 37°C for 7 days. The cysts were harvested, washed with normal saline solution, and adjusted to a final concentration of 10<sup>4</sup> cells/ml. Pipetted 50 µl of *Acanthamoeba* cysts (1x10<sup>4</sup> cells/ml) in each of the 1<sup>st</sup> to 4<sup>th</sup> well of 96 well plate. Dissolves Anthocyanin of F2 (5 mg) in 1 ml of Tween 20. Add 100 µl of F2 in the 1<sup>st</sup> well with 100 µl of Tween 20, then pipette 50 µl from the 1<sup>st</sup> to the 2<sup>nd</sup> well with another 100 µl of Tween 20, and the serial dilution were done to the fourth well. Prepare the *Acanthamoeba* cysts in normal saline solution at the concentration of 1x10<sup>4</sup> cells/ml. The *Acanthamoeba* cysts solution were pipetted 50 µl (1x10<sup>4</sup> cells/ml) and added into each well of 96 wells plate, incubated at 37°C for 24 h. The procedures were repeated for 48 and 72 h. The *Acanthamoeba* protozoa cysts were stained by toluidine blue were reference. *Acanthamoeba* cysts and were checked by under light microscope and the percentage of dead cysts



calculated by dead cysts x 100/total cysts. The 50 % inhibitory concentration values were calculated by a linear equation curve. The activities corresponding to each fraction evaluated in the *vitro* assay.

## RESULTS AND DISCUSSION

### Phytochemical Scanning by TLC

The dried flower of CT were extracted water (200 ml), water: ethanol in ratio 1:1 (100:100 ml) and 1:2 (70:130 ml) gave F1, F2, and F3 respectively. TLC showed the phytochemical components of Anthocyanin by 10%  $H_2SO_4$  in ethanol using spray reagent and heat at  $110^{\circ}C$  were red. In planar chromatography in particular, the retardation factor  $R_f$  is defined, retardation value calculated by formula:

$$R_f = \frac{\text{migration of distance of substance(cm)}}{\text{migration of distance of solvent front}}$$

NP/PEG spray reagent was activated flavonoids under ultraviolet spectrometer at 366 nm. The authentic standard were anthocyanin and quercetin. TLC screening the chemical constituents of CT flowers in F1-F3 were summarized in Table 1.

Table 1 ATN of flower of CT in F1-F3 detected by TLC screening and UV spectrometer

| Extracted fraction (200ml) | Weight of dried crude (g) | % yield | Rf of ATN | Concentration of ATN (mg/ml) |
|----------------------------|---------------------------|---------|-----------|------------------------------|
| F1 : water                 | 1.8                       | 18      | 0.67      | 9                            |
| F2: water:ethanol (1:1)    | 2.2                       | 22      | 0.67      | 15                           |
| F3: water:ethanol (1:2)    | 3.5                       | 35      | 0.67      | 5                            |

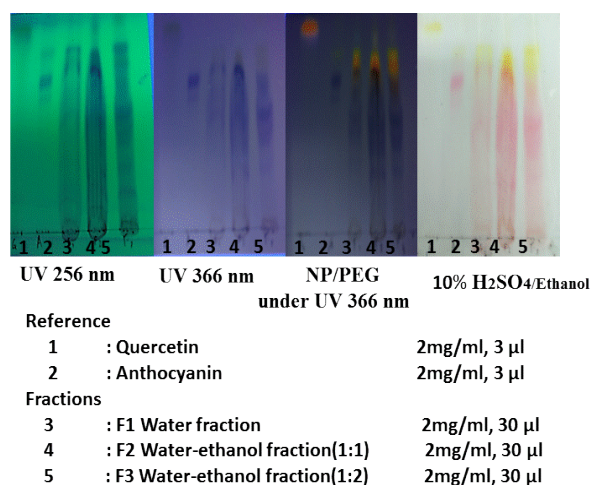


Fig 4 Chemical constituents of F1-F3 detected by UV spectrometer at 256, 366 nm and reagent of NP/PEG detected flavonoids and 10% H<sub>2</sub>SO<sub>4</sub>/ethanol detected ATN.

TLC showed extracted of F2 was extracted ATN components clearly and F3 have flavonoids which have polarity more than quercetin.

## Antioxidant Activity

F1 F2 and F3 were extracted with the order of polarity, water gave the polar compounds as glycosides. The mixed organic reagents by ethanol which is the polar organic reagent and could extracted the organic compounds. Results, F2 was extracted anthocyanin is the high yields and IC<sub>50</sub> was the active in 13.40 (µg/ml). F1-F3. These results are in agreement of F1-F3 were tested antioxidant activity used DPPH reagent, and were IC<sub>50</sub> of F1-F3 were 34.66, 13.40 and 28.77µg/ml, respectively (Table 2).

Table 2 IC<sub>50</sub> of inhibited DPPH radical scavenging on F1-F3 of CT flower.

| Extracted                      | 50% Inhibited of<br>DPPH radical<br>scavenging (µg/ml) |      |      | average | S.D.  | IC <sub>50</sub><br>(µg/ml) |
|--------------------------------|--|------|------|---------|-------|-----------------------------|
|                                | 1  | 2    | 3    |         |       |                             |
| F1 :<br>water                  | 34   | 35   | 35   | 34.66   | 0.06  | 34.66<br>±0.06              |
| F2 :<br>water:ethanol<br>(1:1) | 13.2   | 13.6 | 13.4 | 13.4    | 0.020 | 13.40<br>±0.02              |
| F3 :<br>water:ethanol<br>(1:2) | 28.6   | 28.5 | 29.5 | 28.87   | 0.06  | 28.77<br>±0.06              |

F2 prepared in serial concentration; 1:2, 1:4, 1:8, and 1:16 (250, 125, 62.5 and 31.25 µg/ml) were treated on the *Acanthamoeba* cyst. Preparing *Acanthamoeba* cyst in concentrated  $1 \times 10^4$  cells/ml of normal saline solution. Pipette 50 µl of cysts solution in serial concentration of F2, incubated at 37°C for 24 h. After that studied the morphological changed of *Acanthamoeba* cyst by Anthocyanin dyne staining and counted the dead cyst under light microscopy. The studied of *Acanthamoeba* cyst were treated with F2 for 48 and 72 h. Toluidine dyne stained living *Acanthamoeba* cyst for reference (Fig 5).

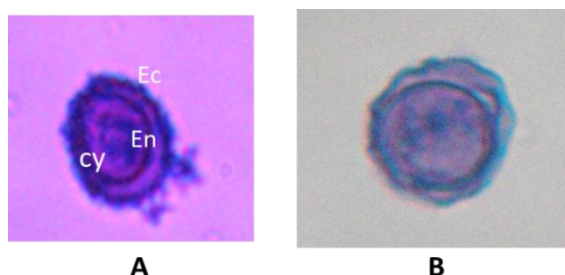


Fig 5 Living *Acanthamoeba* cyst detected by A.Toluidine dyne

### B. Anthocyanins components

The morphological and structural changes of the *Acanthamoeba* cysts after treated with F2 the minimum



cysticidal concentration of 1:16 (31.25 µg/ml) are investigated. The double cyst walls compose of the wrinkled ectocyst and damaged endocyst walls. Most cysts showed the shrinkage of cytoplasm with the cytoplasmic clumps, while no typical cysts are visible. Some cysts showed the empty content within the double-walls cyst with wrinkled ectocyst and enlarged endocyst (Fig 6).

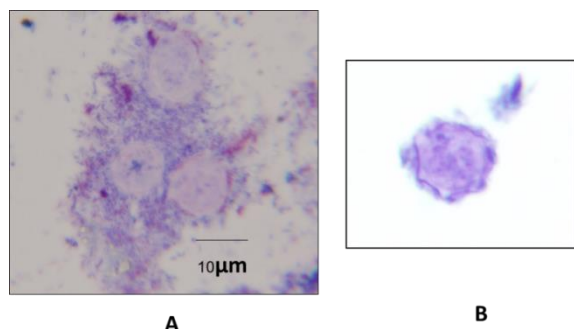


Fig. 6 The dead *Acanthamoeba* cyst showed morphological and structural changes by the double cyst walls compose of the wrinkled ectocyst and damaged endocyst walls which stained by ATN under light microscope.

Anthocyanins extracted from F2 in concentration (250, 125, 62.5, and 31.25 µg/ml) killed the cysts higher than 50% were antiamoebic. The experiment treated Anthocyanins compounds and incubated for 24, 48 and 72h which were active in 140.4, 113.3 and 90 µg/ml, respectively. F2 in 72h was the active for antiamoebic showed  $IC_{50}$   $90.0 \pm 0.03$  % (Fig 7).

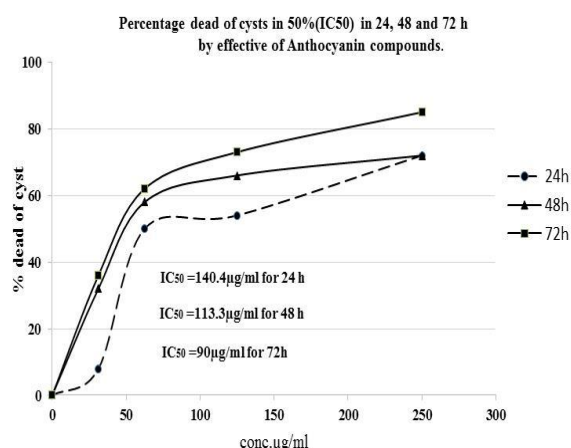


Fig 7.  $IC_{50}$  of Anthocyanin for antiamoebic test of F2 for 24, 48 and 72h.

## CONCLUSIONS

For searched the medicinal plants for kill *Acanthamoeba* cysts, CT is the folk medicinal used

for inflammatory and immunotherapy can kill cancer. CT flowers have deep blue color of Anthocyanins and selected for stained the cell of *Acanthamoeba* cysts which have activity for antiamoebic test. The research aimed to natural color for stained and used the Anthocyanin components for eye drop drug for *Acanthamoeba* keratitis. Reported, used ATN for ingredient in eye drop drug for antibacterial. The study showed Anthocyanin can kill the *Acanthamoeba* cyst by  $IC_{50}$  90 µg/ml in 72 h in vitro. CT is studying in the other conditions for antiamoebic test.

## ACKNOWLEDGMENTS

I am grateful for Assist.Prof. Kosol Roongruangchai Department of Parasitology Mahidol University Bangkok Thailand for providing the *Acanthamoeba* spp. for antiamoebic test

## Conflicts of Interest

The authors declare that they do not have conflict of interest

## REFERENCES

- [1] Morris J. Characterization of butterfly pea (*Clitoria ternatea* L.) accessions for morphology phenology, reproduction and potential nutraceutical, pharmaceutical trait utilization. Genetic Resources and Crop Evolution, 56(3): 2009, pp. 421-427.
- [2] Mukherjee P.K., Kumar, V., Mal, M., Houghton, P.J. Acetyl cholinesterase inhibitors from plants. Phytomedicine 14, 2007, pp. 289-300.
- [3] Sangsuwon C. Developing the film shampoo from sodium alginate and ingredients of the *Clitoria ternatea* extracted for carried on ICBTS conferece, 2018, Zurich Switzerland. 2018, pp. 83-86.
- [4] Ohama P., Kumpun, S. Ultrasonic assisted enhancement in cotton dyeing with natural colorant extracted from *Excoecaria bicolor* Key Engineering Materials, 2016, pp. 683-689.
- [5] Kamkaen N., Wilkinson J.M. The antioxidant activity of *Clitoria ternatea* flower petal extracts and eye gel. Phytother Res.; 23(11): 2009, pp. 1624-5. doi: 10.1002/ptr.2832.
- [6] Saito N., Abe K., Honda T., Timberlake, C.F., Bridle P. Acylated delphinidin glucosides and flavonols from *Clitoria ternatea*. Phytochemistry 24, 1985, pp. 1583-1586.
- [7] Reinoso B.D., Couto D., Moure A., Fernandes E. Optimization of antioxidants Extraction from *Castanea sativa* leaves. Chemical Engineering Journal. 203: 2012, pp. 101-109.
- [8] Terahara N., Oda M., Matsui T., Osajima Y., Saito N., Toki K., et al. Five new anthocyanins, ternatins A3, B4, B3, B2, and D2, from *Clitoria*

- ternatea flowers. Journal of Natural Products, 59, 1996, pp. 139-144.
- [9] Guohua C. and Ronald L. Anthocyanins Are Detected in Human Plasma after Oral Administration of an Elderberry Extract. Clinical chemistry. 45(4), 1999, pp.574-576.
- [10] Page F.C.A. Light- and electron microscopic study of *Protoacanthamoeba bicaledonica* sp., type-species of *Protoacanthamoeba* g. (Amoebozoa, Acanthamoebidae). J. Protozool., 28, 1981, pp.70-78.
- [11] Visvesvara G.S., Moura H., Schuster F.L. Pathogenic and opportunistic free-living amoebae: Acanthamoeba spp., Balamuthia mandrillaris, Naegleria fowleri, and Sappinia diploidea. FEMS Immunol Med Microbiol, 50, 2007, pp. 1–26.
- [12] Gagnon M.R., Walter K.A. A case of Acanthamoeba keratitis as a result of a cosmetic contact lens. Eye Contact Lens, 32:2006, pp. 373-8.
- [13] Tirado-Angel J., Gabreil MM, Wilson L.A., Ahearn D.G. Effects of Polyhexamethylene biguanide and chlorohexidine on four species of Acanthamoeba in vitro. Curr Eye Res 15, 1996, pp.225-228.
- [14] Roongruangchai K., Roongruangchai, J., Pilakasiri K., Sookkua T., et.al. Povidone-Iodine induced changes in the cyst of Acanthamoeba spp.: Transmission Electron Microscopic study. Siriraj.Med.J., 60(5), 2006, pp.251-253.
- [15] Sangsuwon C., Jirujcharyakul W., Roongruangchai K. Chemical constituents and anti-amoebic of methanolic fraction from P. pellucida (Linn.) Kunth. Applied and Mechanics and Materials, 709, 2015, pp.417-421.
- [16] Anthika B., Kusumocahyo S.P., Sutanto H. Ultrasonic approach in Clitoria ternatea (butterfly pea) extraction in water and extract sterilization by ultrafiltration for eye drop active ingredient. Procedia chemistry, 16, 2015, pp. 237-244.

## EFFECT OF TRADITIONAL THAI MASSAGE ON MUSCLE OXYGEN SATURATION IN LOW BACK PAIN PATIENTS: A PRELIMINARILY STUDY

Ketsarakon Oatyimprai<sup>1</sup>, Wichai Eungpinichpong<sup>2</sup>, Orawan Buranruk<sup>3</sup> and Kurusart Konharn<sup>4</sup>  
<sup>1,2,3,4</sup> Research center in Back Neck Other Joint Pain & Human Performance (BNOJPH), Thailand  
<sup>2,3,4</sup> Faculty of Associated Medical Sciences, Khon Kaen University, Thailand

### ABSTRACT

Low Back Pain (LBP) is common disease found in every age that affects daily life. LBP may cause poor posture of lumbar spine, and decrease muscle performance which lead to muscle fatigue, reduce blood circulation and reduce muscle oxygen saturation. Traditional Thai Massage (TTM) has been used to treat patients with LBP for long time with some evidence that it could increase muscle flexibility, improve blood circulation and decrease pain. However, its effect on muscle oxygen saturation has not been explored. This study uses one group pretest-posttest design to preliminary determine this effect. Twenty-three subjects (6 males and 17 females) who had non-specific LBP participated. Each of them was measured on muscle oxygen saturation, perceived muscle fatigue, visual analog scale (VAS) and Sorensen's test before and immediately after having a 15-minute session of TTM. These measures were compared before and after those of 15-minute rest period. The results showed significantly increase in muscle oxygen saturation ( $p < 0.01$ ), decrease VAS ( $3.45 \pm 1.87$ ) ( $p < 0.01$ ) and increase endurance of back extension ( $p < 0.05$ ) in the TTM group. In conclusion, TTM could improve muscle oxygen saturation level, decrease pain scale and increase duration of hold while performing back muscle endurance test.

*Keywords: Low Back Pain (LBP), Traditional Thai Massage (TTM), muscle oxygen saturation*

### INTRODUCTION

Lower back muscles are the part of body structure that used to stabilize the body in upright position where the main muscle that acts in this position is erector spinae (ES) muscle. ES muscle is responsible for thoracic and lumbar flexion from the upright position since its acts as antagonists to the gravity [1]. Low back pain (LBP) is one common disease resulting from disorder of lower back muscle and lumbar spine [2]. LBP has high prevalence in adult population (70-85 %), especially rate of incidence in females was higher than males in all age group [3][4][5].

The individual with LBP which effects on daily life can developed chronic low back pain (CLBP) [6]. LBP could be divided into two types as specific and non-specific base on pathology where most of the cases are non-specific LBP [7][8]. CLBP can affect poor posture of lumbar spine, poor balance in sitting position. Causes of LBP may induce inefficient muscular stabilization of spine, psychological distress and prolong workload is promoting muscle fatigue, reduce blood flow and reduce muscle oxygenation [9][10][11][12] Nowadays, many kinds of treatments have been suggested to treat low back pain such as massage, stretching exercise, strengthening exercise, etc., because they could improve muscle flexibility, muscle activity, blood circulation and oxygen saturation.

Oxygen are the most important to body work in

each working process. Oxygen is transported in hemoglobin and myoglobin. Therefore, oxygen saturation separated two type as arterial oxygen saturation and muscle oxygen saturation. From previous study, Murthy, G. [13] reported that importance of muscle oxygen saturation when muscle ischemia that affect to decrease blood volume and muscle oxygenation, it causes of muscle fatigue. The study of Bengtsson, A. [14] reported that "hypoxia in combination with muscle work causes pain as well as energy depletion" and when oxygen is raising, it can delay onset of muscle fatigue [15].

At the present, there are several studies that show therapeutic evidence base about traditional Thai massage, but none of the studies has provide the level of muscle oxygen saturation of TTM on lower back muscle. Thus, TTM still need more evidences to support the beneficial effects such as treatment guidelines. Therefore, this study will preliminarily determine effects of traditional Thai massage on level of muscle oxygen saturation and muscle endurance of lower back muscles in low back pain patients.

### METHODOLOGY

This study used one group pretest-posttest design, conducted in the department of Physical therapy, faculty of Associated Medical Sciences, Khon Kaen university, Khon Kaen Province, Thailand. This study was approved by Ethics Committee of Khon Kaen university.

## Participants

Male and female participants with LBP age between 20 – 45 years old were recruited by using bulletin boards and oral requests. They were screening by researcher according to the inclusion criteria; subacute (3 weeks to 3 months) or chronic low back pain of non-specific low back pain (> 3 months), body mass index (BMI) =  $18.5\text{--}24.9\text{ kg/m}^2$  [16], visual analog scale  $\geq 3/10$ , good communication and cooperation, no contraindication to either TTM, no fracture, non-smoking [17] and adipose tissue thickness (ATT)  $\leq 6.7\text{ mm}$ . All participants must refrain from drinks containing alcohol and caffeine before attending in 24 hours.

Twenty-three participants ( $26.70 \pm 6.18$  years of age; height  $1.63 \pm 0.09\text{ m}$ ; weight  $56.14 \pm 8.99\text{ kg}$ ; BMI  $20.88 \pm 1.71\text{ kg/m}^2$ ; ATT  $4.37 \pm 1.49\text{ mm}$ .) were signed inform consent before joining in this study.

## Procedure

Twenty-three participants were measured physical examination (e.g. heart rate, blood pressure, severity of pain and level of exhausted at that time), anxiety level by STAI-Y1, Visual analog scale (VAS), muscle oxygen saturation ( $\text{SmO}_2$ ) and endurance of back extension by Sorensen's test for baseline. After that they received TTM for 15 minutes per session on lower back muscle in prone position. The participants rest 15 minute before receive TTM.

Massage points including 2 lines and in this study performed along energy lines or Sen-sib which is call "Ping-kha-la" or "Ei-tha" [18] depends on pain side. The massage therapist was measure 2 fingers base from spine and pressed at T1 to S1 to apply gentle, gradually increasing, pressure through the massage therapists thumb or palmar. Pressure applied until the participants begin to feel slight uncomfortable then hold 5-10 seconds per time. The massage therapist applied in several times until 15 minutes [19]. The participants can request to stop the massage therapists or researcher at any time if they feel pain. And re-measured in same baseline after finished TTM (Fig.1).

## Measurements

### Muscle oxygen saturation ( $\text{SmO}_2$ ) using MOXY

Muscle oxygen saturation choose as a primary outcome measure in this study and used MOXY for measure muscle oxygen saturation. The participants were lying in prone position; the researcher clean up on lower back at L1 to L5. Then the researcher palpated L3 for place MOXY monitor on the center of erector spinae [20] (Fig.2). The data recorded in peripedal (software of MOXY) and exported in Microsoft excel. Validity of this tool are considerably strong (ICC;  $r = 0.773\text{--}0.992$ ) [21]. The researcher has intra-class correlation coefficient at 0.98.

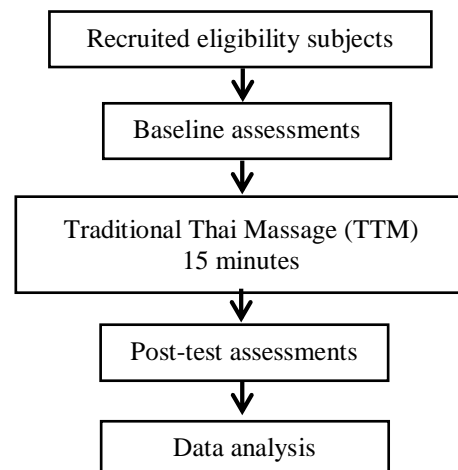


Fig.1 Overview of study design



Fig.2 The location of Moxy monitor placed on low back muscle

### Endurance of back extension using Sorensen's test

The participants were prone by lower part of body on bed and anterior superior iliac spine place on edge of bed after that the researcher strapped to the three point: level of greater trochanter of the femur, knee creases and level of lateral [22]. The chair placed in front of participant for support upper part of body and participant placed both hand on the chair for starting position. Beginning the participant lift the upper part and hand from the chair and both arms crossed on the chest. The upper part of body was horizontal to the bed. They hold horizontal position until fatigue or the body can't lift to horizontal (Fig.3). The researcher measured the time by stopwatch. [23] [22] [24]. Validity of Biering-Sorensen test has 0.77 [22]. This assessment time was 5 minutes approximately.



Fig.3 Sorensen's test

### Pain intensity using Visual analog scale (VAS)

Pain intensity was assessed by 10 cm. visual analog scale. Range 0-10 which 0 is “no pain” and 10 is “most pain”. The participants were mark on the scale of pain intensity.

#### Anxiety level by STAI-Y1 (Thai version)

The participants requested to state trait anxiety inventory Y1 has 20 item State anxiety items include: ‘Not at all; I fell a little bit; I fell quite a lot’ and I fell very so much’. Higher scores mean greater anxiety. Score of STAI-Y1 separate to 3 level of anxiety, there are including; 20-39 scores: Low anxiety, 40-59 scores: Moderate anxiety and 60-80 scores: High anxiety.

#### Statistical analysis

Data analysis was using by SPSS version 23 in this study. Descriptive data of continuous data such as age, weight, etc., are presented in terms of mean and standard deviation. The categorical data such as gender, occupation, etc., are presented in proportion and percentages. Demographic data are presented as mean  $\pm$  standard deviations (SD) and percentage. Mean and standard deviations of the values were calculated for each variable. This study aimed to analyze each outcome in the period before and after treatment, the difference times by immediate effect of each outcome. Paired t-test and Wilcoxon used to compare outcome variables at baseline with outcome variables after received treatment immediately within group. Friedman’s 2-way ANOVA used to compare the change of outcome measure in difference times within group. This study estimates the adjusted mean difference and the 95 percentages confidence interval for each outcome measure.

## RESULTS

#### Muscle oxygen saturation

Table 1 showed that the immediately after received TTM had significantly increasing between Soren1-Recovery, TTM-Recovery and Base5M-Recovery ( $p$  value  $< 0.001$ ). In addition, there are three pairs that have significantly different at  $p$  value  $< 0.05$ : Rest1-Recovery, Soren2-Recovery and Rest2-Recovery.

Muscle oxygen saturation represented the data of twenty-three participants.  $SmO_2$  showed changes of muscle oxygen saturation in each period with the

follow changes: In Soren1 when the participant extend back in Sorensen’s test, the muscle oxygen saturation was decreasing from baseline and increasing after resting 15 minutes. Next, the massage therapist applied massage on affected side, the muscle

oxygen saturation was decreasing again and increasing after resting 15 minutes. In the same result of Soren1 in Soren2 but the muscle oxygen saturation decreased lower than Soren1. The last recovery period was increasing more than all period and significant increasing after received the treatment.

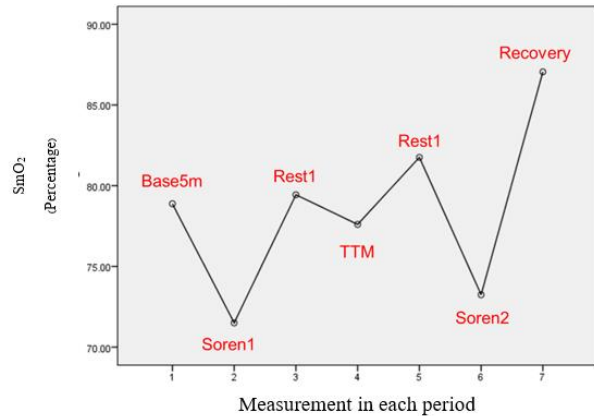


Fig.4 The change of muscle oxygen saturation ( $SmO_2$ ) baseline until recovery.

#### Endurance of back extension muscle

Endurance of back extension was 0.015, significantly improved at  $p$  value  $< 0.05$ .

Endurance of back extension muscle has significantly increasing after received TTM and it's not normal distribution because some participants had decreasing of time when doing Sorensen test 2 (Fig.5).

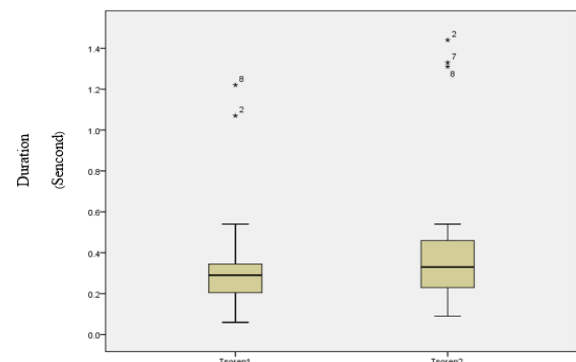


Fig.5 The change after received TTM of endurance of back extension

#### Pain intensity and anxiety level

Pain intensity was significantly decreased at  $p$  value  $< 0.001$  and anxiety level was significantly improving at  $p$  value  $< 0.001$  after received TTM from baseline.

Table 2 Comparison outcome of pain intensity and anxiety level

| Item                      | Baseline<br>(Mean $\pm$ SD) | Post-test<br>(Mean $\pm$ SD) | Difference<br>(95% CI) | P<br>value |
|---------------------------|-----------------------------|------------------------------|------------------------|------------|
| Visual<br>analog<br>scale | 5.67 $\pm$ 1.52             | 2.22 $\pm$ 2.04              | 3.46<br>(2.65 to 4.27) | 0.001      |
| STAI-<br>Y1               | 33.61 $\pm$ 5.46            | 29.57 $\pm$ 4.83             | 4.04<br>(2.30 to 5.78) | 0.001      |

## DISCUSSIONS

This study was preliminarily determining the immediate effects of traditional Thai massage (TTM) on level of the muscle oxygen saturation (SmO<sub>2</sub>), Visual analog scale (VAS), State trait anxiety Y1 (STAI-Y1) and muscle endurance of lower back muscle in low back pain (LBP) patients. The results showed that SmO<sub>2</sub>, muscle endurance, VAS and STAI-Y1 had significant increasing. The result showed the traditional Thai massage can increase level of the muscle oxygen saturation and muscle endurance of lower back muscles in low back pain patients in immediately after received treatment. Beside pain scale and anxiety level have improve in the same way.

### *Immediate effect on increasing muscle oxygen saturation level*

Previous study [25] presented the occlusion technique in TTM could improve blood flow and [26] Swedish massage on calf muscle could improve tissue blood flow. In normally contracting skeletal muscle has increasing of blood flow and oxygen extraction, the oxygen also binds with hemoglobin and myoglobin in blood. It's may cause of increasing of muscle oxygen saturation. [27]

This study showed that changes in real time of muscle oxygen level in 7 periods (Base5m, Soren1, Rest1, TTM, Rest2, Soren2 and recovery), finding that in each period there were different changes. First baseline measurement was measured 5 minutes and the SmO<sub>2</sub> level was high or low depending on the muscle tension and blood flow on lower back in each person. According to previous study, who had myofascial trigger point or muscle spasm often had vasoconstriction that affect to poor blood circulation, poor oxygenation and fatigue easily [28].

Next, Sorensen's test 1 showed SmO<sub>2</sub> was decreasing for baseline because they had muscle contraction when performed back extension, causing the vessels were occluded. So, the SmO<sub>2</sub> level was increasing after resting 15 minutes in period 1. Afterthought, the massage therapist applied the pressure and while doing massage had changes of SmO<sub>2</sub> rise and fall because when she applied the pressure, had compress to vessel in the muscle and then the massage therapist slowly released pressure,

causing the blood vessels to gradually relaxed and increased blood circulation. Then, the participants were resting 15 minutes showed the SmO<sub>2</sub> level was higher than baseline, causing muscle relaxation that improved blood circulation and improved oxygenation. In Sorensen's test 2 showed the SmO<sub>2</sub> level had decreased while doing back extension but it's decreasing less than Sorensen's 1.

The last recovery period showed that the SmO<sub>2</sub> level had significantly increased with each period. Since, there were both relaxing massage and increasing the strength of isometric back extension that effect of the possible mechanism might be promoted parasympathetic to relaxation, improve vasodilation to good blood circulation and exchanges deoxygenation

### *Immediate effect on improving endurance of back extension*

This study found that endurance of back extension was significantly improved after received TTM according to massage could be decreased muscle spasm, muscle tension and improved flexibility, causing there were improved blood flow [25] [29] and improved oxygen saturation. In addition, Sorensen's test was isometric exercise of back extension, it could be improved strengthening cause of participants could be hold the upper body longer from baseline.

### *Immediate effect on reducing pain intensity*

This study showed that the level of pain intensity was significant decreased after the treatment. Previous study, Study of Chatchawan [18] showed that participants received TTM had decreased pain intensity after treatment 3 weeks and one month follow up. There might be explained by gate control theory. The touch sense could decrease pain sensitivity by inhibition of small fiber, so that lead to block the signal to the brain [30]. In addition, TTM promoted vasodilation, exchanges oxygen and decreased lactic acid cause of fatigue

### *Immediate effect on improving state trait anxiety Y1 level*

The study found that after the participants received the massage, there was a better anxiety condition before received massage. In previous study, Buttagat, V. found that the immediately of TTM on back muscle 30 minutes could improve pain intensity and improve level of anxiety which accordance with this study. TTM were promote relaxation, activated parasympathetic and decreased sympathetic. Moreover, [31] massage whole body in pregnancy could increase serotonin (5HIAA), increased dopamine, decreased cortisol that might be explained about improving of anxiety.

The researcher was followed up the participants about pain intensity and adverse effect after received the treatment 1 day. This study didn't found any

participants who had side effects from treatment.

This study has some limitations. First, this study has small sample size because there used preliminary study and non-control group for compare with treatment. Second limitation was no blind for the assessor and patients. Third limitation from muscle oxygen monitor was when doing activities that were moving or sweating. Sometimes the device can't read oxygen saturation in muscle. In some participants who sweat easily, there is a problem while doing Sorensen's test, causing the information to be lost and can't be analyzed. The last limitation was duration of treatment because this study was measuring immediate effect. Although, this study measures immediate effect and in the future study may use randomize control trial (RCT) or crossover design for long term effect of TTM on pain scale and anxiety except for SmO<sub>2</sub> and muscle endurance.

## CONCLUSIONS

TTM on lower back muscle in LBP patients for 15 minutes could improve level of SmO<sub>2</sub>, decrease pain scale, decrease anxiety and increase duration of hold while performing back muscle endurance test. Treatment technique in this study has no side effect and provide relaxation of anxiety. Consequently, this TTM for 15 minutes on pain area can serve as an alternative treatment of LBP patients.

## ACKNOWLEDGMENTS

Financial support in this research were authorized by the Research and Training Center for Enhancing Quality of life of working Age People and the Research Center in Back Neck Other Joint Pain and Human Performance (BNOJPH). Location support in this research has been approved by the Research Center in Back Neck Other Joint Pain and Human Performance (BNOJPH) at the research room 5<sup>th</sup> floor, Faculty of Associated Medical Sciences, Khon Kaen University, Thailand.

## REFERENCES

- [1] Floyd, W. F., & Silver, P. H. S. (1955). The function of the erectores spinae muscles in certain movements and postures in man. *The Journal of physiology*, 129(1), 184-203.
- [2] Colloca, C. J., & Hinrichs, R. N. (2005). The biomechanical and clinical significance of the lumbar erector spinae flexion-relaxation phenomenon: a review of literature. *Journal of manipulative and physiological therapeutics*, 28(8), 623-631.
- [3] Andersson, G. B. (1999). Epidemiological features of chronic low-back pain.

Table1 Participants outcome of Muscle oxygen saturation (SmO<sub>2</sub>)

| Item              | Standard Error (S.E) | P value |
|-------------------|----------------------|---------|
| Base5m – Soren1   | 0.637                | 1.000   |
| Base5m – Rest1    | 0.637                | 1.000   |
| Base5m – TTM      | 0.637                | 1.000   |
| Base5m – Rest2    | 0.637                | 1.000   |
| Base5m – Soren2   | 0.637                | 1.000   |
| Base5m – Recovery | 0.637                | 0.000** |
| Soren1 – Rest1    | 0.637                | 1.000   |
| Soren1 – TTM      | 0.637                | 1.000   |
| Soren1 – Rest2    | 0.637                | 0.510   |
| Soren1 – Soren2   | 0.637                | 0.785   |
| Soren1 – Recovery | 0.637                | 0.000** |
| Rest1 – TTM       | 0.637                | 1.000   |
| Rest1 – Rest2     | 0.637                | 1.000   |
| Rest1 – Soren2    | 0.637                | 1.000   |
| Rest1 – Recovery  | 0.637                | 0.003*  |
| TTM – Rest2       | 0.637                | 1.000   |
| TTM – Soren2      | 0.637                | 1.000   |
| TTM – Recovery    | 0.637                | 0.000** |
| Rest2 – Soren2    | 0.637                | 1.000   |
| Rest2 – Recovery  | 0.637                | 0.022*  |
| Soren2 – Recovery | 0.637                | 0.012*  |

The lancet, 354(9178), 581-585.

- [4] Jones, G. T., & MacFarlane, G. J. (2005). Epidemiology of low back pain in children and adolescents. *Archives of disease in childhood*, 90(3), 312-316.
- [5] Taylor, J. B., Goode, A. P., George, S. Z., & Cook, C. E. (2014). Incidence and risk factors for first-time incident low back pain: a systematic review and meta-analysis. *The Spine Journal*, 14(10), 2299-2319.
- [6] Meucci, R. D., Fassa, A. G., & Faria, N. M. X. (2015). Prevalence of chronic low back pain: systematic review. *Revista de saude publica*, 49
- [7] Minematsu Akira (2012). *Epidemiology, Low Back Pain*, Dr. Ali Asghar Norasteh (Ed.), ISBN:978-953-51-0599-2, InTech, Available from: <http://www.intechopen.com/book>



- s/low-back-pain/epidemiology
- [9] Radebold, A., Cholewicki, J., Polzhofer, G. K., & Greene, H. S. (2001). Impaired postural control of the lumbar spine is associated with delayed muscle response times in patients with chronic idiopathic low back pain. *Spine*, 26(7), 724-730.
  - [10] Hodges, P. W., & Richardson, C. A. (1996). Inefficient muscular stabilization of the lumbar spine associated with low back pain: a motor control evaluation of transversus abdominis. *Spine*, 21(22), 2640-2650.
  - [11] Bansevicius, D., Westgaard, R. H., & Jensen, C. (1997). Mental Stress of Long Duration: EMG Activity, Perceived Tension, Fatigue, and Pain Development in Pain - Free Subjects. *Headache: The Journal of Head and Face Pain*, 37(8), 499-510.
  - [12] Feyer, A. M., Herbison, P., Williamson, A. M., de Silva, I., Mandryk, J., Hendrie, L., & Hely, M. C. (2000). The role of physical and psychological factors in occupational low back pain: a prospective cohort study. *Occupational and environmental medicine*, 57(2), 116-120.
  - [13] Albert, W. J., Sleivert, G. G., Neary, J. P., & Bhambhani, Y. N. (2004). Monitoring individual erector spinae fatigue responses using electromyography and near infrared spectroscopy. *Canadian journal of applied physiology*, 29(4), 363-378.
  - [14] Murthy, G., Hargens, A. R., Lehman, S., & Rempel, D. M. (2001). Ischemia causes muscle fatigue. *Journal of Orthopaedic Research*, 19(3), 436-440.
  - [15] Bengtsson, A. (2002). The muscle in fibromyalgia. *Rheumatology*, Volume 41, Issue 7, 1 July 2002, Pages 721-724
  - [16] Hepple, R. T. (2002). The role of O<sub>2</sub> supply in muscle fatigue. *Canadian journal of applied physiology*, 27(1), 56-69.
  - [17] Heuch, I., Hagen, K., Heuch, I., Nygaard, Ø., & Zwart, J. A. (2010). The impact of body mass index on the prevalence of low back pain: the HUNT study. *Spine*, 35(7), 764-768.
  - [18] Özdal, M., Pancar, Z., Çinar, V., & Bilgiç, M. (2017). Effect of Smoking on Oxygen Saturation in Healthy Sedentary Men and Women. *EC Pulmonology and Respiratory Medicine*, 4(6), 178-182.
  - [19] Chatchawan, U., Thinkhamrop, B., Kharmwan, S., Knowles, J., & Eungpinichpong, W. (2005). Effectiveness of traditional Thai massage versus Swedish massage among patients with back pain associated with myofascial trigger points. *Journal of Bodywork and Movement Therapies*, 9(4), 298-309.
  - [20] Buttagat, V., Eungpinichpong, W., Chatchawan, U., & Kharmwan, S. (2011). The immediate effects of traditional Thai massage on heart rate variability and stress-related parameters in patients with back pain associated with myofascial trigger points. *Journal of bodywork and movement therapies*, 15(1), 15-23.
  - [21] Yoshitake, Y., Ue, H., Miyazaki, M., & Moritani, T. (2001). Assessment of lower-back muscle fatigue using electromyography, mechanomyography, and near-infrared spectroscopy. *European journal of applied physiology*, 84(3), 174-179.
  - [22] Crum, E. M., O'Connor, W. J., Van Loo, L., Valckx, M., & Stannard, S. R. (2017). Validity and reliability of the Moxy oxygen monitor during incremental cycling exercise. *European Journal of Sport Science*, 1-7.
  - [23] Latimer, J., Maher, C. G., Refshauge, K., & Colaco, I. (1999). The reliability and validity of the Biering-Sorensen test in asymptomatic subjects and subjects reporting current or previous nonspecific low back pain. *Spine*, 24(20), 2085.
  - [24] Sánchez-Zuriaga, D., López-Pascual, J., Garrido-Jaén, D., & García-Mas, M. A. (2015). A comparison of lumbopelvic motion patterns and erector spinae behavior between asymptomatic subjects and patients with recurrent low back pain during pain-free periods. *Journal of manipulative and physiological therapeutics*, 38(2), 130-137.
  - [25] Champagne, A., Descarreaux, M., & Lafond, D. (2008). Back and hip extensor muscles fatigue in healthy subjects: task-dependency effect of two variants of the Sorensen test. *European Spine Journal*, 17(12), 1721-1726.
  - [26] Eungpinichpong, W. (2002). Effects of femoral artery temporarily occlusion on skin blood flow of foot. *Journal of Medical Technology and Physical Therapy*, 14(2), 151-159.
  - [27] Munk, N., Symons, B., Shang, Y., Cheng, R., & Yu, G. (2012). Noninvasively measuring the hemodynamic effects of massage on skeletal muscle: a novel hybrid near-infrared diffuse optical instrument. *Journal of bodywork and movement therapies*, 16(1), 22-28.
  - [28] Miura, H., McCully, K., Nioka, S., & Chance, B. (2004). Relationship between muscle architectural features and oxygenation status determined by near infrared device. *European*

- journal of applied physiology, 91(2-3), 273-278.
- [29] Buttagat, V., Narktro, T., Onsrira, K., & Pobsamai, C. (2016). Short-term effects of traditional Thai massage on electromyogram, muscle tension and pain among patients with upper back pain associated with myofascial trigger points. *Complementary therapies in medicine*, 28, 8-12.
- [30] Viravud, Y., Apichartvorakit, A., Mutirangura, P., Plakornkul, V., Roongruangchai, J., Vannabhum, M., ... & Akarasereenont, P. (2017). The anatomical study of the major signal points of the court-type Thai traditional massage on legs and their effects on blood flow and skin temperature. *Journal of integrative medicine*, 15(2), 142-150.
- [31] Melzack, R., & Wall, P. D. (1965). Pain mechanisms: a new theory. *Science*, 150(3699), 971-979
- [32] Field, T., Diego, M. A., Hernandez-Reif, M., Schanberg, S., & Kuhn, C. (2004). Massage therapy effects on depressed pregnant women. *Journal of Psychosomatic Obstetrics & Gynecology*, 25(2), 115-122. Islam M.R., Conference proceedings, in Proc. 2nd Int. Conf. on GEOMATE, 2011, pp. 8-13.

## PROBIOTICS ENCAPSULATED FRUIT JUICE PEARLS AS FUNCTIONAL FOOD PRODUCT

Palida Tanganurat<sup>1</sup>, Intira Lichanporn<sup>1</sup>, Nunchanok Nanthachai<sup>1</sup> and Charoen Charoenchai

<sup>1</sup>Department of Food Science and Technology, Faculty of Agricultural Technology, Rajamangala University of  
Technology Thanyaburi, Pathum Thani, 12130, Thailand

### ABSTRACT

This experimental research investigates encapsulation of *Pediococcus pentosaceus* ARG-MG12 in pure orange juice pearls. In the study, four tropical fruit juices: guava, watermelon, pineapple, and orange, were first evaluated in terms of sensory characteristics: color, odor, flavor, texture, overall acceptance, using a 9-point hedonic scale; and orange juice whose sensory scores were statistically highest was selected for further development into probiotic fruit pearls. The physicochemical properties of probiotic orange pearls were examined and the sensory evaluation undertaken. Furthermore, the probiotic pearls were subjected to gastric juice (pH 2.0) and bile salt (0.6% w/v) environment for 3 h to simulate human gastrointestinal tract and to variable storage durations (0, 3, 5, 7, 14 days) at 6 °C to assess cell viability. The findings showed that the probiotic orange pearls had 390.71 g/sec of stiffness, DPPH radical-scavenging activity of 294 µg ascorbic acid eq./ml, and L-ascorbic acid content of 0.095 mg/ml. Meanwhile, the survival rates of bacterial cells in low pH environment and bile salt were 83.27% and 94.24%, respectively. At day 14, the remaining bacteria were above 8 log CFU/g, given that the minimum concentrations of probiotics are 10<sup>6</sup>–10<sup>7</sup> CFU/ml at the end of product's shelf life. Moreover, sensory testing panelists were unable to differentiate between non-probiotic and probiotic orange pearls.

*Keywords: Probiotic, Encapsulation, Fruit pearl*

### INTRODUCTION

First invented in Taiwan in the 1980s [1], bubble tea is a trendy drink popular among teenagers. The colorful beverage is concocted from green or black tea mixed with milk and fruit syrup. As a marketing gimmick, the drink contains small spherical tapioca starch balls of 10 -15 mm in diameter (also known as bubbles, pearls, or boba), and is served with a wide colorful straw through which the bubbles are sucked up [2].

Encapsulation involves the entrapment of active substance within another substance acting as coating material. The encapsulation technology is commonly used by the food industry for preservation and delivery of flavors, dyes, stabilizers, antioxidants, enzymes, probiotics, lipids, mineral salts, and vitamins [3]. For probiotics, encapsulation protects microorganisms against environmental stresses. Specifically, microcapsules create an anaerobic environment conducive to probiotics growth and provide protection against harsh environment, including acidic fruit juice, freezing, and gastric conditions, thereby mitigating cell injury [4,5].

Of particular interest is the survival of probiotics in food products given that significant proportions of cells deteriorate during processing and storage. According to the International Dairy Federation, the minimum concentrations of probiotics should be 10<sup>6</sup>–10<sup>7</sup> CFU/ml at the end of product's shelf life [6]. The health benefits of probiotics include, for example, bio-availability of macro- and micro-nutrients, antioxidant activity, and production of anti-microbial

compounds [7],[8].

Despite widespread encapsulation of probiotics in a variety of food products, research on probiotics encapsulation for fruit juice pearls is limited and rare. Thus, this research aims to develop fruit pearls containing probiotics encapsulated with sodium alginate as functional food product. In the study, four tropical fruit juices: guava, watermelon, pineapple, and orange, were first evaluated in terms of sensory features (i.e., color, odor, flavor, texture, overall acceptance) using a 9-point hedonic scale and the fruit juice with statistically highest scores selected for further development into probiotic fruit pearls. The physicochemical properties of the probiotic fruit pearls were then characterized in terms of size, texture, antioxidant activity, and L-ascorbic acid content; and the sensory evaluation undertaken in comparison with commercially non-probiotic fruit pearls. In addition, the probiotic fruit pearls were subjected to simulated human gastrointestinal tract and variable storage durations at 6 °C to determine the cell viability.

### MATERIALS AND METHODS

#### Preparation of Fruit Pearls

Fresh tropical fruits were acquired from a local fresh market in Thailand's Pathum Thani province, consisting of 10 kg each of guava, watermelon, pineapple, and orange. The fruits were washed, peeled, and ground by a blender for 5 min at maximum speed (Philips, HR-2118). The slurry was

manually squeezed through a muslin cloth for juice, and pH values were measured by pH meter (Sartorius PB-20, Germany) and titratable acidity determined [9].

In this research, the encapsulation followed Krasaekoopt and Kitsawad [11] whereby 1% sodium alginate (w/w) was mixed with 1000 ml fruit juice and heated at 70 °C for 10 min. The mixture was extruded dropwise through 8-mm needle into sterile 0.1 M CaCl<sub>2</sub> as hardening solution and left for 10 min. The fruit juice pearls were cleaned by potable water and particle sizes measured using Vernier caliper.

The sensory attributes (color, odor, flavor, texture, overall acceptance) of pearls of four fruit juices: guava, watermelon, pineapple, and orange, were evaluated by a team of 30 untrained panelists using a 9-point hedonic scale, where 1 denotes extremely dislike and 9 extremely like. Randomized complete block design was utilized to select the fruit juice with statistically highest sensory scores ( $p \leq 0.05$ ) for subsequent experiment [10].

### Preparation of Inoculum

*Pediococcus pentosaceus* ARG-MG12 was cultured in 10 ml de Man, Rogosa and Sharpe (MRS) broth (Merck, Darmstadt, Germany), followed by overnight incubation at 37 °C. The culture was transferred to 100 mL MRS broth and incubated overnight at 37 °C. Cultures were harvested by centrifugation at 3000 g at 25 °C for 10 min and washed with sterile saline, and the procedure was repeated prior to the collection of cultures.

### Encapsulation of *Ped. pentosaceus*

In encapsulation, *Ped. pentosaceus* ARG-MG12 bacterial cultures ( $10^{11}$  CFU/ml) were aseptically suspended in the selected sodium alginate-mixed fruit juice (i.e., the fruit juice with statistically highest sensory scores). The suspensions were extruded dropwise through 8 mm needle into sterile 0.1 M CaCl<sub>2</sub> as hardening solution and left for 10 min. The probiotic fruit pearls were then washed by potable water.

To determine the bacterial survival, 10 g of the probiotic fruit pearls was mixed with 90 ml of sterile phosphate buffer in mixer bag and broken up by stomacher (Seward, UK) at room temperature for 1 min. The mixture was diluted and the number of viable cells determined by pour plate count (log CFU/ml) in MRS agar after incubation at 37 °C for 48 h. The survival rate (%) was then calculated using Eq. (1):

$$\text{Survival rate (\%)} = (N/N_0) \times 100 \quad (1)$$

where N is the number of viable cells in the fruit pearl (log CFU/ml) and N<sub>0</sub> is the number of free viable cells in suspension containing sodium alginate,

fruit juice, and bacterial culture (log CFU/ml).

### Texture Profile Analysis

Texture profile analysis of fruit pearls was carried out using Texture Analyser (Model TA. XT. Plus, Make: Stable Micro Systems, UK) equipped with 10 kg load cell. The data from the texture profile (force-time) curve was used to determine chewiness (g), energy to chew (g.%), and stiffness (g/sec) [12].

### Antioxidant Activity and L-Ascorbic Acid

The antioxidant activity of probiotic fruit pearls was determined according to [13] using free radical 2,2-diphenyl-1-picrylhydrazil (DPPH), whereby 0.2 ml of the suspension (containing sodium alginate, fruit juice, and bacterial culture) and 3.8 ml of 0.1 mM DPPH in ethanol were briefly mixed in test tube, and retained in darkness for 30 min. The absorbance was measured at 517 nm by visible light spectrophotometer (772s, Precision and Scientific Instrument Co., Shanghai, China). L-ascorbic acid was used as standard and ethanol as blank. The antioxidant activity was expressed in µg of ascorbic acid eq./ml. Meanwhile, the Association of Official Agricultural Chemists (AOAC)'s titrimetric method was used to determine L-ascorbic acid content [9].

### Tolerance of Probiotic Fruit Pearls to Simulated Human Gastrointestinal Tract

In this research, the tolerance of probiotic fruit pearls was characterized under simulated gastric juice (pH 2.0) and bile salt (0.6% w/v) conditions. The simulated gastric and intestinal juices were to mimic human gastrointestinal (GI) tract [14]. In the experiment, fruit pearls were introduced into the simulated gastric juice and incubated at 37 °C for 3 h. Afterward, 10 g of fruit pearls was mixed with 90 ml of sterile phosphate buffer and broken up by the stomacher for 1 min at room temperature. The mixture was diluted and the number of viable cells determined by pour plate count (log CFU/ml) in MRS agar after incubation at 37 °C for 48 h [15]. The survival rate (%) was then determined.

For bile salt tolerance, the probiotic pearls were submerged in the bile salt (Sigma, USA) and incubated at 37 °C for 3 h. Afterward, 10 g of the sample was mixed with 90 ml of sterile phosphate buffer and disintegrated for 1 min at room temperature using the stomacher. The mixture was diluted and the number of viable cells determined by pour plate count (log CFU/ml) in MRS agar after incubation at 37 °C for 48 h [15]. The survival rate (%) was then determined.

### Sensory Evaluation

Color, odor, flavor, texture, and overall

acceptance of probiotic fruit pearls were evaluated by a team of 30 untrained panelists. Two sets of fruit pearls, i.e. commercially non-probiotic (Ding Fong Foods, Thailand) and probiotic fruit pearls, were served to the panelists who subsequently scored on the sensory features (color, odor, flavor, texture, and overall acceptance) using a 9-point hedonic scale, where 1 denotes extremely dislike and 9 extremely like. Randomized complete block design was used to assess the statistical difference between the non-probiotic and probiotic fruit pearls ( $p \leq 0.05$ ) [10].

### Statistical Analysis

All the experiments were carried out in triplicate and the results expressed as mean  $\pm$  standard deviation and average percentage for the survival rate. Analysis of variance (ANOVA) was used to analyze the data and Duncan's multiple-range test to compare means. Statistical significance was based on the 5% significance level ( $p \leq 0.05$ ).

Use at most three levels of headings that correspond to chapters, sections and subsections. The first level headings for chapter titles should be in 10pt, bold, justified, and upper case font. Leave one blank line before and after the first level headings, respectively.

Table 2 Sensory evaluation of four experimental fruit pearls

| Fruit pearls | Sensory evaluation            |                              |                              |                       |                              |
|--------------|-------------------------------|------------------------------|------------------------------|-----------------------|------------------------------|
|              | Color                         | Odor                         | Flavor                       | Texture <sup>ns</sup> | Overall acceptance           |
| Guava        | 5.56 $\pm$ 1.38 <sup>c</sup>  | 4.43 $\pm$ 1.71 <sup>c</sup> | 4.63 $\pm$ 1.62 <sup>c</sup> | 5.76 $\pm$ 1.13       | 5.33 $\pm$ 1.53 <sup>b</sup> |
| Watermelon   | 6.86 $\pm$ 1.47 <sup>bc</sup> | 5.23 $\pm$ 1.52 <sup>b</sup> | 5.36 $\pm$ 1.40 <sup>b</sup> | 5.93 $\pm$ 1.17       | 5.80 $\pm$ 1.32 <sup>b</sup> |
| Pineapple    | 6.40 $\pm$ 1.49 <sup>b</sup>  | 6.46 $\pm$ 1.65 <sup>a</sup> | 6.13 $\pm$ 1.54 <sup>a</sup> | 6.03 $\pm$ 1.62       | 6.46 $\pm$ 1.61 <sup>a</sup> |
| Orange       | 7.40 $\pm$ 1.42 <sup>a</sup>  | 7.13 $\pm$ 1.45 <sup>a</sup> | 6.46 $\pm$ 1.35 <sup>a</sup> | 5.93 $\pm$ 1.38       | 6.90 $\pm$ 1.44 <sup>a</sup> |

The experiments were carried out in triplicate, and the results are expressed as mean  $\pm$  standard deviation. Different superscripts in the same column indicate significant difference ( $p \leq 0.05$ ). ns denotes not significant ( $p > 0.05$ ).

because fruit juices normally have low pH (3.0-4.5), which affects the stability of probiotics. In Table 1, pH of fruit juices, except watermelon, were below 4.5, which is uncondusive to bacterial viability.

Sensory features of fruit pearls are also important in formulating probiotic food products. Table 2 presents the sensory evaluation of the four fruit pearls on color, odor, flavor, texture, and overall acceptance.

The results indicated that the evaluation scores of orange pearls were statistically highest in nearly all sensory characteristics ( $p \leq 0.05$ ). Orange fruit juice (i.e., 100% genuine orange juice) was thus selected for subsequent development into probiotic fruit pearls.

### Characteristics of Probiotic Orange Pearls

Table 3 tabulates the average size, texture profile, L-ascorbic acid, and antioxidant activity of probiotic orange pearls. The average size of probiotic pearls was 11.4 $\pm$ 0.05 mm, as opposed to 0.5-3 mm for conventionally probiotics-encapsulated beads using

## RESULTS AND DISCUSSION

### Comparison of Fruit Pearls

Table 1 tabulates the pH and total acidity of four fruit juices (guava, watermelon, pineapple, and orange) mixed with sodium alginate.

Table 1 pH and total acidity of fruit juices

| Fruit pearls | pH                           | Titrateable acidity (%)      |
|--------------|------------------------------|------------------------------|
| Guava        | 4.31 $\pm$ 0.02 <sup>b</sup> | 0.70 $\pm$ 0.07 <sup>c</sup> |
| Watermelon   | 5.73 $\pm$ 0.04 <sup>a</sup> | 0.62 $\pm$ 0.15 <sup>c</sup> |
| Pineapple    | 4.12 $\pm$ 0.02 <sup>d</sup> | 1.65 $\pm$ 0.80 <sup>a</sup> |
| Orange       | 4.23 $\pm$ 0.03 <sup>c</sup> | 1.23 $\pm$ 0.10 <sup>b</sup> |

The experiments were carried out in triplicate, and the results are expressed as mean  $\pm$  standard deviation. Different superscripts in the same column indicate significant difference ( $p \leq 0.05$ ).

According to Gandomi, Abbaszadeh, Misaghi, Bokaie and Noori [16], formulating probiotic fruit juices presents greater challenges than dairy products

extrusion method [18]. In addition, the beads were spherical in shape given that sphericity plays a crucial role in preventing cell overgrowth in encapsulated beads [18].

Table 3 Characteristics of probiotic orange pearls

| Characteristics  | Value                 |
|--|-----------------------|
| Size (mm)  | 11.4 $\pm$ 0.05       |
| Texture  |                       |
| Chewiness (g)  | 220.03 $\pm$ 26.02    |
| Energy to chew (g.%)   | 3,400.57 $\pm$ 421.92 |
| Stiffness (g/sec)  | 390.71 $\pm$ 25.66    |
| L-ascorbic acid (mg/ml)  | 0.095 $\pm$ 0.01      |
| DPPH radical-scavenging activity ( $\mu$ g ascorbic acid eq./ml) | 294 $\pm$ 22.13       |

The experiments were carried out in triplicate, and the results are expressed as mean  $\pm$  standard deviation.

Based on the bead/pearl size, encapsulation is classified into two categories: macroencapsulation (mm to cm) and microencapsulation (1-1000  $\mu$ m) [8],[17]. The probiotic fruit pearls of this experimental research belong to the macro-encapsulation group. Figure 1 illustrates the experimental probiotic orange fruit pearls.



Figure 1 The experimental probiotic orange pearls

Table 3 also presents the texture of probiotic orange pearls, including chewiness, energy to chew, and stiffness. The texture of fruit pearls was positively correlated with sodium alginate concentrations. Elevated sodium alginate concentrations induced a higher degree of cross-linkage between gel networks, resulting in denser and more rigid gel structure. Specifically, sodium alginate gelation developed as  $\text{Ca}^{2+}$  gelling ions crosslinked with sodium alginate whose optimal concentrations for probiotics encapsulation were 0.5 - 4% (w/v). Sodium alginate is preferable for probiotics encapsulation due to ease of use, biocompatibility, economy, non-toxicity, rapid gel matrix formation around bacterial cells, and mild processing [18]. In Table 3, the DPPH antioxidant activity and L-ascorbic acid content indicated adequate antioxidant capacity of the probiotic orange pearls.

#### Viability of Probiotics in Fruit Pearls under Simulated Gastrointestinal Condition

For health benefits, probiotics must be able to survive during gastrointestinal transition and exist in high proportions in the intestines ( $10^6$  -  $10^8$  CFU/g of intestinal content) [19]. In this research, the viability of *Ped. pentosaceus* ARG-MG12 encapsulated in orange pearls was investigated in the simulated gastric juice (pH 2.0) and bile salt (0.6% w/v) environments for 3 h each. Table 4 tabulates the assay results, where control denotes the initial condition at 0 h.

Encapsulation of probiotics in hydrocolloid beads protects the bacterial cells against damage caused by external environment and during gastrointestinal transition [18]. In Table 4, the bacterial stability decreased in both stimulated gastric juice ( $8.96 \pm 0.06$  log CFU/g) and bile salt ( $10.14 \pm 0.04$  log CFU/g), vis-à-vis the control ( $10.76 \pm 0.12$  log CFU/g), with the corresponding survival rates of 83.27% and 94.24%. In comparison, unencapsulated *Ped. pentosaceus* strains in the simulated gastric juice suffered a reduction in the bacterial stability by two logarithmic cycles after 1h incubation [21].

Table 4 Viability and survival rate of probiotics under simulated gastrointestinal conditions

| Conditions                           | Viability<br>(logCFU/g) | Survival<br>rate (%) |
|--------------------------------------|-------------------------|----------------------|
| Control                              | $10.76 \pm 0.12^a$      | 100.00 <sup>a</sup>  |
| Stimulated gastric<br>juice (pH 2.0) | $8.96 \pm 0.06^c$       | 83.27 <sup>c</sup>   |
| Bile salt (0.6%)                     | $10.14 \pm 0.04^b$      | 94.24 <sup>b</sup>   |

The experiments were carried out in triplicate, and the results are expressed as mean  $\pm$  standard deviation. Different superscripts in the same column indicate significant difference ( $p \leq 0.05$ ).

In this research, 83.27% of *Ped. pentosaceus* ARG-MG12 survived after 3 h in low pH environment, a time period sufficient for the probiotics to reach their action site in the intestine [20]. In addition, 94.24% of the bacteria were capable of surviving high bile salt concentration (0.6% w/v). In [21], unencapsulated *Ped. pentosaceus* strains exhibited abundant growth at 0.5% concentration of bile salt but poor growth rates at 1-2% concentrations, suggesting that encapsulation contributes to the enhanced viability of probiotics in gastrointestinal tract.

#### In Storage Cell Survival and Sensory Evaluation

Table 5 tabulates the viability and survival rates of *Ped. pentosaceus* stored at 6 °C for 0, 3, 5, 7, and 14 days. The cell viability decreased with extended storage time ( $p \leq 0.05$ ). According to Ding and Shah [22], encapsulated *Ped. pentosaceus* could survive in orange and apple juices for six weeks in refrigerated storage (4 °C), whereas free cells (unencapsulated) lost their viability within five weeks.

Table 5 Viability and survival rate of probiotics during storage at 6 °C

| Storage<br>(days) | Viability<br>(logCFU/g) | Survival rate<br>(%) |
|-------------------|-------------------------|----------------------|
| 0                 | $11.38 \pm 0.05^a$      | 100.00 <sup>a</sup>  |
| 3                 | $9.02 \pm 0.04^b$       | 79.26 <sup>b</sup>   |

|    |                        |                    |
|----|------------------------|--------------------|
| 5  | 9.12±0.02 <sup>b</sup> | 80.14 <sup>b</sup> |
| 7  | 9.11±0.02 <sup>b</sup> | 80.05 <sup>b</sup> |
| 14 | 8.58±0.20 <sup>c</sup> | 75.40 <sup>c</sup> |

The experiments were carried out in triplicate, and the results are expressed as mean ± standard deviation. Different superscripts in the same column indicate significant difference ( $p \leq 0.05$ ).

Table 6 Sensory evaluation of commercial (non-probiotic) and probiotic orange pearls

| Fruit pearls             | Sensory evaluation  |                        |                      |                       |                                  |
|--------------------------|---------------------|------------------------|----------------------|-----------------------|----------------------------------|
|                          | Color <sup>ns</sup> | Odor                   | Flavor <sup>ns</sup> | Texture <sup>ns</sup> | Overall acceptance <sup>ns</sup> |
| Commercial orange pearls | 7.77±1.13           | 6.53±1.87 <sup>b</sup> | 7.23±1.59            | 7.60±1.35             | 7.40±1.27                        |
| Probiotic orange pearls  | 7.57±1.04           | 7.67±1.26 <sup>a</sup> | 7.20±1.62            | 7.13±1.47             | 7.50±1.13                        |

The experiments were carried out in triplicate, and the results are expressed as mean ± standard deviation. Different superscripts in the same column indicate significant difference ( $p \leq 0.05$ ). ns denotes not significant ( $p > 0.05$ ).

In Table 5, the viability of probiotics in the orange pearls steadily declined from day 0 through to termination (day 14). At termination, the remaining bacteria in the probiotic orange pearls were still above 8 log CFU/g, given that the minimum concentrations of probiotics are  $10^6$ – $10^7$  CFU/ml at the end of product's shelf life [6].

Table 6 presents the sensory evaluation of commercially non-probiotic (15% orange juice) and probiotic orange (100% orange juice) pearls by 30 untrained panelists.

The results revealed that, except for odor where the probiotic orange pearls received higher scores, the participants were unable to differentiate between the non-probiotic and probiotic orange pearls ( $p > 0.05$ ). Essentially, the orange pearls containing *Ped. pentosaceus* ARG-MG12 possess health and economic potential as a functional food product.

## CONCLUSIONS

This research investigated the encapsulation of *Ped. pentosaceus* ARG-MG12 in pure orange juice pearls as a functional food product. The probiotic pearls also underwent gastric juice (pH 2.0) and bile salt (0.6% w/v) conditions for 3 h each to simulate human gastrointestinal tract; and variable storage times at 6 °C for 14 days to assess cell viability. The experimental results showed that the probiotic orange pearls containing *Ped. pentosaceus* ARG-MG12 had 390.71 g/sec of stiffness, DPPH radical-scavenging activity of 294 µg ascorbic acid eq./ml, and L-ascorbic acid content of 0.095 mg/ml. The remaining bacteria at termination were above 8 log CFU/g, given that the minimum concentrations of probiotics should be  $10^6$ – $10^7$  CFU/ml at the end of product's shelf life. Moreover, the sensory evaluation revealed that the participants were unable to differentiate between the non-probiotic and probiotic orange pearls ( $p > 0.05$ ).

## ACKNOWLEDGMENTS

The authors would like to extend deep gratitude to the Faculty of Agricultural Technology, Rajamangala University of Technology Thanyaburi, for the research grant.

## REFERENCES

- [1] Martin, L.C., Tea: The drink that changed the world, Rutland: Tuttle Publishing, 2007, pp. 219-220.
- [2] The Federal Institute for Risk Assessment (BfR), FAQs about the trendy drink Bubble Tea, 2012, pp. 1-2.
- [3] Estevinho B.H., Rocha F., Santos L., and Alves A., Microencapsulation with chitosan by spray drying for industry applications: A review. Trends Food Science Technology, Vol. 31, 2013, pp. 138-155.
- [4] Antunes A.C.E., Liserre A.M., Coelho A.L.A., Menezes C.R., Moreno I., Yotsuyanagi K., Azambuja N.C., Acerola nectar with added microencapsulated probiotic. LWT – Food Science Technology, Vol. 54, 2013, pp. 125-131.
- [5] Ozyurt, V.H. and Ötles, S., Properties of probiotics and encapsulated probiotics in food, Acta Scientiarum Polonorum. Technologia Alimentaria, Vol. 13, Issue. 4, 2014, pp. 413-424.
- [6] Nualkaekul, S., Cook, M.T., Khutoryanskiy, V.V. and Charalampopoulos, D., Influence of encapsulation and coating materials on the survival of *Lactobacillus plantarum* and *Bifidobacterium longum* in fruit juices, Food Research International, Vol. 53, 2013, pp. 304-311.
- [7] Marco, M. L., Heeney, D., Binda, S., Cifelli, C. J., Cotter, P. D., Foligné, B., & Smid, E. J., Health benefits of fermented foods: Microbiota and beyond. Current Opinion in Biotechnology,



- Vol. 44, 2017, pp. 94–102.
- [8] Kavitate, D., Kandasamy, S., Devi, P.B., and Shetty, P.H. Recent developments on encapsulation of lactic acid bacteria as potential starter culture in fermented foods – A review. *Food Bioscience*, Vol. 21, 2018, pp. 34-44.
- [9] AOAC., Official methods of analysis of the Association of Official Analytical Chemists, 17th ed., Association of Official Analytical Chemists, Arlington VA, 2000, pp. 1058-1059.
- [10] Yang, M., and Li, L. Physicochemical, textural and sensory characteristics of probiotic soy yogurt prepared from germinated soybean characteristics of probiotic soy yogurt. *Food Technology and Biotechnology*, Vol. 48, Issue. 4, 2010, pp. 490-496.
- [11] Krasakoopt, W., and Kitsawad, K., Sensory characteristics and consumer acceptance of fruit juice containing probiotics beads in Thailand, *Australian Journal of Technology*, Vol. 14, 2010, pp. 33-38.
- [12] Kumar, P., and Mishra, H. N. Mango soy fortified set yoghurt: effect of stabilizer addition on physicochemical, sensory and textural properties. *Food Chemistry*, Vol. 87, 2004, pp. 501-507.
- [13] Brand-Williams, W., Cuvelier, M., and Berset, C., Use of a free radical method to evaluate antioxidant activity, *LWT - Food Science and Technology*, Vol. 28, 1995, pp. 25-30.
- [14] Charteris W.P., Kelly P.M., Morelli L. and Collins J.K., Development and application of an in vivo methodology to determine the transit tolerance of potentially probiotic *Lactobacillus* and *Bifidobacterium* species in the upper human gastrointestinal tract, *Journal of Applied Microbiology*, Vol. 84, 1998, pp. 759-768.
- [15] Hyronimus B., Marrec C.L., Sassi A.H. and Deschamps A., Acid and bile tolerance of spore-forming lactic acid bacteria. *International Journal Food Microbiology*, Vol. 61, 2000, pp. 193-197.
- [16] Gandomi, H., Abbaszadeh, S., Misaghi, A., Bokaie, S., and Noori, N., Effect of chitosan-alginate encapsulation with inulin on survival of *Lactobacillus rhamnosus* GG during apple juice storage and under simulated gastrointestinal conditions, *LWT - Food Science and Technology*, Vol. 69, 2016, pp. 365-371.
- [17] Heidebach, T., Först, P., and Kulozik, U., Microencapsulation of probiotic cells for food applications, *Critical Reviews in Food Science and Nutrition*, Vol. 52, 2012, pp. 291–311.
- [18] Krasakoopt, W., Bhandari, B., and Deeth, H., Evaluation of encapsulation techniques of probiotics for yogurt. *International Dairy Journal*, Vol. 13, 2004, pp. 3–13.
- [19] Marteau, P., and Rambaud, J. C. Potential of using lactic acid bacteria for therapy and immunomodulation in man. *FEMS Microbiology Reviews*, Vol. 12, Issue. 1-3, 1993, pp. 207-220.
- [20] Fernandez, M., F. Boris, S., and Barbés, C., Probiotic properties of human *lactobacilli* strains to be used in the gastrointestinal tract. *Journal of Applied Microbiology*, Vol. 94, 2003, pp. 449-455.
- [21] Ramirez-Chavarin, M.L., Wachter, C., Eslava-Campos, C.A. and Perez-Chabela, M.L., Probiotic potential of thermotolerant lactic acid bacteria strains isolated from cooked meat products, *International Food Research Journal*, Vol. 20, Issue. 2, 2013, pp. 991-1000.
- [22] Ding, W. K., & Shah, N. P. Survival of free and microencapsulated probiotic bacteria in orange and apple juices. *International Food Research Journal*, Vol. 15, Issue. 2, 2008, pp. 219–232.
- [23] Park, J.K., and Chang, H.N., Microencapsulation of microbial cells. *Biotechnology Advances*, Vol. 18, 2000, pp. 303–319.

## EFFECT OF ENVIRONMENTAL FLUCTUATIONS ON INCIDENCE OF MYCOFLORA

H.N.P. Singh, Sunita Kumari and M.M. Prasad  
Post Graduate Department of Biotechnology  
T.M.Bhagalpur University, Bhagalpur-812007, Bihar, (India)

### ABSTRACT

The value of medicinal plants on great extent depends on their potential ability to cure diseases. Usually these are collected from the forest or from the natural habitats by the local people of that area and are stored in gunny bags or dumped on the floor of kaccha store house. The faulty storage techniques makes the plants or plant parts victim of several micro-organisms which in turn results in the deterioration of their therapeutic value. Keeping this in view four drug plants viz. *Ricinus communis* (Andi), *Carthamus tinctorius* (Kusum), *Datura alba* (Safed datura) and *Solanum xanthocarpum* (Kateli) was undertaken from field, storage centres and markets of Bhagalpur (Bihar) and its suburbs to record their fungal flora. The results revealed that composition of storage fungi fluctuated on account of the change in the atmospheric condition and the hosts. The fungi was maximum during rainy season due to high humidity, suitable temperature and heavy rainfall. However less incidence of fungi was recorded during winter season when the temperature, R.H. and rainfall was minimum. A large number of fungi was also observed in summer. But in winter; fungal incidence was noted minimum as compared to summer season.

*Keywords: Effect, Environment, Incidence, of, Mycoflora.*

### INTRODUCTION

Rheumatism is a serious problem of Indian mass. Early literature reveals that a large number of plants and plant parts, like seed, leaf and roots are used for the treatment of this disease. Some of the most important ones are *Ricinus communis*, *Carthamus tinctorius*, *Solanum xanthocarpum* and *Datura alba*. The traditional method of using these plants, plant parts, seeds as well as fruits as antirheumatic diseases has been practiced since long in the tribal areas. The unscientific collection, storage, handling and marketing of these drug plants by the unskilled people could not establish their efficacy against diseases. So, that present investigation deals with the effect of Environmental Fluctuations on Incidence of Mycoflora associated with various medicinal plants.

### MATERIALS & METHODS

Different parts of four medicinal plants i.e. *Ricinus communis* (seed), *Carthamus tinctorius* (seed), *Solanum xanthocarpum* (leaf) and *Datura alba* (leaf) which are commonly used against

rheumatism by the local practicers and Hakims. Those are collected from natural habitats markets and store houses of Bhagalpur and its adjoining area. The samples were brought to the laboratory in separate polyethylene bags for detailed study.

Mycoflora associated with the collected samples were isolated following the standard technique recommended by International Seed Testing Association (1966) after sterilizing the samples by 2% sodium hypochloride (NaOCl) solution.

### Blotter Test

Sterilized seeds/leaves of approrimately equal size were placed aseptically on moistened blotters by the sterilized distilled water in petri plates .The plates were incubated for 7days at room temperature ( $25 \pm 2^{\circ}\text{C}$ ). The moisture level of the blotters was maintained by adding sterilized distilled water. Samples were examined regularly from 4<sup>th</sup> days onward under microscope .The fungi appeared on the samples

were isolated and purified and maintained on Potato Dextrose Agar (PDA) as well as Asthana and Hawker agar solid slants. The identification of fungi were also done regularly.

## RESULTS

A comparative accounts of plants/parts with their therapeutic value as well as fungi associated with them during different seasonal variation has been presented in Table 1.

A perusal of Table illustrates that *Aspergillus candidus*, *A. flavus*, *A. niger*, *Fusarium oxysporum*, *Penicillium* sps, *Chaetomium* – *globossum*, *C. cristatum*, *C. cochloides*, *Curvularia lunata*, *Alternaria alternata* and *Colletotrichum* sp. were common fungal flora on all the samples during winter season (November to February) when the temperature and RH ranged from 7.5 to 23.6 °C and 50-97% respectively, the rainfall ranged between 1.4 to 8.0 mm. Besides above listed fungi *Papulospora* sp. and *Rhizopus stolonifer* were listed from *C. tinctorius* seed while *Helminthosporium spiciferum* was recorded from *S. xanthoxarpum* leaves.

The nature and number of fungi varied with the changes in the temperature (10.5-37.2 °C Humidity (31-83% RH) and rainfall (0-0.77mm) during the summer season (March to June). Presence of *Aspergillus flavus*, *A. niger*, *A. candidus*, *A. ochraceus*, *Rhizopus stolonifer*, *Chaetomium cochloides*, *C. globossum*, *Fusarium moniliforme*, *F. oxysporum*, *Penicillium citrinum*, *Curvularia lunata*, *Alternaria alternata*, *Helminthosporium spiciferum*, *Colletotrichum dematium* and *Botryodiplodia theobromae* were recorded on all the selected samples. Besides, these *Rhizopus nigricans* was isolated from the seeds of *C. tinctorius* while *Papulospora* sps, was recorded on *Ricinus communis* seeds.

During rainy season i.e. July to October the environmental temperature, humidity and rainfall ranged between 21.5-24.5°C, 71-91% and 30.5-33.2 mm respectively. It was also noted that the number of myoflora was maximum during the rainy season. *Aspergillus flavus*, *A. niger*, *A. candidus*, *Fusarium moniliforme*, *F. equiseti*, *Chaetomium cochloides*, *C. cristatum*, *C. globossum*, *Penicillium citrinum*, *Colletotrichum dematium*, *Cercospora* sps, *Cladospora cladosporioides*, *Rhizopus stolonifer*, *Curvularia lunata* and *Botryodiplodia theobromae* were isolated from all the selected samples.

## DISCUSSION

The above findings reveal that the medicinal plants/ parts are highly colonized by a large number of fungi. *A. flavus*, *A. niger*, *Fusarium moniliforme*, *F. oxysporum*, *Penicillium citrinum*, *Rhizopus stolonifer*, *Chaetomium cochloides*, *C. globossum*, *Alternaria alternata*, *Curvularia lunata* were regularly recorded on almost all the hosts throughout the year.

A comparative review of Table-1 indicates that composition of storage fungi fluctuated on account of the change in the atmospheric condition and was found maximum during the rainy season. Lesser incidence of fungi was recorded during winter when the temperature, RH and rainfall were minimum. However in the summer season minimum number of fungi was observed in comparison to winter season where maximum number of fungi was noted. Roy *et al.* (1987), Dutta (1988), Chourasia (1990), Chavan *et al.* (1995) and Singh *et al.* (2012) have also observed the similar trend when they worked with various hosts.

The variation in the fungal incidence in different seasons was obviously due to their different level of tolerance to grow under variable environmental conditions. Singh (1992), Prasad *et al.* (1995) observed that maximum number of fungi was found during July to September when temperature, humidity and Rainfall was maximum when they worked with different host. Kadians (1989) observed maximum disease incidence during the rainy season while working on urad bean.

The early literature also shows that higher level of relative humidity favored the luxuriant fungal growth on stored commodities (Christensen 1973 and Wallace *et al.* 1976). The view was also supported by Bhatt and Chauhan (1985), Kumari and Roy (1990) and Singh (1992) who worked on environmental conditions.

## CONCLUSION

Preliminary survey of field, store houses and markets have revealed that drug plants, plant parts and seeds were contaminated by a number of fungi of different groups. However, the nature of mycoflora varied with the chemical composition of the hosts as well as with condition of storage.

The seasonal variations like temperature, humidity and rainfall plays major role on the incidence of fungi (Awasthi and Kolte 1994).

Table 1: Mycoflora Associated with Drug Plants/Parts

| Name of the Plant/Family | Winter Season (November-February) | Summer Season (March-June) | Rainy Season (July-October) |
|--------------------------|-----------------------------------|----------------------------|-----------------------------|
| Ricinus                  | Aspergillus flavus                | A. flavus                  | A. flavus                   |
| Cobbunis                 | A. niger                          | A. candidus                | A. niger                    |
| (Euphorbiaceae)          | A. candidus                       | A. ochraceus               | A. candidus                 |
|                          | Chaetomium globosum               | Chaetomium cochloides      | A. nidulans                 |
|                          | C. cochloides                     | C. cristatus               | Chaetomium globosum         |
|                          | Curvularia sp.                    | Rhizopus stolonifer        | Colletotrichum sp.          |
| C. luntea                | Colletotrichum sp.                | Botryodiplodia theobromae  |                             |
|                          | Fusarium oxysporum                | F. moniliforme             | Fusarium equiseti           |
|                          | Penicillium sp.                   | F. equiseti                | F. oxysporum                |
|                          |                                   | Papulospora sp.            | F. oxysporum                |
|                          |                                   | Penicillium citrinum       | Penicillium citrinum        |
| Carthamus                | A. flavus                         | A. flavus                  | A. nidulans                 |
| Tinctorius               | A. niger                          | A. ochraceus               | A. flavus                   |
| (Coarctatae)             | C. lunata                         | Curvularia lunata          | A. niger                    |
|                          | F. moniliforme                    | Chaetomium globosum        | A. candidus                 |
|                          | F. equiseti                       | C. cochloides              | C. globosum                 |
|                          | Papulospora sp.                   | Colletotrichum dematium    | C. cochloides               |
|                          | Alternaria alternata              | F. moniliforme             | C. indicum                  |
|                          | Rhizopus stolonifer               | F. oxysporum               | F. moniliformae             |
|                          |                                   | Penicillium citrinum       | F. equiseti                 |
| Solanum                  | Actinospora sp.                   | A. alternata               | Actinospora sp.             |
| Xanthocarpum             | Alternaria alternata              | A. flavus                  | A. flavus                   |
| (Solanaceae)             | Aspergillus flavus                | Chaetomium cochloides      | A. niger                    |
|                          | Chaetomium globosum               | C. globosum                | A. candidus                 |
| B. theobromae            | Colletotrichum sp.                | Colletotrichum dematium    |                             |
|                          | Fusarium oxysporum                | Curvularia lunata          | Chaetomium globosum         |
|                          | Helminthosporium                  | Fusarium moniliforme       | C. cochloides               |
|                          | Speciferum                        | F. oxysporum               | Fusarium moniliforme        |
|                          |                                   | H. spiciferum              | F. equiseti                 |
|                          |                                   |                            | Nigrospora oryzae           |
|                          |                                   |                            | Papulospora sp.             |
|                          |                                   |                            | Helminthosporium sp.        |
| Datura alba              | Fusarium equiseti                 | Fusarium oxysporum         | Aspergillus sp.             |
| (Solanaceae)             | Curvularia lunata                 | E. equiseti                | A. flavus                   |
|                          | Alternaria alternata              | Curvularia lunata          | Colletotrichum sps.         |
|                          | Aspergillus flavus                | Alternaria alternata       | Chaetomium indicum          |
| C. globosum              | A. niger                          | Colletotrichum dematium    |                             |
|                          | A. candidus                       | Cladosporium               | C. cochloides               |
|                          |                                   | Cladosporoides             | Cercospora sp.              |
|                          |                                   | Aspergillus flavus         | Botryodiplodia sp.          |

|  |  |          |               |
|--|--|----------|---------------|
|  |  | A. niger | Papulospo sp. |
|--|--|----------|---------------|

However, periodical observation and survey of the samples showed that *Aspergillus flavus*, *A. niger*, *Fusarium moniliforme*, *Rhizopus stolonifer* and *Alternaria alternata* were most common fungal flora on all the samples throughout the year whereas *Curvularia lunata*, *Chaetomium globosum*, *Fusarium oxysporum* and *Penicillium citrinum* remained confined to specific seasons. Some of the fungi like *A.candidus*, *F. semitectum*, *H. spiciferum* *Papulospora* sps. *Cercospora* sps. *Nigrospora* sps. were rare on all the samples. The maximum incidence of fungi was noted between July and October when atmospheric temperature, humidity and rainfall are quite suitable for the presence of fungal incidence. While minimum incidence noted between November to February. These periods are safest for the storage of medicinal plants/ parts as well as seeds due to minimum temperature, humidity and scanty rainfall.

## REFERENCES

- [1] Singh, H.N.P., Studies on disease of Banana: A pathological and Biochemical approach Ph.D. Thesis, 1992, pp. 26-32, 33-43.
- [2] Singh, H.N.P., Kumari, S. and Prasad, M.M. Influence of Meteorological conditions on diseases development of Banana fruits. 2012 Proceeding volume, Glimpses of Phythology for sustainable Agriculture, A.B. Publication New Delhi, Edited Dr. H.K. Chaurasia, Dr. A.K. Roy & Dr. Usha Kumari pp. 227-232.
- [3] Geetika and Ahmad, Mushtaq. Influence of abiotic factors on the bio-control efficacy of trichoderma against *Fusarium proliferatum* under in vitro. Journal of Mycology & plant pathology. 2018, Vol. 48 No. 3 pp. 348-356.
- [4] Singh, H.N.P. and Prasad M.M. Effect of temperature and humidity on fungal spoilage of two varieties of banana Indian Botanical Reporter. 1992, Vol. 6(1) pp. 85-86.
- [5] Prasad, M.M., Singh, H.N.P. Roy, A.K. and Sinha, R.K. Microbial spoilage of silk cocoons in storage centres of Bihar and their control 1995, Final Technical Report U.G.C. Govt. of India, New Delhi, Code No. F 3-22/91(RBB-1) pp. 33-56.
- [6] Roy, A.K., Chourasia, H.K. and Kumari N. Seasonal Variation in mycoflora associate with store medicinal fruits and seeds Biol. Bull. India 1987, Vol. 9 No. 2, pp. 111-116.
- [7] Gutta, G.R. and Roy A.K. Mycoflora associate with strychnos seeds and deterioration of their active principles under storage Ind. Phytopathi 1987, Vol. 40 No. 4, pp. 520-524.
- [8] Chourasia, H.K. Pathological and Biochemical investigation of some common drug plants with special reference to Mycotoxin eleaboration. Ph.D. Thesis, Bhagalpur University, 1990.
- [9] Chavan, S.B., Khandge, S.V., Varshneya, M.C. and Patil, J.D. Influence of weather parameters on conidia formation in powdery mildew of grope. 1995 Indian phytopath Vol. 48. No. 01 pp. 40-44.
- [10] Kadian, O.P. Effect of environment on incidence and development of leaf crinkle disease in urid seed. 1989 Indian phytopath 42(2) pp. 273.
- [11] Bhatt, J.C. and Chauhan, V.S. Epidemiological studies on neck blast of rice in U.P. hills. Indian Phytopath 1985, Vol. 38 No. 1 pp. 126-130.
- [12] Kumari, V. and Roy, A.K. Biodeterioration of Embelia ribes seeds under the influence of different relative humidity. 1990 National Academy Science Letters. Vol. 13 No. 05 pp. 167-169.
- [13] Christensen, C.M., Loss of viability in storage microflora. 1973 Seed Science and Technology 1:547-562.
- [14] Wallace, H.A.H., Sinha, R.N. and Mills, J.J. Fungi associated with small wheat bulks during prolonged storage in Manitoba. 1976. Chad. J. Bot. 54(12) 1332-1343.
- [15] Awasthi, R.P. and Kolte. Epidemiological factors in relation to development & prediction of Alternasia blight of repeseed & mustard 1994. Indian. Phytopath 47(4) pp. 395-39.

## EFFECT OF KNEADING AND FERMENTATION TIME ON CHEMICAL QUALITY OF HERBAL TEA FROM MANGO PEEL

Nunchanok Nanthachai<sup>1</sup>, Intira Lichanporn<sup>1</sup>, Palida Tanganurat<sup>1</sup> and Pradit Kumnongphai<sup>1</sup>

<sup>1</sup>Faculty of Agricultural Technology, Rajamangala University of Technology Thanyaburi, Thailand

### ABSTRACT

This research aimed to develop herbal tea from agricultural by-product such as mango peel. The study was conducted using a 3x3 Factorial in completely randomized design. Two factors were investigated; the kneading time of mango peel at 10, 20 and 30 minutes and the fermentation time of mango peel at 15, 30 and 45 minutes. The result showed that total phenolic content and antioxidant activity of the unripe mango peel were 8.48 mg/g and 18.34%, respectively. And those contents were significantly higher than that ripen mango ( $p \leq 0.05$ ). The kneading and fermentation time were affected on total phenolic content and antioxidant activity of the peel. Mango peel kneaded for 20 minutes had 20.83 – 28.50% antioxidant activity which significantly higher than that kneaded for 10 and 30 minutes ( $p \leq 0.05$ ). And mango peel fermented for 15 minutes had 21.96 – 23.01 mg/g total phenolic compounds that significantly higher than fermentation time at 30 and 45 minutes ( $p \leq 0.05$ ). Sensory evaluation showed that the score of color, flavor and taste of tea from mango peel kneaded and fermented for 10 and 15 minutes, respectively significantly higher than other kneading and fermentation times ( $p \leq 0.05$ ).

**Keywords:** Mango, Herbal tea, Total phenolic compounds, Antioxidant activity

### INTRODUCTION

Tea is an aromatic beverage prepared by pouring hot water over leaves of the *Camellia sinensis*. Tea is a popular beverage, consumed by people worldwide. It is rich in polysaccharides, caffeine, polyphenols and amino acids, as well as antioxidants, which are beneficial for human health [1]. Herbal teas also called tisanes are defined as water-based infusions prepared with herbal ingredients other than *Camellia sinensis*. Such teas are popular amongst health-conscious people as they are rich in minerals and antioxidants [2], [3]. Tisanes are caffeine free and can be served hot or cold. Tisanes were drunk for both enjoyment and medicinal purposes. Plant phenolic, also called polyphenols, are a class of chemical compounds that consist of one or more hydroxyl groups (OH) bonded to one or more benzene rings. In recent years, quantifying the phenolic content and evaluating its contribution to the antioxidant capacity have become important [4]. Phenolic compounds are produced through the secondary metabolism of plants and are essential for their growth. This group of biologically active molecules has been extensively studied due to their multiple biological effects, such as anti-inflammatory, antimicrobial and antioxidant activity [5].

Mango (*Mangifera indica* L.) is one of the most popular and best known tropical fruits due to its production and consumer acceptance [6]. Mango is a highly prized fruit due to its attractive color and flavor, delicious taste and high nutritional value [7],

[8]. Mango is normally used for direct consumption, as well as for the processing of dried fruit, fruit juice and etc [9]. During mango processing, the peel is one of the most important by-products, which constitutes about 15-20 g/100g of the fresh fruit weight [10]. In fact, mango peel has various nutrients, including dietary fiber, protein, fat, and phytochemicals like polyphenols, carotenoids, tocopherols and ascorbic acid etc. [11] - [14]. Bioactive compounds such as polyphenols, carotenoids and anthocyanins present in fruits and vegetables are receiving increased attention because of their potential antioxidant activity. Therefore, mango peel is a potential healthy food ingredient that could be used to improve the functional properties of food [9]. The application of mango peel powder has been reported in biscuits, bread and macaroni etc., and the products showed elevated polyphenol and dietary fiber contents, as well as improved antioxidant ability [15], [16]. However, mango peel has not been applied in beverages. In this study, mango peel was imitated the process of making tea. Kneading and fermentation of the mango peel probably increase phenolic compounds and flavor. Thus, the objective of this research was to develop herbal tea from mango peel by investigated the optimization of kneading and fermentation times of the peel.

### MATERIALS AND METHODS

#### Experimental Materials

In this research, unripe (immature) and ripe (mature) mangos were of *Numdokmai* variety and acquired from a local fresh market in Thailand. Harvesting index of unripe and ripe mango were 70 – 90 and 95 – 105 days after fruiting, respectively [17]. Unripe and ripe mangos were presented in Fig. 1. The fruits were first washed with tap water and then rinsed with distilled water before left to dry and peels removed.

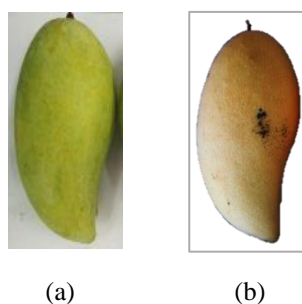


Figure 1 Physical appearance of: (a) unripe and (b) ripe mango

## Experimental Methodology

### *Mango peel drying process*

The mango peels were cut into smaller pieces (1 x 3 cm) and kneaded by a kneader mixer (EMS-200LP, Japan) at a moderate speed for 10 minutes. The kneaded peels were transferred to stainless steel containers and covered with straining cloth to ferment for 10 minutes at room temperature. The fermented peels were then oven-dried at 60°C for 3 hours (BINDER GmbH, Germany). The dried unripe and ripe mango-peel tea products were retained in a concealed airtight container at room temperature.

### *Optimization of kneading and fermentation times*

Prior to optimization, total phenolic content and antioxidant activity of unripe and ripe dried mango-peel tea products were characterized and compared. The tea product possessing higher total phenolic content and antioxidant activity was selected for subsequent experiment.

The kneading and fermentation durations of chosen dried mango peel tea product were optimized with regard to the chemical properties and sensory characteristics using a 3x3 factorial design, giving rise to 9 experimental runs (i.e., nine dried mango peel tea products). The kneading time was varied between 10, 20, and 30 minutes; and the fermentation time between 15, 30, and 45 minutes. The chemical properties of interest were total phenolic content and antioxidant activity and the

sensory characteristics included color, aroma, and taste.

### *Characterization of chemical properties*

In this research, total phenolic content was determined using Folin-Ciocalteu method [18] with minor modifications. In the analysis, 0.3 milliliters of tea infusion was first mixed with 2.25 milliliters of 10% Folin-Ciocalteu reagent dissolved in distilled water, and with 2.25 milliliter of 6% sodium carbonate solution. The mixture was then incubated for 90 minutes at room temperature. The absorbance was measured at 725 nanometers using a spectrophotometer, and total phenolic content expressed as milligram/gram (mg/g).

Antioxidant activity was determined by (1,1-diphenyl-2-picrylhydrazyl) radical scavenging activity [19] with minor modifications, whereby 0.1 milliliter of tea infusion was added to 1.9 milliliter of 0.1 milliliter 1,1-diphenyl-2-picrylhydrazyl solution dissolved in ethanol, shaken and incubated in the dark for 30 minutes at room temperature. The absorbance was measured at 517 nanometers using the spectrophotometer. The 1,1-diphenyl-2-picrylhydrazyl scavenging activity was calculated by

$$\text{Antioxidant activity (\%)} = \frac{A_{\text{control}} - A_{\text{sample}}}{A_{\text{control}}} \times 100$$

where  $A_{\text{control}}$  and  $A_{\text{sample}}$  are the absorbances of reference and tea infusion sample, respectively.

### *Sensory evaluation of mango peel tea*

The sensory evaluation of dried mango peel tea infusions was carried out using a 9-point hedonic scale, where 1 denotes extremely unfavorable and 9 extremely favorable. The dried mango peel tea (3 grams) was brewed in 200 milliliters hot water (80-90°C) for 5 minutes. Then, 20 milliliter of the tea infusions was transferred to tea cups for sensory test where a group of 30 untrained panelists evaluated the tea solution samples on color, aroma, taste, and overall acceptance, based on 9-point hedonic scale.

### *Statistical analysis*

All experiments were carried out in triplicate and the results expressed as mean  $\pm$  standard deviation. Analysis of variance (ANOVA) was used to analyze the data and Duncan's multiple range test to compare means. Statistical significance was based on the 5% significance level ( $p \leq 0.05$ ).



## RESULTS AND DISCUSSION

### Chemical qualities of tea from unripe and ripe mango peel

Figures 2 (a)-(d) respectively illustrate the physical appearance of unripe and ripe dried mango peel tea products and their respective tea infusions. By comparison, unripe mango peel tea possessed a darker color and stronger scent than ripe mango peel tea.

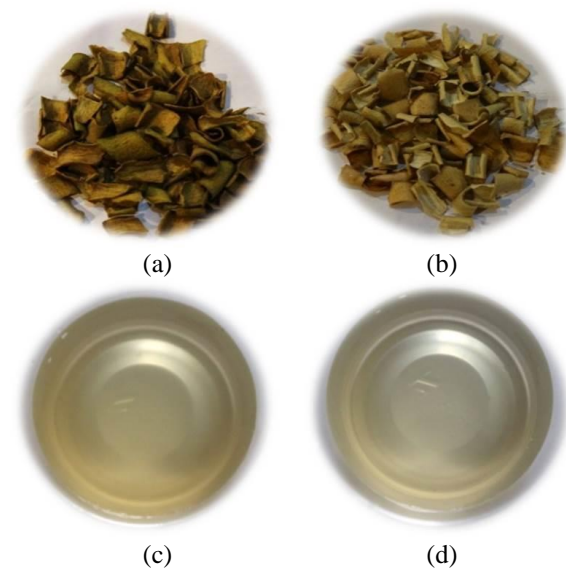


Figure 2 Physical appearance of: (a) unripe and (b) ripe dried mango peel tea products, (c) unripe and (d) ripe mango peel tea infusions

Chlorophyll and carotenoid of mango peel tea were shown in Table 1. Total phenolic content and antioxidant activity of tea from unripe mango peel were 8.48 mg/g and 18.34%, respectively (Table 2). And those contents were significantly higher than that ripe mango ( $p \leq 0.05$ ). The total phenolic content and antioxidant activity of mango peel var. Raspuri and Badami have been reported. The total polyphenols content in 80% acetone extract of raw mango peels ranged from 90 to 110 mg/g peel, whereas it ranged from 55 to 100 mg/g in ripe peels depending on the variety [20]. In the present study, the phenolic content and antioxidant activity were lower than those reported previously; a possible reason could be that the peel was diluted into ready-to-drink-solution before the measurements. However, in this present study also found that total phenolic content and antioxidant activity of the solution from unripe peel higher than product from ripe peel. Thus, the unripe mango peel was selected for the next

experiment.

Table 1 Chlorophyll and carotenoid of tea from unripe and ripe mango peel.

| Tea product       | Chlorophyll (mg/g) | Carotenoid (mg/g) <sup>ns</sup> |
|-------------------|--------------------|---------------------------------|
| Unripe mango peel | 3.33 <sup>a</sup>  | 12.24                           |
| Ripe mango peel   | 0.12 <sup>b</sup>  | 12.80                           |

Mean of the same column with different superscripts indicating significantly differences ( $p \leq 0.05$ ).

ns mean not significant

Table 2 Total phenolic content and antioxidant activity of tea from unripe and ripe mango peel.

| Tea product       | Total phenolic content (mg/g) | Antioxidant activity (%) |
|-------------------|-------------------------------|--------------------------|
| Unripe mango peel | 8.48 <sup>a</sup>             | 18.34 <sup>a</sup>       |
| Ripe mango peel   | 5.85 <sup>b</sup>             | 11.00 <sup>b</sup>       |

Mean of the same column with different superscripts indicating significantly differences ( $p \leq 0.05$ ).

### Optimization of kneading and fermentation times

Kneading and fermentation probably did not affect chlorophyll of mango peel tea (Table 3). Although, chlorophyll of processed mango peel was lower than unprocessed, this might be due to chlorophyll damaged while drying in high temperature. The central Mg atom is replaced by hydrogen ions. This affects the energy levels within the molecule, causing its absorbance spectrum to alter. Thus processed mango peel changed color, becoming a paler, insipid yellowy green. Carotenoid trended to increase after the process (Table 3).

Table 3 Chlorophyll and carotenoid of unripe mango peel teas.

| Kneading & Fermentation (minutes) | Chlorophyll (mg/g) <sup>ns</sup> | Carotenoid (mg/g)   |
|-----------------------------------|----------------------------------|---------------------|
| 10 & 15                           | 0.09                             | 16.22 <sup>bc</sup> |
| 10 & 30                           | 0.08                             | 15.90 <sup>cd</sup> |
| 10 & 45                           | 0.11                             | 14.35 <sup>de</sup> |
| 20 & 15                           | 0.10                             | 19.44 <sup>a</sup>  |
| 20 & 30                           | 0.09                             | 18.94 <sup>a</sup>  |
| 20 & 45                           | 0.09                             | 17.56 <sup>ab</sup> |
| 30 & 15                           | 0.05                             | 16.26 <sup>bc</sup> |
| 30 & 30                           | 0.12                             | 13.25 <sup>e</sup>  |
| 30 & 45                           | 0.08                             | 15.14 <sup>d</sup>  |

Mean of the same column with different superscripts indicating significantly differences ( $p \leq 0.05$ ).

ns mean not significant

In Table 4, total phenolic of unripe mango peel tea were positively correlated with the fermentation time, and the antioxidant activity initially rose with increase in the kneading time and declined beyond 20 minutes. Specifically, the moderate kneading time (20 minutes), for all fermentation durations (15, 30, 45 minutes), achieved significantly higher antioxidant activity (20.83 – 28.50%), compared with short (10 minutes; 16.65 – 19.20%) and long (30 minutes; 15.93 – 18.70%) kneading time ( $p \leq 0.05$ ). Meanwhile, the short fermentation time (15 minutes) yielded significantly higher total phenolic compounds (21.96 – 22.62 mg/g), vis-à-vis moderate (30 minutes; 17.34 – 20.01 mg/g) and long (45 minutes; 17.35 – 19.78 mg/g) fermentation times ( $p \leq 0.05$ ). Generally, total phenolic contents of herbal teas were between 0.08 - 28.97 g/100g dry weight, averaging 4.52 g/100g dry weight [21].

Table 4 The total phenolic content and antioxidant activity of unripe mango peel teas.

| Kneading & Fermentation (minutes) | Phenolic (mg/g)    | Antioxidant activity (%) |
|-----------------------------------|--------------------|--------------------------|
| 10 & 15                           | 21.96 <sup>a</sup> | 19.20 <sup>b</sup>       |
| 10 & 30                           | 18.13 <sup>c</sup> | 17.30 <sup>b</sup>       |
| 10 & 45                           | 17.35 <sup>c</sup> | 16.65 <sup>c</sup>       |
| 20 & 15                           | 22.21 <sup>a</sup> | 28.50 <sup>a</sup>       |
| 20 & 30                           | 20.01 <sup>b</sup> | 25.80 <sup>a</sup>       |
| 20 & 45                           | 19.78 <sup>c</sup> | 20.83 <sup>a</sup>       |
| 30 & 15                           | 22.62 <sup>a</sup> | 18.43 <sup>b</sup>       |
| 30 & 30                           | 17.34 <sup>c</sup> | 15.93 <sup>c</sup>       |
| 30 & 45                           | 18.25 <sup>c</sup> | 18.70 <sup>b</sup>       |

Mean of the same column with different superscripts indicating significantly differences ( $p \leq 0.05$ ).

It was obvious that processed mango peel had phenolic content and antioxidant activity significantly higher than mango peel without any process ( $p \leq 0.05$ ). The results in this study were consistent with the previous study [22]. They found that Japanese-style-green-tea-process-young (JGTP-Y) coffee leaves and black-tea-process-mature (BTP-M) coffee leaves exhibited antioxidant and anti-inflammatory activities that reflected both the phenolic concentration and specific composition. Tea fermentation is usually referred as the atmospheric oxidation of catechins (flavanols) catalyzed by the tea leaf endogenous enzymes, which produces polyphenol pigments [23].

The process of mango peel tea in this study was modified from oolong tea processing since it used short oxidation period. The kneading action of mango peel probably caused some of the sap, essential oils, and juices inside the skin to ooze out, which further enhances the taste of the tea. And in

the fermentation process probably induced the phytochemical compounds and enzymes in mango peel broken down, and its antioxidants are released or transformed. Oxidation is highly important in the formation of many taste and aroma compounds, which give a tea has specific color, strength, and briskness.

The correlation between the total phenolic content and antioxidant property of mango peel teas were calculated as shown in Figure 3. There was no significant correlations detected between the total phenolic compounds and antioxidant activity ( $r^2 = 0.31$ ). Many studies indicated that total phenolic compounds were highly positively correlated with antioxidant activity [24]-[26]. However, the result in this study was difference from other studies; the possible reasons could be that this result was based on the determination and statistical analysis of a small number of samples. Meanwhile, the correlation between the carotenoid content and antioxidant property of mango peel teas showed the strongly relation ( $r^2 = 0.87$ ). Carotenoids also have antioxidant properties. The antioxidant activity of these compounds can shift into a prooxidant effect, depending on such factors as oxygen tension or carotenoid concentration. Mixtures of carotenoids alone or in association with others antioxidants can increase their activity against lipid peroxidation [27].

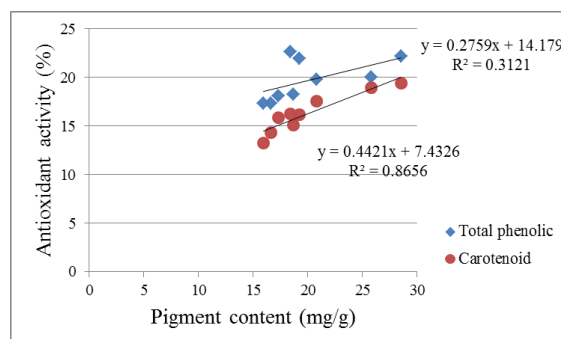


Figure 3 The regression and correlation between the total phenolic compounds and antioxidant activity of the mango peel tea product.

Color of mango peel tea and the infusions were shown in Figure 4 and 5, respectively. Color of infusions of mango peel kneaded for 10 minutes and fermented for 10 and 30 minutes were slightly darker than other treatments. The aroma and taste of infusions were green and a bit astringent. The hedonic test on parameters such as color, flavor, taste and overall acceptance of mango peel tea infusion were presented in Table 3. Sensory evaluation showed that the score of color, flavor and taste of tea from mango peel kneaded and fermented for 10 and 15 minutes, respectively significantly

higher than other kneading and fermentation times ( $p \leq 0.05$ ).

Table 5 Sensory attributes evaluation such as color, flavor, taste and overall acceptance of mango peel tea infusion.

| Kneading & Fermentation (minutes) | Sensory evaluation |                   |                   |                    |
|-----------------------------------|--------------------|-------------------|-------------------|--------------------|
|                                   | Color              | Flavor            | Taste             | Overall acceptance |
| 10 & 15                           | 6.70 <sup>a</sup>  | 6.73 <sup>a</sup> | 6.67 <sup>a</sup> | 6.67 <sup>a</sup>  |
| 10 & 30                           | 5.70 <sup>b</sup>  | 5.97 <sup>b</sup> | 5.90 <sup>b</sup> | 6.00 <sup>b</sup>  |
| 10 & 45                           | 5.77 <sup>b</sup>  | 5.97 <sup>b</sup> | 5.77 <sup>b</sup> | 5.87 <sup>b</sup>  |
| 20 & 15                           | 6.00 <sup>b</sup>  | 5.70 <sup>b</sup> | 5.70 <sup>b</sup> | 5.97 <sup>b</sup>  |
| 20 & 30                           | 6.10 <sup>b</sup>  | 5.67 <sup>b</sup> | 5.73 <sup>b</sup> | 5.90 <sup>b</sup>  |
| 20 & 45                           | 5.93 <sup>b</sup>  | 5.77 <sup>b</sup> | 5.93 <sup>b</sup> | 5.90 <sup>b</sup>  |
| 30 & 15                           | 6.03 <sup>b</sup>  | 5.73 <sup>b</sup> | 5.90 <sup>b</sup> | 5.90 <sup>b</sup>  |
| 30 & 30                           | 5.87 <sup>b</sup>  | 5.90 <sup>b</sup> | 5.90 <sup>b</sup> | 5.93 <sup>b</sup>  |
| 30 & 45                           | 6.10 <sup>b</sup>  | 5.90 <sup>b</sup> | 5.67 <sup>b</sup> | 5.87 <sup>b</sup>  |

Mean of the same column with different superscripts indicating significantly differences ( $p \leq 0.05$ ).



Figure 4 Physical appearance of mango peel tea that kneaded and fermented at different time: (a) 10 and 15 minutes (b) 10 and 30 minutes (c) 10 and 45 minutes (d) 20 and 15 minutes (e) 20 and 30 minutes (f) 20 and 45 minutes (g) 30 and 15 minutes (h) 30 and 30 minutes and (i) 30 and 45 minutes.

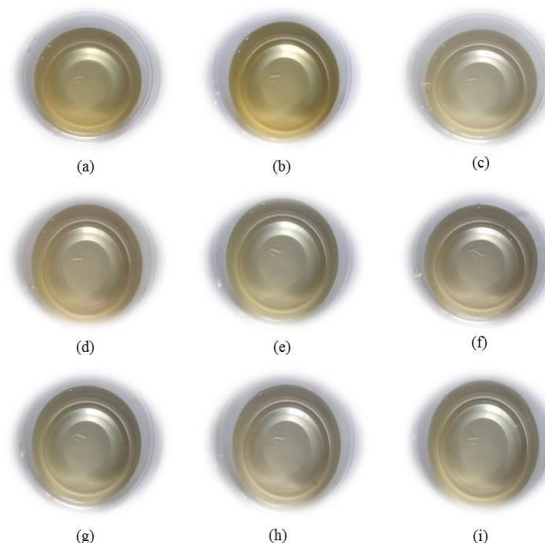


Figure 5 Color of mango peel tea infusions. Mango peels were kneaded and fermented at different time: (a) 10 and 15 minutes (b) 10 and 30 minutes (c) 10 and 45 minutes (d) 20 and 15 minutes (e) 20 and 30 minutes (f) 20 and 45 minutes (g) 30 and 15 minutes (h) 30 and 30 minutes and (i) 30 and 45 minutes.

## CONCLUSION

Total phenolic content and antioxidant activity of tea from unripe mango peel were significantly higher than that ripe mango ( $p \leq 0.05$ ). Kneading time had effect on antioxidant activity of the tea product, while, fermentation time had effect on total phenolic content of the tea. The result showed that mango peel kneaded for 20 minutes had antioxidant activity significantly higher than kneading time at 10 and 30 minutes ( $p \leq 0.05$ ). And mango peel fermented for 15 minutes had total phenolic compounds significantly higher than fermentation time at 30 and 45 minutes ( $p \leq 0.05$ ). Sensory evaluation showed that the score of color, flavor taste and overall acceptance of the infusion from mango peel tea kneaded and fermented for 10 and 15 minutes, respectively significantly higher than other kneading and fermentation times ( $p \leq 0.05$ ).

## ACKNOWLEDGEMENTS

This work was supported by National Research Council of Thailand (NRCT) and Faculty of Agricultural Technology, Rajamangala University of Technology Thanyaburi (RMUTT).

## REFERENCES

- [1] Das, S., Oliveira, L.M., Silva, E., Liu, Y. and Ma, L.Q. Fluoride concentrations in traditional and herbal teas: Health risk assessment, *Environmental Pollution*, Vol. 231, 2017, 779-784.
- [2] Fu, Y., Yanga, J., Cunningham, A.B., Towns, A.M., Zhanga, Y., Hua-ying Yang, H., Li, J. and Yanga, X. A billion cups: The diversity, traditional uses, safety issues and potential of Chinese herbal teas, *Journal of Ethnopharmacology*, Vol. 222, 2018, 217-228.
- [3] Atoui, A.K., Mansouri, A., Boskou, G. and Kefalas, P., 2005. Tea and herbal infusions: their antioxidant activity and phenolic profile. *Food Chemistry*, Vol 89, 2005, 27-36.
- [4] Cai, Y.Z., Xing, J., Sun, M., Zhan, Z.Q. and Corke, H. Phenolic antioxidants (hydrolyzable tannins, flavonols, and anthocyanins) identified by LC-ESI-MS and MALDI-QIT-TOFMS from *Rosa chinensis* flowers. *Journal of Agricultural and Food Chemistry*, Vol. 53, Issue 26, 2005, 9940-9948.
- [5] Rafiee, Z., Barzegar, M., Ali, M. and Maherani, B., Nanoliposomal carriers for improvement the bioavailability of high valued phenolic compounds of pistachio green hull extract, *Food Chemistry*, Vol. 220, 2017, 115-122.
- [6] Ribeiro, S.M.R., Barbosa, L.C.A., Queiroz, J.H., Knödler, M. and Schieber, A. Phenolic compounds and antioxidant capacity of Brazilian mango (*Mangifera indica* L.) varieties, *Food Chemistry*, Vol. 110, Issue 3, 2008, 620-626.
- [7] Mitra, S.K. and Baldwin, E.A. Mango. In: *Postharvest Physiology and Storage of Tropical and Subtropical Fruits*. Mitra, S.K. (Ed.), CAB International, Wallingford, Oxon, 1997, pp. 85-122.
- [8] Lalel, H.J.D., Singh, Z. and Tan, S.C. Glycosidically-bound aroma volatile compounds in the skin and pulp of 'Kensington Pride' mango fruit at different stages of maturity, *Postharvest Biology and Technology*. Vol. 29, 2003, 205-218.
- [9] Chen, Y., Zhao, L., He, T., Ou, Z., Hu, Z. and Wang, K., Effects of mango peel powder on starch digestion and quality characteristics of bread, *International Journal of Biological Macromolecules*. Vol 140, 2019, 647-652.
- [10] Ajila, C.M., Jaganmohan, Rao, L. and Prasada Rao, U.J.S., Characterization of bioactive compounds from raw and ripe *Mangifera indica* L. peel extracts, *Food and Chemical Toxicology*, Vol. 48 Issue 12, 2010, 3406-3411.
- [11] Ajila, C.M., Bhat, S.G. and Prasada Rao, U.J.S., Valuable components of raw and ripe peels from two Indian mango varieties, *Food Chemistry*, Vol. 102 Issue 4, 2007, 1006-1011.
- [12] Hockeng, K., Prasad, K.N., Ismail, A. and Mohdesa, N., Carotenoids from *Mangifera pajang* and their antioxidant capacity, *Molecules*, Vol. 15 Issue 10, 2010, 6699-6712.
- [13] Marina, Z. and Noriham, A., Quantification of total phenolic compound and in vitro antioxidant potential of fruit peel extracts, *International Food Research Journal*, Vol. 21, 2014, 1925-1929.
- [14] Dhital, S., Bhattarai, R.R., Gorham, J. and Gidley, M.J., Intactness of cell wall structure controls the in vitro digestion of starch in legumes, *Food and Function*, Vol. 7 Issue 3, 2016, 1367-1379.
- [15] Ajila, C.M., Leelavathi, K. and Prasada Rao, U.J.S., Improvement of dietary fiber content and antioxidant properties in soft dough biscuits with the incorporation of mango peel powder, *Journal of Cereal Science*, Vol. 48 Issue 2, 2008, 319-326.
- [16] Ajila, C.M., Aalami, M., Leelavathi, K. and Prasada Rao, U.J.S., Mango peel powder: a potential source of antioxidant and dietary fiber in macaroni preparations, *Innovative Food Science and Emerging Technologies*, Vol. 11 Issue 1, 2010, 219-224.
- [17] Maturity index, [online] <http://elearning.yru.ac.th/pluginfile.php>. July 3, 2019.
- [18] Bakar, M.F.A., Mohamed, M., Rahmat, A., and Fry, J. Phytochemicals and antioxidant activity of different parts of bambangan (*Mangifera pajang*) and tarap (*Artocarpus odoratissimus*). *Food Chemistry*, Vol 113, 2009, 479-483.
- [19] Brand-Williams, W., Cuvelier, M.E. and Berset, C. Use of free radical method to evaluate antioxidant activity. *LWT-Food Science and Technology*, Vol.28, Issue 1, 1995, 25-30.
- [20] Ajila, C.M., Naidu, K.A., Bhat, S.G. and Prasada Rao, U.J.S. Bioactive compounds and antioxidant potential of mango peel extract. *Food Chemistry*, Vol, 105, 2007, 982-988.
- [21] Atoui, A.K., Mansouri, A., Boskou, G., Kefalas, P. Tea and herbal infusions: their antioxidant activity and phenolic profile. *Food Chemistry*, Vol. 89, Issue 1, 2005, 27-36.
- [22] Chen, X.M., Ma, Z. and Kitts, D.D. Effects of processing method and age of leaves on phytochemical profiles and bioactivity of coffee leaves. *Food Chemistry*, Vol. 249, 2018, 143-153.
- [23] Feng, Z., Li, Y., Li, M., Wang, Y., Zhang, L., Wan, X. and Yang, X., Tea aroma formation from six model manufacturing processes. *Food Chemistry*, Vol 285, 2019, 347-354.
- [24] Jin, L., Li, X.B., Tian, D.Q., Fang, X.P., Yu,

- Y.M., Zhu, H.Q., Ge, Y.Y., Ma, G.Y., Wang, W.Y., Xiao, W.F. and Li, M. Antioxidant properties and color parameters of herbal teas in China. *Industrial Crops and Products*, Vol 87, 2016, 198-209.
- [25] Chan, E.W.C., Lim, Y.Y., Chong, K.L., Tan, J.B.L., Wong, S.K. Antioxidant properties of tropical and temperate herbal teas. *Journal of Food Composition and Analysis*, Vol. 23, Issue 2, 2010, 185-189.
- [26] Deetae, P., Parichanon, P., Trakunleewatthana, P., Chanseetis, C., Lertsiri, S. Antioxidant and anti-glycation properties of Thai herbal teas in comparison with conventional teas. *Food Chemistry*, Vol. 133, Issue 3, 2012, 953-959.
- [27] Zakyntinos, G., and Varzakas, T. Carotenoids: from Plants to Food Industry. *Current Research in Nutrition and Food Science*, Vol. 4 (Special Issue 1), 2016, 38-51.

## FORMULATION, ANTIOXIDANT AND ANTIBACTERIA ACTIVITIES OF PEEL-OFF GEL MASK, ENRICHED WITH *BIDARA* LEAF (*ZIZIPHUS SPINA-CHRISTI* L.) EXTRACT

Hendrawati<sup>1</sup>, Aziza<sup>1</sup>, La Ode Sumarlin<sup>1</sup>, Yulyani Nur Azizah<sup>1</sup>

Department of Chemistry Faculty of Science and Technology  
State Islamic University Syarif Hidayatullah Jakarta  
Jl. Ir. H Djuanda no. 95 Ciputat Tangerang Selatan Banten Indonesia

### ABSTRACT

Bidara Leaves (*Ziziphus spina-christi* L.) is the one of the herbs that already known by people to repair the broken cell and acne's problem. The bidara leaves extract can be formulated into a peel-off gel mask for facial skin. The objective of this research is to formulate the peel-off gel mask from ethanol extract of bidara leaves. The peel-off gel mask expected effective in reducing the adverse effects of free radicals and inhibits the growth of acne-causing bacteria on the face. Identification of bioactive compounds in bidara leaves extract with phytochemical test and Liquid Chromatography-tandem Mass Spectrometry (LC-MS/MS) instrument. Antioxidant activity test using 1,1-diphenyl-2-picrylhydrazil (DPPH) method and IC<sub>50</sub> value determination. Testing of antibacterial activity of ethanol extract of bidara leaf against *Propionibacterium acne* bacteria by diffusion method. Preparation of gel mask peel-off using variation of concentration 15, 25 and 35%. Peel-off gel mask characterization by organoleptic test, physical appearance, pH value, homogeneity test, dispersion test, drying time test and microbial contamination. Ethanol extract of bidara leaves has very strong antioxidant activity with IC<sub>50</sub> 23,382 ppm and antibacterial activity with inhibition of bacteria *P. acne* at a concentration  $\geq 0.25$  g/mL. The results of LC-MS/MS analysis showed that there were routine compounds at retention time of 5.13 which had the potential as antioxidants and antibacterial. Peel-off gel masks obtained have antioxidant and antibacterial activity and are included in the quality requirements category of SNI 16-6070-1999 and SNI 16-4380-1996.

**Keywords:** antibacterial, antioxidant, bidara leaves, peel-off gel mask

### INTRODUCTION

The utilization of natural substances as antioxidant and antibacterial agents for health product and personal care has been increasingly developed to support human basic needs. Plants as natural substances have been considerable used for health, medicine, and beauty products. In global health's context, natural source and its outcome prove that all plants contain compounds, which are clinically proven beneficial for health [1]. *Bidara* is one of the plants that is beneficial for human health. According to hadith by Bukhari and Muslim, Rasullullah presented the commendable deed to utilize *bidara* leaves in performing Islamic ritual ablution and purification on a dead body. This ritual performance gives basic knowledge to human that *bidara* leaf has beneficial effects to purify.

*Bidara* leaf extract has been utilized in medicines development in addition to pharmacology activities in Middle East, South East, and East Asia. *Bidara* leaf is believed to have medicinal properties to cure various diseases. *Bidara* has been used as an

alternative medicine for self- purify and to cure fever, pain, dandruff, wound, inflammation, asthma, and sore eyes [2]. In traditional medicines, all parts of *bidara*, namely root, leaf, fruit, seed, and stem were used to cure [3]. *Bidara* leaf extract has been analyzed by using LC-MS instrument. Soleh Putri, 2017 obtained the highest concentration of two suspected rutin compounds, which classified as one of the active flavonoid compounds [4]. Kusriani *et al.* (2015) stated that bidara leaf extract contained phenolic compounds, in total  $7.192\% \pm 0.0198$  [5]. Meanwhile, the ethanol extract of bidara leaves showed antioxidant activities with IC<sub>50</sub> value 127,87 ppm [6].

Research conducted by Haeria *et al.* (2016) suggested that the ethanol extract of bidara leaves contained high concentration of antioxidant, with flavonoid compounds 1,5312% in total and IC<sub>50</sub> value 90,9584 ppm [7]. Ali *et al.* (2015) revealed that *bidara* leaf extract shows antibacterial activities to prevent pathogen-bacteria growth, i.e. *Proteus vulgaris*, *Escherichia coli*, *Bacillus subtilis*, *Staphylococcus aureus*, and *Pseudomonas aeruginosa* that can be

potentially added into the active substances in facial-cosmetic product [8].

Facial cosmetic can be produced in various forms. One of those forms is peel-off mask, which is practically used and easy to clean [6]. Ariani and Wigati (2019) used the formulation of peel-off mask as acne cream with Polyvinyl alcohol (PVA) as the main formula of gelling agent; hydroxypropyl methylcellulose (HPMC) as viscosity-increasing agents; and propylene glycol (PG) as humectant agent [9]. The formulation of peel-off gel mask with selected basis substances, i.e. PVA with higher concentration than HPMC, did produce the most excellent characteristic of peel-off gel mask [10]. Therefore, a research on peel-off gel mask, enriched with ethanol extract of *bidara* leaf (*Z. spina-christi* L.) with various concentrations, is supposed to conduct. This new formula is expected to increase antioxidant and antibacterial activities of peel-off gel mask.

## RESEARCH METHOD

### Materials and Equipments

*Bidara* leaves used in this research (approximately 1 kg), were obtained from *bidara* farm in Sumenep, East Java and identified in Herbarium Bogoriense, LIPI Bogor. A solvent used was 96% technical grade ethanol. Bacterial isolate of *P. acne* was obtained from Laboratorium Biologi, Universitas Indonesia (Biology Laboratory, University of Indonesia). Tryptic Soy Agar was used as a medium to culture antibacterial compounds. DPPH was used to analyze antioxidant activities. PVA, HPMC, propylene glycol, and aquades, as well as commercial product to compare, were used to form peel-off gel mask. The equipments used in this research were Spectrophotometer UV Vis, LC-MS/MS, analytical weighing balance, laboratory glassware, pH meter, oven, vacuum rotary evaporator, incubator, and autoclave.

### Extraction and Phytochemical Analysis of *Bidara* Leaves

*Bidara* leaves (*Z. spina-christi* L.) were grinded, weighed and put into a container to be macerated. Afterwards, the macerated *bidara* leaves were added with 96% ethanol until the leaves were completely soaked. After the soaking procedure, the soaked *bidara* leaves were stirred for 30 min. The container was covered and kept for 24 h at room temperature. The filtration of *bidara* leaf extract was collected and condensed in a vacuum rotary evaporator. The solvent was further evaporated to obtain thick-ethanol extract of *bidara* leaves. Afterwards, the ethanol extract of *bidara* leaves were ready to use as the test samples. Phytochemical analysis on *bidara* leaf

extract to examine steroid/triterpenoid, flavonoid, alkaloid, phenolic, tannin, and saponin compounds, was conducted by using proper reagents.

### Identification of Active Compounds of Ethanol Extract of *Bidara* Leaves using LCMS/MS Method

Ethanol extract of *bidara* leaves (1 mg) was weighed and diluted in methanol. Leaf samples (10 µL) were taken and injected to LCMS/MS through column C-18 (2 x 150 mm) with the flow rate 0,2 mL/min. Chromatography analysis and mass spectrophotometry were observed by using a software program, MassLynx (Version 4.1), to identify the suspected chemical structures.

### Formulation of Peel-Off Gel Mask

Polyvinyl alcohol (PVA) was added with aquades four times and heated until the PVA was transparent and homogenous. Hydroxypropyl methylcellulose (HPMC) was grown with aquades for 30 min. PVA and HPMC were mixed in a mortar and grinded until the mixture was homogenous. The mixture was added with propylene glycol, gradually diluted with ethanol and odour, and then homogenized. The peel-off gel mask was formulated with varied concentration of *bidara* leaf extract, 25, 30, and 35% (b/v).

### Antioxidant Activity Testing

A 2 mL sample was put into a culture tube, then added with 2 mL of DPPH 0,002%. The mixture was homogenized then incubated in a dark room, at room temperature for 30 min. The absorbance was measured by using UV-Vis Spectrophotometry and obtained wavelength 516 nm. A percentage inhibition was calculated and equated into a linear regression analysis to obtain IC<sub>50</sub> value.

### Antibacterial Activity Testing

Antibacterial activity testing of *bidara* leaves was conducted by performing preliminary test on ethanol extract of *bidara* leaves, with the following steps: (i) TSA medium (25 mL) was inserted into petri dish; (ii) added with bacterial suspension (0,25 mL); (iii) homogenized until the medium was solid and firm. Furthermore, holes were made in medium and applied with 100 µL extract, then incubated at 37°C for 24 h. Ethanol extract testing of *bidara* leaves was conducted on thick extract, with extract concentration 1; 0,5 ;0,25; 0,125g/mL. Inhibition zone formed was observed; diameter of inhibition zone was measured.

### Characterization of Peel-Off Gel Mask

The analysis of formulation result from ethanol extract of peel-off gel mask of *bidara* leaves includes:



organoleptic test or testing on panellist's preference, physical appearance, pH value, dispersion test, drying-time test, viscosity test, and microbial pollution test to identify the gel mask quality.

## RESULT AND DISCUSSION

### Extraction and Phytochemical Analysis on *Bidara* Leaves

*Bidara* leaves were grinded and extracted by using maceration method with 96% ethanol, resulted thick and dark green extract (Figure 1); yield percentage 19%. Phytochemical screening test of ethanol extract of *bidara* leaves showed positive results on the six reagents with colour change when added with reagents, proved that bidara leaf extract contains steroid, flavonoid, alkaloid, tannin, phenolic, and saponin compounds (Table 1). Ethanol extract of *bidara* leaves was expected to have potential antioxidant and antibacterial activities.

Table 1. Phytochemical screening test

| Class of Compounds | Reagent                        | Colour Change      | Conclusion |
|--------------------|--------------------------------|--------------------|------------|
| Steroid            | Lieberman Burchard             | Green              | +          |
| Flavonoid          | Mg+HCl                         | Orange             | +          |
| Alkaloid           | Wagner                         | Precipitated Brown | +          |
| Phenolat           | Akuades + FeCl <sub>3</sub> 1% | Black              | +          |
| Tannin             | FeCl <sub>3</sub> 1%           | Blackish Green     | +          |
| Saponin            | Aquades                        | Foamed             | +          |



Figure 1. Ethanol extract of bidara leaves

### Identification of Active Compounds in Ethanol Extract of *Bidara* Leaves using LCMS/MS Method

The analysis of the suspected compounds was carried out by comparing the similarity of mass spectra samples and mass spectra compounds, using online database Mass Bank, The Human Metabolome Database, and Mass Bank of North America. Chromatogram in figure 2 illustrated some peaks of

ethanol extract compounds from *bidara* leaves. The m/z value 611,1687 was fragmented to be m/z 303,0536 at retention time 5,15. Ionization used in this research was [M+H]<sup>+</sup> to determine the real m/z value 610,1687. The prediction of compound molecular formula was C<sub>27</sub>H<sub>30</sub>O<sub>16</sub>. Compared with online database Mass Bank, the findings showed some similarities of mass spectra as a result from rutin mass spectra measurement, i.e. m/z 611; 465; 303. Phytochemical screening test showed flavonoid compounds. Thus, the compound appeared at retention time 5,15 was suspected as flavonoid compound, namely rutin.

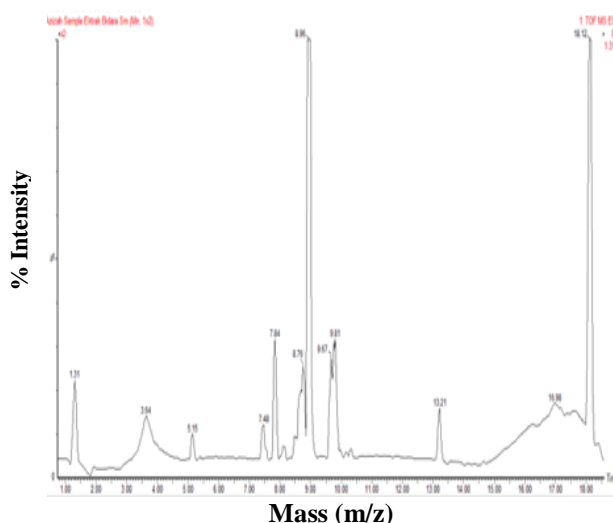


Figure 2. Chromatogram of ethanol extract

### Extract of *bidara* leaves

Rutin is a derivative compound from flavonoid, i.e. flavonol. Rutin is a condensation result between quercetin and glycone rutinose. Quercetin-3-O-rutinoside and quercetin have antioxidant activities [11]. Flavonoid prevents free radicals through free radical scavenger process by donating hydrogen atom to alter radicals being inactive [12]. According to Pelczar dan Chan (2006), quercetin may also act as antibacterial because its phenolic group performs protein denaturation and damage microbial cell membranes [13]. Quercetine and its derivative compounds were first reported to have antiviral activities [14].

### Antioxidant Activity of Ethanol Extract on *Bidara* Leaves

Ascorbic acid was used to observe antioxidant activities. Research found that ascorbic acid showed strong antioxidant activity, with IC<sub>50</sub> value 3,606 ppm. Antioxidant activity of bidara leaf extract (*Z. spina-christi* L.) also classified into highly-strong

antioxidant activity, with  $IC_{50}$  value 23,382. However, antioxidant activity of ethanol extract of *bidara* leaves is lower than ascorbic acid.

Table 2. Antioxidant activity test on ethanol extract of *bidara* leaves

| Concentration Of bidara (ppm) | Ads   | % Inhibition       | Linear Regressi        | $IC_{50}$ (ppm) |
|-------------------------------|-------|--------------------|------------------------|-----------------|
| 0                             | 0,264 | 0                  |                        |                 |
| 2,5                           | 0,185 | $29,92 \pm 0,0042$ |                        |                 |
| 5                             | 0,172 | $35,04 \pm 0,0007$ | $y = 0,7921x + 31,479$ | 23,382          |
| 10                            | 0,156 | $40,90 \pm 0,0014$ | $R^2 = 0,9911$         |                 |
| 20                            | 0,134 | $49,43 \pm 0,0007$ |                        |                 |
| 40                            | 0,093 | $64,96 \pm 0,0007$ |                        |                 |
| 80                            | 0,018 | $93,37 \pm 0,0007$ |                        |                 |

Note: Means  $\pm$  Standard Deviation (SD)

### Antibacterial Activity of Ethanol Extract of *Bidara* Leaves

Antibacterial test was conducted on thick extract without dilution process and some varied concentrations, i.e. concentration 1; 0,5; 0,25, and 0,125g/mL, respectively. Positive control was antibiotic, generated inhibition zone 37,80 mm. Negative control was sterilized aquades, generated inhibition zone 8 mm.

Table 3. Antibacterial activity test on ethanol extract of *bidara* leaves

| Concentration of Bidara (g/mL) | Inhibition Diameter (mm) |
|--------------------------------|--------------------------|
| 0,125                          | $8 \pm 0$                |
| 0,250                          | $14,40 \pm 1,56$         |
| 0,500                          | $15,90 \pm 1,98$         |
| 0,100                          | $17,50 \pm 1,70$         |
| Pekat                          | $18,85 \pm 2,76$         |
| Kontrol (+)                    | $37,80 \pm 1,56$         |
| Kontrol (-)                    | $8 \pm 0$                |

Note: Means of inhibition diameter  $\pm$  Standard Deviation; Control (+) is tetracycline and Control (-) is sterilized aquades

Results of antibacterial test of *bidara* leaf extract at concentration 0,125 g/mL showed the same inhibition

zone with negative control; proved that leaf extract at that concentration did not show inhibition activities against *P. acne* bacteria. Concentration extract of 0,25 g/mL showed diameter of clear zone 14,40 mm; Concentration 0,5 g/mL resulted inhibition diameter 15,90 mm; Concentration 1 g/mL resulted inhibition diameter 17,50 mm and thick extract without dilution process 18,85 mm. *Bidara* leaf extract (*Z. spinachristi* L.) showed inhibition activities against *P. acne* at concentration  $\geq 0,25$  g/mL. Results obtained from responses of substances in diffusion holes, marked by the area clearness or diameter of inhibition zone at each concentration.

### Formulation of Peel-Off Gel Mask of Ethanol Extract of *Bidara* Leaves

The homogenized substances of peel-off gel mask was added with extract concentration, 0,25, 30, and 35%, respectively. The concentration was taken from the results of antibacterial activity test on *bidara* leaf extract, which showed inhibition power at concentration  $\geq 0,25$  g/mL.

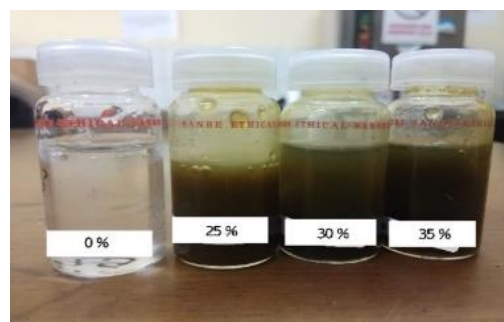


Figure 3. Formulation of peel-off gel mask

The peel-off gel mask obtained was F0 with extract concentration 0%, resulted transparent or clear cream; F1 with 25% extract concentration in faded green colour; F2 with 30% extract concentration in light green colour; F3 with 35% extract concentration in dark green colour (Figure 3). The green colour in peel-off gel mask was resulted from *bidara* leaf extract. The thickness of green colour in peel-off gel mask increased equally with the adding of *bidara* leaf extract.

### Antioxidant Activity of Peel-off Gel Mask of *Bidara* Leaf Ethanol Extract

Based on the results of antioxidant activity test on peel-off gel mask, the higher amount ethanol extract of *bidara* leaves (*Z. spinachristi* L.) added into the peel-off gel mask, the higher antioxidant activities performed. It was in accordance with the increasing inhibition percentage value of peel-off gel mask and

the increasing ethanol extract concentration of *bidara* leaves. The inhibition percentage was lower compared with the ethanol extract of *bidara* leaves. The smaller amount of extract concentration than the amount of peel-off gel mask used in this research led to low percentage of inhibition. The decrease of inhibition percentage might be caused by the amount of ethanol extract of *bidara* leaves that was not sufficient or less, hence the active compounds did not optimally work. However, the peel-off gel mask showed high antioxidant potentials, compared with commercial product with the lowest inhibition value.

**Table 4. Antioxidant activity test of peel-off gel mask**

| Sample                                | Inhibition percentage (%) |
|---------------------------------------|---------------------------|
| Commercial (F0)                       | 18,389 ± 0,737            |
| (Sample without additional extract)   | 3,163 ± 0,847             |
| (Sample added with 25% extract) F2    | 38,638 ± 3,876            |
| (Sample added with 30% extract) F3    | 50,862 ± 1,219            |
| (Sample added with 35% extract)       | 65,743 ± 3,227            |
| Thick extract of <i>bidara</i> leaves | 80,823 ± 3,823            |
| Ascorbic acid                         | 94,568 ± 0,415            |

Note: Means of inhibition percentage ± standard deviation

#### Antibacterial Activity of Peel-off Gel Mask of Ethanol Extract of *Bidara* Leaves

Antibacterial activity test on peel-off gel mask of ethanol extract of *bidara* leaves showed results that the higher concentration the ethanol extract of *bidara* leaves added into the peel-off gel mask, the larger the inhibition activities against *P. Acne* performed. Results were obtained from responses of substances in diffusion holes, marked by the area clearness or diameter of inhibition zone. The difference of extract concentration added to each samples led to different clear zones. The higher extract concentration of *bidara* leaves added, the larger amount antibacterial compounds contained. The larger amount antibacterial compounds obtained from *bidara* leaf extract, the larger amount *P. acne* bacteria damaged, either the structure or metabolic system. Research found bacteria interrupted by antibacterial compounds were killed or inhibited. Findings showed that formulation with the largest width of inhibition zone was peel-off gel mask of *bidara* leaf extract, formula F3 added with 35% extract, which showed

inhibition zone 9,10 mm. The sample with the smallest width of inhibition zone was commercial peel-off gel mask, with inhibition zone 6 mm, same with peel-off gel mask without additional extract as the negative control. Antibacterial activity test showed that peel-off gel mask formula added with ethanol extract of *bidara* leaves performed antibacterial activities against *P. acne*. The result was relatively small compared with the inhibition zone of ethanol extract of *bidara* leaves before formulated in peel-off gel mask. The low inhibition zone in peel-off gel mask was found to be caused by high viscosity, led to a lower antibacterial activities. The bond between gel bases and high viscosity was tighter, hence the active compounds were more difficult to diffuse [15].

**Table 5. Antibacterial test on peel-off gel mask**

| Formulation | Inhibition Diameter (mm) |
|-------------|--------------------------|
| Commercial  | 6 ± 0                    |
| F1          | 7,65 ± 0,49              |
| F2          | 8,50 ± 1,13              |
| F3          | 9,10 ± 0,85              |
| Control (+) | 32,30 ± 0,42             |
| Control (-) | 6 ± 0                    |

Note: Means of inhibition diameter ± standard deviation; Control (+) is t tetracycline and Control negative (-) is peel-off gel mask without additional extract.

#### Characterization of Gel Mask and Hedonic Test on Panellists

Characterization on formula of peel-off gel mask of ethanol extract of *bidara* leaves includes physical appearance, pH value, viscosity test, dispersion test, drying-time test, and microbial pollution test to study the characteristic of each peel-off gel mask sample. Characterization test showed that all samples have fulfilled the requirements of SNI 16-6070-1999, concerning facial-mask quality and SNI 16-4380-1996, concerning facial-cleanser product.

Furthermore, statistical hedonic test on panellist preference showed peel-off gel mask formula F1 indicated the highest level of preference, with the average value 3,87. Commercial peel-off gel mask showed the same subset-class, with the preference level 3,84. Peel-off gel mask formula F0 showed preference value 3,78 on second subset-class. Peel-off gel mask formula F2 and F3 were on first sub-set with preference value 3,02 and 2,64. These values were significantly different with second subset-class, suspected it was due to the colour change, odour, and texture [16].

**Table 6. Activity and charateristic of peel-off gel mask**

| Charac<br>teristic                                  | Comm<br>ercial                    | F0                                | F1                                | F2                                | F3                                |
|---|-----------------------------------|-----------------------------------|-----------------------------------|-----------------------------------|-----------------------------------|
| Physic<br>al  | Homog<br>enous,<br>steriliz<br>ed | Homog<br>enous,<br>steriliz<br>ed | Homog<br>enous,<br>steriliz<br>ed | Homog<br>enous,<br>steriliz<br>ed | Homog<br>enous,<br>steriliz<br>ed |
| pH<br>Value   | 6,56                              | 6,62                              | 5,62                              | 5,53                              | 5,43                              |
| Dispers<br>ion<br>(cm)                              | 5,3                               | 5,5                               | 5,25                              | 4,765                             | 4,53                              |
| Drying<br>Time<br>(min)                             | 25                                | 29                                | 26                                | 24                                | 22,5                              |
| Viscosi<br>ty (cP)                                  | 6020                              | 8141                              | 12039                             | 13367                             | 16653                             |
| Microb<br>ial<br>Polluti<br>on<br>(coloni<br>/gram) | N/A                               | N/A                               | N/A                               | N/A                               | N/A                               |

The panellists preferred white colour and fresh odour. However, moderate addition of extract in formula F1 (25%) still could be accepted by the panellists because the green colour was not very thick; the odour was not too sour; and the thickness texture was sufficient. Therefore, based on organoleptic test, formula F1 was chosen as the best formulation.

## CONCLUSION

Ethanol extract of *bidara* leaves was expected to contain (i) rutin compounds, (ii) IC<sub>50</sub> value 23,382 ppm, and (iii) antibacterial activity of *P. acne* against ethanol extract of *bidara* leaves (*Z. spina-christi* L.) at concentration  $\geq 0,25$  g/mL. Based on organoleptic test, the best formulation of peel-off gel mask of ethanol extract of *bidara* leaves was formula F1 with 25% extract addition. The formulation, which showed antioxidant activity 38,638% and inhibition zone against *P. acne* 7,65 mm, has fulfilled the quality requirement of SNI 16-6070-1999 and SNI 16-4380-1996.

## REFERENCES

- [1] Thalbah, H. 2009. *Ensiklopedia Mukjizat Al-Qur'an dan Hadist* [Encyclopedia of Miracles in Al-Qur'an and Hadith]. Jakarta: Perpustakaan Nasional.
- [2] Asgarpanah J, Haghighat E. 2012. Phytochemistry and pharmacologic properties of *Ziziphus spina christi* (L.) Willd. *African Journal of Pharmacy and Pharmacology*, 6(31), 2332-2339. doi.org/10.5897/AJPP12.509.
- [3] Dragland SM, Senoo H, WakeK, HolteK, Blomhoff R. 2003. Antioxidant activity of terpenoids. *Journal Nutrition*, 1(1), 133.
- [4] Putri RAZ. 2017. [Testing Anticancer Activity of Arabic *Bidara* Leaves in Colony Cells (WiDr) through MIT Method and Identification Active Compounds using LC-MS Method] [Skripsi]. Malang: Universitas Islam Negeri Maulana Malik Ibrahim Malang.
- [5] Kusriani RH, Nawawi A, Machter E. 2015. [Determination of Total Phenolic Content and Antioxidant Activity of *Bidara* Leaf, Fruit, and Seed Extract]. *Prosiding SNaPP2015 Kesehatan*.
- [6] Vieira RP, Fernandes AR, Kaneko TM, Consiglieri VO, Pinto CASDO, Pereira CSC, Velasco MVR. 2009. Physical and physicochemical stability evaluation of cosmetic formulations containing soybean extract fermented by *Bifidobacterium animalis*. *Brazilian Journal of Pharmaceutical Sciences*, 3(45), 515–525. doi.org/10.1590/S1984-82502009000300018.
- [7] Haeria, Hermawati, Dg. PineATU. 2016. [Determination of Total Flavonoid Content and Antioxidant Activity and Ethanol Extract of *Bidara* Leaves]. *Pharmascience*, 1(2), 57–61.
- [8] Ali AB, Almagboul AZ, Mohammed OM. 2015. Antimicrobial Activity of Fruits, Leaves, Seeds and Stems Extracts of *Ziziphus spina-christi* L. *Arabian Journal of Medicinal and Aromatic Plants*, 1(2), 94–107
- [9] Ariani LW, Wigati D. 2009. [Formulation of Peel-off Gel Mask of Ethanol Extract of Sweet Orange Skin as Acne Cream]. *Media Farmasi Indonesia*, 11(2), 1084–1092.
- [10] Syarifah RS, MulyantiD, Gadri, A. 2015. [Formulation of Peel-off Gel Mask of Papaya Leaves as Antiacne and Efficacy Test against *Propionibacterium Acne*]. *Prosiding Penelitian SPeSIA Unisba 2015*, 1(1), 662–670.
- [11] Aderogba MA, Ogundaini AO, Eloff JN. 2006. Isolation of Two Flavonoids From *Bauhinia monandra*(Kruz) Leaves and their Antioxidative Effects. *Afr.J.Tradisional CAM*, 3 (4): 59 - 65.
- [12] Burda S, Oleszek W. 2001. Antioxidant and Antiradical Activities of Flavonoids. *Journal of*

- Agric Food Chemistry*, 49(1), 2774-2779.
- [13] Pelczar MJ, Chan ECS. 2006.*Dasar-Dasar Mikrobiologi 2* [Basic Principles of Microbiology 2]. Jakarta : UI Press
- [14] Santos, Alda E, KusterRM., YamamotoKA, SallesTS, CamposR., Meneses, Marcelo DF, SoaresMR, Ferreira D. 2014. Quercetin and Quercetin 3-O-glycosides from *Bauhinia longifolia* (Bong.) Steud. Show Anti-mayora Virus Activity. *Parasites and Vectors*, 7(1), 130.doi: 10.1186/1756-3305-7-130.
- [15] Cahyana M, EkaprasadaT,HerryA.2002. [Isolation of Antioxidant Compounds of Cinnamon Bark Skin]. *Jurnal Indonesia*, 3(1), 50–58.
- [16] NingsihW, Nofiandi D, DeviarnyC, RoselinDR. 2017. [Formulation and Antibacterial Effect of Peel-off Gel Mask of Dewa Leaf Extract Against *Staphylococcus epidermidis*] . *Scientia*, 7(1), 61–66.

# **A STUDY ON ELECTRICAL IMPEDANCE IN RIPENING AMBON-BANANAS (MUSA PARADISIACA VAR. SAPIENTUM) PROCESSES STIMULATED BY ETHREL (2-CHLOROETHYL PHOSPHONIC ACID)**

Chomsin S Widodo<sup>1</sup>, Didik Rahadi Santosa<sup>1</sup>, Wahyu Sugianto<sup>1</sup>, Arinto Yudi P Wardoyo<sup>1</sup>

<sup>1</sup> Faculty of Mathematics and Natural Science, Brawijaya University, Malang, Indonesia

## **ABSTRACT**

The use of ethrel (2-chloroethyl phosphonic acid) is faster fruit maturity. Excessive use of ethrel in the ripening of bananas causes damage to the fruit and people who consume it. The principle of measurement based on electrical impedance spectroscopy can detect changes that occur in biological material. This paper discusses the comparison of the electrical impedance values of the ripeness of bananas, which marinated using various ethrel concentrations and natural maturity. The electrical impedance measurement system uses four needle electrodes made of pure silver, which are supported by the use of the V to I module and signal generator from PICOSCOPE 5244B. The system injects a current of one mA into the sample. The sample consisted of bananas through the ripening process using three ethrel concentrations of 1000 ppm and 2000 ppm. Observation of changes in fruit and impedance measurements in the range of 1 Hz to 1 MHz carried out every two days for nine days. The impedance value that correlates with the maturity of the banana well observed in the frequency range between one to 100 kHz. Increasing the impedance value describes the fruit maturity, which indicated by increasing the acidic until peak-phase and increasing sugar content until the fruit rot. The maturation process using ethrel provides the effect of shifting the peak impedance value. The higher the ethrel concentrations that used the electrical impedance value of the banana will be higher.

*Keywords: Electrical Impedance, Bananas, Ethrel,*

## **INTRODUCTION**

Consumer attention to healthy food products is still a concern until now, while food producers are trying to find a profit that is as big as possible. Processing products that are faster and cheaper is still the choice of producers, although it has the potential to harm consumers in terms of health. One of the processes used by traders is to speed up the ripening of bananas using ethrel (2-chloroethyl phosphonic acid).

Some studies use ethrel in the process of accelerating fruit with observations based on physiological changes in the fruit. The ethrel mango ripening at a dose of 1000 ppm, gives a good taste and is still acceptable to the market [9], etrel spray effect on postharvest mango with a different concentration of 600 ppm accelerates uniform maturation in 4 days [7], at maturation of Guava [5], maturity of winter tomato fruit harvested [10]. Physiological changes in biological media (e.g., fruits) indicate a difference in the properties of these materials. Changes in the properties of compositions that affect the electrical properties observed using a system of electrical impedance spectroscopy (EIS).

The EIS-based study has been applied to various fields, for example, observing changes in physiological properties in fruits: apples, mango, bananas, and avocado [1, 2, 8, 12, 13]. Also, the EIS application used to detect additives, or additional

food ingredients identify the concentration of salt solutions [6, 15–18]. Until now, various forms and quantities of EIS electrodes have been developed [4, 19].

The study aimed to apply EIS to Ambon banana with a ripening process using various concentrations of ethrel. Electrical parameters obtained from measurements clarified with maturity observed from changes in skin color

## **MATERIAL AND METHODS**

### **Samples of Bananas Ambon**

Ambon banana (*Musa paradisiaca* var. *Sapientum*) obtained from the local market. The selection of bananas based on its size and the banana fruit washed thoroughly.

Banana fruit includes climacteric fruit, which has a different sudden period where during this process, a series of biological changes occur, beginning with the formation of ethylene [11], as shown in Fig. 1. The ripening process starts with the occurrence of cell metabolism that develops towards the beginning of the ripening process (Climacteric Respiration Minimum phase). At that time, acid formation dominated the banana starch. After going through the minimum Climacteric Respiration phase, the transformation of starch into sugar occurs, the transformation of tannin compounds which can

dissolve into insoluble forms, a significant reduction in the amount of acid, softening of woody tissue and increasing fluid levels.

The grouping of Ambon Banana used as a sample based on the treatment group and labeled. The treatment on bananas using ethrel carried out on day 0 for each concentration at room temperature, by dipping the banana into a container containing ethrel solution for 30 seconds then remove it and stored without cover for nine days. Physiological observation of banana skin carried out on the first, third, fifth, seventh, and ninth days.

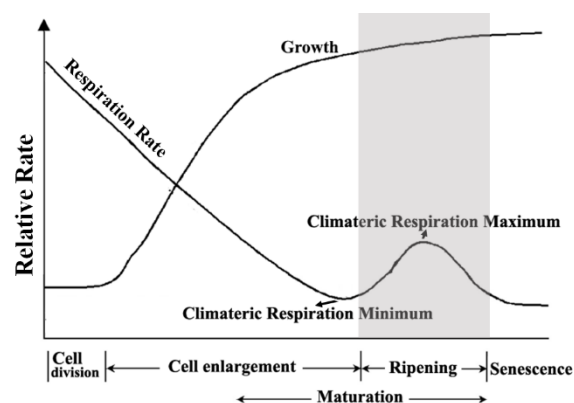


Fig. 1 Generalized patterns of growth and respiration during development, maturation, and senescence of climacteric fruits.

### Electrical Impedance Measurements

The EIS system consists of four silver needle electrodes with a diameter of 1 mm ((length of 10 mm), two electrodes used to inject current (3.6 mm apart) and two others used for measuring the output voltage (8 mm distance). Picoscope type 5244B supports the system as an AC voltage generator, and the injection of 1 mA sinusoidal current in a banana sample uses a V to I converter circuit, as shown in Fig 2.

Measurement of electrical impedance in the frequency range of 1 Hz to 1 MHz using needle electrodes by plugging all parts of the needle electrode into the middle part of the banana. Impedance measurements carried out in room conditions (temperature, humidity, and atmospheric pressure). The data obtained is the value of the output voltage. Calculation of the impedance value by dividing the number of tops and bottom peak voltages, and then the results divided by a current of 1 mA. Calculation of phase difference from input and output voltages by measuring the difference in peak voltage displacement from input and output.

The research subject in the form of biological material is usually analogous to an electrical circuit, which consists of resistors and conductors, and there can be inductors depending on the content. The electrical impedance of banana like any other plant

tissues, does not contain any inductive components but consists of the resistive and capacitive elements [2], as shown in Fig. 3.

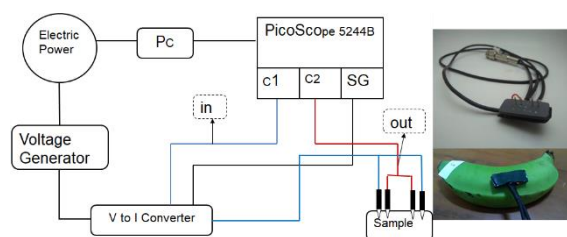


Fig. 2 System of Electrical Impedance Measurements

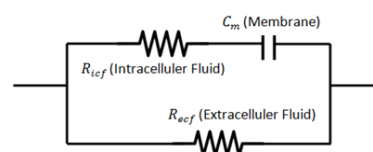


Fig. 3 Equivalent circuit model based on cell tissue according to the modified Hayden Model,  $C_m$  is Capacitance of the membrane,  $R_{eef}$  is the resistance of apoplectic fluids, and  $R_{ief}$  is intracellular resistance [3, 14].

Analysis of the effect of frequency on impedance by application Bode plot to determine the extent of the impact of phase difference on real value and imaginary impedance to frequency. Effect of ethrel treatment by applying the Nyquist curve, as shown in Fig 4.

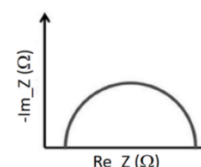


Fig. 4 Nyquist plot analysis for the modified Hayden Model

## RESULTS AND DISCUSSIONS

### Ethrel Effect on Banana Skin Color

Ripening of bananas using ethrel affects the maturity of bananas. Observations on the physiological properties of color, it appears that the yellow color of the fruit skin shows the level of sophistication, the faster it forms in the immersion of 2000-ppm ethrel, as shown in Fig. 5. Control banana (natural ripening process) in 9 days still shows greenish-colored skin, and different results occurred in bananas with a concentration of 1000-ppm ethrel, which was yellow on the fifth day, while an ethrel concentration of 2000 ppm caused a more yellow color to occur on the third day.



The characteristic of the maturity of a banana is that the skin color of the fruit changes from green to turn yellow with the increasing formation of ethylene gas. During the ripening process of bananas, there is an increase in sugar levels and a decrease in flour content or softening of banana meat. This condition causes by an insoluble remodeling of the protopectin to become soluble. These substances are derivatives of Polygalacturonic acid and are present in the form of protopectin, pectin, pectinic acid, and pectic acid.

When the fruit ripens, the soluble pectate and pectinate content increases, while the total amount of pectate decreases. In the change in pectin, the fruit's toughness decreases, so the fruit becomes soft. Hydrolysis Amylum is perfect by acids or specific enzymes on polysaccharides producing mono-saccharides or their derivative compounds, and there is a slight increase in sucrose, glucose, and fructose during maturation.

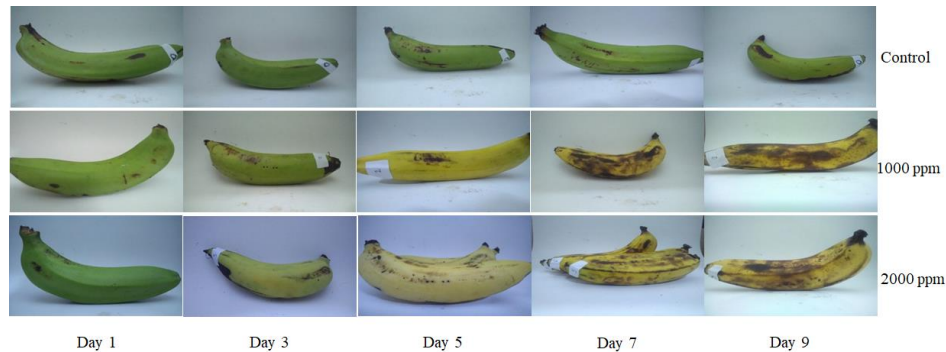


Fig. 5 Display of banana color for all days at various ethrel concentrations.

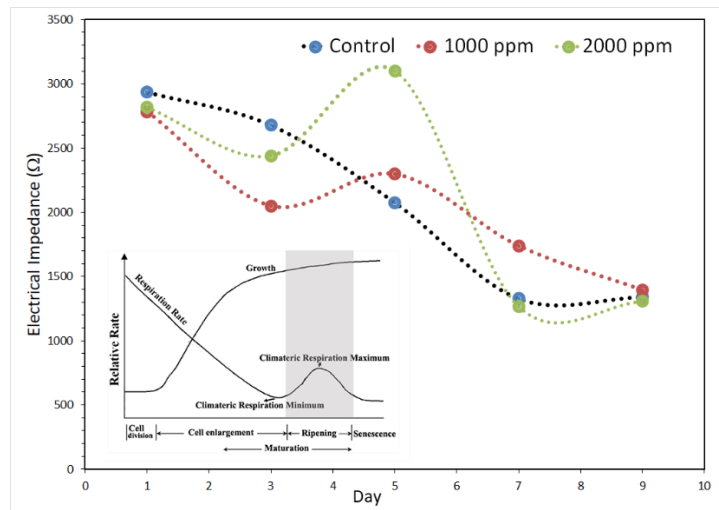


Fig. 6 Plot Graph of electrical impedance measurements at a frequency of 100 Hz in various concentrations, the results compared with climacteric fruit charts.

The results showed a similar pattern, where the impedance value suddenly decreased with increasing time, as shown in Fig. 6. The maturation process in the control sample until the ninth day passes through the minimum climacteric maturation phase and will lead to the formation of sugar. The measurement results show a decreasing impedance value until the minimum climacteric respiration phase.

The formation of sugar in the ripening process will increase the impedance value of the banana [18]. The 1,000 ppm ethrel concentration shifted the time of sugar formation compared to the control, where on the third day, the maximum maturity level occurred, and this also happened at a concentration of 2000 ppm. After the peak phase, the process will enter the

hydrolysis phase, where this phase will reduce the impedance value. The interesting thing happens is that at a concentration of 2000 ppm there is a sharper decline compared to 1000 ppm, the hydrolysis process occurs more so that the banana decomposes more quickly.

Fig. 7 shows the Bode plots for all treatment, where at low frequencies (up to 100 Hz), all graphs show a relatively constant phase angle, and the impedance value shows a linear relationship. Dispersion occurs at a frequency of 1000 Hz and above. At that time, the impedance value more influenced by the presence of resistive and capacitive properties of the material. Plotting Nyquist curves show apparent differences between treatments for all

days. Suitability between extractions results for each element obtained with the model used is very high, as shown in Fig. 8. The measurement on the first day

proved a shift in the imaginary-value and real value of electrical impedance as the concentration of ethrel increased and at 2000 ppm shifted further.

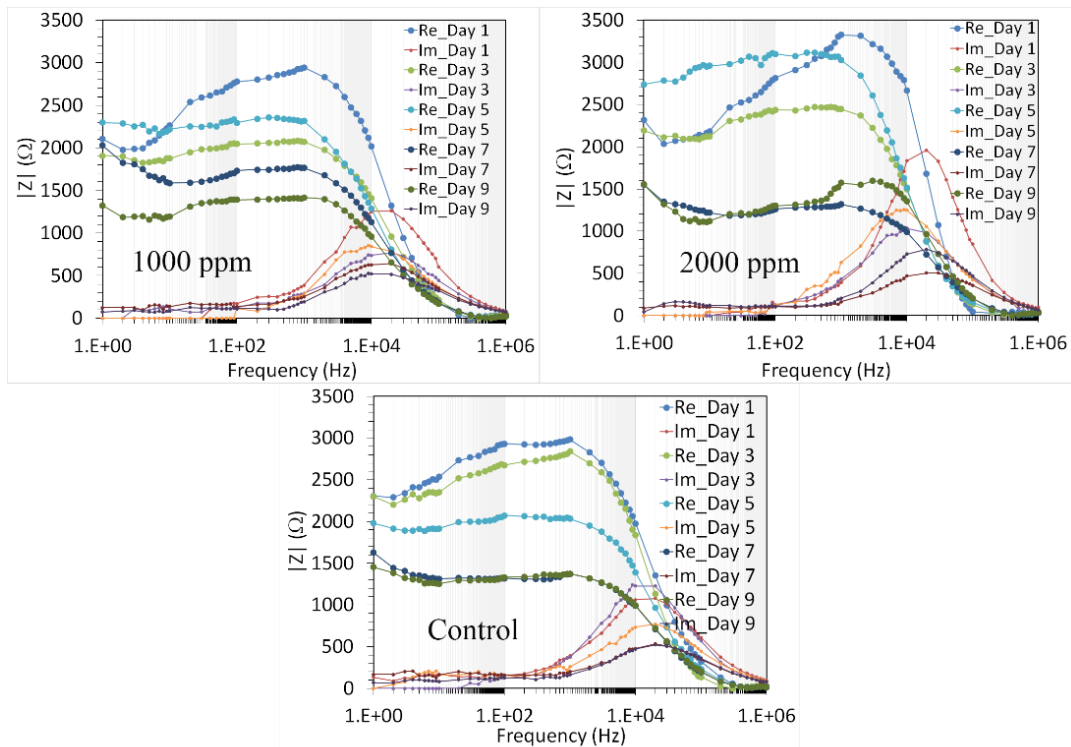


Fig. 7 An analysis of Bode-plots results for real and imaginary of impedance values in all treatments.

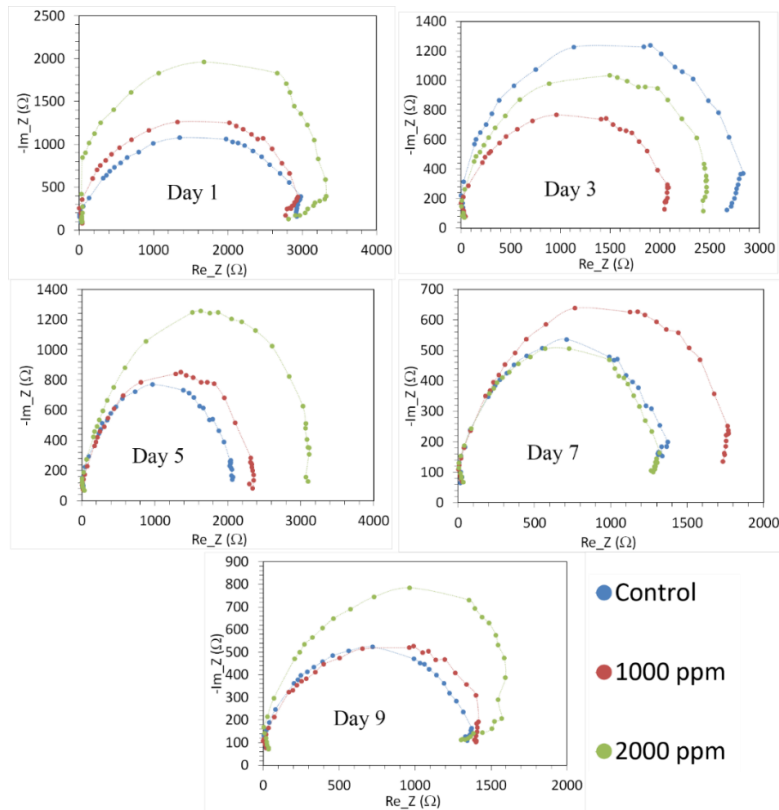


Fig. 8 The results of the Nyquist plot analysis for all treatments.

Table 1 The simulation results using EIS Spectrum Analyzer Freeware [20] for the equivalent circuit in Fig. 3, with the fitting of the Nyquist plot results in Fig. 8.

| Day | Element            | Control | 1000    | 2000    |
|-----|--------------------|---------|---------|---------|
| 1   | $R_{icf} (\Omega)$ | 50.57   | 50.93   | 50.64   |
|     | Error (%)          | 18.20   | 16.63   | 21.70   |
| 1   | $C (nF)$           | 3.22    | 3.07    | 2.11    |
|     | Error (%)          | 3.58    | 3.58    | 11.00   |
| 1   | $R_{ecf} (\Omega)$ | 2986.90 | 2914.00 | 3307.60 |
|     | Error (%)          | 2.30    | 1.52    | 1.24    |
| 3   | $R_{icf} (\Omega)$ | 50.19   | 50.21   | 50.55   |
|     | Error (%)          | 6.78    | 10.19   | 5.33    |
| 3   | $C (nF)$           | 3.30    | 3.72    | 3.33    |
|     | Error (%)          | 3.01    | 3.43    | 16.06   |
| 3   | $R_{ecf} (\Omega)$ | 2756.50 | 2015.40 | 2470.30 |
|     | Error (%)          | 2.13    | 3.30    | 1.94    |
| 5   | $R_{icf} (\Omega)$ | 50.77   | 50.77   | 50.21   |
|     | Error (%)          | 10.06   | 7.18    | 6.86    |
| 5   | $C (nF)$           | 3.72    | 3.72    | 3.69    |
|     | Error (%)          | 3.84    | 19.04   | 9.48    |
| 5   | $R_{ecf} (\Omega)$ | 2323.60 | 2323.60 | 3078.20 |
|     | Error (%)          | 10.99   | 2.80    | 3.07    |
| 7   | $R_{icf} (\Omega)$ | 50.68   | 50.02   | 50.09   |
|     | Error (%)          | 7.09    | 7.98    | 7.23    |
| 7   | $C (nF)$           | 3.83    | 3.79    | 3.86    |
|     | Error (%)          | 9.80    | 14.77   | 5.81    |
| 7   | $R_{ecf} (\Omega)$ | 1367.00 | 1802.00 | 1289.30 |
|     | Error (%)          | 3.52    | 2.29    | 3.52    |
| 9   | $R_{icf} (\Omega)$ | 50.69   | 50.76   | 50.76   |
|     | Error (%)          | 8.51    | 14.96   | 14.96   |
| 9   | $C (nF)$           | 3.84    | 3.73    | 3.73    |
|     | Error (%)          | 18.96   | 6.01    | 6.01    |
| 9   | $R_{ecf} (\Omega)$ | 1353.80 | 1624.50 | 1624.50 |
|     | Error (%)          | 2.46    | 1.48    | 1.48    |

On the third day, a noticeable change occurred in bananas with an ethrel concentration of 2000 ppm, where there was a shift in the real and imaginary values of electrical impedances. Whereas, the result for a 1000 ppm shifts only its imaginary-value. As shown in Table 1, the error is around 7.5% for all elements in all treatments, where the lowest error is 1.24%, and the biggest is 21.70%.

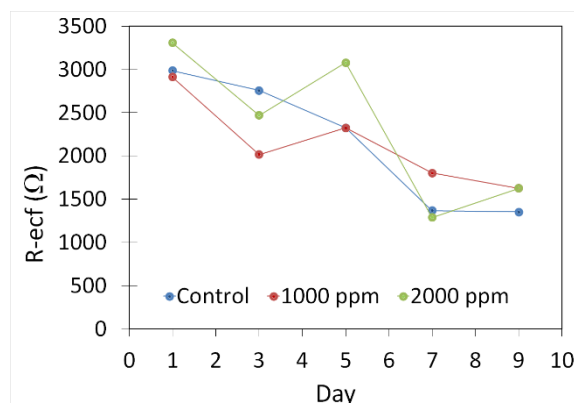


Fig. 9 The value of  $R_{ecf}$  obtained by the Nyquist curve at various concentrations from Table 1.

The value of  $C$  is relatively constant at around 3.5 nF, and similar results obtained for the  $R_{icf}$ , which is approximately 50.5 Ohm. On the other hand,  $R_{ecf}$  results of the curve tend to follow the maturation level of bananas, as shown in Fig 9. The extraction results for all elements in all treatments turned out to be similar to the curves of the measured electrical impedance values, as shown in Fig. 6. Changes in the composition of ingredients in the ripening process of bananas, for example, sugar content, acid content, salt, amount of liquid due to hydrolysis affect the resistivity level of the material.

## CONCLUSIONS

Ethrel stimulation accelerates the ripening process of Ambon banana fruit. On the fifth day, bananas with ethrel have reached the maximum climatic respiration phase, while natural fruit ripening is still in the minimum climacteric respiration phase. Impedance spectroscopic system can detect banana ripening process, where on a fifth day of maturation due to 2000 ppm ethrel has a maximum impedance value of 3101.83  $\Omega$  higher than 1000 ppm with an impedance value of 2297.67  $\Omega$ . The electrical impedance value during the ripening process of bananas is more influenced by the nature of extra cell fluid resistance due to the formation of sugar solution which has resistive properties, with resistance values at the maturity peak of 3078.60  $\Omega$  and 2323.6  $\Omega$  for 2000 ppm and 1000 ppm respectively.

## ACKNOWLEDGMENTS

This research funded by the PTUPT-Grant 2019 from Directorate of Research and Community Service, Directorate General for Research and Development at the Ministry of Research Indonesia, Technology and Higher Education with contract number 332.45/UN10.C10/PN/2019.

## REFERENCES

- [1] Chowdhury A., Datta S., Bera T.K., Ghoshal D., and Chakraborty B., Design and development of microcontroller based instrumentation for studying complex bioelectrical impedance of fruits using electrical impedance spectroscopy, *J. Food Process Eng.*, Vol. 41, 2018, pp. e12640.
- [2] Chowdhury A., Kanti Bera T., Ghoshal D., and Chakraborty B., Electrical Impedance Variations in Banana Ripening: An Analytical Study with Electrical Impedance Spectroscopy, *J. Food Process Eng.*, Vol. 40, 2017, pp. e12387.
- [3] Chowdhury A., Singh P., Bera T.K., Ghoshal D., and Chakraborty B., Electrical impedance spectroscopic study of mandarin orange during ripening, *J. Food Meas. Charact.*, Vol. 11, 2017, pp. 1654–1664.
- [4] Chung J., Chen Y., and Kim S.-J., High-density impedance-sensing array on complementary metal-oxide-semiconductor circuitry assisted by negative dielectrophoresis for single-cell-resolution measurement, *Sensors Actuators B Chem.*, Vol. 266, 2018, pp. 106–114.
- [5] Elkashif M.E., Hamdoun E.A., Elamin O.M., and Mahmoud H.I., Effects of Ethrel, packaging and waxing on quality and shelf life of guava (*Psidium guajava* L.) fruits, *Gezira J. Agric. Sci.*, Vol. 14, 2016.
- [6] Gowry B., Shahrman A.B., and Paulraj M., Electrical bio-impedance as a promising prognostic alternative in detecting breast cancer: A review, *IEEE*, 2015, pp. 1–6 c.
- [7] Gurjar P.S., Verma A.K., Dikshit A., and Shukla D.K., Effect of ethrel spray on the ripening behaviour of mango (*Mangifera indica* L.) variety 'Dashehari', *J. Appl. Nat. Sci.*, Vol. 9, 2017, pp. 1619–1623.
- [8] Islam M., Wahid K., and Dinh A., Assessment of Ripening Degree of Avocado by Electrical Impedance Spectroscopy and Support Vector Machine, *J. Food Qual.*, Vol. 2018, 2018, pp. 1–9.
- [9] Kaur S., Effect of different treatments of ethrel on ripening behaviour and post-harvest quality of mango (*Mangifera indica* L.) during storage, *J. Appl. Nat. Sci.*, Vol. 9, 2017, pp. 85–93.
- [10] Moniruzzaman M., Khatoun R., Hossain M., Rahman M., and Alam S., Influence of ethephon on ripening and quality of winter tomato fruit harvested at different maturity stages, *Bangladesh J. Agric. Res.*, Vol. 40, 2016, pp. 567–580.
- [11] Paul V., Pandey R., and Srivastava G.C., The fading distinctions between classical patterns of ripening in climacteric and non-climacteric fruit and the ubiquity of ethylene—An overview, *J. Food Sci. Technol.*, Vol. 49, 2012, pp. 1–21.
- [12] Watanabe T., Ando Y., Orikasa T., Kasai S., and Shiina T., Electrical impedance estimation for apple fruit tissues during storage using Cole–Cole plots, *J. Food Eng.*, Vol. 221, 2018, pp. 29–34.
- [13] Watanabe T., Ando Y., Orikasa T., Shiina T., and Kohyama K., Effect of short time heating on the mechanical fracture and electrical impedance properties of spinach (*Spinacia oleracea* L.), *J. Food Eng.*, Vol. 194, 2017, pp. 9–14.
- [14] Watanabe T., Nakamura N., Ando Y., Kaneta T., Kitazawa H., and Shiina T., Application and Simplification of Cell-Based Equivalent Circuit Model Analysis of Electrical Impedance for Assessment of Drop Shock Bruising in Japanese Pear Tissues, *Food Bioprocess Technol.*, Vol. 11, 2018, pp. 2125–2129.
- [15] Widodo C.S., Santoso D.R., and Juswono U.P., Double Layer Impedance Analysis on The Electrical Impedance Measurement of Solution Using Parallel Plate, *J. Environmental Eng. Sustain. Technol.*, Vol. 3, 2016, pp. 65–69.
- [16] Widodo C.S. and Saroja G., A study of application of two probes at frequency 0.1 to 10 kHz in electrical impedance measurement system for various fats, *IEEE*, 2017. 86–91 c.
- [17] Widodo C.S., Sela H., and Santosa D.R., The effect of NaCl concentration on the ionic NaCl solutions electrical impedance value using electrochemical impedance spectroscopy methods, *AIP Publishing LLC*, 2018.
- [18] Widodo C.S., Sugianto W., Effendi A.M., and Saroja G., Study on the effect of sugar canes and saccharin to the value of electrical impedance of apple cider manalagi (*Malus sylvestris mill*), *J. Phys. Conf. Ser.*, Vol. 1153, 2019, pp. 012121.
- [19] Xu Y., Xie X., Duan Y., Wang L., Cheng Z., and Cheng J., A review of impedance measurements of whole cells, *Biosens. Bioelectron.*, Vol. 77, 2016, pp. 824–836.
- [20] Bondarenko A.S. and Ragoisha G.A., in *Progress in Chemometrics Research*, Pomerantsev A.L., 2005, pp. 89–102.

## DNA EXTRACTION METHODS FOR FIN OF MACKERELS IN THAILAND

\*Walaiporn Makkapan, Patcharaporn Narkthewan and Kaewalee Viboonkit  
King Mongkut's Institute of Technology Ladkrabang Prince of Chumphon Campus,  
Pathiu, Chumphon, Thailand

### ABSTRACT

The quality and quantity of DNA are crucial aspects for fish studies based on the molecular techniques. Extraction method of genomic DNA is depended on tissue types and organism species. This research aimed to identify an appropriate extraction method for gDNA from fin of three popular mackerel species in Thailand; short-bodied mackerel (*Rastrelliger brachysoma*), island mackerel (*R. faughni*) and Indian mackerel (*R. kanagurta*). Four different methods for gDNA extraction were compared based on time, quality and quantity of extractable gDNA for PCR technique. Method III showed the highest quantity of gDNA in *R. brachysoma* and *R. kanagurta*. Nevertheless, the highest purity of gDNA for both species was obtained by method II and IV, respectively. The gDNA from method IV was successful to amplify the intense band of  $\beta$ -actin fragment. The highest concentration and purity of gDNA from *R. faughni* were received using method II. However,  $\beta$ -actin gene fragment amplified from gDNA of method IV showed intense bands. These results indicated that method IV was suitable for gDNA extraction from fin of three mackerel species because of fastest, high quality and quantity for PCR amplification.

*Keywords: DNA extraction, Fin, Mackerel, Fish*

### INTRODUCTION

Extraction of genomic DNA is an important step of fish studies based on the molecular techniques. Several reports related DNA extraction from various fish suggested quality and quantity of extracted gDNA were depended on fish species, tissues types and extraction methods [1]-[5]. Nowadays, attempt to extract gDNA from fish tissue without or less invasive sampling method was investigated in many fish. Several reports demonstrated the different protocols of DNA extraction from the external organs of fish, such as fins [1], [5], and scales [3]. There is little information related molecular studies in three popular mackerel species in Thailand, including *R. brachysoma*, *R. faughni* and *R. kanagurta*. Therefore, the objective of this study was to identify an appropriate method for gDNA extraction from fin of three mackerel species for PCR-based techniques. The result data will be as a beneficial knowledge for further mackerel research such as genomic analysis, biomarker study and genetic species identification, etc.

### MATERIALS AND METHODS

#### Fish Sample and Extraction Methods

*R. brachysoma*, *R. faughni* and *R. kanagurta* were obtained from port in Chumphon Province,

Thailand. Caudal fin was isolated and subjected for gDNA extraction using four different methods composed of method I-V.

Method I was modified from urea treatment method [6]. Fin tissue (20 mg) was mixed with 300  $\mu$ l of extraction buffer (10 mM Tris-HCl pH 8.0, 10 mM EDTA, 0.5% SDS, 4 M Urea) with 5  $\mu$ l of RNase (10 mg/ml). The mixture was homogenized and incubated at 42°C with shaking at 200 rpm. After incubation for 1 h, the mixture was gently mixed with 10  $\mu$ l of Proteinase K (10 mg/ml) and then incubated at 42°C with shaking at 200 rpm for 16-18 h. Equal volume of phenol:chloroform:isoamyl alcohol (25:24:1) was then added into the mixture and inverted for several times. The mixture was centrifuged at 11,000 rpm for 15 min. The upper phase was collected to the new tube, and mixed with 1 M NaCl and equal volume of absolute ethanol. The mixture was centrifuge at 11,000 rpm for 15 min. The supernatant was discarded. The 70% ethanol was added to DNA pellet and then centrifuged at 11,000 rpm for 5 min. The DNA pellet was air-dried and re-suspended in sterile water.

Method II was modified from report of [1]. Fin tissue (20 mg) was homogenized in 300  $\mu$ l of extraction buffer (50 mM Tris-HCl pH 8.0, 100 mM NaCl, 50 mM EDTA, 1% SDS) with 7.5  $\mu$ l of Proteinase K (10 mg/ml). The mixture was incubated in the shaking incubator at 55°C for 16-18 h with oscillation of

200 rpm. Subsequently, 300  $\mu$ l of 5 M NaCl was mixed with the mixture and centrifuged at 11,000 rpm for 10 min. The supernatant was collected and inversely mixed with equal volume of phenol:chloroform:isoamyl alcohol (25:24:1). The mixture was then centrifuged at 11,000 rpm for 10 min. The upper phase was collected and mixed with equal volume of absolute ethanol for DNA precipitation. The mixture was centrifuged at 11,000 rpm for 15 min. The supernatant was discarded. The 70% ethanol was added to DNA pellet and then centrifuged at 11,000 rpm for 5 min. The DNA pellet was air-dried and re-suspended in sterile water.

Method III was followed by Rapid MT method [4]. The fish fin (20 mg) was homogenized in 660  $\mu$ l of extraction buffer (100 mM Tris-HCl pH 8.0, 5 mM EDTA, 0.2% SDS, 200 mM NaCl) and then 1  $\mu$ l of Proteinase K (10 mg/ml) was added. The mixture was incubated in the shaking incubator at 55°C for 24 h with oscillation of 200 rpm. After incubation, the sample was centrifuged at 12,000xg for 15 min. The supernatant was taken in the new tube and inversely mixed with equal volume of phenol:chloroform:isoamyl alcohol (25:24:1). After centrifugation at 12,000xg for 10 min, the upper phase was collected and mixed with equal volume of isopropanol, and then centrifuged at 12,000xg for 10 min. The supernatant was decanted and the DNA pellet was washed with 70% ethanol. The DNA pellet was air-dried and re-suspended in sterile water.

Method IV was modified from report of [5], [7]. Fin sample (20 mg) was homogenized in 400  $\mu$ l of extraction buffer (200 mM Tris-HCl pH 8.0, 100 mM EDTA, 250 mM NaCl, 1.2% SDS, 200  $\mu$ g/ml Proteinase K) and incubated in the shaking incubator at 48°C for 3 h. Equal volume of phenol:chloroform:isoamyl alcohol (25:24:1) was added into the mixture and mix by inversion for several time. After centrifugation at 11,000 rpm for 15 min, the upper layer was taken into new tube. Equal volume of isopropanol and 0.2 volume of 10 M ammonium acetate was added and mixed. The sample was centrifuged at 11,000 rpm for 15 min. The supernatant was removed and the DNA pellet was washed in 70% ethanol, air-dried and re-suspended in sterile water.

#### Quality and Quantity of gDNA Analysis

The quality and quantity of gDNA from each method were determined by agarose gel electrophoresis and spectrophotometer. The DNA sample was visualized in 1% agarose gel stained with SYBR Safe DNA Gel Stain. The concentration and purity were evaluated using UV/visible

spectrophotometer with absorbance of 260 and 260/280 nm, respectively. The data was presented as a mean  $\pm$  standard deviation (mean $\pm$ SD; n=5). The statistical significance was examined using the One-Way Analysis of Variance followed by a Tukey's HSD test at a significance level of  $\leq 0.05$ .

#### Polymerase Chain Reaction

The quality of gDNA was further confirmed by amplification in conserved region of  $\beta$ -actin gene, consisting of 1244 bp, using specific primers: Forward 5' ATGAAATCGCCGCACTGG 3' and Reverse 5' TGGATGGCAACGTACATGGC 3'. PCR reaction was performed in total volume of 50  $\mu$ l mixture consisting of 100 ng of gDNA, 1X Standard Taq Reaction buffer, 1 mM MgCl<sub>2</sub>, 0.2 mM dNTPs mixture, 0.4  $\mu$ M of forward and reverse specific primers, and 1.25 U Taq DNA polymerase. Amplification conditions were 95°C for 3 min followed by 30 cycles at 95°C for 30 s, 53°C for 30 s, 72°C for 30 s and then subjected to a final extension of 72°C for 3 min. The amplified products were analyzed through 1.5% agarose gel stained with SYBR Safe DNA Gel Stain.

#### RESULTS AND DISCUSSION

This study identified the appropriate extraction method for gDNA from fin tissue of three popular species mackerels in Thailand based on extraction time, quality and quantity of gDNA. The gDNA extraction method should be rapid and efficient for achieving the high quantity and quality of gDNA [8], [9]. The fin gDNA was extracted from four different methods: method I-IV. For the extraction time, the method I-III needed more than 20 h for whole process, whilst the time requirement for method IV was not more than 6 h. Extraction buffer of all methods was generally used SDS and proteinase K as a detergent for tissue digestion process, which was varied the concentration of those. Moreover, urea and RNase were added into extraction buffer of method I for protein and RNA denaturation [5], [6], respectively. The extraction buffer of method II-IV was additionally mixed with NaCl used for extracting protein [4]. The temperature in tissue lysis step in all methods was carried out at 42-55°C. Subsequently, phenol: chloroform: isoamyl alcohol was required to remove the proteins and DNA was precipitated by either absolute ethanol or isopropanol. Interestingly, DNA precipitation step of all did not take additional times.

The quantity and quality of gDNA from fin of *Rastrelliger* sp. obtained from different four methods was summarized in Table 1.

Table 1 Quantity and quality of extracted DNA from different extraction methods

| Extraction Method | <i>R. brachysoma</i>     |                          | <i>R. faughni</i>      |                        | <i>R. kanagurta</i>    |                          |
|-------------------|--------------------------|--------------------------|------------------------|------------------------|------------------------|--------------------------|
|                   | Concentration (µg/µl)    | Purity (A260/A280)       | Concentration (µg/µl)  | Purity (A260/A280)     | Concentration (µg/µl)  | Purity (A260/A280)       |
| Method I          | 0.45±0.18 <sup>a</sup>   | 1.48±0.03 <sup>a</sup>   | 0.62±0.08 <sup>a</sup> | 1.49±0.07 <sup>a</sup> | 0.49±0.03 <sup>a</sup> | 1.67±0.08 <sup>a</sup>   |
| Method II         | 0.64±0.12 <sup>a,b</sup> | 1.61±0.07 <sup>b</sup>   | 1.10±0.07 <sup>b</sup> | 1.77±0.05 <sup>b</sup> | 0.70±0.08 <sup>b</sup> | 1.75±0.06 <sup>a,b</sup> |
| Method III        | 0.98±0.10 <sup>c</sup>   | 1.54±0.02 <sup>a,b</sup> | 0.94±0.12 <sup>b</sup> | 1.66±0.09 <sup>b</sup> | 0.84±0.07 <sup>c</sup> | 1.70±0.02 <sup>a</sup>   |
| Method IV         | 0.74±0.10 <sup>b</sup>   | 1.59±0.03 <sup>b</sup>   | 1.05±0.14 <sup>b</sup> | 1.74±0.08 <sup>b</sup> | 0.70±0.07 <sup>b</sup> | 1.83±0.04 <sup>b</sup>   |

Note: Concentration and purity were represented as mean±SD (n=5). The different letters indicated the significant difference between extraction methods within same species. The significant difference was analyzed by Tukey's HSD at  $P<0.05$ .

The extractable gDNA concentration from different methods varied in each species. The concentration of gDNA from *R. brachysoma* was shown in range of 0.45-0.98 µg/µl. The highest concentration of gDNA from *R. brachysoma* was found from method III (0.98±0.10 µg/µl), followed by method IV (0.74±0.10 µg/µl), method II (0.64±0.12 µg/µl), and method I (0.45±0.18 µg/µl), respectively. The concentration of gDNA of *R. faughni* was obtained in range of 0.62-1.10 µg/µl. The gDNA of *R. faughni* was shown the highest concentration obtained from method II (1.10±0.07 µg/µl). This was followed by method IV (1.05±0.14 µg/µl), method III (0.94±0.12 µg/µl), and method I (0.62±0.08 µg/µl), respectively. The concentration of gDNA of *R. kanagurta* was extractable in range 0.49-0.84 µg/µl. The highest concentration of gDNA from *R. kanagurta* was found in method III (0.84±0.07 µg/µl), followed by method IV (0.70±0.07 µg/µl) and method II (0.70±0.08 µg/µl). The lowest concentration of extracted gDNA was observed from method I (0.49±0.03 µg/µl). This study found the significantly lower values were attained from method I supplemented with urea in extraction buffer, suggesting this method did not suitable for DNA extraction from fin of three mackerel species.

The quality of the gDNA was indicated by A260/A280 ratio. The purity of extracted DNA is generally accepted a yield of A260/A280 ratio in range of 1.8-2.0 [10]. The gDNA of *R. brachysoma* from all extraction methods expressed a low purity, which had a value in range of 1.48-1.61. The highest purity in this species was exhibited in the extracted DNA obtained by method II (1.61±0.07). This was followed by the gDNA attained from method IV (1.59±0.03), method III (1.54±0.02), and method I (1.48±0.03), respectively. The gDNA of *R. faughni* showed the purity values in range of 1.49-1.77. The

gDNA obtained from method II showed the highest purity for *R. faughni* (1.77±0.05), following by method IV (1.74±0.08), method III (1.66±0.09), and method I (1.49±0.07), respectively. Meanwhile, the gDNA of *R. kanagurta* showed the purity values in range of 1.67-1.83. The highest purity in this species was shown in the extracted DNA obtained by method IV (1.83±0.04), following by method II (1.75±0.06), method III (1.70±0.02), and method I (1.67±0.08), respectively. These results suggested the method II produced the highest quality of gDNA for *R. brachysoma* and *R. faughni* compared to other methods. The method IV was able to extract the highest quality of gDNA for *R. kanagurta*. Corresponding with quantity result, the quality of gDNA extracted from method I was lowest for all species. Report of [1] revealed the purity of fin DNA extracted from modified salt method showed in range of 1.83-2.19. These results of showed the similar results of reports from [4], [5] demonstrated the purity of fish DNA was in range of 1.6-2.0.

Subsequently, the quality of gDNA was considered by using as a template for PCR amplification of *β-actin* gene fragment. The amplified products of *β-actin* gene analyzed by 1.5% agarose gel electrophoresis were shown in Fig. 1. The PCR products in *R. brachysoma* as well as *R. kanagurta* were achieved from gDNA obtained from all methods. The intense band of PCR products was represented from the gDNA obtained from method I and IV. Whereas, some of gDNA obtained from method II and III showed the light band of the amplified PCR fragment. The PCR amplification in *R. faughni* was attained by using gDNA extracted from all methods. The PCR products of gDNA from method IV showed the intense band. The gDNA from method I, II and III were amplified the PCR products with light band.



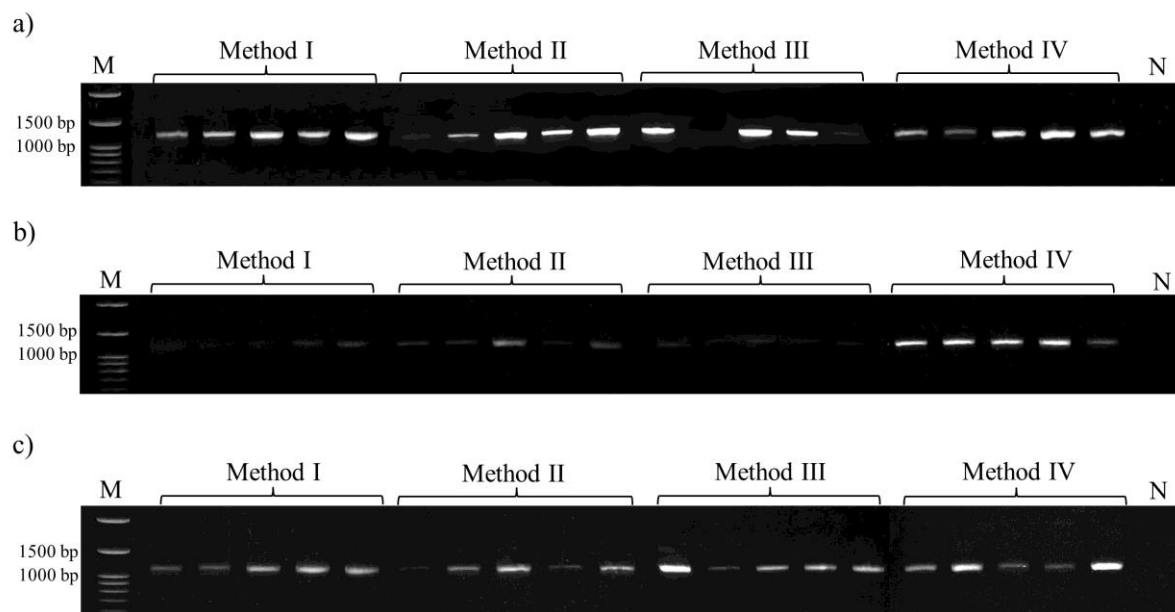


Fig. 1  $\beta$ -Actin fragments amplified from gDNA extracted from fin of a) *R. brachysoma*, b) *R. faughni*, and c) *R. kanagurta* by using different methods (method I-IV). M = 100 bp DNA ladder marker and N = negative control.

## CONCLUSIONS

The quality and quantity of gDNA from fin varied according to fish species and extraction methods. The method IV was the appropriate method for DNA extraction from fin of three mackerel species in Thailand. It indicated that the advantage of method IV was rapid, good quantity and quality of gDNA for PCR amplification.

## ACKNOWLEDGMENTS

This work was financially supported by National Research Council of Thailand. The facilities were supported by King Mongkut's Institute of Technology Ladkrabang Prince of Chumphon Campus, Thailand.

## REFERENCES

- [1] Lopera-Barrero N. M., Povh J. A., Ribeiro R. P., Gomes P. C., Jacometo C. B., and Lopes, T. S., Comparison of DNA Extraction Protocols of Fish Fin and Larvae Samples: Modified Salt (NaCl) Extraction. *Ciencia e Investigación Agraria*, Vol. 35, Issue 1, 2008, pp.65-74.
- [2] Mukhopadhyay T., and Bhattacharjee, S., Standardization of Genomic DNA Isolation from Minute Quantities of Fish Scales and Fins Amenable to RAPD-PCR. *Proceedings of the Zoological Society*, Vol. 67, Issue 1, 2014, pp.28-32.
- [3] Li Y., Gul Y., Cui L., Cao X., and Wang, W., Comparative Analysis of Different Protocol for Extraction of DNA from Fish Scales of *Cyprinus carpio*. *Indian Journal of Biotechnology*, Vol. 14, Issue 3, 2015, pp. 382-387.
- [4] Chowdhury M. M., Rahman A. S. M. S., Nahar L., Rahman M., Reza H. A., and Ahmed Md. S., Efficiency of Different DNA Extraction Methods for Fish Tissues: A Comparative Analysis. *IOSR Journal of Pharmacy and Biological Sciences*, Vol. 11, Issue 3, 2016, pp. 11-15.
- [5] Muhammad H., Iqbal Z., Iqbal M. U., Younas T., and Bashir Q., An Efficient Method for DNA Isolation from Fish Fin. *Pakistan Journal of Agricultural Sciences*, Vol. 53, Issue 4, 2016, pp. 843-850.
- [6] Wasko A. P., Martins C., Oliveira C., and Foresti F., Non-destructive Genetic Sampling in Fish. An Improved Method for DNA Extraction from Fish Fins and Scales. *Hereditas*, Vol. 138, Issue 3, 2003, pp.161-165.
- [7] Kumar R., Singh P. J., Nagpure N. S., Kushwaha B., Srivastava S. K., and Lakra, W. S., A Non-invasive Technique for Rapid Extraction of DNA from Fish Scales. *Indian Journal of Experimental Biology*, Vol. 45, Issue 11, 2007, pp. 992-997.
- [8] Sika K. C., Kefela T., Adoukonou-Sagbadja H., Ahoton L., Saidou A., Baba-Moussa L., Baptiste L. J., Kotconi S. O., and

- Gachomo E. W., A Simple and Efficient Genomic DNA Extraction Protocol for Large Scale Genetic Analyses of Plant Biological Systems. *Plant Gene*, Vol. 1, 2015, pp. 43-45.
- [9] Shafi N., Rauf A., Akhtar T., Minhas R. A., Ulfat, and Bibi S., Comparative Isolation and Amplification of *Cytochrome oxidase I* DNA from *Oncorhynchus mykiss* (Rainbow Trout) of Azad Jammu & Kashmir. *International Journal of Fisheries and Aquatic Studies*, Vol. 4, Issue 6, 2016, pp. 196-199.
- [10] Boesenberg-Smith K. A., Pessarakli M. M., and Wolk D. M., Assessment of DNA Yield and Purity: an Overlooked Detail of PCR Troubleshooting. *Clinical Microbiology Newsletter*, Vol. 34, Issue 1, 2012, pp. 1, 3-6.

## ANGIOTENSION CONVERTING ENZYME (ACE) INHIBITORY ACTIVITY OF PROTEIN EXTRACT OF MUNG BEANS (*Vigna radiata* L.) TEMPEH FERMENTED BY *Rhizopus* sp.

Sri Yadiyal Chalid<sup>1</sup>, Siti Nurbayti<sup>2</sup>, Zelda Zein Zunaedi<sup>3</sup>

<sup>1,2,3</sup>Chemistry dept. Faculty of Science and Technology, Islamic State University Syarif Hidayatullah,  
Jakarta, Indonesia

### ABSTRACT

One of the roles of Angiotensin Converting Enzyme (ACE) is as a narrowing factor of blood vessels by changing angiotensin I to angiotensin II. Prevention of narrowing of arteries can be done by inhibiting ACE work. ACE inhibitorys are derived from synthetic drugs, proteins and active ingredients in food ingredients. Protein-rich fermented foods and bioactive peptides can be used to inhibit ACE and protein tempeh is one of the foods that can inhibit ACE. Mung beans (*Vigna radiata* L.) were fermented with *Rhizopus* sp to produce tempeh. The amount of *Rhizopus* sp used was 0.2 and 0.4% (w/w) with various time variations of 6 hours interval, namely 0, 6, 12, 18, 24, 30, 36 and 42 hours. The physical properties of tempeh were analyzed including the growth of mycelium, color and aroma according to the Indonesian National Standard (SNI). Protein tempeh was extracted by the precipitation method at the isoelectric point, the dissolved protein was measured, and the ability of the protease to hydrolyze the protein into peptide was determined by the degree of hydrolysis (DH). The activity of tempeh protein extract in ACE inhibitory was measured based on the amount of hippuric acid produced in the reaction between hippuryl-histidyl-leucine (HHL) and ACE enzyme. The best ACE inhibitory activity was obtained by mung beans tempeh fermented for 24 hours with a yeast amount of 0.4% and dissolved protein content of 351 mg/mL. The results of the SDS-PAGE analysis showed the presence of proteins with molecular weights of 12, 54, 98 and 125 kDa. The degree of hydrolysis produced was 18.68% and ACE inhibitory activity was 75%. Therefore, mung beans tempeh has the potential to be developed to be functional antihypertensive foods.

**Keywords:** Protein extract, Mung beans tempeh, Functional food, Antihypertensive

### INTRODUCTION

Angiotensin-converting enzyme (ACE) is zinc metallopeptidase which plays a role in changes in angiotensin I to angiotensin II. Angiotensin II is an octapeptide capable of stimulating aldosterone secretion resulting in retention of extracellular sodium and stimulating the secretion of Anti-Deuretic Hormone (ADH) which plays a role in decreasing the amount of urine excreted from the body. This condition causes blood to become thick [1], [2]. Formation of angiotensin II is one of the mechanisms of the cause of hypertension [3]. Some treatments that can be done as therapy and prevention of hypertension are medical treatment, regulating lifestyle, losing weight, consuming foods rich in potassium and calcium, low sodium, rich in fiber, and fruits, doing physical activities, and not consuming alcohol. This balanced lifestyle is according to DASH (diet dietary approaches to stop hypertension) [4].

Medical drugs classified as ACE inhibitorys include katopril, enalapril, and lisinopril [5], yet these synthetic drugs have side effects such as nausea, headache, diarrhea, dry cough, no appetite and kidney problems [6] and allergy [7]. Thus, non-medical

hypertension therapy should be done to avoid the side effects mentioned above.

Some components of food have antihypertensive functional properties such as fermented foods. Tempeh is one of the fermented foods that is widely developed in Indonesia. Consumption of food or functional foods as ACE inhibitorys stimulates the secretion of bradykinin hormones which vasodilate blood vessels thereby reducing blood pressure [8]. Consumption of soybeans tempeh can reduce blood pressure in humans [9].

The objective of the study was to produce mung beans tempeh as a new breakthrough in functional antihypertensive foods. Mung beans was fermented using *Rhizopus* sp [10], the protein was extracted at isoelectric point [11], dissolved protein content [12], hydrolysis degree [13], protein characteristics using sodium dodecyl sulfate polyacrylamide gel electrophoresis (SDS-PAGE) [14] were measured, and angiotensin converting enzyme (ACE) inhibitory activity was tested based on the amount of release of hippuric acid from substrathippuryl-L-histidyl-L-leucine [15, [16].

## METHOD

### Preparation of Mung beans Tempeh

A total of 400 g of mung beans were peeled and soaked for 2 hours with an acid solution (pH 4) by adding vinegar, then steamed for  $\pm 8$  minutes, drained and cooled. Dried mung beans were inoculated with *Rhizopus* sp. inoculum with a concentration of 0.2% (w/w) and stirred evenly. The amount of yeast of 0.2% (w/w) used is based on the amount of yeast to ferment soybeans. A total of 50 grams of mung beans were put into clean propylene plastic bags measuring 5 cm in width and 10 cm in length. These plastic bags had been given several small holes first.

Mung beans fermentation was carried out at room temperature with a 6 hour interval of 0, 6, 12, 18, 24, 30, 36, and 42 hours. Every 6 hours, fermentation was stopped and an organoleptic test was carried out including physical properties, mycelium growth, aroma, color, texture and growth of mycelium [10].

### Protein Extraction of Mung Beans Tempeh

A total of 50 gram mung beans tempeh was mashed using a blender with the addition of distilled water (1:10 w/v). The suspension was added with 1M NaOH until it reached pH 9.8 while stirring using a stirrer for 1 hour. The suspension was centrifuged at 6,000 x g for 20 minutes at 4°C. Supernatant was added with 1M HCl solution gradually while stirring until it reached pH 4.5 (isoelectric point). The solution was centrifuged again at 6,000x g for 20 minutes at 4°C. The resulting deposits are called tempeh protein extracts and were stored in a freezer with a temperature of -20°C or preserved by freeze drying [11].

### Dissolved Protein Content Analysis

A total of 0.1 gram of tempeh protein extract from each time of fermentation was homogenized with 2 mL of distilled water while rotating with vortex. The protein extract suspension was centrifuged at a speed of 12,000 x g at a temperature of 4°C for 20 minutes. Supernatant protein content was determined by Bradford [12] and bovine serum albumine (BSA) methods as standard.

### Degree of Hydrolysis Analysis (DH)

A total of 2 mg of tempeh extract of mung beans were added with a 20% TCA solution (b/v) of 2 mL while stirring to obtain a dissolved and non-soluble fraction in 10% (w/v) TCA. The mixture was left to stand for 30 minutes to precipitate, then centrifuged at a speed of 7,800 x g with a temperature of 4°C for 15 minutes. The nitrogen content of supernatant and

precipitated nitrogen was analyzed using the Kjeldahl method [13] and the degree of hydrolysis was calculated using the formula:

$$\text{DH (\%)} = \frac{\text{Dissolved nitrogen in 10\% TCA}}{\text{Total nitrogen of sample}}$$

### Characterization of Protein Profiles of Mung beans Tempeh using SDS-PAGE Analysis

The profile of protein extract of mung beans tempeh was analyzed by electrophoresis using acrylamide gel. The gel consists of two parts, namely stacking gel and separating gel. The acrylamide concentration on stacking gel was 5% and separating gel was 12%. The injected sample volume was 40  $\mu\text{L}$  and the marker was 5 $\mu\text{L}$  as a standard, namely the Precision Plus Protein TM Dual Color Standard marker. Running was carried out at a constant voltage of 90 volts for 150 minutes. The gel was stained with coomassie brilliant blue G-250 and color removal was carried out by destaining solution [14]. The protein molecular weight was analyzed using the Gel Analyzer 2010a software.

### Analysis of Angiotensin Converting Enzyme Inhibitory Activity

Enzyme activity was determined using Hip-His-Leu (HHL) synthetic peptide as a substrate based on the method developed [15], [16]. A total of 15  $\mu\text{L}$  of a protein extract solution was added with 125  $\mu\text{L}$  of a 100 mM sodium borate solution (pH 8.3) containing 7.6 mM Hip-His-Leu and 608 mM NaCl, and was preincubated for 5 minutes at 37°C. The reaction begins with the addition of 50  $\mu\text{L}$  ACE enzyme which are dissolved in distilled water. The mixture was incubated for 30 minutes at 37°C. A total of 50  $\mu\text{L}$  of aquades were used as blanks.

The reaction was stopped with the addition of 125  $\mu\text{L}$  HCl 1N. The hypuric acid released by ACE was extracted by adding 750  $\mu\text{L}$  of ethyl acetate to the mixture and shaken using the vortex immediately. The mixture was centrifuged at 13,760 x g for 10 minutes, 500  $\mu\text{L}$  of the top layer of the supernatant was collected and dried at 90°C for 30 minutes. Then hypuric acid was dissolved in 1 mL distilled water and the absorbance was measured by a spectrophotometer at a wavelength of 228 nm.

$$\% \text{ ACE Inhibitory Activity} = [(C-A)/(C-B)] \times 100\%$$

Where A is absorbance of the sample, B is absorbance of the blank and C is absorbance of the control (sample replaced with aquades).

## RESULTS AND DISCUSSION

### Characteristics of Mung Beans Tempeh

Mung beans were fermented at intervals of 6 hours namely 0, 6, 12, 18, 24, 30, 36 and 42 hours with yeast concentrations of 0.2% (w/w). The fermentation time was determined by observing the physical properties of tempeh including the texture, aroma and growth of mycelium in accordance with Indonesian National standards. The best fermentation time for mung beans with a yeast concentration of 0.2% (w/w) was 24 hours, where the characteristics of tempeh are in accordance with the Indonesian National Standard (Fig. 1).

The growth of fungi was evenly distributed on the surface of tempeh, sporulation has not occurred or black spores on the surface of tempeh have not yet appeared. The texture of mung beans tempeh was compact and it had a distinctive aroma of tempeh. The distinctive aroma of tempeh is determined by the activity of molds which break down macro molecules into simpler and volatile compounds such as ammonia, aldehyde and ketones [17].

Mung beans fermented less than 24 hours produced tempeh that does not meet Indonesian standards where the growth of mycelium had not been flat, the texture was not compact (crushed when cut) and did not have the distinctive aroma of tempeh. The characteristics of mung beans tempeh are similar to the characteristics of soybeans tempeh [10]. “[18] states that the optimum time and ideal conditions for producing good mung beans tempeh are 24-36 hours at 30 °C”. In this study, mung beans fermented for 36 and 42 hours produced tempeh that began to rot where the mycelium began to blacken on the surface of the tempeh (Fig. 1). In this study, mung beans fermented for 36 and 42 hours produced tempeh that began to rot where the mycelium began to blacken on the surface of the tempeh (Fig. 1).



Fig 1. The physical appearance of mung beans tempeh with varying fermentation times (H)

After obtaining the optimum fermentation time, which is 24 hours, the fermentation of mung beans was continued by varying the concentration of yeast which was 0.1; 0.2; 0.3; and 0.4% (w/w). Each mung beans with varying amounts of yeast was incubated for 24 hours at room temperature. The resulting

tempeh is shown in Figure 2. The optimum amount of yeasts was not determined from the analysis of the physical properties of tempeh but from the measurement of inhibitory activity on optimum ACE (Table 2), namely fermented mung beans with a yeast concentration of 0.4% (w/w).

Physical observations for mung beans tempeh generally showed that the mycelium growth was almost evenly distributed in all tempeh, the presence of distinctive aroma of tempeh with a compact texture, yellow-colored and had almost the same color as soybeans tempeh. Fermented mung beans with a yeast concentration of 0.1% (w/w) showed uneven growth of mycelium on the surface and tempeh crushed when cut. Mycelium growth of the mold was spread evenly on the surface of tempeh with a yeast concentration of 0.2% (w/w) yet the texture is not compact when cut. The same was found in tempeh with yeast concentrations of 0.3% and 0.4% (w/w) (Fig. 2).

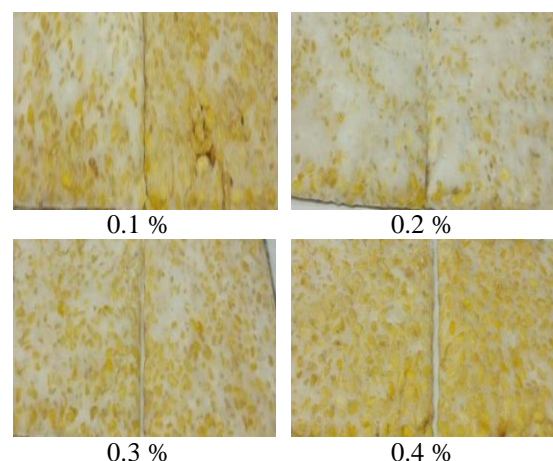


Fig 2. Optimization of yeast concentration of mung beans tempeh (% w/w)

The further parameters measured are the degree of hydrolysis (DH) and dissolved protein content. DH is a parameter that shows the ability of proteases to hydrolyze proteins into peptides and amino acids. The protease in this study derived from *Rhizopus* sp. and the ability of proteases to hydrolyze proteins was determined from DH values. The amount or concentration of tempeh protein extracted by water was determined by the Bradford method [12]. The results of the calculation of DH and dissolved protein are shown in Table 1.

Table 1. Degree of hydrolysis and protein content of Mung beans tempeh with varying yeast concentrations

| % (w/w) | Degree of Hydrolysis (%) | Protein Concentration (mg/L) |
|---------|--------------------------|------------------------------|
| 0.1     | 18.68±0.23               | 62.81±0.31                   |
| 0.2     | 11.27±0.30               | 85.53±0.07                   |

|     |           |             |
|-----|-----------|-------------|
| 0.3 | 8.51±0.28 | 144.19±0.20 |
| 0.4 | 9.02±0.19 | 351.00±0.00 |

Fermented mung beans with a yeast concentration of 0.1% (w/w) were the most optimum treatment in hydrolyzing proteins with a hydrolysis degree value of 18.68%. Some of the enzymes produced by *Rhizopus oligosporus* are lipase, amylase and protease, and the most active enzyme is protease [19]. Enzymatic hydrolysis is better than chemical hydrolysis because enzymatic hydrolysis can produce free amino acids and varied short chain peptides that have functional activities.

### Protein Profile of Mung Beans Tempeh

The profile and molecular weight of protein extract of mung beans tempeh was determined by SDS PAGE electrophoresis. In unfermented mung beans, 10 protein bands were found with molecular weights of 148, 140, 103, 84, 80, 60, 34, 28, 21 and 9 kDa. The same amount of protein bands and protein molecular weight was also found in 6 hours fermented mung beans. The data showed that in 6 hours fermentation, protease enzyme has not been released into the mung beans media or there is a possibility that other protease enzymes have not been active. The 12 hours fermentation of mung beans showed that the hydrolysis reaction had occurred of which the number of protein bands was reduced into 7 bands with a molecular weight of 148, 140, 60, 34, 28, 21 and 9 kDa. Whereas proteins with molecular weights 103 and 84 kD did not appear in 12 hours fermentation.

The fermentation of mung beans for 18 hours obtained only 4 protein bands with molecular weights 84, 71.41 and 10 kDa. Whereas fermentation for 36, 42 and 48 hours obtained only 1 protein band with a molecular weight of 9 kDa. This data shows that proteases have a high activity to degrade large molecules into smaller molecules so that several small molecules are not detected in the electrophoresis gel. Large molecules no longer appear (electrophotogram is not shown).

### ACE Inhibitory Activity of Protein Extract of Mung Beans Tempeh

Measurements of ACE inhibitory activity were carried out on the extracts of mung beans tempeh with variations in yeast concentrations of 0.2% (w/w) and 0.4% (w/w) which fermented for 24 hours. The results of the analysis are shown in Table 2. The highest ACE inhibitory activity of protein extract was 75% for mung beans fermented with a yeast concentration of 0.4% (w/w). Fermented tempeh with yeast concentration of 0.1% (w/w) was 68%. Several studies have shown that fermentation increases ACE inhibitory activity, wherein in this study fermented

soybeans with a yeast amount of 0.2% (w/w) had ACE inhibitory activity of 67.43% [20].

Organoleptic tests (data are not shown) of fermented tempeh with a yeast concentration of 0.4% (w/w) showed that the tempeh was not suitable for consumption because the aroma of tempeh was highly strong so that it was not liked by panelists yet it had a high ACE inhibitory activity in vitro. In contrast, panelists preferred fermented mung beans tempeh with a yeast concentration of 0.1% (w/w) but ACE inhibitory activity was lower.

Table 2. ACE Inhibitory Activity of Protein Extract of Mung Beans Tempeh

| No | Yeast Concentration % (w/w) | ACE Inhibitory Activity (%) |
|----|-----------------------------|-----------------------------|
| 1  | Without yeast               | 50.00±0.36                  |
| 2  | 0.1                         | 68.85±0.21                  |
| 3  | 0.4                         | 75.00±0.08                  |
| 4  | Captopril                   | 80.00±0.02                  |

Fermented mung beans had ACE inhibitory activity of 50%. The data show that consumption of mung beans is good for body health for people with hypertension because it can inhibit ACE activity.

Some grains have ACE inhibitory activity, such as *Mucuna pruriens* Linn seeds which traditionally could control high blood pressure with ACE inhibitory activity of 38.44% [21]. Melinjo fruit extracted using water had ACE inhibitory activity of 89.90% [22].

The further analysis was an analysis of the chemical content of mung beans and mung beans tempeh through the highest ACE inhibitory activity, namely mung beans fermented for 24 hours using a yeast concentration of 0.4%. The results of the analysis are shown in Table 3.

Table 3. Chemical characteristics of mung beans and mung beans tempeh

| Parameter (%) | Type of Sample |                   | Quality of Tempeh Requirements* (%) |
|---------------|----------------|-------------------|-------------------------------------|
|               | Mung Beans     | Mung Beans Tempeh |                                     |
| Water         | 9.36±0.41      | 46.66±0.16        | At most 65                          |
| Ash           | 4.11±0.26      | 2.61±0.36         | At most 1.5                         |
| Fat           | 3.07±0.08      | 2.54±0.42         | At most 7                           |
| Protein       | 20.37±0.19     | 19.85±0.18        | At most 15                          |

\* Indonesian National Standard for soybeans tempeh

The standard used in this study is the Indonesian National standard for soybeans tempeh because Indonesia does not yet have a reference for tempeh from seeds other than soybeans

Fermentation decreased the ash content and the fat content of tempeh yet increases the water content. The moisture content of mung beans tempeh in this study meets Indonesian national standards. The

increase in water content derived from soaking and boiling process during tempeh preparation. Similar results were also obtained [23] wherein fat content was 1.2g, protein content was 22.2g and carbohydrate content was 62.9g each in 100 grams of mung beans. [24]” stated that the fermentation of beans produces tempeh with protein content of 28.85%, fat content of 28.85%, and ash content of 2.10%.

The nutritional content of tempeh made from a mixture of mung beans and jackfruit seed was 13.77%, 0.66% and 2.18% for protein, ash and fat content [25], respectively. Cowpea tempeh contained ash content of 0.83%, protein content of 16.04% and fat content of 1.37%, while gude beans tempeh contained ash content of 1.19%, protein content of 16.04% and fat content of 0.96% [26]. The fat content of mung beans tempeh (2.54%) in this study was lower than that of mung beans (3.07%), thus it can be concluded that the lipase enzyme actively hydrolyzes the fat in mung beans. The fat content of mung beans obtained was 2.61% [27]. The fat content of mung beans and germinated mung beans obtained was 1.3% and 0.6%, respectively [28]. The fat content of mung beans tempeh in this study was low so that tempeh is free from bad odor due to the degradation of fatty acids into low chain fatty acids.

Mung beans protein content (20.37%) in this study was higher than the protein content of mung beans tempeh (19.85%). The decrease in protein content of mung beans tempeh is suspected because some of the decreased protein is used by *Rhizopus* as a nutrient source for its growth. The mung beans protein content obtained was 23.25% [27], this value did not differ greatly from the content of mung beans protein in this study.

## CONCLUSION

Mung bean is a type of beans that can be used as raw material for soybeans tempeh preparation and has ACE inhibitory activity. Mung beans fermented for 24 hours with 0.4% yeast concentration had the best ACE inhibitory activity. ACE inhibitory activity of protein extract of mung beans tempeh was 75% so that mung beans tempeh has the potential to be developed into functional antihypertensive foods.

## ACKNOWLEDGMENTS

The authors thank the Rector of Syarif Hidayatullah Islamic State University Jakarta, Indonesia, for the assistance of research funding.

## REFERENCE

- [1] Piepho R. W., Overview of the angiotensin-converting-enzyme inhibitory. American journal of health-system pharmacy, Vol 57, 2000 (Supplement-1), pp. S3-S7.
- [2] Carter B. L., Zillich, A. J., and Elliott, W. J. How pharmacists can assist physicians with controlling blood pressure. The Journal of clinical hypertension, Vol. 5, Issue 1, 2003, pp.31-37.
- [3] Siswandono S. B., Kimia medisinal, 1<sup>st</sup> ed. Vol. 2, Airlangga Univ. Press. Surabaya, 2000, pp.30-35.
- [4] Sacks F. M., Svetkey L. P., Vollmer W. M., Appel L. J., Bray G. A., Harsha, D., and Karanja, N. Effects on blood pressure of Approaches to Stop Hypertension (DASH) diet. New England Journal of Medicine, Vol. 344 Issue 2001, pp.3-10.
- [5] Natesh R., Schwager, S. L., Evans H. R., Sturrock E. D., & Acharya K. R. Structural details on the binding of antihypertensive drugs captopril and enalaprilat to human testicular angiotensin I-converting enzyme. Biochemistry, Vol 43 Issue 27, 2004, pp.8718-8724.
- [6] Gantenbein M. H., Bauersfeld U., Baenziger O., Frey B., Neuhaus T., Sennhauser F., & Bernet V. Side effects of angiotensin converting enzyme inhibitory (captopril) in newborns and young infants. Journal of perinatal medicine, Vol. 36, Issue 5, 2008, pp. 448-452.
- [7] Pan S., Wang S., Jing L., & Yao, D. Purification and characterisation of a novel angiotensin-I converting enzyme (ACE)-inhibitory peptide derived from the enzymatic hydrolysate of *Enteromorpha clathrata* protein. Food Chemistry, Vol. 211, pp. 423–430.
- [8] Siltari A., Korpela R., and Vapaatalo H. Bradykinin-induced vasodilatation: Role of age, ACE1-inhibitory peptide, mas-and bradykinin receptors. Peptides, Vol 85, 2016, pp.46-55.
- [9] Ansarullah A., Marliyati S. A., and Astawan M., The effect of tempeh drink intervention on blood pressure in hypertension and hypercholesterolemia subjects. Jurnal Gizi dan Pangan, Vol.12, Issue 2, 2017, pp.101-108.
- [10] Radiati A., and Sumarto, S. Analysis of Physical Properties, Organoleptic Properties, and Nutritional Values of Tempeh From Non-Soybeans Legumes. Jurnal aplikasi teknologi pangan, Vol. 5, Issue 1, 2015, pp.16-22
- [11] Wu H., Wang, Q., Ma, T., and Ren, J., Comparative studies on the functional properties of various protein concentrate preparations of peanut protein. Food Research International, Vol. 42, Issue 3, 2009, pp. 343–348.
- [12] Bradford, Marion M., A rapid and sensitive method for the quantitation of microgram quantities of protein utilizing the principle of protein-dye binding. Analytical biochemistry, Vol. 72, 1976, pp. 248–254.
- [13] Hoyle N. T., and Merritt, J. H. Quality of Fish Protein Hydrolysates from Herring (*Clupea harengus*). Journal of Food Science, Vol. 59,



- Issue 1, 1994, pp.76–79.
- [14] Laemmli U. K. Cleavage of structural proteins during the assembly of the head of bacteriophage T4. *Nature*, Vol. 227, Issue 15, 1970, pp. 680-685.
- [15] Cushman D. W., and Cheung H. S. Spectrophotometric assay and properties of the angiotensin-converting enzyme of rabbit lung. *Biochemical pharmacology*, Vol. 20 Issue 7, 1971. pp 1637-1648.
- [16] Arihara K., Nakashima Y., Mukai T., Ishikawa S., and Itoh M., Peptide inhibitorys for angiotensin I-converting enzyme from enzymatic hydrolysates of porcine skeletal muscle proteins. *Meat Science*, Vol. 57, Issue 3, 2001, pp. 319–324.
- [17] Shurtleff W., and Aoyagi, A. The book of tempeh, Soyinfo Center, 1979, pp. 160-164.
- [18] Halifah, P. Laju Pertumbuhan Jamur *Rhizopus* sp. pada Tempeh Kacang Hijau (*Phaseolus radiatus* L.). *Bionature*, Vol.10, Issue 2. 2009.
- [19] Karmini M. and Sutopo D., Aktivitas Enzim Hidrolitik Kapang *Rhizopus* Sp Pada Proses Fermentasi Tempeh. *Jurnal litbang*. ([Http://ejournal litbang. depkes. go. id](http://ejournal.litbang.depkes.go.id). 2007, pp 94-102.
- [20] Chalid S. Y., Hermanto S., & Rahmawati. Angiotensin Converting Enzyme Inhibitory Activity of the Soybeans Tempeh Protein as Functionasl Food, *International Journal of GEOMATE*, Vol. 16, Issue 56, 2019, pp 73-78.
- [21] Chaudhary S. K., De A., Bhadra S. and Mukherjee P. K. Angiotensin-converting enzyme (ACE) inhibitory potential of standardized *Mucuna pruriens* seed extract, *Pharmaceutical biology*, Vol 53, Issue 11), 2015, pp.1614-1620.
- [22] Mun'im A., Munadhil M. A., Puspitasari N. and Yanuar A. A., Angiotensin converting enzyme inhibitory activity of Melinjo (*Gnetum gnemon* L.) seed extracts and molecular docking of its stilbene constituents. Vol. 10, Issue 3, 2017, pp.1-6.
- [23] Radiati A. and Sumarto S., Analisis sifat fisik, sifat organoleptik, dan kandungan gizi pada produk tempeh dari kacang non-kedelai. *Jurnal aplikasi teknologi pangan*, Vol 5 Issue 1. 2016, pp 16 – 20.
- [24] Abu-Salem F. M., and Abou-Arab, E. A., Physico-chemical properties of tempeh produced from chickpea seeds. *Journal of American science*, Vol.7, Issue 7, 2011, pp. 107-118.
- [25] Hutagalung T. Y., Nainggolan R. J. and Nurminah M. The Effect of Ratio of Germinated Mung beans and Jackfruit's Seed and Concentration of Tempeh Inoculum on the Quality of Tempeh. *Jurnal Rekayasa Pangan dan Pertanian*, Vol. 4, Issue 3, 2016, pp. 371-378.
- [26] Dewi R. and Wahyu, I. Sensory characteristic, nutrient value and antioxidant activities of pigeon pea tempeh (*Cajanus cajan*) and cow pea tempeh (*Vigna unguiculata*) with variations of fermentation time. *Biofarmasi*, Vol. 2, Issue 2, 2010, pp.73-82.
- [27] Ekafitri R., and Isworo, R. The Utilization of Beans as Protein Source for Emergency Food. *Jurnal Pangan*, Vol. 23, Issue 2, 2014, pp. 134-145.
- [28] Lopes L., Martins M., Farias, L., Brito, A., Lima, G., Carvalho V., and Silva K.. Cholesterol-Lowering and Liver-Protective Effects of Cooked and Germinated Mung Beans (*Vigna radiata* L.). *Nutrients*, Vol. 10, Issue 7, 2018, pp.1-13.

# ESTIMATION OF PROPENSITY SCORE USING LOGISTIC REGRESSION (CASE STUDY: BREASTFEEDING DATA IN SELOPURO SUB-DISTRICT BLITAR REGENCY)

Hilwin Nisa<sup>1</sup>, Maria Bernadetha Theresia Mitakda<sup>2</sup>, and Suci Astutik<sup>3</sup>

<sup>1</sup>Faculty of Math and Science, Brawijaya University, Indonesia; <sup>2,3</sup> Brawijaya University, Indonesia

## ABSTRACT

Propensity score is a method to estimate the effect of receiving treatment when subjects cannot be treated randomly. Propensity score can be estimated using logistic regression or Classification and Regression Tree Analysis (CART). Logistic regression is the most common method to estimate propensity score. Generally, there are four methods of propensity score, they are matching, stratification, weighting, and regression adjustment. In a breastfeeding case study, random assignments to mothers as subjects are not feasible. So, it will be difficult to estimate the effect of receiving treatment. In Selopuro Sub-District Blitar Regency, many mothers still do not give exclusive breastfeeding for their babies [1]. It is important to know what is factor causes exclusive breastfeeding. Propensity score can help us to estimate the effect of receiving treatment in this breastfeeding case. Before we analyze the propensity score, we need to estimate the propensity score. In this paper, we will estimate the propensity score of breastfeeding data in Selopuro Sub-District Blitar Regency using logistic regression.

*Keywords: Propensity score, Logistic regression, Random, and Exclusive breastfeeding.*

## INTRODUCTION

In conducting research, sometimes the examples which we used cannot be taken randomly. It can be found in observational and non-experimental studies. This condition can cause bias when we evaluate the effects of treatment given. To reduce bias in these kinds of research, we can use propensity score method. Propensity score can help to evaluate the effects of treatment given [2].

No randomization in observational study causes different group on confounding variable. It potentially has significant effect on result [3]. Propensity score helps to make groups more similar. So that, it will reduce bias of estimating treatment effect in observational study.

Research to know factors of exclusive breastfeeding can be conducted by observation. In Selopuro Sub-District Blitar Regency, many mothers still do not give exclusive breastfeeding to their babies. In other side, we know how important exclusive breastfeeding for baby is. World Health Organization (WHO) suspected 53% of acute pneumonia cases and 55% of infant deaths from diarrhea are caused by poor feeding in the first six months of birth [4].

Propensity score can be estimated by several methods. Generally, the methods are Classification and Regression Tree Analysis (CART) and logistic regression. The most familiar method is logistic regression [5]. By logistic regression, we can also predict the probability of an event [6].

Before estimating propensity score, we need to

choose the treatment that we will evaluate the effect. The treatment which we will use in this research is a confounding variable. We use Chi-Square test to know the confounding variable. Then, we will estimate the propensity score using logistic regression. Propensity score can be analyzed after being estimated using logistic regression.

## METHODS

To estimate the propensity score, we use logistic regression. Thus, the function of propensity score is [6]:

$$e(X_i) = P(z_i = 1|X_i) = \frac{\exp(\beta_0 + \beta_1 x_1 + \dots + \beta_k x_k)}{1 + \exp(\beta_0 + \beta_1 x_1 + \dots + \beta_k x_k)} \quad (1)$$

The breastfeeding data which we use is data primer. The data is gotten by conducting survey in March 2019 and the respondents are mothers in Selopuro Sub-District Blitar Regency who have six months until eleven months baby.

In Selopuro Sub-District Blitar Regency, there are 195 mothers who have six-eleven months babies. Using this formula:

$$n = \frac{N}{[1 + N(e)^2]} = \frac{195}{1 + 195(0.05)^2} = 131.092 = 131 \quad (2)$$

we can determine the number of samples. To make the research more valid, we add the number of samples in this research. We use 188 samples in this

research.

Independent variable (Y) in this research is exclusive breastfeeding graduation status (Yes/No) and there are ten dependent variables, they are:

$X_1$  = mother's age

$X_2$  = the last education of mother

$X_3$  = mother's job

$X_4$  = where the mother gives birth

$X_5$  = practice of early breastfeeding initiation

$X_6$  = when the mother starts breastfeeding

$X_7$  = whether the first breastfeeding is colostrum

$X_8$  = mother's knowledge about breastfeeding

$X_9$  = mother's attitude about breastfeeding

$X_{10}$  = mother's reason in first time gives her baby besides breast milk.

## RESULT AND DISCUSSION

Breastfeeding data in Selopuro Sub-District Blitar Regency shows that 105 mothers do not give their babies exclusive breastfeeding and 83 mothers give their babies exclusive breastfeeding. Mothers who give exclusive breastfeeding is 55.9% from 188 respondents. It can be seen in this following table.

Table 1 Classification table

| Observed           |           | Predicted |         |                    |
|--------------------|-----------|-----------|---------|--------------------|
|                    |           | Y         |         | Percentage Correct |
|                    |           | Unsuccess | Success |                    |
| Y                  | Unsuccess | 105       | 0       | 100.0              |
|                    | Success   | 83        | 0       | .0                 |
| Overall Percentage |           |           |         | 55.9               |

Source: Processed using SPSS

Table 2 Model Fitting Information

| Model          | Model Fitting     |            |                        |      |
|----------------|-------------------|------------|------------------------|------|
|                | Criteria          |            | Likelihood Ratio Tests |      |
|                | -2 Log Likelihood | Chi-Square | df                     | Sig. |
| Intercept Only | 258.043           |            |                        |      |
| Final          | 110.358           | 147.685    | 10                     | .000 |

Source: Processed using SPSS

Table 2 shows the result when independent variables have not been in the model.

Table 3 Pseudo R-Square

|               |      |
|---------------|------|
| Cox and Snell | .544 |
| Nagelkerke    | .729 |
| McFadden      | .572 |

Source: Processed using SPSS

Table 3 shows the capability independent variable explain dependent variable. The value of Nagelkerke R Square is 0.729, it means independent variables can explain 72.9% dependent variable and 27.1% of dependent variable is explained by other variable which is not in the model.

Then, the treatment which we use in this research is confounding variable. Confounding variable can be found by Chi-Square test. Based on Chi-Square test, confounding variable is  $X_5$  (practice of early breastfeeding initiation).

The result of Chi-Square test can be seen in this following table.

Table 4 Test of correlation between  $X_5$  and other variables

| Variable       | P-Value | Decision     |
|----------------|---------|--------------|
| $X_5 * X_1$    | 0.905   | Accept $H_0$ |
| $X_5 * X_2$    | 0.076   | Accept $H_0$ |
| $X_5 * X_3$    | 0.96    | Accept $H_0$ |
| $X_5 * X_4$    | 0.000   | Reject $H_0$ |
| $X_5 * X_6$    | 0.000   | Reject $H_0$ |
| $X_5 * X_7$    | 0.358   | Accept $H_0$ |
| $X_5 * X_8$    | -       | -            |
| $X_5 * X_9$    | 0.641   | Accept $H_0$ |
| $X_5 * X_{10}$ | 0.256   | Accept $H_0$ |

Source: Processed using SPSS

where, hypothesis of this test is:

$H_0$ : there is no correlation between  $X_5$  and another variable, versus

$H_1$ : there is a correlation between  $X_5$  and another correlation.

Based on the test, variable which has the most correlation with other variables is  $X_5$ . So, we can say that confounding variable is  $X_5$ . Confounding variable  $X_5$  divides the data become two groups, control and treatment. Control group is a group of mothers who do not practice early breastfeeding initiation and treatment group is a group of mothers who practice early breastfeeding initiation.

Then, we can estimate the propensity score by the function at Eq. (1). There are two groups of propensity score estimation, one is for control group and other for treatment group.

Table 5 Variables in the equation of control group

|    | B     | S.E. | Wald  | df | Sig. | Exp(B) |
|----|-------|------|-------|----|------|--------|
| X1 | .048  | .101 | .229  | 1  | .632 | 1.049  |
| X2 | -.149 | .849 | .031  | 1  | .861 | .862   |
| X3 | -.030 | .485 | .004  | 1  | .951 | .971   |
| X4 | -     | 1.00 | 3.959 | 1  | .047 | .136   |
|    | 1.998 | 4    |       |    |      |        |
| X6 | -.661 | .651 | 1.032 | 1  | .310 | .516   |

|          |                 |                   |       |   |           |                    |
|----------|-----------------|-------------------|-------|---|-----------|--------------------|
| X7       | .149            | 2121<br>0.06<br>3 | .000  | 1 | 1.00<br>0 | 1.161              |
| X9       | 21.21<br>5      | 9313<br>.514      | .000  | 1 | .998      | 1634994<br>733.532 |
| X10      | .656            | .270              | 5.910 | 1 | .015      | 1.928              |
| Constant | -<br>21.99<br>1 | 1905<br>5.84<br>6 | .000  | 1 | .999      | .000               |

Source: Processed using SPSS

Based on Table 5, we can obtain model to estimate propensity score for control group. The model is

$$e(X_i) = P(z_i = 1|X_i) = \frac{\exp(-21.991 + 0.048x_1 + \dots + 0.656x_{10})}{1 + \exp(-21.991 + 0.048x_1 + \dots + 0.656x_{10})} \quad (3)$$

Table 6 Variables in the equation of treatment group

|          | B               | S.E.          | Wald       | df | Sig.      | Exp(B)             |
|----------|-----------------|---------------|------------|----|-----------|--------------------|
| X1       | .030            | .054          | .312       | 1  | .577      | 1.031              |
| X2       | .302            | .316          | .914       | 1  | .339      | 1.353              |
| X3       | -.507           | .178          | 8.067      | 1  | .005      | .602               |
| X4       | -.197           | .333          | .351       | 1  | .554      | .821               |
| X6       | .251            | .488          | .264       | 1  | .607      | 1.285              |
| X7       | -.843           | 26284.<br>863 | .000       | 1  | 1.00<br>0 | .430               |
| X9       | 21.81<br>8      | 6855.7<br>66  | .000       | 1  | .997      | 2989682<br>111.448 |
| X10      | .522            | .135          | 14.99<br>6 | 1  | .000      | 1.686              |
| Constant | -<br>26.10<br>2 | 25375.<br>035 | .000       | 1  | .999      | .000               |

Source: Processed using SPSS

Based on Table 6, we can obtain model to estimate propensity score for treatment group. The model is

$$e(X_i) = P(z_i = 1|X_i) = \frac{\exp(-26.102 + 0.03x_1 + \dots + 0.522x_{10})}{1 + \exp(-26.102 + 0.03x_1 + \dots + 0.522x_{10})} \quad (4)$$

Then, Eq. (2) and Eq. (3) are used to calculate estimation of propensity score like in the following tables.

Table 7 Estimation of propensity score for control group

| Respondent | $E(y z = 0)$ |
|------------|--------------|
| 1          | 0.00538      |
| 2          | 0.00000      |
| 3          | 0.94420      |

|    |         |
|----|---------|
| 4  | 0.97038 |
| ⋮  | ⋮       |
| 58 | 0.91942 |
| 59 | 0.00482 |

Source: Processed using SPSS

Table 8 Estimation of propensity score for treatment group

| Respondent | $E(y z = 1)$ |
|------------|--------------|
| 1          | 0.79124      |
| 2          | 0.40892      |
| 3          | 0.24421      |
| 4          | 0.88427      |
| ⋮          | ⋮            |
| 128        | 0.83864      |
| 129        | 0.48296      |

Source: Processed using SPSS

Based on Table 7 and Table 8, we can know that probability mother give exclusive breastfeeding of treatment group is bigger than control group.

Then, the value of propensity score estimation can be analyzed based on one of four methods propensity score, like matching, weighting, stratification and sregression adjustment.

## CONCLUSION AND RECOMMENDATION

Propensity score of breastfeeding data in Selopuro sub-district Blitar regency can be estimated using logistic regression by Eq. (3) for control group and Eq. (4) for treatment group. For the next research can analyze propensity score using one of propensity score methods.

## ACKNOWLEDGMENTS

This work would not have done well without the financial support of LPDP (Lembaga Pengelola Dana Pendidikan - Indonesia Endowment Fund for Education) who has given me scholarship in my master degree. I am grateful to my lecturers, Dr. Ir. Maria Bernadetha Theresia Mitakda and Dr. Suci Astutik, S. Si., M. Si., who have supported and guided me. I would like to thank my parents and my beloved family whose love and prayers are always for me. All of my friends who always supported me, I am so thankful.

## REFERENCES

- [1] Arum D. N. A., Interviewed by Researcher, in January 2019, Selopuro Health Center.
- [2] Daniel F. M. C., Greg R., and Andrew R. M., Propensity Score Estimation with Boosted Regression for Evaluating Causal Effects in Observational Studies, Psychological Methods, Vol. 9, Issue 4, 2004, pp. 403-425.

- [3] Reeve, B. B., Smith, A. W., Arora, N. K., and Hays, R. D., Reducing Bias in Cancer Research: Application of Propensity Score Matching, *Health Care Financing Review*, Vol. 29, Issue 4, 2008, pp. 69-80.
- [4] Arun G., Shoba S., and Jai P. D., How Can Global Rates of Exclusive Breastfeeding for the First 6 Months be Enhanced? *ICAN: Infant, Child, and Adolescent Nutrition*, Vol. 5, Issue 3, 2013, pp. 133-140.
- [5] Shenyang G. and Mark W. F., *Propensity Score Analysis (Statistical Methods and Application)*, SAGE, 2010, pp. 127-210.
- [6] David W. H. and Stanley L., *Applied Logistic Regression*, John Wiley & Sons, Inc., 2000, pp. 31-43.
- [7] Wei P. and Haiyan B., Propensity Score Interval Matching: Using Bootstrap Confidence Intervals for Accommodating Estimation Errors of Propensity Scores, *BMC Medical Research Methodology*, Vol. 5, Issue 1, pp. 1-9.

# THE MORPHOLOGY AND PHENOLOGY OF YELLOW COMMON BEAN (F<sub>7</sub>) AS OFFSPRING OF INTRODUCED AND LOCAL VARIETY CROSSING

Fathiyyah<sup>1</sup>, Sumeru Ashari<sup>2</sup> and Andy Soegianto<sup>3</sup>  
<sup>1,2,3</sup>Agriculture Faculty, Brawijaya University, Indonesia

## ABSTRACT

Common beans (*Phaseolus vulgaris* L.) are plants from legumes or *Fabaceae* family that are very popular within the society. Crossing between varieties is a method to produce desired trait or produce new trait in the improvement of a plant character. One of them is crossing introduced varieties and local varieties. Some common bean varieties in Indonesia are introduced varieties and crosses between introduced and local Indonesian varieties. Offspring from introduced (Cherokee sun) and local Indonesian varieties (Gogo kuning) in the F<sub>6</sub> generation have shown good adaptation to the medium plain. Morphological and phenology studies on the accession of plant breeding results are needed to determine the similarity of offspring's appearance to its parents. The two accessions obtained have the character of yellow pod having a different type of growth which is dwarf and climbing. Both parents have several differences in morphological and phenological characters. Type of growth, colour (leaves, stems, flowers, and pods), flowering time, the initial appearance of pods is a character observed in six plants at each accession. The yellow character of the pod on the two accessions is a new appeal for consumers. Yellow pigment in plants as an identification of the carotene content in these plants.

*Keywords: Morphology, Phenology, Common Bean, Offspring, Introduced and local variety*

## INTRODUCTION

Common bean (*Phaseolus vulgaris* L.) is a species of *Fabaceae* family that is preferred for consumption. The content of protein and minerals such as K, Ca, Mg, Zn, Cu, P, Fe, vitamin B<sub>6</sub>, folic acid, thiamine, riboflavin, niacin, and essential amino add value to the feasibility of consuming Common beans [1]. High nutrition is also an added value for Common beans and is recommended as an alternative food for diet [2].

Common bean is not only developed in Indonesia but also in various other countries. Common Bean delivered by different countries has different characters and become an advantage for Common beans themselves. Hybridization is the crossing of two individuals of the same species or which has a close relationship [3]. Plant crossing can be one way to combine the two superior traits of each parent into one offspring that has a superior trait or more from both parents. The crossing can be done one of them by hybridizing between introduced varieties and local varieties.

Cherokee Sun variety is introduced variety from Hawaii which has superior yellow pod trait. Gogo Kuning is a local variety of Surakarta Indonesia which has a high yield. The results of both crosses can be seen through morphological and phenology studies on the accession of the results of the crossing of the two parents on the appearance of the offspring.

## METHOD

Two parents are introduced varieties (Cherokee Sun) and local varieties from Surakarta (Gogo Kuning). The crossing is done on two parents which are then selected to get the yellow pod character. Furthermore, several selected lines in the F<sub>7</sub> generation were cultivated in green houses located in Tegal Weru village, Dau sub-district, Malang Regency, East Java, at latitude 7°56'32"S-112°33'51"E with an altitude of 722. Every 6 plants of the parent (Cherokee sun) and 2 accessions of the offspring are planted to determine the differences and similarities between them. Observations were made visually to find out the all appearance of the accession to continue the next selection stage. Morphology observation is done on the colour of leaves, stems, and flowers. Observation of phenology is carried out on the initial character of flowering and pods appearing. The colour of pods and seeds become interesting characters which are then also observed.

## RESULT AND DISCUSSION

The selection of parent is an important aspect for the initiation of plant breeding programs [4]. Crossing between varieties of introduced and local varieties can be good genetic material to change a plant trait. Local common bean varieties display an important

variety of potential characters related to productivity such as the number of pods per plant [5]. The presence of Cherokee sun as introduced varieties and Gogo Kuning as local varieties are expected to be parents that can inherit and improve the character of common beans through crossing both and the results can be seen on the offspring.

In this breeding program Cherokee Sun varieties as female parents and Gogo Kuning local varieties as male parents. The aim of this program is to produce new common bean varieties with high yielding yellow pods [6]. After selection up to F<sub>6</sub>, a number of lines have been found that have known yellow pod trait. Morphological and phenology studies on the lines resulting from the crossing of both were carried out to determine the desired trait appearance for the next selection process.

The colour of leaves and stems between parent (Cherokee sun) and two offspring (CSxGK 1 and 2) both have the green. CSxGK 1 is dwarf bean while CSxGK 2 is climbing bean. Flowers of all them are also purple and white as in Fig.1. Flower initiation in CSxGk 1 and 2 appears early than its parents. Early flower in Cherokee sun appeared on 32 DAP (Days After Planting) and CSxGk 1 and 2 respectively 26-28 and 28-31 DAP. Early pods appeared on the Cherokee sun 37-40 DAP and at CSxGk 1 and 2 respectively 33-35 and 35-37 DAP. Each phenotype in an individual affects the expression of a trait in its offspring. Even in flower phenology, the maternal effect is very influential. Phenology in reproduction is one example of a character from a parent that influences its intergeneration. The effect of maternal reproduction on phenology will influence the time of offspring germination if there is a relationship between flowering time and fruit cooking time [7].



Fig. 1 a) Flower of Cherokee Sun, b) Flower of CSxGK 1, and c) Flower of CSxGK 2.

Table 1 Flowering Time and Pod Initiation of Cherokee Sun and The Offspring

| Lines        | Flowering time (DAP) | Pod Initiation (DAP) |
|--------------|----------------------|----------------------|
| Cherokee Sun | 32                   | ±39                  |
| CSxGk 1      | ±28                  | ±34                  |
| CSxGk 2      | ±30                  | ±36                  |

CSxGK 1 and 2 has yellow pods as seen in Fig.2. The content and composition of pigments in plants

are one of the goals of the initiation program. The pigment determines the colour and shows the visual appearance of parts of the plant. The colour of fresh vegetables or fruit is one of the people's assessments for consuming these foods [8]. Green in vegetables, yellow to orange and red in tomatoes, white to yellow, orange, red and purple is a pigment that identifies the content of carotene, betalain, and anthocyanin. Yellow pods are one of the goals of this preliminary program. The yellow colour of the pod is indicated by the carotene content of the pod. Cherokee sun has a weak degree of curvature and CSxGK 1 and 2 has a medium and strong degree of curvature.

Seed colour on both offspring and parent is Dark brown to black (Fig 4). Dark coloured seeds contain 3.8% ash, 0.1-1.1% fat, 0.5-17.7% protein, 77.4% carbohydrates, 3.4-21.5% fiber [9]. The maternal effects are also a form of phenotypic plasticity across generations, caused by the maternal environment [10]. The direct maternal effects can physically change the appearance of phenotypic offspring as it develops as in the effects of cytoplasmic and seed size [11].

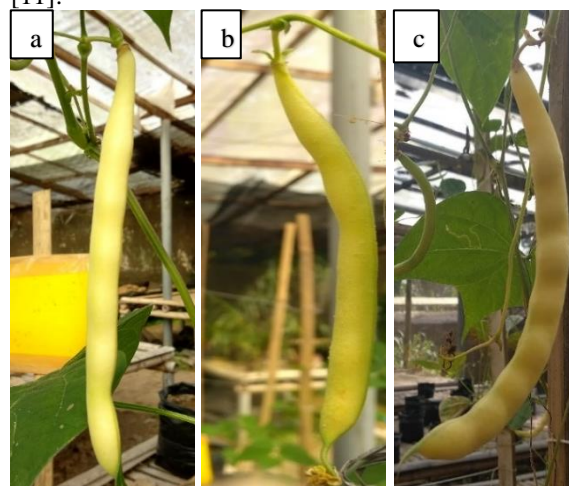


Fig. 2 a) Pod of Cherokee Sun, b) Pod of CSxGK 1, and c) Pod of CSxGK 2

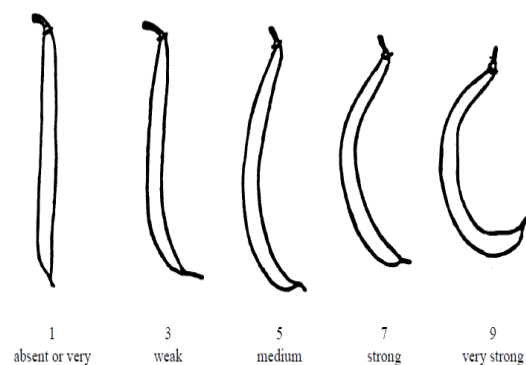


Fig. 3 Curvature Degree of Pod Base on UPOV Assessment TG/12/9 Rev.2.



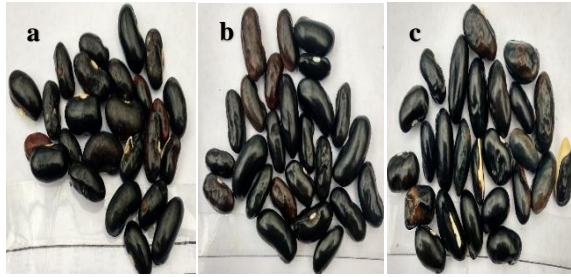


Fig. 4 a) Seed of Cherokee Sun, b) Seed of CSxGK 1, and c) Seed of CSxGK 2

F<sub>1</sub> crosses with parent (Backcross) in the breeding process are considered successful in displaying yellow pod characters. The backcross method is a crossing generation of F<sub>1</sub> with one of the parents. The benefit of the backcross method is to maintain all the positive traits found in the parent variety. This method is part of the convergent breeding method. Where convergent breeding is a method of crossing that is carried out if there are only one or two traits which want to be repaired and will be gathered into existing superior varieties. The results of this method are important traits in superior varieties can still be preserved [12]. Yellow pod trait as a trait from female parent and high yields as a trait from Gogo Kuning which.

Yellow-orange vegetables and fruits as major dietary source of carotene also providing most of the  $\beta$ -carotene and the  $\alpha$ -carotene [13]. One of them is carrots which have *Beta* and high *Alpha* carotene, it's caused by two major locus, namely *Y* and *Y<sub>2</sub>* which are dominant and capable of expressing carotene accumulation. Another case is tomatoes. the *Beta* and *Delta* content of tomatoes is controlled by *CYC-b* and the overexpressed *LCY-e* allele during fruit ripening [14]. Carotene content and carotenogenic expression of the gene as a control response to biotic and abiotic stress such as during growth, photomorphogenesis, photosynthesis, flowering time and fruit ripening [15].

Yellow, orange and red are expressions of chromoplast which depend on the combination of carotene and xanthophyll content. The color appears on the differentiated chromoplast which is deposited in plastoglobules. when chromoplast development, carotenoid accumulation in color plastoglobules confers in fruits and flowers. The development of chromoplast is accompanied by the induction of enzymes that catalyze carotene biosynthesis. although inactive, the enzyme is found in the stroma, active forms occur in plastids which have lipophilic (carotene precursors). Biosynthesis and ability of Carotenoid accumulation in some fruits is controlled by genetic influences, suggesting some rate-limiting carotenogenic step as responsible for the carotenoid accumulation during fruit ripening. Carotenoids were always present in higher quantities than chlorophylls in the flesh of both yellow and red skinned [16]. Color is also influenced by the high quantity and quality of

light absorbed by plants. Light becomes one of the factors that stimulate carotene content in plants [17].

## CONCLUSION

The two lines in the F<sub>7</sub> generation have a morphologically similar appearance to their female parent. This shows the success of a character's decline from the female parent in its derivatives. The presence of yellow pod in common beans can be a new variation in the genetic diversity of common beans. Furthermore, it is necessary to conduct selection and fulfillment the requirements for registration and varieties release of yellow pod-common beans in order to be widely commercialized.

## ACKNOWLEDGMENT

I am enormously grateful to LPDP (Lembaga Pengelola Dana Pendidikan-Indonesia Endowment Fund for Education) for continuous encouragement on my study and funding to participate in this conference. I am thankful for all my lecturer for kindly advices throughout my study.

## REFERENCES

- [1] Tugce C., Hatice S.D., Huseyin C., Duygu S., Alper A.I.D., Tuba E. and Cengiz T., The Nutritional Content of Common Bean (*Phaseolus vulgaris* L.) Landraces in Comparison to Modern Varieties, J.Agron, Volume.8, No.166, pp.1-9.
- [2] Romero A.O., Damian H.M.A., Rivera T.J.A., Baez S.A., Huerta L.M. and Cabrera H.E., The Nutritional value of Beans (*Phaseolus vulgaris* L.) and its importance for Feeding of Rural communities in Puebla-Mexico. Int.Res.J.Biological Sci, Vol.2, No.8, 2013, pp.59-65.
- [3] Acquah G., Principles of Plant Genetics and Breeding, Wiley Blackwell US, pp.132-134.
- [4] Correa A.M., De Souza L.A.R., Braga D.C., Ceccon G., Teodoro P.E., Da Silva J.C.A. and Da Silva F.A., Agronomic performance and genetic variability among common bean genotypes in savanna/pantanal ecotone. J. Agron, Vol.14, 2015, pp.175-179.
- [5] Daria S., Fernando R., Juan J.R., Rosa R. and Giandomenico C, Morphological and genetic diversity among and within common bean (*Phaseolus vulgaris* L.) landraces from the Campania region (Southern Italy), Scientia Horticulturae, Vol.180, 2014, pp.72-78.
- [6] Soegianto A., and Sri L.P., Perakitan Varietas Tanaman Buncis (*Phaseolus vulgaris* L.) Berdaya Hasil Tinngi Dengan Sifat Warna Polong Ungu dan Kuning. Seminar Nasional PERIPI 2014, p.1-8.

- [7] Galloway L.F, The effect of maternal phenology on offspring characters in the herbaceous plant *Campanula Americana*, J. of Eco, Vol.9, 2002, pp. 851-858
- [8] Barrett D.M., Beaulieu J.C. and Shewfelt R., Color, flavor, texture, and nutritional quality of fresh-cut fruits and vegetables: desirable levels, instrumental and sensory measurement, and the effects of processing, Crit.Rev.in Food Sci and Nut. Vol.50, No.5, 2010, pp.369–389.
- [9] Francine G.B.L., Aca C.A.F.Z., Jose P.W., Alessandro N. and Ivo M.D, Beans (*Phaseolus vulgaris* L.): whole seeds with complex chemical composition, Review Current Opinion in Food Science 2018, Vol.19, 2018, pp.63–71.
- [10] Wolf J.B. and Wade M.J, What are maternal effects (and what are they not)?, Philos.Trans.R.Soc.B-Biol.Sci Vol.364, 2009, pp.1107–1115
- [11] Roach D.A. and Wulff R.D., Maternal effects in plants, Annu.Rev.Ecol.Syst, Vol.18, 1987, pp.209–235
- [12] Syukur M., Sujiprihati S. and Yuniarti R., Teknik Pemuliaan Tanaman. Jakarta:Penebar Swadaya, 2012, pp. 96-102
- [13] Amorim K.T., Cepeda A., Fente C. and Regal R, Review of Methods fo analysis of carotenoids. 2014 Trends in analytical chemistry, No.56, 2014, pp.49-73.
- [14] Giuliano G., Provitamin A biofortification of Crop plants: a gold rush with many miners, Current Opinion in Biotechnology, No.44, 2017, pp.269-180
- [15] Hannoufa A., and Hossain Z, Regulation of caretonoid accumulation in plants, Biocatalysis and agricultural Biotechnology, 2012, pp.198-202
- [16] Delgado-Pelayo R., Guerrero L.G., and Mendez D.M., Chlorophyll and carotenoid pigments in the peel and flesh of commercial apple fruit varieties, Article, Food Research International, 2014, pp.1-10
- [17] Rodrigo, M.J. Alquezar B. Alos E. Lado J. Zacarias L., Biochemical bases and molecular regulation of pigmentation in the peel of Citrus fruit. Sci. Hortic, 2013, pp.1-17

## FORWARD MODELING FOR SUBSURFACE SYNTHETIC SEISMOGRAM

Wasis Wasis<sup>1</sup>, Adi Susilo<sup>1</sup>, Musthofa Nuh<sup>1</sup>.

<sup>1</sup>Faculty of Mathematics and Natural Sciences, Brawijaya University, Malang, Indonesia

### ABSTRACT

The relationship between the subsurface geological model and the synthetic seismogram record, could be identified visually. One of the method to identify seismic response is seismic forward modeling that makes seismic survey more efficient. This study is to identify subsurface synthetic seismogram characteristics based on the configuration, frequency, and velocity. Data used in this study are synthetic, including depth, distance/offset, velocity, density, and ricker wavelet. The configurations are Off-end spread and Split spread. Ricker wavelet's frequencies are 20 Hz and 40 Hz. Forward modeling method applied by convoluting the wavelet and the reflection coefficient to gain a synthetic seismogram that represent subsurface structure. Based on the model, the seismic responses were obtained 8 synthetic seismograms with the different responses, which is obtained by variation of configuration, frequency, and velocity. Five reflectors with a different reflection coefficient were obtained. The results show that the largest value is fourth reflector, because of the high contrast of acoustic impedance between sandstone and limestone. Beside that, variation of configuration, frequency, and velocity resulting different synthetic seismograms (wiggles) especially in wave response and arrival time.

*Keywords: Subsurface structure, Forward modeling, Synthetic seismogram, Reflector.*

### INTRODUCTION

Seismic forward modeling is a method of applying seismic waves to actual geological models [1]. The two main components in seismic modeling are the making of numerical and computational geological models of seismic responses. The modeling illustrates the process of propagating seismic waves from the source to the subsurface and return to the receiver. Models can be made based on actual field conditions and can be either 1D, 2D or 3D [2]. Advanced seismic reflection modeling is a computational process in the subsurface geological model (with parameters: horizontal distance, vertical depth, acoustic impedance) which is transformed into synthetic seismic recordings. Vertical depth is converted to two-way travel time. Acoustic impedance contrast (the result of speed and density) is converted into a reflection coefficient. Often, the relationship between geological models and synthetic seismic recordings can be inferred through visual observation [3].

One method that is useful for identifying seismic responses is forward modeling (seismic forward modeling). The reason why advanced modeling is used in seismic surveys is because it can save time and money. If this work is done by a computer, it can make savings rather than using a seismic survey vessel. A seismic ship must conduct a new survey for each target area, while a computer has the ability to carry out different acquisition processes

simultaneously in an area. The synthetic seismic generated from the entire acquisition process will be completed faster and the acquisition parameters that will be used in the actual measurements can be immediately determined so that it can save costs. Synthetic seismic are only predictions to identify what might be beneath the surface. However, acquisitions directly in the field must still be carried out. Synthetic seismic will never be able to replaces actual seismic, but only helps understand it [4].

One form of model that can be made as an initial prediction is the modeling of subsurface synthetic seismograms. This modeling utilizes the convolution process between seismic source wavelets and reflection coefficients (RC) from rock layers. This model can later also be used as an ideal model that is useful for assisting understanding of seismic wave propagation before conducting data acquisition in the field.

### METHODS

#### Input Data

As an initial step, data is collected from related references. This data is in the form of depth, distance ( offset ), velocity, density, and wavelet . Data on depth, distance ( offset ), and velocity are used for calculation of travel time, while data on velocity and density are used for calculation of reflection coefficients. The results of the reflection coefficient

are convoluted with the wavelet so that the data is in the form of a synthetic seismogram. This synthetic seismogram is displayed on a graph of shot gather between time and distance.

### Geology Model

This geological model is based on the predetermined density and velocity data. This model is an approach model to the actual conditions in the field. In this study, two geometry of seismic sources were used, namely Off-end and Split spread.

This geological model will later provide a general picture of subsurface lithology and its interactions with seismic waves so that they can produce a synthetic seismograms.

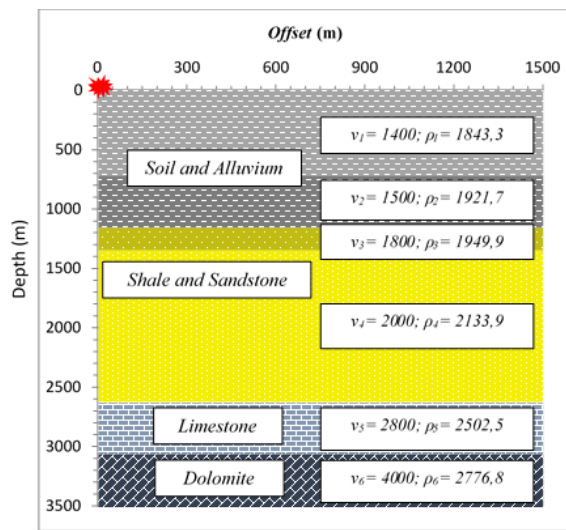


Fig. 1. Off-end spread geology model

### Travel Time Calculation

The travel time calculation phase starts from the process of entering the required data into MATLAB software. Data needed include depth, distance (offset), and velocity.

$$t(x)^2 = \frac{x^2}{v_1^2} + t_0^2 = \frac{x^2}{v_1^2} + \frac{4h_1^2}{v_1^2} \quad (1)$$

### Reflection Coefficient Calculation

The reflection coefficient was obtained from the results of the AI calculation. Based on the calculation, the RC value will be found in the range between -1 and +1. This value is related to the contrast value of AI. The bigger the AI value, the greater the RC value (close to +1), and vice versa.

$$AI = \rho v \quad (2)$$

$$RC = \frac{AI_2 - AI_1}{AI_2 + AI_1} = \frac{\rho_2 v_2 - \rho_1 v_1}{\rho_2 v_2 + \rho_1 v_1} \quad (3)$$

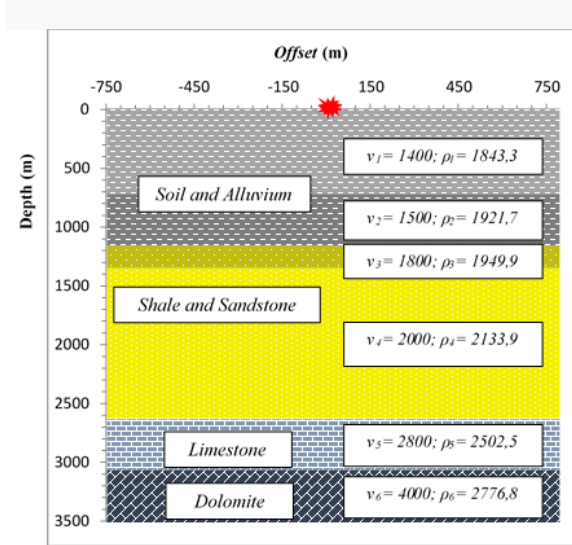


Fig. 2. Split-spread geology model

### Making of Synthetic Seismograms

The synthetic seismogram in this study was carried out by the convolution process between wavelets and reflection coefficients

$$S(t) = W(t) * r(t) \quad (4)$$

### Ricker Wavelet

Ricker wavelets have frequency values of 20 Hz and 40 Hz. in the time domain. The x axis is a time parameter in second, and the y axis is an amplitude parameter.

### Data Plotting

The result of this data plotting is a shot gather graph that describes subsurface synthetic seismograms. The synthetic seismogram in the form of a plot curve between distance (offset) as the x axis and time as the y axis.

## RESULTS AND DISCUSSION

### Research Results

The results obtained from this study are a model of subsurface synthetic seismograms. This synthetic seismogram is obtained from the convolution process between the earth reflection coefficient (RC) and the seismic source wavelet [5].

The value of the velocity and density of each rock layer will produce an acoustic impedance (AI). The greater the velocity and density value, the greater the acoustic impedance value. Comparison of AI values between two rock layers will produce a reflection coefficient (RC) which is located in the boundary plane between layers, and have a value



between -1 and +1. This RC value is convoluted (\*) with wavelets using Matlab.

## Discussion

### Analysis of RC

The reflection coefficient was obtained from the contrast of AI in each layer.

Table 1. Reflection Coefficient on each reflector

| No. | Reflector   | Value of RC |
|-----|-------------|-------------|
| 1   | Reflector 1 | 0.0553      |
| 2   | Reflector 2 | 0.0981      |
| 3   | Reflector 3 | 0.0975      |
| 4   | Reflector 4 | 0.2429      |
| 5   | Reflector 5 | 0.2264      |

### Analysis of Synthetic Seismograms

This synthetic seismogram was obtained from the results of convolution between wavelets and reflection coefficients (RC). Red line or known as wiggle, is the amplitude produced by the convolution process. In seismic fields, the amplitude of this wave is often called a reflector. A strong and bright reflector can be interpreted that the reflector consists of large amplitudes. In the picture you can see there are 6 lines that have different shapes. The red line that is located at the top is interpreted not as a reflector, but the amplitude generated from direct waves. Meanwhile, the other five lines are seismic reflectors, where each of these reflectors has different shapes and amplitude values.

Figure 3 is the result of synthetic seismograms resulting from the Off-end spread configuration geological model and the ricker wavelet frequency of 20 Hz. This off-end spread configuration has a distance / offset ranging from 0 m - 1500 m with seismic sources at the end (zero offset). The five reflectors have different RC values as in Table 1. Figure 4 is a synthetic seismogram that is produced on the same configuration with a different frequency, which is 40 Hz. When observed, both have a significant difference in the waveform. On synthetic seismograms with a frequency of 20 Hz, the resulting waves are larger and wider than those on synthetic seismograms with a frequency of 40 Hz.

On synthetic seismograms with a frequency of 20 Hz, the resulting waves are larger and wider than those on synthetic seismograms with a frequency of 40 Hz. This is also based on the reason for the difference in the location of the wave peak at a frequency of 20 Hz and 40 Hz.

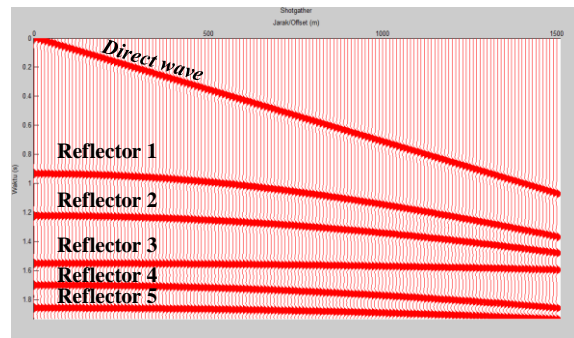


Fig. 3 Synthetic Seismogram (Off-end spread, f=20 Hz, velocity=Data 1).

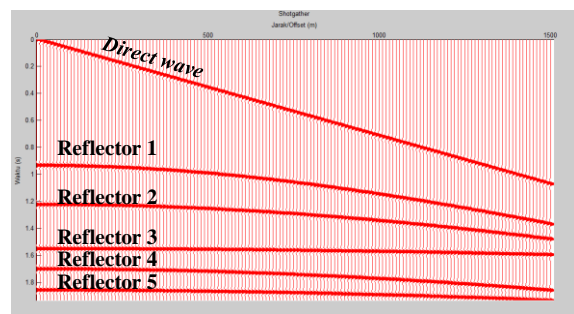


Fig. 4 Synthetic Seismogram (Off-end spread, f=40 Hz, velocity=Data 1).

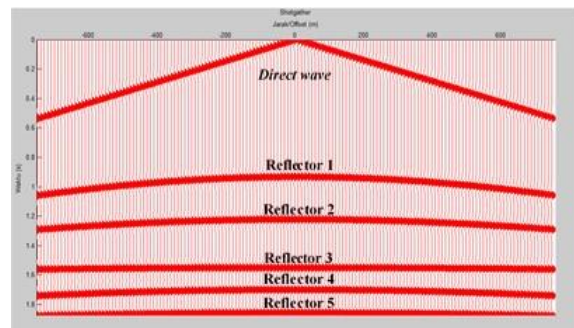


Fig. 5 Synthetic Seismogram (Split spread; frequency= 20 Hz, velocity= Data 1).

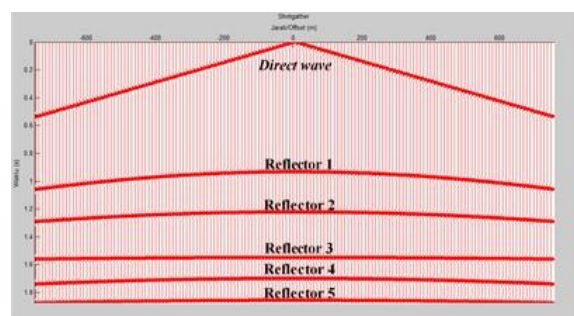


Fig 6 Synthetic Seismogram (Split spread; frequency= 40 Hz, velocity= Data 1).

Figure 5 and Figure 6 are the results of synthetic seismograms resulting from the geological model of the Split spread configuration and the ricker wavelet frequency of 20 Hz and 40 Hz. Both also have a significant difference in the waveform. On synthetic seismograms with a frequency of 20 Hz, the resulting waves are larger and wider than those on synthetic seismograms with a frequency of 40 Hz. This is also based on the reason for the difference in the location of the wave peak at a frequency of 20 Hz and 40 Hz. The difference in the Split spread configuration with the previous configuration (Off-end spread) is where the seismic source is located. In this configuration, the source is located right in the middle so that the synthetic seismogram produced is also different.

In general, split spread configuration is more often used in data acquisition in the field, because the synthetic seismograms produced are better than the results of the off-end spread configuration. This is based on the reason that seismic sources that are in the middle of the range of receivers can better distribute their energy to the near offset and far offset, because the distance traveled by the wave is only half the part. Meanwhile in the off-end configuration spread, the energy must be distributed to all parts of the offset with a distance of 2 times, because the seismic source is at the end. Generally this will result in the farthest distance or far offset not getting enough wave energy distribution so that the resolution of the synthetic seismogram produced is not good enough. Therefore, choosing the right configuration greatly affects the results of synthetic seismograms.

All forms of synthetic seismograms produced from frequency variations (20 Hz and 40 Hz) have advantages and disadvantages. The frequency value of 20 Hz will produce a larger and wider waveform, but if a layer has a low thickness (thin), this frequency is less suitable for use. At that moment, a higher frequency (40 Hz) is needed, because the smaller waveforms can show and separate thin layers that cannot be done by a frequency of 20 Hz. Therefore, the right frequency selection must be considered.

If the RC value is different for each layer, then the wave amplitude will be different from the seismic cross section. This will apply to actual seismic data obtained from measurements directly in the field. But in this study, where the data used is synthetic data (without making direct measurements) and only an approach model, the amplitude produced will appear to have the same value in each layer. Because the RC value cannot be known directly from a synthetic seismogram, to find out the difference it can be seen

from the reflector which has the greatest amplitude value, that is in the result of the reflection coefficient in Table 1. The reflection coefficient that approaches the +1 value has the highest amplitude value.

This can be proven from the type of layer in the geological model. Layers 1 through 6 are rock types that have different velocity and density values, where both parameters increase with increasing depth.

The fifth reflector has a deviation in the form of a wave peak, where the amplitude of the wave will be a peak if the AI value in the lower layer is greater than the layer above it.

## CONCLUSIONS

1. From the results of synthetic seismogram forward modeling, obtained five reflectors. Reflector 4 has the highest value of the reflection coefficient (0.2429) because of the high acoustic impedance contrast between sandstone and limestone.
2. Configuration change, frequency, and velocity show significant difference on the synthetic seismogram form.
  - Configuration change from Off-end spread to Split spread yields a better synthetic seismogram resolution.
  - Frequency change from 20 Hz to 40 Hz gives a thinner and smaller wiggle.
  - Velocity change from data 1 to data 2 yields a shorter wave travel time on the near offset part.

## REFERENCES

- [1] Fagin, S. W. 1991. Seismic Modeling of Geologic Structures: Applications to Exploration Problems (Geophysical Development series, 2 ed.). Society of Exploration Geophysicists.
- [2] Ellison, A. 1993. Modeling, Philosophy and Limitation. Computing & Control Engineering(4), 190-192.
- [3] Anderson, N., & Cardimona, S. 2002. Forward Seismic Modeling: The Key to Understand Reflection Seismic and Ground Penetrating Radar (GPR) Techniques. Rolla: University of Missouri-Rolla.
- [4] Sæther, O.-P. 2013) Seismic Forward Modeling of Deltaic Sequences. Trondheim: Norwegian University of Science and Technology.
- [5] Lillie, R. J. 1999. Whole Earth Geophysics: An Introduction Textbook for Geologist and Geophysics. Prentice-Hall: USA.

## THE PERFORMANCE OF INDONESIAN AGRICULTURAL EXTENSION WORKER

Siti Rochaeni<sup>1</sup>, Muchlis R. Luddin<sup>2</sup>, Mansyur Ramly<sup>3</sup>, and Dewi Susita<sup>4</sup>

<sup>1</sup>Faculty of Science and Technology, State Islamic University Syarif Hidayatullah Jakarta, Indonesia

<sup>2,3,4</sup> State University of Jakarta, Indonesia

### ABSTRACT

The purpose of this study was to determine whether there were a positive direct impact of (1) variations of tasks to rewards, (2) career promotion to rewards, (3) variations of tasks to performance, (4) career promotion to performance, (5) rewards to performance for agricultural extension worker in Banten Province. The research design used is a structural equation model of factors that influence the performance of agricultural extension workers. The collected data were analyzed by using reliability test using Cronbach Alpha coefficient, and then analyzed using Structural Equation Model with the help of Smart PLS software version 3.2.7. The results showed that: (1) there is a significant positive direct impact on the variable variation of the task to reward, (2) there is a significant positive direct impact on the variable of career promotion to rewards (3) there is a significant positive direct impact on the variable variation of the task to performance, (4) there is a positive direct impact not significant variable career promotion to performance, (5) there is a significant positive direct impact on rewards to performance.

*Keywords: Task variety, Career promotion, Rewards, Performance, Agricultural extension worker*

### INTRODUCTION

The agricultural extension worker has a wide range of task variety, especially as a development agent. The wide range of task variety should be managed altogether at the same time by the agricultural extension worker. Task variety refers to the degree to which a job requires employees to perform a wide range of task on the job [1]. Task variety refers to the number and frequency of exceptional, unexpected, or novel events that occur in the task. With high variety, employees typically have difficulty predicting problems or activities in advance. Task analyzability refers to the extended to which a task can be broken into small, well defined components and is concerned with how employees respond to problems that occur. Typically, with highly analyzable tasks, employees follow an objective, well defined procedure to solve problems, and are more likely to pursue knowledge in a formalized and written form. Significant correlations were found between work-life balance and task variety and task autonomy. The employees with high task variety showed lesser interference of work with personal life, lesser personal life interference with work and higher overall work-life balance than the employees with low or average task variety. The employees with high task autonomy also showed higher work-life balance [2].

Self-development for the agricultural extension worker has become the important aspect to make a better agricultural extension management. The

agricultural extension worker can get a promotion to a higher level position if the minimum cumulative credit point is acquired. The performance of the agricultural extension worker is determined by the conformity of the job description and the actual work. The work should be reported as a proof of accountability for the organization. The purpose of this study was to determine whether there were a positive direct impact of (1) task variety to rewards, (2) career promotion to rewards, (3) task variety to performance, (4) career promotion to performance, (5) rewards to performance for agricultural extension worker in Banten Province.

### METHODS

Use at most three levels of headings that correspond to chapters, sections and subsections. The first level headings for chapter titles should be in 10pt, bold, justified, and upper case font. Leave one blank line before and after the first level headings, respectively.

This research conducted in Banten Province, Indonesia, that consisted of five districts: Serang, Serang City, Tangerang, Pandeglang, and Lebak for four months from 2018 February to June. In this research, the variables were: (1) Performance (Y) as endogenous variable; and (2) Task Variety (X1), Career Promotion (X2), and Reward (X3) as exogenous variable.

The design of the research used structural equation model of factors that influence the



performance of agricultural extension worker. The construct validity used to test the validity of the questionnaire through determined the conceptual framework, constructed the operational standard, determined the indicators of each variable, and the field test of the instrument. The reliability of data collected was tested with Cronbach alpha.

The data was analyzed using model Structural Equation Models (SEM). The data processing was done with software Smart PLS 3.2.7 ver. The research variable consisted of observer variable and unobserved variable – a variable that cannot be measured directly but the score could be obtained through observed variable. Based on the relationship direction, there were endogenous variable (influenced by other variable) and exogenous variable (influences other variable). In this research, the variables were: (1) Performance (Y) as endogenous variable; and (2) Task Variety (X1), Career Promotion (X2), and Reward (X3) as exogenous variable. The causality relationship between those four variables could be explained by Figure 1.

The number of samples was determined with Slovin formulation, using simple random sampling technique with 10% of error level. The population of agricultural extension worker in Banten Province was 643 people, so in 10% of error level, the number of sample obtained was 87 people. For a better data distribution, the sample taken was increased to 100 people.

Performance (Y) indicators consisted of: (1) Preparation of agricultural assistance, consisted of 4 parameters; (2) Implementation of agricultural assistance, consisted of 9 parameters; (3) Evaluation and reporting, consisted of 3 parameters. For every parameter, there were 5 answer choices available from a to e. The scoring criteria for every choices was as follow: select “yes” for a,b,c,d = 5 points; select “yes” for b and d = 4 points; select “yes” for a and d = 3 points; select “yes” for a and d = 2 points; select “yes” for d = 1 point. Those parameters were adopted from Republic of Indonesia’s Agricultural Ministry Regulation (Peraturan Menteri Pertanian RI) No.91 in 2013.

Task Variety (X1) indicators consisted of: (1) Integrate various skills at the same time, consisted of 3 parameters; (2) Do various different tasks, consisted of 4 parameters; (3) Do a large scope task, consisted of 4 parameters; (4) Do various tasks at the different times, consisted of 4 parameters. The scoring criteria used Likert scale from 1 to 5 as

follow: 1 = never; 2 = rarely; 3 = sometimes; 4 = often; 5 = always. The indicators and parameters were constructed and developed based on Morgeson and Humphrey (2006).

Career Promotion (X2) indicators were developed based on Gaol (2014) [3]. In other hand, Reward (X3) indicators consisted of: (1) Salary, consisted of 4 parameters; (2) Allowance, consisted of 4 parameters; (3) Appreciation, consisted of 4 parameters; (4) Retirement guarantee, consisted of 4 parameters. The scoring criteria used Likert scale from 1 to 5 as follow: 1 = strongly disagree; 2 = disagree; 3 = doubt; 4 = agree; 5 = strongly agree. The indicators of Reward were developed based on Malik et al. (2015) [4].

## RESULTS AND DISCUSSIONS

### Result of Parametric Estimation Revised Model

Below is the path diagram of Structural Equation Models (SEM) along with the estimation parameters of the initial model with Partial Least Square (PLS) estimation method which describes the relationship between indicators with their latent variables and the effect of exogenous latent variables task variety and endogenous latent variables career promotion and performance.

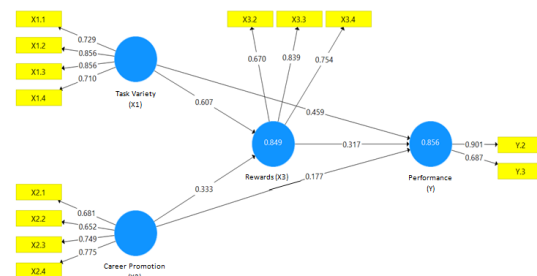


Fig. 1 Path Diagram Result of Parametric Estimation Revised Model.

### The Direct Impact and Indirect Impact of Task variety (X1) to Reward (X3)

The table below showed that the direct impact of Task variety (X1) to Reward (X3) was 36.84%. On the other hand, the indirect impact of Task variety (X1) to Reward (X3) through Career Promotion (X2) was 18.52%. The total value of the impact of Task variety (X1) to Reward (X3) was 55.36%.

Table 1 The Direct Impact and Indirect Impact of Task variety (X<sub>1</sub>) to Reward (X<sub>3</sub>)

| Impact   | Task variety (X <sub>1</sub> ) to Reward (X <sub>3</sub> ) |                                 |          |       |
|--|--|---------------------------------|----------|-------|
|  | Variable   | Calculation                     | Weighted | %     |
| Direct   | Task variety (X <sub>1</sub> )                             | (0.607)*<br>(0.607)             | 0.3684   | 36.84 |
| Indirect through   | Career Promotion (X <sub>2</sub> )                         | (0.607)*<br>(0.916)*<br>(0.333) | 0.1852   | 18.52 |
| Total impact of Task variety (X <sub>1</sub> ) to Reward (X <sub>3</sub> ) |  |                                 | 0.5536   | 55.36 |

Task variety of agricultural extension worker was the degree when the workers need some variations of activity. The high degree of variation needed the use of different skill and talent, that is to encourage the farmers to learn about how to innovate, also to listen to their complaints, then observing farmer's needs, lastly to analyze and take the right steps according to the farmers problem in the same time or different locations. Besides, agricultural extension worker needs to mastered in several aspects, that is (1) crop and livestock production, (2) agriculture as a business, (3) agriculture development process, (4) farmers and their learning style, (5) rural society. Agricultural extension worker had to mastering these aspects all at once in educating process.

While they had a complex tasks to complete, agricultural extension workers are also a social being that need reward for their work. The reward could be attained in form of wage, appreciation, and pension guarantee. The reward would motivate to do a better work. So when we expect someone to do tasks with different variations, we also need to concern about the reward. The reward should be decided along with the sacrifice of tasks delivery.

#### The Direct Impact and Indirect Impact of Career Promotion (X<sub>2</sub>) to Reward (X<sub>3</sub>)

The Direct Impact and Indirect Impact of Career Promotion (X<sub>2</sub>) to Reward (X<sub>3</sub>) showed in this table below.

Table 2 The Direct Impact and Indirect Impact of Career Promotion (X<sub>2</sub>) to Reward (X<sub>3</sub>)

| Impact  | Career Promotion (X <sub>2</sub> ) to Reward (X <sub>3</sub> ) |                                 |          |       |
|---|--|---------------------------------|----------|-------|
|   | Variable   | Calculation                     | Weighted | %     |
| Direct  | Career Promotion (X <sub>2</sub> )                             | (0.333)*<br>(0.333)             | 0.1109   | 11.09 |
| Indirect through  | Task variety (X <sub>1</sub> )                                 | (0.333)*<br>(0.916)*<br>(0.607) | 0.1852   | 18.52 |
| Total Direct Impact and Indirect Impact of Career Promotion (X <sub>2</sub> ) to Reward (X <sub>3</sub> ) |  |                                 | 0.2961   | 29.61 |

According to table above, the direct impact of Career Promotion (X<sub>2</sub>) to Reward (X<sub>3</sub>) was 11.09%, while the indirect impact of Career Promotion (X<sub>2</sub>) to Reward (X<sub>3</sub>) was 18.52%. The total impact of Career Promotion (X<sub>2</sub>) to Reward (X<sub>3</sub>) was 29.61%. Self-improvement of agricultural extension worker was an important element in the agricultural extension changing process. In carrying out the more participative process, the changes in contents and method of staff improvement were needed, both in training and leadership style that inclined to self-improvement of agricultural extension worker. Self-improvement was not only in skill, but also in character development that can be applied in work.

#### The Direct Impact and Indirect Impact of Task Variety (X<sub>1</sub>) to Performance (Y)

The Direct Impact and Indirect Impact of Task Variety (X<sub>1</sub>) to Performance (Y) can be seen in table below:

Table 3 The Direct Impact and Indirect Impact of Task Variety (X<sub>1</sub>) to Performance (Y)

| Impact  | Task Variety (X <sub>1</sub> ) to Performance (Y) |                                 |          |       |
|---|---|---------------------------------|----------|-------|
|   | Variable  | Calculation                     | Weighted | %     |
| Direct  | Task Variety (X <sub>1</sub> )                    | (0.459)*<br>(0.459)             | 0.2107   | 21.07 |
| Indirect through  | Career Promotion (X <sub>2</sub> )                | (0.459)*<br>(0.916)*<br>(0.177) | 0.0744   | 7.44  |
|   | Reward (X <sub>3</sub> )                          | (0.459)*<br>(0.911)*<br>(0.317) | 0.1325   | 13.25 |
| Total Impact of Task Variety (X <sub>1</sub> ) to Performance (Y) |   |                                 | 0.4176   | 41.76 |

The table above showed that the direct impact of Task Variety (X1) to Performance (Y) was 21.07%. The indirect impact of Task Variety (X1) to Performance (Y) through Career Promotion (X2) was 7.44%, and the indirect impact of Task Variety (X1) to Performance (Y) through Reward (X3) was 13.25%. The total value of the impact of Task Variety (X1) to Performance (Y) was 41.76%.

Task Variety is a level where tasks need variation in each different activity. The higher variation in worker tasks would require the use of different skill and talent. The application of different skill and talent would help to increase the productivity of workers. When productivity increased, it was hoped to give impact to reward accepted, so the performance would also increase. Task Variety had a positive impact to worker's performance. This means that if there is a positive change in Task Variety, then the performance will also increase.

#### The direct impact and indirect impact of Career Promotion (X2) to Performance (Y)

The direct impact and indirect impact of Career Promotion (X2) to Performance (Y) could be seen in table below.

Table 4 The Direct Impact and Indirect Impact of Career Promotion (X2) to Performance (Y)

| Impact   | Career Promotion (X2) to Performance (Y) |                                 |          |       |
|--|--|---------------------------------|----------|-------|
|  | Variable                                 | Calculation                     | Weighted | %     |
| Direct   | Career Promotion (X2)                    | (0.177)*<br>(0.177)             | 0.0313   | 3.13  |
| Indirect through   | Task Variety (X1)                        | (0.177)*<br>(0.916)*<br>(0.459) | 0.0744   | 7.44  |
|  | Reward (X3)                              | (0.177)*<br>(0.888)*<br>(0.317) | 0.0498   | 4.98  |
| Total Impact of Career Promotion (X2) to Performance (Y) |  |                                 | 0.1555   | 15.55 |

The table above showed that the direct impact of Career Promotion (X2) to Performance (Y) was 3.13%. The indirect impact of Career Promotion (X2) to Performance (Y) through Task Variety (X1) was 7.44%, and the indirect impact of Career Promotion (X2) to Performance (Y) through Reward (X3) was 4.98%. The total value of the impact of Career Promotion (X2) to Performance (Y) was 15.55%.

Promotion was an advance level position to a higher salary, responsibilities, organization level, usually as appreciation for the performance.

Agricultural extension worker got the promotion opportunity if they could fulfill the required of minimum cumulative credit point. Career promotion refers to things related planned work that carried out to achieve mastering in skill, knowledge, and attitude of the worker. The improvement was focused more on decision making skill. Career promotion had a direct and positive impact to performance. It means that if there was positive change in career, then the performance will also increase.

#### The Direct and Indirect Impact of Reward (X3) to Performance (Y)

The direct influence and indirect effect of the Rewards (X3) variable on the Performance variable (Y) in detail is presented in table 5 below.

Table 5 The Direct and Indirect Impact of Reward (X3) to Performance (Y)

| Impact   | Reward (X3) to Performance (Y) |                                 |          |       |
|--|--------------------------------|---------------------------------|----------|-------|
|  | Variable                       | Calculation                     | Weighted | %     |
| Direct   | Reward (X3)                    | (0.317)*<br>(0.317)             | 0.1005   | 10.05 |
| Indirect through                               | Task Variety (X1)              | (0.317)*<br>(0.911)*<br>(0.459) | 0.1326   | 13.26 |
|  | Career Promotion (X2)          | (0.317)*<br>(0.888)*<br>(0.177) | 0.0498   | 4.98  |
| Total Impact of Reward (X3) to Performance (Y) |                                |                                 | 0.2829   | 28.29 |

From table 5 above it can be seen that the direct impact of the Rewards (X3) variable on the Performance variable (Y) is 0.1005 or 10.05%, while the indirect impact of the Rewards variable (X3) on the Performance variable (Y) through the Task Variety variable (X1) is 0.1326 or 13.26%, and indirect impact through Career Promotion variables (X2) is equal to 0.0498 or 4.98%. So that the total impact is given by the Rewards variable (X3) on the Performance variable (Y) is 0.2829 or equal to 28.29%.

The level of income is the amount of rupiah value of income earned on the outlays of agricultural extension workers and their families in one month. The income of the agricultural extension worker is not only used for daily basic needs but if possible, can still be used for secondary purposes. Thus the income of an agricultural extension worker influences the ability to carry out basic tasks so that the higher the incoming level of an agricultural extension worker, the higher his ability to carry out

basic tasks properly. Rewards for agricultural extension worker have a direct positive impact on the performance of agricultural extension workers. This means that if there are positive changes in the rewards of agricultural extension workers, it will lead to an increase in the performance of agricultural extension workers.

## CONCLUSIONS

Based on the results of data analysis in this study, it can be concluded as follows:

1. There is a significant positive direct impact on the variable task variety of the agricultural extension worker in Banten Province, meaning that if there is a positive change in the task variety of agricultural extension worker, it results in an increase in the agricultural extension service.
2. There is a significant positive direct impact on career promotion variables on the rewards of agricultural extension workers in Banten Province, meaning that if there is a positive change in the rewards of agricultural extension worker, it will result in an increase in the rewards of agricultural extension worker.
3. There is a significant positive direct impact on the variable of task variety on the performance of agricultural extension workers in Banten Province, meaning that if there is a positive change in the task variety of the agricultural extension worker, it will lead to an increase in the performance of agricultural extension workers.
4. There is a positive direct impact not significant on career promotion variables on the performance of agricultural extension workers in Banten Province, meaning that if there is a positive change in the agricultural extension career promotion, it does not result in an increase in the performance of agricultural extension workers.
5. There is a significant positive direct impact of reward variables on the performance of agricultural extension workers in Banten

Province, meaning that if there is a positive change in rewards, then it results in an increase in the performance of agricultural extension workers.

## REFERENCES

- [1] Morgeson, F. P. & Humphrey, S. E.. The work design questionnaire (WDQ): Developing and validating a comprehensive measure for assessing job design and the nature of work. *Journal of Applied Psychology*, 2006. 91: 1321-1339.
- [2] Walia, Parminder. "Work-Life Balance in Relation to Task Variety and Task Autonomy: A Study of Bank Employees," *Journal of Strategic Human Resource Management*. <http://www.publishingindia.com/jshrm/32/work-life-balance-in-relation-to-task-variety-and-task-autonomy-a-study-of-bank-employees/283/2073/>
- [3] Gaol, J. L. *A to Z Human Capital*, 2014, PT. Gramedia Widiasarana Indonesia, Jakarta: Indonesia.
- [4] Malik, M. A. R., Butt, A. N., & Choi, J. N. Rewards and employee creative performance: Moderating effects of creative self-efficacy, reward importance, and locus of control. *Journal of Organizational Behaviour*, 2015. 36: p. 59-74.
- [5] Lee, S. Y. & Ohtake, F. The effect of personality traits and behavioral characteristics on schooling, earnings and career promotion. *Journal of Behavioral Economics and Finance*, 2012. 5: p. 231-238.
- [6] Morgeson, F. P. & Humphrey, S. E. The work design questionnaire (WDQ): Developing and validating a comprehensive measure for assessing job design and the nature of work. *Journal of Applied Psychology*, 2006. 91: 1321-1339.

## DETERMINATION OF HISTAMINE-FORMING BACTERIA, TOTAL COLIFORM AND ESCHERICHIA COLI IN FERMENTED FOODS

Patcharaporn Narkthewan<sup>1</sup> and Walaiporn Makkapan<sup>1</sup>

<sup>1</sup>Food and Agricultural Biotechnology Program, Department of General Science and Liberal Arts,  
King Mongkut's Institute of Technology Ladkrabang Prince of Chumphon Campus, Thailand

### ABSTRACT

Fermented fishery food products have been generally sold in the local market, Thailand. These products were frequently contaminated with various microorganisms due to raw material and unhygienic production process. Determination of microbial contamination of fermented food products helps to assure safety for consumers. Therefore, the aims of the study were to determine total bacteria, total coliform, *Escherichia coli* and histamine producing bacteria from fermented fishery food products commercially distributed in several regions of Chumphon and Surat Thani provinces. Twenty-two samples of fermented fishery food products were randomly collected for bacterial contamination assay. All samples revealed the levels of pH and salt content in range of 3.67-7.46 and 8.46%-29.69%, respectively. The bacterial contamination of the samples was tested by total plate count method. Determination of coliform bacteria and *E. coli* was examined by multiple-tube fermentation technique. Total bacteria, total coliform and *E. coli* of all samples were in the range of 2.15-7.54 log CFU/g, <3-460 MPN/g and <3-93 MPN/g, respectively. In addition, thirteen histamine-forming bacteria were found on histamine-forming bacteria isolation agar after incubation at 37°C for 4 days. Five isolates of histamine-forming bacteria named M1, M3, M9, M11 and M13 were selected to identify by molecular techniques. M1 and M3 were obtained from shrimp paste (Kapi) and M11 was obtained from fermented fish (Pla Pang Dang). They were identified as *Enterobacter* sp. M9 and M13 isolated from fermented fish (Pla Som and Pla Ra) were identified as *Citrobacter farmeri* and *Staphylococcus kloosii*, respectively.

**Keywords:** Fermented food, Histamine, *Enterobacter* sp., *Citrobacter farmeri*, *Staphylococcus kloosii*

### INTRODUCTION

Fermented fishery food products such as fermented fish products (Pla Som, Pla Pang Dang and Pla Ra), fermented fish entrails, fermented molluscs and shrimp pastes are the Thai traditional fermented products. Fermented fish entrails and shrimp pastes (Kapi) are mainly consumed in southern parts of Thailand. However, Pla Ra is normally consumed in the northeastern regions of Thailand.

Biogenic amines are formed mainly through the decarboxylation of specific amino acids. They are basic nitrogenous compounds occurring in foods, especially fermented foods such as kimchi [1], mustard pickle products [2], fermented soybean products (miso, douchi, natto and soybean paste) [3]-[6], fermented meat [7], and fermented seafood products [8]-[11]. The quantity and types of biogenic amines formed in fermented food products are strongly influenced by the food composition, microflora and by other factors which allow bacterial growth during food processing and storage [12].

Histamine, a biogenic amine is causative toxin of scombroid (a food-borne chemical agent). Scombroid poisoning causes of a variety of symptoms including rash, urticaria, nausea, vomiting, diarrhea, flushing and itching of the skin [13]. Free amino acid, histidine was catalyzed to histamine through by exogenous

decarboxylases produced by many bacterial strains. Histamine-forming bacteria were found in fermented food products such as *Bacillus coagulans* [9], *B. megaterium* [9], [11], *B. subtilis*, *Staphylococcus pasteuri* [4], [5], *S. capitis* [4], [5], *Enterobacter* sp. [14].

The high amounts of biogenic amine (mainly histamine) and pathogenic bacteria in fermented foods also increase consideration on food safety. However, a few reports have been presented in histamine-forming bacteria and pathogenic bacteria in fermented fishery food products in Thailand. The objective of this research was, therefore, to extensively determine the contamination of bacterial pathogens in traditional fermented food fishery products sold in the local market of southern areas (Chumphon and Surat Thani provinces).

### MATERIALS AND METHODS

#### Sample Collection

Twenty-two samples of fermented fishery food products, including 8 shrimp pastes (Kapi), 1 fermented shrimp, 8 fermented fish (1 Pla Som, 2 Pla Pang Dang and 5 Pla Ra), 2 fermented green mussel and 2 fermented fish entrails (Tai Pla) were purchased from the local market in Chumphon and

Surat Thani provinces, Thailand. After purchase, they were immediately transported to the laboratory for chemical and microbiological analysis.

#### Determination of pH Measurement and Salt Content

Each fermented food product (10 g) was homogenized in 10 ml of distilled water with the sterile blender to make the slurry product. The pH of slurry product was measured using pH meter. Salt content of each sample was investigated according to the AOAC method [15]. Two grams of samples were homogenized in 18 ml of distilled water. Then, the homogenate was titrated with 0.1 M silver nitrate ( $\text{AgNO}_3$ ) using 10% w/v potassium dichromate ( $\text{K}_2\text{CrO}_4$ ) solution as an indicator

#### Microbial Analysis and Isolation of Histamine-forming bacteria

Twenty-five grams of fermented food products were added into 225 ml of 0.05 M potassium phosphate buffer (pH 7.0) and homogenized with sterile blender for 2 min. The homogenates were serially diluted (1:10) with a sterile potassium phosphate buffer (pH 7.0) in triplicate. The suspension (1 ml) was poured onto Petri dishes (9 cm diameter). Then, 15-20 ml of plate count agar (PCA) containing 0.5% NaCl was added and gently mixed. After solidification of agar plate at room temperature, total bacterial colonies were determined after the plates were incubated at 37°C for 48 h. The bacterial numbers were then expressed as logarithm of colony forming unit per gram (log CFU/g). Total coliform and *E. coli* in fermented food samples were performed using the three-tube most probable number (MPN) method [16].

For histamine-forming bacteria isolation, 0.1 ml of the diluted sample was spread on histamine-forming bacterium isolation agar (HBI agar) supplemented with L-histidine according the method of [17]. After 4 days of incubation at 37°C, colonies with blue or purple color on the plates were picked and further streaked on trypticase soy agar (TSA) to obtain pure colonies.

#### Molecular Identification of Histamine-forming isolates

The identity of the presumptive histamine-forming isolates was carried out by amplifying and sequencing approximately 1400 bp of 16S ribosomal DNA (rDNA). The 16S rDNA gene was amplified with the universal primers: F27 (5' AGAGTTTGATC(A/C)TGGCTCAG3') and R1492 (5'TACGG(C/T)TACCTTGTTACGACTT3') [18].

The selected presumptive histamine-forming isolates were inoculated into 2 ml of trypticase soy

broth (TSB) and incubated at 37°C for 16-24 h. After incubation, the culture was centrifuged at 11,000 rpm for 10 min. The cell pellet was mixed with 1 ml of TE buffer (10 mM Tris-HCl; 1 M EDTA; pH 8.0) and lysozyme. The mixture was incubated at 37°C for 90 min. Then, 200 µl of 10% (w/v) sodium dodecyl sulphate (SDS) was added into the mixture and the reaction was incubated at 60°C for 30 min. The 20 µl of Proteinase K was added into the mixture and incubated at 37°C for 30 min. The equal volume of phenol: chloroform: isoamyl alcohol was mixed with the mixture and centrifuged at 11,000 rpm for 10 min. The supernatant was collected and mixed with the 2 volumes of isopropanol to precipitate the genomic DNA at -20°C for 30 min. The mixture was centrifuged at 11,000 rpm for 10 min. The DNA pellet was washed with 200 µl of 70% ethanol. The air-dried DNA pellet was resuspended in 100 µl of the sterile water. The quality and quantity of extracted DNA were analyzed by measuring the absorbance at 260 and 280 nm and using agarose gel electrophoresis.

The PCR reaction was performed by using 10 ng of extracted DNA in a reaction volume of 25 µl, containing a final concentration of 0.2 µM of each primer, 1X TE buffer, 10 µM of each dNTP, and one unit of Taq DNA polymerase. Amplification conditions were 98°C for 3 min followed by 30 cycles at 98°C for 10 s, 55°C for 10 s, 72°C for 30 s, and then subjected to a final concentration of 72°C for 5 min. The PCR products were then analyzed with an automatic sequencing system (Apical Scientific Sdn Bhd, Malaysia). Sequence homology was aligned using the BLAST tool (NCBI). Phylogenetic tree was conducted by MEGA 7.0 using neighbor-joining method.

## RESULTS AND DISCUSSION

Twenty-two fermented fishery food products were categorized into 2 groups (salty taste and salty and sour taste) based on the taste of fermented food products. The fermented food products with salty taste were Kapi, Pla Ra and Tai Pla. The products with salty and sour taste were Pla Som, Pla Pang Dang, fermented shrimp and fermented green mussel. The levels of pH, salt content, total bacteria, total coliform and *E. coli* in all products were in the range from 3.67-7.46, 8.46%-29.69%, 2.15-7.54 log CFU/g, <3-460 MPN/g, and <3-93 MPN/g, respectively as shown in Table 1.

The average pH value (6.03) and the average salt content (24.40%) of the fermented food products with salty taste was higher than the average pH value (4.27) and the average salt content (15.39%) of the products with salty and sour taste. However, pH value and salt content of fermented food products did not relate with the quantity of total bacteria, total coliform and *E. coli*. Thai Community Product Standards are requirement of quality that makes the reliable and

Table 1 Values of pH and salt content of fermented fishery food products, total bacteria, total coliform and *E. coli*

| Category of fermented food samples   | No. of Samples | pH                  | Salt content (%)      | Total bacteria (log CFU/g) | Total coliform (MPN/g) | <i>E. coli</i> (MPN/g) |
|--|----------------|---------------------|-----------------------|----------------------------|------------------------|------------------------|
| Salty taste<br>- Shrimp paste (Kapi)<br>- Fermented fish (Pla Ra)<br>- Fermented fish entrails   | 15             | 4.49-7.46<br>(6.03) | 18.02-29.69<br>(24.4) | 2.15-7.54                  | < 3-460                | < 3-43                 |
| Salty and sour taste<br>- Fermented fish (Pla Som)<br>- Fermented shrimp<br>- Fermented fish (Pla Pang Dang)<br>- Fermented green mussel | 7              | 3.67-4.76<br>(4.27) | 27.14-8.46<br>(15.39) | 2.79-7.52                  | < 3-53                 | < 3-93                 |

Note: the value in the parenthesis is the average value of each data.

acceptable community products and increases the confidence to consumers. The standard regulation of some fermented food products according to Thai Community Product Standards reveals that the pH value of Pla Som and fermented shrimp must not exceed 4.6. In addition, the salt content of Kapi, Tai Pla and Pla Ra are not lower than 12%. The results of pH value and salt content in this study were similarity with the several previous reports. Values of pH and salt content in fish sauce, fish paste and shrimp paste were 4.8-6.5 and 16.2%-45.3%, respectively [9]. The

traditional fermented products (soybean and black bean douchi products) had the pH values and salt contents of 4.7-5.9 and 4.4%-14.0%, respectively [4]. The level of pH and salt content in fish sauces were in the range of 4.8-5.7 and 15.6%-25.7%, respectively [19]. The traditional soybean pastes of Doenjang had the pH values in the range of 4.8-6.0 [6]. The traditional Rihaakuru (fish paste) from the Maldives had the pH values of 5.62-6.18, whereas salt content of 1.4%-1.6% was lower than this study [10]. The pH values and salt contents in salted seafood products

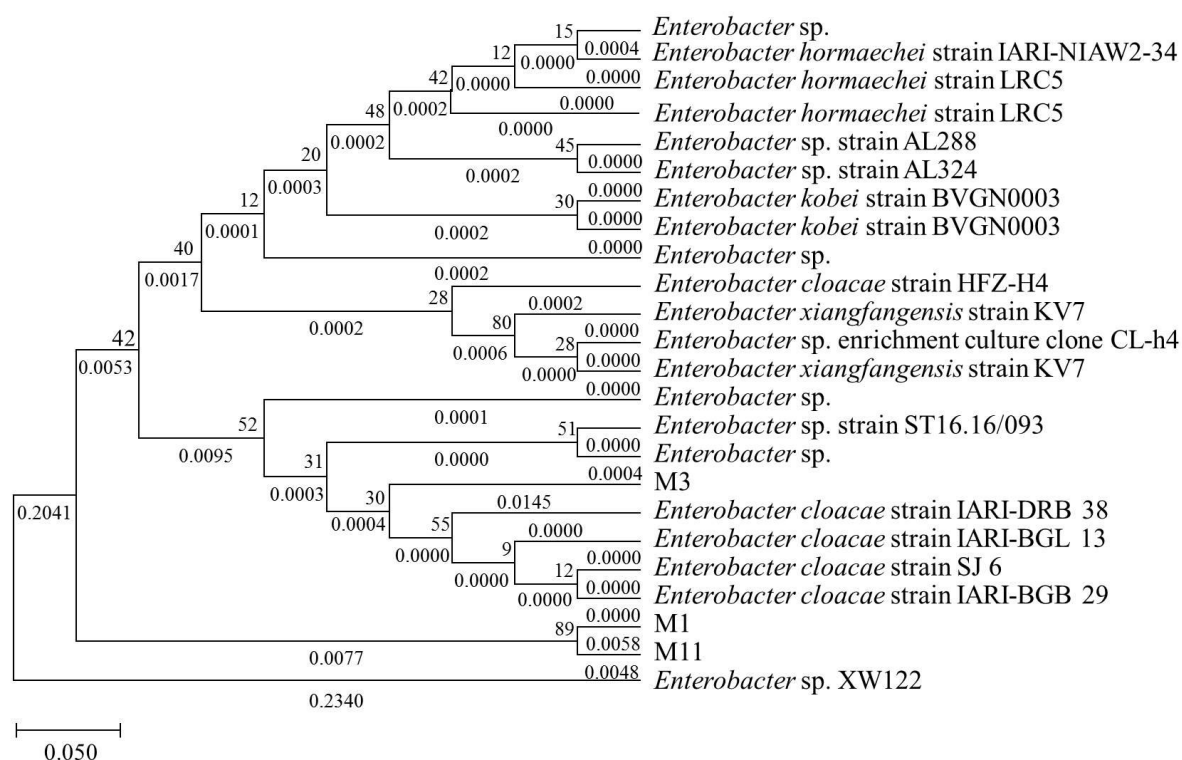


Fig. 1 Phylogenetic analysis of M1, M3 and M11 was constructed based on 16S rDNA sequences using the neighbor-joining method in the MEGA 7.0. The numbers in the phylogramnodes indicated the bootstrap value (%).



were in the range from 3.58-7.47 and 2.34%-21.51%,

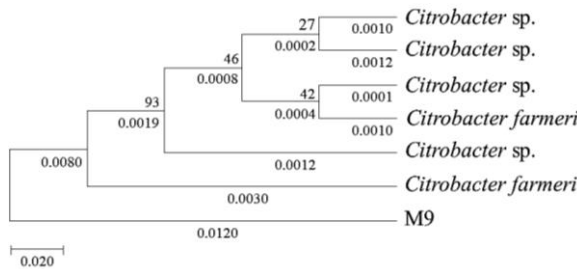


Fig. 2 Phylogenetic analysis of M9 was constructed based on 16S rDNA sequences using the neighbor-joining method in the MEGA 7.0. The numbers in the phylogram nodes indicated the bootstrap value (%).

respectively [11]. The pH is an important factor for fermentation and formation of biogenic amines because amino acid decarboxylase activity remains stronger in an acidic condition [20].

The quantity of total bacteria was 2.15-7.54 log CFU/g obtained from fermented food products in this study. However, the standard regulation of total bacteria in fermented food is not reported in Thai Community Product Standards. Several previous studies determined aerobic plate count (APC) in fermented food products. Fermented fish products were obtained 1.0-4.2 log CFU/g of APC [9]. Soybean douchi and black bean douchi showed 6.6 log CFU/g of APC and 7.5 log CFU/g of APC, respectively [4]. Moreover, salted seafood products had 1.08-7.2 log CFU/g of APC [11].

Total coliform and *E. coli* in all tested samples were <3-460 MPN/g and 3-93 MPN/g, respectively as shown in Table 1. Twelve fermented food samples was found <3 MPN/g of total coliform and *E. coli*. The quantities of *E. coli* in the fermented foods according to Thai regulatory level must be <3 MPN/g whereas the quantity of total coliform in these products is not reported. Comparison with fermented food products in the previous studies such as mustard pickle products, soybean douchi products, salted seafood products, none of these products contained total coliform and *E. coli* [2], [4], [11]. The results of the study indicated that the bacterial contamination of fermented fishery food products may be caused from bacterial flora in the raw materials and the bacterial contamination during fermentation process.

From twenty-two fermented fishery food samples, thirteen histamine-forming bacteria were obtained after incubation at 37°C for 4 day. Five bacterial isolates (M1, M3, M9, M11 and M13) were selected to identify by the universal primers targeted to the 16S rDNA gene. The 1400-bp amplicons obtained from each isolate were analyzed and compared with other reference strains from GenBank using the BLAST tool. Bacterial isolates (M1 and M3) were isolated from Kapi. The other isolates (M9, M11 and M13) were isolated from Pla Som, Pla Pang Dang and

Pla Ra, respectively. The M1, M3 and M11 isolate were identified as *Enterobacter* sp. (Fig. 1). The M9 isolate was highly homologous to *Citrobacter farmeri* (Fig. 2). The M13 isolate had a homology with *Staphylococcus kloosii* (Fig. 3). The *Enterobacter* sp. was identified as histamine former isolated from tuna dumpling [14]. *E. cloacae* isolated from salted mackerel were found to be weak histamine former [8]. *E. cloacae* were also identified as weak histamine former isolated from mustard pickle products [2]. *Staphylococcus* sp. was mostly found as histamine formers in fermented foods. *S. capitis* and *S. pasteurii* were found as a histamine former in the mustard pickle products [2] and douchi [4].

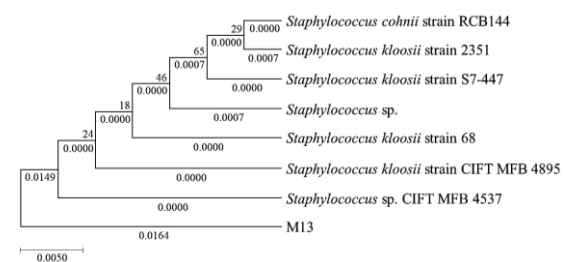


Fig. 3 Phylogenetic analysis of M13 was constructed based on 16S rDNA sequences using the neighbor-joining method in the MEGA 7.0. The numbers in the phylogramnodes indicated the bootstrap value (%).

## CONCLUSIONS

Total bacteria, total coliform, *E. coli* and histamine forming bacteria were determined in fermented fishery food products. The presence of *E. coli* found in some products were out of Thai regulatory level (<3 MPN/g). Moreover, the study of the research demonstrated the incidence of histamine-forming bacteria (*Enterobacter* sp., *C. farmeri* and *S. kloosii*) in fermented fishery food products. Therefore, further studies are to determine the quantity of histamine contents in fermented fishery food products for food safety assessment.

## ACKNOWLEDGMENTS

The authors greatly appreciate Biotechnology Laboratory, King Mongkut's Institute of Technology Ladkrabang Prince of Chumphon Campus for providing the laboratory facilities and Miss Suwanan Sangthong for assisting the research.

## REFERENCES

- [1] Tsai Y.H., Kung H.F., Lin Q.L., Hwang J.H., Cheng S.H., Wei C.I., and Hwang D.F., Occurrence of Histamine and Histamine-Forming Bacteria in Kimchi Products in Taiwan. Food Chemistry, Vol. 90, 2005b, pp. 635-641.

- [2] Kung H.F., Lee Y.H., Teng D.F., Hsieh P.C., Wei C.I., and Tsai Y.H., Histamine Formation by Histamine-Forming Bacteria and Yeast in Mustard Pickle Products in Taiwan. *Food Chemistry*, Vol. 99, 2006, pp. 579-585.
- [3] Kung H.F., Tsai Y.H., and Wei C. I., Histamine and Other Biogenic Amines and Histamine-Forming Bacteria in Miso Products. *Food Chemistry*, Vol. 101, 2007, pp. 351-356.
- [4] Tsai Y.H., Kung H.F., Chang S.C., Lee T.M., and Wei C.I., Histamine Formation by Histamine-Forming Bacteria in Douchi, a Chinese Traditional Fermented Soybean Product. *Food Chemistry*, Vol. 103, 2007a, pp.1305–1311.
- [5] Tsai, Y.H., Chang S.C., and Kung H.F., Histamine Contents and Histamine-Forming Bacteria in Natto Products in Taiwan. *Food Control*, Vol. 18, 2007b, pp. 1026-1030.
- [6] Shukla S., Park H.K., Kim J.K., and Kim M., Determination of Biogenic Amines in Korean Traditional Fermented Soybean Paste (Doenjang). *Food and Chemical Toxicology*, Vol. 48, 2010, pp. 1191-1195.
- [7] Ekici K. and Omer A.K., The Determination of Some Biogenic Amines in Turkish Fermented Sausages Consumed in Van. *Toxicology Reports*, Vol. 5, 2018, pp. 639-643.
- [8] Tsai Y.H., Lin C.Y., Chang S.C., Chen H.C., Kung H.F., Wei C.I., and Hwang D.F., Occurrence of Histamine and Histamine-Forming Bacteria in Salted Mackerel in Taiwan. *Food Microbiology*, Vol. 22, 2005a, pp. 461-467.
- [9] Tsai Y.H., Lin C.Y., Chien L.T., Lee T.M., Wei C.I., and Hwang D.F., Histamine Contents of Fermented Fish Products in Taiwan and Isolation of Histamine-Forming Bacteria. *Food Chemistry*, Vol. 98, 2006, pp. 64-70.
- [10] Naila, A. Flint S., Fletcher G.C., Bremer, P.J., and Meerdink G., Chemistry and Microbiology of Traditional Rihaakuru (Fish Paste) from the Maldives. *International Journal of Food Sciences and Nutrition*, Vol. 62, Issue 2, 2011, pp. 139-147.
- [11] Lin C.S., Liu F.L., Lee Y.C., Hwang C.C., and Tsai, Y.H., Histamine Contents of Salted Seafood Products in Taiwan and Isolation of Halotolerant Histamine-Forming Bacteria. *Food Chemistry*. *Food Chemistry*, Vol. 131, 2012, pp. 574-579.
- [12] Carelli D., Centonze D., Palermo C., Quinto M., and Rotunno T., An Interference Free Amperometric Biosensor for the Detection of Biogenic Amines in Food Products. *Biosensors and Bioelectronics*, Vol. 23, Issue 5, 2007, pp. 640-647.
- [13] Taylor S.L. Histamine Food Poisoning: Toxicology and Chemical Aspects *Critical Reviews and Toxicology*, Vol. 17, 1986, pp. 91-128.
- [14] Chen H.C., Kung H.F., Chen W.C., Lin W.F., Hwang D.F., Lee Y.C., and Tsai Y.H., Determination of Histamine and Histamine-Forming Bacteria in Tuna Dumpling Implicated in a Food-Borne Poisoning. *Food Chemistry*, Vol. 106, 2008, pp. 612-618.
- [15] AOAC. Official methods of analysis of AOAC international, 16th ed., Arlington, VA: AOAC International, 1995.
- [16] Standard Methods for Food Analysis., Department of Medical Sciences, Thailand, Vol. III, 2015.
- [17] Niven C.F., Jeffreg M.B., and Corlett D.A., Differential Plating Medium for Quantitative Detection of Histamine-Producing Bacteria. *Applied and Environmental Microbiology*, Vol. 41, 1981, pp. 321-322.
- [18] Heuer H., Krsek M., Baker P., Smalla K., and Wellington E.M.H., Analysis of Actinomycete Communities by Specific Amplification of Genes Encoding 16S rRNA and Gel-Electrophoretic Separation in Denaturing Gradients. *Applied and Environmental Microbiology*, Vol. 3, Issue 8, 1997, pp. 3233-3241.
- [19] Zaman M.Z., Baker F.B., Seleamat, J., and Baker J. Occurrence of Biogenic Amines and Amines Degrading Bacteria in Fish Sauce. *Czech Journal of Food Sciences*, Vol. 28, Issue 5, pp. 440-449.
- [20] Silla Santos, M.H., Biogenic Amines: Their Importance in Foods. *International Journal of Food Microbiology*, Vol. 29, 1996, pp. 213-231.

## VITAMIN AND MINERAL CONTENT OF SIX NATIVE VARIETIES OF RICE IN THAILAND

Intira Lichanporn<sup>1</sup>, Nanchanok Nantachai<sup>1</sup>, Palida Tunganurat<sup>1</sup>, Unchalini Singkhum<sup>1</sup>, Nowapor Lapsongphon<sup>1</sup>, Anchalee Sawatthum<sup>1</sup>, Ratchata Tonwitawat<sup>1</sup>, Tongmee Mosom<sup>1</sup> and Purin Akkarakultron<sup>1</sup>  
<sup>1</sup> Faculty of Agriculture and Technology, Rajamangala University of Technology Thanyaburi, Phatumthani 12130

### ABSTRACT

The objective of this research was to examine the vitamin and mineral contents present of the native varieties of six rice varieties (Sangyod, Khaw kin, Mali nil surin, Khaw heniyw lump haw, Khaw kla heniyw and Thabthim chumphae) in Thailand. Results showed that Mali nil surin had the highest vitamin E content (0.25 mg/100 g) and Khaw kin had higher iron (5.08 mg/100g) than that other rice. Khaw kla heniyw had the high folic acid content (88 mcg/100g) and niacin content (4.12 mg/100g). Folic acid and niacin of Khaw heniyw lump haw had the lowest (9 mcg/100g and 3.11 mg/100g) while, Khaw kin and Khaw kla heniyw had the lowest vitamin E and iron (0.09 and 0.30 mg/100g). Therefore, rice is a good candidate for natural sources of nutritional and medicinal properties and may hold the potential for the development of rice-based beauty products, functional foods, drugs, and natural food preservatives.

*Keywords: Native varieties of rice, folic acid, iron*

### INTRODUCTION

Rice (*Oryza sativa*), is known as the grain of life and is similar to food for Asians [1]. Over 2 billion people in Asia alone arise 80% of their energy needs from rice, which contains 80% carbohydrates, 7-8% protein, 3% fat, and 3% fibre [2]. Paddy rice is a good specialist of thiamine (vitamin B1), niacin (vitamin B3), and vitamin B6 [3]. The B-complex vitamins, especially thiamin, riboflavin and niacin presented by natural brown rice promote youthful energy and nourishment to skin and blood vessels [1]. Rice bran also holds beneficial anti-oxidations like tocopherols and tocotrienols (of the Vitamin E family) and oryzanols [4]. Red and black rice are full in iron (Fe), zinc (Zn) and minerals [5]. Zinc and iron are required by the human body for enzymatic processes and haemoglobin production, respectively [1]. Iron is a considerable factor affecting its absorption and hence affects iron status. In cereal foods, phytate is the most important absorption inhibitor, binding nonheme iron, zinc, and calcium in an insoluble complex in the intestine, making it unavailable for absorption [6][7]. Folates are an essential nutrition component (an important B vitamin) in the human diet, concerned in many metabolic pathways, mainly in carbon transfer reactions such as purine and pyrimidine biosynthesis and amino acid inter-conversions [8]. Folates survive as vitamers (one carbon folate derivatives) that are polyglutamate with varying oxidation states and substituents [9]. Folates survive in two forms- Naturally occurring folates are found in foods and

metabolically active forms in the human body [10]. The synthetic form of folic acid is the folate found in supplements and fortified foods. This is the more stable form and occurs unusually in foods or the human body [8]. The aim of the research was to examine the vitamin and mineral contents present of the native varieties of six rice varieties (Sangyod, Khaw kin, Mali nil surin, Khaw heniyw lump haw, Khaw kla heniyw, and Thabthim chumphae) in Thailand, they're a good candidate for natural sources of nutritional and medicinal properties.

### EXPERIMENTAL METHODS

#### 1. Preparation of Paddy

Rice, six varieties of Sangyod, Khaw kin, Mali nil surin, Khaw heniyw lump haw, Khaw kla heniyw, and Thabthim chumphae, Thailand were used. Rice grains were ground by the mortar and pestle and analyzed according to the technique described above.

#### 2. Vitamin E

The following vitamin E was measured by high performance liquid chromatographic methods. Vitamins E (a-tocopherol) were determined after alkaline saponification [11].

#### 3. Iron

Iron content was measured by the method described by AOAC, 2016. 984.27 [12]

#### 4. Folic acid

Folic acid was determined by In house

method based on AOAC 2016. 960.46 [13].

#### 5. Niacin (Vitamin B3)

Niacin was determined by the colorimetric method (AOAC 2016. 961.14) [14].

## RESULTS AND DISCUSSION

The color of the varieties is deep red (Sangyod), light red (Khaw kin), purple rice (Mali nil surin and Khaw heniyw lum phaw), red and purple (Khaw kla heniyw) and light red (Thabthim chum phae) (Figure 1A-F). The deep red and purple colors of varieties are comparable more nutritious. The red/purple or brown unpolished rice is a healthy food because it provides with rice bran, thin brown coating between rice kernel and protective hull provides mankind greatest nutritional needs [15]. In Chhattisgarh of India, Layacha variety is effectively used to cure boil caused on scalp of the newly born child. The mother of the child eats cooked rice of the variety, useful to heal the boil of the child who consumes mother milk. Cooked grains of Layacha variety is beneficial for pregnant women to prevent unborn children from contracting Laicha disease (skin infection) [15].



Figure 1. Characterizes of paddy in Pathum Thani Rice Province; Sangyod (A), Khaw kin (B), Mali nil surin (C), Khaw heniyw lum phaw (D), Khaw kla heniyw (E) and Thabthim chumphae (F).

The rice Mali nil surin had the highest vitamin E content (0.25 mg/100g) and Khaw kin had the lowest vitamin E content (0.09 mg/100g) (Table 1). Studies have confirmed beneficial qualities such as the high biological value of vitamin E in brown rice (0.90-2.50 mg/100g) and milled rice (0.75-3.00 mg/100 g) [2]. Rice also holds beneficial anti-oxidants like tocopherols and tocotrienols (of the “Vitamin E family”) and oryzanols [4]. Researchers have explored the anti-cancer activities of tocopherols [16]. While the color of red and purple rice is full in anthocyanin and tannins which possess antioxidant and anti-inflammatory properties [1]. Mali nil surin of the varieties is purple color and high rich antioxidant of anthocyanin. Khonkaen rice seed center [17] have also found that antioxidants and anthocyanins of Mali nil surin were at 117 mg/kg sample and 219.03 mg/kg. Bioavailability of iron is a considerable factor affecting its absorption and

hence affects iron status [1]. For rice levels of phytate informed in the literature range from 0.87 to 3.7 mg/g of dry matter, which equals 0.09-0.37% [18] [19] [20]. In table 1, the iron of Khaw kin was highest as 5.08 mg/100g, while Khaw kla heniyw was lower than the other samples as 0.30 mg/100 g. Iron is demanded by the human body for enzymatic processes and hemoglobin production, respectively [1].

Table 1. Vitamin E and Iron of six native varieties of rice

| Native varieties of rice | Vitamin E (mg/100g) | Iron (mg/100g) |
|--------------------------|---------------------|----------------|
| Sangyod                  | 0.11                | 0.99           |
| Khaw kin                 | 0.09                | 5.08           |
| Mali nil surin           | 0.25                | 0.78           |
| Khaw heniyw lum phaw     | 0.18                | 1.31           |
| Khaw kla heniyw          | 0.14                | 0.30           |
| Thabthim chumphae        | 0.11                | 0.51           |

Khaw kla heniyw had highest folic acid, compared with Sangyod, Khaw kin Mali nil surin, Khaw heniyw lump haw and Thabthim chumphae (Table 2). Folic acid is to prevent neural tube defects (NTDs), which are an important cause of perinatal mortality and infantile paralysis worldwide [21].

Table 2. Folic acid and Niacin of six native varieties of rice

| Native varieties of rice | Folic acid (mcg/100g) | Niacin (mg/100g) |
|--------------------------|-----------------------|------------------|
| Sangyod                  | 31                    | 4.18             |
| Khaw kin                 | 32                    | 3.71             |
| Mali nil surin           | 44                    | 3.95             |
| Khaw heniyw lum phaw     | 9                     | 3.11             |
| Khaw kla heniyw          | 88                    | 4.12             |
| Thabthim chumphae        | 41                    | 3.19             |

Niacin of Sangyod and Khaw kla heniyw had 4.18 and 4.12 mg/100g, while Khaw kin, Mali nil surin, Khaw heniyw lump haw, and Thabthim chumphae had 3.71, 3.95, 3.11 and 3.19 mg/100 g, respectively. Niacin is the vitamin B3 and has basic roles as part of reduction/oxidation coenzymes involved in energy metabolism, amino acid metabolism, and detoxification reactions for drugs and other substances. Niacin comes from in any forms: (1) nicotinic acid (pyridine-3- carboxylic acid) [22], (2) nicotinamide (nicotinic acid amide), and (3) other derivatives (e.g., inositol hexanicotinate) “that exhibit the biological activity of nicotinamide” [23].

## CONCLUSIONS

Thailand is many rice varieties that have medicinal properties and Khaw kla heniyw had higher the folic acid and niacin than other variety rice. While, Khaw kin was high the rich of iron and a much of vitamin E as Mali nil surin.

## ACKNOWLEDGMENTS

Financial support for this work was provided the Plant Genetic Conservation Project under the Royal Initiative of Her Royal Highness Princess Maha Chakri Sirindhorn, Thailand. We thank the Faculty of Agricultural Technology and Institute of Research and Development, Rajamangala University of Technology Thanyaburi. Finally, we would like to thank Pathumthani Rice Research Center for the native varieties of rice in Pathum Thani Province.

## REFERENCES

- [1] Chaudhari P.R., Tamrakar N., Singh L., Tandon A., and Sharma D., Rice nutritional and medicinal properties: A review article, *Journal of Pharmacognosy and Phytochemistry*, Vol. 7, Issue 2, 2018, pp. 150-156.
- [2] Juliano B.O., *Rice Chemistry and Technology*, American Association of Cereal Chemists, USA. 1985, pp. 757.
- [3] Kennedy G., Burlingame B., and Nguyen N., Nutrient impact assessment of rice in major rice-consuming countries, *International Rice Commission Newsletter* 5. Rome: Food and Agriculture Organization. 2002.
- [4] Lloyd B.J., Siebenmorgen T.J., and Beers K.W., Effects of commercial processing on antioxidants in rice bran, *Cereal Chemistry*, Vol. 75, Issue 5, 2000, pp. 551-555.
- [5] Ahuja U., Ahuja S.C., Thakrar R. and Singh R.K., Rice a Nutraceutical, *Asian-Agri History*, Vol. 12, Issue 2, 2008; pp. 93-108.
- [6] Gibson R.S., Bailey K.B., Gibbs M., and Ferguson E.L., A review of phytate, iron, zinc, and calcium concentrations in plant-based complementary foods used in low-income countries and implications for bioavailability, *Food and Nutrition Bulletin*, Vol. 31, Issue 2 (supplement), 2010, pp. S134-S146.
- [7] Hurrell R.F., Phytic acid degradation as a means of improving iron absorption, *International Journal For Vitamin and Nutrition Research*, Vol. 74, 2004, pp. 445-52.
- [8] Arya S.S., and Pavitra K., Folate: sources, production, and bioavailability, *Agro Food Industry Hi Tech*, Vol. 23, Issue 4, 2012, pp. 23-27.
- [9] Kariluoto S., Edelmann M., Herranen M., Lampi, A.M., Shmelev, A., Salovaara, H., et al., Production of folate by bacteria isolated from oat bran, *International Journal of Food Microbiology*, Vol. 143, Issue 1-2, 2010, pp. 41-47.
- [10] Food and Nutrition Board, Institute of Medicine, Folate, 1998, pp. 196-305
- [11] Speek A.J., Schrijver J., and Schreurs W.H.P., Vitamin E composition of some seed oils as determined by high-performance liquid chromatography with fluorometric detection, *Journal of Food Science*, Vol. 50, 1985, pp. 121-124.
- [12] AOAC., AOAC Official Method 984.27 Calcium, Copper, Iron, Magnesium, Manganese, Phosphorus, Potassium, Sodium, and Zinc in Infant Formula Inductively Coupled Plasma Emission Spectroscopic Method. AOAC Official Methods of Analysis. 20th ed. AOAC International. Gaithersburg. MD.2016.
- [13] AOAC., AOAC Official Method 960.46 Vitamin assays, Microbiological Method. AOAC Official Methods of Analysis. 20th ed. AOAC International. Gaithersburg. MD.2016.
- [14] AOAC., AOAC Official Method 961.14 Niacin and niacinamide in drugs, foods and feeds. The colorimetric method, Final action 1962, in the official. AOAC Official Methods of Analysis. 20th ed. AOAC International. Gaithersburg. MD. 2016.
- [15] Rahman S., Sharma M.P., and Sahai S., Nutritional and medicinal values of some indigenous rice varieties, *Indian Journal of Traditional Knowledge*, Vol. 5, Issue 4, 2006, pp. 454-458.
- [16] Kline K., Yu W., and Sanders B.G., Vitamin E and Breast Cancer, *The Journal of Nutrition*, Vol. 134, Issue 12 suppl, 2004, pp. 3458S-3462S.
- [17] Khon Kaen rice seed center, Mali nil surin, Cited June 3, 2019. <https://www.thairicedb.com/rice-detail.php?id=17>, 2007.
- [18] Prynne C.J., McCarron A., Wadsworth M.E.J., and Stephen A.M., Dietary fibre and phytate; a balancing act. Results from 3-time points in a British birth cohort. *British Journal of Nutrition*, Vol. 103, 2010, pp. 274-280.
- [19] Do M.S., Lomeda R.A.R., Cho Y.E., and Kwun. I.S., The decreased molar ration of phytate:zinc improved zinc nutriture in SouthKoreans for the past 30 years (1969-1998), *Nutrition Research and Practice*, Vol. 1, 2007, pp. 356-362.
- [20] Michaelsen K.F., Hoppe C., Roos N., et al., Choice of foods and ingredients for moderately malnourished children 6 months to 5 years of age, *Food and Nutrition Bulletin*. Vol. 30, 2009, pp. S434-S405.

- [21] Berry R.J., Bailey L., Mulinare J., and Bower, Fortification of flour with folic acid, *Food and Nutrition Bulletin*, Vol. 31, 2010, pp. S22–S35.
- [22] Burgeois C, Cervantes-Laurean D., and Moss J., Niacin, In Shils M.E., Shike M., eds. *Modern Nutrition in Health and Disease*. 10th ed. Philadelphia: Lippincott, Williams & Wilkins, 2006, pp. 442.
- [23] Institute of Medicine (IOM), *Dietary Reference Intakes for Thiamin, Riboflavin, Niacin, Vitamin B6, Folate, Vitamin B12, Pantothenic Acid, Biotin, and Choline*. Washington, DC: National Academy Press, 1998.

# AFM VISUALIZATION OF PHYTOPLASMA DNA IMMOBILIZATION AND HYBRIDIZATION EVENT ON CHITOSAN MODIFIED SPCE SURFACE

Porntip Wongkaew<sup>1</sup>, Buddhapala Wongkaew<sup>2</sup>  
<sup>1</sup>Faculty of Agriculture, KhonKaen University, Thailand,  
<sup>2</sup>Metropolitan Waterworks Authority,

## ABSTRACT

The evidence of DNA immobilization and hybridization on a functional surface is demonstrated in this presentation following the high resolution atomic force microscopic (AFM) direct observation. A planar functional surface was fabricated by self-assembly of a biopolymer chitosan onto screen-printed carbon electrode (SPCE) concerning to its excellent covalent bonding binding of biomolecules. The target DNA molecules were extracted from important phytoplasma diseased plants such as sugarcane white leaf (SCWL), burmuda grass white leaf (BGWL) and sesame phyllody (SP). The real image in actual posture of long chain natural DNA and the well-known structure of the DNA double helix were obviously visualized following the DNA immobilization and subsequent transitional hybridization with their complementary DNA. The coordinate quantitative parameters of AFM images such as line profile analysis, surface roughness, power spectrum density (PSD) algorithm and fractal dimension were also determined. The width size of double stranded DNA and the specific hybrid DNA were apparently almost 2 folds bigger than their single stranded DNA. Whereas an aggregation and growth mechanism of those DNAs on chitosan modified SPCE surfaces were mainly stacked in vertical direction and grown beyond a diffusion limited model as indicated by their fractal dimension values around 2 to 3. This phenomenon is hence valuable for the verification and the efficient development of diagnostic DNA-based devices.

*Keywords: Atomic force microscope, Chitosan modified SPCE, DNA immobilization and hybridization, Realactual image*

## INTRODUCTION

At present, biosensing technology has perceived a profound attention due to human life necessity for accurate, specific, ultrasensitive and speedy automatic point of care diagnostic tools. Ubiquitous applications including healthcare monitoring of human, animal husbandry, plant production, food and environment security are growing adopted [1]-[4]. For decades, researches on coupling biomolecules with electronic detection devices have been pursued for effective sensing application. Several biological elements and molecules such as cells, antibodies, enzymes, receptor proteins, lectins, and nucleic acids are considerably competent. Among these, DNA (Deoxyribonucleic acid) has attracted intensive focus according to its structural versatility and genetic functionality that makes a top capacity for target discrimination. Typically, DNA based biosensing system is manipulated through functional surface sensor containing the selected single stranded DNA molecule attached onto an electroactive transducer. The target detection is subsequently operated on the most selective reactions in nature basis of nucleic acid hybridization that allows several readout strategies such as colorimetry, spectroscopy, electrophoresis and especially the electrochemical signalling [1], [2],

[5]. Therefore immobilization and hybridization of the DNA on transducer surface is exactly critical for desirable sensitivity and specificity including overall measurable electronic signal generation of the biosensor.

A direct physical anchor of DNA on the capture molecules at a basal electrode surface is one of the most common immobilization approaches. This procedure involves the simple electrostatic self-assembled layer by layer technique [1], [2], [5]. Selection of a proper working platform is crucial for this type of DNA immobilization and fabrication of the DNA sensor. Previous studies on the establishment of high conductivity and bioaffinity modified electrodes using the versatile chitosan biomaterial have been sequentially reported [1]-[5], [7], [8]. However, a study in more criteria details both quantitatively and morphologically is still needed to elucidate the reality of hybridization dynamics especially the classical double helix forming postulated by Watson and Crick [10] that no one could actually see it ever.

With reference to those excellent advantages of the chitosan modified electrodes previously reports, this current study was further motivated using three genomic DNA, each, from phytoplasma pathogens that cause important plant diseases in Thailand [11] such as sugarcane (*Saccharum officinarum* L.) white



leaf (SCWL), burmuda grass (*Cynodon dactylon* L.) white leaf (BGWL) and sesame (*Sesamum indicum* L.) phyllody (SP) as representative illustrations for a close investigation of the actual hybridization event. The AFM was employed for the intensive speculation due to its superb efficiency in imaging at micro and nanoscale over than other devices at this moment. This microscopy not only offers the capacity to visualize nanometric features in two and three dimensions but also the physicochemical characteristics including its spatial distribution mapping of surfaces at different stages of the molecular assembly. Moreover, observation can be directly performed without any special preparation requirement [3], [4], [7], [8], [12]. In a while, successful direct visual evidence of DNA immobilization and hybridization phenomena could be captured and ascertained by the AFM imaging and corresponding quantitative topographic parameters. The first real image of the being tie in helical posture of the complementary DNA couple during a hybridization event could also be validated in this article.

## MATERIALS AND METHODS

### Materials

Screen printed carbon electrode (SPCE) model DRP-150 consisting of 4 mm spot carbon as working electrode surrounded with a counter electrode platinum line and a reference electrode silver line was provided by DropSens, S.L. Llanera (Asturias) Spain. Chitosan at 85% degree of deacetylation with a molecular weight of 0.28 kDa was obtained from Bioline Lab, Co., Thailand. Analytical graded chemicals for reagent preparation were purchased from Sigma-Aldrich Co. LLC, USA and Ajax Finechem Pty, Ltd., Australia. High purity deionized water of 18.2 M $\Omega$  from Milli-Q RG system (Millipore Corporation, MA, USA) was used in all solutions. The diseased samples, sugarcane white leaf (SCWL), burmuda grass white leaf (BGWL), and sesame phyllody (SP) from collection maintained in the insect proof disease nursery of Plant Pathology Division of the Faculty of Agriculture, KhonKaen University, were used for a pure source of each causal phytoplasma DNA extraction. Healthy sugarcane, burmuda grass and sesame maintaining far apart in another insect proof nursery were brought as the challenge controls. Preliminary confirmation for the absence or existence of each causal phytoplasma was done by PCR with a set of specific primer pair of both the 16S rDNA and 16-23S rDNA reported earlier [9].

### Preparation of Chitosan modified electrode platform

Chitosan solution (1%, w/v) was done by dissolving 1 g chitosan in 100mL of 1% (v/v) acetic acid solvent and the solution was filtered to remove insoluble materials. A self-assembled monolayer of chitosan was formed on carbon working spot of screen-printed carbon electrode (SPCE) by applying a 3.0  $\mu$ L drop of chitosan solution and naturally dried up at room temperature. The modified working surface was then fixed with a 10 $\mu$ L drop of 0.1 M NaOH for 30 min and left it dried again prior to use.

### Nucleic Acid Extraction

The phytoplasma DNA from diseased SCWL, BGWL and SP, each was extracted following the CTAB-phenol-chloroform method [13] from midrib of the leaves, the plant sieve elements where most phytoplasma cells are colonized [11]. The extracted DNA was purified by repeating this procedure again to get at least the purity index of 1.8 at A260/A280 ratio for a suitable direct use in the immobilization and hybridization trials. Its concentration was then quantified spectrophotometrically from the value measured at A260. The Challenging target nucleic acid from healthy plants was also extracted from midrib of the leaves by similar method. Stock solution of each nucleic acid sample was maintained in 10 mM Tris HCL pH 8.0 containing 1 mM Sodium EDTA (TE buffer) and kept frozen. The ssDNA was achieved by denaturing its native dsDNA in 100°C water bath for 10 min and followed by rapid cooling in ice bath. This type of ssDNA was also prompted for subsequently used as probe to its complementary DNA hybridization.

### Immobilization of DNA

The chitosan modified SPCE surface was employed as working platform for every challenging DNA immobilization experiments. Each DNA sample was immobilized by dropping 2  $\mu$ L of its 10  $\mu$ M in TE buffer onto the chitosan-modified SPCE platform and allowed to incubate overnight at room temperature. This functionalized surface was rinsed with 0.1% SDS phosphate buffer (pH 7.0) three times to remove the unbound DNA and dried at room temperature prior for the next manipulation.

### DNA hybridization

Hybridization, a reaction that is commonly recommended as an indication for specific recognition of the complementary DNA strand was due in this investigation. The reaction was performed by overspreading the ssDNA probe-

functionalized spot surface of chitosan modified SPCE with a 3  $\mu\text{L}$  droplet of  $2 \times \text{SSC}$  solvent containing 10 ng/ $\mu\text{L}$  challenging target ssDNA and kept incubating at 42°C for 40 min. Afterward it was rinsed three times with 0.1% SDS phosphate buffer (pH 7.0). The testing hybridization performance was then ready for inspection after a minute of natural drying in air at room temperature.

### AFM imaging and analysis

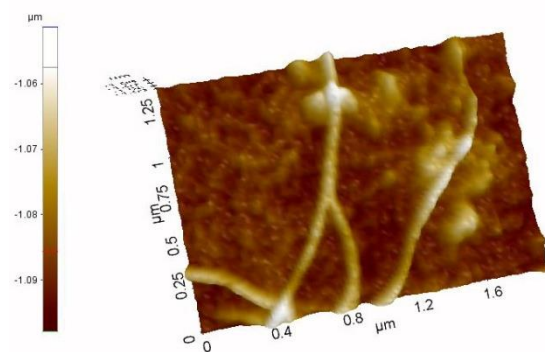
A nanoscale imaging for the DNA immobilization and progressive hybridization event was carried out by an atomic force microscope model XE-70 (Park Systems Corp., Suwon, Korea) through a true non-contact mode. The observation was done under ambient conditions with standard PPP-NCHR silicon cantilever consisting of a < 10 nm tip radius (Nanosensors TM, Neuchâtel, Switzerland) with a spring constant of 42 N/m force constant and resonant frequency of 320 kHz. An x-y accessible  $1 \times 1$  up to  $5 \times 5$   $\mu\text{m}$  area with a Z scanner at 0.5 Hz scan rate was inspected with XEP software for data acquisition and XEI software for image processing and quantitative analysis of the surface topography. Relevant parameters such as line profile, an average roughness  $R_a$  (nm), standard deviation of the height value  $R_q$  (nm), skewness ( $R_{sk}$ ), kurtosis ( $R_{ku}$ ), power spectrum density (PSD) algorithm, and fractal dimension were then successively identified.

## RESULTS AND DISCUSSION

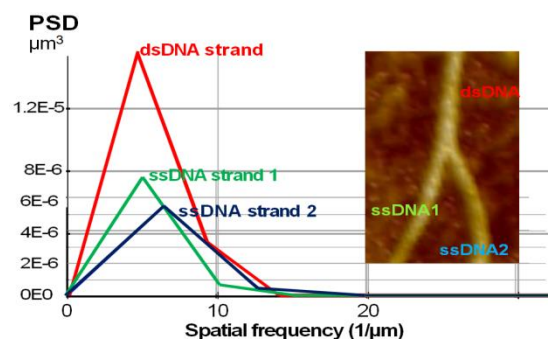
### AFM image and characterization of the dsDNA and ssDNA immobilized on chitosan modified SPCE

A striking atomic force microscopy image of the intact double-stranded DNA (dsDNA) and its correlative two Single-stranded DNA (ssDNA) during the DNA strand separation consequence is perfectly manifested in Fig.1. This picture, in the mean time, declares a fiduciary distinguishing feature between the dsDNA and ssDNA molecules. Observation in all cases of the phytoplasma DNA from SCWL, BGWL and SP similarly and consistently presented the duplex dsDNA and ssDNA profiles as well (data not shown). In general, differentiation in UV light absorption measurement is the only technique for notifying the separation of the DNA strands [14]. The attained AFM image could thus be considered as the first direct visual evidence revealing a DNA separating posture simultaneously after the common denaturation process by heating. An important prerequisite one for this successful imaging is on account of a steady immobilization strategy. In our investigation, a DNA containing TE buffer droplet was simply deposited

on the working surface of chitosan modified SPCE which adequately allowed stable and good quality AFM image without any complicate treatment. It is indeed due to an excellent affinity of the natural chitosan polymer consisting of polycation function compatible for biological molecules including proteins, enzymes and DNA [1]-[5], [7], [8]. This multiple cation site chitosan matrix has been proved highly effective for immobilization of the DNA molecule in our previous experiments [1], [2], [5]. Its electrochemical capability has also been subsequently approved [7]. Affirmation on the DNA incident on the platform surface was proceed by the line analysis of AFM image using power spectral density (PSD) function of the waveguide algorithm. The PSD outcome is as illustrated in Fig. 2 that the density peak size of each DNA strand type could be obviously differentiated, the biggest PSD wave from dsDNA and the smaller two PSD waves from the other two ssDNA.



**Fig. 1** Three-dimensional AFM image at  $1 \times 1$   $\mu\text{m}$  scan size revealing surface morphology of dsDNA and the two ssDNA strands splitting from the dsDNA.



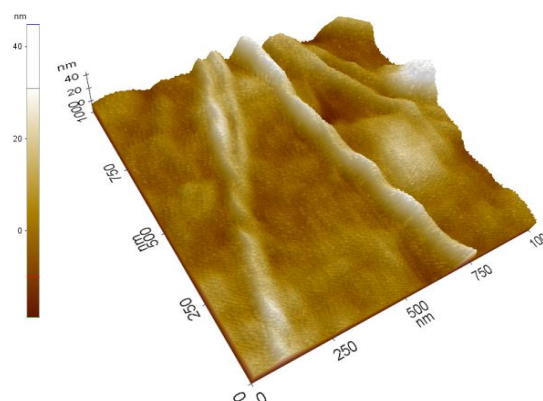
**Fig. 2** Power spectral density (PSD) function of the waveguide analyzed along a line in the AFM image of dsDNA and the two ssDNA strands splitting from the dsDNA at  $1 \times 1$   $\mu\text{m}$  scan size.

### AFM image revealing the conformation of complementary DNA strands upon hybridization

The hybridization scheme was performed on chitosan modified SPCE working surface. This presentation represents a generous process gained from SCWL, BGWL and SP phytoplasma genomic DNA. The ssDNA recognition probe was firmly immobilized and subsequently hybridized with its complementary ssDNA target to form complete dsDNA molecule that can be detected simultaneously by an appropriate read-out systems such as the electrochemical voltammetry and the AFM in our cases [1], [2], [5], [7], [9]. By means of the non contact mode AFM observation, the hybridization incidence was directly visualized showing the duplex helical DNA tile forming clearly (Fig. 3). This AFM image indicates a dynamic of DNA hybridization since the beginning of the well-known Watson-Crick double helix state. The two complementary nucleotide strands were being tie to each other like a two ply rope with a right hand appearance. Herein, to our knowledge this captured image should also be the first direct visible double helix structure forming during the DNA hybridization. Successful direct imaging of the DNA hybridization in this simple technique was obtained by no harm or any damage to the DNA specimen which probably due to an excellent bioaffinity and protective effect of chitosan scaffold. Acceleration in DNA hybridization rate by two orders through facilitation of a nucleation step; a major rate determining step of hybridization was previously demonstrated in cationic polymer such as poly(L-lysine)-graft-dextran copolymer employing fluorescence-based assay [15]. The multiple cationic nature of chitosan polymer was therefore assumed to be an important factor accelerating the DNA hybridization which was found almost complete within 45 min in our observation. Meanwhile the combination trials of phytoplasma ssDNA with ssDNA from their healthy sugarcane, burmuda grass and sesame plants yielded no sign of couple pairing or tying frame, hence referring to a mismatching nature of these non complementary strands.

### AFM surface parameters concerning the DNA morphological configuration

To determine the morphological configuration of the DNA, interpretation of the measured data was performed with reference to our previous reports [7], [8]. Important amplitude features were resolved by relevant statistical parameters as shown in Table 1.



**Fig. 3** The tying complementary ssDNA strands into two-ply strand of the renowned double helix DNA captured image by AFM at  $1 \times 1 \mu\text{m}$  scan size.

The DNA statures appeared in AFM images were estimated by their  $\Delta x$ ,  $\Delta y$  and  $^\circ A$  values from different cross sections lines to define a differentiation between the dsDNA and ssDNA including the tying hybrid ssDNA pair. These values were remarkably 1.4 to 1.75 fold higher in dsDNA and the hybridized DNA than that of the ssDNA. The PSD values gained from dsDNA and hybridized DNA were also higher by 2 to 3 folds. Therefore the form of double stranded DNA is apparently bigger than ssDNA by at least 1.4 orders. The fractal dimension parameter values obtained as 2.37 of the dsDNA and 2.47 of the hybridized DNA explicated their bigger size in comparison to 2.26 of the ssDNA. On the other hand, the fractal dimension values on the surface between 2 and 3 are the values suggesting a top up aggregation of deposit molecule following a 3D diffusion limited model [16]. In the course of roughness profiles  $Ra$  and  $Rq$ , values gained from the dsDNA and the hybrid DNA immobilized surfaces were about 1.34 - 1.73 folds rougher than the ssDNA. A negative  $Rsk$  acquired in the hill top cases represents a good bearing platykurtic surface of the DNA while a more negative value from the whole platforms indicates dominant valley surface underneath the DNA tile. The  $Rku$  values at the DNA hill top cases were all less than 3.00 which imply for a gradually varying feature of the surface. Whereas the values over than 3.00 were from  $Rku$  of the whole immobilized platform and thus explicate an evidence of a high DNA hill laid over the basal surfaces.

The results in this direct visual observation substantiate a success on steady immobilization and subsequent progressive hybridization of the long chain genomic DNA along with their measurable geographical characteristics. The non contact mode AFM has delivered considerably excellent resolution

showing both the distinction between two types of DNA strands and the dynamic of complementary hybridization event. Although a bit limitation on an exact assessment was existed owing to the confine performance of a 10 nm radius standard AFM tip available at present-day which probably make inevitable over estimate in the DNA width that has been formerly reported to be about 2 nm according to crystallographic X-ray diffraction analysis [17]. More sophisticate AFM techniques were suggested for better scaling of DNA configuration such as the miniaturization of AFM cantilevers [18]; the use of frequency modulation AFM [19] and the use of peak force tapping mode including a typical tapping mode [20]. These techniques were found suitably operated with DNA aqueous solution samples. However the procedure of direct non contact mode AFM imaging in air is generally preferred still due to its simplicity and non-invasiveness, improvement concerning the non contact mode hardware including appropriate cantilever and its software combination is thus necessary. Notwithstanding the confinement of a simplest AFM model used in our investigation, a virtual image of the DNA and its differentiation is clearly demonstrated and sufficiently verified a real hybridization event empowering the effective of DNA biosensor performance.

## CONCLUSIONS

The present work shows the first image capturing a striking posture of dsDNA separation and hybridization dynamic through a common non-contact mode AFM observation. A well known double helix forming state between two complementary ssDNA strands could be seen directly following hybridization process. All the trials with SCWL, BGWL and SP phytoplasma genomic DNA yielded similar performance from a very simple immobilization protocol employing the self assembled mechanism of the DNA containing 3  $\mu$ l droplet onto chitosan modified SPCE basal surface. This successful direct imaging of the DNA dynamics was simply obtained in air at room temperature without any deteriorate effects to the observing DNA. The apparent size of dsDNA and hybridized one seemed to be almost 2 folds wider than ssDNA. Their aggregation and growth mechanism on the basal platform surface were mainly directed vertically beyond a diffusion limited model according to the line analysis results. By virtue of this finding, the reality of DNA immobilization and hybridization occurring event empowering an efficacy of the DNA biosensor can easily be verified and encouraged further development of real practicable diagnostic devices.

**Table 1** Surface profile analyzed from AFM nanographs of the dsDNA, ssDNA and completely hybridized DNA at 1x1  $\mu$ m scan size on chitosan modified SPCE platform.

| Parameters               | Ds DNA               | ssDNA                | Hybridized DNA       |
|--------------------------|----------------------|----------------------|----------------------|
| $\Delta x$ (nm)          | 121.2<br>$\pm 11.96$ | 87.6<br>$\pm 11.93$  | 112.67<br>$\pm 6.43$ |
| $\Delta y$ (nm)          | 9.33<br>$\pm 2.08$   | 6.4<br>$\pm 2.41$    | 11.19<br>$\pm 2.45$  |
| $^{\circ}A$              | 27.7<br>$\pm 3.23$   | 16.56<br>$\pm 1.02$  | 28.74<br>$\pm 0.72$  |
| PSD (nm <sup>3</sup> ) 1 | 0.033<br>$\pm 0.01$  | 0.01<br>$\pm 0.001$  | 0.007<br>$\pm 0.001$ |
| 2                        | -                    | -                    | 0.015<br>$\pm 0.008$ |
| Fractal dimension        | 2.37<br>$\pm 0.12$   | 2.26<br>$\pm 0.05$   | 2.47<br>$\pm 0.06$   |
| $Ra$ (nm)                | 9.11<br>$\pm 1.3$    | 5.26<br>$\pm 0.14$   | 7.74<br>$\pm 0.04$   |
| $Rq$ (nm)                | 9.92<br>$\pm 1.26$   | 6.71<br>$\pm 0.17$   | 8.96<br>$\pm 0.86$   |
| $Rsk$ hill surface       | -0.39<br>$\pm 0.15$  | -0.75<br>$\pm 0.085$ | -0.77<br>$\pm 0.06$  |
| $Rsk$ whole surface      | -0.88<br>$\pm 0.15$  | -0.94<br>$\pm 0.62$  | -1.05<br>$\pm 0.09$  |
| $Rku$ hill surface       | 2.21<br>$\pm 0.05$   | 2.06<br>$\pm 0.042$  | 2.24<br>$\pm 0.13$   |
| $Rku$ whole surface      | 3.48<br>$\pm 0.05$   | 3.28<br>$\pm 0.3$    | 3.99<br>$\pm 0.04$   |

Note:  $^{\circ}A$  = angle degree of a hill slope,  $\Delta x$  = horizontal distance  $\Delta y$  = vertical distance, PSD = power spectral density,  $Ra$  = roughness average,  $Rq$  = root mean square roughness,  $Rsk$  = skewness,  $Rku$  = kurtosis.

## ACKNOWLEDGMENTS

The authors gratefully acknowledge KhonKaen University's Division of Research and Technology Transfer Affair for partial funding and the KKU Research Instrument Center for instrumental facilitation. We also thank Mr. SupatrChuaymee and Mr. VorrayuthMekarkat for their AFM technical assistances.

## REFERENCES

- [1] Wongkaew P., and Poosittisak S., Direct electrochemical DNA sensor for sugarcane white leaf disease diagnosis using label free DNA probes and oligochitosan self

- assembled monolayer-modified glassy carbon electrodes, in Proc. 2nd Int. Conf. on Technology and Innovation for Sustainable Development, 2008, pp. 504-507.
- [2] Wongkaew P., and Poosittisak S., Diagnosis of sugarcane white leaf disease using the highly sensitive DNA based voltammetric electrochemical determination. *Amer. J. of Plant Sciences*, Vol. 5, Issue 4, 2014, pp. 2256-2268.
- [3] Sunon P., Wongkaew P., Johns J., and Johns N., Characterization of cerium oxide-chitosan nanocomposite-modified screen printed carbon electrode and application in melatonin determination. *International Journal of GEOMATE*, Vol. 14, Issue 42, 2018, pp.151-157.
- [4] Wongkaew P., Wongkaew B., Saepaisan S., and Thanutong Pa., Development of specific electrochemical biosensor based on chitosan modified screen printed carbon electrode for the monitoring of captan fungicide. *International Journal of GEOMATE*, Vol. 14, Issue 43, 2018, pp. 55-62.
- [5] Wongkaew P., and Poosittisak S., Electro-affinity of SCWL-dsDNA on different high deacetylation degree chitosans deposited glassy carbon electrode, *Advances in Developing Affordable In-Vitro Molecular Diagnostics*, Puri C.P., Abidi N., Bhanushali, P., Pere A., Gupta S.K., Eds., Mumbai: Yashraj Research Foundation, 2012, pp. 249-258.
- [6] Sliwak A., Diez N., EwaMiniach E., and Gryglewicz G., Nitrogen-containing chitosan-based carbon as an electrode material for high-performance supercapacitors. *Journal of Applied Electrochemistry*, Vol. 46, Issue 6, 2016, pp. 667-677.
- [7] Wongkaew P., and Poosittisak S., Atomic force microscopic and electrochemical characterization of the modified screen printed carbon electrode by self assembled deposition of chitosan and activated carbon. *International Journal of GEOMATE*, Vol. 11, Issue 24, 2016, pp. 2356-2362.
- [8] Wongkaew B, Wongkaew P., Thanutong Pa., and Thanutong C., Nanostructural characterization of glutathione-s-transferase immobilizing chitosan modified screen printed carbon electrode by atomic force microscopy. *International Journal of GEOMATE*, Vol. 14, Issue 43, 2018, pp. 132-139.
- [9] Wongkaew P., Sugarcane white leaf disease characterization, diagnosis development, and control strategies. *Func. Plant Sci. Biotechnology*, Vol. 6 (Special Issue 2, Sugarcane Pathology), 2012, pp. 73-84.
- [10] Watson J.D. and Crick F.H., Molecular structure of nucleic acids: A structure for deoxyribose nucleic acid. *Nature*, Vol. 171, Issue 4356, 1953, pp. 737-738.
- [11] Wongkaew P., Plant diseases caused by phytoplasma. *Biosensing Technology for Sustainable Development Research Group's book publishing*, KhonKaen University, 2013, pp. 1-235.
- [12] Variola F., Atomic force microscopy in biomaterials surface science. *Phys. Chem. Chem. Physics*, Vol. 17, Issue 5, 2015, pp. 2950-2959.
- [13] Kollar A., Seemuller E., Bonnet F., Saillard C. and Bove J.M. Isolation of the DNA of Various Plant Pathogenic Mycoplasma-like Organisms from Infected Plants. *Phytopathology*, Vol. 80, No. 3, 1990, pp. 233-237.
- [14] Ackerman M.M., Ricciardi C., Weiss D., Chant A., and Kraemer-Chant C.M., Analyzing Exonuclease-Induced Hyperchromicity by UV Spectroscopy: An Undergraduate Biochemistry Laboratory Experiment. *Journal of Chemical Education*, Vol. 93, Issue 12, 2016, pp. 2089-2095.
- [15] Wu L, Shimada N, Kano A, Maruyama A, "Poly(L-lysine)-graft-dextran copolymer accelerates DNA hybridization by two orders", *Soft Matter*, Vol. 4, Issue 2, 2008, pp. 744-747.
- [16] Țălu S., Stach S., Ikram M., Pathak D., Wagner T., and Nunzi J-M., Surface roughness characterization of ZnO: TiO<sub>2</sub>-organic blended solar cells layers by atomic force microscopy and fractal analysis. *Int. J Nanoscience*, Vol. 13, No. 03, 2014, 12 pp.
- [17] Fuller W., Wilkins W. H. F., Wilson H. R., and Hamilton L. D., The molecular configuration of deoxyribonucleic acid: IV. X-ray diffraction study of the A form. *Journal of Molecular Biology*, Vol. 12, Issue 1, 1965, pp. 60-76.
- [18] Leung C., Bestembayeva A., Thorogate R., Stinson J., Pyne A., Marcovich C., Yang J., Drechsler U., Despont M., Jankowski T., Tschöpe M., Bart W., and Hoogenboom B.W., Atomic force microscopy with nanoscale cantilevers resolves different structural conformations of the DNA double helix, *Nano Letter*, Vol.12, Issue 7, 2012, pp. 3846-3850.
- [19] Ido S., Kimura K., Oyabu N., Kobayashi K., Tsukada M., Matsushige K., and Yamada H., Beyond the helix pitch: direct visualization of native DNA in aqueous solution. *ACS nano*. Vol. 7, No. 2, 2013, pp. 1817-1822.
- [20] Pyne A., Thompson R., Leung C., Roy D., and Hoogenboom B.W., Single-molecule reconstruction of oligonucleotide secondary structure by atomic force microscopy. *Small*, Vol. 10, Issue 16, 2014, pp. 3257-3261.

## IMPROVEMENT THE PROPERTIES OF POLY(L-LACTIDE) FILMS WITH CELLULOSE FIBER FROM RICE STRAW WASTE IN AGRICULTURAL PRODUCTS

Chutima Banthao<sup>1</sup>, Patcharin Kumpolsan<sup>1</sup>, Yodthong Baimark<sup>1</sup>, Sujitra Wongkasemjit<sup>2</sup>, and Kansiri Pakkethati<sup>1</sup>

<sup>1</sup> Department of chemistry, Faculty of Science, Mahasarakham University, Mahasarakham 44150, Thailand;

<sup>2</sup> The Petroleum and Petrochemical College and the National Center of Excellence for Petroleum, Petrochemicals and Advanced Materials, Chulalongkorn University, Bangkok 10330 Thailand

### ABSTRACT

The poly(L-lactide) films properties were improved by using cellulose from rice straw. The cellulose was extracted by hydrolysis method and that was confirmed the property by using Fourier transforms infrared spectroscopy (FT-IR). The sample films were prepared by mixing poly(L-lactide) with cellulose at different weight ratios (100/0, 98/2, 96/4, 94/6, 92/8, 90/10). Physical, mechanical and thermal properties of the films were analyzed by X-Ray diffraction (XRD), Scanning Electron Microscope (SEM), Thermogravimetric Analysis (TGA) and Tensile testing. It was found that after increasing the concentration of the cellulose to 2 %wt, the tensile strength increase from 24.949 to 37.108 MPa and Young's Modulus slightly increase from 0.111 to 0.119 GPa. The thermal stability of the sample films increased slightly. These results showed that cellulose from rice straw was enhanced to develop the thermal and mechanical properties of poly(L-lactide) film. The water uptake increased with the addition of cellulose.

**Keywords:** *Poly(L-lactide), Cellulose fiber, Rice straw*

### INTRODUCTION

Nowadays, polymers are used in the daily life of human which used mostly from petroleum. Because the polymers are lightweight, inexpensive and high strength but it is hard to be degradable. Therefore, the biodegradable polymer is one choice to substitute polymer from fossil fuel. The biodegradable polymers are classified according to their origin into two groups which are natural polymers for example chitosan[1], chitin[2], starch[3] and silk fibroin[4] and synthetic biodegradable polymers such as poly(glycolic acid)[5], poly(caprolactone)[6] and poly(l-lactide). In the decade the researchers are interested in poly(l-lactide) due to nearby properties with the petrochemical origin. The outstanding properties of poly(l-lactide) are renewable[7], biodegrading[8], transparent properties[8]. However, poly(l-lactide) is very brittle[9] and low toughness, which limits in applications that need plastic deformation under high stress[10]. Thus, the disadvantages of poly(l-lactide) were improved by composite with bamboo charcoal[11], cotton gin waste [12], oil palm [13] and cellulose fiber[14]. Thailand is one of rice country so there is a lot of leftover rice straw after the harvest of rice. Although the straw is useful for animal feeding or used as a material for cultivation of straw mushroom however the quantity of rice straw is still rested a lot. Therefore, farmers need to get rid of rice straw by burning, which resulted in the environmental impact. As rice straw is a marginal feed compared to other cereal grain straw

and a problematic fuel source due to high ash generation, exploring more viable options to utilize rice straw is pressing, particularly as an environmental concern. The composition of rice straw is cellulose (38.3%), hemicellulose (31.6%), lignin (11.8%) and silica (18.3%)[15]. In this work reducing the problems of the environment and adding value to the rice straw was studied. Improvement the mechanical properties and thermal properties of the poly(l-lactide) films with cellulose fiber from rice straw was studied in different ratios (0%, 2%, 4%, 6%, 8% and 10% of cellulose fiber).

### MATERIALS AND METHODS

#### Materials

The poly(l-lactide) (PLLA, molecular weight = 100,000), used in this study was supplied by Assoc. Prof. Dr. Yodthong Baimark. Sodium hydroxide (NaOH, AR grade, Ajax Finechem), hydrogen peroxide (H<sub>2</sub>O<sub>2</sub>, 30-32%, ANAPURE), sulfuric acid (H<sub>2</sub>SO<sub>4</sub>, 98%, ANAPURE) and Chloroform (CHCl<sub>3</sub>, AR grade, LLC) were used as received.

#### Preparation of cellulose from rice straw

Rice straw from agriculture was cut in the length of 1-2 cm, washed 3-4 times with tap water for removing dust and dried at 100 °C for 24 hours. NaOH (2M) was added to rice straw (1 g/NaOH 20 ml) and boiled under constant stirring at 80 °C for 1



hour. After that, it was washed with distilled water. Fibers were bleached with 18.5%  $\text{H}_2\text{O}_2$  (v / v) for 3 hours, then washed with distilled water. The cellulose fibers were hydrolyzed using 50%  $\text{H}_2\text{SO}_4$  (v/v) at 45°C for 1 hour under constant stirring as a previously reported method [7]. After hydrolysis, it was diluted with cold water to stop the hydrolysis reaction. Then the samples were washed with water until neutral pH to remove the excess sulfuric acid. The suspension was sonicated [7] at 45 °C for 30 minutes and evaporated in an oven at 100 °C for 12 hours. Then, it was ground into a powder, the powdered cellulose fibers were selected in the size 150-250  $\mu\text{m}$  before stored in a desiccator.

#### Fabrication of poly(l-lactide)/cellulose composite film

Adding the chloroform 15 ml into poly(l-lactide) and stirred until 1 hour. Then it was mixed with cellulose for 30 minutes. It was poured into the petri dish and dried in an oven at 50°C for 1 hour. After that, it was also deeply dried in a vacuum oven at 50°C for 24 hours and then it was stored in a desiccator. The ratio of poly(l-lactide)/cellulose was 100/0, 98/2, 96/4, 94/6, 92/8 and 90/10 (w/w).

#### Characterization of poly(l-lactide)/cellulose composite film

FT-IR spectra were obtained using Fourier Transform Infrared Spectroscopy; FTIR (Perkin Elmer model Spectrum GX). The measurements were scanned in the range 400 - 4000  $\text{cm}^{-1}$ . X-ray diffraction; XRD was widely used for the identification of unknown crystalline materials and measured by the machine models D8 ADVANCE (Bruker). The crystallinity of cellulose was extracted from rice straw, films sample were scanned by scattering 2 angles from 5-40 degree with a rate of 0.2 sec/degrees. Scanning Electron Microscope; SEM (JEOL, JSM-64606V) was used to study surface and morphology (shape, pattern, size) of the samples. The cellulose powder samples were prepared into the carbon tape on the stub and coated with gold. The film samples were prepared by immersion in liquid nitrogen before it was broken to study the cross-section morphology. The film pieces were also mounted on the stub to study morphology. Thermogravimetric Analysis; TGA samples were heated from 40 to 800 °C at a rate of 10 °C/min under nitrogen atmosphere. Tensile testing of the film samples was studied on a universal testing machine (LLOD INSTRUMENTS, AS500) at room temperature. The film samples were cut 1 × 8 cm. (repeat 5-10 times). The water uptake capacity [16] of each film was studied by cut the film to size 1 x 1 cm and was immersed into distilled water at room temperature for 90 minutes. Then it was taken off

from water and weighed. The water uptake was determined using this equation

$$\% \text{ Water uptake} = \frac{M_2 - M_1}{M_1} \times 100$$

where  $M_1$  is the weight of the dry film before immersion and  $M_2$  is the weight of the film after immersion.

## RESULTS AND DISCUSSION

The extracted cellulose was filtered with the sieves and the size of cellulose was 150-250  $\mu\text{m}$ . The result was showed in Fig 1. The result of FT-IR was presented in Fig 2, the 3500-3000  $\text{cm}^{-1}$  range characterized by a broad spectrum and high intensity of OH stretching and 1650  $\text{cm}^{-1}$  was OH bending showed at a lower range than adsorbed water. At 1450-1420  $\text{cm}^{-1}$  was C-H stretching and the range of 1382-1375  $\text{cm}^{-1}$  was CH bending. At 902-893  $\text{cm}^{-1}$  was associated with cellulosic  $\beta$ -glycosidic linkages, at 1155  $\text{cm}^{-1}$  was C-C ring stretching, and C-O-C at 953  $\text{cm}^{-1}$  was glycosidic ether. The results were similar to Ping Lu's *et al* [17] results.



Fig. 1 Rice straw cellulose powder

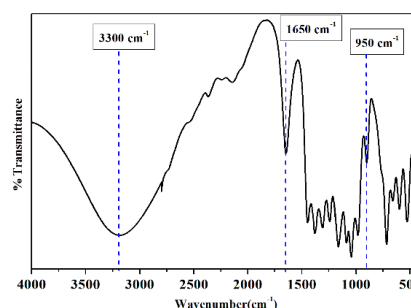


Fig. 2 FT-IR spectrum of rice straw cellulose

The XRD results (Fig. 3) showed that the crystalline peaks of cellulose were at 15.3°, 22.5°, and 34.5°. It could be asserted that the extraction of cellulose could be accomplished by hydrolysis. Lignin and hemicellulose were amorphous structure. The crystalline peaks are found in the same area as the research by Anuj Kumar *et al* [18]. It was also found that when the improved chemical was increased the crystallization was also increased due to



the amorphous removal. Fig 4 shows that the appearance of cellulose powder was small and uncertain shape may be due to the hydrolysis process.

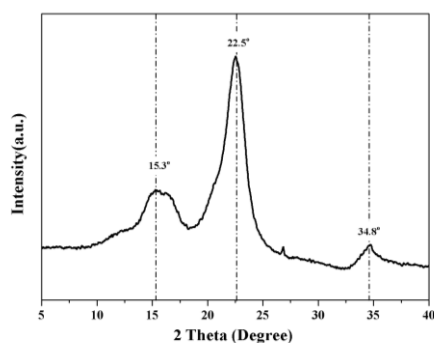


Fig. 3 XRD spectrum of rice straw cellulose

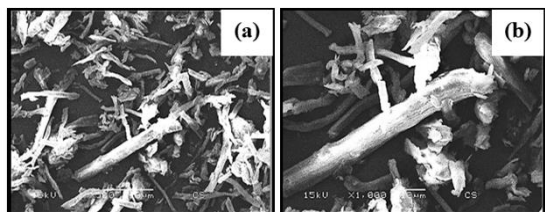


Fig. 4 Morphology of rice straw cellulose powder from SEM 500X (a) and 1000X (b)

#### Characterization of poly(l-lactide) films mixed with rice straw cellulose fiber

The physical appearance of the poly(l-lactide) films (Fig. 5) was smooth and clear. The best cellulose distribution compared to other ratios was PLLA98/CS2. When adding more cellulose, the film became darker and the cellulose was clumped due to the polarity of the cellulose. The results obtained by FT-IR analysis (Fig. 6) show that (a) was a 100% cellulose spectrum. The dominant function of the 3500-3000  $\text{cm}^{-1}$  spectrum was broad spectrum and high intensity of OH stretching. The range of 1450-1420  $\text{cm}^{-1}$  was C-H stretching and at 950  $\text{cm}^{-1}$  was C-O-C glycosidic ether and (g) was the spectrum of poly(l-lactide) film. The 1750  $\text{cm}^{-1}$  function group was a function of C=O and the range of 1450-1420  $\text{cm}^{-1}$  was C-H stretching. The (b-f) spectrum was poly(l-lactide) film mixed with cellulose. The range of 3500 - 3000  $\text{cm}^{-1}$  was OH stretching. It has broad-spectrum and high intensity compared to poly(L-lactide) film (spectra g). As a result, there was a large number of hydroxyl groups (OH) in cellulose. The 1750  $\text{cm}^{-1}$  was a function of carbonyl (C=O), which was prominent in poly(l-lactide). C-H stretching was a common group of poly(lactic acid) and cellulose (950  $\text{cm}^{-1}$ ). C-O-C was a glycosidic ether that was prominent in cellulose. The range of 1450-1420  $\text{cm}^{-1}$

was C-H stretching, which was found in poly(l-lactide) and cellulose. As 950  $\text{cm}^{-1}$  was a C-O-C glycosidic ether that is prominent in cellulose. The results of FT-IR can be confirmed that the sample film (b-f) were contained cellulose. [17]

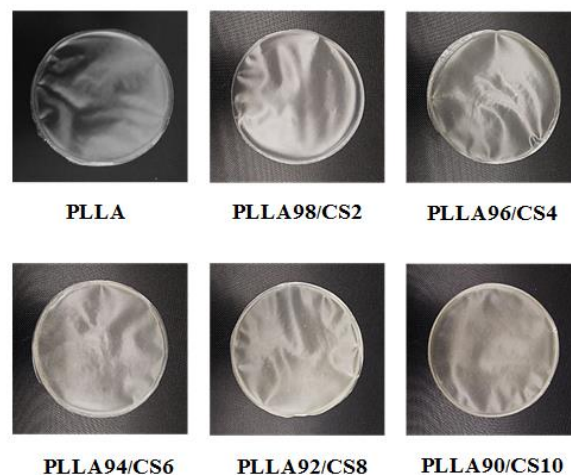


Fig. 5 Physical characteristics of films

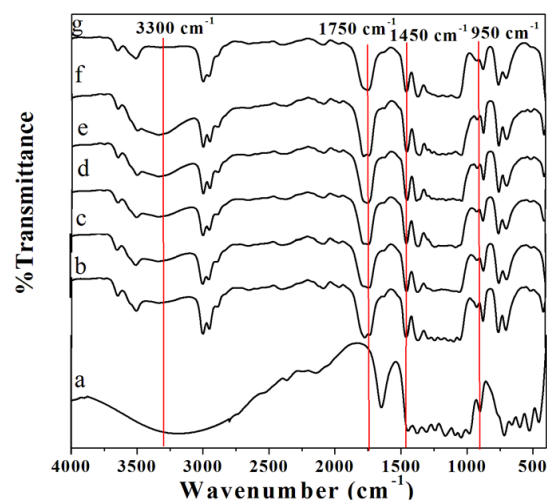


Fig. 6 FT-IR spectra of the film in various ratios (a) CS100, (b) PLLA98 / CS2, (c) PLLA96 / CS4, (d) PLLA94 / CS6, (e) PLLA92 / CS8 (f) PLLA90 / CS10 and (g) PLLA 100.

The crystallinity of polylactide film at 16.7° and 22.6° was shown in Fig. 7. According to Ping Lu *et al.* [18], 2θ values of cellulose were found at 15.3° 22.5° and 34.5°. When the cellulose was mixed into the poly(l-lactide), it was observed that the crystallinity of the film was increased and the highest increase was the PLLA98 / CS2 ratio film. Surface characteristics of films were shown in Fig.8. It was found that the surface appearance of poly (l-lactide) film was smooth and less rough which was different to the films that mixed with cellulose, which were more

roughly textured, the ratio of cellulose increases. However, PLLA98/CS2 was a good dispersion of the cellulose, making the least rugged surface film when compared to the others. The poorly distributed cellulose, resulting in a rough surface. The cross-section of ratio each film were investigated. It was found that the poly(l-lactide) contains rough surface texture somewhat less than film mixed with cellulose. The results were in the same direction as the surface characteristics of the film, as shown in Fig. 9. The cellulose was inserted into the films. It was known that poly(l-lactide) and cellulose were not homogeneous because non-polar properties of poly(l-lactide) and that the cellulose was polar properties. So it was less homogeneous. But it can be seen that the cellulose can be inserted into the poly(l-lactide) as a result of adhesion. It could be said that cellulose has a rough surface when poly(l-lactide) melts into a liquid and could be inserted into the gap in the roughness of the cellulose when the poly(l-lactide) solidifies it causes adhesion. It also described the adhesion of the chemical bonding. Many hydroxyl groups of cellulose could build up hydrogen bond between molecules of cellulose and poly(l-lactide) [19], [20]

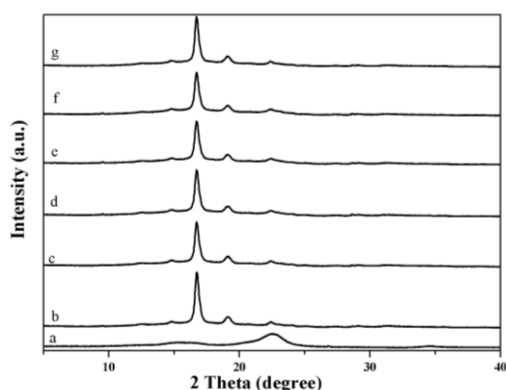


Fig. 7 XRD spectra of the film in various ratios (a) CS100, (b) PLLA98 / CS2, (c) PLLA96 / CS4, (d) PLLA94 / CS6, (e) PLLA92 / CS8 (f) PLLA90 / CS10 and (g) PLLA 100.

Thermogram analysis was shown in Fig.10. The decomposition of poly(l-lactide) at 320 °C and cellulose decomposition showed at 360 °C, so it was showed only one component. Decomposition of hemicellulose (250 °C) and lignin (365 °C) were not found. The results were similar to the article of Su-Hwa Jung[21]. When the cellulose was mixed into the poly(l-lactide), the degradation was 1 stage at 300-400 °C. The decomposition of each ratio varies. It was noted that when the cellulose content increases, the temperature of the decomposition of the film increases slightly as shown in Table 1

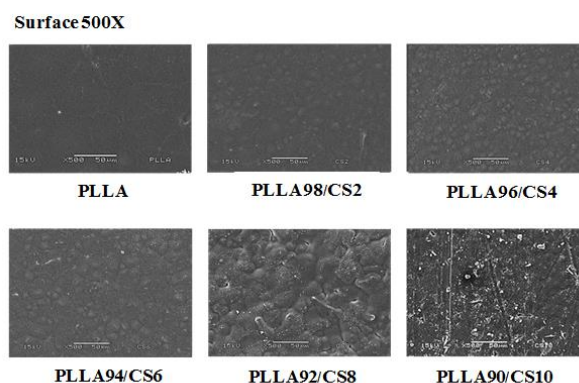


Fig. 8 The surface of PLLA, PLLA98 / CS2, PLLA96 / CS4, PLLA94 / CS6, PLLA92 / CS8 and PLLA90 / CS10 500X

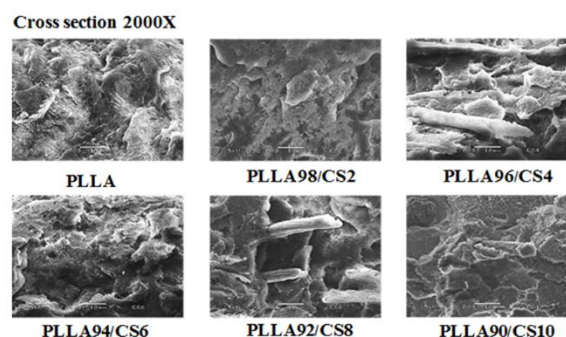


Fig.9 The cross section of PLLA, PLLA98 / CS2, PLLA96 / CS4, PLLA94 / CS6, PLLA92 / CS8 and PLLA90 / CS10 2000X

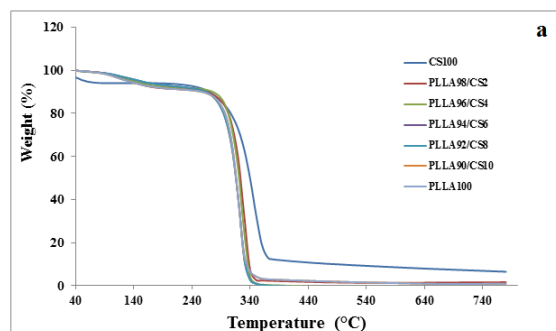


Fig. 10 TG thermograms (a) and DTG thermograms (b) of PLLA100, PLLA98 / CS2, PLLA96 / CS4, PLLA94 / CS6, PLLA92 / CS8, PLLA90 / CS10 and CS100.

Tensile testing of poly(l-lactide) film and cellulose mixed films in various ratios were found that cellulose affects the mechanical properties of poly(l-lactide) films. When mixing the cellulose in the poly(l-lactide) films, the tensile strength, elongation at break and Young's modulus of films were increased. These values indicated the strength of the film (The results are shown in Table 2). However,

the highest test values were from PLLA98/CS2 film. This may be due to the amount and dispersion of cellulose in the film, which affected the strength. The results of this study were consistent with the findings of Sanyang ML *et al.* [16] and also consistent with SEM results. The good dispersion of cellulose resulted in a stronger film. Due to the uniform dispersion, the mixed film was very strong adhesion. Thus the mixed films were better tensile properties than the poly(l-lactide) film without cellulose blends. However, when the amount of cellulose mixture was increased at more than 2% the films were reduced strength. Because the more cellulose, the formation of cellulose was poor dispersion and less adhesion between poly(l-lactide) and cellulose.

Table 1 Temperature decomposition of cellulose and films

| Sample      | T <sub>d</sub> (max) (°C) |
|-------------|---------------------------|
| CS100       | 360                       |
| PLLA        | 320                       |
| PLLA98/CS2  | 340                       |
| PLLA96/CS4  | 340                       |
| PLLA94/CS6  | 330                       |
| PLLA92/CS8  | 330                       |
| PLLA90/CS10 | 330                       |

Table 2 Tensile testing of the films

| Sample      | Tensile strength (MPa) | Elongation at break (MPa) | Young's Modulus (MPa) |
|-------------|------------------------|---------------------------|-----------------------|
| PLLA100     | 24.95<br>±3.95         | 6.47<br>±1.36             | 1112.99<br>±38.31     |
| PLLA98/CS2  | 37.92<br>±1.03         | 13.55<br>±3.45            | 1198.47<br>±45.28     |
| PLLA96/CS4  | 35.46<br>±1.12         | 10.70<br>±2.04            | 1184.18<br>±77.58     |
| PLLA94/CS6  | 34.31<br>±1.51         | 10.31<br>±1.22            | 1141.26<br>±61.27     |
| PLLA92/CS8  | 30.60<br>±1.09         | 10.31<br>±0.96            | 1023.97<br>±88.79     |
| PLLA90/CS10 | 29.98<br>±1.39         | 7.12<br>±2.06             | 1154.50<br>±94.63     |

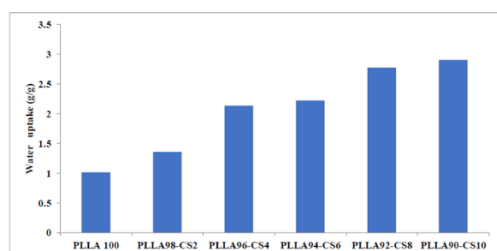


Fig. 11 The water absorption ratio of films

The water absorption results were present in Fig. 11. The poly(l-lactide) film was the lowest water absorption while the water absorption of mixed films was increased because of the hydroxyl groups of cellulose. The water absorption increased with an increasing amount of cellulose. When comparing PLLA with PLLA98/CS2, the values were slightly different[16].

## CONCLUSIONS

The rice straw cellulose was mixed in poly(l-lactide) by the solvent method. The ratio of poly(l-lactide)/cellulose was 100/0, 98/2, 96/4, 94/6, 92/8 and 90/10. Physical characteristics of the film were darker color when cellulose content was increased. The surface fracture of the films was more uneven surface as the ratio of cellulose increased. The thermal stability of the films was slightly increased with the addition of cellulose blends. The cellulose content increased also increasing the tensile strength, Elongation at break, and Young's Modulus. However, when the amount of cellulose is increased, the formation of cellulose results in poor distribution and less adhesion between the poly(l-lactide) and the cellulose. It could be concluded that the cellulose extracted from rice straw was used as a reinforcement to increase the thermal and mechanical properties of poly(l-lactide). The film with 2% cellulose blend was the best thermal and mechanical properties due to the addition of ingredients in the right proportion and well dispersed in the poly(l-lactide) of cellulose.

## ACKNOWLEDGEMENTS

This research was supported by the Department of Chemistry Faculty of Science Mahasarakham University and was financially supported by Thailand Reserch Fund (Senior Research Scholar).

## REFERENCES

- [1] J. Bonilla, E. Fortunati, M. Vargas, A. Chiralt, and J. M. Kenny, "Effects of chitosan on the physicochemical and antimicrobial properties of PLA films," *J. Food Eng.*, vol. 119, no. 2, pp. 236–243, 2013.
- [2] R. Nasrin *et al.*, "Bioactive Materials Preparation of Chitin-PLA laminated composite for implantable application," *Bioact. Mater.*, vol. 2, no. 4, pp. 199–207, 2017.
- [3] M. A. Shirai, M. V. E. Grossmann, F. Yamashita, P. S. Garcia, and C. M. O. Müller,

- “Development of biodegradable flexible films of starch and poly ( lactic acid ) plasticized with adipate or citrate esters,” *Carbohydr. Polym.*, vol. 92, no. 1, pp. 19–22, 2013.
- [4] S. L. Jackman *et al.*, “Silk Fibroin Films Facilitate Single-Step Targeted Expression of Optogenetic Proteins Resource Silk Fibroin Films Facilitate Single-Step Targeted Expression of Optogenetic Proteins,” *CellReports*, vol. 22, no. 12, pp. 3351–3361, 2018.
- [5] K. Lee, K. U. K. R. O. Yoon, S. I. H. L. Woo, and I. S. Choi, “Surface Modification of Poly ( glycolic acid ) ( PGA ) for Biomedical Applications,” vol. 92, no. 5, pp. 933–937, 2003.
- [6] T. Patrício, M. Domingos, A. Gloria, and P. Bártolo, “Characterisation of PCL and PCL / PLA scaffolds for tissue engineering,” *Procedia - Soc. Behav. Sci.*, vol. 5, pp. 110–114, 2013.
- [7] M. Kaseem, “Properties and medical applications of polylactic acid : A review,” no. May, 2015.
- [8] M. Murariu and P. Dubois, “PLA composites : From production to properties,” *Adv. Drug Deliv. Rev.*, vol. 107, pp. 17–46, 2016.
- [9] L. T. Lim, R. Auras, and M. Rubino, “Processing technologies for poly(lactic acid),” *Prog. Polym. Sci.*, vol. 33, no. 8, pp. 820–852, 2008.
- [10] R. M. Rasal, A. V. Janorkar, and D. E. Hirt, “Progress in Polymer Science Poly ( lactic acid ) modifications,” *Prog. Polym. Sci.*, vol. 35, no. 3, pp. 338–356, 2010.
- [11] M. Ho, K. Lau, H. Wang, and D. Hui, “Improvement on the properties of polylactic acid ( PLA ) using bamboo charcoal particles,” *Compos. Part B*, vol. 81, pp. 14–25, 2015.
- [12] R. M. Bajracharya, D. S. Bajwa, and S. G. Bajwa, “ScienceDirect ScienceDirect Mechanical properties of polylactic acid composites reinforced with cotton gin waste and flax fibers,” *Procedia Eng.*, vol. 200, pp. 370–376, 2017.
- [13] M. K. M. Haafiz, A. Hassan, Z. Zakaria, I. M. Inuwa, M. S. Islam, and M. Jawaid, “Properties of polylactic acid composites reinforced with oil palm biomass microcrystalline cellulose,” *Carbohydr. Polym.*, vol. 98, no. 1, pp. 139–145, 2013.
- [14] H. Kyutoku, N. Maeda, H. Sakamoto, H. Nishimura, and K. Yamada, “E ff ect of surface treatment of cellulose fi ber ( CF ) on durability of PLA / CF,” *Carbohydr. Polym.*, vol. 203, no. June 2018, pp. 95–102, 2019.
- [15] A. Ecology, M. Tayyab, F. Agriculture, S. Waheed, and F. Agriculture, “Bioethanol production from lignocellulosic biomass by environment-friendly pretreatment methods : A review BIOETHANOL PRODUCTION FROM LIGNOCELLULOSIC BIOMASS BY ENVIRONMENT-FRIENDLY PRETREATMENT METHODS : A REVIEW,” no. December, 2017.
- [16] M. L. Sanyang, S. M. Sapuan, M. Jawaid, M. R. Ishak, and J. Sahari, “Development and characterization of sugar palm starch and poly (lactic acid) bilayer films,” *Carbohydr. Polym.*, 2016.
- [17] P. Lu and Y. Lo Hsieh, “Preparation and characterization of cellulose nanocrystals from rice straw,” *Carbohydr. Polym.*, vol. 87, no. 1, pp. 564–573, 2012.
- [18] A. Kumar, Y. S. Negi, V. Choudhary, and N. K. Bhardwaj, “Characterization of Cellulose Nanocrystals Produced by Acid-Hydrolysis from Sugarcane Bagasse as Agro-Waste,” no. February 2016, pp. 0–8, 2014.
- [19] C. Miao and W. Y. Hamad, “Alkenylation of cellulose nanocrystals (CNC) and their applications,” *Polymer (Guildf.)*, 2016.
- [20] E. Luiz, D. Paula, V. Mano, E. Aparecida, R. Duck, and F. Vargas, “HYDROLYTIC DEGRADATION BEHAVIOR OF PLLA NANOCOMPOSITES REINFORCED WITH MODIFIED CELLULOSE NANOCRYSTALS,” vol. 38, no. 8, pp. 1014–1020, 2015.
- [21] S. Hyun, Y. Chang, and J. Han, “Development of polylactic acid nanocomposite films reinforced with cellulose nanocrystals derived from coffee silverskin,” *Carbohydr. Polym.*, vol. 169, pp. 495–503, 2017.

## **SUSTAINABLE AQUACULTURE MANAGEMENT OF VANAMEI SHRIMP (*Litopenaeus vannamei*) IN BATUKARAS VILLAGE, PANGANDARAN, INDONESIA**

Andrian Achmad<sup>1</sup>, Dewi Susiloningtyas<sup>2</sup> and Tuty Handayani<sup>3</sup>

<sup>1</sup>Marine Sciences FMIPA Universitas Indonesia, <sup>2</sup> Universitas Indonesia; <sup>3</sup> Universitas Indonesia, Indonesia

### **ABSTRACT**

Vaname shrimp is a superior commodity in aquaculture which continues to increase in demand. The farming of vaname shrimp in Batukaras Village, Cijulang Subdistrict, Pangandaran Regency is carried out with semi-intensive technology, the application of this technology is not sustainable due to lack of supporting facilities. This study aims to analyze the physical aspects and the quality of production and the sustainability status also determine the priority strategy for sustainable management of vaname shrimp. Analysis of sustainability status is carried out by surveys and interviews with farmers then processed using the RAPFISH method (The Rapid Appraisal of The Status Fisheries), for physical aspects measurement of water quality is carried out in situ and testing in the laboratory with measured parameters, namely temperature, salinity, DO, pH, nitrite and ammonia. While the preparation of priority programs is processed using the AHP (Analytical Hierarchy Process) method using Expert Choice software. The results of the research are water quality parameter values for temperature, salinity, pH, DO and nitrite and the quality of shrimp according to standard values, but ammonia parameters are far from normal limits. The multidimensional sustainability level of vaname shrimp management in Batukaras Village has a sustainability index of 60.00 which means it is quite sustainable. The choice of the main priority program for the sustainability of vaname shrimp cultivation is the rehabilitation program for fishpond infrastructure with a value ratio of 0.29.

Keywords: AHP, aquaculture, Pangandaran, Rapfish, vaname shrimp.

### **INTRODUCTION**

Aquaculture has a considerable diversity of potential superior commodities. According to data from the Ministry of Marine Affairs and Fisheries in 2016, the potential for marine aquaculture is 8.3 million ha which consists of 20% for fish farming, 10% for shellfish farming, 60% for seaweed farming, and 10% for others, the potential of brackish water aquaculture or ponds is 1.3 million ha, and the potential of 2.2 million ha of freshwater aquaculture consisting of fish pond with an area of 526.40 thousand ha, public waters (lakes, reservoirs, rivers and swamps) covering 158.2 thousand ha, and rice fields for minapadi covering 1.55 million ha. In 2012, Indonesia ranks 2nd for capture fisheries production and ranks 4th for aquaculture production in the world.

Pangandaran Regency is one of the districts in West Java Province. Pangandaran Regency has only been a District Government since 2012. This district has an area of 1,680 Km<sup>2</sup> consisting of 10 sub-districts with 12 urban villages with 81 villages with a population of 422,586. The district is strategically located, because it is on a provincial road lane, located on the seashore with a beach length of 91 km. Based on its position, Pangandaran is bordered by Ciamis Regency and Banjar City in the north, Cilacap Regency in the east, Indian Ocean in the south, and Tasikmalaya Regency in the west.

According [8], Freshwater aquaculture has a production target of 120 tons consisting of 40 tons of

gourami commodities, 30 tons of tilapia, 15 tons of catfish, 15 tons of carp, 10 tons of tawes, 5 tons of prawns and 5 tons of other fish. From the achievements of production in 2016, Freshwater farming achieved a production realization of 110.79 tons or equal to 92.32% of the production target. Whereas for brackish water farming, the production target is set at 101.5 tons consisting of 70 tons of vaname shrimp, 10 tons of black shrimp, 10 tons of milkfish, 5 tons of crab, grouper of 1 ton, white snapper and other types of fish of 0.5 tons and 5 tons. The achievement of brackish water farming has succeeded in getting production in 2016 of 122.31 tons or equal to 120.5% of the achievement of the production target. For the main commodity of brackish water farming is vaname shrimp from the target set at 70 tons which exceeded the target by successfully obtaining a production of 110.43 tons.

The purpose of this study is to determine the suitability of general water parameters and the quality of production, know the sustainability status of aquaculture in terms of ecological, social, economic, technological and institutional dimensions and determine the priority strategy program for the management of white shrimp farming in Batukaras Village, Cijulang District, Pangandaran Regency. The results of this study will provide an illustration, whether the pond area in Batukaras Village can be continued for shrimp farming production or not. If not, inputs are needed to improve the condition of the pond area to be an ideal pond area for vaname shrimp

farming.

## REVIEW OF REFERENCES

### Biological Vaname Shrimp

The classification of vaname shrimp according to [10] is included in the Kingdom: Animalia, Sub-Kingdom: Metazoa, Genus: Litopenaeus, and Species: Litopenaeus Vannamei.

Generally the body of shrimp can be divided into two parts, namely the head and body parts. The head is fused with the chest part called the cephalothorax which consists of 13 segments, namely 5 segments in the head and 8 segments in the chest section. Body parts and abdomen consist of 6 segments each segment (segment) has a pair of limbs (swimming legs) that are segmented [13].

The vaname shrimp habitat is in the tropical sea with a water temperature of more than 20 °C. They lay eggs in the open sea and at the post larval stage will migrate to the coast to the juvenile stage.

### Potential and Management

The potential for shrimp farming has a very large business opportunity. The utilization of shrimp farming in 2012 was 22.2%. There are 87.8% or 2.3 million hectares of land that are very potential to be used as farms for ponds, especially shrimp. Utilization of shrimp farming in ponds is 22.2% with the consideration that the majority use traditional and semi-intensive cultivation technology. However, if applying advanced technology (intensive and supra-intensive) the opportunity to develop ponds can be even greater, considering that even marginal and sandy land can be utilized.

### General Aquatic Parameters

#### 1. Temperature

Some observers have found that shrimp cannot live at temperatures less than 15°C or more than 40°C. The optimal temperature for shrimp is 28-30 °C. In addition to the lethal direct effect, the temperature also indirectly affects metabolism, the solubility of gases, including oxygen and various water chemical reactions [15].

#### 2. Salinity

Salinity is the total ion concentration found in the waters [3]. Salinity describes the total solids in water, after all carbonates are converted to oxide, all bromides and ionides are replaced by chloride and all organic material has been oxidized. Salinity units are expressed in units of permits (‰).

#### 3. pH

pH shows the activity of hydrogen ions in the solution and is expressed as the concentration of hydrogen ions (in moles per liter) at a certain

temperature [15]. The normal range of water pH for shrimp ranges from 7.5 to 8.5. The direct effect of low pH is that it causes the shrimp skin to become porous and always soft because it cannot form new skin [6].

#### 4. DO

The amount of oxygen needed for respiratory aquaculture depends on the size, temperature and level of activity with a minimum limit of 3 ppm. The oxygen content in water is considered optimum for aquatic biota cultivation is 4-10 ppm, depending on the type. The respiration rate is seen to remain at the oxygen solubility limit between 3-4 ppm at a temperature of 20-30 °C [11].

#### 5. Ammonia

Ammonia is a chemical compound in the form of a gas with a distinctive sharp odor. Ammonia sources in aquaculture containers originate from the waste of fish metabolism and leftovers that are not eaten. [14] states that NH<sub>3</sub> in cultivation media must be lower than 0,8 mg/L.

#### 6. Nitrite

Nitrite is the result of metabolism from the nitrogen cycle. The mid form of nitrification and denitrification. Nitrite is a nitrogen-containing component that binds to two oxygen atoms. In natural waters the nitrite content is in small amounts, because it is not stable in the presence of oxygen. High nitrite content can result in disruption of the oxygen binding process by blood hemoglobin, which in turn forms methemoglobin which is unable to bind oxygen [9].

### Sustainable Development

The concept of sustainable development was first published by The World Conservation Strategy in 1980 in Gland, Switzerland and became the center of thought for development and the environment.

According to [7], the sustainability of fisheries development contains four basic components that must be met. The basic components include:

1. Ecological sustainability is a concern to ensure that crops continue to be sustainable, and that there is no reduction in fish stock depletion.
2. Socio-economic sustainability is maintaining and increasing overall long-term socio-economic well-being.
3. Community sustainability is focused on the desire to defend the community as a human system that has its own rights over its natural resources.
4. Institutional sustainability includes maintaining the suitability of financial, administrative, and organizational capabilities throughout all time, as a prerequisite for the three components of sustainability above.

## RESEARCH METHODS

### Research Data



Measurements of physical aspects were carried out on water quality parameters including temperature, pH, DO, salinity, nitrite and ammonia content and production for shrimp weight and length. This physical data retrieval was carried out in 10 farm plot points which were currently producing vaname shrimp with the taking time on the 0<sup>th</sup>, 30<sup>th</sup> and 60<sup>th</sup> days. Measurement of water quality parameter data is carried out in situ except the measurement of nitrite and ammonia content. Measurements of ammonia and nitrite content were carried out by taking 200 ml of water samples using plastic sample bottles to be analyzed at the Laboratory of UPTD of Brackish and South Sea Water Fisheries, Pangandaran.

The sustainability status of vaname shrimp was analyzed by Rapfish software with data sources derived from respondents who were farmers (pond owners) in the Batukaras Village pond area. The implementation of the interview is assisted by a questionnaire list as a tool for collecting data. The total number of farmers (pond owners) of vaname shrimp in Batukaras Village is 18 people. Calculation of the number of respondents with Slovin method obtained a minimum number of respondents as much as 15.25 rounded up to 15 respondents. Cultivators who are active in aquaculture chosen as respondents.

### Data Processing Method

The results of the analysis of recapitulated water quality parameters in the data tabulation are then compared with the maximum / minimum standard values of each water quality parameter. The vaname shrimp during production was taken as many as 5-10 tails from each sample plot point to measure the average weight or ABW (Average Body Weight) then it will be compared with the standard value.

Rapfish is the latest technique developed by the University of British Columbia Canada, which is an analysis to evaluate the sustainability of multidisciplinary fisheries. Rapfish is based on ordination techniques (placing something on a measured sequence of attributes) using MDS (Multi-Dimensional Scaling). MDS itself is basically a statistical technique that tries to make multidimensional transformations into lower dimensions. The dimensions in Rapfish concern aspects of sustainability from ecology, social, economic, technological and institutional. Rapfish analysis in this study was carried out through several stages, namely:

1. Scoring by referring to the literature (ecology, social, economic, technological, and institutional) of Rapfish by using MS Excel.
2. Perform MDS analysis to determine the ordination and stress values through ALSCAL Algorithm.
3. Perform "rotation" to determine the position of the fishery in ordination of bad and good with MS Excel.

Goodness of Fit in MDS is reflected in the amount of S-Stress value calculated from the value of S. Low stress values indicate good fit, while high S values indicate bad fit. In Rapfish, a good model is shown if the stress value is smaller than 0,25 ( $S < 0,25$ ).

4. Perform sensitivity analysis (leverage analysis) and Monte Carlo analysis to take into account aspects of uncertainty.

The sustainability analysis used in this study refers to [16] who divides sustainability into 4 categories, namely: unsustainable (0-25%), less sustainable (25-50%), fairly sustainable (50-75%), and sustainable (75-100%).

Analytical Hierarchy Process (AHP) is a method for solving a complex situation that is not structured into several components in a hierarchical arrangement, by giving subjective values about the importance of each variable relative, and determining which variable has the highest priority to influence the outcome of the situation.

## RESEARCH RESULTS AND DISCUSSION

### Physical Condition of Ponds

Table 1. Results of Water Quality Parameters [12]

| No | Parameter    | Average Value | Standard Value | Results*)    |
|----|--------------|---------------|----------------|--------------|
| 1  | Temperature  | 29,52 °C      | 28-31,5 °C     | Matching     |
| 2  | Salinity     | 17,53 g/l     | 10-35 g/l      | Matching     |
| 3  | pH           | 8,11          | 7,5-8,5        | Matching     |
| 4  | DO           | 6,7 mg/l      | 4-6 mg/l       | Matching     |
| 5  | Nitrite      | 0,6 ppm       | ≤ 1 ppm        | Matching     |
| 6  | Ammonia      | 0,26 mg/l     | ≤ 0,1 mg/l     | Not matching |
| 7  | Soil texture | Sandy soil    | -              | Matching     |

(Source: Data Processing, 2019)

In this study, the data was taken from a sample of 10 plots of shrimp ponds located in the Shrimp Village of Batukaras Village. The total sample area of the shrimp ponds studied was 14,500 m<sup>2</sup>. From these samples, it is expected to represent the results of the research carried out for the whole shrimp farm. The results of the observation of shrimp farms are shown in Table 1.

### Shrimp Quality

Based on Table 2, the results of the measurement of shrimp quality, the majority of shrimp seed stocked were 9-day post larvae (PL.9), except for plot number 4 ponds using PL.8. The average shrimp weight at the 60<sup>th</sup> day of production was 11.84 grams. This average weight has met the SNI 01-7246-2006 standard which explains that in 61-75 day old shrimp shrimp have a weight range of 8.1-14.0 grams. Shrimp that are around 61 days old have a minimum weight of 8.1 grams. However, there are 3 plots of pond ponds that



have not been able to reach the minimum limit, namely in plots P1, P2, and P3. In the three plots of ponds the development of shrimp appears to be hampered from the 30<sup>th</sup> day to the 60<sup>th</sup> day.

According to the results of interviews in the field with farm owners, this is likely to occur because of the threat of shrimp disease which makes shrimp appetite decrease. Allegedly high levels of ammonia are a cause of decreased appetite for shrimp so that shrimp do not develop. This is also seen when feeding, food that is in the container (anco) is still much left.

Tabel 2. Shrimp Quality Measurement Results

| No. Ponds | Size of Fries | Weight (gr)          | Long (mm) |
|-----------|---------------|----------------------|-----------|
|           |               | 60 <sup>th</sup> day |           |
| P.1       | PL.9          | 7                    | 94        |
| P.2       | PL.9          | 6,4                  | 87        |
| P.3       | PL.9          | 6,5                  | 90        |
| P.4       | PL.8          | 9,3                  | 115       |
| P.5       | PL.9          | 13,4                 | 130       |
| P.6       | PL.9          | 13                   | 130       |
| P.7       | PL.9          | 10                   | 125       |
| P.8       | PL.9          | 12                   | 130       |
| P.9       | PL.9          | 13,2                 | 134       |
| P.10      | PL.9          | 11,5                 | 130       |
| Average   |               | 10,23                | 116,5     |

(Source: Data Processing, 2019)

### Status of Sustainability of Shrimp Pond Aquaculture

#### Dimension Sustainability

The sustainability status of the vaname shrimp pond aquaculture in Batukaras Village, Cijulang District, Pangandaran Regency was determined by analyzing 5 (five) dimensions used in the Rapfish method, namely the ecological, social, economic, technological and institutional dimensions. Based on the analysis of the five dimensions, we obtained a sustainability index for shrimp pond aquaculture in Batukaras Village, Cijulang District, Pangandaran Regency. The assessment of the five dimensions is as follows by Table 3:

Tabel 3. Rapfish Ordination Result

| No | Dimension     | Nilai Indeks | R <sup>2</sup> | Status             |
|----|---------------|--------------|----------------|--------------------|
| 1  | Ecological    | 51,41        | 0,92           | Fairly Sustainable |
| 2  | Social        | 52,32        | 0,91           | Fairly Sustainable |
| 3  | Economi       | 51,62        | 0,92           | Fairly Sustainable |
| 4  | Technological | 76,98        | 0,95           | Sustainable        |
| 5  | Institutional | 66,13        | 0,91           | Fairly Sustainable |

(Source: Data Processing, 2019)

The status of sustainability of vaname shrimp cultivation in Batukaras Village, Pangandaran

Regency is seen from the ecological dimension, social dimension, economic dimension and institutional dimensions having index values of 51.41, 52.32, 51.62 and 66.13 respectively. The four dimensions fall into the fairly sustainable category. While the dimensions of technology include a sustainable category with an index value of 76.98. From these five dimensions, the technology dimension is the dimension with the best level of sustainability. This means that technologically, vaname shrimp farming is a benchmark for the sustainability of vaname shrimp management in Batukaras Village.

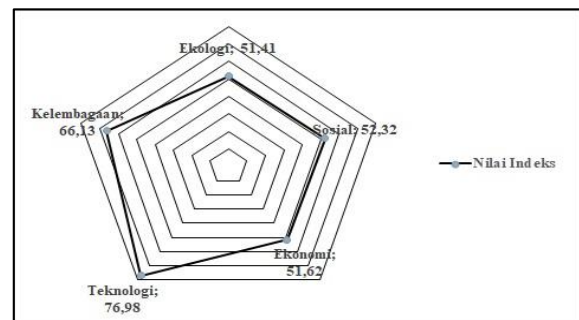


Figure 1. Sustainability Status Diagram

#### Multidimensional Sustainability

According to [5], the assessment of the sustainability status of fisheries management cannot be done by looking at the averages of the five dimensions used as indicators, but it must be done by pairwise comparison tests. Pairwise comparison must be done because each dimension assessed has different weights. Based on the assessment that has been done, a weighted score is obtained as shown in Table 3 above. The results of pairwise comparison by weighing index values as in Table 3 obtained a weighted index value of 60.00 which is in the range of values 50-75. This means that vaname shrimp farming activities in Batukaras Village, Pangandaran Regency are in a fairly sustainable condition.

Tabel 4. Multidimensional Sustainability Index Value

| No                 | Dimension     | Values |       |                |
|--------------------|---------------|--------|-------|----------------|
|                    |               | Weight | Index | Weighted Index |
| 1                  | Ecological    | 0,06   | 51,41 | 3,08           |
| 2                  | Social        | 0,14   | 52,32 | 7,33           |
| 3                  | Economi       | 0,43   | 51,62 | 22,20          |
| 4                  | Technological | 0,27   | 76,98 | 20,79          |
| 5                  | Institutional | 0,10   | 66,13 | 6,61           |
| Total              |               |        |       | 60,00          |
| Fairly Sustainable |               |        |       |                |

(Source: Data Processing, 2019)

The results of the Rapfish analysis show that all the attributes assessed for the sustainability status of vaname shrimp farming are quite accurate. This can be seen from the stress values ranging from 0.20-0.27 with a relatively large degree of determination coefficient ( $R^2$ ), which is 0.91-0.95 for all dimensions assessed. Based on these values it can be illustrated that the attributes used to assess the sustainability status of each dimension are sufficient, as shown in Table 5.

Tabel 5. Value of Rapfish, Stress and Coefficient

| No | Dimension     | Values |        |       | Status             |
|----|---------------|--------|--------|-------|--------------------|
|    |               | Index  | Stress | $R^2$ |                    |
| 1  | Ecological    | 51,41  | 0,24   | 0,92  | Fairly Sustainable |
| 2  | Social        | 52,32  | 0,27   | 0,91  | Fairly Sustainable |
| 3  | Economic      | 51,62  | 0,22   | 0,92  | Fairly Sustainable |
| 4  | Technological | 76,98  | 0,20   | 0,95  | Sustainable        |
| 5  | Institutional | 66,13  | 0,26   | 0,91  | Fairly Sustainable |

(Source: Data Processing, 2019)

## CONCLUSION

a. Water quality and quality of shrimp production in shrimp ponds in Batukaras Village, Cijulang District, Pangandaran Regency have conformed to the standard guidelines for vaname shrimp farming using semi-intensive technology. Suitable water quality parameters include temperature, salinity, pH, DO, and nitrite, while ammonia levels are above the maximum limit for vaname shrimp cultivation.

b. The status of sustainability of vaname shrimp cultivation in Batukaras Village which was analyzed by the Rapfish method is in a fairly sustainable state. With the technology dimension at the highest level because this dimension is a leverage factor for increasing the production of vaname shrimp cultivation in Batukaras Village.

## ACKNOWLEDGMENTS

Dr. Dewi Susiloningtyas, M.Sc as Chair of the Marine Sciences Master Program, also as the 1<sup>st</sup> mentor and Dra. Tuty Handayani, M.S as the 2<sup>nd</sup> mentor who have provided much suggestion and guidance during the implementation of the research and preparation of the thesis. Directorate General of Aquaculture, and head of the Marine and Fisheries Service Pangandaran District which has helped a lot in providing the data needed. My beloved wife Yesha Ayudiana, (Alm.) My Mom, My Dad and in-laws and younger siblings who have given encouragement and enthusiasm so i can complete this thesis. Also, thanks

to University of Indonesia for Hibah Publikasi Internasional Terindeks Tugas Akhir (Hibah PITTA B) in 2019 in accordance with the agreement letter No. NKB-0624/UN2.R3.1/HKP.05.00/2019.

## REFERENCES

- [1] Badan Standarisasi Nasional, (2006). SNI 01-7246-2006: Produksi udang vaname (*litopenaeus vannamei*) ditambah dengan teknologi intensif, Jakarta.
- [2] Bappeda Pemerintah Provinsi Jawa Barat, (2016). Penyusunan rencana kebutuhan investasi pusat pertumbuhan pangandaran raya 2016. Laporan Akhir.
- [3] Boyd C. E, (1988). Water quality management for pond fish cultura. Elsever. Amsterdam.
- [4] BPS Jawa Barat, (2016). Provinsi Jawa Barat dalam angka 2016.
- [5] Budiharsono, S., (2005). Teknik analisis pembangunan dan pesisir. Pradnya Paramita, Jakarta.
- [6] Buwono, I. D., (1993). Pedoman udang windu sistem pengelolaan berpola intensif. Kanisius. Yogyakarta.
- [7] Charles, Anthony T, (2001). Suistainable fishery system, Saint Mary's University, Halifax, Nova Scotia, Canada.
- [8] Dinas Kelautan dan Perikanan Kabupaten Pangandaran, (2016). Laporan Tahunan Perikanan Budidaya.
- [9] Effendi, H, (2003). Telaah kualitas air bagi pengelolaan sumber daya dan lingkungan perairan, Kanisius, Yogyakarta.
- [10] Effendie, M, I, (1997). Biologi perikanan, Yayasan Pustaka Nusantara, Yogyakarta.
- [11] Ghufuran, M dan Kordi K. (2004). Penanggulangan hama dan penyakit ikan. Penerbit Bina Adiaksa dan Rineka Cipta. Jakarta. 190 hal.
- [12] Kementerian Kelautan dan Perikanan, (2006). Peraturan Menteri Kelautan Dan Perikanan Republik Indonesia Nomor. 75/PERMEN-KP/2016 Tentang Pedoman Umum Pembesaran Udang Windu (*Penaeus Monodon*) dan Udang Vaname (*Litopenaeus Vannamei*).
- [13] Kordi, M. G. H. K., dan A. B. Tancung. (2007). Pengelolaan kualitas air dalam budidaya perairan. Rineka Cipta, Jakarta. 210 hlm.
- [14] Stickney RR, (2005). Aquaculture: An introductory text, USA: CABI Publishing.
- [15] Sumeru, U dan S, Anna, (1992). Pakan udang windu, Kanisius, Yogyakarta.
- [16] Susilo, S, B, (2003). Keberlanjutan pembangunan pulau-pulau kecil: studi kasus kelurahan Pulau Panggang dan Pulau Pari, Kepulauan Seribu, DKI Jakarta, *Disertasi*, Program Pascasarjana Institut Pertanian Bogor.

## EVALUATION OF THE TOXIC EFFECTS OF SMOKELESS TOBACCO CHEWING MIXTURES BASED ON BIOLUMINESCENCE TESTING USING THE EXAMPLE OF NASWAR

Dianna B. Kosyan<sup>1,2</sup>, Olga V. Kvan<sup>1</sup>, Elena A. Rusakova<sup>1</sup>, Inara E. Larjushina<sup>1</sup>, Elena V. Kiyaeva<sup>1</sup>,  
Galimzhan K. Duskaev<sup>1</sup>

<sup>1</sup>Laboratory of Nanotechnology and Technogenic Nanomaterial, Federal Research Centre of Biological  
Systems and Agro-technologies of the Russian Academy of Sciences, 9<sup>th</sup> Yanvarya St., 29, 460000,  
Orenburg, Russia; <sup>2</sup>Department of Microbiology and Contagious Disease, FGBEA Orenburg State Agrarian  
University, Chelyuskintsev St., 18, 460000, Orenburg, Russia

### ABSTRACT

The tobacco market includes a wide range of smoking and smokeless products. Previously, cigarettes and other kinds of smoking mixtures mainly comprised tobacco consumption, but with stricter smoking bans in Russia, there has been an expected increase in smokeless tobacco product consumption. The surging use of naswar is of a particular significance. One possible method for rapid toxicity assessment involves bioluminescence analysis using microorganisms that contain different types of sensory cell structures. To conduct bioluminescence analyses, researchers use genetically engineered luminescent microorganisms. For our study, we chose lyophilised, commercially available "Ecolum", a genetically engineered luminescent strain of *Escherichia coli* K12 TG1 that constitutively expresses luxCDABE genes from *Photobacterium leiognathi* 54D10. We also examined *E. coli* K12 MG1655 strains with inducible luminescence through plasmids with the gene mergers soxS lux and katG lux. Our results allow one to consider a basic toxic mechanism due to oxidative stress formation: damage to intracellular structures, namely DNA.

*Keywords: Bioluminescence, Microorganism, Naswar, Oxidative stress, Toxicity*

### INTRODUCTION

The tobacco market includes a wide range of smoking (cigarettes, cigars, cigarillos etc.) and smokeless (chewing, sucking and snuff tobacco) products. Previously, cigarettes and other smoking mixtures mainly accounted for tobacco consumption, but with stricter smoking bans in Russia, there has been an expected increase in smokeless tobacco product consumption [1, 2]. A surge in the use of naswar is of particular significance. Naswar is a multi-component nicotine mixture that contains different plants (such as talkan and sirach) and non-food components (plant ash, quicklime and avian or camel dung); these components represent potential carcinogens. Naswar production is usually artisanal and different detected components may have negative effects on the body [3-5].

Currently, there is a major push to develop methods that assess chewing tobacco product safety because of issues with present diagnostic and testing methods [6]. Almost all existing toxicological methods have several drawbacks: 1) they are not intended to assess tobacco and tobacco smoke toxicity; 2) they do not allow quantification of tobacco products with varying degrees of complexity in their chemical structure; 3) they are designed primarily for screening chemicals to identify possible human carcinogens [7]. Thus,

existing methods should be evaluated and new assays developed to evaluate the safety of tobacco products. However, this research is virtually non-existent in Russia [8, 9].

One possible method for rapid toxicological assessment could be bioluminescence analysis using microorganisms that contain different types of sensory cell structures [10]. Indicators of toxicity from a sample will alter luminescence intensity compared to the control. Bacterial bioluminescence is extremely sensitive to the effects of various inhibitors and is therefore used to analyze many anesthetics, drugs, industrial poisons, insecticides, toxic and medicinal substances [11]. Based on the need to develop new analysis methods, the purpose of this work was to evaluate the use of bioluminescence analysis to evaluate the toxicity of smokeless tobacco mixtures (naswar)

### MATERIALS AND METHOD

#### Test substance preparation

We analyzed four samples (A through D) of smokeless chewing tobacco blend 1 (naswar). An aqueous extract of the test material was performed according to a methodology used in similar studies by foreign researchers [12]. One thousand µl of distilled water was added to 1 g naswar (a 1:1 ratio). The solution was thoroughly mixed and incubated

for 24 h at room temperature.

### Test organism characteristic

Bioluminescence analyses utilize genetically engineered luminescent microorganisms with different types of luminescence. We utilized the commercially available lyophilized "Ecolum" ("Immunotech", Moscow, Russia), a genetically engineered luminescent strain of *Escherichia coli* K12 TG1 that constitutively expressed luxCDABE (lux) genes from the marine microorganism *Photobacterium leiongnathi* 54D10. Naswar toxicity was determined by the degree by which bacterial luminescence was inhibited.

We also examined bacteria with an inducible glow, namely *E. coli* K12 MG1655 that carried plasmids with lux gene mergers for soxS or katG (GosNIIGenetika, Russia). This strain was characterised by initially low luminescence, but was induced specifically upon exposure to the superoxide anion and hydrogen peroxide

### Test strain preparation

Lyophilized "Ecolum" was reconstituted by the addition of chilled distilled water. The bacterial suspension was incubated at 2-4°C for 30 min and then allowed to reach 15-25°C. One hundred µl was add to wells of opaque plastic 96-well plates pre-filled with an equal volume of naswar mixtures.

The *E. coli* pSoxS lux and pKatG lux strains were grown for 18-24 h on Luria Broth (LB) agar in the presence of 100 µg/ml of ampicillin, transferred into fresh LB broth and then grown to the early exponential phase ( $OD_{540} = 0.35$ ). Bacteria was collected by centrifugation, slurred in 0.85% NaCl solution and 50 µl bacteria was added to wells of opaque plastic 96-well plates, pre-filled with an equal volume of the naswar mixture. The mix was incubated for 15 min and then an additional 150 µl LB broth was added..

### Bioluminescent analysis protocol

Bacterial luminescence inhibition was performed on 96-well opaque plastic plates. Sample wells contained a 1:1 mixture of naswar and luminescent

bacteria; control wells contained distilled water and luminescent bacteria. Plates were placed in an Analyzer Infinite PROF200 (TECAN, Austria), which dynamically registered the luminescence intensity for each well over 180 min (5 min intervals) in relative light units (RLU).

The data were analyzed using the software provided with the instrument. Quantification of the bioluminescence inhibition index (I) due to nanoparticle toxicity was calculated by the following algorithm (1).

$$I = RLU_{c0} \times RLU_{tn} / RLU_{cn} \times RLU_{t0} \quad (1),$$

where c and t are the RLU values of the control and test samples at the 0 and nth minute of the measurement.

### Statistical processing

All experiments were performed in triplicate. Statistical analysis was performed using a one-way analysis of variance (ANOVA) followed by the Newman-Keuls test when appropriate. Values of  $p < 0.05$  were considered statistically significant. Factor inhibition ( $F_i$ ) was calculated at the most effective concentration used.

## RESULTS

### Bioluminescent analysis results

Overall, our bioluminescent results showed differences in the level of toxicity of each naswar sample with regards to the test organism depending upon the concentration and type of luminescence.

Sample A, at concentrations from 1 to 0.031 mg/ml mixed with "Ecolum", inhibited bacterial luminescence compared to control, a result that indicated the development of a toxic effect. At 0.015 mg/ml, sample A initially slightly inhibited "Ecolum" bioluminescence, but after 130 min, luminescence was inhibited by 70%. Dilutions from 0.008 mg/ml to 0.001 mg/ml did not inhibit luminescence and thus did not promote toxic effects (Figure 1).

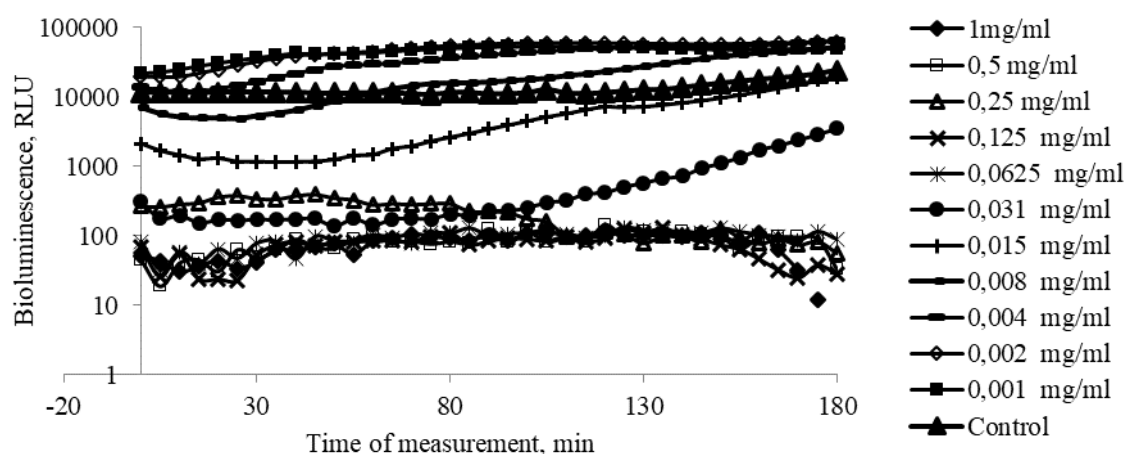


Fig. 1 Luminescence dynamics for "Ecolum" when in contact with sample A

Results from sample B also revealed concentration-dependent negative effects. Concentrations of 1, 0.5 and 0.25 mg/ml reduced luminescence by 95% over the experimental period (180 min). These results represented the greatest toxic effects. Subsequent dilution of sample B from 0.125 to 0.0625 mg/ml suppressed 75% of "Ecolum"

bioluminescence by 110 min. At 0.031 mg/ml, luminescence was decreased after 60 min incubation, but it returned to the control level as incubation time progressed. This finding indicated acute toxicity without prolonged action. Subsequent dilutions of sample B did not alter luminescence and thus did not promote toxic effects (Figure 2).

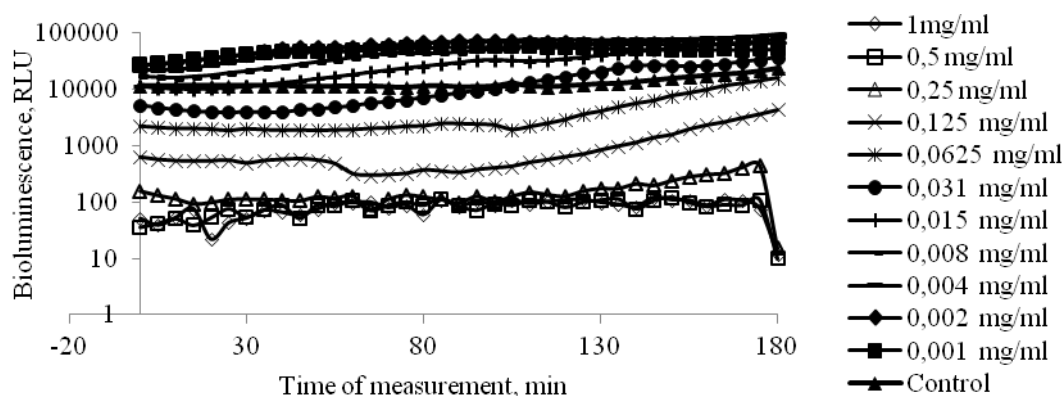


Fig. 2 Luminescence dynamics for "Ecolum" when in contact with sample B

In pilot testing, sample C markedly reduced "Ecolum" luminescence by 90%, and subsequent dilutions (1, 0.5, 0.25 and 0.0625 mg/ml) reduced the intensity by 50-80% compared to control. These results indicated high toxicity from this test material. The 0.031 mg/ml concentration reduced bioluminescence by 55%. At 0.015 mg/ml,

luminescence was suppressed over the first 100 min, but gradually returned to the control level. Thus, this concentration promoted acute toxicity. Finally, subsequent sample C dilutions did not alter luminescence and thus did not promote toxicity (Figure 3).

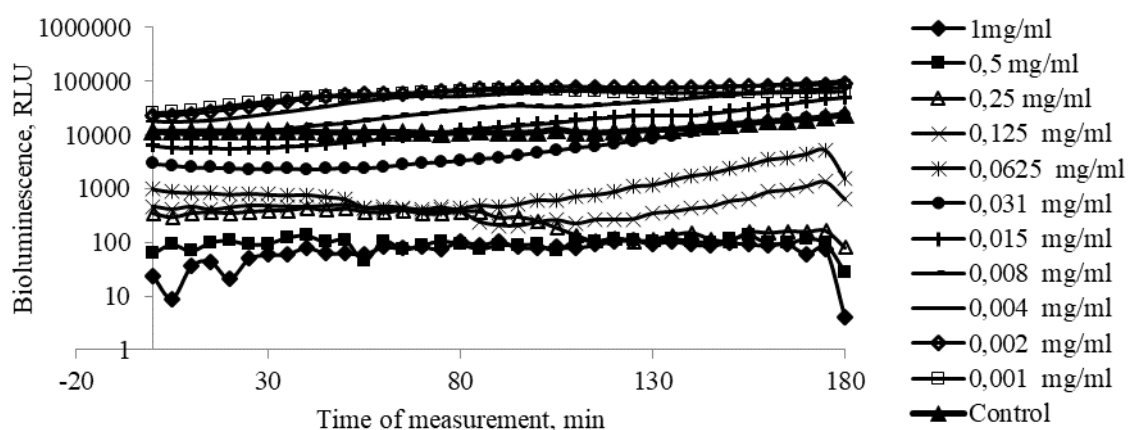


Fig. 3 Luminescence dynamics for "Ecolum" when in contact with sample C

Concentrations of sample D from 1 to 0.031 mg/ml inhibited "Ecolum" bacterial luminescence to 68% relative to the control, a result that indicated acute toxic action. At 0.015 mg/ml, luminescence

was suppressed by 35%, but only after 70 min incubation. Subsequent sample D dilutions (0.008 mg/ml to 0.001 mg/ml) did not promote toxic effects (Figure 4).

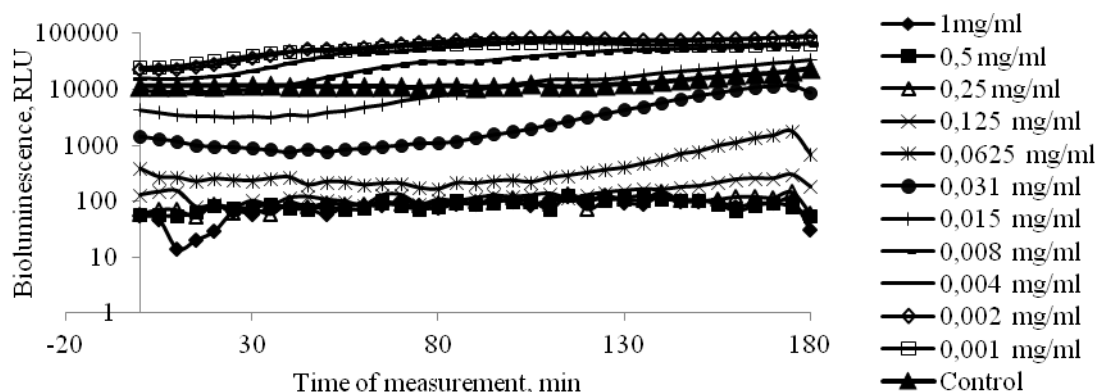


Fig. 4 Luminescence dynamics for "Ecolum" when in contact with sample D

Our data indicated that the four naswar samples promoted differential toxicity. We used this data to calculate the EC50, a measurement that corresponded to the concentration that caused 50% bacterial bioluminescence inhibition compared to

control after 180 min of exposure. The EC50 concentrations (Table 2) were: 0.125 mg/ml for sample A, 0.031 mg/ml for sample B, 0.008 mg/ml for sample C and 0.0625 mg/ml for sample D.

Table 1 Percentage of surviving bacteria (%) after exposure to naswar mixtures

| Sample | Concentration, mg/ml |       |       |        |        |       |      |      |      |
|--------|----------------------|-------|-------|--------|--------|-------|------|------|------|
|        | Control              | 0.008 | 0.015 | 0, 031 | 0.0625 | 0.125 | 0.25 | 0.5  | 1    |
| A      | 100                  | 97,3  | 84,2  | 74,5   | 58,7   | 51,4  | 35,5 | 19,6 | 10,2 |
| B      | 100                  | 63,0  | 58,6  | 50,2   | 43,1   | 36,9  | 25,6 | 19,4 | 7,8  |
| C      | 100                  | 65,1  | 50,9  | 48,9   | 35,6   | 19,4  | 12,8 | 8,2  | 4,5  |
| D      | 100                  | 89    | 78    | 65     | 50,4   | 47,3  | 30,1 | 24,5 | 16,7 |

We next examined the effect of the four naswar samples on bacterial strains with inducible

bioluminescence. The *E. coli* psoxS lux strain luminesces in response to increased superoxide

anion. Measuring glow intensity for this strain would allow us to assess whether the naswar samples caused and/or affected stress and the regulation of its dynamics

Our findings indicated that contact of the bacteria with the analysed substances led to reactive oxygen species formation, specifically through activation of the *psoxS* promoter cassette and transcription of the reporter *luxCDABE* genes (Figure 5).

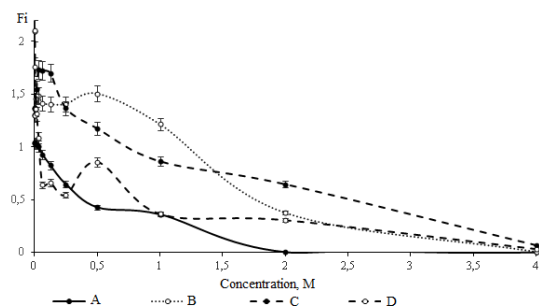


Fig. 5 Factor induction of luminescence (Fi) for *E. coli* K12 MG1655, which carried a plasmid with *pSoxS lux*, after contact with naswar samples.

The most pronounced luminescence induction occurred with exposure to sample B. This finding indicated that sample B likely led to superoxide anion formation presumably due to electron transfer from molecular oxygen and subsequent transformation of the peroxide hydrogen. There was only minimal luminescence induction for sample A

We confirmed the observations with the *E. coli* *psoxS lux* strain using *E. coli* *pkatG lux* (Figure 6). *pkatG* is a stronger promoter than *psoxS*, and thus this experiment allowed us to rule out luminescence induction due to sample peculiarities.

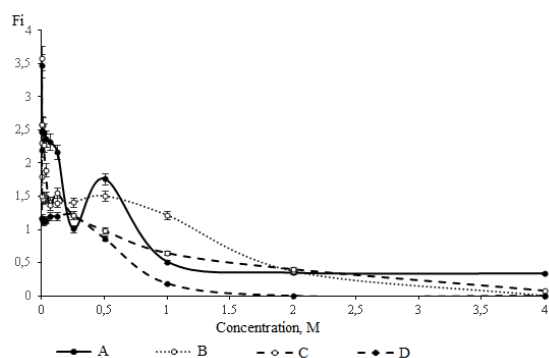


Fig. 6 Factor induction of luminescence (Fi) for *E. coli* K12 MG1655, which carried a plasmids with *pkatG lux*, when in contact with naswar samples.

Finally, we examined luminescence induction in *E. coli* *pRecA lux* bacteria. In this strain, luminescence induction occurs due to the SOS response as a result of DNA damage formed during oxidative stress (Figure 7).

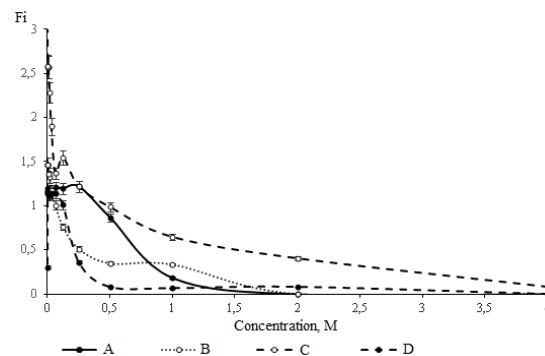


Fig. 7 Factor induction of luminescence (Fi) for *E. coli* K12 MG1655, which carried a plasmid with *pRecA lux*, when in contact with naswar samples.

We found that a wide range of naswar sample concentrations promoted similar luminescence induction as a result of oxidative-stress-induced DNA damage. Sample C produced the most pronounced effect compared to the other samples, whereas sample D promoted minimal damage. Thus, sample C especially promoted the development of oxidative stress cascades, effectively generating hydroxyl radicals that led to pronounced damage to the genetic apparatus of target cells.

## DISCUSSION

To address environmental challenges, as well as for studies in medicine and agriculture, basic biology requires fast and convenient analysis methods substance toxicity [13]. Bioluminescent analysis is one of the most promising methods for biological environmental monitoring. Biotests on luminescent bacteria provide a quantitative toxicity measure and often surpass older, famous biotests with regards to speed, accuracy, sensitivity and simplicity, and allow researchers to examine a considerable number of toxicants [14, 15]. Using the *lux* genes as a marker for gene expression is important in the study of pathogenicity, virulence, adaptation and secondary metabolism. There are several examples in the literature of how to use this method to study transcription. Recombinant bioluminescent strains were created and used to determine toxicity of different antibiotics and heavy metals [16, 17]. There were also reported strains with high specificity to a particular toxic agent [18, 19]. Further, there is evidence of the benefit of bioluminescent reporters to determinate toxicity of



heavy metals and phenols in water and soil samples [20-22].

## CONCLUSIONS

Our data suggest the possibility of using this type of research to analyse tobacco chewing blends. The results obtained here allow us to consider one of the basic negative toxic mechanisms, namely oxidative stress formation with consequent damage to intracellular structures, particularly DNA. Manifestation of this biological activity severely alters target cell energy metabolism and results in bacterial growth inhibition and dysregulated luminescence. The main cause of this effect could be reduced transmembrane electrochemical potential with subsequent bacterial luminescence diminution. Thus, naswar toxicity results from critical damage to cell structures and subsequent cell death.

Studying the bioluminescence intensity of "Ecolum" allowed us to assess the quantitative and dynamic components of several naswar samples. Indeed, we observed a general dose-dependent reduction in bioluminescence. Overall, bioluminescent analysis will first provide data about possible substance toxicity that can serve as the basis for follow-up examinations.

## REFERENCES

- [1] Salomatin V., Filipchuk O., MirgorodSKAYA A., Shkidjuk M., Modeling multicomponent tobacco products reduced toxicity: Uglich, 2010. 150 p.
- [2] Rogain M., Zetterstrom U., Lindholm K., Quantitative and qualitative chemical analysis of securitising tobacco naswar. Science and health. Vol. 1. 2016, pp.15-20.
- [3] Ullah N., Asif A., Azam Khan M., Ahmad W., Ali N., Khan T., Shah A., Chemical analysis of Naswar and Cigarettes. A comparative study. International Journal of Basic and Clinical Research. Vol. 1(1). 2011, pp. 13-15.
- [4] Sajid F. and Bano S., Effects of smokeless dipping tobacco (Naswar) consumption on antioxidant enzymes and lipid profile in its users. Pak J. Pharm Sci. Vol. 28(5). 2015, pp. 1829-1833.
- [5] Ullah A., Khan A., Iqbal Z., Khan I., Evaluation of Serum Copper Level in Naswar (Smokeless Tobacco) Addicts Using Flame Atomic Absorption Spectroscopy. Archives of Iranian Medicine. Vol. 20(10). 2017, pp. 649-651.
- [6] Willis D., Popovch M., Gany F., Hoffman C., Blum J., Zelikoff J., Toxicity of Gutkha, a Smokeless Tobacco Product Gone Global: Is There More to the Toxicity than Nicotine? International Journal of Environmental Research and Public Health. Vol. 11(1). 2014, pp.919-933.
- [7] Sun J., Jin J., Beger R., Cerniglia C., Yang M., Chen H., Metabolomics evaluation of the impact of smokeless tobacco exposure on the oral bacterium *Campylobacter sputigena*. Toxicol. In Vitro. Vol. 30. 2016, pp.133-141.
- [8] Avti P., Kumar S., Pathak C., Vaiphei K., Khanduja K., Smokeless tobacco impairs the antioxidant defense in liver, lung, and kidney of rats. Toxicol. Sci. Vol. 89.2006, pp.547-553.
- [9] Richter P., Hodge K., Stanfill S., Zhang L., Watson C., Surveillance of moist snuff: Total nicotine, moisture, pH, un-ionized nicotine, and tobacco-specific nitrosamines. Nicotine Tob. Res. Vol. 10. 2008, pp.1645-1652.
- [10] Minekawa T., Ohkuma H., Abe K., Maekawa H., Arakawa H., Practical application of bioluminescence enzyme immunoassay using enhancer for firefly luciferin-luciferase bioluminescence. Luminescence. Vol. 26(3). 2010, pp. 167-171.
- [11] Lomakina G., Modestova Y., Ugarova N., Bioluminescence assay for cell viability. Biochemistry (Mosc). Vol. 80(6). 2015, pp.701-713.
- [12] Deryabin D., Alyoshina E., Deryabina T., Efremova L., Biological activity of ions, Nano- and micro-particles of Cu and Fe in the test of inhibition of bacterial bioluminescence. Questions of biological, medical and pharmaceutical chemistry. Vol. 6. 2011, pp. 31-36.
- [13] Osimani A., Garofalo C., Clementi F., Tavoletti S., Aquilanti L., Bioluminescence ATP Monitoring for the Routine Assessment of Food Contact Surface Cleanliness in a University Canteen. Tchounwou PB. International Journal of Environmental Research and Public Health. Vol. 11(10). 2014, pp. 10824-10837.
- [14] Meighen E., Bacterial bioluminescence: organization, regulation, and application of the lux genes. FASEB J. Vol. 7(11). 1993, pp.1016-1022.
- [15] Robinson G., Tonks K., Thorn R., Reynolds D., Application of bacterial bioluminescence to Assess the efficacy of fast-acting biocides. Antimicrobial Agents and Chemotherapy. Vol. 55(11). 2011, pp.5214-5219.
- [16] Perego P., Fanara L., Zilli M., Del Borghi M., Applications of Luminous Bacteria on Environmental Monitoring, Chem. Biochem. Eng. Q. Vol. 16 (2). 2002, pp.87-92.
- [17] Kun J. and Rodica E., Measurement of Bacterial Bioluminescence Intensity and Spectrum: Current Physical Techniques and Principles. Adv. Biochem Eng Biotechnol. Vol. 154. 2016,

- pp.19–45.
- [18] Tavares A., Dias S., Carvalho C., Faustino M., Tome J., Neves M., Tome A., Cavaleiro J., Cunha A., Gomes N., Mechanisms of photodynamic inactivation of a gramnegative recombinant bioluminescent bacterium by cationic porphyrins. *Photochem Photobiolog Sci.* Vol. 10(10). 2011, pp.1659–1669.
- [19] Cronin M., Akin A.R., Collins S., Meganck J., Kim J.-B., Baban C., Joyce S., Van Dam G., Zhang N., Van Sinderen D., High resolution in vivo bioluminescent imaging for the study of bacterial tumour targeting. *PLoS One.* Vol. 7(1). 2012, pp.30940-30949.
- [20] Charrier T., Durand M., Affi M., Jouanneau S., Gezekel H., Thouand G., Bacterial bioluminescent biosensor characterization for on-line monitoring of heavy metals pollutions in waste water treatment plant effluents. In: “Biosensors” book. Vol. 11. 2010, pp. 217-223.
- [21] Ranjitha P., Karthy E., Detection of heavy metal resistance bioluminescence bacteria using microplate bioassay method. *Elixir Pollution.* Vol. 40. 2011, pp.5108-5112.
- [22] Thakre N. and Shanware A., Promising Biological Indicator of Heavy Metal Pollution: Bioluminescent Bacterial Strains Isolated and Characterized from Marine Niches of Goa, India. *Indian Journal of Microbiology.* Vol. 55. No. 3. 2015, pp.327-332.

# THE MODIFIED DECOMPOSITION METHOD FOR SOLVING VOLTERRA FREDHOLM INTEGRO-DIFFERENTIAL EQUATIONS USING MAPLE

Dalal Adnan Maturi<sup>1</sup>

<sup>1</sup>Departement of Mathematics, Faculty of Science, King Abdulaziz University, P.O.Box 42664,Jeddah 21551, Saudi Arabia

## ABSTRACT

In this paper, Vito Volterra studied the phenomenon of population growth, and new types of equations have been developed and termed as the integro–differential equation. Here we will address the Mixed Volterra Fredholm integro-differential equation. We introduce some basic idea of Modified Decomposition method (MDM) to solve the Volterra-Fredholm integro-differential equation. The modified decomposition method (MDM) is applied to solve the Volterra Fredholm integro-differential equation. Based on the proposed after treatment technique, the truncated series solution obtained by the Modified Decomposition method (MDM) can be expressed as another series in terms of the independent sine and cosine trigonometric functions. In addition, examples that illustrate the pertinent features of this method is presented, and results of the study is discussed. Also, we compare the result with exact solution, and we investigate the error between numerical solution and exact solution and draw the graph of function by using Maple18. Finally, the results reveal that the Modified Decomposition method is very effective and convenient for solving Volterra Fredholm integro-differential equation.

*Keywords: Volterra Fredholm Integro-Differential equation, Modified Decomposition method, Maple18 .*

## INTRODUCTION

Integrated stems from the mathematical modeling of many complex real-life problems of differential. Has been formulated many scientific equations phenomena using integrated differential equations. Solution integrative non-linear equation is [5,6] much more difficult than the linear equation of the Therefore, the use of different types of analytical numerical methods to obtain an approximate solution effective [1-4]. Numerical solution of Volterra integral equation of second kind using Implicit Trapezoidal [7,11]. Adomian Decomposition method of Fredholm integral equation of the second kind using Maple and MATLAB[8,10]. Application of Adomian Decomposition method for solving of Fredholm Integral Equation of the Second Kind [9].

The Modified Decomposition Method for Solving Volterra Integral Equation of the Second Kind Using Maple [12].

The main goal in this article is to apply the Modified Decomposition method (MDM) to the Volterra Fredholm integro-differential equation using Maple and then compare the exact solution results with the approximate results obtained from the algorithm Maple. By showing some examples we see how this method gives the best results.

## THE MODIFIED DECOMPOSITION METHOD

To illustrate the basic idea of this method, we consider the following general non-linear differential

equation:

$$u^{(n)}(x) = f(x) + \lambda_1 \int_a^x K_1(x,t) u(t) dt + \lambda_2 \int_a^b K_2(x,t) u(t) dt. \quad (1)$$

And the mixed form

$$u^{(n)}(x) = f(x) + \lambda \int_0^x \int_a^b K(r,t) u(t) dt dr, \quad (2)$$

where  $u^{(n)}(x) = \frac{d^n u(x)}{dx^n}$ .

$$u(x) = \sum_{k=0}^{n-1} \frac{1}{k!} b_k u^k + L^{-1}(f(x)) + L^{-1} \left( \lambda \int_0^x \int_a^b K(r,t) u(t) dt dr \right), \quad (3)$$

where  $L$  is assumed invertible and  $L^{-1}$  is an

The standard Adomian method defines the solution  $u(x)$  by the series  $u(x) = \sum_{n=0}^{\infty} u_n(x)$ .

The modified decomposition method

$$u_0(x) = f_1(x)$$

$$u_1(x) = f_2(x) + L^{-1} \left( \lambda \int_0^x \int_a^b K(r,t) u_0(t) dt dr \right),$$

$$u_{n+1}(x) = L^{-1} \left( \lambda \int_0^x \int_a^b K(r,t) u_n(t) dt dr \right). \quad (4)$$

The use of the modified decomposition method not only minimizes the computations but avoids the use of the higher order Adomian polynomials for such cases.

$$u(0) = 1, u'(0) = 0.$$

**EXAMPLE**

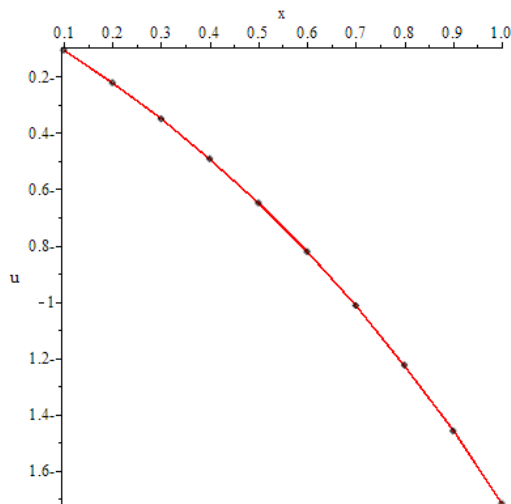
**Example1.** Consider the Volterra Fredholm integro differential equation

$$u'(x) = \frac{1}{4}x^2 - e^{-x} + \int_0^x \int_0^1 rtu(t)dt dr, \quad u(0) = 0$$

Applying the Modified Decomposition Method using Maple we find

Table 1 Numerical results and exact solution of Volterra Fredholm integro differential equation for example 1

| $x$     | $u(x)$     | $Exact$<br>$= 1 - e^x$ | $Error$   |
|---------|------------|------------------------|-----------|
| 0.10000 | -0.1051709 | -0.1051710             | 0.0000001 |
| 0.20000 | -0.2214028 | -0.2214035             | 0.0000007 |
| 0.30000 | -0.3498588 | -0.3498613             | 0.0000025 |
| 0.40000 | -0.4918247 | -0.4918306             | 0.0000059 |
| 0.50000 | -0.6487213 | -0.6487328             | 0.0000116 |
| 0.60000 | -0.8221188 | -0.8221388             | 0.0000200 |
| 0.70000 | -1.0137527 | -1.0137845             | 0.0000318 |
| 0.80000 | -1.2255409 | -1.2255883             | 0.0000474 |
| 0.90000 | -1.4596031 | -1.4596706             | 0.0000675 |
| 1.00000 | -1.7182818 | -1.7183744             | 0.0000926 |



**Fig.1** Plot 2D of the exact solutions result Of Volterra Fredholm integro differential equation for example 1.

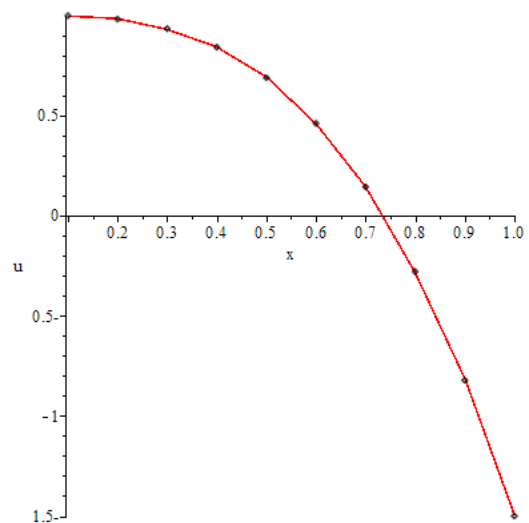
**Example2.** Consider the Volterra integral equation of second kind

$$u''(x) = -15x + \int_0^x \int_0^1 rtu(t)dt dr,$$

Applying the Modified Decomposition Method using Maple we find

Table 2 Numerical results and exact solution of Volterra Fredholm integro differential equation for example 2

| $x$     | $u(x)$     | $Exact$<br>$= \frac{1}{5}x^3 - \frac{1}{2}x^3$ | $Error$   |
|---------|------------|--|-----------|
| 0.10000 | 0.9975000  | 0.9975000                                      | 0.0000000 |
| 0.20000 | 0.9800000  | 0.9800000                                      | 0.0000000 |
| 0.30000 | 0.9325000  | 0.9325000                                      | 0.0000000 |
| 0.40000 | 0.8400000  | 0.8400000                                      | 0.0000000 |
| 0.50000 | 0.6875000  | 0.6875000                                      | 0.0000000 |
| 0.60000 | 0.4600000  | 0.4600000                                      | 0.0000000 |
| 0.70000 | 0.1425000  | 0.1425000                                      | 0.0000000 |
| 0.80000 | -0.2800000 | -0.2800000                                     | 0.0000000 |
| 0.90000 | -0.8225000 | -0.8225000                                     | 0.0000000 |
| 1.00000 | -1.5000000 | -1.5000000                                     | 0.0000000 |



**Fig. 2** Plot 2D of the exact solutions result Of Volterra Fredholm integro differential equation for example 2.

**Example 3.** Consider the Volterra Fredholm integro differential equation

$$u''(x) = 2x^3 - \frac{1}{3}x^2 + \int_0^x \int_{-1}^1 (rt^2 - r^2t)u(t)dt dr, \quad u(0) = 1, u'(0) = 1.$$

Applying the Modified Decomposition Method using Maple we find

Table 3 Numerical results and exact solution of Volterra Fredholm integro differential

equation for example 3.

| $x$     | $u(x)$     | $Exact$<br>$= 1 + 9x$ | $Error$   |
|---------|------------|-----------------------|-----------|
| 0.10000 | 1.9000000  | 1.9000000             | 0.0000000 |
| 0.20000 | 2.8000000  | 2.8000000             | 0.0000000 |
| 0.30000 | 3.7000000  | 3.7000000             | 0.0000000 |
| 0.40000 | 4.6000000  | 4.6000000             | 0.0000000 |
| 0.50000 | 5.5000000  | 5.5000000             | 0.0000000 |
| 0.60000 | 6.4000000  | 6.4000000             | 0.0000000 |
| 0.70000 | 7.3000000  | 7.3000000             | 0.0000000 |
| 0.80000 | 8.2000000  | 8.2000000             | 0.0000000 |
| 0.90000 | 9.1000000  | 9.1000000             | 0.0000000 |
| 1.00000 | 10.0000000 | 10.0000000            | 0.0000000 |

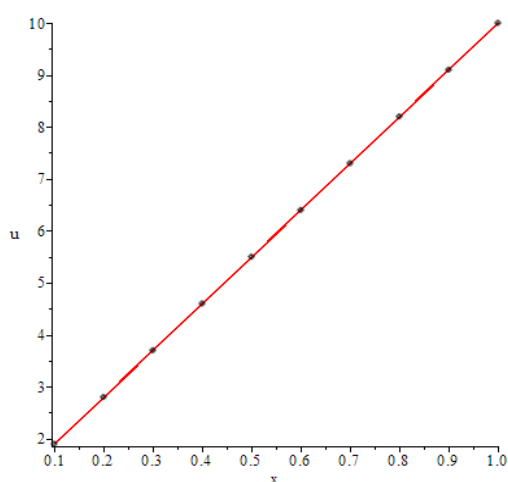


Fig. 3 Plot 2D of the exact solutions result Of Volterra Fredholm integro differential equation for example 3.

## CONCLUSION

In this paper, the Modified Decomposition Method to the solution of Volterra Fredholm integro differential equation numerical results demonstrate that our method is an accurate and reliable numerical technique for solving Volterra Fredholm integro differential equation. Note that the results of examples 1, 2 and 3 show that the exact solution is very close to the approximate solution and that the error rate between them is very small, which proves the efficiency of the method used. This is shown in the tables and graphics from 1-3. Finally, The Modified Decomposition Method using Maple can be easily extended and applied to linear or nonlinear Fredholm and Volterra integral equations of the first or second kind.

## ACKNOWLEDGEMENTS

This paper was supported by the Deanship of Scientific Research (DSR), King Abdulaziz University, Jeddah.

## REFERENCES

- [1] Abdul-Majid. W., A reliable Modification of Adomian Decomposition Method, Applied Mathematics and Computation, Vol. 102, No.1, 1999, pp.77-86.
- [2] Abdul-Majid. W., and Said. A. El-S., A new Modification of the Adomian Decomposition Method for Linear and Nonlinear Operators, Applied Mathematics and Computation, Vol. 122, No.3, 2001, pp.393-405.
- [3] Abdul-Majid. W., Linear and Nonlinear Integral Equations, Higher Education Press, Beijing, China, 2011.
- [4] Peter. L., Analytical and Numerical Methods for Volterra Equations, Studies in Applied Mathematics 7, SIAM, Philadelphia, 1985.
- [5] David M. Doddrell, Lawrence K. Forbes, and Stuart Crozier, "Calculating current densities and fields produced by shielded magnetic resonance imaging probes," SIAM Journal on Applied Mathematics, vol.57, no.2, pp.401-425, 1997.
- [6] Parand .K., Abbasbandy. S., Kazem. S, and Rad J. A., "A novel application of radial basis functions for solving a model of first-order integro-ordinary differential equation," Communications in Nonlinear Science and Numerical Simulation, vol. 16, no. 11, pp. 4250-4258, 2011.
- [7] Dalal A.M, Amani..Z.B.I, Badreeh..M. G., Numerical Solution of Volterra Integral Equation of Second Kind Using Implicit Trapezoidal, Journal of Advances In Mathematics, Vol8, No.2, pp.1540-1553, 2014.
- [8] Dalal .A. M., Adomian Decomposition Method of Fredholm Integral Equation of the Second Kind Using Maple, Journal of Advances In Mathematics, Vol9, No.1, pp.1868-1875, 2014.
- [9] Dalal. A.M., Application of Adomian Decomposition Method for Solving of Fredholm Integral Equation of the Second Kind, European Journal of Science and Engineering, Vol9, No.2, pp.1-9, 2014.
- [10] Dalal .A.M., Adomian Decomposition Method for Solving of Fredholm Integral Equation of the Second Kind Using Matlab, International Journal of GEOMATE, Dec. 2016, Vol. 11, Issue 28, pp.2830-2833. Special Issue on Science, Engineering and Environment, ISSN: 2186-2990, Japan.
- [11] Dalal A.M. and Honida M.M., Numerical

Solution of System of Three Nonlinear Volterra Integral Equation Using Implicit Trapezoidal, Journal of Mathematics Research, Vol.10, No. 1, February 2018,ISSN 1916-9795 E-ISSN 1916-9809.

[12] Dalal .A.M., The Modified Decomposition Method for Solving Volterra Integral Equation

of the Second Kind Using Maple, International Journal of GEOMATE, Oct., 2019, Vol. 17, Issue 62, pp.23-28.Special Issue on Science, Engineering and Environment, ISSN: 2186-2982, Japan.

## STUDY OF ELECTRON FLUXES IN IONOSPHERE-PLASMASPHERE COUPLING FROM WHISTLERS OBSERVED AT LOW LATITUDE GROUND STATION JAMMU L= 1.17

M. Altaf

Department of Physics, GDC Pattan, Govt. Higher Education Department J&K, India

### ABSTRACT

The downward flux of the ionization are measured by whistlers recorded at low latitude ground station Jammu (geomag lat  $22^{\circ} 26'$ ) and  $L= 1.17$ , on 5 June 1997. The whistler data shows a variation in dispersion with time. This decrease in dispersion is interpreted in terms of a corresponding decrease in the electron content of tubes of ionization and is compared with that obtained by Park (1972, Technical Report, Stanford university) for mid latitudes. By Park's (1972) expressions the equatorial electron density and electron tube content  $N_T$  values were computed. Our measurements from whistlers show an average downward flux  $2.8 \times 10^8$  electrons  $\text{cm}^{-2} \text{S}^{-1}$ . The simple diffusion equation which relates the flux to the ionization gradient by the ambipolar diffusion coefficient is again computed shows that the flux computed is within an order of magnitude less than that derived from the dispersion data. It is, therefore, argued that other processes like  $E \times B$  drifts should play a dominant role in controlling the transport of ionization at low latitudes.

*Keywords:- flux of the ionization, equatorial electron density, electron tube content, Plasmasphere, Ionosphere, dispersion*

### INTRODUCTION

An important characteristic of low latitude whistler propagation is the low value of the maximum heights reached by the associated L-values are very low. Thus for Gulmarg  $L=1.2$ , for Nainital  $L=1.12$  and Jammu  $L=1.17$ . It shows that the path for whistlers observed at Jammu is within the upper boundary of the F-layer, this boundary is not well defined but is identified as the level where light ions (hydrogen, helium) becomes more numerous than the heavier ions (Chiefly oxygen). Even though, this upper boundary is found to exhibit diurnal and geographical height variations in the range of 600-2000 km (Mayer et al., 1967, Somayajulu, 1968, Brinton et al., 1969). It is fact to identify it at 1000 km, which is taken as the lower boundary of the plasmasphere. Thus, a study of whistler at Jammu gives us information about the top of the F-layer of the ionosphere.

In addition to the production and loss mechanism, the important problem is the study of the upper F-layer which is the transport of ionization. In general, transport of ionization in the top side F-region may result from (1)  $E \times B$  drifts (2) ambipolar diffusion along the magnetic field (3) interaction between ionization and neutral winds. The combination at the equator of (1) and (2) explains the well known anomaly called the "equatorial anomaly".

The important problem is the maintenance of the nocturnal F-layer, in which several effects are supposed to contribute for this. The wind in the

neutral atmosphere drive the ionization up the magnetic field lines where the loss rate of ionization by dissociative recombination is reduced (Hansen and Patterson, 1964, Park 1970, Carpenter and Bowhill, 1971, Risbeth, 1968). It is found that a night-time production rate of  $1 \text{ cm}^{-3} \text{ s}^{-1}$  contribute to the maintenance of the night-time F-layer to go along with the critical flux of  $1.5 \times 10^7 \text{ cm}^{-3} \text{ s}^{-1}$  (Risbeth, 1968). It appears that the nocturnal F-layer cannot be explained satisfactorily without involving downward diffusion of ionization of the order of  $10^8 \text{ cm}^{-3} \text{ s}^{-1}$  which appears to be sufficient for the night-time production rate of ionization of  $1 \text{ cm}^{-3} \text{ s}^{-1}$  due to the charge exchange with H-ions from plasmasphere (Carpenter and Bowhill, 1971). In many techniques, whistler methods yield reliable data on the morphology and dynamics of the plasmasphere, on magnetospheric electric fields and on coupling fluxes between ionosphere-plasmasphere (Carpenter, 1966, Park, 1972). Mid-latitude whistler study of the electron content of magnetospheric tubes of ionization reported the upward daytime fluxes of  $3 \times 10^8$  electrons  $\text{cm}^{-2} \text{ s}^{-1}$  across 1000km level and downward flux at night of the order of  $\sim 1.5 \times 10^8$  electrons  $\text{cm}^{-2} \text{ s}^{-1}$ , an amount is sufficient to maintain the nocturnal F-layer (Park, 1970). The propagation characteristics and association of plasma behavior of low latitude whistlers have been extensively studies by Hayakawa and Tanaka (1978). The low latitude whistlers are very useful for studying the unsolved problem in this field which is more susceptible to propagation conditions like duct excitation,



ionospheric transmission etc. Hayakawa et.al (1990) on night time low latitude whistlers and their propagation mechanism, pointed out that the propagation of whistlers in the earth-ionosphere wave-guide after ionospheric transmission is more likely to be towards higher latitudes than towards the equator, and sub-ionospheric propagation seems to exhibit a horizontal beaming around the magnetic meridian plane. These characteristics of the observation have interpreted either in terms of nonducted or field aligned propagation and are strongly of the opinion that this is inductive of field-aligned propagation for very low latitude whistlers localized in geomagnetic latitude of  $10^\circ - 14^\circ$ .

In this paper an attempt has been made to determine the downward flux of ionization from the whistler studies at low latitude. The data showed a smooth variation in dispersion with time. This variation in dispersion is interpreted in terms of a corresponding decrease in the electron content of tubes of ionization. At low latitudes the main difficulty in whistler analysis is to determine the nose frequency ( $f_n$ ) and nose time delay ( $t_n$ ) with a reasonable degree of precision. For the analysis of non nose whistlers, the downward flux of ionization is computed by means of an accurate curve fitting method developed by Tarcsai (1975) from the whistlers recorded on 5 June 1997 at our low latitude Jammu and is compared with that obtained by Park (1972) for mid latitudes. The magnetospheric electric field along with protonosphere coupling fluxes using simultaneous phase and group path measurements on whistler mode signals (Andrews et al. 1978). The flux of ionization is computed again from the simple diffusion equation which relates the flux to ionization gradient through the ambipolar diffusion coefficient. It is shown that the flux computed is within an order of magnitude less than that derived from the dispersion data. It is argued that the  $E \times B$  drifts play a very important role in controlling transport of ionization at low latitudes.

### Data Selection and Method of Analysis

At low latitudes, the whistler occurrence rate is low and sporadic. But once it occurs, its occurrence rate becomes comparable to that of mid-latitudes (Hayakawa et al., 1988). Similar behavior has also been observed at our low latitude Indian stations. All the Indian stations are well equipped for measurements of VLF waves from natural sources. For the present study, the whistler data chosen corresponds to June 5, 1997 for Jammu, On 5 June 1997 at Jammu station whistler activity started around 2140 h IST (Indian Standard Time) and lasted upto 2245h IST. During this period about 100

whistlers have been recorded (Lalmani et al., 2001). Altogether more than hundred whistlers were recorded and the occurrence rate showed a feeble but discernible periodicity (Rao and Lalmani, 1975). During this period several whistlers were recorded (Singh et al., 2000).

Fig.1 (a) presents dynamic spectrum of short whistlers (marked A, B, C, D, E, F and G, selected for the analysis) in the frequency band 3-4.5 KHz recorded at Jammu at 2212 IST on June 5, 1997. In the frequency band 1.7-3 KHz large number of frequency components are missing and signals resemble more like emissions rather than whistlers. Further, VLF waves in both the frequency bands do not appear simultaneously, rather they appear alternately. Fig.1 (b) shows dynamic spectrums of short whistlers (marked 1, 2, 3 and 4, selected for the analysis) and VLF emissions recorded at Jammu at 2147 IST. Whistlers are banded and diffused in the frequency range 2.7-3.7 KHz and are repeated in time. The time interval between the 55 events is not constant. Unusual VLF noises are also seen in the spectrum.

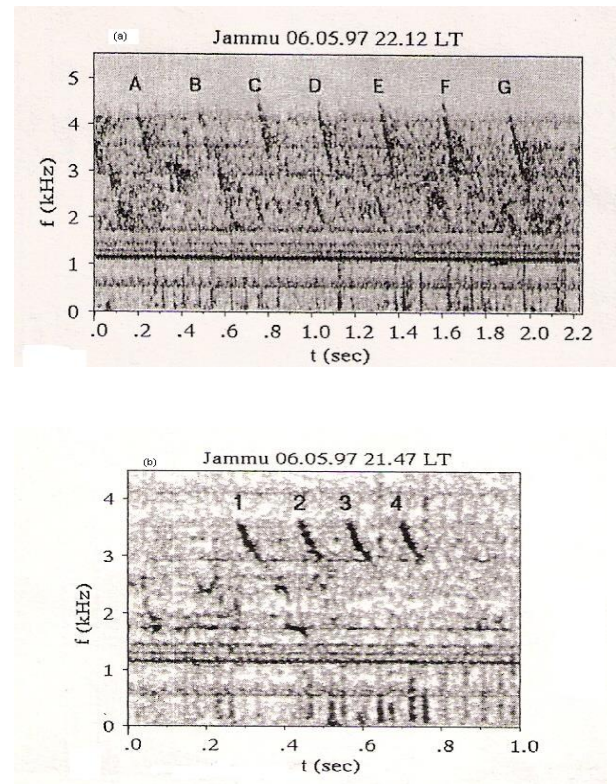


Fig. 1. (a) Dynamic spectrum of whistlers recorded at Jammu June 5, 1997. Whistlers are marked by A,B,C,D,E,F and G. (b) Dynamic spectrum of whistler recorded at Jammu June 5, 1997. Whistlers are marked by 1, 2, 3 and 4.

Tarcsai (1975) has developed a curve fitting technique for the analysis of middle and high latitude whistlers. This technique has also been applied successfully to those low latitude whistlers whose propagation path are low below  $L = 1.4$  (Singh, 1997; Sonwalker and Inan, 1995; Ohta et al., 1996; Tarcsai, 1975). Further technique is found suitable not only for long and good quality whistlers but also for short and faint whistlers. The computer programme written for the purpose requires input data such as frequency time ( $f$ ,  $t$ ) values scaled at several points along whistler trace appropriate for F2, zero frequency dispersion ( $D_o$ ), and a suitable ionospheric model etc. The output results include the  $L$ -value of propagation, equatorial electron density, total tube content etc. we have adopted this programme for the analysis of nighttime whistlers recorded at our station Nanital, Varanasi and Jammu during quiet days.

At low  $L$ -values, the curve fitting method of Tarcsai (1975) would not change too much the equatorial electron density and total electron content values compared to the systematic errors which are inherent in all of the existing nose extension methods. These systematic errors originate from the approximations used for the refractive index and for the ray path in the derivation of the analytic expressions for the dispersion and from the difference between the theoretical and actual distribution plasma along the field lines (Tarcsai et al., 1989). To examine its validity we analyzed few whistlers recorded at Jammu using this method as Dowden Allcock (1971) Q- technique. Both methods yielded results within  $\pm 10\%$ . Further, it is to be noted that the Tarcsai's method has successfully been used in the analysis of low latitude whistlers (Singh et al., 1992).

For the determination of  $D_o$ ,  $f_n$  and  $t_n$  Ho and Bernards (1973) approximate function for the dispersion of whistlers is given by (Tarcsai 1975)

$$D(f) = t(f)f^{1/2} = D_o \left[ \frac{(f_{Heq} - Af)}{f_{Heq} - f} \right] \quad (1)$$

Where

$D_o$  = zero frequency dispersion  
 $f_{Heq}$  = equatorial electron

gyrofrequency

$f$  = Wave frequency

$t(f)$  = travel time at frequency  $f$ ,

and

$$A = \frac{3\Lambda_n - 1}{\Lambda_n(1 + \Lambda_n)}$$

(2)  
Here

$$\Lambda_n = \frac{f_n}{f_{Heq}}$$

Where  $f_n$  is the nose frequency for which travel time  $t_n$  is written as

$$t_n = \left[ \frac{D_o}{f_n^{1/2}} \right] \left[ \frac{2}{(1 + \Lambda_n)} \right] \quad (3)$$

If the causative spheric is unknown, and the travel times at different frequencies of the whistler traces are measured with respect to an arbitrary time origin, then it is necessary to introduce a new parameter  $T$ ,

$$t^*(f) = t(f) - T = \frac{D_o}{\sqrt{f}} \frac{(f_{Heq} - Af)}{(f_{Heq} - f)} - T$$

$$= \left[ \frac{D_o}{\sqrt{f}} \frac{f_{Heq}f_n(f_{Heq} + f_n) - f(3f_n - f_{Heq})}{f_n(f_{Heq} - f)(f_{Heq} + f_n)} \right] - T$$

which gives the difference in time between the chosen origin and the actual causative spheric. Using  $T$  and equation (1) the measured travel time  $t^*(f)$  can be written as

(4)

In this equation there are four unknown parameters;  $D_o$ ,  $f_{Heq}$ ,  $T$  and  $f_n$ . In the following we proceed in two different ways; either we assume  $f_n$  to be an independent parameter or we adopt a model for the electron density distribution. This helps us in reducing the number of unknowns to three. In the present study, the latter procedure is followed. Thus those values of  $D_o$ ,  $f_{Heq}$ , and  $T$  searched for, which fit best to the measurements in the least square sense, i.e., which minimize the sum of the weighted squares of residuals

$$M = \sum_{k=1}^n W_k \left[ t_{mk}^* - t_{ck}^*(D_o, f_{Heq}, T) \right]^2 \quad (5)$$

Where the subscripts  $m$  and  $c$  refer to the measured and computed  $t^*$  values, respectively,  $w_k$  the

weights given to the individual measurements, and the summation is to be taken over the points of the whistler trace scaled at frequency  $f_k$ . As is known from the theory of least squares estimation, in a nonlinear case the determination of the parameters which correspond to the condition  $M = \text{minimum}$ , can be accomplished through linearization by expanding the residuals into a Taylor series and then using an iteration procedure (Tarcsai, 1975), we have done exactly this. Let us introduce the vector  $X$  whose components are

$$\begin{aligned} X_1 &= D_o \\ X_2 &= f_{Heq} \\ X_3 &= T \end{aligned} \quad (6)$$

Then assuming that the values of  $D_o$ ,  $f_{Heq}$  and  $T$  are known at iteration

(i-1), the improved solutions at the  $i$ th step can be obtained as

$$X_i = X_{i-1} + \Delta X_i \quad (7)$$

Where the vector differential corrections  $\Delta X_i$  is given in each step of the iteration by

$$\Delta X = A' W Y (A' W Y)^{-1} \quad (8)$$

In equation (8) the prime indicates matrix transposition  $A$  is then  $n \times 3$  matrix of the partial derivatives of  $t^*$  with respect to the unknown parameters, whose elements can be computed, using equation (4)

$$a_{kj} = \left( \frac{\partial t^*}{\partial x_j} \right)_{f=f_k} \quad (9)$$

$W$  is  $n \times n$  square matrix of the measurement weights, which is diagonal for uncorrected measurement errors, and  $Y$  is the column vector of residuals with elements

$$Y_k = t_{mk}^* - t_{ck}^* \quad (10)$$

In evaluating the matrix formula of equation (8), those values of  $D_o$ ,  $f_{Heq}$  and  $T$  are to be used, of course, which have been obtained in the previous step of the iteration. No weighting has been used in general ( $w_{kk} = 1$ ,  $w_{kj} = 0$ ,  $k \neq j$ ). The value of  $f_n$  has also been improved in each step, in the following manner. According to Park (1972) for typical

diffusive equilibrium model, (DE-1) of the electron density distribution,  $\Lambda_n$  can be calculated from  $f_n$  as

$$\Lambda_n = (3.5475 - 0.47351F + 0.065879F^2)^{-1} \quad (11)$$

Where  $F = \log_{10} f_n$

Also as  $\Lambda_n = f_n / f_{Heq}$ , we can write

$$f_{n,i+1} = \Lambda_{ni} f_{Heq,i+1} \quad (12)$$

Where,  $\Lambda_{ni}$  is computed from equation (11) with  $f_{ni}$  obtained in the preceding step of the iteration. Thus, for a converging,  $f_{ni}$ , the nose frequency also converges. From this it is clear that in the course of iteration the value of  $A$  is also changed successively but in general rather weakly, and it converges very fast. The iteration procedure outlined can be stopped, if the magnitude of the corrections decreases below a certain fixed level, or the sum of weighted squares of the residuals stabilizes. After the criterion of convergence has been fulfilled, i.e., the iteration has been finished,  $t_n$  can be computed from equation (3). In order to ensure the procedure against divergence it is necessary to introduce a multiplier  $m$  into equation (7) we have

$$X_i = X_{i-1} + m \Delta X_i \quad (13)$$

Where  $0 < m \leq 1$  and the actual value of  $m$  is properly varied in the course of iteration. Generally  $m \leq 0.1 - 0.3$  at the first two steps and it is increased to unity. Using values of  $D_o$  and  $f_{Heq}$  (or  $f_n$  and  $t_n$ ) obtained by the curve fitting method, we can compute the equatorial radius of the whistler duct ( $L$ ) the local electron density at the geomagnetic equator ( $n_{eq}$ ) and at a height of 1000km ( $N$ ); and the tube electron content ( $N_T$ ). After Park (1972) and Tarcsai (1975), and using equation (3) for  $t_n$  we can write

$$L = 8.735 \times 10^5 f_{Heq}^{-1/3} \quad (14)$$

Where  $f_{Heq}$  is in  $Hz$ .

$$n_{eq} = K_e f_n t_n^2 L^{-5} = K_e' D_o^2 f_{Heq}^{5/3} \quad (15)$$

$$N_T = K_T f_n t_n^2 L^{-1} = K_T' D_o^2 f_{Heq}^{1/3} \quad (16)$$

$$N = K_1 f_n t_n^2 L^{-5} = K_1' D_o^2 f_{Heq}^{5/3} \quad (17)$$

Where the constants  $K_e'$  and  $K_T'$  are weakly dependent on  $f_n$  and  $\Lambda_n$  Tarcsai (1975).

TABLE 1. Parameters of whistlers observed at Jammu ground station estimated from the whistler dispersion analysis using accurate curve fitting technique. W is the whistler number, IST is the Indian Standard Time,  $D_o$  is the dispersion of whistler,  $f_n$  is the whistler nose frequency,  $f_{Heq}$  is equatorial gyro frequency, L-value is in earths radii,  $n_e$  is the equatorial electron density.

| W  | Station | Dates&Year  | IST      | $D_o$ (sec <sup>1/2</sup> ) | $f_n$ (KHz) | $f_{Heq}$ (KHz) | L Value    | $n_e$ (cm <sup>-3</sup> ) | $N_T$ (cm <sup>-2</sup> ) |
|----|---------|-------------|----------|-----------------------------|-------------|-----------------|------------|---------------------------|---------------------------|
| 1  | Jammu   | 05June 1997 | 21:40:25 | 65.5±1.0                    | 4.2±0.03    | 11.37±0.07      | 4.25±0.01  | 159±3                     | 1.9×10 <sup>13</sup>      |
| 2  | Jammu   | 05June 1997 | 21:47:42 | 81.9±1.1                    | 3.39±0.013  | 10.59±0.034     | 4.35±0.005 | 220±5                     | 2.9×10 <sup>13</sup>      |
| 3  | Jammu   | 05June 1997 | 22:47:50 | 88.9±1.8                    | 3.82±0.02   | 10.27±0.05      | 4.39±0.07  | 247±8                     | 1.9×10 <sup>13</sup>      |
| 4  | Jammu   | 05June 1997 | 22:47:55 | 87.6±1.4                    | 3.85±0.01   | 10.37±0.03      | 4.38±0.00  | 244±6                     | 3.4×10 <sup>13</sup>      |
| 5  | Jammu   | 05June 1997 | 22:12:20 | 28.8±1.2                    | 8.15±0.72   | 21.98±1.95      | 3.41±0.10  | 93±6                      | 3.3×10 <sup>12</sup>      |
| 6  | Jammu   | 05June 1997 | 22:12:51 | 28.9±0.9                    | 6.29±8.21   | 16.96±0.55      | 3.72±0.04  | 61±1                      | 4.5×10 <sup>12</sup>      |
| 7  | Jammu   | 05June 1997 | 22:13:22 | 35.5±1.7                    | 6.13±0.25   | 16.51±0.66      | 3.75±0.05  | 88±2                      | 4.2×10 <sup>12</sup>      |
| 8  | Jammu   | 05June 1997 | 22:13:53 | 38.3±1.9                    | 4.61±0.10   | 12.42±0.28      | 4.12±0.03  | 63±4                      | 6.3×10 <sup>12</sup>      |
| 9  | Jammu   | 05June 1997 | 22:14:24 | 26.1±0.6                    | 5.76±0.13   | 15.53±0.35      | 3.83±0.02  | 43±4                      | 3.3×10 <sup>12</sup>      |
| 10 | Jammu   | 05June 1997 | 22:14:55 | 22.8±1.7                    | 5.99±0.41   | 16.17±1.10      | 3.78±0.08  | 35±1                      | 2.6×10 <sup>12</sup>      |
| 11 | Jammu   | 05June 1997 | 22:15:26 | 38.9±1.2                    | 5.06±0.09   | 13.62±0.24      | 4.00±0.02  | 76±3                      | 7.1×10 <sup>12</sup>      |

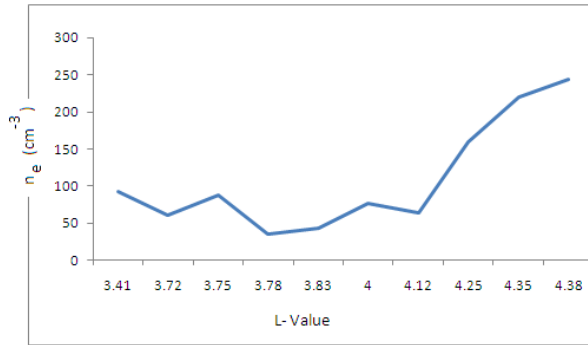


Fig. 2. Variation of equatorial electron density ( $n_e$ ) with L.

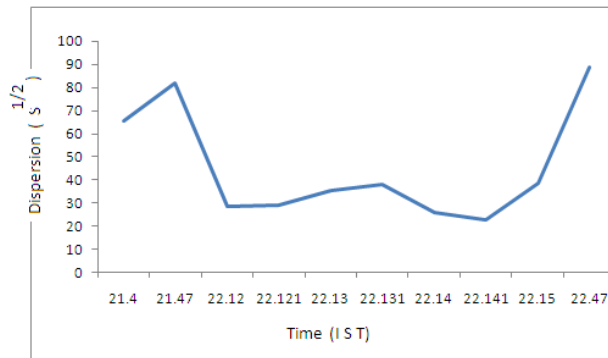


Fig.3. Variation of dispersion with time.

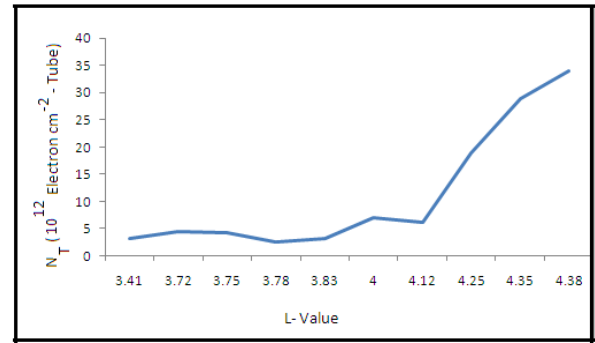


Fig. 4. Variation of Electron tube content with L-Value

### Transport of Ionization and Ambipolar Diffusion

The observed flux of ionization at 500km can be explained by ambipolar diffusion. The ambipolar diffusion coefficient ( $\delta_a$ ), the gradient of electron density ( $\nabla n$ ) and the flux of ionization ( $F$ ) are related by (Carpenter and Bowhill, 1971)

$$F = \delta_a \cdot \nabla n \quad (18)$$

The ambipolar diffusion coefficient  $\delta_a$  (i.e parallel to magnetic field) is approximately given by

$$\delta_a \approx \delta_i \left( 1 + \frac{T_e}{T_i} \right) \quad (19)$$

Where  $\delta_a$  = diffusion coefficient of ions =  $K(T_i/m_i v_{in})$ ,

Here

$T_e$  = electron Temperature,

$T_i$  = Ion temperature,

$K$  = Boltzman Constant,

$m_i$  = mass of ion

and  $\nu_{in}$  = collision frequency between ions and neutral particles.

The value of  $\delta_a$  can be easily calculated with the reasonable values of  $T_e$ ,  $T_i$  and  $\nu_{in}$ . The determined value of  $\delta_a$  at a height of 500 km is  $2 \times 10^{11} \text{ cm}^2 \text{ s}^{-1}$  (Okuzawa et al, 1971). To compute the magnitude of  $\nabla n$  which can be determined from the electron density distributions derived from whistler observations. At a height of 500km this gradient is around  $5.4 \times 10^{-3} \text{ cm}^{-3}$ . Thus the magnitude of flux is about  $14.6 \times 10^7 \text{ cm}^{-2} \text{ s}^{-1}$  which is within one order of magnitude less than the value of  $2.8 \times 10^8 \text{ cm}^{-2} \text{ s}^{-1}$  obtained earlier.

## DISCUSSION OF RESULTS

It is useful information to compare the above results of total electron content and the flux with the values of Park (1970) whose computations for the L-values between 3.5 – 5. The total electron content of tubes for the given L- values are according to Park (1970, 1972) of the order of  $10^{13}$  electrons  $\text{cm}^{-2}$ . Our results are shown in the Table 1. which cannot make any direct comparison with Park (1970, 1972). For the L-values between 3.8 – 4.4, of our observations, the equatorial electron density ( $n_e$ ) and tube electron content ( $N_T$ ) are  $2 \times 10^2$  electron  $\text{cm}^{-3}$  and  $10^{12}$  -  $10^{13}$  electron  $\text{cm}^{-2}$  –tube respectively. This error at low latitudes as compared with high latitudes may be due to the use of the nose extension method of a non nose whistler recorded at our low latitude station Jammu. During the night time due to interchange of ionization between the ionosphere and protonosphere and downward flux of ionization from 500 km to 1000km at mid latitude. Similar downward flux of ionization is observed by our observations recorded at low latitude station.

As per our calculations a downward flux of ionization is of the order of  $2 \times 10^8$  electron  $\text{cm}^{-2} \text{ s}^{-1}$  which is in agreement with Park (1970). The main factor which render our result inaccurate is due to the non-nose low latitude whistlers are observed. In the top-side F-region the present studying of the transport of ionization is still worthwhile. If the measurements of the F-layer by other methods simultaneously (Such as incoherent scatter) are available then our studies would have found much more valuable and physically significant results. However, the value of flux of ionization obtained by ambipolar diffusion process is  $14.4 \times 10^7$  electron  $\text{cm}^{-2} \text{ s}^{-1}$  which is less one order of magnitude than the value of  $2 \times 10^8$  electron  $\text{cm}^{-2} \text{ s}^{-1}$ . This shows that ambipolar diffusion alone cannot explain the observed results. The conclusion is consistent with that of Okuzawa et. al. (1971), who

attempted to explain the duct spreading in terms of the diffusion process.

However, most of the mid-latitude observations of whistlers suggest strongly that  $E \times B$  drifts plays an important role in the transport of ionization (Angerami and Carpenter, 1966, Park, 1970, 1972). Therefore, it is concluded that the transport processes like  $E \times B$  drifts must be operating at these latitudes. In terms of  $E \times B$  drifts the downward movement of ionization have been interpreted and the electric field inferred are westward in the morning sector (Park and Meng, 1971, Altaf and Ahman, 2014). Tube content profiles undergo complex and rapid changes during the substorm (Park, 1970, 1971, 1972) probably because of combination of  $E \times B$  drifts and fluxes along field lines, for this a westward electric field of  $\sim 1 \text{ mVm}^{-1}$  is required. The westward electric field estimated by whistler data is about  $1 \text{ mVm}^{-1}$  (Misra, 1979, Altaf and Ahmad, 2014) from the radial motions of discrete field-aligned whistler ducts as indicated by changes in nose frequency (Block and Carpenter, 1974; Hayakawa and Tanaka, 1978) studied in favour of ducted propagation of low latitude whistlers on the basis of theoretical and experimental results. In the geomagnetic latitude of  $10^\circ$ - $14^\circ$  Hayakawa et. al (1990) have shown that the localization of field-aligned propagation of low latitude whistlers with the help of a speed direction finding method. The computed results reported by other workers lie well within the range (Carpenter et. a., 1972, Block and Carpenter, 1974, Andrews et. al, 1978, Park, 1978) from the ground based observations, although their result refer to higher latitudes. This study shows the important relationship between vertical drifts and protonospheric fluxes and shows both are important in the night-time ionosphere. Hence, it shows that  $E \times B$  drifts plays an essential role in controlling transport of ionization at low latitudes.

## ACKNOWLEDGEMENT

The Author is thankful to the Govt Higher Education Department J&K India and Principal GDC Pattan for their keen interest to the present research.

## REFERENCES

- [1] Park, C G, Methods of determining electron concentration in the magnetosphere from nose whistlers. Technical Report No. 3454-1 Radio sci. Lab, Stanford Electronics Lab. Stanford University, Stanford. (1972)
- [2] Mayar, H C; Bruce, L H and Dunham G S. Ion composition and temperature in the topside ionosphere, J. Geophys. Res. 72, 4391. (1967)

- [3] Samayajulu, V V. Ph. D Thesis, B. H. U, Varanasi, India. (1968)
- [4] Brinton, H C; Pharo, M W, III; Mayar, H C and Taylor H A, Implications for ionospheric chemistry and dynamics of a direct measurement of ion composition in the F2 region, J. Geophysics, Res. 74, 2941. (1969)
- [5] Park, C G and Carpenter, D I, Whistler evidence of large Scale electron density irregularities in the plasmasphere. J. Geophysics. Res. 75, 3825. (1970)
- [6] Carpenter D L and Bowhill, S A, Aeronomy Rept. No. 44. Univ. Of Illinois, Urbana IL (1974)
- [7] Riebeth, H. The effect of winds on the ionospheric F2 peak-II. J. Atmos. Terr. Phys. 30, 63. (1968)
- [8] Carpenter, D L. Whistler studies of the plasmapause in the magnetosphere-I. Temporal variation in the position of the knee and some evidence on plasma motions near the knee. J. Geophys. Res. 71, 693. (1966)
- [9] Hayakawa, M. And Tanaka, Y. On the propagation of low latitude whistlers. Rev. Geophys. Space Phys. 16, 111. (1978)
- [10] Hayakawa, M; Ohta, K and Shimakura M. S. Spaced directions finding of night time whistlers at low and equatorial latitudes and their propagation mechanism. J. Geophys. Res. 95, 15091. (1990)
- [11] Tarcsei, G. Routine whistler analysis by means of accurate curve fitting. J. Atmos. Terr. Phys. 37, 1447. (1975)
- [12] Dowden, R.L., and Allcock, G. Mak., Determination of nose frequency of non-nose whistlers. J. Atmos. Terr. Phys., 33, 1125-1129, (1971).
- [13] Tarcsei, G., Strangeway, H.J and Rycroft, M.J., Error Sources and travel time residuals in plasmaspheric whistler interpretation. J. Atmos. Terr. Phys., 51, 249-258, (1989)
- [14] Singh, U P; Singh, A K; Lalmani; Singh, R P and Singh, R N. Hybrid mode propagation of whistlers at low latitude. Ind. J. . Radio space Phys. 21, 246-250, (1992)
- [15] Singh, B. Middle and High latitude whistlers observed simultaneously in a low latitude station at Agra. J. Geomag. Geoelectricity., 49, 995-1000, 1997.
- [16] Sonwalkar, V.S, Inan, U.S, Angerson, T.L, Farrell, W.M. Pfaff, R.J. Geophys. Res. 100, 7783-7790, 1995.
- [17] Ho, D and L.C. Bernard, A fast method to determine the nose frequency and minimum group delay of whistlers when the causative spheric is unknown., J. Atmos. Terr. Phys. 35, 881-887. (1973).
- [18] Ohta, K; Kitagawa, T; Shima, K; Hayakawa, M and Dowden, R.R. Characteristics of mid latitude whistler ducts as deduced from ground based measurements. Geophys. Res. Lett., 23, 3301-3304, (1996).
- [19] Andrews, M K; Knox, F B and Thomson, N R. Magnetospheric electric fields and protonospheric coupling fluxes inferred from simultaneous phase and group path measurements on whistler mode signals. Planet space Sci. 26, 171. (1978)
- [20] Altaf, M and Ahmad, M M. Estimation of magnetospheric plasma parameters from whistlers observed at low latitudes CURRENT SCIENCE, VOL. 106, NO. 3, 10. (2014)
- [21] Okuzawa, T ; Yamanka, K and Yashino, T. Characteristics of low latitude whistler propagation associated with magnetic storms in March 1970, Rept. Ionospace. Res. Japan. (1971)
- [22] Park, C G. Whistler observations of the interchange of ionization between the ionosphere and the protonosphere. J. Geophys. Res. 75, 4249. (1970)
- [23] Park, C.G. Westward electric fields as the cause of night time enhancements in electron concentrations in mid latitude F regions. J. Geophys. Res. 76, 4560. (1971)
- [24] Block, L P and Carpenter, D L. Derivation of magnetospheric electric field from whistler data in a dynamic geomagnetic field. J. Geophys. Res. 79, 2783. (1974)
- [25] Misra, K D; Singh, B D and Misra, S P. Effect of the parallel electric field on the whistler mode instability in the magnetosphere. J. Geophys. Res. 84, 5923. (1979)
- [26] Carpenter, D L; Stone, K; Siren, J C and Crystal, T L. Magnetospheric electric fields deduced from drifting whistler paths. J. Geophys. Res. 77, 2819. (1972)
- [27] Park, C G. Whistler observations of substorm electric fields in the night side plasmasphere. J. Geophys. Res. 83, 5773. (1978)

## METAL PLASTICITY AND PERIODIC TABLE

Lev B. Zuev<sup>1</sup>, Svetlana A. Barannikova<sup>1</sup> and Albina M. Zharmukhambetova<sup>1</sup>

<sup>1</sup>Strength Physics Laboratory, Institute of Strength Physics & Materials Science SB RAS, Russia

### ABSTRACT

We consider the autowave mechanism of evolution of a localized plastic deformation of crystalline solids of different origins. It is found that localization of the plastic flow is determined by the relation between elastic and plastic phenomena in deforming materials. It is shown that parameters of plastic flow localization at the stage of linear strain hardening in the process of solid body deformation are closely related to characteristics of the electronic structure of metals. Inverse of the product of wavelength and velocity of the localized plasticity autowave grows linearly with the number of conduction electrons per unit cell of the metal. The obtained data directly indicate that the nature of the electron-gas contribution to hindering of dislocations is more complicated. Thus, the parameters of plastic flow localization are defined by the position of metal in the Mendeleev periodic table.

*Keywords: Plastic deformation, Autowave, Pattern, Electronic structure, Periodic Table*

### INTRODUCTION

Plastic deformation of solids is a complex physical phenomenon the evolution of which depends on the crystal lattice and crystal structure defects. The process of plastic flow is usually described by the dependence  $\sigma(\varepsilon)$  of the deforming stress on the strain. It is important that at all its stages from the beginning of plastic flow (yield stress) to fracture (ultimate strength), this process is accompanied by plastic strain localization [1].

The model of evolution of localized plastic strain proposed in [1] presumes that self-organization of the defect structure [2] occurs in the form of autowaves of a localized plastic flow [1], [3], which appear in the deforming medium as a result of interaction of elastic waves and relaxation events of breaking of elastic stress concentrators. Each relaxation event contributes to the overall plastic deformation and generates new stress concentrators. The autowave pattern of localized plasticity distribution regularly changes in accordance with the stage nature of the  $\sigma(\varepsilon)$  curve so that the deformation process can be treated as a natural evolution of localized plasticity autowaves [1].

Therefore, autowaves (localized plasticity) and wave (elastic) deformation phenomena coexist in a plastically deforming medium. The former are characterized by wavelength  $\lambda$  of the localized plasticity autowave and velocity  $V_{aw}$  of its propagation, while the latter are determined by the interplanar distance  $\chi$  in the crystal lattice of the tested material and the velocity  $V_t$  of propagation of transverse elastic waves.

It was noted in earlier experiments with a number of metals [1], [4], [5] that dimensionless ratio

$\lambda V_{aw}/\chi V_t$  formed by these four characteristics is the same for all cases of straining of different metals at the stages of linear strain-hardening when  $\sigma \sim \varepsilon$ . This suggested that ratio  $\lambda V_{aw}/\chi V_t$  is invariant in general. This study aims at the verification of this regularity not only for metals, but also for other materials with a linear law hardening. It is also important to clarify the origin of this relation using general thermodynamic concepts.

### EXPERIMENTAL DATA

Experimental investigations of localized plastic flow were carried out for different metals related to periods 3–6 of Mendeleev's Periodic Table (see Table 1). The quantitative data on the localized plasticity patterns were estimated experimentally for linear stages of the processes at which the deforming stresses and strains are connected by a linear relation. In these cases, a phase localized plasticity autowave corresponding to the condition of the constancy of phase  $2\pi(t/T - x/\lambda) = \text{const}$  is observed, where  $T$  is the period of oscillations in the wave,  $x$  is the coordinate, and  $t$  is the running time. The localized plasticity pattern formed in such cases is stable and can be observed relatively easily [1].

For estimating ratio  $\lambda V_{aw}/\chi V_t$  characterizing various materials, the range of metals under investigation was extended. In addition, we studied the localization of plastic deformation in alkali-halide crystals (KCl, NaCl, and LiF) and rocks such as sandstone ( $\text{SiO}_2$ ) and marble ( $\text{CaCO}_3$ ). The method for observing the patterns of a localized plastic flow in deforming materials, which was based on speckle photography, was described in detail earlier [1] and will not be discussed here. For illustrating the potentialities of this method, Fig. 1 shows a typical



pattern of local plasticity distribution for sequential stages of easy slip and linear strain-hardening during tension with a constant rate for a single crystal sample of alloy Fe-12 wt %Mn ( $\gamma$ -Fe).

Table 1 Metals under study

| Period | Metals        |    |    |    |    |    |    |    |
|--------|---------------|----|----|----|----|----|----|----|
| 3      | Element       | Mg | Al |    |    |    |    |    |
|        | Atomic number | 12 | 13 |    |    |    |    |    |
| 4      | Element       | Ti | V  | Fe | Co | Ni | Cu | Zn |
|        | Atomic number | 22 | 23 | 26 | 27 | 28 | 29 | 30 |
| 5      | Element       | Zr | Nb | Mo | Cd | In | Sn |    |
|        | Atomic number | 40 | 41 | 42 | 48 | 49 | 50 |    |
| 6      | Element       | Hf | Ta | Pb |    |    |    |    |
|        | Atomic number | 72 | 73 | 82 |    |    |    |    |

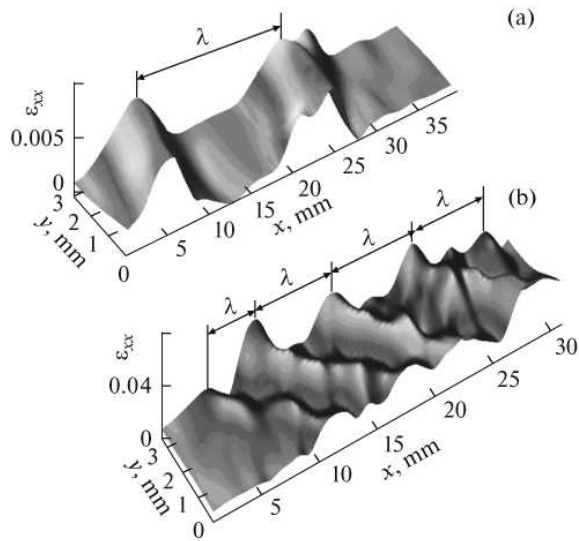


Fig. 1 Strain distribution over a sample of Fe-12 wt %Mn alloy (a) at the easy slip state and (b) at the linear work hardening stage.

The quantitative characteristics  $\lambda$  and  $V_{aw}$  required for analyzing the data on the evolution of localized plasticity were determined from the processing of the so-called  $X-t$  diagrams proposed in [1] for such purposes and shown in Fig. 2. It can be seen from the figure that the values of autowave wavelength  $\lambda$  and period  $T$  can be determined from the vertical and horizontal sections of families of the  $X(t)$  curves. Characteristics  $\lambda$  and  $V_{aw} = \lambda/T$  of localized plasticity autowaves were determined for linear

work-hardening of metals, easily slip in metal single crystals, compression of rock samples, and the phase-transformation straining of the NiTi single crystal.

Let us analyze the data obtained in these experiments. The values of products  $\lambda V_{aw}$  for 19 tested metals are given in Table 2. It can be seen that the results differ insignificantly and the mean value of the product of these quantities is  $\langle \lambda V_{aw} \rangle_{lwh} = (2.52 \pm 0.36) \times 10^{-7} \text{ m}^2/\text{s}$ .

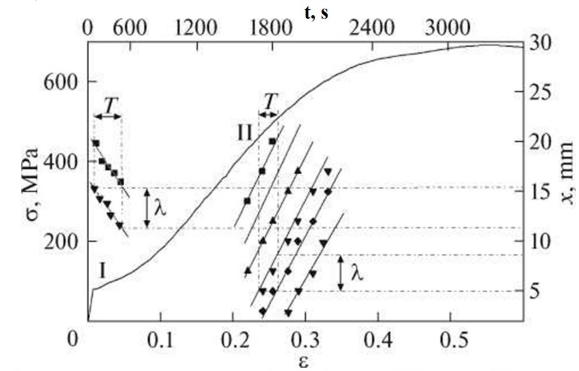


Fig. 2  $X-t$  diagram for Hadfield steel single crystal, plotted for the case shown in Fig. 1.

We managed to supplement these data with the results of analogous processing of localized plasticity patterns observed at the easy slip stages in Cu, Ni,  $\alpha$ -Fe,  $\gamma$ -Fe, Zn, and Sn single crystals for which the proportionality  $\sigma \sim \varepsilon$  also holds and a phase autowave is observed. For this stage, we have  $\langle \lambda V_{aw} \rangle_{eg} \sim (2.95 \pm 1.05) \times 10^{-7} \text{ m}^2/\text{s}$  (see Table 2).

The stage of linear work-hardening and corresponding localized plasticity phase autowaves were observed for compressed samples of alkali-halide crystals and rocks [6], [7]. The results of these experiments given in Table 3 lead to  $\langle \lambda V_{aw} \rangle_{abc} = (3.44 \pm 0.49) \times 10^{-7} \text{ m}^2/\text{s}$  and  $\langle \lambda V_{aw} \rangle_{rock} = (1.44 \pm 0.34) \times 10^{-7} \text{ m}^2/\text{s}$ .

In the case of staining due to the slip of individual dislocations, the process is usually characterized by dislocation path length  $l$  and dislocation velocity  $V_{disl}$ ; these parameters were determined from analysis of the available data on the mobility of individual dislocations in single crystals [8]-[12] in the quasi-viscous flow regime, in which  $V_{disl} \sim \sigma$  [13]. In such conditions, the characteristic dislocation path lengths lie in the interval  $10^{-5} \text{ m} \leq l \leq 10^{-4} \text{ m}$  and the velocities of dislocations belong to the range  $10^{-3} \text{ m/s} \leq V_{disl} \leq 10^{-2} \text{ m/s}$ . The product of these quantities was estimated using the relation  $lV_{disl} = V_{disl}^2 \tau$ , where  $\tau$  is the duration of the load pulse acting during the crystal loading. The results of calculations of products  $lV_{disl}$  in these cases are given in Table 4. It can be seen that  $\langle lV \rangle_{disl} = (3.2 \pm 0.35) \times 10^{-7} \text{ m}^2/\text{s}$  in this case.

Table 2 Comparison of quantities  $\chi V_t$  and  $\lambda V_{aw}$  for metals

| $\times 10^7 \text{ m}^2/\text{s}$ | Linear strain hardening stage |      |     |      |     |      |      |                 |              |      |     |     |      |
|------------------------------------|-------------------------------|------|-----|------|-----|------|------|-----------------|--------------|------|-----|-----|------|
|                                    | Cu                            | Zn   | Al  | Zr   | Ti  | V    | Nb   | $\alpha$ -Fe    | $\gamma$ -Fe | Ni   | Co  | Mo  |      |
| $\lambda V_{aw}$                   | 3.6                           | 3.7  | 7.9 | 3.7  | 2.5 | 2.8  | 1.8  | 2.55            | 2.2          | 2.1  | 3.0 | 1.2 |      |
| $\chi V_t$                         | 4.8                           | 11.9 | 7.5 | 11.9 | 7.9 | 6.2  | 5.3  | 4.7             | 6.5          | 6.0  | 6.0 | 7.4 |      |
| $\lambda V_{aw}/\chi V_t$          | 0.75                          | 0.3  | 1.1 | 0.3  | 0.3 | 0.45 | 0.33 | 0.54            | 0.34         | 0.35 | 0.5 | 0.2 |      |
| $\times 10^7 \text{ m}^2/\text{s}$ | Linear strain hardening stage |      |     |      |     |      |      | Easy slip stage |              |      |     |     |      |
|                                    | Sn                            | Mg   | Cd  | In   | Pb  | Ta   | Hf   | $\alpha$ -Fe    | $\gamma$ -Fe | Cu   | Zn  | Ni  | Sn   |
| $\lambda V_{aw}$                   | 2.4                           | 9.9  | 0.9 | 2.6  | 3.2 | 1.1  | 1.0  | 7.4             | 2.9          | 1.9  | 1.0 | 1.3 | 3.3  |
| $\chi V_t$                         | 5.3                           | 15.8 | 3.5 | 2.2  | 2.0 | 4.7  | 4.2  | 6.5             | 6.0          | 4.7  | 5.0 | 6   | 4.9  |
| $\lambda V_{aw}/\chi V_t$          | 0.65                          | 0.63 | 0.2 | 1.2  | 1.6 | 0.2  | 0.24 | 1.1             | 0.49         | 0.4  | 0.2 | 0.2 | 0.67 |

The experimental estimation of the parameters of a localized plasticity autowave for plastic deformation of TiNi intermetallide single crystal of the equiatomic composition (strain-induced phase transformation [14]) resulted in the value  $\langle \lambda V_{aw} \rangle_{pt} \approx 0.85 \times 10^{-7} \text{ m}^2/\text{s}$ .

Table 3 Comparison of quantities  $\chi V_t$  and  $\lambda V_{aw}$  for alkali- halide crystals [6] and rocks [7]

| $\times 10^7 \text{ m}^2/\text{s}$ | KCl  | NaCl | LiF | Marble | Sandstone |
|------------------------------------|------|------|-----|--------|-----------|
| $\lambda V_{aw}$                   | 3.0  | 3.1  | 4.3 | 1.75   | 0.6       |
| $\chi V_t$                         | 7.0  | 7.5  | 8.8 | 3.7    | 1.5       |
| $V_{aw}/\chi V_t$                  | 0.43 | 0.4  | 0.5 | 0.5    | 0.4       |

Comparing pairwise the above data by calculating the Student t-test [15], we can conclude that the resultant values differ insignificantly (i.e., belong to the same general population). This leads to

$$\langle \lambda V_{aw} \rangle_{lwh} \approx \langle IV \rangle_{disl} \approx \langle V_{aw} \rangle_{pt} \approx \langle V_{aw} \rangle_{abc} \approx \langle V_{aw} \rangle_{rock} \quad (1)$$

Elastic processes in the tested materials were characterized by interplanar distances  $\chi$  in the crystal lattice [16] and velocities  $V_t$  of propagation of transverse elastic waves [17]. As follows from Tables 2-4, we have  $\langle \chi V_t \rangle_{el} = (5.8 \pm 0.3) \times 10^{-7} \text{ m}^2/\text{s}$  for all tested materials.

Table 4 Comparison of quantities  $\chi V_t$  and  $IV_{disl}$  determined by measuring of path lengths of individual dislocations

| $\times 10^7 \text{ m}^2/\text{s}$ | NaCl [8] | LiF [9] | CsI [10] | KCl [11] | Zn [12] |
|------------------------------------|----------|---------|----------|----------|---------|
| $IV_{disl}$                        | 4.1      | 4.1     | 1.9      | 4.1      | 1.8     |
| $\chi V_t$                         | 7.3      | 8.6     | 4.0      | 6.8      | 4.0     |
| $IV_{disl}/\chi V_t$               | 0.56     | 0.47    | 0.47     | 0.6      | 0.45    |

Analysis of the data array obtained for stages of linear strain hardening made it possible to establish that the dependence of  $\lambda V_{aw}$  on atomic number of the

element  $Z$  oscillates with respect to the average value with increasing number of the element within the limits of  $13 \leq Z \leq 82$ . It has been found that these oscillations correlate with regularities in the behavior with an increase in  $Z$  of some independently determined lattice characteristics such as, e.g., characteristic Debye temperature  $\Theta_D \approx \hbar \omega_D / k_B$  ( $\hbar = h/2\pi$  is the Planck constant,  $\omega_D$  is the Debye frequency, and  $k_B$  is the Boltzmann constant) [16], density, melting temperature, elastic moduli, and ionization potential [17]. As an example, correlation of the discussed dependences is illustrated by the common mode behavior of the quantities  $\lambda V_{aw}$  binding energy  $E_b$  and  $\Theta_D$  as functions of the atomic number of the elements under study (Fig. 3).

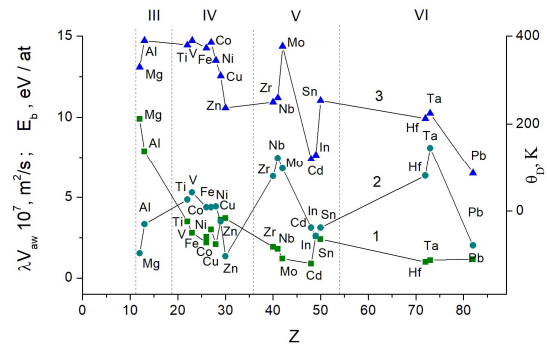


Fig. 3 The quantity (1)  $\lambda V_{aw}$ , binding energy  $E_b$  (2) and (3) Debye temperature  $\Theta_D$  as functions of atomic number of elements  $Z$  (III, IV, V, and VI are numbers of periods)

In addition, in analyzing the behavior of the product  $\lambda V_{aw}$  within the limits of each period of Mendeleev's periodic law, it has been found that the quantity  $(\lambda V_{aw})^{-1}$  grows linearly with the number of conduction electrons per unit cell of the metal  $n$  [18]; therefore, the relation

$$(\lambda V_{aw})^{-1} = A + B \cdot n \quad (2)$$

where  $A$  and  $B$  are constants different for periods 3, 4, 5, and 6, is valid in each period. The dependences

established for the abovementioned periods are shown in Fig. 4.

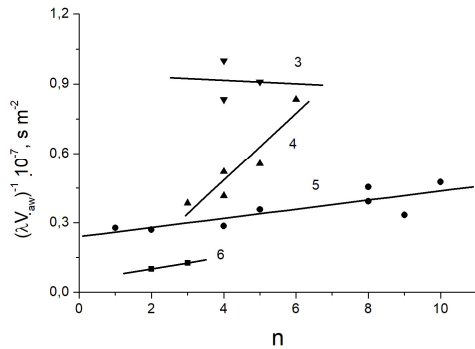


Fig. 4 The quantity  $(\lambda V_{aw})^{-1}$  as a functions of number of conduction electrons per unit cell  $n$  (3, 4, 5, and 6 are numbers of periods)

It was also noted that the parameter of plasticity  $\lambda V_{aw}$  correlates with different physical properties, as shown in Fig.5 a-b.

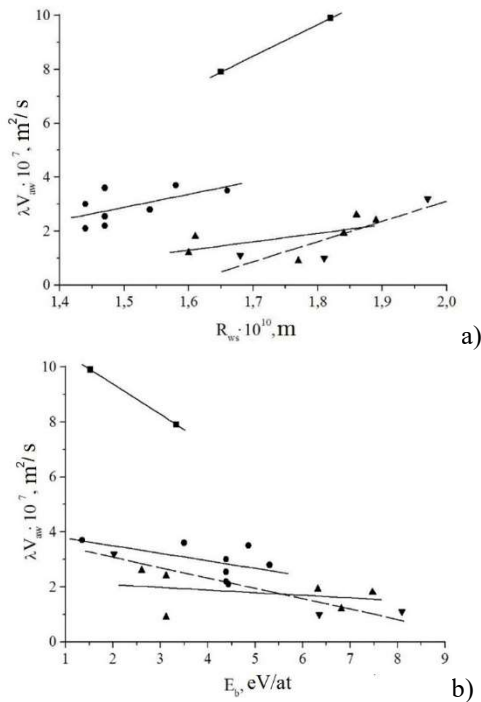


Fig. 5 The dependence of parameter of plasticity on Wigner-Seitz radius (a), the bond energy (b), ■ – elements of the 3rd period (Mg, Al), ● – elements of the 4th period (Ti, V,  $\alpha$ -Fe,  $\gamma$ -Fe, Co, Ni, Cu, Zn), ▲ – elements of the 5th period (Zr, Nb, Mo, Cd, In, Sn); ▼ – elements of the 6th period (Hf, Ta, Pb). The correlation coefficient: (a)  $R=1; 0,6; 0,6; 0,9$ ; (b)  $R=1; 0,53; 0,4; 0,95$

In this case, the dependencies are presented in the form of four linear dependencies, which covers a metals related to the 3rd, 4th, 5th and 6th periods of

Mendeleev periodic table respectively.

The existence of a linear relation such as (Eq.2) was already noted in [19]; however, the separation by periods of Mendeleev's Table was not observed earlier. Processing of experimental data for elements of periods 4–6 shows that,

$$B = A \cdot \exp(\beta/N), \quad (3)$$

where  $A$  and  $B$  are constants. In relation (3),  $N = 4, 5$ , and  $6$  is the period number in Mendeleev's periodic law (it is well known [20] that the number of the period coincides with the number of electron shells of its atoms) and  $\beta$  is a constant.

It has been found that the quantity  $\lambda V_{aw}$  grows linearly with normalized the Debye temperature  $\Theta_D$  [17, 18]; therefore, the relation

$$\lambda V_{aw} = A \cdot \Theta_D \cdot \frac{k_B}{E_b}, \quad (4)$$

where constant  $A = 4.42 \cdot 10^{-5} \text{ m}^2/\text{s}$ ,  $E_b$  is binding energy and  $k_B$  is the Boltzmann constant. The dependence established for the abovementioned periods is shown in Fig. 6.

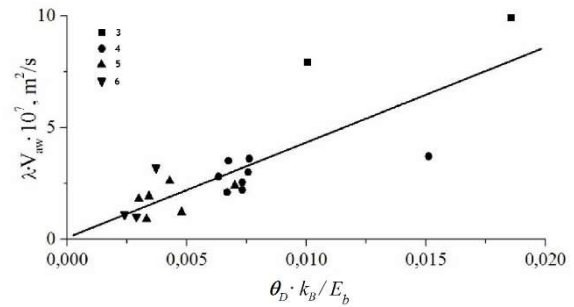


Fig. 6 The quantity  $\lambda V_{aw}$  as a functions of normalized the Debye temperature  $\Theta_D$  (3, 4, 5, and 6 are numbers of periods)

The coefficient of correlation between the quantities presented in Fig. 5 is  $\sim 0.96$ , which indicates the existence of a functional relationship between them [15].

## CONCLUSIONS

The obtained data testify that parameters of plastic flow localization at the stage of linear work hardening in the process of solid body deformation are closely related to characteristics of the electronic structure of metals. This relation manifests itself as a dependence of macroscopic characteristics of localized plasticity autowave propagation at the stage of linear strain hardening on the period number in Mendeleev's Table. In addition, these characteristics depend on the number of valence electrons; for most metals but transition ones, it coincides with the group number in the periodic system. The obtained data directly

indicate that the nature of the electron-gas contribution to hindering of dislocations is more complicated than is envisaged in existing theories [21] of this effect.

The elastic-plastic invariant necessitates the allowance for the role played by elastic (lattice) characteristics of materials and is important in the development of models [22-32] and mechanisms of evolution of a plastic flow [33-42].

## ACKNOWLEDGMENTS

This work was performed by the financial support of RSF, grant no. 16-19-10025 P.

## REFERENCES

- [1] Zuev L.B., Danilov V.I., Barannikova S.A., Zykov I.Y., A new type of plastic deformation waves in solids, *Applied physics A-Materials Science & Processing*, Vol.71, Issue 1, 2000, pp. 91-94.
- [2] Seeger A. and Frank W., Structure Formation by Dissipative Processes in Crystals with High Defect Densities, *Non-Linear Phenomena in Material Science*, Ed. by L. P. Kubin and G. Martin, New York, Trans Tech, 1987, pp. 125-138.
- [3] Davydov V. A., Davydov N. V., Morozov V. G., Stolyarov M. N., and Yamaguchi T., Autowaves in moving excitable media. *Condensed Matter Physics*, Vol. 7, Issue 3, 2004, pp.565-578.
- [4] Barannikova S.A., Nadezhkin M.V., Mel'nichuk V.A., Zuev L.B., Tensile plastic strain localization in single crystals of austenite steel electrolytically saturated with hydrogen, *Technical Physics Letters*, Vol. 37, Issue 9, 2011, pp. 793-796.
- [5] Barannikova S., Zuev L., Li Y., Plastic flow heterogeneity and failure of bimetal material, *International Journal of GEOMATE*, Vol. 14, Issue, 43, 2018, pp. 112-117.
- [6] Barannikova S. A., Nadezhkin M. V., and Zuev L. B., Relationship between burgers vectors of dislocations and plastic strain localization patterns in compression-strained alkali halide crystals, *Technical Physics Letters*, Vol. 37, 2011, p. 750.
- [7] Zuev L. B., Barannikova S. A., Nadezhkin M. V., and Gorbatenko V. V., On the Observation of Slow Wave Processes in Deforming Rock Sample, *Journal of Mining World Express*, Vol.2, Issue 1, 2013, pp. 31-39.
- [8] Kurilov V. F., Zuev L. B., Gromov V. E., Sergeev V. P., and Gershtein G. I., Dynamic Deceleration of Dislocations in NaCl Crystals of Different Purity, *Kristallografiya* 22, 1977, pp. 653-654.
- [9] Darinskaya E. V., Urusovskaya A. A., Opekunov V. N., Abramchuk G. A., and Alekhin V. F., Study of Viscous Deceleration of Dislocations in LiF Crystals Based on the Mobility of Individual Dislocations, *Fizika Tverdogo Tela*, Vol. 20, 1978, p. 1250-1252.
- [10] Darinskaya E. V. and Urusovskaya A. A., Viscous Deceleration of Dislocations in CsI Crystals at a Temperature of 77–300 K, *Fizika Tverdogo Tela*, Vol. 17, 1975, pp. 2421-2422.
- [11] Zuev L. B., Gromov V. E., and Aleksankina O. I., Dependence of Dislocation Velocity on Electric Field Intensity, *Kristallografiya*, Vol. 19, 1974, pp. 889-891.
- [12] Zuev L. B., Gromov V. E., Kurilov V. F., and Gurevich L. I., Mobility of Dislocations in Zn Single Crystals Under the Action of Current Pulses, *Dokl. Akad. Nauk SSSR*, Vol. 239, 1978, pp. 874-876.
- [13] Al'shits V. I. and Indenbom V. L., Dislocations in Solids, Ed. by F. R. N. Nabarro, Amsterdam Elsevier, 1986, p. 1-43.
- [14] Otsuka K. and Shimizu K., Pseudoelasticity and shape memory effects in alloys, *International Metals Reviews*, Vol. 31, Issue 3, 1986, pp. 93.
- [15] Hudson D. J., Lectures on Elementary Statistics and Probability, Geneva CERN, 1963, pp.1-105.
- [16] Newnham R. E., Properties of Materials, Oxford Univ. Press, 2005, pp. 1-391.
- [17] Grigorovich V. K., Metallography and Heat Treatment, The Handbook, Ed. by M. L. Bernshtein and A. G. Rakhshadt, Moscow, Metallurgizdat, 1961, in Russian, p. 387.
- [18] Cracknell A. P. and Wong K. C., The Fermi Surface, Oxford, Clarendon Press, 1973, pp. 1-565.
- [19] Zuev L. B., The linear work hardening stage and de Broglie equation for autowaves of localized plasticity, *International Journal of Solids and Structures*, Vol. 42, 2005, pp. 943-949.
- [20] Shpol'skii E. V., Atomic Physics, Vol. 1, Moscow, Nauka, 1974, in Russian, pp. 1-571.
- [21] Suzuki T., Takeuchi S., and Yoshinaga H., Dislocation Dynamics and Plasticity, Berlin, Springer, 1991, pp. 1-227.
- [22] Naimark O.B., Defect induced transitions as mechanisms of plasticity and failure in multifield continua, *Advances in Multifield Theories of Continua with Substructure*, Boston, Birkhauser Inc., 2003, pp. 75–114.
- [23] Zbib H.M., de la Rubia T.D., A multiscale model of plasticity, *International Journal of Plasticity*, Vol. 18, Issue 7, 2002, pp. 1133–1163.
- [24] Ohashi T., Kawamukai M., Zbib H., A multiscale approach for modeling scale-dependent yield stress in polycrystalline metals, *International Journal of Plasticity*, Vol. 23, Issue 5, 2007, pp. 897–914.

- [25] Zaiser M., Aifantis E.C., Randomness and slip avalanches in gradient plasticity, *International Journal of Plasticity*, Vol. 22, Issue 8, 2006, pp. 1432–1455.
- [26] Bilalov D. A., Sokovikov M. A., Chudinov V. V., Oborin V. A., Bayandin Y. V., Terekhina A. I., Naimark O. B., Numerical Simulation and Experimental Study of Plastic Strain Localization under the Dynamic Loading of Specimens in Conditions Close to a Pure Shear, *Journal of Applied Mechanics and Technical Physics*, Vol. 59, Issue 7, 2018, pp. 1179-1188.
- [27] Naimark O. B., Bayandin Y. V., Zocher M. A., Collective properties of defects, multiscale plasticity, and shock induced phenomena in solids, *Physical Mesomechanics*, Vol. 20, Issue 1, 2017, pp. 10-30.
- [28] Zhelnin M., Iziumova A., Vshivkov A., Plekhov O., Experimental study of an effect of plastic deformation on thermal properties of stainless steel, *Quantitative InfraRed Thermography Journal*, Vol. 16, Issue 1, 2019, pp. 74-86.
- [29] Moretti P., Renner J., Safari A., Zaiser M., Graph theoretical approaches for the characterization of damage in hierarchical materials, *European Physical Journal B*, Vol. 92, Issue 5, 2019, pp.97:1.
- [30] Wu R., Tüzes D., Ispánovity P. D., Groma I., Hochrainer T., Zaiser M., Instability of dislocation fluxes in a single slip: Deterministic and stochastic models of dislocation patterning, *Physical Review B*, Vol.98. Issue 5, 2018, pp. 054110:1.
- [31] Valdenaire P. L., Le Bouar Y., Appolaire B., Finel A., Density-based crystal plasticity: From the discrete to the continuum, *Physical Review B*, Vol. 93, Issue 21, 2016, pp. 214111:1.
- [32] Xia S., El-Azab A., Computational modelling of mesoscale dislocation patterning and plastic deformation of single crystals, *Modelling and Simulation in Materials Science and Engineering*, Vol. 23, Issue 5, 2015, pp. 055009:1.
- [33] Lebyodkin M. A., Kobelev N. P., Bougherira Y., Entemeyer D., Fressengeas C., Gornakov V. S., Lebedkina T. A., Shashkov I. V., On the similarity of plastic flow processes during smooth and jerky flow: Statistical analysis, *Acta Materialia*, Vol. 60, Issue 9, 2012, pp. 3729-3740.
- [34] Fressengeas C., Taupin V., A field theory of strain/curvature incompatibility for coupled fracture and plasticity, *International Journal of Solids and Structures*, Vol. 82, 2016, pp. 16-38.
- [35] Lebyodkin M.A., Zhemchuzhnikova D.A., Lebedkina T.A., Aifantis E.C., Kinematics of formation and cessation of type B deformation bands during the Portevin-Le Chatelier effect in an AlMg alloy, *Results in Physics*, Vol. 12, 2019, pp. 867-869.
- [36] Zuev L. B., Barannikova S. A., Lunev A. G., Kolosov S. V., Zharmukhambetova A. M., Basic Relationships of the Autowave Model of a Plastic Flow, *Russian Physics Journal*, Vol. 61, Issue 9, 2019, pp. 1709-1717.
- [37] Zuev L. B., Lunev A. G., Barannikova S. A., Staskevich O. S., Plastic Flow Localization and Strain Hardening of Metals, *Russian Metallurgy*, Vol. 2019, Issue 4, 2019, pp. 273–280.
- [38] Zuev L. B., Barannikova S. A., Maslova O. A., The features of localized plasticity autowaves in solids, *Materials Research*, Vol. 22, Issue 4, 2019, pp. e20180694:1-12.
- [39] Zuev L. B., Barannikova S. A., Li Yu. V., The kinetics of deformation localization nuclei for the coarse-grained Fe-3%Si alloy, *Materials Today: Proceedings*, Vol. 5, Issue 1P1, 2018, pp. 1121-1124.
- [40] Lunev A. G., Nadezhkin M. V., Barannikova S. A., Zuev L. B., Acoustic Parameters as Criteria of Localized Deformation in Aluminum Alloys, *Acta Physica Polonica A*, Vol. 134, Issue 1, 2018, pp. P. 342-345.
- [41] Barannikova S., Li Yu., Zuev L., Research of the plastic deformation localization of bimetal, *Metallurgija*, Vol. 57, Is. 4, 2018, pp. 275-278.
- [42] Li Yu. V., Zharmukhambetova A. M., Barannikova S. A., Zuev L. B., On the macroscopic phenomena of plastic flow localization and solids microscopic characteristics, *Journal of Physics: Conference Series*. Vol. 1115, 2018, pp. 042037:1-5.

## *Engineering*

## ECONOMICAL ANALYSIS OF THE GEOGRID REINFORCED RAILWAY TRACK

Saad Farhan Ibrahim<sup>1</sup>, Ali Jabbar Kadhim<sup>2</sup> and Harith Basim Khalaf<sup>2</sup>

<sup>1</sup>Faculty of Engineering, Isra University, Amman, Jordan;

<sup>2</sup>Faculty of Engineering, Al-Mustansiriya University, Baghdad, Iraq

### ABSTRACT

One of main challenges in the development of railway transportation is the Reduction of the track costs. The reduction of track costs is crucial for competitiveness of railway operators, since competing modes of transportation (e.g. aviation, automotive) have seen a tremendous reduction in LCC in the last 30 years, while railway maintenance costs have not significantly decreased during the same period. The main objective of this study is to investigate the reduction in the cost of railway track due to the use of geogrid reinforcement. The results of reduction of track cost for the simulated models were for the sub-ballast reinforced model (4.1%), and ballast reinforced model (6.5%) and double reinforced model (3.73%) as compared to the unreinforced track.

*Keywords: Railway transportation, geogrid, reinforcement*

### INTRODUCTION

The total cost of railway transportation is derived from construction, maintenance and operation of infrastructure, manufacturing and maintenance of vehicles, as well as fuel production. Since maintenance, costs for the conventional ballasted railway track could be significantly reduced if the developed settlement under loading decreased. There is a few existing data concerning the lifetime of the geosynthetics in the construction of railway. Because the knowledge about the usage of geosynthetics on railway constructions is only distinguished in the past (20) years, so we can state that the experience and practice of the lifetime of various constructions methods are still aren't enough define them properly. Only little estimates availably from the manufacturers of geosynthetics who announced that the geosynthetics that they produce could rise the ballast lifetime for (2 – 4) times its original value. Since of the deficiency in pervious data, the calculation of maintenance and renovation work of railway were very few. In addition, Federici (2003) noticed that the available studies on railway track system that take in consideration the infrastructures in detail are very seldom and largely focused on vehicles construction. Therefore, the effect of geogrid reinforcement on reducing the cost of railway track will be studied [1].

Life cycle cost could be functional for project through a wide variety of industries, containing the railway. Railway track cost has not considerably changed since the past (30) years with comparison to other rival transportation modes [2]. European Commission (2011) on Sustainable Transportation settled targets for the reduction of railway life cycle cost in 2020 by 30%. Therefore, there is a noteworthy focusing on the analysis of life cycle cost application on railway [3].

The Geogrid was used as part of the INNOTRACK project through numerical simulations

and laboratory tests. This approaches confirmed that the reinforcement using geogrid would cause a reduction in operational disturbances and the life cycle cost. Hall and Sharpe (2007) used a British Railway case study was done in (1988) where geogrid was introduced for the renewal of railway track in the Derby– Leeds line at Shirland. The site was constructed with 100mm blanketing sand and 300mm of ballast over it, a separation layer composed from a heat bonded geo-textile and a geogrid with a small mesh to stop the particles of ballast from the penetration the geotextile. A geogrid with large mesh was furtherly added in order to support the soft subgrade. The project condition was monitored through the long-term general performance and ballast operational life. The result of monitoring showed that the geogrids decreased the requirements of maintenance to a fraction of their past level thus reducing the life cycle cost [4].

Without doubt, the decision-making, maintenance and operation costs are significantly more important initial constructions cost. These costs need to be studied throughout their lifetime so they match their performance threshold [5]. It is important that the making of decisions be based on a life-cycle basis. This will led to choosing more cost-effective strategies in the extended time and are cooperated with the available finance. Latest researches about railway constructions with the use of geosynthetics indicated a positive effect. The maintenance requirements reduced and ballast strength of the ballast increases when geosynthetic were used. Settlement of the track was 37 to 65 percent less than settlement of the equivalent portion of the unreinforced test section [6].

The geosynthetics manufacture company Tensar claims that the usage of their geosynthetics products will led to an increase in maintenance cycle by 3 times from its original value after a railway track case study; the railway track is located between Scotland and London. The railway line has been



under speed restriction for many times in spite of it was maintained regularly 2 times a year. The intrusion of geogrid in that line led to substantial decrease in the deterioration rate of the railway track without speed restrictions or maintenance [7].

## METHODOLOGY

The Life cycle cost (LCC) and the Whole life cost (WLC) are well known approaches used to compute all the associated cost with the whole life of design for a specific asset. The Life cycle cost (LCC) and the Whole life cost (WLC) can be used interchangeably while in the (BS ISO 15685-8:2008) international standard for life cycle costing of buildings and constructed stated that the two have difference meaning [8]:

- Life cycle cost is well defined, as “is the cost of a part or its divisions during its cycle life, though accomplishing the performances requirement”.
- Whole life cost is well defined as “is the procedure of regular economic aspects for the benefits and whole life cost of a known analysis period”. Whole life cost contains extra costs such as support cost related to activity in assets, Land cost and the incomes produced by the assets. The connection between LCC and WLC is displayed in Figure 1.

In order to make the appropriate choices on the economical benefits of the enhancement works that include using new technology the life cycle cost and (LCC) must be studied before and after the use of the technology. The tool were developed within the project “SMARTRAIL”, and available on smartrail.fehrl.org, was used to verify the benefits in cost related to the use of geogrid in railway track system for this research. The smart rail LCC tool was developed with consideration of ISO EN 15686-5 standard for LCC.

The following costs were used in the tool:

- Construction costs
  1. The Ballast
  2. The Sleepers
  3. Fastening and Rails systems
  4. Elastomeric [Resilient] pads
  5. Geogrid
- Routine maintenance costs:
  1. Stabilization and Tamping
  2. Milling of rail

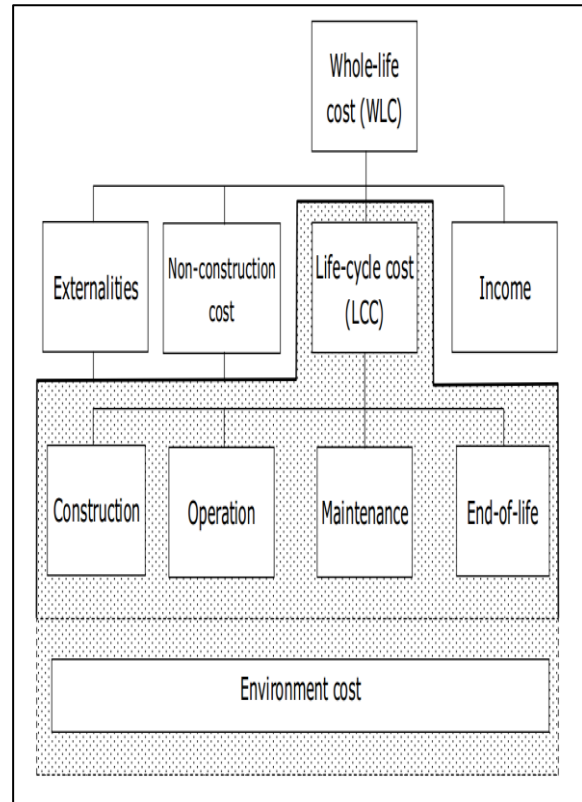


Fig. 1: Scope of life cycle and whole-life costing (Adapted from BS ISO 15685-8:2008).

Geogrid has been progressively used in railroads to offer reinforcement and confinement pressure to the layers of railway track. Four models were tested experimentally in order to calculate the increase in the life of the railway track after using geogrid reinforcement. The model dimensions are (800\*800\*600 mm), subgrade layer is 400 mm thick and sub-ballast layer and ballast layer are 100 mm thick. The tested models are unreinforced model, sub-ballast reinforced model, and ballast reinforced model and double reinforced model consisting of geogrid reinforcement in sub-ballast layer and ballast layer. The result showed that using reinforcement layer would reduce model settlement. The model tested look like the sketch in figure (2).

A Cumulative figure (3) used to show the difference in result of settlement between all tested models.

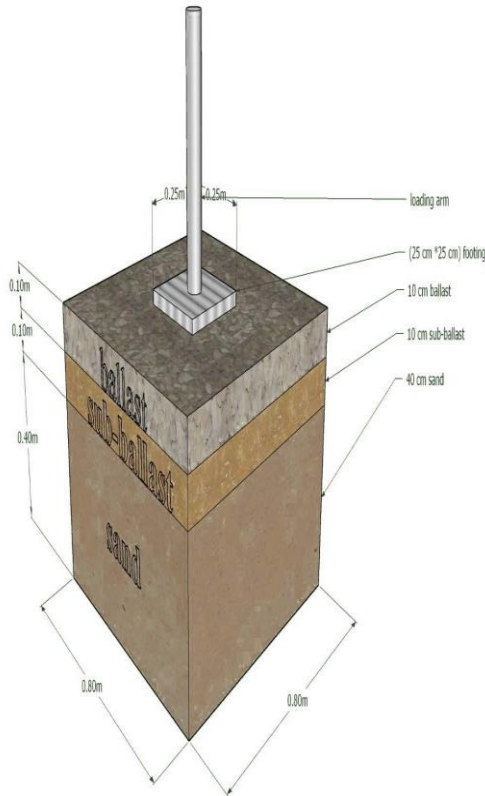


Fig. 2: Sketch to show the experimentally tested model.

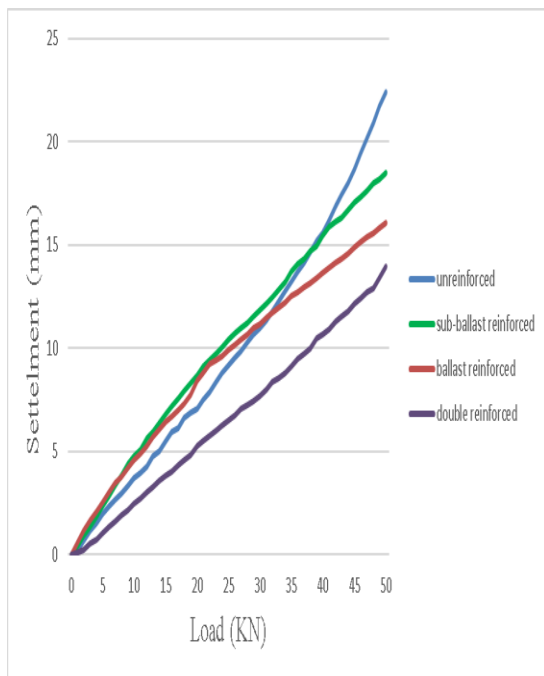


Fig. 3: Load-Settlement relationship for all models at every loading stages.

The purpose of this tool is to let the user to explore the effects of different maintenance option on the life cycle cost of for a railway asset. The assessment of life cycle cost is a way to estimate the over-all costs of maintaining an asset with a specified period for analysis, to be used as an input into a decision-making procedure. Discounting rate and the costs in the Future were converted to be Net Present Value (NPV) to simplify the judgement in maintenances regimes from total cost point of view in the present day.

The data input was gathered from “Hajama – Sawa” Railway Project by Ministry of Transportation Iraqi Republic Railways Company and “Transportation & Telecommunications of Iraq” report by United Nations World Bank [9]. It assumed that the project life span would be for 60 years. In addition, due to the difficultness of predicting the increase in the ballast lifetime of due to the use of geogrid, a number of scenarios were simulated, and all of these scenarios indicate that the use of geogrid in the construction will be cheaper in the end. In addition, this indicate that the maintenance requirement of the tack will be decreased. The tool layout and the used data for evaluated models are shown in figures (4) (5) (6) (7) (8) accordingly.

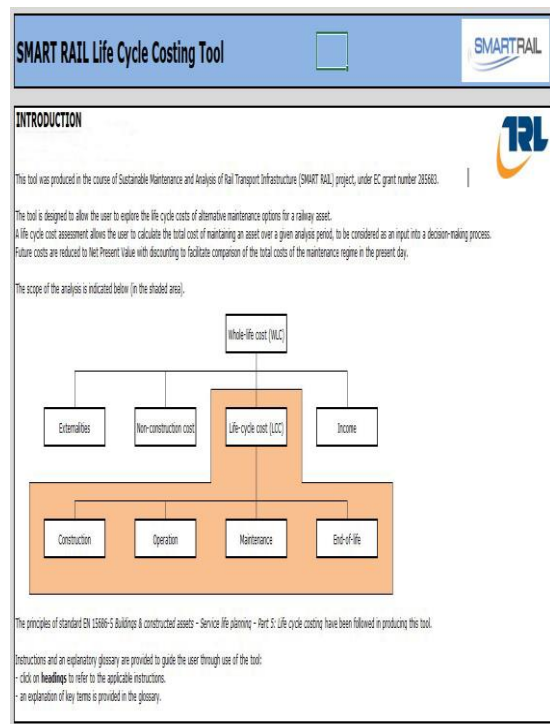


Fig. 4: the LCC tool-starting page.

| Remediation                  |   |                 |                        |            |                       |           |
|------------------------------|---|-----------------|------------------------|------------|-----------------------|-----------|
| Name                         | Description                                 | Cost (€ per km) | Delay (minutes per km) | First year | Expected life (years) | Last year |
| 1 Ballast                    | Replace ballast at end-of-life              | € 771,105.00    | 0                      |            | 25                    | 60        |
| 2 Sleepers                   | Replace sleepers at end-of-life             | € 396,185.00    | 0                      |            | 20                    | 60        |
| 3 Rails and fastening system | Replace rails and fastenings at end-of-life | € 594,278.00    | 0                      |            | 30                    | 60        |
| 4 Elastomeric pads           | Replace elastomeric pads at end-of-life     | € 517.00        | 0                      |            | 30                    | 60        |
| 5                            |   |                 |                        |            |                       |           |
| 6                            |   |                 |                        |            |                       |           |
| 7                            |   |                 |                        |            |                       |           |
| 8                            |   |                 |                        |            |                       |           |
| 9                            |   |                 |                        |            |                       |           |
| 10                           |   |                 |                        |            |                       |           |

| Routine maintenance              |                     |                 |                        |            |                              |           |
|----------------------------------|---------------------|-----------------|------------------------|------------|------------------------------|-----------|
| Name                             | Description         | Cost (€ per km) | Delay (minutes per km) | First year | Average frequency (per year) | Last year |
| 1 Ballast tamping and stabiliser | Routine maintenance | € 1,107.00      | 0                      |            | 0.75                         | 60        |
| 2 Rail milling                   | Routine maintenance | € 5,813.00      | 0                      |            | 0.25                         | 60        |
| 3                                |                     |                 |                        |            |                              |           |
| 4                                |                     |                 |                        |            |                              |           |
| 5                                |                     |                 |                        |            |                              |           |
| 6                                |                     |                 |                        |            |                              |           |
| 7                                |                     |                 |                        |            |                              |           |
| 8                                |                     |                 |                        |            |                              |           |
| 9                                |                     |                 |                        |            |                              |           |
| 10                               |                     |                 |                        |            |                              |           |

Fig. 5: the input data for unreinforced model.

| Remediation                  |   |                 |                        |            |                       |           |
|------------------------------|---|-----------------|------------------------|------------|-----------------------|-----------|
| Name                         | Description                                 | Cost (€ per km) | Delay (minutes per km) | First year | Expected life (years) | Last year |
| 1 Ballast                    | Replace ballast at end-of-life              | € 771,105.00    | 0                      |            | 32                    | 60        |
| 2 Sleepers                   | Replace sleepers at end-of-life             | € 396,185.00    | 0                      |            | 20                    | 60        |
| 3 Rails and fastening system | Replace rails and fastenings at end-of-life | € 594,278.00    | 0                      |            | 30                    | 60        |
| 4 Elastomeric pads           | Replace elastomeric pads at end-of-life     | € 517.00        | 0                      |            | 30                    | 60        |
| 5 Geocomposite membrane      | Replace membrane at end-of-life             | € 20,000.00     | 0                      |            | 35                    | 60        |
| 6                            |   |                 |                        |            |                       |           |
| 7                            |   |                 |                        |            |                       |           |
| 8                            |   |                 |                        |            |                       |           |
| 9                            |   |                 |                        |            |                       |           |
| 10                           |   |                 |                        |            |                       |           |

| Routine maintenance              |                     |                 |                        |            |                              |           |
|----------------------------------|---------------------|-----------------|------------------------|------------|------------------------------|-----------|
| Name                             | Description         | Cost (€ per km) | Delay (minutes per km) | First year | Average frequency (per year) | Last year |
| 1 Ballast tamping and stabiliser | Routine maintenance | € 1,107.00      | 0                      |            | 0.75                         | 60        |
| 2 Rail milling                   | Routine maintenance | € 5,813.00      | 0                      |            | 0.25                         | 60        |
| 3                                |                     |                 |                        |            |                              |           |
| 4                                |                     |                 |                        |            |                              |           |
| 5                                |                     |                 |                        |            |                              |           |
| 6                                |                     |                 |                        |            |                              |           |
| 7                                |                     |                 |                        |            |                              |           |
| 8                                |                     |                 |                        |            |                              |           |
| 9                                |                     |                 |                        |            |                              |           |
| 10                               |                     |                 |                        |            |                              |           |

Fig. 7: the input data for ballast reinforced track.

| Remediation                  |   |                 |                        |            |                       |           |
|------------------------------|---|-----------------|------------------------|------------|-----------------------|-----------|
| Name                         | Description                                 | Cost (€ per km) | Delay (minutes per km) | First year | Expected life (years) | Last year |
| 1 Ballast                    | Replace ballast at end-of-life              | € 771,105.00    | 0                      |            | 30                    | 60        |
| 2 Sleepers                   | Replace sleepers at end-of-life             | € 396,185.00    | 0                      |            | 20                    | 60        |
| 3 Rails and fastening system | Replace rails and fastenings at end-of-life | € 594,278.00    | 0                      |            | 30                    | 60        |
| 4 Elastomeric pads           | Replace elastomeric pads at end-of-life     | € 517.00        | 0                      |            | 30                    | 60        |
| 5 Geocomposite membrane      | Replace membrane at end-of-life             | € 20,000.00     | 0                      |            | 35                    | 60        |
| 6                            |   |                 |                        |            |                       |           |
| 7                            |   |                 |                        |            |                       |           |
| 8                            |   |                 |                        |            |                       |           |
| 9                            |   |                 |                        |            |                       |           |
| 10                           |   |                 |                        |            |                       |           |

| Routine maintenance              |                     |                 |                        |            |                              |           |
|----------------------------------|---------------------|-----------------|------------------------|------------|------------------------------|-----------|
| Name                             | Description         | Cost (€ per km) | Delay (minutes per km) | First year | Average frequency (per year) | Last year |
| 1 Ballast tamping and stabiliser | Routine maintenance | € 1,107.00      | 0                      |            | 0.75                         | 60        |
| 2 Rail milling                   | Routine maintenance | € 5,813.00      | 0                      |            | 0.25                         | 60        |
| 3                                |                     |                 |                        |            |                              |           |
| 4                                |                     |                 |                        |            |                              |           |
| 5                                |                     |                 |                        |            |                              |           |
| 6                                |                     |                 |                        |            |                              |           |
| 7                                |                     |                 |                        |            |                              |           |
| 8                                |                     |                 |                        |            |                              |           |
| 9                                |                     |                 |                        |            |                              |           |
| 10                               |                     |                 |                        |            |                              |           |

Fig. 6: the input data for sub-ballast reinforced track.

| Remediation                  |   |                 |                        |            |                       |           |
|------------------------------|---|-----------------|------------------------|------------|-----------------------|-----------|
| Name                         | Description                                 | Cost (€ per km) | Delay (minutes per km) | First year | Expected life (years) | Last year |
| 1 Ballast                    | Replace ballast at end-of-life              | € 771,105.00    | 0                      |            | 35                    | 60        |
| 2 Sleepers                   | Replace sleepers at end-of-life             | € 396,185.00    | 0                      |            | 20                    | 60        |
| 3 Rails and fastening system | Replace rails and fastenings at end-of-life | € 594,278.00    | 0                      |            | 30                    | 60        |
| 4 Elastomeric pads           | Replace elastomeric pads at end-of-life     | € 517.00        | 0                      |            | 30                    | 60        |
| 5 Geocomposite membrane      | Replace membrane at end-of-life             | € 40,000.00     | 0                      |            | 35                    | 60        |
| 6                            |   |                 |                        |            |                       |           |
| 7                            |   |                 |                        |            |                       |           |
| 8                            |   |                 |                        |            |                       |           |
| 9                            |   |                 |                        |            |                       |           |
| 10                           |   |                 |                        |            |                       |           |

| Routine maintenance              |                     |                 |                        |            |                              |           |
|----------------------------------|---------------------|-----------------|------------------------|------------|------------------------------|-----------|
| Name                             | Description         | Cost (€ per km) | Delay (minutes per km) | First year | Average frequency (per year) | Last year |
| 1 Ballast tamping and stabiliser | Routine maintenance | € 1,107.00      | 0                      |            | 0.75                         | 60        |
| 2 Rail milling                   | Routine maintenance | € 5,813.00      | 0                      |            | 0.25                         | 60        |
| 3                                |                     |                 |                        |            |                              |           |
| 4                                |                     |                 |                        |            |                              |           |
| 5                                |                     |                 |                        |            |                              |           |
| 6                                |                     |                 |                        |            |                              |           |
| 7                                |                     |                 |                        |            |                              |           |
| 8                                |                     |                 |                        |            |                              |           |
| 9                                |                     |                 |                        |            |                              |           |
| 10                               |                     |                 |                        |            |                              |           |

Fig. 8: the input data for double reinforced track.

## RESULTS

LCC Analyses displayed provision economically aimed at the choice to use geogrid under in the railway track as shown in figure (8). This has been proven for all the reinforced models because the lifetime is increasing from the use of the geogrid and thus led to a condition that was extra cheaper and more profitable to use the reinforcement into the tracklayers. The costs differences for the three variants and the baseline for the railway track is shown in the net present value of the three variants is lesser than that of the baseline in spite of initial cost is higher; rising from considerably lesser rate of maintenances.

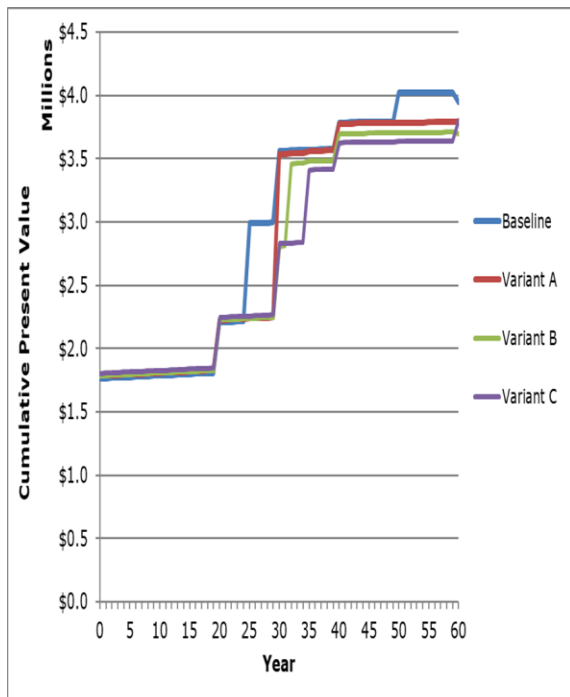


Fig. 4: The Cumulative Present Value and time relationship where  
Baseline: Unreinforced,  
Variant A: The sub-ballast reinforced  
Variant B: ballast reinforced  
Variant C: double reinforced

## CONCLUSION

The economical evolution indicated that the use of geogrid proved to be a feasible and cost-effective in reducing the intervals of maintenance of railway track. Despite of slightly higher initial construction cost of railway track when the geogrid used, the lifetime cost will reduced significantly As the ballast reinforced was the most effective in the reduction of total cost by(6.5%)and the sub-ballast reinforced was (4.1%) and the double reinforced was (3.73%) as compared to the unreinforced track.

## REFERENCES

- [1] Federici, M., S. Ulgiati, et al. (2003). "Efficiency and sustainability indicators for passenger and commodities transportation systems. The case of Siena, Italy." *Ecological Indicators* 3: 155-169.
- [2] Paulsson B, Platzer M and Ekberg A (2006) "INNOTRACK – Innovative Track System – A unique approach of infrastructure managers and competitive track supply industry for developing the innovative products of the future", 7th World Congress on Railway Research.
- [3] European Commission (2011) "White Paper: Roadmap to a single European Transport Area – Towards a competitive and resource efficient transport system".
- [4] Hall C D and Sharpe P (2007) "Review of geogrid stabilisation of railway ballast with reference to performance and durability".
- [5] European Commission (2013) "Sustainable steel-composite bridges in built environment (SBRI)", Final Report
- [6] Parsons R., Jowkar M., Han J., 2012. Performance of Geogrid Reinforced Ballast under Dynamic Loading. Report # MATC-KU: 363, Final Report.
- [7] Tensar (2013) "Railways: Mechanical stabilization of track ballast and sub ballast", March 2013, Issue 11.
- [8] British Standards Institution (2008) BS ISO 15685-8:2008, Buildings and constructed assets – Service life planning – Part 5: Life cycle costing.
- [9] Project "Hajama – Sawa", cost estimate, Ministry of Transportation of Iraq, Iraqi Republic Railways Company.

## A STOCHASTIC MODEL OF THE MRO SPARE PARTS PROCUREMENT PLANNING PROBLEM FOR AIRCRAFT MAINTENANCE SERVICE PROVIDER

Yichen QIN<sup>1,2</sup>, Felix T.S. CHAN<sup>2</sup>, S.H. CHUNG<sup>2</sup> and T. QU<sup>1</sup>

<sup>1</sup>School of Electrical and Information Engineering, Jinan University (Zhuhai Campus), Zhuhai 519070, China;

<sup>2</sup>Department of Industrial and Systems Engineering, The Hong Kong Polytechnic University, Hung Hum, Hong Kong

### ABSTRACT

Increasing number of outsourcing maintenance requests from different airlines has brought great challenge to the independent aircraft maintenance service provider to timely complete the maintenance request. From the perspective of aircraft maintenance service provider, having a long-term sustainable MRO procurement practice in aircraft maintenance service provider ensures the smoothness of implementation of maintenance activities. Given that procurement of consumables and materials varies according to different aircraft maintenance checks, maintenance company need to maintain the continuously availability of parts and components for maintenance activities while minimizing the holding cost of expensive inventory. Considering the uncertainties of maintenance requests from different clients (airlines), a stochastic model is proposed to formulate the problem. The stochastic model aims to alleviate the negative impact of the uncertain maintenance demands on the inventory management operations, and provide a robust procurement strategy while implementing the maintenance operations in real situations.

*Keywords: MRO, Procurement, Stochastic Programming, Aircraft Maintenance, Mixed-integer Linear Programming*

### INTRODUCTION

Outsource the MRO operations to the professional maintenance service provider has become the trend in aviation industry. It is estimated by Marcontell [1] that there is a 45% increase of MRO outsource rose from the mid-1990s to 2012. Receiving increasing demands of MRO service with various aircraft configurations, independent aircraft maintenance service company are faced with great challenge to fulfilling these demands. Having respective aeronautical parts are perquisite before implementing different aircraft maintenance tasks. Procurement of the MRO parts can lead to high inventory holding cost and long lead time. In this regard, maintaining sufficient MRO parts and minimizing inventory cost are critical for the aircraft maintenance enterprise. Moreover, the uncertainties of demands may interrupt the original planning within the maintenance company. In reality, maintenance demands of different clients are difficult to predict since each airline carries out its own flight plan respectively. In addition, the supplying capacity of aeronautical component suppliers are limited, and the stability of the supply chain can be affected by the uncertainties during the productions and transportation process.

The deterministic procurement planning model is unable to handle the uncertainties during the

implementation of maintenance activities as the optimal procurement planning solution can become infeasible. In this connection, it is necessary to incorporate the uncertainty of maintenance demands into the procurement planning problem. Therefore, the contribution of this paper is that: 1) the procurement planning problem for maintenance service provider is studied; 2) the uncertainties in aeronautical component supply and demand are incorporated in the MRO procurement planning problem. Specifically, the uncertainties are characterized as discrete scenarios, and the randomness of different scenarios are associated with probabilities based on the problem.

### LITERATURE REVIEW

Large equipment oriented maintenance, repair and operation (MRO) is significant to asset-intensive industries like aeronautics, which involves substantial investment to maintain sophisticated equipment and spare parts [2]. From the perspective of airlines, maintenance outsourcing is an important way to reduce the business costs, maintain competitive advantages in the market and achieve satisfactory MRO service [1, 3]. With the increasing trend of maintenance outsourcing decisions from different

airlines, efficiently fulfill maintenance requests associated with respective aircraft model becomes a great challenge.

Specifically, the MRO spare parts procurement planning is vital to maintenance checks that are conducted on the aircraft received from different clients. All aircraft maintenance activities associated with MRO spare parts shall be arranged in advanced to ensure that the availability of spare parts can fulfill the maintenance demands. From other side, the inventory of spare parts has to be maintained within suitable level. Therefore, fulfilling maintenance demands with the constraint of limited resources is a common problem in MRO industry. Zhen and Wang [4] developed a two-phase stochastic programming model on the component replenishment decisions for an assemble-to-order (ATO) manufacturer. A multi-objective model for the preventive replacement of a spare part over a planning horizon is proposed by Nosoohi and Hejazi [5]. A two non-linear programming models that is used to predict impending demands based on installed spare parts failure distribution is developed by Gu et al. [6]. Aircraft maintenance checks shares some similarities with the assemble-to-order manufacturing practices and the product configuration problem. Product configuration problem selecting components to constitute a personalized product with specified configurations [7], and aircraft maintenance checks consume different MRO spare parts to during respective maintenance operations. Somarin et al. [8] studied the emergency resupply policy that helps to improve the MRO service providers' flexibility while the shortage of spare parts occurs.

It is common that the maintenance service providers are involved in a global MRO supply chain and they have to purchase necessary spare parts from different supplier globally, instead of producing the spare parts their own. The product configuration parameters, spare part demands, and lead time have to be considered and these data may fluctuate in real-world implementation. Therefore, these uncertainties can have the negative impact on the MRO operations. In literature, the uncertainties maintenance demands, transportation lead-time and suppliers' capacities are less considered in MRO spare part procurement problem. A stochastic programming model is developed, which considers uncertain supplying capacity and maintenance requirement into the procurement planning. Furthermore, the framework of the mathematical formulation envisions the direction of algorithmic design for further research on this topic.

## **MATHEMATICAL MODEL FOR MRO SPARE PARTS PROCUREMENT PROBLEM WITH UNCERTAINTY**

### **Problem Description**

Aircraft maintenance check can be classified as line maintenance and hangar maintenance. Line maintenance get its definition from "on line" maintenance, referring to the light maintenance activities (e.g. A- and some B- checks) that can be conducted at a gate or apron during a turnover between two flights, while other maintenance activities, i.e. some B-check, C check and D-check, are categorized as "hangar" maintenance carried out when the aircraft is taken out of service and sent to the maintenance hangar for heavy maintenance. MRO spare parts are indispensable for the aircraft heavy maintenance checks, and different maintenance checks requires respective MRO spare parts to conduct the maintenance operations on the aircraft. Moreover, for different types of aircraft model, it is the case that the MRO spare parts are different for the same type of maintenance check.

The maintenance service provider has to obtain sufficient dedicated MRO spare parts before conducting any maintenance checks on aircraft from the clients. To control the inventory level and avoid holding excessive MRO spare parts, the maintenance service provider adopts Procure-To-Order (PTO) practice and the service provider receives maintenance order related to aircraft to be serviced with respective configurations. In reality, the supply chain is affected by the uncertain maintenance demands and capacity of suppliers. In particular, the maintenance demands may fluctuate as some urgent unscheduled maintenance requests arrive at maintenance company without short notice period, and the maintenance company does not necessarily have sufficient components to satisfy the additional maintenance request. In this connection, the decision of the maintenance company is to determine the spare part's selection and respective supplier's selection, so as to satisfy the additional maintenance requests such that the total cost of procurement and operations is minimized within the context of uncertainty.

To reduce the cost of putting urgent procurement order that induces significant amount of ordering cost, the pre-procuring practice is used. The maintenance company may purchase some mutual spare part in advance, such that they can be shared with different aircraft type and minimize the negative effects induced by uncertain MRO spare parts requirement and stochastic supply capacity. If the advanced procurement of MRO spare parts cannot meet the real demands, the maintenance company is able to procure additional spare parts to meet the remaining requirements of MRO parts. In this regard, spare part procurement considering uncertainties: 1) identify and select the MRO spare parts required by the client's maintenance requirement, and select the spare



part suppliers; 2) pre-procure spare parts from selected suppliers; 3) conduct the maintenance service on the receiving maintenance request with the pre-procure spare parts and deliver the finished aircraft; 4) if the maintenance demand cannot be fulfilled by the pre-procure spare parts, the maintenance company initiates additional procurement from the suppliers; 5) conduct the maintenance service by using the additional procured spare parts and finished the maintenance requests.

### Mathematical Model

The MRO spare parts procurement problem is formulated as a stochastic model. The advanced procurement process is modeled in the first phase, including spare part and suppliers' selections, is conducted before considering the stochastic demand and supply. In the second phase, the additional procurement is determined under different scenarios to fulfill the unexpected maintenance requests.

The notations of the mathematical model are listed as follows:

| Notations   | Meanings   |
|-------------|--|
| $i, h, l$   | Aircraft to be served, $i, h, l \in I$   |
| $j$         | MRO spare parts, $j \in J$   |
| $m$         | Maintenance module, $m \in M$  |
| $k$         | Spare part provider, $k \in K$   |
| $s$         | Scenario, $s \in S$  |
| $I$         | Set of Aircraft associated with maintenance requirements   |
| $J$         | MRO spare parts set  |
| $M$         | Maintenance module set   |
| $K$         | Spare part provider set  |
| $S$         | Scenario set   |
| $SC_m$      | Set of MRO spare parts belong to maintenance module $m$  |
| $d_i^s$     | Demand of maintenance request $i$ under scenario $s$   |
| $hc_j$      | Inventory holding cost of unused spare part $j$  |
| $ns_{ij}$   | Number of spare part $j$ required for the maintenance request $i$ , if $j$ is selected           |
| $cs_{ij}$   | Cost of spare part $j$ in maintenance request  |
| $mc_j$      | Maximum storage capacity for spare part $j$  |
| $SC_{jk}^s$ | Capacity of supplying spare part $j$ from provider $k$ under scenario $s$                        |
| $ts_{jk}$   | Unit cost of transporting spare part $j$ from spare part provider $k$ to the maintenance company |
| $cp_{ij}$   | Unit cost of advanced procurement component $j$ from spare part provider $k$                     |

|           |   |
|-----------|---|
| $ca_{jk}$ | Unit cost of extra procurement of spare part $j$ from spare part provider $k$ |
| $Pb^s$    | Probability that scenario $s$ occurs  |

### Decision Variables

| Notation    | Meanings  |
|-------------|---|
| $x_{ij}$    | Binary decision variable. 1 indicates that spare part $j$ is used in fulfilling maintenance request $i$ |
| $pp_{jk}$   | Number of procurement spare part $j$ from spare part provider $k$ in advanced                           |
| $ap_{jk}^s$ | Number of additional spare part $j$ from spare part provider $k$ under scenario $s$                     |
| $es_j^s$    | Number of unused spare part $j$ inducing inventory holding cost under scenario $s$                      |

$$\begin{aligned} & \text{Min} \sum_{i \in I} \sum_{j \in J} cs_{ij} \cdot ns_{ij} \cdot x_{ij} + \sum_{j \in J} \sum_{k \in K} (cp_{jk} + ts_{jk}) \cdot pp_{jk} \\ & + \sum_{s \in S} Pb^s \left\{ \sum_{j \in J} \sum_{k \in K} (ca_{jk} + ts_{jk}) \cdot ap_{jk}^s + \sum_{j \in J} hc_j \cdot es_j^s \right\} \quad (1) \end{aligned}$$

$$\sum_{j \in SC_m} x_{ij} = 1, i \in I, m \in M \quad (2)$$

$$\sum_{i \in I} d_i^s \cdot ns_{ij} \cdot x_{ij} \leq \sum_{k \in K} pp_{jk} + \sum_{k \in K} ap_{jk}^s, j \in J, s \in S \quad (3)$$

$$\sum_{k \in K} pp_{jk} \leq mc_j, j \in J \quad (4)$$

$$\sum_{k \in K} pp_{jk} - \sum_{i \in I} d_i^s \cdot ns_{ij} \cdot x_{ij} \leq es_j^s, j \in J, s \in S \quad (5)$$

$$ap_{jk}^s \leq SC_{jk}^s, j \in J, k \in K, s \in S \quad (6)$$

$$x_{ij} \in \{0, 1\}, i \in I, j \in J \quad (7)$$

$$pp_{jk}, ap_{jk}^s, es_j^s \geq 0, i \in I, j \in J, k \in K, s \in S \quad (8)$$

Objective function (1) minimizes the total spare part cost, including the configuration cost, cost of procurement, cost of transportation and cost of inventory holding. Constraint (2) prescribes that one option of spare part can be chosen from the available spare part combination in the dedicated module. Constraint (3) makes sure that that the demands of the MRO spare parts are met by the procurement. Constraint (4) impose the storage capacity limit, meaning that the number of pre-procure and additional procure spare part cannot exceed the capacity of the storage house. Constraint (5) determines the number of excessive spare part. Constraint (6) regulates that the additional procurements of spare parts is below the maximum capacity of the supplier. Constrains (7-8) determine the type of decision variables.



## CONCLUSION

Outsource the aircraft heavy maintenance to a professional maintenance company is becoming a trend in aviation industry, and the spare parts are essential for conducting the maintenance operations on the aircraft. Moreover, procurement of the MRO parts can lead to high inventory holding cost and long lead time. Maintaining sufficient MRO parts and minimizing inventory cost are critical for the aircraft maintenance enterprise. To better resolve the spare part procurement planning problem, a stochastic programming model for the MRO spare parts procurement planning problem is developed in this paper, which assists the maintenance service company better arrange the maintenance procurement plan that aligns with the maintenance schedule for fulfilling the maintenance request from clients. The future research of this topic can be the development of efficient exact algorithm to solve this decomposable structure mathematical model.

## ACKNOWLEDGEMENTS

The work described in this paper was supported by grants from The Natural Science Foundation of China (Grant Nos. 71471158, 71571120, 71271140); The Research Committee of Hong Kong Polytechnic University (Project Number G-UADM); and The Hong Kong Polytechnic University under student account code RUF1.

## REFERENCES

- [1] Marcontell D. MRO's offshore edge shrinking. *Aviation Week & Space Technology*. 2013;175(22):56.
- [2] Li L., Liu M., Shen W.M., Cheng G.Q. An improved stochastic programming model for supply chain planning of MRO spare parts. *Applied Mathematical Modelling*. 2017;47:189-207.
- [3] Qin Y., Chan F.T.S., Chung S.H., Qu T., Niu B. Aircraft parking stand allocation problem with safety consideration for independent hangar maintenance service providers. *Computers & Operations Research*. 2018;91:225-36.
- [4] Zhen L., Wang K. A stochastic programming model for multi-product oriented multi-channel component replenishment. *Computers & Operations Research*. 2015;60:79-90.
- [5] Nosoochi I., Hejazi S.R. A multi-objective approach to simultaneous determination of spare part numbers and preventive replacement times. *Applied Mathematical Modelling*. 2011;35(3):1157-66.
- [6] Gu J.Y., Zhang G.Q., Li K.W. Efficient aircraft spare parts inventory management under demand uncertainty. *Journal of Air Transport Management*. 2015;42:101-9.
- [7] Li X.H., Yang D., Hu M.Q. A scenario-based stochastic programming approach for the product configuration problem under uncertainties and carbon emission regulations. *Transportation Research Part E-Logistics and Transportation Review*. 2018;115:126-46.
- [8] Somarin A.R., Asian S., Jolai F., Chen S.L. Flexibility in service parts supply chain: a study on emergency resupply in aviation MRO. *International Journal of Production Research*. 2018;56(10):3547-62.

## COMPUTING PROGRAM FOR EVALUATING PRESSUREMETER TEST RESULTS OF CLAY

<sup>1</sup> Radhi Alzubaidi and <sup>2</sup> Athra Al-Kanim

<sup>1</sup> College of Engineering, University of Sharjah, UAE

<sup>2</sup> MSc Student, College of Engineering, AlNarain University, Iraq

### ABSTRACT

Due to the increasing importance of the results of pressuremeter testing and their reliable applications for determining the engineering properties of soils. Different methods and theories been used to analyze and interpret the pressuremeter parameters, many assumptions reflect the uncertainties of soil properties, where some assumed the soil is elastic perfectly plastic and the tests insured plain strain conditions, the horizontal at rest pressure and limit pressure represent a great value in the design of foundations, a computer program been developed to explore the results of, conventional and theoretical limit pressure using different methods of analysis, the importance of the computer program is to simplify the methods of determining the conventional and theoretical limit pressure without drawings the curves that necessary to determine the different parameters usually used in the analysis and unified all the symbols of different methods. The results of conventional and theoretical limit pressure showed distinctive discrepancies when using different methods of analysis.

*Keywords: Site investigation, Conventional limit pressure, Theoretical limit pressure, Pressuremeter*

### INTRODUCTION

Laboratory testing for soil samples have already been subjected to a number of disturbance effects like boring operation, act of sampling, transport, removal from the sampler, stress relief and trimming and others. There is much to be said in favor of in-situ testing when many of these disturbance effects are eliminated. The pressuremeter testing seems to receive a great application in site investigation and foundation design where the deduced results predict many valuable parameters from one test. Moayed, Kordnaei and Mola-Abasi [1] used the limit pressure to calculate the settlement and bearing capacity of foundation. They proposed various empirical relations to correlate the limit pressure and the Modulus to other soil parameter like the moisture content, plasticity index and SPT counts ( $N_{60}$ ). Tezel, Hacialioglu, Onal, and Ozmen [2] compared the results of pre-bored pressuremeter and high pressure pressuremeter tests conducted in soil to construct a high rise tower project. They conclude that the net limit pressure values that could be reached in the HyperPAC test are higher than the values that can be reached by Menard Pressuremeter. Lukas [3] used Menard pressuremeter to predict the results of the limit pressure in different type of soils to evaluate the settlement, with experience, reliable data was obtained that allowed for more reliable settlement predictions. Agan and Algin [4] conducting several pressuremeter testing in clay soil and used non-linear

regression analysis for generating empirical equation between the shear strength obtained from unconfined shear strength tests and limit pressure deduced from pressuremeter testing, they concluded that the presented equations based on the nonlinear regression analysis may be valuable for similar soils. Ahmadi and Keshmiri [5] presented a numerical finite difference model of self-boring pressuremeter test (SBPM) using FLAC software. Therefore, determination of limit pressure usually needs extrapolation. They suggested to use cavity pressure at 10% strain ( $P_{10}$ ) for the interpretation of in situ horizontal stress from SBPM test rather than limit pressure. Hamidi, Varaksin and Nikraz [6] studied the established empirical relationships between the limit pressure and Menard Modulus, they concluded that for practical purpose this method is able to provide Menard Modulus values of the correct magnitude. The present research developed a computer program to evaluate the theoretical and conventional limit pressure using different methods. All the symbols of different method for evaluating the conventional and theoretical methods been unified.

### PRESSUREMETER TESTS RESULTS

The site for carrying the pressuremeter tests located on Baghdad - Kut road at Al-Rashid University proposed site. The soil consists mainly of brown silty clay layers with different consistencies and different

gypsum contents, the analysis and application of the computer program in the present study carried out by Al-kanim [7], used the test results of Al-Rawi[8] Menard pressuremeter tests carried out on the same site, Fig.1 shows the pressure increment with volume change reading at 60 second after application of the pressure. The pressure readings recorded during the tests were adjusted to compensate for both, the head of water in the central cell tubing of the probe and the inertia of the rubber.

### THE COMPUTER PROGRAM

The computer is designed to predict the values of the horizontal at rest pressure and the limit pressure using different methods of interpretation. The computer program evaluates the horizontal at rest pressure using the inflection point method, while the computer program predicts the values of the conventional limit pressure using five method and the theoretical limit pressure using three methods. The methods used to evaluate the conventional limit are as follows:

- 1- Expansion P-  $\Delta V$  curve method.
- 2- The upside -down curve method.
- 3-P-  $\ln (\Delta V/V)$  method
- 4- The relative volume method
- 5- Log-log method

The methods used to evaluate the theoretical limit pressure as follows

- 1- The up side -down method
- 2- The P-  $1/\varepsilon_0$  method
- 3- The P- $\ln \Delta V/V$  method

The values of the horizontal at rest pressure evaluated using the inflection point method

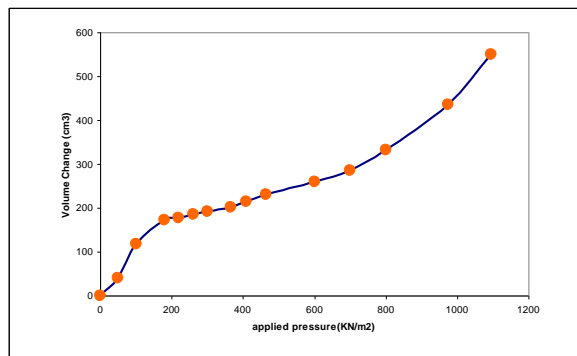


Fig.1 Pressuremeter test curve at al-rashid university site (AlRawi,1985)

### The Results Of The Conventional Limit Pressure

The values of the conventional limit pressure evaluated using five methods of analysis ,these methods as follow

- 1- Expansion P-  $\Delta V$  curve method.
- 2- The upside -down curve method.
- 3-P-  $\ln (\Delta V/V)$  method
- 4- The relative volume method
- 5- Log-log method

The results are shown in Fig.2 to Fig.5 for four bore holes at different depths, it seems that the P- $\Delta V$  method predicted higher values for the conventional limit pressure ,while the up-side down curve method and P-  $\ln (\Delta V/V)$  method deduced the lower values ,the log-log method and relative -volume method are in between. The values of the conventional pressure in BH.No.87 (Fig.2) deduced from the P- $\Delta V$  method are higher than those deduced from up-side down curve method, P-  $\ln (\Delta V/V)$  method, log-log method and Relative volume method in range from 5% to 48% , 1% to 48% ,3% to 24% , 5% to 25% respectively . The same trend found in BH. No. 62 as can be seen in Fig.3 ,the values of the conventional limit pressure deduced from P- $\Delta V$  method are higher than those deduced from up-side down curve method, P-  $\ln (\Delta V/V)$  method, log-log method and Relative volume method in range of 1% to 42% , 1% to 36% ,0.5% to 19% , 0.4% to 20% respectively .

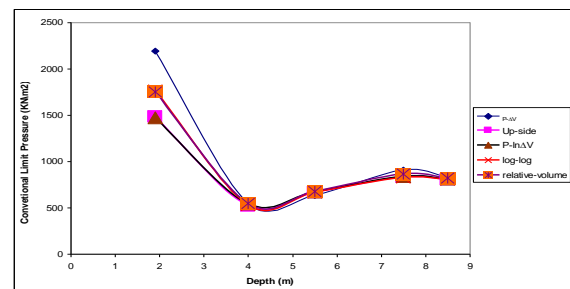


Fig.2 Conventional limitp pressure using different methods bh.no.87

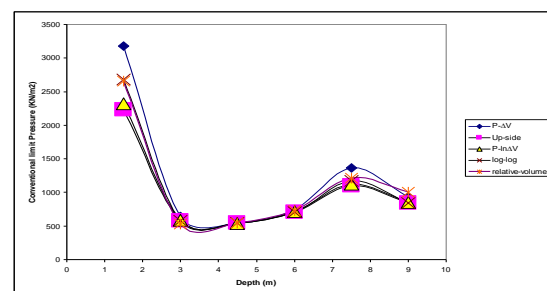


Fig.3 Conventional limit pressure using different methods bh.no.62

Also in Fig.4 the values of the conventional of BH.61 evaluated from P- $\Delta V$  method are higher than those deduced from up-side down curve method, P- $\ln (\Delta V/V)$  method, log-log method and Relative volume method in range of 4% to 28% , 4% to 29% ,3% to 26% , 3% to 16% respectively. In BH.No.92 ,the results of the conventional limit pressure using different methods are shown in Fig. 5 , the values of the conventional evaluated from P- $\Delta V$  method are higher than those deduced from up-side down curve method, P- $\ln (\Delta V/V)$  method, log-log method and Relative volume method in range of 2% to 25% , 3% to 24% ,3% to 26% , 0.5% to 14% respectively. Manual calculations of the conventional limit showed good agreements with results evaluated from the computer program for the all methods of interpretation.

#### *The results of the theoretical limit pressure*

The values of the theoretical limit pressure interpreted using three methods of analysis ,these are as follow

- 1- The up side -down method
- 2- The P-  $1/\epsilon_0$  method
- 3- The P- $\ln \Delta V/V$  method

The results of theoretical limit pressure using the three methods for the four boreholes are shown in Fig.6 to Fig.9 .

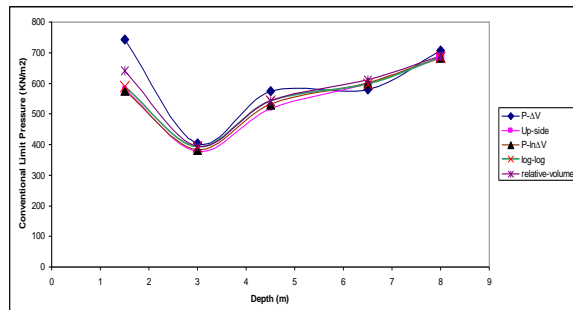


Fig.4 Conventional limit pressure using different methods bh.no.61

As can be seen from the results, the values of the theoretical limit pressures yield from the P- $\ln \Delta V/V$  method are little higher than the other two methods ,in BH.No.87 as shown in Fig.6 ,the results of theoretical limit pressure evaluated using P- $\ln \Delta V/V$  method are higher than those evaluated using up side -down method and P-  $1/\epsilon_0$  method in the range of 2% to 17% and 3% to 12 % respectively.

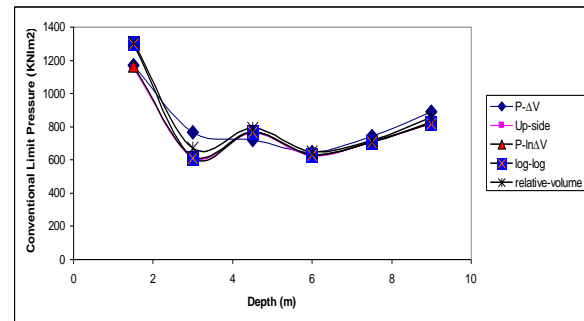


Fig.5 Conventional limit pressure using different methods bh.no.92

Fig.7 represents the results in BH.No.62 , the results of theoretical limit pressure analyzed using P- $\ln \Delta V/V$  method are higher than those evaluated using up side -down method and P-  $1/\epsilon_0$  method in the range of 9% to 12% and 2% to 11 % respectively . The results of theoretical limit pressure in BH.No.61 can be seen in Fig.8, analyzed using P- $\ln \Delta V/V$  method are higher than those evaluated using up side -down method and P-  $1/\epsilon_0$  method in the range of 3% to 21% and 2% to 13 % respectively. The same trend found in BH.No.92 as can be seen in Fig.9, the results of the theoretical limit pressure deduced using P- $\ln \Delta V/V$  method are higher than those evaluated using up side -down method and P-  $1/\epsilon_0$  method in the range of 4% to 15% and 1% to 8 % respectively. Manual calculations of the theoretical limit showed good agreements with results evaluated from the computer program for the all methods of analysis.

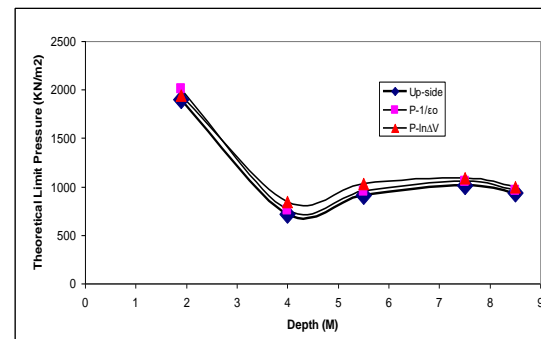


Fig.6 Theoretical limit pressure using different methods bh.no.87

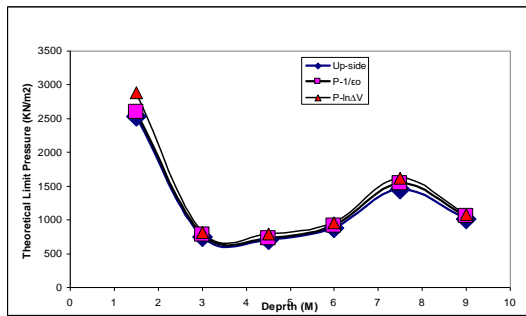


Fig.7 Theoretical limit pressure using different Methods BH.No.62

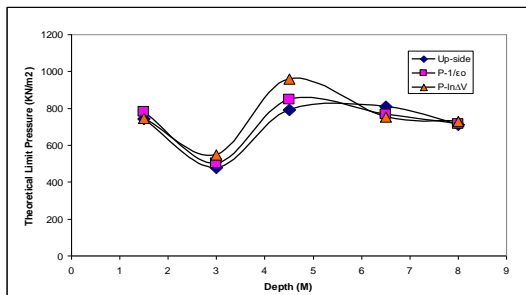


Fig.8 Theoretical Limit Pressure Using Different Methods BH.No.61

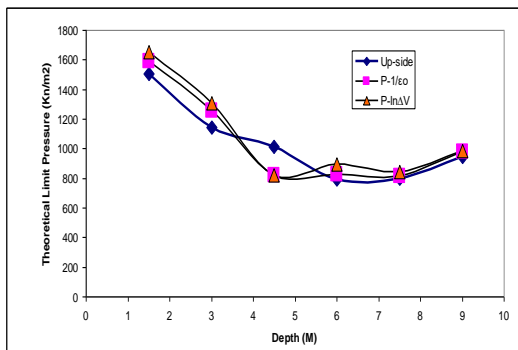


Fig.9 Theoretical Limit Pressure Using Different Methods BH.No.92

## CONCLUSIONS

This research focused on developing a new computer program to be considered when analyzing the pressuremeter tests data to deduce the values of the conventional and theoretical limit pressure using different methods of analysis. Based on the present research results, some conclusions can be drawn as follow:

1- A computer program has been developed using different methods of analysis to evaluate the conventional and theoretical limit pressure, after unifying all the symbols of all methods.

- 2- A manual calculation been carried out to calculate the values of the conventional and theoretical limit pressure in order to confirm the calculation from the computer program and the results showed distinctive consistency.
- 3- The conventional limit pressure evaluated using five methods of analysis using the results of four boreholes in brown silty clay soil.
- 4- The values of the conventional pressure deduced from the P- $\Delta V$  method are higher than those deduced from up-side down curve method, P-  $\ln (\Delta V/V)$  method, log-log method and Relative volume method in range from 1% to 48% , 1% to 48% ,0.5% to 26% , 0.4% to 25% respectively.
- 5- The values of the theoretical limit pressure using three methods of analysis using the results of four boreholes of the same soil.
- 6- The results of theoretical limit pressure evaluated using P- $\ln \Delta V/V$  method are higher than those evaluated using up side -down method and P-  $1/\epsilon_0$  method in the range of 2% to 21% and 1% to 13 % respectively.

## REFERENCES

- [1]. Moayed, R ., Kordnaeij, A. and Mola-Abasi, H "Pressuremeter Modulus and Limit Pressure of Clayey Soils Using GMDH-Type Neural Network and Genetic Algorithms. Geotechnical and Geological Engineering · August 2017, DOI: 10.1007/s10706-017-0314-9
- [2]. Tezel G, Hacialioglu E, Onal O, and Ozmen G "Comparison of High Pressure Pressuremeter (HyperPac) and Pre-Bored Pressuremeter Test Results - A Case Study.Proceedings of the 18th International Conference on Soil Mechanics and Geotechnical Engineering, Paris 2013
- [3]. Lukas R "Pressuremeter Testing in Stiff to Hard Cohesive Soils "Seventh International Conference on Case Histories in Geotechnical Engineering - Apr 29th - May 6<sup>th</sup>, 2013 Missouri University of Science and Technology Scholars' Mine.
- [4]. Agan, C and Algin, H "Determination of Relationships between Menard Pressuremeter Test and Standard Penetration Test Data by Using ANN model: a Case Study on the Clayey Soil in Sivas, Turkey". Geotechnical Testing Journal 37, no. 3, 2014, pp 412-423.
- [5]. Ahmadi, M. and Keshmiri ,E "Interpretation of in situ horizontal stress from self-boring pressuremeter tests in sands via cavity pressure less than limit pressure: a numerical study, Environmental earth sciences, Vol.76, No.9, 2017

- [6]. Hamidi, B., Varaksin, S and Nikraz, H  
"Predicting Menard Modulus using Dynamic  
Compaction Induced Subsidence. International  
Conference on Advances in Geotechnical  
Engineering, Perth, Australia Nov.7-9, 2011,  
ISBN: 978-0-646-55142-5
- [7]. Al-kanim , A " Pressuremeter Theories in Clay  
Testing" ,MSc thesis ,College of Engineering Al  
Nahrain University, Baghdad, Iraq ,1999.
- [8]. Al-Rawi, R " Comparison of Shear Strength  
Between Different In Situ and Laboratory Tests"  
MSc Thesis University of Baghdad ,Iraq,1985

## ANALYSIS OF PROBLEMS AND SOLUTIONS IN THE HEAT INSULATING GLASS MANUFACTURING INDUSTRY USING FMEA

Natsuda Paiboon<sup>1</sup>, Nipalai Inplaeng<sup>2</sup>, Wisitsree Wiyaratn<sup>3</sup> and Anucha Watanapa<sup>4\*</sup>

<sup>1,2,4</sup> Production Technology Education, Industrial Education and Technology, King Mongkut's University of Technology Thonburi University, Thailand; <sup>3</sup>Industrial Education and Technology, King Mongkut's University of Technology Thonburi University, Thailand

### ABSTRACT

This research project was aimed to analyze the problems and solutions in the heat insulating glass manufacturing industry by using technical fault analysis, and to conduct an impact analysis to the application when dead time that occurs in the process of insulating glass units. This research was done with several tasks to reduce the problem based on risk priority number analysis. The 3 problems with the highest RPN value were presented in Pareto diagram. The problems were as follows: the glass was dirty, the employees took a long time to inspect the glass, and the employees took a long time to clean the glass. The team brainstormed ways to resolve the problem and then measured the effect. The result of the adjustment showed that the problem of the dirtiness in the glass manufacturing process decreased by 40%. The employees decreased their inspection time and their cleaning time by 42%. The total amount of time for the whole manufacturing process in the past was 7.39 minutes per sheet. After the adjustment, the manufacturing time reduced to 6.30 minutes. In other words, it decreased by 1.09 minutes, or 14.75%.

*Keywords: Heat Insulation Glasses, Failure Mode and Effects Analysis, Pareto Diagram, Cause and Effect Diagram*

### INTRODUCTION

Float glass manufacturing system is a modern system for manufacturing a sheet of glass which can be used in households and buildings. It can be converted to become heat insulation glass for houses and buildings. Generally, heat insulation glass contains two layers of glass, one internal and one external; hence, the ability to reduce the heat into the building. The space between the two layers helps push the heat outside the building [2]. The manufacturing process starts with Phase 1 which is the preparation in which 2 sheets of glass are loaded to the machine to reduce the sharpness at the margin by approximately 40% of the whole sheet and then they are loaded to the cleaning machine. In Phase 2, the frame will be fixed to the glass. The frame will be checked again to meet the requirements and the glass will be cleaned before the unit is loaded to the glass compressor. In Phase 3, silicon will be applied to the frame and the glass to make them sealed and then the glass will be put aside to leave it until the silicon dries. Then, the glass will be checked for 100% accuracy before it is stored in the warehouse, ready for dispatch to customers.

Because there are many repetitions as mentioned above, the bottleneck problem occurs in Phase 2, the frame being fixed to the glass, resulting in waste time. The researchers were interested in such problem and collected the data as well as presented the data in Pareto diagram in order to find out the problem. Then,

the data were analyzed using Failure Mode and Effect Analysis (FMEA) in order to resolve problems in Phase 2. By doing so, the effectiveness increased and the manufacturing cost decreased. Moreover, the working hour decreased and there were fewer unnecessary jobs. Therefore, FMEA was useful in this study because it could reduce the waste in the manufacturing process. This study would look at the problems in the manufacturing process and solutions in the heat insulating glass manufacturing industry using FMEA.

### LITERATURE REVIEW

The research studies into FMEA started in 1977 when Ford Motors introduced FMEA to address the potential problems in the Research and Development (R&D) in the early stage of production and published the Potential Failure Mode and Effects Analysis Handbook in 1984 to promote the method. The FMEA model was applied in salmon processing and packing industry in collaboration with ISO 22000 and there were valuable results from the implementation [7]. FEAM was also used in order to improve the quality continuously and there were multiple case studies in automobile SMEs. The implementation of those improvement points shows the definite signs of continuous improvement of the quality of process and product as well. The FMEA and subsequent implementations had reduced the quality rejections by around 3% to 4% in companies in the case study



conducted by Tejaskumar S. Parsana and Mihir T. Patel who conducted “A Process FMEA Tool to Enhance Quality and Efficiency of Manufacturing Industry”.

## THEORY

FMEA is a technique which increases the reliability of a product, decreases an interruption period in the initial and normal stages because it focuses on the prediction of problems and analyzes the solutions in order to show risk priority number (RPN).

## METHODOLOGY

According to the research study, the waste from the manufacturing process would be reduced in the heat insulating glass manufacturing industry using the following steps:

1. Current state would be examined and then goal would be set in order to improve the manufacturing process.
2. Steps and procedures to improve would be based on the principles of FMEA.
3. Steps and procedures would be implemented after the data collection in accordance with the setup.
4. The results before and after the intervention would be compared.

## RESULTS

### 3.1 A study into the current state of heat insulating glass manufacturing process

During the heat insulating glass manufacturing process, from the loading of glass and transferring to the other steps, there were 3 sets of procedure. The first set of procedures involved loading. The second set involved assembly and the third set involved sealing as shown in Fig.1.

Procedure 1 or the loading could be analyzed using Man-Machine Chart as shown in Table 1 and the total amount of time was 1.75 minutes or equal to 2.15 minutes when increasing the cleaning work since bringing the glass into the process. The effectiveness was compared to the man labor and it was 95.43% out of 100%. That means humans worked effectively. Regarding the efficiency of Machine 1, it was 71.43% because there was dead time as it waited for the loading. The efficiency of machine 2 was 34.29% because it waited for the loading and for Machine 1 to complete the task. The efficiency of Machine 3 was 23.43% because the dead time was the longest as it waited for two machines to complete their tasks.

Procedure 2 or the assembly involved Process Chart because it was about human labor. It was found that the total amount of time for Procedure 2 was 4.54

minutes and the longest amount of time was for cleaning the first sheet of glass, or 2.59 minutes, namely 57.05% of the total time. The amount of time for cleaning the second sheet of glass was 1.12 minutes, or 24.67% of the overall time.

Procedure 3 or the sealing as shown in Man-Machine Chart had no difficulty. If there was a difficulty, it was due to the fact that the silicon was not sealed properly on the glass. This last set of procedure for the heat insulating glass manufacturing process took 1.10 minutes to complete.

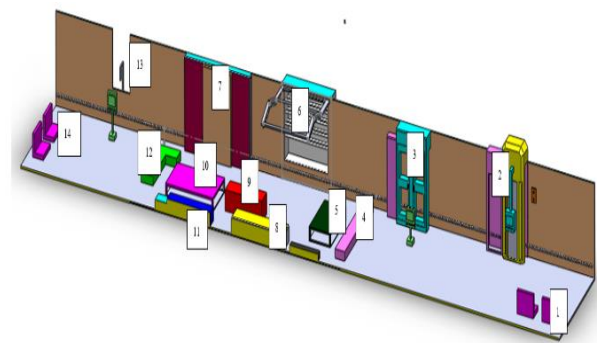


Fig. 1 Layout of machines and devices in the heat insulating glass manufacturing process at the current state

### Position

#### Procedure 1 involves Loading

- Number 1 is Pallet for two sheets of glass
- Number 2 is Arising Machine
- Number 3 is Watching Machine

#### Procedure 2 involves Assembly

- Number 4 is Elevation / Arising Platform?
- Number 5 is area for unused frame
- Number 6 is Inspection area
- Number 7 is Pressing Machine
- Number 8 is Desiccant filling machine
- Number 9 is Butyl sticking machine
- Number 10 is Table for frame
- Number 11 is Cabinet and Bin
- Number 12 is Table for documents

#### Procedure 3 involves Sealing

- Number 13 is Silicone injector
- Number 14 is Pallet for finished glass

Table 1 Man-Machine Chart for Loading Glass (Former)

| Man-machine working chart                  |               |                                |               |   |                     |                                |               |  |  |
|--|---------------|--------------------------------|---------------|---|---------------------|--------------------------------|---------------|--|--|
| Man  | time<br>(min) | Machine<br>1 Suck<br>the glass | time<br>(min) | Machine 2<br>Clear glass                | time<br>(min)       | Machine<br>3<br>Clean<br>glass | time<br>(min) |  |  |
| Glass preparing                            | 0.2           | No working                     | 0.2           |   |                     |                                |               |  |  |
| Forced glass suction machine into conveyor | 0.25          | Suck the glass                 | 0.25          | No working                              | 0.45                | No working                     | 0.75          |  |  |
| prepare the second mirror                  | 0.22          | No working                     | 0.3           | Clear glass                             | 0.3                 |                                |               |  |  |
| No working                                 | 0.08          |                                |               |   |                     |                                |               |  |  |
| Forced glass suction machine into conveyor | 1             | Suck the glass                 | 1             | No working<br>Clear glass<br>No working | 0.11<br>0.3<br>0.59 | Clean glass<br>No working      | 0.41<br>0.59  |  |  |
| total                                      | 1.75          | total                          | 1.75          | total                                   | 1.75                | total                          | 1.75          |  |  |

NOTE: Total time is 1.75 minutes or equal to 2.15 minutes

It was found that the amount of time for Procedure 1 was 2.15 minutes and that the amount of time for Procedure 2 for cleaning was 4.11 minutes. The amount of time for Procedure 3 was 1.10 minutes. The total amount of time for the whole glass manufacturing process was 7.39 minutes per sheet. It was found that the amount of time for cleaning glass in Procedure 2 and for inspection was quite long. It needed to be reduced because in the heat insulating glass manufacturing process there was already a machine for cleaning/washing the glass. Therefore, it was an unnecessary repetition when the glass had to be cleaned again. This problem would create a bottleneck and the amount of time was collected and measured and then presented in a Pareto Chart in order to show the problem as seen in Fig. 2.

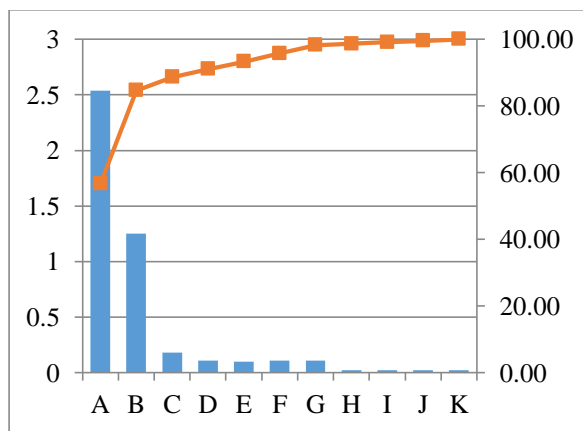


Fig. 2 Pareto Chart showing the heat insulating glass manufacturing process

- A. Clean the glass plate 1
- B. Clean the glass plate 2
- C. Assembling the frame
- D. Go to process 3
- E. Wait for the second mirror.
- F. Go to the mirror compression machine
- G. Wait for the mirror sheet 1
- H. Walk to pick up the frame.
- I. Grab the frame
- J. Walk back
- K. Compress the mirror

According to the data analysis of the Pareto Chart, the dead time for the process was found during the following steps: 1) cleaning the first sheet of glass, and 2) cleaning the second sheet of glass, which is the main reason for dead time and unnecessary waiting time. If 2 sheets of glass needed to be cleaned and the amount of time was combined, it would be 81.72 per cent. The dead time was over 50% and it was for cleaning the first sheet of glass because the first sheet of glass was laminate; hence, the longer time for cleaning. In order to reduce the time and to clean both sheets of glass, the principles of FMEA were used in order to analyze and resolve the real cause of the problem in the heat insulating glass manufacturing process.

*Results from the adjustment to the heat insulating glass manufacturing process based on FMEA*

According to FMEA, the main problem in the heat insulating glass manufacturing process was the time

spent on cleaning sheets of glass as shown in the Table 2. The amount of time for Procedure 1 was 2.15 minutes. After the implementation of the adjustment, Procedure 1 took a longer time to become 3.15 minutes or 2 minutes longer because the glass was cleaned from the beginning. However, Procedure 2 took 1.31 minutes instead of 4.11 minutes. In other words, the amount of time reduced by 2.8 minutes or 68.13%. The total amount of time for the whole manufacturing process in the past was 7.39 minutes per sheet. However, the adjustment brought the manufacturing process down to 6.30 minutes. In other words, the manufacturing process reduced by 1.09 minutes or 14.75%.

glass and the amount of time to clean and inspect remained the same. The other cause of problem which was not as severe as the first one was that the machine stopped suddenly, resulting in the glass getting stuck inside the machine and the new operation time.

The problem could be resolved after the adjustment and the evaluation of the new RPN showed that that the severity (S) remained the same because the dirtiness needed to be cleaned. The Occurrence (O) decreased from 9 to 7, or 77.78% and the ability to detect (D) decreased from 9 to 7, or 77.78%.

After the adjustment to the heat insulating glass manufacturing process based on FMEA, the researchers collected the data of the samples of the

Table 2 Man-Machine Chart for the heat insulating glass manufacturing process (Adjustment)

| Man-machine working chart                  |            |                             |            |   |                     |                           |            |  |              |
|--|------------|-----------------------------|------------|---|---------------------|---------------------------|------------|--|--------------|
| Man  | time (min) | Machine 1<br>Suck the glass | time (min) | Machine 2<br>Clear glass                | time (min)          | Machine 3<br>Clean glass  | time (min) |  |              |
| Glass preparing                            | 1.2        | No working                  | 1.2        |   |                     |                           |            |  |              |
| Forced glass suction machine into conveyor | 0.25       | Suck the glass              | 0.25       | No working                              | 1.65                | No working                |            |  | 1.95         |
| prepare the second mirror                  | 0.22       | No working                  | 0.3        | Clear glass                             | 0.3                 |                           |            |  |              |
| No working                                 | 0.08       |                             |            |   |                     |                           |            |  |              |
| Forced glass suction machine into conveyor | 1          | Suck the glass              | 1          | No working<br>Clear glass<br>No working | 0.11<br>0.3<br>0.59 | Clean glass<br>No working |            |  | 0.41<br>0.59 |
| total                                      | 2.75       | total                       | 2.75       | total                                   | 2.75                | total                     | 2.75       |  |              |

Note \*\* Total time is 2.75 minutes or equal to 3.15 minutes

The main problem of FMEA is Risk Priority Number (or RPN). If a problem has a high level of RPN, that problem needs to be resolved quickly. In this case, the problem with the highest RPN was the fact that the glass was dirty and therefore it took a long time for employees to clean it. The principles of FMEA are useful because the results are obvious. In this case, the value of RPN based on the Severity (S) of the problem due to the dirtiness of the glass decreased from 10 to 6 or decreased by 60%. The total amount of time for cleaning and inspection reduced from 10 to 6, or 60%. The Occurrence (O) of the glass for dirtiness reduced from 10 to 5 or reduced by 50%. The amount of time for cleaning and inspection decreased from 10 to 7 or decreased by 70% because the cleanliness improved from the first Procedure. The ability to detect (D) the dirtiness of

old glass sheets and collected the new data from Procedure 1. Because there were more tasks in Procedure 1 to reduce the unnecessary tasks in Procedure 2, the amount of time for Procedure 1 increased to 3.15 minutes for 1 pair of glass. The effectiveness in comparison to human labor was 97.10% because the cleaning task was added. The efficiency of Machine 1 was 45.45% because there was dead time while it waited for the loading. The efficiency of Machine 2 was 21.82% because it waited for the loading and Machine 1 to complete the tasks. The efficiency of Machine 3 was 14.91% because the dead time was the longest.

The amount of time for Procedure 2 in the past was 2 minutes 5 seconds and after the adjustment it was 1 minute 7 seconds. It decreased by 32.68%. The amount of time for cleaning the second sheet of glass

decreased to 1 minute 4 seconds, or by 31.22%. It can be seen that Procedure 2 after the adjustment to the cleaning task which was taken out and put in Procedure 1 made the first Procedure work longer for 1 minute. However, the problem of cleaning was difficult and there were limitations as follows:

1. The washing machine contained a system which cannot be replaced inside. The cloth inside the machine can be used with any type of glass. If the cloth can be replaced to meet the requirements of each glass, it will take a longer time to set up and to check the quality of the glass sheet.

2. Employees during the assembly procedure needed to be trained to assemble and clean the glass. The distance for viewing is 2 meters and the external environment must be adjusted every minute in accordance with the situation.

3. Check Sheet needs to be used to monitor and control mistake and error. It can also indicate the past errors.

After the adjustment based on FMEA, it was found that the severity (S) and the occurrence (O) decreased but the detection (D) remained the same. According to the analysis, when a sheet of glass is dirty or contains a stain, it cannot be used in the next procedure because it needs to be cleaned and inspected, which can take a long time. The glass for customers must meet the requirements. Therefore, the glass needs to be checked to reduce the chance of dirtiness, the time for cleaning and the time for inspection. After the adjustment with the new values of RPN, it was found that the severity (S) of the product decreased to moderate level. In other words, the dirtiness of the glass decreased from 10 to 6, or by 60%. The amount of time for cleaning and inspection decreased from 10 to 6, or by 60%. The occurrence (O) of error and mistake was high or higher than 1 out of 20 in the past but after the adjustment it was at a moderate level, or 1 out of 1,000 or 1 out of 80. The dirtiness of the glass decreased from 10 to 5, or by 50%. The amount of time for cleaning and inspection decreased from 10 to 7 or by 70% because the cleaning task was done in Procedure 1. The ability to detect (D) the dirtiness of the glass and the amount of time to clean and inspect the glass remained the same because the glass still needed to be cleaned and checked for any cracks and dirtiness. The washing machine could cause stain or dirty spots. According to the analysis, it was found that when the washing machine stopped suddenly and one sheet of glass got stuck inside the machine, the pieces of glass would make stain on the glass sheet. This is the limitation which this machine cannot resolve. After the adjustment based on FMEA with RPN, it was found that the severity (S) remained the same but the effect of the error on the product was at

a moderate level because the stain and the dirtiness can be cleaned. The occurrence (O) for any error was quite high or higher than 1 out of 20 in the past but after the adjustment it became 1 out of 1,000 or 1 out of 80. In other words, it decreased from 9 to 7, or 77.78%. The ability to detect (D) was low in the past but after the adjustment the detection was at a moderate level

## CONCLUSIONS

This research was aimed to analyze the problems and solutions in the heat insulating glass manufacturing industry using FMEA to analyze the dead time in the heat insulating glass manufacturing industry. The faults with the top three highest values of RPN were presented in a Pareto Chart and they were fixed. The main problems were the fact that the glass was dirty, that the employees took a long time to inspect the sample, and that the employee took a long time to clean the sheet of glass. After the adjustment it was found that the dirtiness in the glass manufacturing process decreased by 40%. The employees decreased their inspection time and their cleaning time by 42%. The total amount of time for the glass manufacturing process was 7.39 minutes per sheet. After the adjustment, the total amount time decreased to 6.30 minutes. In other words, it decreased to 1.09 minutes or by 14.75%.

## ACKNOWLEDGMENTS

The authors would like to thank the National Research Council of Thailand for financial support.

## REFERENCES

- [1] Moghal A. A. B., Dafalla M. A., Elkady T. Y., and Al-Shamrani M.A., Lime Leachability Studies on Stabilized Expansive Semi-Arid Soil. International Journal of GEOMATE, Vol. 9, Issue 18, 2015, pp.1467-1471.
- [2] Awal A.S.M.A, Hosseini H. and Hossain M.Z., Strength, Modulus of Elasticity and Shrinkage Behaviour of Concrete Containing Waste Carpet Fiber, International Journal of GEOMATE, Vol. 9, Issue 17, 2015, pp. 1441-1446.
- [3] Hossain M.Z., For Chapter in a Book, Soil Mechanics, 4th ed. Vol. 2, Sakai, Ed. Sankeisha Publisher's Name, Year, pp. 11-60.
- [4] Author H., A Book New York Publisher, Year, pp.1-200.
- [5] Annnn B., Unpublished Work but Accepted, Vol., Issue, Year.
- [6] Kimura S., Journal Paper Title, J. of Computer Science, Vol. 1, Issue 2, 1987, pp. 23-49.
- [7] Islam M.R., Conference proceedings, in Proc. 2nd Int. Conf. on GEOMATE, 2011, pp. 8-13.

- [8] Hossain M.Z. and Awal A.S.M.A., Experimental Validation of a Theoretical Model for Flexural Modulus of Elasticity of Thin Cement Composite, *Const. Build. Mat.*, Vol.25, No.3, 2011, pp.1460-1465.

## APPLICATION OF DEAGGREGATION OF SPATIAL PROBABILISTIC SEISMIC HAZARD TO DISASTER PREPAREDNESS

Takayuki Hayashi<sup>1</sup> and Harumi Yashiro<sup>2</sup>

<sup>1</sup> Tokio Marine & Nichido Risk Consulting Co. Ltd., Japan;

<sup>2</sup> National Defense Academy, Japan

### ABSTRACT

In considering regional disaster prevention, it is important to understand the occurrence area of the strong ground motion and its occurrence probability. Spatial probabilistic seismic hazard analysis (SPSHA) proposed by the authors can provide the such information. In SPSHA, the results are expressed by the relation between the area where a given seismic intensity is generated and the exceedance probability. Results based on such a probabilistic approach include the effects of various seismic sources. Therefore, to clarify the earthquake scenario that should be the target of regional earthquake countermeasures, it is necessary to grasp the impact of each earthquake source. In this study, we propose the seismic hazard deaggregation for SPSHA and show a method for quantitatively grasping earthquakes that affect the target region. In the application example, SPSHA is conducted for Kanagawa prefecture in Japan. We also conduct seismic hazard deaggregation for whole area and sub-area inside and discuss the differences of dominant earthquake for each area and the application to such information to disaster prevention.

*Keywords: PSHA, Seismic hazard deaggregation, Spatial Correlation, Disaster prevention plan*

### INTRODUCTION

In recent years, many big earthquakes have occurred in Japan. In the near future, there are concerns about the occurrence of megathrust earthquake around the Nankai Trough, Tokyo inland earthquake and so on, and earthquake countermeasures are urgently needed. Local governments are considering the measures in advance such as the emergency plan, emergency restoration at the time of disasters, and the reconstruction plan, and conclude them as their regional disaster prevention plans. In establishing the regional disaster prevention plan, they will carry out earthquake damage assessment. Select the earthquake scenarios that occur in the area, and quantify building damage, casualty, economic damage, etc. This is a necessary study to make the measures effective and specific.

In this earthquake damage assessment, some target earthquakes are often selected after discussions by the expert committee in consideration of large earthquakes that occurred in the past and earthquake activity areas around the target region. The outcome of the earthquake selection may depend on the knowledge and experience of the expert or the situation of the discussion. In addition, the way of selecting target earthquakes by local governments across the country is diverse in their studying, and no unified way of selection is shown. Authors believe that the criteria for earthquake and earthquake scenario selection should be based on a more objective process.

Several studies have been conducted on the selection of target earthquakes in regional earthquake

damage assessment in the past. Okada et al.[1] have reported that the uncertainty of target earthquake scenario setting greatly affects the estimated damage. Also, Tomatsu et al. [2] have proposed a method to select the target earthquakes using Analytic Hierarchy Process (AHP) based on the estimated damage. These are based on a deterministic approach, and the image of earthquake scenario such as the earthquake source and magnitude are clear. However, since a small number of scenarios are basically targeted, it cannot be denied the scenario that an unexpected earthquake occurs. In addition, when considering the whole area, appropriate target earthquakes are selected for the entire region, but there is a possibility that a high impact scenario for a specified sub-area inside may not be selected.

Alternatively, a probabilistic approach covers all earthquakes affecting the region comprehensively and is superior in that it can consider the occurrence probability of earthquakes and earthquake hazards simultaneously. In the past, such Probabilistic Seismic Hazard Analysis (PSHA) have been studied for specific sites, so the authors have proposed a method that extends PSHA throughout the area. Spatial Probabilistic Seismic Hazard Analysis (SPSHA) [3] proposed by the authors is a method of calculating the relationship between the occurrence area of given ground motion intensity and its exceedance probability in the target area taking into consideration the correlation of spatial ground motions. In this method, the earthquake motion prediction equation is corrected based on the earthquake observation records obtained in the target area, and the spatial correlation of ground motion

intensity is taken into consideration. However, since the result is expressed by the area of the seismic ground motion and the occurrence probability, there is a problem that the image of earthquake scenario that generates the seismic hazard is hard to recognize.

In this study, in order to grasp the image of results by SPSHA, we propose the method of deaggregation of seismic hazard by SPSHA and the method of selection of the suitable target earthquake scenario for earthquake damage assessment for the region. In addition, we apply this method to Kanagawa Prefecture and discuss the application for regional disaster prevention.

## OUTLINE OF SPSHA

In Spatial Probabilistic Seismic Hazard Analysis (SPSHA) proposed by the authors [3], the probability  $P(A > a; t, y)$  that area  $A$  (or area ratio) of the area exceeding the strong ground motion intensity  $y$  exceeds  $a$  in  $t$  years due to earthquakes in a certain area is calculated by the following equation.

$$P(A > a; t, y) = 1 - \prod_k \{1 - P_k(A > a; t, y)\} \quad (1)$$

Where,  $P_k(A > a; t, y)$  is area  $A$  (or area ratio) of the area exceeding the strong ground motion intensity  $y$  exceeds  $a$  in next  $t$  years due to the  $k$ -th earthquake.  $P_k(A > a; t, y)$  is expressed by Eq. (2) if the updating process is adopted for the  $k$ -th earthquake occurrence probability, and Eq. (3) if the Poisson process is adopted.

$$P_k(A > a; t, y) = P(E_k; t)P(A > a; y|E_k) \quad (2)$$

$$P_k(A > a; t, y) = 1 - \exp\{-\nu(E_k)P(A > a; y|E_k) \cdot t\} \quad (3)$$

Where,  $P(E_k; t)$  is the occurrence probability of the  $k$ -th earthquake in next  $t$  years, and  $P(A > a; y|E_k)$  is a conditional probability that the area  $A$  (or area ratio) of the area where the strong ground motion that exceeds the ground motion intensity  $y$  occurs exceeds  $a$ , when the  $k$ -th earthquake occurs.

We calculate the seismic ground motion distribution samples for the target area by Monte-Carlo simulation (MCS) using the Ground Motion Prediction Equation (GMPE) corrected by the earthquake observation records obtained in the target area and the spatial correlation model regressed from these data. Then, the ground motion intensity at each site is treated probabilistically by the following equation in consideration of the spatial correlation of the seismic intensity between sites.

$$\log(x_{ij}) = \hat{x}_i + \beta_i + \varepsilon_{ej}(0, \sigma_e) + \varepsilon_{cj}(0, \sigma_c) \quad (4)$$

Where, the subscript  $i$  represents the site, and  $j$

represents a sample number.  $x$  is a ground motion intensity sample,  $\hat{x}$  is a log median value of ground motion intensity calculated by the GMPE, and  $\beta_i$  is a site correction coefficient of the GMPE obtained from data analysis of earthquake observation records.  $\varepsilon_{ej}(0, \sigma_e)$  and  $\varepsilon_{cj}(0, \sigma_c)$  are random variables with an average 0 and a standard deviation of  $\sigma_e$  and  $\sigma_c$ , respectively.

$\sigma_c$  represents inter-event variation and assumes common and perfect correlation at all sites.  $\sigma_e$  indicates intra-event variation and gives spatial correlation by the following equation.

$$\rho = \exp(-\gamma \cdot z^\delta) \quad (5)$$

Where,  $z$  is a separation distance (km) between two sites,  $\rho$  is a correlation coefficient, and  $\gamma$  and  $\delta$  are regression constants obtained from data analysis of earthquake observation records.

By the way,  $\beta_i$  in Eq. (4) is calculated only at earthquake observation sites. Therefore, after sampling the ground motion intensity at the sites by Eq. (5), the ground motion intensity at the center points of the meshes obtained by spatially discretizing the target area are calculated by spatial interpolation using the simple kriging method. The relationship between the area and the exceedance probability exceeding the given ground motion intensity  $y$  calculated from the above is hereinafter referred to as a seismic area hazard curve.

## EARTHQUAKE SENARIO SELECTION BY SEISMIC HAZARD DEAGGREGATION

### Deaggregation of the Seismic Area Hazard

Seismic hazard deaggregation in PSHA is a method to measure the contribution of each seismic source on the seismic hazard for a given exceedance probability. The deaggregation of seismic hazard at a specific site is shown by Kameda et al. [4] and McGuire [5]. First, the magnitude of the influence of each seismic source on the seismic hazard with a certain exceedance probability is expressed by the contribution index. Expected values of magnitude and source distance are derived from the results of hazard deaggregation to get the image of seismic source corresponding to the probabilistic seismic hazard. This is the expected target scenario for various damage assessment based on PSHA. In SPSHA, target is the area, so the source distance cannot be determined as same way. Therefore, the degree of contribution is calculated by the following procedure, and the earthquakes that affect the earthquake hazard are identified from the source model of PSHA.

### STEP1: SPSHA for the target region

Conduct SPSHA for the target region to be evaluated and calculate the seismic area hazard curve.



For the risk level  $R(a; yt)$  where the area of the region exceeding the earthquake ground motion intensity  $y$  exceeds  $a$  for next  $t$  years, the exceedance probability  $P(a; yt)$  is obtained.

STEP2: Contribution index for each seismic source

For the risk level  $R(a; yt)$ , the contribution index of each earthquake in the source model are calculated. The contribution index  $c_k$  of earthquake  $k$  to  $R(a; yt)$  is defined by Eq.(6).  $c_k$  means the conditional probability that the event is earthquake  $k$  when the area of the region exceeding the seismic intensity  $y$  in the area exceeds  $a$ .

$$c_k(R_{a;yt}) = P_k(A > a; t, y) / \sum_k P_k(A > a; t, y) \quad (6)$$

### Earthquake Scenario Selection by Seismic Area Hazard Deaggaregation

The earthquakes in the source model used in SPSHA are divided into several groups in terms of activity, area, and type, and the contribution to the risk level  $R(a; yt)$  is summed up by group. From the group with the highest contribution value, let the earthquake with the highest contribution rate be the representative scenario of the risk level  $R(a; yt)$ . If contributions indexes are similar among multiple groups, it is also necessary to adopt representative scenarios from multiple groups. According to this way, earthquakes that affect the region can be selected by probabilistic approach. Target earthquake scenarios for regional disaster prevention can be selected objectively for an optional probability.

## APPLICATION

### Conduction of SPSHA

SPSHA is conducted for Kanagawa Prefecture shown in Fig. 3. There are six subareas in Kanagawa Prefecture, these are based on administrative divisions. As shown in Table 1, approximately 57% of the total population in the prefecture lives in Yokohama City (A1) and Kawasaki City (A2).

According to the proposed method, correction term of GMPE and spatial correlation model of ground motion intensity are set based on the earthquake observation records of K-NET/KiK-net in Kanagawa Prefecture and ground motion intensity is sampled at observation stations site. We perform surface interpolation of the ground motion intensity distribution of the target area by Simple Kriging method using ground motion intensity samples at observation sites. The target area is discretized into a mesh of about 1 km<sup>2</sup> and Peak ground velocity (PGV) on engineering bedrock at the center point of the mesh is estimated. Ground motions intensity distribution is calculated on a mesh of about 250m<sup>2</sup>. The earthquake source model, earthquake ground motion prediction

equation on engineering bedrock, and shallow soil amplification factor are referred to Japanese National Seismic Hazard Map by HERP [6]. Probability characteristics of ground motion intensity is sampled by MCS, considering perfect correlation for inter-event error and the spatial correlation for intra-event error for GMPE based on the author's study [3]. Standard deviation of Inter-event variation and Intra-event variation are 0.192, 0.160, respectively. The number of earthquake ground motion distribution samples of each earthquake by MCS is 1,000 times. Finally, the area of a given ground motion intensity is summed up as seismic area hazard curve.

The earthquake environment of Kanagawa Prefecture is diverse according to the subarea inside. The Philippine Sea plate subducts toward the northern part of Tokyo Bay, and inter-plate and intra-plate earthquakes have occurred in this area. In addition, from the eastern part, the Pacific plate subducts to a deeper place than the Philippine Sea plate, and this area is also active seismic source area. Furthermore, in the area of A3, A4, A5 and A6, there are many active shallow crustal faults such as the Miura Peninsula fault zone with a relatively high probability of occurrence among active faults around Japan.

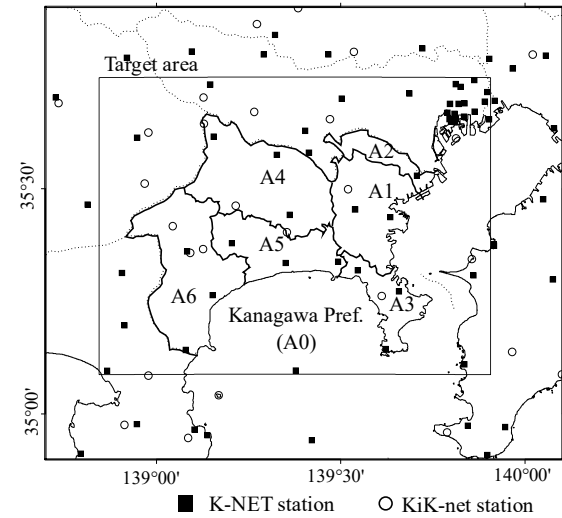


Fig. 1 Target area for this study

Table 1 Areas and the populations (As of March 2019.)

| Area  | Cities   | Area(km <sup>2</sup> ) | Population |
|-------|--|------------------------|------------|
| A1    | Yokohama   | 437                    | 3.74 mil.  |
| A2    | Kawasaki   | 143                    | 1.52 mil.  |
| A3    | Yokosuka, Kamakura, Zushi, Miura, Hayama   | 207                    | 0.70 mil.  |
| A4    | Sagami-hara, Atsugi, Kiyokawa, Yamato, Zama, Ebina, Ayase, Aikawa,                         | 621                    | 1.57 mil.  |
| A5    | Hiratsuka, Fujisawa, Oiso, Chigasaki, Hatano, Isehara, Aikawa, Ninomiya                    | 372                    | 1.31 mil.  |
| A6    | Odawara, Nakai, Oi, Hakone, Minami-Ashigara, Matsuda, Yamakita, Kaisei, Manazuru, Yugawara | 635                    | 0.34 mil.  |
| Total | Kanagawa prefecture  | 2,416                  | 9.18 mil.  |

Table 2 Area ratio corresponding to EP30 by SPSHA

| PGV<br>(cm/s)     | Area | Area ratio |            |            |             |             |
|-------------------|------|------------|------------|------------|-------------|-------------|
|                   |      | EP30<br>1% | EP30<br>3% | EP30<br>6% | EP30<br>14% | EP30<br>26% |
| 50<br>or<br>more  | A0   | 0.76       | 0.65       | 0.57       | 0.45        | 0.34        |
|                   | A1   | 0.93       | 0.83       | 0.73       | 0.57        | 0.42        |
|                   | A2   | 0.94       | 0.90       | 0.78       | 0.67        | 0.57        |
|                   | A3   | 0.92       | 0.80       | 0.66       | 0.44        | 0.27        |
|                   | A4   | 0.81       | 0.62       | 0.52       | 0.38        | 0.27        |
|                   | A5   | 0.94       | 0.88       | 0.82       | 0.72        | 0.59        |
| 100<br>or<br>more | A6   | 0.82       | 0.68       | 0.59       | 0.46        | 0.30        |
|                   | A0   | 0.35       | 0.25       | 0.18       | 0.11        | 0.06        |
|                   | A1   | 0.53       | 0.36       | 0.27       | 0.17        | 0.09        |
|                   | A2   | 0.64       | 0.54       | 0.50       | 0.38        | 0.21        |
|                   | A3   | 0.41       | 0.23       | 0.14       | 0.05        | 0.02        |
|                   | A4   | 0.34       | 0.23       | 0.16       | 0.09        | 0.05        |
|                   | A5   | 0.66       | 0.52       | 0.41       | 0.25        | 0.13        |
|                   | A6   | 0.33       | 0.20       | 0.13       | 0.06        | 0.02        |

Table 2 shows the results of SPSHA for 50 cm/s or more and 100 cm/s or more of PGVs for the whole region and sub-regions in the prefecture. EP30 means the exceedance probability in the next 30 years. The area ratio here indicates the ratio of the area where each ground motion occurs to the area of each region. In addition, Fig.2 shows the seismic area hazard curve. The larger seismic hazard curves express that the region has a high hazard that ground motion will be widespread. In recent big earthquakes in Japan, it is known that a great damage occurs when PGV exceeds 100 cm/s. So, we compare the seismic area hazard curves of PGV:100 cm/s or more. The seismic area hazard curves show that the whole region (A0) and A4 are equivalent. A1, A2 and A4 in the west of the prefecture have a high hazard of PGV 100 cm/s or more in a wide area compared to A0. Table 2 shows that strong ground motion occur in the range of more than twice when the PGV exceeds 50 cm / s, compared with the case of 100 cm / s or more. Table 2 shows that in any region, an area with a PGV of 50 cm/s or more is more than twice as large as an area of 100 cm/s or more, with the same EP30. And, in the case of EP30:6% which is equivalent to about 1/475 for the annual occurrence frequency, the A2 area has the highest hazard, resulting in strong motions in excess of 100 cm/s in half of the A2 area.

On the other hand, in the case where EP30 is 1%, A5 area has the highest hazard. Depending on EP30, seismic area hazard has different results. These are caused by the difference in earthquake environment in each region.

### Conduction of Hazard Deaggregation

Seismic hazard deaggregation for the results of SPSHA in the previous section are conducted to grasp quantitatively the contribution of each seismic source for the seismic area hazard. When deaggregate the seismic area hazard, it is necessary to set earthquake groups by referring to the seismic source data of

SPSHA. In the grouping, first, earthquakes are classified into two categories: the identified earthquakes and the unidentified earthquakes. The former is called the characteristic earthquakes and the latter is called the background earthquakes in PSHA. Next, they are classified into the earthquakes associated with the plate subduction earthquake of Pacific plate and Philippine sea plate and inland crustal earthquakes. Characteristic earthquakes of the Philippine sea plate are further classified into M8 class earthquake around Sagami Trough (hereinafter called "Sagami Trough earthquake") and M8 class Nankai Trough earthquakes (hereinafter called "Nankai Trough earthquake"). Characteristic earthquakes of the crustal inland faults are classified into major active faults and other active faults. Subclassification of background earthquakes includes inter-plate earthquakes, intra-plate earthquakes around the Pacific and Philippine sea plate, and crustal faults. However, according to the long-term evaluation for the earthquakes around Sagami Trough [7] by HERP, the M7 class earthquakes due to Philippine sea plate subduction (hereinafter called "Tokyo inland earthquake") have about 70% chance for next 30 years. It is considered to have a large impact on the target region, so this is classified as an independent group. Tokyo inland earthquake is modeled as a background earthquake (area No.6/7) of the Philippine Sea plate in the Japanese National Seismic Hazard Map. Magnitude of these earthquake is M6.7 or higher.

Figure 3 shows the results of hazard deaggregation for seismic area hazard of 50 cm/sec or more and 100cm/sec or more in area A0. The vertical and the horizontal axis represents the contribution of each earthquake group and the area ratio of Area A0, respectively. Figure 3 shows quantitatively what kind of earthquake groups have the greatest effect on the extent of strong ground motion. The lower part of the thick solid line indicates the contribution of the characteristic earthquakes and the upper part indicates the that of the background area earthquakes. Overall, the contribution of the characteristic earthquakes is larger than that of the background earthquakes, as the strong ground motion becomes wider. Therefore, when considering earthquake disaster prevention in a region, an earthquake scenario which strong ground motion occurs in a narrow area is expected to set as a hypothetical seismic source, and earthquakes scenario that generate strong ground motion in a wide area should be select from characteristic earthquakes.

Next, Table 3 shows the result of deaggregation of seismic area hazard of EP30:6% for the entire area(A0) and sub-area (A1-6). The Nankai Trough earthquake (C11) with a contribution of 0.36 has the greatest impact on the risk of strong ground motion exceeding 100 cm/s in an area of 18% of A0 once every 475 years. The background earthquakes

corresponding to the Tokyo inland earthquake are the intra-plate earthquake (B25) and the inter-plate earthquake (B26). These contributions are 0.16 and 0.35, respectively. The sum of them is 0.51, which has a greater impact on A0 than the Nankai Trough earthquake. Therefore, when selecting an earthquake scenario for A0, it is important to select the inter-plate and intra-plate type earthquakes of the Tokyo inland earthquake, and the Nankai Trough earthquake.

Figure.4 shows the relationship between the contribution of seismic sources and the extent of strong ground motion, for each area, as in Fig.3. From Fig.4 and Table 3, it turns out that the tendency of the contribution is greatly different in each region. From A1 to A5, the intra-plate earthquake (B26) of the Philippine sea plate has a large impact, from small to large area ratios. Since these are classified as background earthquakes where the epicenter cannot be identified, the earthquake damage scenario by virtually placing the epicenter directly under the region should be consider in the regional earthquake risk assessment for these areas. In A3, earthquakes due to major active faults (C13) have a major impact. In this area, there is the Miura Peninsula Fault Zone, which is considered to have a high probability of occurrence among active faults in Japan. Since The influence of this fault zone is significant for A3, it is important to understand the damage scenario caused by this fault. A4, A5 and A6 are located west of Kanagawa Prefecture and close to the Nankai Trough, so they are greatly affected by the Nankai Trough Earthquake (C11). Especially in A6, the Nankai Trough earthquake has a remarkable influence from a small area to a wide area. In risk assessment, it is expected to examine seismic hazards that consider the spread of such various strong ground motion distributions caused by the Nankai Trough earthquake. In any area, as the area of strong ground motion becomes wider, the contribution of the Sagami Trough earthquake (C10) increases. In particular, A4 is most affected by the Sagami Trough earthquake. It is necessary to adopt it as a risk scenario for A4 and A0.

In the report of earthquake damage assessment of Kanagawa prefecture [8], the targets of characteristic earthquakes are follows: the Sagami Trough Earthquake, the Nankai Trough Earthquake, the Miura Peninsula Fault Zone Earthquake, and the Tokai Earthquake. In addition, it is assumed that there are M7 class earthquakes in the south of central Tokyo and in western Kanagawa prefecture, as earthquake scenarios of background earthquakes. According to above mentioned study, although the target earthquakes selected by Kanagawa Prefecture are appropriate, it is considered that there are not enough earthquake scenarios that occur under these areas from the viewpoint of damage scenarios for A1 and A2. Thus, this method is effective in the review of earthquake scenario selection in the target area.

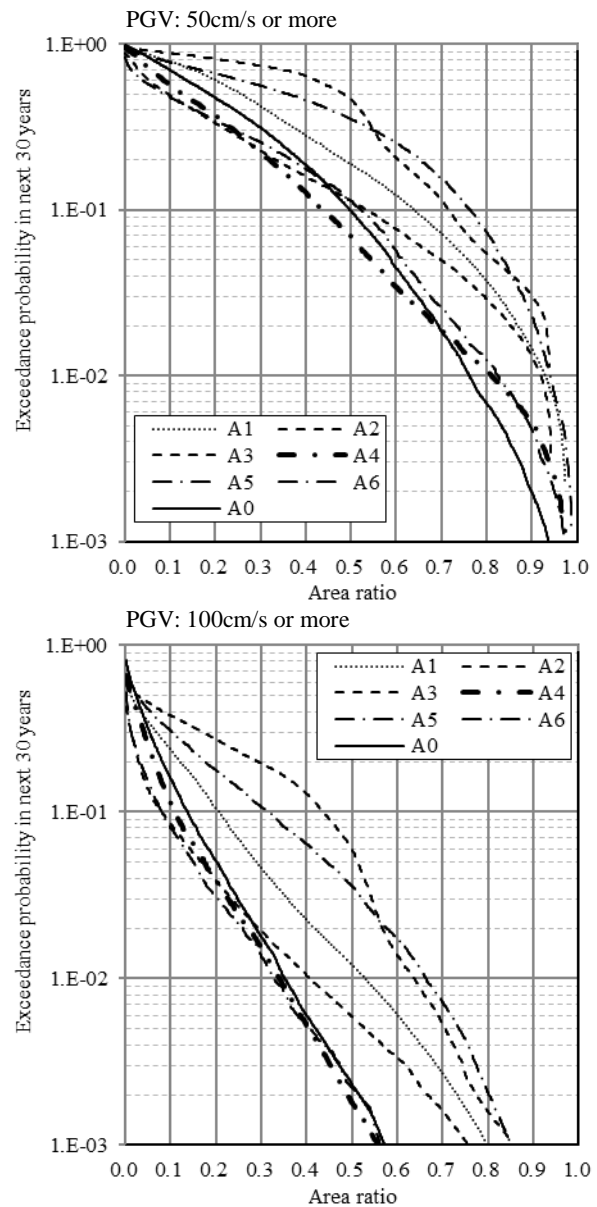


Fig. 2 Seismic area hazard curves of each area

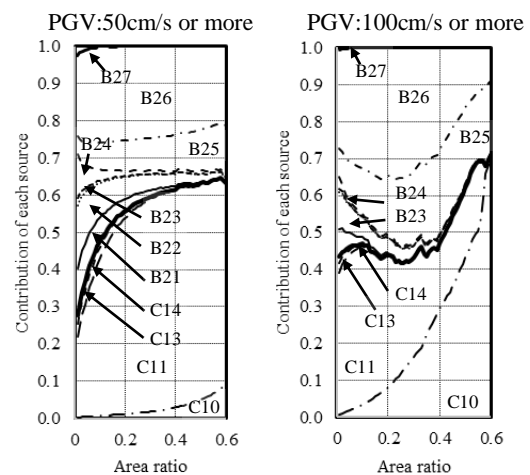


Fig.3 Results of hazard deaggregation of area A0

Table 3 Result of seismic area hazard deaggregation : PGV:100cm/s, Exceedance Probability in next 30 years (EP30): 6%

| Category                   | Class                | Earthquake group                             | Group ID | Area ratio of each area corresponding to EP30:6% |      |      |      |      |      |      |
|----------------------------|----------------------|--|----------|--|------|------|------|------|------|------|
|                            |                      |  |          | A0   | A1   | A2   | A3   | A4   | A5   | A6   |
| Characteristic earthquakes | Philippine sea plate | Sagami Trough Earthquakes                    | C10      | 0.07   | 0.02 | 0.01 | 0.02 | 0.02 | 0.01 | 0.02 |
|                            |                      | Nankai Trough Earthquakes                    | C11      | 0.36   | 0.25 | 0.21 | 0.27 | 0.50 | 0.54 | 0.76 |
|                            | Pacific plate        | Specified Earthquakes                        | C12      | 0.00   | 0.00 | 0.00 | 0.00 | 0.00 | 0.00 | 0.00 |
|                            | Crustal faults       | Major faults                                 | C13      | 0.00   | 0.02 | 0.01 | 0.11 | 0.00 | 0.01 | 0.00 |
|                            | Crustal faults       | Other faults                                 | C14      | 0.00   | 0.00 | 0.00 | 0.02 | 0.01 | 0.03 | 0.01 |
| Background earthquakes     | Pacific plate        | Inter-plate earthquakes                      | B21      | 0.01   | 0.09 | 0.13 | 0.05 | 0.02 | 0.02 | 0.00 |
|                            | Pacific plate        | Intra-plate earthquakes                      | B22      | 0.04   | 0.14 | 0.18 | 0.09 | 0.05 | 0.04 | 0.00 |
|                            | Philippine sea plate | Inter-plate earthquakes (Except area No.6/7) | B23      | 0.00   | 0.00 | 0.01 | 0.01 | 0.01 | 0.01 | 0.00 |
|                            |                      | Intra-plate earthquakes (Except area No.6/7) | B24      | 0.01   | 0.02 | 0.04 | 0.02 | 0.02 | 0.02 | 0.01 |
|                            |                      | Inter-plate earthquakes (Area No.6/7)        | B25      | 0.16   | 0.11 | 0.09 | 0.10 | 0.09 | 0.08 | 0.05 |
|                            |                      | Intra-plate earthquakes (Area No.6/7)        | B26      | 0.35   | 0.34 | 0.31 | 0.31 | 0.27 | 0.24 | 0.12 |
|                            | Crustal faults       | Unknown faults                               | B27      | 0.00   | 0.00 | 0.01 | 0.00 | 0.00 | 0.01 | 0.01 |

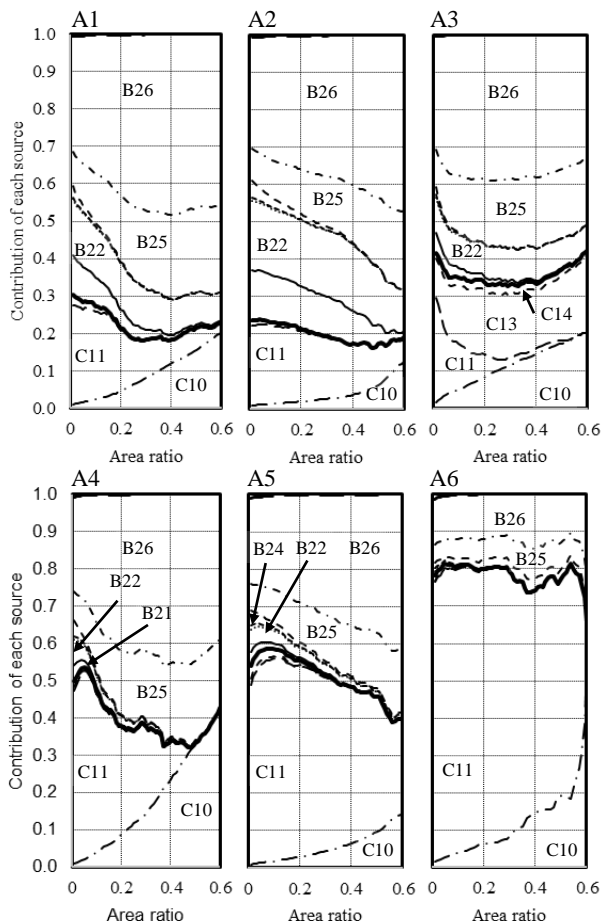


Fig. 4 Results of hazard deaggregation of each area (Case of PGV 100cm/s or more)

## CONCLUSIONS

In this study, the method of seismic area hazard deaggregation of SPSHA has proposed. In addition, based on the application to the region of Kanagawa Prefecture, utilization in regional disaster prevention is discussed.

## REFERENCES

- [1] Okada, S., Tomatsu, M.: Regional Disaster Prevention Planning Guide Based on Seismic Risk Assessment for Earthquakes Occurring near Urban Districts, Journal of Structural and Construction Engineering (Transactions of AIJ), No.530, 2000., pp. 37-44 (in Japanese)
- [2] Tomatsu, M., Okada, S.: Study on the Priority of Measuring against Scenario Earthquakes Based on Seismic Risk Estimation, Journal of Japan Association for Earthquake Engineering. 2011, Vol.11, No.2, 2011, pp. 1-19 (in Japanese)
- [3] Kameda, H., Ishikawa, Y., Okumura, T., Nakajima, M.: Probabilistic Scenario Earthquakes. Definition and Engineering Applications, Transactions of the Japan Society of Civil Engineers. 1997, Vol.577 / I-41, 1997, pp. 75-87 (in Japanese)
- [4] McGuire, R. K.: Probabilistic Seismic Hazard Analysis and Design Earthquake. Closing the Loop, Bulletin of the Seismological Society of America, Vol.85, No.5, 1995, pp. 1275-1284.
- [5] Hayashi, T., Yashiro, H.: Proposal of Spatial Probabilistic Seismic Hazard Analysis and the Application to the Disaster Prevention, Journal of Structural and Construction Engineering (Transactions of AIJ), 2019. (in press) (in Japanese)
- [6] The Headquarters for Earthquake Research Promotion: National Seismic Hazard Maps for Japan (2018 Edition), 2018. (in Japanese)
- [7] Headquarters for Earthquake Research Promotion: Long Term Evaluation for the Earthquakes Around Sagami Trough (2nd Edition), 2014. (in Japanese)
- [8] Kanagawa Prefecture: Report of Earthquake Damage Assessment in Kanagawa Prefecture, 2015. (in Japanese)

## A CONCRETE WALL ELEMENT TEST TO EVALUATE COMPRESSIVE FRACTURE ENERGY

Tetsuya Ohmura<sup>1</sup>, Kyouhei Iwasaki<sup>1</sup> and Hiroaki Matsufuji<sup>1</sup>

<sup>1</sup>Faculty of Architecture, Tokyo City University, Japan;

### ABSTRACT

Concrete walls are significantly effective seismic elements to resist lateral force due to an earthquake, because they have much stiffness and strength. A building with a number of concrete walls would be generally designed for just the strength. On the other hand, a building with a few of concrete walls would be designed for not only the strength but also the ductility. In other words, the ductility of a concrete wall is the key thing considering the survey reports of concrete walls damaged by an earthquake. Generally speaking, the ductility of a concrete building depends on the ductility of the concrete with rebar. According to some previous studies, the fracture energy was focused to evaluate the ductility. However, their test specimen were cylindrical columns, not to target for a concrete wall. In this paper, the ductility of a concrete wall is focused and test the specimen of a concrete wall element. The fracture energy of a concrete wall element was examined, the thickness of a wall and the amount of their rebar were evaluated.

*Keywords: Concrete wall, Ductility, Element test, Concrete strain*

### INTRODUCTION

Lateral strength and ductility significantly depend on the property of the concrete strain softening. It is well-known that the stress decreasing is controlled even in the post peak in the confined concrete with rebar. The column well-confined by rebar has great ductility and hardly collapsed even after a maximum considered earthquake (MCE). The strength of the girder well-confined by rebar is not decreased as well. Those are based on a number of technical reports, and the amount of the rebar is estimated due to the Japanese code.

The depth of the concrete wall is much larger than one of the concrete column. Therefore, the concrete strain at the end of the compressive area at the peak is significantly large, and the compressive area would be developed at the post peak.

The accurate concrete model considered the strain softening is needed to estimate the lateral strength and the ductility of a concrete wall, and the way to estimate the rest of the lateral and axial strength after MCE is expected.

FE analysis is often used to simulate the lateral strength, damage and ductility under an earthquake loading, and to easily have the data that is hard to measure at the test. In addition, parametric analyses could be performed after being verified.

Not to mention, the concrete model is consequence in a FE analysis and sufficient verification must be needed for the material property with compressive fracture energy

For example, Drucker Prager fracture criterion and Mohr-Coulomb fracture criterion were well-known to estimate their maximum compressive stress.

Rots <sup>[1]</sup> defined the effective band width with integrated point of 4 was two times of root of the element area.

Nishiyama and Watanabe et al. <sup>[2]</sup> examined the relationship between stress and strain of the axial and transverse for the concrete cylinder with 135mm of diameter in the concrete strength of 25 to 83 N/mm<sup>2</sup>.

Priestley and Park <sup>[3]</sup> suggested the model with strain softening for a concrete cylinder and a cuboid with enough transverse rebar under one-way cyclic loading.

Higai and Nakamura <sup>[4]</sup> suggested the compressive fracture energy was 8.8 times of concretes strength and the compressive fracture zone length of 1,300 divided by the root of the concrete strength based on the test data of cylinder with no transverse rebar, concrete strength of 11 to 52 N/mm<sup>2</sup> and the diameter of 100 to 150mm and height of 100 to 600mm.

Niwa et al. <sup>[5]</sup> suggested the equation of the fracture zone length and compressive fracture energy based on the test data of cylinder with no transverse rebar, concrete strength of 26 to 48N/mm<sup>2</sup> and the diameter of 100mm, the height of 200 to 800mm.

Koshikawa et al. <sup>[6]</sup> suggested compressive zone length and compressive fracture energy based on the test data of cylinder with no transverse rebar, concrete strength of 29 to 36N/mm<sup>2</sup> and diameter of 100 to 200mm, height of 200 to 600mm.

Their specimen shape mentioned above were cylinder and cuboid for making not a wall but a column concrete model. The fracture energy and fracture zone length of wall in former studies haven't been referred and they are not obvious.

Moreover, the confined effect of the transverse rebar in their cylinders might be definitely different from the one of the vertical and horizontal rebar in a wall.

In this paper, several wall element tests were performed for a concrete wall. The concrete strain softening property was examined and the fracture energy was focused for a wall element with vertical and horizontal rebar.

## TEST

## Specimen

Specimen are shown in Table 1. The number of all of specimen was four. The common factors are concrete material, the width and depth. The parameters are the wall thickness and the rebar ratio ( $p_w$ ). The wall thickness is 150 or 180mm. The rebar is located single or double.  $p_w$  is 0.24 to 1.11 percent. The diameter of rebar is #3 to #5.

Specimen geometrics are shown in Fig. 1. The wall consists of the confined area (Focused area), the extra area and stub. The concrete was cast from top.

Table 1 Specimen

| # | Name       | t (mm) | $f'_c$<br>(N/mm <sup>2</sup> ) | $p_w$ (%) | Rebar         |
|---|------------|--------|--------------------------------|-----------|---------------|
| 1 | 150-21-024 | 150    | 20.7                           | 0.24      | #3(D10)@200-S |
| 2 | 180-21-039 | 180    |                                | 0.39      | #3(D10)@200-D |
| 3 | 180-21-071 |        |                                | 0.71      | #4(D13)@200-D |
| 4 | 180-21-111 |        |                                | 1.11      | #5(D16)@200-D |

Note : S and D indicate single and double rebar respectively. t : Thickness

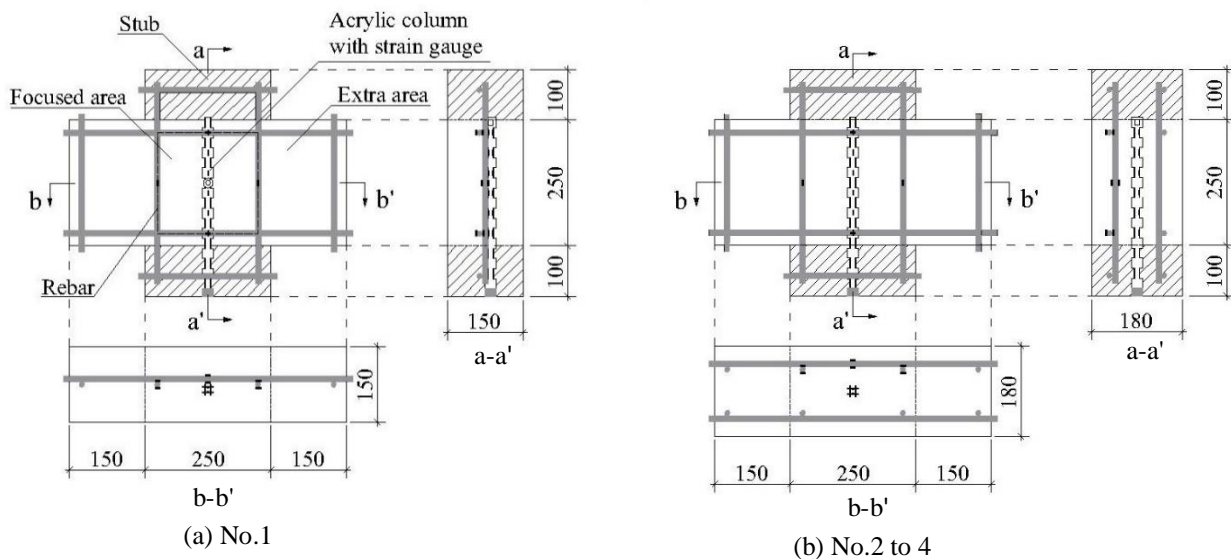


Fig. 1 Specimen geometrics

Table 2 The material property

| a) Concrete |                                |                         |  | b) Rebar |                                      |                     |  |  |
|-------------|--------------------------------|-------------------------|--|----------|--------------------------------------|---------------------|--|--|
|             | $f'_c$<br>(N/mm <sup>2</sup> ) | Strain at $f'_c$<br>(%) | Young modulus<br>(kN/mm <sup>2</sup> ) | Rebar    | Yield stress<br>(N/mm <sup>2</sup> ) | Yield strain<br>(%) | Young modulus<br>(kN/mm <sup>2</sup> ) | Tensile strength<br>(N/mm <sup>2</sup> ) |
| Wall        | 20.7                           | 0.1955                  | 20.9                                   | #3 (D10) | 362                                  | 0.2123              | 170                                    | 495                                      |
| Stub        | 43.4                           | 0.1982                  | 29.4                                   | #4 (D13) | 352                                  | 0.1998              | 176                                    | 481                                      |
|             |                                |                         |  | #5 (D16) | 351                                  | 0.2056              | 171                                    | 501                                      |

## Material property

The material property of concrete and rebar is shown in Table 2. The compressive strength of the cylinder with 100mm of the diameter and 200mm of the height ( $f'_c$ ) was 20.7 N/mm<sup>2</sup> for the wall and 43.4N/mm<sup>2</sup> for the stub.

## Loading

Repeated compressive load was applied via the rigid body of the top and bottom of the specimen by 2,000kN amsler testing machine.

Loading plan is shown in Fig. 2. The repeated compressive load was unloaded at the one-third and two-third of the  $f'_c$  on the material test. Next, it was unloaded at every 10% decreased load after the maximum load.

## Measurement

The measurement plan is shown in Fig. 3. The compressive load ( $P$ ) and the vertical displacement at the center of the specimen were measured by the load

cell and the displacement gage, respectively. The acrylic column with the strain gages was located at the center of the specimen. The strain gages were measured via a data logger as the same strain of the concrete, because of the ruggedness shape of the acrylic column.

## TEST RESULTS

### Load and displacement

The enveloped curve of the relationship between the compressive load and the displacement are shown in Fig. 4. The compressive displacement ( $\delta$ ) of the specimen was defined as the two time of the displacement at the center without the elastic displacement of the rigid body.

The comparison of the enveloped curve between No.1 and 2 are shown in Fig. 4(a). The displacement at the maximum load ( $P_{max}$ ) of No.1 with 150mm thickness and single rebar was larger than one of No.2 with 180mm thickness and double rebar.

For No.1, the displacement of 2.1mm was meas-

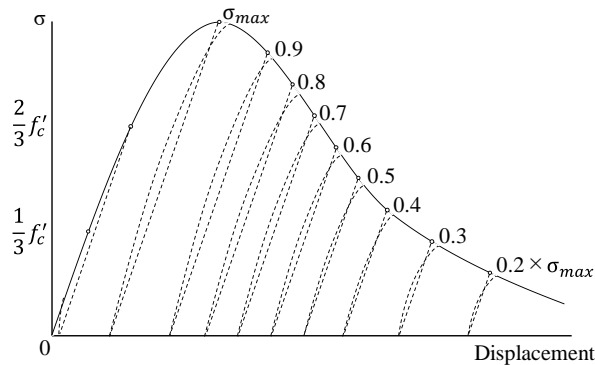


Fig. 2 Loading plan

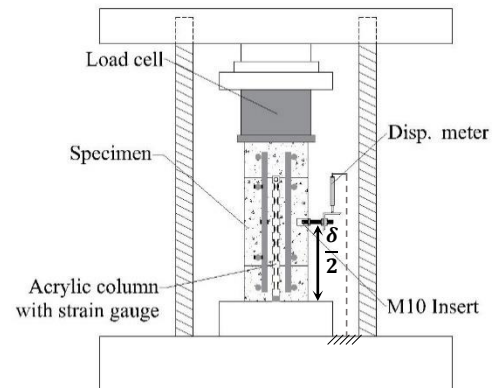
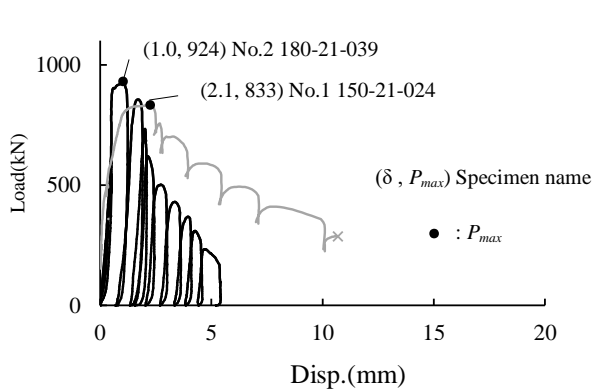
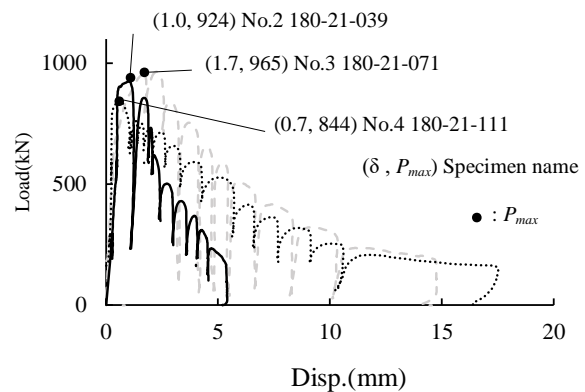


Fig. 3 The measurement



(a) No.1, 2



(b) No.2 to 4

Fig. 4 The enveloped curve of the relationship between the compressive load and the displacement



ured at the  $P_{max}$  of 833kN and the crack width developed and the eccentricity of damage was observed at the displacement of 10.7 and load of 286kN, and then the test was stopped.

For No.2, the displacement of 1.0mm was measured at the  $P_{max}$  of 924kN and the significant damage was observed with 82 % of the decreased load, and then the test was stopped. The eccentricity of damage as well as No.1 was not observed and stable compared with No.1.

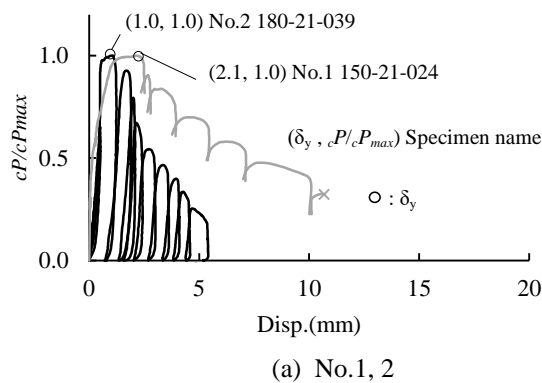
The enveloped curves of No2 to 4 are shown in Fig. 4(b). Their wall thickness was 180mm with double rebar of the  $p_w$  of 0.39 to 1.11%.

For No.3 and 4, the displacement of 1.7 and 0.7 mm at the  $P_{max}$  of 965 and 844kN were observed, respectively. The eccentricity of damage was not observed as well as No.2.

The enveloped curve of the load of the concrete resisted ( $cP$ ) and  $\delta$  is shown in Fig. 5.  $cP$  was defined as the  $P$  without the load of rebar resisted ( $sP$ ). And then the relative load was defined as  $cP$  divided by  $cP_{max}$ .

The strain of the vertical and horizontal rebar showed approximately yield at around  $cP_{max}$  in all specimens.

The displacement at the yield was defined as the



minimum displacement at the  $cP_{max}$  or 0.01 time of the elastic stiffness.

The same tendency was shown in Fig. 4 and 5, and the concrete confined effect was not observed even in the specimen with the rebar ratio of 0.71%.

### Damage and Cracking

The final crack behavior was shown in Fig. 6. For all specimen, about 0.2mm of the crack width was observed before  $P_{max}$ , the crack was developed and the crack width was increased following increase of the displacement.

Crack was hardly observed in the extra area and stub.

For No.1 with the wall thickness 150mm and single rebar, the crack width surrounded by dashed ellipse shown in Fig. 6(a) was significantly developed and the eccentricity of the rebar strain and crack damage were observed, then the fragile behavior was shown.

For No.2 to 4 with the wall thickness 180mm and double rebar, the difference of the crack behavior was not observed independent of the rebar ratio.

### Concrete Strain Distribution

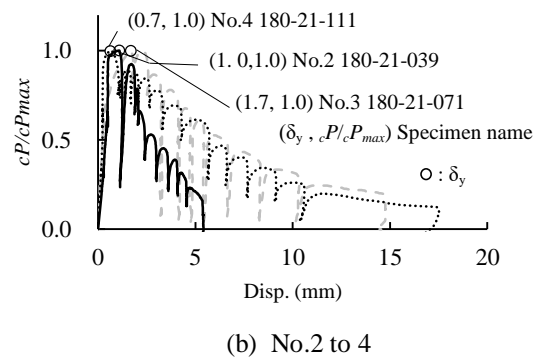
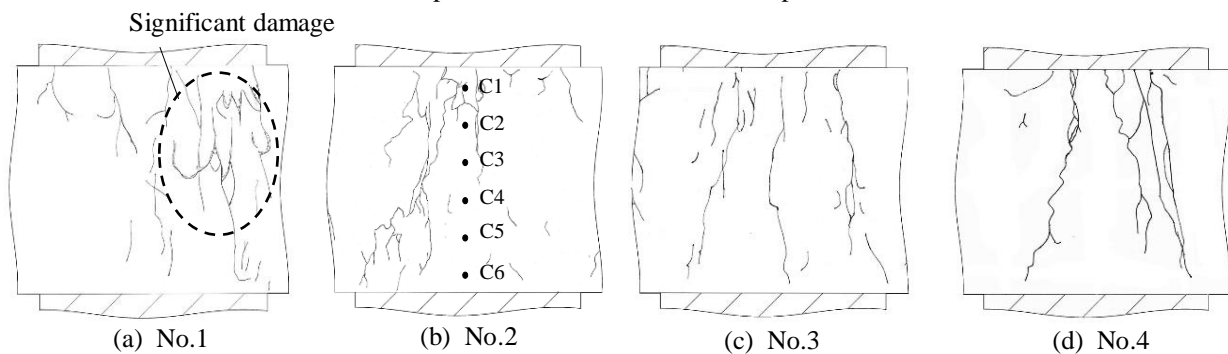


Fig. 5 The enveloped curve of the relationship between the compressive relative load and the displacement

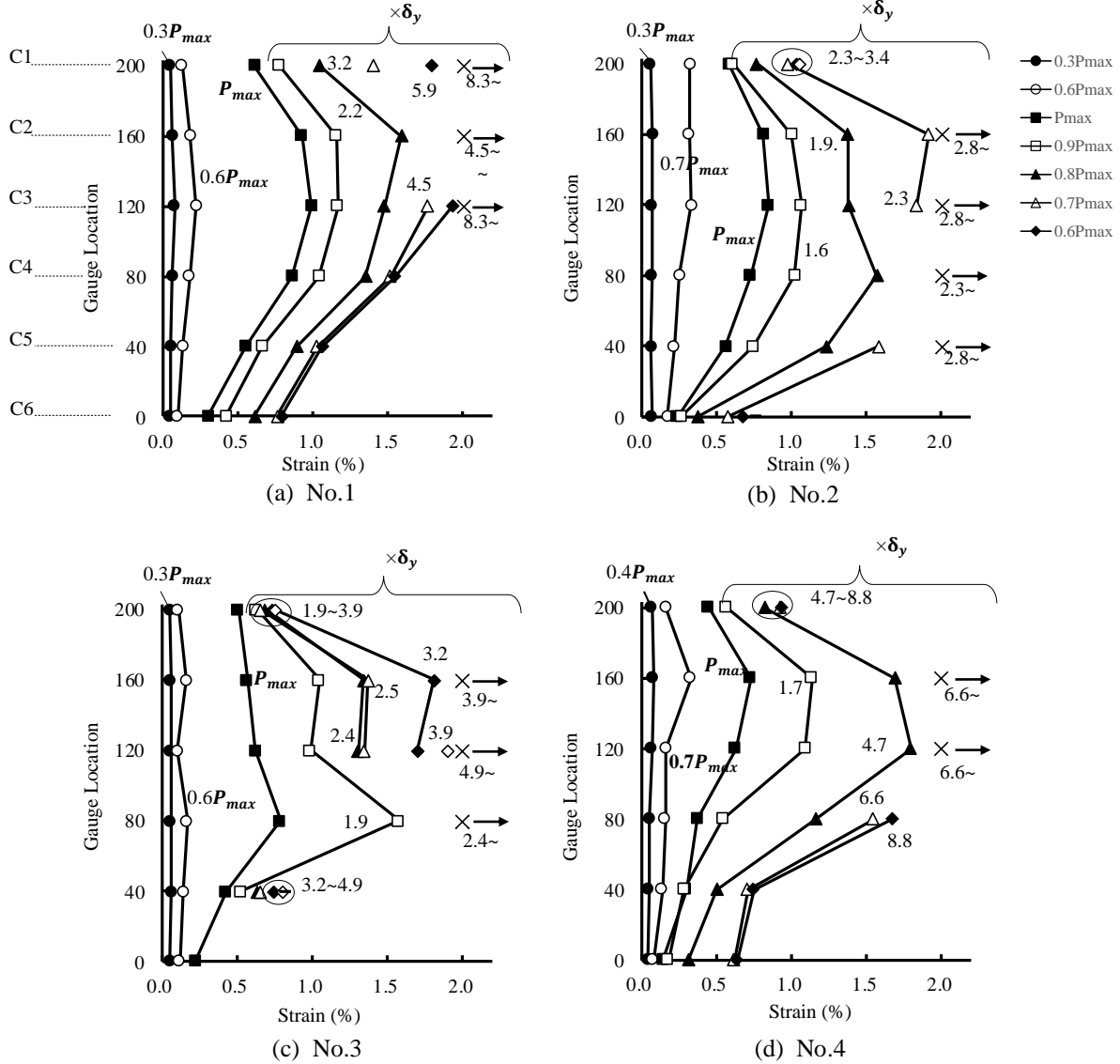


Note: C1 to C6 indicate the gauge location.

Fig. 6 The final crack behavior

The concrete strain distribution was shown in Fig. 7. The strain gages location number of C1 to C6 were indicated the location in Fig. 6(b). For all specimen, it was assessed that up to 2 % of the concrete strain

was appropriate. The amount of over 2% of the stain was estimated as 2% over. The concrete strain at the center of the wall was larger than one of the top and bottom due to the concrete confined effect by rebar.



Note: × → indicates 2% or more.

Fig. 7 The concrete strain distribution

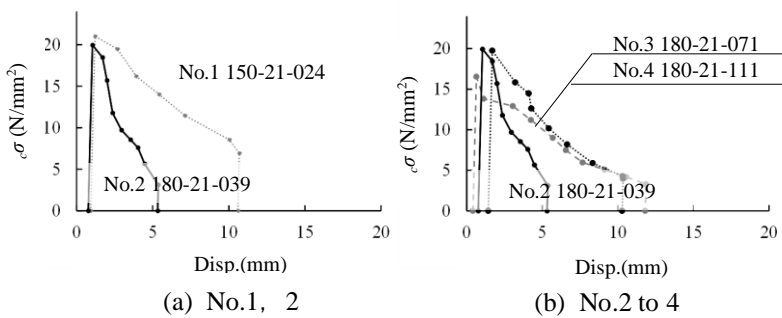


Fig. 8 The envelopment curve between the stress and the displacement

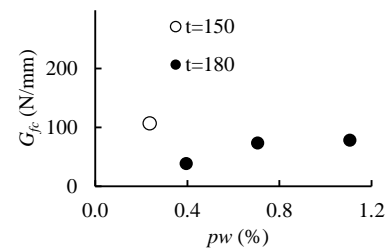


Fig. 9 The relationship between  $G_{fc}$ , wall thickness, and  $p_w$

### Compressive Fracture Zone Length

As mention above, the eccentricity of the concrete strain distribution was not shown along the wall height due to concrete confined effect by the wall rebar. In addition, the all concrete strain in all specimens was the strain at the  $f'_c$  or more at the  $P_{max}$ , therefore the compressive fracture zone length in this paper was defined as 200mm.

### Compressive Fracture Energy

The envelopment curve between the concrete stress and the displacement is shown in Fig. 8. The concrete stress was the  $cP$  divided by the wall thickness and 250mm. The compressive fracture energy ( $G_{fc}$ ) [6] was estimated as the area.

The relationship between  $G_{fc}$ , wall thickness, and  $p_w$  is shown in Fig. 9.

The displacement for  $G_{fc}$  ( $\delta_{conf}$ ) was calculated as the displacement of the focused area i.e. confined area as below.

$$\delta_{conf} = \frac{h_{conf}}{h} \cdot \delta$$

Where  $h$  is the wall height 200mm,  $h_{conf}$  is focused area i.e. confined area 200mm.

For the specimen with the wall thickness of 180mm and double rebar in No.2 to 4,  $G_{fc}$  was increased following increasing of the  $p_w$  and the confined effect.

However, for the specimen with the  $p_w$  of 0.71% more in No.4,  $G_{fc}$  was slightly increased, because the concrete strain was gradually increased.

For the specimen with the wall thickness of 150mm and single rebar in No.1, the  $G_{fc}$  of No.1 was largest. It should be examined in our future study.

### Equivalent Compressive Fracture Zone Width

The test result is shown in Table 3. The equivalent compressive fracture zone width ( $e b_p$ ) was defined as  $P_{max}$  divided by the wall thickness and  $f'_c$ .

$cP$  was decreased following increasing of  $p_w$ , because the  $sP$  was increased.

In other word,  $e b_p$  was decreased following increasing of  $p_w$ .

### CONCLUSION

Basic concrete walls with rebar test was performed applying compressive stress to estimate their compressive fracture energy for a concrete wall element model with rebar.

We reached several conclusions as below.

1) For the specimen with the wall thickness of 150mm and single rebar, the eccentricity of the rebar strain and crack damage were observed, then the fragile behavior was shown. For specimen with the wall

Table 3 The test result

| #    | $P_{max}$<br>(kN) | $cP_{max}$<br>(kN) | $\delta$ at $cP_{max}$<br>(mm) | $\delta_y$<br>(mm) | $A'$<br>(cm <sup>2</sup> ) | $e b_p$<br>(mm) |
|------|-------------------|--------------------|--------------------------------|--------------------|----------------------------|-----------------|
| No.1 | 833               | 807                | 2.1                            | 1.2                | 389                        | 260             |
| No.2 | 924               | 898                | 1.0                            |                    | 433                        | 241             |
| No.3 | 965               | 889                | 1.7                            |                    | 429                        | 238             |
| No.4 | 844               | 747                | 0.7                            | 0.6                | 361                        | 200             |

Note:  $P_{max}$  : Maximum load

$cP_{max}$  : Maximum load of concrete

$\delta$  : Displacement

$\delta_y$  : Displacement at Minimum ( $P_{max}$  or  $0.01 \cdot K_0$ )

$A'$  :  $cP_{max}$  divided by  $f'_c$

$e b_p$  :  $A'$  divided by thickness

thickness 180mm and double rebar, the difference of the crack behavior was not observed independent of the rebar ratio.

2) The concrete strain at the center of the wall was larger than one of the top and bottom due to the concrete confined effect by rebar.

3) For all test specimens the compressive fracture zone length was defined as 200mm.

4) For the specimen with the  $p_w$  of 0.71% more in No.4,  $G_{fc}$  was slightly increased, because the concrete strain was gradually increased.

5)  $e b_p$  was decreased following increasing of  $p_w$ .

### REFERENCES

- [1] ROTS, J. G. : Computational Modeling of Concrete Fracture, PhD thesis, Delft University of Technology, 1988.
- [2] Naoki Takamori, Benny Benni Assa, Minehiro Nishiyama, Fumio Watanabe : Confined Stress concrete - Strain Relationship formulation Fundamental Study, Proceedings of the Japan Concrete Institute, Vol.18, No.3, pp.395-400, 1996.
- [3] J. B. Mander, M. J. N. Priestley, R. Park, Fellow, ASCE : Theoretical Stress-strain Model for Confined Concrete, J. Struct. Eng, Vol.114, Issue.8, pp 1804-1826, Sep.1998.
- [4] Hikaru Nakamura, Takeshi Higai : Compressive Fracture Energy and Fracture Zone Length of Concrete, JCI-C51E Seminar on Post-Peak Behavior of RC Structures Subjected to Seismic Loads, Vol.2, pp.259-272, 1999.10.
- [5] Ken Watanabe, Junichiro Niwa, Hiroshi Yokota, Mitsuyasu Iwanami : Formulation of Stress-strain Relationship of Concrete Considering The Localized Compressive Failure Zone, Journal of JSCE, Vol.58, No.725, pp 197-211, 2003.2.
- [6] Shinya Muramatsu, Koshikawa Takeaki, Takatori Saito, Takuya Hasegawa : Quantitative Evaluation of Strain Softening Characteristics of Concrete Subjected to Uniaxial Compression, Architectural Institute of Japan Hokkaido Branch research report, No.83, pp.81-84, 2010

## THE EFFECTS OF BATANG KANDIS RIVER FLOOD CONTROL IN PADANG CITY-PALAPA METROPOLITAN AREA

Benny Hidayat, #Bambang Istijono, Irwan Irwan, Taufika Ophiyandri and Akhmad Junaidi  
Civil Engineering Department, Universitas Andalas, Padang, Indonesia

### ABSTRACT

Floods often occur in Lubuk Buaya residential housing in Padang city, which has a population of 6,500 citizens per km<sup>2</sup>. These natural phenomena happen due to sea level water rises and the change in the new river mouth of the Batang Kandis river. The construction of a 500 m floodway and a 700 m dike of Batang Kandis river were proposed to control flooding. The floodway was then damaged during the earthquake on September 30th, 2009, and wiped out by a flood on March 24th, 2016. Theoretically, to solve flood conditions downstream of Batang Kandis river with 70 km<sup>2</sup> of watershed area, the floodway is expected to be able to discharge 307 m<sup>3</sup>/s. This study uses a numerical simulation using HEC-RAS software with three scenarios. The first scenario uses the existing condition of the river width of 50 m and a depth of 1 m, it experienced an inundated area of 0.60 km<sup>2</sup> for 5 hours. The second scenario is done by increasing 2.50 m embankment height, which gave the result of 2x700 m<sup>2</sup> flood inundation in several locations. The third scenario also carried out dredging of the river up to the elevation of 0.00 m above sea level, and there was no flood inundation. Thus, the third scenario is the best result that has been carried out to control the floods downstream of Batang Kandis river.

*Keywords: inundation area, floodway, river mouth, simulations.*

### INTRODUCTION

Structural flood control has long been carried out in the city of Padang in the Padang Metropolitan Urban Area, Lubuk Alung and Pariaman (abbreviated as Palapa Metropolitan Area). This activity began in the Dutch era, which was marked by the construction of the Banda Bakali river. This activity was carried out to divert a portion of the flow from the Batang Arau river which passed the Padang City trade center at that time.

Given the frequent occurrence of floods in the city of Padang, a more comprehensive study was conducted for flood prevention in 1983. This study was conducted by JICA (Japan International Cooperation Agency) under the name of the Padang Area Flood Control Project. This activity aims to conduct in-depth studies on flood control, drainage plans, and feasibility studies to identify and prioritize actions to be immediately implemented. The results of this study are the basis for flood control projects in the city of Padang [1].

Some of the activities that have been carried out for flood control in the city of Padang include the normalization of Canal Floods (Banda Bakali river) and the Batang Arau River in 1992-1997; normalization of the Batang Kuranji river, the Air Dingin river (widening, deepening and strengthening of concrete cliffs) and repairing the Padang coast in 1997-2001 [2] [3].

Pinang Bungkok area in Lubuk Buaya Village, Padang City with a population density of 6,500 people per km<sup>2</sup> is an area that is often flooded. High

rainfall and rising sea levels cause natural flood events at the confluence of the Batang Kandis river and the Batang Kasang river. The possibility of flooding, together with the construction of the Batang Kandis River floodway, can increase the risk of tidal flooding in the lowlands around the new inlet in Pinang Bungkok with a distance of about 500 m upstream of the new inlet of the Batang Kandis river.

The flood control effort that has been carried out is the construction of a 500 m sea floodway and embankment at approximately 700 m to the left of the Batang Kandis river flow. The floodway condition was severely damaged by the 7.9 Richter scale earthquake on September 30<sup>th</sup>, 2009, and flooding on March 24<sup>th</sup>, 2016. To overcome the flooding that occurred in the lower reaches of the Batang Kandis river with a 70 km<sup>2</sup> river basin area, rehabilitation is being conducted on the floodways with numerical simulations using HEC-RAS software so that later it is expected that the river can discharge as much as 307 m<sup>3</sup>/s.

The catchment area of Batang Kandis is located in the Koto Tangah sub-district of Padang city. The upstream part of the Batang Kandis river originates from the western part of Bukit Barisan (elevation +1.249 m) and has a catchment area of 56 km<sup>2</sup>. The old Batang Kandis river flows westward through new residential areas and then joins the Batang Kasang river which has a catchment area of 14 km<sup>2</sup> in the area of Pasir Jambak village. The figure below shows the location of the latest Batang Kandis river estuary and the location of the research area.



Fig. 1 Location of Batang Kandis River.

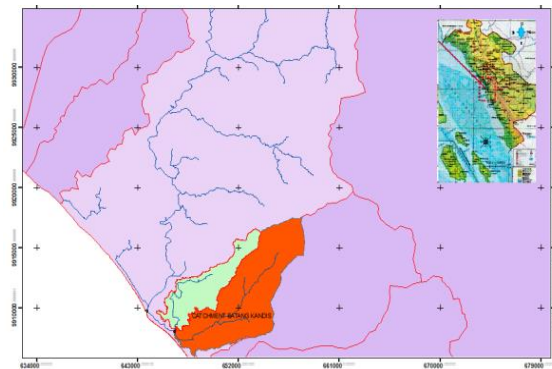


Fig. 2 Area of study in Batang Kandis river.

## LITERATURE REVIEW

Corry Eriza [4] examined the alternative performance of the flood control of the Batang Anai river and Batang Kandis river in West Sumatra. The study aims to review various alternatives in planning the control of the floods of the Batang Anai river and Batang Kandis river over the current condition of the watershed. His research uses the HEC-RAS (Hydrological Engineering Center, River Analysis System) with three alternatives which were based on data availability. Alternative 1 requires the repair of grooves and widening of the face (with embankments) in both rivers and the addition of floodways on the Batang Kandis river. Alternative 2 is similar to Alternative 1, except for the removal of dikes on the Batang Anai river and additional sluices on the Batang Kandis river. Alternative 3 for the Batang Anai river is similar to Alternative 2, and the appearance along the Batang Kandis river is widened. The analysis includes calculation of the flow adequacy in flowing the design and analysis of sediment transport for the best performance alternatives. From the three alternatives, the best alternative was found as alternative 3 because it was able to drain the design discharge  $Q_{50}$  ( $1471 \text{ m}^3/\text{s}$ ) on the Batang Anai river and  $Q_{25}$  ( $293 \text{ m}^3/\text{s}$ ) on the

Batang Kandis river. Sediment transport simulation on the Batang Anai river with the application of Alternative 3 shows the most significant trend of erosion and deposition in a location next to the National Bridge downstream.

The narrowing of the river channel accompanied by siltation and sediment accumulation causes the volume of the plan to be incompatible with the coming discharge, as a result when the rainy season comes there is some run off and flooding can no longer be overcome.

Simulations with HEC-RAS are also used to review the flow of the Cilember river in West Java, also in Segamat town, Malaysia and on the Batang Takung Sijunjung river, West Sumatra [5] - [7]. Based on the simulation results using HEC-RAS software in the Cilember river in West Java, the overflow of Cilember River clearly influences the inundation height on Jalan General H. Amir Machmud which connects the city of Bandung and the city of Cimahi.

## Hydraulics Analysis

The approach performed by HEC-RAS is to divide the cross-sectional area based on the value of  $n$  (Manning roughness coefficient) as the basis for cross-section distribution. Each flow that occurs is calculated using the Manning equation.

$$Q = A \times \left(\frac{1}{n}\right) R^{2/3} \cdot S^{1/2} \quad (1)$$

Where :

$Q$ : discharge ( $\text{m}^3/\text{s}$ )

$n$ : manning roughness coefficient

$A$ : cross-section area ( $\text{m}^2$ )

$R$ : hydraulic radius (m)

$S$ : energy slack.

For steady flow in the HEC-RAS device, energy equations are used except in places where the depth of flow exceeds the critical depth [8]. The energy equation between two cross sections is as follows:

$$Y_2 + Z_2 + \frac{\alpha_2 v_2^2}{2g} = Y_1 + Z_1 + \frac{\alpha_1 v_1^2}{2g} + h_e \quad (2)$$

Where :

$Y_1, Y_2$ : flow depth (m)

$Z_1, Z_2$ : channel base elevation (m)

$V_1, V_2$ : average speed (m/s)

$\alpha_1, \alpha_2$  : speed coefficient

$g$ : gravity acceleration ( $\text{m/s}^2$ )

$h_e$ : lost energy (m)

## Modeling with HEC-RAS

Analysis of the existing cross section using HEC-

RAS aims to determine the condition of the actual river (existing) and water level profile during a flood. HEC-RAS software is integrated with graphical user interfaces, hydraulic analysis, management and data storage, graphics, and reporting.

- Graphical User Interface is the link between users and HEC-RAS. Things that can be done using this feature include file management, inputting and editing data, doing hydraulic analysis, displaying input data and analysis results in the form of tables and graphs, preparing reports and accessing online help.
- Hydraulics analysis. The hydraulic analysis provided includes two analyses, namely, steady flow, and unsteady flow.
- Data storage and data management. Storage of input data in HEC-RAS can be grouped into projects, plans, geometry, steady flow, unsteady flow, and sediment data.
- Graphs and reporting. The graphics facilities provided by HEC-RAS include X-Y river flow graphs, cross-views, curves rating, hydrographs, and other graphs which are X-Y plots of various hydraulic variables.

## RESEARCH METHODOLOGY

This study is conducted in the following stages:

- Collected data on bathymetry maps and discharge data for the Batang Kandis river obtained from the Sumatra V River Basin Office [8].
- Calculated speed using the Manning formula
- Calculated debit using the Rational formula
- Conducted simulation in HEC-RAS by plotting previously calculated data and inputting existing river flow and geometry data.
- Compared the results of the calculation of the bathymetry measurement data so that the inundation height is obtained based on the measurement data and the results of running the application.
- Identified flood control efforts towards the opening of a new estuary on the Batang Kandis river.

## RESULTS AND DISCUSSION

In this research, we developed three scenarios of flood simulation as described below. We set up benchmark stations along the rivers, abbreviated as BKS for Batang Kandis river and BKSG for Batang Kasang river.

### Scenario 1: existing conditions

The simulation results of scenario 1 are for conditions that do not experience flooding starting from the downstream, namely BKS 0 to BKS 4A along 315 m (from the new estuary of the Batang Kandis river to the meeting with the Batang Kasang river) and BKS 4 to BKS 10 along 562 m (the existence of flood dam buildings built in the 2007 and 2008 fiscal years), while the other parts are generally affected by the flood inundation of the Batang Kandis and Batang Kasang rivers [9]. The following are examples of the existing conditions of the flow that did not occur with flooding.

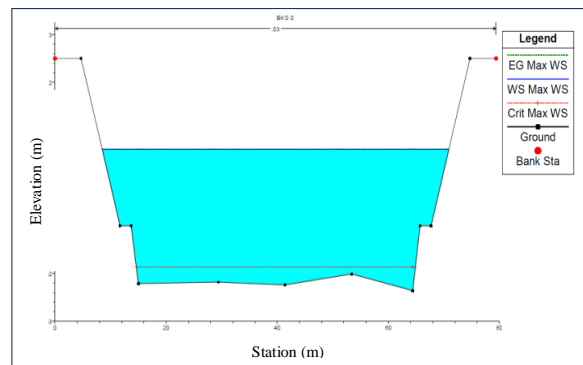


Fig. 3 BKS 0 (no flooding occurs)

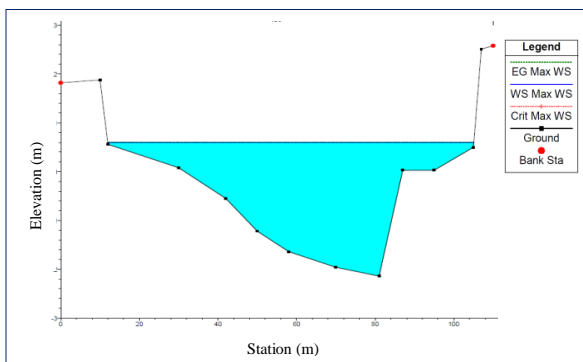


Fig. 4 BKS 1 (no flooding occurs)

The following is an example of the existing conditions of the flow that occurred in flood runoff.

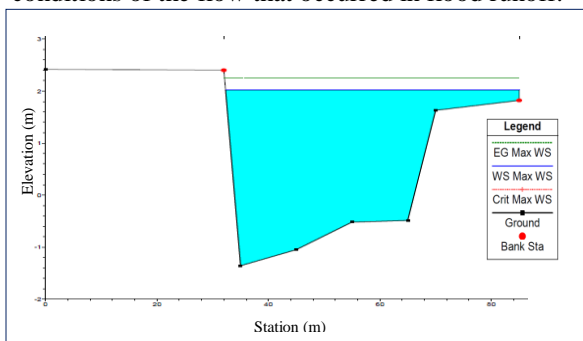


Fig. 5 BKS 16 (in the left part of the flow there is a flood)



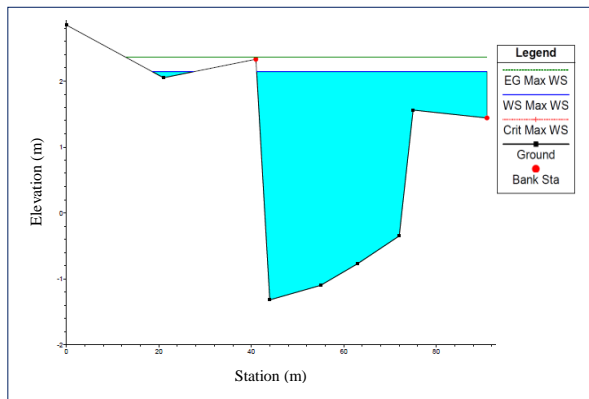


Fig. 6 BKS 17 (on the left side of the flow there is a flood)

**Scenario 2: given the left and right embankments of the flow without any river dredging or flowing**

Scenario 2 is simulated by installing embankments on flood banks. At the flood point, embankments were made both on the banks of the river's left-hand flood, the riverbanks of the right-hand floods and the two floodplains by the conditions of the flooding. From the simulation results of scenario 2 it can be seen that from BKS station 0 to BKS 13 along 1,227 m Batang Kandise river and BKSG 1 to BKSG 6 along 491 m Batang Kasang river there is no flood inundation; while at BKS station 14 to 17 BKS along 250 m of the Batang Kandise river is still flooded, this is caused by the inadequate cross-section of the river to pass the flood discharge of the Batang Kandise river. The following is an example of the existing conditions of the flow that did not occur with flooding.

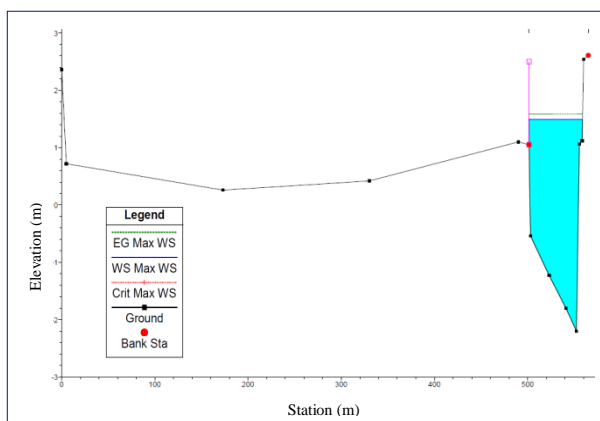


Fig. 7 BKS 6 (no flooding occurs)

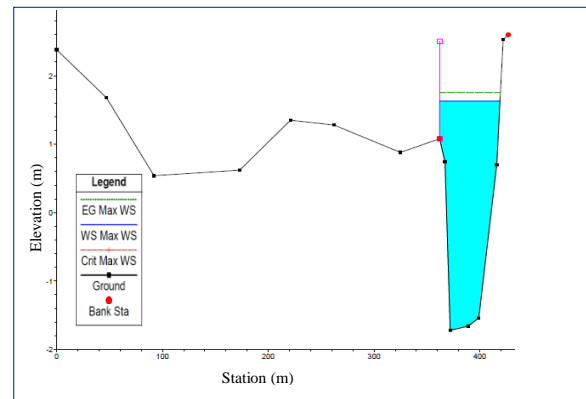


Fig. 8 BKS 10 (no flooding occurs)

The following is an example of the existing conditions of the flow that occurred in flood runoff.

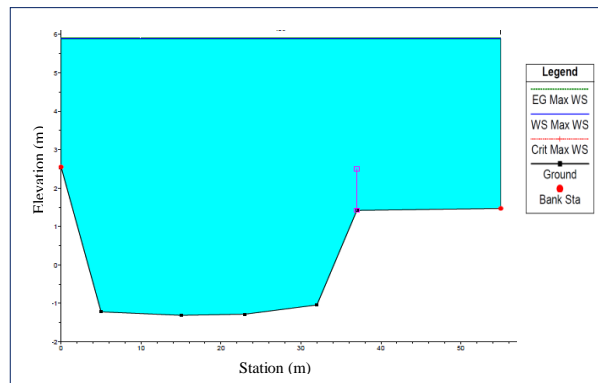


Fig. 9 BKS 15 (flood inundation in the upstream part)

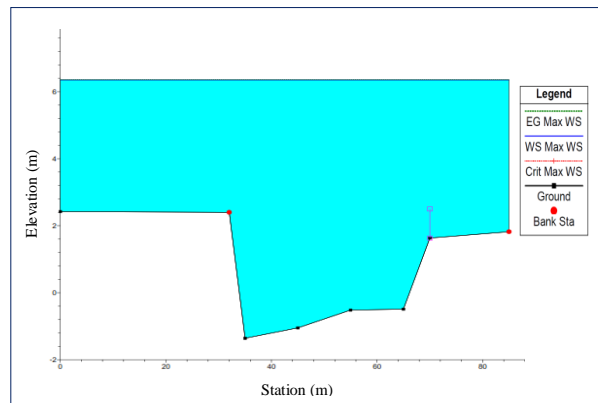


Fig. 10 BKS 16 (flood inundation in the upstream part)

**Scenario 3: given the left and right embankments of the flow with the dredging and widening of the river**

In scenario 3 it is simulated by combining the installation of the left and right embankments with river dredging and widening. The embankment height was taken at an elevation of 2.50 m above sea level as high as the peak height of the Jetty building at the new estuary of the Batang Kandise river and the peak of the



existing embankment on the left flow between BKS 3 to BKS 10 along 676 m. The width and depth of dredging are adjusted to the existing conditions by referring to 0.00 m above sea level. From the simulation results in scenario 3, it can be seen that from the BKS 0 to BKS 17 stations along the 1,583 m Batang Kandise river and BKSG 1 to BKSG 6 along the 810 m Batang Kasang river there is no visible flood inundation. Therefore, to identify flood handling in the lower reaches of the Batang Kandise river, there is no need to do another scenario simulation.

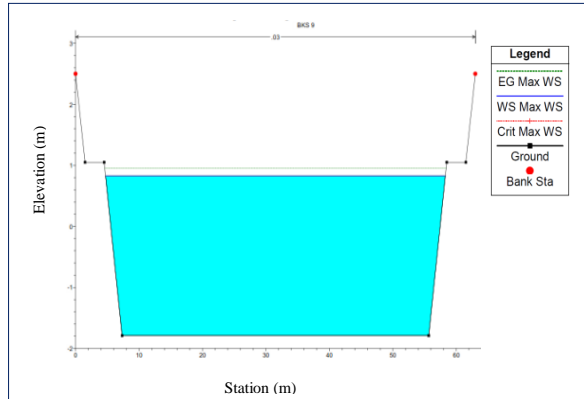


Fig. 11 BKS 9 (no flooding occurs)

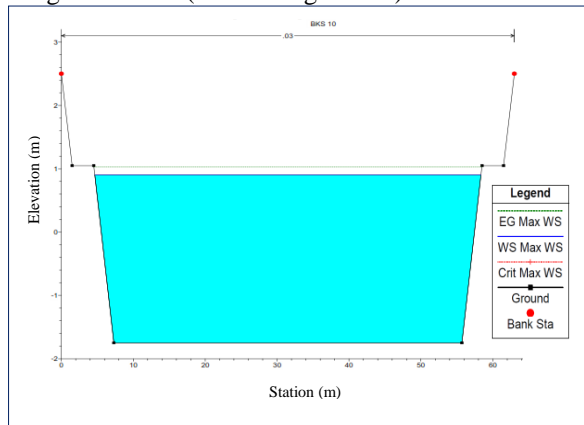


Fig. 12 BKS 10 (no flooding occurs)

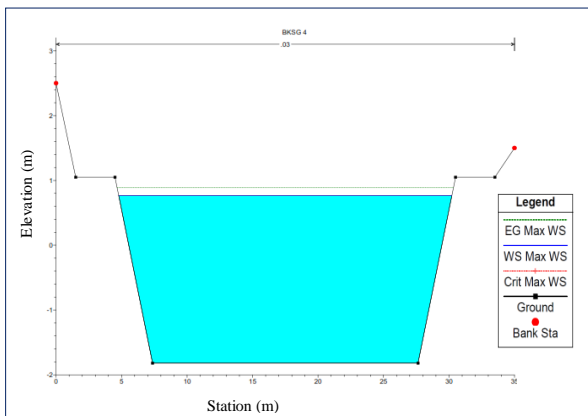


Fig. 13 BKSG 4 (no flooding occurs)

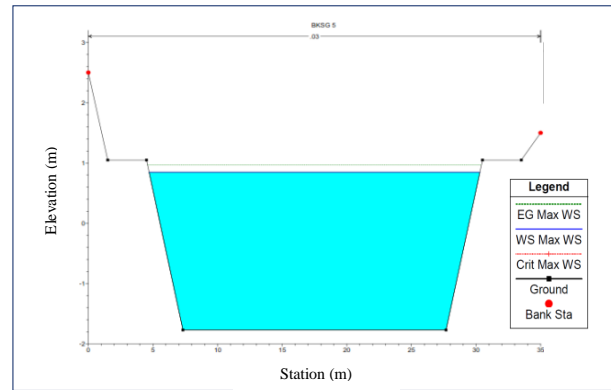


Fig. 14 BKSG 5 (no flooding occurs)

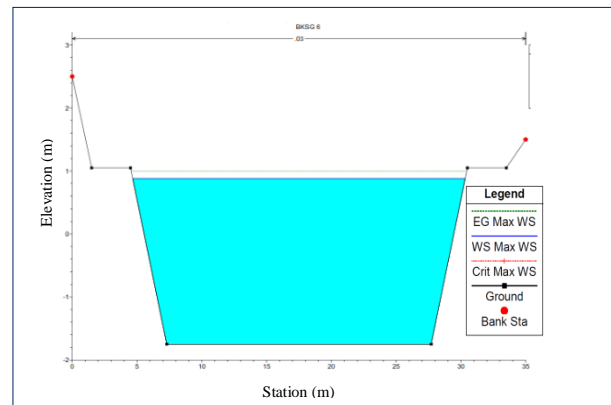


Fig. 15 BKSG 6 (no flooding occurs)

## CONCLUSIONS AND RECOMMENDATIONS

### Conclusion

1. The first scenario with the existing conditions shows that the existing cross-section of the river segment is not flooded as it is in the downstream part of the river, namely: BKS 0 to BKS 4 A (from the new estuary the Batang Kandise river to the meeting with the Batang Kasang river), and in BKS 4 to BKS 10 left flow (the presence of flood embankments built in the 2007 and 2008 fiscal years by the Sumatra V River Basin Office, while the other parts in general are affected by the flood inundation of the Batang Kandise river and the Batang Kasang river).
2. From the simulation results in scenario 2 it can be seen that from BKS station 0 to BKS 13 and BKSG 1 to BKSG 6 there is no flood inundation on the Batang Kandise river, while at the BKS station 14 to BKS 17 there is still a flood inundation on the river of Batang Kandise. This condition is caused by the inadequate cross-section of the river to pass the flood discharge of the Batang Kandise river in the condition of  $Q_{10}$  (Rational Method).

3. From the simulation results in scenario 3, it can be seen that from the BKS station 0 to BKS 17 in the Batang Kandis river and BKSG 1 to BKSG 6 the Batang Kasang river has not seen any inundation. Therefore, to overcome the inundation that occurs at the meeting between the Batang Kandis river and the Batang Kasang river, it is necessary to handle flooding in the lower reaches of the Batang Kandis river by simulating scenario 3.

Based on the simulated scenario at this conclusion, it is stated that scenario 3 is the best result of three scenarios that have been carried out to overcome flooding in the Batang Kandis river due to the opening of the new estuary of the Batang Kandis river.

### Suggestion

1. To overcome flooding in the Batang Kandis river and the Batang Kasang river, serious attention needs to be paid from the Sumatera V River Basin Office.
2. For more optimal and proper handling of the meeting between the Batang Kandis river and the Batang Kasang river, further research is needed on the effect of sea tides on agricultural land.

### ACKNOWLEDGMENTS

This research was funded by University of Andalas under Research Grant Number: T/24/UN.16.17/PP.IS-KRP1GB/ LPPM/2019 dated 13 May 2019.

### REFERENCES

- [1] JICA.1983. Study Report on Padang Area Flood Control Project. Japan International Cooperation Agency (JICA)
- [2] Istijono B, Aprisal, Ophiyandri T and Nurhamidah. 2019. A Study of The Quality of Soil Infiltration at The Downstream of Kuranji River, Padang City. International Journal of GEOMATE, Month April, Year 2019 Vol. 16, Issue 56. Geotec., Const. Mat. & Env., DOI: <https://doi.org/10.21660/2019.56>. Paper ID ISSN: 2186-2982 (Print), 2186-2990 (Online), Japan.
- [3] Istijono B. 2014. Environmentally Friendly Flood Control Construction (Case Study: Controller of Banjir Batang Anai, West Sumatra) (in Bahasa), Teknik, Vol.21(2), pp.1-7.
- [4] Coorri E. 2008. Alternative Performance of Batang Anai and Batang Kandis Flood Control in West Sumatra (in Bahasa: *Unjuk Kerja Alternatif Pengendalian Banjir Batang Anai dan Batang Kandis Sumatera Barat.*) Tesis, Program Studi MPBA Sekolah Pasca Sarjana, Universitas Gadjah Mada, Yogyakarta.
- [5] Karnisah I, Yackob A, Bambang SB, Fitra RA and Reynaldy PH. 2019. Analysis of Drainage Capacity to Resolve Inundation Problem on Jend. H. Amir Machmud Street, Cimahi City West Java Province. International Journal of GEOMATE, Vol. 16, Issue 57. Geotec., Const. Mat. & Env., DOI: <https://doi.org/10.21660/Year.Issue>. Paper ID ISSN: 2186-2982 (Print), 2186-2990 (Online), Japan.
- [6] Romali NS, Yusop Z and Ismail AZ. 2018. Application of HEC-RAS and Arc GIS for Floodplain Mapping in Segamat Town, Malaysia. International Journal of GEOMATE, Vol. 15, Issue 47. Geotec., Const. Mat. & Env., DOI: <https://doi.org/10.21660/Year.Issue>. Paper ID ISSN: 2186-2982 (Print), 2186-2990 (Online), Japan.
- [7] Komalasari N. 2017. Flood Control Simulation of the Batang Sumani River using the HEC-RAS model (in Bahasa: *Simulasi Pengendalian Banjir Sungai Batang Sumani dengan menggunakan HEC-RAS model*). Proceeding of Andalas Civil Engineering Conference, Andalas University.
- [8] Istiarto. 2014. 1-Dimensional Flow Simulation with the help of the HEC-RAS Hydrodynamics Program package. Training Module, basic level, Simple Geometry River (in Bahasa: *Simulasi Aliran 1-Dimensi dengan bantuan paket Program Hidrodinamika HEC- RAS. Modul Pelatihan, jenjang dasar, Simple Geometry River*), page 1-23. [https://www.academia.edu/8781887/HEC-RAS.Dasar\\_Simple\\_Geometry\\_River](https://www.academia.edu/8781887/HEC-RAS.Dasar_Simple_Geometry_River), Juli 2014 (accessed at 29 August 2014).
- [9] Sumatra V River Basin Office. 2001. Anai-Kandis River Improvement, Design Note and Design Report in Padang area flood control project (II) West Sumatra (in Bahasa: *Proyek Pengendalian Banjir dan Pengamanan Pantai Provinsi Sumatera Barat*).

# FATIGUE STRENGTH OF HEADED STUDS WELDED WITH IMPROVED FERRULE IN CONCRETE UNDER UNIDIRECTIONAL CYCLIC LOADING

Hiroshi Higashiyama<sup>1</sup>, Kenji Yoshida<sup>2</sup>, Satoshi Banba<sup>3</sup> and Shigeyuki Matsui<sup>4</sup>

<sup>1</sup>Faculty of Science and Engineering, Kindai University, Japan; <sup>2</sup>Kawada Industries, Inc., Japan;

<sup>3</sup>Nippon Stud Welding Co., Ltd., Japan; <sup>4</sup>Osaka Institute of Technology, Japan

## ABSTRACT

In hybrid and composite structures using steel and concrete materials, shear connectors such as headed studs are generally employed. The authors aim to improve the welding ferrule configuration to increase the fatigue strength of headed studs. The measuring results for 20 specimens of headed studs welded with conventional and improved ferrules reveal that the improved headed stud increased the diameter at the weld root and the height of the weld collar up to the tip of the separated portion between the stud shank and the weld collar in comparison with the conventional headed stud. In this study, the fatigue tests were carried out under unidirectional cyclic loading on single headed studs with a diameter of 16 mm and a height of 60 mm in concrete to determine the fatigue strength. From the fatigue test results, S-N curves were obtained for the headed studs. The improved headed stud has higher fatigue strength than the conventional headed stud. Furthermore, in concrete with normal strength, a fatigue crack initiated from the tip of the separated portion between the stud shank and the weld collar due to the notch effect and progressed into the stud shank. In concrete with higher strength, a fatigue crack initiated from the weld toe and progressed into the steel base plate along the heat affected zone.

*Keywords: Headed studs, improved welding ferrule, fatigue strength, unidirectional cyclic loading*

## INTRODUCTION

In hybrid and composite structures using steel and concrete materials, shear connectors such as headed studs are generally employed. Many researchers have investigated the mechanical behavior and/or the fatigue strength of headed studs [1]-[9]. Hiragi and Matsui [10] have attempted to improve the shape of welding ferrules to increase the fatigue strength of headed studs. For a conventional welding ferrule, high-temperature gas during welding spouts out of the castellation placed at the bottom of the welding ferrule, causing welding burrs to remain radially at the welding toe. They improved the welding ferrule configuration by closing the castellation at the bottom of the welding ferrule to allow high-temperature gas to spout out upward. The weld toe had a smooth shape without welding burrs. The authors have investigated to improve the welding ferrule configuration further to increase the fatigue strength of headed studs. The fatigue strength of headed studs using improved welding ferrules (improved headed studs) has been verified in comparison with conventional headed studs under a rotating shear force to employ the headed studs in steel-concrete composite bridge decks [11-13]. In these research works, depending on the concrete strength and the shear stress range applied, the fatigue life of the improved headed studs under the rotating shear force increased to about three times

more than that of the conventional headed studs.

The mechanical behavior and the fatigue strength of headed studs are generally examined using standard push-out test specimens. Each standard push-out specimen consists of an H-shape steel beam welded with two or four headed studs on each side of the beam flange and concrete slabs. In the experiments using such specimens, the mechanical behavior and the fatigue strength are affected by the group effect of headed studs. This study aims to compare the fatigue strength of single improved and conventional headed studs in concrete under unidirectional cyclic loading and to evaluate the fatigue strength of the improved headed studs in concrete with different concrete strength levels. In the cyclic loading tests, a single headed stud welded on a steel base plate was used without the group effect as Ref. [4]. In this study, the test equipment was setup to apply shear force to be transferred at the interface between a steel plate and concrete without bending moment. The fatigue strength of individual headed studs can then be simply evaluated and compared.

In this study, the fatigue tests carried out on the improved and the conventional headed studs in concrete/mortar under unidirectional cyclic loading to compare the fatigue strength. The shear stress ranges were varied to obtain S-N curves for the headed studs. The concrete/mortar specimens used had two different strengths to compare the fatigue

strength of each headed stud and to observe the failure condition. Also, the S-N curves depending on the concrete strength were determined for the improved headed studs at three different concrete strengths.

## EXPERIMENTAL PROGRAM

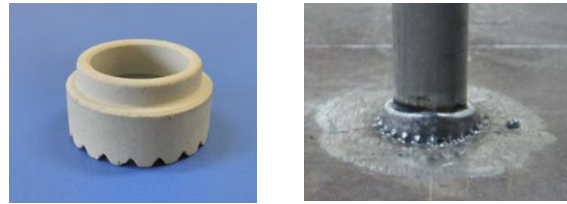
### Specimens and materials

Specimens used in the fatigue tests consist of a steel base plate of  $170 \times 270$  mm with a thickness of 22 mm, a single headed stud, and a square shape steel pipe of  $100 \times 100$  mm with a height of 100 mm and a thickness of 3.2 mm as shown in Fig. 1. The square shape steel pipe, which was simply placed on the steel base plate without any mechanical restraint during the fatigue tests (round bars shown in Fig. 1 were to keep the position of the square shape steel pipe and were removed before testing), functions as a mold for concrete/mortar in casting and as the protection for cracking and/or crushing of concrete/mortar at the loading point. The concrete or non-shrinkage mortar was cast in the square shape steel pipe. Each headed stud had a height of 60 mm and a diameter of 16 mm. The conventional and the improved ferrules and their appearance after welding are shown in Fig. 2. The closing castellation at the bottom of the improved ferrule allows high-temperature gas to spout upward. As can be seen from Fig. 2(b), the weld toe of the improved headed stud was smooth. The proper welding condition was selected in each headed stud. From the size measurement of 20 weld collars for the conventional and the improved headed studs, as given in Table 1, the average diameter (D) was larger and the average separated height between the stud shank and the weld collar (H1–H2) was shorter for the improved headed stud than for the conventional headed stud. These headed studs both had the weld collar with almost the same height.

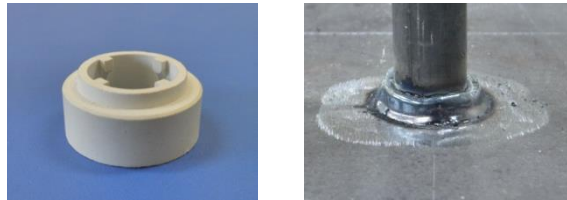
The headed stud used in this study was made of



Fig. 1 General view of specimen before concrete casting.



(a) Conventional headed stud.

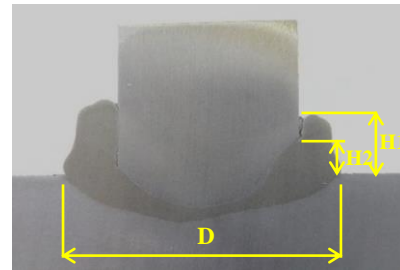


(b) Improved headed stud.

Fig. 2 Ferrules and weld collars.

Table 1 Weld collar dimensions

| Measuring part | Conventional headed stud | Improved headed stud |
|----------------|--------------------------|----------------------|
| D (mm)         | 22.6                     | 24.2                 |
| H1 (mm)        | 5.5                      | 5.6                  |
| H2 (mm)        | 2.1                      | 3.7                  |
| H1–H2 (mm)     | 3.4                      | 1.9                  |



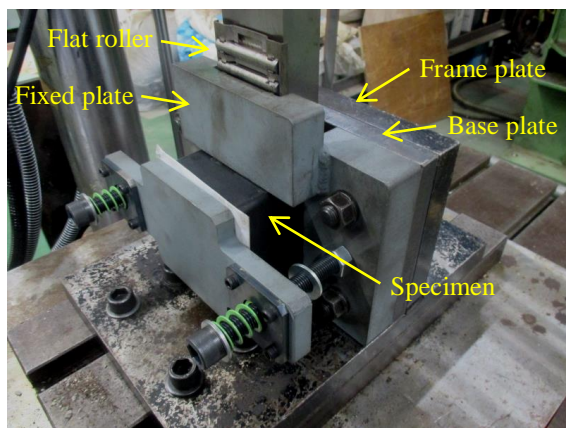
mild steel with yield strength and ultimate strength of  $364 \text{ N/mm}^2$  and  $477 \text{ N/mm}^2$ . The compressive tests for the concrete/mortar were carried out to determine the compressive strength. Three cylindrical concrete specimens of 100 mm in diameter and 200 mm in height and three cylindrical mortar specimens of 50 mm in diameter and 100 mm in height were tested. The compressive strength at the beginning of each fatigue test, the shear stress ranges, and the number of specimens are summarized in Table 2. Herein, one mortar specimen with a compressive strength of  $57.1 \text{ N/mm}^2$  was used for each shear stress range as the pilot test.

### Test method

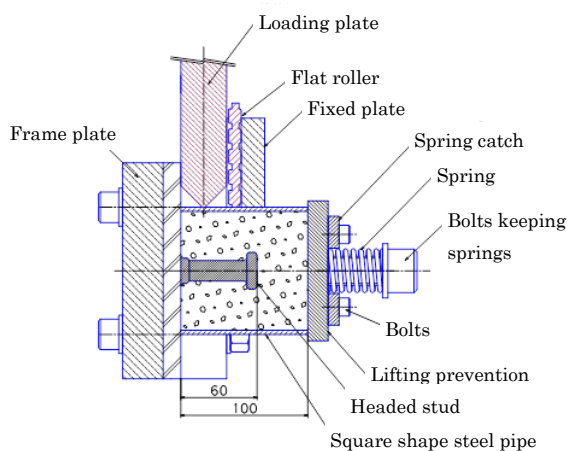
The test setup in the fatigue tests and details of

Table 2 Summary of shear stress ranges

| Headed stud  | Shear stress range (N/mm <sup>2</sup> ) | Number of specimens | Compressive strength (N/mm <sup>2</sup> ) |
|--------------|---|---------------------|---|
| Conventional | 150                                     | 3                   | 23.8                                      |
|              | 120                                     | 3                   |   |
|              | 100                                     | 3                   |   |
|              | 80                                      | 3                   | 57.1                                      |
|              | 140                                     | 1                   |   |
|              | 130                                     | 1                   |   |
| Improved     | 120                                     | 1                   | 23.8                                      |
|              | 150                                     | 3                   |   |
|              | 120                                     | 3                   |   |
|              | 100                                     | 3                   | 31.8                                      |
|              | 80                                      | 3                   |   |
|              | 120                                     | 3                   |   |
|              | 100                                     | 3                   | 57.1                                      |
|              | 90                                      | 3                   |   |
|              | 150                                     | 1                   |   |
|              | 140                                     | 1                   |   |
|              | 120                                     | 1                   |   |



(a) Test setup.



(b) Details of test equipment.

Fig. 3 Test setup and details of test equipment.

the test equipment are shown in Fig. 3. Each specimen was fixed to a frame plate with four bolts. A shear force was vertically applied to the specimen through a loading plate with a thickness of 36 mm. Then, the loading position was 18 mm apart from the surface of the steel base plate of the specimen as close as possible to the root of the headed stud. A fixed steel plate was welded to the test equipment because the shear force transferred at the interface between the steel base plate and the concrete/mortar was applied without bending moment when the headed stud deformed due to a fatigue crack. Moreover, a flat roller was installed between the loading plate and the fixed steel plate to keep the loading position constant and to prevent the frictional resistance between those. In this study, the cyclic load was applied to the specimen by a 200 kN hydraulic actuator. The minimum loading level was kept at 5 kN and the maximum loading level was varied according to the shear stress ranges given in Table 2. As the loading condition, a sine wave with a load frequency of 3 or 5 Hz was applied in the load control.

## RESULTS AND DISCUSSION

### Failure modes

Fig. 4 shows failure conditions after the fatigue tests. In this study, two failure modes were observed as with the previous study on the fatigue tests under the rotating shear force [13]. In the specimens with low and middle compressive strengths of 23.8 and 31.8 N/mm<sup>2</sup>, as shown in Fig. 4(a), a fatigue crack (Type S in Fig. 5) initiated at the tip of the separated portion between the stud shank and the weld collar due to the notch effect and progressed into the stud shank. In this failure mode, the concrete around the weld collar was crushed during the fatigue tests. This phenomenon also depends on the applied loading level. The crushing of the concrete leads to changes in the stress distribution along the headed stud. This stress redistribution was analytically observed by Xu and Sugiura [14] in their push-out specimens.

On the other hand, in the specimens with a higher compressive strength of 57.1 N/mm<sup>2</sup>, as shown in Fig. 4(b), a fatigue crack (Type P in Fig. 5) initiated at the weld toe and progressed into the steel base plate along the heat affected zone. This type of failure mode was also observed in the previous study [13]. Then, the mortar did not crush around the weld collar because the mortar had the higher strength. The concrete/mortar with higher strength and without crushing tends to have more stress concentration at the weld toe than in the separated portion between the stud shank and the weld collar.





(a) Failure mode of Type S.



(b) Failure mode of Type P.

Fig. 4 Failure conditions.

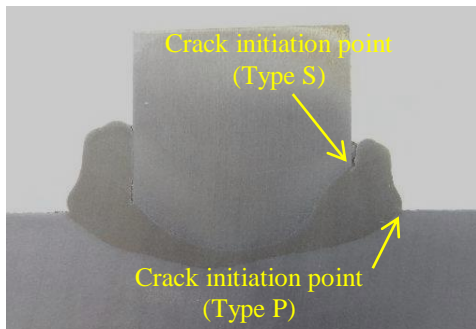


Fig. 5 Macro view of weld collar.

### Comparison of fatigue strength

The relationships between the shear stress range and the number of cycles, namely S-N curves are shown in Fig. 6 to compare the fatigue life between the conventional and the improved headed studs with the compressive strength of 23.8 and 57.1 N/mm<sup>2</sup>. The improved headed stud is about 1.4 times higher at the compressive strength of 23.8 N/mm<sup>2</sup> and is about 2.7 times higher at the compressive strength of 57.1 N/mm<sup>2</sup> than the conventional headed stud. The S-N curves can be expressed using the following equations.

For the improved headed stud,

$$\log N = -4.504 \log(\Delta\tau) + 14.29 \quad (\text{at } 23.8 \text{ N/mm}^2) \quad (1)$$

$$\log N = -11.92 \log(\Delta\tau) + 31.40 \quad (\text{at } 57.1 \text{ N/mm}^2) \quad (2)$$

For the conventional headed stud,

$$\log N = -4.376 \log(\Delta\tau) + 13.89 \quad (\text{at } 23.8 \text{ N/mm}^2) \quad (3)$$

$$\log N = -14.65 \log(\Delta\tau) + 36.84 \quad (\text{at } 57.1 \text{ N/mm}^2) \quad (4)$$

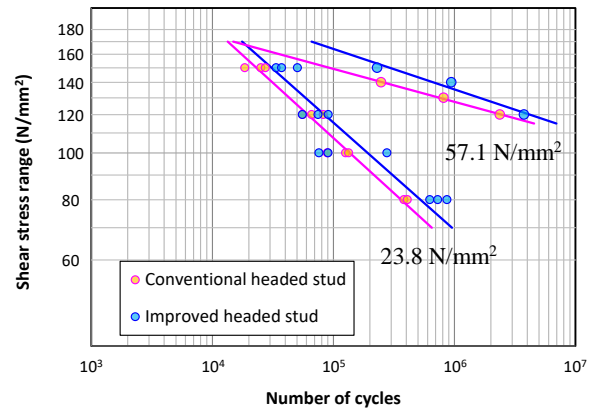


Fig. 6 S-N curves for headed studs.

In the failure mode of Type S, the height up to the tip (H2 shown in Table 1) of the separated portion between the stud shank and the weld collar is higher in the improved headed stud than in the conventional headed stud. This means that the length from the loading point to the tip of the separated portion is shortened and the maximum principal stress is decreased. Consequently, the fatigue life of the improved headed stud increased. In contrast, in the failure mode of Type P, the diameter (D shown in Table 1) of the weld collar is larger in the improved headed stud than in the conventional headed stud. This means that the fatigue crack progresses in a larger path than in the conventional headed stud. Consequently, the improved headed stud has a longer fatigue life.

### S-N curve and compressive strength

The fatigue test data of the improved headed stud were obtained at three different compressive strengths of concrete/mortar. The results are plotted in Fig. 7. When the improved headed studs having the compressive strengths of 23.8 and 31.8 N/mm<sup>2</sup> are compared, the S-N curves crossed in the higher shear stress range. This phenomenon may be considered because in the higher shear stress range, the concrete around the weld collar was crushed at a certain stage during the fatigue test, and a fatigue crack initiated at the tip of the separated portion between the stud shank and the weld collar and progressed into the stud shank as discussed above. Then, the two headed studs showed a similar fatigue life because each headed stud has the stud shank of the same diameter. In contrast, in the lower shear stress range, the headed stud with the higher compressive strength of concrete showed a longer fatigue life. This caused a difference in time taken before the concrete was crushed. Mia and Bhowmick [15] analytically showed that an increase in concrete strength leads to an increase in the fatigue strength of headed studs as in this study.

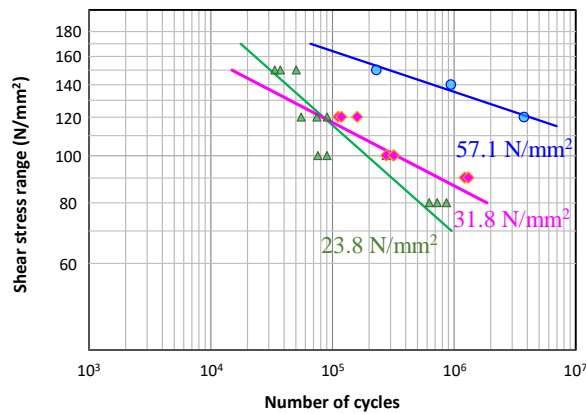
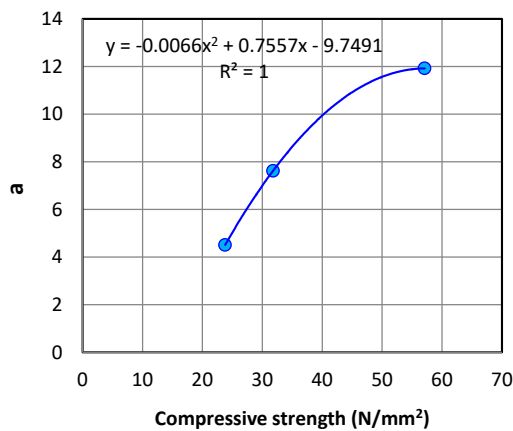
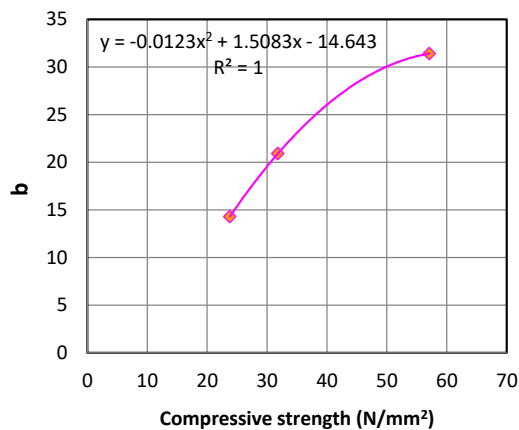


Fig. 7 S-N curves for improved headed stud.



(a) Relationship between the slope and the compressive strength of concrete/mortar.



(b) Relationship between the intercept and the compressive strength of concrete/mortar.

Fig. 8 The slope and the intercept of the S-N curve for the improved headed stud.

The S-N curve for the improved headed stud with the compressive strength of 31.8 N/mm<sup>2</sup> is as follow.

$$\log N = -7.619 \log(\Delta \tau) + 20.89 \quad (5)$$

From Eqs. (1)-(2) and (5), as shown in the following Eq. (6), the slope,  $a$ , and the intercept,  $b$ , with respect to the compressive strength of concrete/mortar, are shown in Fig. 8 and are presented in the following formulas.

$$\log N = -a \log(\Delta \tau) + b \quad (6)$$

$$a = -0.0066f_c'^2 + 0.7557f_c' - 9.7491 \quad (7)$$

$$b = -0.0123f_c'^2 + 1.5083f_c' - 14.643 \quad (8)$$

Although further data collection is needed, the slope and the intercept of the S-N curve for each improved headed stud are best fit to the compressive strength of concrete/mortar by each secondary function approximation. At higher compressive strength, the slope and the intercept have a tendency to approach certain values, respectively. Namely, at a higher compressive strength level, the fatigue strength of the improved headed stud is close to a certain value caused by the failure mode without concrete crushing in which a fatigue crack initiates at the weld toe and progresses into the steel base plate along the heat affected zone. At a lower compressive strength, the fatigue strength is significantly affected by the compressive strength of concrete/mortar.

## CONCLUSIONS

The fatigue tests were carried out for single headed studs in concrete/mortar in this study. The fatigue strength of the improved headed stud was compared with that of the conventional headed stud and the S-N curve of the improved headed stud depending on the compressive strength of concrete/mortar was proposed. The following conclusions were drawn from this study.

- (1) From the fatigue tests, two failure modes of headed studs were observed. In one failure mode, a fatigue crack initiated at the tip of the separated portion between the stud shank and the weld collar and progressed into the stud shank. In the other failure mode, a fatigue crack initiated at the weld toe and progressed into the steel base plate along the heat affected zone.
- (2) The fatigue strength of the improved headed stud was higher than that of the conventional headed stud in concrete/mortar with each compressive strength. The elongation of the fatigue life depends on the compressive strength, the shear stress range, and the failure mode.
- (3) The slope and the intercept of S-N curve for the improved headed stud have a secondary function with respect to the compressive strength of concrete/mortar. At higher compressive strength,



the slope and the intercept tend to approach certain values. At a higher compressive strength level, the fatigue strength of the improved headed stud is close to a certain value in the failure mode without concrete crushing around the weld collar in which the fatigue crack initiates at the weld toe and progresses into the steel base plate along the heat affected zone.

## REFERENCES

- [1] Thürlimann B., Fatigue and Static of Stud Shear Connectors, *ACI Journal*, Vol. 30, No. 12, 1953, pp. 1278-12301.
- [2] Mainstone R.J. and Menzies J.B., Shear Connectors in Steel-concrete Composite Beams for Bridges; Part 1, Static and Fatigue Tests on Push-out Specimens, *Concrete*, Vol. 1, No. 9, 1967, pp. 291-302.
- [3] Ollgaard J.G., Slutter R.G. and Fisher J.W., Shear Strength of Stud Shear Connectors in Lightweight and Normal Concrete, *AISC Engineering Journal*, Vol. 8, No. 2, 1971, pp. 55-64.
- [4] Naithani K.C., Gupta V.K. and Gadh A.D., Behavior of Shear Connectors under Dynamic Loads, *Materials and Structures*, Vol. 21, 1988, pp. 353-363.
- [5] Gattesco N. and Giuriani E., Experimental Study on Stud Shear Connectors Subjected to Cyclic Loading, *Journal of Constructional Steel Research*, Vol. 38, No. 1, 1996, pp. 1-21.
- [6] Johnson R.P., Resistance of Stud Shear Connectors to Fatigue, *Journal of Constructional Steel Research*, Vol. 56, No. 2, 2000, pp. 101-116.
- [7] Hanswille G., Porshe M. and Ustundag C., Resistance of Headed Studs Subjected to Fatigue Loading Part I: Experimental Study, *Journal of Constructional Steel Research*, Vol. 63, No. 4, 2007, pp. 475-484.
- [8] Hanswille G., Porshe M. and Ustundag C., Resistance of Headed Studs Subjected to Fatigue Loading Part II: Analytical Study, *Journal of Constructional Steel Research*, Vol. 63, No. 4, 2007, pp. 485-493.
- [9] Matsui S., Hiragi K. and Fukumoto Y., Derivation of Strength of Headed Stud Shear Connectors – Fatigue Strength –, *Journal of Structural Engineering, JSCE*, Vol. 35A, 1989, pp. 1233-1244 (in Japanese).
- [10] Hiragi K. and Matsui S., Investigation on Remarkable Improvement of Fatigue Strength for Headed Studs, *Proceedings of Developments in Short and Medium Span Bridge Engineering*, Calgary, 1998, pp. 1681-1693.
- [11] Yoshida K. Inamoto K. Matsui S., Higashiyama H. and Kaido H., Development of Headed Stud with High Fatigue Strength for Steel-concrete Composite Deck, *Journal of Structural Engineering, JSCE*, Vol. 58A, 2012, pp. 908-919 (in Japanese).
- [12] Yoshida K., Higashiyama H., Inamoto K., Matsui S. and Kaido H., S-N curve for Durable Headed Stud under Rotating Shear Force, *Journal of the Society of Materials Science, Japan*, Vol. 62, No. 10, 2013, pp. 621-626 (in Japanese).
- [13] Higashiyama H., Yoshida K., Inamoto K., Matsui S. and Kaido H., Fatigue of Headed Studs Welded with Improved Ferrules under Rotating Shear Force, *Journal of Constructional Steel Research*, Vol. 92, 2014, pp. 211-218.
- [14] Xu C. and Sugiura K., FEM Analysis on Failure Development of Group Studs Shear Connector under Effects of Concrete Strength and Stud Dimension, *Engineering Fail Analysis*, Vol. 35, 2013, pp. 343-354.
- [15] Mia M.M. and Bhowmick A.K., A Finite Element Based Approach for Fatigue Life Prediction of Headed Shear Studs, *Structures*, Vol. 19, 2019, pp. 161-172.

## DESIGN AND ANALYSIS OF FORMULA SPACE FRAME CHASSIS WITH SIDE IMPACT

Boonthum Wongchai

Faculty of Engineering at Sriracha, Kasetsart University, Thailand

### ABSTRACT

Space frame chassis is one of the popular types of formula car chassis. There are many subjects to design and analyze formula car chassis. Side impact is the main subject for design and analysis with accurate and safety for driver. In this article, the 2017-2018 formula SAE (the Society of Automotive Engineers) rules is used for analysis. The CAD models of formula car chassis are constructed using SolidWorks 2016. Finite element method (FEM) is used to analyze the CAD models using SolidWorks Simulation. The results show that all formula car chassis models satisfy the 2017-2018 formula SAE rules. The maximum stress and the maximum deflection are not significant affected by varying the distance of the front member joint. While varying the distance of the side impact member joint affects both of the maximum stress and the maximum deflection. The relationship of the distance of the side impact member joint and the maximum stress is increasing linear function. While the relationship of the distance of the side impact member joint and the maximum deflection is the upside down parabolic function. Using the goals of the formula car chassis design are low maximum stress and low maximum deflection, the distance from the side impact members joint and the front roll hoop should be as low as possible.

*Keywords: Formula, Space Frame Chassis, Side Impact, FEM Design and Analysis*

### INTRODUCTION

Nowadays the Formula Society of Automotive Engineers (Formula SAE) main activity is a student-level design competition of formula car which is the beginning event of the Formula One car racing; the most popular car racing event in the world. There are many issues to design formula car such as chassis, suspension, break system, power train, aerodynamics, impact attenuator, materials, engine and electronic system [1]-[6].

Formula car chassis is one of the most important part of the formula car. There are many types of the formula car chassis. Space frame chassis, ladder frame chassis and composite monocoque are the popular types of the formula car chassis [6]-[9]. The space frame chassis is constructed from the circular or square tube by welding. The ladder frame chassis has a shapes of the ladder style. Meanwhile, the composite monocoque is made from composite material.

For the car design, torsional rigidity, modal analysis, vibration analysis, front impact and side impact are the main analysis. Finite element method (FEM) are usually used for these analysis [10]-[11].

Torsional rigidity or torsional stiffness can be determined using FEM. The formula car chassis is fixed at one end and the torque is applied at the other end. The torsional deflection and the torque are applied to determine the torsional stiffness [8].

Modal analysis is conducted to determine the mode shapes and the natural frequencies of the formula car chassis for avoiding the resonant frequency [7]. High vibration occurs at resonant

frequency when the engine frequency equals the natural frequency.

The mass-spring-damper with the road shapes are used in the vibration analysis of the formula car. The quarter-car model is performed for determination the vibration of the tire deflection, the suspension deflection and the car acceleration [12].

The front impact and the side impact are the impact analysis in FEM. Impact analysis can be simplified to static analysis using the relation of the force due to the formula car chassis in a short time and the changing of the formula car momentum [13]

$$F\Delta t = m(v_2 - v_1), \quad (1)$$

where  $F$  is the impact force,  $\Delta t$  is the time duration of the impact force due to the formula car chassis,  $m$  is the total formula mass (with the driver),  $v_1$  is the car velocity before crashing, and  $v_2$  is the car velocity after crashing ( $v_2 = 0$ ).

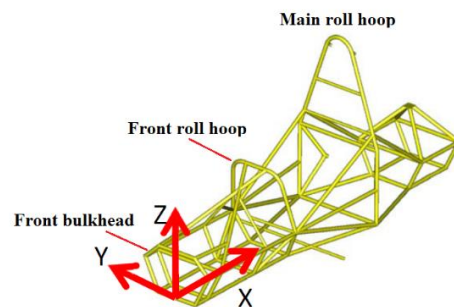


Fig. 1 Formula SAE space frame chassis [1].

The stress and the deflection of the formula car chassis must not over the allowable limit of the chassis materials. Figure 1 shows the Formula SAE space frame chassis. For side impact, the 2017-2018 formula SAE rules define that  $F_y = 7.0$  kN applied at all structural locations between front roll hoop and main roll hoop of the formula car [1]. For boundary conditions, the bottom nodes of both side of the front and main roll hoops are fixed. Failure must not occur at anywhere and the maximum allowable deflection of 25 mm

In this study, the space frame chassis is performed. The shapes of all member locations between front bulkhead and main roll hoop will be investigated with the best condition of stress and deflection of the formula car.

## CHASSIS DESIGN

Figure 2(a) and Figure 2(b) show the 3d view and the side view of the formula car chassis used in this study respectively.

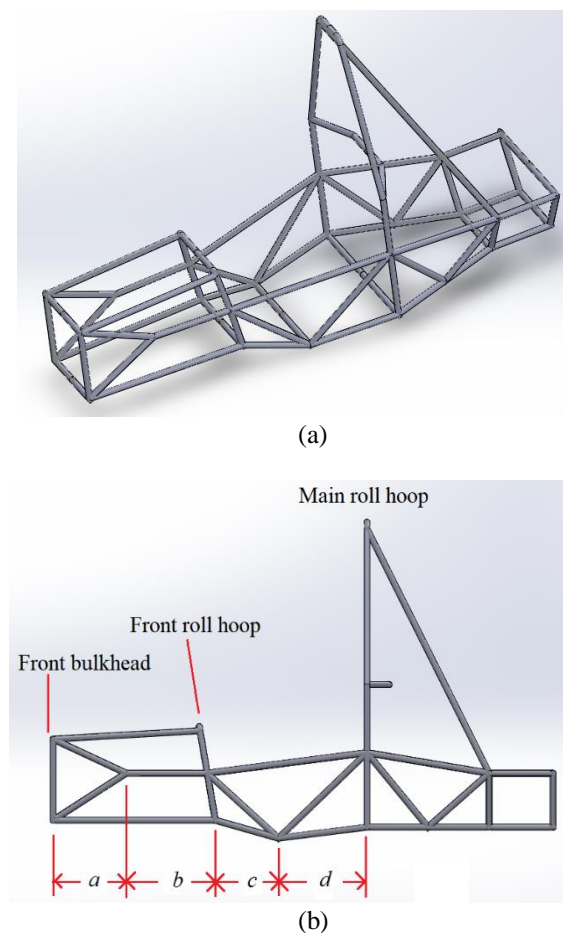


Fig. 2 (a) 3d view (b) side view.

Six of front members between front bulk head and front roll hoop are changed by varying the distance of  $a$  as show in Table 1.

Nine members of side impact members between front roll hoop and main roll hoop are changed by varying the distance of  $c$  as show in Table 2.

Table 1 Design of members between front bulk head and front roll hoop.

| Front members $Fa$ | $a$        |
|--------------------|------------|
| F1                 | $(a+b)/6$  |
| F2                 | $2(a+b)/6$ |
| F3                 | $3(a+b)/6$ |
| F4                 | $4(a+b)/6$ |
| F5                 | $5(a+b)/6$ |

Note:  $a+b = 700$  mm.

Table 2 Design of members between front roll hoop and main roll hoop.

| Side impact members $Sc$ | $c$          |
|--------------------------|--------------|
| S1                       | $(c+d)/12$   |
| S2                       | $2(c+d)/12$  |
| S3                       | $3(c+d)/12$  |
| S4                       | $4(c+d)/12$  |
| S5                       | $5(c+d)/12$  |
| S6                       | $6(c+d)/12$  |
| S7                       | $7(c+d)/12$  |
| S8                       | $8(c+d)/12$  |
| S9                       | $9(c+d)/12$  |
| S10                      | $10(c+d)/12$ |
| S11                      | $11(c+d)/12$ |

Note:  $c+d = 654$  mm.

## MATERIAL SELECTION

All members of the formula car chassis are made of carbon steel pipe with the outer diameter of 25.4 mm and the thickness of 2.5 mm. The mechanical properties of the carbon steel are shown in Table 3.

Table 3 Material properties of carbon steel pipe

| Property         | Value | Units |
|------------------|-------|-------|
| Elastic modulus  | 205   | MPa   |
| Poisson's ratio  | 0.29  | -     |
| Shear modulus    | 80    | GPa   |
| Tensile strength | 365   | MPa   |
| Yield strength   | 305   | MPa   |

## FINITE ELEMENT METHOD

In this study, the side impact members are the dominant factor for side impact. The side impact force acts directly on the side impact members as shown in Fig. 3. While the front members are not acted directly by the side impact force. The CAD

models of the formula car chassis are modeled using SolidWorks 2016. For finite element method, SolidWorks Simulation is applied to analyze the stress and the deflection of the formula car chassis in some cases of the front member; F1, F3, and F5 combining with all cases of the side impact members in Table 2; S1 to S12 with the abbreviation FaSc. For example, the F1Sc is the combination of the front member F1 and all cases of the side impact members Sc. The FaS5 is the combination between the front members F1, F3, and F5 and the side impact member S5. Moreover, the F5S1 is the combination of F5 and S1.

For load and boundary conditions, this study uses the 2017-2018 Formula SAE Rules [1]. For side impact, the force of 7 kN is applied at all members between front roll hoop and main roll hoop with the direction toward the driver. The bottom nodes of both side of the front roll hoop and the main roll hoop are fixed displacement ( $x, y, z$ ) but not rotation as shown in Fig. 3.

The CAD models are meshed with beam element. The upper bound axial and bending stress ( $\sigma$ ) is used to compare the yield strength ( $\sigma_y$ ).

Failure not occur anywhere in structure for  $\sigma < \sigma_y$ . The upper bound axial and bending stress can be computed from

$$\sigma = \frac{P}{A} + \frac{(M_y I_z + M_z I_{yz})z + (M_z I_y + M_y I_{zy})y}{I_y I_z - I_{yz}^2}, \quad (2)$$

where  $P$  is the axial force,  $A$  is the beam cross section area,  $M_y$  and  $M_z$  are the moment in the direction  $y$  and  $z$ , respectively,  $I$  is the moment inertia of area of the beam cross section and the subscript indicates its rotation direction as shown in Fig 4.

The beam deflection can be computed from

$$u = \sqrt{u_x^2 + u_y^2 + u_z^2}, \quad (3)$$

where  $u$  is the beam deflection,  $u_x$ ,  $u_z$  and  $u_y$  are the beam deflection in  $x$ ,  $y$  and  $z$  directions, respectively. The beam deflection is used to compare the allowable deflection of 25 mm.

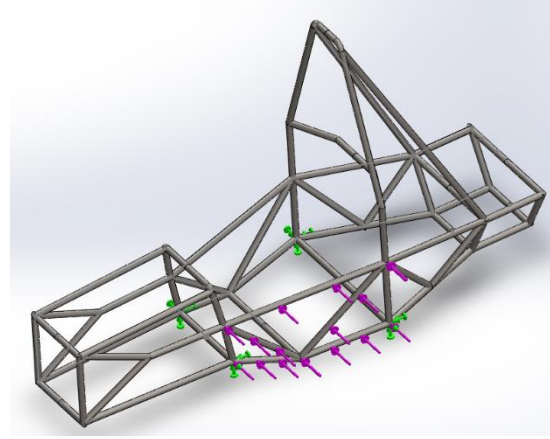


Fig. 3 Load and boundary condition.

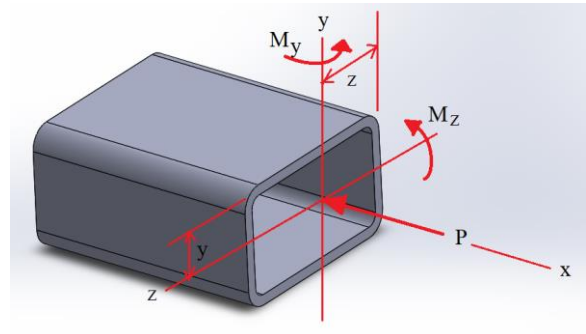


Fig. 4 Combine loading in beam element.

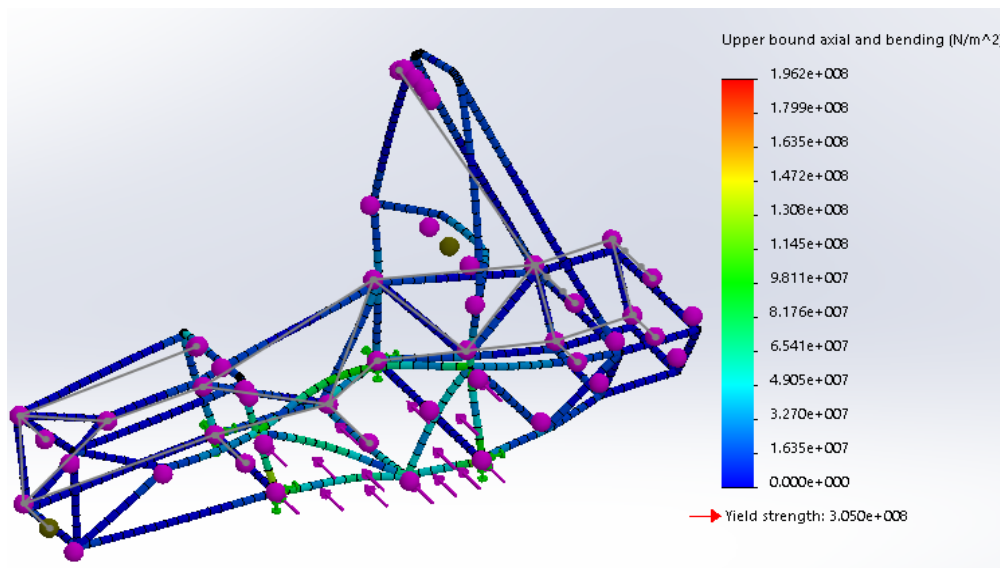


Fig. 5 The upper bound axial and bending stress

## RESULT AND DISCUSSION

Figure 5 shows the upper bound axial and bending stress in the formula car chassis in case F3S5.

For all cases of  $FaSc$  ( $a = 1, 3$ , and  $5$  as shown in Table 1 and  $c = 1, 2, \dots, 11$  as shown in Table 2, respectively), the results of the maximum stress  $\sigma_{\max}$  can be plotted with  $c$  as shown in Fig. 6 to Fig. 8.

From Fig. 6 to Fig. 8, the results show that the relationships of the maximum stress and the distance  $c$  are increasing linear equation with  $R^2$  more than  $0.9$  except the case of F5Sc has  $R^2$  of  $0.8363$ . The maximum stress will be increased by varying the distance  $c$ . The lowest maximum stress occur at cases FaS3 ( $c = 3(654)/12 = 163.5$  mm). For comparing with yield strength ( $\sigma_y = 305$  MPa), failure not occurs anywhere in structure for all cases.

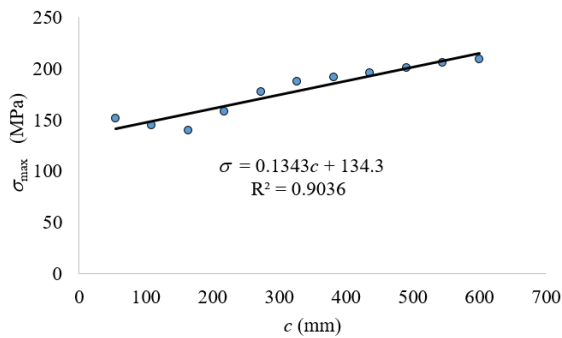


Fig. 6 Maximum stress in case F1Sc ( $a = 700/6$  mm).

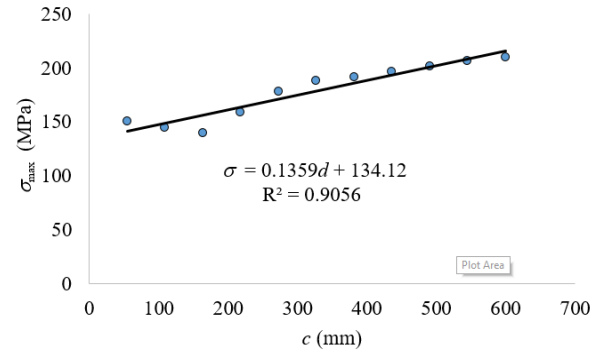


Fig. 7 Maximum stress in case F3Sc ( $a = 3(700)/6$  mm).

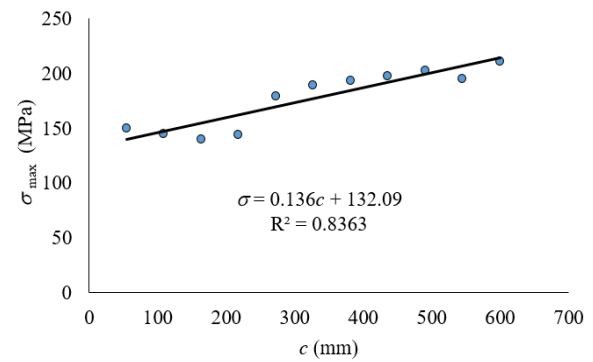


Fig. 8 Maximum stress in case F5Sc ( $a = 5(700)/6$  mm).

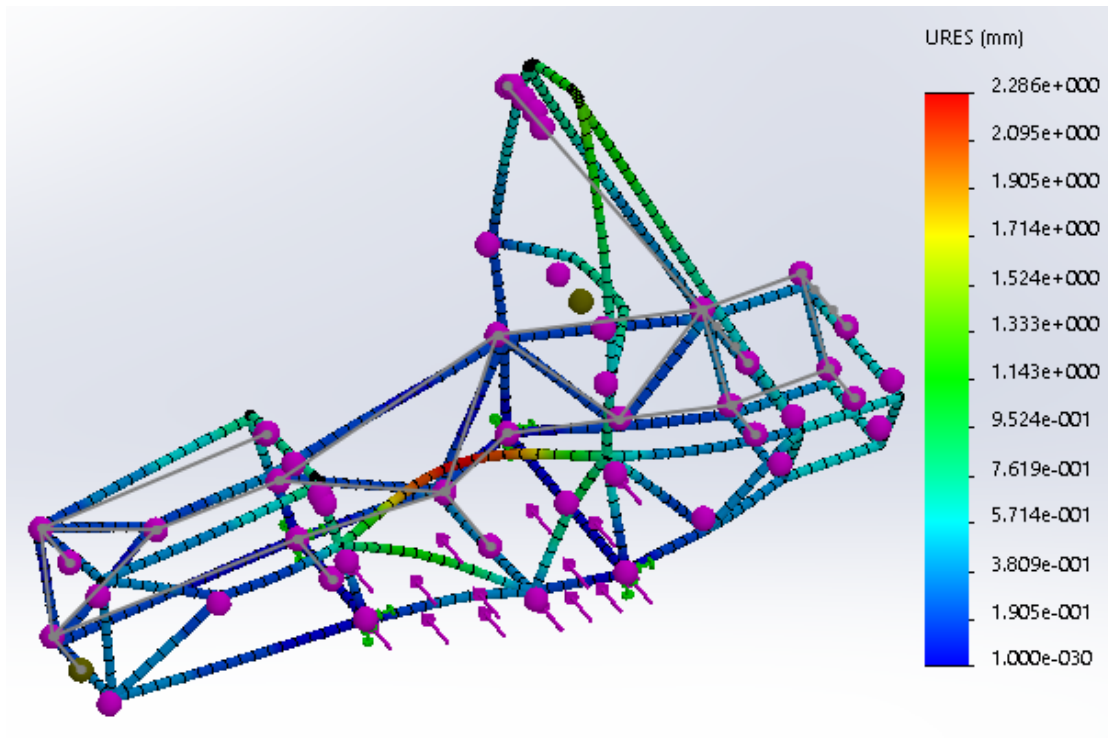


Fig. 9 Deflection of the formula car chassis.



Figure 9 shows the deflection of the formula car chassis of case F3S5. The maximum deflection and the distance  $c$  can be plotted with the upside down parabolic equation with  $R^2$  more than 0.87 as shown in Fig. 10 to Fig. 12.

The maximum values of the maximum deflection occur in cases FaS5 ( $c = 5(654)/12 = 272.5$  mm). The minimum values of the maximum deflection occur in cases FaS11 except case F5Sc occurs in case F5S10. All cases do not exceed the allowable deflection of 25 mm.

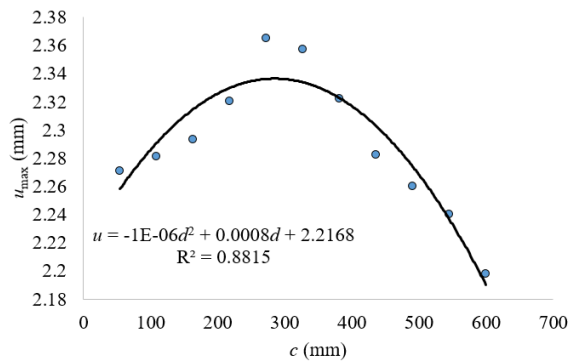


Fig. 10 Maximum deflection in case F1Sc ( $a = 700/6$  mm).

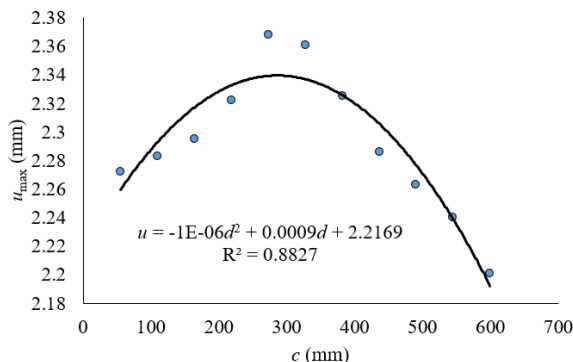


Fig. 11 Maximum deflection in case F3Sc ( $a = 3(700/6)$  mm).

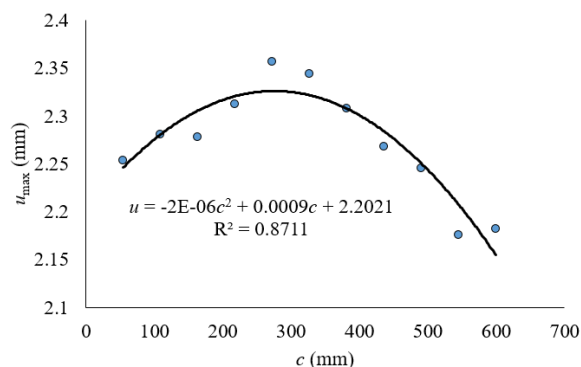


Fig. 12 Maximum deflection in case F5Sc ( $a = 5(700/6)$  mm).

From the maximum stress graph and the maximum deflection graph, using the goal of the formula car chassis design with low stress and low deflection, the distance  $c$  should be as low value as possible. For this study, case F5S1 with lowest value of  $c$  is the best choice.

By varying the distance  $a$ , the results show that the distance  $a$  is not the main factor that affect the maximum stress and the maximum deflection.

## CONCLUSIONS

This paper presents the formula space frame chassis design and analysis subjected on side impact. By varying the distance  $c$  of the side impact members joint, the results show that the relationships between the maximum stress and the distance  $c$  are increasing linear equation for all cases. The maximum stress can be increased by increasing the distance  $c$ . The relationships between the maximum deflection and the distance are the upside down parabolic equation. The distance of the front member joint  $a$  insignificantly affects the maximum stress and the maximum deflection.

The distance  $c$  should be as low as possible by using the goal of the formula car chassis design with low stress and low deflection. Case F5S1 is the best design for this study.

## REFERENCES

- [1] 2017-2018 Formula SAE Rules. <https://www.fsaonline.com/content/2017-18%20FSAE%20Rules%209.2.16a.pdf>, Access on 10, December 2018.
- [2] Chepkasov S., Markin G. and Akulova A., Suspension Kinematics Study of the "Formula SAE" Sports Car, Procedia Engineering, Vol. 150, 2016, pp. 1280-1286.
- [3] Mariani F., Poggiani C., Risi F. and Scappaticci L., Formula-SAE Racing Car: Experimental and Numerical Analysis of the External Aerodynamics. Energy Procedia, Vol. 81, 2015, pp. 1013-1329.
- [4] Hetawal S., Gophane M., Ajay B.K and Mukkamala Y., Aerodynamic Study of Formula SAE Car. Procedia Engineering, Vol. 97, 2014, pp. 1198-1207.
- [5] Savage G., Formula 1 Composites Engineering. Engineering Failure Analysis, Vol. 17, 2010, pp. 92-115.
- [6] Guimaraes A.V., Brasileiro P.C., Giovanni G.C., Costa L.R.O. and Araujo L.S., Failure analysis of a half-shaft of a formula SAE racing car. Case Studies in Engineering Failure Analysis, Vol. 7, 2016, pp. 17-23.

- [7] Anas M.N., Nandu N.C., Anjai K., Arjun R.N. and Pramod S., Design, Analysis, Fabrication and Testing of a Formula Car Chassis. *Materials Today*, Vol. 5, 2018, pp. 24944-24953.
- [8] Limwathanagura T., Sithananun C., Limchamroon T. and Singhanart T., The Frame Analysis and Testing for Student Formula, *International Journal of Mechanical and Mechatronics Engineering*, Vol. 6, 2012, pp. 998-1002.
- [9] Mat M.H. and Ghani A.R.Ab., Design and Analysis of 'Eco' Car Chassis. *Procedia Engineering*, Vol. 41, 2012. pp. 1756-1760.
- [10] Chandan S.N., Sandeep G.M. and Vinayaka N., Design, Analysis and Optimization of Race Car Chassis for its Structural Performance , *International Journal of Engineering Research & Technology* , Vol. 5, 2016, pp. 361-367.
- [11] Patil R.V., Lande P.R., Reddy Y.P. and Sahasrabudhe A.V., Optimization of Three Wheeler Chassis by Linear Static Analysis, *Materials Today*, Vol. 4, 2017, pp. 8806-8815.
- [12] Saurabh S.Y., Kumar S., Jain K.K., Behera S.K., Gandhi D., Raghavendra S. and Kalita K. Design of Suspension System for Formula Student Race Car, *Procedia Engineering*, Vol. 144, 2016, pp. 1138-1149.
- [13] Sood A. and Singh P., Analysis of Space Frame of formula SAE at High Speed with Ergonomic and Vibrational Factors. *International Journal of Mechanical Engineering and Technology*, Vol. 6, 2015, pp. 202-212.



## PUBLIC TRANSPORT INITIATIVES IN WEST AFRICA, A CASE STUDY OF ABIDJAN

Leonard Johnstone<sup>1</sup> and Vatanavongs Ratanavaraha<sup>2</sup>

<sup>1,2</sup>Institute of Engineering, Suranaree University of Technology, Thailand

### ABSTRACT

Abidjan is the principal city of the West African Republic of Côte d'Ivoire. It is the gateway city to West Africa. In 2014, the population of the city was estimated at four million people. Over the next fifteen years, this is projected to rise to nearly seven and a half million people. This continuing growth has an associated projected strong economic growth. This paper addresses the challenges associated with the provision of equitable public transport services to address the needs of the growing population. Public transport currently in Abidjan is complex consisting of both formal transport in the form of public bus services and several forms of informal public transport. In order to understand the existing travel trends and especially the declining public transport proportion in Abidjan, a series of surveys were undertaken for the development of an analytical methodology. This included amongst others an interview survey of people at the household level and public transport opinion surveys. The methodology thus developed allowed an understanding of the impact of new proposed infrastructure. The introduction of new infrastructure in the form of a higher level of public transport and an enhanced regulatory format will enable the implementation of an environmentally friendly public transport with a growing market share.

*Keywords: Public Transport, Côte d'Ivoire, Mode Split, Environment*

### INTRODUCTION

Abidjan is a city of lagoons and parks, a colorful city of blue and green as represented in Fig. 1. The Abidjan vision and long-term city development are based around three main goals of transportation system enhancement namely:

- Efficiency;
- Equity, and
- Better Environment.

An efficient transportation system should be developed to strengthen urban functions, to enhance people's quality of life, to facilitate economic activities, and to sustain stable economic growth in Abidjan. It is of great significance to achieve efficiency by decreasing negative externalities such as economic loss of travel time caused by increasing traffic. The efficiency in transportation is achievable by balancing the growing travel demand within the city and the transportation infrastructure supply.

An enhanced transport system with a diversion from the private to the public leads to a better green environment in a similar structure as with the diversion of cargo to green cargo transport[1].

There are three ways to balance the demand and the supply: 1) by increasing and recovering the infrastructure capacity to meet the demand; 2) by optimizing utilization of the existing transport infrastructure through efficient transportation control measures; and 3) by decreasing excessive vehicular traffic demand through transportation demand management and diverting private vehicle users to public transport.

Equity means that a certain minimum level of mobility should be assured and provided for all members of society. Not only automobiles but also all modes of transport should have a right to share the public space and move around the city freely and safely.

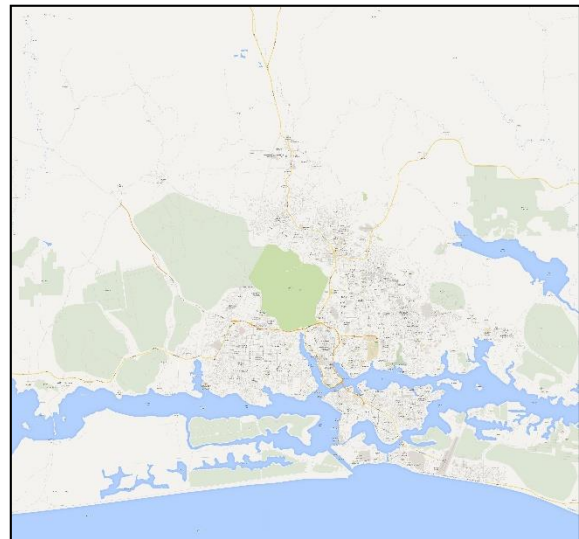


Fig. 1 The city of lagoons.

On the other hand, some low-income people cannot afford to pay for expensive transportation cost. Some socially vulnerable people including the aged and the handicapped have difficulties in their mobility. Affordable and sufficient level of transportation services should be provided for those

people especially by the improvement of the public transport system.

The vision for Greater Abidjan is about, “providing quality living environments,” air pollution and noises caused by automobiles should be minimized by promoting public transport use and controlling the traffic demand. At the same time, air pollution and noises should be reduced by applying stricter vehicle emission standards to reduce air pollutant emissions and this is enshrined in the Paris climate accords[2].

The city of Abidjan is divided into administrative regions or communes. These communes serve in addition as boundaries for physical transportation. In some incidences, there is modal restriction between communes. Some modes of the informal transportation system are not allowed to enter certain communes or there is restricted travel between communes.

## THE CURRENT SITUATION

During the year, 2013, there was an update of the Abidjan transport master plan [3]. Significant surveys were undertaken during this revision including detailed public transport and home interview surveys. The home interview survey sample size was a little over two percent of all households in Abidjan. Some 20,000 households were included in the survey.

One key result from the survey was the confirmation of the importance of both the walk mode and the informal transport sector in the city namely in the form of the Woro-woro and Gbaka as reported in Table 1. The private or car mode is still relatively low but significant growth has been seen in this mode.

As these informal public transport modes are likely unfamiliar, photos of the vehicles associated with these informal modes are provided in Fig 2. The commonly used Gbakas service is provided by minibus vehicles with a capacity of between 14 and 32 seats, and are subject to transport authorization issued by the government for a particular line of operation.

Table 1 City wide modal distribution of traffic

| Mode            | Percentage |
|-----------------|------------|
| Walk            | 53         |
| Car             | 5          |
| Taxi with meter | 2          |
| Woro-woro       | 20         |
| Gbaka           | 11         |
| Bus             | 6          |
| Oher            | 3          |

During the review of the transport master plan study[3], it was estimated that there were 2,900 Gbakas operational during a single day. They may

operate anywhere with the exception of the central business area, the commune of the Plateau.

The Woro-woro or intra-communal taxis are required to perform local services of proximity existed for several years. They have developed significantly in recent years due to some of their competitiveness compared to other modes, and secondly thanks to the shortage in supply of Buses available to the public transport company.

Whilst there are some arguments for the desirability [4] of the informal sector, it does not meet the aspiration associated with the overall improvement of public transport in the city.



Fig. 2 Informal transport modes.

## Historical Activity Levels

These informal modes of transport have risen in percentage terms in recent time by providing a desired service to the public. The public bus service company locally referred to as SOTRA(Société des transports Abidjanais) has seen its ridership fall from a peak of 700,000 passengers per day to 400,000, a decline of forty percent as depicted in Fig 3.

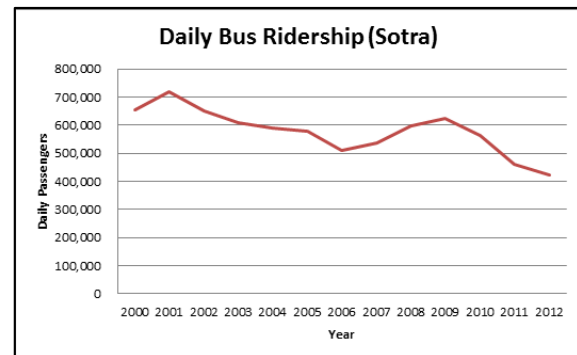


Fig. 3 Public bus patronage

In 1998[5], the modal share of non- walk trips for SOTRA bus was twenty-four percent with Gbaka accounting for a further twenty-five percent whilst seventeen percent of trips were made by Woro-woro. By 2013, the modal proportion of bus and Woro-woro was reversed as reported in Table 2. Woro-woro then accounted for thirty- two percent of mechanized person trips with public bus accounting for a reduced mode split of only twelve percent.

The earlier studies on urban transport conducted revealed a total of 2.2 million person trips per day for

the inhabitants of Abidjan who at the time were more than 8 years old in the inner communes. Public transit at that time consisted of a healthy share of around fifty percent consisting of both the bus and Gbaka.

The mode split within other selected major African cities is reported in Fig 4. Although the informal modal share of mechanized trips is high in other African cities [6], only Abidjan with an informal modal share of nearly fifty percent is second only to Dar Es Salam.

Table 2 Historical mode split of motorized travel

| Mode                            | Percentage |       |
|---------------------------------|------------|-------|
|                                 | 1998       | 2013  |
| Private<br>(Car and Motorcycle) | 14.0       | 11.7  |
| SOTRA                           | 24.0       | 11.7  |
| Gbaka                           | 25.0       | 25.1  |
| Woro-Woro                       | 17.0       | 31.7  |
| Meter Taxi                      | 16.0       | 17.5  |
| Employee Bus                    | 4.0        | 2.3   |
| Total                           | 100.0      | 100.0 |

It must be admitted that the physical city landscape is not so attractive to the provision of long bus routes and could be considered more conducive to the informal sector with an emphasis on shorter trips.

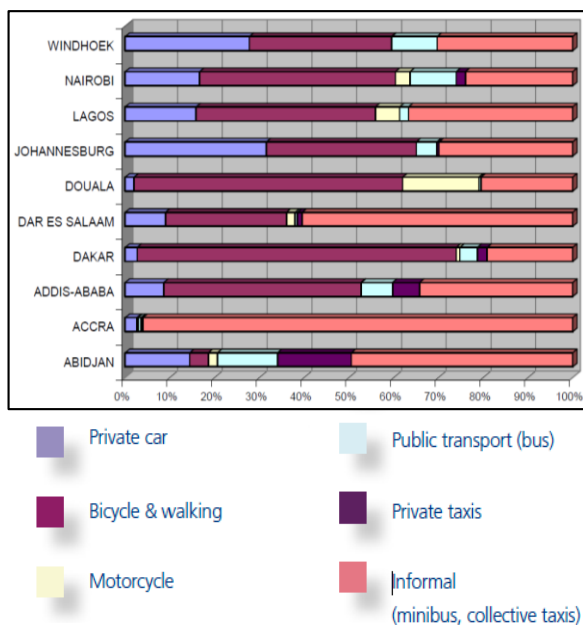


Fig. 4 Public transport city modal share

The landscape of Abidjan District is punctuated by many valleys called thalwegs, surrounded by very steep slopes that are not even conducive to a good road system.

The thalwegs create natural boundaries to quarters and are most of the time uninhabited as people are reluctant to live in those areas that are used as illegal landfill and can be flooded instantly during raining days. Planners have used this free space to design roads inside those thalwegs as the land was available.

### The Urban structure today

In administration terms, Abidjan, as previously mentioned is divided into communes. The key inner communes are depicted in Fig. 5 which also highlights the proposed transit infrastructure. The Plateau commune functions as the central area of the city with the communes of Adjame and Abobo to the north. Whilst in the west of the city there are the communes of Attecoubé and Yopougon. In the east, there are the communes of Cocody and Bingerville.

In the south, north of the southern waterway are the communes of Treichville, Marcory, and Koumassi. Then there are the communes of Port Bouet and Grand Bassam. The later two communes border the Atlantic Ocean.

The road network has been mainly developed without any consideration of Public Transport. Although public transport has been declining in recent years as discussed earlier, the proposals of the updated master plan 2030 have as one of its main objective a restoration the credibility of public transport lost during the previous ten years.

In order to integrate public transport inside the road network, and in particular a mass-transit system, the first step is to secure sufficient space for both road users and public transport facilities along the targeted roads.



Fig. 5 Proposed future transit

Around Abidjan, fast urban development can be seen, in particular between Cocody and Bingerville where large residential areas have been built at a very fast pace. To meet the growing demands in habitation, large residential areas are under development. The

transport master plan and thus the road master plan must take into account all this latest urban development to ensure consistency between land use and infrastructure development.

As the main roads have a high capacity, many private vehicles take the primary urban roads. Moreover, since the primary urban roads connect the major industrial areas in Abidjan such as Yopougon, Treichville, and Koumassi, via the primary urban roads to Abidjan Port and other major cities in Cote d'Ivoire, these roads also serve as a freight transportation corridor. Based on the result of the traffic count surveys undertaken during the master plan review, compositions of trucks to all traffic are documented, and the major truck routes have been identified as part of this analysis. The access from the northwest and the west can be regarded as the heavy vehicle corridors. These corridors then serve the dual purposes of regional connectivity for cargo plus local city traffic.

Some key issues are:

- Congestion points around the central area or Plateau;
- Absence of any high capacity public transport such as a metro system (previously recommended but never constructed) or Bus Rapid Transit;
- Limited access routes to the Plateau which is likely to grow in importance;
- Residents in new developments areas in Abobo and Yopougon (both expected to attract an additional one million people over the next two decades) must access the Plateau in a north-south movement. There is no direct east-west link from central Yopougon to the Plateau; and
- Dependence on the private car and informal public transport.

The key planning issues for public transport is that the public transport service is currently provided largely by the informal sector. Bus services are concentrated on routes originating from suburban areas and ending in several city terminals such as Adjame or the Plateau terminal. The informal sector accounting for eighty-five percent of public transport trips is provided across the following modes namely:

- Gbaka;
- Intra Communal Taxis or Woro-woro;
- Inter Communal Taxis;
- Fixed Route taxis; and
- Meter Taxis.

Bus routes are often categorized into four types from a planning point of view, namely, line-haul bus services on high capacity corridors, circulator bus services within major centers such as the central area,

circumferential routes and suburban feeder bus services. Alternatively, one may consider three levels of public transport namely a primary, secondary and tertiary level. With both the circulator and feeder services set into the later category.

The circumferential routes would provide linkages between major activity hubs without the need for coming into the center to access an adjacent hub. The viability of a bus route re-structure needs consideration in light of existing and future travel demand. Thus a methodology or a tool is needed to understand the impact of future demand in relation to the proposed future land use planning in order to ensure the maintenance of the earlier specified transport goals.

The analysis needs to define a role for all the city transport modes. Most line haul routes can become the prerogative of the formal public transport structure. The role of the informal sector such as Gbaka, Intra Communal Taxi or Woro-woro then focuses on Circulator and Feeder routes and possibly the need or otherwise for circumferential routes. Whilst it is common to have a circular route in the central area, in Abidjan consideration should be given as well for the need for such routes within the individual communes.

## METHODOLOGY

A classic four step transport model is developed as the analytical tool for the understanding of the movement of the people throughout the city as depicted in Fig. 6.

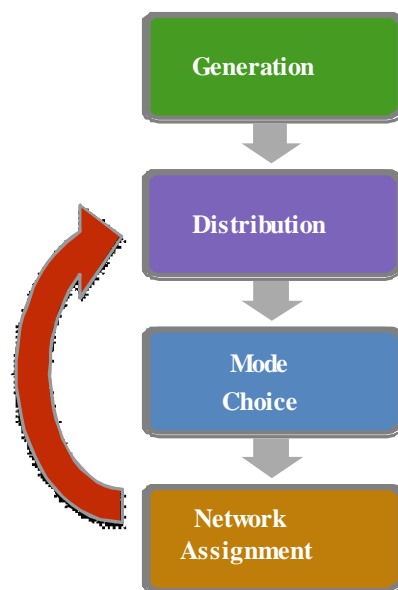


Fig. 6 The city model structure.

The first step is to address the starting and ending point of each person trip. The number of trips



generated in each small area or traffic zones is linked to socio-economic characteristics. In this analysis, the city of Abidjan was divided into 168 traffic zones.

The second step is the distribution of trips throughout the city. This distribution is linked to the impedance of travel between any two traffic zones. whilst the third step, the focus of this project, is the assignment of the person trip to the various walk, private or public transport mode. The public transport mode is then split into the formal and informal sector. This modal choice considers the cost of travel between any two traffic zones.

The network assignment combines all movement across all transport network infrastructure and thus provides an understanding of the movement of people including the priority and type of infrastructure proposals[7]. The focus of this research paper is on the movement of people and the probability of modal shift.

### Data Preparation

The base input data are a collation of databases available from the detailed survey program undertaken during the Abidjan master plan with particular reference to the aforementioned extensive home interview survey. In the model development, a master transport network is first prepared that includes all known and proposed transport projects with particular reference to public transport proposals.

### The Key Inputs – the Drivers of Future Demand

The key planning inputs are the distribution by small area or traffic zone of population, household, employment, student enrolments, and household income. The population of Abidjan is predicted to grow from 5.8 million in 2015 to 8.8 million in 2030 whilst the city economic growth is forecast to increase by seven percent per annum over the same time period.

The emphasis here is on the effort to achieve modal shift from the private sector to the public sector via infrastructure improvement or at the very least to reduce the trend away from the public sector. The model structure under discussion is the mode split segment of the overall Abidjan transport model. Other methods of modal shift for Abidjan other than improvement in the city modal structure may include the introduction of area pricing [8]. Other such alternatives are possible for evaluation within the transport model structure.

### Model Structure

The nested logit model[9] is often used in mode city analysis for both city wide transport and even in the case of long distance transport[10]. The model

structure with four levels of mode split analysis including the walk mode is depicted in Fig 7. Each model level has its own logit mode split curve.

The first curve separates the mechanized trips from the walk trips whilst at the next level, there is a choice between the public and private modes including special school buses. On the private side, there is a distinction between the private car and motorcycle.

On the public side, there is a distinction between the non-fixed route and fixed route transit modes whilst the final level of fixed route transit includes modal allocation within the phase of the public transit assignment.

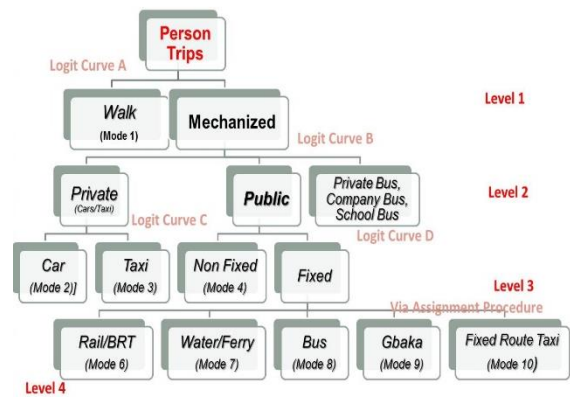


Fig. 7 Mode split structure.

### The Equations

The modal shift equation takes the following form:

$$1/(1+\exp(-\lambda(C_{ij}^2 + \delta - C_{ij}^1))) \quad (1)$$

Equation (1) defines the probability of using mode 1 as opposed to mode 2 whereas  $\lambda$  is the scale parameter and  $\delta$  is the bias as defined in Table 3;  $C_{ij}^1$  is the generalized cost of travel for hierarchical mode choice 1 between any two traffic analysis zones  $i$  and  $j$ ; and  $C_{ij}^2$  is the generalized cost of travel for hierarchical mode choice 2 between any two traffic analysis zones  $i$  and  $j$ .

The generalized cost is a function of travel cost and travel time. For public transport, the cost is the total fare including any access fare to the main transport mode. Travel time is the total time from the start of the trip to the end of the trip.

The mode split parameters for only the work trips representing twenty percent of all trips in Abidjan are depicted in Table 3. All four logit curves, A through to D are described for the four levels of economic activity level in Abidjan. In the model development, both trip generation and trip distribution were also prepared for three additional trip purposes namely school, shopping, and non-home trips. Each curve as

referenced in Table 4 is prepared four levels of economic activity. The levels of economic activity are directly related to the different levels of household income.

The measure of goodness of fit, in this case, is in the form of the  $R^2$  value which is considered within acceptable ranges for this form of model calibration.

Table 3 Mode split parameters for work trips

| Economic Activity Class | Curve A       |          |       | Curve B            |          |       |
|-------------------------|---------------|----------|-------|--------------------|----------|-------|
|                         | (Mode 1=walk) |          |       | (Mode 2=private)   |          |       |
|                         | $\lambda$     | $\delta$ | $R^2$ | $\lambda$          | $\delta$ | $R^2$ |
| Class 1                 | 0.46          | 3.9      | 0.60  | 0.01               | -32.6    | 0.62  |
| Class 2                 | 0.35          | 4.4      | 0.60  | 0.01               | -15.7    | 0.63  |
| Class 3                 | 0.44          | 2.7      | 0.60  | 0.01               | 72.6     | 0.60  |
| Class 4                 | 0.22          | 1.9      | 0.63  | 0.01               | -49.0    | 0.64  |
|                         | Curve C       |          |       | Curve D            |          |       |
|                         | (Mode 3=car)  |          |       | (Mode 4=non fixed) |          |       |
|                         | $\lambda$     | $\delta$ | $R^2$ | $\lambda$          | $\delta$ | $R^2$ |
| Class 1                 | .005          | -478     | 0.63  |                    | -234     | 0.59  |
| Class 2                 | .019          | 200      | 0.85  | 5*                 | -48      | 0.58  |
| Class 3                 | .005          | 152      | 0.61  | $10^{-3}$          | 184      | 0.58  |
| Class 4                 | -.01          | 183      | 0.57  |                    | -252     | 0.99  |

#### Model Calibration

Before a model is usable, it must reproduce the existing situation. If it can reproduce the existing situation within reasonable limitations, it is thus deemed a calibrated model.

In the case of the Abidjan modal split model, as seen in Table 4, there is a close estimation of both the mode split at the macro level for public transport and the three individual sub- modal levels. The maximum difference even at the sub-modal level is only seven percent.

Table 4 Calibration Comparison

| Mode       | Percentage Difference |
|------------|-----------------------|
| Walk       | 0.3                   |
| Private    | -4.8                  |
| All Public | 6.3                   |
| Bus        | 4.8                   |
| Gbaka      | 2.2                   |
| Woro-Woro  | 7.2                   |

In addition, in the calibration phase, it is common to compare traffic movement across a screenline. Four such screenlines were defined within the city. All four screenlines reflected a good match between observed and estimated traffic. The comparison was within ten percent.

## THE ANALYSIS

The focus of this research is on the modal shift or in overall terms the maintenance of the modal balance by the reversal of the decline in public transport share. However, prior to the modal allocation step, there is as previously discussed the trip generation and distribution of the movement of people. Person movements are estimated by traffic zone via a relationship linking population and economic activity.

The cost and time of travel are the key inputs into the mode split model, Eq. (1). The travel time includes all portions of the public transport travel thus incorporating travel by the main mode in addition to access, waiting time, transfer time and any modal boarding penalties.

The movement pattern that meets the objective of improvement in transport within Abidjan is the incorporation of corridor movements and a local ladder pattern providing residential access from the main corridor movements. This combination forms an integrated pattern as depicted in Fig 8. is then the input for analysis within the structure of the transport model.

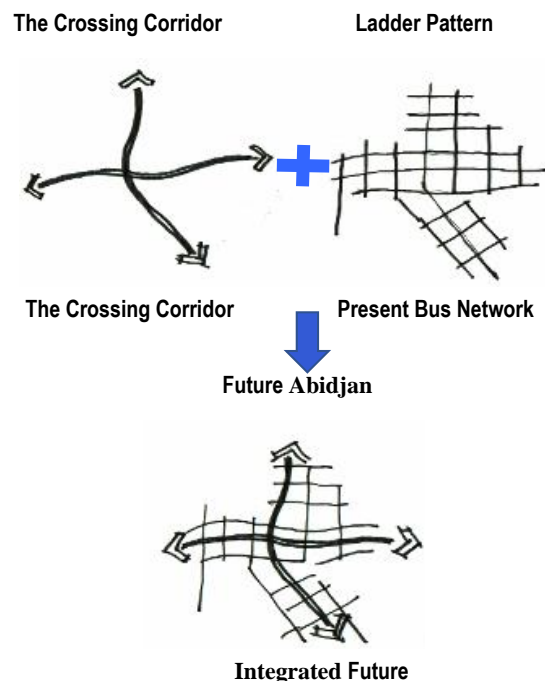


Fig. 8 Future public transport integration.

The decline in public transport is halted in the future as reported in Table 5 resulting from an integrated approach to public transport. In terms of physical infrastructure, this is achieved in the additional investment in public transport of the East-West transit corridor linking the communes of Yopougon and the Plateau and the North-South corridor linking the communes of Abobo and Port

Bouet as depicted in the earlier Fig. 5.

Table 5 Modal shift

| Mode    | 2015 | 2030 |
|---------|------|------|
| Walk    | 39.8 | 34.8 |
| Private | 10.1 | 13.8 |
| Public  | 50.1 | 51.4 |

The informal sector is also reduced in the future with the forecasted estimated modal share of Woroworo by nearly thirty percent. This is a result of a better environment and improved transit efficiency.

## RESULTS AND CONCLUSIONS

The trigger for the upgrading of public transport services in Abidjan is the introduction of the high capacity transit corridors namely the introduction of Bus Rapid Transit (BRT) and a Bus Higher Level of Service (BHLS) as depicted in Fig. 9. Without these services, there will be little incentive for public transport improvement. The purchase of additional SOTRA buses will improve the status of SOTRA.

This purchase will enable additional services on their existing line haul routes in the short term. Whilst at later stages of the public transport timeline when buses are released from this role as the high capacity transit corridors come on line, SOTRA will then have the ability to use buses to access these high capacity transit corridors. SOTRA will provide new services to access as well as outlying centers not served by BRT or BHLS.

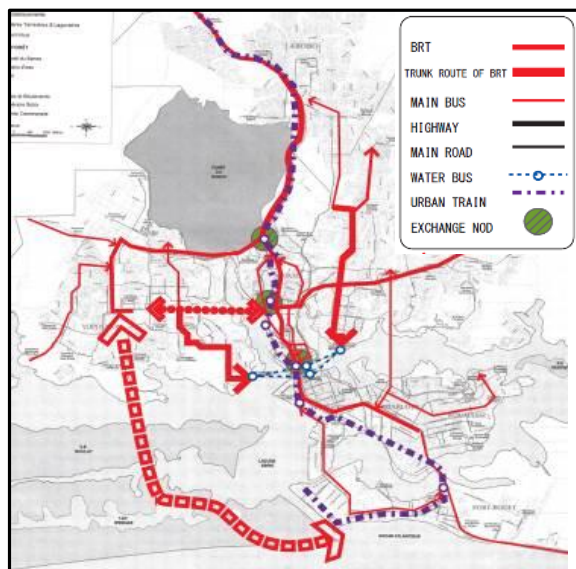


Fig. 9 Future public transport structure.

A new proposed regulatory authority will not only be responsible for the standard of operational service and ensure service. It must also have a role in the

insurance of the safety and maintenance of public transport in Abidjan. The future will demand a high level of training of staff of the new services in Abidjan. It is thus recommended that the new operators and relevant agencies provide a high level of in-house training.

Additional infrastructure in conjunction with an updated regulatory framework will move Abidjan towards the maintenance of public transport mode.

## Feasibility of Green Modal Shift

There is an anticipation of halting the decline in public transport in the future as a result of the introduction of a more efficient and environmentally friendly or greener form of transport for Abidjan. The movement towards an efficient and greener transport system is also in accordance with supporting the Paris climate accords.

## ACKNOWLEDGEMENTS

The authors acknowledge the support of the government of Côte d'Ivoire and the Japan International Cooperation Agency (JICA) in the preparation of existing datasets and the development of the analytical tools.

All ideas and views expressed in this paper are those of the authors. They do not necessarily reflect any of the sponsoring authorities of projects discussed in this paper or any organizations associated with the respective authors.

## REFERENCES

- [1] Johnstone L. and Ratanavaraha V, Green Freight Movement: The Dilemma of the Shifting of Road Freight to Alternatives. *Transportation Research Procedia*, 2017. 21: p. 154-168.
- [2] Klein D.R., Carazo M.P., Doelle M., Bulmer J. and Higham A., The Paris agreement on climate change: analysis and commentary. 2017, Oxford, United Kingdom: Oxford University Press. xxxii, 435 pages.
- [3] Japan International Cooperation Agency (JICA), and Ministry of Construction, Sanitation, and Urban Development (MCLAU) of Cote d'Ivoire, The Project of the Urban Master Plan in Greater Abidjan (SDUGA). 2014.
- [4] Arvin-Rad H., Basu A.K., and Willumsen M., Economic reform, informal-formal sector linkages and intervention in the informal sector in developing countries: A paradox. *International Review of Economics & Finance*, 2010. 19(4): p. 662-670.
- [5] World Bank, Project Information Document/ Integrated Safeguards Data Sheet (PID/ISDS). 2013.
- [6] Union Internationale des Transports



- Publics( UITP), Public Transport in Sub-Saharan Africa Major Trends and Case Studies. 2010.
- [7] Johnstone L.C. and Chanchaen N., Workshop & Lectures on Sustainable Multimodal Transport & Urban Development: with Evaluation of Transport Projects, Land Use Mix and Supply Controls 2010, Griffith University, Australia.
- [8] Yagi S. and Shiraishi H., Policy Analysis for New Commuter Rail and Road Pricing Alternatives Using an SP Survey in Abidjan. 2017. 25: p. 2524-2539.
- [9] Ortuzar J. de D., On the development of the nested logit model. Transportation Research 2001. 35B: p. 213-216.
- [10] Johnstone L. and Ratanavaraha V., Viability of high speed rail alternatives in southern India Proceedings of 2016 Australian Transport Research Forum Conference, 2016.

## PRELIMINARY RESULTS OF SITE-SPECIFIC GROUND RESPONSE ANALYSIS

Bambang Setiawan<sup>1</sup>, Taufiq Saidi<sup>2</sup> and Mark B. Jaksa<sup>3</sup>

<sup>1</sup>Program Studi Teknik Geologi, Fakultas Teknik, Universitas Syiah Kuala, Indonesia

<sup>2</sup>Jurusan Teknik Sipil, Fakultas Teknik, Universitas Syiah Kuala, Indonesia

<sup>3</sup>School of Civil, Environmental and Mining Engineering, the University of Adelaide, Australia

### ABSTRACT

The city of Banda Aceh-Indonesia is extremely exposed to a significant seismic hazard. There are three main seismic sources around the city which are the tectonic subduction, the great Sumatran fault, and the West Andaman fault. Thus, seismic microzonation study of the Banda Aceh city is urgently required for any mitigation efforts. Site-specific ground response analysis was carried at eleven sites in the city of Banda Aceh. An analytical model of the equivalent-linear model was used to achieve ground response analysis. This analytical model of the equivalent-linear approach has demonstrated that they can simulate reasonably well the alteration of seismic ground motions on the ground surface. Three actual historical time histories recorded at rock site nearby the city of Banda Aceh and eleven developed sub-surface models in the city of Banda Aceh were used to estimate the seismic characteristics i.e. the peak ground acceleration, peak ground velocity, fundamental frequency, and estimated site amplification of the investigated sites. Furthermore, both spectral velocity and acceleration of the investigated sites also are proposed.

*Keywords: Seismic, Peak ground acceleration, Fundamental frequency, Site amplification, Banda Aceh*

### INTRODUCTION

The city of Banda Aceh-Indonesia is a coastal capital city of the Province of Aceh located in Northern tip of Sumatra. It is a moderately sized city with an area of 59 km<sup>2</sup> and a population of 300,000 people. The city is located on the delta of Krueng Aceh river. It is surrounded by the district of Aceh Besar on the North-East to South-West and Malacca Strait on the North-West. The city is relatively close to three seismic source zones of the tectonic subduction of Indo-Australian and Eurasian Plates, the great Sumatran fault, and the West Andaman fault. Recently the tectonic subduction seismic source zone has produced several seismic strong events such as the 2004 Aceh earthquake (9.2 Mw), 2005 Nias earthquake (8.7 Mw), 2007 Bengkulu earthquake (8.5 Mw), and 2010 Mentawai earthquake (7.8 Mw). The 2004 Aceh earthquake is suggested by National Geographic as the second worst hazard of all the time [1]. This event affected 14 countries, caused more than 220.000 casualties, caused displacement of more than 1.5 million people, and caused economic losses of 10 billion USD [1]. The subduction of Indo-Australian plate under the Eurasian plate at the west of Sumatra has produced 19 main fault segments with a length of 60 ~ 200 km on the shore of Sumatra [2] which is well known as the great Sumatran fault (GSF) [3]. This fault is identified as a dextral-lateral fault with an estimated length of ±1900 km stretched from Banda Aceh to Sunda Strait. Several

earthquakes along this GSF are 1892 earthquake around Lembah Batang Gadis and Batang Angkola, 1903 Kerinci earthquake [4]. The displacement of each GSF's segment has been measured and calculated using GPS geodetic. A raw estimation of the segments near the city of Banda Aceh i.e. Seulimeum-Aceh-Tripa segments is between about 20 mm/year and 16 mm/year [1].

The tectonic setting of Andaman and the surrounding area is very complex and under research scrutiny [5]-[7]. West Andaman Fault was interpreted as a lateral fault by [8] but proposed as thrust fault by [9]. This West Andaman fault can be correlated to Deligent fault at north and Mentawai fault at the south [10], [11]. Thus, these three faults form a fault zone along Andaman-Sumatra.

The city of Banda Aceh is founded on thick Holocene Alluvium [12] and classified in highly seismic hazard risk [1]. In a recent study on Indonesian seismic hazard assessment [1], the city of Banda Aceh can experience high peak ground accelerations during an earthquake [1]. Furthermore, based on the deterministic seismic hazard analysis studies, the city of Banda Aceh exposes to disastrous onshore seismic with 7.5 magnitude potential value [13]. Therefore, detailed estimation of local site effects is required for the city of Banda Aceh. For this, microtremor measurement at 11 locations across the city of Banda Aceh was carried out. Subsurface and geotechnical data collected from various agencies were collected. These data were used to develop the

sub-surface profiles in the study.

Commonly local ground response effect is examined using one dimensional (1D) model to investigate the sub-surface local characteristics during an earthquake. The basic assumption of this 1D model is the propagation of seismic waves in vertical directions through the horizontal layers of the soil which can be solved using Equivalent-linear or nonlinear analyses. In practice, equivalent-linear ground response analysis is widely used to simulate true nonlinear soil behavior because the model requires small computational effort and few input parameters [14]. The computational process of this equivalent-linear analysis is outlined in [15]. In this study, the effects of local soil conditions on earthquake ground motions have been estimated by carrying out detailed 1D equivalent linear wave propagation analysis using EERA software [14]. The results are useful for structural engineers, town planners, and the government in any mitigation strategy. The results also can be used for carrying out more advance soil-structure dynamic analysis.

## REVIEW OF PREVIOUS STUDIES

Polom et al. [16] carried out shallow shear wave reflection seismic measurements in Krueng Aceh River basin under the project Management of Georisk (MANGEONAD) of the Federal Institute for Geosciences and Natural Resources (BGR), Hanover, German. Several near-surface shear wave velocity profiles of the city of Banda Aceh were produced. Setiawan & Kusuma [17] was enhancing the results of [16] to estimate local ground response during the 2004 Aceh earthquake. A detailed study of the near-surface shear wave velocity of the city of Banda Aceh was carried out by [18] using multichannel analysis of surface waves (MASW) method at 49 locations. Seismic site classification based on Indonesian standard of SNI 1726-2012 for the city of Banda Aceh was deduced and proposed. Most of the sites in the city of Banda Aceh are classified as seismic site class between E and D in accordance to SNI 1726-2012, which suggests class D for  $V_{s,30}$  less than 175m/s and D for  $V_{s,30}$  from 175 m/s to 350 m/s.

In 2018 Saidi et al. [19] simulated typical shophouse buildings in the city Banda Aceh using response spectra curve. Yunita et al. [20] investigated the seismic site amplification of the city of Banda Aceh's soft soil. This investigation suggested the ground motions amplification of Banda Aceh's soils of up to 4.3.

## METHODOLOGY

The methodology of this study in the simplest procedure can be outlined in the following main steps: (1) to collect the secondary and primary data,

(2) to develop the sub-surface profile models for computer programs, (3) to run the computer program, and (4) to deduce and interpret the results. The overall methodology is outlined in Fig. 1. Several main input data are required in the ground response analysis. In this study these inputs are classified into three categories:

- Site sub-surface model development includes soil type, thickness, unit weight, shear wave velocity, and water level. In this study one-dimensional (1D) sub-surface model is developed for the site response analysis at 11 locations in the city of Banda Aceh. Field ambient noise measurements were carried out at the 11 sites from which the sub-surface profiles at the measured site were deduced (Fig. 2). Other related sub-surface data in the city of Banda Aceh are also elaborated in the development of the 1D sub-surface profile.
- Dynamic soil type characterization includes the assessment of dynamic soil properties either by laboratory experimentations of the soil taken from the investigated site or by standard curves and correlations. Modulus reduction and damping ratio curves have been selected based on the different type of soil properties. In the absence of the development of the site-specific modulus reduction and damping ratio curves, standard curves proposed in EERA were applied.
- Earthquake ground motion time histories justification comprises the selection of acceleration time histories based on either factual time histories or the generation of the synthetic ones. Generally, the selected time histories are in line with the expected earthquake hazard in the study area. The selection of the factual earthquake ground motion or the generation of synthetic seismic ground motion is the final step in ground response analysis. This generating or selecting an acceleration time history must be compatible with the expected maximum dynamic loading at the site of interest. The selection of the suitable acceleration time histories can be based on expected peak ground acceleration (PGA) value, maximum earthquake magnitude, distance of the expected most disastrous seismic or seismic site class. This study is based on the factual acceleration time histories data and ignoring this selection of the suitable acceleration time history process. Three recorded at rock site near the city of Banda Aceh acceleration time histories of 2012 Simeulue earthquake, the 2013 Mane-Geumpang earthquake, and the 2013 Bener Meriah earthquake were collected from BMKG earthquake data repository (Table 1). The distance of these seismic events from the city of

Banda Aceh are 613km, 45km, and 181km for 2012 Simeulue earthquake, the 2013 Mane-Geumpang earthquake, and the 2013 Bener Meriah earthquake, consecutively.

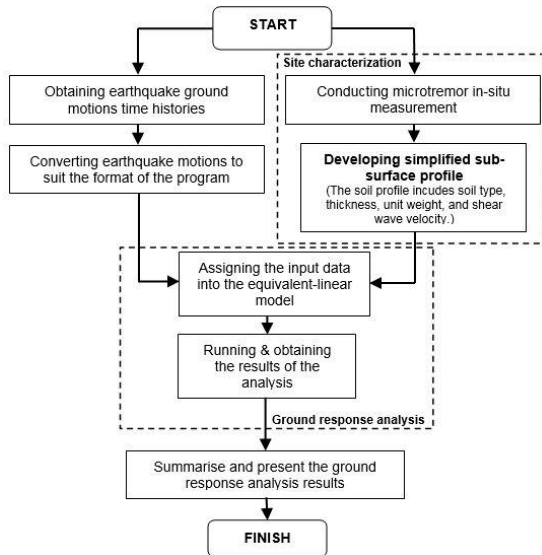


Fig. 1 The methodology of site response analysis.



Fig. 2 Microtremor field measurement campaign in the city of Banda Aceh.

Table 1 Three historical seismic Events Used in This Site Response Analysis

| Event name                             | Epicenter coordinates | Magnitude | Depth (km) |
|--|-----------------------|-----------|------------|
| 7:43:11 on 11-04 2012<br>Simeulue      | N 0.82 & 92.42 E      | 8.1       | 24         |
| 05:22:42 on 22-01-2013<br>Mane-Gempang | N 5.49 & 95.21 E      | 6.0       | 84         |
| 14:37:03 on 02-07-2013<br>Bener Meriah | N 4.70 & 96.61 E      | 6.2       | 10         |

## RESULTS

The results presented in these following sections are deduced from the ambient noise data analysis and seismic ground response analysis.

## Seismic Site Classification

Generally, it is recommended to use the actual near-surface shear wave velocity in seismic site classification [21]. These factors are based on the average shear wave velocity of the top 30m of the soil profile ( $V_{s,30}$ ). Average  $V_{s,30}$  for the soil profile can be calculated using the following equation:

$$\overline{V_{s,30}} = \sum V_{si} \times \left( \frac{d_i}{30} \right) \quad (1)$$

where  $V_{si}$  is shear wave velocity at the  $i$ -th layer and  $d_i$  is the thickness of the  $i$ -th layer.

As aforementioned the near-surface shear wave velocity is inverted using joint inversion of HVSr curve and site fundamental frequency. It has been observed in this study that all of the investigated sites come under site class D based on SNI-1726-2012 with the average  $V_{s,30}$  value for the profiles ranging from 203 to 235 m/s. These seismic site classification outputs were compared with the results of a study by [18]. This study is slightly overestimated the seismic site classes of [18]. This study classifies seismic site class D for all the investigated sites, but [18] suggested seismic site class E for sites #2-Jaw, #3-Smk, #5-Lam, #08-Pad, and #10-Lon. The detailed comparison is presented in Table 2.

Table 2 Results of the site response analysis

| Site name | $V_{s,30}$ in m/s, (Seismic site class) |     |                   |       |
|-----------|---|-----|-------------------|-------|
|           | This study                              |     | Muzli et al. [18] |       |
| #1-Tib    | 205                                     | (D) | 196 or 142        | (D/E) |
| #2-Jaw    | 218                                     | (D) | 173               | (E)   |
| #3-Smk    | 235                                     | (D) | 148               | (E)   |
| #4-Uns    | 203                                     | (D) | -                 | -     |
| #5-Lam    | 213                                     | (D) | 151               | (E)   |
| #6-Ill    | 217                                     | (D) | 175               | (D)   |
| #7-Bat    | 219                                     | (D) | 201               | (D)   |
| #8-Pad    | 210                                     | (D) | 148               | (E)   |
| #9-Inie   | 227                                     | (D) | 238 or 220        | (D)   |
| #10-Lon   | 205                                     | (D) | 151               | (E)   |
| #11-Pie   | 227                                     | (D) | -                 | -     |

Note: The seismic site classification is based on SNI 1726-2016.

## Seismic Ground Response Analysis

Seismic ground response analysis was carried out for 11 sites in the city of Banda Aceh. The main results of site-specific ground response analysis using the EERA model are presented in Tables 3 to 5. The highest peak ground velocity (PGV) of 0.5m/s is estimated at Site #08-Pad. The most peak ground acceleration (PGA) of 0.07g is predicted at two sites of Site #03-Smk and Site #10-Lon. Site fundamental

frequency for the city of Banda Aceh is estimated between 0.2 to 1.1 Hz. The highest maximum spectral velocity and maximum spectral acceleration are estimated at Site #03-Smk of 0.26cm/s and Site #10-Lon of 0.29g, respectively. In this study, the seismic motion acceleration at the ground surface was compared with the acceleration at the expected site's basement. The result is to deduce the site amplification which suggests from 3.5 to 4.9 in the city of Banda Aceh. The spatial distribution of the site-specific ground response analysis results at the city of Banda Aceh is presented in Fig. 3 to Fig. 8.

Table 3 Results of the site response analysis

| Site name | PGV Soil<br>(m/s) | PGA Soil<br>(g) |
|-----------|-------------------|-----------------|
| #1-Tib    | 0.04-0.08         | 0.03-0.06       |
| #2-Jaw    | 0.03-0.04         | 0.03-0.06       |
| #3-Smk    | 0.03-0.04         | 0.03-0.07       |
| #4-Uns    | 0.4               | 0.03-0.06       |
| #5-Lam    | 0.3-0.4           | 0.02-0.06       |
| #6-III    | 0.3-0.5           | 0.03-0.06       |
| #7-Bat    | 0.3-0.4           | 0.03-0.06       |
| #8-Pad    | 0.4-0.5           | 0.03-0.06       |
| #9-Inie   | 0.3               | 0.03-0.06       |
| #10-Lon   | 0.3-0.4           | 0.04-0.07       |
| #11-Pie   | 0.3               | 0.03-0.06       |

Table 4 Results of the site response analysis

| Site name | Max. spectral<br>velocity<br>(cm/s) | Max. spectra<br>acceleration<br>(g) |
|-----------|-------------------------------------|-------------------------------------|
| #1-Tib    | 0.09-0.18                           | 0.12-0.22                           |
| #2-Jaw    | 0.10-0.15                           | 0.11-0.22                           |
| #3-Smk    | 0.12-0.26                           | 0.11-0.23                           |
| #4-Uns    | 0.14-0.25                           | 0.11-0.23                           |
| #5-Lam    | 0.15-0.22                           | 0.10-0.22                           |
| #6-III    | 0.14-0.24                           | 0.10-0.25                           |
| #7-Bat    | 0.11-0.17                           | 0.10-0.24                           |
| #8-Pad    | 0.16-0.22                           | 0.10-0.21                           |
| #9-Inie   | 0.10-0.15                           | 0.10-0.27                           |
| #10-Lon   | 0.14-0.23                           | 0.13-0.29                           |
| #11-Pie   | 0.11-0.15                           | 0.10-0.20                           |

## CONCLUSIONS

Local site effect on earthquake ground motions has been investigated for sites in the city of Banda Aceh (Indonesia) by carrying out detailed 1D equivalent linear ground response analysis. Actual acceleration time histories of Simeulue earthquake (2012), Mane-Geumpang earthquake (2013), and

Bener Meriah earthquake (2013) have been taken as input ground motions. Based on the analysis of the results obtained in this study, the following conclusions have been drawn:

- All the 11 sites have been classified as per the provisions SNI 1726-2012. All the measured sites have been classified as seismic site class D.
- The site fundamental frequency has been observed from 0.2 and 1.1 Hz.
- The amplification factors of the soils in the city of Banda Aceh have been observed in the range of 3.5 and 4.7.

The site fundamental frequency and amplification factor developed in this study can be used for the dynamic analyses of important structures in the city of Banda Aceh.

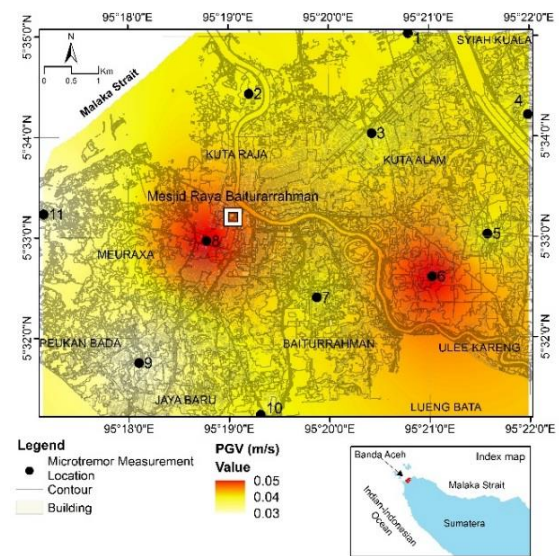


Fig. 3 Estimated maximum peak ground velocity at the city of Banda Aceh.

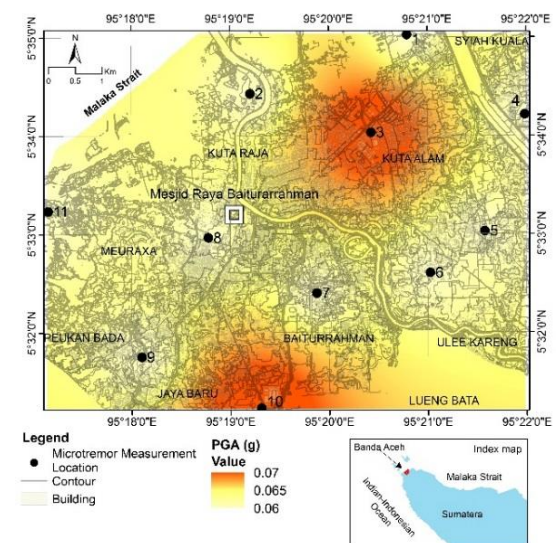


Fig. 4 Estimated maximum peak ground acceleration at the city of Banda Aceh.



Table 5 Results of the site response analysis

| Site name | Fund. Frequency (Hz) |      | Max AF |
|-----------|----------------------|------|--------|
|           | Theoretical          | Exp. |        |
| #1-Tib    | 0.4                  | 0.3  | 4.2    |
| #2-Jaw    | 0.4                  | 0.4  | 3.9    |
| #3-Smk    | 0.4                  | 0.4  | 4.0    |
| #4-Uns    | 0.4                  | 1.1  | 3.6    |
| #5-Lam    | 0.4                  | 0.6  | 3.6    |
| #6-Ill    | 0.4                  | 0.4  | 3.5    |
| #7-Bat    | 0.4                  | 0.4  | 4.1    |
| #8-Pad    | 0.4                  | 0.2  | 4.6    |
| #9-Inie   | 0.4                  | 0.4  | 4.0    |
| #10-Lon   | 0.4                  | 0.6  | 4.7    |
| #11-Pie   | 0.4                  | 0.4  | 3.5    |

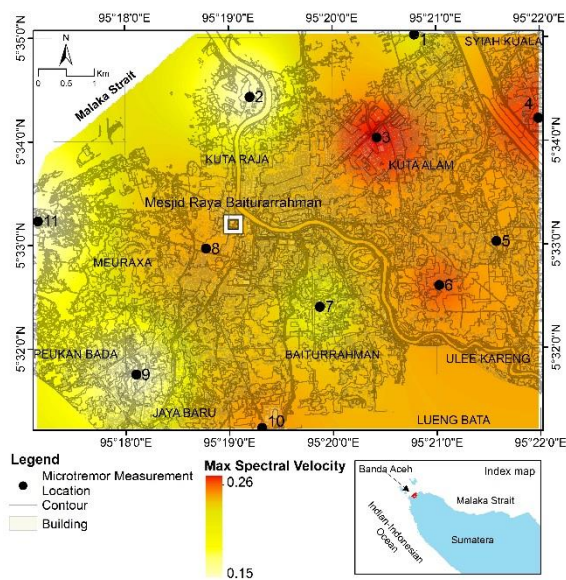


Fig. 5 Estimated maximum spectral velocity at the city of Banda Aceh.

## ACKNOWLEDGMENTS

We acknowledge the help and assistance given by Universitas Syiah Kuala for the study under H-Index Research Scheme Year 2019 of Universitas Syiah Kuala (Contract No. 523/UN11/SPK/PNPB/2019 on date 8 February 2019). Also, the authors are grateful to the Fakultas Teknik Universitas Syiah Kuala for their support

## REFERENCES

- [1] M. Irsyam, S. Widiyanto, D. Natawidjaja, I. Meilano, A. Rudyanto, S. Hidayati, W. Triyoso, N. Hanifa, D. Djarwadi, L. Faizal, S. Sunarjito. Peta Sumber & Bahaya Gempa Indonesia tahun 2017. Pusat Penelitian & Pengembangan Perumahan dan Permukiman, Badan Penelitian

& Pengembangan, Kementerian Pekerjaan Umum & Perumahan Rakyat, 2017, ISBN: 978-602-5489-01-3.

- [2] K. Sieh, D. Natawidjaja, Neotectonics of the Sumatran fault, Indonesia, J. Geophys. Res. 105 (28), 2000, pp.295-326.
- [3] O. Bellier, S. Sébrier, T. Pramumijoyo, H. Beaudouin, I. Harjono, Bahar, O. Fomi. Paleoseismicity and seismic hazard along the Ornat Sumatran Fault (Indonesia), J. Geodyn., 24, 1997, pp.169-183.
- [4] S. G. Wichmann. Die erdbeben des indischen Archipels bis zum Jahre 1857. Amsterdam, Muller, 1918.

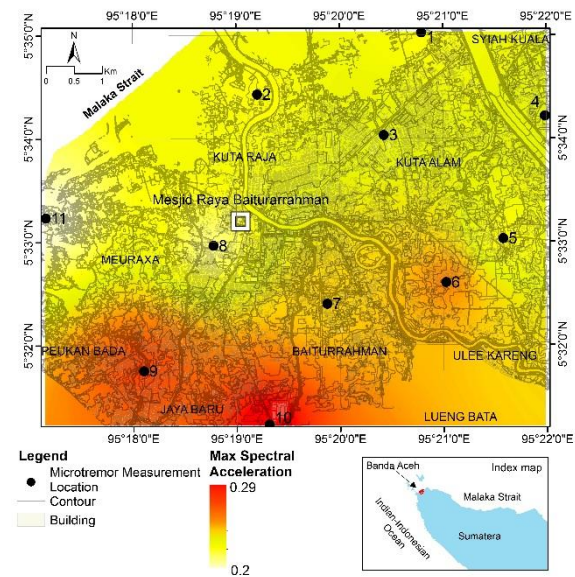


Fig. 6 Estimated maximum spectral acceleration at the city of Banda Aceh.

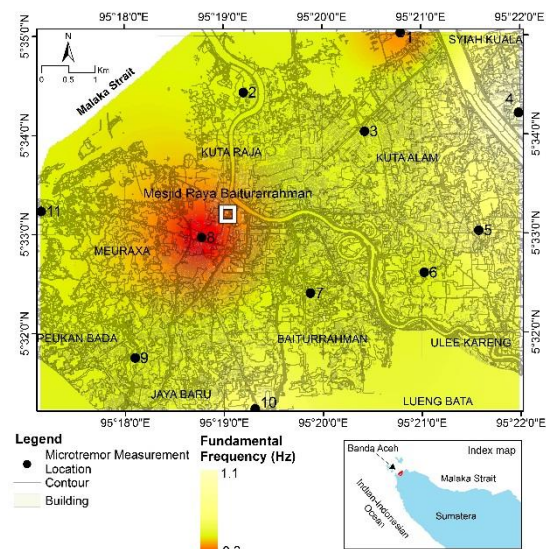


Fig. 7 Estimated site fundamental frequency at the city of Banda Aceh.

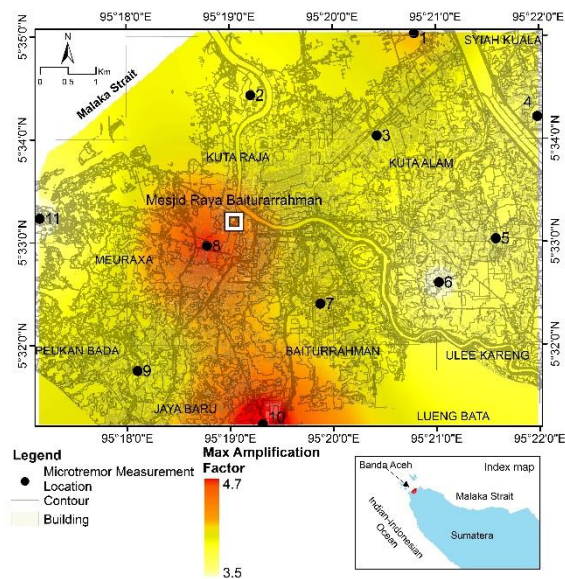


Fig. 8 Estimated maximum amplification factor at the city of Banda Aceh.

- [5] J. R. Curray. Tectonics and history of the Andaman sea region. *J. Asian Earth Sci.* 25(1), 2005, pp. 187-232.
- [6] S. C. Singh, R. Moeremans, J. McArdle, K. Johansen. Seismic images of the sliver strike-slip fault and backthrust in the Andaman-Nicobar region. *J. Geophys. Res.* 118, 2013, pp.1-17.
- [7] C. K. Morley, A. Alvey. Is spreading prolonged, episodic or incipient in the Andaman sea? Evidence from deepwater sedimentation. *J. Asian Earth Sci.* 98, 2015, pp.446-456.
- [8] A. Izart, B. M. Kemal, J. A. Malod. Seismic stratigraphy and subsidence evolution of the northeast Sumatra fore-arc basin. *Mar. Geol.* 122, 1994, pp.109-124.
- [9] A. P. Chauhan, S. C. Singh, N. D. Hananto, H. Carton, F. Klingelhoefer, J. -X. Dessa, H. Permana, N. J. White, D. Graindorge. Seismic imaging of forearc backthrust at Northern Sumatra subduction zone. *Geophys. J. Int.* 179(3), 2009, pp.1772-1780.
- [10] S. C. Singh, N. D. Hananto, A. P. Chauhan, H. Permana, M. Denolle, A. Hendriyana, D. Natawidjaja. Evidence of active backthrusting at the NE Margin of Mentawai Islands, SW Sumatra. *Geophys. J. Int.* 180(2), 2010, pp.703-714.
- [11] M. Mukti, S.C. Singh, I. Deighton, N. D. Hananto, R. Moeremans, H. Permana. Structural evolution of backthrusting in the Mentawai fault zone, offshore Sumatran forearc, *Geochem. Geophys. Geosystems*, 13(12), 2012, pp.1-12.
- [12] B. Siemon, D. Ploethner, J. Pielawa. Hydrogeological Reconnaissance Survei in the Province Nanggroe Aceh Darussalam Northern Sumatra, Indonesia Survei Area: Banda Aceh/Aceh Besar 2005, Report C1, BGR (Federal Institute for Geosciences and Natural Resources), 2006.
- [13] M. Petersen, J. Dewey, S. Hartzell, C. Mueller, S. Hansen, A. Frankel, K. Rukstales. Probabilistic seismic hazard analysis for Sumatra, Indonesia and across the southern Malaysian peninsula, *Tectonophysics*, 390, 2001, pp.141-158.
- [14] J. Bardet, K. Ichii, C. Lin. EERA a computer program for Equivalent-linear Earthquake site Response Analyses of layered soil deposits. Department of Civil Engineering, University of Southern California, 2000.
- [15] P. Schnabel, J. Lysmer, H. Seed. A computer program for earthquake response analysis of horizontally layered sites, *Earthquake Engineering Research Center (EERC) Report 72-12*, 1972, Berkeley, California: University of California.
- [16] U. Polom, I. Arsyad, H. Kumpel. Shallow shear-wave reflection seismics in the tsunami struck Krueng Aceh River Basin, Sumatra. *Adv. Geosci.*, 14, 2008, pp.135-140.
- [17] B. Setiawan, W. B. Kusuma. Propagation of seismic waves in an anisotropic media due to a point source. Seventh International Conference in Geotechnical Engineering, Chicago, USA, 29 April – 4 May 2012, 2012.
- [18] Muzli, A. Rudyanto, A.P. Sakti, F. S. Rahmatullah, K. R. Dewi, E. Santoso, M. Muhajirin, S. Pramono, R. P. Mahesworo, A. Jihad, T. Ardiyansyah, L. A. Satria, R. N. Akbar, R. Madijono. Studi klasifikasi tanah permukaan untuk wilayah Banda Aceh. *Prosiding Seminar Nasional Aplikasi Sain dan Teknologi pada Pengurangan Resiko Bencana*, Banda Aceh, 22 November 2014, 2014.
- [19] T. Saidi, T. B. Aulia, B. Setiawan, N. Abdullah, M. Hasan. Spectral displacement (SD) of banda aceh's soft soil for seismic vulnerability assessment. *MATEC Web of Conferences*, 197, 10001, 2018.
- [20] H. Yunita, B. Setiawan, T. Saidi, N. Abdullah. Site response analysis for estimating seismic site amplification in the case of Banda Aceh – Indonesia. *MATEC Web of Conferences*, 197, 10002, 2018.



## STUDY OF SEEPAGE THROUGH AN EARTH DAM CASE STUDY (AJDABIYA RESERVOIR)

Prof . Salem Al- Sanusi, Mervat J. M. Alarosh  
FACULTY OF ENGINEERING , University of Benghazi, LIBYA

### ABSTRACT

The objective of this study is to determine how leakage through a lining system would affect the design of blanket toe drains in an earth dam. Toe drains decrease the pore pressure at the downstream face and keep the seepage line (or phreatic surface) below the downstream boundary. Simulations will be conducted to determine the location of the phreatic surface in a homogeneous dam due to the presence of defects in liner. Numerical simulations will be performed using GEOSTUDIO to determine the length of the toe drain needed to prevent seepage from occurring on the downstream face of the dam. In addition, the effect of the elevation of the phreatic surface within the dam on the stability of the downstream face of the dam will be considered in analysis. The study will also provide the benefits of using a geomembrane liner regarding the stability and toe drain in the earth dams.

*Keywords: leakage, Seepage, Homogeneous, Numerical simulations, Geostudio.*

### INTRODUCTION

Seepage within and under the embankment must be controlled to prevent concealed internal erosion and migration of fine materials, or external erosion and sloughing. With the homogeneous embankment of dam, the buildup of excess pore pressures within the embankment and seepage has been a problem, especially for a reservoir having high, or rapidly fluctuating water levels for long periods; or for a dam having impervious foundation. If seepage is excessive, this can lead to instability and eventual failure of all or part of the downstream face [1]. Seepage through an earth dam is the continuous movement of water from the upstream face toward its downstream face. The top seepage line of percolating water is known as the phreatic surface. In order to allow adequate embankment and to eliminate seepage problems in the downstream areas of an embankment on impervious foundation, the phreatic surface should be kept within the dam by providing a horizontal drainage filter. The amount of water seeping through and under an earth dam, together with the location of the phreatic surface, can be estimated by considering the flow through porous media. The Laplace equation which governs water seepage cannot be solved analytically, except for cases with very simple and special boundary conditions. Therefore, researchers have invoked to empirical, graphical and recently numerical methods. Several methods have been developed to solve exactly or approximately Laplace's equation for various cases of seepage. One of the most widely used methods, the flow net, can be adapted to many of the under seepage and through-seepage problems found in dams and other projects involving hydraulic structures. The seepage of flow through earth dams was studied analytically by a number of researchers

[2,3,4]. Numerical models are used to make acceptable approximations for the Laplace equation in complex flow conditions. The methods of numerical solution, such as finite element finite difference, finite volume and boundary element, were used to analyze the phenomenon of seepage through earth dams. [5,6,7].

### LITERATURE REVIEW

Darcy (1856) gave the basic law of flow through porous media through his series of experiments on vertical pipe filled with sand. Darcy's Law was originally derived for saturated soil, but later research has shown that it can also be applied to the flow of water through unsaturated soil (Richards, 1931 and Childs & Collins-George, 1950). The only difference is that under conditions of unsaturated flow, the hydraulic conductivity is no longer a constant, but varies with changes in water content and indirectly varies with changes in pore water pressure. Various methods are available for seepage analysis which may be classified as analytical, experimental and numerical methods. various computer softwares are used nowadays which facilitates researcher to simulate the actual field conditions for performing seepage. Shivdakumar S. Athani et al. (2015) have presented the results of finite element modeling of the stability and seepage analyses of the earth dam using PLAXIS 3D software. Imran Arshad et al. (2014) have stated that seepage analysis of earth dam can be efficiently performed using finite element based SEEP/W software. This software is capable to estimate various parameters of flow net such as seepage discharge, exit gradient, seepage velocity, pore water pressure, uplift pressure at any desired point in flownet. Hasani et al reviewed safety of earthen dam

by performing using GEOSTUDIO software sub product Slope/W . G.V.Panthulu et al. (2001) have suggested that Geophysical methods can also be efficiently used for mapping seepage paths and monitoring the changes of the seepage with time. Kamanbedast et al. (2011) focused on need of using different methods to investigate the safety of dam so as to decrease any errors in calculation due to maintenance of water storage especially hydro structure of the dam.

## METHODOLOGY

According to the case study we classify the cases into lining or without lining .with max operation level of 8 m height .the dam used with toe draining system. the case study is then checked for different values of  $k$  from range of  $1E-06$  to  $1E-04$ . The methodology of the work is as shown in Fig(1).

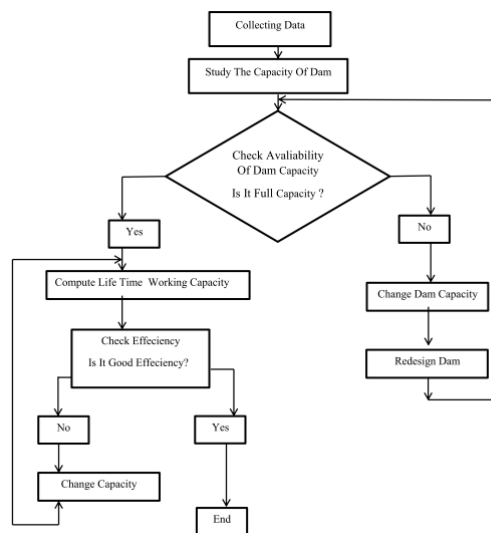


Fig. 1 The methodology

## SOFT WARE (SEEP/W Program)

SEEP/W (which is a sub-program of Geo-Studio) is a finite element software product for analyzing groundwater seepage and excess pore-water pressure dissipation problems within porous materials such as soil and rock. Its comprehensive formulation allows you to consider analyses ranging from simple, saturated steady-state problems to sophisticated, saturated and unsaturated time-dependent problems. SEEP/W can be applied to the analysis and design of geotechnical, civil, hydrogeological, and mining engineering projects . Many previous works studied different seepage problems by using SEEP/W program [4,5,6].

### Case Study Of Reservoir

In the following figures show the current state of the dam fig (2) , fig (3) does show the soil profile lining under reservoir and fig (4) does show the layered structure of the inner of the dam.

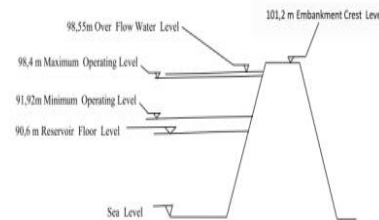


Fig. 2 Current state of the dam

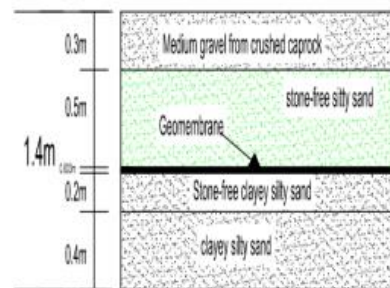


Fig. 3 Soil profile lining under reservoir

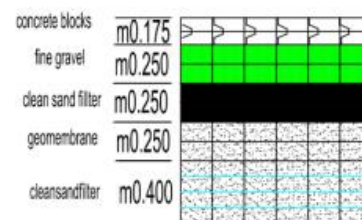


Fig. 4 Layered structure of the inner of the dam

## GOVERNING EQUATIONS

Following partial differential equation (PDE) is the governing equation used for modeling of SEEP/W program:

$$\frac{\partial}{\partial x} \left( k_x \frac{\partial H}{\partial x} \right) + \frac{\partial}{\partial y} \left( k_y \frac{\partial H}{\partial y} \right) + Q = \frac{\partial \theta}{\partial t} \quad (1)$$

Where,

$H$  = Hydraulic head

$K_x$  = hydraulic conductivity in  $x$  direction

$K_y$  = hydraulic conductivity in  $y$  direction

$Q$  = applied boundary flux

$t$  = time domain

$\theta$  = volumetric water content.

The Eq. (1) is time variant and states that 'the difference between the flow entering an elemental volume and leaving an elemental volume at a point is equal to the change in the volumetric water content in a particular time'.

If the volume of influx equals to the volume of out flux then the equation caters for steady state conditions, thus the right hand of the equation changes to zero.

$$\frac{\partial}{\partial x} \left( kx \frac{\partial H}{\partial x} \right) + \frac{\partial}{\partial y} \left( kx \frac{\partial H}{\partial y} \right) + Q = 0 \quad (2)$$

## RESULT DISCUSSION

In the operation of the Seep / W program in a earth dam containing a horizontal discharge system at a maximum operating level of 8 m using three different values of permeability ( $k$ ) (0.000001, 0.00001 and 0.0001 m / s) and its effect on leakage, pore water pressure , hydraulic gradient line and hydraulic conductivity

The change in the value of  $K$  for the different values affect the values of  $I$  ,  $P$  ,  $d$  and  $q$ . The next figures shows the variation of each variables.

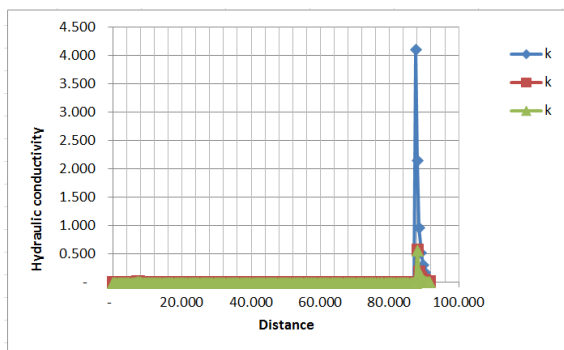


Fig.5. Variation of hydraulic conductivity along distance.

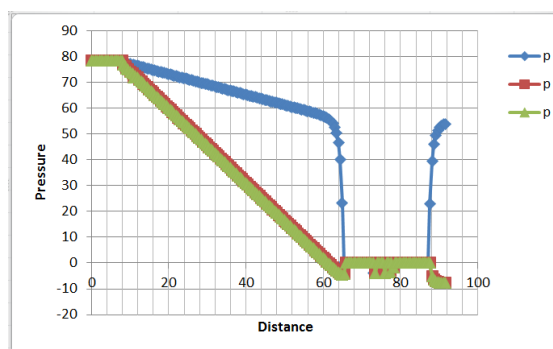


Fig.6. Variation of pressure along distance.

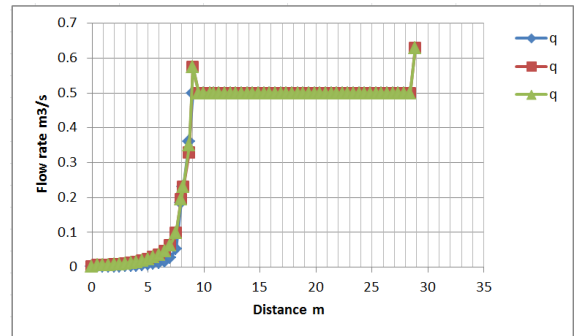


Fig.7.variation of flow rate along distance

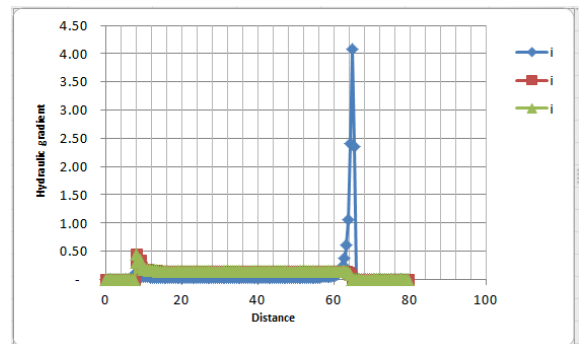


Fig.8. Variation of hydraulic gradient.

We note the following points for the variation of  $k$

1. The hydraulic conductivity is increased to about 4.3 at beginning point of filter zone.
2. The pressure dropped in the zone of filter .
3. The flow rate is gradually increased to the filter zone and then remain constant.
4. The hydraulic gradient is reach value of 4.4 at the start point of filter.

## CONCLUSIONS

From the study of the case study we conclude that.

- 1- The change of hydraulic conductivity is affect the hydraulic gradient , flow rate, pressure by effective value.
- 2- The flow rate under the dam is gradually changed under dam until it reaches certain value ( 0.5 m³/s).
- 3- The pressure is suddenly dropped in the draining system.
- 4- The hydraulic gradient is suddenly increased in the filter zone.

- 5- The max operation level of dam (8m) lead to max leakage of dam. So the more safe state operation of the system is advised to be 5m .
- 6- The increasing of the value of the filter zone the drop in pressure and the less critical values of each of flow rate and hydraulic gradient.

## REFERENCES

- [1] Imran Arshad and M.M. Baber ,“Finite Element Analysis of Seepage through an Earthen Dam by using Geo-Slope (SEEP/W) software, International Journal of Research (IJR), Vol-1, Issue-8, September 2014. ISSN: 2348- 6848.
- [2]Ms. Abhilasha P. S. And T. G. Antony Balan, “Numerical Analysis of Seepage in Embankment Dams”,IOSR Journal of Mechanical and Civil Engineering (IOSR-JMCE) e-ISSN: 2278-1684, p-ISSN: 2320-334X PP 13-23
- [3] Hasani, J. M’amizadeh and H. Karimi , “Stability of Slope and Seepage Analysis in Earth Fills Dams Using Numerical Models (Case Study: Ilam Dam- Iran), World Applied Sciences Journal 21 (9): 1398- 1402, 2013,ISSN 1818-4952.
- [4] Geo-Slope Software Example (2007),” Seepage through A Dam Embankment”.
- [5]Geo-Slope International Ltd, Calgary, Alberta, Canada.
- [6]Carastoian Andrea ,“Unsaturated Slope Stability and Seepage Analysis of a Dam” , Sustainable Solutions for Energy and Environment, EENVIRO - YRC 2015, 18-20 November 2015, Bucharest, Romania
- [7]Shivakumar S. Athani , Shivamanth, C. H. Solanki and G. R. Dodagoudar ,“Seepage and Stability Analyses of Earth Dam Using Finite Element Method”, International Conference On Water Resources, Coastal And Ocean Engineering (Icwrcoe 2015)

## **ANALYSIS OF SLOPE STABILITY (AJDABIYA RESERVOIR)**

Prof. Salem Al- Sanusi, Abier J. M. Alarosh  
FACULTY OF ENGINEERING, University of Benghazi, LIBYA

### **ABSTRACT**

The ability of geotechnical engineers to accurately model slope performance is affected by a variety of factors. This paper research explained about slope stability of earthen dams using GEOSTUDIO software. The main problem is that the exact behavior of slopes cannot be accurately predicted. Hence, geotechnical engineers resort to a factor of safety approach to reduce the risk of slope failure. Although, the factor of safety approach can not quantify the probability of failure associated with the design situation, it offers a conservative way to treat slope stability uncertainties. The uncertainties can be related quantitatively to the design reliability of a slope. The study of the factor of safety based design procedure, in which engineers can combine practical experience, judgment, and statistical information is beneficial for analyzing the stability of slopes for an allowable risk criterion. The objective of this research is to develop a general model of slope stability analysis [1] and the safety of dam in bearing and the settlement. The study is performed through different methods of analysis, the sensitivity analysis is then applied to the output factor of safety with variables to determine the slope design parameters that have apparent effect on the factor of safety (FOS) is a measure used in engineering design to represent how much greater the resisting capacity of a structure or component is relative to an assumed load. For example a dam with a FOS of (1.4) does not necessarily have a higher probability of failure than a dam with a FOS of (1.6). To demonstrate the application of the method developed during this research, the methodology was applied to case study (Ajdabya Reservoir) to present the effect of each variable on the factor of safety. The factor of safety is studied for a circular failure surface using different methods of analysis. The study evaluated four methods for calculating slope stability. We will use the Morgenstern- price method, which is considered an accurate method for calculating the factor of safety. The software which will be used for analysis of the model is GEOSTUDIO package. The procedure was performed in scenarios with different soil groups according to the Unified Soil Classification System (USCS) (ASTM 2011), heights and slope inclinations, and under conditions of reservoir subject to fast and slow emptying.

*Keywords: Slope Stability, allowable risk, factor of safety (FOS), slope inclinations, Earthen Dam, GEOSTUDIO Software.*

### **INTRODUCTION**

In olden days, designing of slopes are based on the experience of Geotechnical Engineers and design approach was based on prevailing site conditions. This approach of designing slopes has resulted in extensive property damage and occasionally resulted in the loss of life.

Now a day's there is an increased demand for engineering cut and fill slopes on construction projects. The construction of finite height sloped embankments is a common practice in dams, highways and railway projects. The finite element analysis of stability failures and seepage analysis demands increased to handle complex problems in the construction field[2].

Stability and seepage analysis for earthen dams are very important to maintain the stability of the structure. Embankments of earthen dams must be designed to construct stable against any type of force conditions which develops in the life of the structure.

Mostly loading conditions are critical like sudden

drawdown and steady seepage which can cause piping through the foundation or within the embankment [1].

To derive factor of safety, slope stability analysis of the embankment may be carried out for the 10m height of the homogeneous dam. The analysis has been performed using Mohr-Coulomb constitutive model. There are many analysis methods such as Method of Slices, Bishop's method, Janbu's method and Morgenstern Method etc. using any of the methods we can determine the stability analysis [3].

GEOSLOPE is developed by GEO-SLOPE International, Canada, based on the principle of limit equilibrium which incorporates a finite element method which is developed specially for the deformation and stability of embankment structures. It includes modeling of stability with (SLOPE/W), modeling of seepage with (SEEP/W), modeling of stress.

SLOPE/W and SEEP/W has been used with "Morgenstern method" to do the stability analysis. It is designed and developed to be a general software

tool for the stability analysis of earth structures for the proposed project of the raw water reservoir.

## METHODOLOGY

In this study, two loading conditions studied like steady state seepage and sudden drawdown analysis. SEEP/W has been applied together with SLOPE/W. Two types of slip surface searching techniques: “Entry-exit” and “Grid-radius” were used. The most common limit equilibrium (LE) based method used is Morgenstern-Price method (M-PM), which is incorporated in SLOPE/W to analyze the model with all four cases to find out the factor of safety on both upstream and downstream sides of the earthen dam contains over all height 22 m and maintained water level at 19 m on upstream other details shown in Figure no. 1 .

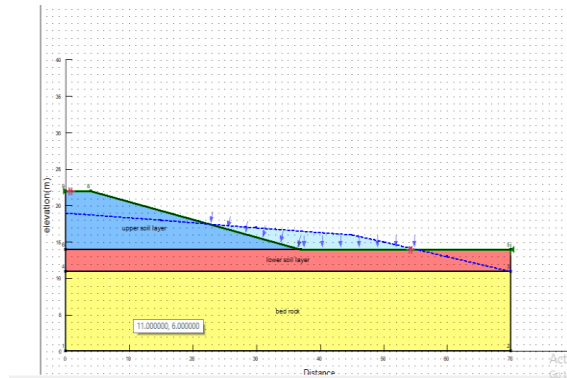


Fig. 1 Earthen dam model.

SLOPE/W uses the SOLVE process to calculate the FOS. Each slip surface is processed in 3 steps:

1. Initially, no forces are considered between the slices.
2. Normal forces are then considered, with no shear. An iterative process is used to calculate the FOS within a specified convergence
3. Then normal and shear force relationship is considered in Morgenstern-Price method.

The steps of the research work can be shown in the following flow chart Figure no. 2.

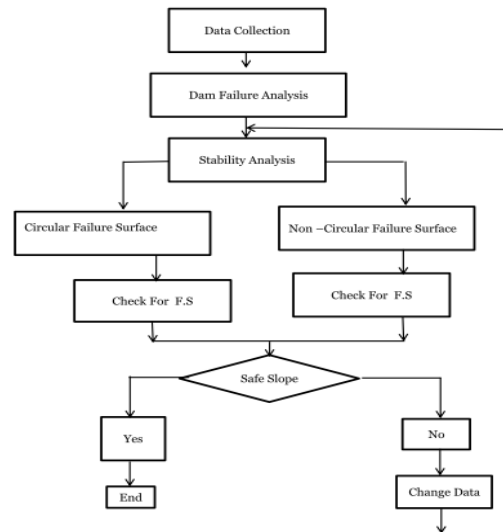


Fig. 2 The steps of research work.

## CASE STUDY

This research studies some of the phenomena occurring in the Ajdabiya reservoir located 20 km southeast of the city of Ajdabiya, in a high position to provide the natural flow of water for both the Gardabiya reservoir and Omar Mohktar reservoir. Water flows by gravity from Sarir and Tazerbo well field ,through a 4m diameter pipe-line (381-667Km ),to Ajdabiya holding reservoir which is designed to hold million cubic meters of water .The reservoir is considered as a storage facility from which water can be distributed to other systems . Materials used in the construction of this circular embankment were obtained from borrow adjacent to the site.

### Characteristics of Ajdabiya Reservoir

storage volume in the reservoir is  $4.2 \text{ M m}^3$  /day at the maximum level of 98.4 m (about mean sea level) and a minimum of 91.92 m . The ultimate in- flow was given as  $3.68 \text{ M m}^3$  /day , but it was safe for  $4.5 \text{ M m}^3$  /day , The reservoir has no natural catchment and contained by a circular embankment of diameter 923.2m to the inner crest . The reservoir operating range is 6.48 m.

### SOFTWARE USED IN STABILITY MODELING AND SEEPAGE ANALYSIS OF EARTHEN DAMS

Many numerical software's are developed from last six decades to evaluate engineering complex problems. Based on modeling approach, various numerical models are determined using software.

In our study, SLOPE/W and SEEP/W are

components of a complete suite of geotechnical products called GEOSTUDI. SLOPE/W can effectively analyses both simple and complex problems like Geometry, soil strength, pore water pressure, analysis methods and loading conditions like Steady state seepage and rapid or sudden drawdown condition applied on both upstream and downstream sides of the dam.

SLOPE/W is framed in terms of force and moment equilibrium to get a factor of safety equations.

The Morgenstern – Price method (1965) defines both moment and force equilibrium. To analyses the seepage of ground water, SEEP/W tool is used and also it helps to find the excess of pore water pressure dissipation problems within rock and soils called porous materials. Foundation material has a saturated hydraulic conductivity equal to  $1 \times 10^6$  m/sec. To define the hydraulic conductivity function over a range of positive and negative pressure to adequately reflect the decrease in

Hydraulic conductivity that occurs as the soil becomes unsaturated.  $K_{sat}$  Upper soil =  $1E-6$  m/day,  $K_{sat}$  Lower soil =  $1E-9$  m/day.

According to IS 7894 – 1975, a) “steady seepage with the reservoir full on downstream side”, the minimum factor of safety is 1.5 and (Duncan & Wright 2005, p.199) explains about a factor of safety provides a “quantitative indication of slope stability”. They are:

(i) A calculated factor of safety value equal to 1.5 (FOS = 1.5) represents the forces on the slope being in equilibrium; that is the forces within the slope causing stability (resisting forces) are in balance with those which cause the slope to be unstable (driving forces).

(ii) A calculated factor of safety value greater than 1.5 (FOS > 1.5) represents the slope being stable under the given conditions (resisting forces > driving forces), and

(iii) A calculated factor of safety value less than 1.0 (FOS < 1) represents the slope is unstable (failing); that is the driving forces out the way the resisting forces.

According to IS 7894 – 1975, b) “sudden drawdown condition the maximum head water to minimum with tail water at maximum on upstream side”, the minimum desired factor of safety is 1.3.

Geostudio software is one of geotechnical program that is based on the finite element and can do analysis such as, stress-strain, seepage, slope stability, dynamic analysis. SEEP/W (seepage for

windows) is a finite element software product that is coming under Geostudio, used to model the movement and pore-water pressure distribution within porous materials like soil and rock. It is formulated on the basis that flow of water through saturated soil follows Darcy’s Law. The SEEP/W model is constructed to solve 2-dimensional flow situations with multiple soil layers. Flow directions of groundwater can be analyzed. Under steady state conditions, the difference between input flux and output flux is zero at all times. for finite element calculations, the SEEP/W model is divided by nodes. The elevation of water level at each node is calculated. In the SEEP/W models, the following assumptions are made:

- (1) The aquifer is homogeneous and isotropic,
- (2) The aquifer is partly confined and partly unconfined.

Good quality output graphics allows a visual display of equipotential lines and flow paths, and contours can be plotted for different properties like pore pressures, seepage velocities, and gradients. Computations include flow quantities and uplift pressures at user-selected locations in the model.

## Equations

The Morgenstern-Price method is a rigorous method also based on limit equilibrium formulation (GEO-SLOPE International Ltd, 2012). [4]

The method considers both shear normal inter slice forces and satisfies both moment and force equilibrium. Two equations are used for calculating the factor of safety one with respect to moment equilibrium,  $F_m$ , and the other with respect to horizontal force equilibrium  $F_f$  see Equation (1) and (2). All input parameters described below and also

Illustrated in Figure 3.

$$F_m = \frac{\sum (C' \beta R + (N - U \beta) R \tan \phi')}{\sum W x - N f + \sum k W e \pm D d \pm \sum A a} \quad (1)$$

$$F_f = \frac{\sum (C' \beta \cos \alpha + (N - U \beta) \tan \phi' \cos \alpha)}{\sum N \sin \alpha + \sum K W - \sum D \cos \alpha \pm \sum A} \quad (2)$$

The variable are defined as follow:

- $C'$  = effective cohesion
- $\phi'$  = effective friction angle
- $U$  = pore water pressure
- $W$  = the total weight of a slice
- $N$  = the total normal force on the base of a slice
- $D$  = an external point load
- $kw$  = the horizontal seismic load applied through the centroid of each slice
- $R$  = the radius for a circular slip surface



$F$  = the perpendicular offset of the normal force from the center of rotation

X = the horizontal distance from the centerline  
of each slice to the center of rotation

$e$  = the vertical distance from the centroid of each slice to the center of rotation

$d$  = the perpendicular distance from a point load to the center of rotation

a = the perpendicular distance from the resultant water force to the center of rotation

A = the resultant external water forces

$\omega$  = the angle of the point load from the horizontal

$\alpha$  = the angle between the tangent to the center of the base of each slice and the horizontal

$\beta$  = the base length of each slice

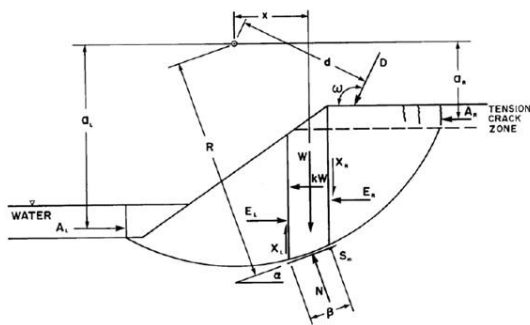


Fig.3. The forces acting on a slice for a circular slip surface. (GEO-SLOPE International Ltd. 2012). The ratio between the interstice forces is iterated until the two factors of safety  $F_m$  and  $F_f$  are equal (GEO-SLOPE International Ltd2012) [4]. In the case of composite slip surface a rigorous method generally produce more accurate results that also err on the safe side. This is illustrated in Figure 4 which shows a slice force polygon with good closure

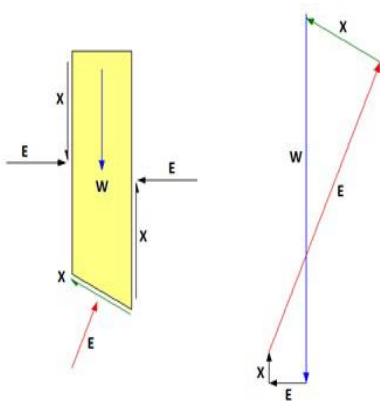


Fig. 4 A free body diagram of a slice and to the right the corresponding force polygon (GEOSLOPE International Ltd. 2012) (modified by the authors). The Morgenstern-Price method allows for the user to

select the interstice force function (GEO-SLOPE International Ltd2012). There are five different inter slice force functions available in Slope with the constant function, the half-sine function, the trapezoidal function and data point specified function. Only half-sine function is considered in this research.

## RESULTS AND DISCUSSIONS

The results of the case study was performed using GEO-SLOPE software to evaluate the critical point of the slip surface then the investigating about the critical safety factor. The critical factor of safety is taken for the most critical case with  $\lambda$ . Fig.(5) shows the distribution of slip surfaces with the coordinate of the center point of slip surface.

The most critical safety factor is at point  $x=35.48$  m and  $y=70.865$  m with radius of  $R=59.808$ . this factor of safety is considered in safe side. (i.e  $F.O.S > 1.50$  ).

The F.O.S is then studied for seepage case which gives value of 1.382.

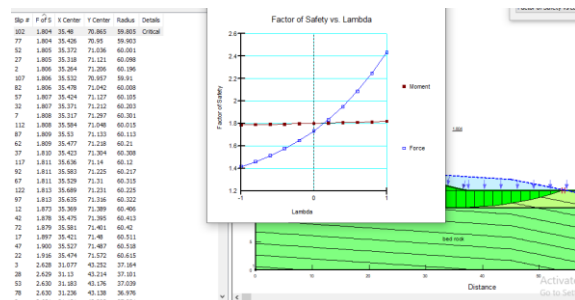


Fig.5.critical factor of safety

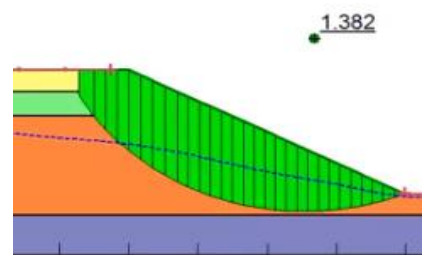


Fig.6 critical factor of safety

The water flows from upstream slope to downstream slope of the earthen dam.

The Graphs are generated same as like “Entry & Exit” technique.

factor of safety improved compared to above three conditions.

The failure of slip circles was generated by specifying the entry of the slip circle at the toe and exit at the top bank of the embankment.

The critical slip circle locates the corresponding factor of safety as shown in Figure 5 (SLOPE/W with critical slip surface) which is 1.804 and Figure 6 (SEEP/W critical slip surface) shows the factor of safety 1.382.

## CONCLUSION

1-The factor of safety is increased on downstream side after providing the drain on the downstream side is 1.804 which is higher than a minimum factor of safety (FOS) specified by IS 7894 (1975) for steady seepage condition with a full reservoir.

2-In this analysis, the factors of safety values of all cases have been analyzed to find out the stability of the earthen dam. Out of all four cases, with drain case is more suitable to stabilize the homogeneous earthen dam with a higher factor of safety (FOS).

3-Provision of a drain on downstream side improves the factor of safety (FOS) on the upstream side.

4- It is possible to create new methods of calculating the factor of safety against sliding by adding more variables to the commonly used limit equilibrium methods.

5-Empirical equations can be derived by assuming different soil conditions in the earth-dam's body.

6-There is no need to use the same soft wares (SLOPE/W and SEEP/W) in performing seepage

and slope stability analysis for earth-dams, which have similar dimensions of the case study.

7- One simple equation is enough to give factor of safety results without using software's because it is already derived through numerical modeling (finite elements) so there is no need to repeat the numerical modeling procedures.

## REFERENCES

- [1] Devi, D. D. N. L., & Anbalagan, R. (2017). Study on Slope Stability of Earthen Dams by using GEOSTUDIO Software.
- [2] Hasani, H., Mamizadeh, J., & Karimi, H. (2013). Stability of slope and seepage analysis in earth fills dams using numerical models (Case Study: Ilam Dam-Iran). *World Applied Sciences Journal*, 21(9), 1398-1402.
- [3] Lowe, J. III, "Stability Analysis of Embankments", *Journal of the Soil Mechanics and Foundations Division, ASCE*, vol.93, No. SM 4, Proc. Paper 5305, July 1967, pp. 1-33.
- [4] Mishal, U. R., & Khayyun, T. S. (2018). Stability Analysis of an Earth Dam Using GEO-SLOPE Model under Different Soil Conditions. *Engineering and Technology Journal*, 36(5 Part (A) Engineering), 523-532.

## PREDICTION OF FLEXURAL STRESS IN UNBONDED POST-TENSIONED STEEL AT DIFFERENT LOADING STAGES

Nazar Oukaili<sup>1</sup> and Iqbal Peera<sup>2</sup>

<sup>1</sup>Professor, University of Baghdad, Iraq; <sup>2</sup>Ph.D. Candidate, University of Baghdad, Iraq

### ABSTRACT

One of the methods for prestressing the structural concrete members is the use of unbonded tendons which is more economical and simpler in the construction of concrete members. This paper presents the analytical formulation of a methodology that proposed to predict the flexural stress in unbonded prestressed steel and in turn assess the strength and deformability of prestressed concrete members which are subjected to different types of static loading (axial force only, uniaxial bending moment, or biaxial bending moment with/without axial force). The suggested methodology uses the real constitutive relationships for each of concrete, non-prestressed and prestressed steel. Since there is no strain compatibility between concrete and prestressed steel due to the lack of bond between these two materials, the stress increase beyond the effective prestress is estimated depending on the total member deformation. A uniform stress distribution along the length of the unbonded tendon is assumed. The methodology is verified using previous experimental data for other researchers.

*Keywords: Internal unbonded tendon, Post-tensioning, Flexural stress, Constitutive relationship, Stiffness matrix*

### INTRODUCTION

Several equations have been suggested for predicting the flexural stress at ultimate  $f_{ub}$  in unbonded prestressed steel based on the experimental works that carried out by different researchers depending on a number of variables as Warwaruk et al. [10], Pannell [8], Mattock et al. [6] and Mojtahedi and Gamble [7]. As a result of these works, different proposals were recommended for the flexural stress at ultimate  $f_{ub}$  and consequently to the methodologies adopted in international practice codes.

The ACI 318M-14 code [1] adopted the following expressions to estimate  $f_{ub}$  in MPa. when  $l/h \leq 35$

$$f_{ub} = f_{pe} + 70 + \frac{f'_c}{100 \rho_{ps}} \quad (1)$$

$$f_{ub} \leq \text{the least of } (f_{pe} + 420) \text{ and } (f_{py})$$

when  $l/h > 35$

$$f_{ub} = f_{pe} + 70 + \frac{f'_c}{300 \rho_{ps}} \quad (2)$$

$$f_{ub} \leq \text{the least of } (f_{pe} + 210) \text{ and } (f_{py})$$

where  $l$  is the length of the clear span measured face to face of support in mm,  $h$  is overall thickness, height or depth of member in mm,  $f_{pe}$  effective stress in prestressing reinforcement after all prestress losses in MPa,  $f'_c$  is specified compressive strength

of concrete in MPa,  $f_{py}$  is specified yield strength of prestressing reinforcement in MPa, and  $\rho_{ps}$  is the prestressing steel ratio ( $\rho_{ps} = A_{ps}/bd_p$ ) in which  $A_{ps}$  is the area of the prestressed reinforcement in tension zone in mm<sup>2</sup>,  $b$  is the width of compression flange of the member in mm, and  $d_p$  is the distance from the extreme compression fiber to the centroid of prestressing reinforcement in mm.

The main objective of this work includes the proposal of an analytical methodology to estimate the stress in internal unbonded prestressed steel at different stages of monotonic static loading and consequently predict the strength and deformability of the structural concrete members under different types of static loading. Also, verification of the proposed methodology with the available experimental previous studies will be carried out using results from Pannell [8], Du and Tao [3], Harajli and Kang [4], Campbell and Chouinard [2]. Results of the proposed methodology will be compared to the results of ACI 318M-14 prediction equations.

### CONSTITUTIVE RELATIONSHIPS

Non-linear stress-strain relationships proposed by Karpenko [5] were used for concrete in tension and compression and for steel. These relationships are based on the secant modulus of elasticity of the material  $\bar{E}_m$  as formulated below

$$f_m = \bar{E}_m \cdot \varepsilon_m \quad (3)$$

$$\bar{E}_m = E_m \cdot v_m \quad (4)$$

$$v_m = \hat{v}_m + (v_o - \hat{v}_m) \sqrt{1 - e_{1m}\eta_m - e_{2m}\eta_m^2} \quad (5)$$

where  $\hat{v}_m$  is the value of  $v_m$  at the vertex of the stress-strain diagram,  $v_o$  is the value of  $v_m$  at the start of the stress-strain diagram,  $e_1$  and  $e_2$  are diagram curvature parameters in which ( $e_{2m} = 1 - e_{1m}$ ) and  $\eta_m$  is the stress level beyond the proportional limit

$$\eta_m = \frac{f_m - f_{m,el}}{\hat{f}_m - f_{m,el}}, \quad 0 \leq \eta_m \leq 1 \quad (6)$$

For more information about Eq. (5), see Ref. [5].

### LOAD-DEFORMATION RELATIONSHIPS

According to the Bernoulli's assumption in which the plane section before bending remains plane after bending, the strain at any fiber can be calculated according to the following expression

$$\varepsilon_m = \varepsilon_{mi} + \varepsilon_o + \psi_x y_m + \psi_y x_m \quad (7)$$

where  $\varepsilon_{mi}$  is the initial strain in the material;  $\varepsilon_o$  is the axial strain;  $\psi_x$  is the curvature of the member longitudinal axis in the OYZ plane;  $\psi_y$  is the curvature of the member longitudinal axis in the OXZ plane. Equation (7) can be rewritten in matrix form as follows

$$\varepsilon_m = Z \{\bar{\varepsilon}\} \quad (8)$$

$$Z = \{1 \quad y \quad x\} \quad (9)$$

$$\{\bar{\varepsilon}\} = \{\varepsilon_o \quad \psi_x \quad \psi_y\}^T \quad (10)$$

Since the force vector can be expressed as

$$\{F\} = \begin{Bmatrix} N \\ M_x \\ M_y \end{Bmatrix} = \begin{Bmatrix} \int_{A_m} f_m dA_m \\ \int_{A_m} f_m y_m dA_m \\ \int_{A_m} f_m x_m dA_m \end{Bmatrix} \quad (11)$$

Substituting Eq. (3) and Eq. (8), Eq. (11) takes a new form

$$\{F\} = \begin{Bmatrix} N \\ M_x \\ M_y \end{Bmatrix} = \begin{bmatrix} C_{11} & C_{12} & C_{13} \\ C_{21} & C_{22} & C_{23} \\ C_{31} & C_{32} & C_{33} \end{bmatrix} \begin{Bmatrix} \varepsilon_o \\ \psi_x \\ \psi_y \end{Bmatrix} \quad (12)$$

where  $C_{ij}$  is the element of the stiffness matrix that depends on the geometry of the section and the attained stress-strain condition under the applied load.

$$C_{11} = \bar{E}_m \int_{A_m} dA_m, C_{12} = C_{21} = \bar{E}_m \int_{A_m} y_m dA_m, \\ C_{13} = C_{31} = \bar{E}_m \int_{A_m} x_m dA_m, C_{22} = \int_{A_m} y_m^2 dA_m, \\ C_{23} = C_{32} = \int_{A_m} y_m x_m dA_m, C_{33} = \int_{A_m} x_m^2 dA_m.$$

The stiffness matrix in Eq. (12) depends on the value of  $\{\bar{\varepsilon}\}$  which has not determined yet. So an iteration process should be performed in which

$$\{\bar{\varepsilon}\}_i = [C(\{\bar{\varepsilon}\}_{i-1})]^{-1} * \{F\} \\ \{\bar{\varepsilon}\}_0 = 0, \quad i = 1, 2, 3, \dots \quad (13)$$

In each iteration the new value of the strain vector  $\{\bar{\varepsilon}\}_i$  should be compared to the value of the previous iteration until the convergence process is reached.

Whenever the strain vector is determined, the strain in each concrete fiber and in each bonded steel reinforcement element can be estimated depending on the strain compatibility using Eq. (7). In case of the internal unbonded steel reinforcement element, due to the lack of bonding and in turn the violation of the strain compatibility, the strain is determined by integrating the strain value of concrete at the level of the unbonded steel along its length and dividing this value on its length between anchorages.

$$\Delta\varepsilon_{ub} = \frac{1}{\ell_{ub}} \int_0^{\ell_{ub}} \Delta\varepsilon_{cub}(x) \cdot dx \quad (14)$$

where  $\Delta\varepsilon_{ub}$  is the change in the strain in the unbonded steel due to the applied load,  $\ell_{ub}$  is the length of unbonded steel between anchorages, and  $\Delta\varepsilon_{cub}$  is the change in strain in concrete fiber at the level of unbonded steel. The value of  $\Delta\varepsilon_{ub}$  is considered as the average change of strain along the unbonded steel. Adding  $\Delta\varepsilon_{ub}$  to the initial prestrain  $\varepsilon_{ubi}$  that induced in this steel reinforcement element and by consequently using the constitutive relationship that represents the mentioned steel element, the total stress can be determined.

$$\varepsilon_{ub} = \varepsilon_{ubi} + \Delta\varepsilon_{ub} \quad (15)$$

$$f_{ub} = f(\varepsilon_{ub}) \quad (16)$$

where  $f$  is the nonlinear function that relates the unbonded steel stress with the unbonded steel strain.

The ultimate stress value is determined when the force vector in Eq. (12) represents the ultimate strength that the critical section can resist.

### VERIFICATION OF THE PROPOSED METHODOLOGY

To verify the proposed methodology for predicting the stress in unbonded steel elements and in turn

the load carrying capacity of the structural concrete member, experimental data for 60 flexural members with different effective parameters were collected from other researchers and treated in the present study. Tam and Pannell [9] tested eight simply supported beams with straight unbonded prestressed reinforcement. The approximate (overall length) to effective depth  $d_p$  ratio ranged from 20 to 45. All these beams were exposed to a single concentrated load at midspan. The experimental and analytical results are shown in Table (1). Du and Tao [3] tested 20 simply supported beams with straight unbonded steel reinforcement. All beams were with the rectangular cross-sectional configuration of (160x280) mm and a span of (4200) mm. The main variables were  $A_{ps}$ ,  $f'_c$ , and the amount of nonprestressed reinforcement  $A_s$ . Tested specimens were exposed to third point static loading up to failure. The span to depth ratio of the beams was 19.1. Table (2) shows the experimental and the calculated, according to the proposed methodology and the ACI 318M-14 approach, results for the stress in unbonded prestressed

steel and the failure moments. Harajli and Kanj [4] tested 26 simply supported beams with three groups having span to depth ratios  $S/d_p$  equal to 20, 13 and 8, respectively in which  $S$  was defined as the span length measured from anchorage to anchorage of the simply supported member. Three different contents of tension reinforcement were used. Thirteen beams were subjected to a single concentrated load at midspan, while the other 13 specimens were exposed to third-point loading. The comparison of the experimental and the analytical results for the stress in unbonded prestressed steel and the failure moments are shown in Table (3). Campbell and Chouinard [2] tested six simply supported beams of a rectangular cross-section of (160x220) mm dimensions and (3300) mm span length. All beams were subjected to third-point loading. The span to depth ratio was 15 for all the beams. The main variable was the amount of bonded nonprestressed reinforcement. Table (4) shows the comparison of the experimental and analytical outcomes. The above comparisons also are represented in Fig. 1 to Fig. 4.

Table 1 Experimental and proposed results for Tam and Pannell tests [9]

| Beam ID   | $\frac{\ell}{d_p}$ | Stress at ultimate in unbonded steel, MPa |                      |                                     |                      |                                     | Failure moment, kN.m |                      |                               |                      |                               |
|---|--------------------|---|----------------------|-------------------------------------|----------------------|-------------------------------------|----------------------|----------------------|-------------------------------|----------------------|-------------------------------|
|   |                    | test record                               | proposed methodology |                                     | ACI 318M-14 approach |                                     | test record          | proposed methodology |                               | ACI 318M-14 approach |                               |
|   |                    | $f_{ub}^{exp}$                            | $f_{ub}^{est}$       | $\frac{f_{ub}^{est}}{f_{ub}^{exp}}$ | $f_{ub}^{est}$       | $\frac{f_{ub}^{est}}{f_{ub}^{exp}}$ | $M_u^{exp}$          | $M_u^{est}$          | $\frac{M_u^{est}}{M_u^{exp}}$ | $M_u^{est}$          | $\frac{M_u^{est}}{M_u^{exp}}$ |
| B1  | 18.0               | 962.19                                    | 914.74               | 0.951                               | 944.08               | 0.981                               | 40.13                | 39.92                | 0.995                         | 42.75                | 1.065                         |
| B2  | 23.5               | 898.43                                    | 857.36               | 0.954                               | 877.01               | 0.976                               | 60.65                | 55.68                | 0.918                         | 69.91                | 1.153                         |
| B3  | 27.5               | 1046.40                                   | 993.13               | 0.949                               | 1036.38              | 0.990                               | 30.75                | 35.00                | 1.138                         | 35.96                | 1.169                         |
| B4  | 28.6               | 969.68                                    | 963.9                | 0.994                               | 984.20               | 1.015                               | 38.38                | 40.24                | 1.048                         | 47.94                | 1.249                         |
| B5  | 29.3               | 1071.84                                   | 1079.08              | 1.007                               | 1097.42              | 1.024                               | 22.14                | 25.57                | 1.155                         | 29.46                | 1.331                         |
| B6  | 31.4               | 944.74                                    | 964.39               | 1.021                               | 983.07               | 1.041                               | 22.47                | 27.54                | 1.226                         | 36.07                | 1.605                         |
| B7  | 38.8               | 859.97                                    | 884.335              | 1.028                               | 902.43               | 1.049                               | 22.84                | 25.67                | 1.124                         | 31.97                | 1.400                         |
| B8  | 43.0               | 732.67                                    | 772.5                | 1.054                               | 833.02               | 1.137                               | 21.01                | 18.59                | 0.885                         | 16.21                | 0.772                         |
| Average of ( $f_{ub}^{est}/f_{ub}^{exp}$ ) or ( $M_u^{est}/M_u^{exp}$ ) |                    |   |                      | 0.995                               |                      | 1.027                               |                      |                      | 1.061                         |                      | 1.218                         |
| Standard of deviation ( $\sigma$ )                                      |                    |   |                      | 0.040                               |                      | 0.052                               |                      |                      | 0.121                         |                      | 0.247                         |
| Coefficient of variation (COV)  |                    |   |                      | 0.040                               |                      | 0.051                               |                      |                      | 0.114                         |                      | 0.203                         |

Table 2 Experimental and proposed results for Du and Tao tests [3]

| Beam ID | $\frac{\ell}{d_p}$ | Stress at ultimate in unbonded steel, MPa |                      |                                     |                      |                                     | Failure moment, kN.m |                      |                               |                      |                               |
|---------|--------------------|---|----------------------|-------------------------------------|----------------------|-------------------------------------|----------------------|----------------------|-------------------------------|----------------------|-------------------------------|
|         |                    | test record                               | proposed methodology |                                     | ACI 318M-14 approach |                                     | test record          | proposed methodology |                               | ACI 318M-14 approach |                               |
|         |                    | $f_{ub}^{exp}$                            | $f_{ub}^{est}$       | $\frac{f_{ub}^{est}}{f_{ub}^{exp}}$ | $f_{ub}^{est}$       | $\frac{f_{ub}^{est}}{f_{ub}^{exp}}$ | $M_u^{exp}$          | $M_u^{est}$          | $\frac{M_u^{est}}{M_u^{exp}}$ | $M_u^{est}$          | $\frac{M_u^{est}}{M_u^{exp}}$ |
| A1      | 19.1               | 1458                                      | 1500                 | 1.029                               | 1213                 | 0.832                               | 31.1                 | 30.1                 | 0.968                         | 24.6                 | 0.791                         |
| A2      | 19.1               | 1430                                      | 1362                 | 0.952                               | 1084                 | 0.758                               | 46.8                 | 41.3                 | 0.882                         | 36.6                 | 0.782                         |
| A3      | 19.1               | 1176                                      | 1242                 | 1.056                               | 959                  | 0.815                               | 63.6                 | 54.3                 | 0.854                         | 50.8                 | 0.799                         |
| A4      | 19.1               | 1465                                      | 1447                 | 0.988                               | 1122                 | 0.766                               | 38.3                 | 34.1                 | 0.890                         | 29.3                 | 0.765                         |
| A5      | 19.1               | 1315                                      | 1303                 | 0.991                               | 1017                 | 0.773                               | 51.2                 | 46.8                 | 0.914                         | 43.4                 | 0.848                         |
| A6      | 19.1               | 1063                                      | 1142                 | 1.074                               | 993                  | 0.934                               | 72.4                 | 67.9                 | 0.938                         | 66.5                 | 0.919                         |
| A7      | 19.1               | 1436                                      | 1329                 | 0.925                               | 1230                 | 0.857                               | 41.5                 | 39.9                 | 0.961                         | 37.9                 | 0.913                         |

|   |      |      |      |       |      |       |       |      |       |       |       |
|---|------|------|------|-------|------|-------|-------|------|-------|-------|-------|
| A8  | 19.1 | 1290 | 1325 | 1.027 | 1162 | 0.901 | 59.4  | 56.2 | 0.946 | 54.1  | 0.911 |
| A9  | 19.1 | 1108 | 1099 | 0.992 | 1064 | 0.960 | 102   | 90.3 | 0.886 | 90.0  | 0.882 |
| B1  | 19.1 | 1645 | 1679 | 1.021 | 1352 | 0.822 | 30.3  | 33.5 | 1.106 | 26.8  | 0.884 |
| B2  | 19.1 | 1564 | 1595 | 1.020 | 1221 | 0.781 | 50.4  | 47.3 | 0.938 | 40.4  | 0.802 |
| B3  | 19.1 | 1361 | 1443 | 1.060 | 1128 | 0.829 | 61.0  | 62.8 | 1.030 | 57.6  | 0.944 |
| B5  | 19.1 | 1520 | 1538 | 1.012 | 1250 | 0.822 | 53.4  | 52.5 | 0.983 | 48.1  | 0.901 |
| B6  | 19.1 | 1402 | 1409 | 1.005 | 1181 | 0.842 | 75.8  | 74.3 | 0.980 | 71.4  | 0.942 |
| B7  | 19.1 | 1603 | 1583 | 0.988 | 1422 | 0.887 | 42.5  | 43.9 | 1.033 | 40.7  | 0.958 |
| B9  | 19.1 | 1346 | 1402 | 1.042 | 1295 | 0.962 | 89.7  | 93.5 | 1.042 | 92.4  | 1.030 |
| C1  | 19.1 | 1396 | 1423 | 1.019 | 1173 | 0.840 | 33.6  | 35.9 | 1.068 | 28.6  | 0.851 |
| C3  | 19.1 | 1316 | 1249 | 0.950 | 969  | 0.736 | 67.3  | 59.5 | 0.884 | 54.2  | 0.805 |
| C7  | 19.1 | 1411 | 1398 | 0.991 | 1322 | 0.937 | 44.6  | 50.5 | 1.132 | 44.3  | 0.993 |
| C9  | 19.1 | 1109 | 1096 | 0.988 | 1047 | 0.944 | 101.0 | 98.0 | 0.970 | 101.6 | 1.006 |
| Average of $(f_{ub}^{est}/f_{ub}^{exp})$ or $(M_u^{est}/M_u^{exp})$ |      |      |      | 1.007 |      | 0.850 |       |      | 0.970 |       | 0.886 |
| Standard of deviation ( $\sigma$ )                                  |      |      |      | 0.038 |      | 0.071 |       |      | 0.078 |       | 0.079 |
| Coefficient of variation (COV)                                      |      |      |      | 0.038 |      | 0.084 |       |      | 0.080 |       | 0.089 |

Table 3 Experimental and proposed results for Harajli and Kanj tests [4]

| Beam ID   | $\frac{\ell}{d_p}$ | Stress at ultimate in unbonded steel, MPa |                      |                                     |                      |                                     | Failure moment, kN.m |                      |
|---|--------------------|---|----------------------|-------------------------------------|----------------------|-------------------------------------|----------------------|----------------------|
|   |                    | test record                               | proposed methodology |                                     | ACI 318M-14 approach |                                     | proposed methodology | ACI 318M-14 approach |
|   |                    | $f_{ub}^{exp}$                            | $f_{ub}^{est}$       | $\frac{f_{ub}^{est}}{f_{ub}^{exp}}$ | $f_{ub}^{est}$       | $\frac{f_{ub}^{est}}{f_{ub}^{exp}}$ | $M_u^{est}$          | $M_u^{est}$          |
| PP2R3-3   | 19.0               | 1261.3                                    | 1284.6               | 1.018                               | 1247.7               | 0.989                               | 21.2                 | 17.9                 |
| PP2R3-0   | 19.0               | 1245.6                                    | 1178.4               | 0.946                               | 1238.0               | 0.994                               | 19.3                 | 15.6                 |
| PP3R3-3   | 19.0               | 1106.9                                    | 1155.7               | 1.044                               | 1066.1               | 0.963                               | 32.7                 | 30.2                 |
| PP3R3-0   | 19.0               | 1068.9                                    | 1002.1               | 0.938                               | 1068.9               | 1.000                               | 32.7                 | 32.5                 |
| P1R3-3  | 19.0               | 1280.0                                    | 1348.7               | 1.054                               | 1365.8               | 1.067                               | 14.0                 | 7.0                  |
| P1R3-0  | 19.0               | 1351.7                                    | 1351.1               | 1.000                               | 1366.1               | 1.011                               | 14.4                 | 7.0                  |
| P2R3-3  | 19.0               | 1212.4                                    | 1262.0               | 1.041                               | 1055.0               | 0.870                               | 20.3                 | 15.2                 |
| P2R3-0  | 19.0               | 1206.9                                    | 1147.9               | 0.951                               | 1046.9               | 0.867                               | 19.6                 | 15.0                 |
| P3R3-3  | 19.0               | 1160.7                                    | 1178.1               | 1.015                               | 1033.8               | 0.891                               | 25.5                 | 20.5                 |
| P3R3-0  | 19.0               | 1127.6                                    | 1107.6               | 0.982                               | 990.3                | 0.878                               | 24.4                 | 19.7                 |
| PP1R2-3   | 12.0               | 1281.3                                    | 1231.0               | 0.961                               | 1224.0               | 0.955                               | 33.21                | 30.9                 |
| PP1R2-0   | 12.0               | 1229.7                                    | 1218.7               | 0.991                               | 1187.6               | 0.966                               | 33.6                 | 29.7                 |
| PP2R2-3   | 12.0               | 1217.2                                    | 1227.5               | 1.009                               | 1098.8               | 0.903                               | 41.8                 | 37.9                 |
| PP2R2-0   | 12.0               | 1259.3                                    | 1154.6               | 0.917                               | 1077.9               | 0.856                               | 41.2                 | 37.6                 |
| PP3R2-3   | 12.0               | 1086.2                                    | 1160.5               | 1.068                               | 1057.7               | 0.974                               | 63.1                 | 61.2                 |
| PP3R2-0   | 12.0               | 1157.2                                    | 1124.9               | 0.972                               | 1089.2               | 0.941                               | 63.75                | 61.7                 |
| P1R2-3  | 12.0               | 1400.0                                    | 1415.2               | 1.011                               | 1231.5               | 0.880                               | 24.1                 | 18.1                 |
| P1R2-0  | 12.0               | 1205.5                                    | 1210.7               | 1.004                               | 1036.8               | 0.860                               | 26.8                 | 19.8                 |
| P2R2-3  | 12.0               | 1233.1                                    | 1234.8               | 1.001                               | 1014.4               | 0.823                               | 34.3                 | 27.0                 |
| P2R2-0  | 12.0               | 1186.2                                    | 1169.9               | 0.986                               | 1009.5               | 0.851                               | 34.4                 | 26.9                 |
| PP1R1-3   | 9.6                | 1200.0                                    | 1240.4               | 1.034                               | 1185.8               | 0.988                               | 49.2                 | 42.7                 |
| PP1R1-0   | 9.6                | 1281.3                                    | 1155.4               | 0.901                               | 1213.0               | 0.947                               | 49.9                 | 44.5                 |
| PP2R1-3   | 9.6                | 1217.2                                    | 1203.0               | 0.988                               | 1140.9               | 0.937                               | 75.1                 | 68.0                 |
| PP2R1-0   | 9.6                | 1182.8                                    | 1161.9               | 0.982                               | 1103.6               | 0.933                               | 65.0                 | 56.7                 |
| PP3R1-3   | 9.6                | 1120.7                                    | 1169.5               | 1.044                               | 1053.2               | 0.940                               | 79.7                 | 71.0                 |
| PP3R1-0   | 9.6                | 1079.3                                    | 1102.9               | 1.022                               | 1043.3               | 0.967                               | 79.6                 | 70.7                 |
| Average of $(f_{ub}^{est}/f_{ub}^{exp})$ or $(M_u^{est}/M_u^{exp})$ |                    |   |                      | 0.995                               |                      | 0.933                               |                      |                      |
| Standard of deviation ( $\sigma$ )                                  |                    |   |                      | 0.042                               |                      | 0.060                               |                      |                      |
| Coefficient of variation (COV)                                      |                    |   |                      | 0.042                               |                      | 0.064                               |                      |                      |

Table 4 Experimental and proposed results for Campbell and Chouinard tests [2]

| Beam ID   | $\frac{\ell}{d_p}$ | Stress at ultimate in unbonded steel, MPa |                      |                                     |                      |                                     | Failure moment, kN.m |                      |                               |                      |                               |
|---|--------------------|---|----------------------|-------------------------------------|----------------------|-------------------------------------|----------------------|----------------------|-------------------------------|----------------------|-------------------------------|
|   |                    | test record                               | proposed methodology |                                     | ACI 318M-14 approach |                                     | test record          | proposed methodology |                               | ACI 318M-14 approach |                               |
|   |                    | $f_{ub}^{exp}$                            | $f_{ub}^{est}$       | $\frac{f_{ub}^{est}}{f_{ub}^{exp}}$ | $f_{ub}^{est}$       | $\frac{f_{ub}^{est}}{f_{ub}^{exp}}$ | $M_u^{exp}$          | $M_u^{est}$          | $\frac{M_u^{est}}{M_u^{exp}}$ | $M_u^{est}$          | $\frac{M_u^{est}}{M_u^{exp}}$ |
| 1   | 15                 | 1476                                      | 1420                 | 0.962                               | 1228                 | 0.832                               | 45.5                 | 42.3                 | 0.930                         | 48.5                 | 0.801                         |
| 2   | 15                 | 1467                                      | 1411                 | 0.962                               | 1212                 | 0.826                               | 63.3                 | 55.7                 | 0.880                         | 63.5                 | 0.832                         |
| 3   | 15                 | 1381                                      | 1320                 | 0.956                               | 1194                 | 0.865                               | 81.1                 | 68.4                 | 0.843                         | 76.5                 | 0.828                         |
| 4   | 15                 | 1348                                      | 1332                 | 0.988                               | 1254                 | 0.930                               | 98.0                 | 85.4                 | 0.871                         | 92.7                 | 0.866                         |
| 5   | 15                 | 1274                                      | 1263                 | 0.991                               | 1240                 | 0.973                               | 105.5                | 97.8                 | 0.927                         | 103.5                | 0.929                         |
| 6   | 15                 | 1269                                      | 1223                 | 0.964                               | 1245                 | 0.980                               | 120.2                | 109.4                | 0.910                         | 113.2                | 0.916                         |
| Average of $(f_{ub}^{est}/f_{ub}^{exp})$ or $(M_u^{est}/M_u^{exp})$ |                    |   |                      | 0.970                               |                      | 0.901                               |                      |                      | 0.894                         |                      | 0.980                         |
| Standard of deviation ( $\sigma$ )                                  |                    |   |                      | 0.015                               |                      | 0.070                               |                      |                      | 0.034                         |                      | 0.049                         |
| Coefficient of variation (COV)                                      |                    |   |                      | 0.0156                              |                      | 0.077                               |                      |                      | 0.038                         |                      | 0.050                         |

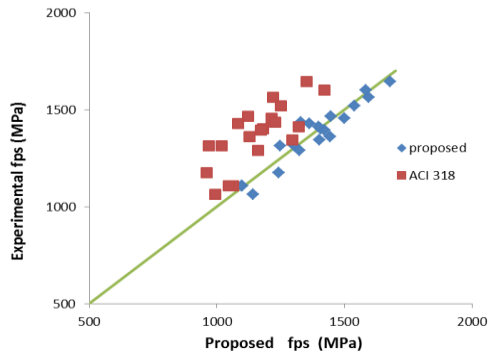


Fig. (1) Experimental and proposed stress relationship for Tam and Pannell tests

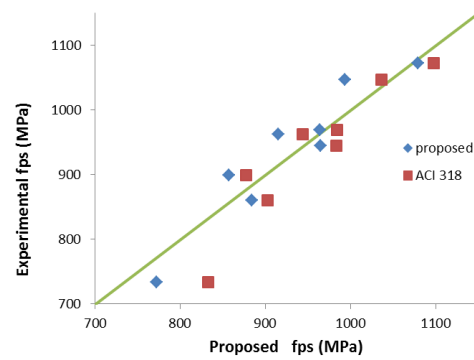


Fig. (2) Experimental and proposed stress relationship for Du and Tao tests

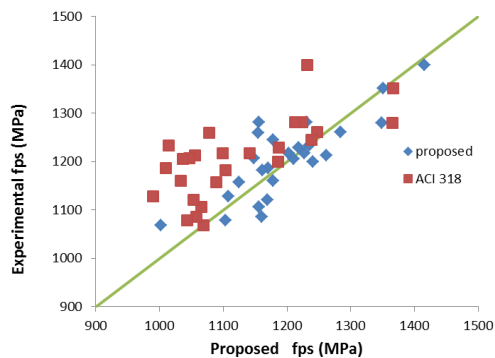


Fig. (3) Experimental and proposed stress relationship for Harajli and Kanj tests

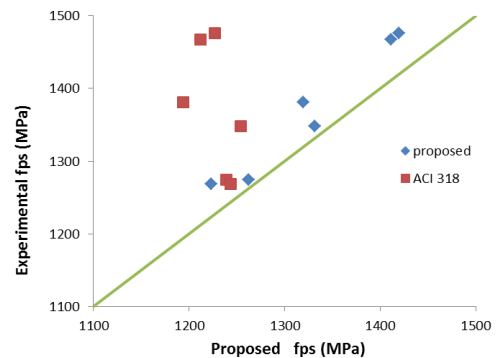


Fig. (4) Experimental and proposed stress relationship for Campbell and Chouinard tests

## CONCLUSIONS

The proposed methodology described in this paper focuses on the determination of the stress in prestressing steel at nominal flexural strength in unbonded members depending on the average strain in

the concrete fiber located at the centroidal axis of the prestressing steel. The proposed methodology adopts the fact that the stress in unbonded prestressing steel is a member-dependent and considers the span-to-depth ratio in a uniform manner without any limitations.



## REFERENCES

- [1] ACI Committee 318, Building Code Requirement for Reinforced Concrete (ACI 318-2014), American Concrete Institute, 2014, pp1-506.
- [2] Campbell, I.T. and Chouinard, K.I., Influence of non-prestressed reinforcement on the strength of unbounded partially prestressed concrete members, *ACI Structural Journal*, Vol.88, No.5, 1991, pp. 546-551.
- [3] Du G. and X. Tao, Ultimate Stress in Unbonded Tendons of Partially Prestressed Concrete Beams, *PCI Journal*, Vol. 30, No. 6, November-December, 1985, pp. 72-91.
- [4] Harajli, M., and Kanj, M., Ultimate Flexural Strength of Concrete Members Prestressed with Unbonded Tendons, *ACI Structural Journal*, V. 88, No. 6, Nov.-Dec. 1991, pp. 663-673.
- [5] Karpenko, N.I., Mukhamediev T.A. and Petrov A.N. ,The Initial and Transformed Stress-strain Diagrams of Steel and Concrete, Special Publication, Stress-Strain Condition for Reinforced Concrete Construction, Reinforced Concrete Research Center, Moscow, 1986, pp. 7-25.
- [6] Mattock, A. H., J. Yamazaki, and B.T. Kattula, Comparative Study of Prestressed Concrete Beams, With and Without Bond, *ACI Journal*, Vol. 68, No. 3, Feb. 1971, pp. 116-125.
- [7] Mojtahedi S. and Gamble W. L., Ultimate Steel Stresses in Unbonded Prestressed Concrete, *ASCE*, V. 104, No. ST7, July 1978, pp. 1159-1165.
- [8] Pannell F. N." The ultimate moment of resistance of unbonded prestressed concrete beams" *Magazine of concrete research*: Vol. 21, No. 66, March 1969, pp. 43-54.
- [9] Tam A. and Pannell F. N., The ultimate moment of resistance of unbounded partially prestressed reinforced concrete beams, *Magazine of concrete research*, Vol. 28, No. 97 December 1976, pp. 203-208.
- [10] Warwaruk, J., M.A. Sozen, and C.P. Siess, Investigation of Prestressed Reinforced Concrete for Highway Bridge, Part III: Strength and Behavior in Flexure of Prestressed Concrete Beams, University of Illinois Engineering Experiment Station Bulletin No. 464, Urban, III, August 1962, pp. 1-105.

## THE DURABILITY OF LIME STABILIZED EXPANSIVE SOIL

Yulvi Zaika<sup>1</sup>, Eko Andi Suryo<sup>2</sup>

<sup>1,2</sup>Engineering Faculty, University of Brawijaya, Indonesia

### ABSTRACT

The failure was caused by expansive soil at the base of the structure can lead to enormous losses and soil using additives (chemical agents) sometimes still indicate the problem of premature failure. This problem is due to the difficulty of understanding complex reactions between clay minerals and chemical agents. The results of this chemical reaction will determine how substantial the swell /shrinkage reduction and strength improvement. In this study, the effects of several treatments will be analysed on expansive soils that have been stabilised with lime, both behaviours that will enhance and reduce their stability. Sample treatment is one way to improve the durability of soil mixtures, while immersion and dry-wet processes are a way to reduce durability. Strength measurements on each treatment were tested with CBR value and measurement of swell potential was carried out by analyzing changes in the sample volume. Dry-wet cycle treatment increases the potential for expansion even though it is still smaller than untreated soil; in this case, it is still below 5% with three cycles and does not indicate a tendency to increase. Lime treated expansive soil could increase durability as subgrade of pavement structure at the limit certain time.

*Keywords: Durability, Lime, Dry, Wet, Cycle.*

### INTRODUCTION

The problems associated with the expansive soils are not yet widely appreciated outside area of the occurrence. The amount of damage caused by expansive soil should be a warning. Several methods can be done to build structure on it such as using deep foundations, remove the troublesome ground and replace it with suitable material, soil reinforcement [1], using additive material that is produced higher strength and lower compressibility than natural soil. Soil improvement methods are often used in road projects rather than using deep foundations because they cover a large area.

The most important binder are limes [2-9] because it can improve expansive soil properties with increasing strength and reduce the shrinkage properties although there are other materials that are also often used such as fly ash [9-11] cement [8], gypsum [12-13] or waste material such as steel slag [14], rice husk ash [15], bagasse ash [16], nanocomposite [17] or other ingredients. Some considerations in choosing additives include:

1. Availability of materials
2. The influence of these materials on changes in soil properties
3. Workability
4. Costs
5. Durability

In this study, it will discuss the expansive soil with lime because of the considerations. Lime is very widely available in Indonesia and is commonly used as an additive soil so that it will not get difficulties in the implementation. The thing that must be investigated is the optimum percentage that will give

maximum results, so further research is needed on the durability of the lime-improved expansive soil as subgrade of pavement structure due to environmental conditions.

Previous studies on soil durability and additives were carried out by [8] which analyzed the effect of curing time on cohesive soil mixtures with lime and natural pozzolan on shear strength which showed that the effect of lime was more dominant than natural pozzolan on changes in friction angle and cohesion. Investigated the occurrence of cracks in the soil due to environmental changes which is one of the factors in the occurrence of slope failure.

The researchers [18] analyzed the effect of dry-wet cycles on the physical and mechanical properties of expansive soils that were improved with 0.3% OTAC and 6% KCL. OTAC-KCL is ameliorant that can be soluble in water or other solvents. The addition of these additives provided unconfined compressive strength and reduced free swell by almost fifty percent (55% to 25%). Strength development is crucial in the study of strength characteristics of soils treated with stabilizers as the structure of such materials evolves with time due to continuing hydration/pozzolanic reaction. The dry-wet cycle process which was carried out 14 days with 1 to 4 cycles showed that even though the development still occurred in the improved soil but it was still much bigger than the natural expansive soil. Direct shear test on natural soil and improved soil with dry-wet cycle showed a decrease in parameters shear strength with the increase of the second dry-wet cycle of the soil but the parameters of the shear strength of the improved soil are still higher than the natural soil. The improved soil with lime is considered resistant to

the dry-wet cycle[3] which is use to stabilize subgrade layer [19].

## MATERIAL AND MECHANISM

### Material

Expansive soil used in this study is from Ngasem Bojonegoro village, East Java, Indonesia. This is soil that is categorized as that is easy to swell and shrink due to changes in water content, which causes damage to the pavement structure in the area. Several experiments were carried out to determine soil characteristics, carrying capacity and swell potential.

### Mechanism

Expansive soil is clay soil containing montmorillonite minerals. This mineral structure consists of one sheet of gibbsite, which is between the silica sheets. Because the inter-crystal bond by the Van Der Waals style between the silica sheets is weak and there is a shortage of negative ions in the octahedral so that water and other ions easily enter and release the bond. Montmorillonite crystals have very small size and very large interest in water. This is the reason why this clay mineral is easy to swell and shrink due to changes in water content.

Additive substances that are mixed with soil result in the process of exchanging alkali cations ( $\text{Na}^+$  and  $\text{K}^+$ ) from the soil replaced by cations from additives so that the size of the clay grains increases (flocculation). After flocculation process occurred, pozzolanic and hydration process follows in soil stabilization. The pozzolanic process occurs between calcium hydroxide from soil reacting with silicates ( $\text{SiO}_2$ ) and aluminate ( $\text{AlO}_3$ ) from additives to form a binding material consisting of calcium silicate or aluminate silicate. The reaction of  $\text{Ca}^{2+}$  ions with silicates and aluminate from the surface of clay particles forms a cemented (hydrated gel) paste that binds soil particles. The cementation reactions that occur in soil mixtures with additives form new grains that are harder so that they are more resistant to the load given.

## TESTING PROGRAM AND RESULT

Durability test specified for lime stabilized soil is specimens are compacted at OMC into molds using either standard or modified Proctor compaction effort immediately after mixing, placed in sealed containers, and then cured for 7 days. After curing, specimens are then placed in a chamber that is subsequently evacuated to a pressure of 24 in. Hg (11.8 psi). After that the chamber is flooded with distilled water and specimens are allowed to soak. Dry wet cycle is carried out in 4 days of submerged conditions and 4 days of dry conditions. The

difference in sample height will be calculated as a change in volume and calculated as potential swell. The carrying capacity of the soil will be measured after dry conditions in one cycle

### Durability of natural soil

Natural soil test result are presented in Table 1. Based on USCS and AASHTO classifications, the soil is classified as high plasticity clay and a poor soil type as a road subgrade layer which the value of soil activity (A) is very high swell potential. The value of un-soaked California Bearing Ratio is 14.7% and soaked CBR is 4.6% at 21.9% moisture content and dry density of  $0.82 \text{ gram/cm}^3$ .

Table 1 Physical properties of expansive soil

| No | Parameters               | Value |
|----|--------------------------|-------|
| 1  | Specific Gravity (Gs)    | 2.68  |
| 2  | Liquid Limit (LL), %     | 81.5  |
| 3  | Plastic Limit (PL), %    | 35.6  |
| 4  | Shrinkage Limit (SL), %  | 6.7   |
| 5  | Plasticity Index (PI), % | 45.9  |

The sample height increased rapidly on the first day and grew slowly the following day. Although the sample was air dried for 4 days but could not evaporate the absorbed water when soaked, so that the water content after drying was still higher than before soaking. CBR decline in the first cycle is very large as in Figure 1. The dry-wet cycle shows a tendency to reduce the strength of the soil until 87%.

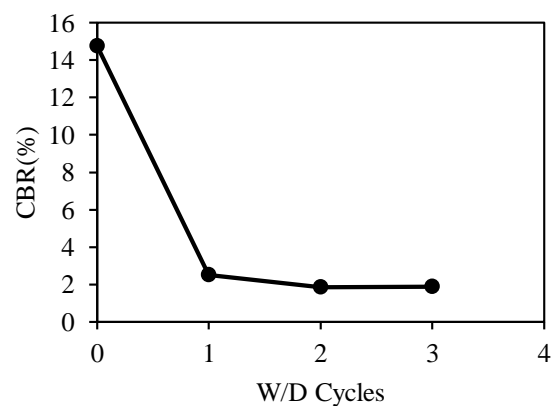


Fig. 1 Influence wetting-drying cycle of natural soil to CBR

The same phenomenon also occurs in the swell as shown in Figure 2. Because the immersion on the first day is already very large (Figure 3), the binding of water to the next increment in cycles two and three becomes insignificant. This shows the soil during the first rainy season every year has decreased the ability to withstand the load and show corrugation on the

road surface. If the swell potential test is obtained at a value of 5.5%, then the wet-dry cycle turns up to 7.1%.

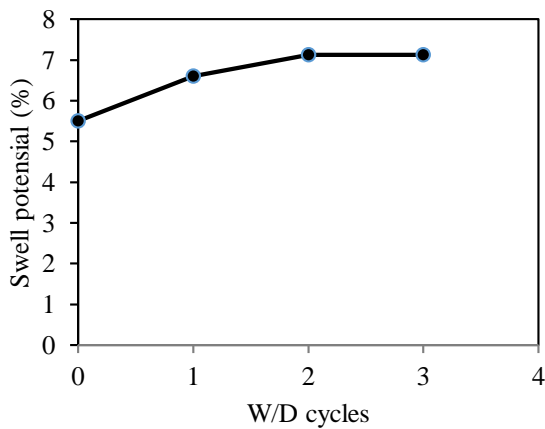


Fig. 2 Influence wetting-drying cycle of natural soil to swell potential

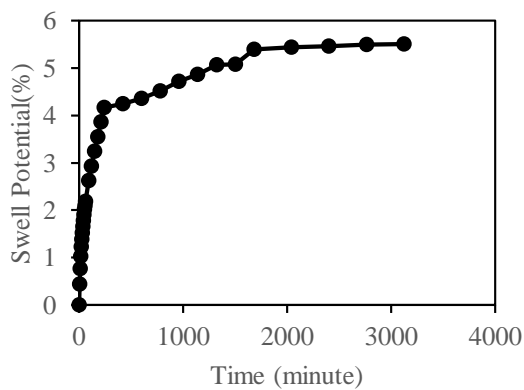


Fig. 3 Swell potential in first cycle

### The durability of lime improved soil

Local lime was used in this study as additive agent. Thus, five different lime content of 0, 6, 8, 9, 10% by soil weight were investigated the optimal lime content. Optimization of lime content is needed to determine the minimum amount of lime needed in stabilized soils to achieve adequate levels of rigidity to withstand environmental conditions and prevent solubility (Figure 4).

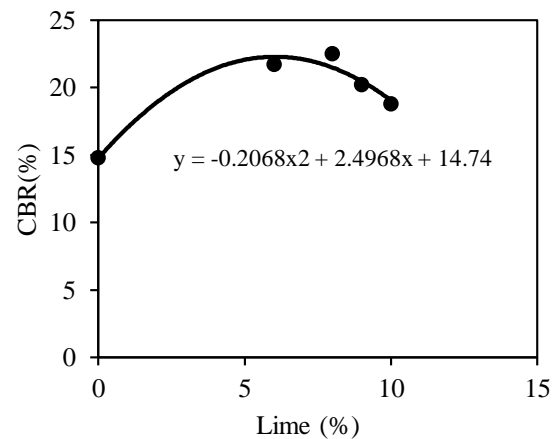


Fig. 4 Changes in CBR Value based on improved soil

The second set was tested for swell potential to analyze the changes due to differences in the dosage of lime mixed with the soil as shown in Figure 5. Swell potential could be reach less than 0.5% at 4% lime.

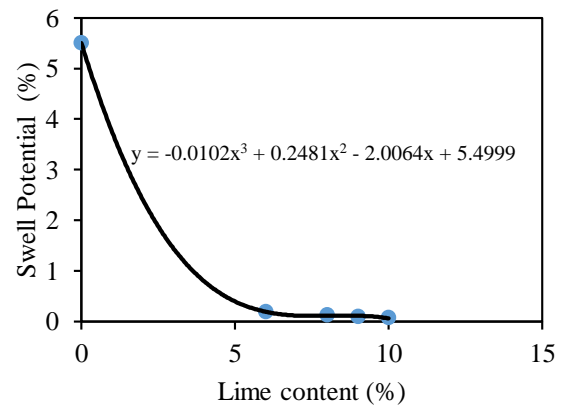


Fig. 5 Decrease in swell potential of expansive soil due to lime

In this study soil mixtures and lime at a dosage of 4% have increased strength by 62% and reduced swell potential by 90%. W / D testing will be carried out.

Harichane et al.[8] investigated effect of different curing time for lime improved soil on shear stress. Addition of lime has a significant effect on shear stress particularly beyond 28 days and in samples containing 8% lime for both grey and red soils tested. There is a significant difference in the strength of soil shear mixed with lime, natural pozzolana and a combination of lime-pozzolana. The difference in the content of additive material other than the characteristics of the original soil will determine curing time.

In this study curing time was also carried out in lime improved soil for seven days. During this time lime and soil are expected to undergo a process of flocculation, hydration and cementation.

After treatment, the initial step of the dry-wet cycle is carried out on the sample. The initial CBR was 23.7% had decreased after the first wet cycle so that its strength was reduced to 42% where there was a decrease of up to 13.6% (Figure 6). The CBR values of untreated and treated samples for different wet-dry cycle times are presented in Table 1.

However, improved soil has a limit of reliability to environmental changes. The time needed to produce a durable mixture is highly recommended by several factors such as the type of additive and the time needed to achieve maximum strength before being utilized, environmental changes that affect the mixture.

Table 1 Result CBR during cyclic wetting-drying process

| Type of soil  | Cycles | CBR (%) | Strength loss (%) |
|---------------|--------|---------|-------------------|
| Natural soil  | 0      | 14.76   |                   |
| Improves soil | 0      | 23.7    |                   |
|               | 1      | 13.60   | 42.62             |
|               | 2      | 7.6     | 67.93             |
|               | 3      | 7.6     | 67.93             |

Based on the Chittoori BCS at al. [20] study, all the soils dominated by clay minerals will fail early in the lower additive content. The content of montmorillonite determines the technical characteristics of stabilized soil. Clay soils with the same plasticity will have different properties when given the same dose of additive. In this study, the dosage of lime was indeed under the optimum mixture so that only 3 cycles of strength degradation had occurred.

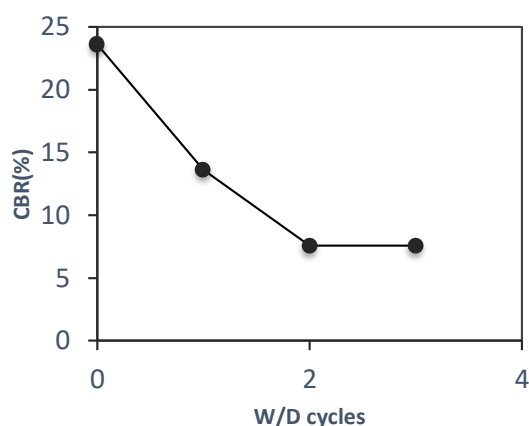
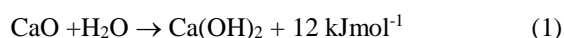


Fig. 6 CBR value in wetting-drying cycle

Due to the subsequent dry-wet process, the soil strength has decreased, which shows that the lime

bonding is not strong, so it is easily removed, so the CBR drops.

In the early stages of adding lime will cause the hydration process of quicklime.



Mixing of soil and lime will increase  $\text{Ca}^{+2}$  and pH, cation exchange modification of clay particles that cause aggregation of clay particles. Short-term results are improvements in workability and reduced swell potential (also shrinkage).

Furthermore, the physic-chemical stabilization process depends on the time of treatment. The measure of acidity (pH) will cause the release of Si and Al so that the reaction will occur as follows:



This is the basic process of the hydro setting reaction where the clinker reaction with water will form a cementitious compound (CSH CASH, etc.). The presence of some chemicals can change the reaction settings:

- Sulphur lead the formation of ettringite which causes swelling
- Nitrate causes a decrease in USCS
- Phosphate can interfere with the hydration process
- Chloride accelerates hydration but leads to the salt formation and reduces the strength
- Other minerals (mica) prevent reactions and cause swelling of swelling

The treated soil is in the first submerging in water causes a potential swell increase of up to 0.5% , then increase until 3% in first cycle. The following dry-wet cycle of two soil types showed insignificant changes after the first cycle (Figure 7).

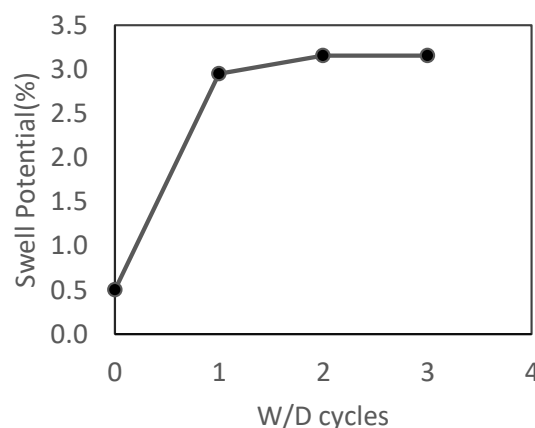


Fig. 7 Swell potential in the wetting-drying cycle of lime improved soil

Guney et al. [7] conducted a cyclic wetting-drying experiment to observe the effects of lime stabilization

on the swell potential. In that study, both potential swelling tests and swell pressure were performed on soil specimens that were not treated and treated with lime, subject to cyclic wetting-drying. It observed that the main advance of lime stabilization disappeared after the first wetting-drying cycle, and the potential for swelling increased for the next cycle.

## CONCLUSIONS

Natural soil is an active expansive soil with very high swell potential which effect to pavement structure in this area that damaged every year due to high rainfall. The addition of lime increases expansive soil strength and reduces the shrinkage properties. Improved lime soil with sufficient curing time will have higher mechanical properties than without curing. The environment also changes such as changes in water content and the presence of certain chemicals can reduce strength and increase the swelling in the soil. The durability of improved soil is determined by the optimum lime content, the time needed for maximum cementation in addition to environmental disturbances that can cause degradation. The same soil can have different durability due to different environmental changes. Untreated specimens have poor water stability, which will collapse after immersion in water at the first cycle. The strength reduce 83% and almost loss it in second cycle. Although in the modified soil there was also a decrease in strength in the first cycle but still in a fairly good soil condition ( $\text{CBR} > 10\%$ ), but in the second cycle collapsing occurred. The same thing happens to swell potential, although swelling increases but is still lower than natural soil. The collapse occurs earlier due to a low additive content. It is recommended to increase the percentage of additives in modified soil.

## REFERENCES

- [1] Parihar N.S, Shukla R.P. and Gupta A.K., Shear strength of medium plastic expansive soil reinforced with polyester fibers, *Slovak journal of civil eng.*, Vol. 26, no.2, 2018, pp. 1-8.
- [2] Addison M.B. and Polma F.A., Extending Durability of Lime Modified Clay Subgrades With Cement Stabilization, *GSP 172 Soil Improvement*, Geo-Denver, February 18-21, 2007 | Denver, Colorado, United States.
- [3] Aldaood A., Bouaskera M. and Al-Mukhtar M. , Impact of wetting–drying cycles on the microstructure and mechanical properties of lime-stabilized gypseous soils, *Engineering Geology*, Elsevier, Vol 174, 2014, pp. 11-21.
- [4] Al-Kiki I.M., Al-Atalla M.A. and Al-Zubaydi A.H., Long term strength and durability of clayey soil stabilized with lime, *Eng. & Tech. Journal*, Vol.29, No.4, 2011.
- [5] Bell .F.G, Lime stabilization of clays minerals and soils, *Engineering Geology*, Elsevier, Vol.42, 1996, pp 223-237.
- [6] Calik U. and Sadoglu E., Classification, shear strength, and durability of expansive clayey soil stabilized with lime and perlite, *Nat Hazards* , 71, 2014, pp.1289–1303.
- [7] Guney, Y., Sari, D., Cetin, M., and Tuncan, M., Impact of cyclic wetting–drying on swelling behaviour of lime-stabilized soil." *Building and Environment*, 42(2),2007, pp. 681-688.
- [8] Harichane K., Ghrici M. and Kenai S., Effect of curing time on shear strength of cohesive soils stabilized with combination of lime and natural pozzolana, *International Journal of Civil engineering, geotechnical engineering*, Vol. 9, No. 2, 2011.
- [9] Mir B.A., Some studies on the effect of fly ash and lime on the physical and mechanical properties expansive clay", *IJCE*, 13, 2015, pp.203- 212.
- [10] Kathrik S., Soil Stabilization by Using Fly Ash, *IOSR Journal of Mechanical and Civil Engineering (IOSR-JMCE)*, Vol.10, Issue 6, 2014.
- [11] Zaika Y, Rachmansyah, A, 2017, The estimation of bearing capacity and swell potential of deep soil mixing on expansive soil by small scale model test, *International Journal of Geomate*, Vol.13, Issue 38, pp.09-15.
- [12] Ahmed A. and Ugai K., Environmental effects on durability of soil stabilized with recycled gypsum, *Cold Regions Science and Technology*, Elsevier ,Vol. 66,2011, pp. 84-92.
- [13] Yilmas I and Civelekoglu.I, Gypsum: An additive for stabilization of swelling clay soils, *Applied clay science*, Elsevier, 44, 2009, pp.166-172.
- [14] Rahmansyah, A, Zaika. Y. Improvement of expansive soil of east java, Indonesia by using industrial solid waste, *Proc. Int. Conf. on unsaturated soil UNSAT*, 2014, Sydney, Australia
- [15] Zaika Y, Soeharjono A and Anwar R, Improving Expansive Soil by Using Combination of Rice Husk Ash and Fly Ash, 2015, *EJGE*, vol. 20, no. 8, pp. 2055 – 2063.
- [16] Zaika Y and Soeharjono A, 2016, Bagasse Ash (BA) and Additive Materials treated Expansive soil, *EJGE*, Vol.21, No. 20, pp. 7085-7094.
- [17] Azzam W.R., Durability of expansive soil using advanced nanocomposite stabilization, *International Journal of Geomate*, Vol. 7, No. 1, 2014 , pp. 927-937.
- [18] Wang B., Zhang C., Qiu X, Ji, E and Zhang, W., (2015) Research on Wetting-Drying Cycles' Effect on the Physical and Mechanical Properties of Expansive Soil Improved by OTAC-KCl, *Advances in Materials Science and Engineering*, 2015, Hindawi Publishing Corporation.
- [19] Razali N., Sa'don N.M. and Karim A.R, Strength and durability effect on stabilized subgrade soil,

- Journal of Civil Engineering, Science and Technology Vol. 7, Issue 1, 2016.
- [20] Chittoori B.C.S, Puppala A.J. and Pedarla A., Addressing clay mineralogy effects on performance of chemically stabilized expansive soils subjected to seasonal wetting and drying, Journal of geotechnical and geoenvironmental engineering, Vol. 144, Issue 1, 2018.



## **DURABILITY OF CONCRETE CONTAINING RECYCLED ASPHALTIC CONCRETE AGGREGATE AND HIGH CALCIUM FLY ASH**

Prinya Chindapasirt<sup>1</sup>, Pornnapa Kasemsiri<sup>2</sup>, Sompron Leekongbub<sup>3</sup> and Patcharapol Posi<sup>4\*</sup>

<sup>1</sup>Sustainable Infrastructure Research and Development Center, Department of Civil Engineering,  
Faculty of Engineering, Khon Kaen University

<sup>2</sup>Sustainable Infrastructure Research and Development Center, Department of Chemical Engineering,  
Faculty of Engineering, Khon Kaen University.

<sup>3,4</sup>Department of Civil Engineering, Faculty of Engineering, Rajamangala University of Technology Isan

### **ABSTRACT**

In this research, the durability of concrete containing recycled asphaltic concrete (RAC) aggregate and fly ash were studied. The concrete was made from ordinary Portland cement (OPC), fly ash, water, sand and combination of natural limestone and RAC aggregates. The RAC aggregate was obtained from the discarded asphaltic pavement. After its service life, the asphaltic concrete is replaced with the new material and this results in a large amount of discarded old asphaltic concrete. The RAC aggregate was used to replace natural limestone aggregate at the replacement levels of 0, 10, 20, and 30 % of the total weight of aggregate. In addition, the high calcium fly ash from Mae Moh power station in the north of Thailand was used to partially replace OPC at the dosages of 0, 20, and 40 % by mass. The compressive strength, water absorption, porosity, flexural strength, modulus of elasticity and resistance to sulfuric acid were tested. The results showed that concretes with 28-day compressive strengths between 22.5 and 33.0 MPa, water absorption between 5.3-5.9 %, porosity between 12.2 and 13.5 %, flexural strength between 4.4 and 5.5 MPa, modulus of elasticity between 25.6 and 30.0 GPa were obtained. The replacement levels of RAC at 10 % and fly ash at 20 % gave the optimum compressive strength and mechanical properties of concrete for use as pavement concrete. In addition, the using of RAC aggregate together with fly ash in concrete work improved water absorption, porosity and sulfuric acid resistance. It has thus been shown that RAC and high calcium fly ash could be used in the manufacturing of concrete with the emphasis on the use of waste material and reduction in OPC which in turn would increase the sustainability of construction industry.

*Keywords: Fly ash, Concrete, Durability, Recycled asphaltic concrete, Surface abrasion*

### **INTRODUCTION**

The economic development and urban growth increase the utilization of energy and natural resources in the industrial, agricultural and transportation sector. The energy consumption in industrial sector is around 36 percent, and the transportation sector is around 35 percent with the majority is in the road transport (87 percent). The consumption of energy causes air pollution and environmental problems,

The road transportation usually consists of good networks and facilities. The highways in Thailand cover a distance of over 71,470 kilometers per 2 traffic lanes and are mostly (92 percent) asphalt road. These roads require maintenance and restoration to stay in good condition for convenience, speed and safety. The restoration of asphalt concrete pavement is done using the reclaim asphalt pavement (RAP). The original pavement was recycled by mixing with cement and used for the pavement layer. The new asphalt concrete is then laid to replace the original

pavement. A large amount of RAP materials are obtained from the scraping off the original pavements to maintain the pavement level, scraping of from the bulging of original pavement due to the wheel track, or from the construction of new pathway. These RAP materials are piled up as discarded asphalt as shown in Fig. 1. Some of this RAP material are reused by mixing with asphalt cement to repair road, or mixed with cement to make concrete products in the pathway, such as concrete curb, concrete barrier, but there are a lot of RAP materials waiting to be utilized.

In the construction industry, Portland cement is used as the main binding material and a large amount of cement production is thus required each year [1]. The manufacturing process involves rock blasting, digesting, conveying, burning and fine grinding. This results in large amount of carbon dioxide emissions and thus increases the greenhouse effect, which affected the environment negatively [2]. Moreover, the Portland cement production process consumes enormous energy. Previous researched had shown that class C high calcium fly ash with some cementing

property could be used successfully as partial replacement of Portland cement [3, 4] and as starting material in geopolymer [5].



**Figure 1.** Discarded asphalt pavement storage area.

This research, therefore, aims to investigate the reuse of RAP materials as a coarse aggregate in the concrete mixture and also the use of high calcium fly ash to partially replace Portland cement. The RAP material was sorted to obtain the required size and is called Recycle Asphalt Concrete Aggregate (RAC aggregate). It was used to replace natural coarse aggregates. High calcium fly ash was also used to partially replace Portland cement to improve the concrete quality. The suitable proportions for concrete pavements were obtained with cost saving due to the use of RAC aggregate and fly ash with the reduced amount of natural aggregate and Portland cement. It is also a conservation of the environment, reduce the amount of waste and reduce the use of natural resources.

## EXPERIMENTAL PROGRAM

### Materials

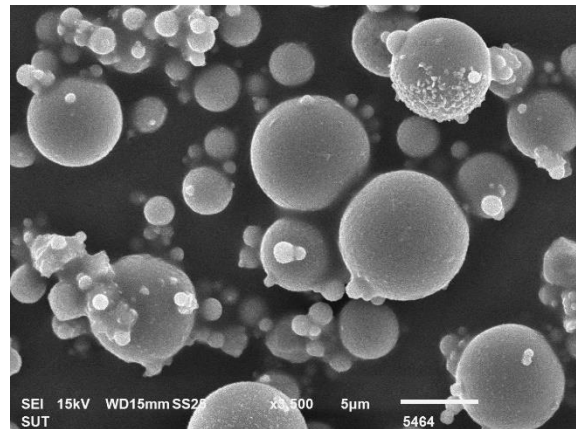
Materials used in this research consisted of ordinary Portland cement (OPC), river sand, crushed lime stone aggregate, water, fly ash (FA) and RAC aggregate. The FA was a class C high calcium from Mae Moh power station in Lampang province, northern Thailand. The RAC aggregate with the particle size between 4.75-19.10 mm and 3.5 % asphalt was from reclaimed asphalt pavement as shown in Fig. 2. The physical properties of materials are shown in Table 1. The morphology of FA by SEM as shown in Fig. 3 indicated that the shape of FA was spherical with smooth surface. The chemical compositions of FA are shown in Table 2. The specific gravity of FA was 2.66 with median particle size of 18.6  $\mu\text{m}$ . The FA consisted of a high content of 36.20%  $\text{SiO}_2$ , 15.52%  $\text{Al}_2\text{O}_3$ , 14.25%  $\text{Fe}_2\text{O}_3$ , and 22.57%  $\text{CaO}$  with the loss on ignition (LOI) of 0.88%. The high calcium content in fly ash gave its cementing property. The XRD of FA as shown in Fig. 4 indicated the high amorphous content with relatively large hump around 22-38  $^{\circ}2\theta$ .



**Figure 2.** RAC aggregate.

**Table 1.** The physical properties of materials

| Materials                              | Sand | OPC  | FA   | RAC<br>agg. | Natural<br>coarse<br>agg. |
|--|------|------|------|-------------|---------------------------|
| Specific gravity                       | 2.61 | 3.15 | 2.66 | 2.39        | 2.7                       |
| Median particle size ( $\mu\text{m}$ ) | -    | 14.6 | 18.6 | -           | -                         |
| Fineness modulus                       | 2.65 | -    | -    | -           | -                         |
| Unit weight ( $\text{kg/m}^3$ )        | 1360 | 1440 | -    | 1266        | 1598                      |
| Abrasion Loss (%)                      | -    | -    | -    | 29.5        | 22.4                      |
| Water absorption (%)                   | 1.17 | -    | -    | 0.36        | 0.46                      |

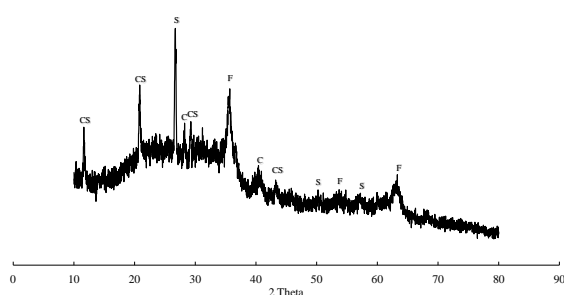


**Figure 3.** The morphology of FA by SEM

### Mix proportion

#### FA and RAC aggregate contents

To study the durability of concrete containing recycled asphaltic concrete (RAC) aggregate and high calcium fly ash, the OPC was replaced with FA at the levels of 0, 20, and 40 % by weight and the natural lime stone aggregate was replaced with RAC aggregate at the replacement levels of 0, 10, 20, and 30 % by weight. The compressive strength, water absorption, porosity, modulus of elasticity, flexural strength and sulfuric acid resistance of concrete containing recycled asphaltic concrete (RAC) aggregate and FA were determined. In order to obtain adequate data, three series of mixes totaling 12 mixes as shown in Table 3 were tested.



**Figure 4.** The XRD of FA. F-Maghemite:  $\text{Fe}_2\text{O}_3$ ;  $\text{Fe}_2\text{O}_3$ ; C-Anhydrite; CS-Gypsum:  $\text{CaSO}_4$ ; S-Quartz:  $\text{SiO}_2$ .

**Table 2.** Chemical composition of materials (by weight)

| Chemical compositions (%) | FA    | OPC  |
|---------------------------|-------|------|
| $\text{SiO}_2$            | 36.20 | 20.8 |
| $\text{Al}_2\text{O}_3$   | 15.52 | 4.7  |
| $\text{Fe}_2\text{O}_3$   | 14.25 | 3.4  |
| CaO                       | 22.57 | 65.3 |
| $\text{K}_2\text{O}$      | 1.63  | 0.4  |
| $\text{Na}_2\text{O}$     | 0.33  | 0.1  |
| $\text{SO}_3$             | 8.9   | 2.7  |
| LOI                       | 0.88  | 0.9  |

#### Details of Mixing

For mixing, OPC and FA were firstly mixed together until the mixture was homogenous. Next, sand was added and mixed for 5 min. Next, crushed lime stone aggregate and RAC aggregate were added and mixed for 5 min. Finally, water was added and mixed for another 5 minutes to obtain a homogenous mixture.

The fresh concrete was placed into 150x300 mm cylindrical molds, 100x100x100 mm cube molds and 150x150x500 mm prism molds. The specimens were demolded at 1 day and stored in water.

#### Details of test

##### Compressive strength

The cylindrical specimens size 150x300 mm were tested to determine the compressive strength in accordance with ASTM C39/C39M-18 [6]. The reported compressive strength was the average of three samples.

**Table 3.** Mixture of concrete by weight. ( $\text{kg}/\text{m}^3$ )

| Table 3: Mixture of concrete by weight. (kg/m <sup>3</sup> ) |        |    |      |        |     |       |
|--|--------|----|------|--------|-----|-------|
| Mix  | Cement | FA | Fine | Coarse | RAC | Water |
|  |        |    | Agg. | Agg.   |     |       |
| 0F - 00R   | 394    | -  | 590  | 1138   | -   | 213   |

|          |     |     |     |      |     |     |
|----------|-----|-----|-----|------|-----|-----|
| 0F - 10R | 394 | -   | 590 | 1024 | 114 | 213 |
| 0F - 20R | 394 | -   | 590 | 910  | 228 | 213 |
| 0F - 30R | 394 | -   | 590 | 797  | 341 | 213 |
| 20F-00R  | 315 | 79  | 590 | 1138 | -   | 213 |
| 20F-10R  | 315 | 79  | 590 | 1024 | 114 | 213 |
| 20F-20R  | 315 | 79  | 590 | 910  | 228 | 213 |
| 20F-30R  | 315 | 79  | 590 | 797  | 341 | 213 |
| 40F-00R  | 236 | 158 | 590 | 1138 | -   | 213 |
| 40F-10R  | 236 | 158 | 590 | 1024 | 114 | 213 |
| 40F-20R  | 236 | 158 | 590 | 910  | 228 | 213 |
| 40F-30R  | 236 | 158 | 590 | 797  | 341 | 213 |

0F-00R = fly ash of 0 % and RAC aggregate of 0 %,

Fine Agg. = fine aggregate, Coarse Agg. = coarse aggregate.

#### Porosity and water absorption

The cube specimens size 100x100x100 mm were tested to determine the porosity and water absorption in accordance with ASTM C642-13 [7]. The reported porosity and water absorption were the average of three samples.

#### Modulus of elasticity

The cylindrical specimens size 150x300 mm were tested to determine the modulus of elasticity in accordance with ASTM C469/C469M-14 [8]. The reported modulus of elasticity was the average of three samples.

#### Flexural strength

The prism specimens size 150x150x500 mm were tested to determine the flexural strength in accordance with ASTM C293-02 [9]. The reported flexural strength was the average of three samples.

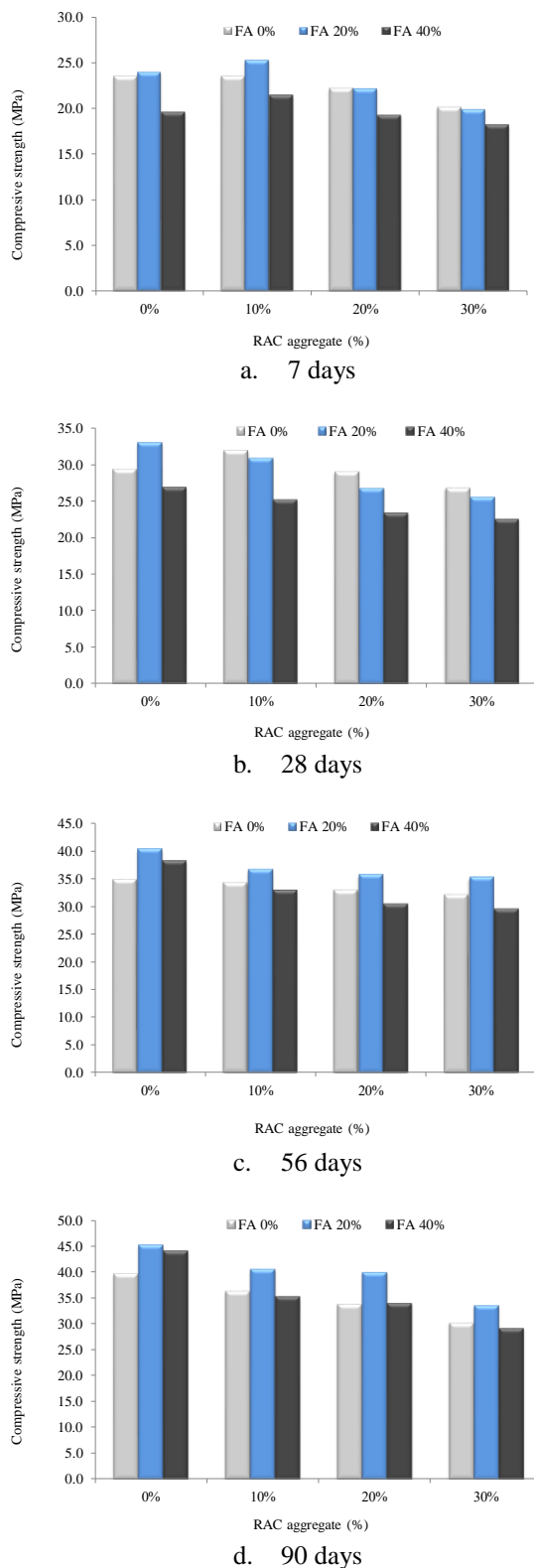
#### The resistance to sulfuric acid

The cube specimens size 100x100x100 mm were tested to determine the resistance to sulfuric acid in accordance with ASTM C267-01 [10]. The reported resistance to sulfuric acid was the average of three samples.

## RESULTS AND DISCUSSIONS

#### Compressive strength

The results of compressive strength of concrete containing RAC aggregate and fly ash are shown in Fig. 5. The compressive strength decreased with increasing RAC aggregate content. For example, the compressive strength at 28 days of mixes with 20 % FA by weight with 0, 10, 20, and 30 % RAC aggregate were 32.9, 30.8, 26.7, and 25.5 MPa, respectively.



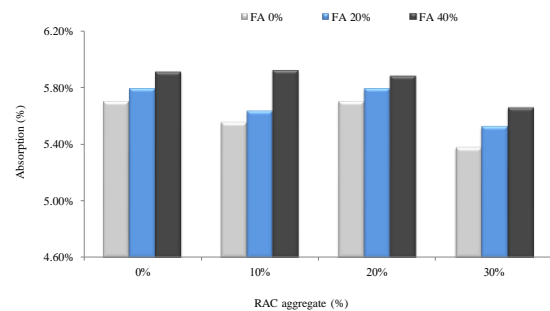
**Figure 5.** Compressive strengths at 7, 28, 56 and 90 days

The RAC aggregate was partly covered with asphalt and its use thus resulted in the reduced bond between cement paste and RAC aggregate compared

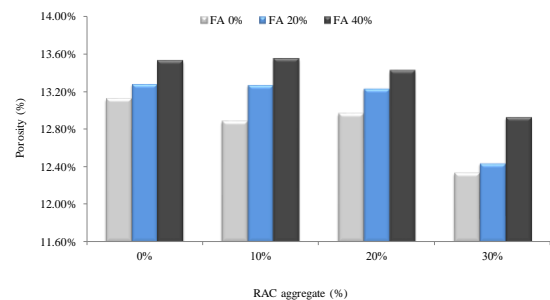
with that of natural lime stone aggregate. This negatively affected the aggregate bonding and reduced the strength of concrete.

With regards to the effect of fly ash content, the compressive strength development of concrete containing fly ash was quite good. The general trend was that the replacement level of 20% improved the compressive strength of the mixes. This was in line with the reported result that normally the strength of concrete with proper amount of fly ash could slightly increase compared with that of normal concrete [3, 4]. The incorporation of fly ash increased the workability of the mix and also resulted in the increases in pozzolanic reaction and filling of the void [11, 12]. Especially when the concrete age was more than 28 days, the pozzolanic effect was more noticeable as indicated by the increases in compressive strengths at 56 and 90 days as shown in Fig. 5(c) and 5(d). For example, the compressive strengths at 56 days of mixes with 10 % RAC aggregate and 0, 20, and 40 % FA were 34.2, 36.6, and 32.9 MPa, respectively.

#### Porosity and water absorption



**Figure 6.** Water absorption at 28 days



**Figure 7.** Porosity at 28 days

The results of water absorption and porosity of concrete containing RAC aggregate and fly ash are shown in Figs. 6 and 7. With regards to the effect of content of fly ash, both water absorption and porosity at 28 days increased with the increasing content of fly ash. The use of fly ash to partially replace OPC resulted in changes in paste content, pore size and

pore structure. However, the early reactions depend on OPC, as a result the pore of fly ash cement paste was increased compared to that of the mixture without fly ash. But the distribution of the pore was improved because the fly ash with circular particles made the dispersion better in cement paste. This resulted in the smaller average size of pore with increasing amount of fly ash [13]. This affected directly and increased the porosity of the samples at the early age. For example, the porosities of mixes with 10 % RAC aggregate and 0, 20, and 40 % fly ash were 12.88, 13.26, and 13.54 %, respectively. In contrast, the increase in RAC aggregate improved the water absorption characteristics and reduced the porosity of concrete. This was due to the fact that the surface of RAC aggregate was partially coated with asphalt (Fig. 1) and this lowered its water absorption (Table 1). For example, the water absorptions of mix with 40 % fly ash and 0, 10, 20, and 30 % RAC aggregate were 5.91, 5.92, 5.88, and 5.66 %, respectively.

### Modulus of elasticity

The results of modulus of elasticity of concrete containing RAC aggregate and fly ash are shown in Fig. 8. The modulus of elasticity tended to decrease with the increasing in the content of RAC aggregate and this trend was similar to the reduction in compressive strength. For example, the moduli of elasticity at 28 days of the 40 % fly ash mix with 0, 10, 20, and 30 % RAC aggregate were 29.20, 27.10, 26.05, and 25.65 GPa, respectively. The modulus of elasticity is affected by the properties of aggregate, water to binder ratio and compressive strength [14, 15]. Normally, a higher value of modulus of elasticity for a given concrete strength indicates the better quality.

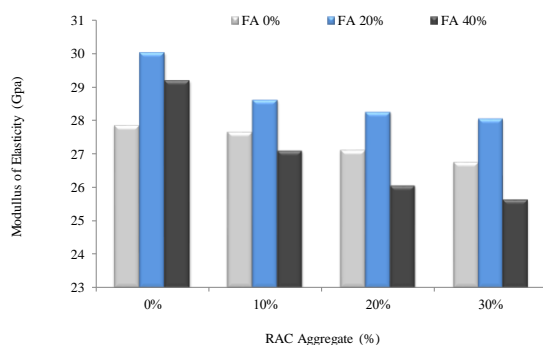


Figure 8. Modulus of elasticity at 28 days

### Flexural strengths

The results of flexural strength of concrete containing RAC aggregate and fly ash are shown in Fig. 9. With regards to the effect of content of fly ash, the flexural strengths increased with the incorporation of fly ash at the 20 % replacement levels but at the

content of fly ash beyond 20 %, the flexural strengths started to decrease. In general, the increase of flexural strength was due to the increase in the reaction products from OPC and fly ash. This was associated with the improvement of compressive strength and modulus of elasticity of fly ash concrete which led to the improvement in flexural strength [3, 16]. For example, the flexural strength at 28 days of the mixes with 20 % RAC aggregate and 0, 20, and 40 % fly ash were 4.66, 4.99, and 4.61 MPa, respectively. With regards to the effect of RAC aggregate content, the flexural strength decreased with increasing RAC aggregate content due to the increase in the amount of weak bond between the RAC aggregate and the matrix. For example, the flexural strengths at 28 days of mixes with 40 % FA and 0, 10, 20, and 30 % RAC aggregate were 4.64, 4.63, 4.61, and 4.40 MPa, respectively.

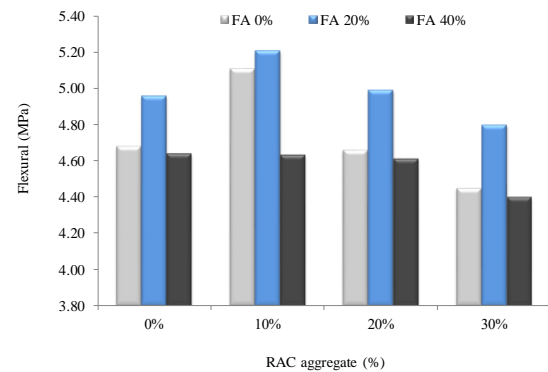
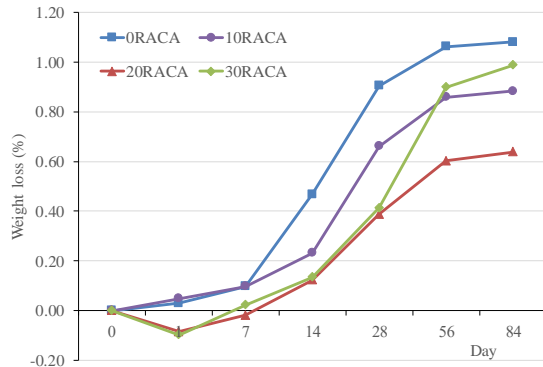


Figure 9. Flexural strengths at 28 days

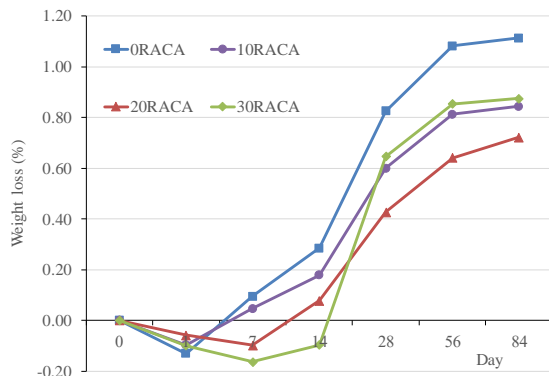
### Sulfuric acid resistance

The results of weight losses in sulfuric acid of concrete containing RAC aggregate and fly ash are shown in Fig. 10. All concrete specimens were immersed in the 1 % sulfuric acid solution for 84 days to study the durability in an acidic environment. The results indicated that the resistance to acid increased slightly with the increasing fly ash content, which was in line with previously reported results [17]. The increase in fly ash reduced the amount of calcium hydroxide in the mix. The reduced calcium hydroxide and the resulting calcium silicate hydrate with low calcium made the sample more durable in the acid environment [17]. In addition, the acid resistance of the cement paste was shown to be dependent on the continuous pore and the acid neutralization capacity of matrix [18]. At the low content of fly ash, the weight loss was high due also to the presence of a large amount of continuous pore in the concrete (Fig. 9a) which were conducive to the attack from sulfuric acid. For example, the weight losses after 84 days in sulfuric acid of the mixes with 10 % RAC aggregate and 0, 20, and 40 % fly ash were 0.88, 0.84, and 0.79 %, respectively. However, the increase in porosity was associated with the pore refining resulting and

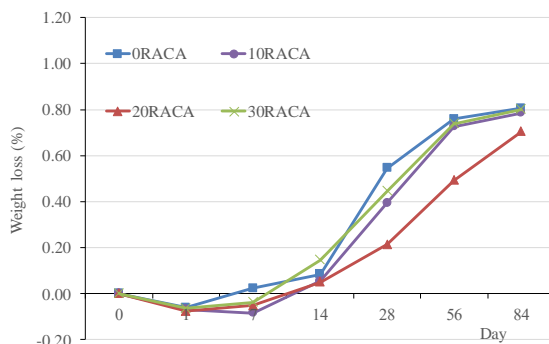
the reduction in the average pore size of paste [13]. The high replacement level of fly ash also resulted in the strength reduction. The resistance to sulfuric acid attack was, therefore, increased but only slightly due to some of the negative effect as well.



a. FA 0 %



b. FA 20 %



c. FA 40 %

**Figure 10.** Sulfuric acid resistance at 28 days

The results also indicated that the resistance to sulfuric acid increased with the incorporation of RAC and the optimum RAC content was 20%. The weight losses after 84 days in sulfuric acid of the mixes with 20 % fly ash and 0, 10, 20, and 30 % RAC aggregate were 1.11, 0.84, 0.72, and 0.87 %, respectively.

Although the incorporation of 20% RAC resulted in a slight reduction in strength of sample, the porosity and water absorption were reduced and this increased the resistance to acid attack as opposed to the reduction in strength and modulus of elasticity of the samples.

The increase in the resistance to acid attack of concrete containing RAC was thus due to the reduced porosity of the sample as a result of the presence of asphalt adhered to the aggregate surface. But the excessive amount of RAC aggregate at 30 % resulted in the increased weight loss due to the adverse effect on the compressive strength.

However, the use of RAC aggregate can improved some of the important engineering properties including impermeability, flexibility, and resistance against erosion as also reported by other researchers [19].

## CONCLUSIONS

Based on the obtained data, the following conclusions can be drawn:

1. The replacement of natural limestone aggregate with RAC aggregate at the level of 0-30% resulted in the reduction in compressive strength, modulus of elasticity and flexural strength due to the decrease in the bonding of cement paste and aggregate as a result of the attached asphalt at the surface of aggregate.

2. The incorporation of RAC aggregate resulted in the improvement of water absorption, porosity and sulfuric acid resistance of concrete.

3. The weight losses from the attack of sulfuric acid decreased and the optimum content of RAC aggregate was 20 % replacement level. The replacement beyond this level resulted in the high weight losses due to the reduction in the strength of the sample.

4. The results showed that the concrete containing 10 % RAC aggregate and 20 % fly ash had 28-day compressive strength of 31.0 MPa, flexural strength of 5.2 MPa and modulus of elasticity of 28.6 GPa with improved water absorption, porosity and durability in terms of acid resistance. It can be used to make concrete pavements in areas with low and light traffic. It can also be used to make simple concrete structures such as concrete barrier and barrier curb.

Moreover, it has also been shown that the use of RAC and fly ash can increase the waste material utilization, reduce the cement usage and increase the sustainability of construction industry.

## ACKNOWLEDGEMENT

This research is financially supported by the Faculty of Engineering, Rajamangala University of Technology Isan Khon Kaen Campus. The support of the Thailand Research Fund (TRF) under the TRF



Distinguished Research Professor Grant No. DPG6180002 is also gratefully acknowledged here.

## REFERENCES

- [1] Wongkvanklom, A., et al., Structural lightweight concrete containing recycled lightweight concrete aggregate, *KSCE Journal of Civil Engineering*, Vol.22, Issue 8, 2018, pp. 3077-3084.
- [2] Malhotra, V.M., Introduction: sustainable development and concrete technology. *Concrete International*, 2002, pp. 22-24.
- [3] Posi, P., et al., effect of fly ash fineness on compressive, flexural and shear strength of high strength-high volume fly ash jointing mortar, *International Journal of GEOMATE*, Vol.16, Issue 54, 2019, pp. 36-41.
- [4] Chindapasirt, P., et al., Influence of fly ash fineness on the chloride penetration of concrete, *Construction and Building Materials*, Vol.21, Issue 2, 2007, pp. 356-361.
- [5] Heng, K., N. Areemit, and P. Chindapasirt, , Behavior of concrete cylinders confined by a ferro-geopolymer jacket in axial compression, *Engineering and Applied Science Research*, Vol.44, Issue 2, 2017, pp. 90-96.
- [6] ASTM C39/C39M-18, Standard test method for compressive strength of cylindrical concrete specimens, *Annual Book of ASTM Standard*, 2018, Vol.04.02.
- [7] ASTM C642-13, Standard Test Method for Density, Absorption, and Voids in Hardened Concrete, *Annual Book of ASTM Standard*, 2013, Vol.04.02.
- [8] ASTM C469/C469M-14, Standard Test Method for Static Modulus of Elasticity and Poisson's Ratio of Concrete in Compression, *Annual Book of ASTM Standard*, 2014, Vol.02.01.
- [9] ASTM C293-02, Standard Test Method for Flexural Strength of Concrete (Using Simple Beam with Center-Point Loading), *Annual Book of ASTM Standard*, 2002, Vol.04.02.
- [10] ASTM C267-01(2012), Standard test methods for chemical resistance of mortars, grouts, and monolithic surfacings and polymer concretes, *Annual Book of ASTM Standard*, 2012, Vol.06.02.
- [11] Chindapasirt, P., S. Homwuttiwong, and V. Sirivivatnanon, Influence of fly ash fineness on strength, drying shrinkage and sulfate resistance of blended cement mortar, *Cement and Concrete Research*, Vol.34, Issue 7, 2004, pp. 1087-1092.
- [12] Chindapasirt, P., C. Jaturapitakkul, and U. Rattanasak, Influence of fineness of rice husk ash and additives on the properties of lightweight aggregate, *Fuel*, Vol.88, Issue 1, 2009, pp. 158-162.
- [13] Chindapasirt, P., C. Jaturapitakkul, and T. Sinsiri, Effect of fly ash fineness on compressive strength and pore size of blended cement paste. *Cement and Concrete Composites*, Vol.27, Issue 4, 2005, pp. 425-428.
- [14] Khan, M.Z.N., et al., Mechanical properties of ambient cured high strength hybrid steel and synthetic fibers reinforced geopolymer composites. *Cement and Concrete Composites*, Vol.85, 2018, pp. 133-152.
- [15] Chi, J.M., et al., Effect of aggregate properties on the strength and stiffness of lightweight concrete. *Cement and Concrete Composites*, Vol.25, Issue 2, 2003, pp. 197-205.
- [16] Phoo-ngernkham, T., et al., High calcium fly ash geopolymer mortar containing Portland cement for use as repair material. *Construction and Building Materials*, Vol.98, 2015, pp. 428-488.
- [17] Sata, V., A. Sathonsaowaphak, and P. Chindapasirt, Resistance of lignite bottom ash geopolymer mortar to sulfate and sulfuric acid attack. *Cement and Concrete Composites*, Vol.34, Issue 5, 2012, pp. 700-708.
- [18] Dulsang, N., et al., Characterization of an environment friendly lightweight concrete containing ethyl vinyl acetate waste. *Materials & Design*, Vol.96, 2016, pp. 305-356.
- [19] Tajdini, M., R. Mahinroosta, and H. Taherkhani, An investigation on the mechanical properties of granular materials in interface with asphaltic concrete. *Construction and Building Materials*, Vol.62, 2014, pp. 85-95.



## WALKING AUTHENTICATION BASED ON POWER SPECTRUM DENSITY OF ACCELERATION AT LUMBER PART

Masahiro Yoneda<sup>1</sup>

<sup>1</sup>Department of Civil and Environmental Engineering, Kindai University

### ABSTRACT

Gait analysis is used to assess and treat individuals with conditions affecting their ability to walk. It is also commonly used in sports biomechanics to help athletes run more efficiently and to identify posture-related or movement-related problems in people with injuries. On the other hand, a lot of gait analyses for healthy subjects have been conducted in order to investigate the resonant vibration problem of pedestrian bridge in the bridge engineering field. In the design of the pedestrian bridge, a dynamic walking load that acts on the bridge surface is necessary. A major feature of gait analysis in the bridge engineering is to calculate the dynamic load factor (DLF). Therefore, in this study, for the six subjects, DLF in three directions (vertical, fore and after, lateral directions) was calculated using the power spectrum density of the acceleration measured at lumber part. As a result, it could be said that a walking authentication of all six subjects was able to be done correctly using the RMS 3 summed up with the root mean square (RMS) value of DLF in three directions. The calculated results clearly demonstrated that the walking authentication using DLF was one of convenient and useful methods.

*Keywords: Walking authentication, Dynamic load factor, Accelerometer, Power spectrum density*

### INTRODUCTION

Gait analysis is utilized not only in medical fields such as orthopedic surgery and rehabilitation but also in form correction of athletes and is also being conducted as a biometric identification technology capable of identifying individuals [1],[2]. On the other hand, in the civil engineering field, a lot of gait analyses for healthy subjects are carried out in order to investigate the resonant vibration problem of pedestrian bridge. A major feature of gait analysis in the civil engineering is to calculate a dynamic walking load that acts on the bridge surface as dynamic load factor (DLF). This DLF is obtained by dividing the body mass acceleration  $a$  by the gravity acceleration  $g$ , and dynamic walking load can be obtained when DLF is multiplied by the weight of the pedestrian [3],[4].

Evaluation of gait characteristics using DLF has not yet been carried out in other fields including medical field. Therefore, in this study, for the six subjects, DLF in three directions (vertical, fore and after, lateral directions) was calculated using the power spectrum density of the acceleration measured on the right lumber part in order to investigate the usefulness of the walking authentication method based on DLF.

### METHOD

#### Subjects

The subjects were six university students (average age: 21 years old), all of whom are healthy

persons who do not have trouble walking. The parameters of the subjects are shown in Table 1, but S6 with the lowest height is a female student. The experiment was conducted with approval from the ethical review committee established at Graduate School of Kindai University (3-4-1 Kowakae Higashi-Osaka, Osaka, Japan).

Table 1 Subject details

| Subject | Sex    | Height | Weight |
|---------|--------|--------|--------|
| S1      | Male   | 183 cm | 706 N  |
| S2      | Male   | 179 cm | 669 N  |
| S3      | Male   | 165 cm | 588 N  |
| S4      | Male   | 170 cm | 637 N  |
| S5      | Male   | 175 cm | 784 N  |
| S6      | Female | 157 cm | 569 N  |

#### Experiment method

##### Measurement method

In healthy subjects, since there is no significant difference in movement between the left and right lumber part, small accelerometers were installed on the right lumber part as shown in Photo 1. The sampling time for the measurement was  $\Delta t = 0.005$  s, and the 10 Hz analog low-pass filter was applied to remove the high frequency component at the right lumber part. In the experiment, the subject walked a distance of 20 m in accordance with the dial tone of the electronic metronome (102 times / minute = 1.700 Hz and 117 times / minute = 1.950 Hz). One

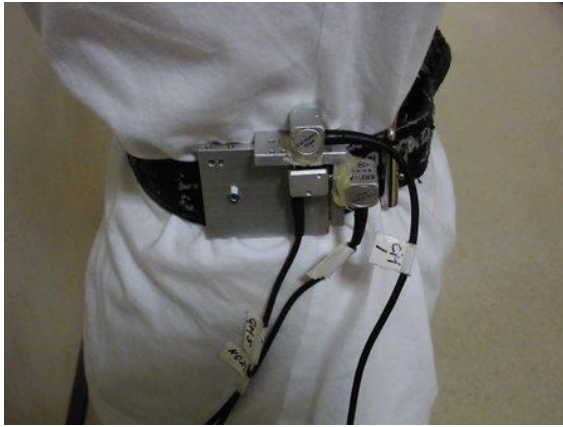


Photo 1 Setup accelerometers on a person being tested.

week later after the first experiment, similar walking experiments were also carried out for the same subject wearing the same shoes.

#### Analysis method

Spectral analysis called Fast Fourier Transform (FFT) was conducted for the acceleration data (2,049 data from 2 seconds after start of walking) measured in the vertical, fore and after and lateral directions of the lumbar part. Since the magnitude of the acceleration corresponding to each frequency component can be obtained by FFT analysis, the difference from the control person was calculated as RMS (Root Mean Square) after obtaining the DLF described in the next chapter for each dominant frequency of 10 Hz or less.

### EVALUATION INDICES

#### Walking load factor DLF in the vertical direction

When a pedestrian passes through the pedestrian bridges, a large vibration that the user feels uncomfortable sometimes occurs due to resonance phenomenon. Therefore, in the field of bridge vibration engineering, a lot of research to estimate the dynamic walking load (the load excluding the static weight component) focusing on the pace component most related to the resonance phenomenon has been conventionally carried out. Specifically, the method using the spectrum analysis result is concretely described below.

The walking vertical force can be estimated as shown in equation (1) using the dynamic load factor (DLF) when the measured vertical acceleration  $a$  on the lumbar part is assumed to be a uniform sinusoidal wave.

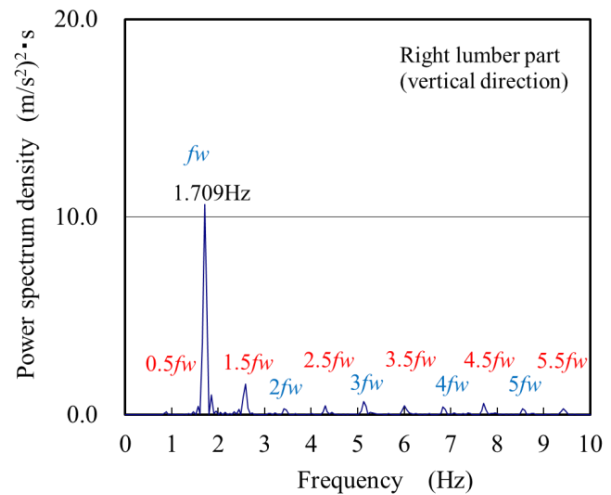


Fig.1 Power spectrum density obtained by FFT analysis.

$$F_d = m \times a \sin 2\pi ft = \frac{W}{g} \times a \sin 2\pi ft = W \times \frac{a}{g} \sin 2\pi ft = W \times \text{DLF} \times \sin 2\pi ft \quad (1)$$

Here,  $F_d$  is the dynamic component of the walking load,  $m$  is the mass of the pedestrian,  $W$  is the weight of the pedestrian,  $g$  ( $\approx 9.81 \text{ m/s}^2$ ) is the gravity acceleration, and  $f$  is the pace frequency.

As described above, considering the vibration problem of the pedestrian bridge, DLF corresponding to the pace frequency component  $fw$  is generally considered to be the most important. When FFT analysis is conducted for the acceleration measured at the right lumbar part, not only the  $fw$  component but also many frequency components including  $0.5fw$ ,  $1.5fw$ ,  $2fw$ ,  $2.5fw$ ,  $3fw$  are also observed as shown in Fig. 1. Here, the component with ".5fw" such as the  $0.5fw$  component, the  $1.5fw$  component, the  $2.5fw$  component and the like is a component that is in opposite phase on the left and right. As a matter of course, these opposite phase components can't be observed if a healthy person wears an accelerometer in the midline.

#### Nondimensionalized acceleration in the fore and after, and lateral directions

Many frequency components are observed in the same way as the vertical direction when FFT analysis is conducted for the measured acceleration in the fore and after, and lateral directions. Therefore, the dimensionalized acceleration in both directions can be estimated by dividing sinusoidal acceleration amplitude  $a$  by the gravity acceleration  $g$ . Although it is impossible to calculate the walking load by multiplying these factors (nondimensionalized acceleration) by the body weight of the subject, the acceleration standardized by the gravity acceleration

$g$  is also expressed using DLF as well as vertical direction.

## ANALYSIS RESULT AND CONSIDERATION

After calculating DLF in three directions for the subject S1, the first (walking speed: 1.25 m/s) and second time results (one week later; walking speed: 1.27 m/s) were compared. The results are shown in Figs. 2 to 4. Although slight differences are observed in the DLF at the first and the second time results even for the same subject, it can be seen from these figures that both results are fairly in good agreement.

Next, focusing on subjects S1 and S2 (control), the DLF obtained from the first experimental results of each are compared. The results are shown in Figs. 5 to 7. It is appended that the walking speed of S2 (first time experiment) was 1.42 m/s. It can be seen from these figures that the DLF in the fore and after, and lateral directions clearly differ from each other, although the DLF in the vertical direction is fairly in good agreement in both subjects S1 and S2.

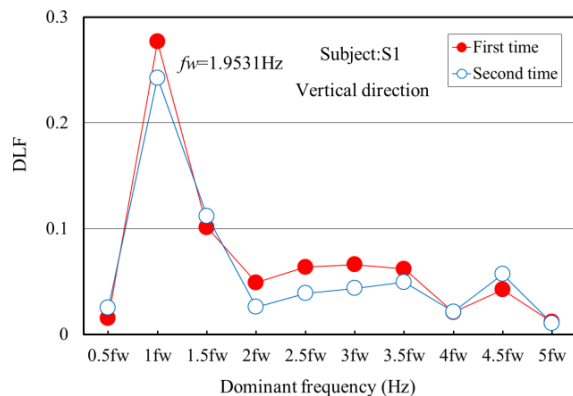


Fig.2 The results of the first and second experiments of subject S1 (Vertical direction).

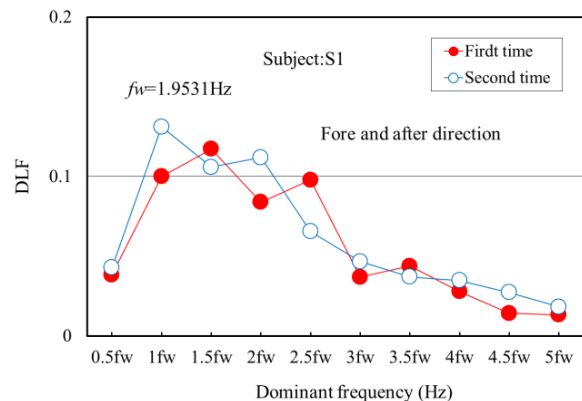


Fig.3 The results of the first and second experiments of subject S1 (Fore and after direction).

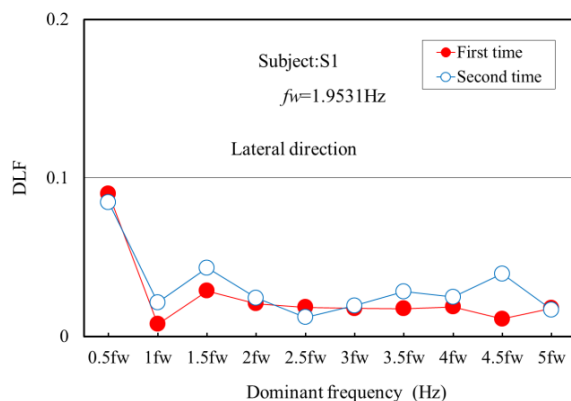


Fig.4 The results of the first and second experiments of subject S1 (Lateral direction).

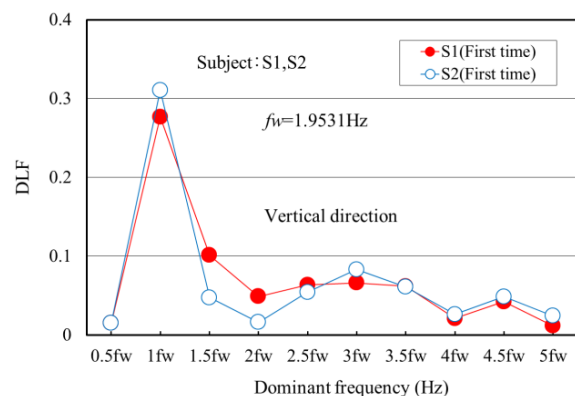


Fig.5 Comparison of experimental results of subjects S1 and S2 (Vertical direction).

Based on the experimental results mentioned above, the DLF in three directions is obtained for all dominant frequencies below 10 Hz. Then, the difference between the principal and the control person is calculated as RMS, and when the total value  $RMS\ 3$  ( $= RMS$  in the vertical direction +  $RMS$  in the fore and after direction +  $RMS$  in the lateral direction) becomes minimum, it is considered to be walking of the same person.

$RMS\ 3$  was determined for the subject S1 and the control person  $S_i$  ( $i = 1, 2, \dots, 6$ ) including the principal. The results are shown in Fig.8. It can be seen from Fig.8 that S1S1 (2) represents the smallest  $RMS\ 3$  for the both pace frequencies of 1.709 Hz and 1.953 Hz, expressing S1 (2) as the second time result of S1. Although the estimation accuracy is higher at the pace frequency of 1.953 Hz, it seemed to be related to the fact that the pace of each subject when walking at comfortable speed was all close to 1.95 Hz.  $RMS\ 3$  was also determined for subjects S3 and S5 as the principal. The results are shown in Figs. 9 and 10. It can be seen from these figures that the combination of S3S3 (2) and S5S5 (2) shows the

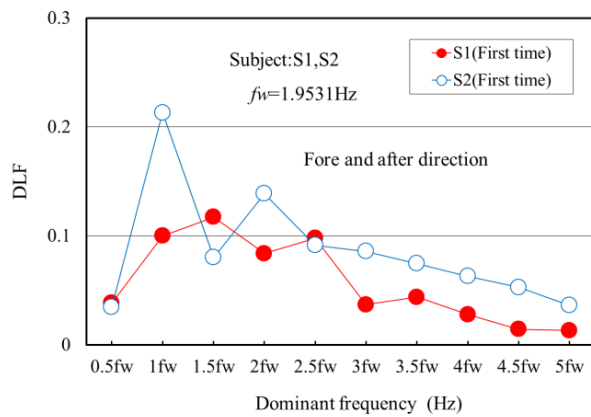


Fig.6 Comparison of experimental results of subjects S1 and S2 (Fore and after direction).

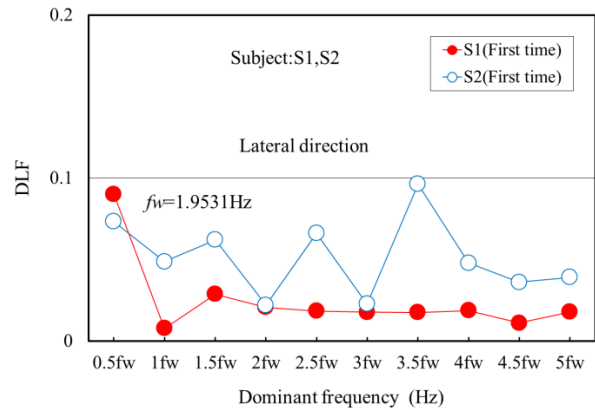


Fig.7 Comparison of experimental results of subjects S1 and S2 (Lateral direction).

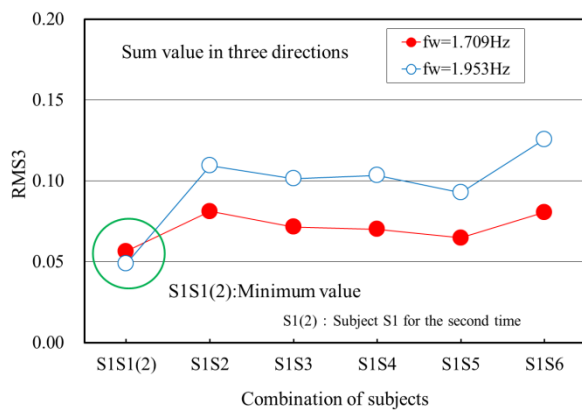


Fig.8 The sum of RMS in three directions when focusing on subject S1.

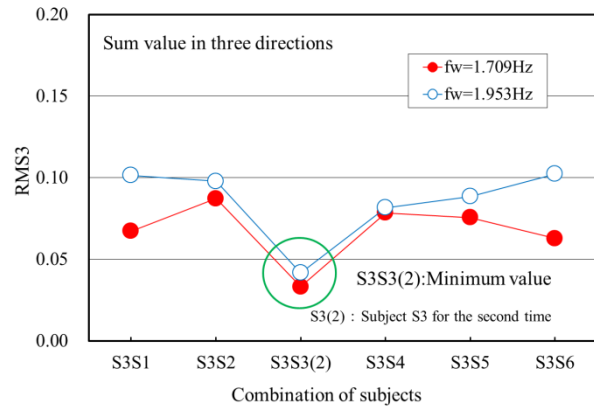


Fig.9 The sum of RMS in three directions when focusing on subject S3.

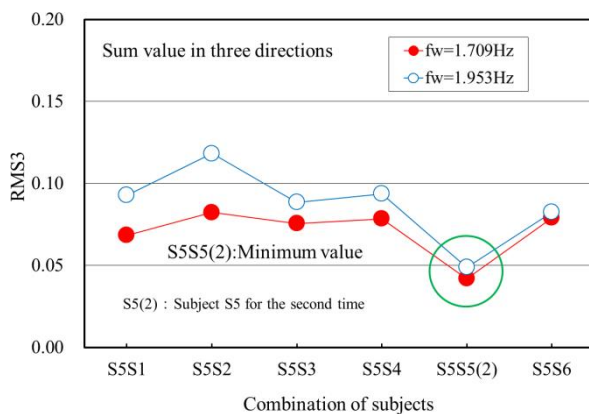


Fig.10 The sum of RMS in three directions when focusing on subject S5.

minimum value.

On the other hand, although the results for the subjects  $S_i$  ( $i = 2, 4, 6$ ) as the principal are omitted, it was verified that the combination of first and second experiments for the same subject showed the smallest RMS 3 in all subjects.

As a result, it could be said that walking authentication of all six subjects was able to be done correctly using the RMS 3 summed up with the root mean square (RMS) value of DLF in three directions. The calculated results clearly demonstrated that the walking authentication using DLF was one of convenient and useful methods.

## CONCLUDING REMARKS

This study investigated the walking authentication method using power spectrum density of acceleration measured at the right lumbar part. As a result, it could be said that walking authentication of all six subjects was able to be done correctly using the RMS 3 summed up with the root mean square (RMS) value of DLF in three directions. The calculated results clearly demonstrated that the walking authentication using DLF was one of convenient and useful methods.

However, since comfortable walking pace is generally decided for each subject, DLF may change when walking pace is different. Therefore, when applying this method to individual walking

authentication, it seems to be necessary to prepare some basic data in advance by changing some walking paces.

On the other hand, there seems to be a desire for women to walk beautifully like a model potentially. However, quantification of model walking has not been done up until now. It can be expected that the beautiful walking style of famous models including pace can be digitized by using DLF. So, I would like to apply this method also to the field of walking lessons aiming to acquire a beautiful way of walking.

## REFERENCES

- [1] Kagaya H, Watanabe , A., Matsuda F. and Kato Y. , Simple motion analysis for ataxia patients, The Japanese Journal of Rehabilitation Medicine, Vol.47, No.9, 2010,pp.612-614 (in Japanese).
- [2] Imano S., Nakamura Y., Shiraishi Y. and Takahashi O., Personal identification method by walking motion using wearable sensor, Information Processing Society of Japan, Vol.25, 2015, pp.1-8 (in Japanese).
- [3] Yoneda M., A simplified method to identify human walking force based on the body response spectrum obtained by FFT analysis, Journal of Japan Society of Civil Engineers, Ser. A1 (Structural Engineering & Earthquake Engineering) ,Vol.67, No.3, 2011, pp.539-544 (in Japanese).
- [4] Yoneda M., Some considerations on higher components of human walking vertical force measured by using FFT power spectrum, Journal of Structural Engineering, Vol.59A, 2013, pp.332-339 (in Japanese).

# EFFECT OF SALT CONTENTS ON COMPRESSIVE STRENGTH OF DMM IN SALINITY CLAY SOFT SOILS FOUNDATION IN VIET NAM

Tran Thi Nguyen Hao<sup>1</sup>, Tran Thi Thanh<sup>2</sup> and Vo Phan<sup>3</sup>

<sup>1</sup>Faculty of construction, University of Architecture HCM City, Vietnam;

<sup>2,3</sup> Southern Institute of Water Resources Research, Vietnam.

## ABSTRACT

The deep mixing method (DMM) has been applied in many construction projects for various improvement purposes. Can Gio is a coastal suburban district of Ho Chi Minh City, Southeast region, Vietnam. It is characterized by a wetland biosystem dominated by mangrove, waterlogged mud and marine shorelines. Stable conditions on construction background in the area of salinity soft soils have to consider unit weight, as soft clay is much harder undisturbed sampling. The analysis is conducted to study the influence of salinity soft soils, water and cement contents on Deep Mixing strength, deformability and workability. Therefore, in this paper presents correlation between soil unit weights to resulting from CTPu have mentioned pore water pressure at the time and deals with mechanical behavior of the Deep Mixing. The results showed that the exact value of salinity unit weight influenced variation of the unconfined compressive strength and the wet unit weight of DMM. Relations and nomograms linking those parameters are proposed, making the results presented directly usable for design methods and on site applications.

*Keywords: Salinity, Soft soils, Deep mixing, Unconfined compressive strength.*

## INTRODUCTION

Deep mixed (DMM) columns have been commonly used as a soil-improvement technique to increase stability and to reduce settlement of embankment. Research on failure modes of DM columns owing to embankment fill and surcharge has been the subject of interest for a number of investigators (Miyake 1991; Kitazume 2000; Han 2005; 2006).

The potential failure modes of DM column include bending, inclination, shearing, rotating, soil flowing and a combination of these modes (Kitazume and Terashi 1991; Broms 1999). Many researchers have found that bending failure of DM columns was more critical than the shear failure. A centrifuge test was performed by Kitazume (2000) and the results showed that the columns failed in bending before shear failure.

In this duty, the determined values of unit weight for salinity clayey silt to silty clay in Can Gio can be obtained by indirectly from correlations based on the CPTu measurement from probings at the depths from 20 to 30m in situ. Values measured in the test ( $q_c$ ,  $f_c$  and  $u_2$ ) are valuable data for qualitative and quantitative assessment of the soft soil. In addition, the ground improvement execution was carried out by DMM at a depth 16m below the ground surface. The results show that the influence of salinity silty clay, water and cement contents on unconfined compressive strength (UCS).

## SOIL CONDITIONS AT TEST SITE

Can Gio is a coastal suburban district of Ho Chi Minh City, Southeast region, Vietnam. It is characterized by a wetland biosystem dominated by mangroves, waterlogged mud and marine shorelines. High tide brings in salt water, and when the tide recedes solar evaporation of the seawater in the soil leads to further increases in salinity.

The geotechnical engineer drilled five exploratory holes with the depth of 20m at the planned building site in “Fig. 1” to retrieve soil samples for the pre-construction lab mixing test program. Data from the lab testing program were used to confirm the design cement dosage and to provide a guideline of the soilcrete UCS.



Fig.1 The pilot test in CanGio District,Vietnam.



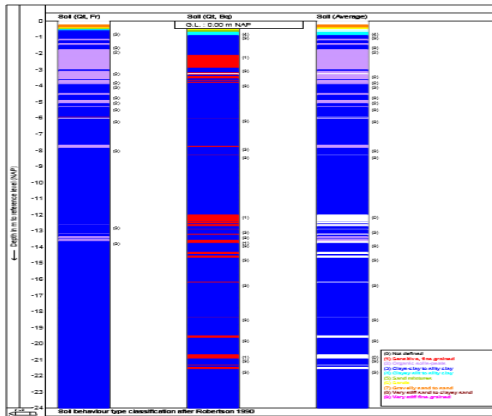


Fig. 2 Typical CPT soil profile in Can Gio District.

The pilot test site location in Can Gio District Ho Chi Minh City, includes four communes Binh Khanh, Tam Thon Hiep, Ly Nhon, Long Hoa and the town of Can Thanh. The piezocone penetration test (CTPu) static probing is a common research technique applied in identifying soil sub-base in situ.

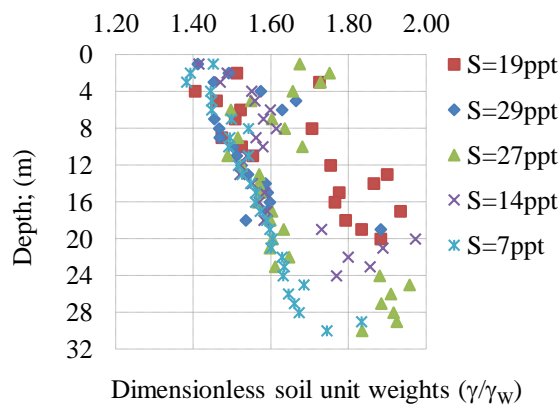


Fig. 3 Unit weight variability depending on salinity and depth for clayey silt in Can Gio District HCMC.

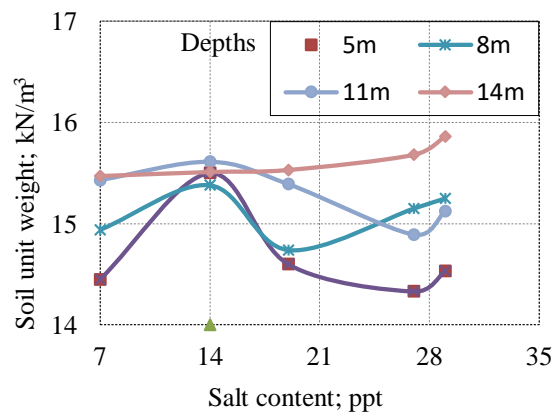


Fig. 4 Unit weight variability in depths depending on salt contents.

The first proposal for determining the unit weight on the basis of CPT probings was presented by Lunne (1997), based on SBT zones in the classification of Robertson. In subsequent publication Robertson and Cabal (2010) updated the procedure for determining unit weight.

## TESTING PROCEDURE

### The Lab Mixing Test

The designed water – cement ratio for the cementitious slurry was 0.7 with 220, 240 kg/m<sup>3</sup> cementitious material.

Table 1 Results of 28 day UCS (MPa) laboratory testing– Strength vs salinity contents S; ppt.

| Depth; (m) | 7ppt | 19ppt | 29ppt |
|------------|------|-------|-------|
| 2 - 3      | 0.75 | 0.85  | 0.63  |
| 5 - 6      | 1.18 | 1.21  | 1.14  |
| 12-13      | 1.25 | 1.38  | 1.18  |

Note: Cement dosage of 220 kg/m<sup>3</sup>

| Depth; (m) | 7ppt | 19ppt | 29ppt |
|------------|------|-------|-------|
| 3 - 4      | 0.91 | 1.14  | 0.76  |
| 5 - 6      | 1.15 | 1.25  | 0.99  |
| 13 - 14    | 1.18 | 1.17  | 1.06  |

Note: Cement dosage of 240 kg/m<sup>3</sup>

### The Deep Mixing Method

Deep soil mixing is a ground improvement technique that improves the characteristics of weak soils by mechanically mixing them with cementitious binder, such as cement, slag, lime, etc. To construct columns, a powerful drill advances drill tooling with radial mixing paddles located near the bottom of the drill string. Binder is injected through the drill steel as it advances and additional soil mixing is achieved as the tool is withdrawn. The technique has been used to increase foundation capacity, decrease static or seismic settlement, increase global stability, and mitigate liquefaction potential for planned structures, tanks, embankments and levees.

Binder content of columns was pure cement, it was designed to add 200 and 240 kg/m<sup>3</sup>.

Undisturbed sampling with coring technique using core pack sampler (diameter of sample is 70mm) were carried out as quality assurance test. Undisturbed samples were taken continuously from top (-2.0 m) to bottom of column after a minimum age of 7 days after installation. Then three specimens were prepared at depths, with electric



cutter. Specimens were wrapped in plastic film and cured in a temperature controlled box with 20 degree Celsius until tested for 28-day UCS.



Fig.5 DMM installation.

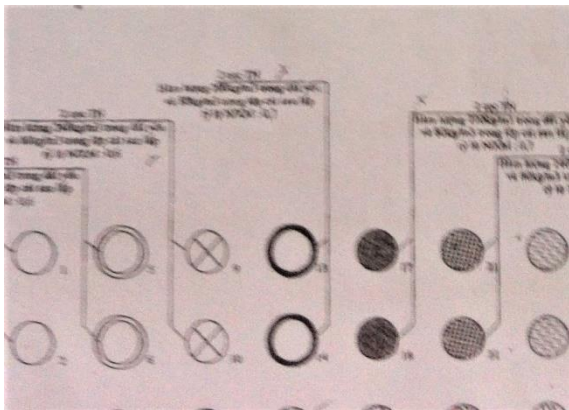


Fig. 6. Typical plan view of the DMM.

Fig. 7 Core samples from soilcrete columns.

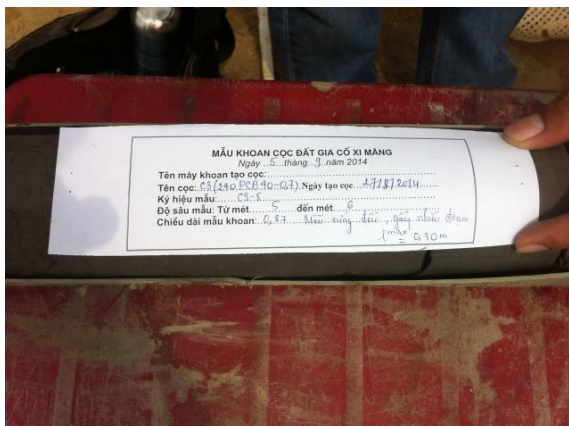


Fig. 8 Unconfined compression test.

In addition, undisturbed samples were sunk in salinity water for over 2 years. The result shown in “Fig. 9” that disturbing the edge-to-face structure in a zone around samples, so may assess influence of USC for DMM in salinity clay soft soils foundation.



Fig. 9 Specimens sunk in salinity water after 2 years

## TEST RESULTS

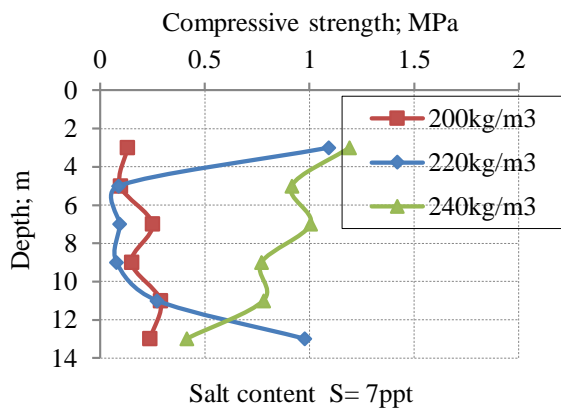


Fig. 10 Results UCS of core soil cement; S=7ppt.

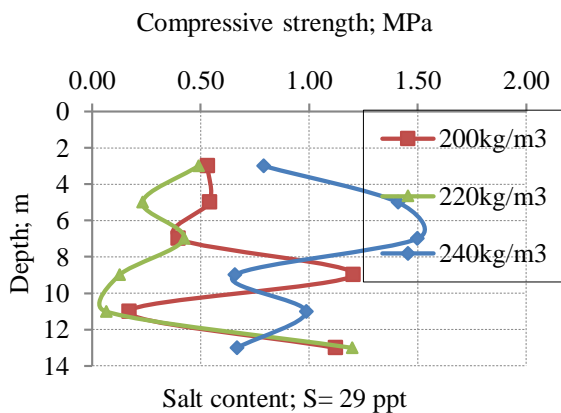


Fig. 11 Results UCS of core soil cement; S= 29ppt.

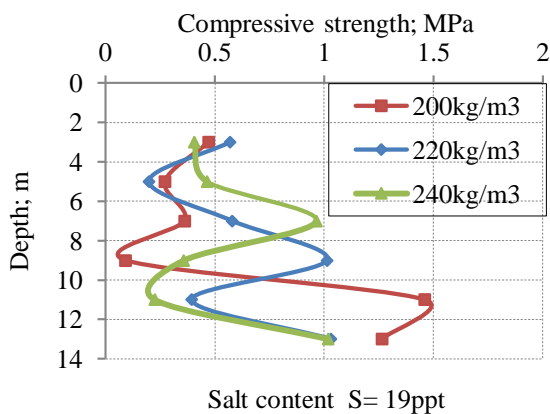


Fig. 12 Results UCS of core soil cement; S= 19ppt.

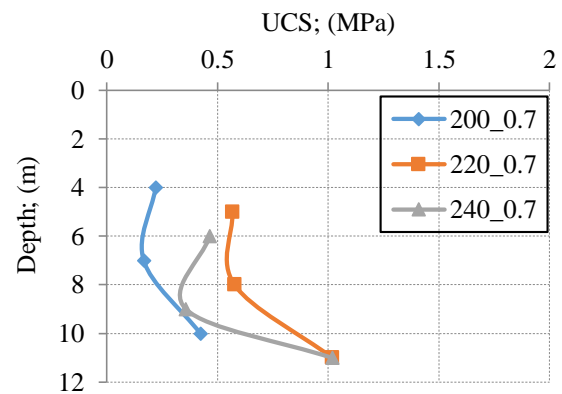


Fig. 13 Results UCS of core soil cement before sinking.

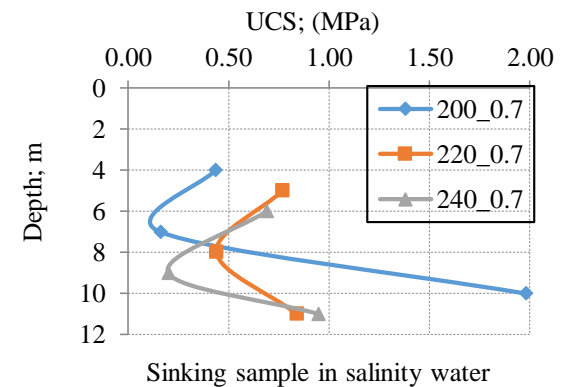


Fig.14 Results UCS of core soil cement after sinking 27 months.

## CONCLUSIONS

In this study, influence of salt contents on the soft foundation improved by DMM was analyzed through the exact value of salinity in depth clay soft soil unit weight. The following conclusions can be drawn from numerical results:

Correlation between unit weight and results CPT of clayey silt in Can Gio district Ho Chi Minh City. The unit weight evaluation with actual values variability depending on salinity and depth are presented in "Fig. 3".

An increase of the pore fluid salinity causes a decrease of the moisture content, decrease of the liquid limit, decrease of the compressibility. The wet unit weight is almost within the range 14 to 16 kN/cm<sup>3</sup>. This trend is inverted with a decrease in UCS of DMM in the case of thick clayey silt deposits with elevated pore fluid salinity. It must be considered that the Can Gio site could be significantly altered by construction practices. For instance, installation of DMM may disturb the edge-to-face structure in a zone around the columns, and the foundation performance could be affected accordingly.

## ACKNOWLEDGMENTS

Funding for this study was provided by the Southern Institute of Water Resources Research (SIWRR) and University of Architecture HCM City, Vietnam. The above supports and assistance are greatly appreciated.

## REFERENCES

- [1] Test according to ASTM 5778.
- [2] Test methods: ASTM\_D2166\_06 .
- [3] Robertson. P. K.; (2009) CPT-DMT Correlations, Geotechnical Journal, ASCE.
- [4] Burke, G.K. and Sehn, A.L., An Analysis of Single axis Wet mix performance, 2005, pp. 41-46.
- [5] Filz, G., Adams, T., Navin, M., and Templeton, A.E., Design of Deep Mixing for Support of Levees and Floodwalls, 2012, pp. 89–133.

## CORRELATION BETWEEN VIBRATION SIGNALS AND SOUND SIGNALS OF A PERSONAL CAR WITH GASOLINE ENGINE

Suphattharachai Chomphan, Boonthum Wongchai  
Faculty of Engineering at Sriracha, Kasetsart University, Thailand

### ABSTRACT

In the present time, the number of petroleum-fuel vehicles is continuously increasing despite of the arising of electric vehicles. Because of the environmental concerns, the EV is being developed in both of its performance and cost reduction. However, petroleum-fuel vehicles are still popular thanks to their more economical sale prize, low-cost maintenance, and widely after-sale services. This paper studies the correlation between the vibration and sound signals of a personal gasoline engine car, since the important interface of the car user are the perceived vibration and sound. In the experimental design, the three vibration sensors and the condensed microphones at different positions have been allocated systematically according to the most perception of car users. A quantity of the engine vibration and sound signals have been measured and collected as signal databases. The signal feature of first pitch is considered due to its indication of main engine frequency. The fast Fourier transform (FFT) is applied the extracted the frequency spectrum of the signal in all databases. Subsequently, the first dominant peak occurring in the spectrum is selected and recorded for both of its frequency and its magnitude. These attributes are then analyzed as comparison with different engine speeds. Finally, the correlations of these attributes between the vibration and sound signals are presented. From the proposed correlation function, some pairs of the signal features expose significant relationships, for example, the sound signal at the exhaust pipe and the vibration signal at the seat when considering the magnitudes at the emerging dominant frequencies.

*Keywords: Correlation study, Vibration, Sound, Fast Fourier transform, Gasoline engine*

### INTRODUCTION

Nowadays, a number of alternative sources of energy are being developed to utilize in the industry, business, and transportation sectors. The energy such as gasohol, biodiesel, Hydrogen, and electricity are very dominant in the incoming future. However, the production cost of these alternative sources of energy is still expensive comparing with the petroleum resources. Therefore, the gasoline and diesel oil production are still being developed in both the quality and the efficiency.

Investigating the reviews on the detection and diagnosis the faults in rotating machinery, it has been found that the mechanical vibration-based studies have been widely conducted [1]-[3]. The related studies are seldom applied with the gasoline or diesel engines. The utilizations of vibration-based techniques to these engines are considerably burdensome due to the transient and non-stationary nature [1]. The application of vibration signals of engines brings about the dynamic movement of the mechanical system condition. A number of powerful signal processing techniques have been studied for fault diagnosis [2]. The power spectrum with high order, cepstrum, and neural network were investigated in the specified-type induction motor

fault diagnosis and indication [4]. The discrete wavelet transform was exploited efficiently with the vibration signal of the diesel engine and the gearbox for the engine fault diagnosis [2]-[3]. The power of signal analysis was adaptively conducted due to its less time consumption and low complexity [5]-[6]. Since the different temperatures of the engine combustion make the working condition of the engine changed, the problems of LPG-installation cause the variation in engine vibration and sound. [7]-[10]. Consequently, the vibration and sound signals are investigated to distinguish between the LPG-installation engine and the normal gasoline engine, because they are ones of important measurable attributes to indicate the causes of irregular conditions of engines [11]-[12].

A study of vibration and sound signal analysis for a gasoline engine with LPG-installation and fault simulations was performed recently, the findings summarized that, LPG-installation and engine faults cause degradations in engine efficiency which can be concretely evidenced by using the proposed signal processing technique [13]-[15].

The correlation of vibration and sound signal attributes has been introduced in the study of this paper. It is expected from the proposed approach that some significant relations are found and

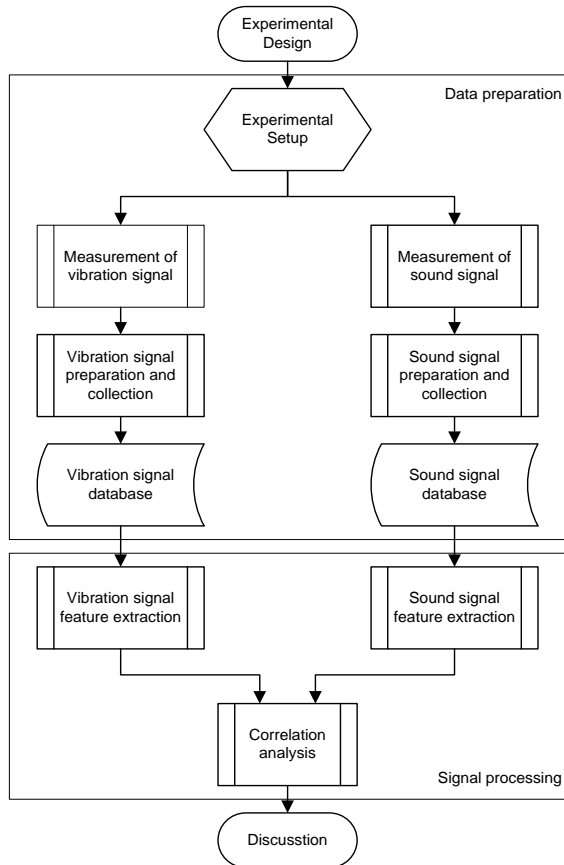


Fig. 1 Experimental Procedure

summarized.

In this paper, the experiment is divided into two stages including data preparation and signal processing. At the first stage of the experiment, the experimental setup has been performed firstly. Subsequently the signal measurement for all designed cases has been done. Finally the signal preparation and collection has been conducted to construct the signal database. The vibration and sound signal databases have been implemented in parallel in this stage.

In the second stage of this experiment, the signal processing has been applied. At the beginning, the signal feature extraction has been performed. The frequency spectrum of this prepared corresponding signal has been conducted by using fast Fourier transform technique. A number of frequencies at the dominant peak points in the frequency spectrum and their corresponding amplitudes have been extracted. The highest peak is assumed to represent the fundamental frequency generated from the moving machine. These features are therefore analyzed and subsequently used in the correlation analysis. It has been stated that the correlation analysis is to measure the level of correlations between corresponding vibration and sound signals by setting a function criteria. Finally, the discussion of this study has been conducted.



Fig. 2 A position of the vibration sensor : the surface of the engine pistons



Fig. 3 Two positions of the vibration sensors : the backrest and the bottom seat of the cushion beside the driver.

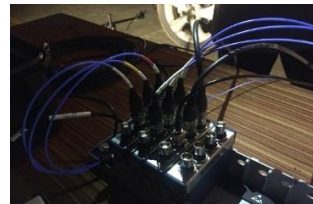


Fig. 4 Connection of all sensors with the NI cards, NI rack

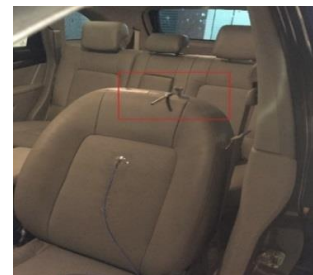


Fig. 5 A position of the microphone : a position at the neck of the backrest of the cushion beside the driver



Fig. 6 A position of the microphone : a position beside the front wheel with 0.5-meter far distance





Fig. 7 A position of the microphone : a position at the rear of the exhaust pipe with a 45-degree angle to that pipe and a 0.5-meter far distance

## MATERIAL AND METHODS

In this section, the material and the methods are presented by using the experimental procedure as illustrated in Fig. 1. The explanation is reviewed step by step as follows.

### Experimental Design

At the beginning, the experimental design process has been inaugurated. All experimental equipment includes a personal gasoline engine car (Chevrolet Captiva brand with 2.4 liter engine, Double CVC, 4 cylinders, and 16 valves), vibration sensors and their accessories, condensed microphones and their complementary parts, NI card for interfacing with computer, and a computer for signal processing. In parallel, these vibration and sound signal retrieving setups are designed to allocate at the specimen car simultaneously.

### Data Preparation

At the data preparation, the experimental setup is conducted to retrieve the vibration and sound signal from the specimen car in a number of engine speeds at the parking stage in parallel. Subsequently, the measurement, preparation and collection, and database implementation are performed respectively.

### Experimental Setup

At the experimental setup, the vibration and sound signal retrieving setups have been prepared. Three sets of high-frequency vibration sensors and three condensed microphones are allocated at different positions within and nearby the car. The corresponding signals are then transferred into the processing computer through a group of NI interfacing cards.

#### *Vibration signal retrieving setup*

Three sets of high-frequency vibration sensors are located at three positions including the surface of the engine pistons as depicted in Fig. 2, the backrest and the bottom seat of the cushion beside the driver

as depicted in Fig. 3. All vibration signal wire are connected with the NI cards which are attached with the NI rack as depicted in Fig. 4. The rack is also connected to the computer which the signals are retrieving into the Labview program.

#### *Sound signal retrieving setup*

The sound signal retrieving setup is almost the same as that of vibration signal retrieving setup. The three positions installing the microphones are including a position at the neck of the backrest of the cushion beside the driver as shown in Fig. 5, a position beside the front wheel with 0.5-meter far distance as shown in Fig. 6, a position at the rear of the exhaust pipe with a 45-degree angle to that pipe and a 0.5-meter far distance as shown in Fig. 7.

#### *Measurement of vibration signal*

The vibration signals of the specimen car are measured at three different points as depicted in Figs. 2 and 3. The sampling frequency is at 50,000 Hz. Ten samples with 5 seconds of the vibration signal are measured for 6 different engine speeds of idle, 1500, 2000, 2500, 3000, and 3500 rpm, respectively.

#### *Vibration signal preparation and collection*

When the signal samples are retrieved through Labview program, the preliminary process of signal segmentation are conducted. The collection of signal from all distinguished sensor positions and all different engine speeds are categorized.

#### *Vibration signal database*

Before entering into the signal processing stage, the database of the categorized signal is implemented. Three subsets of categorization are including the signals from the surface of the engine pistons, the signals from the backrest of the cushion, and the signals from cushion seat. In each subset, the signal portions are dividing into six groups corresponding to each engine speeds as described earlier.

#### *Measurement of Sound signal*

The sound signals of the specimen car are measured at three different points as depicted in Figs. 5-7. The sampling frequency of the sound is also set at 50,000 Hz. Ten samples with 5 seconds of the sound signal are measured for 6 different engine speeds as same as those of vibration signal.

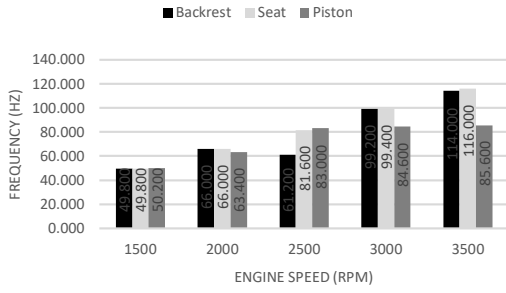


Fig. 8 The emerging dominant frequencies of the vibration signal at five different engine speeds

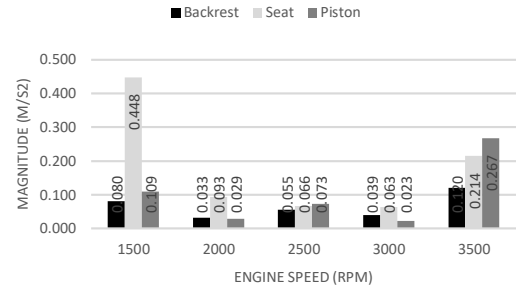


Fig. 10 The magnitudes of the FFT at the emerging dominant frequencies of the vibration signals at five different engine speeds

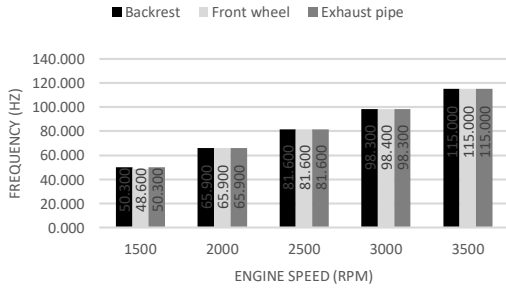


Fig. 9 The emerging dominant frequencies of the sound signal at five different engine speeds

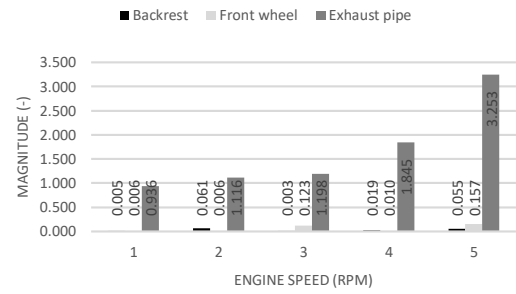


Fig. 11 The magnitudes of the FFT at the emerging dominant frequencies of the sound signals at five different engine speeds

#### Sound signal preparation and collection

The sound signal samples are retrieved through Labview program, and then the preliminary process of signal segmentation are also conducted. The collection of sound signal from all three sensor positions and all different engine speeds are also categorized.

#### Sound signal database

The database of the categorized sound signal is implemented at the end of data preparation stage. Three subsets of categorization are including the signals from the position at the neck of the backrest of the cushion, the position beside the front wheel, and the position at the rear of the exhaust pipe. In each subset, the signal portions are also dividing into six groups of different engine speeds.

#### Signal Processing

At the signal processing, the feature extraction and correlation analysis are performed respectively.

#### Vibration signal feature extraction

Fast Fourier transform (FFT) has been applied

with all of the portions of the vibration signals for all groups within the database. From the output frequency spectrum, the most dominant peak appearing the frequency domain is extracted. The frequency and magnitude at the peak are analyzed and used in the correlation analysis subsequently.

#### Sound signal feature extraction

The feature calculation for sound signals is as same as that of the vibration signals.

#### Correlation analysis

A product function in the same sense as the cross correlation function has been adopted. A summation of the multiplication of between two set of signal features at all engine speeds is calculated and used as this product function. The higher the function value, the more the mutual relation is. The functions are defined as follows,

$$cf(sf_i, vf_j) = \sum_{N=1500}^{N=3500} (sf_i \cdot vf_j), \quad (1)$$

where  $sf_i$  is the peak frequency dominated in the sound spectrum at the  $i^{th}$  position,  $vf_j$  is the peak



frequency dominated in the vibration spectrum at the  $j^{\text{th}}$  position,  $N$  denotes the engine speed ranging from 1500 to 3500 rpm, and

$$cm(sm_i, vm_j) = \sum_{N=1500}^{N=3500} (sm_i \cdot vm_j), \quad (2)$$

where  $sm_i$  is the magnitude at the peak frequency dominated in the sound spectrum at the  $i^{\text{th}}$  position,  $vm_j$  is the magnitude at the peak frequency dominated in the vibration spectrum at the  $j^{\text{th}}$  position,  $N$  is the same as that of Eq.1.

### Discussion

The interpretation of the output correlation is performed. Finally the discussion for all aspects has been completed.

## EXPERIMENTAL RESULTS

### Emerging Dominant Frequency

As for the vibration signal analysis, the FFT is an efficient tool to determine the frequency spectrum. The emerging dominant frequencies at the peak point at five different engine speeds are extracted and plotted in the following bar chart in Fig. 8. Meanwhile figure 9 represents the emerging dominant frequencies for the sound signal analysis.

From Figs. 8 and 9, it can be obvious seen that the emerging dominant frequencies of the vibration and sound signals are approximately directly proportional to the engine speeds. These emerging frequencies reflect the fundamental frequencies of the engine which correspond to the relation  $f = \frac{iN}{2 \times 60}$ , where  $i$  is the number of engine pistons which is 4 for this study, meanwhile  $N$  denotes the engine speed in rpm.

### Magnitude of the FFT at the Emerging Dominant Frequency

At the peak points of the frequency spectrum of vibration signal, the magnitudes are extracted for all five different engine speeds. Subsequently the corresponding averaged values are plotted as a bar chart and depicted in Fig. 10. Moreover, figure 11 shows the magnitudes for the sound signal.

From Fig. 10, it can be noticed that the magnitudes of the FFT at the emerging dominant frequencies of the vibration signals are relatively high at the engine speeds of 1500 and 3500 comparing with the other speeds. Moreover these magnitudes are roughly increased when the engine speed is raised. In Fig. 11 where the magnitudes of

Table 1 The correlation evaluation by using the emerging dominant frequencies

| cf(sf <sub>i</sub> ,vf <sub>j</sub> ) | sf <sub>1</sub> | sf <sub>2</sub> | sf <sub>3</sub> |
|---------------------------------------|-----------------|-----------------|-----------------|
| vf <sub>1</sub>                       | 34709.620       | 34634.880       | 34709.620       |
| vf <sub>2</sub>                       | 36623.920       | 36549.200       | 36623.920       |
| vf <sub>3</sub>                       | 31636.100       | 31559.220       | 31636.100       |

Table 2 The correlation evaluation by using the magnitudes of the FFT at the emerging dominant frequencies

| cm(sm <sub>i</sub> ,vm <sub>j</sub> ) | sm <sub>1</sub> | sm <sub>2</sub> | sm <sub>3</sub> |
|---------------------------------------|-----------------|-----------------|-----------------|
| vm <sub>1</sub>                       | 0.010           | 0.027           | 0.641           |
| vm <sub>2</sub>                       | 0.021           | 0.046           | 1.416           |
| vm <sub>3</sub>                       | 0.018           | 0.052           | 1.133           |

the FFT at the emerging dominant frequencies of the sound signals are focused, it can be explicitly observed that those of the exhaust pipe are highest, meanwhile those of the backrest are lowest. Last but not least, the magnitudes tend to increase, when the engine speed is raised.

### Cross Correlation Analysis

The cross correlation function are applied to measure the correlation between vibration and sound signals of the specimen car. Firstly, the correlation evaluation by using the emerging dominant frequencies is conducted and depicted in Table 1. Secondly, correlation evaluation by using the magnitudes of the FFT at the emerging dominant frequencies is presented Table 2.

From Table 1, it can be noticed that correlation of the emerging dominant frequencies of the vibration signals with the emerging dominant frequencies of the sound signals is relatively highest at the position 2 or at the seat, meanwhile it is lowest at the position 3 or at the piston. As for Table 2, it can be observed that the magnitudes of the FFT at the emerging dominant frequencies of the sound signals with the magnitudes of the FFT at the emerging dominant frequencies of the vibration signals is relatively highest at the position 3 or at the exhaust pipe, meanwhile it is lowest at the position 1 or at the backrest. Moreover, the sound signal at position 3 or the exhaust pipe and the vibration signal at position 2 or the seat disclose the maximum correlation function value, when considering all pairs of signals.

## CONCLUSIONS

This paper proposes a study of the correlation analysis between the vibration and sound signals of

a personal gasoline engine car. Three vibration sensors and three microphones are located at different positions according to the most perception of car users. The correlations of these attributes between the vibration and sound signal are finally presented. FFT has been used with the vibration and sound signals. From the output frequency spectrum, the most dominant peak appearing the frequency domain is extracted. The frequency and magnitude at the peak point are analyzed and used in the correlation analysis. From the proposed correlation function, some pairs of the signal features reveal significant relationships, for example, the sound signal at the exhaust pipe and the vibration signal at the seat when considering the magnitudes of the FFT at the emerging dominant frequencies. In the future research, the other derivatives of the correlation functions should be developed to obtain more efficient indications of relationship between the considered signals.

#### ACKNOWLEDGEMENTS

The research was partly sponsored by Kasetsart University, Faculty of Engineering at Sriracha's Fund.

#### REFERENCES

- [1] Yujun L., Peter W. T., Xin Y., Jianguo Y., EMD-based fault diagnosis for abnormal clearance between contacting components in a diesel engine, *Mechanical Systems and Signal Processing*, Vol. 24, Issue 1, 2010, pp.193–210.
- [2] Xia W., Changwen L., Fengrong B., Xiaoyang B., Kang S., Fault diagnosis of diesel engine based on adaptive wavelet packets and EEMD-fractal dimension. *Mechanical Systems and Signal Processing*, Vol. 41, Issue 1-2, 2013, pp. 581–597.
- [3] Binqiang C., Zhousuo Z., Chuang S., Bing L., Yanyang Z., Zhengjia H., Fault feature extraction of gearbox by using over complete rational dilation discrete wavelet transform on signals measured from vibration sensors. *Mechanical Systems and Signal Processing*, Vol. 33, Issue 11, 2012, pp. 275–298.
- [4] Liang B., Iwnicki S. D., Zhao Y., Application of power spectrum, cepstrum, higher order spectrum and neural network analyses for induction motor fault diagnosis. *Mechanical Systems and Signal Processing*, Vol. 39, Issue 1-2, 2013, pp. 342–360.
- [5] Chomphan S., Chaimanatsakun A., Sakornsin R., Khumneungratavongsa S., Rattanasat K., A Comparative Study of LPG-modified Engine and Normal Oil-usage Engine. in *Proc. Int. Conf. On Engineering and Applied Sciences*, 2016, pp. 219-225.
- [6] Akhand R., Upadhyay S. H., A review on signal processing techniques utilized in the fault diagnosis of rolling element bearings, *Tribology International*, Vol. 96, Issue 4, 2016, pp. 289-306.
- [7] Ahmad T. A., Barat G., Teymour T. H., Seyed S.M., Vibration analysis of a diesel engine using biodiesel and petro diesel fuel blends, *Fuel*, Vol. 102, Issue 12, 2012, pp. 414–422.
- [8] Zunmin G, Jin C., Barry H., Analysis of engine vibration and design of an applicable diagnosing approach. *International Journal of Mechanical Sciences*, Vol. 45, Issue 8, 2003, pp. 1391–1410.
- [9] Xianhua L., Randall R. B., Jerome A., Blind separation of internal combustion engine vibration signals by a deflation method. *Mechanical Systems and Signal Processing*, Vol. 22, Issue 5, 2008, pp.1082–1091.
- [10] Xianhua L., Randall R. B., Blind source separation of internal combustion engine piston slap from other measured vibration signals. *Mechanical Systems and Signal Processing*, Vol. 19, Issue 6, 2005, pp. 1196–1208.
- [11] Zbigniew S., Jan W., Application of vibration signals in the diagnosis of combustion engines – exploitation practices. *Journal of KONES Powertrain and Transport*, Vol. 18, Issue 3, 2011, pp. 405-412.
- [12] Carlucci A. P., Chiara F. F., Laforgia D., Analysis of the relation between injection parameter variation and block vibration of an internal combustion diesel engine. *Journal of Sound and Vibration*, Vol. 295, Issues 1–2, 2006, pp. 141–164
- [13] Boonsit S., Chomphan S., Vibration Signal Analysis for LPG-modified Engine and Normal Oil-usage Engine with Different Engine Speeds and Faults. in *Proc. International Congress on Engineering and Information*, 2017, pp. 102-107.
- [14] Chomphan S., Vibration Signal Analysis of A Motorcycle, *International Journal of GEOMATE*, Vol.16, Issue 56, pp. 27-32.
- [15] Chomphan S., Kingrattanasat T., Boonsit S., Signal Analysis for LPG-modified Gasoline Engine with Engine Faults, *International Journal of GEOMATE*, Vol.16, Issue 56, pp. 65-72.

## STRESS ANALYSIS OF EMBANKMENT DUE TO DIFFERENT IN CONSTRUCTION CONDITIONS

Shin-ichi Kanazawa<sup>1</sup> and Satoe Suzuki<sup>2</sup>

<sup>1,2</sup>National Institute of Technology, Fukushima College, Japan

### ABSTRACT

In recent years, many examples of soil structure collapse due to heavy rainfall have occurred. Because of this, it is urgent to establish a method to evaluate and examine long-term embankment structure quality. Japan's conventional design method insufficiently evaluates embankments. Although this method is shifting to a performance-based design to cope with recent abnormal weather, an effective design method has not yet been established.

Therefore, this research performs an initial stress analysis of embankment, accounting for differences in construction conditions. Notable in this study, is the comparative analysis of results, considering the initial water content ratio, one layer of discharge thickness, rolling compaction, and other given structural conditions that differed from conventional design standards. To do this, first the initial moisture content ratio was determined by reproducing the compaction by analysis. Second, based on the dynamics of unsaturated soil, the rainfall intensity was analyzed in order to confirm the variation of the initial stress due to rainfall. Lastly, and most critically, the dynamic change in embankment performance was analytically expressed, and the optimal structural conditions of embankment, grouped by rainfall history, was examined.

*Keywords: Embankment, Unsaturated soil, Construction condition, Compaction, Finite element analysis*

### INTRODUCTION

Soil compaction tests are carried out to improve embankment construction engineering characteristics, such as stability and deformation. In selecting the soil compaction level to use at a construction site, the water ratio (optimum water ratio) is necessary. This is most efficiently obtained from the relationship between the dry density and the water content of the soil for compaction by changing the water content of soil. From this, the soil structure is constructed using the compaction soil. In recent years, however, many cases of embankment collapse have been reported in Japan due to excessive rainfall and torrential downpours caused by typhoons. Take for example, the torrential rain in the northern part of Kyushu in July 2017 and typhoon No. 18 that hit the Kanto and Tohoku regions in 2015. The river embankments and roads collapsed, and a landslide on the general national highway occurred due to the record heavy rain. At present, the mechanisms of embankment collapse due to such natural disasters are not sufficiently clarified. According to guidelines, the stability of embankment against heavy rain is strongly dependent on four factors: treatment of the underlying ground, quality of embankment material, degree of compaction, and drainage. There are many cases where a drainage issue, in particular, has led to embankment collapse. It is worth mentioning that the construction and maintenance of embankment is developed based on empirical engineering rules and

that the strength of embankment is lowered by intermittent heavy rain. The soil is composed of three phases: solid, liquid, and air. Embankment soil below the groundwater level often exists in the unsaturated state containing air or dissolved air. As pore air pressure changes due to rainfall infiltration, the dissolution and release of air into the liquid phase occurs, seeming to compress the soil volume. As a result of not accounting for this factor, present construction guidelines may not provide sufficient embankment drainage countermeasures for the concentrated rain observed of late, coupled with the given construction compaction management. Furthermore, the civil engineering evaluation of performance-based design, essential to meeting the required performance of engineered structures, is also changing. When an earthquake struck Hyogo Prefecture in 1995, many buildings escaped destruction but became unusable. This is because performance-based design, in which the performance for the assumed load is considered during design, was not sufficiently implemented. Taking this type of disaster as an opportunity for change, structural plans and details have been developed for soil structures, shifting the field to performance-based design to ensure that the required performance is satisfied throughout the service life of the design. It is urgent to establish the techniques that can evaluate and examine the long-term quality of embankment structures and what elements of performance design will be important in the future. Based on the above,

this study attempted to analyze the effects of rainfall intensity to grasp the fluctuation due to rainfall of each initial stress, based on the dynamics of unsaturated soil. In addition, changes in the dynamic behavior of the embankment were expressed analytically, and the optimum construction condition for embankment structure at a given rainfall history were investigated.

## RESEARCH METHOD

### Mathematical model used for soil/water/air coupled finite element analysis

The finite element analysis code [1] (DACSAR-MP) used in this study formulates the unsaturated soil constitutive model proposed by Ohno et al [2]. This model is framed as the soil/water/air coupled problem using the three-phase mixture theory. Equation (1) shows the effective stress. Equation (2) shows the base stress tensor and suction stress. Equation (3) shows suction.

$$\boldsymbol{\sigma}' = \boldsymbol{\sigma}^{\text{net}} + p_s \mathbf{1} \quad (1)$$

$$\boldsymbol{\sigma}^{\text{net}} = \boldsymbol{\sigma} - p_a \mathbf{1}, \quad p_s = S_e s \quad (2)$$

$$s = p_a - p_w, S_e = \frac{S_r - S_{rc}}{1 - S_{rc}} \quad (3)$$

Here,  $\boldsymbol{\sigma}'$  is the effective stress tensor;  $\boldsymbol{\sigma}^{\text{net}}$  is the base stress tensor;  $\mathbf{1}$  is the second order unit tensor;  $\boldsymbol{\sigma}$  is the total stress tensor;  $s$  is the suction;  $p_s$  is the suction stress;  $p_a$  is the pore air pressure;  $p_w$  is the pore water pressure;  $S_r$  is the degree of saturation;  $S_e$  is the effective degree of saturation; and  $S_{rc}$  is the degree of saturation at  $s \rightarrow \infty$ . Equations (4), (5), (6) and (7) provide the yield function.

$$f(\boldsymbol{\sigma}', \zeta, \varepsilon_v^p) = MD \ln \frac{p'}{\zeta p_{sat}} + \frac{MD}{n_E} \left( \frac{q}{Mp'} \right)^{n_E} - \varepsilon_v^p = 0 \quad (4)$$

$$\zeta = \exp \left[ (1 - S_e)^{n_s} \ln a \right], MD = \frac{\lambda - \kappa}{1 + e_0} \quad (5)$$

$$p' = \frac{1}{3} \boldsymbol{\sigma}' : \mathbf{1}, q = \sqrt{\frac{3}{2} \mathbf{s} : \mathbf{s}} \quad (6)$$

$$\mathbf{s} = \boldsymbol{\sigma}' - p' \mathbf{1} = \mathbf{A} : \boldsymbol{\sigma}', \mathbf{A} = \mathbf{I} - \frac{1}{3} \mathbf{1} \otimes \mathbf{1} \quad (7)$$

Here,  $n_E$  is the shape parameter;  $\varepsilon_v^p$  is the plastic volume strain;  $M$  is the  $q/p'$  in the limit state;  $D$  is the dilatancy coefficient;  $p'_{sat}$  is the yield stress at saturation;  $a$  and  $n_s$  are the parameters representing the increase in yield stress due to unsaturation;  $\lambda$  is the compression index; and  $\kappa$  is the expansion index. Equation (8) shows pore water velocity. Equation (9) shows air velocity. Pore water and air flow follow Darcy's law.

$$\tilde{v}_w = -\mathbf{k}_w \cdot \text{grad} h \quad (8)$$

$$\tilde{v}_a = -\mathbf{k}_a \cdot \text{grad} h_a, h_a = \frac{p_a}{\gamma_w} \quad (9)$$

Here,  $\tilde{v}_w$  is the pore water velocity;  $\tilde{v}_a$  is the air velocity;  $\mathbf{k}_w$  is the hydraulic conductivity;  $\mathbf{k}_a$  is the coefficient of air permeability;  $h$  is the total head;  $\gamma_w$  is the unit weight of water; and  $h_a$  is the pneumatic head. Equations (10)-(11) show hydraulic conductivity and the coefficient of air permeability by way of Mualem's [3] formula and the Van Genuchten [4] formula.

$$\mathbf{k}_w = k_{rw} \mathbf{k}_{wsat} = S_e^{1/2} \left[ 1 - \left( 1 - S_e^{1/m} \right)^m \right]^2 \mathbf{k}_{wsat} \quad (10)$$

$$\mathbf{k}_a = k_{ra} \mathbf{k}_{ares} = (1 - S_e)^{1/2} \left( 1 - S_e^{1/m} \right)^{2m} \mathbf{k}_{ares} \quad (11)$$

Here,  $k_{rw}$  is the ratio of hydraulic conductivity;  $k_{ra}$  is the ratio of coefficient of air permeability;  $m$  is the Mualem constant;  $\mathbf{k}_{wsat}$  is the hydraulic conductivity at saturation;  $\mathbf{k}_{ares}$  is the coefficient of air permeability in dry conditions. Equations (12)-(13) show the continuous formula of pore water and air using three-phase mixture theory.

$$n \dot{S}_r - S_r \dot{\varepsilon}_v + \text{div} \tilde{v}_w = 0 \quad (12)$$

$$(1 - S_r) \dot{\varepsilon}_v + n \dot{S}_r - n(1 - S_r) \frac{\dot{p}_a}{p_a + p_0} - \text{div} \tilde{v}_a = 0 \quad (13)$$

Here,  $n$  is porosity;  $\dot{\varepsilon}_v$  is volumetric strain; and  $p_0$  is atmospheric pressure. The elasto-plastic constitutive model obtained from Equation (4) and

the equilibrium equation [Equations (12) - (13)] are formulated as the soil/water/air coupled problem.

### Moisture characteristic curve used by analysis

For a soil-water characteristic curve model, a model capable of hysteresis expression, as proposed by Kawai et al. [5], is used. In addition, to determine the logistic curve in the case of DRY and WET, derived from arbitrary suction and the degree of saturation, the logistic curve equation of Sugii and Uno [6] was used. This makes it possible to grasp the moisture conditions of sloped ground where complex water balance occurs. Figure 1 exhibits the soil-water characteristic curve used in this study.

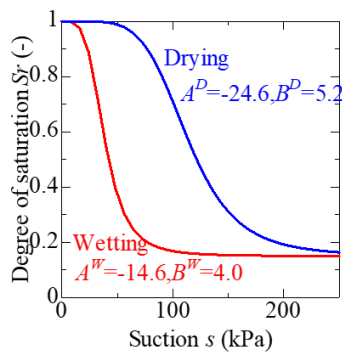


Fig. 1 Soil water characteristic curve

### Compaction analysis

In this study, embankment analysis considering compaction was carried out using the unsaturated soil/water/air coupled finite element analysis code (DACSAR-MP). In addition, rainfall and evapotranspiration conditions, as well as different construction conditions were applied to the analysis. Initial stress in this study indicates the stress state at completion of embankment construction. Table 1 shows material parameters.

Table 1 Material parameters

| $\lambda$ | $\kappa$ | M    | m    | $S_{r0}$ | $k_a(\text{m/day})$ | $p'_{sat}(\text{kPa})$ |
|-----------|----------|------|------|----------|---------------------|------------------------|
| 0.13      | 0.013    | 1.33 | 0.8  | 0.15     | 1.0                 | 20.0                   |
| n         | $n_E$    | a    | v    | $G_s$    | $k_w(\text{m/day})$ | $e_0$                  |
| 1.0       | 1.3      | 10.0 | 0.33 | 2.7      | 0.01                | 1.0                    |

Using these parameters, a compaction test simulating a 13cm high  $\times$  10cm wide mold was analytically conducted to grasp the optimum moisture content of sandy soil. The following are the analysis conditions. The initial water content ratio was set to  $w = 10$  to 28% at a 2% interval. The loading was set at 500 kPa, and the time required for loading and unloading was set at 1 minute. Figure 2 shows the loading condition.

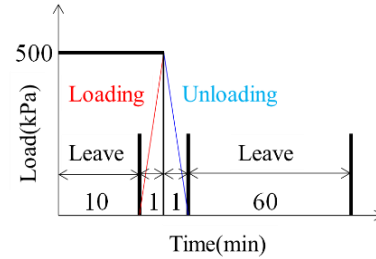


Fig. 2 Loading conditions

From the compaction curve shown in Figure 3, the optimum water content was obtained as  $w = 18\%$ . The degree of compaction was set to 95% or greater, and the initial water content was set to three different water content ratios: the optimum water content  $\pm 2\%$  ( $w = 16\%$ ;  $w = 20\%$ ) and the optimum water content ( $w_{opt}$ ).

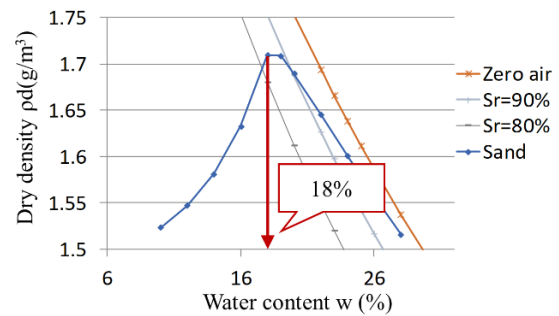


Fig. 3 Compaction curve

### Construction analysis of embankment

Figure 4 shows the analysis mesh. The three water content ratios obtained from Figure 3 in the previous section were used as the initial water contents for analyzing embankments with construction conditions that differed from convention.

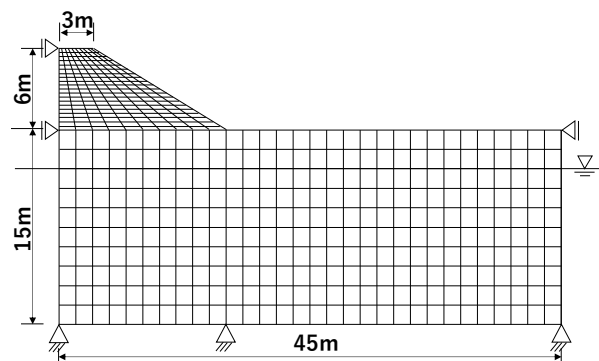


Fig. 4 Analysis mesh

The annual rainfall history of Hikone City, Shiga Prefecture in 2005 was used to simulate the average rainfall in Japan. The soil-water characteristic curve

used for the embankment analysis in the previous section was again employed. The analysis condition was set at a rolling compaction strength of 500kPa after a layer of 0.3m of spreading. The compaction was reproduced by statically loading and unloading each layer. The plane strain analysis was carried out on the displacement boundary with the lower end of the foundation soil fixed vertically and horizontally. The hydraulic boundary is set to an undrained condition above, below, and to the left and right. The above analysis condition is referred to as Case 1. It is assumed to be a conventional construction method. Case 2 is an analysis condition in which the spreading lift of one layer is changed from 0.3m to 0.5m. In addition, the embankment analysis was also carried out under the conditions of Case 3, in which the spreading lift of one layer was changed to 0.6m. The above construction conditions used in Cases 1-3 are assumed as conventional construction conditions. The conditions in Cases 4-6, in which only the compaction speed was doubled, were assumed. In addition, the construction conditions as conventional construction are Case1 only, and Case2-Case6 change construction conditions from the conventional construction. Analysis was carried out considering construction conditions for a total of 6 cases.

## ANALYSIS RESULTS

No large difference in stress change for the foundation soil in any of the analytical conditions occurred, but the stress change of the embankment division is apparent. Figure 5 shows the effective stress under normal construction conditions, and Figure 6 shows the void ratio, also under normal construction conditions.

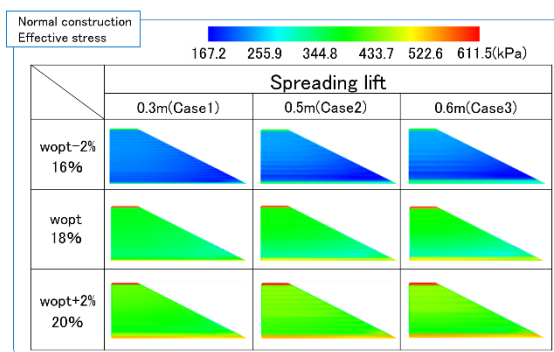


Fig. 5 Normal construction (Effective stress)

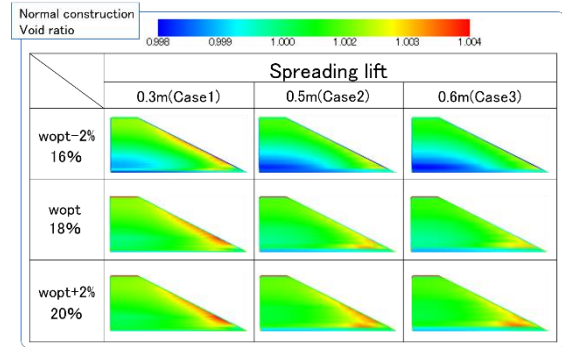


Fig. 6 Normal construction (Void ratio)

Comparing the results of Figures 5 and 6 shows that the distribution of effective stress and the void ratio under normal construction (Case 1 through Case 3) at the optimum moisture content ( $w_{opt} = 18\%$ ) expands at the surface of the embankment, and the value of the effective stress tends to decrease when the spreading lift of one layer was 0.3m. Furthermore, as the thickness of each layer is increased from 0.3m to 0.5m and 0.6m, it expands toward the toe of the slope, and the effective stress tended to decrease. Since the rolling strength of compaction was unified to 500kPa, it is thought that the rolling compaction was not sufficiently transmitted to the soil as the thickness of one layer gradually increased from 0.3m to 0.5m and 0.6m. This was likely caused by the difficulty of air discharging from the soil. Results from the embankment with water content  $w = 20\%$  show the same tendency as the embankment with the optimum moisture content. The consolidation effect in the embankment was demonstrated, and the part which shows the expansion tendency tended to be distributed most widely as the thickness of one layer increased. Furthermore, the effective stress of embankment is low when the water content is 16%, the effective stress showed low value, and the void ratio concentrated in the embankment surface layer and showed the expansion tendency. The reason why the effective stress tended to be low is considered to be the decrease of suction by rainfall infiltration and the increase of pore water pressure. Figure 7 shows the distribution of effective stress under the shortened construction period, and Figure 8 shows the distribution of void ratio under the shortened construction period.

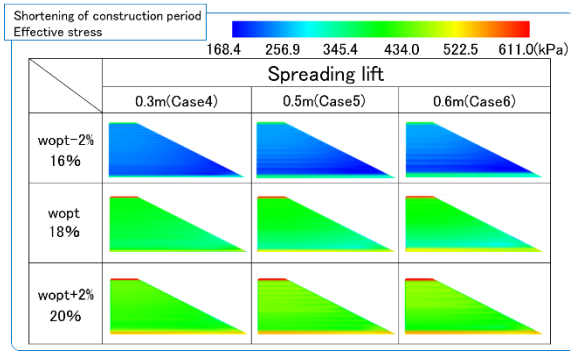


Fig. 7 Shortening of construction period (Effective stress)

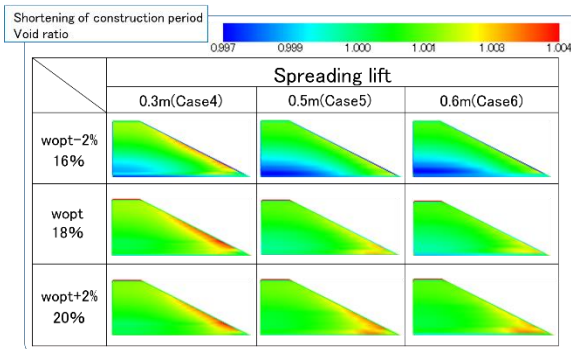


Fig. 8 Shortening of construction period (Void ratio)

The tendency mentioned above is also observed in the analysis of a construction period shortened from the conventional time period (change of compaction speed to twice that of normal compaction).

Figure 9 shows the distribution of shear strain under normal construction conditions.

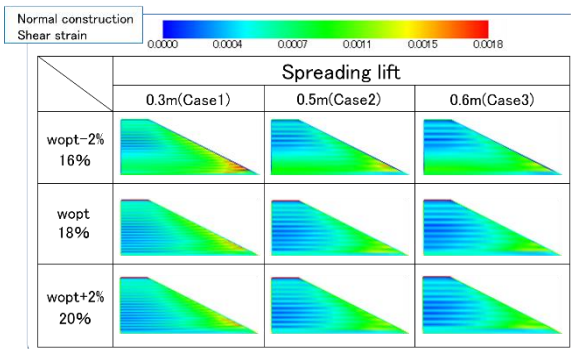


Fig. 9 Normal construction (Shear strain)

The results of embankment analysis using the optimum water content ( $w = 18\%$ ) as the initial water content show that shear strain predominantly occurs from the surface to the tip of the embankment when the thickness of one layer was 0.3 m (Case 1). Case 1 is most likely to demonstrate the compaction effect, because the layer thickness is thinner than other construction conditions. Since sand is used for the

embankment material, drainage is higher than when silt or viscous soil are used. It is thought that this result is obtained because drainage water flows easily in the embankment surface layer. In the case of the construction condition in which one layer's spreading lift was 0.3m, drainage water concentrates in the tip due to the height of drainage. From these results, the compaction effect is easily detected. When the spreading lift of each layer was changed from 0.3m to 0.5m and 0.6m, the shear strain appears predominantly inside the embankment, not in the surface layer. Results for embankment with other water contents ( $w = 16\%$ ,  $w = 20\%$ ) shows the same tendency. This can be due to the fact that the compaction effect decreases as the layer thickness increases because the rolling compaction was kept constant. Additionally, Figure 10 shows the distribution of shear strain when the construction period was shortened to half the normal time period (twice the compaction speed of normal construction).

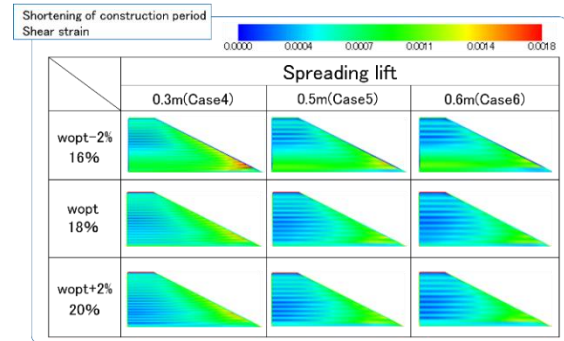


Fig. 10 Shortening of the construction period (Shear strain)

In comparing the results from Figures 9 and 10, the distribution of embankment shear strain in Cases 5 and 6 is slightly larger than for embankment under normal construction. It is likely that the rolling strength was not well transmitted to the soil and the inside of the embankment was not sufficiently compacted with thicknesses increasing 0.3m to 0.5m and 0.6m when the compaction speed increased. Figure 11 shows the critical condition judgement ratio for normal construction.

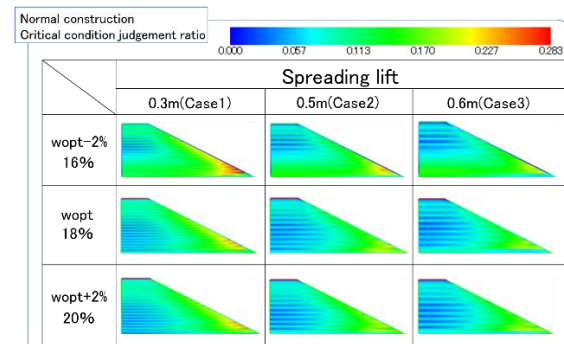




Fig. 11 Normal construction (Critical condition judgement ratio)

The critical condition judgment ratio is an index indicating the possibility of destruction of a structure due to low stability when the maximum value exceeds 1.33. In Case 1, the results of embankment analysis using the optimum water content as the initial water content shows excellent values from the surface to the tip of the embankment. The maximum value of 0.283 is not large enough to indicate destruction in the analytical result of this study, but it does indicate that surface layer slip may occur depending on future environmental changes at the periphery of the embankment. Case 2 and Case 3 also shows a similar tendency, and it seems that the toe of the embankment slope becomes weak at the time of embankment completion. The results of the embankment analysis using  $w = 16\%$  and  $w = 20\%$  as the initial water content are similar to those of embankments with optimum water content. Furthermore, Figure 12 shows the critical condition judgment ratio in the case of shortening the construction period to half of the normal construction time period.

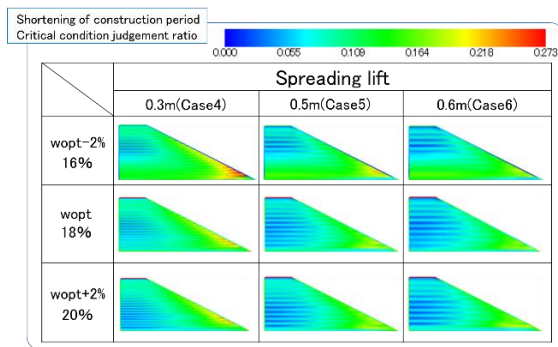


Fig. 12 Shortening of the construction period (Critical condition judgement ratio)

A comparison between Figure 11 and Figure 12 shows that there is no significant difference in performance even if the construction period is shortened, as the same tendency is observed in all analytical conditions.

## DISCUSSION AND CONCLUSIONS

Under the conditions of this study, the strength of the embankment interior was more

pronounced when the embankment was constructed with  $w = 16\%$  than with  $w_{opt} = 18\%$ , when comparing the three water contents obtained from the compaction analysis. Furthermore, a difference in rainfall infiltration quantity was generated by the different construction conditions, as differences in the construction period were generated considering multiple conditions and spreading lifts. Resultingly, effective stress and shear strain, factors causing embankment collapse, were greatly affected. Under this study, the embankment analysis considered differences in water content and construction conditions. However, there were no major performance issues due to either construction conditions or water content at the time of the completion of the embankment. The results of this study support shifting to a performance-based design method.

In the future, it will be possible to evaluate the long-term quality of precision embankment structures by numerically understanding stress change during embankment service life.

## REFERENCE

- [1] Kanazawa, S., Toyoshima, K., Kawai, K., Tachibana, S. and Iizuka, A.: Analysis of mechanical behavior of compacted soil with F.E. method, *Journal of JSCE*, No.68 (2), pp.291-298, 2012.
- [2] Ohno, S., Kawai, K. and Tachibana, S.: Elastoplastic constitutive model for unsaturated soil applied effective degree of saturation as a parameter expressing stiffness, *Journal of JSCE*, Vol.63/No.4, pp.1132-1141, 2007.
- [3] Mualem, Y.: A new model for predicting the hydraulic conductivity of unsaturated porous media, *Water Resources Research*, Vol.12, No.3, pp.514-522, 1976.
- [4] Van Genuchten: A closed-form equation for predicting hydraulic of unsaturated soils, *Soil Science Society American Journal*, Vol.44, pp.892-898, 1980.
- [5] Kawai, K., Wang, W. and Iizuka, A.: The expression of hysteresis appearing on water characteristic curves and the change of stresses in unsaturated soils, *Journal of applied mechanics*, Vol.5, pp.777-784, 2002.
- [6] Sugii T. and Uno T.: Modeling the New Moisture Characteristic Curve, *Journal of JSCE*, pp.130-131, 1995.

# INVESTIGATION OF OPTIMAL CONTACT TYPE ULTRASONIC COLLECTING DEVICE FOR MEASURING ROUGHNESS USING AERIAL ULTRASONIC SENSOR

\*Seiya Nagaoka<sup>1</sup>, Kenji Okajima<sup>1</sup>, Mohammad Raihanul Islam<sup>2</sup>, Ryoei Ito<sup>1</sup> and Ken Watanabe<sup>3</sup>

<sup>1</sup> Graduate school of Bioresources, Mie University, Japan

<sup>2</sup> Department of Farm Structure and Environmental Engineering, Bangladesh Agricultural University, Bangladesh

<sup>3</sup> Maruei Concrete Industry Co., Ltd., Japan

## ABSTRACT

Japan has many concrete irrigation channels with total length of about 400,000 km. Most of these channels are now too old for continued use. The concrete surfaces of channels have been abraded by the flow of water and sand. The roughness of the concrete surface causes a decline in the water flow function. Measurement method of the aerial ultrasonic sensor with 42 kHz is considered to be effective. In this study, we proposed optimal contact type ultrasonic collecting device. The 2 type shape collecting devices of column and cone were used. The columnar type were made of PVC (polyvinyl chloride) pipe. The height are 20-100 cm. The inner diameter are 20 and 30 cm. The conical type were made of plastic traffic cone. The height are 20, 30, 40 and 50 cm. The apex angle are 16 and 20°. We considered relationship between the peak to peak by the aerial ultrasonic with collecting device and the arithmetical mean roughness of a concrete surface. The result, relationship indicated high correlation. Except for the columnar type of diameter 30 cm of height 20 cm, the coefficient of determination was indicated over 0.7. Therefore, the result revealed application for roughness measurement. The gradient of the approximation line from relationship the peak to peak and the arithmetical mean roughness was indicated measuring accuracy. The gradient of conical type tend to be larger than the columnar type. In particular, the shape of the largest gradient was the conical type of apex angle 16° of height 40cm.

*Keywords: Aerial ultrasonic, Irrigation channel, Surface roughness*

## INTRODUCTION

Japan has many concrete irrigation channels, which have a total length of about 400,000 km. These were constructed in the 1954-1973 period of high economic growth. As canals become too old for continued use they are repaired. Hydraulic performance malfunctions are especially considered as the repair factor. A hydraulic performance malfunction is evaluated using the roughness coefficient of Manning's equation. However, previous research has suggested that measuring the roughness coefficient is difficult. The hydraulic performance is affected by the roughness of concrete surfaces due to abrasion. Therefore, considerable attention has been paid to the study of measuring the roughness of concrete surfaces. Scientists have proposed the following methods.

The sand patch test is described in ASTM E965-96 Standard Test Method for Measuring Pavement Macrottexture Depth Using a Volumetric Technique. A quantity of sand is spread in a circular shape on the measurement surface. The roughness of the surface is evaluated by the sand diameter of the expanded circle. It can be used for concrete surface roughness measurements [1].

The laser displacement meter [2] method is done by measuring the distance between the sensor head

and the measurement surface with a laser at 0.1mm intervals. A roughness curve is drawn from the measured distance. Its use in agricultural channels has been investigated, achieving high accuracy measurements. However, it is expensive because it is an exclusive sensor design.

A moulage gauge [3] is made of a plurality of needles. It is pressed against the measurement surface and copies the shape of the surface. This method uses a cheap tool and applies a simple principle. However, analysis based on this method is time- consuming and labor-intensive.

An aerial ultrasonic wave [4] reflected from the concrete surface is diffusely reflected by the concrete surface roughness. Therefore, when roughness is severe, the peak-to-peak voltage is lowered.

Method of the aerial ultrasonic sensor is economical and wide range measuring system. However, there are some issues. Nagaoka [5] proposed that influence of windy velocity and as the wind velocity was increased, the peak to peak was decreased. Therefore, it is desirable to install a windshield. Okajima [4] indicated it is necessary to keep the distance constant and set perpendicularity of the measurement surface and the sensor. We focused on the contact type ultrasonic collecting device to solve the problem. By installing the collecting device as a measuring jig between a measurement surface

and a sensor, it becomes to enable a windshield and easy installation. However, few study have focused on an aerial ultrasonic sensor was installing with collecting devices. The purpose of this study is application for roughness measurement and investigation optimal contact type ultrasonic collecting device.

## MATERIALS AND METHOD

### Aerial Ultrasonic Sensor

The LV-Maxsonar-EZ1 (Maxbotic, Inc.) was used as the aerial ultrasonic sensor. The frequency is 42 kHz. Input voltage is 5.5 V. The sensor was designed as a distance meter. The aerial ultrasonic wave was acquired by oscilloscope. Fig. 1 shows the reflected wave from a concrete surface. We calculated a peak to peak voltage. A peak to peak was indicated reflection intensity.

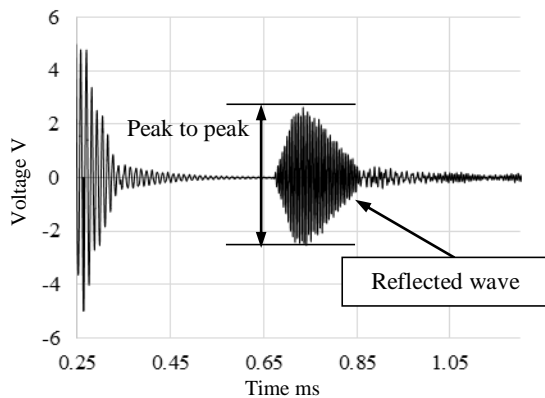


Fig. 1 Sample of reflected ULTRASONIC wave

### Contact type ultrasonic collecting devices

The contact type ultrasonic collecting devices were used shape of column and cone. The Fig. 2 shows diagram of the collecting devices. The columnar type were made of PVC (polyvinyl chloride) pipe. The inner diagram are 20 and 30 cm. The height of diagram 20 cm are 20, 30, 40, 50, 60, 70, 80, 90 and 100 cm. The height of diagram 30 cm are 20, 30, 40 and 50. The conical type were made of plastic traffic cone. The height are 20, 30, 40 and 50 cm. The apex angle are 16 and 20°.

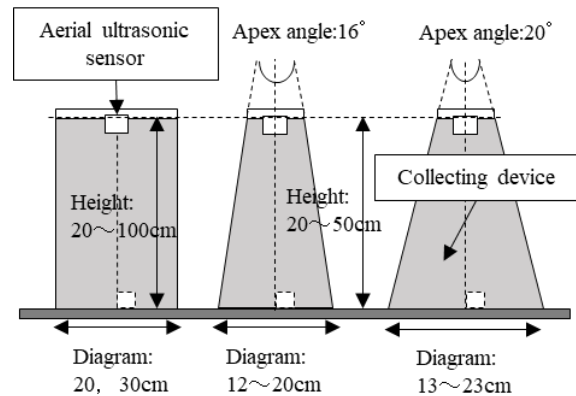


Fig. 2 Diagram of collecting devices

### Concrete samples and previous study results

The concrete samples were made for this study. Fig. 3 shows the picture of the concrete samples. The concrete samples are reproduced the abrasion of irrigation channel. The dimensions were a length of 700 mm, a width of 700 mm and a height of 50 mm. We prepared three types of roughness condition. The first type is a smooth concrete surface. The second and third types were rough concrete surfaces. A roughness is quantified by an arithmetic mean roughness ( $R_a$ ). An arithmetic mean roughness is described in JIS B 0601. An arithmetic mean roughness indicates average of absolute value along the measuring length. We used the moulage gauge as the previous method. The length of the moulage gauge is 150 mm. The number of steel sticks is 180, and the measurement interval is 0.8 mm. Fig. 4 shows a sample graph of an arithmetical mean roughness. The  $f(x)$  is transcribed a roughness curve of a concrete surface by the moulage gauge. The  $Y(x)$  is a liner approximation that is calculated by the  $f(x)$ . The  $R_a$  is calculated integral value of  $|f(x) - Y(x)|$  from 0 to  $l$  divided by length of the moulage gauge. We measured four directions for each measuring point. The Fig. 5 shows the result of the arithmetical mean roughness. The arithmetical mean roughness was used the average value of four directions. The average value of 9 points of the first type was 0.0 mm, the second type was 0.32 mm, and the third type was 1.11 mm. The third type has a variation of roughness.

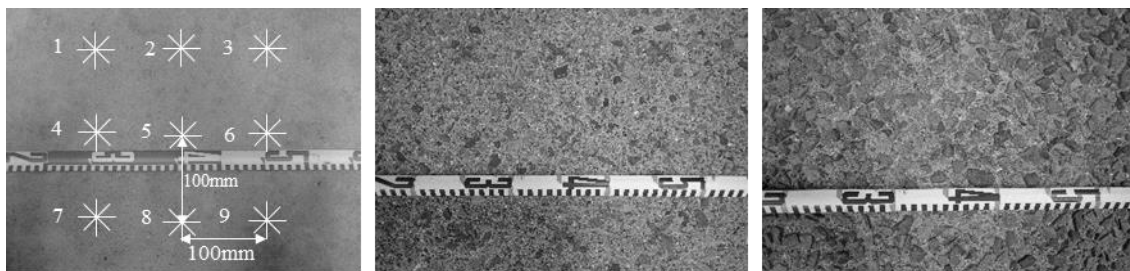


Fig. 3 Picture of concrete samples (first,  $R_a$ : 0.04, second,  $R_a$ : 0.32, third,  $R_a$ : 1.11)

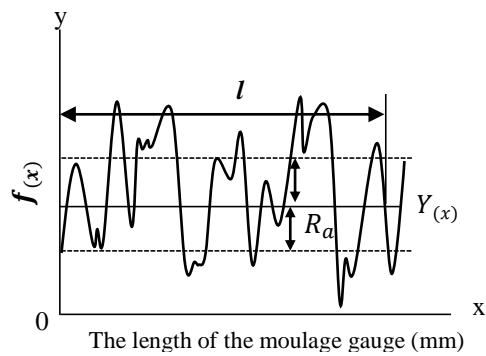


Fig. 4 Sample graph of arithmetical mean roughness

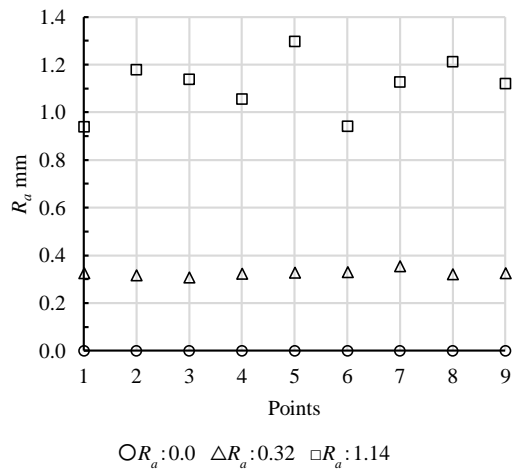


Fig. 5 Result of arithmetical mean roughness

## RESULTS AND DISCUSS

### Application for roughness measurement

We investigated the relationship between the peak to peak and the arithmetic mean roughness ( $R_a$ ) by. The peak to peak was acquired by the aerial ultrasonic with the collecting devices. The  $R_a$  was acquired by the moulage gauge. We measured 3 concrete samples and 9 points in shown Fig. 3. The Fig. 6 shows the state of experiment.

The Fig. 7 shows the result of the columnar type of diameter 20 cm. This peak to peak is an average of 9 measuring points. The standard deviation was showed by the error bar. The peak to peak was decreased as the roughness was increased at all. Except for 20 cm, the peak to peak of  $R_a$  0.0 mm was decreased from 30 to 60 cm and similarly was decreased from 70 to 100 cm. Ihara [6], the reflection intensity due to irregular reflection can be evaluated by the Kirchhoff model. This model indicates that reflected wave intensity decreased due to the roughness of the concrete surface. The results in Fig. 7 showed a similar phenomenon. Therefore, this device of columnar type of diameter 20 cm was revealed application for roughness measurement. The

collecting device becomes heavier in proportion as the measurement distance becomes longer, therefore we consider up to 50 cm.

The Fig. 8, 9 shows result of columnar type of diameter 20 and 30 cm. This peak to peak is 9 points in Fig. 5. The dispersion of the peak to peak was larger in the second type concrete sample than in the first type. Therefore the third type has variation in roughness, the peak to peak has variation. The peak to peak was decreased as the roughness was increased at all height. As the roughness increase, the difference in the peak to peak due to the height tended to decrease, that is, the gradient of approximate line became gradually decrease. The Fig. 8, 9 shows the peak to peak of height 20 was the smallest value.

The Fig. 10, 11 shows the result of conical type of apex angle 16 and 20°. The graph shape of conical type is similar to the columnar type. The peak to peak of the conical type tended to be larger than the peak to peak of columnar type. As the roughness increased, the peak to peak decreased at all height. As the roughness increased, the difference in the peak to peak due to the height tended to decrease. The Fig. 10, 11 shows the peak to peak of height 50 was the smallest value.

The Fig. 7-11 revealed all collecting devices could be application for roughness measurement. The Table 1 shows the coefficient of determination. The coefficient of determination was calculated from the approximate straight line. The example is shown in Fig. 8 of H30. Except for the column30 of H20, the coefficient of determination was showed high value over 0.7. When collecting devices was set H40, the coefficient of determination was indicated over 0.9. This result was revealed that almost collecting devices applicate roughness measurement with high accuracy.

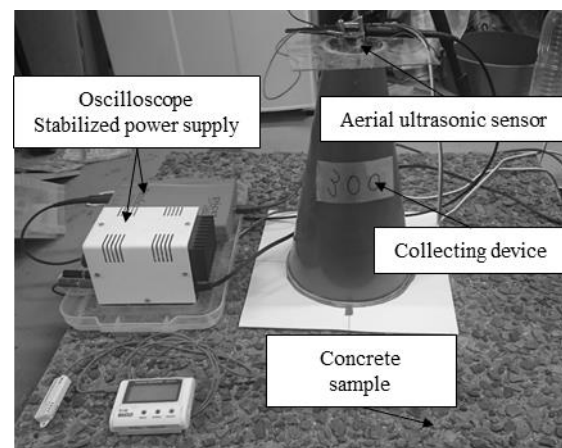


Fig. 6 Picture of experiment by aerial ultrasonic

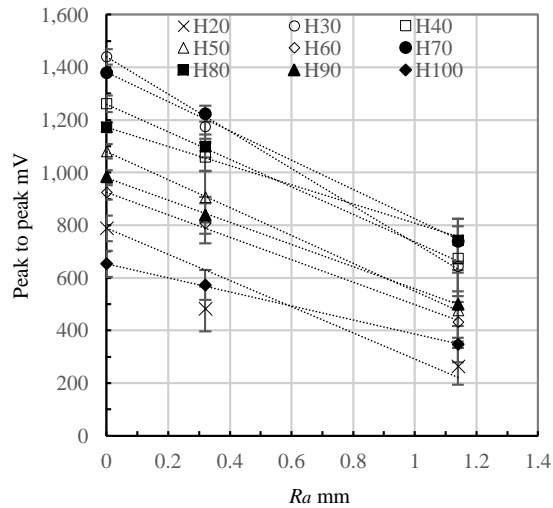


Fig. 7 Relationship between peak to peak and  $R_a$  by columnar type of diameter 20 cm

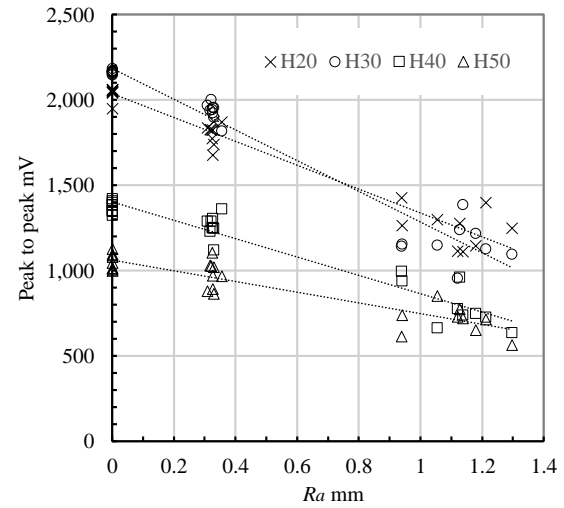


Fig. 10 Relationship between peak to peak and  $R_a$  by conical type of apex angle  $16^\circ$

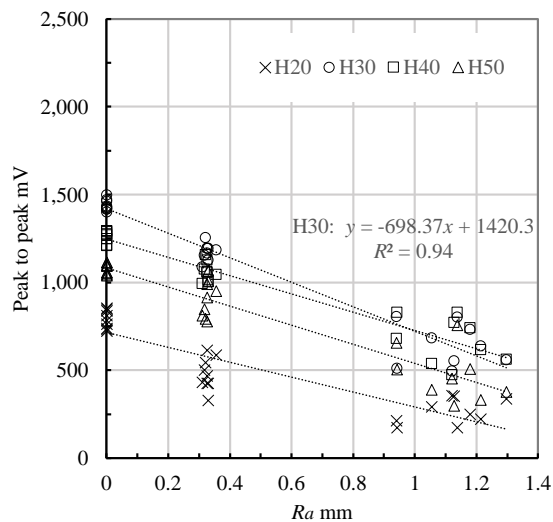


Fig. 8 Relationship between peak to peak and  $R_a$  by columnar type of diameter 20 cm

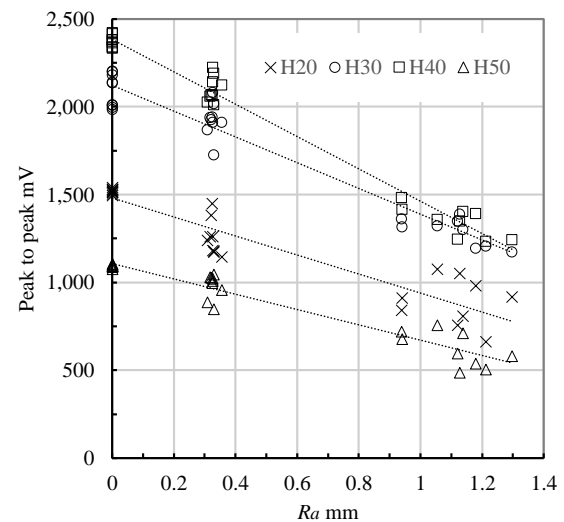


Fig. 11 Relationship between peak to peak and  $R_a$  by conical type of apex angle  $20^\circ$

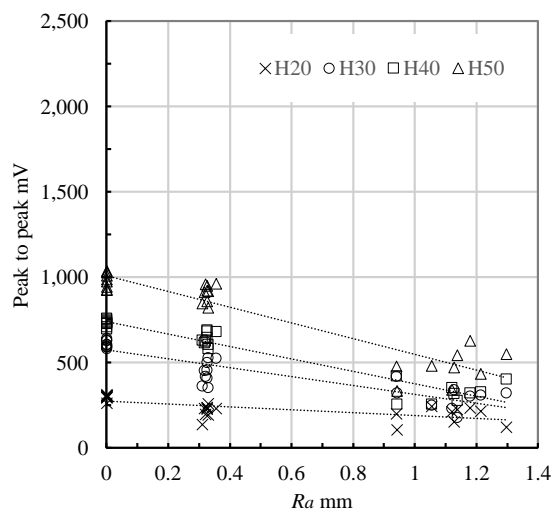


Fig. 9 Relationship between peak to peak and  $R_a$  by columnar type of diameter 30 cm

Table 1 Coefficient of determination

|     | Column20 | Column30 | cone16 | cone20 |
|-----|----------|----------|--------|--------|
| H20 | 0.77     | 0.46     | 0.82   | 0.86   |
| H30 | 0.94     | 0.79     | 0.95   | 0.93   |
| H40 | 0.90     | 0.91     | 0.92   | 0.98   |
| H50 | 0.87     | 0.86     | 0.95   | 0.92   |

### Investigation of optimal collecting device

The Fig. 7-11 and Table 1 revealed all collecting devices could be application for roughness measurement. The relationship the peak to peak and the roughness are highly correlated by approximate line. For example in columnar type of diameter 20 cm height 30 cm, the approximate line was “ $y = -698.37x + 1420.3$ ”. In order to consider the optimal collecting device, we focus on the absolute value of gradient and the intercept of the approximate line.

The gradient affects the measurement accuracy. As the gradient is larger, the accuracy is higher. The intercept influences the sound collecting effect of ultrasonic.

The Fig. 12 shows the absolute value of gradient by collecting devices. The gradient of the conical type was relatively larger than the columnar type. The largest gradient was the conical type of apex angle  $16^\circ$  of height 40 cm. The peak of the gradient by columnar type of diameter 20 cm was height 30 cm. The peak of the gradient by columnar type of diameter 30 cm was height 50 cm. Therefore, when the diameter of collecting device is spread, the peak of gradient tends to shift to higher height of collecting device. The conical type became similar results. The peak of the gradient in apex angle  $16^\circ$  was 30 cm. The peak of the gradient in apex angle  $20^\circ$  was 40 cm. When the apex angle of collecting device is spread, the peak of gradient tends to shift to higher height of collecting device.

The Fig. 13 shows the intercept by collecting devices. The intercept of conical type was relatively larger than the columnar type. Except for height 50 cm, the graph shape of intercept became close to the result of the gradient. The sound collecting effect and the gradient had high correlation. Therefore, a collecting device with high sound collecting effects tends to be a collecting device with high accuracy.

In this study case, the optimal collecting device was the conical type of apex angle  $16^\circ$  of height 40 cm.

## CONCLUSION

This study carried out to investigate the optimal contact type ultrasonic collecting device. By installing this device as a measuring jig between the measurement surface and the sensor, it becomes to enable the windshield and easy installation. We studied application for roughness measurement and investigation optimal contact type ultrasonic collecting device.

The peak to peak was decreased as the roughness was increased at all collecting devices. All collecting devices could be application for roughness measurement. It was found that the coefficient of determination of between the peak to peak and the  $R_a$  was high value. Except for the column30 of H20, the coefficient of determination was indicated over 0.7. When collecting devices was set H40, the coefficient of determination was indicated over 0.9 for all collecting devices.

In order to consider the optimal contact type ultrasonic collecting device, we focus on the absolute value of gradient and intercept of the approximate straight line. The gradient of conical type was relatively larger than the columnar type. The largest gradient was the conical type of apex angle  $16^\circ$  of height 40. The intercept of conical type was relatively

larger than the columnar type. Except for height 50 cm, the intercept became close to the result of the gradient. In this study case, the optimal collecting device was the conical type of apex angle  $16^\circ$  of height 40 cm. However, if the sensor characteristics change, the optimal shape of collecting device also change. Further studies are needed in order to adapt to various sensor characteristics.

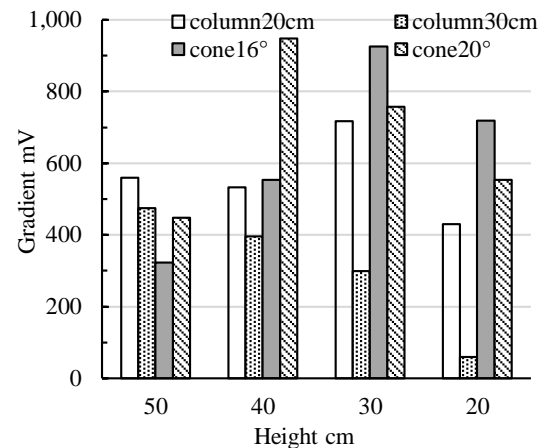


Fig. 12 Gradient of approximate line by collecting devices

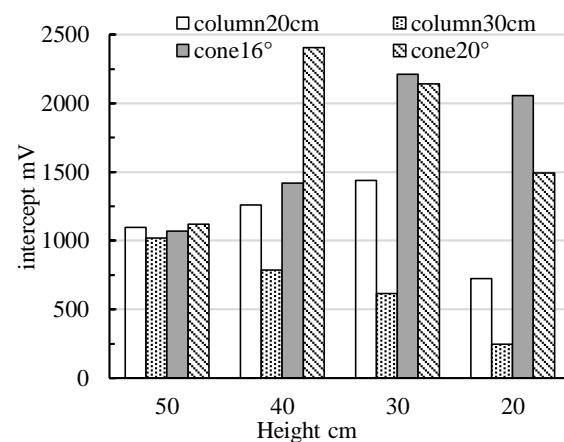


Fig. 13 Intercept of approximate line by collecting devices

## REFERENCE

- [1] ASTM E 2380, Standard test method for measuring pavement texture drainage using an outflow meter, West Conshohocken (PA) ASTM International, 2005.
- [2] Asano I., Tokashiki M., Mori M. and Nishihara M., Development of Erosion Monitoring System on Laser Displacement Meter for Cementitious Surface Coating Method, Irrigation, Drainage and Rural Engineering, Vol. 82, No. 5, 2014, pp. 285-296.

- [3] Kitamura K., Honma S. and Kato T., Quantitative Evaluation for Forecast of Irrigation Canal Abrasion, *Irrigation, Drainage and Rural Engineering*, Vol. 76, No. 9, 2008, pp. 823-828.
- [4] Okajima K., Nagaoka S., Ishiguro S., Ito R., Watanabe K and Ito T, Measurement of the Roughness of the Concrete Surface by the Peak to Peak Value of the Aerial Ultrasonic Wave, *Irrigation, Drainage and Rural Engineering*, Vol. 84, No. 3, 2016, pp. 233-240.
- [5] Nagaoka S., Okajima K., Ito R., Raihanul. I. M, Watanabe K. and Ito T., Influence of Wind Velocity on Measurement of Concrete Surface Roughness Using Aerial Ultrasonic Sensor, *Irrigation, Drainage and Rural Engineering*, Vol. 86, No. 2, 2017, pp. 197-204
- [6] Ihara I. and Sukmana. D. D., Surface Roughness Characterization through the Use of Diffuse Component of Scattered Air-Coupled Ultrasound” *The Japan Society for Precision Engineering*, Vol. 74, No. 7, 2008, pp. 691-695.



## Experimental Investigation of Multi-axial Mechanical Behavior of Rubber Materials for Base-Isolated Bridges

Hiromichi Narita<sup>1</sup>, Junji Yoshida<sup>2</sup>, and Kouichi Takeya<sup>3</sup>

<sup>1</sup> Faculty of Engineering, University of Yamanashi, Japan;

<sup>2,3</sup> Faculty of Engineering, Graduate School, University of Yamanashi, Japan.

### ABSTRACT

Civil engineering structures representing road bridges frequently use laminated rubber bearings for seismic isolation. In recent earthquakes, there have been damages of the bearings in some bridges. In order to investigate behavior of those bridges during the earthquakes and causes of the damage of the bearings, an accurate constitutive model of rubber is required. However, mechanical properties of the rubber such as stress-strain relations under multi-axial deformation is not generally open to the public.

This research provides sufficient material test data for accurately modeling the rubber. Three types of material tests are done. The first one is dynamic simple shear test under multi-axial deformation with several loading frequencies. The experimental results show that the influence of strain amplitudes on stress-strain relation is significant, and that the influence of the loading frequencies is very small. The second one is tensile and compressive test of a thin rubber sheet, which is adhered to plates in upper and lower plane, in order to investigate relation between volumetric deformation and hydro-static pressure of the rubber. The third one is static tensile test. In the test, uniaxial and equi-biaxial tensile test were carried out under quasi-static loading condition, and relations between stretch and nominal stress are obtained. Using these data, we would be able to identify material constants of complex constitutive models, such as visco-elastic damage model and visco-elasto-plastic damage model.

*Keywords: Rubber materials, laminated rubber bearings, Base-isolated bridges, stress-strain relations*

### INTRODUCTION

The 1995 Kobe Earthquake triggered an increase in earthquake countermeasures such as laminated rubber bearings for seismic isolation. With the increase of countermeasures, a large number of laminated rubber bearings have been used in civil engineering structures representing road bridges. However, in the 2011 off the Pacific coast of Tohoku earthquake and the 2016 Kumamoto earthquake, some damages were found in rubber bearings of road bridges. In order to investigate the cause of the damages, it is necessary to approximate the behavior of those bearings with using the accurate constitutive model [1] for the rubbers. However, mechanical properties of those rubbers, which are necessary for modeling, have not been published and, therefore, it is difficult to precisely trace behavior of the devices during the earthquakes by numerical simulation.

In this research, the mechanical properties of rubber material for base-isolated bridges are examined in detail by several loading experiments,

which are required in simulations using accurate constitutive models [2],[3].

### MATERIAL TESTING OVERVIEW

We picked up a popular natural rubber material for laminated rubber bearings of base-isolated bridges, and three types of loading experiments were conducted for the rubber: dynamic simple shear test, tensile and compressive test of a constrained rubber layer, and standard static tensile tests. In the following part of the paper, those tests are called simply as *shear test*, *constrained tensile/compressive test*, and *static tensile test*, respectively.

#### Shear test

In the shear test, the effects of strain levels, frequencies, and loading paths to stress-strain relations were investigated. For this test, we developed a loading machine, which can give arbitrary dynamic displacements to specimens simultaneously in the tri-axial directions.

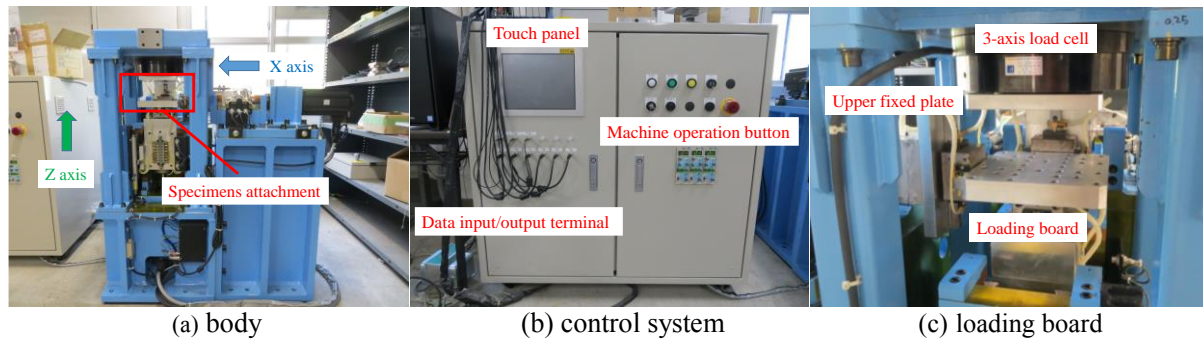


Fig.1 Dynamic triaxial loading machine

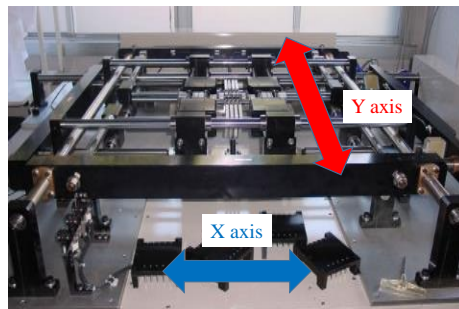


Fig.2 Biaxial tensile testing machine

### Constrained tensile/compressive test

In the constrained tensile and compressive test, a specimen is a thin circular rubber layer sandwiched by steel plates. In the test, the upper plate is fixed, while cyclic displacements with several small amplitudes are given to the lower plate. In spite of the small displacement, the corresponding load is not so small, because high hydrostatic pressure is generated at the central part of the rubber layer, due to slight compressibility of the rubber.

It is noted that those experimental results would need a comparison with its numerical simulation by, for example, FEM, in order to identify material constants related to volumetric deformation. Therefore, in the strict sense, this is not a material test, since deformation of the test is not uniform.

### Static tensile tests

It is known that parameters of even some simple constitutive models for rubber, such as Mooney-Rivlin model or Ogden model [1], can not be identified only from results of uniaxial tensile tests, because some parameters have little sensitivity to uniaxial tensile deformation.

Therefore, in the static tension tests, two types of tension tests are conducted. One is a standard uniaxial tension test to grasp the static behavior in a large strain range of 500% or more. Another is an equibiaxial tensile test to investigate the coupled effect of deformation in two directions.

## EXPERIMENTAL METHODS

### Loading machine

In this sub-section, the loading machines of each test is explained.

We developed a dynamic tri-axial loading machine for the shear test and the constrained tensile/compressive test. Fig.1 shows the outline of the machine. As shown in the figure, three actuators can control the displacements of the central lower plate according to signals given from outside. The maximum stroke is 20 [mm] in the two horizontal directions (X and Y axis), and 50 [mm] in the vertical direction (Z axis). The most characteristic feature of the machine is the maximum speed of the loading. The machine has the ability to perform a sine wave excitation at a frequency of 100 [Hz] with an amplitude of 0.1 [mm] in both X and Y directions.

Fig.2 shows a biaxial loading machine employed for the static tensile test. This machine can give arbitrary two directional displacements for a sheet-type specimen, which is grabbed at the center of the machine. The maximum stroke is 360 [mm] in the horizontal X direction and 240 [mm] in the horizontal Y direction. The maximum velocity and load are 20 [mm/s] and 2000 [N], respectively.

### Specimens

The specimens for the shear test and the constrained tensile / compressive test are both cylindrical, and they are adhered to two steel plates by vulcanization. Drawings of those specimens are shown in Fig3.

In the static tensile test, we employ two types of specimens. One is a dumbbell shape specimen for the uniaxial tensile test and, the other is a square thin sheet for the biaxial tensile test. Both specimens are designed to have different thickness at a part of the edges, at which the machine can tightly grab. Detailed size of those specimens are shown in Fig4.

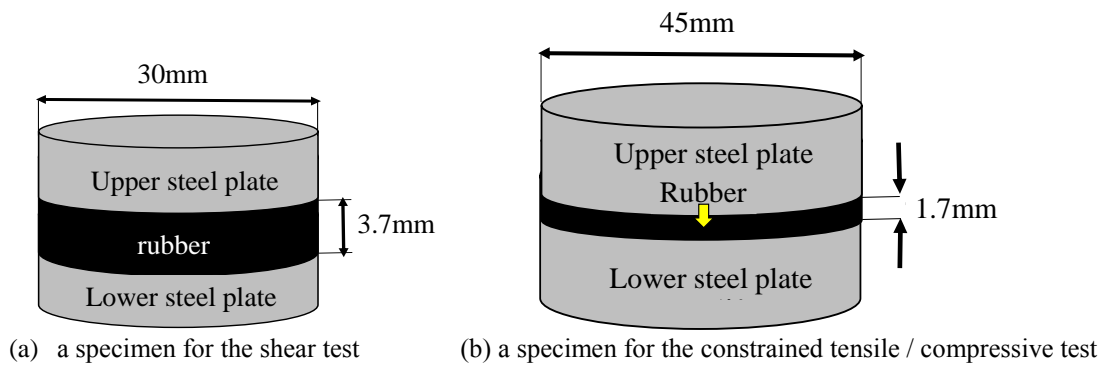


Fig.3 Drawing of the specimens for the shear test and the constrained tensile / compressive test

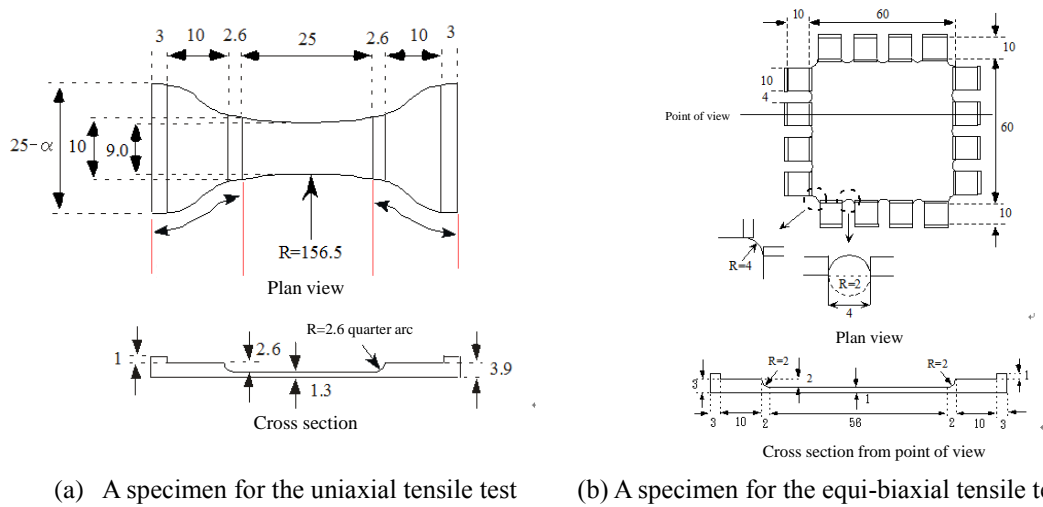


Fig.4 Size of the specimens for the static tensile tests

Table.1 Detailed loading conditions for each test

|                              | Loading directions | Input wave                   | Amplitude (strain/displacement) | frequency           |
|------------------------------|--------------------|------------------------------|---------------------------------|---------------------|
| shear test                   | Uniaxial           | Sine wave                    | 25.50.100.150.200.250[%]        | 0.25,0.50,1,2,4[Hz] |
|                              | Biaxial            | 8-shape, circle, square path | 25.50.100.150.200[%]            | 0.25,0.50,1,2,4[Hz] |
| Constrained tensile test     | Uniaxial           | Sine wave                    | 0.05-1.0[mm]                    | 1[Hz]               |
| Constrained compressive test | Uniaxial           | Sine wave                    | 0.05-0.25[mm]                   | 1[Hz]               |
| Static tensile test          | Uniaxial           | Triangle wave                | 100-750[%]                      | 0.02[Hz]            |
|                              | Biaxial            | Triangle wave                | 100-300[%]                      | 0.02[Hz]            |

## Experimental methods

In each test, cyclic sinusoidal displacement of more than three cycles is given to the specimen at different amplitudes and different frequencies. Detailed loading conditions of each test are summarized in table.1.

## MATERIAL TEST RESULTS AND DISCUSSION

### Shear test

Fig.5 shows a comparison of stress-strain relations at different strains. The shape of hysteretic loops at load reversal points becomes sharp as the amplitude

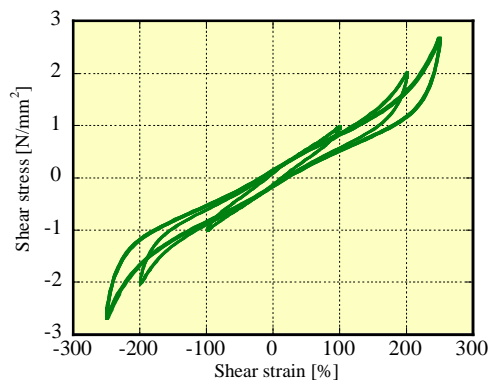


Fig.5 A comparison of stress-strain relations at frequency 1 [Hz]

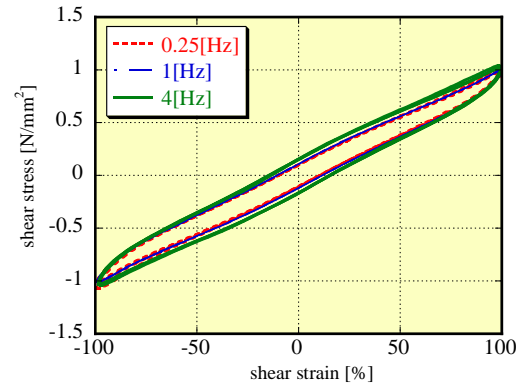


Fig.6 A comparison of stress-strain relations at strain 100 [%]

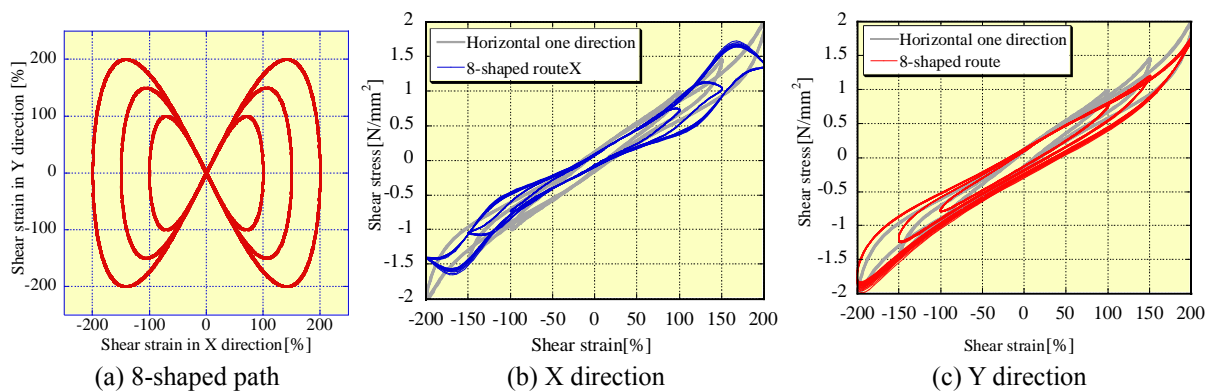


Fig.7 Stress-strain relationships in the shear test

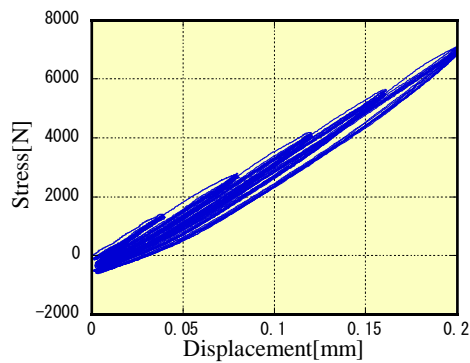


Fig.8 A result of the constrained compressive test

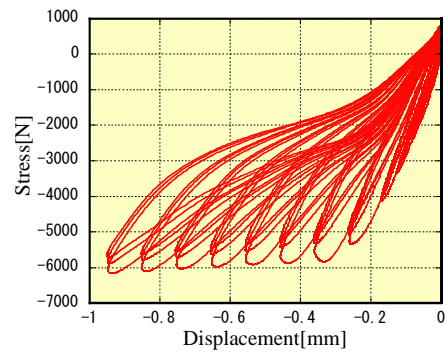


Fig.9 A results of the constrained tensile test

increases. It is clear from this fact that the amplitude has a large effect on the stress-strain relationship. Fig.6 shows a comparison of stress-strain relations at different loading frequencies. From Fig.6, hysteretic loops at different frequencies seem to be similar. Consequently, it is found that the influence of the frequency on the stress-strain relationship is small.

Fig.7 shows a stress-strain relation (in the X direction) of the 8-shaped bi-directional path, in comparison with the one in the unidirectional loading.

The graph shows that the shape of the hysteretic loops is significantly different from the one in unidirectional loading. From this fact, it is understood that the hysteretic loops are affected by coupling effects of bidirectional deformation. Similar results are observed in the circular and square paths. In this paper, the 8-shaped path is taken as an example of two-directional loading paths.

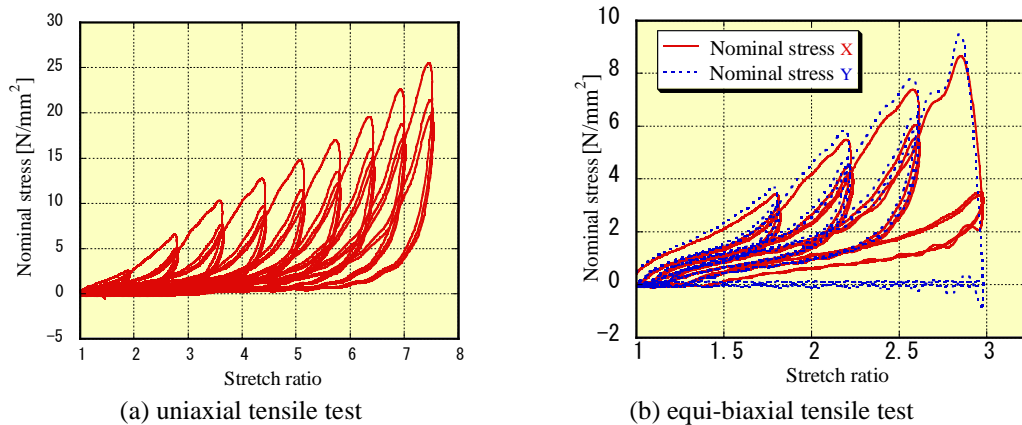


Fig.10 Results of the static tensile test

### Constrained tensile/compressive test

#### Compressive test

The result of the compressive test is shown in Fig.8. The figure indicates that the load-displacement relations were almost elastic. This fact shows that a relation between shrinking deformation and hydrostatic pressure might be elastic.

#### Tensile test

A result of the tensile test is shown in Fig.9. The figure indicates that when deformation is very small, load-displacement relations are almost elastic. However, when the deformation exceeds a limit value, the relations suddenly become nonlinear and irreversible. From this fact, it is supposed that a relation between dilational deformation and hydrostatic pressure would be nonlinear and irreversible.

### Static tensile tests

Those standard tensile tests were done for capturing static uniaxial and biaxial stress-strain relations in various strain ranges. Some examples of the results are shown in Fig.10 as relations between nominal stress and stretch in various strain ranges. The Fig.10 shows typical mechanical properties of rubbers, such as Mullins' effect, hardening, and small energy absorption by hysteresis loops [4].

### CONCLUSION

In this study, we conducted a variety of material tests required for identifying parameters of complex constitutive models of rubber materials.

From the dynamic simple shear test, it is found that the effect of the frequency on stress-strain relations is small, while the effect of the strain amplitude is large.

From the constrained compressive test of rubber layer, it is found that load-displacement relations are almost elastic. On the other hand, the relations in the

constrained tensile test became highly nonlinear, especially in the large deformation range.

In the standard static tensile test, cyclic stress-strain relations in several large strain levels are obtained in the uniaxial and biaxial deformation cases.

From those experimental data, it is expected that we could identify parameters even for complex constitutive models, such as visco-elastic damage models [2] or visco-plastic damage models [3].

### ACKNOWLEDGEMENTS

The specimens used in the material tests are manufactured and provided by the Japan Rubber Bearing Association. We extend our most sincere thanks.

### REFERENCES

- [1] Holzapfel, G. A.: *Nonlinear Solid Mechanics – A Continuum Approach for Engineering*, Wiley, 2000.
- [2] Simo, J. C.: On a fully three-dimensional finite-strain viscoelastic damage model: formulation and computational aspect, *Computer Methods in Applied Mechanics and Engineering*, Vol.60, pp.153-173,1987.
- [3] Miehe, C. and Keck, J.: Superimposed finite elastic- viscoelastic-plastoelastic stress response with damage in filled rubbery polymers. Experiments, modeling and algorithmic implementation, *Journal of the Mechanics and Physics of Solids*, Vol.48, pp.323-365, 2000.
- [4] Treloar, L. R. G: *The Physics of Rubber Elasticity*. 3rd ed., Oxford University Press, 1975.

# HIGHLY ACCURATE ESTIMATION OF DAILY SUSPENDED SEDIMENT LOAD USING MULTIVARIATE HYDROLOGICAL

Phakawat LAMCHUAN, Adichai PORNPROMMIN, Jiramate CHANGKLOM  
Department of Water Resources Engineering, Faculty of Engineering, Kasetsart University, Thailand

## ABSTRACT

Sediment rating curves (SRCs) have been applied to estimate daily suspended sediment load ( $Q_s$ ) worldwide because of its simplicity. In this method, a current  $Q_s$  was estimated by a power function of a sole variable, a current daily water discharge at the same measurement station. However, many studies found that its accuracy is not very high. In this study, we developed a new approach to estimate  $Q_s$  using multivariate hydrological data at the same station and other upstream stations. Using correlation analysis, the additional variables were selected such as upstream water discharges, rainfall at the current or antecedent day. Therefore, spatial and temporal variability was simply considered in our new approach. Then, five methods, a multiple linear regression (MLR), a multiple nonlinear regression (SLR, QLR, and PLR) and an artificial neural network model (ANNs), were applied. The comparison between the SRC method and our new five methods were done using the  $Q_s$  data at three measurement stations in three basins of Thailand between 2000 and 2017. The results showed that our new approach (SLR, QLR, PLR, and ANNs) except MLR gave better satisfaction with the observed data than the traditional SRC method. ANN estimated  $Q_s$  with the highest accuracy (the  $R^2$  and EI of 0.96 and 0.96, respectively) while SRC gave the lowest accuracy (the  $R^2$  and EI of 0.89 and 0.71, respectively). Thus, the more complexity of the model structure and the consideration of the spatial and temporal variability can provide a higher accurate estimation of  $Q_s$ .

*Keywords: Suspended sediment load, Artificial neural networks (ANNs), Sediment Rating Curve, Multiple Linear Regressions, Multiple Non-Linear Regressions*

## INTRODUCTION

Sediment load data is useful for the design of a reservoir storage. Before initiating any water resource projects, we must know water discharge and sediment load to estimate dead storage, useful storage and surcharge of a reservoir. However, it is difficult to measure sediment load daily. Thus, it is common to calculate sediment load using a relationship with water discharge or other hydrological data. Since sediment load is critical to indicate the lifespan of a reservoir, the underestimation of sediment load results in insufficient volume of dead storage and, consequently, a rapidly decrease of reservoir capacity while the overestimation will lead to higher construction and management costs. Therefore, it is important to determine suspended sediment load accurately.

The measurement of suspended sediment load consumes more time and costs higher than other types of hydrological data. Thus, in Thailand, suspended sediment load at one station is measured approximately 8-20 times per year. These data are used to estimate two parameters in the traditional sediment rating curve (SRC) equation in the form of the power function of water discharge at the same station. Although the SRC is very simple and depends on a sole variable, its accuracy is not high. Campbell

and Bauder [1] studied 60 months of record from the Red River, Texas, USA, was found between rating curve derived load estimates and the measured values for seven sub-periods. The errors for the individual periods varied between -20 and +14.8% while the error for the total period was only +1.5 per cent.

Many researchers have proposed other methods to estimate suspended sediment load instead of SRC. Jain [2] showed that the artificial neural networks (ANNs) method provided the results much better than SRC at Mississippi River, USA. Kumar et al. [3] studied suspended sediment load at Kopili River basin, India. They used a machine learning approach to construct six models and found that the least square support vector regression (LS-SVR) and ANNs provided the best satisfactory. In their model, rainfall was included and gave a better accuracy. Melesse et al. [4] predicted suspended sediment load of three major rivers (Mississippi, Missouri and Rio Grande) in USA using four models. From their results, ANNs again provided the highest accuracy for both daily and weekly simulations.

In previous studies, water discharge and sediment load at the same station and rainfall were used as independent variables to build models to estimate suspended sediment load. However, there were no studies using hydrological data of upstream measurement stations to estimate suspended sediment



load. In this study, we investigated the significance of upstream water discharge in estimating sediment load. Five mathematical rainfall-runoff-sediment models were tested and their performances were discussed and compared with the traditional SRC.

## STUDY AREA

Figure 1 shows a map of the study area of 6,350 km<sup>2</sup> which includes P1, P21, P67, and R070391. P1 is a discharge and suspended sediment station located at 18° 47' 09" N and 99° 00' 29" E flow into the Ping Basin in Thailand. P21 and P67 are the discharge station located at 19° 01' 11" N, 98° 57' 42" E and 18° 55' 29" N, 98° 56' 34" E respectively. R070391 is a rainfall station located at 19° 05' 09" N and 98° 45' 29" E.

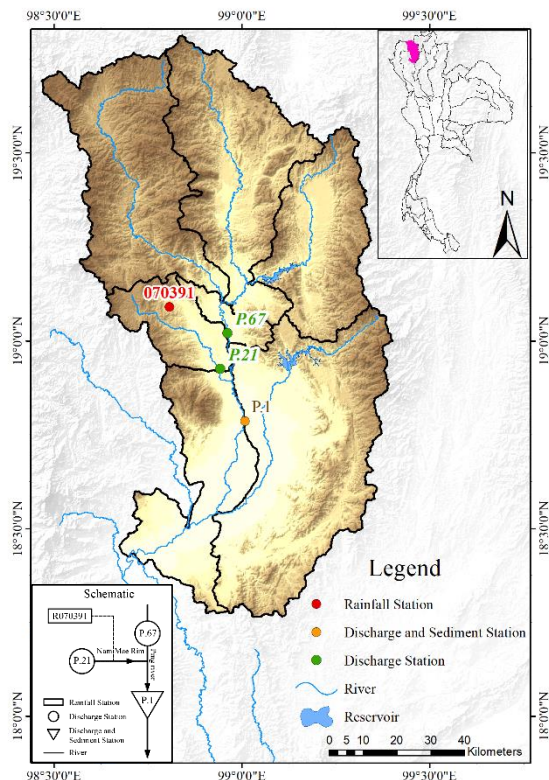


Fig. 1 Map of the study area

## METHODOLOGY

### Sediment Rating Curve

The maximum sediment concentration may not coincide with the flood peak and may either precede or lag behind the maximum water discharge. [5]

The Sediment rating curve is a non-linear relationship between the water discharge and suspended sediment load. [6] SRC is expressed as:

$$Q_s = a \cdot Q_w^b \quad (1)$$

where  $a$  and  $b$  are coefficients obtained by regression.  $Q_s$  is suspended sediment load (Tons/day) and  $Q_w$  is the discharge (m<sup>3</sup>/s).

### Input data selection

Model input for the estimation for the suspended sediment load are P1, P21, P67, and R070391. There are 371 data sets in the period 2000-2017.

The cross-correlation between the various input variables are presented in Table 1. It indicated the output variable  $S_{P1,t}$  has a strong correlation with input variables  $Q_{P1,t}$ ,  $Q_{P21,t}$ ,  $Q_{P67,t}$ , and  $R_{070391,t-2}$

Table 1 Correlation matrix of input variables

|             | $Q_{P1,t}$ | $Q_{P21,t}$ | $Q_{P67,t}$ | $R_{t-2}$ | $S_{P1,t}$ |
|-------------|------------|-------------|-------------|-----------|------------|
| $Q_{P1,t}$  | 1.00       |             |             |           |            |
| $Q_{P21,t}$ | 0.85       | 1.00        |             |           |            |
| $Q_{P67,t}$ | 0.97       | 0.80        | 1.00        |           |            |
| $R_{t-2}$   | 0.50       | 0.49        | 0.46        | 1.00      |            |
| $S_{P1,t}$  | 0.85       | 0.65        | 0.90        | 0.44      | 1.00       |

Note:  $R_{t-2} = R_{070391,t-2}$

From Table 1, we selected the input data in the study according to the equation.

$$S_{P1,t} = f(Q_{P1,t}, Q_{P21,t}, Q_{P67,t}, R_{t-2}) \quad (2)$$

### Model Training and Testing

It is common on several studies to use 70% of the data for training and 30% for testing and validation of the model (The 70-30). Due to the limitations of the data collection, the suspended sediment load is observed at least 6 times a month on a random basis. This study focuses on developing models to estimate high value suspended sediment load to ensure that it can be used to estimate accurately.

High values of suspended sediment load do not occur often and do not occur throughout the whole data set. If we selected the 70-30, those high values would be missing for the test data set. Hence, we decided to use 50% of the date for training and 50% for testing.

### Sliding Window Validation

This study has been validated for the reliability of data for all of the models by using window sliding validation. A model is trained using a training window and applied on the testing window to compute the performance for the first run. For the next run, the training window is slide to a new set of training records and the process is repeated until all the training windows are used. [7] In this study divided whole data were 2 set data (Initial 50% and



Second window 50%) then sliding window 1 iteration per data set. This process repeated until the number of iteration equal to the total amount of whole data. The process of sliding window is shown in Fig. 2

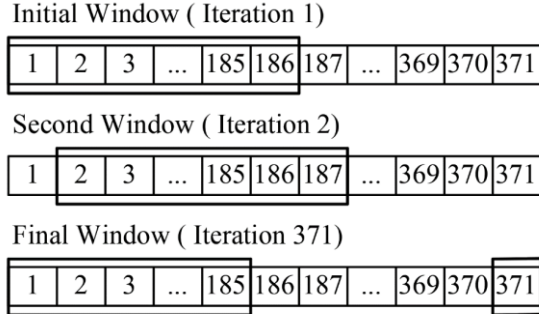


Fig. 2 Sliding window validation process

### Performance Evaluation of Various Models

The data sets were divided into 2 groups, one for training and the other testing. Four indices are used to determine model performance which are the coefficient of determination ( $R^2$ ), the root mean squares of errors (RMSE), the mean absolute percentage error (MAPE), Nash–Sutcliffe coefficient (EI).

### Multiple linear regression (MLR)

Multiple linear regressions (MLR) analysis was performed on the same data set to estimate sediment load and compare the results with output from the SRC model. The MLR equation is defined as:

$$S_{P1,t} = a + bQ_{P1,t} + cQ_{P21,t} + dQ_{P67,t} \quad (3)$$

, where  $a, b, c$  and  $d$  are the regression coefficients.

### Multiple Non-linear regression (MNLR)

Various forms of non-linear equations are used for regression to compare the ability to estimate the suspended sediment load. This study uses three forms of multiple non-linear equations i.e. Squared linear regression (SLR), Quadratic linear regression (QLR), and Power linear regression (PLR).

### Squared linear regression (SLR)

The SLR equation can be written as

$$S_{P1,t} = a + bQ_{P1,t}^2 + cQ_{P21,t}^2 + dQ_{P67,t}^2 \quad (4)$$

, where  $a, b, c$  and  $d$  are the regression coefficients.

### Quadratic linear regression (QLR)

The QLR equation can be written as

$$S_{P1,t} = a_1 + a_2Q_{P1,t} + a_3Q_{P21,t} + a_4Q_{P67,t} + b_1Q_{P1,t}^2 + b_2Q_{P21,t}^2 + b_3Q_{P67,t}^2 \quad (5)$$

, where  $a_1, a_2, a_3, a_4, b_1, b_2$  and  $b_3$  are the regression coefficients.

### Power linear regression (PLR)

The PLR equation can be written as

$$S_{P1,t} = a \cdot Q_{P1,t}^b \cdot Q_{P21,t}^c \cdot Q_{P67,t}^d \quad (6)$$

where  $a, b, c$ , and  $d$  are the regression coefficients.

### Artificial neural networks (ANNs) overview

The Artificial neural networks consist of three layers of the node: Input layer, Hidden layer, and Output layer. The data from the input layer was calculated and passed through the transform function from the hidden layer to the output layer. The principal learning process of the model is changing the weight value of each connection to adjust the results of the model to be as close to the true value as possible by the back-propagation method.

The theory of ANNs has been described in several papers, this study is described here as briefly. The numbers of hidden layer were found using trial and

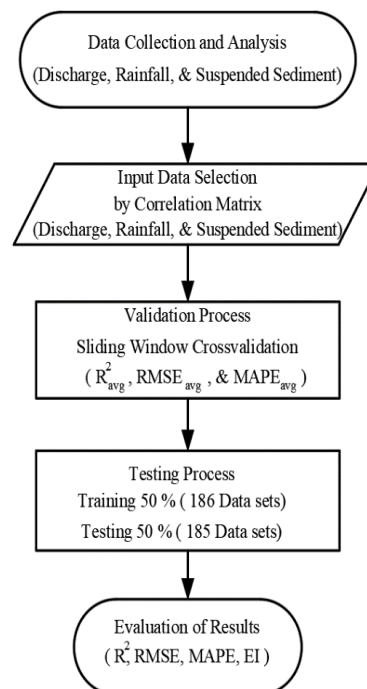


Fig. 3 Workflow for the whole process of

Table 2 Results of Sliding window validation 50-50 of MLR, SLR, QLR, PLR, and ANNs 371 Days

| Input Variables   | Model | $R^2_{avg}$ | RMSE <sub>avg</sub> | MAPE <sub>avg</sub> |
|---|-------|-------------|---------------------|---------------------|
| $S_{P1,t} = f(Q_{P1,t}, Q_{P21,t}, Q_{P67,t}, R_{t-2})$ | MLR   | 0.81        | 3003                | 165                 |
|   | SLR   | 0.94        | 1960                | 217                 |
|   | QLR   | 0.89        | 2518                | 189                 |
|   | PLR   | 0.91        | 3958                | 80                  |
|   | ANNs  | 0.87        | 1765                | 402                 |
| Input Variables   | Model | $R^2_{avg}$ | RMSE <sub>avg</sub> | MAPE <sub>avg</sub> |
| $S_{P1,t} = f(Q_{P1,t}, Q_{P21,t}, Q_{P67,t})$          | MLR   | 0.78        | 3227                | 1427                |
|   | SLR   | 0.94        | 2013                | 204                 |
|   | QLR   | 0.90        | 2624                | 207                 |
|   | PLR   | 0.89        | 4280                | 80                  |
|   | ANNs  | 0.88        | 1657                | 438                 |

Table 3 Results of SRC, MLR, SLR, QLR, PLR, and ANNs during testing period 185 Days (50% of all Data)

| Input Variables                                | Model | $R^2$ | RMSE | MAPE | EI   |
|--|-------|-------|------|------|------|
| $S_{P1,t} = f(Q_{P1,t})$                       | SRC   | 0.89  | 1980 | 150  | 0.71 |
| $S_{P1,t} = f(Q_{P1,t}, Q_{P21,t}, Q_{P67,t})$ | MLR   | 0.70  | 2493 | 3107 | 0.54 |
|  | SLR   | 0.96  | 800  | 588  | 0.95 |
|  | QLR   | 0.95  | 866  | 192  | 0.94 |
|  | PLR   | 0.91  | 1553 | 138  | 0.82 |
|  | ANNs  | 0.96  | 769  | 207  | 0.96 |

error method. The subsampling of all the data for training and validation was conducted using the function 'divideblock' of MATLAB.

## RESULT AND DISCUSSIONS

The results of the sliding window validation are shown in Table 2. The SLR model performed better than other models ( $R^2_{avg} = 0.94$ , RMSE<sub>avg</sub> = 1960, MAPE<sub>avg</sub> = 217) but other models provided satisfactory model performance as well.

The Rainfall data has been removed from the testing data because it provided correlation with suspended sediment lowest (0.44) as shown in Table 1. Also, we have compared estimation performance on all model with and without the rainfall data and the estimation performance is indifference. Therefore, the input data remained only the discharge data ( $Q_{P1,t}$ ,  $Q_{P21,t}$ ,  $Q_{P67,t}$ ). All performance indices, except for the MAPE, are indifferent whether the model contains rainfall data as a predictor variable or not (as shown in table 2). In addition, the process of the sliding window validation verified that the selected data in this study can be used to further divide the training period and the testing period.

The results of SRC, MLR, SLR, QLR, PLR, and ANNs during the testing period is shown in Table 3. The result from SRC has derived from the relationship between the discharge ( $m^3/s$ ) and suspended sediment load (Tons/day) at station P1

only by using the data in 2000-2005, 2007-2010 (186 data sets) for the training period, the equation was  $Q_s = 2.0259Q_w^{1.4856}$  to be used in the testing period. Although the SRC provides good results ( $R^2 = 0.89$ , RMSE = 1980, MAPE = 150, EI = 0.71) from Fig. 4(a), it can be seen that SRC was unable to estimate the high sediment at all peaks suspended sediment load and also it underestimates low values suspended sediment load.

The MLR provided the regression coefficients  $a_0$  (constant),  $a_1$ ,  $a_2$ ,  $a_3$ , and  $a_4$  during training period are found to be -1971.25, -75.74 and 138.72, respectively. The Observed and estimated suspended sediment graph is shown in Fig. 4(b). It was found that the MLR model performs poorly on estimation of suspended sediment load. The performance indices of the MLR were  $R^2 = 0.70$ , RMSE = 2493, MAPE = 3107, EI = 0.54 respectively.

The performance of the SLR model was also evaluated and presented in Table 3. It provided a highly of EI = 0.95 because it can capture almost every peak of suspended sediment load but it provided too high estimation for the low suspended sediments. Moreover, it was shown that the SLR is unable to estimate the low suspended sediments. The estimates for the low sediments are found to be around 400 tons/day. It was shown that the SLR cannot estimate for the low suspended sediments.

The QLR model was found to be relatively accurate. During the testing period, the values of  $R^2$ ,

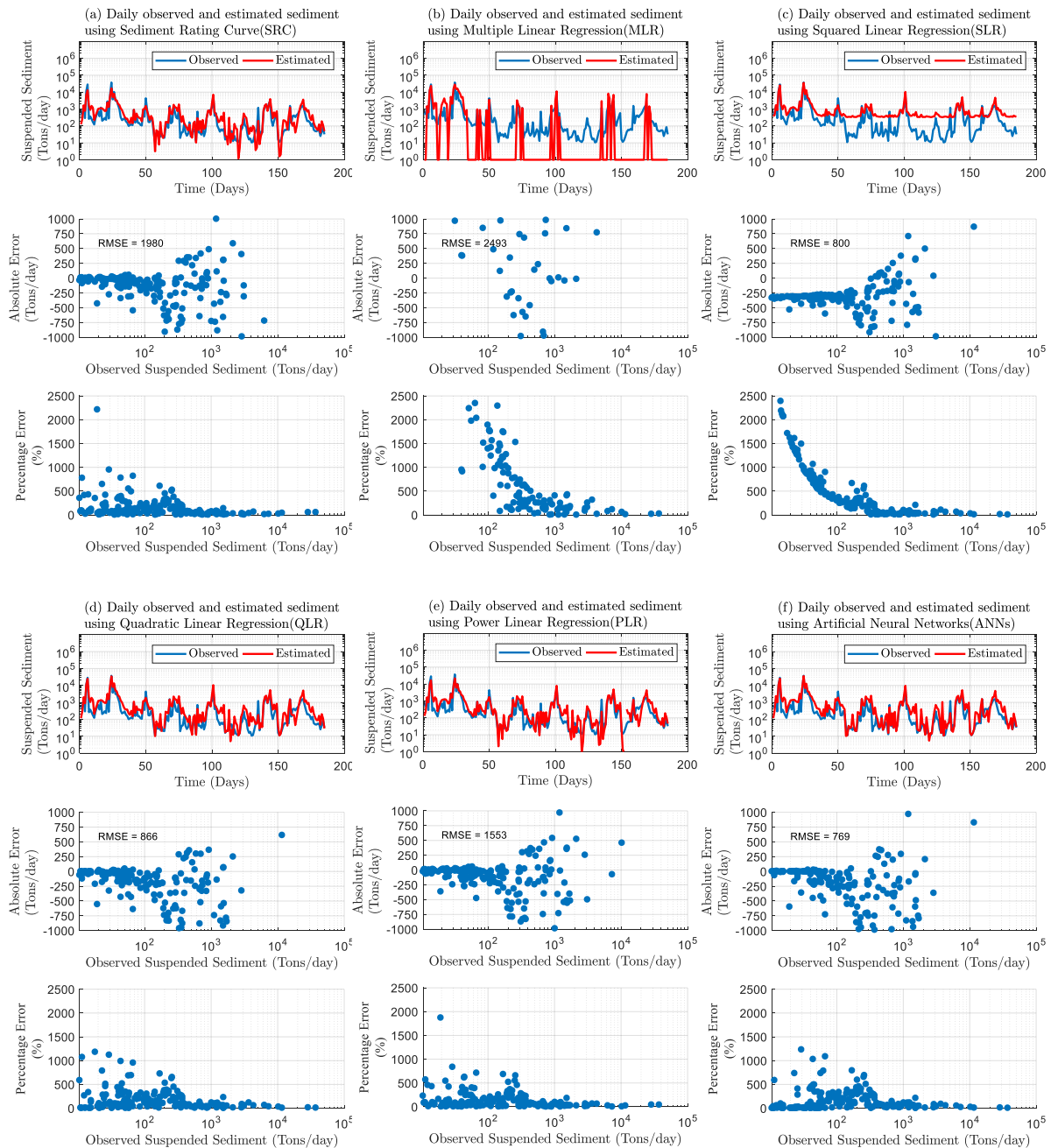


Fig. 4 Estimation results of various model (a) The SRC, (b) The linear (MLR), (c) The squared linear (SLR), (d) The quadratic (QLR), (e) The power (PLR) and (f) The ANNs.

RMSE, MAPE, EI were found to be 0.95, 866, 193 and 0.94, respectively. From Fig. 4(d), it was found that the QLR captured every suspended sediment load peak accurately including the low suspended sediment load. The error suspended sediment load is shown in Fig. 4(d). and it was found that errors are relatively low.

The PLR model provided similar level of accuracy to the SRC. In comparison of both models, the SRC generated suspended sediment from only one variable (discharge at P1) but PLR model consists of 3 variables (discharge at P1, P21, and P67). The values

of  $R^2$ , RMSE, MAPE, EI of the PLR model were found 0.91, 1553, 138, 0.82 respectively.

The ANNs model presented in Fig. 4(f), it can be observed that the model converges well and tends to capture almost all the peaks. The values of RMSE, MAPE of the ANNs model were found 769 and 206 respectively, compared with the RMSE, MAPE of the QLR model (866 and 193) it was found that the ANNs model provides an accurate prediction on high value of suspended sediment load. The errors are less than those obtained from the QLR.

## CONCLUSIONS

According to our investigations, we firstly found that rain data has very little impact on the estimation of the suspended sediments. Therefore, we decided to take the rain data out for the testing process. From the testing results, The ANNs model, the SLR model, the QLR model, and the PLR model provided better estimation results than using sediment rating curves (SRC; the traditional method), given the input data from nearby stations together.

However, it was found that the MLR model is not a suitable model for this estimation as most of the estimates are negative (72.97%). The SLR model estimates well on high values of suspended sediment but provides too high estimation for the low suspended sediments. Although the SLR model can estimate suspended sediment as accurate as the ANNs, it has the highest errors in the low suspended sediment compared to other models.

The QLR model provides a lower EI value than the SLR model but can estimate the suspended sediment well throughout the testing period. It is clear that the QLR model provides lower RMSE and MAPE values than the SLR.

The PLR model fails to estimate peaks suspended sediment accurately, and also it underestimates low values suspended sediment. The estimation of suspended sediment loads is significant for water resource projects, for example, dam reservoir constructions.

The results of this study show that mathematical models such as Multi-linear regression, Multi non-linear regression, and ANNs can be used on multivariate Hydrological data to estimate the suspended sediment load.

## ACKNOWLEDGMENTS

The authors gratefully thank to the Royal Irrigation Department (RID) for the data used in the study, and Mr.Thienchart Suwawong, researcher of the Remote Sensing Research for Water Resources

the Management (SENSWAT) Kasetsart University and Mr.Wachira Surin, Irrigation Engineer of the Smart Operation Center (SWOC) for helpful suggestion and constructive comments.

## REFERENCES

- [1] Campbell, F. B. and Bauder, H. A. 1940 A rating-curve method for determining silt-discharge of streams. Trans. Amer. Geophys. Un. 21, 603-607.
- [2] Jain, S.K., 2001. Development of integrated sediment rating curves using ANNs. J.Hydral. Eng. 127 (1), 30–37
- [3] Dheeraj Kumar, Ashish Pandey, Nayan Sharma, Wolfgang-Albert Flügel, Daily suspended sediment simulation using machine learning approach, CATENA, Volume 138, March 2016, Pages 77-90
- [4] Assefa M. Melesse, Sajjad Ahmad, Michael E. McClain, Xixi Wang, Yeo Howe Lim, Suspended sediment load prediction of river systems: An artificial neural network approach, Agricultural Water Management, Volume 98, Issue 5, March 2011, Pages 855-866
- [5] D.E. Walling, Limitations of the rating curve technique for estimating suspended sediment loads, with particular reference to British rivers, Symposium on Erosion and Solid Matter Transport in Inland Waters, Paris, France, 1977
- [6] Anurag Malik, Anil Kumar, Jamshid Piri, Daily suspended sediment concentration simulation using hydrological data of Pranhita River Basin, India, Computers and Electronics in Agriculture, Volume 138, 1 June 2017, Pages 20-28
- [7] Vijay Kotu, Bala Deshpande, Data Science Concepts and Practice, 2th ed, Morgan Kaufmann Publisher, 2019, Page 443

# **FATIGUE STRENGTH OF HEADED STUDS UNDER ROTATIONAL SHEAR LOADING FOCUSING ON WEIGHT REDUCTION OF STEEL-CONCRETE COMPOSITE BRIDGE DECK**

Kenji Yoshida<sup>1</sup>, Hiroshi Higashiyama<sup>2</sup>, Hideki Ogomori<sup>3</sup> and Shigeyuki Matsui<sup>4</sup>

<sup>1</sup>Kawada Industries, Inc., Japan; <sup>2</sup>Faculty of Science and Engineering, Kindai University, Japan;

<sup>3</sup>Nippon Stud Welding, Co., Ltd., Japan; <sup>4</sup>Osaka Institute of Technology, Japan

## **ABSTRACT**

Headed studs as shear connectors are widely used in steel-concrete composite bridge decks. When vehicles run on the steel-concrete composite bridge deck, horizontal shear force rotationally acts on the headed studs. The authors have investigated durable headed studs by improving the welding ferrule configuration. In Japan, reinforced concrete decks that are likely damaged by fatigue and salt attack have been recently replaced by rehabilitating highway bridges. To use steel-concrete composite bridge decks for those constructions, it is necessary to reduce the dead weight of the bridge decks. Such weight reduction can be achieved by reducing the thickness of the bottom steel plate to, for example, 6 mm in the steel-concrete composite bridge deck. A conventional headed stud with a diameter of 16 mm can weld on the 6 mm thick bottom steel plate, whereas an improved headed stud with a diameter of 16 mm cannot weld on the 6 mm thick bottom steel plate because the bottom steel plate melts with higher heat input during welding. An improved headed stud with a diameter of 13 mm is thus used for the thin bottom steel plate. However, little data is available on the fatigue strength of such combination under rotational shear force. In this study, headed studs welded on the thin bottom steel plate under rotational shear force were experimentally investigated. This paper reports the fatigue durability of a headed stud with an improved headed stud with a diameter of 13 mm welded on the 6 mm thick bottom steel plate.

*Keywords: Headed studs, improved welding ferrule, fatigue strength, rotational shear loading*

## **INTRODUCTION**

Traditionally in Japan, reinforced concrete decks (RC decks) have been widely used for highway bridges. As many highway bridges constructed in the last five decades are getting old, the maintenance of these bridges has become the most serious problem to extend their service life with appropriate rehabilitation works. For bridges with RC decks, replacement of severely deteriorated decks is a recent trend to minimize the Life Cycle Cost (LCC).

Under these circumstances, the steel-concrete composite decks have been developed in recent years as an alternative to RC decks. The steel-concrete composite decks are more used nowadays not only for new bridges, but also for existing bridges by replacing RC decks.

The steel-concrete composite deck is mainly used at the span length of 4 m to 8 m, while the span length of the RC deck is limited up to 4 m in the Japanese Specification of Highway Bridges. This is because the steel-concrete composite deck less than 4 m long is less economical than the RC deck. Furthermore, when replacing the RC deck with the steel-concrete composite deck, the main girder supporting the deck is often kept. Therefore, the weight of the steel-concrete composite deck should be reduced to as light as the existing RC deck.

The steel-concrete composite deck targeted in this study is a Robinson type steel-concrete composite deck (SC deck). The SC deck shown in Fig. 1 consists of a bottom steel plate, headed studs, transverse ribs and reinforced concrete. A number of researches have been performed to develop such steel-concrete composite decks. As shown in Fig. 2, the fatigue failure of headed studs in the SC deck was observed in the wheel load running tests conducted by Matsui et al [1]. Their research work has revealed that the fatigue life of headed studs in the SC deck is significantly shorter than that in the standard push-out fatigue tests. They have also revealed that the headed studs break down earlier because shear force rotationally and repeatedly acts on headed studs while changing its amplitude. This phenomenon is peculiar to the SC deck. Matsui et al. [2-4] also carried out the fatigue tests on a headed stud under rotating shear force. They successfully simulated the reduction of the fatigue strength.

Based on these findings, the fatigue design method for headed studs in steel-concrete composite decks was standardized in Design Code for Steel Structures PART B [5].

In this study, for saving the cost and reducing the weight of the SC deck, specimens with the reduced thickness of the bottom steel plate from 8 mm to 6 mm and the diameter of the headed stud from 16

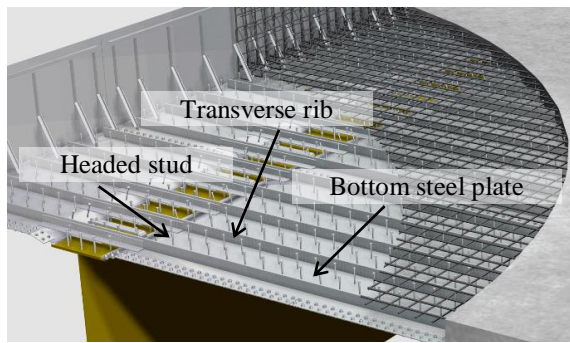


Fig. 1 Steel-concrete composite deck (SC deck).

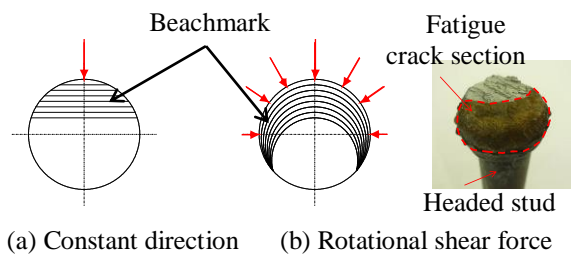


Fig. 2 Rotational shear force and fatigue failure condition acting on stud weld.

mm to 13 mm are manufactured, and the rotational shear fatigue test was conducted to confirm the fatigue strength of the headed stud.

## EXPERIMENTAL PROGRAM

### Specimens and Materials

The general view and dimensions of a specimen are shown in Fig. 3, Fig. 4 and Table 1. The headed studs used in this study have diameters of 16 mm and 13 mm, and a height of 120 mm, which is usually employed in the SC deck. A headed stud was welded on a circular steel plate at a distance of 24 mm from the center. The circular steel plate was with a diameter of 350 mm and thicknesses of 9 mm and 6 mm. A steel tube with a diameter of 232 mm, a height of 150 mm and a thickness of 15 mm was simply placed on the circular steel plate without any mechanical connections. It functions as a mold for concrete in casting and as the protection for wear of concrete when the specimen is horizontally loaded through a loading roller. The compressive strength of the used concrete was 30.8 N/mm<sup>2</sup> after 28 days of curing.

The conventional and the improved ferrules and the state of each headed stud after welding are shown in Fig. 5. The closing castellation at the bottom of the improved ferrule allows the high



Fig. 3 General view of specimen before casting concrete.

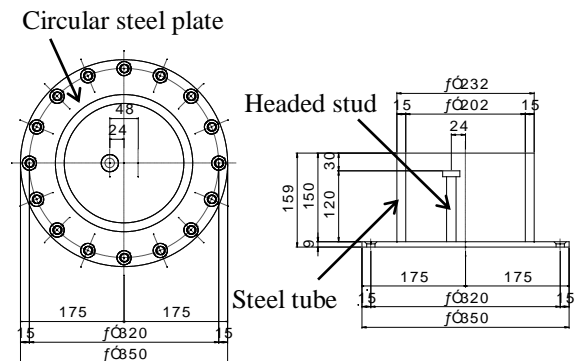


Fig. 4 Dimensions of specimen.

Table 1 Structural dimensions of specimen

|                      |           | Unit              | Structural dimension |
|----------------------|-----------|-------------------|----------------------|
| Concrete             | Thickness | mm                | 150                  |
|                      | Strength  | N/mm <sup>2</sup> | 30.8                 |
| Circular steel plate | Diameter  | mm                | 350                  |
|                      | Thickness | mm                | 6                    |
| Stud                 | Dimension | mm                | φ16×120              |
|                      |           | mm                | φ13×120              |
| Steel tube           | Diameter  | mm                | 232                  |
|                      | Height    | mm                | 150                  |
|                      | Thickness | mm                | 15                   |



(a) Conventional headed stud.



(b) Improved headed stud.

Fig. 5 Ferrules and state of weld collar.



temperature gas to spout upwards. As shown in Fig. 5(b), the weld toe of the improved headed stud is smoothed.

### Test Method

A rotating shear fatigue testing machine used in this test is shown in Fig. 6. This machine can rotationally apply shear force to a headed stud by using four horizontal elastic springs and turn a rotating table by 360 degrees with a rotary actuator. The specimen is fixed on the rotating table by bolts. The maximum contraction of these horizontal springs is fixed to 48 mm in this test. Additionally, vertical force was applied to the specimen by an elastic spring through a free bearing to prevent up-lift of the specimen during loading. In advance, the relationship between the vertical force and the horizontal shear force was computed by FEM analysis and was verified in the previous research [6]. The loading step of rotating shear force ranging from rotation angles of 0 to 180 degrees can be explained as shown in Fig. 7. As the headed stud position is at a rotating center, at STEP-1 (0 degree), the contracted length of the springs is 48 mm, in which the maximum horizontal shear force is applied to the headed stud. Turning by 60 degrees (STEP-2), 120 degrees (STEP-3) and 180 degrees (STEP-4), when the contracted length becomes 0 mm, no horizontal shear force acts on the headed stud. Thus, changing the contracted length of the springs by rotation of the specimen varies the horizontal shear force. As shown in Table 2, in this test, the shear stress applied to the headed stud ranged from 57.0 to 104.1 N/mm<sup>2</sup> using the various elastic springs with different spring constants.

## RESULTS AND DISCUSSION

### Failure Mode

Fig. 8 shows the failure conditions after the fatigue tests. In this study, two failure modes were observed as in the previous study on the fatigue tests under rotating shear force [6]. Fig. 9 shows the incidence of two failure modes classified by three types of specimen and the ranges of shear stress applied to headed studs. In I-6-13 specimens and I-9-16 specimens with a middle compressive strength of 30.8 N/mm<sup>2</sup>, as shown in Fig. 8(a), the fatigue crack (Type S in Fig. 10) initiated at the tip of the separated portion between the stud shank and the weld collar due to the notch effect and progressed into the stud shank. This phenomenon also depends on the applied loading level.

In N-6-13 specimens, as shown in Fig. 8(b), the fatigue crack (Type P in Fig. 10) penetrated from the

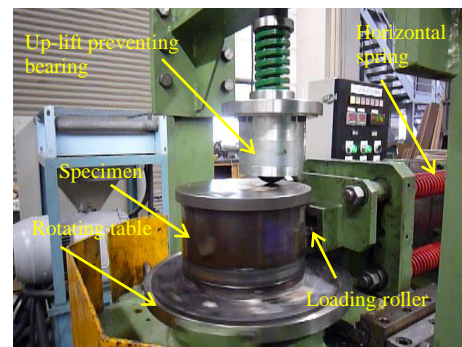


Fig. 6 Rotating shear fatigue testing machine.

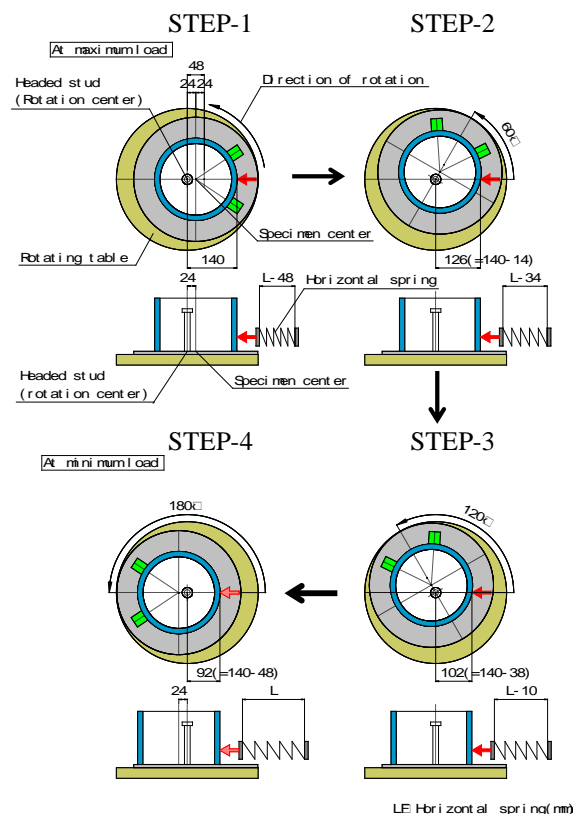


Fig. 7 Load step of rotating shear force.

Table 2 Summary of shear stress ranges

| Specimen | Circular steel plate thickness (mm) | Headed stud dimension (mm)        | Shear stress range (N/mm <sup>2</sup> ) | Number of specimens | Compressive strength (N/mm <sup>2</sup> ) |
|----------|-------------------------------------|-----------------------------------|---|---------------------|---|
| I-6-13   | 6                                   | Improved $\phi 13 \times 120$     | 104.1                                   | 3                   | 30.8                                      |
|          |                                     |                                   | 86.4                                    | 3                   |   |
|          |                                     |                                   | 78.5                                    | 3                   |   |
|          |                                     |                                   | 72.0                                    | 2                   |   |
| N-6-16   | 6                                   | Conventional $\phi 16 \times 120$ | 90.3                                    | 3                   | 30.8                                      |
|          |                                     |                                   | 82.5                                    | 4                   |   |
|          |                                     |                                   | 68.7                                    | 2                   |   |
|          |                                     |                                   | 57.0                                    | 4                   |   |
| I-9-16   | 9                                   | Improved $\phi 16 \times 120$     | 90.3                                    | 3                   | 30.8                                      |
|          |                                     |                                   | 82.5                                    | 3                   |   |
|          |                                     |                                   | 68.7                                    | 4                   |   |



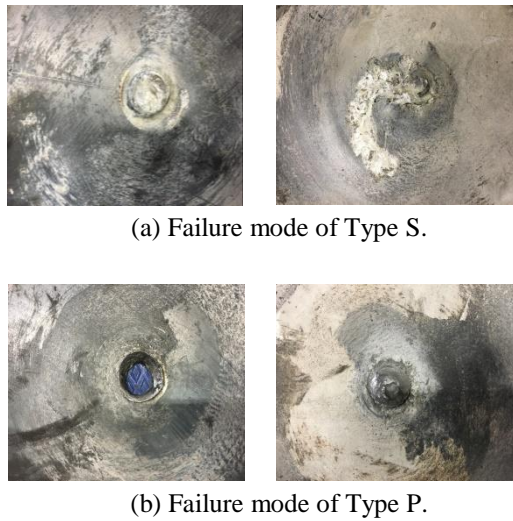


Fig. 8 Failure conditions.

|        |     | Shear stress range                  |
|--------|-----|-------------------------------------|
| I-6-13 | S   | $\Delta\tau = 72.0 \text{ N/mm}^2$  |
|        | S   | $\Delta\tau = 78.5 \text{ N/mm}^2$  |
|        | P S | $\Delta\tau = 86.4 \text{ N/mm}^2$  |
|        | S   | $\Delta\tau = 104.1 \text{ N/mm}^2$ |
| N-6-16 | P   | $\Delta\tau = 57.0 \text{ N/mm}^2$  |
|        | P   | $\Delta\tau = 68.7 \text{ N/mm}^2$  |
|        | P   | $\Delta\tau = 82.5 \text{ N/mm}^2$  |
|        | P S | $\Delta\tau = 90.3 \text{ N/mm}^2$  |
| I-9-16 | S   | $\Delta\tau = 68.7 \text{ N/mm}^2$  |
|        | S   | $\Delta\tau = 82.5 \text{ N/mm}^2$  |
|        | S   | $\Delta\tau = 90.3 \text{ N/mm}^2$  |

Fig. 9 Incidence of two failure modes classified by three type specimens and shear stress ranges applied to headed studs.

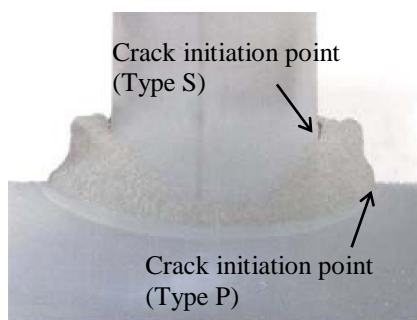


Fig. 10 Macro view of weld collar.

weld toe and progressed into the steel base plate along the heat affected zone. The fatigue crack passed through the steel plate, and the headed stud was wrested due to the thin steel plate.

### Comparison of Fatigue Strength

The relationships between the shear stress range and the number of cycles, namely S-N curves, are shown in Fig. 11 and Fig. 12 to compare the fatigue life between the conventional and the improved headed studs with different stud diameters. The S-N curves of I-6-13 specimens (circular steel plate of thickness 6 mm and improved headed studs of diameter 13 mm) and N-6-16 specimens (circular steel plate of thickness 6 mm and conventional headed studs of diameter 16 mm) are shown in Fig. 11 with the Design Code of Japan Society of Civil Engineers [6], which is the fatigue design standard for headed studs.

For I-6-13 specimen and N-6-16 specimen,

$$\text{I-6-13} \quad \log N = -11.74 \log(\Delta\tau) + 27.41 \quad (1)$$

$$\text{N-6-16} \quad \log N = -2.223 \log(\Delta\tau) + 9.142 \quad (2)$$

$$\text{PART B} \quad \log N = -19.27 \log(\Delta\tau) + 39.88 \quad (3)$$

The fatigue life of I-6-13 specimen was longer when the stress amplitude was lower than  $80 \text{ N/mm}^2$ , and the fatigue life of N-6-16 specimen was longer in the higher stress range. The comparison of the fatigue life under a stress range of  $50 \text{ N/mm}^2$ , which is at the practical level, reveals that the fatigue life of I-6-13 specimen is longer than the fatigue life of PART B [5]. The slope of the S-N curve is steeper for N-6-16 specimen than for I-6-13 specimen seemingly because of the effect of plate bending of the circular steel plate. The local stress at the weld collar increases as the larger diameter of the headed stud tends to induce more bending moment on the thin steel plate. As the influence of plate bending of a circular steel plate is greater, the failure mode of type P is more likely to occur, and as the effect of plate bending is less, the failure mode of type S is more likely to occur.

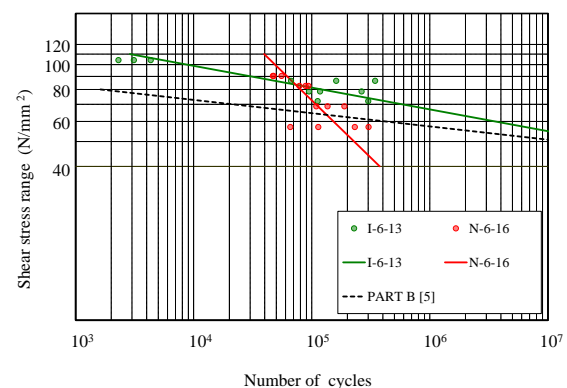


Fig. 11 S-N curves of improved headed studs. (I-6-13 and N-6-16)

On the other hand, the S-N curves of I-6-13 specimens and I-9-16 specimens (circular steel plate

of thickness 9 mm and conventional headed stud of diameter 16 mm) are shown in Fig. 12 with PART B [5].

For I-9-16 specimen,

$$\log N = -7.098 \log(\Delta \tau) + 18.70 \quad (4)$$

The test results show that the S-N curves of these two specimens are almost parallel. By reducing the thickness of the steel plate, the local stress at the weld collar increases due to the influence of the bending of the steel plate. However, the failure mode of both specimens was type S, and under a stress range of 50 N/mm<sup>2</sup>, which is at the practical level, the fatigue life of I-9-16 specimen is shorter than that of I-6-13 and PART B [5]. This will continue to be tested for judgments based on data accumulation.

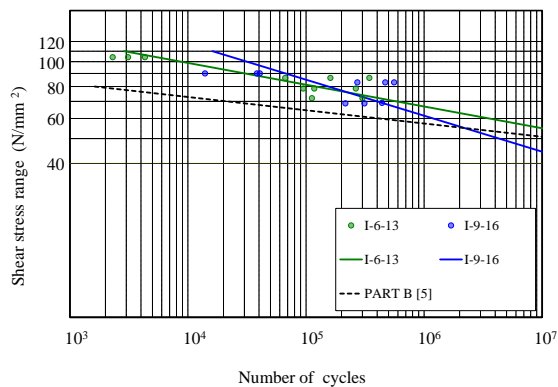


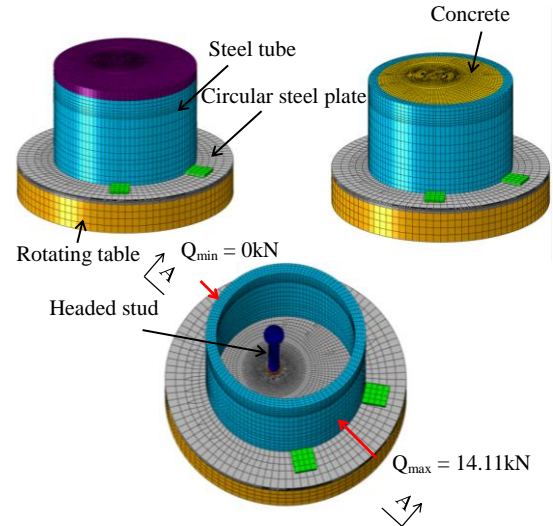
Fig. 12 S-N curves of improved and conventional headed studs. (I-6-13 and N-6-16)

### Verification by FEM Analysis

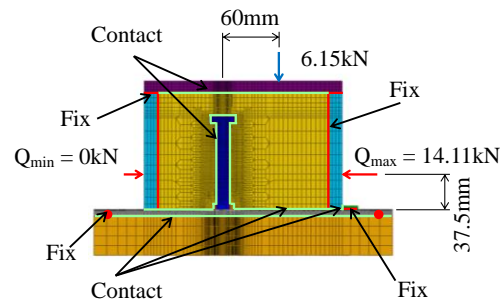
#### Outline of FEM analytical model

FEM analysis is carried out to verify the influence of plate bending due to the difference in thickness of circular steel plates. The basic model for three-dimensional elastic FEM analysis is shown in Fig. 13. Concrete, studs, and a circular steel plate with the thicknesses of 6 mm and 9 mm, conventional and improved headed studs with a diameter of 16 mm, a steel tube, and a bearing plate are assumed to be solid elements. For the boundary condition, the adhesion between the concrete and the steel members such as the studs, the circular steel plate, the steel tube, and the bearing plate was ignored. However, the contact and the non-contact conditions between them were considered in the FEM analysis. In addition, the interface between the circular steel plate and the rotating table and between the steel tube and the bearing plate was fixed at the points of bolts. As the material properties of the concrete, the Young's modulus was

$E = 2.86 \times 10^4$  N/mm<sup>2</sup> and the Poisson's ratio was  $\nu = 0.195$ . For the steel members, the Young's modulus was  $E = 2.0 \times 10^5$  N/mm<sup>2</sup> and the Poisson's ratio was  $\nu = 0.3$ .



(a) General view of FEM analysis model.



(b) Contact condition and load condition. (A-A cross section)

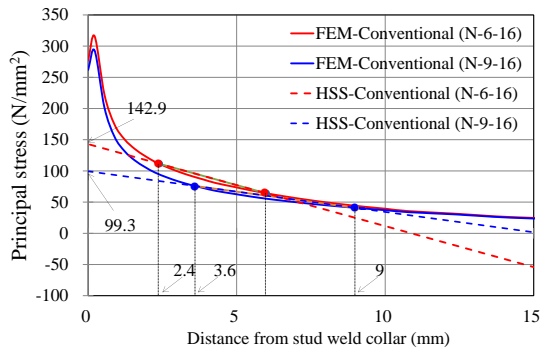
Fig. 13 FEM analytical model.

#### Analytical results

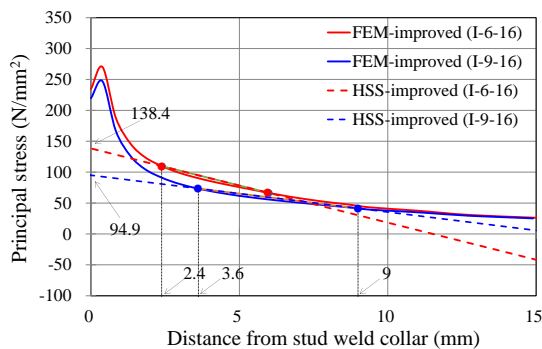
This analysis is elastic analysis, and the analytical stress is used as a reference value to compare the fatigue life from the stress ratio. To verify fatigue, hot spot stress is applied as nominal stress. In this research, the stress at a distance of 0.4T and 1.0T (T: thickness of circular steel plate) from the weld toe is recommended by IIW [7]. Using this calculation method, the stress extrapolated straight to the weld toe was considered as hot spot stress (HSS).

The HSS and FEM analytical stress at the weld collar of the circular steel plate side of the conventional and improved studs are shown in Fig. 14. When the thickness of the circular steel plate is

reduced from 9 mm to 6 mm, HSS at the weld collar on the 6 mm thick steel plate is increased by about 45% in comparison with the 9 mm thick steel plate.



(a) Conventional headed studs.



(b) Improved headed studs.

Fig. 14 Hot spot stress (HSS) on the side of circular steel plate.

## CONCLUSIONS

The following conclusions can be drawn from the fatigue test results:

- (1) In the fatigue tests, two failure modes of headed studs were observed: the fatigue crack initiated at the tip of the separated portion between the stud shank and the weld collar and progressed into the stud shank; and the fatigue crack initiated at the weld toe and progressed into the steel base plate along the heat affected zone.
- (2) The local stress at the weld collar increases seemingly because the larger diameter of the headed stud tends to induce more bending

moment on the thin steel plate. As the influence of plate bending of a circular steel plate is greater, the failure mode of type P is more likely to occur, and as the effect of plate bending is less, the failure mode of type S is more likely to occur.

- (3) The failure mode of I-6-13 and I-9-16 specimens was type S, and the fatigue life of I-9-16 specimen is shorter than that of I-6-13. This will continue to be tested for judgments based on data accumulation.

Based on the above test results, rotational shear fatigue of the headed stud can be secured by reducing the bottom steel plate from 9 mm to 6 mm and changing the conventional headed stud of 16 mm to the improved headed stud of 13 mm. In addition, the weight of SC decks can be reduced.

## REFERENCES

- [1] Matsui S., Moon T., Fukumoto Y., Watanabe H., Kajikawa Y., Fatigue strength of steel plate–concrete composite deck, IABSE Symposium, Brussels, 1990, pp. 191–196.
- [2] Matsui S., Moon T., Fukumoto Y., Fatigue failure mode of studs in steel plate–concrete composite decks of highway bridges, Journal of Structural Engineering, JSCE, Vol. 39A, 1993, pp. 1303–1311 (in Japanese).
- [3] Yoshida K. Inamoto K. Matsui S., Higashiyama H. and Kaido H., Development of Headed Stud with High Fatigue Strength for Steel–concrete Composite Deck, Journal of Structural Engineering, JSCE, Vol. 58A, 2012, pp. 908–919 (in Japanese).
- [4] Yoshida K., Higashiyama H., Inamoto K., Matsui S. and Kaido H., S–N curve for Durable Headed Stud under Rotating Shear Force, Journal of the Society of Materials Science, Japan, Vol. 62, No. 10, 2013, pp. 621–626.
- [5] JSCE, Design Code for Steel Structures PART-B: Composite structures, 9B, 1997 (in Japanese).
- [6] Higashiyama H., Yoshida K., Inamoto K., Matsui S. and Kaido H., Fatigue of Headed Studs Welded with Improved Ferrules under Rotating Shear Force, Journal of Constructional Steel Research, Vol. 92, 2014, pp. 211–218.
- [7] International Institute of Welding (IIW), XIII-1539-96/XV 845-96, 1996.

## LABORATORY EXPERIMENT OF CHANNEL HEAD BIFURCATION BY RADIAL OVERLAND FLOW

Adichai Pornprommin<sup>1</sup>, Ravicha Thaisiam<sup>2</sup> and Wandee Thaisiam<sup>3</sup>

<sup>1,2,3</sup>Department of Water Resources Engineering, Faculty of Engineering, Kasetsart University, Thailand

### ABSTRACT

Many studies have shown that incipient channelization can be explained by the interaction between flow and an erodible bed. Our recent theoretical study has shown that an eroding channel head by overland flow can maintain its shape without bifurcation if the flow depth is sufficiently large comparing to the channel head radius. Here, we performed nine experimental runs using three sediment sizes to provide better understanding of the bifurcation. A circular pan was filled with sand except at the center, where there were a sink hole and a drain installed at the pan bottom. When water had been filled over the sand to a desirable level, the drain was opened and unsteady radial overland flow accelerated toward the hole. After a while, water formed a downward-concave profile, leading to strong bed erosion in the vicinity of the hole and, as a result, the hole size expanded. In the initial development where flow depth was sufficiently large, the hole maintained its circular shape without channel incision while expanding. As the flow depth and discharge reduced and the hole radius increased, the hole started to lose its circular shape. Thus, the experimental results confirmed the condition of channel bifurcation proposed by our previous study. Main incised channels with large spacing were firstly initiated and elongated upstream in the radial direction while small rills were generated later between main channels. Using the network circularity as an indicator, we propose the new four phases of channel network development (unchannelization, initiation, extension and abstraction).

*Keywords: Erosion, Channel head bifurcation, Overland flow, Experiment, Channel network development*

### INTRODUCTION

Channel head bifurcation, sometimes called branching, is one of the most important processes of channel network formation because it leads to a higher complexity in the geometry of the channel networks. Recently, researchers have tried to study its mechanics. Perron et al. [1] investigated the branching river networks of two field sites, the Allegheny Plateau in Pennsylvania and Gabilan Mesa in California. Using the landscape evolution model based on soil creep and channel incision equations, they found good agreement between their model and the field data. Using a groundwater flow equation, Petroff et al. [2] studied stream bifurcation by seepage. They compared their model with field observation at the Panhandle in Florida and found good agreement between them. Thus, both studies showed that channel head bifurcation should be initiated by hydrophysical mechanisms (processes due to water forces such as erosion), not as a consequence of random topology. Pornprommin et al. [3] performed a linear stability analysis using the flow equations in the polar coordination system to investigate incipient channel head bifurcation. Circular holes were assumed to be channel heads, toward which radial overland flow accelerates. Then, channel bifurcation is defined as the holes lose their circular shapes when they are unstable to the imposed perturbations. They

estimated that channel head does not bifurcate if channel head radius is not larger than 10 times the Froude-critical depth of overland flow divided by the friction coefficient [3].

A few experiments have been conducted to investigate the development of the channel head. Pornprommin et al. [4] performed an experiment of channel inception by seepage erosion on a rectangular basin with an adjustable bed slope. The sediment layer was built by coarse sand and water was fed upstream. They found that an increase in the slope led to a larger channel width but more difficulty in channel bifurcation. A higher discharge also caused a larger channel width but easier initiation of the bifurcation. Thus, they hypothesized that the geometry of groundwater flow and the resistibility of sediment material to slope failure play an important role in channel head bifurcation. Berhanu et al. [5] studied channel head shapes in a rectangular box filled with glass beads. Groundwater was fed by an upstream reservoir or rain. They found that the different sources of groundwater led to change in the groundwater flow nets and, consequently, impacted the shape of the channel heads. Their finding was consistent with the hypothesis of Pornprommin et al. [4]. A more comprehensive experiment of channel formation by seepage due to different groundwater flow patterns was conducted by [6]. However, to the authors' knowledge no experimental studies have

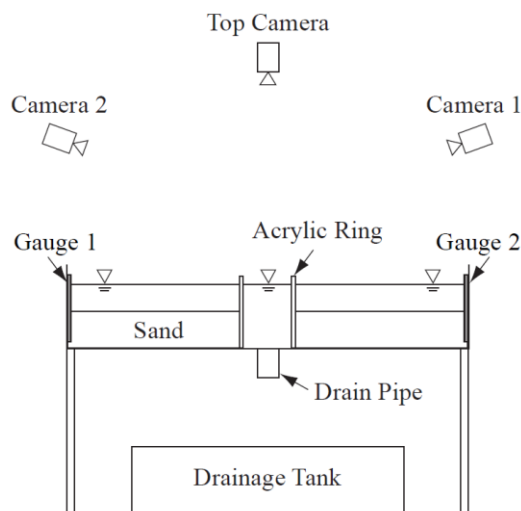


Fig. 1 Experiment setup.

tried to investigate channel head bifurcation from the perspective of surface sheet flow in detail.

In this paper, we conducted a laboratory experiment of channel inception by overland flow in a circular chamber following the concept of channel bifurcation proposed by [3]. Our two main objectives in this study were; (i) to examine the early stage of channel network evolution (channel inception); and (ii) to compare the experimental results with the theoretical study [3].

## EXPERIMENTAL SETUP

The experiment was performed in an apparatus chamber with 120 cm in diameter and 28.5 cm in height as shown in Fig. 1. The apparatus was modified from a class A evaporation pan and placed on a table. The center of the pan and the table under it were drilled and fitted with a PVC pipe drain of 5 cm diameter and 5 cm length. This drain was used to let water and sediment flow in the radial direction toward the center of the apparatus and down into the drainage tank under the table during operation.

In the preparation stage, the drain was closed with a plug, and an acrylic ring of 28 cm height was placed at the center. The ring had many small holes in it to allow water to pass through. Sand was gently filled between the ring and the edge of the apparatus to the design height and it formed a donut-like sediment layer. Then, water was gradually filled inside the ring and flowed into the sediment layer through the small holes until the sand was saturated and the water level reached the height of the layer. Based on the horizontal water surface, the saturated sand layer surface was delicately adjusted. After that, water was filled again to 17 cm depth from the chamber bed to complete the preparation stage.

Table 1 Experimental runs.

| Run | Type           | $d_{50}$<br>(mm) | $d_{10}$<br>(mm) | Thickness<br>(cm) |
|-----|----------------|------------------|------------------|-------------------|
| A-1 | Medium<br>sand | 0.49             | 0.30             | 10                |
| A-2 |                |                  |                  | 10                |
| A-3 |                |                  |                  | 5                 |
| B-1 | Medium<br>sand | 0.30             | 0.12             | 10                |
| B-2 |                |                  |                  | 10                |
| B-3 |                |                  |                  | 5                 |
| C-1 | Fine sand      | 0.18             | 0.07             | 10                |
| C-2 |                |                  |                  | 10                |
| C-3 |                |                  |                  | 5                 |

Three sizes of industrial, sieved sand were used in this study as shown in Table 1. Their grain size distributions were analyzed using sieve analysis and a hydrometer test. The first two coarser sizes (sands A and B) were a non-cohesive, medium sand with medium diameters ( $d_{50}$ ) of 0.49 and 0.30 mm, respectively. The last and smallest size (sand C) was fine sand with  $d_{50}$  of 0.18 mm and had a small proportion of silt and clay (~8% smaller than 62.5  $\mu\text{m}$ ) providing some cohesion. We conducted three experimental runs for each sand type. The first two runs were conducted under the same conditions using a layer thickness of 10 cm. The third run used a thickness of 5 cm. Thus, we performed a total of nine runs. Sand was not reused to ensure the same properties of sediment in each run.

Before the operation, the ring was removed very slowly to keep a symmetrical circular front of the sand layer at the center, and some debris floating on water surface was removed. A video camera was installed above the apparatus to record the evolution of the sand layer from the top view (Top Camera), and two video cameras were placed near the chamber edge to record the water levels at the two gauges attached to the inner edge (Cameras 1 and 2). When the set up was completed, the drain plug was opened. The video records ended when there was no further significant change in the sand layer. Two types of results were digitized from the records: the evolution of the sand layer crest from the Top Camera and the time variation of water levels at the gauges from Cameras 1 and 2.

## EXPERIMENTAL RESULTS

Figure 2 shows the top view of the final drainage networks from the Top Camera. The lines with dots show the digitized hole circumferences according to the uneroded crest lines of sand layers. Since water flowed in the radial direction and converged on the center drain of our circular apparatus, overall there



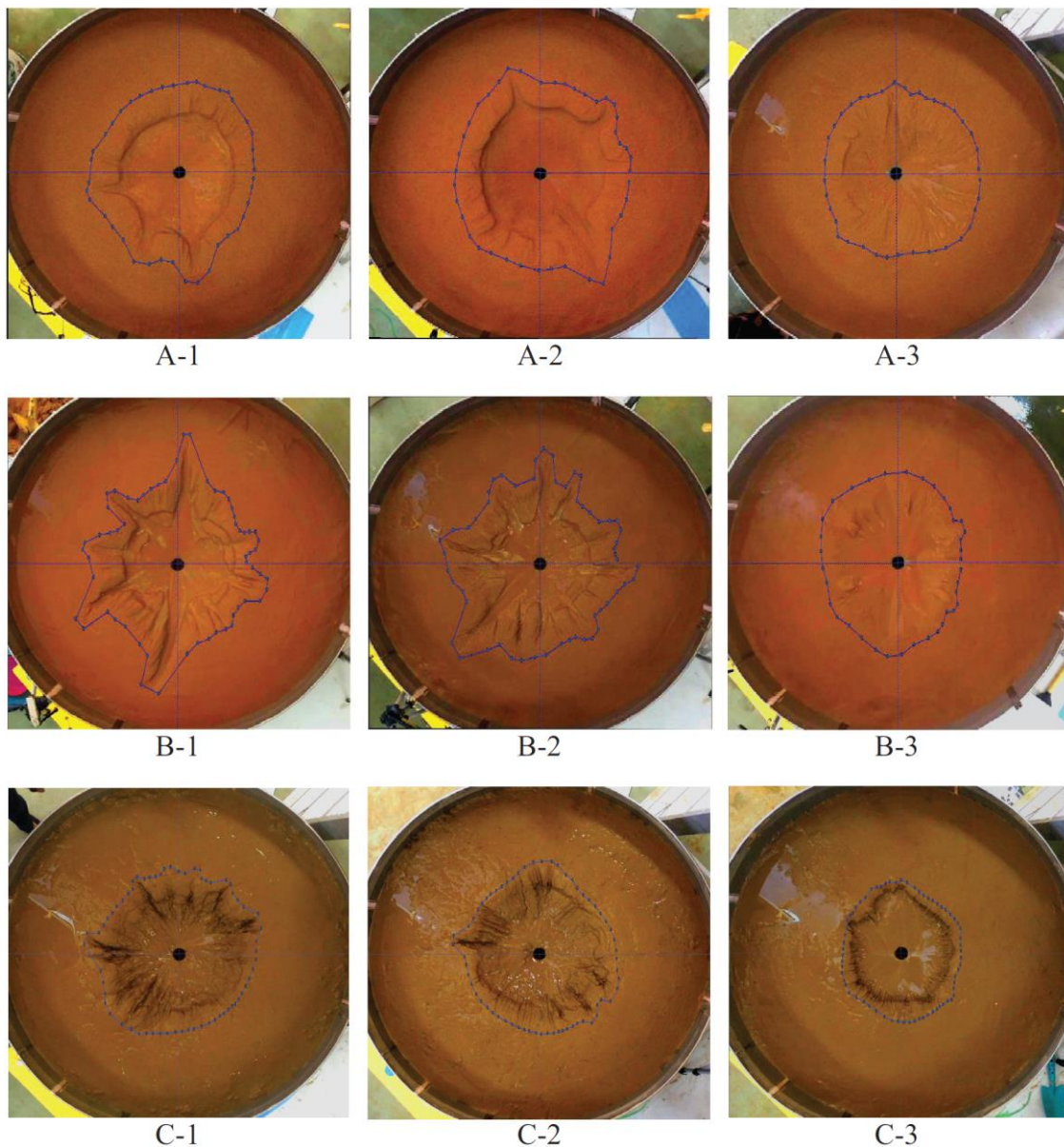


Fig. 2 Photographs of drainage networks in the final stage. Lines with dots show digitized hole circumferences.

was a centripetal drainage pattern. In every run, fluvial erosion (sheet and rill erosion) and mass wasting processes always occurred repeatedly and randomly in the vicinity of the crest and front of sand layers. Thus, incised channels were initiated at the crests, where velocities are highest, and extended upstream. Because the experimental runs happened on short timescales, weathering processes such as abrasion did not affect our results, and, thus, we limited our consideration to the sand type and layer thickness, causing different channel patterns. It can be seen that the runs with sub numbers 1 and 2 of the same sand type have similar channel patterns. For the case of the runs with sub number 3, where the thickness was cut by half, less development of

channel pattern was noticed. A shallower layer caused less seepage and mass wasting and also a milder slope of the front at the end. These induced less erosion and consequently shallower and shorter incised channels.

For sand A, short incised channels were observed with smaller rills in the eroded area. Several incised channels were able to tap the surface water from upstream and developed into longer main channels. In runs A-1 and A-2, long and steep cliffs with cavities at the toes were detected in the area where the overland flow stopped more rapidly than in other places and main channels were not found. The front subjected to seepage erosion can be divided into three zones [7]. The sapping zone is the small area near the

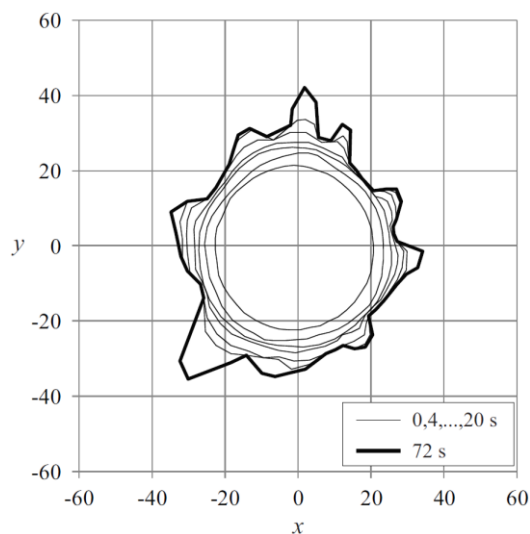


Fig. 3 Time variation in center hole circumference of run B-2.

toe where seepage emerges and the strong force of the effluent seepage initiates sediment detachment and removal from the face. Then, slope failure occurs in the undermining zone on top of the sapping zone due to losing its stability. Finally, sediment transported by fluvial processes in the fluvial zone downstream from the sapping zone helps a repeat of the processes. Thus, the cavities might be generated by seepage erosion in the sapping zone and surface tension between water and sand tends to hold the steep cliffs in the wet undermining zone. In run A-3, a not very long cliff was detected due to thinner thickness. The cavities were less in the experimental runs of sand B, and they were not found in sand C.

Compared with sand A, more main channels were observed in sand B, and they extended further upstream. Channel formation was very symmetrical in the radial direction. In addition, more small rills were also spotted caused by an increase in the strength of channel incision by overland flow because a smaller sediment size leads to lower threshold shear stress for erosion. Since a smaller diameter of sand B provides lower hydraulic conductivity corresponding to less infiltration, surface sheet flow erosion was stronger in the runs of sand B. Again, steep cliffs were detected in runs B-1 and B-2 due to seepage erosion and slump blocks, but it was not detected in run B-3 because of the lower height of the sand layer. Mass wasting is commonly assumed to be a diffusive-type process that smoothens topographic perturbations, while channel incision due to water flow amplifies perturbations. Thus, more extensive incised channels in sand B than in sand A were possibly the results of the stronger process of channel incision by overland

flow related to mass wasting.

Sand C contains a small percentage of mud. Due to having the smallest diameter and the presence of mud, the lowest hydraulic conductivity can be expected. Also, physical cohesion imparted by the mud can significantly influence and reduce the erosive properties of sediment. Many deep, incised rills of narrow width were found. In sand C, we did not observe steep cliffs with cavities as were found in sands A and B. However, soil creep and large-scale block slump were observed during the final stage of the runs when water at the drain had almost disappeared. The failure was possibly due to the low permeability of sand C so that it took a long time for water in the soil to drain. An increase in the soil weight due to the high water content without a counter-balance pressure force by the water level above the drain would be the main factor causing the large-scale failure. In addition, we observed a few step-like, upstream-migrating headcuts within some eroding channels by overland flow. However, they were decaying and finally disappeared as the surface water supplying their channel heads became weaker and finally ceased.

An example of the evolution of the center hole by digitizing sand layer crest lines is illustrated in Fig. 3. It shows the expansion of the hole circumference of the experimental run B-2 from 0 s to 20 s with two-second intervals, and at 72 s as the final pattern. The crest line is defined as the edge of the uneroded top surface of sand layer. We set time 0 when we first detected the start of erosion on the crest line. An initial, almost perfect circular circumference gradually developed into an irregular shape for the crest line due to the presence of main channels. At 72 s, we counted nine rounded corners from the digitized line, but the number of incised channels in the eroded area in the center photo of Fig. 2 was found to be greater than nine because some adjacent incised channels shared the same corner. Thus, the initiation of incised channels in the eroded area and the evolution of the crest line of the uneroded top surface may be generated by the same erosional process by overland flow and interact with each other, but their morphological processes and features can be different.

## ANALYSIS OF CHANNEL HEAD EVOLUTION

At the commencement of drainage evolution in our experiment, the hole expanded while it still maintaining its circular shape. This implied that the hole was stable from perturbations. However, after expanding for a while, the hole became unstable and



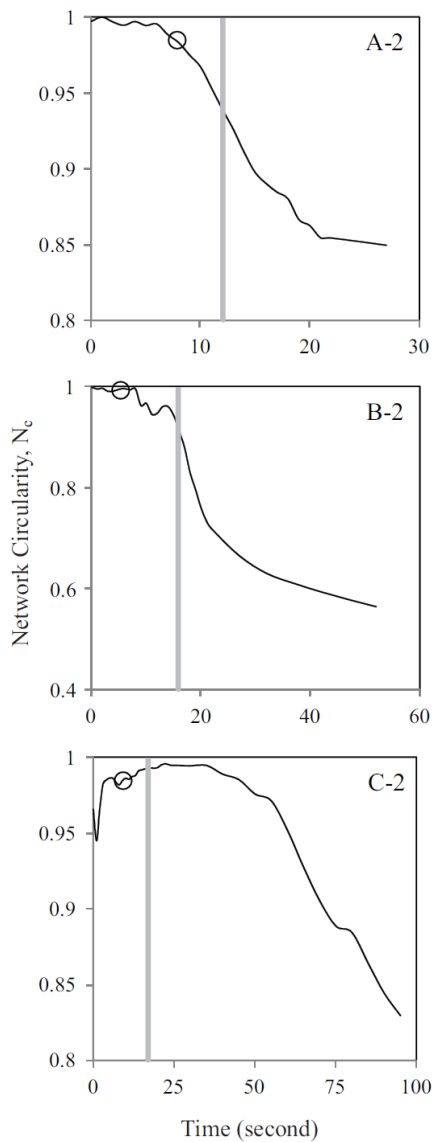


Fig. 4 Time series variations in network circularity. Shaded vertical lines show predicted time of no uniform sheet surface flow, and circles show time of bifurcation predicted by the theory [3].

incised channels were initiated and grew upstream. Thus, there should be a threshold condition whereby an initially circular hole transforms into a channelized drainage. To investigate the threshold condition, we adopted the recent linear stability analysis [3].

Gomez and Mullen [8] performed an experiment on channel networks by considering groundwater flow. To describe the shape of their experimental drainage networks, they adopted the concept of circularity by [9] that has been used to quantify the shape of a whole drainage basin. They called it network circularity ( $N_c$ ) defined as the ratio between the eroded network area and the circle area of the

same perimeter as follows:

$$N_c = A/A_c = A/\pi(P/2\pi)^2 \quad (1)$$

where  $A$  and  $P$  are the eroded area and perimeter of channel network, respectively, and  $A_c$  is the circle area computed using  $P$ .

Network circularity  $N_c$  has a value between 0 and 1 where  $N_c = 1$  means that the shape of the channel network is perfectly circular. Using  $N_c$ , three phases of channel network development was proposed as follows [8]. (1) Initiation is the first stage during which the main channels elongate upstream rapidly.  $N_c$  decreases steeply in this stage. (2) Extension is the second stage in which the channel heads expand laterally and bifurcate into tributary channels.  $N_c$  still continues reducing but at a lower rate. (3) Abstraction is the last stage in which the channel heads continue widening and cause divide decay and consequently  $P$  may reduce while  $A$  still increases.  $N_c$  thus begins to increase.

Figure 4 shows an example of the variation in network circularity with time for runs A-2, B-2 and C-2. In general, the initial  $N_c$  was close to unity and remained so for some period before reducing rapidly. With sands A and B, the reduction in  $N_c$  occurred before the uniform overland flow had disappeared, while for sand C, it occurred after that and took quite a long time of about 1 min. As the sand size decreased, evolution took longer. In run C-2, during the beginning period,  $N_c$  abruptly dropped and then regained because there were small, initial, irregular perturbations along the crest line before the operation. The perturbations disappeared later because the eroding crest neighboring them migrated upstream at a faster rate, and thus the crest lines around the perturbations became rounder and wider. This implied that the network dynamics favored maintaining a circular shape. If we assume that channel inception can be indicated by the slope transition of  $N_c$ , it can be said that in the cases of sands A and B, channelization took place during active, uniform overland flow while it happened later with sand C. Comparing the slope transition with the prediction by the theory shown in circles, we found qualitative agreement for sands A and B. Due to the largest threshold erosion of sand C, it was possible that the active erosion time was too short to generate channelization during the uniform overland flow period. The channelization in runs using sand C was due to some incised channels being able to tap water from depressions on the layer surface.

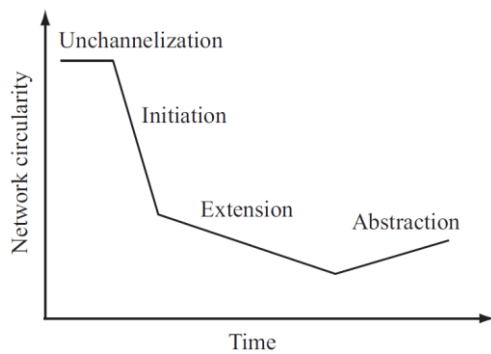


Fig. 5 Revised phases of network evolution classified by network circularity by including unchannelization phase.

In the phases of network evolution proposed by [8], the first phase in our experiment where the network circularity  $N_c$  maintained its value cannot be explained. However, this phase was detected in other experiments. Hancock and Willgoose [10] studied network development in a landscape simulator. They described the first phase in their experiment where surface water flowed to and concentrated at the basin outlet, and it caused the expansion of an unchannelized, large, semi-circular eroded area. Channelization then took place at this eroded area and the channel network developed from there upstream in later phases. Thus, we proposed to include this phase of the development of unchannelized area into the original phase diagram. Figure 5 shows the revised phases of network evolution. The first phase, where the shape of eroded area remains or  $N_c$  keeps constant, was added and was called the “unchannelization” phase.

## CONCLUSION

The experiment of channel bifurcation on a circular hole was performed with three sand diameters ( $d_{50} = 0.49, 0.30$  and  $0.18$  mm) and two layer heights (10 and 5 cm). The smallest size had a small proportion of silt and clay and showed the presence of cohesion and the lowest erodibility. In the runs of the two largest sizes, the combination of slope failure processes of an upper slump motion and a transformed lower flow was observed. However, slow soil creep and earth flow with large-scale slump block failure were found in the case of the smallest size due to cohesion, and step-like upstream-migrating headcuts (cyclic steps) were also detected during the runs. Seepage and seepage erosion were strongest for the largest size due to the highest hydraulic conductivity. The middle-sized sand showed the greatest extension of channelization with

radial symmetry due to high erodibility.

According to [8], network evolution can be divided into three phases (initiation, extension and abstraction). The initiation phase was the first phase of the evolution when main channels elongate rapidly. However, from our experimental runs, circular holes were not incised by main channels unless the hole radii were sufficiently large compared with the flow discharge. Thus, we proposed a new first phase called the unchannelization phase where the shape of the eroded area remains unchanged. The transition between the unchannelization phase and the initiation phase is then expected to be the time of incipient channelization according to the theory by [3].

## REFERENCES

- [1] Perron, J. T., P. W. Richardson, K. L. Ferrier, and M. Lapo tre (2012), The root of branching river networks, *Nature*, 492, 100-103.
- [2] Petroff, A. P., O. Devauchelle, H. Seybold, and D. H. Rothman (2013), Bifurcation dynamics of natural drainage networks, *Philos. T. Roy. Soc. A*, 371 (2004).
- [3] Pornprommin, A., N. Izumi, and G. Parker (2017), Initiation of channel head bifurcation by overland flow, *J. Geophy. Res.: Earth Surface*, 122.
- [4] Pornprommin, A., Y. Takei, A. M. Wubneh, and N. Izumi (2010), Channel inception in cohesionless sediment by seepage erosion, *J. Hydro-env. Res.*, 3, 232-238.
- [5] Berhanu, M., A. Petroff, O. Devauchelle, A. Kudrolli, and D. H. Rothman (2012), Shape and dynamics of seepage erosion in a horizontal granular bed, *Physical Review E*, 864.
- [6] Marra, W. A., S. J. McLelland, D. R. Parsons, B. J. Murphy, E. Hauber, and M. G. Kleinhans (2015), Groundwater seepage landscapes from distant and local sources in experiments and on Mars, *Earth Surf. Dynam.*, 3, 389-408.
- [7] Howard, A. D., and C. F. McLane III (1988), Erosion of cohesionless sediment by ground water seepage, *Water Resour. Res.*, 24 (10).
- [8] Gomez, B., and V. T. Mullen (1992), An experimental study of sapped drainage network development, *Earth Surf. Proc. Land*, 17 (5), 465-476.
- [9] Miller, V. C. (1953), A quantitative geomorphic study of drainage basin characteristics in the Clinch Mountain area, Virginia and Tennessee, Columbia University Technical Report 3, Project NR 389-042, 68 pp., New York.
- [10] Hancock, G., and G. Willgoose (2001), The interaction between hydrology and geomorphology in a landscape simulator experiment, *Hydrol. Process.*, 15, 115-133.

# IDENTIFICATION OF DRAINAGE SYSTEMS CAPACITY USING EPA-SWMM 5.1 VERSION MODELING IN GUNUNG PANGILUN OF PADANG CITY-PALAPA METROPOLITAN AREA

Taufika Ophiyandri, Bambang Istijono, Milania, Benny Hidayat, and Aprisal  
Faculty of Engineering, University of Andalas, Padang, Indonesia

## ABSTRACT

Floods have often occurred in the city of Padang in recent years, this is generally caused by high rainfall and poor drainage capabilities. NVivo software is utilise to analyse the online news which reported floods occurrence. Based on the news collected from 2009–2018, it was found that Gunung Pangilun Village, Padang Utara Subdistrict was often flooded when it rained for more than 3 hours. This area is a densely populated area (1,000 people / km<sup>2</sup>). The cause of inundation in this area is that drainage is not able to accommodate water and high rainfall intensity with the parent river in the Batang Kuranji watershed. The flooding that occurred in this area caused several schools, offices and hospitals to be flooded, a number of houses and a number of points on the local road were flooded. Therefore, it is necessary to know the large drainage capacity that is able to accommodate the amount of runoff discharge when the rain occurs using the 5-year return EPA SWMM software modelling.

*Keywords: flood inundation, drainage, EPA-SWMM, NVivo*

## INTRODUCTION

### Background

The metropolitan Urban Area of Padang, Lubuk Alung, Pariaman (MUA PALAPA) as a National Activity Center is oriented to encourage the development of priority production sectors such as industry, marine fisheries, tourism, trade and services. MUA PALAPA is a priority location for the national urban strategic area as the centre of regional growth in the Sumatra region.

For this reason, problems need to be identified that cause damage to the urban environment, which needs alternative solutions and immediate treatment. Environmental damage problems include drainage conditions, flooding, rainwater inundation, coastal abrasion and the provision of water resources infrastructure with good maintenance and environmentally conscious communities.

One of the disasters often faced by Padang City is flooding [2]. Floods are generally caused by high rainfall [3, 4] and poor drainage capabilities [5, 6]. By using NVivo software news from online media can be evaluated. Based on the news from 2009–2018, it was found that the location of the frequent flooding in Padang City is Gunung Pangilun Subdistrict, especially when it was raining for more than 3 hours (Fig. 1). This area is a densely populated area which is 1,000 people / km<sup>2</sup>. The cause of inundation in this area is that drainage is not able to accommodate water and high rainfall intensity with the main drainage in the Batang Kuranji watershed. The floods that occurred in this area caused inundation in several schools, offices and hospitals, houses, and local road as well.

Therefore, this research aims to identify the ability of the Gunung Pangilun (Fig. 1) drainage network against flood using the EPA SWMM (Environmental Protection Agency Strom Water Management Model).



Location of flood in  
Primary School No.  
17 Gunung Pangilun  
in 2017



Location of flood at  
surrounding Alfaiz  
Mosque in 2018

Fig. 1 Visualization of the Gunung Pangilun Area  
(Source: Google Earth)

## Literature Review

Rossman [7] states EPA SWMM is a rainfall-runoff simulation program commonly used for

quantity simulation and surface runoff quality in urban areas.

NVivo is a software commonly used for qualitative research. Usually qualitative research aims to explore and understand data more deeply. Qualitative data is in-depth and detailed, so it is also lengthy. As a result, the analysis of qualitative data is specific, especially to summarize data and unify it in an analytical flow that is easily understood by others.

A Digital Elevation Model (DEM) is a form of presentation of the height of the earth's surface digitally. It can be seen from the distribution of points representing the shape of the earth's surface that it can be distinguished in a regular, semi-ordered, and random form.

Hidayat [8] in his research on Understanding flood disasters in the city of Padang with the content analysis of the news article explained that, articles were searched using the google.co.id search engine site with the search term 'flood field site: www.padangekspres.co.id' which produced articles about floods in the city of Padang that have been published by the Padang Ekspres website. One by one the articles were opened and explored whether each one was related to flooding in the city of Padang. Articles that met the requirements were stored in the form of Ms-word documents where one article was stored as an Ms-word file. After the articles have been collected in the form of Ms-word files, the files are processed and analysed using NVivo software version 8.

Legowo, et al. [9] stated that the DEM appeared in soil surface morphological information was used to represent the surface runoff hydrology process. Topographic structure extraction algorithms will be sloped and current direction is an important factor in describing drainage networks.

Vinay, et al. [10] said that SWMM modelling played an important role in examining problems such as urban flash floods. SWMM has become an effective tool for flood simulation in urban areas. Frequency analysis is done using the most appropriate distribution, namely, the Gumbel distribution for different return periods and the frequency value used for the development of the IDF curve (intensity frequency duration). The intensity of rain derived from the IDF curve for different return periods is used to estimate the peak runoff of each sub-watershed used as an input parameter in a runoff simulation in SWMM. The GIS methodology is used to handle spatial data simultaneously.

Waikar, et al. [11] explained that urban floods were basically caused by damaged and inefficient urban drainage systems, and caused damage to public and private buildings and disrupted public life. In order to understand the complexity associated with urban flood management, the EPA SWMM application is used. Furthermore, daily rainfall data was obtained from Asarjan closest to the rain gauge station. Arc-GIS (10.1) is used to process DEM

(Digital Elevation Model) and LULC (Land Closure of Land Use) data to obtain height and water resistance respectively. Topographic data such as area, width, length, etc. Also taken from Arc-GIS. The selected extreme daily events are separated into hourly events using the reduction formula. After that, EPA SWMM was used to simulate catch response to rainfall events where runoff, water depth profiles, and outflow hydrographs were obtained. Runoff is also obtained from rational formulas for comparison purposes.

Fairizi [12] in his research used short-term rainfall data from 2001 to 2012. Rainfall data is tested according to normal, Normal log, Pearson III log, and Gumbel distribution. Select one result from the distribution with the smallest standard deviation. Then, it was tested by the Smirnov-Kolmogorov test to find the rainfall intensity equation. Later, the equation will be used to find the drainage dimension. To analyse inadequate drainage, SWMM Program is utilised.

### Hydrological Analysis

Hydrological analysis was used for the calculation of rainfall with a five-year return period, calculation of rainfall intensity, and hyetograph count of planned rain using the Alternating Block Method (ABM) method.

### Rainfall Analysis

If the rain data used in the calculation is in the form of a sample (limited population), then the calculation of the rain plan based on the Gumbel Probability distribution is carried out by the following formulas [13].

$$X_T = \bar{X} + S \times K_T \quad (1)$$

where :

- $X$  : rain plan with a return period  $T$  (mm)
- $\bar{X}$  : Average value of  $X$  (mm)
- $K$  : Gumbel frequency factor, depends on the data  $Y_t, Y_n, S_n$ .

### Rainfall Intensity

Calculation of rainfall intensity uses the Mononobe method with the following formula :

$$I = \frac{R_{24}}{24} x \left( \frac{24}{t} \right)^{\frac{2}{3}} \quad (2)$$

where :

- $I$  : rainfall intensity (mm/hour)
- $R_{24}$  : bulk plan in a return period (mm)
- $t$  : rain duration (hour)



### ***Hyetograph Rain Plan***

Rain distribution models that have been developed to change daily rainfall into rainy days - the uniform rain distribution model using the Alternating Block Method (ABM) method [14].

### **EPA SWMM Version 5.1**

EPA SWMM (Environmental Protection Agency Storm Water Management Model) is a rainfall-runoff simulation program commonly used for simulating the quantity and quality of surface runoff in urban areas. The ability of this software is to be able to calculate the hydrological process that produces runoff from urban areas such as rainfall, evaporation, infiltration and determine the flood point and calculation in runoff discharge. The objects used in this research are:

1. Rain gauge includes rainfall intensity data, observation time intervals, and rainfall data sources in the form of a time series.
2. Sub-catchment includes determining the outlet of the sub-catchment, determining land use, determining the probable and impervious sub-area, determining the slope or slope of the sub-catchment, determining the width of sub-catchment, determining the manning number for surface flow, determining the percentage of impervious sub-areas, determining the depression and impervious regions, determining the percentage of impervious area without depression.
3. Junction is the point of the drainage system where the channels join. The data needed is elevation, maximum depth, storage area when there is a flag (if any), flow from outside the drainage system (if any).
4. Channels (conduit), parameters to be used are shape (channel shape), max-depth (depth), length (channel length), roughness (channel roughness coefficient).
5. Storage unit is the point of the drainage system which is a storage volume. Safety storage units include: elevation or altitude, maximum depth, initial depth, potential evaporation, seepage parameters (if any), external inflow data (if any).

### **RESEARCH METHODOLOGY**

This study is carried out by:

1. Gather news about floods in the MUA PALAPA from 2009 - 2018.
2. Processing flood news using NVivo software.
3. Determine locations that often occur in MUA PALAPA based on NVivo output.
4. Determine the slope of watershed by using DEMNAS data.
5. Check and measure drainage in the field.

6. Calculate the planned rainfall and do a match test using the Chi Kaudrat method.
7. Calculate rain intensity using the Mononobe method.
8. Calculate the hyetograph of the rain plan using the Alternating Block Method (ABM) method.
9. Simulation of the EPA SWMM 5.1 program using data that has been analysed.
10. The program simulation results in the form of runoff discharge that is accommodated by the channel and the location of the flood points that occur along the drainage canal.

### **RESULTS AND DISCUSSION**

#### **Processing News Using Nvivo**

This research uses a news article that discusses waste that occurs in the city of Pariaman, Lubuk Alung, Padang (MUA PALAPA), using news data from 2009 - 2018. As for the publication of news in 1 event a lot, the news taken has very clear information, especially the location affected by the flood. In the quotations obtained, flooding in the MUA PALAPA area was more dominated by poor drainage, and damaged river basins.

From the results of NVivo processing, the area that is very often flooded is the Gunung Pangilun sub-district, Padang City, with 8 times the number of occurrences in the period (2012-2018) from the articles obtained. The problems that occur in this region are drainage which is not functioning optimally, and so on. One example of a quote taken from the article is as follows: Sewerage in the Gunung Pangilun area [15], Jalan Gajah Mada, Padang City, spilled over to cause a number of residents' houses and several points of the road in the local area to be flooded. For this reason, the researcher conducted a study to identify the ability of Gunung Pangilun's drainage, which is more precisely in the Jalan Gajah Mada area.

#### **Conduct Field Investigations**

Field investigations aim to take secondary data such as locations affected by floods, and measurements of existing dimensions, and are used in data processing and guidelines for SWMM 5.1 modelling.

#### **Hydrological Calculation**

##### **Rainfall Calculation Plan**

From the rainfall station map obtained, the station closest to the study location is the Khatib Sulaiman rain station (Table 1), with a total data of 10 years. This data will be used in the calculation of planned rainfall.

Table 1. Rainfall data of the Khatib Sulaiman Station

| Year | Rainfall<br>(mm/day) | Year | Rainfall<br>(mm/day) |
|------|----------------------|------|----------------------|
| 2009 | 160                  | 2014 | 100                  |
| 2010 | 220                  | 2015 | 206                  |
| 2011 | 330                  | 2016 | 270                  |
| 2012 | 143                  | 2017 | 195                  |
| 2013 | 128                  | 2018 | 147                  |

For the calculation of rainfall using the Gumbel Method, Normal, Normal Log, Persion Type III Log, and the suitability of the planned rain data. With the results of the compatibility test using the Chi Square method with the results as shown in Table 2.

Table 2. Chi Square

| Distribution Probabilities  | X <sup>2</sup> | X <sup>2</sup> cr | Information  |
|-----------------------------|----------------|-------------------|--------------|
| Gumbel Method               | 1.00           | 5.99              | Accept       |
| Normal Method               | 1.00           | 5.99              | Accept       |
| Log Normal Method           | 1.00           | 5.99              | Accept       |
| Log Pearson Type III Method | 9.00           | 5.99              | Not Accepted |

#### Compatibility Test Results

The results of the calculation can be seen in Table 3.

Table 3. Recapitulation of planned rainfall with the Gumbel Method

| PUH | XT<br>(mm/day) |
|-----|----------------|
| 2   | 180            |
| 5   | 264            |
| 10  | 319            |
| 25  | 389            |
| 50  | 441            |
| 100 | 492            |

#### Calculation of Rainfall Intensity

After obtaining rainfall values the calculation of rainfall intensity was carried out using the Mononobe method with a 5-year return period of rain. The results of the calculation of rain intensity in the form of an IDF curve (Fig. 2) which will be used in the preparation of the Hyetograph rain plan with the Alternating Block Method (ABM). The calculation of rainfall intensity using the Mononobe formula is attached to the Table 4 below.

Table 4. Recapitulation of the intensity of the 5-year rainy season with the Mononobe method

| Duration |      | 5 Year Period |
|----------|------|---------------|
| Minute   | Hour | 263.95        |
| 30       | 0.5  | 145.26        |
| 60       | 1    | 91.51         |
| 90       | 1.5  | 69.83         |
| 120      | 2    | 57.65         |
| 150      | 2.5  | 49.68         |
| 180      | 3    | 43.99         |

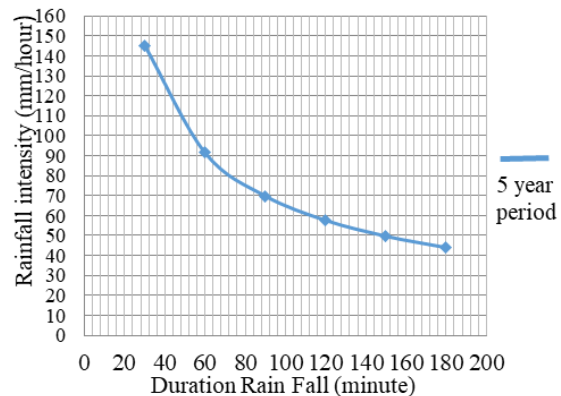


Figure 2. Curve Intensity Duration Frequency (IDF)

#### Hyetograph calculation of rain plan

The calculation of the hourly rain distribution pattern use the Alternating Block Method (ABM) with the data taken from the results of the calculation of rainfall intensity in Table 3 with the duration of the rain event taken for 3 hours (Table 5 and Fig. 3).

Table 5. Hourly rainfall distribution patterns using the ABM method

| Durati<br>on (t)<br>Hour | Intensit<br>y (I <sub>t</sub> )<br>mm/h | Rainfall<br>(I <sub>t</sub> x t)<br>mm | Cum.<br>Rainfall<br>mm | P<br>% | Hyetograph |       |
|--------------------------|---|--|------------------------|--------|------------|-------|
|                          |   |  |                        |        | %          | mm    |
| 1.0                      | 91.5                                    | 91.5                                   | 91.5                   | 69.3   | 18.0       | 47.6  |
| 2.0                      | 57.6                                    | 115.3                                  | 23.8                   | 18.0   | 69.3       | 183.0 |
| 3.0                      | 44.0                                    | 132.0                                  | 16.7                   | 12.6   | 12.6       | 33.4  |
| Total                    | 193.1                                   | 338.8                                  | 132.0                  | 100.0  | 100.0      | 264.0 |

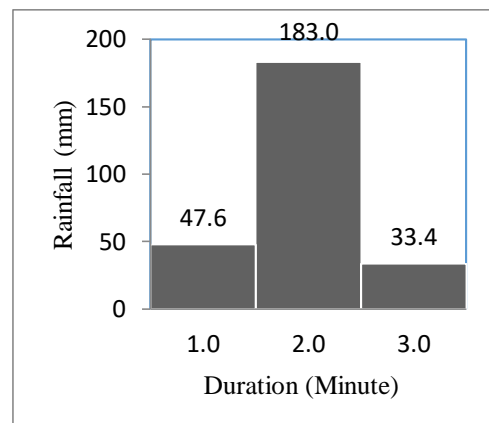


Fig. 3 Rain plan hyetograph with the ABM method

Furthermore, the results of this rain distribution will be used to calculate runoff discharge in EPA SWMM 5.1 simulations.

#### Simulation results with EPA SWMM 5.1

##### Runoff discharge

From the simulation, the results are good, where the continuity error for surface runoff and flow tracing is -0.19% and -1.62% respectively. The

quality of the simulation is not good if the continuity error is  $> 10\%$ . From the 13 Subcatchment found in this model, the highest peak runoff occurs at the subcatchment6, which is  $6.91\text{M}^3 / \text{second}$  which is seen at 3:00 in Fig. 4 below. This is the peak condition of rain. While the Subcatchment with the smallest flowrate is Subcatchment12 with a flow of  $0.62\text{m}^3 / \text{sec}$ .

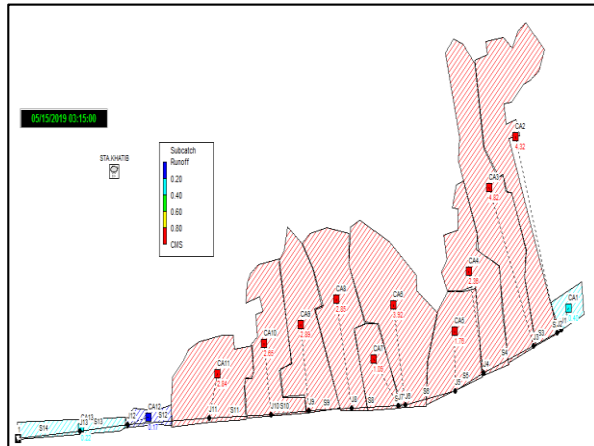


Fig. 4 Sub-catchment runoff of Gunung Pangilun area

#### Location of flood points

Table 6 below shows the location of the flooded cross section. In addition, the duration of flooding and the volume of flooding that occurs in the affected area can also be known. Junction 6 is the longest point experiencing flooding with a duration of 4.72 hours. Junction 6 is the location of Gunung Pangilun Elementary School 17, which is almost a flood area that is in accordance with the field review. While the largest volume occurs at J3 junction is a link between catchment area 3 and drainage channel Jl. Gajah Mada and is the location of the Alfa Mosque's flood permit in 2018 from news articles.

Table 6. Node Flooding Summary

| Node | Hours Flooded | Max Rate CMS | Hour of Max Flooding | Total Flood Volume $10^6 \text{ ltr}$ |
|------|---------------|--------------|----------------------|---------------------------------------|
| J1   | 1.04          | 0.456        | 3:00                 | 1.312                                 |
| J2   | 3.9           | 6.573        | 3:00                 | 31.6                                  |
| J3   | 4.68          | 6.5          | 3:00                 | 41.05                                 |
| J4   | 2.48          | 3.095        | 3:00                 | 12.14                                 |
| J5   | 3.33          | 4.457        | 3:00                 | 21.1                                  |
| J6   | 4.72          | 5.584        | 3:00                 | 21.33                                 |
| J7   | 3.72          | 3.614        | 3:00                 | 31.92                                 |
| J8   | 3.49          | 5.211        | 3:00                 | 23.74                                 |
| J9   | 1.77          | 4.065        | 3:00                 | 13.22                                 |
| J10  | 3.56          | 5.518        | 3:00                 | 30.91                                 |
| J11  | 0.83          | 1.502        | 3:00                 | 2.47                                  |
| J12  | 1.13          | 1.765        | 3:00                 | 4.17                                  |

In Fig. 5, the overflow channel is shown by a red line, the channel that is not overflowing is shown in blue, and the channel that returns to normal or recedes after overflowing is shown in green. From the simulation results it can also be seen that there is almost along the drainage channel of the Jalan Gajah Mada area, Gunung Pangilun Sub-District (Table 7) cannot accommodate runoff that occurred at the 03.30 simulation. This is caused by the dimensions of the channel that cannot accommodate runoff flow.

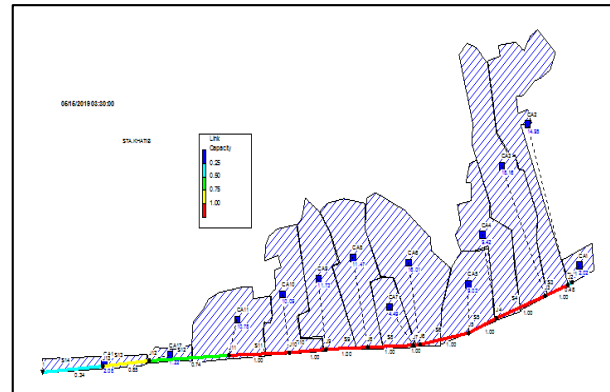


Fig. 5 The channel that overflows at the EPA SWMM 5.1 of Gunung Pangilun area

Table 7. Conduit surcharge Summary

| Conduit | Hours Both Ends Full | Hours Upstream Full | Hours Downstream Full | Hours Above Normal Flow | Hours Capacity Limited |
|---------|----------------------|---------------------|-----------------------|-------------------------|------------------------|
| S2      | 1.03                 | 1.03                | 1.03                  | 0.07                    | 1.03                   |
| S3      | 3.89                 | 3.89                | 3.89                  | 0.12                    | 3.89                   |
| S4      | 4.68                 | 4.68                | 4.68                  | 4.58                    | 4.68                   |
| S5      | 2.48                 | 2.48                | 2.48                  | 2.51                    | 2.48                   |
| S6      | 3.32                 | 3.32                | 3.32                  | 3.28                    | 3.32                   |
| S7      | 2.33                 | 2.33                | 2.33                  | 0.32                    | 2.33                   |
| S8      | 4.72                 | 4.72                | 4.72                  | 4.66                    | 4.72                   |
| S9      | 3.48                 | 3.48                | 3.48                  | 0.5                     | 3.48                   |
| S10     | 1.76                 | 1.76                | 1.76                  | 1.78                    | 1.76                   |
| S11     | 3.54                 | 3.54                | 3.54                  | 3.54                    | 3.54                   |
| S12     | 0.82                 | 0.82                | 0.82                  | 0.82                    | 0.82                   |
| S13     | 1.11                 | 1.11                | 1.11                  | 1.17                    | 1.11                   |

## CONCLUSIONS

From the simulation results using the NVivo application, the location of frequent flooding was found in the MUA PALAPA area (Padang, Lubuk Alung, Pariaman), namely the Gunung Pangilun Padang area.

Furthermore, the floods were calculated in the Gunung Pangilun area where the largest peak runoff occurred at sub-catchment 6, which amounted to  $6.91\text{m}^3 / \text{second}$ , which was the location of Gunung Pangilun Primary School No. 17, which was almost flooded according to the field review, and the news obtained was carried out. Sub-catchment with the



smallest runoff peak flow is sub-catchment 12 with a flow of 0.622 m<sup>3</sup>/sec.

There are 8 channels that are the location of flood points during the simulation hours of 3:30, namely channels S3, S4, S5, S6, S7, S8, S9, S10, while the channels that do not overflow during flood are channels S2, S11, S12 and S13. The overflow of water in the channel occurs because of the capacity of the channel that cannot accommodate runoff discharge, the waste contained in the channel, and the accumulation of sediment in the canal.

Risk flood can be minimised by: normalize the drainage, widened the dimensions of drainage, and create a retention pool in a sub-catchment area that has a large impact discharge.

## ACKNOWLEDGEMENTS

This research was funded by University of Andalas under Research Grant Number: T/24/UN.16.17/PP.IS-KRP1GB/ LPPM/2019 dated 13 May 2019.

## REFERENCES

- [1] Book III of National Mid-term Development Planning 2015-2019.
- [2] Istijono, B., Ophiyandri, T., Aprisal and Nurhamidah. 2019. The Effect of Flood to Quality Index of Soil Physical Properties at the Downstream of Kuranji River Watershed, Padang City. *International Journal of GEOMATE*, Feb., 2019 Vol.16, Issue 54, pp.74 – 80.
- [3] Khan, A. N. (2013). Analysis of 2010-flood causes, nature and magnitude in the Khyber Pakhtunkhwa, Pakistan. *Natural hazards*, 66(2), pp. 887-904.
- [4] Gale, E. L., & Saunders, M. A. (2013). The 2011 Thailand flood: climate causes and return periods. *Weather*, 68(9), pp. 233-237.
- [5] Adelekan, I. O. (2011). Vulnerability assessment of an urban flood in Nigeria: Abeokuta flood 2007. *Natural Hazards*, 56(1), pp. 215-231.
- [6] Douglas, I., Alam, K., Maghenda, M., McDonnell, Y., McLean, L., & Campbell, J. (2008). Unjust waters: climate change, flooding and the urban poor in Africa. *Environment and urbanization*, 20(1), pp. 187-205.
- [7] Rossman, Lewis A. 2015. Storm Water management Model User's Manual Version 5.1. U.S Environmental Protection Agency, USA.
- [8] Hidayat, B, 2017, Understanding Flood Disasters in Padang ity with Content Analysis of News Articles (in bahasa: Memahami Bencana Banjir di Kota Padang dengan Content Analysis Artikel Berita), *Civil Engineering Journal*, Andalas University.
- [9] Legowo, S., Hadihardaja, I. K., Enung, T. S. H., 2019. Application of the Digital Elevation Method for Flood Estimates on the Ciliwung River in West Java, *International journal of GEOMATE*, July 2019, Vol.17, Issue 59, pp.154-165.
- [10] Vinay, R., Umamahesh, N., Sriramoju, P. S., Kumar, P. A. 2018. Simulation of the Urban Drainage System using the Storm Water Management Model (SWMM). National Institute of Technology, Warangal, Andhra Pradesh, India.
- [11] Waikar, L, M and Namita, U. 2015. Model of Flood Transfer using EPA SWMM 5. Department of Civil Engineering and Water Management, Technical Institute and Guru Shri Guru Gobind Singhji Teknologi Nanded, (M.S) India.
- [12] Fairizi, D, 2015. Drainage Channels Analysis and Evaluation in Talang Kelapa Housing Area in Sub watershed Lambidaro, Palembang City. University of Sriwijaya.
- [13] Kamiana, I Made. 2011, Debit Calculation Techniques for Infrastructure (in bahasa: Teknik Perhitungan Debit Rencana Bangunan Air), Graha Ilmu, Yogyakarta
- [14] Chow, V.T., Maidment, D.R. & Mays (1988) *Applied Hydrology*. New York: Mc Graw-Hill Book Company.
- [15] Istijono, B., Aprisal, Ophiyandri T., and Nurhamidah. 2019. A Study of the Quality of Soil Infiltration at the Downstream of Kuranji River, Padang City. *International Journal of GEOMATE*, April 2019, Vol.16, Issue 56, pp. 16-20

# **SIMULATION OF THE COLLAPSE PROCESS OF INFRASTRUCTURE USING GENERAL-PURPOSE PHYSICS ENGINE**

Yoshihiro Kabeyama<sup>1</sup>, Sunao Fujimura<sup>2</sup> and Shinichiro Okazaki<sup>3</sup>

<sup>1,2</sup>Graduate School of Engineering, Kagawa University, Japan;

<sup>3</sup>Faculty of Engineering and Design, Kagawa University, Japan;

## **ABSTRACT**

In recent years, tsunamis caused by earthquakes and flooding associated with heavy rainfall have occurred in Japan. It has often been reported that bridges collapsed because of the outflow of the bridge superstructure and the scouring of the bridge pier resulting from these causes. However, to simulate these phenomena, it is necessary to carry out coupled analysis of three types of behavior of the structure, ground, and fluid, and the calculation cost is very large. Therefore, the examination of this phenomena has not currently achieved much progress. The purpose of this research was to perform a fluid-ground-structure simulation (such as for the collapse of a bridge pier because of flooding) at low cost, using a general-purpose physics engine. In this study, the focus was on the simulation of large deformations of the fluid, ground, and structure, and all objects were modeled with particles. First, the parameters that can simulate the behavior of the fluid were set appropriately by using the dam break problem. Subsequently, the flooding phenomenon in a river and the scouring phenomenon on a bridge pier on the ground were simulated using these parameters.

*Keywords: Physics simulator, Scouring phenomenon, SPH method*

## **INTRODUCTION**

In recent years, damage such as deep deformation of the lower structure has frequently occurred in Japan, along with damage of the upper structure of river bridges due to floods and tsunamis [1]. Heavy rains in the western Japan region that occurred in July 2018 caused damage to many bridges in the Japan Railway Shikoku area. This forced the trains to be shut down and affected many users. In the case of the Saita River Bridge between the Yosano Line Motoyama and Kannonji Temple, the bridge pier sloped because of the scouring, causing deformation of the superstructure. The Saita River Bridge is built on a river that usually has a small amount of water. However, on the day of heavy rains, the water flow was higher than expected. As a result, the ground was scoured by the river flow, and the bridge pier was inclined. This kind of damage has been experienced frequently since ancient times, and it is thought that it is possible to avoid damage by studying disaster cases. In recent years, with the development of numerical calculators, the study of disaster risk by machine learning has been carried out, and it is currently possible to extract a pier having a high risk of scouring with high accuracy. However, the construction of a more accurate forecasting model requires a high-level understanding of the scouring phenomenon, and studies considering changes in the varied topography of the river, ground conditions, and the river flow are necessary. The method of numerical calculation makes it possible on a computer. To

simulate these phenomena, it is necessary to couple the three-phase behavior of the fluid-ground-structure, and the time and load required for modeling and calculation are very large. The examination of this phenomenon using numerical analysis has not significantly progressed, especially in three dimensions. Handling river flow is very important, and plays an important role in revetment work and the design of the bridge.

In particular, it is difficult for the finite-element method (FEM) to reproduce complicatedly changing free surfaces in fluid simulation. In addition, it is necessary to reproduce the fluctuation of the riverbed caused by the river flow scooping the ground. Moreover, in this research, more-complicated analysis is required, because the calculation data for the bridge are included. Although three-dimensional software that can easily simulate such a large deformation has been developed, it is expensive. Therefore, in this research, an attempt was made to solve the soil-fluid-structure interaction problem, which has been difficult to study because of the large computational load, at low cost and in a relatively short time by using a physical simulator that can be used free of charge and has high versatility.

## **SIMULATION METHOD**

### **Software**

In this study, a general-purpose physics simulator (Blender) was used. Blender is equipped with a

physics engine called Bullet, and this software can simulate an object from rigid body to soft body as a discrete body or a continuum. In addition, it supports optimization to the GPU using CUDA and can perform three-dimensional simulation at high speed [2]. This simulator is based on the smoothed-particle hydrodynamics (SPH) method, and can simulate large deformation of both fluids and solids. However, the setting of the parameters that govern the behavior between particles is very different from general numerical analysis, such as the FEM. Therefore, to perform accurate simulation, it is necessary to confirm the validity of the behavior of the fluid, which is originally a continuum, as a connected particle group, and it was examined by comparison with the existing experimental results when simulating.

## REPRESENTATION TECHNIQUE OF MODEL

### Particle and Grid Methods for Rigid-Body Simulations

When simulating a rigid body, it is common to use polygons to calculate and express accurately. However, as the shape becomes more complex, the amount of information processed by the model becomes larger, and complex calculations are required for continuum collision calculation. In the process of calculating such complicated behavior, the deformation of the mesh may break the calculation. Therefore, by using particles instead of polygons for rigid-body representation, mesh problems do not occur, because the interaction between particles is calculated. It is also possible to reduce the cost of computation by limiting the range of interaction. By this means, physical simulation close to reality is performed at high speed [3].

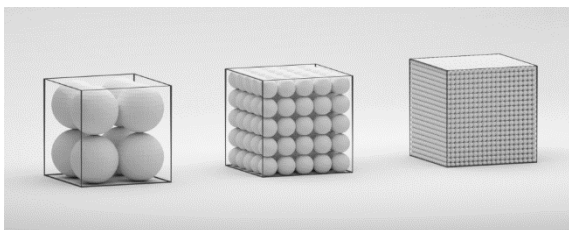


Fig. 1. Structure of cubes

### SPH Method

In this research, the aim was to solve the ground–fluid–structure coupled problem of slope by scouring of the bridge by creating a fluid model, soil particle model, and bridge pier model using the SPH method.

The SPH method is a numerical analysis method and is classified as a meshless method. Among the meshless methods, the SPH method can replace the behavior of a continuum with the motion of a discrete

body by expressing the continuum with a finite number of particles by the Lagrange method. The SPH method is suitable for problems with large-scale changes in objects, and it is used in such fields as structural mechanics and fluid dynamics [4], [5]. In general, calculation of simulation by a continuum requires enormous time, and it frequently cannot be calculated by a general-purpose PC. The method using discrete fields is possible without incurring much time. However, the calculation accuracy of the SPH method itself, and the handling of boundary conditions, are not well established. Further, it is difficult to reproduce the fluid by discrete bodies; hence, it is not performed very often. It is necessary to verify the validity by combining an infinite number of parameters (with the result of the element experiment in each component), and the experimental result in which the interaction between the components is considered, considering the setting of parameters, etc.

### Particle System

Blender is equipped with Particle System. Particle System is a computer graphics technology, and very small objects called “particles” can represent irregularly shaped materials that exist in the natural world. By placing an object called Emitter in Blender, one can release and control particles from there. Also, particles can be influenced by gravity and other external forces, and the effects of interference of different particles can also be expressed. In other words, it is considered that the simulation of scouring can be expressed by interacting different fluid and soil particles represented by particles.

## PARTICLE MODEL SETTING

Blender particles have various parameter settings. The Bullet installed in Blender has features that allow parallel computation by a CPU or GPU, and it can solve various physical phenomena very fast. However, the code is a black box, and viscosity, stiffness, and mass parameters governing particle motion are unitless, so it is impossible to divert actual fluid and solid parameters as they are. Therefore, in the case of fluid simulation, for example, it is necessary to set parameters that can simulate this behavior appropriately after conducting element experiments to understand the characteristic behavior of the fluid.

In this research, the focus is on the behavior of the fluid among the phases that describe the scour phenomenon first, and the fluid-related parameters are set to be able to reproduce the dam breaking problem with high accuracy. Subsequently, a model was constructed that can reproduce the behavior of soil particles under the action of fluid appropriately.

## SIMULATION RESULT

### Dam Break

#### Simulation method

The dam break problem is often used to verify the validity of a model that describes the free surface flow field. In this study, the fluid was represented by particles, and the experimental device was created by a mesh frame. The scale of the model to be created was  $50 \times 100 \times 60$  mm, as shown in Fig. 2. Then, the fluid was set to a portion 30 mm from the bottom in the model, the weir was removed at once, and the flow was tracked. This frame ignores the friction with the particle. In the particle parameter settings, the initial settings were set with reference to books or the Internet site of simulation [6]-[8]. Above all, size and rest density had a large influence on the interaction range and fluid behavior, and other parameters were set based on these. Figure 3 shows the simulated

results for each set value of each parameter. The validity of this simulation was confirmed by image comparison with experimental fluid behavior.

Table 1 show the values that are closest to the experimental fluid behavior as a study of parameter value.

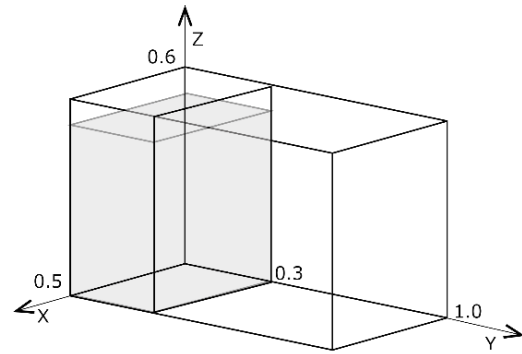


Fig. 2. Mesh frame model

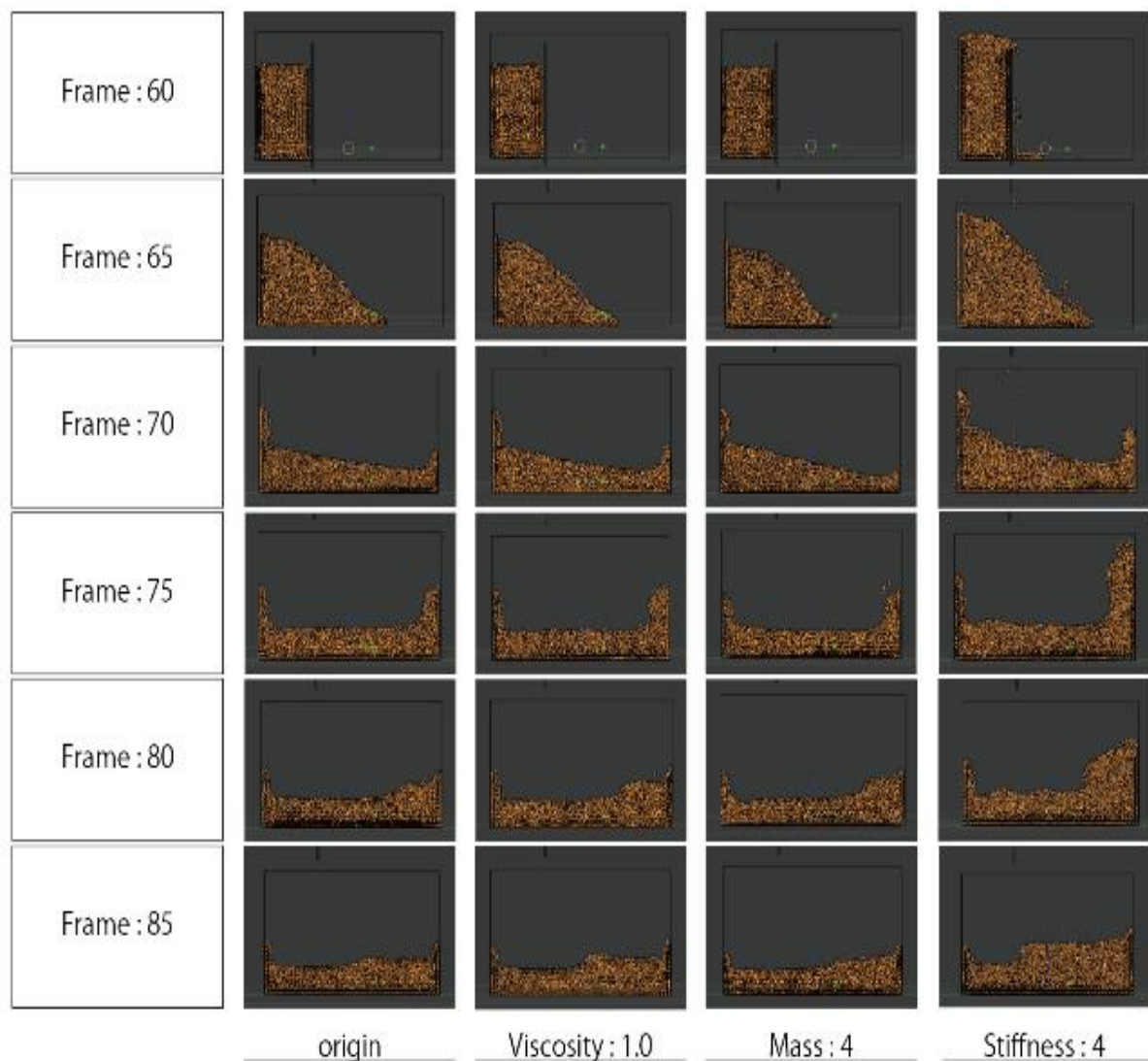


Fig. 3. Comparing dam break simulation result with parameter

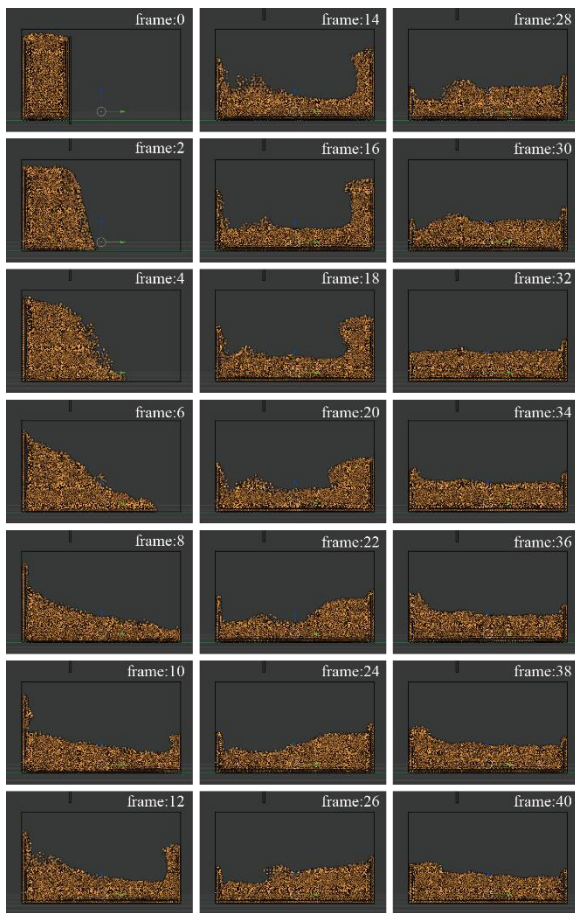


Fig. 4. Result of dam break simulation

The simulated result of the dam break using this setting is shown in Table 1. At frame 0, the stored fluid drains by removing the weir. At the frame 8, The fluid collides with the opposite wall and bounces up. Then the fluid bounces back and is approaching equilibrium. This simulation of frame rate is 24 fbs.

Table 1. Setting of fluid

| Fluid        |       |
|--------------|-------|
| Particles    | 7000  |
| Size         | 0.011 |
| Rest Density | 0.5   |
| Mass         | 4.0   |
| Stiffness    | 4.0   |
| Viscosity    | 1.4   |

#### Simulation results

In Fig. 5, the left side of the figure is the experimental behavior of the fluid, and to the right is the result of the simulation by Blender. Comparing these shows that the fluid did not bound significantly at 0.6 s, but at other times it showed almost the same behavior as the experiments. This value was applied

in the following simulations.

### Collapse Simulation

#### Simulation method

Infiltration, overflow, erosion, earthquakes, etc. can be mentioned as factors that cause the dike and bridge of the river to be destroyed. The scouring phenomenon is included in the erosion. Scouring is a phenomenon in which local erosion, which did not occur in steady-state water flow, happens when the river flow increases because of floods associated with heavy rainfall and the water flow is disrupted. Scouring makes the superstructure unstable because of settlement and outflow of the foundation part. The progress of such scouring may cause the bridge pier to slope, and even collapse.

In the simulation of the scouring phenomenon, three types of particle (fluid, foundation, and bridge structure) were set to solve the fluid–ground–structure interaction problem. Here, to express the foundation and the pier, Molecular Script was used as the setting of particle. In Molecular Script, there is a method called activated particle linking that connects particles, and it is possible to determine the strength of the connection (search length) and the number to be connected (max links) as the setting value among them. These settings are shown in Table 2.

Table 2. Settings of understructure and pier

|               | Foundation | Bridge pier |
|---------------|------------|-------------|
| Search length | 1.7        | 4.0         |
| Max links     | 2          | 16          |
| Broken        | 5.0        | 100.0       |
| % linking     | 0.06       | 0.0         |

#### Mesh frame model

The experimental equipment for simulation was created in the same way as a dam break. In this model, the water flow path, the foundation to be the ground, and the bridge pier installed on this foundation were set. In past research, experiments on such conditions were not conducted, so, in consideration of the performance of the PC used (Intel Core i7-7820X CPU @ 3.60 GHz, System x64 base processor, Compute Device: CUDA GeForce GTX 1080 Ti(Display)), a model was set up and solved, as shown in Fig. 6. Figure 6 shows the setting values of the mesh frame.



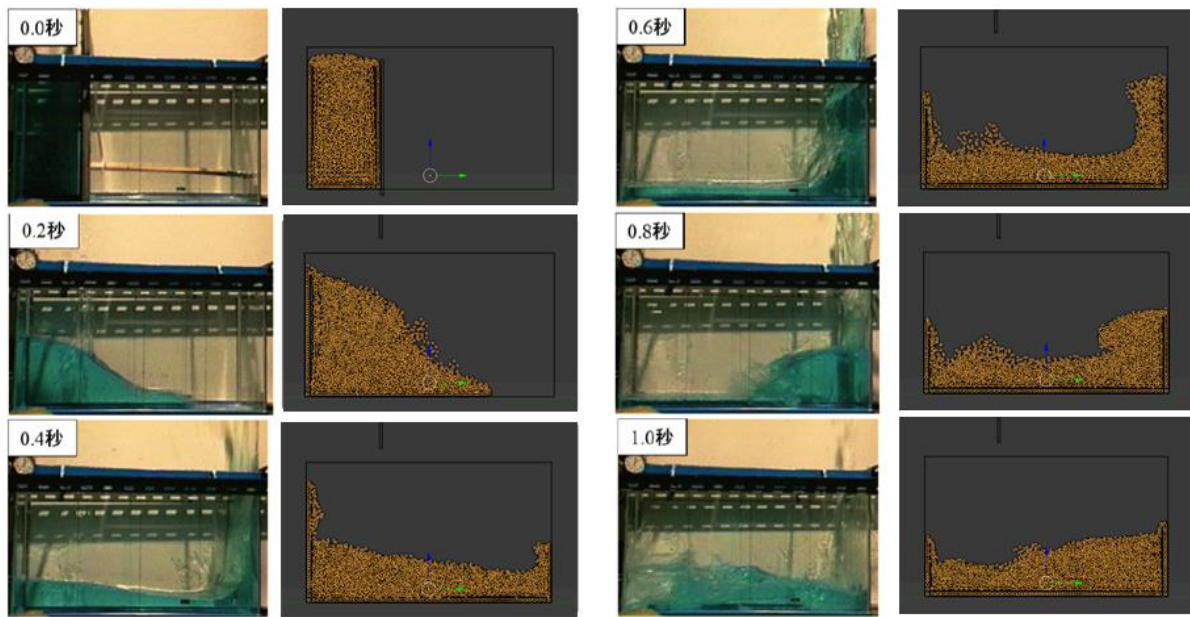


Fig. 5. Comparing dam break simulation result with experiment

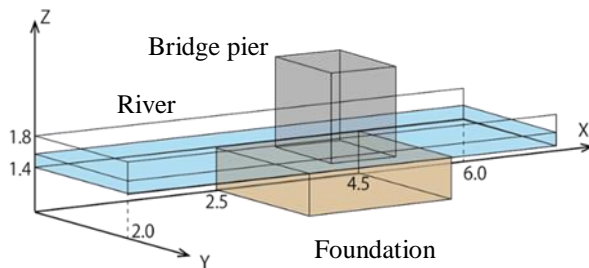


Fig. 6. Mesh frame model

Water channel:

Height 0.4 m, width 2.0 m, length 6.0 m

Foundation:

Height 1.4 m, width 2.0 m, length 2.0 m

Bridge pier:

Height 2.0 m, width 1.2 m, length 0.9 m

### Simulation Results

The foundation was excavated by the running water, and it was confirmed that the bridge piers were eventually inclined. In addition, it was confirmed from the calculation process that the collapse of the bridge pier did not stop and became unnatural. Therefore, it was decided to handle new linking as a new setting. With this setting<sup>6</sup>, the disconnected particles can be rejoined, and the bridge was successfully made to collapse gently. The results are shown in Fig. 7. It was also confirmed that the connection between particles with these settings affects not only the set particles, but also other particles. To improve the simulation accuracy, it is inevitable to reduce the size and increase the number of particles. In the future, it will be necessary to study the object in a more subdivided model by particles.

### CONCLUSIONS

In this study, the problem of the scouring of a bridge pier by a flood was addressed using a general-purpose physics simulator. To carry out the simulation at low cost, an attempt was made to solve the fluid-ground-structure three-phase coupled problem using the SPH method. The physics engine Bullet used in Blender does not disclose the physics formula, so it is very difficult to control the parameters used in the computation. An attempt was made to confirm the validity by comparing a dam break with an experiment to reproduce water by particles. Although the characteristic movement of the fluid could be captured partially, it was not possible to reproduce the surface tension of the water and the associated bounce. In the simulation of scouring, three kinds of particle (fluid, ground foundation, and bridge structure) were treated at the same time. The aim was to solve the fluid-ground-structure interaction problem by this. Here, to express the foundation and the bridge pier, New links was used as the setting of the particles. New links (% linking) can reconnected particles disconnected by fluid impact. It transpired that New links not only works on the particle that has been activated, but also on other particles. Although there was a limit to the segmentation of the model because of the performance of the PC, it was possible to simulate the inclination of the bridge pier by scouring.

As a result, although valid parameters were obtained, when the basic part was subdivided to perform a more accurate simulation, the correct simulation could not be calculated with the same

setting. In other words, the size of the particle and each parameter value are considered to have a strong relationship with each other.

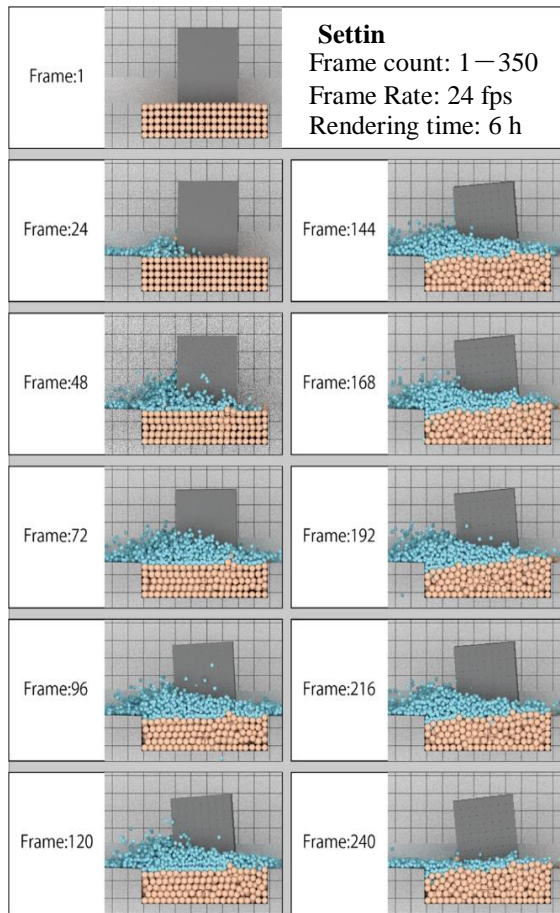


Fig. 7. Collapse simulation result

## ACKNOWLEDGMENTS

The authors would like to express gratitude to a

Grant-in-Aid for Young Scientists (A) and the Cross-ministerial Strategic Innovation Promotion Program (SIP) for their financial support.

## REFERENCES

- [1] Kazuo Ishino et al., A collapse factor and the measures of the bridge by the heavy rain that occurred in Japan after 2004, 安全問題研究論文集, Vol. 5, 2010.
- [2] Tomihisa Yuki, CPUとGPUの性能比較 ～ 行列計算およびN体問題を用いて ～, 2011, pp.1-28.
- [3] Tanaka Masayuki. et al., Particle-based Rigid Body Simulation and Coupling with Fluid Simulation, Transaction of JSCES, Paper No.20070007, 2007.
- [4] Seiichi KOSHIZUKA, Numerical Analysis of Flow using Particle Method, Flow21, 2002, pp.230-239.
- [5] Tanabe syoiti. et al., A FLUID-RIGID BODY SIMULATION BY USING THE SPH METHOD AND ITS APPLICATION TO BRIDGE RUNOFF SIMULATIONS, J.JSCE, Ser.A2 (Applied mechanics) Vol.70, No.2 (JSCE Vol.17), (2014), pp.329-338.
- [6] Todo++, Blender 2.7 Master Book Sculpt & Simulation. Tokyo, Cut system Inc., 2015.6, 459p
- [7] Tony Mullen, Physics simulation Blender, Tokyo, ASCII Media Works Inc., 2008, 12. 458p.
- [8] Introducing particle fluids parameters, available from <https://farsthary.wordpress.com/2010/03/19/introducing-particle-fluids-parameters-function/>, (accessed 2018-07-22)



## MOTORCYCLE-RELATED DEATHS AND HELMET USAGE SITUATION IN THAILAND

Jetsada Kumphong<sup>1</sup>, Thaned Satiennam<sup>1</sup> and Wichuda Satiennam<sup>1</sup>

<sup>1</sup>Department of Civil Engineering, Faculty of Engineering, Khon Kaen University, Thailand.

### ABSTRACT

The high death of motorcycle riders than drivers of other vehicles and low helmet wearing rate is a serious problem in Thailand. This study aimed to evaluate the effects of helmet wearing on motorcycle riders' death rates nationwide. Data were collected from 77 provinces in Thailand between 2012 and 2016. These data included number of police stations, helmet usage percentage, motorcycle-related death rates per 100,000 population and motorcycle-related death rates per 10,000 motorcycles registered in each province. Pearson correlation analysis was used to test the correlations between studied variables. The correlation between helmet usage percentage and motorcycle-related death rate was almost significant. The helmet usage percentage was significantly consistent with number of police stations. Helmet usage was the significant with variable affecting motorcyclists' death rates, leading to the conclusion that wearing a motorcycle helmet reduces the head injury and risk of death from a motorcycle crash. Helmet law enforcement should be effectively supported by the motorcycle safety plan of the Royal Thai Police.

*Keywords: Fatality, Motorcycle, Safety, Helmet usage*

### INTRODUCTION

According to the traffic fatality data surveyed by the World Health Organization (WHO) [1-4], the outcomes of motorcycle-related accidents are categorized as ASEAN countries' social as well as health problems. Motorcycles are widely used for transportation and sport activities in these countries, and the number of motorcycles at present is greater than the number of cars [5-8].

Thailand has a higher motorcycle-related death rate than other countries. Motorcyclists are more than 70% likely [3] to die in road accidents than drivers of other vehicles and low helmet wearing rate as shown in Table 1 and Table 2

Head injury is a major cause of motorcycle-related deaths from road accidents. However, there are clear indications that helmets can reduce the severity of head injuries during crashes [9-10].

Table 1 shows the motorcycle-related death rates per 100,000 population and the motorcycle-related death rates per 10,000 motorcycles registered from the years 2012 to 2016. It can be seen that during this period, the death rates per 10,000 motorcycles registered in Thailand has an increasing trend every year.

Likewise, when the type of motorcycle groups in Thailand was considered, it was found then the motorcycles over 150 CC and 126-150 CC became increasingly popular among the new generation. In Table 3, it can be seen that motorcycles over 150 CC registration continued to increase from 2014, while the data remained consistent with the motorcycle-related deaths.

Table 1 Thailand motorcycle-related death rates between 2012 and 2016

| Year | No. of motorcycle-related deaths | The motorcycle-related death rates per 100,000 | The motorcycle-related death rates per 10,000 motorcycles registered |
|------|----------------------------------|--|--|
| 2012 | 5798 <sup>a</sup>                | 9.00 <sup>a,c</sup>                            | 25.71 <sup>a,b</sup>   |
| 2013 | 5593 <sup>a</sup>                | 8.58 <sup>a,c</sup>                            | 26.38 <sup>a,b</sup>   |
| 2014 | 5394 <sup>a</sup>                | 8.28 <sup>a,c</sup>                            | 29.67 <sup>a,b</sup>   |
| 2015 | 5863 <sup>a</sup>                | 8.92 <sup>a,c</sup>                            | 32.40 <sup>a,b</sup>   |
| 2016 | 6083 <sup>a</sup>                | 9.17 <sup>a,c</sup>                            | 31.81 <sup>a,b</sup>   |

Sources: <sup>a</sup>The Bureau of Non Communicable Diseases of the Ministry of Public Health [11];

<sup>b</sup>Department of Land Transport, 2012-2016[12].

Table 2 Helmet usage rates between 2012 and 2016

| Year | Helmet usage percentage (Mean %) | Helmet usage percentage of riders (Mean %) | Helmet usage percentage of passengers (Mean %) |
|------|----------------------------------|--|--|
| 2012 | 43 <sup>d</sup>                  | 52 <sup>d</sup>                            | 20 <sup>d</sup>                                |
| 2013 | 43 <sup>d</sup>                  | 51 <sup>d</sup>                            | 19 <sup>d</sup>                                |
| 2014 | 42 <sup>d</sup>                  | 51 <sup>d</sup>                            | 19 <sup>d</sup>                                |
| 2015 | 43 <sup>d</sup>                  | 51 <sup>d</sup>                            | 20 <sup>d</sup>                                |
| 2016 | 43 <sup>d</sup>                  | 51 <sup>d</sup>                            | 20 <sup>d</sup>                                |

Sources: <sup>d</sup>Thai Roads Foundation, 2012-2016 [13]

Table 3 The motorcycles registered and number of motorcycles registered

| Year | No. of motorcycles registered (126-150 cc) | No. of motorcycles registered (>150 cc) |
|------|--|---|
| 2012 | 28970 <sup>b</sup>                         | 47948 <sup>b</sup>                      |
| 2013 | 25900 <sup>b</sup>                         | 69777 <sup>b</sup>                      |
| 2014 | 68706 <sup>b</sup>                         | 48703 <sup>b</sup>                      |
| 2015 | 109166 <sup>b</sup>                        | 53930 <sup>b</sup>                      |
| 2016 | 153290 <sup>b</sup>                        | 80551 <sup>b</sup>                      |

Sources: <sup>b</sup>Department of Land Transport, 2012-2016 [12].

There are 77 provinces and 5 regions in Thailand, including the North, Northeast, Central, West and South, as illustrated in Table 4.

| Table 4 Thailand provinces |   |
|----------------------------|---|
| Region                     | Provinces   |
| North                      | Chiangrai, Chiangmai, Nan, Phrae, Phayao, Mae Hong Son, Lampang, Lamphun, Uttaradit.  |
| The North-East             | Khon Kaen, Chaiyaphum, Nakhon Phanom, Nakhon Ratchasima, , Mukdahan, Yasothon, Roi Et, Loei, Sisaket, Sakon Nakhon, Surin, Nong Khai, Nong Bua Lam Phu, Udon Thani, Ubon Ratchathani, Amnat Charoen.  |
| Central                    | Bangkok, Kamphaengphet, Chai Nat, Nakhon Nayok, Nakhon Pathom, Nakhon Sawan, Nonthaburi, Pathum Thani, Phra Nakhon Si Ayutthaya, Phichit, Phitsanulok, Phetchabun, Lop Buri, Samut Prakan, Samut Songkhram, , Sukhothai, Suphan Buri, Ang Thong, Uthai Thani. |
| East                       | Chanthaburi, Chachoengsao, Chonburi, Trat, Prachin Buri, Rayong, Sa Kaeo.   |
| West                       | Kanchanaburi Tak, Prachuap Khiri Khan, Phetchaburi, Ratchaburi.   |
| South                      | Krabi, Chumphon, Trang, Nakhon Si Thammarat, Narathiwat, Pattani, Phangnga, Phatthalung, Phuket, Yala, Ranong, Songkhla, Satun, Surat Thani.  |

The above problem is aggravated by other problems. On the one hand, helmet law enforcement in Thailand is relatively low. The other involves low percentage of helmet usage [1-4, 14]. Many studies similarly show the correlation between high fatality

rates – among motorcyclists – and low percentages of helmet usage [7, 15]. In this research, the first objective was to study the differences of helmet usage percentage between riders and passengers, and the second was to study the correlation between the helmet usage percentage, motorcycle-related deaths and number of police stations. The data collected covered all of the 77 provinces in the country, from 2012 to 2016.

## METHODOLOGY

### Data retrieval and entry

This study investigated the secondary data on motorcycle accident numbers obtained from the Bureau of Non Communicable Diseases of the Ministry of Public Health, 2016 [11]; helmet usage percentage report by Thai Roads Foundation, 2016[13]; the size of population by the National Statistics Bureau, 2016 [16]; the number of motorcycles registered from the Department of Land Transport, 2016[12]; and the number of police stations from the Royal Thai Police, 2016 [17]. All of the data were separated into their respective provinces. The variables were motorcycle-related deaths, helmet usage percentage, population size, number of motorcycles and number of police stations.

### Statistics

T-test was used to test the differences of helmet usage percentage between the rider group and the passenger group [18]. Logarithmic transformation of motorcycle-related death per 100,000 populations per 10,000 motorcycles registered was performed as it was the best applicable method [15]. A Pearson correlation test was used to correlate different variables [19].

## RESULTS AND DISCUSSION

### Test of differences of helmet usage percentages

Table 5 shows t-test significant level of differences between results obtained from helmet usage percentage of riders and helmet usage percentage of passengers by province in Thailand. As shown in the table, the significant levels ( $p < 0.001$ ), are less than 0.05. Hence, the significant level of differences is said to be at 0.05. The t-test analysis indicated that the helmet usage percentage of riders and helmet usage percentage of passengers has 0.05 significant differences.

### Correlations between the studied variables

The result of correlations analysis indicates that the helmet usage percentage has a significant and

negative correlation with the log transformation of motorcycle-related death rate/100,000 population at the 95 % confidence level ( $R = -0.224, p < 0.001$ ). The helmet usage percentage of riders has a significant and negative correlation with the log transformation of motorcycle-related death rate/100,000 population at the 95% confidence level ( $R = -0.187, p < 0.001$ ). Similarly, the helmet usage percentage of passengers has a significant and negative correlation with the log transformation of motorcycle-related death rate/100,000 population at the 95% confidence level ( $R = -0.243, p < 0.001$ ). The number of police stations also has a significant and negative correlation with the log transformation of motorcycle-related death rate/100,000 population at the 95 % confidence level ( $R = -0.174, p = 0.001$ ).

Table 5 Significant level of differences between results obtained from helmet usage percentage of riders and helmet usage percentage of passengers by province in Thailand

|   | Difference |       |                 | t     | Sig.   |
|---|------------|-------|-----------------|-------|--------|
|   | Mean       | SD.   | Std. Error Mean |       |        |
| (Helmet usage percentage of riders) – (Helmet usage percentage of passengers) | 28.90      | 10.27 | 0.52            | 55.23 | <0.001 |

In addition, the result of correlations analysis indicates that the helmet usage percentage of riders? has a significant and negative correlation with the log transformation of motorcycle-related death rate/10,000 motorcycles registered at the 95% confidence level ( $R = -0.117, p = 0.022$ ). The helmet usage percentage of passengers has a significant and negative correlation with the log transformation of motorcycle-related death rate/10,000 motorcycles registered at the 95% confidence level ( $R = -0.267, p < 0.001$ ). The number of police stations has a significant and negative correlation with the log transformation of motorcycle-related death rate/10,000 motorcycles registered at the 95% confidence level ( $R = -0.349, p = 0.001$ ).

Moreover, the result of correlations analysis indicates that the overall helmet usage percentage has a significant and positive correlation with the number of police stations at the 95% confidence level ( $R = 0.299, p < 0.001$ ). The helmet usage percentage of riders has a significant and positive correlation with the number of police stations at the 95% confidence level ( $R = 0.253, p < 0.001$ ). The helmet usage percentage of passengers also has a significant and positive correlation with the number of police stations at the 95% confidence level ( $R = 0.365, p < 0.001$ ) as shown in Table 6, 7, 8, 9, 10 and Table 11. It can be

concluded that the laws related to helmet wearing can reduce the fatality rates. Some provinces have a low number of motorcycle-related deaths, possibly owing to high helmet usage percentage. Also, high helmet usage percentage results from the high degree of helmet enforcement efficiency which in turn is based on the number of police stations in each province.

Table 6 Correlations between the motorcycle-related death rate/100,000 population and other variables.

|   |                              | Log transformation of motorcycle-related death rate/100,000 population |
|---|------------------------------|--|
| Log transformation of motorcycle-related death rate/10,000 motorcycles registered | Pearson correlation.<br>Sig. | 0.620 <sup>***</sup><br><0.001   |
| Helmet usage percentage (Overall)   | Pearson correlation.<br>Sig. | -0.224 <sup>***</sup><br><0.001  |
| Helmet usage percentage of riders   | Pearson correlation.<br>Sig. | -0.187 <sup>***</sup><br><0.001  |
| Helmet usage percentage of passengers   | Pearson correlation.<br>Sig. | -0.243 <sup>***</sup><br><0.001  |
| Number of police stations   | Pearson correlation.<br>Sig. | -0.174 <sup>***</sup><br>0.001   |

\*Statistically significant at 5%.

\*\*\* Statistically significant at 1%.

Table 7 Correlations between the motorcycle-related death rate/10,000 motorcycles and other variables

|  |                              | Log transformation of motorcycle-related death rate/10,000 motorcycles |
|--|------------------------------|--|
| Log transformation of motorcycle-related death rate/100,000 population | Pearson correlation.<br>Sig. | 0.620 <sup>***</sup><br><0.001   |
| Helmet usage percentage (Overall)                                      | Pearson correlation.<br>Sig. | -0.117 <sup>*</sup><br>0.022   |
| Helmet usage percentage of riders                                      | Pearson correlation.<br>Sig. | -0.058<br>0.254  |
| Helmet usage percentage of passengers                                  | Pearson correlation.<br>Sig. | -0.267 <sup>***</sup><br><0.001  |
| Number of police stations  | Pearson correlation.<br>Sig. | -0.349 <sup>***</sup><br><0.001  |

\*Statistically significant at 5%.

\*\*\* Statistically significant at 1%.

Table 8 Correlations between the helmet usage percentage (Overall) and other variables.

|   |                              | Helmet usage percentage (Overall) |
|---|------------------------------|-----------------------------------|
| Log transformation of motorcycle-related death rate/100,000 population            | Pearson correlation.<br>Sig. | -0.224 <sup>αα</sup><br><0.001    |
| Log transformation of motorcycle-related death rate/10,000 motorcycles registered | Pearson correlation.<br>Sig. | -0.117 <sup>α</sup><br>0.022      |
| Helmet usage percentage of riders   | Pearson correlation.<br>Sig. | 0.976 <sup>αα</sup><br><0.001     |
| Helmet usage percentage of passengers   | Pearson correlation.<br>Sig. | 0.752 <sup>αα</sup><br><0.001     |
| Number of police stations   | Pearson correlation.<br>Sig. | 0.299 <sup>αα</sup><br><0.001     |

\*Statistically significant at 5%.

<sup>αα</sup> Statistically significant at 1%.

Table 9 Correlations between the helmet usage percentage of riders and other variables.

|   |                              | Helmet usage percentage of riders |
|---|------------------------------|-----------------------------------|
| Log transformation of motorcycle-related death rate/100,000 population            | Pearson correlation.<br>Sig. | -0.187 <sup>αα</sup><br><0.001    |
| Log transformation of motorcycle-related death rate/10,000 motorcycles registered | Pearson correlation.<br>Sig. | -0.058<br>0.254                   |
| Helmet usage percentage (Overall)   | Pearson correlation.<br>Sig. | 0.976 <sup>αα</sup><br><0.001     |
| Helmet usage percentage of passengers   | Pearson correlation.<br>Sig. | 0.633 <sup>αα</sup><br><0.001     |
| Number of police stations   | Pearson correlation.<br>Sig. | 0.253 <sup>αα</sup><br><0.001     |

\*Statistically significant at 5%.

<sup>αα</sup> Statistically significant at 1%.

Table 10 Correlations between the helmet usage percentage of passengers and other variables.

|   |                              | Helmet usage percentage of passengers |
|---|------------------------------|---------------------------------------|
| Log transformation of motorcycle-related death rate/100,000 population            | Pearson correlation.<br>Sig. | -0.243 <sup>αα</sup><br><0.001        |
| Log transformation of motorcycle-related death rate/10,000 motorcycles registered | Pearson correlation.<br>Sig. | -0.267 <sup>αα</sup><br><0.001        |
| Helmet usage percentage (Overall)   | Pearson correlation.<br>Sig. | 0.752 <sup>αα</sup><br><0.001         |
| Helmet usage percentage of riders   | Pearson correlation.<br>Sig. | 0.633 <sup>αα</sup><br><0.001         |
| Number of police stations   | Pearson correlation.<br>Sig. | 0.356 <sup>αα</sup><br><0.001         |

\*Statistically significant at 5%.

<sup>αα</sup> Statistically significant at 1%.

Table 11 Correlations between the number of police stations and other variables.

|   |                              | Number of police stations      |
|---|------------------------------|--------------------------------|
| Log transformation of motorcycle-related death rate/100,000 population            | Pearson correlation.<br>Sig. | -0.174 <sup>αα</sup><br>0.001  |
| Log transformation of motorcycle-related death rate/10,000 motorcycles registered | Pearson correlation.<br>Sig. | -0.349 <sup>αα</sup><br><0.001 |
| Helmet usage percentage (Overall)   | Pearson correlation.<br>Sig. | 0.299 <sup>αα</sup><br><0.001  |
| Helmet usage percentage of riders   | Pearson correlation.<br>Sig. | 0.253 <sup>αα</sup><br><0.001  |
| Helmet usage percentage of passengers   | Pearson correlation.<br>Sig. | 0.356 <sup>αα</sup><br><0.001  |

\*Statistically significant at 5%.

<sup>αα</sup> Statistically significant at 1%.

The results of this study show that deaths of motorcycle riders in Thailand have tended to increase every year. This may be a problem related to relaxed law enforcement among motorcycle riders, resulting in low rates of helmet wearing in Thailand. Moreover, it was found that the rate of helmet usage among motorcycle passengers was lower than 20% on average in each province.

From the problems mentioned above and from the data available, the relation of variables can be shown and consequently solutions recommended. The

results of the analysis demonstrate that the problem of increasing motorcycle fatalities can be managed by encouraging, or enforcing, riders to wear a helmet. As such, fatal head injuries can be reduced.

Motorcyclists riding without helmets show a 44% higher chance of the head injuries being intracranial injuries [20]. The severity of head injuries is significantly lower when wearing a motorcycle helmet according to the Glasgow coma scale [15, 21]. Present studies suggest that the life of one person per million can be saved each year with a 10% increase in motorcyclists wearing helmets. Riders are reluctant to wear helmets, citing that wearing a helmet causes discomfort and the use is unsafe [15, 22]. According to a research study from China, Li et al. (2008) [23] found 70% of motorcyclists perceive wearing a helmet as uncomfortable. Approximately 40% of motorcyclists claim that wearing a helmet impairs the vision. 75% of riders only wore a helmet to escape fines from the authority. McKnight et al. (1995) [24] carried out a comprehensive study on the impairment of sound and vision whilst wearing a helmet. Riders wearing helmets need to pivot their heads more to expand the range of vision.

In this research, the number of police stations in each province was taken as a variable of law enforcement. The analysis clearly indicates that if the number of police stations were to increase in each province, there would be more officers to effectively enforce the law in that area and the helmet wearing rate would almost certainly increase. However, in reality, certain technologies could also be used to enforce law such as CCTV helmet camera detectors that operate 24 hours a day [25-26]. Helmet usage percentage not only depends on the existence of legislation but also on the effectiveness of law enforcement. Kumphong et al. (2017) [27] studied the social norms and Perceived Behaviour Control (PBC) and found that both are significant and affect the intention of helmet use. However, some studies have found Descriptive Norm and Injunctive Norm were the highest influencing factors that could account for 25% and 38% of variance of helmet use intention by Theory of Reasoned Action (TRA) model and Theory of Planned Behavior (TPB) model. This is consistent with a study conducted on students in the city of Ho Chi Minh, Vietnam and Vientiane, Laos [28-29]. To conclude, it is not only the matter of law enforcement over motorcyclists' use of helmet, but the attitudes and environmental factors also play an important part in their intention to wear a helmet.

## CONCLUSIONS AND RECOMMENDATIONS

This study has shown that helmet usage percentage was the most significant factor affecting motorcyclists' death rate. Wearing a motorcycle helmet reduces the head injury and risk of death from a motorcycle crash. Helmet law enforcement should

be effectively supported by motorcycle safety programs of the Royal Thai Police. This finding is useful as a guideline to set a policy for reducing motorcycle-related deaths. The available helmet law issueless if it is not enforced effectively on motorcyclists all over the country. In addition, the helmet law should also have a control over the passengers, as the study found that the motorcycle death rates correlated significantly with the percentage of helmet use among the passengers, which found the percentage all over the country was significantly very low, i.e. 15%.

This study did not investigate other factors that cause mortality in motorcycle accidents, i.e., speed and alcohol level. Nonetheless, further studies should be conducted on the enforcement of law that is effective on motorcyclists' wearing of helmet.

## ACKNOWLEDGEMENTS

This research received a Research Fund for Supporting Lecturer to Admit High Potential Student to Study and Research on His Expert Program Year 2016, Graduate School, Khon Kaen University, Khon Kaen, Thailand.

## REFERENCES

- [1] World Health Organization, Global Status Report on Road Safety 2009, Geneva, Switzerland, 2009.
- [2] World Health Organization, Global Status Report on Road Safety 2013, Geneva, Switzerland, 2013.
- [3] World Health Organization, Global Status Report on Road Safety 2015, Geneva, Switzerland, 2015.
- [4] World Health Organization, Global Status Report on Road Safety 2018, Geneva, Switzerland, 2018.
- [5] Tanaboriboon Y., and Satiennam T., Traffic accidents in Thailand. IATSS RESEARCH, Vol. 29, No. 1, 2005, pp. 88-100.
- [6] Kumphong J., Satiennam T., and Satiennam W., A correlation of traffic accident fatalities, speed enforcement and the gross national income of Thailand and its cross-border countries. International Journal of Technology, Vol. 7, 2016, pp. 1141-1146.
- [7] Kumphong, J., Satiennam, T., and Satiennam, W., Correlations among motorcycle-related deaths, helmet law enforcement and helmet usage for ASEAN countries. International Journal of GEOMATE, Sept. 2018, Vol.15, Issue 49, pp. 72-77.
- [8] Kumphong, J., Satiennam, T., Satiennam, W., and Tirapat, S., Change of motorcycle speed under speed enforcement camera on urban arterial in Khon Kaen City, Thailand. International Journal of GEOMATE, April. 2019, Vol.16, Issue 56, pp. 159-164.
- [9] Ichikawa M., Chadbunchachai W., and Marui E., Effect of the helmet act for motorcyclists in

- Thailand. Accident Analysis and Prevention, Vol. 35, 2003, pp. 183-189.
- [10] Nakahara S., Chadbunchachai W., Ichikawa M., Tipsuntornsak N., and Wakai S., Temporal distribution of motorcyclist injuries and risk of fatalities in relation to age, helmet use, and riding while intoxicated in Khon Kaen, Thailand. Accident Analysis and Prevention, Vol. 37, 2005, pp. 833-842.
- [11] The Bureau of Non Communicable Diseases of the Ministry of Public health, Injuries and Deaths Report 2012-2016, Thailand, 2016. (In Thai)
- [12] Department of Land Transport , Motorcycle Report 2012-2016.Thailand, 2016. (In Thai)
- [13] Thai Roads Foundation, Helmet Usage Rates Report 2012-2016 ,Thailand, 2016. (In Thai)
- [14] Kumphong J., Satiennam T., and Satiennam W., The determinants of motorcyclists helmet use: Urban arterial road in Khon Kaen City, Thailand. Journal of Safety Research, Vol. 67, 2018, pp. 93-97.
- [15] Alaa K.A., Ashraf F.H., Fikri M.A.Z., Does wearing helmets reduce motorcycle-related death? A global evaluation. Accident Analysis and Prevention, Vol. 49, 2012, pp. 249-252.
- [16] National Statistics Bureau. Population Report 2012-2016.Thailand; 2016. (In Thai)
- [17] Royal Thai Police. Police Stations Report 2012-2016.Thailand; 2016. (In Thai)
- [18] Park H M., Comparing Group Means: The T-test and One-way ANOVA Using STATA, SAS, and SPSS. The Trustees of Indiana University, 2005. ([http://stat.smmu.edu.cn/DOWNLOAD/ebook/statistics\\_course.pdf](http://stat.smmu.edu.cn/DOWNLOAD/ebook/statistics_course.pdf))
- [19] Sedgwick P., Pearson's correlation coefficient. University of London, London, UK, 2012. (<https://doi.org/10.1136/bmj.e4483>)
- [20] Hossain M., and Iamtrakul P., Medical investigation of motorcycle accidents in Thailand. Journal of the Eastern Asia Society for Transportation Studies, Vol. 7, 2007.
- [21] Ankarath S., Giannoudis P V., Balow I., Bellamy M C., Matthews S J., and Smith R M., Injury patterns associated with mortality following motorcycle crashes. Injury, Vol. 33, 2002, pp. 473-477.
- [22] Skalkidou A., Petridou E., Papadopoulos F C., Dessypris N., and Trichopoulos D., Factors affecting motorcycle helmet use in the population of Greater Athens, Greece. Injury Prevention, Vol. 5, 1999, pp. 264-267.
- [23] Li L P., Li G L., Cai Q E., Zhang A L., and Lo S K., Improper motorcycle helmet use in provincial areas of a developing country. Accident Analysis and Prevention, Vol. 40, 2008, pp. 1937-1942.
- [24] Mcknight A J., and Mcknight A S., The effects of motorcycle helmets upon seeing and hearing. Accident Analysis and Prevention, Vol. 27, 1995, pp. 493-501.
- [25] Kumphong J., Satiennam T., and Satiennam W., Preliminary evaluation of helmet law enforcement by CCTV camera: Case of the phatumuang intersection, Khon Kaen City, Thailand. Injury Prevention, Vol. 24 - Suppl 2 (Safety 2018 abstracts). (<http://dx.doi.org/10.1136/injury-prevention-2018-safety.234>)
- [26] Wonghabut P., Kumphong J., Satiennam T., Ung-arunyawee R., and Leelapatra W., Automatic helmet-wearing detection for law enforcement using CCTV cameras. IOP Conference Series: Earth and Environmental Science, Vol.143, 2018.
- [27] Kumphong J., Satiennam T., and Satiennam W., A Study of Social Norms and Motorcycle Helmet Use Intentions among Student Riders in University: A comparison of the Theory of Reasoned Action and the Theory of Planned Behavior. Conference proceedings, in Proc. 12th Int. Conf. on the Eastern Asia Society for Transportation Studies, Vol. 11, 2017, pp. 1-14.
- [28] Kumphong J., Satiennam T., Satiennam, W., and Tu Anh Trinh. Psychological models for the development of motorcycle helmet use among students in Vietnam, IOP Conference Series: Earth and Environmental Science, Vol.143, 2018.
- [29] Kumphong J., Satiennam, T., Satiennam W., Inthavongsa P., and Pramualsakdikul S. Motorcycle helmet use and the theory of traffic psychology for behavior change in Lao PDR. International Journal of GEOMATE, April. 2019, Vol.16, Issue 56, pp. 203 -208.

## STUDY ON SEISMIC LOAD ON BUILDINGS CONSIDERING RESIDUAL RISK

Sei'ichiro Fukushima<sup>1</sup>, Takayuki Hayashi<sup>2</sup> and Mitsuo Tsuzuki<sup>3</sup>

<sup>1</sup> RKK Consulting Co., Ltd, Japan; <sup>2</sup> Tokio Marine & Nichido Risk Consulting Co., Ltd, Japan;

<sup>3</sup> Nagoya University, Japan

### ABSTRACT

The concept of performance-based design introduces the multi-level seismic design loads so that the given performances with proper reliability are assured. However, the seismic design cannot secure the safety against the ground motions greater than specified levels, since no consideration is required for the situation. So, Authors insist the necessity of introducing the concept of residual risks into seismic design and examine the seismic loads considering the residual risks. Two different seismic design loads are considered based on the seismic hazard curve; one called VaR (Value at Risk) corresponds to the given exceedance probability, and the other called CVaR (Conditional VaR) corresponds to the centroid of probability distribution greater than VaR. VaR and CVaR are calculated for 47 sites in Japan to characterize the seismic hazard. The risks of buildings using VaR and CVaR as design seismic loads are also evaluated. In case that uses VaR as design seismic load, the risks scatter largely around the mean. On the contrary, the scattering of risks remains small when using CVaR. This tendency leads to the setting procedure of design seismic loads that realize uniform risk.

*Keywords: Performance-based design, Seismic load, Residual risk, Value at risk, Conditional value at risk*

### INTRODUCTION

Recently the concept of performance-based design has made it common to introduce multi-level seismic design loads so that the given performances with proper reliability are assured. For example, The term for seismic load in "Recommendation for Loads on Buildings [1]" illustrates the procedure to obtain the loads for given recurrence periods based on seismic hazard analysis, so that engineers can conduct the performance-based structural design by combining the level of seismic load and building's performance in case of earthquake.

By the way, the social requirement to secure safety against ground motions larger than ones given for specified recurrence period has risen since 2011 off the Pacific coast of Tohoku Earthquake. Though the current seismic design code can assure the performance against the ground motions specified, it is unknown that the performance will be maintained against the larger ground motion. Namely, there exists the residual risk as stated in Wenzel et al. [2] and Hayashi et al. [3].

This paper examines the method to obtain the seismic load based on the residual risk.

### SEISMIC LOAD BASED ON RESIDUAL RISK

Authors propose the procedure to determine the seismic load from the probabilistic seismic hazard curve (hereinafter called PSHC).

### Effect of Seismic Hazard Curve on Residual Risk

Figure 1 shows two PSHCs which give the identical seismic load  $x_R$  for a given annual exceedance probability  $p_R$ .

Since seismic load is identical to the building at site A and to one at site B, the capacity of the buildings are also same. However the annual exceedance probability of ground motion greater than  $x_R$  at site B is larger than one at site A, so that the residual risk of building at site B as also larger than one at site A.

It is concluded that "tail" of seismic hazard curve affects the residual risk. Namely, if "tail" is small, the residual risk is small, and vice versa.

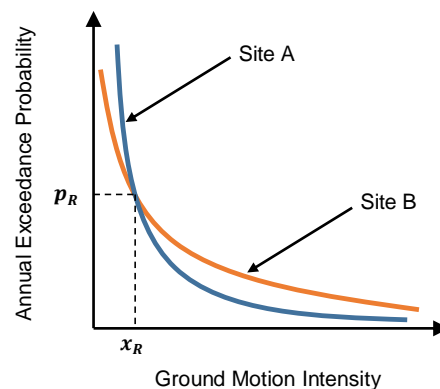


Fig. 1 Shape of PSHC and residual risk



## Seismic Load Considering “Tail” of PSHC

Since larger “tail” of PSHC gives larger residual risk, authors introduces the seismic load considering the shape of “tail”. Specifically, the seismic load corresponding to the centroid of “tail” is proposed, since the centroid is the representative variable of probabilistic distribution.

Let  $h(x)$  be annual probabilistic density function of ground motion. It is noted that seismic hazard curve  $H(x)$  is related to  $h(x)$  by Eq.(1).

$$H(x) = 1 - \int_0^x h(t)dt \quad (1)$$

Let the ground motion intensity corresponding to the centroid of “tail” be  $x_T(x_R)$  as given by Eq.(2).

$$x_T(x_R) = \frac{\int_{x_R}^{\infty} xh(x)dx}{\int_{x_R}^{\infty} h(x)dx} = \frac{1}{p_R} \int_{x_R}^{\infty} xh(x)dx \quad (2)$$

By the way, seismic hazard is often given by the seismic hazard curve  $H(x)$  rather than probabilistic density function  $h(x)$  as illustrated in Ebeling [4], so it is convenient to express  $x_T(x_R)$  by  $H(x)$ . Eq.(2) can be rewritten by Eq.(3)

$$x_T(x_R) = x_R + \frac{1}{p_R} \int_{x_R}^{\infty} H(x)dx \quad (3)$$

Eq.(3) is expressed by the area, which is surrounded by  $x$ -axis,  $y$ -axis, line that  $x = 1$ , and PSHC normalized by  $p_R$ , as illustrated by Fig. 2. In Fig.2, area “A” corresponds to ground motion  $x_R$ , and area “A+B” corresponds to  $x_T(x_R)$ .

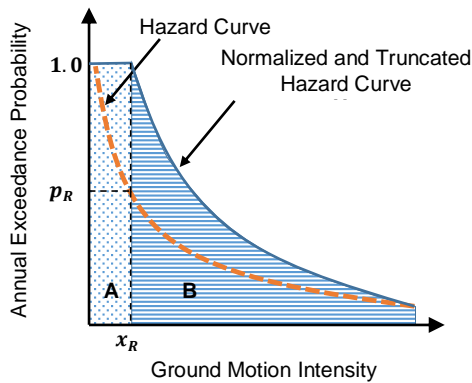


Fig. 2 Ground motion intensity derived from seismic hazard curve

## Seismic Hazard Analysis

In order to examine the characteristics of the shape of PSHC and increment of design seismic load, seismic hazard analysis was conducted.

### Analysis conditions

Seismic source zone model was established by using source zone database prepared by NIED [5]. In order to obtain time-independent result, Poisson's process was employed to characterize recurrence interval of characteristic earthquakes such as large active faults earthquakes and inter-plate earthquakes. (Hayashi et al. [6])

Kanno et al. [7] was referred as ground motion prediction equation. The peak ground acceleration (PGA) at engineering bedrock, where averaged shear velocity is 292m/s, was employed as ground motion parameter.

The locations of 47 sites are shown in Fig. 3. Each site is the prefectural capital.

### Results

For each site, calculated were ground motion intensity  $x_R$  corresponding to reference annual exceedance probability, ground motion intensity  $x_T(x_R)$  corresponding to the centroid of “tail” of seismic hazard curve, and increment of design ground motion intensity  $z(x_R)$ . It is noted that  $z(x_R)$  is given by the ratio of  $x_T(x_R)$  to  $x_R$ .

Figure 4 shows the ground motions in each site. From the figure it can be seen that ground motions in the sites located along the Pacific coast are larger than those in other sites, since the seismic hazards at the sites are affected by large earthquakes in Sagami trough and/or Nankai trough whose recurrence periods are about 500 years. The ground motion intensity at site #8 is the largest since the site is affected large earthquakes such as ones in Sagami trough, Ibaraki off shore earthquake, and so on. The tendency of  $x_R$  and  $x_T(x_R)$  are similar.

Figure 5 shows the increment of ground motion intensity for each site. It is apparent that the larger ground motion intensity  $x_R$  is, the smaller increment of ground motion intensity  $z(x_R)$  is.

This is because the area “B” in Fig.2 decreases with the increasing  $x_R$ . This suggests that employing small ground motion intensity for design may give large residual risk. Concretely, combination of large design load and large threshold is better than the combination of small design load and small threshold from the viewpoint of avoiding residual risk.

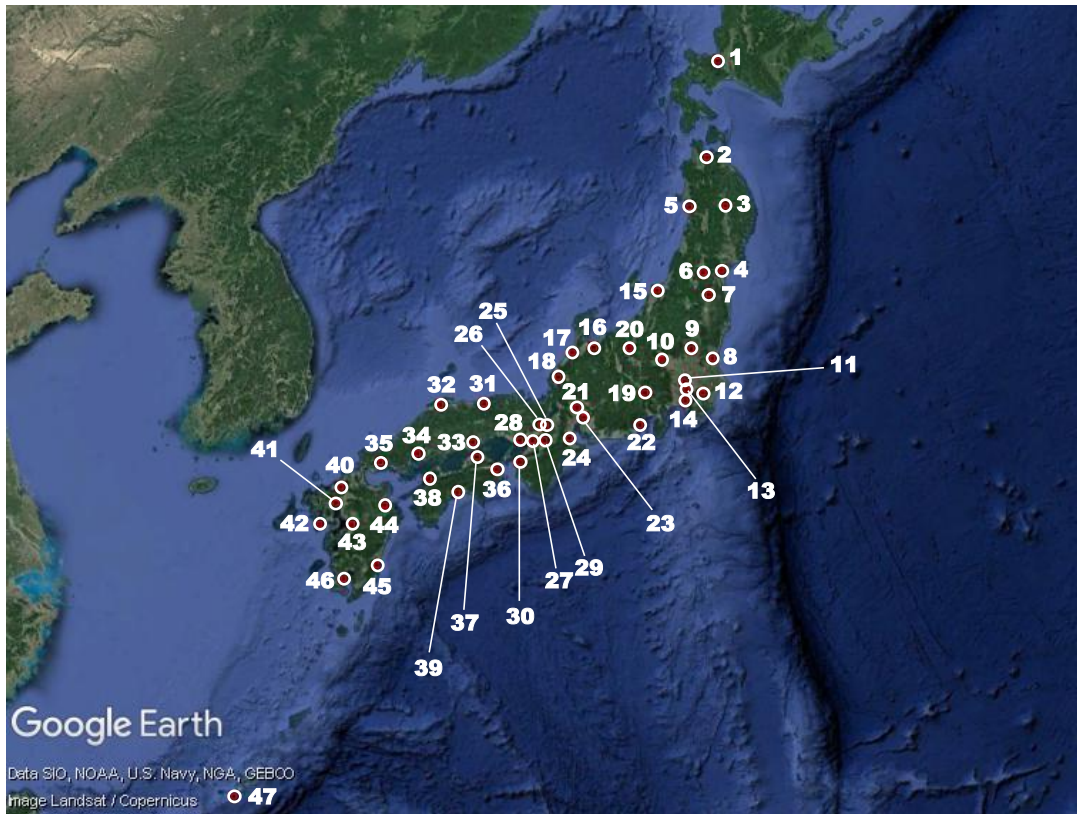


Fig. 3 Location of sites for seismic hazard analysis

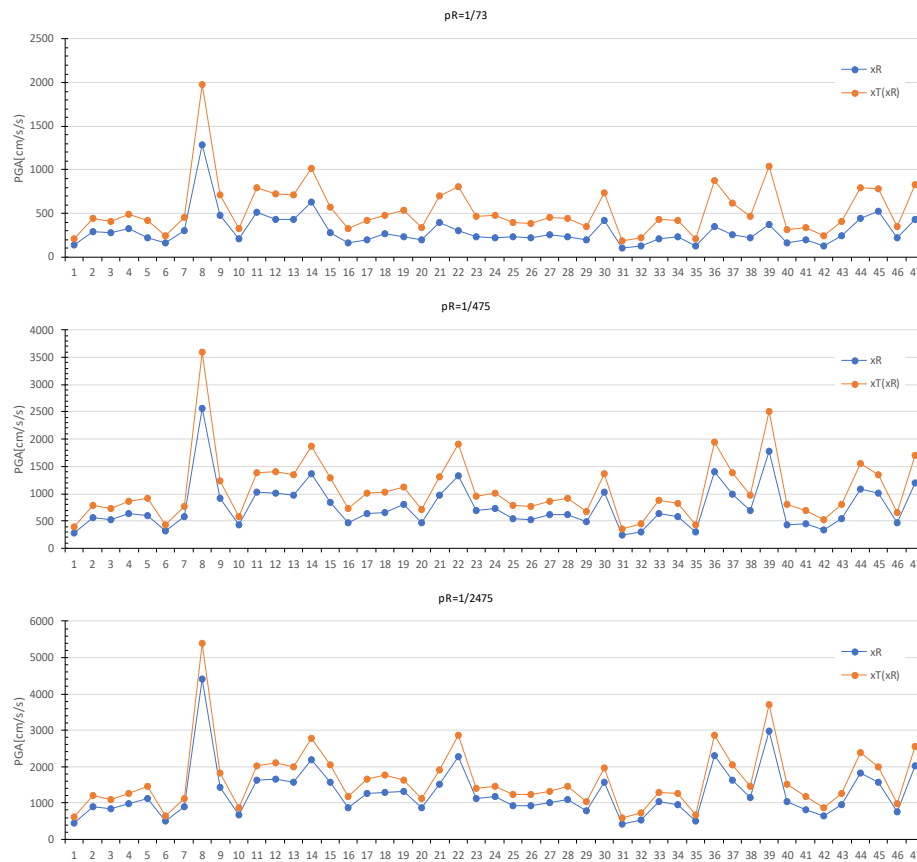


Fig. 4 Comparison of ground motion for given annual exceedance probability

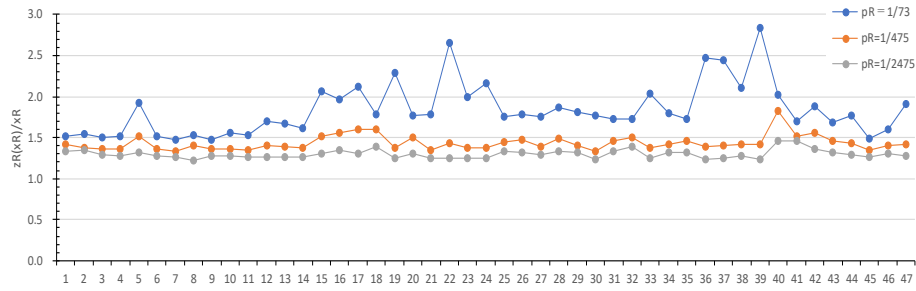


Fig. 5 Comparison of increment of ground motion for given annual exceedance probability

Table 1 summarizes  $x_R$ ,  $x_T(x_R)$  and their ratio  $z(x_R)$  corresponding to  $p_R$  of 1/475 for some sites. From the table it can be seen that the ratios  $z(x_R)$  for the sites located in the Pacific coast are small comparing with other site, since the seismic hazard of sites along the Pacific coast are dominated by large inter-plate earthquakes with high annual exceedance probability. On the contrary, other sites are dominated by large active faults.

Table 1 Design seismic loads for some major prefectural capital in Japan

| No | Pref.     | $x_R$ | $x_T(x_R)$ | $z(x_R)$ |
|----|-----------|-------|------------|----------|
| 1  | Hokkaido  | 272   | 386        | 1.42     |
| 4  | Miyagi    | 628   | 856        | 1.36     |
| 13 | Tokyo     | 968   | 1345       | 1.39     |
| 15 | Niigata   | 850   | 1293       | 1.52     |
| 23 | Aichi     | 694   | 957        | 1.38     |
| 27 | Osaka     | 623   | 868        | 1.40     |
| 34 | Hiroshima | 574   | 816        | 1.42     |
| 40 | Fukuoka   | 436   | 798        | 1.83     |

## QUANTIFICATION OF RISK

Authors proposed the seismic load  $x_T(x_R)$  considering residual risk in the previous section. This section examines the risks of buildings designed by  $x_R$  and  $x_T(x_R)$ .

### Seismic capacity of building

Authors employ fragility curve to express the capacity of building. The fragility curve is assumed to be log-normally distributed, so that two(2) parameters are needed to express the curve; median and log-normal standard deviation.

Though median of fragility curve is always greater than design seismic load by conservativeness in design, it is assumed that the median is identical to design load  $x_R$  or  $x_T(x_R)$  for simplicity. The log-normal standard deviation is set 0.4 in natural logarithm based on Fukushima and Yashiro [8].

### Definition of risk

Annual expected failure probability which is given from the seismic risk curve expressing the relationship between failure probability and annual exceedance probability as illustrated in Fig. 6. It is noted the annual expected failure probability can be given as an area surrounded by risk curve, x-axis and y-axis.

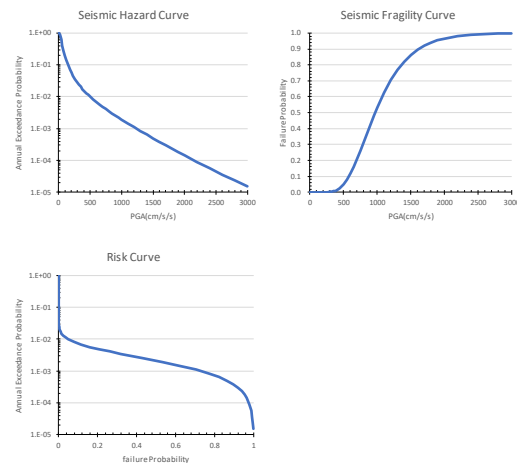


Fig. 6 Outline to obtain risk curve from PSHC and seismic fragility curve

### Calculation of risk

For some annual exceedance probabilities, the expected failure probabilities were calculated. Figure 7 shows the risks of two(2) types of buildings; one designed using  $x_R$ , and the other using  $x_T(x_R)$ . Since design load  $x_T(x_R)$  is greater than  $x_R$ , the risks of buildings designed using  $x_T(x_R)$  are smaller.

And it is remarkable that the scattering of risk along the sites is also smaller when  $x_T(x_R)$  is used as design load. In order to examine this tendency, the relationship between the increment of ground motion  $z(x_R)$  and the risk is arranged as shown in Fig. 8.

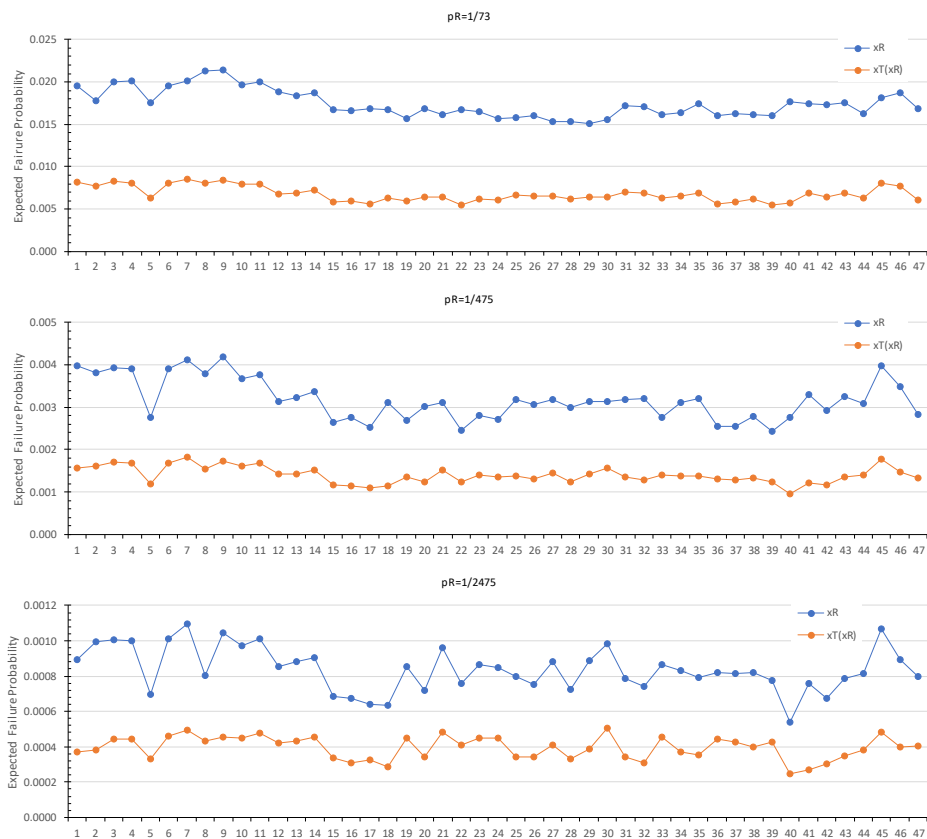


Fig. 7 Comparison of expected failure probabilities for given annual exceedance probability

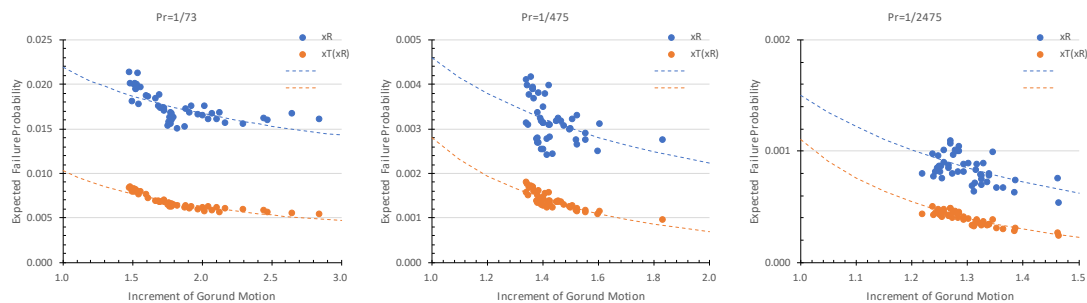


Fig. 8 Relationship between increment of ground motion intensity and expected failure probability

In the figure, also indicated by dashed line are the regression curves. So it is seen that scattering of expected failure probability around the regression curves is smaller in case that  $x_T(x_R)$  is used as design seismic load.

Table 2 summarizes the risks with the ratio  $z(x_R)$  for the major prefectures in Japan in case that buildings are designed by ground motion intensity when  $p_R$  is 1/475. It can be seen that the larger  $z(x_R)$  is, the smaller the risk is, if the buildings are designed by  $x_T(x_R)$ . However, such a tendency can be observed when the buildings are designed by  $x_R$ .

Table 2 Comparison of expected failure probability of major prefectural capital in Japan

| No | Pref.     | Ground Motion |            | $z(x_R)$ |
|----|-----------|---------------|------------|----------|
|    |           | $x_R$         | $x_T(x_R)$ |          |
| 1  | Hokkaido  | 0.398%        | 0.157%     | 1.42     |
| 4  | Miyagi    | 0.391%        | 0.170%     | 1.36     |
| 13 | Tokyo     | 0.324%        | 0.144%     | 1.39     |
| 15 | Niigata   | 0.265%        | 0.116%     | 1.52     |
| 23 | Aichi     | 0.245%        | 0.123%     | 1.38     |
| 27 | Osaka     | 0.319%        | 0.146%     | 1.40     |
| 34 | Hiroshima | 0.310%        | 0.139%     | 1.42     |
| 40 | Fukuoka   | 0.276%        | 0.096%     | 1.83     |

## CONCLUSION

Employing the seismic design load for the given exceedance probability is the rational way to realize the uniform performance in case of earthquake. However, the value is not always a good index since the effect of the “tail” of PSHC on the risk cannot be ignored, especially in case that large earthquake with low occurrence probability is dominant.

In order solve the problem above, authors proposed to employ the ground motion intensity corresponding to the centroid of “tail” of the probabilistic density function of ground motion intensity, where “tail” is defined as the portion greater than the ground motion intensity corresponding to the given annual exceedance probability. It was seen that less scattered risk is obtainable by introducing this new intensity.

Also derived was the monotonic relationship between the increment of ground motion intensity (ground motion intensity ratio)  $z(x_R)$  and the risk. This suggests the possibility to realize the setting of ground motion intensity by which the risk of the buildings will be uniform.

It is noted that above results are given on some assumption. For example, log-normal standard deviation of fragility curve is set 0.4, seismic load is identical to median of fragility curve, and so on. So authors will obtain robust conclusion through further numerical simulations. Identifying better index than  $x_T(x_R)$  is still of concern.

## REFERENCES

- [1] Architectural Institute of Japan, Recommendation for Loads on Buildings, AIJ, 2015. (in Japanese)
- [2] Wenzel et al., Measuring residual risk in earthquakes, Transaction of Second European Conference on Earthquake Engineering and Seismology, EAEE & ESC, 2014
- [3] Hayashi et al., Study on the Seismic Load Considering Residual Risk, Part1: Ground Motion Considering Residual Risk, Transaction of annual meeting of AIJ, AIJ, 2016. (in Japanese)
- [4] Ebeling, C. E., An Introduction To Reliability and Maintainability Engineering, McGraw-Hill, 2000.
- [5] National Research Institute for Earth Science and Disaster Prevention, Improved Seismic Hazard Assessment after 2011 Great East Japan Earthquake, Technical Note of NIED No.399, NIED, 2015. (in Japanese)
- [6] Hayashi et al., Study on Application of Uniform Hazard Spectrum into Seismic Design, Part1: Uniform Hazard Spectrum, Transaction of annual meeting of AIJ, AIJ, 2015. (in Japanese)
- [7] Kanno et al., A new attenuation relation for strong ground motion in Japan based on recorded data, Bulletin of Seismological Society of America, Vol.96, No.3. 879-897, 2006.
- [8] Fukushima, S., H. Yashiro, Seismic Risk Analysis on Portfolio of Buildings, Journal of Architecture, Planning and Environmental Engineering, No.552, 169-176, AIJ, 2002. (in Japanese)

# CONSTRUCTION OF DAMAGE FUNCTION FOR AN ANALYSIS OF THE ECONOMIC DAMAGE BY EARTHQUAKES WITH A FOCUS ON THE RECONSTRUCTION OF SHARED HOUSING

Norikazu Sakaba<sup>1</sup>, Yashiro Harumi<sup>2</sup>

<sup>1</sup>Tokio Marine & Nichido Risk Consulting Co., Ltd., Japan, <sup>2,3</sup> National Defense Academy of Japan, Japan

## ABSTRACT

Conventional economic housing damage estimation methods quantitatively estimate the damage amount from the structural damage of the building, cannot consider variability for the repair costs that the decision making of the victim gives it to. Therefore, in the assessment of economic housing damage, there is a concern that a large deviation may occur between the estimated value and the actual value. In this research, we will focus on what kind of system the governments or local government can build for the victims, and the quick rebuilding will be possible. Economic housing damage was estimated in line with the actual damage situation, in particular by considering the diversity of housing reconstruction methods for apartments. We focused on the damage states and restoration examples provided in the Act on Special Measures concerning Reconstruction of Condominiums Destroyed by Disaster, constructed a damage function in line with the actual situation by constructing a restoration pattern model for housing reconstruction of an apartment house. As a result of the earthquake simulation, we quantitatively showed that the diversity of housing reconstruction methods of collective housing gives a large variation to the damage amount. In addition, we showed that the current measures and measures that governments and local governments assumed were not sufficient, and pointed out the issues regarding effective measures and measures in the future.

*Keywords: Earthquake, Economic damage Analysis, Damage Function, Housing Reconstruction*

## INTRODUCTION

Many earthquakes that have taken place in recent years have been caused by inland active faults, including the Kumamoto Earthquake in April 2016, the Northern Osaka Prefecture Earthquake in June 2018, and the Hokkaido Eastern Iwate Earthquake in September 2018. Earthquakes caused by inland active faults have a smaller scale than trench-type earthquakes. When major local earthquakes occur near cities, there is a risk of great damage to the livelihoods of the local residents. For this reason, the government and municipalities implement damage estimation measures in advance in order to take measures for disaster prevention and mitigation. In estimating damage, the number of buildings that can be totally or partially destroyed is clarified. This information helps protect the lives of victims. Economic damage is monitored to help survivors of a disaster to restore their lives and to contribute toward the reconstruction of the economy. Economic damage may include direct damage to the building and the funds required for the reconstruction of damaged housing. In this study, economic damage is defined as the funds required for housing reconstruction. Using the number of totally and partially destroyed buildings, the economic damage analysis of the government and municipalities <sup>example</sup> <sup>1</sup> assumes that the rate of economic damage is 100% in the case of total destruction, and 50% in the case of partial destruction. However, in recent cases of

earthquake damage, buildings that were judged as being totally destroyed were restored, while buildings that were judged as partially destroyed were reconstructed. Since shared housing units have many unit owners, housing reconstruction is carried out based on diverse values, such as livelihood rehabilitation and asset formation. Accordingly, if economic damage is calculated mainly based on the structural damage of buildings, such as the current damage estimation, it is impossible to properly grasp the extent of funding necessary for the reconstruction of shared housing. The proportion of shared housing, especially in urban areas, is large. The economic forecast that is necessary for restoration and reconstruction of housing can be considered inadequate. Another issue is that the categories of total and partial destruction, which are assumed in the current damage estimation process, are not linked to the categories of damage that are used in various support systems that implemented by the government and municipalities. It is not possible to measure the funds required for various support systems quantitatively, because the mode of categorizing damage varies. Funding is necessary to provide various types of support. If planned reserves are not made, there is a risk that the support system may become bankrupt. To take disaster prevention and mitigation measures in the future, it is important to quantitatively indicate the reconstruction costs that may be required by the victims and the funding support that may be necessary for various support

Table. 1 List of building damage survey

| No. | Survey name  | Purpose   | Investigator               | Damage category name  |
|-----|--|---|----------------------------|---|
| 1   | Damage certification survey  | Issuance of disaster certificates                               | Municipality               | Partial destruction, large-scale partial destruction, and total destruction   |
| 2   | Damage survey  | Earthquake insurance  | Non-life insurance company | Partial loss, small and partial loss, large loss, and total loss  |
| 3   | Damage degree classification survey  | Understanding the degree of damage, judgment for continuous use | Architect                  | Insignificant damage, small damage, intermediate damage, large damage, and collapse                                     |
| 4   | Act on Disaster-Affected Condominiums  | Research for clarifying the causes of disaster                  | Researcher                 | Small damage, intermediate damage, large damage, collapse or partial damage, partial destruction, and total destruction |
| 5   | Research survey by the Architectural Institute of Japan and the Japan Society of Civil Engineers | Understanding the extent of damage                              | Municipality               | Partial damage, partial destruction, total destruction  |

Table. 2 Classification and criteria of the Act on Disaster-Affected Condominiums

| Unit                     | State  | Requirement                 | Condominium Ownership Act            | Act on Disaster-Affected Condominiums Buildings |
|--------------------------|--|-----------------------------|--------------------------------------|---|
| Total loss               | State in which the main part has disappeared, and the overall utility of the building has been lost from a social and economic viewpoint | Reconstruction              | Consent of everyone is required      | Consent of four-fifths is required              |
| Large-scale partial loss | In cases where the part corresponding to more than half the building price is lost   | Reconstruction              | Consent of four-fifths is required   |   |
|                          |  | Restoration                 | Consent of three-fourths is required |   |
|                          |  | Sale of building and site   | Consent of everyone is required      | Consent of four-fifths is required              |
|                          |  | Demolition and sale of site | Consent of everyone is required      | Consent of four-fifths is required              |
| Small-scale partial loss | In cases where the part corresponding to less than half the building price is lost   | Reconstruction              | Consent of everyone is required      | Consent of everyone is required                 |
|                          |  | Restoration                 | Consent of half of the people        |   |

systems.

In this study, we focus on the different kinds of economic disaster prevention and mitigation measures that the state and the municipalities can take in order to achieve speedy reconstruction. We review the evaluation of shared housing that provides an element of uncertainty in economic damage, and create a damage function by considering the diversity in the approaches toward the reconstruction of shared housing. The damage function should be created in harmony with the classification of various support systems, in keeping with the quantitative evaluation of each of these support systems. We also present an example of an economic damage analysis of an earthquake for Tokyo using the damage function so created.

## BUILDING DAMAGE AND RECONSTRUCTION

### Classification of Building Damage

After an earthquake, several surveys are conducted to understand the extent of damage to the building. There are various ways of detecting damage to buildings based on the purpose and the method used in the survey. Table 1 summarizes the main surveys conducted after a disaster and the categories of damage under each. As shown in the table, there are various categories for each survey,

and the names, definitions, and number of categories vary. Number 1 in the table is implemented relying on the Act on the Support for Reconstructing Houses of Disaster Victims and the Emergency Repair System. This legislation covers buildings ranging from total destruction to large-scale partial destruction, and the Emergency Repair System provides funding support in cases of total and partial destruction. Number 2 in the table is implemented while using earthquake insurance. In earthquake insurance cases, the insurance amount is paid for total and partial loss. Number 3 in the table is implemented when shared housing is affected and a resolution of reconstruction methods is carried out. The number of votes necessary to decide upon a reconstruction method and the resolution of reconstruction methods varies based on the category of damage. Numbers 4 and 5 are voluntary surveys of academic societies and municipalities. The survey is conducted in cases of total and partial destruction. The damage function used in the damage estimation by the government and municipalities has been created based on the results of this survey. Even if the degree of damage is the same, the names, definitions, and number of categories vary based on the surveyor. This estimation uses two categories, total and partial destruction, but these categories do not correspond to the categories for the investigations under the Act on Support for Reconstructing Houses of Disaster Victims, the



| Damage Ratio                                    | 0.0                            | 0.1                | 0.2                      | 0.3                           | 0.4 | 0.5                             | 0.6                      | 0.7          | 0.8 | 0.9        | 1.0 |
|---|--------------------------------|--------------------|--------------------------|-------------------------------|-----|---------------------------------|--------------------------|--------------|-----|------------|-----|
| Damage estimation                               | No Damage                      | Semi-destruction   |                          |                               |     |                                 | Total destruction        |              |     |            |     |
| Damage certification survey                     | No Damage/Insignificant damage |                    |                          | Partial-destruction           |     | Large-scale partial-destruction | Total destruction        |              |     |            |     |
| Damage survey                                   | No Damage                      | Partial damage     |                          | Small and partial-destruction |     | Large-scale partial-destruction | Total destruction        |              |     |            |     |
| Damage degree classification assessment         | No Damage                      | Partial damage     |                          | Small damage                  |     | Intermediate damage             |                          | Large damage |     | Collapse   |     |
| Emergency risk assessment                       | Safety                         |                    |                          |                               |     | Attention needed                |                          | Danger       |     |            |     |
| Act on Disaster-Affected Condominiums Buildings | No Damage                      | Insignificant loss | Small-scale partial loss |                               |     |                                 | Large-scale partial loss |              |     | Total loss |     |

Figure 1. Survey of damage and arrangement of damage category

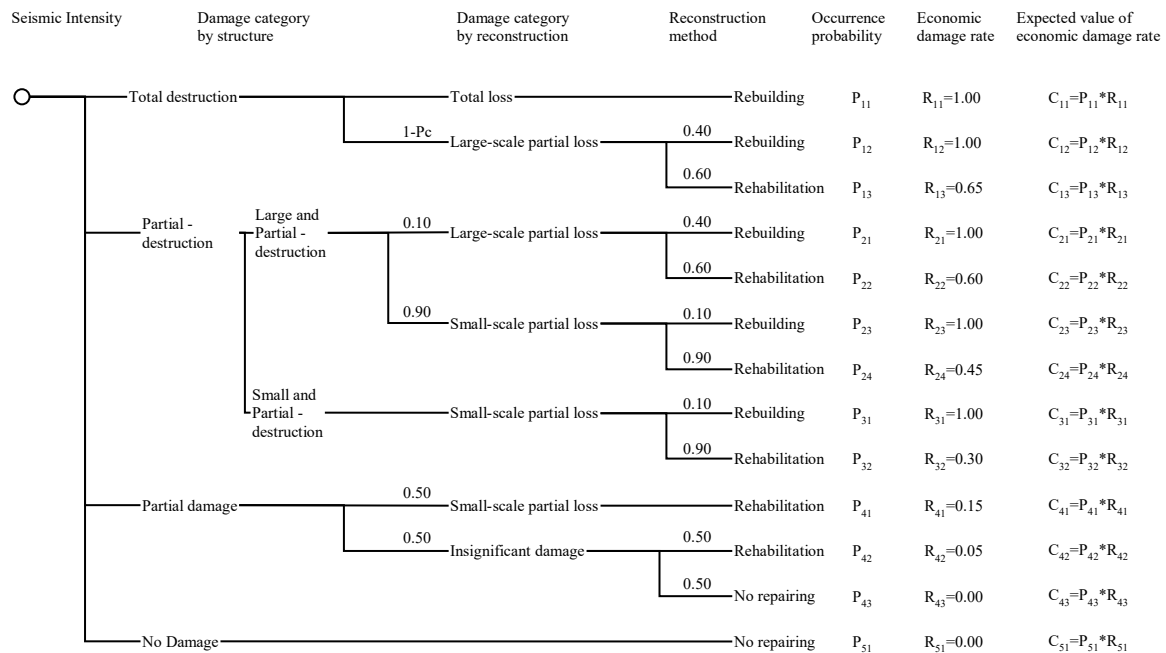


Figure 2. Event tree related to damages to shared housing

Emergency Repair System, and the earthquake insurance system. Therefore, it is not possible to quantify funds necessary for these support systems when different assumptions of damage are made. To estimate damage, it is necessary to set categories of damage that are consistent with various support systems.

### Housing Reconstruction Process

In case of damage to detached houses, decisions are made to reconstruct or restore such houses mainly for the purpose of the rehabilitation of livelihood. This judgment can be made by the owner of the building at his own discretion. However, when shared housing is damaged, the decision on whether to opt for reconstruction or restoration is made not only based on the rehabilitation of livelihood, but also on diverse values such as asset formation. This decision must be determined by the consensus of the unit owners since the building or site becomes a part of a condominium ownership

system. The decision to rebuild shared housing is provided by the Condominium Ownership Act of the Civil Code or the Act on Disaster-Affected Condominiums. Here, the Act on Disaster-Affected Condominiums applies only to shared housing damaged by large-scale disasters as specified by government decree. Table 2 shows the damage categories and criteria based on the Condominium Ownership Act and the Act on Disaster-Affected Condominiums.

As shown in the table, when shared housing is affected, it is divided into four categories: complete loss, large-scale partial loss, small-scale partial loss, and others (minor or no damage). Here, complete loss means that the utility of the entire building has been lost, and partial loss means that the utility is lost for some parts, but the utility as a whole is maintained. The loss of utility indicates the loss of utilization value and not market price. Among the partial losses, large-scale partial loss indicates a loss of more than half of the building price, and the small-scale partial loss indicates a loss of less than

half of the building price. The reconstruction resolution is different for each damage category, and it is necessary to proceed with each resolution according to the method of reconstruction. However, in these resolutions, it is difficult for the unit owners to arrive at a consensus. In the case of the Kumamoto earthquake, nearly half of the 18 shared houses that had applied for public funded demolition had difficulties in arriving at a consensus among the unit owners, and the need for demolition was not established sufficiently. In other words, the selection of the building reconstruction method varies widely among the unit owners as well. It is quite possible to take a decision on restoration instead of rebuilding when a large-scale partial loss occurs, and to take the decision of rebuilding instead of restoration when a small-scale partial loss occurs.

## DAMAGE FUNCTION FOCUSED ON RECONSTRUCTION OF SHARED HOUSING

### Event Tree

In the previous chapter, we showed the classification of building damage based on the housing damage survey and presented the process of reconstruction of apartment houses. In this chapter, we create a damage function based on the review of damage categories and the reconstruction method based on the Act on Disaster-Affected Condominiums. First, the differences in the economic damage rates of buildings in each damage survey are summarized in Figure 1. The economic damage rates shown in the figure are organized with reference to Okada et al. (1999)<sup>2</sup>. Damage assessment surveys used in damage certification and damage surveys used in earthquake insurance have four damage categories, although the category names are different. The economic damage rates assumed for each category are similar. On the other hand, the damage estimates implemented by the government and municipalities set two categories: total and partial destruction. Partial destruction in damage estimation includes partial destruction and large-scale partial destruction. Partial damage is not considered. The two main systems that can be used for housing reconstruction are livelihood rehabilitation support and earthquake insurance. The damage category set in the current damage estimation is not appropriate while considering the formulation of policies for measures and response for recovery and reconstruction from earthquake damage after the estimation of such damage. Therefore, we set four damage categories in this study: total destruction, large-scale partial destruction, small-scale partial destruction, and partial damage.

Next, we look at the method of reconstruction of houses. If a detached house is damaged, the reconstruction will be considered first with the goal

of returning it to the current status. Therefore, the funds required for housing reconstruction should correspond sufficiently to the degree of structural damage. In this study, following the earthquake insurance payment rate, the economic damage rate is set to 100% for total destruction, 60% for large-scale partial destruction, 40% for small-scale partial destruction, and 5% for partial damage. In the case of shared housing, it is necessary to determine the reconstruction method through discussions among unit owners. As seen in the previous chapter, in shared housing, various methods of housing reconstruction are selected based on the diverse values held by the unit owners. The funds required for housing reconstruction may show a response different from what the degree of structural damage requires. Therefore, in this study, we created a model of the damage function using the event tree as seen in Figure 2. After damage categorization based on the structure, we branched out the damage categories based on the Act on Disaster-Affected Condominiums. We also branched out the methods

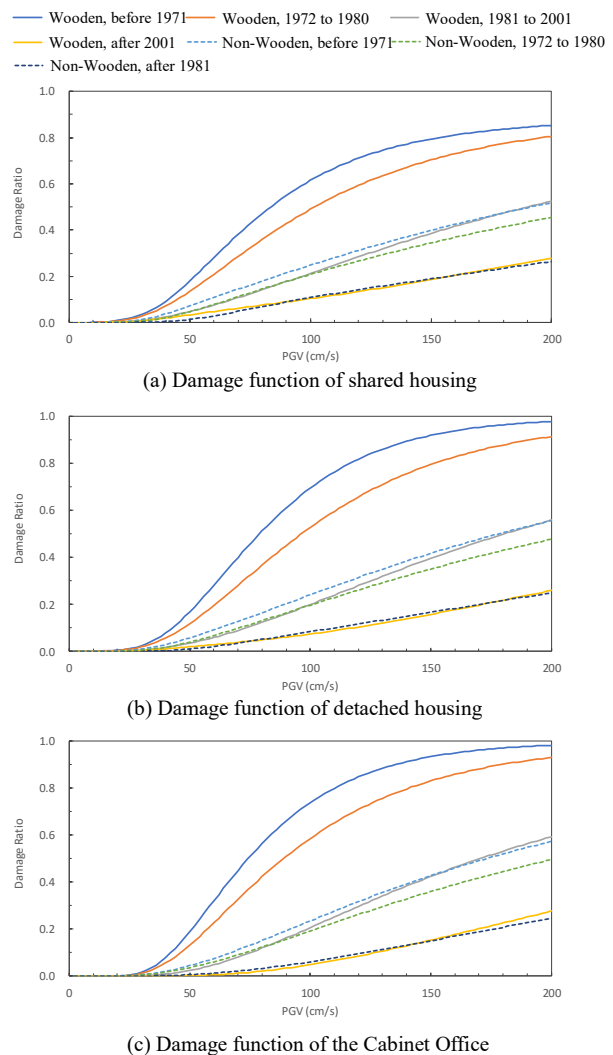


Figure 3. Damage function

Table 5. Number of households in Tokyo and asset amount data (number of households, 1 billion yen)

| Structure            |                  | Wooden      |         |           |           | Non-wooden  |         |           |           | Total     |
|----------------------|------------------|-------------|---------|-----------|-----------|-------------|---------|-----------|-----------|-----------|
| Building Age         |                  | Ancient old | Old     | New       | Subtotal  | Ancient old | Old     | New       | Subtotal  |           |
| Number of households | Shared housing   | 52,558      | 77,565  | 627,643   | 757,767   | 181,667     | 460,141 | 2,949,199 | 3,591,007 | 4,348,774 |
|                      | Detached housing | 254,013     | 281,379 | 1,313,299 | 1,848,691 | 5,456       | 7,209   | 53,621    | 66,285    | 1,914,976 |
|                      | Total            | 306,571     | 358,944 | 1,940,942 | 2,606,457 | 187,123     | 467,350 | 3,002,820 | 3,657,293 | 6,263,750 |
| Asset amount         | Shared housing   | 1,808       | 2,690   | 21,753    | 26,252    | 8,194       | 20,754  | 132,967   | 161,916   | 188,167   |
|                      | Detached housing | 6,836       | 7,573   | 35,345    | 49,753    | 211         | 279     | 2,077     | 2,568     | 52,321    |
|                      | Total            | 8,644       | 10,263  | 57,098    | 76,005    | 8,405       | 21,033  | 135,045   | 164,483   | 240,489   |

Table 6. Number of households damaged by the Tachikawa fault zone

| Structure             |                  | Wooden structure |         |           |           | Non-wooden structure |         |           |           | Total     |
|-----------------------|------------------|------------------|---------|-----------|-----------|----------------------|---------|-----------|-----------|-----------|
| Building Age          |                  | Ancient old      | Old     | New       | Subtotal  | Ancient old          | Old     | New       | Subtotal  |           |
| Proposed method       | Shared housing   | 33,855           | 50,334  | 330,375   | 414,564   | 106,846              | 197,996 | 1,027,438 | 1,332,279 | 1,746,843 |
|                       | Detached housing | 164,014          | 181,057 | 695,434   | 1,040,505 | 2,891                | 3,019   | 17,817    | 23,726    | 1,064,231 |
|                       | Total            | 197,870          | 231,391 | 1,025,809 | 1,455,070 | 109,736              | 201,014 | 1,045,255 | 1,356,005 | 2,811,075 |
| Cabinet Office method | Shared housing   | 25,796           | 36,374  | 79,365    | 141,535   | 37,128               | 70,374  | 190,441   | 297,943   | 439,479   |
|                       | Detached housing | 126,182          | 131,628 | 183,611   | 441,421   | 904                  | 1,061   | 3,202     | 5,167     | 446,587   |
|                       | Total            | 151,978          | 168,001 | 262,976   | 582,956   | 38,032               | 71,435  | 193,643   | 303,110   | 886,066   |

Table 7. Economic damage by the Tachikawa fault zone (billion yen)

| Structure             |                  | Wooden structure |       |       |          | Non-wooden structure |       |       |          | Total  |
|-----------------------|------------------|------------------|-------|-------|----------|----------------------|-------|-------|----------|--------|
| Building Age          |                  | Ancient old      | Old   | New   | Subtotal | Ancient old          | Old   | New   | Subtotal |        |
| Proposed method       | Shared housing   | 599              | 825   | 2,356 | 3,780    | 1,302                | 2,361 | 8,042 | 11,705   | 15,485 |
|                       | Detached housing | 2,449            | 2,420 | 3,605 | 8,473    | 26                   | 29    | 98    | 154      | 8,627  |
|                       | Total            | 3,048            | 3,245 | 5,961 | 12,254   | 1,329                | 2,390 | 8,140 | 11,859   | 24,112 |
| Cabinet Office method | Shared housing   | 570              | 770   | 1,563 | 2,903    | 994                  | 1,866 | 4,765 | 7,624    | 10,527 |
|                       | Detached housing | 2,596            | 2,613 | 3,388 | 8,597    | 25                   | 29    | 82    | 136      | 8,733  |
|                       | Total            | 3,167            | 3,382 | 4,951 | 11,501   | 1,019                | 1,895 | 4,847 | 7,760    | 19,261 |

of reconstruction that can be used after the classification of damage based on the Act on Disaster-Affected Condominiums. From this, we set it to select reconstruction and restoration even in cases of total destruction. We assumed that the branching probability  $P_c$  of total loss and large-scale loss after total destruction is the state where all buildings are lost, and no buildings exist. We adopted the damage grade of Okada et al. (1999)<sup>2</sup> and used the ratio of D5 level damage (equivalent to collapse) to D4 level damage or above (equivalent to total destruction.) We set other branching probabilities based on the relationship with the economic damage rate as seen in Figure 2. However, it may be possible to update the approach using statistical data such as damage results in the future.

### Damage Function

We create a damage function based on the event tree drawn up in the previous section. To create the damage function, it is necessary to define the damage rate function of total destruction, large-scale

partial destruction, small-scale partial destruction, and partial damage. In this study, the damage rate function for partial damage uses data from the Non-Life Insurance Rating Organization of Japan,<sup>4</sup> partial destruction and total destruction use data from the Cabinet Office on damage estimation.<sup>1</sup> Further, while dividing the partial destruction into large-scale and small-scale partial destruction, we use data on the number of damaged buildings for each damage category according to Nagao and Yamazaki (2011).<sup>3</sup> Using the ratio of the number of damaged buildings that were completely destroyed, largely partially destroyed and partial destroyed as indicated in the literature, we created a damage function of large-scale partial destruction by combining the damage functions of total and partial destruction. From the above, the damage function obtained is shown in Figure 3. The damage function used in the damage estimation of the Cabinet Office is also shown as a reference. From the figure, because of the diversity in the methods of reconstruction, the damage function of share housing has a damage rate that is

slightly larger than that of the detached houses and the Cabinet Office in areas where the seismic intensity is small, and the damage rate is smaller than that of detached houses and the Cabinet Office in areas where the seismic intensity is large.

## EXAMPLE OF ECONOMIC DAMAGE ANALYSIS

### Analysis Condition

Using the damage function created in the previous chapter, we try to determine the number of damaged households and the funds necessary for housing reconstruction. We evaluate Tokyo, which is densely populated with a large number of buildings, many of which are shared housing units. We make predictions assuming that an earthquake was caused by the Tachikawa fault, which has raised concerns of causing significant damage to Tokyo.

### Result of Analysis

Table 5 shows the number of households and the asset amount as a summary of the asset data for Tokyo. Table 6 shows the number of damaged households after damage estimation and Table 7 shows the prediction of the economic damage. The number of damaged households indicates the number of households affected by such damage. Tables 6 and 7 also show the results of the damage function as adopted by the Central Disaster Management Council of the Cabinet Office<sup>1</sup> for comparison.

Based on the results, the total number of damaged households in the proposed method is about 2.80 million, which is about 3.1 times more than the results of the Cabinet Office method. The proposed method considers the damage category of partial damage, but the Cabinet Office method does not consider this category. Instead, it considers partial destruction as a category. As a result of this difference, the number of damaged households in the proposed method has significantly increased. While looking at recent earthquake damage, although non-wooden buildings rarely result in complete or partial destruction, there are many cases in which partial damage has occurred. We think that using the proposed method can predict a number of damaged households that is closer to the actual situation.

Next, based on the results, the total economic damage of the proposed method is approximately 24 trillion yen, which is approximately 1.3 times the result of the Cabinet Office method.

The breakdown of economic damage was approximately 1.30 times for shared housing comprising wooden structures, 1.54 times for shared houses comprising non-wooden structures, 0.99 times for detached houses comprising wooden

structures, and 1.13 times for detached houses comprising non-wooden structures. As the main difference between the proposed method and the Cabinet Office method, we can say that shared housing takes into consideration the diversity of reconstruction methods and the damage cost because of partial damage, and also that detached houses take into consideration the damage cost because of partial damage. Shared housing is significantly affected when the diversity of reconstruction methods is taken into consideration.

## CONCLUSION

In the case of shared housing being affected by a disaster, housing reconstruction is selected according to the diverse values of unit owners. Therefore, the funds needed for reconstruction do not necessarily coincide with the degree of structural damage. Also, as shown in the case of the Kumamoto Earthquake, resolutions for the reconstruction and restoration of shared housing are complex and require a lot of time to rebuild. The reconstruction process is complicated when there are many options such as large-scale partial loss. It is necessary to take measures in advance so as not to interfere with rapid restoration and reconstruction.

In this study, we focused on the damage classification and reconstruction methods that are related to the Act on Disaster-Affected Condominiums, and created the damage function of shared housing by using the event tree of restoration. By using this damage function, economic damage analysis can be performed according to the actual condition of the restoration cost of buildings. We also used damage categories linked to the support system for the subsequent restoration and reconstruction measures and because of this, it is possible to evaluate the costs and effects required for various support systems, as well as to evaluate economic damage. In future studies, we plan to examine the sufficiency of the current support system, as well as effective measures and responses to these economic damages.

## REFERENCES

- [1] The Disaster Management in Japan Report, Cabinet Office Japan, 2013, [http://www.bousai.go.jp/jishin/syuto/taisaku\\_wg/](http://www.bousai.go.jp/jishin/syuto/taisaku_wg/)
- [2] Okada, S. and Takai, N. (1999). Classifications of Structural Types and Damage Patterns of Buildings for Earthquake Field Investigation, Journal of Structural and Construction Engineering, Vol. 524, pp.65–72 (in Japanese)
- [3] Nagao, T. and Yamazaki, F. (2011). Analysis of Building Damage in Kashiwazaki City due to the 2007 Niigata-Ken Chuetsu-Oki Earthquake, Journal of social safety science, Vol. 15, 2011, pp. 249-254

## GROUND SURVEY BASED ON THE DISTRIBUTION OF SURFACE WAVE VELOCITY AND ELECTRICAL RESISTIBILITY

Katsuyuki Kawai<sup>1</sup>, Ryosuke Hamada<sup>2</sup> and Koji Nakashima<sup>3</sup>

<sup>1,3</sup> Dept. of Civil and Environmental Engineering, Kindai University, Japan; <sup>2</sup> Toyo Construction Co., Ltd., Japan

### ABSTRACT

Geophysical exploration, which can explore the distribution of material properties underground, has, for less than the last half a century, been applied for prospecting groundwater and bedrock. Though simulation techniques have improved with greater sophistication of the constitutive model for soil material, comprehension of current soil conditions is important for accurately predicting the behavior of earth structures. Therefore, the importance of geophysical exploration is growing. Soil parameters are indirectly identified from physical parameters, such as wave velocity, electric conductivity and so on. In geophysical exploration, calibrating physical parameters with necessary soil parameters is required for individual soil material and has thus prevented the application of geophysical exploration at the site level. In this study, surface wave and electric prospecting were conducted at a site first investigated circumstantially by borings and other soundings. Then, the applicability of surface wave and electric prospecting were validated through their comparison. Next, geophysical explorations were conducted on a large-size embankment. Consequently, the applicable scope of this type of exploration was demonstrated, proving its applicability for geotechnical engineering sites.

*Keywords: Geophysical Exploration, Surface Wave Velocity, Electrical Resistibility, Embankment*

### INTRODUCTION

Recently, a constitutive model for soil has improved, and numerical computing techniques have become more sophisticated (e.g. Sugiyama et al., 2016). Therewith, numerical simulation has become more reliable in geotechnical engineering and has been used for designing and maintaining earth structures. When we conduct numerical simulation, the initial condition is needed. In the case of an existing earth structure, the current condition within the earth structure is the initial condition for simulation. Therefore, ground surveys, such as borings and soundings, are important. However, these ground surveys cannot be conducted at a fine scale due to economic constraints. Geophysical exploration is effective for knowing material properties of the ground through non-destructive inspection to develop in-depth cross-sectional information. On the other hand, in geophysical exploration, necessary soil

parameters, such as the N-value and soil moisture, have to be converted from elastic wave velocity and electric resistibility. These material properties are influenced by other soil parameters. Consequently, geophysical exploration is only used as a supplement.

In this study, surface wave and electric prospecting were conducted in ground first surveyed by borings and various soundings for calibration. Based on the calibration, geophysical exploration techniques were applied to a large-size embankment.

### GEOPHYSICAL EXPLORATION

#### Surface wave prospecting

When the ground is hit by a hammer, the surface wave, called a Rayleigh wave, is transmitted along the ground surface. A Rayleigh wave has more vertical vibration and 0.9 to 0.95 times velocity of a shear wave. Since the energy of vibration occurs

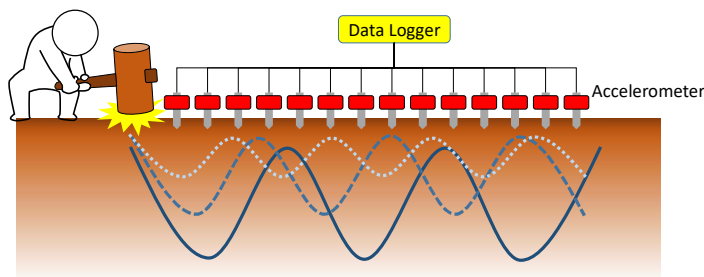


Figure 1 Surface wave prospecting



Photo 1 Surface wave prospecting

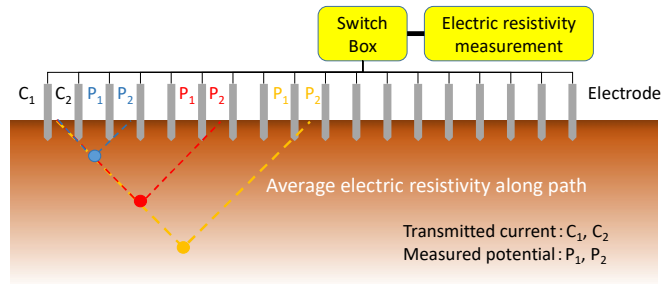


Figure 2 Electric prospecting



Photo 2 Electric prospecting

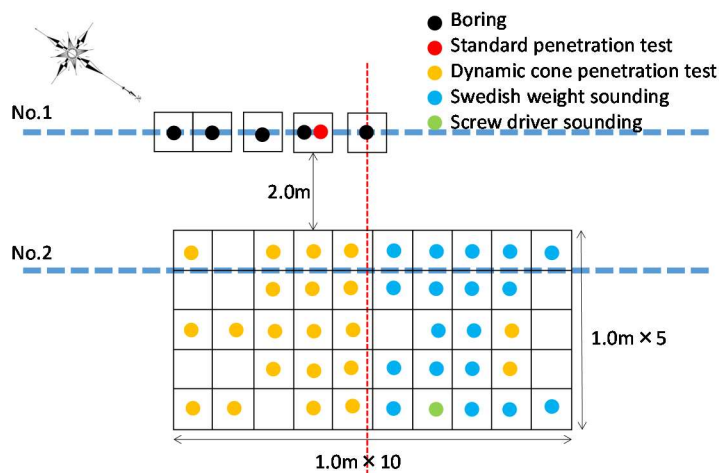


Figure 3 Location of borings and soundings

mostly at the ground surface and dampens with depth, shear wave in shallower depth than wavelength can be measured. With surface wave prospecting, we can know the distribution of shear wave velocity within the ground by catching waves with accelerometers aligned on the ground surface (as in Figure 1 and Photo 1). All wave shapes measured by each accelerometer are applied to frequency analysis, and the relationship between phase velocity and frequency are obtained (Park, 1999). It is said that the shear wave velocity correlates well with the stiffness of soil material and that it is applicable for estimating ground properties. Various correlation equations between the shear wave velocity and N-value have been proposed. Imai and Tonouchi (1982) proposed the following equation.

$$N = \left( \frac{V_s}{97} \right)^{\frac{1}{0.314}} \quad (1)$$

Here,  $N$  is the N-value obtained from the standard penetration test, and  $V_s$  is shear wave velocity (m/s).

### Electric prospecting

The potential response on the ground surface is generated by passing an electric current through the ground. In electric prospecting, the distribution of

| Level (m) | Thickness (m) | Soil           |
|-----------|---------------|----------------|
| 0.00      | 0.90          | Gravel         |
| 0.90      | 1.70          | Silty sand     |
| 1.80      | 1.90          | Sandy silt     |
| 3.70      |               | Silt           |
| 5.60      | 4.70          | Gravel         |
| 10.30     | 5.30          | Silt           |
| 15.60     | 5.30          | Silt           |
| 20.90     |               | Sand with silt |
| 26.20     | 5.30          | Sandy silt     |
| 31.50     | 11.40         | Silty clay     |
| 42.90     | 11.40         | Silty clay     |
| 54.30     | 11.40         | Clay with silt |
| 65.70     | 11.40         | Clay with silt |
| 77.10     | 11.40         | Clay with silt |
| 88.50     | 11.40         | Clay with silt |
| 100.00    | 11.40         | Clay with silt |

Figure 4 Stratigraphic column

electric resistivity can be identified from this potential response (as in Figure 2 and Photo 2). The apparent electric resistivity can be calculated by attenuation from the potential difference between transmission electrodes ( $C_m$ ,  $C_n$ ) to the potential difference between receipt electrodes ( $P_m$ ,  $P_n$ ). Here, apparent electric resistivity means average electric resistivity along the path from transmission electrodes to receipt electrodes. The distribution of true electric resistivity can be obtained by back analysis. The finer electrodes are aligned, the higher the resolution of the electric resistivity distribution that can be obtained. The obtained electric resistivity reflects porosity, soil moisture, mineral content, temperature and so on. Electric resistivity is said to correlate to soil moisture in homogeneous material ground.

### COMPARISONS OF GEOPHYSICAL EXPLORATION WITH BORINGS AND SOUNDINGS

To verify the results from geophysical exploration, surface wave and electric prospecting explorations were conducted at a centrally located site in Osaka city. There, detailed ground surveys, including five borings and various soundings, were conducted. Figure 3 shows the locations of the ground surveys. Here, the dynamic cone developed by some

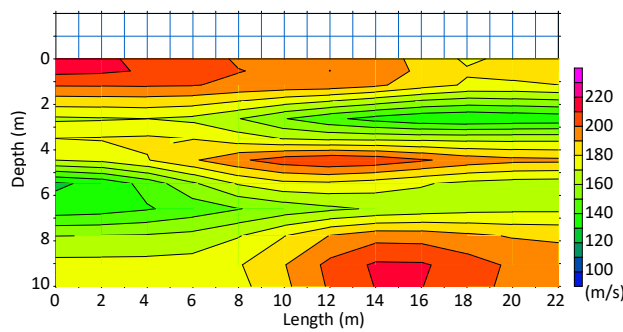


Figure 5 Shear wave velocity distribution (Line No.2)

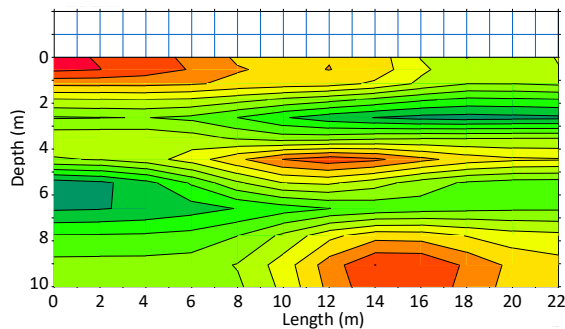


Figure 7 N-value distribution (Line No.2)

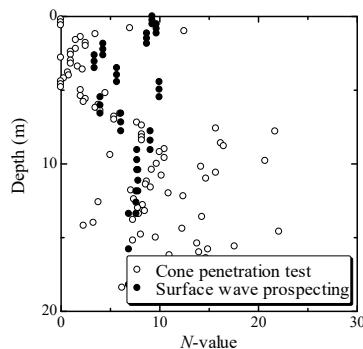


Figure 9 Comparison with a cone penetration test

companies was included and their specifications are various. Both the surface wave and the electric prospecting were conducted along survey Lines No.1 and No.2 shown in Figure 3. Figure 4 shows the stratigraphic column obtained from one boring. It indicates a thick alluvial clayey soil layer under an alluvial sandy soil layer near the ground surface. Diluvial sand and clay layers repeatedly appear under the alluvial layer, and this ground exhibits West Osaka's typical plain stratigraphy. The groundwater level appears around 2.0m deep.

Figure 5 shows shear wave velocity distribution obtained from surface wave prospecting along Line No.2. The green areas indicate small wave velocity and low stiffness. On the other hand, red areas indicate relatively higher stiffness. In this site, PS logging was conducted at one boring hole. The results of PS logging and surface wave prospecting are compared in Figure 6. A similar tendency can be seen

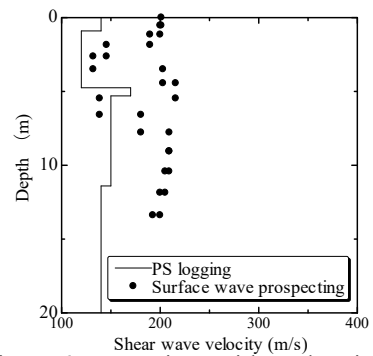


Figure 6 Comparison with PS logging

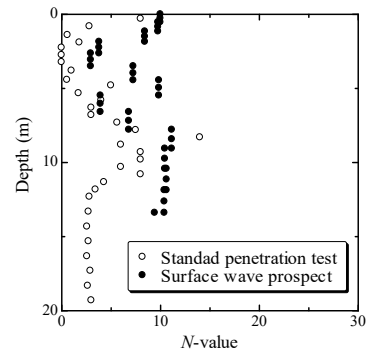


Figure 8 Comparison with a standard penetration test

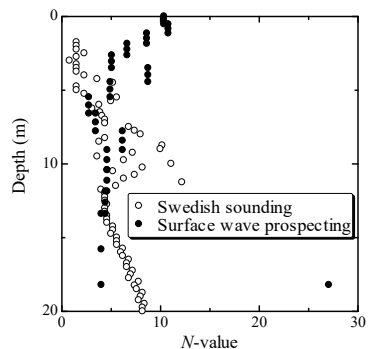


Figure 10 Comparison with Swedish sounding

near the ground surface. It is generally said that surface wave prospecting is applicable until 15m deep. Moreover, the results from PS logging show 2 to 3 times of the results from surface wave prospecting. This is because the shear wave velocity can be directly obtained from PS logging, while shear wave velocity is converted from Rayleigh wave velocity in surface wave prospecting. In soundings, the ground stiffness is expressed by the N-value. Figure 7 shows N-value distribution calculated from Figure 5 by equation (1). Figures 8, 9 and 10 show comparisons of the N-value expressed in Figure 7 with the N-value obtained by each of the soundings. They show good agreement. However, as seen in the comparison with PS logging, some difference between surface wave prospecting and soundings appear, and surface wave prospecting is applicable only at depths shallower than 10m.

In electric prospecting, measurable area and



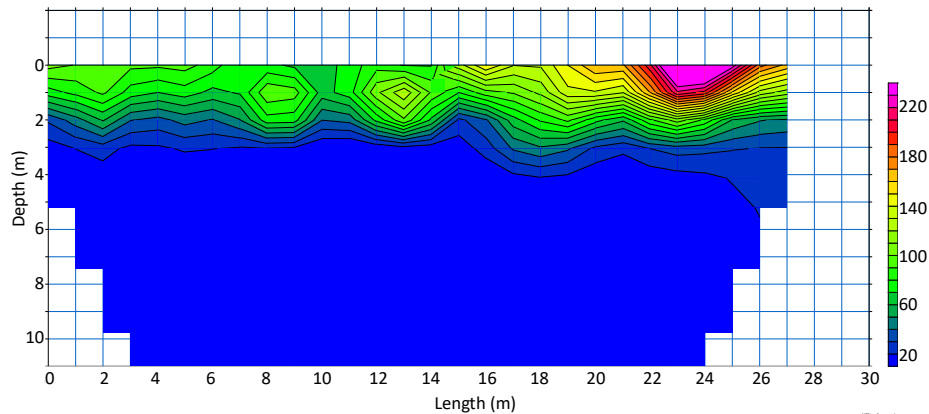


Figure 11 Electric resistivity distribution with Pole-Pole Array (Line No.2)

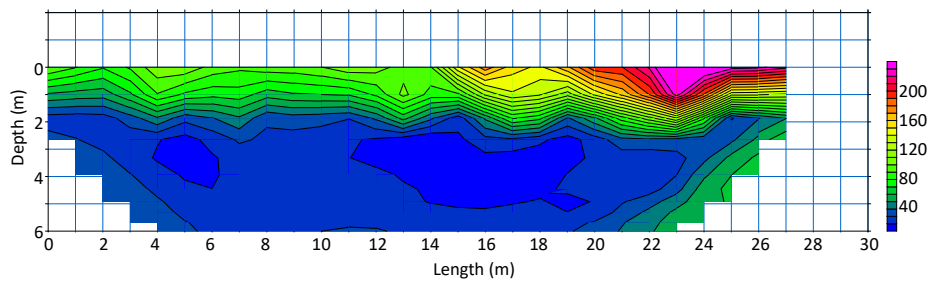


Figure 12 Electric resistivity distribution with Dipole-Dipole Array (Line No.2)

resolution is dependent not only on electrode separation but also on the array of transmission and receipt electrodes. Here, electrodes were placed 1.0m apart. Both the two-electrode method (Pole-Pole Array) and the four-electrode method (Dipole-Dipole Array) were applied as electrode alignment. It is said that relatively deeper ground can be explored with Pole-Pole Arrays and that Dipole-Dipole Arrays show higher resolution. Moreover, when we apply a Pole-Pole Array, two reference potential points are needed, and two electrodes are placed at 5 times the maximum measurement length apart from the measurement line. Figures 11 and 12 show the electrical resistivity distribution obtained from the Pole-Pole Array and the Dipole-Dipole Array, respectively. The bluer area shows lower electrical resistivity. In this site, the groundwater level is about 2.0m deep. The contour of  $40\Omega\cdot\text{m}$  electrical resistivity corresponds to the groundwater level. As detailed before, the electrical resistivity depends not only on soil moisture but also on mineral and ionic contents. However, differences in soil properties apparent deeper than the groundwater level in Figure 4 cannot be identified. We can say that soil moisture is a dominant factor for electrical resistivity in this site. Moreover, though the water pressure distribution, indicating existence of perched groundwater, was found in borings, it cannot be found in the electrical resistivity distribution. The difference between Figures 11 and 12 is not large, and both arrays are applicable for the site condition.

Though geophysical explorations, surface wave

and electric prospecting exhibit some differences from soundings, they show good agreement qualitatively. Because of this, we can say that they are effective for comprehensively characterizing relatively shallow ground.

#### APPLICATION OF GEOPHYSICAL EXPLORATION FOR EMBANKMENT

To test the applicability of geophysical exploration to embankment, surface wave and electrical prospecting were conducted at a large earthmoving construction site. Figure 13 shows the geography of the site and the locations of geophysical exploration. Lines a, b and c are located in what was originally a valley area and surrounding a sand basin for construction. In this area, a 40m high embankment was constructed. Lines d and e are in a cut area and on the construction site access road. The surface wave

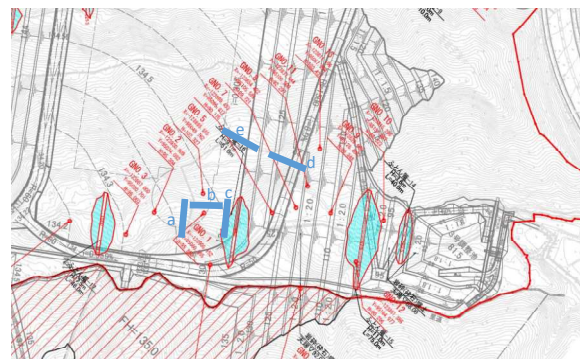
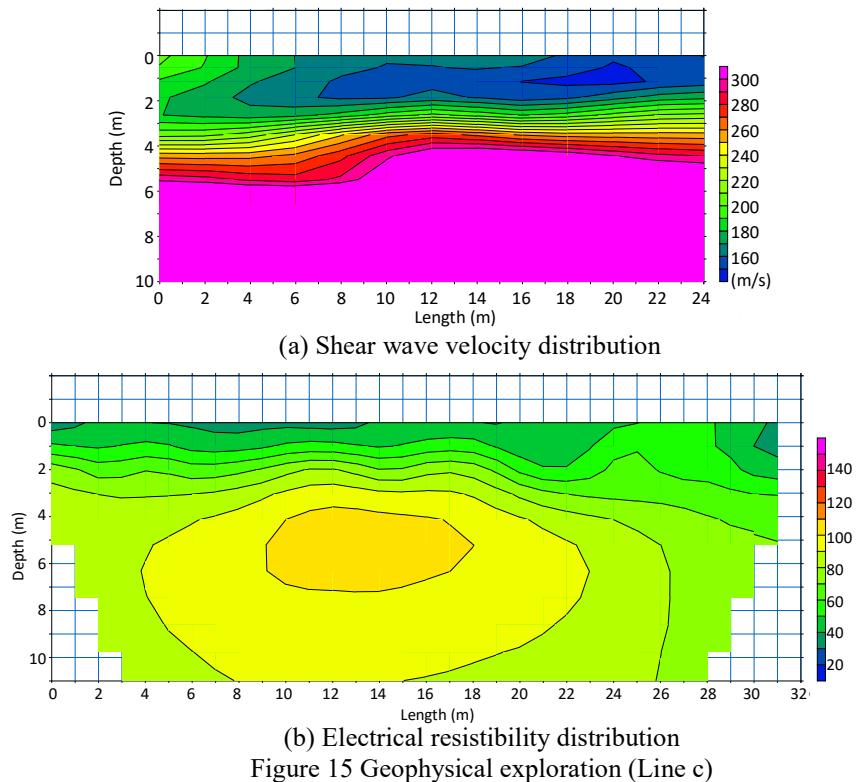
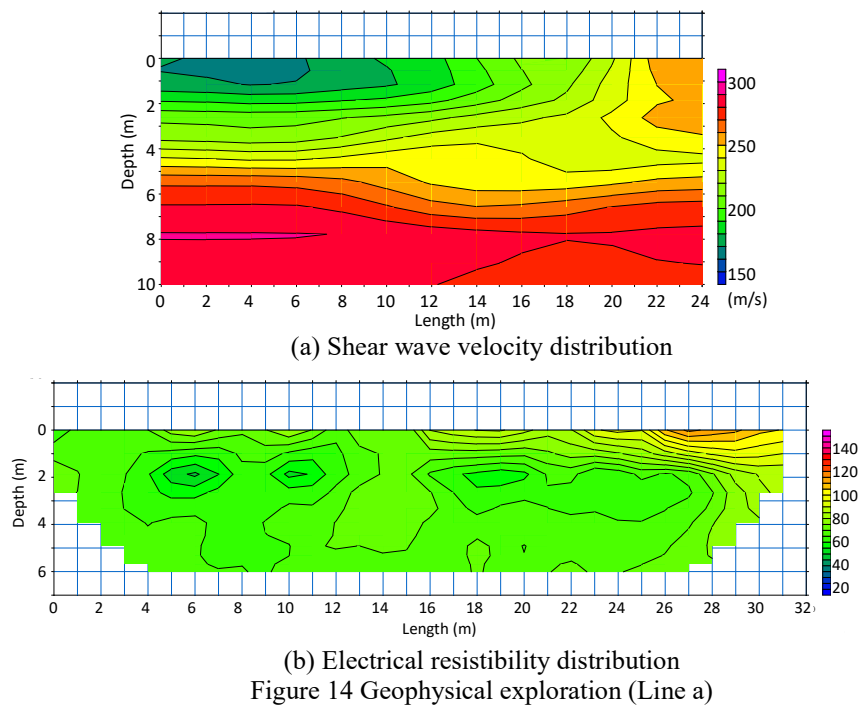


Figure 13 Construction site and exploration lines



prospecting was conducted in September 2018, and the electric prospecting was conducted in November 2018. The embankment was built up to 5m high around the sand basin at the time of the surface wave prospecting. As the construction progressed afterwards, the embankment had reached 10m high at the time of the electric prospecting. Figures 14 and 15 show results of geophysical exploration in Line a and c, respectively. Redder areas indicate that higher

shear wave velocity and higher stiffness exists at depth. A shear wave velocity of 250m/s can be converted to an N-value of 20. If this is regarded as the boundary between embankment material and original ground, then it corresponds to about 5m depth for both Lines a and c, showing good agreement with the actual construction process. Moreover, in this site, the valley is inclined from the left to the right side of Figure 13. Therefore, the embankment of Line

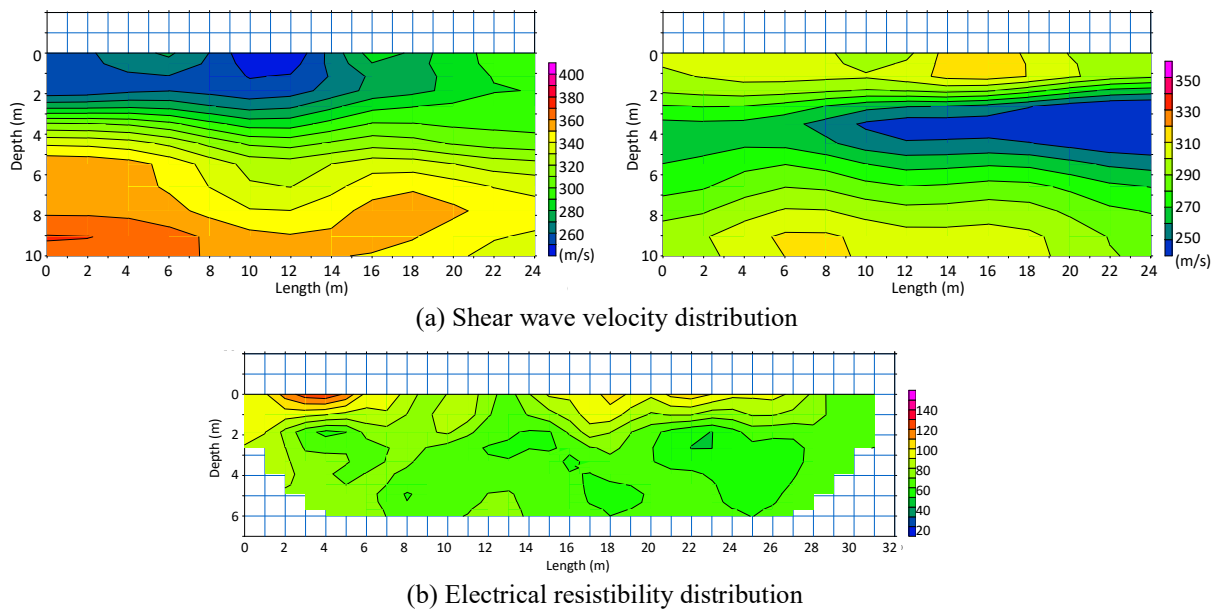


Figure 16 Geophysical exploration (Line e: left and d: right)

a is thicker than that of Line c, and this difference is captured in the results of surface wave prospecting. Considering the construction process, the exploration area for the electric prospecting, shown in Figure 14 (b) and 15 (b), indicate an embankment area. Kawai et al. (2017) monitored soil moisture distribution of embankment and clarified seepage behavior within embankment. They said that water contained in embankment material redistributes due to potential head difference within embankment after construction and that it finally forms the phreatic surface at the bottom of the embankment. The electrical resistibility shown here indicates the redistribution process of water within embankment. The difference in electric resistibility between Lines a and c can be regarded as the difference in time elapsed during construction.

Figure 16 shows the results of geophysical exploration conducted in Lines d and e. This area is a cut slope. Therefore, fairly high shear wave velocity distributions are seen. The minimum shear wave velocity in the exploration area is 250m/s, and this corresponds to the boundary between embankment and original ground, as shown in Figure 14 and 15. The results of electric prospecting illustrate the tendency of higher electrical resistibility at depth. This tendency is more apparent than in Lines a and c.

Consequently, it appears that geophysical exploration can express the ground conditions of the construction process well, and it is applicable for ground surveys.

## CONCLUSIONS

In this study, investigating the applicability of geophysical explorations to embankment, surface wave and electric prospecting were conducted at a site investigated in detail by borings and various

soundings. In addition, applicability was also investigated at a huge earth moving construction site. Consequently, the following conclusions were determined:

- (1) Comparing the results of geophysical exploration with borings and soundings found good agreement. However, limits in the measurable area of the geophysical exploration were discovered. In the case of surface wave prospecting, the applicable limit is about 10m depth from the ground surface.
- (2) Electric prospecting shows good agreement with the groundwater level. However, it only indicates soil moisture and cannot resolve pressure differences within saturated ground, such as those caused by perched groundwater.
- (3) Geophysical exploration can express the process of embankment construction.

## REFERENCES

- [1] Sugiyama, Y., Kawai, K. and Iizuka, A., Effects of stress conditions on B-value measurement, *Soils and Foundations*, Vol.56, No.5, 2016, pp.848-860.
- [2] Imai, T. and Tonouchi, K., Correlation of N-value with S-wave velocity and shear modulus, *Proc. of the second European symposium on penetration testing*, 1982, pp.67-72.
- [3] Kawai, K., Hazama, D. and Nose, R., Behavior of the air phase within embankment due to rainfall, *Proc. of 2nd PanAm-UNSAT2017*, 2017, pp.1-10.
- [4] Park, C. B., Miller, R. D. and Xia, J., Multichannel analysis of surface waves, *Geophysics*, 64, 1999, pp.800-808.

## BASIC STUDY ON BRIDGE WEIGH-IN-MOTION USING OPTICAL FLOW ANALYSIS

Kouichi Takeya<sup>1</sup>, Junji Yoshida<sup>2</sup>

<sup>1,2</sup> Faculty of Engineering, Graduate School, University of Yamanashi, Japan

### ABSTRACT

Understanding traffic loads on bridges is essential since traffic-induced vibration is a primary factor of damage in bridge structures. Bridge Weigh-in-Motion (B-WIM) is a method to measure vehicle axle loads by inverting the analysis of bridge structural responses. In various studies into B-WIM, the influence line of girder deflection and strain were mainly used and obtained results, especially on highway bridges. However, the accuracy decreased on regular road bridges since vehicle speeds are variable on bridges due to traffic conditions. In this study, optical flow analysis was applied using a video camera to precisely measure the location of vehicles on a bridge. A foreground mask using the Gaussian mixture model and a Kalman filter was then applied to identify the vehicles. Using results of measurements on a road bridge, first, an influence line of girder deflection was estimated considering vehicle locations for the initial calibration. The deflection responses of local buses and passenger vehicles were used in the initial calibration. Next, the vehicle axle loads were analyzed by monitoring the location of vehicles using the video camera. Compared with conventional methods, which estimate vehicle locations from average speeds, the proposed method has demonstrated higher adaptability in variable traffic conditions.

*Keywords: Bridge, Bridge Weight-In-Motion, Optical flow, Variable speed*

### INTRODUCTION

Monitoring bridge traffic is critical to bridge maintenance since heavy or overloaded vehicles cause significant impact to bridge deterioration. Static weigh stations have thus been installed for monitoring the weight of vehicles, especially on highways. However, these static weigh stations have disadvantages of interrupting regular traffic and measuring costs.

Bridge Weigh-in-Motion (B-WIM) is a method to determine the weights of vehicles traveling on bridges by using the dynamic response of bridges. B-WIM can be securely implemented without interrupting regular traffic, since B-WIM is installed under existing bridges and installation work is not required on traffic lanes. The concept of B-WIM was introduced as a feasibility study for an agency within the U.S. Department of Transportation (the Federal Highway Administration) by Moses in 1979 [1]. The definition of the influence line, which is the structural response of bridges proportional to the magnitude and position of loads, was used to calculate vehicle axle weights. Other B-WIM methods, such as the influence area method [2] and the reaction force method [3], have also been developed for several decades. B-WIM performs calibration by running a weight-known reference vehicle. However, calibration is periodically required since structural response changes due to bridge deterioration and environmental changes and so costs the organization of the reference vehicles.

Technical problems in many B-WIM approaches include weight estimation errors when the vehicle speed is variable, since the vehicle traveling speed is assumed constant in the calculation of vehicle weights. Moreover, in the calculation of influence lines, approximation is often based on numerical analysis and beam theory from the structural response when the test vehicle is traveling, but it has been noted that accuracy can be further improved if influence lines that are based on actual measurements can be used. O'Brien et al. proposed a method to calculate the influence line from direct strain measurements [4]. The difference between the two curves, the measured strain and influence line, is minimized using the least squares method to obtain the axle loads of traveling vehicles.

However, a disadvantage of the aforementioned B-WIM algorithms is an assumption of constant vehicle speed. Vehicles travel at a non-constant speed on bridges, in congested urban areas, or near intersections or traffic lights. To address this issue, Takeya et al. proposed a method to measure the positions of traveling objects by analyzing video images and applying a basic B-WIM using structural responses of peak deflection [5]. Andrew et al. proposed a correction method to B-WIM to adapt non-constant vehicle speed by a re-sampling process [6].

In this study, a new B-WIM using video images and deflection responses was devised, and it performs calibration using local buses and regular traffic vehicles. In particular, local buses can be treated as

reference vehicles in the calibration process, as these vehicle types are easy to identify and are relatively heavy. In addition, it is possible to recreate a system which adapts to various traffic conditions such as variable traveling speed by using video images. In this study, axle weights were calculated from deflection measurements and the analysis of video images of traveling vehicles on an existing bridge.

## CALCULATION OF INFLUENCE LINE USING REGULAR TRAFFIC RESPONSE

### Target Bridge and Measurement Instruments

The target bridge is a general road bridge of nine continuous simple steel girders and RC decks, located in Kofu City, Yamanashi Prefecture, Japan. The cross-section of the bridge is shown in Fig. 1. The length of each span is ten meters. Figure 2 shows the target bridge and the installation of measurement instruments. The deflection at the center of the second girder was measured with a laser displacement meter (Keyence, LK-500) installed on a tripod (Fig. 3). The measured deflection was recorded by the data logger (Keyence, NR-HV04). The frame size and frame rate of the video camera (Sony, FDR-AX55) were 1080p and 30 fps respectively.

### Vehicle Detection with Optical Flow Analysis Based on Background Subtraction Algorithm

To date, the authors have constructed a method for tracking objects in video images using a stationary camera and acquiring their locations [5]. This study improves the previous method by detecting multiple vehicles on bridges using a Kalman filter.

### Motion-Based Object Tracking

Motion-based object tracking is divided into three parts:

- 1) detecting moving objects in each video frame;
  - 2) associating the detections corresponding to the same object over time; and
  - 3) calculating the location of each object over time.
- MATLAB 2016b was used for this analysis.

The detection of moving objects uses a background subtraction algorithm based on the Gaussian mixture model. To determine whether individual pixels are part of the background or the foreground, a foreground mask using the Gaussian mixture model compared a grayscale video frame to a background model. The parameters used in the background subtraction algorithm using the Gaussian mixture model are shown in Table 1 and Table 2. Sixty or more video frames were used for initial learning of the background. Clouds tended to be noise in the background subtraction. Therefore, the learning ratio for adapting the background subtraction to the

changes in background and the number of Gaussian modes was manually tuned, as shown in Table 1. The image erosion and morphological operations were applied to the resulting foreground mask to eliminate noise. Table 2 shows the tuned parameters of these noise canceling filters.

Second, blob analysis detects groups of connected pixels, which are likely to correspond to vehicles. The association of detections to the same object is estimated by a Kalman filter [7]. The Kalman filter is used to predict the location in each frame and determine the likelihood of each detection being assigned to each track. If an object is detected, the Kalman filter first predicts the objects state in the current video frame. In this study, constant velocity is assumed for prediction. The filter uses the newly detected location to correct the state, producing a filtered location. Finally, the location of each moving

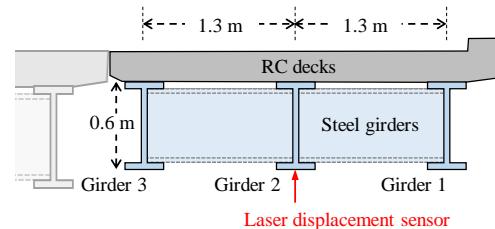


Fig. 1 Cross section of the target bridge and the measuring point of the deflection

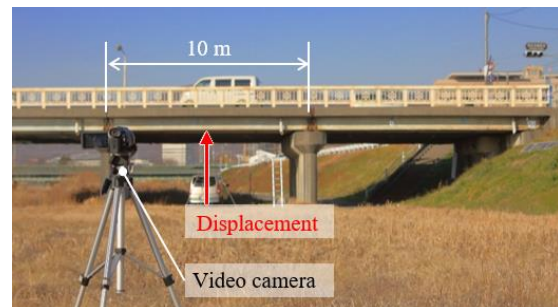


Fig. 2 Target bridge and installation of the video camera

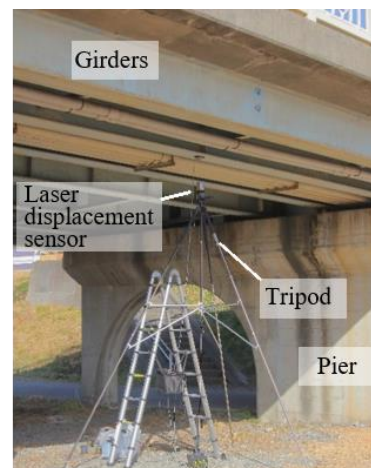


Fig. 3 The target bridge and measuring equipment for the deflection of bridge



object is calculated. Figure 4 shows how the location of the vehicle and axle were defined. First, the detected blob of the vehicle is enclosed in a bounding box, and the center position of the vehicle is obtained using the front and rear positions. Next, all axle positions are manually selected from each detected vehicle image, and the locations of the axles are calculated. An example of an analysis result is shown in Fig. 5. In this study, the location start point is the edge of the second span of the target bridge. After automatically extracting the center position of the vehicle, the time history data of the axle location is

Table 1 Parameters of the Gaussian Mixture Model for the background subtraction

| Gaussian modes | Number of learning frames | Learning ratio |
|----------------|---------------------------|----------------|
| 5              | 60 frames or more         | 0.005          |

Table 2 Parameters of the morphological image processing for noise elimination

| Process              | Image erosion    | Morphological closing | Morphological opening |
|----------------------|------------------|-----------------------|-----------------------|
| Structuring elements | Line-shaped      | Disk-shaped           | Disk-shaped           |
| pixels               | 15 px (vertical) | 100 px (radius)       | 10 px (radius)        |

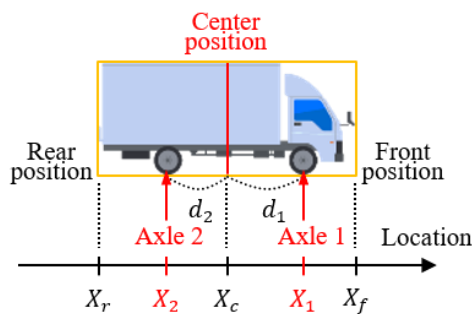


Fig. 4 Definition of the location of the target vehicle and its axle.

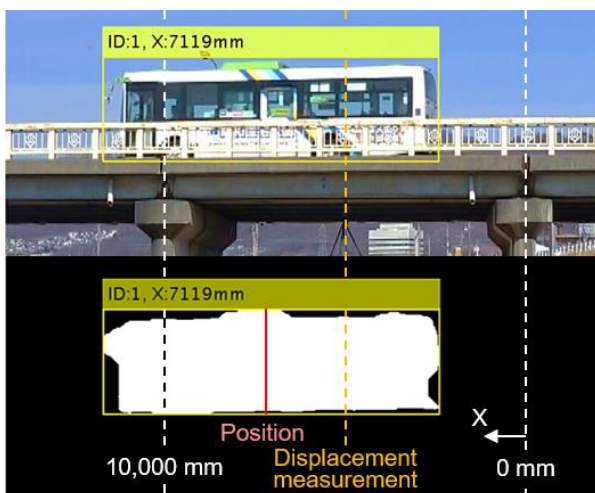


Fig. 5 Example of the result of the background subtraction using GMM analysis.

obtained using the information of the axle position judged by visual observation.

### Consideration

The proposed optical flow analysis based on the background subtraction method acquires the time history of the location of traveling vehicles on the bridge. However, it does not consider two-way traffic, namely cases where vehicles are mutually traveling in both directions, since the vehicles are detected as silhouettes. Although the target bridge had two-way traffic with one lane on each side, the main target was only when there was traffic on the front lane (vehicles traveling from right to left in the photo). When the target vehicle was much larger than others, their silhouette could be tracked even for two-way traffic. Convolutional Neural Networks (CNN) could improve the ability of tracking, including two-way traffic and multiple lanes.

### CALCULATION OF INFLUENCE LINE BASED ON MEASUREMENT

In this study, the influence line of deflection was calculated by synchronizing the time history of the axle position from optical flow analysis and the time history of deflection. Instead of using a reference vehicle in the calibration process, local buses and vehicles detected from video images were used. A diagram of the necessary steps to predict the influence line is shown in Fig. 6. First, the initial values of the influence line  $L(x)$  and axle weight  $W$  are approximately estimated. Next, the influence line is converted in time domain for each axle ( $L(t)$ ), as shown in Fig. 7. Deflection is calculated from a convolution of each converted influence line  $L(t)$  multiplied by the axle weight  $W$ . The Euclidean distance between the calculated distance and measured deflection  $D(t)$  is evaluated, and the influence line and axle weight are modified to minimize the evaluation function by the direct search method. The evaluation function is expressed by the following equation using the influence line converted in time domain.

$$f(L(t), W, D(t)) = \|L(t) \cdot W - D(t)\| \quad (1)$$

To avoid convergence to the local solution, search for the influence line and the axle weight were repeated three times in this study. The initial value of the influence line is based on beam theory. The initial axle weight is estimated by dividing the total weight of the vehicle by the number of axes. The vehicles used were two medium-sized local buses and two passenger cars. The passengers on the buses or cars were not observed from the video images. The model of the passenger cars was estimated from the video images, and the approximate average weight was

used as the initial axle weight. Figure 8 shows the modified influence line  $L^*(x)$  obtained as a result of the aforesaid method, and the modified axle weight  $W^*$  is shown in Table 3. Although the target bridge is a series of simple girders, the influence line is still affected even when the vehicle is traveling on the girders that are further than the measurement span for this study. Figure 9 shows the time history of deflection obtained from the convolution of influence

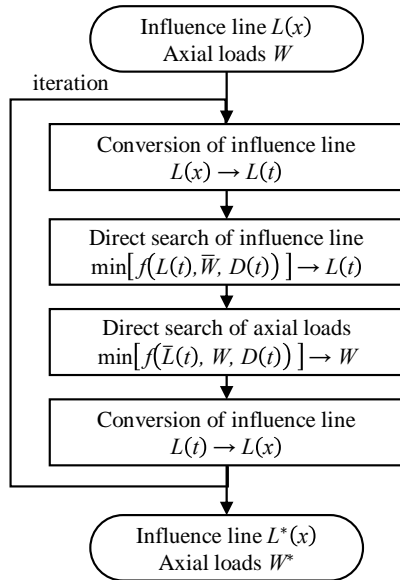


Fig. 6 Analysis diagram of the influence line based on measurements

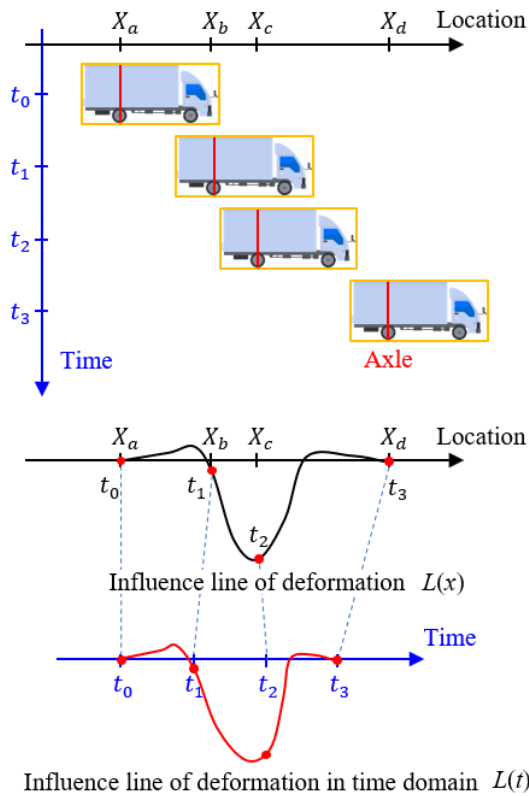


Fig. 7 Explanation of domain exchange of the influence line

lines and axle weights. The deflection estimated from the modified influence lines and axle weights is considered to correspond with the measured deflection.

### Consideration

Since the proposed method calculates the influence line based on actual measurements, it could be applied to continuous bridges where deflection occurs in the negative direction. On the other hand, one problem in the analysis is time synchronization between evaluating the video images of the traffic and the deflection data of the bridge. Time synchronization error accumulated since the internal clocks of the measuring instruments were different. This error depends on the span of the bridge and the speed of vehicles however, it is necessary to synchronize the time to the order of 50 ms or less, as determined from experiment, to calculate the correct influence line.

In this study, beam deflection was measured using a laser displacement meter. Nonetheless, if it was possible to use an accelerometer and obtain deflection by integrating acceleration, the B-WIM system could operate with greater ease. The sampling moiré method is another method considered able to measure deflection using video images [9].

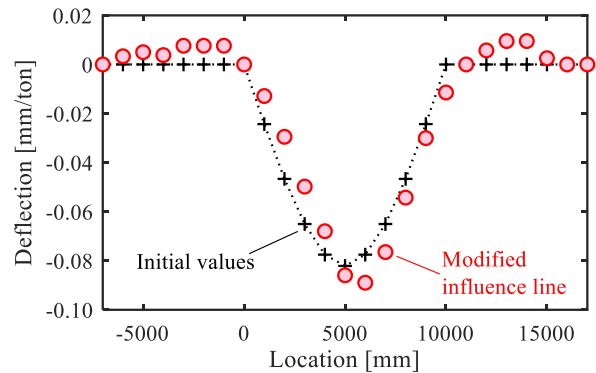


Fig. 8 Modified influence line calculated through the iterative analysis

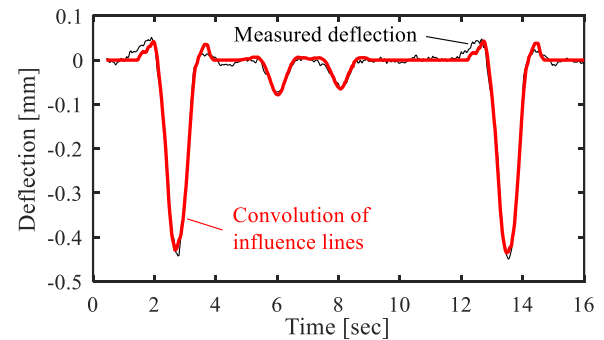


Fig. 9 Comparison of Measured and calculated influence line



## AXLE WEIGHT ESTIMATION

In previous sections, calibration was performed to calculate the influence line using local buses and vehicles by processing the data of deflection and video images. By combining the obtained influence line, vehicle location, and beam deflection data, the axle weights of traveling vehicles were estimated. Figure 10 shows the calculation process for the axle weights. The influence line is converted to time domain using the time history of the vehicle location of each axle obtained from the video images. The axle weights are determined so that the difference between the deflection calculated from the influence lines of each axle weight and measured deflection is minimized using the direct search method. The objective function is a nonnegative linear least squares problem.

The results obtained are shown in Table 4. As a result of estimating the axle weights of medium-sized local bus C, the difference between the calculated vehicle weight and the nominal weight was 5.7 %. Although the speed of another local bus (bus D, shown in Fig. 11) changed on the bridge due to traffic congestion (shown in Fig. 12), the difference between the total vehicle weight calculated from each axle weight and the nominal weight was less than 1 %. The time history of deflection obtained from the convolution of the influence lines of the axle weights,

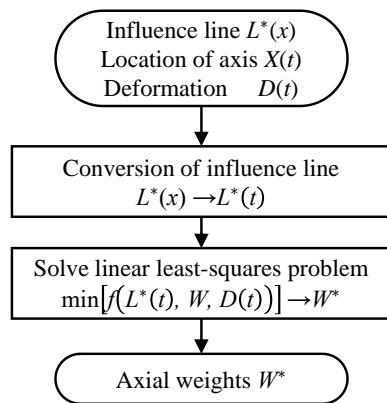


Fig. 10 Calculation process of axle weights

which approximately matches the measured deflection is shown in Fig. 13. This proposed B-WIM using video images could estimate the axle weights and the total vehicle weight with small errors even for low or variable speeds, which was a difficult condition for many conventional B-WIM systems.

The time history of a dump truck location, which was traveling on the bridge (Fig. 14), determined by blob analysis is shown in Fig. 15. The dump truck has three axles and traveled at an approximately constant speed of 35 km/h. The time history of measured deflection and the fitted deflection from the convolution of the influence lines is shown in Fig. 16. As a result of calculating the weight of the dump truck, it was possible to estimate each axle weight.

In this study, there were no patterns where large vehicles traveled on the same girder since the girder span was relatively short. However, the proposed method could in principal, estimate each axle weight even under continuous traffic conditions on the same girder.

## CONCLUSIONS

In this study, by devising a new B-WIM method, which performs image analysis based on a calculation process using multiple general local buses and passenger vehicles, the following findings were obtained.

Image subtraction based on the Gaussian mixture model determined the location of traveling vehicles on the target bridge. The location of all axles in each vehicle was acquired by manual selection from the vehicle images. A calibration process was proposed using the iteration process to optimize the axle weight of reference vehicles and the influence line of deflection. The total vehicle weights could be calculated even under variable traffic speed.

The proposed method could estimate each axle weight even under continuous traffic on the same girder. If the deep learning method is incorporated into the proposed system, vehicles under various traffic conditions, including two-way traffic, could also be identified.

Table 3 Comparison of initial and modified axle weights through the analysis process of the influence line

| Vehicles        | Initial weights $W$  |                      | Modified weights $W^*$ |                      |
|-----------------|----------------------|----------------------|------------------------|----------------------|
|                 | 1 <sup>st</sup> axle | 2 <sup>nd</sup> axle | 1 <sup>st</sup> axle   | 2 <sup>nd</sup> axle |
| Local bus A     | 3,650 kg             | 3,650 kg             | 3,534 kg               | 3,699 kg             |
| Local bus B     | 3,650 kg             | 3,650 kg             | 3,416 kg               | 3,970 kg             |
| Passenger car A | 500 kg               | 500 kg               | 569 kg                 | 462 kg               |
| Passenger car B | 400 kg               | 400 kg               | 284 kg                 | 537 kg               |

Table 4 Calculated axle weights and total weight of vehicles

| Vehicles (Nominal weight) | 1 <sup>st</sup> axle | 2 <sup>nd</sup> axle | 3 <sup>rd</sup> axle | Total     | Error |
|---------------------------|----------------------|----------------------|----------------------|-----------|-------|
| Local bus C (7,315 kg)    | 2,809 kg             | 4,090 kg             | -                    | 6,899 kg  | -5.7% |
| Local bus D (10,630 kg)   | 4,118 kg             | 6,433 kg             | -                    | 10,551 kg | -0.7% |
| Dump truck (unknown)      | 3,548 kg             | 4,812 kg             | 2,692 kg             | 11,052 kg | -     |

## ACKNOWLEDGMENTS

This research was supported by Grants-in-Aid for Scientific Research for Early-Career Scientists from Japan Society for the Promotion of Science (JSPS).

## REFERENCES

- [1] Moses F., Weigh-in-Motion System Using Instrumented Bridges, Transportation Engineering Journal of ASCE, Vol. 105, Issue 3, 1979, pp. 233-249.
- [2] Ojio T, Yamada K., Bridge Weigh-in-Motion Systems using Stringers of Plate Girder Bridges, Third International Conference on Weigh-in-Motion, 2002, pp. 209-218.
- [3] Ojio T, Yamada K., Bridge WIM by Reaction Force Method, Fourth International Conference on Weigh-in-Motion, 2005, pp.97-108.
- [4] O'Brien E. J., Quilligan M. J., Karoumi R., Calculating an Influence Line from Direct Measurements, Proceedings of the institution of civil engineers - Bridge Engineering, Vol. 159, Issue 1, 2006, pp. 31-34.
- [5] Takeya K., Ota K., Takagi S., and Yoshida J., Analysis of Traffic Environment and Dynamic Behavior of Bridge Girders based on Image Sensing Techniques, Fourth International Conference on Science, Engineering and Environment, No. 4721, 2018, pp. 1-6.
- [6] Lansdella A., Songa W., and Dixon B., Development and Testing of a Bridge Weigh-in-Motion Method Considering Nonconstant Vehicle Speed, Engineering Structures, vol. 152, 2017, pp. 709-726.
- [7] Welch G., and Bishop G., An Introduction to the Kalman Filter, University of North Carolina at Chapel Hill, Department of Computer Science, 2006.
- [8] Ri S., Numayama T., Saka M., Nanbara K., and Kobayashi D., Noncontact Deflection Measurement for Large-Scale Structures by Advanced Image Processing Technique, Materials Transactions, Vol. 53, No. 2, 2012, pp. 323-329.



Fig. 11 Out view of the local bus D

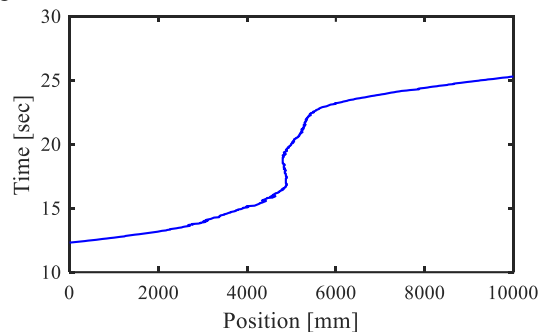


Fig. 12 Time history of the location of the local bus D on the target bridge

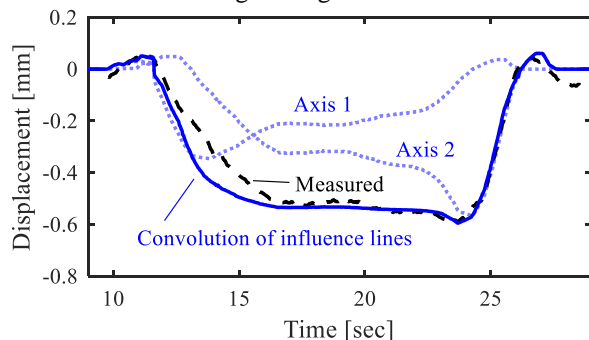


Fig. 13 The measured and calculated deflection when the local bus D was traveling on the bridge



Fig. 14 Out view of the dump truck

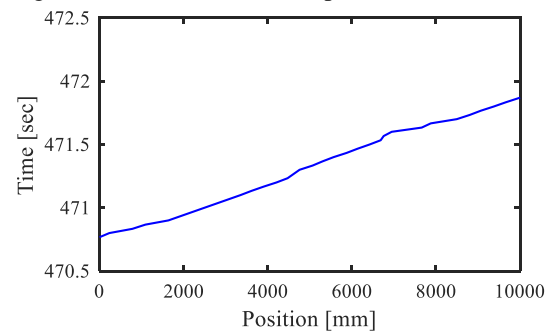


Fig. 15 Time history of the location of the dump truck on the target bridge

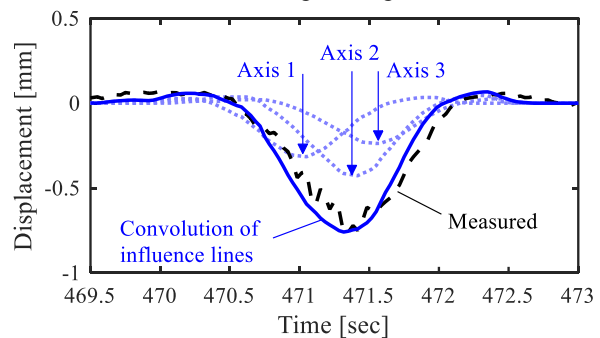


Fig. 16 The measured and calculated deflection when the dump truck was traveling on the bridge

# EFFECT OF REINFORCEMENT STIFFNESS ARRANGEMENT ON SEISMIC PERFORMCANCE OF GEOGRID REINFORCED SOIL WALLS

Albano Acacio Ajuda<sup>1</sup>, Jiro Kuwano<sup>2</sup> and Kosuke Hoshina<sup>3</sup>

<sup>1,2,3</sup>Department of Civil and Environmental Engineering, Saitama University, Japan

## ABSTRACT

It is well known that geosynthetics reinforced soil walls are much cheaper and stable compared to traditional retaining wall. However, most of the existing studies were conducted using a uniform reinforcement stiffness along the wall height. Very few studies have been conducted regarding the effect of multiple reinforcement stiffness along the reinforced soil wall height. This type of configuration can be used for construction cost reduction maintaining adequate seismic response. In order to evaluate the behavior of wall with different stiffness arrangement, a series of shaking table test were conducted on segmental walls with two different geogrid stiffness material. The geogrid stiffness arrangement was alternating and grouped schemes. Image analysis based on FEM allowed shear bands to be identified within the reinforced soil zone. Results showed that wall residual displacement, shear deformation was dependent on the geogrid stiffness arrangement and despite application of multiple stiffness the failure surfaces angles observed in the model test remained the same. Additionally, simple shearing and strain localization was observed within the reinforcement layers. Further results showed that wall with alternated geogrid stiffness was similar to wall with uniform stiffness in both magnitude and shape. However, by grouping a less stiff geogrid either in upper half or lower half of the wall the magnitude of wall displacement and shear strain was larger and bulging deformation was observed at mid-height of the wall before reaching critical acceleration.

*Keywords: Earthquake, Shaking table test, Retaining wall, Stiffness arrangement*

## INTRODUCTION

Geosynthetics reinforced soil wall are well known to be cost-effective and able to resist earthquake-induced damage as compared to the traditional retaining wall, for this reason, the number of constructed walls has been increasing over the years as reported in [1], [2]. Most of the existing literature focuses on the application of one type of reinforcement stiffness or geosynthetics material along the wall height. According to [3] reinforcement material can cost about 30 % of the total construction cost of reinforced soil walls depending on wall height, backfill type, and design loading condition. A possible solution to further reduce the construction cost maintaining an adequate seismic behavior could be by constructing the wall with multiple reinforcement stiffness or by using different geosynthetics material.

In the field of full-scale models, [4] investigated the performance of geosynthetic reinforced soil walls by monitoring the wall behavior over a period of 1 year. The walls were 3.6 m high seated on a clay foundation, the backfill was constructed using recycled construction waste to minimize the construction cost as well to reduce the environmental impact. They reported that greater displacement can be observed in walls constructed with more extensible nonwoven geotextile as compared to walls with woven polyester (PET) layers and the maximum

displacement amount was about 6% and 3% respectively.

In the field of reduced-scale models, [5]-[7] conducted series of shaking table test on geosynthetics reinforced soil walls using FHR facing, parameters such as L/H ratio, reinforcement stiffness, wall inclination was investigated. Their results showed that wall horizontal displacement decreased with increase in L/H ratio and wall reinforced with higher reinforcement stiffness generated a shallower displacement-acceleration response curve compared to walls reinforced with a less stiff reinforcement. [8] reported that placing longer reinforcement layer at a higher elevation in the backfill it is possible to increase substantially the resistance against overturning failure.

In the field of numerical analysis, [8] investigated the influence of reinforcement length arrangement along the wall height. It was found that the deformation behavior of the surrounding ground was totally different, by placing shorter reinforcement length in the upper half and longer in the lower half of the wall a zone of large shear deformation was formed in an arc-shaped which extended from the foundation layer towards the top of the backfill in the retaining area and slippage occurred, on the other hand it was found that the formation of failure surface was interrupted by the shorter reinforcement layers. The maximum shear strain observed in the models was concentrated at the end of

the reinforcement layers. [10] performed numerical analysis using a computer program FLAC on wrap-around walls subject to static loading. They reported that wall deformation of walls with alternated reinforcement stiffness values along the wall height was consisted with walls with one type of reinforcement stiffness in shape and magnitude, by grouping the reinforcement stiffness either in the upper or lower part of the wall large deformation occurred in the region where less stiff reinforcement was placed.

[11] showed three case studies of reinforced soil walls which were damaged due to heavy rainfall in Japan. The geosynthetic reinforced soil walls were constructed with a steel frame facing with a total height of 9.5 m and 10.7 m. in one of the reinforced soils walls the reinforcement layers were a combination of two different material, geogrid, and geotextile, which was placed in alternated manner. Another wall was constructed with two different lengths, a primary reinforcement with a longer length and a secondary with shorter length also placed in alternated manner.

The investigation of multiple reinforcement stiffness or material type along the geosynthetic reinforced soil wall is still limited. According to [10] no currently guideline directly considers the influence of different reinforcement stiffness layers on the distribution of tensile load in reinforced soil walls systems. Additionally, for the author best knowledge no current physical model test of this type of arrangement is available in the literature. Taking this into account, the present experimental work consisted of a series of shaking table test to investigate the seismic response of walls constructed with different reinforcement stiffness along the wall height. Image analysis technique was used to observe the wall residual displacement and the failure mechanism at different levels of ground motion amplitudes.

## PHYSICAL MODEL TEST

In the present experimental work six segmental geogrid reinforced soil wall were tested considering the effect of reinforcement length, layout and stiffness arrangement on seismic performance using a shaking table test which was conducted at Saitama University, Japan.

The shaking table is compromised on a plan dimension of 1300 by 1000 mm controlled by a computer. The shaking table is seated on a pair of low friction bearing rails which are constrained in the horizontal direction equivalent to a single degree of freedom. The soil was poured in a rigid container with the following dimension: 1300 mm (L), 300 mm (W) and 650 mm (H). One of the sides of the rigid box was constructed using a transparent Plexiglas so that wall and backfill deformation can be visualized and compute by a CCD camera. The far end boundary of the rigid container was mad of steel which could induce reflective waves and magnification of the structure dynamic response during model testing as demonstrated by [14]. However, according to [15] the effect of reinforcement in reducing the deformation is independent of container boundary type.

### Model Soil and Geogrid

The model soil was Toyoura sand with the following properties:  $e_{max} = 0.973$ ,  $e_{min} = 0.609$ ,  $D_{50} = 0.19 \text{ mm}$ . The soil foundation and backfill were constructed using air pluviation method (raining) to achieve a desired relative density of 90%.

Two types of biaxial geogrid were used in the present study: a) high tensile strength (stiff) geogrid and b) low tensile strength (soft) geogrid. The geogrid was placed horizontal in the reinforced zone with a total of eight layers spaced at 60 mm vertically.

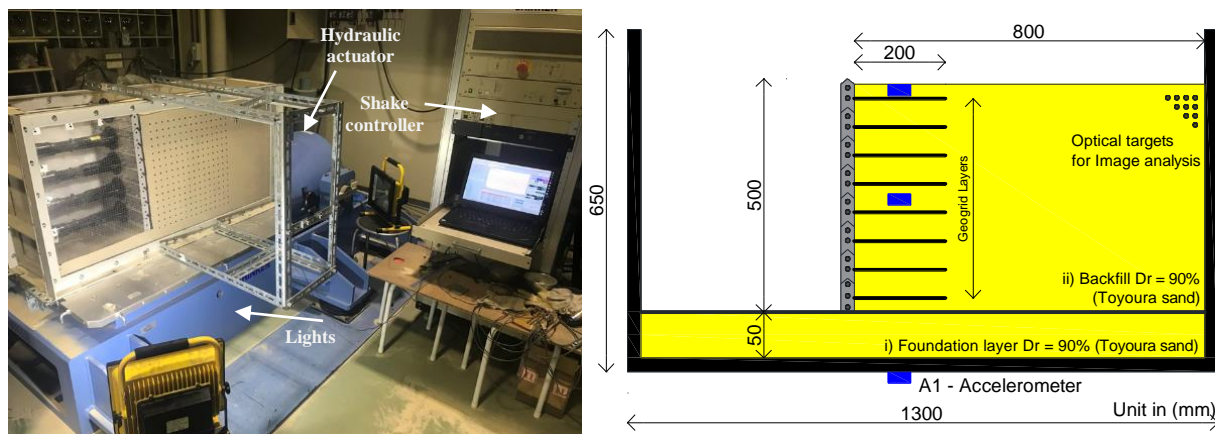


Figure 1. Typical model test setup

Table 1. Summary of the tested cases

| Test cases | Reinforcement length (mm) | Reinforcement arrangement | Vertical spacing (mm) |
|------------|---------------------------|---------------------------|-----------------------|
| Wall 1     | 300                       | Uniform                   | 60                    |
| Wall 2     | 200                       | Uniform                   |                       |
| Wall 3     | 300/200                   | Alternated lengths        |                       |
| Wall 4     | 200                       | Alternated stiffness      |                       |
| Wall 5     |                           | Grouped                   |                       |
| Wall 6     |                           | Grouped                   |                       |

### Facing Panels

The wall was built vertically with a total of eight acrylic panels each with the following dimension: 300 mm (W), 75 mm (H) and 30 mm thick, each panel was stacked on top of each other up to a total height of 500 mm, without any additional connection between the panels. On both sides of the wall panels Teflon sheets were used to minimize friction between the soil container and the wall panels. Similar wall height has been investigated by [8], [12]. The toe of the wall can slide freely to the horizontal direction since the first panel is seated on the sand foundation.

The geogrid reinforcement layers were rigidly connected between two steel clamps with the same length and width as the wall panels, this arrangement prevented slippage of the reinforcement layers during model test and finally, the connection was bolted to each wall panel as illustrated in Figure 2.

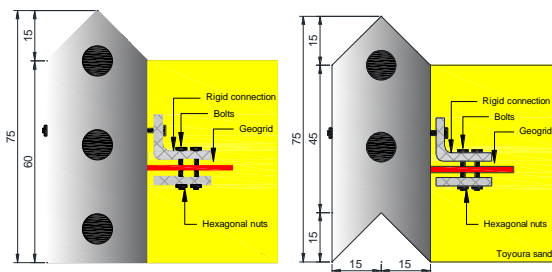


Fig. 2 Details of wall panels

### Model Instrumentation

Two different types of instrumentation were used in each model to record the seismic response. The instrumentation consisted in three accelerometers where the first was attached to the shaking table to record the input ground motion and one at the mid-height and one at the top of the wall in the reinforced zone and at 100 mm away from the wall to record the soil dynamic response. Twelve optical targets made of cartoon was glued to the wall panels to record the wall displacement and 240 optical targets with 8 mm in diameter made of rubber sponge glued with short nails was placed in the backfill in a 30 mm by 30 mm grid to obtain soil displacement for subsequent calculation of shear strain.

### Model Construction

The first construction stage consisted in building the foundation layer which was made of 50 mm layer. Then the wall panels were placed into the appropriate position and braced to prevent wall lateral movement during backfilling. The backfill was then constructed in 30 mm layers to allow optical targets to be placed, after the backfilling finished unbracing stage started from the wall top toward the bottom. Finally, the last stage consisted in bolting the light steel frame to the soil container as well to the shaking table to accommodate the CCC camera.

### Input Ground Motion

The seismic wave was applied using a sinusoidal wave with a predominant frequency of 5 Hz. Each shaking stage was held for 10 seconds corresponding to a total of 50 cycles/step. The models were subjected to different amplitudes which started from the lowest 1m/s<sup>2</sup> with steady increments of 1m/s<sup>2</sup> until fully collapsed.

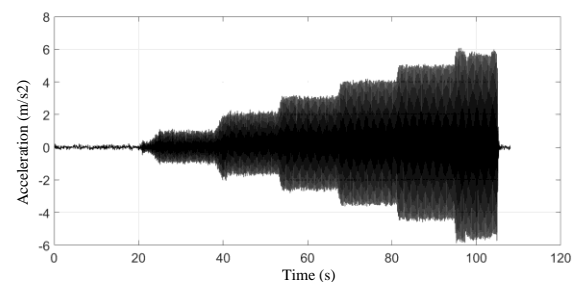


Fig. 3 Input ground motion

### Similitude Rules

Geogrid reinforced soil walls model test was carried out using 1g shaking table test. The stress levels in the experiments do not truly represent the stresses in the field because of the gravity and boundary effects in model studies. In the present experimental program similitude laws proposed by [16] was used with a geometric scaling factor of 10 between model and prototype scale.



## EXPERIMENTAL RESULTS AND DISCUSSION

Regarding seismic deformation of geogrid reinforced soil walls, previous researchers [13], [17] showed a displacement of 5% which the reinforced zone suffered a backfill strength deterioration. In the present experimental test, the wall displacement increased with base acceleration and when the top displacement reached 3% of the wall height which is here defined as the critical accretion at this stage unrecoverable deformation of the backfill was observed, at this stage clear failure surfaces was observed within the reinforced zone and retained zone. [7] defined critical acceleration as the sudden change in the rate of wall rotation and [12] as acceleration at which a sharp increase in incremental displacement takes place.

Figure 4 shows the progressive deformation of the backfill for wall 2 reinforced with a uniform high stiffness reinforcement from 4m/s<sup>2</sup> to 5m/s<sup>2</sup>. The failure extended from the wall top toward the bottom in the lowest reinforcement layer and inclined failure surfaces the wall toe towards the end of the first reinforcement layer from this location it inclined upwards towards the backfill surface in the retained zone allowing a creation of an active failure wedge where the soil mass slide downward to the back of the wall, at this point large backfill settlement can be observed with a “U” shape geometry and drag-down

forces at the end of the reinforcement layers as well at the end of the retained area can observed. For all cases the failure surfaces penetrated the reinforced soil block suggesting that the bottom reinforcement did not constrain the sliding component efficiently. Once the critical acceleration was reached the failure surfaces angles remained the same throughout the model shaking. [18] reported that the exact position of the failure surfaces changes as the amplitude of shaking increases using Geo-PIV.

In the present work simple shearing and strain localization along the reinforcement layers was observed during model testing. For instance [19] defined strain localization as a high gradient of shear strain associated with high displacement gradient, it is possible to notice from Figure 4 a concentration of high magnitude of shear strain along the reinforcement layers especially in the upper half of the wall during 5 m/s<sup>2</sup> at 15 and 30 cycles since large deformation of the wall and backfill occurs in this region due to overturning, therefore pullout displacement of the reinforcement layers was larger. [20] conducted pull out test to investigate the soil-geogrid interface mechanism, they reported that the maximum shear strain occurred close to the soil-geogrid interface and that under pullout condition passive resistance is the main contributor of soil resistance to pullout particularly under low confining pressures.

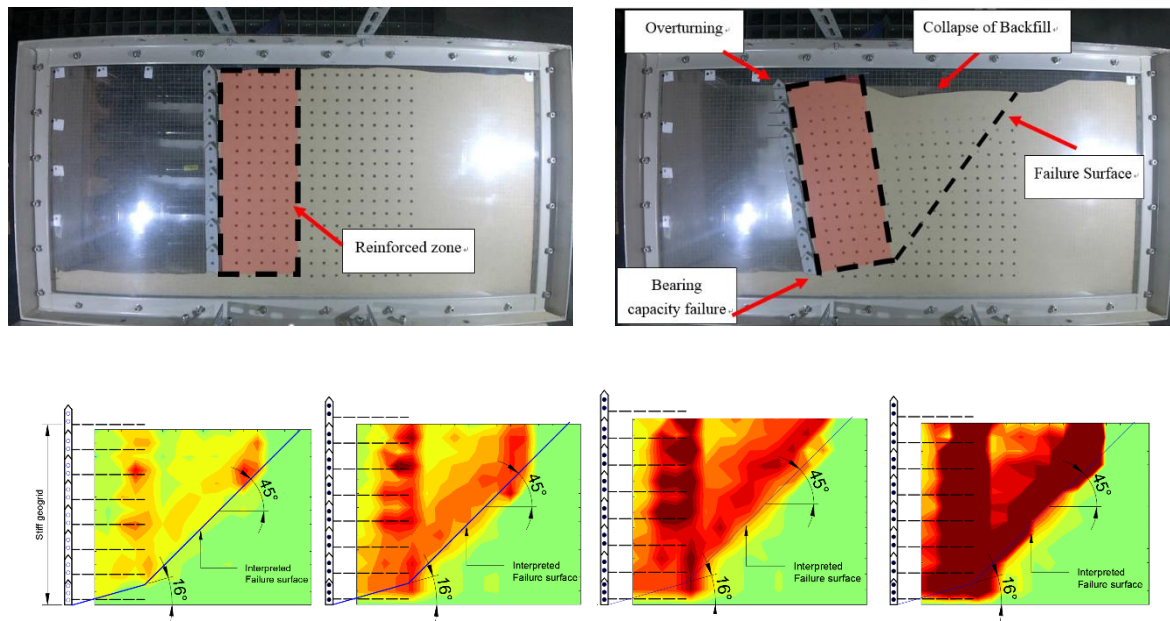


Fig. 4 Progressive deformation wall 2 a) 4 m/s<sup>2</sup> b) 5 m/s<sup>2</sup> (15 cycles) c) 5 m/s<sup>2</sup> (30 cycles) d) end of 5 m/s<sup>2</sup>

By increasing the geogrid reinforcement length shallower top displacement-acceleration curve is observed, therefore less deformation and higher acceleration the wall can sustain. It is possible to notice that Wall 1 with longer geogrid reach the

critical acceleration at around 500 gal while Wall 2 with shorter geogrid length reached critical acceleration at 400 gal, suggesting that shorter reinforcement length reach the instability stage at smaller base shaking. However, by alternating longer

and shorter reinforcement along the wall height Wall 3, the wall showed an intermediate behavior between Wall 1 and Wall 2 and the critical acceleration was observed to be the same as Wall 1. This behavior could indicate that the wall can maintain serviceability and performance during seismic shaking.

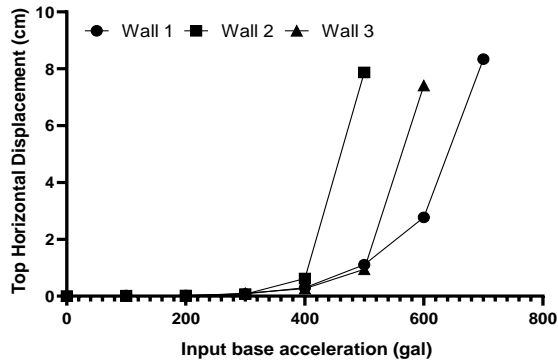


Figure 5 Wall residual displacement against base acceleration

In Figure 7 are plotted the relationship of top displacement with the base acceleration of the tested walls. It is possible to notice that wall with stiff uniform reinforcement Wall 2 showed an increase in stability. However, by substituting half of the stiff geogrid with soft geogrid in an alternating manner Wall 4, the wall showed almost the same amount of displacement and shape to Wall 2 constructed with stiff geogrid. By grouping the reinforcement stiffness Wall 5 or Wall 6 it showed an increase in the top horizontal displacement and bulging phenomena was observed at mid-height before reaching critical stages as illustrated in Figure 7. It is possible to notice the difference in the deformation along the wall elevation, for example at 300 gal in Wall 2 the deformation tends to be linear from to wall toe up to the wall top, this deformation shape was also observed in the case of Wall 4, while in grouped schemes the wall deformation is less in the region where the stiff geogrid is placed, however, when reaching the mid-height of the wall where the geogrid stiffness changes to a soft geogrid the horizontal displacement increases considerable. Wall 6 showed an increase in sliding component because of this movement the wall top displacement also increased considerably. It is possible to notice that in the bottom part of the wall where soft geogrid is placed the displacement in this region tends to increase with elevation up to the mid

height of the wall where the stiff geogrid is placed, from this location the wall horizontal displacement tends to reduce with increase with increase in wall elevation. However, due to large amount of sliding component, the wall top continually moved to the outward direction.

The shear strain magnitude in the backfill was dependent on the geogrid stiffness arrangement as illustrated in Figure 6, the lowest values of shear strain were observed for wall with stiff geogrid Wall 2, similar variation on shear strain can be observed in Wall 4. However, walls with grouped schemes Wall 5 and Wall 6 showed larger movement of the backfill, consequently large values of shear strain can be seen compared to Wall 2. From the same figure it is possible to see the angles of failure surface observed in shaking table test for walls with multiple reinforcement stiffness. Interesting, even by mixing or grouping the reinforcement stiffness along the wall height, failure surfaces were depended only on the high stiffness reinforcement and reinforcement length. For instance, [21] demonstrated that failure surfaces have different geometry under different geogrid tensile strength using centrifuge test and two-wedge method. This behavior could indicate that reinforced soil wall constructed with different tensile strength along the wall height can be designed using high tensile strength value only especially for walls with alternating schemes. Additionally, according to [21] if the tensile stiffness of the geogrid is insufficient, strain is concentrated in the reinforced area because the geogrid reinforcement cannot restrict the deformation of the backfill. Therefore, wall with stiff geogrid in this experiment was able to resist most of the backfill shear deformation as can be seen through the magnitude of the shear strain distribution, followed by wall with alternating stiffness which showed about 20% increase in the magnitude of shear strain. However, wall with grouped schemes showed very large backfill shear deformation with shear strain of about 80 % increase as compared to stiff geogrid wall. This behavior may suggest that grouping the lower reinforcement stiffness either in the upper or lower part of the wall may not be appropriate for construction cost reduction of GRSW.



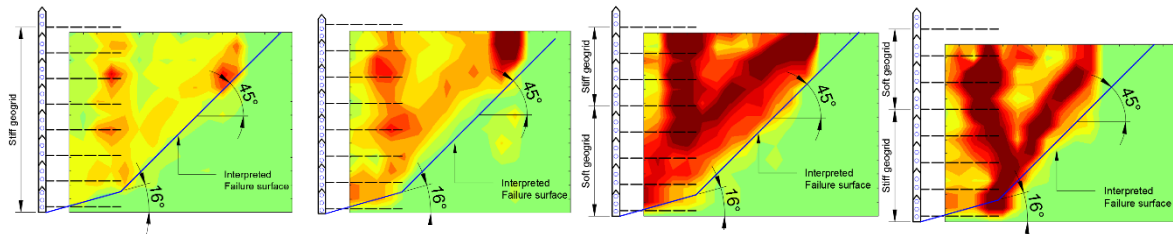


Fig. 6 Maximum shear strain after 4 m/s<sup>2</sup> base acceleration a) wall 1 b) wall 2 c) wall 3 and d) wall 4

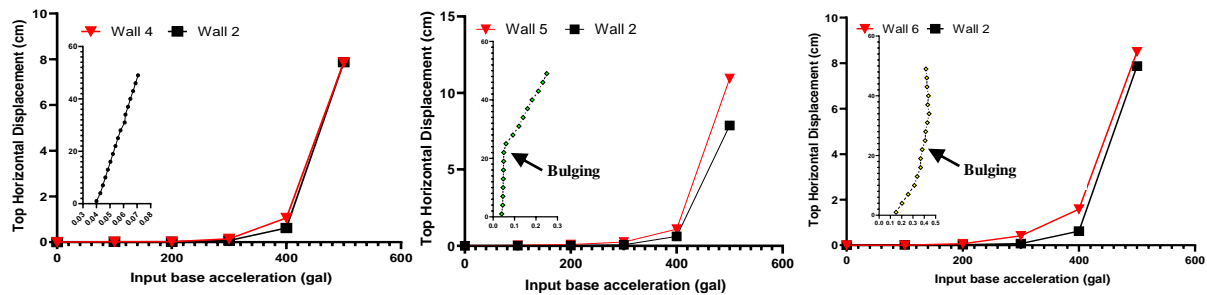


Fig. 7 Top horizontal displacement with ground acceleration and displacement profile at 3 m/s<sup>2</sup>.

## CONCLUSION

Reduced-scale shaking table tests were performed to investigate the seismic response of segmental geogrid reinforced soil retaining wall constructed with multiple reinforcement stiffness along the wall height in different configuration. The progressive failure, shear strain distribution in the backfill and lateral displacements of the wall were compared under different ground motions amplitudes. The following conclusions could be drawn:

- I. Wall residual displacement decrease with increase of reinforcement length; By mixing shorter and longer reinforcement it was found that the critical acceleration was almost same as the wall with longer geogrid (300 mm) which could indicate that the wall may still work at service level;
- II. The predominant failure mode was overturning accompanied with sliding and bulging deformation; Failure surface were formed when the wall horizontal displacement reached 3 percent of the wall height;
- III. Results showed that alternating reinforcement stiffness along the wall height similar wall deformation and shear strain magnitude to walls with a single reinforcement stiffness can be observed;
- IV. Grouped schemes clearly showed larger wall deformation together with an increase of shear strain magnitude compared to wall with single reinforcement stiffness;
- V. Failure surface angles was observed to be independent on the reinforcement stiffness

arrangement; and failure surfaces angles observed in the backfill were almost the same to wall with single reinforcement stiffness;

## ACKNOWLEDGEMENT

This research project has been sponsored by JSPS KAKENHI Grant Number 16H04406 and Monbukagakusho Scholarship (MEXT)

## REFERENCES

- [1] Kuwano J., Miyata Y., and Koseki J. Performance Of Reinforced Soil Walls During The 2011 Tohoku Earthquake, *Geosynthetics International*, Vol. 21, Issue 3, 2014, pp.179-196.
- [2] Koseki J., Bathurst, R.J., Guler, E., Kuwano, J. and Maugeri M., *Seismic Stability Of Reinforced Soil Walls*, 8<sup>th</sup> International Conference of Geosynthetics, 2006.
- [3] FHWA, *Mechanically Stabilized Earth Walls And Reinforced Soil Slopes Design & Construction Guidelines*, No. 132042. 2001.
- [4] Santos E. C. G., Palmeira E. M., and Bathurst R. J., *Performance of Two Geosynthetic Reinforced Walls With Recycled Construction Waste Backfill and Constructed on Collapsible Ground*, Vol. 21, Issue. 4, 2014, pp. 256-269.
- [5] El-Emam M. M. and Bathurst R. J., *Experimental Design , Instrumentation And Interpretation of Reinforced Soil Wall Response Using A Shaking Table*, Vol. 4 Issue 4, 2004, pp. 13-32.
- [6] El-Emam M. M. and Bathurst R. J., *Facing Contribution To Seismic Response Of Reduced-Scale Reinforced Soil Walls*, Vol. 12, Issue 5, 2005, pp. 215-238

- [7] El-Emam M. M. and Bathrust R. J., Influence of Reinforcement Parameters on the Seismic Response of Reduced-Scale Reinforced Soil Retaining Walls, Vol. 25, Issue 1, 2007, pp. 33-49
- [8] Watanabe K., Munaf Y., Koseki J., Tateyama M., Kojima K., Behaviors Of Several Types Of Model Retaining Walls Subjected To Irregular Excitation, Soils and Foudnations, Vol. 43 Issue 5, 2003, pp. 13-27.
- [9] Kikumoto, M., Nakai, T., Shahin, H. M., Watanabe, A., Ishii, K. and Zhang, F., Mechanical behaviour of geosynthetic-reinforced soil retaining wall, ASCE Geotechnical Special Publication (Ground Improvement and Geosynthetics) 207, pp. 310-317
- [10] Hatami K., Bathrust R. J. and Di Pietro P., Static Response of Reinforced Soil Retaining Walls With Nonuniform Reinforcement, The International Journal of Geomechanics, Vol. 1, Issue 4, 2001, pp. 477-506.
- [11] Miyata Y. and Shinoda M., A case study of damages of geogrid reinforced soil walls triggered by rainfall, 6th Asian Regional Conference on Geosynthetics, 2016.
- [12] Matsuo O., Tsustumi T., Yokoyama K. and Saito Y., Shaking Table Tests and analyses of Geosynthetic-Reinforced Soil Retaining Walls, Geosynthetics International, Vol. 5, 1998, pp. 97-126.
- [13] Koseki J., Munaf Y., Tatsuoka F., Tateyama M., Kojima K. and Sato T., Shaking and Tilt Table Tests of Geosynthetic Reinforced Soil walls and Conventional-Type Retaining Walls, Geosynthetics International Vol. 5, 1998, pp. 73-96.
- [14] Bathrust R. J. and Hatami K., Seismic Response Analysis of a Geosynthetic-Reinforced Soil Retaining Wall,” Vol. 5, Issue 1-2, 1989, pp. 127-166.
- [15] Krishna A. M. and Gali M. L., Container Boundary Effects In Shaking Table Tests On Reinforced Soil Wall Models, International Journal of Physical Modelling in Geotechnics, 2009, pp. 1-14.
- [16] Lai S., Similitude For Shaking Table Tests on Soil-Structure fluid Models in 1G Gravitational Field, Soils and Foundtion, Vol. 29, Issue 1, 1989 pp. 105-118.
- [17] Huang C. and Wu H., Seismic Displacement Analysis of a Reinforced Soil Model Wall Considering Progressive Development of Reinforcement Force, Geosynthetics International, Volume 16, Issue. 3, 2009, pp. 222-234.
- [18] Bowman E. T., Jackson P., Cubrinovski M., and Fannin R. J., Progressive Failure And Shear Band Development Within Model-Scale Reinforced Soil Walls Subject To Seismic Shaking, Géotechnique Letters, Vol. 1, No. 3, 2011, pp. 53-57.
- [19] Wood D. M., Some Observations Of Volumetric Instabilities In Soils, International Journal of Soilds and Structures, Vol. 39, 2002, pp. 3429-3449.
- [20] Abdi M. R. and Mirzaeifar H., Experimental And Piv Evaluation Of Grain Size And Distribution On Soil-Geogrid Interactions In Pullout Test, Soils and Foundtion., Vol. 57, Issue. 6, 2017, Pp. 1045-1058.
- [21] Izawa J. and Kuwano J. Centrifuge modelling of geogrid reinforced soil walls subjected to pseudo-static loading, International Journal of Physical Modelling in Geotechnics, Vol. 10, Issue. 1, 2010, pp.1-18.

## THE IMPACT AGGREGATE QUALITY MATERIAL AS A LINEAR REGRESSION STUDY ON MIXTURE CONCRETE

Ranti Hidayawanti<sup>1</sup>, Dicki Dian Purnama<sup>2</sup>, Tommy Iduwin<sup>3</sup>, Supriadi Legino<sup>4</sup> and Fahdun Ibnu Wachid<sup>5</sup>  
<sup>1,2,3</sup>Department of Civil Engineering, Sekolah Tinggi Teknik PLN, Indonesia; <sup>4</sup>Department of Informatic Engineering, Sekolah Tinggi Teknik PLN, Indonesia; <sup>5</sup>PT.Pembangkitan Jawa Bali, Indonesia

### ABSTRACT

Fine aggregate and coarse aggregate are important components in making concrete for light and structure concrete. These mixture concretes are one of the elements as structural component in building construction. Generally, this aggregate is easy to find both coarse and fine aggregates beside the aggregate can be used as a component on concrete in the building which needs strong support. The objectives of this study are adding mixture aggregate with compared to designed result (theory) mixture concrete by using the method of fine modulus and linear regression. Those two methods will be found out theoretically in optimizing certain components (economic). In order to get the presentation of aggregate and meet the requirement of standard quality concrete, are used the comparison of fine and coarse aggregate at 60% - 40%. The method that is used to pass the screening is fine modulus and the counting of mixture aggregate used statistic formula calculation which is regression linear method to find the percentage comparison between coarse and fine aggregate in designing of a mix that can be used in making concrete. By knowing the maximum aggregate limit, it is expected to find out the limitation aggregate of fine and coarse accurately so that the result of concrete that is used is better because the raw material is correct for the construction composition. From the test results for fine aggregate  $R^2 = 0.9444$  and coarse aggregates  $R^2 = 0.9541$  with linear regression formulation is and compressive strength shows the value of  $R^2 = 0.9627$ , then the strength of the relationship between variables can be expressed by the magnitude of the correlation coefficient value on the linear function.

*Keywords: fine aggregate, coarse aggregate, fine modulus, concrete, linear regression*

### INTRODUCTION

Aggregate is a basic material used in buildings ranging from the lowest structure to the uppermost structure, both as fine aggregates and coarse aggregates used in each mixture of concrete mixtures. It is commonly known that 70% of the building is concrete[1]. According to SNI 03-2847-2002, concrete is a material obtained by mixing Portland cement or other hydraulic cement, fine aggregates, coarse aggregates and water, with or without additives forming solid mass. The use of material from concrete can also be used with waste[2]. Besides that there are still many other uses of fine and rough aggregates in building use such as filling in building columns, making foundations and road infrastructure.

In determining and grouping the size and type of fine and coarse aggregates, it is important to note that the quality of the building blocks of building materials is suitable and ideal. For this reason, it is necessary to test the gradation in each aggregate to be used as a mixture.

The index used to show the fineness / coarseness of aggregate grains is MHB, and the factors that can influence the search for fine grain modulus (MHB) are the sieve size used and the size of aggregate

grains[3], where the formulation is as follows :

$$w = \frac{k-c}{c-p} \times 100\% \quad (1)$$

w = Percentage of fine aggregate (sand) in the mixture

k = Fine modulus of coarse aggregate

p = Fine modulus of sand

c = Fine modulus mixture

Gradation can be said as smooth or rough modulus in an aggregate, this difference will affect the use of aggregate as a building material. All types of aggregates taken from the source must be processed before use. Washing and filtering is a processing process that must be carried out and has been required for its use.

In order to get gradations that are in accordance with the standard concrete mix, an experiment needs to be carried out then the results of the experiment will be processed. Data processing is done using linear regression formulations.

$$\hat{y} = a + bx \quad (2)$$

$\hat{y}$  = Estimate value of the dependent variable

a = Intersection point of the regression line on the y axis or the estimated value if x = 0

- b = Gradient of the regression line (change in the estimated value per unit change in the value of x)
- x = Free variable value

The formula of linear regression [4] is the data taken based on the dependent and independent variables.  $R^2$  is the coefficient of determination (coefficient of multiple determination) of a regression model that can be defined, as follows :

$$R^2 = \frac{SSR}{SSTO} = 1 - \frac{SSE}{SSTO} \quad (3)$$

$$0 \leq R^2 \leq 1$$

The greater value of  $R^2$ , the better model used and the result  $R^2$  is the value of regression analysis while approaching 1 means the data can be used.

This study aims to determine the effect of aggregate grain size on compressive strength and modulus of elasticity of concrete. Compressive strength of concrete with a larger grain size has a lower compressive strength value than concrete with a smaller size. A good aggregate gradation and small aggregate size will be able to produce maximum density and minimum porosity.

$$f'c = \frac{P}{A} \quad (4)$$

$f'c$  = Value of Concrete Compressive Strength (MPa)

P = Compressive Force that occurs (N)

A = Test Surface Area ( $\text{mm}^2$ )

## MATERIALS



Fig. 1 Mix Design Laboratory

In the laboratory test the sample used are :

- Fine Aggregates (Bangka Sand)
- Coarse Aggregates
- Cement
- Water

Laboratory supporting equipment for the sample

above are :

- Sieve diameter (9.60mm; 4.80mm; 2.40mm; 1.2mm)
- Cup; 0.60mm; 0.30mm; 0.15mm and PAN)
- Trays
- Filters
- Pedestals
- Sieve shaker tools
- Sieve cleaning brush



Fig. 2 Supporting Equipment

## METHODOLOGY

In order to get the quality of the uniformity of the concrete according to what is required, the implementation of concrete making must be done well and in accordance with the standard code procedures. Elaborate on test method used. The test results are implemented into statistical formulations with linear regression formulas. The stages in the design are: Analysis of fine aggregate and coarse aggregate, examination of specific gravity and absorption of fine aggregate and coarse aggregate, examination of aggregate content weight, and compressive strength testing on concrete samples and checking linear regression formulations.

## TEST RESULT AND DISCUSSION

Sieve analysis is a grouping of large items of coarse aggregate analysis and fine aggregate into a composite composition that is reviewed based on the filter.

The goal of sieve analysis are :

- a. To obtain concrete that easy to be worked and has a high level of workability.
- b. To obtain economical price of concrete and high durability.
- c. To obtain a solid concrete.
- d. To obtain a gradation limit from aggregate
- e. To obtain a mix composition of coarse and fine aggregate analysis in the ideal form.

The mixed aggregate is a comparison between fine aggregate and coarse aggregate in the

manufacture of concrete in both light and structural concrete. The purpose of adding the aggregate of this mixture is to compare the theoretical results of the planned concrete mixture using a linear regression formulation to obtain fine modulus.

Fine modulus is a value that is used to show the smoothness and roughness of the aggregate items that are left / held above the sieve set. The greater the value of fine modulus, the greater the aggregate items. The following are the results of the STT PLN laboratory test :

Table 1 Fine Aggregate Data with Bangka Sand

| Sieve | Upper Side | Lower Side | Result |
|-------|------------|------------|--------|
| 9.6   | 100        | 100        | 100    |
| 4.8   | 90         | 100        | 99.7   |

|      |    |     |       |
|------|----|-----|-------|
| 2.4  | 85 | 100 | 98.95 |
| .2   | 75 | 100 | 94.35 |
| 0.6  | 60 | 79  | 67.85 |
| 0.3  | 12 | 40  | 12.7  |
| 0.15 | 0  | 10  | 0     |
| pan  | 0  | 0   | 0     |

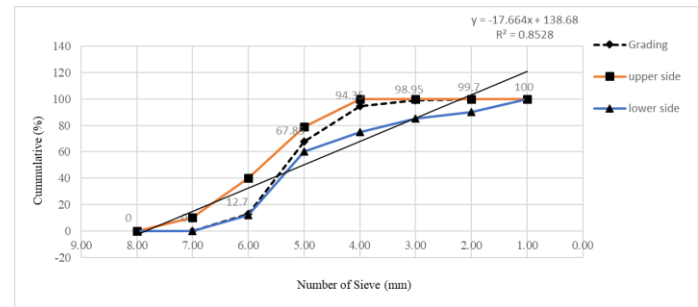


Fig. 3 Analysis of Linear Regression

The strength of the relationship between variables  $x$  and  $y$  is measured by the correlation coefficient. Correlation coefficient values are in the range  $-1$  hingga  $1$  ( $-1 \leq r \leq 1$ ). When the coefficient is  $-1$  or  $1$ , then the data is said that the relationship between variables is perfect where events in variable  $y$  can be explained or predicted by variable  $x$  without errors.

Table 2 Percentage Cummulative

| Particle size<br>(mm) | Percentage Cummulative (%)  |                           |         |       |        |         | Specifications of Mixed<br>Aggregate Gradation Maximum<br>Grain Size 40 mm |         |         |
|-----------------------|-----------------------------|---------------------------|---------|-------|--------|---------|--|---------|---------|
|                       | Coarse<br>Aggregates<br>(K) | Fine<br>Aggregates<br>(P) | 1,5 x K | 1 x P | d + e  | f/(P+K) | Curve 1  | Curve 2 | Curve 3 |
| a                     | b                           | c                         | d       | e     | f      | g       |  |         |         |
| 38                    | 100                         | 100                       | 150     | 100   | 250    | 100     | 100  | 100     | 100     |
| 19                    | 53.14                       | 100                       | 79.71   | 100   | 179.71 | 72      | 74   | 86      | 93      |
| 9.6                   | 2.64                        | 100                       | 3.96    | 100   | 103.96 | 42      | 47   | 70      | 82      |
| 4.8                   | 1.38                        | 99                        | 2.07    | 99    | 101.07 | 40      | 28   | 52      | 70      |
| 2.4                   | 0                           | 96.4                      | 0       | 96.4  | 96.4   | 39      | 18   | 40      | 57      |
| 1.2                   | 0                           | 83                        | 0       | 83    | 83     | 33      | 10   | 31      | 46      |
| 0.6                   | 0                           | 40.6                      | 0       | 40.6  | 40.6   | 16      | 6  | 21      | 32      |
| 0.3                   | 0                           | 11.2                      | 0       | 11.2  | 11.2   | 4       | 4  | 11      | 19      |
| 0.15                  | 0                           | 1                         | 0       | 1     | 1      | 0       | 0  | 1       | 4       |



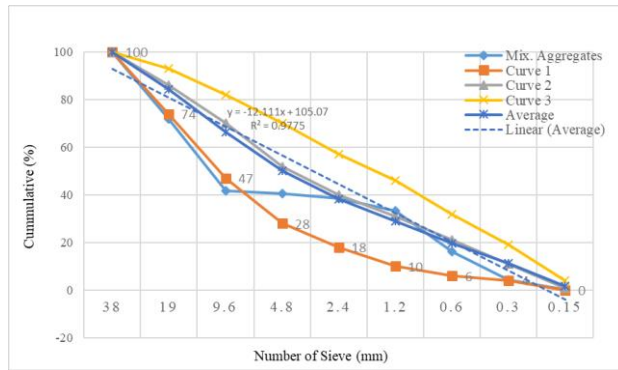


Fig. 4 Mixed Aggregate Gradation

Calculations are carried out statistically to obtain the amount or  $\Sigma$  of each calculation. The amount of each calculation data above will be used in the calculation of fine modulus on sand and gravel, the results of the fine modulus obtained must be in accordance with SNI standards. Where SNI requirements for fine modulus of sand are 1.5 - 3.8 and fine aggregate modulus is 6.5 - 7.5. From Fig. 4 above obtained in the calculation in accordance with the standard. So the fine modulus of the mixture and the results of the ratio of the percentage of fine aggregate: coarse aggregate = 60%: 40%. The specification data is based on SNI provisions so that data for curve 1, curve 2 and curve 3 are obtained.

From Fig.4 shows that the aggregate gradation combined for the maximum grain of data obtained is the amount of fine aggregate (sand) and coarse aggregate of 40mm, so that the curve obtained has met the standard. From the calculation of the data using a linear regression formula, which is through the set collected data which is illustrated through the scatterplot [5] to get results that are more accurate and in accordance with the results, namely  $R^2 = 0.9875$ .

Table 3 . Compressive Strength Test Results

| Test Object (code) | Age (Days) | Cross-Sectional Area (mm) | Load (kN) | Compressive Strength (Mpa) |
|--------------------|------------|---------------------------|-----------|----------------------------|
| RH 1               | 3          | 17622.5                   | 150       | 8.512                      |
| RH 2               |            | 17622.5                   | 130       | 7.377                      |
| RH 3               |            | 17622.5                   | 140       | 7.944                      |
| RH 1               | 7          | 17622.5                   | 170       | 9.647                      |
| RH 2               |            | 17622.5                   | 175       | 9.930                      |
| RH 3               |            | 17622.5                   | 160       | 9.079                      |
| RH 1               | 14         | 17622.5                   | 200       | 11.349                     |
| RH 2               |            | 17622.5                   | 210       | 11.917                     |
| RH 3               |            | 17622.5                   | 220       | 12.484                     |

|      |    |         |     |        |
|------|----|---------|-----|--------|
| RH 1 |    | 17622.5 | 230 | 13.051 |
| RH 2 | 21 | 17622.5 | 240 | 13.619 |
| RH 3 |    | 17622.5 | 250 | 14.186 |
| RH 1 |    | 17622.5 | 260 | 14.754 |
| RH 2 | 28 | 17622.5 | 270 | 15.321 |
| RH 3 |    | 17622.5 | 280 | 15.889 |

The magnitude of the correlation coefficient can be determined based on the distribution of the coordinates of the x and y variables. If the distribution of points is in a perfectly straight line, it can be said that the correlation value is 1 or -1 (positive and negative values depend on the direction of the distribution of points). Through correlation analysis, it can be informed that X and Y are closely related

## ANALYSIS

### Gradation Analysis of Fine Aggregate

The fine aggregate (sand) used in this study is bangka sand, in general the quality of bangka sand has fulfilled the requirements to be used as building material. However, the testing phase needs to be carried out before it is used for concrete mixture. The following is the result of a sand inspection carried out in a concrete technology laboratory.



Fig. 5 Result of Sand Gradation

In fine aggregate grading testing using a set of sieves from sieves with particle size 9.6 mm in diameter, 4.8 mm, 2.4 mm, 1.2 mm, 0.6 mm, 0.3 mm, 0.15 mm. The sieve with the largest diameter particle size is placed at the top then the smallest diameter sieve is placed at the bottom. After that, the sand is sieve using a sieve shaker and the sieve is weighed.

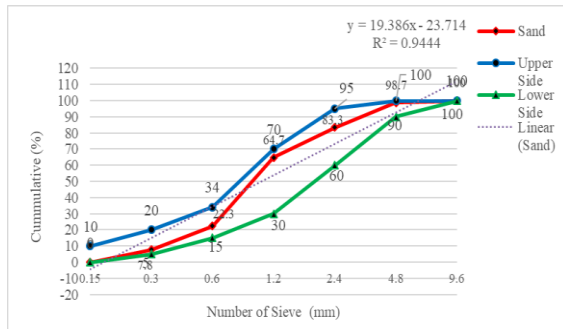


Fig. 6 Fine Aggregate Gradation Analysis

$$\text{Modulus of Sand Fineness} = \frac{\text{Total \% Cumulative Left Weight}}{100\%}$$

To find out the zone and category of sand types, it can be seen in the table below :

Table 3 Limits and Results of Test Sand Gradations[5]

| Number of Sieve (mm) | % fine aggregate through a sieve |                         |                        |                |
|----------------------|----------------------------------|-------------------------|------------------------|----------------|
|                      | Coarse (Zone I)                  | Rather Coarse (Zone II) | Rather Fine (Zone III) | Fine (Zone IV) |
| 9.6                  | 100                              | 100                     | 100                    | 100            |
| 4.8                  | 90 -                             | 90 - 100                | 90 -                   | 95 - 100       |
| 2.4                  | 60 - 95                          | 75 - 100                | 85 - 100               | 95 - 100       |
| 1.2                  | 30 - 70                          | 55 - 90                 | 75 - 100               | 90 - 100       |
| 0.6                  | 15 - 34                          | 35 - 59                 | 60 - 79                | 80 - 100       |
| 0.3                  | 5 - 20                           | 8 - 30                  | 12 - 40                | 15 - 50        |
| 0.15                 | 0 - 10                           | 0 - 10                  | 0 - 10                 | 0 - 15         |

To find out the zone and type of sand category, it can be seen in the table above:

Based on the results of testing that Bangka sand is included in the fine sand category (Zone I) with a modulus of sand fineness obtained at 3.232 This fineness modulus fulfills the requirements specified in SNI 03-6820-2002, namely with the modulus of smoothness of sand 2 - 3 and Bangka sand can be used as the main material of concrete mixture.

#### Gradation Analysis of Coarse Aggregate



Fig. 7 Coarse Aggregate Gradation Results

Coarse aggregate in the form of gravel as shown in Fig. 7 is an aggregate that all the grains are left above the 4.8mm sieve. From the results of the coarse aggregate lab test calculations, the graph calculations are as follows :

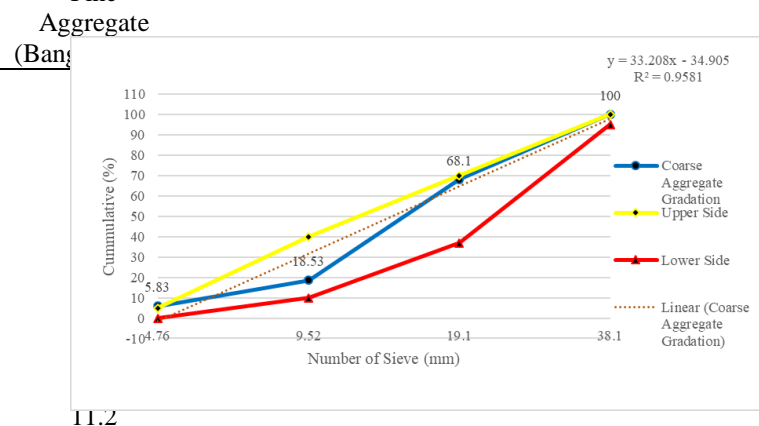


Fig. 8 Coarse Aggregate Gradation Analysis

Characterization of quality of materials is important to ensure good use of resources from environmental and economic perspectives. Particle size distribution of materials is one of the widely used tests in geotechnical engineering to evaluate quality of materials. Sieve analysis test has been used as the main method to determine particle size distribution of granular materials including coarse materials for many decades[6]. Based on the results (fig.8) of the gravel gradation analysis test shows that it has varying size shapes with 38.10 mm filter size. The result for fineness modulus obtained is 7.62 where the value of the modulus of fineness meets the requirements according to SNI 03-6820-2002[7] is the value of the modulus of fineness is not more than 8% with size around 5-8 mm and this coarse aggregate



can be used as the main material for concrete mixture.

### Concrete Compressive Strength Analysis

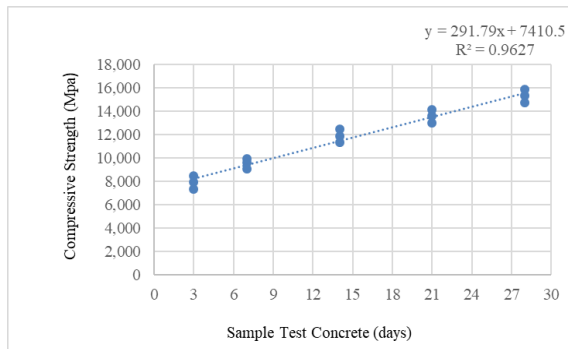


Fig. 9 Compressive Strength

Simple linear regression is a linear relationship between one independent variable (X) with a dependent variable (Y). These analyzes are used to determine the direction of the relationship between the independent variable and dependent whether positive or negative and to predict the value of the dependent variable if the value of the independent variable increases or decreases in value[8][9]. Data used is usually interval scale. Regression analysis aims to explain or model the relationships between variables.

Table 4. The value of the Linear Regression correlation coefficient according to Gelford [10]

| No. | Correlation Coefficient Values | Notes   |
|-----|--------------------------------|---|
| 1   | 0 - < 0.2                      | Very small correlation can be considered no correlation |
| 2   | $\geq 0.2$ - < 0.4             | Small relationship / not close                          |
| 3   | $\geq 0.4$ - < 0.7             | Moderate / Medium relationship                          |
| 4   | $\geq 0.7$ - < 0.9             | Close relationship                                      |
| 5   | $\geq 0.9$ - < 1               | Very close relationship                                 |

Correlation analysis aims to determine whether there is a relationship between variables and the closeness of the relationship. Correlation is a number that shows the direction and strength of the relationship between the variables studied. The direction of the relationship between variables can be positive and negative and 0 (zero) if there is no relationship at all. The strength of the relationship between variables can be expressed by the magnitude of the correlation coefficient value on the linear function. From Fig. 3 Fig.4, Fig.6, Fig.8 (regression results) can be concluded that the two X variables

and Y variable can be said to have a positive relationship if the increase in X variable is followed by an increase in Y variable, while the X variable and Y variable can be said to have a negative relationship if for every increase in X variable followed by a decrease in Y variable.

The Pearson values correlation (r) can describe the extent to which the data cluster around a straight line. Therefore from Figure 9 scatterplot correlation follows the line with a positive slope, it can be said that there is a high positive correlation between the two variables X and Y

### CONCLUSIONS

From the results of data processing for laboratory testing results is aggregate gradation affects the nature of concrete produced by mixing coarse aggregates and fine aggregates should take into account their gradations. Therefore:

1. With the use of mixed aggregate comparisons, the quality of concrete is guaranteed.
2. Fine modulus of the grains obtained is in accordance with SNI, the result is fine aggregate modulus is 3.232 and coarse aggregate modulus is 7.62
3. Bangka sand is included in zone I (coarse) and coarse aggregate is passed requirement according to SNI 03-6821-2002.
4. From calculations for the results of Linear Regression R2 for fine aggregate = 0.9441, for coarse aggregate = 0.9581 and for compressive strength = 0.9627 it means that it has a strong relationship for each variable and can be accounted for the implementation of concrete for good quality.

### RECOMENDATION

It is better to do with a sample with more variation so that it ensures whether the application of linear regression can be applied.

### ACKNOWLEDGMENTS

The author would like to thanks the Ministry of Research and Technology of Higher Education for providing funding grants for 2019 based on SK : 7/E/KPT/2019 and 225/SP2H/LT/DRPM/2019; 9/AKM/PNT/2019. Chairman of the STT PLN with SK: 0168.SK/2/A0/2019 and Head of LPPM with No. Contract; 012/1 / A01 / 2019 concerning Dikti Research Beginner Lecturer Grants.

### REFERENCES

- [1] R. Hidayawanti, S. Legino, and D. Harjanto, "Optimizing the Utilization Cement Slag and Fly

- Ash of Concrete Quality,” in *The IIER International Conference*, 2018, no. March, pp. 14–18.
- [2] R. Hidayawanti, S. Legino, I. Sangadji, R. Panca, and A. Widodo, “The Efficiency Of Fly Ash And Cement Slag To Development Building,” *Geomate*, vol. 16, no. 57, pp. 95–100, 2019.
- [3] M. Velay-Lizancos, I. Martinez-Lage, M. Azenha, J. Granja, and P. Vazquez-Burgo, “Concrete with fine and coarse recycled aggregates: E-modulus evolution, compressive strength and non-destructive testing at early ages,” *Constr. Build. Mater.*, vol. 193, pp. 323–331, 2018.
- [4] J. Sun, J. Zhang, Y. Gu, Y. Huang, Y. Sun, and G. Ma, “Prediction of permeability and unconfined compressive strength of pervious concrete using evolved support vector regression,” *Constr. Build. Mater.*, vol. 207, pp. 440–449, 2019.
- [5] National Standard Indonesia, “Fine Aggregate Analysis Test Method SNI 03-1968-1990,” pp. 1–17, 1990.
- [6] G. H. A. J. J. Kumara, K. Hayano, and K. Ogiwara, “Image analysis techniques on evaluation of particle size distribution of gravel,” *Int. J. GEOMATE*, vol. 3, no. 1, pp. 290–297, 2012.
- [7] SNI 7656: 2012, “Mix Design - SNI 7656 - 2012,” vol. 2012, pp. 2–7, 2016.
- [8] S. Palaniraj, “Evaluation of Compressive Strength of Mineral Admixed Recycled Aggregate Evaluation of Compressive Strength of Mineral Admixed Recycled Aggregate Concrete Using Multiple Linear Regression Model,” no. June, 2018.
- [9] R. Neves, A. Silva, J. De Brito, and R. V Silva, “Statistical modelling of the resistance to chloride penetration in concrete with recycled aggregates,” *Constr. Build. Mater.*, vol. 182, pp. 550–560, 2018.
- [10] B. W. Silverman, *Generalized Linear Models*, 2nd ed. London, 2018.

## DEVELOPMENT OF A MICROBIAL-BASED GROUTING MATERIAL WITH CALCIUM CARBONATE PRECIPITATES

Yoko Sakakihara<sup>1</sup>, Yoshihiro Kabeyama<sup>2</sup> and Shinichiro Okazaki<sup>3</sup>

<sup>1,2</sup> Graduate school of engineering, Kagawa University, Japan;

<sup>3</sup> Faculty of engineering and design, Kagawa University, Japan

### ABSTRACT

Bio-concrete, which is a concrete with self-repair capability provided by microorganisms, is attracting much attention. In recent years, crack repair grouts based on microbial metabolism have been studied. Because such grouts are flowable aqueous solutions, they differ greatly from grouts based on inorganic or organic compounds and are expected to penetrate into cracks in concrete by capillary action. Therefore, press fitting of bio-grouts is unnecessary. As an additional advantage, these grouts do not impose a load on the environment. In this study, we performed benchtop experiments using conical tubes with a large amount of calcium source. The experimental results show that the addition of a large amount of calcium shows no substantial change in the amount of precipitate. In addition, the amount of precipitated crystals did not substantially differ even when the type of calcium salt was varied. Prolonging the standing time was led to crystal growth, and the amount of precipitates obtained increased. As a result of scanning electron microscopy observations of the crystals obtained under each growth condition, we confirmed that many yeast cells were mixed in the crystals. However, difference was observed in the crystal structure when calcium salt was varied. Moreover, Calcium carbonate formation was observed on concrete as a preliminary experiment for the crack repair of concrete. Crystals were generated even at room temperature, and better results were obtained when the temperature was set to 40 °C.

*Keywords: Grout, Calcium carbonate, Calcite, Microbial metabolism*

### INTRODUCTION

Concrete is designed to undergo cracking, and some cracking is considered acceptable to some extent. However, cracking of concrete enables water and carbon dioxide to flow in at the gaps; the concrete becomes carbonated, and the cracks provide channels for the penetration of chloride ions that corrode rebar.

Grouting has been investigated as a crack repair method; however, concerns have arisen about that environmental load imposed by grouting because of the chemical agents involved. Odor at the time of construction has also been mentioned as a problem. Such concerns have spurred recent research into biomaterials, including bio-grouts.

Last year, we examined the formulation conditions of bio-grout using the simulation software PHREEQC, which can be used to carry out geoscience calculations. Recently, on the basis of our previous results, we have conducted experiments that consider biological conditions and crystallographic phenomena. [1] - [7]

### IN VITRO EXPERIMENTS

In our recent work, the amount of calcium carbonate generated from bio-grout was examined in a conical tube, and the results were discussed.

### Outline of Experiments

The experimental conditions were assembled with reference to the conditions selected from the previous research and the results obtained by simulation last year [1], [7]. Table 1 shows the compounding conditions used in our previous study.

Table 1 Formulation of bio-grout as reference.

|          | Materials                           | Conc.   |
|----------|-------------------------------------|---------|
| Microbe  | Yeast                               | 6.0 g/L |
| Nutrient | D-Glucose                           | 0.40 M  |
| Calcium  | Calcium lactate                     | 0.20 M  |
| Buffer   | Tris(hydroxymethyl)<br>aminomethane | 0.75 M  |

Note: The pH was set to 9.0, and the experimental temperature was 20 °C.

The simulation results indicated that the precipitation amount of calcium carbonate can be increased by setting the temperature high and preventing a decrease in pH. Yeast is an organism and, as such, has an optimum temperature for growth. Yeast is killed at temperatures greater than 40 °C; thus, the setpoint temperature in these experiments was 40 °C, and a comparative experiment was performed at room temperature.

We speculated that the amount of precipitated

calcium carbonate would increase with increasing amount of calcium salt. We therefore conducted experiments in which the concentration of the calcium salt was varied. In addition, we investigated whether the results differ depending on the calcium salt used in the bio-grout. Table 2 shows the experimental materials. The experimental conditions are summarized in Table 3.

Water (40 ml) as a solvent was placed in a 50 ml conical tube. The buffer and calcium salt were dissolved, the pH was adjusted to 9.0, and the experiment was started by simultaneously dissolving glucose and dry yeast in the solution. Both solutions were covered with silicon, leaving air holes to prevent the evaporation of water.

Table 2 Proposed formulation of bio-grout.

|          | Material                         | Conc.   |
|----------|----------------------------------|---------|
| Microbe  | Yeast                            | 6.0 g/L |
| Nutrient | D-Glucose                        | 0.4 M   |
| Calcium  | Various                          | Various |
| Buffer   | Tris(hydroxymethyl) aminomethane | 0.75 M  |

Table 3 Different experimental conditions using the components from Table 2.

|        | Calcium salt      | Conc. |
|--------|-------------------|-------|
| Case 1 | Calcium acetate   | 0.2 M |
| Case 2 | Calcium acetate   | 0.3 M |
| Case 3 | Calcium acetate   | 0.4 M |
| Case 4 | Calcium lactate   | 0.2 M |
| Case 5 | Calcium ascorbate | 0.2 M |

## Experimental Procedure

To observe the progress of the experiment, we observed the aqueous solution with a microscope on the second day after the start of the experiment to observe whether calcium carbonate crystals had formed.

### Microscopic observations

A biological microscope was used for observations. The objective lens was 40 $\times$ , the eyepiece was 10 $\times$ , and the image was taken at a magnification of 4 $\times$  with a digital camera attached to the lens barrel.

An image of the aqueous solution in which calcium lactate was used as the calcium salt is shown in Fig. 1. The small circles are yeast cells, and the darker objects with shadows are crystals. Although the amount of precipitates was small, they could be observed by optical microscopy.

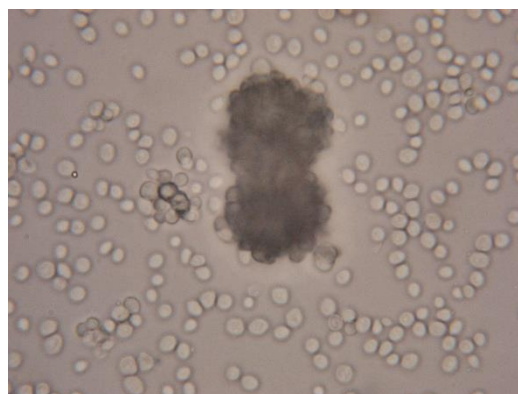


Fig. 1 Microscopic image (magnification: 1600 $\times$ ) corresponding to Case 4 with calcium lactate as the calcium salt.

## Experimental Results

The experiment was conducted for 3 days. The pH change was confirmed every 24 h, and the amount of precipitates was measured. Room temperature was between 24 and 28  $^{\circ}\text{C}$  throughout the experiment.

### pH change

The decrease in pH was greater for the samples maintained at 40  $^{\circ}\text{C}$ . We attributed this lower pH to the enhanced activity of the yeast at the higher temperature, which caused it to breathe more and discharge more carbon dioxide than the yeast at room temperature.

### Measurement of precipitation amount

The precipitate generated in the experiment was collected by vacuum filtration using filter paper (No. 5C). The amounts of precipitates obtained from the samples maintained at room temperature and from those maintained at 40  $^{\circ}\text{C}$  are shown in Fig. 2 and Fig. 3, respectively. Even when no crystal was observed on the filter paper, approximately 0.1 g of material was recovered. We speculated that approximately 0.1 g of yeast remained on the filter paper.

In general, the results of this study show that the addition of a large amount of calcium salt did not lead to a large amount of precipitate. This outcome is attributable to two possible causes. First, the experimental period may have been too short for appreciable precipitate growth. Second, the concentration and, therefore, the osmotic pressure may have been too high for the yeast to survive. These possibilities are currently being investigated further.

When calcium ascorbate was added, the amount

of precipitates increased slightly. The product was confirmed by X-ray diffraction (XRD) and scanning electron microscopy (SEM). Then, we confirmed that the crystals grew and the amount of precipitates increased with increasing standing time.

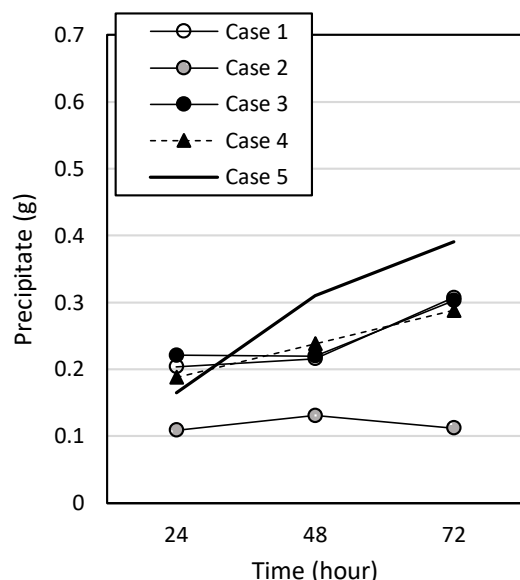


Fig. 2 Amount of precipitates collected from samples maintained at room temperature.

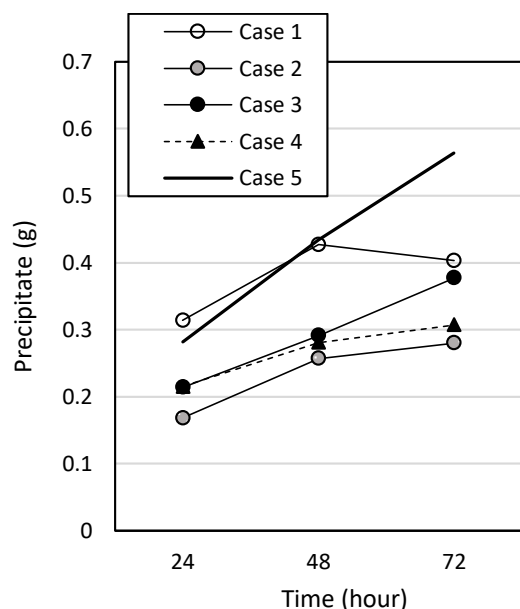


Fig. 3 Amount of precipitates collected from the samples placed in a constant-temperature bath at 40 °C.

### XRD analysis

The crystal structure of the precipitate obtained in the experiment was analyzed by XRD. The results, presented in Fig. 4, show that the precipitated crystals are mainly composed of calcite.

In Cases 1-3 and 4, in addition to calcite, vaterite was detected. In Case 5 to which calcium ascorbate was added, only calcite was precipitated.

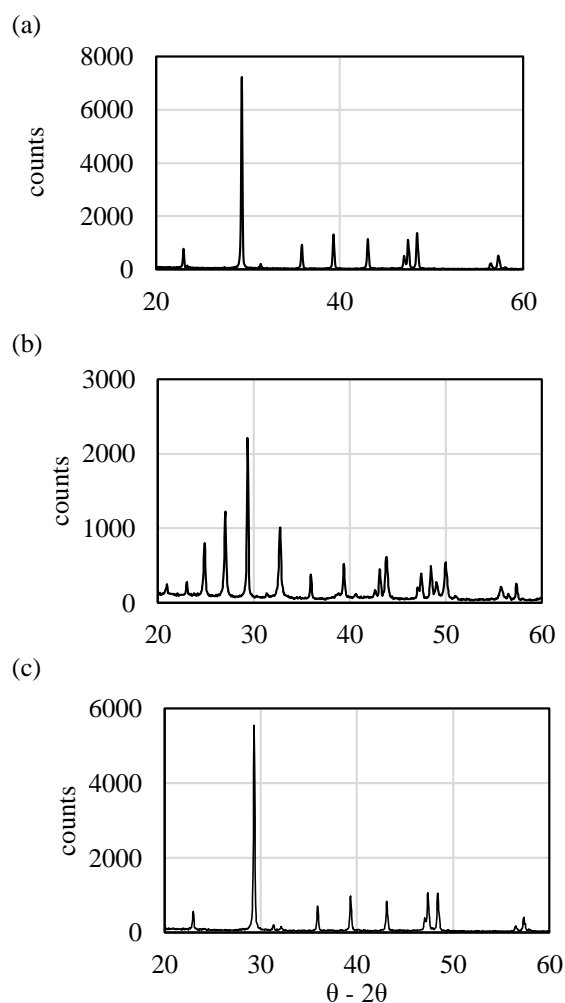


Fig. 4 XRD patterns: (a) Calcite; (b) Case 1: 0.2M Calcium acetate; (c) Case 5: 0.2M Calcium ascorbate

### SEM analysis

The crystals obtained under each condition were observed by FESEM, and SEM. The images confirmed that many yeast cells were mixed with each crystal. The crystals themselves were spherical. It is speculated that this is because the crystal takes on a vaterite structure at the formation stage. The SEM images of the precipitates corresponding to Cases 1 and 3, where numerous crystals were obtained, are shown in Fig. 5.

Although experiments were conducted in two systems (one at room temperature and the other in a constant-temperature bath at 40 °C) and the amounts of precipitates differed, no significant difference was found in the crystal structures of the precipitates.

In Case 5 to which calcium ascorbate was added,

a peak of only calcite was observed in the XRD, however aragonite was also confirmed in the SEM image. But, the amount is very small. From the SEM image, it was found that many cavities were found in the crystal, and it took longer standing times for crystal growth.

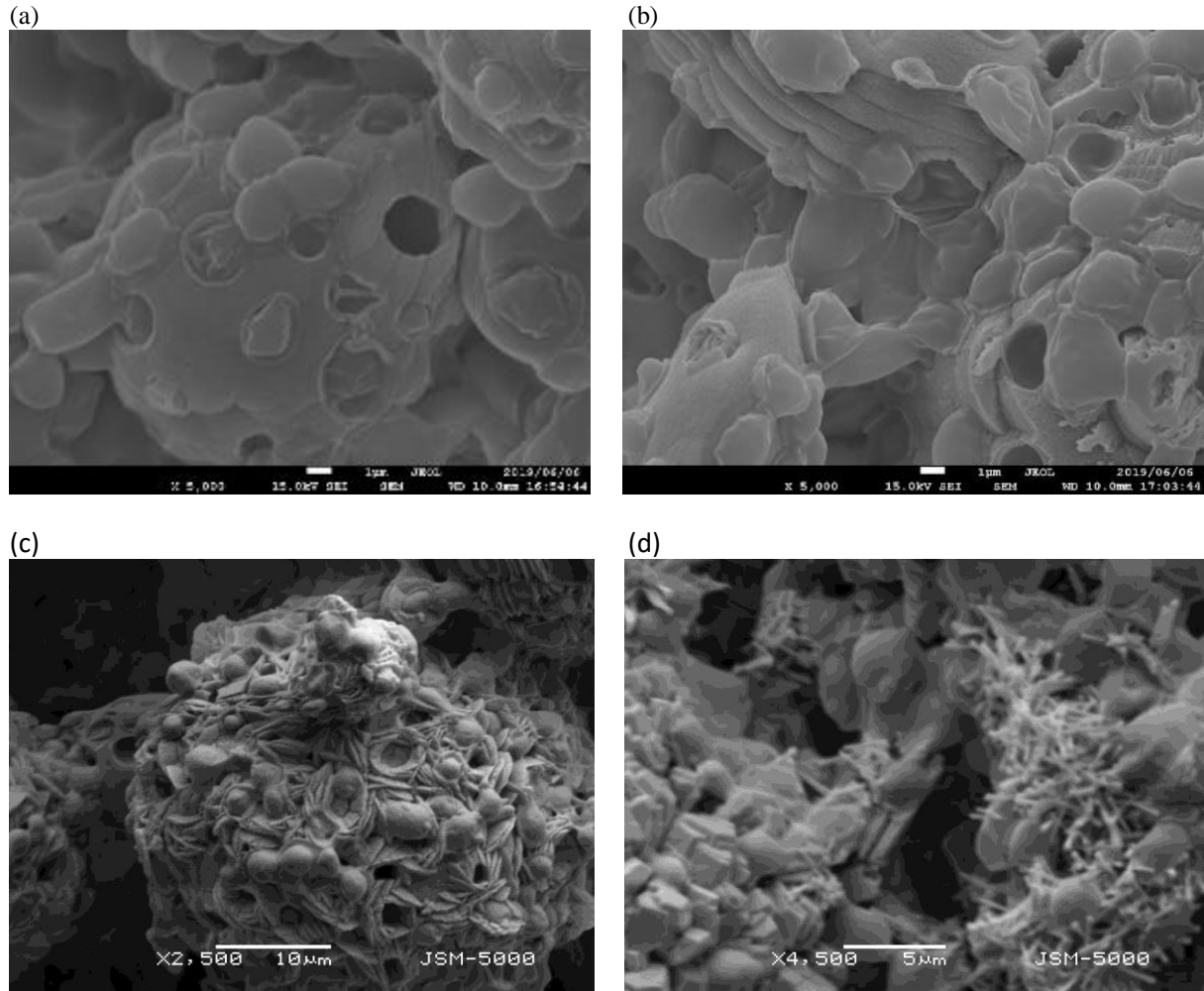


Fig. 5 FESEM, and SEM micrographs: (a) Case 1, room temperature (5000×); (b) Case 1, 40°C (5000×); (c) Case 3, 40 °C (2500×); (d) Case 5, 40 °C (4500×).

## ADAPTATION TO CONCRETE

The optimum environment for the yeast strain used in this work is approximately pH 4-6; thus, the yeast prefers slightly acidic conditions [8]. However, concrete is alkaline, with a pH of approximately 11. Bacteria that grow under basic conditions are usually selected for use in bio-concrete and bio-grout.

Our rationale for selecting yeast is that they are inexpensive, easily obtainable anywhere in the world, and ubiquitous.

## Preliminary Experiment

Before repairing cracks using bio-grout, to understand the growth conditions of the yeast and the generation of crystals, we conducted experiments on the concrete. A silicon was placed as a wall on top of a 10 cm × 10 cm mortar specimen, and the grout was poured into it. The selected grout was that of Case 1.

After the start of the experiment, only water was added as necessary to prevent dehydration because an aqueous solution placed on the concrete would be lost immediately by evaporation and absorption. The concrete was covered with a wrap to prevent excessive drying.



Two specimens were prepared. One was placed indoors at room temperature, and the other was placed in a thermostatic chamber at 40 °C.

### Experiment Result Day 2

Crystal growth was checked 2 days after the start of the experiment. A biological microscope was used for the observation; the magnification was 1600×.

As a result of microscopic observation, crystals were suspended on the water surface of a solution placed in concrete installed at room temperature. The solution immediately above the concrete was also collected and observed. However, mostly yeast cells were observed, with very few crystals.

### Experimental Result 5th Day

Five days after the start of the experiment, the solution was removed and the concrete surface was observed.

### Microscopy

A microscope was used for the observation; the images were collected at approximately 200× magnification.

Pure calcium carbonate crystals appeared on the concrete surface in the specimen maintained at room temperature (Fig. 6 (a)). These crystals were observed over the whole concrete surface and in the holes.

For the sample maintained at 40 °C, the crystals apparently aggregated into large flocks (Fig. 6 (b)). An image of the side not in contact with the aqueous solution is shown in Fig. 6 (c). This image was collected by expanding the innumerable small holes in the concrete surface; however, the interior of the holes was empty, and the surface was flat.

For the sample maintained at 40 °C, the locations of the crystals on the concrete surface were difficult to determine; however, the crystals clearly grew large, as revealed by observation of the interior of the holes (Fig. 6 (d)).

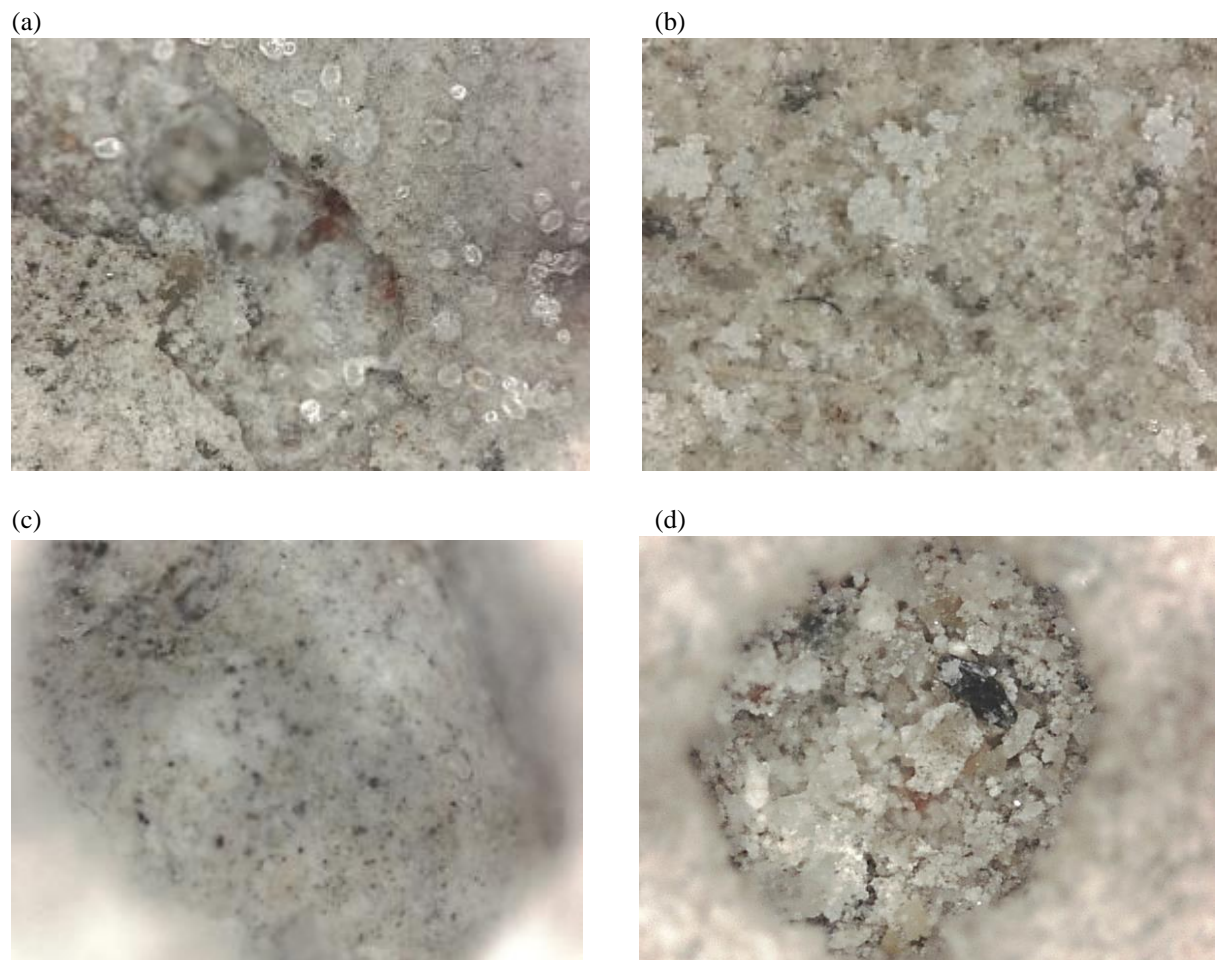


Fig. 6 Microscopic images (200×): (a) crystals generated on the concrete surface at room temperature; (b) crystals generated on the concrete surface at 40 °C; (c) a hole in an untested concrete surface; and (d) crystals formed in the hole at 40 °C.



### Laser Raman spectroscopy

When the crystal which precipitated on concrete was analyzed by laser Raman spectroscopy, the peak of calcium carbonate was confirmed. The image of the Raman spectrum is shown in the Fig. 7.

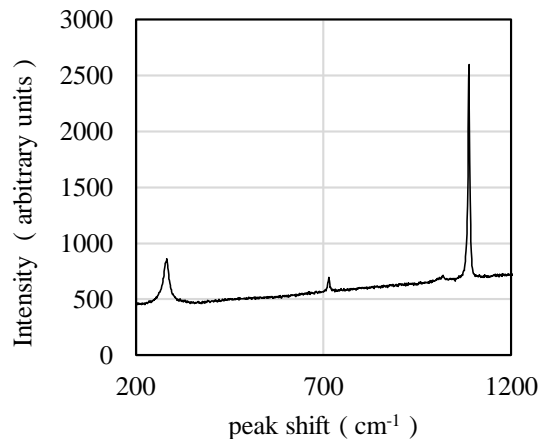


Fig. 7 Raman spectrum of precipitates

### CONCLUSIONS

In in vitro experiments, we expected that a large amount of calcium carbonate could be obtained by adding a large amount of calcium salt; however, no change was observed. Experiments confirmed that the amount of calcium carbonate obtained was almost the same irrespective of the type of calcium salt. Prolonging the standing time led to crystal growth, and the amount of precipitates increased. SEM observations of the crystals obtained under each condition confirmed that many yeast cells were mixed with the crystals. Difference was observed in the crystal structure when calcium salt was varied.

A preliminary experiment was carried out to adapt the bio-grout to concrete, and the process was observed via optical microscopy, and the precipitates were observed via microscope and laser Raman spectrophotometer. The precipitating calcium carbonate on the concrete surface could be confirmed. Crystals were generated even at room temperature, and better results were obtained in experiments conducted at 40 °C.

In the future, we will conduct more practical experiments for crack repair, repeat follow-up observations, and further consider optimal combinations of grout materials..

### ACKNOWLEDGMENTS

We appreciate the support for this research provided by the JSPS Grant-In-Aid for Scientific Research (B) task number 15h04025.

### REFERENCES

- [1] Putri P. Y., Kawai K., Ujike I., and Yamamoto S., Effect of temperature on precipitation rate of calcium carbonate produced through the microbial metabolic process of bio materials, *Civil Engineering Dimension*, 18(2), 2016, pp. 103-108
- [2] Kawaai K., Ujike I., Putri P.Y., and Yamamoto S., Some considerations on precipitation rate of calcium carbonate in bio-based materials used for concrete repair, *Concrete Solutions 2016: Proceeding of 6th International Conference on Concrete Repair*, Aristotle University of Thessaloniki, Greece, June 20-22, 2016, pp. 580-587
- [3] Kawasaki S., Muaro A., Hiroyoshi N., Taunekawa M., and Kaneko K., Fundamental study on novel grout cementing due to microbial metabolism, *Journal of Japan Society of Engineering Geology*, 47(1), 2006, pp. 2-12
- [4] Kubo K., Okazaki S., and Ujike I., Development of microbial metabolic processes to repair concrete joint leakage, *Advanced Material Research*, 845, 2013, pp. 158-162
- [5] Ujike I., Kubo F., Kawai K., and Okazaki S., Influencing factors affecting microbial metabolic processes of biomaterials used for leakage repairs, *Concrete Solutions*, 2014, pp. 127-133
- [6] Akiyama M. and Kawasaki S., Application of numerical simulation of microbial reaction to biogrout with ureolytic bacteria, *Japanese Geotechnical Journal*, 12(3), 2017, pp. 337-349
- [7] Sakakihara Y., and Okazaki S., Development of a crack repair method using yeast-induced calcium carbonate precipitation, *International Journal of GEOMATE*, May 2019, Vol.16, Issue 57, pp.89 – 94.
- [8] Watanabe S., Shinohara N., Kanai S. and Iizuka Y., Properties of natural yeast isolated from raisin as a baker's yeast, *Bulletin of Seitoku University Junior College of Nutrition*, 2005, Vol.36, pp.1-6

## EVALUATION OF LARGE DIAMETER JET GROUTING TECHNIQUE USED FOR TUNNEL CONSTRUCTION IN BANGKOK

Kuo Chieh Chao, Ph.D., P.E.<sup>1</sup>, Sasirada Seepim<sup>2</sup>, Ricky K. N. Wong<sup>3</sup>, Takeshi Iwakubo<sup>4</sup>, and Morris Wang<sup>5</sup>

<sup>1,2</sup> Geotechnical and Earth Resources Engineering, Asian Institute of Technology, Pathumthani, Thailand

<sup>3,4</sup> Sanshin Construction (Thailand) Co., Ltd., Bangkok, Thailand

<sup>5</sup> ISEKI Engineering (Thailand) Co., Ltd., Bangkok, Thailand

### ABSTRACT

This paper presents the use of a large diameter jet grouting technique for installation of jet grout piles for 2 different tunnel projects in Bangkok. The first project where the large diameter jet grouting technique was used is the MRTA Blue Line Extension Project in Bangkok, Thailand. The jet grouted piles were used to seal off the base of excavation at the ITD TBM retrieval shaft from the high-water pressure. The second project where the large diameter jet grouting technique was used is the MRTA Orange Line-East Project in Bangkok, Thailand. Preceding beams with a thickness of 3.0 m were designed and constructed to reduce the overstress that could happen to the pile foundation of the adjacent Srirat Expressway. The procedure and design parameters of the large diameter jet grouting technique are provided in the paper. The required design parameters for the grouted materials were verified by conducting laboratory testing of coring samples obtained at the site. Moreover, the required design parameters were further verified by conducting a pumping test and an electrical resistivity test at the site. The results of the laboratory and field tests indicate that the design requirements of the treated materials can be met effectively using the large diameter jet grouting technique in Bangkok. Furthermore, the construction time and the associated cost were reduced using the large diameter jet grouting technique.

*Keywords: jet grouting; soil improvement; TBM; underground structure; electrical resistivity; case study*

### INTRODUCTION

Jet grouting technique has been widely used for soft ground improvement in various underground projects to form water-proof base seals and buried grout supports for deep excavations and tunnel construction. The process of jet grouting technique is relating high-pressure erosion, grout injection and mixing of in-situ soil, resulting in both replacement and reduction of the soil and the construction of a treated soil mass which in most illustrations has the form of a jet grout column. Over the past few decades, significant progress has been made in the jet grouting technology, especially in increasing the diameter of the jet grout column and improving the jet grouting equipment (Yoshida, 2010; Burke, 2012, and Cheng et al., 2017). The diameter of the jet grout column is controlled by the grouting parameters including grout slurry selection, jet grouting pressure, flow rate of a jetting fluid, jetting time, jet nozzle size, grouting layout, withdraw rate, etc. The diameter of the jet grouting columns constructed in Bangkok by local contractors is approximately 0.8 to 1.2 m. Constructing jet grouting columns with a larger diameter has certain advantages, especially for the ground improvement work in a limited construction

space and sensitive ground conditions in Bangkok. The advantages of using the large diameter jet grouted technique instead of the traditional method include to minimize the required number of boreholes, to save drilling time, and to provide higher strength and lower permeability of the treated materials.

A large diameter jet grouting technique called Rapid-Jet Method was developed in the jet grouting industry within the last decade. The Rapid-Jet Method utilizes high-pressured grout slurry to erode and mix the in-situ soil to form soil-cement mixture columns with a diameter up to approximately 3.5 m. A double-tube grouting system with two nozzles on the opposite side of the jetting device can carry out efficient grouting with large-diameter and high-speed construction. Fig. 1 shows the sketch of the large diameter jet grouting system.

This paper presents the use of the large diameter jet grouting technique for installation of jet grout piles for two different tunnel projects in Bangkok. The first project that the large diameter jet grouting technique was used is the MRTA Blue Line Extension Project in Bangkok, Thailand. The jet grouted piles were used to seal off the base of an excavation of the ITD TBM retrieval shaft from the high-water pressure. The second project that the large diameter jet grouting technique was used is the MRTA Orange Line-East Project in Bangkok, Thailand. Jet grouted preceding beams with a

thickness of 3.0 m were designed to reduce the overstress that could happen to the pile foundation of the adjacent Srirat Expressway.

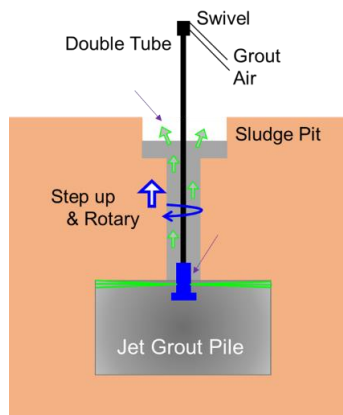


Fig. 1 Sketch of large diameter jet grouting system

The design parameters and procedure of the large diameter jet grouting technique were provided in the paper. The required design parameters for the grouted materials were verified by conducting laboratory testing of coring samples obtained at the site. Moreover, the required design parameters were further verified by conducting a pumping test and an electrical resistivity test at the site. The results of the laboratory tests and the field tests were discussed in the following sections.

## COMPARISON OF JET GROUTING PRACTICE IN THE INDUSTRY

Jet grouting technique has been used for soil improvement method for many projects in Thailand. The most well-known project for using jet grouting as the ground improvement technique is the Suvarnabhumi International Airport (SBIA) Drainage Project. The construction of jet grouting at this project has a total length of about 5 kilometers and include 85,300 jet grouted piles with a diameter of 0.8 m. The single tube jet grouting system was used for the project.

Another example project of using jet grouting for ground improvement is the Pak Phanang Diversion Dam Project located in Nakornsrihammarat, Thailand (Jaritngam, 2003). Jet grouting piles were used for the project to minimize settlement and increase the stability of the dam. The double tube system was adopted to install the 1.6-m diameter jet grouted piles with a jet grouted volume of approximately 144,600 m<sup>3</sup>. The jet grouting parameters for this project are presented in Table 1.

Table 1 The optimum jet grouting operating parameters (Jaritngam, 2003)

| Parameters            |     | Unit                |
|-----------------------|-----|---------------------|
| Jet grouting pressure | 20  | MPa                 |
| Grout flow rate       | 60  | Liter/min           |
| Air pressure          | 700 | kPa                 |
| Air flow rate         | 3   | m <sup>3</sup> /min |
| Withdrawal rate       | 18  | min/m               |
| Rotation rate         | 10  | rpm                 |
| Mix proportion        | 700 | kg/m <sup>3</sup>   |

Table 2 presents the common jet grouting parameters that are used in Thailand. For comparison purposes, existing grouting methods that are used in the industry within the region are also included in Table 2. Furthermore, Table 2 shows the grouting parameters for the Rapid-Jet Method that were used for both of the MRTA projects. Table 2 indicates that, in general, the jet grouting practice in Thailand uses a single-tube grouting system with one nozzle. The diameter of a grout pile can be only installed up to 1.2 m. For the JSG and CJG methods, the diameter of a grout pile can be installed up to 2 m, whereas the diameter of a grout pile for the RJP method can be constructed up to 3 m. Similar to the JSG method, the Rapid-Jet Method uses a double-tube grouting system with two nozzles on the opposite side of the monitor. The latter also uses air and jet stream to cut and mix the in-situ soil with grout. The grouting parameters that are used are as follows: grouting pressure = 33 ~ 37 MPa, grouting rate = 180 or 360 L/min, rod rotation = 2 ~ 5 rpm, and withdrawal rate = 10 ~ 18 min/m. Using these parameters, the grouting capacity can be increased to 35.3 m<sup>3</sup>/hr. So, it can rapidly install a grout pile with a diameter up to 2.5 ~ 3.5 m at a depth up to 50 m below the ground surface.

## APPLICATIONS OF LARGE DIAMETER JET GROUTING TECHNIQUE

### MRTA Blue Line Extension Project

#### Site conditions

For the MRTA Blue Line Extension Project, the IDT TBM retrieval shaft is located at the Northern end of the Sanam Chai (BS12) Station, which is the extension of Chaloem Ratchamongkhon (or the Blue Line) of the Bangkok MRT. The Blue Line Extension Project is 16.51 m long, 9.60 m wide, and 32.5 m deep. The subsoil conditions at the site are shown in Fig. 2. The groundwater level was measured at a depth of 10 m below the ground surface. As indicated in Fig. 2, the site has mostly soft clay to stiff clay and sand interlayers. A soft clay layer is located within the

Table 2 Comparison of different jet grouting methods (modified from Yong et al., 1996; Yoshida et al., 1996)

| Item \ Method         |                 | Common Grout Parameters in Thailand | Jet Special Grout (JSG method)     | Column Jet Grout (CJG method)      | Rodin Jet Pile (RJP method)        | Rapid-Jet Method                   |
|-----------------------|-----------------|-------------------------------------|------------------------------------|------------------------------------|------------------------------------|------------------------------------|
| Effective diameter    |                 | $\phi$ 0.8 ~ 1.2 m                  | $\phi$ 1.0 ~ 2.0 m                 | $\phi$ 1.2 ~ 2.0 m                 | $\phi$ 2.0 ~ 3.0 m                 | $\phi$ 2.5 ~ 3.5 m                 |
| Geological condition  | Sand            | SPT-N $\leq$ 100                    | SPT-N $\leq$ 50                    | SPT-N $\leq$ 200                   | SPT-N $\leq$ 100                   | SPT-N $\leq$ 100                   |
|                       | Clay            | SPT-N $\leq$ 5                      | SPT-N $\leq$ 4                     | SPT-N $\leq$ 9                     | SPT-N $\leq$ 5                     | SPT-N $\leq$ 5                     |
| Design strength       | Sand            | 2 ~ 3 MPa                           | 2 ~ 3 MPa                          | 2 ~ 3 MPa                          | 2 ~ 3 MPa                          | 2 ~ 3 MPa                          |
|                       | Clay            | 0.3 ~ 1 MPa                         | 0.3 ~ 1 MPa                        | 0.3 ~ 1 MPa                        | 0.3 ~ 1 MPa                        | 0.3 ~ 1 MPa                        |
| Drill hole diameter   |                 | -                                   | 0.12 ~ 0.15 m                      | 0.14 ~ 0.25 m                      | 0.14 ~ 0.25 m                      | 0.14 ~ 0.25 m                      |
| Drill rod diameter    |                 | single-tube                         | 0.06 m (double-tube)               | 0.06 m or 0.09 m (triple-tube)     | 0.09 m (triple-tube)               | 0.06 m or 0.09 m (double-tube)     |
| Number of nozzles use |                 | 1                                   | 1                                  | 2                                  | 2                                  | 2                                  |
| Jet grouting          | material        | Binder                              | Binder                             | Water                              | Water                              | Binder                             |
|                       | total pressure  | 20 ~ 40 MPa                         | 18 ~ 22 MPa                        | 35 ~ 40 MPa                        | 20 MPa                             | 30 ~ 35 MPa                        |
|                       | total flow rate | -                                   | 60 L/min                           | 70 L/min                           | 50 L/min                           | 180 or 360 L/min                   |
| Total air pressure    |                 | -                                   | 0.6 ~ 0.7 MPa                      | 0.6 ~ 0.7 MPa                      | 0.7 ~ 1.05 MPa                     | 0.7 ~ 1.05 MPa                     |
| Binder                | total pressure  | -                                   | -                                  | 2 ~ 5 MPa                          | 40 MPa                             | -                                  |
|                       | total flow rate | -                                   | -                                  | 140 ~ 180 L/min                    | 190 L/min                          | -                                  |
| Rod rotation          |                 | 6 - 15 rpm                          | < 10 rpm                           | < 6 rpm                            | < 6 rpm                            | 2 ~ 5 rpm                          |
| Withdrawal rate       |                 | 3 ~ 5 min/m                         | 16 ~ 40 min/m                      | 16 ~ 25 min/m                      | 15 ~ 20 min/m                      | 8 ~ 16 min/m                       |
| Grouting capacity     |                 | -                                   | 4.0 m <sup>3</sup> /hr             | 11.8 m <sup>3</sup> /hr            | 18.5 m <sup>3</sup> /hr            | 35.3 m <sup>3</sup> /hr            |
| Binder consumption    |                 | -                                   | 0.9 m <sup>3</sup> /m <sup>3</sup> | 0.9 m <sup>3</sup> /m <sup>3</sup> | 0.6 m <sup>3</sup> /m <sup>3</sup> | 0.5 m <sup>3</sup> /m <sup>3</sup> |
| Amount of sludge      |                 | -                                   | 1.3 m <sup>3</sup> /m <sup>3</sup> | 1.8 m <sup>3</sup> /m <sup>3</sup> | 1.0 m <sup>3</sup> /m <sup>3</sup> | 0.7 m <sup>3</sup> /m <sup>3</sup> |

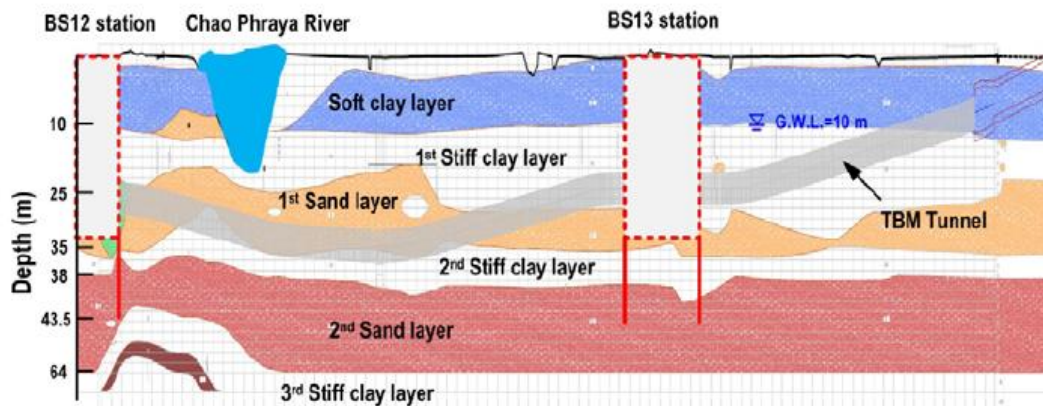


Fig. 2 Soil profile and the locations of BS12 station and IDT shaft

upper 10 m. The 1<sup>st</sup> stiff clay layer is located at depths of 10 to 25 m. The 1<sup>st</sup> sand layer is located at depths of 25 to 35 m. The 1<sup>st</sup> sand layer has the SPT-N values of about 20 to 35 and a fine content of  $\approx 0$  to 10%. The 2<sup>nd</sup> stiff clay layer is located at depths of 35 to 38 m. The 2<sup>nd</sup> stiff clay layer has the SPT-N values of about 20 to 60 and a fine content of approximately 70%. The 2<sup>nd</sup> sand layer is located below a depth of 38 m and is more than 20 m thick. Hence, when excavating to the designed depth, the impermeable 2<sup>nd</sup> stiff clay layer (only 0 ~ 4 m thick) is unable to resist the artesian water pressure from the permeable 2<sup>nd</sup> sand layer and might cause the risk of uplift and piping in the 2<sup>nd</sup> stiff clay layer (refer to Fig. 3).

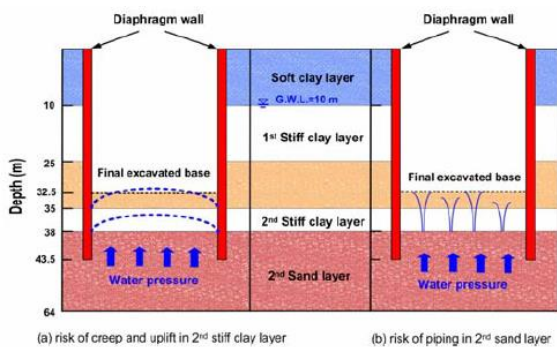


Fig. 3 Construction risk of IDT shaft and the purposed jet grouting

When excavating an extremely deep ground and the groundwater level is relatively high, the thickness of the impermeable layer under excavation base is the key factor that influences the safety of construction. In order to improve construction safety, base seal grouting, as a compensation measure, is often applied to increase the thickness of the impermeable layer and to improve the strength and water tightness of excavation base. This can also reduce the uplift pressure from the artesian water.

#### *Jet grouting at the base of the excavation*

Jet grouting was conducted at the base of the excavation to prevent the risk of uplift and piping in the 2<sup>nd</sup> stiff clay layer. Fig. 4 shows the grouting plan and cross-section view of the rapid-jet grouting dimensions. A total of 30 JGP columns with a diameter of 3.2 m were installed at the site. The grouting thickness was about 9.86 m and the depth of drilling was 43.81 m below the ground surface. The grouting parameters are provided as follows: grout pressure = 35 MPa; grout flow = 360 L/min; withdraw rate = 14 min/m; and rod rotation = 4 rpm. The water-cement ratio is 758 kg (water):750 kg (cement).

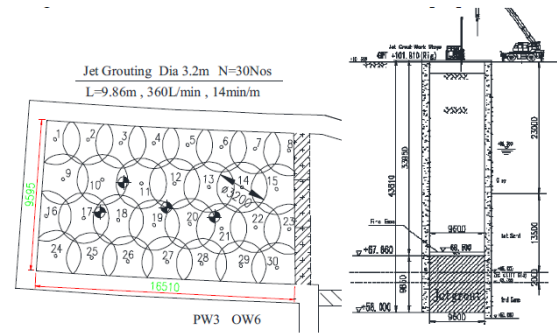


Fig. 4 Jet grouting layout and cross section

#### *Quality control*

Four verticality tests were carried out to check the verticality. The results of the verticality tests indicate that the verticality was less than 1/250 at a depth of 44 m. One coring test was conducted at the intersection of grout points 4, 5, and 12. The unconfined compression strengths for the core samples were measured to be on the average of 6 MPa, which meets the design requirement strength of 3.0 MPa. A field pumping test was carried out, and the results of the pumping test showed that there was no water in the IDT shaft. The required hydraulic conductivity of the sandy layer was  $5 \times 10^{-5}$  cm/sec after grouting. Fig. 5 shows that the base of the excavation was in a dry condition after grouting. Consequently, the design requirement for hydraulic conductivity was met for the MRTA underground retrieval shaft.



Fig. 5 Final excavation base at a depth of 32.5 m for IDT shaft

### **MRTA Orange Line East Project**

#### *Site conditions*

The Pradit Manutham Station (OR15) is an underground station along the MRTA Orange Line East (Contract E1) Project, which consists of 3 underground stations (OR13: Thailand Cultural Center, OR14 MRTA, and OR15: Pradit Manutham). The portion of this project is approximately 6.3 km in length. The area under consideration lies within relatively flat terrain where the ground level varies from 100.0 to 102.0 mRL. The location of the MRTA Orange Line East Project is presented in Fig. 6. Along the MRTA Orange Line East Project, the OR15 Station is considered to have a high-risk potential to



the nearby Srirat Expressway. Therefore, the OR15 Station was chosen for the jet grouting study. The plan view of the OR15 Station and the Srirat expressway is presented in Fig. 7.

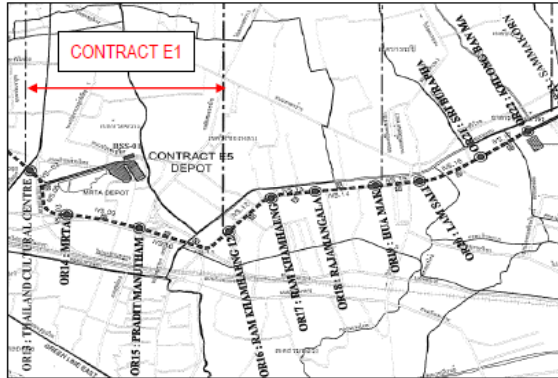


Fig. 6 MRTA Orange Line East (Contract E1)



Fig. 7 Plan view of OR15 station and Srirat expressway

Without any protection measures for the Srirat Expressway viaduct, it was estimated that the deflection at the base slab of the diaphragm wall could increase up to 66 mm with an unsatisfied estimated moment in the piles. To avoid the excessive amount of deflection, it was determined to install 2 preceding beams with a thickness of 3.5 m using the large diameter jet grouting technique. The first preceding beam is constructed at a depth of 15 m below the ground level in a medium clay layer. The second preceding beam was installed in a sand layer, which is at a depth of 26.5 m below the ground surface. The layout plan of the preceding beams at the OR15 Station is shown in Fig. 8.

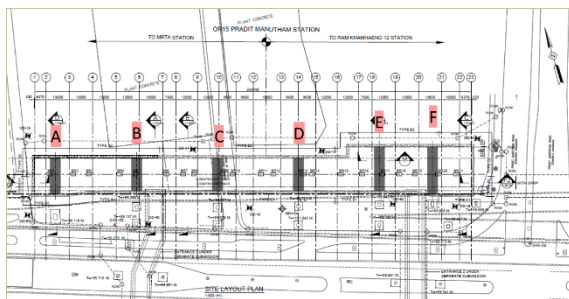


Fig. 8 Layout plan of preceding beams at OR15

station

#### *Jet grouting for preceding beams*

The Rapid-Jet Method was used to form the preceding beams at the site. Fig. 9 shows the design plan of the jet grouted preceding beam. Fig. 9 indicates that the designed width of the preceding beam within the grout treated zone ranges from 5 to 6 m. The grouting parameters used at the site are provided as follows: grouting pressure = 30 ~ 34 MPa, grouting rate = 360 L/min, rod rotation = 4 rpm, and withdrawal rate = 10 ~ 12 min/m. The grouting parameters allowed the contractor to rapidly install grouting piles with a diameter up to approximately 3.5 m at a depth of up to 50 m below the ground surface.

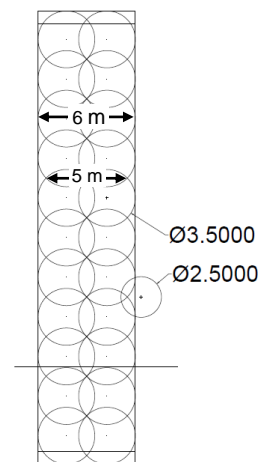


Fig. 9 Design plan of the jet grouted preceding beam (Block F)

#### *Quality control*

An electrical resistivity testing was adopted to verify the constructed width of the preceding beam with the jet grouted piles installed in the medium clay layer underneath the OR15 Station. The electrical resistivity testing was conducted at Block F of the station, as shown in Fig. 8. The testing was conducted with probes spaced at a distance of 18.8 m across the beam.

To determine the resistivity values of the grout treated and untreated soils at the site, the resistivity test was conducted in the laboratory for soil samples obtained from the site. The resistivity values of the untreated clay samples were determined to range from 1.5 to 1.6 Ohm-m. The resistivity values of the grout treated clay samples were determined to range from 7.0 to 30.0 Ohm-m. The resistivity value for the transition zone between the completely treated clay and untreated clay was assumed to be 4.25 Ohm-m, which is the average value of the resistivity values for the grout treated clay samples and the untreated clay samples. The resistivity value of 4.25 Ohm-m was used to determine the effective diameter of the jet

grouting.

The results of the electrical resistivity test performed at Block F are shown in Fig. 10. Fig. 10 indicates that the measured resistivity values for the entire cross section range from 0.6 to 22 Ohm-m. Using the resistivity value of 4.25 Ohm-m for the transition zone, the constructed width of the preceding beam was estimated to be approximately 6.4 m. Field observation was conducted to measure the constructed width of the preceding beam when the preceding was exposed. The constructed width of the beam was measured to range from 5.8 to 6.3 m. The visual observation confirmed the estimated width of the beam obtained from the resistivity test. Therefore, it is concluded that the constructed preceding beam meets the requirement of the designed width.

## CONCLUSIONS AND RECOMMENDATIONS

This paper presented the usage of the large diameter jet grouting technique for two tunnel projects in Bangkok. The following conclusions were drawn from the study of the projects:

1. The field pumping test that was conducted for the MRTA Blue Line Extension Project indicated that there was no water at the excavated base of the IDT shaft. Therefore, the large diameter jet grouting conducted at the site successfully prevented the risk of uplift and piping in the 2<sup>nd</sup> stiff clay layer. Furthermore, the base of the

excavation was in a dry condition after grouting. Consequently, the design requirement for hydraulic conductivity was met for the IDT shaft.

2. The electrical resistivity test and the field observation performed at Block F of the MRTA Orange East Project indicated that the large diameter jet grouting technique could be utilized to meet the width requirement of the preceding beam constructed in the medium clay layer underneath the OR15 Station. It is recommended that the effectiveness of the large diameter jet grouting technique be verified for sandy Bangkok soils.
3. This study demonstrates that the design requirements of the treated materials can be met effectively using the large diameter jet grouting technique. Furthermore, the construction time and the associated costs were reduced using the large diameter jet grouting technique.

## ACKNOWLEDGMENTS

The authors wish to thank the following organizations: Sanshin Construction (Thailand) Co., Ltd. and ISEKI Engineering (Thailand) Co., Ltd. for carrying out the field work of the large diameter jet grouting; Geotechnical & Foundation Engineering Co., Ltd; CKST Joint Venture, and Mass Rapid Transit Authority, Thailand for providing valuable construction records for conducting this evaluation.

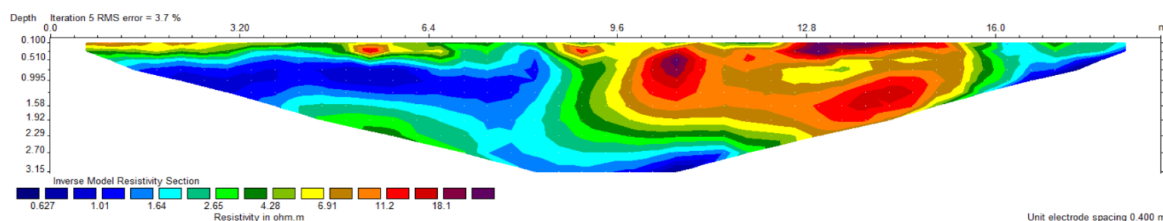


Fig. 10 Results of electrical resistivity test for Block F

## REFERENCES

- [1] Cheng S.H., Risky K.N., Liao H.J., and Hsieh Y.H., A Large Diameter Jet Grouting Method for Arrival of Shield Tunnelling Machine. ISSMGE - TC 211 International Symposium on Ground Improvement IS-GI, Brussels, 2012.
- [2] Jaritngam S., Design Concept of The Soil Improvement for Road Construction on Soft Clay. Eastern Asia Society for Transportation Studies, Vol. 4, 2013.
- [3] MRTA, OR15 Pradit Manutham Station Detailed Design: Diaphragm Wall including Impact Assessment and Protection Measures for Sirat Expressway viaduct, 2017.
- [4] Sompong R., Soil Properties Effect on Construction of Soil-Cement Column: Case Study on Drainage System Suvarnabhumi International Airport Project, 2009.
- [5] Yong, D. M., Hayashi, K. and Chia, B. H., Jet grouting for construction of a RC canal in soft marine clay. Grouting and deep mixing: Procds., IS Tokyo 96, 2<sup>nd</sup> International Conference on Ground Improvement Geosystems Tokyo, Japan, 1996. pp. 375-380.
- [6] Yoshida, H., Jimbo, S. and Uesawa, S., Development and practical applications of large diameter soil improvement. Grouting and deep mixing: Procds., IS Tokyo 96, 2<sup>nd</sup> International Conference on Ground Improvement Geosystems Tokyo, Japan, 1996. pp. 721-726.



## STRUCTURAL BEHAVIOR OF NON-DUCTILE REINFORCED CONCRETE COLUMNS

Ari Wibowo<sup>1</sup>, Rizki Amalia Tri Cahyani<sup>2</sup>

<sup>1</sup>Department of Civil Engineering, Faculty of Engineering, Brawijaya University, Malang, Indonesia

<sup>2</sup>Department of Civil Engineering, Muhammadiyah University, Malang, Indonesia

### ABSTRACT

Confinement of columns with non-seismic detailing is prevalent in many old buildings and common in current detailing practice in many developing countries. This type of columns is believed to have a very low drift capacity from a conventional design perspective. To investigate the lateral load-drift behavior and the collapse mechanism of such columns, the experimental tests on four lightly reinforced concrete columns with light transverse reinforcement ratio have been undertaken. The quasi-static tests were applied on concrete columns with various longitudinal reinforcement ratio, transverse reinforcement ratio, and lap splice position. Interestingly, the results showed that the total drift capacities could reach up to 7% well beyond the required maximum drift suggested by many codes despite the low detailing. Reasonably, the closer the stirrups spacing, the higher the ductility of the columns. Whereas, it appeared that the higher the longitudinal reinforcement ratio, the lower the ductility ratio. Furthermore, the theoretical analyses have been conducted to estimate investigate the lateral load-deflection behavior of the columns which were in a good agreement with the test results.

*Keywords: Lightly reinforced columns, Transverse reinforcement, Seismic performance*

### INTRODUCTION

Lightly reinforced concrete columns are commonly found on construction practices in low seismic region countries and many developing countries [1]. The practices generally include one or the combination of some parameters, i.e., low longitudinal reinforcement ratio, low transverse reinforcement ratio, inadequate development length of steel reinforcement, and lap splice position. Some studies have studied the effect of several parameters affecting the seismic performance of reinforced concrete columns as follows:

- Sezen [2] examined four columns using both the axial load ratio and loading history as the variables in order to investigate the axial load failure of structures with light transverse reinforcement, typical of buildings designed before the requirements for ductile detailing were introduced in the USA. It was observed that by increasing the axial load, the lateral strength increased and the displacement capacity decreased whilst the loading history did not appear to affect the column lateral drift capacity.
- Rodsin [3] tested three columns S1, S2, and S3 with aspect ratios of 3.75, 2.75 and 2.25 respectively. The specimens were composed of cantilever columns having 1.4% longitudinal steel ratio, 0.24% transverse reinforcement area ratio and a constant axial load ratio of 0.20. Interestingly, the drift capacities of the

specimens with smaller aspect ratios were similar or even larger than specimens with the larger aspect ratio. It was shown that this was due to additional rotation at shear cracks which increased the drift capacity of the columns.

- Griffith et al [4] investigated the retrofitted RC columns including two slender columns (without retrofitting) with low to mid steel reinforcement ratio. It was observed that the slender columns were still able to sustain axial load even after extensive concrete crushing and effectively zero lateral load capacity.
- Nakamura and Yoshimura [5] analyzed four column specimens by varying two parameters; axial load ratio (0.18 and 0.27) and lateral loading type (monotonic and cyclic loading) to investigate the intermediate-story collapse found in many structures during 1995 Kobe earthquake. The effect of the axial load ratio on the shear-dominated column was found very significant. Increasing the axial load ratio from 0.18 to 0.27 decreased the lateral drift capacity from 20.6% to 3.0% for monotonic lateral loading and from 10.4% to 4.8% for cyclic lateral loading.
- Yoshimura et al [6] conducted a test on eight specimens representing short columns which may fail in shear or flexural-shear. Some of the conclusions were: a) the decrease of longitudinal reinforcement ratio from  $\rho_v = 1.69\%$  to  $0.94\%$  increased the axial load drift

capacity significantly from 2.0% to 17.8%; b) interestingly, the research showed that short columns with 0.21% transverse reinforcement could provide considerable drift capacity compared with flexure-dominated columns.

- Kogoma et al [7] studied three parameters (transverse reinforcement ratio, axial load ratio, and lateral loading type) in order to study the reinforced concrete column damage pattern and the maximum strength and displacement capacities. The axial load failure drift capacity and failure mode were considerably affected by the amount of transverse reinforcement ratio with a reduction in the stirrup spacing. An increase in transverse steel ratio increasing the drift capacity and shifting the failure mode from a shear failure to a flexure-dominant failure mode.

It appeared from those studies that the lateral load-carrying capacity and collapse mechanism of such columns are mainly affected by longitudinal reinforcement ratio, transverse reinforcement ratio, axial load ratio, and aspect ratio. The first two parameters became the main focus of this research.

## EXPERIMENTAL TEST

Eight column specimens have been designed to represent structural columns commonly found in developing countries with three parameters studied: longitudinal reinforcement ratio, transverse reinforcement ratio and location of lap splice. This study was the extension of previous studies [8,9] which investigated the aspect ratio, the longitudinal reinforcement ratio and the axial load ratio on seismic performance of such columns.

Eight concrete columns specimens had a cross-section area of 150×160 mm and height of 640 mm (to the location of lateral load point, with the aspect

ratios of  $a=4.3$ ). Each four column specimens were reinforced with 4D8 and 4D10 corresponding to the longitudinal reinforcement ratios of 0.75% and 1.1% respectively. All stirrups with a diameter of 6mm were used for the transverse reinforcements which were spaced at 150mm and 250 mm (equivalent to 0.61% and 0.36% of volumetric transverse reinforcement ratio respectively).

Concrete strength ranging 22-27 MPa (an average of 25 MPa) were observed from concrete compression strength of cylinder concrete and hammer tests on column specimens. The measured yield strength of steel bar with a diameter of 6mm, 8mm, and 10 mm were about 378MPa, 433 MPa, and 536 MPa respectively, whereas, the corresponding steel ultimate strength were 538MPa, 646 MPa, and 824 MPa respectively. The column properties and reinforcement configurations are shown in Table 1 and Fig. 1.

Table 1 Column specimen properties

| Col.  | $\rho_v$<br>(%) | $\rho_h$ |      | $n$ | Lap<br>Splice<br>Region | $l_d$<br>(mm) |
|-------|-----------------|----------|------|-----|-------------------------|---------------|
|       |                 | Area     | Vol. |     |                         |               |
| L15C  | 0.76            | 0.35     | 0.61 | 0.1 | -                       | -             |
| L25C  | 0.76            | 0.21     | 0.36 | 0.1 | -                       | -             |
| M15C  | 1.10            | 0.35     | 0.61 | 0.1 | -                       | -             |
| M25C  | 1.10            | 0.21     | 0.36 | 0.1 | -                       | -             |
| L15SB | 0.76            | 0.35     | 0.61 | 0.1 | Plastic                 | 200           |
| L15SM | 0.76            | 0.35     | 0.61 | 0.1 | Elastic                 | 200           |
| M15SB | 1.10            | 0.35     | 0.61 | 0.1 | Plastic                 | 250           |
| M15SM | 1.10            | 0.35     | 0.61 | 0.1 | Elastic                 | 250           |

Note:  $\rho_v$  = longitudinal reinforcement ratio,  $\rho_h$  = transverse reinforcement ratio,  $n$  = axial load ratio,  $l_d$  = lap splice length

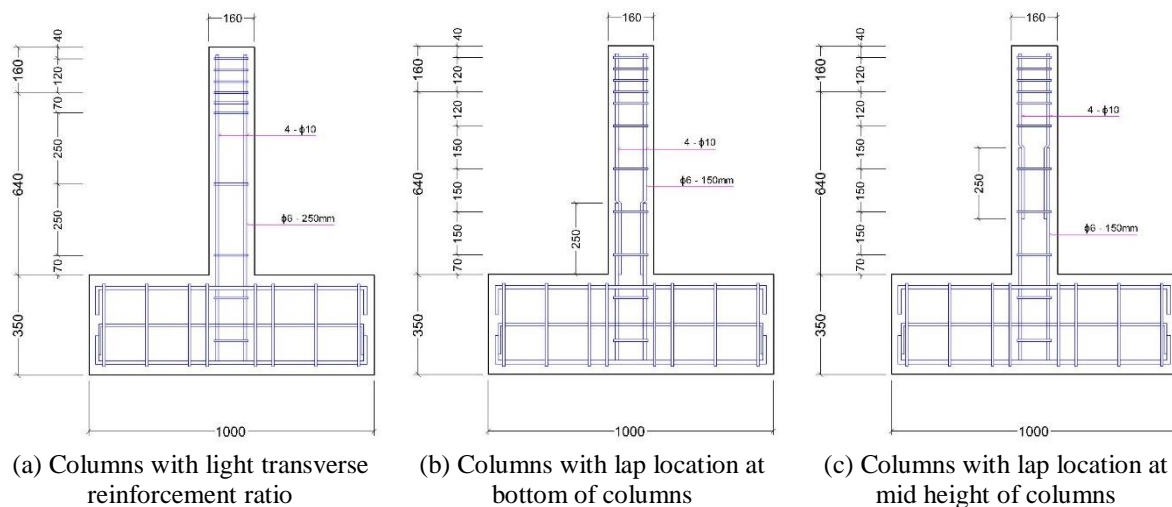


Fig. 1 Typical column specimens with various parameters tested.

The lateral quasi-static loading tests were conducted as per ASTM E2126 code. The displacement control sequence was applied by using drift increment of 0.25% up until reaching drift of 2.0% and then followed by drift increment of 0.5% until the occurrence of lateral load failure which was taken at about 20% load drop of peak strength. On each defined discrete drift, the displacement components were measured (consisting of flexural, shear and total displacement) using LVDTs and dial gauges, and crack propagation recorded.

The LVDTs and dial gauges were set to monitor and measure three components of column deformation, i.e., flexural, yield penetration, and shear with configuration as shown in Fig. 2, i.e., no 1-5 for flexural deformation, no 5-6 for total lateral deformation, and no. 8-9 for shear deformation.

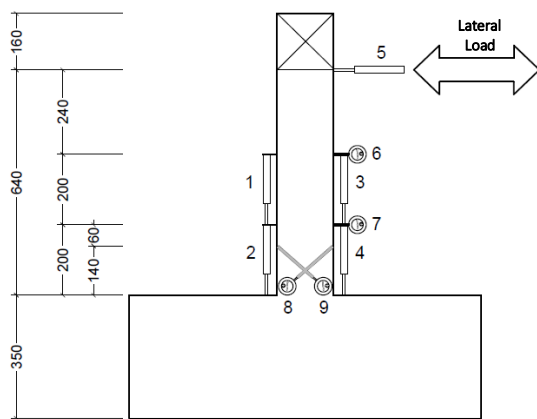


Fig. 2 LVDTs and dial gauges Measurement Setup.

## TEST RESULTS

### Peak Strength and Ductility Ratio

The test findings showed interesting results as follows (refer to Fig. 3 and Table 2):

- Specimens with a lower ratio of longitudinal reinforcement ratio tended to have higher ductility ratio. The increase of the longitudinal reinforcement ratio increases the peak strength but decrease the ductility ratio.
- The lateral peak strengths of columns with lap splice located at the half height of the cantilever columns were relatively similar to those of columns with continuous reinforcement. On the other hand, the columns with lap splice located at plastic hinge region showed the smallest of peak lateral strength capacity.
- The continuous reinforcement bar reasonably provided the larger drift capacity, followed by the lap-splice location at column mid-height (elastic region) and bottom (plastic hinge

region) respectively.

- The closer the spacing of transverse reinforcement, the higher the ductility ratio due to the higher the confining effect provided by the stirrups.
- From the curvature distribution over the column height (refer Fig. 4-5), it shows clearly that by placing the lap splice at column mid-height, the plastic region tends to spread over to the second region from the column-foundation interface. Whilst columns with the continuous bars and lap splice at the bottom of the column had the curvature distribution concentrated more in the plastic hinge area.

### Load-Displacement Behavior and Collapse Mechanism

The collapse mechanisms and crack propagations of column specimens were observed as follows (refer Fig. 6-7):

- All column specimens exhibited flexural-dominant behavior particularly at the ascending part of the load-displacement curve.
- However, columns with a larger spacing of stirrups tended to developed shear cracks at a later stage following the initial flexural cracks. It showed that the shear strength of columns started to decrease after a certain point and triggered the shear cracks once it is below the flexural strength of columns. It can be attributed to the flexure-shear-critical mechanism of the columns (refer Fig. 6) where the shear strength  $V_n$  is higher but relatively close to the flexural strength ( $M_n/L$ ) [7]. On the contrary, the flexure-critical columns with the closer stirrups spacing could maintain the shear strength of columns higher than the flexural capacity despite the shear strength reduction with the progression of drift.

Table 2 Ductility ratio of all column specimens

| Specimens | Yield Drift | Failure Drift | Ductility Ratio |
|-----------|-------------|---------------|-----------------|
| L15C      | 0.72        | 4.00          | 5.55            |
| L25C      | 0.8         | 3.67          | 4.59            |
| M15C      | 1.19        | 4.00          | 3.36            |
| M25C      | 1.15        | 3.35          | 2.91            |
| L15SB     | 0.92        | 3.67          | 3.99            |
| L15SM     | 0.63        | 3.35          | 5.32            |
| M15SB     | 0.56        | 2.50          | 4.46            |
| M15SM     | 0.68        | 3.00          | 4.41            |

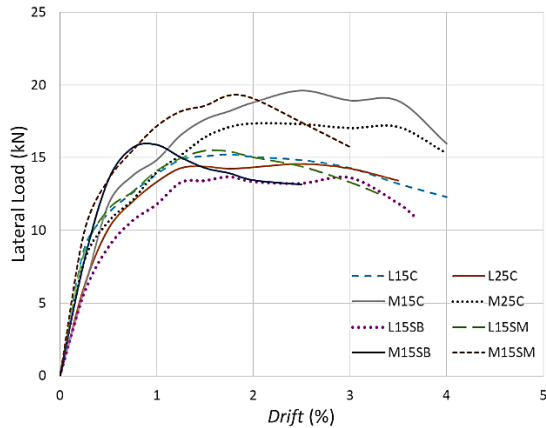


Fig. 3 Lateral load-drift behavior for all column specimens.

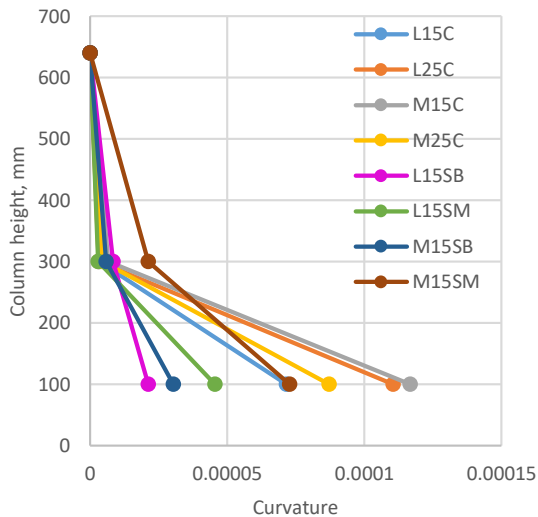


Fig. 4 Curvature distribution over the column height at peak load.

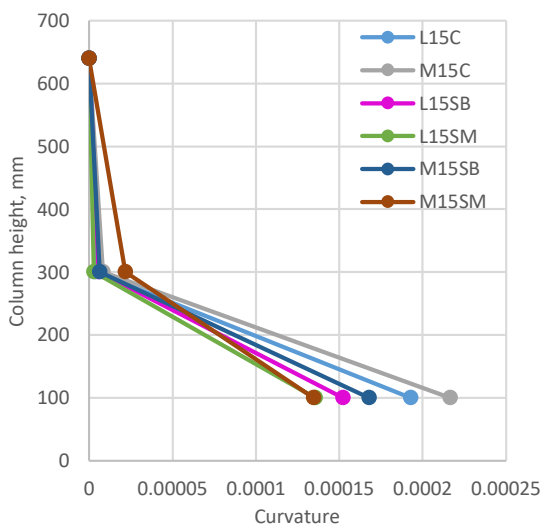


Fig. 5 Curvature distribution over the column height at lateral load failure.

- The columns with lap splice at mid-height of column showed wider cracking area and more severe concrete spalling compared to columns with lap splice located at the plastic hinge region. The double amount of reinforcement at lap splice location provided higher effectiveness when it was placed at the plastic hinge region (where the maximum moment occurs) compared with if it was located within the elastic area of column (outside the plastic hinge region).
- On the other hand, all columns with lap-splice connection developed higher damage degree compared to columns with continuous bars. It can be attributed to the lack of proper lap splice development lengths in all columns which were purposely designed less than the minimum code requirement in order to investigate the effect of such connection.

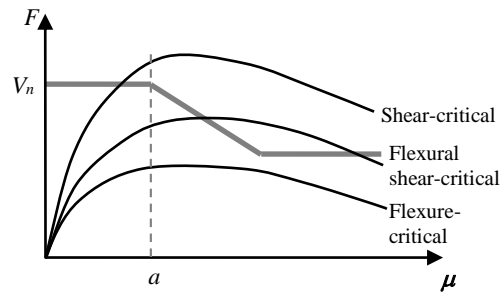


Fig. 6 Curvature distribution over the column height at peak load.

### Displacement Components

Furthermore, the measurement of the displacement components of columns (flexural, yield penetration, and shear) showed the different effect of each studied parameters as follows (refer Fig. 8-9):

- The shear deformation was the least component observed in all column specimens up to 5% of total deformation. It was reasonable since all specimens were designed with light longitudinal reinforcement. However, columns L25C and M25C with lower transverse reinforcement ratio showed larger shear deformation after reaching peak strength. It corroborated the observation of collapse mechanism and crack propagation on column specimens.
- The yield penetration deformation took about 20%-50% of the total deformation. The larger percentage of those was found on columns with lower longitudinal reinforcement. The smaller the diameter of the longitudinal bar, the higher the yield force developed at the bar for the same amount of bending moment, and hence the earlier the slip occurrences between concrete



- and steel.
- And certainly, the flexural deformations were reasonably the largest component of

deformation ranging 50%-70% of the total deformation due to the nature of flexure-dominant columns.

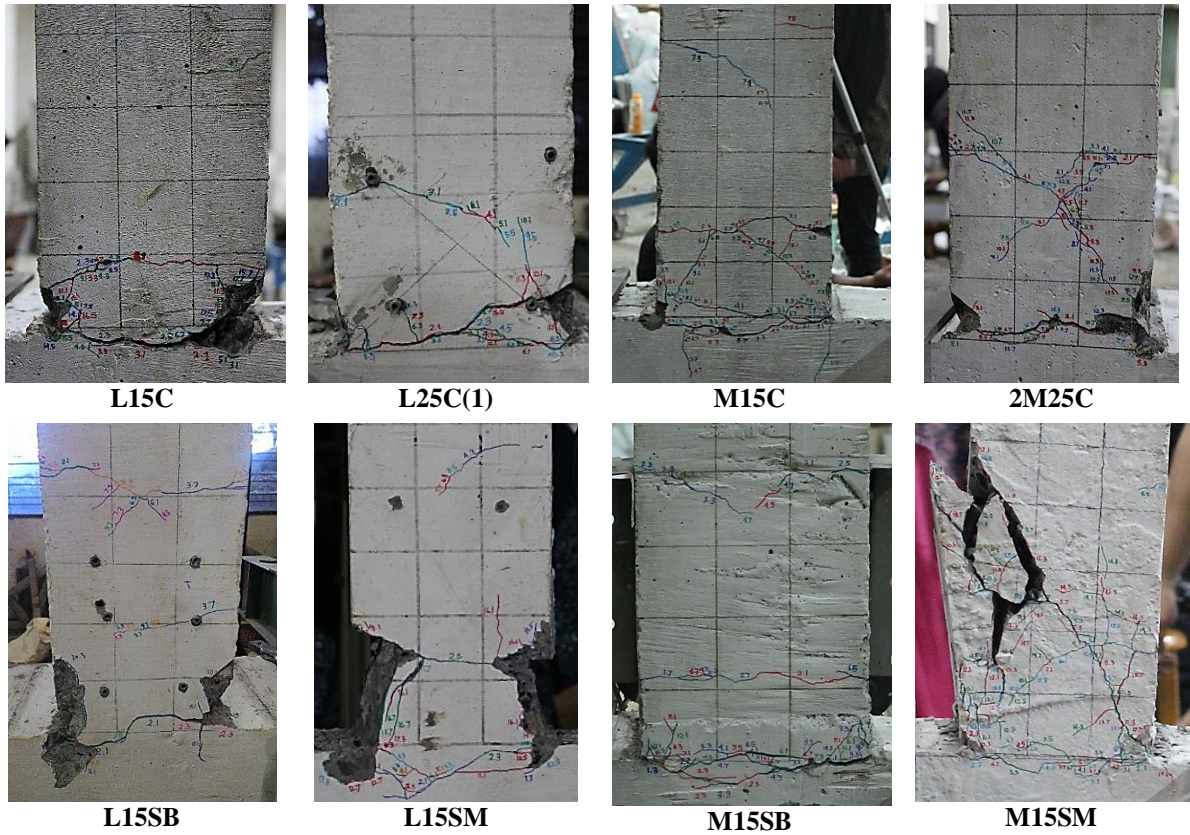


Fig. 7 Crack Propagation and collapse mechanism of all column specimens.

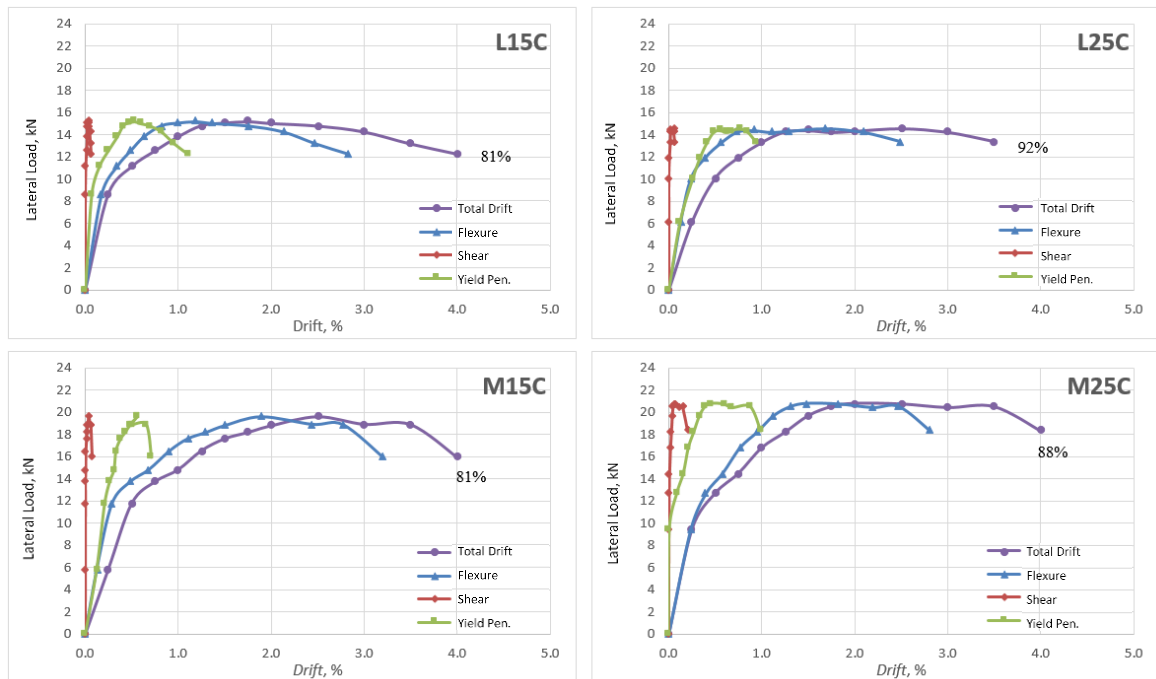


Fig. 8 Displacement components for columns with continuous reinforcement.

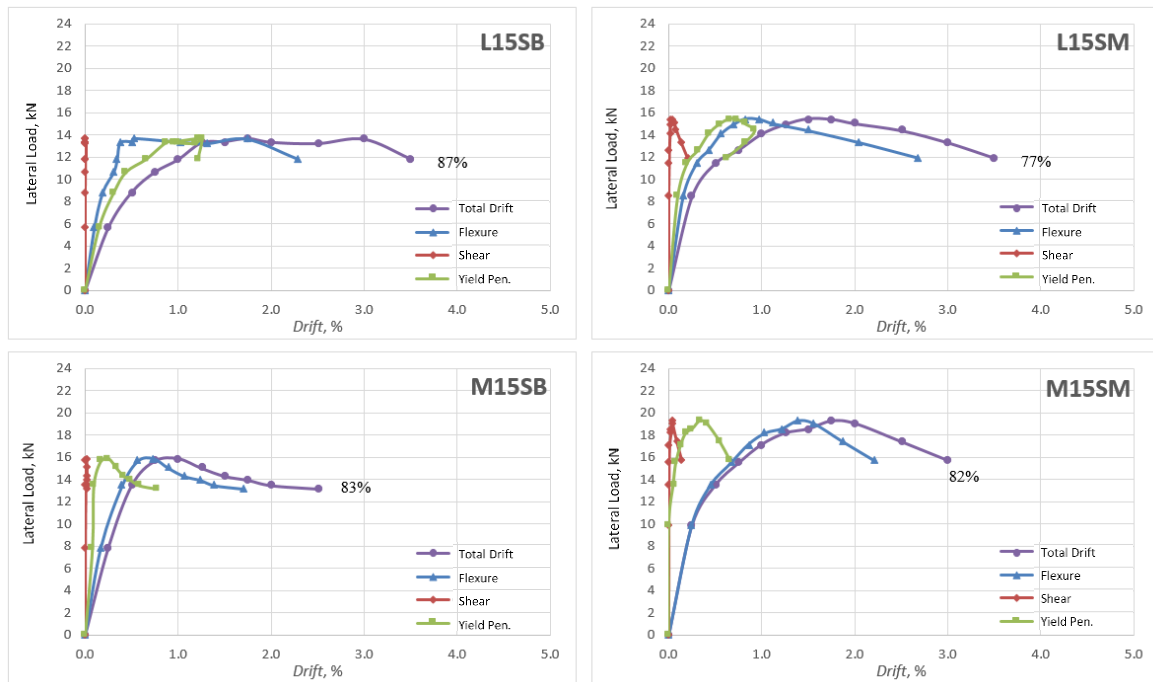


Fig. 9 Displacement components for columns with reinforcement lap-splice.

## CONCLUSIONS

Reinforced concrete columns with light reinforcement are commonly found in developing countries and low-to-moderate seismic region. An experimental test has been conducted for investigating the seismic performance of such columns. The effect of longitudinal reinforcement ratio, transverse reinforcement ratio, and placing of reinforcement lap splice were the main parameters for studying the load-displacement behavior and collapse mechanism of lightly reinforced concrete columns when subjected to quasi-static lateral load. The findings were as follows:

- The increase of longitudinal reinforcement ratio increases the lateral peak strength, but decrease the ductility ratio, resulted in more flexural-dominant behavior and reduce the yield penetration deformation.
- The increase of transverse reinforcement ratio the higher the ductility ratio, the smaller the shear deformation observed. The closer the shear strength to the flexural strength, columns tend to developed flexure-shear dominant behavior marked with shear collapse mechanism following the initial flexural crack development.
- Placing the lap-splice closer to the plastic hinge region resulted in more concentrated curvature distribution and flexural damage to the bottom of the column which leads to a smaller displacement at the column top. And certainly, the largest displacement capacity can be obtained by using continuous reinforcement bars.

## REFERENCES

- [1] Kafle, B., Mohyeddin-Kermani, A., Wibowo, A., A Report on the Visit to the Region Stricken by the Wenchuan Earthquake, Electronic Journal of Structural Engineering, Vol 1, No 1, Appendix B, 2008, pp. 1-40
- [2] Sezen, H., "Seismic Response and Modeling of Reinforced Concrete Building Columns, Ph.D. Dissertation, Department of Civil and Environmental Engineering, University of California, Berkeley, 2002.
- [3] Rodsin, K., Seismic Performance of Reinforced Concrete Soft-storey Buildings in Low to Moderate Seismicity Regions, Ph.D. Dissertation, Department of Civil and Environmental Engineering, University of Melbourne, Melbourne, 2007.
- [4] Griffith, M.C., Wu, Y.F., Oehlers, D.J., Behaviour of Steel Plated RC Columns Subject to Lateral Loading, Advances in Structural Engineering, Vol. 8, No. 4, 2005, pp 333-347.
- [5] Nakamura, T., Yoshimura, M., Gravity Load Collapse of Reinforced Concrete Columns with Brittle Failure Modes, Journal of Asian Architecture and Building Engineering, Vol 1, No. 1, 2002, pp. 21-27. (2002)
- [6] Yoshimura, M., Takaine, Y., Nakamura, T., Collapse Drift of Reinforced Concrete Columns, PEER Report 2003/11, Fifth US-Japan Workshop on Performance-Based Earthquake Engineering Methodology for Reinforced Concrete Building Structures, Hakone, Japan, 2003, pp. 239-253.

- [7] Kogoma, I., Hayashida, T., Minowa, C. Experimental Studies on the Collapse of RC Columns During Strong Earthquake Motions, Tenth World Conference on Earthquake Engineering, Rotterdam, Holland, 1992, pp. 3013-3017.
- [8] Wibowo A, Wilson JL, Lam NTK, Gad EF. Drift Performance of Lightly Reinforced Concrete Columns. Engineering Structures Journal, Elsevier, Volume 59, February 2014, pp 522–535.
- [9] Wibowo A, Wilson JL, Lam NTK, Gad EF., Drift Capacity of Lightly Reinforced Concrete Columns”. Australian Journal of Structural Engineering, Vol. 15, No. 2, 2014, pp. 131-150.



# STATISTICAL ANALYSIS OF THE INFLUENCE OF TRAFFIC AND ENVIRONMENTAL DISTURBANCES ON DAMPING IN A BRIDGE

Koharu Ota<sup>1</sup>, Kouichi Takeya<sup>2</sup>, Junji Yoshida<sup>3</sup>

<sup>1,2,3</sup> Faculty of Engineering, Graduate School, University of Yamanashi, Japan;

## ABSTRACT

To maintain and improve the performance of infrastructures, Structural Health Monitoring (SHM) has been studied in the past few decades. Vibration-based SHM is mainly used for bridge health monitoring that focuses on structural parameters including the natural frequency, deflection, and damping. Among these parameters, damping can be considered as an index of the deterioration of structures, since damping is influenced by changing the energy distribution in bridge structural systems. However, there is difficulty in the long-term monitoring of damping as it is also influenced by external disturbances such as traffic and temperature. In this study, the damping of bridges was statistically analyzed by considering the influence of traffic and temperature. In particular, a solar-powered monitoring system using MEMS accelerometers was constructed and installed on a steel girder bridge. The Random Decrement method was applied, and the appropriate data length and window size were considered to measure the damping ratio with high accuracy. The measured damping ratio from traffic-induced vibrations and micro-tremors of bridge girders were statistically compared by considering a probability density distribution. Moreover, the influence of temperature on the damping ratio was also analyzed. Based on the results, generalized linear models of the measured damping ratio were estimated considering the influence of these external disturbances.

*Keywords: Bridge, Random Decrement method, Modal analysis, Damping ratio*

## INTRODUCTION

Bridge Health Monitoring (BHM) using the structural response of bridges is carried out to promptly detect bridge deterioration and efficiently manage bridge maintenance.

In BHM, structural parameters such as damping, deflection, and natural frequency are identified by the inverse analysis of vibration response data. Damping influences the energy flow in bridge components, including upper structures such as bridge decks as well as main girders, supports, piers, and abutments. Since deterioration or damage changes the energy flow in bridge components, a change in damping can be observed. [1]-[5] However, damping is a variable parameter since the energy flow changes due to environmental disturbances such as temperature and traffic on bridges.

Moreover, measurement equipment and calculation methods also influence the results. The half power method, the Random Decrement (RD) method, and the Eigen-system Realization Algorithm (ERA) method are generally used to calculate the damping ratio.

The half-power method estimates the damping ratio from the frequency response function of a structure which has been excited by base motion or an applied force. This method calculates the approximation damping ratio but can only be applied when the damping ratio is small (about 0.1 or less), and the frequency-amplitude characteristic shows an evident single-peak characteristic. [6]

The RD method calculates the damping ratio using the free vibration waves obtained by convolution of micro-tremor vibrations. The damping ratio is calculated from the envelope of the peaks of free vibration waves. [7] This method is generally used when the damping ratio is small. In addition, this method has low enough calculation cost to be calculated by a microcomputer and so data processing is possible at the measurement location.

In the ERA method, first, free vibrations are calculated from micro-tremor observation data by forming a cross-correlation function using the Natural Excitation Technique (NExT).

Next, the ERA is used to obtain natural frequencies, mode shapes, and damping ratios based on the singular value decomposition of a Hankel matrix of the free vibrations. [8] This method can estimate the vibration characteristics even in adjacent modes. However, the calculation cost is remarkably high compared to other methods, thus it is difficult to implement the ERA method to microcomputers. Considering the ease of implementing the analysis unit to microcomputers, the RD method was selected as the analysis method for this study.

To date, various types of statistical processing, such as Bayesian estimation, have been studied for evaluating the variations of structural parameters. [9], [10] This study looked at statistical analysis using probability density and histograms as an evaluation method of damping ratio.

Furthermore, to evaluate the damping ratio using the vibration response from bridges, the factor of the

variation of the damping ratio was organized and the influence of temperature and traffic was quantitatively evaluated. Long-term monitoring on a road bridge was conducted and the analysis method of the damping ratio was examined. Statistical evaluation of the damping ratio considering the influence of environmental disturbance was then investigated.

## ACCELERATION MEASUREMENT ON A STEEL GIRDER BRIDGE

### Target Bridge

The target bridge is a nine-span girder bridge; and each span length is 10m. This bridge was built in Kofu City, Yamanashi Prefecture, Japan in 1958. This bridge is made of a Reinforced Concrete (RC) deck with I-shaped steel girders. The traffic on the bridge is two-way traffic, with a single lane in each direction. Fig. 1 (a) shows an overview of the bridge and Fig. 1 (b) shows sensor positions in the cross-section of the bridge.

### Monitoring System

A monitoring system was constructed to monitor damping in the long term. Figure 2 shows an overview of the monitoring system. Three Micro Electro Mechanical System (MEMS) type accelerometers (EPSON, M-A550AC) were used for acceleration measurement with high precision. The measured acceleration data was logged by a data logger (KEYENCE, NR-600). Solar panels and shield batteries supplied electricity to the monitoring system. Table 1 shows the specification of the accelerometer. The accelerometer was attached on a plastic base plate with neodymium magnets for installation on steel bridge components, as shown in Fig. 3.

### CALCULATION OF DAMPING RATIO

Acceleration data obtained from long-term measurements was used to calculate the damping ratio. In this study, the measured data was analyzed using MATLAB 2017a. The proposed analysis method could be implemented in the monitoring system with microcomputers as it followed the RD method of analysis. The flowchart of the proposed analysis method is shown in Fig. 4. First, the baseline of the acceleration data is corrected by extracting the drift component. Second, micro-tremors and traffic-induced vibrations are classified using the threshold of the vibration amplitude. Third, dominant frequencies are analyzed by the Fast Fourier

Transform (FFT). Band-pass filters are designed and applied to focus on the target dominant frequency, and free vibrations are calculated by the RD method. Finally, the damping ratio is calculated by curve fitting and the weighted average.

### Baseline Correction of Acceleration Data

Acceleration data contains drift components which influences the acquisition of micro-tremors and the calculation of the damping ratio. The moving average filter is therefore applied to the acceleration data to extract drift components. Figure 5 shows the moving average of acceleration data between 7<sup>th</sup> and

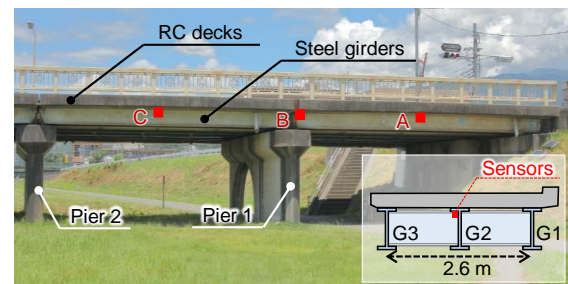


Fig. 1 (a) Overview of the bridge.  
(b) Installation location of accelerometers.

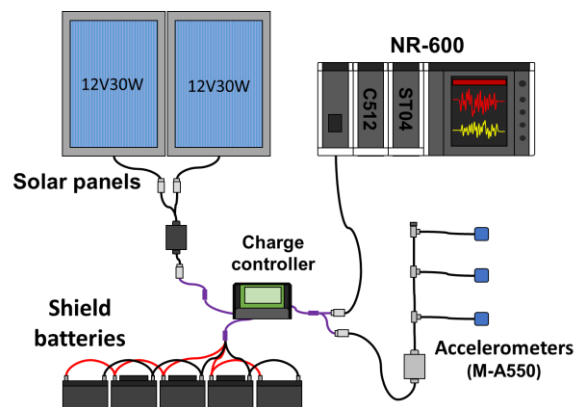


Fig. 2 Overview of the monitoring system.

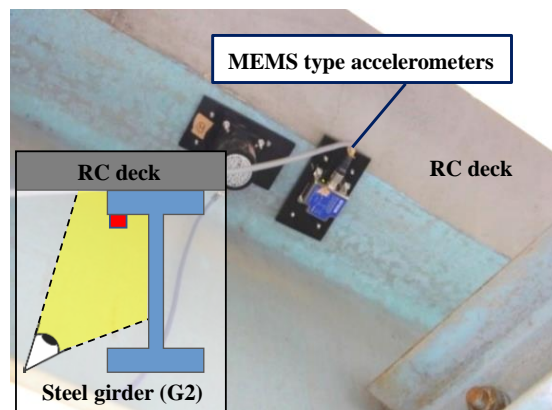


Fig. 3 MEMS type accelerometer

Table 1 Specification of the accelerometers

| Model    | Range | Sampling | Resolution   |
|----------|-------|----------|--------------|
| M-A550AC | ±5 G  | 100 Hz   | 0.06 $\mu$ G |

13<sup>th</sup> August 2018. The baseline of the acceleration data appears to drift with temperature change. The baseline is corrected by subtracting the temperature drift component from acceleration data.

### Data Classification

Micro-tremors are generally used to analyze structural parameters of bridges. In this study, micro-tremors and traffic-induced vibrations are separated to analyze the influence of traffic-induced dynamic load on structural parameters. When the maximum absolute acceleration in each data segment of 100 samples is 70% or less of all absolute peaks, the data segment is classified as a micro-tremor. This percentage acts as a threshold for the absolute acceleration. On the contrary, when the maximum absolute acceleration is higher than the threshold, the data segment is classified into traffic induced vibration. The image of the data classification process is shown in Fig. 6.

### Acquisition of the Dominant Frequencies

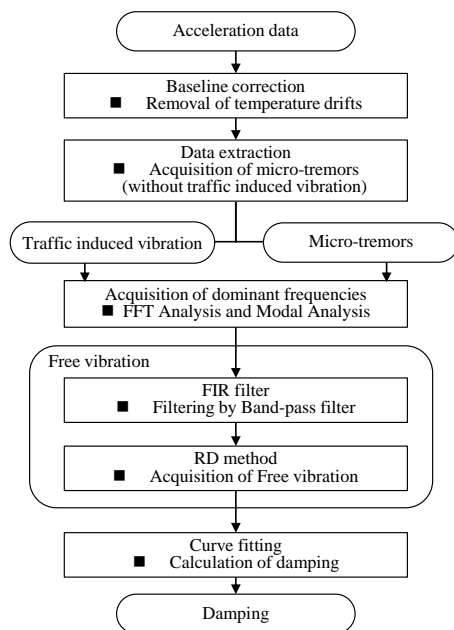


Fig. 4 Flowchart of calculating damping ratio

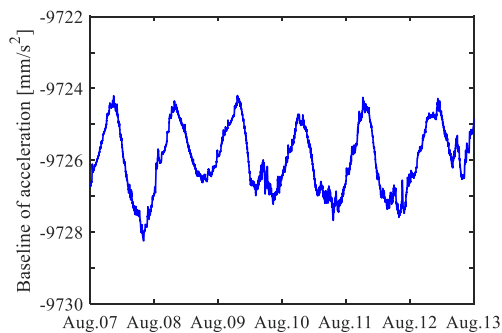


Fig. 5 Moving average of the acceleration data

In the aforementioned process, the dominant frequencies are determined by modal analysis and the target frequency is decided. First, the dominant frequencies of the bridge were calculated using FFT of acceleration data. Figure. 7 shows the power spectral density of acceleration data at measurement position A in Fig. 1.

Next, modal analysis is conducted. The Frequency Domain Decomposition (FDD) technique uses the fact that modes can be estimated from the spectral densities calculated with the assumption of white noise input. FDD can estimate mode shapes directly from signal processing calculations using Singular Value Decomposition (SVD) of each spectral density matrices [11], [12]. The spectral transfer function which is the ratio of the output power spectrum to the reference power spectrum, was calculated at each measuring position. The reference measurement position was not on a node of a vibration mode. In this study, there were three accelerometers; one was fixed as a reference measuring point and the remaining two were attached on all measurement positions, one by one. The

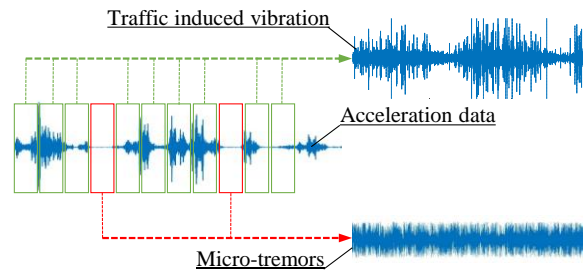


Fig. 6 Example of the data classification process

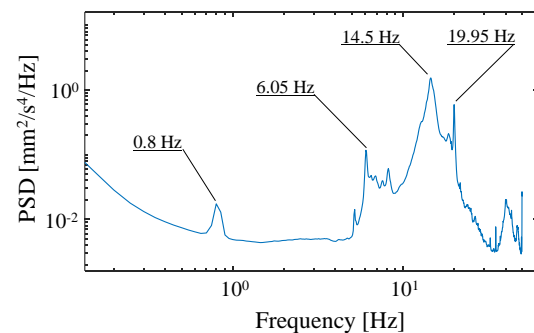


Fig. 7 Power spectral density of acceleration and natural frequencies of the bridge

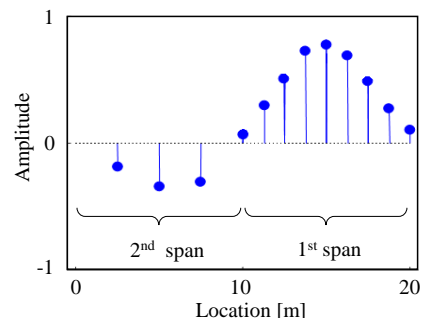


Fig. 8 First vertical vibration mode shape (14.5Hz).

measurement period was 5 minutes.

As a result, it was estimated that 14.5 Hz was close to the state of the first vertical mode. There were four significant dominant frequencies, and the main frequencies were 0.8 Hz, 6.05 Hz, 14.5 Hz, and 19.95 Hz. Figure 8 shows a mode shape of the first and second span of the target bridge in 14.5 Hz.

### Acquisition of Free Vibration

A Finite Impulse Response (FIR) band-pass filter was applied to eliminate noise and focus on the natural frequency of the first vertical vibration mode. Bandwidth frequencies were automatically determined with the two closest negative peaks from the target frequency, as shown in Fig. 10.

The damping ratio determined from the free vibration waveform and curve fitting was affected by the analysis process of the RD method. Therefore, it is necessary to analyze the influence of the analysis parameters, the data length, and the window length in the RD method. The acceleration data at measurement position A was analyzed to observe changes in the damping ratio. Figure 11 shows the relationship between the number of data and the attenuation ratio. The gray line is the attenuation ratio  $m(n, m)$  at different time data  $m$ , the black dot is the average attenuation ratio  $\bar{\zeta}(n)$  per data number  $n$ , and the red line is the overall average attenuation ratio  $\bar{\zeta}_{all}$ . When  $n$  is sufficiently large,  $\bar{\zeta}_{all}$  is taken as the convergence value  $\bar{\zeta}^*$  of the damping ratio. The average damping ratio proposed here is a weighted average weighted by the determination coefficient  $R^2$  given by the following equation.

$$\bar{\zeta}_{all} = \frac{\sum_n \sum_m R_{(n,m)}^2 \bar{\zeta}_{(n,m)}}{\sum_n \sum_m R_{(n,m)}^2} \rightarrow \bar{\zeta}^* \quad (1)$$

The damping ratio converges as the data length increases. As a result of the analysis, the data length was set to  $1 \times 10^6$  samples, and so if the window length is set to 69 samples, 10 cycles of target vibrations are included. Table 2 shows the conditions under which the RD method is applied.

Table 2 Condition of RD method application

|                    |  |
|--------------------|--|
| Vibration mode     | 1 <sup>st</sup> vertical mode          |
| Dominant frequency | 14.5 Hz                                |
| Filter type        | Band-pass                              |
| Window             | Kaiser                                 |
| Filter order       | 128                                    |
| Sampling rate      | 100 Hz (samples/sec.)                  |
| Window length      | 10 cycles (69 samples)                 |
| Data length        | $1 \times 10^6$ samples ( $10^4$ sec.) |
| Overlap ratio      | 0.8                                    |

### Calculation of Damping Ratio (Curve fitting)

The damping ratio was obtained using curve fitting of the free vibration peaks. Curve fitting calculated in the RD method process is represented in Fig. 9. Data from 1<sup>st</sup> December to 22<sup>nd</sup> December 2018 were used, and the damping ratio was 5.51%. The determination coefficient at this time was 0.887.

### STATISTICAL ANALYSIS OF DAMPING RATIO

Histograms and probability density distribution analysis was applied to consider the variance of the damping ratio against both temperature and traffic. First, histograms were calculated with the frequency on the vertical axis and the damping ratio on the horizontal axis. Next, probability density distributions of the damping ratio were calculated

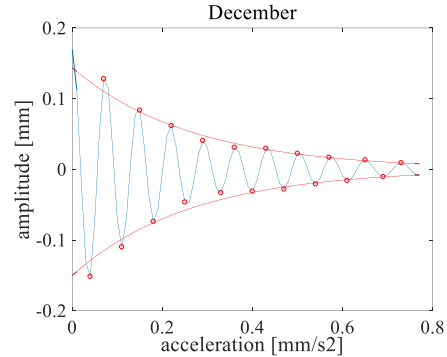


Fig. 9 Free vibration and curve fitting to calculate the damping ratio

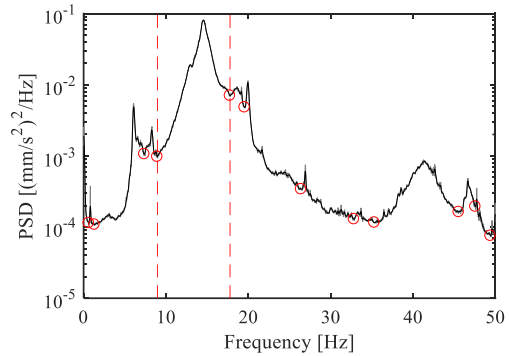


Fig. 10 Power spectral density of acceleration and the bandwidth frequencies

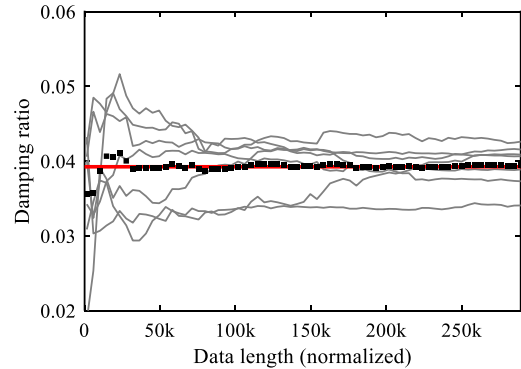


Fig. 11 Convergence of damping ratios along the data length

using the Gaussian distribution model.

To consider the influence of traffic on the damping ratio, damping ratio distributions were compared by analyzing traffic induced vibrations and micro-tremors. Moreover, damping ratio distributions in each month were also compared to consider the seasonal effect.

### Traffic Effect on the Damping Ratio

Figure 12 shows the distribution of damping ratio with and without traffic effect. Analysing the histograms, traffic distribution (Fig. 12(a)) is concentrated at a damping ratio of around 3.5%, while the non-traffic distribution (Fig. 12(b)) is concentrated at around 4.8%. In addition, the variance of the damping ratio calculated from the traffic induced vibrations is higher than that from the micro-tremors. Traffic increases the variance of the damping ratios, which can be seen from the amplitude dependence of the structural damping and the effect of truck dampers traveling on the bridge.

### Seasonal Effect on the Damping Ratio

The seasonal effect on the damping ratio was analyzed, and the results of the damping ratio distribution in August and December are shown in Fig. 13 (a) and (b), respectively. Comparing the damping ratio distribution in other months show that the damping ratio fluctuated and variances in the damping ratios are high.

In the probability density distribution, the variance of damping ratios from micro-tremors was small however, the variance and average of the damping ratios changed between seasons. The seasonal effect on the damping ratio likely encompasses temperature effect rather than deterioration of the bridge over time.

### Temperature Effect on the Damping Ratio

Micro-tremors in the acceleration data were classified based on air temperature and damping ratio distributions were analyzed using the RD method. Figure 14 shows the damping ratio distribution of different temperature ranges, 0 to 10 °C, 10 to 20 °C, and 20 to 30 °C. The damping ratio increased as temperature decreased. Compared to the damping ratio distribution considering seasonal changes, the variance of the damping ratio against air temperature is small.

Figure 15 shows the damping ratio distribution against air temperature. Orange circles show the damping ratio distribution at a given temperature and red circles express the mean value of the damping ratio. The mean value of the damping ratio changed with temperature. Damping ratio and temperature variations were formulated by the least squares

approximation as follows, where air temperature  $T$  represents the weighted average of damping ratio  $\zeta$ .

$$\zeta = 0.0087T^3 - 0.3308T^2 + 2.386T + 51.49 (\times 10^{-3}) \quad (2)$$

### CONCLUSIONS

In this study, statistical analysis of the damping ratio of a bridge was conducted to identify the factor that causes variance and quantitatively evaluate the

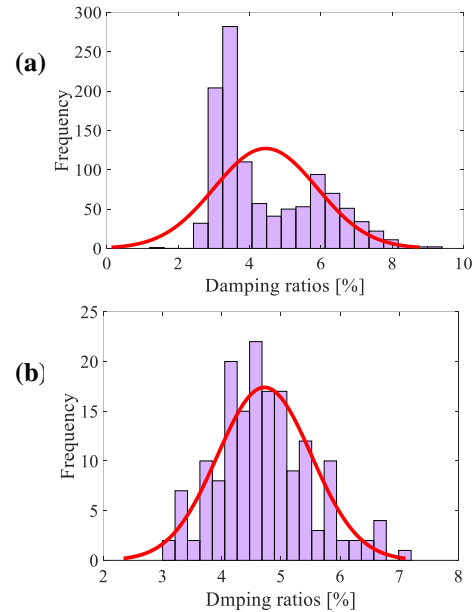


Fig. 12 Comparison of histograms and probability density distributions of damping ratios (a) from vibration induced vibrations, and (b) micro-tremors

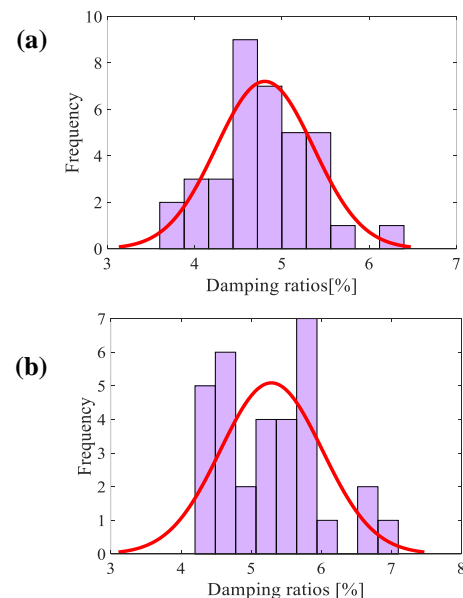


Fig. 13 Comparison of histograms and probability density distributions of damping ratios (a) from acceleration in August, and (b) December.



influence by temperature and traffic. The following findings were obtained.

The damping ratios of a road bridge were calculated from measured acceleration data. Modal analysis determined the target mode at 14.5 Hz.

Data classification using the threshold of peak acceleration was incorporated into the proposed analysis process to consider the influence of the traffic load on the damping of the bridge. It was found that traffic load influences the variance of damping ratios.

It was also clarified that the damping ratio is affected by air temperature. The relationship between the damping ratio and air temperature was formulated.

If the cause of variation in damping ratio along with temperature and traffic is further clarified, it could assist SHM to evaluate the structural state from structural parameters.

## REFERENCES

- [1] Yamamoto K., Isemoto R., Oshima Y., Kim C W., and Sugiura K., Evaluation of Acceleration Responses in a Steel Truss Bridge and Passing Vehicle Before and After Member's Breakage, Journal Society of Civil Engineers (JSCE), Vol. 58A, 2013, pp. 180-193.
- [2] Mastuoka K., Kaito K., Tokunaga M., Watanabe T., Sogabe M., Identification of the Vibration Properties of Bridge Using the Axle Acceleration Response of a Running Train, Journal Society of Civil Engineers (JSCE) F4(Construction management), Vol. 68, No. 3, 2012, pp. 175-192.
- [3] Takeda T., Yamanobe S., and Nihara Y., Damping Property of Prestressed Concrete Cable-Stayed Bridges Based on Measured Data, Journal Society of Civil Engineers (JSCE) No. 626/1-48, 1999, pp. 147-161.
- [4] Watanabe G., Tomohiro Fumiya., Goto S., and Emoto H., Health monitoring and identification of dynamic characteristic of a skewed bridge based on the vibration test using a moving vehicle, Journal Society of Civil Engineers (JSCE), Journal of structural engineering Vol.60A, 2014.
- [5] Yoshioka T., Yamaguchi H., Ito S. and Harada M., Identification of vibration characteristic of the steel truss bridge and influence of diagonal member damage on damping, Journal Society of Civil Engineers (JSCE), Journal of structural engineering Vol.55A, 2009, pp. 295-305.
- [6] Okabayashi T., Yamamori K., Sanuki Y., and Tamura T., Estimation of Dynamic Characteristics for Structures with Closely Spaced Eigenvalues, Journal Society of Civil Engineers (JSCE), No. 633/1-49, 1999, pp. 93-102.
- [7] Chiu Jen Kua., Jack Edward Cermak., Li-Shu Chou., Random decrement based method for modalparameter identification of a dynamic system using acceleration responses., Journal of Wind Engineering and Industrial Aerodynamics 95, 2007, pp. 389-410.
- [8] Prasenjit Mohanty, Daniel J. Rixen., Modified ERA method for operational modal analysis in the presence of harmonic excitations, Mechanical Systems and Signal Processing 20, 2006, pp. 114-130.
- [9] Goi Y., Kim C W. and Au S K., Investigation of Operational Modal Identification of a Cable-Stayed Bridge Based on Bayesian Estimation Considering Stochastic Uncertainty, Journal Society of Civil Engineers (JSCE) A2(Applied mechanics), Vol. 72, No. 2 (Journal of applied mechanics Vol. 19), 2016, pp. 751-762.
- [10] Nishino M., and Fujino Y., Bayesian Inference Based Uncertainty Quantification and Calibration of Numerical Models of Existing Structures, Journal Society of Civil Engineers (JSCE) A2(Applied mechanics), Vol. 69, No. 2, 2013, pp. 711-718.
- [11] Kaito K., Matsuoka K., Watanabe T., Sogabe M., and Fujino Y., Vibration Monitoring for Railway Bridges Using Passing Train Load, Journal Society of Civil Engineers (JSCE) F, Vol. 66, No. 3, 2010, pp. 382-401.
- [12] Mehdi Batel, Brüel & Kjær, Norcross, Georgia Operational Modal Analysis – Another Way for Doing Modal Test.

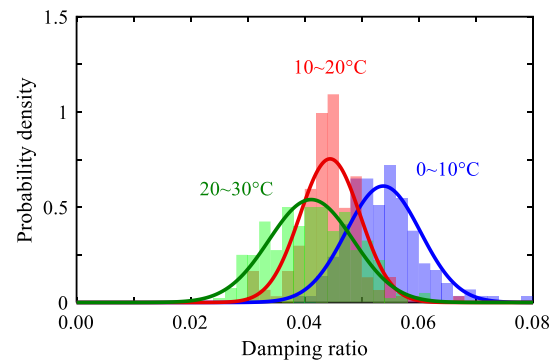


Fig. 14 Histogram of each temperature range.

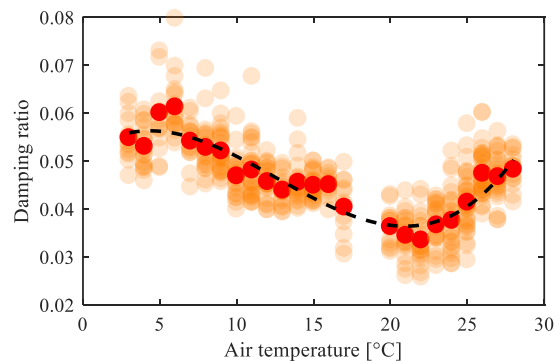


Fig. 15 Damping distribution by temperature.

## REDUCTION IN BEARING CAPACITY OF GYPSEOUS SOILS WITH CAVITIES

Ahmed A. Al-Obaidi<sup>1</sup> and Reem S. Najim<sup>2</sup>  
<sup>1,2</sup>Engineering College, Tikrit University, Iraq

### ABSTRACT

The presence of gypsum in the soil will cause problems if the source of fresh water is available and permeable soil permitting significant movement of water is to take place. The solubility of gypsum by excess water from irrigation or localized leak into the gypseous soil may cause cavity formation. In this research, a model was developed for governing the mass-transport to assess the variation of gypsum content of the soil during dissolution. A general three-dimensional finite element program (PLAXIS TUNNEL) was selected for the numerical analysis method to generate the solution. Parameters that affect the bearing capacity of a square footing represented by the gypsum content, the cavity volume, and the location of the cavity which represent by three offset distances from the footing center to the cavity center (X, Y, and Z), where (X) represents the horizontal distance, (Y) represents the vertical (depth) distance, and (Z) represents the diagonal distance. The main results show that the cavity location found to be the most parameter that affects the bearing capacity ratio (BCR). The minimum values are found when the cavity locates at the center of the footing base, and the lowest one (0.211) when the gypsum dissolved equal to 40%, also there is no effect of the cavity location when the ratio of (X/B) and (Z/B) exceed (3.0) for any depth and when the gypsum dissolved less than 10%. For high gypsum dissolution (more than 30%), the dimensionless ratios (X/B), (Z/B) and (Y/B) of the cavity must be more than 5.0.

*Keywords: Gypseous soil, Cavity location, Cavity volume, Gypsum dissolution, BCR.*

### INTRODUCTION

The development programs of many areas within the last years were faced with a problem due to the existence of the various amount of gypsum. In most of these areas, the gypsum found as partially gypsum stratum or soil containing an amount of gypsum.

In Iraq gypseous soils covered wide areas, (more than 20% of the total area) sometimes with high gypsum content exceeds the soil content, and yet today engineering properties of these soils in some areas are unknown.

Many major projects have suffered from several problems related to construction on or by gypseous soils such as cracks, tilting, collapse and leaching the soil. These problems could happen due to seepage of water into these soils, causing the dissolution of gypsum, which provides the cementing bonds between the soil particles. This process leads to the collapse of soil structure and progressive compression, and the problem becomes more complicated if flow occurs, causing continuous loss of soil mass and the formation of serious cavities.

Several cases in the world were recorded in the literature associated with problems of structures due to cavity formation [1]. In Iraq, many injuries were recorded in the buildings due to the existing of cavities. In 2004, a sudden collapse of the pumping room and surrounding areas (tanks and stores) in the Educational Hospital in Saladin was an example.

After site investigation, it was found that a shallow cavity with dimensions about 5.5m × 2.0m. Also, many problems have been noticed in different structures constructed on gypseous soils in the last three decades among them, Samarra tourist hotel, Tikrit training center, Kerbala elevated water tank, and the excessive settlement and cracks in Al-Anbar University Main building, as shown in Plate (1).

The presence of gypsum will cause problems if the source of fresh water is available and permeable soil permitting significant movement of water is to take place, [2]. The solubility of gypsum by excess water from irrigation or localized leak into the gypsiferous layer (Solubility of gypsum 2.6 g per one liter of water at 20 °C and 1 atm.) will cause sudden settlement. Degree and amount of settlement is not a function only of the amount of gypsum but also the structure of gypsum (whether powder or large crystals) and also the distribution of gypsum as well as the quality of water. The solubility of gypsum may cause sinkholes formation and serious damage to the structures.

The cavity formation often occurs where excess water infiltrating (soaking and leaching) beneath foundations into the gypsum-rich layer. This water will attack and dissolve gypsum particles which act as cementing bond in soil, and transportation of soil mass will occur that mass will plug down, and by these techniques, a collapse of sinkholes occurs as the bridging material over a subsurface carven cannot



support the overlying material. The cover collapses into the cavern and large, funnel-shaped depressions forms. The cover collapse happens suddenly in small, focused locations. Leaking utility pipes near the building can accelerate this process and may also cause differential settlement, as shown in Figure (1), [2].



Plate 1 Collapse of a Building in Al-Ramadi City

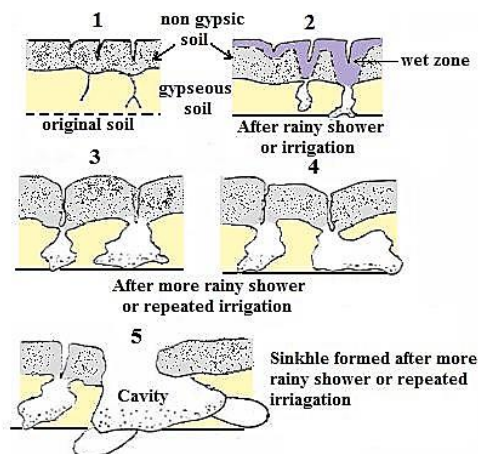


Fig. 1 Sinkhole formation in highly gypsiferous soils, [2].

Al-Tabba et al., [3] presented an analysis of the deformation and failure of cavitated ground when subjected to surface loading using model tests resting on an artificial cohesive-frictional soil containing a single circular or square cavity. Charles et al., [4] studied the undrained stability of submerged cavities that lead to sinkhole formation using finite element analysis techniques in order to obtain upper and lower bound values of suitable load parameter and the cavity was assumed to be spherical, of diameter  $D$  and cover  $C$ . The effects of the cavity on the bearing capacity of footing were investigated by [5] using a two dimensional elasto-plastic finite element method using PLAXIS software. On the other hand, other

researchers investigate the compressibility and collapsibility of gypseous soils without considering the existence of cavities, [6] [7], excluding the relation between the amount of gypsum dissolved and cavity volume. Thus, in this study, the authors aimed to present an analytic model to simulate the behavior of gypseous soil as the cavity formed related to the amount of gypsum dissolved, to estimate the reduction of the bearing capacity due to this phenomenon.

## THE FINITE ELEMENT MODELING

A general finite element program (PLAXIS 3D TUNNEL) was selected to generate the solution. The gypseous soils idealized as an elastic-perfect plastic material and follow Mohr-Coulomb failure criterion. The tensile strength is used as one half of the adhesive strength. The dilatancy angle is given to be zero so that the volumetric strain does not change after the yield failure, and the plastic strain is obtained according to the non-associated plastic flow rule.

The soil layer extends by a range equal twenty times of the footing width in the all horizontal directions measured from the edge of the footing, the depth of this layer extends four times the footing width measured from the surface. The purposes of these dimensions are to make the model is sufficiently large to allow any possible collapse mechanism to be developed and to avoid any influence from the model boundaries. The vertical and horizontal displacements are fixed along the bottom, while the horizontal displacements are fixed along the side. Summary of the parameters used is shown in Table 1. A square footing with dimensions of  $1.0\text{m} \times 1.0\text{m}$  and  $0.25\text{m}$  thickness was selected. These dimensions kept constant in exam all other parameters. The footing is assumed as a linear elastic body, and the physical properties are given with typical values of concrete in order to concede the footing as perfectly rigid with material modulus,  $E_c = 26 \text{ GPa}$ , a unit weight,  $\gamma_c = 24 \text{ kN/m}^3$ , and a Poisson's ratio,  $\nu = 0.2$ .

## Parameters Studied

In order to examine the effect of gypsum dissolution and cavity formation on the bearing capacity and settlement of the foundation, and from researches mentioned about the cavity formation [2], [8], [9], and [10], the following model is developed:

As the excess water from pipe leakage, irrigation, and rainfall will percolate through gypseous soil, the soil wet, the amount and shape of the wetting pattern depend on soil type, [11]. In granular soil, the shape of the wetting pattern will be parabola with approximately horizontal line at the bottom, where the water diffused in three dimensions, as shown in Fig. 2. The water in this zone will soak and leaches the gypseous soil dissolving the gypsum and create a

cavity.

The first case in this study represents a dry gypseous soil with gypsum content of 60%. As the water seepage through the soil (second case), the wetting reign will appear, and a cavity represents a size equal to the dissolving of 10% of gypsum will be formatted. Consequently, other cases represent dissolving of gypsum of 20%, 30%, and 40% respectively, as shown in Fig. 2.

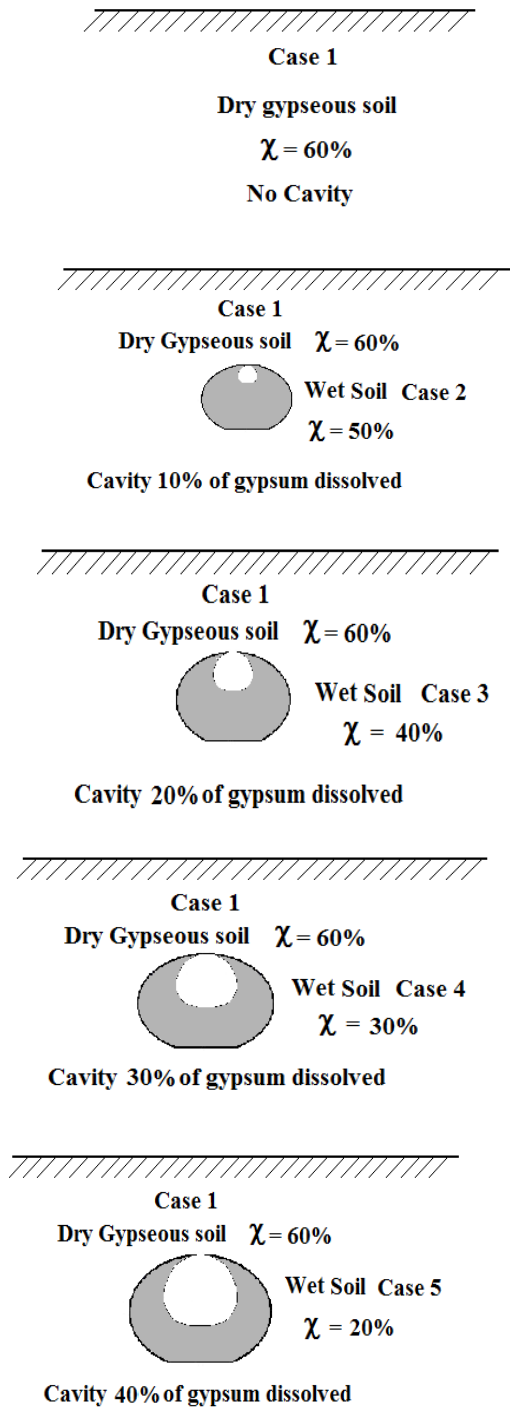


Fig. 2 Cavity shape and cases studied

Table 1 Soil properties used in finite element analysis

| Soil property                                  | Case 1          | Case 2          | Case 3          | Case 4          | Case 5          |
|--|-----------------|-----------------|-----------------|-----------------|-----------------|
| Gypsum content                                 | 60%             | 50%             | 40%             | 30%             | 20%             |
| Apparent cohesion $c$ (kN/m <sup>2</sup> )     | 23              | 17              | 15              | 12              | 9               |
| Angle of internal friction $\phi^\circ$        | 41.2            | 35              | 30              | 25              | 19              |
| Modulus of elasticity $E$ (kN/m <sup>2</sup> ) | $6 \times 10^5$ | $5 \times 10^5$ | $4 \times 10^5$ | $3 \times 10^5$ | $2 \times 10^5$ |
| Poisson's ratio $\nu$                          | 0.35            | 0.33            | 0.30            | 0.30            | 0.25            |

Knowing these values represent the weight of the gypsum mass from the total soil mass, and indicated as a variable ( $\chi\%$ ).

In order to examine the effect of cavity position on the bearing capacity, three offset distances from the footing center to the cavity center are considered (X, Y, and Z) as shown in Fig. 3. where (X) represents the horizontal distance, (Y) represents the vertical (depth) distance, and (Z) represents the diagonal distance. Since the cavity shape has a negligible effect on the bearing capacity for practical purposes, [5] and [12]. Moreover, cavities that forming in gypseous are almost like a loaf. This cavity is characterized in PLAXIS program with three parts (crown, bench, and invert) as shown in Fig. 4. The cavity shape kept loaf with equivalent radius ( $r$ ). The volume of the cavity is changed depending on the amount of gypsum dissolution, as shown in Table 2.

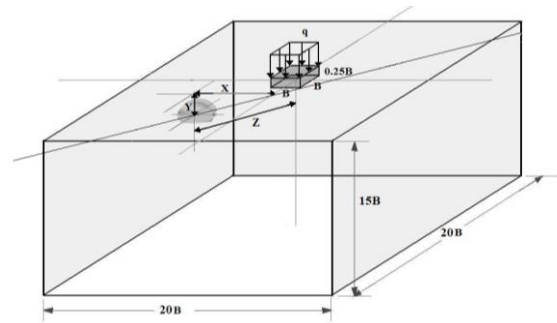


Fig. 3 The geometric configuration of the problem

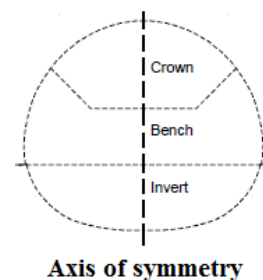


Fig. 4 Geometry of loaf cavity shape

Table 2 Cavity volume related to gypsum dissolution

| Dissolution Rate | Equivalent Cavity Radius (r) (m) | Cavity Length (m) | Cavity Volume (m <sup>3</sup> ) |
|------------------|----------------------------------|-------------------|---------------------------------|
| 10%              | 0.2                              | 0.2666            | 0.0335                          |
| 20%              | 0.3                              | 0.3997            | 0.1130                          |
| 30%              | 0.4                              | 0.5332            | 0.2680                          |
| 40%              | 0.5                              | 0.6666            | 0.5236                          |

A quarter shape configuration for the finite element was used, as shown in Fig. 5

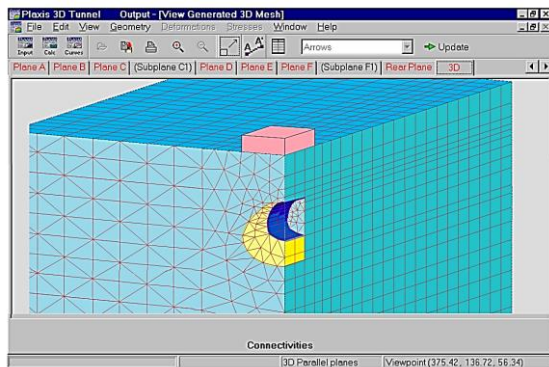


Fig. 5 Finite element model of the wet zone and cavity (quarter shape)

### CAVITY EFFECTS ON THE BEARING CAPACITY FOR THE FOOTING

The effect of the cavity on the bearing capacity is evaluated by using the Bearing Capacity Ratio (BCR), which is the ratio between the ultimate bearing capacity of the footing foundation with cavity and without a cavity.

#### Effect of the Cavity Location on the Bearing Capacity

Table 3 shows the effect of cavity location on the bearing capacity ratio; the cavity position was expressed by the dimensionless ratio (X/B) as the cavity move in a horizontal direction and (Y/B) which represent the cavity location in vertical (depth) direction. From these figures, it seems that BCR decreases with decreasing of (X/B), or (Y/B).

Table 4 shows the values of the bearing capacity for different locations (Z/B) and (Y/B) of the cavity due to gypsum dissolution.

The behavior of the above relationships are reasonable, since that the reduction in bearing capacity found when the cavity located in the active and passive zone in soil that affects the bearing capacity, also when the cavity found in deep layers of soil, the effect may be disappearance, which confirms the stress distribution in the soil.

Table 3 Values of the BCR for different cavity locations (X/B) and (Y/B) due to gypsum dissolution.

| Y/B \ X/B | 0.0  | 2.0  | 2.5  | 3.0  | 3.5  | 4.5  | Gypsum dissolved |
|-----------|------|------|------|------|------|------|------------------|
| 0         | 0.69 | 0.84 | 0.89 | 0.93 | 0.97 | 0.98 | 10%              |
| 1         | 0.87 | 0.94 | 0.96 | 0.97 | 0.98 | 0.98 |                  |
| 2         | 0.96 | 0.98 | 0.99 | 0.99 | 1.00 | 0.99 |                  |
| 3         | 0.98 | 0.99 | 0.99 | 1.00 | 1.00 | 1.00 |                  |
| 4         | 0.98 | 0.99 | 0.99 | 1.00 | 1.00 | 1.00 |                  |
| 0         | 0.47 | 0.73 | 0.79 | 0.87 | 0.93 | 0.98 | 20%              |
| 1         | 0.69 | 0.82 | 0.87 | 0.92 | 0.95 | 0.99 |                  |
| 2         | 0.84 | 0.90 | 0.92 | 0.95 | 0.97 | 0.99 |                  |
| 3         | 0.92 | 0.94 | 0.95 | 0.96 | 0.98 | 1.00 |                  |
| 4         | 0.94 | 0.96 | 0.97 | 0.98 | 0.99 | 1.00 |                  |
| 0         | 0.34 | 0.65 | 0.74 | 0.84 | 0.90 | 0.98 | 30%              |
| 1         | 0.67 | 0.79 | 0.85 | 0.90 | 0.93 | 0.99 |                  |
| 2         | 0.83 | 0.86 | 0.91 | 0.93 | 0.96 | 0.99 |                  |
| 3         | 0.89 | 0.91 | 0.94 | 0.96 | 0.97 | 0.99 |                  |
| 4         | 0.92 | 0.94 | 0.96 | 0.97 | 0.99 | 1.00 |                  |
| Y/B \ X/B | 0.0  | 2.0  | 2.5  | 3.0  | 4.0  | 5.0  |                  |
| 0         | 0.21 | 0.53 | 0.64 | 0.74 | 0.87 | 0.96 | 40%              |
| 1         | 0.49 | 0.65 | 0.75 | 0.82 | 0.92 | 0.97 |                  |
| 2         | 0.68 | 0.79 | 0.84 | 0.90 | 0.95 | 0.98 |                  |
| 3         | 0.81 | 0.87 | 0.91 | 0.95 | 0.97 | 0.99 |                  |
| 4         | 0.85 | 0.90 | 0.94 | 0.96 | 0.98 | 1.00 |                  |

Table 4 Values of the BCR for different cavity locations (X/B) and (Y/B) due to gypsum dissolution

| Y/B \ Z/B | 0.0  | 2.0  | 2.5  | 3.0  | 3.5  | 4.5  | Gypsum dissolved |
|-----------|------|------|------|------|------|------|------------------|
| 0         | 0.69 | 0.84 | 0.89 | 0.93 | 0.97 | 0.98 | 10%              |
| 1.5       | 0.89 | 0.95 | 0.97 | 0.98 | 0.98 | 0.99 |                  |
| 2.5       | 0.96 | 0.98 | 0.99 | 0.99 | 0.99 | 0.99 |                  |
| 3.5       | 0.98 | 0.99 | 0.99 | 1.00 | 1.00 | 1.00 |                  |
| 0         | 0.47 | 0.73 | 0.79 | 0.87 | 0.93 | 0.98 | 20%              |
| 1.5       | 0.73 | 0.85 | 0.89 | 0.93 | 0.96 | 0.99 |                  |
| 2.5       | 0.87 | 0.93 | 0.95 | 0.96 | 0.98 | 0.99 |                  |
| 3.5       | 0.93 | 0.96 | 0.98 | 0.99 | 1.00 | 1.00 |                  |
| 4.5       | 0.94 | 0.97 | 0.98 | 0.99 | 1.00 | 1.00 | 30%              |
| 0         | 0.34 | 0.65 | 0.74 | 0.84 | 0.90 | 0.98 |                  |
| 1.5       | 0.71 | 0.82 | 0.87 | 0.91 | 0.95 | 0.99 |                  |
| 2.5       | 0.85 | 0.90 | 0.93 | 0.95 | 0.98 | 0.99 |                  |
| 3.5       | 0.91 | 0.93 | 0.96 | 0.98 | 0.99 | 1.00 | 40%              |
| 4.5       | 0.93 | 0.96 | 0.97 | 0.99 | 1.00 | 1.00 |                  |

Table 4, cont.

| $\frac{Y/B}{Z/B}$ | 0.0  | 2.0  | 2.5  | 3.0  | 4.0  | 5.0  |     |
|-------------------|------|------|------|------|------|------|-----|
| 0                 | 0.21 | 0.53 | 0.64 | 0.74 | 0.86 | 0.92 |     |
| 1.5               | 0.54 | 0.71 | 0.78 | 0.85 | 0.93 | 0.96 |     |
| 2.5               | 0.72 | 0.83 | 0.88 | 0.92 | 0.96 | 0.99 | 40% |
| 3.5               | 0.81 | 0.92 | 0.95 | 0.97 | 0.98 | 1.00 |     |
| 4.5               | 0.85 | 0.94 | 0.97 | 0.98 | 0.99 | 1.00 |     |

From these Tables, it is clear that as the amount of gypsum dissolved increased, the BCR decreased. The reason behind this behavior can be attributed to the amount of gypsum dissolved, which leads to reduce the bonding between particles and the reduction in strength parameters. The reduction in the BCR is almost low when the amount of the gypsum dissolved less than 10% and when the cavity located at depth more than three times the foundation width. However, if the cavity position is shallow ( $Y/B$  less than 2.5) and the amount of gypsum dissolved more than 20%, the value of BCR may reach 0.6. The dangerous case may be found when the cavity formed near the footing center ( $X/B$  and  $Y/B$  less than 2.0) and when the amount of gypsum dissolved exceeds 30%.

#### Effect of the Cavity Volume on the Bearing Capacity

The variation of the BCR with the cavity volume and ratios ( $Y/B$ ) and ( $X/B$ ) were shown in Figs. 6 to 9, while the variation of the BCR with the cavity volume and ratios ( $Y/B$ ) and ( $Z/B$ ) were shown in Figs. 10 to 13. The curves in these figures show a reduction in the BCR as the dimensionless value ( $Y/B$ ) decreased, this foundation for all cases of ( $X/B$ ) and ( $Z/B$ ). Also, these figures indicated that the volume of the cavity has little effect on BCR when the value of ( $X/B$ ) and ( $Z/B$ ) more than 4.0.

#### CONCLUSIONS

Based on the main results obtained from non-linear analysis using the finite element method in this study, the following conclusions are drawn:

The cavity location found to be the most parameter that affects the BCR. The minimum values are found when the cavity locates at the center of the footing base, and the lowest one (0.211) when the gypsum dissolved equally to 40%. There is no effect of the cavity location when the ratio of ( $X/B$ ) and ( $Z/B$ ) exceed (3.0) for any depth and when the gypsum dissolved less than 10%. For high gypsum dissolution (more than 30%), the dimensionless ratios ( $X/B$ ), ( $Z/B$ ) and ( $Y/B$ ) of the cavity must be more

than 5.0, so that the BCR may be reached 1.0. The amount of gypsum dissolution affect the BCR, and the dangerous case may be found when the cavity formed near the footing center ( $X/B$  and  $Y/B$  less than 2.0) and when the amount of gypsum dissolved exceeds 30%. The cavity size has a significant effect on the BCR; low values of BCR were found for large cavities. The volume of the cavity has little affect on BCR when the value of ( $X/B$ ) and ( $Z/B$ ) more than 4.0. From the results of this study, the minimum values of factor of safety for the foundation design in gypseous soils must be not less than 1.5, 2.5, 3.0, and 4.75 when the gypsum contains these soils are 10%, 20%, 30%, and 40% respectively.

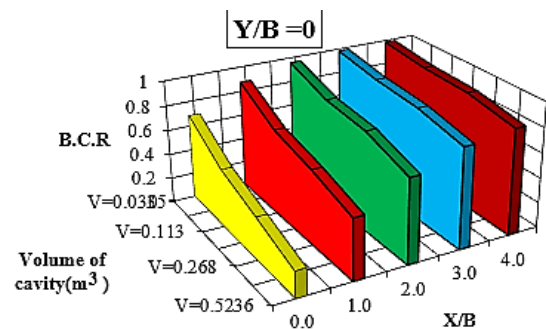


Fig. 6 Variation of BCR with cavity volume and cavity position ( $X/B$ ) for depth ratio ( $Y/B=0$ ).

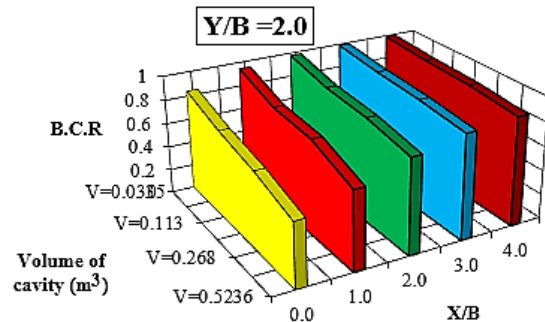


Fig. 7 Variation of BCR with cavity volume and cavity position ( $X/B$ ) for depth ratio ( $Y/B=2$ ).

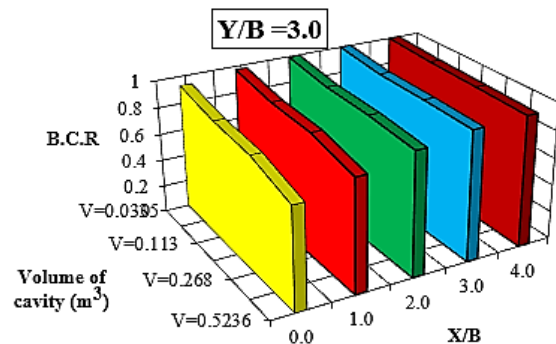


Fig. 8 Variation of BCR with cavity volume and cavity position ( $X/B$ ) for depth ratio ( $Y/B=3$ ).



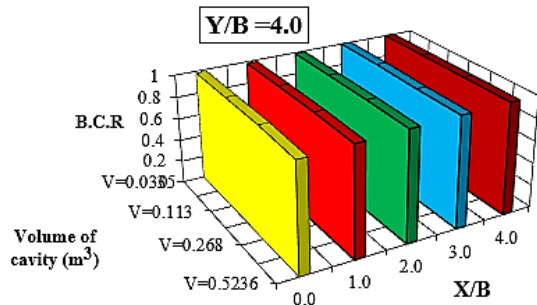


Fig. 9 Variation of BCR with cavity volume and cavity position (X/B) for depth ratio (Y/B=4).

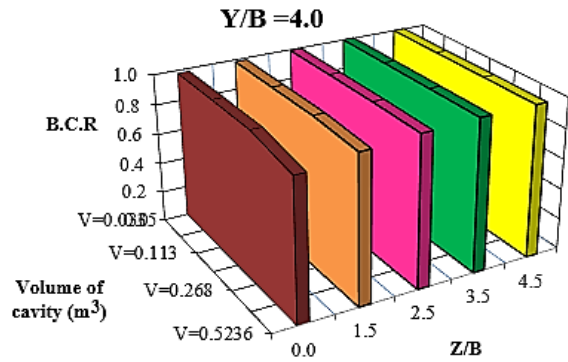


Fig. 13 Variation of BCR with cavity volume and cavity position (Z/B) for depth ratio (Y/B=4).

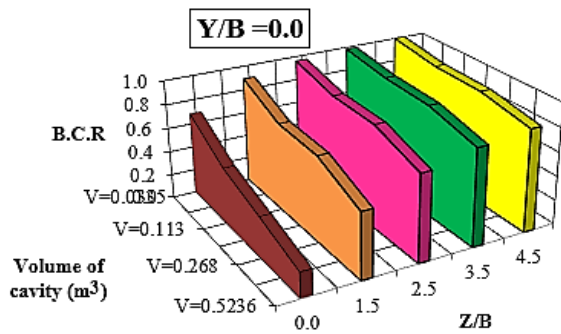


Fig. 10 Variation of BCR with cavity volume and cavity position (Z/B) for depth ratio (Y/B=0).

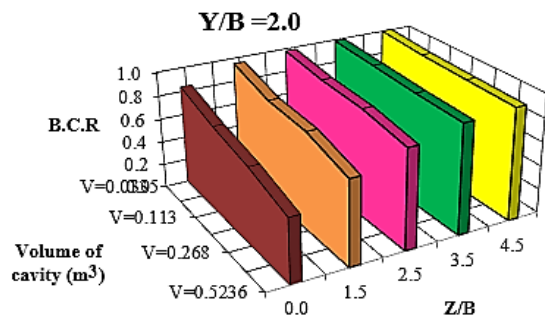


Fig. 11 Variation of BCR with cavity volume and cavity position (Z/B) for depth ratio (Y/B=2).

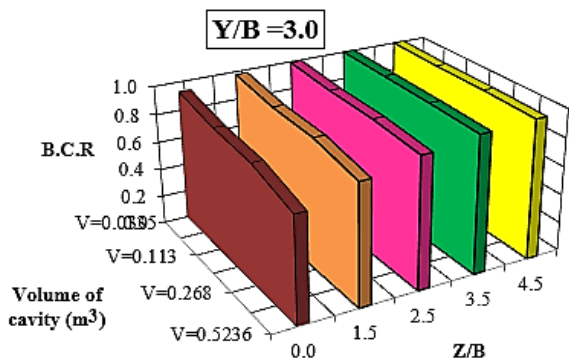


Fig. 12 Variation of BCR with cavity volume and cavity position (Z/B) for depth ratio (Y/B=3).

## REFERENCES

- [1] Wang, M. C., and Badie, A., Effect of Underground Void on Foundation Stability. *Journal of Geotechnical Engineering, ASCE*, Vol. 111, No. 8, 1985, pp. 1008-1019.
- [2] Al-Khafaji, A.N., Some Chemical Properties of South Al-Jazira Irrigation Project. Soil Report Submitted to Dijla Irrigation Center, Mosul, Iraq 1990.
- [3] Al-Tabbaa, A. and Russell, L. and O'Reilly, M., Model Test of Footings above Shallow Cavities, *Ground Engineering*, October 1989, pp. 39-41.
- [4] Charles, E. A., Lyamin, A. V., and Scott W. S., Prediction of Undrained Sinkhole Collapse. *Journal of Geotechnical & Geoenvironmental Engineering, ASCE*, Vol. 129, No. 3, 2003, pp.197-205.
- [5] Peng, F. L., Kiyosumi, M., Ohuchi, M., & Kusakabe, O., Cavity Effects on the Bearing Capacity of Footing Foundations and the Calculation Method. *ASCE, Underground Construction and Ground Movement (GSP 155)*, 2006, pp.50-57.
- [6] Al-Obaidi, A. A. H. and Al-Mafragei, I. H. S., Settlement and Collapse of Gypseous Soils. *Tikrit Journal of Engineering Sciences*, Vol. 23, No. 1, 2016, pp. 20-31
- [7] Fattah, M. Y., Al-Ani Mohammad M., and Al-Lamy M. T. A., Wetling and Drying Collapse Behavior of Collapsible gypseous Soils Treated by Grouting. *Arabian Journal of Geosciences*, 2015 8:2035-2049.
- [8] Sputo, T. Sinkhole Damage to Masonry Structures. *Journal of Performance of Constructed Facilities, ASCE*, Vol.7, No.1, 1993, pp. 67-73.
- [9] Augarde, C. E., Lyamin, A. V. and Sloan, S W., Prediction of Undrained Sinkhole Collapse.

- Journal of Geotechnical and Geoenvironmental Engineering, ASCE, Vol. 129, No. 3, 2003, pp. 197-205.
- [10] Kaufmann J. E., Sinkholes. A study Submit to U.S. Department of the Interior. Geological Survey. Mid-Continent Geographic Science Center, 1400 Independence Road. Rolla, Missouri 65401, 2007.
- [11] Al-Dulaymi A. A., A Laboratory Study of Water Movement in Homogeneous Soils from a Deep Irrigation Pipe Hole with Constant Flow Rates. PhD Thesis, Water Resource Engineering Department, University of Mosul, Iraq, 2007.
- [12] Baus, R. L., and Wang, M. C, Bearing Capacity of Strip Footing above Void. Journal of the Geotechnical Engineering Division, ASCE, Vol. 109, No. 1, 1983, pp. 1-14.

## A STUDY OF THE EFFECTS OF THE FLOOD IN 2554 ON AGRICULTURAL MACHINERY USE IN RICE PADDY FIELDS IN PATHUMTHANI PROVINCE

Dowroong Watcharinrat<sup>1</sup>

<sup>1</sup>Faculty of Agricultural Technology ,Division of Crop Production,  
Rajamangala University of Technology Thanyaburi ,Thailand

### ABSTRACT

In the year 2554, Thailand experienced devastating flooding in the northern and central regions of the country. The objective of this research was to study the effects of this flooding on agricultural machinery use in rice paddy fields. The sample population were farmers from seven districts in Pathumthani Province: Muang, Lamlukka, Nong Suea, Sam Khok, Thanyaburi, Klong Luang and Lad Lum Kaew. The research was conducted from January to April 2014. A group of 100 rice farmers were randomly selected by district. Each district provided a group of 14 to 15 farmers for a total of 100. The questionnaire was created by the researcher with the help of three experts in agricultural machinery and research. The questionnaire consisted of general background information about the farmers as well as the tools they used, such as soil preparation tools, maintenance tools, harvesting tools and post-harvesting tools. Seven students functioned as research assistants and were trained in methods of data collection, questionnaire development and interviewing in order to solicit answers from the farmers. The results of this study showed that the farmers were primarily males between the ages of 41 and 60 with secondary education as the highest education level reached. Most of the farmers in the random sample of 100 used some sort of agricultural machinery. The use of agricultural machinery was widespread and 94% of the farmers made a direct link between the use of machinery and the profitability of their rice paddy fields. It was found that 95% of these farmers claimed that the productivity in rice farming before and after the flood showed no difference.

*Keywords: Rice field, Agricultural machinery, Farm machinery, Flood effect*

### INTRODUCTION

The major flood which occurred in 2554 had a great impact on a wide area of agricultural fields around the lowland areas of Thailand. Especially rice fields in these areas were severely affected. The areas covered by Pathum Thani Province, which includes 7 districts, namely Muang District, Klong Luang District, Thanyaburi District, Nong Suea District, Lat Lum Kaew District, Lam Luk Kaew District and Sam Khok District, were classified as areas that were affected by the flood at that time.

Besides affecting the general condition of the environment, rice yields in these areas were also affected. As the rice paddy fields were flooded, they were not able to meet their expected production. Therefore, farmers lost huge amounts of revenue as a result of the flood. However, once the flood waters receded, farmers started farming again to generate income for their families. In the efforts to restore the affected areas, it was necessary to understand the patterns of usage of agricultural machinery. Effective tool usage became a critical factor in preparing the areas once again and maximizing those areas' productivity. By recognizing these factors, farmers were able to fulfill their needs as a whole.

So in order to reclaim these rice paddy fields and

effectively regain previous yield levels, the methods of production employed by the farmers needed to be studied. These studies revealed those aspects of the farmers' operations that best affected the quality and yield production of rice. Moreover, this information could lead to a sustainable career in farming by developing a variety of agricultural methods and management processes based on a community's needs. The farmers should be involved in the consideration of and decision-making about how to manage the rice production process most efficiently and effectively. This will lead to the cooperation of all sectors that have a role in this process.

Therefore, this research analyzed rice production factors that affected the model of utilization of agricultural tools. The knowledge that was gained from this survey can be used to plan the development of rice production in the areas that were affected by the flood. This will lead to a stable self-reliance.

### PURPOSE/ OBJECTIVE

1. To know the patterns of agricultural machinery use in paddy fields before and after the flood.



2. To evaluate the efficiency of agricultural machinery for rice field management and rice production.

## LIMITS OF THE RESEARCH PROJECT

This research studied only rice paddy fields that were farmed with agricultural machinery in Pathum Thani Province.

## EXPECTED BENEFITS

To understand the patterns of agricultural machinery use in farmers' rice paddy fields, such as the methods of selection, purchase and efficient use of this machinery for farming.

## EQUIPMENT AND METHODS

This study relied on a survey on agricultural machinery use in flooded paddy fields in Pathum Thani province which covers 7 districts, namely Muang District, Klong Luang District, Thanyaburi District, Nong Suea District, Lat Lum Kaew District, Lam Luk Kaew District and Sam Khok District.

## STUDY METHODS

1). Studied opinions and patterns of utilization of agricultural machines used in rice fields and their impact on rice production.

2). Collected survey data via a questionnaire from a random sample of 100 rice farmers from 7 districts with 14 to 15 farmers in each district to represent the study area.

3). Produced a questionnaire which consisted of farmers' general information and their use of agricultural machinery in rice farming. All of this covered 5 options such as soil preparation tools, cultivation tools, maintenance tools, harvesting tools and other tools. This survey tool was developed by asking and getting advice from experts in agricultural machinery and research.

4). Analyzed the data obtained by using statistics, percentage and mean. Other factors analyzed were agricultural machinery use in rice farming, patterns of efficient agricultural machinery use and participation in selecting, purchasing and using agricultural machinery.

## DATA ANALYSIS

Data were presented in the form of tables, frequencies and percentages together with narration based on the questionnaire results for each item.

## LOCATION AND DURATION

The area of this study was in Pathum Thani

province and covered seven districts which have agricultural farming groups. The data collected spanned a four month period, from January to April 2014.

## EXPERIMENTAL RESULTS

The research questionnaire was given to a total of 100 respondents from the following seven districts in Pathumthani province: Muang, Samkhok, Lamlukka, Thanyaburi, Klong Luang, Nong Suea and Lad Lum Kaew. The results can be summarized as follows:

Table 1 Questionnaire data on agricultural machinery utilization in rice paddy fields classified by gender (sex)

| Men | Women | Total |
|-----|-------|-------|
| 71  | 29    | 100   |

From Table 1: Based on the 100 respondents to the research questionnaire, it was found that most of them were male (71 males to 29 females).

Table 2 Questionnaire data on agricultural machinery utilization in rice paddy fields classified by age

| Less than 30 | 31-40 year | 41-50 year | 51-60 year | 61-70 year | More than 70 year | Total |
|--------------|------------|------------|------------|------------|-------------------|-------|
| 2            | 13         | 30         | 40         | 14         | 1                 | 100   |

From table 2: According to the answers from the 100 respondents to the research questionnaire, most were in the age group of 51-60 year olds (40 people). The next largest group were the 41-50 year olds (30 people). The rest of the groups were as follows in descending order: 61-70 year olds (14 people), 31-40 year olds (13 people), less than 30 years old (2 people) and more than 70 years old (1 person).

Table 3 Questionnaire data on agricultural machinery utilization in rice paddy fields classified by education

| Primary school | Secondary-High School | Diploma | Bachelor's Degree or above | Total |
|----------------|-----------------------|---------|----------------------------|-------|
| 48             | 33                    | 12      | 7                          | 100   |

From Table 3: According to the answers from the 100 respondents of the research questionnaire, 48 of the respondents completed primary school, 33 completed secondary-high school, 12 completed a diploma, and 7 completed a Bachelor's degree.

Table 4 Questionnaire data on agricultural machinery utilization in rice paddy fields classified by the number of household members

| Less than 3 people | 3-5 people | 6-8 people | 9-11 people | More than 11 people | Total |
|--------------------|------------|------------|-------------|---------------------|-------|
| 4                  | 51         | 38         | 6           | 1                   | 100   |

From Table 4: According to the answers from the 100 respondents of the research questionnaire, 51 families had 3-5 members, 38 families had 6-8 members, 6 families had 9-11 members, 4 families had less than 3 members and 1 family had more than 11 members in the family.

Table 5 Questionnaire data on agricultural machinery utilization in rice paddy rice fields classified by other occupations than farming

| Farmers | Contractors | Trading / Business | Employees | Government officials / state enterprises | Others ..... | Total |
|---------|-------------|--------------------|-----------|--|--------------|-------|
| 26      | 39          | 16                 | 12        | 7  |              | 100   |

From Table 5: According to the answers from the 100 respondents of the research questionnaire, 39 were general hired contractors, 26 were employed in the field of agriculture, 16 were in trading/private business, 12 were company employees and 7 were government officials / state employees.

Table 6 Questionnaire data on agricultural machinery utilization in rice paddy fields classified by farm size

| Less than 20 rai | 20-40 rai | 41-60 rai | 61-80 rai | 81-100 rai | 101-120 rai | 121-140 rai | 141-160 rai | More than 160 rai | Total |
|------------------|-----------|-----------|-----------|------------|-------------|-------------|-------------|-------------------|-------|
| 26               | 37        | 25        | 8         | 2          | 1           | 1           | 0           | 6                 | 100   |

From Table 6: According to the answers from the 100 respondents of the research questionnaire, 37 had a farming area of 20-40 rai, 26 had less than 20 rai, 25 had 41-60 rai, 8 had 61-80 rai, 6 had more than 160 rai, 2 had 81-100 rai, 1 had 101-120 rai and no one had 121-140 rai.

Table 7 Questionnaire data on agricultural machinery utilization in rice paddy fields classified by net income / year

| Less than 100,000 baht | 100,000-200,000 baht | 200,001-300,000 baht | 300,001-400,000 baht | 400,001-500,000 baht | 500,001-600,000 baht | 600,001-700,000 baht | 700,001-800,000 baht | More than 800,000 baht | Total |
|------------------------|----------------------|----------------------|----------------------|----------------------|----------------------|----------------------|----------------------|------------------------|-------|
| 3                      | 10                   | 26                   | 28                   | 13                   | 9                    | 6                    | 2                    | 3                      | 100   |

From Table 7: According to the answers from the 100 respondents of the research questionnaire, 28 had a net income of 300,001-400,000 baht, 28 had a net income of 200,001-300,000 baht, 13 had a net

income of 400,001-500,000 baht, 10 had a net income of 100,000-200,000 baht, 9 had a net income of 500,001-600,000 baht, 6 had a net income of 600,001-700,000 baht, 3 had a net income of less than 100,000 baht and 3 others had a net income of more than 800,000 Baht and 1 had a net income of 700,001-800,000 baht.

Table 8 Questionnaire data on agricultural machinery utilization in rice paddy fields classified by number of times farming / year

| 1. time | 2. time | 3.time | More than 3 time | Total |
|---------|---------|--------|------------------|-------|
| 0       | 18      | 79     | 3                | 100   |

From Table 8: According to the answers from the 100 respondents of the research questionnaire, 79 farmers farm 3 times a year, 18 famers farm 2 times a year, and 3 farmers farm more than 3 times a year.

Table 9: Questionnaire data on agricultural machinery utilization in rice paddy fields classified by profitability in farming

| Loss | Profit | The same | Total |
|------|--------|----------|-------|
| 1    | 94     | 5        | 100   |

From Table 9: According to the answers from the 100 respondents of the research questionnaire, 94 made a profit from farming, 5 said that profit and investment were equal and 1 farmer made no profit in rice farming.

Table 10 Questionnaire data on agricultural machinery utilization in rice paddy fields classified by farming yield.

| Before the flood better | After the flood better | not different | Total |
|-------------------------|------------------------|---------------|-------|
| 2                       | 3                      | 95            | 100   |

From Table 10: According to the answers from the 100 respondents of the research questionnaire, 95 farmers answered that there was no significant difference between the pre-flood and post-flood periods, 3 farmers said the post- flood period was better than the pre-flood period and 2 said the pre-flood period was better than post-flood period.

Table 11 Questionnaire data on agricultural machinery utilization in rice paddy fields classified by the type of property used for farming

| Own | Hire | Own and rent | Total |
|-----|------|--------------|-------|
| 81  | 4    | 15           | 100   |

From Table 11: According to the answers from the 100 respondents of the research questionnaire, most of the respondents, 81 had their own property for rice farming, 15 had their own and rented property for farming and 4 farmers rented property for farming.

Table 12 Questionnaire data on agricultural machinery utilization in rice paddy fields classified by efficiency of agricultural machinery utilization for rice farming.

| Excellent | Good | Fair | Little | Least | Total |
|-----------|------|------|--------|-------|-------|
| 72        | 25   | 3    | 0      | 0     | 100   |

From Table 12: According to the answers from the 100 respondents of the research questionnaire, 72 commented that the efficiency of using agricultural machinery in production was excellent, 25 commented that it was good and 3 commented that that the efficiency of using agricultural machinery in rice production was fair.

Table 13 Questionnaire data on agricultural machinery utilization in rice paddy fields classified by district

| District        | Number |
|-----------------|--------|
| 1. City         | 15     |
| 2. Lum Lukka    | 14     |
| 3. Thanyaburi   | 14     |
| 4. Klong Luang  | 14     |
| 5. Nong Sua     | 14     |
| 6. Lard lumkaew | 14     |
| 7. Sam khok     | 15     |
| Total           | 100    |

From Table 13: According to the answers from the 100 respondents of the research questionnaire, the 7 districts in Pathum Thani Province were divided as follows: 15 farmers were from Muang district and Sam Khok district, and 14 farmers were from Lam Lukka, Thanyaburi, Khlong Luang, Nong Sua and Ladlumkaew districts.

Table 14 Test data for using and purchasing agricultural machinery classified by participation

| Participation  | Number |
|--|--------|
| 1. Think by themselves   | 47     |
| 2. Ask fellow farmers in the community.                        | 3      |
| 3. Think by themselves and ask fellow farmers in the community | 46     |
| Total  | 100    |

Table 14: According to the answers from the 100 respondents of the research questionnaire, 47

farmers thought by themselves, 3 farmers asked fellow farmers in the community and 46 farmers both thought by themselves and asked fellow farmers in the community.

Table 15 Patterns of agricultural machinery utilization in rice farming classified by type of tillage tool

| Tillage Equipment                    | Usage pattern of agricultural machinery |            |                     |           |                                |
|--------------------------------------|---|------------|---------------------|-----------|--------------------------------|
|                                      | use                                     | Do not use | hiring a contractor | Their own | Hire contractors and their own |
| 1. Two-wheeled tractor               | 65                                      | 35         | 7                   | 58        | 0                              |
| 2. 4 wheel tractor, 2 wheel drive    | 32                                      | 68         | 4                   | 28        | 0                              |
| 3. Four-wheel-drive tractor          | 36                                      | 64         | 5                   | 31        | 0                              |
| 4. E-mill (rollers, mixers, rollers) | 100                                     | 0          | 19                  | 81        | 0                              |
| 5. Plow head                         | 4                                       | 96         | 0                   | 4         | 0                              |
| 6. Plow                              | 9                                       | 91         | 0                   | 9         | 0                              |
| 7. Plow chisel                       | 0                                       | 100        | 0                   | 0         | 0                              |
| 8. Scoop                             | 12                                      | 88         | 0                   | 12        | 0                              |
| 9. Twist                             | 99                                      | 1          | 7                   | 92        | 0                              |
| 10. Spinning                         | 100                                     | 0          | 25                  | 69        | 6                              |
| 11. Capital drag (Lube Lane board)   | 100                                     | 0          | 8                   | 85        | 7                              |
| 12. Rake                             | 100                                     | 0          | 23                  | 69        | 8                              |

From Table 15: The use of agricultural machinery for rice farming type of tillage tool showed that 65 farmers used two-wheel walking tractors, 35 didn't use walking tractors, 7 farmers hired a contractor with a 2-wheel tractor pattern and 58 had their own. There were 32 farmers who used 4 wheel tractors with 2 wheel drive, 68 farmers didn't use 4 wheel tractors with 2 wheel drive, 28 farmers used the pattern of hiring a contractor with a 4 wheel tractor with 2 wheel drive and 1 farmer already had a 4 wheel tractor with 2 wheel drive. There were 36 farmers who used a 4 wheel tractor with 4 wheel drive, 68 farmers didn't use a 4 wheel tractor with 4 wheel drive, 5 farmers used the pattern of hiring a contractor with a 4 wheel tractor with 4 wheel drive and 31 farmers had their own 4 wheel tractor with 4 wheel drive. There were 19 farmers who used e-rolls (rollers, mixers, rollers) all forms use e-rolls (rollers, mixers, rollers), 19 farmers hired a contractor and 81 had their own. Four farmers used plow heads and 96 did not use plows with heads. Nine farmers used plows without heads, 91 farmers did not use plows without heads and 9 farmers used the plow pattern. Twelve farmers used scraping dishes, 88 farmers did

not use them and 12 farmers had their own. There were 99 farmers who used a twist, 1 farmer did not, 7 farmers hired a contractor pattern and 92 had their own. All farmers used spinning, 25 farmers hired, 69 had their own and 6 hired and had their own. All farmers used the capital to drag (Lube Lane boards). For use of capital drag (Lube Lane Board), 8 farmers hired, 85 had their own and 7 farmers hired and had their own. All farmers used rakes, 23 farmers used a hire pattern, 69 had their own and 8 farmers hired and had their own.

Table 16 Patterns of agricultural machinery utilization in paddy cultivation

| Planting Equipment           | Usage pattern of agricultural machinery |            |                     |           |                                 |
|------------------------------|---|------------|---------------------|-----------|---------------------------------|
|                              | Use                                     | Do not use | Hiring a contractor | Their own | Hire a contractor and their own |
| 1. Seeder machine            | 0                                       | 100        | 0                   | 0         | 0                               |
| 2. Sowing machine            | 100                                     | 0          | 38                  | 54        | 8                               |
| 3. Transplant rice seedlings | 11                                      | 89         | 3                   | 8         | 0                               |

From Table 16: The use of agricultural machinery for rice cultivation found that no farmers used a seeder, 38 hired a seeder pattern, 54 had their own seeder and 8 hired and had their own. There were 11 farmers who used drones, 89 did not use drones, 3 farmers hired a contractor and 8 had their own.

Table 17 Patterns of agricultural machinery concerning maintenance tools used in rice farming

| Crop Protection and Fertilizing Equipment | Usage pattern of agricultural machinery |            |                     |           |                                 |
|---|---|------------|---------------------|-----------|---------------------------------|
|   | Use                                     | Do not use | Hiring a contractor | Their own | Hire a contractor and their own |
| 3.1 Sprayer                               | 98                                      | 2          | 37                  | 54        | 7                               |
| 3.2 Manure spreader                       | 99                                      | 1          | 38                  | 54        | 7                               |
| 3.3 Pump                                  | 96                                      | 4          | 18                  | 78        | 0                               |
| 3.4 Lawn mower                            | 93                                      | 7          | 4                   | 89        | 0                               |
| 3.5 Harvesting weeds                      | 4                                       | 96         | 0                   | 4         | 0                               |

From Table 17: The use of agricultural machinery concerning maintenance tools in rice farming found that there were 98 farmers who used a sprayer, 2 did not, 37 hired a contractor, 54 had their own and 7 hired a contractor and had their own. There were 99 farmers who used manure spreaders,

1 did not, 38 farmers hired manure spreaders and 54 hired contractors and had their own. There were 96 farmers who used pump units, 4 farmers did not, 18 used a hire pattern and 78 had their own. There were 93 farmers who used lawn mowers, 7 farmers did not, 4 used hire pattern and 89 had their own. There were 4 farmers who used weeding machines, 96 farmers did not, 4 farmers used a pattern of hiring weeding machines.

Table 18 Agricultural machinery utilization in rice fields classified by type of harvest tool

| Harvesting Equipment | Usage pattern of agricultural machinery |            |                     |           |                                 |
|----------------------|---|------------|---------------------|-----------|---------------------------------|
|                      | Use                                     | Do not use | Hiring a contractor | Their own | Hire a contractor and their own |
| 1. Combine harvester | 3                                       | 97         | 0                   | 3         | 0                               |
| 2. Threshing machine | 3                                       | 97         | 0                   | 3         | 0                               |
| 3. Harvester         | 97                                      | 3          | 89                  | 8         | 0                               |
| 4. Turbine           | 5                                       | 95         | 0                   | 5         | 0                               |

Table 18: Agricultural machinery utilization in rice fields classified by type of harvest tool found that 3 farmers used combine harvesters, 97 farmers did not, 3 farmers used a hire pattern. There were 3 farmers who used threshing machines, 97 farmers did not, 3 used the pattern of hiring threshing machines. There were 97 farmers who used combine harvesters, 3 farmers did not, 89 used a pattern of hiring a contractor and 8 farmers had their own. There were 5 farmers who used milling machines, 95 did not and 5 farmers used their own milling machines.

Table 19 Patterns of agricultural machinery use in rice farming classified by other types of tools

| Other Equipment | Usage pattern of agricultural machinery |            |                   |           |                                 |
|-----------------|---|------------|-------------------|-----------|---------------------------------|
|                 | use                                     | Do not use | Hire a contractor | Their own | Hire a contractor and their own |
| 1. Rice mill    | 11                                      | 89         | 4                 | 7         | 0                               |
| 2. Dehumidifier | 2                                       | 98         | 0                 | 2         | 0                               |
| 3. Mower        | 7                                       | 93         | 0                 | 7         | 0                               |

Table 19: Patterns of agricultural machinery used in rice farming classified by other types of tools: 11 farmers used rice mills, 89 did not use rice mills, 4 hired and 7 farmers had their own. There were 2 farmers who used two desiccators, 98 did not and 2 had their own desiccators. There were 7 farmers who used rice straw mills, 93 did not and 7 farmers had their own rice straw mills.

## EXPERIMENTAL RESULT CONCLUSION

According to this study on rice planting with

agricultural machinery, it was found that most farmers, around 81%, had an education background that included primary and secondary schools, around 62% had a planting area of between 20-60 rai, around 81% had their own planting area, around 55% of the farmers had a net income of between 200,000-400,000 and around 79% planted rice 3 times per year. Agro-based agricultural machinery was seen as performing better than other methods. And the process of choosing agricultural machinery or buying agricultural machinery was conducted both by the farmers thinking for themselves and consulting a farmer in the community about issues such as a tractor walks, the tractor seat drive (clutching rollers), the drag capital (lump lane) maintenance tools such as fertilizer spreaders and sprayers. The villagers bought machinery for themselves and usually hired a contractor rather than buying for themselves.

### RECOMMENDATIONS

1. Study the effects of using farm machinery that is produced domestically versus from abroad
2. Study the benefits of using agricultural machinery for drowning and sowing
3. Study the economic returns on using agricultural machinery three times a year and two times a year

### DISCUSSION

According to this study on the impact of using agricultural machinery when planting rice, it was found that 81% of farmers finished primary and secondary school. If their education was greater than this, they would be counted in the industrial or service sector which requires more knowledge to find money for funds for labor costs in rice planting. Some rice farming families worked in rice fields only on the weekends and used charter methods in every stage rather than doing it by themselves. About 62% of rice farmers used agricultural machinery, farmed a planting area of 20-60 rai and farmed around 2-4 times a year in Pathumthani province. This province which is in the central region of Thailand has many rice fields because it is a low-lying area suitable for rice planting. This area is located in an irrigation zone that does not have many water issues and can therefore offer a main career or part time job in farming. This vast amount of rice farming areas is suitable for using agricultural machinery. Many rice farmers replied

that using agricultural machinery over other methods was more efficient and had greater rice production as well as saved time, expenses and reduced labor issues. Moreover, agricultural machinery contributed to more frequent planting (3-4 times a year). The flood conditions in 2554 had no effect on rice production. Farmers said that before and after the flood, their yield did not change in Pathumthani province. They mostly relied on irrigation on both the left and right sides of the Chaopraya river which includes the Rapeepat and Rangsit canals. Most farmers had their own tractors which could also be used in other capacities, such as a trucks for tillage or pumping and even for travel. For harvesting machines, farmers commonly rented more than they purchased due to the relatively high prices.

### REFERENCES

- [1] Department of Agriculture .2012. Rice research srtagety .2012-2016. Source : [www.it.doa.go.th/kasikorn/year-53/jan\\_feb.../part-1.pdf](http://www.it.doa.go.th/kasikorn/year-53/jan_feb.../part-1.pdf), 14 May 2013.
- [2] Kasem Jankaew . 2011. Environmental Science. 5th. Kasetsart University, Bangkok.
- [3] Chayan Wattanaphuti . 1991 .Concept of Research,Research for Job Development,Institute of Research and Development,Kkon khaen University
- [4] Parichart Walaisatien. 2000. Process of Development. Office of Research Fund, Bangkok.
- [5] Rungreung Kalsirisilk .2004. Using of Agricultural Machinery in Pathumthani Province,Research Report of Agricultural Machinery Department,Rajamangala University of Technology Thanyaburi
- [6] Financial of Pathumthani Province,2011,*Report of Econmics for Pathumthani,2012,Source:* [www.klang.cgd.go.th/ptt/cfo\\_doc/economy/mcq3-](http://www.klang.cgd.go.th/ptt/cfo_doc/economy/mcq3-)
- [7] Rice Research Institute [http://www.arda.or.th/kasetinfo/rice/rice\\_cultivate\\_machine/rice-cultivate\\_cultivate\\_machine\\_index.html](http://www.arda.or.th/kasetinfo/rice/rice_cultivate_machine/rice-cultivate_cultivate_machine_index.html)
- [8] Samerkwan Tantikul.2007. Farm Machinery,.Bangkok.The Knowledge Center,December,2007.
- [9] Rawat Phitaksakul2 . 003.Using of Agricultural Machinery in Lopburi Province,Kasetsart University.

## DESIGN AND IMPLEMENT A MONITORING SYSTEM OF TRAFFIC SIGNAL USING MICROCONTROLLER DEVICES

Aleksander Purba<sup>1</sup>, Rahayu Sulistyorini<sup>1</sup>, Agung Ilhami<sup>1</sup> and Ageng Sadnowo Repelianto<sup>1</sup>

<sup>1</sup>Faculty of Engineering, University of Lampung, Lampung Indonesia

### ABSTRACT

This project focused on designing traffic signal monitoring tools, based on ideas and concepts developed previously. Authors used the Arduino Nano module with ATmega328P as the microcontroller, which was chosen because it simplifies the scenario of traffic signal anomalies, short messages service (SMS) news content, and time settings. A microcontroller was used to process data from the interference detection result, and processing the SMS content, therefore, it is able to quickly inform the types of traffic signal disruptions. Based on result findings it is possible to utilize this development in building an integrated traffic signal monitoring system services, in the form of mobile applications in the near future.

*Keywords: Monitoring system, Traffic signal, Microcontroller, Malfunctioning, Short message service*

### INTRODUCTION

Traffic signal infrastructure is responsible for assigning the right of way to vehicular and pedestrian passage at intersections. Meanwhile, its management and operations requires the proper design, location, operation and maintenance, to provide safe and efficient movements. A lot of mysteries surround its mechanism of action, although they are relatively simple as the installation comprises of traffic signal heads, detection and a controller, which is the 'brains' behind the equipment, containing the information required to force the lights through various sequences. These signals run under a variety of modes, dependent on location and time of day, which under fixed time operation, displays green to each approach for the same amount of time per cycle, regardless of the traffic conditions.

This may be adequate in heavily congested areas, while instances where a lightly trafficked side road is included within the sequence, the system becomes very wasteful, as no vehicles are waiting in some cycles, and the time could be better allocated to the busier approach. Vehicle actuation is one of the most common modes of operation, and as the name suggests, it takes into account demands on all approaches and also adjusts the green time accordingly. Furthermore, the requirements to actualize this mechanism are registered through the detection installed, either in the carriageway or above the signal heads, which the controller processes and further allocates the green time in the most appropriate way.

However, minimum and maximum periods are specified, and this cannot be violated, therefore, a vehicle passing a detector demands a certain phase and once that phase is green, any subsequently

passing automobile, causes the phase to extend. This continues as such up to the point where either the traffic demand ceases and another approach gains green, or a conflicting demand causes the maximum timer to count down. Moreover, while vehicle actuation mode is more responsive than fixed time it also has the propensity of being inefficient in instances where long queues build up on conflicting approaches. The setting of maximum timers is then difficult due to changes in traffic patterns through junctions over time, which should therefore be regularly updated, in order to maintain effective operation. This is a labor intensive task for a local transportation authority, which is often not undertaken, thus leading to the signals becoming less effective over time.

As all electronic equipment, these devices are subject to breakdowns, malfunctions, and power outages, which could lead to safe intersections becoming dangerously congested and confusing, therefore resulting in needless accidents. However, a study on the city of Boston calculated that simply reconfiguring the timings of 60 intersections in one district of the city could save US\$1.2 million per year, in terms of person-hours, safety, emissions, and energy costs [1]. In situations where malfunctioning occurs, the entity responsible for maintaining the signal may be held accountable, as regions and municipalities have a statutorily imposed duty, which ensure roads are safe for users. Furthermore, the Province of Ontario has set up certain minimum requirements for the maintenance of roadways, which include standards related to traffic signals, according to Regulation 239/02, which states the Minimum Maintenance Standards for Municipal Highways, under the Municipal Act. However, section 13 of the O.Reg 239/02 stipulates that in cases where a

malfunctioning traffic control signal system occurs, the minimum guideline is to “deploy resources as soon as practicable after the awareness of the defect, in order to commence repairs or replacements” [2]. Meanwhile, most regions and municipalities have no statutory in this regards as Ontario, and due to the fact that most of the traffic signals are categorized as isolated intersections, the surveillance system is therefore highly dependent on road users report. Hence, response time needed is longer, especially during out of work hours.

This project focused on designing traffic signal monitoring tools, based on ideas and concepts developed from the research conducted by Sivarao et al. [3] and Anita Ahmad et al. [4], as well as self-diagnosis techniques, using the Reed-Solomon Codes by Tang and Wang [5]. Furthermore, a monitoring system with Proteus advancement tool, developed in Africa, was also used [6]. However, activities including designing concepts, materials selection, assembling tools, and traffic signal monitoring systems testing are rarely performed.

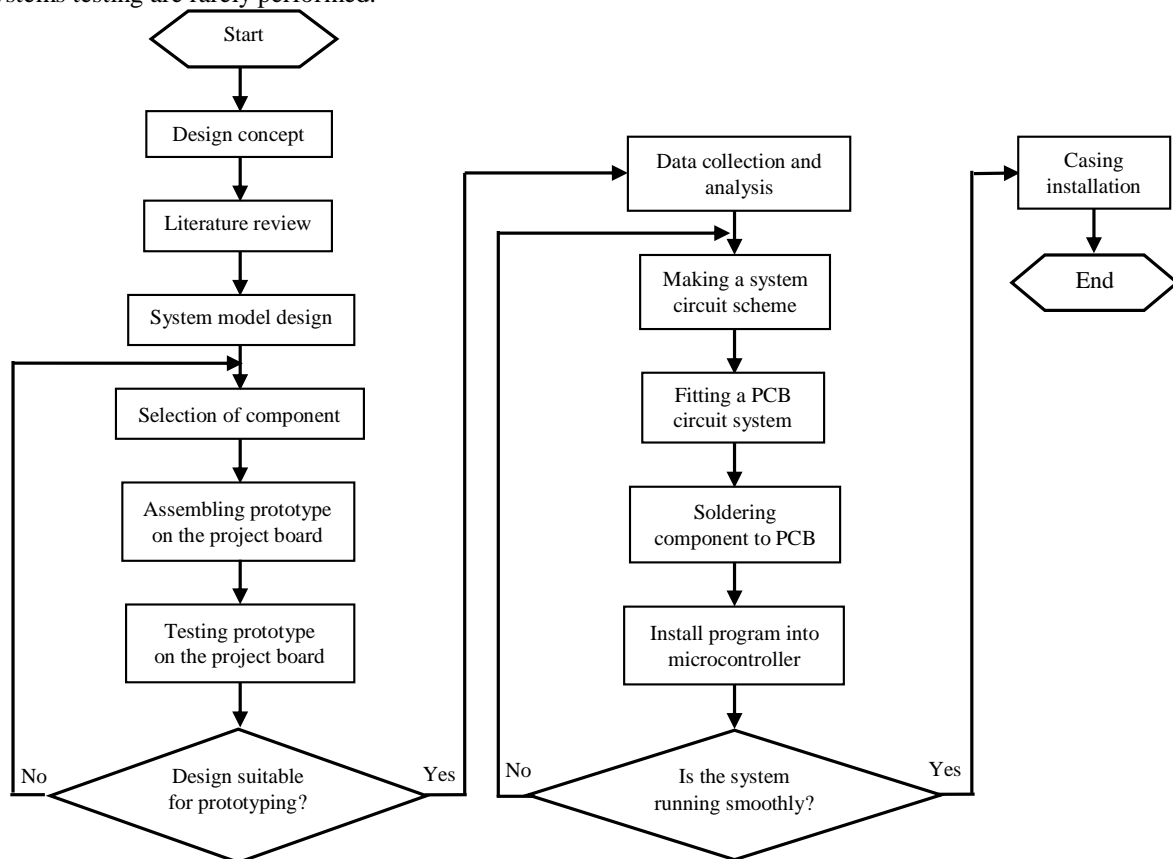


Fig. 1 Design circuit flow chart

## RESULT AND DISCUSSION

Each traffic signal display is equipped with a form of light sensor, positioned in a way, in order to detect beams from the traffic signal. This is then processed by the logic gate and microcontroller to be diagnosed,

## RESEARCH METHODOLOGY

The product was designed based on electronic circuit plan, where all blocks were arranged on the project board and tested individually, and also a combination on printed circuit board (PCB) was conducted, at periods of proper function. This study used the Arduino Nano module with ATmega328P as the microcontroller, which was chosen because it simplifies the scenario of traffic signal anomalies, short messages service (SMS) news content, and time settings.

This also facilitates programming, possesses a memory capacity that is capable of accommodating program scripts, it is affordable, readily available, and is relatively small in size.

However, programming was carried out using the built-in Arduino IDE open-source software, and the general description of electronic circuit design is seen in Fig. 1 as developed previously [7, 8, 9].

based on the rational state, guard time and verification of the programming anomaly scenario. Furthermore, the microcontroller recognizes the anomaly and immediately turns all traffic signal display (red, yellow and green) off. Meanwhile, during the termination process, the microcontroller instructs the A6 GSM module to dispatch an SMS, at certain time



intervals, according to the program (e.g., once every hour). Therefore, the emergency light flashes periodically, serving as a visual marker, which indicates that the signal is under repair. Hence, mobile or smartphones can be used as an SMS receiver by entering the recipient's number from the traffic signal in the microcontroller program.

Switching mode power supply (SMPS) with DC 12V 10A voltage was used as the main source. This

voltage was chosen to supply the relay and a series of LED lights on the traffic display and emergency flash. In addition, step-down DC to DC buck converter was also applied by reducing the DC 12 Volt voltage from SMPS to DC 5V 3A, which was further used to supply logical state, guard time, data latch, reflected light sensor, GSM A6 module, and the microcontroller as shown in Fig. 2.

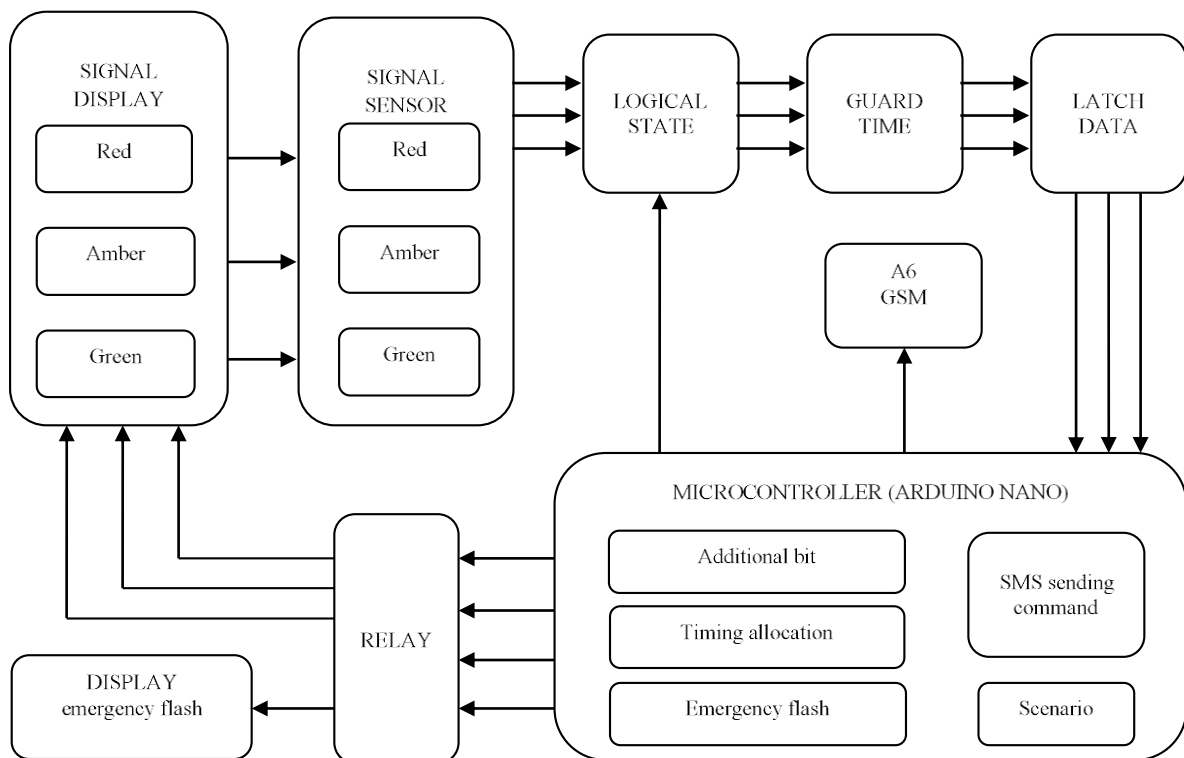


Fig. 2 Devices diagram block

Referring to Fig. 2, a design of electronic series consists of some blocks:

1. The traffic signal display block consists of the combination of a series of light emitted diode (LED) illuminations (red, amber and green), and placed between them are three light dependent resistor sensors (LDRs), used to detect reflections produced by LEDs and other reflectors.

2. The emergency flash display block consists of a combination of LED beams, functioning as visual markers, and the main traffic signal, during the repair process.

3. Reflection sensor block. The readings of each LDR (red, amber, and green) are entered into three voltage comparator circuits. Therefore, if it obtains reflected light, the sensor produces a LOW logic, and on the contrary, a HIGH logic is emitted in the absence of reflected light.

4. The logical state block is an electronic path, which uses an integrated circuit (IC) type CD4028 (BCD to decimal decoder), designed to identify different bits of each sequence of statement traffic signals, in cases of anomaly. Furthermore, the input pin of this IC is a 4-bit binary number (from 0000 to 1111), while the output pin is represented by 10 digits (Y0 to Y9). The following are some identity bits designed for each traffic signal anomaly statement:

- 4.1. the red display is given the 0101-bit, characterized by pin Y5.

- 4.2. the amber demonstration specifies the 0011-bit, represented by pin Y3.

- 4.3. the green exhibition is allotted the 0111-bit, denoted by pin Y7.

5. Guard time block: Anomalous data Y5, Y3, and Y7 cannot be considered valid when in the guard time series, which was allotted a time period of 1 second in this study. For example, if Y5 sends an

under-1 second-anomalous signal, it is not considered an anomaly and vice versa.

6. Latch data block: After the validity of the anomaly signal has been considered, the block is then locked (latch). This is further processed by the microcontroller, at the end of a cycle of traffic signal.

7. Microcontroller block: This is divided into five sub-blocks with their respective functions, including:

7.1. timing traffic signal functions as a time allocator per cycle.

7.2. Provision of additional bit function for CD4028 IC input (logical statement block), in determining bit during an anomaly.

7.3. Anomaly data verification scenario, through the process of matching results of processing data latch blocks with anomalous scenarios, which have been programmed in the microcontroller.

7.4. SMS sending command, when a change in the traffic signal anomaly was considered a malfunction (through the verification process) to be forwarded as news to the A6 GSM module block.

7.5. emergency flash: This sub-block works by flashing, depicting a sign that the main traffic signal is under maintenance.

8. The GSM block A6 module works by sending SMS on the processing results, from the microcontroller to the operator. This occurs because the unit has been recognized by the Arduino library,

therefore, it is easily programmed in the IDE, with the AT command instruction set.

9. Relay block is a series, consisting of 4 types of transmissions, while the ULN2803A IC and optocoupler turns ON or OFF the traffic signal display and emergency flash. These conditions for the four types of relay, follow the order of the microcontroller sub-block timing functions.

The traffic signal cycle in this study followed the sequence as shown in Fig 3.

1. Red OFF, Amber ON, Green OFF;
2. Red ON, Amber OFF, Green OFF;
3. Red ON, Amber ON, Green OFF;
4. Red OFF, Amber OFF, Green ON;
5. The second cycle (restarts from Red OFF, Amber ON and Green OFF).

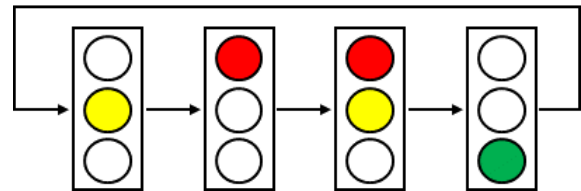


Fig. 3 Traffic signal cycle

Hence, the implementation of a monitoring system completely as combined work of Fig. 1 and Fig. 2 respectively, shown in the Fig. 4 below.

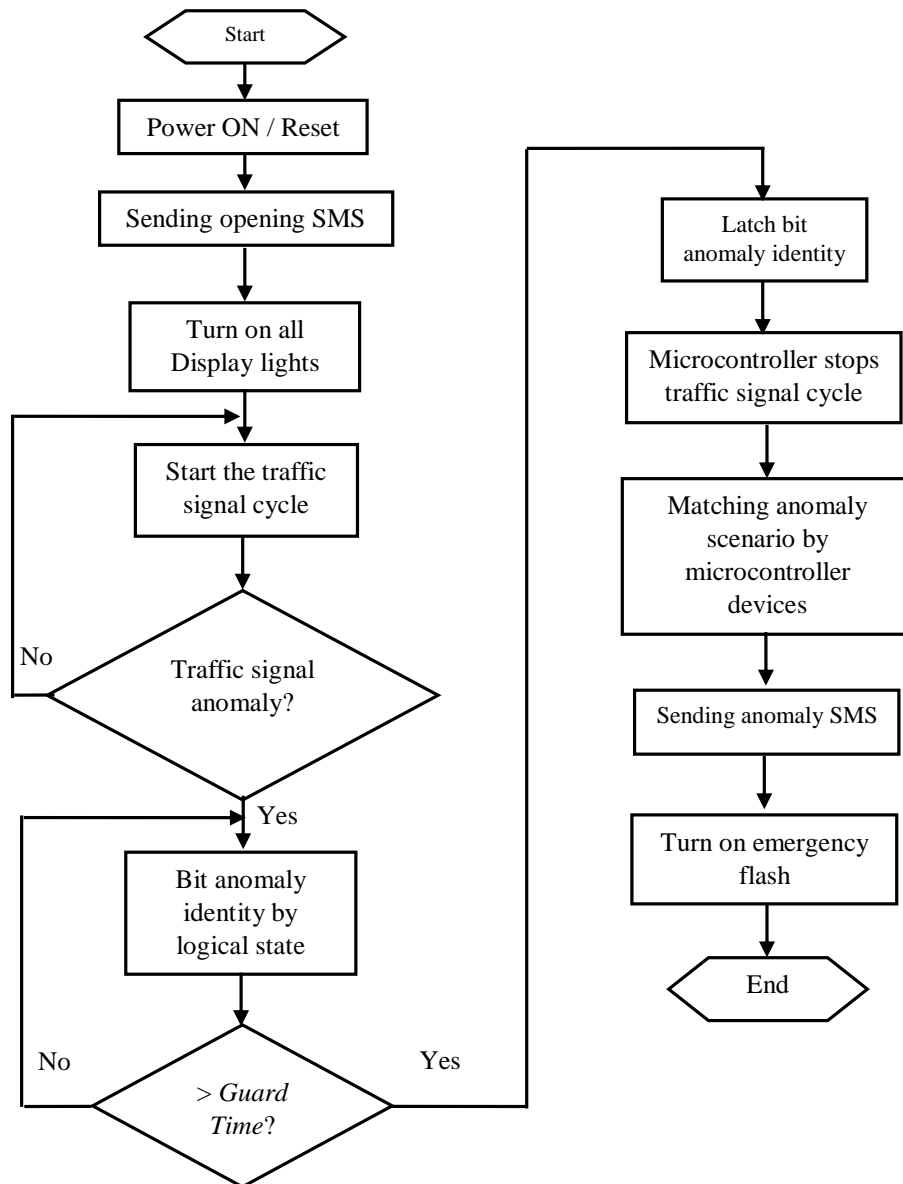


Fig. 4 Flow chart of signal monitoring system

## CONCLUSION

This research highlights the ability to autonomously diagnose traffic signal device systems, especially in its work function, with the intent to detect interference on the device, and provide report via short message service (SMS) to a monitoring unit. Furthermore, this can be placed in any area covered by the Global System for Mobile Communication (GSM) wireless communication service. Meanwhile, a microcontroller was used to process data from the interference detection result, and processing the SMS

content, therefore, it is able to quickly inform the types of traffic signal disruptions. Hence, it is possible to utilize this development in building an integrated traffic signal monitoring system services, in the form of mobile applications.

## ACKNOWLEDGMENTS

Authors would like to express our special thanks of gratitude to Ministry of Research and Higher Education of Republic of Indonesia through DRPM (Penelitian Terapan) for providing research funds during 2017 – 2019.

## REFERENCES

- [1] Boston Transportation Department. The benefits of retiming/rephasing traffic signals in the Back Bay, 2010.
- [2] [http://www.cityofboston.gov/images\\_documents/The%20Benefits%20of%20Traffic%20Signal%20Retiming%20Report\\_tcm3-18554.pdf](http://www.cityofboston.gov/images_documents/The%20Benefits%20of%20Traffic%20Signal%20Retiming%20Report_tcm3-18554.pdf)
- [3] Sivarao, S. K. Subramanian, M. Ezro and T. J. S. Anand, Electrical & Mechanical Fault Alert Traffic signal System Using Wireless Technology, International Journal of Mechanical & Mechatronics Engineering IJMME-IJENS, August, 2010, 10(4), pp.15-18.
- [4] M. Z. A. Marzuki, A. Ahmad, S. Buyamin, K. H. Abas and S. Hj. M. Said, Fault Monitoring System for Traffic signal, Jurnal Teknologi (Science and Engineering), 2015, 73(6), pp. 59-64.
- [5] X. Tang and S. Wang, A Low Hardware Overhead Self-Diagnosis Technique Using Reed-Solomon Codes for Self-Repairing Chips, IEEE Transactions on Computers, October, 2010, 59(10), pp. 1309-1319.
- [6] P. I. Okwu, E. S. Mbonu, C. G. Ezekwe and C. U. Ajuzie, Quick Prototyping of Real Time Monitoring System Using Proteus Development Tool: A Case for Self Diagnostic Traffic signal System, December, 2013, 6(5), pp. 147-154.
- [7] P. Aleksander, S. Rahayu, S. R. Ageng and I. Agung, Developing Monitoring System of Traffic Signal Using Microcontroller Device by SMS of GSM Network, Proceeding of Seminar Nasional SINTA FT UNILA, 2018, Vol. 1, pp. 273-277.
- [8] F. K. Rasha, Traffic Light Control System Using Microcontroller, AL-Qadisiyah Journal of Pure Science, 2018, 23(2), pp. 269-280.
- [9] T. A. Kareem and M. K. Jabbar, Design and Implementation Smart Traffic Light Using GSM and IR, Iraqi Journal for Computers and Informatics, 2018, 44(2), pp. 1-5.

## **ENHANCING THE ROLE OF BENT-UP BARS IN SHEAR BEYOND THE CODE REQUIREMENTS BY USING PLANE-CRACK INTERCEPTOR-CROSS DIAGONAL FORM**

Ms. Naim Asha  
AL QUBA ENGINEERING OFFICE

### **ABSTRACT**

Swimmer bars are new type of shear reinforcement; these are small inclined bars, with its both ends bent horizontally for a short distance; welded to both top and bottom flexural steel reinforcement, or welded to hanger bars when compression reinforcement is absent. Regardless of the number of swimmer bars used in each inclined plane, the system forms with the added horizontal bars plane-crack interceptor instead of bars-crack interceptors. The results obtained from testing of beams provided with this system, and the effectiveness of this new system is discussed. The width of the shear cracks were much smaller than the width of the shear cracks in beams reinforced by the traditional stirrups system. The equivalent steel amount used to replace the conventional steel for the same purposes showed a superior performance of this system over the conventional system; especially when a smaller amount of reinforcement was used by the new system preventing shear failure that took place for the beams which are reinforced with the conventional shear reinforcement. The system used to replace the congestion of stirrups when high shear forces exist.

### **INTRODUCTION**

Beams carry loads primarily by internal moments and shears. In the design of a reinforced concrete member, flexure is usually considered first, leading to the size of the section and the arrangement of reinforcement to provide the necessary resistance for moments. Limits are placed on the amounts of flexural reinforcement to ensure ductile type of failure, beams are then designed for shear. Since shear failure is frequently sudden with little or no advanced warning, the design for shear must ensure that the shear strength for every member in the structure exceeds the flexural strength. The shear failure mechanism varies depending upon the cross-sectional dimensions, the geometry, the types of loading, and the properties of the member. Reinforced concrete (RC) beams are important structural elements that transmit the loads from slabs to columns. Beams must have an adequate safety margin against bending and shear forces, so that it will perform effectively during its service life. At the ultimate limit state, the combined effects of bending and shear may exceed the resistance capacity of the beam causing tensile cracks. The shear failure is difficult to predict accurately despite extensive experimental research. The behavior of reinforced concrete beams at failure by shear is distinctly different from their behavior by bending, which may be unsafe. The shear failure of beams is usually sudden without sufficient advanced warning, and the diagonal cracks that develop are considerably wider than the flexural cracks.

### **OBJECTIVES**

In general, the purpose of this research is to investigate the behavior of rectangular beams in shear, using special forms of "Swimmer bars" as

single swimmer bar.

### **Scope of the study**

The scope of study is limited by the:

- a) The study was based on experimental investigation of two rectangular reinforced concrete beams.
- b) All specimens were of the same size and reinforced with identical amount of longitudinal steel.
- c) The beams were tested to fail due to two point loads by shear given the ratio of a shear span to effective depth of 2.5.
- d) The concrete compressive strength of the specimens on the testing day was in the range of 25 N/mm<sup>2</sup> to 36 N/mm<sup>2</sup>.
- e) The variables in these specimens are the shear reinforcement systems

### **Experimental Investigation**

Experimental works were carried out at the Structure Laboratory of the Civil Engineering Department at the University of Jordan. Different types of shear reinforcement were used. In general, the objective of this study is to explore the shear structural behaviors in beams. In this investigation, all of the tested beams were designed to fail by shear, thus adequate amount of tension and compression reinforcements were provided to give sufficient bending moment strength in these beams

### **MODEL OF SHEAR REINFORCEMENT SYSTEM**

To achieve the objectives of this study, one stage of experimental work was done; this stage has different types of reinforced concrete beams which

contained different types of shear reinforcement. These beams were designed and prepared for laboratory testing to serve the main purpose of this study. The dimensions of these tested beams are 200 mm in width, 250 mm in height x 2000 mm in length. All of these beams were the same grade of concrete.

### Beams Detail

Figures 1 - 4 shows design detailing of 'B1-5, ' B2-5

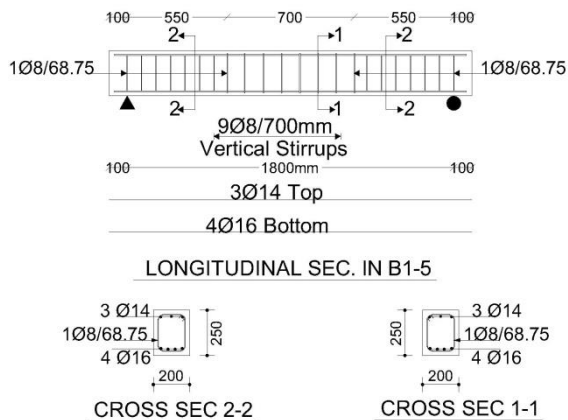


Fig. 1: Details of Beam 'B1-5

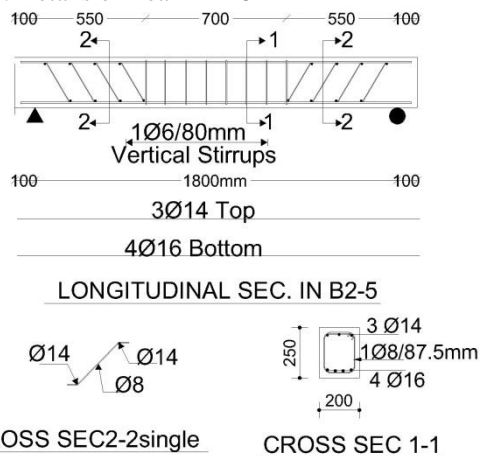


Fig. 2: Details of Beam 'B2-5

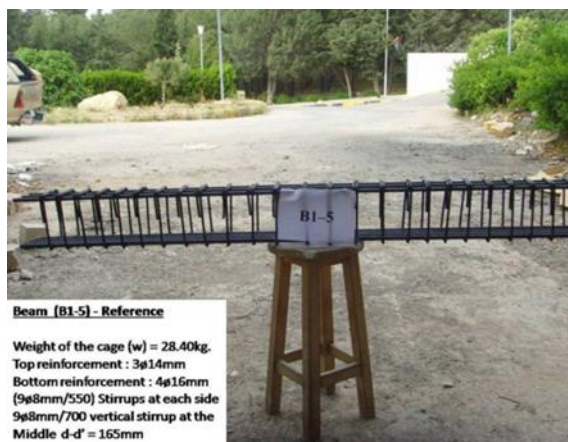


Fig. 3: Steel Cage Reinforcement of Beam 'B1-5



Fig. 4: Steel Cage Reinforcement of Beam 'B2-5

### Casting of Specimens

Each specimen was marked carefully to insure that each of the specimens would satisfy the strength specification. Several steps were carried out in making structural concrete beam such including, reinforcement installation, mixing, concreting and curing. Installation of steel reinforcement was carried out in the early stage before concreting works. Shear and nominal links were fastened together with top and bottom reinforcement. To ease the fastening works, wire and welding were used. It is important to ensure that cutting and bending process was prepared with adequate length and anchorage. Before the bars were placed in the moulds, they were first cleaned of any dirt and thin layer of oil was applied on its surface. Stable temporary woods supports were provided to hold the loaded end of the bars in place, while the other end was placed in the base of the mould. These are referred as hanging concept. The spacers were withdrawn slowly during the compaction process. All the materials for concrete such as, fine aggregate, coarse aggregate, cement and water were provided according to concrete mix design. The concrete was prepared in a rotated pan mixer. Water was added to the materials depends on the aggregate condition and mixed between two to three minutes to produce a uniform color and consistency mixes. Forklift truck was used to carry the fresh concrete from rotating mixer to formwork. The concrete was placed in formwork steel mould manually in two layers. The concrete was compacted by an internal vibrator of 25 mm diameter. After leveling and smoothing the surface, the specimens were covered with polythene sheeting for at least three days. After the concrete harden or after 3 days, the moulds were stripped. Control specimens comprising of six 150 mm cubs, were also prepared from the same batch of concrete. They were all air cured in the same manner as the test specimens.

### Compression Tests: Cube Test

The compressive strength is the most important property of concrete. To determine the compressive strength of the concrete, the compression test was

carried out for each concrete mix proportion. The fresh concrete was cast in steel or cast-iron moulds with standard size 150 mm x 150 mm x 150 mm cube the mould and its base should be clamped together during casting to reduce leakage of mortar. The use of a rigidly connected base is essential when compaction is effected by means of vibration. About 10 samples of cube concrete were prepared for each concrete mix prepared for each concrete mix proportion. The standard practice prescribed by A.S.T.M C 192-57 is to fill the mould in three layers and each layer of fresh concrete was compacted by not less than 35 times of 25mm square steel. After the top surface of the cube has been finished by means of a trowel, all of cube concretes were curing by water. The curing process for cube concrete only takes 7 days. After the concrete hardens, the moulds were tested on 7 days and 28 days to measure the strength of concrete. The graph for compressive strength of cubes concrete is given in Table 1, and Figure 5

Table 1: Compressive Strength Cubes Results.

| Days    | Sample | Cubes result<br>N/mm <sup>2</sup> | Average cubes result<br>N/mm <sup>2</sup> | $f'_c = 0.80$<br>cubes result<br>N/mm <sup>2</sup> |
|---------|--------|-----------------------------------|---|--|
| 7 days  | 1      | 34.9                              | 35.60                                     | 28.50  |
|         | 2      | 36.2                              |   |  |
|         | 3      | 35.8                              |   |  |
| 28 days | 4      | 37.1                              | 37.0                                      | 29.60  |
|         | 5      | 36.7                              |   |  |
|         | 6      | 37.2                              |   |  |

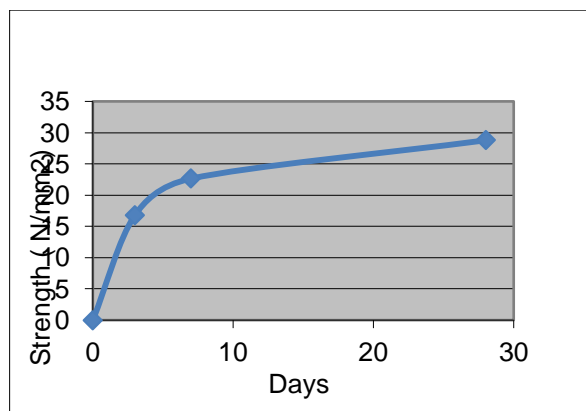


Fig. 5: Compressive Strength of Concrete vs. Days

### Test Procedure

Prior to testing, the surface of the specimens was painted with white emulsion so that the detection of the cracks during the test was easier and their making become clearer. At age 28 days reinforced concrete beams were prepared for testing. The lines position of point load, support and the middle of beam span were marked to ease the installation of beam in testing frame. In this experimental investigation, hydraulic jack was used and the arrangement of test setup. The test was carried out with the specimen placed horizontally in a simple loading arrangement. The beam was supported by solid round steel on their two edges as simply supported member. The effective length of each beam was 1800 mm that is from support to support, but the total length of the beam was 2000 mm. All the beams were designed to ensure the beams will only fail in shear rather than in flexure. To ensure that shear cracks will occur near the support, two point loads were applied symmetrically to the beam with  $a_v$  less than  $2.5d$ . In this testing,  $a_v \approx 550$  mm, where  $a_v$  is shear span (the distance from the point of the applied load to the support), and  $d$  is the effective depth of a beam. A loading jack was placed at the mid-span position above the beam. The load was applied by jacking the beam against the rig base member at a constant rate until the ultimate load capacity of the beam was reached. A universal column section was used to transfer the load to the beam at two point loads via transfer girder. A reasonable time interval was allowed in between 20.0 kN load increments for measuring deflections, marking cracks, measuring the shear reinforcement strain and recording the ultimate load. Each beam took about two hours to test.

### Test Results

Program presents the test result of each specimen, covering the specimen behavior, cracks formation, deflections, strains of mid-section and ultimate loads. The concrete compressive strength of the specimens was obtained by concrete sampling carried out on the same day of casting. The concrete compressive strength of the tested samples ranged from 25 to 36 N/mm<sup>2</sup>.

#### Behavior of Beam 'B1-5

This beam is a reference beam, which is reinforced with stirrups as shear reinforcement. Before starting the test, strain and deflection gages were fixed as shown in Figure 6 Initially the readings of strain and deflection gages were taken, then the beam was loaded by 20 kN, and the



readings of the strain and deflection gages were taken again. By raising the load up to 40 kN, hair cracks appeared at the bottom face between two concentrated loads. At the loading of 60 kN more hair cracks appeared, and the deflection was 3.4mm. When loading reached up to 100 kN there weren't any cracks at shear region as shown in Figure 9. When loading reached 140 kN, hair shear cracks appeared in the shear zone at the right side, and at 200 kN load more shear cracks appeared. As the loading increased up to 240 kN, more and more shear cracks appeared at both sides of this beam. At each loading, all strains and deflection gages were taken as listed in Table 2. Finally, at the load of 280 kN, the beam failed by shear at right side and the maximum deflection of the beam was measured to be 14.54 mm as shown in Figure 10.

### Test Results of Beam 'B1-5

The ultimate loads, deflections and strains measurements for beam 'B1-5 were listed in Table 1. Figure 7 shows the load deflection curve and the maximum deflection of 14.54 mm at the load of 260 kN. Figure 8 shows load - strain data

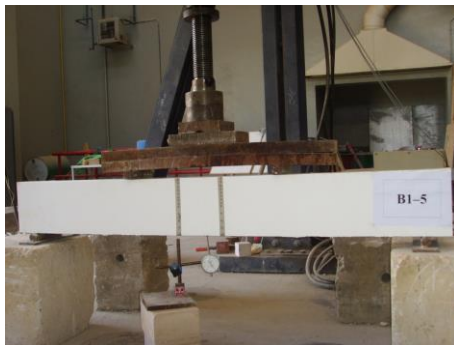


Fig. 6: 'B1-5 beams Before Test

Table 2: Test Results for Beam 'B1-5

| kn  | Def-lection<br>mm | Strain x 10 <sup>-5</sup> mm/mm |      |      |      |      |     |      |      |      |
|-----|-------------------|---------------------------------|------|------|------|------|-----|------|------|------|
|     |                   | 9                               | 8    | 7    | 6    | 5    | 4   | 3    | 2    | 1    |
| 0   | 0                 | 0                               | 0    | 0    | 0    | 0    | 0   | 0    | 0    | 0    |
| 40  | 2.78              | 26.4                            | 21.6 | 18.4 | 15.2 | 12.8 | 4.8 | 1.6  | -2.4 | 9.6  |
| 80  | 4.65              | 56                              | 45.6 | 36   | 28   | 23.2 | 8   | 1.6  | 13.6 | 0.8  |
| 120 | 6.47              | 87.2                            | 71.2 | 53.6 | 44   | 34.4 | 12  | -2.4 | -20  | 22.4 |

|     |       |       |       |       |       |      |      |       |       |       |
|-----|-------|-------|-------|-------|-------|------|------|-------|-------|-------|
| 160 | 8.28  | 124.8 | 102.4 | 78.4  | 64    | 44.8 | 20   | -31.2 | 54.4  | -64.8 |
| 200 | 10.11 | 164   | 133.6 | 103.2 | 84    | 48.8 | 28   | 2.4   | 29.6  | -84   |
| 240 | 12.51 | 204   | 168   | 133.6 | 106.4 | 67.2 | 38.4 | 8.8   | -31.2 | -100  |
| 260 | 14.54 | 229.6 | 190.4 | 152   | 121.6 | 70.4 | 46.4 | 14.4  | -28   | -104  |

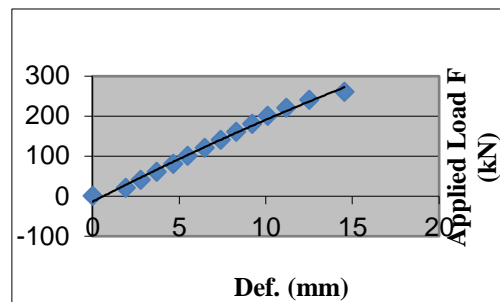


Fig. 7: Load vs. Deflection for 'B1-5'

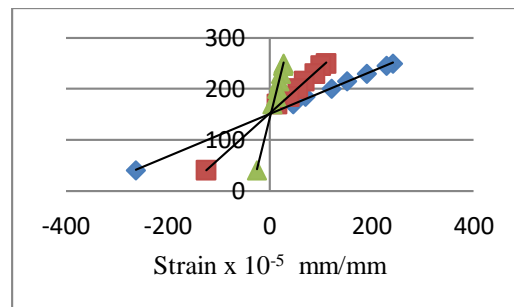


Fig. 8: Strain Diagram for 'B1-5



Fig. 9: 'B1-5 Cracks at the Load of 100 kN



Fig. 10: 'B1-5' Shear Failure at the Load of 280 kN

#### 4.1.3 Behavior of Beam 'B2-5'

This beam was reinforced with four single swimmer bars of  $\phi 8\text{mm}$  diameter as shear reinforcement at each side of the beam. At the initial load of 20 kN as shown in Figure 13, there wasn't any evidence or appearance of cracks, but when the load reached 40 kN, hair cracks appeared at the bottom of face between the two concentrated loads. After taking all deflection and strain gage readings, the load was increased up to 60 kN, then to 80 kN load where there weren't any shear cracks, but when loading reached up to 120 kN as shown in Figure 4.9, shear cracks appeared at shear regions at both sides of the beam and the deflection at this load was measured to be 4.56 mm. When loading reached 140 kN more shear cracks appeared at both sides, and at the load of 160 kN, shear cracks were increased in length and width. Finally, when the load reached 181 kN applied load this beam failed in shear as shown in Figure 15. After removing concrete cover off the failed beam, it was noticed that the swimmer bars were loaded beyond the point of necking stage, which means that this type of shear reinforcement resist high shear forces.

#### Test Results of Beam 'B2-5'

Measurements of ultimate loads, deflections and strains are listed in Table 3. From this table the deflection was measured to be 6.77 mm at the load of 160 kN and the maximum strain was measured to be (0.0011). Figure 11 shows loads – deflections data and Figure 12 shows strains data through the cross section of beam at a specific load, for example the maximum compression strain at load 160 kN.

Table 3: Test Results for Beam 'B2-5'

| Load<br>F<br>kn | Def-<br>lection<br>n<br>mm | Strain $\times 10^{-5}$ mm/mm |   |   |   |   |   |   |   |   |
|-----------------|----------------------------|-------------------------------|---|---|---|---|---|---|---|---|
|                 |                            | 9                             | 8 | 7 | 6 | 5 | 4 | 3 | 2 | 1 |

|     |      |       |      |      |      |      |      |      |       |       |
|-----|------|-------|------|------|------|------|------|------|-------|-------|
| 0   | 0    | 0     | 0    | 0    | 0    | 0    | 0    | 0    | 0     | 0     |
| 40  | 1.48 | 24.8  | 20.8 | 16.8 | 12.8 | 7.2  | -2.4 | 0    | -4    | -5.6  |
| 80  | 3.05 | 53.6  | 44   | 36   | 26.4 | 13.6 | 6.4  | -2.4 | -11.2 | -19.2 |
| 120 | 4.56 | 80.8  | 68   | 56   | 41.6 | 25.6 | 12   | 0.8  | -12   | -24.8 |
| 160 | 6.77 | 111.2 | 94.4 | 78.4 | 58.4 | 38.4 | 21.6 | 1.6  | 12.8  | -32.8 |

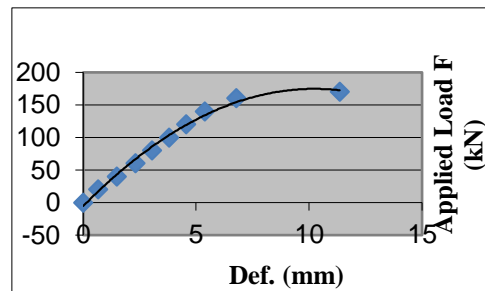


Fig. 11: Load vs. Deflection for 'B2-5'

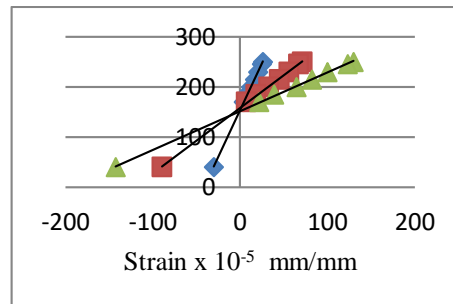


Fig. 12: Strain Diagram for 'B2-5'

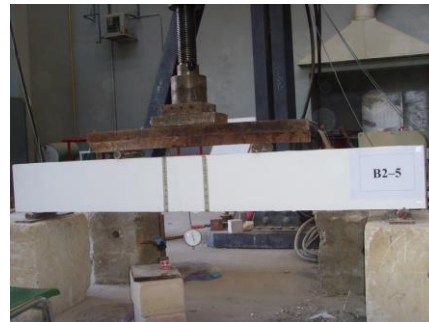


Figure 13: 'B2-5' The Experimental Setup

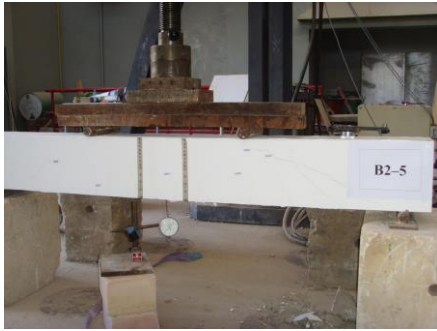


Fig. 14: 'B2-5 Shear Cracks at the Load of 80 kN

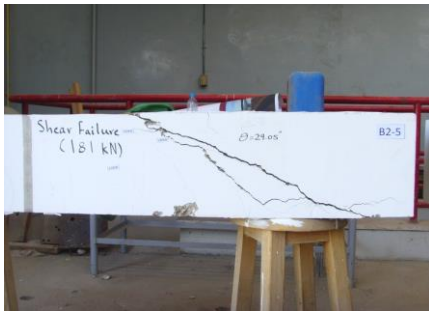


Fig. 15: 'B2-5 Shear Failure at the Load of 181 kN

### Analysis

The results from two beams of reinforced concrete beams were analyzed and presented. The performance of each specimen in terms of its behavior, crack formation; shear resistance, deflection, strain and cost of the shear reinforcement were discussed. It was found that the use of swimmer bars as a shear reinforcement performed better than the use of conventional shear reinforcements such as stirrups. Although variation among different casts in the same testing was unavoidable, they were relatively small.

### Cracks

It was observed that beams showed several cracks once the stresses exceeded the cracking moment, and with the increase in the applied load the length and width of these cracks were increased.

### Crack Pattern of Beams

It was observed that initial flexural cracks appeared in the bottom face of these beams between the two applied loads. By increasing the loads, diagonal cracks were developed in the shear region at approximately  $31^\circ$  angle with respect to the longitudinal axis of these beams. The length and width of these shear cracks increased gradually until shear failure took place. The width of shear cracks of beams, 'B2-5', were relatively smaller than the width of the shear cracks of beam 'B1-5' as shown in Figure 16 and Figure 17. In beams 'B2-5', the width

of the shear cracks were relatively smaller than the width of the shear cracks of the beam 'B1-5', which means that by using swimmer bars as shear reinforcement reduce the control cracks.

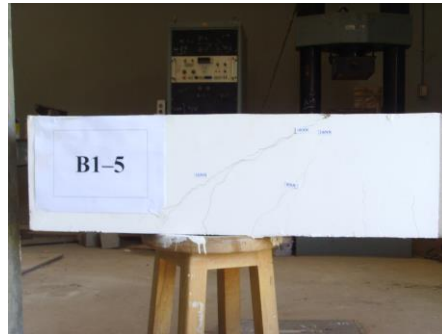


Fig. 16: Cracks Pattern of Beam 'B1-5



Fig. 17: Cracks Pattern of Beam 'B2-5

### Shear Resistance

All beams were tested by one - third concentrator load as shown in previous. Loads used in this study are listed in tables in 2 and 3. Each of these beams failed at its ultimate load.

### Shear Resistance of Beams B1-5 and B2-5

All shear resistance of these beams from experimental results and the theoretical values are listed in Table 2. The beam 'B1-5' which is used as a reference beam failed at 280 kN total applied load, which is 15% higher in value than the theoretical shear value. Beam 'B2-5' failed at 181 kN which is 25% higher than the theoretical value.

Table 4: The Differences in Shear Resistance between Theory and Test Results of

| Beam | Shear Resistance Theory (kN) | Shear Resistance Results (kN) | % Test / Theory | Note         |
|------|------------------------------|-------------------------------|-----------------|--------------|
| B1-5 | 91.44                        | 104                           | 115%            | -            |
| B2-5 | 72.4                         | 90.5                          | 125%            | Necking of a |

|  |  |  |  |                |
|--|--|--|--|----------------|
|  |  |  |  | swimmer<br>bar |
|--|--|--|--|----------------|

### Deflection

The beam tested in this study showed different values of deflection. The value varies from stage to stage.

### Deflection in Beams B1-5 and B2-5

Table 5 shows the deflection of Beam 'B1-5' at given loads. The deflection of this beam at the load of 100 kN is 5.48 mm and the deflection at the load of 160 kN is 8.28 mm and the maximum deflection at the load of 240 kN is 12.51mm. Beam 'B2-5' deflected at the load of 100 kN by 3.8 mm and at the load of 160 kN by 6.77 mm which is the maximum deflection. The summary of the deflection of these beams in this stage is listed in Table 5.

Table 5: Deflection in Beams

| Load<br>kN | B1-5            | B2-5 |
|------------|-----------------|------|
|            | Deflection (mm) |      |
| 100        | 5.48            | 3.8  |
| 160        | 8.28            | 6.77 |
| 240        | 12.51           | 9.60 |

### Strain

Strain is the change in length of the cross section of the beam at the middle. The beams divided into nine spacing from center line of beam to the top face as shown in Figure 18. All strains – loads values are listed in Tables.



Fig.18: Distribution of Strain Gages

### Strains for Beams B1-5 and B2-5

Maximum strain of beam 'B1-5' is 0.00124 at the load of 160 kN but the maximum strain of beam 'B2-5' at the load of 160 kN is 0.00111 which is smaller

than the strain in beam 'B1-5'. These data are shown in Table 6. In summary, Beam which used swimmer bar system exhibit higher values of stiffness in comparison with Beam 'B1-5' which used stirrups.

Table 6: Strains in Beams

| Load<br>kN | B1-5    | B2-5    |
|------------|---------|---------|
|            | strains |         |
| 100        | 0.00072 | 0.00054 |
| 160        | 0.00124 | 0.00111 |

### CONCLUSION AND RECOMMENDATION

This study presented a new type of shear reinforcement called swimmer bar system. This type of shear reinforcement can be formed in many shapes such as a single swimmer and rectangle with cross similar to the types of shear reinforcement. The following are the major highlights of this study.

1. The use of swimmer bar system improved the shear capacity in the reinforced Concrete beams.
2. The use of swimmer bar system reduced the beam deflection in reinforced concrete beams
3. The width and length of the cracks in beams with swimmer bar system under loads are relatively smaller than the width and length of the cracks in beams with traditional stirrups.
4. The cost of reinforced concrete beams reinforced with swimmers bar system is less than the cost of reinforced concrete beams reinforced with traditional stirrups.

### REFERENCES

- [1] Abdul Hamid, Noor A. (2005), The Use of Horizontal and Inclined Bars as Shear Reinforcement, (Electronic Version) Dissertation, University Technology Malaysia.
- [2] American Concrete Institute (2008), ACI Committee 318 Building Code Requirements for Structural Concrete, Farmington Hills, MI.
- [3] Nawy, Edward G., (2009), Reinforced Concrete: A Fundamental Approach, by Person Education, Inc., New Jersey.
- [4] Nilson, Arthur H., (1997), Designed of Concrete Structure, (Twelfth Edition), McGraw Hill.
- [5] Piyamahant, Asohgkram (2002), Shear Behavior of Reinforced Concrete Beams with Small Amount of Web Reinforcement, (Electronic Version) Adissertation Kochi University of Technology Kochi, Japan.

# EFFECT OF EXCESS PORE WATER PRESSURE IN SATURATED SANDY SOIL FOR EVALUATING LIQUEFACTION POTENTIAL DURING EARTHQUAKE DURATION

Hua Thanh Than<sup>1</sup>, Nguyen Ngoc Phuc<sup>2</sup> and Tran Thi Thanh<sup>3</sup>

<sup>1</sup>Quy Nhon University, Binh Dinh Province, Vietnam

<sup>2,3</sup>Industrial University of Ho Chi Minh City, Vietnam

## ABSTRACT

The content of this paper is about establishment the ground acceleration record for random phase variations in saturated sandy soil during earthquake duration by using cosine function method. Then, the ground acceleration spectrums are calculated for many differ damping ratio values. The correlation between the ground acceleration with uniform cycle numbers (N) and moment magnitude (M) are established for evaluating liquefaction potential, excess pore water pressure with time history (in cases of N = 15 for M = 6.5 and N = 12 for M = 8.0). At time of 30s in case N=12 for M=8.0, the ratio  $r_u$  of excess pore water pressure is 0.61 in 3 m depth and zero from 4 m to deeper of the depth.

*Keywords: Sand foundation, Ground acceleration record, Acceleration spectrum, Excess pore water pressure, Earthquake duration.*

## INTRODUCTION

Most earthquake damage to urban areas is directly or indirectly related to ground vibration, ie ground vibration occurring during earthquakes. In fact, earthquake vibration due to earthquakes is a complex process that depends on many factors, of which the most important factor is the ground conditions at the location of the earthquake. The most commonly used is the peak horizontal ground acceleration during earthquakes.

Currently, In Vietnam, Design Standards of Civil Engineering (TCVN 9386-2012) [13] are the ones for earthquake resistant, that is compiled from the design standard in Eurocode 8 [5], the content shows the elastic reaction spectrum for substrates from A to E type base and the peak design ground acceleration values for each specific area. However, this the peak design ground acceleration value of the standard sites are not compatible with some construction sites. Therefore, in order to perform dynamic analysis time history, there should be ground accelerators record which are the input data used for each construction survey site with values consistent of the elastic response spectrum amplitudes and different random phase shift phase fluctuations.

The Kanai-Tajimi (1960) [9] model has been widely used in modelling earthquake ground motions due to its physical meaning and simplicity. From the power spectral density function (PSDf) of the ground acceleration record is obtained by passing a band-limited white noise through a filter that represents the soil layer above the rock level.

Kiureghian (1996) [10] developed Tajimi-Kanai power spectrum density model, the results of the calculation are the parameters of model such as the damping ratio, the undamped actural frequencies and power spectral density for soft, medium and stiff soil, respectively.

On the significance of phrase content in earthquake ground motion with the value of random phase angle by Osaki (1979) [11].

Amico (2012) [1] has suggested that the value of the ground acceleration record can be expressed as a set of lognormal distributed random variable and correlated Gaussian random variables.

According to Glaser (1996) [7], the correlation between the ground acceleration spectrum and the time history with the undamped natural frequency is established. The ground acceleration spectrum is increased, the excess pore water pressure is also increased and the modal contribution factor is established.

Recently, Taciroglu (2016) [12] has built up the ground acceleration record funtion according to the original accelerator grid, the modal contribution factor and the infinite impulse response function. The value of these modal contribution factors is determined by Glaser (1996) [7].

And, Doan Thanh Nha (2017) [4] studied the simulation model of ground accelerated record according to sin function by Kanai - Tajimi model, Clough model - Penzien (1993), and the results are suggested about the value of base gound type A and C.

By Idriss et al., (2006) [8], semi-empirical procedures for evaluating the liquefaction potential of saturated cohesionless soils during earthquakes are re-examined. The earthquake magnitude scaling factor for cyclic stress ratios (MSF), number of equivalent stress cycles (N) versus earthquake magnitude (M) is established and revised relations for use in practice are recommended.

Due to the complex features of ground motion time histories, relative duration does not depend on the peak values. It is the time interval between the points at which 5% and 95% of the total energy has been recorded. Bracketed duration is the measure of time between the



first and last exceedance of a threshold acceleration 0.05g by Choudhury [3].

Chiaradonna A., et al., (2015) [2] proposed that build-up of excess pore water pressure in sandy soils during seismic loading causes reduction in stiffness and strength and can lead to liquefaction. An increase of maximum accelerations and strains is observed within the layers where the pore pressure ratio is above 0.4 in the coupled analysis.

Than et al., (2018) [14] suggested that is the liquefiable soils of  $M = 8.0$  and no liquefaction soil of  $M = 6.5$  by Dixit method, this liquefaction resistance coefficient is greater than 1 for sandy soil at construction sites of arear in Quy Nhon city, Binh Dinh province.

The numerical method by Geostudio 2007 software [6] calculated some problems such as ground acceleration coredo establishment by NewMark method, cyclic shear stress, strain - stress, excess pore water pressure, ... versus time history.

This content presents for methods using the technique transformation of the cos function is simulated the ground acceleration record with the elastic response spectrum acceleration amplitude as specified in Eurocode 8 [5] with different phase shift phase variations. At the same time, the correlation between the power spectral density with different for the undamped natural frequency is established, the harmonic ground acceleration relation with time radution, the peak shear strain history and depth, excess pore water pressure and time history.

## 2. BASIS OF CALCULATION THEORY

### 2.1 Establishment of Ground Acceleration Record from the Elastic Reaction Spectrum Acceleration

#### 2.1.1. Determination of the power spectral density $S(\omega)$

The Tajimi-Kanai model [9] for the earthquake ground motion is based on the observation that the absolute acceleration of the ground may be sought as a white noise process (acceleration at bedrock) filtered through superimposed soil deposit modeled as a single degree of freedom system (DOFs) as in Fig. 1.

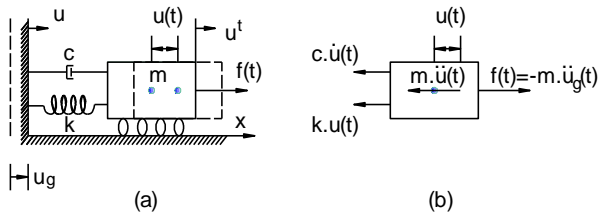


Fig. 1. DOFs by Tajimi (1957)-Kanai (1960) model [9]

The degree of DOFs of the mass  $m$  is given as

$$m \ddot{u}'(t) + c \dot{u}(t) + k u(t) = 0 \quad (1)$$

$$m [\ddot{u}(t) + \ddot{u}_g(t)] + c \dot{u}(t) + k u(t) = 0 \quad (2)$$

$$m \ddot{u}(t) + c \dot{u}(t) + k u(t) = -m \ddot{u}_g(t) \quad (3)$$

$$\ddot{u}(t) + \ddot{u}_g(t) = -\frac{c}{m} \dot{u}(t) - \frac{k}{m} u(t) \quad (4)$$

Then, since the absolute acceleration is given in the form:

$$u'(t) = \ddot{u}(t) + \ddot{u}_g(t) = -2\xi \dot{u}(t) - \omega^2 u(t) \quad (5)$$

where  $m$ ,  $k$ ,  $c$  is the mass of the oscillator, the stiffness, the damping coefficient of the dashpot connecting the mass and the bedrock, respectively.  $u_g(t)$  is the absolute displacement of the bedrock,  $u(t)$  is the relative displacement between the mass  $m$  and the bedrock,  $u'(t)$  is the absolute displacement of the mass  $m$  with  $u'(t) = u(t) + u_g(t)$ . Here  $u(t)$ ,  $\dot{u}(t)$ ,  $\ddot{u}(t)$  is the displacement, the velocity and the acceleration with time, respectively.

The frequency domain analysis, leads to conclude that the power spectral density function (PSDf) of the absolute acceleration of the ground is simply given as:

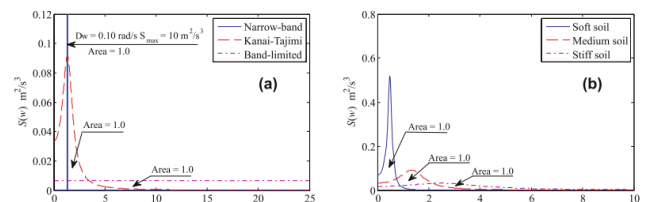
$$S_{\ddot{u},t}(\omega) = S_0 \cdot \frac{1 + 4\xi_{g,t}^2 \left( \frac{\omega}{\omega_{g,t}} \right)^2}{\left[ 1 - \left( \frac{\omega}{\omega_{g,t}} \right)^2 \right]^2 + 4\xi_{g,t}^2 \left( \frac{\omega}{\omega_{g,t}} \right)^2} \quad (6)$$

where  $S_0$  is the (constant) power spectral density of the acceleration at the bedrock, and  $\xi_{g,t}$ ,  $\omega_g$ ,  $\omega$  is the damping ratio, the undamped and damped natural frequencies of the soil layer, respectively with  $\omega = \omega_g \sqrt{1 - \xi_{g,t}^2}$ ,

$\omega_g = 2\pi/T_g = 2\pi f_g$ ,  $\omega_g = \sqrt{k/m}$  and  $2\xi = c/m$  - damping ratio,  $f_g$  - frequency. The parameters of Tajimi-Kanai power spectrum density model (Kiureghian .D 1996) [10] and the numerical results are shown in Table 1.

Table 1 Parameters of Tajimi-Kanai power spectrum density model (Kiureghian D., 1996) [10]

| Soil type | $f_g$ (Hz) | $\omega_g$ (rad/s) | $\xi_g$ | $S_0$ ( $m^2/s^3$ ) |
|-----------|------------|--------------------|---------|---------------------|
| Soft      | $0.5\pi$   | $\pi$              | 0.02    | 0.26                |
| Medium    | $1.5\pi$   | $3\pi$             | 0.04    | 0.53                |
| Stiff     | $\pi$      | $6\pi$             | 0.06    | 0.72                |



Frequency (Hz)

Frequency (Hz)

Fig. 2. Power spectral density function for ground acceleration (Kanai-Tajimi) [10]

In this regard, the matching can be achieved by adopting the following iterative scheme applied to the stationary component  $S_0$ .

$$S_0 = \alpha \cdot \left( \frac{GPA}{GPA_{G_0=1}} \right) \quad (7)$$

here  $\alpha$  is the correction factor for  $\alpha \geq 1$ ; GPA is the acceleration of the region's ground acceleration;  $GPA_{G_0=1}$  is the peak ground acceleration when the value of  $S_0 = 1$ , the value  $GPA_{G_0=1} = 1.6599g$  of ground type C. At the same time, Doan Thanh Nha (2017) [4] suggested that the value of  $GPA_{G_0=1} = 2.1750g$  for ground type A with the correction factor  $\alpha = 1$  (Clough - Penzien model) and  $3.0063g$  for ground type C with the correction factor  $\alpha = 1.51$  (Kanai - Tajimi model).

### 2.1.2. Determination of the response spectrum $S_e(t)$ according to Eurocode 8

The proposed method for generating fully nonstationary spectrum compatible earthquakes is applied to the target response spectrum defined in Eurocode 8 [5]. Specifically, for a 5% damping ratio, the response spectrum of elastic acceleration is written as:

$$S_e(t) = a_g S \left[ 1 + \frac{t}{t_B} (\eta 2.5 - 1) \right] \text{ for } 0 \leq t \leq t_B \quad (8)$$

$$S_e(t) = a_g S \eta 2.5 \text{ for } t_B \leq t \leq t_C \quad (9)$$

$$S_e(t) = a_g S \eta 2.5 \left[ \frac{t_C}{t} \right] \text{ for } t_C \leq t \leq t_D \quad (10)$$

$$S_e(t) = a_g S \eta 2.5 \left[ \frac{t_C t_D}{t} \right] \text{ for } t_D \leq t \leq 4s \quad (11)$$

The parameters defined for ground type A have been used for the applications. Namely,  $S = 1.0$ ,  $t_B = 0.1$ ,  $t_C = 0.4$  s and  $t_D = 3.0$  s; furthermore, the maximum ground acceleration  $a_g$  it has been set equal to  $1 \text{ m/s}^2$ ,  $\eta$  is the damping resistance coefficient with the reference value of  $\eta = 10/(5 + \xi) \geq 0.55$  and  $\eta = 1$  for  $\xi = 5\%$ .

According to Eurocode 8, consistency is considered to be achieved if the condition:

$$[\Delta] = \max \left\{ \frac{S(\omega_i) - S_e(t)}{S_e(t)} 100 \right\} \leq 10\% \quad (12)$$

is satisfied over the range of periods between  $0.2t_1$  to  $2t_1$ ,  $t_1$  being the fundamental period of the structure under study in the direction where the ground acceleration record is applied and

$$S_e(0) > a_g S \quad (13)$$

where  $S(\omega_i)$ ,  $S_e(t)$  is the design response spectrum modeled, the response spectrum from at least three simulated earthquakes, respectively. To illustrative purpose the variability of the response spectrum has been set as

$$S^{+\sigma}(\omega_i) = 1.5S(\omega_i) \quad (14)$$

### 2.1.3. The random phase $\varphi_n$

The determination of the random phase  $\varphi_n$  is based on the random probability variable  $EE(p)$  with uniformly distributed in the range (0,1) and the value of random phase angle can determined in the interval  $(0 \pm 2\pi)$  by Osaki (1979) [11] derived from Fig. 3, as follows:

$$\varphi_{n+1} = \varphi_n + \Delta\varphi = \varphi_n + 2\pi EE(p) \quad (15)$$

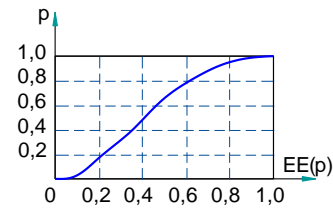


Fig. 3. Correlations between  $EE(p)$  with  $p$  [11]

### 2.1.4. The spectrum acceleration function $E(t)$

The value of the spectrum acceleration  $E(t)$  is a function with a linear with time history in Eurocode 8 [5]:

$$E(t) = \frac{5t}{T_{gn}} \text{ for } 0 \leq t \leq 0.05T_{gn} \quad (16)$$

$$E(t) = \frac{15t}{T_{gn}} - 0.5 \text{ for } 0.05T_{gn} \leq t \leq 0.10T_{gn} \quad (17)$$

$$E(t) = 1 \text{ for } 0.10T_{gn} \leq t \leq 0.30T_{gn} \quad (18)$$



$$E(t) = 2.5 - \frac{15t}{3T_{gn}} \text{ for } 0.30T_{gn} \leq t \leq 0.35T_{gn} \quad (19)$$

$$E(t) = \frac{4}{3} - \frac{5t}{3T_{gn}} \text{ for } 0.35T_{gn} \leq t \leq 0.50T_{gn} \quad (20)$$

$$E(t) = 0.75 - \frac{t}{3T_{gn}} \text{ for } 0.50T_{gn} \leq t \leq T_{gn} \quad (21)$$

where  $T_{gt}$  is the the influence duration of the ground motion of  $T_{gt} = 30$  s,  $\alpha$  is the random variable,  $\alpha = [0.01 \div 0.1]$  and  $T_{gn} = T_{gt} / (1.5 - 2\alpha)$ .

### 2.1.5 Background acceleration band $a_g(t)$ with time

Simulation of the background acceleration band  $a_g(t)$  and time  $t$  with random amplitude  $A_n$  and phase deviation angle  $\varphi_n$  [10]:

$$a_g(t) = E(t) \cdot \sum_{n=1}^N A_n \cos(\omega_n t + \varphi_n) \quad (22)$$

In which  $E(t)$  is the spectrum acceleration function in Eurocode 8 [5],  $A_n$  is determined by the power spectrum density  $S(\omega_n)$  at each equally divided interval  $\Delta\omega$  with  $\Delta\omega = 0.005$  rad/s and  $A_n = \sqrt{2S(\omega_n)\Delta\omega}$ ,  $N$  is the total number of time steps divided with  $t$  for time period steps ( $\Delta t = 0.01$  s).

## 2.2. Horizontal Ground Acceleration Record $a_g(t)$ with Time According to Harmonic Oscillator Functions

Earthquake shaking is highly variable and irregular which in turn causes highly variable and irregular shear stresses  $\tau_{peak}$  in the ground. However, the laboratory tests are usually done by repeatedly applying a uniform stress cycle  $\tau_{cycle}$ . So our understanding of soil behavior under dynamic loading comes from the application of uniform stress cycles.

According to Seed et al. (1975b) [6], the most common procedure is to set the uniform cyclic shear amplitude to 65% of the peak shear stress in the irregular shear stress time history or 0.65 is a weighting factor to calculate the equivalent uniform stress cycles required to generate same pore water pressure during an earthquake. In equation form:

$$\tau_{cycle} = 0.65 \tau_{peak} \quad (23)$$

The value of  $\tau_{peak}$  is defined as follows

$$\tau_{peak} = \left( \frac{a_{max}}{g} \right) r_d \sigma_v \frac{1}{MSF} \quad (24)$$

Similarly, the value of  $\tau_{cycle}$  can expressed as

$$\tau_{cycle} = \left( \frac{a_{cycle}}{g} \right) r_d \sigma_v \frac{1}{MSF} \quad (25)$$

$$a_{cycle} = 0.65 a_{peak} \quad (26)$$

In the above expression,  $MSF$  is the magnitude scaling factor, based on the data obtained by Idriss and Boulanger [8] may be approximated by the equation:  $MSF = 6.9 \exp(-M/4) - 0.058$  and  $MSF \leq 1.8$  at small earthquake magnitudes ( $M \leq 5.5$ ), here  $M$  is the moment magnitude,  $a_{max}$  is the peak horizontal ground acceleration,  $a_{cycle}$  is the equivalent uniform stress cycles ground acceleration in the laboratory tests,  $g$  is the acceleration of gravity,  $g = 9.81$  m/s<sup>2</sup>,  $r_d$  is depth dependent stress reduction factor,  $r_d = 1 - 0.015z$ , where  $z$  is the depth,  $\sigma_v$  is the total vertical overburden stress at a given depth below the ground surface.

In addition, Seed also studied actual ground motions and the resulting increase in pore water pressures, and then correlated this with the number  $N$  of  $0.65 \tau_{peak}$  uniform stress cycles that produced similar pore - pressures [6]. The equivalent number of cycles  $N$  is presented in Fig. 4.

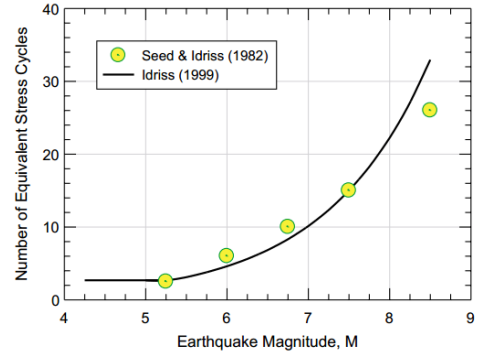


Fig. 4. Number of equivalent stress cycles versus earthquake magnitude (Seed et al., 1975) [8]

## 3. TEST RESULTS AND CORRELATION CALCULATION

### 3.1. Test Results

Test at construction sites of arear in Quy Nhon city, Binh Dinh province.

Quy Nhon Plaza project, Item for 9-storey house, No. 10-12-14-16 Do Doc Bao street, Quy Nhon City, Binh Dinh Province, as shown in Table 2.

Location of project is in Quy Nhon city, Binh Dinh province, according to Vietnamese Design Standards of Civil Engineering 9386-2012 [13], the area corresponding

to earthquake level  $M = 6.5$  ( $M$  is the moment magnitude) and the peak horizontal ground acceleration  $a_{\max}$  for the types A of soil is  $0.0941g$ , in which  $g$  is the acceleration of gravity.

The characteristics of soil type C with base factor  $S = 1.15$ , the values of cycle spectral acceleration  $T_B = 0.2$  s,

$T_C = 0.6$  s and  $T_D = 2.0$  s, importance factor  $\gamma_I = 1$ . The peak horizontal design ground acceleration is  $\bar{a}_g = \gamma_I \cdot a_{gr} \cdot S = (1)(0.0941)(1.15) = 0.1082$  g

Table 2. Test results of soil physics - Quy Nhon Plaza project

| Layer soil | Depth (m) | SPT $N_{30}$ | $\gamma_w$ (kN/m <sup>3</sup> ) | $\phi$ (°) | $c$ (kN/m <sup>2</sup> ) | $p_c$ (kN/m <sup>2</sup> ) | $f_s$ (kN/m <sup>2</sup> ) | Types soil         |
|------------|-----------|--------------|---------------------------------|------------|--------------------------|----------------------------|----------------------------|--------------------|
| 1          | 0 ÷ 10    | 8 ÷ 16       | 17,3                            | 29         | -                        | 24000                      | 2267                       | Medium sand        |
| 2          | 11 ÷ 13   | 2            | 17,2                            | 4          | 10                       | 3000                       | 750                        | silty sandy, loose |
| 3          | 14 ÷ 24   | 10 ÷ 20      | 17,3                            | 30         | -                        | 31000                      | 3000                       | Medium sand        |
| 4          | > 24      | 25           | 18,5                            | 16         | 22                       | 20000                      | 1900                       | Clay, dense        |

Underground water at 2,5 m

### 3.2. Correlation Calculation

#### 3.2.1 Ground acceleration relation for cos method and Geostudio software

Calculation for the cos method with  $\Delta t = 0.01$  s the influence duration of the ground motion  $T_d = 30$  s, the value of the horizontal design ground acceleration sequence with the time history as shown in Fig.5 (a). The peak of the design background acceleration of cos function is  $0.1168g$  at time  $t = 6.31$  s. Form that, the difference  $\Delta(\%)$  calculation value between cos function and Vietnamese Design Standard is 7.94% ( $M = 6.5$ ).

The first exceedance time is the 3 seconds and the last exceedance time is the 23 seconds, the value of ground acceleration record is  $0.05g$ . And, Suitable to select the time history duration of influence  $T_d = 30$  s (Kramer 1996) [3]. The reduction in peak ground acceleration (PGA) value indicates the improvement effectiveness of densification in soil liquefaction by restraining the acceleration record.

In Geostudio 2007 software, the determination of the design ground acceleration sequence with time steps of  $\Delta t = 0.06$  s and 500 steps, the influence duration  $T_d = 30$  s by the NewMark method in Fig. 5 (b). The value of the peak design ground acceleration  $a_{\max, g} = 0.1189g$  with time history periods  $t = 6.42$  s.

The duration of the consideration is  $T_d = 30$  s, the time of peak acceleration is time = 6.31 s for cos method and 6.42 s according to NewMark method by Geostudio software. The cos method is shorter time period by NewMark method.

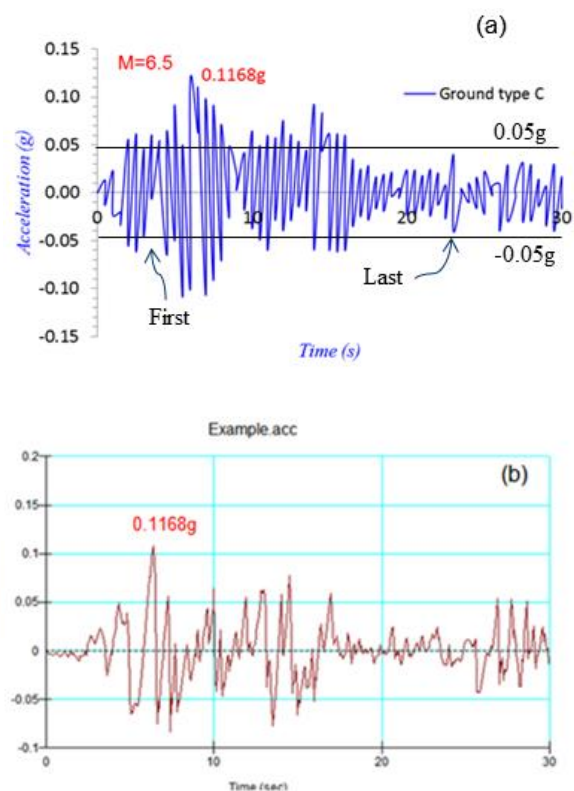


Fig. 5. Correlation between ground acceleration with time history ( $M = 6.5$ ), (a) cos function, (b) Geostudio software

#### 3.2.2. Relationship between ground acceleration spectra with different damping ratio

The accuracy of the proposed procedure is manifested in Fig. 6 (a) by the positive matching between simulated and target response spectra. Interestingly, it can be noted in all the case considered the mean target response spectra in perfectly matched, so to satisfy the response-spectrum compatibility criteria imposed by the seismic Eurocodes. The value of the peak horizontal spectral acceleration is  $0.39g$  of target spectrum and  $0.27g$  of simulated spectrum with time period 0.4 s.

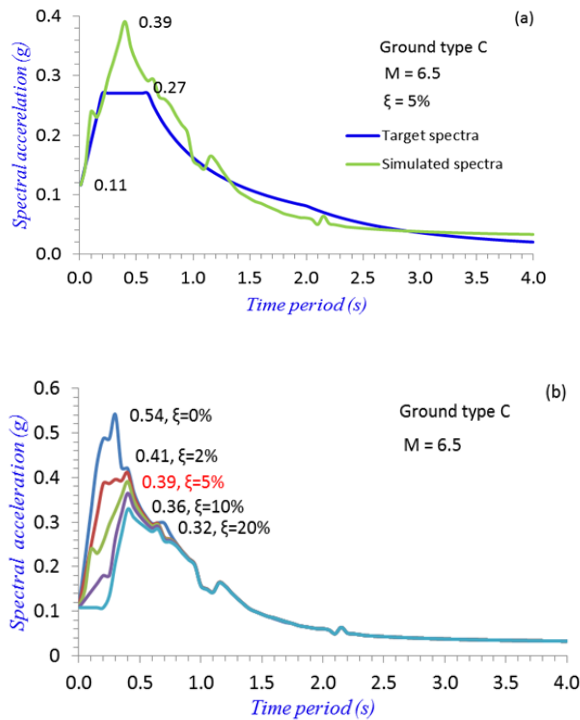


Fig. 6. Correlation between spectral acceleration with time period

As shown in Fig. 6 (b), the damping ratio is small, the spectral acceleration value is large and specific, the spectral acceleration value is 0.54 with the damping ratio of 0%, 0.41 with the damping ratio of 2%, 0.39 with the damping ratio of 5%, 0.36 for the with the damping ratio of 10% and 0.32 with the damping ratio of 10% of the earthquake level 6.5, respectively.

### 3.2.3. Establish ground acceleration record according to harmonic oscillator function

According to the simulation results in Fig. 7 for earthquake level  $M = 6.5$  and  $M = 8.0$  by Geostudio 2007 software, the results show that in the area with horizontal axis from 24 m to 34 m and depth from 0 to 3 m, the excess water pressure pores will appear. In addition in Fig. 7, the hydrostatic water line (blue lines, a-b) is pushed up, the highest position with a horizontal axis is 32 m. Therefore, at a horizontal position of 32 m is considered because of the largest pore water pressure value. However, it is difficult to identify the direction of migration.

With the same construction site, the building will collapse faster when the building is affected by the larger earthquake leves.

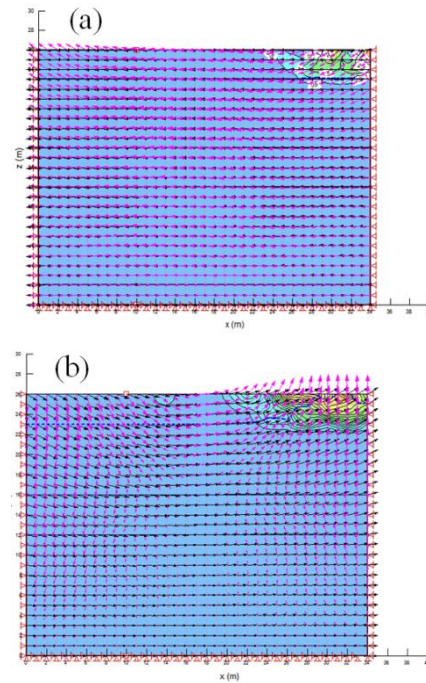


Fig. 7. Ground model for the project by Geostudio 2007 software of the excess pore water pressure shape with  $M = 6.5$  (a),  $M = 8.0$  (b)

When  $M=6.5$

To assess the efficiency of the ground model by Geostudio 2007 software, at depths of 1 m, 2 m and 3 m with a horizontal axis position of 16m is determined conduction, respectively. The results of the cycle shear strees are 5.25 kPa, 6.072 kPa and 7.254 kPa, cycle peak acceleration are 0.1789g, 0.1829g and 0.19g, respectively. After calculating, results of the average earthquake level  $M$  is 7.68, the number of cycle  $N$  is 15 in Fig. 8.

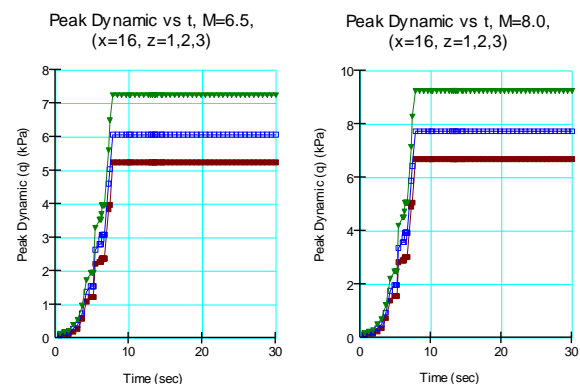


Fig. 8. Correlations between peak dynamic and time duration

Instead, as shown by the Fig. 9 (a), the harmonic ground acceleration relation fuction with time radution can expressed as follows  $a_g(t) = 0.1168 g \cos(\pi t - \pi/2)$  where numbers of cycles  $N = 15$ , influence time total  $T_d =$

30 s, time of a cycles  $T = 2$  s, undamped natural frequencies  $\omega_n = 2\pi/T = \pi$  rad/s, respectively.

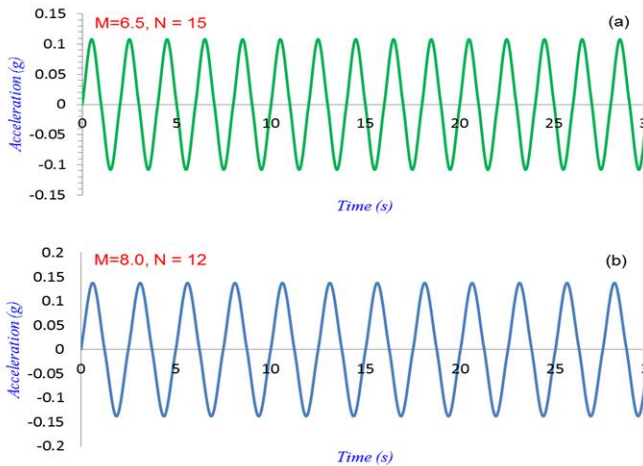


Fig. 9. Time histories of harmonic ground acceleration (a)  $M = 6.5$ , (b).  $M = 8.0$

When  $M=8.0$

As described in Fig. 8, the cycle shear stress values are significant between 1 m, 2 m and 3 m depths with 16 m horizontal axis position, respectively. The results of the cycle shear stress are 6.69 kPa, 7.74 kPa and 9.25 kPa, the cycle peak acceleration are 0.406g, 0.413g and 0.416g, respectively. From that, results of average earthquake level  $M$  is 7.68, the number of cycle  $N$  is 12.

Here, the number of cycle of  $M = 8.0$  is bigger than the number of cycle of  $M = 6.5$ , the difference about the number of cycle of  $M = 8.0$  and  $M = 6.5$  is 3 cycle.

In Fig. 9 (b), the harmonic ground acceleration relation function with time radution can be given as follows  $a_g(t) = 0.1381 g \cos(2.512t - \pi/2)$  here numbers of cycles  $N = 12$ , influence time total  $T_d = 30$  s, time of a cycles  $T = 2.5$  s, undamped natural frequencies  $\omega_n = 2\pi/T = 2.512$  rad/s, respectively.

### 3.2.4. Maximum acceleration, shear strain and depth relations

The results of decoupled analysis are plotted in Fig. 10, in terms of vertical profiles of peak ground acceleration (PGA) with depth, strain with depth for different earthquake levels ( $M = 6.5$  and  $M = 8.0$ ). The distribution of the maximum strain shows the highest value at depth of 1 m is 0.355% for  $M = 6.5$ , PGA = 0.1167g at 11.8 m depth and 1m is 0.452% for  $M = 8.0$ , PGA = 0.1461g at 12 m depth, respectively. The value of PGA, the strain with earthquake level  $M = 8.0$  is greater than the value of PGA, earthquake stress level ( $M = 6.5$ ), the value of the difference strain is 27.3% at 1m depth. At the same time, the value of shear strain is reduced with depth.

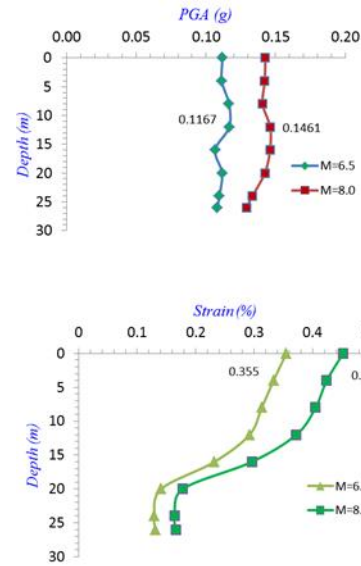


Fig. 10. Correlation between maximum acceleration, shear strain and depth

### 3.2.5. Shear strain, excess pore water pressure and time relations

When earthquake level  $M = 6.5$ , the liquefaction phenomenon has not appeared, the value of pore water pressure is 6.8 kPa for zero depth of the time of 30 s, the value of excess pore water pressure is 13.5 kPa for 3 m depth of the time of 30 s, too and the value of the excess pore water pressure is zero for a depth of more than 4m, as shown in Fig. 11.

According to the evaluation of liquefaction capacity by Than et al., (2018) [14] for sand soil type in Quy Nhon city. Secifically, when earthquake level increase, the peak horizontal ground acceleration increase too (values -  $a_{max}$ ). The liquefiable soils occurs completely by Dixit method of  $M = 8.0$  and no liquefaction soil of  $M = 6.5$ , this liquefaction resistance coefficient is greater than 1. For silty sandy soil, the values of  $FS_{lip} < 1$  calculated according to the methods for earthquake level, here  $FS_{lip}$  is the liquefaction resistance factor of method as shown above.

As shown in Fig. 12, when the depth value is smaller, the value of the excess pore water pressure is bigger over time. At the time of 30 s, the value of the excess pore water pressure is 35 kPa with a depth of zero and the value of excess pore water pressure is zero with depth from 4 m to deeper. At the time of 30 s, the excess pore water pressure ratio  $r_u$  is 0.61 of 3 m depth and from 4 m to deeper of the depth, the excess pore water pressure ratio  $r_u$  is zero, too.



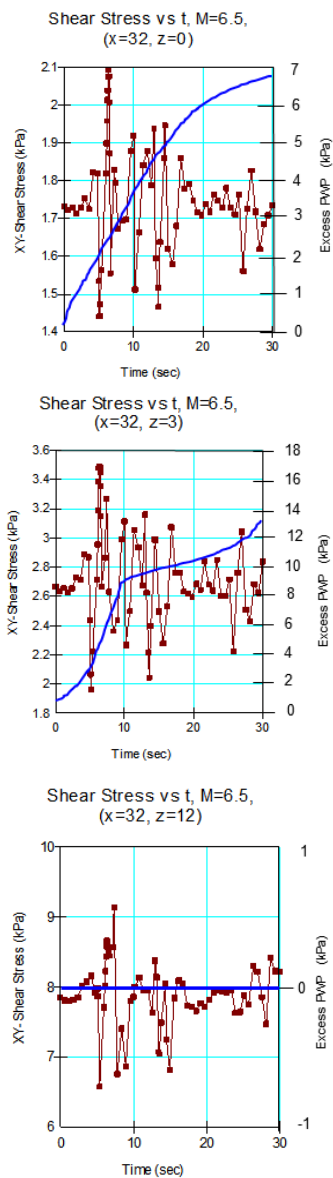


Fig. 11 Correlation between shear stress and excess pore water pressure with time history at 0 m, 3 m and 16 m depth of  $M = 6.5$

#### 4. CONCLUSION

- In the value  $0.05g$  ( $M = 6.5$ ) of ground acceleration record for C type soil, the influence duration gets start from 3<sup>rd</sup> second to end of 23<sup>th</sup> second.
- In period  $0.4s$  of the peak horizontal acceleration spectrum for  $0.39g$  of target spectrum or  $0.27g$  of simulated spectrum, the spectral acceleration value is largest and the damping ratio is smallest (Fig.6).
- Relations between the harmonic ground acceleration and time radution are set up. The cycle number  $N=15$  of the harmonic ground acceleration fits with  $M = 6.5$  of ground acceleration and  $N = 12$  fits with  $M = 8.0$

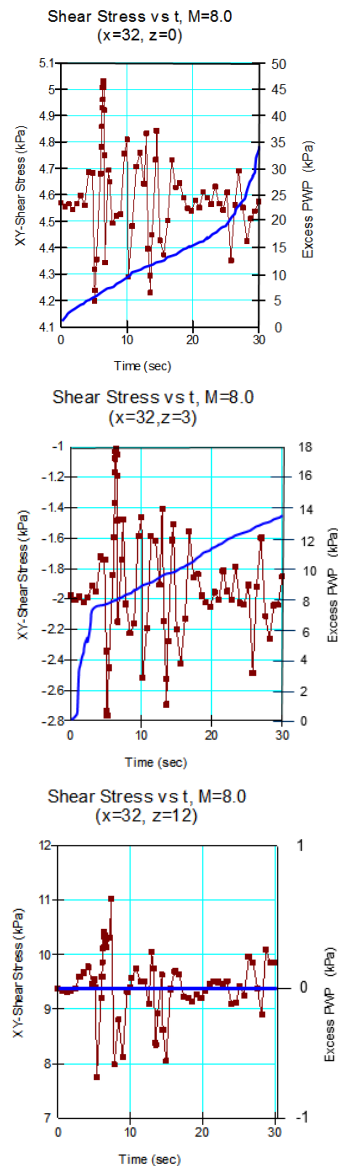


Fig. 12 Correlation between shear stress and excess pore water pressure with time history at 0 m, 3 m and 16 m depth of  $M = 8.0$

- At the PGA (peak of ground acceleration), strain of ground in earthquake level  $M = 8.0$  is greater than  $M = 6.5$ . The different strain value is about 27.3%.
- In depth from 0m to 3m, the value of the excess pore water pressure increases in case of  $M = 6.5$  but decreases in case of  $M = 8.0$ . The value of excess pore water pressure is 13.5 kPa at 3m depth in case of  $M = 6.5$  and 35 kPa at the surface of ground in case of  $M = 8.0$ . At time of 30<sup>th</sup> second in case  $N=12$  for  $M=8.0$ , the ratio  $r_u$  of excess pore water pressure is 0.61 in 3 m depth and zero from 4 m to deeper of the depth.

## REFERENCES

- [1] Amico L.D. et al., Simulation of Spectral-Acceleration Correlated and Response-Spectrum-Compatible Ground Motion Accelerograms, No 15, WCEE, 2012, pp. 1-10.
- [2] Chiaradonna A., et al., Application of a Simplified Model for the Prediction of Pore Pressure Build-up in Sandy Soils Subjected to Seismic Loading, 6th International Conference on Earthquake Geotechnical Engineering, New Zealand, 2015, pp 1-9.
- [3] Choudhury D., Geotechnical Earthquake Engineering, Department of Civil Engineering, India, <http://www.civil.iitb.ac.in>, 2019, pp 1-10.
- [4] Doan Thanh Nha, Simulation of Ground Acceleration Record from Elastic Reaction Spectrum during Earthquake, Master thesis, Department of Civil Engineering, Bach Khoa University, Ho Chi Minh City, Viet Nam, 2016, pp 79-89.
- [5] EN1998, " Eurocode 8: Design of Structures for Earthquake Resistancee," ed: European Union, 2004.
- [6] Geostudio 2007, Dynamic Modeing with Quake/W 2007, Geo - Slope Intrenational Ltd., 2008, Alberta, Canada, <http://www.geo-slope.com>, <https://www.youtube.com/watch?v=XVgY6tUXMS>.
- [7] Glaser .S, Insight into liquefaction by system identification, Geotechnique, 46, No. 4, 1996, pp. 641-655.
- [8] Idriss I.M, Boulanger R.W, Semi-empirical Procedures for Evaluating Liquefaction Potential During Earthquakes, Soil Dynamics and Earthquake Enguneering, 2006, pp. 115 - 130.
- [9] Kanai, K. (1957), "Semi Empirical Formula for the Seismic Characteristics of the Ground Motion", Bull. Earthq. Res. Inst.-Univiversity of Tokyo 35, 1957, pp. 309–325.
- [10] Moustafa A., Identification of Resonant Earthquake ground Motion, Vol. 5, Part 3, Indian Academy of Sciences, 2010, pp. 355-371.
- [11] Osaki Y., "On the Significance of Phrase Content in Earthquake Ground Motion", EESD, Vol.7, 1979.
- [12] Taciroglu E., Ghahari S.F., Identification of Spatial Variability in Bridge Foundation Input Motions: Theoretical basis, Irvine, Cliforna, 2016, pp. 111-139.
- [13] TCVN 9386-2012, Design of structures for earthquake resistances, 2012.
- [14] Thanh-Than Hua, Ngoc-Phuc Nguyen, Thi-Thanh Tran, Effecton of Liquefaction by Earthquake due to Pore Water Pressure in Sand, Numerical Analysis in Geotechnics, NAG2018, Ho Chi Minh City, Vietnam, 2018.

# PREDICTION OF GROUNDWATER LEVEL USING A DISCRETE SPACE-STATE MODEL AS AN ALTERNATIVE TO PHYSICALLY BASED GROUNDWATER MODELLING

Dilip Kumar Roy<sup>1</sup>, Sujit Kumar Biswas<sup>1</sup> and Khandakar Faisal Ibn Murad<sup>1</sup>

<sup>1</sup>Bangladesh Agricultural Research Institute, Bangladesh

## ABSTRACT

Reliable and accurate prediction of groundwater level is an essential component of sustainable water resources management and designing remediation plans. Groundwater simulations and predictions are often performed by employing physically based models, which are not applicable in many parts of the world especially in developing countries like Bangladesh due to data limitations. On the other hand, data-driven statistical methods have proven their applicability in modeling complex and nonlinear hydrological processes with a view to forecasting short-term and long-term groundwater levels. The purpose of this effort is to develop a non-physical based approach by utilizing a discrete Space-State model as a prediction tool for future scenarios of groundwater level forecasting. In Space-State modelling approach, a model is identified to accurately compute a dynamic system with response to an input. The present study utilizes the prediction focused approach of the system identification process in which the overall goal is to create a realistic dynamic system model. The performance of the proposed approach is evaluated for groundwater level data at three observation wells of Tanore upazilla of Rajshahi district, Bangladesh. Historical weekly time series of water level data from the three observation wells for 39 (1980-2018) years is used to develop the time series model, which is used for future water level predictions for a period of the next 22 years (up to 2040). The results of the present study indicate the potential applicability of the proposed discrete Space-State modelling approach in forecasting future groundwater levels in the observation wells of the study area.

*Keywords: Groundwater level prediction, Data-driven methods, Discrete Space-State modelling, Dynamic system model, Bangladesh*

## INTRODUCTION

Groundwater is one of the major sources of water supply for domestic, urban, agricultural and industrial purposes, especially in the Barind area of Bangladesh. However, many problems occur due to overexploitation of groundwater and unsustainable groundwater use and management, such as major water-level declines, drying up of wells, water-quality degradation, increased pumping costs, land surface subsidence, loss of pumpage in residential water supply wells, and aquifer compaction [1]. Reliable and accurate prediction of groundwater level is an essential component of suitable water resources management, predicting contaminant transport, and designing remediation plans. Groundwater simulations and predictions are often performed by employing physically based models (e.g. MODFLOW, FEEFLOW, FEMWATER etc.), which are not applicable in many parts of the world especially in developing countries like Bangladesh due to data limitations. On the other hand, data-driven statistical methods have proven their applicability in modeling complex and nonlinear hydrological processes with a view to forecasting short-term and long-term groundwater levels. The purpose of this effort is to develop a non-physical based approach with limited data availability for highly accurate

groundwater level forecasting that can be used to help water managers, engineers, and stake-holders manage groundwater in a more effective and sustainable manner.

The complexity of aquifer and hydrological systems makes accurate physical process simulations challenging due to the large agricultural and hydrogeological data requirements for model development and calibration. Thus, it is appealing to consider data-driven and machine learning methods based on nonlinear interdependencies that may be able to predict groundwater level change without deep knowledge of the underlying physical parameters. The data-driven models attempt to identify a direct mapping between the inputs and outputs of the system without reaching an understanding of the internal structure of the physical process. That is to say, the data-driven approach recognizes the hidden patterns in historical data and then apply those patterns to predict future scenarios. The commonly used data-driven methods for forecasting groundwater heads are based on the time series method [2], Kalman filter [3], artificial neural network method [4]-[6], and co-kriging technique [7]. Assessments of data-driven modelling applications in hydrology suggest that such methods can achieve performance comparable to, or even more accurate than, that of numerical models of physical transport



[8]-[10]. Overall, these studies have demonstrated the ability of statistical and data-driven machine learning methods for capturing the nonlinear relation between climate variables and groundwater, particularly in areas in which physically based models would be challenging to implement. Keeping these in mind, this effort seeks to implement discrete Space-State modelling approach as a prediction tool for future scenarios of groundwater level forecasting in selected observation wells of Tanore upazilla in Rajshahi district of Bangladesh.

## METHODOLOGY

### Study Area and Data

The study area is located at Tanore upazilla of Rajshahi district in the division of Rajshahi, Bangladesh. It is located between 24°28'N and 24°44'N latitudes and between 88°24'E and 88°39'E longitudes. The study area has an aerial extent of 295.40 km<sup>2</sup>, which is surrounded by Niamatpur Upazila and Manda Upazila of Naogaon District to the north, Mohanpur Upazila of Rajshahi district to the east, Paba Upazila and Godagari Upazila of Rajshahi district to the south, Chapai Nawabganj Sadar Upazila and Nachol Upazila of Chapai Nawabganj District to the west. The Shiba river flows through Tanore upazilla providing insufficient quantity of water for irrigation purposes. The geology of Tanore is composed of Barind Tract (81.8%), Old Gangetic Floodplain (3%) and Tista Floodplain (4.8%). The rest 10.4% of the total area consists of homestead, wetland, ponds, and rivers [11]. Clay loam (46%), Loam (35%), and Clay (8%) are the main constituents of land formation in Tanore upazilla [12]. The irrigated agriculture in Tanore upazilla mainly depends on groundwater resources, which is declining gradually as a result of excessive withdrawal of water for irrigating crops. Barind area is basically a flood free zone in Bangladesh because of high elevation with respect to mean sea level. Therefore, rainfall is the only source of water for groundwater recharge. Nevertheless, thick sticky clay surface of Barind area in combination with scanty rainfall hinders the natural aquifer recharge in this area. As a result, groundwater level is continuously falling in response to increasing amount of water abstracted for irrigation purposes.

Secondary data of weekly groundwater level fluctuations at selected observation wells are collected from Bangladesh Water Development Board. Historical weekly groundwater level data from January 1980 to September 2018 of three observation wells of Bangladesh Water Development Board are used. Observation well GT 8194046 is located at 24.68°N latitude and 88.53°E longitude. Observation well GT 8194048 is situated at 24.57°N latitude and 88.55°E longitude whereas the observation well GT

8194049 is located at 24.063°N latitude and 88.58°E longitude.

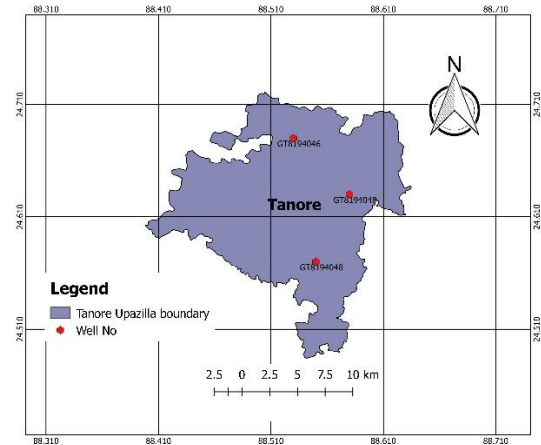


Fig. 1 Locations of the observation wells in the study area.

Historical weekly time series of water table data for 38 years is used for developing the time series model, which is used for future water level predictions for a period of the next 22 years (up to 2040).

The original time series of groundwater table data is divided into identification (training) and validation data. Eighty percent of the entire time series data is used to train the model whereas the rest 20% is used to validate the developed model. After satisfactory training of the models, the trained and validated models are used for future predictions.

### Modelling Technique

This study utilizes a discrete Space-State model as a prediction tool for future scenarios of groundwater level forecasting. The groundwater table can be modelled as a State-Space system with noisy input and measured water table date as output. The measured water table is proportional to the system state, i.e.

$$\mathbf{x}_{n+1} = \mathbf{A}\mathbf{x}_n + \mathbf{K}\mathbf{e}_n \quad (1)$$

$$\mathbf{y}_n = \mathbf{C}\mathbf{x}_n + \mathbf{e}_n \quad (2)$$

Where,  $\mathbf{x}_n$  is the state vector, contains the weekly water table values;  $\mathbf{y}_n$  is the output from the model;  $\mathbf{e}_n$  is the noise and  $\mathbf{A}, \mathbf{C}, \mathbf{K}$  are the parameters to be identified.

In Space-State modelling approach, a model is identified to accurately compute a dynamic system with response to an input. Two different approaches exist to generate an identified model response: (a) Simulation, which computes model response using

input data and initial conditions, and (b) Prediction, which computes the model response at some specified amount of time in the future using the current and past values of measured input and output values, as well as initial conditions. The present study utilizes the prediction focused approach of the system identification process in which the overall goal is to create a realistic dynamic system model that can be used or handed off for an application goal. During the model identification process, a one-step prediction focus is used as it generally produces the best results. By using both input and output measurements, one-step prediction accounts for the nature of the disturbances. Accounting for disturbances provides the most statistically optimal results.

#### Prediction focused approach

Prediction means projecting the model response  $k$  steps ahead into the future using the current and past values of measured input and output values.  $k$  is called the prediction horizon, and corresponds to predicting output at time  $kT_s$ , where  $T_s$  is the sample time. In other words, given measured inputs  $\mathbf{u}_m(t_1, \dots, t_{N+K})$  and measured outputs  $\mathbf{y}_m(t_1, \dots, t_N)$ , the prediction generates the final output  $\mathbf{y}_p(t_{N+K})$ . For example, if the input and output signals of a physical system are  $\mathbf{u}_m(t)$  and  $\mathbf{y}_m(t)$ , respectively, then the first order equation of this system can be represented by

$$\mathbf{y}_p(t+1) = \mathbf{a}\mathbf{y}_m(t) + \mathbf{b}\mathbf{u}_m(t) \quad (3)$$

where  $\mathbf{y}$  is the output and  $\mathbf{u}$  is the input. In general, to predict the model response  $k$  steps into the future ( $k \geq 1$ ) from the current time  $t$ , one must know the inputs up to time  $t+k$  and outputs up to time  $t$  such that

$$\begin{aligned} \mathbf{y}_p(t+k) \\ = \mathbf{f}(\mathbf{u}_m(t+K), \mathbf{u}_m(t+k-1), \dots, \mathbf{u}_m(t), \mathbf{u}_m(t-1), \dots, \mathbf{u}_m(0), \mathbf{y}_m(t), \mathbf{y}_m(t-1), \mathbf{y}_m(t-2), \dots, \mathbf{y}_m(0)) \end{aligned} \quad (4)$$

Where,  $\mathbf{u}_m(0)$  and  $\mathbf{y}_m(0)$  are the initial states.  $\mathbf{f}(\cdot)$  represents the predictor, which is a dynamic model whose form depends on the model structure.

A MATLAB command is used to identify a discrete state-space model from the measured data.

#### Performance Evaluation Criteria

##### Akaike's final prediction error (FPE)

FPE criterion provides a measure of model quality by simulating the situation where the model is tested on a different data set. According to Akaike's theory,

the most accurate model has the smallest FPE. Akaike's FPE is defined by the following equation

$$FPE = \det \left( \frac{1}{N} \sum_{t=1}^N \mathbf{e}(t, \hat{\boldsymbol{\theta}}_N) (\mathbf{e}(t, \hat{\boldsymbol{\theta}}_N))^T \right) \left( \frac{1 + d/N}{1 - d/N} \right) \quad (5)$$

Where,  $N$  is the number of values in the estimation data set,  $\mathbf{e}(t)$  is a  $n_y$ -by-1 vector of prediction errors,  $\boldsymbol{\theta}_N$  represents the estimated parameters,  $d$  is the number of estimated parameters. If number of parameters exceeds the number of samples, FPE is not computed when model estimation is performed.

##### Mean squared error (MSE)

$$MSE = \frac{1}{N} \sum_{i=1}^N (\text{Actual}_i - \text{Predicted}_i)^2 \quad (6)$$

#### MODEL DEVELOPMENT

As the first step of the model development, a 1-step ahead prediction is performed for all the three observation well locations. For observation well GT8194046, the system identifies 440 numbers of free coefficients to develop a Space-State model for which estimation data fit is found to be 91.35% (prediction focus). The FPE and MSE values of 0.07358 and 0.06796, respectively are found, which indicates a very good prediction model. The corresponding values of free coefficients, FPE and MSE values of observation wells GT8194048 and GT8194049 are presented in Table 1.

Table 1 Prediction performance of the developed models at observation wells GT8194048 and GT8194049

| Observation Well | Fit to estimation data (prediction focus), % | FPE  | MSE  |
|------------------|--|------|------|
| GT8194048        | 81.42  | 0.29 | 0.27 |
| GT8194049        | 89.98  | 0.07 | 0.07 |

The identified models minimize the 1-step ahead prediction. Then, the model is validated using a 10-step ahead predictor, i.e., given  $\mathbf{y}_0, \dots, \mathbf{y}_n$ , the model is used to predict  $\mathbf{y}_{n+10}$ . Note that the measured and predicted values,  $\mathbf{y}_0 - \hat{\mathbf{y}}_0, \dots, \mathbf{y}_n - \hat{\mathbf{y}}_n$ , are used to make the  $\mathbf{y}_{n+10}$  prediction. The 10-step ahead prediction results for the identification and the validation data for observation wells GT8194046, GT8194048, and GT8194049 are presented in Figs. 2, 3, and 4, respectively.

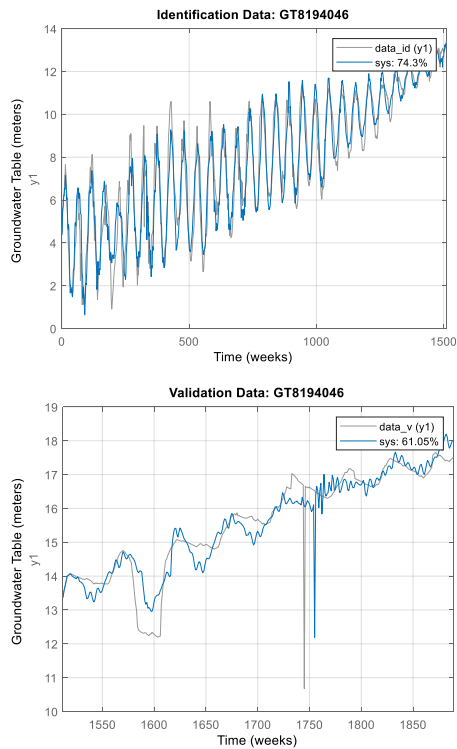


Fig. 2 10-step ahead prediction results for the identification and validation data at observation well GT8194046.

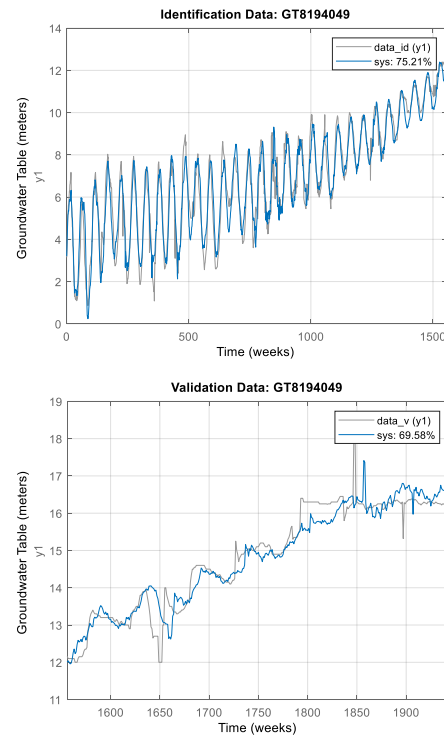


Fig. 4 10-step ahead prediction results for the identification and validation data at observation well GT8194049.

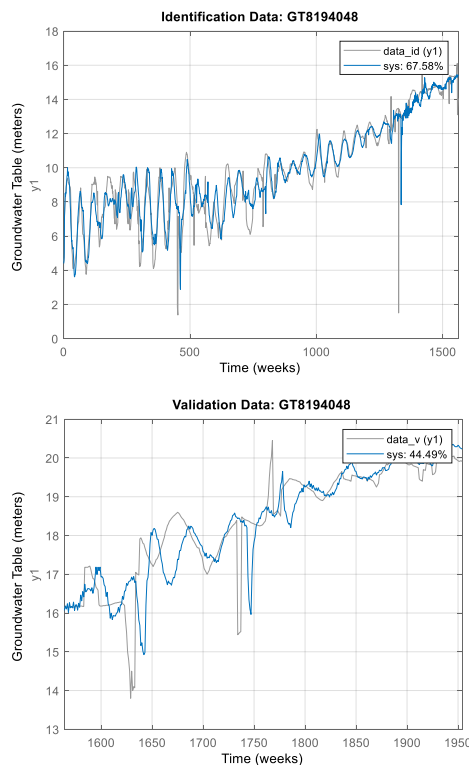


Fig. 3 10-step ahead prediction results for the identification and validation data at observation well GT8194048.

It is observed from Figures 2, 3, and 4 that for both identification and validation datasets at all observation wells the predictor matches well with the measured data. Then to further verify the developed prediction model, forecasting within the range of the validation data is performed. Forecasting uses the measured data record  $y_0, y_1, \dots, y_n - \hat{y}_n$  to compute the model state at time step  $n$ . This value is used as initial condition for forecasting the model response for a future time span. We forecast the model response over the time span of the validation data and then compare the two.

## RESULTS AND DISCUSSION

Predicted response over the validation data's time span at observation wells GT8194046, GT8194048 and GT8194049 are illustrated in Fig. 5.

The plots show that the model response overlaps the measured value for the validation data. The combined prediction and forecasting results indicate that the model represents the measured water level data quite accurately. Figure 5 shows that there are relatively good agreements between the simulated and observed groundwater level for all the three models. Thus, it is practically possible to develop groundwater forecasting models using this data-driven approach. However, there are discrepancies in matching some of the peak events, where the events may be under predicted or over predicted values.

The forecasting results also show that over large horizons the model variance is large and for practical purposes future forecasts should be limited to short horizons. For the water level prediction model, a horizon of 22 years is appropriate given the previous data available is only for 38 years.

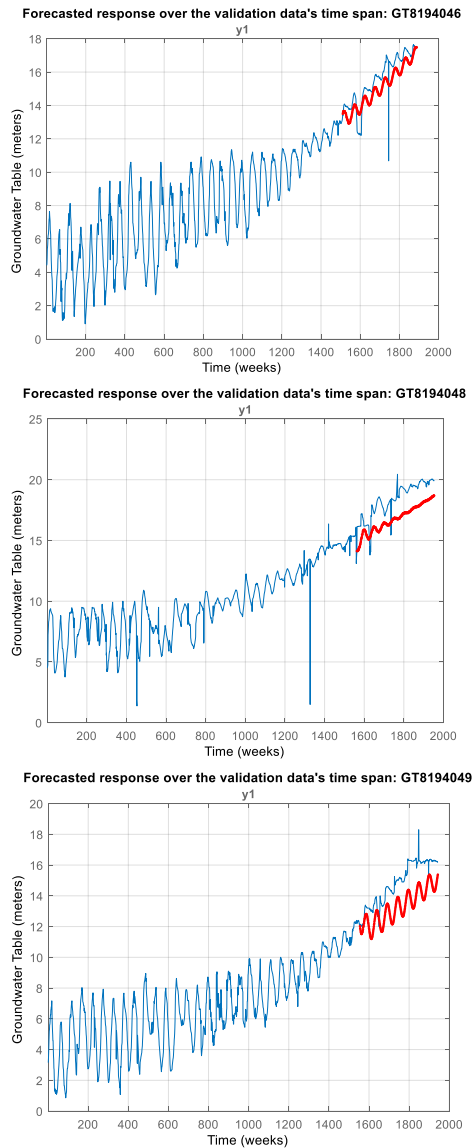


Fig. 5 Predicted response over the validation data's time span at observation wells GT8194046, GT8194048 and GT8194049.

The properly trained and validated models are then used to forecast the response 1105 steps into future for the time span of 22 years (From 25/09/2018 to 24/09/2040). The forecasted results are presented in Fig. 6.

The green curve shows the measured identification data whereas the blue curve shows the measured validation data that spans over 1-1900 weeks. The red curve is the forecasted response for 1105 weeks beyond the measured data's time range.

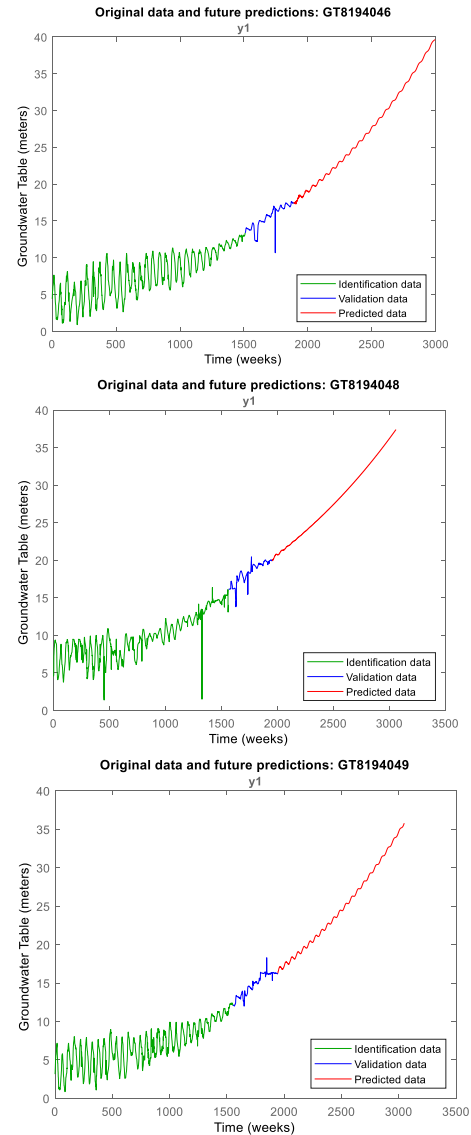


Fig. 6 Original and future predicted groundwater levels at observation wells GT8194046, GT8194048 and GT8194049.

Figure 7 illustrates groundwater level at the selected three observation wells on 24/09/2018 and the projected (model predictions) groundwater table on 24/09/2040. It is perceived from Figure 7 that groundwater level declination almost doubled at all three observation wells for the next 22 years if the present rate of abstraction continues. It is concluded that the proposed modeling framework can serve as an alternative approach to simulating groundwater level change and water availability, especially in regions where subsurface properties are unknown.

Of note, the forecasting results are entirely based on the historical groundwater level data based on the previous abstraction and recharge rates. As the increasing demand of water is triggering more and more groundwater abstraction from the aquifer and the recharge rate is decreasing due to scanty rainfall

in that area, the groundwater level declination might be even more dangerous than the projected ones if corrective measures are not taken. Moreover, the sticky clay subsurface of the study area slows down the natural recharge to the aquifer. Therefore, groundwater abstraction should be judiciously optimized in the study area to protect the already vulnerable groundwater resources.

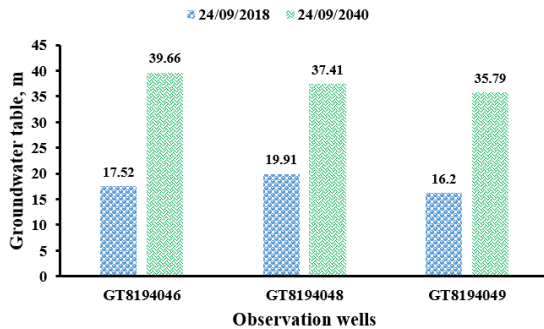


Fig. 7 Present and future scenarios of groundwater levels at three observation wells.

## CONCLUSIONS

The present study investigates the accuracy of the discrete Space-State modelling approach for forecasting weekly groundwater levels. The core idea is to develop a dynamic prediction model using the prediction focused approach to accurately forecast future groundwater levels at specified observation wells. The models are developed using the historical groundwater level data of the study area. The combined training, validation and forecasting results indicate that the model represents the measured water level data quite accurately. Therefore, the modelling approach presented in this paper can be used as an alternative to the complex numerical simulation models in data scarce situations. A univariate time series of groundwater level has been performed and presented in this paper. Future studies may aim to consider a multivariate time series analysis that considers the effects of other hydrogeological parameters for groundwater level predictions.

## ACKNOWLEDGMENTS

The authors gratefully acknowledge the financial support provided by National Agricultural Technology Program: Phase II Project, Bangladesh Agricultural Research Council, Bangladesh.

## REFERENCES

- [1] Banerjee P., Prasad R. K., and Singh V. S., Forecasting of Groundwater Level in Hard Rock Region Using Artificial Neural Network. *Environmental Geology*, Vol. 58, Issue 6, 2009, pp. 1239-1246.
- [2] Kontur I., Long-Range Groundwater Level Prediction Based on Time Series Analysis. In: Jones G. P., editor. *Improvements of Methods of Long Term Prediction of Variations in Groundwater Resources and Regimes due to Human Activity*, 1982, pp. 187-193.
- [3] Knotters M., and Bierkens M. F. P., Accuracy of Spatio-Temporal RARX Model Predictions of Water Table Depths. *Stochastic Environmental Research and Risk Assessment*, Vol. 16, Issue 2, 2002, pp.112-126.
- [4] Coulibaly P., Anctil F., Aravena R., and Bobée B., Artificial Neural Network Modeling of Water Table Depth Fluctuations. *Water Resources Research*, Vol. 37, Issue 4, 2001, pp. 885-896.
- [5] Daliakopoulos I. N., Coulibaly P., and Tsanis I. K., Groundwater Level Forecasting Using Artificial Neural Networks. *Journal of Hydrology*, Vol. 309, Issue 1, 2005, pp. 229-240.
- [6] Shigidi A., and A. Garcia L. A., Parameter Estimation in Groundwater Hydrology Using Artificial Neural Networks. *Journal of Computing in Civil Engineering*, Vol. 17, Issue 4, 2003, pp. 281-289.
- [7] Ahmadi S. H., and Sedghamiz A., Application and Evaluation of Kriging and Co-Kriging Methods On Groundwater Depth Mapping. *Environmental Monitoring and Assessment*, Vol. 138, Issue 1, pp. 357-368.
- [8] Coppola E., Szidarovszky F., Poulton M., and Charles E., Artificial Neural Network Approach for Predicting Transient Water Levels in a Multilayered Groundwater System under Variable State, Pumping, and Climate Conditions. *Journal of Hydrologic Engineering*, Vol 8, Issue 6, 2003, pp. 348-360.
- [9] Parkin G., Birkinshaw S. J., Younger P. L., Rao Z., and Kirk S., A Numerical Modelling and Neural Network Approach to Estimate the Impact of Groundwater Abstractions On River Flows. *Journal of Hydrology*, Vol 339, Issue 1, 2007, pp. 15-28.
- [10] Nikolos I. K., Stergiadi M., Papadopoulou M. P., and Karatzas G. P., Artificial Neural Networks as an Alternative Approach to Groundwater Numerical Modelling and Environmental Design. *Hydrological Processes*, Vol 22, Issue 17, 2008, pp. 3337-48.
- [11] SRDI. Upazila Land and Soil Resource Utilization Guide: Tanore, Rajshahi. SRDI (Soil Resource Development Institute), Dhaka, 2000. P.10.
- [12] SRDI. Land and Soil Statistical Appraisal Book of Bangladesh. SRDI (Soil Resource Development Institute), Dhaka, 2010. P. 155.



## EXPERIMENTAL INVESTIGATION OF RESPONSE OF SEGMENT LINING DUE TO ADJACENT PILE UNDER LOADING

Pattanasak Chaipanna<sup>1</sup>, Kisada Trakoonjannak<sup>2</sup> and Pornkasem Jongpradist<sup>3</sup>

<sup>1</sup>Faculty of Industry and Technology, Rajamangala University of Technology Isan, Thailand

<sup>2</sup>Geotechnical & Foundation Engineering Co., Ltd (GFE), Thailand

<sup>3</sup>Faculty of Engineering, King Mongkut's University of Technology Thonburi, Thailand

### ABSTRACT

The effect of adjacent pile under loading on the existing tunnel is one of the serious concerns in urban environment. In this study, the deformation and internal forces of segmental lining due to an adjacent loaded pile, are investigated through a series of physical laboratory tests. Special attention is paid on the relative positions between the key segment and the pile tip. The experimental results show that the relative pile tip level to the key-segment position plays a crucial role. The key-segment position at 90 degree (measured from tunnel crown) should be realized in assessment of lining response when the pile tip level is at the tunnel springline. For the pile tip at springline, the key-segment positions at 90 and 142 degrees should be taken into consideration.

*Keywords: Key-segment, Physical model test, Tunnel deformation, Pile-tunnel interaction*

### INTRODUCTION

In the urban areas, some pile foundations are closely located to the existing tunnel. The pile load transfers to the surrounding soil media and induces the additional internal force and deformation on the tunnel lining. The induced loading can contribute to possible damage to operational safety to the existing tunnel. Especially, tunnels for transport networks can often tolerate only minimal movement. A grasp of pile-soil-tunnel interaction is imperative for effect of pile loading on the functional safety of existing tunnel.

There are several studies on the effects of pile loading effect on the existing tunnel [1-3]. The most of them model the lining still using continuous element, which can not response the essential aspect of the segmental lining

The aim of this paper is to investigate the internal force and deformation of segmental lining via a series of physical model test.

### DESIGN OF THE MODEL

The prototype of this test is the universal subway tunnel, which generally made by reinforce concrete segments and connected them together with the steel bolts. The elastic moduli of concrete and steel bolt of the prototype tunnel are equal to  $3.45\text{E}+7$  and  $2.00\text{E}+8$  Pa, respectively. The segment are straggly assembled along the tunnel axis. The prototype tunnel consists of one key, two adjacent and three standard segments. The similarity method [4] is used to scale down the model test. The scaling factor of 30 is selected for performing the test. The high density

polyethylene (HDPE) and nylon sheet are employed to represent the segment and joints, respectively. The elastic moduli of HDPE and nylon sheet are equal  $1.18\text{E}+9$  and  $6.13\text{E}+8$  Pa, respectively. The configuration of the model tunnel is shown in Fig. 1(a). Table 1 shows the geometry of prototype and model tunnels. The HDPE is also represented the pile. The diameter of the model pile is 33 mm which scale down from 1.0 m diameter of prototype pile. The figure of pile model is shown in Fig. 1(b).

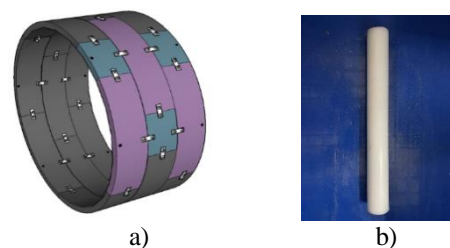


Fig. 1 a) configuration of tunnel model, b) pile model

Table 1 Geometry of prototype and model segments (mm).

| Items     | Outside diameter | Thickness | Width |
|-----------|------------------|-----------|-------|
| Prototype | 6200             | 350       | 1000  |
| Model     | 210              | 12        | 33    |

## PROCEDURE OF PHYSICAL MODEL TEST

### The test preparation

Fig 2 shows the determination of the ultimate capacity of the pile model from the experimental load-settlement curve from axial load test using De beer's method (1970)[5]. The service load of 121.5 N was used in the subsequent test. Series of physical tests are performed in acrylic test box (Fig.3) which is filled with KMUTT sand. Both lateral sides of the test box in the longitudinal direction are bored for facilitating the installation of both the model tunnel and measuring devices. To control the density and uniform leveling of sand within the test box, the sand is free fallen from the multiple sieving pluviation apparatus (Fig.4).

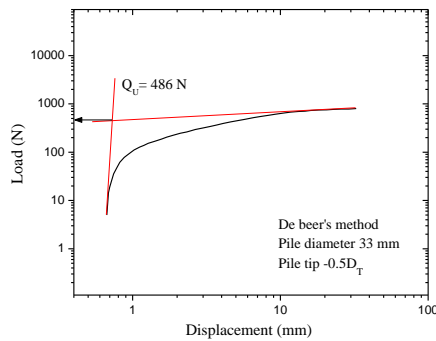


Fig. 2 Determination of the pile capacity

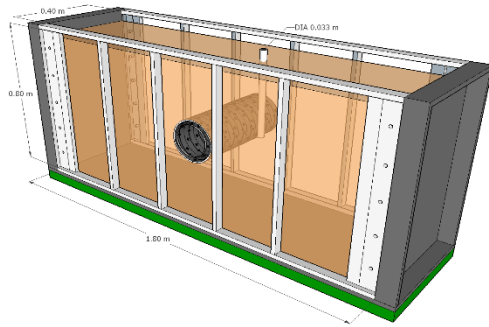


Fig.3 Arrangement of the experimental test

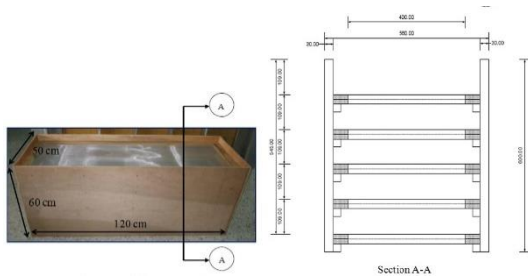


Fig.4 a) the pluviation apparatus, b) section A-A multiple sieve layers

### Monitoring and loading control

The strain gauges are installed on both external and internal surfaces of lining, as shown in Fig. 5. Strain obtained from strain gauges are used to compute the bending moment ( $M$ ) and normal force ( $N$ ) of the segment as expressed in Eq. 1 and 2, respectively.

$$M = \frac{(\varepsilon_{in} - \varepsilon_{ex})EI}{t} \quad (1)$$

$$N = \frac{(\varepsilon_{in} + \varepsilon_{ex})EA}{2} \quad (2)$$

where  $\varepsilon_{in}$  and  $\varepsilon_{ex}$  are internal and external strains which measure in tangential direction.  $E$  is modulus of elasticity.  $A$  is sectional area.  $I$  is moment of inertia of section.  $t$  is the lining thickness.

The deformation of the lining is measured by a laser transducer. The white laser targets are attached on internal surface of both ends of each segment, as shown in Fig. 5.

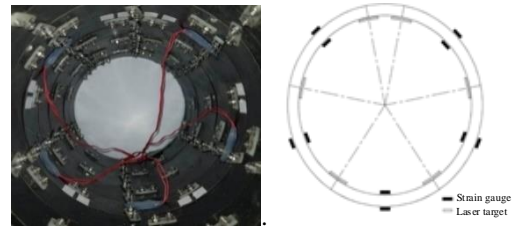


Fig. 5 a) installation of strain gauge, b) positions of strain gauge and laser target.

During testing, the pile loads and settlement are measured via the load cell and linear variable differential transformation (LVDT), respectively. The pneumatic control system is used to control the pile loading, which is shown in Fig6.

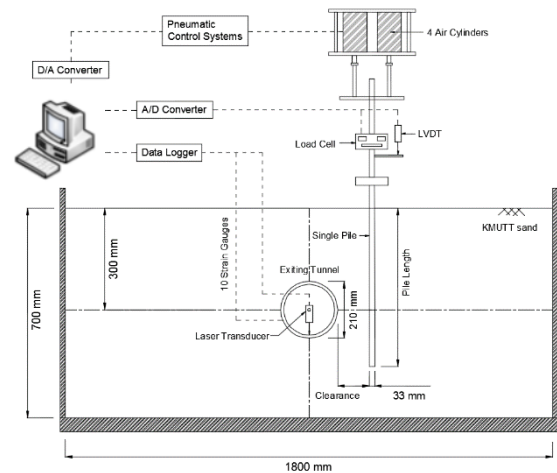


Fig. 6 Schematic of the physical model test



The strain gauge, laser transducer, load cell and LVDT are connected to the acquisition device to interpret and log the data.

## EXPERIMENTAL RESULTS

In order to obtain a better understanding of the influence of pile tip level on the tunnel response, two levels of pile tip were considered.

The measured data are distinguish in term of effect of key-segment position and effect of the pile tip level. In the test series of various key-segment position, the pile tip level is set at the springline. The key-segments are set at the 38, 90 and 142 degree measuring clockwise from the tunnel crown. For various pile tip levels, the key-segment is set at the 38 degree. The pile tip levels are set at the tunnel crown and springline.

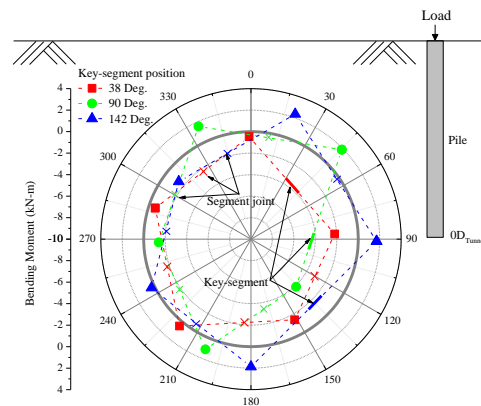
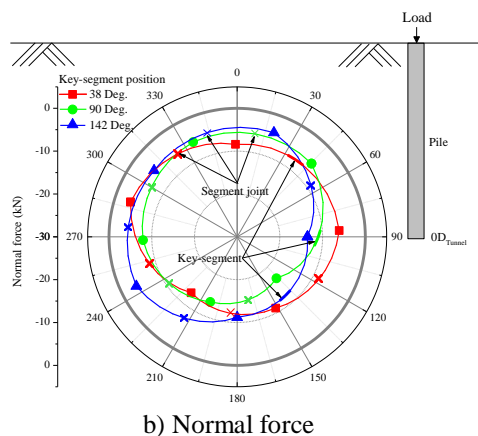
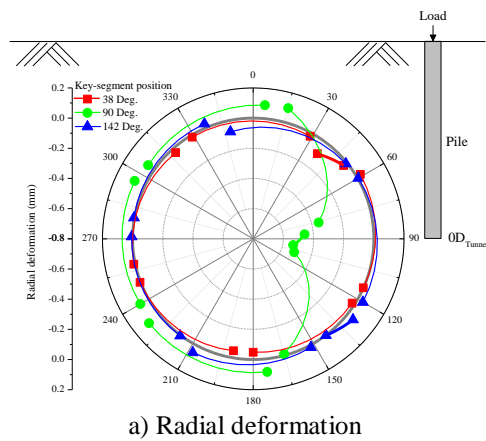


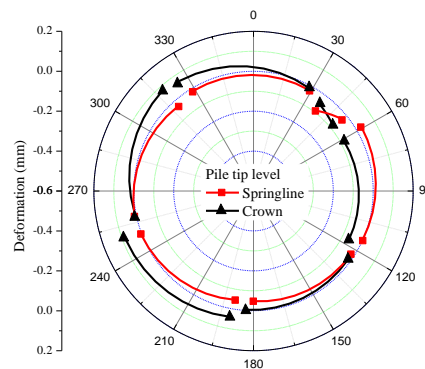
Fig. 7 Influence of key-segment position

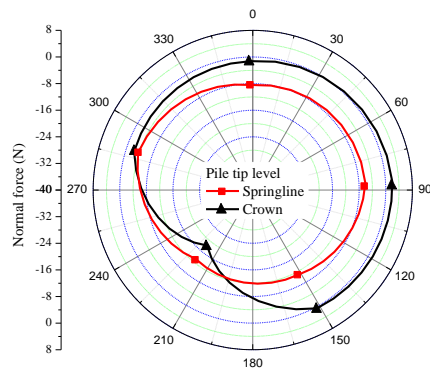
### Effect of key-segment position

Fig.7(a) shows the radial deformation measured at different of the key-segment position. The maximum radial deformation occurs in case of key-segment 90 degree occurring at the key-segment. Due to this case, the key-segment is locate near the pile tip. The induced load push the lining moving away from the pile. Moreover, case of key-segment locate at 90 degree shows the maximum normal force which appears at the 135 degree, as show in Fig.7(b). The measured bending moment is shown in Fig.7(c). The maximum (+) bending moment appears in case of the key-segment locating at the 142 degree, which occur at around the tunnel crown. The minimum (-) bending moment occurs at the springline.

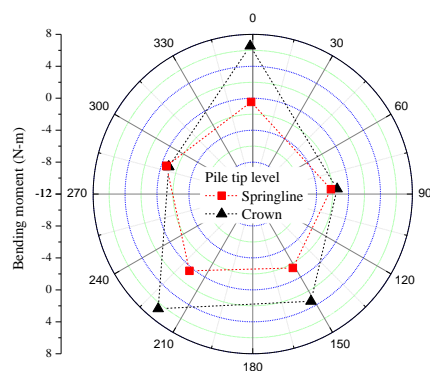
### Effect of pile tip level

The effect of pile tip levels are shown in Fig.8. In case of the pile tip level is at the crown, the induced force pushes the tunnel moving down away the pile greater than that of pile level at springline, as shown in Fig.8(a). As can be seen in Fig.8(b), the normal force increase with the increasing of pile length. In Fig.8(c), the pile tip level at the tunnel crown introduce the positive bending moment in the lining (compression on outer and tension on inner surfaces)





b) Normal force



c) Bending moment

Fig. 8 Influence of pile tip level.

## CONCLUSION

In the present paper, the results of tests performed in a laboratory with reduced-scale of tunnel response due to adjacent pile loading is presented. The objective of the test is to provide element of understanding about influence of the

relative position between the key-segment and pile tip position on the behavior of the existing tunnel lining. Based on the experimental observations and measurements, the following conclusions may be drawn:

- (1) The induced deformation will increase if the key-segment is closely the pile tip position.
- (2) The longer pile induces the normal force greater than that of short pile.
- (3) When the pile tip is at the crown level, the pile loading significantly induces the positive bending moment at the crown and invert of the lining.

## REFERENCES

- [1] Lueprasert, P., Jonpardist, P., Jonpardist, P. and Suwansawat, S., Numerical investigation of tunnel deformation due to adjacent loaded pile and pile-soil-tunnel interaction. *Tunnelling and Underground Space Technology*, Vol. 40, 2017, pp. 166-181
- [2] Lueprasert, P., Jongpradist, P., Suwansawat, S., Tunneling simulation in soft ground using shell elements and grouting layer. *International Journal of GEOMATE*, Vol.12, Issue 31, 2017, pp.51-57
- [3] Schroeder, F.C., Potts D.M., Addenbrooke, T.I., The influence of pile group loading on existing tunnels, *Geotechnique*, Vol.54, No.6, 2002, pp.351-362
- [4] Ye, F., Gou, C.F., Sun, H.D., Liu, Y.P., Xia, Y.X., and Zhou, Z., Model Test Study on Effective Ratio of Segment Transverse Bending Rigidity of Shield Tunnel. *Tunnelling and Underground Space Technology*, Vol. 41, 2014, pp.193-205.
- [5] De Beer, E., Experimental Determination of the Shape Factors and the Bearing Capacity Factors of Sand *Geotechnique*, Vol. 20, No 4, 1996, pp. 387-411.

## THE STUDY ON EFFECT OF LIGHTWEIGHT CONCRETE BLOCK BY WATER HYACINTH ADDING

Prang Subpa-Asa<sup>1</sup>, Laemthong Laokongthavorn<sup>2</sup>, Shigeyuki Date<sup>3</sup>

<sup>1</sup>Faculty<sup>1</sup>Graduate student, Civil Engineering Department, Faculty of Engineering, King Mongkut's Institute of Technology Ladkrabang, Bangkok, Thailand, 10520.

<sup>2</sup>Associate professor, Civil Engineering Department, Faculty of Engineering, King Mongkut's Institute of Technology Ladkrabang, Bangkok, Thailand, 10520.

<sup>3</sup>Professor, Civil Engineering Department, Faculty of Engineering, Tokai University, Kanagawa-pref., Japan, 259-1292.

### ABSTRACT

The objective of this study is to find out the pattern of water hyacinth which is suitable for making light-weighted concrete and use sand replacing in light-weighted concrete production. The proportion of cement: sand: water: foam is 1: 1: 0.65: 44.08 and the proportion of water hyacinth that will replace the sand by cement's weight is 0%, 2.5%, 5%, 7.5% and 10%, to study the density, water absorption, compressive strength (by the standard of TIS 1505-2541) and heat conduction at 14 days. The results of compressive strength of lightweight concrete (LC) and cellular lightweight concrete (CLC) are 167.56 ksc and 284.94 ksc, respectively. Compressive strength of cellular lightweight concrete mixed water hyacinth (CLCH) and lightweight concrete mixed water hyacinth (LCH) were investigated. The compressive strength of CLCH and LCH are 156.37 ksc and 172.45 ksc. The percentage loss of CLC and LC compressive strength are 6.68% and 39.83%. The physical properties which are density and thermal conductivity decrease. In contrast, water absorption increases by the percentage of water hyacinth by sand replacement. The optimal of water hyacinth ratio in this study is 5%. Moreover, CLC block is specified by Thai Industrial Standards Institute 1505-2541 and classified as C16 of CLC block. of your paper will be formatted further at International Journal of Computer Theory and Engineering. Define all symbols used in the abstract. Do not cite references in the abstract. Do not delete the blank line immediately above the abstract; it sets the footnote at the bottom of this column.

*Keywords: Water hyacinth, Lightweight concrete, concrete block, Construction materials*

### INTRODUCTION

The growing demand of construction in Thailand has increased usage of construction materials as lightweight concrete block which many types of building as residential and warehouse construction. The benefits of using lightweight aggregate concrete are 1) reduce in dead loads making savings in foundations and reinforcement, 2) improved thermal properties, 3) improved fire resistance, 4) save transporting and handling precast units on site and 5) reduce in formwork and propping. On the other hand, convention concrete making is not entirely environmentally-friendly, and this has enthused research on seeking greener alternative material for concrete.

Light-weight concrete has less density than a normal concrete. It's a new type of concrete that create from a natural material such as Portland cement, sand, lime, gypsum, water and air bubble disperser component in a right amount. Property of lightweight concrete: heat proof, sound proof, fire proof, hardened, light weight, easy to use, energy saving, reliable size and long age for usage [1]

Water hyacinth (WH) has known as one of the fastest growing plant. Its primary means of reproduction is by way of runners or stolons, which

eventually form daughter plants. It also produces large quantities of seeds that are viable for up to 30 years. Because of water hyacinth's ability to quickly reproduce, populations often double in size in just two weeks. [2]

Water hyacinth (WH) is a floating perennial plant that is native to the Amazon and has spread to of the southern united states. It prefers warmer climates and has board, thick, and glossy leaves that are 10-20 cm across. The hanging roots of the plant feathery and purplish-black in color.

Once it escapes into waterways, however, water hyacinth becomes an aggressive invasive species. In fact, it has been named one of the 10 worst weeds and the most widespread and damaging aquatic plant species in the world. But even without seeds, its growth rate is among the highest in the plant world, as it reproduces vegetative by short runner stems that branch out from the base of the plant.

Therefore, Water hyacinth (WH) are many advantages. However, there has huge effect to environment life cycle. Thus, it will be great which use weed as cement replacement or concrete aggregate were supported in concrete properties

According to using biomass as cheap insulation concrete block materials admixture with difference of mix proportion by using water hyacinth dried

cellulose, sawdust and stone dust by 1:9 ratio which compressive strength test was half of standard concrete blocks. Heat conduction coefficient was 0.105 W/m. K so concrete blocks made from mixing of sawdust and stone dust are not suitable for construction. [3]

Fiber cement material were made of cement paste containing coconut coir fibers and oil palm residues which used as roof sheet and siding materials to reduce heat transfer through buildings and energy conservation. The investigation focused mainly on the effects of both cellulose fibers on the physical mechanical and thermal properties of products which the results, the mixtures of fiber cement products containing 5% of both cellulose fibers by weight of Portland cement yielded optimal physical and mechanical properties. The thermal conductivity of the fiber cement pastes was 66% less than that of the control specimens. [4]

According to previous researches which use natural fibers derived from agricultural residues to develop fiber cement products with better sound insulation properties. To study the parameters that affect the density, compressive strength, flexural strength and sound insulation of the fiber cement materials. The fiber cement specimens consisted of Portland cement type 1, limestone powder, water, sand, natural fibers, including coconut coir fiber and oil palm fiber, at the levels of 5%, 10%, 15% and 20% by weight replacement and casting fiber cement specimens of 8, 12 and 16 mm thickness. Increasing the percentage replacement of the natural fibers, the density, compressive strength and flexural strength of the materials have decreased. Physical and mechanical properties of the fiber cement boards containing coconut fibers were better than containing oil palm fibers. [5]

Similarly, the research which investigated on the behavior of concrete with rice husk ash after exposed to different high temperatures (200, 300 and 400 °C). Then, samples were measured compressive strength and water permeability of concrete. The results showed that the strength of concrete reduced after exposure to high temperatures compared with control concrete and tended to decrease with increasing percentage of replacement of Portland. [6]

In particular, the research that study on the property of lightweight concrete block made from expanded clay pellets and fly ash by focusing on the mortar's compressive strength to the various mixing of fly ash and cement. The result shows that an increased proportion of fly ash resulted to mortar's low compressive strength. Mixtures of fly ash at proportion of 10% and 20% exhibited at 225 and 224 ksc. respectively which it is higher than compressive strength of cement. [7]

Hence, the research was focusing on the possibility of making a lightweight concrete with a water hyacinth that pass the qualification from

Thailand industrial standard institute (TIS) [1] and this paper will be researching on the physical and mechanical property of lightweight concrete that mix with a water hyacinth.

## METHODOLOGY

### Part 0: Materials and mix properties

Water hyacinth was located in Ladkrabang district, a suburb area in Bangkok, Thailand. The water hyacinth was cut into about 5 mm in length using long knife and then dried in a hot air oven at 60° C for 48 hours. [8] and divided into 2 parts as was blended and not blend (by a bender). There were classified in 3 classes 1) 0.5 cm of length, 2) do not pass through sieves NO.50 and 3) pass through sieves NO.50 which show in fig 1. The material used and its quality was show in table 1.



a) b) c)

Fig.1. The classification of water hyacinth in 3 class

- Water hyacinth dried powder pass through sieves NO.50 (WH NO.50)
- Water hyacinth dried powder do not pass through sieves NO.50 (WHnpNO.50)
- Water hyacinth dried 0.5 cm of length (WH 0.5 cm)

### Part 1: Compressive strength testing by Trial size of water hyacinth

In first part of the research, to find the optimal size of water hyacinth dried was used to determine the trend of maximum compressive strength. The water hyacinth specimens were tested in three sizes as show in fig 1 and mixed proportion show in table 2. The result was found that mortar by non-water hyacinth adding, mortar with water hyacinth dried powder which pass through sieves NO.50 adding, mortar with water hyacinth dried powder do not pass through sieves NO. 50 adding, mortar with water hyacinth dried 0.5 cm of length adding were 369.02, 233.27, 216.15 and 165.39 ksc of compressive strength, respectively and were presented in table 3. The water hyacinth dried powder pass through sieves NO. 50 was optimal size for this part of research

### Part 2: The experiment for finding optimal ratio of water hyacinth dried powder pass through sieves NO.50

In second part, after found optimal size of water hyacinth dried powder was used to determine the trend of maximum compressive strength for using in the research. The ratio of water hyacinth by sand

replacement were classified in 5 states as 0%, 2.5%, 5.0% 7.5% and 10%.

Table 2: Mixed proportions

|  | Description  | Ratio |      |      |      |
|--|--|-------|------|------|------|
|  |  | C     | S    | WH   | W    |
| A  | Cement plate   | 1.00  | 2.00 | -    | 0.60 |
| Adding Water Hyacinth 3% by mass of cement |  |       |      |      |      |
| B1-B5                                      | Cement plate with water hyacinth dried powder pass through sieves NO.50        | 1.00  | 2.00 | 0.03 | 0.60 |
| C1-C5                                      | Cement plate with water hyacinth dried powder do not pass through sieves NO.50 | 1.00  | 2.00 | 0.03 | 0.60 |
| D1-D5                                      | Cement plate with water hyacinth dried 0.5 cm of length                        | 1.00  | 2.00 | 0.03 | 0.60 |

Table 3: Result of compressive strength Test by Trial size of water hyacinth

| Description   | Weight (g) | Cross-sectional Area (cm <sup>2</sup> ) | Age (days) | Compressive Strength (ksc) |
|---|------------|---|------------|----------------------------|
| Mortar by non-water hyacinth adding   | 258.01     | 25.10                                   | 14         | 369.02                     |
| Mortar with water hyacinth dried powder pass through sieves NO.50 adding        | 251.52     | 25.47                                   | 14         | 233.27                     |
| Mortar with water hyacinth dried powder do not pass through sieves NO.50 adding | 252.08     | 25.35                                   | 14         | 216.58                     |
| Mortar with water hyacinth dried 0.5 cm of length adding                        | 247.29     | 25.32                                   | 14         | 165.39                     |

Table 4: Mixed proportions of mortar with water Hyacinth dried powder pass sieves NO.50 adding

|       | Description  | Ratio |      |       |      |
|-------|--|-------|------|-------|------|
|       |  | C     | S    | WHSR* | W    |
| A     | Mortar   | 1.00  | 1.00 | 0%    | 0.65 |
| B1-B5 | Mortar with water hyacinth dried powder pass through sieves NO.50 adding | 1.00  | 1.00 | 2.5%  | 0.65 |
| C1-C5 |  | 1.00  | 1.00 | 5.0%  | 0.65 |
| D1-D5 |  | 1.00  | 1.00 | 7.5%  | 0.65 |
| E1-E5 |  | 1.00  | 1.00 | 10%   | 0.65 |

Table 5: Mixed proportions of mortar with water Hyacinth dried powder pass through sieves NO. 50 adding and CLC foaming agent

|       | Description  | Ratio |      |       |      |        |
|-------|--|-------|------|-------|------|--------|
|       |  | C     | S    | WHSR* | W    | CLCFA* |
| A     | Mortar   | 1.00  | 1.00 | 0%    | 0.65 | 44.08% |
| B1-B5 | Mortar with water hyacinth dried powder pass through sieves NO.50 and CLC foaming agent adding | 1.00  | 1.00 | 2.5%  | 0.66 | 44.08% |
| C1-C5 |  | 1.00  | 1.00 | 5.0%  | 0.67 | 44.08% |
| D1-D5 |  | 1.00  | 1.00 | 7.5%  | 0.68 | 44.08% |
| E1-E5 |  | 1.00  | 1.00 | 10%   | 0.69 | 44.08% |

Table 1: Materials and properties

| Materials         | Symbol | Properties               |
|-------------------|--------|--------------------------|
| Cement            | C      | Ordinary Portland cement |
| Fine aggregate    | S      | River sand               |
| Water hyacinth    | WH     | WH NO.50                 |
|                   |        | WHnp NO.50               |
|                   |        | WH 0.5 cm                |
| CLC Foaming agent | AD     | Protein based            |

Part 2.1: The sample of mortar with water hyacinth dried powder pass through sieves NO.50 adding.

Mixed proportion of mortar with water Hyacinth dried powder which pass through sieves NO.50 adding was shown in table 4.

Part 2.2: The sample of mortar with water hyacinth dried powder pass through sieves NO.50 and CLC foaming agent adding.

Mixed proportion of mortar with water Hyacinth dried powder pass through sieves NO.50 and CLC foaming agent adding was show in table 5.

### Part 3: Physical properties Testing

#### Part 3.1: Compressive strength testing

The sample, which passed 14 days, were tested its compressive strength according to Thailand industrial standard institute TIS. 1505- 2541 by compressive load was controlling between 0.05 - 0.20 N/mm<sup>2</sup>/sec until failure.

#### Part 3.2: Dry density testing

The dry density of mortar testing was according to Thailand industrial standard institute TIS. 1505-2541 by measured volume sample then dried in a hot air oven at 105±5 °C for 24 hours, weight after dried and follow the equation 1.1.

$$\text{dry density} = \frac{\text{mass of sample}}{\text{Volume of sample}} \quad (1.1)$$

#### Part 3.3: Water absorption testing

Water absorption testing also followed by Thailand industrial standard institute TIS. 1505-2541 which the sample dried in a hot air oven until constant weight more than 24 hour at 105±5 °C then cool down to room temperature more than 4- hour, measured mass. Therefore, curing sample in the water, after 24

hours, wipe surface and harden mortar measured mass in 3 minutes, follow the equation 1.2

$$\% \text{Absorption} = \frac{W_s - W_d}{W_d} \times 100 \quad (1.2)$$

Ws : Wet weight (Kg)

Wd : Dry weight (Kg)

## RESULTS

Result of part 3.1 Compressive strength testing of WHSR mortar and WHSR and CLCFA mortar.

The representative of compressive strength of WHSR mortar were measured by compressive load tester in the Table 4 which mass of cement and water cement ratio were controlled by mortar cement ratio 1 : 1 (Portland cement type 1 : river sand). The general mortar (non- WHSR) is on dimensional specimens of 10x10x10 cm were 284.94 ksc of compressive strength. Fig 2 was presented result of this study as WH sand replacement ratio 2.5%, 5%, 7.5% and 10% were 225.99 ksc, 171.45 ksc, 6.09 ksc and 4.23 ksc of compressive strength, respectively.

On the other hand, the CLCFA mortar (non-WH) on dimensional specimens of 10x10x10 cm were 167.56 ksc of compressive strength. WHSR and CLCFA mortar were present on fig 2 as WH sand replacement ratio 2.5%, 5%, 7.5% and 10% and CLCFA adding were 136.85, 156.37, 5.39 and 6.26 ksc of compressive strength, respectively.

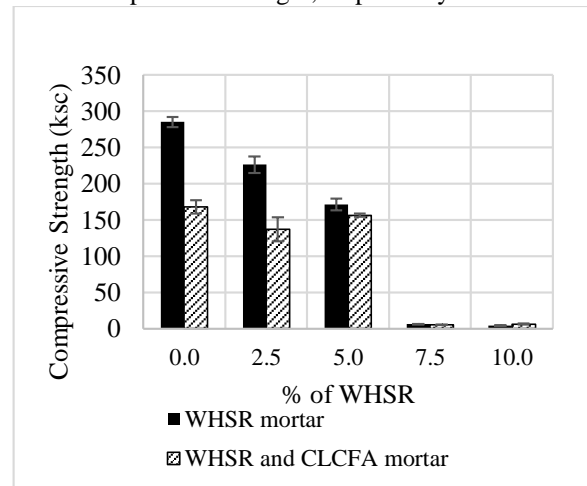


Fig.2. Compressive strength Test

Result of part 3.2: Dry density testing of WHSR mortar and WHSR and CLCFA mortar.

The representative of dry density of WHSR mortar were measured and followed by equation 1.1. The general mortar (non- WHSR) is on dimensional specimens of 10x10x10 cm were 1696.57 kg/m<sup>3</sup> of dry density. Fig 3 was presented result of this study as WH sand replacement ratio 2.5%, 5%, 7.5% and



10% were 1656.59, 1533.52, 1388.49 and 1347.14 ( $\text{kg/m}^3$ ) of dry density, respectively.

In the same way, the CLCFA mortar (non-WHSR) is on dimensional specimens of 10x10x10 cm were 1526.98 ( $\text{kg/m}^3$ ) of dry density. Fig 3 was presented result of this study as WH sand replacement ratio 2.5%, 5%, 7.5% and 10% were 1445.57, 1460.66, 1373.41 and 1324.31 ( $\text{kg/m}^3$ ) of dry density, respectively.

Result of part 3.3: Water absorption testing of WHSR mortar and WHSR and CLCFA mortar.

The representative of water absorption of WHSR mortar were measured and followed by equation 1.2. The general mortar (non-WHSR) is on dimensional specimens of 10x10x10 cm were 16.29% of water absorption. Fig 4 was presented result of this study as WH sand replacement ratio 2.5%, 5%, 7.5% and 10% were 14.64%, 17.84%, 30.73% and 33.89% of water absorption, respectively.

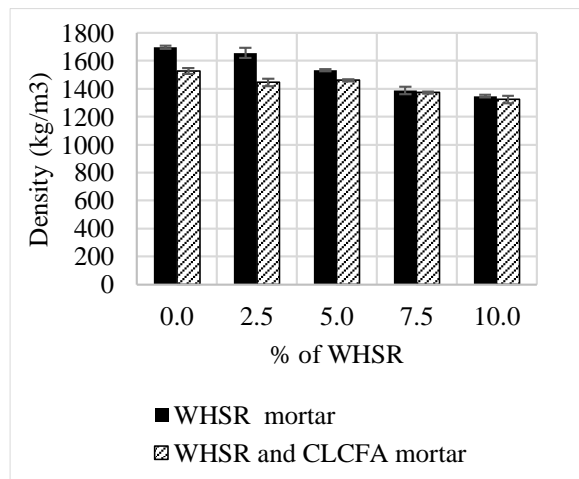


Fig.3. Density Test

Similarly, the CLCFA mortar (non-WHSR) is on dimensional specimens of 10x10x10 cm were 16.95% of water absorption. Fig 4 was presented the result of this study as WH sand replacement ratio 2.5%, 5%, 7.5% and 10% were 17.09%, 18.15%, 30.8% and 34.2% of water absorption, respectively.

## CONCLUSIONS

The study has been investigated the possibility of making a lightweight concrete with a water hyacinth which was qualified from Thailand industrial standard institute (TIS) and the physical and mechanical properties. The main result can be concluded as follow:

1) The compressive strength was decrease when the percentage of water hyacinth dried sand replacement was increase. It was found that the compressive strength was significantly reduced by water hyacinth dried sand replacement on 7.5. the optimum percentage of water hyacinth dried sand

replacement ratio both of WHSR mortar and WHSR and CLCFA mortar at 5% of water hyacinth dried sand replacement were 171.45 and 156.37 ksc of compressive strength, according to TIS 2601-2556.

2) The percentage of water hyacinth dried sand replacement was increase and it caused density decreasing. The lowest density was obtained for WHSR mortar, WHSR and CLCFA mortar on 10% as 14.1347 and 21.1342 ( $\text{kg/m}^3$ ) respectively. Nonetheless, there was not pass the standard of TIS 2601-2556. Hence, the optimum percentage of water hyacinth dried sand replacement ratio was 5% as WHSR mortar, WHSR and CLCFA mortar, with a density of 1533.52 and 1460.66  $\text{kg/m}^3$ , respectively which be able to classify in lightweight concrete block type C16 according to TIS 2601-2556.

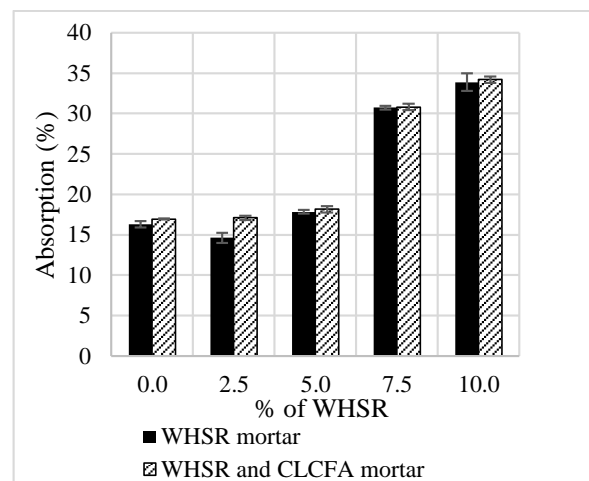


Fig.4. Water absorption Test

3) Water absorption was increased by the percentage of water hyacinth dried sand replacement increasing. The lowest Water absorption was obtained for WHSR mortar, WHSR and CLCFA mortar on 2.5% as 14.64% and 17.09% respectively which lower than mortar. For this result, the optimum percentage of water hyacinth dried sand replacement ratio was 5% as WHSR mortar, WHSR and CLCFA mortar, with a density of 1533.52 and 1460.66  $\text{kg/m}^3$ , respectively which according to TIS 2601-2556.

This study investigated the mixing of water hyacinth dried sand replacement ratio, size of water hyacinth dried sand, compressive strength testing, dry density and water absorption testing were carried out in a ratio can be summarized that the optimal size and ratio in this study were water hyacinth dried powder which pass through sieves NO.50. As a result, the compressive strength much higher than standard of TIS 2601-2556 as 20.4 ksc, WHSR mortar which have 7.5 and 10% of water hyacinth dried sand replacement do not pass the standard. Hence, 2.5 and 5.0% of water hyacinth dried sand replacement were optimal conditions for producing lightweight concrete block. The mortar which contain 2.5% of

WHSR was 225.99 ksc of compressive strength, which is the highest in this study compared with 5.0% of WHSR and CLCFA was 156.37 ksc of compressive strength. In contrast, the density and water absorption of 5.0% of WHSR and CLCFA were 1460.66 kg/m<sup>3</sup> and 18.15% which is the best condition. The optimal condition does not necessary to have high compressive strength load, it have to be over qualification of the Thailand Institute Standard and focus on eliminated more water hyacinth volume. As a result, 5.0% of WHSR and CLCFA mortar was an optimal condition. Furthermore, it would be reduced water hyacinth in 1 m<sup>2</sup> in the canal by standard size of lightweight concrete block production which is an environmentally-friendly material.

## REFERENCES

- [1] Thai industrial standard institute, Ministry of industry, “ Aerated lightweight concrete elements” , Thailand Institute Standard (TIS.2601-2556), vol. 4562, 2013.
- [2] Ekasilp, W. and Boonthanomwong, C. , “ Thermal Insulator Performance of Water Hyacinth and Sawdust Hollow Concrete Block”, National Research Conference, 2014.
- [3] Budnumpecth, T. and Tanpaiboonkul, N. , “Properties of lightweight concrete containing crumb rubber and cement replacing with fly ash from coal power plant”, Veridian E- Journal, Science and Technology, Silpakorn University, vol. 3 (4), 2016.
- [4] Lertwattanakruk, P. and Suntijitto, A. , “Properties of natural fiber cement materials containing coconut coir and oil palm fibers for residential building applications”, Construction and Building Materials, vol. 94, pp. 664- 669, 2015.
- [5] Lertwattanakruk, P. and Masuwan, K. , “Investigation of sound Insulation Properties of Fiber Cement Board Containing Natural Fiber”, KMUTT research and development Journal, vol 38(1), 2015.
- [6] Ladbhat, N. , Ongwandee, M. , and Homwuttiwong, S., “Compressive strength and permeability of concrete with rice- husk ash exposed to various temperatures, Mahasarakham University Research Conference, 2014.
- [7] D. G. Roy, S. P. Mehrotra and P. C. Kapur, “ Lightweight masonry blocks from fly ash pellets” , Resources and Conservation, vol.11(1), pp.63-74, 1984.
- [8] Ouensanga, A., “Variation of fiber composition in sugarcane stalks”, Wood and fiber science, vol.21(2), pp.105-111, 1989.

# STUDY ON THE PROPERTIES OF CEMENT MILK ADDED WITH BAKING SODA -COMPRESSION STRENGTH ESTIMATION FROM BLEEDING REDUCTION AND INITIAL ELECTRICAL RESISTIVITY

Yasuhide Mochida <sup>1</sup>, Joshua O. Ogunbiyi <sup>2</sup>, Makoto Minemoto<sup>2</sup>, and Keisuke Funato<sup>3</sup>

<sup>1</sup> Prof. Ritsumeikan University, Japan

<sup>2</sup>Graduate School of Science and Engineering, Ritsumeikan University, Japan

<sup>3</sup>Associate Prof. National Institute of Technology, Ishikawa, Japan

## ABSTRACT

Cement milk is used for earth retaining structures, pile construction and also for ground improvement through cement deep mixing and other methods. However, it is quite difficult to estimate or evaluate the compressive strength of concrete mix during curing phase of the construction process. Excessive bleeding also remains a pertinent issue. Excessive absorption of moisture eventually leads to expansion, cracks, and causes reduction in concrete strength. This research was focused on reducing bleeding of cement solidified materials by adding baking soda. Baking soda acts as a catalyst and promotes hydration of cement through hydrolysis reaction. An alkali silica reaction occurs within the cement milk to form alkali silica gel. This shortens the setting time, and curtails excess moisture. The Laboratory experiments revealed that addition of about 3% of backing soda was the most effective. Furthermore, from the electrical resistivity and the compressive strength of 24 hours of the cement solidified material to which 1 to 4% of sodium bicarbonate was added, the compressive strength of 28 days of the material was also accurately estimated.

*Keywords: Cement milk, Bleeding, Baking soda, Electrical resistivity, Compressive strength*

## INTRODUCTION

Cement milk or slurry is generally considered as liquefied cement. It is a mixed liquid that is composed of cement, water and other relative chemical additives. Cement milk has varied densities depending on the applied degree of mix. Cement milk has unique mechanical properties as it can flow under gravity and are also capable of being pumped. It can also be used in under water projects. In the past few decades, the use of cement milk in relative construction projects has greatly increased.

In Japan, cement milk is used for earth retaining structures, pile construction and also for ground improvement through cement deep mixing. The Cement Deep Mixing (CDM) method is a technique to chemically solidify and strengthen soft ground by in-situ mixing of the soil with cement slurry. This method of ground improvement is environmentally friendly and cost effective.

This method has been repeatedly used in ground improvement applications to prevent embankment instability and settlement, improve ground stability for construction projects, as countermeasures against liquefaction, and as reinforcement of ground to improve earthquake-response of superstructures [5].

The use of cement milk as a construction material is widely acceptable. However, bleeding has been a major constraint to the efficiency of this material in construction projects. Bleeding is an important phenomenon in construction process. This occurs

majorly in freshly mixed concrete. Bleeding is widely described as the upward movement of moisture towards the surface as a result of the uneven settlement of heavier particles constituent of the mix.

Although various researches have been conducted on the possibilities of controlling bleeding including the use of slag as additive, bleeding still remains a concern with regards to quality assurance of the use of cement milk especially in marine.

The purpose of this study is to examine and ascertain the hypothesis that backing soda can be used as additive in cement milk to control the bleeding rate of the material during construction process. It is expected to stabilize the hydration reaction of the cement.

## LITERATURE REVIEW

Real time monitoring and control of high-quality execution is an important aspect in construction management. Development of techniques and technology with such features has been a growing concern. Ground improvement processes are also not left out of these concerns.

For example, while using cement milk material for in-situ cement deep mixing, it will be important to monitor the flow rate of the cement slurry, penetration and retrieval speed, and the rotation speed of the mixing shaft including the accuracy of degree mix of the constituents.

Different technology has been developed to

monitor such processes including the use of computer aided monitor system for real time monitoring and analysis of the construction process. The use of electrical resistivity has also been engaged to provide instant feedback on the mixing degree between constituents of the cement milk during placement. This is accurately deduced from the change in resistivity of the resulting compound.

During the mixing process of concrete or cement slurry in our previous experiments, it has been established that with regards to the ion concentration of the primary materials, the electrical resistivity of the compound is adequately lower when properly mixed and increase in cases where the compound is incompletely stirred [3].

Aside the aforementioned issues, another factor that relatively affects cement mixture is bleeding. Bleeding is equally important in construction process. This occurs majorly in freshly mixed concrete. Bleeding is widely described as the upward movement of moisture towards the surface as a result of the uneven settlement of heavier particles constituent of the mix.

In structures using cement milk such as piles, ground improvement and cement soil mixture, the occurrence of excessive bleeding results to the formation of a weak hardened cement milk layer and cause problems relative to level control.

Although bleeding plays an important role during concrete setting as it replaces evaporated moisture and thus prevents excessively early hardening. Excessive bleeding leads to strength loss by producing laitance at the surface of the concrete. This also leads to wear resistance and poor bonding between the layers of the concrete.

Aside the cement water ratio, cement type and the corresponding size of the fine aggregate also indicates the bleeding rate to a large extent. In the cases of grouting, factors such as pressure and height also affect the rate and percentage of bleeding.

Although Addition of supplementary binding materials, use of finer cements including the introduction of an air entraining admixture can be effective in controlling bleeding rate however, care must be taken to ensure that the rate of chemical composition of the mix does not end up increasing the bleeding rate.

In this study, we experimentally verified the possibility of controlling bleeding by adding baking soda to cement milk. The purpose is to examine the behavior of baking soda as a catalyst to promote the hydration reaction of cement.

The effect of the additive on bleeding rate of cement milk including the electrical resistivity was also monitored relatively to the compressive strength.

A method of estimating the 28-day compressive strength of cement milk from the initial electrical resistivity and the compressive strength, using a strength prediction based on the electrical resistance

of the cement milk was proposed.

In this way, we aim to realize a construction management method which is easy to operate with higher precision and quality assurance.

## MATERIALS

Materials used for this study includes cement, water and baking soda. In the experiment, sodium bicarbonate was mixed with cement milk in four different ratios. The bicarbonate and cement ratio (B / C) was at 1%, 2%, 3% and 4%. These were mixed with 70% water and marked as the W / C ratio. The detail of each of these samples including the total weight of each specimen is as shown on Table 1.

Table 1 Recipe of the specimens

| Water | Weight (Kg) |        |       | W/C (%) | B/C (%) |
|-------|-------------|--------|-------|---------|---------|
|       | Baking soda | Cement | Total |         |         |
| 14    | 0.2         | 19     | 33.2  | 70      | 1       |
| 14    | 0.4         | 19     | 33.4  | 70      | 2       |
| 13    | 0.6         | 19     | 32.6  | 70      | 3       |
| 13    | 0.8         | 19     | 32.8  | 70      | 4       |

## EXPERIMENTAL EVALUATIONS

### Bleeding Test

In cases where concrete retains excess moisture, cracks could occur. This results to a decrease in strength of the concrete. In this study, the impact and influence of baking soda through the soda cement ratio was noticed.

The bleeding rates were noted at the initial age of 0-24 hours including 15 minutes, 30 minutes, and 1 hour. The bleeding rate was also recorded at day 1, 3, 5, 7, 14, 21 and 28.

Table 2 Bleeding Test Results

|     | B/C | Volume    |      |       | Bleeding |    |
|-----|-----|-----------|------|-------|----------|----|
|     |     | Immediate | 1day | 2days |          |    |
| No1 | 1%  | 585       | 560  | 570   | 4%       | 3% |
| No2 | 2%  | 590       | 571  | 581   | 3%       | 2% |
| No3 | 3%  | 670       | 660  | 660   | 1%       | 1% |
| No4 | 4%  | 660       | 650  | 660   | 2%       | 0% |

Table 2 shows the results of bleeding experiments at each baking soda cement ratio (B / C) within the first 48hours of the experiment. Although there is no much difference in the result recorded from the specimens, the material with more bicarbonate shows the least amount of bleeding.

Baking soda acted as a catalyst and the hydrolysis reaction promotes the continuous hydration of the cement. Alkali silica reaction occurred within the cement milk to form alkali silica gel. This reaction shortened the setting time and bleeding was reduced.

### Electrical Resistivity

In this experiment, instant feedback on the mixing degree of the cement milk was achieved using electrical resistivity.

Electrical resistivity quantifies the extent of resistance of a material to the flow of current. The sensor is made up of electrodes that measures both current and voltage when inserted into a compound. Using the Ohms law, the resistance to current flow can be calculated.

During the mixing process of constituents of ground improvement bodies, or cement slurry in previous experiment, the relationship between the ion concentration of the primary materials relative to the electrical resistivity of the compound was established by comparing the resulting values when the compound is properly mixed and cases where the compound is incompletely stirred [3]. This has further improved the quality assurance during construction management.

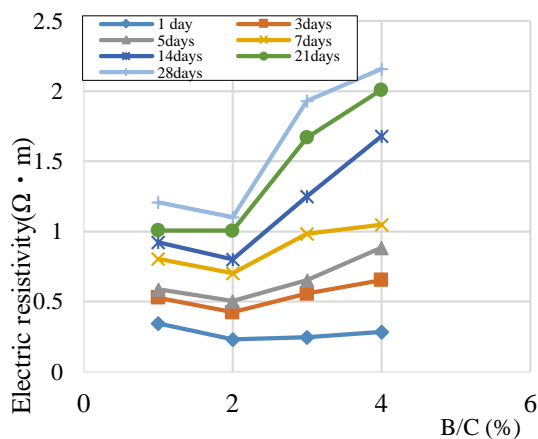


Fig. 1 Relationship between the B/C ratio and the electrical resistivity of the specimens

In this study, the Electrical resistivity of the concrete mix was recorded at day 1, 3, 5, 7, 14, 21 and 28 of curing. Fig. 1 shows the relationship between sodium bicarbonate cement ratio (B/C) and electrical resistivity at each day.

At the age of 1 to 7 days, the specific resistance value increased only moderately regardless of the baking soda cement ratio, but after 14 days, the specific resistance value increased remarkably with

the increase of the baking soda cement ratio as shown in Fig. 2. The values at B/C of 1% and 2% showed similar tendency until the 28th day. But at B/C of

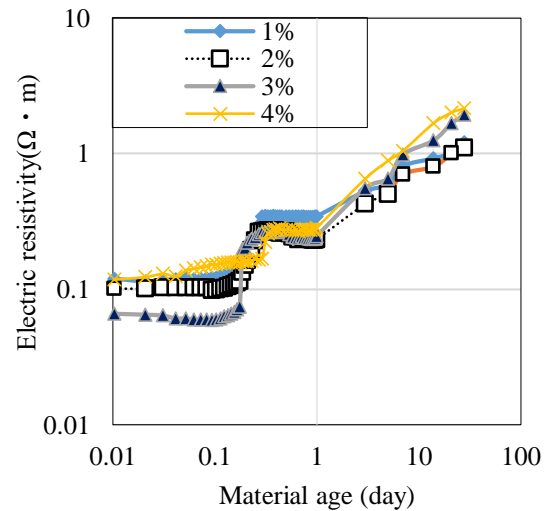


Fig. 2 Relationship between age and the electrical resistivity of the specimens

3% and 4%, there was steady increase in the electrical resistivity values within the first 14 days. However, there was a sharp increase in values afterwards and through the curing age.

### Uniaxial Compressive Test

In this study, the compressive strength test of each experimental sample with different ratio of baking soda was also conducted.

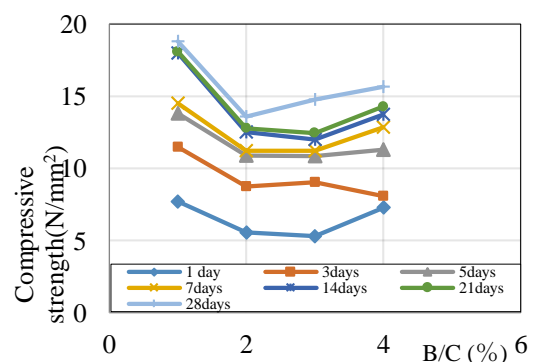


Fig. 3 Relationship between B/C ratio and compressive strength of the specimens

As shown in Fig. 3 the compressive strength of specimens with B/C of 1%, 2%, and 3%, shows only slight difference in increment between the day 5-21 and rises steadily till the 28<sup>th</sup> day. However, there was a huge difference with the 1% B/C specimen. There was a sharp rise in the compressive strength from the first 24 hours to the 7<sup>th</sup> day. A much higher strength

was recorded at the 28<sup>th</sup> day compared to the other specimens.

### Temperature

The corresponding temperature differences of the specimens were monitored during the course of the experiments.

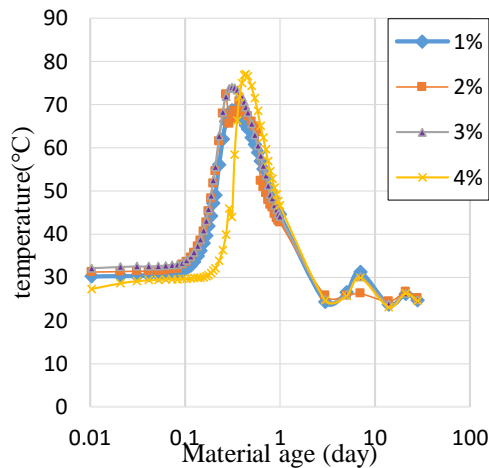


Fig. 4 Relationship age and temperature of the specimens

As shown in Fig. 4, the temperature peaked at about 75 °C after 10 hours and showed the same tendency in all baking soda ratios. However, the specimen with B/C 4% showed a rise in temperature slightly later than the other samples. Generally, the temperature dropped back at a drastic rate within the following 15 hours after attaining the peak temperature.

Also from Fig. 2, it will be observed that each specimen increased in specific resistance with rapid temperature change 5 hours after the start of the experiment. After 7 hours, the specific resistance value gradually increased.

### Relationship between Compressive Strength and Electric Resistivity

As shown in Fig. 5, the compressive strengths of all the specimens increase with increase in electrical resistivity although the response followed different trends. For instance, specimen with B/C of 1% shows a rapid increment in Compressive strength to attain the peak value compare to others.

### EXPERIMENTAL CONSIDERATION AND EVALUATION

Formulas (1) and (2) are used with reference to the evaluation method of prior research [1]. From the

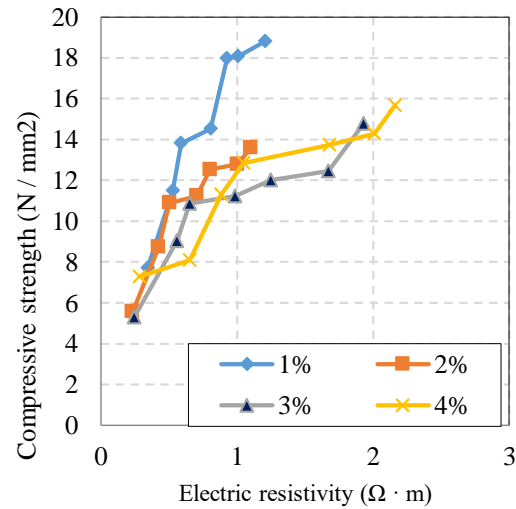


Fig. 5 Relationship compressive strength and electric resistivity

results of these experiments, evaluation equations were proposed by setting the constants **a** and **b** of Eq. (1) and the coefficients K1 and K2 of Eq. (2).

The relationship between material age and electrical resistivity is shown in Fig. 6. Since the material age and the specific resistance value are close to a linear relationship, it can be expressed by the near-form equation of  $Y = aX^b$  (X: material age, Y: specific resistance value) based on material age and specific resistance value.

Since the value of **a** does not have a big difference in B / C, an average value is used this time. Since the value of **b** varies depending on the amount of baking soda blended, an approximate expression was used from the tendency of the inclination

$$\rho(X) = aX^b + \{\rho(1) - \rho(1ave)\} \quad (1)$$

$\rho(X)$  : Electric resistivity of the material at age X day( $\Omega \cdot m$ )

$\rho(1)$  : Measured electrical resistivity of the material at age 1 day ( $\Omega \cdot m$ )

$$\rho(1AVE) = 0.27675[\Omega \cdot m]$$

$\rho(1AVE)$  : the average value of 1 day of the materials as shown in Table 3

$$a = 0.292925 \quad b = 0.3656B^{0.3984}$$

B: Baking soda cement ratio [%]

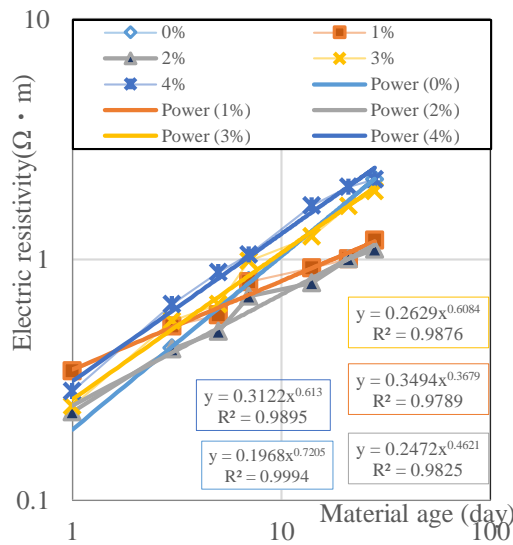


Fig. 6 Evaluation of material age and electrical resistivity

The electrical resistivity at 1 day of material age in Fig. 6 shows a somewhat constant value regardless of B / C. As shown in Fig. 7, in the trends of material ages 1 to 28 days, changes in specific resistance value and compressive strength ratio were almost constant at each B / C. As mentioned above, the evaluation formula was proposed with reference to the following coefficients K1 and K2.

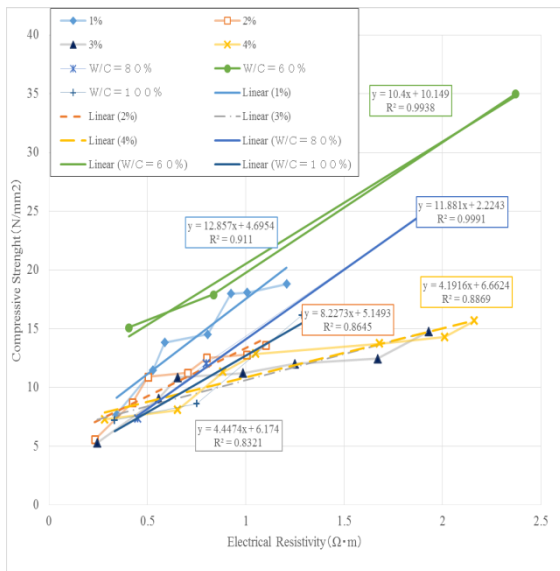


Fig. 7 Evaluation of electrical resistivity and compressive strength

$$qu(28) = K1 \cdot \{ \rho(28) - K2 + qu(1) \} \quad (2)$$

$qu(28)$ : Compression strength of the material at age 28 day (N/mm<sup>2</sup>)

$qu(1)$ : Measured compression strength of the material at age 1 day (N/mm<sup>2</sup>)

$\rho(28)$ : Estimated electrical resistivity of the material at 28 days of age (Ω·m)

$$K1 = 13.278B^{(-0.868)} \{ N / mm^2 \cdot (\Omega \cdot m) \} \quad (3)$$

K2:  $\rho(1)$

※This time, using the measured electrical resistivity (Ω·m) of 1 day of material age

Table 3 Electric resistivity and average value for 1-day material

|     | 1%   | 2%   | 3%   | 4%   | Average value |
|-----|------|------|------|------|---------------|
| 1da | 0.34 | 0.23 | 0.24 | 0.28 | 0.2767        |
| y   | 4    | 3    | 6    | 4    | 5             |

## SUMMARY AND CONCLUSION

As shown in Fig. 7 and Fig 8, the electrical resistivity of the specimens within the material age of 28days which was measured and recorded during the course of the experiment was verified according to Eq. (1) and was compared with the estimated value of the compressive strength according to Eq. (2). It was deduced that both are highly similar.

Table 4 Validity of evaluation formula

|    | Experimental value (N/mm <sup>2</sup> ) | Evaluation formula (N/mm <sup>2</sup> ) |
|----|---|---|
| 1% | 18.811                                  | 18.075                                  |
| 2% | 13.593                                  | 13.846                                  |
| 3% | 14.771                                  | 13.624                                  |
| 4% | 15.668                                  | 15.889                                  |

Also, the electrical resistivity at 1 day of the specimens was derived using Eq. (1) and used with the measured compression at 1 day of material age in Eq. (2). The strengths were used to correctly estimate the 28-day compressive strength of cement milk mixed with baking soda.



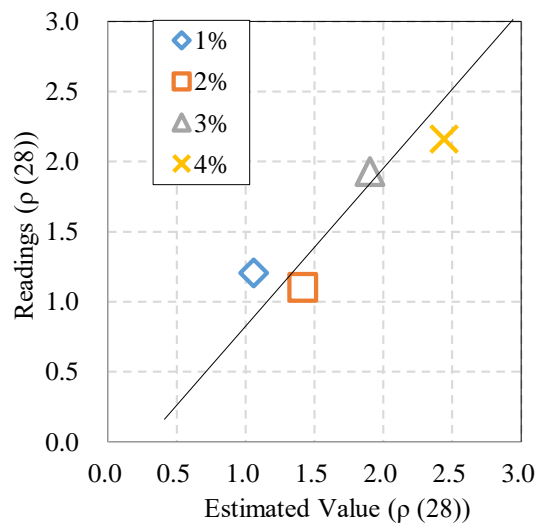


Fig. 8 Relationship between estimated values and measured electrical resistivity values

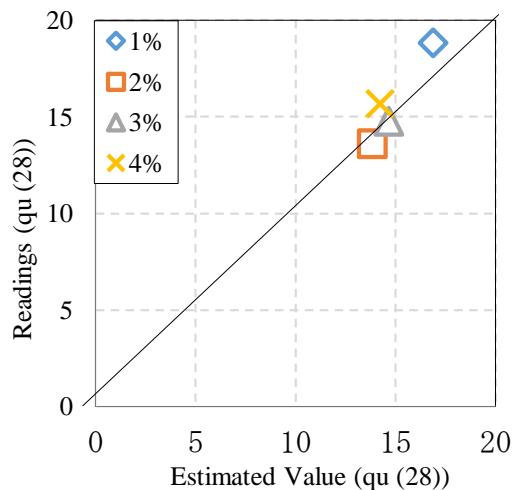


Fig. 9 Relationship between estimated values and measured compressive strength values

It was finally deduced that baking soda can be used as a catalyst in controlling the bleeding rate of cement milk or a cement soil mixture. Through an alkali silica reaction within the cement milk to form alkali silica gel, backing soda can shorten setting time and reduce bleeding rate while fostering the continuous hydration of the cement milk.

In addition, it has been verified that this method can be used to estimate the 28-day compressive strength of cement milk from the initial electrical resistivity and the compressive strength. This is achieved using strength prediction based on the electrical specific resistance of the cement milk. This method can also be used as a tool in preempting likely behavior of the resulting material from the cement milk mixture towards fostering quality assurance in construction management.

## REFERENCES

- [1] Mochida Y., M. Matsuura, Study on Strength Estimation of Soil Cement Used In the Embedded Pile Method by Electrical Resistivity Measurement. International Journal of GEOMATE, 17/59, 74-81, 2018/7
- [2] Mochida Y., Fujii M., Study on the control of construction quality of the fixed solution around the pile of embedded pile using electrical resistivity survey Part 1) Estimation of compressive strength by electrical resistivity of cement milk. Meeting of the Architectural Institute of Japan Abstracts of Academic Lectures, 845-846, 2016/8
- [3] Mochida Y., Indra H. Promotion of ICT utilization by electric resistivity management in fluidization treatment process for ground improvement. International Journal of GEOMATE (2016)
- [4] Mochida Y., Tsukamoto M., Development of fluidization ground improvement method using cement-based solidifying material and local soil (Part 1, Construction and management method), Technical Report of the Architectural Institute of Japan, 19/42, 485-490, 2013/06
- [5] Aly A., Nabil M., Mohamed H., Takeshi K Stabilisation of soft soil with recycled plaster admixtures. Ice proceedings, Volume 171 (2018) Issue G11, Page 12-20 <https://www.icevirtuallibrary.com/doi/10.1680/jgrim.16.00038>
- [6] Cement Deep Mixing Association. Corporate Journal on Cement Deep Mixing, 2015. [www.cdm-gr.com](http://www.cdm-gr.com)

## **SHEAR STRENGTH AND PERMEABILITY ANALYSIS OF GEOTEXTILE FROM PINEAPPLE LEAVES AND LUFFA**

INZ Baharuddin<sup>1</sup>, Hairin Taha<sup>2</sup>, RC Omar<sup>3</sup>, R.Roslan<sup>4</sup> and S.Nadirah<sup>5</sup>

<sup>1,2,3,4</sup> Institute of Energy Infrastructure,

<sup>5</sup> College of Engineering, Universiti Tenaga Nasional, Malaysia.

### **ABSTRACT**

Geotextiles are commonly utilized in many geotechnical and civil engineering applications for soil reinforcement, erosion control, drainage, filtration and separation. The market trend for geotextiles nowadays dominates more on synthetic materials such as polyethylene and polyamide. However, synthetic geotextiles can be costly when the application involves major construction and larger area. In term of environmental concern, geosynthetic materials may contain chemical additives that could leak into the surroundings. Geotextile products from natural fiber such as jute and coir are commonly available especially in India but the market for natural geotextiles is very competitive against polymeric geotextiles. In view of that, this study was aimed to design natural geotextile from local plants. Pineapple leaves were used as the main fibre for the fabrication of geotextile together with luffa and coconut flakes. Four types of designs were developed based on the seam type and number of rows of stitching. The strength and permeability of the geotextiles were tested using direct shear box test and falling head method. Results showed that the geotextile design with J seam and two rows of stitches has the higher strength and lower permeability. This study demonstrated the beneficial use of agricultural waste from pineapple leaves that can be recycled into sustainable product.

*Keywords: geotextile; pineapple leaves; luffa; shear strength; permeability*

### **INTRODUCTION**

Geotextile is mainly used for soil reservation especially in soil reinforcement, erosion control and reducing surface run-off. Other applications of geotextile include separation and filtration between different type of materials, drainage and containment [1]. Geotextile can be defined as permeable textile used together with soil, rock, earth, foundation or geo-engineering materials. Some of the typical materials used to produce geotextile include polypropylene, polyethylene, polyamides or polyester [2].

There are two categories of geotextile; woven and non-woven. The woven geotextiles are manufactured on a loom through the process of weaving or knitting textiles which has two sets of parallel threads [3]. This type of geotextile has excellent tensile strength. Most geosynthetics are woven type. The non-woven geotextiles are made from the process of mechanical or chemical interlocking or thermal bonding of non-woven fabric. The materials are pressed together using adhesive or heat treatment. However, this type has lower tensile strength compared to that of the woven type.

Several factors need to be considered when designing geotextile such as the type of geotextile, seam and stitch type, thread type, numbers of rows of stitching and sewing equipment [4]. The strength of geotextile was mainly influenced by the seam strength and this can be tested using cross machine

direction based on ASTM D4595 "Standard Test Method for Tensile Properties of Geotextiles by the wide width strip method". Another test based on ASTM D4884 can also be done to test the seam strength [5].

In general, there are two types of seam commonly used to produce geotextile, the superimposed seam (S seam) or prayer seam, and J seam. The S seam is made by stitching two fabrics together with one or more row of stitching. This is the easiest type of seam. The J seam is more difficult to make. It is done by superimposing two fabrics and folded to produce a thickness of four plies which contributes to higher seam strength [6]. This type of seam has more strength compared to other type of seam. For fabric geotextile, the seam is sewn 1 to 1.5 inches from the edge and folded to create a double plies thickness. The thread type also affects the strength of the geotextile. It should have similar or higher durability. Numbers of rows of stitching serve as the seam type colleague.

Geotextile should have higher mechanical strength due to the applied load of soil which is directly transferred to it. The occurrence of soil erosion and landslide is mostly caused by the weakening soil that has losses its strength [7]. Several factors that affect soil failure include rainfall, erosion, construction activities and external loading. Soil cannot resist tension but can withstand compression. The shear strength of soil will decrease when there is excessive water content in the soil.

When the water overflow, the soil structure will become loose and this results in soil erosion or landslide. Natural geotextile from plant fiber can help reinforce and fertilize the soil at the same time, unlike geosynthetics [8-9].

In this study, pineapple leaves waste and luffas were used to produce the natural geotextiles for soil reinforcement [10]. The concept was to utilize plant fibers which are acquired from local resources such as the local farms and markets. Malaysia produces more than one million tonnes of agricultural waste annually [11]. Instead of burning the agro waste that highly contribute to greenhouse gas emission, the agro waste could be recycled into sustainable products or converted into biomass as renewable energy.

Pineapple (*Ananas comosus* L.Merr) or known locally as 'Nenas' is a tropical plant native to South East Asia and planted as commodity crop in Malaysia. Pineapple industry contributes significantly to the country's economy and the fiber from the leaves can be developed into commercial products [12]. Pineapple leaf is rich in cellulose and biodegradable. A study on pineapple leaf fiber showed that they are suitable for building and construction materials due to its highest cellulosic content [13-14]. The fibers of pineapple leaves also have the potential as alternative raw materials in paper industries due to its good mechanical properties and high cellulose contents [15]. In recent development, pineapple leaves were also found to be suitable alternative natural acoustic material for sound absorption due to the characteristics of its fiber [16].

*Luffa acutangula* is extensively used throughout the world as materials for hybrid biodegradable geopolymer composites and sound absorbing [17-18]. Luffa fiber has high cellulose content, low cost, biodegradable and absorbs water easily. It has a thick texture that prevents the water to pass through easily [19]. For this research, pineapple leaves waste were obtained from a pineapple plantation in Johor, Malaysia and Luffa fibers were obtained from Sarawak, Malaysia.

The objective of this research was to design natural geotextile from local plant fibers, and evaluate the strength of the geotextile through permeability and direct shear box test. The chosen design based on seam type and number of rows of stitching will be used to develop the natural geotextiles and tested on site to observe the effectiveness of the geotextiles against erosion.

## 2. EXPERIMENTAL

### 2.1 Design of Natural Geotextile

The natural geotextile was designed from natural fibre consist of pineapple leaves and luffa (Fig. 1).

Four samples of geotextile designs arranged in three layers were developed based on seam type and rows of stitching (Fig.2). First, the pineapple leaves and luffa were dried outside for 72 hours until the leaves and the luffa turned brown in color and completely dried. This is important to ensure that there was no water contained in the leaves. When the fiber is fully dried, the mechanical strength of the fiber will also increase. Dried coconut flakes were then added as moisture absorber. Jute thread (5.0 mm thick) was used to stitch the geotextiles. Table 1 shows the types of geotextile design according to seam type and number of rows of stitching which will be tested.

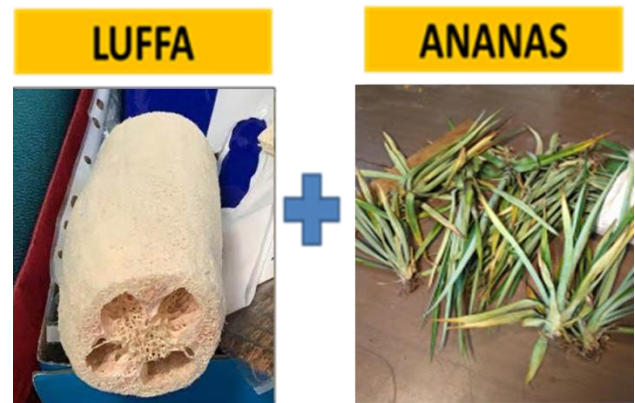


Fig.1 Natural geotextile from luffa and pineapple leaves



Fig. 2 Three layers of geotextile

Table 1. Designs of geotextile

| Samples | Seam Type | Number of rows of stitching |
|---------|-----------|-----------------------------|
|---------|-----------|-----------------------------|

|   |   |   |
|---|---|---|
| A | J | 2 |
| B | J | 1 |
| C | S | 2 |
| D | S | 1 |

## 2.2 Direct shear box test

Laboratory testing was carried out to determine the most appropriate design of geotextile for soil reinforcement. The strength of the geotextile sample was tested using direct shear box test following ASTM D5321 guidelines. The test equipment consists of a metal box (100 mm x 100 mm) in which the soil specimen and the geotextile will be placed. The geotextile sample was placed on the top and below the soil specimen. The strength between the original soil and soil together with geotextile sample was compared. The direct shear box test was done using different weights (5.0, 10.0 and 15.0 kg). The type of soil used was sandy SILT with intermediate plasticity.

## 2.3 Permeability test

The permeability of the geotextile was determined through permeability test of falling head method (ASTM D4491) as described in previous study [16]. The test consists of flow of water passing through soil sample connected to a standpipe that provides the water head and measures the volume of passing water through the sample. The standpipe diameter is governed by the permeability of the tested soil specimen. Water was allowed to flow through the sample until it reached the lower limit and the time was recorded when the water in the standpipe dropped from the upper to the lower level.

## 2.4 Experimental application

The geotextile was tested at the selected area. The soil at the experimental site was classified as sandy SILT with intermediate plasticity. The geotextile (20 cm x 20 cm) was arranged on the eroded surface inside a grid measured 600 mm x 800 mm. Prior to that, the subsurface was cleared first to remove foreign objects. The geotextiles was properly arranged on the surface. The sites with geotextiles were observed for 35 days to monitor the progress.

## 3. RESULTS AND DISCUSSION

### 3.1 Shear Box Test

The shear strength of the geotextile was influenced by the seam type and the number of row of stitching. The results of shear stress at failure against normal stress for Samples A, B, C and D are shown in Table 2. Observation showed that the value of cohesion has decreased, while the friction angles had similar values but for Sample A, the cohesion value was 0.00043 and the value for friction angle was 36.9°. This showed that Sample A has the higher shear strength compared to that of other samples.

Table 2. Cohesion and friction angle values

| Sample | Cohesion | Friction angle |
|--------|----------|----------------|
| A      | 0.0043   | 36.9           |
| B      | 0.0025   | 29.5           |
| C      | 0.0022   | 28.6           |
| D      | 0.002    | 28.4           |

The results of the direct shear box test showed sample A has higher strength compared to other samples, which were 25.83 N/m<sup>2</sup>, 47.5 N/m<sup>2</sup> and 69.44 N/m<sup>2</sup> for 5.0, 10.0 and 15.0 kg weight respectively (See Figure 3-5). The shear strength has decreased from sample A to D. The shear strength of the geotextile was influenced by the number of rows of stitching for sample A and C because the stitches were stronger to hold the fabric together from shearing.

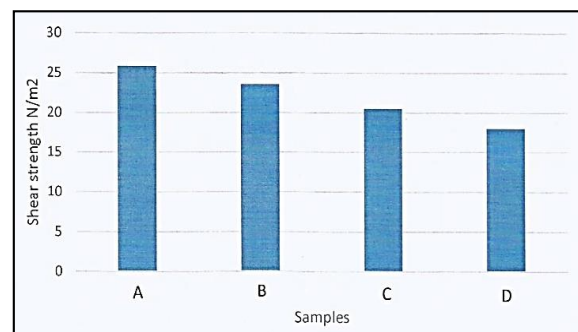


Fig. 3 Shear strength using 5.0 kg weight

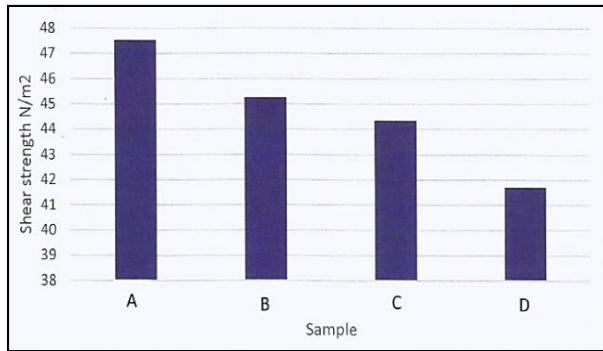


Fig. 4: Shear strength using 10.0 kg weight

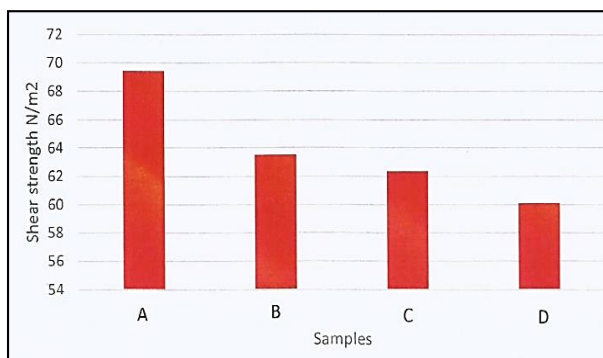


Fig. 5 Shear strength using 15.0 kg weight

### 3.2 Permeability Test

The results of permeability test showed that Sample A has low permeability due to the J seam type design. Sample A has four plies with two rows of stitching compared to S seam type which only has two plies. The test demonstrated that the soil specimen with geotextile was more impermeable. The value of coefficient of permeability,  $k$ , has increased when the geotextile samples were applied (Table 3). This showed that the presence of geotextile has decreased the permeability of the soil specimen. The flow of water through the geotextile took longer time to pass through compared to that of original soil.

Table 3. Percentage of permeability increment

| Sample        | Seam type | Coefficient of permeability (k) | Increment (%) |
|---------------|-----------|---------------------------------|---------------|
| Original soil |           | $7.2 \times 10^{-4}$            | -             |
| A             | J         | $2.16 \times 10^{-7}$           | 98.98         |
| B             | J         | $2.26 \times 10^{-7}$           | 99.87         |
| C             | S         | $2.33 \times 10^{-7}$           | 99.85         |
| D             | S         | $2.36 \times 10^{-7}$           | 99.8          |

### 3.3 Geotextile Application

The results of permeability and shear box test showed that the design of Sample A geotextile based on J seam and two rows of stitching has higher strength compared to other designs. Based on these criteria, the natural geotextile was assembled for experimental site test against soil erosion. The geotextiles were arranged on the eroded surface and observed for 35 days. The observation was documented on day 7, 14, 28 and 35 as shown in Figure 6-9. After 35 days of geotextile application, new batch of grass has grown through the natural geotextile, and the geotextile has integrated with the soil. The eroded surface has been covered with vegetation. This study has demonstrated that the geotextile from pineapple and luffa has performed as protective cover for the exposed area.



Fig. 6: Geotextile application on Day 7





Fig 7: Geotextile application on Day 14



Fig. 8: Geotextile application on Day 28



Fig 9: Geotextile application on Day 35

#### 4. CONCLUSION

In this work, natural geotextile was designed and developed using pineapple leaves waste and luffa for soil reinforcement. The geotextile was tested based on the strength and permeability using shear box test and falling head method. From the results, it was demonstrated that the geotextile design with J seam and two rows of stitching had the higher shear strength to encounter the application of

friction force. The fiber from pineapple and luffa also has lower permeability, thus, suitable for soil reinforcement.

This study demonstrated the capability of pineapple leaves and luffa as renewable resource for natural geotextile. Thus, this innovative method is cost-effective and can be developed as commercial product that would contribute to the economy. On top of that, natural geotextile from pineapple leaves and luffa can provide green solution for sustainable soil reinforcement and slope stabilization. The design of geotextile from pineapple leaves and luffa can encourage the recycling and processing of agricultural materials into sustainable products. Hence, the newly developed natural geotextile from pineapple leaves and luffa can be used to control soil erosion.

#### ACKNOWLEDGMENTS

This study was supported by UNITEN grants J510050884 (UNIIG 2018) and 201901001YCU/02.

#### REFERENCES

- [1] Zornberg, JG (2017), Functions and applications of geosynthetics in roadways. *Procedia engineering*, 189, pp.298-306.
- [2] Stepanovic, JM, Trajkovic D, Stojiljkovic D & Djordjic D, (2016), Predicting the behavior of nonwoven geotextile materials made of polyester and polypropylene fibers. *Textile Research Journal*, 86(13), pp.1385-1397.
- [3] Mishra SR, Mohapatra SR, Sudarsanan N, Rajagopal K & Robinson RG (2017), A simple image-based deformation measurement technique in tensile testing of geotextiles. *Geosynthetics International*, 24(3), pp.306-320.
- [4] Mudgal A, Sarkar R & Shrivastava AK (2018), Influence of geotextiles in enhancing the shear strength of Yamuna sand. *International Journal of Applied Engineering Research*, 13(12), pp.10733-10740.
- [5] Allen JM, Ferreira JA and Athanassopoulos C (2017), Laboratory study of geosynthetic clay liner panel shrinkage forces and seam strength. *Geotechnical Frontiers*, pp. 11-21.
- [6] Guo W, Chu J & Zhou B (2015), Method to increase seam efficiency for woven geotextile materials. *Geosynthetics International*, 22(6), pp.404-410. Annnn B., Unpublished Work but Accepted, Vol., Issue, Year.
- [7] Haeri SM, Noorzad R & Oskoorouchi AM (2000), Effect of geotextile reinforcement on

- the mechanical behavior of sand. *Geotextiles and Geomembranes*, 18(6), pp.385-402.
- [8] Kalibová, J, Jačka, L, & Petrů, J. (2016). The effectiveness of jute and coir blankets for erosion control in different field and laboratory conditions. *Solid Earth*, 7(2), pp. 469-479.
- [9] Müller, W. W., & Saathoff, F. (2015). Geosynthetics in geoenvironmental engineering. *Science and technology of advanced materials*, 16(3), pp. 034605.
- [10] Omar RC, H. Taha, R.Roslan & Baharuddin INZ (2019). GEOTEXTILE FROM PINEAPPLE LEAVES AND BIO-GROUT FOR SLOPE STABILIZATION AND EROSION CONTROL. *International Journal*, 17(60), 219-224.
- [11] Saili, R., Muhamad, Z., & Aziz, N. H. (2017). A Preliminary Study on Sustainable Management of Pineapple Waste: Perspective of Smallholders. *International Journal of Academic Research in Business and Social Sciences*, 7(6), pp. 2222-6990.
- [12] Yusof, Y., Yahya, S. A., & Adam, A. (2015). Novel technology for sustainable pineapple leaf fibers productions. *Procedia CIRP*, 26, pp.756-760.
- [13] Laborel-Préneron A, Aubert JE, Magniont C, Tribout C & Bertron A (2016), Plant aggregates and fibers in earth construction materials: A review. *Construction and building materials*, 111, pp.719-734.
- [14] Asim M, Abdan K, Jawaid M, Nasir M, Dashtizadeh Z, Ishak MR & Hoque ME (2015), A review on pineapple leaves fibre and its composites. *International Journal of Polymer Science*.
- [15] Laftah WA & Wan Abdul Rahman, WA (2016), Pulping process and the potential of using non-wood pineapple leaves fiber for pulp and paper production: A review. *Journal of Natural Fibers*, 13(1), pp.85-102.
- [16] Putra, A., Or, K. H., Selamat, M. Z., Nor, M. J. M., Hassan, M. H., & Prasetyo, I. (2018). Sound absorption of extracted pineapple-leaf fibres. *Applied Acoustics*, 136, pp. 9-15.
- [17] Koruk H & Genç G (2015), Investigation of the acoustic properties of bio luffa fiber and composite materials. *Materials Letters*, 157, pp.166-168.
- [18] Alshaaer M, Mallouh SA, Al-Faiyz Y, Fahmy T, Kallel A & Rocha F (2017), Fabrication, microstructural and mechanical characterization of Luffa Cylindrical Fibre-Reinforced geopolymer composite. *Applied Clay Science*, 143, pp. 125-133.
- [19] Chen Y, Su N, Zhang K, Zhu S, Zhu Z, Qin W, Yang Y, Shi Y, Fan S, Wang Z (2018), Effect of fiber surface treatment on structure, moisture absorption and mechanical properties of luffa sponge fiber bundles. *Industrial crops and products*, 123, pp. 341-352.



## APPLICATION OF WASTE WATER AND GREEN ALGAE TO STRENGTHEN SOIL

R.Roslan<sup>1</sup>, RC Omar<sup>2</sup>, INZ Baharuddin<sup>3</sup>, Hairin Taha<sup>4</sup> and M.Syafiq<sup>5</sup>

<sup>1,2,3,4</sup> Institute of Energy Infrastructure, Universiti Tenaga Nasional, Malaysia.

<sup>5</sup> College of Engineering, Universiti Tenaga Nasional, Malaysia.

### ABSTRACT

The engineering technology has evolved with the combination of microbiological and geotechnical engineering knowledge. In the past years, ecological approach has been applied to improve the strength of liquefiable soil for ground improvement. Traditional methods include chemical and cement grouting require heavy machinery, and are often costly and not environmental friendly. The potential of biological approach have been investigated by many researchers. One study showed that the green alga has the potential to clog soil particles by creating impermeable layer on soil surface. It was also observed that the accumulation of bacterial biomass and insoluble bacterial slime or known as extrapolsaccharides make the soil more impermeable to water. This study was aimed to analyze the effect of waste water and algae in improving the soil permeability and shear strength. The permeability of the soil was evaluated before and after the treatment with waste water and algae. The results showed that the coefficient of permeability of the treated soil has reduced by 26% and the shear stress increased by 29.5%. Observation using Scanning Electron Microscope showed that the void spaces of the soil particles were filled up and bonded together. This concludes that algae and waste water has the capacity to improve the mechanical properties of soil.

*Keywords: Waste water; Green algae; Bio-grout; Liquefied soil; Ground improvement*

### INTRODUCTION

The civil engineering field has progressively advanced with the introduction and integration of biotechnology into geotechnical engineering applications which utilize microorganisms to strengthen, stabilize and reinforce engineering properties of soils [1]. The applications of bio-mediated method to improve the mechanical properties of liquefied soil have been demonstrated in many studies such as improving the shear strength and reduce the permeability of soils [2-4]. The bio-mediated soil improvement technology has successfully improved the geotechnical properties of granular soils through calcite precipitation on soil particles [5]. Chemical or cement grouting techniques are often costly and environmentally unfriendly which require heavy machinery and disturb urban infrastructure. Moreover, chemical grouts can pollute the environment with its toxic effect. Though these methods work very effectively to strengthen the soil and reduce its permeability, they may hinder groundwater flow and limits the injection distance which is not feasible for large-scale treatment [6].

Accumulation of bacterial biomass, insoluble bacterial slime, and poorly soluble biogenic gas bubbles in soil will make the soil more impermeable for water. Production of bacterial exopolymers in situ can be used to modify soil properties by

clogging the soil and reducing porosity and permeability [7-8]. The accumulation of bacterial biomass and insoluble bacterial slime will make the soil more impermeable for water. This has been adopted for enhancing oil recovery or soil bioremediation. The groups of microorganisms that produce insoluble extracellular polysaccharides to bind the soil particles and fill in the soil pores are oligotrophic bacteria from genus *Caulobacter*, aerobic Gram-negative bacteria from genera *Acinetobacter*, *Agrobacterium*, *Alcaligenes*, *Arcobacter*, *Cytophaga*, *Flavobacterium*, *Pseudomonas*, and *Rhizobium* [9]. Apart of that, Exopolysaccharide-producing bacteria may be used to modify the soil matrix in situ. After growth of these bacteria in soil, its permeability for water will be greatly reduced [10]. Nitrifying bacteria that produce exopolysaccharides can also be used in soil bioclogging technique. These bacteria are commonly found in soil and waste water [11]. It was found that microalgae was capable in precipitating calcite through photosynthesis process that can be used as bio-cement to bind soil particles together [12]. Microbial exopolymers have strong potential to replace cement as sustainable soil treatment material [13].

In this study, laboratory scale experiment was conducted to investigate the effect of waste water and algae in improving the strength and texture of the soil. The shear strength and permeability of the

untreated and treated soil were analyzed using The Falling Head Method and Triaxial Test. The micro images of the soils were observed by Scanning Electron Microscope (SEM).

## EXPERIMENTAL

The soil samples were collected from a landslide area outside the university's campus where the slope has failed due to water saturation. The soil characteristics of the original soil sample collected from the experimental site were analyzed in the laboratory based on Wet Sieve and Dry Sieve analysis, Liquid Limit test, Plastic Limit test, Coefficient of Permeability test and Triaxial with Unconsolidated Undrained test (Fig. 1). For the bio-mediated treatment, waste water was obtained from the drainage system on the campus and green algae were acquired from the local aquatic supplier. In this experiment, the soil samples were divided into 2 containers (7.0 kg each), one treated with algae and waste water (treated) and the other container as a control (untreated). In the first container, the soil was mixed with 2 L of waste water and algae (3.0 kg) were added on top of the soil (Fig. 2). These containers were then left at room temperature for 54 days. Occasionally, waste water was sprinkled on the soil to maintain the moisture content.



Fig. 1 Original soil



Fig. 2 Treated soil with waste water and algae

## Falling head test

The Falling Head method was applied to determine the Coefficient of Permeability of the soil. Permeability of soil is defined as the ability of water to flow through soil. As the water permeability increases, the water seepage also increases. The permeability test was conducted to analyze the effects of algae as impermeable layer on the soil surface against the rate of water seepage.

## Triaxial test-CU

The triaxial test was carried out to determine shear strength of undisturbed or remolded soil sample in the triaxial compression apparatus by consolidation undrained test without the pore measurement. This test was conducted on untreated and treated soil samples. Comparison was made to study the effects of waste water and algae applied on soil towards the shear stress. Each sample was tested 3 times with pressures of 100kPa, 200kPa and 400kPa. Reading was taken at every 3mm of deformation interval until soil failure occurred. After that, Mohr Coulombs was plotted from the results to calculate and compare the shear stress and factor of safety of the soil.

## Scanning Electron Microscope (SEM)

The morphology and structure of the inner surface of the soil samples were observed by Scanning Electron Microscope (SEM).

## RESULTS AND DISCUSSION

### Soil Characteristic

The wet sieve and dry sieve analyses showed that the original soil consists of 1.745 % of Gravel, 7.018 % of sand, 88.596 % of Silt and Clay. From the graph of Percentage passing versus Sieve Size plotted, the coefficient of uniformity,  $C_u$ , and coefficient of gradation,  $C_z$ , were equal to 2.87 and 0.620, respectively. The result of Atterberg limit test showed that the liquid limit was 47.5% whereby the plastic test equaled to 28%. Under the Plasticity Chart, the soil sample was categorized under the group of OL or ML known as Organic soil of low plasticity or Silt of Low plasticity which have  $WL < 50$ . From the tests, it can be concluded that the soil was classified as Silty Sand.

### Falling Head Test

Table 1 shows the results of Falling Head test carried out on the original sample (untreated). The

tests were conducted thrice to obtain more accurate results at 400mm of water elevation difference ( $h_1-h_2$ ). For the first determination,  $k$  equals to 0.0022mm/s, while for the second and the third determination,  $k$  are 0.0022mm/s and 0.0025mm/s. Thus, the average coefficient of permeability,  $k$  equals to  $2.3 \times 10^{-3}$  mm/s.

Table 1 Falling head test results of untreated sample

| Determination No.      | 1      | 2      | 3      |
|------------------------|--------|--------|--------|
| Time interval, t (sec) | 210    | 210    | 185    |
| $h_1$ , (mm)           | 1000   | 1000   | 1000   |
| $h_2$ , (mm)           | 600    | 600    | 600    |
| $k = 2.3026 aL$        | 0.0022 | 0.0022 | 0.0025 |
| $\log_{10} h_1$        |        |        |        |

Table 2 shows the results of Falling Head test of treated soil with waste water and algae after 54 days. The tests were conducted 3 times to obtain more accurate results at 400mm of water elevation difference ( $h_1-h_2$ ). For the first determination,  $k$  equals to 0.0015mm/s, while for the second and the third determination,  $k$  are 0.0015 mm/s and 0.0014mm/s. Thus, the average coefficient of permeability,  $k$  equals to  $1.47 \times 10^{-3}$  mm/s.

Table 2. Falling head test results of treated sample

| Determination No.    | 1      | 2      | 3      |
|----------------------|--------|--------|--------|
| Time interval, (sec) | 310    | 308    | 320    |
| $h_1$ , (mm)         | 1000   | 1000   | 1000   |
| $h_2$ , (mm)         | 600    | 600    | 600    |
| $k = 2.3026 aL$      | 0.0015 | 0.0015 | 0.0014 |
| $\log_{10} h_1$      |        |        |        |

The results showed that the coefficient of permeability decreased by 36% which is 10% of reduction. From the original sample, time taken for the water to seep into the soil in 400mm of water elevation difference is 200 seconds in average. The time taken for water to seep into the soil in 400mm of water elevation difference is 313 seconds in average. This shows that the extracellular polysaccharides (bacterial slime) produced by the microorganisms have attached the soil particles together and filled the soil pores thus greatly reduced the permeability of the soil.

Table 3 displays the summary of results of the 3 Triaxial tests carried out on the untreated sample at different cell pressures. At cell pressure of 100

kN/m<sup>2</sup>, the deviator stress at failure was 51.25 kN/m<sup>2</sup> and by calculations, the major principle stress,  $\sigma_1$  was 151.25 kN/m<sup>2</sup>. At cell pressure of 200 kN/m<sup>2</sup> and 400 kN/m<sup>2</sup>, the soil failed at 104.9 kN/m<sup>2</sup> and 120.8 kN/m<sup>2</sup> where the major principal stresses were 304.9 kN/m<sup>2</sup> and 520.8 respectively.

Graph of deviator stress against axial strain for the 3 samples were plotted and illustrated in Figure 3. Based on the graph, the soil compressed with 400 kPa of cell pressure having the highest deviator stress at failure. The soil had the lowest deviator stress at failure when tested with 100 kPa of cell pressure.

Table 3. Summary of results for original soil

| No. | Cell pressure (kN/m <sup>2</sup> ) | Deviator stress (kN/m <sup>2</sup> ) | Major principal stress (kN/m <sup>2</sup> ) |
|-----|------------------------------------|--------------------------------------|---|
| 1   | 100                                | 51.25                                | 151.25                                      |
| 2   | 200                                | 104.9                                | 304.9                                       |
| 3   | 400                                | 120.8                                | 520.8                                       |

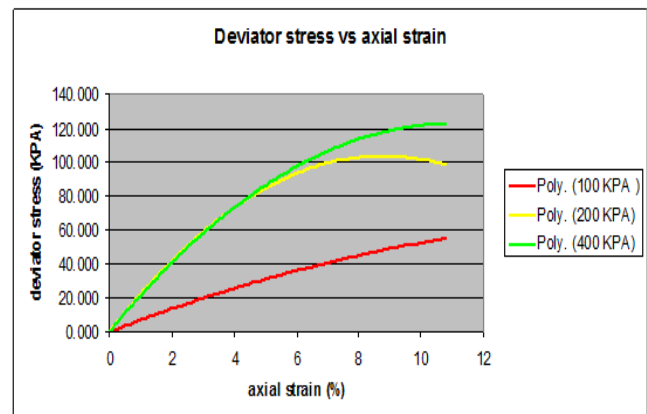


Fig. 3 Graph of deviator stress against axial strain (untreated soil)

Table 4 shows the summary of results of the 3 Triaxial tests carried out on the treated sample at different cell pressures. At cell pressure of 100 kN/m<sup>2</sup>, the deviator stress at failure is 88.7 kN/m<sup>2</sup> and by calculations, the major principle stress,  $\sigma_1$  is 188.7 kN/m<sup>2</sup>. At cell pressure of 200 kN/m<sup>2</sup> and 400 kN/m<sup>2</sup>, the soil failed at 166.208 kN/m<sup>2</sup> and 146.283 kN/m<sup>2</sup> whereby the major principal stresses are 366.208 kN/m<sup>2</sup> and 546.283 respectively. Graph of deviator stress against axial strain for the 3 samples were plotted and shows in Figure 4. Based on the graph, the soil compressed with 200 kPa of cell pressure having the highest deviator stress at failure.

Table 4. Summary of results for treated soil

| No. | Cell pressure (KN/m <sup>2</sup> ) | Deviator stress (KN/m <sup>2</sup> ) | Major principal stress (KN/m <sup>2</sup> ) |
|-----|------------------------------------|--------------------------------------|---|
| 1   | 100                                | 88.7                                 | 188.7                                       |
| 2   | 200                                | 166.208                              | 366.208                                     |
| 3   | 400                                | 146.283                              | 546.283                                     |

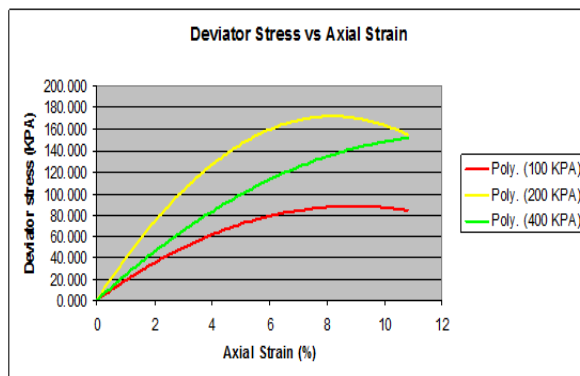


Fig. 4 Graph of deviator stress against axial strain (treated soil)

Figure 5 and 6 show the Mohr circle of the original soil and treated soil respectively. The Mohr Circle was developed from the deviator stress results to calculate the shear strength of both of the soil. From the plotted Mohr Circles, the shear strength parameters were referred to as the cohesion intercept and the angle of shearing resistance. The Cohesion of the soil is equal to 0 whereby the angle of resistance is 17°. By calculation, the shear strength of the original soil was 43 kN/m<sup>2</sup>. Moreover, the shear strength of the soil treated with waste water and algae was equaled to 61 kN/m<sup>2</sup>. This shows an increase in the shear stress of the treated soil by 29.5%.

The shear strength of the treated soil has increased due to the existence of slimy liquid produced by the bacteria from the waste water which filled up the soil pores. Therefore, it has reduced the soil permeability as well as increased the shear strength of the soil. However, the shear strength was not greatly improved due to the short time duration of the experiment.

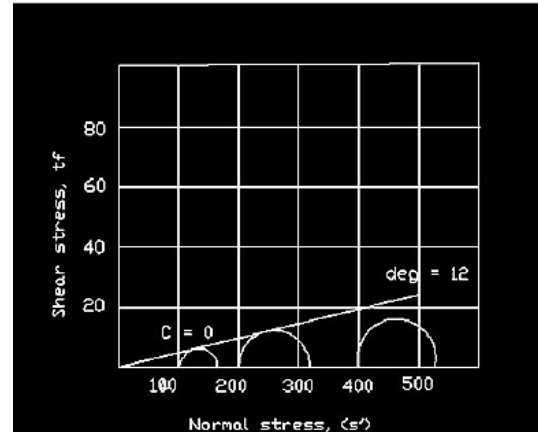


Fig. 5 Stress condition at failure of untreated soil

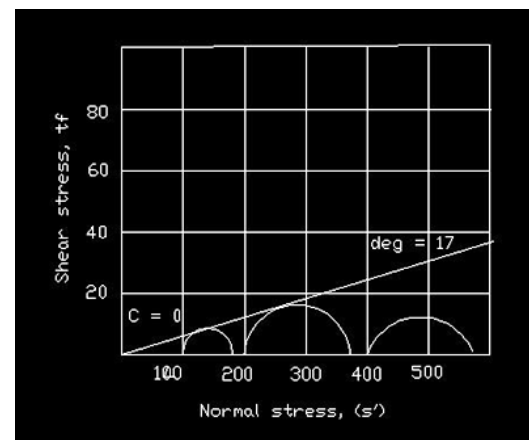


Fig. 6 Stress condition at failure of treated soil

### Scanning Electron Microscope (SEM)

Figure 7 shows the microscope image of the original soil sample before it was treated with waste water and algae. From the analysis, it was observed that the soil contains two types of minerals typically found in clay which are Kaolinite,  $2\text{Al}_2\text{Si}_2\text{O}_5(\text{OH})_4$  and Hallosite,  $2\text{Al}_2\text{Si}_2\text{O}_5(\text{OH})_4 \cdot 4\text{H}_2\text{O}$ . The Hallosite is a mineral that has cylindrical shape and same chemical formula with Kaolinite but it contains  $\text{H}_2\text{O}$ . Hallosite is normally has length about 1.0 to 15.0  $\mu\text{m}$  with diameter from 10 to 150 nm.

The Kaolinite mineral found in the original soil formed almost a complete and well organized layer on top of each other (Figure 8). However, the formation of these Kaolinite were not well compacted and not resting completely on top of each other, therefore allowing water to flow through the pore or void. The amount and velocity of water seeping through the soil will be minimized by decreasing the void size of the Kaolinites. Thus, it can reduce the velocity of groundwater that might lead to a landslide.



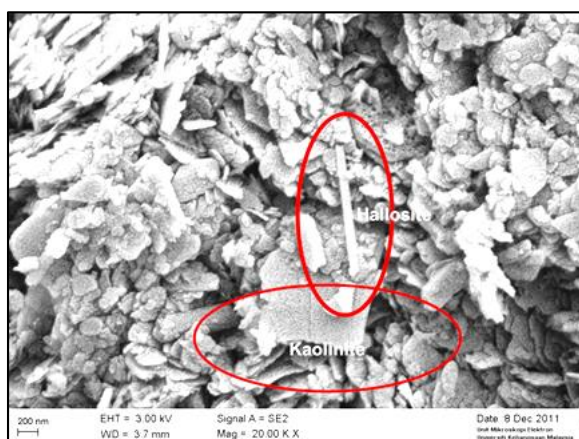


Fig. 7 SEM image of untreated soil

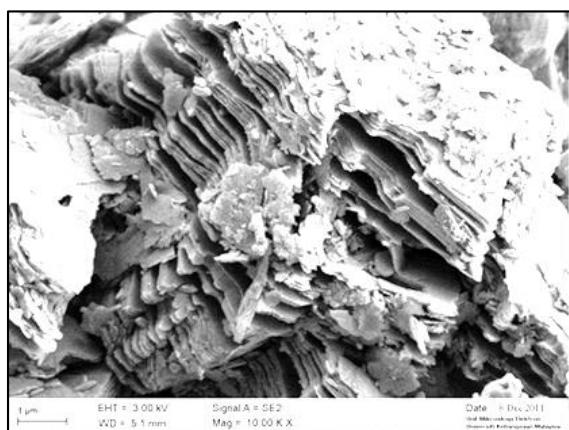


Fig. 8 SEM image of Kaolinite layers in original soil

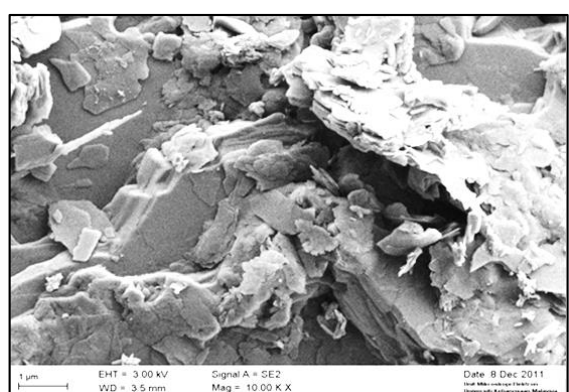


Fig. 9 SEM image of Kaolinite layers in treated soil

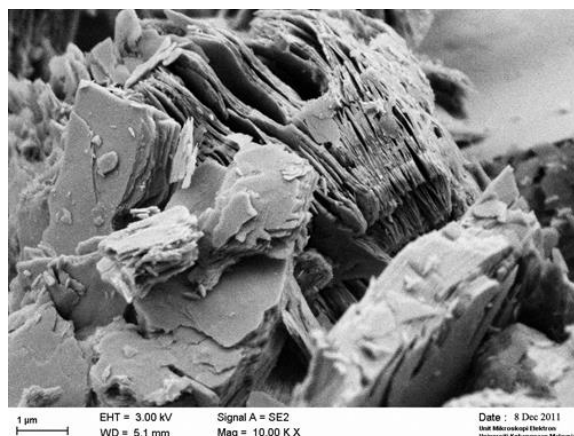


Fig. 10 SEM image of bounded Kaolinite layers

Figure 9 and 10 show the layers of Kaolinites that have bound together which has significantly reduced the soil pores. The pieces of Kaolinite have almost completely closed the pores and become compacted. Furthermore, the distance between the minerals is hardly seen. However, there was still some Kaolinite that has not closed down the distance between each layer. This was probably due to the shorter period of experiment. Most bio-mediated treatment takes a longer period to achieve the expected results due to the natural biological process of the microorganisms [14].

From this analysis, it can be assumed that the natural microorganisms in the soil and waste water have produced a biological substance such as the exopolymer which have closed down the distance between the minerals. The slime produced by the bacteria have spread in some parts of the soil particles and created sticky liquid substance that bound the soil particles together, thus reducing the permeability of the soil and increasing the shear strength. Despite that, there are areas where the mineral distances are not completely close down. This is probably because the bacteria did not distribute into that particular area and therefore longer time and higher amount of bacteria are required to accomplish a better result. The microbial activity in the soil could be incomplete by the limitation of nutrients needed [15].

## CONCLUSION

In this study, it was demonstrated that waste water and algae managed to reduce soil permeability by 26% and increased shear stress by 29.5%. This showed that waste water and algae could be applied to improve the mechanical properties of soil in situ. These methods can replace the more energy demanding mechanical compaction methods or the expensive and environmentally unfriendly chemical grouting methods. However, since the application of

green algae and waste water as the catalyst are still at early stage, to adopt this method effectively, an integration of engineering, microbiological and ecological studies and design consideration are required. Besides that, further experiment about waste water application in bioclogging must be done to fully utilize its potential in biogeotechnical engineering. Other waste materials such as food waste and sewage water may also be used and explored due to its bigger potential of producing microbes that grow by consuming inorganic nitrogen compounds such as *Nitrosomonas*, *Nitrosococcus*, *Nitrospira* and *Nitrosolobus*.

## ACKNOWLEDGMENTS

We would like to thank UNITEN grant for conference and publication fund.

## REFERENCES

- [1] Hamdan, N., Kavazanjian Jr, E., Rittmann, B. E., & Karatas, I. (2017). Carbonate mineral precipitation for soil improvement through microbial denitrification. *Geomicrobiology journal*, 34(2), 139-146.
- [2] Zhao, Q., Li, L., Li, C., Li, M., Amini, F., & Zhang, H. (2014). Factors affecting improvement of engineering properties of MICP-treated soil catalyzed by bacteria and urease. *Journal of Materials in Civil Engineering*, 26(12), 04014094.
- [3] Soon, N. W., Lee, L. M., Khun, T. C., & Ling, H. S. (2014). Factors affecting improvement in engineering properties of residual soil through microbial-induced calcite precipitation. *Journal of Geotechnical and Geoenvironmental Engineering*, 140(5), 04014006.
- [4] Umar, M., Kassim, K. A., & Chiet, K. T. P. (2016). Biological process of soil improvement in civil engineering: A review. *Journal of Rock Mechanics and Geotechnical Engineering*, 8(5), 767-774.
- [5] DeJong, J. T., & Kavazanjian, E. (2019). Bio-mediated and Bio-inspired Geotechnics. In *Geotechnical Fundamentals for Addressing New World Challenges* (pp. 193-207). Springer, Cham.
- [6] Kumari, D., & Xiang, W. N. (2019). Review on biologically based grout material to prevent soil liquefaction for ground improvement. *International Journal of Geotechnical Engineering*, 13(1), 48-53.
- [7] Costa, O. Y., Raaijmakers, J. M., & Kuramae, E. E. (2018). Microbial extracellular polymeric substances: ecological function and impact on soil aggregation. *Frontiers in microbiology*, 9.
- [8] Farah, T., Souli, H., Fleureau, J. M., Kermouche, G., Fry, J. J., Girard, B., & Harkes, M. (2016). Durability of bioclogging treatment of soils. *Journal of Geotechnical and Geoenvironmental Engineering*, 142(9), 04016040.
- [9] Xia, L., Zheng, X., Shao, H., Xin, J., Sun, Z., & Wang, L. (2016). Effects of bacterial cells and two types of extracellular polymers on bioclogging of sand columns. *Journal of Hydrology*, 535, 293-300.
- [10] Ivanov, V., & Stabnikov, V. (2017). Soil surface biotreatment. In *Construction Biotechnology* (pp. 179-197). Springer, Singapore.
- [11] Cydzik-Kwiatkowska, A., & Zielińska, M. (2016). Bacterial communities in full-scale wastewater treatment systems. *World Journal of Microbiology and Biotechnology*, 32(4), 66.
- [12] Ariyanti, D. and Handayani, N.A., 2012. Hadiyanto (2012) Feasibility of Using Microalgae for Biocement Production through Biocementation. *J Bioprocess Biotechniq*, 2(111), p.2.
- [13] Chang, I., Im, J., & Cho, G. C. (2016). Introduction of microbial biopolymers in soil treatment for future environmentally-friendly and sustainable geotechnical engineering. *Sustainability*, 8(3), 251.
- [14] Saad, A. H., Nahazanan, H., Yusoff, Z. M., Huat, B. K., & Mustafa, M. (2018). Properties of Biomineralization Process in Various Types of Soil and Their Limitations. *International Journal of Engineering & Technology*, 7(4), 4973-4979.
- [15] Castle, S. C., Sullivan, B. W., Knelman, J., Hood, E., Nemergut, D. R., Schmidt, S. K., & Cleveland, C. C. (2017). Nutrient limitation of soil microbial activity during the earliest stages of ecosystem development. *Oecologia*, 185(3), 513-524.



# QUANTITATIVE INTERPRETATION OF LANDSLIDE OCCURENCE SITE BY AI TECHNOLOGY OF IMAGE CLASSIFICATION AND TOPOGRAPHICAL ANALYSIS MAP CREATED BY AERIAL LASER DATA

Koki Sakita<sup>1</sup>, Satoshi Nishiyama<sup>1</sup>, Teruyuki Kikuchi<sup>2</sup>, Junsheng Song<sup>3</sup> and Yuzo Ohnishi<sup>4</sup>

<sup>1</sup> Graduate School of Environmental and Life Science, Okayama University, Japan;

<sup>2</sup> JP Design Co. Ltd. Japan;

<sup>3</sup> School of Mechanics and Civil Engineering, China University of Mining and Technology, China;

<sup>4</sup> Kyoto University, Japan;

## ABSTRACT

It is very important from the point of view of disaster prevention inspection to fully understand the landslide occurrence site. In the current inspection work, it has been a problem that the information used to predict the site is insufficient, and the results may vary depending on the skill of the engineer. Therefore, in this research, a two-dimensional map is created based on aerial laser surveying and an attempt was made on doing a quantitative interpretation for the site of the landslide by applying Artificial Intelligence (AI) technology specialized for image classification, which is called Convolutional Neural Network (CNN), to the map. There are a variety of maps that can be made from aerial laser data. In order to effectively interpret the topographical features, the topographical analysis map was used that transparently combined the slope map and the wavelet analysis map in this study. In the target site, dozens of landslides have occurred due to Typhoon Talus, which occurred in 2011, and in the analysis of CNN, the AI model was trained on the map before the occurrence of the landslide on the concerned site. As a result, the interpretation had an accuracy exceeding 80% and it was considered that the topography, such as scarplets and gravitational deformation, could be the pertinent information needed for the interpretation. This suggests that the extraction of topography, which is an inherent factor of landslides, has been successfully performed in the interpretation of AI, and the method can be used to predict future landslides.

*Keywords: Landslide, Artificial intelligence, Aerial Laser Surveying, Terrain analysis filter*

## INTRODUCTION

Many landslides have occurred due to the influence of climate change and heavy rainfall in recent years. Therefore, the importance of disaster countermeasures on slopes is increasing. In the inspection work for dealing with slope disasters up to now, interpretation has been carried out by experts using maps such as aerial photographs. However, it has been a problem that the method of selection and judgment of the suspicious area is qualitative and that the result differs depending on each expert's interpretation. In the first place, the information for predicting a landslide area is insufficient. The task is to organize the information such as what topographic features contribute to the landslide and what were the main contributing factors so it is necessary to establish a quantitative inspection method based on these criteria.

With regard to these problems, the utilization of aerial laser survey is used as a technology for solving these problems. In the survey, which can be measured from the sky, it is suitable for measurements over wide areas such as slopes and rivers, using many utilization methods for the measurements [1]. Moreover, by using a method called a terrain analysis filter, feature properties are extracted from the survey

data, and they are emphasized and visualized in two-dimensional maps. Furthermore, in recent years, with advances in Artificial Intelligence (AI) technology there have been remarkable, and various applications such as the classification of images and the extraction of regions.

In this study that was conducted, a verification of the quantitative interpretation of a landslide was done by extracting the occurrence site and organizing the topographical information contributing to it using an aerial laser survey, terrain analysis filter, and AI technology.

## METHODS FOR QUANTITATIVE INTERPRETATION

In order to establish the inspection method, an aerial laser survey, topography analysis filter, and AI technology were utilized. Below, each technology that was used is described.

### Aerial Laser Surveying

The technology of aerial laser surveying is one of the mobile measurement methods, and it performs measurements using a combination of three sensors: Global Navigation Satellite System (GNSS), Inertial

Measurement Unit (IMU), and a laser range finder. As mentioned above, it is suitable for measurement in a wide area and has been used in various applications such as the measurement on slopes or river dikes. The measured data is acquired as data having a three-dimensional shape composed of points which are spatially defined by three-dimensional coordinates. However, in the wide area measurement, unnecessary information is also measured at the same time such as vegetation. In the case of extracting topographical features, information of vegetation is unnecessary because the direction and the unevenness of the slope are targeted. The unnecessary information from the aerial laser data is removed by filter processing, and the data is converted into a form that can be handled easily. The data obtained by the process is called ground data. I show ground data in the mountainous area in Fig.1. A river flows in the center, and mountains cover both sides of Fig. 1. The data is expressed by a set of points having three-dimensional coordinates and is called a point cloud.

### Terrain Analysis Filter

Although the aerial laser data was subjected to a filtering process, so that the necessary information is left in, the measurement range is so wide that there is still too much information to handle as it is. Therefore, it is necessary to further extract information to be focused on and to use it in a more manageable form. In this study, a method called terrain analysis filter is used for the purpose of feature extraction and visualization of the data and the analysis is performed using the topographical analysis map.

#### Topographical analysis map

In this method, two different terrain analysis filters are used, and they are created by performing transmission synthesis so as to use the respective features that complement both filter methods. The two terrain analysis maps are wavelet analysis and slope maps.

#### Slope map

The slope map is a terrain analysis map that uses the degree of inclination as a feature amount. Using the 8 points around arbitrary points (a, b) in the measurement data, the slope amount S of the local slope can be calculated by Eq. (1), and the map is created by allocating light and dark according to those values. Each value in the following equation corresponds to the elevation value of each point in the relationship of Fig. 2.

#### Wavelet analysis map

The wavelet analysis map is developed for the purpose of emphasizing the unevenness of the slope and is created according to the wavelet coefficient C (s, a, b) calculated by Eq. (2) where s indicates the shift amount and (a, b) indicates x and y coordinates at an arbitrary point.  $\phi$  is called a mother wavelet function, it is shown in Eq. (3), and the magnitude of the product between the function and the data relates to the expression of unevenness. Figure 3 shows an example of the function when s = 1 and a wavelet analysis map.

$$S(a, b) = \sqrt{S_x(a, b)^2 + S_y(a, b)^2} \quad (1)$$

$$S_x(a, b) = \frac{H11 + H21 + H31 - (H13 + H23 + H33)}{6 * D_x}$$

$$S_y(a, b) = \frac{H11 + H12 + H13 - (H31 + H32 + H33)}{6 * D_y}$$

$$C(s, a, b) = \frac{1}{s} \iint z(x, y) \phi\left(\frac{x-a}{s}, \frac{y-b}{s}\right) dx dy \quad (2)$$

$$\phi(x, y) = (2 - x^2 - y^2) \exp\left\{-\frac{1}{2}(x^2 + y^2)\right\} \quad (3)$$

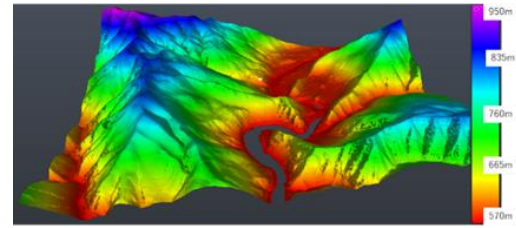


Fig. 1 Example of the ground data obtained by the aerial laser survey

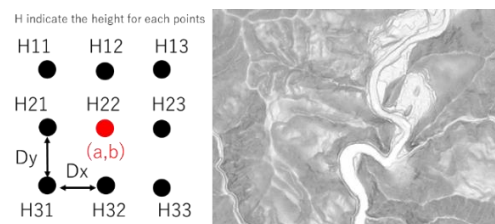


Fig. 2 Chart of the relationship between the points to calculate the slope amount and slope map

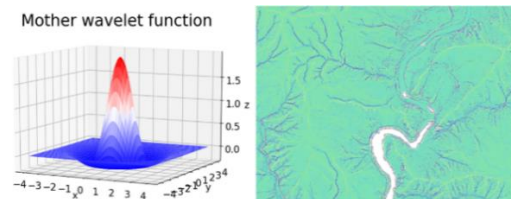


Fig. 3 Graph of mother wavelet function for s=1 and wavelet analysis map example

## Image Classification by AI

Recent advances in AI technologies are remarkable, and as computer performance has improved, the time to compute the analysis has become shorter, and opportunities for use in many fields have increased. In particular, image classification technology is expected to be used in a variety of applications, and it has received a high degree of attention. Recently a model has been released that performs classification with an accuracy of 96.43% in recognition of images classified into 1000 categories [2]. Among such AIs, is a model specialized for image classification called Convolutional Neural Network (CNN), CNN automatically performs the extraction of the feature quantities in an image and the inference based on the extracted feature is quantified. In this research, the AI was trained on identifying landslides using the topographical analysis map created from the aerial laser survey data, and binary classification of whether the map has the features characteristic of landslides in the image. Instead of using the general CNN model that has already been proposed for the AI model, a specific model for interpreting the landslide was created. Therefore, the most suitable model in the interpretation of the landslide site is searched for amongst the combination of model and data. At that time, Sony's "Neural network Console" is used as the software for AI analysis.

## CONTENT OF EXPERIMENT

### Proposed method

First, an overview of the method is given. In this method, the AI trains using the maps made from the aerial laser data and then the AI extracts landslide features automatically based on the given data and classifies them.

The data used to let the AI train is a map before the occurrence of landslides. Therefore, two types of data across the area are required: 1) before the landslide; 2) and, after the landslide. It is necessary to create a topographical analysis map from each of the survey data and compare the two types of maps to know where the landslide site is located on the pre-landslide map.

The scale value of the wavelet analysis maps must be determined in order to create the topographical analysis map. Here, it is set as  $s = 1$ . As an example of this map, Fig. 4 shows a topographical analysis map before and after the landslide. On the AI analysis part, a CNN model is used. As mentioned above, the interpretation model is searched in order to obtain a more optimal solution in this study. In this method, the survey data generated before landslide is required to train the AI. However, this data cannot be obtained

at every landslide site. Therefore, as a proposed method, tile images are created as shown in Fig. 5 to increase the number of training data. First, by comparing the data before and after the landslide, the place to be the landslide is extracted and cut out of the map. Thereafter, the extracted parts are divided into square tiles without overlapping. In this research, the length of one side is set to 50 pix, and a rotation process at 90 degrees and inversion processing of left/right and top/bottom are performed for each tile finally. Then, the amount of data is expanded by six times. By tiling the map in this manner, the number of images to be used as training data increases. This is expected to improve classification accuracy. In addition, the tile images created from other sites is used as the no-landslide site image.

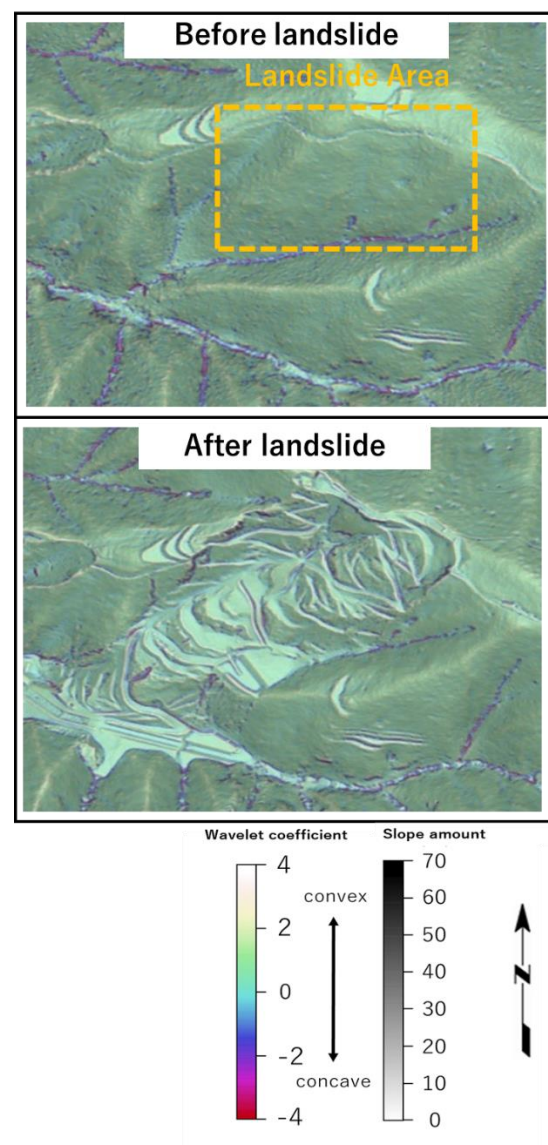


Fig. 4 Topographical analysis map before and after the Landslide and two color bars representing map colors

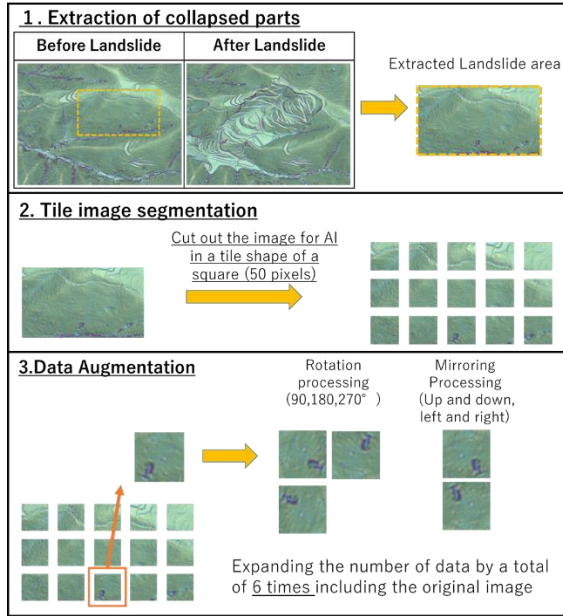


Fig. 5 Creation flow of tile images from the original map

### Observation Site

Here, the site information is described as it relates to the analysis of this research. The target area of this study is the Kii Mountains which is the middle basin of the Totsu river and it is also the Kumano river water system which was damaged by Typhoon Talus in 2011. This Typhoon caused heavy rainfall over 2000 mm in the Kii Mountains and caused more than 50 landslides. For countermeasure of this event, aerial laser surveys were conducted by a national organization, and data of 1 m mesh size was maintained. Even more, fortunately, similar surveys were conducted in 2009 in this area. Therefore, the data before and after the landslide are available, making it ideal data for this research.

### Verification Content

The analysis is performed in three steps. The first two of them are related to the search of the model. The first step is training. In the training, the AI model is allowed to train the map having the features of the landslide or not. As mentioned above, the CNN model is used in this research. Therefore, the CNN model which is designated trains the landslide and the non-landslide tiles, with their respective labels. Next step is evaluation. In the evaluation, the training result is evaluated for the accuracy of the classification. For the trained model, new image sets are given that have already been labeled as landslide / no-landslide and is different from the training images, and its accuracy is evaluated by comparing the classification results of the label and the AI. In this research, the most suitable model for classification is searched for by performing

these two steps while rearranging the CNN model. From the results of these two steps, the model with the highest accuracy is determined as the optimum model, and the process proceeds to the last step. The final step is to validate the model. In the model verification, the new image sets for the verification is given to the optimal model and verification is performed to verify the model accuracy. Each of these three steps requires a separate set of data. Therefore, the 3 sets of tile images need to be prepared. The number of data sets is shown in the table. The data sets for learning and evaluation are created by dividing the generated 9,205 tile images so that the ratio of the number of data sets for learning and evaluation is 8: 2.

Table 1 Number of data sets for each category and types

| Data type  | Landslide | No-Landslide | Total |
|------------|-----------|--------------|-------|
| Training   | 3,348     | 4,016        | 7,364 |
| Evaluation | 858       | 983          | 1,841 |
| Total      | 4,206     | 4,999        | 9,205 |
| Validation | 249       | 527          | 776   |

## RESULTS

### Accuracy Indicator

Here, three accuracy indices are defined in Eq. (3) to (5) as indices for quantitatively evaluating the classification. TP, FP, FN, and TN in the equation are determined by the correspondence between the true label of the image and the classification result of AI. For images in which the true label is a landslide, the number of AI classified as landslide is TP (True Positive), and conversely, the number of no-Landslide is TN (True Negative). Furthermore, when the true label is a non-landslide site, the number of images in which the classification results are similar to non-landslide sites is FN (False Negative), and the number of landslide images that are classified as no-Landslide is FP (false positive).

$$Recall = \frac{TP}{TP + FN} * 100, \frac{TN}{FP + TN} * 100 \quad (4)$$

$$Precision = \frac{TP}{TP + FP} * 100, \frac{TN}{TN + FN} * 100 \quad (5)$$

$$Accuracy = \frac{TP + TN}{TP + FP + FN + TN} * 100 \quad (6)$$



## Model Structure Searching

In the structure search of the model, the model was recombined, and the accuracy verification using the evaluation data was performed each time to determine the optimum model. Here, it was decided that the optimal model is a model that maximizes Recall. The classification results at that time are shown in Table 2 below. Further, Fig. 6 shows an optimal model at that time.

Table 2 Accuracy evaluation results in optimal AI model by using evaluation data sets

|                          |           |              |
|--------------------------|-----------|--------------|
|                          | Landslide | No-Landslide |
| Inferred as Landslide    | TP:688    | FP:77        |
| Inferred as No-landslide | FN:170    | TN:906       |
| Total                    | 858       | 983          |
| Recall                   | 80.2%     | 92.2%        |

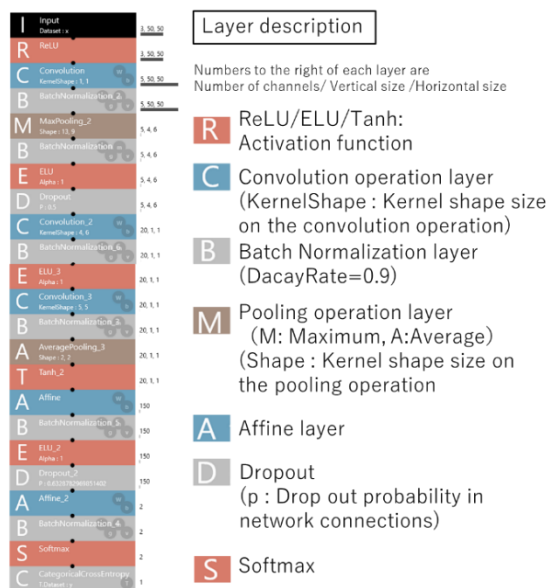


Fig. 6 Best classification model in the structure searching

## Validation

The accuracy was verified using the data set for verification and the searched model. The accuracy verification results are shown in Table 3. About 88% of the recalled and non-collapsed sites are read, and the accuracy of the entire data set is 88.5%. The precision was 78.3% in the collapsed area and 94.3% in the non-collapsed area.

Table 3 Validation result in optimal AI model by using validation data sets

|                          | Landslide | No-landslide | Precision       |
|--------------------------|-----------|--------------|-----------------|
| Inferred as landslide    | Tp:221    | FP:61        | 78.3%           |
| Inferred as No-Landslide | FN:28     | TN:466       | 94.3%           |
| Recall                   | 88.8%     | 88.4%        | Accuracy: 88.5% |

### Estimation of classification basis by AI

Here, the topography will be considered which is the basis for the classification by AI from the results obtained by validation. As mentioned earlier, the information in the interpretation of landslides is still insufficient, and it is necessary to reorganize what should be focused on in the inspection. In this case, by using the images classified as TP and FN in Table 3, reasons the AI classified landslides and non-landslides are considered based on the basis, and on the results, the topography is organized resulting from the landslide phenomenon. At the time of the basis estimation, the middle layer visualization technique of the CNN model was used. The model comprises feature quantity extraction in an image and a neural network, and feature quantity extraction corresponds to filtering processing in the image processing field. Therefore, by executing only feature quantity extraction processing in the searched optimum model and forcibly outputting in the middle of the network, it is possible to obtain an image in which feature quantities for estimation in the network are extracted for each image. It is called the interlayer visualization tile. Note that since the image being used is a tile image, it is not possible to evaluate the entire landslide area as it is. Therefore, the interlayer visualization tile is returned to the original arrangement, and one landslide area image is generated. In addition, since each tile image has a result classified as Landslide or no-Landslide according to classification by AI, the interlayer visualized tiles with a probability of belonging to each class at the time of classification over 80% are highlighted in red. The images generated from these results are called mid-layer visualization images. These are shown in Fig. 7.

In Fig. 7, two places in the landslide area in the data set used in Table 3 are shown. The original image and the mid-layer visualization image are displayed, and the original image includes the topographic interpretation comment of the expert. The first

original image can be seen to have gravitational deformation and multiple scarplets. On the other hand, it can be seen that the mid-layer visualization image is emphasized by black and white. Further, the tiles in which they appear are classified as landslides. Next, looking at the second set, the arc-shape unclear scarplet found in the center of the original image is also classified as a landslide in the mid-layer visualization image. On the contrary, it can be seen that a relatively gentle slope having an inclination angle of about 5 degrees or a ridge having a wide inclination angle of 10 degrees, which is seen in the upper and lower parts of the image, is not classified as a landslide.

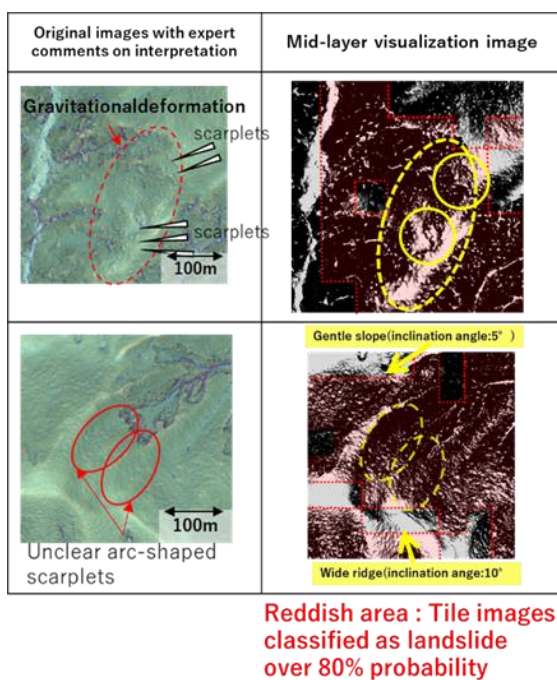


Fig. 7 Comparison table between original images and mid-layer visualization image

## CONCLUSIONS

In this study, automatic extraction of the slope landslide was tried by using an aerial laser survey and AI technology as an attempt to improve efficiency and quantification of slope disaster inspection. The topographical analysis maps are created from survey data using aerial laser survey and terrain analysis filters. Detailed information of topography was extracted from 3D survey data, and this topography information was expressed on the maps. Furthermore, by applying a model which specialized in image classification called CNN to these maps, the maps were classified into the landslide or other topography. As a result, the study succeeded in the classification by Recall and Accuracy of over 80%.

In addition, it was considered that topography such as gravitational deformation and scarplets are the most important elements for the interpretation of the landslide by the estimation of the judgment basis of AI based on the interpretation result. In addition, it was found that terrains with relatively gentle inclination tend to be classified as terrains other than the landslide site.

This is the result of judgment based on the inherent factor that causes a landslide. However, it is reported that the information of triggering rainfall is also an important factor that causes a landslide [3], [4]. That is, in order to carry out further quantitative and accurate interpretation, it is necessary to develop an analysis system that interprets AI taking into consideration both rainfall information and topographic information. In addition, in the preparation of this map, the dataset is created with the landslide site in the rainfall of the 2011 Typhoon Talus as the landslide site. However, not only the predisposition for promoting landslide is included in the whole landslide area in the first place, but it may be considered that analysis by AI in the case where unnecessary information was originally included. This is also the case with no-landslide data sets, and data sets classified as no-landslide areas may also include the inherence as landslide areas. That is, depending on events such as future rainfall, landslides may occur even at locations classified as no-landslide areas. Therefore, it is an urgent task to organize measurement data and topographical information and quantitatively clarify the relationship between the topography and landslide represented in the survey data.

## REFERENCES

- [1] Suwa. T, Nikaido. R, Hamaguchi. K, Harada. T, Watanabe. K, Nakazono. D, Hara. F, Aoki. S, Analysis of Topographic Change Using Aviation Laser Survey due to the 2001 Tohoku Tsunami, Journal of Japan Society of Civil Engineers, Ser. B3, Vol.72, No.2, 2016, pp.I\_181-I\_186
- [2] He. K, Zhang. X, Ren. S, Sun. J, Deep Residual Learning for Image Recognition, arXiv preprint arXiv:1512.03385, 2015
- [3] Chigira. M, Civil engineering laboratory manual Creek extraction manual (draft) that could cause a collapse of the deep layer, Journal of Japan Society of Civil Engineers, Ser. C, Vol.62, No.4, 2006, pp.722-735
- [4] Chigira. M, Prediction of Potential Sites of Deep-Seated Catastrophic Landslides and its Future Research, Jour. Japan Soc. Eng. Geol, Vol.56, No.5, 2015, pp.200-209



# LIQUEFACTION MAPPING PROCEDURE DEVELOPMENT: DENSITY AND MEAN GRAIN SIZE FORMULATIONS

Abdul Hakam<sup>1</sup>, Bayu Martanto Adji<sup>1</sup> and Junaidi<sup>1</sup>  
<sup>1</sup>Engineering Faculty, Andalas University, Indonesia

## ABSTRACT

The assessment of liquefaction potential is very important and is the main step in making a map of liquefaction hazard in a certain area. The assessment methods of liquefaction potential have been proposed by researchers since last eight decades. Each method is based on the purposes and completeness of the data obtained by the developer. In this study, these methods then were modified to propose the new method that is easier and technically cheaper. Furthermore, the method will be applied in making liquefaction hazard maps. The method as a result of this study is a new procedure that is more practical to be applied. This method is associated with soil parameters that are commonly and easy obtained in general soil investigation. The soil parameters used to assess the potential of liquefaction in this procedure are the density and mean size of soil particles. Soil density and particle mean size needed for analysis of liquefaction potential can be obtained from laboratory tests or the correlation results from the value of field tests, namely the standard penetration test or cone penetration test. This new procedure is expected to be more applicable and reliable in making liquefaction hazard maps.

*Keywords: Liquefaction, Assessment method, Grain size, Density, Nspt, CPT*

## INTRODUCTION

An evaluation procedure of soil liquefaction potential using the simplified method [1] based on both a liquefaction resistance factor (FL) and a liquefaction potential factor, (PL) has been proposed in 1981 [2]. The procedure tried to introduce the factor FL and PL which are is the liquefaction potential at a calculated depth and at the surface respectively. The factor PL then used with the famous name as liquefaction potential index (LPI) by researchers in Korea, India and Bangladesh [3] - [5]. The LPI becomes interesting since it indicates the damage level at the surface at the site of interest related to the factors of safety of liquefaction potential at the deeper point underneath.

The first LPI is introduced for only 20m of depth with the formula of:

$$LPI = \int_0^{20} F(z) W(z) dz \quad (1)$$

where  $F(z) = 1 - FS$  with the minimum 0.0,  $W(z) = 10^{-1/2 z}$  with the minimum 0.0,  $z$  and  $dz$  are the depth the incremental depth respectively. The modified term of severity level of LPI has also been introduced by the other researcher [Luna 1995] as:

$$LPI = \sum_{i=1}^n F_i W_i H_i \quad (2)$$

where  $n$  denotes the number of discretized layers,  $H_i$  denotes the thickness of the discretized layer,  $W_i$  weighting function and  $F_i$  is the liquefaction severity for layer  $i$ . The liquefaction severity assessed based

on the liquefaction potential index (LPI) is shown in Table 1.

Table 1 The liquefaction severity - potential index

| LPI  | Iwasaki<br>[2] | Luna-Forest<br>[6] | Chung et al<br>[7] |
|------|----------------|--------------------|--------------------|
| 0    | Very Low       | Little to None     | None               |
| 0-5  | Low            | Minor              | Little to None     |
| 5-15 | High           | Moderate           | Moderate           |
| . 16 | Very High      | Major              | Severe             |

In order to show the severity liquefaction from the liquefaction potential index (LPI), the typical illustrations based on field observations in the New Zealand are presented in Fig. 1 [8].

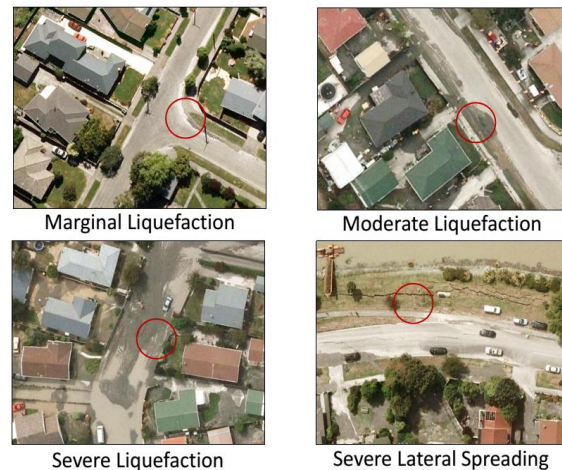


Fig. 1 Bird-eye observed liquefaction [8]

## LIQUEFACTION ASSESSMENT

The liquefaction potential assessment is an important aspect for mapping the earthquake related hazard for certain area. Since Niigata earthquake in 1964 the simplified method [1] has been widely used. However this continuously improved method became complex since it involves many parameters that rarely used in geotechnical engineering and not as simple as it was named [10] [11]. The method also has been modified for assessing liquefaction potential based on Cone Penetration Test results [12].

The liquefaction potential in the soil layer can be assessed based on the mean grain size ( $D_{50}$ ) and its relative density ( $Dr$ ) [13]. This method has been applied to real cases in the field and gave satisfactory results [14]. The liquefaction potential at certain point in the soil layer can be determined by plotting the value of the relative density and the average grain size (Fig. 2).

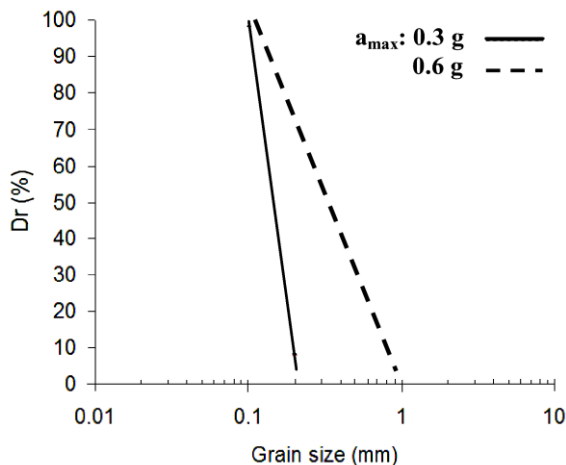


Fig. 2  $Dr - D_{50}$  for liquefaction assessment

Based on the authors' experience so far, the most popular direct in field tests used in Indonesia for civil works are the Standard Penetration Test (SPT) and Cone Penetration Test (CPT). The Standard Penetration Test provides a soil parameter value in the form of  $N$  or  $N_{spt}$ . The Standard Penetration Test usually follows the drilling works that include soil samples that can involve sieve analysis in advanced. While the Cone Penetration Test often produces cone tip resistance parameters ( $q_c$ ) and friction ratio ( $Fr$ ). Both of these filed tests have no relative density value involved in. In order to develop a general method for using  $Dr$  and  $D_{50}$

Liquefaction assessment, it will be written the simple procedure to obtain the relative density estimation based on the correlation of those filed tests. In addition it is also given an estimated mean of grain size based on those filed tests' results.

## FIELD TEST CORRELATION

Obtaining of soil parameter generally require laboratory tests that take time and cost. Fortunately past engineers and researchers have done a number of precious works to obtain soil parameters from soil field test report. This approach is taken in this study to correlate soil parameters with based on the results of the most commonly used soil field investigation CPT and SPT. The correlation of CPT and SPT test results also has been proposed by many researcher as recently it is done [15]. However, each test has its own advantageous and restriction in engineering practices.

### $Dr$ from SPT

In a laboratory, relative density can be calculated as a relationship result of maximum density,  $\gamma_{max}$  minimum density  $\gamma_{min}$  and at present state of soil density  $\gamma_d$ , as follows:

$$Dr = \frac{\gamma_d - \gamma_{min}}{\gamma_{max} - \gamma_{min}} \times \frac{\gamma_{max}}{\gamma_d} \times 100\% \quad (3)$$

However, in the absence of relative density test of soil samples in laboratory test as it is usually, the value of  $Dr$  can be taken from the  $N$  correlation. In the past, the researchers then made relationship between the laboratory test values of  $Dr$  with the number of blows from SPT ( $N$ ).

The first relative density and penetration resistant correlation was revealed in 1948 [16]. Later on a researcher [17] has conducted the sophisticated laboratory investigation on  $N$  and  $Dr$  relationship using a 1.2 m high heavy steel tank with the diameter of 1 m. The more important feature of this test is it had two different soil grain sizes that are the coarse sand with  $D_{50}$  of 1.5mm and fine sand with  $D_{50}$  of 0.3 as shown in Fig. 3.

General result of that study is given in graphs of relationship between penetration resistant,  $N$  and relative density,  $Dr$  for cohesionless sands as shown in Fig. 4. It seems that for air dry sand, the grain size of sand has no significant effect to the penetration resistant and relative density relationship. However, for saturated sands, the gain size of the sand contributed very important effect to the penetration

resistant and relative density relationship. It indicates that the grain size of sand is a very important parameter to effect on the behavior of the soil. So, it must be considered in soil mechanic analysis. Then, for liquefaction potential analysis based on Standard Penetration Test results, it must include the sieve analysis of soil samples that taken from the same drilling hole to obtain the grain size of the soil.

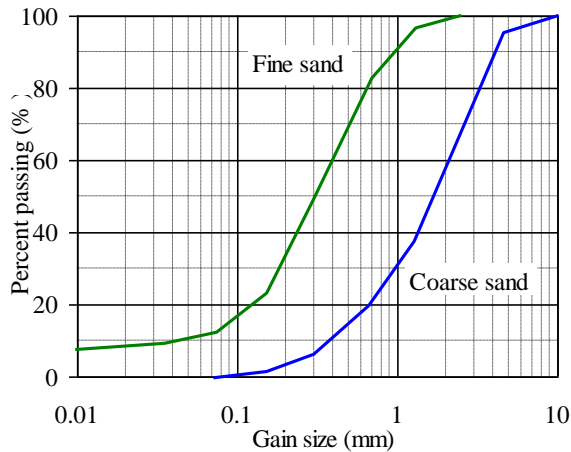


Fig. 3 Gradation of sand used in the Dr-N tests, reconstructed from [17]

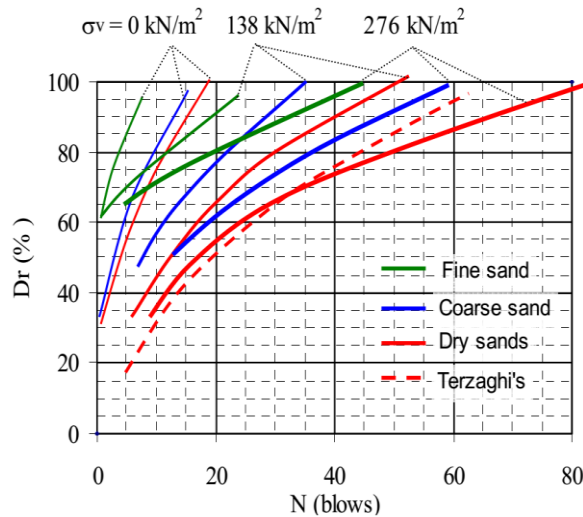


Fig. 4 Relative density and penetration resistance relationship for fine and coarse sands, reconstructed from [17]

#### Dr from CPT

Different from the Standard Penetration Test, the Cone Penetration Test give two soil parameter; cone tip resistance ( $q_c$ ) and skin resistance ( $q_s$ ). The ration of those two values is named a friction ratio (Fr). This ratio is very important value that can be

used to estimate the type of soil.

The first relative density, Dr correlation from CPT cone resistance,  $q_c$  was published in 1975 [18]. The Dr -  $q_c$  correlation then was updated and published in 1978 [19]. Both correlations take into account the effect of vertical effective stress,  $\sigma_v'$  as they are shown in Fig. 5.

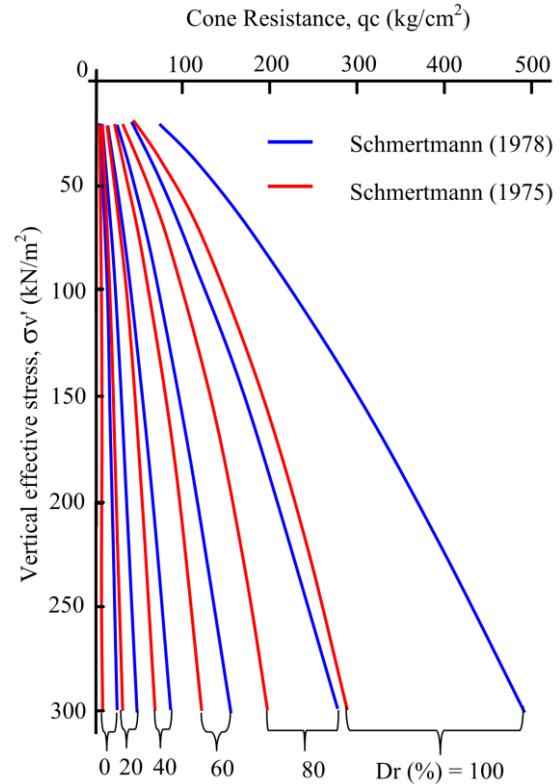


Fig. 5 Relative density -  $q_c$  relationships for sandy soil, reconstructed from [19]

In Indonesia, the Cone Penetration Test is very famous in engineering practice, then Dr -  $q_c$  relationship become very important for liquefaction potential analysis. It has been known that the  $q_c$  is effected by sand density, in-situ effective stress and sand compressibility. Sand compressibility depends on grain size, grain shape and mineralogy. For the liquefaction potential analysis purpose, the relative density of the soil can be taken from the cone resistant correlation in the equation as follows [20]:

$$Dr = C_2^{(-1)} \ln Q/C_0 \quad (1)$$

Where  $C_0=15.7$ ,  $C_2=2.41$  and  $Q=(q_c/p_a)/(\sigma_v'/p_a)^{-0.5}$ . Here  $p_a$  is reference pressure taken as 100kPa, in the same unit as  $q_c$  and  $\sigma_v'$ .

Using the above equation, the liquefaction assessment of sand deposit in Pasir Jambak due to Padang earthquake 2009 has been demonstrated [10].

This formulation is practically simple and gave good estimation of the liquefaction potential in sand deposits.

### D50 from CPT

Although it is widely used for soil investigation works, unfortunately CPT is usually not followed by drilling for soil sampling. So the test of the grain size of the soil is not possible. But fortunately CPT also provides information on the skin resistance of  $q_s$ , where in the terms of the comparison with the  $q_c$  resulting in the value of  $Fr$ .

The CPT test result generally can be used to form soil profiling as well as soil type. The cone resistance, ( $q_c$ ) is generally higher in sands and lower in clays. Then, the friction ratio,  $Fr$  consequently is lower in sands and higher in clays. The  $Fr$  value can not to provide exact estimation of grain size but it may provide a guide to soil type which has particular characteristic and behavior.

Many researcher had observed soil grain size using CPT and confirmed that sandy soils tend have high cone resistance,  $q_c$  where consequently gave low friction ratio  $Fr$ , and the reverse for soft clay soils [21] [22]. Fig. 6 presents the  $D_{50}$  and  $R_f$  correlation, the CPT data were taken from mechanical and electrical cones.

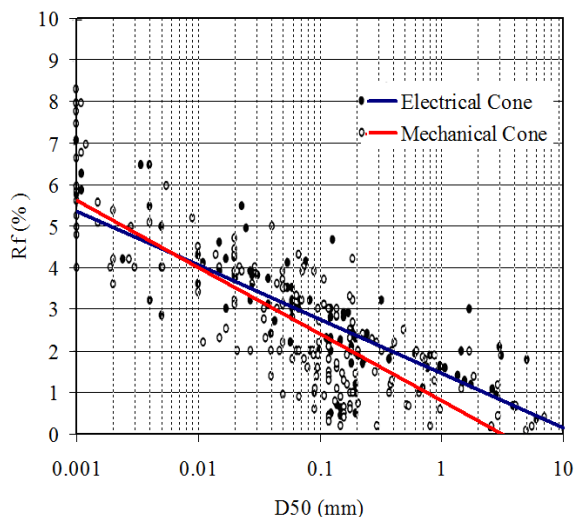


Fig. 6 Dr- $R_f$  correlation [21]

The best fit equation for the  $Dr$ - $R_f$  correlation of [21] is:

$$R_f = 1.45 - 1.3 \log(D_{50}) \text{ for electrical cone} \quad (2)$$

and,

$$R_f = 0.78 - 1.61 \log(D_{50}) \text{ for mechanical cone} \quad (3)$$

For estimating  $D_{50}$  from  $R_f$ , the Eq. (2) and Eq. (3) turn into Eq. (4) and Eq. (5) as follows:

$$D_{50} = 3.056 e^{-1.4302 R_f} \text{ for electrical cone} \quad (4)$$

and respectively,

$$D_{50} = 13.043 e^{-1.7712 R_f} \text{ for mechanical cone} \quad (5)$$

In addition, the past studies on soil grain size distribution had been conducted using SPT and CPT resistances [22] and [23]. The SPT data is presented in the terms of  $N_{60}$  values which is corresponding to the energy ratio of about 60%. They concluded that the  $q_c$ - $N$  ratio is strongly related to the soil grain size and expressed by the mean grain size ( $D_{50}$ ) as shown in Fig.7. It is very useful in practice if both CPT and SPT are performed in soil investigation.

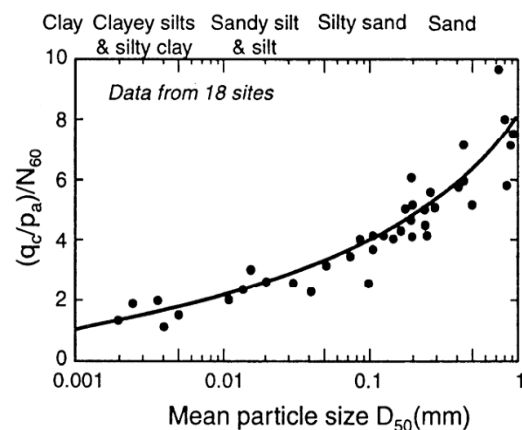


Fig. 7 CPT-SPT correlation with  $D_{50}$  [23]

### ASSEESMENT FORMULA DEVELOPMENT

Based on the previous description, the procedure for liquefaction potential assessment of soil layers then can be developed based on the  $Dr$ - $D_{50}$  parameters obtained from the correlation of the test results of soil investigation in the field using CPT and SPT. Each penetration test procedure can be made in the form of a flow chart as shown in Fig. 8 for CPT and Fig. 9 for SPT respectively. Specifically for SPT testing, soil samples from the soil layer must be taken to determine the grain size of the soil, or there must be a companion CPT test to determine the correlation of soil grains.

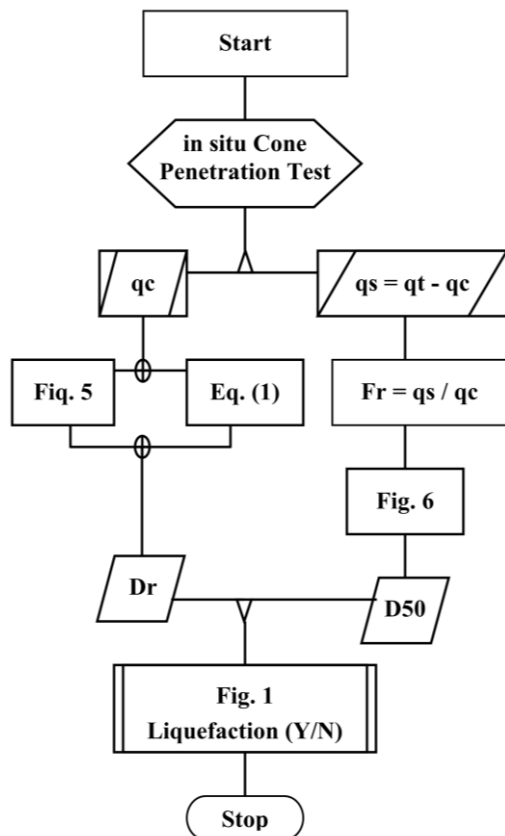


Fig. 8 Dr-D50 Procedure for CPT test results

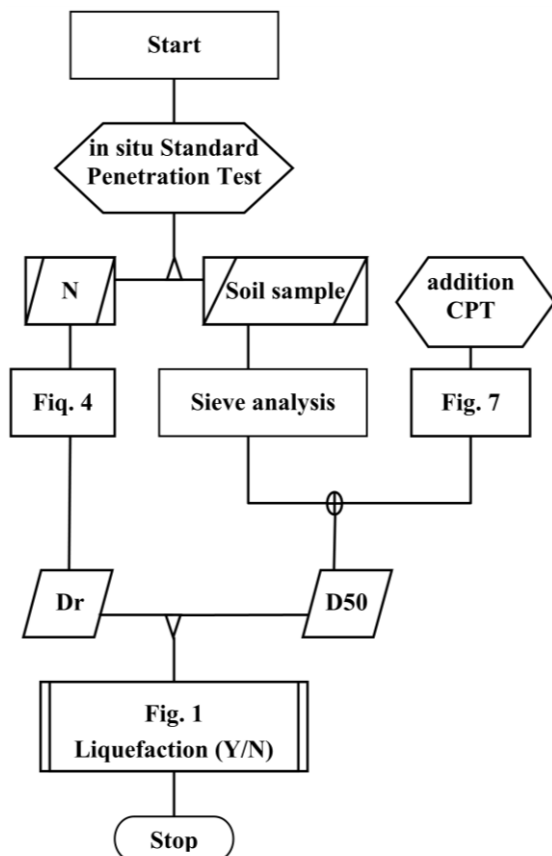


Fig. 9 Dr-D50 Procedure for SPT test results

## CONCLUSIONS

In order to produce a liquefaction hazard map of a specific area, the assessment of liquefaction potential is very important and become the main step. Some liquefaction potential assessment methods have been proposed by researchers since the last century. Every method is developed based on the purposes and the completeness of available data. The modified method in here is based on soil relative density and mean grain size which are obtained from laboratory tests.

In this paper a modified new method that is easier and technically cheaper is proposed. The method is developed based on the penetration resistance data of the standard penetration test, SPT and/or cone penetration test, CPT. The method is a new procedure that is more practical to be applied for general soil investigation test results. This method is associated with soil parameters that are obtained from the available correlation from soil investigation test results that turned into the relative density and mean grain size of the soil layer. This new procedure is expected to be more applicable and reliable in making liquefaction hazard maps. The application of the purposed method is under process and the results in terms of liquefaction potential of Padang City area will be published soon.

## ACKNOWLEDGMENTS

The authors greatly express thank to Andalas University which provided any support in the process of finishing this research.

## REFERENCES

- [1] Seed H.B. and Idriss I.M., Simplified procedure for evaluating soil liquefaction potential, J. Soil Mech. Foundation Division, 97, 1249–1273, 1971
- [2] Iwasaki, T., Tokida, K. and Tatsuoka, F., Soil Liquefaction Potential Evaluation with Use of the Simplified Procedure, International Conferences on Recent Advances in Geotechnical Earthquake Engineering and Soil Dynamics. 12. April 26th - May 30th, 1981, <http://scholarsmine.mst.edu/icrageesd/01icrageesd/session02/12>
- [3] Kim H.S., Cho N.G. and Chung C.K., Real-time LPI-based Assessment of the Liquefaction Potential of the Incheon Port in Korea, 15 WCEE, Lisboa 2012
- [4] Dixit, J., Dewaikar, D.M. and Jangid R.S., Assessment of liquefaction potential index for

- Mumbai city, Nat. Hazards Earth Syst. Sci., 12, 2759–2768, 2012
- [5] Sarker D. and Ansary M.A., Assessment of Liquefaction Potential Index for Approach Road of Padma Multipurpose Bridge, IOSR Journal of Mechanical and Civil Engineering (IOSR-JMCE), Vol. 12, Issue 2 Ver. VI (Mar - Apr. 2015), PP 132-138
- [6] Luna, R. and Frost, J. D.: Spatial liquefaction analysis system, J. Comput. Civil Eng., 12, 48–56, 1998
- [7] Chung, J.W. and David Rogers J., Simplified Method for Spatial Evaluation of Liquefaction Potential in the St. Louis Area, Journal of Geotechnical and Geoenvironmental Engineering. 137:5,505-515, 2011
- [8] Maurer B.W., Green R.A., Cubrinovski M. and Bradley B.A., Evaluation of Liquefaction Potential Index (LPI) for Assessing Liquefaction Hazard: A Case Study in Christchurch, New Zealand, Poster UC, Christchurch, NZ, <https://core.ac.uk/download/pdf/35471699.pdf> (Accessed, May 2019)
- [9] Hakam, A., Laboratory Liquefaction Test of Sand Based on Grain Size and Relative Density, J. Eng. Technol. Sci. Vol. 48, No. 3, 2016, 334-344
- [10] Seed, H. Bolton dan Idriss I.M., Ground Motion and Soil Liquefaction During Earthquake, Earthquake Engineering Research Institute, Berkeley, 1982
- [11] Youd, T. L. and Idriss, I. M., Liquefaction resistance of soils: Summary report from the 1996 NCEER and 1998 NCEER/NSF workshop on evaluation of liquefaction resistance of soils, J. Geotechnical and Geoenvironmental Engg., ASCE, April 2001, pp. 297-313
- [12] Shibata, T. and Teparaksa, W., Evaluation of liquefaction potential of soils using cone penetration tests, J. Soils and Foundations, Vol. 28, NO. 2, 1998, pp. 49-60
- [13] Hakam A., Laboratory Liquefaction Test of Sand Based on Grain Size and Relative Density, J. Eng. Technology and Science, Vol. 48, No. 3, 2016, 334-344
- [14] Hakam A., Ismail F.A., Fauzan, Liquefaction Potential Assessment Based On Laboratory Test, International Journal of GEOMATE, Oct., 2016, Vol. 11, Issue 26, pp. 2553-2557
- [15] Urmi Z.A. and Ansary M.A., Interpretation of geotechnical parameters from CPT and SPT for the reclaimed areas of Dhaka, Bangladesh, Conference:CPT18 At Netherlands, November 2017.
- [16] Terzaghi K. and Peck R.B. (1948) Soil Mechanics in Engineering Practice, Wiley, New York, USA
- [17] Gibbs K.J. and Holtz W.G. (1957), Research on determining the density of sands by spoon penetration testing, Proceedings of the 4th International Conference on Soil Mechanics and Foundation Engineering, London, 35–39
- [18] Schmertmann J.H. (1975) State of the art paper: measure of in situ strength. Proceedings of ASCE Conference on in situ Measurements of Soil Properties, Raleigh, North Carolina, pp. 57–138.
- [19] Schmertmann J.H. (1978), Guidelines for Cone Penetration Test, Performance and Design. Federal Highway Administration, Washington, DC, USA, Vol. 145, Report FHWA-TS-78–209.
- [20] Robertson P. K. and Cabal K.L., Guide to Cone Penetration Testing, GREGG inc., 2010
- [21] Douglas, B. J. and Olsen, R. S. (1981), Soil classification using electric cone penetrometer Cone Penetration Testing and Experience, Proc. of the ASCE National Convention, St. Louis, 209-27, American Society of Civil Engineers (ASCE)
- [22] Muromachi T. (1981), Cone penetration testing in Japan, Proc. Symposium on Cone Penetration Testing and Experience, Geotechnical Engineering Division, ASCE, St. Louis, Missouri, pp. 49–75.
- [23] Robertson, P.K., Campanella, R.G. and Wightman, A., SPT-CPT correlations, Journal of Geotechnical Engineering, ASCE, Vol. 109 (11), 1983, pp. 1449–1459



## COMPARISON STUDY ON DAMAGE PATTERN OF TWO STORIES BUILDING: SIMULATION VS FIELD RECORD

Febrin Anas Ismail<sup>1</sup>, Abdul Hakam<sup>1</sup>, Hendri Gusti Putra<sup>1</sup>, M Maisaquddus Hape<sup>2</sup>, M Sofian Asmirza<sup>3</sup>  
<sup>1</sup>Engineering Fac., Andalas University, Indonesia; <sup>2</sup>Civil and Environmental Engineering Fac., Institute  
Technology of Bandung, Indonesia, <sup>3</sup>Engineering Fac., North Sumatra University, Indonesia

### ABSTRACT

Study on damage pattern of the two-story building is needed for quick assessment soon after the earthquake. In Indonesia, quick assessment is needed at least for two reasons: to determine Government subsidies Fund and to retrofit the damaged houses. The previous article has been analyzed and simulated the case study of the two-story building due to earthquake load base on Indonesia Earthquake Code by considering the soil conditions. It shows that the influence of soil conditions as well as column properties especially at a lower level are an important factor in determining the damage patterns. However, that study was not verified yet with the damage data of the two stories building in the field. This paper discussed the comparison between the simulation results with the field record of two stories building damage in Indonesia. The data are collected base on the recent earthquakes in Indonesia: Padang Earthquake, Lombok Earthquake, Solok Selatan Earthquake, and Padang Panjang Earthquake. It shows that they are confirmed the damage patterns are in line with the simulation results. Base on this study, the guidance for quick assessment of two-story building then is developed.

*Keywords: Earthquake, Quick assessment, Non-engineered two-story building, Indonesian code*

### INTRODUCTION

This study is the continuation of the previous study regarding quick assessment of two stories building [1]. Two stories building model has been analyzed including the soil-structure interaction.

The soil categories are differed based on the average of soil strength in terms either Standard penetration value,  $N_{spt}$ , Shear wave velocity,  $V_s$ , or, Soil strength,  $S_u$ . Based on those values, the numerical simulation then is conducted to take the advances of soil-structure interaction methods.

The structural elements of the building are designed as reinforced concrete with the minimum reinforcement. This design then gives the minimum capacity required for two-story building and will be discussed in the results section. The typical soil-structure interaction model for numerical simulation are shown in Fig. 2

The geometry of the finite element model shown in Fig. 2 has a height of 3.5m every level and 4.0m between columns.

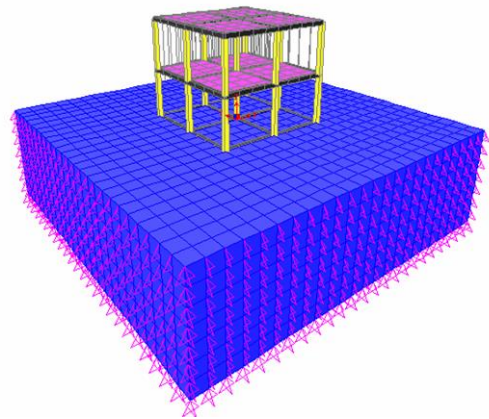


Fig. 2 Typical soil-structure model for analysis

The applied loads on the models are the self-weight load, live load, and earthquake load. The earthquake load is adopted from the calculation results by Ministry of Public Service of Indonesia. The values of Acceleration Spectrum in a unit of  $g$  are plotted on Y-axis respect to the period,  $T$  in second on X-axis.

The displacement pattern due to the earthquake load is shown in Fig. 4. Meanwhile, the typical internal moment is shown in Fig. 5. The values of displacement and internal forces due to the applied load are given in Table 3.

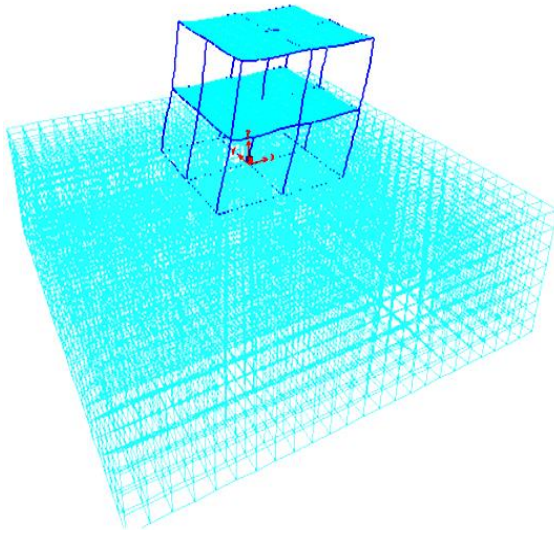


Fig. 4 Typical displacement of the models due to applied earthquake load.

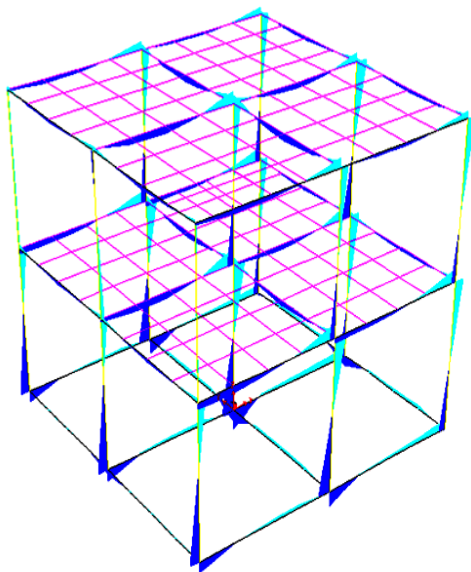


Fig. 5 Typical internal moment due to loads.

Table 3. Internal force values in column

| Hard soil site  |        |       |        |
|-----------------|--------|-------|--------|
| Column position | Axial  | Shear | Moment |
| Edge 2nd storey | -3497  | 306   | -1068  |
| Edge 1st storey | -5704  | 2876  | 5879   |
| Side 2nd storey | -10455 | -345  | -977   |
| Side 1st storey | -18904 | 2744  | 5800   |

| Middle 2nd storey | -28915 | 2778  | -5281  |
|-------------------|--------|-------|--------|
| Middle 1st storey | -56483 | 4559  | 8236   |
| Medium soil site  |        |       |        |
| Column position   | Axial  | Shear | Moment |
| Edge 2nd storey   | -3661  | 208   | -918   |
| Edge 1st storey   | -5973  | 2937  | 5918   |
| Side 2nd storey   | -10474 | -490  | -1261  |
| Side 1st storey   | -18821 | 2913  | 6132   |
| Middle 2nd storey | -28095 | 2777  | -5305  |
| Middle 1st storey | -54976 | 4708  | 8429   |
| Soft soil site    |        |       |        |
| Column position   | Axial  | Shear | Moment |
| Edge 2nd storey   | -3990  | -36   | -569   |
| Edge 1st storey   | -6739  | 2720  | 5505   |
| Side 2nd storey   | -10625 | -805  | -1776  |
| Side 1st storey   | -19247 | 2761  | 5920   |
| Middle 2nd storey | -27204 | 2506  | -4807  |
| Middle 1st storey | -53316 | 4359  | 7744   |

From the numerical results, it can be seen that even though the applied earthquake loads for medium soil site and hard soil site are the same, but the response of the structure give different values. The medium site gives larger internal forces in general. Furthermore, the earthquake load applied to the structure in the soft soil is 10% less than the others. But the responses regarding internal forces give bigger in some points.

The numerical simulations then will be compared to the strength of the structural element to give the idea for built the quick assessment procedure. This work is still under the investigation and will be reported soon after it ready to be presented. However, these preliminary results have given the idea to see the soil characteristic in the location of the building during investigating the building assessment, especially soon after the earthquake.

The purpose of this study is to compare between the simulation results with the field record of two stories building damage in Indonesia.

### Methodology

The methodology used in this comparison study, as shown in Fig. 6. First, check the earthquake intensity. There are 3 categorizes of earthquake intensity: small, medium, and high. The criteria are used base on MMI scale. Second,

the soil type is checked. There are 3 types of soil: soft, medium, and hard. Third, the column condition is identified. In this case, there are 3 position of column to be checked: edge, side, and middle, including first and second floor.

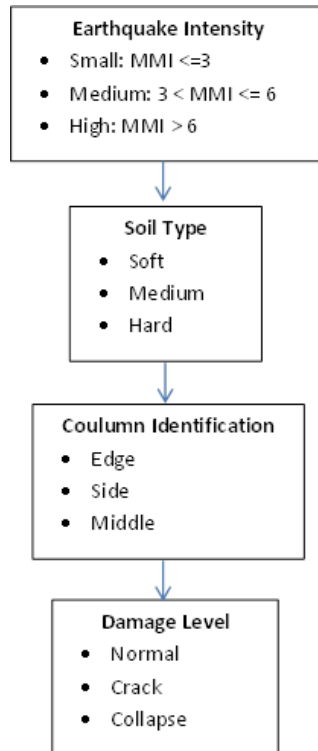


Fig. 6 Field Assessment Procedure

## RESULT AND DISCUSSION

In this study, there are a number of two stories building are evaluated. The taken samples of two stories building are collected from earthquake impacted area in Indonesia, that are, Aceh earthquake 2006 (M6.0), Padang earthquake 2009 (M7.9), Lombok earthquake 2017 (M7.0), and Palu earthquake 2017 (M6.1). Each building selected is located in 3 types of soil, that is, soft, medium, and hard. Building evaluation then applied using procedure in Fig.4.

### A. Earthquake Intensity

In general, the bigger the intensity of the earthquake, the heavier the damage of building. In case of un-proper constructed building, it will collapse severely. It can be seen during Padang earthquake (M7.9) with intensity in certain area reach MMI 7. The same thing happens during

earthquake in Aceh, Lombok and Palu.

### B. Soil Type

Soil type will influence the shaking of the earthquake. The softer the soil, the bigger the shaking. Building on the soft soil will experience more vibration due to its amplification. Fig. 5 shows how the building collapse built on soft soil.



a. Soft Soil



b. Medium Soil



c. Hard Soil

Fig. 7 Damaged building in Assessment

In case of medium soil, due to big earthquake, the building still survived especially its structural component. However, its non structural components are collapse since they are not design



to withstand to the big earthquake load. Fig 7 shows the non structural component are collapse due to earthquake.

Most building stayed on hard soil and properly design according to earthquake code, can withstand against the earthquake load. Hard soil will keep the shaking constant and the good design can absorb the earthquake energy properly.



a. Edge Column



b. Middle Column



c. Side Column

Fig. 8 Damaged structural components.

### C. Damage Analysis

Damage analysis can be seen from the detail damage of each building. Fig. 8 shows the damage of structural component. It shows that the edge column will first damage due to the shaking. It is in line with simulation analysis where the internal forces are bigger in this area. The next damage will experience the side column and the last is the middle column.

### Conclusions

Padang is the capital city of the West Sumatra is a very earthquake-prone city in Indonesia. The city has experienced from many big during the last years in this century. There are two main sources of the earthquake in Padang, first is coming from the subduction boundary in the west part and the second source is the great fault of Sumatra the eastern part. Many big earthquakes have resulted damages in the West Sumatra province from that sources.

In purpose of build quick assessment tool, it is very important to accomplish numerical simulations of typical building structures in the different soil type sites. Two stories building generally destroyed by the earthquake, in this paper the earthquake loaded building in Padang become the main point. The numerical results show that for the medium soil site and hard soil site with the same load, give different responses to the structure. Furthermore, for the soft soil with 10% less earthquake load, the responses regarding internal forces give bigger in some points.

The comparison field's data and analysis result in this study showed a good correlation between them. More samples of damaged building to be compared to the analysis are still needed. This work is still under further investigation but these preliminary results have given a good idea to develop a quick procedure in conducting the building assessment due to the earthquake.

### ACKNOWLEDGEMENTS

The authors greatly express thank to our colleagues who have helped in the process of finishing this research.

### REFERENCES

- [1] Aydan, Ö., Imamura F., Suzuki T., Ismail F.A., Hakam A., Masmera, Devi P.R., A Reconnaissance Report On The Bengkulu Earthquake Of September 12, Japan Society of Civil Engineers (JSCE) and Japan Association for Earthquake Engineering (JAEE) With the collaboration of Andalas University, October 2007

- [2] Hakam, A, "Laboratory Liquefaction Test of Sand Based on Grain Size and Relative Density", J. Eng. Technol. Sci., Vol. 48, No. 3, 2016, 334-344
- [3] SNI-1736-2012, Indonesian Earthquake code, Indonesian Public Service Ministry, 2012
- [4] Wahyuni E., Vulnerability Assessment of Reinforced Concrete Building Post-Earthquake, Procedia Earth and Planetary Science, Volume 14, 2015, Pages 76-82
- [5] Sarmah T., Earthquake Vulnerability Assessment for RCC Buildings of Guwahati City using Rapid Visual Screening, Procedia Engineering Volume 212, 2018, Pages 214-221
- [6] Local Disaster Management Agent, BPBD, pictures of damages due to Padang earthquake in 2009. taken in 2018
- [7] Tumeo R., Soil-Structure Interaction Effects on the Seismic Performances of Reinforced Concrete Moment Resisting Frames Procedia Engineering Volume 199, 2017, Pages 230-235
- [8] Menglin L., Structure-Soil-Structure Interaction: Literature Review, Soil Dynamics and Earthquake Engineering Volume 31, Issue 12, December 2011, Pages 1724-1731

#### **AUTHOR'S BIOGRAPHY**

Dr. Febrin Anas Ismail is an Associate Professor in the Civil Engineering Department of

Andalas University, Indonesia. He was graduated and got Master from Institute Technology of Bandung. His Doctor is from Yokohama University, Japan. His research interests include the general problem in structural engineering and dynamics of the structure. His contact E-mail is febrin@eng.unand.ac.id.

#### **AUTHOR'S CONTRIBUTIONS**

Dr. Febrin Anas Ismail: Conception, design, acquisition, final approval of the version to be submitted. Dr. Abdul Hakam: Conception, design, final approval of the version and submit the paper. Dr. M Sofian Asmirza and Hendri G Putra: Critical reviewing, analysis. M Maisaquddus H: Summarizing and Interpretation of data as well as conducting numerical model.

#### **ETHICS**

This article is original and contains unpublished material. The corresponding author confirms that all of the other authors have read and approved the manuscript and no ethical issues involved.

## LIQUEFACTION POTENTIAL MAPPING OF THE CITY OF VALENZUELA, PHILIPPINES

Angelo S. Enoria, Jr.<sup>1</sup>, Sophia Joy Q. San Juan<sup>1</sup>, Hiyasmin F. Ubaldo<sup>1</sup>,  
Jordan N. Velasco<sup>1</sup> and John Lemar M. Tirao<sup>1</sup>

<sup>1</sup>Department of Civil Engineering, Pamantasan ng Lungsod ng Valenzuela, Philippines

### ABSTRACT

The city of Valenzuela in the Philippines has provided several preparedness plans and contingency measures in anticipation of the 7.2-magnitude earthquake, dubbed as the “Big One”. In studying the movements along the country’s Valley Fault System, the said plans and measures were not accomplished. The consideration of the soil’s potential to liquefy was not included—which is significant in providing hazard maps for the city. The researchers assessed the soil in Valenzuela using soil investigation reports done from 2008 to 2017. The geotechnical properties were utilized to calculate liquefaction potential using Idriss and Boulanger’s Semi-empirical Method for Factor of Safety against Liquefaction and the formula from Iwasaki, *et al.* for Liquefaction Potential Index. Liquefaction potential maps were produced corresponding to moment magnitudes 6, 7, and 8. Based on the results, 67.65% of the city has the potential and probability to liquefy at magnitudes 6 and 7, while 70.59% for magnitude 8. On the same hand, about 32.35% of the city are the least susceptible to liquefaction during earthquake magnitudes 6 and 7, while 29.41% for magnitude 8. It is therefore concluded that the majority of the soils in Valenzuela is highly susceptible to liquefaction.

*Keywords: Semi-empirical method, Liquefaction, Factor of safety, Liquefaction potential map*

### INTRODUCTION

When the pore-water pressure in a saturated soil increases in a great amount, soil deposits behave like a viscous liquid that causes the soil to suspend in water. Earthquake shaking further reduces soil strength and stiffness, triggering a phenomenon called liquefaction. Failure in ground capacity happens, added by ground deformations and slope instability which generates substantial structural damage. The highly urbanized city of Valenzuela in northern Metro Manila, Philippines, consists of thirty-three (33) barangays (or wards), has a population of 653,441 as of 2019, and a land area of 47.02 square kilometers, and is one of the many cities near the West Valley Fault. Liquefaction, in these areas, is more probable to happen after a massive earthquake shaking which will greatly affect several communities alongside the coastal areas of Taguig, Pasig, Marikina, Muntinlupa, Pasay, Las Piñas, Pateros, Caloocan, Malabon, Navotas, and Valenzuela. (PHIVOLCS 2011) These coastal areas are most likely to be prone to soil liquefaction.

The main objective of this research is to develop an earthquake liquefaction potential map of Valenzuela that can inform the local government of the liquefaction susceptibility of different barangays to plan in advance for any liquefaction-related disasters in the future.

The researchers will apply Idriss and Boulanger’s semi-empirical approach of assessing liquefaction potential in incorporation with the weighting scheme of Iwasaki et al. using gathered geotechnical surveys to evaluate liquefaction resistance of soils in a deposit, or the cyclic shear stress ratio at a particular depth beneath a level ground surface, determine the maximum or equivalent cyclic shear strength likely to be induced in the soil deposit, and estimate the liquefaction potential index of the soil. (IB reference) Utilizing a semi-empirical approach, the data outputs will be computed as the factor of safety against liquefaction, the liquefaction potential index, and the production of liquefaction potential map of Valenzuela City.

### EXPERIMENTAL PROGRAM

The conceptual framework is presented in Fig. 1. This discusses the process of determining whether the soil in Valenzuela is susceptible to liquefaction under earthquakes of magnitudes 6, 7, and 8.

In order to satisfy the objectives of this research, geotechnical properties taken from several soil investigation reports collections were assessed using a spreadsheet program. Idriss and Boulanger’s simplified approach of liquefaction analysis in Fig. 2 was then utilized to determine the factor of safety against liquefaction. Liquefaction potential index was then computed using the formula from Iwasaki et al.



Geologic maps and production of a liquefaction potential map were made using ArcGIS®.

|                           |     |
|---------------------------|-----|
| $FS = \frac{CRR_m}{CSR}$  | (1) |
| $LPI = \sum w(z) * F * H$ | (2) |

Where

$FS$  is the factor of safety;

$CRR_m$  is the corrected cyclic resistance ratio;

$CSR$  is cyclic shear stress ratio;

$LPI$  is the liquefaction potential index;

$w(z) = 10 - 0.5z$ , where  $z$  is the average depth of soil layer and its preceding layer from the ground surface;

$F = 1 - FS$ ;

$H$  is the thickness of the soil layer

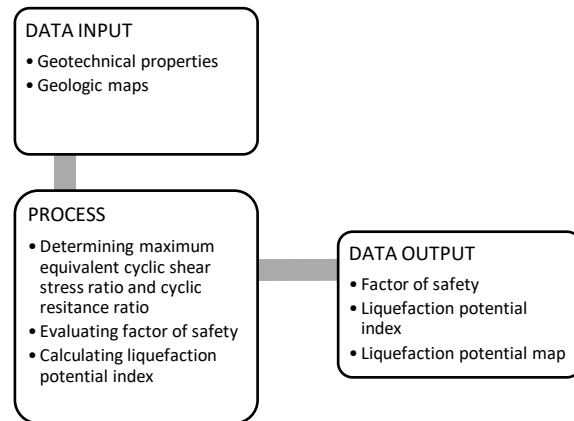


Fig. 1 Conceptual framework

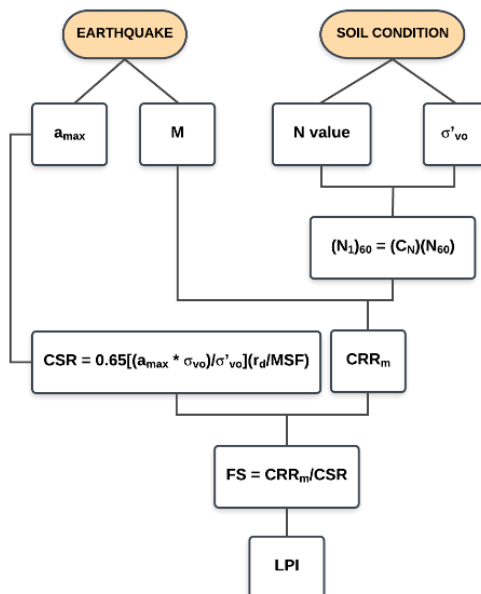


Fig. 2 Idriss and Boulanger (2004) semi-empirical method for evaluating liquefaction potential.

## RESULTS AND DISCUSSION

### Geotechnical Assessment

The map of Valenzuela and its barangays is shown in Fig. 3.

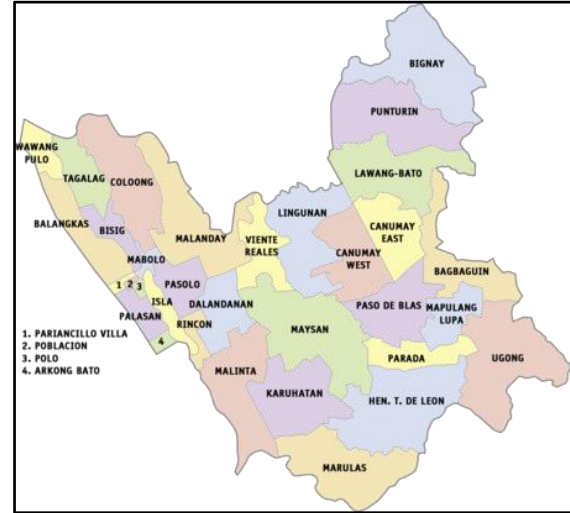


Fig. 3 The city of Valenzuela and its barangays.

Considering water content, N-value (number of blows required for 12-inch penetration resistance of the soil during Standard Penetration Test, or SPT), and depth of soil penetration, collected data from the local government of the were analyzed. After careful considerations, only 34 borehole logs were able to deliver the necessary requirements for this research, as shown in Table 1.

Table 1 List of accepted soil investigation reports/borehole logs for Valenzuela

| Barangay name   | Number of borehole logs |
|-----------------|-------------------------|
| Arkong Bato     | 3                       |
| Bagbaguin       | 2                       |
| Balangkas       | 1                       |
| Bignay          | 2                       |
| Dalandanan      | 3                       |
| Gen. T. de Leon | 1                       |
| Karuhatan       | 2                       |
| Mapulang Lupa   | 2                       |
| Marulas         | 1                       |
| Maysan          | 4                       |
| Palasan         | 4                       |
| Parada          | 1                       |
| Pasong de Blas  | 2                       |
| Rincon          | 1                       |
| Ulong           | 1                       |
| Veinte Reales   | 4                       |
| <b>TOTAL</b>    | <b>34</b>               |

For calculating moist unit weight and dry unit weights from the soil reports water content and

specific gravity per soil depth were used, as shown in a sample computation in Table 2. The depth and computed unit weights were then used to calculate the total vertical pressure, pore water pressure, and effective vertical pressure.

Table 2 Geotechnical properties calculation (Bignay, Valenzuela)

| Depth (m) | Water content (%) | N-value | Specific gravity | Moist unit weight (kN/m <sup>3</sup> ) | Dry unit weight (kN/m <sup>3</sup> ) |
|-----------|-------------------|---------|------------------|--|--------------------------------------|
| 1.00      | 18.66             | 1       | 2.65             | 20.6408                                | 17.3949                              |
| 1.50      | 71.24             | 3       | 2.65             | 15.4150                                | 9.0020                               |
| 3.00      | 42.03             | 9       | 2.65             | 17.4676                                | 12.2985                              |
| 4.50      | 23.27             | 12      | 2.65             | 19.8223                                | 16.0804                              |
| 6.00      | 30.21             | 21      | 2.65             | 18.7997                                | 14.4380                              |
| 7.50      | 22.34             | 32      | 2.65             | 19.9773                                | 16.3294                              |
| 9.00      | 20.34             | 35      | 2.65             | 20.3275                                | 16.8917                              |

### Semi-Empirical Method

Values of the stress reduction coefficient  $r_d$ , magnitude scaling factor  $MSF$ , standard penetration resistance  $N_{1(60)}$ , cyclic shear stress ratio  $CSR$ , cyclic resistance ratio  $CRR_m$ , and factor of safety  $FS$  at magnitudes 6, 7, and 8 respectively, were calculated using the previously computed values. Furthermore, if  $FS \leq 1.0$ , the soil layer is identified as susceptible to liquefaction, otherwise, that layer has a low potential to liquefy.

Table 3 Results of factor of safety calculations at magnitude 6

| Depth (m) | Unit weight (kN/m <sup>3</sup> ) | $N_{1(60)}$ | $M = 6$ |       |       |         |       |
|-----------|----------------------------------|-------------|---------|-------|-------|---------|-------|
|           |                                  |             | $r_d$   | $MSF$ | $CSR$ | $CRR_m$ | $FS$  |
| 1.00      | 17.395                           | 3.218       | 0.994   | 1.482 | 1.711 | 0.112   | 0.065 |
| 1.50      | 9.002                            | 11.719      | 0.986   | 1.482 | 2.403 | 0.188   | 0.078 |
| 3.00      | 12.298                           | 22.987      | 0.959   | 1.482 | 2.825 | 0.357   | 0.126 |
| 4.50      | 16.080                           | 22.535      | 0.929   | 1.482 | 2.674 | 0.346   | 0.129 |
| 6.00      | 14.438                           | 36.574      | 0.896   | 1.482 | 2.816 | 2.445   | 0.868 |
| 7.50      | 16.329                           | 47.309      | 0.861   | 1.482 | 2.628 | 338.300 | 1.000 |
| 9.00      | 16.892                           | 46.734      | 0.824   | 1.482 | 2.520 | 226.400 | 1.000 |

### Liquefaction Potential Index

To compute for the liquefaction potential index, factor of safety is needed. Iwasaki et al. established a condition where the liquefaction susceptibility for soils with  $LPI = 0$  is very low,  $0 < LPI \leq 5$  is low,  $5 < LPI \leq 15$  is high, and  $LPI > 15$  is very high. It can be inferred from the results that as the earthquake magnitude increases, the LPI also increases. Most of the locations rendered LPI values greater than 15 which denotes high levels of liquefaction severity.

Table 6 Computation of liquefaction potential index (LPI) at magnitude 6

| Depth (m)                       | $z$ (m) | $H$ (m) | $w(z)$ | $M = 6$   |                |
|---------------------------------|---------|---------|--------|-----------|----------------|
|                                 |         |         |        | $F$       | $w(z) * F * H$ |
| 1.00                            | 0.50    | 1.00    | 9.75   | 0.935     | 9.112          |
| 1.50                            | 1.25    | 0.50    | 9.375  | 0.922     | 4.321          |
| 3.00                            | 2.25    | 1.50    | 8.875  | 0.874     | 11.631         |
| 4.50                            | 3.75    | 1.50    | 8.125  | 0.871     | 10.612         |
| 6.00                            | 5.25    | 1.50    | 7.375  | 0.132     | 1.457          |
| 7.50                            | 6.75    | 1.50    | 6.625  | 0.000     | 0.000          |
| 9.00                            | 8.25    | 1.50    | 5.875  | 0.000     | 0.000          |
| LPI                             |         |         |        | 37.134    |                |
| Level of liquefaction severity: |         |         |        | Very high |                |

### Liquefaction Potential Mapping

Contour maps of liquefaction potential indices of each location were generated to indicate liquefaction variability triggered by the effects of earthquake magnitudes 6, 7, and 8.

LPI values greater than 15 correspond to a very high level of liquefaction severity, values between 5 and 15 are high, values between 0 and 5 are low, and values of 0 indicate a very low chance of liquefaction. The identification of liquefaction severity in the maps corresponds to specific colors of the shaded contours which are based on the LPI values, as shown in Figures 4 to 6.

Based on the gathered soil investigation reports, most of the areas that exhibit high liquefaction potential were found to have soft soils and are in areas in which groundwater tables are at shallow depths. It can be observed based on these maps that there is a very high probability of liquefaction in majority of the areas in Valenzuela.

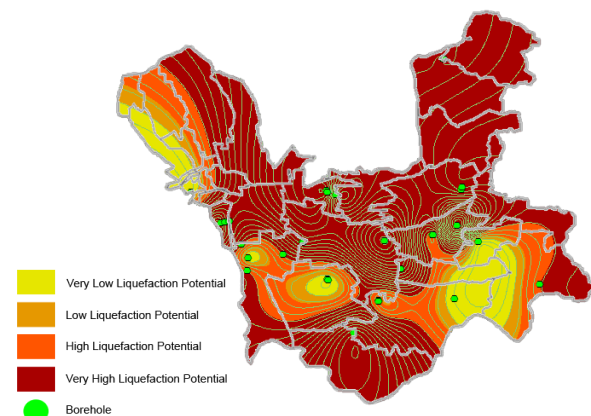


Fig. 4 Liquefaction potential map at magnitude 6.

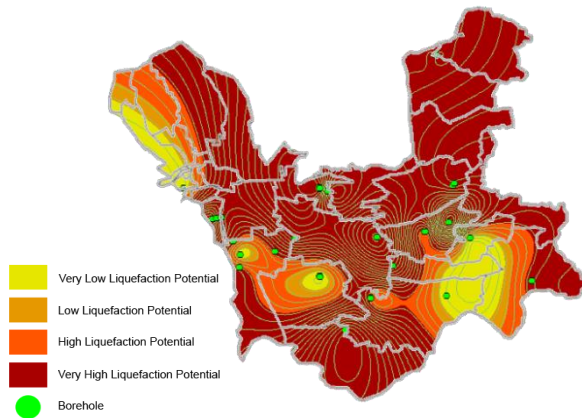


Fig. 5 Liquefaction potential map at magnitude 7.

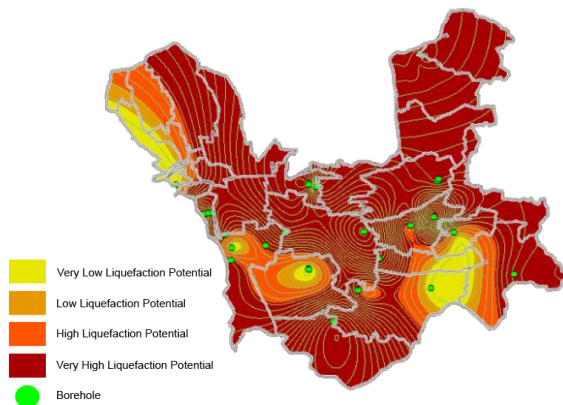


Fig. 6 Liquefaction potential map at magnitude 8.

## CONCLUSION

Majority of the areas in Valenzuela gave liquefaction potential indices greater than 15 which indicate very high liquefaction potential. About 67.65% of the total land area exhibited possibility of high potential to liquefy while 32.35% of the city are the least susceptible to liquefaction at magnitudes 6 and 7. For magnitude 8, about 70.59% of the total land area has high probability to liquefy and 29.41% have low potential to liquefy. With the aid of ArcGIS®, liquefaction potential maps were easily generated to provided rapid analysis of various locations, and in turn, may provide vital information

to structural designers and engineers.

Considering soil liquefaction potential is important in design and construction. Ground improvement and strengthening techniques of building's foundation systems are recommended for areas that are exhibiting probabilities of liquefaction to reduce it susceptibility. Suggested approaches for ground improvement are vibro-compaction, dynamic deep compaction, excavation and disposal of liquefiable soils, and jet grouting or using structural fills. The use of deep foundations and well-reinforced or post-tensioned mats are also advisable.

## ACKNOWLEDGMENTS

The researchers would like to acknowledge the Local Government of Valenzuela City for allowing them to obtain the borehole logs needed to complete this study. To the professors who took their time to guide and advise, a heartfelt thanks. To the researchers' families and friends, sincerest thanks for all the patience and support that you have given. Ultimately, to the One who is able to sustain the energies of the weary authors, to Him be all the glory.

## REFERENCES

- [1] G. Castro, S. Poulos, "Factors affecting liquefaction and cyclic mobility," *Journal of Geotechnical Engineering Division, ASCE*, 1977; Vol.103, No.GT6: 501-506.
- [2] E. Dela Vega, "Liquefaction susceptibility plot of Gerona, Central Luzon Philippines," *Tarlac City, Tarlac, Philippines: Tarlac State University*, 2016.
- [3] I. Garcia, J. Go, P. Suspine, N. Concha, "Earthquake liquefaction susceptibility mapping of Pasig City," *Sampaloc, Manila, Philippines: Far Eastern University Institute of Technology*, 2017.
- [4] I. Idriss, R. Boulanger, "Semi-empirical procedures for evaluating liquefaction potential during earthquakes," *Berkeley, California, USA: University of California*, 2004.
- [5] T. Iwasaki, T. Arakawa, and K. Tokida, "Simplified procedures for assessing soil liquefaction during earthquakes," *International Journal of Soil Dynamics and Earthquake Engineering*, 3(1), 49-58, 1984.

# THE PROPERTIES OF POROUS CONCRETE PAVING BLOCKS

Nurul Rezuana Buyung<sup>1</sup> and Abdul Naser Abdul Ghani<sup>2</sup>

<sup>1,2</sup>School of Housing, Building and Planning, Universiti Sains Malaysia, Malaysia

## ABSTRACT

Porous concrete paver is a mixture of Portland cement, coarse aggregate or gravel and water. Higher porosity is achieved by removing the finer particles such as sand from the concrete mixture. This research study the properties of readymade porous concrete paver blocks. The density and void content of porous concrete pavers were presented in this study by using 33 samples of porous concrete pavers and were analyzed using statistical analysis. Then, all samples are divided into four groups to study the infiltration rate and analyzed with different design of joint and void content. This study shows the consistency on measurement of density and void content where all the reading were nearer to the average value. Basically, porous concrete pavers usually contains 15 percent to 25 percent of void content. However, these porous pavers in individual form did not achieve the 15 percent to 25 percent of void content where the highest void content is 6.5 percent. But, the void requirements are satisfactory when they are placed together on the ground. The joint gap provides for the voids requirement. While, the infiltration rate shows a different reading between two design where there is a different length of joint.

*Keywords: Porous concrete pavers, Density, Void content, Infiltration rate*

## INTRODUCTION

Interconnected void in the porous pavement would allow water to go through the pavement especially during rainfall seasons. Conventional impermeable asphalts and concrete pavements are replaced by porous asphalt and porous concrete. Through porous pavements, water could pass through and leaves the pavements and it is called as exfiltrate. Most of the porous pavements type has the similar general structure as shown in Fig. 1 [1].

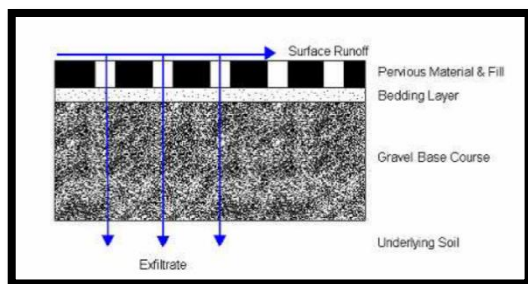


Fig. 1 Cross section of a typical block paver permeable pavement installation without underdrains

Basically, porous pavements are used as an alternative to conventional impermeable pavement which allows stormwater to stream into it and into a stone reservoir [2]. Porous pavement usually have rough surface which could reduce the flows of stormwater runoff and also improved the quality of the stormwater [3]. Porous pavements are usually used for low traffic load, car parks, footpaths, walkways and driveways [2],[3].

## POROUS CONCRETE PAVERS

Porous concrete is a mixture of Portland cement, coarse aggregate or gravel and water. Void content of porous pavement is about 15 percent to 35 percent or in average of 20 percent and this is achieved by removing the finer particles such as sand from the concrete mixture. This void allows water to infiltrate underlying soil and the water either pooling on the surface or being discharge as runoff [4].

Permeable concrete pavement contain of aggregates and a Portland cement binder. The omission of fine aggregates provides the porosity in permeable pavements. Modular interlocking concrete blocks of the internal drainage cell type are pre-cast or cast-in-place lattice or castellated pavers of concrete or plastic, which contain open cells. The filling of the cells usually soil mixed with grass or porous aggregates [5]. Permeable paver units such as stone, concrete or another durable material fixed within and above a base rock. Water infiltrated to the sub-soils through voids provided by gaps between pavers [6].

## Density

The density of pervious concrete depends on the properties and proportion of the materials used, and the compaction procedures used in placement. In-place densities on the order to 1600 kg per cubic meter to 2000 kg per cubic meter are common, which is in the upper range of lightweight concretes [7]. The density of the specimens ranged from 1650 kg per cubic meter to 1943 kg per cubic meter [8].



### Void content

Typically, around 15 percent to 25 percent voids are achieved in hardened concrete (Pervious concrete pavements). A lot of study has been conducted by other researcher and usually, the ranges of voids percentage are within 15 percent to 30 percent [7] (ASTM C1754) The void content of the specimens ranged from 22.6 percent to 37.0 percent [8].

### Infiltration rate

Porous pavements are designed to infiltrate rainfall falling directly onto the surface [6]. A pavement's surface infiltration rate is measured with water ponded on top of the pavement [9]. The standards on infiltration tests for two types of permeable pavement systems: ASTM C1701 and C1781 were developed for porous concrete and interlocking concrete pavers, respectively [10]. The surface infiltration rates of some porous pavements change over time, due to processes such as compaction, sedimentation, migration of pavement binder, and aggregation of soil particles by growing vegetation [9].

The infiltration rate of a specific pavement surface at a given moment in time depends on the quality of materials and construction, and the history of compaction and sedimentation. The infiltration rate assigned for the design of a surface should be a typical value which will apply for the life of the pavement [9]. It can be seen from previous research, the infiltration rate ranges are from the lowest 0.08 cm per second to the highest 1.33 cm per second. However, based on ASTM C 1781, the average infiltration rates ranging from 30 to 1600 inch per hour (0.21 cm per second to 1.13 cm per second) and the average result difference between two location averages 19.1 percent with a median value of 12.2 [11].

## MATERIAL AND METHODS

This research study on the properties of readymade porous concrete pavers. The density, void content and infiltration rate of readymade porous concrete pavers. The reading of density and void content are taken to review the consistency of porous concrete pavers' production. While, the infiltration rate reading is taken with different design of jointing of porous concrete pavers.

### Material

The readymade porous concrete pavers with hexagonal shape were used for this experiment. The pavers were produced in the factory with controlled environment and production. This pavers have a rough texture compared to normal concrete pavers where it is allow water to go through the pavers.



Fig. 2 Porous concrete pavers

### Density and void content

Density and void content test was carried out using standard test ASTM C642 (Standard Test Method for Density, Absorption, and Voids in Hardened Concrete). The calculation for density and void content are as follow:-

$$\text{Bulk density} = [A/(C - D)] \rho = g_1 \quad (1)$$

$$\text{Apparent density} = [A/(A - D)] \rho = g_2 \quad (2)$$

Where A is the weight of oven-dried sample measured in grams, B is the weight of surface-dry sample after immersion measured in grams, C is the weight of surface-dry sample after immersion and boiling measured in grams and D is the apparent mass of sample in water after immersion and boiling measured in grams. While,  $\rho$  is the density of water which  $1 \text{ Mg/m}^3 = 1 \text{ g/cm}^3$ .

Moreover, the void content is a percentage of the volume of permeable pore space (voids) as in Eq. 3.

$$\text{Void content, \%} = (g_2 - g_1)/g_2 * 100 \quad (3)$$

Where,  $g_1$  is the bulk density, dry, ( $\text{Mg/m}^3$ ) and  $g_2$  is apparent density ( $\text{Mg/m}^3$ ).

### Infiltration rate

Infiltration rate test was carried out using standard test ASTM C1781 (Standard Test Method for Surface Infiltration Rate of Permeable Unit Pavement Systems). A single infiltration ring is used for this test.

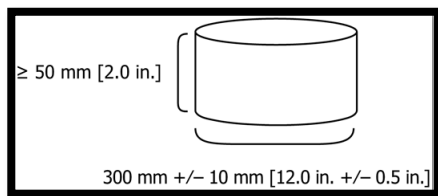


Fig. 3 Dimension of single infiltration ring.



Fig. 4 Infiltration ring

The calculation for infiltration rate is as follow:-

$$I = KM/(D^2 * t) \quad (4)$$

Where, I is the infiltration rate measured in mm/h (in./h), M is the mass of infiltrated water measured in kg (lb), D is the inside diameter of infiltration ring measured in mm (in.), t is the time required for measured amount of water to infiltrate the surface measured in second (s) and K is 4 583 666 000 in SI units or 126 870 in (inch-pound) units.

### RESULT AND DISCUSSION

The density and void content of readymade porous concrete pavers were taken and analyzed using statistical analysis by measuring the mean and standard deviation in order to measure the consistency during production of the pavers. While, infiltration rate reading is taken too compared between different designs of jointing.

#### Consistency of density of porous concrete pavers

The result shows the mean of density is 2.05 Mg cubic meter with standard deviation 0.041. Based on Fig. 5, the value of densities are spread out near the mean of the samples and Fig. 6 shows the samples are

normally distributed. These showed the samples are consistent in their densities.

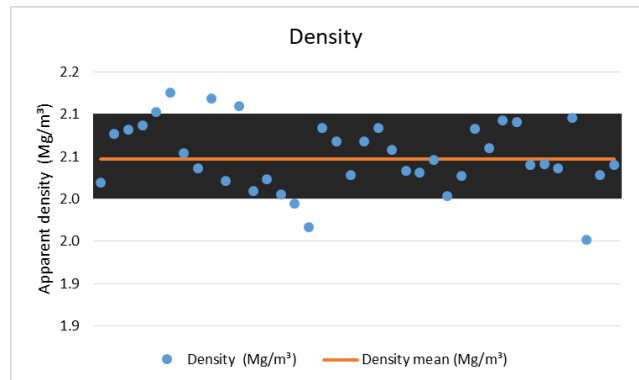


Fig. 5 Standard deviation graph of density

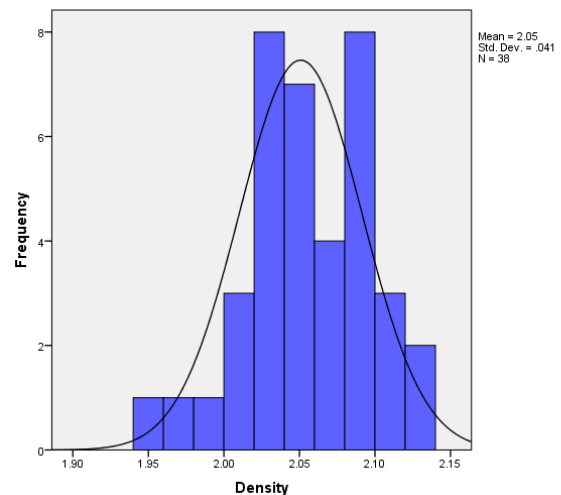


Fig. 6 Normal distribution graph of density

#### Consistency of void content of porous concrete pavers

The result shows the mean of void content is 5.65 percent with 0.432 standard deviation. The values of void content are spread out near the mean value as shown in Fig. 7. it is also shown the void content of porous concrete pavers are normally distributed and this shows they are consistent in their void content as shown in Fig. 8.



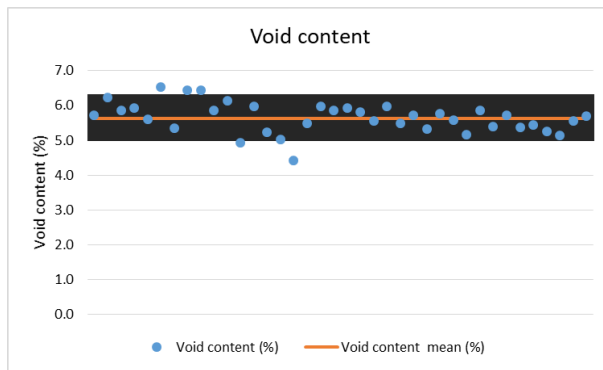


Fig. 7 Standard deviation graph of void content

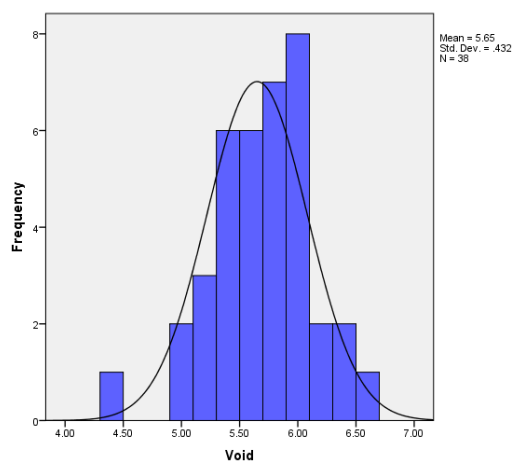


Fig. 8 Normal distribution graph of void content

### Effects of jointing design on infiltration rates

Fig. 9 and Fig. 10 shows the design of jointing and location of infiltration ring for infiltration rates test.



Fig. 9 Joint design A



Fig. 10 Joint design B

Table 1.1 shows the result of infiltration rate and length of jointing. As shown in Table 1.1, the infiltration rate for Design B is higher compared to infiltration rate for Design A. It can be seen the infiltration rate is higher with the longer length of jointing. Longer length of joint will infiltrated more water compared to short length of joint.

Table 1 Infiltration rates and length of joint

| Design | Group   | Infiltration rate (in/h) | Length of joint (mm) |
|--------|---------|--------------------------|----------------------|
| A      | Group 1 | 1199                     | 544                  |
|        | Group 2 | 1175                     | 544                  |
| B      | Group 3 | 1496                     | 867                  |
|        | Group 4 | 1415                     | 873                  |

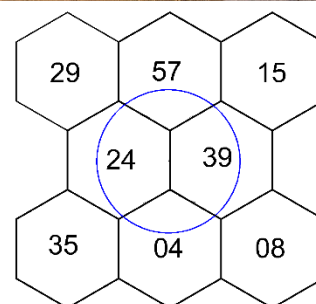


Fig. 11 Infiltration test for Design A Group 1

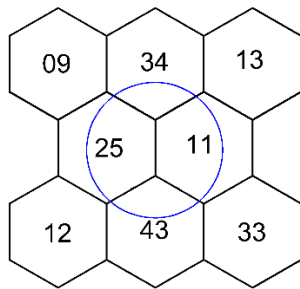


Fig. 12 Infiltration test for Design A Group 2

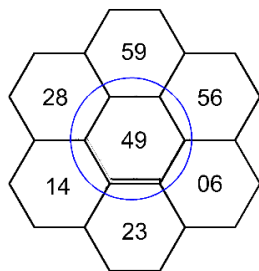


Fig. 13 Infiltration test for Design B Group 1

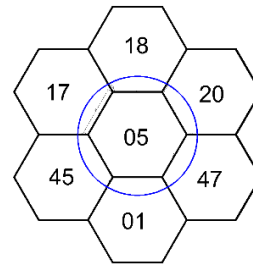


Fig. 14 Infiltration test for Design B Group 2

The length of jointing were measured by using AutoCAD 2017 program based on actual arrangement during infiltration test. The schematic layout

## CONCLUSIONS

The result of the experimental test for density and infiltration rate for porous concrete paver were acceptable where the range density are 1600 kg per cubic meter to 2000 kg per cubic meter and the density of readymade porous concrete pavers range are between 2000 kg per cubic meter to 2100 kg per cubic meter. While the infiltration rate of these samples are acceptable where the value of infiltration rates are between 1175 inch per hour to 1496 inch per hour. As mention in ASTM 1781, the range of infiltration rates are between 30 inch per hour to 1600 inch per hour. However, the void content of these porous concrete pavers does not achieve the void content required for porous ranged are between 15 percent to 30 percent. While in ASTM C1754 mentioned the void content ranged from 22.6 percent to 37.0 percent. However, the void content of these porous concrete pavers are between 4.4 percent to 5.6 percent. This shows a large different between standard void content and actual void content of pavers. More investigation need to be done on the variety of arrangement and how they compensate the deficiency in the individual block. Future study can be conducted to measure the void content where the spaces of jointing will be included in the void content measurements.

## REFERENCES

- [1] I. Abustan, M. O. Hamzah, and M. A. Rashid, 'Review of permeable pavement systems in Malaysia conditions', *OIDA Int. J. Sustain. Dev.*, vol. 4, no. 02, pp. 27–36, 2012.
- [2] J. Sansalone, M. Asce, X. Kuang, and V. Ranieri, 'Permeable Pavement as a Hydraulic and Filtration Interface for Urban Drainage', *J. Irrig. Drain. Eng.*, vol. 134, no. October, pp. 666–674, 2008.
- [3] C. Pagotto, M. Legret, and P. L. E. Cloirec, 'COMPARISON OF THE HYDRAULIC BEHAVIOUR AND THE QUALITY OF HIGHWAY RUNOFF WATER', *Water Res.*, vol. 34, no. 18, pp. 4446–4454, 2000.
- [4] M. Giguère, *Urban Heat Island Mitigation Strategies*. 2009.
- [5] E. P. A. EPA, 'Reducing Urban Heat Islands : Compendium of Strategies Cool Pavements', United State, 2005.
- [6] M. Cahill, D. C. Godwin, and M. Sowles, 'Porous Pavement', *Low Impact Dev. Fact Sheet*, p. 12, 2011.
- [7] P. D. Tennis, M. L. Leming, and D. J. Akers, *Pervious Concrete Pavements*. 2004.
- [8] I. ASTM, 'Standard Test Method for Density and Void Content of Hardened Pervious Concrete', pp. 1–3, 2018.
- [9] K. F. Bruce, *Porous Pavements*. 2005.
- [10] C. Valeo and R. Gupta, 'Determining Surface Infiltration Rate of Permeable Pavements with Digital Imaging', *Water*, vol. 10, no. 133, pp. 1–22, 2018.
- [11] A. International, 'Standard Test Method for Surface Infiltration Rate of Permeable Unit Pavement', pp. 3–8, 2018.

# CONSTRUCTING AN ARTIFICIAL INTELLIGENCE MODEL FOR WATER ENVIRONMENT EVALUATION

Shengping Zhang<sup>1</sup> and Jie Qi<sup>2</sup>

<sup>1</sup>Professor, Meijo University, Japan; <sup>2</sup> Professor, Utsunomiya University, Japan

## ABSTRACT

This study constructs an artificial intelligence (AI) model to evaluate water environments, and applies an artificial neural network system to this AI model construction. This AI model has been tested in a real urban river basin. The evaluation results based on the model reveal that most parts of the river are not suitable to its management goal. Therefore, a sensitivity analysis based on the AI Model is carried out to select and rank the river environment improvement measures in terms of the effectiveness of improvement. This study has shown that an AI Model is able to reveal and simulate the complicated relationships between river management goals and diverse river environment factors and also is able to make the sensitivity analysis and the selecting of effective river environment improvement measures much more convenient and reliable. This study will contribute to establishing a more reliable river environment planning and management methodology.

*Keywords: Water Environment Evaluation, Artificial Intelligence (AI), Neural Network, Sensitivity Analysis*

## INTRODUCTION

Water environment evaluation is necessary not only for water environment planning but also for selecting the most effective and most efficient water environment improvement measures. The traditional water environment evaluation methods can be classified into three groups [1]-[3].

The most-widely applied water environment evaluation method is the one based on the physical, chemical or biochemical indexes of river water quality, such as PH, Dissolved Oxygen (DO), Biochemical Oxygen Demand (BOD), and total coliforms. Objectivity is considered to be the most significant and most important character of this method which, however, also leads to critiques that relatively subjective resident/human demands for water environments have not been taken into consideration with this method.

In order to maximize the utility of the residents in a river basin, the water environment evaluation method based on the satisfaction of all residents has been applied quite frequently, particularly in urban river planning in which resident satisfaction is the main water environment management goal. Questionnaire survey is the central tool of this method.

The third common method for water environment evaluation is based on the biodiversity of the water environment, which takes the perspective that the water environment is not only for human beings but also for the entire ecosystem.

Every method is suitable for some specific water environment planning goals, and there are no particular standards or characteristics that can be used to distinguish one from the others as good or bad. But

there is one very strong common criticism which applies to all three methods [3]: each method has only evaluated the final water quality/environment. No direct connections between evaluation results and the causes or related environmental factors inside the river basins have been taken into any consideration in all of the methods although water environment is necessarily considered as a whole system.

Artificial intelligence (AI) has achieved great successes in a broad range of fields such as image recognition, automatic driving, and gaming due to AI's strong capability to identify causal relations [3], [4]. An AI model is expected to be a powerful analytic tool for water environment evaluation when the water environment of a specific river is considered to be a result caused by all possible water-environment-related factors in the river basin. This study will construct an AI model specifically for water environment evaluation and establish a more reliable methodology for river environment planning and management.

## ARTIFICIAL INTELLIGENCE MODEL

An artificial intelligence model, specifically a neural network model has been adopted to compose a water environment evaluation method for evaluation or prediction problems due to the suitability of neural network models [4], [5].

### Structure of A Neural Network [5]

A neural network is a network system constructed artificially by idealizing the neurons (nerve cells), and consists of a number of nodes and lines that are called

units and connections (or links) respectively. Based on the differences in network structures, neural networks generally are classified into two types: layered networks and interconnected networks. It has been shown that a layered network is suitable for evaluation/prediction problems due to its abilities in learning (self-organization) and parallel processing of information.

Figure 1 shows the structure of a typical layered neural network, which has a layer of input units at the top, a layer of output units at the bottom, and a number of hidden layers between the input layer and the output layer. Connections exist only between the units in the adjacent layers, and connections within a layer or from a higher to lower layers are forbidden.

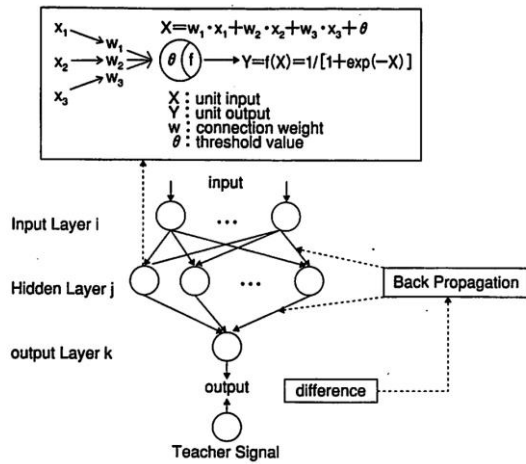


Fig. 1 Structure of a layered neural network.

### Modelling A Neural Network

For the sake of simplicity, consider a neural network consisting of three layers.

Let the unit numbers of the input layer, hidden layer and output layer be  $N$ ,  $M$ , and  $1$ , respectively. When an input  $\{I_i, i = 1, 2, \dots, N\}$  is given to the units of the input layer, the inputs and outputs of the hidden layer units as well as the output layer units are represented as follows.

$$Y_j = f(X_j), \quad j = 1, 2, \dots, M \quad (1)$$

$$X_j = \sum_{i=1}^N w_{ij} I_i + \theta_j, \quad j = 1, 2, \dots, M \quad (2)$$

$$O = f(Z) \quad (3)$$

$$Z = \sum_{j=1}^M w_j Y_j + \theta \quad (4)$$

Where  $Y_j$  : output from the unit  $j$  of the hidden layer.

$X_j$  : input the unit  $j$  of the hidden layer.

$f(\cdot)$  : unit output function.

$w_{ij}$  : connection weight between the input layer unit  $i$  and hidden layer unit  $j$ .

$\theta_j$  : threshold value of the hidden layer unit  $j$

$O$  : output from the output layer unit.

$Z$  : input to the output layer unit.

$w_j$  : connection weight between the hidden layer unit  $j$  and the output layer unit.

$\theta$  : threshold value of the hidden layer unit  $j$

For the unit output function  $f(\cdot)$ , some expressions have been proposed. The following Sigmoid function has been applied frequently. However, it is not necessarily the best one in terms of learning efficiency. A testing process for different output functions is strongly suggested.

$$f(x) = \frac{1}{1 + e^{-x}} \quad (5)$$

Theoretically, the neural network model expressed by Eqs. (1) through (5) is able to approximate any non-linear relationship between inputs and outputs with any degree of accuracy by using enough hidden layer units and setting connection weights and thresholds to be appropriate through proper learning processes [5].

### Learning Process of Neural Network Model

For a neural network model, the process of setting the connection weights unit thresholds is called *learning*. The term *learning* here means the self-organization process through which the neural network model automatically adjusts all the parameters (i.e. all the connections and thresholds) to the appropriate values, when a series of samples of input-output data (called teacher data or teacher signals) are shown to the model. If we consider the information processing in a neural network model as a transformation of input data to output data, then model learning can be considered to be a process through which the neural network model gradually becomes capable of imitating the transforming patterns represented by the teacher data.

A lot of learning algorithms have been proposed, and among them the Error Back Propagation Algorithm is the most widely used and most successful algorithm. The following is the summary of the Error Back Propagation Algorithm [6].

Suppose  $T$  sets of teacher data are given.

$$\{I_1^{(t)}, I_2^{(t)}, \dots, I_N^{(t)}, O^{(t)}; t = 1, 2, \dots, T\} \quad (6)$$

Notice that the teacher data consists of two parts: the input part  $\{I_1^{(t)}, I_2^{(t)}, \dots, I_N^{(t)}; t = 1, 2, \dots, T\}$  and

the output part  $\{O^{(t)}; t = 1, 2, \dots, T\}$ .

Now consider an initial value

$$w_{ij}^{[k]}, w_j^{[k]}, \theta_j^{[k]}, \theta^{[k]}, k = 0 \quad (7)$$

for each of the connection weights and threshold values, respectively. Notice that the superscript  $[k]$  indicates the number of learning iterations and  $[k=0]$  means the initial values for all the parameters directly preceding the start of the learning process. Then the outputs corresponding to the inputs of the teacher data  $\{I_1^{(t)}, I_2^{(t)}, \dots, I_N^{(t)}; t = 1, 2, \dots, T\}$  can be obtained from Eq. (1) ~ Eq. (5). Let these outputs be  $\{U^{[k](t)}; t = 1, 2, \dots, T \text{ and } k = 0\}$ . Clearly,  $\{U^{[k](t)}; t = 1, 2, \dots, T \text{ and } k = 0\}$  are different from the outputs of the teacher data  $\{O^{(t)}; t = 1, 2, \dots, T\}$ , and an error function can be defined with the two different kinds of outputs as follows.

$$R^{[k]} = \sum_{t=1}^T (O^{(t)} - U^{[k](t)})^2, k = 0 \quad (8)$$

Obviously,  $R^{[k]}$  is a function of connection weights and threshold values because  $\{U^{[k](t)}; t = 1, 2, \dots, T \text{ and } k = 0\}$  are calculated after all  $w_{ij}^{[k]}$ ,  $w_j^{[k]}$ ,  $\theta_j^{[k]}$  and  $\theta^{[k]}$  are given.

The Error Back Propagation Algorithm makes use of the connection weights and threshold values that minimize the above error function  $R^{[k]}$ . Usually a non-linear programming method is required to solve the optimization problem along with an iteration process in order to obtain the optimal (but possibly suboptimal) connection weights and threshold values. The final iteration procedures derived from a non-linear programming method known as the Method of Gradient Descent are as follows.

$$w_j^{[k+1]} = w_j^{[k]} - \eta \cdot \sum_{t=1}^T (\delta^{[k](t)} \cdot Y_j^{[k](t)}) \quad (9)$$

$$\theta^{[k+1]} = \theta^{[k]} - \eta \cdot \sum_{t=1}^T \delta^{[k](t)} \quad (10)$$

$$w_{ij}^{[k+1]} = w_{ij}^{[k]} - \eta \cdot \sum_{t=1}^T (\delta^{[k](t)} \cdot w_j^{[k+1]} \cdot Y_j^{[k](t)} \cdot I_i^{(t)}) \quad (11)$$

$$\theta_j^{[k+1]} = \theta_j^{[k]} - \eta \cdot \sum_{t=1}^T (\delta^{[k](t)} \cdot w_j^{[k+1]} \cdot Y_j^{[k](t)}) \quad (12)$$

where the superscript  $[k]$  indicates the number of learning iterations as mentioned earlier, and  $\eta$  is a small positive number that indicates the step size of the Method of Gradient Descent for optimization iteration process, and we have set  $\eta = 0.25$  in this

study. The other variables which occurred in the final learning procedures are defined as follows.

$$\delta^{[k](t)} = (O^{(t)} - U^{[k](t)}) \cdot O^{(t)} \cdot (1 - O^{(t)}) \quad (13)$$

$$Y_j^{[k](t)} = Y_j^{[k](t)} \cdot (1 - Y_j^{[k](t)}) \quad (14)$$

In order to avoid the overfitting (or over-learning) problem, a criterion is usually required to make a judgement when the iterative learning process should be terminated. In this study the learning process will be stopped when the Mean Relative Error (MRE) of the outputs is less than a specified relative error expectation for prediction/evaluation results, which is a common treatment for a learning process of teacher data with random errors (i.e. white noise). In this study we have set the error expectation to 2%, which is considered an accuracy that is good enough for the expected result in this study. Needless to say, this error expectation should be set according to the required accuracy of the problem which is being dealt with.

### Verification of Neural Network Model

The proposed neural network model has been verified by applying it to an urban daily water demand prediction problem [7], which has been studied with several different models, and for which there is clarity regarding what is a good or an acceptable prediction for daily water demand. We will examine whether the proposed neural network model is able to predict daily water demand with the same or even higher accuracy by using the same information as the other prediction models used.

Specifically, the neural network model has been compared with three different prediction models: Multiple Regression Model [8], ARIMA (Auto-Regressive Integrated Moving Average) Model [9], [10] and Kalman-Filtering Model [10]. All the models used the same daily water delivery records from April 1982 to March 1990 for a city in Japan, the weather information during the same time period and each day's characteristics (weekday or weekend/national holiday) to calibrate or identify the model parameters. This historical data is used because the comparison models are composed with these data. For the neural network model, these records are used as the teacher data to train the model. As for the weather information, the records of daily high temperature, weather (sunny, cloudy or rainy) and daily precipitation are included.

Three accuracy indexes have been applied to compare the models to identify which model is able to give the most accurate prediction for daily water demands. Mean Relative Error (MRE, %) is a very straight index: the smaller the Mean Relative Error is, the better the predictions are. Correlation Coefficient (CC) between predictions and records indicates how



good the predictions are: the predictions are perfect when  $CC=1.0$ , and the predictions are totally random when  $CC=0$ . Relative Root Mean Square Error (RRMSE) are similar to CC and reflect how good the predictions are:  $RRMSE=0$  for perfect predictions and  $RRMSE=1$  when all the predictions are equal to the mean of the records.

Table 1 shows the prediction accuracies of daily water demands over the course of a year for the same city from April 1991 to March 1992 by different models. The neural network model gave the best predictions by far in terms of all the three accuracy indexes. The improvement magnitudes of prediction accuracy in each index show the reliability and the potential of the neural network model.

Table 1 Prediction accuracy comparison of different models.

| Model                     | MRE(%) | CC    | RRMSE |
|---------------------------|--------|-------|-------|
| Multiple Regression Model | 2.90   | 0.764 | 0.659 |
| ARIMA Model               | 2.80   | 0.794 | 0.623 |
| Kalman Filtering Model    | 2.69   | 0.808 | 0.599 |
| Neural Network Model      | 2.13   | 0.877 | 0.483 |

In order to understand the error structure of the predictions given by the neural network model, the prediction error distribution is shown in Table 2, and the possible causes have been examined for the 5 days which have a prediction relative error greater than 10%, which is shown in Table 3. Per Table 3, the largest prediction error was yielded when important information that affected daily water demands was missed. In other words, prediction accuracy is expected to be further improved when this missed information, such as typhoon, continuous rain periods, extreme weather events or atypical days, are taken into consideration by including all of them into the teacher data for neural network training. This demonstrates that careful teacher data hunting is important in artificial intelligence application research.

Table 2 Relative error distribution of the predictions made by the Neural Network Model

| Relative Error Range (%) | No. of Days | Composition (%) |
|--------------------------|-------------|-----------------|
| [0.0, 3.0)               | 278         | 76.2            |
| [3.0, 5.0)               | 61          | 16.7            |
| [5.0, 8.0)               | 19          | 5.2             |
| [8.0, 10.)               | 2           | 0.5             |
| [10. , $\infty$ )        | 5           | 1.4             |

Based on these results, it is reasonable to conclude that the proposed neural model is a reliable and capable tool in information processing of data. In the next section we will apply this neural network model to river environment evaluations and predictions in order to provide better information for water

environment planning and management.

Table 3 The possible causes for the days with a relative error more than 10%.

| Date     | Demand prediction (m <sup>3</sup> /day) | Delivery record (m <sup>3</sup> /day) | Relative error (%) | Possible causes  |
|----------|---|---------------------------------------|--------------------|--|
| May 5    | 354.5                                   | 320.0                                 | 10.8               | The last day of Japanese holiday "Golden Week" and sunny after a rainy week. |
| Sept. 17 | 364.9                                   | 319.5                                 | 14.2               | Hit by typhoon.  |
| Oct. 5   | 362.9                                   | 315.0                                 | 15.2               | Heavy rain. (105.5mm/day)  |
| Oct. 7   | 361.4                                   | 404.4                                 | 10.6               | Sunny after 5 continuous rainy days.   |
| Jan. 2   | 358.5                                   | 315.0                                 | 13.8               | New Year Holiday and sunny.  |

## TRAINING OF NEURAL NETWORK MODEL

### Teacher Data

The neural network model proposed above is now ready to be applied to a water environment evaluation problem, which is the purpose of this study. As for the water environment evaluation index, the habitability of a water environment to Genji fireflies (*Luciola cruciate*) is adopted. Genji fireflies are highly prized in Japanese culture, and are widely regarded as a symbol for a good water environment. Firefly habitability has even been adopted as a river environment management goal in many urban river basins in Japan.

As for the factors that affect the habitability of fireflies, five highly critical factors have been selected to be included in the teacher data although there are many factors that impact firefly habitability [11]. Additionally, these five factors have been selected because they are the main changeable factors through common river environment improvement measures. The five factors are 1) Concentration of Dissolved Oxygen (DO), 2) Brightness of lighting during nighttime, 3) Inflow of sewage, 4) Riverbed situation, and 5) Type of revetment construction.

### Quantification of Habitability and Factors

Firefly habitability and related factors have been quantified by utilizing information and knowledge about Genji fireflies from existing research [11], [12].

First, firefly habitability is treated as a continuous variable which ranges from 0.0 (for extremely unlivable water environments) to 1.0 (for an idealistic water environment). Then, all the factors are categorized although most are usually measured quantitatively as a continuous figure. This resolves the issue that the same number can mean different

things for different rivers. For example, the sewage inflow rate 1.0 *ton/hour* is an extremely strong pollution source for small urban rivers, but could mean almost nothing for a river with a flow rate of more than 100  $m^3/s$ .

As an example, Concentration of Dissolved Oxygen (DO) is categorized as 1 for a DO saturated situation, 0 for the DO concentration above 6.8 *mg/l* (which means a livable environment for fireflies), and -1 for the DO concentration below 6.8 *mg/l* (which means an undesirable/deadly living environment). In the same way, the other four factors are also categorized as shown in Table 4.

Table 4 Factor Quantification

| Factor                                 | Category | Meaning                                      |
|--|----------|--|
| Concentration Of Dissolved Oxygen (DO) | 1        | DO saturated                                 |
|  | 0        | $\geq 6.8 \text{ mg/l}$ , livable            |
|  | -1       | $< 6.8 \text{ mg/l}$ , undesirable           |
| Inflow of sewage                       | 1        | No sewage inflow                             |
|  | 0        | A small amount of inflow                     |
|  | -1       | Constant inflow                              |
| Brightness Of lighting                 | 1        | Dark (no artificial light)                   |
|  | 0        | Relatively dark                              |
|  | -1       | Bright                                       |
| Riverbed situation                     | 1        | Natural riverbed with soil, sands or pebbles |
|  | -1       | Artificial riverbed                          |
| Type of revetment construction         | 1        | Natural                                      |
|  | 0        | Partially natural                            |
|  | -1       | Artificial                                   |

The firefly habitability and the five related factors together make the teacher data. Samples of teacher data which are used in this study are shown in Table 5. 162 teacher data have been collected from a variety of research references on Genji firefly habitability [11], [12].

Table 5 Teacher data samples.

| Concentration of DO | Inflow of sewage | Brightness of lighting | Riverbed situation | Type of revetment | Habitability |
|---------------------|------------------|------------------------|--------------------|-------------------|--------------|
| 0                   | 1                | 1                      | 1                  | 0                 | 0.915        |
| -1                  | 1                | 1                      | 1                  | 0                 | 0.000        |
| 1                   | 0                | 1                      | 1                  | 0                 | 0.875        |
| 0                   | 0                | 1                      | 1                  | 0                 | 0.865        |
| -1                  | 0                | 1                      | 1                  | 0                 | 0.000        |
| 1                   | -1               | 1                      | 1                  | 0                 | 0.000        |
| 1                   | 1                | 1                      | 1                  | 1                 | 1.000        |

### Training of Neural Network Model

The neural network model has been trained (put under a learning process) with the collected teacher data. The training process is based on the learning procedures as explained before, but it is still a process of trial and error because there are still a lot of details that remain undecided, such as a suitable step size of optimization, a suitable output function, an efficient

order to present the teacher data to the neural network model, and a proper initial network size (layers and units in each layers). An experienced AI engineer may be able to assist in accelerating the learning process.

Figure 2 shows the reproduction accuracy of the teacher data with the trained neural network model. Here the reproduction accuracy is represented by the absolute error between the habitability in the teacher data and the habitability generated with the trained neural network model. Based on the results in Fig. 2, there are only 6 out of 162 teacher data that have the same order of absolute error as the smallest significant figure ( $\pm 0.001$ ) of habitability, and all the 156 teacher data have an error less than the smallest significant figure, which means that the trained neural network model is able to reproduce the teacher data with almost no errors. In the next section, this well-trained neural network model will be used to evaluate the firefly habitability of an urban river.

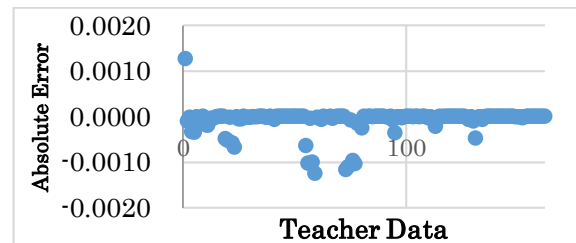


Fig. 2 Reproduction accuracy of teacher data

## WATER ENVIRONMENT EVALUATION

### Firefly Habitability of Aise River

The trained neural network model has been applied to evaluate the firefly habitability of Aise River. Aise River passes through Inuyama City in Aichi prefecture, Japan, and is a typical urban river which receives sewage and urban drainage. Aise River also receives fresh water inflow at its uppermost location from Kisogawa River, a regional water supply source with a high flow rate. The fresh water from Kisogawa River has improved the water environment of Aise River in its upper segments significantly, but the improvement effects have been gradually cancelled out by the constant sewage inflow when the river runs downstream. In this study, Aise River has been divided into four segments according to the present water environment: upper, mid-upper, mid-lower and lower. Fig. 3 shows the images of the four segments of Aise River.

The present water environment factors of Aise River and its firefly habitability yielded by the trained neural network model are shown in Table 6. The evaluation results can be summarized as follows.

- The upper segment of Aise River is a habitat very suitable to Genji fireflies.
- The habitability has decreased sharply

downstream.

- The mid-lower and the lower segments of Aise River are no longer habitable to Genji fireflies.

The above conclusions derived from the evaluation results that are given by the trained neural network model match well with the observation that there are no fireflies during summer along the mid-lower and lower segments of Aise River for many years.



(a) Upper Segment



(b) Mid-Upper Segment



(c) Mid-Lower Segment



(d) Lower segment

Fig. 3 Images of Aise River

Table 6 The firefly habitability of Aise River

| Location  | Concentration of DO | Inflow of Sewage | Brightness of lighting | Riverbed situation | Type of revetment | Habitability |
|-----------|---------------------|------------------|------------------------|--------------------|-------------------|--------------|
| Upper     | 1                   | 1                | 1                      | 1                  | 1                 | 0.999        |
| Mid-Upper | 1                   | 1                | 0                      | 1                  | 0                 | 0.874        |
| Mid-Lower | 1                   | 0                | 0                      | 1                  | -1                | 0.471        |
| Lower     | 1                   | -1               | -1                     | -1                 | -1                | 0.003        |

## Sensibility Analyses of Factors

The trained neural network model has also been used to carry out a sensibility analysis for all the factors related to firefly habitability. The sensibility coefficient of a factor is defined as the partial derivative of the habitability regarding the factor as follows.

$$S_i = \frac{\partial O(X_1, X_2, \dots, X_N)}{\partial X_i} \Big|_{\text{present factor values}} \quad (15)$$

$S_i$  is the sensitivity coefficient of factor  $X_i$  at the present factor values. For all the factors, the sensitivity coefficients have been calculated and shown in Table 7. The whole number 0 means a coefficient value less than the smallest significant figure.

Table 7 Sensibility coefficients of factors.

| Location  | Concentration of DO | Inflow of Sewage | Brightness of lighting | Riverbed situation | Type of revetment |
|-----------|---------------------|------------------|------------------------|--------------------|-------------------|
| Upper     | 0.0003              | 0.0042           | 0.0016                 | 0.0002             | 0.0016            |
| Mid-Upper | 0.0749              | 0.0585           | 0.4608                 | 0.1195             | 4.4079            |
| Mid-Lower | 0.0010              | 0                | 0.0002                 | 0.0002             | 0.0011            |
| Lower     | 0                   | 0                | 0                      | 0                  | 0                 |

For the upper segment of Aise River, all the factors have a relatively small sensibility coefficient, which is because the present values of all the factors are good enough and there is no room for further improvement.

For the mid-lower and lower segments, all the factors also have a relatively small sensibility coefficient, which is because the present values of all the factors are so poor that a small improvement will not make a meaningful change in firefly habitability along these river segments.

For the mid-upper segment, the revetment has a large sensitivity coefficient, this indicates that improving the present revetment (partially natural) will increase the firefly habitability significantly. The brightness factor also has a large sensitivity coefficient, which means that removing all the artificial lighting will improve the firefly habitability. The other three factors all have a relatively small sensitivity coefficient, which is because the present values of these factors are already good, and there is no need for further improvement.

## Selecting Improvement Measures

The evaluation results of firefly habitability along with the sensibility analysis results have drawn a clear picture about the most effective water environment improvement measures, which can be summarized as follows.

- For the upper segment, no improvement measures are necessary because the present situation is already good enough.
- For the mid-upper segment, changing the revetment into natural revetment and removing all the artificial lighting are expected to raise firefly habitability significantly.
- For the mid-lower and lower segments, significant improvement for all factors are necessary because a small change for either factor is not expected to cause any meaningful improvement in firefly habitability due to the poor situation at present.

## CONCLUSIONS

With the purpose of developing a better methodology for water environment planning and management, a neural network model has been proposed for water environment evaluation in this study.

The neural network model was tested with the daily water demand prediction problem, a well-studied problem suitable for testing. The test has shown the reliability and potential of an artificial intelligence model.

The verified neural network model was applied to a water environment evaluation problem, specifically the Genji firefly habitability problem. The application results have shown that, with a neural network model, not only can the environment of an urban river be evaluated with a high level of accuracy and detail, but also that the most effective environment improvement measures can be clearly identified. These results demonstrate that artificial intelligence is an effective and efficient tool for water environment evaluation.

The firefly habitability was studied with only select critical factors in this study, which is insufficient for genuine habitability research because there are many other factors which affect firefly habitability. The factors were limited to the critical ones due to the limitations of data hunting. This illustrates that one of the significant challenges of

practical research on artificial intelligence applications will be the gathering of teacher data. In spite of these difficulties, artificial intelligence is a promising tool for water environment planning and management.

## REFERENCES

- [1] Hagihara R., Takahashi K. and Hagihara K., Urban Environment and Waterfront Planning, Keisoshobo Publisher, 1998.
- [2] Hagihara Y. and Hagihara K., Methodology of Planning for Water and Green, Kyoto University Publisher. 2010.
- [3] Zhang S. P. and Kido Y., A Study on the Environment Evaluation method for Aise River and the Effectiveness of River Environment Improvement Measures, Urban Science Studies, No. 21, 2016, pp. 45-56.
- [4] IPA, WHITE PAPER Artificial Intelligence 2019, Kadokawa publisher, 2018.
- [5] Asou H., The Information Processing by Neural Network Models, Sangyo Publisher, 1988.
- [6] Rumelhart D. E., Hinton G. E., and Williams R. J., Learning Representations by Back-propagating Errors, Nature, Vol. 323, No. 9, 1986, pp. 533-536.
- [7] Zhang S. P., Watanabe H., and Yamada Y., prediction of Daily Water Demands by Neural networks, Stochastic and Statistical Methods in Hydrology and Environmental Engineering, Vol. 3, 1994, pp. 217-227
- [8] Tsunoi M., An Estimate of Water Supply Based on Weighted Regression Analysis Using a Personal Computer, Journal of Japan Water Works Association, Vol.54, No. 3, 1985, pp.2-6.
- [9] Koizumi A., Inakazu T., Chida K., and Kawaguchi S., Forecasting Daily Water Consumption by Multiple ARIMA Model, Journal of Japan Water Works Association, Vol. 57, No. 12, 1988, pp. 13-20.
- [10] Yamada R., Zhang S. P., and Konda T., An Application of Multiple ARIMA Model to Daily Water Demand Forecasting, Annual Report of NSC, Vol. 18, No.1, 1992, pp. 126-136.
- [11] Furukawa Y., Encyclopedia of Fireflies, Tokyo Institute of Firefly Researches, 2001
- [12] Murada Y., A Study on the Water Qualities for Firefly Habitats, Proc. Of the 50<sup>th</sup> Annual Meeting of the Civil Engineering Associations of Japan. 2005.

# INFLUENCE OF ERRORS THAT RESULT FROM CONSIDERATION OF WATER IN-FLOW DIMENSION DIFFERENCES BASED ON OBSERVATION METHOD FOR MOUNTAIN TUNNEL CONSTRUCTION

Yasuyuki Kubota<sup>1</sup>, Moritada Mori<sup>2</sup>, Toru Yasuda<sup>3</sup>, Satoshi Nishiyama<sup>4</sup>

<sup>1</sup>Environmental Science and Technology, Okayama University, Japan; <sup>2</sup>Takenaka Civil Engineering & Construction, Japan; <sup>3</sup> Pacific Consultants Co., Ltd, Japan; <sup>4</sup>Graduate School of Environmental and Life Science, Okayama University, Japan

## ABSTRACT

Groundwater infiltration during mountain tunnel construction can lead to several problems, including tunnel face collapses and environmental impacts. To address these issues, it is necessary to be able to evaluate groundwater flow rapidly and accurately, and hence, Sequential Data Assimilation – System on Water Information of Ground (SDA-SWING) method was developed. It enables inverse analysis using a simplified model and reflects observational data from the site. However, groundwater inflow control during tunnel excavation is generally difficult, as it depends on the heterogeneity of the geological structure. According to the equations for Dupuit quasi-uniform flow and Bear associated rainfall penetration rate, the SDA-SWING method incorporated a certain error, in that flow in the vertical and depth directions is not considered, strictly speaking, as isotropic hydraulic conductivity is assumed. In this study, we conducted numerical experiments on simulated tunnels and were able to verify how the error, which was caused by flow dimension difference, affected Ensemble Kalman Filter (EnKF) processing. As a result, the error in the SDA-SWING method was small enough compared to each analysis method, which is considered two-dimensional and three-dimensional flow, and the difference could be incorporated into the analysis at the initial stages of excavation when performing EnKF processing. For this reason, we reported that the method has the potential to be a system, which is able to evaluate groundwater flow quickly and accurately.

*Keywords: Tunnel excavation, Groundwater, EnKF, SDA-SWING*

## INTRODUCTION

There are various problems associated with groundwater in mountain tunnel construction, including collapse of the tunnel face, delays to excavation schedule, damage to excavation machinery, and environmental impact. To address these problems, it is necessary to be able to evaluate groundwater flow quickly and accurately. Prediction analysis is necessary and important, to reduce risks related to tunnel excavation, such as unexpected groundwater inflow to the tunnel. Numerical simulations by the finite element method (FEM) have been commonly used as the primary method for predicting and evaluating groundwater inflow into a tunnel and the impact of excavation on the surrounding groundwater environment. For better predictions and estimations, sophisticated numerical three-dimensional models, using suitable geological data obtained from field measurements, are required. However, as there are always limits to field investigations-mostly due to economic and technical issues, these predictions are not always correct. Inverse analysis, using value observations from the field, would be useful, although the three-dimensional models for FEM are not compatible with

this type of inverse analysis, and it is difficult to apply data obtained from observations such as tunnel inflow and groundwater level, due to numerical model complexities. Hence, the SWING (System on Water Information of Ground) method was developed as an evaluation method for groundwater flow. This model facilitates inverse analysis using a simplified model, and applies site-based observation data. Control of the groundwater inflow during tunnel excavation is a difficult issue, because it depends on the heterogeneity of the geological structure. The SWING method is an evaluation system that follows the tunnel excavation process, by reconstructing model steps using data obtained from observations made at the construction site. In this reconstructing process, you can determine parameters for the updated models by using an optimization method. In the original SWING method, parameter optimization was performed using trial-and-error, and required highly skilled personnel, so the method was modified using an Ensemble Kalman Filter (EnKF)-which is a data assimilation technique. Introduction of the EnKF allowed automatic optimization of hydraulic parameters, and the modified. The developed SWING method has been called SDA-SWING (Sequential Data Assimilation-SWING). According to the

equations for Dupuit quasi-uniform flow and Bear associated rainfall penetration rate, the SWING method introduce a certain amount of error, by not considering flow in both the vertical and depth directions, and assuming isotropic hydraulic conductivity. The SDA-SWING method is an approach to find the optimal solution considering the error. In this study, we conducted numerical experiments on simulated tunnels and verified how the error that was caused by flow dimension differences, affected the EnKF processing.

### THE SWING METOHD CONCEPT

The SWING method uses slice volumes, reflects site observation data, and enables inverse analysis using the simplified model and so is able to improve prediction accuracy. For develop the SWING method, this analysis should be satisfied with the strength and weakness of conventional tunnel groundwater inflow prediction methods.

#### Slice volumes during tunnel excavation

A slice volume is the tunnel excavation area divided at equal intervals (see Fig. 1). For each slice, we analyzed groundwater flow, assuming Dupuit quasi-uniform flow (see Fig. 2). The groundwater level at slice 1 is lowered after tunnel excavation; i.e., at the end of slice 1's excavation, the groundwater level is lowered, but only in slice 1. The new slice volume (slice 2) was added at the time when slice 2 became the analysis point. The analysis continued while accumulating slice volumes sequentially, as excavation progressed.

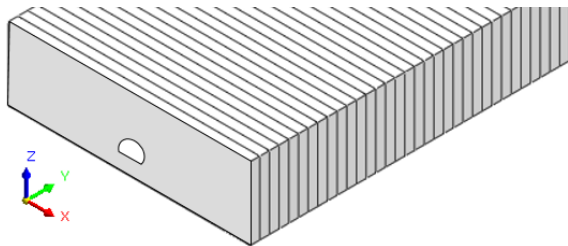


Fig. 1. Slice volume during tunnel excavation.

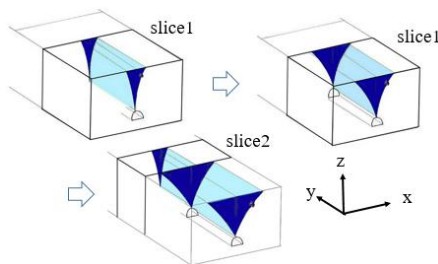


Fig. 2. Summation of slice volumes during tunnel excavation.

### Calculation of groundwater inflow and the range of groundwater level reduction

The SWING method incorporates some assumptions (see Fig. 3). (1) The tunnel is excavated in an aquifer that is above an impermeable layer. (2) The size of the excavated tunnel is relatively small compared to the analytical domain. (3) The initial groundwater table is horizontal above the tunnel (the location of the initial groundwater table is  $H_o$  from the upper boundary of the impermeable layer). (4) The rainwater infiltration rate,  $\varepsilon$ , is considered in the model. The SWING method follows the equations for Dupuit quasi-uniform flow, which the equations, the groundwater inflow to the tunnel per unit length,  $q(t)$ , and the groundwater level,  $h(x, t)$ , can be calculated using Eq. (1), as follows:[3]

$$\begin{cases} \frac{h(x, t)^2 - h_o^2}{H_o^2 - h_o^2} = \frac{x}{R(t)} \\ q(t) = k \frac{H_o^2 - h_o^2}{2R(t)} \end{cases} \quad (1)$$

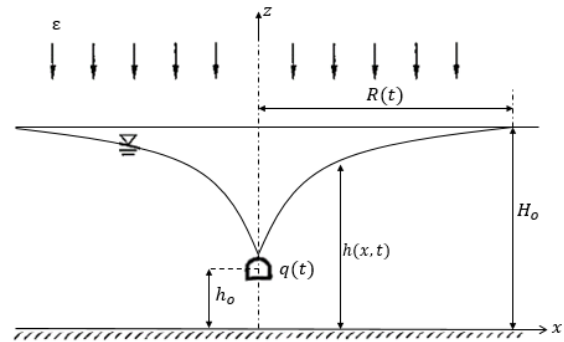


Fig. 3. Schematic of groundwater level variation caused by tunnel excavation.

In Eq.(1),  $\varepsilon$  is rainfall infiltration rate,  $k$  is stratum hydraulic conductivity,  $h(x, t)$  is groundwater level at position  $x$  as a function of time  $t$ ,  $H_o$  is initial groundwater level,  $h_o$  is the distance of the tunnel from the impermeable layer,  $q(t)$  is the amount of tunnel groundwater inflow for each slice volume, and  $R(t)$  is the range of influence (where the groundwater level is lowered as a result of tunnel excavation) for each slice volume.

Using Eq. (1), the groundwater level at any position, and its time evolution during the excavation process,  $h(x, t)$ , can be calculated as shown in Eq.(2).

$$h(x, t) = \sqrt{\frac{x}{R(t)} (H_o^2 - h_o^2) + h_o^2} \quad (2)$$

Considering the water balance, the amount of groundwater inflow to the tunnel should equal the sum of the groundwater lost in the aquifer plus



rainwater infiltration (see Fig. 4). This relationship is expressed in Eq. (3)-which is the Bernoulli equation- in which  $\lambda_e$  and  $\varepsilon$  are the porosity and rainfall infiltration rate, respectively.

$$qdt = k \frac{H_o^2 - h_o^2}{2R(t)} dt = \lambda_e \frac{H_o - h_o}{3} dL + \varepsilon R dt \quad (3)$$

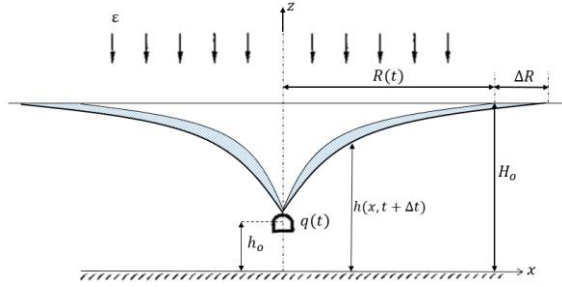


Fig. 4. Calculation method for groundwater inflow into the tunnel with each slice volume.

In terms of time,  $t$ , with the initial conditions of  $R(t) = 0$  at  $t = 0$ , Eq. (3) can be integrated between limits, to yield Eq. (4).

$$R(t) = \left[ \frac{k(H_o^2 - h_o^2)}{2\varepsilon} \left\{ 1 - e^{-\frac{6\varepsilon t}{\lambda_e(H_o - h_o)}} \right\} \right]^{\frac{1}{2}} \quad (4)$$

The range of influence at  $t = \infty$  can be calculated as shown in Eq. (5).

$$R(\infty) = \left[ \frac{k(H_o^2 - h_o^2)}{2\varepsilon} \right]^{\frac{1}{2}} \quad (5)$$

The instantaneous groundwater inflow (per unit of length) for each slice volume can then be calculated.

$$q(t) = \frac{k(H_o^2 - h_o^2)}{2R(t)} \quad (6)$$

From the above equations, the amount of groundwater inflow to the tunnel and the range of influence of the groundwater table can be calculated for each tunnel excavation stage (every slice volume), as shown in Fig. 2. The calculated groundwater inflow to the tunnel in each slice volume can be summed for the slice volumes' total, and the total calculated amount of groundwater inflow can be compared with observational data. The hydraulic conductivity for each slice volume is then back-calculated, based on the observation data. This process is repeated for each excavation stage and the hydraulic conductivity field can be continually updated hydraulic conductivity field can then be used to predict groundwater inflow to the tunnel. In the

SWING method, rainwater infiltration is considered using the rainfall infiltration rate,  $\varepsilon$ , which can be determined using a multi-tank model.

### INCORPORATING ENKF INTO THE SDA-SWING METHOD

EnKF processing is a form of the data assimilation, and incorporating it into the SWING method improved prediction accuracy and enabled automatic parameter optimization. However, according to the equations for Dupuit quasi-uniform flow and the associated Bear rainfall penetration rate, the SDA-SWING method incorporated an error, in that it didn't strictly consider flow in both the vertical and depth directions, as it assumed isotropic hydraulic conductivity. In addition, it included errors associated with both observation data, and caused by variations in hydraulic conductivity. These various errors are found in the governing equation, and so EnKF processing was incorporated into the SDA-SWING method, to derive optimal solutions based on observation data.

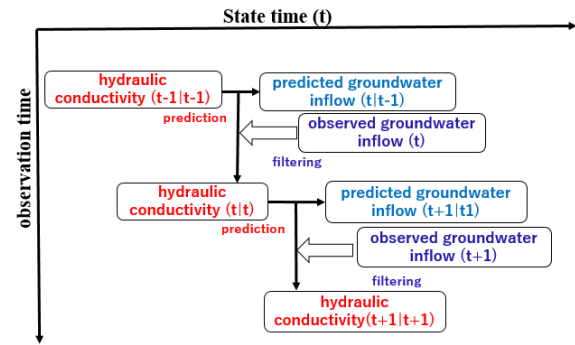


Fig. 5. The SDA-SWING method incorporating EnKF processing.

Data assimilation has two distinct phases-“predict” and “update”. The predict phase uses the state estimate of the previous time step,  $t-1$ , to produce an estimate of the state at the current time step,  $t$ . Although, it does not include observation information from the current time step, it is an estimate of the state at the current time step. In the update phase, the current prediction is combined with current observation information to refine the state estimate.

System model

$$x_t = f_t(x_{t-1}) + v_t \quad , \quad v_t \sim N(0, Q) \quad (7)$$

Observation model

$$y_t = h_t(x_t) + w_t \quad , \quad w_t \sim N(0, R) \quad (8)$$

In (7) and (8), vectors  $x_t$  and  $y_t$  indicate the state of a system and observed data at a discrete time, and

vectors  $v_k$  and  $w_k$  denote system noise and observation noise. Operation  $f_i$  represents the temporal evolution of a state from time  $t_{k-1}$  to time  $t_k$ , according to the system model based on the simulation, while  $H_k$  projects the state vector  $x_k$  to the observation space.

When performing optimization using observation data, we sought to combine state models that could reproduce observation data under the assumption that noise ( $v_t$ ,  $w_t$ ) was included in the system state and observed data vectors. Therefore, the system model is as shown in Eq. (9), where it is assumed that the state transition matrix does not exist and that system noise is included.

System model

$$x_t = x_{t-1} + v_t, \quad v_t \sim N(0, Q) \quad (9)$$

The state variable vector in the SDA-SWING method is hydraulic conductivity,  $k$ , and rainfall infiltration rate,  $\varepsilon$ . The observation variable vector is the groundwater flow. However,  $v_t$  is applied only to any  $k$  that has a significant effect on the system state analysis results. In the EnKF, the closer the probability distribution of the system state to a Gaussian distribution, the better the accuracy. The logarithmic value of hydraulic conductivity follows a Gaussian distribution, so therefore, system noise is given to the logarithmic value of the hydraulic conductivity. From this, the state space model in the SDA-SWING method can be described as shown in Eqs. (10) and (11), where  $\Sigma q_t(x_t)$  is the amount of groundwater.

$$x_t = \left\{ \begin{matrix} K_t \\ \lambda_{et} \end{matrix} \right\} + \left\{ \begin{matrix} v_t^{K_t} \\ 0 \end{matrix} \right\} \quad \Sigma K_t = \ln(k_t) \quad (10)$$

$$y_t = h_t(x_t) + w_t = \sum q_t(x_t) + w_t \quad (11)$$

The state space model is updated when the observation values are obtained, and the parameters are estimated using the maximum likelihood method.

## ANALYTICAL METHOD

In this study, in order to verify how the error caused by the difference in the flow dimension in the SDA-SWING method affected identification of hydraulic conductivity by the EnKF, we considered comparison using the following three analyses.

- (a) SWING method: quasi-uniform flow (horizontal)
- (b) Two-dimensional: two-dimensional flow (horizontal and vertical)
- (c) Three-dimensional: three-dimensional flow (horizontal, vertical and depth)

The Bear formula, which is the basic equation of the SWING method, is a formula for the area of influence associated with tunnel excavation.

Therefore, only the horizontal flow was considered in method (a). On the other hand, methods (b) and (c) accounted for flow in the vertical or depth direction. The error caused by flow dimension differences was included in calculations (a) to (c). Method (c) was expected to be able to reproduce the actual phenomenon, calculating the groundwater flow with hydraulic conductivity set as a constant. We applied the data assimilation by EnKF to the inverse calculation of the hydraulic conductivity when the groundwater flow of (c) represented is the observation information of (a) and (b). Thus, there was neither system noise,  $v_k$ , nor observation noise,  $w_k$ . Therefore, comparing the calculated hydraulic conductivity inverses, each value would differ by the error caused by flow dimension difference. By comparing these, the effects of the difference in each analysis method can be directly calculated.

## Consideration of two-dimensional flow

To consider two-dimensional flow with vertical direction, it was necessary to carry out two-dimensional seepage flow analysis. Herein, an equation (Nishigaki Formula) has been proposed to allow for two-dimensional flow (horizontal and vertical). In this study, this equation was verified as equivalent to two-dimensional FEM analysis. In (12) and (13),  $q(t)$  is the amount of groundwater inflow to the tunnel for each slice volume, and  $R(t)$  is the range of influence (where the groundwater level is lowered as a result of tunnel excavation) for each slice volume.

$$R(t) = 1.22 \left[ \left( \frac{k}{\varepsilon} \right)^{\frac{1}{2}} - 1 \right] H_o \left[ 1 - \left( \frac{h_o}{H_o} \right)^2 \right] \quad (12)$$

$$q(t) = \frac{0.72 H_o^{-1} k (H_o^2 - h_o^2) \left( \frac{k}{\varepsilon} \right)^{-0.35}}{\left[ 1 - e^{-\frac{6 \varepsilon t}{\lambda_e (H_o - h_o)}} \right]^{\frac{1}{2}}} \quad (13)$$

## Consideration of three-dimensional flow

### Quasi-two and quasi-three dimensional analysis methods

The SWING method considers horizontal flow, while the Nishigaki Formula considers horizontal and vertical flows. In order to consider three-dimensional flow, it is necessary to consider the groundwater level lowering in front of the tunnel face. The  $R(t)$  occurs in each slice in front of the face, and it is necessary to add the amount of groundwater in this range, applying the assumption that the water level reduction range in front of the face is equivalent to the horizontal direction.

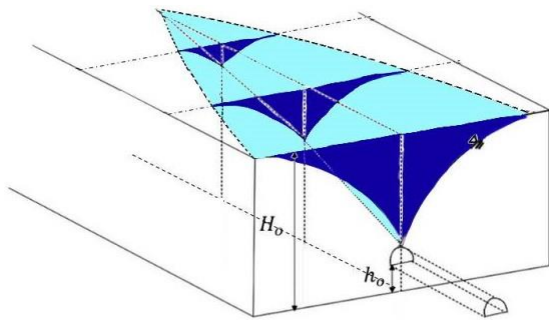


Fig. 6. Groundwater level lowering in the front of the tunnel face.

#### The three-dimensional seepage flow analysis method

This analysis doesn't consider full three-dimensional flow, so it is necessary to conduct three-dimensional FEM analysis, as shown in Fig. 7. We analyzed the amount of groundwater associated with tunnel excavation based on the Bear equation assumption that it was equal to the well flow rate if a well had been excavated in slice units just above the tunnel.

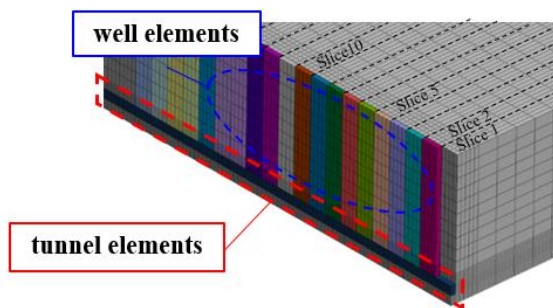


Fig. 7. Three-dimensional FEM analysis model (during slice 1 drilling).

#### ANALYTICAL CONDITIONS

We compared the groundwater inflow calculated using each method as drilling progressed, with the inverse analyzed hydraulic conductivity. The purpose of the study was to identify how flow dimension differences affected EnKF processing, so we compared groundwater inflow using the parameters listed in Table 1. Based on the volume of groundwater inflow calculated by three-dimensional seepage flow analysis, we conducted hydraulic conductivity inverse

Table. 1. Input parameters

| Input data                                 | Value                            |
|--|----------------------------------|
| $\varepsilon$ : rainfall infiltration rate | $5.0 \times 10^{-8}(\text{m/s})$ |
| $k$ : stratum hydraulic conductivity       | $5.0 \times 10^{-7}(\text{m/s})$ |
| $\lambda_e$ : porosity                     | 0.1                              |
| $H_o$ : initial groundwater level          | 30(m)                            |
| $h_o$ : elevation above impermeable layer  | 10(m)                            |

using each method, and then compared the error caused by the differences in flow dimensions. For this exercise, we made  $\lambda_e$  and  $\varepsilon$  constant, according to the assumptions previously described.

#### ANALYTICAL RESULTS

The calculation results from each method described above were compared, in order to evaluate the error caused by the differences in the flow dimensions. Figure 8 shows a comparison of groundwater inflow to the tunnel during the tunnel excavation on day-50. Table 2 shows  $Q_1$ ,  $Q_2$  and  $Q_5$ , which are the maximum amounts of the slices 1, 2 and 5, and  $k_1$ ,  $k_2$  and  $k_5$ , which are the inverse analyses of hydraulic conductivity from the other method, based on the  $Q_1$ ,  $Q_2$  and  $Q_5$  achieved by three-dimensional seepage flow analysis. For slice 1, groundwater inflow tended to increase as the flow dimension increased, in all cases. However, for slices 2 and 5, groundwater inflow in Case 5 was similar to Case 1. In order to verify the cause, Fig. 9 was prepared, and shows the groundwater level reduction in Case 5, when slice 10 was excavated. Fig. 10 shows the range of groundwater level reduction in the unexcavated section, focusing on slice 1 and slice 2, and from this, it was seen that groundwater level reduction in the unexcavated section unexcavated section did not occur just before slice 1 excavation. On the other hand, in the excavation after slice 2, groundwater level reduction was seen in the unexcavated section. We thought that the groundwater level reduction range would become larger, through excavation, and that the amount of groundwater inflow after excavation would be small. In the Case 2 and Case 4, this effect is not take into account.

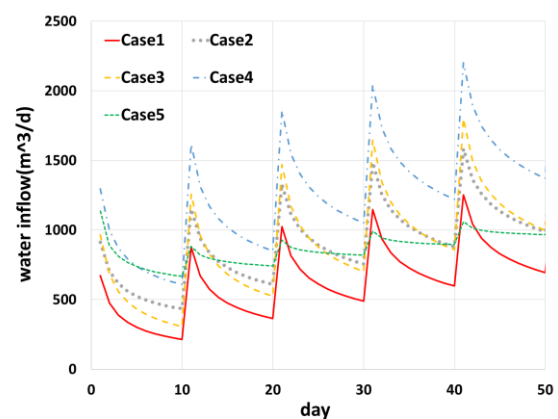


Fig. 8. Groundwater inflow predicted by each method.

As a result, it is considered that the amounts of groundwater inflow in Case 1 and Case 5 were close to actual values, after slice 2. In Table 2, as a result of

Table. 2. Analysis results

| Analysis step |   |              | slice 1               |                       |        | slice 2               |                      |        | slice 5               |                      |        |
|---------------|---|--------------|-----------------------|-----------------------|--------|-----------------------|----------------------|--------|-----------------------|----------------------|--------|
| Case          | Formula                                 | dimensional  | Q1(m <sup>3</sup> /d) | k1(m/s)               | ln(k1) | Q2(m <sup>3</sup> /d) | k2(m/s)              | ln(k2) | Q5(m <sup>3</sup> /d) | k5(m/s)              | ln(k5) |
| Case1         | SDA-SWING method                        | one          | 672.3                 | 13.6×10 <sup>-7</sup> | -5.87  | 876.0                 | 5.1×10 <sup>-7</sup> | -6.29  | 1253.4                | 3.6×10 <sup>-7</sup> | -6.44  |
| Case2         | SDA-SWING method                        | quasis-two   | 911.4                 | 7.1×10 <sup>-7</sup>  | -6.15  | 1151.4                | 3.0×10 <sup>-7</sup> | -6.52  | 1583.9                | 2.4×10 <sup>-7</sup> | -6.62  |
| Case3         | Nishigaki Formula                       | two          | 964.8                 | 6.4×10 <sup>-7</sup>  | -6.19  | 1257.1                | 2.9×10 <sup>-7</sup> | -6.54  | 1798.8                | 2.2×10 <sup>-7</sup> | -6.66  |
| Case4         | Nishigaki Formula                       | quasis-three | 1294.8                | 3.8×10 <sup>-7</sup>  | -6.42  | 1617.4                | 2.2×10 <sup>-7</sup> | -6.66  | 2201.2                | 1.8×10 <sup>-7</sup> | -6.74  |
| Case5         | Three-dimensional seepage flow analysis | three        | 1136.5                | 5.0×10 <sup>-7</sup>  | -6.30  | 883.4                 | 5.0×10 <sup>-7</sup> | -6.30  | 1059.8                | 5.0×10 <sup>-7</sup> | -6.30  |

※ We set the hydraulic conductivity  $k=5.0 \times 10^{-7}$  (m/s) when calculating  $Q_1$ ,  $Q_2$  and  $Q_5$ .

※ We back calculated  $k_1, k_2$ , and  $k_5$  on the basis of Case 5's  $Q_1$ ,  $Q_2$ , and  $Q_5$ .

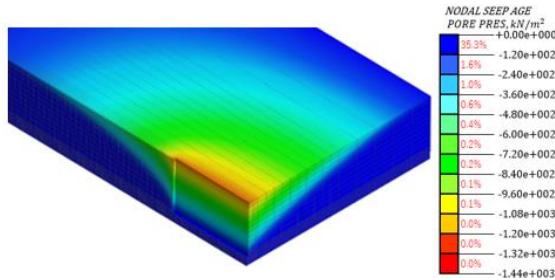


Fig. 9. Groundwater lowering range for Case 5 (slice 10).

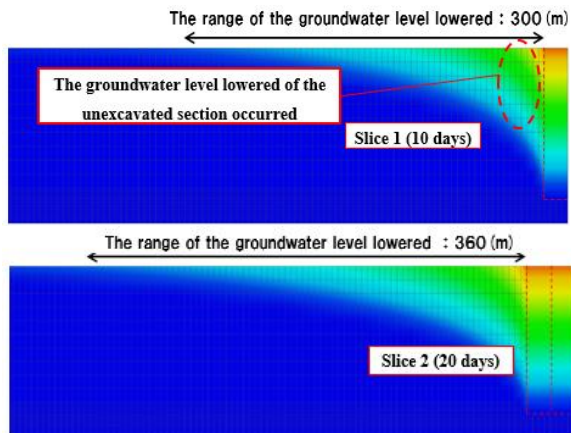


Fig. 10. Groundwater lowering range, focusing on slices 1 and 2.

conductivity analysis in Case 1-5, the error caused by the flow dimension difference of slice 1 became about 0.6, becoming 0.4 after slice 2. Generally, a difference  $<1$  in the hydraulic conductivity was considered very small. Considering EnKF processing, we concluded therefore, that the errors caused by the analysis method differences converged at the initial stage of the excavation.

## CONCLUSIONS

In this study, the error caused by flow dimension difference in the SDA-SWING method was acceptably small, when compared using analysis methods that considered, two-dimensional and three-dimensional flow, and the small difference converged at the initial excavation stage in the analysis, when

performing EnKF processing, based on observation data. In this study, we used one type of virtual tunnel. It is necessary to confirm that similar outcomes can be obtained in tunnels with different overhead structure and hydraulic conductivity. Moreover, field verification of our method in a real tunnel is very important. Therefore, in the future, we intend to improve the SDA-SWING method analysis accuracy, and to field-test the method.

## REFERENCES

- [1] Takahashi, K., Ohnishi, Y., Yasuda, T., and Xiong, J., Simplified seepage analysis system applied to tunnel excavation for assessment of water inflow. Proceedings of the Symposium on Underground Space, Vol. 13, 2008, pp. 147- 150.
- [2] Kogiso, J., Koyama T., Takahashi, K., Yasuda, T., and Ohnishi, Y., Development of SWING method with sequential data assimilation, Proceeding of the Japan Society of Civil Engineers F1 (Tunnel Engineering) Vol. 66, No. 1, 2012, pp. 9- 15.
- [3] Bear, J., Dynamics of Fluid in Porous Media, Dover Publications, 1998, pp. 420- 422.
- [4] Nishigaki, M., Komatsu, M., Irie, Akira., Yano, K., and Ota, T., Simple Method for Predicting Changes of Groundwater Caused by a Construction of a Mountain Tunnel Digging and its Applicability, Proceeding of the Japan Society of Civil Engineers, No.778, III-69, 2004, pp. 125- 137.
- [5] Higuchi, T., Ueno, G., Nakano, S., Nakamura, K., and Yoshida, J., Introduction to Data Assimilation-Simulation Technology for the Next Generation, Asakura Shoten, 2011.
- [6] Awaji, T., Kamachi, M., Ikeda, M., and Ishikawa, Y., Data Assimilation, Kyoto University, 2009, pp. 63- 92.
- [7] Umeda, K., Yanagisawa, K., and Yoneda, S., Creation of hydraulic conductivity database for Japanese ground, Journal of Japan Society of Engineering Geology, No.37, 1995, pp. 69- 77.
- [8] Tomofumi K., Junya, K., Kenji, T., Toru, Y., and Yuzo, O., Development of swing method with sequential data assimilation (SDA-SWING) and its application to groundwater problems in real tunnel construction, Tunneling and Underground Space Technology, No.28, 2012, pp. 229- 237.

## THE USE OF SAWDUST WASTE ON PHYSICAL PROPERTIES AND THERMAL CONDUCTIVITY OF FIRED CLAY BRICK PRODUCTION

Nonthaphong Phonphuak<sup>1,2\*</sup>, Anuwat Srisuwan<sup>3</sup>, Must Srila<sup>2</sup>, Siriwan Artbumrung<sup>2</sup> and Panuwat Ruenruangrit<sup>1</sup>

<sup>1</sup>Department of Engineering Management, Faculty of Engineering, Rajabhat Maha Sarakham University, Maha Sarakham 44000, Thailand

<sup>2</sup>Department of Industrial Technology, Faculty of Engineering, Rajabhat Maha Sarakham University, Maha Sarakham 44000, Thailand

<sup>3</sup>Faculty of Liberal Art and Science, Sisaket Rajabhat University, Muang, Sisaket 33000, Thailand

### ABSTRACT

In this paper, the effects of incorporation of sawdust waste on the properties of fired clay bricks were investigated. Clay bricks fabricated with 0, 2.5, 5, 7.5 and 10% by weight sawdust waste were tested. The clay brick specimens were fired at 900, 1000 and 1100 °C to study for water absorption, bulk density, apparent porosity and compressive strength of the fired clay brick specimens were investigated. It was found that the use of sawdust waste reduced the bulk density and compressive strength of the specimens. It was observed their apparent porosity ratios up to 30% improved with increasing of sawdust waste up to 10% by weight fired at 900 °C. The compressive strength of brick specimens with 2.5% by weight sawdust waste fired at 1100 °C were higher than the required strength values as pre ASTM C62-13a with beneficial reduced density and increased apparent porosity. Thermal conductivity of the porous fired clay brick specimens with 2.5-10% by weight sawdust waste produced at 1000 °C compared to the fired clay brick specimens without additive, decreased from 0.47 to 0.22 W/mK. The results thus showed that sawdust waste was a potential material for use as a pore former additive to raw clay-brick production.

*Keywords: Physical properties, Clay brick, Pore forming, Thermal insulation, sawdust waste*

### INTRODUCTION

One of the oldest construction materials is brick, and it continues to be one of the most popular building materials because it is durable, easy to handle, aesthetic in look, and inexpensive. Today, clay bricks are still being used for the same purpose. Fired clay brick should also contain high amount of pores to give it a lighter weight and associated low thermal conductivity [1]-[4]. New construction materials with friendly environment are interested in current research. Therefore, the improvement of fired clay bricks incorporating sawdust waste that is especially the development approach [5], [6]. For environmental protection and sustainable development, a number of researchers have investigated the use of waste materials to produce clay bricks. A wide variety of waste materials have studies, including sawdust, coal, coke, papermaking sludge, grass and coconut shell, corn cob, rice husk, and inorganic ones are polystyrene, perlite and dolomite or calcite [7]-[11]. Firing temperature is an important factor in clay brick making industry. It influences the mineralogical, textural and physical formation of clay bricks [12]. The porosity of material is a major factor influencing its thermal conductivity, but no simple relationship can be formulated to cover the complexity of various factor. Air is a very good insulating material, so that a highly porous body

material will have a lower conductivity than the same material with solid body. The advantage and application of high porosity bricks are the light weight structure and better thermal insulation [13]-[14]. Sawdust is a waste from the primary woodworking and timber industry. As it possesses a firing capacity, it is normally used as a fuel source in the thermal processes (biomass). The main chemical components of sawdust are; C (60.8%), H (5.2%), O (33.8%) and N (0.9%). Dry wood is primarily composed of cellulose, lignin, hemicelluloses, and minor amounts (5-10%) of extraneous materials [15]-[8]. The sawdust waste can be incorporated in clay as a pore-forming agent in clay brick technology. Furthermore, such combined products give the fired clay a more porous microstructure. Okunade (2008) investigated the use of wood ash and sawdust as admixtures in laterite-clay bricks. Sawdust (for burning out) and wood ash admixtures with ratio of 70:30 by weight laterite-clay were investigated. The admixtures were added in various combinations of proportions by volume (from 0 to 10%). This had resulted in denser products with high compressive strengths (with 0% sawdust and 10% wood ash), high softening coefficient, low water absorption rates, low saturation coefficient, low abrasion index, especially with addition of wood ash admixture solely. Conclusively, the results revealed that wood ash on its own would also result in production of lightweight



and more porous products [16]. In this research, the effects due to the use of sawdust waste were investigated in laboratory and the firing behavior, physical properties and thermal conductivity of fired clay bricks were discussed.

## EXPERIMENTAL

### Characterization of raw materials

The clay body is taken from one of the local plants. The average particle size distribution of clay body was analysed by diffraction (Mastersizer 2000+Hydro2000 MU, Melvern Instrument Ltd, UK), the average particle size distribution of 1 to 200  $\mu\text{m}$ , with D [4,3] of 14.91  $\mu\text{m}$  (Figure 1). The mineralogical composition of clay body was achieved using an X-ray diffractometer technique (XRD: X' Pert PRO MPD, Philips, Netherland). The major crystalline phases found in clay body were quartz, muscovite, rutile and hematite (Figure 2). Chemical analysis of the clay was carried out using X-ray fluorescence (XRF) elemental analysis spectrometer (Horiba Mesa-500 w). Chemical compositions of clay body are given in Table 1.

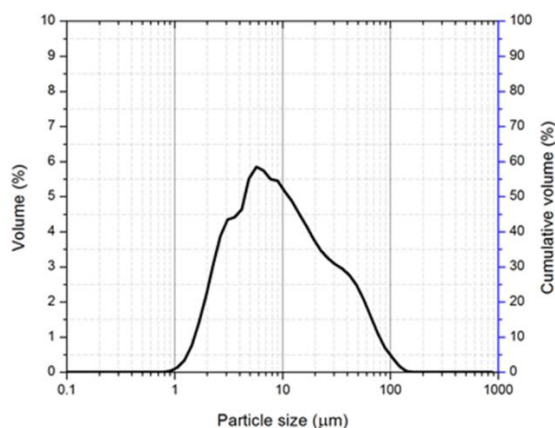


Fig. 1 Particle size distribution of clay body.

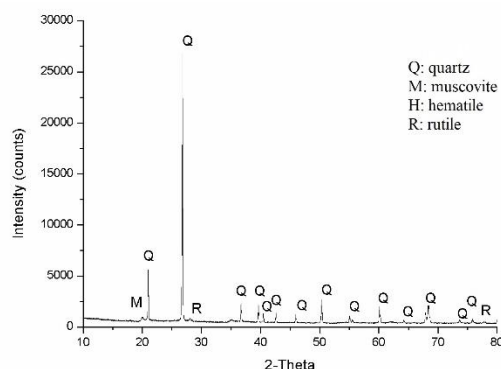


Fig. 2 XRD pattern of clay body.

Table 1 Chemical compositions of clay body.

| Oxide content                  | Clay body (wt.%) |
|--------------------------------|------------------|
| SiO <sub>2</sub>               | 58.76            |
| Al <sub>2</sub> O <sub>3</sub> | 21.34            |
| Fe <sub>2</sub> O <sub>3</sub> | 5.10             |
| CaO                            | 0.21             |
| K <sub>2</sub> O               | 3.10             |
| Na <sub>2</sub> O              | -                |
| P <sub>2</sub> O <sub>5</sub>  | -                |
| TiO <sub>2</sub>               | 0.93             |
| MnO                            | 1.18             |
| MgO                            | -                |
| LOI                            | 8.74             |
| (Loss on ignition)             |                  |

### Preparation of brick specimens

In order to determine the extent of the pore-forming effect of the use sawdust waste, additive was dry sieved through No. 45 mesh and finally the sawdust waste particle sizes was obtained in the range of 0.5 to 1.0 mm. Then, they were added in to the raw-brick clay body in different proportions (0, 2.5, 5, 7.5 and 10% by weight), for specimens of internal dimension of 14 cm x 6.5 cm x 4.0 cm were molded with hand. Specimens were dried at 110 °C for 24 hrs then, fired at 900, 1000 and 1100 °C (soaking time of 30 min).

Fired shrinkage was measured in accordance with the standard ASTM C326-09 [17]. The water absorption, bulk density and apparent porosity of brick specimens were tested using the Archimedes method in accordance with ASTM C373-14a [18]. The mechanical strengths of fired clay bricks were measured using the methods specified in ASTM C773-88 [19] and a digital camera was used to study the surface texture of fired clay bricks. Thermal conductivity measurement test was conducted according to an adapted experimental procedure of international standards ASTM C177-97 [20]. The thermal conductivity was calculated by using the following equation:

$$\frac{dq}{dA} = k \frac{dT}{dx} \quad (1)$$

Where  $q$  is the rate heat flow in direction normal to surface (W),  $k$  is the thermal conductivity (W/m K),  $A$  is the surface area (m<sup>2</sup>),  $dT$  is the temperature difference, the thickness (K) and  $dx$  are the distance measured normal to surface (m). Fired brick specimens mixed with increasing amount of sawdust waste 0%, 2.5%, 5.0%, 7.5% and 10%. All specimens were fired at 1000 °C with the size of 30 cm wide, 30 cm long and 25 mm thick for the measurement of thermal conductivity respectively.



## RESULTS AND DISCUSSION

### Firing Shrinkage

Firing shrinkage of clay bricks occurred due to the loss of water from clay structure during firing process. Clay particles were then moved closer that affected on higher shrinkage [3], [8]. However, the degree of shrinkage could be controlled by firing process. Figure. 3(a) shows the firing shrinkage of clay bricks with sawdust waste additions after fired at 900-1100 °C. In firing factor, shrinkage was increased with higher firing temperature because of the elimination of the pores. It was observed that the firing shrinkage tended to increase with increasing amount of sawdust waste in clay mixture at the same temperature. This was explained that carbon phase was eliminated from sawdust residues structure, leading to high driving force to improve surface area during firing process. In general, an increase in firing shrinkage. Generally, a good quality of fired clay bricks exhibits shrinkage below 8% [11]. The results showed that the firing shrinkage occurred in the fired clay brick was in the range of 4.27-7.31% and were within the limit of ASTM standard C62-13a. The control samples without any sawdust waste addition had comparable firing shrinkage of 4.72-6.36%.

### Bulk Density

The bulk density of fired clay bricks is an important parameter on the performance of the fired clay bricks. This is beneficial in terms of reduction of the overall dead load and the improvement of thermal behavior of structure. As the bulk density of clay bricks decreases, its strength also decreases, while its water absorption increases. In this study, the bulk density of fired clay bricks was inversely proportion to the quantity of sawdust waste added in the mixture. The bulk density of clay bricks was decreased with increasing sawdust waste content in the clay bricks. This behavior was associated some generated pores from sawdust waste combustion could not be eliminated in clay structure. The results indicated that the values of bulk density of specimens containing sawdust waste varied from 1.41 to 1.83 g/cm<sup>3</sup> (Figure. 3b). The bulk density is related to durability and water absorption characteristics of clay bricks. The high bulk density indicated the denseness of the clay brick with usually increased durability and reduced water absorption.

### Water Absorption

The durability of clay brick is related to the water absorption of clay brick. The durability of clay brick can be reduced when the brick absorbs water. It is important that the brick should be dense to reduce

the water absorption in the brick body [21]. According to Figure 3c, it could be seen that the water absorption slightly increased when sawdust waste increased in the range of 12.3-22.5%. In the part of different firing temperatures, it was found that water absorption of clay bricks decreased with increasing firing temperature where the bricks got stronger. Reduction in water absorption rate in brick structure associated with an increase in compressive strength [22], [23]. The control specimens without sawdust waste addition had comparable water absorption of 10.8-14.5%. The results of water absorption normally confirmed with the results of porosity.

### Apparent Porosity

Apparent porosity is an important characteristic of fired clay brick and related to the capacity of water absorption [22]. The high porosity of clay brick affected on the reduction of thermal conductivity that is required for insulating materials. The study results that fired clay bricks showed various apparent porosity depending on the amount of sawdust waste addition. The highest porosity was about 32.40% for 10% sawdust waste addition after fired at 900 °C. The lowest porosity of 22.80% was obtained in the bricks containing 2.5% sawdust waste and fired at 1100 °C, as shown in Figure 3d. Thus, porosity in fired clay bricks was caused when sawdust waste addition was burnt out during firing process. Therefore, the higher the amount of sawdust waste in clay brick, the higher the open porosity and hence the more porous clay brick as a result.

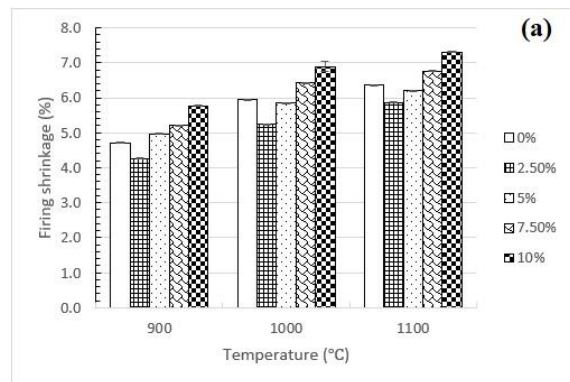


Fig. 3 Physical properties of fired clay brick fired at 900 to 1100 °C: (a) firing shrinkage, (b) bulk density, (c) water absorption and (d) apparent porosity.

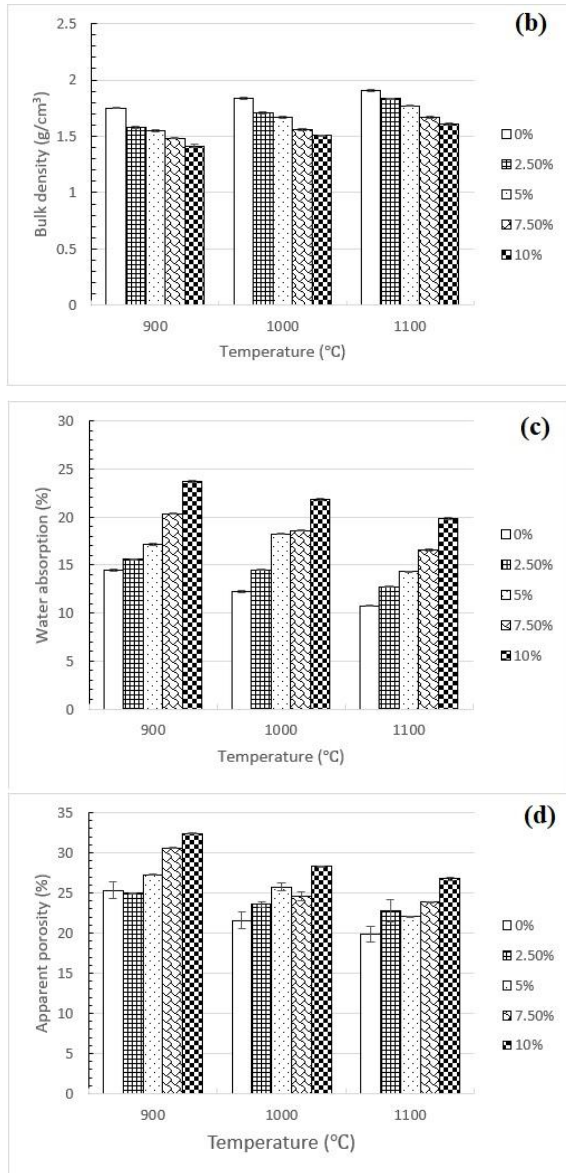


Fig. 3 (continued).

### Compressive Strength

The compressive strength of clay brick is the most important engineering-quality index for building materials [22]. According to ASTM C62-13a, the Grade MW bricks must have minimum compressive strength of 17.2 MPa [24]. In this study, the compressive strength of specimens fired at 900 to 1100 °C by varied sawdust waste in different compositions, as shown in figure 4. With increasing firing temperature, the strength of the bricks increased due to a decrease in porosity and an increase in density. The results showed that the compressive strengths of the specimens varied from 4.35 to 18.2 MPa with corresponding 2.5 to 10 wt.% sawdust waste. The results in figure 5 showed that bricks with 2.5 % sawdust waste fired at 1100 °C had adequate strength of 18.2 MPa compared to 17.2 MPa as required by ASTM standard. Moreover, high

porosity of brick has the advantage in the lightweight and improved thermal conductivity.

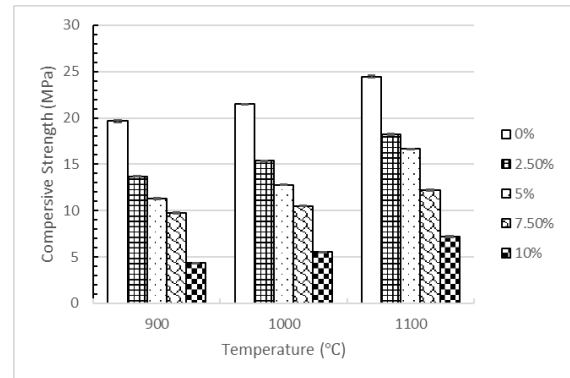


Fig. 4 Compressive strength of fired clay bricks.

### Thermal Conductivity of Fired Clay Bricks

The thermal conductivity analyzed was performed on fired clay bricks mixed with sawdust waste 0 to 10% by weight and fired at 1000 °C, as shown in figure 5. The results showed that higher percentages of sawdust waste (10% by weight) induced low thermal conductivity to the specimens. From the results, it could be explained that thermal conductivity decreased with a decrease in density and increased with an increase in fired clay bricks porosity. It was shown that the thermal conductivity was directly proportional to the density of the fired clay bricks. An understanding of conduction process indicated that the determining factor was porosity which was related to density.

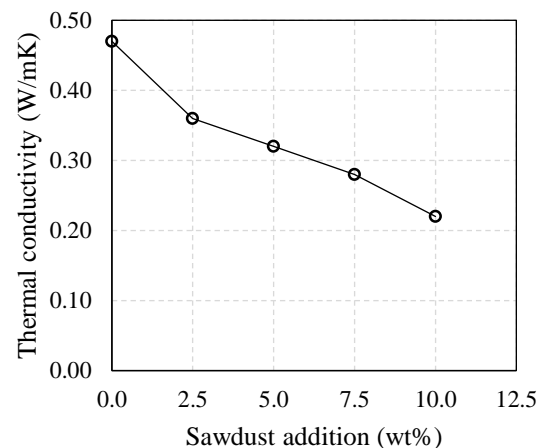


Fig. 5 Thermal conductivity of fired clay bricks at 1000 °C

### Surface Texture of Fired Clay Bricks

Surface texture of fired clay bricks with 2.5, 5, 7.5 and 10 wt% sawdust waste are presented in figure 6. The fired clay bricks specimens with sawdust waste contained visible pores when fired

from 900 to 1100 °C. The results revealed the effect of mixing sawdust waste on the fired clay brick specimens which can be seen in the cross-section a view. The results correlated well with the water absorption, porosity and density of the fired clay brick. The fired clay bricks with high content of sawdust waste also showed high level of visible pores. Beside the firing method, the chemical composition of clay and the firing temperature also affected with the color of fired clay bricks. The color of fired clay bricks also became darker with the increasing firing temperature. In our study, the bricks fired at high temperature (1000 and 1100 °C) were reddish-brown caused of iron oxide. The compressive strength of the fired clay bricks was reduced with the increase in the sawdust waste content due to the increased porosity. However, the compressive strength was also found to increase with firing temperatures. The increase in firing temperature from 1000 to 1100 °C substantially increases the compressive strength of fired clay bricks.

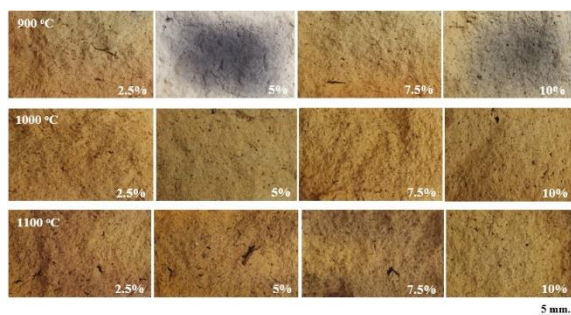


Fig. 6 Surface texture of fired clay bricks specimens fired at 900 to 1100 °C with different percentages of sawdust waste.

## CONCLUSIONS

In conclusion, the results showed that sawdust waste could be used as pore forming additive in making fired clay bricks. The results indicated that the addition of sawdust waste does have a reduction effect on compressive strength. However, good strength bricks which meet the ASTM strength requirement of 17.2 MPa could be obtained with 2.5 % sawdust waste fired at 1100 °C. The sawdust waste -clay bricks had lower density due to the pore forming characteristics of sawdust waste when compared to the control bricks without sawdust waste. The more porosity is the more thermal performance. Thermal conductivity of the porous fired clay brick specimens with 2.5-10% by weight sawdust waste produced at 1000 °C compared to the fired clay brick specimens without additive, decreased from 0.47 to 0.22 W/mK. Consequently, these clay bricks produced with addition of sawdust waste can be used as a heat insulation building materials. The reduced density was the added beneficial property of fired clay and lightweight bricks.

## ACKNOWLEDGMENTS

The authors also would like to acknowledge the financial supports from Rajabhat Maha Sarakham University.

## REFERENCES

- [1] Duggal, S.K., Building materials, 3rd revised ed. New Age International (P) Ltd., Publishers. 2008, pp.1.
- [2] Phonphuak, N. and Chindaprasirt, P., Types of waste, properties and durability of pore forming waste-based fired masonry bricks 1st End, Woodhead Publishing, 2014, pp, 103-127.
- [3] Karaman, S., Gunal, H. and Ersahin, S., Quantitative analysis of pumice effect on some physical and mechanical properties of clay bricks. Appl. Clay Sci. Vol.8(7), 2008, pp. 1340-1345.
- [4] Madurwar, M.V. Ralegaonkar, R.V. and Mandavgane, S.A., Application of agro-waste for sustainable construction materials: A review, Const. Build. Mat., Vol.38, 2013, pp.872-878.
- [5] Bories, C., Borredon, M.E. and Vedrenne, E., Development of eco-friendly porous fired clay bricks using pore-forming agent: A review, J. of Environ. Manag. Vol.143, 2014, pp.168-196.
- [6] Algin, H.M. and Turgut, P., Cotton and limestone powder wastes as brick material, Const. Build. Mat., Vol.22, 2008, pp.1074-1080.
- [7] Kazmi, S.M.S., Abbas, S., Saleem, M.A., Munir, M.J. and Khitab, A., Manufacturing of sustainable clay brick: Utilization of waste sugarcane bagasse and rice husk ashes, Const. Build. Mat., Vol.120, 2016, pp.29-41.
- [8] Eliche-Quesada, D., Corpas-Iglesias, F.A., Pérez-Villarejo, L. and Iglesias-Godino, F.J., Recycling of sawdust, spent earth from oil filtration, compost and marble residues for brick manufacturing, Const. Build. Mat., Vol.34, 2012, pp.275-284.
- [9] Al-Fakih, A., Mohammed, B.S., Liew, M.S. and Nikbakht, E., Incorporation of waste materials in the manufacture of masonry bricks: An update review, J of Build. Eng., Vol.21, 2019, pp.37-54.
- [10] Zhang, L., Production of bricks from waste materials – A review, Const. Build. Mat., Vol.47, 2013, pp.643-655.
- [11] Phonphuak, N. and Thiansem, S., Using charcoal to increase properties and durability of fired test briquettes, Const. Build. Mat., Vol.29, 2012, pp.612-618.
- [12] Mansaray, K.G. and Ghaly, A.E., Physical and thermochemical properties of rice husk. Energy Sources Part A: Recovery Utilization and Environmental Effects, Vol.19, 1998, pp.989-1004.
- [13] Ganesan, K., Rajagopal, K. and Thangavel, K., Evaluation of bagasse ash as supplementary

- cementitious material. *Cem. Concr. Comp.*, Vol.29, 2007, pp.515-524.
- [14] Phonphuak, N. and Chindaprasirt, P., Utilization of sugarcane bagasse ash to improve properties of fired clay brick. *Chiang Mai J of Sci*, Vol.45(4), 2018, pp.1855-1862.
- [15] Horisawa, S., Sunagawa, M., Tamai, Y., Matsuoka, Y., Tohru Miura, T. and Terazawa, M., Biodegradation of nonlignocellulosic substances II: physical and chemical properties of sawdust before and after use as artificial soil. *J. Wood. Sci*, Vol.45, 1999, pp.492-497.
- [16] Okunade, E.A., The effect of wood ash and sawdust admixtures on the engineering properties of a burnt laterite-clay brick, *J of Eng. Appl. Sci.* Vol.8, 2008, pp.1042- 1048.
- [17] ASTM C326-09., Standard Test Method for Drying and Firing Shrinkages of Ceramic Whiteware Clays, West Conshohocken, Pennsylvania. ASTM Book of Standards. Vol. 15.02., 2014.
- [18] ASTM C373-14a., Standard Test Method for Water Absorption, Bulk Density, Apparent Porosity, and Apparent Specific Gravity of Fired Whiteware Products, Ceramic Tiles, and Glass Tiles, West Conshohocken, Pennsylvania. ASTM Book of Standards. Vol. 15.02., 2014.
- [19] ASTM C773-88., Standard Test Method for Compressive (Crushing) Strength of Fired Whiteware Materials, West Conshohocken, Pennsylvania. ASTM Book of Standards. Vol. 15.02., 2011.
- [20] ASTM C177-97., Standard test method for steady-state heat flux measurements and thermal transmission properties by means of the guarded-hot-plate apparatus. West Conshohocken, Pennsylvania. ASTM Book of standard. Vol. 04.06., 2000.
- [21] Demir, I., Reuse of waste glass in building brick production, *Waste. Manag. Res.*, Vol.27, 2009, pp.572-577.
- [22] Phonphuak, N., Kanyakam, S. and Chindaprasirt, P., Utilization of waste glass to enhance physical-mechanical properties of fired clay brick, *J of Cleaner. Prod.*, Vol. 112, 2016, pp. 3057-3062.
- [23] Görhan, G. and Şimşek, O., Porous clay bricks manufactured with rice husks, *Const. Build. Mat.*, Vol.40, 2013, pp.390–396.
- [24] ASTM C62-13a., Standard Specification for Building Brick (Solid Masonry Units Made From Clay or Shale), West Conshohocken, Pennsylvania. ASTM Book of Standards. Vol. 04.05., 2013.



# THE VERIFICATION OF DIFFERENCE ANALYSIS IN THE HIGH PRECISION INSPECTION TECHNOLOGY FOR SLOPE SURFACE, USING MOBILE MAPPING SYSTEM

Naoto Samori<sup>1</sup>, Satoshi Nishiyama<sup>2</sup>, Koki Sakita<sup>3</sup>, Michinari Fuziki<sup>4</sup>, Naoya Ono<sup>5</sup> and Junsheng Song<sup>6</sup>

<sup>1</sup>Faculty of environmental science and technology, Okayama University, Japan,

<sup>2,3</sup>Graduate school of environmental and life science, Okayama University, Japan,

<sup>4,5</sup>Kokusai Kogyo Co.,Ltd, Japan,

<sup>6</sup>Disaster prevention research institute, School of mechanics and civil engineering,  
China University of mining and technology, Beijing. China

## ABSTRACT

In recent years, deterioration of road slope has become a problem and deterioration monitoring of road slope is required. However, it is challenging how to maintain road slope efficiently for local governments because they don't have enough civil engineers or financial resources sometimes. ICP (Iterative Closest Points) which is difference analysis method was tried to verify in the road slope monitoring using MMS (Mobile Mapping System). ICP, difference analysis method can quantify the deformation of road slope from group points data image. MMS is a system vehicle equipped with GNSS, IMU, digital camera, laser scanner and trip odometer. MMS can get laser point cloud data, surrounding image of 360 degrees and spot image. Road slope where there is potential bulging was monitored by MMS, and the road slope was set to force displacement by setting 10mm~ thick sheet on the slope or chipping the surface of the slope wall. At a result, accuracy of ICP method by using MMS seemed to be good and the monitored slope has confirmed that there is no deformation which is more than 1cm this time.

*Keywords: Road slope, MMS, ICP, Difference analysis*

## INTRODUCTION

Japan has experienced a period of high economic growth in the last 40 to 50 years during which large number of roads were constructed. However, at present, the aging of these structures poses a significant problem. Although regular inspection is carried out once in every five years, the inspection rate of the monitored structures is less than 50%. Therefore, this study focuses on the issue of deterioration of the slope of road structures.

Although several inspection points are considered in the existing inspection method of road slopes, visual inspection throughout the entire road slope must be performed. Furthermore, in Japan, it is difficult to efficiently check, maintain, and manage these structures due to the shortage of engineers and lack of financial resources in the local governments. At present, techniques using laser measurement equipment are gaining importance, and methods of quantifying the displacement and deformation by point cloud analysis are necessary for the maintenance and management of structures. In this study, to increase efficiency and to quantify the inspection of road slopes, the MMS and a difference analysis method conducted two verifications processes. It was verified whether the analysis method for slope monitoring using the MMS was practically feasible.

In the first verification process, the accuracy of the analysis method was checked. In the second verification, it was determined if there was a deformation of the slope between two periods.



Fig.1 Photograph of slope observation using the MMS

## METHODS OF STUDY

The MMS, difference analysis method, and equipment used in this study are described below.

### Mobile Mapping System(MMS)

The MMS is a vehicle equipped with a global navigation satellite system (GNSS), inertial measurement unit (IMU), digital camera, laser scanner, and odometer. Using this vehicle, the positions and orientations of the vehicle can be determined, and point cloud data (Fig. 2), of all the surrounding images, and spot images can be acquired.

The point cloud data is a three-dimensional data of the topography and shape around the road having coordinates X, Y, and Z (H). By comparing the first and second periods of this data, it is possible to quantitatively determine the deformations and fluctuations between the two periods.

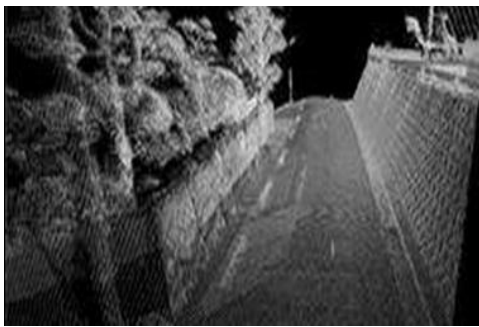


Fig.2 Reference image of 3D point cloud data

The MMS does not require a large number of inspectors, but only one driver, to acquire and survey the point cloud data, and it can be used even if the volume of traffic is large on the road in front of the slope. It is a measurement technology that is expected to replace conventional maintenance and management of the road.

### Difference Analysis

The difference analysis method applies a point cloud matching algorithm, known as the ICP.

ICP uses the point cloud data of two periods acquired by laser scanners and digital cameras, divides them into meshes of a certain size, and associates the points in the mesh that minimize the distance between the first and second period points. By repeating the rotational and parallel movements, the position where the corresponding point group of the two periods matches the most is calculated. This process is repeated to estimate the position where the two points match the most. A displacement vector is subsequently determined using which the data of the second period comes closest to first period, and the displacement can be obtained (Fig.3).

The difference analysis method using the ICP was utilized in the present study as it was expected to quantify the displacement and deformation of the 3D point cloud data obtained by the MMS.

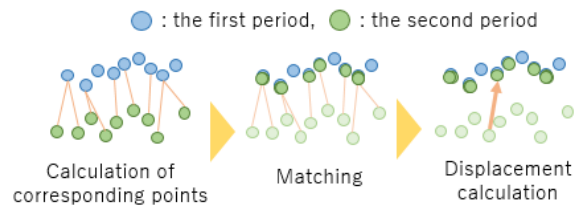


Fig.3 Simplified diagram of ICP analysis

### Equipment Used for Verification

In the verification processes, they were used, the MMS equipped with a laser scanner, GNSS receiver, an odometer, IMU, and eight spot cameras (Figs. 4 and 5). This laser scanner was not permeability type, and scans one million points per second by phase difference type. In addition, in the second verification, they were used, total station (TS), a stationary laser scanner for obtaining point cloud data as true values. The TS is a phase difference type scanner, with approximately 30million acquisition points.

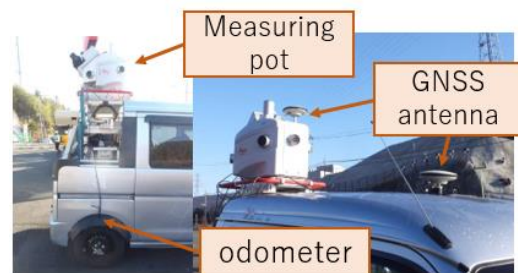


Fig.4 State of the MMS used in the study (1)



Fig.5 State of the MMS used in the study (2)

### METHODS OF VERIFICATION

The objective of conducting the two verifications processes is to verify the analysis method for slope monitoring using the MMS was practically feasible. The two verifications were conducted in the following manner.

Verification 1 checked the accuracy of the analysis method by either placing sheets or dropping off slope on the slope, causing forced displacement,



and thereafter analyzing the same.

Verification 2 ascertained whether monitoring of the slope could be performed by acquiring the point cloud data of the slope the first and second periods by the MMS, and analyzing the data obtained whether the slope in the two periods could be monitored.

### Verification 1: “Accuracy Verification”

It was verified that the accuracy of the method by determining the deformation when displacement is forcibly caused to the slope with the possibility of bulging (Fig. 6). The first measurement period was January 12, 2018, and the second measurement period was May 28, 2018. It has not given the slope deformation in the first period. In the second period, as shown in Fig. 7, it has not given any deformation to 1. In 2, it has given the slope a dropping off approximately 40 mm deep. In 3 and 4, sheets of thicknesses 10mm and 20mm were installed, respectively. Each of the sheets had an area of 50 mm<sup>2</sup>



Fig.6 Slope to be verified and road

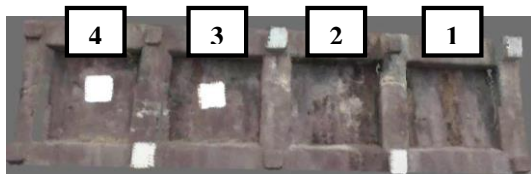


Fig.7 Forced deformation given to slope

For the survey by the MMS, the car with the MMS ran in the lane marked in red in Fig. 6, at a speed 50 km/h to obtain high density data with few missing 3D point cloud data. To improve the self-position accuracy of the MMS, the survey was conducted at time when the dilution of precision (DOP), of satellite arrangement) was good, i.e., less than 2.

The method of drawing the analysis results is shown in Fig. 8. The Y-axis component which is generally in the direction across the slope was extracted from the displacement vector of each mesh obtained by comparison by the ICP method twice. The method was adopted that is able to visualize the presence or absence of displacement such as bulging of the slope, peelings, or floating.

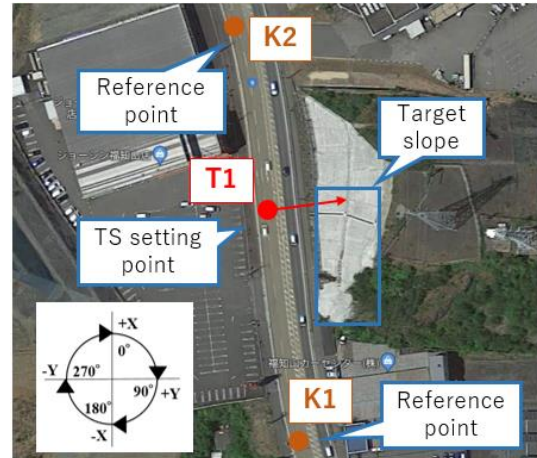


Fig.8 The map around the slope and surveying coordinate system

### Verification 2: “Slope Monitoring”

This verification process was monitored on the same slope that was considered during verification 1 (Fig. 6).

The survey conditions were also the same as in verification 1. We checked the possibility of monitoring the slope using this method by conducting the following test:4.

The first test compared the point cloud data of the targets placed on the slope in the first and second periods obtained by the TS, and investigated whether the slope was actually changing.

The second test compared the data obtained by the TS with that obtained by the MMS at the same time, i.e., we determined the difference between the true data by the TS and that data obtained by the MMS.

The third test compared the data obtained by the TS with that obtained from the MMS at the same time. The data of the second test were adjusted. Based on this comparison, there was an improvement in the accuracy due to the adjustment calculation.

Finally, the fourth test compared the adjustment calculated data obtained from the MMS in the first and second periods. The results of the fourth and first tests were then compared to verify if they agreed with each other.

#### *First Test “Comparison for examining slope deformation”*

This verification process used targets for the purpose of assessment. The targets point cloud data were obtained for each of the first and second periods by the TS.

As there are fewer sources of error for data by the TS than for that by the MMS, the former were assumed to be the true values. Therefore, when there was a change in the data obtained by the TS between the first and second periods, it could be seen that the

slope was actually changing.

In this test, the target was measured with reference point T1 (Fig. 8). The installation method of T1 was a GNSS surveying machine where static surveying was performed for 2 h near both ends of the slope (K1, K2 in Fig. 8) and a reference point was installed. Subsequently, the position of T1 was observed by the backward intersection. The point cloud of the target was obtained from T1 by the radiation method, and we tried to reduce the error by counter-observation.

A total of eight targets were set for this test as shown in Fig. 9. At the same time, 6 displacement verification points were set up.



Fig.9 State of target setting

#### *Second Test “Comparison for absolute accuracy verification”*

In this test, the point cloud data of the TS target obtained in first test were assumed to be true values, and compared with the point cloud data obtained by the MMS which was not calculated for adjustment and the difference was determined. Based on this difference, the adjustment calculations were added to the point cloud data obtained by the MMS, and the third test was performed.

#### *Third Test “Comparison for improvement of absolute accuracy”*

Based on the true values obtained by the TS survey of the first and second tests, the data obtained by the MMS were compared with the values given by the adjustment calculations. This test improved the absolute accuracy obtained in the second test.

The accuracy of adjustment calculations was verified by using two methods: The first method was a conventional method that performed adjustment calculations by using the features on the ground surface such as white lines or curbs, for localization. The second method was by placing a target placed on the slope for localization. These two methods were compared to improve the absolute accuracy.

#### *Fourth Test “Two period comparison by difference analysis method”*

The point cloud data obtained by the MMS in the first and second periods that was calculated for adjustment was subjected to a difference analysis. It was verified that the state of the change would be the same as in the first test which is the true value.

## VERIFICATION RESULTS

### Verification 1: “Accuracy Verification”

A difference analysis was performed on the point cloud data between two periods, and the data was compared. The results are shown in Fig 10.

At point 1, no displacement is observed, as forced displacement was not given during the second period. On the other hand, there was a displacement at point 2 (shown blue in the figure). This is because in the second period, the slope was dropped off and was given a negative displacement. As a result of this dropping off, a maximum displacement of about 40 mm occurred, it appeared to be approximately 40 mm (Fig. 10) where the negative displacement was large. Therefore, it is observed that the displacement was accurately extracted. In places where sheets of thickness 10 mm and 20 mm were installed at 3 and 4, respectively, the displacement was observed in places where the sheets were installed in the same manner as that of 2. The result clearly confirmed the change in the forced displacement point, whereas the other minute displacements were ignored and considered that the difference analysis method confirms a negative displacement of approximately 40 mm and positive displacement of approximately 20 mm.

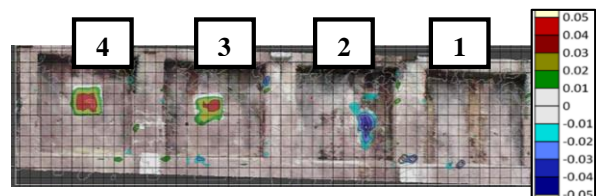


Fig.10 Comparison of forced displacement given to slope, (unit: m)

### Verification 2: “Slope monitoring”

#### *First Test “Comparison for examining slope deformation”*

The results of the comparison of the data obtained by the TS in the first and second periods were as follows.

The absolute values of the coordinates of the target in each axial direction were 1 mm on an average, and the difference between the coordinates of the verification point was 2 mm on an average, and the difference between the coordinates of the verification point was 2 mm on an average in the X direction, 0 mm in the Y direction, and 1 mm in the Z

direction (Table. 1).

Table. 1 Comparison of the point cloud data obtained by TS in the first and second period

| Measured value             | 2 period data - 1 period data |              |              |               |
|----------------------------|-------------------------------|--------------|--------------|---------------|
| point name (TG)            | dx(m)                         | dy(m)        | dxy(m)       | dh(m)         |
| TG01                       | -0.001                        | -0.001       | 0.001        | -0.002        |
| TG02                       | -0.002                        | -0.001       | 0.002        | -0.002        |
| TG03                       | 0.001                         | 0.000        | 0.001        | -0.002        |
| TG04                       | 0.001                         | 0.003        | 0.003        | -0.002        |
| TG05                       | 0.003                         | 0.000        | 0.003        | -0.001        |
| TG06                       | -0.001                        | 0.003        | 0.003        | -0.002        |
| TG07                       | 0.001                         | 0.000        | 0.001        | 0.000         |
| TG08                       | 0.003                         | 0.003        | 0.004        | 0.001         |
| <b>ave</b>                 | <b>0.001</b>                  | <b>0.001</b> | <b>0.002</b> | <b>-0.001</b> |
| <b><math>\sigma</math></b> | <b>0.002</b>                  | <b>0.002</b> | <b>0.001</b> | <b>0.001</b>  |

When the observation distance was 30 to 100 m, the accuracy of the TS machine was  $2 \text{ mm} + 2 \text{ ppm} * D$  ( $\pm 2.2 \text{ mm}$ ) and the angle 3 was sec ( $\pm 1 \text{ mm}$ ) in the distance measurement, at the observation distance of approximately 12 m. Therefore, the difference between the two periods depends on the accuracy of the TS machine, and there was no significant change corresponding to the deformation. It was observed that the surface of the subject did not change between January 12, 2018 and May 28, 2018.

#### Second Test "Comparison for absolute accuracy verification"

The point cloud data obtained by the TS in the first test was compared with that obtained by the MMS.

It was observed that the data obtained by the MMS differ by a maximum value of 0.077 m, and minimum value of 0.001 m in the horizontal direction (dxy) and maximum value of 0.091 m, and minimum value of 0.000 m in the vertical direction (dh), with respect to the value measured by the TS. This difference was less than 0.1 m (Table. 2). And reached the accuracy of 0.15 m of the map information level 500. Thus, it can be stated that the accuracy of measurement by the MMS was generally good.

Table.2 Comparison of point cloud data obtained by MMS with that obtained by TS

| Summary       |        |       |
|---------------|--------|-------|
|               | dxy(m) | dh(m) |
| Maximum value | 0.077  | 0.091 |
| Minimum value | 0.001  | 0.000 |

#### Third Test "Comparison for improvement of absolute

accuracy"

The point cloud data obtained by the TS in the first test were compared with that obtained by the MMS which was calculated for adjustment based on the second test.

As shown in the first test as a criterion for comparison, the difference between the observations in the first and second periods was dependent on the accuracy of the machine, therefore, we assumed that no significant change had occurred in the target. To prevent the error accompanying the measurement, the measured values obtained by the TS in the first period were adopted as the true values in the second period.

Consequently, for accuracy in the position after the adjustment calculations, the difference in the coordinates when the target was used averages to 0.001 m in the X, Y directions (horizontal direction with respect to the ground) in the first period, Z direction (height) The average was 0.001 m, in the X and Y directions in the second period, and 0.001 m in the Z direction. The difference in the coordinate values when using one of the conventional features was 0.035 m on an average in the X and Y directions in the first period, 0.004 m in the Z direction, and 0.011 m on an average in the X and Y directions in the second period. The difference was 0.008 m in the Z direction (Table. 3).

Table.3 Comparison of point cloud data obtained by adjusted MMS in the first period and point cloud data obtained by TS (partial)

| point name (TG)            | Adjust using TG |              | Adjust using features |              |
|----------------------------|-----------------|--------------|-----------------------|--------------|
|                            | dx(m)           | dy(m)        | dxy(m)                | dh(m)        |
| TG01                       | 0.000           | 0.000        | 0.109                 | -0.002       |
| TG03                       | 0.000           | 0.000        | 0.098                 | 0.000        |
| TG04                       | 0.000           | 0.000        | 0.102                 | 0.013        |
| TG05                       | 0.000           | 0.000        | 0.089                 | 0.001        |
| TG06                       | 0.000           | -0.001       | 0.089                 | -0.009       |
| TG07                       | 0.000           | 0.000        | 0.085                 | 0.003        |
| TG08                       | 0.000           | 0.001        | 0.085                 | 0.002        |
| <b>ave</b>                 | <b>0.000</b>    | <b>0.000</b> | <b>0.094</b>          | <b>0.001</b> |
| <b><math>\sigma</math></b> | <b>0.000</b>    | <b>0.001</b> | <b>0.009</b>          | <b>0.006</b> |

It was observed that the accuracy of position after the adjustment calculations improved in the method when the target was used compared to the method when the conventional features were used. Therefore, the adjustment calculations were performed in our method using the target.

#### Fourth Test "Two period comparison by difference analysis method"

A variation in the slope was observed by comparing the data of the first and second periods in which the adjustment calculations were added to the



point cloud data obtained by the MMS by the difference analysis method.

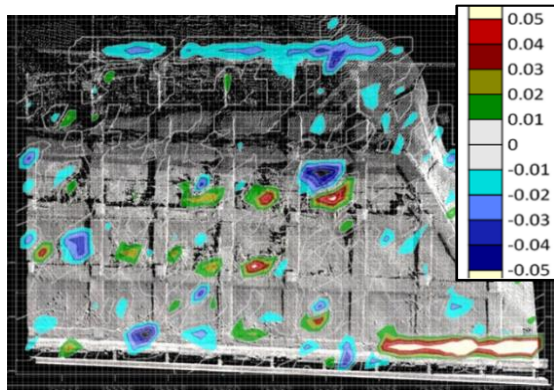


Fig.11 Comparison of one or two seasons of MMS data after adjustment calculation

The results are as shown in Fig. 11. The colored portions indicate the parts where the slope was deformed. However, it to be noted that there was vegetation, safety cones, and nets along the slope. The appearance of the slope was considered to be local noise, as the deformation appears locally. This anomaly was ignored this in this study. By ignoring local anomalies, as well as not having widespread anomaly on the slope, it was found that the present slope changed by the point cloud data by MMS after the adjustment calculation and the difference analysis method.

## CONCLUSION

In this study, two verification processes were conducted with the aim of establishing an analysis method for slope monitoring using the MMS.

### Verification 1: “Accuracy Verification”

In this verification, the accuracy of the analysis method used in this research was checked.

As a result of this verification, it was concluded that displacement was confirmed when there was positive displacement and negative displacement, and it was not confirmed when the displacement was not given. Therefore, information regarded the deformation could be extracted from the slope using this method. In addition, the deformation was determined to be approximately 40 mm for negative displacement and 20 mm for positive displacement.

### Verification 2: “Slope Monitoring”

In this verification, the slope monitoring process was checked to confirm whether there could be a

deformation of the slope between the two periods. From the point cloud data of first test by the TS, it was observed that the slope did not change, and from the point cloud data by the MMS after adjustment calculations of the fourth test, it was established that the slope did not change. As the conditions of the first and fourth tests were consistent, it was concluded that this method could monitor the slopes that could be judged quantitatively.

From the verification processes, it was confirmed that the analysis method for slope monitoring by the MMS was practically feasible.

In addition, the height of the slope was approximately 7 to 8.5 m in the verifications processes, and the measurement distance from the MMS to the present slope was almost 12 m. Although it was possible to make measurements at the upper part of the slope at a distance of almost 12 m from the slope, point cloud data cannot be obtained perpendicular to the slope. The angle becomes steep, the footprint of the point cloud data obtained becomes large, the quality of the data declines, and the number of available point clouds decreases. For example, in this survey, in the case of guard fences and targets, point cloud data would be acquired at an angle of almost 60 degrees at a distance of approximately 15 m. As the conditions of measurements in the lower and upper parts of the slope differ, the difficulty lies in maintaining the accuracy of measurement by the MMS.

## ACKNOWLEDGMENT

This study was supported by KAKENHI (16K01329).

## REFERENCES

- [1] Besl, P.J and McKay, N.D. (1992): A Method for Registration of 3-D Shapes, IEEE Pattern Analysis and Machine Intelligence, Vol.14, No. 2, pp. 239- 256.
- [2] Is this good? Infrastructure Specialist, Necessary things for infrastructure repaired period, Gyosei, pp.130~132.
- [3] Doctoral dissertation, Research on Rationalization of Road Tunnel Inspection Method Utilizing Traveling Measurement Technology, Takashi Mizuguchi, 2017, pp.3-1~3-5.
- [4] Accuracy verification of analysis method for slope monitoring method using mobile measuring vehicle, Koki Sakita, 2018.

# LESSON LEARNED IN MAINTAINING THE PRECAST CONCRETE BUILDINGS

Zul-Atfi Ismail

Civil Engineering Program, School of Environmental Engineering, Universiti Malaysia Perlis, Malaysia

## ABSTRACT

The contemporary practice of conventional methods in the Precast Concrete (PC) building maintenance entails many issues due to poor service delivery and defect repetition. A key problem impeding the widespread adoption of emerging technologies is the lack of competent contractor supporting the effectiveness of implemented Information and Communication Technology (ICT) than conventional methods and the returns on investment. The shortcomings of conventional methods are assessed from the perspective of PC buildings. Data were collected through a case study of eight PC buildings from two type of design which were high-rise and complex building. The conventional methods had significantly little emphasis on defect diagnosis tools. It had also increased the inadequate strategic decision making to analyse information in improving the maintenance project outcomes for PC building. Building Information Modelling (BIM) tools is suggested from findings and lessons learned as a good practice to reduce the repetition of defect on the design specification used and construction practiced.

*Keywords: Maintenance Management, Conventional Method, Maintenance Management System, Building Information Modelling, Malaysian PC Building*

## INTRODUCTION

Maintenance management is paramount in ensuring the effective and efficient monitoring process of maintenance activities, and Information and Communication Technology (ICT) could play fundamental role in delivering that maintenance management. Precast Concrete (PC) building maintenance depends on the design type (e.g. complex and high-rise building), size and building usability that require quality maintenance in order to achieve life-span prolongation. Structural repairing practice in managing PC building maintenance activities has been a hot issue in recent years due to lack of progress in the area of computer-aided maintenance management and difficulties with accessing information and data in maintenance support systems such as Computerised Maintenance Management System (CMMS) and Computerised Aided Facility Management (CAFM) [1]. Clients and contractors should use the high-quality building information from an emerging application of computerbased technology during the maintenance activities of the PC building's lifecycle. In response to the challenges of dynamic maintenance operations and the need for improving the quality of maintenance process in complex and high-rise structural building components, clients and contractors could change their method from conventional practices to more enabling technology to increase productivity and a new level of interoperability and collaboration. The conventional modus operandi (paper-based reports/unsystematic

database), which is commonly being conducted in a sequential manner using CAFM and CMMS tools replaced to new business model which integrates various sources of data and knowledge such as CMMS with the Building Information Modelling (BIM) of the PC building in the maintenance activities [2, 3, 4].

Maintenance staff generally introduces ICT into PC building maintenance management for providing maintenance inspection records and results, including checklists, specification, and maintenance procedure by using software such as CMMS and CAFM. The CMMS and CAFM application provides various paper-based reports (such as inventory confirmation) related to maintenance and repair issues [3]. Furthermore, the traditional 2D Computer-Aided Design (CAD) technology is widely used for maintenance information illustration and even integrating related data for PC building construction design history purposes [5]. Despite the fact that the use of ICT solutions in assessing, planning or process execution takes place at a different scale and function, the emerging trend such as using sophisticated or innovative tools and techniques could improve productivity in PC building maintenance activities and have a great potential to redefine and re-engineer the conventional setting. The conventional method (paper-based reports/unsystematic database) is lack of knowledge support in coordination, maintenance monitoring, maintainability, automation and robot control systems. The PC building maintenance has different training or maintenance information to

address the issue of defects for particular component compared to the conventional building maintenance. The connection of PC component such as by using corbel and PCB need the expert knowledge to improve the quality and reliability of PC scheme in order to avoid any defect repetition in the long-term of life cycle building services. Failure to capture the data acquisition and monitor the defects effectively will influence the assessment process including maintenance planning and execution. This can contribute poor quality, productivity and performance in PC building construction projects [6, 7]. There is also give problematic and inefficient in the handling of information and integration of data of maintenance components within a post-construction site activity [8].

### BIM FOR PC BUILDING MAINTENANCE

Recently on PC construction sites, there are many efforts to improve the efficiency of maintenance management activities through the use of more ICT-based systems (i.e. BIM). With the development of emerging technology such as BIM, maintenance management improvements in PC building construction has become possible [9]. Several other industry projects worldwide, for example real estate, waste management, transportation, supply chain and facility management, have been successfully completed by implementing BIM technology [10, 11, 12]. BIM can assist clients to determine the appropriate technology strategy and scope of each deliverable, with the intention of reducing redundancy and rework while improving performance and productivity of an operation and maintenance processes effectively in the future [13, 14]. Whereas BIM related studies mainly focus on utilising sophisticated tool and efficient technique, associating decision making support in diagnosis principles can help in achieving new levels of efficiency in PC building maintenance performance.

### CASE STUDY

The case studies on the eight PC buildings were undertaken in order to identify the maintenance management problems, the current approaches to addressing the problems, the ICT implementation, use of emerging technologies and the maintenance management system (MMS) to obtain information relating to the maintenance identification, assessment, planning and execution processes. Eight maintenance clients/contractors are selected based on major problems of using conventional method (paper-based reports/unsystematic database) in the comparison to investigate the maintenance management practices in each PC building. There are around 51 contractors of Industrialised Building System (IBS) building maintenance from a classification of PC system have

the highest of IBS building maintenance projects in Malaysia according to CIDB and almost are using conventional method and inadequately use of modern ICT tools. The number is considered very big indicating that the use of modern ICT is still very limited for PC system classification in IBS building maintenance management in Malaysia. The adopted synthesis of good practices of maintenance operations is based on the findings of the interviews and case studies conducted with professional engineers working in PC building maintenance departments [15]. This paper is part of a larger research and will only introduce and discuss the entire finding of the case study. This finding is illustrated in the following sections.

The interviews consisted of two types of PC building, namely, "Residential" and "Non-Residential". The case study was based on eight cases (Case A-Case H) of PC buildings in Malaysia. There were two case studies (Cases A and E) on "Residential" due to housing maintenance operation such as the Putrajaya Quarters. In addition, six more case studies (Cases B, C, D, F, G and H) were classified as "Non-Residential" which manages the maintenance operation with fully equipped office buildings. The interviews reached a saturated point after the eighth interview session. The justifications for the selected case studies were according to the following main criteria: exposed to the conventional method used and major problems, attempted to implement computerised technology and the willingness of staff to share their experiences in improving the maintenance management processes at the PC building. The differences between the types of the PC building project provided an opportunity to explore variations in maintenance management issues for complex and high-rise PC building projects. The type of PC building under study for maintenance project were all varied from Quarters to Integration News Centre. The summary on the eight case studies is presented in Table 1.

Table 1 List of Case Studies

| Interviewee                  | A  |
|------------------------------|--|
| Type of IBS Building Project | Quarters   |
| Type of Building             | Residential  |
| Design of IBS Building       | High-rise  |
| Interviewee                  | B  |
| Type of IBS Building Project | Malaysian Institute of Pharmaceuticals and Nutraceuticals (IPHARM) |
| Type of Building             | Non-Residential  |



|                              |   |
|------------------------------|---|
| Design of IBS Building       | High-rise   |
| <b>Interviewee</b>           | <b>C</b>  |
| Type of IBS Building Project | National Youth Skills Institute (IKBN)            |
| Type of Building             | Non-Residential                                   |
| Design of IBS Building       | Complex   |
| <b>Interviewee</b>           | <b>D</b>  |
| Type of IBS Building Project | Anti-Corruption Agency Office Complex and Housing |
| Type of Building             | Non-Residential                                   |
| Design of IBS Building       | Complex   |
| <b>Interviewee</b>           | <b>E</b>  |
| Type of IBS Building Project | Double Storey Super link House                    |
| Type of Building             | Residential                                       |
| Design of IBS Building       | Complex   |
| <b>Interviewee</b>           | <b>F</b>  |
| Type of IBS Building Project | Inland Revenue Board Of Malaysia Complex          |
| Type of Building             | Non-Residential                                   |
| Design of IBS Building       | High-rise   |
| <b>Interviewee</b>           | <b>G</b>  |
| Type of IBS Building Project | National Audit Department Office                  |
| Type of Building             | Non-Residential                                   |
| Design of IBS Building       | Complex   |
| <b>Interviewee</b>           | <b>H</b>  |
| Type of IBS Building Project | Integration News Centre                           |
| Type of Building             | Non-Residential                                   |
| Design of IBS Building       | High-rise   |

The semi-structured interviews were conducted with the engineers who were responsible for the maintenance management of the entire PC's building structure under the Facility Management and Development Unit (UPPF) and Maintenance and Development Unit (UPS) including maintenance contractor. The interview sessions took around five hours to accumulate the data on the maintenance processes including the demonstration of the current maintenance management system with the implementation of the ICT tools by the engineer. All the data from the interviews were recorded using video camera and transcribed verbatim.

## KEY FINDINGS

The eight case studies involved in this research were to identify the maintenance management problems,

the approaches to address problems, ICT implementation, use of emerging technologies including the maintenance management system at the selected PC building. The problems identified from the eight case studies revealed that each case study experienced similar problems with defect repetition at the specific component part of PC building and are summarised and presented as below. The discussion involves a cross-case analysis and has been grouped into five main 'embedded units of analysis' identified which are (1) Maintenance Management Problems, (2) Approaches to Address Problems, (3) ICT Implementation, (4) Use of Emerging Technologies and (5) Maintenance Management System.

Table 2 Cross-Case Analysis

| Case   | Element of Analysis: Maintenance Management Problems   |
|--------|--|
| Case A | <p><i>Lack of commitment for handling defect</i></p> <ul style="list-style-type: none"> <li>-Report delay and undelivered</li> <li>-Unsystematic database</li> </ul> <p><i>Less competent contractor staff</i></p> <ul style="list-style-type: none"> <li>-Less engineer competency</li> <li>-Technician's report is in general description</li> <li>-Technician's failure to identify defect problem</li> </ul> <p><i>Defects repetition (surface cracking, leaking, scaling and jointing)</i></p> <ul style="list-style-type: none"> <li>-Fault design</li> </ul> <p><i>Poor quality work by contractor</i></p> <ul style="list-style-type: none"> <li>-Less material quality</li> </ul> <p><i>Poor buildability (M&amp;E coordination)</i></p> <ul style="list-style-type: none"> <li>-Lack coordination between design and maintenance team</li> </ul> <p><i>Poor maintainability</i></p> <ul style="list-style-type: none"> <li>-Unspecific accessibility to the defect location</li> </ul> <p><i>Poor waterproofing</i></p> <ul style="list-style-type: none"> <li>-Poor maintenance method</li> </ul> |
| Case B | <p><i>Poor quality work by contractor</i></p> <ul style="list-style-type: none"> <li>-Low repair requirements of the structure component</li> </ul> <p><i>Lack of staff</i></p> <ul style="list-style-type: none"> <li>-Lack of supervision</li> </ul> <p><i>Limited Budgets</i></p> <ul style="list-style-type: none"> <li>-Budget constraint</li> </ul> <p><i>Defects repetition (surface cracking and aircond belting)</i></p> <ul style="list-style-type: none"> <li>-Lack of technician</li> <li>-Less defect detection technologies</li> </ul> <p><i>Less competent contractor staff</i></p> <ul style="list-style-type: none"> <li>-Less engineer/technician competency</li> </ul>  |
| Case C | <p><i>Defects repetition (surface cracking, leaking and jointing)</i></p> <ul style="list-style-type: none"> <li>-Low quality design control</li> </ul>  |

|             |  |
|-------------|--|
|             | <i>Surface cracks due to improper jointing</i><br>-Less quality of joint material<br><i>Deep cracks due to settlement</i><br>-Less suitable soil<br><i>Less competent contractor staff</i><br>-Less engineer/technician competency   |
| Case D      | <i>Defects repetition (leaking and jointing)</i><br>-Design performance for concrete durability requirements<br>-Structural installation method<br><i>Poor waterproofing</i><br>-Poor installation of the waterproof membrane<br><i>Poor quality work by contractor</i><br>-Lack of uniform standard<br>-Poor material quality<br><i>Less competent contractor staff</i><br>-Less engineer/technician competency |
| Case E      | <i>Defects repetition (surface cracking, leaking and jointing)</i><br>-Fault design<br>-Poor material quality<br>-Time gap of building repairs<br><i>Poor plumbing fitting</i><br>-Plumbing installation method  |
| Case F      | <i>Defects repetition (leaking and jointing)</i><br>-Design performance for concrete durability requirements<br><i>Less competent contractor staff</i><br>-Less engineer/technician competency   |
| Case G      | <i>Defects repetition (leaking, jointing and overload current trip)</i><br>-Fault design<br>-Contractor ethics issues-Interested in making profits   |
| Case H      | <i>Defects repetition (heavy leaking)</i><br>-Poor quality of design<br>-Less technician competency<br><i>Deep cracking on structure</i><br>-Limited experience by engineer<br>-Poor maintenance method by contractor<br><i>Less competent contractor staff</i><br>-Less engineer/technician competency  |
| <b>Case</b> | <b>Element of Analysis: Approaches to Address Problem</b>  |
| Case A      | -Improve the maintenance assessment for the building works did by contractor   |
| Case B      | -Provide more quality staff in managing the maintenance of critical defect<br>-To replace the conventional defect detection method (e.g. visual inspection) with the sophisticated ICT application (e.g. CMMS)   |

|             |   |
|-------------|---|
| Case C      | -Improve the maintenance effectiveness for the building works did by contractor   |
| Case D      | -Proper supervision of work for the building works did by contractor  |
| Case E      | -Improve the building control for the building works did by main contractor   |
| Case F      | -Critical plan on maintenance repairs   |
| Case G      | -Conduct the maintenance assessment for evaluating the building works performance did by contractor   |
| Case H      | -Conduct the maintenance assessment for evaluating the building works performance did by contractor   |
| <b>Case</b> | <b>Element of Analysis: ICT Implementation</b>  |
| Case A      | <i>mySPATA</i> -Data inventory for immobile facilities (e.g. building)<br><i>mySPA</i> -Data inventory for mobile facilities (e.g. furniture)<br><i>mySMS System</i> -for managing complaints   |
| Case B      | -Conventional (e.g. MS Word, MS Excel)  |
| Case C      | <i>mySPATA</i> -Data inventory for immobile facilities (e.g. building)<br><i>mySPA</i> -Data inventory for mobile facilities (e.g. furniture)   |
| Case D      | -Conventional (e.g. MS Word, MS Excel)  |
| Case E      | -Conventional (e.g. MS Word, MS Excel)  |
| Case F      | -Conventional (e.g. MS Word, MS Excel)  |
| Case G      | -Conventional (e.g. MS Word, MS Excel)  |
| Case H      | <i>Building Automation System (BAS)</i> -for detected building's heating, ventilation and air conditioning systems<br><i>Supervisory Control and Data Acquisition System (SCADA)</i> -to ensure that the building systems (e.g. fire alarm) were in good condition<br><i>E-Aduan</i> -for managing complaints |
| <b>Case</b> | <b>Element of Analysis: Use of Emerging Technologies</b>  |
| Case A      | -No   |
| Case B      | -No   |
| Case C      | -No   |
| Case D      | -No   |
| Case E      | -No   |
| Case F      | -No   |
| Case G      | -No   |
| Case H      | -No   |
| <b>Case</b> | <b>Element of Analysis: Maintenance Management System</b>   |
| Case A      | -Conventional (e.g. paper-based reports/unsystematic database)  |

|        |  |
|--------|--|
| Case B | -Conventional (e.g. paper-based reports/unsystematic database) |
| Case C | -Conventional (e.g. paper-based reports/unsystematic database) |
| Case D | -Conventional (e.g. paper-based reports/unsystematic database) |
| Case E | -Conventional (e.g. paper-based reports/unsystematic database) |
| Case F | -Conventional (e.g. paper-based reports/unsystematic database) |
| Case G | -Conventional (e.g. paper-based reports/unsystematic database) |
| Case H | -Conventional (e.g. paper-based reports/unsystematic database) |

### SYNTHESIS OF GOOD PRACTICES

Table 3 below represents the suggested solutions from the case studies to improve the current practices on the maintenance management by implementing three approaches at the PC building. Case A, B, C, D, F, G and H suggested improving the transfer of knowledge in the defect diagnosis by combining with the related software technology such as CMMS and CAD. In fact, the problem of knowledge transfer in the defect diagnosis delivery also does affect the other PC buildings to some extent and the significance of this factor is quite obvious. The maintenance contractors will use the inadequate knowledge to handle the defect problem and less detail of the defect source explanation to gather accuracy information record for inspection and planning works. The other suggestion from the client/contractor was to provide the transfer of knowledge to improve the maintenance quality of structure and facility at the PC building (Case A, B, D, F, G and H). All the related cases are facing the impact of problems for the quality knowledge management, which are associated to the defect repetition for handling the defect of structures and facilities with IBS score usage about 70% on its structure development of PC building.

Case C, D, E, F and G suggested on efficient controlling of building performance based design and monitoring the defect diagnostic operation in maintenance through implementation of emerging technology (BIM) on the PC building maintenance. These are also recommended by Case A, B and H to integrate the design/construction and maintenance's database in order to facilitate better decision support and coordination within and across multiple field (e.g. civil, mechanical and electrical) for effective management of the PC building maintenance. This suggested solution is ranked as the most important solution due to suggest from almost case studies in order to manage the large and critical maintenance services for the PC building structure and facility. The using of emerging technology is also the lowest in terms of existing practice for better managing PC building components including mechanical and

electrical control systems. As the overall results indicated in Table 3, it was deemed necessary to analyse the use of emerging technology further. Therefore, the systematic system with the emerging technology, defect diagnosis and decision making process should be developed to improve the building structure and facility performance by conducting effective knowledge transfer on the structure component maintenance defects.

Table 3 Suggested Solutions from Case Studies

| Case            | Suggested Solutions  |
|-----------------|--|
| A,B,C,D,F,G,H   | Provide more transfer of knowledge in defect diagnosis   |
| A,B,D,F,G,H     | Provide more transfer of knowledge to improve the maintenance quality in maintenance execution   |
| A,B,C,D,E,F,G,H | Implementation of emerging technology (BIM) (efficient control of building performance based design/ monitor the defect diagnostic operation in maintenance) |

### LESSON AND ENLIGHTMENTS

- 1) The PC building maintenance and the application of diagnosis techniques should be paid highly attention. Because of the defect repetition of structure components and limitation of understanding about the PC knowledge, the maintenance approach is very important. The application of modern ICT tools such as BIM integration can avoid or alleviate the defect of critical structure.
- 2) The appropriate modern ICT tools should be selected in assessment areas (diagnosis and decision making process on the design specification used and construction practiced) for PC buildings. The high-rise or complex structure should be given the priority for these types of PC buildings.
- 3) The maintenance quality of PC buildings should be strictly guaranteed.
- 4) The deficiency of PC buildings knowledge affected the quality of competent maintenance staff in Malaysia. The future work should be strengthened to guarantee the quality and knowledge in case of defect repetition.

The repetition of defect was frequent at PC building. The maintenance inspection and assessment was not able to address the building structure defect problems at the particular location due to the less knowledge transfer between all members in maintenance

management. Furthermore, the less competent contractor caused the maintenance faults to be increased to encourage the deterioration of the IBS building structure and facility.

In this research, the frontline approaches (new system development with BIM) is intended to counter the maintenance management problems on PC building which are:

- a) Defect repetition information and knowledge due to failure to identify the actual reason of structure defect;
- b) Defect repetition (leaking, jointing and cracking) information and knowledge due to design defect; and
- c) Less competent contractor due to lack of knowledge regarding with materials, method and design of structure repair.

## CONCLUSIONS

The data obtained in the case studies revealed that the PC buildings are using the conventional method such as paper-based reports in managing the maintenance processes for building structure and facility. This arise a problematic situation such as defects repetition (leaking, jointing and cracking) and poor quality work by contractor that need sophisticated tools towards a solution. Presently, the implementation of ICT tools in the new system is the better improvement to lead the tremendous saving in budget, time planning and to receive the precise data in handling the defect diagnosis and control. The suggestion for good practices was through the implementation of BIM to reduce the repetition of defect on the design specification used and construction practiced for the building structure and facility.

## REFERENCES

- [1] Duran, O. (2011). Computer-aided Maintenance Management Systems Selection based on a Fuzzy AHP Approach. *Advances in Engineering Software*, 42(2011), 821-829.
- [2] Espindola, D. B., Fumagalli, L., Garetti, M., Pereira, C. E., Botelho, S. S. C., & Henriques, R. V. (2013). A Model-based Approach for Data Integration to Improve Maintenance Management by Mixed Reality. *Computers in Industry*, 64(2013), 376-391.
- [3] Motamedi, A., Hammad, A., & Asen, Y. (2014). Knowledge-assisted BIM-based Visual Analytics for Failure Root Cause Detection in Facilities Management. *Automation in Construction*, 43(2014), 73-83.
- [4] Nawi, M. N. M., Salleh, N. A., & Anuar, H. S. (2014). A Review Study of Maintenance and Management Issues in IBS Commercial Building. *International Journal of Computer Informatics & Technological Engineering*, 1(1), 42-46.
- [5] Su, Y., Lee, Y. C., & Lin, Y. C. (2011). Enhancing Maintenance Management using Building Information Modeling in Facilities Management. 2011 Proceedings of the 28th International Symposium on Automation and Robotics in Construction (ISARC), IAARC, Seoul, Korea, 752757.
- [6] Vaha, P., Heikkila, T., Kilpelainen, P., Jarviluoma, M., & Gambao, E. (2013). Extending Automation of Building Construction-Survey on Potential Sensor Technologies and Robotic Applications. *Automation in Construction*, 36(2013), 168-178.
- [7] Kamaruddin, S. S., Mohammad, M. F., Mahbub, R., & Ahmad, K. (2013). Mechanisation and Automation of the IBS Construction Approach: A Malaysian Experience. *Procedia Social and Behavioral Sciences*, 105(2013), 106-114.
- [8] Babic, N. C., Podbreznik, P., & Rebolj, D. (2010). Integrating Resource Production and Construction using BIM. *Automation in Construction*, 19(2010), 539-543.
- [9] Nawari, N. O. (2012). BIM Standard in Off-Site Construction. *Journal of Architectural Engineering*, 18(2), 107-113.
- [10] Cheng, J. C. P. & Ma, L. Y. H. (2013). A BIM-based System for Demolition and Renovation Waste Estimation and Planning. *Waste Management*, 33(2013), 1539-1551.
- [11] Irizarry, J., Karan, E. P. & Jalaei, F. (2013). Integrating BIM and GIS to Improve the Visual Monitoring of Construction Supply Chain Management. *Automation in Construction*, 31(2013), 241-254.
- [12] Love, P. E. D., Matthews, J., Simpson, I., Hill, A. & Olatunji, O. A. (2014). A Benefits Realization Management Building Information Modeling Framework for Asset Owners. *Automation in Construction*, 37(2014), 1-10.
- [13] Love, P. E. D., Simpson, I., Hill, A. & Standing, C. (2013). From Justification to Evaluation: Building Information Modeling for Asset Owners. *Automation in Construction*, 35(2013), 208-216.
- [14] Volk, R., Stengel, J. & Schultmann, F. (2014). Building Information Modeling for Existing Buildings-Literature Review and Future Needs. *Automation in Construction*, 38(2014), 109-127.
- [15] Ismail, Z., Mutalib, A. A., & Hamzah, N. (2016). Case Study to Analyse Problems and Issues in IBS Building Maintenance. *International Journal of Applied Engineering Research*, 11(1), 226-232.

## ON THE SEASONAL COLORS AND SMELLS ANALYZING SOCIAL NETWORKING SERVICE

Tatsuya Matsuura<sup>1</sup>, Momoko Tanaka<sup>2</sup>, Hayate Deguchi<sup>3</sup> and Kazunari Tanaka<sup>4</sup>

<sup>1</sup>Graduate Course in Architecture, Civil Engineering and Urban Design, Graduate School, Osaka Institute of Technology, Japan; <sup>2</sup>Ohba & co.,ltd, Japan; <sup>3</sup>Chuoh consultants co.,ltd, Japan ; <sup>4</sup>Osaka Institute of Technology, Japan

### ABSTRACT

The purpose of this study is to examine a method to extract the “sense of the season” through colors and smells. The research method is based on the Twenty-four Divisions of the Solar Year as units to extract and categorize colors and smells from photos and posts on SNS; Twitter and Facebook, where people post about the seasons. We collect the data using *geospatial information system* and *text mining* (KH coder) software. First, we collected yearly tweets from 2017 posted on Twitter. The photo accompanied in the tweet is subjected to extract the colors at that point in the season. Sentences are subjected to text mining to extract “smells”. In this research, we try to extract not just a few typical colors and smells of the seasons, but all colors and smells. The results show that there are from 64 to 77 seasonal colors. The smells of the season occur in the first half of February, the second half of May, the second half of June, the first half of July, the second half of September, and October. Outside of this we cannot significantly detect the seasonal smells.

*Keywords: colors, smells, Twenty-four Divisions of the Solar Year, SNS*

### INTRODUCTION

Japan has four distinct seasons, but traditionally in Japan, the seasons were actually divided into 24. So, the Japanese people were always very sensitive to the changing seasons. Natural phenomena that change daily such as seasonal food and events have always enriched the lives and minds of Japanese people. However, in the present era it is difficult for Japanese people to feel these more subtle changes in the seasons. The modern lifestyle does not allow people to feel the seasons in the same way as the past. So, I would argue that Japanese people are missing an opportunity to enrich their minds. However, at present, with the spread of electronic devices, it can be said that Japanese people now feel the seasons through TV and Internet, especially with a focus on SNS where individual people can post their pictures and feelings. If one can express a sense of season through information channels, we can use this for analyzing in the real world.

### PURPOSE AND METHOD OF RESEARCH

In this research, the purpose is to capture the present-day colors and smell of the seasons. The method is by using the images and comments on SNS to extract this information. The share of information acquired by the human five senses is overwhelmingly vision-based at 87%. In recent years, many people are using photos to transmit information and convey feeling via SNS, indicating that the relationship

between modern people and visual information is high. Therefore, we focus on the vision part of the five senses. Also, olfactory information has a strong relationship with emotion and memory in the brain, and information collected from this method is retained for a long time. For this reason, we also focus on the sense of smell along with as the sense of sight. We also plan to incorporate an additional sense after this examination.

### COLOR ANALYSIS

We collected images from Twitter to extract seasonal colors. We collected 50 images per period. We set three conditions such as images not including illustrations, image of object including background and image not edited. And we resized the image to 60 x 60 pixels (for uniformity of resolution and aspect ratio). We then convert RGB values per pixel to the XYZ color system (to  $L^*a^*b^*$  color system.[1]), to easily express the results of image analysis. This time, the colors extracted from multiple images were divided into the same color system, and the  $\Delta E_{2000}$  color error formula [2] was used to calculate the colors and proportions (Figure-1, Figure-2, Figure-3). Extraction results were not consistent in color order, hence we used the Munsell color system to arrange the results. From the results, the proportion of green lines increase from May to August, and the proportion of red lines was dominant in October and November. Although there are events such as beach and pools

opening in July and August, the proportion of blue and light blue is not significant. Going against what we originally thought, that Japanese people would feel a sense of the summer season with the color of the water, such as sea etc. This indicates that Japanese people feel summer from various other things.

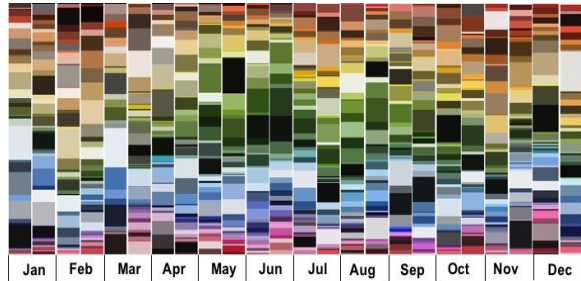


Fig. 1 Extraction result of color of the all season.

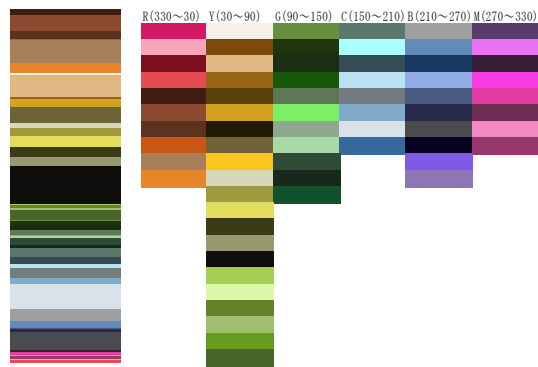


Fig. 2 Extraction result of color of the first half of October [3].

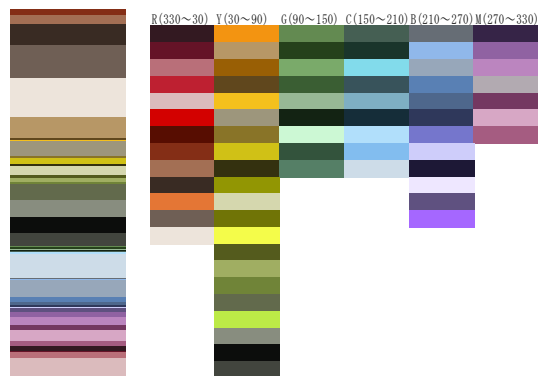


Fig. 3 Extraction result of color of the late March [3].

## ANALYSIS USING TEXT INFORMATION

As with color analysis, we collected 10 text tweets/day using Twitter to represent the “smells”. They were random selected by the Twitter search system on website. Next, the URL contained in the text data was deleted and the collected data was organized

by half months. We used text mining software to analyze the data, and finally created a co-occurrence network. As an example, the results of the same month as color analysis. From the results of the Late of March, we could extract the words of morning, perfume and person have an influence in the season. From the results of the first half of October, we could extract the smell of fragrant olive (osmanthus) has a great influence in the season (Figure-4, Figure-5). We selected the necessary parts of speech, set the minimum number of co-occurring words, and corrected co-occurring words when creating a co-occurrence network. As a result of this analysis, it was found that seasonal words appeared at the turn of the season, and that changes in the seasonal smells were present. However, it can be seen that there are few months when season-specific smells appeared. From the results of the co-occurrence network, we made the graph as the number of occurrences of the word on the vertical axis and on the horizontal axis as the first half and late of the month. Light blue line is words about seasonal, red line is words about related to people, gray line is words about food, yellow line is words about nature, blue line is words about place (Figure-6). When the smell of one season starts to transition to the

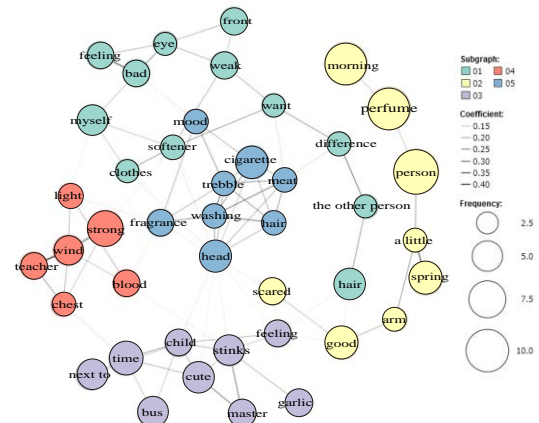


Fig. 4 Late of March co-occurrence

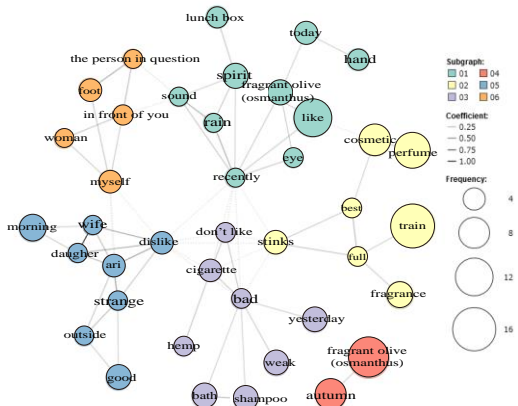




Fig. 5 First half of October co-occurrence

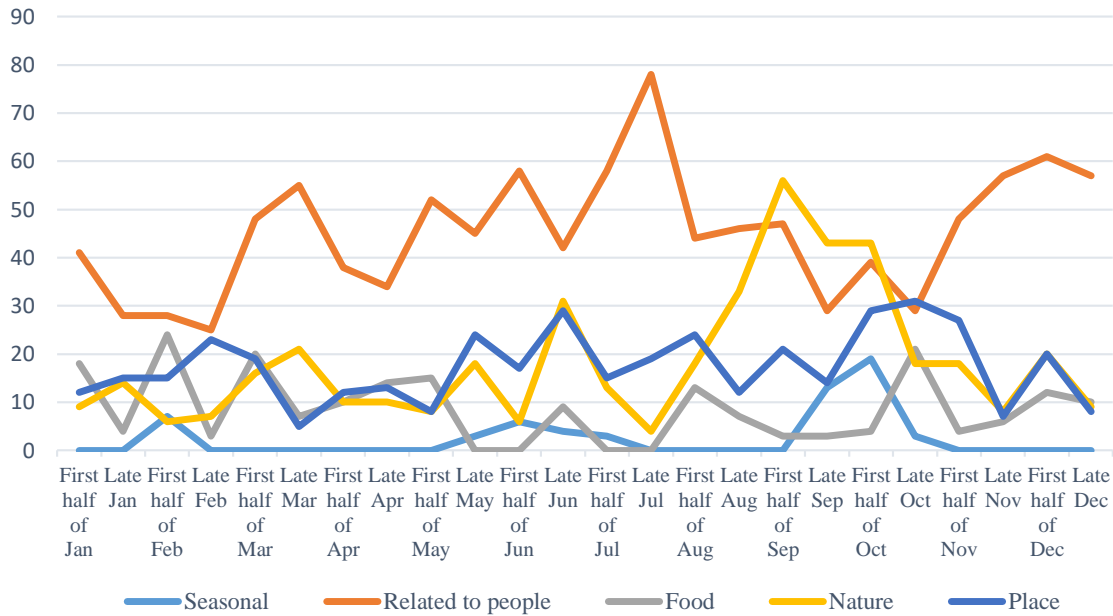


Fig. 6 Change of smell of each month

next season based on the categorization of the co-occurrence word, the influence of other smells becomes small. With regards to the months that do not emit season-specific smells, it can be considered that the season is sensed from a variety of smells rather than specific smells.

## CONCLUSIONS

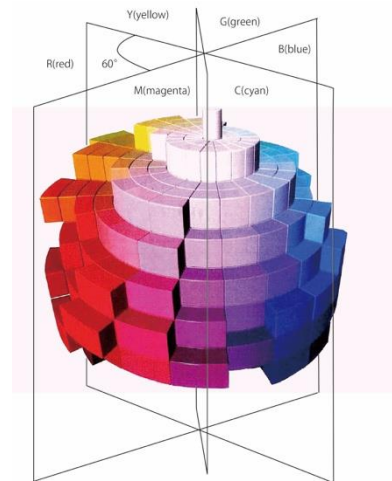
In this research, seasonal color extraction results revealed that there are many different colors present than the standard seasonal colors we imagine. Not only the main subjects, but also the colors of the sub-subjects influenced the surrounding environment when the seasonal colors were extracted. Regarding the results of the smells of the season, changes with the seasons and smell became clear. Although we could infer smell from objects, we found that the smells that are easy to feel and communicate are food and seasonal goods, and that they are greatly influenced by nature. As a future subject, when collecting photos and text data from Twitter, we will try to further extract the sense of seasons by region. Furthermore, by increasing the amount of data collected, we will discover sensory relationships including additional sensations in each season.

## ACKNOWLEDGMENTS

I would like to thank Hikaru NISHIHATA for useful discussions. I am grateful to Nobuaki TANAKA and Hiroki KOMAI for assistance with the numerical simulations.

## REFERENCES

- [1]  $L^*a^*b^*$  is a color space defined by the International Commission on Illumination (CIE) in 1976. It expresses color as three values:  $L^*$  for the lightness from black (0) to white (100),  $a^*$  from green (-) to red (+), and  $b^*$  from blue (-) to yellow (+).
- [2]  $\Delta E_{2000} = \sqrt{\left(\frac{\Delta L^*}{k_L \cdot S_L}\right)^2 + \left(\frac{\Delta C^*}{k_C \cdot S_C}\right)^2 + \left(\frac{\Delta H^*}{k_H \cdot S_H}\right)^2} + \left(R_T \left(\frac{\Delta H^*}{k_H \cdot S_H}\right) \left(\frac{\Delta H^*}{k_H \cdot S_H}\right)\right)$   
 $L' = L^*, a' = a^* \cdot (1 + G) \quad G = 0.5 \left(1 - \sqrt{\frac{C^* a b^7}{C^* a b^7 + 25^7}}\right)$   
 $b' = b^*, C' a = \sqrt{(a')^2 + (b')^2}, h' = \tan^{-1} \left(\frac{b'}{a'}\right)$
- [3] We divided the Hue-ring 6 categories of colors every 60 degrees from the center color (red).



## PROPOSED ANGAT RIVER WATER IMPOUNDING AND FLOOD MITIGATION PROJECT

Bon Ryan P. Aniban<sup>1</sup>, Roniel C. Naungayan<sup>1</sup>, Sheina R. Pallega<sup>1</sup>

Jordan N. Velasco<sup>1</sup>, and John Lemar M. Tirao<sup>1</sup>

<sup>1</sup>Pamantasan ng Lungsod ng Valenzuela, Valenzuela, Philippines

### ABSTRACT

Along the Angat river in Bulacan, central Philippines, three existing dams (Ipo, Bustos, and Angat, dams) are installed which serve different purposes. These dams release huge volume of water which contributes to the floods downstream the reservoir. This research aims to reduce flood water downstream and to impound flood water from Ipo and Angat dams. The researchers conducted data gathering, preliminary investigations and flood simulations using Global Mapper, ArcGIS and HEC-HMS respectively to compute the maximum decision flood (MDF) for the basis of the dam. The proposed structure is a gated spillway-gravity dam subdivided into 15 flood storages where water surface elevations were set as critical levels. Decision floods are formed by dividing the MDF into 15 sub-hydrographs. As a result of routing simulations of the decision floods, a set of 15 spillway gate openings is identified where all floods from very small magnitudes to the MDF may be routed without overpassing the crest of dam. A 15-stage operation rules are then identified where the gate openings of the primary stages are decreased as the critical levels increased step by step, with the objective of attenuating smaller floods more effectively and releasing higher outflows for larger floods close to and including the MDF.

*Keywords: Maximum decision flood, Flood mitigation, Gated spillway gravity dam, Water impounding*

### INTRODUCTION

The province of Bulacan, in central Philippines, is largely affected by heavy rainfall and strong winds which caused worst floods and landslides in the area. Huge volume of water coming from the nearby Sierra Madre mountain range, drainage capacity constraints and low-lying area elevations are also reasons of flooding in the province. Because of these, the need to develop strategies in flood mitigation is considered a priority. One of the long-term solutions that can be applied is the construction of flood-regulating dams.

There are three existing dams in Bulacan, the Ipo, Bustos, and Angat dams, that serve different purposes. Each dam is operated by a specific water control plan, but due to extreme weather conditions, may contribute to an impending huge flood. According to Bulacan's Provincial Risk Reduction and Management Council, Angat dam is the only impounding dam that can store large amount of water among the three. If Angat dam reached its critical level, flood water starts to overflow its radial gates and subsequently inundates vast areas of the province.

This study mainly deals with designing a dam that will reduce destructive flood impacts in extreme events and provide alternative water source as well. This also focuses only in determining good location of the water impounding and flood mitigation dam, most efficient dimensions and stability, and designing the operational openings of the gated spillways during different flood events. The design of dam and gated

spillways will be base flood on the upstream of proposed location of the dam. This will not cover soil exploration and studies for the foundation, as well as the bill of quantities of the design.

### RELATED STUDIES

Throughout history, dams and reservoirs have been used successfully in collecting, storing and managing water supplies needed to sustain life. It is also used as a water impounding structure during heavy rains that reduces flooding [1]. However, Schultz stated that dams should not be constructed without considering the location, choice and size, and storage capacity [2]. In line with this, the US Department of Interior published a design manual for gravity dams presenting instructions, examples and standards for the design of dams.

Hydrology and hydraulics analysis are required in dam design and several applications are made available for the process. Blue Marble Geographic created Global Mapper which handles vector, raster and elevation data that provides viewing conversion and other geographic information systems (GIS) [3]. Another GIS software that was produced, called the ArcGIS, works with maps that can calculate and provide properties of land cover [4]. For flood modelling, the US Army Corps introduced the use of HEC-HMS for simulating precipitation-runoff processes of dendritic watershed systems [5].

For efficient flood mitigation, inundation dams

with gated spillways are commonly used, however, the operation of such gates is difficult, due to its inconsistency to predict the true magnitude of an incoming flood [6]. Linsley observed that discharge regulation from these types of dams is regulated by gates and valves are operated on the basis of the judgment of a project engineer [7]. Sakakima also made a similar comment that for extremely large flood, a reservoir operator has to control the gates to protect the reservoir and the downstream reference point by relying on his judgment [8]. With these problems, numerous solutions were suggested for the spillway gate operations. For example, Afshar and Salehi [9] proposed a modification of the 6-stage model presented by Acanal, et al. [10], which takes into account additional real-time information of the inflow hydrograph measured at a gauging station installed at the reservoir entrance [10]. Afshar and Saheli also coded another operation method which assigns 3 critical water surface elevations associated with 3 control discharges with the objective of minimizing downstream flooding [9]. Haktanir and Citakoglu modified the said 6-stage model into a 15-stage model [11]. On their model, the flood retention of a dam having a gated spillway is divided into 15 sub-storages whose surface elevations are identified as critical levels.

## METHODOLOGY

### Preliminary Data and Investigations

#### *Location of dam, catchment area, lag time and curve number*

Google Earth© was used to determine the possible location of the proposed dam, should be along Angat river with a narrowing channel, away from major towns and cities, and the area upstream is suitable for a reservoir. To verify if the location is in a narrowing river, SRT-DEM was setup using Global Mapper software. Contours and elevations are generated in the SRT-DEM to determine the catchment area and perimeter of the chosen location.

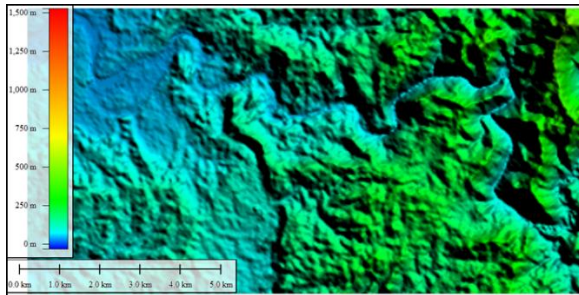


Fig. 1 Digital elevation model of Angat River.

To determine lag time, the soil conservation service (SCS) formula, adopted by DHI 2009 was used:

$$T_{lag} = \frac{(L \times 3.28 \times 10^3)^{0.8} \times \left(\frac{1000}{CN} - 9\right)^{0.7}}{3.42 \times Y^{0.5}} \quad (1)$$

Where

$T_{lag}$  is the lag time (hour);

$CN$  is the curve number within the catchment area;

$L$  is the hydraulic length of the catchment (kilometer); and,

$Y$  is the average catchment slope

The values of the parameters used in SCS for lag time calculation were obtained from ArcGIS. Curve number, on the other hand, was determined from the hydrologic soil group and land use [12].

#### *Design flood*

The proposed dam is categorized according to failure hazard and dam height. Design flood and minimum freeboard is then determined.

#### *Elevation-storage relationship*

To calculate the change in storage in relation to elevation and area, the following equation is used:

$$\Delta S = \left(\frac{A_1 + A_2}{2}\right)(h_2 - h_1) \quad (2)$$

Where

$\Delta S$  is the change in storage;

$A_1$  is the surface area of water at previous elevation  $h_1$ ; and

$A_2$  is the surface area of water at current elevation  $h_2$

#### *Spillway design*

In designing spillways, the capacity of water flowing and time must be considered. To check if discharge will satisfy the time, the following equation is used:

$$t = \frac{1}{3600} \int_0^H \frac{0.75A}{\frac{2}{3} C \sqrt{2gLH^2}} dh \quad (2)$$

Where

$t$  is the time required to discharge water (hour);

$A$  is the area (square meter) of water surface at certain height  $h$  (meter);

$H$  is the height of water from crest of spillway (meter);

$L$  is the length of spillway (meter); and,

$g$  is the acceleration due to gravity ( $9.81 \text{ m/s}^2$ )

## HEC-HMS Simulation

HEC-HMS model components are used to simulate the hydrologic response in a watershed. A simulation calculates the precipitation-runoff response in the basin model given by the input from the meteorological model. In this study, to compute the total inflow on the dam location, the rainfall-runoff from the catchment area given by the 100-year return period and the discharge of Ipo dam during the 2009 Typhoon Ketsana. During the simulation, SCS curve number method is used for the loss rate, SCS unit hydrograph for transform of sub-basin, and discharge method for the flow or source creation.

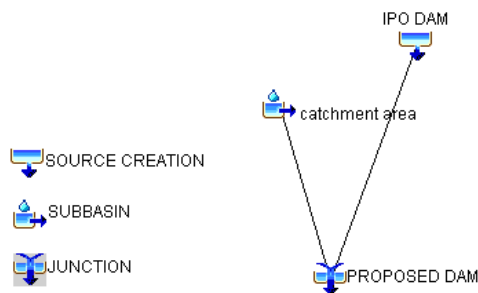


Fig. 2 Model of the study area in HEC-HMS.

## Fifteen-stage Routing Model

### Computation of spillway flow

The spillway discharge for the fully-opened and partially opened gates is computed by the following equations,

$$Q = \frac{2}{3} C \sqrt{2gL} H^{1.5} \quad (4)$$

$$Q = \frac{2}{3} C \sqrt{2gL} (H_1^{1.5} - H_2^{1.5}) \quad (5)$$

Where

- $Q$  is the total discharge;
- $C$  is the discharge coefficient;
- $L$  is the length of the spillway;
- $H_1$  and  $H_2$  are the pressure head at the bottom of the weir respectively; and,
- $g$  is the acceleration due to gravity ( $9.81 \text{ m/s}^2$ )

### Flood routing simulation

The flood routing simulation is performed stepwise at fixed-time intervals, such as  $0.25h$  by solving the continuity equation,

$$\left( \frac{I_1 + I_2}{2} \right) \Delta t - \left( \frac{O_1 + O_2}{2} \right) \Delta t = \Delta S \quad (6)$$

Where

$I_1$  and  $I_2$  are the inflows at previous and current time steps respectively;

$O_1$  and  $O_2$  are the outflows at previous and current time steps respectively;

$\Delta S$  is the change in storage (cu.m.),  $\Delta S = S_2 - S_1$ ; and,

$\Delta t$  is the change in storage in time.

For 15-stage routing mode, stepwise routing simulations at pre-defined time increments, such as  $t = 0.5 \text{ hr}$ , each of the 15-decision hydrographs from 5% to 250% of the 100-year flood are repeated as many times as required. The large loop of routing computations begins by allocating  $1/15^{\text{th}}$  of the flood-retention storage to all of the 15 decision floods. The top elevations of sub-portions of the flood retention storage are known as the critical levels ( $H_{cr_i}$ ) is shown in Figure 3.

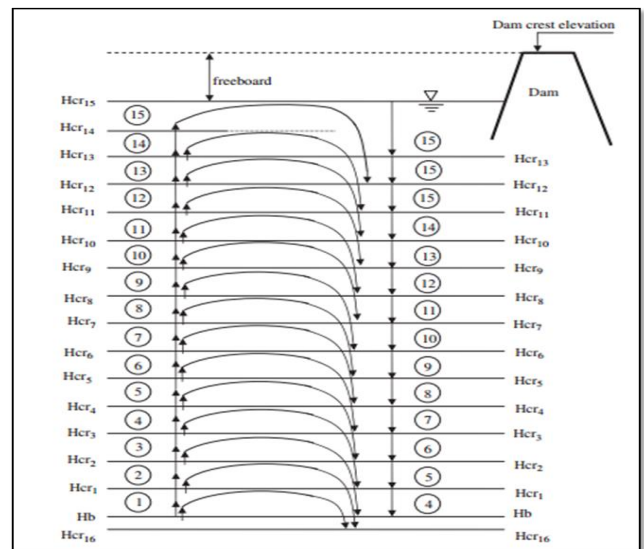


Fig. 3 The 15-stage routing model scheme. The circles on the left and right show the stages during the rising and recession limbs respectively of the outflow hydrograph.

## General Dimensions and Stability of Dam

The general dimension of the dam includes height, width and the downstream slope, and a batter, if necessary. All dimensions must be designed satisfying stability and factor of safety. In this study, the factor of safety (FS) used is 1, as stated to be the minimum FS of gravity dams [13]. The downstream slope in this study followed the 1:2 vertical-horizontal ratio rule in designing gravity dams [14].

In the design of concrete gravity dams, it is essential to determine the loads required for stability. The following loads may affect the design: dead load,

head water and tail water pressures and uplift. It is also important to check the dimension of the dam if it will satisfy FS against sliding and overturning.

$$W = \gamma_c V \quad (7)$$

$$F = \frac{9.81 H^2 L}{2} \quad (8)$$

$$F = 9.81 H B \quad (9)$$

$$FS_s = \frac{\mu R_y}{R_x} \quad (10)$$

$$FS_o = \frac{RM}{OM} \quad (11)$$

Where

W is the concrete weight in kN;  
 $\gamma_c$  is the unit weight of concrete, 23.6 kN/m<sup>3</sup>;  
 V is the volume of concrete;  
 F is the force acting on the dam laterally;  
 H is the height of either head or tail water;  
 L is the length of dam, usually considering 1-meter strip length of the dam;  
 B is the length of the base of the dam;  
 $FS_s$  is the factor of safety against sliding;  
 $FS_o$  is the factor of safety against overturning;  
 $R_y$  is the totality of all forces acting vertically to the dam;  
 $R_x$  is the totality of all forces acting horizontally to the dam;  
 $\mu$  is the coefficient of friction;  
 OM is the overturning moment; and,  
 RM is the righting moment

## RESULTS AND DISCUSSION

The proposed dam should be located at 14°53'41.75"N, 121°07'05.80"E, or in barangay San Mateo, Bulacan, with a catchment area of 18.063 km<sup>2</sup>.

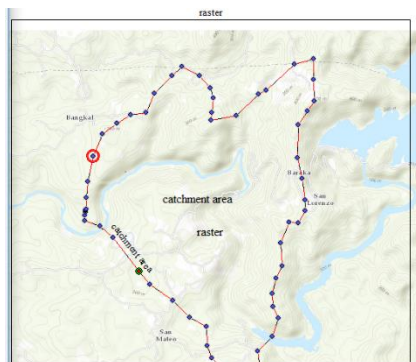


Fig. 4 Catchment area from the dam axis.

The general dimensions of the proposed dam were determined using trial and error, such that the most desirable and most efficient dimension must produce the smallest volume (Fig. 5). The height of the dam

was determined with the use of contours that close the reservoir from the axis of the dam. It was found that the maximum surface elevation is 99 m and the lowest elevation on the dam location is 56 m. The dam is classified as Class IV and the design flood is 225% of 100-year flood with a minimum freeboard of 1.25 m. With the assessment of stability, it was found that the factors of safety against sliding and overturning is 1.21 and 1.38, respectively.

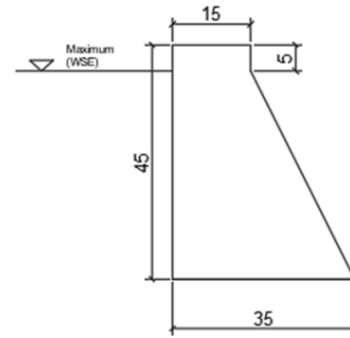


Fig. 5 General dimension of the dam, in meters.

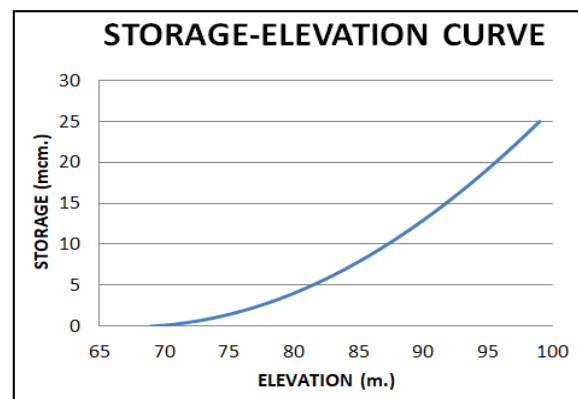


Fig. 6 Storage-elevation curve

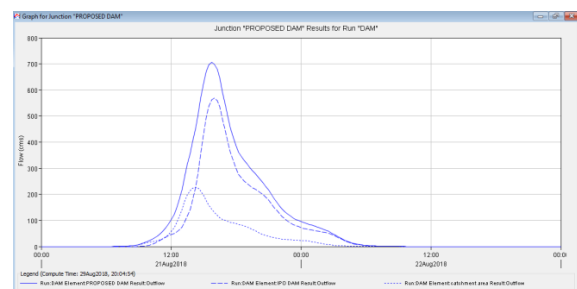


Fig. 7 Outflow hydrograph generated in HEC-HMS.

Figure 7 shows the hydrograph of the 100-year flood at the dam axis. It is the combination of the discharges from the nearby Ipo dam and the rainfall runoff produced by a 100-year flood from the catchment area itself. The 15-decision floods shown in Fig. 8 are prepared for optimum management during flood events.



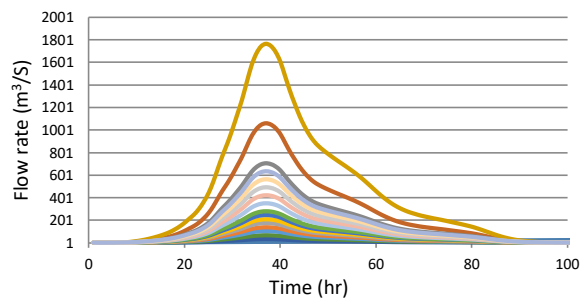


Fig. 8 The 250% of 100-year flood of the proposed dam, the 15<sup>th</sup> decision flood hydrograph along with the other 14 decision hydrographs.

Table 1 summarizes the first operation option along with two other options referred to the methodology. Table 2 shows the summary of 15 rules for the spillway gate openings.

Table 1 Spillway gate opening and critical lake levels for the 1<sup>st</sup>, 2<sup>nd</sup> and 3<sup>rd</sup> options of operations.

|                   | Critical Levels and Gate Openings (m) |               |              |
|-------------------|---------------------------------------|---------------|--------------|
|                   | First Option                          | Second Option | Third Option |
| Hb                | 88.76                                 | 88.76         | 88.76        |
|                   | 0.1                                   | 0             | 0            |
| Hcr <sub>1</sub>  | 89.17                                 | 89.39         | 89.39        |
|                   | 0.2                                   | 0             | 0            |
| Hcr <sub>3</sub>  | 89.64                                 | 90.1          | 90.1         |
|                   | 0.4                                   | 0             | 0            |
| Hcr <sub>4</sub>  | 89.95                                 | 90.8          | 90.8         |
|                   | 0.6                                   | 0             | 0            |
| Hcr <sub>5</sub>  | 90.24                                 | 91.47         | 91.47        |
|                   | 0.8                                   | 0.8           | 0            |
| Hcr <sub>6</sub>  | 90.51                                 | 91.52         | 92.13        |
|                   | 0.9                                   | 0.9           | 0            |
| Hcr <sub>7</sub>  | 91.25                                 | 91.79         | 92.85        |
|                   | 1                                     | 1             | 0            |
| Hcr <sub>8</sub>  | 91.97                                 | 92.33         | 93.95        |
|                   | 1.2                                   | 1.2           | 0            |
| Hcr <sub>9</sub>  | 92.57                                 | 92.89         | 95.77        |
|                   | 1.4                                   | 1.4           | 1.6          |
| Hcr <sub>10</sub> | 93.12                                 | 93.39         | 95.83        |
|                   | 1.8                                   | 1.8           | 3            |
| Hcr <sub>11</sub> | 93.54                                 | 93.77         | 96.11        |
|                   | 2                                     | 3             | 4            |
| Hcr <sub>12</sub> | 94.05                                 | 93.89         | 96.15        |
|                   | 2.6                                   | 3.2           | 6            |
| Hcr <sub>13</sub> | 94.28                                 | 94.17         | 96.51        |
|                   | 3.8                                   | 5             | Fully Open   |
| Hcr <sub>14</sub> | 96.01                                 | 95.61         | 97.83        |
|                   | 6.5                                   | 6.5           | Fully Open   |
| Hcr <sub>15</sub> | 99.00                                 | 99.00         | 99.00        |
| Maximum WSE       | 98.99                                 | 98.99         | 98.97        |

Table 2 Summary of spillway gate opening step numbers for 15-operation rule sets, given by the 15-stage routing for the proposed dam.

| Operation Option | Gate opening numbers (*) for stages 1-15 |   |   |   |   |   |    |    |    |    |    |    |    |    |    | Maximum WSE (m) |
|------------------|--|---|---|---|---|---|----|----|----|----|----|----|----|----|----|-----------------|
|                  | 1  | 2 | 3 | 4 | 5 | 6 | 7  | 8  | 9  | 10 | 11 | 12 | 13 | 14 | 15 |                 |
| 1                | 1  | 2 | 3 | 5 | 7 | 9 | 10 | 11 | 12 | 13 | 15 | 16 | 19 | 25 | 34 | 98.99           |
| 2                | 1  | 1 | 3 | 5 | 7 | 9 | 10 | 11 | 12 | 13 | 15 | 17 | 21 | 27 | 34 | 98.99           |
| 3                | 1  | 1 | 1 | 5 | 7 | 9 | 10 | 11 | 12 | 13 | 15 | 18 | 21 | 28 | 34 | 98.99           |
| 4                | 1  | 1 | 1 | 1 | 7 | 9 | 10 | 11 | 12 | 13 | 15 | 18 | 21 | 29 | 34 | 98.99           |
| 5                | 1  | 1 | 1 | 1 | 1 | 9 | 10 | 11 | 12 | 13 | 15 | 21 | 22 | 31 | 34 | 98.99           |
| 6                | 1  | 1 | 1 | 1 | 1 | 1 | 10 | 11 | 12 | 14 | 20 | 22 | 23 | 31 | 34 | 98.99           |
| 7                | 1  | 1 | 1 | 1 | 1 | 1 | 1  | 11 | 12 | 14 | 21 | 23 | 24 | 31 | 34 | 98.98           |
| 8                | 1  | 1 | 1 | 1 | 1 | 1 | 1  | 1  | 12 | 16 | 21 | 23 | 26 | 31 | 35 | 98.92           |
| 9                | 1  | 1 | 1 | 1 | 1 | 1 | 1  | 1  | 1  | 16 | 21 | 26 | 33 | 34 | 37 | 98.96           |
| 10               | 1  | 1 | 1 | 1 | 1 | 1 | 1  | 1  | 1  | 1  | 24 | 27 | 33 | 35 | 38 | 98.94           |
| 11               | 1  | 1 | 1 | 1 | 1 | 1 | 1  | 1  | 1  | 1  | 1  | 26 | 29 | 33 | 35 | 98.68           |
| 12               | 1  | 1 | 1 | 1 | 1 | 1 | 1  | 1  | 1  | 1  | 1  | 30 | 34 | 36 | 39 | 98.69           |
| 13               | 1  | 1 | 1 | 1 | 1 | 1 | 1  | 1  | 1  | 1  | 1  | 1  | 35 | 37 | 40 | 98.52           |
| 14               | 1  | 1 | 1 | 1 | 1 | 1 | 1  | 1  | 1  | 1  | 1  | 1  | 1  | 41 | 42 | 97.89           |
| 15               | 1  | 1 | 1 | 1 | 1 | 1 | 1  | 1  | 1  | 1  | 1  | 1  | 1  | 1  | 42 | 98.67           |

Figure 9 shows the inflow and outflow hydrographs of the dam. It also reveals that the 2<sup>nd</sup> and 3<sup>rd</sup> options of encroaching the spillway gates for smaller floods, and having to open them wider for higher floods, yield outflow hydrographs for the maximum design flood (MDF) peaks greater than that of the 1<sup>st</sup> option (much greater for the 3<sup>rd</sup> option), while peaks of an intermediate flood, the 7<sup>th</sup> decision flood, are considerable smaller than that of the 1<sup>st</sup> option as expected. The 2<sup>nd</sup> or 3<sup>rd</sup> options may be preferred than the 1<sup>st</sup> option if mitigation of moderate severity floods is the desired target. The flood retention storage of the proposed dam is fairly large, while the total discharge is also high; therefore, the 3<sup>rd</sup> option, which aims at keeping the spillway gates closed as much as possible for smaller decision floods, results in closed gates up to the 7<sup>th</sup> decision flood. However, this defiant policy necessitates large gate openings after the 10<sup>th</sup> decision flood (half of MDF) and fully opened gates beyond the 13<sup>th</sup> decision flood to the MDF. This implies that effective mitigation of moderate floods is paid for by heavy damage downstream in case a severe flood is arriving to the reservoir.

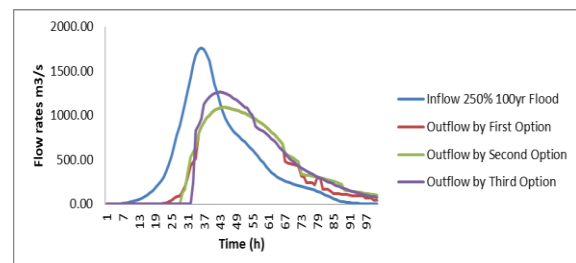


Fig. 9 Hydrographs for the 1<sup>st</sup>, 2<sup>nd</sup> and 3<sup>rd</sup> operation options resulting from routing the parabolic 250% of 100-year flood of the proposed dam using the 15-stage routing model.



Figure 10 illustrates the variations in water surface elevation (WSE) together with the critical levels during routing of MDF during the 1<sup>st</sup>, 2<sup>nd</sup> and 3<sup>rd</sup> options.

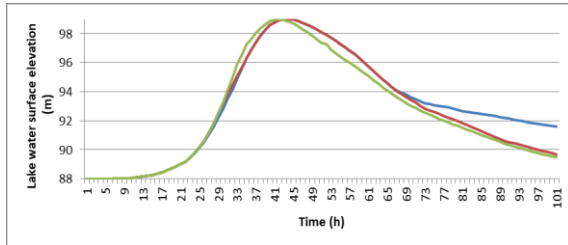


Fig. 10 Rate of change of the lake WSE during the MDF routing of proposed dam using 1<sup>st</sup>, 2<sup>nd</sup> and 3<sup>rd</sup> operation options.

## CONCLUSION

The proposed Angat river water impounding and flood mitigation project located at San Mateo, Bulacan is a viable long-term solution to the recurring problem flooding in the downstream areas of Ipo and Angat dams. The infrastructure system is envisioned to provide a solution to the flood-disaster prone low-lying areas in southern Bulacan.

The implementation of 15-stages of fixed operational gate opening will eliminate the need to predict the occurrence of flood event by management. Since it has a fixed set of gate opening values on different floods, it gives the most efficient routing method and may avoid flash floods during and after extreme rainfall events.

## RECOMMENDATION

The proposed project is envisioned to provide a long-term solution to the flooding in Bulacan. Within the framework of sustainable development, it is recommended to adopt the principles of integrated water resource management and river basin approach. This shall ensure that the outcomes of the project are consistent with the general intent and master plan of the government for a sustainable and functional built environment.

There are a number of collateral issues and challenges that concerned government agencies may face at the implementation of this kind of projects. Notwithstanding these issues, it is recommended that the project be immediately implemented after a validation and detailed feasibility studies are undertaken, such as soil explorations. The socio-political repercussions should have special attention to ensure smooth implementation of this project.

## REFERENCES

- [1] International Commission on Large Dams, Benefits and Concerns about Dams, Committee on Public Awareness and Education, July 1999.
- [2] Shultz A., Dam Construction, 2010
- [3] Blue Marble Geographics – LIDAR Module, Unpublished Master's Thesis, 2016.
- [4] Environmental Systems Research Institute (ESRI 2001-2004), Master's thesis, 2004.
- [5] Hydrologic Engineering Center (HEC), HEC-5 Simulation of Flood Control and Conservation Systems, US Army Corps of Engineers, 1998.
- [6] Japan International Cooperation Agency, Feasibility Study on Flood Control, Forecasting and Warning System for Seyhan River Basin: Final Report, Summary, General Directorate of State Hydraulic Works and Nippon Koei Co., Ltd., 1994, pp. 3-39.
- [7] Linsley R.K., Water Resources Engineering, 4th ed., McGraw-Hill, 1992.
- [8] Sakakima S., Kojiri T., and Itoh K., Real-time Reservoir Operation with Neural Nets Concept, Proceedings of the 7<sup>th</sup> International Conference on Applications of Artificial Intelligence in Engineering (AIENG/92), Computational Mechanics Publications, pp. 501-514.
- [9] Afshar A., and Salehi A., Gated Spillways Operations Rules Considering Water Surface Elevation and Flood Peak: Application to Karkheh Dam, Proceedings of the World Environmental and Water Resources Congress, 2011, pp. 3007-3015.
- [10] Acanal N., Yurtal R., and Haktanir T., Multi-Stage Flood Routing for Gated Reservoirs and Conjunctive Optimization of Hydroelectricity Income with Flood Losses, Hydrological Sciences Journal, Vol. 45, Issue 5, 2000, pp. 675-688.
- [11] Haktanir T., Citakoglu H., and Nese A., Fifteen-Stage Operation of Gated Spillways for Routing Management Through Artificial Reservoirs, Hydrological Sciences Journal, Vol. 58, Issue 5, pp. 1013-1031.
- [12] National Engineering Handbook, National Resources Conservation Service, US Department of Agriculture, Part 630 Hydrology, Chapter 7, n.d.
- [13] Bureau of Reclamation, US Department of Interior, Design of Gravity Dams, 1976.
- [14] New York State Department of Environmental Conservation, Guidelines for Design of Dam, 1989.

## A RISK ASSESSMENT FRAMEWORK FOR HIGH-RISE SCHOOL BUILDING PROJECT IN METRO MANILA, PHILIPPINES

Michael V. Almeida<sup>1</sup> and Andres Winston C. Oreta<sup>2</sup>  
<sup>1,2</sup>De La Salle University, Philippines

### ABSTRACT

The rapid increase of school building construction in the country was brought by the implementation of a nationwide reform in pre-university education cycle from 10 to 12 years in June 2012. The change demanded a significant increase in school buildings. However, construction of high-rise school building project is unique due to its varying characteristics as compared to other types of building construction project. Construction of such buildings depends on variables such as site, surrounding, size, structure, student population, resources and culture. As a result, it is subject to numerous risk and weakness, which invariably have significant negative impact on its overall performance. Therefore, risk assessment tools for school buildings must be modified to fit these varying characteristics. However, there are three major challenges during the planning stage of project risk management of such buildings, first is the correct identification of the sources and type of risks, second the necessary statistical information and third, the selection of methods that will successfully estimate the potential impacts and probabilities of occurrence. Presently, school administrators are experiencing difficulty in dealing with risk assessment process due to no formal risk management structure in place and the lack of knowledge in risk management theories and techniques. The skills gap resulting to ambiguity in risk decision making process during project risk assessment must be bridged. This paper proposed a conceptual framework for developing a decision support tool which allows correct factor identification and assessment of risk associated in high-rise school building construction in Philippines.

*Keywords: High-rise school building, Risk Factor, Risk identification, Risk Assessment*

### INTRODUCTION

School building construction in the Philippines becomes prevalent since the implementation of a nationwide reform in pre-university education cycle from 10 to 12 years in June 2012 (Figueroa, Lim, and Lee, 2016). However, such building construction compared from other types is not simple and differs in terms of built environment (private or public). School building construction methods consist of both physical and metaphysical factors. The physical factors that will influence the outcomes are financial resources, limitations of the proposed project site due to its controlled environment, nature of the education program and framework of the age class groups. The metaphysical nature on the other hand is a critical factor before its realization. Compared to other building construction the stakeholders are not limited only to designers, contractors, and project managers but also the participation of school administrators, teachers, parents and age structure of students to be served as well. According to Lunenburg & Ornstein (2008), schools buildings deteriorates faster compared to other buildings because the physical facilities such as plumbing, sewer, electric, roof, masonry and carpentry are out of date and below the standard code. For example, according to a Commission on Audit (COA) report

dated 2017 (coaweb@coa.gov.ph) that some school buildings constructed by the Department of Public Works and Highways (DPWH) cannot be utilized due to construction issues such as incomplete utilities, structural defects, and delayed completion and turnover of buildings.

Project risk management approach for building new schools is different from a private school to that of a public school. The rules from public schools are not simple, stakes are higher and considerations are political. Compared in private school projects there are clear answers to questions on the number of students that will be accommodated, location of building site, environmental issues, companies and contractors to hire, funding, attendance boundaries and no voters reaction to deal with (Lunenburg, 2010). Risk conditions are practices or aspects of school building construction environment that may result to risk occurrence. In January 2009, the Center for Research on Epidemiology of Disaster mentioned that approximately 1.2 billion students are enrolled in primary and secondary school; of these, 875 million school children live in high seismic risk zones and hundreds of millions more face regular flood, landslide, extreme wind and fire hazards. School buildings constructed without considering these risks during planning phase not only injure or kill children, but also destroy the physical infrastructure where the cost of repair and

reconstruction can be a great economic burden (INEE and GFDR, 2009). For instance, super typhoon Durian (2006) in the Philippines caused 20m USD damage to school, including 90-100% of school buildings in three cities and 50-60% of school buildings in two other cities (INEE and GFDR, 2009). The failure of the people responsible to consider the threat of constructing school buildings in hazard prone areas resulted not only damages to properties but also loss of lives.

The increasing awareness of the need to establish a best approach for treating these problems has put the focus of stakeholders to consider the various potential risk and impact to prevent any financial losses. However, there are three major challenges during the planning stage of project risk management of such buildings, first is the correct identification of the sources and type of risks, second the necessary statistical information and third, the selection of methods or tools that will be used to successfully estimate the potential impacts and probabilities of occurrence. Presently, professionals in the project organization are experiencing difficulty in dealing with risk assessment process due to no formal risk management structure in place and the lack of knowledge in risk management theories and techniques. Intuition and experience were used for risk decision making which is inadequate for a controlled construction such as school buildings resulting to cost overruns, delays, claims, and disputes. The skills gap resulting to ambiguity in risk decision making process during project risk assessment must be bridged.

There are few published local researches of formal risk assessment techniques challenging the traditional approach of assessing risk factors for school building construction projects in the Philippines such as Oreta and Brizuela (2013) used a computer-aided earthquake risk management tool that would allow school administrators to participate in the decision making process. Miyamoto and Gilani (2015) also used computer models, to estimate losses of hazard risks in public school buildings. Figueroa, Lim and Lee (2016) utilized geographic information system to assess the condition of school building quality affected by geography, climate and societal factors. Also, there are some foreign researchers that developed risk assessment models for school buildings to improve the traditional approach, such as Global Facility for Disaster Reduction and Recovery introduced in 2015 an innovative partnership-based approach an open source mapping platform to provide a global baseline to ensure safety of all school facilities at risk (INEE and GFDR, 2009). Theunynck (2008), revealed that one of the most economical and effective approaches to a hazard resilient school construction in Africa and Asia is a community driven development approach (CDD). Finn & Dexter

(2012), applied the probability-impact (PI) matrix in identifying, prioritizing and segregating highly potential risks for a school building projects. The Institute of Risk Management (2015), also proposed a systematic risk analysis to evaluate risk factors in terms of likelihood of occurrence or probability and consequence of impact using traffic light system or probability impact diagram. The United States Department of Education (2008), stated that risk identification on vulnerability assessment for school can be done by various techniques such as brain storming, interview/expert opinion, past experience and checklists which can minimize cost overruns and scheduling problems. Grant, D.N. et al. (2006), carried out vulnerability assessment using score-and index-based methods to define the earthquake resistance of school buildings. Coronel & Lopez (2012), developed a computational tool based on geographical information system (GIS) using modern seismic attenuation relationships to estimates damages and losses of seismic event on school buildings. Mudiyansele & Marasingha (2013), proposed the incremental dynamic analysis (IDA) to assess the performance of a two storey school building for seismic event using nonlinear finite element model. Wetterneck, Sass & Davies (2005), assessed risk factors for school buildings using multivariate analyses of variance (MANOVA). Panahi, Rezale & Meshkani (2014), developed a seismic vulnerability map of school buildings using on analytic hierarchy process (AHP) and geographical information system (GIS). Mazilgüney, L. et al (2012), performed ATC 21 (FEMA 154) seismic vulnerability assessment method for reinforced concrete school buildings to evaluate performance of school buildings. The Construction Industry Institute (CII) developed the project definition rating index (PDRI) as tool to support school administrators in decision making process during the planning stage (Pope, et al. 2016). This tool attempts to identify uncertainty before school building construction (Cho & Gibson, 2000).

Following these developments there is no single technique that can be considered the best technique capable of measuring and treating these uncertainties and risks that affect school building project outcome. The study will attempt to address the gap of traditional risk assessment approach of private school building projects and the limitations of cited techniques by developing a weighted simulation decision support tool using Analytic Network Process and Monte Carlo Simulation technique.

## FRAMEWORK

The theoretical framework underpinning this study, is anchored on building elements which govern its development from design to completion namely: codes and regulations, structural system,

walls, windows and façade, service system and financing. Fig. 1 shows that a risk cannot be accurately analysed and controlled unless its nature and components are first identified and understood.

Standard codes and regulation are indispensable project requirement that all site works be planned and executed in such a manner so as to avoid the risk of danger to site personnel and construction area and the effect to the environment, that all such operations are performed in accordance with the following accepted rules and regulations where the project is located.

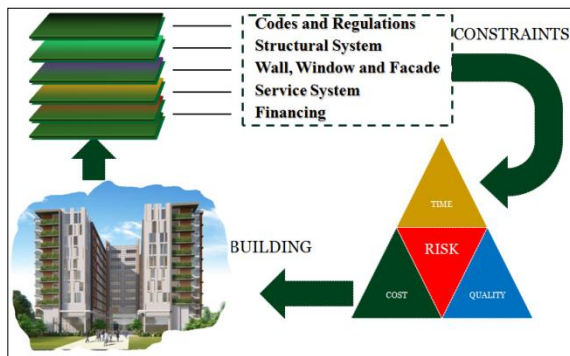


Fig. 1 Building risk framework

The possibility of design errors to occur in today's building construction projects is high due to its time of discovery. The failure to review the plans and specification makes errors to be discovered when works has reached its advanced stage. The attempt to correct the design errors will delay the project and incur additional cost burden to the owner unless otherwise at the account of the designer through the professional indemnity insurance prescribe in other countries. Because of the high level of seismicity here in the Philippines, earthquake loads govern the structural design of all building, in which wind loads assume prime importance. The structural system of a building is designed to transmit vertical and horizontal loads from the point of application to the foundations by the most efficient path with minimum impact on the economy and function of the other elements of the building. The structural engineer must consider many different factors before selecting the final structural system of a school building project. Basic building properties such as height, shape, and usage as well as local economic conditions that affect the materials and labor costs; construction schedule, design loads both vertical and lateral; building behavior and occupant behavior; foundation considerations and coordination with mechanical systems (Cohen, 1986) are factors that influence the structural system of a building structure. Generally, structural systems are flexible and limitations only come from the material used in the construction. Typical materials used for structural systems are

steel and concrete.

Buildings today utilize service system and facilities as required by the National Building Code of the Philippines and other related legislature. These facilities are included in the design and construction of a building and are provided for the comfort and safety of the occupants. The following service system in building projects are vertical transportation, electrical systems, HVAC systems (heating, ventilating and air conditioning) and fire protection systems. When specialist designer specifies the materials to be installed and construction details to execute, the contractor should conform to the use of these materials and details. However, it is difficult or impossible for the contractors to determine if the materials and details specified by the designer are suitable and correct. For example, unsuitable materials and connections in plumbing installation will result to damages due to bursting of pipes; unsuitable materials for insulation which can produce toxic gases in case of fire; incorrect sizes of fixtures suspended in ceilings or façade components which can cause injury or damage to property if they fall down. The consequential losses for the damages and efforts in the repair works will add on the financial burden of the owner.

Lastly, the element of financing the costs for the construction of a building project is the sole responsibility of the developer. Costs of construction of a buildings range to hundreds of millions of dollars. Financing of building project depends on what type of business is going to be established. Basic sources of capital can be through equity finance, debt finance or internally generated funds. The owner of the building will rarely be willing to shoulder the construction costs without the assistance of outside financial institution. Without sufficient financing during the periods of rapid construction of the building when additional capital is needed to cover operation, to maintain equipment, to procure materials, to pay salaries and wages, to cover storage, transportation and reserve will result to conflicts, disputes and claims which jeopardize the primary aim of the owner to complete the building on time. On the other hand, any delay in completion affects the target date of use producing loss of profit for its owner.

### Developing Risk Assessment Framework for High-Rise School Building Project

The traditional risk assessment revealed by the literature such as brain storming, Delphi technique, interview/expert opinion, past experience, check lists, influence diagram produced level of uncertainty which are not suitable for projects like school buildings. This traditional approach assumes that precise decisions are provided and there is no venue

for statistical interpretation of results on similar or close decisions. Hence, the uncertainties underpinning the risk assessment process in school building environment, both explicit and implicit should be dealt appropriately (David, 1996). Most of the studies concluded in the improvement of these traditional approach using qualitatively and quantitatively methods. This methods when combined allows the quantification of risk in terms of magnitude/impact and frequency or time frame of each event (Mills, 2001) as well its probability of occurring (Shunmugam and Rwelamila, 2014). Therefore, this study will attempt to develop an effective risk assessment using qualitatively and quantitatively methods such as Analytic Network Process and Monte Carlo Simulation as shown in Fig. 2.

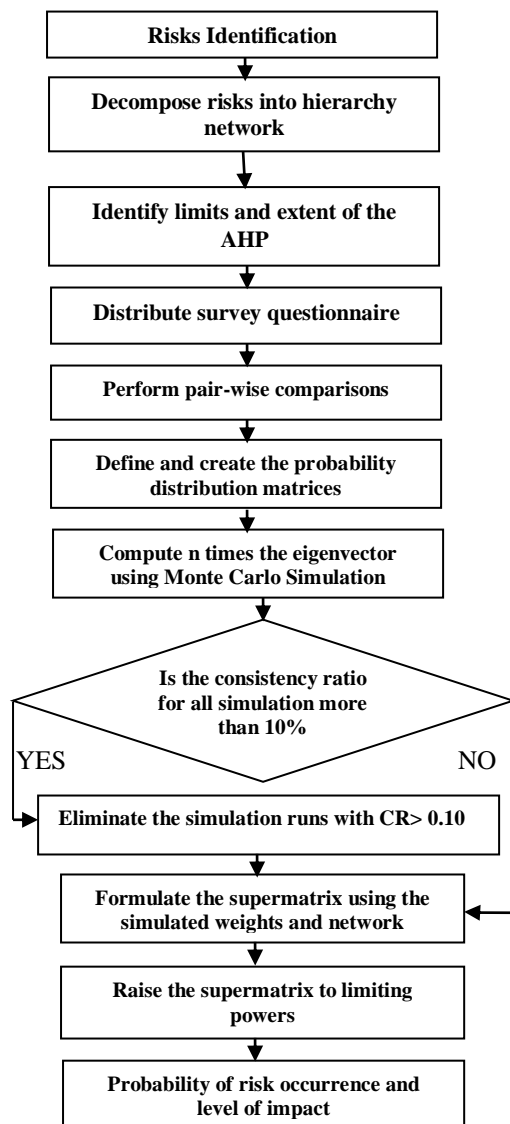


Fig. 2 MCANP weighted simulation framework

The combination of Analytic Network Process a multiple criteria decision-making method and Monte

Carlo a simulation method will produce the following advantages:

1. Provide a more systematic approach;
2. Will handle subjectivity in weighing risks brought by human factors like personal experience, intuition and judgment;
3. Will derive potential relation and level of riskiness between risk factors;
4. Will improve applicability for both quantitative and qualitative features of risk;
5. Will manage uncertainty in the judgments of decision makers by testing the statistical significance of the final rankings of risk factors.

Furthermore, the proposed method will address the following limitations of cited risk assessment techniques such as:

1. inability to model epistemic uncertainty due to lack of enough information,
2. inability of measuring and including the intangible factors,
3. limitation in representing interdependencies between different risks and the assumptions that they are independent,
4. and inability to consider both qualitative and non-monetary risk.

The use of this method will fill the skills gap among practitioners in determining the probability and impact values of potential risks in school building projects.

## METHODOLOGY

The theoretical framework will set the foundation in formulating the research questions to be answered. A mixed method approach will be used in this study to utilize the strengths of both qualitative and quantitative methods. Lee (1999) believed that mixed methods are very powerful when carried out correctly for a single research study. The study will first review sources of related literatures that identify and classify various types of risk which are commonly associated in school building projects. Based from these reviews, a classification method will be adopted to arrange risk factors into groups and sub-groups for the purpose of risk identification and modelling as illustrated in Fig. 3.

In this study school building construction risk are divided into two categories: external risks and internal risks and 6 risk factors consisting of sub-risk factors are derived. Based from the presented literatures, risk in a construction projects are generally based from two sources, the external risk which are originated due to the project environment or usually unique to the country while internal risks are initiated inside the project (Flanagan & Norman, 1993; Aleshin, 2001; Fang et al., 2004; Ling & Hoi, 2006; El-Sayegh, 2008).

In the second stage of data collection, selection



of group subject matter experts. The group will be defined first according to skills, knowledge and unique qualities and the sample subject matter expert will be selected using a probability sampling process. The subject matter should have undertaken and completed school construction projects for the past 10 years and held administrative position in the institution. The data acquired from this group will play a vital role in the successful application of MC-ANP technique. Therefore, the right people will be selected for best results. Finally, once the group of subject respondents are selected, a survey questionnaire will be administered.

This study will perform pairwise comparisons at every level using the numeric preference of the subject matter experts judgement as input data from the survey questionnaire. Using Analytic Network Process (ANP) will utilize the derivation of potential relation and the level of riskiness of between potential risks factors as illustrated in Fig. 3 is the proposed risk breakdown network for school building. Assuming the factors are interdependent and there is a feedback loop from elements in level of risk (High, Medium and Low) to factor elements. Judgment consistency ratio(CR) of  $CI = (\lambda_{max} - n) / (n - 1)$ ,  $n$  is the matrix size with the appropriate value in Table 4. If CR is more than 0.10, the judgment matrix is inconsistent (Saaty, 1990).

Table 4 Random consistency index (RI)

| n  | 1 | 2 | 3   | 4   | 5    | 6    | 7    | 8    | 9    | 10   |
|----|---|---|-----|-----|------|------|------|------|------|------|
| RI | 0 | 0 | .58 | .90 | 1.12 | 1.24 | 1.32 | 1.41 | 1.45 | 1.49 |

The local priority vectors from pair-wise comparisons on the elements of the cluster and sub-cluster levels will be adopted to achieve a supermatrix, which in turn obtain global priorities. After entering the sub-matrices into the supermatrix and adjusting its values to achieve column stochastic. The supermatrix is raised to limiting powers until weights have converged and remain stable (Saaty, 1996; Meade and Sarkis, 1998; Promentilla et al., 2005). The proper decomposition of the problem into a network is vital for the successful application of MC-ANP technique.

To address the ambiguity gap that occurs during the judgement of the selected group of subject matter experts in answering the survey questionnaires, this different judgement will be collected to define the probability distributions in order to create the probabilistic pair-wise comparison matrix. Fig. 4 illustrates an example of the proposed probabilistic distribution matrix. Since probabilistic judgment uses random variables the computation of eigenvectors and eigen-values cannot be done in a traditional way, the Monte Carlo simulation technique will be used.

## RESULTS AND DISCUSSION

### The ANP model for risk assessment

This study proposes a multi-criteria decision model for assessing overall riskiness of school building construction project as shown in Fig. 3.

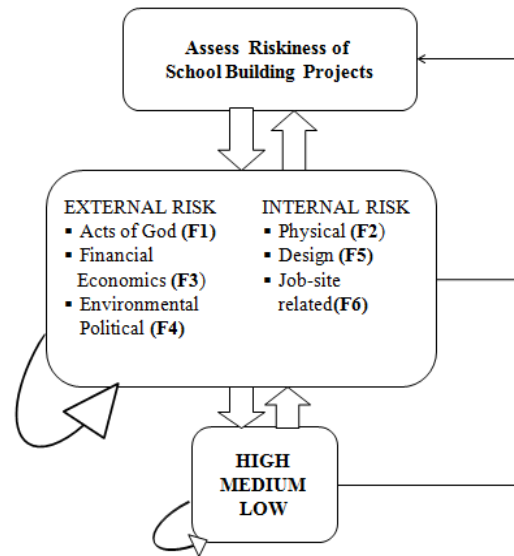


Fig. 3 Risk breakdown network model

The proposed model will evaluate potential risk factors associated in school building projects. There are several conflicting, weighted, and incommensurable risk factors involved besides the interrelationships among these factors such as dependencies and feedbacks. Because of this complicated nature of the problem on hand, it can be modeled as a network and treated with a network based multi criteria decision making approach.

The ANP is a multi-criteria theory of measurement used to determine weights of numeric preference from decision maker's judgements at the same time allows the assumptions of relative influence of higher level elements from the lower level elements (Saaty, 2006). Saaty (1996) proposed ANP approach that can be utilized for examining network model representations. The power of ANP lies in its use of special ratio scales (Saaty, 1996) to capture all kinds of interactions between external and internal risk factors for making accurate predictions and better decisions. Because of interactions among criteria, the criteria that are less important individually might turn out to be more important when evaluated collectively in a network (Saaty and Vargas, 2006). Moreover, two types of interactions are illustrated in the proposed ANP model, the outer dependence which is represented by straight arrows and inner dependence which is represented by loops. Furthermore, the decision problem is characterized by three aspects namely



the goal, risk factors and level of impact. Thus, the overall goal of this study is to assess the risk of school building construction projects.

### The probability distribution matrix

During the traditional ANP, the pairwise comparisons in the decision clusters and respective elements represented by  $a_{ij}$  are deterministic, where  $a_{ij}$  indicates how much more important the  $i$ th alternative/criteria is than the  $j$ th alternative/criteria and this will lead to the construction of the composite priority vector of alternatives' importance. In the MCANP, the  $a_{ij}$  values are represented by the  $p_{ij}$  probabilistic judgments. The most rigorous and suitable method to select the appropriate distribution of  $p_{ij}$  is using the statistical principles. From the central limit theorem, it can be seen that for almost all populations, the sample distribution can be approximated closely by a normal distribution, provided the sample size is sufficiently large (Kiemele et al. 1997). However, it can be difficult to obtain a large sample size of subject-matter experts to perform the pair-wise comparison (Banuelas & Antony, 2004). Another method can be use according to Banuelas & Antony (2004) is the chi-squared goodness-of-fit test to investigate whether an underlying distribution (or population) from which the data have been taken is of a specified form or not. Hauser and Tadikamalla (1996) suggest that in the extreme case the decision-makers are not 'n' times. Thus, to quantify variation due to uncertainty of the decision maker's judgements the use of random variable with a uniform probabilistic distribution between 1/9 and 9 in the pair-wise comparison matrix as shown in Table 1.

Rosenbloom (1996) recommended the use of Monte Carlo simulation to estimate the composite priority vector from the probabilistic judgment ( $P_{ij}$ ). Therefore, each replication would be a realization of all the  $a_{ij}$ s in the decision hierarchy followed by the standard ANP calculation of eigenvectors and eigen values. Replicating  $n$  times will provide estimates of the probabilities associated with the priority vector as shown in Table 2 and Table 3.

The probability distribution function,  $F(x)$  is the mathematical equation that describes the probability that a random variable  $X$  is less than or equal to  $x$ , given by Eq. (1) (David, 1996):

$$F(x) \approx P(X \leq x) \quad (1)$$

where  $P(X \leq x)$  means the probability of the event  $X \leq x$ . Therefore, in order to meet the Saaty's pairwise comparison scale the probability distribution of the random variable  $X$  is equal to or greater than 1/9 and not greater than 9. If  $X$  are random variables it follows that final ratings are also random variables. To test the statistical significance of the final ratings

the use of Monte Carlo simulation is recommended. Simulation according to Albright (2010) is a useful tool for modeling random variables. Thus, constructing a simulation of iterations  $n$  will provide estimates of the probabilities associated with the vector of priorities (Banuelas and Anthony, 2004).

Table 1 Normalized probability distribution matrix

|   | F1 | F2 | F3   | F4 | F5   | F6   | $\omega$ |
|---|----|----|------|----|------|------|----------|
| F1  | 1  | .2 | .111 | 1  | .166 | .142 | .0297    |
| F2  | 5  | 1  | .125 | 5  | .500 | .250 | .0951    |
| F3  | 9  | 8  | 1    | 9  | 7    | 4    | .5345    |
| F4  | 1  | .2 | .111 | 1  | .333 | .500 | .0420    |
| F5  | 6  | 2  | .142 | 3  | 1    | 1    | .1316    |
| F6  | 7  | 4  | .250 | 2  | 1    | 1    | .1672    |
| $\lambda_{\max}= 6.605$ , CI= 0.12, RI=1.25, CR= 0.097 < 0.10 OK. |    |    |      |    |      |      |          |

Table 2 Simulated priority weights

|               | HIGH   | MED    | LOW    |
|---------------|--------|--------|--------|
| F1(0.0297)    | 0.1692 | 0.3874 | 0.4434 |
| F2(0.0951)    | 0.1311 | 0.6608 | 0.2081 |
| F3(0.5345)    | 0.7928 | 0.1312 | 0.0760 |
| F4(0.0420)    | 0.0890 | 0.3234 | 0.5876 |
| F5(0.1316)    | 0.0881 | 0.7172 | 0.1947 |
| F6(0.1672)    | 0.7626 | 0.1662 | 0.0726 |
| Overall Level | 0.5840 | 0.2802 | 0.1360 |

Table 3. Overall priority weights

| Risk Factors & Levels | Final Ratings |
|-----------------------|---------------|
| F1                    | .0451         |
| F2                    | .0478         |
| F3                    | .1646         |
| F4                    | .0300         |
| F5                    | .0520         |
| F6                    | .0604         |
| HIGH                  | .1000         |
| MEDIUM                | .0640         |
| LOW                   | .0400         |

In the proposed MCANP method compared to traditional approach that assumes precise decisions are provided and there is no venue for statistical interpretation of results on similar or close decisions. MCANP can quantify the error of uncertainty in the judgements through the probabilistic judgements with a confidence level of 95%.

### CONCLUSION

Classification of all types of potential risks for high-rise school building construction according to probability of occurrence and consequence was suggested. The objective of this classification is to identify the impact of each risk factors on the construction of the school buildings For example,

the total construction cost for structural works in a typical high-rise building is PhP 300M but due to Financial risk factor (F1) as shown in Table 3 the probability of occurrence if not considered during the planning stage is 16.46% and the level of riskiness is HIGH with a possible impact in cost of 10% which translate in a risk value of 1.65% amounting to PhP 4.95M. This cost of risk will be the maximum value of damage according to the impact in percent of the construction cost. Therefore, it is important to determine the potential damage or value of losses of each risk factor in the project. The value of risk is the potential amount of damages when the event occurs. Thus, the method allows to estimate the probable value of losses and the degree of influence in the project.

## ACKNOWLEDGMENTS

The author would like to thank De La Salle University, particularly Dr. Andres Winston Oreta in his support in completing this paper.

## REFERENCES

- [1] Albright, B. (2010). Mathematical modeling with excel. The Jones and Bartlett Publishers International Series in Mathematics.
- [2] Aleshin, A. (2001). Risk management of international projects in Russia. *International Journal of Project Management*, 19(4), 207-222.
- [3] Banuelas, R., & Anthony, J. (2004). Modified analytic hierarchy process to incorporate uncertainty and managerial aspects. *International Journal of Production Research*, 42(18), 3851-3872.
- [4] Commission on Audit Report 2017. <https://www.coa.gov.ph/index.php/national-government-agencies/2017/category/6994-department-of-public-works-and-highways>.
- [5] Cho, C. and Gibson, E. (2000). "Development of a Project Definition Rating Index (PDRI) for general building projects," in *Proceedings of the Construction Research Congress*, pp. 343-352.
- [6] Coronel, G.D. & Lopez, O.A. (2012). Regional Seismic Damage, Loss and Risk Scenarios. Institute of Materials and Structural Models (IMME), 15 WCEE LISBOA 2012
- [7] El-Sayegh, S. M. (2008). Risk assessment and allocation in the UAE construction industry. *International Journal of Project Management*, 26(4), 431-438.
- [8] Fang, D., Li, M., Fong, P. S.-W., & Shen, L. Y. (2004). Risks in Chinese construction market-Contractors' perspective. *Journal of Construction Engineering and Management*, 130(6).
- [9] Figueroa, L.L., Lim, S. & Lee, J. (2016). Spatial analysis to identify disparities in Philippine public school facilities, *Regional Studies, Regional Science*, 3:1, 1-27.
- [10] Flanagan, R., and Norman, G. (1993) *Risk management and construction*, Blackwell Publishing, Oxford, UK.
- [11] Grant, D. N., Bommer, J. J., Pinho, R. & Calvi, G. M. (2006). *Defining Priorities and Timescales for Seismic Intervention in School Buildings in Italy*.
- [12] Hauser, D. and Tadikamalla, P., 1996, The analytic hierarchy process in an uncertain environment: a simulation approach. *European Journal of Operation Research*, 91, 27-37.
- [13] <https://www.rappler.com>. School buildings costing P326 million' incomplete, defective'-COA
- [14] Inter-Agency Network for Education in Emergencies & Global Facility for Disaster Reduction and Recovery. (2009). *Guidance Notes on Safer School Construction: Global Facility for Disaster Reduction and Recovery*. Washington, D.C.: International Bank for Reconstruction and Development – The World Bank.
- [15] Kiemle, M., Schmidt, S. and Berdine, R., 1997, *Basic Statistics: Tools for Continuous*
- [16] *Improvement* (Colorado Springs: Air Academic Press).
- [17] Lee, T. W., 1999. *Using qualitative methods in organisational research*. London: Sage Publications.
- [18] Liam Finn, W.D. and Dexter, A. *Risk Management Plan for School Seismic Mitigation Program*.
- [19] Ling, F. Y. Y., & Hoi, L. (2006). Risks faced by Singapore firms when undertaking construction projects in India. *International Journal of Project Management*, 24(3), 261-270.
- [20] Lunenberg, F.C. (2010). *School Facilities Management*. National Forum of Educational Administration & Supervision Journal Volume 27, Number 4, 2010.
- [21] Lunenburg, F. C., & Ornstein, A. O. (2008). *Educational administration: Concepts and practices*. Belmont, CA: Wadsworth/Cengage Learning.
- [22] Mazılıgüney, L., Yakut, A., Kadaş, K. & Kalem, İ. (2012). Evaluation of Preliminary Assessment Procedures for Reinforced Concrete School Buildings in Turkey. 10th International Congress on Advances in Civil Engineering, 17-19 October 2012 Middle East Technical University, Ankara, Turkey
- [23] Meade, L. and Sarkis, J. (1998) Strategic analysis of logistics and supply chain management systems using the analytic network process. *Transportation Research Part E*:

- Logistics and Transportation Review, 34(3), 201–15.
- [24] Mills, A. (2001). A systematic approach to risk management for construction. *Structural survey*, 19(5), 245–252.
- [25] Miyamoto, K. H. and Gilani A.S.J. Comprehensive Seismic Risk Reduction Program for Public Buildings in Metro Manila, Philippines
- [26] Mudiyansele, M. & Marasingha, J.K. (2013). Seismic Assessment of School Buildings in Sri Lanka
- [27] Oreta, A. and Brizuela, K. (2017). A Semi-Quantitative Seismic Hazard Risk Management Tool To Promote Safe School Communities
- [28] Panahi, M., Rezaie, F., and Meshkani, S.A. (2014). Seismic Vulnerability Assessment of School Buildings in Tehran City based on AHP and GIS, *Nat. Hazards Earth Syst. Sci.*, 14, 969–979.
- [29] Promentilla, M.A.B., Furuichi, T., Ishii, K., Tanikawa, N. (2005). Evaluation of remedial countermeasures using the analytic network process. *Waste Management* 26 (2006) 1410–1421.
- [30] Rosenbloom, E. S., 1996, A probabilistic interpretation of the final rankings in AHP. *European Journal of Operation Research*, 96, 371–378.
- [31] Saaty T.L. (1990). How to make a decision: The Analytic Hierarchy Process. *European Journal of Operational Research*, 48, 9–26.
- [32] Saaty, T. L. (1996). *The Analytic Network Process* (Pittsburgh: RWS).
- [33] Saaty, T.L. and L. Vargas, 2006, “Decision Making with The Analytic Network Process, Economics, Political, Social and Technological Applications with Benefits, Opportunities, Costs, and Risks”, Springer, 2(195),
- [34] Shunmugam, S., and Rwelamila, P.D. (2014). An evaluation of the status of risk management in South African construction projects. *Project Management South Africa (PMSA) Conference*, 2-16.
- [35] Theunynck, S. (2003). Education for all: Building the Schools.
- [36] United States Department of Education Office of Safe and Drug-Free Schools. (2008). A guide to school vulnerability assessments:
- [37] Wetterneck, C., Sass, D.A. and Davies, H.W. (2005). Perceptions of Risk Factors for School Violence: Concordance with FBI Risk Profile. *Journal of School Violence*, Vol. 4(2).
- [38] Pope, C., Marks, E., Back, E., Leopard, T., Love, T. (2016). Renovation versus New Construction and Building Decision Tool for Educational Facilities. *Journal of Construction Engineering* Volume 2016, Article ID 5737160, 10 pages <http://dx.doi.org/10.1155/2016/5737160>

# ASSESSMENT OF DEBRIS FLOW VELOCITY USING A SIMPLE LUMPED MASS MODEL FOR DEBRIS FLOW MOBILIZATION

Thapthai Chaithong<sup>1</sup>

<sup>1</sup>Graduate school of Environmental Studies, Tohoku University

## ABSTRACT

Debris flow is a natural phenomenon that is a flow of a mixture of liquid (water) and solid components (soil, rock or wood debris). Considering the triggering factors, extreme or prolonged rainfall is a significant parameter in this phenomenon. The anatomy of debris flow consists of three main parts: initiation zone, transportation zone and deposition area. The debris flow can destroy infrastructure and housing along its path of flow and deposition area, including causing loss of human lives. In this study, a simple lumped mass model is used to calculate the velocity of debris flow and to estimate the potential deposition area of debris flow. The lumped mass model describes the movement of the centroid of a debris flow. In the analysis, gravity is the driving force and the resistance force is developed based on a combination of Coulomb's friction law and Terzaghi's effective stress principle. A historical debris flow case in Japan is the case study of this analysis. According to calculation, the simple lumped mass can estimate the velocities and deposition areas of debris flows.

*Keywords: Debris flow, Lumped mass model, Extreme rainfall, Landslide, Typhoon*

## INTRODUCTION

Debris flow is a rapid flow of hillslope materials, sediment and other debris mixed with water [1], [2]. In general, debris flow can be divided into three main parts: initiation, flow path and deposition area [2], [3]. Housing and infrastructure such as bridges, railways and highways are greatly damaged by debris flow. Considering the debris flow, it causes harm generally in three different ways, namely deposition, entrainment and direct impact, in which direct impact is the major cause of building destruction [4], [5]. For assessment and design of the building or infrastructure that can resist the debris flow, there are several important parameters, such as volume of debris flow, velocity of debris flow and size of debris fan that need to be considered [6]. In particular, the velocity of debris flow is a significant parameter to calculate the impact force of debris flow because the velocity of debris flow is a parameter in numerous equations of impact force of debris flow [4]–[6]. The velocity of debris flow can be calculated or predicted using the debris flow run-out model. In general, the debris flow run-out models are developed based on two main frames of reference: Lagrangian and Eulerian approaches such as DAN, DMM, EDDA 1.0 or EDDA 2.0 [7]–[10].

Therefore, the aim of this study is to calculate the velocity of debris using a simple lumped mass model for debris flow mobilization. A historical debris flow case in Japan is the example for debris flow velocity calculation.

## SLOPE STABILITY ANALYSIS AND HILLSLOPE HYDROLOGY

The infinite slope stability model is a traditional slope stability model utilised to analyse shallow slope failures or shallow landslides. Shallow slope failures are characterised by a shallow depth and form failure planes parallel to the hillslope surface. These factors are similar to the assumptions of the infinite slope stability model. The stability of the hillslope is presented in the form of a safety factor, as shown in Eq. (1). The safety factor is the ratio of driving stress to resisting stress. Resisting stress is developed based on the Mohr–Coulomb failure criteria.

$$FS = \frac{c' + [(z\gamma_{sat}) + (B - z)\gamma_t - (z\gamma_w)] \cos^2 \beta \tan \phi'}{[(z\gamma') + (B - z)\gamma_t + (z\gamma_w)] \sin \beta \cos \beta} \quad (1)$$

where  $c'$  is the cohesion of soil,  $z$  is the saturated zone (groundwater depth),  $B$  is the depth of soil,  $\beta$  is the slope angle,  $\phi'$  is the effective friction angle,  $\gamma'$  is the effective unit weight of soil,  $\gamma_t$  is the total unit weight of soil,  $\gamma_w$  is the unit weight of water.

Conte [11] proposed the equation for ground water level prediction. Eq. (2) presents the groundwater table height ( $z(t)$ ).

$$z(t) = \frac{P}{n(1 - S_r)} \exp[-k_t \sin \beta \cos \beta (t - t_o)] \quad (2)$$

where  $p$  is precipitation,  $B$  is the channel width,  $k_t$  is ratio of hydraulic conductivity of soil and channel width,  $n$  is the porosity,  $S_r$  is the degree of saturation,  $t_0$  is initial time.

### A SIMPLE LUMPED MASS FOR DEBRIS FLOW MOBILIZATION

To analyse the run-out behaviour of debris flow, the previous research assumed the debris flow as a finite mass (finite boundaries at any position) [7], [12]–[14]. Hence, this study applies the sliding block model to analyse the motion of debris flow. The sliding block model is a lumped mass model utilised to describe the movement of the centroid of a debris flow in which the block is treated as a lumped mass [15]. To analyse the sliding block motion, the acting force is a significant result of the driving force and movement resistance. In this analysis, gravity imposes a driving force and the movement resistance is developed based on a combination of Coulomb's friction law and Terzaghi's effective stress principle. The motion of the sliding block model is described by Newton's law and the momentum change to the sum of the forces. Figure 1 shows the forces assumed in the sliding block model.

$$\frac{d(mv)}{dt} = \text{net force} \quad (3)$$

where net force ( $F_n$ ) is sum of forces of debris flow (net force = driving force – resisting force),  $m$  is the mass of debris flow,  $v$  is the velocity of debris flow and  $t$  is time interval.

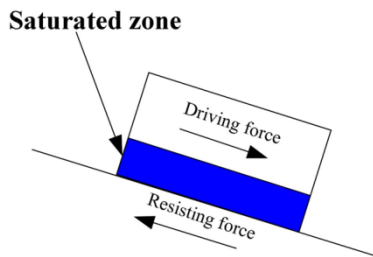


Fig. 1 Schematic of forces assumed in the sliding block model.

The driving force ( $D$ ) can be expressed as follows:

$$D = mg(\sin \beta) \quad (4)$$

where  $g$  is the gravitational acceleration ( $9.81 \text{ m/s}^2$ ) and  $\beta$  is the slope angle.

The resisting force ( $R$ ) is the movement resistance which can be expressed as follows:

$$R = mg(1 - r_u) \tan \phi \cos \beta \quad (5)$$

where  $r_u$  is the pore pressure ratio,  $\phi$  is the friction angle.

$$r_u = \frac{u}{\gamma h} \quad (6)$$

where  $u$  is the pore fluid pressure on the base of block,  $\gamma$  is the unit weight of soil,  $h$  is the height of block slide.

The pore fluid pressure on the base of block can calculate using Eq. (7).

$$u = [z\gamma_{sat} + (h - z)\gamma] \cos^2 \beta \quad (7)$$

where  $z$  is the height of saturated layer,  $\gamma_{sat}$  is the unit weight of saturated soil.

Hutchinson [16] used Terzaghi's one-dimensional consolidation theory to calculate the dissipation of pore fluid pressure. The time  $t$  required for the basal pore fluid pressure to dissipate can be written in Eq. (8). The pore fluid pressure changes with time based on the differential equation of Terzaghi's one-dimensional consolidation theory, which can be written in Eq. (9).

$$t = \frac{T(h)^2}{c_v} \quad (8)$$

$$\frac{\partial u}{\partial t} = c_v \frac{\partial^2 u}{\partial h^2} \quad (9)$$

where  $T$  time factor for the degree of dissipation of the basal pore fluid pressure,  $c_v$  is the coefficient of consolidation.

From Eq. (3), it can be changed the form into Eq. (10) which is based on the equation of motion on a curved path.

$$mv \frac{dv}{ds} + v^2 \frac{dm}{ds} = \text{net force}(F_n) \quad (10)$$

Therefore

$$mv \frac{dv}{ds} = F_n - v^2 \frac{dm}{ds} \quad (11)$$

where  $s$  is the distance of debris flow run-out. Considering the term of  $(dm/ds)$ , it can refer to the changing of mass of debris flow during the run-out such as erosion, entrainment, or deposition.

Equation (11) can be discretized based on the finite difference method as follows:

$$mv \frac{\Delta v}{\Delta s} = F_n - v^2 \frac{\Delta m}{\Delta s} \quad (12)$$

Therefore

$$\Delta v = \frac{g \Delta s (\sin \beta)}{v} - \frac{g \Delta s (1 - r_u) \tan \phi \cos \beta}{v} - \frac{v^2 \Delta m}{mv} \quad (13)$$

Considering the conservation of energy for any sliding block, this study assumed that the velocity is parallel to the slip path at the base of the block at time  $t$ . On motion triggering, the potential energy of the block is converted into kinetic energy [17]. The equation of motion of the sliding block can be expressed as follows:

$$\frac{d}{dt} \left( \frac{1}{2} mv^2 \right) = \frac{d}{dt} (mgh) - \frac{d}{dt} \left( \frac{mg(1 - r_u) \tan \phi h}{\tan \beta} \right) \quad (14)$$

When; the kinetic energy can be rewritten as:

$$\frac{d}{dt} \left( \frac{1}{2} mv^2 \right) = mv \frac{dv}{dt} \quad (15)$$

And; the potential energy can be rewritten as shown in Eq. (16) when  $dh/dt$  represents the velocity ( $v$ )

$$\frac{d}{dt} (mgh) = mg \frac{dh}{dt} = mgv \sin \theta \quad (16)$$

And; the friction at the base of block and slip surface can be written as follows:

$$\begin{aligned} \frac{d}{dt} \left( \frac{mg(1 - r_u) \tan \phi}{\tan \beta} \right) &= \frac{mg(1 - r_u) \tan \phi}{\tan \beta} \frac{dh}{dt} \\ &= \frac{mg(1 - r_u) \tan \phi}{\tan \beta} v \end{aligned} \quad (17)$$

Using Eqs. (15), to (17), Eq. (14) becomes as follows:

$$\frac{dv}{dt} = g \sin \beta - \frac{g(1 - r_u) \tan \phi}{\tan \beta} \quad (18)$$

## CALCULATION FRAMEWORK

There are three main parts to the calculation. First, the initial landslide is calculated using the rainfall-induced shallow slope failure model. The result of the first step is the landslide occurrence time and safety factor. The second step is to calculate the initial velocity of debris using Eq. (18).

Finally, the velocity of debris changing with distance will be calculated using Eq. (13). Table 1 summarises the parameters used in the rainfall-induced shallow slope failure, the sliding block model.

In this study, we examined the historical landslide and flow slide that occurred on the local slope of the town of Iwaizumi, in Japan's Iwate Prefecture, on 30 August 2016. Figure 2 shows the topography of the case study.

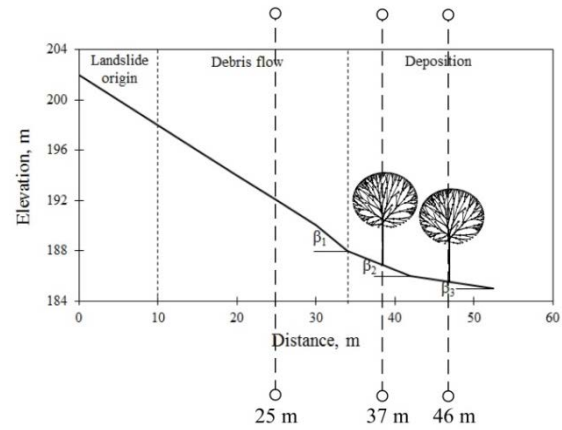


Fig. 2 Topography and elevation of case study.

Table 1 Properties used in this study

| Parameters                    | Unit              | Values |
|-------------------------------|-------------------|--------|
| Hydraulic conductivity        | m/hr              | 0.03   |
| Soil cohesion                 | kN/m <sup>2</sup> | 6.8    |
| Unit weight of water          | kN/m <sup>3</sup> | 9.81   |
| Soil friction angle           | degrees           | 24.7   |
| Saturated unit weight of soil | kN/m <sup>3</sup> | 16.7   |
| Unit weight of debris flow    | kN/m <sup>3</sup> | 24.06  |
| Slope angle 1, $\beta_1$      | degrees           | 22.38  |
| Slope angle 2, $\beta_2$      | degrees           | 14.04  |
| Slope angle 3, $\beta_3$      | degrees           | 5.43   |

## RESULTS AND DISCUSSION

Considering the location of landslide initiation, shallow slope failure occurred at the top of the hillslope and slope angle 1. Figure 3 plots the safety factor and hourly rainfall on 30 August 2016. In this study, we selected the rainfall data detected at the Iwaizumi rain gauge operated by Iwate prefecture because this rain gauge was installed in closest proximity to our case study. The peak hourly rainfall of 63 mm was recorded at 18:00 on 30 August 2016. According to our calculations, we found that the safety factor of the slope was less than 1 between 17:00 and 18:00 on 30 August 2016. The cumulative rainfall during the period when the safety factor was less than 1 was approximately 160 mm.



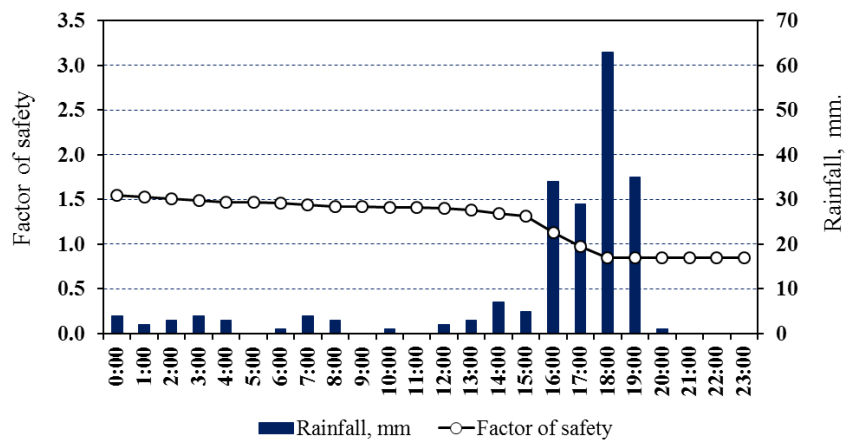


Fig. 3 Safety factor of case study and hourly rainfall at Iwaizumi rain gauge.

Figure 4 shows the plot of the relation between the velocity of the flow slide and time. Figure 5 shows the plots of the relation between the velocity of the flow slide and horizontal displacement. The plots show that the velocity of the flow slide increased at slope angle 1 and decreased slightly at slope angle 2. The velocity of the flow slide sharply decreased at slope angle 3. The flow slide stopped and deposited its debris at a horizontal distance of 51 m. The location of the deposition based on the calculation accords well with our field observations at the site. According to the calculation, the total duration of the flow slide from the origin of the landslide to deposition was approximately 8 seconds. Figure 6 shows a photograph of the site studied in this research.

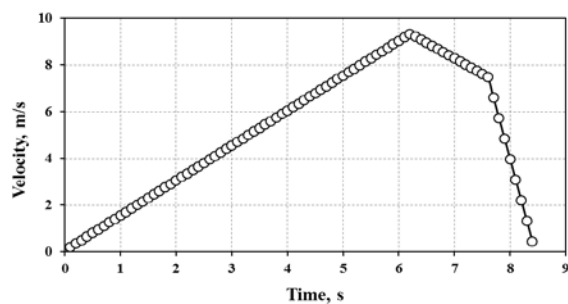


Fig. 4 Velocity of flow slide versus time.

## CONCLUSIONS

The results of the model are a good fit for the data obtained from the field observation. The unknown factors of tree and soil parameters are critical variables in the calculation. The maximum speed is approximately 9 m/s. The unknown parameters of parameters are critical variables in the calculation and an important challenge for back analysis of debris flow.

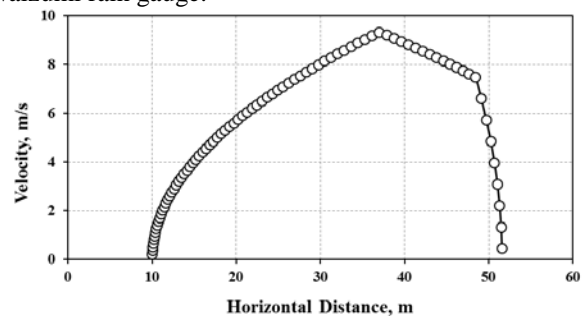


Fig. 5 Velocity and horizontal displacement.

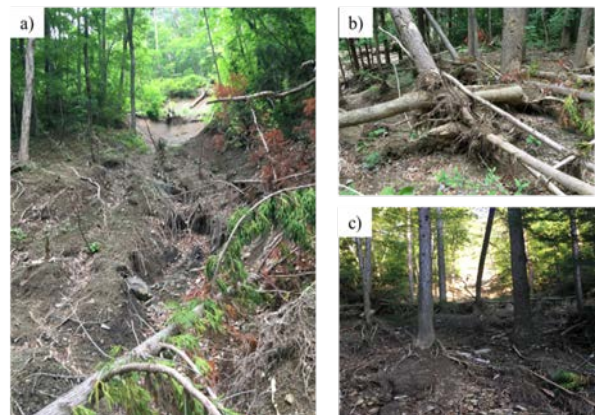


Fig. 6 a) Origin of landslide; b) the condition of trees at 37 m; and c) the condition of trees at 46 m.

## REFERENCES

- [1] Regmi N. R., Giardino J. R., McDonald E. V., and Vitek J. D., Chapter 11-A Review of Mass Movement Processes and Risk in the Critical Zone of Earth. *Developments in Earth Surface Processes*, Vol. 2, 2015, pp. 319-362.
- [2] Gao L., Zhang L. M., Chen H. X., and Shen P., *Simulating Debris Flow Mobility in Urban Settings*. *Engineering Geology*, Vol. 214, 2016, pp. 67-78.

- [3] Franks C. A. M., Characteristics of some Rainfall-induced Landslides on Natural Slopes, Lantau Island, Hong Kong. *Quarterly Journal of Engineering Geology*, Vol. 32, 1999, pp. 247-259.
- [4] Hu K. H., Wei F. Q., and Y L., Real-time Measurement and Preliminary Analysis of Debris-flow Impact Force at Jiangjia Ravine, China. *Earth Surf. Process. Landforms*, Vol. 36, 2011, pp. 1268-1278.
- [5] He S., Liu W., and Li X. P., Prediction of Impact Force of Debris Flows Based on Distribution and Size of Particles. *Environ Earth Sci*, Vol. 75, Issue. 298, 2016, pp. 1-8.
- [6] Gao L., Zhang L. M., and Chen H. X., Two-dimensional Simulation of Debris Flow Impact Pressures on Buildings. *Engineering Geology*, Vol. 226, 2017, pp. 236-244.
- [7] Hungr O., A model for the runout analysis of rapid flow slides, debris flows, and avalanches. *Can. Geotech. J*, Vol. 32, 1995, pp. 610-623.
- [8] Kwan J. S. H., and Sun H. W., An improved landslide mobility model. *Can. Geotech. J*, Vol. 43, 2006, pp. 531-539.
- [9] Zhang L. M., and Chen H. X., EDDA 1.0: integrated simulation of debris flow erosion, deposition and property changes. *Geosci. Model Dev.*, Vol. 8, 2015, pp. 829-844.
- [10] Shen P., Zhang L., Chen H., and Fan R., EDDA 2.0: integrated simulation of debris flow initiation and dynamics considering two initiation mechanisms. *Geosci. Model Dev.*, Vol. 11, 2018, pp. 2841-2856.
- [11] Conte E., Donato A., and Troncone A., A simplified method for predicting rainfall-induced mobility of active landslides. *Landslides*, Vol. 14, 2017, pp. 35-45.
- [12] Perla R., A Two-parameter Model of Snow-avalanche Motion. *Journal of Glaciology*, Vol. 26, No. 94, 1980, pp. 197-207.
- [13] Cannon S. H., and Savage W. Z., A Mass-change Model for the Estimation of Debris-flow Runout. *Journal of Geology*, Vol. 1988, pp. 221-227.
- [14] Savage S. B., and Hutter K., The Motion of a Finite Mass of Granular Material Down a Rough Incline. *J. Fluid Mech*, Vol. 199, 1989, pp. 177-215.
- [15] Ku C. Y., Modeling of Rockfalls Using the Lumped Mass Method and DDA. in *Proc. ISRM SINOROCK*, 2013.
- [16] Hutchinson J. N., A sliding-consolidation model for flow slides. *Can. Geotech. J*, Vol. 23, 1986, pp. 115-126.
- [17] Lorenzini G., and Mazza N., Debris Flow: Phenomenology and Rheological Modelling, 2004, pp. 1-202.

## DYNAMIC ANALYSIS OF NAILED SLOPE

Srinivas Ch<sup>1</sup>, Padmavathi M<sup>2</sup> and Sanjeeva P<sup>3</sup>

<sup>1</sup>P.G student, Jawaharlal Nehru Technological University Hyderabad, India

<sup>2</sup>Associate Professor, Jawaharlal Nehru Technological University Hyderabad, India

<sup>3</sup>Associate Professor, Malla Reddy Engineering College, India

### ABSTRACT

Soil nailing technique has been used in many applications to improve the stability of existing natural slopes and excavated vertical cuts under precarious conditions. Dynamic stability of nailed is required in earthquake prone areas. In the present study, stability analysis is carried out for a nailed slope with 50° slope angle and 20m height. The analysis is carried out by both 2D limit equilibrium and finite element methods using a geotechnical modeling software, GeoStudio. The nailed slope is analysed for stability with respect to static, pseudo- static and dynamic conditions. Dynamic response of nailed slope is analysed against an earthquake with PGA of 0.15g by Finite element method. The acceleration-time history is used as an input to simulate the earthquake in the numerical model. The variation of factors of safety, shear stresses and displacements during earthquake are analysed by dynamic analysis. From the analysis, it is found that the slope is unstable without nails with factor of safety 1.116 in static condition. And the factor of safety increases to about 1.628 by soil nailing. The factor of safety of nailed slope increases on an average of 6% with 1m increase in nail length from 0.5H to 0.7H. The nailed slope experiences 60mm and 33mm displacements in both horizontal and vertical directions at the top of the slope. From the results, it is concluded that the soil nails are efficient in improving the stability of slopes in both static and seismic conditions.

*Keywords: Finite element analysis, Slope stability, Soil nailing, Geo studio, Dynamic analysis*

### INTRODUCTION

Soil nailing has become as an effective stabilization technique especially in case of slope instability. The unstable slopes can now be improved and made stable by the insertion of nails into the slope. The performance of nailed slope is significantly depends on the interaction between soil, nails and facing. Additionally various factors such as the installation method of nails, the construction sequence etc. influences the stability of the nailed slope. Generally, the nailed slopes are analyzed for stability by conventional limit equilibrium methods. Many researchers have developed the limit equilibrium methods to analyze the stability of nailed slopes [1]-[3]. The stability of nailed slope is mainly depends on nail pullout strength and nail tensile strength. The laboratory model tests and field tests are proposed to determine the pullout strength and stability of the nailed slope [4]-[6]. Numerical modeling, limit equilibrium methods and finite element methods (FEM) are used to analyze the stability of nailed slope, failure zone, soil nonlinearity and the staged construction effect to predict the actual site conditions [7]-[10]. Numerical modeling of reinforced slope by finite element methods has proved very useful in prediction of slope deformations, stresses. The effect of nail length, nail spacing, nail inclination on stability of the nailed slope is also analyzed by the numerical models. Mohamed proposed design charts for nailed

walls with different nail lengths, nail spacing's and nail inclinations for different soils [11]. However the slopes are more prone to failure when they are subjected to earthquake loading. So the researchers proposed new methods to analyze the stability of slopes against dynamic loading. The conventional seismic stability of slopes is based on Pseudo-static method [12]. Though it is very simple approach but its applicability in seismic condition is very limited. It considers only the earthquake forces and neglects amplification of waves into soil stratum. Pseudo-dynamic (Steedman & Zeng, 1990) method is the concept which imports amplification of vibrations into the analysis [13]. Numerical methods are used to study the nailed slope failure pattern, deformations and stresses during earthquake by dynamic analysis [14].

### METHODOLOGY

For the purpose of illustration and better understanding, a slope with 50° slope angle and 20m height is considered for the study. The stability analysis is carried out for static, pseudo-static and dynamic conditions. Pseudo-static and dynamic conditions refer to seismic condition in limit equilibrium and finite element analysis respectively. The analysis is carried out by both 2D limit equilibrium and finite element methods using a geotechnical modeling software, GeoStudio. In limit equilibrium analysis, Bishop's simplified method of

slices is used to find the stability of nailed slope by SLOPE/w module of GeoStudio. QUAKE/w module of GeoStudio is used to carry out the analysis by finite element method.

## NUMERICAL MODELLING

### SLOPE/W Modeling for Static Analysis

SLOPE/W is one of the modules of software tool, GeoStudio. In the present study, stability analysis for a slope with 20m height and 50° slope angle is carried with and without nails. SLOPE/W module enables to construct the soil slope by drawing the slope regions. The dimensions of soil slope are scaled down to incorporate into the SLOPE/W to create the numerical model. The slope is modeled at different slope angles by coordinate system present in the SLOPE/W. Materials of slope are defined and assigned to regions, once the slope regions have been determined. The soil properties used in the analysis are summarized in Table 1 [15]. The numerical model of the slope is presented in Fig. 1.

Table 1 Soil properties used in the analysis

| Property                          | Symbol   | Value                     |
|-----------------------------------|----------|---------------------------|
| Unit weight (kN/m <sup>3</sup> )  | $\Gamma$ | 18 kN/m <sup>3</sup>      |
| Cohesion (kN/m <sup>2</sup> )     | C        | 20 kN/m <sup>2</sup>      |
| Friction angle (°)                | $\Phi$   | 28°                       |
| Coefficient of permeability (m/s) | k        | 1.16*10 <sup>-8</sup> m/s |
| Poisson's ratio                   | $\mu$    | 0.35                      |
| Young's modulus (kPa)             | E        | 37000kPa                  |

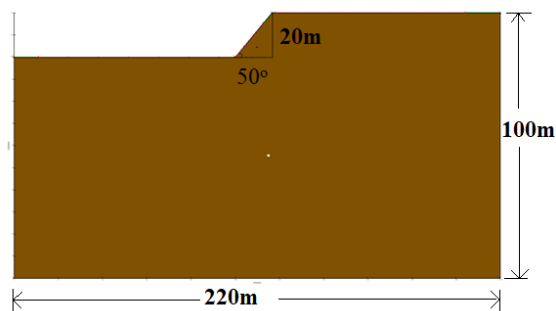


Fig. 1 Numerical model of slope

SLOPE/W module provides the option to input reinforcement in the form of anchors, nails, piles and geosynthetics. Nail element option is used to model reinforcement in the nailed slope. The nail properties used in the analysis are summarized in Table 2. The slip surface is simulated by providing the range of the slip surface along the ground surface. In the

present study, entry- exit option is used to simulate the range of slip surface. SLOPE/W provides different limit equilibrium methods to analyze the problem. Bishop's simplified method is considered in the present analysis.

Table 2 Optimum nail details used in the analysis

| Nail property      | Symbol    | Value                |
|--------------------|-----------|----------------------|
| Yield strength     | $f_y$     | 415N/mm <sup>2</sup> |
| Nail diameter      | d         | 25mm                 |
| Nail length        | $l$       | 12m (0.6H)           |
| Nail inclination   | $\lambda$ | 15°                  |
| Horizontal spacing | $S_h$     | 1m                   |
| Vertical spacing   | $S_v$     | 1m                   |

### SLOPE/W Modeling for Pseudo-Static Analysis

The slope is further analyzed to find the stability against an earthquake of given PGA. Pseudo- static analysis considers seismic loading in terms of horizontal and vertical seismic coefficients of earthquake. The slope modeling and assigning materials in pseudo – static analysis are similar to static analysis. The magnitudes of both horizontal and vertical seismic coefficients of earthquake are given as input once the modeling of slope is done. In the present study, seismic coefficients of  $k_h = 0.15$  and  $k_v = 0.075$  is considered for the analysis. The failure slip circle and Factor of Safety (FOS) are the major results from the pseudo- static analysis.

### QUAKE/W Modeling for Dynamic Analysis

The dynamic analysis is carried out to analyse the stability of the slope during the period of earthquake. The acceleration- time history of the earthquake is taken in to consideration to analyse the behavior of the slope during earthquake. In the present study, the optimum nailed slope obtained in static and pseudo static analysis is considered for dynamic analysis.

In the present study, the dynamic analysis is carried out in 4 phases. The first and second phases are carried out in QUAKE/W and third and fourth phases are carried out in SLOPE/W to find the FOS by considering the first two phases as parent analysis. In first stage initial static stresses are calculated in QUAKE/W. The construction of slope regions by coordinate system and assigning materials to the regions is similar to the process in SLOPE/W. QUAKE/W provides an option to input slope boundaries to the model. History nodes have been selected where the results are required to retrieve after the analysis.

The static stresses obtained in first phase are

considered as input in second stage. The dynamic analysis is carried out by equivalent dynamic method in the present study. The acceleration – time history of the earthquake is given as an input in the second phase. An earthquake of 0.15g PGA is considered for the dynamic analysis. Fig. 2 shows the acceleration –time history used in the analysis. The complete slope model is divided into elements to generate the finite element mesh. Slope deformation and stresses distribution during the earthquake are the primary results in the dynamic analysis.

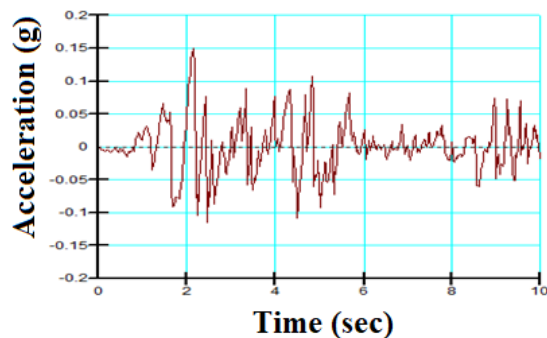


Fig. 2 Earthquake acceleration-time history

The variation of stresses and displacements during the earthquake are stored from the above two phases. These stresses are incorporated into SLOPE/W to find FOS. In third phase, initial static stresses are considered as parent analysis. The range of slip surface is once again specified in this phase like in static condition. The factor of safety before earthquake is obtained in this phase as an output. In final phase, Equivalent linear dynamic analysis is considered as parent analysis. This analysis is performed to find Factor of safety during the earthquake by Newmark's deformation method in SLOPE/W. The nailed slope with history nodes is presented in Fig. 3

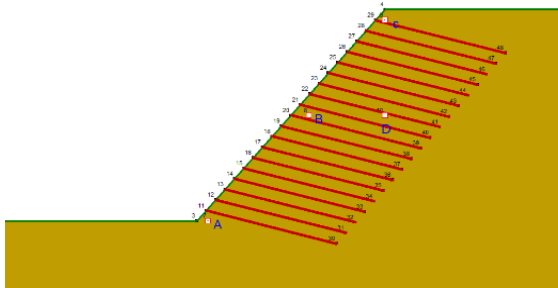


Fig. 3 Nailed slope with history nodes A, B, C and D

## RESULTS AND DISCUSSION

### Results of Static Analysis

The factor of safety of slope without nails in static condition is found to be 1.116 which is far below the safe value of FOS of 1.5 as shown in Fig. 4.

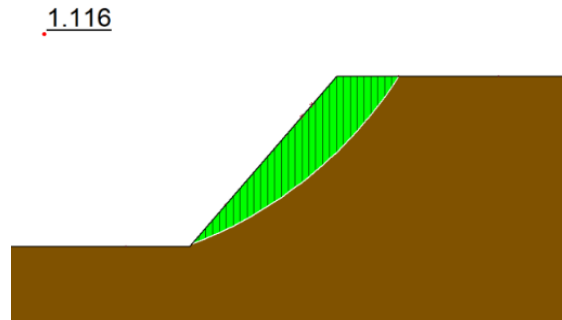


Fig. 4 Critical slip surface of slope without nails in static condition ( $H = 20\text{m}$ ,  $\theta = 50^\circ$ )

Soil nailing technique is employed to stabilize the slope. The nailed slope design is optimized with the optimum values of nail length, nail spacing and nail inclinations. To find the optimum design, the numerical model of nailed slope is analyzed for different combinations of nail lengths from  $0.5H$  to  $0.75H$ , nail inclinations from  $10^\circ$  to  $25^\circ$  and nail spacing from 1m to 2m in both directions.

### Effect of nail inclination

Initially, the nailed slope is analyzed for stability at different nail inclinations of  $10^\circ$ ,  $15^\circ$ ,  $20^\circ$  and  $25^\circ$ . The length and spacing of nails are kept constant with  $0.7H$  and 1.5m respectively to find the optimum nail inclination. Fig. 5 depicts the variation of FOS with nail inclination.

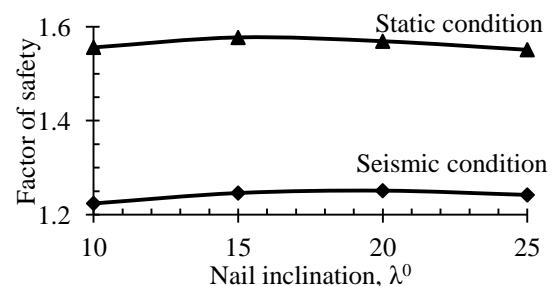


Fig. 5 Influence of nail inclination on factor of safety ( $H = 20\text{m}$ ,  $\theta = 50^\circ$ ,  $l = 0.7H = 14\text{m}$ ,  $S_h = S_v = 1.5\text{m}$ )

From the Fig. 5, it is observed that the nailed slope with  $15^\circ$  nail inclination attains maximum FOS of 1.577 which is more than minimum value of FOS (as per FHWA manual-2015) of 1.5. Hence nail inclination of  $15^\circ$  is considered as optimum nail

inclination for the study.

#### Effect of nail length

The nailed slope is further analyzed for stability at different nail lengths of  $0.5H$ ,  $0.55H$ ,  $0.6H$ ,  $0.65H$ ,  $0.7H$ ,  $0.75H$  and  $0.8H$ . The nail inclination and spacing are kept constant at  $15^\circ$  and  $1\text{m}$  to study the effect of nail length on stability. The results are presented in Fig. 6.

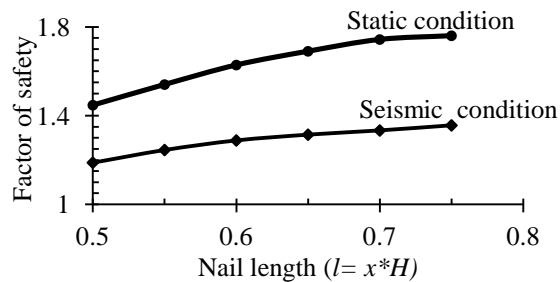


Fig. 6 Influence of nail length on Factor of Safety ( $H=20\text{m}$ ,  $\theta=50^\circ$ ,  $\lambda=15^\circ$ ,  $S_h=S_v=1\text{m}$ )

The factor of safety increases with increase in nail length from up to about  $0.7H$  and then shows an asymptotic variation. Based on the results presented in Fig. 5 and Fig. 6, the nailed slope with  $12\text{m}$  ( $0.6H$ ) length nails at  $15^\circ$  inclination and  $1\text{m}$  spacing in both directions is considered as optimum with FOS of  $1.628$  which is more than minimum recommended value of FOS of  $1.5$ . The critical slip circle of nailed slope is with optimum parameters are given in Fig. 7.

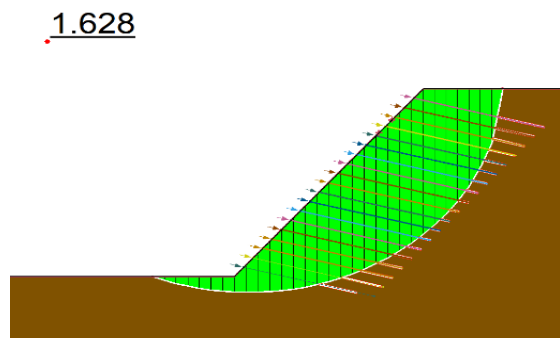


Fig. 7 Nailed slope with critical slip surface ( $l=0.6H$ ,  $S_h=S_v=1\text{m}$ ,  $\lambda=15^\circ$ )

#### Results of Pseudo-Static Analysis

The stability of the nailed slope against an earthquake of  $0.15\text{g}$  PGA is analyzed with the help of numerical model in SLOPE/W module. The horizontal seismic coefficient,  $k_h=0.15$  and vertical seismic coefficient,  $k_v=0.5k_h=0.075$  are used to import the seismic loading into the analysis. Table 3 presents the different values of FOS obtained in the pseudo static analysis.

#### Results of Dynamic Analysis

The dynamic analysis helps to analyze the behavior of slope during earthquake. The variation of FOS, stresses distribution and displacements at history nodes during the earthquake of  $0.15\text{g}$  PGA are studied in the dynamic analysis.

Table 3 Results of static & Pseudo-static analysis

| Slope         | Minimum recommended FOS (FHWA manual-2105) |         | Obtained FOS    |                        |
|---------------|--|---------|-----------------|------------------------|
|               | Static                                     | Seismic | Static analysis | Pseudo static analysis |
| Without nails | 1.5  | 1.1     | 1.116           | 0.881                  |
| Nailed slope  | 1.5  | 1.1     | 1.628           | 1.288                  |

#### Shear stress variation during earthquake

Variation of the maximum shear stresses developed at history nodes during the earthquake of PGA  $0.15\text{g}$  in the slope without and with nails are presented in Fig. 8 and Fig. 9 respectively.

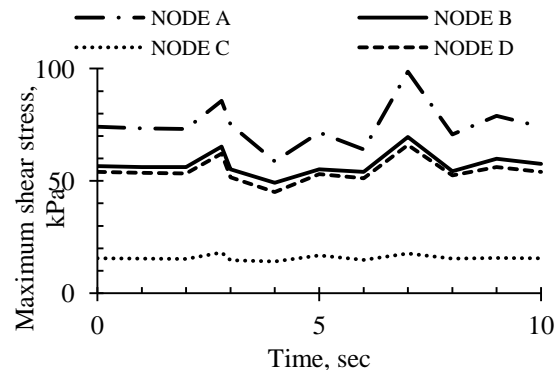


Fig. 8 Variation of shear stresses at history nodes in the slope without nails

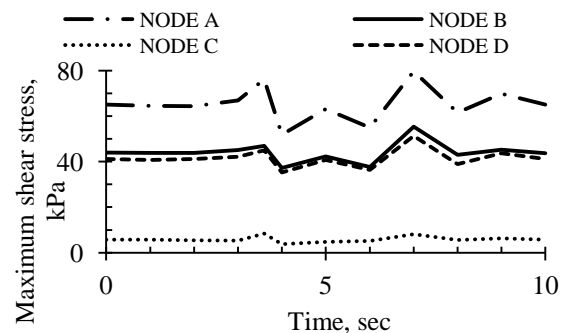


Fig. 9 Variation of shear stresses at history nodes in nailed slope



The maximum shear stress is found at NODE A which is located at bottom of the slope for both the cases of slope with and without nails. It decreases from 98.69kPa to 79kPa by the inclusion of nails into the slope. The minimum shear stress is found at the top of the slope at NODE C with a value of about 10kN in the nailed slope.

#### Nail axial force

The distribution of nail axial force along the length in both bottom and top nail row is depicted in Fig. 10. The maximum nail axial force is developed in bottom nail row.

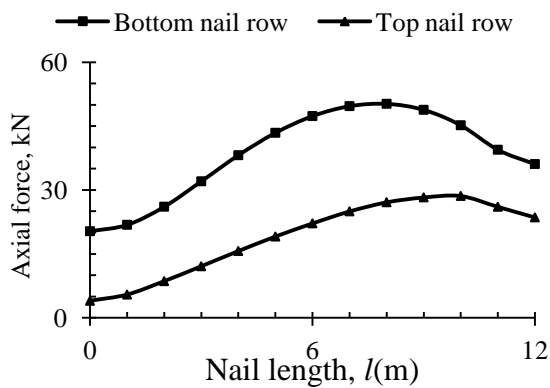


Fig. 10 Variation of nail axial force along the length

Maximum nail axial forces in top and bottom nail rows are 24.44kN and 50.38kN respectively. Nail axial force increases along nail length. It attains maximum in between the lengths of  $0.6L$  (7.2m) to  $0.9L$  (10.8m) from nail head and then decreases towards nail tip. Location of maximum nail force is presented in Fig. 11.

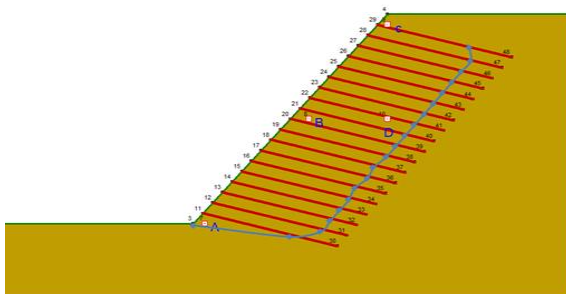


Fig. 11 Location of maximum nail axial force

The variation of horizontal displacements of nailed slope at history nodes during the earthquake of 0.15g PGA are presented in Fig. 12 and Fig. 13.

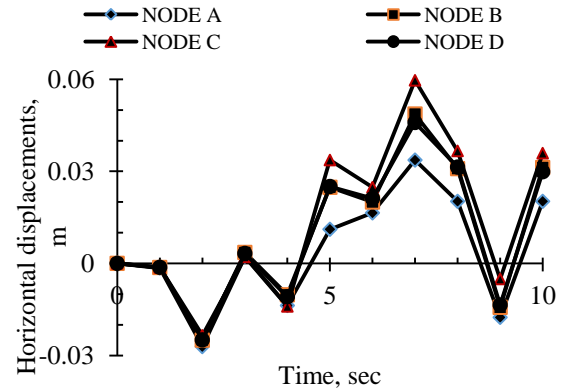


Fig. 12 variation of horizontal displacements in nailed slope ( $H=20\text{m}$ ,  $\theta=50^\circ$ ,  $l=0.6H=12\text{m}$ ,  $\lambda=15^\circ$ ,  $S_h=S_v=1\text{m}$ )

Nailed slope experiences maximum horizontal displacement of 60mm at NODE C which is at the top of the slope. It experiences minimum horizontal displacement of 28mm at the bottom of the slope at NODE A.

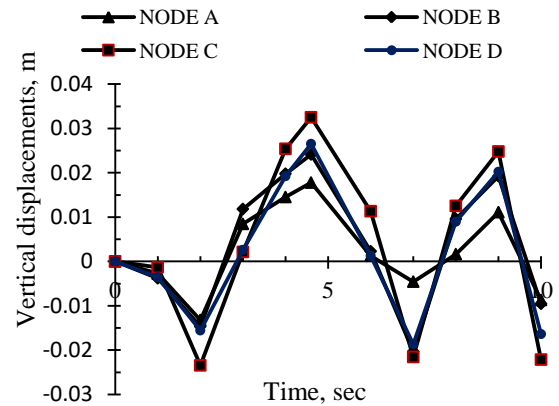


Fig. 13 Vertical displacements of nailed slope ( $H=20\text{m}$ ,  $\theta=50^\circ$ ,  $l=0.6H=12\text{m}$ ,  $\lambda=15^\circ$ ,  $S_h=S_v=1\text{m}$ )

The nailed slope experiences maximum and minimum vertical displacements of 32mm and 17mm at the top (NODE C) and bottom (node A) of the slope respectively.

#### Results of Newmark's deformation analysis

The variation of FOS during the total period of the earthquake (PGA of 0.15g) are presented in Fig. 14

The nailed slope attains minimum FOS of 1.352 at 7<sup>th</sup> second of ground motion which is more than the safe FOS of 1.1 (FHWA manual-2015). Hence the slope with nails of length, 12m inserted at  $15^\circ$  inclination and 1m spacing is stable even during earthquake of PGA 0.15g.

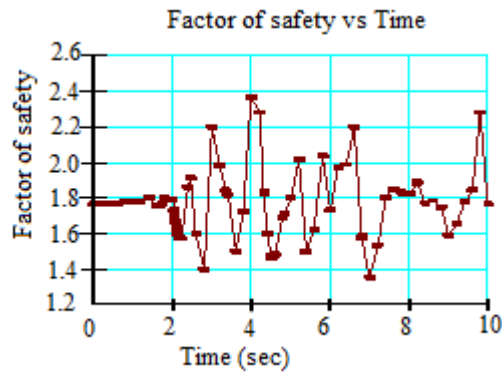


Fig. 14 Variation of FOS with time in nailed slope

## CONCLUSIONS

Following conclusions are made based on the results obtained from the study.

1. The slope is stabilized by the inclusion of nails of length 12m at  $15^\circ$  inclination and 1m spacing in both directions. The FOS increases from 1.116 to 1.628 after nailing.
2. From dynamic analysis, the horizontal and vertical displacements of nailed slope decreases from top to the bottom of the slope. The slope experiences displacement of 60mm and 33mm in both horizontal and vertical directions both at the top of the slope. The inclusion of 12m nails with  $15^\circ$  inclinations at 1m spacing into the slope leads to 20% reduction in shear stress.
3. The nailed slope is safe against an earthquake of PGA, 0.15g with FOS of 1.288 and 1.35 in both pseudo-static and dynamic analyses respectively.

## REFERENCES

- [1] Amit Prasanth and Mousumi Mukherjee, Soil Nailing for Stabilization Steep slopes near Railway Tracks. Research Gate, pp.1-203.
- [2] Federal Highway Administration FHWA. Reference manual, 7<sup>th</sup> Edition, U.S.A. 2015, FHWA-NHI-14-007.
- [3] Basudhar P. K., Anubhav and Lakshminarayana M. R., Three-Dimensional Limit-Equilibrium Stability Analyses of Slopes and Effect of Inclusion of Soil Nails. International Journal of Geo-mechanics, Vol. 17, Issue 9, 2017, pp. 1-11.
- [4] Wong I. H., Low B. K., Pang P.Y. and Raju G.V.R., Field Performance of Nailed Soil Wall in Residual Soils. Journal of Performance of Constructed Facilities, Vol. 11, Issue 3, 1997, pp. 105-112.
- [5] Lok Man Chu and Jain-Hua Yin. Comparison of Interface Shear strength of Soil Nails by both direct shear box Tests and Pull-out Tests. Journal of Geotechnical and Geo Environmental Engineering, Vol. 131, Issue 9, 2005, pp. 1097-1107.
- [6] Seo H. J., Lee and Loizos P., Net Load-Displacement Estimation in Soil-Nail Pullout Tests. Geotechnical Engineering, Vol. 170, 2017, pp. 534-547.
- [7] Chia Cheng Fan and Jiun Hung Luo., Numerical Study on the Optimum Layout of Soil Nailed Slopes. Computers and Geotechnics, Vol. 35, 2008, pp. 585-599.
- [8] Sivakumar Babu G. L. and Vikas Pratap Singh., 2D Numerical Simulations of Soil Nail Walls. Geotechnical and Geological Engineering, Vol. 28, 2009, pp. 299-309.
- [9] Sahoo S., Manna B. and Sharma K. G., Stability Analysis of Un-Reinforced and Reinforced Soil Slopes. Geo-China, Vol. 257, 2016, pp. 74-81.
- [10] Rawat S. and Gupta A. K., Analysis of a Nailed Soil Slope Using Limit Equilibrium and Finite Element Methods. International Journal of Geo-synthetics and Ground Engineering, Vol. 2, Issue 34, 2016, pp. 1-23.
- [11] Ahmed Mohamed, Design Charts for Soil Nailing. Research Gate, pp. 1-221.
- [12] Jonathan D. and Thaleia T., Pseudo Static Slope Stability Procedure. 5<sup>th</sup> International Conference of Earthquake Geotechnical Engineering, Issue 1, 2011, pp. 10-13.
- [13] Kramer S. L., Chapter 10, Seismic Slope Stability, Geotechnical Earthquake Engineering. Pearson Education, 2018, Singapore.
- [14] Rawath P. and Chatterjee K., Seismic Stability Analysis of Soil Slopes Using Soil Nails. Geotechnical Earthquake Engineering and Soil Dynamics. Vol. 293, 2018, pp. 79-87.
- [15] Shrestha S., Ravichandran N., Raveendra M. and Attenhofer J. A., Design and analysis of retaining wall backfilled with shredded tire and subjected to earthquake shaking. Soil Dynamics and Earthquake Engineering, Vol. 90, 2016, pp. 227-239.

## SETTLEMENT OF SILTY SOIL UNDER SATURATION USING MICRO SYNTHETIC FIBERS

Padmavathi, V.<sup>1</sup> and Rao, P. N.<sup>2</sup>

<sup>1</sup>Faculty, JNTUH college of Engg. Hyderabad, India;

<sup>2</sup>Faculty, BITS Pilani, Hyderabad Campus, Hyderabad, India

### ABSTRACT

Loose silty soils are often encountered by the foundation engineers working in semi-arid and arid areas of the world. The silty soil has low water content and high void ratio. The problems concerning loose silty soil are instability and considerable settlement due to minor changes in the water content, which can cause remarkable damages to overlying structures. In dry condition, these soils are strong and appear to provide good support for foundations. The large differential settlements reduce the serviceability of the civil structure and raise the frequency and cost of rehabilitation. To avoid these kinds of settlements, it is necessary to identify the potential settlements and apply mitigation measures. The soil samples are collected at faculty training center near block B, IDBI campus, Gachibowli, Hyderabad, India. The present study is related to the prediction and identification of collapsible nature of silty soil and its behavior under saturation at various loading conditions and quantifying the degree of settlement by finding the collapsible potential. The study also investigates the effect of micro synthetic fibers on soil volume change.

**Keywords:** *Silty soil, Micro synthetic fiber, Collapsible nature, Settlements, Oedometer test*

### INTRODUCTION

The stability of superstructure is statically indeterminate problem when built on soil which has sudden settlement. The collapse of natural ground is due to excessive settlement of soil and causes destruction of structure. The collapse phenomenon can occur in the case of natural soil like loose silts and silty sands. Generally, collapsible soils are defined as metastable soils that contain voids within their soil structure, with grain sizes ranging from silt to fine sand and fewer amounts of clay and salts. In dry state, the cementation between particles is responsible to support heavy loads. However, if the soil becomes wet or saturated, the soil structure will collapse due to the loss of binding strength between soil particles. Experimental and theoretical studies carried out to understand the uncertainties involved in the phenomenon of collapse. The collapsible potential is the difference in the axial strain at an applied stress, after and before saturation. The literature reveals that the majority of the research is on the collapse identification, predictions, mechanism and treatment methods. Momeni et al. (2012) defined the collapsible soils are any unsaturated soils generally characterized by the sudden and the considerable reduction in volume that occurs when subjected to inundation under constant stress. Ayeldeen et al. (2017) studied the collapsible behavior of soil by adding biopolymers under dry and curing conditions and found 20 to 30 % decrease in collapsible potential. Abdelmohsen

and Ali (2017) conducted field and laboratory tests on loose silty soil and found that field collapsible potential values are 15% lesser than the laboratory test values. Eldesouky (2017) reported that the randomly distributed dry loose 0.5% fiber reinforcement inclusion in sand increases the shear strength and dilation of sand as compare to unreinforced moist sand. Abbeche and Ziani (2014) studied the effect of the hydraulic gradient and the vertical load on the collapsible potential of soils and concluded that for 400 kPa of vertical load the collapse reaches to maximum. Nassima Bakir (2017) has conducted an experimental study to evaluate the collapsible potential of loose silty soil with the addition of glass fibers and concluded that 6% addition of glass fibers reduces the collapse without soil disorder. Ziani et al. (2019) studied the stabilization of collapsible soil using industrial waste and natural pozzolan and found that large decrease in suction and higher degree of compaction by addition of 5-7% of industrial waste and natural pozzolan. Lin et al. (2016) depicted enhancing soft subgrade soil with a sewage sludge ash/cement mixture and nano-silicon dioxide. However, the main objective of the present study is to predict and identification of collapsible nature and studying its behavior under saturation at various loading conditions and quantifying the degree of settlement by finding the collapsible potential of loose silts with and without reinforcement of micro synthetic fiber.

## EXPERIMENTAL INVESTIGATION

### Materials used

The soil is collected from block B, Faculty Training Centre, IDBI campus, Gachibowli, Hyderabad, India. The soil properties are determined and presented in the Table 1. The stabilizing material used is micro synthetic fibers and the physical and chemical properties are shown in Table 2.

### Testing Methodology

The dry unit weight of the soil is maintained as 12.8 kN/m<sup>3</sup>, which is about 67% of the maximum dry unit weight of the soil. The percentage of micro synthetic fiber in the testing varied from 0.1 to 1.0 by weight of the soil. It is very difficult to mix more than 1.0 % fiber content in preparing the soil samples due to balling effect.

Table 1 Physical Properties of soil used

| S. No. | Property                                    | Description |
|--------|---|-------------|
| 1      | GRAIN SIZE DISTRIBUTION<br>(% Passing)      |             |
|        | Gravel (>4.75 mm)                           | 05          |
|        | Coarse Sand<br>(2.0 - 4.75 mm)              | 08          |
|        | Medium Sand<br>(0.425 - 2.0 mm)             | 22          |
|        | Fine Sand<br>(0.075 – 0.425 mm)             | 23          |
|        | Silt (0.075 – 0.002 mm)                     | 42          |
|        | Clay (<0.002 mm)                            | 0           |
| 2      | Liquid limit (%)                            | 33          |
| 3      | Plastic limit (%)                           | Non Plastic |
| 4      | IS Classification                           | SM          |
| 5      | Specific gravity                            | 2.64        |
| 6      | Maximum Unit Weight<br>(kN/m <sup>3</sup> ) | 19.3        |
| 7      | Optimum moisture content<br>(%)             | 13          |
| 8      | Cohesion (kPa)                              | 0           |
| 9      | Internal friction (degrees)                 | 31          |

Table 2 Physical and Chemical Properties of Micro Synthetic Fiber

| Property                     | Value             |
|------------------------------|-------------------|
| Diameter of fiber (mm)       | 0.05              |
| Fiber tensile strength (MPa) | 350               |
| Elastic modulus (MPa)        | 1000              |
| Melting temperature (°C)     | 165               |
| Fiber length (mm)            | 12                |
| Type                         | fine monofilament |
| Absorption                   | Nil               |

|                        |              |
|------------------------|--------------|
| Specific gravity       | 0.91         |
| Electric conductivity  | Low          |
| Acid & salt resistance | High         |
| Ignition point (°C)    | 37           |
| Thermal conductivity   | Low          |
| Melt point (°C)        | 324          |
| Alkali resistance      | alkali proof |

Oedometer tests are conducted to determine the settlements under different applied stresses for both soils samples without and with fiber reinforcement. The amount of micro synthetic fibers is taken as 0.1%, 0.3%, 0.5%, 0.7% and 1.0% by weight of the soil. The soil samples for Oedometer test are prepared and saturated at applied stress levels of 50, 100 and 200 kPa to observe the settlements. The test series numbers and particulars are given in Table 3. Three series of tests T<sub>1</sub>, T<sub>2</sub> and T<sub>3</sub> have been conducted on soil and soil with fiber content. Three Oedometer tests are conducted in T<sub>1</sub> series on soil only for 50, 100 and 200 kPa stress levels of saturation. The soil and micro synthetic fiber combination tests are given in second series, T<sub>2</sub> for fiber content of 0.1, 0.3, 0.5, 0.7 and 1% under saturation at 200 kPa stress level. The third test series, T<sub>3</sub> is for optimum content of fiber 0.7% varying with saturation stress levels of 50, 100 and 200 kPa. The shear strength is also obtained by direct shear tests for untreated and treated soil with 0.1%, 0.3%, 0.5%, 0.7% and 1.0% fiber content.

Table 3 Oedometer test program

|                |   |   |
|----------------|---|---|
| T <sub>1</sub> | Samples with compacted unit weight of 12.8 kN/m <sup>3</sup>                            |   |
|                | S <sub>1</sub>  | Saturated at 50 kPa pressure in Oedometer (T <sub>1</sub> S <sub>1</sub> )  |
|                | S <sub>2</sub>  | Saturated at 100 kPa pressure in Oedometer (T <sub>1</sub> S <sub>2</sub> ) |
|                | S <sub>3</sub>  | Saturated at 200 kPa pressure in Oedometer (T <sub>1</sub> S <sub>3</sub> ) |
| T <sub>2</sub> | Samples with compacted unit weight of 12.8 kN/m <sup>3</sup> with micro synthetic fiber |   |
|                | S <sub>1</sub>  | 0.1 % fiber Saturated at 200 kPa pressure in Oedometer                      |
|                | S <sub>2</sub>  | 0.3 % fiber Saturated at 200 kPa pressure in Oedometer                      |
|                | S <sub>3</sub>  | 0.5 % fiber Saturated at 200 kPa pressure in Oedometer                      |
|                | S <sub>4</sub>  | 0.7 % fiber Saturated at 200 kPa pressure in Oedometer                      |
|                | S <sub>5</sub>  | 1.0 % fiber Saturated at 200 kPa pressure in Oedometer                      |
| T <sub>3</sub> | Samples with compacted with micro synthetic fiber of 0.7%                               |   |
|                | S <sub>1</sub>  | Saturated at 50 kPa pressure in Oedometer                                   |
|                | S <sub>2</sub>  | Saturated at 100 kPa pressure in Oedometer                                  |
|                | S <sub>3</sub>  | Saturated at 200 kPa pressure in Oedometer                                  |

## RESULTS AND DISCUSSION

The effect of micro synthetic fibers on settlement or collapsible nature of loose silts upon saturation is observed. The increase of fiber content in silty soils from 0.1 to 1.0 % causes a reduction in the dry unit weight as shown in Fig. 1. This reduction is due to the less weight of the fiber content compared to the replaced soil.

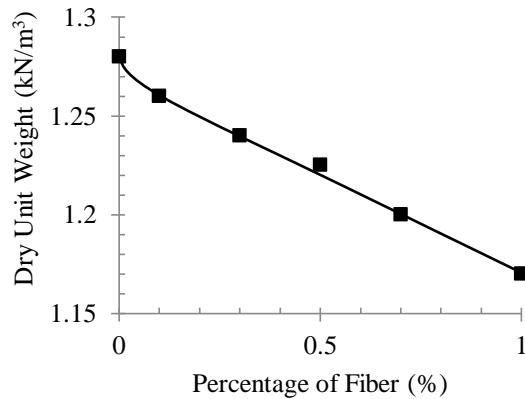


Fig.1 Dry Unit Weight vs Percentage Fiber Content

The oedometer test program is mentioned in Table 3. First test series is nomenclature as T<sub>1</sub>S<sub>1</sub>, T<sub>1</sub>S<sub>2</sub> and T<sub>1</sub>S<sub>3</sub> upon saturation of silty soil at 50, 100 and 200 kPa respectively for a dry unit weight of 12.8 kN/m³ and the results are shown in Fig. 2. There is a sudden decrease in volumetric strain corresponding to stress at which saturation takes place, indicating collapsible nature of the soil. The axial strain in oedometer test is same as volumetric strain as the area is constant. The collapsible potentials are 7.05, 7.15 and 7.5% corresponding to saturation at 50, 100 and 200 kPa applied stresses respectively. The collapsible potentials are almost same even though the applied stress changes from 50 to 200 kPa. It is observed that the settlement in terms of collapsible potential of silty soil is moderately severe. Hence, the stabilization is required and used micro synthetic fibers in present study to reduce the volumetric strains or settlements.

Soil is mixed with micro synthetic fibers and the test series T<sub>2</sub> is conducted. Fig. 3 shows the oedometer test results, when the saturation is done at an applied stress of 200 kPa with 0.1, 0.3, 0.5, 0.7 and 1.0 % fiber content. The collapsible potential at 200 kPa applied stress is observed for the treated samples and found as 4.3, 2.8, 1.35, 1.0 and 0.9 % respectively for 0.1, 0.3, 0.5, 0.7 and 1.0 % fiber content in the soil.

It is observed that the collapsible potential values are progressively decreased with addition of fiber content and the problem of collapse is reduced from

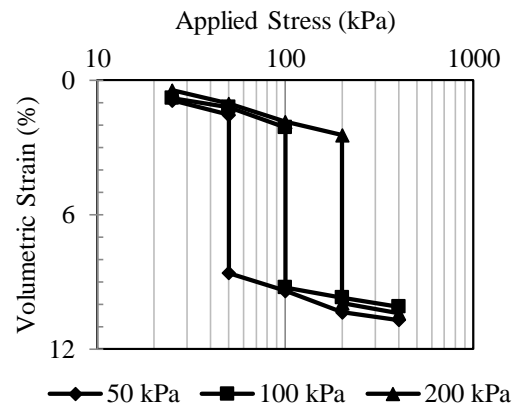


Fig. 2 Volumetric Strain corresponding to 50, 100 and 200 kPa Saturation

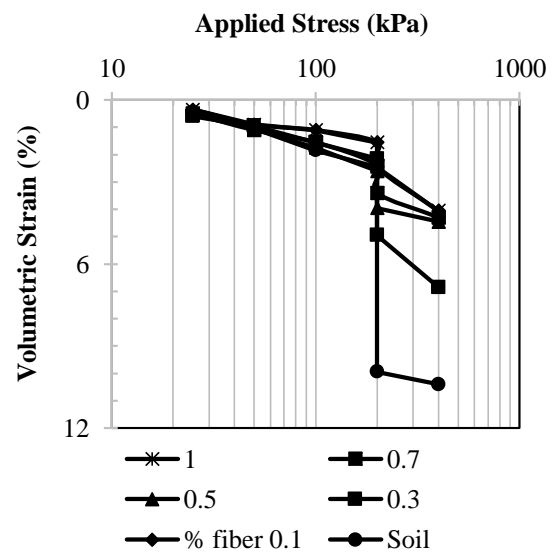


Fig. 3 Effect of Percentage Fiber Content in Soil on Volumetric Strain

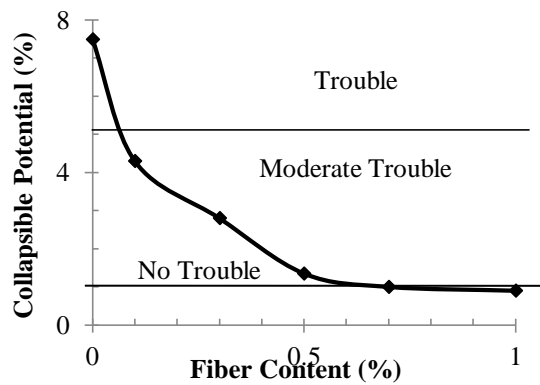


Fig. 4 Percentage of Fiber vs Collapsible Potential  
moderate severity to no trouble. This behavior can be attributed to the reinforcing mechanism of fibers which also reduces the voids in treated soil by binding action of soil particles and fibers.

Fig. 4 shows the variation of collapse potential with percentage of micro synthetic fiber. For a fiber content of 0.7%, the severity degree changes from "moderate Trouble" to "no trouble".

The collapsible potential is observed as 1.0% for treated soil sample with 0.7% of fiber content saturated at 200 kPa stress level. Hence, 0.7% fiber content is considered as optimum percentage of fiber for further testing of test series T<sub>3</sub>. Collapsible potential values are obtained for 50 kPa and 100 kPa stress level saturations with optimum fiber content.

Fig. 5 represents the applied stress verses volumetric strain. The collapsible potentials are 0.3 and 0.75 and 1.0 % respectively for 50, 100 and 200 kPa stress level saturations.

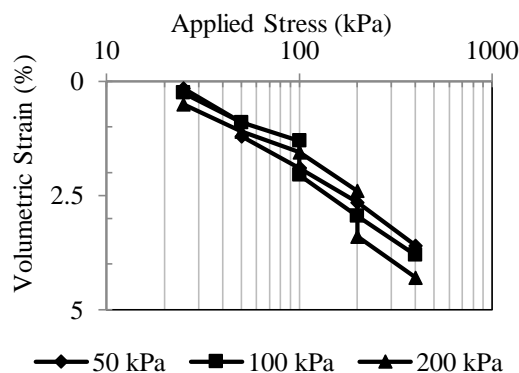


Fig. 5 Effect of Applied Stress in Stabilization

Based on collapsible potential obtained for the treated soil, the final settlement is less when the compaction is done at lower stress level (50 kPa) than when done at higher stress levels 100 and 200 kPa.

The direct shear test results for untreated and treated soil samples for the 12.8 kN/m<sup>3</sup> unit weight and the fiber content of 0.1, 0.3, 0.5, 0.7 and 1.0% fibers are presented in Fig. 6. The angle of internal friction of untreated soil is 31°. The shear strength of the treated soil increases with increase in percentage of fiber content. The increase in shear strength is due reinforcement effect of fiber in soil. There is a development of interlocking mechanism of fiber at higher percentage of fiber content. The angle of internal friction increases with increase in fiber content in soil as shown in Fig. 7. The angle of internal friction corresponding to treated soil with 0.1, 0.3, 0.5 and 0.7% fiber is 32.5, 34.5, 36.0 and 36.5° respectively. The treated soil with 0.7% fiber content shows interlocking of soil and fiber content apparent cohesion or interlocking stress of 2.5 kPa where as it is 14 kPa (Fig. 8) for 1.0% fiber content and angle of internal friction is reduced to 35°.

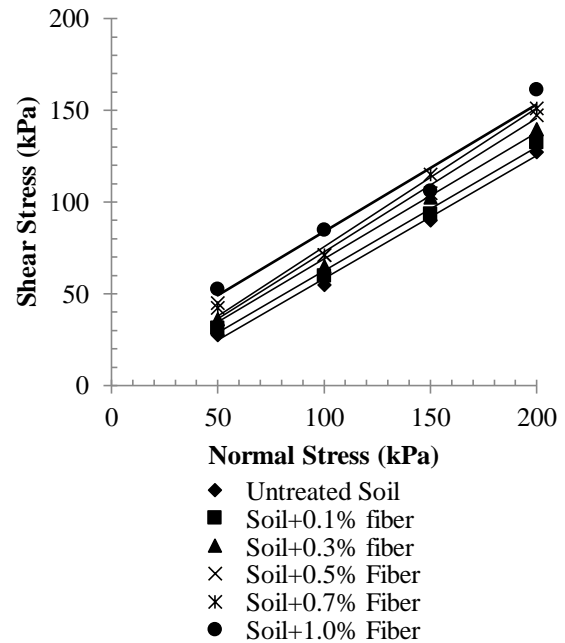


Fig. 6 Shear Strength Variation with increase in Fiber Content

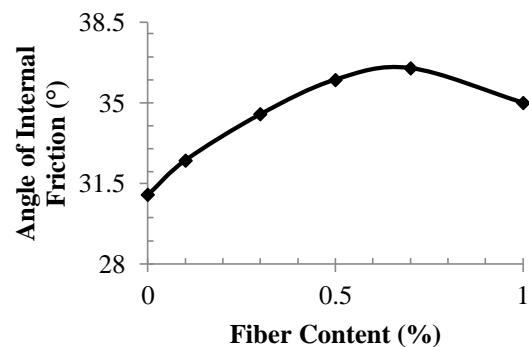




Fig. 7 Effect of Fiber Content on Angle of Internal Friction of Treated Soil

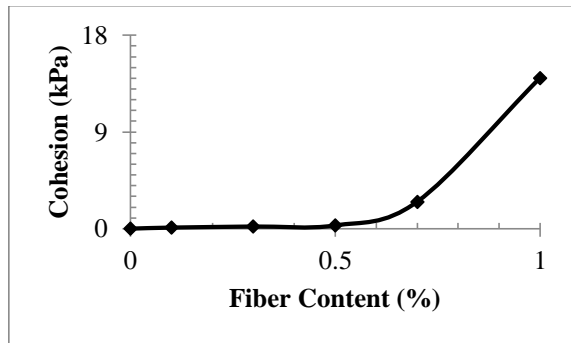


Fig. 7 Effect of Fiber Content on Cohesion of Treated Soil

## CONCLUSIONS

The following conclusions are made based on the experiment results obtained from the laboratory tests.

1. The soil is Silty Sand with no percentage of clay. The soil causes 'trouble' to the foundation as the collapsible potential values lie between 5 and 10.
2. The optimum content of micro synthetic fiber is obtained as 0.7% from compaction test.
3. At 12.8 kN/m<sup>3</sup> unit weight of soil at saturation under 200 kPa applied stress level, with 0.7% of micro synthetic fiber the collapsible potential of soil is 1.0, which comes under 'no trouble' zone.
4. For the soil with unit weight of 12.8 kN/m<sup>3</sup> and 0.7% of micro synthetic fiber, the settlements are calculated at saturation of 50, 100 and 200 kPa stresses as 0.3, 0.75 and 1%. The total settlement of the soil reduces, when the saturation is done at lower stress level (50 kPa) than higher stress levels 100 and 200 kPa.
5. The shear strength of the soil increases with increase in fiber content due to reinforcement and interlocking effect of fibers in soil.

## ACKNOWLEDGEMENTS

The authors acknowledge Central Public Works Department (CPWD), India and Industrial Consultancy Services of JNTU College of Engineering, Hyderabad, India.

## REFERENCES

- [1] Abbeche, K. and Ziani, H. (2014). "Effect Study of the Hydraulic Gradient and the Vertical Load on the Collapse Potential of Soils", Proceedings of Geo-Shanghai, Soil Behaviour and Geomechanics, pp. 173-183.
- [2] Abdelmohsen, H. H. and Ali, N. A. (2014). "Practical Engineering Behavior of Egyptian Collapsible Soils, Laboratory and In-situ Experimental Study", International Conference on Advances in Structural and Geotechnical Engineering, pp. 1-7.
- [3] Ayeldeen, M., Abdelazim, N., Mostafa ES and Masaki, K. (2017). "Enhancing Mechanical Behaviors of Collapsible Soil using Two Biopolymers", Journal of Rock Mechanics and Geotechnical Engineering, Vol. 9, No. 2, pp. 329-339.
- [4] Eldesouky, H. M., Morsy, M. M. and Mansour, M. F. (2017). "Fiber-reinforced Sand Strength and Dilation Characteristics", Ain Shams Engineering Journal, vol. 7, No. 2, pp. 517-526.
- [5] Lin, D. F., Luo, H. L., Chen, C. T., and Cai, M. D. (2016). "Study Properties of Soft Subgrade Soil Stabilized by Sewage Sludge/Lime and Nano-SiO<sub>2</sub>." Geomechanics and Engineering, Vol. 10, No. 6, pp.793-806.
- [6] Momeni, W.M., Shafiee, A., Heidari, M., Jafari, M.K., Madhavifar M.R. (2012). "Evaluation of Soil Collapse Potential in Regional Scale", Natural Hazards, Vol. 64, pp 459-479.
- [7] Nassima Bakir, Khelifa Abbeche and Gerard Panczer, (2017), "Experimental Study of the Effect of the Glass Fibers on Reducing Collapse of a Collapsible Soil", Geomechanics and Engineering, vol. 12, pp. 71- 83.
- [8] Ziani, H., Abbeche, K., Messaoudene, I. and Andrade Pais, L. J. (2019). "Treatment of Collapsible Soils by Additions of Granulated Slag and Natural Pozzolan", KSCE Journal of Civil Engineering, Vol. 23, No. 3, pp. 1028-1042.

## GROUND IMPROVEMENT USING GEOSYNTHETICS ~ A LITERATURE REVIEW

Mohamed Eltaher<sup>1</sup>, Zakaria Hossain<sup>1</sup>, Jim Shiau<sup>2</sup>, and Hajime Takami<sup>3</sup>

<sup>1</sup>Graduate School of Bioresources, Mie University, Japan; <sup>2</sup>School of Civil Engineering and Surveying, University of Southern Queensland, Australia; <sup>3</sup>Tsuchiya TSCO Co., Ltd., Japan

### ABSTRACT

Owing to the rapid growth of population and city urbanization, the need for more development of infrastructures e.g. highways, airports, railways, bridges, and many other engineered structures demands a variety of construction activities. Engineers have to be able to put in place new methods, techniques, and materials for structure sitting on the existing weak and soft soils by improving their strength and other properties. Nowadays, in addition to soil compaction, soil replacement is a convenient ground improvement technique in the construction processes with the aims of increasing the bearing capacity of the soil and reducing the settlement. But it may not be the best financial or technical option for a specific project while in the same time there was a great opportunity in many ways to improve the ground performance e.g. mechanical stabilization, preloading stabilization, sand drain stabilization, physical and chemical modification stabilization, addition and confinement modification stabilization and soil reinforcement using geosynthetics. This paper presents a review on the application of geosynthetics in construction engineering. Various available commercial types of geosynthetics and main functions in field application are discussed with respect to the reinforcement and separation functions, especially in pavement construction. Finally, the environmental and financial benefits of using geosynthetics as a ground improvement technique are discussed.

*Keywords: Geosynthetics, Ground Improvement Technique, Reinforcement, Pavement.*

### INTRODUCTION

In fact, Geosynthetics is a generic name representing a broad range of planar and three-dimensional products manufactured from synthetic polymeric materials. As shown in table 1, Synthetic polymers used in the manufacturing of geosynthetics are generally derived from crude petroleum oils but also rubber, fiberglass, basalt rock in addition to many other materials can be used for manufacturing geosynthetics e.g. natural fabrics but recently organic natural fabrics are not used due to the rapid decomposition [1,2].

Table 1 Materials commonly used for the manufacturing of geosynthetics

| Type of Material                                 | Abbrev. |
|--|---------|
| Polypropylene (polymer)                          | PP      |
| Polyester (polyethylene terephthalate) (polymer) | PET     |
| Polyvinyl chloride (polymer)                     | PVC     |
| Polyamide (polymer)                              | PA      |
| Polystyrene (polymer)                            | PS      |
| Polyethylene (polymer):                          |         |
| Low-Density Polyethylene                         | LDPE    |
| Very-Low-Density Polyethylene                    | VLDPE   |
| Linear Low-Density Polyethylene                  | LLDPE   |
| Medium Density Polyethylene                      | MDPE    |
| High-Density Polyethylene                        | HDPE    |
| Chlorinated Polyethylene                         | CPE     |
| Chlorosulfonated Polyethylene                    | CSPE    |
| In addition to many other materials              | ---     |

### TYPES OF GEOSYNTHETICS

The most common geosynthetics are geotextiles, geotextile-related products (GTP) as geogrids, geonets, geomembranes, geocomposites, etc. in addition to many other types which are used in contact with soil, rock and/or any other civil engineering-related material as an integral part of man-made projects, structures or systems [3]. And they are briefly described below.

#### Geotextile

It is a planar, permeable, polymeric textile product in the form of a flexible sheet.

Currently available geotextiles are classified into four main categories based on the manufacturing process as woven, nonwoven, knitted, and stitched geotextiles [1,4,5].

As shown in Fig. 1, Woven geotextiles are produced by interlacing, usually at the right angles, two or more sets of yarns (made of one or several fibers) or other elements using a conventional weaving process with a weaving loom.

Nonwoven geotextiles like in Fig. 2, are produced from directionally or randomly oriented fibers into a loose web by bonding with partial melting, needle punching, or chemical binding agents (glue, rubber, latex, cellulose derivative, etc.).

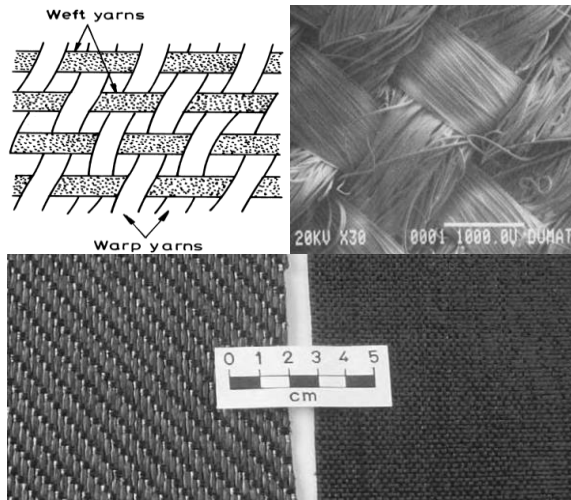


Fig. 1 Typical Woven Geotextile [6,7]

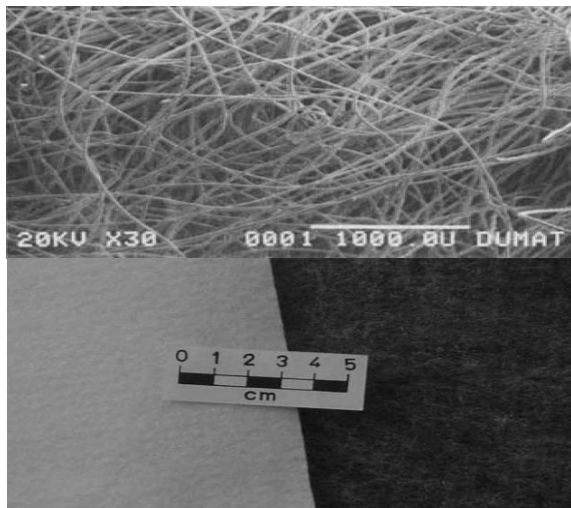


Fig. 2 Typical Nonwoven Geotextile [6,7]

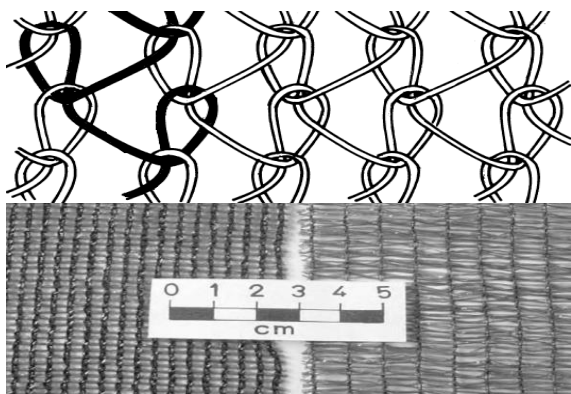


Fig. 3 Typical Knitted Geotextile [6,7]

Knitted geotextiles are produced by interlocking one or more yarns (or any other elements) together with a knitting machine, instead of a weaving loom, see Fig. 3.

Stitched geotextiles are one type of geotextile in which fibers or yarns or both are interlocked/bonded by stitching or sewing.

### Geogrid

It is a planer, polymeric product consisting of a mesh or net-like. Where a regular open network of intersecting tensile-resistant elements, called ribs, integrally connected at the junction. The ribs can be linked by bonding, interlacing, or extrusion. So, the resulting geogrids are respectively called bonded geogrids (Fig. 4), woven geogrids (Fig. 5) and extruded geogrids [8,9].

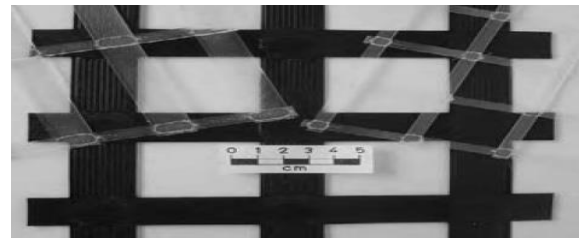


Fig. 4 Typical Bonded Geogrid [7]

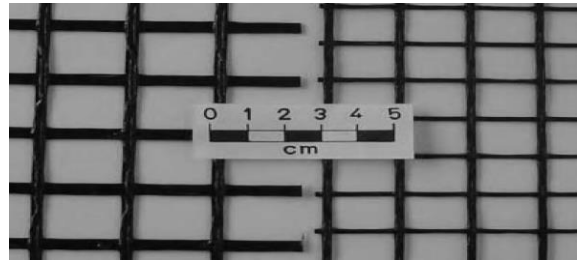


Fig. 5 Typical Woven Geogrid [7]

The extruded geogrids are classified into two categories based on the direction of stretching during their manufacture process as uniaxial extruding geogrids and biaxial extruding geogrids [10].

As shown in Fig. 6, Extruded uniaxial geogrids produced by the longitudinal stretching of a regularly punched polymer sheet, therefore it possesses a much higher tensile strength in the longitudinal direction than the tensile strength in the transverse direction.

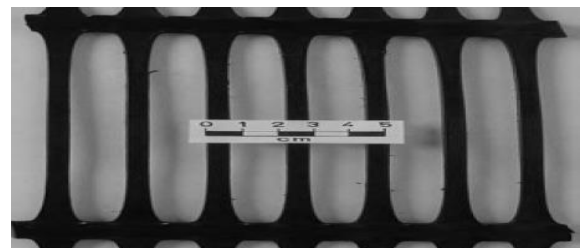


Fig. 6 Typical Extruded Uniaxial Geogrid [7]

Extruded biaxial geogrids produced by stretching in both the longitudinal and transverse directions of a regularly punched polymer sheet, therefore it possesses equal tensile strength in both directions longitudinal and transverse, see Fig. 7.

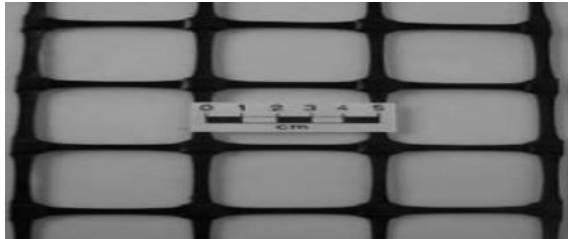


Fig. 7 Typical Extruded Biaxial Geogrid [7]

### Geonet

As Fig. 8 shows, it is a planer, polymeric product consisting of a regular dense network of integrally connected parallel sets of ribs overlaying similar sets at various angles. At first glance, geonets appear similar to geogrids, however, geonets are different from geogrids, not mainly in the materials or their configuration only but also in their functions to perform the in-plane drainage of liquids or gases [11].

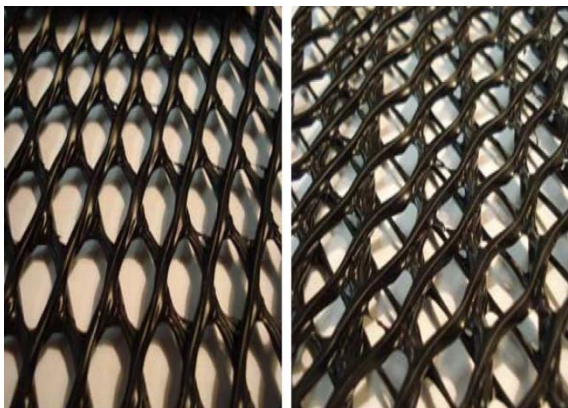


Fig. 8 Typical Geonet [11]

### Geomembrane

It is a planer, relatively impermeable, synthetic sheet manufactured from materials of low permeability to control fluid migration in a project as a barrier or liner, see Fig. 9.



Fig. 9 Typical Geomembrane [7]

The material may be polymeric or asphaltic or a combination thereof. The term barrier applies when the geomembrane is used inside an earth mass while the term liner is usually reserved for cases where the geomembrane is used as an interface or a surface revetment.

### Geocomposite

It is a term applied to the product that is assembled or manufactured in laminated or composite form from two or more material, of which one at least is geosynthetic, which, in combination performs a specific function(s) more effectively than when used separately, as illustrated in Fig. 10 [12].

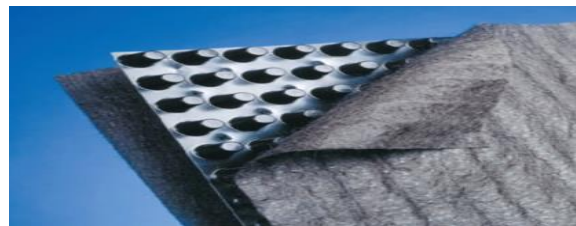


Fig. 10 Typical Geocomposite [13]

### Geocell

Fig. 11 shows a three-dimensional, permeable, polymeric honeycomb or web structure, assembled from geogrids and special bodkins couplings in triangular or square cells or produced using strips of needle-punched Polyester or solid High-Density Poly Ethylene (HDPE) known as geocell.



Fig. 11 Typical Geocell [14]

### Geomesh

It is a geosynthetic or geo-natural generally with planer woven structure having large pore sizes, which vary from several millimeters to several centimeters for use in mainly erosion control works, see Fig. 12.



Fig. 12 Typical Geomesh [7]

# Geomat

As Fig. 13 shows, it is a three-dimensional, permeable, polymeric structure made of coarse and rigid filaments bonded at their junctions used to reinforce roots of vegetation such as grass and small plants and extend the erosion control limits of vegetation for permanent installation.

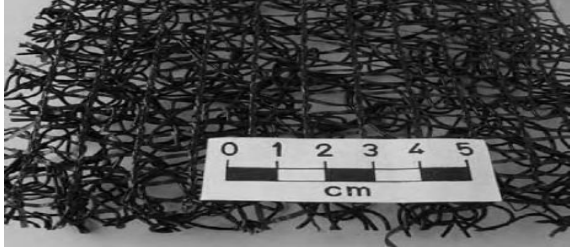


Fig. 13 Typical Geomat [7]

## Geostrip

It is a polymeric material in the form of a strip with different width illustrated in Fig. 14.

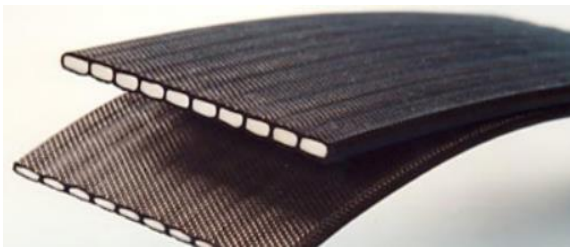
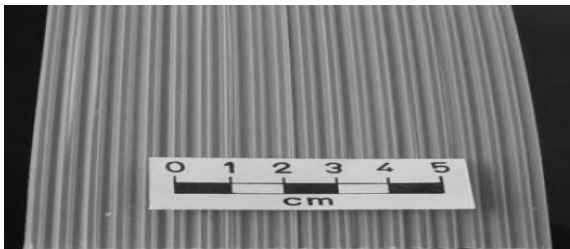


Fig. 14 Typical Geostrip [15]

## Geospacer

It is a three-dimensional polymeric molded structure consisting of cuspidated or corrugated plates with large void spaces, see Fig. 15.



**Fig. 15** Typical Geospacer [7]

## Geopipe

As shown in Fig. 16, It is a plastic pipe (smooth or corrugated with or without perforations) placed beneath the ground surface and subsequently backfilled.



Fig. 16 Typical Geopipe [7]

## Geofoam

It is a polymeric material manufactured by the application of the polymer in semi-liquid form through the use of a foaming agent to have a lightweight material in slab or block form with high void content for use as a lightweight fill, thermal insulators, and drainage channels. Samples are shown in Fig. 17.

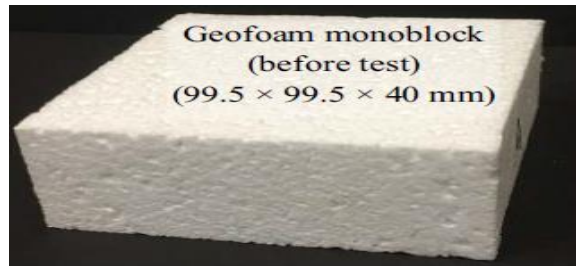


Fig. 17 Typical Geofoam [16]






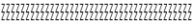

For convenience in making drawings or diagrams of geosynthetic applications with clarity, Geosynthetic products can be represented by abbreviations and/or graphical symbols as recommended by the International Geosynthetics Society (IGS) described in table 2.

Table 2 Abbreviations and graphical symbols of geosynthetic products

[illegible]



Table 2 Continued

|     |  |   |
|-----|--|---|
| GST | Geostrip                                     |  |
| GSP | Geospacer                                    |  |
| GBL | Geoblanket                                   |  |
| GBA | Geobar                                       |  |
| GEC | Surficial<br>geosynthetic<br>erosion control |  |
| GEK | Electrokinetic<br>geosynthetic               |  |
| GMT | Geomattress                                  |  |

Note: as recommended by the International Geosynthetics Society (IGS) [17].

## FUNCTIONS OF GEOSYNTHETICS

Geosynthetic products have numerous application areas in civil engineering. It could be applied for construction of transportation infrastructures e.g. highways, railroads, airports, and ports., water resources management infrastructures e.g. dams, canals, surface and subsurface drainage systems., environmental protection infrastructures e.g. sanitary landfills, coastal erosion control measures., slopes stabilization e.g. natural slopes, embankments stabilization, retaining walls., and/or many other application areas. That is because of geosynthetics usually expected to serve more than one function during its performance life [12,18,19].

The selection of a specific geosynthetic for any field application is highly governed by the function(s) to be performed by the geosynthetic in that specific application. Reinforcement, Separation, Filtration, Drainage, Fluid barrier, and/or Protection are the basic geosynthetic functions when it used in contact with soil, rock and/or any other civil engineering-related material [10,12,18]. Reinforcement for walls and steep slopes in addition to base reinforcement functions using mono-directional and three-dimensional geogrids, woven and nonwoven geotextiles and geocomposites have been achieved and utilized in many projects mainly because of their ability to improve the mechanical performances of the soil adding tensile strength, improve the bearing capacity, reduce the settlements and the formation of holes and ruts.

Separation function is performed when the geosynthetic has the ability to prevent intermixing of adjacent dissimilar soils and/or fill materials during construction and over a projected service lifetime of the application under consideration.

In some applications, a geosynthetic layer is needed as a localized stress reduction layer to prevent or reduce local damage to a geotechnical system. Therefore, a geosynthetic, placed between two materials, performs the protection function as it alleviates or distributes stresses and strains transmitted to the material to be protected against any damage.

Geocells perform the confinement function significantly by preventing the lateral movements of the soil volumes confined inside. In the meanwhile, separation could be achieved using geotextiles and geocomposites which prevent the contamination between two different soils or materials with different granulometry. In addition to that preventing mechanical damage to structures and materials as a protection function is a direct result of using nonwoven geotextiles, geonets, and geocomposites.

A geosynthetic may function as a filter (performing the filtration function) that allows for adequate fluid flow with limited migration of soil particles across its plane over a projected service lifetime of the application under consideration. In the meanwhile, if a geosynthetic allows for adequate fluid flow with limited migration of soil particles within its plane from surrounding soil mass to various outlets over a projected service lifetime of the application under consideration, it is said to perform the drainage function. On the other hand, if a geosynthetic act like an almost impermeable membrane to prevent the migration of liquids or gases over a projected service lifetime of the application under consideration, it is said to perform the fluid barrier function.

Because of their structure geonets and geocomposites can be used to collect and transport rain waters, groundwaters, and other fluids or gas so usually, they are used to perform the drainage function. On the other hand, filtration function could be performed using geotextile and geocomposites because they retain the soil subject to hydrodynamic forces and allow the passage of fluids [10,12]. Furthermore, geomembranes and geocomposites prevent or limit the migration of fluids. So, engineers use these products for their waterproofing function. But in the case of erosion control applications, it is preferable to utilize geomats and geocells which prevent the detachment and transport of the soil caused by meteoric events and allow the vegetation growth. The coming few paragraphs will discuss the functions of reinforcement and separation that can be performed by some commercially available types of Geosynthetics.

## Reinforcement

A geosynthetic performs the reinforcement function by improving the mechanical properties of a soil mass as a result of its inclusion. When soil and geosynthetic reinforcement are combined, a composite material, 'reinforced soil', possessing high compressive and tensile strength (and similar, in principle, to the reinforced concrete) is produced. In fact, any geosynthetic applied as reinforcement has the main task of resisting applied stress or preventing inadmissible deformations in geotechnical structures. [1] In this process, and as shown in Fig. 18 the



geosynthetic act as a tensioned member (a structural element that is subjected to axial tensile forces.) coupled to the soil/fill material by friction, adhesion, interlocking, containment or confinement and thus maintains the stability of the soil mass [12].

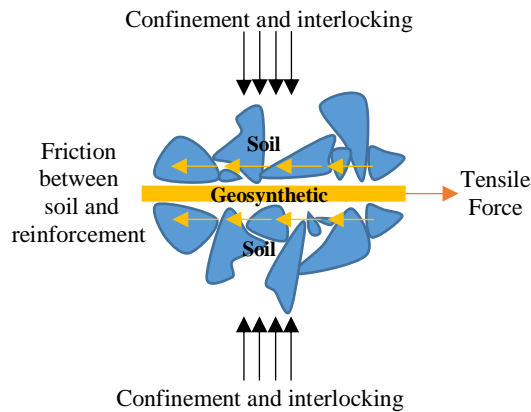


Fig. 18 Basic mechanism in the reinforcement function

Different concepts have been developed to define the basic mechanism of reinforced soils. The effect of inclusion of relatively inextensible reinforcements (such as metals having a high modulus of deformation) in the soil can be explained using either an induced stresses concept [20] (Schlosser and Vidal, 1969) or an induced deformations concept [21] (Bassett and Last, 1978). According to the induced stresses concept, the tensile strength of the reinforcements and friction at soil-reinforcement interfaces give an apparent cohesion to the reinforced soil system. The induced deformations concept considers that the tensile reinforcements involve anisotropic restraint of the soil deformations [2,18].

The behavior of the soil reinforced with extensible reinforcements such as geosynthetics does not fall within these concepts, see Fig. 19. And the difference, between the influences of inextensible and extensible reinforcements, is significant in terms of load-settlement behavior of the reinforced soil system. The soil reinforced with extensible reinforcement (termed ply-soil by McGown and Andrawes (1977) [22]) has greater extensibility and smaller losses of post-peak strength compared to soil alone or even soil reinforced with inextensible reinforcement (termed reinforced earth by Vidal (1969)). [4,23]

However, some similarity between ply-soil and reinforced earth exists in that they inhibit the development of internal tensile strains in the soil and develop tensile stress. Fluet (1988) subdivided the reinforcement function into the following two categories [24]:

1. A tensile member, which supports a planar load, see Fig. 20.

2. A tensioned member, which supports not only a planar load but also a normal load, see Fig. 21.

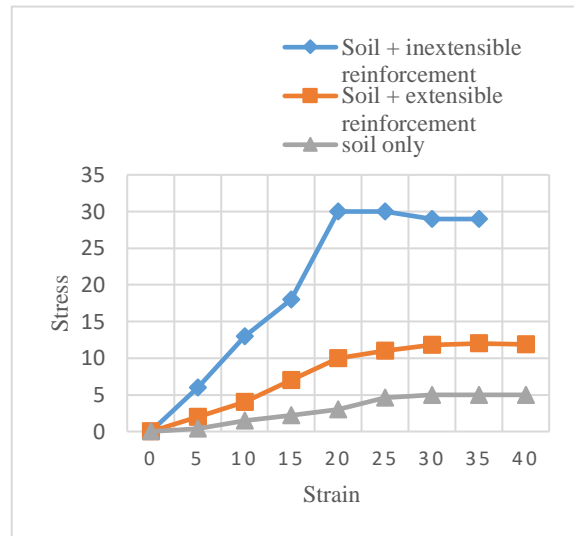


Fig. 19 Stress-Strain relationship for soil only and reinforced soils

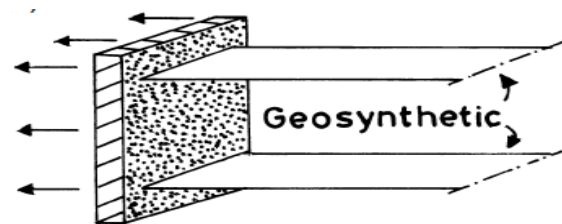


Fig. 20 Reinforcement function as a tensile member [24]

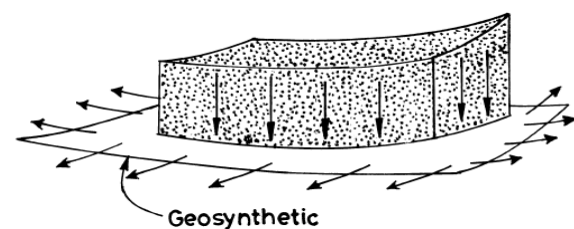


Fig. 21 Reinforcement function as a tensioned member [24]

Jewell (1996) considered not two but three mechanisms for soil reinforcement [2], because when the geosynthetic works as a tensile member it might be due to two different mechanisms: shear and anchorage. Therefore, the three reinforcing mechanisms, concerned simply with the types of load that is supported by the geosynthetic, are:

1. Anchorage also called pullout: The geosynthetic supports a planar load due to its pullout from the soil.

2. Shear, also called sliding: The geosynthetic supports a planar load due to slide of the soil over it.
3. Membrane: The geosynthetic supports both planar and normal load when placed on a deformable soil.

### Separation

In many cases, there is a bad need for separation between two soils or between soil and any other material. The pavement is a clear example since there are deferent layers of aggregate to be separated from each other, as shown in Fig. 22 (subgrade, subbase, base and surface courses) in addition not to permit the loosening of one layer into another [10,18].

And because of the contamination of aggregate base material with the underlying soft subgrade soil is one of the major causes of roadways constructed over soft foundations failure, the geosynthetic is placed between the two different particle-size distributions layers (dissimilar materials) basically for maintaining the functionality and integrity of the two layers which is illustrated in Fig. 23 [18,25].

This contamination occurs because of two main reasons, the first is the penetration of the base aggregate into the weak subgrade soil due to localized bearing capacity failure under wheel-load induced stresses and the second reason is the intrusion of the fine-grained subgrade soils into the base aggregate because of pumping or subgrade weakening due to excess pore water pressure. This results in inadequate structural support due to reduced shear strength and decreased hydraulic conductivity in addition to a reduced base layer thickness, leading to premature failure of the roadway [12,25].

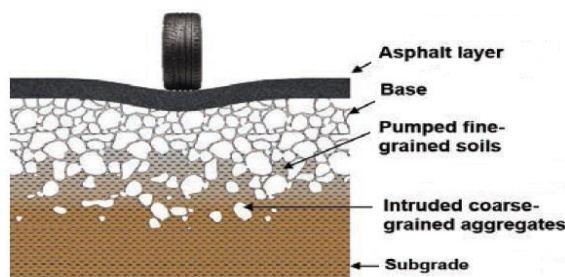


Fig. 22 Roadway designed without geosynthetic

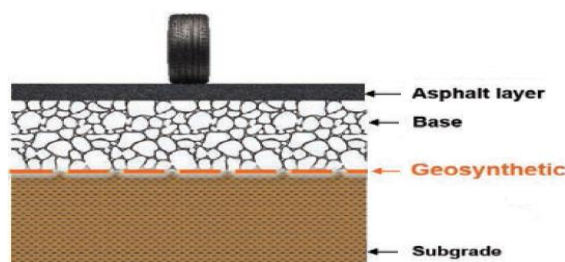


Fig. 23 Roadway designed with geosynthetic

### CONCLUSIONS

From this review it can be concluded that the usage of geotextiles, geotextile-related products (GTP) and the other types of geosynthetics for ground improvement is technically viable and cost-effective solution for soils which are weak in strength in order to make them more suitable for construction because reinforcement is the main function which all types of geosynthetics provide.

The usage of various types of geosynthetics have been tested and its use has been proven in the recent past years for a variety of infrastructure projects e.g. highways, airfields, ports, railways, dams, slope stabilization, tunneling, and other infrastructures facilities. Considering that the selection of a specific geosynthetic is highly governed by the functions to be performed in that specific application.

Ground improvement using geosynthetics has been proved not only to enhance infrastructure quality, performance, and durability but also reduce the infrastructure life-cycle cost, construction and maintenance durations in addition to amounts of natural recourse used which leads to reducing the environmental impacts of constructing and maintaining these projects.

These types of geosynthetics have been used worldwide for reinforcement, separation, filtration, drainage, fluid barrier, and/or protection with a variety of soils e.g. loose sand, silts, clays, and weak rocks. But still, a geosynthetic which suits for routine application, perhaps not available. For future development, it is believed that the characterization of new types of geosynthetics and understanding of soil-geosynthetic interface behavior under different kinds of tests should be explored.

### ACKNOWLEDGMENTS

Thanks to Japan International Cooperation Agency (JICA), African Business Education Initiative for collaboration with International Environment Conservation Lab, Graduate School of Bioresources, Mie University, School of Civil Engineering and Surveying, University of Southern Queensland, Australia, Egyptian Airports Company (EAC) and Tsuchiya TSCO Co., Ltd. for the opportunity which they gave me to proceed in this research.

### REFERENCES

- [1] Hossain M.B., Hossain M.Z., and Sakai T., Interaction Properties of Geosynthetic with Different Backfill Soils. *International Journal of Geosciences*, 3, 2012, pp.1033-1039
- [2] Jewell R.A., *Soil Reinforcement with Geotextiles*, CIRIA, Thomas Telford, 1996.
- [3] Hossain M.B., Hossain M.Z., and Sakai T.,

- Interface Behaviour of Basalt Geosynthetic with Sand Using Direct Shear Device. Proceedings of the 1st International Conference on Geotechnique, Construction Materials and Environment, Mie, 21-23 November 2011, pp.191-196.
- [4] Islam M.A., Hossain M.Z., Shiau J., and Rachmawati S. H., Characterization of Environment-Friendly Geotextiles Embedded in Soil Under Pullout Test. Proceedings of the 7<sup>th</sup> International Conference on Geotechnique, Construction Materials and Environment, Mie, 21-24 November 2017, pp.36-42.
- [5] Juran I. and Chen C.L., Soil-Geotextile Pull-Out Interaction Properties: Testing and Interpretation Transportation Research Record 1188, 1988, pp. 37- 47.
- [6] Koerner R. M., Designing with Geosynthetics, Fifth Edition, Pearson Prentice Hall, Upper Saddle River, New Jersey, 2005.
- [7] Shukla S.K. and Yin J.H., Fundamentals of Geosynthetic Engineering, Taylor and Francis Group, London, UK, 2006.
- [8] Moayed H., Kazemian S., Prasad A., and Huat B. B. K., Effect of Geogrid Reinforcement Location in Paved Road Improvement. Electronic Journal of Geotechnical Engineering, EJGE, Bund. P, Vol. 14, 2009, pp.1-11.
- [9] Lee M.S., Choi Y.S., and Prezzi M. Quality Assessment of Geogrids Used for Subgrade Treatment. Publication FHWA/IN/JTRP-2012/27. Joint Transportation Research Program, Indiana Department of Transportation and Purdue University, Indiana, 2012, pp. 1-28.
- [10] Hufenus R., Rueegger R., Banjac R., Mayor P., and Springman S.M., Brönnimann R., Full-Scale Field Tests on Geosynthetic Reinforced Unpaved Roads on Soft Subgrade. Geotextiles and Geomembranes, 24, 2006, pp.21-37.
- [11] Jeon H.Y., Short-Term Compressive Properties and Transmissivity of Geonets. Korean Textile Engineering Association, Vol. 51, Issue 2, 2014, pp. 96-100
- [12] Zornberg J. G., Functions and Applications of Geosynthetics in Roadways. Procedia Engineering, 189, 2017, pp.298-306.
- [13] Nicholson P. G., Soil Improvement and Ground Modification Methods, 2015
- [14] Mehrjardi G. T. and Motarjemi F., Interfacial Properties of Geocell-Reinforced Granular Soils, Geotextiles and Geomembranes, 46, 2018, pp. 384–395.
- [15] Luo Y., Leshchinsky D., Rimoldi P., Lugli G., and Xu C., Instrumented MSE Wall Reinforced with Polyester Straps, DCT 250, Delaware Center for Transportation, University of Delaware, Delaware, 2015.
- [16] Khan M. I. and Meguid M. A., Experimental Investigation of the Shear Behavior of EPS Geofabric, International Journal of Geosynthetics and Ground Engineering, 2018, pp. 4-12.
- [17] Recommended Descriptions of Geosynthetics Functions, Geosynthetics Terminology, and Graphical Symbols, International Geosynthetics Society, 5th Ed. 2009, pp. 1-31
- [18] Perkins S.W., and Ismeik M., A Synthesis and Evaluation of Geosynthetic-Reinforced Base Layers in Flexible Pavements: Part I. Geosynthetics International, Vol. 4, No. 6, 1997, pp.549-604.
- [19] Mishra B., A Study on Ground Improvement Techniques and Its Applications. International Journal of Innovative Research in Science, Engineering and Technology Vol. 5, Issue 1, 2016, pp.72-86.
- [20] Schlosser F., and Vidal H., Reinforced Earth. Bulletin de Liaison des Laboratoires des Ponts et Chaussées, No. 41, France, 1969.
- [21] Bassett R.H., and Last N.C., Reinforcing Earth Below Footings and Embankments. Proceedings of the Symposium on Earth Reinforcement, ASCE, New York, 1978, pp. 202–231.
- [22] McGown A. and Andrawes K.Z., The Influence of Nonwoven Fabric Inclusions on The Stress-Strain Behavior of a Soil Mass. Proceedings of the International Conference on the Use of Fabrics in Geotechnics, Paris, 1977, pp. 161–166.
- [23] Vidal H., The Principle of Reinforced Earth. Highway Research Record, No. 282, 1969, pp. 1–16.
- [24] Fluet, J.E., Geosynthetics for Soil Improvement: A General Report and Keynote Address. Proceedings of the Symposium on Geosynthetics for Soil Improvement, Tennessee, 1988, pp. 1–21.
- [25] Perkins S.W., and Ismeik M., A Synthesis and Evaluation of Geosynthetic-Reinforced Base Layers in Flexible Pavements: Part II. Geosynthetics International, Vol. 4, No. 6, 1997, pp.605-62

## STATICAL MODEL OF THE PIEZOELECTRIC SELF- ADJUSTINGGYROSCOPE-ACCELEROMETER

ArifPashayev, AnvarHazarkhanov, ToghrulKarimli,VasifNeymatov  
National Aviation Academy of Azerbaijan, Baku

### ABSTRACT

A critical analysis of gyroscopic accelerometers was carried out, the principle of operation of a piezoelectric self-regulating gyroscope accelerometer with advanced technical capabilities was stated, and static characteristics were obtained - depending on the difference in frequency and output voltage of the device on changes in the measured rotation angle of the aircraft. In particular, some existing devices are presented that are more modern inertial mass transducers, their shortcomings are revealed, the essence of the technical solution, design features and principle of operation of the developed new accelerometer gyroscope with piezoelectric sensitive elements. On the basis of an electrical connection scheme in which piezoelectric sensing elements are interconnected in a differential circuit and an input signal conversion sequence - the angle of rotation into an output signal voltage, mathematical equations are developed. On the basis of the composed equations, a computer model was constructed, after the simulation of which the necessary conclusions were drawn on the basis of the obtained oscillograms.

*Keywords:*gyro-accelerometer, inertial mass, resonant frequency, deflection angle, the output voltage

### INTRODUCTION

Inertial navigation system consisting of gyroscopes and accelerometers is intended for determination of coordinates, angles of inclination, stationary and non-stationary objects, and also the direction of movement and angular velocities of various moving elements and objects, submarine and surface ships, aircraft [1-4].

In case of termination or absence of communication between receivers and satellites in the objects on which the corresponding devices are installed, to solve the problems of navigation it is necessary to make correction of systematic errors.

### PROPOSED APPROACH

The value of angular parameters determined by gyroscopes and the values of angles (roll and pitch) measured by accelerometers are received on the element of comparison, the difference signal of which carries information both on the systematic and angular error and serves as the initial information base for auto-correction of corresponding parameters of movement.

The disadvantages of this device include the impossibility of measuring, as well as linear accelerations, the parallel functioning of gyroscopes and accelerometers, resulting in their hardware redundancy.

Fig. 1 shows the Vertical Gyro scheme, which is intended for measuring the course and the spatial position (roll and pitch) of movable objects.

Girovertikal [5], installed on the movable object, contains gyroscopes, accelerometers, the algorithm of the initial exhibition, the Kalman filter algorithm, the integrator, the device of comparison, the computation

of adjusted signals, the computation of angles of orientation (Pitch, roll, yaw). When starting the inertial-navigation system (INS) gyroscopes are not able to determine the initial angular positions. Based on the signals obtained from the accelerometers algorithm of the initial alignment, the initial values of angular positions are set.

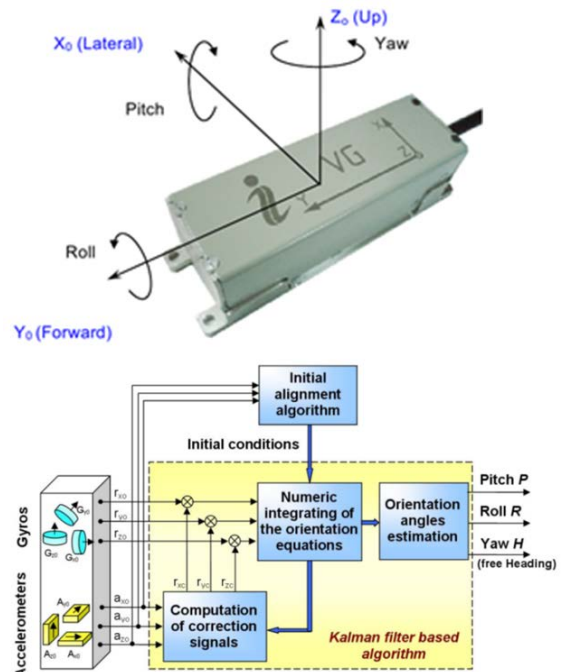


Fig. 1. Vertical Gyro

In the process of moving the objects or flight of the aircraft, the gyro drift is tuned by accelerometers. The Kalman filter is used to optimally evaluate the



INS errors and reduce the measurement noise.

However, this device is also characterized by excessive hardware redundancy of gyroscopes and accelerometers, as well as the need for additional time-consuming for accurate perpendicular adjustment of the axes of the sensitivity of gyroscopes and Accelerometers in a perpendicular plane.

As it is known, at present the fields of application of micromechanical gyroscopes (MG) are very broad. MG are electromechanical systems in which the energy of forced oscillations of inertial masses on the elastic resonator at the appearance of a portable angular velocity is converted into the energy of secondary oscillations. This conversion is carried out due to influence on the resonator of inertia forces of Coriolis at the rotation of a resonator with a portable angular speed.

By the type of movement of inertial masses in motion mode and sensitivity modes, there are MG LL-type (linear-linear), RR-type (rotate-rotate), LR-type. In the LL-types, inertial masses make progressive, in RR-types Rotary, LR (RL)-types of various combinations of progressive and rotary movements [6-8]. A significant drawback of these devices is the redundancy of structural elements, low sensitivity, a large measurement error and the need to introduce the initial angular data on the accelerometer signals.

There are electro-acoustic converters, microaccelerometer on surface acoustic waves [9]. One of the last such developments is presented in the work [10]. Gyroscope-Accelerometer containing the driver, made, for example, from quartz, niobate lithium or piezoceramics with carrying electrodes, as well as connected with each other a sensitive to deformation element and Inertial Mass.

Based on the analysis of the above shortcomings, modern inertial navigation systems can be formed the task of their improvement, providing the possibility of parallel measurement of various parameters (linear and angular acceleration, angular velocity, angular position), increase of linear acceleration measurement range, as well as correction (adjustment) of measured angles of inclination, by using gravitation force [11, 12].

The specificity of the technical solution of this problem lies in the fact that the acceleration-sensitive elements located on the most extreme opposite points of the movable object and fixing the values of linear and angular accelerations, as well as angular Velocity, at its deviation relative to the vertical plane are subjected to maximum displacement, overcoming the maximum differential line. At the same time inertial masses, being exposed to maximal displacement, by the elastic gasket with the greatest force influence on piezoelectric sensors).

To measure such movements proportional to linear and angular acceleration, it is enough to use four intakes of the upper side of two piezoelectric

sensors (two for linear, two for angular) and four inferences of the bottom side of two piezoelectric sensors (two for linear, two for angular), as well as two different (one for linear, one for angular) measuring channels, implemented in a single design, and, the linear acceleration meter has no restriction on Frequency, in static and dynamic modes depending on the angle of inclination under the influence of linear acceleration, and formed angular parameters adjust (tune) measured angles.

The main advantages of piezoelectric self-adjusted gyroscope-accelerometer can be considered: the possibility of simultaneous measurement of linear and angular acceleration, as well as angular velocity, significantly increases the efficiency of measurements, And the lack of frequency limit allows increasing the range of linear acceleration measurements.

1. Measured tilt angles are continuously independently adjusted (adjusted).

The developed device contains 1-case; 2-excitative element; 3- piezoelectric sensors; 4-inertial mass; 5-elastic gaskets; 6-limiter supporting the fixed positions of elements 3 and 4 (Fig. 2).

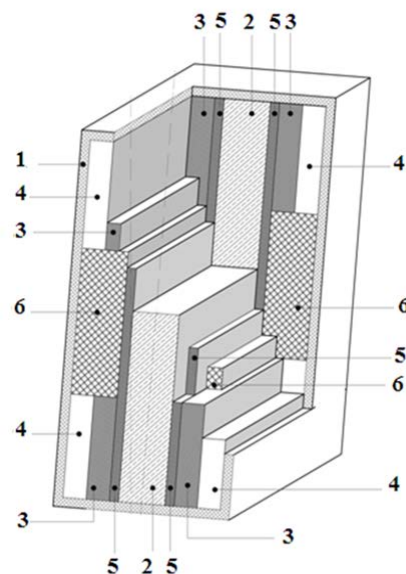


Fig. 2. Piezoelectric Self-adjusting Gyroscope-Accelerometer.

When moving the sensitivity axis from the position from  $OO'$  to the  $OO''$  position (from the vertical position to the right side) under the influence of linear and (or) angular acceleration, angular velocity of displacement of inertial masses 3 on the right side (top and bottom), Perceived by elastic gaskets 4, contribute to increase the clamping force on the third-party piezoelectric sensors, at the same time moving left side inertial masses (top and bottom part), perceived by elastic gaskets, contribute to reducing the clamping force on the left side piezoelectric sensors.

The location of inertial masses, gaskets, piezoelectric sensors at the endpoints excitative piezoelectric elements (drivers) contribute to the greatest linear movement of these points at the rotary motion of the device.

As a result, on the right side piezoelectric sensors (top-  $f_2$  and bottom-  $f'_2$ ) frequencies of oscillations increase, and on the left side of piezoelectric sensors (top -  $f_1$  and bottom-  $f'_1$ ) the frequency of oscillations decreases. Linear and (or) angular acceleration, angular velocity are determined by the difference of frequencies of piezoelectric sensors. By measuring linear accelerations, the initial (initial) angular positions are determined (adjusted) or the drift of the angular velocity channel is corrected.

In case of rest or uniform straight motion, when the object is in a horizontal position (the axis of sensitivity of  $OO'$  is in vertical position) frequency of oscillations in the left side and right-sided (top and bottom) piezoelectric sensors are equal, as inertial masses and elastic strips exert equal pressing forces on piezoelectric sensors, in the upper block of difference of linear accelerations 6 frequency difference is defined as  $a_1 \sim f_1 - f_2 = 0$ ; and in the bottom block of difference of linear accelerations 6 difference frequency is defined as  $a_2 \sim f'_1 - f'_2 = 0$ .

If the object is relative to the horizon at a certain angle  $\varphi$  (as in the case of rest or uniform motion) (corresponds to the position of  $OO''$ ), the influence of gravity left side inertial masses under their elastic gaskets pressed to the left piezoelectric sensors, and the right side inertial masses by means of elastic gaskets apart from the right side. Thus, in the upper and lower part of the left side sensitive piezoelectric the frequency of oscillations increases equally, whereas in the upper and lower part of the right side sensitive piezoelectric the frequency of oscillations decreases accordingly ( $f_1 = f'_1, f_2 = f'_2, f_1 > f_2$ ). In this case, (given the zero values of linear and angular acceleration, angular velocity, based on the condition of  $a_1 = a_2 = 0, \ddot{\varphi}_1 = \ddot{\varphi}_2 = 0, \dot{\varphi}_1 = \dot{\varphi}_2 = 0$  at the top and bottom points of the device the difference of frequencies on piezoelectric sensors changes proportionally to the angle of inclination ( $a_1 = a_2$  linear acceleration,  $\ddot{\varphi}_1 = \ddot{\varphi}_2$  angular acceleration,  $\dot{\varphi}_1 = \dot{\varphi}_2$  angular velocity).

In dynamic mode, when the object is subjected only to linear acceleration, the acceleration of the upper and lower points are equal, the difference of frequencies in the upper and lower units of the difference of linear accelerations 7 are defined as  $f_1 - f_2 \sim a_1, a_1 = a_2, (f_1 - f_2) - (f'_1 - f'_2) = 0$

(here  $a_1$  is determined by the upper block 6,  $a_2$  determined The bottom block 6) (Fig.3)

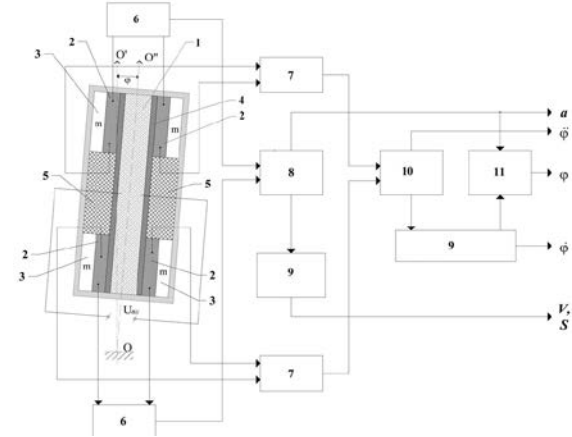


Fig. 3. Functional scheme of the measuring system of the piezoelectric self-adjusting gyroscope-accelerometer

In the dynamic mode, when the object is subjected only to angular acceleration, in the upper block of the difference of angular accelerations 7 the difference of frequencies on piezoelectric sensors is proportional to angular acceleration  $f_1 - f_2 \sim \ddot{\varphi}_1$ , and in the bottom block of the difference of angular acceleration 7, this difference is defined as  $f'_1 - f'_2 \sim \ddot{\varphi}_2$ . Given the unit of time that the top point is subjected to the maximum displacement relative to the bottom point, the acceleration of the top point will be greater, the difference of frequencies in the lower and upper 7 blocks are not equal to zero  $(f_1 - f_2) - (f'_1 - f'_2) \neq 0$ . In other words, the angular position of the movable object is determined by the change of the acceleration difference between the top and bottom points per unit of time:

$$\ddot{\varphi} \sim d \frac{(f_1 - f_2) - (f'_1 - f'_2)}{dt} \neq 0$$

Linear acceleration is formed in the block (computer) of formation of linear acceleration 8 on the basis of signal difference. This signal passing through Integrator 9 is converted into velocity and movement values (after double integration). angular acceleration and angular velocity are formed in the block (computer) of formation of angular acceleration 10 on the basis of the difference of signals,  $\ddot{\varphi}_1 - \ddot{\varphi}_2, \dot{\varphi}_1 - \dot{\varphi}_2$ . Further, this signal passing through the integrator is converted into angular velocity  $\dot{\varphi}$  and angle  $\varphi$  (after double integration). The angle correction block 11 is used to adjust (tune) the angle drift based on the difference of linear accelerations.



In the special case, when the measured angle can be adjusted (tuned) with high precision by means of a signal:  $\varphi \sim f_1 - f_2$ .

In dynamic mode, when the object is subjected to linear and angular accelerations, linear acceleration is formed by block 8, angular acceleration and angular velocity is formed by block 10. In this case in the upper block of the difference of angular accelerations 7 the difference of frequencies on piezoelectric sensors will be described as  $f_1 - f_2 \sim \ddot{\varphi}_1 + a_1$ , and in the bottom block of the difference of angular accelerations 7 as  $f'_1 - f'_2 \sim \ddot{\varphi}_2 + a_2$ , where:

$$a_1 \sim \frac{d(f_1 - f_2)}{dt} \neq 0,$$

$$a_2 \sim d \frac{(f'_1 - f'_2)}{dt} \neq 0,$$

$$\ddot{\varphi} \sim d \frac{(f_1 - f_2) - (f'_1 - f'_2)}{dt} \neq 0$$

An arrangement of the bottom part of sensitive piezoelectric in the center of gravity of the investigated object, the difference of frequencies in the bottom block of the difference of angular accelerations are defined in the form  $f'_1 - f'_2 \sim a_2$ , where  $\ddot{\varphi}_2 = 0$ .

Taking into consideration the wide scope of application of gyroscope-accelerometer with high technical characteristics, we continue to study the developed device for determination of dynamic characteristics by means of modeling in MatlabSimulink Software Environment.

Thus, based on the principle of operation of the device research of the static characteristic for each measured parameter is needed.

Fig. 4 illustrates the functional scheme of conversion of "turn angle of the movable object-output voltage of the scheme", and Fig. 5 illustrates the electrical circuit of the connection of piezoelectric sensitive elements is presented.



Fig. 4. Functional scheme of conversion "turn angle of the movable object-output voltage of the scheme"

The main formula showing the dependence of frequency change on the resonant frequency by force is the expression:

$$f_1 = f_0 \left( 1 - \frac{\nu}{Y_{33}^E S} \Delta F \right)$$

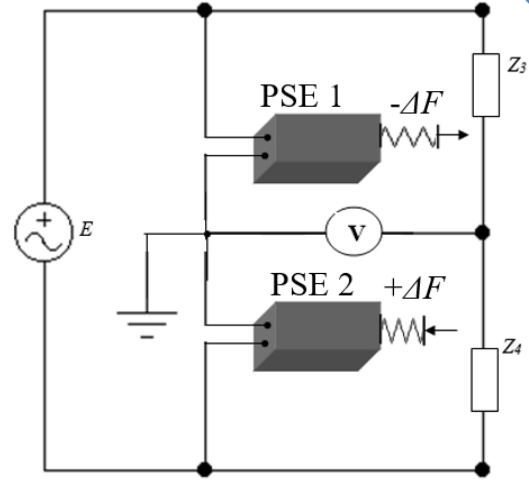


Fig. 5. The electrical circuit of connection of piezoelectric sensitive elements (PSE)

Where  $\alpha$ -resonant frequency;  $E$ -Jung's module;  $S$ -section of the surface on which the force acts;  $\nu$ -Poisson coefficient;  $\alpha$ -the turn angle of the movable object;  $\Delta F$ -Change of the exerted force;  $\Delta f$ -Frequency difference relative to the resonant frequency;  $\Delta Z(j\omega)$ -Change the value of the complex resistance;  $U(\Delta f)$ -voltage of electric output of the vibration and acceleration sensor;  $K_{\Delta F\omega}$ -coefficient of conversion "turn angle -power";  $K_{\omega\Delta z}$ -coefficient of conversion "power-frequency";  $K_{\Delta F\omega}$ -coefficient of conversion "frequency-resistance";  $K_{\Delta ZU}$ -coefficient of conversion "resistance-tension".

Thus, a mathematical relationship is given by:

$$U(\Delta f) = F(\alpha)$$

## SOLVING THE PROBLEM

According to the theory of measurement of parameters of mechanical motion on the basis of [13-15] work of the researched piezoelectric gyro-accelerometer it is possible to say, that the shift of frequency from the resonant value of frequency under influence of force will be determined by the formula:

$$f = f_0 \left( 1 - \frac{\nu}{Y_{33}^E S} \Delta F \right). \quad (1)$$

This will result in an expression we define the dependence of change of resistance of  $\Delta Z(j\omega)$ -on the difference of frequencies  $\Delta f$ , we define with the help

of a bridge scheme of connection piezoelectric sensitive elements (PSE) which is presented on fig. 1.

Hence the expression:

$$\Delta f = \frac{\nu \omega_0}{2\pi Y_{33}^E S} \Delta F \quad (2)$$

It is known that for the non-loaded piezoelectric converter is:  $\Delta F = 0$ ;  $\Delta Z = 0$ ;  $Z_{0P} = R_{0P}$ ; the resonance frequency will be determined by:

$$\omega_0 = \frac{1}{\sqrt{L_{0P} C_{0P}}}, \quad (3)$$

Where:  $L_{0P}, C_{0P}$  - inductance and capacity. To find a dependency  $\Delta Z(j\omega) = f(\Delta f)$ , it is advisable to use a known formula [16,17]:

$$Z_P = R_{0P} \sqrt{1 + Q^2 \left( n - \frac{1}{n} \right)^2}. \quad (4)$$

Where:  $Q = \omega_0 L / R_{0P}$  - the quality of the scheme of substitution of piezoelectric sensitive elements (PSE);  $n = \omega / \omega_0$  - Relative frequency change.

According to initial conditions  $Z_0 = R_{0P}$ :

$$\Delta Z = R_{0P} \left[ 1 - \sqrt{1 + Q^2 \left( n - \frac{1}{n} \right)^2} \right], \quad (5)$$

and also, taking into account the expression for the relative value of the frequency, composed on the basis of equations (1) and (2)

$$n = \frac{f}{f_0} = \frac{\omega}{\omega_0} = \left( 1 - \frac{\nu}{Y_{33}^E S} \Delta F \right), \quad (6)$$

after the mathematical transformation we get:

$$Z = R_{0P} \sqrt{1 + Q^2 \left( \frac{\nu \Delta F}{Y_{33}^E S} \right)^2 \cdot \left( \frac{Y_{33}^E S}{Y_{33}^E S - \nu \Delta F} + 1 \right)^2}. \quad (7)$$

If we consider the resulting expression (7) if we consider in the expression (5) we will obtain the final expression for Dependencies  $\Delta Z(j\omega) = f(\Delta f)$ :

$$\Delta Z = R_{0P} \left[ 1 - \sqrt{1 + Q^2 \left( \frac{\nu \Delta F}{Y_{33}^E S} \right)^2 \cdot \left( \frac{Y_{33}^E S}{Y_{33}^E S - \nu \Delta F} + 1 \right)^2} \right] \quad (8)$$

Expression of the voltage of the electric output of vibration and acceleration sensor  $U(\Delta f)$ :

$$U = \frac{1}{2} E \frac{\Delta Z}{R_0},$$

$$U = \frac{1}{2} E \left[ 1 - \sqrt{1 + Q^2 \left( \frac{\nu \Delta F}{Y_{33}^E S} \right)^2 \cdot \left( \frac{Y_{33}^E S}{Y_{33}^E S - \nu \Delta F} + 1 \right)^2} \right] \quad (9)$$

Equation (9) is a static characteristic of the device in question, defining the dependence  $U = f(\Delta F)$ .

According to the principle of the device is the force acting on the sensitive elements, more precisely, the gravity of the inertia mass (Figure 3, Position 3):

$$\Delta F = mg - mg \cos(\alpha) = mg(1 - \cos(\alpha))$$

Thus, we get the expression for the static characteristic of the piezoelectric self-adjusting gyro-accelerometer, working in the mode of measuring the turn angle of the object:

$$U = \frac{1}{2} E \left[ 1 - \sqrt{1 + Q^2 \left( \frac{vmg(1 - \cos(\alpha))}{Y_{33}^E S} \right)^2 \cdot \left( \frac{Y_{33}^E S + Y_{33}^E S}{Y_{33}^E S - vmg(1 - \cos(\alpha))} - \frac{vmg(1 - \cos(\alpha))}{Y_{33}^E S - vmg(1 - \cos(\alpha))} \right)^2} \right], \quad (10)$$

$$\omega_0 = \frac{1,58}{c} \sqrt{\frac{Y_{33}^E}{\rho}}, \quad \Delta f = \frac{\nu \omega_0}{2\pi Y_{33}^E S} \Delta F,$$

$$n = \frac{f}{f_0} = \frac{\omega}{\omega_0} = \left( 1 - \frac{\nu}{Y_{33}^E S} \Delta F \right)$$

In Fig. 6,7 the oscillograms obtained after the simulation of the computer model, constructed on the basis of equation (10) in the environment of MATLAB are presented.

We choose Piezoceramics PZT-8 with dimensions:  $a=0,01m$ ;  $b=0,002m$ ;  $c=0,005m$ (the same dimensions for inertial mass), physical and technical parameters, which according to [18]:  $\rho_M=7800\text{ kg/m}^3$ ;  $\rho=7720\text{ kg/m}^3$ ;  $Q=60$ ;  $Y_{33}^E=5.3 \cdot 10^9\text{ Pa}$ ;  $\nu=0.35$ . The supply voltage of the device is selected  $E=24V$ . The numerical results are obtained:  $L_m=41,14\text{ Hn}$ ;  $C_m=8,476e-15F$ ;  $R_m=131,10m$ ;  $f_p=26980\text{ Hz}$ ;  $\alpha=0-90^\circ$ ;  $U=0-0.18\text{ V}$ .

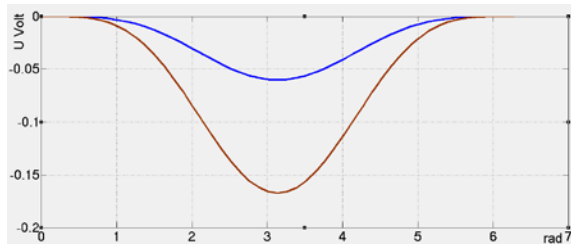


Fig. 6. The oscillograms obtained after the simulation of the computer model :  $U = f(\alpha)$

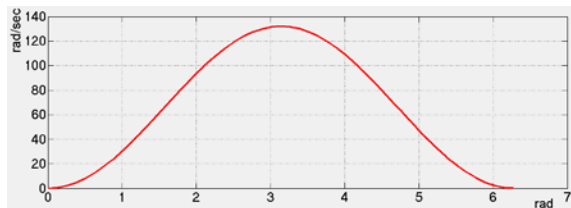


Fig. 7. The oscillograms obtained after the simulation of the computer model :  $\omega = f(\alpha)$

The simulation of measurements was performed when the turn angle of the object changed in the interval  $(0-180^\circ)$ . The main purpose of the choice of such interval was that it was possible to verify the return of the Electric Bridge scheme to the original state. As it can be seen from the obtained characteristics, the output voltage of the device has proportional dependence on the change of the turn angle of the object, as the laws of change of both signals are similar. Due to the large value of Jung's module of the chosen piezoceramics, the output voltage is quite small. This requires the use of a voltage amplifier with a sufficiently large gain.

## CONCLUSION

In this way, the following basic conclusions can be drawn: the proposed constructive solution of the piezoelectric accelerometer-gyroscope allows you to design the device, with relatively smaller mass-size indicators and relatively high sensitivity, due to the use of small materials and the use of piezoelectric converters as sensitive elements; To ensure a proportional change in the output voltage of the

device depending on the measured angle of the piezoelectric sensitive elements must be connected in a consistent-differential scheme; in the range of angular turn measurements of  $0-90^\circ$ , the output signal changes in frequency in the range of  $0-140\text{ Hz}$ , deviation from the resonance frequency is  $0.08\%$ .

## REFERENCES

- [1] David L. Churchill. Inertial measurement system with a self-correction: Patent US 8,010,308 B1 Int. Cl.: G01C 25/00 (2006.01), G06F 19/00 (2011.01). Aug. 30, 2011, p.20.
- [2] Christian Domingues. Challenges for integrating high performance Inertial Measurement Unit (IMU). IP-Embedded System Conference & Exhibition. France, Grenoble: 2013, p.27.
- [3] Honeywell. Micro Inertial Reference System. Product Description. March 2012, p.33.
- [4] Boeing 747-8. Maintenance Training Manual. Navigation1. Boeing Company, 2016. p.393.
- [5] [www.inertiallabs.com](http://www.inertiallabs.com). Vertical Gyro
- [6] Raspopov V.Y. Micromechanical Devices: Training manual. Moscow.: Mashinostroyeniye, 2007, p.400.
- [7] Matveyev V.V. Mathematical models of LL-type micromechanical gyroscopes//Izvestia Tula. Technical Sciences. 2012. Vol. 12, p1, pp. 205-213
- [8] Matveyev V.V., Pogorelov M.G. Analysis of errors of micromechanical gyroscopes by the method of variations of Allan//Izvestia Tula. Technical Sciences, 2015, vol. 3, pp. 123-135.
- [9] Petrov P.N. Acoustics. Electro-acoustic Converters. SpB.: SpBGUAP, 2003, p.80.
- [10] Ansev G.V., Bogoyavlenskiy S.V., Sapojnikov G.A. Gyroscope-Accelerometer. Patent: RU 2381510, 10.02.2010, p.9.
- [11] Qurbanov T.B., Karimli T.I., Karimli V.I. Piezoelectric self-adjusting gyroscope-accelerometer. Patent Application Publication Nea20140107. Azerbaijan, Baku, 20.06.2017.
- [12] Hazarkhanov A.T., Karimli T.I., Neymatov V.A., Karimli V.I. Operating modes of piezoelectric self-adjusting gyroscope-accelerometer//HERALD of the Azerbaijan Engineering Academy. Vol 10, №1. Baku, 2018, pp.7-15.
- [13] Piezoelectric sensors. <https://students-library.com/library/read/48485-pezelektriceskie-datciki>
- [14] Steinem C., Janshoff A. Piezoelectric Sensors. Berlin: Springer-Verlag. 2007, p.484.
- [15] Regtien P., Dertien E. Sensors for mechatronics. 2nd edition. Elsevier, 2018, p.380.
- [16] Resonant properties RLS-chains [http://elar.urfu.ru/bitstream/10995/45632/1/978-5-7996-0831-6\\_2013.pdf](http://elar.urfu.ru/bitstream/10995/45632/1/978-5-7996-0831-6_2013.pdf)
- [17] Thomas R.E., Rosa A.J., Toussaint G.J. The

Analysis and Design of Linear Circuits. 8th edition.  
Hoboken: Wiley, 2016. p.912 .  
[18] Performance of PZT-8 versus PZTT4

piezoceramic materials in ultrasonic transducers  
[sciencedirect.com/science/article/pii/S18753892](https://www.sciencedirect.com/science/article/pii/S1875389216304175)  
16304175

# PROPORTION AND PROPERTY SPECIFICATIONS AND STRENGTH BEHAVIOR OF MORTAR USING WOOD ASH AS PARTIAL REPLACEMENT OF LIME

Robert Michael Tampus<sup>1</sup>, Janine R. Lardizabal<sup>1</sup>, Dennise Linoel M. Acena<sup>1</sup>, Michaela Angelica M. Uy<sup>1</sup>, and  
Kenneth Vance R. Arcenal<sup>1</sup>

<sup>1</sup>Mapúa University Young Innovators Research Center, Mapúa University, Philippines

## ABSTRACT

Wood ash is produced by the incineration of wood and wood products; thus, it is a waste product generated from various sources such as household fireplaces, agricultural activities, or manufacturing plants. By reusing wood ash wastes as lime-replacement additives, the resulting lime mortar would become a more practical building material. This study utilized varying proportions of wood ash (25%, 50%, 75%, and 100%) as partial replacement of lime in manufacturing Type N mortars through the provision of proportion and property specifications that adhere to known industry standards. The proportion specification for Type N Mortar was modified as one part Type 1 Portland cement, one part Type S Hydraulic Lime and/or wood ash, and six parts of coarse sand aggregate (1:1:6). The air content, initial and final setting times, 7- and 28-day compressive strengths of the mixed mortars were shown to be heavily affected by the presence of wood ash within the mortar mix. Furthermore, the use of wood ash as a partial replacement of lime caused an increase in air content and a decrease in setting times of the mortar mix. Mortars with 100% replacement of lime with wood ash showed the highest compressive strength for both 7- and 28-day tests. Therefore, the incorporation of wood ash as a lime replacement was determined to be a viable option for Type N mortars.

*Keywords: Air content, Compressive strength, Mortar, Setting time, Wood ash*

## INTRODUCTION

In construction, mortars are building materials that fill the gaps between blocks of a structure; these materials are typically composed of fine aggregates, a binder, and water. According to [1], different types of mortars can be classified according to the type of binding material: earth mortar, cement-sand mortar, gypsum mortar, and lime mortar. Lime mortar is comparable to other mortar types except for its breathability; this provides flexibility and strength to the structure. In terms of plasticity and workability, a lime mortar can quickly adhere to blocks as it can accommodate changes in moisture within the masonry construction. It also reduces the potential damage caused by the accumulation of salt from the weathering of the blocks [2].

Lime mortar serves as sacrificial layers to preserve structures from excessive exposure against mechanical and environmental influence. These mortars are cohesive and adhesive to the structure. It is necessary to choose the right materials, formulation, and preserving conditions of the mortar to meet functional and aesthetic requirements and fulfill the principles of compatibility, while maintaining the structure's integrity and durability [3]. Lime is a weaker element than stone, brick, or cob, which enables it to resist cracking from a certain amount of movement. When the lime mortar is applied, it is

much easier and simpler to repair [4].

The trend of using lime mortar was certainly altered due to the difficulties experienced regarding the application of lime mortars, such as long setting and hardening times, especially at a very high relative humidity as well as weak mechanical properties [5]. Lime mortar is not water-resistant, but it allows the wall block to breathe. However, segregation of the original material and the lime might occur as the mortar dries and hardens. The resulting mortar will be seriously weakened, with a poorly-formed pore structure leaving it very susceptible to frost damage and deterioration.

This study aimed to fill the gap of previous studies, wherein most literature focused on testing the strength behavior of the mortars using various lime-replacement additives such as slags and ashes. Several studies about wood ash [6] – [8] discovered the potential use of wood ash in several applications such as mortar and concrete production, and forest road construction, but most studies lacked focus on the importance of the proportion and property specifications of wood ash in manufacturing lime mortars.

This study was generally aimed to utilize wood ash as a partial replacement of lime in manufacturing mortars for masonry construction. Specifically, this study addressed the following objectives: (1) to determine the proportion specification of the mortars

with 0%, 25%, 50%, 75%, and 100% replacement of lime by wood ash conforming to the requirements of American Society for Testing and Materials (ASTM) C270, and (2) to compare the property specifications of the mixed mortars in terms of setting time, air content, and compressive strength.

This study had contributed to the development of the masonry construction industry. Wood ash is produced by the incineration of wood and wood products; thus, it is a waste product generated from various sources such as household fireplaces, agricultural activities, or manufacturing plants. By reusing wood ash wastes as lime-replacement additives, the resulting mortar would become a more practical building material. Also, the process of lime production involves the emission of large quantities of carbon dioxide which contributes to global climate change [9]. The partial replacement of lime with wood ash wastes could lessen environmental problems associated with manufacturing mortars, such as air, water and soil pollution. Thus, this study can significantly contribute to achieving sustainable development by reducing the ecological footprint of disposing wood ash and manufacturing lime mortars.

This study is limited only to the concept of specifying the proportion, properties, and compressive strength of the mortars mixed with wood ash as partial replacement of lime. However, this study does not indicate the specific type of wood burnt to generate the wood ashes. The researchers used the American Society for Testing and Materials (ASTM) C270 [10] as the standard specification for mortars used in unit masonry. In conformity with the American Association of State Highway and Transportation Officials (AASHTO) standard specifications, different mortar testing equipment were used such as a flow table to measure air content (AASHTO T 137-04) [11]; a Gillmore needle to record setting time (AASHTO T 154-06) [12]; and a Universal Testing Machine (UTM) to measure the compressive strength of the mortars (AASHTO T 106M/T 106-07) [13]. However, as a consequence of time constraints, the preliminary tests for the compressive strength of the mortars were conducted only after 7 and 28 days of curing.

## METHODOLOGY

In conformity to both American Society for Testing and Materials (ASTM) and American Association of State Highway and Transportation Officials (AASHTO) standard specifications, this section presents the different procedures and equipment used in the study.

### Material Sourcing and Preparation

The mortars were composed of the following components: lime, cement binder, aggregate, and

water. Type S Hydrated Lime conforming to ASTM C-207 was used in the study. Type 1 Portland cement was also used as the binder as specified in ASTM C-150. A well-graded coarse sand aggregate (4.75 mm in diameter) was used. Wood ashes were utilized as partial lime-replacement additives; the ashes were collected from household fireplaces. Water was prepared and kept free from oils, acids, alkalis, salts, organic materials, or other substances that were deleterious to mortar.

### Preparation of Lime Mortar with Varying Proportions of Wood Ash as Lime Replacement

In accordance with ASTM C270 [10], several batches of Type N Mortar were made with a mortar mix ratio of one-part Portland cement, one-part hydrated lime, and six-parts sand (1:1:6). However, the hydrated lime was partially replaced with varying proportions (25%, 50%, 75%, and 100%) of wood ash. Proportion specifications of the mortars were determined depending on the sample weight required by each test. A reference mortar containing 0% wood ash and 100% lime was also evaluated.

### Determination of Air Content (AASHTO T 137-04)

Mortars were mixed using 350 g of cement to 1400 g of 20-30 standard sand and sufficient water to give a flow of  $87.5 \pm 7.5\%$ . A layer of mortar about 25 mm in thickness was placed in the mold and tamped 20 times to ensure uniform filling of the mold. An approximately 20-mm layer of mortar was added to the top of the mold and tamped again. The mortar was separated from the mold and then placed on a planar surface. Prior to determining the air content of the mortar, its flow rate was calculated using Equation (1):

$$R_{flow} = \frac{D_{mold}}{D_{mortar}} \times 100\% \quad (1)$$

where  $R_{flow}$  is the flow rate (in percent),  $D_{mold}$  is the diameter of mold (in mm), and  $D_{mortar}$  is the diameter of mortar (in mm).

The flow table and mold used were conforming to the requirements of AASHTO 152M/M 152 [11]. The flow table should be clean and dry, so any water from around the edge of the mold was removed. After the mixing operation, the flow table was dropped 10 times and the flow rate was recorded as the resulting increase in average diameter of the mortar mass. Several trial mortars with varying percentages of water were made until a desired flow of  $87.5 \pm 7.5\%$  was obtained.

Air content of the mortar was determined using the mass of 400 mL of mortar and the physical



properties of its components used, as shown in Eq. (2) and Eq. (3):

$$D = \frac{W_1 + W_2 + V_w}{\frac{W_1}{S_1} + \frac{W_2}{S_2} + V_w} \quad (2)$$

$$A = 100 - \frac{W_m}{4D} \quad (3)$$

where D is the density of air-free mortar (in g/cm<sup>3</sup>), W<sub>1</sub> is the mass of cement (in grams), W<sub>2</sub> is the mass of sand (in grams), W<sub>m</sub> is the mass of 400 mL of mortar (in grams), V<sub>w</sub> is the millilitres-gram of water used (in mL-g), S<sub>1</sub> is the density of cement (in g/cm<sup>3</sup>), S<sub>2</sub> is the density of standard sand (2.65 g/cm<sup>3</sup>), and A is the volume percent of entrained air (%). The air content was compared to the ratio of mixing water to the binding materials; this ratio is calculated using the volume of mixing water (in mL) divided by the total mass of binding materials (cement ± lime ± wood ash) used (in grams).

#### Determination of Setting Time (AASHTO T 154-06)

Mortars were batched using 650 g of cement with the percentage of mixing water required for normal consistency. To mold the mortars, a pat was made with a flat top by drawing the trowel from the outer edge toward the center. The prepared mortars were tested to meet the required consistency using the needles of the Gillmore apparatus. The time required to obtain the stipulated penetration of the Gillmore needle is the time of setting. The needles were held in a vertical position and applied lightly to the surface of the pat. The initial set was acquired when the initial Gillmore needle touched the surface of the pat without appreciable indentation. The Gillmore initial time of setting was determined when the elapsed time, in minutes, between the time of contact of mortar and the time when the mortar acquired its initial set. The final set was also acquired when the final Gillmore needle touched the surface of the pat without appreciable indentation. The Gillmore final time of setting was determined when the elapsed time, in minutes, between the time of contact of mortar and the time when the mortar acquired its final set.

#### Compressive Strength Testing (AASHTO T 106M/T 106-07)

A compressive strength test was conducted on the mortars that were proportioned, mixed and conditioned in the testing laboratory. Two-inch mortar cubes were used as compressive strength specimens cast in non-absorbent molds and cured in

a moist room and conditioned in the laboratory meeting the requirements of ASTM C511. One-third of the mold was filled with mortar and pressed 25 times with the help of a tampering rod; this procedure of filling and tapping was repeated thrice. A trowel was used to smoothen the upper surface and was kept open air for one day. Afterwards, the cube specimens were cured in a lime bath for 7 and 28 days. To determine the compressive strength of the mortar, the Universal Testing Machine (UTM) was used by applying incremental load to the cube specimen. As the load was applied on the cube, it developed cracks at a certain load. The application of load was stopped when the cube has been crushed. The compressive strength of the mortar was calculated using Eq. (4):

$$f_m = \frac{P}{A} \quad (4)$$

where f<sub>m</sub> is the compressive strength of the mortar (in MPa), P is the total maximum load (in N), and A is the area of loaded surface (in mm<sup>2</sup>). The compressive strength was reported as an average of two trials.

## RESULTS AND DISCUSSION

Five (5) sets of mortars with Type 1 Portland cement, well-graded coarse sand, and gradual replacement of Type S Hydraulic Lime with wood ash were tested to determine the appropriate proportion specification with the right volume of mixing water as well as its mechanical properties such as setting time, air content, and compressive strength.

#### Proportion Specifications of Lime Mortar with Varying Proportions of Wood Ash as Lime Replacement

Modified from ASTM C270 [10], several batches of Type N Mortar were made with a mortar mix ratio of one-part Type 1 Portland cement, one-part Type S Hydrated Lime and/or wood ash, and six-parts coarse sand aggregate (1:1:6). As presented in Table 1, a total sample weight of 800 grams was used in every batch of mortars in the determination of air content and compressive strength conforming to AASHTO T 137-04 [11] and AASHTO T 106M/T 106-0 [13], respectively. Furthermore, a total sample weight of 650 grams was sampled in every batch of mortars for the determination of initial and final setting times in accordance with AASHTO T 154-06 [12], as shown in Table 2. Upon determination of the proportion specifications, Mortar A is the reference mortar having no partial replacement of lime with wood ash.

Table 1 Mortar Mix Proportions for the Determination of Air Content and Compressive Strength Test (AASHTO T 137-04; AASHTO T 106M/T 106-07)

| Sample:<br>800 g | Cement : Lime : Sand = 1:1:6 |             |                 |             |
|------------------|------------------------------|-------------|-----------------|-------------|
|                  | Cement<br>(g)                | Lime<br>(g) | Wood<br>Ash (g) | Sand<br>(g) |
| Mortar A         | 100                          | 100         | 0               | 600         |
| Mortar B         | 100                          | 75          | 25              | 600         |
| Mortar C         | 100                          | 50          | 50              | 600         |
| Mortar D         | 100                          | 25          | 75              | 600         |
| Mortar E         | 100                          | 0           | 100             | 600         |

Table 2 Mortar Mix Proportions for the Determination of Initial and Final Setting Times (AASHTO T 154-06)

| Sample:<br>650 g | Cement : Lime : Sand = 1:1:6 |             |                 |             |
|------------------|------------------------------|-------------|-----------------|-------------|
|                  | Cement<br>(g)                | Lime<br>(g) | Wood<br>Ash (g) | Sand<br>(g) |
| Mortar A         | 81.25                        | 81.25       | 0               | 487.5       |
| Mortar B         | 81.25                        | 60.94       | 20.31           | 487.5       |
| Mortar C         | 81.25                        | 40.625      | 40.625          | 487.5       |
| Mortar D         | 81.25                        | 20.31       | 60.94           | 487.5       |
| Mortar E         | 81.25                        | 0           | 81.25           | 487.5       |

### Air Content

The flow was first determined to identify the ratio of mixing water to the binding materials with the resulting flow of 87.5  $\pm$  7.5%, as stated in AASHTO T 137-04 [11]. In particular, the mixed mortars got the desired flow between 0.65 to 0.80 ratio of mixing water to the binding materials when the volume of mixing water was varied from 130 – 170 mL. The ASTM C91/ C91M-18 property specification provided an allowable range of 8 - 21% for the air content of Type N mortars [14]. All of the set of mortars have an average air content within the standard range; however, Mortar E with 0% lime and 100% wood ash had the highest air content of 14.58%, as shown in Table 3 and graphically presented in Figure 1. Furthermore, the air content of Mortar E will be at its maximum at 0.65 ratio of mixing water to the binding materials. The air content of mixed mortars generally increased as the amount of wood ash increased. A possible explanation was that the angularity of the wood ash particles as described by [6], allocated larger pore spaces between sand aggregates and binding materials.

Table 3 Experimental Results of Air Content

| MW/<br>BM | Air Content of Mortars (%) |       |       |       |       |
|-----------|----------------------------|-------|-------|-------|-------|
|           | A                          | B     | C     | D     | E     |
| 0.65      | 15.89                      | 17.28 | 18.54 | 19.46 | 20.11 |
| 0.70      | 13.15                      | 15.76 | 16.12 | 15.46 | 16.62 |
| 0.75      | 10.98                      | 14.00 | 13.86 | 12.60 | 14.04 |
| 0.80      | 9.52                       | 12.51 | 11.06 | 10.85 | 12.17 |
| 0.80      | 8.16                       | 9.58  | 8.98  | 9.15  | 9.95  |

Note: MW/BM means ratio of mixing water to binding materials (cement  $\pm$  lime  $\pm$  wood ash).

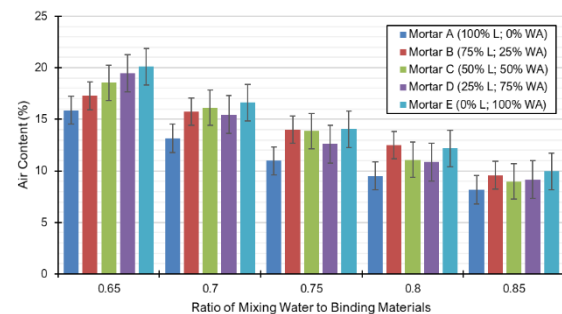


Fig. 1 Relationship between air content and water-to-binding material ratio of the mixed mortars. Error bars represent standard errors. L means lime and WA means wood ash.

### Setting Time

The AASHTO T-154 [12] limits the initial time of setting on samples testing between 100 to 341 minutes. Basically, the mortar with time closest to 100 minutes is said to have the best initial setting time. As shown in Table 4 and Fig. 2, Mortar C with 50% lime and 50% wood ash has an average initial setting time closest to 100 minutes, having 108 minutes. On the other hand, Mortar A with 100% lime has the longest average of initial setting time. This is similar to the study of [5] which stated that lime mortar shows difficulties including slow setting and hardening times. Moreover, the AASHTO T-154 [12] also limits the final time of setting on samples testing between 239 and 561 minutes. Basically, the mortar with time closest to 239 minutes is said to have the best final setting time. Mortar B with 75% lime and 25% wood ash has an average final setting time closest to a minimum of 239 minutes, having 243 minutes, followed by mortar C which had the best initial setting time. On the other hand, Mortar A with 100% lime has the longest average of final setting time. The initial and final setting times of mixed mortars were drastically reduced when gradual replacement of lime by wood ash (25%, 50%, 75%, and 100%) was involved.

Table 4 Experimental Results of Setting Time

| Composition                 | Setting Time (mins) |       |
|-----------------------------|---------------------|-------|
|                             | Initial             | Final |
| Mortar A<br>(100% L; 0% WA) | 162                 | 348   |
| Mortar B<br>(75% L; 25% WA) | 114                 | 243   |
| Mortar C<br>(50% L; 50% WA) | 108                 | 246   |
| Mortar D<br>(25% L; 75% WA) | 123                 | 270   |
| Mortar E<br>(0% L; 100% WA) | 147                 | 321   |

Note: L means lime and WA means wood ash.

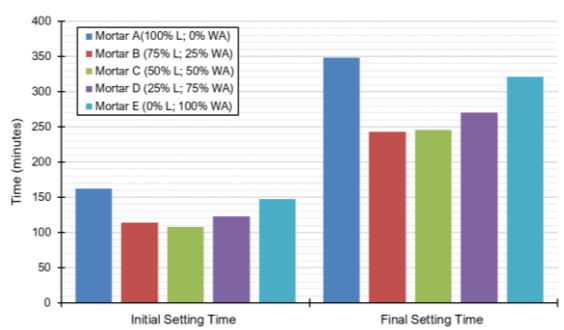


Fig. 2 Relationship between the Initial and Final Setting Times and Wood Ash/Lime Ratio. L means lime and WA means wood ash.

### Compressive Strength

When prepared and tested in accordance with ASTM C91/ C91M – 18 [14], the compressive strength of Type N mortars should be equal or greater than 3.4 MPa for 7-day test and 6.2 MPa for the 28-day test. As presented in Table 5 and Fig. 3, all of the mortars exhibited 7- and 28-day compressive strengths greater than the specified standards; however, Mortar A has a below standard 28-day compressive strength. Mortar E with 100% wood ash and 0% lime yielded the highest compressive strength for both day-tests. The 28-day compressive strength of mixed mortars was significantly enhanced when varying amounts of wood ash were incorporated. The improved 28-day compressive strengths could be attributed to wood ash as a pozzolanic material, similar to the findings of [15]. Mixed mortars with at least 25% partial replacement of lime with wood ash could possibly be sufficient in exhibiting pozzolanic reaction; however, it is notable that the amount of Type 1 Portland cement was kept constant across all mixed mortars.

Table 5 Experimental Results of Compressive Strength Test

| Composition                 | Compressive Strength (MPa) |        |
|-----------------------------|----------------------------|--------|
|                             | 7-day                      | 28-day |
| Mortar A<br>(100% L; 0% WA) | 4.625                      | 5.185  |
| Mortar B<br>(75% L; 25% WA) | 4.59                       | 7.095  |
| Mortar C<br>(50% L; 50% WA) | 4.5                        | 6.91   |
| Mortar D<br>(25% L; 75% WA) | 4.01                       | 6.54   |
| Mortar E<br>(0% L; 100% WA) | 4.935                      | 6.98   |

Note: L means lime and WA means wood ash.

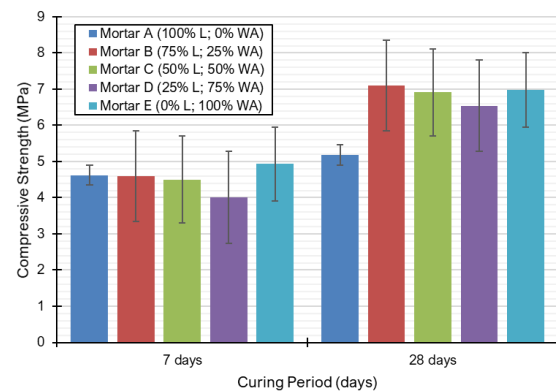


Fig. 3 Variation of Compressive Strength at 7 and 28 days curing period. Error bars represent standard errors. L means lime and WA means wood ash.

### CONCLUSIONS

This study aimed to utilize wood ash as a partial replacement of Type S Hydraulic Lime in manufacturing Type N mortars through the provision of proportion and property specifications that adhere to known industry standards such as American Society for Testing and Materials (ASTM) and American Association of State Highway and Transportation Officials (AASHTO). The air content, initial and final setting times, 7- and 28-day compressive strengths of the mixed mortars were shown to be heavily affected by the presence of wood ash within the mortar mix. Based on the results of this study, the following conclusions were made:

1. Modified from ASTM C270, the proportion specification for Type N Mortar is one part Type 1 Portland cement, one part Type S Hydraulic Lime and/or wood ash, and six parts of coarse sand aggregate (1:1:6). Furthermore, the ideal water-to-binding material ratio was 0.65, wherein

the mixed mortars typically exhibited higher air content.

2. Based on the proportion specification of the mortars with 0%, 25%, 50%, 75%, and 100% replacement of lime by wood ash, the following property specifications were most favorable:
  - a. The value of air content was highest when lime was completely replaced by 100% wood ash. As the amount of wood ash content increased, the air content significantly increased resulting from the angularity of wood ash particles.
  - b. The initial time of setting was fastest when lime was partially replaced by 50% wood ash, whereas the longest initial setting time was observed in the reference mortar. Gradual replacement of wood ash caused the mixed mortars to have significantly faster initial setting times as compared to the reference mortar.
  - c. The final time of setting was fastest when lime was replaced by 25% of wood ash. Gradual replacement of wood ash caused the mixed mortars to exhibit significantly faster final setting times as compared to the reference mortar.
  - d. Mortars with 100% replacement of lime with wood ash showed the highest compressive strength for both 7- and 28-day tests. Thus, the incorporation of wood ash as a lime replacement is a viable option for Type N mortars.

## ACKNOWLEDGMENTS

The authors would like to thank the Soil Mechanics and Material Testing Laboratory and the Universal Testing Machine Laboratory of Mapúa University for providing assistance during experimentation.

## REFERENCES

- [1] Dhir, R., De Brito, J., Lynn, C., and Silva, R., *Sustainable Construction Materials* Cambridge Woodhead Publishing, 2018, pp.139-195.
- [2] Ingham, J. P., *Geomaterials Under the Microscope a Colour Guide: Building Stone, Roofing Slate, Aggregate, Concrete, Mortar, Plaster, Bricks, Ceramics, and Bituminous Mixtures* United States, Academic Press, 2012, pp.7-20.
- [3] Veiga, M. D., Fragata, A., Velosa, A. L., Magalhães, A. C., and Margalha, G., *Lime-based Mortars: Viability for Use as Substitution Renders in Historical Buildings*, *International Journal of Architectural Heritage*, Vol. 4, Issue 2, 2010, pp 177-195.
- [4] Zhang, D., Zhao, J., Wang, D., Xu, C., Zhai, M., and Ma, X., *Comparative Study on the Properties of Three Hydraulic Lime Mortar Systems: Natural Hydraulic Lime Mortar, Cement-aerial Lime-based Mortar and Slag-aerial Lime-based Mortar*, *Construction and Building Materials*, Vol. 186, 2018, pp. 42-52.
- [5] Elert, K., Rodriguez-Navarro, C., Pardo, E. S., Hansen, E., and Cazalla, O., *Lime Mortars for the Conservation of Historic Buildings*, *Studies in Conservation*, Vol. 47, Issue 1, 2013, p. 62.
- [6] Ban, C. and Ramli, M., *The Implementation of Wood Waste Ash as a Partial Cement Replacement Material in the Production of Structural Grade Concrete and Mortar: An overview*, *Resources, Conservation and Recycling*, Vol. 55, Issue 7, 2011, pp. 669-685.
- [7] Ramos, T., Matos, A. M., and Sousa-Coutinho, J., *Mortar with Wood Waste Ash: Mechanical Strength Carbonation Resistance and ASR Expansion*, *Construction and Building Materials*, Vol. 49, 2013, pp. 343-351.
- [8] Oburger, E., Jäger, A., Pasch, A., Dellantonio, A., Stampfer, K., and Wenzel, W., *Environmental Impact Assessment of Wood Ash Utilization in Forest Road Construction and Maintenance — A Field Study*, *Science of the Total Environment*, Vol. 544, 2016, 711-721.
- [9] Gutierrez, A., Caneghem, J., Martinez, J., and Vandecasteele, C., *Evaluation of The Environmental Performance of Lime Production in Cuba*, *Journal of Cleaner Production*, Vol. 31, 2012, pp. 126-136.
- [10] ASTM C270, *Standard Specification for Mortar for Unit Masonry*, ASTM International West Conshohocken, PA, 2019.
- [11] AASHTO T 137- 04, *Air Content of Hydraulic Cement Mortar*, American Association of State Highway and Transportation Officials, Washington, D.C., 2018.
- [12] AASHTO T-154, *Standard Method of Test for Time of Setting of Hydraulic Cement Paste by Gillmore Needles*, American Association of State Highway and Transportation Officials, Washington, D.C., 2018.
- [13] AASHTO T-106, *Standard Method of Test for Compressive Strength of Hydraulic Cement Mortar (Using 50-mm or 2-in. Cube Specimens)*, American Association of State Highway and Transportation Officials, Washington, D.C., 2018.
- [14] ASTM C91 / C91M-18, *Standard specification for masonry cement*, ASTM International, West Conshohocken, PA, 2018.
- [15] Sebastian A., Manapurath, Balachandran, and Sebastian D., *Partial Replacement of Cement with Wood Ash*, *International Journal of Science Technology & Engineering*, Vol. 2, Issue 11, 2016, pp. 666-670.

# IMPACTS OF WEATHER VARIABLES ON URBAN WATER DEMAND AT MULTIPLE TEMPORAL SCALES

Chinnapan Makpiboon<sup>1</sup>, Adichai Pornprommin<sup>2</sup> and Surachai Lipiwattanakarn<sup>3</sup>

<sup>1,2,3</sup>Department of Water Resources Engineering, Faculty of Engineering, Kasetsart University, Thailand

## ABSTRACT

Population growth and urban development have contributed to increase in base urban water demand in a long-term temporal scale. However, if we consider a short-term temporal scale, weather variability is an important factor affecting daily, monthly, seasonal and annually water demands. This study examines the relationship between urban water demand in the Metropolitan Waterworks Authority (MWA) service area, including Bangkok, Nonthaburi and Samut Prakan provinces, and two weather variables; temperature and rainfall at various temporal scales. The growth of water demand was detrended and then normalized. The multiple linear regressions were used for analysis of impacts from weather variables to urban water demand. Temperature had a strong negative impact on the demand and the impacts were stronger for larger time scales. On the other hand, rainfall had a weak positive impact on the demand but also gave more impact for larger time scales. As climate changes will affect both temperature and rainfall, MWA should consider the weather variability for a better management of water production and distribution.

*Keywords: Urban Water Demand, Water Consumption, Multiple Temporal Scales, Weather Impact*

## INTRODUCTION

The global water demand for domestic uses is expected to increase significantly, especially in cities and countries with developing economic growth [14]. In 1900, the global population lived in urban areas just 13% and has been rising to 49% in 2005. As a prediction, the global population lives in urban areas will rise to 60% in 2030. [13]. Bangkok as Thailand capital city and its vicinity provinces (Nonthaburi and Samut Prakan provinces) are growing rapidly, the water demand provided by Metropolitan Waterworks Authority (MWA) has increased from 4.76 million cubic meters per day (MCM/day) in 2007 to 5.38 MCM/day in 2016. Understanding and forecasting the water demand is one of the challenging tasks for MWA.

Urban water demand is influenced by many variables based on whether it is analyzed on temporal or spatial bases. The common explanatory variables for temporal analysis are temperature, precipitation, wind speed, evaporation, water price, rate structure, income and population [4]. For weather related variables, temperature and precipitation are the most common ones. Impacts of climate and weather variables on urban water demand have been studied for nonlinear [7], linear [3] or a combination of both linear and nonlinear effects [11].

Urban water demand is also sensitive to time scale, especially seasonal time scale as pointed out by [4]. The temporal effects on urban water demand whether on daily, monthly, seasonally or annually time scales have not been explicitly studied especially

on large metropolitan water demand in the hot humid tropical climate. One of the models used for time series data analysis is time series linear regression model [1]

In this study, daily, monthly, seasonal and annually weather variables have been related to MWA water demand. We then analyzed the temporal effects with different time scales of these weather variables on the water demand.

## STUDY AREA AND DATA

MWA is a sole water utility agency providing potable water for Bangkok and its vicinity areas with more than 10 million population. MWA provides approximately 1,800 million cubic meters of potable water in 2018. Our study area is the MWA service area covering Bangkok, Nonthaburi and Samut

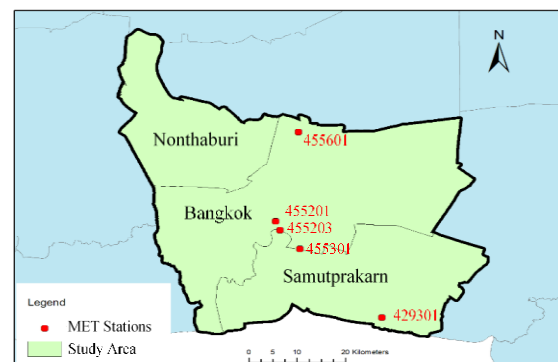


Fig. 1 Study area and weather stations

Table 1 Detailed Information of Urban Water Demand Temporal Scales Dataset

| Urban Water Demand Dataset | Daily                    | Monthly             | Seasonal                  |       |        |
|----------------------------|--------------------------|---------------------|---------------------------|-------|--------|
|                            |                          |                     | Summer                    | Rainy | Winter |
| Period                     | 1 Oct 2007 - 30 Sep 2017 | Oct 2007 - Sep 2017 | Winter 2007 – Summer 2017 |       |        |
| Number of Data             | 3,424 days*              | 116 months*         | 30 seasons*               |       |        |
| Water Demand               |                          |                     |                           |       |        |
| Max (MCM/Day)              | 4.30                     | 4.11                | 4.03                      | 3.90  | 3.80   |
| Min (MCM/Day)              | 3.04                     | 3.23                | 3.54                      | 3.42  | 3.32   |
| Average (MCM/Day)          | 3.67                     | 3.67                | 3.81                      | 3.68  | 3.58   |
| Temperature                |                          |                     |                           |       |        |
| Max ( °c)                  | 34.15                    | 31.90               | 31.10                     | 29.90 | 29.02  |
| Min ( °c)                  | 18.20                    | 25.12               | 28.72                     | 29.06 | 26.80  |
| Average ( °c)              | 29.17                    | 29.19               | 30.24                     | 29.47 | 28.05  |
| Rainfall                   |                          |                     |                           |       |        |
| Max (mm/day)               | 115.90                   | 17.65               | 5.89                      | 10.75 | 3.50   |
| Min (mm/day)               | 0.00                     | 0.00                | 0.72                      | 6.33  | 0.69   |
| Average (mm/day)           | 5.09                     | 5.16                | 2.81                      | 9.00  | 1.86   |

Note:\* exclude long holidays and during a 2011 mega flood (229 days)

Prakan provinces [6] MWA provides water demand dataset consisting of daily water discharge and monthly water demand. To obtain daily demand, we assumed daily water loss by subtracting monthly water discharge with water demand and averaging it for daily water loss. The monthly and seasonal water demand are then based on these daily data. Seasonal data are sum of the daily data during a range of seasons.

Weather dataset obtains from 5 Thai Meteorological Department (TMD) stations, namely Bangkok (455201), Khlong Toei Port (455203), Bangna (455301), Don Muang Airport (455601) and Samut Prakarn (429301). TMD provided daily temperature and rain data. According to TMD, Thailand weather can be divided into 3 seasons. Summer is between 16 February and 15 May, rainy season is from 16 May to 15 October, and winter is from 16 October to 15 February. The period of the data used in this study was between 1 October 2007 to 30 September 2017, totaling of 10 years.

According to the demand data, we found extremely low water demand during October 2011-January 2012 caused by a mega flood in 2011. We also found that during long holidays (more than 3 days) water demand was significantly lower than usual. Therefore, we did not include these unrepresentative demand data in our study. Detailed information of urban water demand temporal scales dataset is described in Table 1. Since our study is in the tropical zone, the daily temperature was between 18.20°C and 34.15°C, and the seasonal water demand and temperature did not vary greatly like those in the temperate zone. However, in the rainy season, the amount of rainfall could be 3-5 times higher than that in other seasons.

## METHODOLOGY

### Normalization

To investigate the impact of weather on water demand, we assumed that all other major variables except weather-related variables present in the water demand as a long-term time series trend. After removing this trend, we then can relate weather data to urban water demand. The time series model of urban water demand can be expressed as:

$$D_t = \alpha_0 + \sum_{j=1}^v \alpha_j t_j \quad (1)$$

where  $D_t$  is water demand at time  $t$ ,  $\alpha_0$  is the regression intercept and  $j$  is a polynomial term in the trend component,  $v$  is a polynomial order and  $\alpha_j$  is the trend coefficient. For our model, we used  $v$  as 1 for a linear trend component. We considered that all growth-related variables such as population, economics, and an urban growth are included in the trend. After the model is constructed with daily data, we removed this trend by subtracting it from water demand such that

$$\hat{D}_t = D_{obs,t} - \alpha_1 t \quad (2)$$

where  $\hat{D}_t$  is the detrended water demand at time  $t$ . We then tested the stationarity of  $\hat{D}$  by using an Augmented Dickey-Fuller (ADF) test [8]. The test is aimed for an unknown lag time autoregressive-moving average model. However, for this study, a k-lag autoregressive model, AR(k), is considered and can be given by the equation:



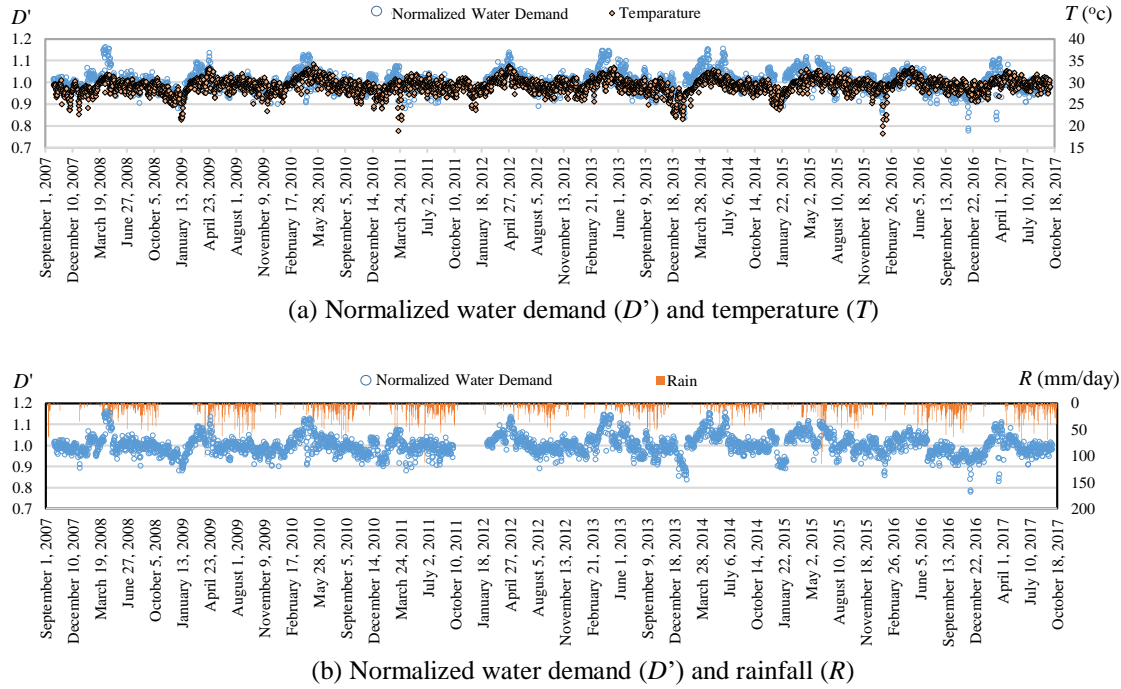


Fig. 2 Temporal changes of daily normalized water demand with (a) temperature and (b) rainfall

$$\Delta \hat{D}_t = \alpha \hat{D}_{t-1} + \sum_{j=1}^{k-1} \beta_j \Delta \hat{D}_{t-1} + e_t \quad (3)$$

where  $\Delta$  is the difference operator,  $e_t$  is a white noise sequence of random variables,  $\alpha$  and  $\beta_j$  are the coefficients. The null hypothesis of the unit root test is that the time series data has a unit root and is not stationary. If the null hypothesis is rejected then the time series data is stationary.

After proving for its stationarity, we normalized the detrended daily water demands by dividing them with  $\alpha_0$  from (1) to analyze the demands as a ratio. This would give an easy understanding on impact of weather variables to the water demand.

$$D'_t = \hat{D}_t / \alpha_0 \quad (4)$$

### Multiple Regression Analysis

A multiple regression is a simple linear regression extension used when we predict two or more the value of a variable. The variables we predict are called dependent variables or target variables. A linear relationship is assumed between two variables. Linear regression is a commonly used statistical analysis in water demand while nonlinear regression is used to various growth models [10]. Results in one variable can be predicted from the others [9].

After removing the long-term trend and normalizing the detrended data, the influences of weather-related variables on normalized water demand can be described by a multiple linear regression model which is based on the basis of relationship between water demand and its determinants. Our model can be expressed as:

$$D'_t = \beta_0 + \sum_{i=1}^n \beta_i x_{i,t} \quad (5)$$

where  $D'_t$  is the normalized water demand at time  $t$ ,  $\beta_0$  is the regression intercept and  $i$  is an index of  $i^{\text{th}}$  independent variable,  $n$  is the number of variables and  $x_{i,t}$  is a value of  $i^{\text{th}}$  independent variable at time  $t$ . Our independent variables are temperature ( $i = 1$ ) and rainfall ( $i = 2$ ).

## RESULTS AND DISCUSSION

### Normalized Water Demand

To find the urban growth trend of daily water demands, a simple time series model (1) was adopted. We found the relationship based on the start of our data (October 2011) to be

$$D_t = 3.3846 + 1.5696 \times 10^{-4} t \quad (6)$$

where  $\alpha_0 = 3.3846$  MCM/day and  $\alpha_1 = 1.5696 \times 10^{-4}$  MCM/day<sup>2</sup>. Thus, the yearly average growth of water demand of MWA for 2007-2017 was roughly 0.0573 MCM/year (+1.7%).

We removed this trend for a zero-slope adjustment by subtracting it from water demand to obtain the detrended water demand  $\hat{D}_t$  in (2). We then normalized  $\hat{D}_t$  by dividing it with  $\alpha_0$  in (4). Consequently, we have the normalized water demand  $D'_t$  that ranged between 0.8 to 1.2 due to temperature ( $T$ ) and rainfall ( $R$ ) as shown in Fig.2.

Table 2 Results of multivariable linear regression of the normalized water demand ( $D'$ ) to the average temperature ( $T$ ) and the rainfall ( $R$ ) in the daily, monthly and seasonally temporal scales.

| Normalized water demand | Coefficients             |                            |                        | t Stat  |         | P-value   |        |
|-------------------------|--------------------------|----------------------------|------------------------|---------|---------|-----------|--------|
|                         | $\beta_1$ for $T$ (1/°C) | $\beta_2$ for $R$ (day/mm) | $\beta_0$ as intercept | $T$     | $R$     | $T$       | $R$    |
| Daily                   | 0.0152                   | -0.00017                   | 0.5571                 | 40.5224 | -2.9464 | 1.23E-293 | 0.0032 |
| Monthly                 | 0.0187                   | -0.00189                   | 0.4656                 | 7.6667  | -2.8275 | 8.54E-12  | 0.0056 |
| Seasonal                | 0.0238                   | -0.00291                   | 0.3224                 | 8.6211  | -3.3784 | 3.09E-9   | 0.0022 |

Note:\*Significant at the 0.01 level

### Weather Variability Analysis

Impacts of weather variables, temperature and rainfall, were analyzed using a multiple linear regression in the following equation:

$$D'_t = \beta_0 + \beta_1 T_t + \beta_2 R_t \quad (7)$$

where  $T_t$  is temperature and  $R_t$  is rainfall.

Table 2 shows the results from the regression. The statistics in the table are composed of coefficients of the regression variables, t Stat and P-value. The coefficient values show how strong the impact of each variable on the normalized water demand. From the results, an increase in 1°C of the temperature caused an increase in 1.52%, 1.87% and 2.38% of the water demands in the cases of the daily, monthly and seasonal time scales, respectively. However, an increase in 10 mm/day of the rainfall caused a decrease in 0.17%, 1.89% and 2.91% of the water demands in the cases of the daily, monthly and seasonal time scales, respectively. In conclusion, temperature generates a higher demand while rainfall leads to a lower demand. Also, the time scale became larger, the impact was stronger.

We tested the significance of the independent variables, the temperature ( $T$ ) and the rainfall ( $R$ ) using t stat and P-value at the 0.01 significance level as shown in Table 2. The t stat values show how large the coefficients compare to the standard error. The larger value of t stat indicates the more significance of the variable. The P-value is the probability that the variables have no effect on the dependent, the normalized urban demand in this case.

For temperature, the T-stat value for daily is much higher than monthly and seasonal values, indicating that the model for daily tends to be more accurate. Also, the P-value for daily is significantly lower than those for monthly and seasonal, indicating the same message. The t Stat and P-value results show that rainfall is less significant than temperature. In addition, the daily, monthly and seasonal models with rainfall tend to have the same accuracy.

### Impact of Weather Variables on Demand

The results of multiple linear regression for daily, monthly and seasonal were compared with the datasets in Figs. 3, 4 and 5, respectively, showing the impact of temperature and rainfall on MWA water demand.

From Fig. 3, the normalized daily water demands ranged between 0.8 and 1.2 with the daily temperature between 21°C and 34°C. A clear trend between temperature and water demand can be seen. The line of rainfall at levels 2, 6 and 10 mm/day are overlapping line. Many previous research studies in the temperate climate have found the temperature and rainfall thresholds for urban water demand. For example, [2] show that residential water use for East Doncaster, Victoria, Australia is not affected by temperature changes at 15.3°C or below and at rainfall level of 4.8 mm or higher. For our study area in the tropical climate, however, we cannot find those thresholds. It is possible that our lowest temperature is still higher than the threshold value.

Fig. 4 shows monthly water demand related to temperature and rainfall. Rainfall line at levels 2, 6 and 10 mm/day show a slight difference. A similar tendency as the daily case that water demand increases with temperature and decrease with rainfall can be found. However, the range of temperature decreases to be between 26°C and 32°C due to monthly averaging.

Rainfall lines at levels 2, 6, and 10 mm/day show clearer differences in Fig 5a and 5b. Then, clearer impact on temperature and rainfall on water demand can be observed in the seasonal case in Fig. 5a. Also, in Fig. 5b where the data were divided according to seasons, it is clear that temperature and rainfall in each season are different. In summer, high water demand is due to high temperature while, in winter, low temperature causes low water demand. As the temperature in rainy season is moderate, water demand is low due to rainfall.

In Fig. 3 shows the amount of data, the data has a high frequency, but there is an unclear relationship with the weather. While Fig. 4 and 5 use the monthly and seasonal solutions, but clearly show the relationship of weather conditions and higher water demand.

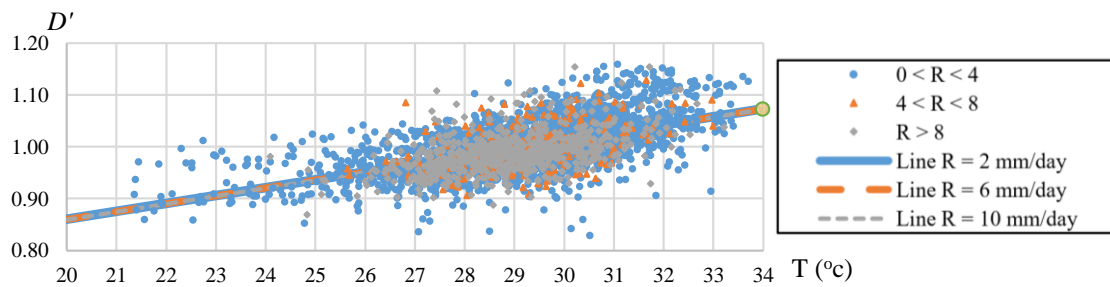


Fig. 3 Relationship between daily normalize urban water demand dataset, temperature and rainfall dataset during winter 2007 – summer 2017

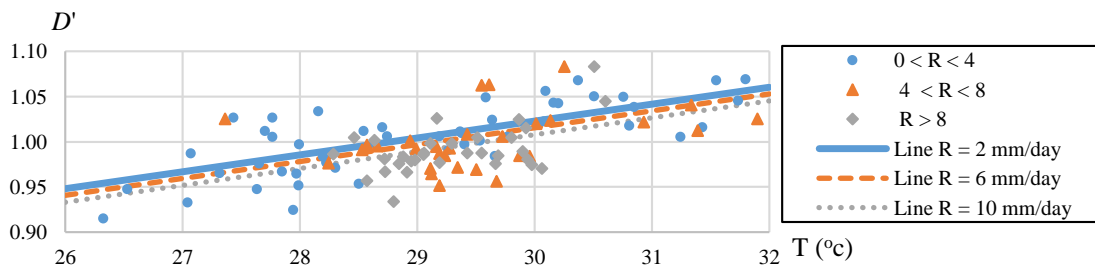


Fig. 4 Relationship between monthly normalize urban water demand dataset, temperature and rainfall dataset during winter 2007 – summer 2017 in the MWA service area

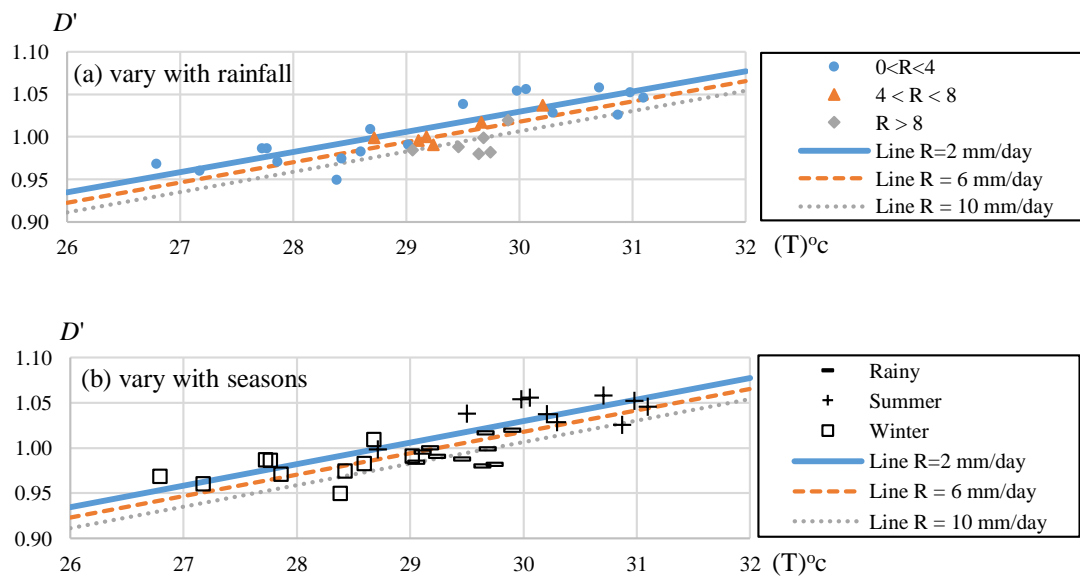


Fig. 5 Relationship between seasonal normalize urban water demand dataset, temperature and rainfall dataset during winter 2007 – summer 2017 (a) and show the amount of rainfall of each season. (b)

## CONCLUSIONS

The average temperature of the world is constantly rising. Thailand is also affected by global warming. Over the past 40 years, between 1970 – 2009, the average temperature in Thailand rose about

0.024 °C per years, especially in the metropolitan areas where the urban temperature is higher than other places due to a dome heat island effect [12]. This condition will increase urban water demand. Statistical analyzes of urban water demand of Bangkok, Nonthaburi and Samut Prakan provinces

showed that temperature and rainfall influence the urban water demand in the daily, monthly and seasonal time scale. While an increase in 1°C of the temperature caused an increase in 1.52%, 1.87% and 2.38% of the water demands in the cases of the daily, monthly and seasonal time scales, respectively, an increase in 10 mm/day of the rainfall caused a decrease in 0.17%, 1.89% and 2.91% of the water demands, respectively. Using t stat and P-value, temperature is a more significant variable than rainfall, especially in the daily time scale. Unlike in the temperate climate, we could not find the temperature and rainfall thresholds for urban water demand in our tropical climate study area. The weather effect to water demand with different scale levels will provide a clear result for evaluating the quantity requirements as well, depending on the purpose of short-term and long-term water demand planning. These weather factors can be accompanied with other urban growth factors, such as population density, immigration or expansion, type of urban land use, the network of transport routes and etc.

#### ACKNOWLEDGEMENTS

The authors would like to thank the Metropolitan Waterworks Authority (MWA) and the Thai Meteorological Department (TMD) for supporting the data used in this study.

#### REFERENCES

- [1] Donkor, E. A., Mazzuchi, T.A., Soyer, R., & Roberson, J.A., (2014), Urban Water Demand Forecasting: Review of Methods and Models, *J. Water Resour. Plann. Manage.*, 140(2): 146-159
- [2] Gato, S., Jayasuriya, N. and Roberts, P. (2007), Temperature and rainfall thresholds for base use urban water demand modelling. *Journal of Hydrology* 337 (3-4), pp.364– 376
- [3] Goodchild, C. W. (2003). Modelling the impact of climate change on domestic water demand. *The Journal*. V17 N1: 5.
- [4] House-Peters, L. A., & Chang, H. (2011). Urban water demand modeling: Review of concepts, methods, and organizing principles. *Water Resources Research*, 47, 15
- [5] Meteorological Department. (2018), Website of Meteorological Department (Thailand), Topic “Academic: Meteorological Book “Season of Thailand””  
<https://www.tmd.go.th/info/info.php?FileID=53>
- [6] Metropolitan Waterworks Authority. (2018), Website of Metropolitan Waterworks Authority (Thailand), Topic “About MWA: The Metropolitan Waterworks Authority’s History”  
[https://www.mwa.co.th/ewtadmin/ewt/mwa\\_internet\\_eng/ewt\\_news.php?nid=349](https://www.mwa.co.th/ewtadmin/ewt/mwa_internet_eng/ewt_news.php?nid=349)
- [7] Miaou, S., (1990), A Class of Time Series Urban Water Demand Model with Nonlinear Climatic Effects, *Water Resources Research*, Vol. 26(2), 169-178.
- [8] Said, E.S. & Dickey, D.A. (1984), Testing for unit roots in autoregressive-moving average models of unknown order, *Biometric*, 71, 3, pp. 599-607.
- [9] Indian Agricultural Statistics Research Institute (IASRI), (2018), Regression Analysis Library Avenue, PUSA, New Delhi - 110 012 (INDIA)  
[www.iasri.res.in/ebook/win\\_school\\_aa/notes/Regression\\_Analysis.pdf](http://www.iasri.res.in/ebook/win_school_aa/notes/Regression_Analysis.pdf)
- [10] Statistics Solution. (2018), website Complete Dissertation by Statistics Solution,  
<http://www.statisticssolutions.com/what-is-multiple-linear-regression/>
- [11] Toth, E., Bragalli, C. & Neri, M. (2018), Assessing the significance of tourism and climate on residential water demand: Panel-data analysis and non-linear modelling of monthly consumptions, *Environmental Modelling & Software*, 103, 2-61.
- [12] Limsakul, S. L. a. A. 2012. Atmospheric Research: Trends in Thailand pan evaporation from 1970 to 2007. ELSEVIER: 6.
- [13] United Nations, (2018), World Urbanization Prospects: The 2018 Revision [Key Facts]. United Nations.
- [14] WWAP (United Nations World Water Assessment Programme) (2014), The United Nations World Water Development Report 2014: Water and Energy (Paris: UNESCO)

## GROUNDWATER LEVEL RISE IN MUSCAT AIRPORT AREA AND WAYS OF MANAGING THE ISSUE

Luminda Gunawardhana<sup>1</sup>, Mahad Baawain<sup>2</sup> and Ahmed Sana<sup>3</sup>

<sup>1,2,3</sup>Civil and Architectural Engineering Department, Sultan Qaboos University, Oman

### ABSTRACT

Despite the arid climate and scarce water resources, groundwater level rises in some areas of Muscat, the capital city of Oman. Consequent impacts have already been detected in manholes around the new runway, where groundwater seepage into basements of utility lines. The objective of this study is to simulate the groundwater flow in the airport area, which then can be used to propose countermeasures for lowering the groundwater levels as applicable. There are 8 pumping wells and 16 monitoring wells were drilled around the runway and the terminal building to conduct pumping test and to estimate the aquifer properties such as the transmissivity and specific yield. Estimated aquifer properties were then used to develop a three-dimensional groundwater flow model using MODFLOW software. Steady state model calibration and verification were done using two independent data sets in 15 monitoring wells in 2017 and 2018. Four pumping scenarios were considered for lowering the average groundwater level by 0.5m. Model results show that potential water volume that can be withdrawn from existing pumping wells with highest pumping rates is about 8.4% of water coming into the model from the upstream mountain area. It was estimated that altogether 24 pumping wells with the pumping rates vary from 222 to 1564 m<sup>3</sup>/day, are required to achieve the expected reduction. Two pumping scenarios were proposed to guide the operations in different situations. It is expected to carry out further investigations to calibrate the proposed pumping rates and to understand aquifer response for long-term pumping.

*Keywords: Pumping test, Neuman method, MODFLOW, Numerical modeling*

### INTRODUCTION

Over the past decades, economic development, rapid population growth and agricultural activities have increased the stress on groundwater aquifers in Gulf Cooperation Council (GCC) countries. Sultanate of Oman is no exception to this. Annual total rainfall averaged over the country is approximately 130mm, which is about 10% of the global average annual rainfall [1]. Consequently, over exploiting aquifers became vulnerable to the seawater intrusion. For example, the total land area affected in the governorates of Batinah, which locates next to the Muscat governorate, grew from 840 hectares in 1995 to 6930 hectares in 2010 [2].

Muscat airport area, which is located in the heart of the Muscat city, however experiences opposite phenomenon over the last decade. Oman Airport Management Company (OAMC) was alarmed when the groundwater level rises over 1.5m in most of its observation wells since 2010. This effect is likely a result of the groundwater recharge from extreme rainfall events occurred in 2007 (Cyclone Gonu) and 2010 (Cyclone Phet), decline in agricultural activities in the area due to increase urbanization and water leakage from sewer lines and septic tanks.

The potential impacts of rising groundwater levels include, increase in uplift forces on buried water infrastructure and buildings, increase risk of

birds strike during runway operations, flooding of underground tunnels and low-lying infrastructures, erosion into underground utilities lines and cables and decrease groundwater quality due to contaminants in shallow subsurface layers and inter-aquifer leakage [3].

In recent years, continuous increase in shallow groundwater table has been observed in many manholes installed in the Muscat International Airport. Under drains beneath the foundation of the structures and groundwater pumping wells are common strategies apply to prevent underground flooding. For example, groundwater within 1m of the ground surface was a major challenge to the runway operations in Munich airport, West Germany. Two longitudinal ditches and a system of drains between the runways were able to lower the groundwater table by around 2m [4]. Mohamed [5] used finite difference numerical modeling approach to show that the local groundwater level can be lowered by means of pumping wells operate in the vicinity of the area of interest.

Current problems and anticipated issues with rising groundwater level can be prevented by pumping adequate amount of water from the shallow aquifer. The objective of this study is to simulate the groundwater flow in the Muscat airport area and propose operational plans to lower the groundwater level around the runway.

## STUD AREA AND DATA COLLECTION

Muscat is the capital city of Oman located at the southeast tip of the Arabian Peninsula. It is a coastal city where the Muscat International Airport is located in the vicinity of the coast. Upstream side of the catchment area consists of a series of rugged mountains and Ophiolite hills run parallel to the coastline. According to the rainfall records during 1991 to 2010, annual total rainfall is approximately 87mm with 73% of that occurred from November to April when the cold frontal troughs are active [6]. Tropical cyclones such as Cyclone Gonu in 2007 and Cyclone Phet in 2010 are rare but brings extreme rainfall causing substantial damages.

There are 15 observation wells maintained by the OAMC to monitor the groundwater level inside the airport (Fig. 1). Among them, 11 wells have the monthly observations from 2010 to 2018 (W1-W11). Of these 11 wells, four wells (W8-W11) are located adjacent and parallel to the coastline. Observation wells W13-W15 have the observations from 2017 to 2018.

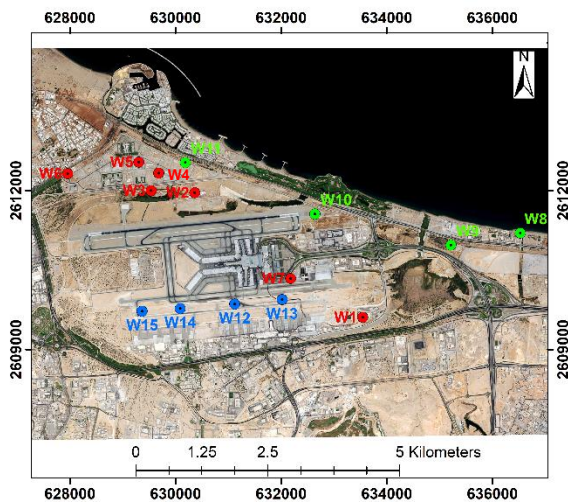


Fig. 1 Study area and the location of wells.

Figure 2 shows the change in groundwater level compared to the monthly averaged water level in 2010. All the wells in the interior (W1-W7) show a similar pattern where groundwater levels rise significantly between 2010 and 2015. When the water level changes were averaged in seven wells (W1-W7), Fig. 2a depicts nearly a 1.5m rise over 5 years. The large mass of seawater body with a constant head is acting as a barrier for groundwater level variation near to the coastal line. Therefore, groundwater level rise in W8-W11 (Fig. 2b) is not as significant as in interior wells.

Simulation of the groundwater level requires proper understanding of aquifer properties such as hydraulic conductivity and specific yield. Therefore, a series of pumping tests were conducted by drilling

8 production wells and 16 monitoring wells (Fig. 3). Each production well (PW) is 25m deep and consists with 2 monitoring wells at 10m and 50m distances.

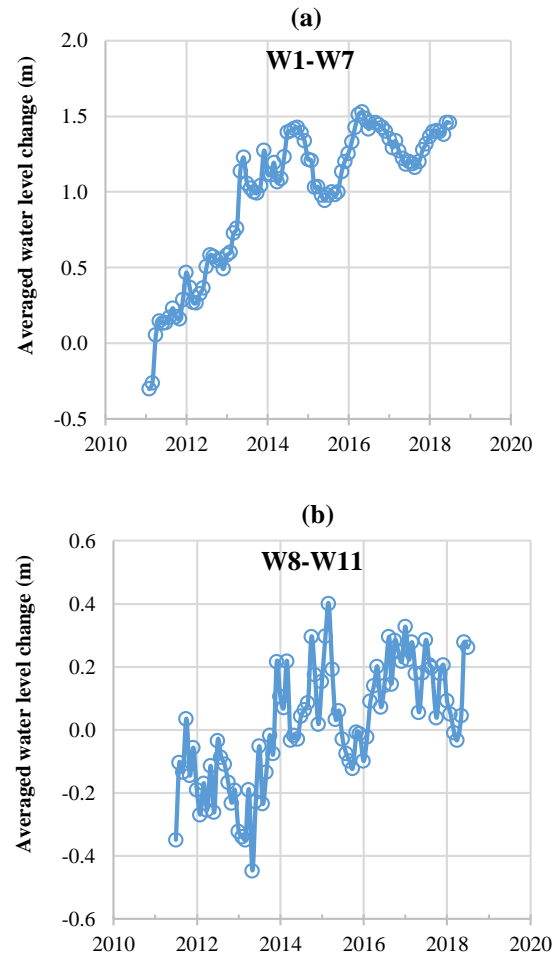


Fig. 2 Averaged water level changes in W8-W11.

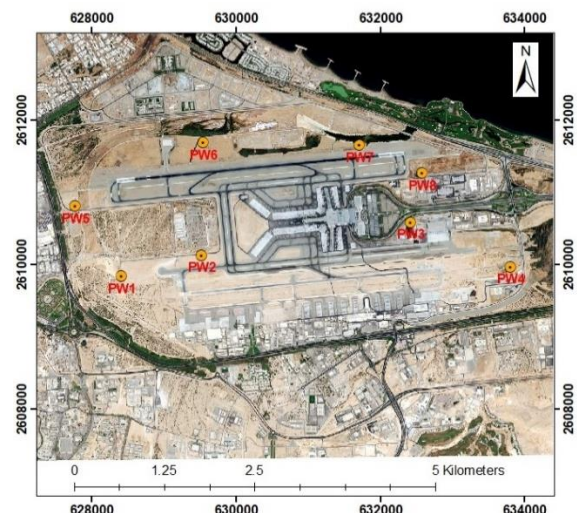


Fig. 3 Production wells used for the pumping test.



Figure 4 shows the groundwater levels recorded in an observation well during the one and half daylong test. The observation well is located at a 10m distance from the production well (PW6). Water was pumped at a constant rate of 18 liters/second in PW6 for 24 hours and recovery test was conducted for another 12 hours. Water levels were recorded in all three wells (production well and two observation wells) at 15 seconds interval at the beginning of the test. The time interval was gradually increased to 1-hour during the later stage of the test. The drawdown is significant in the production well (4.18m in PW-6) but decreases greatly towards the observation wells (1.56m and 0.78m at 10m and 50m wells, respectively).

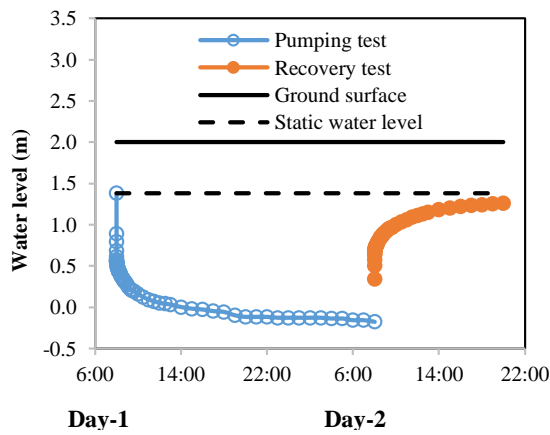


Fig. 4 Groundwater levels in the observation well.

## THEORY AND METHOD

The recovery test is used to estimate the transmissivity of the aquifer. It is assumed that if a well is pumped for a known period of time and then shutdown, the drawdown thereafter (known as the residual drawdown) will be identically the same as if the pumping had been continued and a hypothetical recharge well with the same flow rate were superposed on the pumping well at the instant the actual pumping is stopped [7]. Accordingly, transmissivity ( $T$  in  $\text{m}^2/\text{day}$ ) can be written as:

$$T = \frac{2.3Q}{4\pi s'} \log\left(\frac{t}{t'}\right) \quad (1)$$

where,  $Q$  is the pumping rate ( $\text{m}^3/\text{day}$ ),  $s'$  is the residual drawdown (m),  $t$  (min) is the time since the pumping test was started and  $t'$  (min) is the time since the recovery test was started. The gradient of a plot of  $s'$  versus the logarithm of  $t/t'$  is used to estimate  $T$ .

Neuman [8] theory on unsteady radial flow in unconfined aquifer can be used to estimate the hydraulic conductivity and specific yield. The drawdown ( $s$ ) subjected to a constant pumping rate is given as follows.

$$s = \frac{Q}{4\pi T} W(u_a, u_y, \eta) \quad (2)$$

here,

$$u_a = \frac{r^2 S}{4Tt} \text{ (applicable for early drawdown data)} \quad (3)$$

$$u_y = \frac{r^2 S_y}{4Tt} \text{ (applicable for later drawdown data)} \quad (4)$$

$$\eta = \frac{r^2 K_z}{b^2 K_h} \quad (5)$$

where,  $r$  is the distance from the pumping well to the observation well,  $S_y$  is the specific yield,  $b$  is the initial saturated thickness of the unconfined aquifer and  $K_h$  and  $K_v$  are the horizontal and vertical hydraulic conductivity, respectively. Plotting the graph of drawdown versus time and matching it with the Neuman's theoretical curves, hydraulic conductivities and the specific yield can be estimated.

Aquifer properties found from the pumping tests were used for simulating the groundwater flow in the study area. A three-dimensional groundwater flow model was developed using the MODFLOW software. The principal governing equation used to simulate the water flow is as follows [9].

$$\frac{\partial}{\partial x} \left[ k_x \frac{\partial h}{\partial x} \right] + \frac{\partial}{\partial y} \left[ k_y \frac{\partial h}{\partial y} \right] + \frac{\partial}{\partial z} \left[ k_z \frac{\partial h}{\partial z} \right] - W = S_s \frac{\partial h}{\partial t} \quad (6)$$

where,  $k_x$ ,  $k_y$  and  $k_z$  are hydraulic conductivities ( $\text{m/day}$ ) in  $x$ ,  $y$  and  $z$  directions, respectively,  $h$  (m) is the groundwater head,  $W$  is the groundwater recharge or discharge per unit volume ( $\text{day}^{-1}$ ) and  $S_s$  is the specific storage ( $\text{m}^{-1}$ ).

The aquifer is an alluvial, unconfined layer with an average thickness of 70m from the mean sea level. The modeled area is approximately 12.5 km long and 5 km wide (Fig. 5). The entire area was divided into 294092 active square cells of size 20 by 20 m. The top elevations of the cells were assigned based on topography contour maps prepared by OAMC. The western and eastern boundaries of the model were assumed to follow the catchment boundary and assigned no-flow boundary condition (Fig. 5). A constant head boundary condition was used for the coastal side boundary. The upstream boundary condition was determined based on water level data in the observation well maintained by the Ministry of Regional Municipality and Water Resources (MRMWR). An automated parameter calibration was carried out to estimate the recharge rate and to fine-tune the hydraulic conductivity values obtained from pumping test data. Steady state model calibration and verification were done using two independent data sets in 2017 and 2018. For this, observations in 15 monitoring wells shown in Fig. 1 were used.

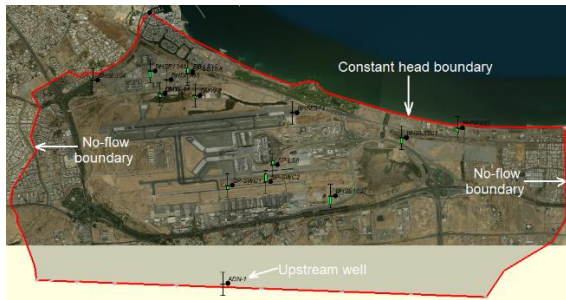


Fig. 5 Boundary conditions of the model.

## RESULTS AND DISCUSSION

Figure 6 shows the drawdown in the pumping well PW-6 and in two observation wells at 10m and 50m distances away (MW-15 and MW-16, respectively) from the pumping well. It was observed that the drawdown is significant closer to the pumping well, but decays exponentially as the distance from the pumping well increases. The recovery test was carried out for 24 data sets (8 PWs and 16 MWs). Figure 7a shows the relation between residual drawdown ( $s'$ ) and the logarithm of  $t/t'$  ratio for the observations in MW-15. The gradient of the best-fit line along with the Eq. (1) were used to calculate the transmissivity and the corresponding hydraulic conductivity.

Similarly, drawdown data and residual drawdown data in 24 wells were used to fit the Neuman type curves using AQTESOLV software. Figure 7b shows the fitted curve for the observations in MW-15 well. Based on results of two tests and observation in three wells, the estimated hydraulic conductivity ranges from 37 m/day to 49 m/day for the pumping test in PW-6. The average hydraulic conductivity estimated from all the wells range from 6.4 m/day in PW-1 to 169 m/day in PW-7. These values were used for defining different hydrological zones in the study area and further adjusted during the calibration process of the MODFLOW model.

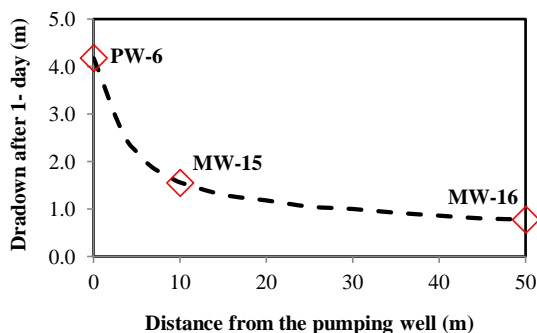


Fig. 6 Change in drawdown with the distance.

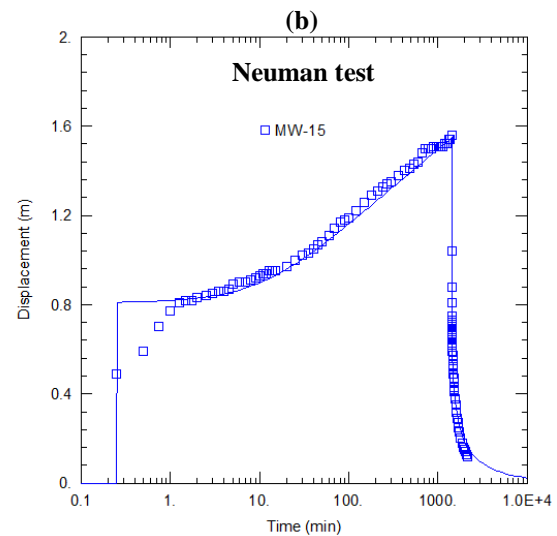
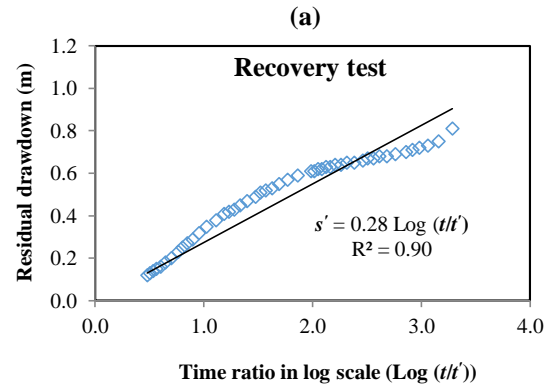


Fig. 7 Pumping test results at MW-15

## MODFLOW model calibration and verification

Figure 8 shows the comparison of observed and simulated groundwater levels during model calibration (2017) and verification (2018) stages. In general, calibration standards for numerical groundwater flow simulation agree that the number of observation wells with an absolute error level less than 0.5m in simulation must be greater than 70% of all observation wells [10]. Model results indicate that 93% of all wells have absolute error less than 0.5m with estimated RMSE of 0.14m during calibration stage. Two wells in 2018 simulation show a significant error approximately equals to 1.5m. This can be attributed to the local pumping in the airport. Consequently, model verification depicts that about 69% of the wells have absolute error less than 0.5m with estimated RMSE of 0.47m.

Contour lines drawn for the simulated groundwater levels indicates that the dominant groundwater flow is from southwest to northeast direction of the study area (Fig. 9). Total water volume that can be withdrawn from the PWs (Fig. 3) when they are operated at the highest yield is about

7943 m<sup>3</sup>/day. It is approximately equals to 8.4% of the water enters to the study area through the upstream boundary (94091 m<sup>3</sup>/day). By applying a proper strategy, it is expected to lower the groundwater level by 0.5m around the runaway. Therefore, an additional set of wells with an appropriate operational plan would be required to achieve the above reduction in groundwater levels.

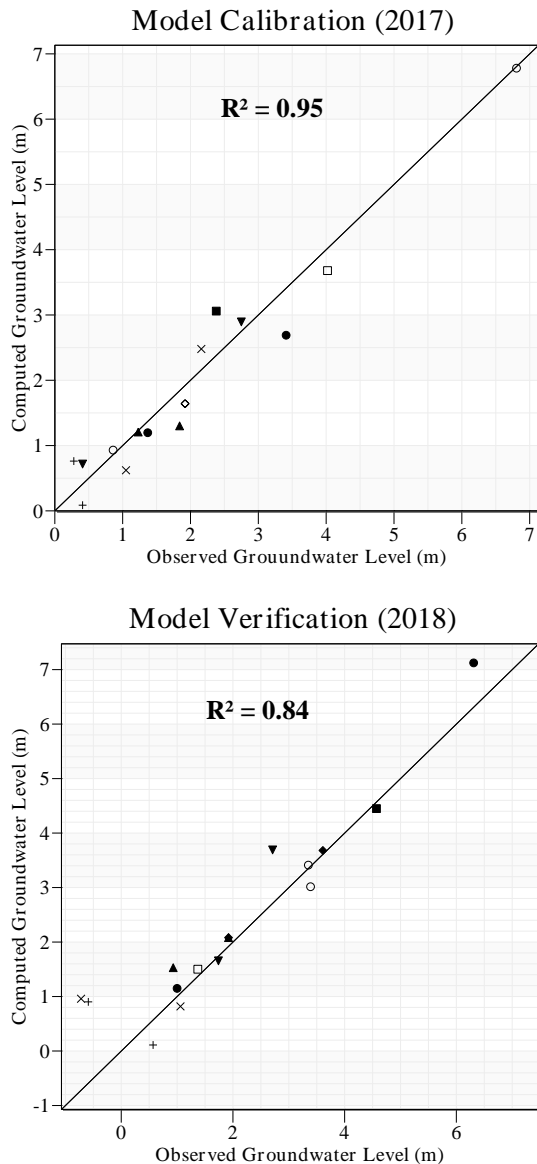


Fig. 8 Observed and simulated water levels.

### Pumping Scenarios

Due to the significant amount of water enters to the study area through the upstream boundary, 16 new production wells (NPWs) were added around the runaway and the terminal building. Three pumping scenarios were considered as follows.

1. Pumping with maximum yield (range from 222 m<sup>3</sup>/day to 1564 m<sup>3</sup>/day) in existing eight

production wells (PWs) continuously for two weeks and recovery for one week. Repeat the same steps for four more times.

2. Two-week pumping and one-week recovery from all 24 wells (8 PWs and 16 NPWs). An average pumping rate of 1500 m<sup>3</sup>/day was assigned for the NPWs.
3. Two Set of pumps with only one set operating at a time. All 24 wells were divided to two equal sets with each set covering the entire focused area. While the first set of pumps operates for two weeks, the other set remained nonoperational. While the recovery is started for the first set of pumps for one-week, the other set of pumps operate.

All three scenarios were continued for four more pumping sessions extending the total model simulations for 98 days. Figure 9a shows a comparison of groundwater level change between initial stage (prior to the pumping starts) and after five sessions of pumping according to Scenario 2. When the runaway area is considered, Point A in Fig. 9a showed the highest groundwater level of 3.8m, which according to Scenario 2 can be reduced to 3.1m after five pumping sessions (Fig. 9b). The lowest groundwater level of 1m was simulated in the runaway area at Point B. This water level can be reduced to 0.6m during the same time.

Model results show that pumping only from existing wells with the highest yield (Scenario 1) is not sufficient to lower groundwater level by 0.5m. It was able to lower the groundwater levels by 0.11m and 0.13m at points A and B, respectively. Scenario 3 explores the possibility of shutting down some pumps for the maintenance purposes while maintaining the lowered water levels. Model results estimated that approximately 0.57m and 0.34m water level reduction can be expected at points A and B, respectively with operating 50% of the pumps at a time.

### CONCLUSION

This study was conducted to simulate the groundwater flow in the Muscat airport area for proposing countermeasures to lower the water levels about 0.5m near the runaway area. According to the model results, drawdown due to pumping from existing eight production wells is significant only near to the pumping wells. Reducing water level over a large area surrounding the runaway therefore requires additional set of wells. Among the three pumping scenarios were simulated, two of them with an additional set of pumps indicated the possibility of achieving the required water level reduction. However, further studies with actual field testing pumping sessions are required to understand the long-term pumping effects on reducing the groundwater levels.



(a) Initial groundwater levels from steady state



Fig. 9 Groundwater levels in Scenario 2.

## REFERENCES

- [1] Gunawardhana L. N., Al-Rawas G. A., Kwarteng A. Y., Al-Wardy M., and Charabi Y., Potential Changes in the Number of Wet Days and ITS Effect on Future Intense and Annual Precipitation in Northern Oman. *Hydrology Research*, Vol. 49, Issue 1, 2018, pp. 237-250.
- [2] ICBA., Oman Salinity Strategy. International Center for Biosaline Agriculture. 2012, pp. 1-130.
- [3] Washington State Department of Transportation Aviation Division, Guidance for Developing a Stormwater Management Manual for Washington State: Mitigating Hazards due to Wildlife Attractions at Airports. Technical Memorandum, Arlington, Washington, 2007.
- [4] Munich Airport Environmental Statement (2008). [https://www.munich-airport.de/media/download/general/publikationen/en/Umwelterkl\\_rung\\_2008\\_englisch.pdf](https://www.munich-airport.de/media/download/general/publikationen/en/Umwelterkl_rung_2008_englisch.pdf)
- [5] Mohamed H. I., Effect of Dewatering Schemes on Uplift Pressure and Groundwater Variation Under Buildings. *International Journal of Applied Engineering Research*, Vol. 9, 2014, pp. 9989-10003.
- [6] Gunawardhana L. N., and Al-Rawas G. A., A Comparison of Trends in Extreme Rainfall Using 20-Year Data in Three major Cities in Oman. *The Journal of Engineering Research*, Vol. 13, Issue 2, 2016, pp. 137-148.
- [7] Todd D. K., and Mays L. W., *Groundwater Hydrology*, John Wiley & Sons, 2004, pp. 170-172.
- [8] Neuman, S. P., Theory of Flow in Unconfined Aquifers Considering Delayed Response of the Water Table. *Water Resources Research*, Vol. 8 1972, pp. 1031-1045.
- [9] McDonald M. G., and Harbaugh A. W., *A Modular Three-Dimensional Finite-Difference Ground-Water Flow Model*. Techniques of Water-Resources Investigations of the United States Geological Survey, 1988.
- [10] Du X., Lu X., Hou J., and Ye X., Improving the Reliability of Numerical Groundwater Modeling in a Data-Spares Region. *Water*, Vol. 10, paper 289, 2018, pp. 1-15.

## LIGHTWEIGHT FOAMED CONCRETE INTERLOCKING BLOCK UTILISING UNGROUND OIL PALM ASH

Hanizam Awang<sup>1</sup>, Mohammed Zuhear Al-Mulali<sup>2</sup> and Wenny Arminda<sup>3</sup>

<sup>1,3</sup>School of Housing, Building and Planning, Universiti Sains Malaysia, Malaysia;

<sup>2</sup>Department of Civil Engineering, Al-Mustaqbal University College, Babylon, Iraq

### ABSTRACT

This study examines the properties of lightweight foamed concrete interlocking block with a density of 1300kg/m<sup>3</sup> and containing 35% unground oil palm ash (UOPA) as cement replacement. The UOPA foamed concrete interlocking blocks were produced in three shapes including stretcher, base and the half block. From the testing conducted, it was found that the compressive strength of the stretcher, half block, and the base block is 3.75, 4.29 and 3.00 MPa, respectively. The UOPA foamed concrete interlocking block achieved a higher strength than the specified minimum strength of 2.8MPa by BS 5628.

*Keywords: Foamed concrete, Oil palm ash, Cement replacement, Interlocking block*

### INTRODUCTION

Foamed concrete is a mortar based or slurry material with mechanically entrained air bubbles that have a minimum volume of 20%. In foamed concrete, air bubbles are introduced to the base mix (mortar or cement slurry) by mixing a stable pre-formed foam which, in itself, is a mixture of compressed air and a suitable foaming agent [1]. Due to its energy saving and environmentally friendly features, the construction industry is currently paying considerable attention to foamed concrete [2]. Foamed concrete is becoming an innovational product because it offers a better fire protection, superior heat and sound insulation as well as diverse range of densities lower than that of conventional concrete (1000 kg/m<sup>3</sup> to 1600 kg/m<sup>3</sup>) [3]. However, to improve the properties of foamed concrete and cost saving, many studies have endeavored to use supplementary cementing materials as cement replacements [4]. One of the potential supplementary cementing materials is oil palm ash.

Oil palm ash (OPA) is an agriculturally based waste material existing in countries with a booming palm oil industry. As an alternative fuel source, palm oil mills use the biomass (shell and fibres) as boiler fuel for producing steam [5] and electricity for the mill's internal use [6]. In Malaysia alone, about 4 million tonnes of OPA are produced annually and the amount increase every year [7] [8]. OPA amounts are deemed to rise in Malaysia due to the implementation of a project introduced by the Malaysian government which utilises the biomass produced by the palm oil industry to generate power [9]. OPA is commonly disposed of by either spreading the waste over the premises of the mill or dumping it in low

economic value dumps or selected types of land such as swamp lands and abandoned sand quarries [10]. These disposal methods are conducted without taking into consideration the surrounding environment or taking precautions to compact, cover and prevent the spreading of pollutants into the ground water levels [11]. In addition, due to its fine particles, OPA can be easily carried away causing smog in humid days [12].

Although OPA is a relatively new pozzolanic material, a number of researchers have used it as a cement replacement or as a filler replacement in the production of concrete [13], high strength concrete [14], aerated concrete [15] and lightweight concrete [16]. The OPA used has been processed by either grinding to achieve a higher fineness, by heat treatment to reduce the amount of carbon content or using both treatments. Although these enhancements are beneficial in making OPA a good pozzolanic material, they considerably increase the cost [17]. As a result of this utilisation, the prospect of broadening the recycling methods of this waste is increased.

This study introduced the OPA to manufacture a new designed interlocking block. Interlocking block systems are known to be made from conventional concrete. As a result, these blocks are heavy and poor in thermal insulation properties. The newly design will be made out of OPA foamed concrete, hence, it is lightweight and possess all the good properties of thermal and fire resistance. The block system is environmentally friendly due to the utilisation of a waste material in its fabrication.

In this study, the foamed concrete specimens using unground OPA (UOPA) passing through a 300 µm sieve were cast into three different shape of interlocking block. This study was conducted to

investigate the strength and failure mechanism of the foamed concrete interlocking blocks.

## MATERIALS AND MIXTURE DESIGN

The foamed concrete having design density of  $1300\text{kg/m}^3$  and filler to binder ratio of 1.5 has been cast using Type I cement complying with BS EN 196 [18] and unground oil palm ash (UOPA) as cement replacement.

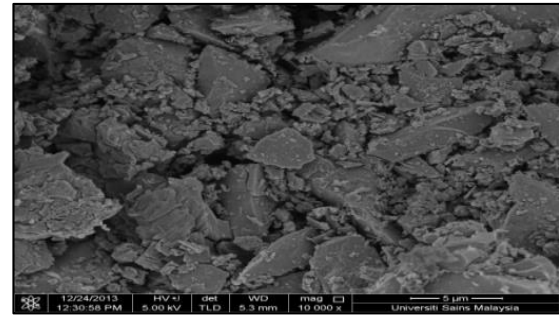
The raw UOPA that was collected from a nearby oil palm mill is a product from the combustion of palm oil biomass at the temperatures exceeding  $1000^\circ\text{C}$ . The UOPA was dried in an oven for 24 hours at a temperature of  $105^\circ\text{C}$  then sieved through a  $300\text{ }\mu\text{m}$  sieve to remove any unburned fibrous and large size particles. Table 1 lists the chemical composition and physical properties of both cement and UOPA used in this study.

Table 1 Chemical and physical properties of cement and UOPA

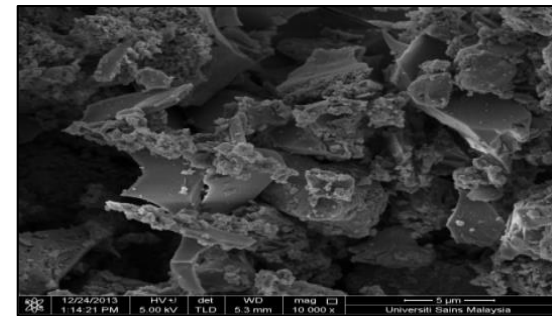
| Chemical Composition (%)                                       | Cement | UOPA   |
|--|--------|--------|
| Silicon Dioxide ( $\text{SiO}_2$ )                             | 19.98  | 66.64  |
| Aluminium Oxide ( $\text{Al}_2\text{O}_3$ )                    | 5.17   | 3.82   |
| Iron Oxide ( $\text{Fe}_2\text{O}_3$ )                         | 3.27   | 3.69   |
| Calcium Oxide ( $\text{CaO}$ )                                 | 63.17  | 5.23   |
| Magnesium Oxide ( $\text{MgO}$ )                               | 0.79   | 2.29   |
| Sulphur Trioxide ( $\text{SO}_3$ )                             | 2.38   | 0.43   |
| Alkalis ( $\text{Na}_2\text{O}$ )                              | --     | 0.15   |
| Loss on Ignition (LOI)   | --     | 6.09   |
| $\text{SiO}_2 + \text{Al}_2\text{O}_3 + \text{Fe}_2\text{O}_3$ | --     | 74.15  |
| Median particle size $d_{50}$ ( $\mu\text{m}$ )                | 5.73   | 101.81 |
| Specific gravity   | 2.85   | 1.65   |
| Loose bulk density ( $\text{kg/m}^3$ )                         | 1180   | 833.6  |
| Blaine surface area ( $\text{cm}^2/\text{g}$ )                 | 3924   | 1952   |

Fine sand from a local river bed was used as filler. The foaming agent that was used to produce the pre-formed foam is a locally made protein-based foaming agent. The foaming agent was diluted in water at a percentage of (1:30) enabling it to produce table foam with a density of  $65\text{ kg/m}^3$ .

From the SEM image, UOPA particles tend to be angular and irregular in shape (Fig. 1). Hence, these particles require more water to lubricate their surface for the purpose of maintaining the needed consistency. Therefore, a naphthalene based super-plasticiser with a pH number of 7.5 was used with foamed concrete mixes containing UOPA to produce a mixture with reduced water demand and higher flowability.



(a) SEM imagery of cement particles at a 10000X magnification



(b) SEM imagery of UOPA particles at a 10000X magnification

Fig. 1 SEM imagery for (a) cement and (b) UOPA

## INTERLOCKING BLOCK PRODUCTION

The foamed concrete interlocking block was produced using 35% UOPA (by the weight of binder) to replace cement and the filler-to-binder ratio of 1.5. The mixture design is shown in Table 2.

Table 2 Calculated mix constituents ( $\text{kg/m}^3$ )

| Constituent Material |        |
|----------------------|--------|
| Cement               | 315.06 |
| UOPA                 | 169.65 |
| Sand                 | 727.06 |
| SP                   | 4.85   |
| Water                | 218.12 |

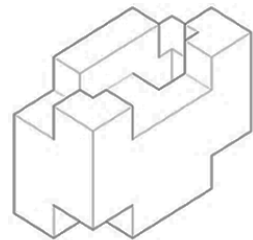
The compressive strength of UOPA foamed concrete was tested using cube specimen of  $100 \times 100 \times 100\text{ mm}$ . The given mixture achieved the compressive strength of  $7.28\text{ MPa}$ . This mixture has a porosity reading of  $55.23\%$ .

## Block design consideration and sizes

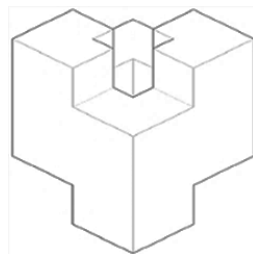
The design philosophy for the interlocking block is that it should have an interlocking mechanism that allows self-alignment and mortarless, has dimensions that agree with the modular system and can be used to build none, semi and



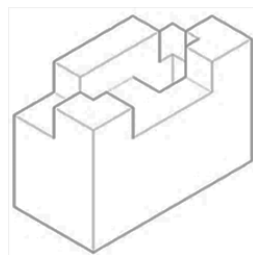
loadbearing walls. The interlocking mechanism depends on intrusions and protrusions on the upper and lower face of the block. The newly designed system is called BTechLiTe Block (Fig. 2) with the dimension is shown in the Table 3.



(a) Stretcher Block



(b) Half Block



(c) Base Block

Fig. 2 BTechLite Block

Table 3 Physical characteristics of the individual blocks

| Block type                             | Stretcher | Half  | Base  |
|--|-----------|-------|-------|
| Dimension (mm)                         |           |       |       |
| • Length                               | 300       | 150   | 300   |
| • Width                                | 150       | 150   | 150   |
| • Height                               | 200       | 200   | 200   |
| Average mass (kg)                      | 7.72      | 4.22  | 9.14  |
| Volume ( $\text{m}^3 \times 10^{-3}$ ) | 5.56      | 3.0   | 6.5   |
| Bearing area ( $\text{mm}^2$ )         | 37500     | 20000 | 37500 |

### Experimental program

The blocks were tested for their compressive strength using a universal testing machine with a maximum capacity of 3000 kN and a loading cell of a 500 kN capacity. In the case of the stretcher

block, two linear variable differential transformers (LVDTs), one vertical and one horizontal were placed on top and perpendicular to the face of the block. In addition to the two LVDTs, three strain gauges were placed on the face and side of the stretcher block. The testing setup is illustrated in Fig. 3.



(a) Stretcher block test set-up



(b) Prism test set-up



(c) Wall panel test set-up

Fig. 3 Experimental setup for block, prism and panel

The prisms have the dimensions of three blocks high (600 mm) and a width of one block (150 mm) giving them a slenderness ratio of 4. The standard prisms usually can be built to various heights ranging between 1.5 and 5 times the thicknesses of the block (ASTM C90-75). As in the case of the individual block, the stability of the prisms was investigated using two LVDTs. A vertical LVDT to investigate the prism's vertical displacement and a horizontal LVDT was located at the centre of the middle course of the prism. The panel selected had a dimension of 0.8 m in height and 0.9 m in length. The panel consists of base blocks, stretcher and half blocks. The panels were tested using a loading cell of a maximum load capacity of 1000 kN and a

loading frame. The test was conducted by increasing the load until total failure occurred.

## RESULTS AND DISCUSSION

### Strength and failure mechanism

The average maximum loads that the stretcher, base and half blocks reached are 82.07 kN, 84.5 kN and 37.5 kN respectively (Table 4). The stretcher block have the same shape on the top and bottom; therefore, the area that resists the load is 22500 mm<sup>2</sup>, hence, the strength is 3.75 MPa. The half block has a smaller area than the stretcher block of 8750 mm<sup>2</sup>; hence, the stress is determined as 4.29 MPa. Meanwhile, the base block has two different top and bottom faces; therefore, top and bottom stress are determined and then the average is taken [19]. The stress that the base withstands is 3.00 MPa.

Since the blocks are made out of foamed concrete; therefore, they have to be compared to aerated concrete blocks. The most common strength that the aerated concrete blocks possess is 2.8 MPa [20]. So, it is safe to say that the newly designed block is higher in compressive strength than aerated concrete blocks. In addition, the minimum requirement for a load bearing concrete block is 2.9 MPa [21]; hence, the newly designed block system can be used in constructing walls that can bear medium loads.

Table 4 Compressive strength of the individual blocks

| Block shape                   | Stretcher | Half | Base |
|-------------------------------|-----------|------|------|
| Maximum Load (kN)             | 84.27     | 37.5 | 84.5 |
| Strength (N/mm <sup>2</sup> ) | 3.75      | 4.29 | 3.00 |

The vertical deformation detected at the maximum load of 84.27 kN was 0.82 mm. Once failure occurs, the load drops and the displacement continues to occur. When the load is subjected onto the upper protrusions, the compressive stresses extend downwards. The load tends to push the block downwards; hence, expanding the lower part of the block. The expansion movement translates to tensile stresses near the connection point of the lower protrusions and the body of the block. Maximum tensile stresses occur at the connection points at in-plane and out-of-plane connection areas of between the lower protrusions and the upper body of the block. These connection points will be the areas where cracks will first appear when loaded. Fig. 4 shows the cracks exhibited by the stretcher block when loaded until failure.



(a) Face



(b) Back

Fig. 4 Cracking of the stretcher block

It is obvious that cracks occur at the area where the compressive stresses transform to tensile stresses. Therefore, a shear line is created in the transformation area; hence, creating the exhibited crack lines shown in Fig. 5. The cracks started at the small protrusions on top then extended towards the lower parts of block. The cracks moved in line with the end of a protrusion to the beginning of the protrusion beneath it. At the centre of the distance between the two protrusions, a crack appeared which extended towards the centre of the block's face then divided itself into two smaller cracks.

The prisms' compressive strengths were determined using a loading cell with a maximum capacity of 500 kN. The average compressive strength of the prism was 3.69 N/mm<sup>2</sup> with the maximum load of 110.66 kN. Once the load compresses the first block, the load divides into two because of the two half blocks that lie underneath. The load coming down from the two half blocks is transferred through the protrusions and intrusions of the upper facial of the base block then goes across to the base of the base block. The staggered joints helped in enhancing the load transfer from the top block through the halves and then to the base block. After loading, prism showed the first cracks at a load of 60 kN (54% of the maximum load). The cracks occurred in the centre of the half block which extended upwards and at the base of the protrusion of the base block which extended downwards. A crack occurred at a load of 80 kN which extended from the joint in the middle

course upwards towards the stretcher block on top. At 109.5 kN the cracks which were previously observed on the single block appeared but on the first stretcher block only. The reduction in the compressive strength of the prism compared to the individual stretcher block unit was due to the effect of the slenderness of the prism specimen. Fig. 5(a) shows the cracks that occurred when testing prism.



(a) Cracks on prism



(b) Cracks on the panel

Fig. 5 Cracks on the prism and panel

In the case of maximum load and strength obtained, wall panels achieved an average load of 130 kN and a compressive strength of 1.16 MPa. The higher slenderness ratio and larger number of interlocking joints may have been responsible for this further reduction in the compressive strength capacity of the panel. The first cracking occurred in the area where lower strain readings were detected. However, the cracks did not extend upwards or downwards and they did not threaten the integrity of the wall panel in whole. Reaching failure, chips from the wall panel started to shave off at the areas connecting the high strain with the

lower strained areas. Figure 5(b) shows the failure mode exhibited by wall panel.

### Strength correlations

From analysing the cracking patterns that occurred in the individual, prisms and wall panels, similar patterns of cracks occur in the three types. When testing the blocks individually, the crack extended from the end of a protrusion towards the beginning of the protrusion beneath it. It seems that the crack is following a path which separates two areas. The first area, when loading the upward protrusions, the area beneath the protrusion is pushed downwards. The second area is the opposite case, when loading the downward protrusion pushes the area above it upwards. Hence, a shear failure occurs between the two areas.

The strength correlations between block, prism and panel are investigated. The stretcher block achieved a compressive strength ( $f_{cB}$ ) of 3.75MPa, and Prism achieved a compressive strength ( $f_{cP}$ ) of 3.69 and Panel achieved a compressive strength ( $f_{cW}$ ) of 1.16MPa. From the numbers mentioned, it is obvious that  $f_{cB} > f_{cP} > f_{cW}$  the same observations were made by [19]. The following equations describe the relationship between block, prism and wall.

$$f_{cP} = 0.98 f_{cB} \quad (1)$$

$$f_{cW} = 0.314 f_{cP} \quad (2)$$

$$f_{cW} = 0.309 f_{cB} \quad (3)$$

### CONCLUSIONS

The BTechLiTe block has a number of good properties such as its lightweight (average weight of stretcher block is about 7 kg), it has the dimensions that agree with the modular system and its interlocking mechanism insures that the block interlocks with other blocks in all directions. The block has achieved an average strength of 3.75 MPa for the stretcher block, 4.29 MPa for the half block and 3.00 MPa for the base block, a higher strength than the specified minimum strength of 2.8 MPa stated by BS 5628. The newly designed block showed that the stretcher block achieved a compressive strength of 3.75MPa, higher than the prism (3.69 MPa). Meanwhile the compressive strength of prism was higher than the panel which achieved 1.16 MPa.

The failure mode that was observed while testing the newly designed block system is that it cracking occurs due to shear. The cracks occurred

in a region where areas on the block move in opposite sides of each other due to the loading of the protrusions.

Eventually, the fabrication of BTechLite blocks with 35% UOPA as the cement replacement offers a lighter blocks with superior compressive strength which resulting in further cost reductions and environmentally friendly.

## ACKNOWLEDGMENTS

The authors gratefully acknowledge the financial support of the Universiti Sains Malaysia under the Research University Grant (RUI) (Ref. No. 1001 / PPBGN / 8014015).

## REFERENCES

- [1] Ramamurthy K., Nambiar E.K.K., Indu Siva Ranjani G. A classification of studies on properties of foam concrete. *Cem Concr Compos*, Vol 31, 2009, pp. 388–396.
- [2] Bing C., Zhen W., Ning L. Experimental Research on Properties of High-Strength Foamed Concrete. *J Mater Civ Eng*, Vol 24, 2012, pp. 113–118.
- [3] Lim S.K., Tan C.S., Lim O.Y., Lee Y.L. Fresh and hardened properties of lightweight foamed concrete with palm oil fuel ash as filler. *Constr Build Mater*, Vol 46, 2013, pp. 39–47..
- [4] Yang K.H., Lee K.H., Song J.K., Gong M.H. Properties and sustainability of alkali-activated slag foamed concrete. *J Clean Prod*, Vol 68, 2014, pp. 226–233.
- [5] Mahlia T.M.I., Abdulmuin M.Z., Alamsyah T.M.I., Mukhlisshien D. An alternative energy source from palm wastes industry for Malaysia and Indonesia. *Energy Convers Manag*, Vol 42, 2001, pp. 2109–2118..
- [6] Sumathi S., Chai S.P., Mohamed A.R. Utilization of oil palm as a source of renewable energy in Malaysia. *Renew Sustain Energy Rev*, Vol 12, 2008, pp. 2404–2421
- [7] Foo K.Y., Hameed B.H. An overview of landfill leachate treatment via activated carbon adsorption process. *J Hazard Mater*, Vol 171, 2009, pp. 54–60.
- [8] Hassan U.J., Noh M.Z., Zainal A.A. Effects of palm oil fuel ash composition on the properties and morphology of porcelain-palm oil fuel ash composite. *J Teknol (Sciences Eng)*, Vol 70, 2014, pp. 5–10.
- [9] Shuit S.H., Tan K.T., Lee K.T., Kamaruddin A.H. Oil palm biomass as a sustainable energy source: A Malaysian case study. *Energy*, Vol 34, 2009, pp. 1225–1235.
- [10] Foo K.Y., Hameed B.H.. Value-added utilization of oil palm ash: A superior recycling of the industrial agricultural waste, Vol 172, 2009, pp. 523–531.
- [11] Khankhaje E., Hussin M.W., Mirza J., Rafieizonooz M., Salim M.R., Siong H.C., Warid, M.N.M. On blended cement and geopolymer concretes containing palm oil fuel ash. *Mater Des*, Vol 89, 2016, pp. 385–398.
- [12] Tay J.H., Show K.Y. Use of ash derived from oil-palm waste incineration as a cement replacement material. *Resour Conserv Recycl*, Vol 13, 1995, pp. 27–36.
- [13] Sata V., Jaturapitakkul C., Rattanasotinunt C. Compressive Strength and Heat Evolution of Concretes Containing Palm Oil Fuel Ash. *J Mater Civ Eng*, Vol 22, 2010, pp. 1033–1038.
- [14] Zeyad A.M., Megat Johari M.A., Tayeh B.A., Yusuf M.O. Pozzolan reactivity of ultrafine palm oil fuel ash waste on strength and durability performances of high strength concrete. *J Clean Prod*, Vol 144, 2017, pp. 511–522.
- [15] Abdullah K., Hussin M. Fire Resistance Properties of Palm Oil Fuel Ash Cement Based Aerated Concrete. *Concr Res Lett*, Vol 1, 2010, pp. 1–5.
- [16] Islam M.M.U., Mo K.H., Alengaram U.J., Jumaat M.Z. Mechanical and fresh properties of sustainable oil palm shell lightweight concrete incorporating palm oil fuel ash. *J Clean Prod*, Vol 115, 2015, pp. 307–14
- [17] Chao-Lung H., Anh-Tuan B.L., Chun-Tsun C. Effect of rice husk ash on the strength and durability characteristics of concrete. *Constr Build Mater*, Vol 5, 2011, pp. 3768–72.
- [18] BSI. 2005. BS EN 196-2. UK: British Standards Institution.
- [19] Ali M., Gultom R.J., Chouw N. Capacity of innovative interlocking blocks under monotonic loading. *Constr Build Mater*, Vol 37, 2012. pp. 812–821.
- [20] Arya C. Design of Structural Elements : Concrete, Steelwork, Masonry and Timber Designs to British Standards and Eurocodes. Oxford, UK: Taylor & Francis, pp. 239-278.
- [21] BSI. 2002. BS EN 5628-1. UK: British Standards Institution.

## FINANCIAL AND INSTITUTIONAL ASPECT FOR APPLICATION OF A CENTRALIZED DOMESTIC WASTEWATER MANAGEMENT SYSTEM IN SUKOLILO DISTRICT, SURABAYA, INDONESIA

Dwi Agustiang Ningsih<sup>1</sup>, Eddy Setiadi Soedjono<sup>2</sup> and Nurina Fitriani<sup>3</sup>

<sup>1,2</sup> Environmental Engineering Department, Institut Teknologi Sepuluh Nopember (ITS), Surabaya, Indonesia, <sup>3</sup>Study Program of Environmental Engineering, Department of Biology, Universitas Airlangga, Surabaya, Indonesia

### ABSTRACT

Sukolilo district is one of the sub-districts in Surabaya City which still uses the on-site system for its wastewater treatment. This sub-district is one of the areas that designate for the centralized domestic wastewater management system (CDWMS) plan. The application of CDWMS itself based on the strategic plan of system and infrastructure development of Surabaya City 2015-2034, namely the provision of centralized Wastewater Treatment Plan. Reflecting on these policies and strategies, in the future there will be efforts to shift the localized (on-site) wastewater treatment and management infrastructure into the centralized one. For this reason, it is necessary to conduct a study of the application of CDWMS in terms of technical aspects and community involvement. The community involvement aspect is examined with real demand survey method related to the participation, willingness, and ability to use the CDWMS. The result of this study indicates that the community readiness in the CDWMS implementation plan shows that the community still does not know the procedures as well as the benefits of it. Hence, even though the community shows vast willingness to use this system, it is not backed with the community's ability to pay the pipeline connections and the charges of retribution. The community is only able to pay pipeline connections at < IDR 500,000 and pay charge of retribution at IDR 6,000 - IDR 10,000.

*Keywords: Domestic wastewater, community involvement, CDWMS, Sukolilo*

### INTRODUCTION

Based on the Surabaya City Sanitation Strategy in 2016, the city of Surabaya is currently planning centralized domestic wastewater management system (CDWMS) with a long-term target of regional scale use of CDWMS reaching 21.52% and city-scale reaching 67.20%. Sukolilo District is one of the locations to execute this plan [1].

Sukolilo District consists of seven sub-districts. The environmental conditions of the settlements in this district can be categorized as dense residential neighborhoods. The wastewater management in Sukolilo District is currently using the on-site system. One of the sub-district not declared yet as open defecation free (ODF). The largest number of people who still practice open defecation is in Keputih Sub-district [2]. Most of the residents use shared toilets, private toilets, and septic tanks. The blackwater is treated in the septic tanks while the greywater will be discharged to the nearest drainage [1].

Looking at these policies and strategies, in the future, there will be an effort to transform the on-site wastewater infrastructure and management system into a centralized system. To implement the CDWMS in Sukolilo district in accordance to the Surabaya Sanitation Strategy, build of community support is also needed to maintain the sustainable implementation of CDWMS [3]. This is related to the

obligation that must be borne by the community to maintain a sustainable CDWMS service [4].

This community support is in the form of awareness in using a centralized system, given that most people today have used the local system [5]. Community is assigned to collect retribution, operation and maintenance of physical infrastructure [6].

Community preparation must be done correctly and precisely because it refers to the Surabaya City Regulation which mentioned the obligations of the community [7]. The application of CDWMS requires support from the community in order to realize the sustainability of the system. Based on the reason, in this study will identify the level of community readiness in the use of CDWMS both in terms of willingness and ability.

### METHOD

Community surveys were conducted at selected locations for the application of CDWMS. Analysis of the participation aspects of the community emphasized the involvement of the community in relation to their participation to CDWMS pipeline connection, willingness, and the ability to use CDWMS.

To find out the community participation in the management of domestic wastewater, data collection



was carried out using questionnaires. The number of sample questionnaires use the formula [3]:

$$n = \frac{N \cdot p(1-p)}{(N-1)D + p(1-p)} \quad (1)$$

$$D = \frac{B^2}{t^2} \quad (2)$$

Where: n = number of samples, N = number of population (house hold), p = element ratio in the sample that have desirable properties (0.5), B = allowable error rate for each sample 5%, and t = level of confidence (1-B)

The selection of respondents in this study is based on the distribution of samples by stratified random sampling because the study area has a heterogeneous population.

## RESULTS AND DISCUSSION

Based on the calculation refer to Eq. (1) and Eq. (2) the number of questionnaires was 80 questionnaires distributed in the study area. The study area is presented in the Fig. 1.

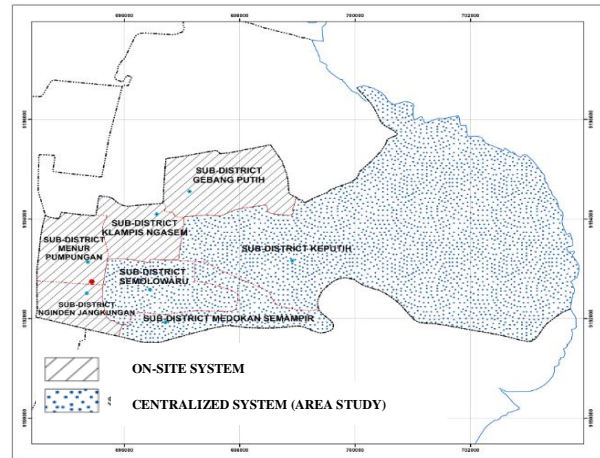


Fig. 1 Map of Area Study in Sukolilo District

### Correlation between Education Levels, Public Counseling and Knowledge About CDWMS

Apart from public counseling, knowledge of wastewater management can be obtained through formal education. The results of the analysis of the relationship between education levels, public counseling and the level of public knowledge of the CDWMS implementation plan can be seen in Table 1.

Table 1. Availability of Public Counseling \* Knowledge of the Definition, Benefit, and Ways of Work of CDWMS \* Education Level of the Head of the Family Cross Tabulation

| Education Level of the Head of the Family |                                   |                     | Knowledge of the definition, benefit, and ways of work of CDWMS |                       |             | Total |
|---|-----------------------------------|---------------------|---|-----------------------|-------------|-------|
|   |                                   |                     | Know the benefit and the ways of work                           | Know the ways of work | Do not know |       |
| Elementary school                         | Availability of Public Counseling | Not available       | 0   | 2                     | 12          | 14    |
|   |                                   | Available           | 0   | 0                     | 2           | 2     |
|   | Total                             |                     | 0   | 2                     | 14          | 16    |
| Junior high school                        | Availability of Public Counseling | Not available       | 0   | 0                     | 4           | 4     |
|   |                                   | Available           | 1   | 1                     | 0           | 2     |
|   | Total                             |                     | 1   | 1                     | 4           | 6     |
| Senior High school                        | Availability of Public Counseling | Not available       | 1   | 3                     | 25          | 29    |
|   |                                   | Sometimes available | 0   | 1                     | 0           | 1     |
|   | Total                             | Available           | 0   | 1                     | 2           | 3     |
| Bachelor                                  | Availability of Public Counseling | Sometimes available | 1   | 5                     | 27          | 33    |
|   |                                   | Available           | 0   | 1                     | 18          | 19    |
|   | Total                             |                     | 0   | 1                     | 18          | 19    |
| Total                                     | Availability of Public Counseling | Not available       | 2   | 1                     | 0           | 3     |
|   |                                   | Sometimes available | 2   | 0                     | 1           | 3     |
|   | Total                             | Available           | 4   | 2                     | 19          | 25    |
| Total                                     |                                   |                     | 1   | 6                     | 59          | 66    |



|       |                     |   |    |    |    |
|-------|---------------------|---|----|----|----|
|       | Sometimes available | 2 | 2  | 0  | 4  |
|       | Available           | 3 | 2  | 5  | 10 |
| Total |                     | 6 | 10 | 64 | 80 |

Based on the results of the analysis in Table 1, it can be seen that all levels of education do not know the definition, benefit, and ways of work of CDWMS. The lack of community knowledge is due to the absence of public counseling carried out by the CDWMS implementation program. This can be proven in the number of criteria of not knowing the definition, benefit and how CDWMS works is relatively large when there is no counseling. Thus the public counseling program is very influential on people's knowledge about the definition, benefit and how CDWMS works.

#### **Correlation between Public Counseling, Knowledge about CDWMS, and Community Willingness to Use CDWMS**

Although many people answered that they did not know about CDWMS, after a brief explanation about the benefits of CDWMS, the community was interested and willing to participate in using it. The relationship between extension programs, the level of community knowledge, and community willingness to use CDWMS can be seen in Table 2.

Table 2. Knowledge of The Definition, Benefit, and Ways of Work of CDWMS \* Availability of Public Counseling Cross Tabulation

|                                   |   |                                       | Willingness to use CDWMS |                | Total |
|-----------------------------------|---|---------------------------------------|--------------------------|----------------|-------|
| Availability of Public Counseling |   |                                       | Unwilling to use         | Willing to use |       |
| Not available                     | Knowledge of the definition, benefit, and ways of work of CDWMS | Know the benefit and the ways of work | 0                        | 1              | 1     |
|                                   |   | Know the ways of work                 | 3                        | 3              | 6     |
|                                   |   | Do not know                           | 26                       | 33             | 59    |
|                                   |   | Total                                 | 29                       | 37             | 66    |
| Sometimes available               | Knowledge of the definition, benefit, and ways of work of CDWMS | Know the benefit and the ways of work | 1                        | 1              | 2     |
|                                   |   | Know the ways of work                 | 1                        | 1              | 2     |
|                                   |   | Total                                 | 2                        | 2              | 4     |
|                                   |   |                                       |                          |                |       |
| Available                         | Knowledge of the definition, benefit, and ways of work of CDWMS | Know the benefit and the ways of work | 0                        | 3              | 3     |
|                                   |   | Know the ways of work                 | 0                        | 2              | 2     |
|                                   |   | Do not know                           | 0                        | 5              | 5     |
|                                   |   | Total                                 | 0                        | 10             | 10    |
| Total                             | Knowledge of the definition, benefit, and ways of work of CDWMS | Know the benefit and the ways of work | 1                        | 5              | 6     |
|                                   |   | Know the ways of work                 | 4                        | 6              | 10    |
|                                   |   | Do not know                           | 26                       | 38             | 64    |
|                                   |   | Total                                 | 31                       | 49             | 80    |

Based on the results of the analysis in Table 2, can be seen that overall the community is more willing to use CDWMS even though many do not receive counseling. Through a brief explanation of what CDWMS is and its benefits, many people are willing to use CDWMS, especially if a routine public counseling program is held. In this condition, it means that counseling is needed to increase public knowledge about the benefits and how CDWMS works thus encourage the availability of people to use it.

One of the basic factors in the sustainability of the

sanitation system is community preparation that needs to be done properly. This means that the meaning is not just public counseling, but the community really has the need for sanitation facilities [8].

#### **Correlation between Income Level, Willingness to Tap to CDWMS Network, and Ability to Tap to CDWMS**

The sustainability of a program and the usefulness of infrastructure will succeed if it is supported by

community participation both in terms of willingness to use and the ability to use it. The level of community ability can be seen from the amount of income. The relationship between the three criteria is presented in Table 3.

Based on the results of the analysis in Table 3, it is known that the greater the level of income, the more willing to pay the CDWMS connection fees. However, in majority only willing to pay the network tapping fee if the amount is less than IDR 500,000.00.

The willingness of the community to use CDWMS is extensive, however, it is not supported by the community's ability to pay. This is indicated by the majority of people in the study who only willing to pay around IDR 500,000.00 even though the connection costs itself range from IDR 1,500,000.00 - IDR 4,000,000.00 [9]. The community obligations are to contribute to the thinking, time, and finances both for construction (minimum cost of home connections), and maintenance operations through the payment of regular monthly contributions [10].

Table 3. Ability to Connect to CDWMS Sewerage Network \* Willing to Pay the CDWMS Network Tapping Cost \* Income Level Cross Tabulation

| Income level (IDR) |  |                     | Willing to pay the CDWMS network tapping cost |                | Total |
|--------------------|--|---------------------|---|----------------|-------|
|                    |  |                     | Unwilling to pay                              | Willing to pay |       |
| <1 million         | Ability to connect to CDWMS sewerage network | <500,000            | 0   | 1              | 1     |
|                    |  | Unwilling           | 2   | 0              | 2     |
|                    | Total  |                     | 2   | 1              | 3     |
| 1-2.5 million      | Ability to connect to CDWMS sewerage network | <500,000            | 0   | 12             | 12    |
|                    |  | 600,000-1,000,000   | 0   | 3              | 3     |
|                    |  | Unwilling           | 15  | 0              | 15    |
|                    | Total  |                     | 15  | 15             | 30    |
| 2.6-4.5 million    | Ability to connect to CDWMS sewerage network | <500,000            | 0   | 6              | 6     |
|                    |  | 600,000-1,000,000   | 0   | 4              | 4     |
|                    |  | 1,100,000-2,000,000 | 0   | 3              | 3     |
|                    |  | Unwilling           | 12  | 2              | 14    |
|                    | Total  |                     | 12  | 15             | 27    |
| 4.6-6.5 million    | Ability to connect to CDWMS sewerage network | <500,000            | 0   | 4              | 4     |
|                    |  | 600,000-1,000,000   | 0   | 4              | 4     |
|                    |  | Unwilling           | 4   | 0              | 4     |
|                    | Total  |                     | 4   | 8              | 12    |
| 6.6-8.5 million    | Ability to connect to CDWMS sewerage network | <500,000            | 0   | 1              | 1     |
|                    |  | 600,000-1,000,000   | 0   | 1              | 1     |
|                    |  | 1,100,000-2,000,000 | 0   | 1              | 1     |
|                    |  | Unwilling           | 1   | 0              | 1     |
|                    | Total  |                     | 1   | 3              | 4     |
| >8.5 million       | Ability to connect to CDWMS sewerage network | 600,000-1,000,000   | 0   | 3              | 3     |
|                    |  | Unwilling           | 1   | 0              | 1     |
|                    | Total  |                     | 1   | 3              | 4     |
| Total              | Ability to connect to CDWMS sewerage network | <500,000            | 0   | 24             | 24    |
|                    |  | 600,000-1,000,000   | 0   | 15             | 15    |
|                    |  | 1,100,000-2,000,000 | 0   | 4              | 4     |
|                    |  | Unwilling           | 35  | 2              | 37    |
|                    | Total  |                     | 35  | 45             | 80    |

#### Correlation between Income Level, Willingness to Pay Operation and Maintenance Cost, and Ability to Pay CDWMS Retribution Fee

In addition to the importance of considering the ability of the community to connect to CDWMS,

measuring the ability of the community to pay retribution for the sustainability of CDWMS must also be considered. The results of the analysis of the relationship between income levels, willingness to pay for O & M, and the ability to pay retribution can be seen in Table 4.

Based on the results of the analysis in Table 4 it can be seen that the higher the income, more are the people willing to pay. The majority of this group are those who have the ability to pay fees less than or

equal to IDR 6,000.00 - 10,000.00. The value of the ability to pay levies is still in the range of the value of CDWMS retribution, which ranges from IDR 5,000.00 - 20,000.00 [9].

Table 10. Ability To Pay CDWMS Retribution \* Willingness To Pay The Operation And Maintenance Cost  
\* Income Level Cross tabulation

|                    |                                  |                                  | Willing to pay the O & M cost |                | Total |
|--------------------|----------------------------------|----------------------------------|-------------------------------|----------------|-------|
| Income Level (IDR) |                                  |                                  | Unwilling to pay              | Willing to pay |       |
| <1 million         | Ability to pay CDWMS retribution | <5,000                           | 0                             | 1              | 1     |
|                    |                                  | Unwilling                        | 2                             | 0              | 2     |
|                    | Total                            |                                  | 2                             | 1              | 3     |
| 1-2,5 million      | Ability to pay CDWMS retribution | <5,000                           | 0                             | 6              | 6     |
|                    |                                  | 6,000-10,000                     | 0                             | 3              | 3     |
|                    |                                  | 11,000-15,000                    | 0                             | 1              | 1     |
|                    |                                  | 16,000-20,000                    | 0                             | 5              | 5     |
|                    | Total                            | Unwilling                        | 13                            | 2              | 15    |
| 2,6-4,5 million    | Ability to pay CDWMS retribution | <5,000                           | 0                             | 2              | 2     |
|                    |                                  | 6,000-10,000                     | 0                             | 9              | 9     |
|                    |                                  | 11,000-15,000                    | 0                             | 2              | 2     |
|                    |                                  | Unwilling                        | 13                            | 1              | 14    |
|                    | Total                            |                                  | 13                            | 14             | 27    |
| 4,6-6,5 million    | Ability to pay CDWMS retribution | <5,000                           | 0                             | 1              | 1     |
|                    |                                  | 6,000-10,000                     | 0                             | 3              | 3     |
|                    |                                  | 11,000-15,000                    | 0                             | 2              | 2     |
|                    |                                  | 16,000-20,000                    | 0                             | 2              | 2     |
|                    | Total                            | Unwilling                        | 4                             | 0              | 4     |
| 6,6-8,5 million    | Ability to pay CDWMS retribution | <5,000                           | 0                             | 1              | 1     |
|                    |                                  | 11,000-15,000                    | 0                             | 2              | 2     |
|                    |                                  | Unwilling                        | 1                             | 0              | 1     |
|                    |                                  | Total                            |                               | 1              | 3     |
|                    | >8,5 million                     | Ability to pay CDWMS retribution | <5,000                        | 0              | 1     |
| 6,000-10,000       |                                  |                                  | 0                             | 1              | 1     |
| 16,000-20,000      |                                  |                                  | 0                             | 1              | 1     |
| Unwilling          |                                  |                                  | 1                             | 0              | 1     |
| Total              |                                  |                                  | 1                             | 3              | 4     |
| Total              | Ability to pay CDWMS retribution | <5,000                           | 0                             | 12             | 12    |
|                    |                                  | 6,000-10,000                     | 0                             | 16             | 16    |
|                    |                                  | 11,000-15,000                    | 0                             | 7              | 7     |
|                    |                                  | 16,000-20,000                    | 0                             | 8              | 8     |
|                    | Total                            | Unwilling                        | 34                            | 3              | 37    |
|                    |                                  |                                  | 34                            | 46             | 80    |

## CONCLUSIONS

Conclusions from this study are:

- 1) The community readiness in the centralized domestic wastewater treatment implementation plan shows that the community still does not know the procedures as well as the benefits of it. Hence, even though the community shows vast willingness to use this system, it is not backed with the community's ability to pay the pipeline connections and the charges.

- 2) The community is only able to pay pipeline connections at < IDR 500,000 and pay charge of retribution at IDR 6,000 - IDR 10,000.

## REFERENCES

- [1] City of Surabaya Sanitation Working Group. 2016. Sanitation Strategy in Surabaya. Surabaya: Health Agency of Surabaya City.
- [2] Tucunan, K.P., Ridwan, Y.H., Putri, A.S., Soedjono, E.S.. 2018. Sustainable kampung model in Kelurahan Keputih, Kejawan Putih

- Tambak and Gebang Putih of Surabaya City. IOP Conference Series: Earth and Environmental Science. Sci. 202 012075: 1-8.
- [3] Directorate General of Human Settlements. 2016. Technical Guidance on Preparation of Feasibility Study of Sewerage System.
- [4] Soedjono, S.S., Fitriani, N., Setiawan, A. Mulia, G. J. T., Ningsih, D.A. 2019. Study on Communal Wastewater Treatment Plants (CWWTPs) in Gresik, Indonesia. International Journal Of Integrated Engineering. 11 (2): 236 - 242
- [5] Mazaya, G.I., Noya, H., dan Soedjono, E.S. 2015. Study on Open Defecation Free in Kelurahan Kelayan Tengah Banjarmasin City. Prosiding of International Conference on Science, Technology, and Humanity: Surakarta.
- [6] The Center Regulation Policy and Governance and Institute for Sustainable Future. (2015). Review of Regulatory Framework for Local Scale —Air Limbahl. (Sydney: Institute for Sustainable Futures, University of Technology Sydney).
- [7] Surabaya City Regulation No. 12 of 2016 about The Management Of Water Quality And Control Of Wastewater
- [8] Iskandar, S., Fransisca, I, Arianto, E., dan Ruslan, A.. 2016. Centralized Domestic Wastewater Management System, Volume 3. Minister For Public Works and Human Settlements: Jakarta
- [9] Japan International Cooperate Agency. 2012. Project for Capacity Development of the Wastewater Sector Through Review of the Wastewater Management Master Plan in DKI Jakarta, Indonesia.
- [10] Sunarti. 2003. Community Participation in Group Housing Development. Jurnal Tata Loka. Semarang: Planologi UNDIP

# ANALYSIS OF CHANGES IN SHEAR STRENGTH AND STIFFNESS OF HO CHI MINH CITY' SOFT SOIL UNDER THE UNLOADING STRESS PATHS FOR DEEP EXCAVATIONS CALCULATION

Trung Ngo Duc<sup>1</sup>, Phan Vo<sup>2</sup> and Thanh Tran Thi<sup>3</sup>

<sup>1</sup> Civil Engineering Department, Van Hien University, Ho Chi Minh City, Vietnam,

<sup>2</sup> Ho Chi Minh City University of Technology, Vietnam,

<sup>3</sup> The Industrial University of Ho Chi Minh City, Vietnam

## ABSTRACT

In urban areas, underground space are growing demand and deep excavations are often used to solve this problem. In Ho Chi Minh City, deep excavation is often constructed in areas close to existing buildings, infrastructure or public services, so limiting the displacement of the retaining wall and surface subsidence is very important to ensure that the surrounding works are not affected or affected by the level of permission. In order to analyze the displacement and deformation of the excavation pit, it is necessary to determine the soil characteristics of the excavation pit foundation for inclusion in the soil models. However, the construction design of the project is mainly taken from normal geological experiments, yet it does not describe the behavior of the surrounding soil. Therefore, the problem is to use an experimental model with a reasonable stress path to determine input parameters that are appropriate to the behavior of the ground around the pit, expressed by the change the stiffness of the soil during the excavation work, which the current experimental process is considered unchanged. This paper uses triaxial tests to evaluate the shear strength behavior of soft soil in Ho Chi Minh City with stress paths for calculation deep excavations. The experiments were carried out on a undraining fixture scheme of 50, 100, 200kPa pressure ratings to determine the shear strength and deformation modulus parameters of the  $E_{50}$  during the unloading process.

*Keywords: strain, stress paths, nonlinearity, deep excavation, soil model, unloading*

## INTRODUCTION

In recent years, the demand for underground space has been increasing in urban areas. Deep excavations are often used to solve this problem. In Ho Chi Minh City, deep excavations has usually constructed in areas close to existing buildings, infrastructure or public services, so it is important to limit the displacement of retaining walls and surface settlement. to ensure the surrounding buildings are not affected or affected by the permitted level.

Due to the lack of laboratory data in the room, engineers often use conventional geological test data or correlate design parameters from available parameters and are often limited to simple model land in design of deep excavations. In fact, the construction of excavation can be considered a loading and unloading problem for the ground, this unloading changes the deformation stress state in the ground. If the correlation is irrelevant or determine parameters from test with improper stress paths, the engineer often faces the problem of deformation the actual deep excavations will be different from the predicted value.

Deep excavations is influenced by geotechnical conditions, the most important calculation is the control of horizontal displacement of the retaining

wall at the lowest level, so it is necessary to determine the actual stress state of the soil around the deep excavations.

Many studies [4][5] have divided the area affected by the excavation process into four parts, as shown in Figure 1.

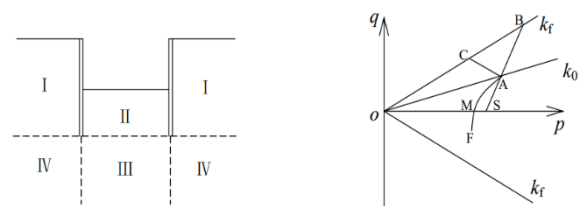


Fig. 1 Area of influence of deep excavation and stress paths

Zone I: when removing soil out of the excavation, horizontal displacement of the retaining wall will occur and horizontal stress decreases while vertical stress remains unchanged. Stress paths as the AC segment in Figure 1.

Zone II: during excavation, vertical stress decreases and lateral stress increases due to wall displacement, reduced soil strength, and ductile region may appear at the bottom of the pit. The stress path for this region is represented by the AMF segment in Figure 1.

Zone III: During the excavation process, vertical stress decreases continuously; horizontal stress changes a little; and stress path is shown in the AS segment in Figure 1.

Region IV: Vertical stress is basically constant; there is a slight change in horizontal stress; the main shaft of the stress is deflected by shear; and the stress path is still near the AC segment in Figure 1.

The most significant effect on the deformation of the deep excavation is Zone I and Zone II, in which Zone I is the main factor causing horizontal displacement and Zone II causing bottom heave, which has important effects on deformation of deep excavation. Zone I and Zone II correspond to stress paths AC and AMF. In the AMF, the AM part is the unloading part and the MF part is loaded, which can be analyzed by a general geotechnical model. The AC line is the horizontal unloading stress line. Unlike AB stress lines in conventional experiments, there are different behaviors and stress paths.

In practice, the soil productivity change is very complicated. It can be seen that in order to analyze the behavior of Zone I (behind the retaining wall) and Zone II (at the bottom of the excavation pit), the analysis of soil strength and stiffness parameters of these two areas is a major issue focus on solving.

In order to have accurate data on the deformation of the excavation, it is necessary to have the soil characteristics of the area around the excavation to provide input data to be included in the calculation models. However, the current design of construction activities is mainly taken from normal geological tests, not describing the behavior of the land around the excavation pit. Therefore, the question is to use an experimental model with a reasonable stress path to determine the input parameters in accordance with the behavior of the ground around the excavation, expressed through change soil stiffness during excavation, which the current experimental procedure is considered to be constant.

In this study, the author performed a series of three undrained triaxial tests (CU) on 27 soft soil samples with a depth of 4 to 24m with load levels of 50, 100, 200 kPa, respectively, with the stress paths. Different stresses for evaluating shear and stiffness behavior of soft soil in Ho Chi Minh City.

## APPARATUS

The test was carried out with the load frame system of Humboldt (USA) according to ASTM D4767. This system includes pressure, deformation, pressure and volume sensors connected to ADAM View 32-channel datalogger system. Advantech Adam view software allows collecting data from sensors over time. The system is connected to the computer via a network card to allow chamber pressure control and testing to be performed automatically from the beginning to the end.



Fig. 2 Humboldt tri-axial equipment system

Principles for design of the compression cell of the experiment with loading models based on Bishop and Wesley's hydraulics (1975) [1][2][3] to control the different stresses during the unloading experiment.

Testing samples and testing parameters according to different stress paths shows in Table 2. A total of 27 soft soil samples were tested, of which 18 samples of very soft clays and 9 samples of soft clays, experimented according to the stress paths. The stress program is as follows:

- Conventional triaxial compression model (CTC - increase  $\sigma_1$  and fixed  $\sigma_3$ ): Saturated soil samples are isotropic consolidation and undrained samples according to the usual compression schedule: 9 samples;
- Triaxial drag model (RTE - reduced  $\sigma_1$  and fixed  $\sigma_3$ ): Saturated soil samples are isotropic consolidation and non-draining samples according to vertical stress reduction schedule: 9 samples;
- Model of cell pressure reduction (RTC - reduction  $\sigma_3$  and fixed  $\sigma_1$ ): Saturated soil samples are isotropic consolidation and non-draining samples according to horizontal stress reduction schedule: 9 samples;

Table 2 Soil parameters for soft soil in Ho Chi Minh City and the stress paths in the tri-axial test

| Depth [m]              | Stress paths | Test No. | $W_n$ [%] | $\gamma_n$ [kN/m <sup>3</sup> ] | $\sigma_c$ [kPa] |
|------------------------|--------------|----------|-----------|---------------------------------|------------------|
| <i>Very soft clays</i> |              |          |           |                                 |                  |
| 4÷6                    | CTC          | 1        | 88.55     | 15.7                            | 50               |
|                        |              | 2        | 88.38     | 16.0                            | 100              |
|                        |              | 3        | 81.47     | 15.9                            | 200              |
|                        | RTE          | 4        | 88.55     | 15.7                            | 50               |
|                        |              | 5        | 88.38     | 16.0                            | 100              |
|                        |              | 6        | 81.47     | 15.9                            | 200              |
|                        | RTC          | 7        | 88.55     | 15.7                            | 50               |
|                        |              | 8        | 88.38     | 16.0                            | 100              |
|                        |              | 9        | 81.47     | 15.9                            | 200              |
| 12÷14                  | CTC          | 10       | 78.87     | 15.6                            | 50               |
|                        |              | 11       | 78.70     | 15.4                            | 100              |
|                        |              | 12       | 75.80     | 15.9                            | 200              |



|                   |     |    |       |      |     |
|-------------------|-----|----|-------|------|-----|
|                   | RTE | 13 | 78.87 | 15.6 | 50  |
|                   |     | 14 | 78.70 | 15.4 | 100 |
|                   |     | 15 | 75.80 | 15.9 | 200 |
|                   | RTC | 16 | 78.87 | 15.6 | 50  |
|                   |     | 17 | 78.70 | 15.4 | 100 |
|                   |     | 18 | 75.80 | 15.9 | 200 |
| <i>Soft clays</i> |     |    |       |      |     |
| 18÷20             | CTC | 19 | 71.83 | 15.6 | 50  |
|                   |     | 20 | 62.86 | 15.7 | 100 |
|                   |     | 21 | 65.89 | 15.6 | 200 |
|                   | RTE | 22 | 71.83 | 15.6 | 50  |
|                   |     | 23 | 62.86 | 15.7 | 100 |
|                   |     | 24 | 65.89 | 15.6 | 200 |
|                   | RTC | 25 | 68.45 | 15.8 | 50  |
|                   |     | 26 | 65.76 | 15.7 | 100 |
|                   |     | 27 | 65.76 | 15.9 | 200 |
| 24÷26             | CTC | 28 | 50.14 | 16.4 | 50  |
|                   |     | 29 | 66.27 | 16.6 | 100 |
|                   |     | 30 | 54.21 | 16.7 | 200 |
|                   | RTE | 31 | 50.14 | 16.4 | 50  |
|                   |     | 32 | 66.27 | 16.6 | 100 |
|                   |     | 33 | 54.21 | 16.7 | 200 |
|                   | RTC | 34 | 50.14 | 16.4 | 50  |
|                   |     | 35 | 66.27 | 16.6 | 100 |
|                   |     | 36 | 54.21 | 16.7 | 200 |

## ANALYSIS AND EVALUATION OF TESTING RESULTS

### Stress and strain relationship ( $q$ - $\epsilon$ )

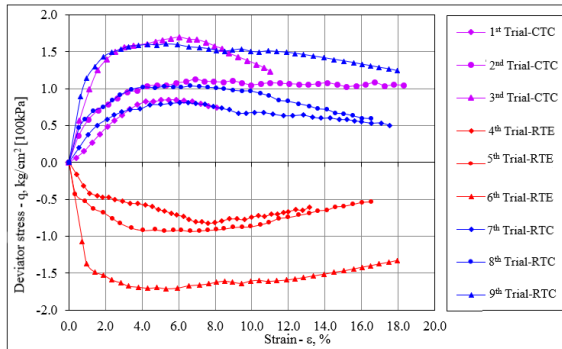


Fig. 3 Relationship ( $q$  -  $\epsilon$ ) of stress paths at depths 4-6m

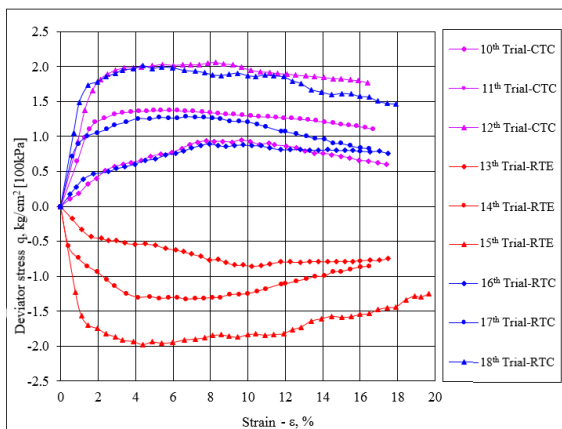


Fig. 4 Relationship ( $q$  -  $\epsilon$ ) of stress paths at depths 12-14m

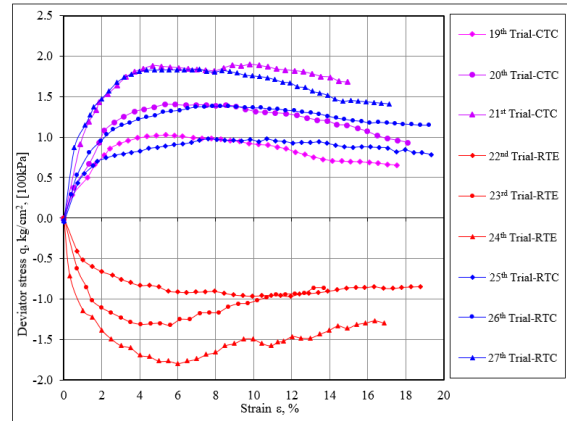


Fig. 5 Relationship ( $q$  -  $\epsilon$ ) of stress paths at depths 18-20m

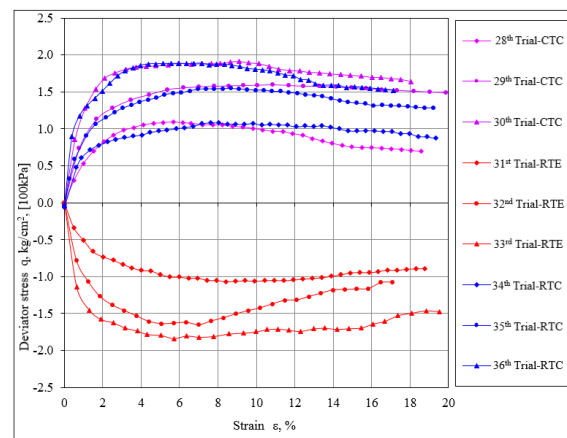


Fig. 6 Relationship ( $q$  -  $\epsilon$ ) of stress paths at depths 24-26m

In the above section, the triaxial test according to the three stresses CTC, RTE and RTC is performed with the CU diagram. The relationship of stress - deformation and change of pore water pressure with deformation with the above 3 stress paths at the cell pressure levels ( $\sigma_3$ ) are respectively 50kPa, 100kPa and 200kPa are shown from Figure 3 to Figure 6.

In conventional triaxial compression test with CTC stress curve, stress relationship - deformation is progressively nonlinear and deformed with increasing deviation stress until the sample is destroyed, value maximum deviation stress increases with cell pressure level. The pore water pressure is always positive and also increases immediately along with the deformation in the axial stress increase process.

In contrast, for the RTE stress paths in a triaxial tensile test, the pore water pressure decreases at low stress levels and gradually increases at higher stress levels. The initial pressure of the pore water is negative and the positive sign is changed according to the increase of the deviation stress due to the reduction of  $\sigma_1$ . Therefore, the destructive stress and the change of pore water pressure for triaxial tensile tests also depend on the stress paths. Experimental results with RTE stress paths show that axial strain corresponding to maximum stress increases with cell

pressure and pore water pressure represents elasticity, which corresponds to the corresponding. The expansion of volume of ground soil outside reality when unloading during construction of excavation pits. This expansion behavior may be partly explained by the change in the pore water pressure of the soil sample at the end of the saturation and consolidation period during shear stress. In most cases, these soil samples were damaged by declining deformation. The destruction of the sample is seen in the middle of the sample like the bottleneck shape as shown in Fig. 7. It can be seen that, during the increase in stress, the pore water pressure also increases similarly corresponding to each stress paths. The destructive pattern when deforming is about  $6 \div 8\%$ .

Testing results show that in the axial stress strain RTE paths, it increases more slowly than CTC stress paths, especially shown at the maximum cell pressure level, which means that the initial tangent modulus is higher in the RTE stress paths and has a lower value for the CTC stress paths. From this, it can be concluded that the elastic parameters depend on the initial stress and strain modulus paths in the process of unloading.

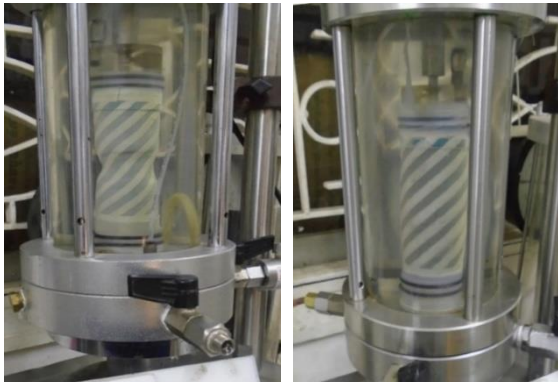


Fig. 7 Sample destruction by RTE (left picture) and RTC stress path (right picture)

With the triaxial compression stress paths reducing horizontal stress RTC, when the horizontal stress is reduced during the sample cutting process, the deformation also increases but is slower than the deformation compared to CTC stress paths, so the strain deformation modulus. The intention to calculate deep excavation by HS model has much greater results than CTC stress paths due to the curvature of stress strain relationship with greater slope. The pore water pressure in the RTC route is opposite to the CTC stress path but has a significantly smaller magnitude and has a different nonlinearity, this pressure gradually increases to the destructive threshold of the sample and decreases when the sample starts destructive. Testing results indicate that the parameter values determined from the strain stress relationship of the ground soil depend on the stress path of the triaxial test. Different stress paths will give different shear strength values and the deformation

characteristics of soil samples will change as cell pressure increases. The initial deformation module  $E_i$  in experiments with unloading path is also of different value than when determining from the usual tri-axial compressive stress paths. Therefore, with the problem of designing deep excavations, the determination of input parameters with appropriate stress paths will give economical and safety results.

#### Analysis of deformation modules of stress paths

The relation ( $q, \varepsilon_1$ ) Figure 3 to Figure 6 calculate the deformation module  $E_{50}$  of soft clays samples at different depths and different cell pressures as determined stiffness parameters of HS model. The results are shown in Table 3.

The magnitude of the  $E_{50}$  strain module increases gradually with depth. At the same depth, the distortion module will also have a greater value if tested with a larger cell pressure level.

Testing results show that the stiffness of soil depends on the stress paths. With HDS, the selection of stiffness parameters in the displacement calculation should be taken from the test with the unloading stress paths.

Table 3  $E_{50}$  deformation modules from CTC, RTE and RTC stress paths

|                        |            | RTE      | RTC      | CTC      |                                 |                                 |
|------------------------|------------|----------|----------|----------|---------------------------------|---------------------------------|
| Depth                  | $\sigma_c$ | $E_{50}$ | $E_{50}$ | $E_{50}$ | $\frac{E_{50,RTE}}{E_{50,CTC}}$ | $\frac{E_{50,RTC}}{E_{50,CTC}}$ |
| [m]                    | [kPa]      | [kPa]    | [kPa]    | [kPa]    |                                 |                                 |
| <i>Very soft clays</i> |            |          |          |          |                                 |                                 |
| 4÷6                    | 50         | 3611     | 3494     | 2085     | 1.73                            | 1.68                            |
|                        | 100        | 8202     | 7495     | 4774     | 1.72                            | 1.57                            |
|                        | 200        | 14528    | 13997    | 8553     | 1.70                            | 1.64                            |
| 12÷14                  | 50         | 2750     | 2968     | 1853     | 1.48                            | 1.60                            |
|                        | 100        | 11575    | 9427     | 5981     | 1.94                            | 1.58                            |
|                        | 200        | 15194    | 17774    | 9389     | 1.62                            | 1.89                            |
| <i>Soft clays</i>      |            |          |          |          |                                 |                                 |
| 18÷20                  | 50         | 5811     | 5391     | 3673     | 1.58                            | 1.47                            |
|                        | 100        | 8640     | 6442     | 4510     | 1.95                            | 1.48                            |
|                        | 200        | 14652    | 14121    | 9273     | 1.58                            | 1.52                            |
| 24÷26                  | 50         | 4579     | 4201     | 2861     | 1.60                            | 1.47                            |
|                        | 100        | 7765     | 7026     | 4922     | 1.58                            | 1.43                            |
|                        | 200        | 16688    | 15107    | 9161     | 1.82                            | 1.65                            |

The difference in the value of the elastic modulus according to the stress paths can be explained by the dependence of the elastic modulus according to each stress paths on the plastic strain level. The magnitude of plastic deformation depends on the flexible potential function and flexible flow function. Thus, the elastic modulus of the ground at some point has only one value in the state without deformation. When the ground is deformed, the value of the elastic modulus decreases with a degree of dependence on the stress path. The value of the elastic modulus of the ground soil is determined by the initial slope of the

strain-strain relationship curve in such a conventional tri-axial compression test that results in a large error in the calculation. Therefore, it is recommended to use the value of the elastic module from the unloading tri-axial compression test.

With triaxial test according to RTE and RTC stresses, the results of the deformation modulus are much larger than those calculated from the test results according to the normal tri-axial compressive stress path:

$$\frac{E_{50,RTE}}{E_{50,CTC}} \approx \frac{E_{50,RTC}}{E_{50,CTC}} = [1.48 \div 1.57] \quad (1)$$

### Strength resistance of soil with different stress paths

From the above diagrams of stress-strain relationship (Figure 3 to Figure 6), destructive contour lines can be drawn to determine the effective shear resistance parameters for soil layers as follows:

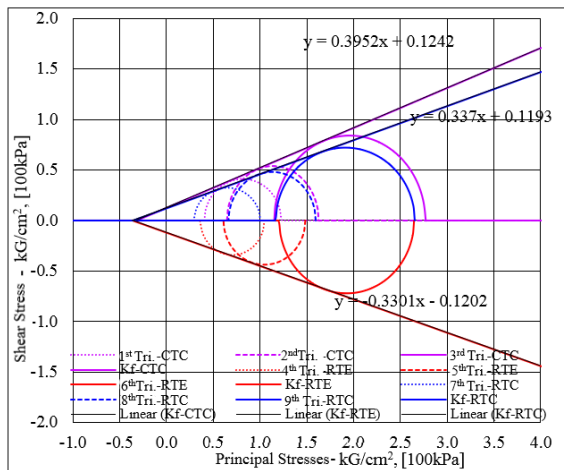


Fig. 8 Mohr circle according to stress paths at depth of 4-6m

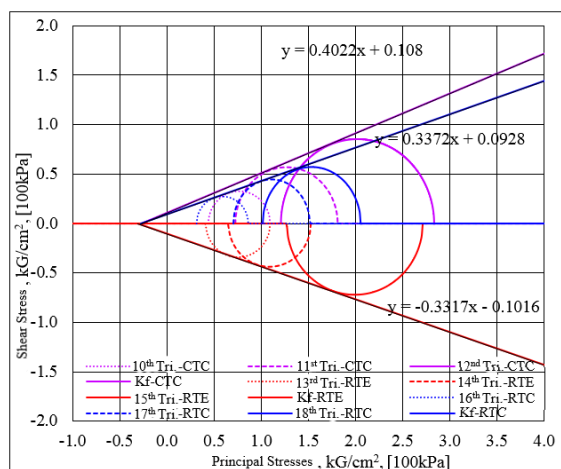


Fig. 9 Mohr circle according to stress paths at depth of 12-14m

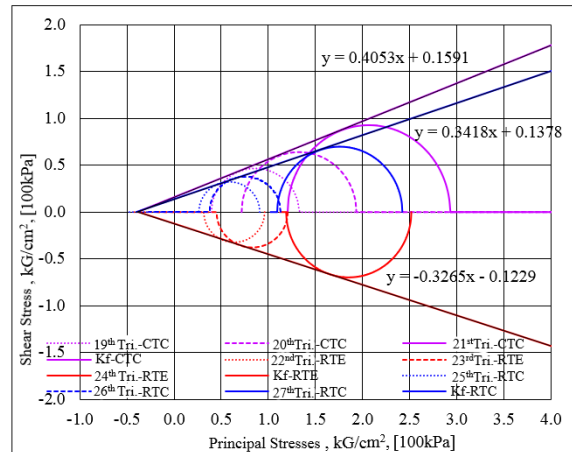


Fig. 10 Mohr circle according to stress paths at depth of 18-20m

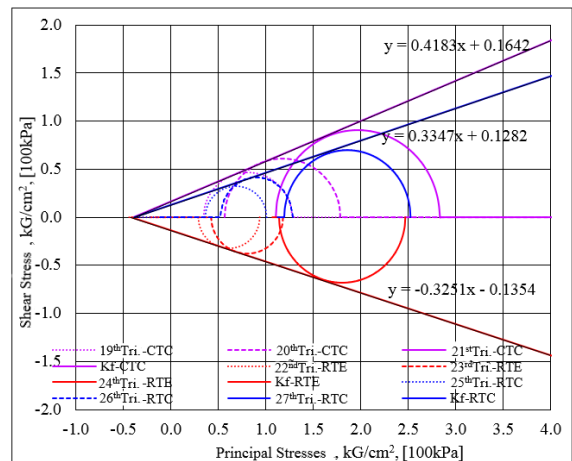


Fig. 11 Mohr circle according to stress paths at depth of 24-26m

The slope of the  $K_f$  destructive lines according to the stress paths is clearly different.

The effective friction angle of the RTE and RTC unloading route is similar and smaller than the CTC schedule. For each load level, the stress circle of RTE and RTC routes is back to the origin of the coordinates compared to the normal tri-axial compression stress paths CTC.

From the diagrams of Figure 8 to Figure 11, determine the effective shear strength parameters of the soil as shown in Table 4.

Table 4 Value of  $c'$  and  $\phi'$  of soft soil in HCMC. according to stressed paths

| Depth [m]              | Stress paths | $c'$ [kPa] | $\Delta c'$ [%] | $\phi'$ [°] | $\Delta \phi'$ [%] |
|------------------------|--------------|------------|-----------------|-------------|--------------------|
| <i>Very soft clays</i> |              |            |                 |             |                    |
| 4÷6                    | CTC          | 13.58      |                 | 21.56       |                    |
|                        | RTC          | 11.21      | 0.83            | 18.62       | 0.86               |
|                        | RTE          | 11.17      | 0.82            | 18.26       | 0.85               |
| 12÷14                  | CTC          | 13.87      |                 | 21.90       |                    |
|                        | RTC          | 11.12      | 0.80            | 18.63       | 0.85               |

|                   | RTE | 11.39 | 0.82 | 18.35 | 0.84 |
|-------------------|-----|-------|------|-------|------|
| <i>Soft clays</i> |     |       |      |       |      |
| 18÷20             | CTC | 15.32 |      | 22.00 |      |
|                   | RTC | 12.45 | 0.81 | 18.87 | 0.86 |
|                   | RTE | 12.17 | 0.79 | 18.08 | 0.82 |
| 24÷26             | CTC | 14.94 |      | 22.70 |      |
|                   | RTC | 11.72 | 0.78 | 18.51 | 0.82 |
|                   | RTE | 11.64 | 0.78 | 18.01 | 0.79 |

From the results of the analysis, it can be seen that the effective friction angle of the ground ( $\phi'$ ) in the three-axis test calculated by RTE and RTC is similar and smaller than that determined by the usual triaxial compression stress paths (CTC), this value is about 15% to 23% smaller:

$$\frac{\phi'_{RTE}}{\phi'_{CTC}} \approx \frac{\phi'_{RTC}}{\phi'_{CTC}} = 0.77 \div 0.85 \quad (2)$$

Experimental results show that the effective shear strength ( $\phi'$ ) of soft soil in HCMC declined from 15% to 23% under the unloading stress schedule in case of deep excavations.

## CONCLUTIONS

- Behavior of soil depends greatly on stress paths. Determining the shear strength parameters as well as the stiffness parameters for the deep excavation problem should be determined from the tri-axial experiment with the unloading stress paths because these experiments describe the actual working state of the ground during the construction process
- In the experiment with the unloading schedule, the shear resistance of the soil is significantly reduced compared to the conventional tri-axial compression test, because the excavation process is the process of unloading so the horizontal displacement of the soil will cause the soil to deteriorate (soft soil when digging).

- The effective friction angle of the ground ( $\phi'$ ) in the tri-axial test calculated by RTE and RTC is similar and smaller, determined by the usual tri-axial compression stress path (CTC), which is smaller between 15% and 23%:

$$\frac{\phi'_{RTE}}{\phi'_{CTC}} \approx \frac{\phi'_{RTC}}{\phi'_{CTC}} = 0.77 \div 0.85$$

- Deformation modulus of soil also depends on stress paths. The linear sand deformation module of the triaxial test reduces the stress greater than the conventional triaxial test. Triaxial test according to RTE and RTC stresses results in equivalent modulus of modulus but larger than conventional tri-axial CTC stress path. With soft soil, scale ranges from  $[1.48 \div 1.57]$  times:

$$\frac{E_{50,RTE}}{E_{50,CTC}} \approx \frac{E_{50,RTC}}{E_{50,CTC}} = 1.48 \div 1.57$$

## REFERENCES

- [1] Bishop, A. W. and Garga, V. K., Drained Tension Tests on London Clay, Géotechnique Volume 19 issue 2, June 1969, pp. 309-313;
- [2] Bishop, A.W. and Henkel, D.J., The measurement of soil properties in the triaxial test, London : E. Arnold, 1962, ©1957.
- [3] Bishop, A.W. and Wesley, L.D. (1975), A Hydraulic Triaxial Apparatus for Controlled Stress Path Testing, Geotechnique, vol. 25(4), pp. 657–670;
- [4] Taha, M.R., Mofiz, S.A., Hossain, M.K. and Asmirza, M.S. (1999). Model simulation of residual soil in triaxial extension tests. Proc. of the Fifth Geotechnical Eng. Conference, Geotropika-99, pp. 105–114.
- [5] Wong, K. S. (2009), A Short Course on Deep excavations, New Zealand;

## SELF-SUPPORT SHELTER AS AN ALTERNATIVE SOLUTION IN THE TSUNAMI-PRONE AREA

Anas Febrin Ismail<sup>1</sup> \*, Taufika Ophiyandri<sup>1</sup>, Abdul Hakam<sup>1</sup>, Afdilla Yofianda<sup>1</sup>, Dicky Kurnia Adha<sup>1</sup>, Tria Yuli Anggraini<sup>1</sup>

<sup>1</sup>Civil Engineering of Andalas University, Padang, Indonesia

### ABSTRACT

Padang City, as the capital of West Sumatra province, has the potential to be hit by tsunamis. It is located about 200 km from subduction zone near Mentawai island. History shows that the city has experienced the tsunami in 1797 and 1833. This situation has been realized by all stakeholders in the area, including the Government, Private Sector, NGOs, and Communities. Today, there are approximately 600,000 residents exposed to the tsunami. So far, tsunami mitigation efforts have been carried out by many parties. The Government, with a limited budget, has built five shelters with a capacity of 2000-3000 people. This number is still far from enough. As a solution, the Government invites the owners of multi stories buildings to function their building as shelters. However, this invitation is not responding well since a lot of costs to strengthen the building to meet the shelter criteria. One promising alternative is Self-Support Shelters that are built by the community. The Self-Support Shelters are utilizing the existing public facilities such as Mosques or *Mushollas* (small mosque) where they are closed to community residence. The shelter may be built a base on the concept of upgrading the quality and capacity of the Mosque or Musholla. The construction costs are based on the *infaq*, that is, a kind of charity or donation by the Moslem to build religious facilities that will be rewarded by God in the hereafter. With this concept, the construction of shelters that require high costs can be done hand in hand by the community. This paper discusses the procedures for building Self-Support Shelter in terms of its capacity, accessibility, management, and construction methods. The results may be adopted as the guidance in building the Self-Support Shelters in Indonesia.

*Keywords: tsunami, public facilities, self-support shelter, procedures*

### INTRODUCTION

The series of big earthquakes in the last two decades have stricken the western part of Sumatra Island. Those earthquakes, so far, do not trigger a tsunami. However, experts still predict a big earthquake that can generate a tsunami is very potential to happen in the near future [1, 2, 3]. It is due to what so-called seismic gap that available near the Mentawai Islands. Padang City as the capital of West Sumatra province, where is about 200 km from the Mentawai Islands, has the potential to be destroyed by this tsunami. This information has been well understood by stakeholders in the area including Government, Private Sector, NGOs and Communities. There are approximately 600,000 residents exposed to the tsunami, as shown in Fig. 1.

Tsunami mitigation efforts have been carried out [4,5,6]. The Government with a limited budget has built five shelters with a capacity of 2000-3000 people. This number is still far from enough. As a solution, the Government invites the owners of multi stories buildings to function their building as shelters. This effort requires an assessment process to make sure the buildings are reliable [7, 8, 9, 10]. Unreliable buildings must be retrofitted to meet the shelter requirements [4, 5]. The expensive additional cost for retrofitting results rejection the Government proposal.



Fig. 1. Tsunami exposed area of Padang City

Therefore, it is necessary to find an alternative shelter that can be built in a massive and fast way without the Government budget. One alternative is what so-called the Self-Support Shelter. The Self-Support Shelter is a shelter that built and operated by the community. It is utilizing the existing public facilities such as Mosques or *Mushollas* (small mosque) where are close to houses. In



Padang City, each RW (a community group of about 100-200 households) at least has one *Musholla* located on an area about 100 to 400 m<sup>2</sup>. So, the Mosque and Musholla are easy to be found in the Muslim community like in Padang City.

At least there are three advantages using Mosque or Musholla as shelter. First, the land is already available, so it does not need to buy new land that is quite expensive. Second, Mosque or Musholla close to community so it can accommodate the surrounding community as a tsunami evacuation shelter, in time. Third, to build shelters require substantial funds, therefore, if the concept of upgrading the quality and capacity of the Mosque or Musholla, people are interested in donating their money because they will get a reward from God in the hereafter. Although it requires a long time period in its construction, however, using step by step concept depending on the incoming donation, the shelter finally will be completed. By using proper construction method, the existing Mosque or Musholla no need to be destroyed before the shelters completed.

This paper discusses the procedures for building Self-Support Shelter in terms of its capacity, accessibility, management, and construction methods. The procedure may be adopted as the guidance to build the Self-Support Shelters in Indonesia.

## METHODOLOGY

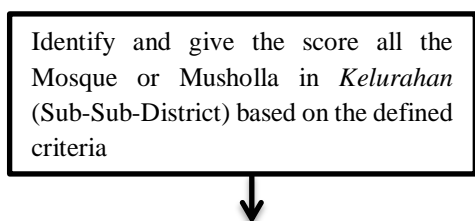
The study is conducted in the selected *Kelurahan* (Sub-Sub-District) which is the the lowest level unit of Government authority. It is chosen because the *Kelurahan* coordinates the grass root of the community. Under *Lurah* (Head of Sub-Sub District), there is *Ketua RW* (Coordinator several blocks of residence). Under *Ketua RW*, there is *Ketua RT* (Coordinator one block of residence). Both *Ketua RW* and *Ketua RT*, chosen by the community. Meanwhile, *Lurah*, is chosen by the Government.

The procedure in building the Self Supported Shelter then is applied as seen in the Flow Chart in Fig.2. *Kelurahan Pasie Nan Tigo* is selected as the case study for Self Supported Shelter. It is one out of 104 *Kelurahan* in Padang City. Its location can be seen Fig. 3.

### Identification of Mosque or Musholla

Each of Mosque or Musholla within Kelurahan Pasie Nan Tigo was surveyed and identified. After identifying all Mosques or Musholla, the next step is giving the score base on the defined criteria. The defined criteria are including the population distribution, land area, distance from the beach, accessibility, and the availability of the administrators.

Fig 2. Procedure in building Self Support Shelter





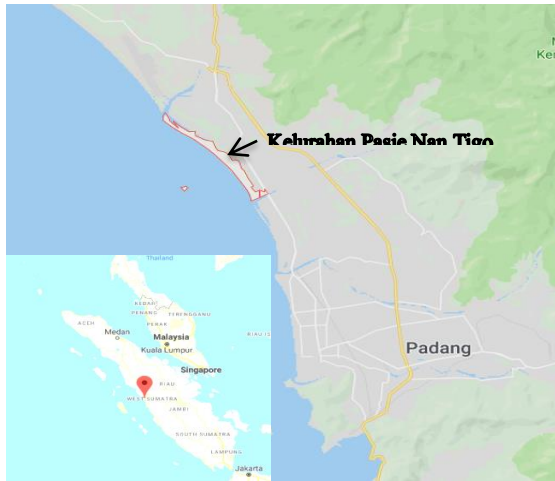


Fig 4. Map of Kelurahan Pasie Nan Tigo

Each of the criterion then is scoring. Population Distribution has score 4, 3, and 2 for Large, Medium, and Small, respectively. Land Area has score 3 and 0 for  $>600 \text{ m}^2$  and  $< 600 \text{ m}^2$ , respectively. Distance from the beach has score 2 and 0 for  $> 200 \text{ m}$  and  $< 200 \text{ m}$ , respectively. Accessibility has score 2 and 0 for high and low, respectively. Administrator has score 2 and 0 for available and unavailable, respectively.

There are twenty one Mosque or Musholla spreading in Kelurahan Pasie Nan Tigo have been identified. Eight of them including their attributes can be seen in Fig 5. The scoring result for all the Mosque and Musholla are summarized in Table 1.

It can be seen that there are 10 Mosque or Musholla that has the highest score. The ten Mosques and Musholla can be as seen in Table 2.

The next step is to ask the approval of each Mosque or Musholla administrator. Out of the 10 Musholla or Mosque, 4 of them are objection to be shelter due to some reasons. One reason is the birocracy process among the administrators. Therefore, only six are nominated to be Self Support Shelter as seen in Fig.2

| NO | MOSQUE NAME                                    | PHOTO | NOTES  |
|----|--|-------|--|
| 1  | Masjid Al Furqan                               |       | Address : Muaro Pengaliran<br>Kelurahan Pasie Nan Tigo<br>Building Area : $322 \text{ m}^2$<br>Land Area : $1345 \text{ m}^2$<br>Distance from Shore Line : $980 \text{ m}$<br>Ownership Status : Community<br>At Evacuation Route : Yes<br>Administrator : Available<br>Located at Dense Residence : Yes        |
| 2  | Masjid Nurul Falah                             |       | Address : Kompleks Kuala Nyiur II<br>Kelurahan Pasie Nan Tigo<br>Building Area : $245 \text{ m}^2$<br>Land Area : $666 \text{ m}^2$<br>Distance from Shore Line : $647 \text{ m}$<br>Ownership Status : Government<br>At Evacuation Route : Yes<br>Administrator : Available<br>Located at Dense Residence : Yes |
| 3  | Masjid Baiturrahmah                            |       | Address : Kelurahan Pasie Nan Tigo<br>Building Area : $216 \text{ m}^2$<br>Land Area : $390 \text{ m}^2$<br>Distance from Shore Line : $480 \text{ m}$<br>Ownership Status : Government<br>At Evacuation Route : Yes<br>Administrator : Available<br>Located at Dense Residence : Yes                            |
| 4  | Masjid Darul Islah                             |       | Address : Jalan Pasir Sebelah<br>Kelurahan Pasie Nan Tigo<br>Building Area : $318 \text{ m}^2$<br>Land Area : $537 \text{ m}^2$<br>Distance from Shore Line : $232 \text{ m}$<br>Ownership Status : Government<br>At Evacuation Route : Yes<br>Administrator : Available<br>Located at Dense Residence : Yes     |
| 5  | Masjid Universitas Muhammadiyah Sumatera Barat |       | Address : Kelurahan Pasie Nan Tigo<br>Building Area : $710 \text{ m}^2$<br>Land Area : $3465 \text{ m}^2$<br>Distance from Shore Line : $367 \text{ m}$<br>Ownership Status : Government<br>At Evacuation Route : Yes<br>Administrator : Available<br>Located at Dense Residence : Yes                           |
| 6  | Masjid TabiYestul 'Ulum                        |       | Address : Kelurahan Pasie Nan Tigo<br>Building Area : $377 \text{ m}^2$<br>Land Area : $671 \text{ m}^2$<br>Distance from Shore Line : $212 \text{ m}$<br>Ownership Status : Government<br>At Evacuation Route : Yes<br>Administrator : Available<br>Located at Dense Residence : Yes                            |
| 7  | Musala Darussalam                              |       | Address : Kelurahan Pasie Nan Tigo<br>Building Area : $250 \text{ m}^2$<br>Land Area : $347 \text{ m}^2$<br>Distance from Shore Line : $328 \text{ m}$<br>Ownership Status : Government<br>At Evacuation Route : Yes<br>Administrator : Available<br>Located at Dense Residence : Yes                            |
| 8  | Masjid Darul Muttaqin                          |       | Address : Kelurahan Pasie Nan Tigo<br>Building Area : $184 \text{ m}^2$<br>Land Area : $597 \text{ m}^2$<br>Distance from Shore Line : $224 \text{ m}$<br>Ownership Status : Government<br>At Evacuation Route : Yes<br>Administrator : Available<br>Located at Dense Residence : Yes                            |

Fig 5. Some of the Mosques or Mushollas in Kelurahan Pasie Nan Tigo

Table 1. Recapitulation of Mosque or Musholla score

| Mosque/<br>Musala<br>Code | Name of Mosque/Musala              | Population Distribution |             |            | Land Area<br>> 600 m <sup>2</sup> |         | Distance from<br>the beach ><br>200 m |         | Access    |            | Administrators |         | Total<br>Score |
|---------------------------|------------------------------------|-------------------------|-------------|------------|-----------------------------------|---------|---------------------------------------|---------|-----------|------------|----------------|---------|----------------|
|                           |                                    | Large<br>4              | Medium<br>3 | Small<br>2 | Yes<br>3                          | No<br>0 | Yes<br>2                              | No<br>0 | High<br>2 | Lower<br>0 | Yes<br>2       | No<br>0 |                |
| 1                         | Masjid Al Furqan                   | 1                       |             |            | 1                                 |         | 1                                     |         | 1         |            | 1              |         | 12             |
| 2                         | Masjid Nurul Falah                 | 1                       |             |            | 1                                 |         | 1                                     |         | 1         |            | 1              |         | 13             |
| 3                         | Masjid Baiturrahman                | 1                       |             |            | 1                                 |         | 1                                     |         | 1         |            | 1              |         | 10             |
| 4                         | Masjid Darul Islah                 |                         | 1           |            | 1                                 |         | 1                                     |         | 1         |            | 1              |         | 9              |
| 5                         | Masjid Cahaya Rohani<br>UMSB       | 1                       |             |            | 1                                 |         | 1                                     |         | 1         |            | 1              |         | 13             |
| 6                         | Masjid Tarbiyatul 'Ulum            |                         | 1           |            | 1                                 |         | 1                                     |         | 1         |            | 1              |         | 12             |
| 7                         | Musala Darussalam                  |                         | 1           |            | 1                                 |         | 1                                     |         | 1         |            | 1              |         | 9              |
| 8                         | Masjid Darul Muttaqin              |                         | 1           |            | 1                                 |         | 1                                     |         | 1         |            | 1              |         | 9              |
| 9                         | Masjid Iqra'                       |                         | 1           |            | 1                                 |         | 1                                     |         | 1         |            | 1              |         | 9              |
| 10                        | Musala Al Muqarrabin               |                         |             | 1          | 1                                 |         | 1                                     |         | 1         |            | 1              |         | 6              |
| 11                        | Musala Al Ikhlas                   |                         | 1           |            | 1                                 |         | 1                                     |         | 1         |            | 1              |         | 12             |
| 12                        | Masjid Asra                        |                         |             | 1          | 1                                 |         | 1                                     |         | 1         |            | 1              |         | 11             |
| 13                        | Musala Ihdinasshiratol<br>Mustaqim |                         | 1           |            | 1                                 |         | 1                                     |         | 1         |            | 1              |         | 12             |
| 14                        | Masjid Al Mannar                   | 1                       |             |            | 1                                 |         | 1                                     |         | 1         |            | 1              |         | 13             |
| 15                        | Musala Nurul Ikhlas Taho<br>Sapek  |                         | 1           |            | 1                                 |         | 1                                     |         | 1         |            | 1              |         | 9              |
| 16                        | Musala Darul Iman                  |                         | 1           |            | 1                                 |         | 1                                     |         | 1         |            | 1              |         | 7              |
| 17                        | Musala Nurul Ikhlas                | 1                       |             |            | 1                                 |         | 1                                     |         | 1         |            | 1              |         | 8              |
| 18                        | Musala Muslimin                    |                         |             | 1          | 1                                 |         | 1                                     |         | 1         |            | 1              |         | 9              |
| 19                        | Musala Al Falah                    |                         | 1           |            | 1                                 |         | 1                                     |         | 1         |            | 1              |         | 12             |
| 20                        | Masjid At Taubah                   |                         |             | 1          | 1                                 |         | 1                                     |         | 1         |            | 1              |         | 11             |
| 21                        | Musala As salam                    |                         |             | 1          | 1                                 |         | 1                                     |         | 1         | 0          |                | 1       | 9              |

Table 2. The highest score of Mosque or Musholla

| No. | Name of Mosque/Musala     | No. | Name of Mosque/Musala           |
|-----|---------------------------|-----|---------------------------------|
| 1   | Masjid Al Furqan          | 6   | Masjid Asra                     |
| 2   | Masjid Nurul Falah        | 7   | Musala Ihdinasshiratol Mustaqim |
| 3   | Masjid Cahaya Rohani UMSB | 8   | Masjid Al Mannar                |
| 4   | Masjid Tarbiyatul 'Ulum   | 9   | Musala Al Falah                 |
| 5   | Musala Al Ikhlas          | 10  | Masjid At Taubah                |

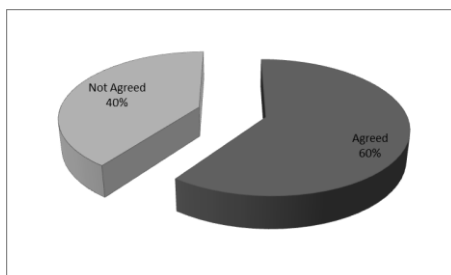


Fig 2. Approval Mosque or Musholla

The name of the approval Mosque or Musholla are

1. Masjid Al Furqan
2. Masjid UMSB
3. Musholla Al Ikhlas
4. Masjid Asra
5. Mushala Ihdinasshiratol Mustaqim
6. Masjid Tarbiyatul Uloom

The location of the Mosque and Musholla can be seen in Fig.3.



Fig 3. The distance between the mosque

Furthermore, comparing the six Mosque or Musholla based on its land capacity and its location to the community will come up with the best Self Support Shelter or the determined Self Support Shelter. They are

1. Masjid Al-Furqan (Land Area: 1345 m<sup>2</sup>)
2. Masjid UMSB (Land area: 3465 m<sup>2</sup>)
3. Musholla Al Ikhlas (Land area: 945 m<sup>2</sup>)
4. Masjid Asra (Area of land: 1355 m<sup>2</sup>)

Each Mosque or Musholla above has its own cluster. Cluster 1, Cluster 2, Cluster 3, and Cluster 4 are belong to Masjid Al-Furqan, Masjid UMSB, Musholla Al Ikhlas, and Masjid Asra, respectively. The next step is to determine the RW included in each cluster. Table 3 shows the distribution of the population represents by RW for each cluster. The air view of cluster can be seen in Fig.4.

Table 3. Cluster Distribution

| Zone      | Name of<br>RW | Total<br>Population | Total<br>population per-<br>Cluster |
|-----------|---------------|---------------------|-------------------------------------|
| CLUSTER 1 | RW 01         | 1141                | 3153                                |
|           | RW 02         | 865                 |                                     |
|           | RW 14         | 679                 |                                     |
|           | RW11          | 468                 |                                     |
| CLUSTER 2 | RW 03         | 641                 | 4904                                |
|           | RW04          | 1195                |                                     |
|           | RW13          | 558                 |                                     |
|           | RW08          | 1613                |                                     |
|           | RW12          | 457                 |                                     |
| CLUSTER 3 | RW05          | 440                 | 2410                                |
|           | RW 09         | 910                 |                                     |
|           | RW 06         | 1059                |                                     |
| CLUSTER 4 | RW 07         | 743                 | 1476                                |
|           | RW 10         | 733                 |                                     |

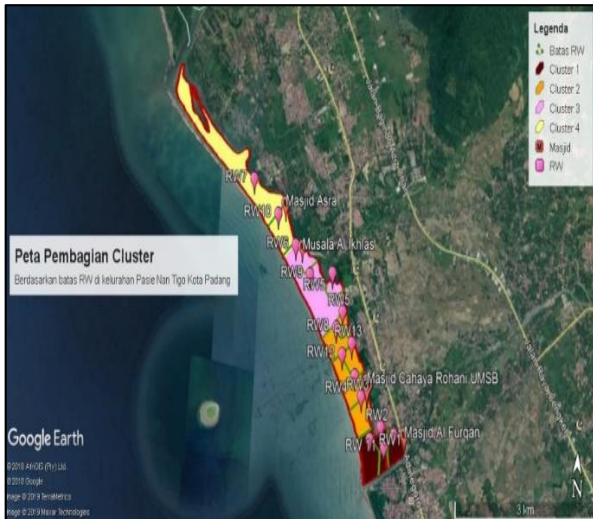


Fig 4. Cluster Division

### Shelter Capacity Calculation

According to FEMA 2012 [7], the tsunami evacuation space requirement is 3 ft<sup>2</sup> per person or about 1 m<sup>2</sup> per person. Based on this data, then, the capacity of the shelter floor can be calculated. The following is the procedure of calculation in Cluster 1.



Fig 5. Planning Shelter in Al Furqan

The total population of Cluster 1 is RW 01 + RW 02 + RW14+ RW11= 1141 + 865 + 679 + 468 = 3153 population. If 1 m<sup>2</sup> at the shelter can accommodate one person, then the total area required is 3153 m<sup>2</sup>. The Mosque or Musholla located in this cluster is Masjid Al Furqan with the availability of the land is 1345 m<sup>2</sup>. Shelter to be built is a rectangular shape with area 30 m x 28 m. It means that this mosque will be built 4 floors which are 3 floors functioned as evacuation place with area 840 m<sup>2</sup> per floor.

### Detail Engineering Design and Construction Method

Detail Engineering Design (DED) must be carried out according to the current Standard or Code [11, 12, 13]. Structural analysis must be conducted using proper model and structural analysis software [14]. All the loads

especially earthquake and tsunami must be applied [15, 16]. Space function analysis must be designed according to the shelter need.

In building the shelter, the construction methods is important. Since the existing Mosque or Musholla is still function during the construction process, therefore, the construction procedure must be convinced not to disturb the daily services. To meet these criteria, then, the selected material, the step of construction, the supported equipment, as well as safety criteria, must be considered.

### Evacuation Accessibility Analysis

The analysis of evacuation accessibility is conducted to find an effective and efficient evacuation route to the shelter. Some studies have been done [17]. All infrastructure and facilities within the cluster must be identified and analyzed. Fig.5 shows the infrastructure within Cluster 1. The study of accessibility is still in progress.

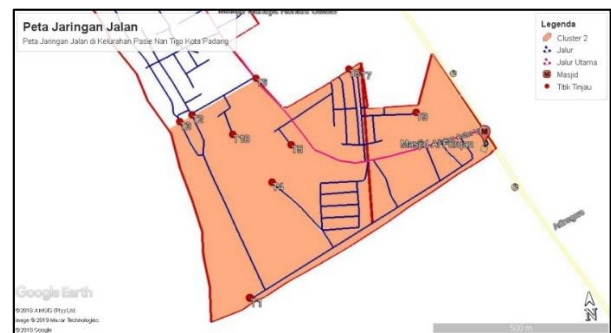


Fig 4. Infrastructure in Cluster 1

### Evacuation Systems

To evacuate the people within cluster need the system and procedure base on local wisdom. Some model has been developed in a certain area [9, 10]. However, it need to be reviewed in order to be implemented in different area. The agreement among all stakeholders to select the proper system is necessary. Coordination and discussion among stakeholders are needed. The study of the evacuation system is still in progress.

### CONCLUSIONS

From the study has been conducted, it can be concluded as follows:

1. The Self Support Shelter is the promising alternative shelter to fulfill the limited Government capacity in providing the shelters in a tsunami-prone area
2. Mosque or Musholla is the best public facilities to be designed as a shelter since it has some advantages: land free, donation scheme for construction, availability of Administrator, and availability in almost all *Kelurahan* (Sub-Sub District) in Moeslim Community that means close to the residential area.
3. The selection of the Mosque or Musholla needs some procedure in order to get the best designed shelter.

4. The evacuation system must be established in operating of Self Support Shelter base on local wisdom.

## REFERENCES

- [1] Natawidjaja, D.H., Sieh, K., Chlieh, M., Galetzka, J., Suwargadi, B.W., Cheng, H., Edwards, R.L., Avouac, J.-P., and S.N. Ward. Source parameters of the great Sumatran megathrust earthquakes of 1797 and 1833 inferred from coral microatolls, *Journal of Geophysical Research* 111, B06403, , 2006.
- [2] Sieh, K., D. H. Natawidjaja, A. J. Meltzner, C. Shen, H. Cheng, K. Li, B. W. Suwargadi, J. Galetzka, B. Philibosian, R. L. Edwards. Earthquake Supercycles Inferred from Sea-Level Changes Recorded in the Corals of West Sumatra, *Science* 322, 1674 – 1678, 2008.
- [3] Omer AYDAN, Seismic and Tsunami Hazard Potentials in Indonesiawith a special emphasis on Sumatra Island, *Journal of The School of Marine Science and Technology, Tokai University*, Vol.6, No.3, pp.19-38, 2008
- [4] V Cedillos, N Canney, G Deierlein, S Henderson, F Ismail, A Syukri, J Toth, K Wood, An Evaluation of Infrastructure For Tsunami Evacuation In Padang, West Sumatra, Indonesia, 2010.
- [5] Febrin Anas Ismail, Jafril Tanjung, Syah Bintang Aruan, On The Use Of A Simple Tuned Mass Damper Model For Reducing The Excessive Vibration Of Tsunami Evacuation Suspension Footbridge, *MATEC Web of Conferences* **229**, 01013 (2018)
- [6] Hannes Taubenböck<sup>1</sup>, Joachim Post, Ralph Kiefl, Achim Roth, Febrin A. Ismail, Günter Strunz and Stefan Dech, Risk and Vulnerability Assessment To Tsunami Hazard Using Very High Resolution Satellite Data: The Case Study Of Padang, Indonesia, *EARSeL eProceedings* 8, 1/2009
- [7] U.S. Guidelines for Design and Construction of Cyclones / Shelter Tsunamis, 2006
- [8] Fauzan, Febrin Anas Ismail, Nurpadila Siregar, and Zev Al Jauhari, The Effect Of Tsunami Loads On Pasar Raya Inpres Block III Building In Padang City Based On FEMA P-646
- [9] E. Rita, R. Permata, H. Yonne, and N. Carlo, Tsunami shelter in Padang city: Location suitability and management issue, *Proceedings of the 3<sup>rd</sup> ICONBUILD* (2017)
- [10] F. Ashar, D. Amaratunga, R. Haigh, The analysis of tsunami vertical shelter in Padang city, *4<sup>th</sup> International Conference on Building Resilience*, (Salford Quays, United Kingdom 2014)
- [11] National Standardization Agency of Indonesia, Design Method of Earthquake Resistance for Buildings and Other Structures SNI 1726-2012, Jakarta, Indonesia (2012)
- [12] Federal Emergency Management Agency, FEMA P-646 (April 2012): Guidelines for Design of Structure for Vertical Evacuation from Tsunami 2nd edition, Washington D.C, USA (2012)
- [13] National Standardization Agency of Indonesia, Minimum load for the design of buildings and other structures SNI 1727:2013, Jakarta, Indonesia (2013)
- [14] Computers and Structures Inc., Manual ETABS (Integrated Building Design Software), California, USA (2016)
- [15] Y. Nakano, Structural Design Requirements for Tsunami Evacuation Buildings in Japan, Volume: 313, Date: 3/1/2017, ACI (American Concrete Institute) Journal. First ACI & JCI Joint Seminar.
- [16] K. H. Pacheco, Evaluation of Tsunami Loads and Their Effect on Reinforced Concrete Buildings, A Thesis Master of Science in Civil Eng., University of Hawai'i Library (2005)
- [17] Yosritzal, BM Kemal, Purnawan, and H Putra, An Observation of the Walking Speed Evacuation in a Simulated Tsunami Evacuation in Padang Indonesia: IOP Conference Series: Earth and Environmental Science, 2018.



## GREEN CONCRETE HOLLOW BLOCKS UTILIZING BASIC OXYGEN FURNACE STEEL SLAG

Santiago, Karen Joyce B.<sup>1</sup>; and Juan, Jose Arnel P.<sup>2</sup>

<sup>1</sup>Faculty, Mariano Marcos State University, Philippines; <sup>2</sup>Faculty, Mapua University, Philippines

### ABSTRACT

This study presented the effects of replacement of fine aggregates with high percentages of steel slag (BOF) on the properties of Concrete Hollow Blocks (CHB). The mix proportions of 1:3:4, 1:4:3, and 1:3.5:3.5 (cement: fine aggregates: coarse aggregates) incorporating various percentages of steel slag were designed. Fine aggregate was replaced 25, 50, 75, and 100 percentages of BOF steel slag by volume of fine aggregate. Elemental and chemical tests were conducted to determine the toxicity of BOF slag to the environment and its use as a partial replacement of fine aggregates thru optical microscopy and xrf spectrometer. Compressive test and statistical inference reveal that inclusion of steel slag as partial replacement with fine aggregates in CHB has a greater compressive strength than the conventional CHB. Moreover, the results of the xrf indicates the presence of calcium and iron oxides. Iron oxides, which are non-toxic, have inert, opaque, and water resistant properties. In raw cement manufacturing, calcium oxide and silica oxides are components and considered to be non-toxic.

*Keywords: BOF Steel Slag, Compressive Strength, Green Concrete Hollow Blocks, Toxicity*

### INTRODUCTION

In the Philippines, Concrete Hollow Blocks (CHB) are commonly used for exterior and interior walls of buildings especially residential projects [1]. It is also used for perimeter fence, tank, septic vault, drainage canal, and many more. Fajardo [2] adds that CHBs are classified as bearing and non-bearing blocks. Load bearing blocks are those which thickness ranges from 15 cm to 20 cm and are used to carry load aside from their own weight. Non-bearing blocks, on the other hand, have thickness ranging from 7.5 cm to 10cm blocks and are intended for walls and partition fences carrying their own weight.

Hua-dong and Liu's [3] study as cited in Yi, Xu, Cheng, Wang, Wan and Chen [4] stated that basic oxygen furnace (BOF) steel slag is a solid waste from steel production. This slag is formed when scrap metals, molten iron, and various fluxes like lime are oxidized by injecting large amounts of pure oxygen into the molten mix to create molten steel and molten slag [5].

In the construction industry, concrete is one of the most commonly used material in variety of environment such as dry, water, underground and even in hot or cold climate zones. One of the advantages of concrete is the material's possibility to change its properties depending on the requirements of the construction project and the price. Concrete consists of three components: binder, filler, and water. Natural aggregates with different proportions are the most common filler. However, the status of depleting

natural resources especially on natural aggregates is under question. This led to the conduct of studies using alternatives and replacements of natural aggregates using solid waste.

A global sand importer, Omnico Natural Resources (ONRI), has been exporting construction sand from Ilocos Norte, Philippines to Japan and Singapore since 2009. It has also been importing furnace slag aggregates from Taiwan since 2015 to develop a 112 hectare seaport reclamation project in Currimao, Ilocos Norte [6]. However, the use of this slag for embankment and backfilling materials has been stopped by the Ilocos Norte Provincial Quarry Council due to the alleged toxic slag elements. The council needed the slag to be re-examined in its toxicity and threat to the marine ecosystem of Currimao [7]. Due to the discontinue of the use of the BOF steel slag, which appears like mixed gravel and sand and furnace slag steel, wastes are stockpiled in the northern portion of ONRI seaport complex, measuring as high as 20 meters [8].

Yildirim and Prezzi [9] stated that it is essential to have knowledge of the chemical, mineralogical, and morphological properties of steel slag to utilize BOF steel slag as a replacement material in concrete development to produce green concrete. The use of the Currimao BOF steel slag will take care of the environmental issue as well as the scarcity of the use of natural aggregates for concrete. The use of the slag as a partial replacement for fine aggregates will lessen and eventually eliminate the stockpiled BOF steel slag in Currimao. It will address the problem in industrial

waste and apply the recycle, reuse, and recover implementing rules and regulation of the Philippine's Ecological Solid Waste Management Act of 2000 (RA 9003)[10].

The study focused on the utilization of the BOF steel slag as a partial replacement of fine aggregates to produce green concrete hollow blocks. Establishment of proportions for the BOF as a partial replacement of fine aggregates was observed and its possibility as a substitute for natural aggregates.

## METHODOLOGY

### Concrete Mix Design

Sample design mixes of proportions 1:3:4; 1:3.5:3.5; and 1:4:3 (cement: fine aggregates: coarse aggregates) were used as presented in Table 1. The fine aggregates were replaced by BOF steel slag with various percentage replacement of 25%, 50%, 75%, and 100%, respectively.

### Elemental Test by Optical Microscopy

Natural aggregates and BOF slag were collected, sorted, and dried before undergoing elemental analysis using OEM optical microscope.

Table 1. Concrete Mix Design

| Mixture<br>(Cement : Fine :<br>Course) | Natural Fine<br>Aggregates<br>% | BOF Slag<br>Aggregate<br>% |
|--|---------------------------------|----------------------------|
| 1:3:4                                  | 0                               | 100                        |
|  | 25                              | 75                         |
|  | 50                              | 50                         |
|  | 75                              | 25                         |
|  | 100                             | 0                          |
| 1:3.5:3.5                              | 0                               | 100                        |
|  | 25                              | 75                         |
|  | 50                              | 50                         |
|  | 75                              | 25                         |
|  | 100                             | 0                          |
| 1:4:3                                  | 0                               | 100                        |
|  | 25                              | 75                         |
|  | 50                              | 50                         |
|  | 75                              | 25                         |
|  | 100                             | 0                          |

### Material Characterization

Natural aggregates and BOF steel slag were pulverized and characterized by the handheld X-Ray Fluorescence Spectrometer.

### Slump Test

All procedures and test methods conducted were in accordance with ASTM C143, "Standard Test Method for Slump of Hydraulic-Cement Concrete" specification. Slump was maintained at 5 inches for all mix designs.

### Compressive Strength of Cylindrical Concrete Specimens

One hundred fifty (150) 4 x 8 inches concrete cylinders have been tested in the uni-axial compressive test in order to obtain compressive strength. Every five (5) concrete cylinders was tested, respectively, on the same age set to 14<sup>th</sup> and 28<sup>th</sup> day period. The development of compressive strength of BOF steel slag aggregate at the age of 14 and 28 days was investigated.

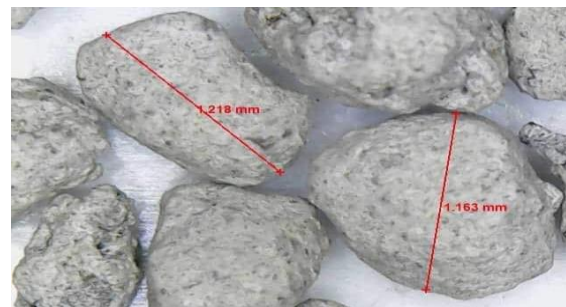
### Green Concrete Hollow Blocks Development

BOF steel slag was incorporated in the production of CHB to produce green concrete hollow blocks. Based on the results of the compressive test of the cylindrical samples, the mixture with the highest compressive strength value served as the proportion to be used in the fabrication of the green concrete hollow blocks.

## RESULTS AND DISCUSSIONS

### Optical Microscopy

The results obtained from the optical microscopy shows that the sample coarse aggregate had a 12.21mm diameter. This value conforms to the standard size used in concrete mix wherein the usual range employed is between 9.5mm and 37.5mm in diameter. Likewise, the sample fine aggregate had 1.432mm and 1.064mm diameter, respectively. Lastly, the result obtained for BOF steel slag aggregate had 1.218mm and 1.163mm diameter, as shown in Fig. 1. These values of fine aggregates and BOF steel slag conforms to the standard size of fine aggregate used in concrete mix with a range less than 9.5mm.



690 Figure 1. BOF steel slag



Table 2. Traced Chemical Composition of BOF Steel Slag

| Element | PPM    | +/-     |
|---------|--------|---------|
| Ca      | 37.61% | 0.3706% |
| Fe      | 23.99% | 0.2423% |
| LE      | 16.32% | 0.2215% |
| Si      | 7.72%  | 0.1664% |
| Mg      | 7.10%  | 0.8808% |
| Al      | 3.38%  | 0.1362% |
| Mn      | 1.90%  | 0.0305% |
| P       | 1.34%  | 0.0266% |
| Ti      | 3072   | 286.68  |
| Cr      | 1010   | 81.84   |
| S       | 936    | 61.47   |
| V       | 509    | 123.64  |
| Sr      | 259    | 6.57    |
| Zn      | 178    | 14.08   |
| Cu      | 142    | 17.84   |
| Nb      | 93     | 5.11    |
| Zr      | 82     | 4.54    |
| Ni      | 69     | 21.12   |
| Pb      | 25     | 7.30    |
| Mg      | 21     | 3.64    |
| Se      | 9      | 2.89    |

### Material Characterization

Table 2 shows the weight percentage of the element present on BOF steel slag. Its main chemical constituents are CaO, FeO/ Fe<sub>2</sub>O<sub>3</sub>, and SiO<sub>2</sub>. The iron oxide (FeO/ Fe<sub>2</sub>O<sub>3</sub>) content of BOF slag was 23.99% which could be as high as 31%. This is the amount of oxidized iron that cannot be recovered during the conversion of molten iron into steel. The silica (SiO<sub>2</sub>) content of BOF slag was 7.72% ranging from 6.9449% to 8.4951%. The Al<sub>2</sub>O<sub>3</sub> and MgO contents were 3.38% and 7.10% ranging from 2.92-3.84% and 0.84-13.35%, respectively. Large quantities of lime were used during the process of conversion from iron to steel; hence, the CaO content of BOF steel slag was 37.61%, which was typically very high (CaO>35%).

In Table 3, Calcium oxides (ranges from 52.25 % to 72.15% parts per million) and iron oxide (ranges from 25.99 % to 42.61% parts per million) are the two major chemical constituent of BOF steel slag. According to Egrani, Latif, Poyi, Wessey and Acharjee [11] as discussed by Ohimain [12], oxides of iron ore are highly values and possess non-toxic, inert, opaque and water resistant properties. Calcium oxide and silica oxides are likewise non- toxic substances since these oxides are raw materials in producing raw cement [13].

Table 3. Oxides present in BOF Steel Slag

| Oxides                         | Range Percentage (%) |       |
|--------------------------------|----------------------|-------|
|                                | Low                  | High  |
| CaO                            | 33.12                | 72.13 |
| Fe <sub>2</sub> O <sub>3</sub> | 25.99                | 42.61 |
| SiO <sub>2</sub>               | 13.77                | 19.26 |
| MgO                            | 1.40                 | 22.15 |
| Al <sub>2</sub> O <sub>3</sub> | 5.52                 | 7.26  |
| MnO                            | 2.38                 | 2.53  |
| P <sub>2</sub> O <sub>5</sub>  | 2.99                 | 3.15  |

### Compressive Strength Test

One hundred fifty cylindrical samples were subjected to compressive test. On the 14<sup>th</sup> and 28<sup>th</sup> days of curing, the cylindrical samples were tested at the Universal Testing Machine (UTM) to determine their compressive strength. The 150 samples comprised of 3 mixture proportions, namely 1:3:4, 1:4:3, and 1:3.5:3.5 (cement: fine sand: coarse aggregate) with different percentages of fine aggregates replaced by BOF steel slag of percentages 0%, 25%, 50%, 75%, and 100%, respectively.

Five samples on different percentages of slag (0%,25%,50%,75% and 100%) on the different proportions of cement, fine sand, and coarse aggregate (1:3:4, 1:4:3, and 1:3.5:3.5) were subjected to compressive test as presented in Table 4. From Fig. 2, it was presented that the proportion 1:3:4 (cement: fine sand: coarse aggregate) with 25% partial replacement of BOF slag had the highest compressive strength of 4.34 MPa. Furthermore, five samples on different percentages of slag (0%, 25%, 50%, 75%, and 100%) on the different proportions of cement, fine sand, and coarse aggregate (1:3:4,1:4:3, and 1:3.5:3.5) were subjected to compressive test as presented in Table 4 for 28 days curing. It presented that the proportion 1:3:4 (cement: fine sand: coarse aggregate) with 75% partial replacement of BOF slag had the highest compressive strength of 5.38 MPa.

The proportion of 1:3:4 (cement: fine sand: coarse aggregate) significantly presents a higher compressive strength compared to the conventional mix. In the mixture, the 25% BOF steel slag replacement attained the highest value of compressive strength for a 14-day-old concrete while a 75% BOF steel slag replacement attained the highest compressive strength for a 28-day-old concrete. Results indicate that the use of BOF steel slag in the 1:3.5:3.5 proportion yields a lower compressive strength than

those of the conventional mix made from the similar mix proportions.

In addition, there was a difference among the compressive strength of concrete which depended upon the percentage of BOF steel slag it contained. There was also a significant increase of the mean compressive strength between the 14 day age and 28 day age. The highest compressive strength of concrete was considered for the 28 day age since their mean values were significantly higher than the mean compressive strength of the 14 day age. For the mixture 1:3:4, 75% replacement of BOF steel slag showed the highest compressive among the different replacement with the value 5.38 MPa. In the mixture 1:4:3, 50% replacement of BOF steel slag presented the highest compressive strength of 4.39 MPa. While in the 1:3.5:3.5 mixture, 100% replacement of BOF steel slag had the highest mean compressive strength of 5.33 MPa. Although the value of the mean compressive strength of the 100% BOF steel slag replacement was high, the values presented in the 1:3.5:3.5 proportions were not recommended since the values were all lower than the compressive strength of the control sample (0% BOF steel slag replacement) which was 5.53 MPa.

Table 4. Comparison of Compressive Strength

| Mixture   | Percentage Replaced by BOF (%) | Compressive Strength, MPa |            |
|-----------|--------------------------------|---------------------------|------------|
|           |                                | 14 day Age                | 28 day Age |
| 1:3:4     | 0% BOF                         | 2.76                      | 4.84       |
|           | 25% BOF                        | 4.34                      | 5.28       |
|           | 50% BOF                        | 3.06                      | 5.31       |
|           | 75% BOF                        | 2.86                      | 5.38       |
|           | 100%BOF                        | 2.84                      | 4.44       |
| 1:4:3     | 0% BOF                         | 3.11                      | 3.65       |
|           | 25% BOF                        | 2.47                      | 4.25       |
|           | 50% BOF                        | 3.01                      | 4.39       |
|           | 75% BOF                        | 2.71                      | 4.34       |
|           | 100%BOF                        | 2.47                      | 4.29       |
| 1:3.5:3.5 | 0% BOF                         | 3.21                      | 5.53       |
|           | 25% BOF                        | 2.32                      | 3.31       |
|           | 50% BOF                        | 2.42                      | 3.85       |
|           | 75% BOF                        | 2.57                      | 4.74       |
|           | 100%BOF                        | 3.31                      | 5.33       |

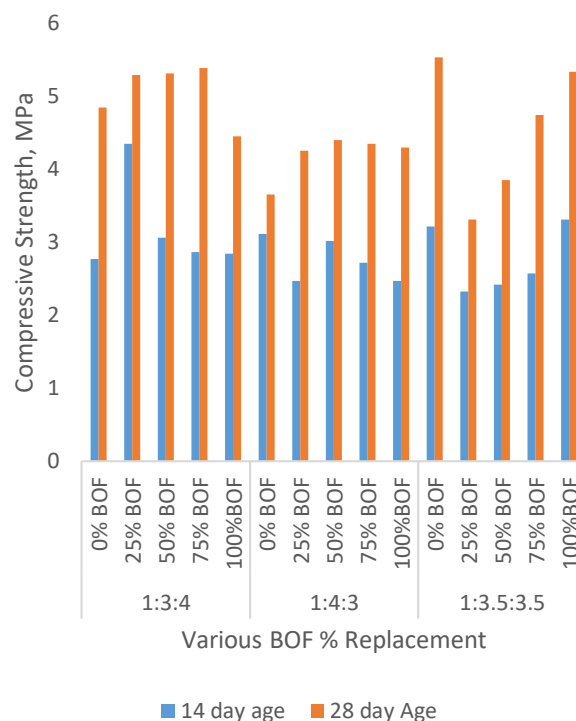


Figure 2. Comparison of compressive strength of various BOF percentages

### Statistical Analysis T Test

The t-test analysis with 95% confidence is presented in Table 5. In the design mix 1:3:4, the t critical 2.54 was higher than the t actual 1.20 and the p value of 0.28 was higher than the level of significance. There was no significance between the control mix and the highest compressive strength generated of the design mix 1:3:4. However, this design mix actually generated the highest compressive strength among the mixes. Likewise, the two design mixes of 1:4:3 and 1:3.5:3.5, showed that most of the t actual was greater than the t critical ( $t_{\text{actual}} > t_{\text{critical}}$ ). Moreover, the p values of these two design mixes were less than 0.05, the level of significance. Hence, the results show that there is a significance difference between the control mix and the fine aggregates replaced by BOF steel slag in the design mix 1:4:3 and 1:3.5:3.5. Likewise, the presence of BOF slag in the mixture of concrete increases the compressive strength of the concrete.

Table 5 Statistical Analysis T test for the compressive strength of concrete of all design mixes

| Parameters                                    | Mix Design |       |           |
|---|------------|-------|-----------|
|   | 1:3:4      | 1:4:3 | 1:3.5:3.5 |
| Compressive Strength, Control Design Mix, MPa | 4.84       | 3.65  | 5.53      |
| Highest Compressive Strength, MPa             | 5.38       | 4.39  | 5.33      |
| Fine aggregates replaced by BOF steel slag, % | 75         | 50    | 100       |
| T actual                                      | 1.20       | 20.91 | 2.71      |
| T critical                                    | 2.45       | 2.45  | 2.45      |
| P value                                       | 0.28       | 0     | 0.04      |



Figure 3. Green CHB

### Development of Green Concrete Hollow Blocks

The proportion 1:3:4 served as the basis for the fabrication of the green concrete hollow blocks since it generated the highest compressive strength of 5.38 MPa. Conventional procedure in the fabrication of hollow blocks was implemented. Fine aggregates were replaced by 75% BOF steel slag. After the molding of green CHB, a maximum of 10 days curing was observed to attain its maximum strength.

### CONCLUSION

Green concrete, also known as a sustainable or 'high performance' concrete, uses sustainable materials which are made from recyclable materials or green materials. They are more efficient than the traditional products because they require fewer resources to produce. Green concrete is a material that exhibits better functional performance and capabilities than ordinary concrete. It is considered a maintainable construction material as it consumes less natural resources and less energy and emits a smaller amount of carbon dioxide. The concrete wastes are slag, power plant wastes, recycled concrete, mining and quarrying wastes, waste glass, incinerator residue, red mud, burnt clay, sawdust, combustor ash and foundry sand.

The results obtained from the optical microscopy shows that the BOF steel slag conforms to the standard size of fine aggregate used in concrete mix with a range less than 9.5mm. In determining the elements and oxides present in pure BOF steel slag specimen, it was found out that it contained oxides that had similar elements to the results of the previous studies. Calcium oxides (ranges from 52.25 % to 72.15% parts per million) and iron oxide (ranges from 25.99 % to 42.61% parts per million) are the two major chemical constituent of BOF steel slag. Iron oxides, which are non-toxic, have inert, opaque, and water resistant properties. In raw cement manufacturing, calcium oxide and silica oxides are components and considered non-toxic. Thus it can be concluded that the BOF steel slag treated specimen does not contain any toxic and harmful elements that can harm the environment. The slag can then be used as a suitable material for replacement of natural aggregates and can be categorized as a sustainable material to produce green concrete products.

This study attempts to optimize and develop proportions that can include steel slags as an ingredient for concrete hollow block. BOF slag replaced a certain percentage of fine natural aggregates and the specimens were tested according on the specimens curing days. Concrete hollow block proportion 1:4:3 has the highest value for compressive strength of a fourteen-day old CHB having a value of 4.34 MPa with 50% fine aggregate replacement by BOF steel slag. Likewise, concrete hollow block proportion of 75% replacement from the 1:3:4 proportion governed the value for compressive strength of a twenty-eight-day old concrete hollow block with a compressive strength of 5.38 MPa.

Based on statistical analysis, there was a great significance of the replacement of BOF steel slag in the concrete mixture. There was a significant increase of the compressive strength of concrete as the percentage

of BOF replacement also increases until it reaches its maximum strength. Also, the three mixture proportions were treated independently and presented increase of compressive strength as its age from 14 to 28 days, as well as the addition of BOF steel slag as a replacement of fine sand. As the percentage of fine aggregates replaced by steel slag increased, compressive strength of concrete samples slowly increased.

It can be concluded that BOF steel slag can be used as an aggregate in the manufacture of concrete hollow blocks. It can reduce the solid wastes present in Currimao, Ilocos Norte as well as environmental impacts. Moreover, the use of BOF steel slag makes it possible to reduce the consumption of natural sand which causes potential environmental damage in riverbeds.

## REFERENCES

- [1] Rabena, A. R. & Aman, N. V.. (2010). Analysis on the Strength of 5" CHB with Oyster Shell as Component of the Aggregates. *UNP Research Journal*, 19(1). Retrieved from <http://ejournals.ph/form/cite.php?id=6891>
- [2] Fajardo, M. B. (1980). *Simplified Construction Estimate*. National Bookstore.
- [3] Hua-dong, M. E. N. G., & Liu, L. I. U. (2009). Stability processing technology and application prospect of steel slag [J]. *Steelmaking*, 25(6), 74.
- [4] Yi, H., Xu, G., Cheng, H., Wang, J., Wan, Y., & Chen, H. (2012). An overview of utilization of steel slag. *Procedia Environ Sci* 16: 791–801.
- [5] Shi, C. (2004). Steel slag—its production, processing, characteristics, and cementitious properties. *Journal of Materials in Civil Engineering*, 16(3), 230-236.
- [6] Ilocos Norte's Global Sand Exporter Pushes Private Seaport Reclamation Project. (2015). *Northbound Philippines News Online*. Retrieved from <http://northboundasia.com/2015/12/07/ilocos-nortes-global-sand-exporter-pushes-private-seaport-reclamation-project/>
- [7] Ilocos Norte Gov't Halts Importation of Alleged Toxic Materials for Port Expansion Project. (2015). *Balita*. Retrieved from <http://balita.ph/2015/04/17/ilocos-norte-govt-halts-importation-of-alleged-toxic-materials-for-port-expansion-project/>
- [8] Adriano, Leilanie. (2015, April 17). Entry of 'toxic' materials for port project stopped. *Inquirer*. Retrieved from <http://newsinfo.inquirer.net/685993/entry-of-toxic-materials-for-port-project-stopped#ixzz58NurPQsT>
- [9] Yildirim, I., & Prezzi, M. (2011). Chemical, Mineralogical, and Morphological Properties of Steel Slag. *Advances in Civil Engineering*, 1-13.
- [10] Sapuay, G. P. (2005, July). Ecological Solid Waste Management Act of 2000 (RA 9003): a major step to better solid waste management in the Philippines. In *International Conference on Integrated Solid Waste Management in Southeast Asian Cities, Siem Reap* (pp. 51-59).
- [11] Egirani, D. E., Latif, M. T., Poyi, N. R., Wessey, N., & Acharjee, S. (2018). Genesis, Uses and Environment Implications of Iron Oxides and Ores. In *Iron Ores and Iron Oxide Materials*. IntechOpen.
- [12] Ohimain, E. I. (2013). Scrap iron and steel recycling in Nigeria. *Greener Journal of environmental Management and public safety*, 2(1), 1-9.
- [13] Li, X., Yu, H., & Yuan, M. (2012). Modeling and optimization of cement raw materials blending process. *Mathematical Problems in Engineering*, 2012.

## RESPONSE OF A SINGLE PILE LOCATED ON SLOPING GROUND UNDER DYNAMIC LOADING

Deendayal Rathod<sup>1</sup>, D. Nigitha<sup>2</sup> and Krishnanunni K T<sup>3</sup>

<sup>1</sup>Asst.Professor, National Institute of Technology (NIT), Tiruchirappalli (Trichy),  
India; <sup>2,3</sup> Research Scholars, National Institute of Technology (NIT), India

### ABSTRACT

Pile foundations are extensively used to support the laterally loaded structure. The structures like high-rise building, transmission tower, power station and offshore structures are subjected to lateral load in addition to the vertical load. The behavior of the piles on sloping ground under earthquake loading is different from the behavior of the pile located on the horizontal ground surface because of the large permanent displacement. In the present study, the numerical analysis has been carried out by using PLAXIS 2D. The analyses are carried out on single model pile under dynamic loading to determine the behavior of the soil-pile system. A single pile of embedment length to diameter ratio (L/D) of 16, 25 and 33 were located on the horizontal ground surface and slope angle of 1V:1.5H, 1V:2H and 1V:3H. The pile was subjected to dynamic loading (Bhuj earthquake, Gujarat) at its base. From the analysis, the acceleration, displacement and bending moment of the pile under each case was studied. Based on the results, it is concluded that as L/D ratio increases, the acceleration and maximum displacement and bending moment of the pile decreases

*Keywords: Dynamic loading; Numerical analysis; Sloping ground; Single pile, PLAXIS 2D.*

### INTRODUCTION

A study of laterally loaded piles under dynamic loading has received considerable attention from the designers and researchers for more than three decades. The dynamic response of a pile subjected to external excitation is a complex phenomenon resulting from the interactions between the pile and the surrounding soil. The structures like high rise buildings, transmission towers and offshore structures are subjected to large lateral loads due to strong winds or earthquakes. The behavior of pile foundations under earthquake loading is an important issue that widely affects the performance of the structure. And also, many big cities in the world are built on sloped ground. Most of the structures which are constructed on soft clay with sloped ground surface are subjected to large displacements due to high lateral loads. Most of the coastline have surface which are sloping towards the waterfront. The design of pile foundation in coastal region to resist lateral load is primarily based on the limiting deflection criterion, considering the safe operation of the superstructure. Lateral loading on pile foundations due to wave and earthquake loadings are cyclic in nature, which bring additional complexity to the soil-structure interaction problem. In such cases, studying the interaction between the soil and the pile foundation due to lateral load is essential. In this paper, the numerical analysis are carried out to determine the effect of acceleration, displacement and bending moment for piles of different embedment length to diameter ratio (L/D) installed on various sloping ground conditions.

### LITERATURE REVIEW

The dynamic response of pile subjected to horizontal excitation is a complex matter involving the non-linearity at large displacements, pile separation and slippage. Gaul (1958) conducted static and dynamic model tests on instrumented aluminium pipes embedded in bentonite soil medium. The dynamic load is applied by means of a mechanical oscillator and highly amplified strain variations during the vibrations are recorded. Their study shows that at relatively low frequency, magnitude and location of maximum bending moment does not vary significantly as compared with static case. Hayashi and Miyajima (1962) performed tests on vertical steel H-piles installed in sand of different relative density. Forced vibration tests are conducted and bending moment, lateral deflection of pile head and acceleration response is measured. Frequency response curves of single piles are plotted and natural frequency of single pile is obtained from these tests. However, the results of such dynamic 1-g model tests are affected by the 'box effect' and inappropriate stress levels. Prakash and Aggarwal (1965) reported that the zone of influence of a dynamically loaded pile can extend to greater distances such as 30 times the width of pile in the direction of loading and 15 times the pile width in the orthogonal direction. Tajimi (1969) proposed an analytical model considering the pile to support a concentrated mass and the underlying soil is assumed as viscoelastic (linearly elastic material with frequency dependent viscous damping). Nogami and Novak (1977) obtained closed form solutions for the same problem neglecting the

effect of superstructure on the pile head response but considering hysteretic type material damping of the soil layer. Nogami and Konagai (1988) worked on the analytical expression in frequency-domain for the dynamic response of a single pile assumed as a massless cylinder embedded in an elastic infinite medium. El Naggar and Novak (1996) developed a computationally efficient model that accounts for non-linear behavior of soil, discontinuity conditions like slippage and gapping at soil-pile interface and energy dissipation through different types of damping. Dou and Byrne (1996) applied dynamic loading through shake table test and preserved the stress levels of the prototype for the model through hydraulic gradient similitude technique. It is observed that the bending moment in model pile reached its peak value when the frequency applied is close to the resonant frequency. It is also found that the location of maximum bending moment shifted downwards as the pile head load is increased. In addition to this, dynamic p-y curves in dense sand are also presented which exhibited highly non-linear characteristics up to a depth of four times the pile diameter for a strong level shaking. Dou and Byrne (1997) demonstrated that wave reflections at the boundary walls are negligible when the loading frequencies are far below the fundamental frequency of the soil layer. Bentley and El Naggar (2000) used 3D FE program ANSYS to develop a model that can account for kinematic soil-structure interaction of piles and used it to evaluate the dynamic pile response with respect to input ground motion. It is shown that for an elastoplastic soil with separation allowed, the lateral response of pile head is very close to the free field response at very low frequency of seismic excitation. Abdoun and Dobry (2002) discuss the critical locations in shear and bending response of deep foundations in liquefied soil based on the reported case history. Maheshwari et al. (2003) studied the effects of plasticity and work hardening of soil on the free field response and also the kinematic response of single piles using the advanced plasticity-based model in a finite element formulation. Maheshwari et al. (2004) confirmed that the material non-linearity significantly affects seismic response of pile foundation which in turn is dependent on the frequency of excitation. Boominathan and Ayothiraman (2007) carried out a comprehensive investigation on single piles installed in soft clay under static and dynamic lateral loads. It is noted that the dynamic magnification factor reduces with an increase in magnitude of load due to large hysteretic damping originating from the extreme non-linear behaviour of soft clay. The active length under dynamic lateral load is increased by about 1.5 times compared to that under static lateral load. Maiorano et al. (2009) performed 3D finite element analysis on a pile subjected to dynamic lateral load to examine the kinematic bending moments in different subsoil

conditions. The piles are represented as elastic beams while the soil is modelled using linear elastic constitutive model. The results are used to predict the transient peak bending moments at the soil layer interface. Yang et al. (2011) through his shaking table test demonstrates that the dynamic p-y curves are highly affected by the input acceleration amplitude. Di Laora and Rovithis (2015) carried out a numerical treatment using the rigorous finite element technique to evaluate the kinematic bending moment of long piles embedded in a continuously non-homogenous soil resting over a rigid base. During the analysis, soil stiffness is allowed to vary with depth in a parabolic fashion with its initial value at the ground surface to be zero or a finite quantity. The active length of pile in non-homogenous soil layer is finally proposed considering the effect of kinematic interaction. Deendayal et al. (2016) investigated the effect of the earthquake on a single pile located on the sloping ground. A single pile was located on varying slope with different length to diameter (L/D) ratios. It is observed that the acceleration, displacement and bending moment decreases with the increase in L/D ratio. And also, the displacement and bending moment increases significantly as slope increases from horizontal ground surface to the slope under consideration.

## NUMERICAL MODELING

### Governing Factor

Finite element method requires several approximations to obtain the solution during numerical modeling. The suitability of the approximation used in the modeling approach is based on the conditions in the field. Plane strain conditions are assumed to hold in the plastic deformation regime developed during the dynamic loading. The problem being modeled is complex and has to be simplified to obtain a solution. Two major factors affecting the lateral response of piles are: (1) the properties of the soil (2) soil-pile interaction at the interface.

### Constitutive Model

A constitutive model to be satisfactory it must be able to define the material behavior for the concerned range of stress and strain, identify the model parameter by standard material test and physically represent the material response to change in applied stress and strain. In the present study, a two dimensional finite element program PLAXIS 2D is used for the analysis. PLAXIS automatically imposes a set of general boundary conditions (standard fixities) to the actual geometry model. The Mohr-Coulomb model is used for depicting the soil behavior. The Mohr-Coulomb model is straightforward and quick and accounts for the



elastoplastic behavior of the soil with utmost simplicity.

### Geometry Model

A geometry model is a composition of points, lines and cluster. Points and lines are created in the draw area by entering the coordinates in the command line. Then the clusters are generated by program. Each cluster gives the properties to simulate the behavior of soil. The clusters are divided into soil element during mesh generation. In addition to this, structural object such as the beam representing a pile can be assigned to the geometry. Once the geometry model has been created, the pile parameters are assigned to the corresponding geometry component. When the full geometry model is defined and all geometry components have their initial properties, then the finite element mesh is generated. Fig. 1 shows the typical models in case of L/D 33 for sloping ground.

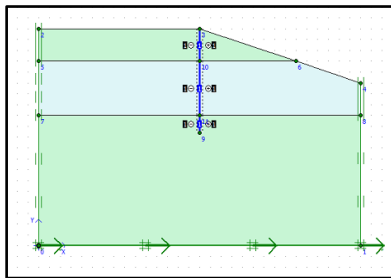


Fig. 1 Geometric model for L/D = 33, 1V:3H.

### Soil-Pile Interaction

The Mohr-coulomb model describes the behavior of interfaces for the modeling of soil-pile interaction. The pile consists of the beam element with special interface elements providing the interaction between the pile and the surrounding soil. The pile is considered as linear elastic and its behavior is represented by using stiffness properties. The interface strength reduction factor accounting for the effect of soil-structure interaction at the interface is chosen on a conservative basis in the current study.

### Boundary Condition

An absorbent boundary is aimed to absorb the increasing stress in the boundaries caused by the dynamic loading; otherwise, it will be reflected inside the soil body. In this model, the absorbent boundaries are generated at the left, right and the bottom boundary.

### Material Properties

The parameter values for soil and pile are adopted from (Abdoun, T and Dobry R, 2002). A single concrete pile of diameter 0.6 m is used for the FEM analysis in the present study. An axial modulus (EA) is taken as  $3.56 \times 10^5$  (kN/m) and Rigidity modulus (EI) is taken as 8000 (kN/m<sup>2</sup>). An embedment pile consists of a beam element and it provides the interface between the beam and the soil enclosed by the pile. The angle of internal friction ( $\phi$ ) and dilatancy angle ( $\psi$ ) for sand-1 is 32 and 2, and for slightly cemented sand-2 is 35 and 5 respectively. The detailed properties of soil and pile used for modeling are listed in Table 1 and 2.

Table 1 Values of soil and interface properties.

| Description   | Sand - 1     | Slightly cemented sand -2 |
|---|--------------|---------------------------|
| Unit weight ( $\gamma$ ) (kN/m <sup>3</sup> )       | 25           | 28                        |
| Material model                                      | Mohr-coulomb | Mohr-coulomb              |
| Young's modulus ( $E_s$ ) (kN/m <sup>2</sup> )      | 38000        | 49000                     |
| Poisson's ratio ( $\mu$ )                           | 0.25         | 0.3                       |
| Angle of internal friction ( $\phi$ )               | 32°          | 35°                       |
| Dilation angle ( $\psi$ )                           | 2°           | 5°                        |
| Interface strength reduction factor ( $R_{inter}$ ) | 0.67         | 0.8                       |

Table 2 Values of pile properties.

| Description                                | Pile               |
|--|--------------------|
| Axial modulus (EA) (kN/m)                  | $3.56 \times 10^5$ |
| Rigidity modulus (EI) (kN-m <sup>2</sup> ) | 8000               |
| Equivalent thickness (t) (m)               | 0.519              |
| Diameter (D) (m)                           | 0.6                |

### Finite Element Mesh Generation and Calculation

The geometry of the soil-pile model is divided into finite elements forming the mesh. After generating the finite element mesh, the actual finite element calculations are executed. The calculation involves two phases. First, the prescribed displacement is activated while defining the calculation phases. Second, the earthquakes have been simulated in the dynamic analysis. The displacements are reset to zero in order to analyze the effect of the earthquake in detail. Earthquake loads

are usually applied by means of prescribed horizontal displacements. The earthquake loading is applied at the bottom of the pile. In the present study, aftershock of the Bhuj Earthquake (Gujarat) data presented in Fig. 2 is used. The analysis has been carried out for all cases and variation of bending moment and maximum displacement is observed. Fig. 3 shows the deformed mesh for L/D ratio 33 on 1V:3H slope.

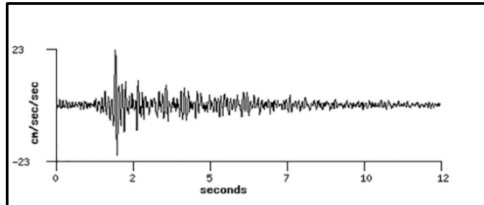


Fig. 2 Acceleration-time data for the Bhuj/Kachchh aftershock recorded at the Bhuj station.

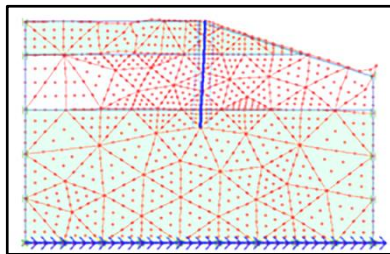


Fig. 3. Deformed Mesh for L/D = 33, 1V:3H

## RESULTS AND DISCUSSIONS

The lateral load behavior of a single pile due to dynamic loading is studied by using lateral load – deflection curves. The variations of acceleration are determined for different L/D ratio in case of horizontal and sloping ground. The effect of slope and L/D ratio on maximum bending moment and maximum displacement is also analyzed.

### Effect of L/D Ratio on Acceleration Curves For Horizontal And Sloping Ground.

The pile head/cap is more vulnerable to failure due to reduction in soil resistance along its shaft and also due to high slenderness of pile. In the present study, maximum acceleration is measured at pile head. Fig. 4 shows the variation of acceleration versus time graphs of a pile (at pile head) for different L/D ratios (16, 25 and 33) for horizontal ground surface. From the results, it is observed that as L/D ratio increases, the maximum acceleration decreases. When L/D ratio changes from 16-25, the maximum acceleration is observed to decrease by 59.82%. This behavior is observed due to increase in embedded length of pile or increase in the flexibility of soil-pile system. Fig. 5 shows the variation of acceleration with time for a

pile (at pile head) with different L/D ratios (16, 25 and 33) installed at the crest of 1V:1.5H slope. The percentage decrease in maximum acceleration with change in L/D ratio 16-25, 25-33 and 16-33 for the horizontal ground and slope of 1V:3H and 1V:1.5H are shown in Table 3, Table 4 and Table 5 respectively. From the results, it is observed that as L/D ratio increases, the maximum acceleration decreases irrespective of slopes. When L/D ratio changes from 16-33, the maximum acceleration is observed to decrease by 61.50% and 43.25% on slopes of 1V:3H and 1V:1.5H respectively. The magnitude of maximum acceleration recorded on relatively steeper slope of 1V:1.5H is much higher for L/D ratio of 33. This is because of the reduced passive wedge of soil in front of the pile which may lead to lower inertial resistance from the soil present in the region of active pile length. This can cause the net earthquake force to predominate over the weaker resistance forces resulting in higher acceleration at the pile head.

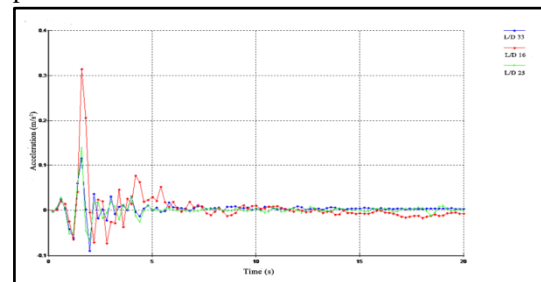


Fig. 4. Acceleration-time response for different L/D ratio's on horizontal ground

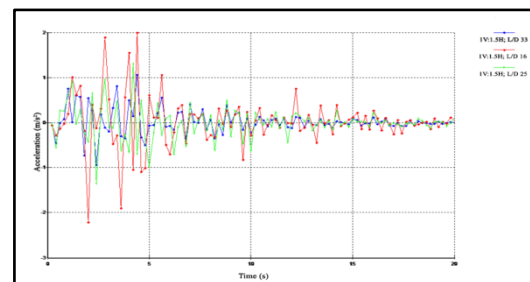


Fig. 5. Acceleration-time response for different L/D ratio's on 1V:1.5H slope

Table 3. Percentage decrease in maximum acceleration due to change in L/D ratio for horizontal ground.

| Horizontal ground Surface             |        |        |        |
|---------------------------------------|--------|--------|--------|
| L/D ratios                            | 16     | 25     | 33     |
| Max. Acceleration (m/s <sup>2</sup> ) | 0.326  | 0.131  | 0.110  |
| Change in L/D ratios                  | 16-25  | 25-33  | 16-33  |
| % Decrease                            | 59.82% | 16.03% | 66.25% |

Table 4. Percentage decrease in maximum acceleration due to change in L/D ratio for 1V:3H slope

| Slope 1V:3H                           |        |        |        |  |
|---------------------------------------|--------|--------|--------|--|
| L/D Ratio                             | 16     | 25     | 33     |  |
| Max. Acceleration (m/s <sup>2</sup> ) | 1.46   | 0.985  | 0.562  |  |
| Change in L/D ratio                   | 16-25  | 25-33  | 16-33  |  |
| % Decrease                            | 32.53% | 42.94% | 61.50% |  |

Table 5. Percentage decrease in maximum acceleration due to change in L/D ratio for 1V:1.5H slope

| Slope 1V:1.5H                         |        |        |        |  |
|---------------------------------------|--------|--------|--------|--|
| L/D Ratio                             | 16     | 25     | 33     |  |
| Max. Acceleration (m/s <sup>2</sup> ) | 2.00   | 1.459  | 1.135  |  |
| Change in L/D ratio                   | 16-25  | 25-33  | 16-33  |  |
| % Decrease                            | 27.05% | 22.20% | 43.25% |  |

### Effects of L/D Ratio and Slope on Displacement

Table numbers and labels should be placed on top of the table, hanging by 12.5 mm, and left- and right-justified. Number the tables consecutively and locate them after and close to where they are first referenced. Leave at least one line space between the table, label and the text. Tables should be auto-fit to a single column or the whole width over two columns and no vertical lines or borders are needed. Fig. 6 shows the variation of maximum displacement with slope for different L/D ratios. From the graph, it is observed that as L/D ratio increases, the maximum displacement decreases. It is also noted that as slope increases from horizontal ground surface to steeper 1V:3H, 1V:2H and 1V:1.5H slope, the maximum displacement increases significantly. The maximum displacement observed on a slope of 1V:1.5H for L/D=16 increased considerably for the present dynamic loading considered at the pile base. This is mainly due to the heavy reduction in inertial resistance from the soil in the wedge. The present result is found to be good agreement with the literature results (Deendayal R and Sitharam T G, 2016).

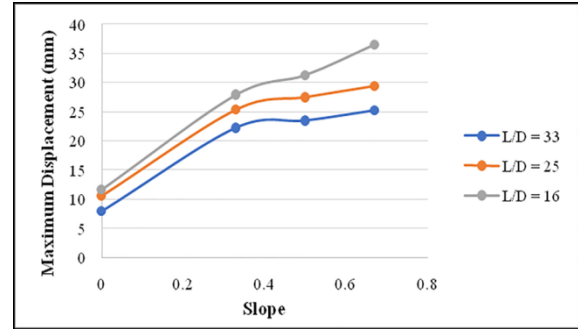


Fig 6. Maximum Displacement vs Depth curve for L/D = 16 with different slope.

### Effects of L/D Ratio and Slope on Bending Moment

The effect of slope on the maximum bending moment is shown in Fig.7 for different L/D ratio. From the graph, it is observed that the increase in embedment length to diameter ratio, the maximum bending moment of the pile decreases. This behavior is due to the increased depth of fixity arising from the larger relative stiffness of the soil-pile system. And also, if the slope increases from ground surface (zero slope) and becomes steeper (1V:1.5H), the bending moment also increases. This is due to the reduction in the passive resistance of the soil in front of the pile. It can be noted that the bending moment increases by 50-80% as the slope approaches 1V:1.5H for the range of L/D ratio's (16-33) considered in the study.

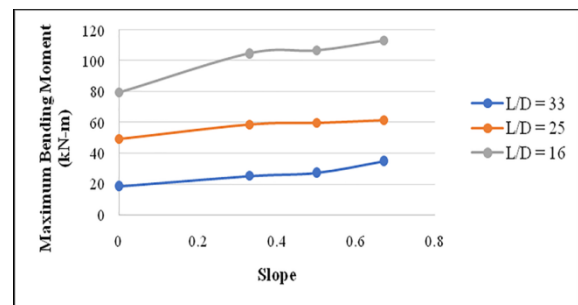


Fig 7. Variation of maximum bending moment with slope for different L/D ratio.

### CONCLUSIONS

A finite element analysis has been performed to evaluate the seismic response of a single pile installed on slopes. The developed analysis has been validated with the similar study carried out by Deendayal et al. (2016). The major conclusions from the study are presented below.

1. As L/D ratio increases, the maximum acceleration decreases irrespective of slopes. When L/D ratio increases from 16-25, 25-33 and 16-33 the maximum acceleration observed a percentage reduction of 16.03-66.25%, 32.53-61.50% and 27.05-

43.25% for horizontal ground surface, 1V:3H slope and 1V:1.5H slope respectively. This behavior was due to the increase in embedded length that enhanced the flexibility of soil-pile system.

2. From the study, it is very clear that as L/D ratio increases, the maximum displacement has been reducing. This is due to the decrease in active pile length that contributes to deflection as L/D ratio increases. And also, when ground surface changes from horizontal to steeper slopes, the maximum displacement increases tremendously especially for the case of L/D = 16.

3. It is noted that the bending moment decreases significantly with increase in L/D ratios. It is also observed that steeper slopes like 1V:1.5H has a considerable effect on increasing the bending moment.

## INFERENCE

A Kinematic soil-pile interaction study is conducted to evaluate the effect of slenderness ratio (L/D) of long piles installed on sloping ground. The dynamic loading of pile affecting the free-field motion of the soil and their combined response as soil-pile system is studied through a finite element package Plaxis 2D. It may be inferred that as the pile becomes more flexible as a result of enhancement of length, it is able to deform and rather bend more freely with the soil thus attracting less forces. The consequences of this has been evidently shown through a reduction in acceleration, displacement amplitude and bending moment. However, the study shows that the effect of steeper slopes like 1V:1.5H on increasing the maximum displacement and bending moment of relatively lower flexible piles (L/D = 16) is still alarming and requires caution through proper design considering the dynamic parameters. It is also noted that increasing the L/D ratio has only a marginal effect on such steep slopes.

## REFERENCES

- [1] T. Abdoun and R. Dobry, "Evaluation of pile foundation response to lateral spreading," *Soil Dyn. Earthq. Eng.*, vol. 22, pp. 1051–1058, 2002.
- [2] R. M. S. Maiorano, L. de Sanctis, S. Aversa, and A. Mandolini, "Kinematic response analysis of piled foundations under seismic excitation," *Can. Geotech. J.*, vol. 46, no. 5, pp. 571–584, 2009.
- [3] A. Boominathan and R. Ayothiraman, "An experimental study on static and dynamic bending behaviour of piles in soft clay," *Geotech. Geol. Eng.*, vol. 25, no. 2, pp. 177–189, 2007.
- [4] R. Di Laora and E. Rovithis, "Kinematic Bending of Fixed-Head Piles in Nonhomogeneous Soil," *J. Geotech. Geoenvironmental Eng.*, vol. 141, no. 4, p. 04014126, 2014.
- [5] Huaren Dou and Peter M. Byrne, "Dynamic response of single piles and soil-pile interaction," *Can. Geotech. J.*, vol. 33:80-96, p. 43, 1996.
- [6] H. Dou and P. M. Byrne, "Model studies of boundary effect on dynamic soil response," *Can. Geotech. J.*, vol. 34, no. 3, pp. 460–465, 2012.
- [7] R. Deendayal, T. G. Sitharam, and K. Muthukkumaran, "Effect of earthquake on a single pile located in sloping ground," *Int. J. Geotech. Earthq. Eng.*, vol. 7, no. 1, pp. 57–72, 2016.
- [8] M. H. El Naggar and M. Novak, "Nonlinear analysis for dynamic lateral pile response," *Soil Dyn. Earthq. Eng.*, vol. 15, no. 4, pp. 233–244, 1996.
- [9] B. K. Maheshwari, K. Z. Truman, P. L. Gould, and M. H. El Naggar, "Three-Dimensional Nonlinear Seismic Analysis of Single Piles Using Finite Element Model: Effects of Plasticity of Soil," *Int. J. Geomech.*, vol. 5, no. 1, pp. 35–44, 2005.
- [10] T. Nogami and M. Novak, *Resistance of soil to a horizontally vibrating pile*, vol. 5. 1977.
- [11] K. K. Toyoaki Nogami, "Time Domain Flexural Response of Dynamically Loaded Single Piles," *Am. Soc. Civ. Eng.*, vol. 114, no. 9, pp. 1512–1525, 1989.
- [12] S. L. A. Shamsheer Prakash, "Study of vertical pile under lateral load.pdf," *Proc. Third World Conf. Earthq. Eng.*, vol. 1, pp. 215–229, 1965.
- [13] H. Tajimi, "Dynamic analysis of a structure Embedded in an Elastic Stratum," *Proc. 4th World Conf. Earthq. Eng. Santiago*, vol. 3, pp. 54–69, 1969.
- [14] E. K. Yang, J. I. Choi, S. Y. Kwon, and M. M. Kim, "Development of dynamic p-y backbone curves for a single pile in dense sand by 1g shaking table tests," *KSCE J. Civ. Eng.*, vol. 15, no. 5, pp. 813–821, 2011.
- [15] Gaul, R. D. "Model study of a dynamically laterally loaded pile," *Journal of the Soil Mechanics and Foundations Division*, 84(1), pp. 1–33, 1958.
- [16] Hayashi, S and Miyajima, N. "Dynamic lateral load tests on steel H-piles," *Proceedings, Japan National Symposium on Earthquake Engineering*, Tokyo, Japan, 1962.

# BIM-BASED SIMPLIFIED APPROACH TO AUTOMATICALLY ESTIMATE BUILDING COSTS FOR PROJECTS IN THAILAND

Suon Tokla<sup>1</sup>, and Kumpon Subsomboon<sup>2</sup>

<sup>1</sup>Faculty of Engineering, Naresuan University, Thailand

## ABSTRACT

Cost estimating is a significant and critical phase of construction projects. Traditional cost estimating methods count on 2D drawings and human interpretation result in time-consuming and prone to errors. Emerging Building Information Modeling (BIM) is a process that can enhance the quantity takeoff and cost estimating with a higher level of accuracy. BIM-based cost estimating approaches can be done by integrating 3D BIM with BIM-based estimating software. These approaches are complicated, expensive, and required skilled-personnel to reap the full benefits from every estimating tools integrating with the external database. This research presents a developed BIM algorithm that is capable of automatically estimating building costs. 3D BIM intelligent objects were integrated with a custom built database with specialized templates, thereby providing ease of use while eliminating the need to manually re-enter cost changes. This algorithm creates a list of the specialized work breakdown structure (WBS) containing construction specifications, and unit costs, based on the Thai standard system. A typical BOQ was generated from the 3D BIM case study, and linked to the specialized templates that automatically estimate building cost. Estimating costs of the traditional and BIM-based approaches were compared and showed approximately closed value. This research offers a simplified but essential BIM-based cost estimating algorithm for Small and Medium Enterprises (SMEs) with a simple, fast and accurate process.

*Keywords: Building information modeling, Bill of quantity, Quantity takeoff, Cost estimates*

## INTRODUCTION

Construction cost estimating is a complicated, time-consuming and error-prone process. It is one of a significant and critical phase of construction projects. Traditionally applied cost estimating methods are performed that the process relied heavily on 2D drawings and human interpretations for generating the quantity takeoff (QTO): every single building element is measured and counted then inputted onto excel platforms to keep an inventory of all items and produce a bill of quantity (BOQ) [1]. Eastman [2] mentioned that using traditional methods are usually missed interpretations and incorrect inputs because of the hard process and complex relationships between large amounts of building elements.

In Thailand, traditional cost estimating method is still using manually quantity takeoff based on a spreadsheet of BOQ according to Thailand's Comptroller General Department (CGD), Ministry of Commerce's format. The BOQ based on the CGD format is still required for bidders in every government building work.

In the modern information technology, Building Information Modeling (BIM) is a high tech process being used in different construction aspects such as visualization, simulation, cost estimation, facility management, and construction project lifecycle [3]. As a visualized database of building elements, BIM

is able to offer an accurate QTO process as well as facilitate to decrease the variation of the cost estimations [4].

This research presents a BIM algorithm that automatically estimates building costs based on BIM 3D models that integrate with custom built database and specialized templates. This approach will facilitate ease of use without the needs of updating unit costs in BIM applications; also it is capable of enhancing BIM-based QTO process and automatically estimating costs. This research offers a BIM-based simplified approach with an essential process based on the CGD format for AEC industry and SMEs use to implement in their building construction projects in order to increase accuracy, minimize time and costs.

The following sections in this paper will present the overview of related researches, custom built database and specialized templates, develop objects properties and model a 3D building in BIM application, link typical BOQ with specialized templates for automatically generating total cost estimation.

## LITERATURE REVIEW

### Cost Estimation

Cheng [5] defined the cost estimate as an essential task for all projects because it affects

planning, bidding, design, and budget. The accurate cost estimating is a crucial aspect of any organization liable for budget submission, contract negotiation, and financial decision making [6]. The benefit of estimation is that it allows decision makers to select adequate alternatives as well as to decrease misjudged solutions [7]. The significant goal of doing cost estimating is to assist owners and other decision makers to clearly visual the detailing information of the construction projects that based on this, they can consider to continue or alter the process according to the suitable budget and time period requirements for project completion.

#### *Traditional cost estimation*

The traditionally applied methods of cost estimating start during clients got preliminary 2D drawings from designers and then offered to contractors for manually calculating a summary QTO and brief cost estimate [8]. The traditional process of QTO is involved the design objects measurement and other related documents such as 2D shop drawings that contain top views, left and right views, and section views of building specifications. These 2D based documents, either hand designed or facilitated by CAD software, are used for extracting the materials quantities by human interpretation to produce BOQ [9]. In the organized BOQ, material and labor unit costs then will be inputted manually by estimators for multiplying with the quantities in order to get the final costs. The traditional estimating process is time-consuming and low level of accuracy.

#### *BIM-based cost estimation*

Building Information Modeling (BIM) is a high prototype technology and process in architecture, engineering, and construction industry. BIM is capable of enhancing visualization, simulation, cost estimation, and facility management in the construction project lifecycle. BIM visualization and simulation of construction specification analysis offers design alternatives for decision makers communicate with stakeholders to avoid reworks and conflicts when the design is changed [10]. BIM can fulfill a process-related requirement series, non-geometric data, interoperability and automated digital data sharing for a successful facility management [11]. BIM can enhance interoperation between project teams in the AEC industry as well as facilitate the construction performances and decrease project expense [12].

BIM applications allow users to access 3D building models with quickly analyze, select, and apply the material specifications for every building component in order to create the intelligent objects that will support a BIM-based QTO process. The 3D

building that is modeled by using smart objects can enhance of extracting quantities that then link to estimating software for pricing [13]. Linking BIM components to the estimating software is capable of mapping BIM objects and matching with external database to produce estimating costs in their system. Estimating costs using a BIM-based QTO tool is able to extract the data from BIM tools to estimating software by their readable format [14]. BIM-based cost estimating process is capable of providing the accurate QTO with essential effort and time savings.

## METHODOLOGY

This research developed a BIM-based simplified approach for estimating building costs based on BIM tool that integrates with a custom built database and specialized templates. The whole process of this method is illustrated in Fig. 1.

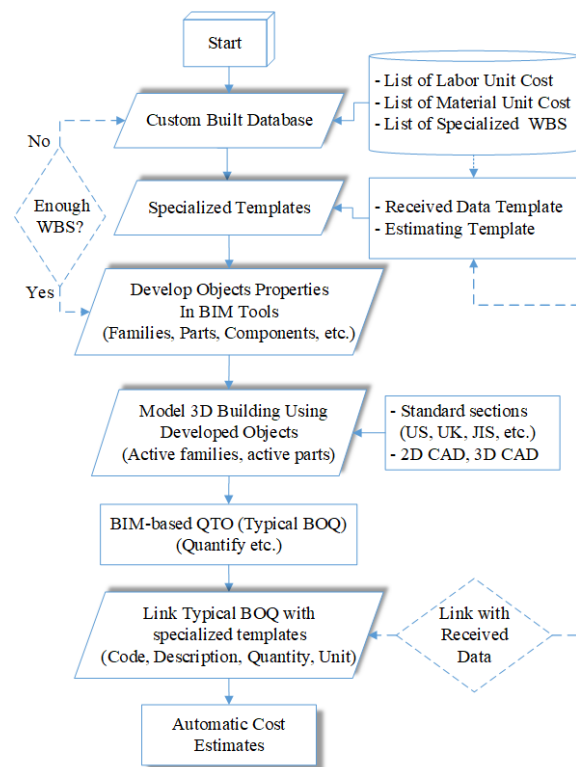


Fig. 1 Flowchart of a BIM-based simplified approach to automatically estimate building costs.

#### **Custom Built Database**

The custom built database represents an excel list of special work breakdown structure (Specialized WBS) that is created based on the combination of labor and material unit cost lists. The Practical Guidelines and Details for Calculating Construction Cost, Thai handbook updated in October 2017, contain lists of labor costs/operations for construction cost calculation that used as an original



basic data for creating the excel labor unit cost list. The excel list of material unit cost is created based on lists of standard materials price, Bureau of Trade and Economic Indices, produced by Thai Ministry of Commerce. The created list of Specialized WBS contains specifications such as codes, descriptions, units, and unit costs. The codes applied to items of the WBS have six levels, which level 1 to level 3 followed the Engineering Institute of Thailand (EIT) standard cost codes and the level 4 to level 6 are manual codes created based on the Thai Standard System as illustrated in Fig. 2.

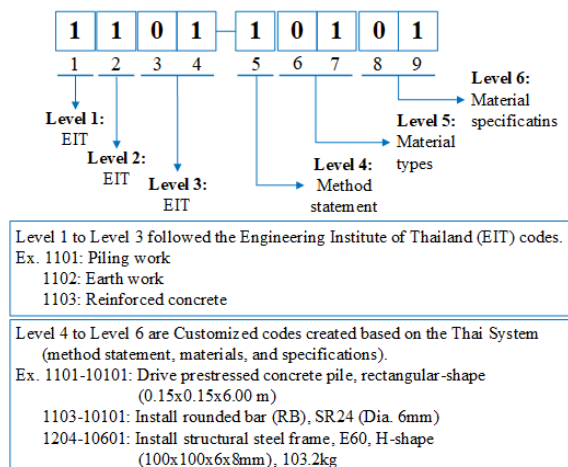


Fig. 2 Schema of the specialized WBS codes.

This research requires the custom built database in order to transfer the labor and material unit costs into the estimating template for automatically generating a total cost. This database is significant and efficient for the BIM-based cost estimating approaches, thereby providing sufficient construction WBS that is easy to observe costing of an original estimate according to cost changes while eliminates re-enter the unit costs multiple times.

### Specialized Templates

The specialized templates (received data and estimating) are created in different excel sheets linking each other by the assigned formulas and functions. The received data template contains the same columns heading with those of the typical BOQ that can facilitate the data exporting process. The estimating template is a special detailing sheet that “if function” and “v-lookup” are assigned into every cell for linking with the received data template and custom built database. Once the received data template got the data such as WBS codes, descriptions, quantities and units from the typical BOQ, that information will be automatically transferred into the estimating template. Especially, based on the WBS codes, this estimating template is capable of automatically searching for unit costs

from the custom built database and generating a completed BOQ and total costs.

### Develop Object Properties in a BIM tool

In this research, AECOsim Building Designer V8i™ is used as the BIM tool for developing the object properties. This BIM application provides “building primary tool” within “dataset explorer” that contains “Parts” and “Components” for users to develop objects geometries depend on their projects’ requirements. The process of the objects properties development is shown in Fig. 3.

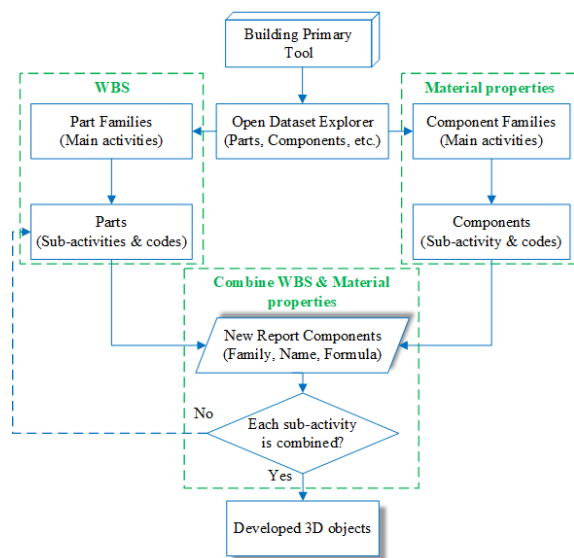


Fig. 3 The system of developing objects properties in a BIM application.

### Part (WBS) and components (materials properties)

AECOsim Building Designer V8i™ allows users to create WBS specifications, which the definitions and rendering properties can be applied by “Families” and “Parts.” This BIM tool also offers “Components” tool that allows users to create materials specifications by applying the density, unit, unit price and level of accuracy to each of them. By using this BIM tool, users can put either the labor or material unit price to the material specifications that will support the QTO process to produce directly an estimating BOQ with unit cost, but all will need to be re-entered again when the costs are changed. Moreover, some of existing objects properties provided by BIM tools contained the incorrect assigned data information even they are not well-organized that this could be complicated and make users difficult to find the existing objects properties as well as cause to be error for the estimating process. So, this present research is trying to resolve those problems by creating well-organized objects properties based on the Thai standard system

that can utilize for construction projects in Thailand. This research creates “Part families” and “Parts” that represent all construction activities in the list of specialized WBS. “Part families” are referred to all main activities that contain codes level 1 to 5. “Parts” are all of the sub-activities that contain codes level 6. The main activities and sub-activities that are created will be shown in “active families” and “active parts” respectively in the “building primary tool.” This can facilitate users to utilize depend on objects specifications during drawing process.

#### *Combine WBS with materials properties*

This is the important part of the objects properties development in order to create the completed smart elements that can affect to the quantity takeoff process. The WBS represent objects definitions and the material properties represent objects specifications. If both are not combined the software will not recognize the materials to be taken off as well as error will happen during the takeoff process. According to the existing objects properties provided by BIM tool are not sufficient for construction projects in Thailand as well as the formulas assigned are not suitable for Thai material specifications. The present mechanism creates the building WBS with material properties based on the Thai standard system and combines them with the data information and formulas assigned are correct as well as adequate due to the Thai construction requirements. The mechanism to combine is to select for “Report component” at “Part view” then open property for one of sub-activity at “Parts groups” that need to be combined. Next, click on “New report component” to show columns of Family, Name, and Formula that users can select respectively for “Component families” and “Components” then assign formula based on the object specifications.

This research creates a schematic database in BIM tool in order to support the 3D building models as well as quantity takeoff process with higher accuracy, thereby providing the adequate intelligent objects based on the Thai material specification. This database is a necessary requirement and sufficient for SME utilizing to estimate their building projects in Thailand.

#### **Model a 3D building Using Developed Objects**

This present research developed the intelligent objects based on the Thai standard system that is a necessary requirement for users utilize for modeling 3D building in BIM tool in order to produce an accurate BOQ. The way to place a 3D object in AECOsim Building Designer V8i™ is by entering data points using “AccuDraw” or by selecting object types from which the shapes are generated. In this

case, users can consider placing the 3D intelligent objects developed by the author in two ways; 1) Select for the developed objects at “Active families” and then “Active parts” respectively during the process of objects placement; 2) Place all the 3D objects to complete the 3D model then modify all of them after the process completion by using either “Apply parts” or “Building element info” tools. Moreover, the shape of every object can be modified by connecting, applying cutbacks or modifying ends.

#### **BIM-based QTO (Typical BOQ)**

BIM tool is capable of extracting material takeoffs from the 3D models and export that data information in the form of spreadsheets, databases, or word processing files. The reported BOQ is based on settings completed using the “Quantify” tool and component definitions defined by the “Families” and “Parts” in the “Dataset explorer” that the level of accurate results is highly affected by the intelligent 3D objects. This present approach modeled a completed 3D building by using the intelligent objects, which contains specific codes that can associate with the Thai material specifications. This completed 3D model is then extracted due to a BIM-based QTO process in order to produce the typical BOQ, which have only building WBS specifications and quantities. So, this algorithm requires linking the typical BOQ with specialized templates that is capable of deriving labor and material unit price and generating a completed BOQ.

#### **Link Typical BOQ with Specialized Templates**

The typical BOQ is a summary of data information in an excel sheet, which is extracted from the completed BIM-based intelligent 3D models. Specialized templates are also the excel sheets that created for linking with the typical BOQ. The received data template contained the same columns heading to those of the typical BOQ in order to facilitate the linking process. All data information in the received data template will be automatically reflected to the estimating template that is capable of deriving unit costs from the custom built database due to the WBS codes then automatically generates for the completed BOQ as well as total costs. Linking between two excel workbooks is a simple process and it is sufficient for the estimators implement in their building construction project in order to get the accurate results and time saving.

#### **RESULTS AND DISCUSSIONS**

As a result, this research offers a BIM-based simplified approach that automatically estimates building costs based on BIM 3D models that

integrate with custom built database and specialized templates. This approach is compared to the traditional and BIM-based estimating software methods as below discussion consecutively.

Traditional cost estimating methods are time-consuming and error-prone because they rely heavily on 2D drawings and human interpretation to generate the BOQ. Zhao [15] mentioned that cost control-based traditional method requires much time, 23% of training time and 77% for implementing cost control process.

Emerging BIM technology provides users with the capability of modeling 3D smart elements and produces a BOQ with unit costs, but that information needs to be inputted manually into the BIM tools or by linking via plug-in/third-party with the estimating software that derives cost data from the iCloud database. To grasp the benefits from BIM based estimating software approaches, the experienced on software using, habitual modeling, and high level of users training are necessary requirements [16]. This method is also time-consuming, 65% for software training and 23% on 3D modeling, and have the causes for inaccuracies; an inadequate classification system of BIM compatibilities; insufficient of construction material definition; incomplete BIM compatible calculating rules properties; and lack effort in a way of operability for data exchange requirements [17].

This research presents a BIM algorithm that the process of QTO is to export the building component quantities from BIM application to Microsoft Excel for producing the typical BOQ. This BOQ does not contain unit prices, so it requires the custom built database and specialized templates to fulfill this gaps. Custom built database is a well-organized list of WBS based on the required CGD's format, which contains construction activities codes, labor and material unit costs. These data then will be transferred to the estimating template that automatically generates a completed BOQ and total costs. The created mechanism provides a simplified, fast and accurate process because it needs only a BIM application and Microsoft Excel, not requires for interoperating with estimating software and iCloud database. This BIM algorithm is capable of facilitating SMEs to implement their building construction projects in order to minimize time and increase the accuracy. A case study, Start-Up and Innovation Building, was estimated for its construction costs by two different methods. The building is located in Faculty of Engineering, Naresuan University, Thailand. It is a mixed of reinforced concrete and steel structure, which has total floor area is 1469.54 m<sup>2</sup>. The estimating cost results using the Thai Manual Method, produced by an estimator of the design team in Faculty of Engineering, Naresuan University, and those results estimated by the author using BIM-based simplified

approach were compared that is shown the approximately close values as illustrated in Table 1.

This proposed method will limit to estimate only a structural and an architectural parts of a building construction project. Users also need to know well BIM software, custom built database, and the Thai cost estimated system.

Table 1 The results of estimating costs produced by the Thai manual method and BIM-based approach

| Building WBS    | Thai Manual Method (Dollars) | BIM Simple Approach (Dollars) | Different Values (%) |
|-----------------|------------------------------|-------------------------------|----------------------|
| Sub-Structure   | 14922.43\$                   | 14,740.38\$                   | 1.22%                |
| Super-Structure | 115117.34\$                  | 116,326.08\$                  | -1.05%               |
| Floor           | 26355.36\$                   | 26,010.11\$                   | 1.31%                |
| Wall            | 30323.71\$                   | 30,008.35\$                   | 1.04%                |
| Ceiling         | 7753.57\$                    | 7,850.50\$                    | -1.25%               |
| Door            | 33197.41\$                   | 32,948.43\$                   | 0.75%                |
| Window          | 22131.61\$                   | 21,965.62\$                   | 0.75%                |
| Stair           | 6851.72\$                    | 6,753.73\$                    | 1.43%                |
| Toilet          | 14140.56\$                   | 14,006.24\$                   | 0.95%                |
| Roof            | 53012.20\$                   | 52,572.19\$                   | 0.83%                |
| <b>Total</b>    | <b>323805.92\$</b>           | <b>323,181.60\$</b>           | <b>0.19%</b>         |

## CONCLUSION

The research provides a BIM-based simplified approach for automatically estimating building costs based on BIM 3D intelligent objects that integrates with custom built database and specialized templates based on the CGD's requirement. This algorithm is capable of enhancing the BIM-based quantity takeoff process and automatic cost estimations. This method created a custom built database on that contains WBS specifications and unit costs. This is a significant list with well-organized information that allows users to update either WBS or unit costs due to their construction projects' requirements in Thailand. The developed objects that are created in a BIM tool is the schematic database, which will support the 3D building models in order to produce a typical BOQ with a higher accuracy. The process is completed by creating the specialized templates to link with the typical BOQ and search for the labor and material unit cost from the custom built database that automatically generates the completed estimating BOQ as well as total costs. This BIM algorithm is capable of contributing the estimators and decision makers to reduce the time and increase accuracy for the process of cost estimation. Resulting from this research, a simplified but essential cost estimating algorithm was created for SME to implement and prepare estimating costs on their governmental building construction projects

based on the Thailand CGD's requirements with a fast, simple, and accurate process in term of time and cost savings. This method is a necessary requirement for the AEC industry that installs their building projects in Thailand. Especially, the industry that interoperated with the Thai government construction sectors, which the projects will need to be estimated with the monthly updated material costs produced by the Ministry of Commerce and the labor unit cost updated by the Comptroller General's Department (CGD).

## ACKNOWLEDGEMENT

The authors gratefully to acknowledge the Royal Scholarship under Her Royal Highness Princess Maha Chakri Sirindhorn Education Project for Cambodia and Naresuan University that offered the full scholarship and supported for this research. And also would like to thanks the Integrated Facility Engineering and Management (iFEM) in the Department of Civil Engineering, Faculty of Engineering, Naresuan University for providing research facilities.

## REFERENCES

- [1] Jadid M. N., and Idrees M. M., Cost Estimation of Structural Skeleton Using an Interactive Automation Algorithm: A Conceptual Approach. *Automation in Construction*, Vol. 6, Issue 16, 2007, pp.797-805.
- [2] Eastman C., Teicholz, P., and Sacks R., *BIM handbook: A guide to building information modeling for owners, managers, designers, engineers and contractors*, John Wiley and Sons, 2011.
- [3] Bryde D., Broquetas M., and Volm J. M., The Project Benefits of Building Information Modeling (BIM). *International Journal of Project Management*, Vol. 7, Issue 31, 2013, pp.971- 980.
- [4] Li J., Hou L., Wang X., Wang J., Guo J., Zhang S., and Jiao Y., A Project-based Quantification of BIM Benefits. *International Journal of Advanced Robotic Systems*, Vol. 8, Issue 11, 2014, pp.123.
- [5] Cheng M. Y., Tsai H. C., and Sudjono E., Conceptual Cost Estimates Using Evolutionary Fuzzy Hybrid Neural Network for Projects in Construction Industry. *Expert Systems with Applications*, Vol. 6, Issue 37, 2010, pp.4224-4231.
- [6] Jade A., and Alkass S., Computer-Integrated System for Estimating the Costs of Building Projects. *Journal of Architectural Engineering*, Vol. 4, Issue 13, 2007, pp.205-223.
- [7] Arafa M., and Alqedra M., Early Stage Cost Estimation of Buildings Construction Projects Using Artificial Neural Networks. *Journal of Artificial Intelligence*, Vol. 1, Issue 4, 2011, pp.63-75.
- [8] Wang S. W., and Park S. M., Building Information Modeling (BIM) for Project Value: Quantity Take-Off of Building Frame Approach. *International Journal of Applied Engineering Research*, Vol. 12, Issue 11, 2016, pp.7749-7757.
- [9] Sattineni A., and Bradford R. H., Estimating with BIM: A Survey of US Construction Companies, in *Proc. 28th Int. Conf. on ISARC*, 2011, pp. 564-569.
- [10] Li J., Hou L., Wang X., Wang J., Guo J., Zhang S., and Jiao Y., A Project-based Quantification of BIM Benefits. *International Journal of Advanced Robotic Systems*, Vol. 8, Issue 11, 2014, pp.123.
- [11] Becerik-Gerber B., Jazizadeh F., Li N., and Calis G., Application Areas and Data Requirements for BIM-Enabled Facilities Management. *Journal of Construction Engineering and Management*, Vol. 3, Issue 138, 2012, pp.431-442.
- [12] Azhar S., Building Information Modeling (BIM): Trends, Benefits, Risks, and Challenges for the AEC Industry. *Leadership and Management in Engineering*, Vol. 3, Issue 11, 2011, pp.241-252.
- [13] Lee N., Dossick C. S., and Foley S. P., Guideline for Building Information Modeling in Construction Engineering and Management Education. *Journal of Professional Issues in Engineering Education and Practice*, Vol. 4, Issue 139, 2013, pp.266-274.
- [14] Nassar K., Assessing Building Information Modeling Estimating Techniques Using Data from the Classroom. *Journal of Professional Issues in Engineering Education and Practice*, Vol. 3, Issue 138, 2012, pp.171-180.
- [15] Zhao P. A., and Wang C. C., A Comparison of Using Traditional Cost Estimating Software and BIM for Construction Cost Control. *ICCREM: Smart Construction and Management in the Construction and Management in the Context of New Technology*, 2014, pp.256-264.
- [16] Choi J., Kim H., and Kim I., Open BIM-Based Quantity Take-Off System for Schematic Estimation of Building Frame in Early Design Stage. *Journal of Computational Design and Engineering*, Vol. 1, Issue 2, 2015, pp.16-25.
- [17] Zhao P. A., and Wang C. C., A Comparison of Using Traditional Cost Estimating Software and BIM for Construction Cost Control. *ICCREM: Smart Construction and Management in the Construction and Management in the Context of New Technology*, 2014, pp.256-264.

# EMOTIONAL QUOTIENT ASSESSMENT PROGRAM FOR STUDENTS

Nualsawat Hiransakolwong<sup>1</sup>

<sup>1</sup>Department of Computer Science, Faculty of Science, KMITL, BKK, Thailand

## ABSTRACT

Emotional Quotient means being able to realize feelings of oneself and others to create self-motivation and can manage various emotions to be good, smart, and happy. Nowadays, most students use smartphones. This research presents Emotional Quotient assessment Program for students aging 12-17 years processing on smartphones with Android OS. There were randomly selected 30 students from the Protpittayapayat School to test this software. The experiment results show that the software can help these students to know their Emotional Quotient assessment results reported to their parents and counselor teachers. At the same time, the executive board of school can use the histogram of Emotional Quotient assessment results to plan suitable for school activities for developing emotional quotient to their students. All users gave an excellent level of satisfaction of this software with an average of 4.88 from 5.

*Keywords: Emotional Quotient, Student, School, Android*

## INTRODUCTION

Emotional Quotient [1-5] is the ability to recognize and understand the emotions of yourself and the emotions of others by playing an important role in social life. Due to the current lifestyle of Thai youth, social and cultural changes that affect emotional development cause problems that young people cannot solve problems on their own. Emotional quotient assessment software for Thai children has a role in assessing emotional quotient that can tell the tester how to develop or improve the emotional quotient.

Nowadays, mobile phones or smartphones have been developed to be able to use the internet and various applications that reach users of all ages. Especially in adolescents, the behavior of this age persons needs convenience, speed, and modernity. But with the change of teenagers both physically and mentally, sometimes they do not dare to ask for advice to adults directly. Smartphone technology may help young people to be enthusiastic and interested in self-assessing emotional quotient. This assessment form is an assessment of emotional quotient from the Department of Mental Health. After users do assessments complexly, there will be a report of the results in three aspects: good, smart and happy, which will be very useful for those who do the assessment. In previous work, there are web applications [6, 7] assessing mental health that can be done and evaluated online. But they cannot record data and results of the assessment. At the same time, teenagers spend most of their time at the school, where is a place for teaching students and teachers give advice to students. This paper presents a mobile application doing Emotional Quotient

assessment that can record the results. Guidance or class teachers can print the evaluation report and attach it in the students' report books to their parents for acknowledging as well. At the same time, guidance teachers are aware of the results of the emotional quotient assessment of students, both individual, and all. Therefore, the executive board of school able to use the information to plan activities [5] to develop emotional intelligence to suit students that will benefit students, academics and the nation.

## ALGORITHM

The Emotional Quotient (EQ) assessment program for students aging 12-17 years. The registration function is divided into 2 statuses; as a teacher or as a student. A teacher can create a classroom and classroom code. Students can do the Emotional Quotient assessment running question randomly with a total of 52 questions. The result of Emotional Quotient assessment is divided into 2 statuses either normal or abnormal. Then suggestions based on the evaluation results are shown also. Students can send their assessment results into the classroom with the classroom code. The Emotional Quotient assessment of students' results will be shown to their counselor teacher.

Teachers can see functions as follows: Students Assessment results in each student or summary table for all students. The Emotional Quotient assessment results will show in both text and graph. Emotional Quotient assessment results can be

printed and also report to their parents as well.

The flowchart of the EQ assessment program is shown in Fig. 1 and its use case diagram is shown in Fig. 2.

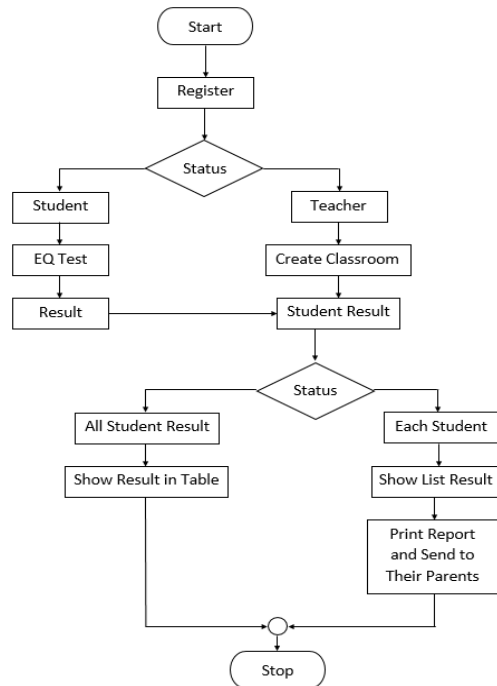


Fig.1 Flowchart for the EQ assessment program

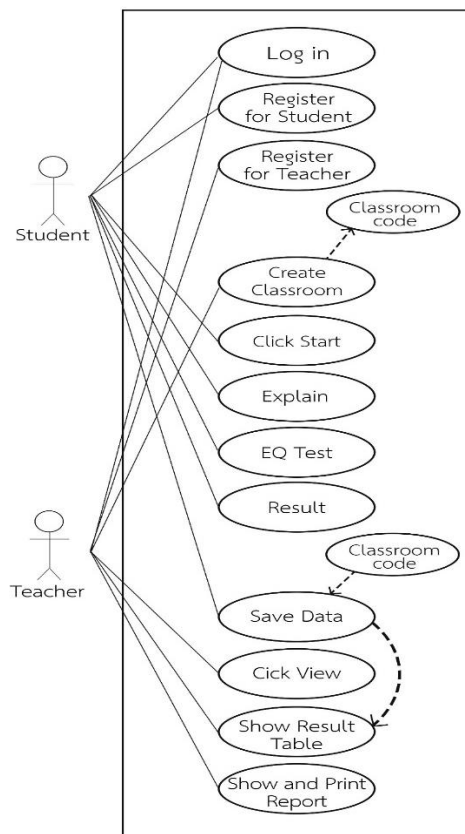


Fig. 2 Use case diagram

## PROGRAM

The Adobe Photoshop CS6 is used for interface design. The EQ Assessment Program is created with Android Studio programming language and the Firebase software is used for handling database. The content of the EQ Assessment comes from the Department of Mental Health, Ministry of Public Health, Nonthaburi 11000 Thailand.

The EQ assessment program for students with aging 12-17 Years is processed on smartphones with Android OS. After installing the EQ assessment program on the smartphone, and then click open the application shown the interface as Fig. 3. This application is called EQ 101.

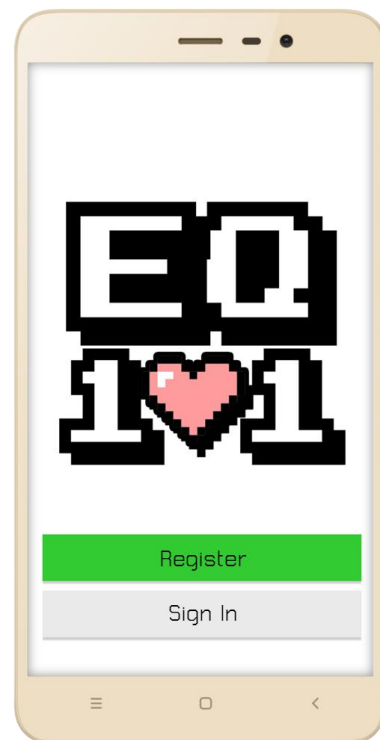


Fig. 3 An interface of the EQ assessment program

For the first time use, users can choose a register button. Then the monitor will ask for the registration status either teachers or students as shown in Fig. 4. If a user clicks on the teacher button, the monitor will ask for private information such as name, surname, school name, email, password, and the confirm password as shown on Fig. 5. If a user clicks on student button, the monitor will ask for more private information such as name, surname, school name, email, password, the confirm password, and more information about their parents. For the next time use, users only click on the Sign In button, and then the monitor will ask only for email and password as on Fig. 6. Then the program will show functions for each type of



registration either teachers or students.

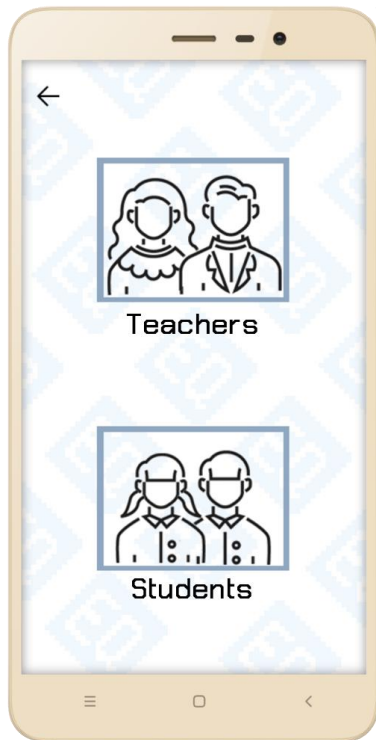


Fig. 4 Registration status either teachers or students



Fig. 6 Sign In after the registration

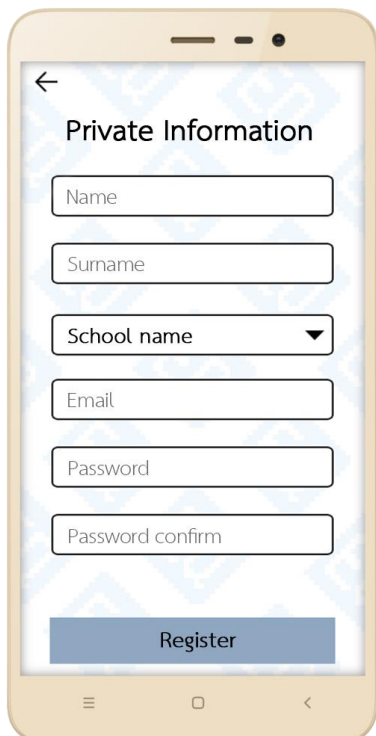


Fig. 5 Private information for registration

In Fig. 7, when a user has a status as a teacher after the user login, the monitor will show functions, such as Classroom for creating a classroom, Information for editing teacher's information, the EQ questions showing 52 questions in the EQ Assessment, Advice for EQ showing examples of advice to develop EQ that teachers can learn, and Assessments showing the EQ assessment results for each student or the all students in a class/school. Teachers can create, edit, and delete classrooms. When a teacher creates a classroom by pressing the + sign on the bottom right in Fig 8, the program will generate a classroom code for a teacher to inform his/her students. Students will use a classroom code to add name and send the EQ assessment results in their classrooms as shown in Fig. 9. Teachers can view and print the EQ assessment results for each student to inform the student's parents. The EQ assessment results will show in a graph with 3 categories such as being good, smart, and happy. In Fig. 10, a teacher view the EQ assessment results in being in the good category of one student who ever did the EQ assessment twice. Its results will show both times: #1 and #2. Being good is consist of self-regulation, empathy, and responsible. The parents will know the EQ assessment results of their children, and then they can adjust activities in the family to develop QE for their children.

When the user has a student status after entering the system of the user, the screen will display functions such as assessments for doing EQ

assessments, assessment results to show the history of QE assessment results, Information for editing his/her information, Advices for EQ showing examples of advice to develop EQ that students can learn.

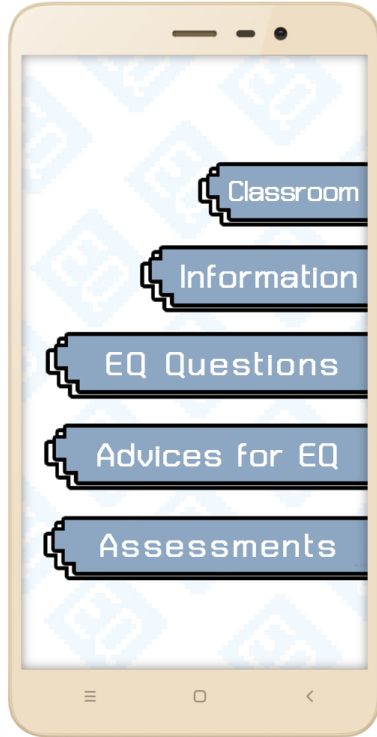


Fig. 7 Functions for teachers



Fig. 8 An example for creating a classroom 101



Fig. 9 The EQ assessment results of each student

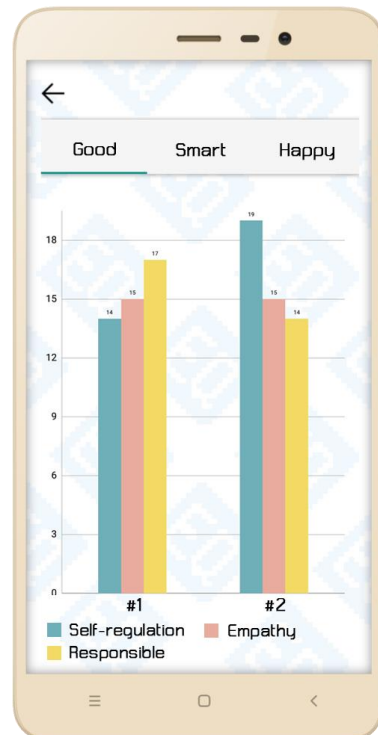


Fig. 10 EQ assessment results in being good

From Fig. 10, the more detail will show in Fig. 11 and Fig. 12. Being good consists of self-regulation, empathy, and responsible. Being smart

consists of motivation one-self, decide the solution, and build relationships. Happiness consists of self-esteem, satisfied in life, and calm. There are totally nine items of the EQ assessment results, such as self-regulation, empathy, responsible, motivation one-self, decide the solution, build relationships, self-esteem, satisfied in life, and calm. From Fig. 11 and Fig. 12, the results of a student whose name is Mr. B Park is shown all of nine items. There is an opening bracket in front of each item. If the opening bracket is blue, the evaluation results of that item are normal and it is written "normal" at the end of the item also. On another hand, if the opening bracket is red, the evaluation results of that item are abnormal and it is written "should improve" at the end of the item also. Fig. 12 is a screen continue from Fig. 11 after sliding its slide bar. There are two buttons of the bottom in Fig. 12. The Advice button will show some advice on how to improve in each abnormal item from the EQ assessment results. The Create PDF button will create the EQ assessment results and advice on how to improve abnormal items into the PDF file. Teachers can print the PDF file and also report to students' parents as well. Teachers and their parents will aware of the EQ assessment results and know how to arrange activities [5] for their children. Teachers can select activities [9-10] that help student's improvement in their EQ. At the same time, their parents can also adjust activities in the family more suitable for improving the EQ of their children.

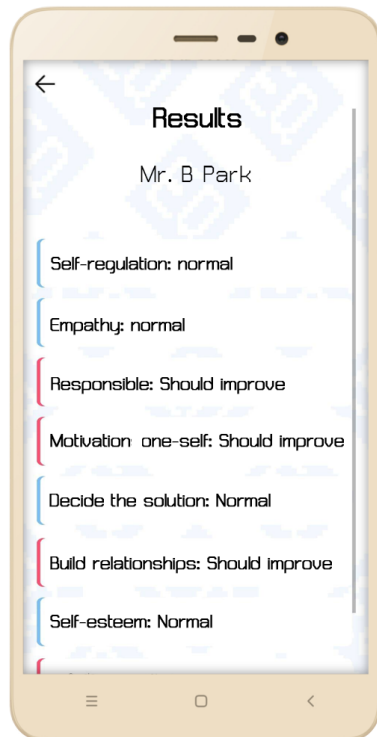


Fig. 11 EQ assessment results of Mr. B Park

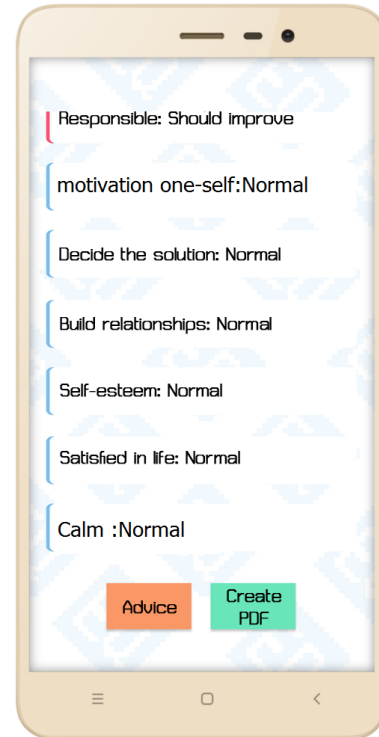


Fig. 12 The EQ assessment results (continue)

Teachers not only know the results of each student's EQ assessment in the classroom but also know the unusual frequency of each item of the EQ evaluation of all students in their school, as shown in Fig. 13. From Fig. 13, the table shows each row is consist of a student name and EQ evaluation in nine columns composed self-regulation, empathy, responsible, motivation one-self, decide the solution, build relationships, self-esteem, satisfied in life, and calm. The EQ assessment result in each column represents color. For example, white means the normal result and red means abnormal or should be improved. At the bottom of the table is a summary of the frequency of irregularities in each column.

| Students     | Self-regulation | Empathy | Responsible    | Motivation one-self | Decide the solution | Build relationships | Self-esteem | Satisfied in life | Calm   |
|--------------|-----------------|---------|----------------|---------------------|---------------------|---------------------|-------------|-------------------|--------|
| Miss A Brown | Normal          | Normal  | Should improve | Should improve      | Should improve      | Should improve      | Normal      | Normal            | Normal |
| Mr. B Park   | Normal          | Normal  | Should improve | Should improve      | Normal              | Should improve      | Normal      | Normal            | Normal |
| Mr. C Pink   | Normal          | Normal  | Should improve | Should improve      | Normal              | Should improve      | Normal      | Normal            | Normal |
| Mr. D Crown  | Normal          | Normal  | Should improve | Should improve      | Normal              | Should improve      | Normal      | Normal            | Normal |
| <b>Total</b> | 1               | 3       | 4              | 1                   | 0                   | 1                   | 1           | 4                 | 1      |

Fig. 13 The EQ assessment results of all students

## EXPERIMENTAL RESULTS

After the EQ 101 was finish coding program, this application was installed into five smartphones on Android OS. There were randomly selected one teacher and ten students from the Protpittayapayat School, a local school to test this software. In the first time, after the application had been used by teacher and students, each user was an interview and gave with some comments to develop the application more benefits, such as creating the EQ assessment results into PDF file that can print to report student's parents and summary results of all students in school, then the executive board of school can use histogram of Emotional Quotient assessment results to plan suitable of school activities for developing emotional quotient to their students. Then the EQ 101 had been adjusted the new version following the comments.

On the second time, there were randomly selected 31 students and 2 teachers from the same local school to test this new version software. After users were finished the test, they did questionnaires and were an interview. The survey results were as follows: For the personal information, users are 10 male (about 30.30 %) and 23 female (about 69.70 %) as shown in Table 1, and there are 2 teachers and 31 students as shown in Table 2. For percentages of the grade level of students, there are 2 students of Grade 9<sup>th</sup>, 11 students of Grade 10<sup>th</sup>, and 18 students of Grade 11<sup>th</sup> as shown in Table 3.

Table 1 Frequency distribution: gender of users

| Gender | Number | Percent |
|--------|--------|---------|
| Male   | 10     | 30.30   |
| Female | 23     | 69.70   |
| Total  | 33     | 100.00  |

Table 2 Frequency distribution: status of users

| Status   | Number | Percent |
|----------|--------|---------|
| Teachers | 2      | 6.06    |
| Students | 31     | 93.94   |
| Total    | 33     | 100.00  |

Table 3 Percentages of grade level for users

| Grade level | Number | Percent |
|-------------|--------|---------|
| Grade 9     | 2      | 6.45    |
| Grade 10    | 11     | 35.48   |
| Grade 11    | 18     | 58.07   |
| Total       | 31     | 100.00  |

Table 4 Average user satisfaction of the EQ 101

| Satisfaction  | Average | Level of satisfaction |
|---|---------|-----------------------|
| 1. Able to study usage quickly and easily                       | 4.52    | excellent             |
| 2. Satisfied with the modernization of application design       | 4.52    | excellent             |
| 3. The application can display correctly                        | 4.45    | excellent             |
| 4. The appropriateness of the font size used in the application | 4.58    | excellent             |
| 5. The suitability of the colors used in the use                | 4.45    | excellent             |
| 6. Response speed   | 4.82    | excellent             |
| 7. The application is useful to users                           | 4.88    | excellent             |
| 8. Satisfaction in using the application                        | 4.79    | excellent             |

$$w = (H - L)/N \quad (1)$$

Where  $w$  = the width of the class

$H$  = the highest value of the scale

$L$  = the lowest value of the scale

$N$  = the number of levels

From [8] Likert scale of five levels will compute the width of the class by using Eq. (1). The highest value of the scale is five and the lowest value of the scale is one. The number of levels is five. Therefore,  $H = 5$ ,  $L = 1$ ,  $N = 5$ , the width of the class is equal to 0.8 ( $w = 0.8$ ). The level of satisfaction can transform as follows:

The value of satisfaction 1.00 – 1.80 means poor.

The value of satisfaction 1.81 – 2.60 means fair.

The value of satisfaction 2.61 – 3.40 means good.

The value of satisfaction 3.41 – 4.20 means very good, and the value of satisfaction 4.21 – 5.00 means excellent.

From Table 4, the average user satisfaction of the EQ 101 was shown. For example, users gave an average of satisfaction with 4.52 for able to study usage quickly and easily means excellent. Users gave excellent satisfaction in all dimensions of using this application. The application is useful to users get the highest satisfaction with the average value 4.88 identifying the high quality of the EQ assessment for students, teachers, and schools.

## CONCLUSION

The Benefits of the applications are as follows:

1. Students can do the EQ assessment more convenient, know their EQ assessment results, and know how to improve their EQ.
2. Teachers can check the EQ assessment results of students either the results for each student or whole students in a class/school more convenient.
3. Students can develop and improve themselves appropriately from the results of the EQ assessment and its recommendations.
4. Teachers and parents know how to organize activities to improve emotional intelligence behavior more suit with students.
5. At the same time, the executive board of school can use the histogram of Emotional Quotient assessment results to plan suitable of school activities for developing emotional quotient to their students that will benefit students, academics and the nation.

## ACKNOWLEDGMENTS

I would like to thank you, Miss. Tharinee Vatesee and Miss. Bongkot Chatchawan to help me coding the program.

## REFERENCES

- [1] Robert K. Cooper (1998), Executive EQ, Texere Publishing, US 1998.
- [2] Cary Cherniss (2000), Emotional Intelligence: What it is and Why it Matters, Consortium for Research on Emotional Intelligence in Organizations, Psychology, New Orleans, LA, April 15, 2000, available online at, <https://www.talentsmart.com/media/uploads/pdfs/eq-what-it-is.pdf>
- [3] Daniel Goleman (1996), Emotional Intelligence: Why It Can Matter More than IQ, Learning, v24 n6 p49-50 May-Jun 1996.
- [4] M.L.Somchai Chakrabhand, Community Mental Health: Thailand Country Report 2008, Department of Mental Health, Ministry of Public Health, Nonthaburi 11000 Thailand, August 2009.
- [5] Project TO BE NUMBER ONE, Practice thinking to solve problems, develop EQ, Event handbook for Volunteers, Kaew Chao Chom Media and Publications Center, Suan Sunandha Rajabhat University, Revised version July 2015.
- [6] Webpage IQEQDEKTHAI is available at <http://rajanukul.go.th/ieeq/index.php>.
- [7] Department of Mental Health is available at <https://www.dmh.go.th/test/>.
- [8] Rensis Likert (1961), New Patterns of Management, New York: McGraw-Hill Book Company Inc.
- [9] Yaowanat P., Sajee S., Kaliyakorn K., Pruksa P., Activity guide to strengthen students' EQ, Department of Mental Health, Ministry of Public Health, Nonthaburi 11000 Thailand, August 2014.
- [10] Yaowanat P., Sajee S., Kaliyakorn K., Pruksa P., Activity guide to strengthen students' EQ, Department of Mental Health, Ministry of Public Health, Nonthaburi 11000 Thailand, August 2018.

# ELECTROMAGNETIC SWITCHING TRANSIENTS IN TRANSMISSION LINE COOPERATING WITH THE LOCAL SUBSYSTEM

Pawel Sowa<sup>1</sup>, Daria Macha<sup>1</sup>

<sup>1</sup>Silesian University of Technology, Gliwice, Poland

## ABSTRACT

The article investigates the overvoltage occurring during switching states in the line cooperating with the local subsystem. Overvoltages appearing in the line connected to the local subsystem during switching operations, forced by the change of network operation conditions. Electromagnetic transients in the unloaded line were tested after its sudden disconnection from the power supply. In the research, particular attention was paid to the conditions of switching off the line (moment and disconnection unity), the influence of surge protection devices, the type of the voltage transformer and the short-circuit power of the power subsystems.

*Keywords: Overvoltages, Switching Surges, Electromagnetic Transients, Equivalent Network*

## INTRODUCTION

In the 400 kV transmission network the overvoltages can occur which are mainly caused by the following factors:

- maintaining normal voltages in relation to the rated voltage of the network,
- expansion of the 400 kV transmission network (lines, especially in low-load states, are a source of reactive power, and as a result, increase the voltage level),
- insufficient equipment of the 400 kV transmission network in devices for capacitive reactive power compensation (parallel reactors),
- development of local production sources that relieve the transmission network.

The waveforms of electrical quantities in the highest voltage lines depend on many factors of which for the steady state the most important are: shunt parameters, short-circuit power and line symmetry. This influence is emphasized in the case of a weak line load or if the line is opened at one end.

However one-side opened transmission line is a source of reactive power (the value of generated reactive power is proportional to the length of the line - 1 km of the 400 kV line generates approx. 0.5 MVar). If the attached end of the line is connected to a weak system, it can cause a large voltage boost.

During transient states there are many important factors affecting the maximum values of electromagnetic transient components.

For a full assessment of critical value, a comprehensive analysis was carried out, including the moment of switching off the line, the nonsimultaneously disconnection, the influence of surge protection devices, the type of the voltage transformer and the short-circuit power of the

subsystems of the power supply.

Figure 1 presents a schematic diagram of the studied system and a graphic model introducing the input data to the MicroTran [1] program (UBC version of the Electromagnetic Transients Program - EMTF) used by simulation. The program provides tabular display, printer plots and high resolution graphic plots as output. The method used in program is based on Bergeron's method for transmission lines and trapezoidal rule of integration for lumped parameters.

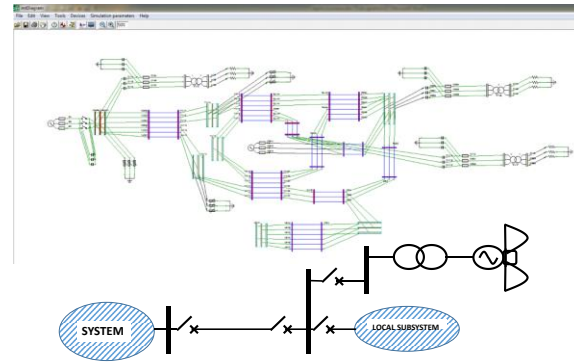


Fig. 1 Diagram of tested system.

Using MicroTran program it is shown that all transients in high voltage system can be determined and the most severe conditions can be modeled without risk and with very flexible possibility to determine the performance of electrical equipment in the high voltage line under all possible fault conditions in transmission system.

Analysis was made for the signals with very high level of high-frequency component. Methods were tested with the help of MicroTran program and NETOMAC – program [2].



## SELECTION OF SIMULATION METHOD

### Transmission line model

Transmission line in real is the only one element of the power system with distributed parameters, and therefore for the simulation the adequate numerical models and methods must be used. Figure 2 shows the elementary dx section of the transmission line.

Line modeling by means of a series of substitute elements connected in series – three-phase PI-gliders taking into account inductive and capacitive couplings - can lead to erroneous results manifested by the presence of artificial components that do not exist in real systems.

For the model of lines with distributed parameters, the dependence of parameters on the frequency is taken into account by the use of the so-called Marti model [3], which is the optimal solution from the point of view of accuracy and speed of calculation.

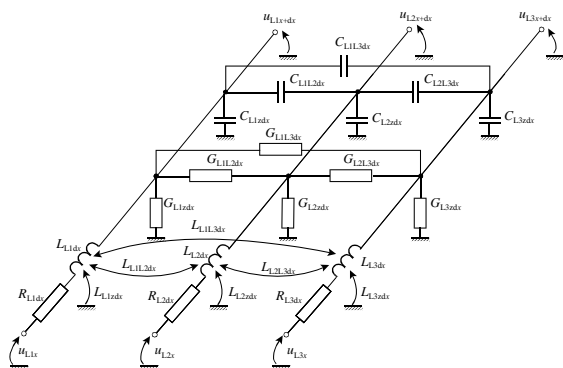


Fig. 2 Representation of the transmission line section length dx.

### Primary equipment models

In order to obtain reliable results of electromagnetic studies of transient phenomena, apart from the overhead line model, it is very important to get the correctly representation of primary equipment such as voltage transformers and surge arresters. There are two constructions of voltage transformers:

- inductive, which are measuring transformers with a primary winding connected directly to the network;
- capacitive, in which the measuring transformer is supplied from a capacitive voltage divider, thanks to which the insulation of the transformer itself can be built to a much lower voltage than in the case of inductive transformers;

In many constructions of inductive voltage

transformer, the effective counteracting of ferroresonance phenomena for both harmonics and subharmonics is protracted. Figure 3 is a substitute diagram of an inductive voltage transformer. The errors in the transfer of the voltage signal transformer to the secondary side can be caused primarily by the impedance values of the load and the magnetization inductance  $L_\mu$  and loss resistance in the  $R_{Fe}$  core.

The schematic diagram of the capacitive voltage transformer is shown in Fig. 4. During transient voltage transformers accurately transmit the voltage signal. The share of a non-periodic component in the voltage signal is small - there is no threat of saturation of the transformer. All significant harmonics are reproduced exactly on the secondary side and the impact of the magnetizing currents appearing during switching the transformers is damped very quickly. Signal transfer errors can only occur for very high frequency.

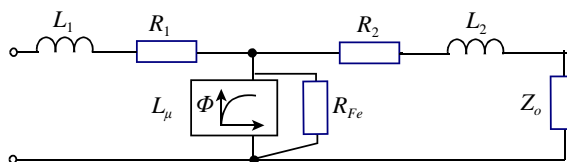


Fig. 3 Model of inductive voltage transformer.

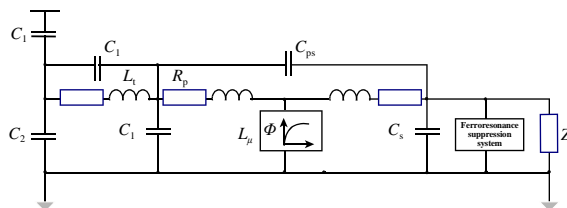


Fig. 4 Model of capacitive voltage transformer.

To protect the electrical apparatus against transient overvoltages, surge arresters (lightning arresters) are used to limit the duration and frequency of the subsequent current. In MicroTran program two models of the surge arrester are available to the user: using non-linear resistance (Fig. 5) and built of a non-linear element - usually ZnO (Fig. 6).

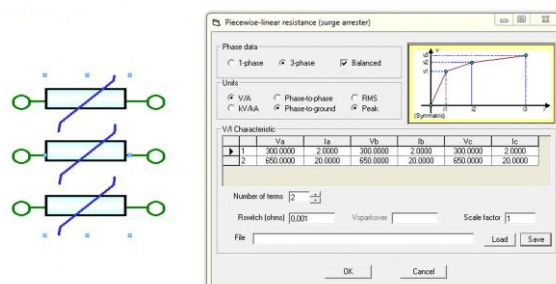


Fig. 5 Representation of surge arrester with non-linear resistance.

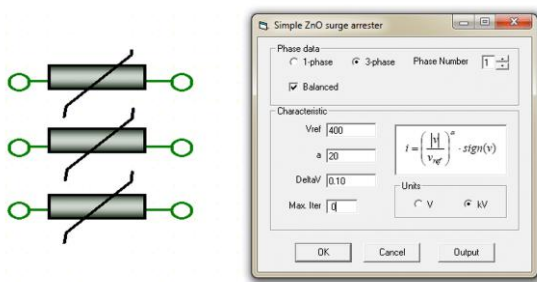


Fig. 6 Model of surge arrester used ZnO element.

### Equivalent system

During analysis in complex system call in question both the necessity of detailed representation of each element and the range of reduction of network and its influence on credibility of results of investigation. Generally to get correct results of calculation in equivalent system is possible only when:

- element of system, for which transient (voltage or current) should be determined, must be modeled in detail without any simplification taking into consideration every factor having influence on result of investigation,
- remaining part of system which will be reduced must be represented by equivalent network but the parameters must be identified with the help of according optimization method.

By process of identification for given transient input signals there are searching the parameters of determined mathematical model representing part of system designed for reduction. For solution of such problem it is assumed at begin unchanged structure of investigated model and possibility of unlimited choice of parameter for equivalent.

By lack of information of identified equivalent system the identification process is going in 4 steps after preparation of input and output data signals:

- determination of structure of equivalent system,
- choice of optimization criterion,
- choice of numerical method and determination of parameters according to chosen criterion,
- testing of structure of model taking into account that for each new structure new parameter identification will be performed.

The choice of structure depend on later application but critical verification must be only after determination of optimal parameters of equivalent system. Very important is optimization method.

The modification of least-square method proposed in [4] was tested for signals with high level of high frequency free components with MicroTran program and for signals with low level of this components with NETOMAC program.

The new idea using artificial neural network (ANN) determine the new direction of search of equivalent solution for the range of electromagnetic transient [5]. The aim is to replace part of systems by suitable universal ANN-based dynamic equivalents.

### SIMULATION TESTS FOR VARIOUS WORK AND DISTURBANCE VARIANTS

#### Verification of computer simulation with the values measured during the fault test

Comparison of computed transient waveforms with those measured on an actual system allow some assessment to be made of the methods of calculation. The measurement techniques must be free of error and comprehensive system data must be provided in order to achieve maximum computational accuracy. In Figure 7 the comparison of two measured voltage transient are presented.

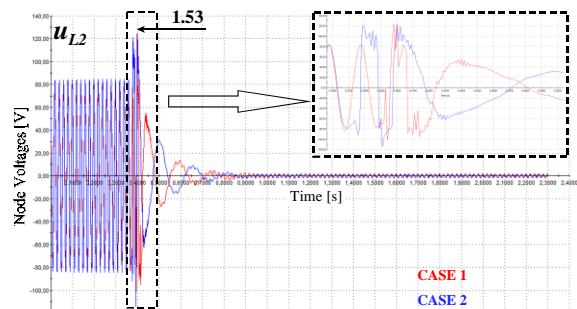


Fig. 7 Recorded voltage waveforms.

The results were recorded during two measurements at the beginning of 260 km line length, during disconnection at the end of line. To be able to use the test results the values measured during the tests have been transferred into a mathematical model for the MicroTran program. The computer simulation was used for very detailed transmission line model and simple equivalents of complex transmission networks. Comparison of the measured and calculated values for the voltage and current transients indicates that the system modeling was precise enough for further transient analyses.

#### Determination of the value and nature of overvoltages occurring for the unloaded line

The research has shown a huge number of factors affecting the surge coefficients, whereby repeatedly

changing individual parameters for a given system configuration does not cause a significant change in the values of these factors, but only a change in "circumstances", e.g. time of peak voltage during an ongoing transient process. numerical analysis to determine the phasing delay times during which maximum overvoltages can occur is very tedious and time-consuming.

The maximum amplitudes of free components occur in the phase whose voltage at the moment of switching off reaches the maximum value. From the extremely different conditions of maximum transient voltage values (maximum overvoltages for the initial moment of the disturbance, when the disconnection phase voltage reaches the maximum) it follows that virtually always during the interferences there are free components with different amplitudes and damping times. Taking into account the phenomenon of superimposition of these components during non-simultaneous disturbances, there is the problem of the increase of these amplitudes and damping times in relation to these values calculated for simultaneous disturbances. The inconsistency of the switching disturbances results in a significant increase of the overvoltage coefficients in relation to the maximum calculated during these disturbances treated as simultaneous.

Figures 8 and 9 show the example of transients on the secondary side of the capacitive and inductive transformers installed at the beginning of the line when the circuit breakers are off at each of the two transmission line systems.

Overvoltage coefficients obtained during non-simultaneous switching off significantly exceed these values (as can be seen in the presented drawings) and despite the fact that overvoltages are transient, but due to the repetition of this phenomenon may pose a threat to the primary apparatus.

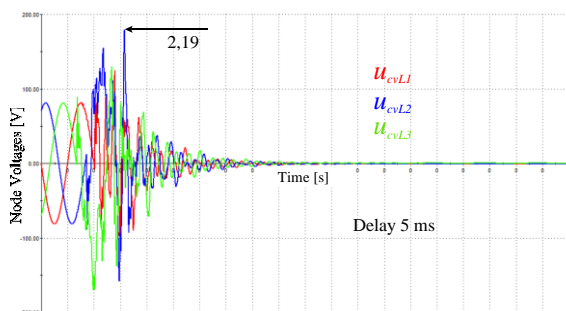


Fig. 8 Waveforms on the secondary side of the capacitive transformer installed at the beginning of the line after 5 millisecond delay of shutting down the second system.

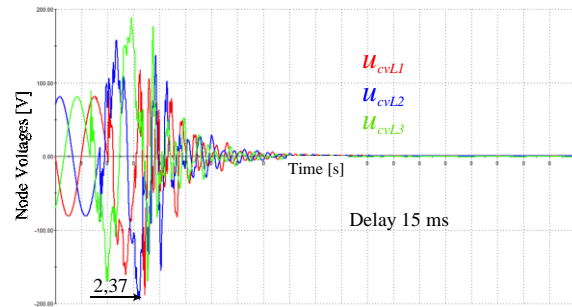


Fig. 9 Waveforms on the secondary side of the capacitive transformer installed at the beginning of the line after 15 millisecond delay of shutting down the second system.

Figure 10 shows the same example of transients but on the primary system.

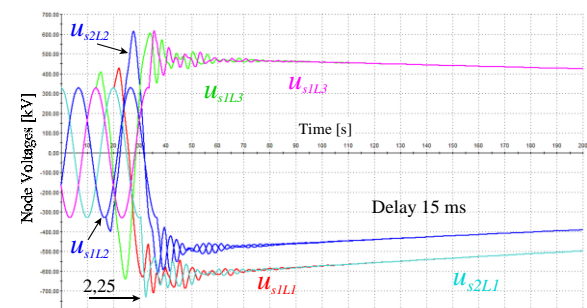


Fig. 10 Waveforms on the primary side of the capacitive transformer installed at the beginning of the line at the 15 millisecond delay of switching off the second system.

### Discussion of the impact of data on test results

Situation in the line after disconnection from the power supply is stable. The voltage remains at a certain level - keeping the instantaneous value as it was before the disturbance. This is due to the fact that the voltage in the line is not possible (or they are minimal) for unloading. Connecting the equipment - voltage limiters on both sides of the line improves this situation.

Note that both types of representation of surge arresters do not contribute to large differences in the values of extreme surge coefficients.

There is clearly faster damping in the case of modeling using a resistive model, but there is no major difference in the obtained surge coefficients, what is illustrated in the Fig. 11 and 12.

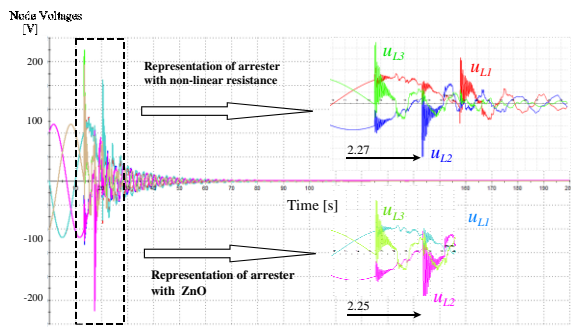


Fig. 11 Comparison of transients calculated on the secondary side of the capacitive transformer with two representation of surge arrester.

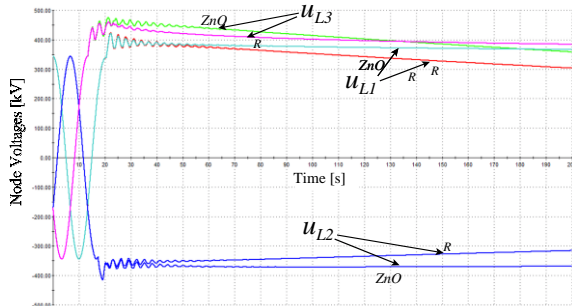


Fig. 12 Comparison of transients calculated on the primary side of the capacitive transformer with two representation of surge arrester.

Transient waveforms occurring on the secondary side of capacitive voltage transformers do not change their character along with a change in the representation of surge arresters in the transmission system on the primary side. In both cases these waveforms are faster suppressed than the primary voltage, but there are oscillations resulting from the free components of the higher frequencies. Overlapping of these components causes a large number of voltages on the secondary side of capacitive voltage transformers. However, this does not pose a threat to the transformer due to the voltage value on the secondary side of the transformer.

## CONCLUSIONS

As stated in the research, the high frequency components that disappear relatively quickly have a significant impact on the peak values of instantaneous voltages on both sides of capacitive voltage transformers. The extreme peak of the instantaneous voltage was noted at both ends of the switched off line with multiples significantly value = 2 in relation to the maximum phase voltage of the line.

There are also free lower frequency components damping very slowly.

During the disturbance state on the primary side of the capacitive transformer, the energy stored in the capacities and inductances results in transient oscillations on its secondary side. Transient waveforms are a combination of low frequency signal oscillation (2-15 Hz) and high frequency oscillation signal (900-4000 Hz). The free frequency component of the higher frequency is suppressed in a short time (less than 10 ms), whereas the low frequency oscillation signal lasts longer.

The overlapping of free components created on the primary side of the transformer and its own oscillations may cause false signals from the secondary side. This mainly applies to free components of higher frequencies that determine the amplitude of induced overvoltages.

The cause of the disturbing phenomena investigated in the paper is the problem of switching overvoltages arising when switching off the unloaded line of considerable length, but still equipped with capacitor voltage transformers. The line with a fairly complex course is over 260 km long, so the power of charging it is about 150 MVar. It follows that the switch is designed to disable the capacitance of significant value.

Therefore, to determine the correct conditions for conducting mergers, one or several of the remedial measures resulting from the analysis should be applied:

- for the suppression of transient states, the simplest remedy could be to replace capacitive transducers with inductive voltage transformers. This is particularly important for the tested line of considerable length.
- it would be advisable to use high-voltage transverse chokes to reduce the overvoltages of the mains frequency (the so-called compensated line).
- discharge resistors, a short-term bypass switch, would be helpful.
- a good damping effect of oscillations after switching off the line could give short-term switching of resistors

Generally, for the elimination or reduction of the overvoltage in the line after disconnection of line - the best and the fastest solution would be to replace the capacitive voltage transformers with the use of inductive voltage transformers.

However, this causes the risk of occurrence of ferroresonance phenomena (in particular chaotic

ones).

The use of controlled energoelectronic regulators system is not - from the point of view of development of network conditions conducive to the generation of ferrozonance chaos - only the risks, but it can be an effective means of great potential to prevent or mitigate the effects of the phenomenon of ferrozonance or ferrozonance chaos in the power system.

Effective and efficient use of energoelectronic controllers, must be preceded by a series of simulation studies and not limited only to determine the presence and impact of regulatory options to change the substitute driver impedance parameters of the network and the resulting possibility of preventing ferrozonance chaos but also taking into account, the impact of network parameters control using energoelectronic devices on systems stability - especially dynamic - power system or selected parts of system.

## REFERENCES

- [1] MicroTran, Transients Analysis Program for Personal Computers, MicroTran Power System Analysis Corporation, June 1991, Vancouver, B.C., Canada
- [2] Kulicke B., Simulationsprogram Netomac: Differenzen - Leitwertverfahren bei kontinuierlichen und diskontinuierlichen Systemen, Siemens Forsch.- und Entwickl. Ber Bd. 10 (1981), 5, pp. 299-302
- [3] Marti J.R., Accurate modelling of frequency-dependent lines in electromagnetic transient simulations, IEEE Trans. PAS-101, 1982 s.147-157.
- [4] Sowa P., Search of Optimum Equivalent Representation for Transient Investigations during non-Simultaneous Faults, Proceedings of the IASTED, Int. Conference Modeling and Simulation, Pittsburgh, USA, 1998, IASTED/ACTA Press, ISBN: 0-88986-252-4, ISSN: 1021-818, pp.466-470.
- [5] Azmy A.M., Erlich I., Sowa P., Artificial Neural Network-Based Dynamic Equivalents for Distribution Systems Containing Active Sources, IEEE Power Systems, 2004.
- [6] Sowa P., Comparison of results of optimization by searching of equivalent system, Power Symposium, NAPS '08, 40th North American, 10.1109/NAPS, 2008, 5307379, pp. 1-4
- [7] Sowa P.: Representation of power system for electromagnetic transient calculation, International Journal of Electrical Power & Energy Systems Engineering, 2008, Vol. 1, No. 3, pp. 152-155.
- [8] Optimization of Equivalent Networks for Transient Simulation in H.V. Transmission Systems, IASTED, International Conference - Modeling, Simulation and Optimization, Gold Coast, Australia, May. 6-9, Paper#: 242-205, 1996.
- [9] Castellanos F., Marti J.R.: Full Frequency-Dependent Phase-Domain Transmission Line Model, IEEE Transactions on Power Systems, Vol. 12, No. 3, August 1997, pp. 1331-1339.



# SAFETY, CONNECTIVITY, AND COMFORTABILITY AS INDICATORS TO IMPROVE WALKABILITY TO THE BUS STOPS IN PENANG ISLAND

\*Nur Sabahiah Abdul Sukor<sup>1</sup> and Siti Fadhlin Muhammad Faisal<sup>2</sup>

<sup>1,2</sup>School of Civil Engineering, Universiti Sains Malaysia, Engineering Campus, Pulau Pinang, Malaysia

## ABSTRACT

Less walkability will result in various negative impacts if not addressed immediately. Among the consequences are increased in private vehicles which contributes to environmental degradation and fatalities. Hence, this study investigates the determinants of walkability by evaluating the assessment indicators concerning one of the active modes of transport i.e., walkability, by constructing a path model from structural equation modeling (SEM) based on on-site data collected in Penang. Based on the path analysis, safety ( $\beta_3=0.598$ ), connectivity ( $\beta_1 = 0.371$ ) and comfort ( $\beta_3 = 0.257$ ) obtained positive impacts towards walkability which safety possessed the strongest correlation with four statistically significant indicators (W6;  $t=15.194$ , W7;  $t=7.149$ , W9;  $t=18.062$ ; W10;  $t=9.115$ ) contributing to walkability. The findings from the study give weight to the related authorities to focus more on enhancing the safety for walking facilities to access the bus stops. Thus it will likely to increase the likeliness to use the public bus services. The findings from this study also reveal the underlying factors to boost the preference of public to adopt walking as an active mode of transport thereby, reducing the dependency on private vehicles.

*Keywords: Walkability, Structural Equation Modelling (SEM), Factor Analysis, Sustainable Transport, Public Transport*

## INTRODUCTION

Walkability is recognized as a sustainable active mode element which has tremendous social and environmental benefits. In terms of health, walkability is proven to be associated with obesity where people are more likely to become obese if settled in a less walkable area [1-6]. Moreover, the previous study stated that walking will not only decreases the risk of obesity but also prevents the incidence of other chronic diseases [7]. In this 21st century, it is noticeable that there is a decline in the walking behavior among people due to increasing reliance on the use of private vehicles. Regardless of the negative health consequences that may arise due to less walking, people still tend to opt and rely more on private vehicles instead of practicing active modes.

Apart from negative health consequences, less walkability gives adverse consequences to the environment as well. Increase in private vehicles will deteriorate the environment by causing air pollution and noise pollution. Moreover, an alarming rate of vehicles also exposes people to fatalities. Statistics from the World Health Organization (WHO) reported that Malaysia was ranked as one of the top three countries in the world with the deadliest roads after Thailand and South Africa [8]. Adding to that, a total of 7,152 deaths from road accidents was recorded in Malaysia in the year 2016 which mainly involved the motorcyclists. One of the

major contribution to this fatalities is none other the high reliance of vehicles. In conjunction to achieve 40:60 modal split by 2030 as per enforced by the government, this issue should be dealt with immediately. Safety and built environment factors should be put forth to encourage walkability. The less walkable area will discourage walkability which in turn causes people to depend on vehicular transportation modes. Thus, an inherent environment is crucial to engage the vibes of walkability in an area.

## LITERATURE REVIEW

The previous study ascertained that the major factor to encourage walkability is the accessibility to a good walking environment [9]. They listed out few determinants of walking behavior such as land use mix, street connectivity, distance to transit stops and destination accessibility. This can also be associated with highly urbanized areas [10], destination types [11] and the aesthetics factors on choosing a route for walking [12]. Another study figured out that connectivity is an important attribute to ensure high-quality public transit, considering the end-to-end connectivity from the origins of the trip to respective destinations [13]. In addition, the physical distances between stations also have an impact on the willingness to walk. Physical connectivity criteria such as continuously connected sidewalks and place-based barriers to segregate with the vehicular traffic



do affect the last-mile trip. It is also claimed that the origin and destination of the walking trip is one of the built-in environmental factors that affect the willingness to walk [14].

Walkability is also affected by the social demographic factors such as walking distance, walking time and the purpose of the trip [15]. In addition to the above factors, gender, age, marital status, income, education, and vehicle ownership were also claimed as contributing factors to walkability [10], [16], [17]. In addition, shorter travel time and travel distance are also among the influencing determinants [12]. Safety is another social feature that has been prioritized by pedestrians. A previous study proved that the majority of motorcycle-taxi users are reluctant to walk because of safety concerns and most of them are afraid of accidents [18]. Similarly, young adults also would likely to have perception towards safety while choosing their preference for transportation modes [19]. A high rate of accidents involving pedestrians is also discouraging their willingness to walk which in turn increase their dependency on vehicles reliance. In addition, comfort is also associated with walkability where most of the people would like to walk if the walkway is comfortable [20]. This is also should be supported by good environmental design, proper space for walking and good surfaces to walk [21]. It is believed that comfortable walkways should also not be obstructed, safe and smooth for stroller and wheelchair users [22].

As a result, this study will focus on identifying the criteria to improve walkability especially for the accessibility to the public buses. The significant criteria will be selected through the path modeling analyses. Next subtopics will explain the methodology used in this study, the indicators for each criteria and the results from data analyses.

## METHODOLOGY

The study was conducted along the alignment of the proposed Bayan Lepas Light Rail Transit (BLLRT) in Penang Island. The objective of selecting the proposed BLLRT alignment as the site location is to explore the futuristic possibility for an integrated transportation network for public conveyance involving both the LRT and the public bus. There are 27 proposed LRT stations altogether, but the study only involves 19 stations on the island as the other 8 stations are on the 3 proposed reclaimed islands which haven't been developed yet. Even though the proposed BLLRT alignment is still in the proposal stage, this study can still be a baseline for the walkability study. 123 bus stops were evaluated along the alignment, and the selected bus stops were located in a radius of approximately

800 meters walking distance from the transit stations as per suggested in previous studies [18], [23], [24]. Fig. 1 shows the site location of the study with a circular radius of 800 meters. The selected bus stops were divided into 19 zones as shown in Table 1



Fig 1 Site location according to BLLRT alignment [25]

The data collection involved two types of on-site data collection, which were traffic volume for private vehicles and transport assessment audit. The traffic count was conducted for 3 working days (Tuesday, Wednesday, Thursday) during 2 peak hours (630-930) and (1715-1930) within 5 months. Meanwhile, the traffic count focused on private cars and motorcycles. Transport Assessment Checklist was designed, and the auditing tasks were done at the selected bus stops. The indicators were audited based on the score options; 1= does not exist, 2= Not following the guidelines and 3= Following the guidelines. The criteria of walkability elements were derived from numerous studies in the literature and reports. The elements were selected based on the frequency of mention by scholars. Table 2 shows the sources for walkability criteria that is considered in this study.

Table 1 Zones and bus stops involved in this study

| Site Zones                           | Number of Bus Stops |
|--------------------------------------|---------------------|
| 1. Komtar Zone (KMZ)                 | 23                  |
| 2. Macallum Zone (MZ)                | 9                   |
| 3. Bandar Sri Pinang Zone (BSPZ)     | 8                   |
| 4. Skycab Zone (SKYZ)                | 7                   |
| 5. East Jelutong Zone (EJZ)          | 6                   |
| 6. The Light Zone (TLZ)              | 7                   |
| 7. Gelugor Zone (GZ)                 | 3                   |
| 8. USM Zone (USMZ)                   | 2                   |
| 9. Batu Uban Zone (BUZ)              | 9                   |
| 10. Pesta Zone (PZ)                  | 9                   |
| 11. Sg. Nibong Zone (SNZ)            | 7                   |
| 12. Bukit Jambul Zone (BJZ)          | 3                   |
| 13. SPICE Zone (SZ)                  | 8                   |
| 14. Jalan Tengah Zone (JTZ)          | 8                   |
| 15. FIZ North Zone (FNZ)             | 2                   |
| 16. FIZ South Zone (FSZ)             | 1                   |
| 17. Sg Tiram Zone (STZ)              | 2                   |
| 18. Penang Airport Zone (PAZ)        | 7                   |
| 19. Permatang Damar Laut Zone (PDLZ) | 2                   |

Table 2 Walkability Criteria based on previous literature reviews

| Indicator ID        | Walkability   | Source/Previous Study        |
|---------------------|---|------------------------------|
| <b>Connectivity</b> |   |                              |
| W1                  | Connecting pedestrian walkways either paved or unpaved to the nearest main attraction within 400 meters to/from bus stop        | [26], [27], [28], [29], [30] |
| W2                  | The walkway should not be obstructed by any things (for ex: trees, shrubs, etc) to the nearest main attractions                 | [30], [31]                   |
| <b>Safety</b>       |   |                              |
| W3                  | Provision of bollards/shrubs/fence/ditch at the end of the walkway to segregate from the car lanes                              | [32]                         |
| W4                  | Provision of bollards at road intersections (if there are intersections)  |                              |
| W5                  | Provision of median refuge island with a minimum of 1.0 meter at crossings for the road that exceed 2 lanes                     |                              |
| W6                  | Provision of crosswalk at road intersections for a pedestrian to cross  | [28]                         |
| W7                  | Well maintained walkways (smooth pavement/not overgrown shrubs and trees/not broken)  | [33]                         |
| W8                  | Signages in good condition (clearly seen/not broken)  | [34], [35]                   |
| W9                  | Crosswalk/markings are clearly seen   | [29], [32]                   |
| W10                 | Pedestrian signals must be in good condition (functional/not broken)  |                              |
| W11                 | Walkways have smooth incline at the end of walkways or towards road intersection which can be used by wheelchairs and strollers | [26], [28]                   |
| <b>Comfort</b>      |   |                              |
| W12                 | Have seats at bus stop  |                              |
| W13                 | Have a rubbish bin at the bus stop  |                              |
| W14                 | Sidewalk width must not less than 1.50m width   |                              |
| W15                 | Availability of street trees/awnings/arcades  | [30], [31]                   |
| W16                 | Provision of signage for a pedestrian walkway   |                              |
| W17                 | Provision of signage to warn motorist about the presence of pedestrian walkway  |                              |
| W18                 | Provision of minimum 1.0-meter divider width (low shrubs/plants/fence/any safety barriers) between road and walkway.            | [28], [34]                   |

### Data Analysis

The aim of the study was to investigate the indicators for walkability by developing a structural equation path model. SPSS software was used for data computation and analysis. Data analysis was conducted in three stages; Exploratory Factor Analysis (EFA), Reliability test and development of PLS Path-Modelling.

#### i. Exploratory Factor Analysis (EFA)

Exploratory factor analysis (EFA) was conducted to investigate the relationship between the indicators and walkability. EFA identifies the individual constructs and explores the consistency of the proposed latent factors with the actual data. The principal component extraction (PCA) method was used to examine the factor loading among the measurement items for each factor. The threshold value for cross-loading of the measurement items should be more than 0.5. For rotated factor analysis, varimax rotation was applied to determine the degree of relationship between variables. The numbers of components in the latent variables were extracted based on the output values of Kaiser-Meyer-Olkin (KMO) measures. The components possessing higher factor loading of Kaiser criterion i.e., more than 0.55 were accepted.

#### ii. Reliability Test

The reliability test was conducted based on Cronbach's alpha value. The acceptable value for Cronbach's alpha is 0.7. However, it is suggested to accept the lower value (0.6) to be adapted in the research model [35].

#### iii. PLS Path-modelling

The path model was constructed with a Structural Equation Model (SEM) by using SmartPLS 3.0 software. In this study, SEM-PLS was chosen because it can be applied for theoretical confirmation or theory development. It is compatible with the aim of the study which is to identify the relationship of connectivity, comfort, and safety towards walkability.

Figure 2 shows the conceptual path model for

walkability. It consists of three latent variables,  $\zeta$  (Connectivity; Comfort; Safety) directing towards "Walkability", and 11 indicators for safety, 7 indicators for comfort and 2 indicators for connectivity

## RESULTS AND ANALYSIS

### Exploratory Factor Analysis (EFA)

Before a model is constructed, factor analysis is implied to summarize the data by assessing the structure of variables for further analysis [36]. Theoretically, factor analysis was used to solve the problem by combining variables that are collinear [37]. A principal component analysis (PCA) was conducted on the 18 walkability indicators with oblique rotation (varimax). Table 3 shows the retained walkability indicators with extraction values more than 0.6 and less than 0.6. The indicators of less than 0.6 were deleted from the model.

Meanwhile, the Kaiser-Meyer-Olkin measure verified the sampling adequacy for the analysis,  $KMO = 0.93$  [38]. Based on Table 4, all KMO values for the items were  $>0.7$ , which is well above the limit of 0.50. Bartlett's test of sphericity ( $105 = 358.275$ ,  $p = 0.000$ ), indicating that the correlations between items were sufficiently large for PCA. Hence, the remaining variables were sufficient to be analyzed. Cronbach's alpha reliability test revealed that all 8 walkability items satisfy the acceptable value of 0.6 ( $\alpha=0.786$ ). Thus, all 8 items were advanced for path model construct.

### Reliability Assessment

Table 5 shows the reliability and validity results applied to the constructed model. Connectivity and safety were found to fulfill all requirements by possessing a value of Cronbach's Alpha higher than 0.6 which has been suggested by previous studies [39], [40] whereas, comfort obtained below than the suggested value (0.284). Meanwhile [41] and [42] suggested  $>0.6$  for indicator loadings and  $>0.6$  for composite reliability [43]. For Average Variance Extracted (AVE),  $>0.5$  is the suggested threshold value [44]. From Table 5, the results for connectivity and safety confirmed the convergent validity and good internal consistency of the measurement model.

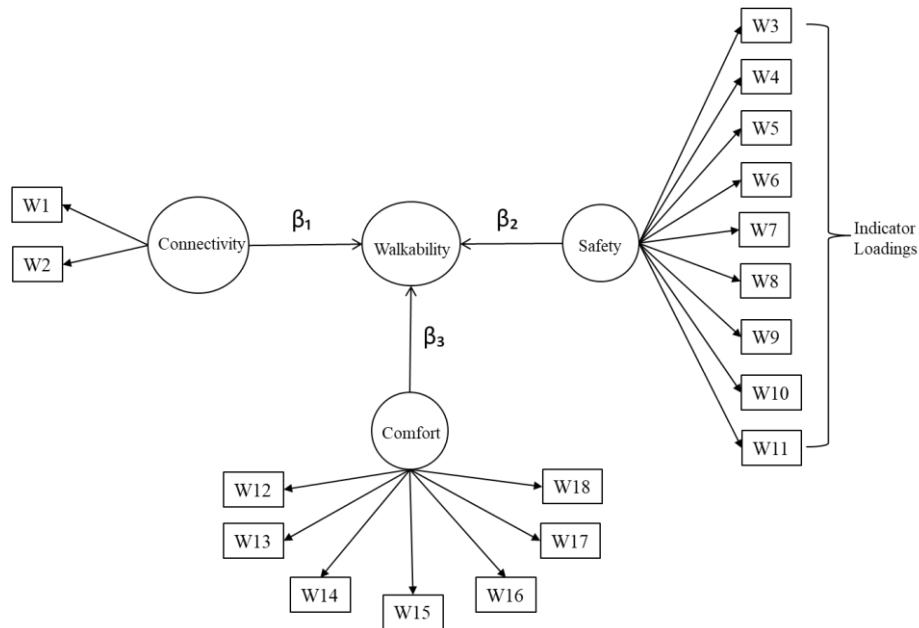


Fig. 2 Conceptual Path Model for Walkability

Table 3 Results of Extraction Communalities

|                       | Extraction Before Variables Deleted | Extraction After Variables Deleted |
|-----------------------|-------------------------------------|------------------------------------|
| WALKABILITY 1         | .731                                | .703                               |
| WALKABILITY 2         | .687                                | .705                               |
| <b>WALKABILITY 3</b>  | <b>.646</b>                         |                                    |
| <b>WALKABILITY 4</b>  | <b>.662</b>                         |                                    |
| <b>WALKABILITY 5</b>  | <b>.702</b>                         |                                    |
| WALKABILITY 6         | .804                                | .734                               |
| WALKABILITY 7         | .627                                | .602                               |
| <b>WALKABILITY 8</b>  | <b>.691</b>                         |                                    |
| WALKABILITY 9         | .817                                | .788                               |
| WALKABILITY 10        | .658                                | .697                               |
| <b>WALKABILITY 11</b> | <b>.586</b>                         |                                    |
| <b>WALKABILITY 12</b> | <b>.399</b>                         |                                    |
| <b>WALKABILITY 13</b> | <b>.689</b>                         |                                    |
| WALKABILITY 14        | .698                                | .685                               |
| <b>WALKABILITY 15</b> | <b>.619</b>                         |                                    |
| WALKABILITY 16        | .679                                | .967                               |
| <b>WALKABILITY 17</b> | <b>.452</b>                         |                                    |
| <b>WALKABILITY 18</b> | <b>.248</b>                         |                                    |

Extraction Method: Principal Component Analysis

Table 4 KMO and Bartlett's test Results

|  |                    |         |
|--|--------------------|---------|
| Kaiser-Meyer-Olkin Measure of Sampling Adequacy.   |                    | .770    |
|  | Approx. Chi-Square | 358.275 |
| Bartlett's Test of Sphericity  | df                 | 28      |
|  | Sig.               | .000    |
| The Standardized Root Mean Square Residual (SRMR) measures the estimated model fit by having the standard value of SRMR=<0.08 for a good fit model and lower than that for a better fit model [45] |                    |         |

Table 5 Assessment results of the model

| Variable/Indicator   | Cronbach's Alpha | Indicator loading | Composite Reliability | Average Variance Extracted (AVE) |
|--|------------------|-------------------|-----------------------|----------------------------------|
| <b>Comfort</b>   |                  |                   |                       |                                  |
| W14: Sidewalk width must not be less than 1.50m width  | 0.284            | 0.798             | 0.736                 | 0.582                            |
| W16: Provision of signage for a pedestrian walkway   |                  | 0.726             |                       |                                  |
| <b>Connectivity</b>  |                  |                   |                       |                                  |
| W1: Connecting pedestrian walkways either paved or unpaved to the nearest main attraction within 500 meters to/from the bus stop                     | <b>0.759</b>     | 0.898             | <b>0.893</b>          | <b>0.806</b>                     |
| W2: The walkway should not be obstructed by physical objects (for ex: trees, shrubs, etc) to the nearest main attractions                            |                  | 0.897             |                       |                                  |
| <b>Safety</b>  |                  |                   |                       |                                  |
| W6: Provision of crosswalk at road intersections for pedestrian to cross   | <b>0.753</b>     | 0.800             | <b>0.846</b>          | <b>0.582</b>                     |
| W7: Well-maintained walkways (smooth pavement/not overgrown shrubs and trees/not broken)   |                  | 0.706             |                       |                                  |
| W9: Crosswalk/markings are clearly seen  |                  | 0.871             |                       |                                  |
| W10: Walkways have smooth incline at the end of walkways or towards road intersection which can facilitate easier wheelchairs and strollers movement |                  | 0.742             |                       |                                  |

#### Path Analysis

As shown in Figure 3, the latent variables namely safety, connectivity, and comfort were related to the latent variable; walkability. Meanwhile, connectivity, safety, and comfort were connected to their indicators respectively. Bootstrapping was performed on the model to test the significance of the relationships between adjacent constructs [46]. Based on figure 3, the t-statistics for all indicators were satisfying the threshold value; ( $t = >1.96$ ), [44]. All of the t-statistics are larger than 1.96 which shows that the variables are highly significant.

Based on the result run by PLS-Algorithm, safety shows a path coefficient value of  $\beta_2=0.598$  ( $t=11.189$ ,  $p = 0.000$ ), comfort ( $\beta_3 = 0.257$ ,  $t = 10.368$ ,

$p = 0.000$ ), connectivity ( $\beta_1 = 0.371$ ,  $t = 9.595$ ,  $p = 0.000$ ). The path analysis shows positive results which depicting direct effect towards walkability. Safety shows strong correlation due to a higher value of the coefficient,  $\beta$  towards walkability compared to connectivity and comfort. This also shows that safety had a greater value of variance and high effect with regard to affecting walkability [45]. Hence, safety had a huge influence on walkability which parallels with had been put forth by the previous studies [47] [48]. Nevertheless, the findings also revealed positive impacts of connectivity and comfort towards walkability. Based on the  $\beta$  values, connectivity possessed the second strongest impact on walkability followed by comfort.

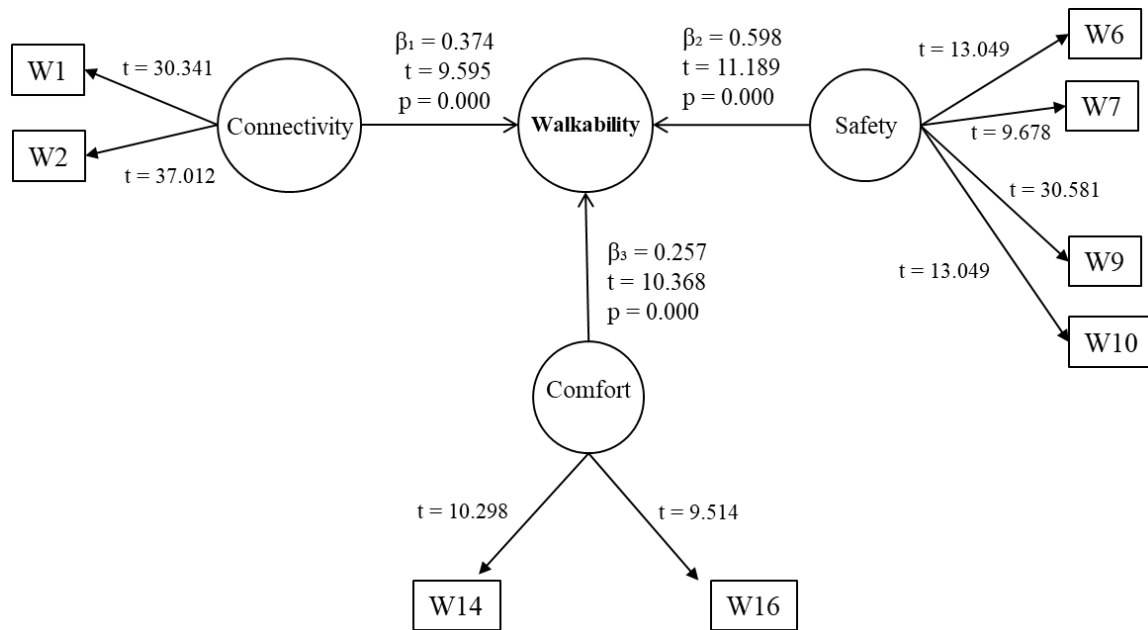


Fig. 3 The constructed path model for walkability

## CONCLUSIONS

Based on the path analysis, it is found that safety ( $\beta_2=0.598$ ,  $t= 11.189$ ,  $p = 0.000$ ), connectivity ( $\beta_1 = 0.371$ ,  $t = 9.595$ ,  $p = 0.000$ ) and comfort ( $\beta_3 = 0.257$ ,  $t = 10.368$ ,  $p = 0.000$ ), possessed positive impacts towards walkability which safety has the strongest correlation depicting that safety should be highly concerned to encourage walkability. Exploratory factor analysis revealed the indicators that are significant to boost safety which are;

- Provision of crosswalk at road intersections for a pedestrian to cross.
- Well-maintained walkways (smooth pavement/not overgrown shrubs and trees/not broken).
- Crosswalk/markings are clearly seen
- Walkways have smooth incline at the end of walkways or towards road intersection facilitate easier wheelchairs and strollers movement.

In conclusion, safety is the top concern by the pedestrian which should be prioritized first compared to other criteria. These indicators were proven to give impact on walkability. Meanwhile, connectivity and comfort were found to affect walkability as well but safety possessed the strongest correlation. Nevertheless, the indicators for both variables can be considered as significant due to the satisfying threshold value of indicator loadings.

All of the indicators can be suggested to be included in the transport assessment guidelines for a more credible policy in the future. Including these indicators could enhance the currently practiced traffic impact assessment (TIA) in yielding a more sustainable transport system. By focusing on the

safety element, walkability criteria in an area can be further improved. The concept of sustainability in transportation system demands more than just social or environmental supports but also an effective engagement in policy. These indicators could be the main elements in encouraging the acceptable mobility paradigm by promoting walkability and indirectly to reduce the reliance on private vehicles.

## ACKNOWLEDGMENTS

This study was funded by the Transdisciplinary Research Grant Scheme (TRGS) from the Ministry of Higher Education, MOHE (203/PAWAM/67610002)

## REFERENCES

- [1] Frank, L. D., Sallis, J. F., Conway, T. L., Chapman, J. E., Saelens, B. E., & Bachman, W. Many pathways from land use to health: associations between neighborhood walkability and active transportation, body mass index, and air quality. *Journal of the American planning Association*, 2006, 72(1), 75-87.
- [2] Giles-Corti, B., Hooper, P., Foster, S., Koohsari, M. J., & Francis, J. Low density development: Impacts on physical activity and associated health outcomes. Melbourne: National Heart Foundation of Australia. 2014
- [3] Glazier, R. H., Creatore, M. I., Weyman, J. T., Fazli, G., Matheson, F. I., Gozdyra, P., ... & Booth, G. L. Density, destinations or both? A comparison of measures of walkability in relation to transportation behaviors, obesity and diabetes in Toronto, Canada. *PloS one*, 2014, 9(1), e85295.



- [4] Booth, G. L., Creatore, M. I., Moineddin, R., Gozdyra, P., Weyman, J. T., Matheson, F. I., & Glazier, R. H. Unwalkable neighborhoods, poverty, and the risk of diabetes among recent immigrants to Canada compared with long-term residents. *Diabetes Care*, 2013, 36(2), 302-308.
- [5] Creatore, Maria I., Richard H. Glazier, Rahim Moineddin, Ghazal S. Fazli, Ashley Johns, Peter Gozdyra, Flora I. Matheson et al. "Association of neighborhood walkability with change in overweight, obesity, and diabetes." *Jama* 315, no. 20 (2016): 2211-2220.
- [6] Chiu, M., Shah, B. R., MacLagan, L. C., Rezai, M. R., Austin, P. C., & Tu, J. V. Walk Score® and the prevalence of utilitarian walking and obesity among Ontario adults: a cross-sectional study. *Health Reports*, 2015, 26(7), 3.
- [7] Rafiemanzelat, R., Emadi, M. I., & Kamali, A. J. City sustainability: the influence of walkability on built environments. *Transportation research procedia*, 2017, 24, 97-104.
- [8] Tang Ruxyn. Death Rates on Malaysia Roads is 3<sup>rd</sup> Highest Globally, More Than China and India. Jne 2017. <https://says.com/my/news/malaysia-s-roads-among-the-world-s-most-dangerous-and-deadliest>. Accessed on 25<sup>th</sup> June 2019
- [9] Vale, D. S., & Pereira, M. Influence on pedestrian commuting behavior of the built environment surrounding destinations: A structural equations modeling approach. *International journal of sustainable transportation*, 2016, 10(8), 730-741
- [10] Corpuz, G., Hay, A., & Merom, D. Walking for transport and health: Trends in Sydney in the last decade. In 28th Australasian Transport Research Forum, Sydney, Australia. 2015
- [11] Townsend, C. and Zacharias, Built environment and pedestrian behaviour at rail rapid transit stations in Bangkok, *Transportation* 27, 2010, 317-330
- [12] Agrawal, A. W., Schlossberg, M., & Irvin, K. How far, by which route, and why? A spatial analysis of pedestrian preference. *Journal of Urban Design*, 2008,13(1), 81-98
- [13] Tilahun, N., Yin, S., Li, M., Keita, Y., Mapping Metropolitan Chicago's Accessibility. Technical Report. The Travel Behavior and Urban Systems Research Group, Department of Urban Planning and Policy, University of Illinois at Chicago, Chicago, IL.2015
- [14] Maghelal, P. K., & Capp, C. J. Walkability: A Review of Existing Pedestrian Indices. *Journal of the Urban & Regional Information Systems Association*, 2011, 23(2).
- [15] Sukor, N. S. A., & Fisal, S. F. M. Factors Influencing the Willingness to Walk To the Bus Stops in Penang Island. *Planning Malaysia Journal*, 2018, 16(5).
- [16] Daniels, R., & Mulley, C. Explaining walking distance to public transport: The dominance of public transport supply. *Journal of Transport and Land Use*, 2013, 6(2), 5-20
- [17] Freeland, A. L., Banerjee, S. N., Dannenberg, A. L., & Wendel, A. M. Walking associated with public transit: moving toward increased physical activity in the United States. *American Journal of Public Health*, 2013, 103(3), 536-542
- [18] Pongprasert, P., & Kubota, H. Switching from motorcycle taxi to walking: A case study of transit station access in Bangkok, Thailand. *IATSS research*, 2017, 41(4), 182
- [19] Simons, D., Clarys, P., De Bourdeaudhuij, I., de Geus, B., Vandelanotte, C., & Deforche, B. Why do young adults choose different transport modes? A focus group study. *Transport policy*, 36, 2014, 151-159.
- [20] Litman, T. A. Economic value of walkability. *Transportation Research Record*, 2003, 1828(1), 3-11.
- [21] Kumar, R. Walkability of neighborhoods: a critical analysis of the role played by zoning codes in creating a walkable environment. LAP Lambert Academic. 2010
- [22] Zakaria, J., & Ujang, N. Comfort of walking in the city center of Kuala Lumpur. *Procedia-Social and Behavioral Sciences*, 170, 2015, 642-652.
- [23] Ji, J., & Gao, X. Analysis of people's satisfaction with public transportation in Beijing. *Habitat International*, 2010, 34(4), 464-470.
- [24] Ker, I., & Ginn, S. Myths and realities in walkable catchments: the case of walking and transit. *Road & Transport Research*, 2003, 12(2), 69.
- [25] Penang Transport Master Plan (2017, February 22) Retrieved from <http://pgmasterplan.penang.gov.my/index.php/ms/2016-02-26-03-12-57>
- [26] West Sussex County Council, West Sussex County Council Transport Assessment Methodology, 2007
- [27] Phillips and Joyce, Transportation Assessment and Management Study, 2016
- [28] Development for Regional Development, Transport Assessment, Guidelines for Development Proposals in Northern Ireland, 2006
- [29] Ford, Glanville Transport Assessment, Granta Park Phase II, 2010
- [30] Institute of Transport and Development Policy (ITDP), TOD Standard, 2017
- [31] New Zealand Government, NZ Transport Agency, Pedestrian Planning and Design Guide, 2009
- [32] McNally, Design Guidelines for Walkable Communities, 2010
- [33] Transport Scotland, Transport Assessment Guidance, 2012

- [34] Jabatan Perancangan Bandar dan Desa Semenanjung Malaysia, Kementerian Perumahan dan Kerajaan Tempatan, *Garis Panduan Perancangan Kejiranan Hijau*, (2012)
- [35] Hair Jr, J. F. Black, WC, Babin, BJ Anderson, RE & Tatham, RL, 2006. *Multivariate Data Analysis*, 6. Prentice Hall, Upper Saddle River, NJ.
- [36] Hair, J. F., Black, W. C., Babin, B. J., & Anderson, R. E. *Pearson New International Edition: Multivariate Data Analysis. In Exploratory Data Analysis in Business and Economics*. 2014. [https://doi.org/10.1007/978-3-319-01517-0\\_3](https://doi.org/10.1007/978-3-319-01517-0_3)
- [37] Field, A. *Discovering statistics using SPSS*. Sage publications. 2009
- [38] F. Hair Jr, J., Sarstedt, M., Hopkins, L., & G. Kuppelwieser, V. Partial least squares structural equation modeling (PLS-SEM) An emerging tool in business research. *European Business Review*, 2014, 26(2), 106-121.
- [39] Hair Jr, J. F., Hult, G. T. M., Ringle, C., & Sarstedt, M. *A primer on partial least squares structural equation modeling (PLS-SEM)*. Sage publications. 2016
- [40] Chin, W. W. *Commentary: Issues and opinion on structural equation modeling*. 1998
- [41] Henseler, J., Ringle, C. M., & Sinkovics, R. R. The use of partial least squares path modeling in international marketing. In *New challenges to international marketing*, 2009, (pp. 277-319). Emerald Group Publishing Limited.
- [42] Hair, J. F., Ringle, C. M., & Sarstedt, M. PLS-SEM: Indeed a silver bullet. *Journal of Marketing theory and Practice*, 2011, 19(2), 139-152.
- [43] Fornell, C., & Larcker, D. F. *Structural equation models with unobservable variables and measurement error: Algebra and statistics*. 1981
- [44] Streukens, S., & Leroi-Werelds, S. Bootstrapping and PLS-SEM: A step-by-step guide to get more out of your bootstrap results. *European Management Journal*, 2016, 34(6), 618-632.
- [45] Hussain, S., Fangwei, Z., Siddiqi, A. F., Ali, Z., & Shabbir, M. S. Structural Equation Model for evaluating factors affecting quality of social infrastructure projects. *Sustainability (Switzerland)*, 2018, 10(5), 1–25. <https://doi.org/10.3390/su10051415>
- [46] Wong, K. K. K. Partial least squares structural equation modeling (PLS-SEM) techniques using SmartPLS. *Marketing Bulletin*, 2013, 24(1), 1-32.
- [47] Leh, O. L. H., Hasri, N. I. Z., & Musthafa, S. N. A. M. Residents' transportation mode preferences in Transit Oriented Area: A case study of Mentari Court, Petaling Jaya, Malaysia. *Geografia-Malaysian Journal of Society and Space*, 2017, 12(1).
- [48] Shay, E., Spoon, S. C., Khattak, A. J., & Center, S. T. *Walkable environments and walking activity. Final Report for Seed Grant Submitted to Southeastern Transportation Center, University of Tennessee*. 2003

# APPLICATION OF CONDITIONAL CULTURE ALGORITHM AND SIMULATION FOR OPTIMAL RESERVOIR RULE CURVES PROJECTS

Anujit Phumiphan<sup>1</sup> and Anongrit Kangrang<sup>2</sup>

<sup>1</sup> Faculty of Engineering, Rajabhat Maha Sarakham University, Maha Sarakham, Thailand, 44000

<sup>2</sup> Faculty of Engineering, Mahasarakham University, Kantarawichai, Mahasarakham, Thailand 44150

## ABSTRACT

The uncertainties of rapid population growth have directly impacted the water resource management. In reservoir operation, rule curves are used to determine water release in response to water demand over long-term operation. This study applied the conditional cultural algorithm (CCA) technique to connect with the reservoir simulation model in order to search optimal reservoir rule curves for Huai Luang reservoir located in Udon Thani province in the northeast of Thailand. Their four hundred samples of generated inflow data of the reservoir were used to evaluate the performance of the proposed technique, and the results were compared with those of genetic algorithm technique (GAs) and current reservoir usage. The results found that the new rule curve patterns produced by the CCA were similar as compared with the rule curves provided by genetic algorithm technique. Moreover, the patterns were different from the existing pattern. The situations of water shortage and flood when using the new rule curves with generated inflow were lower than those of using the existing rule curves. Nevertheless, these situations were close to the situations of using the rule curves of genetic algorithms technique. In conclusion, the proposed model could enhance the performance of the Huai Luang Reservoirs, and it could be applied easily to other reservoirs to modify the objective functions and searching constraints.

*Keywords: Water resource management, Reservoir rule curves, Simulation model, Cultural algorithm, Genetic algorithm.*

## INTRODUCTION

Nowadays, water resource problems such as flood and drought situations are increasing that concern with rapid population growth and economic expansion. Water resource management consists of demand management site and supply management site. Effective reservoir operation is achieved using suitable rule curves to control the release of water following the release criteria. A reservoir operation that uses rule curves to consider release water responds to water demands in long-term operation.

Generally, reservoir operation functions with a water release budget and amount of storage water monthly. The stored water in reservoir is released under certain conditions that are defined by water demand criteria and reservoir rule curves. The rule curves have been improved to provide the best solution for long term operation of reservoir. Typically, reservoir operating system has been large and complex especially area having both drought and flood situations [1]

A searching optimal rule curve is non-linear optimization problem. The optimization technique was applied to search the optimal rule curves that performed with a reservoir simulation model [2]. The rule curves provided by this method are not guaranteed to yield the optimal curves because of human adjustment in the trial and error process during

perform. Later, dynamic programming (DP) was applied to solve non-linear problems in water resource areas including rule curves search. The genetic algorithm (GA) was applied to search rule curves of reservoir subsequently, it has been in several studies [3][4]. The differential evolution (DE) is another search technique that was developed by Storn and Price [5][6]. It uses a simulation of natural evolution, the same as the GA. The DE was applied to search optimal rule curves in several studies. Then, a simulated annealing algorithm (SA) was applied to solve the optimization problem [7][8]. The SA has been applied to connect with simulation for searching the optimal reservoir rule curves [8]. It revealed that the SA could be used to find the optimal rule curves effectively.

Recently, a genetic algorithm (GA) is a metaheuristic inspired by the process of natural selection that belongs to the larger class of evolutionary algorithms (EA). Genetic algorithms are commonly used to generate high-quality solutions to optimization and search problems by relying on bio-inspired operators such as mutation, crossover and selection. John Holland introduced genetic algorithms in 1960 based on the concept of Darwin's theory of evolution. GAs has been widely applied in various problems [9]. Lately, a conditional genetic algorithm technique was applied to search the optimal rule curves of the Huai Luang reservoir. The results

showed that CGAs technique can be use find rule curves. Moreover, the situations of flood and drought when operated by rule curves of both techniques were closed together. Later, there are many alternative tools to solve complex computational problems. The cultural algorithm is a computational model of social evolution based upon a general model of the cultural evolution process. The key idea behind cultural algorithm is to acquire problem-solving knowledge (beliefs) from the evolving population and in return make use of that knowledge to guide the searching process [10][11]. Cultural Algorithms have been successfully applied in a number of diverse application areas [12]. In the process of doing this, five general types of knowledge have been gradually added to the cultural space that represent generic knowledge found in cultural systems. The knowledge sources include normative knowledge, spatial knowledge (topographic), temporal (historic), domain knowledge, and exemplar knowledge.

This study proposed Conditional Cultural Algorithm (CCA) to connect with simulation model for searching the optimal reservoir rule curves. A minimum function for searching procedure. The proposed model has applied to determine the optimal rule curves of the Huai Luang Reservoir in the Northeast region of Thailand. Comparisons of the CCA and the CGA as well as the existing simulation model were shown to demonstrate the effectiveness of the proposed CCA model.

## METHODOLOGY

The culture algorithm was introduced by Reynolds as a vehicle for modeling social evolution and learning in agent-based societies [13]. A cultural algorithm consists of an evolutionary population of agents whose experiences are integrated into a belief space consisting of various forms of symbolic knowledge. The cultural algorithm framework easily lends itself to supporting various types of learning activities including ensemble learning. The various knowledge sources in the belief space can be viewed as an ensemble of classifiers with the acceptance function collecting sample data using techniques such as bagging and boosting from the agent population. The influence function reflects the influence of the ensemble on the agent actions.

As a dual inheritance system, cultural algorithm has two basic components: The population space and the belief space. In each generation, individuals in the population space are first evaluated with a performance function *obj()*. An acceptance function *accept()* is then used to determine which individuals will be allowed to update the belief space. experiences of those chosen individuals are then added to the contents of the belief space via function *update()*. Next, knowledge from the belief space is allowed to influence the selection of individuals for

the next generation of the population through the *influence()* function. This supports the idea of dual inheritance in that the population and the belief space are updated each time step based upon feedback from each other. The CA repeats this process for each generation until the pre-specified termination condition is met. In this way, the population component and the belief space component interact with, and support each other in a manner analogous to the evolution of human culture. Fig. 1 describes such a framework of cultural algorithm is given as follows:

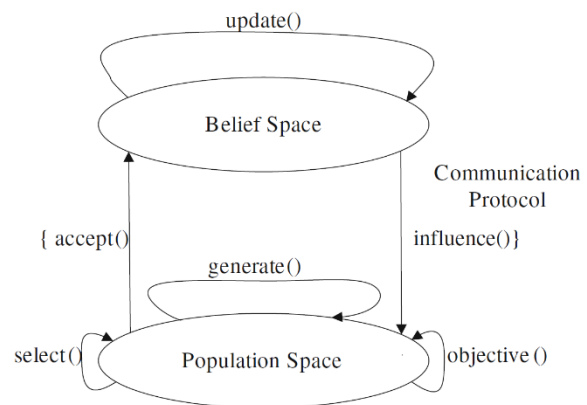


Fig. 1 Framework of the cultural algorithm

The procedure of development model consists of reservoir simulation model and conditional cultural algorithm that combined together for searching the optimal rule curves. The detail of each model will be described as following.

## Reservoir operation model

Generally, reservoir system comprises available water that flows into the reservoir with a single or multipurpose downstream covering watershed area. The reservoirs are usually operated under water usage criteria and reservoir rule curves with monthly data for long term perform. The reservoir rule curves have been found to offer the most equitable solution to all operational problems. A modified reservoir operation model was constructed on the concept of water balance, and it can be used to simulate reservoir operation effectively as well as the Huai Luang Reservoir. The reservoir operation policies are based on the monthly rule curves of individual reservoirs and the principles of water balance equation under reservoir simulation model. The reservoir system is operated along the standard operating policy as expressed equation (1):

$$R_{v,\tau} = \begin{cases} D_\tau + W_{v,\tau} - y_\tau, & \text{for } W_{v,\tau} \geq y_\tau + D_\tau \\ D_\tau, & \text{for } x_\tau \leq W_{v,\tau} < y_\tau + D_\tau \\ D_\tau + W_{v,\tau} - x_\tau, & \text{for } x_\tau - D_\tau \leq W_{v,\tau} < x_\tau \\ 0, & \text{otherwise.} \end{cases} \quad (1)$$

Which  $R_{v,\tau}$  is the release discharges from the reservoir during year  $v$  and period  $\tau$  ( $\tau = 1$  to 12, representing January to December);  $D_\tau$  is the water requirement of month  $\tau$ ;  $x_\tau$  is lower rule curve of month  $\tau$ ;  $y_\tau$  is upper rule curve of month  $\tau$ ; and  $W_{v,\tau}$  is the available water calculated by simple water balance as described in equation (2):

$$W_{v,\tau+1} = S_{v,\tau} + Q_{v,\tau} - R_{v,\tau} - E_\tau - DS \quad (2)$$

Where  $S_{v,\tau}$  is the stored water at the end of month  $\tau$ ;  $Q_{v,\tau}$  is monthly reservoir inflow;  $E_\tau$  is average value of evaporation loss; and  $DS$  is the minimum reservoir storage capacity (the capacity of dead storage).

In the Equation (1), if available water is in the rang of the upper and lower rule level, then demands are satisfied in full. If available water over the top of the upper rules level, then the water is spilled from the reservoir in downstream river in order to maintain water level at the upper rule level. If available water is under the lower rules level, a reduction of supply is required. The policy usually reserves the available water  $W_{v,\tau}$  (for reducing the risk of water shortage in the future, when  $0 \leq W_{v,\tau} < x_\tau - D_\tau$  under long term operation.

After operation for all months along the considered inflow period, all monthly releases of water from the reservoir ( $R_\tau$  for all months) were used to calculate the objective function in the searching procedure. Results of each objective function were recorded and used in the CCA model until met the stop criteria and the optimal rule curves were obtained as described in Fig.2. The details of each objective function will be described in the next section.

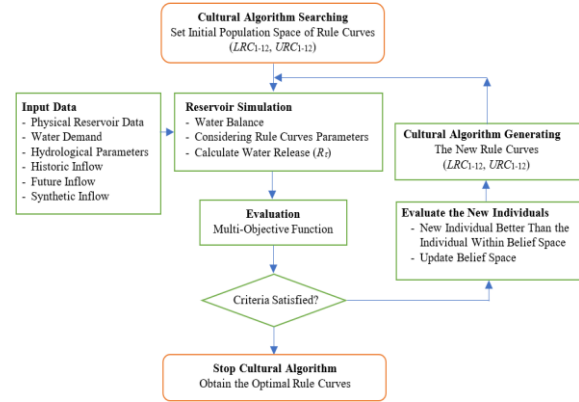


Fig. 2. Conditional cultural algorithm with reservoir simulation for searching rule curves.

Conditional cultural algorithm connected with reservoir simulation

Firstly, the conditional cultural algorithm was created with the reservoir simulation model. The procedure starts from creating an initial population of rule curves, boundary search, probable crossover and mutation, objective function and stopping criteria. Then the population initial rule curves were sent to reservoir simulation model for operating reservoir by considering input data and physical information of the reservoir. The monthly release was calculated using initial rule curves for all months along the inflow period. Then all monthly releases were used to calculate objective function and to evaluate the set of initial rule curves for accepting of first generation. Next, the new accepted rule curves (the selected populations for the first generation after cross over and mutation processes) were used to replace the initial population. This procedure was repeated until the new accepted rule curves were appropriate and the search was stopped [14]. The integrating conditional cultural algorithm and reservoir simulation model for searching optimal rule curves is described in Fig. 2.

Three objective functions were considered. Firstly, the minimum average water shortage per year (H) was used as the objective function of the searching procedure subject to the constraints on the simulation model as in the following:

$$\text{Fitness} = \text{Min } H(Xi) = \left( \frac{1}{n} \sum_{v=1}^n Sh_v \right) \quad (3)$$

$$\text{if } R_\tau < D_\tau; \text{Then } Sh_v = \sum_{\tau=1}^{12} (D_\tau - R_\tau) \quad (4)$$

$$\text{Else } Sh_v = 0$$

where  $n$  is the total number of considered years,  $Sh_v$  is the water shortage during year  $v$  (year that releases does not meet 100% of target demand) and  $i$  is the iteration number.

### Illustrative application of proposed model

In this study the Huai Luang reservoir in Udon Thani province, is located in the Mae Klong Basin with an upstream watershed area of 4,122 km<sup>2</sup> (see Fig. 3). The annual rainfall over the watershed varies from 1,145–2,174 mm which results in an annual average of 1,564 mm and the mean annual temperature is 26.3 °C. The normal storage capacity and average annual inflow are 136 MCM and 165.60 MCM/year, respectively.

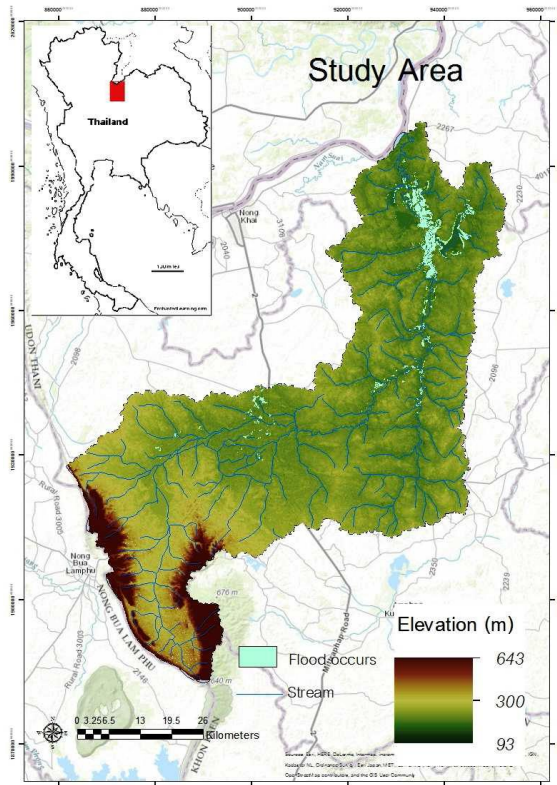


Fig. 3. Location of Huai Luang watershed

The schematic diagrams of above reservoirs are presented in Fig. 4. They indicate that the water demands from reservoirs are electricity generation, irrigation, flood control, industrial demand, domestic water supply and environmental conservation.

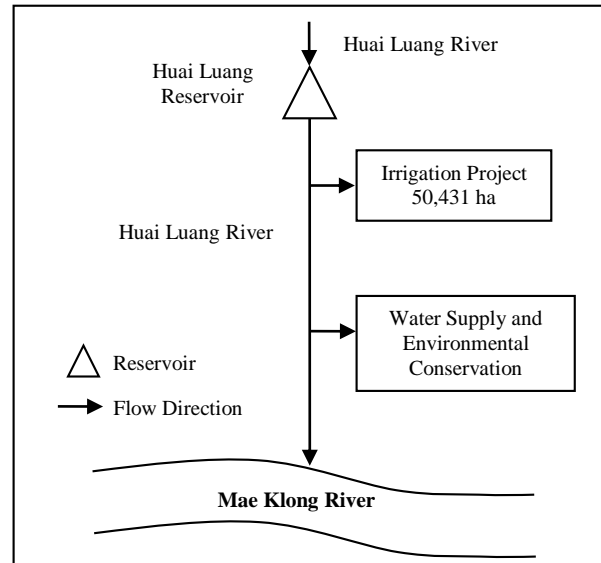


Fig. 4. Schematic diagram of the Huai Luang basin.

The study used CCA in connection with a reservoir operation model to find optimal rule curves through the MATLAB toolbox. The optimal rule curve can then be applied to an actual scenario depending on whether the rule curve can be used to cover every case or event that might occur. Thus, the HEC-4 model was used to create the synthetic inflow data into the monthly inflows as a synthetic data set of 500 events. Then, input synthetic inflow data were used to assess the efficiency of the new rule curves and compare them with the existing rule curves and also between the CCA model, CGA model and the existing SM model under the same conditions (objective function and constraints). Moreover, the new rule curves were assessed in various other situations, i.e., irrigation area increases to judge the impact of how these things will affect future operations.

### RESULTS AND DISCUSSION

The historic data of inflow, evaporation, water requirement and monthly rainfall were imported for processing in the CCA model; the optimal rule curves were obtained. These obtained rule curves are plotted in order to compare them with the rule curves of CGA and existing rule curves of the SM approach as shown in Fig. 5. The results show that the patterns of rule curves obtained from the proposed CCA, The CGA and the SM. Are similar. The obtained rule curves also indicated that the water storage levels of the CCA lower rule curves are lower than the existing rule curves during the dry season (January - May) in order to release more water to reduce water scarcity. In the beginning of rainy season (May - August) the CCA upper curves are lower than their curves of SM in order to add a volume for flood protection. Whereas



during August – November, their upper curves are higher than the curves of SM because of decreasing spill water in order to meet a full capacity at the end of rainy season. This will help alleviate water shortages in the next year. These patterns of the obtained curves are similar to the pattern of the other reservoirs in Thailand on the other studies because of seasonal effect. However, the different points of each reservoir are on lower rule curves during dry season (December - May) and on the upper rule curves during wet season (Jun - November).

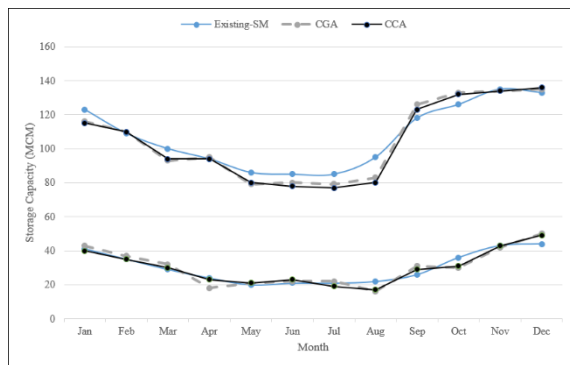


Fig. 5. Optimal rule curves of Huai Luang reservoir.

Table 1 Situations of water shortage and excess release of the system

| Situations     | Rule curves |          | Frequency (times/year) | Magnitude (MCM/year) |         | Duration (year) |         |
|----------------|-------------|----------|------------------------|----------------------|---------|-----------------|---------|
|                |             |          |                        | Average              | Maximum | Average         | Maximum |
| Water shortage | Existing-SM | $\mu$    | 0.955                  | 32.572               | 90.213  | 12.242          | 18.251  |
|                |             | $\sigma$ | 0.171                  | 7.223                | 26.262  | 7.892           | 3.681   |
|                | CGA         | $\mu$    | 0.622                  | 28.218               | 82.821  | 1.452           | 2.788   |
|                |             | $\sigma$ | 0.153                  | 7.105                | 25.425  | 0.624           | 1.715   |
|                | CCA         | $\mu$    | 0.479                  | 25.288               | 77.549  | 19.212          | 14.139  |
|                |             | $\sigma$ | 0.167                  | 3.774                | 3.681   | 0.000           | 0.000   |
| Excess water   | Existing-SM | $\mu$    | 0.876                  | 28.523               | 85.635  | 5.376           | 7.019   |
|                |             | $\sigma$ | 0.107                  | 19.571               | 34.955  | 1.402           | 2.961   |
|                | CGA         | $\mu$    | 0.547                  | 12.475               | 50.840  | 2.537           | 5.161   |
|                |             | $\sigma$ | 0.118                  | 8.249                | 40.273  | 0.846           | 2.160   |
|                | CCA         | $\mu$    | 0.835                  | 30.384               | 44.268  | 7.643           | 6.018   |
|                |             | $\sigma$ | 0.052                  | 119.719              | 26.248  | 5.713           | 3.454   |

## CONCLUSIONS

This study proposed alternative algorithm for searching optimal reservoir rule curves. The conditional shuffled frog leaping (CCA) and reservoir simulation model was applied to search the optimal rule curves of the Huai Luang Reservoir. The results found that the new obtained rule curves are more suitable for reservoir operation than the existing rule curves. The frequency and magnitude of water shortage and excess water release for using new obtained rule curves are lower than their existing rule curves. When comparing the new obtained rule curves with the rule curves of the CGA method as

(new and existing system)

The proposed CCA model is another search optima technique, so the results are near optimality that closed to the results of the results of the other search techniques based on the same condition. However, the efficiency of each technique was carried out on many studies.

The performance of the proposed model was evaluated with monthly synthetic inflow data. These results of the Huai Luang Reservoir are shown in Table 1. The results show that, the average frequency of water shortage was 0.479 per year, the average magnitude of water shortage was 25.288 million cubic meters (MCM) per year and the maximum magnitude of water shortage was 77.549 MCM/year. These are smaller than the results of using rule curves of CGA. The average frequency of excess water release was 0.835 times per year, the average magnitude of excess water release was 30.384 MCM/year and the maximum magnitude of excess water release was 44.268 MCM/year. These are less than the results of using both existing curves but near by the CGA's curves.

well as the existing simulation. The proposed CCA model is an effective method for application to find optimal reservoir rule curves.

## ACKNOWLEDGMENTS

This research was financially supported by Rajabhat Maha Sarakham University Grant 2019; the authors would like to acknowledge Rajabhat Maha Sarakham University.

## REFERENCES

- [1] S. K. Jain, M. K. Goel, and P. K. Agarwal,

- “Reservoir operation study of sabamati system, India,” *Journal of Water Resources Planning and Management*, vol. 124, no. 1, pp. 31–38, 1998.
- [2] M. Azizpour, V. Ghalenoei, M. H. Afshar, and S. S. Solis, “Optimal operation of hydropower reservoir systems using weed optimization algorithm,” *Water Resources Management*, vol. 30, no. 11, pp. 3995–4009, 2016.
- [3] C. Chaleeraktragoon, and A. Kangrang, “Dynamic programming with the principle of progressive optimality for searching rule curves,” *Canadian Journal of Civil Engineering*, vol. 34, pp. 170–176, 2007.
- [4] F. J. Chang, L. Chen, and L. C. Chang, “Optimizing the reservoir operating rule curves by genetic algorithms,” *Hydrological Processes*, vol. 19, pp. 2277–2289, 2005.
- [5] A. Kangrang, S. Compliew, and R. Hormwichian, “Optimal reservoir rule curves using simulated annealing,” *Proceedings of the Institution of Civil Engineers - Water Management*, vol. 164, no. WM1, pp. 27–34, 2011.
- [6] R. Hormwichian, A. Kangrang, A. Lamom, C. Chaleeraktragoon, and P. Patamatamkul, “Coupled-operations model and a conditional differential evolution algorithm for improving reservoir management,” *International Journal of Physical Sciences*, vol. 7, no. 42, pp. 5701–5710, 2012.
- [7] A. Kangrang, and R. Homwichian, “Optimal reservoir rule curves using conditional shuffled frog leaping algorithm and simulation,” *International Journal of Earth Sciences and Engineering*, vol. 6, no. 6, pp. 1392–1399, 2013.
- [8] A. Kangrang, W. Pakoktom, W. Nualnukul, and C. Chaleeraktragoon, “Adaptive Reservoir Rule Curves by Optimization and Simulation”, *Proceedings of the Institution of Civil Engineers - Water Management*, vol. 170, no. WM5, pp. 219–230, 2017.
- [9] Mitchell, Melanie (1996). *An Introduction to Genetic Algorithms*. Cambridge, MA: MIT Press. ISBN 9780585030944.
- [10] Reynolds RG (1994) *An introduction to cultural algorithms*. In: *Proceedings of the 3th annual conference on evolution programming*, Sebalk, A.V. Fogel, World Scientific, River Edge, NJ, pp 131–136.
- [11] Jin X, Reynolds RG (1999) Using knowledge based evolutionary computation to solve nonlinear constraint optimization problems: a cultural algorithm approach. In: *Proceedings of the 1999 Congress on Evolutionary Computation*, Washington DC, IEEE Service Center, pp 1672–1678
- [12] Reynolds, G. R. 1979. *An Adaptive Computer Model of the Evolution of Agriculture for Hunter-Gatherers in the Valley of Oaxaca Mexico*. Ph.D. Dissertation, Department of Computer Science, University of Michigan.
- [13] Reynolds, G. R. 1994. *An Introduction to Cultural Algorithms*. In *Proceedings of the 3<sup>rd</sup> Annual Conference on Evolutionary Programming*, 131–139: World Scientific Publishing.
- [14] A. Kangrang, and C. Lokham, “Optimal reservoir rule curves considering conditional ant colony optimization with simulation model”, *Journal of Applied Sciences*, vol. 13, no. 1, pp. 154–160, 2013.

## A STUDY OF FLOOD FORECASTING AND MAPPING FOR THE ATTANAGALU OYA

W.C.P. Wickramarachchi<sup>1</sup>, N.K. Gunasekara<sup>2</sup>, W.C.D.K. Fernando<sup>3</sup> and S.S. Wickramasuriya<sup>4</sup>  
<sup>1,2,3,4</sup>Faculty of Engineering, General Sir John Kotelawala Defence University, Sri Lanka

### ABSTRACT

This research focuses on developing a hydrological model and a hydraulic model using HEC-HMS and HEC-RAS respectively to enable flood projection in the basin around the only available downstream gauging station at Dunamale. Dunamale is a defective gauging station that gives erroneous readings at high flows. Despite, reliable flood inundation maps were produced and were validated. This study intends to forecast flood for a catchment with minimal data as in many developing countries. Soil Conservation Services Curve Number Method was used as the loss method while the Snyder unit hydrograph was employed as the transform method. Monthly minimum flows were considered as the base flow of the corresponding months from the Dunamale gauging station. 2011 and 2010 daily discharge data were used to calibrate and validate the hydrological model. Nash Sutcliffe coefficients (NSC) of 0.836 and 0.825 were found for calibration and validation respectively. The computed water surface elevation was compared with actual flood levels to calibrate the model. Thus, the Manning's coefficient was determined. The identified rainfall patterns for 25, 50, 100 year return periods were used in the rainfall-runoff model to obtain the corresponding flow hydrographs. Using the hydraulic model, it was observed in the maps that a low lying area of 9.5 km<sup>2</sup> downstream of Dunamale will be inundated. The resulting flood inundation maps can be used to develop a proper mitigation plan to assist the affected people and direct them to safe locations. Thus, the loss of lives and damage to property can be minimized immensely.

**Keywords:** *Dunamale, Flood, Inundation Maps, Hydrological, Modelling*

### INTRODUCTION

Sri Lanka being a small island in the Indian Ocean in the path of two monsoons is frequently affected by tropical hazards such as floods. During the period of 1974-2004, over three million people were affected due to flood disasters which was 48% when compared with other destructive natural disasters [1]. Adverse consequences of flood ranges from direct damages such as loss of lives to indirect damages such as spread of diseases. It was recorded that the flood occurred in 2014 [2] was the most severe and the most destructive hydrological event that occurred after the devastating flood in 1989 [3]. The floods recurred in 2016 [4], 2017 [5] and 2018 as well and severely affected the people settled in the vicinity of the Attanagalu oya. Table 1 illustrates the severity of the recent floods. The occurrence of floods is more frequent in the Attanagalu Oya catchment and hence, rapid and viable solutions are essential to mitigate flood disasters.

Table 1 The severity of floods

| Flood occurred year | People affected |
|---------------------|-----------------|
| 1989                | Over 300000     |
| 2014                | Over 107000     |
| 2016                | Over 425000     |
| 2017                | Over 500000     |

### STUDY AREA

Attanagalu Oya is situated in the Western

Province between two major rivers, Kelani River and Maha Oya with an extent of 727 km<sup>2</sup> [6]. 64% of its basin area are in the lower valley with a mean sea level lower than 30 meters. This basin experiences a mean annual rainfall of 2000 mm-2500 mm. Rainfall received by the basin is well distributed and frequently experienced from April to December [7].

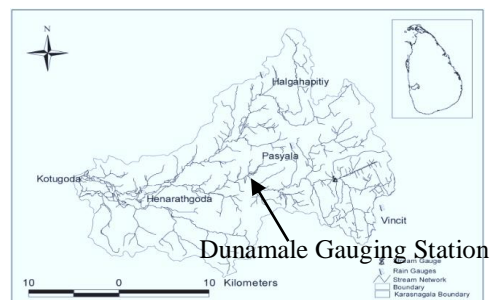


Fig. 1 Study Area

### METHODOLOGY

Daily rainfall data from the Pasyala gauging station was obtained for ten years (2005-2015), daily discharge data and flood level heights were obtained from the Dunamale gauging station for the same years. Land use data was obtained from the Urban Development Authority.

A digital elevation model (DEM) of 2 m accuracy was used to delineate the watershed and was further developed to perform digital terrain

analysis. The generated stream network was overlaid on Google earth pro and was validated.

Figure 2 illustrates the watershed delineated at Dunamale gauge. The area of the watershed is 148 km<sup>2</sup>.

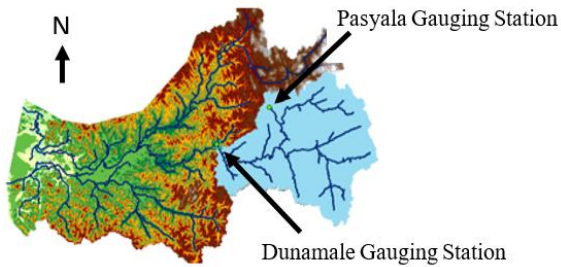


Fig. 2 Delineated Watershed (scale 1:600,000)

These results were subsequently used in the hydrological and hydraulic models. HEC-HMS is a commonly used reliable hydrological modelling software which provide acceptable simulations of flood events when compared with other modelling tools such as WBNM [8]. In the HEC-HMS model, the water budget equation is used in order to compute the precipitation-runoff model.

$$\Delta S = P + R + B - I - E - T \quad (1)$$

Where:

$\Delta S$  - Storage, P - Precipitation, R - rainfall excess or runoff, B - subsurface flow, I - Infiltration, E - Evaporation, T - Transpiration [1]

The precipitation that do not get subjected to ponding or infiltration, will flow overland to a stream channel. Hence, the resultant stream flow at Dunamale gauging station due to runoff, interflow, baseflow and the precipitation is considered as the total watershed outflow for this study.

The study was conducted by using two loss methods, namely Soil Conservation Service Unit Hydrograph method (SCS-UH) and Deficit and Constant loss method. Later a comparison of the two was carried out. The SCS curve number method has been developed using the following equations by estimating excess rainfall as a function of cumulative precipitation, soil cover, land use, and antecedent moisture.

$$Pe = \frac{(P - Ia)^2}{(P - Ia) + S} \quad (2)$$

$$Pe = \frac{(P - 0.2S)^2}{(P + 0.8S)} \quad (3)$$

$$S = \frac{(25400 - 254CN)}{CN} \quad (4)$$

Pe = Accumulated precipitation excess at time t

P = Accumulated Rainfall depth at time t (mm)

Ia = Initial Abstractions (initial loss)

S = potential maximum retention

The Deficit and Constant Loss method is a continuous simulation method which uses a single soil layer to account for continuous changes in moisture content. This method consists of three parameters, namely, Initial Deficit, Maximum Deficit and Constant Rate. Initial condition is referred to as the amount of water initially required to fill the soil layer to the maximum storage. The maximum deficit is the maximum amount of water the soil layer can hold [9]. These three parameters were obtained through trial and error as they require a great amount of data which is unavailable for the Attanagalu Oya catchment.

The direct-runoff model of HEC-HMS facilitates seven transformation methods including Snyder Unit Hydrograph method. The Snyder Unit Hydrograph method simulates flows more reliably than other transformation methods for Attanagalu Oya basin [10]. It requires only two parameters and they are the standard lag ( $t_p$ ) and the peaking coefficient ( $C_p$ ).

The equation proposed for standard lag is as follows;

$$t_p = CC_1(LL_c)^{0.3} \quad (5)$$

$C_1$  = basin coefficient,  $L$  = length of the main stream from the outlet to the divide,  $L_c$  = length along the main stream from the outlet to the nearest point to the centroid,  $C$  = a conversion constant (0.75) [9]. The basin coefficient ( $C_1$ ) has been calibrated to be 3.75 with a Mean Ratio of Absolute Error (MRAE) of 0.2 for the Attanagalu Oya basin. This value has been directly used to calculate the standard lag [11]. The  $C_p$  for the Attanagalu Oya basin was initially estimated as 0.38 as this value was recommended in [11] and was optimized to get the best goodness-of-fit for the simulated and measured hydrographs.

Baseflow of a tropical catchment with year round precipitation is very significant as the groundwater flow contribution is very high. The minimum constant discharge of each month was assumed to be the monthly baseflow [10].

Through a sensitivity analysis it was determined that evaporation has no effect on the results from the model. Daily precipitation data for a duration of seven months were input to calibrate and validate the model. The parameters were estimated and optimized using the Nelder - Mead search algorithm. The goodness of fit was assessed using the NSC as the objective function. The hydraulic model was developed to analyze the extent of inundation and plot the water surface elevations for the selected return period storm events. As it was a river flood analysis, two dimensional unsteady flow modelling was carried out [12]. MIKE11 is another widely used hydraulic. However, HEC-RAS has the advantage over MIKE11 as it is able to generate river flood flow velocity map which is not available in MIKE11. The flood flow velocity is one of the

most important factors that is used, flood mitigation, flood management, classification and evaluation of river flood risk [13].

As the terrain data have been collected using Light Detection and Ranging (LiDAR), certain stream channels may not have bathymetric data. The conventional forms of LiDAR do not penetrate water. Therefore, it is necessary to incorporate cross section data into the terrain for a single comprehensive terrain model that includes bathymetry when carrying out two dimensional modelling. Manning's coefficient was the only parameter that was varied to calibrate and validate the hydraulic model. The Manning's  $n$  value that computes the actual water surface elevation was determined. It is highly dependent on a number of factors such as surface roughness, vegetation, channel irregularities, channel alignment, scour and deposition, obstructions, size and shape of the channel, stage and discharge [14].

The flow hydrograph was given as the upstream boundary condition and the normal depth was considered as the downstream boundary condition. Observed discharge of Dunamale guage was input for the upstream flow hydrograph and the bed slope was considered as the normal depth at the downstream.

The Attanagalu Oya experiences no flow conditions twice a year. Therefore, the simulation was started when the river begins to have any flow in order to consider the initial condition as zero.

A flood frequency analysis was done to determine the storm hydrographs for 25, 50, 100 year return periods using IDF curves developed for Colombo. Obtained rainfall patterns computed were input as precipitation to the developed rainfall-runoff model and the runoff was calculated. The obtained discharge was input at the inlet of Dunamale in order to compute the flood simulation and develop the inundation maps.

## RESULTS AND DISCUSSION

A hydrological model was developed using the SCS Curve Number loss method. The Land use data obtained from the Urban Development Authority valid for the years 2010- 2015 were analyzed and the impervious percentage was calculated as 5.8% with a majority land use cover of rubber and garden. The spatial features of the watershed and the longest path, watershed area, length along the main stream from the outlet to a point nearest the watershed centroid was found using a GIS tools. Hence, the standard lag was calculated as 16.22 hrs. It was observed that the runoff simulation model did not show any sensitivity towards evapotranspiration. Precipitation data of the year 2011, from 01st

January to 31st July were used to calibrate the model and obtain the optimized parameters.

The Figure 3 shows the goodness-of-fit of the simulated and the observed hydrographs which was satisfactory with a NSC of 0.836. Therefore, the parameters obtained from the simulation were accepted and are presented in the Table 2. The SCS CN method is applied for very large watershed areas without considering the substantial transmission losses, which results in overestimation of the runoff [10]. This problem is overcome as the SCS CN loss method is applied only to a sub-catchment of Attanagalu Oya and also transmission losses were accurately calculated and optimized as explained in the methodology. Hence, successful results were obtained for the hydrological model developed using the SCS CN loss method.

However, it was noted that the optimized Curve Number is significantly low. This could be justified by the fault of the gauging station location. It was observed that the Dunamale gauging station is bypassed by a naturally developed bypass channel during periods of high flow. Hence, the observed discharge data are undervalued as it includes the flow measurement of the main channel only. This causes the high flows to be read lower than actual while the other flows are gauged accurately. The Figure 4 shows the Dunamale gauging station and the bypass channel.

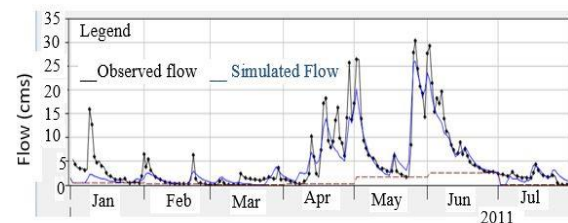


Fig. 3 Runoff Simulation for the year 2011 using SCS CN Loss Method for calibration

Table 2 Parameters used in the hydrological model- SCS CN loss method

| Parameter                 | Optimized values |
|---------------------------|------------------|
| <b>Loss method</b>        |                  |
| Curve number              | 6.5              |
| Impervious Percentage (%) | 6                |
| <b>Transform method</b>   |                  |
| Standard lag (hours)      | 20               |
| Peaking coefficient       | 0.35             |



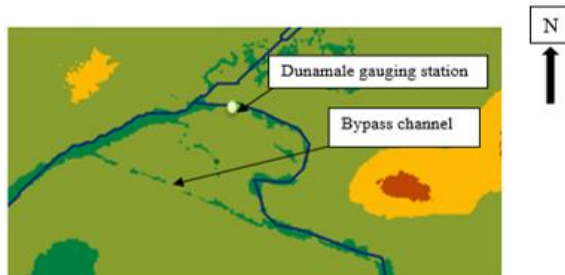


Fig. 4 The Dunamale Gauging Station and the bypass channel (Scale 1:40000)

Curve number 100 represents 100 percent imperviousness of the catchment [1]. Therefore, CN 6.5 suggests high perviousness. Since the observed discharge is under measured, the developed hydrological model attempts to decrease the simulated results to match the defected observed discharge readings by adjusting perviousness to a higher value. Further, the literature reveals that the estimate of stream flows with CN estimations based on

standard tables were of lesser quality when compared with those with the use of average CN value from observed event calibrations [14]. It was also noted that different curve numbers were optimized for the same catchment by different hydrological models. Red Yellow was determined as the major soil type appearing in the Attanagalu Oya basin. Therefore, based on the characteristics of the basin and the soil type 45 was selected for the curve number for the Attanagalu Oya [15]. Another Literature suggests an average CN value of 70.11 was calibrated with a MRAE of 0.4 to model peak flow magnitudes reasonably for Attanagalu Oya [14]. The calibrated hydrological model was validated using rainfall data from 01st January 2010 to 31st July 2010. The modelled runoff matched the measured runoff with a NSC of 0.825. The goodness-of-fit of the observed and the simulated graphs is shown in the Fig 5.

Similarly, the model was run changing the loss method to Deficit and Constant loss method. The loss parameters were estimated and optimized. The simulation was run by keeping the transform parameters and the base flow values same as in the SCS CN method. The simulation obtained a NSC of 0.813. It was observed that the constant rate and the impervious percentage

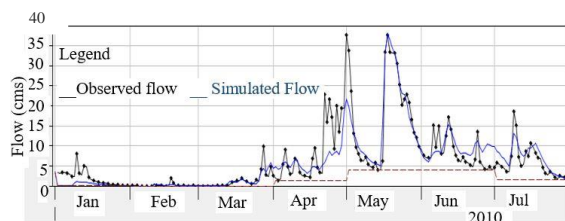


Fig. 5 Model validation for 2010 using SCS CN Loss Method

Table 3 Hydrological model parameters using Deficit and Constant method

| Parameters              | Optimized Values |
|-------------------------|------------------|
| <b>Loss Method</b>      |                  |
| Initial Deficit (mm)    | 0.5              |
| Maximum Deficit (mm)    | 1.2              |
| Constant Rate (mm/hr)   | 1.3              |
| Impervious percentage   | 6                |
| <b>Transform Method</b> |                  |
| Standard lag (hours)    | 20               |
| Peaking coefficient     | 0.23             |

Table 3 Hydrological model parameters using Deficit and Constant method were the only loss parameters that contributed to the goodness-of-fit of the two graphs and the initial deficit and the maximum deficit showed no sensitivity to improve the NSC.

were the only loss parameters that contributed to the goodness-of-fit of the two graphs and the initial deficit and the maximum deficit showed no sensitivity to improve the NSC.

The model was validated for the year 2010 from 1st January to 31st July. The NSC was 0.660. Even though the coefficient is above the threshold of the minimum acceptable value, some peaks are highly overvalued and some are highly undervalued. Moreover, due to the consistency of the high goodness-of-fit of the SCS method, the hydrological model developed using the SCS CN loss method can be justified as more accurate.

The hydraulic model was calibrated in terms of the Manning's coefficient. Dunamale discharge data was input to the model at the upstream inlet and the inundation heights produced by the model were compared also at the same upstream inlet location as observed flood heights were not available in the downstream. The best Manning's value for the model that enabled to obtain the observed heights

Fig. 6 Simulation of the 30/10/2009 Flood event

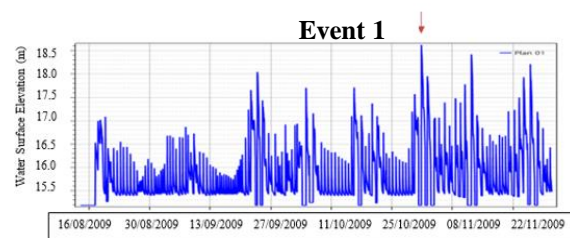




Table 4 Analysis of the Error Percentage of the Simulation for the Year 2009 (Event 1) and in 2008 (Events 2-5)

|         | Error percentage of the simulated and observed flood heights | Error in the date of occurrence in days |
|---------|--|---|
| Event 1 | -2.37%   | 01 day                                  |
| Event 2 | 0.93%  | 02 days                                 |
| Event 3 | -5.47%   | 01 day                                  |
| Event 4 | -1.57%   | 01 Day                                  |
| Event 5 | -2.99%   | -02 Days                                |

from the flood simulation was identified through calibration. The simulation was run for the entire year of 2009 as shown in the Figure 6 and the calibrated Manning's coefficient obtained was 0.02.

The published Manning coefficients for mountain rivers consisting gravel, stones and natural vegetation were ranging from 0.025- 0.035 [16]. The calibrated Manning's coefficient of 0.02 very close although it is not within the range. Manning's coefficients are difficult to be determined for catchments with significant spatial variations and therefore a coefficient with least overall discrepancies between simulations and measurements should be selected [1].

The model was validated by running a simulation for the year 2008 and four flood events were observed for the year. The simulation for the year 2008 were almost the same as measured data and the results are as depicted in the Figure 7.

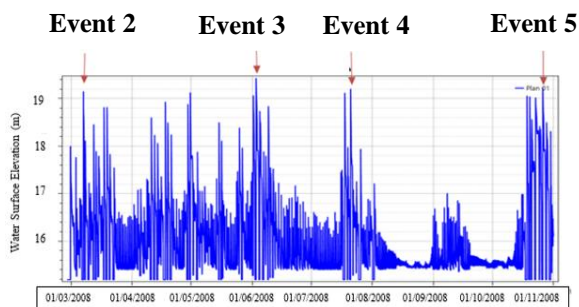


Fig. 7 Simulation of the Four Floods in 2008

It was observed that the error 2 was the only error with a positive error and these errors may have resulted due to temporal changes of the stream bed profile. The Manning's coefficient of 0.02 was accepted after the calibration done for the single event of 2009 and the validation done for the four flood events of 2008.

However, it was notable that the simulated heights were lower than the observed heights and this could be due to several reasons such as the error of the location of the Dunamale gauging station and errors of the digital elevation model.

The runoff simulations for each return period was obtained by using the developed hydrological

model. The parameters which were calibrated and validated using the SCS curve number method were used. The constant monthly base flow method was used in the Basin Model Manager and the average monthly base flow from 2009-2016 was input for all return periods. The values obtained from the hydrological model for the three return periods are shown in the Table 5.

Table 5 Analysis of the Results from the Hydrological Model

| Return Period  | 25-yr | 50-yr | 100-yr |
|--|-------|-------|--------|
| Peak Discharge (m <sup>3</sup> /s)                         | 32.5  | 39.5  | 50     |
| Direct Runoff Volume (10 <sup>6</sup> m <sup>3</sup> )     | 8.82  | 10.70 | 13.91  |
| Flood heights in mean sea level at the gauging station (m) | 20.7  | 20.9  | 21.0   |

The inundation maps which were laid on Google Satellite images shows that the flood is mostly contained in the low lying areas on either sides of the stream. The inundation area was obtained as 9.5 km<sup>2</sup> and by laying the inundation layer on Google Earth the land use types that are inundated can be identified. The inundation map obtained from the hydraulic maps for the 100 year return period is shown in Figure 8.

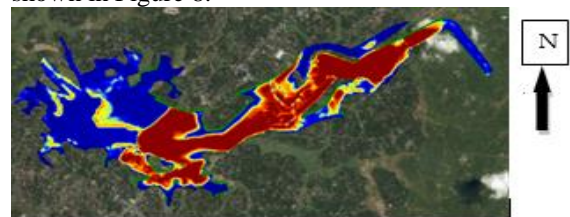


Fig 8 Inundation Map of the 100-Yr Return Period Flood (scale 1: 70000)

## CONCLUSION

Dunamale gauging station from where the discharge data were obtained is a station which gives erroneous discharge rates during high peaks due to the bypass channel. This is an ungagged watershed where many essential data like flood heights in the downstream were not available. However, very reliable results were obtained from the models with satisfactory NSC values.

HEC-HMS model was reliably used to simulate flood flows of Attanagalu Oya using SCS CN loss method and Synder UH method as the transform method. The basic parameters obtained from the calibration were 6.5 as the curve number, 20 hours as the lag time, 0.35 as the peaking coefficient, basin coefficient used to calculate the standard lag was 3.75 and this value was obtained from literature. By

using these parameters, a goodness-of-fit of 0.836 NSC was obtained. The Manning's coefficient for the basin was calibrated to be 0.02.

The results were subsequently used to map the inundation due to 25-yr, 50-yr, 100-yr return period storms and it was observed in the maps that a low lying area of 9.5 km<sup>2</sup> will be inundated. These maps will be contributory for mitigation of future floods and also such maps can be further analysed to devise a proper risk assessment and a risk management plan to support the affected individuals.

As a future direction, the error in the Dunamale gauging station due to the diversion of the channel can be addressed when modelling to obtain more accurate results. Further, a study for a suitable flood mitigation structure for the modelled area can be suggested as another future direction. The flood extents and the intensities can be obtained from this study and a suitable structure can be proposed to minimize the flood damages.

## ACKNOWLEDGEMENT

The authors wish to extend their gratitude to Eng. P.A.A.P.K Pannala, Deputy Project Director of the Climate Resilience Improvement Project (CRIP). The support extended by the Department of Irrigation and the Department of Meteorology for providing the required data is gratefully acknowledged.

## REFERENCES

- [1] "Hazard Profile of Sri Lanka," Ministry of Disaster Management, 21 May 2019. [Online]. Available: [http://www.disastermin.gov.lk/web/index.php?option=com\\_content&view=article&id=57:hazard-profile-of-sri-lanka&catid=73:reports&Itemid=70&lang=en](http://www.disastermin.gov.lk/web/index.php?option=com_content&view=article&id=57:hazard-profile-of-sri-lanka&catid=73:reports&Itemid=70&lang=en). [Accessed 13 June 2019].
- [2] M. Johnney, "The International Federation of Red Cross," 4 June 2014. [Online]. Available: <https://www.ifrc.org/en/news-and-media/news-stories/asia-pacific/sri-lanka/sri-lanka-flash-floods-affect-over-40000-in-western-sri-lanka--66090/>. [Accessed 13 June 2019].
- [3] H. Gehrels, "Protecting Colombo against future floods," Deltares, [Online]. Available: <https://www.deltares.nl/en/projects/protecting-colombo-against-future-floods/>. [Accessed 13 June 2018]
- [4] A. Sathisraja, "Special reports – Floods," The Sunday Times, 22 May 2016. [Online]. Available: <http://www.sundaytimes.lk/160522/news/special-reports-floods-194617.html>. [Accessed 13 June 2018].
- [5] A. Ameen, "News," BBC, 27 May 2017. [Online]. Available: <https://www.bbc.com/news/av/world-asia-40071230/sri-lanka-floods-rescuers-reach-worst-affected-area>. [Accessed 13 June 2019].
- [6] R. Wijesekara and C. Kudahetty, "Preliminary groundwater assessment and water quality study in the shallow aquifer system in the Attanagalu Oya Basin," in *National Conference on Water, Food Security and Climate Change in Sri Lanka. Water Quality, Environment and Climate Change*, 2010.
- [7] I. d. Hydrology Division.
- [8] F. Laouacheria and R. Mansouri, "Comparison of WBNM and HEC-HMS for runoff hydrograph prediction in a small urban catchment," *Water Resources Management*, vol. 29, no. 8, pp. 2485-2501, 2015.
- [9] A. D. Feldman, "Hydrologic Modeling System HEC-HMS: Technical Reference Manual," US Army Corps of Engineers, Hydrologic Engineering Center, 2000.
- [10] D. Halwatura and M. M. M. Najim, "Application of the HEC-HMS model for runoff simulation in a tropical catchment," *Environmental modelling & software*, vol. 46, pp. 155-162, 2013.
- [11] G. Thapa and N. T. S. W. ", "Computation and Optimization of Snyder's Synthetic Unit Hydrograph Parameters," 2018.
- [12] G. W. Brunner, "HEC-RAS, River Analysis System Hydraulic Reference Manual, Version 5," US Army Corps of Engineers, Hydrologic engineering Center, 2016.
- [13] S. Alaghmand, R. bin Abdullah, I. Abustan and S. Eslamian, "Comparison between capabilities of HEC-RAS and MIKE11 hydraulic models in river flood risk modelling (a case study of Sungai Kayu Ara River basin, Malaysia)," *International Journal of Hydrology Science and Technology*, vol. 2, no. 3, pp. 270-291, 2012.
- [14] S. Tobgay, "A CASE STUDY OF ATTANAGALU OYA BASIN-KARASNAGALA, SRI LANKA," *EVALUATION OF RUNOFF ESTIMATION USING SCS METHOD FOR INFRASTRUCTURE DESIGN*, 2015.
- [15] T. Pushpakumara and T. Isuru, "Flood Modelling and Analyzing of Attanagalu Oya River Basin Using Geographic Information System," *International Journal of Advanced Remote Sensing and GIS*, vol. 7, no. 1, pp. 2712-2718, 2018..
- [16] M. Iosub, I. Minea, O. Hapciuc and G. Romanescu, "The use of Hec-Ras modelling in flood risk analysis," *Aerul si Apa. Componente ale Mediului*, p. 315, 2015.

## LAO KHAM'S VARISCITE PROPERTIES AND APPLICATION IN CHEMICALLY BONDED PHOSPHATE CEMENT

Watcharagon Wongkamjan<sup>1</sup> and Thanawat Jumepaeng<sup>2</sup>

<sup>1</sup> Faculty of Liberal Arts and Science, Roi Et Rajabhat University, Thailand

<sup>2</sup> Faculty of Sports and Health Science, Thailand National Sports University Udon Thani Campus, Thailand

### ABSTRACT

This study aims to investigate properties and application of Lao Kham Variscite, LKV, variscite at Lao Kham village, Roi Et province Thailand. The samples were investigated properties included mineral composition analysis, Thin-section analysis and microscopic characteristics analysis with digital stereomicroscope. The applications of LKV in chemically cement were also investigated. The results indicated that LKV is itself a composite with several crystalline in microstructure characterization. It was found that LKV calcined at 600°C has best reactive with NaOH 3M solution and tendency to develop for used as chemically bonded phosphate cement (CBPC).

*Keywords: Variscite, Chemically Bonded Phosphate Cement*

### INTRODUCTION

Aluminum phosphate is an aluminum compound found in natural minerals, including: angelite, coeruleolactite, evansite, lucinite, metavariscite, sterretite, variscite, vashegyite, wavellite, and zepharovicht. According to a recent study, these minerals can be used as an additive in cement by mixing with calcium sulfate and sodium silicate solutions as concrete, flux for ceramics, dental cements, waterproofing and catalyst in organic synthesis [1], [2]

Chemically Bonded Cements/Ceramics (CBCs) have been widely applied, especially radiation protection systems, solid nuclear waste coagulation and encapsulation, active structure in high temperature composites and medical applications, especially chemically bonded phosphate cement/ceramics. CBPCs, which are ceramic materials that have complete mechanical properties from chemical reactions at low temperatures (below 300 degrees Celsius), instead of normal ceramic properties at high temperatures. Practically, this material has both cements and ceramics qualities. The original CBCs were primarily studied and researched in dentistry [3] and since 1970, magnesium phosphate ceramics had been used in construction materials for construction work, started by the Brookhaven National Laboratory (BNL) in the United States. After that, aluminum phosphate (found in the target local material source) has also been applied to CBPCs as well [4].

According to a study of Japakasetr, 1982 [5]; Sheldon, 1984 [6] the phosphate group of aluminum phosphate was found "Variscite"  $(\text{Al}(\text{PO}_4)(\text{H}_2\text{O})_2)$  at Lao Kham Village, Si Kaeo Sub-District, Mueang Roi Et District. However, there are no studies to test

and study the guidelines for use. Guidelines for the development of Variscite at Lao Kham Village or Lao Kham's Variscite; LKV, in material and application, is necessary for further development. In this study, The aim of this work is to apply LKV for chemically bonded phosphate cement (CBPC).

### MATERIALS AND METHODS

#### Materials

The material is a mineral that is composed aluminum phosphate. From Sheldon's study (1984) at the Lao Kham Village area of Roi Et Province, Thailand which was a mineral that is likely to be the secondary mineral of the phosphate group of aluminum phosphate, namely "Variscite"  $(\text{Al}(\text{PO}_4)(\text{H}_2\text{O})_2)$ . The two groups of samples were collected, random sample, which was randomly collected from rocks containing mineral. Also screen sample, which was extracted the mineral from streak in the origin rock. In the screen sample group, the sample will be calcined by heat to determine the effect of the temperature, ie, non- calcining sample (LKV<sub>NOR</sub>), sample calcined at 400, 600, 800 and 1,000 ° C (LKV<sub>400</sub>, LKV<sub>600</sub>, LKV<sub>800</sub> and LKV<sub>1000</sub> respectively). Type I Portland cement, according to ASTM C150-07 [7] was used for a reference cement in this study.

#### Method

##### *Microscope analysis*

The cold mount method was used for prepared the mounted sample and polished section. This is a method for preparing brittle parts and may cause breakage when polishing the surface by applying the

sample in the mold. Then it was applied with epoxy and setting at room temperature for 24 hours. Then removed the sample from the mold and polish until surface was smooth. Indispensable prerequisites for the success of investigations using transmitted or reflected light microscopy [8].

#### *Petrographic analysis*

Thin section petrography was carried out using Olympus BX-41 imaging petrographic microscope equipped with plane and cross polarization illumination mode. The petrographic analysis was used to study the microstructure of the aggregates, to identify the constituent minerals and to classify the aggregates. When placed between two polarizing filters set at right angles to each other, the optical properties of the minerals in the thin section alter the color and intensity of the light as seen by the viewer. As different minerals have different optical properties, most rock forming minerals can be easily identified [9].

#### *Chemical compositions and Mineral analysis*

The chemical compositions were analyzed with X-ray Fluorescence spectroscopy (XRF) and X-ray diffraction spectroscopy (XRD).

#### *Initial Setting Time and Final Setting Time Testing*

Initial setting time and final setting time testing of cement paste and LKV mixed with NaOH 3M were also test in this study with ASTM C 191: Time of Setting of Hydraulic Cement by Vicat needle [10].

#### *Compressive Strength*

Compressive strength index (%) of cement paste and LKV mixing sample were test at the age of 14 days.

## **RESULTS AND DISCUSSION**

### **Random Sample**

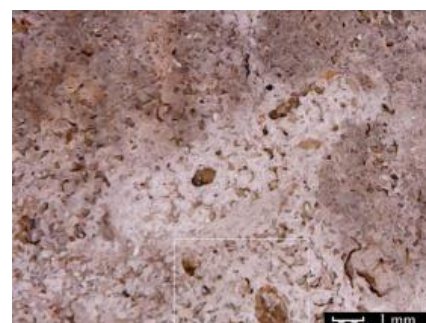
The random sample, which was randomly collected from rocks containing mineral as show in Fig.1.



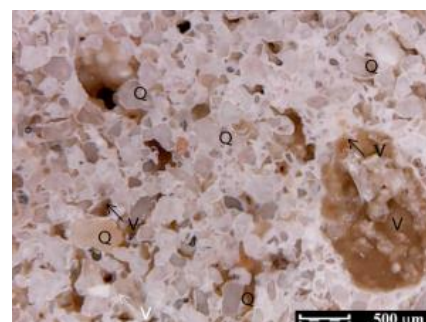
Fig. 1 Random sample.

#### *Microscope analysis*

In the polished section analyzed with a digital microscope, at magnification at 15 times and 35 times, the rock sample has the white mineral line in the red-brown coarse particle of sandstone (Fig. 2a and Fig. 2b). Variscite had a very fine grain size of particle compared to the particle size of the quartz crystals (Quartz,  $\text{SiO}_2$ ) in sandstone. Also iron oxide (Iron, Fe) distributed in the rock with the yellow to dark brown color particles.



(a)



V: Variscite ( $\text{AlPO}_4 \cdot 2\text{H}_2\text{O}$ )  
Q: Quartz ( $\text{SiO}_2$ )

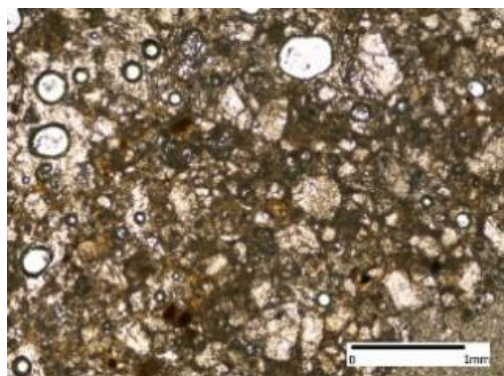
Fig.2 Digital Microscope of Random Sample LKV (a) at 15X (b) at 35X

#### *Petrographic analysis*

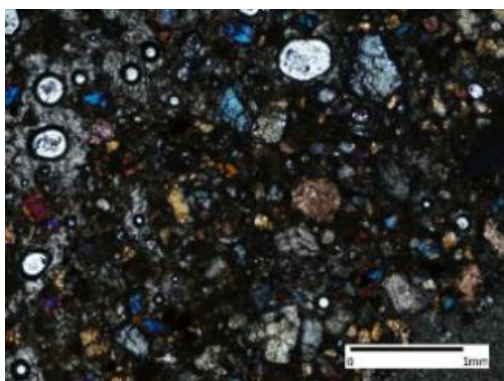
The result of Petrographic analysis, it found that the Nordstrandite and Variscite microscopic texture, both of which consists of quartz mineral



Nordstrandite and Variscite ore as shown in Fig. 2 and 3.



(a)



(b)

Fig. 3 Thin section microscopy of Random Sample LKV the (a) without using polarized light and (b) using polarized light.

#### *X-ray diffraction spectroscopy*

The XRD result shown in Table 1 found that the randomly sample consisting of quartz ( $\text{SiO}_2$ ), mostly (81.0%) making the majority of the elements are sandstone, because the test samples were tested without the separation of the mineral. However 6.9 percent of Variscite ( $\text{Al}(\text{PO}_4)(\text{H}_2\text{O})_2$ ) has been found.

#### *X-ray Fluorescence spectroscopy*

As shown in Table 2, it was found that most of the samples were silica oxide ( $\text{SiO}_2$ ) or Quartz (33.90%), followed by Phosphorus pentoxide ( $\text{P}_2\text{O}_5$ ), with 13.95%.

Table 1 X-ray diffraction of Random Sample LKV

| Mineral | Formula        | Concentration (wt%) |
|---------|----------------|---------------------|
| Quartz  | $\text{SiO}_2$ | 81.0                |

|               |  |     |
|---------------|--|-----|
| Variscite     | $\text{Al}(\text{PO}_4)(\text{H}_2\text{O})_2$ | 6.9 |
| Nordstrandite | $\text{Al}(\text{OH})_3$                       | 7.2 |
| Bayerite, syn | $\text{Al}(\text{OH})_3$                       | 4.8 |

Table 2 X-ray fluorescence of Random Sample LKV

| Formula                 | Concentration (wt%) |
|-------------------------|---------------------|
| $\text{SiO}_2$          | 33.90               |
| $\text{P}_2\text{O}_5$  | 13.95               |
| $\text{Na}_2\text{O}$   | 19.59               |
| $\text{Fe}_2\text{O}_3$ | 11.44               |
| $\text{Al}_2\text{O}_3$ | 10.11               |
| $\text{CaO}$            | 4.73                |
| $\text{MgO}$            | 5.48                |
| $\text{K}_2\text{O}$    | 0.20                |
| $\text{SrO}$            | 0.60                |
| Total                   | 100                 |

#### **Screening Sample**

Based on the polished Section test a white mineral, Variscite, had a very fine grain size compared to the particle size of the sand which could be observed with apparent, as shown in Fig. 4 (a). Therefore this study will separated the mineral from the sandstone to be the main example in the study of screening sample group, Fig. 4 (b).



(a)

(b)

Fig. 4 (a) the mineral from the sandstone texture (b) White mineral obtained from sandstone extraction

#### *X-ray diffraction spectroscopy*

The XRD result shown in Table 3 found that the survey sample consisted of the same amount of quartz ( $\text{SiO}_2$ ) (46.12% - 56.72%). LKVNOR with Variscite ( $\text{Al}(\text{PO}_4)(\text{H}_2\text{O})_2$ ), 23.51%, which was significantly higher than random Sample. While all the calcined samples were not found Variscite, but the mineral composition was changed to Aluminum Phosphate ( $\text{AlPO}_4$ ) altogether. Aluminum Phosphate Hydrate ( $\text{AlPO}_4 \cdot x(\text{H}_2\text{O})$ ) only found in LKV400. When the temperature rises from 600 degrees, some parts of Aluminum Phosphate Hydrate had changed to Aluminum Phosphate ( $\text{AlPO}_4$ ) which was composed of Aluminum Phosphate equal to 34.12%, 34.51% and 30.44% for LKV600 LKV800 and

LKV1000 respectively. In addition, some parts of Phosphate ( $\text{PO}_4$ ) appeared in Calcium Iron Phosphate and Calcium Hydrogen Iron Phosphate for the samples that are calcined with temperatures up to 600 degrees while not found this mineral in the sample calcined at 400 degrees.

Table 3 X-ray Diffractometer of Screening LKV Sample

| Sample                          | Formula  | LKVNOR | LKV400 | LKV600 | LKV800 | LKV1000 |
|---------------------------------|--|--------|--------|--------|--------|---------|
| Quartz                          | $\text{SiO}_2$   | 46.12  | 48.51  | 52.6   | 55.81  | 56.72   |
| Kaolinite                       | $\text{Al}_2(\text{Si}_2\text{O}_5)(\text{OH})_4$                            | 15.61  | 13.1   | -      | -      | -       |
| Variscite                       | $\text{AlPO}_4(\text{H}_2\text{O})_2$  | 23.51  | -      | -      | -      | -       |
| Aluminum Phosphate              | $\text{AlPO}_4$  | -      | 18.42  | 34.12  | 34.51  | 30.44   |
| Aluminum Iron Phosphate         | $\text{Al}_{0.67}\text{Fe}_{0.33}(\text{PO}_4)$                              | -      | 8.6    | -      | -      | -       |
| Aluminum Phosphate Hydrate      | $\text{AlPO}_4 \cdot x(\text{H}_2\text{O})$                                  | -      | 6.24   | -      | -      | -       |
| Crandallite                     | $\text{CaAl}_3(\text{OH})_6(\text{PO}_3(\text{O}_{0.5}(\text{OH})_{0.5}))_2$ | 5.43   | 5.12   | -      | -      | -       |
| Calcium Iron Phosphate          | $\text{Ca}_9\text{Fe}_2(\text{PO}_4)_{14}$                                   | 2.56   | -      | 6.91   | 7.37   | 8.23    |
| Calcium Hydrogen Iron Phosphate | $\text{Ca}_9\text{FeH}(\text{PO}_4)_7$                                       | 6.77   | -      | 6.37   | 2.31   | 4.61    |

### Setting Time

Mixing of NaOH 3M with LKV conducted to find the setting time. While 3M was the amount of NaOH estimated by the chemical equation balance by weight, to make the reaction even with  $\text{AlPO}_4$  in LKV (average of 30%  $\text{AlPO}_4$  in the sample and the mixture ratio of solution and LKV was 0.35). It was found that the non-calcined LKVNOR did not setting when mixed with the 3M NaOH solution while the LKV600 had the fastest formation (initial setting time 15 minutes, and final setting time was 90 minutes), which indicates that the LKV 600 was most likely to react with the NaOH 3M solution, followed by LKV800 LKV1000 and LKV400 respectively, as show in Fig.5.

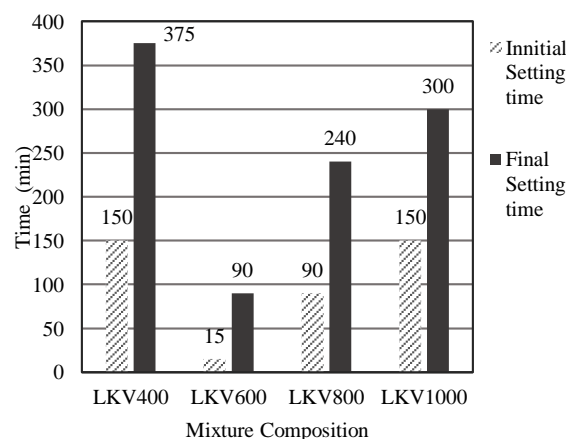


Fig. 5 Setting Time results of calcined LKV

### Compressive Strength

Compressive strength index (%) of cement paste and LKV mixing sample at the age of 14 days found that LKV600 had the highest compressive strength (24.5%) followed by LKV800 LKV1000 and LKV400 respectively (14.9%, 6.2%, and 3.3%). While LKVNOR, no formation was found so the



compressive strength test was not possible. Which corresponds to the previous setting time test results that LKV600 has the fastest formation. However, LKV600 has only 24.5% compressive strength when compared with the reference cement (REF). Therefore, it should be studied in terms of the solution type and the appropriate concentration to optimize solution mixing LKV as show in Fig.6.

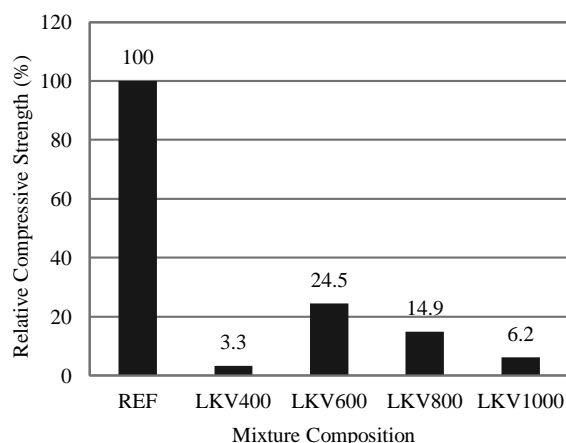


Fig. 6 Compressive strength index (%) of cement paste and LKV mixing sample at the age of 14 days.

## CONCLUSIONS

1. LKV, which was screen sample, had Variscite mineral of 23.5% which was significantly higher than random sample.

2. Calcination affected the mineral state of LKV. All samples that had calcined were not found Variscite, but the mineral composition changed to Aluminum Phosphate ( $\text{AlPO}_4$ ).

3. Non-calcined LKVNOR found no formation when mixed with 3M NaOH solution. While LKV600 had the fastest setting time when mixed with 3M NaOH solution. It indicated that LKV 600 was the most reactive with NaOH 3M.

4. The LKV600 had the highest compressive strength. However, when compared to the reference cement, LKV600 only received 24.5% of compressive strength when compared with the reference cement. There should be a study of the solution and the appropriate concentration to optimize solution mixing LKV.

## ACKNOWLEDGEMENTS

This research was supported by National research council of Thailand (NRCT). We thank our colleagues from Roi Et Rajabhat University who provided insight and expertise that greatly assisted the research, although they may not agree with all of the interpretations/conclusions of this paper.

## REFERENCES

- [1] Kawasaki S. and Akiyama M., Unique Grout Material Composed of Calcium Phosphate Compounds, *International Journal of GEOMATE*, Vol. 4, No. 1, 2013, pp. 429-435
- [2] Pangdaeng S., Sata V. and Chindaprasirt P., Effect of Sodium Hydroxide Concentration and Sodium Silicate to Sodium Hydroxide Ratio on Properties of Calcined Kaolin-White Portland Cement Geopolymer, *International Journal of GEOMATE*, Vol.14, Issue 46, 2018, pp.121-128.
- [3] Colorado H. A., Hiel C., Hahn T., and Yang J. M., Wollastonite-Based Chemically Bonded Phosphate Ceramic Composites, *Metal, Ceramic and Polymeric Composites for Various Uses*, 2011, pp.265-282.
- [4] Wagh A. S., *Chemically Bonded Phosphate Ceramics*, 2016, pp.1-283.
- [5] Japakasetr, T., *Phosphate in Thailand; Economic Geology Division, DMR*, 1982, 7p.
- [6] Sheldon, R.P., 1984, *Phosphate Resource Assessment and Exploration in Thailand*, Thai Department of Mineral Resources, 52 p.
- [7] American Society for Testing and Materials. *Standard Specification for Portland Cement*, 2007, ASTM C150-07.
- [8] Moreland G.G., Preparation of Polished Thin Sections, *American Mineralogist*, Vol. 53, Issue 5-6, 1968. pp. 2070-2074.
- [9] Barber, D.J. 1981. Demountable polished extra-thin sections and their use in transmission electron microscopy. *Mineralogical Magazine* 44:357-359.
- [10] American Society for Testing and Materials. *Time of Setting of Hydraulic Cement by Vicat needle*, 2018, ASTM C 191-18a.

## PERFORMANCE EVALUATION OF CONCRETE WITH RECYCLED WASTE POLYPROPYLENE

N. Haque<sup>1</sup>, M.J Islam<sup>2</sup>, A. Tahsin<sup>3</sup> & T. Mehdi<sup>4</sup>

<sup>1</sup> Department of Civil Engineering, Military Institute of Science and Technology, Dhaka, Bangladesh; <sup>2,3,4</sup>

### ABSTRACT

Production and application of plastic waste has become a severe environmental problem worldwide where polypropylene (PP) possesses around 35% of the total plastic waste. Using recycled PP in concrete could be a solution for the problem. This study aims at evaluating structural and durability performance of various strength concrete mixed with recycled waste polypropylene as a partial replacement of coarse aggregate. Performance of concrete was evaluated in terms of compressive strength, chloride ion penetration and high temperature exposure at different ages. In order to determine the optimum proportion of polypropylene in concrete, samples were prepared with 0%, 10%, & 20% replacement of PP as coarse aggregate for two different w/c ratios (0.35 and 0.40). It was found that for maximum 20% of PP replacement, compressive strength reduction was only 21% which could still produce more than 25 MPa of concrete and at high temperature exposure (more than 200° C) for 1 hour the strength of concrete was still more than 20 MPa. Moreover, PP can also be used to produce light weight concrete due to its lower unit weight, as relative reduction was up to 10% in density for 20% of PP replacement, than regular concrete. Therefore, concrete with optimum proportion of PP as partial replacement of coarse aggregate can produce strong and durable structure concrete.

*Keywords: Concrete, Polypropylene; Compressive strength; Chloride ion penetration; High temperature exposure;*

### INTRODUCTION

With the technological advancement around the world, disposal of wastes and waste management has gotten to be a major natural issue all over the world. Among all these waste materials, plastic-based waste materials are worst as they don't effectively debase or decayed [1]. Plastic is accessible nearly all over and its utilization around the world expanded from 5 million tons to almost 335 million tons amid the year 1950–2016 [2]. Only around 7% of these produced plastics are recycled and rest are polluting the earth. According to statistical report, around 34.20% of these huge plastic wastes are polypropylene found in municipal solid waste [3].

Construction industry is getting a quick expansion every day, so researchers are always working to develop a cleaner, cheaper and energy efficient construction material to cope up with the advancement. Currently, the global concrete consumption is estimated around 25 Billion tons per year and annual coarse aggregate (stone) usage is more than 3.9 billion tones (2016) [4]. The use of waste product like plastics in concrete not only makes it economical but also helps in reducing the plastic waste disposal problems.

The use of polypropylene (PP), due to its low unit weight, reduces the unit weight of concrete

which results in a reduction in the dead load of a structural concrete member of a building. Reduction in the self-weight of a building will help to reduce the seismic risk of the building since the earthquake forces linearly dependent on the dead-weight. Furthermore, it can also be concluded that the use of recycled PP as a partial replacement of coarse aggregate in concrete provides some advantages, i.e., reduction in the use of natural resources, disposal of polymer wastes, low cost alternative to regular aggregates, prevention of environmental pollution, and energy saving.

Polypropylene (PP) is a cheap and plentiful thermoplastic used in a wide variety of applications including food packaging, textiles, laboratory equipment, automotive components, and polymer banknotes. It is slightly harder, more heat resistant, mechanically rugged material; and has a high chemical resistance [5]. It is the second-most widely produced commodity plastic and can be used in making composite concrete for its excellent material property [6]. The melting point of polypropylene is exceptionally high compared to numerous other plastics at 320°F (160°C).

There were several researches done on such types of composites in recent years but in terms of durability, the question still arises if it is durable against chloride ion penetration and high temperature exposure. Chloride penetration refers to

the depth to which chloride ions from the environment penetrate into the concrete which can lead to corrosion in RCC structures [7]. This research emphasizes on finding out compressive strength and durability performance of engineered concrete in terms of Chloride penetration and high temperature exposure with polypropylene replacing coarse aggregates at various proportion.

## MATERIALS

For the experimental work, stone chips and recycled waste PP were used as two different types of coarse aggregates. According to the ASTM C33, the gradation of the coarse aggregates was performed. Ordinary Portland Cement (OPC) has been used as binding material for this research work. River (Sylhet) sand has been collected and used as fine aggregates (FA). Coarse aggregate (CA) as Crushed stones were purchased from local market according to required quantities. Shredded PP aggregate, as shown in Fig. 1, was used as partial replacement of coarse aggregate. Polypropylene was prepared through a process of collection, cleaning and scraping. After that, it had been melted and cooled into certain shape. Those cooled plastic molds were then shredded into specific sizes.



Fig. 1 Processed polypropylene (PP) aggregate



Fig. 2 Coarse and Fine Aggregate

Material properties have been found out by performing specific tests in the laboratory according to the ASTM standards. Materials properties of the aggregates are summarized in Table 1.

Water-reducing admixture following ASTM C-494, for maintaining uniform workability, was used

for all combination of fresh concrete. The specific gravity of admixture was 1.21.

Table 1 Properties of coarse and fine aggregate

| Description          | Crushed Stone | Polypropylene (PP) | Sand |
|----------------------|---------------|--------------------|------|
| Maximum Size (mm)    | 19            | 12                 | -    |
| Specific Gravity     | 2.61          | 0.85               | 2.7  |
| Water Absorption (%) | 0.36          | 0.3                | 2.8  |
| Fineness Modulus     | 8.12          | 6.77               | 2.46 |

## METHODOLOGY

Using Polypropylene (PP) in construction is an economical and green concept of modern civil engineering [8]. To achieve the objectives, a number of experiments have been done in the laboratories. The concrete samples were prepared with 0%, 10% and 20% replacement of PP as coarse aggregate with two different w/c ratios (0.35 and 0.40). Concrete cylinder samples, 100 mm x 200 mm, were prepared as per requirement of the test methods following ASTM C 192. After 24 hours of humidity curing the samples were water cured for 28 days, except for 7 days test. Samples were tested for compressive strength following ASTM C39 at 7, 28 and 90 days. Samples were also tested for chloride ion penetration by surface resistivity meter following AASHTO TP 95 at 28 days and compressive strength test after high temperature exposure (more than 200° C for 1 hour) at 90 days.

## Mix Design

Mix design for the concrete specimens was proposed considering stone chips with three different partial replacement of PP (0%, 10% and 20%) along with two different water cement ratios (0.35 and 0.40). Table 2 shows the mix proportion for 1 m<sup>3</sup> of concrete.

Table 2 Mix design for 1m<sup>3</sup> of concrete

| Designation | Water (kg) | OPC (kg) | CA (kg) | PP (kg) | FA (kg) | Total |
|-------------|------------|----------|---------|---------|---------|-------|
| WC35P0      | 206        | 589      | 977     | 0       | 487     | 4112  |
| WC35P10     | 206        | 589      | 879     | 39      | 474     | 4041  |
| WC35P20     | 206        | 589      | 781     | 78      | 461     | 3969  |
| WC40P0      | 206        | 514      | 975     | 0       | 552     | 3480  |
| WC40P10     | 206        | 514      | 877     | 39      | 539     | 3409  |
| WC40P20     | 206        | 514      | 780     | 78      | 526     | 3337  |

Note: in the designation, WCXPY, “X” stands for the water cement ratio and “Y” stands for percentage of PP replacement.

## RESULTS AND DISCUSSION

For evaluating the physical properties of concrete, relative density reduction, compressive strength reduction and chloride ion penetration test was analyzed. Compressive test of concrete was performed at different stages from 7 to 90 days and chloride ion penetration test using a surface resistivity meter was performed at 28 days of the age of concrete, as shown in Fig. 3.

Also, higher temperature exposure was performed in oven shown in Fig. 4 at 200°C and compressive strength test was performed accordingly.



Fig. 3 Compressive test and Chloride penetration test of concrete



Fig. 4 High temperature exposure in oven

### Effect on Density reduction

The density of concrete was determined for all type of combinations and compared, as presented in Fig. 5, with the standard sample of concrete (without any PP replacement) to measure the relative reduction of density.

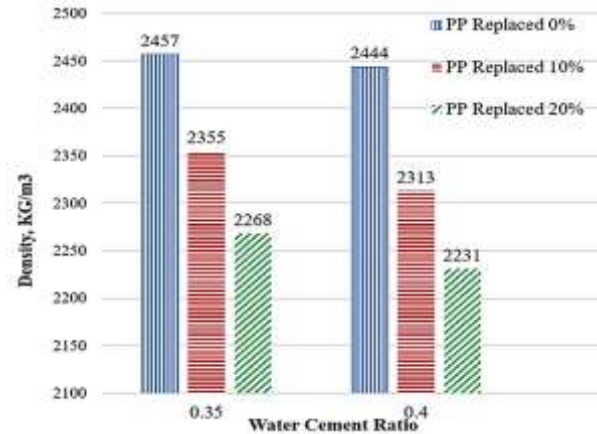


Fig. 5 Comparison of density reduction of PP replaced concrete

Based on the data, it can be said that, maximum relative reduction of density was around 10% for 20 percent PP replaced concrete, which implies that it can produce lighter concrete with reduced dead load and seismic vulnerability.

### Effect on Compressive Strength

The compressive strengths at 7, 28 and 90 days after casting were measured for all type of concretes. Compressive strength test results of w/c ratios 0.35 and 0.40 for various ages are described in Fig. 6 and 7. Based on the test data it can be said that concrete with PP will produce lower strength compare to the regular concrete with no PP content. This is expected as synthetic PP does not bond well with the binding material used in content. However, with increase in concrete age interfacial transition zone between the aggregate and cement matrix gain strength and reduction of compressive strength becomes smaller and smaller.

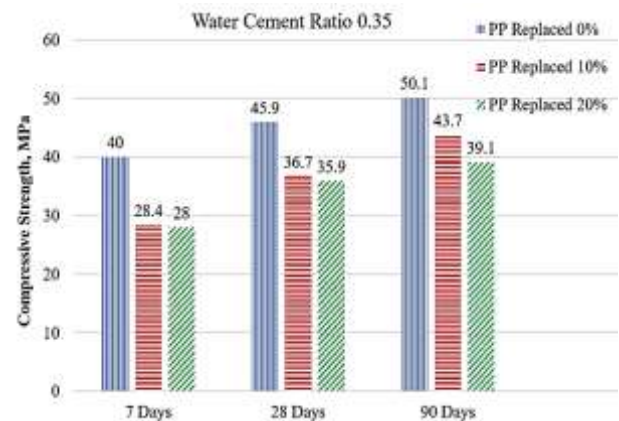


Fig. 6 Compressive strength of concrete at various ages for water cement ratio of 0.35



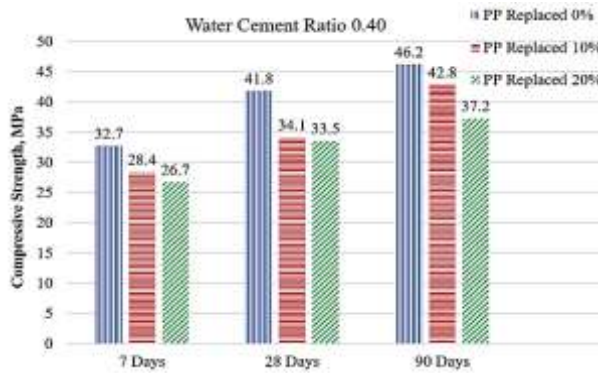


Fig. 7 Compressive strength of concrete at various ages for water cement ratio of 0.40

For the water cement ratio of 0.35, compressive strength reductions for 10% and 20% PP replaced concrete compare to 0% PP replaced concrete is only 12% and 21%, respectively. On the other hand, for the water cement ratio of 0.40 compressive strength reductions for 10% and 20% PP replacement compare to 0% PP replaced concrete is only 7% and 19%, respectively. The results of the PP replaced concrete gives the indication of adequate strength of the concrete even with higher percentage of PP replacement.

#### Effect on Chloride Ion Penetration

The surface resistivity test was performed according to AASHTO TP 95. In this test method, the specific resistance of concrete was measured by surface resistivity meter and the data was correlated to the chloride penetrability classification of the concrete. According to this test method, specific resistance value of 12 KOhm-cm to 21 KOhm-cm is considered as moderate category. Fig. 8 shows the specific resistance in KOhm-cm for two different water-cement ratios and three different PP replacement percentages. For the all the cases, chloride ion penetrability of concrete falls under low to moderate category.

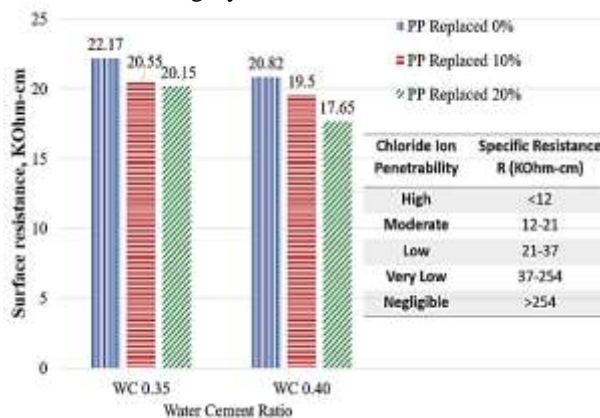


Fig. 8 Chloride ion penetrability of concrete

The results of the chloride ion penetrability of PP replaced concrete gives the indication with replacement of PP there is almost no effect on durability aspect in terms of chloride ion penetration compare to the regular concrete without PP.

#### Effect on High Temperature exposure

For high temperature exposure, the concrete cylinders were heated evenly in an enclosed furnace chamber at the age of 90 days. The temperature loading curve shown in Fig. 9 indicate that the concrete cylinders were exposed to 200°C for over an hour. After the application of temperature, the samples were cooled down to room temperature at the laboratory. Samples were then tested for compressive strength. Compressive strength results, as presented in Fig. 10, are compared with for all three PP replaced concrete (0, 10 and 20%) for w/c ratios of 0.35 and 0.40.

The results of the compressive strength after high temperature exposure indicates that, even after an hour, the PP replaced concrete may retain sustainable compressive strength (more than 24 MPa).

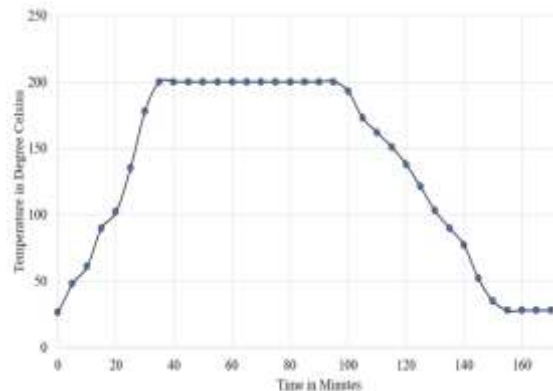


Fig. 9 Temperature loading graph

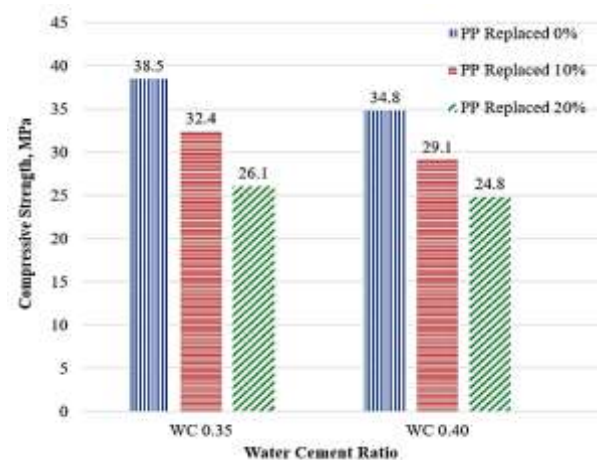


Fig. 10 Compressive strength of concrete after high temperature exposure

## CONCLUSION

Compared to regular concrete, PP concrete has the lower compressive strength as well as the lower durability against high temperature exposure. With the increasing amount of PP percentage in the concrete, both compressive strength and surface resistivity of the concrete is decreasing albeit in lower percentage. It is to be expected as the synthetic nature of the PP provides lesser bonding with the cement mortar compare to the natural stone aggregate. However, at water-cement ratio 0.40 this reduction is about 21% for 20% PP replaced concrete and still it produces concrete with compressive strength higher than 25 MPa.

Furthermore, more than 33 MPa strength for 20% PP replaced concrete gives the indication that PP can be used for structural concrete safely. Furthermore, structure made by PP concrete is lighter than regular concrete due to the lower unit weight of PP. Therefore, it can be concluded that the recycled PP can be adopted as partial replacement of coarse aggregate in concrete used for structural purposes.

## REFERENCES

- [1] Frigione, M. 2010. Recycling of PET bottles as fine aggregate in concrete. *Waste Management*, 30 (6): 1101–1106.
- [2] Statista, 2016. Global production of plastic since 1950. [online]. Available at: <https://www.statista.com/statistics/282732/global-production-of-plastics-since-1950>. [Accessed 12 June 2019].
- [3] Islam, Md, Sarwar, Navid and Al shafian, Sultan, Conference proceeding in International Conference on Recent Innovation in Civil Engineering for Sustainable Development (IICSD-2015), An Investigation of Concrete Properties with Polypropylene (PP) as Partial Replacement of Coarse Aggregate. pp. 1.
- [4] USGS Mineral Commodity Summaries, 2017. [online]. Available at : [https://mineralsmakelife.org/wp-content/uploads/2017/04/Mineral\\_Commodity\\_Summaries\\_2017.pdf](https://mineralsmakelife.org/wp-content/uploads/2017/04/Mineral_Commodity_Summaries_2017.pdf) [Accessed 12 June 2019]
- [5] Whiteley, K. S., Heggs, T. G., Koch, H., Mawer, R. L., & Immel, W. 2005. Polyolefins in Ullmann's Encyclopedia of Industrial Chemistry. Weinheim: Wiley-VCH Verlag GmbH & Co.
- [6] Bagherzadeh R., Pakravan, H. R., Sadeghi, A. H., Latifi, M., & Merati, A. A. 2012. An Investigation on Adding Polypropylene Fibers to Reinforce Lightweight Cement Composites (LWC). *Journal of Engineered Fabrics & Fibers (JEFF)*. 7 (4): 13-21.
- [7] Zhang, J., Shi, C., Li, Y., et al, 2015a. Influence of carbonated recycled concrete aggregate on properties of cement mortar. *Construction and Building Materials* 98, 1–7.
- [8] Islam, M. J., Meherier, M. S., Islam, A. K., M. R. 2016. Effects of waste PET as coarse aggregate on the fresh and harden properties of concrete. *Construction and Building Materials*, 125, 946-951.



## LIFE CYCLE COST ANALYSIS FOR REINFORCED GEOGRID RAILWAY TRACK

Saad Farhan Ibrahim Alabdullah<sup>1</sup>, Ali Jabbar Kadhim<sup>2</sup> and Harith Basim Khalaf<sup>2</sup>

<sup>1</sup>Faculty of Engineering, Isra University, Amman, Jordan;

<sup>2</sup>Faculty of Engineering, Al-Mustansiriya University, Baghdad, Iraq

### ABSTRACT

The development of railway transportation is facing many challenges and one of main challenges is the Reduction of the track costs. The reduction of railway track costs is critical for competitiveness of railway operators, since other competing modes of transportation (e.g. automotive, aviation) have seen a tremendous reduction in life cycle cost in the previous years, while the costs of railway maintenance has not decreased significantly through the same time. The objective of this study is mainly focus on the reduction in of the railway track cost due to the use of geogrids reinforcement. The results showed a redaction of railway track cost for the sub-ballast reinforced model (4.1%), the ballast reinforced model was (6.5%) and the double reinforced model was (3.73%) as compared to the unreinforced track.

*Keywords: Railway, life cycle cost, Geogrid, Reinforcement, maintenance.*

### INTRODUCTION

The entire cost of railway transportation comes from construction, repairing and the operating of facilities, manufacturing and maintenance of railway vehicles, as well as fuel production. Because maintenance, expenses for the traditional ballasted train track might be significantly decreased if the final settlement below loading is reduced. There are a few current data regarding the lifetime of the actual geosynthetics within the construction associated with railway. Since the knowledge about using geosynthetics upon railway tracks is only recognized in the past (20) years, and we can claim that the experience as well as practice from the lifetime of numerous constructions techniques are still are not enough regulate them correctly. Just little estimations available through the geosynthetics manufacturers involving geosynthetics who announced that the materials which they produce might rise the ballast life time by (2 - 4) times the original life. Since of the deficiency within the pervious data, the computation of repairing and renewal work related to railway tracks had been very few. Additionally, Federici (2003) noticed that the main available scientific studies on railway track method that ingest consideration the infrastructures in depth are very hardly ever and mainly focused on cars construction. Consequently, the effect of geogrid support on lowering the cost of train track will probably be studied [1].

Life cycle cost could be functional for project through a wide variety of industries, containing the railway. Railway track cost has not considerably changed since the past (30) years with comparison to other rival transportation modes [2]. European

Commission (2011) on Sustainable Transportation settled goals for the reduction of railway life cycle cost by 30% in 2020. Thus, there is a important focusing on the study of life cycle cost application on railway track [3].

INNOTRACK project used the Geogrid as a part of its numerical simulations and laboratory tests. This approach proved that the geogrid reinforcement would cause a reduction in the life cycle cost and operational disturbances. Hall and Sharpe (2007) used a British Railway case study was done in (1988) where geogrid was introduced for the renewal of railway track in the Derby–Leeds line at Shirland. The railway site was constructed with 300mm of ballast and a 100mm blanketing sand below it, a separation layer composed from a heat bonded geo-textile and a geogrid with a small mesh to stop the particles of ballast from the penetration the geotextile. A new geogrid having large mesh was furtherly added as a way to support often the soft subgrade. The undertaking condition seemed to be monitored over the long-term performance in addition to operational life of the ballast. The end result of monitoring exhibited that the geogrids decreased the requirements of routine maintenance to a tiny proportion of their past level so reducing the cycle cost [4].

the decision-making, maintenance and operation costs Without doubt are significantly more vital than initial cost of constructions. These types of costs have to be studied all through the life time of the project so they match up their overall performance threshold [5].It is necessary that the making of decisions must be based on the life-cycle foundation. This will be resulted in choosing cheaper strategies within the extended

time and cooperated with the available finance. Newest researches concerning railway track improvements with the use of geosynthetics reinforcement indicated a positive effect. The maintenance requirement dropped and the strength of the ballast was boosted when the geosynthetics were applied. Settlement of the track was 37 to 65 percent less than settlement of the equivalent portion of the unreinforced test section [6].

The geosynthetics manufacture company Tensar stated that the using of their geosynthetics products will cause a rise in maintenance cycle by 3 times from its original value after a railway track case study; the railway track was located between London and Scotland. The railway track has been under speed limit for many times in spite of it was maintained frequently 2 times a year. The intrusion of geogrid in that track caused a considerable decrease in the deterioration rate of the railway track without speed restrictions or maintenance [7].

## METHODOLOGY

The Life cycle cost (LCC) and the Whole life cost (WLC) are well known methods used to calculate all the related cost with the whole life of design for a specific asset. The Life cycle cost (LCC) and the Whole life cost (WLC) could be used interchangeably while in the (BS ISO 15685-8:2008) international standard for life cycle costing of buildings and constructed specified that the two have difference meaning [8]:

- Life cycle cost is well defined, as “is the cost of a part or its divisions during its cycle life, though accomplishing the performances requirement”.
- Whole life cost is well defined as “is the process of regular economic aspects for the benefits and whole life cost of a known analysis time”. Whole life cost covers the extra costs such as Land cost, support cost related to activity in assets, and the incomes produced by the assets. The connection between LCC and WLC is showed in Fig.1.

In order to make the suitable choices on the economical profits of the enhancement works that include using an innovative technology the life cycle cost and (LCC) should be calculated before and after the use of the technology. The tool was created within the project SMARTRAIL, and available on [smartrail.fehrl.org](http://smartrail.fehrl.org), was used to validate the cost benefits related to the use of geogrid reinforcement in railway track system for this research. The smart LCC rail tool was developed with Taking into account the ISO EN 15686-5 standard for LCC.

The following costs were used in the tool:

- Construction costs
  1. The Ballast layer
  2. The Sleepers
  3. Fastening and Rails systems
  4. Elastomeric [Resilient] pads
  5. Geogrid
- Routine maintenance costs:
  1. Stabilization and Tamping
  2. Milling of rail

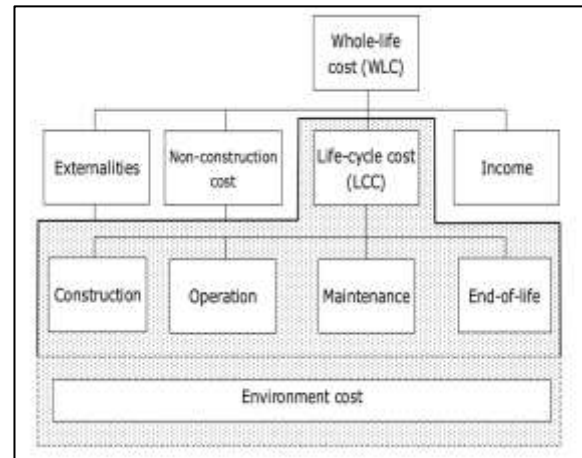


Fig.1 Scope of life cycle and whole-life costing (Adapted from BS ISO 15685-8:2008).

Geogrid has been increasingly used in railroads to offer reinforcement and confinement pressure to railway track layers. Four models were studied experimentally to measure the difference in the life of the railway track after using the geogrid.

The tested model dimensions were (800\*800\*600 mm), the subgrade layer was 400 mm and both ballast and sub-ballast layers were 100 mm thick each. The tested models are unreinforced model, sub ballast-reinforced model, and ballast-reinforced model and double-reinforced model containing a geogrid reinforcement under ballast layer and sub-ballast layer. The result demonstrated that using reinforcement layer would reduce the settlement in models. The tested model looks like the sketch in fig.2. A Cumulative fig.3 used to show the difference in result of settlement between all models that had been tested.

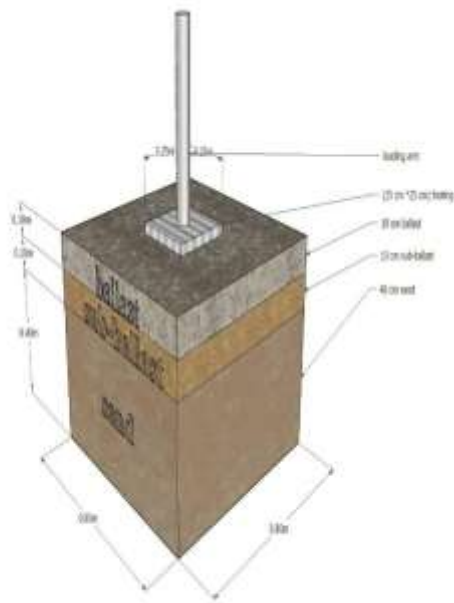


Fig.2 Sketch to show the experimentally tested model.

The used tool let the user to discover the effects of different maintenance choices on the life cycle cost of for a railway track system. The calculation of life cycle cost is a way to estimate the over-all costs of maintaining an asset with a specified period for analysis, to be used as an input into a decision-making procedure. The costs in the Future and Discounting rate were transformed to be Net Present Value (NPV) to make the judgement simpler in maintenances regimes from total cost point of view in the present day.

The input data was collected from “Transportation & Telecommunications of Iraq” report by United Nations World Bank and “Hajama – Sawa” Railway Project done by Iraqi Ministry of Transportation Republic Railways Company [9]. The project life span was assumed would be 60 years. Due to the difficultness of predicting the increase in the ballast lifetime of due to the use of geogrid, a number of scenarios were tested, and all of these scenarios show that the using of the geogrid in the railway track will be more economical in the end. In addition, this mean that the requirement of maintenance of the tack will be reduced. The tool layout and the used data for evaluated models are shown in figs. (4) (5) (6) (7) (8) accordingly.

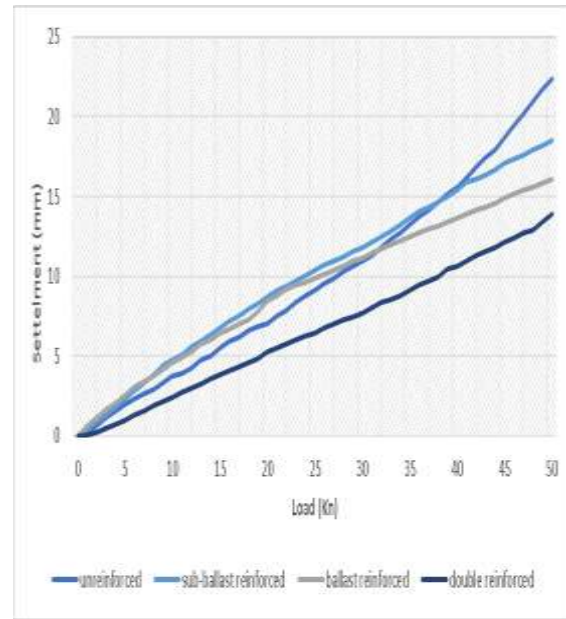


Fig.3 Load-Settlement relationship for all models at every loading stage.

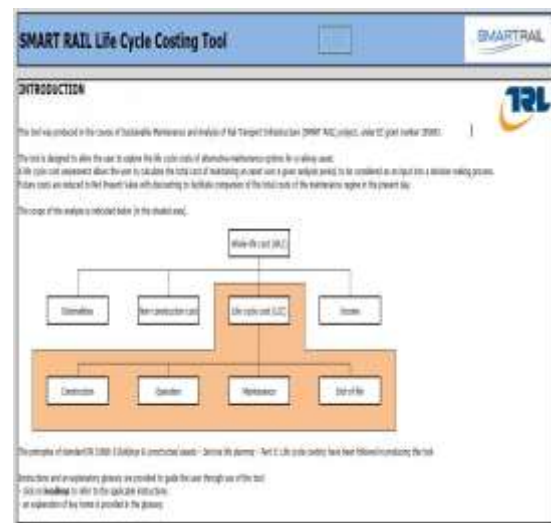


Fig.4 The LCC tool-starting page.

| Remediation  |  |                 |                        |            |                              |           |
|--|--|-----------------|------------------------|------------|------------------------------|-----------|
| Name   | Description                                    | Cost (€ per km) | Delay (minutes per km) | First year | Expected life (years)        | Last year |
| 1 Ballast  | Replace ballast at end of life                 | € 171,005.00    | 0                      | 25         | 60                           |           |
| 2 Sleepers   | Replace sleepers at end of life                | € 396,005.00    | 0                      | 20         | 60                           |           |
| 3 Rails and fastening system                         | Replace rails and fastenings at end of life    | € 594,270.00    | 0                      | 30         | 60                           |           |
| 4 Electromechanical parts                            | Replace electromechanical parts at end of life | € 317.00        | 0                      | 30         | 60                           |           |
| 5 Geotextile membrane                                | Replace membrane at end of life                | € 20,000.00     | 0                      | 25         | 60                           |           |
| 6  |  |                 |                        |            |                              |           |
| 7  |  |                 |                        |            |                              |           |
| 8  |  |                 |                        |            |                              |           |
| 9  |  |                 |                        |            |                              |           |
| 10   |  |                 |                        |            |                              |           |
| Routine maintenance                                  |  |                 |                        |            |                              |           |
| Name   | Description                                    | Cost (€ per km) | Delay (minutes per km) | First year | Average frequency (per year) | Last year |
| 1 Ballast tamping and stabiliser routine maintenance |  | € 1,007.00      | 0                      | 0.75       | 60                           |           |
| 2 Rail milling                                       | Routine maintenance                            | € 3,810.00      | 0                      | 0.25       | 60                           |           |
| 3  |  |                 |                        |            |                              |           |
| 4  |  |                 |                        |            |                              |           |
| 5  |  |                 |                        |            |                              |           |
| 6  |  |                 |                        |            |                              |           |
| 7  |  |                 |                        |            |                              |           |
| 8  |  |                 |                        |            |                              |           |
| 9  |  |                 |                        |            |                              |           |
| 10   |  |                 |                        |            |                              |           |

Fig.5 The input data for unreinforced model.

| Remediation  |  |                 |                        |            |                              |           |
|--|--|-----------------|------------------------|------------|------------------------------|-----------|
| Name   | Description                                    | Cost (€ per km) | Delay (minutes per km) | First year | Expected life (years)        | Last year |
| 1 Ballast  | Replace ballast at end of life                 | € 171,005.00    | 0                      | 25         | 60                           |           |
| 2 Sleepers   | Replace sleepers at end of life                | € 396,005.00    | 0                      | 20         | 60                           |           |
| 3 Rails and fastening system                         | Replace rails and fastenings at end of life    | € 594,270.00    | 0                      | 30         | 60                           |           |
| 4 Electromechanical parts                            | Replace electromechanical parts at end of life | € 317.00        | 0                      | 30         | 60                           |           |
| 5 Geotextile membrane                                | Replace membrane at end of life                | € 20,000.00     | 0                      | 25         | 60                           |           |
| 6  |  |                 |                        |            |                              |           |
| 7  |  |                 |                        |            |                              |           |
| 8  |  |                 |                        |            |                              |           |
| 9  |  |                 |                        |            |                              |           |
| 10   |  |                 |                        |            |                              |           |
| Routine maintenance                                  |  |                 |                        |            |                              |           |
| Name   | Description                                    | Cost (€ per km) | Delay (minutes per km) | First year | Average frequency (per year) | Last year |
| 1 Ballast tamping and stabiliser routine maintenance |  | € 1,007.00      | 0                      | 0.75       | 60                           |           |
| 2 Rail milling                                       | Routine maintenance                            | € 3,810.00      | 0                      | 0.25       | 60                           |           |
| 3  |  |                 |                        |            |                              |           |
| 4  |  |                 |                        |            |                              |           |
| 5  |  |                 |                        |            |                              |           |
| 6  |  |                 |                        |            |                              |           |
| 7  |  |                 |                        |            |                              |           |
| 8  |  |                 |                        |            |                              |           |
| 9  |  |                 |                        |            |                              |           |
| 10   |  |                 |                        |            |                              |           |

Fig.7 The input data for ballast reinforced track.

| Remediation  |  |                 |                        |            |                              |           |
|--|--|-----------------|------------------------|------------|------------------------------|-----------|
| Name   | Description                                    | Cost (€ per km) | Delay (minutes per km) | First year | Expected life (years)        | Last year |
| 1 Ballast  | Replace ballast at end of life                 | € 171,005.00    | 0                      | 25         | 60                           |           |
| 2 Sleepers   | Replace sleepers at end of life                | € 396,005.00    | 0                      | 20         | 60                           |           |
| 3 Rails and fastening system                         | Replace rails and fastenings at end of life    | € 594,270.00    | 0                      | 30         | 60                           |           |
| 4 Electromechanical parts                            | Replace electromechanical parts at end of life | € 317.00        | 0                      | 30         | 60                           |           |
| 5 Geotextile membrane                                | Replace membrane at end of life                | € 20,000.00     | 0                      | 25         | 60                           |           |
| 6  |  |                 |                        |            |                              |           |
| 7  |  |                 |                        |            |                              |           |
| 8  |  |                 |                        |            |                              |           |
| 9  |  |                 |                        |            |                              |           |
| 10   |  |                 |                        |            |                              |           |
| Routine maintenance                                  |  |                 |                        |            |                              |           |
| Name   | Description                                    | Cost (€ per km) | Delay (minutes per km) | First year | Average frequency (per year) | Last year |
| 1 Ballast tamping and stabiliser routine maintenance |  | € 1,007.00      | 0                      | 0.75       | 60                           |           |
| 2 Rail milling                                       | Routine maintenance                            | € 3,810.00      | 0                      | 0.25       | 60                           |           |
| 3  |  |                 |                        |            |                              |           |
| 4  |  |                 |                        |            |                              |           |
| 5  |  |                 |                        |            |                              |           |
| 6  |  |                 |                        |            |                              |           |
| 7  |  |                 |                        |            |                              |           |
| 8  |  |                 |                        |            |                              |           |
| 9  |  |                 |                        |            |                              |           |
| 10   |  |                 |                        |            |                              |           |

Fig.6 The input data for sub-ballast reinforced track.

| Remediation  |  |                 |                        |            |                              |           |
|--|--|-----------------|------------------------|------------|------------------------------|-----------|
| Name   | Description                                    | Cost (€ per km) | Delay (minutes per km) | First year | Expected life (years)        | Last year |
| 1 Ballast  | Replace ballast at end of life                 | € 171,005.00    | 0                      | 25         | 60                           |           |
| 2 Sleepers   | Replace sleepers at end of life                | € 396,005.00    | 0                      | 20         | 60                           |           |
| 3 Rails and fastening system                         | Replace rails and fastenings at end of life    | € 594,270.00    | 0                      | 30         | 60                           |           |
| 4 Electromechanical parts                            | Replace electromechanical parts at end of life | € 317.00        | 0                      | 30         | 60                           |           |
| 5 Geotextile membrane                                | Replace membrane at end of life                | € 20,000.00     | 0                      | 25         | 60                           |           |
| 6  |  |                 |                        |            |                              |           |
| 7  |  |                 |                        |            |                              |           |
| 8  |  |                 |                        |            |                              |           |
| 9  |  |                 |                        |            |                              |           |
| 10   |  |                 |                        |            |                              |           |
| Routine maintenance                                  |  |                 |                        |            |                              |           |
| Name   | Description                                    | Cost (€ per km) | Delay (minutes per km) | First year | Average frequency (per year) | Last year |
| 1 Ballast tamping and stabiliser routine maintenance |  | € 1,007.00      | 0                      | 0.75       | 60                           |           |
| 2 Rail milling                                       | Routine maintenance                            | € 3,810.00      | 0                      | 0.25       | 60                           |           |
| 3  |  |                 |                        |            |                              |           |
| 4  |  |                 |                        |            |                              |           |
| 5  |  |                 |                        |            |                              |           |
| 6  |  |                 |                        |            |                              |           |
| 7  |  |                 |                        |            |                              |           |
| 8  |  |                 |                        |            |                              |           |
| 9  |  |                 |                        |            |                              |           |
| 10   |  |                 |                        |            |                              |           |

Fig.8 The input data for double reinforced track.

## RESULTS

Life cycle cost Analyses showed a provision economically towards the choice of using geogrid under in the railway track as shown in fig.8. This has been confirmed for all the models that have been tested because the lifetime is increasing from the use of the geogrid and thus directed us to a situation that it was cheaper and extra profitable to use the geogrid reinforcement into the railway track layers. The expenses differences for the three variants and baseline variant for the railway track is shown in the net present value of the three variants is lesser than that of the baseline despite of the initial cost is higher; rising from significantly lesser rate of maintenances.

## CONCLUSION

The economical evolution indicated that the use of geogrid proved to be a feasible and cost-effective in reducing the intervals of maintenance of railway track. Despite of slightly higher initial construction cost of railway track when the geogrid used, the lifetime cost will reduced significantly As the ballast reinforced was the most effective in the reduction of total cost by(6.5%)and the sub-ballast reinforced was (4.1%) and the double reinforced was (3.73%) as compared to the unreinforced track.

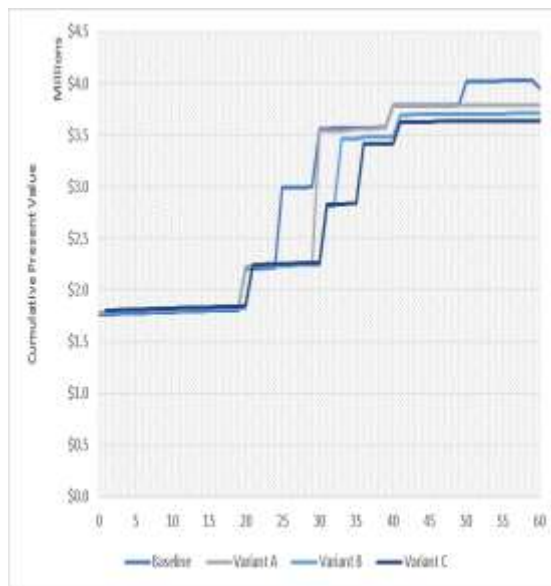


Fig.8 The Cumulative Present Value and time relationship where  
 Baseline: Unreinforced,  
 Variant A: The sub-ballast reinforced  
 Variant B: ballast reinforced  
 Variant C: double reinforced

## REFERENCES:

- [1] Federici, M., S. Ulgiati, et al. (2003). "Efficiency and sustainability indicators for passenger and commodities transportation systems. The case of Siena, Italy." *Ecological Indicators* 3: 155-169.
- [2] Paulsson B, Platzer M and Ekberg A (2006) "INNOTRACK – Innovative Track System – A unique approach of infrastructure managers and competitive track supply industry for developing the innovative products of the future", 7th World Congress on Railway Research.
- [3] European Commission (2011) "White Paper: Roadmap to a single European Transport Area – Towards a competitive and resource efficient transport system".
- [4] Hall C D and Sharpe P (2007) "Review of geogrid stabilisation of railway ballast with reference to performance and durability".
- [5] European Commission (2013) "Sustainable steel-composite bridges in built environment (SBRI)", Final Report
- [6] Parsons R., Jowkar M., Han J., 2012. Performance of Geogrid Reinforced Ballast under Dynamic Loading. Report # MATC-KU: 363, Final Report.
- [7] Tensar (2013) "Railways: Mechanical stabilization of track ballast and sub ballast", March 2013, Issue 11.
- [8] British Standards Institution (2008) BS ISO 15685-8:2008, Buildings and constructed assets – Service life planning – Part 5: Life cycle costing.
- [9] Project "Hajama – Sawa", cost estimate, Ministry of Transportation of Iraq, Iraqi Republic Railways Company.

## CHARACTERIZATION OF NEW TYPES OF GEOSYNTHETICS EMBEDDED IN SOIL USING CALIFORNIA BEARING RATIO TEST

Mohamed Eltaher<sup>1</sup>, Zakaria Hossain<sup>1</sup>, Jim Shiau<sup>2</sup>, and Hajime Takami<sup>3</sup>

<sup>1</sup>Graduate School of Bioresources, Mie University, Japan; <sup>2</sup>School of Civil Engineering and Surveying,  
University of Southern Queensland, Australia; <sup>3</sup>Tsuchiya TSCO Co., Ltd., Japan

### ABSTRACT

Characterizing of geosynthetics is essential for its effective use in various field applications of reinforced soil structures. The success of a reinforced soil structure depends very much on the type of reinforcements used. Therefore, a total of six types of geosynthetics is evaluated in this paper for its bearing capacity using the California bearing ratio (CBR) test. Based on the analyses of the experimental data, the penetration strength and the penetration displacement of specimens due to the variation of the type of geosynthetic are examined. As a result of this study, the load-penetration behavior of the backfill soil with the six types of geosynthetic shows different significant increments in the bearing capacity. It is found that in sandy soil, the embedment of a double layer of eco-friendly geogrids (GGR 1, 2) as a reinforcement displays higher bearing capacity than all the other geosynthetics. Also, geotextile (GTX 2) showed the highest bearing capacity as a single layer reinforcement. Therefore, it would be the most promising one for ground improvement compared to the rest of the tested geosynthetics in this study.

*Keywords: Geosynthetics, Sandy Soil, California Bearing Ratio Test, Bearing Capacity.*

### INTRODUCTION

Airfields, embankments, highways, and many other public facilities are mainly earth-fill structures and they must be stable under all static and dynamic loadings during construction and in-service as well [1]. Resistance to deformation under load is a core requirement of subgrade soils and that is why the strong subgrade soil can reduce the cost of the airfield or highway construction.

Additionally, the required thickness of a flexible pavement using reinforced subgrade (which could be complex depending on the nature and properties of the reinforcement) can be reduced as compared to weaker subgrades [2]. Therefore, this will result in a significant cost saving advantage due to resource-saving and durability [3,4,5]. This is the reason that reinforcing the soft soil using various types of geosynthetics is a well-known technique to improve the ground performance, enhance its bearing capacity and reducing the settlements.

The strength and performance of subgrade soils, sub-base, and base course material for the design of the pavement thickness are widely evaluated by using the California bearing ratio (CBR) test which often forms the basis of pavement design. For this reason, it finds favor with some design and control methods.

Several researchers investigated the bearing capacity of soils reinforced with geosynthetics using the CBR test. They used various types of geosynthetic materials i.e. polypropylene (PP), High-density polyethylene (HDPE), Polyester (PET) yarns, etc. [4]

The present study dealt with new types of

geosynthetics which are made from basalt and plastic fibers. A series of CBR tests on the geosynthetic embedded inside one type of backfill soil have been conducted. Based on the test results, the load-penetration behavior of the reinforced subgrade soil along with different mechanical characteristics has been evaluated and discussed shortly.

### PURPOSE OF THE STUDY

1. To investigate the influence of embedding of new types of basalt and plastic geosynthetics in the effective embedding position(s) of one backfill soil on bearing capacity behavior, through a series of CBR tests.
2. Evaluating load-penetration behavior and soil-geosynthetics California bearing ratio.
3. Characterizing of new geosynthetics.

### MATERIALS AND METHODS

#### Backfill Material

In this study, one type of soil collected from Handa area, Tsu City, Mie Prefecture, Japan was used as backfill material in combination with different geosynthetic materials to evaluate its bearing behavior.

According to the Japanese Geotechnical Society engineering classification system (JGS), this soil is classified as SF (sandy soil). The gradation curve and the major physical properties of this soil are addressed by Eltaher 2019. [5].



## Geosynthetic Materials

The woven and nonwoven geosynthetics used in this study are made of basalt fiber and provided by Tsuchiya TSCO Co., Ltd. The chemical composition and basic characteristics of basalt fiber used for manufacturing these geosynthetics are discussed in detail in another research on the influence of embedding position on the performance of basalt geosynthetics which had been conducted in early 2019 by same authors [5,6]. Also, another geosynthetic made of plastic fiber has been used in this study.

Totally, six types of geosynthetics have been used, two woven basalt fiber geotextiles, one nonwoven basalt fiber geotextile (with soft texture), two woven basalt fiber geogrids (with stiff texture), and one plastic fiber geomat. For the purpose of discussion, the geotextiles are noted as GTX1,2,3, the geogrids are noted as GGR1,2 and the geomat is noted as GMA respectively as shown in Fig. 1.

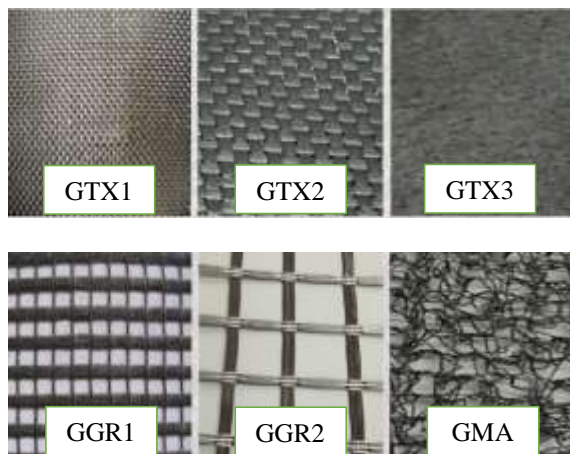
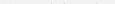
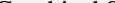
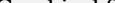


Fig. 1 Types of the six geosynthetics used

For convenience in drawing CBR specimens, the used geosynthetic products were represented by abbreviations and graphical symbols and described in table 1 as recommended by the International Geosynthetics Society (IGS) [7].

Table 1. Abbreviations and graphical symbols of the used geotextile, geogrid, and geomat products

| Abbrev. | Product    | Graphical Symbol  |
|---------|------------|---|
| GTX     | Geotextile |  |
| GGR     | Geogrid    |  |
| GMA     | Geomat     |  |

## CBR Test Apparatus and Equipment

In this research, many tools have been used e.g. CBR stainless steel Mold, and CBR penetration testing machine, etc.

For the convenience of the readers, the important components of the CBR penetration testing machine shown in Fig. 5 are numbered numerically. Additionally, the complete used set of equipment, tools, and its specifications are listed and described by Eltaher 2019 [5].

### CBR Specimen's Preparation

In the beginning, the CBR control specimen (soil only specimen) as shown in Fig. 2 was prepared in the CBR mold.

To prepare the control specimen layers, soil and water (12% of the soil weight) were mixed homogeneously. Then the soil was added into the mold after it had been assembled with the perforated bottom plate, spacer disc, and mold extension. The soil had been added into the mold in three layers and tamped uniformly 67 times per layer using a manual hammer.

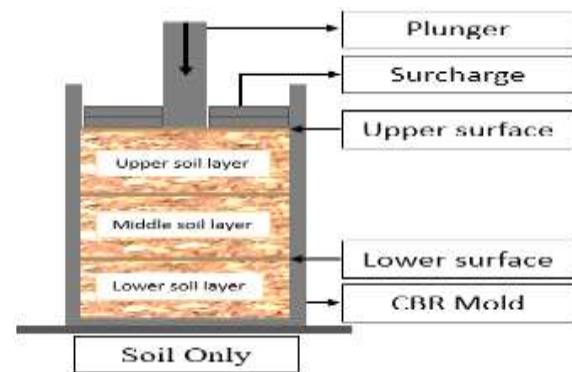


Fig. 2 Typical schematic diagram of CBR control specimen using a divided three layers of soil only with an indication of the surface of layers where geosynthetic(s) will be laid on in the test specimens.

For the preparation of CBR test specimens, in the same way, the mold had been assembled, then the wet soil sample was poured into it. The wet soil sample was divided into three layers then tamped uniformly 67 times per layer. Considering that in these CBR test specimens, the surface of each soil layer was leveled precisely and geosynthetic(s) of the same diameter of the mold was/were laid on the surface of the chosen soil layer(s) which had been tamped before to achieve the best reinforcement and highest CBR value resulting in two patterns of CBR test specimens with a total number of six specimens according to the position and the type of the geosynthetics used.

The two patterns of the CBR test specimens were classified into two groups, in which the first group (pattern I) contained three specimens of one geotextile layer laid on the surface of the lower soil layer (lower GTX 1, lower GTX 2, and lower GTX 3) as shown in Fig. 3, while the second group (pattern II) contained three specimens of two geosynthetic

layers laid on the surfaces of the upper and the lower soil layers (upper and lower GGR 1, upper and lower GGR 2, and upper and lower GMA) as shown in Fig.4.

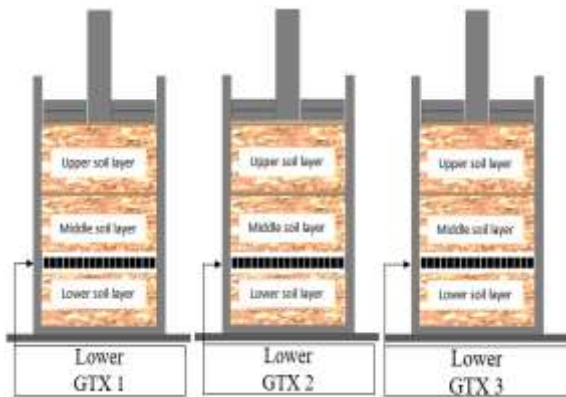


Fig. 3 Pattern I: three different CBR test specimens of one geotextile layer embedded on the surface of the lower layer of compacted soil using three different geotextiles (GTX1, GTX2, and GTX3)

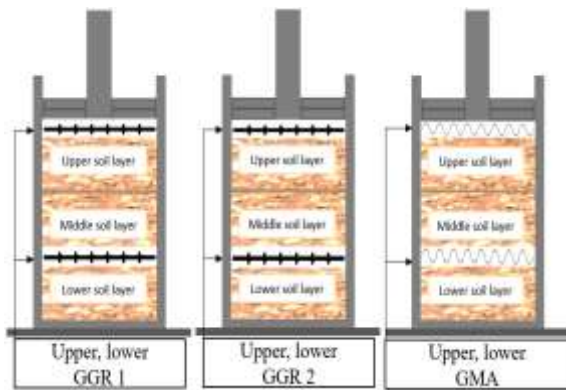


Fig. 4 pattern II: three different CBR test specimens of two geosynthetic layers embedded on the surfaces of upper- and lower-layers of compacted soil using three different geosynthetics (GGR1, GGR2, and GMA)

### CBR Test Setup and Procedures

In 1930 the California Division of highways, USA invented the California Bearing Ratio (CBR) test and it has been widely used all over the world to evaluate the bearing capacity of soils and subgrades since its invention [8]. And in this research, the CBR test was performed as follows:

After the specimen had been set up in the mold then the specimen is placed on the top board of the CBR apparatus jack (No.7, Fig. 5). The tests were conducted.

While operating the CBR testing machine, the load (pounds) was measured using proving ring dial gauge (No.2, Fig. 5) versus depth of penetration (inches) of the piston as it is being pushed into the soil was recorded using penetration measuring dial gauge

(No.6, Fig. 5) considering the penetration depths of 0.5 mm, 1.0 mm, 1.5 mm, 2.0 mm, 2.5 mm, 3.0 mm, 4.0 mm, 5.0 mm, 7.5 mm, 10.0 mm, and 12.5 mm.

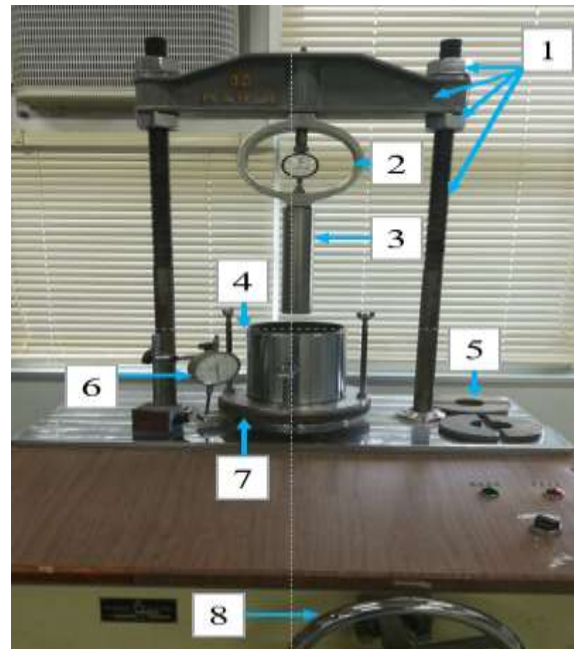


Fig. 5 CBR testing machine and its components

Then the stress (psi) on the piston by dividing the load by the area of the piston was calculated. And a graph for the stress (psi) or load (kN) versus the depth of penetration (inches) relationship was plotted.

The bearing value is the stress (psi) corresponding to a depth of penetration of the piston of 0.10 in. (2.54mm). This bearing value is converted to a ratio by dividing it by 1000 psi, which represents the penetration resistance of compacted standard crushed rock. This bearing ratio, which is a fraction, is multiplied by 100 and reported as the California Bearing Ratio [9].

In this study, the CBR tests were carried out for one control specimen and six test specimens with their repetitions.

The loads were recorded up to a penetration depth of 12.5 mm according to the Japanese Industrial Standards (JIS-A-1211) [10] and the CBR value was calculated according to the following equation:

$$CBR \% = \frac{\text{Load Strength}}{\text{Standard Load Strength}} \times 100 \quad (1)$$

### RESULTS AND DISCUSSION

In the present investigation, six types of new geosynthetics (three basalt geotextiles (GTX1,2,3), two basalt geogrids (GGR1,2), and one plastic geomat (GMA)) were embedded inside soil layers with the purpose of reinforcing the subgrade soil. The CBR test was used for evaluation of the performance

of the non-reinforced and reinforced subgrade specimens. A high CBR value indicates the excellent quality of the material, although other relevant parameters may be necessary to re-confirm the material's performance. Typical CBR values range from less than 5 for soft clays up to 80 for dense sandy gravel as shown in table 2 [11,12].

Table 2. CBR values for soils by the unified soil classification system (USCS) [11].

| Soil type            |                                       | Field CBR value |       |
|----------------------|---------------------------------------|-----------------|-------|
| Coarse-grained soils | Gravel and gravelly soils             | GW              | 60-80 |
|                      |                                       | GP              | 35-60 |
|                      |                                       | GU              | 25-50 |
|                      |                                       | GM              | 40-80 |
|                      |                                       | GC              | 20-40 |
|                      | Sand and sandy soils                  | SW              | 20-40 |
|                      |                                       | SP              | 15-25 |
|                      |                                       | SU              | 10-20 |
|                      |                                       | SM              | 20-40 |
|                      |                                       | SC              | 10-20 |
| Fine-grained soils   | Low compressibility soils<br>LL < 50  | ML              | 5-15  |
|                      |                                       | CL              | 5-15  |
|                      |                                       | OL              | 4-8   |
|                      | High compressibility soils<br>LL > 50 | MH              | 4-8   |
|                      |                                       | CH              | 3-5   |
|                      |                                       | OH              | 3-5   |

As a result of the research on the influence of the embedding position of geotextile and geogrid (GTX1 and GGR1) inside same backfill soil on the CBR value conducted by Eltaher in 2019, it was found that there are effective embedment positions according to the geosynthetic type to increase the bearing capacity to its highest values [5].

Also, Eltaher found that the CBR value for the control specimen (soil only) was 47.93% and it was observed that while using the geogrid type, the highest CBR value (74.61%) was reached by using double layers of GGR1 on the upper-lower layers and while using the geotextile type, the highest CBR value (59.28%) was obtained by using the subgrade soil reinforced with one-layer of GTX1 on the lower soil layer [5].

Considering these results [5], only the most effective position patterns for using geotextiles and geogrids to reinforce the subgrade soil as shown in Fig. 6 were selected in this research for characterizing the new geosynthetics (GTX 1, 2, 3, GGR 1, 2 and GMA). Therefore, two-position patterns forming six different CBR test specimens of subgrade soil reinforced with different geosynthetics were tested in this study to understand their performance response.

Therefore, the types of test specimens in the present study were classified into two groups according to the effective embedding position pattern.

In the first group (pattern I) which contains three specimens, only one layer of geotextile product was embedded inside the subgrade soil layers forming three different specimens according to the used geotextile type which were GTX1, GTX2, and GTX3 on the surface of the lower layer of the subgrade soil as shown in Fig. 3.

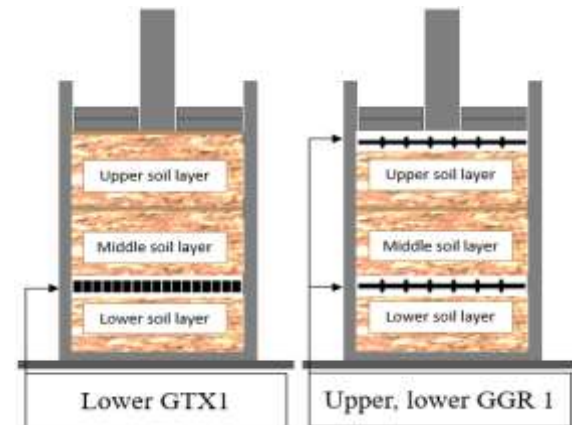


Fig. 6 The most effective position patterns for using geotextiles and geogrids to reinforce the subgrade soil respectively [5].

On the other hand, also the second group (pattern II) contained three test specimens but in which a combined layer of geosynthetics (geogrid or geomat) was embedded inside the subgrade soil layers forming three different specimens according to the used geosynthetic type which were GGR1, GGR2, and GMA on surfaces of upper and on lower layers of the subgrade soil as shown in Fig. 4.

The results for the effects of different geosynthetic types embedded in the effective depths of soil are depicted and a discussion comparing the results with the control specimen is presented.

#### Influence of Embedding Different Geosynthetics Inside Subgrade Soil on CBR Value

A series of CBR tests were conducted to obtain the load-penetration relationship of CBR control and test specimens to understand the Influence of geosynthetic type embedded in the effective position inside subgrade soil on the CBR value.

##### *Influence of reinforcing the subgrade soil with one layer of basalt GTX1,2, or 3*

The CBR test results for the subgrade soil control and test specimens containing one layer of basalt GTX 1, GTX 2, and GTX 3 on the lower soil layer all together are shown in Fig. 7.

From this figure, it can be seen that all curves follow a typical trend of a CBR test. Also, the results of the test specimens especially the woven geotextile



GTX1 and GTX2 display higher trends before and after penetration depth of 2.5 mm than the control specimen.

The calculated CBR test values for penetration depths of 2.5 mm in the subgrade soil reinforced with one layer of GTX1,2, and 3 are given in table 3. From this table, it can be observed that the CBR values increase significantly while using GTX1,2, and 3 on the lower soil layer. As in the GTX2 case, the supporting force was maximized. The CBR values for subgrade soil reinforced with one layer of GTX1, GTX2, and GTX3 on the lower soil layer are 59.28, 69.69, and 64.08% respectively.

The CBR value of the control specimen (soil only) in this research is 47.93%. This means that CBR values can approximately 45.4% higher be achieved by embedding the GTX 2 on the lower subgrade soil layer compared to the CBR value of the control.

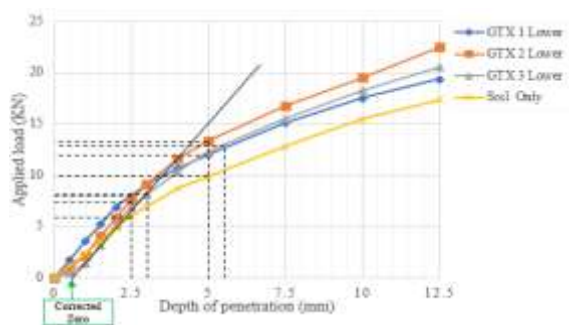


Fig. 7 Load penetration curves of control specimen and three subgrade soil test specimens containing one layer of basalt GTX 1, GTX 2, and GTX 3 respectively on the surface of the lower soil layer.

Also, it is noticed that the stiffer the geotextile (as the used woven GTX2), the higher the bearing capacity and the CBR value increases drastically. In contrast, the softer the geotextile (as the used nonwoven GTX3), the lower the increment in the bearing capacity and therefore the CBR value increases slightly.

#### *Influence of reinforcing the subgrade soil with two layers of GGR1,2, or GMA*

In addition to the CBR control specimen curve, three load-penetration curves obtained from the CBR tests of the three subgrade test specimens containing two layers of geosynthetic in which three different geosynthetics (GGR1, GGR2, and GMA) were laid on the upper and lower soil layers are shown in Fig.8.

The CBR curves for the GGR 1, 2 and GMA double layer in subgrade soil are more pronounced in comparison to the previous group of single layer GTX. It is evident that the penetration load increased for this case.

The CBR values for the penetration depth of 2.5mm penetration are shown in table 3. In

comparison to the previous group (Pattern I) of one layer of geosynthetic (GTX1,2,3), the current CBR results show higher increments especially while using planner products (GGR1 and GGR2) on the upper-lower layers. The CBR values for a penetration depth of 2.5 mm for subgrade double layers of GGR1, GGR2, and GMA upper-lower are 74.61, 71.69 and, 66.94% respectively.

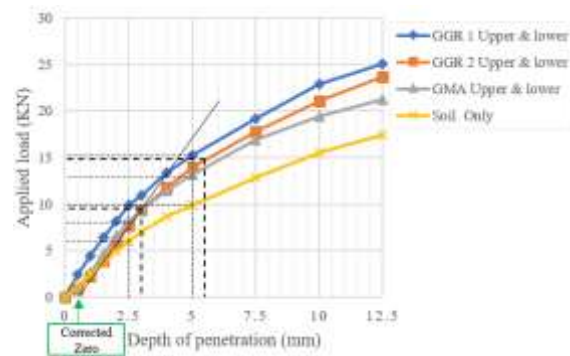


Fig. 8 Load penetration curves of control specimen and three subgrade soil test specimens containing two layers of GGR1, GGR2, and GMA respectively on the surfaces of the upper and lower soil layers

Although GGR 2 is stiffer than GGR 1 which may indicate that GGR 2 might raise the CBR value higher than GGR 1 would do, it is found that the smaller the geogrid apertures (as in the used woven GGR1), the higher the bearing capacity and the CBR value increases drastically. In contrast, the wider the geogrid apertures (as in the used woven GGR2), the lower the increment in the bearing capacity.

Table 3 summarizes the CBR values of control and test specimens with various types of geosynthetics. It shows that embedding the eco-friendly basalt geosynthetic (geogrid and geotextile) and also the plastic geomat inside the subgrade soil at the effective positions has a significant effect on improving the CBR value.

Table 3 CBR values of subgrade soil specimen types

| Specimen type<br>or<br>layering pattern |               |       | CBR<br>Value<br>% |
|---|---------------|-------|-------------------|
| One layer<br>test<br>specimen           | Lower         | GTX 1 | 59.28             |
|   |               | GTX 2 | 69.69             |
|   |               | GTX 3 | 64.08             |
| Two layers<br>test<br>specimen          | Upper & lower | GGR 1 | 74.61             |
|   |               | GGR 2 | 71.69             |
|   |               | GMA   | 66.94             |
| Control specimen (soil only)            |               |       | 47.93             |

Table 3 could be illustrated by a bar graph to compare the difference in the CBR values depending on the geosynthetic type and layering pattern inside

the subgrade soil where the CBR value is plotted on the vertical axis and the specimen type is plotted on the horizontal axis. see Fig. 9.

From Fig. 9, it can be seen that the CBR value of one layer of GTX1 embedded on the lower subgrade soil layer specimen has the lowest value, whilst the specimen of GTX2 flattened on the lower subgrade soil layer has the highest CBR value among the one-layer GTX pattern. At one-layer geotextile embedment in the subgrade soil, the maximum increment in the CBR value was 45.4% in the woven black geotextile GTX2 lower layer case.

On the other hand, changing the one-layer GTX pattern into two layers of GGR or GMA pattern alters the behavior of the ground conspicuously. It is observed that the GGR1 upper-lower double layer in the subgrade soil gave the highest CBR value compared to the other two double-layer cases, whilst the GMA upper-lower double-layer showed the lowest CBR value in this pattern. In the two layers geosynthetic embedment case, the maximum increment in the CBR value was 55.7% in the woven basalt geogrid 1 upper lower layers case.

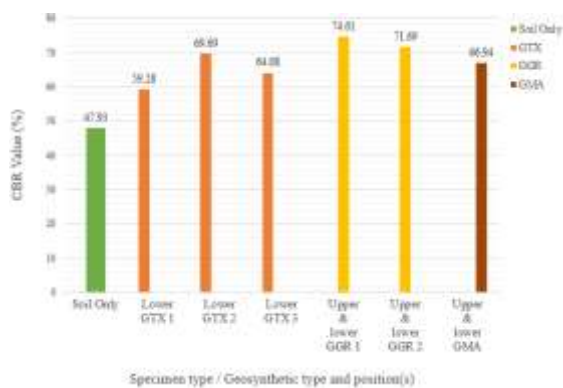


Fig. 9 Comparison between CBR values of control and test specimens.

It was interesting to note that the geosynthetics (GGR1,2, or GMA) double layers embedded inside the subgrade soil layers are not as beneficial as originally expected when compared to a single GTX2 lower layer. Indicating that there is no benefit in using a double GGR1, 2, or GMA layer for the purpose of subgrade soil reinforcement in constructions. In general, even though the double layer gives the highest CBR values, the single layer is more effective and recommended for field application due to economic reasons where it has the benefit on the budgeting aspect for design and construction.

## CONCLUSIONS

Based on the above study, it can be concluded that embedding of these new types of eco-friendly basalt geotextiles, geogrids and the plastic geomat inside the

subgrade soil layers has a significant effect on improving the CBR value. Since it was found that the CBR value increases by a range from 24 to 55 % from the CBR value of the control specimen according to the used geosynthetic type.

It could also be concluded that there are effective embedment positions for these geosynthetics according to its type to increase the bearing capacity where the highest CBR value (74.61%) was reached by using double layer of GGR1 on the upper-lower layers and the lowest CBR value (59.28%) was obtained by using the subgrade soil reinforced with one-layer of GTX1 on the lower soil layer. It was also interesting to note that the double geosynthetic layers patterns are not as beneficial as originally expected when compared to a single lower layer in the case of using GTX2. This conclusion has certain economic implications for optimizing design and construction using these new geosynthetics.

Practically and economically, it is recommended to use the pattern of the GTX2 lower layer for the field application. Even though the GGR1 two layers upper-lower pattern gives the highest CBR value, the GTX2 lower layer is more effective for field application due to materials supplied and economic reasons. It has a benefit on the budgeting aspect for design and construction when using this geosynthetic.

## ACKNOWLEDGMENTS

Thanks to Japan International Cooperation Agency (JICA), for collaboration with International Environment Conservation Lab, Graduate School of Bioresources, Mie University, School of Civil Engineering and Surveying, University of Southern Queensland, and Tsuchiya TSCO Co., Ltd. for the opportunity which they gave me to proceed in this research.

## REFERENCES

- [1] Hossain M.B., Sakai T., and Hossain M.Z., Evaluation of Sand/Geosynthetic Interface Behavior for Earth Reinforcement. *International Journal of Geosciences Engineering*, Vol. 7, No.3, 2013, pp.452-465.
- [2] Shukla, S.K., Discussion of Applications of geosynthetics for soil reinforcement by M.I.M. Pinto, *Ground Improvement*, 7, 2004, pp. 61-72.
- [3] Choudhary A.K., Jha J.N., and Gill K.S., A Study on CBR Behavior of Waste Plastic Strip Reinforced Soil. *Emirates Journal for Engineering Research*, 15 (1), 2010, pp.51-57.
- [4] Eltaher M., Hossain M.Z., Shiao J., and Takami H., Ground Improvement Using Geosynthetics A Literature Review. *Proceedings of the 5th International Conference on Science, Engineering & Environment (SEE)*, Bangkok, 11-13 November 2019, an accepted paper.

- [5] Eltaher M., Hossain M.Z., Shiao J., and Takami H., Influence of Embedding Position on The Performance of The Basalt Geosynthetics. Proceedings of the 9th International Conference on Geotechnique, Construction Materials and Environment (GEOMATE), Tokyo, 20-22 November 2019, an accepted paper.
- [6] Basalt Fiber Products Report, Tsuchiya TESCO Co., Ltd., 2nd Ed., 2018, pp. 1-15.
- [7] Recommended Descriptions of Geosynthetics Functions, Geosynthetics Terminology, and Graphical Symbols, International Geosynthetics Society, 5th Ed. 2009, pp. 1-31.
- [8] Hossain M.Z., and Sakai T., The Effectiveness of Nominal Dosage of Ordinary Cement on Strength and permeability of Clay Soil, Journal of Japanese Society of Soil Physics, No.110, 2008, pp.25-35.
- [9] Yildirim B. and Gunaydin O., Estimation of California Bearing Ratio by Using Soft Computing Systems, Journal of Expert Systems with Applications, Vol.38, 2011, pp: 6381-6391.
- [10] Test Method for the California Bearing Ratio CBR of Soils in Laboratory, Japan Industrial Standards Committee (JIS-A-1211), 2009.
- [11] Yoder E. J., and Witczak M.W., Principles of Pavement Design. John Wiley and Sons, Inc. 2<sup>nd</sup> Ed., 1975.
- [12] Ekeocha N.E., and Egesi N., Evaluation of Subgrade Soils using California Bearing Ratio (CBR) in Parts of Rivers State, Journal of Applied Sciences Environmental Management, Vol.18, 2, 2014, pp.185-187.



## *Environment*

# A STUDY ON HUMAN DAMAGE IN EVACUATION FROM TSUNAMI CONSIDERING STREET-BLOCKADES CAUSED BY DESTROY OF BUILDINGS

Ken-ichi Fujita<sup>1</sup>, Harumi Yashiro<sup>2</sup>

<sup>1</sup> Faculty of Engineering, Nagasaki Institute of Applied Science, Japan;

<sup>2</sup> School of Systems Engineering, National Defense Academy, Japan

## ABSTRACT

Damage estimation and disaster prevention plan for a Nankai megathrust earthquake which occurrence is assumed in the future have been formulated cabinet office of Japan based on lesson learned from the huge human damage caused by the tsunami of The Great East Japan Earthquake in 2011. Damage estimation for earthquake and tsunami is usually evaluated independently. For the damage estimation by tsunami, the human damage in evacuation from tsunami has been carried out. However, any street-blockades have not been considered. When evacuation routes are changed by the street-blockades, configuration of the human damage in evacuation from tsunami seems to be different in no street-blockades. This study presents an evaluation method of human damage in evacuation from tsunami considering street-blockades using area-wide mesh. The author's method considering variances of tsunami run-up speed and walking speed is used to the evaluation. Moreover, the difference in configuration of the human damage by consider the street-blockades and no blockades is discussed.

*Keywords: Tsunami evacuation, Human damage, Street-blockade, Human damage probability, Area-wide mesh*

## INTRODUCTION

In disaster prevention planning for large scaled natural disasters such as mega-class earthquake, tsunami and eruption, estimation of buildings damage and human damage is extremely important. Damage estimation for the natural disaster in cabinet office and local governments of Japan has been usually evaluated independently for each disaster [1], [2]. Using the damage estimation results, disaster prevention planning for both structural measures and non-structural measures are projected.

The disaster prevention planning for tsunami are as follows; construction of tide embankment, relocation to higher ground of town, education on evacuation and so on. Evacuation planning from tsunami is especially important item for tsunami disaster prevention. Evaluation of human damage for tsunami is carried out for evacuation action to safety area. In evaluation of the human damage, difference between evacuation time and tsunami arriving time to evacuation facilities is usually used. In evaluating of human damage in evacuation from tsunami, the effect of damage of buildings by earthquake before arriving tsunami has not been considered in many studies and damage estimation. In evacuation planning from tsunami, to consider street-blockade by destroy of buildings, fallen down of street walls and fire caused by large earthquakes becomes important. Street-blockade has been considered to lifesaving activities and fire-fighting in the disaster estimation for large earthquakes [3]. When street-blockades are caused change of evacuation routes, configuration of the

human damage in evacuation from a tsunami seems to be different in no street-blockades.

This study presents an evaluation method of human damage in evacuation from tsunami considering street-blockades by destroy of buildings. Area-wide mesh is used to the evaluation of the human damage. The author's method [4]-[6] for the human damage taking account of variances of tsunami run-up speed and walking speed is also used to the evaluation considering the street-blockades. Moreover, the difference in configuration of the human damage between the street-blockades and no street-blockades by using the evaluation method.

## EVALUATION FLOW OF HUMAN DAMAGE

The area-wide mesh is used to the evaluation of the human damage. Population composition, height above sea level, tsunami inundation depth, seismic intensity, street-blockade ratio, and evacuation awareness are set up for each mesh based on a real area data. The population composition and the height above sea level of GIS (Geographic Information System) data are used.

Evacuation route from an evacuation mesh to an evacuation facility is defined as the route along the mesh. Evacuation distance including difference of elevation between mesh is assumed to be 1.5 times of length of plane distance. The human damage probability is evaluated by using relation between evacuation time and tsunami arriving time after earthquake occurrence. The human damage ratio to

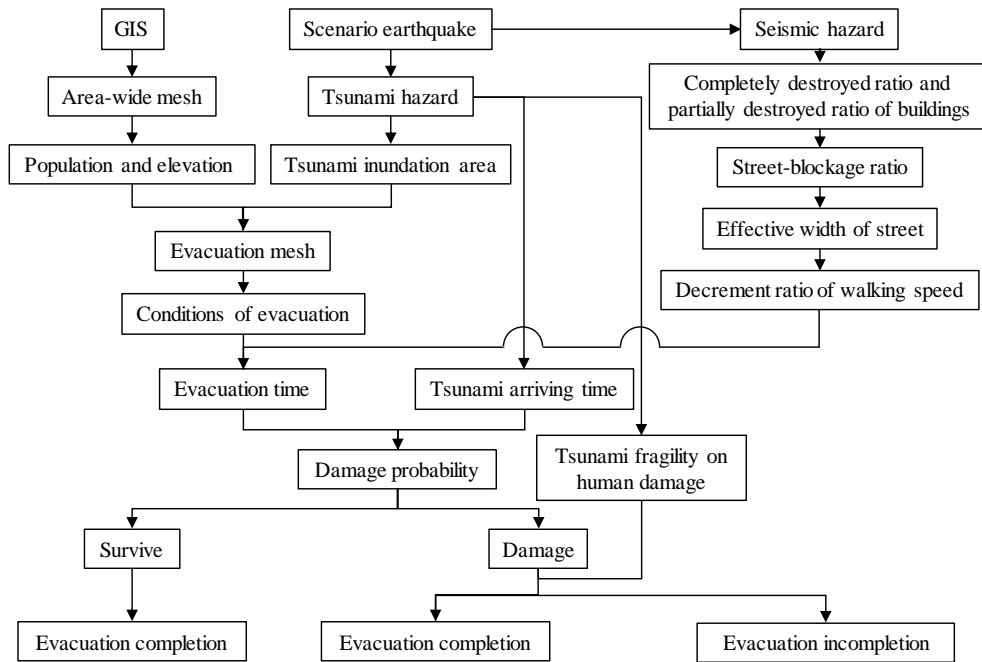


Fig.1 Evaluation flow of human damage in evacuation from tsunami

tsunami inundation depth in each mesh can be obtained by the tsunami fragility curve [7]. The street-blockade is evaluated by the fragility of buildings for earthquakes [8]. Decrement of the walking speed is determined by effective sidewalk width which passing is possible. From the above, the evaluation flow on the human damage can be shown in Figure 1.

The following assumptions are used in this study.

- 1) The human damage is counted when a person is caught up with tsunami.
- 2) The evacuation is only walk. The walking is only permitted on sidewalk.
- 3) The evacuation facility is designated for each evacuation mesh. The facilities are not damaged to earthquakes.
- 4) The street-blockades are occurred by destroy of buildings by large earthquakes
- 5) The evacuation direction is not toward to coast.
- 6) In emergency, to across any railroad crossing is prohibited because crossing gates keeps down.

## HUMAN DAMAGE PROBABILITY

### Damage Probability of Human in Evacuation

The human damage probability is evaluated by the Author's method [5], [6]. The probability is defined by a function of evacuation time and tsunami arriving time after earthquake occurrence. The evacuation time and the tsunami run-up time from coast to evacuation facilities are assumed to follow the normal distribution. The tsunami arriving time is divided into the time of tsunami propagation and run-up. The evacuation time and the tsunami run-up time can be evaluated from walking speed and tsunami

run-up speed, respectively. The variation of the tsunami run-up speed is considered for evaluation of the tsunami arriving time. The tsunami run-up time can be obtained by the relation of the run-up speed and the minimum distance between coast and evacuation facilities. The mean value of the run-up speed can be determined by the tsunami inundation depth [9]. Average tsunami inundation depth from the coast to the evacuation facilities is considered in this study. The standard deviation of the run-up speed is evaluated by the geometric standard deviation [10] which indicates the adaptation between tsunami height marks on land and tsunami simulation results.

In this study, the reliability evaluation method for structures [11] applied to the evaluation of the human damage. The evaluation equation of the human damage can be provided the following equation.

$$P_R = 1 - \Phi(\mu_P / \sigma_P) \quad (1)$$

where,  $\Phi$  is the standard normal distribution function with the mean value 0 and the standard deviation 1. The function of  $\Phi$  is also shown in Figure 2.  $\mu_P$  and  $\sigma_P$  are provided by the following equations, respectively;

$$\mu_P = \mu_T - \mu_E \quad (2)$$

$$\sigma_P = \sqrt{\sigma_T^2 + \sigma_E^2} \quad (3)$$

where,  $\mu_E$  and  $\mu_T$  are the mean value of total evacuation time and the tsunami arriving time to evacuation facilities after earthquake, respectively,  $\sigma_E$  and  $\sigma_T$  are the standard deviation of  $\mu_E$  and  $\mu_T$ , respectively.

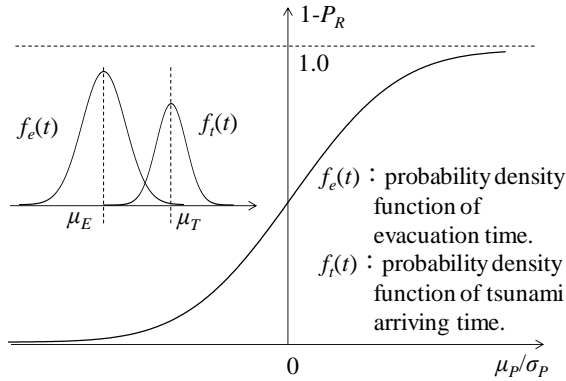


Fig.2 Probability function of human damage

### Street-Blockage by Destroy of Buildings

In this study, the street-blockage is assumed to be caused by completely destruction and partial destruction of buildings. The destroy ratio can be obtained by using fragility of buildings for wooden and non-wooden structures shown in Figure 3 [8]. The partial destruction ratio is also obtained by a difference completely destruction number and partial destruction number of buildings. The street-blockage ratio is evaluated for each mesh by using the completely and partially destruction ratios. Effective sidewalk width  $W_{es}$  by the street-blockage of each mesh can be obtained from the following equation;

$$W_{es} = (1 - R_d)W_s \quad (4)$$

where,  $W_s$  is the sidewalk width in normal period,  $R_d$  is the street-blockage ratio which given for range of  $W_s$  represented by the following equation;

$$R_d = \begin{cases} 1.28D_{rb} & (W_s < 3m) \\ 0.604D_{rb} & (3m \leq W_s < 5.5m) \\ 0.194D_{rb} & (5.5m < W_s \leq 13m) \end{cases} \quad (5)$$

where,  $D_{rb}$  is the destruction ratio represented by the following equation [3];

$$D_{rb} = D_c + D_p / 2 \quad (6)$$

where,  $D_c$  and  $D_p$  are the completely and partially destruction ratio of buildings, respectively.

Deterioration of the walking speed is assumed to be proportional to the effective width. The deterioration ratio of the speed maybe expressed by using consideration of the decrement ratio of walking speed of crowded with people [12]. In this study, the sidewalk width is assumed to be proportional to the crowded with people per area. In evacuation, no deterioration of the walking speed is considered for  $W_{es}$  more than 1.5m, the speed is linearly deteriorated with proportional to  $W_{es}$  within 0.5m to 1.5m and

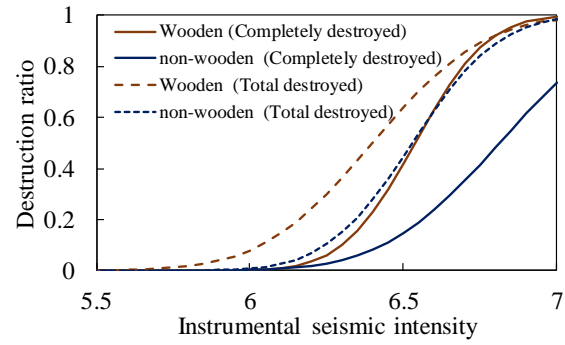


Fig.3 Fragility curves of buildings [8]

impassable for less than 0.5m. The Deterioration ratio  $R_w$  may be evaluated by the following equation;

$$R_w = \begin{cases} 1.0 & (1.5m < W_{es}) \\ 0.8W_{es} - 0.2 & (0.5m \leq W_{es} < 1.5m) \\ 0 & (W_{es} < 0.5m) \end{cases} \quad (7)$$

The walking speed in evacuation is evaluated by multiplying  $R_w$  the walking speed in normal period.

## EVALUATION OF HUMAN DAMAGE

### Evaluation Conditions

The human damage in evacuation from tsunami using the method in this study is discussed under conditions of street-blockage and no street-blockage. The area-wide mesh and population distribution of target area [13] is shown in Figure 4. The mesh size is 250m x 250m and the population is 23,345.

Tsunami inundation depth and seismic intensity used in this study are based on a Meio type scenario earthquake (moment magnitude scale,  $M_w$  8.4) and a scenario earthquake along the Miura peninsula faults ( $M_w$  7.0), respectively. To investigate the maximum case of the human damages considered the effect of the street-blockage, two types scenario earthquakes which are the maximum case of the damage

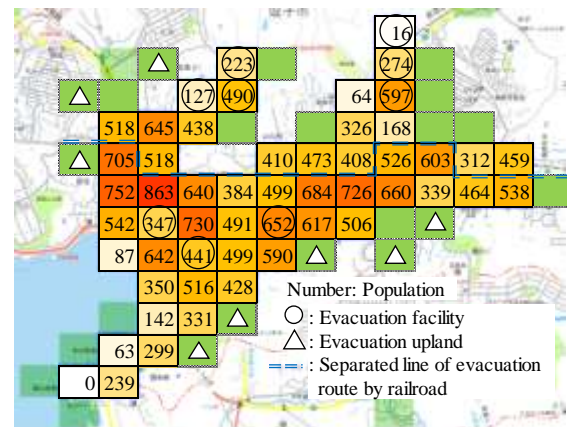


Fig.4 Area-wide mesh

Table 1 Population ratio for evacuation awareness

| Evacuation awareness | Evacuation immediately                 |                                | Urgency evacuation<br>(Weak awareness) | No evacuation<br>(Weak awareness) |
|----------------------|--|--------------------------------|--|-----------------------------------|
|                      | after earthquake<br>(Strong awareness) | after work<br>(Weak awareness) |  |                                   |
| Strong               | 80%                                    | 10%                            | 5%                                     | 5%                                |
| Average              | 50%                                    | 25%                            | 15%                                    | 10%                               |
| Weak                 | 15%                                    | 35%                            | 30%                                    | 20%                               |

Table 2 Start time of evacuation after earthquake occurrence

| Evacuation immediately after an earthquake | Evacuation immediately after finished the | Urgency evacuation    |
|--|---|-----------------------|
| 5 (min.)                                   | 15 (min.)                                 | tsunami arriving time |

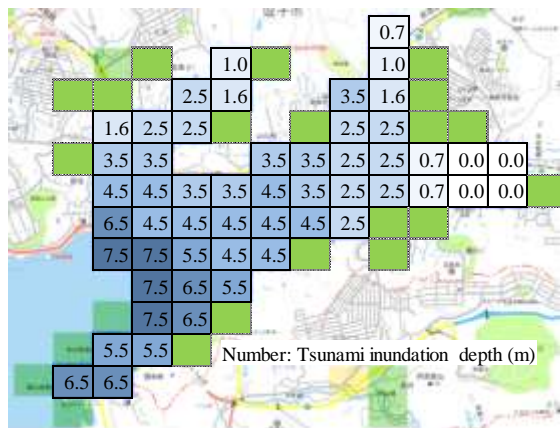


Fig.5 Tsunami inundation depth

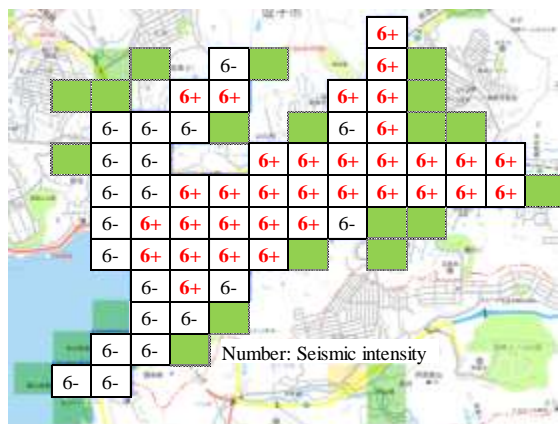


Fig.6 Seismic intensity

estimation in the target area [13] is selected. Tsunami inundation depth and seismic intensity are shown in Figures 5 and 6, respectively. The maximum tsunami height is 8.94m. Though tsunami arriving time to coast is 59 minute [13], to clear the difference of evacuation awareness, tsunami arriving time in this study is set to 20 minute.

Buildings and roads are uniformly allocated to each mesh because of the evaluation to be simplification. Total number of buildings in the area is 9,256 (wooden: 6,664, non-wooden: 2,592). Road area including sidewalk per mesh is 7,375m<sup>2</sup> which is 11.8% of one mesh area.

Population ratio of the evacuation activity is divided into four type; evacuation immediately, evacuation after work, urgency evacuation and no evacuation [14]. The population ratio is set up by combining the following three types evacuation awareness; strong awareness, average awareness and weak awareness. The evacuation awareness and the start time of evacuation after earthquake occurrence are shown in Tables 1 and 2, respectively.

The mean value and standard deviation of walking speed is 1.34m/s and 0.167m/s in normal period [15]. In addition, the mean value is deteriorated by the effect of the street-blockade and the standard deviation is assumed to be not variable for the blockade in this study.

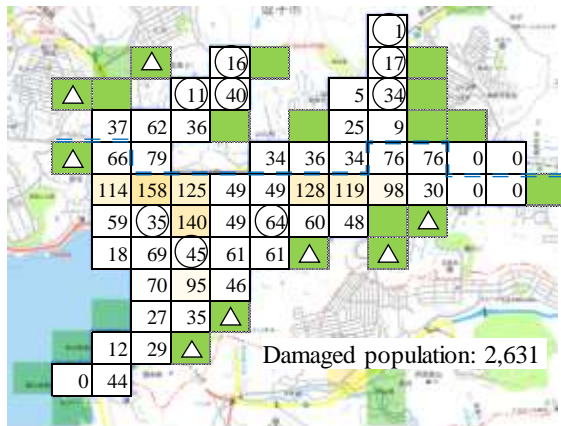
### Evaluation Results without Street-Blockage

The human damage for several evacuation awareness under no street-blockade condition is shown in Figure 7. The large number of the damage is also shown with deep color. The number of the damage with the strong awareness is the minimum. The damage near the evacuation area is less than that of the other mesh. The damage on mesh of the coast and the railroad crossing becomes large.

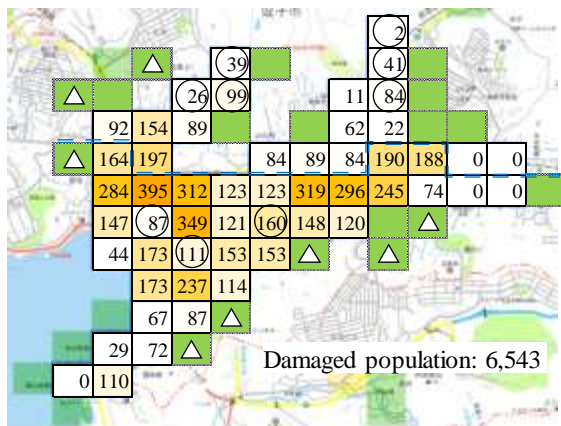
The number of the human damage is shown in Table 3. The human damage with the strong awareness decreased to 22% of the damage with the weak awareness. The evacuation awareness is large influence to decrease the human damage.

### Evaluation Results with Street-Blockage

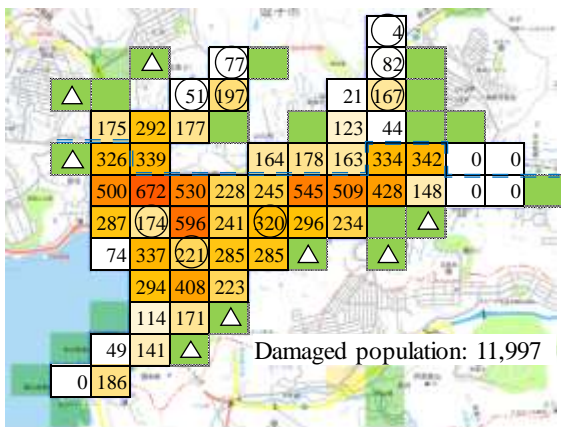
The street-blockages ratio by destroyed of buildings is shown in Figure 8 The ratio becomes large for strong seismic intensity. In addition, the numbers of destroyed buildings simulated in this study are 1,801 for completely destroyed and 1,114 for partially destroyed. The decrement ratio of the walking speed by the blockade is shown in Figure 9 The number shown in the figure represents the destined walking speed ratio for each evacuation



(a) Strong awareness



(b) Middle awareness



(c) Weak awareness

Fig.8 Human damage distribution without street-blockade

mesh population. The ratio is variable with the scale of the blockades.

The human damage for several evacuation awareness under street-blockade condition is shown in Figure 10. The human damage becomes large in spite of the evacuation awareness compared to that of the no blockage. The number of the damage with the strong awareness is the minimum.

Table 3 Total number of human damage

| Evacuation awareness | Damaged population (persons) |          |
|----------------------|------------------------------|----------|
|                      | No blockage                  | Blockage |
| Strong               | 2,631                        | 4,181    |
| Middle               | 6,543                        | 8,401    |
| Weak                 | 11,997                       | 13,857   |

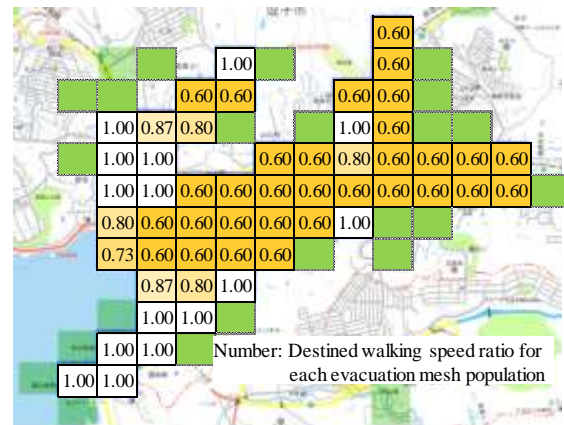


Figure 10 Decrement ratio of walking speed by street blockade

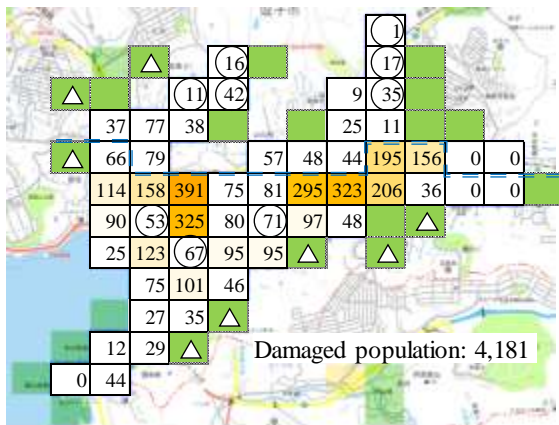
The number of the human damage for the blockade is also shown in Table 3. The damage is increased to 1.58, 1.28 and 1.16 times for the strong, middle and weak awareness, respectively. To consider the decrement of walking speed by the blockade is important for the human damage estimation from tsunami. Enhancing of evacuation awareness as well as seismic strengthening of buildings become the one way to decrease the human damage in evacuation.

## CONCLUSIONS

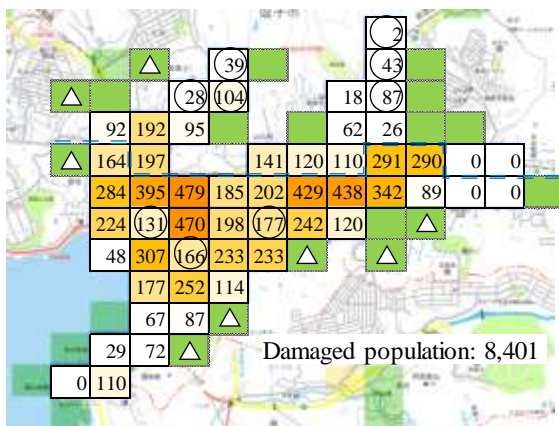
The evaluation method of the human damage considering the street-blockade by destroy of buildings is proposed. The human damage in evacuation from tsunami is discussed for the street-blockade and no street blockade conditions. The following conclusions can be drawn.

- 1) The human damage under the street-blockade becomes large compared to that of no street-blockade because of decrement of the walking speed by the blockade.
- 2) To consider the effect of the street-blockade in evacuation planning is important.
- 3) The human damage in evacuation from tsunami can be decreased by enhancing evacuation awareness for evacuation and education on disaster prevention.
- 4) A Seismic strengthening of buildings is the one way to decrease the street-blockade for large earthquakes.

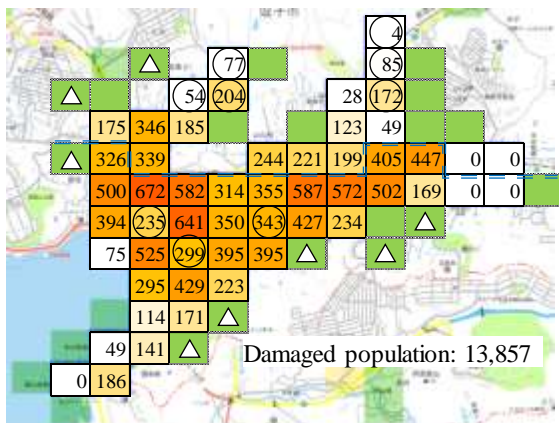




(a) Strong awareness



(b) Middle awareness



(c) Weak awareness

Fig.10 Human damage distribution with street-blockade

## REFERENCES

- [1] Cabinet Office, Damage Estimation of Nankai Trough Earthquake (1st. Report), 2012. (in Japanese)
- [2] Kanagawa Prefecture, Manual of Tsunami

- Inundation Forecast, 2012. (in Japanese)
- [3] Cabinet Office, Damage Estimation of Nankai Trough Earthquake (2st. Report), 2013. (in Japanese)
- [4] Yashiro, H., Fujita, K., Evaluation Method of Evacuation Safety Performance for Tsunami using Area-Wide Mesh, Second European Conference on Earthquake Engineering and Seismology, 2014, CD-ROM.
- [5] Fujita, K., Yashiro, H., A Study on the Number of Installed and Installation Location of Tsunami Evacuation Facilities Using Area-wide Mesh, Journal of Japan Society of Civil Engineers, Ser. F6 (Safety Problem), Vol. 72, No.2, 2016, p.I\_151-I\_156. (in Japanese)
- [6] Fujita, K., Yashiro, H., Evaluation of Human Damage in Tsunami Evacuation Considered the Variance of Walking and Tsunami Run-up Speeds, Internet Journal of Social Management Systems, Issue 11 Vol.1, sms17-8200, 2017, pp.213-223.
- [7] Koshimura, S., Namegawa, Y., Yanagisawa, H., Fragility Functions for Tsunami Damage Estimation, Journal of Japan Society of Civil Engineers, ser. B, Vol.65, No.4, 2009, pp.320-331. (in Japanese)
- [8] Midorikawa, S., Ito, Y., Miura, H., Vulnerability Functions of Buildings Based on Damage Survey Data of Earthquake after the 1995 Kobe Earthquake, Journal of Japan Association for Earthquake Engineering, Vol.11, No.4, 2011, pp.34-43. (in Japanese)
- [9] Shuto, N., *et al.*, eds., Encyclopedia of Tsunami, Asakura Publishing Co., Ltd., 2007. (in Japanese)
- [10] Aida, I., Simulations of Large Tsunamis Occurring in the Past off the Coast of the Sanriku District, Bulletin of the Earthquake Research Institute, Univ. of Tokyo, Vol.52, No.1, 2009, pp.71-101. (in Japanese)
- [11] Hoshiya, M., Ishii, K., Reliability Based Design for Structures, Kajima Institute Publishing Co., Ltd., 1986. (in Japanese)
- [12] Cabinet Office, Simulation results on return home action, 2007. (in Japanese)
- [13] Zushi City Homepage, <http://www.city.zushi.kanagawa.jp/>
- [14] Ministry of Land, Infrastructure, Transport and Tourism, Present State Survey in Tsunami Affected Area of the Great East Japan Earthquake (3rd. Report), Results of Actual Survey on Tsunami Evacuation (Preliminary), 2011. (in Japanese)
- [15] Matsumoto, N., Kiyota, S., Ito, M., Relationship between the Characteristics of Streetscape and Walking Speed, Journal of Architecture and Planning, Vol.74, No.640, 2009, pp.1371-1377. (in Japanese)

## DEVELOPING AGE-FRIENDLY CITY: CASE STUDY FROM DEPOK

Fatmah Fatmah  
Faculty of Public Health, Universitas Indonesia

### ABSTRACT

Depok, as one of the largest cities in Indonesia, has great potential to be an Age-Friendly City (AFC). Before the formation of AFC is established, eight dimensions of AFCs had been studied by the WHO in 2013, but since 2013, these dimensions have not been assessed. The study aimed to assess the preparedness of Depok to be an AFC with a qualitative approach from the stakeholders' point of view. This study used a qualitative design involving 50 informants through in-depth interviews and Focus Group Discussion (FGD) techniques using purposive sampling. The findings indicate that Depok was deemed not yet prepared to be an AFC due to an abundance of infrastructure deficiencies. There were not many changes in the facilities, such as infrastructure improvements in AFC indicators and existing Regional Regulations of AFCs, except for buildings and open green spaces. In general, Depok still needs time to achieve the AFC where the community will have a good place to live, grow, and age in it.

*Keywords: Age-Friendly City, older people, buildings and open green spaces, indicator, infrastructure*

### INTRODUCTION

Increased life expectancy is one of the consequences of development and has an impact on the increasing number of older people in Indonesia. The increase in the population of older people must be balanced with efforts to achieve active ageing goals.<sup>1</sup> Active ageing consists of three main pillars, namely, income security, health, and space to participate. These three pillars are the basis for the formation of an older people-friendly city. The WHO developed eight domains of Age-Friendly Cities (AFCs): housing, transportation, outdoor spaces and buildings; community support and health services; communication and information; civic participation and employment; respect and social inclusion; and social participation.<sup>2</sup> Some studies on developing AFCs in Brussels, Manchester, Australia, and Malaysia described their preparedness and implementation.<sup>3-5</sup> A study on AFCs from community stakeholders in Brussels and Manchester identified key elements and resources needed for an AFC. Another study in Australia mentioned that the impact of AFCs on government mainstream actions has been limited by uncertain political commitment and growing fiscal austerity. A study in Malaysia stated that public transportation and housing, healthcare services, and older people-friendly outdoor spaces and buildings have a role in building an age-friendly environment.

To support the formation of an older people-friendly society, it is necessary to design an AFC, which Indonesia still lacks. This can be

seen with the difficulty that older people have in accessing public facilities. A concrete example is the road to the bus stop, which is built at a very high and steep elevation and is extremely difficult for older people to access. There are still many multiple-story buildings that do not provide lifts and force people to climb stairs. There are eight areas that require special treatment for older people, which are health, social life, environment, information-communication, infrastructure, transportation, law, and art. In Indonesia, the Surabaya City Government, the capital of East Java Province in Indonesia, has local regulations for the service and empowerment of older people.<sup>6</sup> In comparison, Depok, as a suburban city in West Java Province in Indonesia (Figure 1, 2), has been singled out by regional leaders and leaders of care organizations for older people who want to achieve an AFC.

Depok has a growing population of older people. This population is currently estimated to be 114,060 people out of 1,570,949 people. Depok has a life expectancy of 73 years.<sup>7</sup> Therefore, Depok has a great opportunity to become an AFC because of the implementation of the integrated service posts for older people (there are nearly 500 integrated service posts for older people). Currently, there is no pension plan, and there is an insufficient social infrastructure and not enough facilities geared towards older people. The mayor of Depok has supported the existence of Depok as an AFC. One indication that Depok is ready to be an older people-friendly city is the construction of a special crossing in front of both the Bhakti

Yudha Hospital and the Depok Government building. The crossing is equipped with a button to activate a red light if an older people needs to cross the road. In addition, Depok has 344 integrated development posts (the integrated service post for older people) spread across six sub-districts.<sup>7</sup> Depok has great potential to be an Age-Friendly City (AFC) considering the successful implementation of the integrated service posts for older people and the support of the Depok Government for declaring Depok an AFC. However, various preparations need to be made.

Before the formation of DAFC (Depok Age-Friendly City), two previous studies established eight indicators of an AFC in 2010 and 2014.<sup>8-9</sup> These two studies found that the majority of the community and government stakeholders considered Depok to be ready to become a DAFC as long as it was supported by a budget and programmes that prioritize the interests of older people, as well as good coordination among the Depok Government, the community and related institutions. As a result of these stipulations, Depok is not yet ready to fully assume the status of an AFC. The existence of Regional Regulations, laws and policies that regulate the formation of the Depok Local Committee of Older people can indirectly accelerate the realization of DAFC.

With reference to the findings of the two aforementioned studies, there should be a study to evaluate the extent of preparedness of Depok towards becoming an AFC from 2010 to the present based on the eight indicators of an AFC. It is expected that this study can identify the eight indicators of DAFC based on a qualitative assessment by stakeholders and related agencies. The objective was to assess Depok preparedness towards becoming an AFC with a qualitative approach from the viewpoint of stakeholders.

## METHODS

### Design Study and Subjects

The study utilized a qualitative approach by using 10 in-depth interviews with 10 key informants in policy and practices and 4 groups of Focus Group Discussion/FGD (Figure 3). The ten informants for the indepth interviews came from private sectors (*lapaklansia*, Depok Industrial Chamber of Commerce, political parties, The Indonesian Businesswomen Bond of Depok Branch, Depok Center of Small and Medium Enterprises, and Head of Depok Central Family Welfare Program Team). They

have a position as a chairman, operational manager, and head of division who are implementing the program for older person. They were recruited by the research team through formal invitations. The research team made a list of some private and government institutions associated with programmes for older people. Then, the research team visited their offices to conduct in-depth interviews. The key informants from the 4 FGDs ( $n = 40$ ) were recruited on the basis of their institutional roles in empowering programmes and having policies and laws geared towards older people. The research team recruited the informants by sending formal invitations requesting their attendance at the CAS UI office in Depok to develop schedules for the FGDs. The inclusion criteria for the informants were those from private and/or government institutions who were either male or female, who were involved directly as stakeholders and who acted in conjunction with older people, male or female. There were no sample sizes calculated since the study applied a qualitative approach. The exclusion criteria were informants who did not attend the FGD scheduling when invited, who did not fully attend the FGDs due to their business, and who cancelled the interview. Each FGD took 90 minutes and each indepth interview will be finished in 60 minutes. The research team acted as the FGD facilitator and indepth interview enumerator who well-trained before.

### Data Collection

Qualitative data collection involved the research team member as the facilitator/moderator of the FGD and organizer of the in-depth interviews. Recruitment of informants was accomplished through purposive sampling with the help of a research secretary who followed-up on confirmations. In-depth interviews were conducted by direct visits to the informants' offices after an appointment was made. The research goals and purpose of the study explained by the research team at FGD and indepth interview sessions. The questions asked in the FGD covered the following: the definition of an AFC; the description of and opinion about the cleanliness of open spaces and buildings; the housing conditions; and the condition of civic participation and employment for older people. In-depth interview guidelines covered the AFC policies and programmes and the facts and real status of the eight dimensions of the AFC determined by the WHO. The FGDs

and in-depth interview guidelines were validated in a previous study in 2013.<sup>9</sup>

To ensure validity of research, a well-trained and skilled moderator/facilitator was chosen from the research team. Another way to promote internal validity (credibility) was to employ triangulation by using several moderators with different scientific backgrounds and multiple individuals analysing the same data. Method triangulation through FGD and in-depth interviews was also used in the study to increase internal validity. Triangulation method has objective to eliminate or reduce biases and increase the validity of the study. Triangulation can be used to improve the study validity by confirming the analysis results with other methods, such as open or structured interviews, observation, or any alternate research method.<sup>10</sup>

Variation of participants selection from different position such as the cadres of integrated service post of older person, community health centre staffs, sub-district office staffs, and community/organization in older persons was one of the efforts to establish the external validity.

Discussions were held at the Centre for Ageing Studies UI office in Depok. The independent interview process was conducted by the researcher at the informants' offices. All informants were given verbal explanations about the research objectives and data collection procedures. The research team collected all informed consent from each informant in the FGDs and in-depth interviews. Informants were provided with local transportation after participating in the study. All FGDs and in-depth interviews were audiotaped and transcribed, and the quality was confirmed by comparing the transcriptions with the audio recordings by the moderators of the research group.

### Data Analysis

Content analysis was used to analyse the information collected from all informants. Three researchers performed the qualitative analysis (F, VPD, and Y). They read and checked the transcription several times individually and created a single coding for the themes agreed upon. Matrix analysis was performed to summarize the findings from the two methods. An ethical review license for this study was obtained from the Faculty of Public Health, Universitas Indonesia.

## RESULTS

### Socio-demographic of Informants

### Characteristics

Table 1 illustrates the socio-demographic characteristics of the informants, including age, sex, final education, and employment status. The older people (more than 60 years old) comprise one-third of the pre-older people age group (less than 60 years old). The proportion of female informants was four times greater than that of male informants. More than three quarters of all informants graduated from colleges and universities. Some informants even possessed masters (10%) and doctoral degrees (0.4%), and none had a low level of education (0%). The majority of informants worked as civil servants (24%) and private employees (38%).

### Perceptions of Age-Friendly Cities and DAFC Policies

Generally, most informants had heard about AFCs and the DAFC. All the integrated service posts for older informants had heard the term AFC. In their view, an AFC took into account aspects such as the health of older people, facilities for older people such as parks, easy access to health care, absence of neglect, availability of special lines in the sub-district level community health centres, providing priority necklaces for older people in district health centres since 2016, special road crossings, elder care, handrails in offices, and slip-resistant flooring. An older people-friendly city is a city that can support the desires and needs of older people.

Most of the informants stated that an AFC (specifically for older people) means a city in which security and comfort are provided for older people and in which their desires and needs are understood. This could be seen from the availability of facilities and infrastructure that support the comfort of older people and provide special treatment for them given the limitations they encounter in some of their activities. However, an older people-friendly city has not become a priority because the priority is a Depok Healthy City, Depok Child-friendly City, and Depok Cyber City.

Nonetheless, the development of and process towards an AFC continues to this day. What might hamper the formation of DAFC is the absence of data collection on the number of older people and their socio-demographic characteristics by the Depok Social Service Office. Almost all informants from the

political parties said that they did not know about DAFC. They were only familiar with the Depok Child-friendly City programme. The existence of the integrated service posts for older persons at the local level, such as the free-of-charge medical examination for older people, showed that the government of Depok had some active older people programmes.

The older person friendly city is a city that can support the desires and needs of the older person so that the community's stigma about the older people can be changed to good and positive views (older people NGO figure). Yes, Depok Aged Friendly City has no older person feel set aside, still able to be productive, feel they are still being used, and there are no neglected older person. Community health centers have a special counter for older person (the integrated service post cadre)

#### **Depok's Preparedness for Becoming an AFC**

Generally, the informants said that Depok's preparedness to be an AFC was not optimized. Several informants even doubted that this programme would be successful. Depok's unpreparedness to become an AFC was mainly due to the absence of a sufficient budget and of programmes. Becoming an AFC was not yet a priority, and there were still many neglected older people in Depok. In addition, the FGD informants from the community health centre stated that to support DAFC, it was necessary to build several facilities to make it easier for older people to conduct their activities. For example, the government should increase the number of city parks for older people to relax in or take walks through; maintain special treatment for older people, such as the availability of special seats on commuter line trains, an increase in waiting places or the creation of special lines for older person people in hospitals, health centres, banks and other community service places. Even though Depok was not prepared, Depok still has to pioneer the realization of an AFC because the life expectancy in Depok is quite high (79-80 years), and the increase in the population of older people in Depok is quite rapid. Older people should be given special attention in order not to be a burden to the government and society. To prepare for the realization of DAFC, the Depok Government issued Regional Regulation No. 09 in 2017 concerning Depok as a Family Friendly City and Regional Regulation No. 15 in 2013 concerning Depok as a Child-Friendly City. An AFC was contained in the Regional Regulation on Depok as a Family-Friendly City. However, the Depok Government will realize DAFC

in synergy with the concepts of a Depok Cyber City, Depok Healthy City, and Depok Child-friendly City. In addition, the Mayor Regulation has been published regarding the Realization of DAFC.

There were several efforts from the Depok Government in cooperation with the Depok Local Committee of the Older People. Staff members were sent directly to the village level to socialize regarding DAFC. An informant suggested that DAFC be projected as a pilot project because the characteristics of the region were different. Each region would be better prepared if it adjusted to the conditions and needs of each individual territory. Previous surveys were necessary to identify older people's needs, considering that each territory had its own issues. If the social environment supports the programme, perhaps the City Government of Depok can build facilities for older people. For example, if the Depok government were to build a garden for older people, but the social environment did not support this plan, then the park would be used by children for graffiti, causing older people to be reluctant to use the park.

Judging from the preparedness of DAFC, development should be focused on community support, health services and participation because the implementation of these two indicators was the most effective in Depok. Health examination and older people's activities in Depok were going well. Several efforts to improve service facilities for older people aimed at the realization of an AFC by the Depok Government were the socialization of the AFC at the sub-district level within the community and the provision of special lines or counters for older people at the sub-district level community health centre as an older people-friendly health centre. Private hospitals, government hospitals, and village-level community health centres do not yet have special services for older people. In addition, the issues surrounding older people are health related, because those who came were generally still productive and able to work, but these people also needed a place to vent their feelings. Older people also need more attention, not just treatment. Most of the older people were treated alone and were not brought by their families. This showed a lack of attention from families towards older people. According to most informants, when seeking treatment, older people need to be taken by their families as stated by one of the informants:

*For health issues, there are already monthly routine checks for older person*

*people. However, the problem is that there are no families in the home or family members who can take them (sub-district health centre staff)*

Regarding the health of older people, some informants said that they tend to suffer from non-communicable diseases such as hypertension. In addition, most informants said that health services for older people were not optimal because they were not focused only on older people. Other informants stated that there was a lack of understanding about older people, especially about how to communicate with them. Clear cooperation from all involved parties was essential, where monitoring and evaluation for each activity were needed.

### **Social Participation**

The social participation of older people in Depok was considered by most informants to be quite good. Many older people were still actively involved in community activities. However, there was no access to social activities that were specifically for older people, except for activities created by the community, such as volunteering to procure food during elections and engaging in post-disaster activities. Informants stated that many older people did not want to engage in activities even though they were still productive. Some informants said that most of the social activities attended by the older people were recitation or religious activities and sports, such as exercise sports or exercise activities usually carried out at public facilities in housing areas. When asked whether the informants were involved in community activities, most informants stated that they were active in religious activities such as recitation and community meetings. The remaining informants were active in sports activities, the integrated service posts for older people, and the arts.

Social participation has encouraged the participation of older person people. Older person people are specifically involved. In the sub-district, there is the implementation of National Older people' Day, several games, and competitions for older person people. These activities are monitored and evaluated. (by the sub-district community health centre staff)

### **Civil Participation and Employment / Economics**

Most of the informants stated that the older people still had the opportunity to work or

become volunteers, provided that they were physically healthy. The involvement of the older people in volunteer activities was usually personal, such as functioning as a social worker at the mosque, being involved in community service or in a celebration of the birth of the prophet Muhammad), participating in art events, various kinds of competitions (exercise, choir), and helping in landslides, floods, etc. Older people can take part in the community by participating in social activities, such as community service or as entrepreneurs. For work as office staff, only managerial work was available for older people who had not reached the age of 65 years. Non-managerial positions were more focused on a younger and productive age groups.

The study results showed that most informants agreed that there was a need to improve the quality of work of older people in Depok. Furthermore, the informants assessed the need for training opportunities for older people after retirement as well as for policies on the recruitment of workers, promotions, training, and support for entrepreneurship. Some informants agreed on the existence of flexible employment opportunities with good income for older people. However, employment opportunities for older people in both formal and informal sectors were still low due to the lack of expertise and low education. Usually, older people are involved in activities such as cooking, crafts, and reciting the Al Quran. An older people's profession that was still considered suitable was to become a parking attendant or a security guard. The training of older people was truly limited, was only given one time and was not routinely conducted. For example, one government institution conducted recycling of waste (Waste Bank) and offered culinary courses; Depok *Muslimat NU* organized bridal makeup courses for the public, but there were no specified programmes for older people, and after training, kits were provided. Activities specified for the older people were usually health-related, such as exercise, the Healthy Heart Club, Older people Family Development and Increased Income for Families Program. Older people with foot defects in Depok were usually employed in the private sector in administration and not in production. Depok civil servants planning to enter retirement were given training for retirement preparation such as farming, gardening, and baking.

There was no specified economic support for the older people, and only a general programme existed for all age groups. According to the



integrated service posts for older informants, there were several efforts to improve the creative economy by the Depok Government, namely, 1) producing candy, banana chips, star fruit, processed products, cassava chips, and cheese sticks; 2) providing non-interest loan funds in stages starting from IDR 100,000, 200,000, 500,000 and so on; 3) assistance in the form of bazaars can be followed by older people business groups, catering groups (consisting of 4 people, with the number of older people from 1-2 people); and 4) the use of females in heads of household programmes involving 10-20% of older people for the past 2 years to lend funds of IDR 10 million per - group (10 people) for home industries such as vegetables mixed with peanut sauce, fried rice cake, and handicrafts such as sticking and making hand bags from recycled materials.

Until now, all informants revealed that there were no policies or government regulations regarding the age limit of workers, promotions or job training for older people; there was no opportunity to get post-retirement training or to get support in self-employment activities. However, decision-making agencies in Depok such as the Health Office, Representative Office and private companies encouraged the participation and membership of older people, especially in the health sector in the integrated service posts for older persons, venting activities for older people, participation (National Older People Day), etc.

### **Buildings and Open Spaces**

Most people thought that buildings and open spaces were still inadequate for older people. However, there were already some improvements, although not significant, such as better cleanliness in public places (streets, sidewalks, parks, and markets); sufficient and well-preserved seating in parks; the existence of older people-friendly parks; slip resistant sidewalks for pedestrians that were still used by street vendors and motorbike riders; places and buttons for older people at special crossings had not fully functioned, creating the need for officers to help them cross the street; generally continued adherence to crossing signs for older people by car and motorcycle drivers; quite good level of security because security officers were on duty for 24 hours; relatively fewer lighting lamps, especially if the lights were off, which takes a long time to repair; special lines and counters for older people at health

centres; special seats for older people on the train; the absence of a separation between bicycle lanes and pedestrians; and toilets in public places were not older people-friendly. Buildings and open spaces are not yet optimal for older people. There are no older people-friendly parks or green open spaces. Public parks have not prioritized older people (sub-district community health centre staff). Generally, Depok housing is flood free, which is around 70%, except for houses on the banks of rivers. Housing of Ambassador in Cimanggis Sub-district always flooded (the integrated service post cadres)

### **Transportation and Housing**

For transportation facilities, some informants stated that transportation did not support the needs of older people, but some stated that city transportation was relatively comfortable. Public transportation for older people is already being planned. The conditions in public transportation have not supported older people because it is difficult to ride on public transportation.

Transportation in Depok is still lacking, especially long-distance transportation. In the city, there are still minibuses. These models are old, and in my observation, the braking may not be sufficient, which shows that there is no special attention given to transportation (a member of a political party)

For housing indicators in Depok, some informants considered that housing was still not older people-friendly both for private and rental / contracted houses because they did not have a pedestrian walkway. Housing prices were still not affordable for older people. Other informants suggested that the size of the housing should make it free from flooding. If the residents of the house come from a certain socioeconomic group, they are able to usually renovate parts of a room in the house, such as toilets and floors, to meet the needs of an older people.

Currently, the Depok housing developer has not fulfilled the needs of older people because it prioritizes homes for young families. Depok has yet to have flats specifically designed for older people because such housing has not been planned by the government and the developer. However, some informants considered that the construction of flats for older people in Depok was not suitable and was inappropriate because it was better for older people to live with their families. There were no older people-friendly homes because the developer had not designed the house in accordance with the physical needs of older

people, such as flat roads, a wide entrance, and a bathroom, kitchen, and toilet specifically designed for older people. Some housing and apartments in Depok were not older people-friendly because of their location, which is far from public facilities such as public health centres and hospitals, except for motorcycle transportation. In fact, according to the informant from one political party, housing in Depok originally had open spaces, but these spaces were then converted into parking areas. Housing conditions are not older people-friendly. Owners are more responsible for making the house comfortable. The developer has not built an older people-friendly house (sub-district community health centre staff)

### **Communication, Information, and Education**

Communication and obtaining information in the present era were better with the technology of mobile communication. Sunday meetings for older people were quite supportive and, when coupled with social media, allowed older people to keep up with information. Every year, the celebration held talk shows related to National Older people Day. It was expected that seniors received information about various issues when engaged in these activities. However, some informants said that information did not address the needs of older people. There still needed to be an information centre to meet the needs of older people.

### **Community Support and Infrastructure for Older People' Health Services**

The implementation of community support for the older people in Depok was very good. This was revealed by all informants from political parties who expressed concern that the Depok Health Office is improving the quality of life of older people through exercise and health services in the integrated service posts for older people every month. Health services were adequate in terms of access and financing.

Health services are programmes that are quite adequate both from an access and a financial perspective, with the availability of free health checks and health insurance. All first-level community health centres in Depok have already become older people-friendly health centres, while second-level centres are still in the process of developing. Visits to the community health centre were quite high. The types of diseases that commonly affect older people are hypertension and NCDs (Non-Communicable Diseases). According to the

informant, health examination activities should be carried out continuously, but the implementation depends on the condition of the agency. Sometimes people were diligent in checking themselves into the centre, while there were also people who were too lazy to go to the health centre. What I look at is the health aspect. Health access is better in terms of financing and access because this programme is for all levels of society. With government support, financing and access are better. (member of a political party)

### **Social Respect and Inclusion**

Older people should gain respect from their involvement in social activities and their assimilation in the society, but their role was mostly kept at a domestic level, such as taking care of children/grandchildren, which is likely to accelerate the ageing process. Thus far, there has been almost no involvement of older people in official community organizations at the government level because it was considered appropriate for young people, and the youth population was large. The health and physical conditions of older people also declined, causing them to be reluctant to blend in with community organizations/NGOs, etc. Another source of appreciation for older people was their inclusion as community leaders or in activities such as the Independence Day celebration or elections. Other activities seem to depend on their health conditions. According to one informant, older people must be active, and if they were retired, they must be cared for. If you do not manage yourself after retirement, you will become senile. Although older people are physically weak, they need to remain active. Do not just leave our old parents at home; we have to be affectionate and considerate (member of a political party)

### **Discussion**

The increased number of older people has an impact on socio-economics at the family, community and government levels. Therefore, an AFC must be created so that older people can engage in activities and be productive. An AFC will be a testament to the readiness of a nation to face an era that continues to move to reduce the number of dependent people in life. The population of older people is no longer a burden on families, communities, and nations.<sup>11</sup>

When combined with the increasing number of older people, it appears that local regulation

is needed to accommodate regional specificities and improve regional welfare. However, in reality, the Regional Regulation on older people, especially that related to AFCs, which were originally planned to be issued, was cancelled and replaced with the Mayor's Regulation, which is still in the drafting stage. The existence of these policy regulations guarantees that the principles of administrative actions and every event that deals with equality, legal certainty, and actions are based on certain regulations.<sup>12-14</sup>

The large number of older people who choose to go to health care centres makes older people-friendly health facilities the issue that needs to be addressed.<sup>15-16</sup> Visits of older people to community health centres are quite high. All first-level community health centres are older people-friendly, while the second-level community health centres are still in the process of becoming so. In addition, with free treatment for older people and a health insurance programme, it is easier for them to receive treatment. The emergence of health problems and the number of older people who seek treatment at health facilities reflect the demand for health services to meet the needs of older people in a friendly manner so that their health can be guaranteed. The findings in the study are in line with the study in Malaysia that found community health services to be one of the most important for developing an age-friendly environment.<sup>5</sup> Eight dimensions of the older people-friendly city designed by the WHO support a person's life, not just as a friendly place for older people but for all age groups, including children and disabled people.<sup>13</sup> Therefore, within the context of the older people, an AFC is a city that accommodates the needs of older people with all the limitations that accompany them. In addition, Depok City has challenges encountered to realize DAFC such as developing housing friendly city. One of the strength of DAFC readiness is active community participation at the integrated service post. These two findings is supporting by a similar study in Netherland.<sup>17</sup>

The Depok Government has strived to create an older people-friendly area/community/city, but it is not yet optimal because it has to prioritize other facilities. Therefore, policies related to older people-friendly communities and cities, especially for Depok, are very important because of the high population of older people in this region. The preparation of older people programmes in annual activities must be increased and must involve the community so that the programmes that are prepared can respond to

the interests of older people. In addition, it is necessary to prepare the infrastructure, budget (funds), government support (policies), and concern for older people.<sup>18-19</sup>

Older people play roles as job seekers who garner financial income, and they also play an active role in giving to the community in accordance with the capabilities/skills of each older person. However, older people have not been optimally empowered, even though there are still many older people who have potential in their fields. Several factors that Depok's preparedness for DAFC contained were 1) optimized older people programmes and budgets; 2) insufficient infrastructure, primarily buildings and open spaces, transportation, housing, civil participation and employment of older people; and 3) lack of coordination between the Depok Government and related institutions, where each programme is running independently.

Depok's preparedness to become an AFC is not yet optimized because of the lack of realization of the commitment of the Depok Government to focus on the interests of the older people, except for the idea of a healthy city that has been implemented even though older people are not mentioned specifically. Today, Depok focuses more on child-friendly cities than on DAFC. DAFC should also receive special attention and receive its own Special Regional Regulation of DAFC, which is separate from the Depok Regional Regulation on Child-Friendly Cities. The existence of Regional Regulations, national policies, and the law, including the issuance of the Depok Mayor's Regulation concerning the establishment of the Depok Local Committee for the Older People, will bring the realization of DAFC in the future.

The potential for public support in Depok to realize DAFC is quite large. This can be seen from the enthusiastic participation of all age groups, including older people in the integrated service posts for older people activities and healthy heart exercises. The socialization of DAFC is being realized by the AFC. The Working Group from the sub-district to the citizen association level supports the dissemination of information and broad public knowledge about DAFC. When compared with the findings of a similar study in 2013, it was concluded that there had been no significant changes from the 3 indicators of AFCs that were considered unfavourable, namely, open buildings and green spaces, housing, and social and work participation. There is little importance in the 2018's study given to such factors as additional parks for older people, including Lembah Gurame Park, Terapi Lansia Park, and Mekarsari Park. Approximately 33% of Depok's land already has

103 parks<sup>20</sup>, and the issuance of Regional Regulation No. 09 of 2017 concerning Depok as a family-Friendly City includes DAFC. There has been no changes in housing and civil participation or work indicators in the findings of this study.

### Limitations

The study has several limitations, such as the difficulty of determining the timing of in-depth interviews and FGDs for several informants from government stakeholders. As a result, a number of relevant government stakeholders, such as the Housing Agency, the Manpower Office, the SME (Small Medium Enterprises), and Market Office could not attend. Likewise, when they were visited, they refused to participate without giving any explanation. Another limitation was the presence of FGD informants from organizations of older people aged 70 years and over who experienced hearing loss and had difficulty concentrating on moderator questions. They could not answer the questions correctly and tended to provide lengthy explanations that deviated far from the contents of the question.

### CONCLUSIONS

Depok still needs time to achieve the AFC, however, the existence of regional laws and policies regulating the Depok Local Committee for the Older People formation can indirectly accelerate the realization of DAFC. These policies or regulations are designed to ensure local government cares about the population irrespective of age. In addition, there is a regional policy that provides legal certainty for older people that their needs are guaranteed. The best practices that have been carried out by relevant agencies in Depok that relate to older people are the formation of the Local Committee of the Older people by the government and the community health centre *Santun Lansia* that provides good services for older people.

### ACKNOWLEDGEMENTS

We express our appreciation for all the informants for their participation in the study. This study received a specific grant from the Grant of Improving Research Working Group Universitas Indonesia 2018 (No: 5283/UN2.R3.1/HKP 05.00/2018).

### CONFLICT OF INTEREST

The Author(s) declare(s) that there is no conflict of interest.

### ETHICAL APPROVAL

This study was conducted according to the guidelines laid down in the Declaration of Helsinki and all procedures involving human subjects/patients were approved by The Research and Community Engagement Ethical Committee Faculty of Public Health University of Indonesia. Written informed consent was obtained from all subjects. Applicable (approval number of ethical clearance: 666/UN2.F10/PPM.00.02/2018).

### PERMISSION TO REPRODUCE FIGURES OF MAP AND DESCRIPTION OF DEPOK CITY

Depok District Health Office had given permission to reproduce map and the description of Depok City to authors (taken from Depok City Profiles Year 2017, Depok District Health Office).

### FUNDING ACKNOWLEDGEMENT

Directorate of Community Engagement and Research of Universitas Indonesia (UI) for their fund of student final research project grant (No.5283/UN2.R3.1/HKP 05.00/2018). UI had no role in the design, analysis, or writing of this article, except covering the publication/handling cost of the journal publication

### REFERENCES

- [1] Fatmah. *Geriatric nutrition*. Jakarta: Erlangga Publisher, 2010, p.2-3.
- [2] WHO. *Global Age Friendly-Cities: a guide*. France: WHO, 2007, no page.
- [3] Buffel T, McGarry P, Phillipson C, et al. Developing age-friendly cities: case studies from Brussels and Manchester and implications for policy and practice. *J Aging Soc Policy*. 2014;26 (1-2):52-72
- [4] Kendig H., Elias AM., Matwijiw P., Anstey K. Developing age-friendly cities and communities in Australia. *J Aging Health* 2014; 26(8): 1390-414.
- [5] Ming L.M, Shi Y.L., Shiok H.L., Ming L.L. Modeling age-friendly environment, active aging, and social connectedness in an emerging Asian economy. *Journal of Aging Research* 2016; 1-14.

- [6] No author. Surabaya of Age Friendly City. *Gapura XIV*, 2012, page 15.
- [7] Depok City Statistic Center Bureau., *Population growth of Depok City in 2017*. Depok: Depok City Statistic Center Bureau, 2017, no page.
- [8] Survey Meter. One final step into dream on Age Friendly City 2030. Report, Survey Meter Yogyakarta, 2013.
- [9] Fatmah, Vita, Dina, et al. The assessment of Depok as Age Friendly City (AFC). *Journal of Biosciences and Medicines* 2014; 2:1-40.
- [10] Jonsen K, Jehn KA. Using triangulation to validate themes in qualitative studies. *Qualitative Research in Organizations* 2009; 4: 123-150.
- [11] Dewi VP, Raden II, Lindawati. Training program to support preparedness of older persons health services". *ASEAN Journal of Community Engagement* 2018; 2:120-133.
- [12] Older persons Regional Commission of West Java Province. Guidelines for the development of older persons friendly areas in West Java Province. Bandung: Older Persons Regional Commission of West Java Province, 2017, no page.
- [13] Saepudin. Fungsi peraturan daerah pada perundangan Tahun 2011 (Function of regional regulation in legislation 2011), <https://saepudinonline.wordpress.com/2013/05/01/fungsi-perda-dalam-peraturan-perundang-undangan/> (2011, accessed 25 September 2018).
- [14] Ahmad. Fungsi kebijakan peraturan dalam melengkapi sistem legislasi administrasi negara (Function of policy regulations in completing the legislation system of state administration), <http://asaad36.blogspot.com/2010/11/fungsi-peraturan-kebijakan-dalam.html> (2010, accessed 1 October 1 2018).
- [15] UNFPA. Executive summary of aging population in the twentieth century: a celebration and challenge. UNFPA, 2012, no page.
- [16] National Family Planning Coordinating Board. Kota ramah lansia membentuk lansia tangguh (Older persons friendly cities form tough older persons), <https://keluargaindonesia.id/kabar/kota-ramah-lansia-upaya-membentuk-lansia-tangguh/> (2017, accessed 16 September 2018).
- [17] Van Hoof J., Kazak JK, Jolanta MPB, Sebastiaan TMP. The challenges of urban ageing: making cities aged friendly in Europe. *Int. J. Environ. Res. Public Health* 2018; 15 (11): 2473.
- [18] Hermawati. Study on Age Friendly City. In: *Age Friendly City Seminar and Workshop*. Yogyakarta.
- [19] Agustiniingsih, Aryanti P. Pentingnya fasilitas kesehatan yang ramah lansia (The Importance of older persons friendly health facilities), <https://www.kompasiana.com/aryantipuji/592c10349397739b381ff541/pentingnya-fasilitas-kesehatan-yang-ramah-lansia/> (2017, accessed 15 August 2018).
- [20] Berita Satu. Hanya 33% kelurahan di Depok memiliki taman (Only 33% of villages in Depok have parks), [www.beritasatu.com/satu/477652-baru-33-kelurahan-di-depok-yang-miliki-taman.html](http://www.beritasatu.com/satu/477652-baru-33-kelurahan-di-depok-yang-miliki-taman.html) (2018, accessed 1 November 2018).

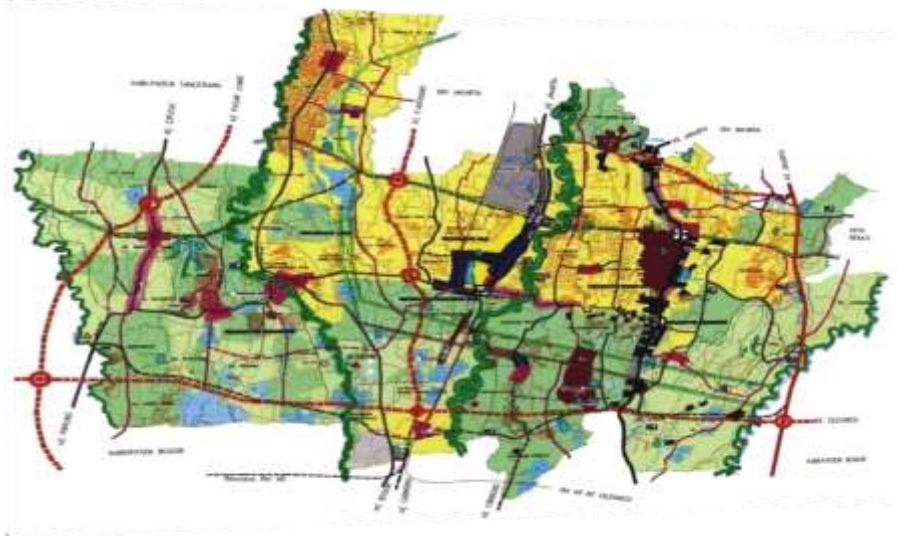


Figure 1. Map of Depok City (reproduce from Profile of Depok City Profile Year 2017, Depok DHO)



Figure 2. Description of Depok City (reproduce from Profile of Depok City Profile Year 2017, Depok DHO)

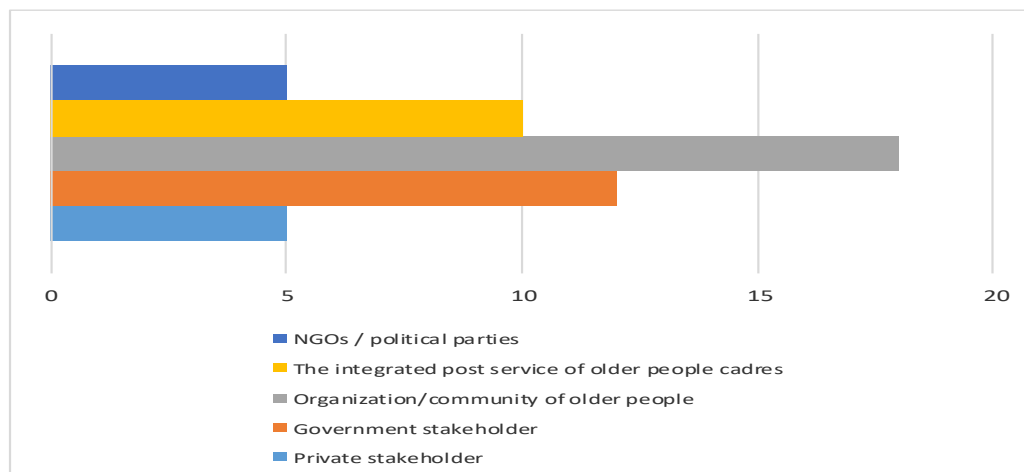


Figure 3. Type of key informant

Table 1 Socio-demographic characteristic of informants (n = 50)

| Variable               | Level                   | n  | %    |
|------------------------|-------------------------|----|------|
| Age (years)            | Pre-older people (< 60) | 37 | 74.0 |
|                        | Older people (>= 60)    | 13 | 26.0 |
| Sex                    | Male                    | 11 | 22.0 |
|                        | Female                  | 39 | 78.0 |
| Educational background | Senior high school      | 11 | 22.0 |
|                        | Academy/University      | 39 | 78.0 |
| Working status         | Yes:                    |    |      |
|                        | Government employee     | 12 | 24.0 |
|                        | Private employee        | 19 | 38.0 |
|                        | No                      | 19 | 38.0 |



## BIOMONITORING OF WATER POLLUTION IN LAKE CHEBARKUL BY THE CONTENT OF HEAVY METALS IN MACROPHYTE ORGANS, RUSSIA

I.V. Mashkova<sup>1</sup>, A.M. Kostryukova<sup>2</sup>, E.E. Schelkanova<sup>3</sup>, V.V. Trofimenko<sup>4</sup> and A.I. Slavnaya<sup>5</sup>

<sup>1, 2, 3, 5</sup>Department of Chemistry, South Ural State University, Chelyabinsk, Russia

<sup>4</sup>Department of Philosophy and Culturology South Ural State Humanitarian Pedagogical University  
Chelyabinsk, Russia

### ABSTRACT

This paper studies bioconcentration of heavy metals (HMs) in macrophytes. The high content of heavy metal compounds in Lake Chebarkul is natural. However, in some parts of the lake higher heavy metal content is observed. This is typical for the areas with an increased man-made impact on the lake. In these areas heavy metals get into the water together with partly treated sewage. The goal of our research is to determine the macrophyte species diversity of Lake Chebarkul, as well as the bioconcentration of heavy metals in macrophytes. In our research we identified species diversity, water flora taxonomic structure for each sampling point. We made flora lists for each profile and lake part and the total lists of differences and similarities of all the studied sites. The final flora list includes about 90 plants. According to the research macrophyte species composition of the studied sites is different. The article discusses the issues of bioaccumulation and bioindication of heavy metals (TM: Cu, Zn, Mn and Fe) in three types of macrophytes - *Potamogeton lucens*, *Phragmites australis* and *Elodea canadensis* of Lake Chebarkul (Russia). The research revealed that HMs in plants were actively accumulated from water. *Potamogeton lucens* and *Phragmites australis* showed higher average HM accumulation values.

*Keywords: Aquatic Macrophytes, Bioaccumulation, Heavy Metals, Biomonitoring*

### INTRODUCTION

Water quality in water-bodies has become of an increased interest. Overland water pollution by heavy metals is one of the main environmental issues [1]. Heavy metals get into water systems in various ways including industrial, municipal and agricultural effluents [2]-[4]. Being very persistent, heavy metals tend to accumulate in soil, water, sediment and pass through trophic chains.

Heavy metal toxicity is explained by their ability to bind with proteins and prevent DNA replication [5]. Most of the metals provoke the production of free radicals and reactive oxygen intermediate (ROI) which leads to oxidative stress [6]. But some elements such as Cu, Fe, Zn, Mn, Ni are necessary for plants to grow. And some macrophytes can accumulate metals and metalloids [7]-[9]. Macrophytes are very important for the community as they take part in oxygen production, nutrient cycle, stabilizing sediments and providing habitat for water life [10], [11]. Macrophytes actively accumulate metals from sediment and water so that they become accessible for epiphytic phytoplankton and other herbivores and detritivores [12]. So, taking into account the importance of macrophytes in ecology, the assessment of heavy metal content in macrophytes presents interest [13]. Macrophytes'

attached mode of life makes them especially effective in bioindicating heavy metal pollution of particular zones. Besides, there is research showing significant differences in heavy metal accumulation by different macrophyte species [14], [15]. Macrophytes take a priority part in the methods of treatment and detoxification of water-bodies. Submergent vegetation accumulate heavy metals more than coastal.

So far, few studies have investigated macrophyte biodiversity in South Ural. Taking into account the fact that the problem has been little investigated in the South Ural region [16], we continued to study the peculiarities of heavy metal accumulation analyzing the macrophyte biodiversity. As there is growing concern to the problem of heavy metal pollution, particularly of water-bodies, the discussions emerged have become timely. The current paper aims to identify macrophyte biodiversity of Lake Chebarkul (Russia) and to study the total concentration of heavy metals in three most dispersed species of macrophytes in the coastal water.

### MATERIALS AND METHODS

#### Study Area

Lake Chebarkul is on the eastern slope of the Urals range of mountains. Its altitude is 320 m above sea level. It is a low-land lake with tough shores overgrown with reeds. The creeks are full of water vegetation. Chebarkul is of tectonic origin. Its eastern part is very deep, the northern and western shores are steep and rocky, eastern and southern are flat flooded in spring. There are rocky promontories. Western coasts are forested. The bottom is covered with silt, sand, pebble and shells. It is the lake where the meteorite fell in 2013 (Chelyabinsky, Fig. 1, point 6). Several small dry in summer rivers fall into the lake. The lake area is 19.8 km<sup>2</sup>, its volume is 0.154 km<sup>3</sup>, the deepest part is 12 m, the average depth is 2.3 m. the water level varies between 1.5 m, the highest water is in June. The lake is frozen early in November, and is opened in May. There are many health resorts and recreation facilities on the lake coasts. It is also of much fishery importance. Lake Chebarkul has extensive resources of quality fresh drinking water of 154 million m<sup>3</sup>. It is a source of drinking water supply for the town of Chebarkul and its neighbouring villages. The water level has dropped almost by 3 m for the last 70 years. As a result, the natural hydrological regime was disturbed. The lake has become shallow, its southern and eastern coasts got swamped, weeds have grown not only on the coasts but also away from them.

### Sample Collection

12 sampling points were chosen to study macrophyte species diversity (Fig. 1).

The samples of water and macrophytes were selected at the points. To determine species diversity all the existing macrophyte species were collected at each sampling point with their further taxonomic identification. Five-grade scale was used to give a quantitative characteristic of species occurrence: 1 - rarely or isolatedly occurred species; 2 - rarely or sporadically occurred; 3 - occurred frequently enough but without dominating; 4 - occurred frequently, able to form communities; 5 - widely occurred species that make coenosis. To measure heavy metal content 3 - 6 samples of the widely occurred macrophyte species were selected at each sampling point: *Potamogeton lucens*, *Phragmites australis* и *Elodea canadensis*.

To remove sediment, roots and rhizomes were cleaned in river water and put into plastic bags. Water samples were kept in one-litre plastic bottles. Climatically identical days were chosen for sampling to eliminate weather impact on the research results. The days were sunny and not windy. Sampling was made in June - September 2017-2018. The period from June to September was chosen deliberately, as this is the vegetation time for macrophyte in the studied area. It is in this period that bioaccumulation tends to reach high concentration in macrophyte. Each sampling point was surveyed twice over the period.

Ten plant samples of each species identical in size were collected.

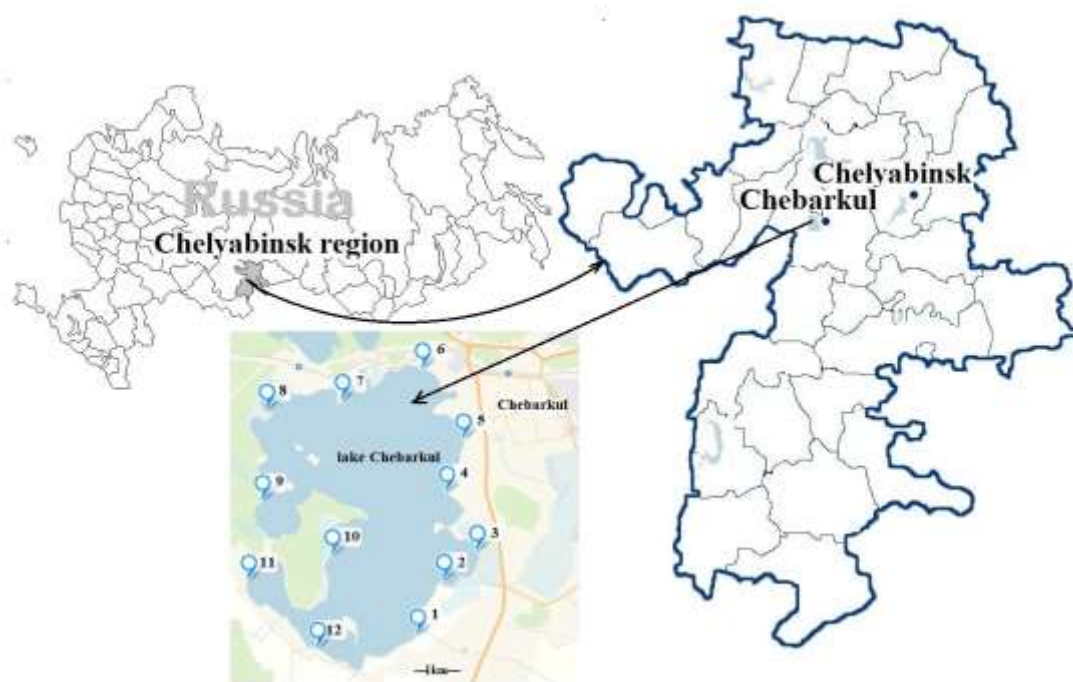


Fig. 1 Map of Lake Chebarkul and location of the sampling stations.

The plants were thoroughly washed with the stream of tub water until they appeared clean. To remove water they were intensively shaken and then were dried under the sun for 3 days. The plants were further packed in paper and delivered into the laboratory, where they were washed with distilled water, air-dried and put into the oven at 700 °C for 6 hours. Microscopy of plant surface did not reveal any evident sediment. To make a composite sample, ten plants of each group were milled with a stainless steel atomizer and then homogenized. Before analyzing the aliquots of the powder were dried again at 700 °C for a night.

### Analytical Determination of Metal Content in Macrophytes

X-ray patterns were registered in the laboratory of the Nanotechnology Centre of the South Ural State University. Spectrometer Rigaku SuperMini200 XRF was used to make an XRF analysis. The following standard samples were used: the standard sample of birch leaves GSO 8922-2007, of the mix of herbs, algae and OSO 10-150-2008 (laminaria) and GSO 8921-2007 *Elodea Canadensis*. Relative standard deviation was not more than 5%.

### Analytical Determination of Metal Content in Water

Water samples were acidized with concentrated HNO<sub>3</sub> as described in APHA [17]. Heavy metal content in water samples was determined with the atomic absorption spectrometer Analyst 400 (Perkin-Elmer) with a flame spraying mode. To get a standard curve in accordance with GOST 51309-99, the standard metal solution was used. All the metal concentrations were measured in the laboratory of the South Ural Public Centre of the Ilmen State Reserve of the Ural Department of Russian Academy of Sciences.

### Data Processing

The total weight of each heavy metal can be calculated on the results of XRF. The data about the content (mkg/g) used in the present study is made of the heavy metal weight divided into the dry weight (DW) of macrophyte samples. Software Microsoft Excel 2013 and SPSS 24.0 was used to manage and analyze data. The difference in heavy metal concentrations between species and lakes was analyzed with the help of ANOVA with subsequent comparison performed using the least significant Fisher difference (LSD).

The data was analyzed using graphs that were made by calculating similarity based on the Serensen coefficient as the affinity index, taking into account the positive matches for the cluster analysis. The

graphs were calculated using a special software module "Graphs" [18].

## RESULTS AND DISCUSSION

The lake vegetation is diverse enough and well-developed. In shallow waters macrophytes are distributed evenly with the zones covering relatively large areas towards the basin (covering up to 100 % locally). The formed communities cover the bottom up to the depth of 3.0-4.0 m in average. Some species such as *Fontinalis antipyretica* and representatives of *Charophytes* are met at the depth of 5 m.

About 90 species of macrophytes of 35 families were identified, 53 (59 %) of them are water plants and 33 (41 %) are coastal. We think that some species were not covered, as we did not take tree species into account. Besides, the given research aimed to study lake ecosystem, so the small rivers and streams entering the lake were not considered.

Analyzing sampling points results in classifying them into four groups according to the common vegetation associations and man-made impact that was described in grades (Fig. 2).

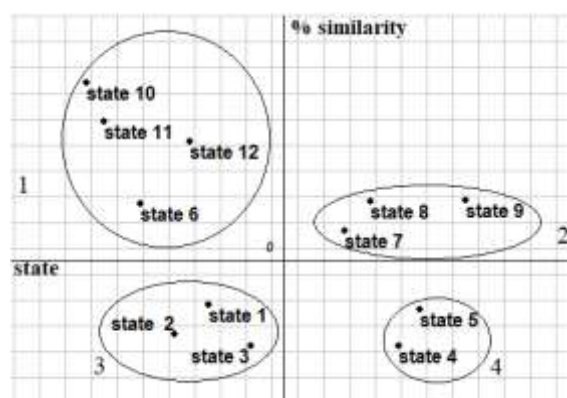


Fig. 2 The four groups of sampling points.

The first group (0 grade) comprises the sampling points that are not under a man-made impact (6, 10-12). The second group (1 grade) presents a recreation territory that is under a significant tourist-made impact (7-9). The third (2 grades) is located in the zone that is affected by the households of small villages on the coasts (1-3). The fourth point (3 grades) is the area under an adverse impact of both domestic and commercial character, its situated within the limits of Chebarkul (a town in the Chelyabinsk region).

Heavy metal concentrations in the sampling points do not exceed the maximum permissible concentration, but their statistically significant differences are marked (Table 1). Heavy metal content in water is not homogenous in space and depends on the proximity to the pollutant.

Table 1 Metal content in lake water, mg·L<sup>-1</sup>

| Metal | Group         |               |
|-------|---------------|---------------|
|       | 1             | 2             |
| Mn    | 0.015±0.002   | 0.028±0.005   |
| Fe    | 0.026±0.006   | 0.031±0.006   |
| Cu    | 0.0018±0.0008 | 0.0012±0.0008 |
| Zn    | 0.002±0.001   | 0.0018±0.001  |
|       | 3             | 4             |
|       |               |               |
| Mn    | 0.021±0.006   | 0.025±0.002   |
| Fe    | 0.028±0.006   | 0.028±0.006   |
| Cu    | 0.0020±0.0006 | 0.0023±0.0008 |
| Zn    | 0.0032±0.001  | 0.0039±0.002  |

Species diversity of some families differs with the groups of sampling points, e.g., *Potamogeton*, *Hydrocharitaceae*, *Polygonaceae*, *Nymphaeaceae*, *Characeae* and *Ranunculaceae*. Unlike groups 3 and 4, groups 1 and 2 have a richer diversity of these species.

The qualitative analysis shows that the studied areas do not significantly differ in taxonomic diversity of water flora. According to the collected data macrophyte species composition of group 1 includes 90 species of 35 families. Many species are met here including *Characeae*, water moss (*Fontinalis*), some species of *Potamogeton*, some species of hygrophytes growing in swamps. The list of macrophytes of this group includes all the registered in the lake Chebarkul species belonging to the general list. Groups 2 (82 species of 34 families) and 1 are 91 % close in species composition. Species composition of group 3 is even lower (71 species of 32 families). Group 4 is characterized by a much poor species diversity (69 % of the general list, 62 species of 26 families, namely). Rare species of some families such as, *Alismataceae*, *Araceae*, *Ranunculaceae*, *Primulaceae*, *Lamiaceae*, *Scrophulariaceae*, *Lentibulariaceae*, *Potamogetonaceae*, *Characeae* are met in groups 1 and 2. That can be associated with natural eutrophication of these sampling points. Overgrowing of the sampling points of group 3 and 4 is accelerated due to the man-made impact of the territory: the flora of sensitive species becomes poor, but weeds do richer, on the contrary.

The analysis shows that the studied lake parts significantly differ in the frequency of occurrence of general species. Overgrowing, which is higher in groups 4 and 5, contributes to it.

The research reveals the abundant growth of *Potamogeton lucens* L., *Phragmites australis* L. and *Elodea canadensis* L. in all the studied lake parts. These species were chosen to study heavy metal content.

Mn > Fe > Cu > Zn is the ratio we got as a result (Table 2).

Table 2 Mean values (±standard errors), mg·kg<sup>-1</sup>DW, for all HM concentrations in macrophytes

| Metal                   | Group    |          |          |           |
|-------------------------|----------|----------|----------|-----------|
|                         | 1        | 2        | 3        | 4         |
| <i>P. lucens</i>        |          |          |          |           |
| Mn                      | 790±121a | 818±104a | 821±58a  | 990±68a   |
| Fe                      | 503±132a | 536±118a | 590±67a  | 689±68a   |
| Cu                      | 36±6a    | 35±5a    | 46±5a    | 49±5a     |
| Zn                      | 22±4a    | 27±6a    | 38±5a    | 39±5a     |
| <i>P. australis</i> L.  |          |          |          |           |
| Mn                      | 890±101a | 857±115a | 921±67b  | 1098±118a |
| Fe                      | 519±32a  | 521±108b | 691±77a  | 789±54a   |
| Cu                      | 37±5a    | 42±5a    | 53±6a    | 58±6b     |
| Zn                      | 26±4a    | 29±4b    | 38±4b    | 38±5a     |
| <i>E. canadensis</i> L. |          |          |          |           |
| Mn                      | 779±119a | 793±125b | 802±117a | 956±61a   |
| Fe                      | 398±108b | 403±82c  | 452±97b  | 487±106b  |
| Cu                      | 35±6b    | 34±5b    | 41±6b    | 45±6c     |
| Zn                      | 21±6b    | 27±5b    | 28±4a    | 28±4b     |

Note: Different letters indicate significant differences among the species according to Fisher's LSD (p<0.05).

Mn content in plant organs is usually from 10 to 25 mg/kg [19], which is enough for most of the plants in terms of physiology. Very high levels of Mn were registered in *P. lucens* (790-990 mg·kg<sup>-1</sup>DW) and *E. canadensis* L. (779-956 mg·kg<sup>-1</sup>DW). Such concentrations in water are known as toxic for most of the plants [20], [21]. But, as it was stated before, water was not polluted by Mn. The higher Mn content in the plant organs can show a positive effect macrophytes have on the purification of the lake water from Mn compounds in relation to physiological needs, and can be a genetic feature [19].

Fe content remains at 398-789 mg·kg<sup>-1</sup>DW. The metal is necessary for the plant metabolism [22]. As a rule, Cu content (36-58 mg·kg<sup>-1</sup>DW) and Zn content (21-39 mg·kg<sup>-1</sup>DW) in the studied macrophytes are within the natural level for water plants [19]. All plants have a high accumulation of manganese and iron (Table 2), while the accumulation of copper and zinc is negligible.

## CONCLUSIONS

Thus, the composition of ecological groups of macrophytes in relation to the water factor is one of the most of water-bodies. The local flora of even one water-body has some differences. The first group has a higher level of taxonomic diversity and the diversity of ecological forms of plants. This is due to the large variety of microbiotopes and the lack of man-made impact. Statistically significant differences were found between the accumulation of

Fe > Cu > Zn in *E. canadensis* L. compared to *P. lucens* L., *P. australis* L. No such trend was found for Mn. There is an urgent need for such studies to identify more species capable of the greatest bioaccumulation.

## REFERENCES

- [1] Bastian R.K. and Hammer D., The Use of Constructed Wetlands for Wastewater Treatment and Recycling, In Constructed Wetlands for Water Quality Improvement, Moshiri, Ed., Lewis Publishers, CRC Press: Boca Raton, FL, 1993, pp. 1-59.
- [2] Guzma H.M. and Jimenez C.E., Contamination of coral reefs by heavy metals along the Caribbean coast of Central America (Costa Rica and Panama), Marine Pollution Bulletin, Vol. 24, 1992, pp. 554-561.
- [3] Gonzalez H., Pomares M., Ramirez M. and Torres I., Heavy metals in organism and sediments from the discharge zone of the submarine sewage outfall of Havana city, Cuba, Marine Pollution Bulletin, Vol. 38, 1999, pp. 1048-1051.
- [4] Echols K.R., Meadows J.C. and Orazio C.E., Pollution of aquatic ecosystems II: hydrocarbons, synthetic organics, radionuclides, heavy metals, acids, and thermal pollution. In Encyclopedia of inland waters, Likens G.E., Ed., Cambridge: Elsevier/Academic Press, 2009, pp. 120-128.
- [5] Kar R.N., Sahoo B.N. and Sukla L.B., Removal of heavy metal from mine water using sulphate reducing Bacteria, Pollution Research, Vol. 11, 1992, pp. 1-13.
- [6] Gratão P.L., Prasad M.N.V., Cardoso P.F., Lea P.J. and Azevedo R.A., Phytoremediation: green technology for the clean up of toxic metals in the environment, Brazilian Journal of Plant Physiology, Vol. 17, 2005, pp. 53-64.
- [7] Mejare M. and Bulow L., Metal-binding proteins and peptides in bioremediation and phytoremediation of heavy metals, Trends Biotechnology, Vol. 19, 2001, pp. 67-73.
- [8] Prasad M.N.V., Freitas H. and Pratas J., Metal tolerant plants and biodiversity prospecting to promote phytotechnologies for cleanup of metals in the environment, in Trace elements in the environment: Biogeochemistry, Biotechnology and Bioremediation, CRC Press, M.N.V. Prasad, K.S.Sajwan, and Ravi Naidu, Eds, 2005, pp. 483-506.
- [9] Vardanyan L.G. and Ingole B., Studies on heavy metal accumulation in aquatic macrophytes from Sevan (Armenia) and Carambolim (India) lake systems, Environment International, Elsevier, Vol. 32, 2006, pp. 208-218.
- [10] Malec P., Mysliwa-Kurczel B., Prasad M.N.V., Waloszek A. and Strzałka K., Role of aquatic macrophytes in biogeochemical cycling of heavy metals—relevance to soil: sediment continuum detoxification and ecosystem health, in Detoxification of Heavy Metals. Soil Biology, I. Sherameti and A. Varma, Eds., Springer-Verlag Berlin Heidelberg, Vol. 30, 2011, pp. 345-368.
- [11] Krupnova T.G., Mashkova I.V., Kostryukova A.M., Schelkanova E.E. and Gavrilkina S.V., Gastropods as potential biomonitors of contamination caused by heavy metals in South Ural lakes, Russia, Ecological Indicators, Vol. 95, 2018, pp. 1001-1007.
- [12] Cardwell A.J., Hawker D.W. and Greenway M., Metal accumulation in aquatic macrophytes from southeast Queensland, Australia, Chemosphere, Vol. 48, 2002, pp. 653-663.
- [13] Mashkova I.V., Krupnova T.G. and Kostryukova A.M., Water quality and aquatic macrophytes interrelationships for selected reserved lakes of south ural, International Multidisciplinary Scientific GeoConference Surveying Geology and Mining Ecology Management, SGEM, Vol. 1, Issue 3, 2015, pp. 763-770.
- [14] Prasad M.N.V. and Freitas H., Metal hyperaccumulation in plants - Biodiversity prospecting for phytoremediation technology. (Review article), Electronic Journal of Biotechnology, Vol. 6, 2003, pp. 275-321.
- [15] Krupnova T.G., Mashkova I.V., Kostryukova A.M. and Artyukov E.V., The distribution and accumulation of chemical elements in the ecosystem of lake Ilmenskoe, International Journal of GEOMATE, Vol. 12, Issue 34, 2017, pp. 82-88.
- [16] Krupnova T.G., Mashkova I.V., Kostryukova A.M., Egorov N.O. and Gavrilkina S.V., Bioconcentration of heavy metals in aquatic macrophytes of South Urals region lakes, Biodiversitas, Vol. 19, Issue 1, 2018, pp. 296-302.
- [17] APHA, Standard Methods for the Examination of Water and Wastewater, American Public Health Association, Washington DC, 1998.
- [18] Nowakowski A.B., Possibilities and principles of operation of the software module "Graphs", Automation of scientific research, Issue 27, 2004, pp. 1-31.
- [19] Parzych A., Cymer A. and Macheta K., Leaves and roots of *Typha latifolia* L. and *Iris pseudacorus* L. as bioindicators of contamination of bottom sediments by heavy metals, Limnol. Rev., Vol. 16, Issue 2, 2016, pp. 77-83.
- [20] Bonanno G., Comparative performance of trace element bioaccumulation and biomonitoring in the plants species *Typha domingensis*, *Phragmites australis* and *Arundo donax*,

- Ecotoxicol Environ Saf, Vol. 97, 2013, pp. 124-130.
- [21] Bonanno G and Lo Giudice R., Heavy metal bioaccumulation by the organs of *Phragmites australis* (common reed) and their potential use as contamination indicators, *Ecol Indic*, Vol. 10, 2010, pp. 639-645.
- [22] Kumari M. and Tripathi B.D., Efficiency of *Phragmites australis* and *Typha latifolia* for heavy metal removal from wastewater, *Ecol Environ Saf*, Vol. 112, 2015, pp. 80-86.



## GROUND REACTION FORCE OF STEP MARCHING: A PILOT STUDY

Pairaya Sitthiracha<sup>1</sup>, Wichai Eungpinichpong<sup>2,3</sup>

<sup>1</sup>Human Movement Science, Faculty of Associate Medical Sciences,  
Khon Kaen University, Thailand

<sup>2</sup>School of Physical Therapy, Faculty of Associated Medical Sciences, Khon Kaen University, Thailand

<sup>3</sup>BNOJHP research center, Khon Kaen University, Thailand

### ABSTRACT

Step marching is rhythmic movement of lower extremity which combines with hip, knee and ankle joints movement. The rhythmic movement requires standing on one leg that involves voluntary action of moving the center of mass over the upcoming stance leg. Step marching has been used for body balance training methods for elderly people because it is relatively simple and save for practicing. The amount and direction of ground reaction force during step marching, that affect standing balance, have not been thoroughly explored. The objective of this study was to compare effect of two difference types of marching (comfortable marching and marching at 90-degree of hip and knee flexion) with walking on vertical ground reaction force (VGRF). Ten healthy subjects (5 males and 5 females), aged  $27.6 \pm 3.9$  years (mean  $\pm$  SD) participated. Each of the subjects underwent tested with step marching with the two conditions for 2 minutes, and 10 rounds of preferred-speed walking on 2 force platforms. VGRF was measured by Smart analyzer®, BTS Bioengineering software. Paired t-test revealed significantly difference in VGRF among the two conditions of step marching and walking where step marching of the 90-degrees hip and knee flexion showed the highest mean value ( $11.23 \pm 0.5$  N/kg) whereas walking condition showed the lowest ( $10.09 \pm 0.6$  N/kg). Two types of step marching provide slightly higher VGRF than walking. They could be used to challenge on balance training for the elderly people in case of weight bearing to bones and joints are required for progressive strength training of the lower limbs.

*Keywords: Marching, Walking, Vertical ground reaction force, Healthy*

### INTRODUCTION

Step marching is rhythmic movement of lower extremity which required hip, knee and ankle joint movement. This movement requires 2 main movements where one leg stands and another one leg raises from the ground. While standing on one leg, center of mass of the body was adjusted by voluntary action of upcoming stance and stand legs [1]. Dingenen investigated muscle activating in double leg stance to single leg stance. The result shows that lower limb muscles are included Vastus lateralis, Tibialis anterior, Peroneus, Vastus medialis, Tensor fasciae latae, Hamstring, Gluteus medius, Gastrocnemius were activated [2]. Similarly, Iverson indicated that performance of single leg standing in relation with the torques of the hip flexors, extensors, and abductor [3]. Step marching, has been applied as a simple field test for assessment for aerobic endurance of the elderly people. Moreover, it has been frequently used as one of balance exercises to reduce falls in the elderly [4]-[6].

While doing step marching, vertical ground reaction will deliver force to the feet into 3 directions including vertical, antero-posterior and medio-lateral [7], [8]. Among these, the vertical ground reaction force (VGRF) has been known to be the most prominent. Ground reaction forces can play in a role in challenging body balance control by

sending shock waves through receptors from lower extremity to central nervous system [9]. Moreover, the ground reaction force in other conditions such as fast walking, jogging and running are 1.15-2.45 BW which could be harmful to the joints of the elderly due to the high speed of movement and body weight [10].

Ground reaction force of step marching was most likely investigated in military field. Carden and colleagues are studied ground reaction force in 24 trained soldiers and 12 untrained civilians in performed marching and five drill maneuvers on 2 separated force platforms foot. They found that ground reaction force of marching range between 1.1-1.3 N/BW [11]. Nevertheless, the amount and direction of ground reaction force during step marching, that may positively affect standing balance, have not been thoroughly explored. The objective of this study was to compare effect of two difference types of marching (comfortable marching and marching at 90-degree of hip and knee flexion) with walking on vertical ground reaction force.

### METHODS

#### Design and Setting

Quasi-experimental study was conducted in laboratory room at College of sport science, Mahidol

University Thailand.

## Participants

Ten healthy subjects (5 males and 5 females), aged  $27.6 \pm 3.9$  years (Mean  $\pm$  Standard deviation) participated in the study. Subjects were interviewed their demographic data and their physical problem by the researcher. Inclusion criteria of the study consists of no pain in lower limb extremity more than three weeks before the experimental, no limit range of motion of hip joint and knee joint, no underlying disease and abnormality of lower limb joint. Subjects were wearing a comfort shirt and shorts to avoid any uncomfortable movement.

## Intervention

Before starting intervention, subjects were sat on the chair for 5 minutes and were asked for any sign and symptoms such as dizziness and vertigo. They were instructed an intervention procedure by the researcher which included 3 trials are comfortable step marching, Marching at 90-degree and walking (Fig. 1).



Fig. 1 Pictures from left to right are comfortable step marching trials including marching at 90-degree trial and walking trial, respectively.

Comfortable step marching trial is participant flexion their hip and knee joint with comfortable speed and raise the knee to the middle of thigh for 2 minutes. The researcher measured thigh length of individual and prepared reference rope that instructed participant to reach the height level while marching. Marching at 90-degree trial is participant flexion hip and knee joints at 90 degrees with their individuals speed for 2 minutes. Walking trial is subjects were instructed to walk barefoot with their preferred walking speed for 10 rounds on 2 force plates. Subjects were instructed to walk placing their side handed foot on first force plate and followed by foot on second force plate. Vertical ground reaction force data was collected by Klistar force plate with sampling rate 100 hertz (Klistar

9260AA3; Klistar Group, Winterthur, Switzerland) and was generated data from Smart analyzer®, BTS Bioengineering software (BTS Bioengineering, Milan, Italy).

## Statistical Analyses

Descriptive statistics were used to describe baseline demographics and findings of the study. A Shapiro-wilk test was used to ensure the normal distribution of the data. Paired t-test was used to determine the differences of VGRF within group. P-value was set as less than 0.05 which defines as significantly difference within group.

## RESULTS

All 10 subjects (5 males and 5 females), aged  $26.9 \pm 4.1$  (Mean  $\pm$  SD) were participated in the study. Subjects demographic data as show in Table 1.

Table 1 Demographic data of ten subjects

| Characteristic           | Mean $\pm$ SD (n=10) |
|--------------------------|----------------------|
| Age (year)               | 26.9 $\pm$ 4.1       |
| Height (cm)              | 170.6 $\pm$ 8.7      |
| Weight (kg)              | 67.6 $\pm$ 12.2      |
| BMI (Kg/m <sup>2</sup> ) | 23.1 $\pm$ 2.5       |

Paired t-test revealed no significantly difference of VGRF (N/Kg) between right and left side in marching 90 degrees (M90\_Rt and M90\_Lt), step marching (SM\_Rt and SM\_Lt), and walking (W\_Rt and W\_Lt). All variables data are normal distribution as show in Table 2.

Table 2 Comparison VGRF between right and left side

| Variables | VGRF (N/Kg)      | p-value |
|-----------|------------------|---------|
| M90_Rt    | 11.25 $\pm$ 0.52 | 0.764   |
| M90_Lt    | 11.23 $\pm$ 0.54 |         |
| SM_Rt     | 10.37 $\pm$ 0.43 | 0.343   |
| SM_Lt     | 10.43 $\pm$ 0.51 |         |
| W_Rt      | 10.13 $\pm$ 0.84 | 0.678   |
| W_Lt      | 10.09 $\pm$ 0.62 |         |

Note: Mean $\pm$ SD., Paired t-test., p-value<0.05

Abbreviation: M90\_Rt and M90\_Lt are VGRF of Marching in 90 degrees of right and left side., SM\_Rt and SM\_Lt are VGRF of step marching of right and left side., W\_Rt and W\_Lt are VGRF walking of right and left side

No difference between VGRF of left and right so the researcher selected VGRF values of right side as a reference value. Step marching in 2 conditions and walking was significantly difference when compare

between each condition as shown in Table 3.

Table 3 Comparison between VGRF of 3 conditions of right side

| Variables        | p-value |
|------------------|---------|
| M90_Rt and SM_Rt | <0.001* |
| M90_Rt and W_Rt  | 0.004*  |
| SM_Rt and W_Rt   | 0.438   |

Note: \*= Significantly difference (p-value<0.05)

## DISCUSSION

The objective of this study is to compare effect of two difference types of step marching with walking on vertical ground reaction force (VGRF). The result shows that average VGRF of marching with 90 degrees has significantly highest when compared with step marching and walking. In addition, no significantly difference between step marching and walking conditions. Previous studied is investigated VGRF and running speed. They founded VGRF increasing due to a speed movement [10]. According to factor that influences VGRF are body mass and acceleration. In marching with 90 degrees, subjects need to move their segment to reach 90 degrees by pushing down against the force plate more than other 2 conditions. According to similarly average VGRF between step marching and walking, it seems to participant exert their force to achieve the movement equally.

The result shows that while marching an average between 1-1.2 bodyweight of impact force in female and male young adults and have per 1 bodyweight on walking. In similarly with previous study, Carden and colleagues founded marching has average VGRF between 1.1 -1.2 percent bodyweight in trained men and women but VGRF has increased to 1.3 percent bodyweight in untrained men [11]. Hamill and colleagues also examined VGRF on running and walking conditions. They revealed that walking with speed 1.36 m/s-1 has average VGRF is 7.78 N/kg [12]. Keller and colleagues demonstrated that maximum VGRF also gradually increase for 1.15-2.45 and 1.23-2.38 of percent body weight in female and male, respectively when speed is also increasing from 1.5-6.0 m/s-1 [10]. The result indicates that marching exercise seem to gain less impact force than jogging which not induces physical activity injurious in the elderly especially in running. There were four limitations in the study. Firstly, the researcher did not use metronome to control speed of marching in both conditions. Secondly, the researcher did not control movement of upper extremity while marching. Thirdly, this study should increase number of subjects to ensure effect of marching on VGRF. Fourthly, the future study should increase sample size and control speed of step marching.

## CONCLUSION

The objective of this study was to compare effect of two difference types of marching with walking on average VGRF. The average VGRF were collected from force plate and computed by software. Marching at 90 degrees has higher average VGRF more than comfortable step marching and walking conditions. Interestingly, the similarity of average VGRF between comfortable step marching and walking may lead to conduct marching (1-1.2 BW) as an exercise for elderly which should not induce physical activity injurious as jogging and running (1.5-2.45 BW) may do.

## ACKNOWLEDGMENT

I would like to grateful thanks to Dr. Wichai Eungpinichpong, Ph.D. for kindly suggest and editor of my study. I would like to appreciate helpful to lab officer for kindly help about the instrumentation in this study and all participants from College of sport science, Mahidol University.

## REFERENCES

- [1] Jonsson E, Henriksson M, Hirschfeld H., Age-related differences in postural adjustments in connection with different tasks involving weight transfer while standing. *Gait & Posture*, Vol. 26, Issue 4, 2007, pp. 508–515.
- [2] Dingenen B, Janssens L, Claes S, Bellemans J, Staes FF., Lower extremity muscle activation onset times during the transition from double-leg stance to single-leg stance in anterior cruciate ligament reconstructed subjects. *Clinical Biomechanics*, Vol. 35, 2016, pp. 116–123.
- [3] Iverson BD, Gossman MR, Shaddeau SA, Turner ME., Balance performance, force production, and activity levels in noninstitutionalized men 60 to 90 years of age. *Physical Therapy*, Vol. 70, Issue 6, 1990, pp. 348–355.
- [4] Sherrington C, Whitney JC, Lord SR, Herbert RD, Cumming RG, Close JCT., Effective Exercise for the Prevention of Falls: A Systematic Review and Meta-Analysis. *Journal of the American Geriatrics Society*, Vol. 56, Issue 12, 2008, pp. 2234–2243.
- [5] Thiamwong L, Suwanno J., Effects of Simple Balance Training on Balance Performance and Fear of Falling in Rural Older Adults. *International Journal of Gerontology*, Vol. 8, Issue 3, 2014, pp. 143–146.
- [6] Sherrington C, Tiedemann A., Physiotherapy in the prevention of falls in older people. *Journal of Physiotherapy*, Vol. 61, Issue 2, 2015, pp. 54–60.

- [7] Tresilian J., *Sensorimotor Control and Learning: An Introduction to the Behavioral Neuroscience of Action*. Macmillan International Higher Education, 2012, pp. 1-192.
- [8] Redfern MS, Cham R, Gielo-Perczak K, Grönqvist R, Hirvonen M, Lanshammar H., *Biomechanics of slips*. *Ergonomics*, Vol. 44, Issue 13, 2001, pp. 1138–1166.
- [9] Nigg BM, Wakeling JM. *Impact Forces and Muscle Tuning, A New Paradigm*. *Exercise and Sport Sciences Reviews*, Vol, 29, Issue 1, 2001, pp. 37.
- [10] Keller T, Weisberger A, Ray J, Hasan S, Shiavi R, Spengler D., *Relationship between vertical ground reaction force and speed during walking, slow jogging, and running*. *Clinical Biomechanics*, Vol. 11, Issue 5, 1996, pp. 253–259.
- [11] Carden PPJ, Izard RM, Greeves JP, Lake JP, Myers SD., *Force and acceleration characteristics of military foot drill: implications for injury risk in recruits*. *BMJ Open Sport Exercise Medicine*, Vol. 1, Issue 1, 2015, pp. 1-7.
- [12] Hamill J, Bates BT, Knutzen KM., *Ground Reaction Force Symmetry during Walking and Running*. *Research Quarterly for Exercise and Sport*, Vol. 55, Issue 3, 1984, pp. 289–293.

## THE EFFECTS OF WATERING RATES USING THE DRIP IRRIGATION METHOD ON THE ROOT MASS GROWTH OF BIRD'S NEST FERNS

Sawat Pimsuwan<sup>1</sup> and Dowroong Watcharinrat<sup>1</sup>

<sup>1</sup> Faculty of Agricultural Technology, Rajamangala University of Technology Thanyaburi, Thailand

### ABSTRACT

The increasing demands of gardeners have made peat moss a popular option as a planting material. However, the price of peat moss has increased recently. Therefore, alternative substances for use as a planting material need to be studied. The root of the bird's nest fern offers a cheaper, easier to produce and more readily available source for a planting material than peat moss. The objective of this research was to increase root mass growth by using drip irrigation. With an experimental design using CRD, two-year old bird's nest ferns with root mass sizes of 5 inches were watered by means of a drip irrigation method at rates of 200, 400, 600, 800 and 1,000 ml every 3 days. The data measured were root mass height, root mass diameter, leaf length, leaf width and canopy width. The data were analyzed by ANOVA and the differences between the means of treatment were compared by DMRT. The research found that the ferns which received water at a rate of 800 ml produced a root mass height of 11.06 cm and a root mass diameter of 11.93 cm. They were significantly different ( $p < 0.05$ ). The ferns which received water at a rate of 200 ml produced a leaf length of 29.52 cm and a leaf width of 9.55 cm. The amount of water causes fern growth to significantly different ( $p < 0.01$ ). The 800 ml rate of drip irrigation also produced the largest canopy width of 48.12 cm.

**Keywords:** Drip irrigation, *Asplenium nidus*, root mass bird-nest fern, peat moss

### INTRODUCTION

The bird's nest fern (*Asplenium nidus*) is an epiphyte fern. It is native to the tropical rain forests in South East Asia and Africa [1]. The fronds (leaves) are slender, like a sword, and grow from the top center of the rhizome in the root mass. The fronds can have many shapes: wide-short, narrow-long or some frond tips are forked. In the rainy season, some fronds can grow to lengths of 150 cm and widths of 20 cm. Fronds are shiny green, smooth, thin leaves with curly, black midribs. Dark brown indusium covered sorus, which develop from sporangium (spore producers), have many parallel lines arranged obliquely toward the center of the back of the fronds [2].

This fern provides an important role for the natural nutrient cycle in tropical rain forest canopies [3], [4], [5]. Moreover, it offers a cool and moist microhabitat for the canopy [6].

The bird's nest fern offers many advantages. It can be used for ornamental plants, potted plants, hanging plants, and even mounted plants on tree branches in gardens. It also possesses medicinal benefits. Its antibacterial qualities justify its usage in traditional medicines [7], [8]. Furthermore, it can be used as food [9].

In its natural state, the root mass of this fern protects the rhizomes which grow in the middle of it. These can attach to large tree branches or other things with root masses.

The roots of the bird's nest fern develop cellulose in cell wall appositions with yellow-brown pigments. There are different shapes and sizes which occur in the epidermal and the cortex of old roots [10]. When considering the benefits of natural materials such as these ferns, it is especially interesting to explore their use in making planting material.

Currently, the most popular plant growing material in horticulture is peat moss. In world production, about 50 percent of peat moss is used for agriculture purposes and the rest is used for energy [11]. In the growing media of almost all commercial greenhouses, peat moss is used because of its nutrient content and low pH [12]. Furthermore, it doesn't damage young plant roots, leaves plenty of air space for oxygen flow and allows for greater absorption of water for plant growth. This is why peat moss is popular for use as a planting material; it offers a high-quality horticultural growing media [13], [14], [15], [16]. Also, peat moss is suitable for fern spore germination in the early development stage of gametophytes and transitioning into the young sporophyte phase [17]. Gardeners can buy peat moss from garden centers or specialty shops but the price has increased rapidly [18]. Peat land is a source of atmospheric methane (CH<sub>4</sub>) and a source of carbon (C) in the form of dissolved organic carbon (DOC) [19], [20]. Greater use of peat moss has been shown to damage the environment [21], [22]. Peat moss extraction is a significant source of greenhouse gases

as well as a user of large amounts of land for its growth [23], [24].

Research objectives need to focus on the possibility of using bird's nest fern roots instead of peat moss. This fern can be easily grown in the general climate [25]. But the roots of this fern can sometimes not be of sufficient size. Increasing root size by watering using the drip irrigation method has been shown to be successful in previous experiments with vegetables [26], [27]. Therefore, applying this methodology to the bird's nest fern roots should produce results that enhance their size.

## METHOD

### Material preparation

*Preparation of plants:* A total of 80 plants were used in this study. All plants were two-year old bird's nest ferns. They were all planted in 6 inch pots.

*Preparation of drip irrigation system:* The system is made up of a drip head, capillary tube, joints and a water tank. All of these parts are connected to create the system, along with a cylinder and a measurement tool.

*Preparation of finely ground of bird nest fern root:* The bird's nest fern is finely ground using a grinder and sieve.

### Method

With an experimental design using CRD, two-year old bird's nest ferns with root mass sizes of 5 inches were watered by means of a drip irrigation method at rates of 200, 400, 600, 800 and 1,000 ml every 3 days. The data measured were root mass height, root mass diameter, leaf length, leaf width and canopy width. The data were analyzed by ANOVA and the differences between the means of treatment were compared by DMRT.

## RESULT

The growth of the root mass of bird's nest ferns as a result of using a drip irrigation method was studied over 12 weeks. The ferns which received water at a rate of 800 ml developed the best root mass height of 11.06 cm and the biggest root mass diameter of 11.93 cm. (Table 2, Fig.4,6,7) They were significantly different ( $p < 0.05$ ). The ferns which received water at a rate of 200 ml produced the longest leaf length of 29.52 cm and the widest leaf width of 9.55 cm. (Table 2, Fig.1,8) The amount of water causes fern growth to significantly different ( $p < 0.01$ ). The ferns which received water at a rate of 800 ml produced the largest canopy width of 48.12 cm. (Table 2, Fig.4,9)

Table 1 The growth of bird's nest ferns by drip irrigation every three days over 12 weeks

| Water rate(ml) | Growth of bird's nest fern ( $\bar{x}$ /cm) |         |
|----------------|---|---------|
|                | RMH   | RMD     |
| 200            | 10.93ab                                     | 11.68b  |
| 400            | 10.70ab                                     | 11.68b  |
| 600            | 10.56b                                      | 11.86ab |
| 800            | 11.06a                                      | 11.93a  |
| 1,000          | 10.98ab                                     | 11.73ab |
| CV%            | 2.78  | 1.14    |
| F test         | *   | *       |

RMH = Root Mass Height, RMD = Root Mass Diameter

\* = significantly different ( $p < 0.05$ )

Table 2 The growth of bird's nest ferns by drip irrigation every three days over 12 weeks

| Water rate(ml) | Growth of bird's nest fern ( $\bar{x}$ /cm) |        |       |
|----------------|---|--------|-------|
|                | LL  | LW     | CW    |
| 200            | 29.52a                                      | 9.55a  | 47.19 |
| 400            | 25.03ac                                     | 8.32c  | 44.81 |
| 600            | 24.72c                                      | 8.12c  | 45.19 |
| 800            | 27.11b                                      | 9.21ab | 48.12 |
| 1,000          | 25.15c                                      | 8.86b  | 46.56 |
| CV%            | 4.68  | 3.95   | 6.55  |
| F test         | **  | **     | ns    |

LL = Leaf Length, LW = Leaf Width, CW = Canopy Width.

ns = non-significant, \*\* = significantly different ( $p < 0.01$ )

## Figures



Fig. 1 watering rate at 200 ml





Fig. 2 watering rate at 400 ml



Fig. 5 watering rate at 1,000 ml



Fig. 3 watering rate at 600 ml

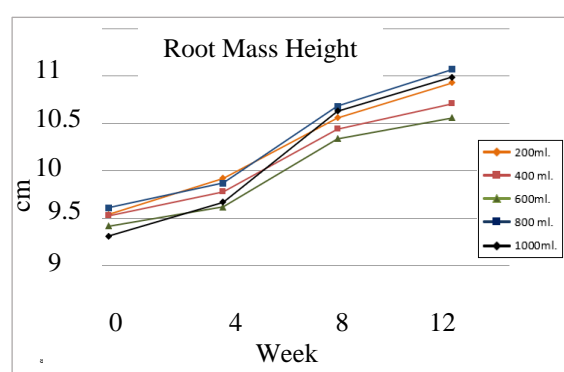


Fig. 6 Root Mass Height



Fig. 4 watering rate at 800 ml

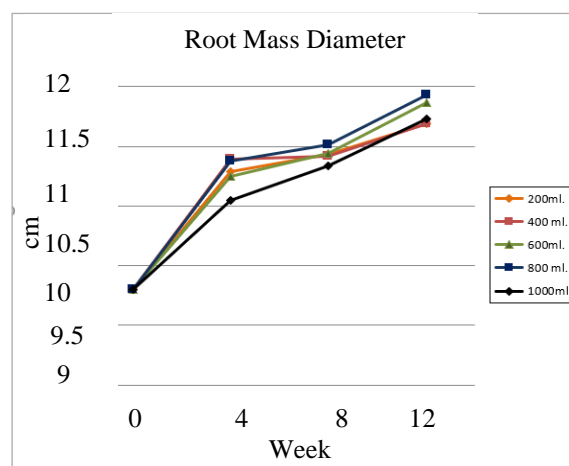


Fig. 7 Root Mass Diameter

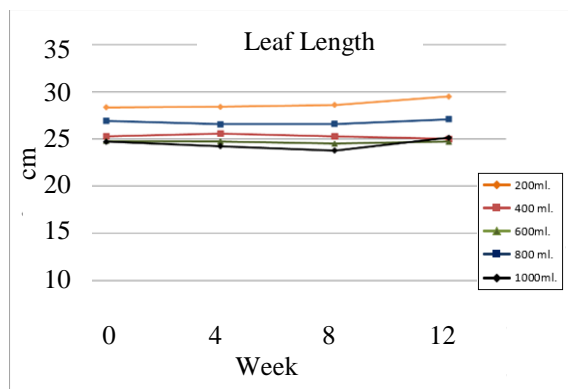


Fig. 8 Leaf Length

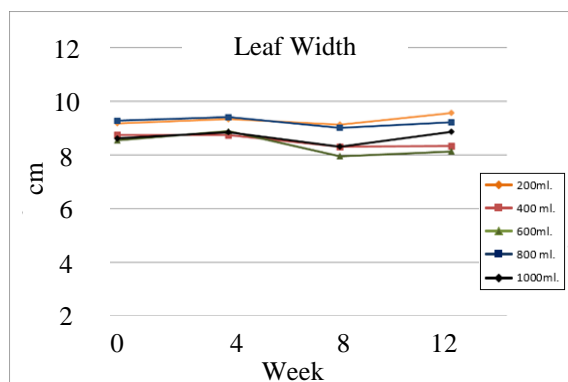


Fig. 9 Leaf Width

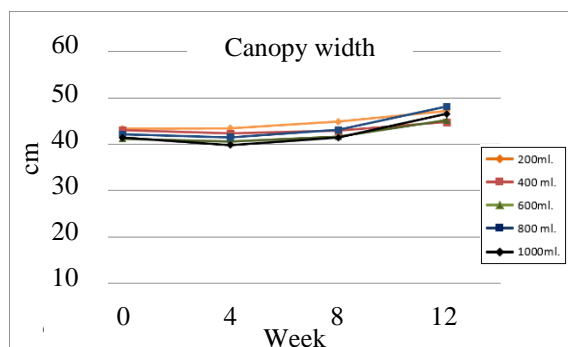


Fig. 10 Canopy Width

## CONCLUSIONS

In this study, the priority was to analyze the growth of the root mass of bird's nest ferns under different rates of watering by the drip irrigation method. The study revealed that the largest root mass height and diameter came from the watering rate of 800 ml every 3 days. Some epiphyte ferns like dry and wet water such as stag horn ferns [17]. In addition, when the root mass of the bird's nest fern becomes dry, it can absorb a lot of water during the rainy

season [28]. The root mass of this fern can be used as a fern planting material [29].

However, drip irrigation is not the best method for increasing the bird's nest fern root mass because the root epiphyte cannot absorb enough water. New studies of other methods of irrigation, including fog or mist watering, should be conducted to look for a better alternative.

## ACKNOWLEDGMENTS

This research was partially funded by The Faculty of Agricultural Technology, Rajamangala University of Technology Thanyaburi, Thailand. And this text was edited by Mr. Bruce Groening.

## REFERENCES

- [1] Liang J-Y. and Chien Y-H., Effects of photosynthetic photon flux density and photoperiod on water quality and crop production in a loach (*Misgurnus anguillicandatus*) - nest fern (*Asplenium nidus*) raft aquaponics system. International Biodeterioration & Biodegradation, Vol.102, 2015, 214-222.
- [2] Haddad S. and Bayerly R., In vitro Propagation of Ferns (*Asplenium nidus*) via Spores Culture Jordan Journal of Agricultural Sciences, Vol.10, No.1, 2014, pp.144-153.
- [3] Ainuddin N.A. and Najwa D.A.N., Growth and Physiological Responses of *Asplenium nidus* to Water Stress. Asian Journal of Plant Sciences, Vol. 8, No.6, 2009, pp.447-450.
- [4] Zhang L, Nurvianto S. and Harrison R., Factors Affecting the Distribution and Abundance of *Asplenium nidus* L. in a Tropical Lowland Rain Forest in Peninsular Malaysia. BIOTROPICA, Vol.42, No.4, 2010, pp.464-469.
- [5] Rahmad, Z. B. and Akomolafe, G. F., Distribution, Diversity and Abundance of Ferns in A Tropical University Campus. Tropical Agricultural Science, Pertanika J. Trop. Agric. Sc., Vol.41, No.4, 2018, pp.1875-1887.
- [6] Scheffers B.R., Phillips B.L. and Shoof L.P., *Asplenium* Bird's Nest Ferns in Rainforest Canopies are Climate-Contingent Refuges for Frogs. Global Ecology and Conservation, Vol.2, 2014, pp.37-46.
- [7] Nath K., Bhattacharya M.K., Sen A. and Kar S., Antibacterial Activity of Frond Extract of *Asplenium nidus* L., A Threatened Ethno-Medicinal Fern of North East India. International Journal of Pharmacognosy and Phytochemistry, Vol.28, Issue.2, 2013, pp.1169-1172.
- [8] Tahir M.M., Wai Y.C., Yaacob W.A. and Ibrahim N., Antibacterial, cytotoxicity and

- antiviral activities of *Asplenium nidus*. Journal of Chemical and Pharmaceutical Research, Vol.7, No.7, 2015, pp.440-444.
- [9] Medina M.N.D. and Cabras A.A., Gametophyte development of In Vitro cultured *Diplazium esculentum* (Retz.) and *Asplenium nidus* L. Univ. of Min. Intl. Mult. Res. Jour., vol.1, No.1, 2016, pp.143-151.
- [10] Leroux O., Leroux F., Bagniewska-Zadworna A, Knox J.P., Claeys M., Bals S. and Vian R.L., Ultrastructure and composition of cell wall appositions in the roots of *Asplenium* (Polypodiales). Micron, Vol.42, 2011, pp.863–870.
- [11] Short P. and Boudreau S., Canadian sphagnum peat moss association (CSPMA), Industry Social Responsibility Report, 2014, pp.1-44.
- [12] Gruda N., Qaryouti M.M. and Leonardi C., Growing Media. in FAO, Good Agricultural Practices for Greenhouse Vegetable Crops Principles for Mediterranean Climate Areas. Food and Agriculture Organization of the United Nations, Rome, 2013, pp.1-600.
- [13] Kern J., Tammeorg P., Shanskiy M., Sakrabani R., Knicker H., Kammann C., Tuhkanen E-M., Smidt G., Prasad M., Tiilikka K., Sohi S., Gascó G., Steiner C. and Glaser B., Synergistic use of peat and charred material in growing media – an option to reduce the pressure on peatlands? Journal of Environmental. Engineering and Landscape Management, Vol. 25, No.02, 2017, pp.160–174.
- [14] Zhao W., Li Z., Hu Y., Wang M., Zheng S., Li Q., Wang Y., Xu L., Li X., Zhu R., Resk R. and Sun Y., Development of a method for protonema proliferation of peat moss (*Sphagnum squarrosum*) through regeneration analysis. New Phytologist, 2018, pp.1-12.
- [15] Truong H.D., Wang C.H. and Kien T.T., Study on Effects of Different Medium Compositions on Growth and Seedling Quality of Two Tomato Varieties Under Greenhouse Conditions. Communications in Soil Science and Plant
- [16] Gungor F. and Yildirim E., Effect of different Growing Media on quality, Growth and Yield of Pepper (*Capsicum annum* L.) Under Greenhouse Conditions, Pakistan Journal of Botany, Vol.45, No.5, 2013, pp.1605-1608.
- [17] Pimsuwan S., Wongsrisakulkaew Y., Jumradjit N., Thumsuk P. and Mulmanee S., The Effects of Watering Frequencies and Slowreleased-fertilizer Levels on the Growth of *Platyserium coronarium* in Young Sporophyte Phase. International Journal of GEOMATE, Vol. 13, Issue 40, 2017, pp.24-28.
- [18] Sendi H, Mohamed M.T.M., Anwar M.P. and Saud H.M., Spent Mushroom Waste as a Media Replacement for Peat Moss in Kai-Lan (*Brassica oleracea* var. *Alboglabra*) Production. The Scientific World Journal, Vol.2013, 2013, pp.1-8.
- [19] Kiely G., Leahy P, McVeigh P, Lewis C, Sottocornola M, Laine A. and Koehler A-K., Peat GHG - Survey of GHG Emission and Sink Potential of Blanket Peatlands. Published by the Environmental Protection Agency, Ireland, 2018, pp.1-48.
- [20] Nawab J., Ghani J., Khan S. and Xiaoping W., Minimizing the risk to human health due to the ingestion of arsenic and toxic metals in vegetables by the application of biochar, farmyard manure and peat moss. Journal of Environmental Management, Vol.214, 2018, pp.172-183.
- [21] Hu Y., Christensen E., Restuccia F. and Rein G., Transient gas and particle emissions from smouldering combustion of peat. Proceedings of the Combustion Institute, Vol.37, 2019, pp.4035–4042.
- [22] Grand-Clement E., Anderson K., Smith D., Angus M., Luscombe D.J., Gatis N., Bray L.S. and Brazier R.E., New approaches to the restoration of shallow marginal peatlands. Journal of Environmental Management, Vol.161, 2015, pp. 417-430.
- [23] Joosten H, Peatlands, Climate Change Mitigation and Biodiversity Conservation. Printed in Denmark, 2015, pp.1-16.
- [24] Swystun K., Chen X., Lewtas K., McCandless M. and Venema H.D., Peatland mining in Manitoba's Interlake: Cumulative Impacts Analysis Focusing on Potential Nutrient Loading and Greenhouse Gas Emissions. Final report. The International Institute for Sustainable Development (IISD), 2015, pp. 1- 45.
- [25] Srivastava R. and Uniyal P.L., *Asplenium nidus*; The Bird's Nest Fern: Developmental Studies and Its Conservation. American Journal of Plant Sciences, Vol.4, 2013, pp. 45-48.
- [26] Donald J., Maxfield P., Murray D. and Ellwood M.D.F., How Tropical Epiphytes at the Eden Project Contribute to Rainforest Canopy Science. The Journal of Botanic Garden Horticulture, No.14, 2016, pp.55-68.
- [27] Al-Ghobari H.M, and Dewidar A.Z., Integrating deficit irrigation into surface and subsurface drip irrigation as a strategy to save water in arid regions, Agricultural Water Management, Vol.209, 2018, pp. 55–61.
- [28] Ainuddin N.A. and Najwa D.A.N., Growth and Physiological Responses of *Asplenium nidus* to Water Stress. Asian Journal of Plant Sciences, Vol. 8, No.6, 2009, pp.447-450.
- [29] Pimsuwan S, Hongthong P., Phattraraporn Krangpanich P. and Suwanpinta C., The Effect of Fertilizer on growth of Staghorn Fern at Seedling Stage. International Journal of GEOMATE, Vol. 11, Issue 28, 2016, pp. 2879-2882

# THE INFLUENCES OF HEAVY METALS AND MAJOR IONS IN STREAM WATERS, RUNNING IN SERPENTINE, LIMESTONE, AND CLOSED-MINE AREAS, ON MACROINVERTEBRATE COMMUNITIES, KINKI AND CHUGOKU, JAPAN

Akio Nishida<sup>1</sup> and Hiroyuki Ii<sup>2</sup>

<sup>1</sup>CLERK Memorial International High School, Hyogo, Japan

<sup>2</sup> Faculty of System Engineering, Wakayama University, Wakayama, Japan

## ABSTRACT

The influences of water chemistry on macroinvertebrate communities were investigated at 24 study sites in four areas with different geological characteristics: closed-mine, serpentine, limestone and reference areas. Our aims of this study were to clarify how macroinvertebrate communities in different geological areas are affected by chemical variables. Based on the results from nonmetric multidimensional scaling and distance-based redundancy analysis data, chemical variables in running waters had the strong relationships to macroinvertebrate communities. In a closed-mine area, they were affected by Zn and Pb, and only *Baetis* spp. was the dominant species in an environment polluted by heavy metals. In serpentine areas, water chemistry was characterized by high concentrations of  $Mg^{2+}$  and Ni, and those chemical variables affected macroinvertebrate communities. From the result of distance-based redundancy analysis, we noted that the communities in this area were classified into three groups: (1) affected by Ni, (2) affected by  $Mg^{2+}$ , and (3) affected by other heavy metals such as Zn. In limestone areas, water chemistry was characterized by a high  $Ca^{2+}$  concentration. However, we could not detect clear influences of this ion on invertebrate communities in this area. As a whole, we saw that macroinvertebrate communities were influenced by the geological characteristics of their habitats, and also saw that those characteristics were a main environmental factor in community construction.

*Keywords: macroinvertebrate, heavy metals, serpentine, limestone, geology*

## INTRODUCTION

Benthic macroinvertebrates in mountain streams, are greatly affected by chemical and physical factors. These factors include the nature of substrates forming streambeds, water temperature, and water quality, especially concerning water pollution. The size of main streambed materials affects their mobility and contributes to greater macroinvertebrate biomass. Especially, the water temperature in running water affects the emergence of aquatic insects such as *stenopsyche marmorata* (Trichoptera), which is a dominant species in Japanese rivers [1]. Water pollution has often been studied as a factor affecting macroinvertebrate community structures. Water pollution arising from drainage of industrial and closed-mine areas has been shown to affect macroinvertebrates [2]. Similar studies have also been conducted in the United Kingdom, Australia and the United States, studies that made clear that macroinvertebrate communities had been influenced by heavy metals such as Zn and Pb [3]. Water quality in running water is impacted by human activities, land use, vegetation, and main drainage. However, studies, especially those focusing on geological characteristics, of how water chemistry affects macroinvertebrate communities have been rarely conducted. Based on the hypothesis that water chemistry in running waters with

serpentine geology influences macroinvertebrate communities, we carried out this study at 24 sites with four geological characteristics: closed-mine, serpentine, limestone and reference areas.

## STUDY SITES

Eight sites (st.1–st.8) were located in the closed-mine area around the Ikuno mine in the central part of Hyogo Prefecture (Fig. 1). That mine was closed in late March, 1973 after operating for about 1200 years. The elevations of sites in this area ranged from 343 m to 513 m. Eleven sites (st.9–st.19) of serpentine geology were mostly located in Yabu City in the northern part of Hyogo Prefecture, with two of these sites (st.11 and st.12) in Oecho, Fukuchiyama City, Kyoto Prefecture (Fig. 1). All of the streambeds of the 11 sites in this area are composed of serpentine rocks and the land around the sites is largely covered by serpentine soils produced after weathering of the rocks.

Serpentine rocks in Japan, described by Suzuki [4], are found along two south–northeast-trending belts in Kyushu, Shikoku, and central and southern Honshu. The serpentine areas in Yabu City and Oecho, are two wide belts in Honshu.

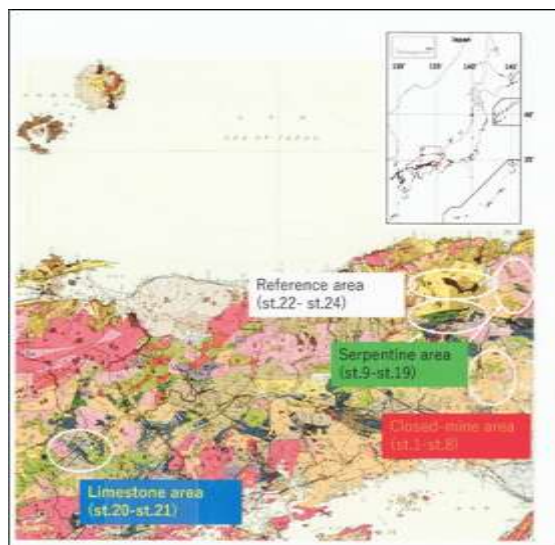


Fig. 1 Twenty-four study sites

Two sites in the limestone area were located in Taishaku Valley, Tojocho, in the northern part of Hiroshima Prefecture (Fig. 1). Two sites, st.20 and st.21, were selected in the Mito and the Taishaku rivers, respectively. The streambeds of the two rivers have substrates of limestone rocks, and are surrounded by huge limestone walls.

In addition to these sites, we selected three reference sites that were established in the Yada River system in the northern part of Hyogo Prefecture. The three sites (st.22, st.23 and st.24) were located in the Yamada, Kumanami and Konyo rivers, respectively (Fig. 1). These sites were chosen for their geological characteristics (Yamada River: sedimentary rocks; Kumanami River; quartz porphyry; Konyo River; basalt).

## SAMPLING AND ANALYTICAL METHODS

### Water Sampling and Analytical Methods

Water samples were collected in spring and autumn from 2010 to 2012. Water temperatures, pH, conductivity (EC), dissolved oxygen (DO) and total dissolved solids (TDS) were measured at the sites using a sensor probe (Horiba W-23XD). Water samples were collected in two polyethylene bottles (100 mL) before transportation to the laboratory. The water samples were analyzed by ICP-AES (inductively coupled plasma atomic emission spectroscopy) (SPS1700HVR) for measurements of heavy metal concentrations. Ion chromatographic analysis (DIONEX ICS-1500) was used to analyze other nonmetallic ions, including  $\text{Ca}^{2+}$  and  $\text{Mg}^{2+}$ . Water samples were stored in a refrigerator at about 10°C until chemical analysis was performed.

### Macroinvertebrate Collection and Identification

Benthic macroinvertebrates were qualitatively collected in spring and autumn, 2012 using a net (mesh size 0.22 mm) with a wire gauze (25 cm × 25 cm). Sampling was replicated four to eight times. The net was placed just downstream and then stones larger than about 5 cm were carefully removed. Stones were washed into the net, and substrates within the area were distributed to depths of 20 to 30 cm so that detached organisms would flow into the net. The organisms collected in the net were removed to a container half-filled with water, and those attached to stones and the net were picked off with tweezers. The contents, including the organisms, were placed into a plastic bag with a stopper and preserved in 5% formaldehyde solution. After removal to the laboratory, the organisms were sorted and counted [5]. Early instar larvae and some other organisms were not identified at species levels.

## Data Analysis

### *Multivariate analysis and ordination of macroinvertebrate communities*

First, macroinvertebrate communities were clustered into several groups by K-medoids (non-hierarchical clustering method) [6]. The number of clusters was decided by maximizing the average silhouette width [6]. Indicator species of each cluster were selected using the indicator values (IndVal) [6]. Second, we performed nMDS (nonmetric multidimensional scaling) to investigate among the 24 invertebrate communities and environmental variables. After carrying out that analysis, we conducted dbRDA (distance-based redundancy analysis) to determine the appropriate analytical method. For investigating the relationship between feeding groups of macroinvertebrates and chemical variables, dbRDA was also carried out. We performed the estimation of species diversity, clustering, nMDS and dbRDA using packages of cluster (pam), labdsv (IndVal) and vegan [7] in the software environment R 3.3.2 [8].

## RESULT

### Faunal Composition and Species Diversity

#### *Faunal composition*

Sixty-two macroinvertebrate taxa were identified from 24 sites, collected in spring and autumn, 2012. A total of 4517 individual species, were collected at 24 sites. We clustered 24 communities into six groups using the K-medoids method [6]. The results of nonhierarchical clustering were as follows: cluster1 (st.1, st.11, st.18 and st.23), cluster2 (st.2, st.3, st.14), cluster3 (st.4, st.5, st.6-st.10, st.15, st.19), cluster4 (st.13), cluster5 (st.16 and st.17) and



cluster6 (st.20-st.22, st.24). Average silhouette values of cluster1 showed a lower value (0.065) than those of other clusters, because cluster1 was represented in a variety of communities. Especially, those values at st.1 and st.11 were  $-0.097$  and  $-0.036$ , respectively. However, the average value of cluster5 was 0.800, indicating a high resemblance of communities within that cluster. Indicator species of each cluster, estimated by the IndVal method, are shown in Table 1. From cluster1 to cluster3, we could not detect a significant species ( $p < 0.05$ ). Significant indicator species from permutations were as follows: *Ephemera orientalis*

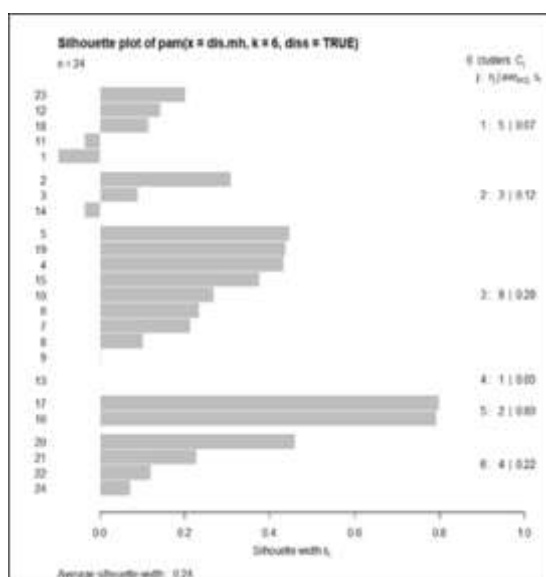


Fig. 2 Silhouette plots of 24 study sites; average silhouette width = 0.24

*Ephemera japonica*, *Epeorus ikanois* and *Epeorus curvatus* (Ephemeroptera); and *Stenopsyche marmorata* (Trichoptera).

### Species Diversity

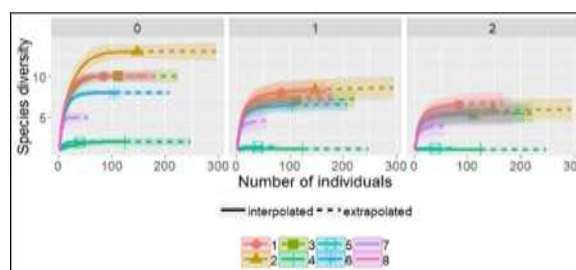
The exponential Shannon–Wiener diversity index (ESI) and Simpson’s inverse diversity index (SDI) were estimated at each site (Fig. 3[A]–[D]). In the closed-mine area, the two indexes are lower than those values in another areas. Especially, the ESI at st.4 and st.5 were quite low, at 1.153 and 1.384, respectively, in comparison with sites in the reference area. In the serpentine area, the highest value of the ESI was 12.057 at st.11, and the lowest value was 2.834 at st.16, with slightly lower values obtained in the reference area sites. In the limestone area, the ESI and SDI at two sites were quite similar with those at sites in reference area. Especially, the ESI of 11.680 at st.20, which was similar to the highest value of 12.340 at st.22.

Table 1. Indicator species of each cluster. The

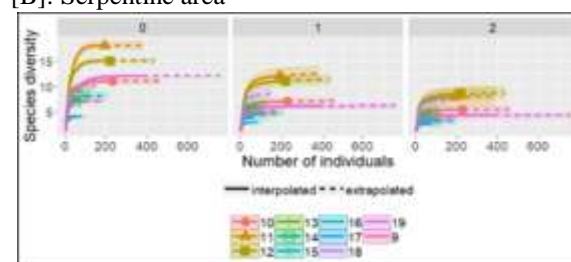
fourth column shows the IndVal values and p-values of permutations

| Cluster  | Number of sites | Average silhouette width | Indicator species (IndVal; permutation $p < 0.05$ )   |
|----------|-----------------|--------------------------|---|
| cluster1 | 5               | 0.007                    |   |
| cluster2 | 3               | 0.121                    |   |
| cluster3 | 9               | 0.280                    |   |
| cluster4 | 1               | 0.000                    | <i>Ephemera orientalis</i> (0.900; $p < 0.0386$ )   |
| cluster5 | 2               | 0.800                    | <i>Ephemera japonica</i> (0.809; $p < 0.0112$ )<br><i>Epeorus ikanois</i> (0.776; $p < 0.0256$ )      |
| cluster6 | 4               | 0.220                    | <i>Epeorus curvatus</i> (0.938; $p < 0.0002$ )<br><i>Stenopsyche marmorata</i> (0.779; $p < 0.0006$ ) |
| Total    | 24              | 0.24                     |   |

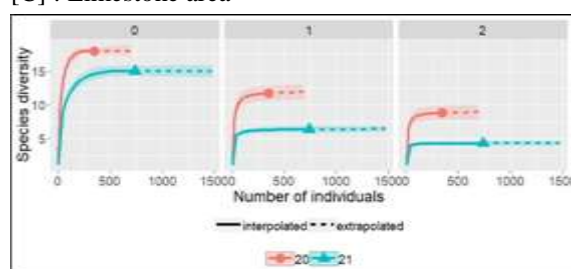
[A]: Closed-mine area



[B]: Serpentine area



[C]: Limestone area



[D] Reference area



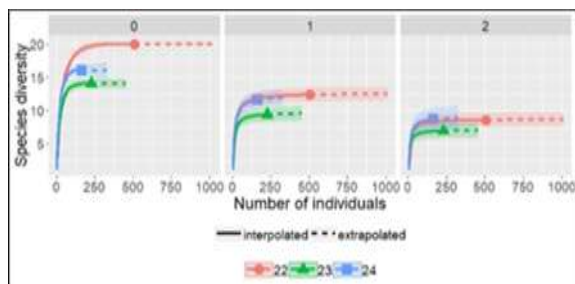


Fig. 3 Left figure (0) shows taxa number sampling at the study sites. Middle figure (1) shows the exponential Shannon–Wiener diversity index  $\{expH' = \exp[-\sum p_i \log_e(p_i)]\}$ , where  $p_i$  is the proportion of abundance for species  $i$ . Right figure (2) shows Simpson's inverse diversity index  $(1/D)$ . The dashed lines express the expectations by attenuation, and the dotted lines express the expectation by extrapolation. The shaded cones show 95% confidence intervals obtained by bootstrap methods. [A] Closed-mine area (st.1–st.8), [B] Serpentine area (st.9–st.19), [C] Limestone area (st.20–st.21). [D] Reference area (st.22–st.24)

### Water Chemistry

Table 2. Chemical variables (mean values) of the 24 study sites, especially for heavy metals, measured from spring 2010 to autumn 2012. The (\*) shows the site samplings and measurements in spring, 2012

| Study sites | Geo-logy | Pb<br>mgL <sup>-1</sup> | Cu<br>mgL <sup>-1</sup> | Zn<br>mgL <sup>-1</sup> | Ni<br>mgL <sup>-1</sup> |
|-------------|----------|-------------------------|-------------------------|-------------------------|-------------------------|
| St.1        | M        | 0.007                   | 0.001>                  | 0.046                   | 0.002                   |
| St.2        | M        | 0.057                   | 0.001>                  | 0.004                   | 0.003                   |
| St.3        | M        | 0.013                   | 0.001>                  | 0.430                   | 0.014                   |
| St.4        | M        | 0.021                   | 0.035                   | 1.273                   | 0.005                   |
| St.5        | M        | 0.116                   | 0.043                   | 1.457                   | 0.005                   |
| St.6        | M        | 0.087                   | 0.001>                  | 0.014                   | 0.002                   |
| St.7        | M        | 0.098                   | 0.138                   | 0.039                   | 0.002                   |
| St.8        | M        | 0.007                   | 0.001>                  | 0.018                   | 0.001>                  |
| St.9        | S        | 0.008                   | 0.001                   | 0.001                   | 0.022                   |
| St.10       | S        | 0.007                   | 0.002                   | 0.003                   | 0.062                   |
| St.11       | S        | 0.014                   | 0.001                   | 0.111                   | 0.011                   |
| St.12       | S        | 0.008                   | 0.001>                  | 0.003                   | 0.010                   |
| St.13       | S        | 0.080                   | 0.082                   | 0.010                   | 0.448                   |
| *St.14      | S        | 0.115                   | 0.764                   | 0.001                   | 0.588                   |
| *St.15      | S        | 0.042                   | 0.001>                  | 0.021                   | 0.019                   |
| *St.16      | S        | 0.207                   | 0.231                   | 0.021                   | 0.568                   |
| *St.17      | S        | 0.110                   | 0.232                   | 0.003                   | 0.838                   |
| *St.18      | S        | 0.129                   | 0.247                   | 0.001                   | 0.532                   |
| St.19       | S        | 0.113                   | 0.253                   | 0.006                   | 0.519                   |

|       |   |        |        |       |        |
|-------|---|--------|--------|-------|--------|
| St.20 | L | 0.004  | 0.001> | 0.001 | 0.002  |
| St.21 | L | 0.002  | 0.001> | 0.002 | 0.001  |
| St.22 | R | 0.004  | 0.001> | 0.001 | 0.001  |
| St.23 | R | 0.004  | 0.001> | 0.001 | 0.001  |
| St.24 | R | 0.001> | 1.30   | 0.001 | 0.001> |

Note: Geology: M = closed-mine area, S = serpentine area, L = limestone area and R = reference area with sedimentary rocks and basalt



Fig.4 Scatter plots between all pairs of environmental variables

Mean pH values at the 24 sites ranged from 7.1 to 8.3 with the highest values of 8.1 and 8.3 at st.20 and st.21 in limestone area. The pH values in the reference area ranged from 7.6 to 7.8, which were slightly higher than in the closed-mine and serpentine areas. The water chemistry at eight sites (st.1–st.8) in the closed-mine area was characterized by high concentrations of heavy metals, such as Zn, Pb, Cu, Fe and Mn, compared with that of three sites (St.22–st.24) in the reference area. Mean concentrations of Zn were 1.27 mgL<sup>-1</sup> at st.4 and 1.46 mgL<sup>-1</sup> at st.5, the highest values of all the sites. The other heavy metals measured at sites in the closed-mine area also were in high concentrations

(Table 2). Water chemistry in the serpentine area was characterized by very high  $Mg^{2+}$  and Ni concentrations (Table 2). In the serpentine area, the maximum concentration was  $21.3 \text{ mgL}^{-1}$  at st.10 and the minimum was  $11.9 \text{ mgL}^{-1}$  at st.19 (Table 2). The water chemistry of the sites in the limestone area was characterized by high calcium ( $Ca^{2+}$ ) concentrations at two sites,  $31.2 \text{ mgL}^{-1}$  at st.20 and  $18.0 \text{ mgL}^{-1}$  at st.21. These values were about three or five times higher than the calcium concentrations of the reference area. Correlations based on Pearson's correlation coefficient ( $r$ ) among chemical variables are shown in Fig. 4. We identified greater values in the relationships between two chemical variables as follows:  $Ca^{2+}$ – $F^-$  ( $r=0.69$ ),  $Mg^{2+}$ –Ni (0.52), Pb–Ni (0.73), Zn– $F^-$  (0.96) and Ni–Cu (0.74) (Fig. 4).

### Ordinations

We carried out nMDS mainly to investigate the relationships among 24 macroinvertebrate communities. Eigenvalues of the two axes were 1.252 (axis 1) and 1.001 (axis 2). We intended to display

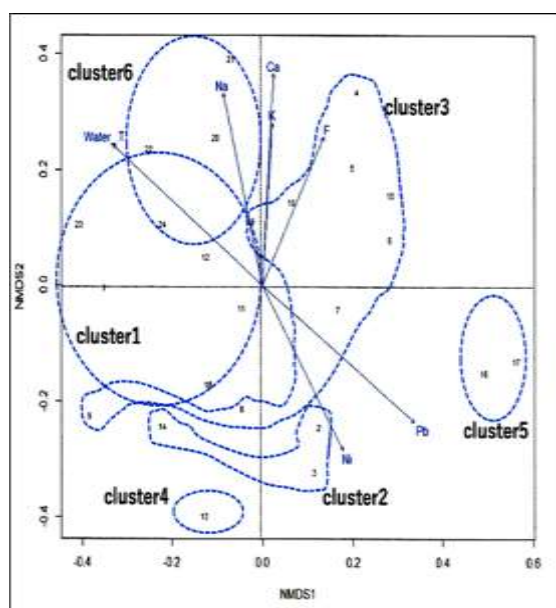


Fig. 5 Ordination by nMDS of 24 sites {distance = Morisita–Horn, stress = 0.152 (three dimension  $k = 3$ )}

six clusters, but they were impossible to describe because of nonhierarchical clustering. This nMDS ordination picked up seven significant ( $Pr < 0.1$ ) chemical variables, pointed out as vectors, such as

water T (water temperature) ( $Pr=0.004$ ),  $F^-$  (0.077),  $Na^+$  (0.023),  $K^+$  (0.100),  $Ca^{2+}$  (0.012), Pb (0.004) and Ni (0.035). Moreover, we performed dbRDA (distance-based redundancy analysis) to investigate in more detail the relationship between two. We constructed the model with six chemical variables

( $Ca^{2+}$ ,  $Mg^{2+}$ , Fe, Zn, Cu and Ni). In this model, the constrained inertia (sum of the squared distance) was 2.613 (51.6% of the total inertia). The Eigenvalues for the constrained axes were 1.381 (axis 1) and 0.708 (axis 2). We evaluated this model by ANOVA, then obtained the significant value ( $Pr(>F)=0.13$ ). In this analysis, the six clusters located separately. Cluster1 and cluster4 were widely spread above axis 1, representing the relationship to  $Mg^{2+}$ . Cluster5, located at the top of right side, showed a strong relationship to Ni. Moreover, cluster3, situated on the opposite side of cluster5, had a strong relationship to Zn.

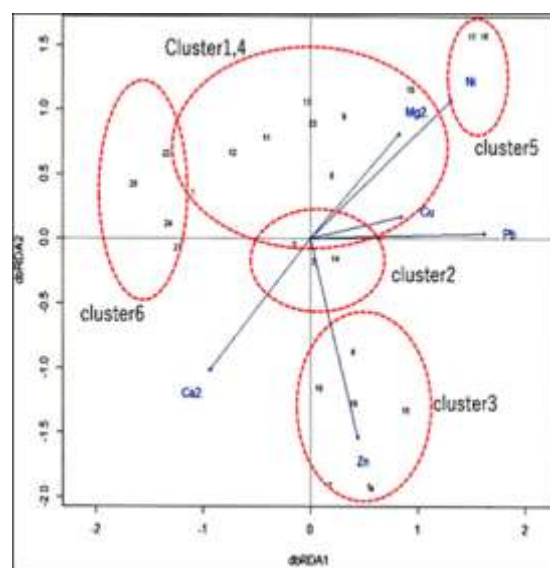


Fig. 6 Ordination by dbRDA with biplots of six chemical variables

### DISCUSSION

In the serpentine area, the richness of the chemical variables, such as  $Mg^{2+}$  and Ni, depend on the process of serpentinization, which involves the conversion of peridotite to a serpentine form mainly by hydration of primary igneous minerals [13]. Under those conditions, it might be said that the communities in serpentine area are divided into three groups: (1) one in which nickel (Ni) influences the construction of the community, (2) one that is affected by the influence of magnesium ions ( $Mg^{2+}$ ), and (3) one that is influenced by other chemical variables, such as Zn and  $SO_4^{2-}$ . From the result of dbRDA, we see that heavy metals have important roles in controlling the construction of invertebrate communities. Ii and Nishida [9] reported that *Protohemes grandis* (Neuroptera) accumulated heavy metals in their bodies. In the limestone area, it is possible that invertebrate communities are slightly affected by  $Ca^{2+}$ . However, we could not detect clear influences on invertebrate communities because of other factors, such as substratum instability, water velocity, suspended solids, and benthic algae. In the

closed-mine area, invertebrate communities might be effected by Zn, as is true in the st.10, st.15, and st.19 communities in the serpentine area. Moreover, these high concentrations probably result from the sphalerite and metal sulfides of the stream beds in this area. Under these conditions, the dominant species were *Baetis* spp. (Phemeroptera) and *Athericidae* spp. (Diptera). These species could be resistant to water pollutions, and might be a possible macroinvertebrate index of water pollution. Therefore, it is clear that most of macroinvertebrate communities in the serpentine, closed-mine and limestone areas are affected by geology, and that the geological characteristics of their habitats are the main factors that define their community structures and feeding methods.

## CONCLUSION

From this study, the water chemistry of running waters in four areas with different geological characteristics contain higher concentrations of chemical variables. Macroinvertebrate communities in the serpentine area were affected by Ni and  $Mg^{2+}$ . Depending on the effectiveness of the two ions, those communities can be classified into three groups. This is very interesting to us when considering the relationship between the community and geology. However, we cannot identify the influence of geology on the construction of communities. On the whole, geological characteristics of habitats are the main factors for the construction of macroinvertebrate communities.

## ACKNOWLEDGEMENTS

We thank Dr. Noboru Nishimura, President of Hyogo Freshwater Biology, for providing us with much useful advice and promoting our study in advance. We also thank Dr. Yoshinari and Dr. Miyahara of Idea Co., Dr. Taniguchi of Wakayama University and Mr. Nobutaka Uemura of Mitsubishi Electric Business Systems Co. for their help with analyzing the concentrations of chemical ions in the running waters and biostatistical analysis.

## REFERENCES

- [1] Nishida A., and Nishimura N., Life history (Stenopsychidae) in the Sugihara River of *Stenopsyche marmorata* Navas (Tricoptera: of Kakogawa River System.1. Voltinism, survival numbers of larvae and pupae and photoperiodic influence on the life cycle, Hyogo Fresh Water Biology, Vol.60, 2008, pp.31-51.
- [2] Watanabe N., Harada S., and Komai Y., Long-term recovery from mine drainage disturbance of a macroinvertebrate community in the Ichi-kawa River, Japan, Hydrobiologia, Vol.429, 2000, pp.171-180.
- [3] Schultheis A.S., Sanchez M., and Hendricks A.C., Structural and functional responses of stream insects to copper pollution, Hydrobiologia, Vol.346, 1997, pp.85-93.
- [4] Suzuki J., Ultramafic rocks and associated ore deposits of Hokkaido Japan, Journal of the Faculty of Science Hokkaido University, Series 5, Vol.8, 1952, pp175-210.
- [5] kawai T., and Tanida K., Aquatic insects of Japan: manual with keys and Illustrations, Tokai university Publishing, 2005, Tokyo.
- [6] Borcard D., Gillet F., and Legendre P., Numerical ecology with R -Second Edition- , Springer, New York, USA, 2011, pp59-160.
- [7] Oksanen J., Blanchet FG., Kindt R., legendre P., Minchin PR., O'Hara RB., Simpson GL., Solymos P., Stevens MHH., and Wagner H., vegan: Community Ecology package. R package version 2.0-10., Available from: <http://CRAN.R-project.org/package=vegan>, 2013.
- [8] R Core Team, R: A language and environment for statistical computing. R Foundation for statistical computing. Vienna, Austria, 2014.
- [9] Ii H., and Nishida A., Effectiveness of using river insect larvae as index of Cu, Zn and As contaminations in rivers, Japan, Second International Conference on Science, Engineering & Environment (proceeding paper), 2016.

## LANDSCAPE OPPORTUNITIES AND PREFERENCES FOR CHOOSING RECREATIONAL PLACES OF MEGALOPOLIS RESIDENTS (ON EXAMPLE OF ST. PETERSBURG)

Pogodina V.<sup>1</sup>, Matveevskaya A.<sup>2</sup>, Filippova I.<sup>3</sup>, Evseeva L.<sup>4</sup> and Evseev V.<sup>5</sup>

<sup>1</sup> Institute of Business Communication, Saint-Petersburg State University of Industrial Technologies and Design, Russia

<sup>2</sup> Department of International Relations, Saint-Petersburg State University, Russia

<sup>3</sup> Institute of Humanities and Social Sciences, Saint-Petersburg University of Management Technologies and Economics, Russia

<sup>4</sup> Humanitarian Institute, Peter the Great St. Petersburg Polytechnic University, Russia

<sup>5</sup> Institute of Physical Culture, Sports and Tourism, Peter the Great St. Petersburg Polytechnic University, Russia

### ABSTRACT

A resident of a large city is increasingly in need of a complete rest in the bosom of nature, enjoy the peace and beauty of landscapes. The administration of megacities is concerned about the problems of preserving the natural environment and creating within the city limits a network of recreational areas where recreational activities can be organized. The necessity and importance of establishing a network of specially protected natural areas within the metropolis is not in doubt. But the status of the created nature reserves implies, for the most part, prohibitions and restrictions for the organization of recreational activities. A detailed description of recreational opportunities for the rational use of individual components of the city's natural environment is presented. The authors conducted a geoecological analysis of the allocation of recreational areas in large cities. Features of nature that should be considered when designing recreational areas in large cities, on example of St. Petersburg, are noted. The process of using network of specially protected natural areas of megacities as destinations for ecological excursion and tourism activities will be optimal if the landscape features of these areas are considered, the use of modern world and domestic experience in the designing of conditions for the stay of recreants and excursionists.

*Keywords: Recreational places, Specially protected natural areas (SPNA), Geoecological analysis, Ecological tourism, Tourism-recreation activity*

### INTRODUCTION

One of the tasks of tourist-recreational activity is to optimize environmental management. Recreation in the lap of nature, using natural resources and conditions, occupies a special place in this regard. Organization of this type of recreation is designed to minimize damage to the environment [1]. Experts, discussing the organization of eco-tourism, use the following terms for its characteristics: "biotourism", "natural", "green", "soft", "quiet", "non-tech". The Russian law on tourism explains ecotourism as travel for the purpose of environmental education and training. At the same time, eco-tourism should consider the protection of local socio-cultural sphere, be economically effective and contribute to the development of those regions where it is organized [2]. Environmental protection activity (for example, garbage-collecting) is not a mandatory feature that should determine the recreational program related to eco-tourism.

The concept of the Federal target program "Development of domestic and inbound tourism in Russian Federation (2019-2025)" was approved by the order of Government of Russian Federation No. 872-p, signed on May 5, 2018. The head of Government Dmitry Medvedev points out the following: "Growing interest in cultural, educational and ecological tourism focused on recreational activities in nature is considered a global trend. This makes Russian Federation an even more attractive tourist destination for Russian and foreign tourists. The main regions for the development of eco-tourism in Russia are concentrated in Siberian, Far Eastern, Volga, Ural, North-Western, North Caucasian and Southern federal districts. The Agency of Tourism Statistics reports that more than 9 million people visit natural national parks and reserves of Russia annually" [3].

Landscape features play a leading role in eco-tourism. Natural parameters are considered as resources and conditions for organization of recreational activities by the nature of the impact on

recreation. Natural components and their combinations are evaluated as factors contributing to the development of certain types of recreational activities. Conducting the estimation of tourist-recreational potential of territory, it is necessary to determine the complex of leading conditions and factors, both contributing to and limiting the ecological and recreational development of the region [4].

St. Petersburg is known as the main center of tourism in Russia. 8.3 million tourists visited the city in 2018 [5]. Unfortunately, only a few visitors seek to re-visit St. Petersburg. At the same time, the number of residents of megapolis and the adjacent Leningrad Region exceeds 7 million people [6]. The city has gained fame as the cultural capital of country with a combination of developed infrastructure and cultural and historical resources. Traditional types of tourism are cultural, educational, business and sports and recreational. A variety of landscape conditions is a necessary and enough potential for development health, ecological, cruise and extreme types of tourism. Rural and ethnic travels are developing.

City parks and urban specially protected natural areas are the most important condition for effective recreation for residents of megalopolises and tourists arriving, and this city with different purposes. Traditional activities for the territory of Large St. Petersburg are visiting recreational natural objects, rest on nature.

## MATERIALS AND METHODS

Landscapes intended for use for recreation are studied by a special type of landscape geography - recreational landscape science. Determination of effective ways of using such complexes is the most important tasks of recreational landscape studies. Many countries worked out and widely apply a variety of techniques that allow to give a comprehensive assessment of projects of tourist and recreational development of territories. Foreign methodologies that are used to assess the projects of tourist and recreational development territories are considered: Environment Impact Assessment (EIA); Assessment of current capacity (Assessment of Carrying); Visitor load accounting (Visitor Impact Management - VIM); Limits of Acceptable Change (LAC) [7].

One of the forms of environmental management is the allocation and development of specially protected natural reservation (SPNR). Such territories have different status. Placing of industrial enterprises and carrying out agricultural work is prohibited in most of them. In some of them recreational activities are allowed. The main task of protected areas, related to nature conservation, is often in conflict with the task of increasing the intensity of tourist visits to the protected area. Recreational development of

protected areas can create a certain socio-cultural load and leads to a change in nature [8], although its scale is usually incomparably smaller compared to those in industrial and agricultural production. Uncontrolled flow of tourists can worsen the environmental situation [9]. Consequently, it minimizes the possibility of further functioning of the territory, not only as protected, but also as recreational.

The following types of assessments are necessary for research of ecological and recreational potential of SPNR:

- ecological (determination of the background ecological state of territories and water areas, identification of local areas attractive for organizing eco-tours and at the same time possessing enough environment sustainability, diagnostics of the level of environmental safety for tourists);
- technological (consideration of the functional suitability of resources);
- physiological (determining the degree of comfort conditions);
- psychological (revealing the level of aesthetic qualities);
- cost (for the calculation of tourist rent) [10].

Modern domestic practice offers tourists as an eco-tourism tours within SPNA - national and natural parks, nature reserves, etc. The objects of ecological excursion show and the territories of visiting within the framework of eco-tourism are not only natural, but also cultural attractions, including natural-anthropogenic landscapes of different genesis [11]. The choice of visited objects is determined not so much by uniqueness, but by the degree of awareness of possible visitors. One of sustainable directions of tourism development is associated with trips to unique natural and geographical objects. Destinations of eco-tourism world level are the objects of the world Natural Heritage List of UNESCO [12].

Modern vacationers are showing increasing interest in areas classified as areas with extreme natural conditions for human life. These can be spaces with a harsh cold climate, with animals that are especially dangerous to human life and health; areas which are particularly affected by the consequences of natural disasters, or anthropogenic accidents, activities that turned the area into a territory dangerous to the life and health of the person on it. Tour operators are looking for new forms of organization in such areas of recreational activities [13].

Modern man especially needs a kind of rest from the intense rhythm of city life [14]. The most common trips using natural resources are recreational (relaxation) and health (rehabilitation). Active, sports recreation takes the second place. These are rafting on rivers and lakes, including yachting, trekking, mountaineering and climbing, skiing tourism, etc. Popular leisure activities among Russian are hunting and fishing, as well as amateur collection of



mushrooms, berries, medicinal plants. Some tourists decide on nature-oriented tours with a desire to test themselves in extreme programs. So-called "survival" tours. Numerous offers on the market of recreational services relate to adventure recreation (diving, caving, visiting the area, the natural features of which are exclusively exotic, etc.) [15].

Visits of the so-called "Norwegian (rope) parks" have become very popular. Norwegian parks are particularly attractive for lowland areas devoid of significant rock formations that can attract climbers to natural obstacles [16]. The most significant problems of the development of a network of such parks are: not mandatory, but voluntary certification; lack of proper control and security; possible aggravation of environmental problems in the area where such parks are created and actively used.

Another trend of our time is the desire to use unconventional types of vehicles. Cycling is one of the available alternatives to the car. Cycling tourism is one of the types of sports tourism, which consists of cycling routes containing bicycle-specific obstacles. The problem for organizing cycling is the lack of the necessary infrastructure, including all the elements that ensure the functioning of cycling: the cycle path or cycle track system, cycle parking, signs, traffic lights, road signs for cyclists, recreation centers, rental centers and the system of supporting bicycle traffic. Cycling is becoming an increasingly popular form of outdoor activities. The growth of its popularity is associated with the fashion for a healthy lifestyle.

Experts consider equestrian tourism as a form of eco-tourism. It is gaining popularity in the global tourism industry. Equestrian tours are a range of services, including horseback riding training, classes in the open arena, rides on equestrian routes of varying degrees of difficulty, equestrian equipment, accommodation, feed and additional services. Riding skills are not required, as beginning of tourist rest is educating to the receptions of handling a horse and training on riding. The organization of equestrian routes can have a negative impact on the natural complexes along which they will pass. Designers need to consider the ecological capacity of landscape, use technologies for cleaning routes from household waste, the appearance of which is inevitable.

## RESULTS

The main feature of the climate of St. Petersburg is the lack of heat and excess moisture. The territory is in area with a shortage of ultraviolet rays. Real opportunities for climate therapy are available on the territory of Large St. Petersburg. However, the optimal period for its implementation is short. Possible strong winds of winter and autumn can be considered negative factors for the development of recreation. Squall winds with considerable power are

observed at times. Changeable mode of atmospheric pressure is determined by the geographical location of the territory. Sudden pressure drops can negatively affect the well-being of even healthy people. People with diseases of the cardiovascular system suffer the most. Variability, instability of weather creates serious difficulties for synoptic forecasting in St. Petersburg [17].

From average data a steady snow cover lies in the suburbs of St. Petersburg for about 140 days. The height of the snow cover is small due to thaws and is 30-40 cm by the end of winter [18]. However, especially warm years were observed repeatedly, when the snow-cover was not formed during all winter. This makes it difficult to predict the organization of recreation for people in the territory in winter. In general, the climatic conditions of St. Petersburg are characterized as relatively favorable: summer rest is short, unstable weather conditions; in winter, frosty weather can be replaced by long thaws.

Therapeutic recreation is organized on a large-hilly or ridge relief, where the slightly hilly or undulating terrain is relatively favorable. The relief of greater part of the described territory is exactly like that. The area, where forested hills are combined with deep hollows, is very picturesque. This nature of the surface contributes to the development of hiking and cycling. The most favorable conditions for therapeutic and recreation are available on the Karelian Isthmus in the Northern and North-Western regions of Greater St. Petersburg.

Urban areas are washed by the Gulf of Finland of the Baltic Sea. Neva connects St. Petersburg with the waters of the largest European lake - Ladoga. In St. Petersburg, the swimming season averages 60 days - from mid-June until the end of August (the duration of the swimming season is determined by the number of days with water temperatures above +170 C) [19]. The shores of the Gulf of Finland are characterized by good sandy beaches and sandy bottoms. Beaches along the Northern coast of the Gulf of Finland are especially popular in St. Petersburg. However, the beaches are not equipped with the necessary infrastructure everywhere. Vacationers accumulate in areas of equipped beaches, as a result of sanitary-hygienic indicators of the beach area are reduced. When designing a recreation area near the water, it is necessary to specify the rate of additional recreational load along the length of the coastline, depending on the specific natural complex.

Conditions for yachting are available in the Gulf of Finland. This is a large area with enough depth (from three meters) and significantly indented coastline (sailing ships can take refuge in a strong wind). However, the infrastructure for maintenance of yachts in the city still does not exist. Large urban water reservoirs are increasingly used for jet skiing, motorboats and windsurfing. The Gulf of Finland,



lakes and rivers of the region are covered with ice for more than four winter months.

Most of the rivers that flow through the territory of St. Petersburg and its suburbs have a calm, balanced character. Rivers and lakes of the suburbs of St. Petersburg allow to develop family tourism on boats and rafts. This type of tourism does not pursue sports goals, it can be practiced by people who love measured rest on the water. Water cruises (including international ones) are one of the priorities of tourism development. Large water areas can be used more intensively for motor ship, cruise tourism (Baltic, Neva, Ladoga, Svir, Onega). Some limitations to the development of ship rest will be in high rates of storm frequency, especially in the autumn months. Short waves are ways to induce a strong pitching on the Baltic and Lake Ladoga. A serious obstacle to the further development of motor ship tours is the lack of appropriate berths along the routes of vessels running. The Central part of St. Petersburg offers tourists especially popular walks on boats, river ships (including those capable of passing under low small bridges of the central part of the city).

Mineral waters and therapeutic muds are available on the territory of St. Petersburg. Sodium chloride sources related to the Cambrian deposits are found almost everywhere. These waters are represented most widely on the Karelian Isthmus (Sestroretsk, Gorskaya, Lysii Nos, Devyatkinno, Vsevolozhsk). These waters are used for balneotherapy in local health resorts, they normalize the body's metabolism, and have a beneficial effect on the activity of the central nervous system. The most famous mineral water - Polyustrovskie located on the right bank of the Neva. Sources were discovered at the beginning of the XVIII century by a court physician of Peter I, L. Blumentrost. One of the first resorts in Russia functioned here from 1721 to 1865. based on these sources [20]. Doctors prescribe the use of this water for some forms of anemia, stomach diseases, as well as a table drink. Conditions for mud therapy are also favorable. Significant reserves of sapropel mud were found on the lakes. Peat mud resources are practically inexhaustible in this territory. The use of medicinal properties of the famous Cambrian clay in St. Petersburg is just beginning.

The predominant type of vegetation is coniferous forests, characteristic of the subzone of the middle and southern taiga. The predominant tree species in the forests are spruce, pine and small-leaved trees: birch, aspen, mountain ash, etc. Taiga forests have a great healing effect on the human body due to the ionization and phytoncidal properties of plants. Pine forests have a high ionization ability, which has a cleansing effect on the human body. They are widely represented on the Karelian Isthmus, along the southern coast of the Gulf of Finland. Pine forests are considered the most favorable for recreation in the suburbs of St. Petersburg. Psychologically, a person

feels more comfortable in the pine forests of heathlands, bilberries, lingonberries [21]. These forests are light, easily passable, they are not for nothing called park forests. Feeling in a spruce, dark, damp, sometimes difficult forest is less comfortable psychologically. Seasonal recreational loads on the forests of St. Petersburg's suburban area are significant, but their intensity varies in different areas. Trampling oppressive effect on taiga species (especially shrubs). Trampling leads to damage and disease of roots and shoots, primarily woody. The oppression and partial destruction of shrubs and trees of lower tier leads to lightening of the forest, which, in turn, leads to the displacement of forest species of plants by meadow turf soils.

Swamp complexes occupy both huge areas and small areas in forest in the taiga zone. Swamps on the territory of the Greater St. Petersburg are rich in berries, can be used for limited extent for picking berries (cranberries, cloudberries, lingonberries, blueberries, etc.), mushrooms or for hunting. Uncontrolled, intensive visits by tourists to swamps causes changes in vegetation cover, as a result of which their biological productivity decreases. Plants that can harm human health grow on this territory. These are, for example, poisonous plants: black henbane, poisonous milestone, crow's eye, wolf's bark, hogweed, etc. Each summer-autumn season registers cases of mushroom poisoning. It is necessary to inform people who decide to relax in nature.

The fauna of the city is rich and diverse. Several hunting species, numerous in the suburbs of St. Petersburg, virtually absent in European countries. About 80 species of fish are found in the waters of rivers and lakes. These are such species of fish, including valuable species, like salmon, brown trout, whitefish, sturgeon, grayling. Nature preserves are designed to preserve fauna. Restrictions on visits to certain areas are introduced during the bird nesting period. Some unfavorable features of individual representatives of the local fauna are also observed here. This is the abundance of bloodsucking insects (midges) in the summer. Some members of the fauna can be dangerous to humans, because they are carriers of various infections. All this is important to consider when organizing various types of recreational activities. Among the actual poisonous animals that are dangerous to human life, we can single out only the common viper. Danger can also come from large animals. Cases of attacks on humans are extremely rare, but collisions with them on the roads, especially with elks, often cause tragedies. Consequently, expressways should be equipped properly (for example, install a special barrier along the tracks).

## DISCUSSION

Recreational programs can be combined with

other activities (sports, recreational, informational, educational, classes of interest) in St. Petersburg [22]. The natural resources of Greater St. Petersburg make it possible to develop health tourism - a sanatorium and resort vacation in order to strengthen or restore health. The nature of the territory of Greater St. Petersburg is largely anthropogenically transformed. However, many landscapes are unique, classified as specially protected. One of the largest megacities in Europe is the five-millionth of St. Petersburg, surrounded by a network of satellite cities with powerful industrial and agricultural potential. Natural systems within a radius of 100–150 km of a city and its suburbs occupy no more than 20% of the entire territory. On the territory of St. Petersburg, specially protected natural areas are allocated. These include areas of land, water surface and air space above them, where natural complexes and objects of special environmental, scientific, cultural, aesthetic, recreational and recreational importance are located. These territories were withdrawn by decisions of public authorities in whole or in part from economic use, for them a special protection regime has been established. Natural reserves and monuments of nature (geological, geomorphological, hydrological, botanical) are located on the territory of Greater St. Petersburg. The possibility of visits by recreants determines the prospects for the further development of ecological tourism.

On the territory of St. Petersburg allocated specially protected natural areas, where areas with high-rise buildings and industrial zones dominate. The organization of a network of specially protected natural areas is the most important condition for the formation of a harmonious urban environment. Such territories improve the aesthetics of urban landscapes, along with the artificially created vegetation of gardens and parks, greenery on the streets [23].

15 protected areas are allocated within the city limits of Greater St. Petersburg. The total area of the fifteen currently existing protected areas in St. Petersburg is 6,140 hectares (more than 4% of the entire city territory). Most of them are close to the coast of the Gulf of Finland. A comparison of the urban landscape map and SPNA located within their boundaries allows to make a conclusion about unequal representation of each landscape. This should be considered when designing new protected areas within the city limits. The first place in terms of the number and area of specially protected natural areas will be taken by the Kurortny district. It is planned that protected areas will occupy 1/10 of its area by 2025.

Eight nature reserves: Yuntolovsky, Gladyshevsky, the Northern coast of the Neva Bay, Lake Shchuchye, the Sestroretsk swamp, West Kotlin island, the Southern coast of the Neva Bay, the Novoorlovsky are of importance for recreation purposes. They are created to preserve or restore

several components of nature and to maintain the overall ecological balance. Some types of economic activities are limited on their territory. It is difficult to overestimate the importance of SPNA within a large city [24], such as St. Petersburg. A program for further expansion of the network of territories with this status exists.

Some park areas need to be given the status of protected areas (for example, by analogy with the nature monument Elagin Island, or the park "Sergievka"). For example, Shuvalovsky Park is located on the Northern outskirts of St. Petersburg. This is a popular holiday destination of citizens.

The authorities failed to implement some decisions on granting the status of protected areas. Here are some examples. In 1996, the decision was made in order to preserve the unique natural complex of the Suzdal Lakes. Establish the status of protected areas for the natural complex of Suzdal Lakes in the Vyborg and Primorsky districts of the city. Suzdal Lakes are a unique natural formation, representing a system of three lakes. Bizarre coastal outlines, flat terrain from the west, hilly from the east, combined with the water surface, predetermine landscape diversity and determine aesthetic appeal. The functional use of the lakes has a wide range, including recreational. The decision is not made.

In 1997, the city government determined the need to establish an integrated (landscape) St. Petersburg state natural reserve of regional significance in the territories of the city of Pavlovsk and the city of Petrodvorets. The decision was not made.

## CONCLUSIONS

The General plan of St. Petersburg provides for the organization of a system of SPNA in order to improve the environmental protection. New SPNA will be created before 2025. Some of them, for example, "Levashovo forest", "Coastal ledge Serovo", "Puhtolova mountain" can be examples of new types of SPNA, that solve both environmental and recreational tasks.

Natural parks of different profiles can be created on the territory of the city. From the point of view of modern scientific approaches, the most promising forms of natural parks should be parks which provide:

- Zones of scientific and educational importance (for scientific ecological and landscape researches with arrangement of ecological trails and routes),
- Recreational zone (with construction of walkways, stops, tent camps and parking for tourists, mini-camp sites, tourist sites);
- Sports tourist parks (with specially organized territories, including facilities and areas for training and amateur qualifying tourism, as well as educational and sports tourist events-tourist rallies, competitions, seminars, etc.).

- Fishing and hunting parks (with specially designated territories for carrying out hunting and amateur fisheries regulated by licenses, as well as ecological, zoological, ichthyological research and activities);

- Water parks (focused on water areas and territories suitable for the development of water tourism-yachting, swimming, boating, relaxing on the beach, etc.);

- Agricultural parks, and in the version of St. Petersburg-natural - historical dacha zones (with dedicated special areas designed for agricultural activities, exhibiting its tourists, as well as the creation of country museums, ethnic museums, museums demonstrating the achievements of modern science and technology in the arrangement of dacha farms, not harmful to the natural environment).

In any case, SPNA should have visit centers equipped in accordance with international experience and modern requirements for the organization of eco-excursion and tourism activities. Eco-tourism can and should become for the economy of St. Petersburg not only an urban, but also a Federal specialization, with a correctly built policy based on the integrated use of tourism and reclamation resources, considering all conditions that can contribute to the development of recreation.

## REFERENCES

- [1] Schirru, M.R. Montalto di Castro, Sustainable tourism as an opportunity for urban and environmental regeneration. (Conference Paper) DOI: 10.1007/978-3-319-92102-0\_70
- [2] Nikolaeva J. V., Bogoliubova N. M., Shirin S. S. Ecological tourism in the state image policy structure. Experience and problems of modern Russia. *Current Issues in Tourism*. Vol. 21, Issue 5, 2018, pp. 547-566 DOI: 10.1080/13683500.2015.1100588
- [3] The Federal target program "Development internal and entrance tourism in Russian Federation (2019-2025)", available at: URL: <https://www.russiaturism.ru> (Accessed 5 May 2019)
- [4] Slater S. J., Tarlov E., Jones K., Matthewa S. A., Wing C. and Zenk S. N., Would increasing access to recreational places promote healthier weights and a healthier nation? *Health and Place*, Vol. 56, 2019, pp. 127-134. DOI: 10.1016/j.healthplace.2019.01.013
- [5] Official website of World Tourism Organization (UNWTO), available at: URL: <http://unwto.org/ru> (Accessed 10 June 2019)
- [6] Official website of Russian Federal Agency for Tourism, available at: URL: <https://www.russiaturism.ru/> (Accessed 7 June 2019)
- [7] Matveevskaya A., Pogodina V., Ermolina M., Geoecological approach to the design of recreational areas in large cities. *MATEC Web of Conferences*, Vol. 265, 2019. DOI:10.1051/mateconf/201926506012
- [8] Paranina A., Archaeological objects as elements of informational life support system and sources of information about the evolution of the environment. *International Journal of GEOMATE*, Vol. 13, Issue 35, 2017, pp.100-107 DOI: 10.21660/2017.35.6722
- [9] Stăfănică M., Butnaru G. I., Research on tourists' perception of the relationship between tourism and environment. *Procedia Economics and Finance*. 2015, pp. 595-600.
- [10] Matveevskaya A. S., Pogodina V. L., Tarakanova T. S., Evseev V. V. and Nesterova I. E., Technologies of Tourism in the Modern Urban Environment. *International Journal of Civil Engineering and Technology (IJCET)* Vol.9, Issue 10, 2018. pp. 1566-1574.
- [11] Paranina A. N., Paranin R. V., Information in geographical space as the basis of cross-disciplinary researches in culture geography. *European Journal of Geography* 8 (3) 2017, pp.67-77
- [12] Baranov A. S., Drapeko E. G., Bogdanov E. I., World Heritage of St. Petersburg in the context of cultural tourism, 2011, pp.42-48.
- [13] Pozdeeva E. G., Trostinskaya I. R., Evseeva L. I., Ivanova R. A., Problems of personality type transformation in current conditions of Russian society. *International conference on research paradigms transformation in social sciences (RPTSS 2017) European Proceedings of Social and Behavioral Sciences*, 35, pp. 1092-1099 DOI: 10.15405/epsbs.2018.02.128.
- [14] Shipunova O. D., Kolomeitsev I. V., Sociotechnical system and socio-cultural environment in modern society. *Scientific and technical statements*, №1 (105), 2010, pp. 15-21.
- [15] The Geography of Tourism of Central and Eastern European Countries. K. Widawski, J. Wyrzykowski (Ed.) 2017, P. 551 DOI: 10.1007/978-3-319-42205-3
- [16] Pogodina V., Filippova I. *Geography of Tourism*, 2015, P. 256.
- [17] Matveevskaya A., Pogodina V. New objects of tourist interest and their reflection in the register of tourist resources of St. Petersburg. *Tourism and Education*, 2017, pp. 44-50.
- [18] Belkina I., Pogodina V. Eco-recreational features of Leningrad region' landscape. *Geology and evolutionary geography*, 2003, pp. 156-166.
- [19] Grigoriev A., Zelyutkina L., Isachenko T., Korostelev E., Paranina A and Sevastyanov D. The Heritage of the North-West of Russia and recreational environment management, 2013, P.152.
- [20] Gaidai A., Pogodina V. Features of the design of ecological trails in protected areas of St.

- Petersburg. Natural and cultural heritage, 2016, pp. 440-445.
- [21] Nutsford, D., Pearson, A.L., Kingham, S. An ecological study investigating the association between access to urban green space and mental health. *Public Health*, 127 (11), 2013, pp. 1005-1011. DOI: 10.1016/j.puhe.2013.08.016
- [22] Problems of development of domestic and inbound tourism in Russian Federation, 2018, P. 223.
- [23] Thongdejsri, M., Nitivattananon, V. Assessing impacts of implementing low-carbon tourism program for sustainable tourism in a world heritage city. *Tourism Review*, Vol. 74, Issue 2, 2019, pp. 138-156. DOI: 10.1108/TR-04-2017-0082
- [24] Kovnova, T., Koleva, V., Dragoeva, A. P. and Natchev N. Peri-urban national parks as green spaces for recreation: A case study of nature park Shumen plateau. *International Journal of Social Ecology and Sustainable Development*, Vol. 10, Issue 1, 2019, pp. 46-58 DOI: 10.4018/IJSESD.2019010104

# ANALYSING THE INFLUENCE OF COGNITIVE, AFFECTIVE, CONATIVE AND MOTIVATION ASPECTS ON TRAIN PASSENGER'S DEVIANT BEHAVIOUR: COMMUTER LINE, INDONESIA

Ahmad Zubair<sup>1</sup>, Chotib<sup>1</sup>

<sup>1</sup>Urban Studies, School of Strategic and Global Studies, Universitas Indonesia, Indonesia

## ABSTRACT

Commuter Line in Jakarta and surrounding cities became the best public transportation for urban choice. However, there are still many problems related to behavior deviations carried out by passengers. These forms of deviant behavior such as pickpocketing, sexual abuse, smoking in the station, aggressive passengers, eating and drinking in the carriage, priority seat abuse and many other passenger behaviors. The purpose of this paper is to analyze whether there is a significant influence between the cognitive, affective, conative and motivation aspects of passengers simultaneously and partially to deviant behavior. A mixed method research is conducted to understand behavior aspects. The Sequential Exploratory research model is used with the main focus is to explore a phenomenon of train passenger deviant behavior. This research model is divided into two stages. The first stage is the collection of qualitative data using observation and in-depth interview methods. The second stage is collecting quantitative data with the survey and distributing questionnaires methods. Multiple linear regression and triangulation analysis are used in this study with several test such as hypothesis test and coefficient of determination test. The results showed some implication about passenger deviant behavior based on four aspects: cognitive, affective, conative and motivation. The conclusions explained cognitive, motivation and conative aspects showing a very strong influence on deviant behavior.

*Keywords: Passenger behaviour, Deviant behaviour, Train passenger, Multiple linear regression, Commuter line*

## INTRODUCTION

Wesley Woodson [1] argued that the transportation space should pay more attention to the characteristics of passengers, it was attitude and behavior. Understanding passenger attitudes and behavior is important to anticipate operational and service problems.

Sears [2] suggested that there were three components to seeing the form of attitudes, including the cognitive, affective and conative. Based on the small findings in the pre-research stage, it showed that the relationship between cognitive, affective and passenger behaviors can be in one direction, but not always compatible [2]. Most of the passengers form an anomie so the use of facilities and regulations in the station sometimes becomes biased. Passengers no longer know which one can be said to be 'correct' and which one is 'wrong' in using the facility. This research was conducted to enrich the patterns of Commuter Line passengers deviant behavior both in stations and train cars based on three components coupled with motivation aspect [3].

The study of train passengers behavior has been carried out starting from how the passengers behavior during boarding [4] and forms of commuter line passenger deviant behavior up the train roof [5] how passengers did affordances and adaptation in Commuter Line trains [6] and how passenger

behavior is viewed from policy implementation of facilities and infrastructure within the station [7]. Research on passenger behavior modeling using regression analysis has also been carried out [8] but the factors used have not been specific regarding deviant behavior itself.

From the various studies above, this paper tries to combine and complement the research of passenger behavior in terms of the passengers deviant behavior aspects. How does the influence of cognitive, affective, conative and motivation aspects on passengers deviant behavior? Do each variable partially influence the deviation? How about its influence simultaneously? If there is any relations, what is the power of the relation? And which variables most influence passengers deviant behavior?

## METHODOLOGY

This study used a quantitative approach. Data collection is done by survey method with questionnaire instruments. The distribution of questionnaires was conducted to complete the analysis of quantitative data. Data is also collected to strengthen data interpretation/tabulation. Respondent data in this study can be analyzed descriptively to find out the characteristics of respondents and deviant

behavior factors based on three components (cognitive, affective & conative) and an additional component, motivation aspect.

The questionnaire was distributed to passengers using the Tangerang-Duri route with the intention that passengers who were given a questionnaire were willing to respond according to the questions asked. The scale used in this study is the Likert scale to measure attitudes, opinions and passenger perceptions of deviant behavior that occurs.

Table 1 Likert Scale Answer Sheet

| Answer | SD | D | Do | A | SA |
|--------|----|---|----|---|----|
| Score  | 1  | 2 | 3  | 4 | 5  |

Note: Strongly Disagree (SD), Disagree (D), Doubtful (Do), Agree (A), Strongly Agree (SA)

### Population and Sample

The population in this study were passengers on weekdays and weekends observed at peak and off-peak hours. The sample in question is a portion of the Commuter Line population of the Tangerang-Duri route whose characteristics are to be investigated and can represent the entire population. Sugiyono [9] explained that one technique in drawing samples must be representative by using the Slovin formula below.

$$n = \frac{N}{1 + N e^2} \quad (1)$$

n = sample/total respondent  
N = population  
e = the percentage of sampling accuracy errors that can still be tolerated

Table 2 Research Population

| Time                                      |          | Average Passenger in Station |                         |
|---|----------|------------------------------|-------------------------|
|   |          | Tangerang                    | Duri                    |
| Weekdays                                  | Peak     | 2670                         | 3751                    |
|   | Off Peak | 1530                         | 2458                    |
| Weekend                                   | Peak     | 1774                         | 1846                    |
|   | Off Peak | 1121                         | 1507                    |
| <b>Average Passenger Population (1+2)</b> |          | <b>1773<sup>1</sup></b>      | <b>2390<sup>2</sup></b> |
|   |          |                              | <b>4163</b>             |

The population in this study was 4163 passengers. The population is the sum of the average passengers at Tangerang and Duri Station on weekdays and weekends. Data was collected through initial observation by manual counting.

Samples taken based on random sampling techniques where researchers provide equal opportunities for each member of the population

(passengers) to be chosen randomly. Sampling data can also be taken incidentally [9] which is the determination of respondents by chance (whoever meets the surveyor can be used as a sample). Percentage of allowance used is 10% and the results can be rounded up so that the number of samples is 110 respondents.

### Variables

In this study there are four independent variables (Cognitive, Affective, Conative and Motivation) and 1 dependent variable (Passenger Deviant Behavior). The variables are operationalized as follows:

Table 3 Variables' Operationalization

| Variable                   | Indicator   |
|----------------------------|---|
| Cognitive                  | a. Knowledge about deviant behavior                     |
|                            | b. Understanding of regulations                         |
|                            | c. Understanding of station and train facilities        |
|                            | d. Understanding of space and time resources            |
| Affective                  | a. Response of deviant behavior                         |
|                            | b. Reaction to deviant behavior                         |
|                            | c. Passenger amenities                                  |
|                            | d. Passenger safety                                     |
| Conative                   | a. Passenger action to deviant behavior                 |
|                            | b. Passenger readiness to deviant behavior              |
|                            | c. Passenger anticipation to deviant behavior           |
|                            | d. Passenger anticipation to deviant behavior           |
| Motivation                 | a. Passenger basic needs fulfillment                    |
|                            | b. Passenger opportunity in committing deviant behavior |
| Passenger Deviant Behavior | a. Understanding of regulation/norms                    |
|                            | b. Regulation socialization                             |
|                            | c. Passenger tolerance                                  |
|                            | d. Station and train facilities                         |
|                            | e. Space and time limitation                            |

### Analysis

The questionnaire data was processed through the tabulation and Statistical Package for the Social Sciences (SPSS) program. The results of processing data will be analyzed using multiple linear regression and hypothesis test. Multiple linear regression is used because of several aspects that will be tested. This analysis is the most suitable for the research model.



### Multiple Linear Regression Analysis

Regression analysis is a method of correlation between cause and effect relations and to make predictions for the topic by using the relation [10]. The multiple linear regression analysis in this study aims to determine the magnitude of the influence of four independent variables namely Cognitive ( $X_1$ ), Affective ( $X_2$ ), Conative ( $X_3$ ) and Motivation ( $X_4$ ) to the dependent variable namely Deviant Behavior ( $Y$ ). The multiple linear regression equation models used in this study are as follows:

$$Y = \alpha + b_1X_1 + b_2X_2 + b_3X_3 + b_4X_4 + \varepsilon \quad (2)$$

$Y$  : Dependent Variable  
 $\alpha$  : Constanta Coefficient  
 $b_{1,2,3,4}$  : Regression Coefficient  $X_1, X_2, X_3, X_4$   
 $X_1$  : Cognitive  
 $X_2$  : Affective  
 $X_3$  : Conative  
 $X_4$  : Motivation  
 $\varepsilon$  : Error

### Hypothesis Test

Hypothesis test is divided into two methods, which are t test (partial) and F test (simultaneous). The t test, known as the partial test, is conducted to determine the effect of the independent variable ( $X$ ) on the dependent variable ( $Y$ ) separately / one by one / each [11]. According to Ghozali [12], the t test is said to be significant if the value of t count > t table or significance value (p value) < probability.

This F test is also often referred to as a simultaneous test, to test whether the independent variables used in the model are able to explain changes in the value of variables [12]. F test is said to be significant if the value of F count > f table or significance value (p value) < probability. The description of the calculation can be seen in the ANOVA table.

## RESULTS AND DISCUSSIONS

The distribution of the questionnaire was carried out for approximately two months (December 2018 until January 2019). The questionnaire was distributed to complement the primary data needs that had been identified through observation and semi interviews with both passengers and PT. KCI. The results of distributing questionnaires can be in the form of characteristics of respondents' profiles and tabular data filling in questions to be tested with multiple linear regression analysis.

### Respondent Profile

Respondent profile data describes the characteristics of 110 respondents. The profile of the respondents can be elaborated through the identity of the respondents based on the characteristics of age, gender, occupation and time of Commuter Line usage.

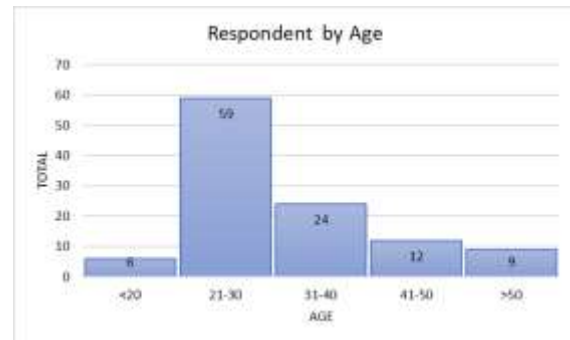


Fig. 1 Total Respondent by Age

Based on the survey results, respondents in this study had the youngest age range of 18 years to the oldest 65 years. Most of the respondents were passengers aged 21-30 years as many as 59 people (53.6%) and passengers aged 31-40 years as many as 24 people (21.8%) and passengers aged 41-50 years as many as 12 people (10.9%). This distribution shows that respondents are dominated by productive age passengers. Productive age passengers usually work in the Jakarta area and come from the suburban area (Tangerang, Depok, Bogor and Bekasi). Based on research from the Ministry of Transportation, most workers in productive age in Jakarta prefer to use public transportation modes rather than private vehicles, most of them using Commuter Line.

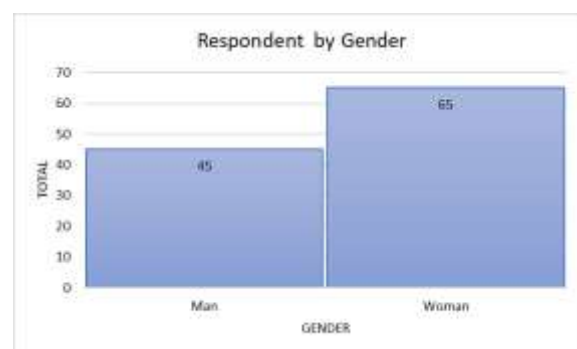


Fig. 2 Total Respondent by Gender

Based on gender, the respondents in this study were dominated by women as many as 65 people (59.1%). Meanwhile, there were 45 male respondents (40.9%). That is, Commuter Line in Indonesia is more used by women. The results of the observation also showed that on the Tangerang-Duri route, woman passengers were dominated especially mothers carrying children during off-peak hours.

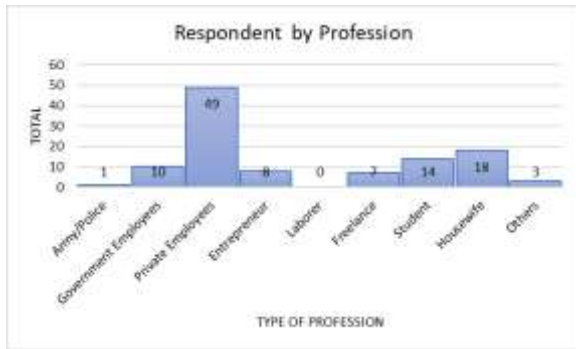


Fig. 3 Total Respondent by Profession

The types of profession identified are Army/Police, Civil Servants (PNS), private employees, entrepreneurs, laborers, freelancers, students/college students, housewives and others. The majority of respondents worked as private employees as many as 49 people (44.5%). The next most respondents were housewives as many as 18 people (16.4%) and students /college students (12.7%). Of the 110 respondents, 75 passengers were daily workers (68.2%) and 35 passengers did not work (31.8%).

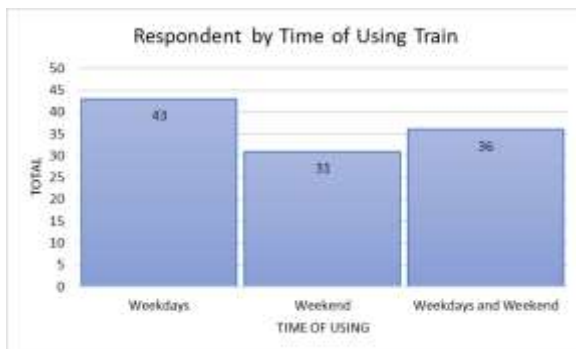


Fig. 4 Total Respondent by Time of Using Train

Time of using train is divided into weekdays (working days), weekends and both (weekdays and weekend). 43 respondents (39.1%) used the Commuter Line only on weekdays. 31 respondents (28.2%) using Commuter Line only on weekend,

these passengers are usually dominated by passengers carrying families. While as many as 36 respondents (32.7%) used Commuter Line on both weekdays and weekend.

### Multiple Linear Regression Model

Based on table, the values in the table output are included in the following terms of multiple linear regression.

$$Y = (\alpha) 28,671 + (X_1) 0,929 - (X_2) 0,019 - (X_3) 0,746 + (X_4) 0,589 \quad (3)$$

Equation (3) shows a constant value of (28,671), it can be interpreted that if the value of other independent variables is 0, then the value of the dependent variable (deviant behavior without being influenced by the independent variable is equal to (28,671).

Cognitive variable coefficient ( $X_1$ ) is 0.929; meaning that every increase 1 unit in Cognitive variable, it will increase deviant behavior by 0.929 units, assuming other independent variables are fixed values. Beta Standardized Coefficients Cognitive variable ( $X_1$ ) of 0.540 means that Cognitive variables have a positive influence of 54% on deviant behavior variables ( $Y$ ).

The Affective variable coefficient ( $X_2$ ) is -0.019; meaning that every increase 1 unit in Affective variable, it will reduce deviant behavior by 0.019 units, assuming other independent variables are fixed values. Beta Standardized Coefficients Affective variable ( $X_2$ ) of -0.016 means that Affective variables have a negative effect of 1.6% on variable deviation behavior ( $Y$ ).

The Conative variable coefficient ( $X_3$ ) is -0.746; meaning that every increase 1 unit in Conative variable, it will reduce deviant behavior by 0.746 units, assuming the other independent variables are fixed values. Beta Standardized Coefficients Conative variable ( $X_3$ ) is -0.320, which means that the Conative variable has a negative influence of 32% on the deviant behavior variable ( $Y$ ). Motivation variable coefficient ( $X_4$ ) is -0.589; meaning that every

Table 4 Multiple Linear Regression Output

| Model        | Unstandardized Coefficients |            | Standardized Coefficients | t      | Sig. |
|--------------|-----------------------------|------------|---------------------------|--------|------|
|              | B                           | Std. Error |                           |        |      |
| 1 (Constant) | 28.671                      | 6.445      |                           | 4.448  | .000 |
| Cognitive    | .929                        | .141       | 0.540                     | 6.610  | .000 |
| Affective    | -.019                       | .095       | -.016                     | -.206  | .837 |
| Conative     | -.746                       | .191       | -.320                     | -3.914 | .000 |
| Motivation   | .589                        | .240       | .229                      | 2.451  | .016 |

increase 1 unit in Motivation variable, it will increase deviant behavior by 0.589 units, assuming other independent variables are fixed values. Beta Standardized Coefficients Motivation variable ( $X_3$ ) of 0.229 means that the Motivation variable has a positive effect of 22.9% on deviant behavior variable (Y).

The multiple linear regression model above shows that Cognitive variable ( $X_1$ ) and Motivation variable ( $X_4$ ) are positively related to deviant behavior. Meanwhile, Affective variable ( $X_2$ ) and Conative variables ( $X_3$ ) are negatively related to deviant behavior. Based on Beta Standardized Coefficients, the most influences variable to deviant behavior is the Cognitive variable ( $X_1$ ). This can be seen in the form of passenger behavior due to a lack of understanding of the rules and norms in the station and train.

After analyzing the independent variables that influence deviant behavior as explained by Sears [2], all variables simultaneously influence behavior deviations. Cognitive variables have the greatest influence indicating that aspects of knowledge and understanding of passengers in implementing rules and norms are important to be discussed further. Imron and Harianto's research [13] also showed that human cognitive factors greatly determine the form of deviations made. Sujatmiko and Harianto's research [5] also showed that there are several motives that cause passengers deviant behavior in train cars. Four of the five motives found by Sujatmiko & Harianto [5] explained that they (passengers) were more influenced by cognitive aspects and passenger motivation than affective aspects. Partially, affective variables show no significant effect on deviant behavior. For this reason, affective variable should be substituted with variable that predominantly influence such as motivation variable. The addition of motivational variable from Maslow [3] can finally explain that deviant behavior was positively carried out to meet the needs of the passengers themselves. Deviant behavior also tends to occur because of the special or urgent motivation of these passengers.

### Coefficient of Determination Test

The coefficient of determination shows how much the percentage of the regression model is able to explain the dependent variable.

Table 5 Coefficient of Determination Test

| Model | R                 | R Square | Adjusted R Square | Std. Error of Estimate |
|-------|-------------------|----------|-------------------|------------------------|
| 1     | .668 <sup>a</sup> | .447     | .426              | 4.08145                |

Note: a. Predictors: (Constant), Motivation, Affective, Cognitive, Conative

The limit of  $R_2$  is  $0 \leq R_2 \leq 1$  so that if  $R_2$  equals zero (0) means that the dependent variable cannot be explained by the independent variable simultaneously, whereas if  $R_2$  is equal to 1 means that the independent variable can explain the dependent variable simultaneously.

Table 5 shows that the correlation between the dependent variables Deviation Behavior and the four independent variables in general is 0.668. This shows that the Cognitive, Affective, Conative and Motivation variables towards Deviant Behavior are in the strong category.

The Adjusted R Square value is 0.426 (42.6%). This shows that the variation of the independent variables used in the model (cognitive, affective, conative and motivation) is able to explain 42.6% of the variation in the behavioral deviation variables, while the remaining 57.4% is explained by other variables not included in this research model.

### Hypothesis Test

The partial test results (t test) can be seen in Table 4. Conclusions can be drawn based on the following requirements: If the t count is greater than t table or p value is smaller than 0.1, then hypothesis 0 is rejected and the initial hypothesis is accepted which means the independent variable affect the dependent variable.

Based on the table 4, the t count of cognitive variables is 6.610, motivation variable is 2,451, conative variable is -3,914 and the significance value is 0,000. The t table value can be seen from the statistical table with a significance of 0.1 and degrees of freedom (df)  $n-k-1$  or  $110 - 4 - 1 = 105$ . With the 2-sided test the results are obtained for t table of 1,289 / -1,289. That is, t count > t table (6.610, 2,451, -3,914 > 1,289 / -1,289) significance value < from  $\alpha$  (0,000 < 0,1). Therefore, it can be concluded that Cognitive and Motivational variables partially influence the deviation of Commuter Line passenger behavior. Positive t count value, meaning that the increasing assessment of the cognitive aspects and motivation of a passenger will increase deviant behavior. The results of calculations on the conative variables show a negative t count, which means that the increased assessment of the conative aspects of a passenger will reduce behavioral deviations.

On the other hand, Affective variable shows the value of t count is -0.206 and the significance value is 0.837. The t table value can be seen from the same statistical table. That is, t count < t table (-0.206 < -1,289) significance value > of  $\alpha$  (0.837 > 0.1). Then it can be concluded that the Affective variable partially does not affect Commuter Line passenger deviant behavior.

In addition to the t test, the F test is used to determine whether the independent variables simultaneously influence the dependent variable or

not. The hypothesis 0 is accepted if  $F_{\text{count}} \leq F_{\text{table}}$ . Hypothesis is rejected if  $F_{\text{count}} > F_{\text{table}}$ . The F test results obtained after the processed data are presented in the following ANOVA table.

Table 6. ANOVA

| Model      | SST  | df  | Mean Squar<br>e | F      | Sig               |
|------------|------|-----|-----------------|--------|-------------------|
| Regression | 1411 | 4   | 352.9           | 21.189 | .000 <sup>b</sup> |
| Residual   | 1749 | 105 | 16.6            |        |                   |
| Total      | 3160 | 109 |                 |        |                   |

Note: a. Dependent Variable: Deviant Behavior, b. Predictors: (Constant), Motivation, Affective, Cognitive, Conative

Based on the ANOVA table above, the calculated F value is 21,189. F table can be seen in the statistical table using a significance level of 0.1 and df 1 (number of variables - 1) or  $4-1 = 3$  and df 2 (nk-1) or  $110-4-1 = 105$ . Results obtained for F table amounting to 2,136. That is, the value of  $F_{\text{count}} > F_{\text{table}}$  (21,189 > 2,136), then hypothesis 0 is rejected and the initial hypothesis is accepted. Therefore, it can be concluded that the cognitive, affective, conative and motivation variables simultaneously influence the Commuter Line passenger deviant behavior.

Based on the F test table above, the significance value of the Cognitive variable ( $X_1$ ), Affective variable ( $X_2$ ), Conative variable ( $X_3$ ) and Motivation variable ( $X_4$ ) is 0,000 < value of  $\alpha$  (0,1) so that all independent variables together has an effect on Commuter Line passenger deviant behavior at stations and train cars.

## CONCLUSIONS

Deviant behaviors in this study are interpreted specifically as all forms of passenger behavior that violate the rules and norms that apply both in the station and train cars. Previous research about deviant behavior discussed irregularities in train cars by linking passenger motives to behavior. There has been no discussion about the relationship between the effects of deviant behavior aspects. Cognitive, motivation and conative aspects show a very strong influence on passenger deviant behavior. The tendency of these deviant behaviors can ultimately show the lack of cognitive abilities of Commuter Line passengers accompanied by strong motivation to fulfill their needs. Future research is expected to be able to include other aspects such as the social,

cultural and economic aspects of passengers which can influence deviant behavior.

## ACKNOWLEDGMENTS

This article is part of Grant of International Publications for Students Final Project of Universitas Indonesia: Urban Public Transportation and Planning.

## REFERENCES

- [1] Woodson W., Human Factors Design Handbook: Information and Guidelines for the Design of Systems, Facilities, Equipment and Products for Human Use. New York, McGraw-Hill, 1981.
- [2] Sears D., Freedman J., Peplau L., Social Psychology 5<sup>th</sup> Ed. Jakarta, Erlangga, 1992.
- [3] Maslow AH., Motivation and Personality: Motivation Theory with a Hierarchy of Human Needs Approach., Jakarta, PT PBP, 1994.
- [4] Oliveira L. CR., Fox C., Birrell S., Cain R., Analysing Passenger's Behaviours when Boarding Trains to Improve Rail Infrastructure and Technology. Robotics and Computer-Integrated Manufacturing, Vol. 57, 2019, pp.282-291.
- [5] Sujatimko., Harianto S., Phenomenology Study of Passenger Behavior on Train Car. Paradigma Journal, Vol. 2, Issue 1, 2014, pp.1-5.
- [6] Basyarah Z., Affordances and Passenger Adaptation on KRL Commuter Line Train. Depok, Universitas Indonesia, 2014.
- [7] Kusumaningtyas B., Railway Implementation Policies (Study of Duri-Tangerang Commuterline Facilities and Infrastructure). Depok, Universitas Indonesia, 2014.
- [8] de Ona J., de Ona R., Eboli L., Forciniti C., Mazzulla G., An Ordered Regression Model to Predict Transit Passengers' Behavioural Intentions. Case Studies on Transport Policy, Vol. 6, Issue 4, 2018, pp.449-455.
- [9] Sugiyono., Quantitative, Qualitative and R&D Research Method. Bandung, Alfabeta, 2011.
- [10] Uyanik G.K., Güller N., A Study on Multiple Linear Regression Analysis. Procedia – Social and Behavioral Sciences, Vol. 106, 2013, pp.234-240.
- [11] Sudjana., Regression and Correlation Analysis Techniques for Researchers. Bandung, Tarsito, 1996.
- [12] Ghozali I., Application of Multivariate Analysis with the SPSS Program, 4<sup>th</sup> Ed. Semarang, Universitas Diponegoro, 2011
- [13] Imron A., Harianto S., Social Deviation and Social Control. Jakarta, Ministry of Education and Culture.

## IMMEDIATE EFFECTS OF THAI MASSAGE ON GAIT SPEEDS AND BALANCE PARAMETERS IN ELDERLY

Nutthanun Tatchananusorn<sup>1</sup>, and Wichai Eungpinichpong<sup>2</sup>

<sup>1,2</sup>Research and Training Center for Enhancing Quality of Life of Working Age People, Khon Kaen  
University, Thailand

<sup>2</sup>Department of Physical Therapy, Faculty of Associated Medical Sciences, Khon Kaen University, Thailand

### ABSTRACT

The purpose of this study was to determine the immediate effects of Thai massage on gait parameters, balance performance, and trunk flexibility in elderly aged 60-80 years. A randomized control trial was used. Sixteen elderly participants (12 females and 4 males) participated. They were divided into a Thai massage group and a control group. Participants in Thai massage group received 1-hour whole body Thai massage while those in the control group were assigned to rest for one-hour. Changes in all parameters after receiving each of the sessions were compared by independent T-test. Within-group comparisons were analyzed by dependent t-test. Significant differences were found for within-group comparison in right gait cycle duration of maximal gait speed (0.0023 s;  $p$ -value = 0.0023), single leg stance of left leg with open eye (15.17 s.;  $p$ -value = 0.034), and close eye conditions (2.3 s.;  $p$ -value = 0.022), and right leg with open eye (12.41 s.;  $p$ -value = 0.0294) and close eye conditions (4.06 s.;  $p$ -value = 0.0087), and trunk flexibility (2.14 cm.;  $p$ -value = 0.0003). However, there are little improvement of gait speed, stride length, gait cycle duration, cadences, and time-up-and-go test. We concluded that one session of Thai massage could provide immediate improvement in some gait parameters, balance performances, and body flexibility.

*Keywords: Elderly, Thai massage, Gait, Balance, Flexibility*

### INTRODUCTION

Worldwide, elderly population is increasing faster. Number of elderly people aged 60 years or over in 2000 and 2012 were 607 and 900 million respectively and it is projected to reach 2,092 million in 2050. The world will be turned to ageing society [1]. The health status of elderly people is degenerated by the physical changes in many systems with decrease in performances and capabilities of physiological processes [2]. Moreover, these changes also influence mobility and activities of elderly people that are affected to health problems and considered as fall risk [3].

Exercise is found to help improve gait and balance performance of elderly by improve muscle strength, delivery and extraction of oxygen to the muscle, and joint range of motion [4]. Furthermore, other treatment that also help improve balance and gait were therapeutic massage [5], [6], and foot massage [7].

Lately, Thai massage is a practicable, and cheap traditional treatment for Thai people. There are many benefits of Thai massage including increasing blood flow, skin temperature, and tissue flexibility, and decreasing pain and muscle spasm. In addition, Thai massage may improve arousal or body awareness in elderly that resulted from response of brain activating. Previous study also found that Thai massage improved walking performances in normal adults [8],

improve physical fitness of soccer players [9], improved recovery performance after fatigue of basketball player, [10] decreased spasticity, and improved quality of life and psychological condition in stroke patients [11]. According to previous study, Thai massage may improve walking and balance performances in elderly people but there is no previous study investigate about this topic. Thus, propose of this study was to investigate the immediate effects of Thai massage on gait speed and balance performances in elderly adults compare with resting or control session.

### METHOD

#### Design and Setting

A randomized control trial was conducted at Nong Wang Community Health Center, Khon Kaen hospital. The study was approved by the ethical committees of Khon Kaen University, and Khon Kaen Hospital

#### Participants

Elderly participants were recruited from Khon Kaen province using bulletin boards and oral requests for participants during 2 months period between November and December 2018. Participants who 60-80 years old with ability to walk equal or more than

10 meters without walking aid and good co-operation were included in this study. They were excluded if they had history of brain injury, acute or unstable chronic illness, uncontrolled hypertension, communicable diseases, osteoporosis, deep vein thrombosis, acute arthritis at upper and lower limb, vestibular, neurological and cardiovascular problem, fracture and dislocation, deformities of lower extremities, pain more than 5/10 on visual analog scale, opened wound at back, upper and lower extremity, and visual problems than could not be solved by glasses.

### Intervention

A whole body of Thai Massage session was used as an intervention in this study. The 1-hour Thai massage protocol consisted of deep pressure massage and stretch on major muscles of the body. Firstly, therapist applied gently and deep thumb pressure massage along the meridian lines that covered neck, back, lower and upper extremities and foot consequently (Fig. 1 – 9). Thumb pressure was maintained at each point on the meridian lines for 5-10 seconds each point and repeated 3 times. The intensity of thumb pressure was not exceeded pressure pain threshold of participants and was adjusted by the therapist. After massage session, the therapist applied gentle stretch for those muscles including calf, hamstring, and quadriceps as shown in Fig. 10 – 12. Participants in control group was assigned to rest on the bed in the same environment as massage group.

### 3. PROCEDURE

#### Randomization

Twenty participants who met the above inclusion/exclusion criteria were recruited and randomly allocated into one of two groups using block-randomized allocation with block sizes of 2 and 4. The groups were assigned using a pre-generated random assignment scheme enclosed in envelopes, which resulted in a total of 11 participants per group.



Fig.1 Massage lines of neck area

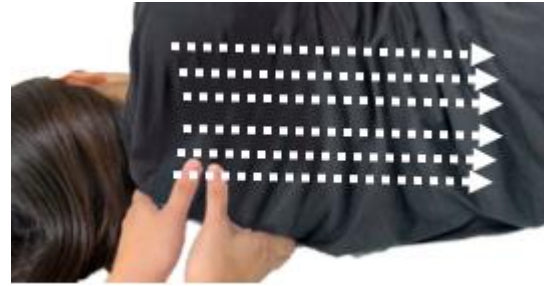


Fig.2. Massage lines of back area.



Fig.3 Massage lines of lower extremity (medial side)



Fig.4 Massage lines of lower extremity (lateral side)



Fig.5 Massage lines of lower extremity (anterior side)





Fig.6 Massage lines of lower extremity (posterior side)



Fig.7 Massage lines of upper extremity (anterior side)



Fig.8 Massage lines of upper extremity (posterior side)



Fig.9 Massage lines of feet



Fig.10 Quadriceps muscle stretching



Fig.11 Hamstrings muscle stretching



Fig.12 Calf muscle stretching

### Treatment

Participants in group A received 2 sessions of one-hour Thai massage per week for 4 weeks. Whereas participants in group B took one-hour rest in supine lying position 2 times per week for 4 weeks.

In keeping with the recommendation of Khon Kaen University's ethical committee and Board in Human Research Khon Kaen Hospital Institute Review, all participants gave informed consent before participation in the study.

### ASSESSMENT

On the baseline session, immediate session after the 1<sup>st</sup> session of treatment, short-term session (before the last session) and follow-up session (after the last session for 1 week), all outcome measures were assessed by one physical therapist. Details of outcome measures and assessments are described below.

### Gait Parameters

Gait parameters were assessed by walking in preferred gait speed and maximal gait speed on 10-meter walkway. Participants were assigned to wear the Opal sensors of APDM at the sternum, posterior lower back, and both foot while walking. Outcomes consisted of gait speed, stride length, cadences, gait cycle duration of preferred gait speed and maximal gait speed. This test was repeated 3 times and calculated for the average values for each speed.

### Static Balance Performance

The Single-leg-stance test (SLS) was assessed static balance over the stance leg. The SLS was measured standing time on each foot in condition of open eyes and close eyes. The assessor started time when participants lifted feet from the floor.

Participant were able to balance their body by move hand or body but they were not allowed to touch anything while controlling their body. Time was stopped when they moved their stance feet or other feet touched the floor [12].

### Dynamic Balance Performance

The time-up-and-go test (TUG) was measured dynamic balance by timing the 5 sequences of test including standing up from armchair, walking 3-meter distance, turning, walking 3-meter distance back to chair, and sitting down. Using stop-watch to time the tasks of 5 sequences. Time was started when assessor said “go” and stopped when participants sit and lean to the back rest of chair [13].

### Body Flexibility

A sit-and-reach box was used to measure body flexibility. Participants sat long-sitting to the sit-and-reach box and reached both hands forward as much as possible to the measuring bar. [14]. Participants were allowed to practice in the 1<sup>st</sup> trial. and they were recorded on the other 2 trials. The value considered as the test result was the best value of 2 trials.

### STATISTICAL ANALYSES

Changes in all parameters between Thai massage session and control session results were analyzed by independent t-test. Changes between pretest and posttest for both sessions were performed by dependent t-test. All statistical analyses were calculated by Stata 10 software (StataCorp LP, 4905 Lakeway Drive College Station, Texas 77845, USA). A *p*-value of less than 0.05 was considered statistically significant.

### RESULTS

Twenty potential participants responded to flyers or word-of-mouth; Four were excluded after screening for eligibility. 16 adults who met the inclusion and exclusion criteria were randomly assigned to the treatment group and the control group. A flow chart of participant progression through the trial is presented in Fig.13 The characteristic of the study population is shown in Table 1. There were 12 females and 4 males. The mean age of control group and massage group were 70.63 and 66.91 years. The mean weight of control group and massage group were 65.93 and 69.09 kilograms. The mean height of control group and massage group were 160.64 centimeters and 159.18 centimeters.

Gait cycle duration of maximal gait speed, single-leg-stance test of all conditions and sit and reach test showed significant improvement after Thai massage session. (Table 2)

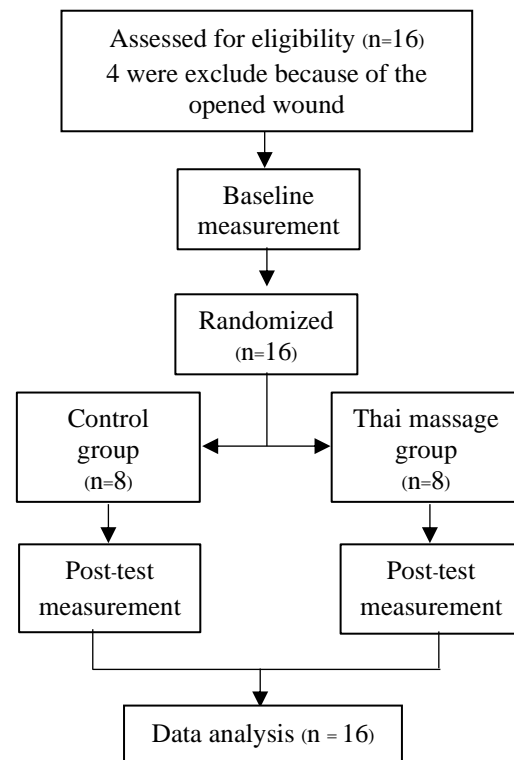


Fig.13 Diagram of study design and participants

### DISCUSSION

This study showed that one session of 1-hour whole body Thai massage could improve walking performance, balance performances and trunk flexibility in elderly on stride lengths of maximal gait speed, gait cycle duration of maximal gait speed, single-leg-stance test, and sit-and-reach test results. Thai massage is to use deep pressure on meridian lines that covers all muscles of the whole body and follow by passive stretching. Possible mechanisms of Thai massage on improving flexibility, gait and balance may base on the neuro-mechanical and mechanical effects. Massage may arouse the proprioceptive nerve endings, adjust sarcomere length, stretch muscle, tendon, and ligament structures that begin reflex muscle relaxation [15][16]. Mechanical pressure of massage may decrease tissue adhesion by lengthen reduced or adhered connective tissue [17]. Thai massage may help improve flexibility as measured by sit-and-reach test [8]. Furthermore, flexibility may help improve stride length and gait cycle duration [18].

Moreover, massage found to affect the somatosensory systems. It may arouse muscle, tendons, joints, and ligaments to provoke the proprioceptors including cutaneous, Golgi tendon organ, joint receptors, and muscle spindles by pressure distribution, muscle tension, changing joint

Table 1. Characteristics of the study population

| Participant Data     | Group A       | Group B       |
|----------------------|---------------|---------------|
| Gender (female/male) | 6/2           | 6/2           |
| Age (year)           | 70.63 ± 6.38  | 66.91 ± 5.52  |
| Weight (kg)          | 65.93 ± 9.1   | 69.09 ± 10.94 |
| Height (cm)          | 160.64 ± 9.48 | 159.18 ± 8.32 |

Table 2. Evaluation of outcome measures (Mean±SD). Variables showing a significant interaction effects between groups have been signed with \* (*p*-value is less than 0.05).

| Parameter                       | Pre-A        | Post-A       | Pre-B        | Post-B       |
|---------------------------------|--------------|--------------|--------------|--------------|
| <b>Maximal gait speed</b>       |              |              |              |              |
|                                 | 1.42         | 1.45         | 1.46         | 1.51         |
| Gait speed (m/s)                | ±0.18        | ±0.16        | ±0.16        | ±0.25        |
| Left stride length (m) *        | 1.25 ±0.11   | 1.26 ±0.11   | 1.27 ±0.17   | 1.3 ±0.17    |
| Right stride length (m) *       | 1.25 ±0.11   | 1.25 ±0.1    | 1.27 ±0.17   | 1.29 ±0.18   |
| Left cadence (bpm)              | 125.5 ±11.87 | 126.4 ±10.7  | 127.9 ±9.27  | 130.4 ±10.87 |
| Right cadence (bpm)             | 125.4 ±11.94 | 126.2 ±11.04 | 127.7 ±9.51  | 130.3 ±11.07 |
| Left gait cycle duration (s)    | 0.96 ±0.08   | 0.97 ±0.06   | 0.94 ±0.08   | 0.93 ±0.08   |
| Right gait cycle duration (s) * | 0.96 ±0.08   | 0.98 ±0.06   | 0.95 ±0.08   | 0.92 ±0.09   |
| <b>Preferred gait speed</b>     |              |              |              |              |
|                                 | 1.1          | 1.11         | 1.07         | 1.12         |
| Gait speed (m/s)                | ±0.15        | ±0.09        | ±0.14        | ±0.19        |
| Left stride length (m)          | 1.12 ±0.09   | 1.12 ±3.39   | 1.1 ±0.12    | 1.12 ±0.11   |
| Right stride length (m)         | 1.1 ±0.09    | 1.11 ±0.07   | 1.09 ±0.12   | 1.12 ±0.11   |
| Left cadence (bpm)              | 111.3 ±7.04  | 109.7 ±6.23  | 112.6 ±6.88  | 114.6 ±9.49  |
| Right cadence (bpm)             | 110.9 ±6.93  | 109.3 ±6.34  | 112.5 ±6.92  | 114.4 ±9.35  |
| Left gait cycle duration (s)    | 1.1 ±0.08    | 1.1 ±0.07    | 1.08 ±0.09   | 1.07 ±0.09   |
| Right gait cycle duration (s)   | 1.1 ±0.09    | 1.1 ±0.07    | 1.08 ±0.09   | 1.07 ±0.09   |
| <b>Single-leg-stance test</b>   |              |              |              |              |
| Opened eye Left side (s) *      | 23.72 ±11.02 | 25.87 ±12.53 | 24.9 ±10.98  | 40.06 ±30.17 |
| Opened eye Right Side (s) *     | 25.68 ±9.95  | 25.47 ±10.59 | 26.16 ±14.12 | 38.57 ±28.27 |
| Closed eye Left side (s) *      | 4.85 ±2.69   | 6.14 ±3.8    | 5.12 ±1.81   | 7.42 ±3.7    |
| Closed eye Right Side (s) *     | 5.48 ±3.33   | 6.32 ±4.55   | 4.48 ±4.85   | 8.55 ±4.53   |
| TUG test (s) *                  | 8.81 ±1.44   | 9.25 ±1.25   | 8.79 ±1.94   | 8.26 ±1.92   |
| Sit and Reach (cm) *            | 1.54 ±9.03   | 1.45 ±9.82   | 1.64 ±11.02  | 3.77 ±10.65  |

angle, and changing muscle length respectively. Massage methods also activated the resetting of unproductive reflex actions [19]. These effects may help improve balance performance.

In addition, our results were related with earlier studies found that Thai massage could improve gait parameters, balance performances, and trunk flexibility. Thai massage might improve stride length and trunk flexibility in normal adult with hamstring tightness [8]. Thai massage on the lower leg might decreased pain and duration of TUGT in elderly with knee pain [20]. Thai foot massage also found to improve TUGT and Single-leg-stance in diabetes patients with peripheral neuropathy [21]. Moreover, many researchers studied the effects of other type of massage which is similar to Thai massage. 15-minute of therapeutic massage might improve gait speed, stride length, and step length in adult with DOMS [22]. 1-hour whole body therapeutic massage might improve balance performance in elderly [5]. 25 minutes of Chinese massage might improve walking speed in elderly with knee osteoarthritis [23]. A small improvement of some gait parameters after 1-hour Thai massage were founded because of a few Thai massage sessions. One session of 1-hour whole body Thai massage could not give a great result. Further study should investigate the multiple sessions with follow-up session on these effects. This study was the pilot study with few participants. Further study also should investigate with proper number of participants.

## CONCLUSIONS

According to the results of this study, we concluded that 1-hour Thai massage session may provide some immediate improvement of gait parameters, balance performance, and trunk flexibility, especially for stride length of maximal gait speed, gait cycle duration of maximal gait speed, single-leg-stance test, time-up-and-go test, and sit-and-reach test. In a further study, long-term treatment with following up are suggested.

## ACKNOWLEDGMENTS

The authors would like to thank Mr. Daniel Seng, product manager of Biofit Technology and Services, for providing equipment, and thank Khon Kaen Hospital for arranging a study visit at Nong Wang Community Health Center. The study was financially supported by the Research and Training Center for Enhancing Quality of Life of Working Age People, Khon Kaen University, Thailand.

## REFERENCES

- [1] United Nations. World Population Ageing 2015. Department of Economic and Social Affairs, Population Division, 2015.
- [2] Boss G.R., Seegmiller J.E. Age-Related Physiological Changes and Their Clinical Significance. *Western Journal of Medicine*. Volume 135, Issue 6, 1981, pp.434-440.
- [3] Tinetti M.E., and Kumar C. The Patient Who Falls: "It's Always a Trade-off." *JAMA*. Volume 303, Issue 3, 2010, pp.258-266.
- [4] Howe T.E., Rochester L., Neil F., Skelton D.A., and Ballinger C. Exercise for improving balance in older people. *the Cochrane Database of Systematic Reviews*. Volume 9, Issue 11, 2011, pp. CD004963.
- [5] Sefton J.M., Yazar C., and Berry J.W. Massage Therapy Produces Short-term Improvements in Balance, Neurological, and Cardiovascular Measures in Older Persons. *The International Journal of Therapeutic Massage & Bodywork*. Volume 5, Issue 3, 2012, pp.16-27.
- [6] Sefton J.M., Yazar C., and Berry J.W. Six Weeks of Massage Therapy Produces Changes in Balance, Neurological and Cardiovascular Measures in Older Persons. *The International Journal of Therapeutic Massage & Bodywork*. Volume 5, Issue 3, 2012, pp.23-40.
- [7] Namkorn P. Effects of Foot Massage on Functional Mobility and Balance Performance in the Elderly [Thesis], Khon Kaen: Khon Kaen University, 2014.
- [8] Tatchananusorn N., Eungpinichpong W., Chatchawan U., and Promkeaw D. Immediate effects of Thai massage on gait parameters in normal adults: A pilot study. *International Journal of GEOMATE*. Volume 15, Issue 49, 2018, pp.118-123.
- [9] Hongsuwan C., Eungpinichpong W., Chatchawan U., and Yamauchi J. Effects of Thai Massage on Physical Fitness in Soccer Players. *Journal of Physical Therapy Science*. Volume 27, Issue 2, 2015, pp. 505-508.
- [10] Kaesaman N. and Eungpinichpong W. The Acute Effect of Traditional Thai Massage on Recovery From Fatigue in Basketball Players. *The International Journal of GEOMATE*. Volume 16 Issue 55, 2019, pp.53-58.
- [11] Thanakiatpinyo T., Suwannatrai S., Suwannatrai U. et al. The efficacy of traditional Thai massage in decreasing spasticity in elderly stroke patients. *Clinical Interventions in Aging*. Volume 9, 2014, pp.1311-1319.
- [12] Jonsson E., Seiger A., Hirschfeld H. One-leg stance in healthy young and elderly adults: a measure of postural steadiness? *Clinical Biomechanics*. Volume 19, Issue 7, 2004, pp.688-694.
- [13] Podsiadlo D. and Richardson S. The timed "Up & Go": a test of basic functional mobility for frail elderly persons. *Journal of the American Geriatrics Society*. Volume 39, Issue 2, 1991, pp. 142-148.
- [14] Mayorga-Vega D., Merino-Marban E., Viciano J. "Criterion-Related Validity of Sit-and-Reach Test for Estimation Hamstring and Lumbar Extensibility: a Meta-Analysis" *Journal of Sports Science and Medicine*. Volume 13, 2014, pp.1-14
- [15] Fritz S. *Mosby's Fundamentals of Therapeutic Massage*, Elsevier, 2013, pp. 184.
- [16] Shin M.S. and Sung Y.H. Effects of Massage on Muscular Strength and Proprioception After Exercise-Induced Muscle Damage. *The Journal of Strength and Conditioning Research*, Volume 29, 2015, pp. 2255-2260.
- [17] Magnusson S. Passive properties of human skeletal muscle during stretch maneuvers. *Journal of Medicine and Science in Sports and Exercise*. Volume 8, 1998, pp. 65-77.
- [18] Christiansen C. The Effects of Hip and Ankle Stretching on Gait Function of Older People. *Archives of Physical Medicine and Rehabilitation*. Volume 89, 2008, pp.1421-1428.
- [19] Fritz S. *Mosby's Fundamentals of Therapeutic Massage*, Elsevier Health Sciences, 2016, pp. 216-218.
- [20] Sansila P., Eungpinichpong W., Buakate L., and Ruangrunsi N. The Efficacy of Court-Type Thai Traditional Massage on Knee Pain Relief in Osteoarthritis Patients. *Journal of Health Research*. Vol.28, Issue 2, 2014, pp.121-126.
- [21] Chatchawan U., Eungpinichpong W., Plandee P., and Yamauchi J. Effects of Thai foot massage on balance performance in diabetic patients with peripheral neuropathy: a randomized parallel-controlled trial. *Medical Science Monitor Basic Research*. Vol.21, 2015 pp. 68-75.
- [22] Han J.H., Kim M.J., Yang H.J., Lee Y.J., and Sung Y.H. Effects of therapeutic massage on gait and pain after delayed onset muscle soreness. *Journal of Exercise Rehabilitation*. Vol.10, Issue 2, 2014 pp.136-140.
- [23] Qingguang Z., Min F., Li G., Shuyun J., Wuquan S., Jianhuan L., and Yong L. Gait analysis of patients with knee osteoarthritis before and after Chinese massage treatment. *Journal of Traditional Chinese Medicine*. Vol.35, Issue 4, 2015, pp.441-446.

## A COMPARISON STUDY BETWEEN CHEMICAL COAGULATION AND ELECTRO-COAGULATION PROCESSES FOR THE TREATMENT OF WASTEWATER CONTAINING REACTIVE BLUE DYE

NIDAA ADIL JASIM, TAMARA KAWTHER HUSSEIN

Faculty of Engineering, Al-Mustansiriyah University, Baghdad, Iraq , nidaa.albayati@uomustansiriyah.edu.iq

### ABSTRACT

This study examined the possibility to remove reactive blue dye from simulated wastewater by chemical coagulation, in comparison with electro-coagulation. Ferric sulphate  $\text{Fe}_2(\text{SO}_4)_3$ , ferrous sulphate ( $\text{FeSO}_4$ ), poly aluminum chloride (PACl) and alum ( $\text{Al}_2\text{SO}_4.5\text{H}_2\text{O}$ ) were used as coagulants. Optimum pH, coagulants dosages and initial concentration were determined by jar tests, and the maximum dye removal was obtained. The maximum removal efficiency were 96%, where the best coagulant was  $\text{Fe}_2(\text{SO}_4)_3$  at optimum pH and dosage of 6, 200 mg/L. On the other hand, electrochemical cell is designed using aluminum plates as the anode and cathode with dimensions of (7\*4\*0.3)  $\text{cm}^3$ . Many experimental runs were done at a different operating conditions (pH, NaCl concentration, initial concentration and electrical supply voltage) to study the removal performance of electro-coagulation for reactive blue dye removal. The results indicated that, the maximum removal were 99 %, at optimum pH of 2 and NaCl concentration of 1000 mg/L, initial concentration of 100 mg/L and 15 volt. The study proved that, the percentage removal of reactive blue is better by electrochemical system than in chemical coagulation.

**Keywords:** Chemical coagulation,  $\text{Fe}_2(\text{SO}_4)_3$ , Electro-coagulation, NaCl, Reactive blue.

### INTRODUCTION

The reuse and recycle are the main factors to face the challenges of depletion of reserves and environmental troubles in the new world age where. Wastewater is not only one of the main pollutant that damages the environment, but also leads to the deficit of the earth water. A lot of industrial processes are managed at the spend of plenty of fresh water, which is haggard as a wastewater, and need to be treated to eliminate or uproot the pollutants and to produce a pure treated water in order to be reused as a sustain environment natural resource [1].

Textile industry wastewater is strongly polluted with many chemical pollutants, its percentage emission to the nature is 70%. The wastewater from textile processing as follows: water bath from preparation, dyeing, finishing, slashing , printing, coloring and other operations, In the textile industries and during the dyeing process a lot of fresh water are used which are the main consumers of synthetic dyes. The industrial wastewater contains many kinds of pollutants: chemical oxygen demand, dyes, suspended solids, high temperature, salts and variable pH. These pollutants damage the environment. Wastewater should be treated before it is drained to the rivers or seas. However , these pollutants could be treated for minimum harmful for the environment or for better behavior after they

flow to the nature. The textile industry utilizes about 10,000 dyes and pigments [2]. In general one method of treatment is not sufficient for a perfect treatment. A combined treatment with physical , chemical and biological treatment are used to remove the heavy pollutants from textile wastewater [3-5].

More recently, studies have focused on color removal from real combined textile wastewater and reactive dye bath effluent [5, 6] as well as aqueous textile dyes [7-10].

It can see that the combination of physical, chemical and biological methods are the most traditional treat the textile wastewater. This attribute to the high molecular weight of dye and presence of aromatic rings. Clearly, there is low and slow degradation when using biological methods [6-8]. Precipitation and adsorption are consume time and money as they are physical methods, on the other hand, most of chemical treatments generate secondary pollutants, such as, adding of aluminum sulfate and chlorine.

Some other advanced technologies such as photo oxidation by  $\text{UV}/\text{H}_2\text{O}_2$  or  $\text{UV}/\text{TiO}_2$  also generate secondary pollutants [9]. Biological treatment of textile wastewater has low efficiency because of the toxicity of dye molecules to active microorganisms.

Electro-coagulation (EC) process has been mostly used to treat many pollutants in wastewaters

because it is a simple and effective method. This process was based on the forming of coagulants via electrolytic reactions at electrode column. The formulization of destabilization agents brings about neutralization of electric charge for removing pollutant [10]. EC process also facilitates flocculation by turbulence generated by oxygen and hydrogen transformation at the cathode and anode electrodes. With the gas evolution, particles are destabilized and they start attracting each other and generate bigger particles. EC process depends on particle size, pH, conductivity, and the concentrations of the continuous phase. These experimental factors affect the results in different ways. EC has some advantages like simple apparatus, easy automation of the process, versatility, environmental compatibility, quick reactions and smaller systems [11, 12].

This study aims is to conduct an experimental investigation on the removal of a reactive blue from the wastewater using the chemical coagulation and electro-coagulation methods. Several fundamental aspects regarding the effects of type of coagulants, pH, coagulants dosage, voltage, pH, electrolyte concentration and dye initial concentration.

## MATERIALS AND METHODS

### Preparation of reactive blue dye

Reactive blue dye (Commercial Name : Forosyn Blue (SE) was supplied from 14 Ramadan factory of textile industries\_ ministry of industry, with molecular weight 1309.87 gm/gmol, molecular formula  $C_{38}H_{28}C_{12}N_{14}O_{18}S_5Na$  was used in this study as model pollutant for textile dyes. Dye stock solution was prepared by dissolving 1 g of dye in 1 liter distilled water, the final concentration is 1000 mg/L. The experimental solutions were obtained by diluting the dye stock solutions in accurate proportions to obtain different initial concentrations.

### Chemicals

Ferrous sulfate  $[FeSO_4]$ , ferric sulfate  $[Fe_2(SO_4)_3]$ , alum  $[Al_2(SO_4)_3 \cdot 5H_2O]$  and polyaluminium chloride or PACl  $[AlCl_3 \cdot 6H_2O]$ , were used as a coagulant using stock solution (1000 mg/L). Sodium chloride NaCl was used as electrolyte. For pH adjustment, sodium hydroxide, NaOH and hydrochloric acid were used. All the chemicals used were supplied from BDH company, England.

### Jar Tests

Jar tests were conducted in the coagulation process to find the optimum pH, initial

concentration, coagulant doses (for each coagulant). Jar tests were done with six bakets size 1000 ml. Reactive blue solution was prepared previously. pH was adjusted to the desired value by the addition of 0.1M HCl or/and 0.1M NaOH solutions as required. The samples were mixed for 2 min, 200 rpm (rapid mixing), then slow mixing for 30 min, 50 rpm. The coagulation process was taken place, with the consistence of flocculants, precipitation and settlements. The mixers were left for 30 min to allow the agglomerates to settle down. Samples were taken from 1-2 mm below the solution surface.

### Electro-coagulation cell

The experiments were conducted in a beaker 1L in capacity. The anode and cathode were positioned vertically and in parallel to each other with an inter electrode gap of 3.5 cm. Both anode and cathode were an aluminum plates 7cm high, 4cm width and 0.3 cm thickness. These electrodes were dipped in the electrolyte solution. Stabilized DC power supply was used as the source of electrical current (Figure. 1). The solution was constantly stirred at 200 rpm using a magnetic stirrer in order to maintain uniform concentration of the electrolyte solution, a stirrer Model LMS-1003 Korea was used.

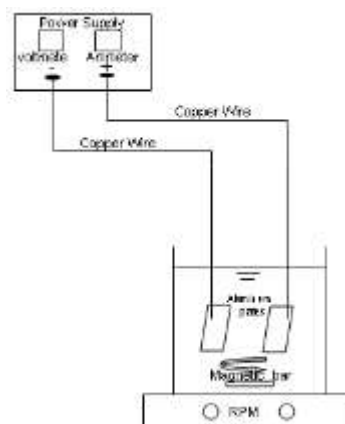


Fig. 1 Experimental set up

### Analytical methods

The mixture of reactive blue dye of the samples was drawn, centrifuged using electrical centrifuge device at 5000 rpm for 20 minutes and un adsorbed supernatant liquid was analyzed for the residual dye concentration using Elico make UV Spectrophotometer (CI 73) at a max wavelength of 592 nm. Reactive blue dye removal efficiencies was calculated by:

$$Removal(\%) = \frac{C_r - C_t}{C_t} \times 100 \quad (1)$$

where,  $C_r$  and  $C_t$  are the concentration in raw



and treated solutions, respectively.

## RESULTS AND DISCUSSIONS

### For chemical coagulation

#### *pH effect's*

pH plays an important role in the coagulation process. The charge percentage for what precipitate from metal hydroxide and hydrolysis product are controlled by pH whatever is increasing or decreasing. Thus, pH must be controlled to establish optimum conditions for coagulation [13]. To examine the effect of pH on reactive blue dye removal efficiency, dosage of 150 mg/L of each coagulants were taken, while varying pH of the samples using 0.1M HCl and/or 0.1M NaOH from (2-12). Reactive blue dye concentration was fixed at 50 mg/L during the experiments.

Figure 2 shows the maximum removal of reactive blue, and they are as follows 86, 75, 35 and 91 % at pH 8, 10, 4 and 6 for alum, PACL,  $\text{FeSO}_4$  and  $\text{Fe}_2(\text{SO}_4)_3$  respectively. The reason for these results can be explained by, that every coagulant had its point of zero charge. Below this pH, the coagulant is protonated and the surface is positively charged; however, attractive of negatively charged ions (for examples, dyes) is favorable. Above this pH, the coagulant surface becomes negatively charged, so in this region of pH, dye ions cannot be attracted effectively. Gaceva et al., 2008 [14] studied the removal of color from wastewater containing water base color using polyaluminium chloride (PACl). The optimal results for reactive dye enabling almost 80% dye removal, were obtained at pH=7.1 and PACl concentration of 20 mg/L [15].

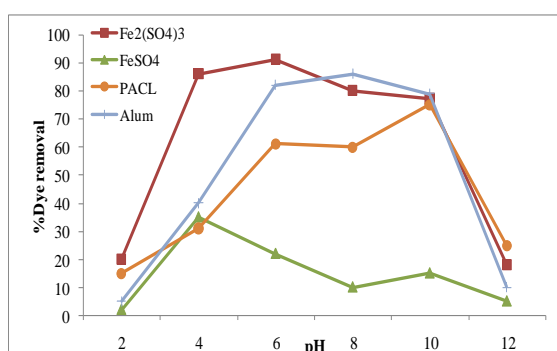


Fig. 2 Reactive blue removal as a function of pH at dye concentration 50 mg/L.

#### *Coagulant dosage effect's*

To study the effect of coagulant dose, the pH was fixed at optimum value from previous experiment and the initial concentration of reactive blue is 50 mg/L. The coagulant doses were varied as

(10, 50, 100, 150, 200 and 300 mg/L). The optimum coagulant dose was found to be 200 mg/L. Above this value there is no increase in the percentage removal of reactive blue. As the coagulant dosage increases, the number of binding sites for the dye also increases. After some point (200 mg/L), coagulant capacity was steady due to a screen effect between coagulant molecules, this produced a block of the coagulant active sites by an increase of coagulant dosage in the system. The maximum removal efficiency is 90, 85, 40 and 94% for alum, PACL,  $\text{FeSO}_4$  and  $\text{Fe}_2(\text{SO}_4)_3$  respectively. The same results were reported by some other researchers [16]. Figure 3 reveals the maximum dye removing versus the optimum coagulant dosage.

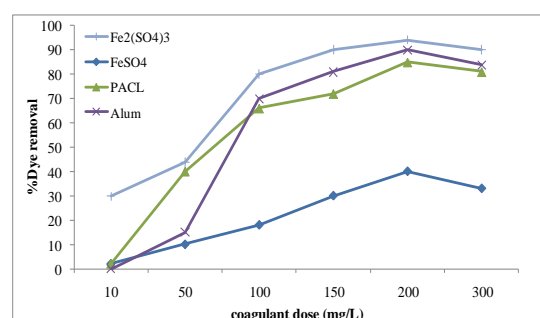


Fig.3 Reactive blue removal as a function of coagulant dosages at optimum pH and dye concentration 50 mg/L.

#### *Initial concentration effect's*

The experiments were performed to determine the effect of initial reactive blue concentration on percentage removal, using a fixed coagulant dosage (the optimum is 200 mg/L). The results are illustrated in Figure 4 for reactive blue, with the increase of initial concentration from 20 -100 mg/l, the removal efficiency, increased suddenly from 81 to 93%, 77 to 87 %, 26 to 41%, 88 to 96% for alum, PACL,  $\text{FeSO}_4$  and  $\text{Fe}_2(\text{SO}_4)_3$  respectively. While, for concentrations more than 100 mg/L, the efficiency goes down and reached to 78, 70, 28 and 79% for the same sequence, for initial concentration of 150 mg/L.

According to the data of Zonoozi group, at the optimum coagulant (polyaluminium chloride and alum) dosage, the removal degree was associated with the initial concentration of the selected dyes, and the smallest removal degree was obtained for smallest concentrations of the dyes [17]. This result is inconsistent with the results obtained for the used coagulants in this study, which showed the smallest values of removal efficiency for smaller initial concentration.

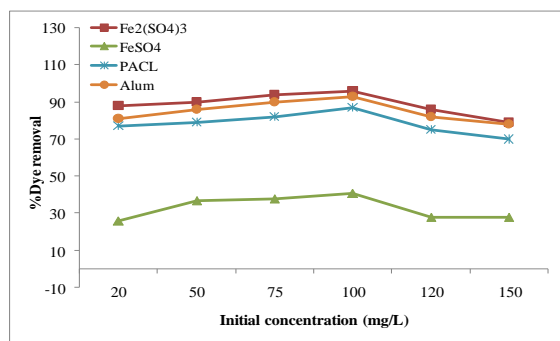


Fig.4 Reactive blue removal as a function of initial concentration at optimum pH and dosage.

### For Electro-coagulation

#### pH effect's

Experiments were conducted under acid, alkaline and neutral conditions as mentioned in chemical coagulation process by adjusting the electrolyte with 0.1M NaOH and/or 0.1M HCl. The observations are given in Figure 5, where the removal of reactive blue increased with decreasing the pH of the solution. The reason may be due to the increasing of the hypochlorite ion in an acidic medium and in low pH solutions the presences of hypochlorous acid (HOCl), which possesses higher oxidation potential than that of hypochlorite ion.

It can be ascertained from Figure 5 that, the maximum removal for reactive blue was 88% at pH 2 for NaCl concentration 500 mg/L and voltage of 5 V after about 30 minutes reaction time. Some researches achieved maximum removal of color in the pH range of 1.5 – 4 [18, 19].

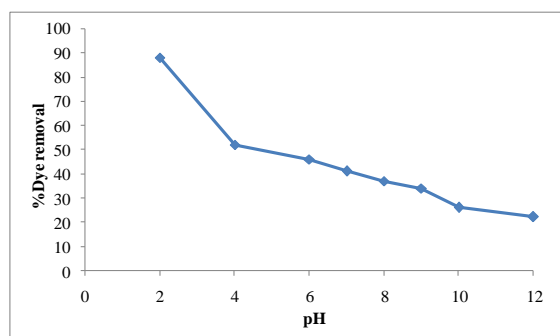


Fig.5 Percentage removal of reactive blue, as a function of pH.

#### NaCl concentration effect's

The effect of changing the electrolyte concentration (200, 500 and 1000 mg/L) on dye removal efficiency at optimum pH obtained from previous experiment, fixed dye and initial

concentration of 50 mg/L and voltage of 5V is illustrated in Figure 6. It is clear from this figure that, the reactive blue removal was increased when NaCl concentration increased from 200 to 500 mg/L, and when NaCl concentration increased up to 1000 mg/L, dye removing increased and equal 95%, because the conductivity of solutions rise when NaCl concentration increased and resistance decreases, so the passed current increases and the produced amount of metallic hydroxide and dye removal increases, also, hypochlorite ions produced at the anode causes the increasing in dye removal by oxidation of dye molecules [20-22].

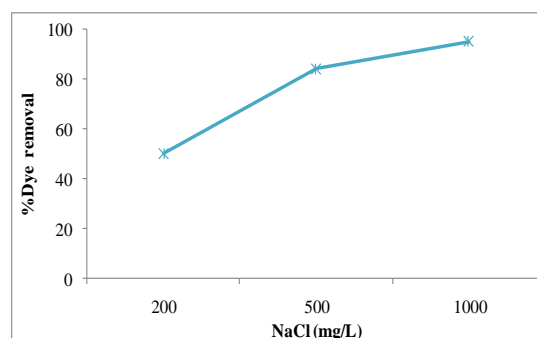


Fig.6 Percentage removal of reactive blue, as a function of NaCl concentration

#### Initial concentration effect's

The reactive blue percentage removal decreases with an increase in the initial concentration, because the number of metal hydroxide flocs formed may be insufficient to absorb all of the pollutant molecules when the initial pollutant concentrations are rather high [23]. Dye solutions with the following concentrations (50, 75, 100, 200, and 300 mg/L) was used in order to test the effect of initial dye concentration on degradation efficiency at optimum pH and NaCl concentration. Results showed that, when dye concentration increased to 100 mg/L, dye removals increased to 96% as shown in Figure 7. However, when the concentration raised up to 300 mg/L, the removal decreased to 51%, because of dye molecule adsorption on metallic hydroxide flocs. At the same voltage, the amount of Al<sup>3+</sup> that released from anode to solution is constant, thus, the amount of flocs is also constant, therefore, a specific amount of dye molecules would adsorbed onto the flocs, no more dye molecule adsorption, therefore, the efficiency of dye removal decreases when concentration increase [24, 25].

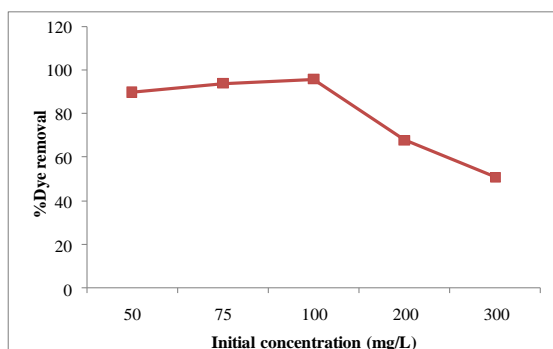


Fig.7 Percentage removal of reactive blue as a function of initial concentration

#### Voltage variation effect's

The effect of varying the voltage in the ranges 5 and 15 V at optimum operation conditions was investigated. Reactive blue removal increases when the voltage increased. The removal efficiency reached to 90% when the voltage is 5, and 99% at 15 V, as shown in Figure 8. The maximum removal is registered at 15 V. However, after 60 min the removal was at a constant rate. It is clear that, dye removal depend on many factors, first of all, aluminum dosage, and this depends on the voltage and time of reaction, because of that, when the voltage increase, coagulants and flocs amount increase, so, dye is removed. The same results were obtained by other researchers [26, 27].

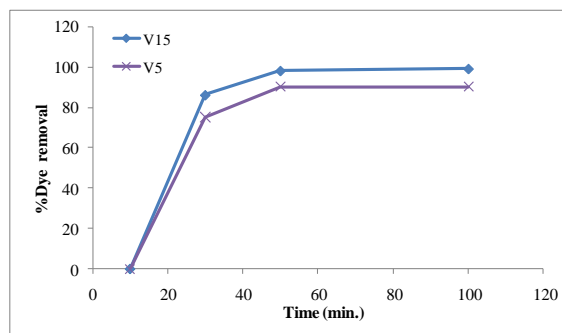


Fig.8 Percentage removal of reactive blue as a function of voltage

#### CONCLUSIONS

After treatment by both electro-coagulation and chemical coagulation processes, the obtained removal efficiency of reactive blue are very high, the values is 96% when chemical coagulation was used, while it's 99% with electro-coagulation treatment. The optimum pH for both processes occurred under acidic condition where the value is 6 and 2 for chemical coagulation and electro-coagulation respectively. The removal efficiency increase with increased dosages of coagulants and

electrolytes to 200 mg/L and 1000 mg/L. The removal efficiency, increased with increase in the initial concentration to certain values then decreased.

The performance of electro-coagulation is relatively better than chemical coagulation. To overcome problems associated with chemical coagulation, EC could be advocated as a novel approach in removing wide range of wastewater pollutants such as dye.

#### ACKNOWLEDGMENTS

The author would like to thank the Mustansiriyah university ([www.uomustansiriyah.edu.iq](http://www.uomustansiriyah.edu.iq)) Baghdad - Iraq for its support in the present work.

#### REFERENCES

- [1] Eddy M.A., Inc Wastewater Engineering, Treatment and Reuse. 4th Edition, 2003. McGraw-Hill, New York, 2003, pp. 545-644.
- [2] Korbahti K.B., Abdurrahman T., Electrochemical Treatment of Simulated Textile Wastewater with Industrial Components and Levafix Blue CA reactive dye , j.haz mat, 2006, pp. 422-31.
- [3] Sheng H.L., Chi M.L., Treatment of textile waste effluents by ozonation and chemical coagulation, Water Research J., Vol. 27, Issue 12, 1993, pp. 1743-1748.
- [4] Ghoreishi R., Chemical catalytic reaction and biological oxidation for treatment of non-biodegradable textile effluent, Haghghi, Chemical Engineering Journal, Vol. 95, Issues 1-3, 2003, pp. 163-169.
- [5] Daneshvar N., Oladegaragoze A., Djafarzadeh, N., Decolorization of basic dye solutions by electrocoagulation: an investigation of the effect of operational parameters, J. Hazard. Mater. B129, 2006, pp. 116-122.
- [6] Shaul G.M., Holdsworth T.J., Dempsey C.R., Dostall K.A., Fate of water soluble azo dyes in the activated sludge process, Chemosphere, Vol. 22, 1991, pp. 107-109.
- [7] Swamy J., Ramsay J.A., The evaluation of white rot fungi in the decoloration of textile dyes, Enzyme and Microbial Technology, 1999, Volume 24, 2004, pp. 130-137.
- [8] Muthukumar M., Sargunamani D., Selvakumar N., Rao, J.V., Optimisation of ozone treatment for colour and COD removal of acid dye effluent using central composite design experiment, Vol. 63, Issue 2, 2004, pp. 127-134.
- [9] Pablo C., Fabiola M., Carlos J., Justo L., and Manuel A.R., Coagulation and Electrocoagulation of Wastes Polluted with Dyes, Environ. Sci. Technol., 2006, Vol. 40, No.

- 20, 2006 pp. 6418–6424.
- [10] Usha N.M., Rekha H.B., Mahaveer D., Contribution of Electrochemical Treatment in Treating Textile Dye Wastewater, World Academy of Science, Engineering and Technology International Journal of Materials and Textile Engineering Vol. 8, No. 2, 2014.
- [11] Guohua C., Electrochemical technologies in wastewater treatment, Separation and Purification Technology, Vol. 38, 2004, pp. 11–41
- [12] Humberto R., Carlos B., Ivonne L., Cheikh F., Bilyeu B., A Combined Electrocoagulation-Electrooxidation Process for Carwash Wastewater Reclamation, Int. J. Electrochem. Sci., Vol. 10, 2015, pp. 6754 – 6767.
- [13] Mitra G., Ahmad, J.J., Niyaz M.M., Dye Removal, Energy Consumption and Operating Cost of Electro-coagulation of Textile Wastewater as a Clean Process, Clean- Soil Air Water, 2011.
- [14] Gaceva G. B., Aleksandra B. and Bojan D., Discoloration of Synthetic Dyeing Wastewater Using Polyaluminium Chloride. G.U. Journal of Science, Volume 2, No.4, 2008, pp. 123-128.
- [15] Baoyou S., Guohong L., Dongsheng W., Chenghong F., Hongxiao T., The performance of preformed polymeric aluminum species, Journal of Hazardous Materials, Vol. 143, Issues 1–2, 2007, pp. 567–574.
- [16] Akshaya K.V., Rajesh R.D., Puspendu B., A review on chemical coagulation/flocculation technologies for removal of colour from textile wastewaters, Journal of Environmental Management, Vol. 93, 2012, pp. 154-168.
- [17] Zonoozi M. H., Mohammad R.A., Mokhtar A., Removal of Acid red 398 dye from aqueous solutions by coagulation/flocculation process, Environmental Engineering and Management Journal, Vol. 7, No.6, 2008, pp. 695-699.
- [18] Chen, G. and Hung, Y.T., Electrochemical Wastewater Treatment Processes, in Handbook of Environmental Engineering, The Humana Press Inc., Totowa, NJ., Vol. 5, 2007, pp. 57-105.
- [19] Li F., Li S., Zhang C., Zhao H., Application of corrosive cell process in treatment of printing and dyeing wastewater, Chem. Eng. Environ. Protect., Vol. 15, 1995, pp. 157–161.
- [20] Yang, Y., Electrochemistrical decolorization of C.I. Reactive black KN-B simulated wastewater, Chin. J. Environ. Sci., 2009.
- [21] Wong H.M, Shang C., Cheung Y.K., Chen G., Chloride Assisted Electrochemical Disinfection, in: Proceedings of the Eighth Mainland-Taiwan Environmental Protection Conference, Tsin Chu, Taiwan, 2002.
- [22] Vinita K., Electrocoagulation for the treatment of textile industry effluent - A review Article in Journal of Environmental Management, 2013.
- [23] Song, S. He, Z., Qiu, J., Chen, X. L., Ozone Assisted Electrocoagulation for Decolorization of C.I. Reactive Black 5 in Aqueous Solution: An Investigation of the Effect of Operational Parameters, Sep. Purif. Technol. Vol. 55, 2007, pp. 238–245.
- [24] Fatiha Z., Patrick D., Brahim L. , Jalila B., Jean, F., Ois B., Said B. , Kacem K., Decolourization of dye containing effluent using mineral coagulants produced by electrocoagulation, Journal of Hazardous Materials, Vol. 155, 2008, pp. 153–163.
- [25] Zhang, Y., Cong, Y., Sun, P., Experiment and kinetic model for methyl orange wastewater removal by electrocoagulation. J. Chem. Ind. Eng. Soc. Chin., 2009.
- [26] Arslan, A., Tuerkoglu, I., Kabdash, G.I., Chemical pretreatment of a spent disperse dyebath analogue by coagulation and electrocoagulation. Fresenius Environ. Bull. Vol. 17, 2008, pp. 1809-1815.
- [27] Jiang J.Q., Development of coagulation theory and pre-polymerized coagulants for water treatment, Separation and Purification Methods, Vol. 30, 2001, pp.127-141.

## INDOOR PLANT SPECIES SURVIVAL UNDER DIFFERENT ENVIRONMENT IN INDOOR VERTICAL GARDEN

Sukanya Chaipong<sup>1</sup>

<sup>1</sup>Faculty of Agricultural Technology, Rajamangala University of Technology Thanyaburi, Thailand

### ABSTRACT

One way to measure the efficacy of a vertical garden is the survival of the plants that cover the growing area, which affects the beauty of a vertical garden. Thus, this research aimed to study the survival of some indoor plant species in with and without air conditioning. We selected plants from 15 families in a total of 20 plant species by review the documents related to the indoor plant and based on duplication of the top 20 plant species, and popular in the market. The study was conducted by incubating in a room with air conditioning (average of temperature and light at 25.6 Celsius and 396.6 Lux, respectively) and without air conditioning (average of temperature and light at 31.9 Celsius and 2,044.1 Lux, respectively), 8 hrs./day average light, watering one time in the initial experiment and noticed the water saturated soil. The survival condition was recorded in 3 levels, namely, the normal condition was 1, the wilted condition was 2 and the dead condition was 3. The data was collected for 15 days. The results were 7 species of plants that tolerated both conditioning included as *Philodendron* 'Moonlight', *Aechmea fasciata*, *Tradescantia zebrina*, *Chlorophytum comosum*, *Dracaena surculosa*, *Tillandsia usneoides* and *Nephrolepis cordifolia*. There were in Araceae, Commelinaceae, Agavaceae, Neprolepidaceae and Bromeliaceae families.

**Keywords:** Indoor plant species, Vertical garden, Plant species survival, Indoor vertical garden

### INTRODUCTION

The limitation on space for landscaping by vertical gardening is a more popular choice, and also has many benefits, especially improving the urban environment. Nowadays, it is popular both inside and outside the building. A living wall with a fabric system is one of the types that is used inside the building. The efficiency of this system depends on the water supply system, structure, and plants that affect the efficacy of cover and beauty. It was found that 5-10 percent of a plant in the indoor living wall death and must be planted to replace. This high-cost was loss by planted to replace [1]. Considerations for choosing plants depend on moisture and light which may not be direct sunlight but it can be light bulbs [2]. Therefore, the efficiency maintenance of living wall which is the plant selection for an aesthetic and living. This research aims to test the survival plants that are arranged in a vertical garden, both with air conditioning and without air conditioning. This information is useful for the landscape designers and gardeners for choosing a plant that anesthetic and living to save on the maintenance cost.

### MATERIALS AND METHODS

1) Establish a vertical garden structure from steel material, box size 1.00 x 2.00 meters, choose the type of plants that are popularly planted on the vertical

garden, 23 species, using the planting sheet (Felt) attached to the structure and penetrate the planting box. Using 4 plants per species, first watering once, until the soil is saturated with water.

2) Place in the interior of the building with air conditioning and without air conditioning turned to the east, both conditions.

3) Recording data for 15 days by temperature and light ( Light intensity meter model TM- 213 TENMARS), which 3 times daily at 9.00 am., 12.00 am. and 16.00 am. and also the survey record in survival landscape ( The survival landscape is the survival plants, which beauty in landscape visibility.) was representative 1 as normal, 2 as wizened (With more than 50% wilted leaves of the leaves) and 3 as dead.



3 = Died                      2 = wizened                      1 = Normal

Fig. 1 Survival landscape status

4) Using the data to analyze with descriptive

statistics and interpretation of values obtained from the average survival conditions in the landscape, there was 1.00 - 1.67 means normal, 1.68 - 2.33 means wilted and 2.34 - 3.00 means death. Comparing the survival conditions of both plant conditions with the Chi-Square hypothesis test.

## RESULTS

### Survival Landscape Survey Results.

Based on the study of ornamental plants that are suitable for use in vertical garden, comprising 16 families [3]-[5] including Araceae, Aspleniaceae, Liliaceae, Commelinaceae, Bromeliaceae, Labiatae, Polypodiaceae, Urticaceae, Gesneriaceae, Apocynaceae, Acroleanidae, Neprolepidaceae, Convallariaceae, Lythraceae, Piperaceae and Agavaceae. There were chosen 23 species of plants that the book recommends, and also considered the popularity and available in the market. 23 Plants experimented with 16 Families as shown in Table 1 and 2.

The results found both landscape survival conditions were "normal" including *Chlorophytum comosum* (*Anthesicum Vittatum*), *Aechmea fasciata*, *Tradescantia zebrina* Loudon ( *Zebrina pendula* Schnizl. ) , *Philodendron 'Moonlight'*, *Dracaena surculosa*, *Nephrolepis cordifolia* and *Tillandsia usneoides*, which are in family of Bromeliaceae Commelinaceae Araceae Agavaceae Neprolepidaceae and Bromeliaceae, respectively. On the other hand, *Fittonia albivenis*, *Pilea cadieri*, *Lectranthus scutellarioides* and *Cuphea hyssopifolia* died in both conditions, which are in family of Acanthaceae Urticaceae Labiatae Lythraceae, respectively. Further, it was found that wizened plants in both conditions, *Platynerium holtumii*, *Asplenium nidus*, *Syngonium podophyllum*, and *Epipremnum aureum*, which are the family of Polypodiaceae, Aspleniaceae, Araceae, respectively.

In additional *Pellionia repens* (Lour.) Merr was found dead in air condition but the normal condition in without air conditioner, which belongs to the Urticaceae and also two species are *Ophiopogon japonicus* ( Convallariaceae) and *Chlorophytum comosum* ( *Anthesicum Picturatum*) ( Liliaceae) , which died in air conditioning but wizened in the without air conditioning. Moreover, there are two types of Araceae; *Epipremnum aureum* 'Marble Queen' and *Philodendron erubescens* K. Koch & Augustin ' Lemon Lime' , and *Dischidia* ' White Diamond' (Apocynaceae), there were normally in air conditioning but wizened in without air conditioning. On the other hand, it was found two species;

*Peperomia obtusifolia* (Piperaceae) and *Episcia* spp. & Hybrid (Gesneriaceae) which is wizened in the air conditioning and normally in the without air conditioning.

It can be seen species that found to survive both conditions is Araceae but found that some species wizened in both conditions in this family include *Syngonium podophyllum* and *Epipremnum aureum*. *Pellionia repens* (Lour.) Merr. and *Pilea cadieri* is in the Urticaceae, were died in both conditioning, but *Pilea cadieri* survived without air conditioning. The air-conditioned rooms have a "dead" plant rather than in a room without air conditioning. While in a room without air conditioners were found less "wilted" plants and also "dead" plants condition than rooms with air conditioning.

Table 1 23 Plant species of experimented

| No. | Scientific name   | Family name     |
|-----|---|-----------------|
| 1   | <i>Fittonia albivenis</i>   | Acanthaceae     |
| 2   | <i>Pilea cadieri</i>  | Urticaceae      |
| 3   | <i>lectranthus scutellarioides</i>                                    | Labiatae        |
| 4   | <i>Cuphea hyssopifolia</i>  | Lythraceae      |
| 5   | <i>Platynerium holtumii</i>   | Polypodiaceae   |
| 6   | <i>Asplenium nidus</i>  | Aspleniaceae    |
| 7   | <i>Syngonium podophyllum</i>  | Araceae         |
| 8   | <i>Epipremnum aureum</i>  | Araceae         |
| 9   | <i>Chlorophytum comosum</i> ( <i>Anthesicum Vittatum</i> )            | Liliaceae       |
| 10  | <i>Aechmea fasciata</i>   | Bromeliaceae    |
| 11  | <i>Tradescantia zebrina</i> Loudon ( <i>Zebrina pendula</i> Schnizl.) | Commelinaceae   |
| 12  | <i>Philodendron 'Moonlight'</i>                                       | Araceae         |
| 13  | <i>Dracaena surculosa</i>   | Agavaceae       |
| 14  | <i>Nephrolepis cordifolia</i>   | Neprolepidaceae |
| 15  | <i>Tillandsia usneoides</i>   | Bromeliaceae    |
| 16  | <i>Ophiopogon japonicus</i>   | Convallariaceae |
| 17  | <i>Pellionia repens</i> (Lour.) Merr.                                 | Urticaceae      |
| 18  | <i>Chlorophytum comosum</i> ( <i>Anthesicum Picturatum</i> )          | Liliaceae       |
| 19  | <i>Epipremnum aureum</i> 'Marble Queen'                               | Araceae         |
| 20  | <i>Philodendron erubescens</i> K.Koch & Augustin 'Lemon Lime'         | Araceae         |
| 21  | <i>Dischidia</i> 'White Diamond'                                      | Apocynaceae     |



| No. | Scientific name              | Family name  |
|-----|------------------------------|--------------|
| 22  | <i>Peperomia obtusifolia</i> | Piperaceae   |
| 23  | <i>Episcia</i> spp. & hybrid | Gesneriaceae |

Table 2 landscape survival status in air-conditioning and without air-conditioning

| No. | Air condition room<br>(Temperature average 25.6) |      |          | Without air condition room<br>(Temperature average 31.9) |      |          |
|-----|--|------|----------|--|------|----------|
|     | landscape survival status (x□)                   | SD   | Mean-ing | landscape survival status (x□)                           | SD   | Mean-ing |
| 1   | 2.69   | 0.24 | D        | 2.73   | 0.59 | D        |
| 2   | 2.40   | 0.26 | D        | 2.57   | 0.67 | D        |
| 3   | 2.58   | 0.26 | D        | 2.35   | 0.88 | D        |
| 4   | 2.47   | 0.27 | D        | 2.57   | 0.77 | D        |
| 5   | 1.76   | 0.14 | w        | 2.20   | 0.51 | w        |
| 6   | 2.32   | 0.26 | w        | 2.08   | 0.86 | w        |
| 7   | 2.24   | 0.24 | w        | 1.77   | 0.73 | w        |
| 8   | 2.30   | 0.23 | w        | 2.00   | 0.93 | w        |
| 9   | 1.00   | 0.00 | N        | 1.60   | 0.51 | N        |
| 10  | 1.00   | 0.00 | N        | 1.15   | 0.58 | N        |
| 11  | 1.00   | 0.00 | N        | 1.40   | 0.51 | N        |
| 12  | 1.00   | 0.00 | N        | 1.40   | 0.51 | N        |
| 13  | 1.48   | 0.13 | N        | 1.53   | 0.52 | N        |
| 14  | 1.00   | 0.00 | N        | 1.13   | 0.52 | N        |
| 15  | 1.00   | 0.00 | N        | 1.23   | 0.42 | N        |
| 16  | 2.34   | 0.27 | D        | 2.20   | 0.94 | w        |
| 17  | 2.47   | 0.21 | D        | 1.62   | 0.31 | N        |
| 18  | 2.54   | 0.17 | D        | 1.98   | 0.93 | w        |
| 19  | 1.67   | 0.17 | N        | 1.93   | 0.88 | w        |
| 20  | 1.11   | 0.06 | N        | 1.68   | 0.71 | w        |
| 21  | 1.00   | 0.00 | N        | 1.83   | 0.94 | w        |
| 22  | 1.77   | 0.20 | w        | 1.52   | 0.59 | N        |
| 23  | 1.77   | 0.20 | w        | 1.52   | 0.59 | N        |

Remarks: D is died, W is wizened and N is Normal

### Hypothesis Results

Comparison of survival landscape of plant species in each condition was found that each plant is not different in both conditions of a survival landscape. There were the same results as 0.317, therefore it was accepted the main hypothesis that each plant not significantly different at the level of 0.05 of survival landscape.

Based on the main hypothesis that plants are in the air-conditioning and without air-conditioning have no difference in a survival landscape. It is found that significance at 1.88, therefore both conditions had no difference in a survival landscape of a significant level at 0.05.

### DISCUSSION

Light temperature and relative humidity were averaged relative rooms with and without air conditioning 25.6, 31.9 degrees Celsius, and 396.6, 2,044.1 lux and 56.45% 51.25%, respectively. There was a light average of 8 hours/day. Gunawardena K. and Steemers K. [6] said that the relative humidity of humans and plants are that occupant comfort in the room is 20-28 degrees Celsius and 30-50% relative humidity and also Blanc P. [7] said that some plant species selected tend to require high canopy humidity to maintain good foliage health (RH85–95%). This comfort level RH may present the risk of foliage water stress. Vertical plant canopies however rare observed to maintain a self-hydrating micro climate that mitigates this risk to an extent. In additional, Jongrunklang N. [8] said that the temperature and humidity in the air is a factor that affects the dehydration of plants. This affects the growth process of plants, and Techawongstien S. "In press" [9] says that moisture in the air is a low effect on a lot of dehydration plants. This is consistent with the results of the study that air-conditioned rooms have a "dead" landscape survival rather than in rooms without air conditioning. Therefore, the relative humidity level in the experiment was at the level that humans and plants are occupant comfort but a relative humidity that likely to be more maintained to good foliage health. As corresponds to the results of the air condition room which the lower relative humidity, was "dead" plant rather than in another.

The study was found that the plants survival landscape both conditions are *Tradescantia zebrina* Loudon ( *Zebrina pendula* Schnizl. ) of the Commelinaceae family which is a plant with crater and leaf similar to succulent characteristics. According to the study Gunawardena K. and Steemers K. [10], one of the most popular plants is succulent plants. This corresponded to Rochanavibhata [11] found that indoor shrub plants that are resistant to low-light environments or light frenzy are mostly succulent plants. The family is similar to succulent plants namely the *Philodendron* in the Araceae and the *Dracaena surculosa* in the Agavaceae which is Semi-succulent plants [12]. In additional plants that tolerate both conditions were

*Nephrolepis cordifolia* in the Neprolepidaceae, *Aechmea fasciata* and *Tillandsia usneoides* in the Bromeliaceae both families are generated with wax leaf. These plants are suitable for planting in a vertical garden especially in a living wall. Due to the leaves can reduce dehydration and also reduce the capture of dust "In press" [13].

## CONCLUSION

The hypothesis test shown that the survival landscape conditions of each plant and both conditions do not differ at the significance level 0.05. These results of temperature and relative humidity have affected the survival of plants. The indoor should have a temperature of 20-28 degrees Celsius and relative humidity of 30-50% so that people and plants are comfortable. It can maintain good foliage health in an indoor vertical garden without air conditioning, which a temperature of 28-32 degrees Celsius and relative humidity at 85-95%. On the other hand, an indoor vertical garden with air conditioning suggests to Commelinaceae, Araceae, Agavaceae, Neprolepidaceae, and Bromeliaceae.

From the results, appropriate plants are recommended in the vertical garden (Living wall), which with and without air conditioning, including *Philodendron* 'Moonlight', *Aechmea fasciata*, *Tradescantia zebrina*, *Chlorophytum comosum*, *Dracaena surculosa*, *Tillandsia usneoides*, and *Nephrolepis cordifolia*.

## ACKNOWLEDGEMENTS

Thank you to the Faculty of Agricultural Technology, Rajamangala University of Technology Thanyaburi for the research budget.

## LITERATURE CITED

[1] Pérez-Urrestarazu L., Fernández-Cañero R., Franco-Salas A. and Gregorio E., Vertical greening systems and sustainable cities. *Journal of Urban Technology*, Vol. 22, Issue 4, 2015, pp. 65-85.

[2] Fernández-Cañero R., Urrestaraz, LP. and Salas FA., Assessment of the Cooling Potential of an Indoor Living Wall Using Different Substrates in a Warm Climate, *Indoor and Built Environment*, Vol. 21, Issue 5, 2012, pp. 642-650

[3] Flower Ornament Club, *Ornamental Plants Manual*. Bangkok: United Books, 1993, pp 1-138.

[4] Promthong W., Bunnak C. and Chaimongkol C., *Indoor Plotted Plant* (2nd edition). Bangkok, Pikanesh Publishing, 2000, pp. 1-103.

[5] Bunnak T., *Vertical Garden Plants* (1<sup>st</sup> edition). Bangkok: Baanlaesuan Publishing, 2012, pp 1-129.

[6] Giordano R., Montacchinia, E., Tedesco, S. and Peronea, A *Living Wall Systems: a technical standard proposal*. *Energy Procedia*, Vol. 111, 2017, pp. 298 – 307.

[7] Blanc P., *The Vertical Garden: from Nature to the City* (Revised Ed), W.W. Norton, New York, 2012, pp. 208.

[8] Jongrunklang N., Crop growth modeling: a novel way to supplement conventional trial. *KHON KAEN AGR. J.*, Vol. 41, Issue 3, 2013, pp. 359-368.

[9] Techawongstien S., *Factors Affecting Plant Growth and Development*, Horticultural field, Department of Plant Science and Agricultural Resources, Faculty of Agriculture, Khon Kaen University, 2017, Available Source: [https://ag.kku.ac.th/suntec/1341/13410120%01Factors%20affecting%20G-D%20note\).pdf](https://ag.kku.ac.th/suntec/1341/13410120%01Factors%20affecting%20G-D%20note).pdf), August 1, 2017.

[10] Gunawardena K. and Steemers K., *Living walls in indoor environments*. *Building and Environment*, Vol. 148, 2019, pp.478-487.

[11] Rochanavibhata S., *Plant Roofing Plates to help reduce heat*. Independent Study, Master of Architecture, Department of Architecture, Kasetsart University, Bangkok, Thailand, 2008.

[12] Chayamrit K., *Key Characters of Plant Families No.3*. Forest and Plant Conservation Research Office, Department of National Parks, Wildlife and Plant Conservation. 90 pages, 2008, pp 1-90.

[13] Shackleton K., Bell N., Smith H. and Davies L., *The role of shrubs and perennials in the capture and mitigation of particulate air pollution in London*, Centre for Environmental Policy, Imperial College London, 2012, Available Source: <https://www.tfl.gov.uk/cdn/static/cms/documents/role-gi-pmpollution.pdf>, August 1, 2017

## THE CONSIDERATIONS FOR URBAN DESIGN REGARDING THE PRESENCE OF ONLINE TAXI BIKE

Heidy Octaviani Rachman<sup>1</sup>, Chotib<sup>2</sup> and Kemas Ridwan Kurniawan<sup>3</sup>

<sup>1,2</sup>School of Strategic and Global Studies, Universitas Indonesia, Indonesia; <sup>3</sup> Department of Architecture, Universitas Indonesia, Indonesia

### ABSTRACT

The online taxi bike gives some convenience to customers since its first launch. The demand for using online taxi bike from the public is quite high. Unfortunately, the high demand is not accompanied by the adaptation of urban space. Streets and circulation nodes begin to be filled with online taxi bike which is hanging or waiting for passengers. This activity causes congestion and misuse of urban infrastructure. This development must be maintained by the government so that the presence of online taxi bike can run optimally without harming any parties. This study will examine how significant the impact of the presence of online taxi bike in urban areas, related to the use of space and urban infrastructure. This study uses qualitative method is done by observing several strategic points in the city and synthesize through the map. The research is complemented by literature studies and enriches the latest information through the city news. The result prove that the existence of online taxi bike can reach the blank spot of the city and complete the public access to the destination. Nevertheless, its existence can lead to conflict especially with other public transportation services. On the other hand, passengers feel great helped by the presence of online taxi bike. The meeting between the two can be arranged by the government in terms of inter-reaching, so that the congestion is reduced and more orderly.

*Keywords: Online Taxi Bike, Demand, Urban Space, Infrastructure, Environmental Behavior.*

### INTRODUCTION

Human activity has been made easier by the presence of technology because space and time can be reduced. With technology, we can now order whatever we need through our hands without stepping out of the house. In terms of transportation, now we no longer need to step into the taxi bike base to get the services, the taxi bike will approach us.

Previously, to get these transportation services, we must walk or visit the terminal or base so that it is easier to get services. But not now, with the sophistication of connectivity technology, certain spaces can turn into close proximity. We know it by the term, online-based transportation.

This research will examine how space can be formed through social processes and also with the intervention of technology. The case study in this issue was an online taxi bike. The formation of online taxi bike spaces is observed from the production process of space in the city, a review of social space and its impact on space.

The area of the study is Margonda street, Depok, agglomeration area from the capital city, Jakarta. In observations on the field, there will be many objective results from the author.

From the book *The Production of Space*, Lefebvre said that space is a product of social activity [1]. Understanding of space production according to Hegelianism is one of which is human beings living

in the world by working to produce history, science, and self-awareness (Lefebvre, 1974). We can understand that the civilization of human life originates from a long and undefined history of space production because humans can only reach the world to the extent that it can be sensed. But we can recognize how space is formed by probing its origin, that is a human social activity.

According to Lefebvre, there are 3 concepts of humans create space according to the way they live in social life. First, perceived space is all physical space that can be sensed by humans. Perceived space or spatial practice is the first space where the occurrence of social interaction between humans formed to human civilization for the first time. Second, conceived space is all space that comes from non-physical aspects or only exists in one's mental state. This second space is only formed after real social interactions occur in physical space. This space develops because humans use their minds to make ideas, make their own perceptions about what they have experienced. With this idea or perception, it will shape the way every human being acts in physical space. Physical space that has been reinterpreted by humans then gradually changes the shape of existing spaces. These spaces are lived space. The three meanings of space do not occur linearly, the process can be intervened by various things, one of them is technology. These three concepts of space are commonly called Triad of Social Space.

If the production of space has reached lived space, then humans will stay in it and eventually become accustomed to interpreting the lived space to become the new perceived space. As proof of this is the development of human history from ancient times to the present. Humans and space are constantly changing. Changes and additions in this space are interpreted as a reproduction of space or can be called the effect of surplus production. The production surplus is not a separate space, but a new idea of man in interpreting his space.

The definition of production here is a process that includes various kinds of activities and forms of space. The production concept is simplified into three concepts, that is an actor (labor), production process (production) and product (product). In this case, space becomes part of a historical production, which includes the intersection of time, space and social beings.

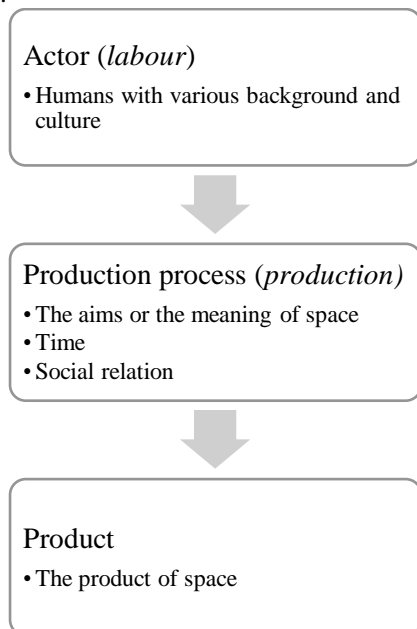


Fig. 1 The process of production space.

Production of space in the city cannot be separated from the social relations between the actors themselves. The conflict that occurred and the driver's personal life in the community certainly had an impact on the space production process that occurred in the city. Personal social relationships of online taxi bike drivers allow them to get a place to stay.

The presence of technology is intended so that humans can make smaller efforts for results that are equal or greater and more accurate. Technology not only facilitates the work of a job, saves time, space and energy, but technology also permeates human activities and changes the pattern of activities and the space it produces. Technology also has the power to change the movements and space produced. The following is a diagram that explains the changes in space that occur in terms of Triad of Social Space.



Fig. 2 The illustration of triad of space with intervention of technology.

According to Lefebvre in *The Production of Space*, in the context of space production, a city is a space formed and invigorated by social activities for a limited period of time and then changed again in the future.

The city consists of physical elements, social systems, and individuals who act in cities (Wirth, 1938). Factors that affect the physical city include economy, social, politics, culture, security and the development of science and technology. The city consists of buildings and activities that are above the ground, sub-surface installations and above-ground activities. City design can control and limit a person's movement, can even decide and intervene (Lynch, 1960). We can experience the city with vision, hearing, smell and another sensing. More than that, the city presents interesting sights and layout to explore (Lynch, 1960).

A city is formed from every activity carried out by the community. They act in it, organize space, work together and try to create a better space for the future. This is what is called the social system in the city. In terms of population, cities generally have densely populated and heterogeneous populations, and have political, economic, religious and cultural organizations (Sirjamaki, 1964).

A good city is a city full of opportunities and expectations. There is room for fulfilling the main, secondary and tertiary needs. Inside is an infrastructure that can connect one place to another, both by walking and riding a vehicle. Without supportive infrastructure, the development of the city becomes slow and human activities become hampered. The network makes all the potential in the city connected to each other and creates greater opportunities for human life.

Each city has spatial planning, but no region is 100% organized by the authorities. This spurred the development of the informal sector in certain areas. Like street vendors and online motorcycle taxi drivers, he has no place so he uses a weak space from power to make a place to stay.

## METHODS

The author begins his research by examining the theory of space production from Lefebvre's perspective. The author shows how social interaction forms a space divided into the triad of social space. Furthermore, Space Production theory is associated with the current conditions, that is the era of technology use. From there it can be seen how space can change because of social activities that are intervened by technology.

Data obtained from direct observation and interviews with objects. Data analysis was carried out by mapping synthesizing field findings.

The area of the study is Margonda Street, Depok, an agglomeration area of Greater Jakarta. The Margonda area is filled with rental and retail housing that continues to grow throughout the year given the existence of 2 major universities around this road. The availability of various needs in this place makes many people visit to buy their needs and just relax. Therefore, the Margonda road should be a pedestrian-friendly road, such as the availability of decent sidewalks and crossing bridges.

## FINDINGS AND RESULT

Taxi bike is a bicycle or motorbike that is added by riding passengers or renters. In this discussion, motorcycle taxi drivers act as central actors forming space. The personal life of actors outside the work area influences the choice of space (Lefebvre, 1988: 78).

### The Base of Conventional Taxi Bike

The taxi bike base is present in an area through a long unplanned process. The process starts with a group of productive-aged citizens who live in an area. They gathered to carry out social interactions including room negotiations until finally they routinely carried out motorcycle taxi activities in the room. The space chosen by the taxi bike base is usually at the end of the road to the fork or intersection and its position can be seen from various angles. This they use so that prospective passengers can easily find their presence. While waiting for customers to arrive, often these motorcycle taxi drivers do other activities.

Taxi bike bases usually operate and deliver passengers around the base area. They rely on space knowledge as a signpost. Passengers who use their services must walk to the base first to get a motorcycle taxi. After arriving at the base, it is likely he will immediately get a taxi bike because usually the base is occupied by more than 3 motorcycle taxi drivers. To get to the destination, the passenger tells the destination by mentioning the spatial code to the driver. The spatial code can be a street name, an

interesting thing or the closest node or the name of a district location. After that, passengers and drivers negotiate prices. When they have reached an agreement, then they leave.

So, the space produced by taxi bike bases is still considering district, lane, knot, interesting things and the edge of an area. Shelters built sometimes do not damage the existing and disturb activities that occur there.

### Online Taxi Bike and Smart Phone Applications

In this digital era, motorcycle taxis have begun to transform. A more modern taxi bike management system has emerged, an application that functions as a means of finding motorbike services provided by third parties (taxi bike drivers). The smartphone application makes online taxi bike drivers work anywhere without having to meet each other and get passengers from the closest radius of their existence. Because of this, online motorcycle taxis can at any time access the territory of the base motorcycle taxi. This is often made as a 'scapegoat' for the reduction in base taxi bike customers, so there have been several conflicts between online taxi bike drivers and conventional taxi bike drivers who maintain power in their territory.

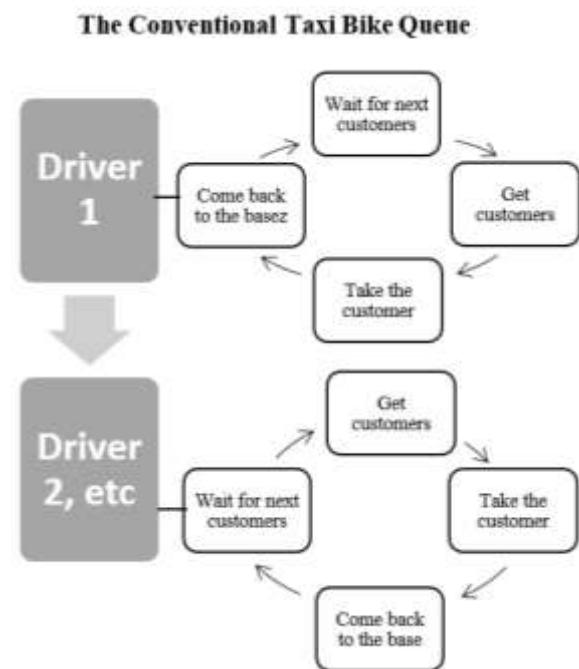


Fig. 3 The cycle of conventional taxi bike.

Online taxi bike drivers can choose to stop somewhere because the place belongs to a friend or the place is not maintained at all so it is easy to stop there.

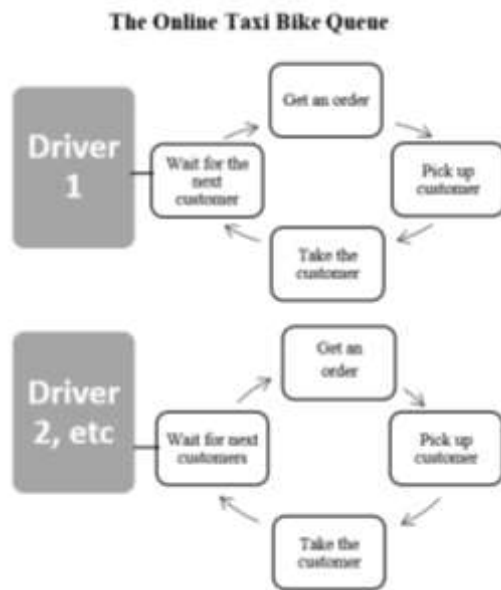


Fig. 4 Travel online taxi bike drivers at a time. Each driver is not related to each other, but his activities can intersect.

### The Comparison between Online and Conventional Taxi Bike

Table numbers and labels should be placed on top of the table, hanging by 12.5 mm, and left- and right-justified. Number the tables consecutively and locate them after and close to where they are first referenced. Leave at least one line space between the table, label and the text. Tables should be auto-fit to a single column or the whole width over two columns and no vertical lines or borders are needed.

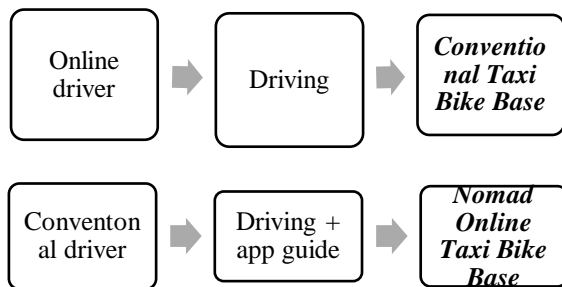
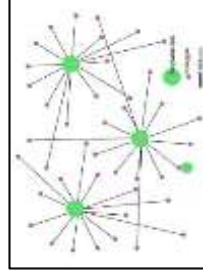
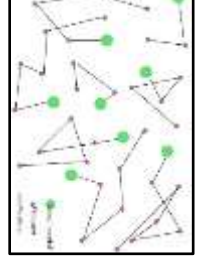


Fig. 5 The comparison of online and conventional taxi bike.

Technology injection in conventional human activities produces a different space than before. Conventional motorbike drivers need a certain amount of space that is fixed for their activities. He needed the space so that his presence in the city space could be realized by the local people, so they could use his services. But for online taxi bike drivers, the function of the base as a media of existence is replaced by smartphone application technology. So the space produced by online motorcycle taxi drivers is not space for residents to realize, but as a place to

rest and wait for the next call. Here is a comparison table of the behavior of online and conventional taxi bike drivers in city spaces.

Table 1. The Comparison between Online and Conventional Taxi Bike

| Variable                | Conventional   | Online  |
|-------------------------|--|---|
| Former                  | Neighborhood   | Company   |
| Base                    | Negotiation with the landlord to make a base   | Negotiation or not  |
| How to get customer     | Rely on existence on the base  | Rely on applications, internet signal access, telephone or sms  |
| Price                   | Standard and flexible prices   | Price depends on distance (km) and congestion level   |
| The destination         | Use spatial code to get to the destination. Usually the destination is still in the surrounding area   | Using spatial code and GPS to get to the destination, no more than 25km.  |
| The location of driving | Operates around the base area and forms a centralized network on the base.<br> | Operate anywhere and form a network not centered in urban space but centralized in cyberspace.<br> |
| Drivers information     | Driver data cannot be obtained directly  | Driver data can be accessed through the smartphone application  |
| The production of space | The resulting space is permanent or semi-permanent with a simple shelter   | The space produced is semi-permanent or just stops (overlaps with other space functions)  |



### The Observation

The observation took place in Margonda Street, Depok which is one of the artery road that connect the agglomeration area and Jakarta.



Fig. 6 The location of observation.

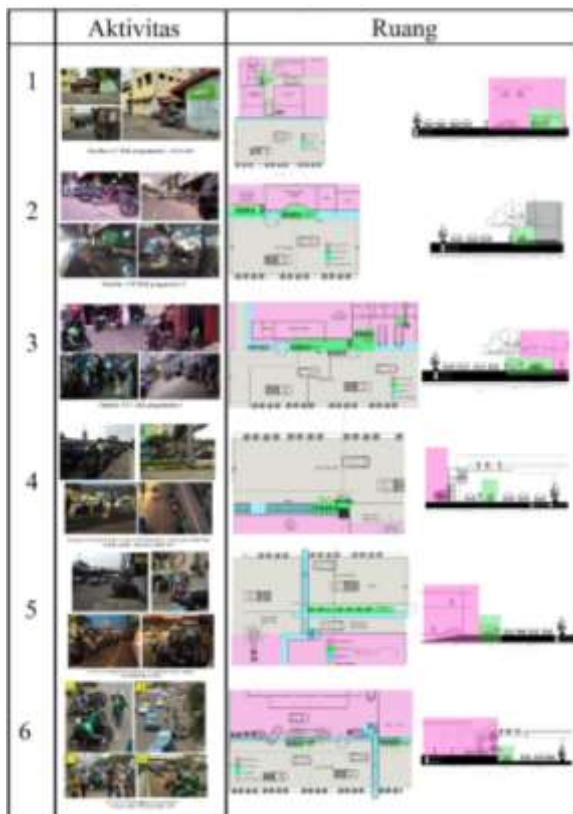


Fig. 7 The space organization by online taxi bike driver.

The presence of information technology that is so easy makes the structure of activities not always centered on physical space. Before the presence of an online taxi bike, we have to walk to the taxi bike base to get a taxi bike. That means the taxi bike base is a center for finding transportation services. Since the presence of online applications, looking for taxi bike services no longer need to walk out, just order via online media, then motorcycle taxis will come to where we are. This indicates that the center is almost merged or decentralized.

Discussion of human activities in the city space certainly depends on where he is. In this study, I focused my observation on Margonda Street, Depok so that I could see the link between space and activity that occurred. Margonda Street is a primary arterial road in the city of Depok which is known for its high density. This road is the main access for the driver to Jakarta or from the direction of Jakarta to Depok. At 07.00-08.30 AM and 16.30-19.00 PM, several points on this road are crowded by passing vehicles. Online motorcycle taxis also colored the traffic on the morning and evening on Margonda Street.

### CONCLUSIONS

The existence of a taxi bike in a crowded place can be done because they are looking for passengers by showing themselves. However, online taxi bike must still order through the application. The purpose of online taxi bike is just to get and get orders because GPS radar will ask for approval in the crowd so that opportunities are needed to get larger orders.

The impact of courageous online taxi bike trips to city space is access to access to go anywhere. No need to leave the house to get what he wants. From the observations made we can conclude that technology really helps human activities that can be done to improve the space carried out both mentally and physically. Social space is formed because of the social activities of the community which are usually hit by conflict because they are not aware of whether the community is aware of the space negotiations that occur. Unlike the social space formed by technological assistance, it can develop in a relatively fast time but can cause pros and cons of the surrounding community because of their impure participation through social activities.

Taxi bike dares to use technology and social relations in forming space in the city. Courageous motorcycle taxi drivers cannot choose as an anti-social space, because attending to it still considers the social aspects. As at the first point, the social relations between former base taxi bike drivers and relations with coffee shop owners make it easy to get a decent shelter.

The choice of online taxi bike is done spontaneously. Weak spaces of guarding or mastery are more likely to be used as transit points. Low guarded space like the courtyard of a building with low sidewalks; shophouse without fence or iron chain barrier; and on the circulation path of vehicles without police/security guards / regional thugs who control vehicles. The production of courageous taxi bike spaces is one of the expressions of adaptation to the environment and response to social relations, which ultimately makes the face of the city more dynamic. However, many courageous taxi bike drivers make traffic jams and pedestrians have to walk on the road instead of on the sidewalk.

#### ACKNOWLEDGMENTS

This article is part of Grant of International Publications for Student Final Project of Universitas Indonesia (Hibah PITMA). Thank you to Mr. Chotib and Mr. Kemas Ridwan Kurniawan for the advice and brainstorming through this topic and being a supportive lecturer. Thank you to Department of Architecture (Faculty of Engineering) and Urban Development Studies (School of Strategic and Global Studies) Universitas Indonesia.

#### REFERENCES

- [1] Lefebvre, H., 1974. *The Production of Space*. Cambridge: Basil Blackwell.
- [2] Wirth, L. 1938. Urbanism as a Way of Life. *American Journal of Sociology*, 44(1), 1-24. Retrieved from <http://www.jstor.org/stable/2768119>
- [3] Lynch, K., 1960. *The Image of The City*. Cambridge: The Technology Press & Harvard University Press.
- [4] Sirjamaki, J., 1964. *The Sociology of Cities*. New York: Random House.
- [5] Arendt, Hannah. (1958). *The Human Condition*. Chicago & London: The University of Chicago Press.
- [6] Atkinson, Robert D., 1998. Technological Change and Cities dalam *Cityscape: A Journal of Policy Development and Research*, Volume 3, Number 3.
- [7] Bloomer, K. C. & Moore, C. W., 1977. *Body, Memory and Architecture*. New Haven: Yale University Press.
- [8] Carmona, M. & Tiesdell, S., 2007. *Urban Design Reader*. Great Britain: Architectural Press.
- [9] Daimtri, 2014. Persepsi Terhadap Ruang (Perkotaan) – 1. [itscomma9.com/persepsi-terhadap-ruang-perkotaan-1/](http://itscomma9.com/persepsi-terhadap-ruang-perkotaan-1/). Oktober 9, 2014. Diakses 19 Agustus 2016.
- [10] Gehl, J., 2011. *Life Between Building*. Washington: Island Press.
- [11] Hardt, M. & Negri, A., 2004. *Multitude: War and Democracy in The Age of Empire*. New York: Penguin.
- [12] Neighborhood Placemaking in Chicago. Chicago: Project for Publik Space (PPS) and Metropolitan Planning Council (MPC).
- [13] Katznelson, Ira., 1992, *Marxism and the City*. New York: Oxford University Press. Reviewed by Robert A. Beauregard, University of Pittsburgh.
- [14] Licara, M., 2010. *Ojek dan Taktik Produksi Ruang dalam Kehidupan Sehari-hari*. Depok: Universitas Indonesia.
- [15] Lynch, K., 1960. *The Image of The City*. Cambridge: The Technology Press & Harvard University Press.
- [16] M, Gottdiener., 1993, *A Marx for Our Time: Henri Lefebvre and The Production of Space*. Ebook.
- [17] National Association of City Transportation Officials. 2012. *Urban Street Design Guide Overview*. Newyork: Ebook.
- [18] Official website of PT. Go-Jek Indonesia. <http://www.go-jek.com/>. Accessed May 19, 2016, 06.15 AM.

## SERVICE QUALITY GAP ANALYSIS OF WATER SUPPLY IN URBAN AREAS: WATER SUPPLY COMPANY, KABUPATEN BOGOR

Armeinita Octavia<sup>1</sup> and Chotib<sup>1</sup>

<sup>1</sup>School of Strategic and Global Studies, Universitas Indonesia, Indonesia

### ABSTRACT

High population growth in urban areas has led to higher activities which increase the needs of clean water. Efforts to provide water in urban areas come from the government known as Water Supply Companies. The increasing demand will affect the quality of clean water itself, because of water resources capacity is limited and could create water service quality gap in the end. The purpose of this thesis is to identify the level of customer satisfaction with the service performance of PDAM Kota Wisata, to identify factors which influence service quality of Water Supply Company, and to analyze service quality gaps between water supply and the benefits received by the users (customers). This research uses a qualitative and quantitative approach, data collection is done through area observation, agency visits, and questionnaires, as well as literature reviews. The assessment of service quality is carried out through weighting based on the Likert scale, data processing and analysis methods are carried out through the Structuring Equation Modelling (SEM) method. The results showed some of the service quality aspects caused by several factors, starts from the water resources capacity, the management of the water supply company, and the operational standards and procedures in serving water to the users. The conclusions can be done by forming irreparable factors and give alternative solution to reduce the gap of service quality between water supply and benefits to the users.

*Keywords: Water supply company, Service quality, Water resources, Gap analysis*

### INTRODUCTION

The increasing of urban population requires the availability of clean water. SDG's number 6 challenge is to ensure the availability and management of sustainable water and sanitation for all, then the Government's target to achieve 100% clean water in 2019 is not an easy thing to do without the help and coordination of various stakeholders, both in government and the community itself, including assistance from the private sector.

The management of Bogor Regency drinking water is managed by the Regional Water Supply Company (PDAM) Tirta Kahuripan which is designated as a water services BUMD (*Permendagri* 2/2007), and the management characteristics is non-rivalry and join consumption, but there are excludability (people will be charged of consuming water, the higher the usage, the higher the cost, and there is a market mechanism). And to achieve service for all, water management must be done properly, from water source, production and distribution system, including providing scales of services.

*Permen PUPR* 19/PRT/M/2016 has regulated cooperation in Drinking Water Supply System (SPAM) implementation related to Government Support (DPP) on SPAM cooperation, procedures for granting Government Support, and management of central/regional assets from Government Support. In case state-owned enterprises (BUMN) or regional

owned enterprises (BUMD) are not able to finance the need for SPAM management with a pipeline network or outside the service area of BUMN and BUMD, it could be done by cooperation with private sector (Public-Private Partnership/KPBU).

PDAM Tirta Kahuripan classify customers as follows: I, IIA, IIB, IIIA, IIIB, IIIC, IVA, IVB, IVC, IVD, IVE, V. PDAM Tirta Kahuripan is a member of International Organization (PERPAMSI) and its performance received rank 10<sup>th</sup> of Healthy PDAM [1]. PDAM performance has been measured from 4 aspects of performance indicators: finance (25%), service (25%), operational (35%), and human resources (15%). The operational aspect gets the highest weight because it is an important factor in revenue generation (coverage of production efficiency, water loss rates, service hours, water pressure on customer connections and replacement/calibration of customer water meters). The other influential thing is the determination of PDAM tariff rates. Based on *Permendagri* 23/2006, tariffs are set based on the principle of affordability and fairness, service quality, cost recovery, efficient use of water, transparency and accountability and protection of raw water/water resource, divided into 4 types of tariffs: 1) low tariff (tariff which value lower than the basic cost; 2) basic tariff (tariff with the same value or equivalent to the basic cost; 3) full tariff (higher value than the basic cost); 4) agreement rates (tariff which are based on agreements between

PDAM and customers).

One of PDAM Tirta Kahuripan service area located in separate watersheds of ground water basins (CAT) Bogor is Gunung Putri and Cileungsi (located in CAT Bekasi-Karawang) with the highest and third highest population in Bogor Regency (7.9% and 6% of the total population in 40 sub-districts of Bogor Regency). The largest service area is managed by PDAM Kota Wisata Services Unit with 400 liters per second capacity, and 120 liters per second to serve Kota Wisata housing area (775 Ha), which is the largest and integrated housing area with PDAM facilitation.

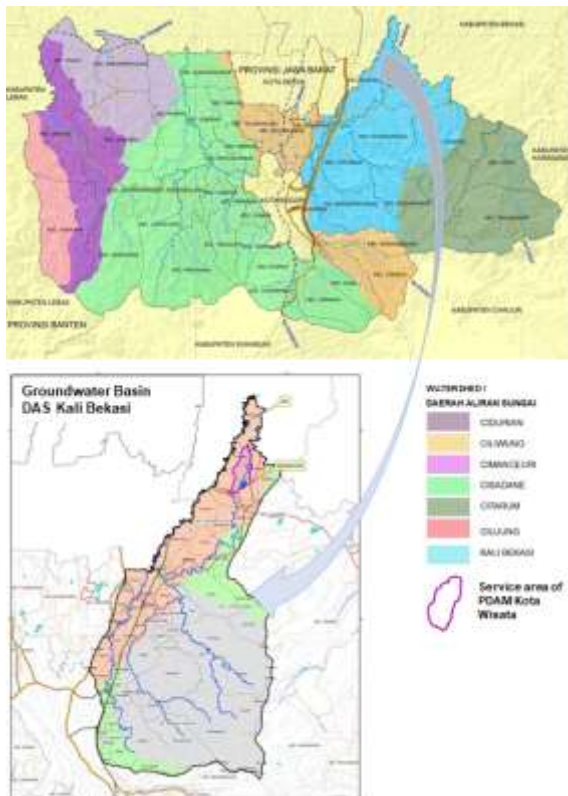


Fig. 1 The research location in the scope of CAT Bekasi-Karawang.

Although PDAM services for Kota Wisata has been integrated, and the group rates are included in IVA (luxury houses), there are still problems, both in water quality and service system that affect customer satisfaction. This has caused the users has switched their source of water from PDAM to other, such as ground water. Some of the alleged problems occur include the water discharge capacity received by users decreases from year to year, frequent turbidity of water (especially during the dry season), and the absence of notification for repairing leaks so it cannot be anticipated by the users. These problems occurred because of the increasing number of PDAM users (debit capacity is still not increasing) and declining infrastructure conditions (maintenance efforts that

need to be improved).

The purpose of this study is to identify the level of customer satisfaction with the service performance of PDAM Kota Wisata, to identify factors which influence service quality of Water Supply Company, and to analyze service quality gaps between water supply and the benefits received by the users (customers). The result of this study will be useful as an input to PDAM Tirta Kahuripan in improving the quality of services, as well as for the local government in terms of regulating water supply policy for PDAM.

## LITERATURE REVIEW

The literature review will start from the explanation regarding drinking water supply system (SPAM), then the urban areas which is the location of the study, and ends with the service quality, factor and gap analysis of the quality service.

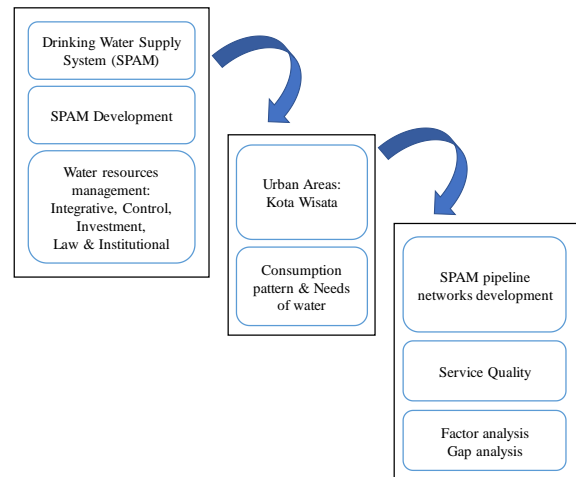


Fig. 2 Literature review concept.

## Drinking Water Supply System (SPAM), SPAM Development, and Water Resources Management

The government regulation 122/2015 has stipulated that the Drinking Water Supply System (SPAM) is provided by the Government to fulfill people's need of water, and to create water services and management with quality and at affordable prices, effective and efficient, balanced between customers and water supply providers.

In urban drinking water supply system, there is 3 components: water resources, water management, and water services distribution. Water resources consists of surface water (*air permukaan*) and ground water (*air tanah*). These water resources are strongly influenced by the water balance in the area (concept of watershed/DAS and sub-watershed/Sub-DAS). And their water flow discharge is strongly influenced by the ground water basin.



And for the water management, Ministry Regulation of Public Works & Housing 27/PRT/M/2016 has explained that SPAM development has to follow the basic processes of management that are interrelated, the principle of implementing based on sustainable development, good governance/corporate governance, including new development, improvement, expansion, management of SPAM (operation and maintenance, improvement, human resource and institutional development). And management of water resources is inseparable from management principles in the form of utilization, protection, control, which are carried out in an integrated manner/multisector (Laws 32/2009).

#### Urban Areas: Kota Wisata, Consumption Pattern and The Needs of Water

In fulfilling clean water needs, the government distinguishes the authority to carry out its implementation. For rural areas more is carried out by local governments (*Pemerintah Daerah*), while for urban areas in general it is left to BUMD, one of them is PDAM. One of the urban areas is Kota Wisata which has the urban characteristics such as located in 1 wide-range area and integrated with the supply of clean water piping systems and managed by the PDAM.

In general, it has regulated how to create sustainable water resources, the procedures for exploiting water resources, the water management including the alternatives of management. But it still does not lead to a management concept whose approach is more to the paradigm (mindset) of people's behavior towards water itself. Based on the directives of existing regulations, all of them emphasize more on treating water as an unlimited resource. Although water pollution control has been regulated, it does not explicitly emphasize that water will be rare at times if it is not managed efficiently and effectively. We all know that the pattern of water consumption needs to be a major concern because the use of water starts from the individual. Water consumption factors are influenced by individual factors (character of each user) and economic factors (income level, family size, etc.) [2].

The Ministry of Public Works and Housing has set the standards for domestic water requirements that currently apply in urban areas according to the size of the population.

Table 1 Standards of Domestic Water Needs [3]

| Population              | City Size    | Needs of Water (liter/person/day) |
|-------------------------|--------------|-----------------------------------|
| > 2,000,000             | Metropolitan | > 210                             |
| > 1,000,000 – 2,000,000 | Metropolitan | > 150 – 210                       |
| > 500,000 – 1,000,000   | Big          | > 120 – 150                       |
| > 100,000 – 500,000     | Big          | > 100 – 150                       |
| > 20,000 – 100,000      | Medium       | > 90 – 100                        |
| > 3,000 – 20,000        | Small        | > 60 – 100                        |

#### SPAM Pipeline Networks Development, Service Quality, Factors and Gap Analysis

The SPAM pipeline network development needs to apply the principles of Water Governance [4]: \*) Approach: open and transparent, inclusive and communicative, coherent and integrative, fair and ethical; \*) Performance and operations: accountable, efficient, responsive and sustainable.

The increasing of water needs will affect the service quality, the problem occurs especially at the quality and quantity aspects. And these problems usually lead to the lack of management in providing services to the customers. One of the descriptive methods to describe customer satisfaction level (in this case is PDAM service quality) is Service Quality (ServQual). Quality of service can also be defined as everything that focuses on the business to meet the needs and desires of consumers which are accompanied by the accuracy in delivering it, so that compatibility is matched with consumer expectations [5]. Thus, Service Quality can be defined as an analysis of the expectation achievement level of customers/consumers of services received.

Service Quality can be identified in 5 dimensions: 1) reliability, 2) responsiveness, 3) assurance, 4) empathy, and 5) tangibles [6] - [8]. The assessment of service quality will be differed in the order of dimensions according to the needs of the study. Related to service quality that affects PDAM customer satisfaction, the order of 5 dimensions are [9]: 1) services are real and show direct evidence including physical facilities, equipment, employees, and means of communication (tangible); 2) trusted and reliable, that is, providing services in accordance with the promised, accurate and satisfying (reliability); 3) responsive in the form of the desire of staff and employees to help and provide services quickly and responsively (responsiveness); 4) can guarantee include knowledge, ability, politeness,

trustworthiness that is owned by staff, free from danger, risk and doubt (assurance); 5) shows sincerity in the form of personal attention to customers (empathy).

To analyze and measure which dimension factors most influence service quality, it will be done by using confirmatory factor analysis in Structural Equation Modeling (SEM) method, through AMOS Statistic Program. There are observed an unobserved variable in SEM, the unobserved variables can be measured from analysis factor indicators.

For the gap analysis, it will be used one of 5 gaps in ServQual [10]: \*) Gap 1: customer expected service vs. company perception of customer expectations; \*) Gap 2: company perceptions of customer expectations vs. design services that are portrayed/driven by customers; \*) Gap 3: service design that is portrayed/customer driven vs. service delivery; \*) Gap 4: external communication vs. service delivery; \*) Gap 5: expected service vs. perceived service.

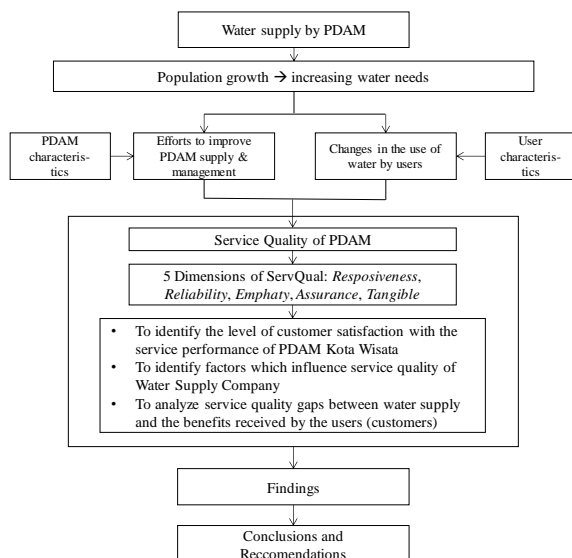


Fig. 3 Research conceptual framework.

## METHODOLOGY

This study used mix-methods (quantitative and qualitative approach) with cross-sectional type of survey. The quantitative approach has been done by questionnaire distribution and structured interview. Choice of sampling came from the population characteristics that had been facilitated by PDAM for providing water. The sample size had been measured by using 90% reliability, which is 100 respondents, using slovin formula from 8.568 population, and the choice of sample is proportional fit to size. The study variables consist of dependent variables (Y) and independent variables (X). The dependent variable is service quality of PDAM Kota Wisata, and the

independent variables are 5 dimensions of ServQual: responsiveness, reliability, emphaty, assurance, and tangible. The measurement of each independent variable is based on certain indicators and using Likert scale from 1 to 4.

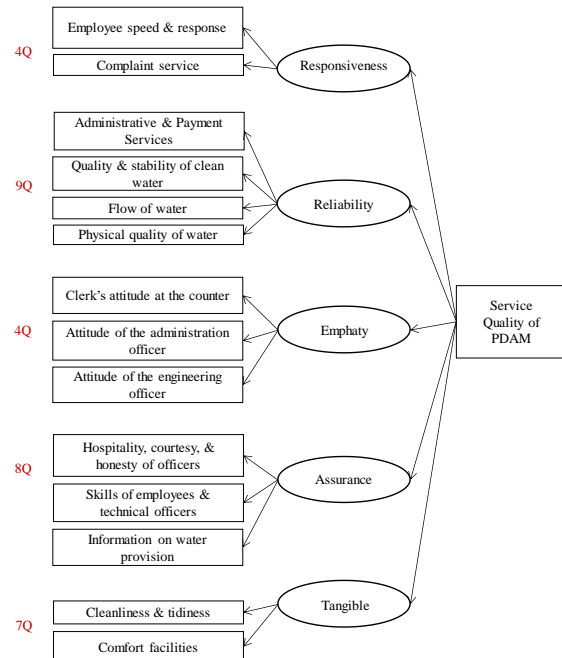


Fig. 4 Framework for analysis of factors affecting PDAM service quality.

The qualitative approach has been done by field observations, in-depth interviews, documentation. The observation consists of passive participation observation, gathering documents from the field related to the study. In-depth interviews consist of semi structure interview with PDAM Kota Wisata, and Gunung Putri Installation (IPA Gunung Putri), using recording and transcription, and it is equipped with documentation.

Data analysis has been done through quantitative data analysis (univariate and multivariate) and qualitative data analysis (triangulation). The statistic data will be analyzed using SEM method with Analysis Moment of Structure (AMOS).

## RESULT AND DISCUSSION

The study location is at the end of DAS Kali Bekasi, CAT Bekasi-Karawang. According to Kabupaten Bogor Spatial Plan, the area is designated as a high intensity urban zone. The low slope rate is only around 0-15%, making the area potential for development especially urban settlements. But according to ground water basins data, the study location is designated as prone zones of greater 40-60% zone drop, with 250-600 mg/l chloride content.



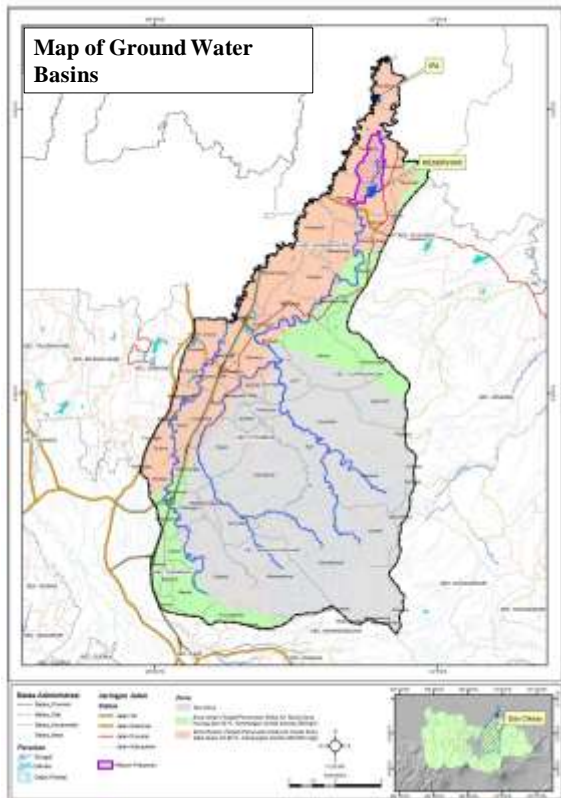


Fig. 5 Map of ground water basins.

PDAM Kota Wisata as one of the service units of PDAM Tirta Kahuripan, Branch Cileungsi, which has 1 installation named IPA Gunung Putri, with Cikeas River as the water resource (surface water). The capacity is 400 liter/second. It served several settlements, and the biggest one is at *Perumahan Kota Wisata*, which has 8.568 active connections (SR/*Sambungan Rumah*).

The number of employees working at PDAM Kota Wisata is 15 people including 1 Head of the Service Unit. The 14 staff consist of: customer relations (including 5 meter-readers), engineering, engineering administration, and cashier/financial administration.



Fig. 6 Scheme for the Implementation of Drinking Water Supply Systems for Kota Wisata.

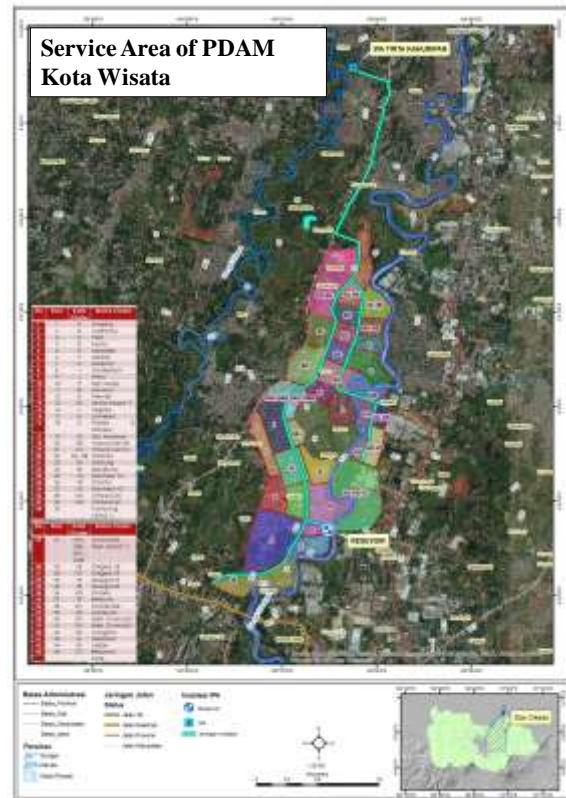


Fig. 7 Service area of PDAM Kota Wisata.

### Identification the Level of Customer Satisfaction with The Service Performance of PDAM Kota Wisata

The most important thing in this study is the respondents' assessment of PDAM service performance. There is a questionnaire has been given to the respondents to measure the service quality based on Likert scale 1 to 4 (lowest to highest). And it will be compared with the level of importance (respondents' expectation). To describe mean score of each item, the indicators and variables are using class intervals based on the equation below:

$$\frac{(\text{Highest answer score} - \text{Lowest answer score})}{\text{Sum of class/categories}} \quad (1)$$

Table 2 Basic Interpretation of Indicator Scores in Research Variables

| No | Score        | Interpretation of Performance Quality |
|----|--------------|---------------------------------------|
| 1  | 1 - 1,75     | Very Low                              |
| 2  | > 1,75 - 2,5 | Low                                   |
| 4  | > 2,5 - 3,25 | High                                  |
| 5  | >3,25 - 4,0  | Very High                             |

| No | Score        | Interpretation of Expectation/Importance |
|----|--------------|--|
| 1  | 1 - 1,75     | Very Low                                 |
| 2  | > 1,75 - 2,5 | Low                                      |
| 4  | > 2,5 - 3,25 | High                                     |
| 5  | >3,25 - 4,0  | Very High                                |

#### Service Performance: Responsiveness

Based on the results of an in-depth survey in carrying out payments, the clerk is quite alert and fast to serve residents who want to pay the PDAM bill at the payment counter. This is also in accordance with the SOP for administrative and financial services for PDAM customers.

On the other side, the importance of item 1 is low because all respondents who have PDAM facilities have never dealt with customer administration services, especially in registering as new customers, because it has been integrated with housing construction, so that when the handover of the house, the PDAM is installed.

Table 3 Distribution of Respondents' Response to the Responsiveness Variable (X1)

| No                                   | Items of Responsiveness (X1)  |   | Satisfaction Level |          |           |            | Mean | Performance Quality |
|--------------------------------------|---|---|--------------------|----------|-----------|------------|------|---------------------|
|                                      |   |   | SP<br>(4)          | P<br>(3) | TP<br>(2) | STP<br>(1) |      |                     |
| 1                                    | The speed and responsiveness of employees in customer administration services | F | 9                  | 126      | 56        | 8          | 2.68 | High                |
|                                      |   | % | 4.5                | 63.3     | 28.1      | 4.0        |      |                     |
| 2                                    | The speed and responsiveness of employees in the payment process              | F | 20                 | 140      | 36        | 3          | 2.89 | High                |
|                                      |   | % | 10.1               | 70.4     | 18.1      | 1.5        |      |                     |
| 3                                    | Speed of employees in resolving complaints at the counters                    | F | 8                  | 106      | 74        | 11         | 2.56 | High                |
|                                      |   | % | 4.0                | 53.3     | 37.2      | 5.5        |      |                     |
| 4                                    | Speed of field officers responds and serves complaints                        | F | 7                  | 105      | 68        | 19         | 2.50 | High                |
|                                      |   | % | 3.5                | 52.8     | 34.2      | 9.5        |      |                     |
| Accumulation of respondents' answers |   | F | 44                 | 477      | 234       | 41         | 2.66 | High                |
|                                      |   | % | 5.53               | 59.92    | 29.40     | 5.15       |      |                     |

#### Service Performance: Reliability

Easiness of payment at the payment counters has the highest satisfaction among others, because there are other alternatives besides the payment counter in the PDAM office, such as paying through Government Bank ATMs (Mandiri, BNI, BRI, BTN), Alfamart and Indomaret, Online (Tokopedia, Bukalapak), etc.

Although it generally shows high quality performance, there are several important and vital items for customer service that are still relatively low, such as the aspect of water quality and quantity. Whereas the PDAM has implemented a Standard, Operational, and Procedure (SOP) for clean water fulfillment in maintaining the quality and stability of clean water, as well as maintaining the smooth running of water and the physical quality of water, including: *Permenkes 492/Menkes/Per/IV/2010* concerning Requirements for Quality of Drinking Water, then the arrangement of water discharge through a distribution pump adjustment for peak and off-peak hours, and water quality monitoring by

laboratory tests (once a month).

With this low satisfaction for water quality and quantity, the result shows that about 20% respondents have switched or added other water resource (ground water).

On the other side, the importance of this reliability dimension is related to easiness for payment system, accuracy of water meter-reading, and the stability of PDAM water quality and quantity.

Table 4 Distribution of Respondents' Response to the Reliability Variable (X2)

| No                                   | Items of Reliability (X2)                     |   | Satisfaction Level |          |           |            | Mean | Performance Quality |
|--------------------------------------|---|---|--------------------|----------|-----------|------------|------|---------------------|
|                                      |   |   | SP<br>(4)          | P<br>(3) | TP<br>(2) | STP<br>(1) |      |                     |
| 1                                    | Easiness in the customer registration process | F | 13                 | 143      | 41        | 2          | 2.84 | High                |
|                                      |   | % | 6.5                | 71.9     | 20.6      | 1.0        |      |                     |
| 2                                    | Easiness of payment at the payment counters   | F | 25                 | 139      | 32        | 3          | 2.93 | High                |
|                                      |   | % | 12.6               | 69.8     | 16.1      | 1.5        |      |                     |
| 3                                    | Meter-reading at the customer's home          | F | 12                 | 111      | 64        | 12         | 2.62 | High                |
|                                      |   | % | 6.0                | 55.8     | 32.2      | 6.0        |      |                     |
| 4                                    | Quality and stability of PDAM water quality   | F | 8                  | 67       | 80        | 44         | 2.20 | Low                 |
|                                      |   | % | 4.0                | 33.7     | 40.2      | 22.1       |      |                     |
| 5                                    | Smooth flow of water during peak hours        | F | 12                 | 81       | 66        | 40         | 2.33 | Low                 |
|                                      |   | % | 6.0                | 40.7     | 33.2      | 20.1       |      |                     |
| 6                                    | Smooth water off-peak hours                   | F | 22                 | 124      | 42        | 11         | 2.79 | High                |
|                                      |   | % | 11.1               | 62.3     | 21.1      | 5.5        |      |                     |
| 7                                    | Physical quality of water (water clarity)     | F | 11                 | 64       | 89        | 35         | 2.26 | Low                 |
|                                      |   | % | 5.5                | 32.2     | 44.7      | 17.6       |      |                     |
| 8                                    | Physical quality of water (water aroma)       | F | 8                  | 73       | 91        | 27         | 2.31 | Low                 |
|                                      |   | % | 4.0                | 36.7     | 45.7      | 13.6       |      |                     |
| 9                                    | Physical quality of water (taste of water)    | F | 5                  | 87       | 89        | 18         | 2.40 | Low                 |
|                                      |   | % | 2.5                | 43.7     | 44.7      | 9.0        |      |                     |
| Accumulation of respondents' answers |   | F | 116                | 889      | 594       | 192        | 2.52 | High                |
|                                      |   | % | 6.48               | 49.64    | 33.17     | 10.72      |      |                     |

#### Service Performance: Empathy

Based on the result of in-depth survey, the respondents felt that they were always will received when making complaints, and the location of the office is very accessible (inside residential area). However, the important item 'Sensitivity of officers in providing information regarding tariff changes' has the lowest quality performance, lots of respondents did not receive notification of the tariff changes. Even though PDAM has the SOP of service to customers related to tariffs: socializing through online media, distributing letter of notification regarding tariff changes, and posting information at the payment counter.

And on the other side, 'Sensitivity of officers in providing information regarding tariff changes' becomes the highest expectations of respondents. This is what most respondents do not feel. This problem may occurred because of the coordination and information delivery system from PDAM to the users are still not optimal, due to conventional style of delivering information (still using letter of notification/non online/non digital), and PDAM does not have all the RW contacts on each cluster in Kota Wisata.

Table 5 Distribution of Respondents' Response to the Empathy Variable (X3)

| No                                   | Items of Empathy (X3)   | Satisfaction Level |              |              |            | Mean | Performance Quality |
|--------------------------------------|---|--------------------|--------------|--------------|------------|------|---------------------|
|                                      |   | SP<br>(4)          | P<br>(3)     | TP<br>(2)    | STP<br>(1) |      |                     |
| 1                                    | Officers' attitudes at the payment counters   | F 15<br>% 7.5      | 139<br>69.8  | 41<br>20.6   | 4<br>2.0   | 2.83 | High                |
| 2                                    | Sensitivity of employees on receiving complaints and gives information                  | F 11<br>% 5.5      | 116<br>58.3  | 63<br>31.7   | 9<br>4.5   | 2.65 | High                |
| 3                                    | Sensitivity of officers in providing information regarding tariff changes               | F 9<br>% 4.5       | 82<br>41.2   | 84<br>42.2   | 24<br>12.1 | 2.38 | Low                 |
| 4                                    | The attitude of the technical officer towards the customer in carrying out their duties | F 9<br>% 4.5       | 117<br>58.8  | 63<br>31.7   | 10<br>5.0  | 2.63 | High                |
| Accumulation of respondents' answers |   | F 44<br>% 5.53     | 454<br>57.04 | 251<br>31.53 | 47<br>5.90 | 2.62 | High                |

### Service Performance: Assurance

The skills of employees and Engineering officers based on the survey results, did not encounter significant problems, but there were problems related to the attitude and friendliness of the officers in resolving complaints. If we compare it with the SOP of recruiting PDAM employees already refers to *Perda Kabupaten. Bogor 7/2007* about the Organizations and Staffing of PDAM Tirta Kahuripan. And it requires that the employees must pegawai Perusahaan Daerah must have the education, skills and expertise needed, with a maximum age of 35 years, and pass the selection, and for the service section it has been facilitated with various types of training.

Item of Assurance which has the lower quality performance is the information of water supply system aspect (condition of water resources, infrastructures, management and monitoring system). It is also in accordance with there is no SOP regarding the information of water supply system, unless there are users who request it. There is also an evidence that around 36% of the respondents did not even know where the water source of PDAM is came from. Even though lots of them can answer the source is from the river, but 42% of them have failed to mention which one is the correct river.

'Honesty of employees regarding new connections paying process' gets the less important item among other, but there still lots of respondents wish to have employees to be honest regarding new connections paying process, considering there was a case with the customer regarding the process of installing a new connection, but the details of the costs are not included in the billing system. This is one of the problems of transparency that occurred and it is become inconsistency with of the principle of water governance.

Table 6 Distribution of Respondents' Response to the Assurance Variable (X4)

| No                                   | Items of Assurance (X4)  | Satisfaction Level |              |              |              | Mean | Performance Quality |
|--------------------------------------|--|--------------------|--------------|--------------|--------------|------|---------------------|
|                                      |  | SP<br>(4)          | P<br>(3)     | TP<br>(2)    | STP<br>(1)   |      |                     |
| 1                                    | Friendliness and politeness of the complaint department officer  | F 15<br>% 7.5      | 136<br>68.3  | 40<br>20.1   | 8<br>4.0     | 2.79 | High                |
| 2                                    | Honesty of employees regarding new connections paying process  | F 10<br>% 5.0      | 146<br>73.4  | 40<br>20.1   | 3<br>1.5     | 2.82 | High                |
| 3                                    | Employee skills in the payment process   | F 14<br>% 7.0      | 154<br>77.4  | 29<br>14.6   | 2<br>1.0     | 2.90 | High                |
| 4                                    | Skills of technical officers in handling technical problems  | F 10<br>% 5.0      | 128<br>64.3  | 54<br>27.1   | 7<br>3.5     | 2.71 | High                |
| 5                                    | PDAM provides information services related to the condition & availability of water sources (water discharge conditions, water source problems, etc.)                                | F 7<br>% 3.5       | 56<br>28.1   | 101<br>50.8  | 35<br>17.6   | 2.18 | Low                 |
| 6                                    | PDAM provides information regarding the condition of PDAM water supply infrastructure (news about the condition of piping networks, pumping equipment, water treatment plants, etc.) | F 8<br>% 4.0       | 54<br>27.1   | 104<br>52.3  | 33<br>16.6   | 2.19 | Low                 |
| 7                                    | PDAM provides information regarding the condition of the PDAM management system (maintenance scheduling information such as water drainage, leak repair, etc.)                       | F 8<br>% 4.0       | 58<br>29.1   | 89<br>44.7   | 44<br>22.1   | 2.15 | Low                 |
| 8                                    | The PDAM provides information regarding the PDAM water use monitoring system   | F 7<br>% 3.5       | 57<br>28.6   | 101<br>50.8  | 34<br>17.1   | 2.19 | Low                 |
| Accumulation of respondents' answers |  | F 79<br>% 4.96     | 789<br>49.56 | 558<br>35.05 | 166<br>10.43 | 2.49 | Low                 |

### Service Performance: Tangible

Based on the survey results, tangible items do not affect the level of satisfaction too much, because there are many alternatives on the payment system. However, for some respondents who still relied on traveling to the payment counter, several assessments of dissatisfaction were more related to the condition of the service office that was less feasible. There is no SOP for service facilities at the PDAM, only adjusting to service requirements, at least having a payment counter and a complaint office.

Although there are many alternative payments that can be done, the respondents' expectations regarding PDAM service office facilities still need to be improved, because some respondents still choose to pay manually to the counters, especially those who do a lot of activities around their houses.

Table 7 Distribution of Respondents' Response to the Tangible Variable (X5)

| No                                   | Items of Tangible (X5)   | Satisfaction Level |              |              |            | Mean | Performance Quality |
|--------------------------------------|--|--------------------|--------------|--------------|------------|------|---------------------|
|                                      |  | SP<br>(4)          | P<br>(3)     | TP<br>(2)    | STP<br>(1) |      |                     |
| 1                                    | Cleanliness of payment counters                                  | F 7<br>% 3.5       | 130<br>65.3  | 57<br>28.6   | 5<br>2.5   | 2.70 | High                |
| 2                                    | Cleanliness and tidiness of clerks/staffs                        | F 12<br>% 6.0      | 147<br>73.9  | 39<br>19.6   | 1<br>0.5   | 2.85 | High                |
| 3                                    | Comfort of the service office waiting room                       | F 8<br>% 4.0       | 102<br>51.3  | 80<br>40.2   | 9<br>4.5   | 2.55 | High                |
| 4                                    | Parking facilities at the service office                         | F 19<br>% 9.5      | 134<br>67.3  | 42<br>21.1   | 4<br>2.0   | 2.84 | High                |
| 5                                    | Public facilities such as toilets                                | F 8<br>% 4.0       | 94<br>47.2   | 80<br>40.2   | 17<br>8.5  | 2.47 | Low                 |
| 6                                    | The easiness of obtaining a guide book about service information | F 9<br>% 4.5       | 93<br>46.7   | 80<br>40.2   | 17<br>8.5  | 2.47 | Low                 |
| 7                                    | The easiness of obtaining information related to PDAM policy     | F 10<br>% 5.0      | 76<br>38.2   | 89<br>44.7   | 24<br>12.1 | 2.36 | Low                 |
| Accumulation of respondents' answers |  | F 73<br>% 5.24     | 776<br>55.71 | 467<br>33.52 | 77<br>5.53 | 2.61 | High                |

### Identification of Factors Which Influence Service Quality of Water Supply Company

To get the key factors and indicators that have major role in Service Quality, the method used is Confirmatory Factor Analysis (CFA), using AMOS software as the analysis tool which is used in one of the SEM (Structural Equation Modeling) procedures.

With this analysis, it can be identified which indicators that can explain a construct/concept/variable.

As we can see at the table and figure below, the aspect on Assurance dimension has the highest loading factor (0.94), with the best indicators forming Assurance variables are the skills of employees and technical officers.

Table 8 Measurement Model Evaluation Phase 2 (2<sup>nd</sup> Order Outer Model)

| Latent Variable     | Manifest Variables  | Loading/Weight | Rule of Thumb | Note         | Rank     |
|---------------------|---------------------|----------------|---------------|--------------|----------|
| Service Quality (X) | Responsiveness (X1) | 0.927          | 0.500         | Valid        | 2        |
|                     | Reliability (X2)    | 0.882          | 0.500         | Valid        | 4        |
|                     | Emphaty (X3)        | 0.926          | 1.500         | Valid        | 3        |
|                     | Assurance (X4)      | <b>0.941</b>   | <b>2.500</b>  | <b>Valid</b> | <b>1</b> |
|                     | Tangible (X5)       | 0.85           | 0.500         | Valid        | 5        |

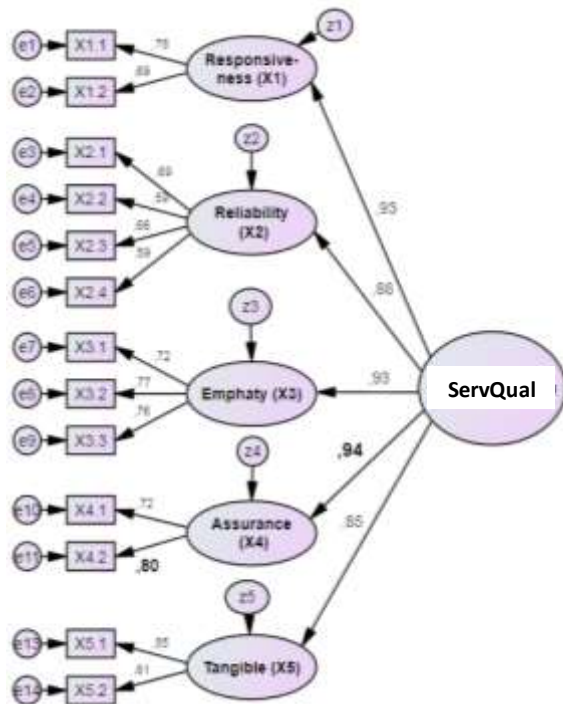


Fig. 7 Diagram of Confirmatory Factor Analysis.

### Service Quality Gap Analysis Between Water Supply and The Benefits Received by The Users (Customers)

This gap analysis will give the information about how much the level of customer satisfaction for Service Quality. This level of customer satisfaction can be determined by means of the average value of expectations then disputed by the average value of performance, which can result 3 categories:

1. Positive (+), category: Very Satisfied
2. Zero (0), category: Satisfied
3. Negative (-), category: Not Satisfied

Table 9 Gap Analysis Between Consumers Satisfaction and Service Quality (Variable: Responsiveness/X1)

| Variable            | Item | Statement   | Mean        |             | Gap   | Category       |
|---------------------|------|---|-------------|-------------|-------|----------------|
|                     |      |   | Performance | Expectation |       |                |
| Responsiveness (X1) | C1   | The speed and responsiveness of employees in customer administration services | 2,68        | 2,46        | 0,22  | Very Satisfied |
|                     | C2   | The speed and responsiveness of employees in the payment process              | 2,89        | 3,33        | -0,44 | Not Satisfied  |
|                     | C3   | Speed of employees in resolving complaints at the counters                    | 2,56        | 3,38        | -0,82 | Not Satisfied  |
|                     | C4   | Speed of field officers responds and serves complaints                        | 2,50        | 3,40        | -0,90 | Not Satisfied  |

Table 10 Gap Analysis Between Consumers Satisfaction and Service Quality (Variable: Reliability/X2)

| Variable         | Item | Statement                                     | Mean        |             | Gap   | Category      |
|------------------|------|---|-------------|-------------|-------|---------------|
|                  |      |   | Performance | Expectation |       |               |
| Reliability (X2) | C5   | Easiness in the customer registration process | 2,84        | 3,32        | -0,48 | Not Satisfied |
|                  | C6   | Easiness of payment at the payment counters   | 2,93        | 3,39        | -0,46 | Not Satisfied |
|                  | C7   | Meter-reading at the customer's home          | 2,62        | 3,36        | -0,74 | Not Satisfied |
|                  | C8   | Quality and stability of PDAM water quality   | 2,20        | 3,55        | -1,35 | Not Satisfied |
|                  | C9   | Smooth flow of water during peak hours        | 2,33        | 3,49        | -1,17 | Not Satisfied |
|                  | C10  | Smooth water off-peak hours                   | 2,79        | 3,40        | -0,61 | Not Satisfied |
|                  | C11  | Physical quality of water (water clarity)     | 2,26        | 3,64        | -1,38 | Not Satisfied |
|                  | C12  | Physical quality of water (water aroma)       | 2,31        | 3,61        | -1,30 | Not Satisfied |
|                  | C13  | Physical quality of water (taste of water)    | 2,40        | 3,61        | -1,21 | Not Satisfied |



Table 11 Gap Analysis Between Consumers Satisfaction and Service Quality (Variable: Empathy/X3)

| Variable        | Item | Statement   | Mean             |                  | Gap   | Category      |
|-----------------|------|---|------------------|------------------|-------|---------------|
|                 |      |   | Perfor-<br>mance | Expect-<br>ation |       |               |
| Empathy<br>(X3) | C14  | Officers' attitudes at the payment counters   | 2,83             | 3,40             | -0,57 | Not Satisfied |
|                 | C15  | Sensitivity of employees on receiving complaints and gives information                  | 2,65             | 3,42             | -0,77 | Not Satisfied |
|                 | C16  | Sensitivity of officers in providing information regarding tariff changes               | 2,38             | 3,45             | -1,07 | Not Satisfied |
|                 | C17  | The attitude of the technical officer towards the customer in carrying out their duties | 2,63             | 3,40             | -0,77 | Not Satisfied |

Table 12 Gap Analysis Between Consumers Satisfaction and Service Quality (Variable: Assurance/X2)

| Variable          | Item | Statement  | Mean             |                  | Gap   | Category       |
|-------------------|------|--|------------------|------------------|-------|----------------|
|                   |      |  | Perfor-<br>mance | Expect-<br>ation |       |                |
| Assurance<br>(X4) | C18  | Friendliness and politeness of the complaint department officer  | 2,79             | 3,43             | -0,64 | Not Satisfied  |
|                   | C19  | Honesty of employees regarding new connections paying process  | 2,82             | 2,51             | 0,31  | Very Satisfied |
|                   | C20  | Employee skills in the payment process   | 2,90             | 3,37             | -0,47 | Not Satisfied  |
|                   | C21  | Skills of technical officers in handling technical problems  | 2,71             | 3,41             | -0,70 | Not Satisfied  |
|                   | D1   | PDAM provides information services related to the condition & availability of water sources (water discharge conditions, water source problems, etc.)                                | 2,18             | 3,37             | -1,19 | Not Satisfied  |
|                   | D2   | PDAM provides information regarding the condition of PDAM water supply infrastructure (news about the condition of piping networks, pumping equipment, water treatment plants, etc.) | 2,19             | 3,36             | -1,18 | Not Satisfied  |
|                   | D3   | PDAM provides information regarding the condition of the PDAM management system (maintenance scheduling information such as water drainage, leak repair, etc.)                       | 2,15             | 3,43             | -1,28 | Not Satisfied  |
|                   | D4   | PDAM provides information regarding the PDAM water use monitoring system   | 2,19             | 3,37             | -1,18 | Not Satisfied  |

Table 13 Gap Analysis Between Consumers Satisfaction and Service Quality (Variable: Tangible/X2)

| Variable         | Item | Statement  | Mean             |                  | Gap   | Category      |
|------------------|------|--|------------------|------------------|-------|---------------|
|                  |      |  | Perfor-<br>mance | Expect-<br>ation |       |               |
| Tangible<br>(X5) | C22  | Cleanliness of payment counters                                  | 2,70             | 3,34             | -0,64 | Not Satisfied |
|                  | C23  | Cleanliness and tidiness of clerks/staffs                        | 2,85             | 3,30             | -0,45 | Not Satisfied |
|                  | C24  | Comfort of the service office waiting room                       | 2,55             | 3,33             | -0,78 | Not Satisfied |
|                  | C25  | Parking facilities at the service office                         | 2,84             | 3,30             | -0,46 | Not Satisfied |
|                  | C26  | Public facilities such as toilets                                | 2,47             | 3,25             | -0,78 | Not Satisfied |
|                  | C27  | The easiness of obtaining a guide book about service information | 2,47             | 3,31             | -0,84 | Not Satisfied |
|                  | C28  | The easiness of obtaining information related to PDAM policy     | 2,36             | 3,37             | -1,01 | Not Satisfied |

The highest quality service gap is found in the quality and stability of clean water; quantity (debit) and physical quality of water (water clarity); sensitivity of officers in providing information on tariff changes; and information regarding the condition of water sources, conditions of water supply infrastructure, conditions of management systems, and supervision of water use; including the easiness of obtaining information related to PDAM policies.

## CONCLUSIONS

PDAM Kota Wisata service is still not able to provide maximum service quality for its customers. Although the planning has been integrated between the developer and PDAM, and has been equipped with several service SOPs, the problem of service quality is still occurred.

There is still customer dissatisfaction especially in the aspect of quality and quantity. This became a concern because of the tariff applied for Kota Wisata area is IVA (luxury houses), which should be able to obtain better services. And with kind of high tariff, it can make PDAM more flexible to manage their financing and budgeting, especially in terms of development and maintenance, as well as providing training to employees and officers.

Aspek utama untuk peningkatan kualitas layanan berdasarkan hasil analisis statistik adalah keterampilan karyawan dan petugas Teknik. Namun hal ini tidak terbatas hanya pada keterampilan saat melaksanakan proses pembayaran dan pelaksanaan teknis di lapangan, namun juga perlu adanya perbaikan sikap dalam melayani pelanggan, untuk menghindari konflik dan kesalahpahaman saat terjadi keluhan. Hal ini sangat berkaitan dengan peningkatan sumber daya manusia terutama petugas yang melayani langsung konsumen PDAM.

The main aspect for improving service quality based on the statistical analysis result is the skills of

employees and technical/engineering officers. But it is not limited only on skills at payment process and technical implementation in the field, but also needs to improve attitudes in serving customers, to avoid conflicts and misunderstandings when complaints occurred. This means it needs to improve the human resources, especially who serve directly to the users (customers).

Di sisi lainnya, penyediaan dan pengelolaan air bersih untuk kawasan perkotaan tidak dapat hanya ditangani oleh PDAM saja, namun perlu koordinasi dari berbagai sektor, mulai dari pemerintah hingga masyarakat penggunaannya, termasuk pelibatan pihak swasta, sehingga prinsip pemerintahan air yaitu accountable, efficient, responsive and sustainable.

On the other hand, the provision and management of clean water for urban areas cannot only be handled by PDAM, but it needs coordination from various sectors, from the government to the user community, including the involvement of private sector, so it can achieve the principle of water governance, which is accountable, efficient, responsive and sustainable.

## ACKNOWLEDGMENTS

This article is part of Grant of International Publication for Students Final Projects of Universitas Indonesia: Urban Clean Water Fulfillment.

## REFERENCES

- [1] BPPSPAM. (2017). Buku Kinerja PDAM 2017. Jakarta: Kementerian Pekerjaan Umum dan Perumahan Rakyat.
- [2] Hendriawan, F., & Cahyadi, A. (2016). Analisis Faktor-Faktor Yang Mempengaruhi Konsumsi Air Bersih Pelanggan Kelompok Rumah Tangga Menengah (K3B) Di PDAM Tirta Kahuripan Kabupaten Bogor Wilayah Cabang Pelayanan XI Cibinong. Kabupaten Bogor: STIE Dewantara.
- [3] Meutia, A. (2013). Arahana Pengembangan Sistem Penyediaan Air Minum Kota Bogor. Bogor: Institut Pertanian Bogor.
- [4] Batchelor, C. (2008). Water Governance Literature Assessment. London: IIED.
- [5] Purnamawati, E. (2012). Analisis Kualitas Layanan dengan Metode Servqual dan AHP di Dinas Kependudukan dan Pencatatan Sipil di Surabaya. Surabaya: FTI - UPN Veteran Jatim.
- [6] Parasuraman, A. P., Berry, L., & Zeuthaml, V. A. (1988). SERVQUAL: A Multiple - Item Scale for Measuring Consumer Perceptions of Service Quality. *Journal of Retailing*, 12-40.
- [7] Nugraha, L., Yuniar, & Harsono, A. (2015). Usulan Peningkatan Kualitas Pelayanan Jasa Pendidikan Bahasa Inggris Menggunakan Metode Service Quality (Servqual) di LBPP Lia Martadinata Kota Bandung. *Jurnal Online Institut Teknologi Nasional*, Vol. 3 No. 1, 61-72.
- [8] Triwibowo, S., Rukmi, H. S., & Harsono, A. (2014). Usulan Peningkatan Kualitas Pelayanan Pada Kawasan Wisata Kawah Putih Perum Perhutani Jawa Barat dan Banten dengan Menggunakan Metode Service Quality (SERVQUAL). *Jurnal Online Institut Teknologi Nasional*, Vol. 2 No. 1, 13-23.
- [9] Affandi, H., Zaki, M., & Azmeri. (2017). Pengaruh Kualitas Pelayanan Terhadap Kepuasan Pelanggan Pada Perusahaan Daerah Air Minum (PDAM) Tirta Mon Pase Kabupaten Aceh Utara. *Jurnal Teknik Sipil Universitas Syiah Kuala*, Vol. 6 No. 3, 297-308.
- [10] Maass, W. (2011). *Servie Management - Service Quality*. Saarbrucken: Chair in Economics - Information and Service Systems (ISS).



## ISOLATION OF HEAVY METAL DEGRADABLE HALOPHILIC BACTERIA FROM SOIL IN SAMUT SAKHON PROVINCE, THAILAND

Jaruwan Chutrtong<sup>1</sup> and Waradoon Chutrtong<sup>2</sup>

<sup>1</sup>Faculty of Science and Technology, Suan Sunandha Rajabhat University, Thailand;

<sup>2</sup> Faculty of Science, Srinarinwirot University, 10110 Bangkok, Thailand Company, Country

### ABSTRACT

This research was conducted to select halophilic microorganisms that can reduce heavy metals in water to be used in wastewater treatment. Halophilic bacteria from salt field soil were isolated in nutrient broth containing 5 heavy metals compound (Zn, Co, Cr, Hg, and Cu). 20 isolates which growth in heavy metal containing media were screened. After that, Experiment was conducted to determine the maximum concentration of heavy metals that the isolated could growth. The concentration of heavy metals was obtained from 50-500 mg/L. In media which add Zn, Co, Cr and Cu compound, the isolated were found to be able to grow at concentrations of 450-500 mg/L but not growth in media which add Hg (50-500 mg/L). To check the heavy metal degrading ability, the isolates were cultured in nutrient broth which add the most concentrated of heavy metal and incubated at 37 ° C for 15 days. Measured the remaining heavy metals and counted the number of microorganisms on days 3, 5, 7, 10 and 15. It was found that microorganisms were capable to reduce two heavy metals, Cr and Co. Cr reduced by the isolated HL7 and 10-20. Co reduced by the isolated HL1, 3, 4, 5, 7, 8, 10, 11 and 15. Zn and Cu decreased at the decimal level, which was not significant. The results of this research showed that the isolated halophilic bacteria had the ability to reduce some heavy metals, which can be applied in wastewater treatment.

*Keywords: Halophilic bacteria, Heavy metal, Isolation, Soil, Thailand*

### INTRODUCTION

In the present situation, chemicals are used increasingly to facilitate life. They are used in many industries such as smelting industry, tannery industry, dying industry, agricultural products' industry (insecticides, pesticides, chemical fertilizers) and household products' industry [1]. These products may contain more or less heavy metal contaminants. Using heavy metal contaminants products can cause contamination in the environment which harmful to life, for example, arsenic from smelting outflow in water resources in Ron Piboon District in Thailand that caused black fever [2]. Because heavy metals are stable substances, they do not decompose by natural processes in a short time. It must be treated before released to environments to reduce toxicity [3]. There are many ways to treat heavy metal contaminated wastewater, but the friendly way is biological treatment using microorganisms, although it takes longer to heal [4]. It can save money and does not cause any chemical contamination.

From the former studies, salinity tolerant microorganisms were able to grow in heavy metals such as copper, lead, cadmium, chromium and zinc [5]. It also found that saline tolerant microorganisms could transform toxic substances into non-toxic substances and absorbed into their cells. *Halomonas* spp., salinity-sensitive bacteria, which isolated from

the San Joaquin community in California, was able to grow in water containing 2M of Selenium (Se). The concentration of Selenium at this level could kill fish and poultry. This type of microorganism could convert Selenium to dimethyl selenite form, non-toxic substance. The rate of change was 1.65 mg/hr. [6]. These show that saline-tolerant microbes have the ability to reduce heavy metals. Therefore, the researcher was interested to find microorganisms that can degrade other heavy metals in water. This is the source of this study by separating the salt tolerant bacteria that is capable to grow in the presence of heavy metals and studying its ability to reduce heavy metals in the water of the microorganisms. If the selected microorganism is highly capable, it will be applied in the treatment of heavy metal contaminated wastewater.

### PROCEDURE

In this research, salt-tolerant microorganisms from soil which collected from salt pan were isolated. Subsequently, cultured the isolates in broth to study the efficiency of heavy metals reducing in liquid environments. The steps are as follows

### Isolation of Halophilic Bacteria in Metallic Conditions

1. Weigh soil, which collected from salt pan in Samut Sakhon province in Thailand, 10 g.
2. Put the weighing soils in flask containing 100 mL of 0.5% NaCl Nutrient broth.
3. Shake flask to mix soil with media.
4. Incubate at 37 °C for 5 days.
5. Take 500 µl of culture from 4. Inoculate in nutrient broth flask which supplemented with 0.05 mg /ml. of Co, Cu, Hg, Cr and Zn.
6. Incubate at 37 °C for 72 hours.
7. Take 100 µl of culture from 6. Inoculate on nutrient agar with 0.5% NaCl. Spread over the plate and then incubated at 37 °C for 24 hours.
8. Select different types of colonies and re-streak on nutrient agar with 0.5% NaCl to get pure colonies.
9. Incubate at 37 °C for 24 h. Study physical character by Gram's stain and microscope.

### Study Resistance of Halophilic Bacteria on Heavy Metal by Plate Diffusion Method

1. Culture the purely isolated bacteria in 0.5% NaCl nutrient broth. Incubated at 37 °C for 18 h for nutrient broth.
2. Divide nutrient agar plate with 0.5% NaCl to 6 equal parts.
3. Spread 100 µl of 18-hour-old broth from 1. on nutrient agar in 2.
4. Drill a hole on 6 divided part of Nutrient Agar plates in 3.
5. Drop 40 µl of  $\text{CoSO}_4 \cdot 7\text{H}_2\text{O}$ ,  $\text{ZnSO}_4 \cdot 7\text{H}_2\text{O}$ ,  $\text{Hg}(\text{NO}_3)_2$ ,  $\text{Cr}(\text{NO}_3)_3 \cdot 9\text{H}_2\text{O}$  and  $\text{CuSO}_4 \cdot 5\text{H}_2\text{O}$  per hole at different concentration (50,100,150, 200, 250, 300, 350,400, 450,500 mg /ml).
6. Incubate at 37 °C for 24 h. Check clear zone around the hole.

### Testing the ability to degrade heavy metals in water

1. Add the highest concentration of heavy metal solution from the plate diffusion method to 0.5% NaCl Nutrient broth.
2. Inoculate 1 ml of 108 CFU/ml of the isolates and incubate at 37 °C for 15 days.
3. Examine the remaining heavy metals in the sample on days 3, 5,7,10 and 15 with Atomic Absorption Spectrophotometer (AA).

## RESULT

### Isolation of Halophilic Bacteria in Metallic Conditions

After a few days of cultivation, bacteria were isolated and purified. Different morphology colonies were selected and re-cultured for purification. Total 20 different pure bacterial isolates were collected. Primary screening was performed by Gram's staining and microscopic examination. Characterization of isolate colonies were carried out and the results are shown in table 1 and 2.

Table 1 Isolate colonies form, elevate and margin.

| sample | form      | elevate | margin   |
|--------|-----------|---------|----------|
| HL 1   | circular  | raised  | undulate |
| HL 2   | circular  | raised  | entire   |
| HL 3   | circular  | raised  | undulate |
| HL 4   | circular  | raised  | undulate |
| HL 5   | circular  | raised  | entire   |
| HL 6   | circular  | raised  | entire   |
| HL 7   | circular  | raised  | entire   |
| HL 8   | circular  | raised  | entire   |
| HL 9   | circular  | convex  | undulate |
| HL 10  | circular  | raised  | undulate |
| HL 11  | circular  | raised  | undulate |
| HL 12  | circular  | raised  | entire   |
| HL 13  | circular  | convex  | undulate |
| HL 14  | circular  | raised  | entire   |
| HL 15  | circular  | raised  | undulate |
| HL 16  | irregular | flat    | undulate |
| HL 17  | irregular | flat    | entire   |
| HL 18  | irregular | convex  | entire   |
| HL 19  | irregular | convex  | entire   |
| HL 20  | circular  | raised  | entire   |

Table 2 Isolate colonies color, Gram and shape.

| sample | color   | Gram     | shape |
|--------|---------|----------|-------|
| HL 1   | creamy  | positive | rod   |
| HL 2   | creamy  | positive | rod   |
| HL 3   | creamy  | positive | rod   |
| HL 4   | greyish | positive | rod   |
| HL 5   | greyish | positive | rod   |
| HL 6   | creamy  | positive | rod   |
| HL 7   | white   | negative | rod   |
| HL 8   | white   | positive | rod   |
| HL 9   | creamy  | positive | rod   |
| HL 10  | greyish | positive | rod   |
| HL 11  | white   | positive | rod   |

Table 2 (continue)

| sample | color   | Gram     | shape |
|--------|---------|----------|-------|
| HL 12  | white   | positive | rod   |
| HL 13  | greyish | positive | rod   |
| HL 14  | creamy  | positive | rod   |
| HL 15  | white   | positive | rod   |
| HL 16  | greyish | positive | rod   |
| HL 17  | white   | positive | rod   |
| HL 18  | white   | positive | rod   |
| HL 19  | greyish | positive | rod   |
| HL 20  | greyish | positive | rod   |

### Resistance of Halophilic Bacteria on Heavy Metal by Plate Diffusion Method

Result of growth performance of 20 isolates in the presence of cobalt, chromium, mercury and zinc are shown in the table 3. and 4.

Table 3 Capability to grow in heavy metal at concentrations 50-250 mg /ml.

| sample | Co | Cr | Hg | Cu | Zn |
|--------|----|----|----|----|----|
| HL 1   | -  | -  | +  | -  | -  |
| HL 2   | -  | -  | +  | -  | -  |
| HL 3   | -  | -  | +  | -  | -  |
| HL 4   | -  | -  | +  | -  | -  |
| HL 5   | -  | -  | +  | -  | -  |
| HL 6   | -  | -  | +  | -  | -  |
| HL 7   | -  | -  | +  | -  | -  |
| HL 8   | -  | -  | +  | -  | -  |
| HL 9   | -  | -  | +  | -  | -  |
| HL 10  | -  | -  | +  | -  | -  |
| HL 11  | -  | -  | +  | -  | -  |
| HL 12  | -  | -  | +  | -  | -  |
| HL 13  | -  | -  | +  | -  | -  |
| HL 14  | -  | -  | +  | -  | -  |
| HL 15  | -  | -  | +  | -  | -  |
| HL 16  | -  | -  | +  | -  | -  |
| HL 17  | -  | -  | +  | -  | -  |
| HL 18  | -  | -  | +  | -  | -  |
| HL 19  | -  | -  | +  | -  | -  |
| HL 20  | -  | -  | +  | -  | -  |

- = do not found clear zone    + = found clear zone

Table 4 Capability to grow in heavy metal at concentrations 250-500 mg /ml.

| sample | Co | Cr | Hg | Cu | Zn |
|--------|----|----|----|----|----|
| HL 1   | -  | -  | +  | -  | -  |
| HL 2   | -  | -  | +  | -  | -  |
| HL 3   | -  | -  | +  | -  | -  |
| HL 4   | -  | -  | +  | -  | -  |
| HL 5   | -  | -  | +  | -  | -  |
| HL 6   | -  | -  | +  | +  | -  |
| HL 7   | -  | -  | +  | -  | -  |
| HL 8   | -  | -  | +  | -  | -  |
| HL 9   | -  | -  | +  | -  | -  |
| HL 10  | -  | -  | +  | -  | -  |
| HL 11  | -  | -  | +  | -  | -  |
| HL 12  | -  | -  | +  | -  | -  |
| HL 13  | -  | -  | +  | -  | -  |
| HL 14  | -  | -  | +  | -  | -  |
| HL 15  | -  | -  | +  | -  | -  |
| HL 16  | -  | -  | +  | -  | -  |
| HL 17  | -  | -  | +  | -  | -  |
| HL 18  | -  | -  | +  | -  | -  |
| HL 19  | +  | -  | +  | -  | -  |
| HL 20  | -  | -  | +  | +  | -  |

- = do not found clear zone    + = found clear zone

\* = found clear zone at 500 mg/ml

### The Ability to Degrade Heavy Metals in Water

Result of ability to degrade heavy metals in water are shown in the table 5 and 6.

Table 5 Heavy metal residue in Nutrient broth

| Sample | Day | Remaining quantity in broth (ppm) |       |       |       |
|--------|-----|-----------------------------------|-------|-------|-------|
|        |     | Zn                                | Co    | Cr    | Cu    |
| HL1    | 3   | 19.73                             | 77.69 | 69.51 | 23.92 |
|        | 5   | 19.72                             | 77.67 | 69.36 | 22.78 |
|        | 7   | 19.75                             | 77.63 | 69.54 | 22.08 |
|        | 10  | 19.73                             | 73.76 | 69.42 | 22.93 |
|        | 15  | 19.73                             | 73.71 | 69.21 | 21.88 |
| HL2    | 3   | 19.59                             | 73.95 | 64.95 | 24.74 |
|        | 5   | 19.57                             | 73.06 | 64.41 | 24.46 |
|        | 7   | 19.56                             | 72.95 | 64.12 | 24.42 |
|        | 10  | 19.55                             | 72.90 | 64.08 | 24.21 |
|        | 15  | 19.53                             | 72.51 | 63.92 | 24.14 |
| HL3    | 3   | 19.45                             | 77.29 | 75.84 | 25.45 |
|        | 5   | 19.44                             | 76.91 | 75.61 | 25.15 |
|        | 7   | 19.43                             | 75.86 | 75.42 | 23.72 |
|        | 10  | 19.43                             | 75.63 | 75.11 | 23.36 |
|        | 3   | 19.41                             | 75.21 | 75.10 | 23.23 |

Table 5 (continue)

| Sample | Day | Remaining quantity in broth (ppm) |       |       |       |
|--------|-----|-----------------------------------|-------|-------|-------|
|        |     | Zn                                | Co    | Cr    | Cu    |
| HL4    | 3   | 19.58                             | 76.64 | 68.62 | 25.91 |
|        | 5   | 19.56                             | 76.05 | 68.51 | 25.61 |
|        | 7   | 19.54                             | 75.99 | 68.45 | 23.78 |
|        | 10  | 19.53                             | 74.93 | 68.44 | 23.17 |
|        | 15  | 19.52                             | 74.16 | 68.19 | 23.07 |
| HL5    | 3   | 19.68                             | 78.49 | 65.91 | 24.44 |
|        | 5   | 19.67                             | 78.28 | 65.81 | 24.04 |
|        | 7   | 19.67                             | 75.51 | 65.47 | 24.27 |
|        | 10  | 19.66                             | 74.63 | 65.41 | 23.55 |
|        | 15  | 19.66                             | 74.19 | 65.27 | 23.54 |
| HL6    | 3   | 19.75                             | 73.68 | 58.88 | 24.81 |
|        | 5   | 19.74                             | 73.66 | 58.71 | 24.72 |
|        | 7   | 19.73                             | 73.53 | 58.55 | 23.40 |
|        | 10  | 19.73                             | 73.25 | 58.52 | 23.81 |
|        | 15  | 19.73                             | 73.16 | 58.28 | 22.37 |
| HL7    | 3   | 19.94                             | 80.85 | 77.38 | 22.88 |
|        | 5   | 19.94                             | 80.82 | 72.49 | 22.60 |
|        | 7   | 19.78                             | 79.14 | 61.42 | 22.36 |
|        | 10  | 19.71                             | 78.21 | 51.19 | 21.38 |
|        | 15  | 19.71                             | 76.09 | 49.78 | 20.05 |
| HL8    | 3   | 19.86                             | 78.37 | 77.64 | 24.64 |
|        | 5   | 19.85                             | 78.28 | 77.36 | 24.46 |
|        | 7   | 19.83                             | 75.66 | 77.37 | 24.15 |
|        | 10  | 19.79                             | 75.18 | 77.04 | 23.74 |
|        | 15  | 19.53                             | 75.10 | 77.02 | 22.31 |
| HL9    | 3   | 19.76                             | 76.73 | 70.59 | 23.76 |
|        | 5   | 19.75                             | 76.23 | 70.49 | 23.40 |
|        | 7   | 19.74                             | 75.98 | 70.74 | 23.13 |
|        | 10  | 19.66                             | 75.61 | 70.18 | 23.10 |
|        | 15  | 19.65                             | 75.15 | 70.07 | 23.08 |
| HL10   | 3   | 20.10                             | 77.73 | 88.93 | 24.52 |
|        | 5   | 19.85                             | 77.13 | 88.51 | 24.21 |
|        | 7   | 19.76                             | 77.05 | 61.31 | 24.41 |
|        | 10  | 19.55                             | 75.31 | 53.05 | 23.15 |
|        | 15  | 19.55                             | 75.71 | 49.66 | 22.06 |
| HL11   | 3   | 19.92                             | 78.98 | 82.71 | 23.63 |
|        | 5   | 19.91                             | 78.24 | 77.93 | 23.19 |
|        | 7   | 19.91                             | 77.53 | 63.64 | 23.16 |
|        | 10  | 19.85                             | 77.10 | 63.92 | 22.52 |
|        | 15  | 19.72                             | 76.72 | 38.89 | 22.33 |
| HL12   | 3   | 19.70                             | 77.72 | 88.13 | 23.91 |
|        | 5   | 19.67                             | 77.12 | 78.20 | 23.08 |
|        | 7   | 19.63                             | 77.47 | 77.02 | 22.98 |
|        | 10  | 19.60                             | 77.05 | 50.57 | 22.41 |
|        | 15  | 19.58                             | 76.84 | 50.45 | 22.01 |
| HL13   | 3   | 19.92                             | 77.18 | 79.37 | 23.16 |
|        | 5   | 19.81                             | 77.09 | 75.97 | 22.95 |
|        | 7   | 19.77                             | 77.08 | 73.46 | 22.91 |
|        | 10  | 19.66                             | 77.04 | 57.34 | 22.56 |
|        | 15  | 19.54                             | 77.01 | 55.40 | 22.51 |

Table 5 (continue)

| Sample | Day | Remaining quantity in broth (ppm) |       |       |       |
|--------|-----|-----------------------------------|-------|-------|-------|
|        |     | Zn                                | Co    | Cr    | Cu    |
| HL14   | 3   | 19.93                             | 77.60 | 76.62 | 23.90 |
|        | 5   | 19.93                             | 77.58 | 75.28 | 23.53 |
|        | 7   | 19.83                             | 77.28 | 70.87 | 23.16 |
|        | 10  | 19.75                             | 77.08 | 70.57 | 22.92 |
|        | 15  | 19.68                             | 76.92 | 70.03 | 22.65 |
| HL15   | 3   | 19.77                             | 78.21 | 79.30 | 22.86 |
|        | 5   | 19.76                             | 76.24 | 73.98 | 22.80 |
|        | 7   | 19.76                             | 76.09 | 71.09 | 22.63 |
|        | 10  | 19.71                             | 76.09 | 59.49 | 22.27 |
|        | 15  | 19.70                             | 76.09 | 56.42 | 22.11 |
| HL16   | 3   | 19.86                             | 77.08 | 82.91 | 23.51 |
|        | 5   | 19.85                             | 77.07 | 82.38 | 23.17 |
|        | 7   | 19.83                             | 77.06 | 76.36 | 23.03 |
|        | 10  | 19.76                             | 77.02 | 62.99 | 22.22 |
|        | 15  | 19.62                             | 77.01 | 62.24 | 22.08 |
| HL17   | 3   | 19.75                             | 76.64 | 75.72 | 24.45 |
|        | 5   | 19.72                             | 76.56 | 74.60 | 23.19 |
|        | 7   | 19.66                             | 76.47 | 72.15 | 22.87 |
|        | 10  | 19.66                             | 76.41 | 66.24 | 22.67 |
|        | 15  | 19.60                             | 76.04 | 63.68 | 22.34 |
| HL18   | 3   | 19.96                             | 76.60 | 76.60 | 22.84 |
|        | 5   | 19.91                             | 76.51 | 76.43 | 22.83 |
|        | 7   | 19.71                             | 76.46 | 76.47 | 22.53 |
|        | 10  | 19.67                             | 76.30 | 59.56 | 22.42 |
|        | 15  | 19.60                             | 76.12 | 58.21 | 22.02 |
| HL19   | 3   | 19.72                             | 76.16 | 84.19 | 24.64 |
|        | 5   | 19.71                             | 75.85 | 84.15 | 24.02 |
|        | 7   | 19.66                             | 75.53 | 75.50 | 23.77 |
|        | 10  | 19.59                             | 75.43 | 63.26 | 22.70 |
|        | 15  | 19.59                             | 74.91 | 62.24 | 22.53 |
| HL20   | 3   | 19.74                             | 77.37 | 87.45 | 21.80 |
|        | 5   | 19.68                             | 77.34 | 74.26 | 21.34 |
|        | 7   | 19.63                             | 76.51 | 74.03 | 21.16 |
|        | 10  | 19.63                             | 76.47 | 70.65 | 21.01 |
|        | 15  | 19.62                             | 76.08 | 70.23 | 20.68 |

## CONCLUSIONS

The major focus of this study is to isolate and identify bacterial that help recovery of surroundings from heavy metal contamination. 20 isolates of halo-tolerance microorganisms which could grow in medium contain 5 heavy metals (Cu, Cr, Co, Zn and Hg) were isolated from salt soil in Samut Sakorn province. Characters of colonies were varied. All of them had rod shape. Only HL 7 was Gram's negative. All of them were tested for the highest concentration of heavy metals that they could tolerance by Plate diffusion method in nutrient agar. Incubated at 37 °C for 15 days. All of the isolates, HL1-20, could not grow on media which had Hg. The best Co reducing isolate was HL1, which reduced Co quantity from 77.68 to 73.76 (5.05 %). Reduction of Co conducted

from the tenth day to the fifteenth day. The best Cr reducing isolate was HL7, which reduced Cr from 77.38 to 49.78 (35.66 %). The decline of Cr was continuous from the beginning to the last day of experiment (15 days). The best Co reducing isolate was HL1, which reduced Co quantity from 77.68 to 73.76 (5.05 %). Reduction of Co conducted from the tenth day to the fifteenth day. For Zn and Cu, all the isolates (HL1-20) reduced heavy metals at the decimal level, which was not significant.

These four heavy metals (Cu, Cr, Co, and Zn) are used in a variety of industries. Exposure to these substances causes harm to health. Getting Zn into the body causes liver and kidney failure and may also cause anemia. Cr causes inflammation of the skin and irritate epithelium of the internal organs. Getting Cu into the body causes red blood cells breaking. If the body has copper accumulated in the amount of 25-30 mg/kg of body weight, the symptoms of cirrhosis and mania may occur. Getting Co into the body can cause allergies, asthma, difficulty breathing and also cause skin allergy. For this reason, wastewater contaminated with these four heavy metals needs to be treated before released to natural water source. Therefore, the microorganisms isolated from this experiment can be utilized to decrease the heavy metal pollutant in future. However, more study on this matter should be executed in order to reconfirm the bioremediation activity by these bacteria, the presence of the bacteria, as well as bacteria identification genotype and the concentration of heavy metal pollution in the environment.

#### ACKNOWLEDGMENTS

This work was supported by Suan Sunandha Rajabhat University. I thank my colleagues who provided insight and expertise that greatly assisted the research, although they may not agree with all of the interpretations/conclusions of this paper.

#### REFERENCES

- [1] Marzan L.W., Hossain M., Sohana Akter , Mina Y.A., and Chowdhury A.M. M.A., Isolation and biochemical characterization of heavy-metal resistant bacteria from tannery effluent in Chittagong city, Bangladesh: Bioremediation viewpoint. *The Egyptian Journal of Aquatic Research*, Vol. 43, Issue 1, 2017, pp. 65-74.
- [2] Meenambigai P., Vijayaraghavan R., Gowri R.S., Rajarajeswari P., and Prabhavathi P., Biodegradation of Heavy Metals: A Review. *International Journal of Current Microbiology and Applied Sciences*, Vol. 5. Issue 4, 2016, pp. 375-383.
- [3] Ayangbenro A.S., and Babalola O.O., A New Strategy for Heavy Metal Polluted Environments: A Review of Microbial Biosorbents. *Int J Environ Res Public Health*, Vol. 14, Issue 1, 2017, pp. 94.
- [4] Chutrtong, J., Comparison of Corncob and Corn Using as Fungal Culture Medium. *Procedia - Social and Behavioral Sciences*, Vol. 197, 2015, pp. 797-800.
- [5] Gupta A., Joia J., Sood A., Sood R., Sidhu C., and Kaur G., Microbes as Potential Tool for Remediation of Heavy Metals: A Review. *J Microb Biochem Technol*, Vol.8, 2016, pp. 364-372.
- [6] Dixit R., and Malaviya D., Bioremediation of Heavy Metals from Soil and Aquatic Environment: An Overview of Principles and Criteria of Fundamental Processes, Sustainability. Vol. 7, 2015, pp. 2189-2212.

# FACTORS AFFECTING COMMUNITY PERCEPTION AROUND BETAWI CULTURE TOURISM ACTIVITIES SETU BABAKAN JAKARTA SELATAN

Dwinanto<sup>1</sup> and Chotib<sup>2</sup>

<sup>1,2</sup> Dept.of Urban Studies, School of Strategic and Global Studies, University of Indonesia, Indonesia

## ABSTRACT

The purpose of this study was to analyze community perceptions of the Setu Babakan Betawi Cultural Village in South Jakarta and find out the significance of the factors that influence it. A total of 345 questionnaires were distributed to the community sample using simple random sampling method and carried out analysis on environmental, economic and social variables using descriptive and quantitative analysis methods. Descriptive analysis is used to determine the frequency distribution of scores and the mean of each variable indicator item. While quantitative analysis uses Structural Equation Modeling (SEM) analysis techniques that aim to measure the effect of the relationship between variables and indicators. Based on the results of path analysis from structural equation models it is known that public perception of the Setu Babakan Betawi Cultural Village is significantly influenced by Economic Factors and Social Factors while environmental factors do not significantly influence people's perceptions. The research findings show that the people who live around the area are very helpful and economically dependent on the activities of the Betawi Cultural Village. In the future it is necessary to develop economic activities in the region so that people are more prosperous and develop existing social networks to improve social ties so that the goal of preserving Betawi culture in this region is sustainable.

*Keywords: community perception, factors that influence perception, social, economic and environmental variables, Betawi Cultural Village*

## INTRODUCTION

The increasing number of people will reduce the land to support the ideal life of urban residents. Geographical conditions in cities, for example in the form of water catchment areas, floodplains, waterfronts and so on will influence and shape the culture of the community and the environment in which they live. The city of Jakarta is a miniature of Indonesia which is home to and activities of various cultures. Castles (1967) [1] mentions Sundanese, Javanese, Batak, Chinese, Arabic and other cultures as one in urban life in Jakarta. Betawi culture is one of the cultures in Jakarta that is formed from the acculturation (mixing) of various cultures that have existed before.

As the development of Betawi culture time will be tested for its existence by the times. To preserve Betawi ethnic arts and culture, the Government has determined the Betawi ethnic conservation efforts by establishing the Setu Babakan Betawi Cultural Village in South Jakarta. The Setu Babakan Betawi Cultural Village is the center of Betawi culture in Jakarta which is quite complete by seeking the development of landscapes, natural and betawi traditions such as religious (religious), Betawi culture and arts. In the area there are typical Betawi activities such as Pencak Silat, Aqiqah, Injek tanah, Ngarak Penganten Circumcision, until Betawi specialties such as Soto Betawi, Pecak Fish, Gabus Pucung, Laksa, Boiled Toge, Egg Crust, beer pletok,

dodol, tape uli, geplak, wajik and others. There are two Setu in the area, namely Setu Babakan and Setu Mangga Bolong which at first this area was overgrown with fruiting trees such as harp, starfruit, rambutan, sapodilla, melinjo, banana, guava and jackfruit.

After fourteen years since the Jakarta Government's establishment of the Betawi Cultural Village, the government's perception of the Betawi Cultural Village has passed, does the implementation of conservation development have the desired impact, Does the program have support from the community with Betawi culture. The Betawi Culture Village can only be successful and sustainable if it receives support from the local community.

The purpose of this study is to analyze community perceptions of the Setu Babakan Betawi Cultural Village in South Jakarta and find out the significance of the factors that influence it. Thus, this study was designed as follows. Based on the previous researches, the section on hypotheses proposed a series of hypotheses on the 4 types of local community involvement in tourism activities namely, participation in decision making, knowledge sharing, empowerment, and community knowledge about tourism on sustainable rural tourism development namely, social, cultural, economic, and environmental sustainability. The methodology section presents the data and the method used to analyse empirically the hypotheses developed in



rural tourism in

## THEORITICAL REVIEWS

### Perception

Perception is a human awareness of the conditions and the surrounding environment . Mulyana : 168 in Sereno and Cohen, (2005) [2] states that perception is knowledge that appears outside its surroundings that determines someone to accept or ignore information or knowledge. The more similarities and similarities of individual perceptions, the more intense and easy it is to interact and communicate. Perception is the result of the accumulation of acceptance of the senses against the conditions of the surrounding environment. Effendy (1984) [3]. Acceptance of perception is influenced by the level of knowledge and experience of a person. The more knowledge and experience a person has, the stronger and complete his perception will be. In general, a person's perception can be influenced by three factors. Siagian (1989) [4] namely, the person concerned (attitude, motivation, interests, experience and expectations); perception goals (people, objects or events); situation (environmental conditions).

Aspects that influence perceptions according to Mulyana are perceptions based on experience, are selective, evaluative, and contextual. The pattern of human behavior towards the subject, object or reaction is the result of past experience and not based on initial assumptions or guesses. In connection with the limitations of the human mind and mind, human interpretation and understanding of all objects or events will be selected and influenced by internal and external factors. Internal factors, such as gender, religion, education level, occupation, income level, behavior patterns, experience, motivation, needs, expectations and so on while external factors, namely intensity, contrast and repetition. Individual perceptions to interpret objects based on information that are often incomplete so that allegations are needed to make conclusions. The perception of each person will vary. Perception is the result of cognitive processes based on individual experiences of attitudes, beliefs, values and expectations of objects or events so that perceptions are personal and subjective. Context is the biggest influence in determining one's perception when seeing objects or events that will affect cognitive structures and ultimately affect one's perception.

### Environmental factor

A person's perception of his living environment is influenced by the five senses, experience, values and ways of life and psychological conditions that

make the perceptions of each individual will be different from an object. The community feels the impact of the quality of life from services and conditions in society on various aspects of life, for example, family, social, entertainment, health, finance, culture, consumers, work, spiritual, and environment. This perception affects the overall perception of society.

Some researchers have conceptualized the satisfaction of staying as an evaluation or feeling of being liked or disliked towards the environment referred to in a sense of values. Therefore, satisfaction with one's residence is captured as a combination of satisfaction with physical and social environmental features - features such as perceived attractiveness of the environment, evaluation of maintenance of housing, similarities with neighbors, and level of noise pollution. The quality of urban life is a result of human and urban environment interactions. The level of satisfaction with the urban environment is one indicator of quality of life (Sirgy and Cornwell, 2001) [5].

### Economic Factors

Economic factors influence perception. looks at the proximity to work locations looks at economic factors from accessibility. Describe the economic aspects of the physical condition of the location that provides income for the population, for example locations that have the opportunity to work, smoothen the business / business, there are people who want to provide financial assistance, including providing loans when needed. Pitana (2005) [6] the influence of tourism on surrounding communities will lead to a relationship between local communities and visitors that causes economic transactions. Relationships are generally unequal because local people tend to feel tourists are more prosperous and more educated. an explanation of the success of tourist areas that are located around community settlements, namely preserving and developing the existing physical environment, Providing economic prosperity to communities around the area, ensuring the quality of services to tourists who come, involving communities around tourist area and development zone.

### Social Factors

In some social science literature, people's perceptions are influenced by social factors which are shown by the intensity of interaction with neighbors, concern when neighbors experience disaster and a sense of togetherness with the people

around them in the neighborhood. Social values such as cooperation, trust or reciprocal relationships between individuals become social capital in society in life.

Participation in decision making has a large impact on individual attitudes, beliefs, and motivations. The theory of participation is widely known from Arnstein (1969) [7], which is eight levels or degrees of community participation. The success and sustainability of government programs depends on the active involvement of the community. Therefore, community participation in decision making can be done because it will increase productivity and profit from certain goals.

Used German Economic data to examine the relevance of environmental aspects to life satisfaction. The study findings revealed a positive relationship between social cohesiveness and life satisfaction. That is, people who are closer to their neighbors tend to report higher levels of life satisfaction than people who are less close show that community involvement is an important determinant in the pride of the neighborhood [5].

## METHODOLOGY

### Hypotheses

From the results of direct observations it can be taken the initial conclusion that the communities around the Setu Babakan Betawi Cultural Village area feel positive social, economic and environmental benefits so that the hypothesis of this study is that social, economic and environmental factors have a significant relationship with the surrounding community perceptions of Settlements Setu Babakan Betawi Culture.

This study uses a mixed quantitative and qualitative methods. Descriptive analysis uses a frequency distribution table that will be used as material to obtain statements from the public on the Setu Babakan Betawi Cultural Settlement area using the Likert scale technique with a score of 1-5 on each questionnaire with a value of 1 means strongly agree; 2 means Disagree; 3 means hesitation; 4 means agree; 5 means Strongly agree. The results of the distribution of questionnaires will be processed and will be discussed in table form. Determination of sample size from the population using the method of simple random sampling randomly with the aim that all members of the population have the same opportunity to be chosen regardless of the strata that exist in the population.

Table 1 Profile of Respondents by place of residence, Gender, Age, Population Status, Education, Employment and Length of Stay

| No                              | Criteria           | Total | (%) |
|---------------------------------|--------------------|-------|-----|
| <b>Gender</b>                   |                    |       |     |
| 1                               | Male               | 172   | 50  |
| 2                               | Woman              | 173   | 50  |
|                                 | Sum                | 345   | 100 |
| <b>Age</b>                      |                    |       |     |
| 1                               | < 30               | 45    | 13  |
| 2                               | 31 – 45            | 141   | 41  |
| 3                               | 46 – 55            | 79    | 23  |
| 4                               | 55 – 64            | 50    | 14  |
| 5                               | > 64               | 30    | 9   |
|                                 | Sum                | 345   | 100 |
| <b>Ethnic</b>                   |                    |       |     |
| 1                               | Betawi             | 237   | 69  |
| 2                               | Non Betawi         | 108   | 31  |
|                                 | Sum                | 345   | 100 |
| <b>Education</b>                |                    |       |     |
| 1                               | Primary school     | 58    | 17  |
| 2                               | Junior High School | 41    | 12  |
| 3                               | Senior High School | 188   | 54  |
| 4                               | Scholar            | 58    | 17  |
|                                 | Sum                | 345   | 100 |
| <b>Housing Ownership Status</b> |                    |       |     |
| 1                               | Right of ownership | 299   | 87  |
| 2                               | Rent/Contract      | 46    | 13  |
|                                 | Sum                | 345   | 100 |
| <b>Neighbourhood</b>            |                    |       |     |
| 1                               | RW 5               | 14    | 3   |
| 2                               | RW 6               | 81    | 24  |
| 3                               | RW 7               | 69    | 20  |
| 4                               | RW 8               | 122   | 36  |
| 5                               | RW 9               | 59    | 17  |
|                                 | Sum                | 345   | 100 |
| <b>Occupation</b>               |                    |       |     |
| 1                               | Private Employee   | 110   | 32  |
| 2                               | Retired            | 7     | 2   |
| 3                               | Scholar Student    | 2     | 1   |
| 4                               | Entrepreneur       | 40    | 12  |
| 5                               | Teacher            | 8     | 2   |
| 6                               | Civil servant      | 10    | 3   |
| 7                               | Housewife          | 136   | 39  |
| 8                               | Others             | 32    | 9   |
|                                 | Sum                | 345   | 100 |

| No  | Criteria    | Total | (%) |
|---|-------------|-------|-----|
| <b>Length of Stay</b>                               |             |       |     |
| 1   | >50 years   | 48    | 14  |
| 2   | 30-50 years | 101   | 29  |
| 3   | 10-30 years | 156   | 45  |
| 4   | <10 years   | 40    | 12  |
| Sum   |             | 345   | 100 |
| <b>Occupation related to Betawi Culture Tourism</b> |             |       |     |
| 1   | Yes         | 97    | 28  |
| 2   | No          | 248   | 72  |
| Sum   |             | 345   | 100 |

### Structural Equation Model (SEM)

According to Sugiyono (2009) [8] Structural equation model (SEM) consists of 2 elements, namely the measurement model (outer model) and the structural model (inner model). Where in SEM three analysis activities were carried out at once in one analysis, namely 1) CFA validity (Confirmatory factor Analysis); 2) Path Analysis 3) Goodness of fit test. Before discussing the results of SEM analysis, it is necessary to test assumptions which in this case include evaluating data normality and evaluating outliers.

The overall suitability test of the model relates to the analysis of GOF statistics produced by the program, in this case AMOS 20. Using the GOF measurement guidelines and GOF statistical results, the overall model compatibility analysis can be carried out as follows:

Table 2 Evaluation of Structural Model Compatibility (After Model modification)

| Goodness of fit Index | Cut of value   | Result  | Note               |
|-----------------------|--|---------|--------------------|
| Chi-Square / CMIN     | < ChiTabel : Good fit<br>> ChiTabel : Poor fit                     | 469,108 | Model Poor Fit     |
| P-value CMIN          | > 0,050 : Good fit<br>< 0,050 : Poor fit                           | 0,000   | Model Poor Fit     |
| CMIN/DF               | < 2,000 : Good Fit<br>< 3,000 : Marginal Fit<br>> 3,000 : Poor Fit | 2,076   | Marginal Fit       |
| RMSEA                 | < 0,080 : Good fit<br>< 0,100 : Marginal Fit<br>> 0,100 : Poor fit | 0,056   | Model Good fit     |
| GFI                   | > 0,900 : Good fit   | 0,909   | Model Good fit     |
| AGFI                  | > 0,800 : Marginal fit   | 0,848   | Model Marginal fit |
| TLI                   | < 0,800 : Poor fit   | 0,933   | Model Good fit     |
| CFI                   |  | 0,957   | Model Good fit     |

Tabel 3 Resume Model Evaluation/Outer Model (Measurement Model)

| Variable Laten           | Variable Manifest | Validity Konvergen |             | Rank | Validity Diskriminant (AVE > 0,5=Valid) |            | Construct Reliability (CR > 0,7) |          |
|--------------------------|-------------------|--------------------|-------------|------|---|------------|----------------------------------|----------|
|                          |                   | Loading Factors    | value       |      | AVE                                     | Conclusion | CR                               | value    |
| Social Network (X1.1)    | X1.1.1            | 0,879              | Valid       | 2    | 0,865                                   | Valid      | 0,896                            | Reliabel |
|                          | X1.1.2            | 0,799              | Valid       | 3    |   |            |                                  |          |
|                          | X1.1.3            | 0,904              | Valid       | 1    |   |            |                                  |          |
| Mutual (X1.2)            | X1.2.1            | 0,800              | Valid       | 2    | 0,783                                   | Valid      | 0,834                            | Reliabel |
|                          | X1.2.2            | 0,890              | Valid       | 1    |   |            |                                  |          |
| Participation (X1.3)     | X1.3.1            | 0,750              | Valid       | 1    | 0,573                                   | Valid      | 0,710                            | Reliabel |
|                          | X1.3.2            | 0,733              | Valid       | 2    |   |            |                                  |          |
| Environment Factor (X2)  | X2.1              | 0,854              | Valid       | 2    | 0,715                                   | Valid      | 0,824                            | Reliabel |
|                          | X2.2              | 0,860              | Valid       | 1    |   |            |                                  |          |
|                          | X2.3              | 0,744              | Valid       | 3    |   |            |                                  |          |
|                          | X2.4              | 0,394              | Tidak Valid | 5    |   |            |                                  |          |
|                          | X2.5              | 0,571              | Valid       | 4    |   |            |                                  |          |
| Economic Factor (X3)     | X3.1              | 0,680              | Valid       | 3    | 0,603                                   | Valid      | 0,782                            | Reliabel |
|                          | X3.2              | 0,620              | Valid       | 4    |   |            |                                  |          |
|                          | X3.3              | 0,527              | Valid       | 5    |   |            |                                  |          |
|                          | X3.4              | 0,684              | Valid       | 2    |   |            |                                  |          |
|                          | X3.5              | 0,711              | Valid       | 1    |   |            |                                  |          |
| Community Perception (Y) | Y1                | 0,632              | Valid       | 6    | 0,790                                   | Valid      | 0,890                            | Reliabel |
|                          | Y2                | 0,681              | Valid       | 4    |   |            |                                  |          |
|                          | Y3                | 0,613              | Valid       | 7    |   |            |                                  |          |
|                          | Y4                | 0,643              | Valid       | 5    |   |            |                                  |          |
|                          | Y5                | 0,545              | Valid       | 10   |   |            |                                  |          |
|                          | Y6                | 0,833              | Valid       | 1    |   |            |                                  |          |
|                          | Y7                | 0,613              | Valid       | 7    |   |            |                                  |          |
|                          | Y8                | 0,558              | Valid       | 9    |   |            |                                  |          |
|                          | Y9                | 0,764              | Valid       | 3    |   |            |                                  |          |
|                          | Y10               | 0,785              | Valid       | 2    |   |            |                                  |          |

The measurement model is a model with calculation results based on calculations using the AMOS 20 program. The method used is Confirmatory Factor Analysis, where using this tool it is known that the existing indicators can really explain a construct. The purpose of the measurement model is to describe how well the indicators in this study can be used as instruments for measuring latent variables. The main concepts used in this case are measurement, validity and reliability. The indicators used to reflect a variable also contain errors, so they must also be considered in statistical analysis.

Based on the table above, it can be seen that most of the Loading factor values  $\geq 0.50$  (Valid), even though there are some items partially declared invalid (item X2.4) but still fixed can be maintained because OverAll is good / feasible, that is with value  $AVE \geq 0.50$  (Valid). Thus it can be concluded that the validity of all manifest variables on the latent variable is good. While the results of reliability calculations show that all values of construct reliability (CR)  $\geq 0.70$  (reliable), thus it can be concluded that all these latent variables have good reliability.

Table 4 Evaluation Model measurement Phase 2  
(2nd Order Outer Model)

| Var Latent  | Variable Manifest    | Loading Factor | Rule of Thum | value | Rank |
|-------------|----------------------|----------------|--------------|-------|------|
| Social (X1) | Network (X1.1)       | 0,926          | 0,500        | Valid | 1    |
|             | Mutual (X1.2)        | 0,880          | 0,500        | Valid | 2    |
|             | Participation (X1.3) | 0,639          | 0,500        | Valid | 3    |

The best aspect in forming the Social variable (X1) is Social Network (X1.1) with the highest loading factor of 0.926. So that if the decision maker wants to increase Social Value (X1), the statistic recommendation is to prioritize the increase in value on the Social Network Aspect (X1.1).

### Structural Model

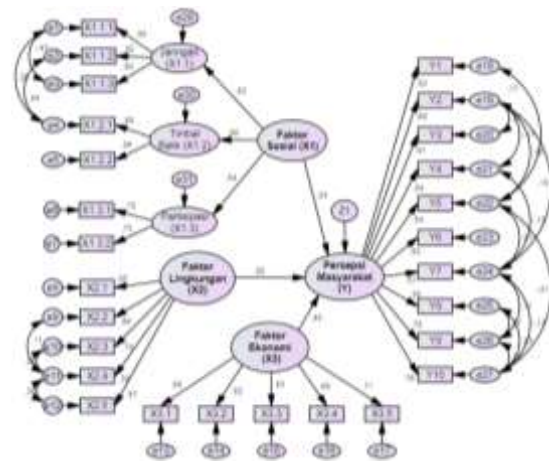
This section deals with evaluating the coefficients or parameters that indicate a causal relationship or the effect of one latent variable on other latent variables. A causal relationship is declared not significant if the value of the critical ratio (C.R.) is between the range -1.96 and 1.96 with a significance level of 0.05. With the help of the AMOS 20 program application, the results of the estimation of the critical ratio of the structural model are obtained.

Table Results of Estimates and Testing of Hypotheses

| Variable                |     |                          | Coefficient Path | Result of Hypotheses |         | Score           |
|-------------------------|-----|--------------------------|------------------|----------------------|---------|-----------------|
| Eksogen                 | --> | Endogen                  |                  | CR                   | p-value |                 |
| Social Factor (X1)      | --> | Community Perception (Y) | 0,237            | 3,249                | 0,001   | Significan      |
| Environment Factor (X2) | --> | Community Perception (Y) | 0,054            | 0,912                | 0,362   | Not Significant |
| Economic Factor (X3)    | --> | Community Perception (Y) | 0,534            | 6,582                | 0,000   | Significan      |

The Social Factor variable (X1) and Economic Factor Variable (X3) have an influence (Path coefficient) on Community Perception (Y) Because the CR value is in the range -1.96 and 1.96 and the p-value <0.05, the statistical hypothesis states  $H_0$  rejected, meaning Social Factor (X1) and Economic Factor (X3) have a significant effect on Community Perception (Y).

The Environmental Factor variable (X2) has an influence (Path coefficient) on Community Perception (Y) of 0.054 with a CR value of 0.912 and p-value of 0.362. Because the CR value is outside the range -1.96 and 1.96 and the p-value is <0.05, the statistical hypothesis states  $H_0$  is accepted, meaning that the Environmental Factor (X2) has no significant effect on Community Perception (Y).

Figure 1 Model Path Diagram  
Structural Equation Modelling (SEM)

In order to facilitate the evaluation of the outer model which is also integrated with path analysis (path analysis), the following are presented in the path diagram of the measurement model (outer model) and structural models (structural models)

The path diagram of the Structural equation model can be converted in the form of equations as follows

$$Y = 0,24 X_1 + 0,05 X_2 + 0,53 X_3 + e_1$$

From the structural equation above it can be seen the relationship of exogenous latent constructs to endogenous latent constructs. it can be seen that the public perception variable (Y) is more dominantly influenced by the latent variable economic factor (X3), which is the highest influence value of 0.53. where the indicator (manifest variable) is best in forming the economic factor variable (X3) is X3.5 (facilities for trading / services) with the highest loading factor of 0.711, so that if the decision maker wants to increase the value of economic factors (X3) then the recommendation statistically is prioritizing the improvement of values on the X3.5 indicator (facilities for trading / services).

### CONCLUSIONS

The validity of all manifest variables on the latent variable is good, where the best aspect in forming the Social variable (X1) is Network (X1.1) with the highest loading factor of 0.926. So that if the decision maker wants to increase Social Value (X1), the statistic recommendation is to prioritize the increase in value on the Network Aspect (X1.1).

Based on the results of path analysis from structural equation models it is known that public perception of the Setu Babakan Betawi Cultural

Village is significantly influenced by Economic Factors and Social Factors while environmental factors do not significantly influence people's perceptions.

The research findings show that the people who live around the area are very helpful and economically dependent on activities from the Betawi Cultural Village. In the future it is necessary to develop economic activities in the region so that the people are more prosperous

Community support for the development of the Betawi Cultural Village area can be strengthened by developing existing social networks to improve social ties so that the objectives and conservation programs of the Betawi culture in the region can be sustainable and supported by the community.

The Social Network intended for the Community has been made by the Community in this case marked by Life in the Community as a Family that Maintain Public Relations Can Be Required to Arrange Plans and Activities That Can Be Done By the Community Alone Can Be Responded to Programs or Assistance Coming from the Government For example by forming a community of cooking experts, Betawi cultural communities or other communities for information and knowledge within the framework of developing activities within the region.

#### ACKNOWLEDGMENTS

The authors wish to acknowledge the grateful acknowledgment that this research is supported

by the publications grant for thesis and dissertation of Universitas Indonesia (PITMA UI grant).

#### REFERENCES

- [1] Castles, Lance. 2007. Ethnic Profil Jakarta. Masup Jakarta.
- [2] Mulyana, Dedy. 2005. Introduction Science of Comunication. Remaja Rosdakarya. Bandung
- [3] Efendi, Usman. 1984. Introduction of Physcology. Bandung : Angkasa
- [4] Siagian, Sondang P. 1989. Theory of Motivation and application. Bina Aksara, Jakarta
- [5] Sirgy, M. J., & Cornwell, T. (2001). Further validation of the Sirgy et al.'s measure of community quality of life. *Social Indikators Research*, 56 , 125–143
- [6] Pitana, I. Gde dan Putu G. Gayatri. 2005. *Tourism Sociology*. Yogyakarta: Andi Offset.
- [7] Arnstein, Sherry R., *Eight Rungs on the Ladder of Citizen Participation* in Edgar S. Cahn and Barry A. Passet, *Citizen Participation: Affecting Community Change*, New York: Praeger Publishers, 1971.
- [8] Wijanto, Hari, Setyo. (2015). *The Research Method use Structural Equation Modeling with Lisrel 9*. Faculty of Economics. University of Indonesia. Jakarta

## QUALITY OF VERMICOMPOST BY *Pheretima peguana* On Different Organic Wastes

Pornpailin Boonna <sup>1</sup>, \*Nipapun Kungskulniti <sup>1,2</sup>, Rochana Tangkoonboribun <sup>3</sup>, Naowarut Charoenca <sup>1,2</sup>

<sup>1</sup> Faculty of Public Health, Mahidol University, Thailand

<sup>2</sup> Center of Excellence on Environmental Health and Toxicology, Thailand

<sup>3</sup> Thailand Institute of Scientific and Technological Research, Thailand

### ABSTRACT

This research studied the quality of compost using earthworms (vermicompost) developed with three different organic wastes: water hyacinth scraps, food wastes, and corncobs as base materials. One kilogram of local Thai earthworms, *Pheretima peguana*, was introduced into wastes of three different organic-based materials (either water hyacinth scraps, food wastes, or corncobs) in the vermibin with a constant ratio of rice bran, and cow dung. Each organic waste was tested for a high, medium and low ratio by weight with rice bran, and cow dung. The set materials were vermicomposted for 45 days. Physico-chemical parameters and phytotoxicity as germination index of the compost were analyzed from vermicompost samples taken from the final day of composting. Values of pH, electrical conductivity, moisture content, total nitrogen, total phosphorus, total potassium, total organic carbon, C/N ratio, and germination index were determined. The vermicompost from all ratios of water hyacinth scraps and food wastes with rice bran and cow dung had acceptable nutrient levels (total nitrogen, total phosphorus, total potassium) as specified by the Thai agricultural standard, National Bureau of Agricultural Commodity and Food Standards, Ministry of Agriculture and Cooperative.

**Keywords:** *Pheretima peguana*, Vermicompost, Organic wastes

### INTRODUCTION

The rapid increase of organic wastes in Thailand with large volumes of water hyacinth wastes cleared from canals generates a major disposal problem. This huge amount of biomass waste produces environmental pollution. Water hyacinths are free-floating offensive aquatic macrophytes rich in organic matter, nitrogen, phosphorus, potassium and micronutrients. Corncobs are also an abundant organic waste particularly after the harvest season. However, composting corncobs takes a longer time than leafy material like cornhusks. Vermicomposting is a suitable biological process for disposing of organic wastes involving interactions between earthworms and microorganisms. The role of earthworms is to convert different types of organic wastes into nutrient-rich manure [1]. Mutual action of earthworms and microorganisms change the biological, physical and chemical properties of waste materials and convert them into vermicompost. Research shows that use of earthworms can compost organic wastes faster than common composting. Physico-chemical and biological properties of soil with ameliorated fertility are obtained from the bio-processing before the reuse of these wastes. Hence,

farmers can reduce the use of chemical fertilizer, which leads to environmental, and health hazards. Earthworms, *Pheretima peguana*, have unique capabilities to disintegrate organic wastes. They produce vermicompost with vermicast, homogeneous, odor-free, peat-like material containing significant quantities of nutrients with a low level of toxicants [2]. Vermicomposting is a suitable technique due to its simplicity, cost-effectiveness and can be used for all types of non-toxic biodegradable wastes. Municipal solid wastes are mostly composed of organic wastes with the highest ratio of around 64% for food wastes. Composting technology has gained interest for large-scale practice and disposal of a wide variety of organic wastes; hence, vermicomposting could be a useful means of handling and treating these organic wastes.

The aim of this study is to investigate organic wastes such as food wastes, corncobs, and water hyacinth scraps as a base material for vermicomposting. The quality of vermicompost derived in this study was determined according to the Thai agricultural standard, National Bureau of



Agricultural Commodity and Food Standards,

### Collection of waste material and earthworms

Food wastes were collected from the municipal landfill at Tandaw subdistrict, Kaengkhoei district, Saraburi province, Thailand by the collector. Water hyacinth scraps were collected from the local canal. Corncobs were collected from local cornfields. Rice bran was collected from the local rice mill. Cow dung was collected from a dairy farm in Saraburi province. Earthworms, *Pheretima peguana*, were obtained from a local vendor in Mae-on, Chiangmai province using cow dung as culture medium.

### Preparation of experimental media

Vermicomposting was carried out in a cement vermibin with dimensions of 80 cm (diameter) and 40 cm (depth). Net fabric covered the top of the vermibin to protect from any animals entering the bin.

### Feedstock materials collection and preparation

Nine sets of treatment were studied with different ratios of the three different organic base materials (water hyacinths, food wastes and corncobs) on layers of rice bran and cow dung in a constant ratio as shown in Table 1. The vermibin was arranged to do vermicomposting with six separate layers of media with rice bran and cow dung as illustrated in Figure 1. One kilogram of local Thai earthworms, *Pheretima peguana*, were introduced in each treatment. The process period of vermicomposting took 45 days with moisture content monitored periodically and maintained at 60-70% by sprinkling water manually.

Table 1. Combination of organic waste materials in vermicomposting

| Treatment | Materials Ratio Quantity (OW:RB:CD) | Total Quantity (Kilogram) |
|-----------|-------------------------------------|---------------------------|
| T1        | 7:4:3                               | 14                        |
| T2        | 6:4:3                               | 13                        |
| T3        | 5:4:3                               | 12                        |
| T4        | 7:4:3                               | 14                        |
| T5        | 6:4:3                               | 13                        |
| T6        | 5:4:3                               | 12                        |
| T7        | 7:4:3                               | 14                        |
| T8        | 6:4:3                               | 13                        |
| T9        | 5:4:3                               | 12                        |

Note: OW = Organic wastes are Base materials for the earthworm

T1-T3 Water hyacinth scraps

Ministry of Agriculture and Cooperative.

### MATERIALS AND METHODS

T4-T6 Food wastes

T7-T9 Corncobs

RB= Rice bran

CD= Cow dung



Figure 1. Illustration of different material layers for vermicomposting in vermibin

### Physico-chemical analysis of vermicompost

Physico-chemical characteristics of the vermicompost were measured for various parameters, including pH, electrical conductivity (EC), organic carbon (OC), organic matter (OM), C/N ratio, total nitrogen (TN), total potassium (K), total phosphorus (P), and Germination Index (%). About 500 grams of each grab sample was collected from six different locations by hand for a representative samples for the analysis [3]. The upper layer produced in the vermibin was analyzed for nutrient elements because the upper layer is changed to vermicast [4]. The pH was determined using a pH meter (AOAC973.04). EC was determined using a Conductivity Meter, BS EN 13038. Organic carbon was determined by organic matter multiplied by 1.72. Organic matter was determined by the Wet Oxidation method. The C/N ratio was determined by organic carbon divided by total nitrogen. Total nitrogen was measured by the Kjeldahl method and colorimetric measurement was done by spectrophotometer. Potassium was detected by colorimetric method using ammonium molybdate in HCl. Phosphorus was determined by spectrophotometer. Germination Index (GI) was tested using mung beans mixed with distilled water at the ratio of 1:10 (vermicompost to distilled). The percentage germination index (GI) were calculated according to the following formula:

$$GI (\%) = \frac{\% \text{ seed germination of compost} \times \% \text{ root growth of compost}}{\% \text{ seed germination of control} \times \% \text{ root growth of control}} \times 100$$

### RESULTS AND DISCUSSION

Among all parameter analyze for organic base materials in Table 2, water hyacinth scraps

contained the highest values, except for total nitrogen and total phosphorus; food waste contained higher values of phosphorus than water hyacinth scraps and corncobs waste. Parameter analysis results of compost materials (cow dung and rice bran) are shown in Table 3, The moisture content of these two compost materials was less than in the study of Kavita Sharma [4] and Zongqi Shoua. [5], but potassium was of incomparable amounts in their studies.

Table 2. The initial physico-chemical characteristics of organic base materials used for vermicomposting

| Parameter            | $\bar{X} \pm SD$ *    |                 |                  |
|----------------------|-----------------------|-----------------|------------------|
|                      | Water hyacinth scraps | Food wastes     | Corncobs         |
| pH                   | 7.70                  | 5.80            | 7.30             |
| Moisture content (%) | 96.18 $\pm$ 0.45      | 92.74 $\pm$ 0.2 | 4.75 $\pm$ 0.2   |
| OC (%)               | 42.75 $\pm$ 0.33      | 28.54 $\pm$ 0.1 | 19.32 $\pm$ 0.34 |
| OM (%)               | 73.70 $\pm$ 0.49      | 49.20 $\pm$ 0.1 | 33.31 $\pm$ 0.33 |
| TN (%)               | 5                     | 95              | 17               |
| TP (%)               | 0.72 $\pm$ 0.0        | 0.88 $\pm$ 0.1  | 0.93 $\pm$ 0.0   |
| TK (%)               | 9                     | 7               | 0                |
| C/N ratio            | 0.57 $\pm$ 0.04       | 1.06 $\pm$ 0.23 | 0.34 $\pm$ 0.17  |
|                      | 3.03 $\pm$ 0.07       | 1.08 $\pm$ 0.3  | 0.95 $\pm$ 0.01  |
|                      | 59.40                 | 32.43           | 20.77            |

Note: \*Mean  $\pm$  Standard Deviation

Table 3. The initial physico-chemical characteristics of compost materials used for vermicomposting

| Parameter            | $\bar{X} \pm SD$ * |                  |
|----------------------|--------------------|------------------|
|                      | Cow dung           | Rice bran        |
| pH                   | 7.80               | 7.35             |
| Moisture content (%) | 10.91 $\pm$ 0.02   | 8.93 $\pm$ 0.80  |
|                      | 45.25 $\pm$ 0.90   | 28.54 $\pm$ 0.02 |
|                      | 78.01 $\pm$ 0.33   | 49.20 $\pm$ 0.00 |
| OC (%)               | 1.32 $\pm$ 0.95    | 0.58 $\pm$ 0.17  |
| OM (%)               | 0.65 $\pm$ 0.55    | 1.38 $\pm$ 0.01  |
| TN(%)                | 2.73 $\pm$ 0.00    | 0.39 $\pm$ 0.27  |
| TP(%)                | 34.27              | 49.20            |
| TK (%)               |                    |                  |
| C/N ratio            |                    |                  |

Note: \* Mean  $\pm$  Standard Deviation

### Physico-chemical changes in the composting process

Moisture content is a key factor for the movement of earthworms since moisture is essential for microorganism survival [6]. After the composting

process, the weight of the compost had fallen to about half of the original amount due to the oxidation reaction of carbon to carbon dioxide and the loss of moisture [7]. The moisture content of the vermicompost is shown in Table 4. During the vermicomposting process for each treatment, moisture content was controlled to between 40 and 60%. Vermicomposting requires optimum moisture content for the microorganisms to grow and support the movement of earthworms. When the moisture content is too high, it will affect the organic matter decomposition process. The moisture content of each treatment product was 30.3%, 32.7% and 34.1% for T1, T2, and T3, respectively; 28.6%, 22.0% and 33.9% for T4, T5, and T6, respectively; 29.7%, 32.2% and 33.3% for T7, T8, and T9, respectively. The moisture content values were acceptable for most treatments. The pH values of compost were 7.9, 7.8, 7.7, 6.7, 6.3, 6.7, 7.1, 7.2, and 7.4 for T1 – T9 respectively. It can be seen that throughout the composting process in all treatments, pH values were slightly alkaline. The increase in pH was caused by the degradation of organic acids and the release of ammonia. The low-molecular-weight fatty acids and CO<sub>2</sub> greatly contributed to the decrease in the pH of the compost [8]. When compared with the standard, the pH values were acceptable in all experiments. The electrical conductivity of compost was 1.53, 2.37, 2.26, 1.56, 1.26, 1.45, 2.07, 2.54, and 1.97 mS/cm. for T1-T9, respectively. When compared with the standard, values of less than 10 dS/m were acceptable in all experiments showing that the vermicompost product is suitable for use in agriculture. The organic matter values of vermicompost were 71.98%, 67.06%, 56.89%, 65.94%, 53.46%, 41.39%, 40.36%, 36.82% and 33.37% for T1- T9, respectively. When compared with the standard, the organic matter percentages were acceptable in all experiments. Further, analysis of organic matter throughout the composting process showed that the trend was in the same direction. The organic matter of the composting process decreased, indicating an increased degradation rate, which corresponds to findings in the study of Benjawan [9]. It was explained that organic carbon and organic matter decreased throughout the composting processes due to the composting process with degradation occurring continuously. When it is stable, organic matter degradation slows which might be due to the temperature, so that the easily degradable organic matter is decreased. This leads to reduced microbial activity [10]. The results of C/N ratios were 30.13, 19.42, 17.90, 13.23, 10.23, 7.84, 16.25, 16.43, and 15.24 for T1-T9, respectively. When compared with the standard, the C/N ratios were acceptable in T2-T9 except for T1 which

exceeded 20. The composting period of T1 should be more than 45 days to adjust its C/N ratio to less than 20 before being used.

#### Major nutrients

The major nutrients analyzed were total nitrogen, total phosphorus and total potassium as shown in Figure 2 with values of 0.59-2.14%, 1.5%-2.93%, 1.80%-2.67%, 1.14%-3.39%, 1.04%-3.03%, 0.94%-3.06%, 0.45%-1.44%, 0.39%-1.3%, and 0.33%-1.27% for T1-T9, respectively. When compared with the standard, total nitrogen and total potassium were acceptable in all experiments. Total phosphorus was unacceptable for T7- T9 (corncoobs) since they were less than the standard of the Thai Agricultural Commodity and Food Standards, 2005. However, this could be resolved by adding some manure to help decrease the decomposition period and increase nitrogen and phosphorus of the vermicompost.

#### Germination index (GI)

Germination index (GI) is the most commonly used parameter to evaluate the phytotoxicity of the final compost and the effect on seed germination [11]. The germination index (GI) test results of compost at 45 days is shown in Table 4. The germination index for T1-T9 was 88.50%, 85.71%, 82.95%, 95.21%, 92.71%, 89.72%, 82.50%, 81.50%, and 80.50% respectively, which corresponds to findings in a study by Ponsa [12] which reported that the germination index in all treatments met the standard. Additionally, Tiquia and Tam [13] reported that the germination index values in their study were more than 80%, phytotoxic-free and were considered to have complete maturity. Therefore, the germination index in this study similarly showed non-phytotoxicity to plant growth.

92.71%, 89.72%, 82.50%, 81.50%, and 80.50% respectively, which corresponds to findings in a study by Ponsa [12] which reported that the germination index in all treatments met the standard. Additionally, Tiquia and Tam [13] reported that the germination index values in their study were more than 80%, phytotoxic-free and were considered to have complete maturity. Therefore, the germination index in this study similarly showed non-phytotoxicity to plant growth.

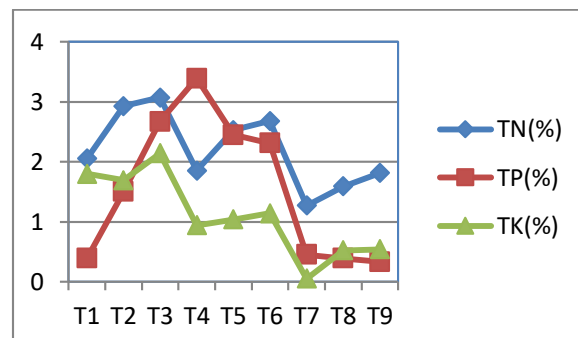


Figure 2. Results of major nutrients after vermicomposting for 45 days.

Table 4. Parameters of vermicompost products compared with the Thai Agricultural Commodity and Food Standards, 2005

| Parameters            | Treatments |          |          |          |          |          |          |         |          | Std.*   |
|-----------------------|------------|----------|----------|----------|----------|----------|----------|---------|----------|---------|
|                       | T1         | T2       | T3       | T4       | T5       | T6       | T7       | T8      | T9       |         |
| Moisture content (%)  | 30.3±0.9   | 32.7±0.1 | 34.      | 28.6±0.4 | 22.0±0.2 | 33.9±0.3 | 29.7±0.0 | 32.2±0. | 33.2±0.5 | ≤ 30    |
| pH                    | 0          | 0        | 1±0.33   | 5        | 1        | 0        | 0        | 03      | 5        | 5.5-8.5 |
| EC (ds/m)             | 7.9        | 7.6      | 7.3      | 6.7      | 6.3      | 6.7      | 7.1      | 7.2     | 7.4      | ≤ 10    |
| Organic carbon (%)    | 1.53±0.1   | 2.37±0.0 | 2.26±0.0 | 1.56±1.0 | 1.26±0.3 | 1.45±0.9 | 2.07±1.0 | 2.54±2. | 1.97±0.5 | ≤ 10    |
|                       | 9          | 6        | 8        | 8        | 2        | 4        | 8        | 08      | 8        |         |
| Organic matter (%)    | 41.75±0.   | 38.90±1. | 33.01±1. | 38.25±1. | 31.01±1. | 24.01±2. | 23.41±0. | 21.36±1 | 19.36±1. | -       |
|                       | 70         | 04       | 25       | 25       | 43       | 25       | 95       | .7      | 75       |         |
| C/N ratio             | 71.98±1.   | 67.06±1. | 56.89±2. | 65.94±0. | 53.46±1. | 41.39±1. | 40.36±1. | 36.82±1 | 33.37±0. | ≥20     |
|                       | 20         | 79       | 15       | 3        | 33       | 05       | 05       | .6      | 05       |         |
| TN (%)                | 30.25±0.   | 19.45±0. | 17.90±0. | 13.23±1. | 10.23±2. | 7.84±1.3 | 16.25±0. | 16.43±1 | 15.24±0. | ≤ 20:1  |
|                       | 97         | 18       | 32       | 95       | 11       | 2        | 97       | .6      | 55       |         |
| TP (%)                | 1.38±0.0   | 2.0±0.88 | 1.84±0.1 | 2.89±0.0 | 3.03±0.9 | 3.06±0.0 | 1.44±0.7 | 1.3±0.0 | 1.27±0.0 | ≥1.0    |
|                       | 5          | 4        | 0        | 0        | 5        | 0        | 1        | 2       | 1        |         |
| TK (%)                | 0.59±0.0   | 1.50±0.0 | 2.67±0.0 | 3.39±1.2 | 2.45±1.5 | 2.31±1.8 | 0.45±1.0 | 0.39±1. | 0.33±0.5 | ≥0.5    |
|                       | 8          | 5        | 6        | 6        | 0        | 5        | 6        | 08      | 5        |         |
| Germination index (%) | 2.14±0.8   | 1.69±0.8 | 1.80±0.9 | 1.14±1.5 | 1.04±0.3 | 0.94±1.9 | 0.54±0.1 | 0.52±1. | 0.49±0.5 | ≥0.5    |
|                       | 8          | 8        | 4        | 8        | 8        | 7        | 1        | 48      | 2        |         |
|                       | 88.50±1.   | 85.71±0. | 82.95±1. | 95.21±0. | 92.71±1. | 89.72±1. | 82.50±1. | 81.50±0 | 80.50±2. | ≥80     |
|                       | 94         | 54       | 30       | 9        | 7        | 1        | 45       | .0      | 06       |         |

Note: \* from Thai agricultural standard, National Bureau of Agricultural Commodity and Food

## CONCLUSION

The vermicompost from all ratios of water hyacinth scraps and food wastes with rice bran and cow dung had acceptable nutrient levels (total nitrogen, total phosphorus, total potassium) as specified by the Thai agricultural standard, National Bureau of Agricultural Commodity and Food Standards, Ministry of Agriculture and Cooperative. The color of vermicompost products by *pheretima* *peaguana* earthworms was brown or black color and had no odor.

Corn cob materials can be employed for vermicomposting but will take a longer time than with water hyacinths and food wastes. Therefore, corn cobs is not considered suitable for composting. The final vermicompost products in this study were soft with rich nutrients. Besides, the organic materials were completely degraded. Moreover, vermicomposting can help reduce the volume of organic wastes while reducing disposal costs and visual pollution.

## ACKNOWLEDGMENTS

The success of this thesis was possible through the kind support of my advisors. Research work is financially supported by the Thailand Institute of Scientific and Technological Research and Mahidol University.

## REFERENCES

- [1] Amouei, Yousefi and Khosrav. Comparison of vermicompost characteristics produced from sewage sludge of wood and paper industry and household solid wastes. Journal of Environmental Health Science and Engineering 2017;15(1)
- [2] Ndegwa and Thompson . Integrating composting ad vermicomposting in the treatment and bioconversion of biosolids. Journal of Bioresource Technology 2011; 76(2):107-12
- [3] Kasamsuk K. Assessment of school composters with different power source of mixing. Department of sanitary engineering, Faculty of Public Health, Mahidol university; 2013.
- [4] Liu N, Zhou J, Han L, Ma S, Sun X, Huang G. Role and multi-scale characterization of bamboo biochar during poultry manure aerobic composting. Journal of Bioresource Technology 2017; 241:190-199.
- Standards, Ministry of Agriculture and Cooperative, 2005.
- [5] Kavita Sharma, V.K. Garga. Comparative analysis of vermicompost quality produced from rice straw and paper waste employing earthworm *Eisenia fetida* (Sav.). Journal of Bioresource Technology 2018; 250:708-715.
- [6] Norliyana Sailila r. Azizi Abu Bakar. Noor Zalina Mahmood. Jaime A. Teixeira da Silva. Noorlidah Abdullahr. Adi Ainurzaman Jamaludin. Nutrient Elements of Different Agricultural Wastes from Vermicomposting Activity. Globalscience Books 2010
- [7] Singh J, Kalamdhad AS. Assessment of bioavailability and leachability of heavy metals during rotary drum composting of green waste (water hyacinth). Journal of Ecological Engineering 2013; 52:59–69.
- [8] FAO. Soil management: compost production and use in tropical and subtropical environment. FAO Soils Bulletin 56. Food and Agriculture Organization of the United Nations, Rome; 1987. p.177.
- [9] Benjawan L, Kaewsuan U, Kungskulniti N, Sihawong S, Chayaprasert W. Development of aerobic organic wastes composter prototypes with automatic mixing for household and community users. National Research Council of Thailand, Thailand; 2012.
- [10] Liu W, Huo R, Xu J, Liang S, Li J, Zhao T, et al. Effects of biochar on nitrogen transformation and heavy metal in sludge composting. Journal of Bioresource Technology 2017; 235:43-49.
- [11] Chan MT, Selvam A, Wong JWC. Reducing nitrogen loss and salinity during struvite food waste composting by zeolite amendment. Journal of Bioresource Technology 2016; 200:838-844.
- [12] Ponsa S, Pagans E, Sanchez A. Composting of dewatered wastewater sludge with various ratios of pruning waste used as a bulking agent and monitored by respirometer. Journal of Biosystems Engineering 2009; 102:433-443.
- [13] Tiquia SM, Tam NFY, Hodgkiss I J. Effect of composting on phytotoxicity of spent pig-manure sawdust Litter. Journal of Environmental Pollution 1996; 93:249-256.

## EVALUATION OF METHANE AND CARBON DIOXIDE EMISSIONS FROM LIVESTOCK WASTE, COMPOST, AND BIOGAS SLUDGE

Ambar Pertiwinigrum<sup>1</sup>, Margaretha Arnita Wuri<sup>2</sup>, Dina Setiyana<sup>3</sup>, Benito Heru Purwanto<sup>4</sup>, Andang Widi Harto<sup>5</sup> and Misri Gozan<sup>6</sup>

<sup>1,3</sup>Faculty of Animal Science, Universitas Gadjah Mada, Indonesia; <sup>1,2,5</sup>Center for Development of Sustainable Region (CDSR), <sup>2</sup>Center of Energy Studies, Universitas Gadjah Mada; <sup>4</sup>Faculty of Agriculture, Universitas Gadjah Mada, <sup>5</sup>Faculty of Engineering, Universitas Gadjah Mada, Indonesia; <sup>6</sup>Faculty of Engineering, Universitas Indonesia, Indonesia

### ABSTRACT

Livestock sector contributes to greenhouse gases (GHGs) emission especially methane and carbon dioxide gases that produced from digestive system and manure of ruminants. GHGs mitigation was conducted by cattle manure waste management through biogas and compost technologies. In this study we evaluated methane and carbon dioxide emissions from untreated and treated cattle manure in cattle farm group of Ngudi Mulyo, Yogyakarta. Test equipment that used in this study is 25-liters chamber to isolate gas emissions from naturally digested untreated and treated cattle manure for eight weeks. Gas samples were analyzed by gas chromatography (GC). The results shows that buried cattle manure produced the highest methane emission of 173100 ppm while compost from cattle manure produced of 2963.33 ppm. There is the decrease in methane emission of compost and sludge biogas from cattle manure of 98.18 and 98.10% respectively compared to fresh cattle manure. The highest carbon dioxide emission was produced by fresh cattle manure of 580215.371 ppm. Conversion of cattle manure to biogas sludge and compost could reduce carbon dioxide emission of 80.85 and 86.23% respectively compared to fresh cattle manure. We concluded that cattle manure waste management by biogas and compost technologies are important role in GHGs mitigation especially in livestock sector.

*Keywords: Cattle manure, Methane, Carbon dioxide, Biogas, Compost*

### INTRODUCTION

Global warming is due to the increase in greenhouse gases (GHGs) like carbon dioxide (CO<sub>2</sub>), methane (CH<sub>4</sub>), chloro-fluoro-carbon (CFC), hydro-fluoro-carbon (HFC), nitrous oxide (NO<sub>x</sub>), and sulfur hexafluoride (SF<sub>6</sub>). All of these gases, carbon dioxide and methane are the most abundant GHGs in the atmospheric. In addition, methane has 21 times higher global warming potential. One of sectors that generate methane and carbon dioxide emissions is livestock sector. In United Nations' books, Livestock Long Shadow in 2016 reported that livestock activities generate 18% from total GHGs emission [1]. Pete et al. [2] were also reported that agriculture sector included livestock sector contributes 10-12% of total anthropogenic emissions of GHGs. CH<sub>4</sub> contributes approximately 50% of total emissions. It means livestock have a substantial impact on climate change. Emissions of methane and carbon dioxide were produced from digestive system of ruminants and livestock waste. Based on Livestock and Animal Health Directorate [3], in Indonesia number of cattle population undergone the increase from year 2013 until 2017. A dramatic expansion livestock sector has been driven by population growth and rising income in Indonesia.

But unfortunately, manure from cattle livestock is just being stockpiled in these cages. And the consequence the accumulation of cattle manure enhances GHGs emission. The high level of emissions opens up large opportunities for climate change mitigation through livestock action.

Mitigation strategic to reduce GHGs emission that generated from livestock manure is utilizing cattle manure as substitute of fossil fuel energies through biogas technology. Cattle manure is the most typical forms of waste that used in as source of biogas production because its composition consists of carbohydrates, proteins, fats, cellulose, and hemicelluloses [4]. Cattle manure is suitable to be converted to biogas and compost because of its high organic content. Methane that produced from cattle manure by biogas technology through three pathways are hydrolysis, acidification and methanogenesis [5]. Hydrolysis pathway is when complex organic content in cattle manure to be converted to monomers or simple organic compounds while acidification is when organic monomers to be converted to organic acids. Last step, methanogenesis pathway, organic acids will be converted to methane by anaerobic bacteria. Livestock waste management by utilizing cattle manure to produced biogas and compost will reduce

methane emission [6]-[8]. Biogas is a clean, efficient, and renewable energy that substitutes coal energy [9].

Evaluation of methane and carbon dioxide is rare studied so in this study we evaluated methane and carbon dioxide emission from untreated cattle manure and treated cattle manure that taken from farmer group in Yogyakarta.

## METHODOLOGY

### Materials

Cattle manure that used in this study was taken from cattle farmer group of Ngudi Mulyo in Yogyakarta. In this study, we evaluated methane and carbon dioxide emissions from untreated and treated cattle manure. Sample of untreated cattle manure were taken from fresh cattle manure and 3 months buried cattle manure. Sample of treated cattle manure were taken from compost which processed for five weeks and biogas sludge which digested for one week.

The test equipment that used to calculate methane and carbon dioxide emissions is 25-liter chambers equipped with fan and thermometer. Each chamber is also equipped with a rubber cap above its surface to take gas sample. The design of chamber can be seen in Fig. 1.

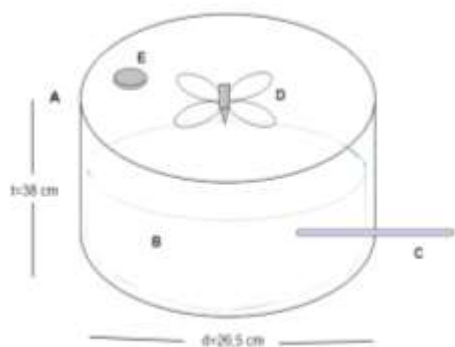


Fig. 1 The design of chamber (A. chamber with height of 38 cm and diameter of 26,5 cm, B. untreated/treated cattle manure, C. thermometer, D. fan, E. rubber cap).

### Methane and Carbon Dioxide Data Collection

Each of fresh cattle manure, buried cattle manure, compost, and biogas sludge was put in a 25-liter chamber. Each sample was naturally digested for 8 weeks. Gas that produced from this chamber was analyzed to calculate of methane and carbon dioxide emissions. Gas samplings were carried out in every week for 8 weeks. The time interval for each gas sampling per week are 10 minutes, 20 minutes, and 30 minutes respectively. In addition, the fan must be

turned out to make homogenized gas when gas sampling was taken by a syringe.

Methane and carbon dioxide concentration in gas samples were analyzed by gas chromatography (GC). Methane or carbon dioxide concentration was used to calculate methane or carbon dioxide flux with formula in Eq. (1) [5].

$$E \left( \frac{\text{mg}}{\text{m}^2 \cdot \text{minute}} \right) = \frac{dc}{dt} \times \frac{V_{ch}}{A_{ch}} \times \frac{mW}{mV} \times \frac{273,2}{273,2+T} \quad (1)$$

Equation (1) is formula to calculate methane or carbon dioxide emission per unit of area and time (E).  $\frac{dc}{dt}$  refers to difference concentration of methane or carbon dioxide per unit time (ppm).  $V_{ch}$  is volume of chamber ( $\text{m}^3$ ) while  $A_{ch}$  is area of top chamber ( $\text{m}^2$ ).  $mW$  is the molecular weight of gas,  $mV$  is the volume of gas molecule (22.4 liters), and  $T$  is average temperature in gas sampling ( $^{\circ}\text{C}$ ). We conducted T-test to analyzed methane and carbon dioxide emission in ppm.

## RESULTS AND DISCUSSION

### Methane and Carbon Dioxide Emissions

In this study, methane and carbon dioxide are GHGs emission that generate from untreated and treated cattle manure. Tubiello [10] reported that methane and carbon dioxide emission are produced from cattle's digestive system and manure. Cattle have a special digestive system which there is methanogenics bacteria in their rumen that convert organic matter to be methane and carbon dioxide gases and carried out together with their manure. To reduce methane and carbon dioxide emissions, cattle manure waste could be managed by biogas and compost technology [6]-[8]. We have evaluated and compared GHGs emission from untreated and treated cattle manure. In this study we reported that management of cattle manure by biogas and compost can reduce GHGs emission. Methane and carbon dioxide total emissions of cattle manure showed in Table 1 and Table 2 respectively.

Table 1 Total emissions of methane from cattle manure

| Sample        | CH <sub>4</sub> emission (ppm) |                            |
|---------------|--------------------------------|----------------------------|
|               | Total CH <sub>4</sub>          | Average of CH <sub>4</sub> |
| Fresh manure  | 162797.10                      | 32559.4±107 <sup>a</sup>   |
| Buried manure | 173101.00                      | 34620.2±981 <sup>a</sup>   |
| Sludge biogas | 3070.55                        | 614.1±981 <sup>a</sup>     |



|         |         |                          |
|---------|---------|--------------------------|
| Compost | 2933.89 | 586.78±43,0 <sup>b</sup> |
|---------|---------|--------------------------|

Note: a, b different superscripts at the same column indicates significant differences (P<0,05).

Table 2 Total emissions of carbon dioxide from cattle manure

| Sample        | CO <sub>2</sub> emission (ppm) |                            |
|---------------|--------------------------------|----------------------------|
|               | Total CH <sub>4</sub>          | Average of CH <sub>4</sub> |
| Fresh manure  | 580215.371                     | 116043.8±197 <sup>a</sup>  |
| Buried manure | 535458.552                     | 107091.6±844 <sup>a</sup>  |
| Sludge biogas | 3070.55                        | 614.11±51,0 <sup>b</sup>   |
| Compost       | 2933.89                        | 586.78±43,0 <sup>b</sup>   |

Note: a, b different superscripts at the same column indicates significant differences (P<0,05).

In this study, fresh and buried cattle manure are not significantly different in producing high methane emissions. When cattle manure was buried, it will make the condition increasingly anaerobic, a good condition to generate more methane gases [11]. But based on the data on Table 1, methane gas emissions from fresh cattle manure is higher significantly compared to cattle manure that converted to be sludge of biogas and compost. In compost production, the surface material was incorporated into the pile while material at the bottom so the chance of CH<sub>4</sub> production by anaerobic condition were minimal [12]. The turning of compost resulted in more uniform and smaller-sized aggregates makes some anaerobic microsites could have not developed inside in the pile [13]. Amanda [9] explained that biogas sludge is product of anaerobic degradation that has lower methane gases emission because it was utilized as resource of renewable energy. Methane is flammable gas that converted to energy for cooking or electricity. Utilization of cattle manure to biogas and compost was proven to be able to reduce methane emission of 98.11 and 98.18% respectively. The same phenomenon also occurred in carbon dioxide emission. Utilization cattle manure to biogas and compost reduced carbon dioxide emission significantly. The significant reducing of carbon dioxide in biogas because anaerobic condition makes carbon dioxide production can be minimized. Anaerobic condition would prefer to convert carbon content in cattle manure to methane gases compared to carbon dioxide. In this study, buried cattle manure reduced 7.71% of carbon dioxide while cattle manure treatment by biogas and

compost were able to reduce carbon dioxide of 80.85 and 86.23% respectively. Many cattle farmers in Indonesia are not capable to manage organic waste to biogas or compost. Some of them still maintain waste management by piling up cattle manure in specific place. So, biogas and compost technologies are recommended as alternative mitigation action in reducing GHGs emission.

### Methane or Carbon Dioxide Flux

Methane or carbon dioxide flux are the differences of methane or carbon dioxide concentration that produced in certain time and area units. In this study, we also investigated methane emissions from untreated and treated cattle manure. Figure 2 is methane flux from fresh and buried cattle manure, biogas sludge, and compost.

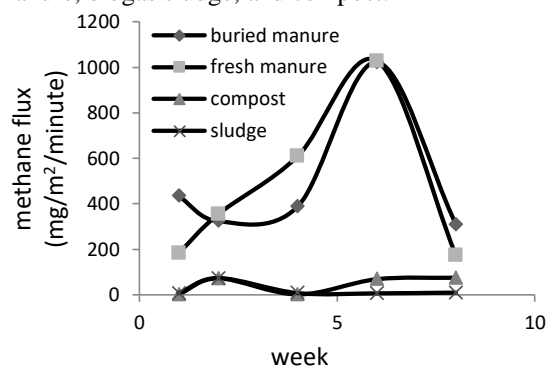


Fig. 2 Methane flux of fresh cattle manure (A), buried cattle manure (B), biogas sludge (C), and compost (D)

Methane flux of fresh cattle manure at the first week was 183.21 mg/m<sup>2</sup>/minute, at the second week was 354.97 mg/m<sup>2</sup>/minute, at the third week was 608.57 mg/m<sup>2</sup>/minute, at the sixth week was 1027 mg/m<sup>2</sup>/minute, and at the eighth week was 173.06 mg/m<sup>2</sup>/minute. There was the increase in methane flux by increasing time of observation. The same trend showed by buried cattle manure. Methane flux of buried cattle manure were 435.19, 324.96, 388.15, 1022.78, 310.53 mg/m<sup>2</sup>/minute at the first, second, fourth, sixth, and eighth week of observation. At first day to 30 days naturally methanogenic bacteria started to convert organic matter in fresh and buried cattle manure to methane gases [14]. In this study, at the last week of observation, production of methane gases was limited because the methane production was optimal until sixth week. At the sixth week, methanogenic bacteria have already multiplied to produce the highest methane gases. After that, methane production would decrease day by day. This phenomenon also was reported by Lise [14] and Puspitasari [15]. Methane flux of cattle manure increased from the first until sixth week and after that, at the eighth week it would decrease.

Lower methane flux was showed by treated

cattle manure, biogas sludge and compost. Methane flux of biogas sludge were 7.66, 72.23, 8.14, 7.01, and 10.29 mg/m<sup>2</sup>/minute at the first, second, fourth, sixth, and eighth week of observation. While methane flux of biogas sludge were 2.68, 73.09, 2.64, 69.32, and 75.80 mg/m<sup>2</sup>/minute at the first, second, fourth, sixth, and eighth week of observation. Methane flux on biogas sludge and compost were relatively stable in the eighth week. It means carbon conversion of cattle manure to biogas and compost have ended.

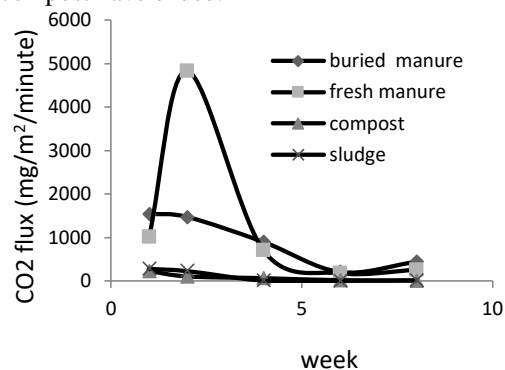


Fig. 3 Carbon dioxide flux of fresh cattle manure (A), buried cattle manure (B), biogas sludge (C), and compost (D)

Beside generating methane, carbon dioxide was also generated after one week observation. In this study carbon dioxide flux decreased with the increasing time. Figure 3 showed that carbon dioxide flux of fresh manure were 1007.36, 4824.73, 700.89, 178.01, and 254.69 at the first, second, fourth, sixth, and eighth week respectively. The highest carbon dioxide flux of fresh cattle manure was occurred at the second week because fresh cattle manure contained high organic matter that used by microorganism to produced carbon dioxide. The decreasing of carbon dioxide flux of biogas sludge and compost were not significant for eight weeks observation. Carbon dioxide flux of biogas sludge were 282.14, 230.56, 11.07, and 5.97 mg/m<sup>2</sup>/minute at the first, second, fourth, sixth, and eighth week respectively while carbon dioxide flux of compost were 226.11, 101.85, 60.15, 12.51, and 5.98 mg/m<sup>2</sup>/minute at the first, second, fourth, sixth, and eighth week respectively. These carbon dioxide flux were relatively stable and lower compared to fresh and buried cattle manure because cattle manure have decomposed and converted to energy and others material content. Decomposition and stabilization of cattle manure by biogas and compost technology would emit GHGs emission [6]-[8],[16].

## CONCLUSIONS

Based on this study, we concluded that conversion of cattle manure by biogas and compost technologies were able to decrease in methane

emission at 98.11 and 98.18% respectively while carbon dioxide emission at 80.85 and 86.23% respectively. Biogas and compost technologies were proven and recommended to be one of actions in GHGs mitigation especially in livestock sector.

## ACKNOWLEDGMENTS

The research was supported by Grant Program from Universitas Gadjah Mada, Indonesia through PTUPT program. We gratefully acknowledge the support from USAID through the SHERA program – Centre for Development of Sustainable Region (CDSR). In year 2017-2021 CDSR is led by Center for Energy Studies - UGM. Authors also would like to thank for students of Faculty of Animal Science that contributed in collecting the data.

## REFERENCES

- [1] Food and Agriculture Organization (FAO), *Livestock's Long Shadow*, FAO, 2011, <http://www.fao.org/3/a-a0701e.pdf>.
- [2] Pete S., Daniel M., Zucong C., Daniel G., Henry J., Pushpam K., Bruce M., Frank O., Charles R., Bob S., and Oleg S., 2007, *Agriculture, Climate Change 2007, Mitigation Contribution of Working Group III to the Fourth Assessment Report Intergovernmental Panel on Climate Change*, 2007, pp.498-540.
- [3] Livestock and Animal Health Directorate, Ministry of Agriculture, 2017, pp. 83.
- [4] Spyridon A., Vasileios A., and Gerrit J.W.E., *A Technological Overview of Biogas Production from Biowaste*, Engineering, Vol.3., 2017, pp.299-307.
- [5] Peter J.J., *Biogas – Green Energy*, Faculty of Agriculture Sciences, Aarhus University, 2009, pp.1-35.
- [6] H. Pathak, N. Jain, A. Bhatia, S. Mohanty, and Navindu G., *Global Warming Mitigation Potential of Biogas Plants in India*, Environ. Monit. Assess., Vol.157, Issue 1-4, 2009, pp.407-418.
- [7] Leila K., Ngudiantoro, M. Faizal, and P.K.S. Halim., *Evaluation of CO<sub>2</sub> and CH<sub>4</sub> Emission at Peat Swamp Forest Under Different Land Cover*, in Proc. 3<sup>rd</sup> International Conference on Chemical, Ecology and Environmental Science, 2013, pp. 185-189.
- [8] Amanda D.C. and Michael E.W., *Cow Power: The Energy and Emissions Benefits of Converting Manure to Biogas*, Environ. Res. Lett., Vol. 3, 2018, pp.1-8.
- [9] Liu Y., Kuang Y., Huang N., Wu Z., and Xu L., *Popularizing Household-Scale Biogas Digester for Rural Sustainable Energy Development and Greenhouse Gas Mitigation*, Renewable Energy,

- Vol.33, 2008, pp.2027-2035.
- [10] F.N. Tubiello, M. Salvatore, R.D. Condor Golec, A. Ferrara, S. Rossi, R. Biancalani, S. Federici, H. Jacobs, and A. Falmini, Agriculture, Forestry and Other Land Use Emissions by Sources and Removals by Sinks, FAO (Food and Agriculture Organization, 2014, pp.1-75.
- [11] Ari M.I., Effect of Maturity of Waste on Methane Gas Production in Putri Cempo Mojosongo Landfill, Postgraduate of Environment Science of Sebelas Maret University, 2007, pp.1-52.
- [12] G.Singh, O.G. Clark, and J. Leonard, Comparison of GHG emissions from A Compost Pile and Manure Stockpile, in Proc. The Canadian Society for Engineering in Agricultural, Food, and Biological Systems, Vol.05, 2005.
- [13] Y.Fukumoto, T. Osada, D. Hanajima, and K.Haga, Patterns and Quantities of Ammonia Nitrous Oxide and Methane Emissions during Swine Manure Composting with Forced Aeration-Effect of Compost Pile Scale, Biores. Technol., Vol.89, 2003, pp.109-114.
- [14] Lise A., Jan B., Jan D., and Raf D., Principles and Potential of The Anaerobic Digestion of Waste-Activated Sludge, Prog. In Energy and Comb. Sci., Vol.34, Issue 6, 2008, pp.755-781.
- [15] R. Puspitasari, Muladno, A. Atabany, and Salundik, Methane Gas Production from Lactating Dairy Cow Feces by Feeding with Elephant Grass and Rice Straw, Jurnal Ilmu Produksi dan Tek. Hasil Peternakan, Vol.3, No.1, 2015, pp.42-44.
- [16] Xiyang H., Chi C., Francis J.L., and Greg R.T., Greenhouse Gas Emissions during Cattle Manure Composting, J. Environ. Qual., Vol.30, 2011, pp.376-386.

## STUDY ON ELUTION REDUCTION OF HEXAVALENT CHROMIUM FROM RECYCLED BASE COURSE MATERIAL USING WASTE SYRUP

Keiichiro Shibata<sup>1</sup>, Hidenori Yoshida<sup>2</sup>, Hiroki Yokoyama<sup>3</sup>, Shinichiro Okazaki<sup>4</sup> and Matsumoto Naomichi<sup>5</sup>

<sup>1</sup> Graduate school of engineering, Kagawa university, <sup>2,3,4</sup> Faculty of engineering and design, Kagawa university, Japan; <sup>5</sup> Technical staff, Kagawa university, Japan

### ABSTRACT

In the civil engineering field, the utilization of recycled materials is promoted so as to reduce environmental burden. In particular, the utilization of concrete accessory product generated by the dismantlement of the concrete construct is an urgent issue in the light of both environment conservation and the shortage of repository site. Most concrete accessory products are recycled as the recycled base course material. However, it is at risk of the elution of the trace of hexavalent chromium from the recycled base course material. A major countermeasure to this problem is the reduction treatment to harmless trivalent chromium by reducing substances. There are many different types of the reducing substances. Among them, low cost is required for the reduction material because the recycled base course material is inexpensive. Therefore, in this study, waste sugar syrup is focused on with attention to two points such as reducibility and low cost. The elution test for the hexavalent chromium in cement paste is conducted, and the reducibility of the sugar contained in the waste syrup is verified. As a result of the reduction test using the waste syrup, it becomes clear that the eluted hexavalent chromium concentration decreases below the effluent standard.

*Keywords: Waste syrup, Hexavalent Chromium, Recycled base course material, Reducing property*

### INTRODUCTION

The utilization of recycled materials for the purpose of environmental loading reduction is promoted in the civil engineering field in Japan which shifts from the mass production, mass consumption and mass disposal society to the recycling society. Especially, the utilization of concrete by-products generated from the demolition of concrete structures is promoted from the viewpoint of environmental conservation and tightening of disposal sites, and most of them are recycled as in [1]. The transition of the recycling rate of concrete by-products is shown in Fig. 1 as in [2]. More than 99 % of the by-products are recycled, and most of them are recycled as roadbed material. The utilization of recycled roadbed material is expected to be promoted in future from the viewpoint of reduction of environmental load by recycling and low material cost. However, trace of hexavalent chromium ( $\text{Cr}^{6+}$ ) contained in the cement may be detected from the recycled roadbed material as in [3], [4]. It is recommended to confirm the degree of the elution in the case of using recycled roadbed material. In addition,  $\text{Cr}^{6+}$  may elute from not only recycled roadbed materials but also cementitious solidification materials used for cement-improved soil, when the soil in which the significant inhibition of hydrate formation is occurred such as a volcanic cohesive soil is improved as in [5], [6]. Hexavalent chromium has very strong toxicity, and is specified as

a harmful substance in the environmental standard by the Ministry of Environment. On the other hand, it is easily reduced to harmless trivalent chromium. Therefore, hexavalent chromium is often detoxified by reduction treatment using a reducing substance. Though the kinds of reducing substances are various, the low cost is also required for reducing substances due to the cheapness of the recycled roadbed material. Thus, in this study, the discarded sugar syrup is focused on with considering two points, i.e., reducing characteristics and low cost.

There is a past research which verified the reduction of  $\text{Cr}^{6+}$  elution from regenerated roadbed material by reducing sugar as in [7]. Concretely speaking, the fruit juice and six kinds of sugar solution including reducing sugar are sprayed or immersed in crushed concrete material. The reduction sugar and the fruit juice containing it are confirmed to have the effect of reducing the elution for  $\text{Cr}^{6+}$ . Among them, fructose and glucose have high reducing ability for  $\text{Cr}^{6+}$ . In this study, two test methods are devised to verify the reduction of  $\text{Cr}^{6+}$  elution from the roadbed material is examined with a view to verification of the reduction of  $\text{Cr}^{6+}$  elution from cement-improved soil in near future. One is a method to immerse crushed concrete in sugar solution as in the past research, and the other is a method to mix sugar solution as admixture in mixing concrete. An availability of the waste syrup on the elution of the  $\text{Cr}^{6+}$  is examined by each different approach.

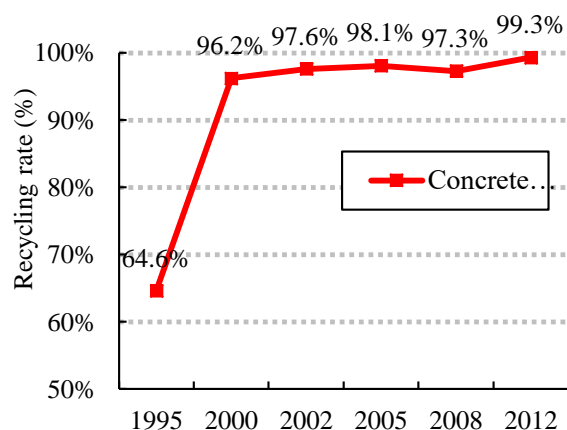


Fig. 1 Transition of recycling rate of concrete by-products

### ELUTION MECHANISM OF HEXAVALENT CHROMIUM

In nature, chromium exists in a trivalent state as well as in cement raw materials. Trivalent chromium ( $\text{Cr}^{3+}$ ) in the raw material is partly changed to  $\text{Cr}^{6+}$  in the cement manufacturing process. Previous studies have shown that  $\text{Cr}^{6+}$  is not only adherent to cement minerals but also present as water-soluble  $\text{Cr}^{6+}$  as in [8]. Water soluble  $\text{Cr}^{6+}$  in the cement is dissolved in the liquid phase during the elution process of the hydration reaction and is fixed to the precipitated hydrate. Therefore, the concentration of  $\text{Cr}^{6+}$  in the liquid phase decreases as the hydrate is formed.

As has described above, the cement contains  $\text{Cr}^{6+}$ , and  $\text{Cr}^{6+}$  is eluted with the hydration reaction. On the other hand, when concrete is crushed and used as a recycled roadbed material,  $\text{Cr}^{6+}$  may be eluted from the recycled roadbed material due to its use under the environment in contact with rain, groundwater, etc., and due to the influence of the particle size of the material. Alternatively, advanced processing such as crushing, grinding and classification is not conducted because there is no regulation in the processing

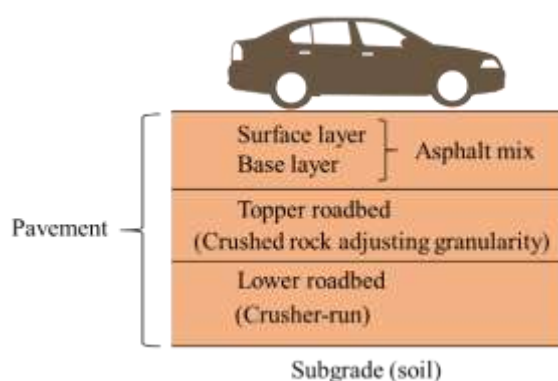


Fig. 2 Materials used for roadbed material

method of recycled roadbed material. According to the past research, the elution amount of  $\text{Cr}^{6+}$  increases as the grain size decreases. Therefore, it is considered that the possibility of  $\text{Cr}^{6+}$  elution increases by the mixture of crushed concrete with extremely small grain size. Furthermore, the using site of recycled roadbed material is mainly the topper roadbed or the lower roadbed (see Fig. 2), and the runoff of  $\text{Cr}^{6+}$  to soil may occur because the recycled roadbed material is in contact with soil. Thus, the elution countermeasure of  $\text{Cr}^{6+}$  before the usage as recycled roadbed material is very important from a safety point of view.

### WASTE SYRUP AND REDUCING ABILITY OF SUGAR

Waste syrup is selected as a reducing agent for  $\text{Cr}^{6+}$  in view of low material costs, reducing ability and waste recycling. The syrup contains several kinds of sugars such as allose, glucose and fructose, and the expired syrup is used in the test. Sugars are divided into reducing and non-reducing sugars. The difference between reducing and non-reducing sugars is the existence or non-existence of reducing group, and it is known that the sugar with aldehyde group in the structure shows reducing property as in [9]. For example, glucose has the structure shown in Fig. 3, in which the aldehyde moiety shows reducing property. On the other hand, the sucrose which is a disaccharide does not show reducing property because the glucose and fructose which belong to the reducing group link together. In the test, the glucose, allose and sucrose are prepared as the reducing agents in addition to the waste syrup in order to confirm the usefulness of the waste syrup and to clarify each reducibility.

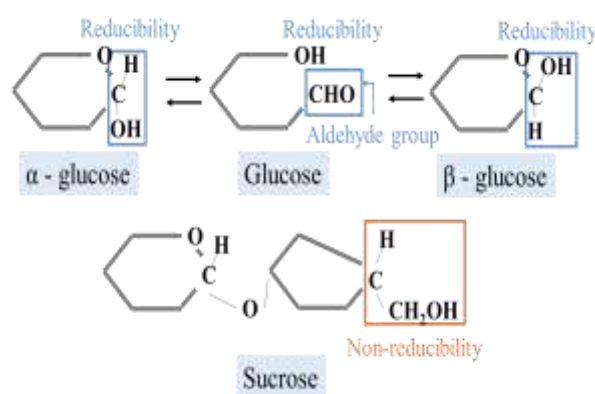


Fig. 3 Examples of reducing sugars and non-reducing sugars

### TEST METHOD

As has already mentioned above, two kinds of tests are conducted to evaluate the reducibility of sugars to  $\text{Cr}^{6+}$ . One is a method to mix sugar in

cement before solidification, and the other is a method to immerse sample after solidification and grinding in sugar aqueous solution. The former is called the mixing method and the latter is called the reduction test by the immersion method. Each test is conducted by reference to the elution test which is noticed by the Ministry of Environment Notification No. 46 as in [10], and three times of each test are conducted under the same conditions to ensure reproducibility.

### Mixture method

The purpose of this method is to reduce the elution amount of  $\text{Cr}^{6+}$  by mixing the sugar which has the reducibility as an admixture. Cement paste of 70 % water-cement ratio is produced, and the mold for cement is removed after 7 days and sealed curing is carried out for 21 days. Samples are prepared by mixing  $\text{Cr}^{6+}$  standard solution and waste syrup. There are nine patterns of specimens, and the test conditions are shown in Table 1. After curing, the specimen is finely crushed with a hammer, and the sample having grain size of less than 2 mm is collected by sieving. Thereafter, the concentration of  $\text{Cr}^{6+}$  in the solution obtained by the elution test is measured. The concentration of  $\text{Cr}^{6+}$  is determined by diphenylcarbazide adsorptiometry coupled with collecting on membrane filter. The mixture method is shown in Fig. 4. The operation added to the mixture

Table 1 Test condition (Mixture method)

|                           |                                 |
|---------------------------|---------------------------------|
| Water-cement ratio        | 70 %                            |
| Formwork size             | $\phi 5 * 10 \text{ cm}$        |
| Form removal              | After 7days                     |
| Sealed curing             | 21 days                         |
| Adding $\text{Cr}^{6+}$   | 0, 1, 2 ppm                     |
| Waste syrup concentration | 0.000, 0.125, 0.250 % (/cement) |

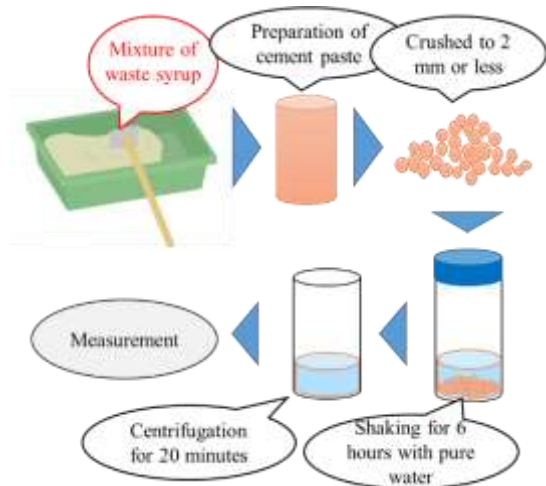


Fig. 4 Mixture method

method is shown in the figure. The  $\text{Cr}^{6+}$  is reduced by mixing in advance before cement is set. The advantage of this method is that there is not necessary to treat for sample after construction.

### Immersion method

The purpose of the immersion test is to reduce  $\text{Cr}^{6+}$  by immersing the crushed sample in a sugar solution. Though the test procedure is almost the same as that described in 4-1, the sugar is not mixed. Four kinds (waste syrup, glucose, allose, and sucrose) of sugar aqueous solution are respectively adjusted at three kinds of concentrations, and the crushed sample is immersed in the sugar solution for 24 hours. There are 12 patterns of specimens. Test conditions in the immersion method are shown in Table 2. Also, the mixture method is shown in Fig. 5. The operation added to the immersion method is shown in the figure. Most of  $\text{Cr}^{6+}$  remains in the concrete by hydration of cement. However, immersion in sugar solution may reduce  $\text{Cr}^{6+}$  which is slightly eluted from the concrete.

Table 2 Test condition (Immersion method)

|                              |                          |
|------------------------------|--------------------------|
| Water-cement ratio           | 70 %                     |
| Formwork size                | $\phi 5 * 10 \text{ cm}$ |
| Form removal                 | After 7days              |
| Sealed curing                | 21 days                  |
| Adding $\text{Cr}^{6+}$      | 0, 1, 2 ppm              |
| Sugar solution concentration | 0.1, 0.5, 1.0 % (/water) |

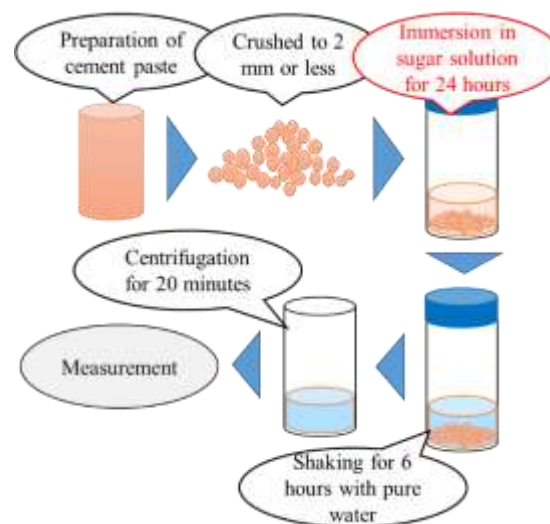


Fig. 5 Immersion method

### TEST RESULTS

The test results for each method are shown in graphs. Each test is conducted three times to ensure a reproducibility, and the average value for three batches is listed in the graphs.



### Test results of mixing method

Fig. 6 shows the results of the elution test on a specimen mixed with waste syrup as a mixture agent.

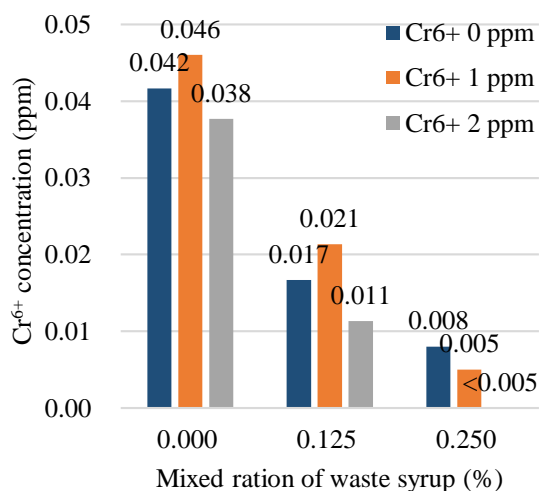


Fig. 6 Test results of elution test by mixture method

The vertical axis of the graph represents the concentration of detected Cr<sup>6+</sup>, and the horizontal axis represents the concentration of mixed waste syrup. Focusing on the concentration of Cr<sup>6+</sup> in the sample without waste syrup, it is revealed that the added concentration of Cr<sup>6+</sup> does not affect the concentration of Cr<sup>6+</sup> eluted from the sample. According to the past research, an amount of water soluble Cr<sup>6+</sup> in cement is about 5 ~ 10 mg/kg, which means that 0.3 -0.6 ppm is contained according to the present test conditions. This suggests that most of the Cr<sup>6+</sup> is immobilized in the cement setting process, and that the elution amount of water-soluble Cr<sup>6+</sup> from the cement does not change. The detected concentration of Cr<sup>6+</sup> decreases in the specimen to which waste syrup is added. Furthermore, the detected concentration of Cr<sup>6+</sup> decreases as the concentration of waste syrup increases. From these results, it is clarified that mixing waste syrup is effective for the reduction of elution amount of Cr<sup>6+</sup>. When waste syrup was mixed by 0.25%, the concentration of Cr<sup>6+</sup> is lower than the environmental quality standards for soil as well as the effluent standard. The waste syrup is a highly effective admixture, because it has sufficient reducibility in a small amount and leads to the recycling of waste. In order to establish the waste syrup as an admixture, it is necessary to examine not only reducibility but also workability factors such as compressive strength and slump value. Alternatively, only the specimen using waste syrup is prepared and the elution test is performed in the mixing method. Therefore, in the future, the test in which other sugar solutions are mixed is conducted in order to investigate the effects of each type of sugar. In

addition, it is necessary to examine the usage as a cement-based solidifying agent since the reduction effect by mixing is confirmed. The detected concentration of Cr<sup>6+</sup> and kinds of immersed sugar solution are shown in the vertical and horizontal axes, respectively. The graph also includes the elution results from the blank test, i.e., the elution results from the test for samples which is not immersed in the sugar solution, as the reference value.

### Test results of immersion method

Fig. 7, 8 and 9 show the results of the elution test of the test specimen which is immersed in each sugar solution. The elution amount of Cr<sup>6+</sup> is summarized in the graph when three kinds of Cr<sup>6+</sup> are added in each RSS addition amount. As in the test of the mixing method, there is no effect of the concentration of Cr<sup>6+</sup> on the elution amount in the immersion test. The Cr<sup>6+</sup> is not reduced regardless of the concentration of sucrose since sucrose is a non-reducing sugar. On the other hand, the concentration of Cr<sup>6+</sup> decreases in all cases and the concentration of Cr<sup>6+</sup> decreased as the concentration of sugar solution increased when the waste syrup, allose and glucose with reducing groups are used. Additionally, the concentration of Cr<sup>6+</sup> decreases as the concentration of sugar solution increases. When the sugar concentration exceeded 0.5%, the concentration of Cr<sup>6+</sup> falls below the detection limit of 0.005 ppm. Among them, the glucose solution has the highest reducing ability, followed by glucose, waste syrup, allose and sucrose in order of decreasing ability. Since most of the components of the waste syrup are glucose, it is considered that the waste syrup has higher reducing ability than the allose solution. In both the mixing method and the immersion method, the elution amount of Cr<sup>6+</sup> is decreased, and it is

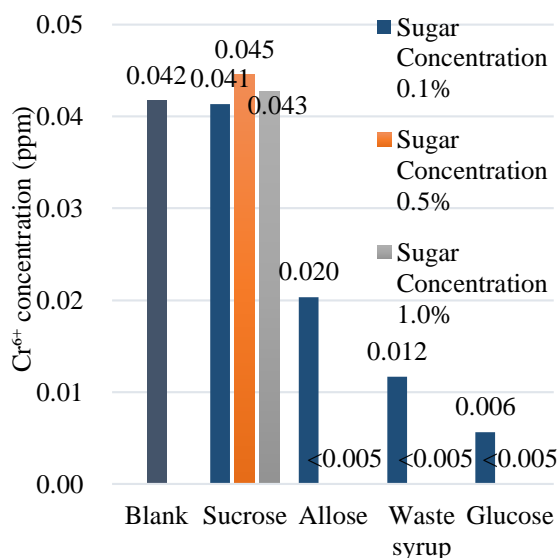


Fig. 7 Test results of elution test by immersion method (adding Cr<sup>6+</sup> concentration of 0 ppm)

clarified that the waste syrup has an enough ability as the elution reducing material for  $\text{Cr}^{6+}$  in the recycled base material.

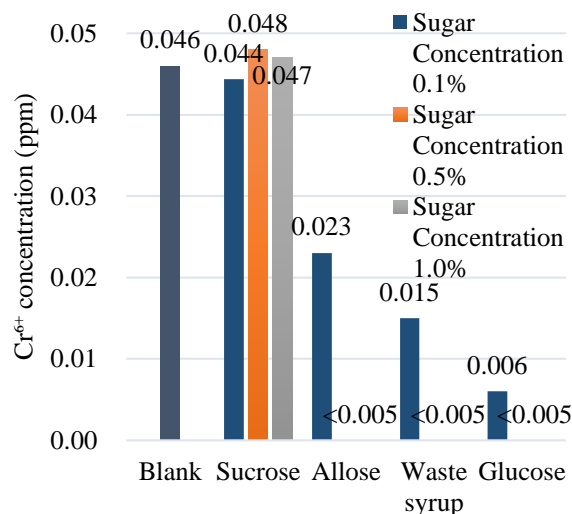


Fig. 8 Test results of elution test by immersion method (adding  $\text{Cr}^{6+}$  concentration of 1 ppm)

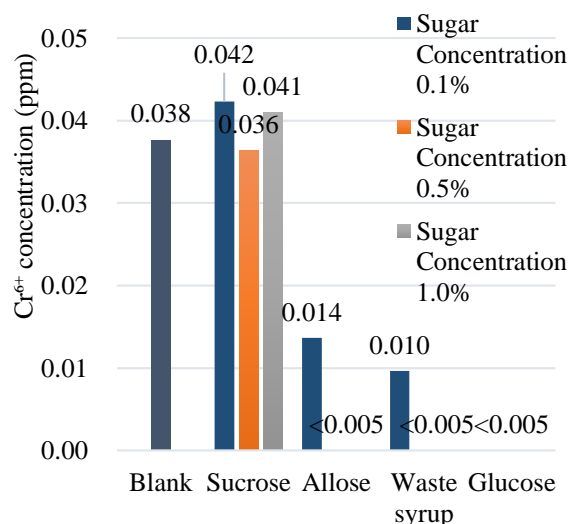


Fig. 9 Test results of elution test by immersion method (adding  $\text{Cr}^{6+}$  concentration of 2 ppm)

## CONCLUSIONS

- The elution amount of  $\text{Cr}^{6+}$  eluted from the cement paste is roughly determined according to the amount of cement, and the elution amount of  $\text{Cr}^{6+}$  does not change even if  $\text{Cr}^{6+}$  is added.
- In the elution test by the mixing method using waste syrup, the detected concentration of  $\text{Cr}^{6+}$  decreased with the increase of the mixed concentration. The reducibility of the waste syrup is confirmed, and the possibility of the application to cement-based fixation agent is suggested.
- In the elution test by immersion method in the sugar

solution, some sugar solutions show reducing property to  $\text{Cr}^{6+}$ . Sucrose solution does not show reducing property, while the waste syrup, allose and glucose solution show high reducing property.

- The relative merits in reducibility are confirmed in the Reducing sugars, and it is necessary to exam its cause.
- The reducing effect is higher test using immersion method than mixing method when the two methods are compared with the specimens using waste syrup. In addition, it is revealed that the waste syrup is the recycled material that has a reducing effect on the elution of  $\text{Cr}^{6+}$  from recycled roadbed material by two methods.

## ACKNOWLEDGMENTS

This work was supported by Japan Society for the Promotion of Science, the Grants-in-Aid for Scientific Research (C) (Grant number: 18J12343). Additionally, this work was Program for Building Regional Innovation Ecosystems (MEXT).

## REFERENCES

- [1] Mikami T., Takahama T., Niihata T., Yamamori K., Yamashita T., Kawamoto Y., Imaoka T., Study on promotion of use of recycled aggregate, Proceedings of the Annual Conference of Japan Society of Material Cycles and Waste Management, No. 28, 2017, pp189-190.
- [2] Ministry of Land, Infrastructure, Transport and Tourism, 2012 construction by-product fact-finding result reference materials, 2012, pp. 1- 15.
- [3] Kuroda Y., Koshiishi N., INFLUENCE OF VARIOUS FACTORS ON LEACHING OF HEXAVALENT CHROMIUM FROM CEMENT CONCRETE, Journal of Structural and Construction Engineering, Vol. 75, Issue 650, 2010, pp. 715-722.
- [4] Ugajin T., The Effects of the Trace Elements in Cement on the Environment, Concrete Journal, Vol. 39, Issue, 2001, pp. 14-19.
- [5] Tsuneoka N., Mori H., Sakamoto H., Itonaga S., Moriya M., INFLUENCE OF ADSORPTION AND REDUCTION BY SURROUNDING SOIL ON HEXAVALENT CHROMIUM LEACHED FROM CEMENT TREATED SOIL, Proceedings of the Japan Society of Civil Engineering, Vol. 2004, Issue 764, 2004, pp. 133-145.
- [6] Yoshida M., Kitamura T., Katsushima H., Kondo K., ELUTION CONTROL OF Cr (VI) FROM VOLCANIC COARSE-GRAINED SOIL IMPROVED WITH CEMENT, Cement Science and Concrete Technology, Vol. 71, Issue 1, 2017, pp. 661-666.

- [7] Niida R., Nitta H., Nishizaki I., METHOD FOR REDUCING HEXAVALENT CHROMIUM ELUTED FROM RECYCLED BASE COURSE MATERIAL USING REDUCING SUGAR, Journal of Japan Society of Civil Engineers, Ser. E1 (Pavement Engineering), Vol. 71, Issue 3, 2015, pp. I\_211-I\_216.
- [8] Sakai E., Hisada M., Sugiyama T., Leaching of Trace Elements and Hydrated Products from Cement and Concrete, Concrete Journal, Vol. 41, Issue. 12, 2003, pp. 18-22.
- [9] Ono T., Experiment to confirm the nature of saccharides, CHEMISTRY & EDUCATION, Vol. 57, Issue 2, 2009, pp. 92-93.
- [10] Ministry of the Environment, Ministry of the Environment notification No. 46, 1991.

## GEOINFORMATICS OF TUBERCULOSIS (TB) DISEASE IN JAKARTA CITY YEAR 2017

\*Titin Siswantining<sup>1</sup>, NPC Purwandani<sup>2</sup>, MHD Susilowati<sup>2</sup> and Adi Wibowo<sup>2</sup>

<sup>1</sup>Department of Mathematics, Faculty of Mathematics and Natural Sciences, Universitas Indonesia, 16424, Depok, Jawa Barat, Indonesia;

<sup>2</sup>Department of Geography, Faculty of Mathematics and Natural Sciences, Universitas Indonesia, Indonesia

### ABSTRACT

Tuberculosis (TB) disease are still become the leading cause of morbidity and mortality in Indonesia. The TB had a relationship between human and their environment, especially in the urban area. The urban area had the highest population and density, that is the way the accurate information about the urban environment of the TB area is critical. The research objective to representing characteristic spatial of TB patients lived in Jakarta year 2017. The research used a method using visual interpretation from superimposed spatial data. Spatial data collection from google earth data, household area (RW boundary), and TB patient addressed from the hospital. The total TB patients in Jakarta City year 2017 was 114 patient from a hospital and distributed in 108 household area (RW boundary). The result of geoinformatics of the urban environment, first building population, building density, vegetated covered, and distance from the main road. The TB area characteristic had two classified high and low, based on total patient TB disease in a household area (RW boundary). The research concluded of the geoinformatics of TB disease in Jakarta City year 2017 with highly classified is high building population and building density, lowest vegetated covered (high temperature) and near the main road.

*Keywords: Geoinformatics, TB disease, Characteristic spatial*

### INTRODUCTION

Tuberculosis (TB) is one of the infectious diseases caused by *Mycobacterium tuberculosis* with the name of acid-resistant bacteria (ARB) [1]. In the year 2017 there have been 6.4 million official new TB cases reported to the WHO, this number increased since 2013 with a total of 5.8 million new cases that occurred in the year 2017, then the country with the top number of cases India (26%), Indonesia (11%), and Nigeria (9%) [2]. Based on the results of primary health research in 2013, DKI Jakarta is one of the provinces that has the highest TB prevalence rate in Indonesia because it occupies the second position of the equivalent to Papua is 0.6 [3]. The case of a positive ARB pulmonary tuberculosis or bacteria that is red and rod-shaped in Indonesia in 2016 according to the most age group found in the age group 45-54 years, and the record that the sufferer occurs at a productive age Compared to non-productive age. In the year 2016, DKI Jakarta recorded the most significant Case Notification Rate number of 241 cases, and the success rate of treatment is only 73% [4].

The tools for dealing with geospatial information, however, have primarily been developed within the context of an emerging discipline, named Geoinformatics, Geomatics, or Geographic

(sometimes Geospatial) Information Sciences [5]. The term Geomatics is derived from the French word *Geomatique*, coined by the French photogrammetrist Dubuisson and widely used in North America [6]. Geoinformatics seems to be popular in Europe, whereas Geographic Information Science usually indicates a Geography background [7], [1]. In the following, the term Geoinformatics will use because it emphasizes a formal scientific approach to handle geoinformation, which Geomatics does not imply. TB disease are still become the leading cause of morbidity and mortality in Indonesia.

A spatial approach can examine the geosphere phenomenon of the complexity of the symptoms with the concept of a regional paradigm [8]. The territory is a characteristic similarity in a part of the Earth's surface [9]. The spatial approach in each region can cope with the health problems that considered as the top priority, with the resources being able to be used more effectively [10]. The TB had a relationship between human and their environment, especially in the urban area with the highest population and density.

The TB had a relationship between human and their environment, especially in the urban area. A person with a history of taking a breaking drug at risk of 5.36 times becomes resistant to TB compared with a history of taking his drug that does not break [11].

The urban area had the highest population and density, that is the way the accurate information about the urban environment of the TB area is critical. The research objective to representing characteristic spatial of TB patients lived in Jakarta year 2017.

## METHODS

The research conduct in Jakarta Province in July until November 2018. The unit of analysis used is the point of the sufferer of TB and the household area administrative boundary (RW boundary) whose recorded as tuberculosis disease in the year 2017. The local characteristic variables in the TB-sufferer or RW in the study include building density, air temperature, and distance from the river, and the quality of the settlement. Data on residential environmental conditions from Google Earth and surveys. The data used includes TB disease sufferers of 114 patients with tuberculosis disease from the National Center General Hospital of Dr. Cipto Mangunkusumo in 2017.

The research used visual interpretation from spatial data collection from google earth data, RW boundary, and TB patient addressed from the hospital. The total TB patients in Jakarta City year 2017 was 114 patient from a hospital and distributed in 108 household area (RW boundary).

## RESULTS AND DISCUSSIONS

### Distribution of Patient with TB Disease

Patients with TB disease in Jakarta in 2017 amounted to 114 sufferers (see fig. 1) which scattered in 35 sub-districts, 80 villages, and 108 pillars. Location of the people of TB is seen by spatial many occur in central Jakarta, South Jakarta, and East Jakarta. Based on the data of TB patients, there are three characteristics of sufferers, including gender, age, and nutritional status. Patients with male tuberculosis disease total 79 sufferers or 69%, and female-sex sufferers total 35 or 31%. Based on age, patients with tuberculosis disease who are productive (15-64 years) total 87 sufferers or 77%, and non-productive age (< 15 and > 64 years) amounted to 27 sufferers or 23%.

Table 1 Number of TB Suffers based on Gender

| Gender                  | Number | Percentage (%) |
|-------------------------|--------|----------------|
| Male                    | 79     | 69             |
| Female                  | 35     | 31             |
| Total                   | 114    | 100            |
| Source: data processing |        |                |

Based on nutritional status, patients with tuberculosis disease who have a lean nutritional status (BMI value < 17-18.4) amounted to 36 sufferers or 32%, normal nutritional status (BMI value 18.5-25) amounted to 63 or 55%, and fat nutritional status (BMI value 25-27) amounted to 15 or 13%.

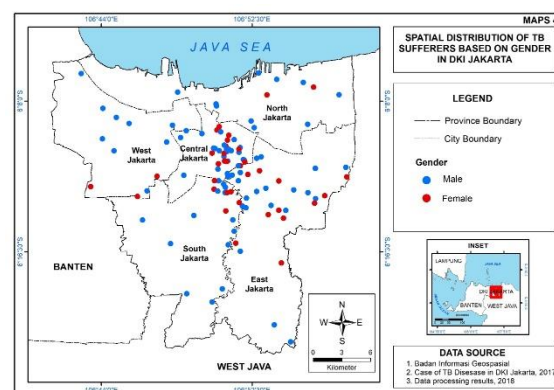


Fig. 1 Spatial Distribution of TB Sufferers in DKI Jakarta year 2017.

Areas with TB disease in DKI Jakarta year 2017 amounted to 108, which includes 114 people with TB (see fig. 2). The lowest area of TB sufferers or 1 TB sufferer per RW as much as 102 regions are in an RW that spreads from the edge to the city center. While in the height of TB sufferers or 2 TB sufferers per RW as many as six regions located in the central to the east side of the city, which precisely located in the village of Malacca Sari, Paseban, Rawasari, Senen, and Tanah Tinggi.

### Spatial Distribution of Building Density

Building Density obtained from the Intersect results of Open Street Map building with the region of TB sufferers, then classified into three namely low density (< 60 units/ha), Moderate (60-100 units/ha), and high (> 100 units/ha). Based on the building density map (see fig. 3), the characteristics of areas with a high density of buildings located in the central and eastern regions. In the downtown area, which TB sufferers have a group of the pattern, as for the east part has a pattern spread from east to southeast.

The density of building Data with TB region done cross-tabulation which produces six classifications, so it is symbolized with six different colors to see the difference of area characteristic of sufferer based on building density (see fig. 4). Based on the explanation, it shown that TB sufferers not only occur at the high density of buildings can even happen at the density of low and medium buildings.



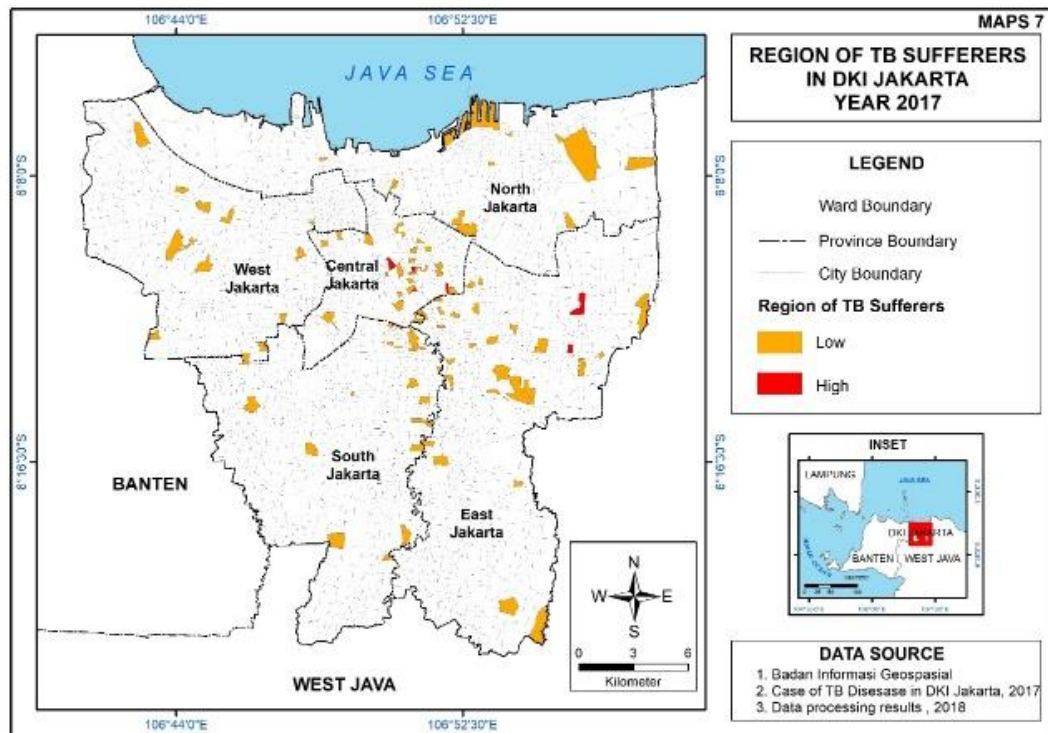


Fig. 2 Spatial Distribution of TB Sufferers Regions in DKI Jakarta year 2017.

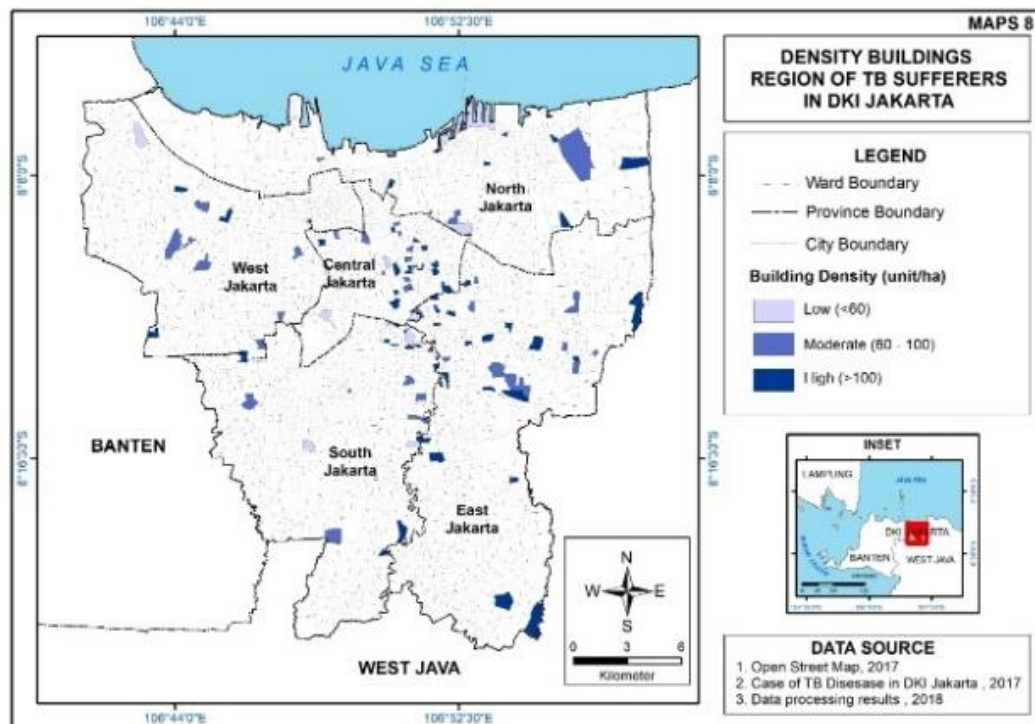


Fig. 3 The Building Density of TB Sufferer in DKI Jakarta.



The density of building Data with TB region done cross-tabulation which produces six classifications, so it is symbolized with six different colors to see the difference of area characteristic of sufferer based on building density (see fig. 4). Based on the explanation, it shown that TB sufferers not only occur at the high density of buildings can even happen at the density of low and medium buildings.

### Environment Quality

The first quality of settlement in parameters is the layout of the building in an RW. The Data shows that people with TB has the orientation of different buildings that are good, moderate and bad so that the condition of the building layout can be infected by TB disease (see fig. 5).

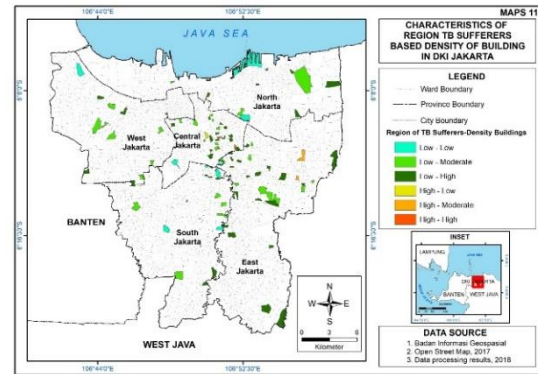


Fig. 4 The Characteristics of TB Sufferers Region Based on Building Density in DKI Jakarta.



Fig. 5 The Building Density.

The people with TB disease have the condition of the building with cold, no air circulation, no sun entry to the building so that terms will be infected by TB disease (see fig. 6).



Fig. 6 The Building Layout of TB Patient.

Second is the protective tree; it has seen that the low or high of TB sufferers have a protective tree condition or the existence of harmful trees or < 25%

(see fig. 7). There was tree cover in the RW, which is assumed to increase the temperature of the air and cause the air cycle is not optimal in the absorption of pollutants. When the air temperature rises, the condition inversely proportional to the humidity of the air decreases, making it easier for germs to breed.

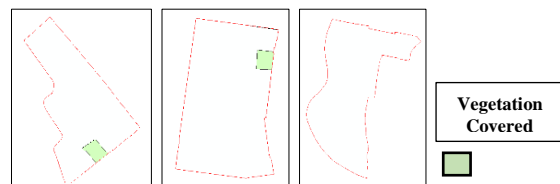


Fig. 7 The Tree Covered in House Hold (RW).

The third is the width of the road; it sees that TB can occur in a residential area that has a category of good or easy to go through two cars, medium or only traversed one car, or harmful or without a vehicle can pass. However, when viewed based on a high area of TB sufferers, tends to occur in the regions that have a

narrow or steep road width traversed with four-wheeled vehicles and they have a moderate to high density (see fig. 8).



Fig. 8 The Road Width.

Fourth, based on the location of the settlement against the source of pollution and activities, poor settlement environment condition following the high area of TB sufferers, it is explained that the closer to the cause of pollution, in this case, the main road will facilitate the occurrence of transmission in TB disease. The result appropriate with previous research by Fitriana [12], which explains that the activity center or source of pollution is a place to interact to facilitate the transmission of TB (see fig. 9).

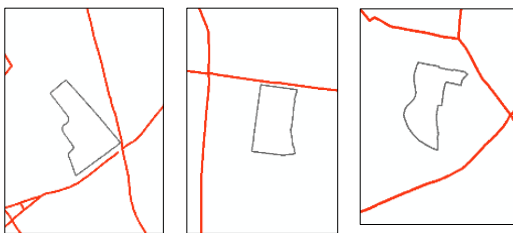


Fig. 9 The Road Density.

Lastly, the health service parameters appear that from the six regions can still be affordable to health facilities because it is in the classification well to moderate. DKI Jakarta is certainly a metropolitan city that has health facilities almost spread evenly so that in TB, people who are close to health services can also occur TB sufferers. Because of not only the treatment factors available but also needed routine in medicine for the sufferer.

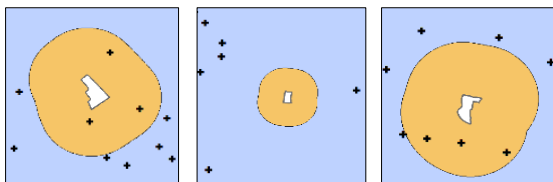


Fig. 10 The Health Facilities Around House Hold.

Based on the explanation, spatial uniqueness that occurred in 6 TB sufferers turned out to have a common characteristic of the region that is irregularities in the layout of buildings, road width tends to narrow, the existence of protective trees and close to the main road as a place of activity or

activities (see fig 10).

## CONCLUSIONS

The research concluded that the geoinformatics of TB disease in Jakarta City year 2017 with highly classified is high building population and building density, lowest vegetated covered, and near the main road.

## ACKNOWLEDGMENTS

The research supported by the University of Indonesia.

## REFERENCES

- [1] Data Center and Information Ministry of Health Republik Indonesia, Tuberculosis. Kementerian Kesehatan RI, 2018, Jakarta Selatan
- [2] World Health Organization, Global Tuberculosis Report, 2018
- [3] The Research Agency and Health Development, Indonesian Ministry of Health, Laporan Riset Kesehatan Dasar (RISKESDAS), 2013, Jakarta
- [4] Ministry of Health Rep. Indonesia, Data and Information Indonesia Health Profile 2016, Pusat Data dan Informasi Kementerian Kesehatan RI, 2017
- [5] Chandarasekaran S.K., and Arivarignan G., Disease mapping using mixture distribution, Indian Journal of Medical Research, Vol. 123, Issue 6, 2006, pp. 788-798.
- [6] Ehler M., Geoinformatics and digital earth initiatives: a German perspective, International Journal of Digital Earth, Vol. 1, Issue 1, 2008, pp. 17-30.
- [7] Goodchild, M. F., Geographical Information Science. International Journal of Geographical Information Systems, Volume 6, Issue 1, 1992, pp. 31-45.
- [8] Yunus, H. S., Metodologi Penelitian Wilayah Kontemporer, 2010, Yogyakarta: Pustaka Pelajar
- [9] Sumaatmadja, N, Studi Geografi: Suatu Pendekatan dan Analisa Keruangan, 1981, Bandung: Alumni
- [10] Fauzan A., Achmadi U. F., and Susanna D., Analisis Spasial Penyakit Tuberkulosis Paru BTA Positif di Kota Sukabumi Tahun 2010-2012, Universitas Indonesia, 2014.
- [11] T Siswantining, A Malyinda, T Kamilia and A Bustamam, Risk factors for resistance tuberculosis, Citation: AIP Conference Proceedings 2023, 020224 (2018); doi: 10.1063/1.5064221.
- [12] Fitriana N., Saraswati E., and Widayani P., Apikasi Penginderaan Jauh dan Sistem Informasi Geografi untuk Pemetaan Tingkat Kerentanan Penyakit Tuberkulosis (TB) di Kecamatan Imogiri, Kab, Bantul, Yogyakarta, Jurnal Bumi Indonesia, Vol. 3, Issue 2, 2014, pp. 110-120.

## SPATIAL AND TEMPORAL PATTERN OF SOIL CONSERVATION IN MOUNTAIN ECOSYSTEM: CASE STUDY OF PATUHA MOUNTAIN, WEST JAVA - INDONESIA

Satia Nisa Firdhauzi<sup>1</sup>, Astrid Damayanti<sup>1</sup>, Jarot Mulyo Semedi<sup>1</sup>, Muhammad Dimyati<sup>1</sup>

<sup>1</sup>Department of Geography - Universitas Indonesia, Indonesia

### ABSTRACT

The Patuha Mountain area located 50 km south of Bandung City and the upstream of the longest river in West Java, The Citarum River. 12% of Patuha Mountain area categorized as the steep slope area ( $>25^\circ$ ). Agriculture and plantations on steep slope locations require appropriate soil conservation methods to reduce erosion rates and avoid the threat of landslides. Land use in The Patuha Mountain area dominated by tea plantations, paddy fields and various agriculture commodities such as coffee, corn, scallion, and beans. The objective of this study is to identify the spatial and temporal patterns of soil conservation applied by farmers from 1990 to 2018 and project it to 2036 to understand the possible impact in the future. The scenario used in the analysis is the Business as Usual (BAU) scenario. The method used to model the changes in agricultural land use is Cellular Automata - Markov Chain by various driving factors, such as distance from the road, river, settlements, forests, and percent slope. The slope and other driving factor are then correlated with agriculture land to identify soil conservation methods and later validated by field survey. The results indicate that the spatial pattern of soil conservation methods carried out by the community is closely related to slope conditions and the changes in agricultural land caused by development pressure and type of commodities planted by farmers. Agricultural land on  $<15\%$  slope adopt chemical and vegetative conservation methods, while agricultural land on  $>40\%$  slopes adopts mechanical, vegetative, and chemical conservation method.

*Keywords: Soil conservation, Agriculture, Spatial and temporal pattern, Markov chain*

### INTRODUCTION

Erosion is the loss of land or parts of the land from a place by wind or water [1]. On a large scale, erosion is a potential landslide disaster that can threaten human life and also capable of damaging facilities and community buildings in various locations. The impact of erosion can be seen in the loss of nutrients located in the topsoil caused by the force of water worn away and removed various soil materials thus resulting in reduced soil productivity [2].

Resisting high soil loss rate and Reducing the impact of damage due to erosion requires soil conservation activities [1]. Based on this, in order to avoid the negative impacts of soil erosion, soil conservation activities are needed not only to prevent disasters but also to increase productivity by optimizing the use of soil. The importance of soil conservation activities is inseparable from land use conversion and physical aspects of it, such as topography and soil type. The relationship built between soil conservation and land use conversion illustrates the importance of information on future land use projections or future trends for a reevaluation of current conservation planning and analysis that have been carried out by stakeholders in the research area.

Increasing developments in society tend to stimulate land conversion as a complex process of

supporting human activities in certain regions. The process mentioned will lead to further escalate erosion process so that land use planning and erosion management are needed to avoid large losses. Therefore, the application of soil conservation needs to be carried out and examined as a solution to problems caused by degraded soil.

The Patuha Mountain area was chosen as a research area because of the existence of physical characteristics such as steep slopes and high rainfall intensity and social processes that could potentially cause disasters. Social factors such as population growth and economic factors often lead to changes in land use. Studies show the increasing population number and changes in population structure inevitably led to land use conversion [3], while numbers of socio-economic factors influence its change like shifting cultivation, increasing demand for forest and farm products and migration [4], to which can also deliver pressure to soil resulting in landslides disaster. It can be seen that the Patuha Mountain Area captured the ecological processes of erosion and its relation to human aspects such as agriculture and hazard. Based on the previous description and the occurrence of landslides and land use dominated by plantations and agriculture in the research area, it is necessary to review conservation actions in the research area, Especially conservation of soil in agriculture of Patuha Mountain area.

## MATERIALS AND METHODS

### Research Area

The Patuha Mountain area is part of the administrative area of Bandung Regency, West Java. Three Districts included in the Patuha Mountain Area, namely Ciwidey, Rancabali, and Pasirjambu Districts. Astronomically, the Patuha Mountain Area located between  $107^{\circ}12''$  E -  $107^{\circ}30''$  E and  $7^{\circ}6''$  S -  $7^{\circ}12''$  S.

The Patuha Mountain covers an area of 43,642 hectares. The Patuha Mountain region which consists of 3 Districts then divided into 22 villages. The Majority of Residents in The Patuha Mountain Area derive their livelihood from agricultural activities or best known as farmers livelihood. Our research area is also known for its agricultural products such as tea and coffee, reaching 550 ton production for coffee in 2017 [5]. The regional policy also states that in 2007 Ciwidey sub-district was set to be an agropolitan area through Ciwidey Agropolitan Masterplan, thus confirming the functionality of the research area [6].

The Patuha Mountain area is still parts of the upstream zone of the Citarum watershed and followed by the physical condition of a relatively steep slope. The slope of the Patuha Mountain area was classified into three classes, namely  $<15\%$ ,  $15-40\%$ , and  $>40\%$ . When viewed from Fig. 1, the dominant steep area is on the Southeast side of the Patuha Mountain Region. The slope class that dominates the research area is class  $15-40\%$  with an area of 21,714 Ha or about 54% of the total area of research, while the slope class with the smallest area is a slope class of  $40\%$  which has an area of 8,179 Ha or 20% of the area scattered research.

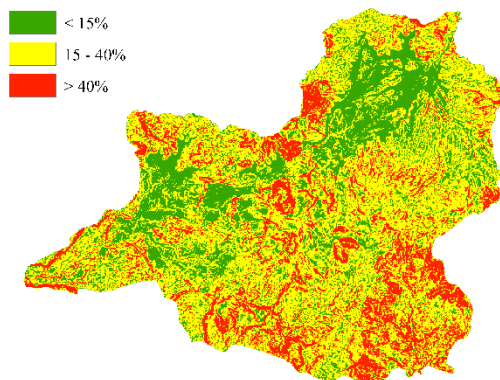


Fig. 1 Slope map of the Patuha Mountain area

### Data and variables

The variables used to analyze and predict land use changes are land use of 1990, 2000, and 2018, slope, distance from the road, distance from the river, distance from the forest, and distance from the settlement. Landsat was used in our research because

of its reliable archive and rich collections spanning from 1972 to recent years globally with 30 m resolution freely available [7]. The need for a long period of data in our research leads us to use Landsat 5 and 8 for land use variables. The gap in data availability was solved by implementing different Landsat imagery because Landsat 5 imagery is only available up to 2012 while Landsat 8 starts from 2013. Landsat 5 was used for deriving land use data in 1990 and 2000. Landsat 8 imagery is used for land use data processing in 2018. Slope, distance from the road, distance from the river, distance from the forest, and distance from the settlement were used as the driving factors for changes in land use.

Land use and slope were overlaid based on recent data to determine survey points. Stratified Random Sampling is used to identify the sampled points, thus population classification is applied based on previous overlaid results. Number of samples is determined by a random selection system [8] and a total of 30 points samples is randomly selected in three sub-districts in the Patuha Mountain Area: Rancabali, Pasirjambu, and Ciwidey District.

### Data Processing

In processing land use data, the initial step taken was to visually interpret the imagery to produce land use maps in 1990, 2000, and 2018, to first acquire the information of land use changes in 1990 to 2018. Visual interpretation with Landsat 5 and Landsat 8 was done in natural colour composite bands of each Landsat image; 321 and 432 respectively, to identify vegetation and other land use. National classification system was used to classify various land use in our research area and 11 class was identified which can be seen in Table 1.

Land use maps in 1990 and 2000 were used for land use modelling in 2018. The land use model in 2018 was tested with the kappa method to determine the accuracy of the predicted results. Kappa validation is done by comparing the 2018 land use prediction from IDRISI software with visually interpret 2018 land use maps. The kappa value threshold according to Landis [9] is  $K > 0.75$  shows a very good agreement,  $0.4 \leq K < 0.75$  shows a pretty good agreement and  $K < 0.4$  indicates a weak agreement. The expected kappa value is  $\geq 75\%$  if it is less than this number, the data repair process must be carried out until it reaches  $\geq 75\%$ . After we obtained the appropriate validation value then we can proceed with predicting land use in 2036 with 2018 as the base year input. The year 2036 was selected for the upper threshold based on the Regional Spatial Plan (RTRW) Bandung Regency which applies from 2016 to 2036.

We used Markov Chain-Cellular Automata model with five driving factors to predict and project the land use in 2036, which is: the distance from the road,

the distance from the river, the distance from the settlement, the distance from the forest, and slope. Variables data was Processed using ArcGIS 10.5 and Idrisi Selva Software was used to analyze land use changes and to perform the accuracy test. The driving factor variable is calculated using the Euclidean distance method to produce distance from plantation and agriculture. Euclidean distance is the physical distance in two or three-dimensional space to multidimensional space [10]. The results of the field survey are used as a basis for determining land conservation parameters and then used to model soil conservation on the land use map.

## RESULTS AND DISCUSSION

### Land Use Changes

Land use in 1990, 2000 and 2018 was used as the basis for analyzing land use changes in the Patuha Mountain Area for the past 28 years. Land use in the Patuha Mountain region in 1990, 2000 and 2018 was dominated by the use of plantation and agricultural land as a whole. Land use in the Patuha Mountain area in 3 Period Year shows that almost all land uses continue to change each year, but not the case with water bodies. Significant changes in land use changes that can be observed from 1990 to 2018 are the plantation and primary forest, resulting in increasing 14,767 Ha of plantation and the declining 4,086 Ha of primary forest in 2018 (Table 1).

Major changes occurred on the south and southeast side of the Patuha mountain area. The central part of the Gunung Patuha area in 1990 was only a small portion of open land, which was 6 ha. However, in 2000 open land increased significantly to 303 ha. This shows that in 1990-2000 there had been a lot of land clearing which would be converted into other land, and it could be proven in 2018 that the land had been turned into plantation land.

Table 1 Land use area in the Patuha Mountain

| Land Use                  | Area (ha) |        |        |
|---------------------------|-----------|--------|--------|
|                           | 1990      | 2000   | 2018   |
| Primary Forest            | 5.068     | 4.828  | 4.087  |
| Secondary Forest          | 5.138     | 5.004  | 5.030  |
| Forest Plantation         | 5.099     | 5.180  | 5.662  |
| Shurbs                    | 892       | 873    | 183    |
| Plantation                | 13.864    | 13.894 | 14.768 |
| Settlement                | 1.693     | 1.752  | 1.817  |
| Water                     | 66        | 66     | 66     |
| Dryland Agriculture       | 1.679     | 1.647  | 2.094  |
| Dryland Mixed Agriculture | 2.124     | 2.137  | 1.910  |
| Paddy                     | 4.450     | 4.395  | 4.450  |
| Bare Land                 | 6         | 303    | 12     |

Source : Analysis Result (2019)

Decreasing rate of Plantation and agricultural land is observed from 1990 to 2000, this is likely to occur because of the impact of the monetary crisis that occurred in that period in Indonesia. In 1997 the industrialization process shifted the agricultural sector resulting in reduced production of basic commodities produced by the agricultural sector so that Indonesia had to import 9 million tons of rice [11]. In 2000-2018 there was an increase of plantation, dryland agriculture and paddy area. Significant changes occurred in plantations and dryland agriculture. This happens because according to the community, plantations, dry land agriculture has a higher economic value compared to rice fields. So that many people use the land as dryland farming compared to rice fields.

In this study, the prediction of land use in 2018 was carried out with an accuracy test with actual land use in 2018 using kappa validation. K standard values show results of 0.9082 or 90% which indicates a high level of accuracy (>75%). High Accuracy test results confirm the model to continue projecting for land use in 2036.

Modelling of land use in 2036 in the process requires the influence of driving factors. The driving factor is the variables used to estimate the probability value of each pixel in the research area. The driving factor estimates the probability value of each pixel to remain or change to another element. Each variable is classified and scored to determine the value of compatibility for plantation and agricultural land use. The variables used are the distance from the road, distance from the river, distance from the settlement, distance from the forest, and slope. Closer the area is to roads, settlements, and forests show that the land is highly prospective to change, while the more it located closer to the river indicates that the land has little chance to change and the more level or flat the land is, it is more likely to change.

Modelling of land use in 2036 is carried out with Business as Usual scenario. BAU scenario refers to the condition given in specific period without any policy applied or regulation intervention [12] which can cause the model to behave differently with various base year or starting points. Modelling of land use in 2036 was used as a reference in determining the spatial distribution of soil conservation methods applied in 2036 prediction model. Can be seen in Fig. 2, in 2036 results predicted that there will be a significant change in the area and distribution of land use, However plantation and agricultural land is still the dominant class in the region. Changes often occur within area nearer to roads and directly adjacent to the forest area. Land use that experienced the most significant increase was dryland agriculture reaching to 2871 Ha or 7% of the total area of research. Meanwhile, the land use which experienced the most significant decline in 2036 was primary forest which was 2,944 Ha.



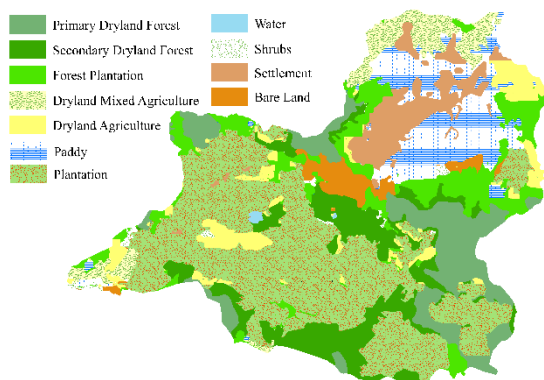


Fig. 2 Land use map in 2036

Figure 3 shows a graph of plantation and agricultural area in 2018 and 2036 in the Patuha Mountain Area. In 2036 results predicted that the area of plantations, mixed dryland agriculture, and paddy fields decreased. However, dryland agriculture experienced a significant increase. This change in the area can cause changes in the area of land conserved in 2036, assuming the physical condition of the slope is fixed.

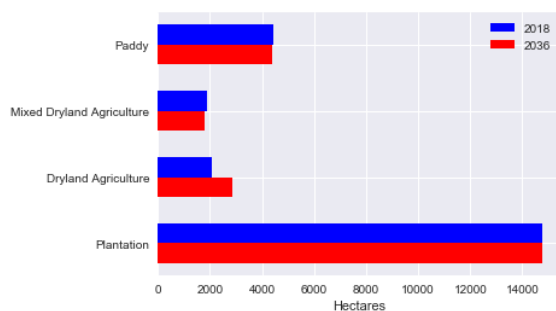


Fig. 3 Plantation and agriculture land area in 2018 and 2036

### Soil Conservation

Vegetative, mechanical and chemical soil conservation methods are applied by the community on plantation and agricultural land in 2018. However, the community does not only apply one conservation method in each field but is divided into 2, namely a combination of two soil conservation methods (vegetative and chemical) and combinations three soil conservation methods (vegetative, mechanical, and chemical). The combination of the two methods is used for plantation and agricultural land on slopes <15% while the combination of the three methods is used for plantation and agricultural land on slopes between 15% and 179% degree. Plantations and agriculture that are on relatively steep slopes (15% - 179%) have a higher risk of landslides, so conservation activities carried out must be

supplemented with mechanical conservation methods to achieve stronger soil structure and reduces the risk of landslides.

In the Patuha Mountain Area, soil conservation with the use of a combination of three methods is the most dominant one, which is an area of 16,005 Ha or 69% of the total area conserved (Table 2). Soil conservation using a combination of three methods requires a greater cost than soil conservation using two combinations. However, using a combination of three methods on steep slopes can better protect the land to avoid landslides.

Table 2 Land Area Conserved in the Patuha Mountain Area in 2018

| Soil Conservation Method             | Area (Ha) | Percentage (%) |
|--------------------------------------|-----------|----------------|
| Vegetative and Chemical              | 7.205     | 31             |
| Vegetative, Mechanical, and Chemical | 16.005    | 69             |

Source : Analysis Result (2019)

The local community has conducted several means to implement vegetative conservation methods i.e by using crop residues, using cover crops, and crop rotation. The method of vegetative soil conservation using plant residues is carried out in the form of mulch which is spread over the surface of the soil. Mulch can be in the form of organic and inorganic (Fig. 4). Organic mulch is like the remains of plants or straw, while inorganic mulch is made of synthetic materials such as plastic. Vegetative soil conservation method using plants to cover the topsoil is done in three ways, by using low soil cover plants (grasses or vines), medium ground cover plants (shrubs), high cover crops (trees). Crop rotation as a vegetative conservation method in the Patuha Mountain Area is identified with three patterns including all season paddy fields, paddy to vegetable crops, and all season vegetables crops.



Fig. 4 Organic mulch and inorganic mulch

Mechanical conservation methods are conducted by the local community in several means, including by making guludan which is a pile of dirt or soil, trenches, terrace, rorak which is a dead-hole to trap and absorb water into the soil and accommodate sediments, and irrigation. Mechanical conservation



method implemented by making guludan is done by making soil piles, the size of it is determined by the type of plant and the structure of the soil. Trenches are carried out in order to accommodate or channel surface flow. Trenches can be made in the direction of contour lines or cutting slopes. Trenches are usually made on areas with long slopes. The terrace is done by cutting contour lines often carried out on land that has a relatively steep slope (Fig. 5). There are two types of terraces, which is wide-based terrace and terrace stairs or bench terraces.



Fig. 5 Mechanical soil conservation method by making the terrace

Mechanical soil conservation method by making rorak is done by making a hole between plants. Large rorak varies greatly depending on needs, but usually rorak has a depth of 50 cm. Rorak is used to store plant debris which can later be used as organic fertilizer, rorak can also be used to hold and absorb water. Irrigation Method is executed to provide and regulate water (Fig. 6). Irrigation channels are made to irrigate plants so that the plants get enough water supply. Irrigation channels are usually used on agricultural wetlands so that the plants remain submerged in water achieving no shortage of water supply.



Fig. 6 Mechanical soil conservation method by making irrigation

Several chemical conservation method carried out by the local people of Mount Patuha is by providing chemical fertilizers such as phonska, Triple Super Phosphate (TSP), Zwavelzure Ammoniac (ZA), urea,

Potassium Chloride (KCl), ZN, and kieserite. The content in each fertilizer is very diverse, such as nitrogen, carbon, hydrograph, oxygen, phosphate, potassium, sulfur, calcium, magnesium, and sulfur.

Soil conservation in the Patuha Mountain Area in 2036 is predicted to continue using two types of combine methods, namely a combination of two (vegetative and chemical) and a combination of three (vegetative, mechanical, and chemical) soil conservation methods (Fig. 7). The land use model in 2036 predicted that plantation and agricultural land in 2036 is still dominating and expanding. Therefore in 2036, the whole region is predicted as having an increased total of conserved soil area by 23,722 hectares or 59% of the total area of the study.

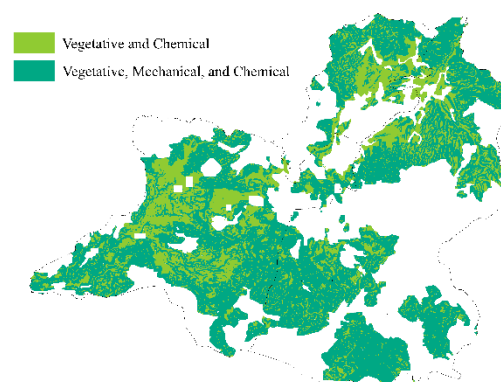


Fig. 7 Soil conservation method in 2036

Can be seen in Fig. 8, is predicted that the combination of three methods of soil conservation used in 2036 still dominates, which expand to 16,584 Ha or 69% of all land that is conserved. While the combination of the two methods in 2036 decreased to 7,200 hectares or 31% of all the land that was conserved in the study area. This shows that plantation and agricultural land on relatively steep slopes (15% - 179%) in 2036 is predicted to increase while plantations and agriculture on relatively flat slopes (15%) decreased, so in 2036 the prediction of combination three methods of soil conservation are mostly carried out compared to the combination of two soil conservation methods.

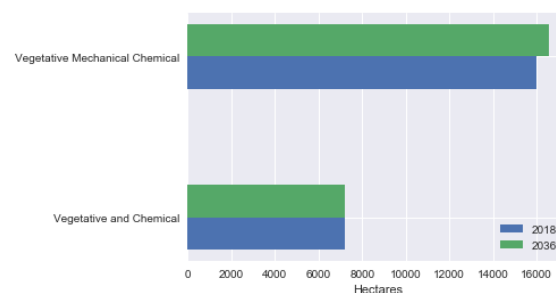


Fig. 8 Soil conservation methods area in 2018 and 2036

## CONCLUSIONS

Land use in the Patuha Mountain area in 1990, 2000 to 2018 experienced significant changes and plantation and agricultural land always dominated every year. Changes in the plantation area and agriculture will affect changes in the land that must be conserved. Vegetative, mechanical and chemical soil conservation methods are applied by the community on plantation and agricultural land in 2018, but the community does not only apply one conservation method in each field but rather a combination of two methods (vegetative and chemical) and a combination of three methods (vegetative, mechanical, and chemical). The combination of the two methods is carried out by the community on the plantation and agricultural land which is on a relatively flat slope (<15%) and a combination of three methods are done on plantation and agricultural land which is on relatively steep slopes (15% - 179%). In 2036 plantation and agricultural land are predicted to increase, resulting in increasing conserved land in 2036. Plantations and agriculture on relatively steep slopes (15% - 179%) increased while plantations and agriculture on relatively flat slopes (<15) decrease, resulting in higher application of three combination methods in our research area rather than two by 2036, this occurs most likely because of the combination of three methods applied on steep slopes that can better protect the soil to avoid landslides and degrade the quality of soil in certain area. .

## ACKNOWLEDGEMENT

The author would like to express our gratitude to the Directorate of Research and Community Service (DRPM) Universitas Indonesia, which has supported this research in PITTA B UI 2019 Grant. This research is also part of soil ecosystem services mapping in Patuha Area under the ongoing PhD research of Jarot Mulyo Semedi with the title 'Quantifying the spatial-temporal impact of geothermal development on ecosystem services in Indonesia.'

## REFERENCES

- [1] Arsyad, S. (2010). *Konservasi Tanah dan Air*. Bogor: Departemen Ilmu-Ilmu Tanah Fakultas Pertanian IPB.
- [2] Suripin. (2004). *Pelestarian Sumber Daya Tanah dan Air*. Yogyakarta: ANDI.
- [3] Lau S S V, Giridharan R, Ganesan S, 2005. Multiple and intensive land use: Case studies in Hong Kong. *Habitat International*, 29(3): 527-546.
- [4] Nzunda, N.G., Munishi, P.K.T., Soka, G.E., Monjare, J.F. (2013). Influence of Socio-economic Factors on Land Use and Vegetation Cover Changes In And Around Kagoma Forest Reservein Tanzania. *Ethiopian Journal of Environmental Studies and Management*, Vol 6 No. 5 2013.
- [5] BPS. (2017). *Kabupaten Bandung dalam Angka*. Kabupaten Bandung: BPS Kabupaten Bandung.
- [6] BAPPEDA. (2007). *Penyusunan Masterplan Pembangunan Ekonomi Daerah (Kawasan Agropolitan Ciwidey)*. Kabupaten Bandung.
- [7] Woodcock, C.E., Allen, R.G., Anderson, M., Belward, A., Bindschadler, R., Cohen, W.B., Wynne, R. (2008). Free access to Landsat imagery. *Science*, 320(5879), 1011.
- [8] Tika, M. P. (2005). *Metode Penelitian Geografi*. Jakarta: Bumi Aksara.
- [9] Landis, J. R., & Koch, G. G. (2012). The Measurement of Observer Agreement for Categorical Data Data for Categorical of Observer Agreement The Measurement. *International Biometric Society*, 33(1), 159–17.
- [10] Greenacre, M. (2008). *Correspondence Analysis and Related Methods*. Barcelona: Department of Statistics, Stanford University.
- [11] Tyas, N. K. (2013). *Dinamika Ekonomi Pabrik Gula Sumberharjo Pematang pada Tahun 1985-2005*. Universitas Negeri Yogyakarta.
- [12] Teng, F., and S.-Q. Xu, 2012: Definition of Business as Usual and its impacts on assessment of mitigation efforts. *Adv. Clim. Change Res.*, 3(4), doi: 10.3724/SP.J.1248.2012.00212 .

## SPATIO-TEMPORAL RICE PHENOLOGY USING UAV IN PARAKAN SALAK, SUKABUMI REGENCY, INDONESIA

Rokhmatuloh<sup>1</sup>, Supriatna<sup>1</sup>, Adi Wibowo<sup>1</sup> and Iqbal Putut Ash Shidiq<sup>1</sup>

<sup>1</sup>Department of Geography, Faculty of Mathematics and Natural Sciences, University of Indonesia,  
Indonesia

### ABSTRACT

Paddy is the primary food source for the Indonesian. Accurate information about the stage of rice or phenology is very crucial. The phenology was land preparation, vegetative, generative, and harvest. The study aims to analyze the spatial and temporal of rice phenology and productivity using unnamed vehicles (UAV) or DRONE in Parakan Salak. In the study used high-resolution imagery and object-based image analysis (OBIA) method to classifying the phenology of the paddy field. The result from image analysis of phenology vegetative until the harvest of NDVI was indicating 0.21 until 0.84. The results from the estimation of rice productivity in Parakan Salak of 5 0 tons/hectares. Finally, the research concluded that the harvest area from UAV (DRONE) imagery could provide an estimation of productivity on the paddy field in Parakan Salak, Sukabumi Regency.

*Keywords: Paddy field, obia, phenology, spatial-temporal*

### INTRODUCTION

According to Statistics Indonesia (or known as Badan Pusat Statistik) in 2015, about 51.69% of the national rice production has been produced in Java island. It is recorded as much as 51.69% of the national rice production in the production by rice fields on the island of Java. However, on the other hand, BPS Data also mentioned that in the last ten years, the population of Java Island increased by 1.15% with a decrease in the rate of the land area of 0.02%. Sukabumi Regency is one of the rice producers and becomes one of the West Java Rice Barn located in the southern region. Sukabumi Regency recorded in BPS has an area of rice farming and horticultural area of  $\pm 3,816$  Ha and produce 64.97 Quintal/Ha rice paddy field. The availability of the rice of West Java will depend heavily on the districts that become the barn.

In general, rice in Indonesia can be harvested twice for irrigated rice fields and one harvest on the rain field. Rice has three phases in one harvest, namely the vegetative phase (0-60 days), the generative phase (60-90 days), and the cooking phase (90-120 days). In irrigated paddy fields, paddy fields have a planting period of 80-90 days. Meanwhile, for rain rice field has planting period 100-130 days.

Before rice seedlings planted, rice fields need to given plenty of water (flooded). Once the seeds are planted or in the germination phase, it takes 25-30 days to reach the initiation stage of the saplings, and the rice leaves begin to grow. The leaf color then transforms from yellow to green in the early phase of the saplings and intermediate stripping phase. The generative phase is plant growth, ranging from

flowering until maturation (harvest). The growth will reach maximum on the initiation of interest where for the initial rice varieties, it takes 55-60 days from the inadequate phase, and for the final variation, it takes 65-75 days. The next stage is the flowering phase, where the rice plants begin to grow flowers, and the leaves of the leaf begin to turn yellow. For the initial rice varieties, this phase reaches 85-100 days after the inadequate phase, and for variations of rice varieties, it takes 100-115 days. The last phase is a harvest, where rice has been developed and ready to harvest. The initial varieties of rice need 130-145 days after the sproachment phase to be harvested, whereas for other varieties it takes 140-165 days (long time).

Satellite utilization in agricultural land monitoring has constraints such as low spatial resolution and depends on the quantity of cloud cover (Moeslah, 2015). The phenology was land preparation, vegetative, generative, and harvest. The study aims to analyze the spatial and temporal of rice phenology and productivity using unnamed vehicles (UAV) or DRONE in Parakan Salak.

### METHODS

The research area took the agricultural land in Parakan Salak District, Sukabumi Regency. Located at coordinates 6.786809 ° LS and 106.699957 ° BT. This region chose due to the different type of land use conditions, namely rice fields mixed with plantations and Tegalan. The condition is ideal to see how well the methods of analysis used able to separate the rice field with other farmland. Besides, the chosen land is a rice field that has a condition of growing age/phase of rice that varies, namely from the vegetative,

generative, and fallow phases.

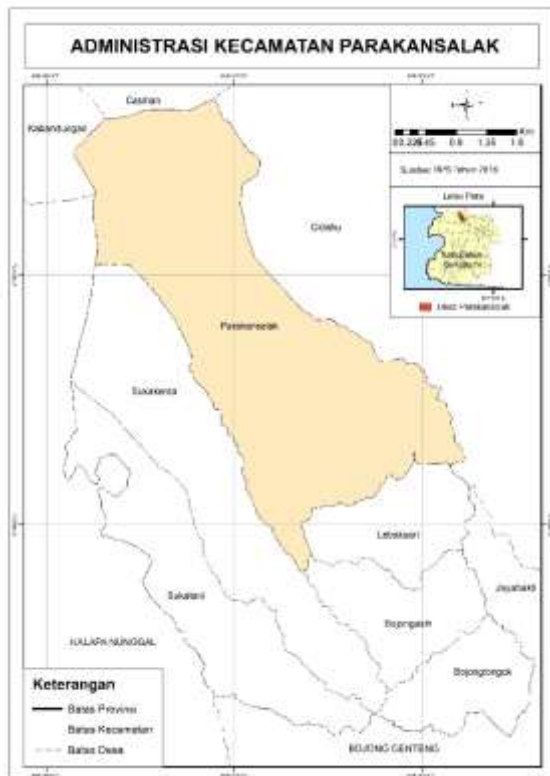


Fig. 1 This is the example for figure formatting.

### The Object-Based Identification Analysis

The photo or image of the drone recording is processed and classification to get the area of paddy fields based on the growth phase. In the classification process, there are two methods, which are the Object-based classification and pixel-based (Pixel based) method. The classification method used in this research is the Object-based Classification method. This method has a characteristic that the smallest unit is not a pixel but a segment, where this segment is a combination of several pixels that have a characteristic resemblance.

Based on the experiments conducted by Weih (Weihl et al., 2010), the classification results using Object-based techniques provide better accuracy than pixel-based methods. Also, some researchers find the pixel-based classification results performed on high-resolution satellite imagery have a "salt and pepper" effect, where this effect describes the emerging noise or pixels with minority classes (Gao and Mas, 2008; Van de Voorde et al., 2004). These noise effects make classification with pixel-based methods less accurate.

In the classification process, the Pixel based method only looks at the parameters of the pixel value, while the object based method not only looks at the pixel value but from the spatial aspect. Object-Based Classification is a classification method that can produce similarity of objects based on segmentation

of spectral values in imagery by creating a homogeneous polygon by considering spectral and space characteristic. Segmenting algorithms not only relies on one single pixel value, but also on the shape, texture, and continuity of the pixels.

Vegetation index was generated using different bands from the sensor. This study used NDVI as a tool to differentiate different types of crop. NDVI has widely used in many applications, and one of them is for identifying plant characteristics in the ground [4,5,6]. NDVI calculated with the following equation (1) [7]:

$$NDVI = \frac{\rho_{NIR} - \rho_{red}}{\rho_{NIR} + \rho_{red}} \quad (1)$$

where  $\rho_{red}$  and  $\rho_{NIR}$  are reflectance value of red and near-infrared bands.

### RESULT AND DISCUSSIONS

Figures or Tables should be sized the whole width of a column, as shown in Table 1 or Fig.1 in the present example, or the whole width over two columns.

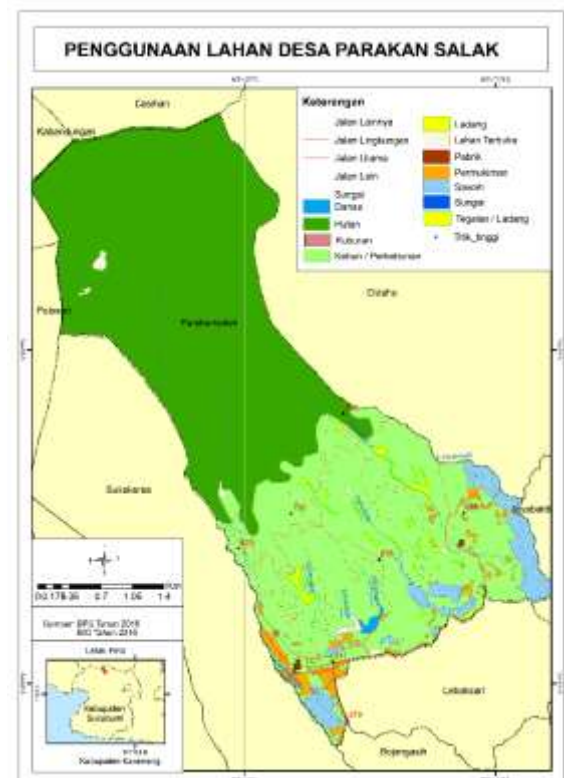


Fig. 2 Land use/Land cover in Parakan Salak.

Based on Fig. 3. Data from google earth shows the Parakan Salak area with land cover rice filed, plantation (tea and oil palm), river, and settlement.





Fig. 3 The Parakan Salak from Google Earth Data.

Figure 4 shows the rice field from a drone on final generative. (planting phase 12-15 weeks/100 days).



Fig. 4 The rice field from UAV.

Table 1 Range of NDVI values for paddy in Parakan Salak

| Rice Field                       | Min  | Max  | Mean | Stdev |
|----------------------------------|------|------|------|-------|
| Paddy                            | 0.21 | 0.85 | 0.61 | 0.25  |
| Sarengui Paddy                   | 0.21 | 0.80 | 0.58 | 0.27  |
| Sarengui Paddy (45 days)         | 0.79 | 0.84 | 0.82 | 0.02  |
| Sarengui Paddy (to be harvested) | 0.38 | 0.85 | 0.66 | 0.25  |
| Super Paddy                      | 0.31 | 0.83 | 0.64 | 0.19  |

Source: Data Processing and Survey

Note: should be placed under the table leaving no space in-between; 10-pt font; and left- and right-justified.

Table 2 Range of NDVI values for paddy in Parakan Salak

| Rice Field                       | Ma<br>x | Area<br>(ha) | productivity |
|----------------------------------|---------|--------------|--------------|
| Sarengui Paddy                   | 0.80    | 10           | 5.6          |
| Sarengui Paddy (45 days)         | 0.84    | 10           | 4.8          |
| Sarengui Paddy (to be harvested) | 0.85    | 10           | 5.3          |
| Super Paddy                      | 0.83    | 10           | 5.2          |
| Average                          | 0.83    | 10           | 5.0          |

Source: Data Processing and Survey



Fig. 5 The final vegetative phase.

Based on Fig. 5, the figure shows information on rice field in final vegetative phase (planting phase 4 - 5 weeks/30 days), characterized by tight plants, soils, and water are barely visible.



Fig. 6 The final generative phase.

Based on Fig. 6, the figure shows information on the rice field in the final generative phase (planting phase 12-15 weeks/100 days) marked with a foam or panicles that start to yellow and immediately enter the harvest period.

## CONCLUSIONS

The result from image analysis of phenology vegetative until the harvest of NDVI was indicating 0.21 until 0.84. The results from the estimation of rice

productivity in Parakan Salak of 5.0 tons/hectares. Finally, the research concluded that the harvest area from UAV (DRONE) imagery could provide an estimation of productivity on the paddy field in Parakan Salak, Sukabumi Regency.

#### ACKNOWLEDGMENTS

The study funded by the Ministry of Research and Higher Education, under the Penelitian Dasar Unggulan Perguruan Tinggi (PDUPT) or the Basic Primary Research for Higher Education with grant number: 378/UN2.R3.1/HKP.05.00/2018.

#### REFERENCES

- [1] Mosleh M.K., Hassan Q.K., and Chowdhury E.H., Application of Remote Sensors in Mapping Rice Area and Forecasting Its Production: A Review. Sensors, Vol. 15, 2015, pp.769-791.
- [2] Richards J.A., and Jia Xiuping, Remote Sensing Digital Image Analysis. An Introduction, 3<sup>rd</sup> revised and enlarged edition. Springer-Verlag Berlin Heidelberg, 1999, pp.
- [3] Rouse Jr. J., Haas R.H., Schell J.A., and Deering D.W., Monitoring vegetation systems in the Great Plains with ERTS. NASA Special Publication 35`, 1974, pp. 309.
- [4] Gnyp A.S.M.A, Hosseini H. and Hossain M.Z., Strength, Modulus of Elasticity and Shrinkage Behaviour of Concrete Containing Waste Carpet Fiber, International Journal of GEOMATE, Vol. 9, Issue 17, 2015, pp. 1441-1446.
- [5] Hossain M.Z., For Chapter in a Book, Soil Mechanics, 4th ed. Vol. 2, Sakai, Ed. Sankeisha Publisher's Name, Year, pp. 11-60.
- [6] Author H., A Book New York Publisher, Year, pp.1-200.
- [7] Jensen J.R., Remote Sensing of the Environment: An Earth Resources Perspective, Prentice Hall, New Jersey, 2000, pp.
- [8] Shidiq I.P.A., Wibowo A., Kusratmoko E., Indratmoko S., Ardianto R., and Nugroho B.P., Urban forest topographical mapping using UAV LIDAR. In *IOP Conference Series: Earth and Environmental Science*, Vol. 98, Issue. 1, 2017, pp. 012034.
- [9] Walter-Shea E.A., and Biehl L.L Measuring Vegetation Spectral Properties, Remote Sensing Reviews, Vol. 5, Issue 1, 1990, pp.179-205.
- [10] Weih Jr. R.C., and Riggan Jr. N.D., Object-Based Classification vs. Pixel-Based Classification Comparative Importance of Multi-Resolution Imagery. The International Archives of the Photogrammetry, Remote Sensing and Spatial Information Sciences, 2010, XXXVIII- 4/C7.



## RICE PRODUCTIVITY ESTIMATION BY SENTINEL-2A IMAGERY IN KARAWANG REGENCY, WEST JAVA, INDONESIA

Suprianta<sup>1</sup>, Rokhmatuloh<sup>1</sup>, Adi ibowo<sup>1</sup> and Iqbal Putut Ash Shidiq<sup>1</sup>

<sup>1</sup>Department of Geography, Faculty of Mathematics and Natural Sciences, University of Indonesia,  
Indonesia

### ABSTRACT

Karawang Regency is the top rice producer within West Java, Indonesia. Accurate information about the number of harvest area is essential in rice production in Indonesia with population majority eat rice. The Sentinel-2A imagery which has a spatial resolution of 10 meters. The study aims to spatial analysis pattern of rice phenology and estimation of rice productivity using Sentinel-2A imagery in Karawang Regency. The NDVI algorithm method used to determine the age of rice plants, which then used to estimate rice productivity. The Karawang Regency had 30 districts with rice field. The stage of rice was land preparation (NDVI=-0.096-0.036), vegetative (NDVI=-0.036-0.24), generative (NDVI=-0.24-0.45) and harvesting (NDVI=-0.45-0.63). The result from the estimation of harvest area is 109,338.27 hectares, and the estimation of rice productivity is 5.5 tons/ha until 6.0 tons/hectares in Karawang Regency. Finally, the research concluded that the harvest area from Sentinel-2A imagery could provide an estimation of productivity on the paddy field in Karawang Regency.

*Keywords: Rice field, Sentinel-2A, phenology, rice productivity*

### INTRODUCTION

West Java province is the largest rice producer in Indonesia, especially Karawang Regency. Based on the national statistic report, in 2014-2015, rice production has been reduced from 11.085.544 to 10.856.438 tons from [1]. From the report, it is possible to acknowledge that efforts to maintain food security in West Java Province are necessary. Karawang Regency is the top rice producer within West Java, Indonesia. Accurate information about the number of harvest area is essential in rice production in Indonesia with population majority eat rice.

Rice phenology defined as the changes that occur within the rice from the moment rice is planted in the ground and proceeds to grow during the harvesting stage [2], [3] (Supriatna, Rokhmat). The detection of rice phenology could be done using a remote sensing ([4]; [5]; [6]; [7];[8]; [9]; [10]; [11]). Spatial information shows that the actual conditions on indicators of food security and food vulnerability can obtain from remote sensing data that has high spectral and temporal resolutions such as LANDSAT 8 data and MODIS [12]. The results of the growth detection [12], indicating that the initial planting time of rice crops can know from the value of the Maximum Of Vegetation Index (EVI Max). By implementing the Vegetation Index (NDVI) value and the temporal analysis of Zheng [13] can determine the dates on the stage in the age of rice crops.

The Sentinel-2A imagery has a spatial resolution of 10 meters. The study aims to spatial analysis pattern of rice phenology and estimation of rice productivity using Sentinel-2A imagery in Karawang Regency.

### METHODS

The Karawang Regency had 30 districts with rice field. The rice field observed in this study is rice paddies planted in rice fields that grow in a cycle of three main periods, which are planting period, growing period, and harvesting period. Five classes took from these three main periods according to a literature study on Sentinel-2A using index vegetation values, which are land preparation, early vegetative, late vegetative, generative, and harvesting/ripening. The spatial analysis approach is used to achieve a spatial pattern of the rice growth phase, and temporal analysis is used to achieve a temporal pattern of the rice growth phase.

The study aims to spatial analysis pattern of rice phenology and estimation of rice productivity using Sentinel-2A imagery in Karawang Regency. The NDVI algorithm method used to determine the age of rice plants, which then used to estimate rice productivity. The stage of rice was land preparation (NDVI=-0.096-0.036), vegetative (NDVI=-0.036-0.24), generative (NDVI=-0.24-0.45) and harvesting (NDVI=-0.45-0.63).

## RESULT AND DISCUSSIONS

Spatial patterns of the rice paddy Vegetation Index show that in June and July, there are different spatial patterns. The spatial distribution of vegetation index in June 2017 saw in Fig 1, and spatial distribution of vegetation index in July 2017 saw in Fig. 2. The high greenish index is in the southern regions of the district of Karawang in June and July. The difference in the relationship pattern occurs based on the area of the high-speed vegetation index.

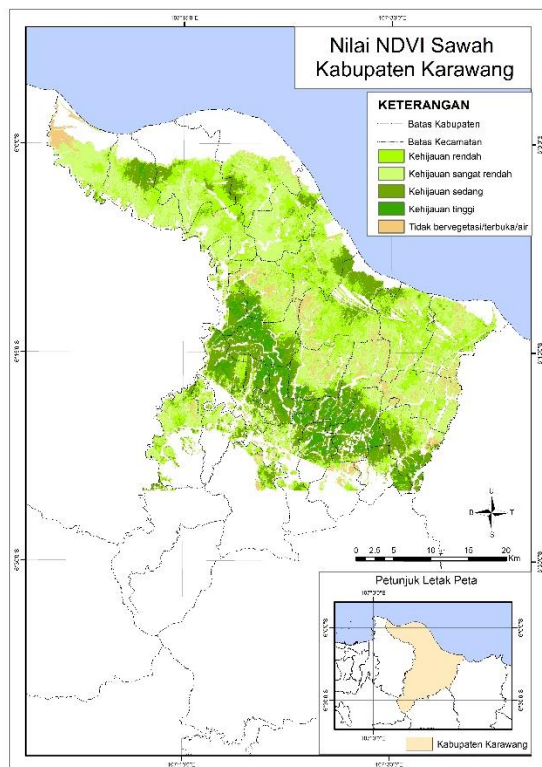


Fig. 1 The NDVI Rice Field in June.

There is a high and medium vegetation index area of 23,335.85 hectares and 6,950.78 hectares. (Table 1). Table 1 shows that the potential rice harvest area in June is 30,186.63 hectares.

Table 1 The NDVI and Vegetation Index in June 2017

| NDVI        | Green Index | Area (Ha)         |
|-------------|-------------|-------------------|
| 0.096-0.036 | No Veg.     | 6,114.98          |
| 0.036-0.240 | Very Low    | 44,560.09         |
| 0.240-0.450 | Low         | 28,376.57         |
| 0.450-0.630 | Medium      | 23,335.85         |
| 0.450-0.630 | Hight       | 6,950.78          |
| Total Area  |             | <b>109,338.27</b> |

Source: Data Processing

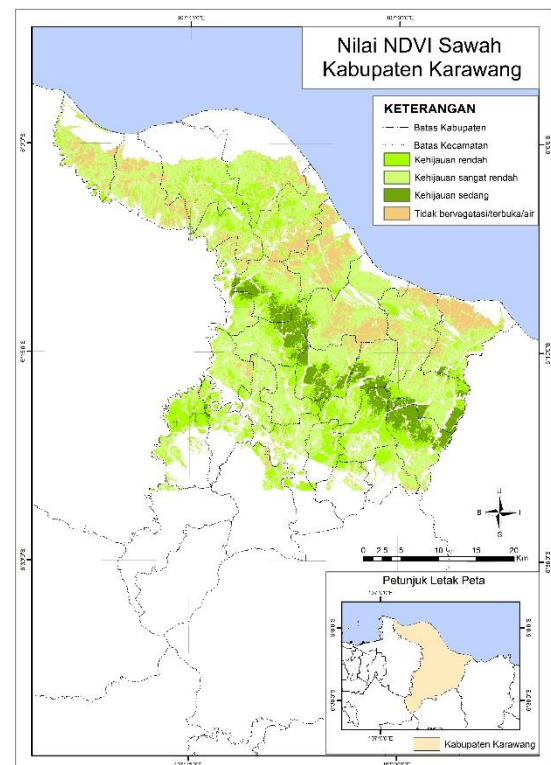


Fig. 2 The NDVI Rice Field on July 2017.

The hight of the vegetation index was not present in July because it was already in the harvest phase. The NDVI July but that was a low vegetation index to an index of 9,077.92 hectares of vegetation. This medium vegetation index area shows the potential of rice harvesting in July (Table 2)

Table 2 The NDVI and Vegetation Index in July 2017

| NDVI        | Green Index | Area (Ha)         |
|-------------|-------------|-------------------|
| 0.096-0.036 | No Veg.     | 15,973.56         |
| 0.036-0.240 | Very Low    | 59,507.50         |
| 0.240-0.450 | Low         | 24,785.00         |
| 0.450-0.630 | Medium      | 9,077.92          |
| Total Area  |             | <b>109,338.27</b> |

Source: Data Processing

Spatial patterns The rice planting phase is associated with the rice field vegetation index showing the different patterns of between in June and July (Fig 1 and Fig. 2)

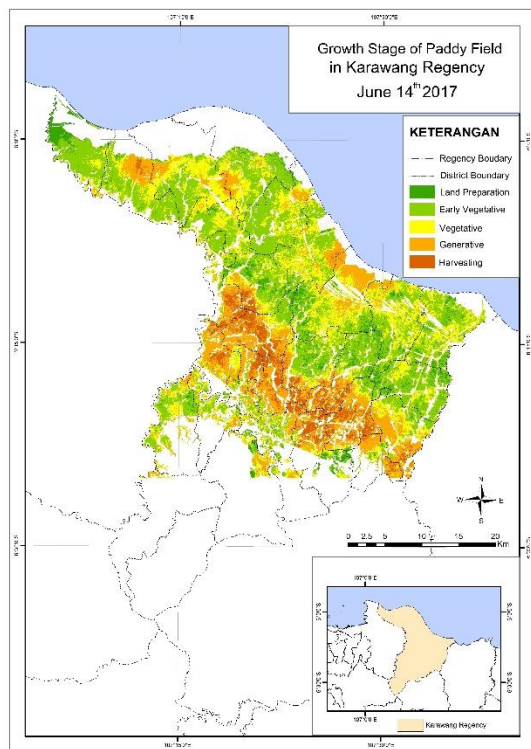


Fig. 3 The phenology based on NDVI in June 2017.

Table 3 The NDVI and Phenology in June 2017

| NDVI        | Phenology | Area (Ha)         |
|-------------|-----------|-------------------|
| 0.096-0.036 | <3        | 6,114.98          |
| 0.036-0.240 | 3-4       | 44,560.09         |
| 0.240-0.450 | 4-6       | 28,376.57         |
| 0.450-0.630 | 6-8       | 23,335.85         |
| 0.450-0.630 | 8-10      | 6,950.78          |
| Total Area  |           | <b>109,338.27</b> |

Source: Data Analysis

The harvest area in June was 30,286.63 hectares with average productivity of 7 ton/hectare then production in June reached 212,006.41 tons. July harvest area of 9,077.92 hectares with 7 tons/hectare productivity will reduce 63,545.44 tons of rice in July.

Table 4 The NDVI and Phenology in July 2017

| NDVI        | Phenology | Area (Ha)         |
|-------------|-----------|-------------------|
| 0.096-0.036 | <3        | 15,973.56         |
| 0.036-0.240 | 3-4       | 59,507.50         |
| 0.240-0.450 | 4-6       | 24,785.00         |
| 0.450-0.630 | 6-8       | 9,077.92          |
| Total Area  |           | <b>109,338.27</b> |

Source: Data Analysis

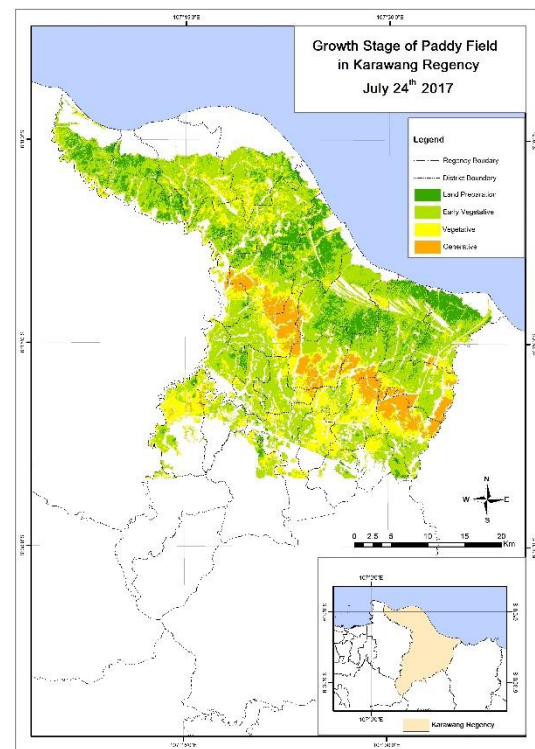


Fig. 4 The phenology based on NDVI in July 2017.

## CONCLUSIONS

The result from the estimation of harvest area is 109,338.27 hectares, and the estimation of rice productivity is 5.5 tons/ha until 6.0 tons/hectares in Karawang Regency. Finally, the result concluded that the harvest area from Sentinel-2A imagery could provide an estimation of productivity on the paddy field in Karawang Regency.

## ACKNOWLEDGMENTS

This study is supported by the Ministry of Research and Higher Education, under the Penelitian Dasar Unggulan Perguruan Tinggi (PDUPT) or the Basic Primary Research for Higher Education Grant based on contract no: 382/UN2.R3.1/HKP.05.00/2018.

## REFERENCES

- [1] BPS – Agency for Statistic. 2015. Rice production report. *Annual Report*.
- [2] Rokhamtuloh, Supriatna, TG Pin, R Hernina, R Ardianto, IPA Shisiq, and A Wibowo, Paddy Field Mapping Using UAV Multi-Spectral Imagery. *International Journal of Geomate* Vol. 17, Issue 61, 2019, pp. 241-247
- [3] Supriatna, Rokhamtuloh, IPA Shidiq, GP Pratama, L Gandharum, and A Wibowo, Spatio-Temporal Analysis of Rice Field Phenology Using Sentinel-1 Image In Karawang Regency,

- West Java, Indonesia. *International Journal of Geomate* Vol. 17, Issue 62, 2019, pp. 101-106
- [4] Lopez-Sanchez J.M., Cloude S.R., and Ballester-Berman J.D., Rice Phenology monitoring by means of SAR polarimetry at X-band. *IEEE Transactions on Geoscience and Remote Sensing*, Vol. 50, Issue 7, 2012, pp. 2695-2709.
- [5] Semedi J.M., Rice Crop Spatial Distribution and Production Estimation using Modis Evi (Case Study of Karawang, Subang, and Indramayu Regency). Master Thesis, Graduate School, Bogor Agriculture University
- [6] Lopez-Sanchez J.M., Vicente-Guijalba F., Ballester-Berman J.D., and Cloude S.R., Polarimetric Response of Rice Fields at C-band: Analysis and phenology retrieval. *IEEE Transactions on Geoscience and Remote Sensing*, Vol. 52, Issue 5, 2014, pp. 2977-2993.
- [7] Nelson A., Setiyono T., Rala A.B., Quicho E.D., Raviz J.V., ....and Thongbai P., Towards an operational SAR-based rice monitoring system in Asia: Example from 13 demonstration sites across Asia in the RIICE project. *Remote Sensing*, Vol. 6, Issue 11, 2014, pp. 10773-10812.
- [8] Dong J., Xiao X., Kou W., Qin Y., Zhang G., Li L., Jin C., Zhou Y., Wang J., Biradar C. and Liu, J., Tracking the dynamics of paddy rice planting area in 1986-201 through time series Landsat images and phenology-based algorithms. *Remote Sensing of Environment*, Vol. 160, Issue 1, 2015, pp. 99-113.
- [9] Küçük Ç., Taşkın G., and Erten, E., Paddy-rice phenology classification based on machine-learning methods using multitemporal co-polar X-band SAR images. *IEEE Journal of Selected Topics in Applied Earth Observations and Remote Sensing*, Vol. 9, Issue 6, 2016, pp.2509-2519.
- [10] Chaparro D., Piles M., Vall-llossera M., Camps A., Konings A.G., and Entekhabi D., L-band vegetation optical depth seasonal metrics for crop yield assessment. *Remote Sensing of Environment*, Vol. 212, 2018, pp.249-259.
- [11] Xu X., Ji X., Jiang J., Yao X., Tian Y., Zhu Y., Cao W., Cao Q., Yang H., Shi Z., Cheng T., Evaluation of One-Class Support Vector Classification for Mapping the Paddy Rice Planting Area in Jiangsu Province of China from Landsat 8 OLI Imagery. *Remote Sensing*, Vol. 10, Issue 4, 2018, pp. 546.
- [12] Domiri, D. D., The method for detecting a biological parameter of rice growth and early planting of paddy crop by using multi temporal remote sensing data. In *IOP Conference Series: Earth and Environmental Science* (Vol. 54, No. 1, pp.012002, 2017). IOP Publishing.
- [13] Zheng, H., Cheng, T., Yao, X., Deng, X., Tian, Y., Cao, W., and Zhu, Y, Detection of rice phenology through time series analysis of ground-based spectral index data. *Field Crops Research*, Volume 198, 2016, pp. 131-139.

## EFFECTS OF OZONE SPARGING ON GROUNDWATER PHYSICAL-CHEMICAL PARAMETERS DURING IN SITU REMEDIATION OF A SITE CONTAMINATED WITH CHLORIDES

Erica Kotani Caram<sup>1</sup> and Maria Eugênia Gimenez Boscov<sup>2</sup>

<sup>1,2</sup>Escola Politécnica da Universidade de São Paulo, Brazil

### ABSTRACT

This paper's objective was to evaluate the effects of in-situ chemical oxidation (ISCO) for groundwater remediation using ozone sparging in a site contaminated with vinyl chloride (VC) and trichloroethene (TCE). The studied area, located in São Paulo, Brazil, has been investigated for over 10 years, and remediation started two years ago. This paper is based on results obtained before the remediation startup and during its operation. Geotechnical and hydrogeological characterization is discussed to support analysis of results. The remediation system includes 86 monitoring wells, 31 vapor extraction wells (above water table) and 33 ozone sparging wells (saturated zone). Periodic monitoring campaigns were executed in 14 monitoring wells, called control points. Groundwater physical-chemical parameters such as: pH, dissolved oxygen (DO), electrical conductivity (EC), oxidation/reduction potential (ORP), temperature and water table, were obtained from low flow samples collected during periodic monitoring campaigns in control points chosen according to their location and hot spot proximity. In general, the control points have shown an ORP elevation, indicating a more oxidative underground environment than before remediation startup, and EC reduction, probably due to a lower ionic concentration in groundwater after remediation started. Dissolved oxygen levels have also increased due to ozone degradation.

*Keywords: Remediation, In Situ Chemical Oxidation (ISCO), Ozone, Groundwater, Physical-chemical parameters.*

### INTRODUCTION

A São Paulo State law defines remediation as a group of techniques used in contaminated sites, that can be classified as treatment or containment techniques [1]. Choice of the proper technique should consider aspects such as geology, contamination data, theoretical efficiency and remediation time [2].

In situ chemical oxidation (ISCO) comprises the mixture of a chemical oxidant in a contaminated matrix, promoting its reaction with the contaminant, mineralizing the contaminant and converting it into water, carbon dioxide and inorganic ions, or even intermediate byproducts formed during the reaction [3]. Oxidants usage has its origin in wastewater treatment, and only in 1990 researchers started exploring its application to soil and groundwater remediation [4].

Among ISCO's positive aspects are high efficiency, absence of direct contact between workers and contaminants, no need for large excavation or civil works, and the fact that the main byproduct is oxygen, non-pollutant and commonly found in subsurface [6], [7]. On the other hand, the short half-life of oxidants, health and safety risks, and possible oxidant consumption by other compounds can be listed as negative aspects [5]. Another worry is the existence of preferable paths

flows in subsurface which can interfere in remediation efficiency [6].

This paper will approach ozone sparging ISCO remediation effects on the subsoil saturated zone in a decommissioned industrial contaminated site. The studied area is located in São Paulo city and presents groundwater contamination by organochlorides, mainly Vinyl Chloride (VC) and Trichloroethylene (TCE). The main objective was to verify ozone range through physical-chemical parameters analysis in groundwater samples collected in control points, considering the presence of fine-grained soils which can impair the technique efficiency.

### SITE CHARACTERIZATION

Field data showed in this paper were obtained from investigation and remediation studies over the past ten years. The area is provided with 86 monitoring wells from 4-6 meters deep (A level) to 30 meters deep (E level).

### Environmental management history

Preliminary assessment of the area identified pasts land uses as an automotive industrial plant between 1930 and 1968, and as a construction deposit from 2001 to 2008. Vehicles were produced in large scale in the 1950s and 1960s, before the creation of São Paulo State Environmental Agency

(CETESB) in 1968. This is the probable reason why no documents have been found that could indicate the location of the primary sources.

However, 2 brickwork oil tanks were found during excavation works in the northwest limit of the studied area. They were both removed in 2009, and the whole area was covered with a 3-meter compacted layer. Investigation of groundwater and contaminated plumes started after that, and 5 studies were carried out in order to define the plumes limits.

During the 5<sup>th</sup> and last investigation study [8], 30 monitoring wells were drilled (in 3 different depths), but still the plumes could not be totally defined. Moreover, new hot spots, detected upstream of the area, couldn't be related to the oil tanks. This study also established health risk due to vapor inhalation in open and closed spaces over the plumes area, based on CETESB risk assessment method.

Following CETESB's Manual for the Management of Contaminated Sites [9], an intervention plan was studied, and a remediation system with ozone sparging and vapor extraction was recommended. Remediation goals were to reduce VC and TCE concentrations, and to eliminate health risks pathways [10].

Remediation of sites contaminated with solvent chlorides is especially difficult and expensive. Different techniques have been developed and applied with a limited success rate. Besides, remediation time can be long and usually measured in decades [5].

### Contaminant characterization

Since 1940, chloride solvents have been used with different purposes, from machinery degreasing and dry-cleaning to chemical industries. Their incorrect disposal has caused a variety of environmental problems such as groundwater and soil contamination, which reflected in the reduction of chloride solvents production and usage [5].

Vinyl chloride (VC) doesn't occur naturally in subsurface and its anthropogenic sources are related to PVC production or VC formation in landfill areas due to organochlorides degradation [11].

However, VC has been detected in groundwater in landfill areas where there was no VC or PVC production nearby. VC can also be formed in anaerobic conditions from the reduction of chloroethylenes: Perchloroethylene (PCE), Trichloroethylene (TCE) and Dichloroethylene isomers (cis-1,2-DCE, trans-1,2-DCE and 1,1-DCE). Some studies indicate that in anaerobic conditions, PCE and TCE can degrade into ethenes by the action of methanogenic, acetogenic and sulfate reduction bacteria. On the other hand, in aerobic conditions a direct or co-metabolic oxidation of DCE and VC can occur. Figure 1 shows contaminants degradation pathways [12].

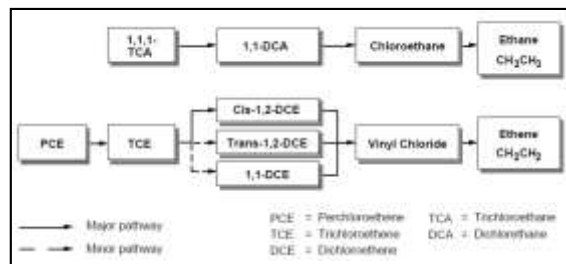


Figure 1: Organochlorides degradation pathways [12].

Depending on primary sources, VC can be released to environment through air, water or soil. The most critical pathways are probably air and groundwater, where VC is most commonly found. When released to air, VC is expected to exist almost exclusively in vapor phase. However, VC half-life in air is limited by its reaction with Oh radicals produced photochemically [11].

VC solubility in water is relatively low but can be raised depending on salts present in water. VC volatilization acts as a significant transport mechanism, considered the most rapid pathway to remove it from superficial water, but an unlikely pathway for groundwater removal [13]. Some parameters such as vapor pressure and Henry's law constant indicate that VC is highly volatile, but in groundwater it can exist for months or years [14].

### Local geological characterization

Site geology is composed by a 3 -meters thick clay layer overlying plastic clay and clay-sand layers up to 15 meters deep [15]. Groundwater flow directions are mainly northwest, north and northeast in shallow (6 meters) and intermediate (9 meters) monitoring wells [15].

In order to understand contaminants behavior in groundwater, slug tests were executed in 7 multilevel monitoring wells (21 in total) to determine hydraulic conductivity (K). These tests were based on USEPA standard [16] and consisted on measurements of the water level in a monitoring well, before and after the introduction of a solid cylinder that causes an artificial elevation of the water level. Hvorslev equation was applied to these data to determine hydraulic conductivity and the results are shown in Table 1.

Location of the monitoring wells is shown in Figure 2. In CM-505A and CM-508C wells, the tests couldn't be finalized in a day period, which can indicate the presence of low permeability soil layers in these wells. CM-504B test presented water table fluctuations possibly related to interferences in the study area (trains and subways nearby). Those occurrences are common in field data, and do not bring important losses to the study.



Table 1. Hydraulic conductivity in monitoring wells

| Well    | Hydraulic Conductivity (cm/s) | Geometric Mean K (cm/s) |
|---------|-------------------------------|-------------------------|
| CM-503A | 3.60E-06                      | 6.60E-05                |
| CM-504A | 3.50E-04                      |                         |
| CM-506A | 2.,30E-04                     |                         |
| CM-507A | 1.60E-05                      |                         |
| CM-508A | 5.20E-04                      |                         |
| CM-509A | 3.50E-05                      | 1.20E-03                |
| CM-503B | 7.40E-04                      |                         |
| CM-505B | 1.50E-02                      |                         |
| CM-506B | 3.60E-04                      |                         |
| CM-507B | 5.90E-03                      |                         |
| CM-508B | 2.20E-04                      | 2.60E-05                |
| CM-509B | 6.60E-04                      |                         |
| CM-503C | 5.10E-06                      |                         |
| CM-504C | 6.20E-06                      |                         |
| CM-505C | 2.60E-04                      |                         |
| CM-506C | 2.60E-06                      |                         |
| CM-507C | 4.20E-05                      |                         |
| CM-509C | 3.50E-04                      |                         |

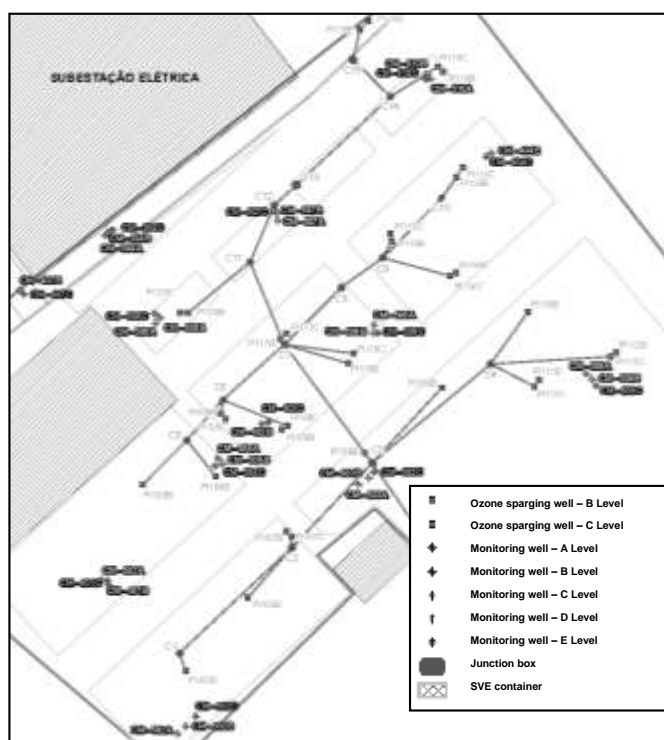


Figure 2. Remediation and monitoring wells

Analyzing the results, deep wells (C level) present lower K, followed by the shallow wells (A level), therefore, the intermediate wells (B level) presented the higher K. Those data are important since organochlorides contaminants (PCE, TCE and DCE) are usually heavier than water and a low K can slow the vertical downwards movement of the contaminants. Moreover, the intermediate layer

presents the higher hydraulic conductivity and also the major part of the contaminant mass.

### Remediation system

The remediation system, composed of 31 vapor extraction wells (in the vadose zone, above the water table) and 33 ozone sparging wells (in the saturated zone, below the water table), operated from April 2015 to November 2017.

Remediation wells were drilled in 8" holes with hollow stem auger, as presented in Fig. 3 (soil vapor extraction wells) and Fig. 4 (ozone sparging wells).

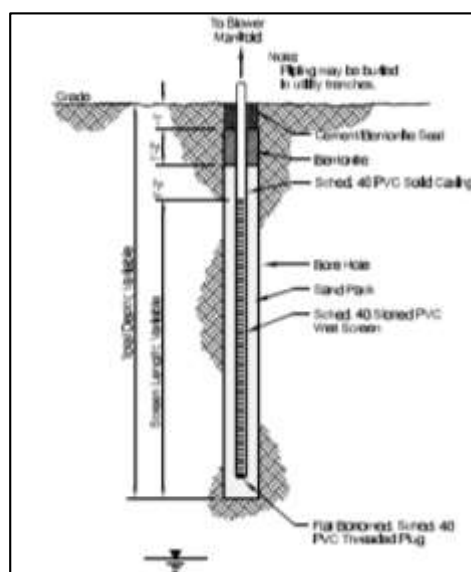


Figure 3: Soil vapor extraction well [17]

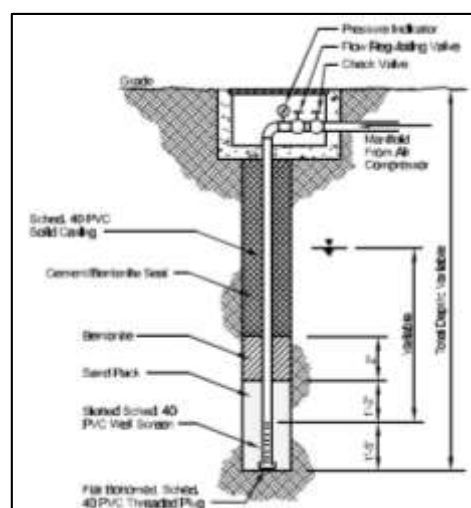


Figure 4: Air sparging well [18]

### Groundwater sampling plan

During remediation, all 86 monitoring wells were sampled at several campaigns to determine TCE and VC concentrations. Sampling campaigns to register physical-chemical parameters were also

carried out at 14 monitoring wells (control points): pH, dissolved oxygen (DO), electric conductivity (EC), temperature and oxidation/reduction potential (ORP). Among the control points, 7 were intermediate wells (B – 9m deep) and 7 profound wells (C – 12m deep), selected accordingly to hot spot and plume configurations.

When groundwater samples were collected to measure TCE and VC concentrations, the remediation system was shut down to avoid interferences in the samples [6]. Groundwater monitoring campaigns were executed by the low flow method, following Brazilian procedures for groundwater sampling [19] and guidelines from CETESB's Manual for the Management of Contaminated Sites [9].

## RESULTS

DO, ORP and EC results are presented to view ISCO remediation effects on groundwater and to verify the extension of the subsoil affected by ozone sparging. Figures 5 to 10 present data from before remediation until 16 months after startup. Results are presented and sorted by depth in order to avoid possible lithology interferences in the results analysis.

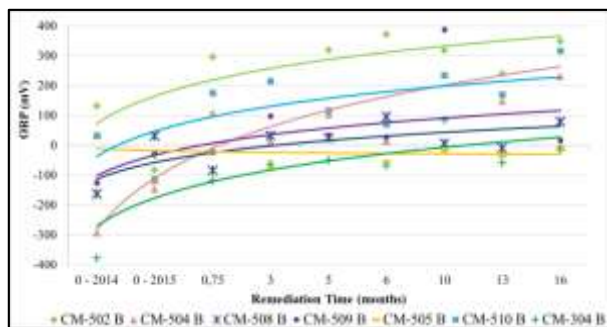


Figure 5: ORP at B level wells (9m deep)

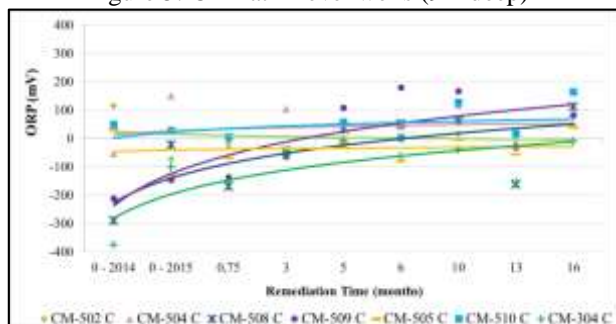


Figure 6: ORP at C level wells (12m deep)

According to the literature and specifically for ozone as oxidant, an increase of groundwater ORP (due to oxidant action) and DO (due to ozone degradation into oxygen) is expected [4], [20], [21].

A tendency to ORP increase can be observed: means in B and C wells were -110,2 mV and -105,5 mV respectively in 2014, and increased to

+103,5mV (B level) and +69,0 (C level) in 2016. Those results were expected since higher ORP solutions tend to oxidize other compounds and lower ORP solutions tend to reduce them, and positive ORP is required for aerobic oxidation of chlorinated solvents and hydrocarbons [22].

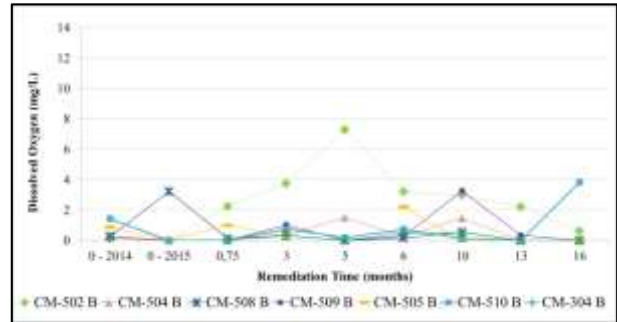


Figure 7: DO at B level wells (9m deep)

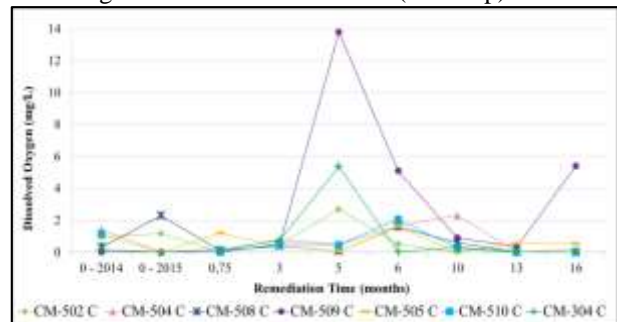


Figure 8: DO at C level wells (12m deep)

DO values showed fluctuation, with results from C level wells slightly higher than B level wells, and an overall trend of DO increase with time. DO in groundwater is usually lower than in surface water, but in this case, oxygen is an ozone byproduct [6], [7]. In Fig. 7 and 8, DO peaks can be observed, probably due to shut down and re-activation of the remediation system during sampling. Besides, DO equipment may have malfunctioned in the campaign carried out 5 months after startup, since all DO data are higher than the other campaigns, especially CM-509C.

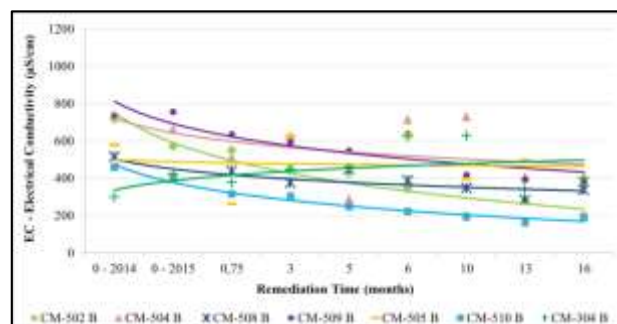


Figure 9: EC at B level wells (9m deep)

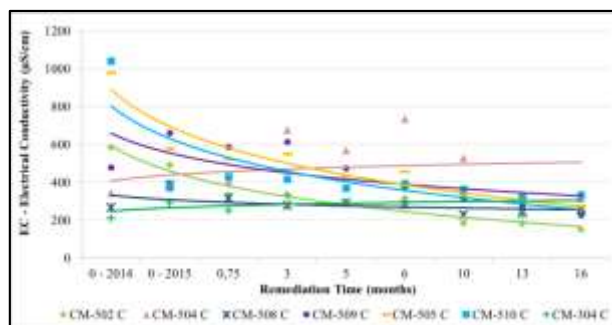


Figure 10: EC at C level wells (12m deep)

A reduction in EC in the control points is also observed, directly related to ionic concentrations and presence of salts in groundwater, representing an indirect measure of pollutants concentration. Groundwater is considered damaged when EC values exceed 100  $\mu\text{S}/\text{cm}$  [23], as presented in Table 2.

Table 2. Physical-chemical parameters results in control points

| Level         | Data        |      | ORP<br>(mv) | DO<br>(mg/L) | EC<br>( $\mu\text{S}/\text{cm}$ ) |
|---------------|-------------|------|-------------|--------------|-----------------------------------|
| B level wells | C.0 (2014)* | Mean | -110,2      | 0,48         | 577,4                             |
|               |             | SD   | -           | 0,48         | 167                               |
|               | C.16**      | Mean | 103,5       | 0,63         | 326,4                             |
|               |             | SD   | -           | 1,42         | 93,1                              |
| C level wells | C.0 (2014)* | Mean | -105,5      | 0,72         | 556,7                             |
|               |             | SD   | -           | 0,56         | 333,5                             |
|               | C.16**      | Mean | 69          | 0,87         | 257,3                             |
|               |             | SD   | -           | 2,01         | 60,35                             |

\* C.0 (2014) - before remediation start-up

\*\* C.16 - 16 months after remediation startup

Temperature and pH parameters were also monitored during remediation, however those results fluctuated more due to seasonality than remediation and ozone action, and therefore they aren't presented in this paper.

## CONCLUSIONS

Analyzing groundwater physical-chemical parameters at control points indicates that the oxidant (ozone) has reached subsurface in all desired depths, since there was in general an increase in oxidation/reduction potential (ORP), dissolved oxygen (DO) growth and electrical conductivity (EC) reduction in groundwater. This behavior was expected for an area with ozone sparging ISCO remediation, according to the literature.

Besides ozone reaching desired depths and since the control points are distributed throughout the contaminated area, it can also be said that chemical oxidation occurred in the subsoil. The research will continue with the analysis of CV concentrations and

discussion of the efficiency of ozone sparging ISCO technique in reducing contaminants concentration.

## Acknowledgments

The authors thank WALM Engenharia e Tecnologia Ambiental Ltda. for the incentive to the development of a M.Sc. program. The authors also thank the owner of the study area for making data and results available and for allowing the publication of data and results.

## REFERENCES

- [1] São Paulo State. Decree n°. 59.263, June, 05<sup>th</sup>, 2013. Regulates the law n° 13.577, July, 08<sup>th</sup>, 2009, which provides guidelines and procedures for the protection of soil quality and management of contaminated áreas and provides related measures. Available in <<http://www.al.sp.gov.br/repositorio/legislacao/decreto/2013/decreto-59263-05.06.2013.html>>. In Aug, 19<sup>th</sup>, 2017.
- [2] Interstate Technology & Regulatory Council – ITRC. Technical / Regulatory Guidance – Integrated DNAPL Site Strategy. November, 2011. 209p.
- [3] Instituto de Pesquisas Tecnológicas do Estado de São Paulo – IPT. Guia para elaboração de Planos de Intervenção para o Gerenciamento de Áreas Contaminadas. BNDS, 2014.
- [4] SIEGRIST, R. L., CRIMI, M., SIMPKIN, T. J. *In situ* Chemical Oxidation for Groundwater Remediation. SERDP, ESTCP, Springer Science, New York, New York, United States of America, 2011.
- [5] STROO, H. F.; WARD, C. H. *In situ* Remediation of Chlorinated Solvent Plumes. SERDP, ESTCP, Springer Science, New York, New York, United States of America, 2010.
- [6] HULLING, S.G.; KO, S.; PIVETZ, B. Groundwater Sampling at ISCO Sites: Binary Mixtures of Volatile Organic Compounds and Persulfate. Groundwater monitoring & Remediation 31 issue 2. 72-79.
- [7] MAHMOUD, A.; FREIRE, R. S. Métodos emergentes para aumentar a eficiência do ozônio no tratamento de águas contaminadas. Centro de Capacitação e Pesquisa em Meio ambiente, Cubatão – SP, 2006. (Química Nova, Vol, 30, n°, 1, 198-205, 2007)
- [8] WALM Engenharia e Tecnologia Ambiental Ltda. RT-2.00.00.00/1Y9-011 – Investigação Ambiental Detalhada – Etapa 5. 2014a.
- [9] CETESB – Companhia Ambiental do Estado de São Paulo. Manual de Gerenciamento de Áreas Contaminadas. São Paulo: CETESB, 2013a. 389p.

- [10] WALM Engenharia e Tecnologia Ambiental Ltda. RT-2.00.00.00/1Y9-013 – Plano de Intervenção e Concepção do Sistema de Remediação. 2014b.
- [11] World Health Organization - WHO. Environmental Health Criteria 215 – Vinyl Chloride. United Nations Environment Programme, International Labour Organization, World Health Organization e Inter-Organization Programme for the Sound Management of Chemicals. Geneva, Switzerland, 1999.
- [12] United States Environmental Protection Agency - USEPA. Natural Attenuation Decision Support System User's Manual. Version 1.0. United States of America. January, 2000.
- [13] SMITH, LR; DRAGUN, J. Degradation of Volatile Chlorinated Aliphatic Priority Pollutants in Groundwater. Environmental International, Vol. 10, pp. 291-298. 1984.
- [14] Agency for toxic substances and disease registry - ATSDR. ATSDR Case studies in environmental medicine: Vinyl Chloride toxicity. Clin. Toxicol, 28: 267-285. United States of America, 1990.
- [15] WALM Engenharia e Tecnologia Ambiental Ltda. RT-2.00.00.00/1Y5-032 – 2º Relatório de Monitoramento da Eficiência e Eficácia dos Sistemas de Remediação. 2016a.
- [16] United States Environmental Protection Agency - USEPA. Standard Operating Procedures # 2046 – Slug tests. United States of America, March, 1994.
- [17] United States Environmental Protection Agency - USEPA. How to evaluate alternative cleanup technologies for underground storage tank sites. A guide for corrective action plan reviewers, Chapter II – Soil Vapor Extraction. United States of America, 2017. (EPA/510/B-17-003).
- [18] United States Environmental Protection Agency - USEPA. How to evaluate alternative cleanup technologies for underground storage tank sites. A guide for corrective action plan reviewers, Chapter VII – Air Sparging. United States of America, 2017. (EPA/510/B-17-003).
- [19] ABNT – Associação Brasileira de Normas Técnicas. NBR-15.487. Amostragem de água subterrânea em poços de monitoramento – métodos de purga, 2010.
- [20] BHUYAN, S. J. e LATIN, M. R. BTEX Remediation under challenging site conditions using in-situ ozone injection and soil vapor extraction technologies: a case study. Soil and Sediment Contamination, 21:545-556, 2012.
- [21] BANHIDI, M. Metal Finishing 93 - pH and ORP. 544;546;548-550. 1995.
- [22] United States Environmental Protection Agency - USEPA.. Introduction to in situ bioremediation of groundwater. Office of Solid Waste and Emergency Response, December, 2013. (EPA/542/R-13-018).
- [23] CETESB – Companhia Ambiental do Estado de São Paulo. Qualidade das Águas Interiores no Estado de São Paulo – Apêndice A. Significado ambiental e sanitário das variáveis de qualidade das águas e dos sedimentos e metodologias analíticas e de amostragem. São Paulo, 2013b. 43p.

## DAIRY WASTEWATER TREATMENT BY VERMI-BIOFILTRATION

Rabee Rustum <sup>1</sup>, Shebin Akbar K <sup>2</sup> and Adebayo J. Adeleye <sup>3</sup>

<sup>1,2</sup> School of Energy, Geoscience, Infrastructure and Society, Heriot-Watt University, Dubai Campus, UAE

<sup>3</sup> School of Energy, Geoscience, Infrastructure and Society, Heriot-Watt University, Edinburgh, UK,

### ABSTRACT

The treatment of dairy wastewater using traditional wastewater treatment plants such as the activated sludge is not feasible as it will require high energy rate to provide the required oxygen. This paper presents experimental results of using Vermi Bio-filtration to treat wastewater from dairy industry. Samples of wastewater were collected from Prasanthi Farms located in a small village of Kollam district, India. The sample characteristics of pH, Total Dissolved Solids, Total Suspended Solids, Chemical Oxygen Demand, Oil & Grease and Dissolved Oxygen were measured before and after vermi bio-filtration treatment. The characteristics were measured at different time intervals of 12 hours (12, 24, 36, 48, and 60 hours). The percentage changes of the above parameters after 60 hours are -18, 79, 75, 67, 69 and -31% respectively. the method is inexpensive, it can capture all organic materials, capital and working expenses are low, there is no foul scent, worm biomass would be used as nourishment for the cows, fish agro-business.

*Keywords: Dairy, Wastewater treatment, Vermi Bio-filtration, Vermi composting.*

### INTRODUCTION

Dairy industry is engaged with the assembling of different sorts of drain items from dairy processing. The largest part of wastewater is generated from cleaning activities. The industry produces between 0.2 to 10 liters of effluent per liter of processed milk with an average distribution of around 2.5 liters of wastewater for every liter of the milk prepared [1]. The planned volumetric load is 1 m<sup>3</sup> of waste for each ton of produced milk [2].

The composition, concentration and effluents volume emerging within dairy plants remain reliant on the nature of products that is handled, plan of the production, operating techniques, processing plan patterns, and the level of management of water use for cleaning the equipments [3]. In general, the dairy wastewater comprises higher biological loadings denoted as BOD (Biological Oxygen Demand), COD (Chemical Oxygen Demand), and total solids that might be in liquefied or colloidal system. It also has high amounts of nitrogen and phosphorus that are, to a great extent, connected with milk proteins [4]. Hence, arrival of untreated dairy wastewater into the stream prompts consumption of dissolved oxygen (DO).

Aerobic & anaerobic techniques are usually used in treating dairy wastewaters because of the very biodegradable contaminants. A review on different aerobic and anaerobic treatment methods in dairy industry wastewater can be found in [5]. However, conventional treatment procedures of dairy wastewater are costly, since they have constant supply of power, which is an issue in developing countries. Thus, several alternatives are proposed for

sustainable wastewater treatment of dairy wastewater such as stabilization ponds [6] and constructed wetlands [7]. Nevertheless, these methods require large area of land. Thus, several researchers undertake researches to use vermi-bio-filtration treatment for dairy wastewater like [8], [9].

The use of night crawlers in wastewater or sludge treatment is called *vermi-bio-filtration* [9]. In this process, dissolved and suspended natural and inorganic solids are caught by adsorption and adjustment through complex biodegradation forms that happen in the "living soil" possessed by worm and the vigorous microorganisms [10]. Microorganisms that are present inside the earthworm helps in biochemical degradation of organic matter present in the wastewater [9].

Thus, *vermi-filtration* have several advantages. It has a low energy dependency; 100% capturing of the organic materials is certain; there is less capital and working expenses, and with the addition of high valued additional finished product (*vermi compost*); there is no foul scent while the worms capture decomposing and decay of every single putrescible matters in the wastewater; large amounts of worm biomass would be accessible as nourishment for the cows, fowls, and fish agro-business, after the principal year of vermi-treatment; sludge is released in the vermi-filter bed as excreta (*vermi compost*) which is a valuable soil added substance for farming and cultivation [11].

Hughes, Nair, and Ho [12] also reported that *Vermi-technology* is reasonable for dispersed wastewater treatment. It is very efficient in regard to eliminating COD, BOD, SS and some N and P. It was also observed that there was no foul odor throughout



the treatment.

Arora, Rajpal, and Kazmi [13] reported that *vermi-filtration* showed a greater potential for chemical pollutants and pathogen removal from wastewater. Higher percentage of BOD, COD, TSS, FC, FS, *Salmonella* and *Escherichia coli* removal was observed to the accepted level for reuse in irrigation purpose. It was seen that *vermi-filter* (VF) diminished biochemical oxygen demand and chemical oxygen demand by 84.8% and 73.9%, respectively.

Sinha, Bharambe, and Chaudhari [9] examined the vermi-filtration of sewage acquired from the Oxley Wastewater Treatment Plant in Brisbane, Australia. Results demonstrated that the worms expelled BOD heaps of sewage by more than 99 % at water powered maintenance time, hydraulic retention time of 1-2 hours. Normal COD expelled from the sewage by night crawlers is more than 50 %. Worms additionally evacuated the total suspended solids (TSS) by more than 90 %.

Patel [14] conducted the analysis on the waste water generated from dairy industry and found a high removal efficiency for most water quality parameters: BOD - 97.95%; COD - 91.64%; TSS -76.39%; TDS - 84.27%; Oil & grease - 84.13%.

However, it is necessary for the wastewater to stay in contact with the worms in the filter bed for some time. This time depends on the flow rate and the porosity of the filter. This paper investigate the effects of retention time on the performance of *Vermi filter* used to treat dairy wastewater.

## MATERIALS AND METHOD

For the ease of comparison, the work used almost the same methodology presented Telang and Patel [14]. The vermi bio-filter was made by using a plastic bucket of 20-liter capacity for the breeding of the worms. Holes are drilled on the curved surface area of the drum for natural aeration. The schematic details of the experiment is shown in Fig. 1.

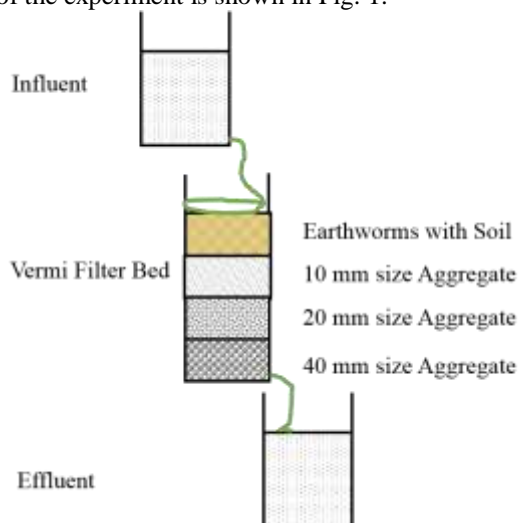


Fig.1 Vermi Bio filter.

Young specimens of *Earthworms*, *Eisiena Fetida* and *Eudrilos eugeniae* were gotten from composting unit kept up at temperature of 25°C in cow dung situated in Kollam, India. Kollam locale is one of 14 regions of the territory of Kerala, India. The region has a cross-segment of Kerala's normal traits; it is invested with a long coastline, a noteworthy Laccadive Sea seaport and an inland lake, Ashtamudi Lake. The area has numerous waterbodies, Kallada stream is one among them, and the east side place where there is waterway is East Kallada and the west side land is West Kallada. As per the 2011 statistics Kollam area has a populace of 2,629,703 [15].

The bio filter consisted of four layers through which the wastewater filtered through. The bottom layer was 6-7 cm of 40 mm size aggregate, over which 20 mm size aggregate was placed at a depth of 4-5 cm. Another layer of aggregate of 10 mm size was set up to a depth of 2-3 cm. The top most layer was the garden soil mixed with earthworms (Fig.2). The different depths of the layers were adopted in order to treat a maximum of 3L of wastewater at a time such that the vermi bed is not submerged. If the vermi bed is submerged, it would prevent the earthworms from obtaining the oxygen they require, since earthworms breathe through their skin.



Fig. 2 Garden soil mixed with earthworms.

The influent was conveyed into the bio filter through an irrigation system, which was made to distribute the water over the entire surface area of the bio-filter. The irrigation system was prepared with the help of a polyvinyl hose into which holes of about 3mm diameter at a spacing of 6 to 7 cm. The experimental procedure was carried out using dairy farm wastewater. The samples were collected from the Prasanthi Farms located in a small village of Kollam district, India. This wastewater is produced from the dairy product manufacturing and washing of the milk containers. This water is found to be simply discarded into the ground without any sort of treatment. The initial characteristics of the wastewater are given in Table 1. The influent characteristics were found out for each trial and then it was subjected to *vermi* bio filtration treatment and the effluent characteristics are noted at different trials. The wastewater samples were retained in the bio-



filter for different durations, that is, 12 hours, 24 hours, 36 hours, 48 hours and 60 hours.

Table 1 Influent and effluent water quality parameters

| Retention time (hours) | Influent/ Effluent | pH  | TDS (mg/l) | TSS (mg/l) | COD (mg/l) | DO (mg/l) | Oil & Grease (mg/l) |
|------------------------|--------------------|-----|------------|------------|------------|-----------|---------------------|
| 12                     | INF.               | 6.5 | 2440       | 120        | 2480       | 9.5       | 560                 |
|                        | EFF.               | 7   | 1990       | 100        | 2280       | 7.9       | 470                 |
| 24                     | INF.               | 6.5 | 2960       | 140        | 3600       | 9.4       | 340                 |
|                        | EFF.               | 7.3 | 1870       | 80         | 2120       | 7.3       | 210                 |
| 36                     | INF.               | 7   | 3080       | 170        | 3200       | 9.6       | 700                 |
|                        | EFF.               | 7.9 | 1340       | 90         | 1200       | 11.3      | 400                 |
| 48                     | INF.               | 6.5 | 2480       | 140        | 2200       | 9.9       | 540                 |
|                        | EFF.               | 7.7 | 540        | 40         | 750        | 12.7      | 240                 |
| 60                     | INF.               | 6.3 | 2680       | 160        | 2560       | 10        | 610                 |
|                        | EFF.               | 7.5 | 560        | 40         | 850        | 13.1      | 190                 |

To ensure the presence of the earthworms in the bio-filter, dry leaves, dried cow dung, fruits and vegetable waste materials are added to enhance the growth of the worms. The container was protected from direct sunlight and was aerated properly. Black soil and dry cow dung are mixed together and are filled to a depth of 3 – 5 cm along with the earthworms. A layer of kitchen waste is filled as the fourth layer above which the dry leaves are placed.

The 20L influent container is placed at a height above bio-filter to ensure continuous flow of wastewater into the filter. The tap was fitted to the base of the influent container and the bio-filter. The irrigation pipe, which allows distributed flow into the bio-filter, is connected to the pipe at the base of the influent container. The effluent is collected in a 20L capacity effluent bucket. About 3L of the wastewater sample was treated for each trial.

## RESULTS AND DISCUSSION

Different parameters have been used to determine the effect of retention time on the removal efficiency of *vermi-filter*.

### Variation in Hydrogen Ion (pH)

As seen from Table 2 and Fig. 3, the pH values has generally increased after the dairy wastewater passed through the filter, and this increase ranges

between 8 and 19%. However, the pH values stays within the range of 7-7.9, and this implies that the earthworms neutralize the dairy wastewater within the vermi bio-filter.

Table 2 Removal efficiency (%) of measured parameters

| Time | pH  | TDS (mg/l) | TSS (mg/l) | COD (mg/l) | DO (mg/l) | Oil & Grease (mg/l) |
|------|-----|------------|------------|------------|-----------|---------------------|
| 12   | -8  | 18         | 17         | 8          | 17        | 16                  |
| 24   | -12 | 37         | 43         | 41         | 22        | 38                  |
| 36   | -13 | 56         | 47         | 63         | -18       | 43                  |
| 48   | -19 | 78         | 71         | 66         | -28       | 56                  |
| 60   | -18 | 79         | 75         | 67         | -31       | 69                  |

### Total Dissolved Solids (TDS)

The TDS values of the raw data used for this experiment ranges from 2440 to 2080 mg/l. These values have been reduced over time as seen from Table 2 and Fig.3 and the maximum removal efficiency achieved after 60 hours was 79%. This imply that the worms can convert the dissolved solids to suspended solids stay in the filter and hence enhance the removal efficiency of the TDS in the vermi-filter.

### Total Suspended Solids (TSS)

The range of TSS values of the raw dairy wastewater introduced to the *vermi-filter* ranges between 120 and 170 mg/l. The results presented in Table 2 shows that the *vermi-filter* reduces the TSS values and this reduction increases with elapsed time and the maximum removal efficiency was 75% over 60 hours. These solids were consumed by earthworms and converted to small particles stayed in the filter or passed with the effluent.

### Chemical Oxygen Demand (COD)

COD values presented to the vermi filter ranges from 2200 to 3600 mg/l. The overall removal efficiencies of the COD increase over time and reached to 67% after 60 hours as seen from Fig. 3. This results are close to the results found by [9] who have done similar experiment for soaking wastewater and found that the COD reduction using earthworm is more than 50%.

Patel [14] reached almost to the same results

(84.27 % removal efficiency), but with a shorter time, 24 hours. However, it is difficult to compare the results as the mass of earthworms has not been determined in both cases, which must have an effect on the removal efficiency of the measured parameters.

Similar removal efficiency were observed by [16] who have also made a research on the up flow anaerobic fixed bed reactor for processing of dairy industry waste utilizing polypropylene pall rings as a pressing media and discovered that regular COD removal efficiency of 87% and highest biogas creation of 9.8 l/d was accomplished. A down flow fixed-film digester was also utilized by [17] for the treatment of deproteinized cheese with a regular chemical oxygen demand of 59,000 mg/L, the digester accomplished a COD decrease of 90–95% at a hydraulic retention time of 2.0–2.5 days.

### Dissolved oxygen (DO) Variation

The behavior of DO in the experiment is different from other parameters. The DO is reduced during the initial stages and then started to increase in the later stages. This reduction is due to other microorganisms that use the DO to consume the organic materials in the sample, and since the oxygen is supplied by the atmosphere to the wastewater, the DO concentration started to increase.

### Oil & Grease

Similar to other organic parameters, the removal efficiencies of the oil & grease using the *vermi-filtration* increases with time as indicated by the result presented in Table 2 and the highest observed value

was 69% after 60 hours. Similar results was observed by [14] who found that the removal efficiency of Oil and Grease was 84.13% after 24 hours.

### CONCLUSION

This study presented the results of an experimental study to investigate the effect of retention time on the performance of *vermi* bio filter used to treat dairy wastewater. The results showed that the removal efficiency of the vermi filter increase over time and the maximum value for TDS, TSS, COD and Oil & Grease after 60 hours were 79, 75, 67 and 69% respectively. The pH buffering ability was attained as the pH of the wastewater was neutralized by the earthworms within the bio filter and increase by 18%. DO value shows some decrease at the first 24 hours and then increases by 31% after 36 hours. Clogs within the filter, due to sludge accumulation, were not witnessed during the experiment. This is due to the action of earthworms that consume the solids and hence clear the path for water. There was no foul smell with *vermi-filtration* unit all through the experiment and there was no sludge development in the vermi-filtration procedure.

The filtered water can be used for irrigation and the produced *vermi* compost can be used as fertilizer. Other design parameters such as the depth and the surface of the filter should be taken into consideration in the future. Also the effect of the mass of earthworms need to be investigated further, which is the next step of this research. Thus, *vermi-filtration* is a viable technology for the treatment of dairy wastewater.

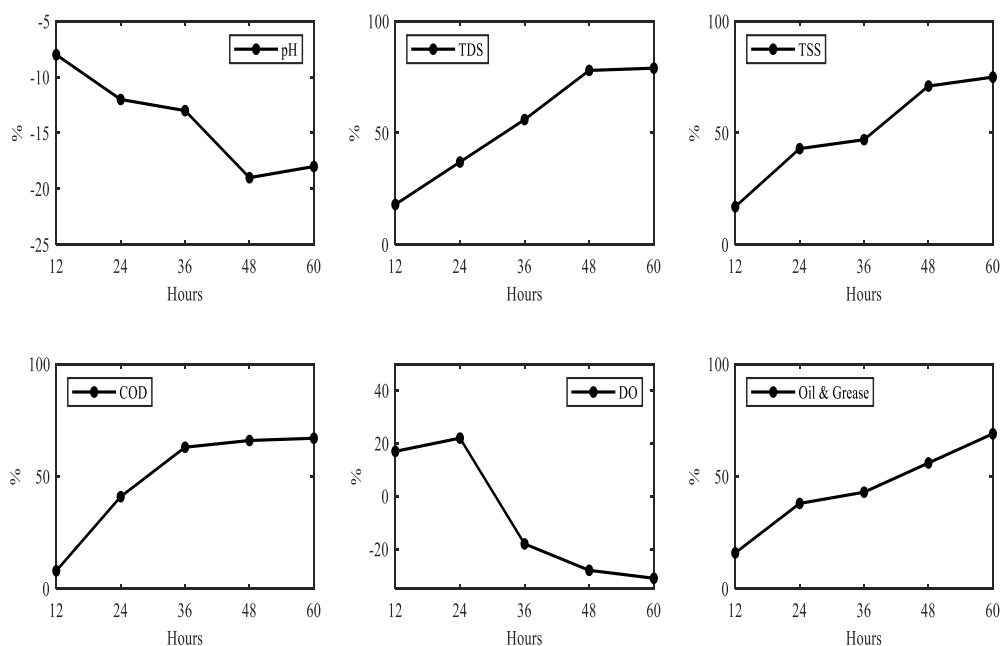


Fig. 3 distribution of water quality parameters over time.

## REFERENCES

- [1] Shete, B.S. and Shinkar, N.P., Dairy industry wastewater sources, characteristics & its effects on environment. *International Journal of Current Engineering and Technology*, Vol. 3, Issue 5, 2013, pp.1611-1615.
- [2] Nadais, M.H.G., Capela, M.I.A., Arroja, L.M.G. and Hung, Y.T., Anaerobic treatment of milk processing wastewater. In *Environmental Bioengineering*, Humana Press, Totowa, NJ., 2010, pp. 555-627.
- [3] Karadag, D., K ro lu, O.E., Ozkaya, B. and Cakmakci, M., A review on anaerobic biofilm reactors for the treatment of dairy industry wastewater. *Process Biochemistry*, Vol. 50, Issue 2, 2015, pp.262-271.
- [4] Vidal, G., Carvalho, A., Mendez, R. and Lema, J.M., Influence of the content in fats and proteins on the anaerobic biodegradability of dairy wastewaters. *Bioresource Technology*, Vol. 74, Issue 3, 2000, pp.231-239.
- [5] Goli, A., Shamiri, A., Khosroyar, S., Talaiekhosani, A., Sanaye, R. and Azizi, K., A Review on Different Aerobic and Anaerobic Treatment Methods in Dairy Industry Wastewater. *Journal of Environmental Treatment Techniques*, Vol. 6, Issue 1, 2019, pp.113-141.
- [6] Boruszko, D., Research of Effective Microorganisms on Dairy Sewage Sludge Stabilization. *Journal of Ecological Engineering*, Vol. 20, Issue 3, 2019, pp.241-252.
- [7] D browski, W., Karolinczak, B., Gajewska, M. and Wojciechowska, E., Application of subsurface vertical flow constructed wetlands to reject water treatment in dairy wastewater treatment plant. *Environmental technology*, Vol. 38, Issue 2, 2017, pp.175-182.
- [8] Kaur, S. and Cheema, P.P.S., Vermifiltration Using Garden Waste as Padding Media for Treatment of Dairy Wastewater. In *International Conference on Sustainable Waste Management through Design*, Springer, Cham, 2018, pp. 51-58.
- [9] Sinha, R.K., Bharambe, G. and Chaudhari, U., Sewage treatment by vermifiltration with synchronous treatment of sludge by earthworms: a low-cost sustainable technology over conventional systems with potential for decentralization. *The Environmentalist*, Vol. 28, Issue 4, 2008, pp.409-420.
- [10] Emamjomeh, M.M., Tahergorabi, M., Farzadkia, M. and Bazrafshan, E., A review of the use of earthworms and aquatic worms for reducing sludge produced: an innovative ecotechnology. *Waste and biomass valorization*, Vol. 9, Issue 9, 2018, pp.1543-1557.
- [11] Louren o, N. and Nunes, L.M., Optimization of a vermifiltration process for treating urban wastewater. *Ecological engineering*, Vol. 100, Issue 1, 2017, pp.138-146.
- [12] Hughes, R.J., Nair, J. and Ho, G., The risk of sodium toxicity from bed accumulation to key species in the vermifiltration wastewater treatment process. *Bioresource technology*, Vol. 100, Issue 16, 2009, pp.3815-3819.
- [13] Arora, S., Rajpal, A. and Kazmi, A.A., Antimicrobial activity of bacterial community for removal of pathogens during vermifiltration. *Journal of Environmental Engineering*, Vol. 142, Issue 5, 2016, pp. 1-10.
- [14] Telang, S. and Patel, H., Vermi-biofiltration-a low cost treatment for dairy wastewater. *Int J Sci Res*, Vol. 4, Issue 7, 2015, pp.595-599.
- [15] Kuruvilla, K., Census towns in Kerala: Challenges of urban transformation. *Research notebooks*, School of Habitat Studies, 2014, pp. 1-12.
- [16] Deshannavar, U.B., Basavaraj, R.K. and Naik, N.M., High rate digestion of dairy industry effluent by upflow anaerobic fixed-bed reactor. *Journal of Chemical and Pharmaceutical Research*, Vol. 4, Issue 6, 2012, pp.2895-2899.
- [17] Canovas-Diaz, M. and Howell, J.A., Stability of a percolating anaerobic downflow fixed film reactor under overloading conditions. *Biotechnology letters*, Vol. 8, Issue 5, 1986, pp.379-384.

## System Dynamic Modelling for Sword and White Pomfret Fish Resources at Depok Coast, Bantul Regency

Dewi Susiloningtyas<sup>1</sup>, Hengki Tasman<sup>2</sup>, Tuty Handayani<sup>3</sup> and Arti Aulia<sup>4</sup>

<sup>1</sup>Department of Geography, Faculty of Mathematics and Natural Sciences, Universitas Indonesia, Indonesia;

<sup>2</sup>Department of Mathematics, Faculty of Mathematics and Natural Sciences, Universitas Indonesia, Indonesia

### ABSTRACT

Depok Coast in Bantul Regency popular for fishing activities. The potential for considerable marine resources in Depok Coast is a major factor in progress of fisheries business. The potential of these marine resources can provide a great opportunity for the development of capture fisheries and raise the economy of coastal communities. Sword and white pomfret fish are the main commodities in capture fisheries households in Depok Coast. However, if the occurrence of continuous arrests without further study is feared to cause the end of the sword and white pomfret fish resources in the future. This study aims to know the policies and the relationship between the ecological, economic and social sub-systems in the resources of sword and white pomfret on the Depok Coast. The method used in this research is the modeling of dynamic systems, where the sub-systems of the ecological, economic and associated social and serve as a model system dynamic of sword and white pomfret fish resources. Data for the ecological sub-system is an inventory of sword and white pomfret fish and the condition of the waters of Depok Coast. Furthermore, for the economic sub-system interviews were conducted by focus group discussion for the fishermen on Depok Coast and results in quantitative form. Data for the social sub-system is the number of fishermen and the population of Depok Village. The results of this modeling shows that overfishing can reduce sword and white pomfret fish resources if it is not compensated by fish preservation.

*Keywords: System Dinamic, Sword Fish, White Pomfret Fish, Depok Coast*

### INTRODUCTION

Fisheries system consists of a human system and a fisheries management system. The natural system consists of subsystems, namely fish, ecosystem and biophysical environment [1]. The human system consists of four subsystems, namely fishers, harvest sector and consumer posts, fishing household and communities and economic / cultural environment. The management system is grouped into four subsystems, namely fishery policy and planning, fishery management, fishery development and fishery research. The three components of the fishery system interact with each other to form a dynamic fisheries system.

The activities of fishermen in carrying out marine fisheries have various obstacles both from physical and non-physical factors. The constraints that many face in Indonesian fisheries and maritime affairs lie in their management systems. The potential of fisheries which is quite large but managed by the people without the knowledge of fisheries conditions is feared that overfishing will occur.

The increasing exploitation of fish resources as a result of increasing demand for these resources will have an impact on the increasing pressure on the sustainability of fish resources [2]. Coupled with the nature of the use of marine resources, which in general are open access, which means that their utilization is open to anyone and their ownership is

general so that the use of these resources tends to be free without any limitations as long as there are benefits / benefits obtained. The above conditions if it is not immediately managed (managed) properly sooner or later it is feared that it will threaten the sustainability of fish resources. It is estimated that 47 percent of the world's fisheries resources have experienced full exploited, 19 percent were declared overexplored, 9 percent have been depleted. Thus 75 percent of fish resources have experienced critical [3].

Depok Coastal is the largest fishery products in Bantul Regency [4]. The potential for considerable marine resources in Depok Coast is a major factor in the progress of fisheries fisheries. High potential of marine resources in Depok Coast made many fishermen from outside Bantul Regency migrate to Depok Coast to find decent income for fish at there.

According to data from TPI MinaBahari 45, the main commodity in Depok Coast are sword and white pomfret. In 2015, sword became the largest catch (32.42%) of the 13 types of fish available. Whereas white pomfret is the most expensive type of fish with the third largest catch result after Sword and Snapper.

Therefore, the management of capture fisheries with characteristics of densely captured and multifunctional waters requires an integrated policy of coastal and marine natural resource utilization and management in order to be able to improve the welfare of fishing communities. To make it happen, a

resource management instrument is needed which focuses more on the ability of carrying capacity of the nature without ignoring the economic interests of the community. This study aims to determine fisheries resources especially Sword and White Pomfret in Depok coast waters with dynamic system models up to 2030.

## METHODS

This research was conducted in Depok coast, Bantul district using secondary data from TPI Mina Bahari 45. The model used was a dynamic system model using Powersim 8 software.

### Production Surplus Model

This surplus production model is used to see carrying capacity and capture capabilities in a fishery waters. This study uses a surplus model produced by Walters and Hilborn (1992). In general the regression form of the Walters and Hilborn production surplus model can be written as follows:

$$Y = \alpha + \beta X_{1t} + \gamma X_{2t} + \varepsilon_t \quad (1)$$

Where :

$$Y_t = \frac{U_{t+1}}{U_t} - 1$$

$$X_{1t} = U_t$$

$$X_{2t} = E_t$$

$$\varepsilon_t = \text{error - term}$$

Equation 1 is a regression equation with dependent or non-dependent variables is the rate of biomass change and independent or independent variables are CPUE and effort (Walters and Hilborn 1992). Those equation can be used to estimate the biological parameters K (carrying capacity) and q (capture ability) separately from the three regression equation coefficients.

### System Dynamics Model

Fisheries resources are dynamic natural resources, as well as pertubasi that occurs in these resources both in the form of a relationship between catch dam effort, Therefore the management of fisheries resources which are relatively dynamic and complex requires a dynamic analysis approach as well. For this reason, dynamic analysis needs to be done to see the interaction between the components of resources and their changes [5].

System Dynamics analysis is carried out through two stages, namely making a causal loop diagram and flow diagram. The causal loop diagram shows the relationship between variables in the system process being examined. The basic principle of making it is a

process as a cause that will produce a condition, or vice versa a situation as a cause will produce a process while a flow diagram is made based on the equation of the dynamic model which includes state variables (level), flow/rate, auxiliary, and constant.

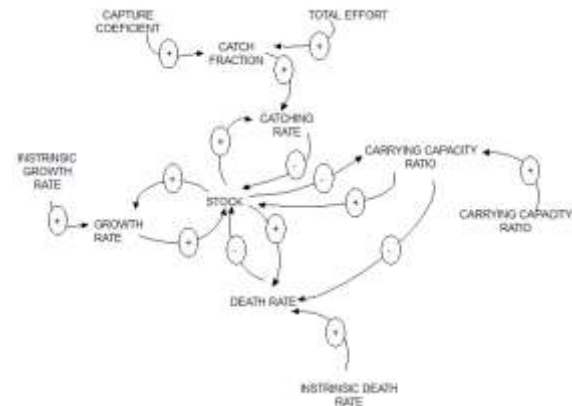


Fig 1. Causal Loop Diagram for Fish Resources

In the end, validation is carried out to determine the compatibility between the simulation results and the simulated symptoms or processes. The model can be stated either if the error or deviation of the simulation results against the symptoms or process is simulated small. The validation of the performance of the model is done by a simple statistical method, namely Average Mean Error (AME) between the simulation data and empirical data. The formula used is:

$$AME = \frac{|(Si - Ai)|}{Ai} \quad (2)$$

$$Si = \frac{\sum Si}{N} \quad (3)$$

$$Ai = \frac{\sum Ai}{N} \quad (4)$$

Where :

A = Actual Value

S = Simulation Value

N = Time Unit

Equation 2 until 4 are validation between simulation and empirical data on model. Model can be declared valid if the deviation between the simulation results and actual data is <30% [6].

## RESULTS

### Model for Sword Resources

Fishing data for Sword is obtained from Tempat Pelelangan Ikan (TPI) Mina Bahari 45. We got 54 months historical data, that is from January 2014 until April 2018. In this 54 months, fishermen went to sea as many as 23.067 trips. Which means that the total effort of fishermen was 23.067 times.

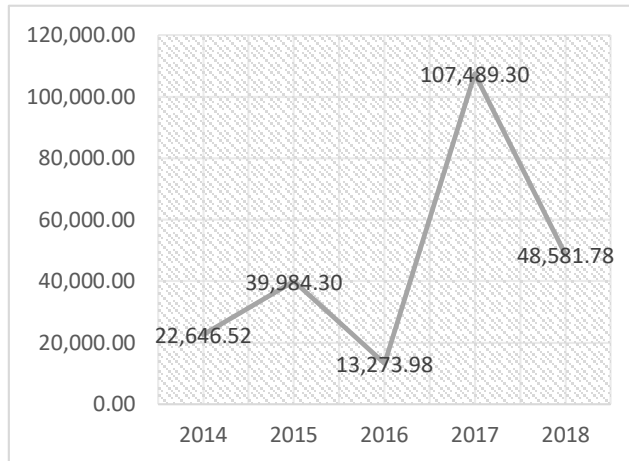


Fig 2. Captured of Sword per Year

Figure 2 is that the highest sword catch is in 2017, which is 107,489,30 kg. While the lowest catch is in 2016, which is 13,273,98 kg. This is because there is a west monsoon that causes strong waves so that it is difficult to sail. The average sword catch per year is 46,395,18 kg.

Results of the production surplus model to see carrying capacity and capture capabilities seen from CPUE data are 0.9986 and 0.9302. Then this value are included in the stock flow diagram for Sword Resources.

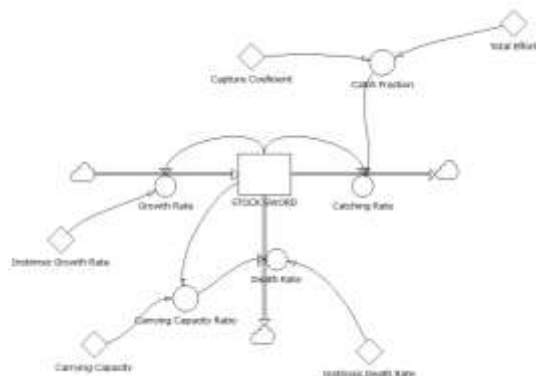


Fig 3. Stock Flow Diagram for Sword Resources

After the Stock Flow Diagram is made, the model is ready to be simulated. The simulation results in Figure 4 show that the stock of swords decreases every year. this is related to the decline in growth and also fish mortality, while the effort made by fishermen continues to increase each year. the fewer fish stocks there are, the less the number of catches obtained by fishermen. In 2030 the growth of sword fish was only 98 kg with a much higher death or capture rate of 105.45 kg and 273.78 kg which would result in the depletion of sword resources on the coast of Depok.

| Time        | STOCK SWORD (kg) | Growth Rate (kg/yr) | Death Rate (kg/yr) | Catching Rate (kg/yr) |
|-------------|------------------|---------------------|--------------------|-----------------------|
| 01 Jan 2014 | 22,646.52        | 126.82              | 126.33             | 353.93                |
| 01 Jan 2015 | 22,285.95        | 124.80              | 124.16             | 348.38                |
| 01 Jan 2016 | 21,931.11        | 122.81              | 122.02             | 342.75                |
| 01 Jan 2017 | 21,581.83        | 120.86              | 120.02             | 337.38                |
| 01 Jan 2018 | 21,238.31        | 118.93              | 117.85             | 331.92                |
| 01 Jan 2019 | 20,900.36        | 117.04              | 125.62             | 326.64                |
| 01 Jan 2020 | 20,567.29        | 115.18              | 123.81             | 321.44                |
| 01 Jan 2021 | 20,239.82        | 113.34              | 122.84             | 316.32                |
| 01 Jan 2022 | 19,917.60        | 111.54              | 119.90             | 311.28                |
| 01 Jan 2023 | 19,600.54        | 109.76              | 117.99             | 306.33                |
| 01 Jan 2024 | 19,288.46        | 108.02              | 116.11             | 301.45                |
| 01 Jan 2025 | 18,981.35        | 106.30              | 114.27             | 296.65                |
| 01 Jan 2026 | 18,679.14        | 104.60              | 112.45             | 291.93                |
| 01 Jan 2027 | 18,381.73        | 102.94              | 110.66             | 287.28                |
| 01 Jan 2028 | 18,089.96        | 101.30              | 108.89             | 282.71                |
| 01 Jan 2029 | 17,801.85        | 99.68               | 107.16             | 278.21                |
| 01 Jan 2030 | 17,517.62        | 98.10               | 105.45             | 273.78                |

Fig 5. Simulation Results for Sword Resources

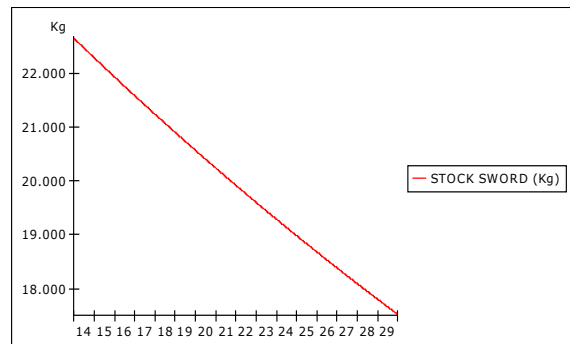


Fig 6. Graphic for Sword Stock in Model

Based on figure 6, we know that stock for sword fish will decrease during the simulation. this indicates that the sword fish will be depleted at a certain time. After the simulation is done. then the AME test is performed to determine the validity of the simulation results of the model and to find out whether the model can be predicted further.

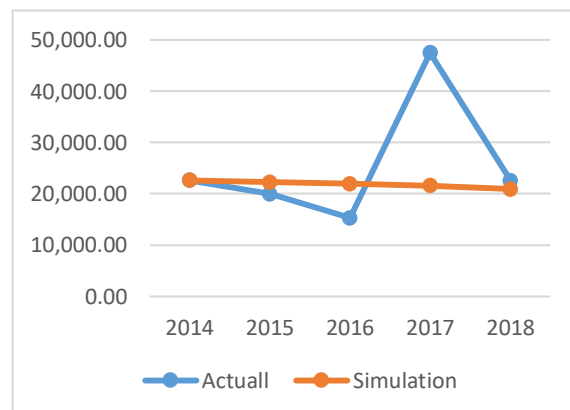


Fig 7. AME for Sword Stock

Results for AME test showed that the simulation results and acute data have a difference of 14.55% which means that the simulation results can be predicted further.



### Model for White Pomfret Resources

The data for white pomfret is also obtained from TPI Mina Bahari 45. With 54 months, and total trips of fishermen went to sea as many as 23.067 trips. Data showed that average white pomfret catch per year is 9.501,92 kg (figure 8). The highest catch in 2015 with a total of 15.198,95 kg. Different from sword fish, in 2017 white pomfret actually got the lowest catch of only 3.569,40 kg. This could be because in that year white pomfret was still migrating due to the existing high waves.

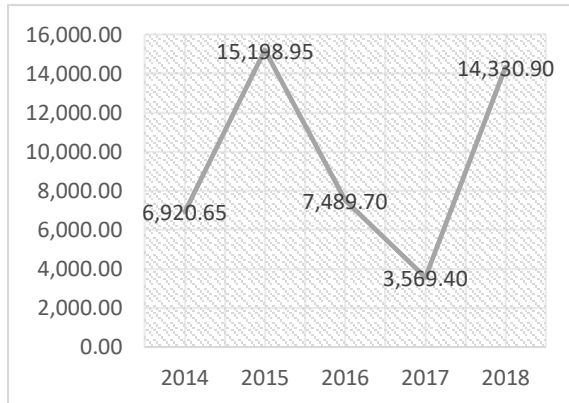


Fig 8. Captured of White Pomfret each Year

Results for production surplus model to see carrying capacity and capture capabilities seen from CPUE data same as the results for sword fish are 0.9986 and 0.9302. It is just the difference is value of intrinsic growth / death for white pomfret which is equal to 0.95 per year.

| Time        | STOCK WP (Kg) | Growth Rate - WP (Kg/yr) | Catching Rate - WP (Kg/yr) | Death Rate - WP (Kg/yr) |
|-------------|---------------|--------------------------|----------------------------|-------------------------|
| 01 Jan 2014 | 6,920.65      | 65.75                    | 106.36                     | 70.68                   |
| 01 Jan 2015 | 6,888.47      | 64.68                    | 106.43                     | 69.53                   |
| 01 Jan 2016 | 6,688.11      | 63.63                    | 104.68                     | 68.40                   |
| 01 Jan 2017 | 6,589.53      | 62.60                    | 102.99                     | 67.29                   |
| 01 Jan 2018 | 6,482.72      | 61.58                    | 101.32                     | 66.20                   |
| 01 Jan 2019 | 6,377.64      | 60.58                    | 99.67                      | 65.13                   |
| 01 Jan 2020 | 6,274.26      | 59.61                    | 98.06                      | 64.07                   |
| 01 Jan 2021 | 6,172.56      | 58.64                    | 96.47                      | 63.04                   |
| 01 Jan 2022 | 6,072.50      | 57.68                    | 94.90                      | 62.01                   |
| 01 Jan 2023 | 5,974.07      | 56.75                    | 93.37                      | 61.01                   |
| 01 Jan 2024 | 5,877.23      | 55.83                    | 91.85                      | 60.02                   |
| 01 Jan 2025 | 5,781.96      | 54.93                    | 90.38                      | 59.05                   |
| 01 Jan 2026 | 5,688.24      | 54.04                    | 88.90                      | 58.09                   |
| 01 Jan 2027 | 5,595.04      | 53.16                    | 87.46                      | 57.15                   |
| 01 Jan 2028 | 5,503.33      | 52.30                    | 86.04                      | 56.22                   |
| 01 Jan 2029 | 5,413.09      | 51.45                    | 84.65                      | 55.31                   |
| 01 Jan 2030 | 5,324.29      | 50.62                    | 83.27                      | 54.41                   |

Fig 9. Simulation Results for White Pomfret Resources

Stock flow diagram for white pomfret is the same as that used for sword fish. The simulation results in Figure 10 showed that the stock of white pomfret decreases every year. This is related to the decline in growth and also fish mortality, while the effort made

by fishermen continues to increase each year. The fewer fish stocks there are, the less the number of catches obtained by fishermen. In 2030 the growth of sword fish was only 50,63 kg, but this difference is not too far from the death rate of only 54,41 kg. But also, the number of arrests is far greater than the death of 83,27 kg.

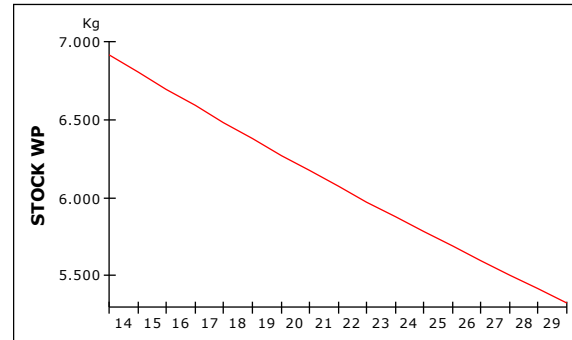


Fig 10. Graphic for White Pomfret Stock

After the simulation is done, result of AME test showed that the simulation results and acute data have a difference of 8,98% which means that the simulation results can be predicted further.

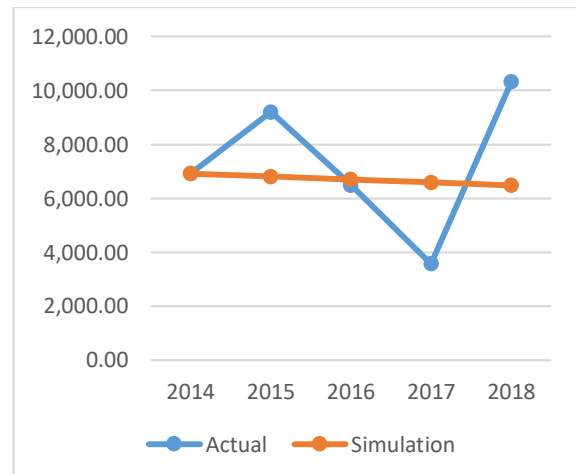


Fig.11 AME for White Pomfret Model

Figure 11 is value of AME in white pomfret model. Graphic showed for simulation white pomfret stock- from 2014 until 2018- stable between 6000-8000 kg, but in reality stock of white pomfret has increased and decreased (fluctuated).

### CONCLUSION

The model shows that both sword fish and white pomfret will decline in stock until 2030. This is also followed by a smaller growth rate than the death rate or catching rate. If this condition still continues it will cause depletion of sword fish and white pomfret resources in the waters of Depok Coast. Therefore it is necessary for government efforts to provide a

balance between the desires of the market and existing resources.

#### ACKNOWLEDGMENTS

We would like to thank for Hibah PDUPT 2019 from DIKTI (1/E1/KP.PTNBH/2019 and 234/PKS/R/UI/2019) have supported in funding of this research.

#### REFERENCES

- [1] Charles AT. 2001. Sustainable Fishery Systems. United Kingdom: Blackwell Science Ltd. 370 p.
- [2] Mulyani, Tri Ayu. 2013. *Economic Development Policy Sustainable Captain Fisheries In Dki Jakarta Province*. Postgraduate. Bogor Agricultur Institute.
- [3] Fauzi A dan S Anna. 2002. Evaluation of Fisheries Development Sustainability Status: Application of Rapfish Approach (Case Study of DKI Jakarta Coastal Waters). Indonesian Coastal and Ocean Journal Vol 4 (2) pp: 36-49.
- [4] Bantul Regency Marine and Fisheries Service. 2015. Bantul Regency Fisheries Production.
- [5] Muhammadi. et. al. 2001. Dynamic System Analysis: Environment, Social, Economy and Management. Jakarta :UMJ Press.
- [6] Hilborn R and CJ Walters. 1992. Quantitative Fisheries Stock Assessment, Choice, Dynamic and Uncertainty.
- [7] Supriatna, Supriatna, J., Koestoer, R. H., & Takarina, N. D. (2016). Spatial Dynamics Model for Sustainability Landscape in Cimandiri Estuary, West Java, Indonesia. Journal Procedia Social and Behavioral Sciences, 227, 19-30.
- [8] Muhammadi, Aminullah, E., Soesilo, B. (2001). Systems Dynamics Analysis: Environmental, Social, Economic, Management. Jakarta: UMJ Press.

## FRESH PROPERTIES PERFORMANCE OF ALKALINE ACTIVATED PALM OIL PASTE

Aidan N<sup>1</sup>, Nuradila Izzaty H<sup>1</sup>, Muhd Norhasri M.S<sup>2</sup>, Sharifah A<sup>2</sup>

<sup>1</sup>Student, Faculty of Civil Engineering, Universiti Teknologi MARA, 40450 Shah Alam, Selangor, Malaysia; <sup>2</sup>Lecturer, Faculty of Civil Engineering, Universiti Teknologi MARA, 40450 Shah Alam, Selangor, Malaysia

### ABSTRACT

Cement powder has been used as the basic construction material throughout the years. As the demand increases, so does the production. Researchers have been trying to find an alternative to replace the usage of cement to reduce the production that resulted in increase of carbon dioxide emission. Palm Oil Fuel Ash (POFA) is one of the alternatives. POFA usage has been proven to be beneficial. However, the use of activator with POFA cement paste might enhance these benefits even more. This research highlights the fresh properties of Palm Oil Fuel Ash cement paste with activator through experimental investigation. In this research, the activator used are sodium-based solution; sodium silicate and sodium hydroxide. This sodium-based solution is generally used in geopolymer cement to improve its mechanical and fresh properties. In this research, cement is replaced by 5% weight of POFA whereas water is partially replaced by alkaline activator with ratio of 1kg of water to 200ml activator. The fresh properties of the paste in this study emphasis on flow, setting time and consistency, which are the important properties to improve effectiveness and efficiency of repairing work such as grouting and patching. Sodium Silicate POFA cement paste tends to have the highest consistency and the fastest setting time for both initial and final. Other than that, the presence of POFA tends to reduce flowability of paste. Sodium Hydroxide POFA cement paste has highest flowability, however Sodium Silicate POFA cement paste decrease in flow percentage compare to OPC.

*Keywords: POFA; Sodium Hydroxide; Sodium Silicate; Flow; Setting Time; Consistency*

### INTRODUCTION

Palm Oil Fuel Ash (POFA) waste has been increasing day by day which contribute to large usage of land disposal. Lately, the use of POFA in sustainability development has open an opportunity to solve this environmental issue. POFA has been used as cement replacement due to its pozzolanic properties. As our economical, technological and ecological advancement grew by days, the usage of pozzolanic material as cement replacement also increases and is expected to continue in years to come [1]. Other than addressing the issue of increase in land disposal usage, the use of POFA also could potentially decrease the effects of carbon footprint due to cement production. Cement production industry has contributed up to 5% of the world's carbon dioxide emission [2]. Tons of carbon dioxide are release into the atmosphere from the decarbonation process of limestone and the combustion of fossil fuel during the cement manufacturing process [3]

Previous studies manage to prove that the usage of POFA in concrete can improve the compressive strength and the durability. High content of silicon dioxide or calcium oxide in POFA can produce extra hydration process that will improve the concrete strength and durability [4]. A denser and durable

cement mortar resulted from high Calcium-Silicate - Hydroxide gel formed from high content of silica in POFA [5]. Other than that, due to its fine particle, POFA can also acts as filler. When used to replace cement in a high amount, the fine particle of POFA has the ability to increases the concrete workability as well as the setting time [5]. Other than mechanical behavior, the usage of POFA also improve the fresh properties of concrete. Improved finishing surfaces and workability is produced by the ability of POFA to absorb water from the mixture and retained it in the system [6]. However, to improve the efficiency of POFA usage in cement replacement, activator is needed.

Since Alkali-activated binders production uses a moderate amount of energy, they are considered environmental friendly [7]. Alkaline activator has the ability to dissolve the acidic oxides of POFA which normal water is not able to do [8]. For this research, sodium-based solution is used as alkaline activator; Sodium Hydroxide and Sodium Silicate. Sodium Silicate has been proven to decrease the setting time of cement. Although there is no increase in strength of concrete, sodium silicate has the ability to make the concrete to undergone fast setting [9]. Whereas, Sodium Hydroxide has the ability to increase the strength of concrete. The compressive strength properties of geopolymer concrete is

improved because the higher concentration of Sodium Hydroxide produced a good bonding of aggregate and paste [10]. A Higher amount of Sodium Hydroxide also reduces the cement setting time [11]. This activator will be a partial replacement for water in the design mix. During the hydration process of cement, small amount of calcium hydroxide is produced when less amount of cement is used. The small amount of calcium hydroxide is insufficient for hydration with large amount of reactive silica. So, in order to activated the reaction of excessive reactive silica, sodium hydroxide is needed [12]. With this, the usage of alkaline activator might be able to enhance the efficiency of POFA replacement in cement.

This research also emphasis on the patching and repair work application. The use of POFA has been proved to enhancing cement properties used in repair works. When POFA is incorporated, the compressive strength of cement grout increased up to 20% [13]. However, better performance can be achieved with the usage of alkaline activators.

This research is conducted in hoping to discover new types of material that can be used in patch and repair work. The goal of this research is to evaluate the fresh properties of POFA cement paste reacted with sodium-based solution. This research also hopes to contribute to the reduction in cement manufacture which resulted in increasing of carbon dioxide release, reduction of the POFA waste which will consume large amount of land for disposal as well as improving concrete repair works material.

## METHODOLOGY

### Sample Preparation

The sample used in this research are prepared based on the design mix shown in table 2.1. OPC has no replacement in cement and water. Whereas, 5P has a 5% replacement of cement with POFA but no replacement in water. For 5P5.2H and 5P5.2S has a 5% cement replacement to POFA and a replacement of water with a ratio of 1kg of water to 200ml of with sodium hydroxide and silicate solution respectively.

Table 1: Design Mix

| Sample | Cement<br>(kg/m <sup>3</sup> ) | POFA<br>(kg/m <sup>3</sup> ) | Water<br>(kg/m <sup>3</sup> ) | Activator<br>(kg/m <sup>3</sup> ) |
|--------|--------------------------------|------------------------------|-------------------------------|-----------------------------------|
| OPC    | 380                            | 0                            | 205                           | 0                                 |
| 5P     | 360                            | 20                           | 205                           | 0                                 |
| 5P5.2H | 360                            | 20                           | 163                           | 42                                |
| 5P5.2S | 360                            | 20                           | 163                           | 42                                |

### Fresh Properties Testing

This research emphasis on the fresh properties of cement paste since it is one of the most important properties that will influence the effectiveness and efficiency of repairing and rehabilitation work. The fresh properties tests are standard consistency test, setting time test and flow table test.

### Standard Consistency Test

Standard consistency test is used to obtained the water demand of the paste. Paste consistency is an important attribute since it could affect the workability of a freshly mixed paste as well as the strength of the paste after it hardens. Too much water could increase workability but reduce the strength and vice versa. In order to get the optimum water demand, this test is needed. This test is conducted accordance to ASTM C191 standards.

### Setting Time Test

Setting time test is conducted after conducting standard consistency test. The optimum water demand obtained in standard consistency test is used in this test. Setting time test consist of initial setting time and final setting time. Initial setting time is obtained to determine the time when the paste started to losses its plasticity. Whereas, the final setting time is obtained to determine the time the paste started to losses its plasticity completely and hardened. Setting time is also an important attribute since in repairing works, paste needed to set quickly so that the repaired structure can be operational again. Since this test is a continuity to standard consistency test, therefore it is also conducted in accordance to ASTM C191 standards.

### Flow Table Test

The workability of the paste is obtained by conducting flow table test. Water cement ratio obtained from the standard consistency test is used in this test. Workability of the paste is essential to be access especially in repairing work since some requires the paste to be injected in cracks. This test is conducted in accordance to ASTM C1437 standards where the flow table will be dropped for 25 times in 15 seconds.

## RESULTS

### Standard Consistency Test

Table 2: Standard Consistency Test Result

| Design Mix | Weight of Cement (g) | Percentage of POFA (%) | Amount of Water (ml) | Amount of Sodium (ml) | Penetration (mm) | Percentage of Water (%) |
|------------|----------------------|------------------------|----------------------|-----------------------|------------------|-------------------------|
| OPC        | 400                  | 0                      | 119                  | 0                     | 6                | 29.8                    |
| 5P         | 400                  | 5                      | 130                  | 0                     | 6                | 32.51                   |
| 5P5.2H     | 400                  | 5                      | 112                  | 28                    | 6                | 35                      |
| 5P5.2S     | 400                  | 5                      | 124                  | 31                    | 5                | 38.8                    |

### Setting Time Test

Table 3: Setting Time Test Result

| Design Mix | Initial Setting Time (min) | Final Setting Time (min) |
|------------|----------------------------|--------------------------|
| OPC        | 178                        | 292                      |
| 5P         | 220                        | 365                      |
| 5P5.2H     | 280                        | 289                      |
| 5P5.2S     | 58                         | 62                       |

### Flow Table Test

Table 4: Flow Table Test Result

| Sample | Ave. diameter (mm) | Flow (%) |
|--------|--------------------|----------|
| OPC    | 172.67             | 69.28    |
| 5P     | 163.00             | 59.80    |
| 5P5.2H | 216.33             | 112.09   |
| 5P5.2S | 102.33             | 0.33     |

## DISCUSSION

Based on the data obtained, a few discussions have been made.

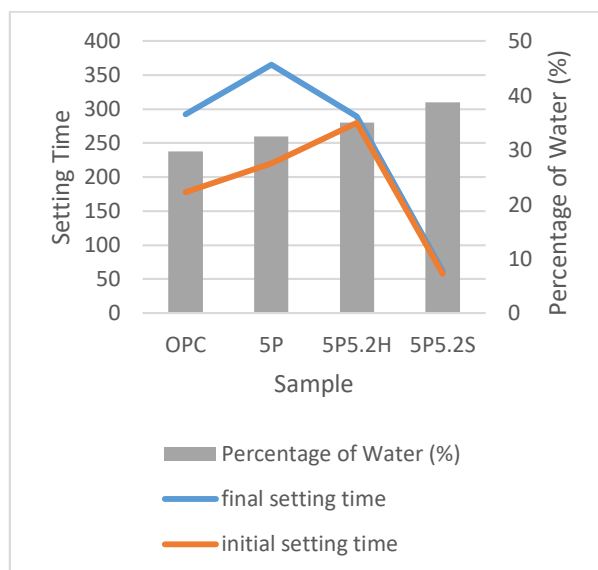


Fig 1: Relationship between Setting Time (min) and Consistency (%)

As cement consistency increase, the it will make the cement setting time to increase as well. However, with activator, it can be seen that it could reduce the setting time. Sodium Silicate could decrease the setting time more compare to Sodium Hydroxide as seen by sample 5P5.2S and 5P5.2H in Fig 1. This shows that both alkaline activators have the ability to accelerate hydration which reduce the setting time of the cement. However, the presence of POFA in cement increases the setting time. This is probably due to the porous particle of POFA that is able to absorb more water hence retaining more water in the system for a longer period of time.

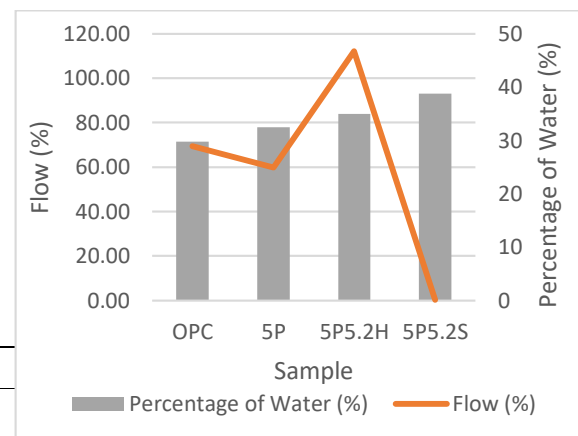


Fig 2: Relationship between Flow (%) and Consistency (%)

Supposedly, the higher the cement consistency will make cement paste to flow better. But as seen in Fig 2, when POFA is partially replace with cement, it tends to reduce the flow. Basically, this is due to the POFA that's absorb the water in the system. But, the presence of Sodium Hydroxide tends to increase the flow due to its ability to disperse the POFA cement particle. On the other hand, Sodium Silicate reacts in a different way. The presence of Sodium Silicate tends to make the paste less flowable. This is probably because Sodium Silicate might have increased the hydration process immediately it has been mixed with POFA cement.

## CONCLUSIONS

Fresh properties have been the focus of this research due to its applications in repairing and rehabilitation works. POFA and sodium-based solution are used to enhance the fresh properties in order for them to fit for their purpose. Based on all the test conducted and data obtained, below are the findings;

1. In consistency test, sodium silicate sample shows to have high water percentage, which

is 38.8% compared to OPC which is 29.8% in order to achieved standard consistency. This is due to the fast hydration reaction between the sodium silicate and the cement when they are in contact.

2. In both initial and final setting time test, sample with sodium silicate activator shows to have fast setting time compared to the other 3 samples with a reading of 58 and 62 minutes respectively. Compare to OPC, sample with sodium silicate has a decrement of 67.41% in initial setting time and 78.76% decrement in final setting time. Since there is fast hydration process after the activator mixed with the cement, therefore this is expected to happen. Fast setting happens when higher rate of hydration occurs. However, fast setting result in poor workability over time. In this case, sodium hydroxide tends to have better workability since it has higher initial setting time.
3. In flow table test, the presence of POFA in the paste stuns the flowability where the flow percentage recorded is 59.80% compare to OPC with 69.28%. However, when POFA cement is reacted with Sodium Hydroxide, it improves the flowability even more compare to OPC with a value of 112.09%. However, Sodium Silicate presence in POFA cement tends to decrease the flow with a reading of 0.33% flow compare to OPC.

Based on the findings above, it is concluded that the uses of sodium silicate as activator is suitable to be used as external repairing work in need of immediate operation. It can be used to seal cracks. However, for internal repairing like cracks filling, sodium hydroxide activator is suitable since it has better ability to flow into the cracks. Other than that, the use of sodium-based solution also proves to improve certain properties of the POFA cement paste.

## ACKNOWLEDGMENTS

I would like to take this opportunity to express my gratitude and most sincere thanks to my supervisor Dr. Muhd Norhasri Bin Muhd Sidek for guiding me throughout this research. I also would like to thank the technicians for their involvement in heavy structure laboratory. Many thanks to my friends and family for supporting me mentally in order for me to complete this research.

## REFERENCES

- [1] A. S. M. Abdul Awal and M. Warid Hussin, "Effect of palm oil fuel ash in controlling heat of hydration of concrete," *Procedia Eng.*, vol. 14, pp. 2650–2657, 2011.
- [2] M. T. Carrasco, "Alkaline activation of different aluminosilicates as an alternative to Portland cement : Alkali activated cements or ... Alkaline activation of different aluminosilicates as an alternative to Portland cement : alkali activated cements or geopolymers La ac," no. August, pp. 4–12, 2017.
- [3] S. V. Joshi and M. S. Kadu, "Role of Alkaline Activator in Development of Eco-friendly Fly Ash Based Geo Polymer Concrete," *Int. J. Environ. Sci. Dev.*, vol. 3, no. 5, pp. 417–421, 2012.
- [4] K. Wi, H. S. Lee, S. Lim, H. Song, M. W. Hussin, and M. A. Ismail, "Use of an agricultural by-product, nano sized Palm Oil Fuel Ash as a supplementary cementitious material," *Constr. Build. Mater.*, vol. 183, pp. 139–149, 2018.
- [5] H. M. Hamada, G. A. Jokhio, F. M. Yahaya, A. M. Humada, and Y. Gul, "The present state of the use of palm oil fuel ash (POFA) in concrete," *Constr. Build. Mater.*, vol. 175, pp. 26–40, 2018.
- [6] N. F. Imran, M. N. Hasri, N. A. K. Fitri, D. Hasan, and M. Z. Ramli, "Effects of palm oil fuel ash ( POFA ) towards consistency and setting time properties of concrete Effects of Palm Oil Fuel Ash ( POFA ) Towards Consistency and Setting Time Properties of Concrete," vol. 020035, no. October 2018, 2020.
- [7] G. F. Huseien, M. M. Tahir, J. Mirza, M. Ismail, K. W. Shah, and M. A. Asaad, "Effects of POFA replaced with FA on durability properties of GBFS included alkali activated mortars," *Constr. Build. Mater.*, vol. 175, pp. 174–186, 2018.
- [8] O. A. Abdulkareem and M. Ramli, "Optimization of Alkaline Activator Mixing and Curing Conditions for A fly Ash-Based Geopolymer Paste System," *Mod. Appl. Sci.*, vol. 9, no. 12, p. 61, 2015.
- [9] A. M. Ifrah Habib Lone, Javid Ahmad, Syed Mohammad Jasim, Mintazir Ali, Mushtaq Ahmad Khan, and Amir Hussain Malik, "Experimental Study of Effect of Sodium Silicate ( $\text{Na}_2\text{SiO}_3$ ) on Properties of Concrete," *Int. J. Civ. Eng. Technol.*, vol. 6, no. 12, pp. 39–47, 2015.
- [10] A. R. M. Ridzuan, M. M. Al Bakri Abdullah, M. F. Arshad, M. F. Mohd Tahir, and A. A. Khairulniza, "The Effect of NaOH Concentration and Curing Condition to the Strength and Shrinkage Performance of Recycled Geopolymer Concrete," *Mater. Sci. Forum*, vol. 803, no. August 2014, pp. 194–200, 2014.



- [11]Y. Huang and Z. Lin, "Effect of sodium hydroxide on the properties of phosphogypsum based cement," J. Wuhan Univ. Technol. Mater. Sci. Ed., vol. 25, no. 2, pp. 342–345, 2010.
- [12]B. Bahadure and N. Naik, "Effect of Alkaline Activator on Workability and Compressive Strength of Cement Concrete with RHA," Int. J. Comput. Eng. Res., vol. 03, no. 5, 2013.
- [13]D. Mujah, "Compressive strength and chloride resistance of grout containing ground palm oil fuel ash," J. Clean. Prod., vol. 112, pp. 712–722, 2016.

## ANALYSIS OF THE PERFORMANCE AND ELEMENTAL ANALYSIS ON LIME ACTIVATOR POFA

Nuradila Izzaty H<sup>1</sup>, Aidan N<sup>1</sup>, Muhd Norhasri M.S<sup>2</sup>, Sharifah A<sup>2</sup>

<sup>1</sup>Student, Faculty of Civil Engineering, Universiti Teknologi MARA, 40450 Shah Alam, Selangor, Malaysia; <sup>2</sup>Lecturer, Faculty of Civil Engineering, Universiti Teknologi MARA, 40450 Shah Alam, Selangor, Malaysia

### ABSTRACT

Utilization of waste products by replacing and additive in cement is growing robustly in the construction industries in order to give a result of high strength of concrete especially by using Supplementary Cementitious Material (SCM) such as Rice Husk Ash (RHA), Slag (SG) and Palm Oil Fuel Ash (POFA). An experimental study is done on the cement paste incorporating Palm Oil Fuel Ash (POFA) and lime activator solution to assess on its performance and elementary analysis for development of aging 1, 3, 7 and 28 days. The 50 mm x 50 mm x 50 mm cube specimens were cast by partially replacing cement with 5% of POFA as pozzolons and partially replacing water with lime activator, with ratio of water to lime activator, 1kg to 200ml. It was observed that cube specimens with 5% partial replacement of cement with POFA with the inclusion of lime activator give contribution on high element of calcium that gives a result on fast hardened cement paste with an adequate compressive strength which can be beneficial on patching and repairing concrete with demand on time constraint in the construction industries.

*Keywords: Lime activator; Compressive strength; Elementary analysis; Repairing*

### INTRODUCTION

Urbanization worldwide has make cement standout as one of the significant building material among other in construction industry. Cement properties that versatile and durable makes it the utmost sustainable choice for both residential and commercial construction. However, the cement production gives negative impact to the environment which releases greenhouse gas emissions both directly through calcination process and indirectly produced by burning fossil fuels to heat the kiln. As a consequence, CO<sub>2</sub> emissions cause harm and pollute the environment. Sooraj VM [1] has states that 5% from total amount of each ton of cement production has release CO<sub>2</sub> emission to the atmosphere and by improving on the production process in cement manufacturing can reduce the emission of CO<sub>2</sub>. Reducing the CO<sub>2</sub> emissions from the calcination process in the cement production means looking to a material that having the same properties as cement. Environmental have concern on the huge amount of CO<sub>2</sub> that have been release from the cement manufacturing that produce expanding widely and this lead an enthusiasm the study on the field of supplemental cementitious materials (SCMs) with a particular ultimate objective to decrease the amount of cement in the concrete production [2].

Palm oil production gives a big contribution in economy of Malaysia as the product comes as the second world's largest producer after Indonesia. As

framed in Ninth Malaysian Plan (RMK-9), palm oil also has is export worldwide as Malaysia is now aiming on biotechnology industry which estimated to generate improved quality of agriculture products [3]. According to study by Mohd Hilton Ahmad & Noor [4], the industrial sector in Malaysia has produced huge number of waste which more than 10 million ton per year. Waste such as POFA, rice husk and fly ashes are the most interest waste to be study among engineers and scientist. The waste can be reuse in construction material as pozzolans. Pozzolans is a siliceous or siliceous and aluminous material when the particles react with the calcium hydroxide from the cement and produce cementitious properties [4]. Several studies have done on the uses of pozzolans as cement replacement in concrete improving on the construction material and encounter waste disposal problem.

Palm Oil Fuel Ash (POFA) is the ash that a product from burning of palm oil husk and palm kernel shell in palm oil mill boiler [5]. POFA ashes are usually disposed with no commercial as the return effect on the environmental pollution. With the contribution of POFA in concrete, the disposal effects of this waste are reducing. In addition, the uses of POFA as a supplementary cementing material in concrete reduces the amount of cement used and makes the concrete mixtures to be more economical.

However, the addition of POFA with alkaline based in the cement paste have enhance the cement

properties. Due to high content of silicon dioxide and calcium oxide in POFA, the concrete strength and durability can be affected [6]. The presence of alkaline activator gives effect on the polymerization in the pozzolanic materials [7]. Silicate, carbonate, and hydroxide, sulphate forms of sodium and potassium ions are some of the alkaline activators that commonly used. However, sodium hydroxide and liquid sodium silicate is a choice of alkaline activator for a geopolymers material [8]. This research was undertaken to analyses the performance and the elemental analysis on Lime activator POFA.

## METHODOLOGY

### Cement Paste Preparation

For this study, cement paste is prepared consist of OPC as control samples, 5PP5.2SH which is 5% replacement of cement with POFA and replacement of water with ratio 1kg: 200ml with sodium hydroxide, and 5PP5.2S which is 5% replacement of cement with POFA and replacement of water with ratio 1kg: 200ml with sodium silicate. Table 2.1 shows the design mix for the cement paste preparation.

Table 1: Design Mix Preparation

| Sample  | Cement<br>(kg/m <sup>3</sup> ) | Water<br>(kg/m <sup>3</sup> ) | POFA<br>(kg/m <sup>3</sup> ) | Lime<br>Activator<br>(kg/m <sup>3</sup> ) |
|---------|--------------------------------|-------------------------------|------------------------------|---|
| OPC     | 380                            | 0                             | 205                          | 0   |
| 5PP5.2H | 360                            | 20                            | 163                          | 42  |
| 5PP5.2S | 360                            | 20                            | 163                          | 42  |

### Material Preparation

#### Palm Oil Fuel Ash (POFA)

There are four steps on the POFA preparation. Firstly, is finding the POFA. The POFA that used for this study is obtained the incinerated palm oil waste from United Palm Oil SDN BHD factory at Sungai Kecil, Nibong Tebal, Pulau Pinang, Malaysia. Next, to remove the coarse particles as small particle that useful to get a better control over the filler effect, the POFA were sieved passing 212 $\mu$ m sieving. After sieving, the POFA will be stored inside a clean, dry and airtight humidity-controlled room inside the laboratory to ensure its purity. The liquidated POFA were used in this study, which is the POFA is liquefied using ratio 1kg total volume of water used in the study with 200ml lime activator solution.

#### Raw material

#### Water

Normal tap water is use in this study in the concrete mix design.

#### Cement

Ordinary Portland cement (OPC) obtained from Tasek Corporation Sdn. Bhd. was used in this study. Due to the replacement of cement with POFA, each mixing used different weight of cement. The percentage of POFA used for this procedure is 5%.

### Mixing, Handling a test on compressive strength and elemental analysis of cement paste.

#### Compression test

The performance of the cement paste is observed through compression test. The compressive strength results are obtained by breaking down the specimen into the compression-testing machine cement. BS 1881-108:1983 was used as reference for this study.

#### XRF Analysis

The elemental analysis of cement paste estimated the proportions of each element present in the sample were performed with the X-Ray Fluorescence (XRF) by S1 TITAN Handheld XRF Spectrometer. The XRF machine uses polarized energy dispersion. The samples of XRF analysis for each condition were four cubes, which each cube per trial mix of 0.000125 m<sup>3</sup>. Each sample will be analyses for 1, 3, 7 and 28 days.

## RESULT AND DISCUSSION

### Compressive strength

Results of compressive strength of this study were shown in the figure and table below.

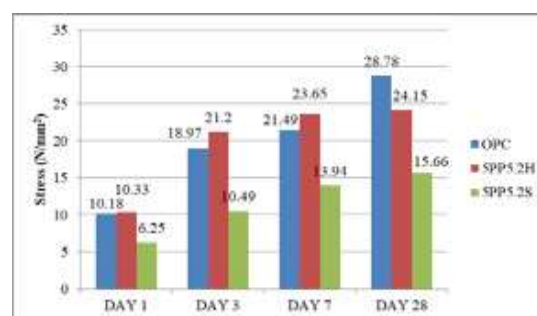


Fig 1: Compressive strength

The compressive strength results for this study are represented in Figure 3.1. The aging effect on the cement paste plays an important role in compressive strength. Based on figure 3.1, it shown that increment in age corresponds to a higher compressive strength. 5PP5.2H give result of high early strength on day 1, day 3, day 7 and day 14 followed by OPC and 5PP5.2S. The explanation behind this rate is due to adhesion mechanisms between CSH and POFA as fillers affect a great significance when it employed as a cement replacement. However, OPC tends to increase its strength on day 28. 5PP5.2S shows the lowest compressive strength compare to others.

### XRF Analysis

Based on the XRF analysis on the elemental analysis, the calcium and silicate element of each design mix is shown in table 3.3, 3.4 and 3.5.

Table 2: Elemental analysis of Calcium and Silica in OPC

|            | CaO   | SiO <sub>2</sub> |
|------------|-------|------------------|
| OPC DAY 1  | 65.04 | 23.38            |
| OPC DAY 3  | 78.69 | 34.25            |
| OPC DAY 7  | 85.12 | 24.52            |
| OPC DAY 28 | 60.49 | 26.63            |

Table 3: Elemental analysis of Calcium and Silica in 5PP5.2H

|                | CaO   | SiO <sub>2</sub> |
|----------------|-------|------------------|
| 5PP5.2H DAY 1  | 74.31 | 25.23            |
| 5PP5.2H DAY 3  | 75.83 | 31.83            |
| 5PP5.2H DAY 7  | 87.29 | 28.72            |
| 5PP5.2H DAY 28 | 91.31 | 25.24            |

Table 4: Elemental analysis of Calcium and Silica in 5PP5.2S

|                | CaO   | SiO <sub>2</sub> |
|----------------|-------|------------------|
| 5PP5.2S DAY 1  | 78.44 | 9.88             |
| 5PP5.2S DAY 3  | 87.41 | 3.18             |
| 5PP5.2S DAY 7  | 87.52 | 3.79             |
| 5PP5.2S DAY 28 | 93.89 | 0.31             |

From results, we can see that Calcium element increase over time for 5PP5.2H and 5PP5.2S. However, the Silica element for OPC and 5PP5.2H give high result on day 1 and increase on day 3, decreasing from day 7 to day 28. Silica element for 5PP5.2S is decreasing over time as this gives an

explanation on the lowest compressive strength. Based on the XRF analysis shown, 5PP5.2H and 5PP5.2S consist of high element of calcium compare to control samples and this gives an explanation on the result on fast setting cement. However, the high element of calcium gives less contribution in affecting the final binder since the silica element in both 5PP5.2H and 5PP5.2S decreasing over time.

### CONCLUSIONS

The conclusions drawn are both 5PP5.2H and 5PP5.2S contribute to accelerate on setting time compare to control sample which the cement paste are harden faster. Even though both 5PP5.2H and 5PP5.2S gives the lower result on compressive strength compared to OPC, but it has a moderate strength that can be used for repairing work such as patching and grouting. This gives a benefit in construction since construction site is normally highlighted on the time constraint for repairing work.

### ACKNOWLEDGMENTS

The author would like express profound gratitude to Dr. Muhd Norhasri bin Muhd Sidek for their guidance during this study. The author also wishes to thank to technicians of Heavy laboratory Universiti Teknologi Mara (UiTM) for their kind assistance in this research.

### REFERENCES

- [1] Sooraj VM, "Effect of Palm Oil Fuel Ash (POFA) on Strength Properties of Concrete," Int. J. Sci. Res. Publ., vol. 3, no. 6, pp. 2250–3153, 2013.
- [2] N. M. Altwair, S. Kabir, and W. Brameshuber, "Palm Oil Fuel Ash (Pofa): an Environmentally-Friendly Supplemental Cementitious Material for Concrete Production," Int. Rilem Conf. Mater. Sci. (Matsci), Vol Iii, vol. 77, pp. 113–126, 2010.
- [3] V. S. Ahamed and A. Pradesh, "STUDY OF STRENGTH OF CONCRETE WITH PALM OIL FUEL ASH AS CEMENT REPLACEMENT," vol. 7, no. 3, pp. 337–341, 2016.
- [4] M. H. Ahmad and N. M. Noor, "Chemical Attack of Malaysian Pozzolans Concrete," pp. 11–24, 2009.
- [5] S. K. Nguong and A. S. M. A. Awal, "FUEL ASH ( POFA ) CONCRETE A SHORT-TERM INVESTIGATION ON HIGH VOLUME PALM OIL FUEL ASH ( POFA ) CONCRETE," 2010.

- [6] K. Wi, H. S. Lee, S. Lim, H. Song, M. W. Hussin, and M. A. Ismail, "Use of an agricultural by-product, nano sized Palm Oil Fuel Ash as a supplementary cementitious material," *Constr. Build. Mater.*, vol. 183, pp. 139–149, 2018.
- [7] U. J. Alengaram and S. M. Alamgirkabir, "Engineering properties of oil palm shell and palm oil clinker based geopolymer concrete," vol. 38, pp. 34–48, 2015.
- [8] D. Hardjito, S. E. Wallah, D. M. J. Sumajouw, and B. V. Rangan, "On The Development of Fly Ash-based Geopolymer Concrete On the Development of Fly Ash-Based," no. October, pp. 467–472, 2015.

## PHYSICAL AND CHEMICAL PROPERTIES OF WATER: CASE OF TAAL LAKE, PHILIPPINES

Merlita C. Medallan<sup>1</sup>, Ed.D. & Enrico Garcia<sup>2</sup>

<sup>1,2</sup>Faculty, Lyceum of the Philippines University Laguna, Philippines

### ABSTRACT

Water quality can affect the ecosystem at several trophic levels. It is very important for an ecosystem to have healthy water bodies as lives of aquatic species depend upon them. Taal, with a small lake located in the southern part of Luzon in the Philippines is teeming with aquatic resources, yet it is observed that its water quality is deteriorating. The lake is surrounded by several municipalities with tributaries contributing to its quality. This study evaluated Taal lake ecosystem in six sample sites in terms of physical and chemical attributes utilizing secondary data obtained from the Department of Environment and Natural Resources (DENR). Mean values of pH, temperature and total soluble solids (TSS) were within the standards set by the agency. However, there was a slight increase in dissolved oxygen (DO) and a low biological oxygen demand (BOD). There is high nitrogen and heavy metal contamination with one highly contaminated site. This was attributed to high municipal and kitchen waste disposal and high amounts of fertilizers used in fields. Taal lake aquatic ecosystem can be classified as severely polluted based on the chemical parameters. Nitrate, phosphate, oil and grease, pH, temperature and DO levels vary significantly from site to site. Levels of arsenic, chromium, TSS and BOD do not show any significant difference among the sites.

*Keywords: Chemical, Physical, Quality, Taal Lake, Water*

### INTRODUCTION

The health condition of every human is co-related to the environment or surrounding where he or she lives. With the rapid urbanization, increasing population, human and industrial activities and more so the extreme climatic condition, the world has seen some drastic changes to acknowledge that our environment is severely affected. Lakes and other freshwater ecosystems provide essential services to the society. Most important of these services is fresh drinking water, power generation, water for bathing, sites for recreational activities and important fisheries.

One of the most important body of water in the southern island of Luzon in the Philippines is Taal Lake. Taal Volcano, a famous site is seated in the middle of the Taal Lake. Taal Lake, formerly known as Bombon Lake, is also the deepest and the third largest Lake in the Philippines. Taal Lake is located in Southern Luzon, Batangas Province, (approximately 60 km. south of Manila) is surrounded by nine (9) towns and two (2) cities translating into 287 barangays. It has a total area: 24,356 hectares, with a circumference of 120 kilometers; a maximum depth of 198 meters or an average of 60 meters (PCCARD, 1981) and a shoreline of 82,500 m.

The lake is a major source of livelihood for most of the local dwellers. Fishing as one of the main jobs provides for the living of the community. Lake fisheries provide livelihood to around 20,000 fisherfolk.

The resource is used for aquaculture, recreation, tourism, navigation, and water source for Tagaytay. The Lake is known for its ecosystem that supports a diverse aquatic fauna comprising of both freshwater and marine species. Records of fish found in the lake by Albert W. Herre revealed 32 families of varied finfish resource, consisting of about 100 species, most (76 species) of which are migratory (BFAR Profile). In 2016, Taal Lake has a total fish production of 80,690MT, a majority of which comes from fish cage production.

A total number of thirty-seven (37) side streams surge into the Lake and its only outlet is the Site F [1]. The lake quality is determined by the effluents discharge in the tributaries. This in turn characterizes the aquatic conditions where fishes and other freshwater lake organisms live.

Global climate change is modifying freshwater productivity by changing the global area of these ecosystems by increasing their temperature and revising stratification. Extreme heating of surface waters between 30° N and S, associated with the high heat of vaporization of water, will result into rise in salinity of inland waters at low latitudes and loss of productivity of key organisms [2].

Water quality monitoring can help researchers predict and learn from natural processes in the environment and determine human impacts in an ecosystem. These measurement efforts can also assist in restoration projects and ensure that environmental standards are being met. Human intervention also has noticeable effects on water quality. Activities that



harm the environment directly by severely polluting them like discharge of domestic, industrial, urban and other wastewaters into the water course, whether intentional or accidental, and the spreading of chemicals on agricultural land in the drainage basin are the most obvious anthropologic destruction brought to the aquatic ecosystem. Any significant changes to the natural water quality are usually disruptive to the ecosystem [3].

The quality of a lake's water depends mostly on their physical, chemical and biological well-being. The degradation of water quality can affect not only the aquatic life but the surrounding ecosystem as well. Thus, a thorough assessment of water quality is an integral part of the lake's environmental monitoring. In this research, water quality was determined by reviewing the physical and chemical properties of water. The physical parameters such as temperature, pH, total dissolved solids, dissolved oxygen and biological oxygen demand was evaluated. Chemical properties include concentration levels of arsenic, chromium, nitrates, phosphates, oil and grease.

The temperature of water has less to do with the type, and more to do with the depth of water. Smaller bodies of water, like ponds, lakes and rivers, fluctuate more easily. This affects what kind of life can live there [4]. The significance of excessive turbidity in water on fish and other aquatic life begins by altering the temperature structure of lakes. Bottom-level temperatures are usually lower in turbid lakes or ponds than in clear ones. Generally, in many lakes, lower temperatures mean lower productivity. Turbidity also prohibits with the piercing of light. This reduces photosynthesis and thereby decreases the primary productivity upon which the fish food organisms survive. As a result, fish production is reduced. Also, by prohibiting light, turbidity makes it difficult for aquatic life to find food. Adversely, some organisms may be similarly protected from predators [5].

In streamlets, increased sedimentation and siltation can take place, which can result in degradation to habitat areas for fish and other aquatic life. Particles also supply attachment places for other pollutants, notably metals and bacteria. For this reason, turbidity readings can be used as an indicator of probable pollution in a water body. The particles of turbidity provide "shelter" for microbes by minimizing their subjection to attack by antiseptics. Microbial attachment to particulate material has been contemplated to aid in microbial existence [6].

pH is a measure of how acidic/basic water is. It ranges from 0 - 14, with 7 being neutral. Total dissolved solids (TDS) comprise inorganic salts (principally calcium, magnesium, potassium, sodium, bicarbonates, chlorides, and sulfates) and some small amounts of organic matter that are dissolved in water.

Dissolved Oxygen is the amount of gaseous oxygen (O<sub>2</sub>) dissolved in the water. Oxygen enters

the water by direct absorption from the atmosphere, by rapid movement, or as a waste product of plant photosynthesis. Water temperature and the volume of moving water can affect dissolved oxygen levels. Biochemical Oxygen Demand is an important water quality parameter because it provides an index to assess the effect discharged wastewater will have on the receiving environment. The higher the BOD value, the greater the amount of organic matter or "food" available for oxygen consuming bacteria.

Arsenic, although being toxic and probably carcinogenic when exposed through drinking water, has received very little attention in these past years. Potential pollution hazard of arsenic comes from ingesting it rather than eating arsenic-containing aquatic organisms. Although arsenic is greatly concentrated in aquatic organisms, it is evidently not progressively concentrated along a food chain. Additionally, arsenic in flesh has low toxicity, in general. Use of arsenic, the burning of fossil fuels, increased erosion of land, and the mining and processing of sulfide minerals have increased the amount of arsenic entering the lakes [7].

A range of 10 to 70 ppm arsenic has been commonly detected in household detergents and pre-soaks. Arsenic is present in detergents in arsenate state (V) and not in arsenide (III), a toxic form that is prepared for pesticide-use available commercially.

Chromium (VI) is a well-known priority polluting as well as highly toxic heavy metal. Maximum allowable concentration of chromium (VI) in drinking water is 0.05 mg/L [8]. Hexavalent chromium forms many soluble salts that can enter body membranes and induce a toxic response. Rats, mice, beagle, aquatic plants and fish species, all are affected adversely because of Cr (VI) pollution [9].

Nitrate is colorless, odorless and tasteless compound present in water. Common sources of nitrogen are fertilizers, manure, municipal wastewater, sludge, animal feedlots, septic systems, etc. Purification of nitrate-contaminated water can be done by treatments of distillation, reverse osmosis, ion-exchange, blending, charcoal filters and water softeners. Other health factors such as diarrhea and respiratory disease have also been associated with high nitrate levels in water [10].

Discharge of organic matter to water is one of the major sources of nutrients to seep through, since aerobic decomposition of such organic matter can result in release of phosphates, nitrates, etc., especially on domestic sewage containing high phosphate concentrations coming from detergents [11]. Agricultural run-offs and food-processing effluents are high in phosphate. Water analysis of water entering and leaving nine commercial trout farms three times during summer showed that concentrations of ortho-phosphate in the water may increase substantially during passage through the farm. Hence, magnetic separation can be applied to

all waterborne contaminants and removing the dissolved orthophosphate from the aqueous slurry [12].

The main cause of oil and grease water pollution is anthropologic activities. Water bodies situated near colleges, parks and other public institutions had high concentration of oil and grease particles in water due to drainage of cafeteria which also cause BOD and TSS value to be higher than normal in the lake. This has now been declared as one of the main factors that cause mass fish death in lake ecosystems [13].

It is important here to note that oil which forms a surface film on the river can coat plants and animals cutting or reducing their supply of oxygen from the above lying atmosphere. Transmission of light is affected due to the formation of oil film that floats above the body of water. This disturbs the photosynthesis process of aquatic plants. In animals, insulating properties of furs and feathers are affected. Mobility is also reduced due to increased stickiness once the oil starts to dry [14]. Eventually, in most cases, this leads to death. Oil bio accumulates in the higher animals and further enters the food chain. Detergents create frothing and can harm invertebrates and fish, as they are a major source of phosphates. Moreover, petroleum or grease spilled over water also produces chemicals that are extremely harmful for marine animals[14].

With the foregoing significance of Taal Lake to the community, it is but noting that quality of its water be monitored. The Department of Environment and Natural Resources (DENR) and the Bureau of Fisheries and Aquatic Resources (BFAR) are the two main government agencies that look after the quality of the Philippine waters. Water monitoring is regularly done to ensure preservation of the water quality and safety of the consumers. The study summarizes the physical and chemical properties of Taal Lake from six different sites where a comparison is also done.

Natural resources are the important wealth of our country, and water is one of them. Water is a wonder of nature. "No life without water" is a common saying given the fact that water is the one of the naturally occurring essential requirement of all life supporting activities [15]. Impurities present in water reduce its quality and its use. This would affect the health of both cultured and wild species as water quality is a major factor controlling them. The quality of water can easily be described by the physical, chemical and biological parameters or characteristics [16]. Physio-chemical variables are important environmental factors of water in which all biological communities live in association with each other [17].

## OBJECTIVES OF THE STUDY

This study aimed to present the water quality of Taal Lake in the Philippines by analyzing the physical

and chemical properties of water from different sites and compare them with the acceptable standards. The physical properties of the water include pH, temperature, total soluble solids, dissolved oxygen and biological oxygen demand. The chemical properties include Arsenic, Chromium, Nitrates, Phosphates, and Oil and Grease were also presented. A comparative analysis of the physical and chemical parameters among sites was done.

## METHOD

This study utilized a descriptive research design aimed to present the concentration level of different chemicals in the locality of Taal Lake's aquatic ecosystem. The study used a mixed method which consists of both quantitative and qualitative data. Secondary data collected from 2013 to 2018 by the Department of Environment and Natural Resources [DENR] in Site A, Batangas was used in the analysis.

Water samples were taken from six different sample sites within the vicinity of Taal Lake. Taal Lake is the third largest lake present in the southwestern region of Luzon in the Philippines. It occupies a volcanic crater with a maximum width of 24 kilometers and is 3 meters above sea level. At least four samples per site was collected for physical and chemical analysis.

Water samples were collected and placed in 1L sample in PET bottle and 1L sample in wide mouth glass bottle. Samples were immediately taken to the laboratory located in local BFAR office for analysis. Some data such as temperature and pH were collected on site.

Water analysis was performed following the procedures in the Standard Methods for the Examination of Water and Wastewater, 22nd ed, APHA, AWWA, WEF, Washington DC 2012. Standard values used for comparison is contained in DAO No. 2016-08 Water Quality Guidelines and General Effluent Standards of 2016. Physical parameters measured were pH, temperature, total soluble solids, dissolved oxygen and biological oxygen demand. Chemical parameters measured were arsenic, chromium, phosphate, nitrate and oil and grease.

All chemical tests collected were compared to the standard parameter table from the Bureau of Fisheries and Aquatic Resources (BFAR). Weighted mean has also been used to identify the average value of different study sites.

## RESULTS AND DISCUSSION

### Physical Properties of the Lake Water.

Physical water quality parameters such as pH, temperature, total soluble solids and dissolved oxygen fall under control set by DENR-EMB whereas levels of biological oxygen demand fall short

to the standards set.

The pH concentration levels were found highest in Site F is more than 8 whereas lowest in Site B counting some less than 7. All sites show acceptable pH levels. Changes in the pH value of water are important to many organisms. Most organisms have adapted to life in water of a specific pH and may die if it changes even slightly. This is especially true of aquatic macroinvertebrates and fish eggs and fry. The pH is a critical factor determining the health of a waterway. The factors that control it are obviously complicated. As with many environmental concerns, we need to be aware of the implications of any impacts we have upon the environment. [18]. Changes in pH is caused by natural conditions

(especially in swamps), dumping of waste (batteries) and farm runoff (lime). Most aquatic life cannot withstand water outside the optimum pH thus resulting in death.

Highest mean temperature recorded was around 27.6 from Site F while lowest was less than 26 from Site B. Site F being the only outlet of the lake and is a large stream, has a larger surface area which also encourages higher temperature compared to other sites [19]. Elements such as sunlight, heat transfer from the atmosphere, stream confluence and turbidity affect water temperature. Shallow and surface waters are more easily influenced by these factors than deep water.

Table 1. Physical Property Measurements

| Physical parameters      | Standard Values by<br>DENR-EMB (for<br>class B) | Site A | Site B | Site C | Site D | Site E | Site F |
|--------------------------|---|--------|--------|--------|--------|--------|--------|
| Sample size              |   | 7      | 5      | 13     | 4      | 5      | 4      |
| pH                       | 6.5 – 8.5                                       | 7.25   | 6.97   | 7.25   | 7.36   | 7.51   | 8.23   |
| Temperature              | 24-27 degree C                                  | 27.35  | 25.92  | 26.47  | 25.96  | 26.96  | 27.58  |
| Total Soluble Solids     | Not more than 30% increase                      | 22.48  | 11.28  | 31.48  | 29.56  | 32.35  | 10.31  |
| Dissolved Oxygen         | 5(minimum)                                      | 4.41   | 3.95   | 6.51   | 5.7    | 6.66   | 6.43   |
| Biological Oxygen Demand | 5(minimum) - 10(maximum)                        | 8      | 2.95   | 3.26   | 3.33   | 2.18   | 3.19   |

Site E, Site C and Site F had most levels of mean dissolved oxygen (DO) which is more than 6 whereas Site B was lowest falling few short of level 4. Just as we need air to breathe, aquatic organisms need dissolved oxygen to respire. It is necessary for the survival of fish, invertebrates, bacteria, and underwater plants.

DO is also needed for the decomposition of organic matter. Water with high concentrations of dissolved minerals such as salt will have a lower DO concentration than fresh water at the same temperature. Low dissolved oxygen (DO) primarily results from excessive algae growth caused by phosphorus. As the algae die and decompose, the process consumes dissolved oxygen [22]. All our sites except site B have good levels of dissolved oxygen which is healthy and no sign of threat. Oxygen enters the water by direct absorption from the atmosphere, by rapid movement, or as a waste product of plant photosynthesis. Water temperature and the volume of moving water can affect dissolved oxygen levels [23]. Dissolved Oxygen is found abundant from each sample that showcases the standard of ecosystem persisting in the premises is in healthy condition.

Ideally, the average level of DO desirable for aquatic habitat is 9.0 ppm (parts per million). This

provides good habitat for abundant fish population. Below 9ppm but higher than 7 ppm supports growth and aquatic activities while 5 ppm can still support spawning. When the level of DO is below 5, the condition becomes stressful for aquatic animals and there is about 12 to 24 hours of tolerance for growth. Below 3 ppm could hardly support fish population.

Site A region of Taal Lake has almost double levels of BOD compared to others and highest at 8 whereas lowest stands in Site E levelling a few more than 2. Oxygen consumption is affected by a number of variables: temperature, pH, the presence of certain kinds of microorganisms, and the type of organic and inorganic material in the water [24]. When the water body has high BOD, aerobic bacteria will utilize the available DO of water. In case of excessive BOD there will be deficiency of DO and water will be in anaerobic condition resulting in mortality of living aquatic organisms; release of ammonia, methane, CO<sub>2</sub> etc. In absence of oxygen, anaerobic bacteria become active. When BOD value is medium, water will possess excessive nutrients causing algal bloom. Such condition is again dangerous because during day time water will be supersaturated with oxygen (due to photosynthesis in presence of sun light), but at late night DO may be zero or close to zero. This is primarily due to utilization of oxygen for respiration

by plants and animals (without any production of oxygen in absence of sunlight). For this purpose, BOD must be maintained up to certain level in any surface waterbody [25]. All other sites except site A falls below the minimum requirement for BOD.

Somehow the physical factors of the Lake Taal have a corresponding influence on each other. Higher amounts of total dissolved solids will lower the temperature because these solids won't allow sunlight to reach enough depth of the water body. The physical properties do not correlate even if they are from same structure since its properties depend upon different factors like the surrounding it is situated or human interaction around. Temperature and pH levels also should be suitable for the life survival existing in the water body with abundant supply of Oxygen. According to Galera & Martinez [26], the water surface temperature, pH, total dissolved solids, total suspended solids, color and dissolved oxygen of Taal lake in 2009 conformed the class C water standards (DENR AO 34, 1990) and was therefore safe for aquaculture use.

**Chemical Parameters of the Lake Water.** In Site A, the levels of arsenic, chromium and nitrogen are found to be over the standard limit set by BFAR with nitrogen levels being almost 6 times higher than the standard limit. The levels of phosphorous, and oil

and grease are within the standard limit but dangerously close to the threshold value. A sampling point has given output of 180 mg/L nitrogen while 7mg/L is the standard set. A sample point shows nitrogen levels of 66mg/L.

Higher nitrogen levels mean possible overstimulation of algae and aquatic plants which could lead to lack of oxygen for fishes. In Site B, every chemical parameter was more or less near the standard limits set by BFAR. Only one sample from the five sampling points had minimal nitrogen pollution. This means that there will soon be an algal bloom and possible eutrophication, if not taken care of. Nitrogen in water comes mainly from fertilizers and insecticides.

Site C shows very unsatisfactory data results with only phosphorous levels being within tolerable standards while all other chemical parameters exceeded the standard limit. Nitrogen pollution was in excess with samples from two sampling points showing levels higher than 30 mg/L. Heavy metal pollution of arsenic and chromium show heavy unregulated industrial discharge which may be a determining source in Site C. Nitrogen in water comes from kitchen wastes and fertilizers and causes eutrophication in water causing death of the lake, if not controlled soon enough

Table 2. Chemical Property Measurements

| Chemical parameters            | Standard Values | Site A | Site B | Site C | Site D | Site E | Site F |
|--------------------------------|-----------------|--------|--------|--------|--------|--------|--------|
| Sample size                    |                 | 7      | 5      | 13     | 4      | 5      | 4      |
| Arsenic                        | .01 mg/L        | 0.025  | 0.03   | 0.028  | 0.021  | 0.024  | 0.025  |
| Chromium                       | .001 mg/L       | 0.029  | 0.03   | 0.034  | 0.023  | 0.052  | 0.024  |
| Nitrogen as NO <sub>3</sub>    | 7 mg/L          | 41.813 | 3.94   | 18.571 | 7.149  | 9.277  | 375.05 |
| Phosphorous as PO <sub>4</sub> | 0.5 mg/L        | 0.435  | 0.245  | 0.084  | 0.416  | 0.072  | 0.587  |
| Oil & Grease                   | 1 mg/L          | 0.939  | 1.46   | 1.519  | 0.781  | 1.62   | 1.081  |

Site D samples show heavy metal pollution with higher levels of arsenic and chromium. Other chemical parameters (nitrates, phosphates, oil and grease) are found to be within standard limits. The levels of arsenic and chromium are not dangerously high as seen in previous sample sites, but still, any situation can amplify if not taken seriously. This means industrial effluents loom in large amount polluting waters near Site D. Constant erosion of volcanic rocks with arsenic and chromium content is another possible source.

Site E is another problematic place as arsenic, chromium, nitrate, and oil and grease levels are all found to be above the standard limit with only phosphorous being within tolerable limit. Most nitrogen and chromium outputs are found from two of the five sampling points. Nitrogen can cause eutrophication and lack of oxygen. Their possible source can be pesticides and insecticides. Chromium

excess happens when volcanic rocks erode and heavy industrial effluents are dumped into the lake water.

Site F had all other chemical parameters in optimum levels except nitrogen. In fact, nitrogen pollution looms at large as values reach as high as 592mg/L (standard is 7mg/L) which indicates high level of eutrophication. Heavy use of fertilizers and pesticides in the area around Site F and domestic sewage could be the reason for excess nitrogen. Highest amount is found in one of the four sampling points (592mg/L), followed by 487mg/L and 420mg/L found at the two other sampling points.

The standard limit for arsenic set by BFAR is 0.01 mg/L. All the sample sites have higher values (highest to lowest: Site C, Site B, Site A, Site F, Site E, Site D) than the standard limit indicating arsenic pollution in Taal Lake. After Metro Manila, Batangas is known for being an industrial growth sector in its region. Site C is known for its booming agriculture and real estate

industries. Hence, industries can be a major contributing arsenic pollutant. Arsenics are used in industrial processes to produce antifungal wood preservatives, cosmetics, for making residential structures, playhouses, decks, fences, picnic houses, insecticides and pesticides [27]. The values, however, do not show significant differences when compared among the sample sites.

Phosphate levels in Taal ecosystem is in better control with only Site F having levels above standard limit. Standard value for phosphate is 0.5mg/L. All other sites have levels lower than that of Site E showing level of just 0.07mg/L. Taal Lake has many illegally built fish cages and this cause eutrophication problem as fishermen would throw nutrients in water without any regulation. But in the recent times, all illegal cages have been removed but Site F still shows low amounts of phosphate contamination, possibly still due to excessive nutrient being laid in water for fishes [28].

Values for oil and grease vary among sites with highest value in Site E (1.6mg/L). The standard value set by BFAR is 1mg/L. Site C had value of 1.5mg/L. The rest of the sample sites are more or less within tolerable value range, with Site F showing levels of 1.08mg/L, followed by Site A with 0.9mg/L and Site D with 0.7mg/L. Again, Site C and Site E have slightly higher levels of oil and grease than the standard parameter set by BFAR. Sources of oil and grease are mostly anthropogenic with most oil and grease accumulating in lakes from residential sewage drains and dumping of industrial byproducts. The more people using automobiles and moving machineries, the more oil and grease are being used, thus, contribute more to the pollution [29].

All physical attributes of water quality of Taal lake were found fit into the criteria set by DENR-EMB except the balance of Oxygen levels which were more than required; hence, lowering biological oxygen demand of water. No significant differences were found in mean measures of total soluble solids and biological oxygen demand whereas mean evaluation of parameters such as pH, temperature and dissolved oxygen show notable differences. Based on the overall results of the study, Taal Lake water can still be classified as Class B (DENREMB, 2005), Recreational Water Class I. The classification is the same with two other river basins in the Philippines (DENR-EMB, 2005). Taal lake aquatic ecosystem can be classified as severely polluted based on the chemical parameters analyzed in this study. Nitrate, phosphate, and oil and grease levels vary significantly from site to site. Values of all other parameters such as arsenic and chromium do not show any significant difference. All the sample sites have heavy metal contamination. Taal Lake shows very high levels of arsenic and chromium with Site C having highest

arsenic levels and Site E having highest chromium levels. When it comes to nitrate levels that determine algal content in a lake, all sample sites, except Site B, have higher values than the set standard levels. Site F shows extremely high levels of nitrogen. Phosphate levels are under control. Site C and Site E also shows high oil and grease levels. This data indicates high industrialization in Site C and Site E. A common contaminant found through this study is nitrogen. This indicates high municipal waste disposal, kitchen waste disposal, and high fertilizers used in fields around Taal Lake.

A major problem that Taal Lake's ecosystem is combating is heavy metal pollution. Arsenic and chromium levels are above standard levels in all sample sites. There are costly methods like ion exchange and membrane technology but local communities in developing countries cannot afford it. Many other alternative methods are available. One of the suggestions is switching from an arsenic-unsafe well to an arsenic-safe drinking water source or use deep tube wells (which are generally arsenic free). Technologies for arsenic removal include oxidation, coagulation-precipitation, absorption, ion exchange, and membrane techniques. There are increasing number of effective and low-cost options for removing arsenic from small or household supplies.

Nitrate pollution looms at large in Taal Lake as levels are extremely high and eutrophication is inevitable. Eutrophication can possibly lead to death of the precious, endangered, endemic species residing in Taal Lake due to lack of sunlight and oxygen. Excess of nitrate also leads to excess oxidation and excess phosphates. Nitration can be treated by adsorption techniques by using best adsorbent according to the location [30]. For preventive measures, nitrogen leaching into water from soil can be prevented by avoiding over-irrigation as it increases the chances of nitrate leaching. Upgrading manure storage sites can reduce manure leaking. Efforts should be made to reduce the amount of nitrogen applied to older sites and collect drainage water instead of allowing it to drain in Taal Lake.

In order to maintain and conserve the condition of water in Taal Lake, safety, security, and environmental management plan should be carried out by concerned local government units (LGUs). This way the best favorable use of the Lake is likely to be encouraged. Likewise, information campaign on the protection and preservation of the Lake has to get in touch with the nearby natives and mountaineers to reduce the quantity of contaminants in the surrounding locale.

## ACKNOWLEDGMENTS

The researchers would like to acknowledge the Philippine government agencies that provided the primary data for the analysis; The Department of Environment and Natural Resource (DENR) and the

Bureau of Fisheries and Aquatic Resources (BFAR) both in Region IV-A. register and make payment after the registration deadline will not be guaranteed that their papers are included in the proceedings. Try to follow the reference style below.

## REFERENCES

- [1] Tan, R. L., Garcia, Y. T., Dator, M. A. L., Tan, I. M. A., & Pemsil, D. E. (2011). Technical efficiency of Genetically Improved Farmed Tilapia (GIFT) cage culture operations in the lakes of Laguna and Batangas, Philippines. *Journal of ISSAAS (International Society for Southeast Asian Agricultural Sciences)*, 17(1), 194-207..
- [2] Downing, J. A. (2014). Productivity of freshwater ecosystems and climate change. In *Global Environmental Change* (pp. 221-229). Springer Netherlands.
- [3] Bhatnagar, A., and Devi, P. (2013). Water quality guidelines for the management of pond fish culture. *International Journal of Environmental Sciences* 3, 1980–2009.
- [4] Bond, N. R., Lake, P. S., & Arthington, A. H. (2008). The impacts of drought on freshwater ecosystems: an Australian perspective. *Hydrobiologia*, 600(1), 3-16.
- [5] Arthington AH, Naiman RJ, McClain ME, Nilsson C. 2010. Preserving the biodiversity and ecological services of rivers: new challenges and research opportunities. *Freshwater Biol.* 55: 1-16
- [6] Dunlop, J., McGregor, G., & Horrigan, N. (2005). Potential impacts of salinity and turbidity in riverine ecosystems. *The State of Queensland*, 72.
- [7] Förstner, U., & Wittmann, G. T. (2012). *Metal pollution in the aquatic environment*. Springer Science & Business Media.
- [8] World Health Organization. (2004). *Guidelines for drinking-water quality: recommendations* (Vol. 1). World Health Organization.
- [9] Mohan, D., & Pittman Jr, C. U. (2006). Activated carbons and low cost adsorbents for remediation of tri-and hexavalent chromium from water. *Journal of hazardous materials*, 137(2), 762-811.
- [10] Ward, M. H. (2005). Workgroup report: drinking-water nitrate and health—recent findings and research needs. *Environmental health perspectives*, 113(11), 1607.
- [11] Förstner, U., & Wittmann, G. T. (2012). *Metal pollution in the aquatic environment*. Springer Science & Business Media.
- [12] Sirés, I., & Brillas, E. (2012). Remediation of water pollution caused by pharmaceutical residues based on electrochemical separation and degradation technologies: a review. *Environment international*, 40, 212-229.
- [13] Lokhande, R. S., Singare, P. U., & Pimple, D. S. (2011). Study on physico-chemical parameters of waste water effluents from Taloja industrial area of Mumbai, India. *International Journal of Ecosystem*, 1(1), 1-9.
- [14] Ashraf, M. A., Maah, M. J., & Yusoff, I. (2010). Water quality characterization of varsity lake, University of Malaya, Kuala Lumpur, Malaysia. *Journal of Chemistry*, 7(S1), S245-S254.
- [15] Simpi, B., SM Hiremath, KNS Murthy. 2011. Analysis of water quality using physico-chemical parameters Hosahalli Tank in Shimoga district. <https://www.researchgate.net/publication/287182663>
- [16] Manjare, S. A., Vhanalakar, S. A. and Muley, D. V. (2010). Analysis of water quality using physio-chemical parameters Tamadolge Tank in KohlaPur district, Maharashtra. *International Journal of Advanced Biotechnology and Research* ISSN 0976-2612. Vol 1. Issue 2, pp 115-119.
- [17] Sharma, R.C., A. Sharma and A. Anthawal. (2008). Surveying of aquatic insect diversity of Chandrabhaga river, Garhwal Himalayas. *Environmentalist.*, doi:10.1007/s10669-007-9155-z.
- [18] Scheffer, M. (2004). The story of some shallow lakes. In *Ecology of shallow lakes* (pp. 1-19). Springer Netherlands.
- [19] Warner, B., & Breon, S. R. (2004). Temperature Scales and Absolute Zero. In *Cryogenics and Fluids Branch*.
- [20] Zeigler, A. C. (2002). Issues Related to the Use of Turbidity Measurements as a Surrogate for Suspended Sediment. In *Turbidity and Other Sediment Surrogates Workshop*.
- [21] Lucas JS, Southgate PC (2012) *Aquaculture: Farming Aquatic Animals and Plants*. Blackwell Publishing. John Wiley and Sons, UK. Pp. 648.
- [22] Katznelson R, (2004). Dissolved oxygen measurement principles and methods. DQM Information Paper 3.1.1. [https://www.waterboards.ca.gov/water\\_issues/programs/swamp/docs/cwt/guidance/311.pdf](https://www.waterboards.ca.gov/water_issues/programs/swamp/docs/cwt/guidance/311.pdf)
- [23] Hargreaves, J. A., & Tucker, C. S. (2002). Measuring Dissolved Oxygen Concentration In Aquaculture. In *Southern Regional Aquaculture Center*.
- [24] Wetzel, R. G. (2001). *Limnology: Lake and River Ecosystems* (3rd ed.). San Diego, CA: Academic Press.
- [25] Dasgupta M, Yildiz Y (2016) Assessment of Biochemical Oxygen Demand as Indicator of Organic Load in Wastewaters of Morris County, New Jersey, USA. *J Environ Anal Toxicol* 6:378. doi:10.4172/2161-0525.1000378



- [26] Galera IC, Martinez FV (2011) Monitoring and evaluation of the water quality of Taal Lake, Talisay, Batangas, Philippines. *Journal of Academic Research* 1 : 229-236.
- [27] Santos, T. G. (2016, July 01). DOH warns vs arsenic in water supply. *Philippine Daily Inquirer*. Retrieved April 19, 2018, from <http://newsinfo.inquirer.net/793616/doh-warns-vs-arsenic-in-water-supply>.
- [28] Martinez, F. B., & Galera, I. C. (2011). Monitoring and evaluation of the water quality of Taal Lake, Talisay, Batangas, Philippines. *Academic Research International*, 1(1), 229.
- [29] McMurtrie, G., Lambert, C., Jason, R. & Pattillo, J. 2011. Deepwater Potential of the NW Palawasn Basin Philippines. *Proceedings of the 2011 South East Asia Petroleum Exploration Society (SEAPEX) Conference*, 2011. Pages 1-24.
- [30] Ivan Shu & Tom Getting. 2012. A review of nitrate reduction using inorganic materials. *Journal Enviromental Technology Reviews*. Vol 1, 2012. Issue 1. <https://www.tandfonline.com/doi/full/10.1080/09593330.2012.706646>

## DURABILITY STUDY OF MALAYSIA ROCK MASS FOR TUNNELLING CONSTRUCTION

RC Omar<sup>1</sup>, R.Roslan<sup>2</sup>, INZ Baharuddin<sup>3</sup>, Hairin Taha<sup>4</sup> and Vigneswaran V<sup>5</sup>

<sup>1,2,3,4</sup> Institute of Infrastructure Energy,

<sup>5</sup> College of Engineering,

Universiti Tenaga Nasional, 43000 Kajang, Malaysia

### ABSTRACT

Malaysia is dominated by forested mountains made up of old igneous and metamorphic rocks with compressive strength less than 50 MPa which are susceptible to weathering which can cause faults, shear zones and thrust zones. These conditions impose a challenging task for rock tunnel constructions in Malaysia. Rapid development and population in Malaysia has generated the constructions of many infrastructure and facilities that include tunnel constructions to facilitate the network system and expand traffic flow. For the safe and economical design of tunnels, it is important to assess the strength and behavior of the rock mass to prevent the ground collapse that can lead to loss of life and property. The main objective of this study is to investigate the durability of Malaysia Rock Mass for tunneling purposes by using the point load test, direct shear test and slake durability test. The results of the study showed that the worse weathering grade for Granite rock and Schist-Phyllite rock were II and II respectively, with all rocks suitable with durability classification of longer span. This study concludes the most suitable place at particular rock mass of each rock type based on durability.

*Keywords: durability study; rock mass; point load test; direct shear test; slake durability test*

### INTRODUCTION

Rock tunneling can be defined as construction in a material which cannot be excavated by ordinary digging tools. In many countries, tunnels were constructed to facilitate transportation and traffic network connection due to rapid population and industrialization including lack of space [1]. Normally, tunnels were built through mountains to connect to areas and cities. Malaysia is one of the countries which embarked on tunnel construction to address problems such as traffic congestion and repeated flooding in the cities [2-3]. Malaysia is a mountainous country covered mostly by old igneous and metamorphic rocks with compressive strength > 50 MPa. However, these rocks suffered with weathering and even earth movement which cause faults, shear zones and thrust zones.

Rock tunneling has great influence on the behavior and type of the rock due to weathering, erosion and tectonic processes. In common term, rocks are described as hard or weak rocks but in engineering term the main classes of rocks are described as igneous, sedimentary and metamorphic rocks. The difference between hard and weak rock tunneling can be estimated when the rock mass strength is greater than the induced stresses imposed by tunneling [4-5]. The rocks have their own local weak zones and discontinuity properties. Normally, weak rock tunneling is hard and its design construction must be carried out carefully. Hard rocks have no loss of strength on actual or closed

conditions unless exposed toward water or climate changes.

Durability factor for tunneling construction in Malaysia needs to be considered since Malaysia rocks narrowed toward igneous and metamorphic rocks only. This is because most of the sedimentary rocks in Malaysia undergo deformation or recrystallization and evolved to metamorphic rocks. Climate changes were one of the major elements that caused irreversible changes in rocks or in other words weathering. Weathering effect on the igneous and metamorphic rock in particular place can be determined by performing study and test on sample of rocks for ensure that the strength of the rock [6-8].

Knowledge of rock and the environments in which they were formed and the way the rocks response toward weathering, erosion and tectonic processes are essential in conducting site investigation survey especially on rock durability of tunneling [9]. Tunnels will be constructed and maintained by taking several mitigations to ensure the tunnel is durable for a long time. The strength of rock strength can indirectly affect the durability of tunnel. Hence, durability of the rock should be evaluated prior to the construction of a tunnel by performing various assessments on the rock itself [10-11].

In this study, laboratory testing such Point Load Test, Schmidt Rebound Hammer Test, Slake Durability test and Uniaxial Compression Test were

done to identify the durability of the rocks and their weathering classification.

### Study Area

Two different areas with different rock characteristics were selected. Granite rock samples originally from igneous family were collected from rock mass of Kajang Silk Highway (KM 17) (Figure 1 and 2) and Schist-Phyllite Rock Mass were collected from Putrajaya which has metamorphic rock (Figure 3 and 4).



Fig.1 Kajang Silk Highway site



Fig. 2 Samples of granite rock mass



Fig 3. Putrajaya Site



Fig 4. Samples of Schist-Phyllite Rock Mass

## METHODOLOGY

### Schmidt Rebound Hammer Test

Schmidt rebound hammer test was done to estimate the unconfined compressive strength and modulus elasticity of the intact rocks to estimate the strength of the rocks. It operates by measuring rebound of the steel hammer mass when propelled with 0.075 kg.m of energy against the rock surface. Energy against a rock surface is proportional to the hardness of the material which is related with strength. Test followed ISRM standard.

### Direct Shear Test

Shear strength test is important to assess the behavior of rock mass. The test was carried out according to ISRM standard (Figure 5)



Fig.5 Direct shear test apparatus

### Point Load Test

Point load test is a tensile based test where uniaxial compressive strength and modulus of elasticity are obtained experimentally (Figure 6). It is a variation of the Brazil tensile strength test. The point load test is useful to determine the maximum and minimum strengths which results due to rock

anisotropy, such as foliated metamorphic rock. The test was done following ISRM code.



Fig 6. Point load test machine

### Slake Durability Test

Slake durability test was carried out to identify the weatherability of the rock samples following the standard methods ISRM and ASTM (Figure 7). Slake durability test consist of placing weighed, oven dried samples of rock in a drum having a 2 mm meshed exterior. Water is placed in a trough at a level below the drum axle and the drum is rotated within specified number of times. The sample that remains in drum is oven dried and the test is repeated for a second cycle. After the second cycle, the slake durability index is obtained, *Id*. Standardized procedures for the slake durability test have been established by the International Society for Rock Mechanics (ISRM, 1979b). If the second cycle index is in between of 0% to 10%, hence first cycle slake durability index is preferred but with the statement provided.



Fig. 7 Slake Durability Equipment

## RESULTS AND DISCUSSION

### Weathering of Rock Samples

The study on rock strength is important to establish its relation to the weathering effect. This is because the weathering grade of rock can be related to rock durability of tunneling. In this study, the

strength of Schmidt Rebound Hammer Test was based on Uniaxial Compression Strength value (UCS).

Table 1. Weathering of Granite Rock Based on Schmidt Hammer Analysis (SHV)

| Type of Rock (Schist-Phyllite) | Discoloration | Mean Schmidt Hammer Value (%) | Texture and Structure | Fractility (fr hand)               | SHV (%) | Prediction on Weathering Grade | Comments (Based on Predicted Weathering Grade) |
|--------------------------------|---------------|-------------------------------|-----------------------|------------------------------------|---------|--------------------------------|--|
| M1                             | Partial       | 48                            | 100% Preserved        | Fragment corners cannot be chipped | >25     | II                             | Acceptable                                     |
| M2                             | Partial       | 54                            | 100% Preserved        | Fragment corners cannot be chipped | >25     | II                             | Acceptable                                     |
| M3                             | Partial       | 48                            | 100% Preserved        | Fragment corners cannot be chipped | >25     | II                             | Acceptable                                     |
| M4                             | Partial       | 50                            | 100% Preserved        | Fragment corners cannot be chipped | >25     | II                             | Acceptable                                     |
| M5                             | Partial       | 49                            | 100% Preserved        | Fragment corners cannot be chipped | >25     | II                             | Acceptable                                     |
| M6                             | Partial       | 50                            | 100% Preserved        | Fragment corners cannot be chipped | >25     | II                             | Acceptable                                     |

The results in Table 1 shows that Granite 1, Granite 4 and Granite 6 satisfied all the parameters with weathering grade of IB due to the rocks experienced discoloration on major discontinuity surfaces. At the same time, the rocks are preserved 100% in texture and structure. Granite 2 and Granite 3 have weathering grade of II, also preserved completely in texture. Granite 5 underwent complete discoloration that should have weathering grade II instead of III.

Table 2. Weathering of Schist-Phyllite Rock Based on Schmidt Hammer Analysis (SHV)

| Type of Rock (Granite) | Discoloration | Mean Schmidt Hammer Value (%) | Texture and Structure | Fractility (fr hand)               | SHV (%) | Prediction on Weathering Grade | Comments (Based on Predicted Weathering Grade) |
|------------------------|---------------|-------------------------------|-----------------------|------------------------------------|---------|--------------------------------|--|
| G1                     | Partial       | 44                            | 100% Preserved        | Fragment corners cannot be chipped | >25     | II                             | Acceptable                                     |
| G2                     | Partial       | 38                            | 100% Preserved        | Fragment corners cannot be chipped | >25     | II                             | Acceptable                                     |
| G3                     | Partial       | 38                            | 100% Preserved        | Fragment corners cannot be chipped | >25     | II                             | Acceptable                                     |
| G4                     | Partial       | 49                            | 100% Preserved        | Fragment corners cannot be chipped | >25     | II                             | Acceptable                                     |
| G5                     | Complete      | 38                            | 100% Preserved        | Fragment corners cannot be chipped | >25     | III                            | Should be II                                   |
| G6                     | Partial       | 43                            | 100% Preserved        | Fragment corners cannot be chipped | >25     | II                             | Acceptable                                     |

Table 2 shows all Schist-Phyllite rock samples (1-6) satisfied all the parameters where partial discoloration was observed. The texture and structure of the rock samples were 100% preserved indicating weathering grade of II.

### Direct Shear Test

Based on the results shown in Table 3, Granite rocks (1-6) shows that the rocks own strength ranged from high to very high. This shows that the rock has

very good strength which indirectly shows that durability of the rock based on shear strength is very good. Similarly, all Schist-Phyllite rocks showed the strength of high indicating that the rock durability is also good (Table 4).

Table 3. Direct Shear Analysis for Granite Rock

| Rock Type | Samples | Peak Shear Stress (kPa) | Average Peak Shear Stress (MPa) | Strength Categories |
|-----------|---------|-------------------------|---------------------------------|---------------------|
| G1        | S1      | 4280                    | 4.660                           | High to Very high   |
|           | S2      | 4150                    |                                 |                     |
|           | S3      | 4850                    |                                 |                     |
| G2        | S1      | 4180                    | 4.310                           | High to Very high   |
|           | S2      | 4850                    |                                 |                     |
|           | S3      | 4950                    |                                 |                     |
| G3        | S1      | 3650                    | 3.650                           | High to Very high   |
|           | S2      | 3100                    |                                 |                     |
|           | S3      | 4250                    |                                 |                     |
| G4        | S1      | 3950                    | 4.387                           | High to Very high   |
|           | S2      | 4280                    |                                 |                     |
|           | S3      | 4780                    |                                 |                     |
| G5        | S1      | 4180                    | 4.267                           | High to Very high   |
|           | S2      | 4850                    |                                 |                     |
|           | S3      | 4850                    |                                 |                     |
| G6        | S1      | 4780                    | 4.387                           | High to Very high   |
|           | S2      | 3950                    |                                 |                     |
|           | S3      | 4350                    |                                 |                     |

Table 4. Direct Shear Analysis for Schist-Phyllite Rock

| Rock Type | Samples | Peak Shear Stress (kPa) | Average Peak Shear Stress (MPa) | Strength Categories |
|-----------|---------|-------------------------|---------------------------------|---------------------|
| S1        | S1      | 2280                    | 2.330                           | High to very high   |
|           | S2      | 2850                    |                                 |                     |
|           | S3      | 2950                    |                                 |                     |
| S2        | S1      | 3050                    | 3.007                           | High to very high   |
|           | S2      | 3450                    |                                 |                     |
|           | S3      | 2280                    |                                 |                     |
| S3        | S1      | 3450                    | 3.377                           | High to very high   |
|           | S2      | 2250                    |                                 |                     |
|           | S3      | 2250                    |                                 |                     |
| S4        | S1      | 3000                    | 3.750                           | High to very high   |
|           | S2      | 2850                    |                                 |                     |
|           | S3      | 3000                    |                                 |                     |
| S5        | S1      | 2850                    | 3.717                           | High to very high   |
|           | S2      | 2450                    |                                 |                     |
|           | S3      | 2850                    |                                 |                     |
| S6        | S1      | 2280                    | 2.450                           | Medium to medium    |
|           | S2      | 2250                    |                                 |                     |
|           | S3      | 2280                    |                                 |                     |

## Point Load Test

Table 5 shows that the rock strength for samples Granite 1-6 was very high due to less weathering effect. The rock samples for Schist-Phyllite 1, Schist-Phyllite 3, Schist-Phyllite 4 and Schist-Phyllite 6 showed extremely high rock strength which has no or less weathering effect (Table 6). Among all the rock types, metamorphic rock showed very strong and extremely quality rock.

Table 5. Strength Classification of Granite Rock Based on Point Load Test Analysis

| Type of Rock   | L <sub>10</sub> (MPa) | Average L <sub>10</sub> (MPa) | Strength Classification |
|----------------|-----------------------|-------------------------------|-------------------------|
| Granite 1 (G1) | 8.147                 | 8.080                         | Very High               |
|                | 8.827                 |                               |                         |
|                | 10.708                |                               |                         |
| Granite 2 (G2) | 7.821                 | 7.983                         | Very High               |
|                | 8.847                 |                               |                         |
|                | 4.283                 |                               |                         |
| Granite 3 (G3) | 7.933                 | 7.324                         | Very High               |
|                | 7.933                 |                               |                         |
|                | 7.933                 |                               |                         |
| Granite 4 (G4) | 7.724                 | 4.887                         | Very High               |
|                | 7.724                 |                               |                         |
|                | 7.724                 |                               |                         |
| Granite 5 (G5) | 7.871                 | 4.243                         | Very High               |
|                | 7.724                 |                               |                         |
|                | 7.724                 |                               |                         |
| Granite 6 (G6) | 7.747                 | 7.338                         | Very High               |
|                | 7.747                 |                               |                         |
|                | 7.844                 |                               |                         |

Table 6. Strength Classification of Schist-Phyllite Rock Based on Point Load Test Analysis

| Type of Rock           | L <sub>10</sub> (MPa) | Average L <sub>10</sub> (MPa) | Strength Classification |
|------------------------|-----------------------|-------------------------------|-------------------------|
| Schist-Phyllite 1 (M1) | 24.668                | 16.197                        | Extremely High          |
|                        | 5.003                 |                               |                         |
|                        | 18.920                |                               |                         |
| Schist-Phyllite 2 (M2) | 7.902                 | 8.060                         | Very High               |
|                        | 6.994                 |                               |                         |
|                        | 9.280                 |                               |                         |
| Schist-Phyllite 3 (M3) | 10.435                | 14.761                        | Extremely High          |
|                        | 14.189                |                               |                         |
|                        | 19.658                |                               |                         |
| Schist-Phyllite 4 (M4) | 10.379                | 10.410                        | Extremely High          |
|                        | 6.870                 |                               |                         |
|                        | 14.177                |                               |                         |
| Schist-Phyllite 5 (M5) | 7.207                 | 9.836                         | Very High               |
|                        | 8.414                 |                               |                         |
|                        | 13.956                |                               |                         |
| Schist-Phyllite 6 (M6) | 21.681                | 23.237                        | Extremely High          |
|                        | 30.709                |                               |                         |
|                        | 17.521                |                               |                         |

## Slake Durability Test

Slake durability test clearly shows that Granite 1- 6 having durability strength of very high which is proportional to Point Load Test and Direct Shear Test results. Visual descriptions of rocks for Granite 1- 6 except for Granite 3 were I and II, respectively. Visual descriptions of I represent that remaining rock pieces were virtually unchanged and visual descriptions of II represents that remaining pieces consist of large and small in size. For Schist-Phyllite rock samples, the results also showed extremely higher in durability strength. This indicates that the rock materials are able to withstand higher strength of load but still maintain its origin and texture of the rock itself. All the Schist-Phyllite rock showed visual description of I except for Schist-Phyllite 2 and Schist-Phyllite 3 which was II (Table 8).

Table 7. Durability Strength of Granite Rock

| Specimen | I <sub>2</sub><br>(End of cycle) |          |          | I <sub>2</sub> (avg) | Visual Description | Durability Classification |
|----------|----------------------------------|----------|----------|----------------------|--------------------|---------------------------|
|          | 2                                | 4        | 6        |                      |                    |                           |
| G1       | 99.3443                          | 99.81915 | 99.69485 | 99.61933             | I                  | Extremely High            |
| G2       | 99.18729                         | 99.8089  | 99.67441 | 99.5587              | I                  | Extremely High            |
| G3       | 99.66228                         | 99.08309 | 99.66579 | 99.4837              | II                 | Extremely High            |
| G4       | 99.19782                         | 99.70368 | 99.5763  | 99.4826              | I                  | Extremely High            |
| G5       | 99.39787                         | 99.75419 | 99.68324 | 99.6117              | I                  | Extremely High            |
| G6       | 99.70873                         | 99.88904 | 99.7168  | 99.7889              | I                  | Extremely High            |

Table 8. Durability Strength of Schist-Phyllite Rock

| Metamorphic | I <sub>2</sub><br>(End of cycle) |          |          | I <sub>2</sub> (avg) | Visual Description | Durability Classification |
|-------------|----------------------------------|----------|----------|----------------------|--------------------|---------------------------|
|             | 2                                | 4        | 6        |                      |                    |                           |
| M1          | 99.17987                         | 99.31389 | 99.41829 | 99.31689             | I                  | Extremely High            |
| M2          | 99.72962                         | 99.66290 | 99.66012 | 99.6843              | II                 | Extremely High            |
| M3          | 99.68879                         | 99.00117 | 99.34172 | 99.00421             | II                 | Extremely High            |
| M4          | 99.71577                         | 99.79329 | 99.73289 | 99.75391             | I                  | Extremely High            |
| M5          | 99.7942                          | 99.88810 | 99.482   | 99.58813             | I                  | Extremely High            |
| M6          | 99.77205                         | 99.77085 | 99.66837 | 99.73122             | I                  | Extremely High            |



## CONCLUSIONS

In this study, two types of rock mass samples were collected from two proposed sites for tunneling construction. They were assessed by Point Load Test, Direct Shear Test and Slake Durability Test to evaluate the strength of rock fragments and its relation to durability and weathering. The results of the laboratory tests verified that the strength of the rock samples was the same as the strength of rock at the rock mass. Hence, if the rock samples are classified as durable, then the rock mass should also have the same durability classification. This indirectly shows that the particular rock mass are very suitable for tunneling construction.

## ACKNOWLEDGMENTS

This study was funded by UNITEN grant.

## REFERENCES

- [1] Chen, Mengchong, and Fusheng Niu. "Reasonable Construction Methods for Tunneling Beneath an Operating Highway." *Stability Assessment for Underground Excavations and Key Construction Techniques*. Springer, Singapore, 2017. 105-121.
- [2] Jeong, H., Ha, S., & Kim, H. (2018). Flood protection cost allocation using cooperative game theory for adapting infrastructure to climate change. *Journal of Water Resources Planning and Management*, 144(4), 04018010.
- [3] Tan, Y. C., Koo, K. S., & Chow, C. M. (2016). Underground stations excavation of up to 45m deep for mass rapid transit in limestone formation, Malaysia. *Japanese Geotechnical Society Special Publication*, 2(2), 170-175.
- [4] Shirlaw, J. N. (2016). *Pressurised TBM tunnelling in mixed face conditions resulting from tropical weathering of igneous rock*. *Tunnelling and underground space technology*, 57, 225-240.
- [5] Liu, L., Rong, Y., Zhang, C. K., Mao, M. Y., & Zhang, L. L. (2017). Instability Mechanism of Du Yun Pass Tunnel Entrance Weathered Stacking Area Analysis. In *Applied Mechanics and Materials* (Vol. 858, pp. 81-85). Trans Tech Publications.
- [6] Momeni, A., Hashemi, S. S., Khanlari, G. R., & Heidari, M. (2017). The effect of weathering on durability and deformability properties of granitoid rocks. *Bulletin of Engineering Geology and the Environment*, 76(3), 1037-1049.
- [7] Abad, S. A. N. K., Tugrul, A., Gokceoglu, C., & Armaghani, D. J. (2016). Characteristics of weathering zones of granitic rocks in Malaysia for geotechnical engineering design. *Engineering geology*, 200, 94-103.
- [8] Yusoff, Z. M., Daud, N. N., Nahazanan, H., Omar, H., Aziz, A., & Ab Razak, M. S. (2017, July). Granites in Malaysia: From Hard Rock to Clay Minerals. In *Global Civil Engineering Conference* (pp. 1295-1305). Springer, Singapore.
- [9] Ko, J., & Jeong, S. (2017). A Study on Rock Mass Classifications and Tunnel Support Systems in Unconsolidated Sedimentary Rock. *Sustainability*, 9(4), 573.
- [10] Sharma, L. K., Vishal, V., & Singh, T. N. (2017). Developing novel models using neural networks and fuzzy systems for the prediction of strength of rocks from key geomechanical properties. *Measurement*, 102, 158-169.
- [11] Prokopov, A., Matua, V., & Akopyan, V. (2016). Monitoring of the Geotechnical State of the Array During the Reconstruction of the Roki Tunnel. *Procedia Engineering*, 150, 2255-2260.



## H<sub>2</sub> PRODUCTION FROM LACTIC ACID RICH MEDIUM AND CASSAVA STARCH WASTEWATER BY *Klebsiella pneumoniae* subsp. *pneumoniae*

Piyawadee Saraphirom<sup>1</sup>, Napapach Chainamom<sup>1</sup>, Piyarat Namsena<sup>1</sup>,  
Ornanong Chaiyachet<sup>1</sup>, Weeranuch Wonkaonoi<sup>1</sup> and Mullika Teerakun<sup>2\*</sup>

<sup>1</sup>Faculty of Science and Technology, Rajabhat Maha Sarakham University, Maha Sarakham, Thailand;

<sup>2</sup>Faculty of Agricultural Technology, Kalasin University, Thailand

### ABSTRACT

H<sub>2</sub> production from lactic acid rich medium and H<sub>2</sub> production from cassava starch wastewater by isolated strains were investigated. The isolation of H<sub>2</sub> producing bacteria from heat treated sludge was carried out. The H<sub>2</sub> production from lactic acid rich medium which used 1.5 g/L sodium acetate, 1.5 g/L sodium lactate and 1 g/L sucrose as carbon sources. The effects of inoculum size of 10, 20, 30 and 40 % (v/v) and incubation temperature of 35, 45 and 55 °C using cassava starch wastewater as substrate on H<sub>2</sub> production by isolation strains were investigated. Results shown 6 isolated strains i.e. isolation code of MK01 to MK06 indicated the H<sub>2</sub> production capability when cultured in lactic acid rich medium. However, 3 isolated strains i.e. MK01, MK04 and MK06 were preferred to use as seed inoculum for further experiment depend on a high H<sub>2</sub> production capacity obtained. Results indicated that the optimal condition of H<sub>2</sub> production from cassava starch wastewater was 30% (v/v) inoculum size of MK06 under 35 °C of incubation temperature. The maximum *P*<sub>s</sub>, H<sub>2</sub> yield and H<sub>2</sub> production rate of 4.20 L H<sub>2</sub>/L medium, 1.47 L H<sub>2</sub>/g substrate consumed, and 14.00 mL H<sub>2</sub>/L/h were obtained. Identification and characterization of MK06 was investigated using 16S rRNA gene sequence analysis followed by phylogenetic analysis. The 100% similarity of 16S rDNA compare with closely related species was indicated *Klebsiella pneumoniae* subsp. *pneumoniae* DSM 30104(T).

**Keywords:** Hydrogen production, Lactic acid rich medium, Cassava starch wastewater.

### INTRODUCTION

H<sub>2</sub> producing bacteria such Clostridiaceae can ferment the carbohydrates in agricultural wastewater to H<sub>2</sub>, CO<sub>2</sub> and volatile organic acids – mainly acetic and butyric acids. However, these bacteria are not able to further break down the organic acids to H<sub>2</sub> due to the positive Gibbs free energy of the reaction [1]. The genus *Clostridium* i.e. *Clostridium butyricum*, *Clostridium diolis* and *C. beijerinckii* have been reported their ability to produce hydrogen from a mixture of acetic acid and lactic acid [2]. A mole ratio of depletion of acetic acid to lactic acid of 1:2 could be obtained from the biological H<sub>2</sub> production from a mixture of acetic and lactic acids by *C. diolis* JCCC H-3 [2]. Cassava starch wastewater is an industrial residue composed mainly of lactic acid bacteria with excess of the genera *Lactobacillus*, and organic acids [3]. The cassava starch wastewater is excluded, and it is returned an effluent with high chemical oxygen demand [4]. However, this residue presents a motivating component for prospective use in innovative products. The cassava starch wastewater has a low pH and it is an organic acid rich wastewater [4]. The major organic acids include lactic acid, acetic acid, butyric acid and other components include starch residual. In dark fermentative H<sub>2</sub> production, the presence of lactic acid as a metabolite during H<sub>2</sub> production is frequently regarded as a sign of lower H<sub>2</sub> production [5, 6, 7]. Lactic acid has been rarely

studied as substrate for H<sub>2</sub> production and despite reports of CH<sub>4</sub> production from lactate [7], no considerable H<sub>2</sub> production was reported when lactate was used as the individual substrate [2].

Although previous report on H<sub>2</sub> production from mixture of lactic acid and acetic acid by *Clostridium diolis* showed the promise on efficient H<sub>2</sub> production process in batch scale but the information on the H<sub>2</sub> production from lactic acid rich wastewater are still lacking. Therefore, this research aims to isolate H<sub>2</sub> producing bacteria which capable to use lactic acid as substrate for H<sub>2</sub> production. Effects of inoculum size and incubation temperature on H<sub>2</sub> production parameters were investigated. Means of H<sub>2</sub> production parameters which indicated the high efficiency of H<sub>2</sub> producing strain were selected to produce H<sub>2</sub> from cassava starch wastewater. The results from this study provided high efficiency of hydrogen producing strain and the optimum condition could improve hydrogen yield from lactic acid rich wastewater.

### MATERIALS AND METHODS

#### Anaerobic Sludge

The anaerobic sludge of UASB was pretreated by dry heating method using hot air oven under 105°C for 2 h for suppressing the methanogen. After heating, the UASB sludge was dispersed into an aqueous suspension by vortexing it in PBS buffer (pH 7.2, 10

mM Na<sub>2</sub>HPO<sub>4</sub>, and 0.13% NaCl) for 5 min. The suspension was diluted serially, plated on an NB medium (pH 6.8, 0.3% beef extract, and 0.5% peptone) and incubated at 30 °C under anaerobic conditions. After incubating for 24-36 h, colonies were selected randomly and transferred to fresh NB plates.

### H<sub>2</sub> Production Confirmation

Each isolated bacterium obtained was used as seed inoculums for the H<sub>2</sub> production confirmation experiment. The experiment was accompanied in 25 mL serum flasks with a working volume of 15 mL. The H<sub>2</sub> production medium was contained 10% (v/v) inoculum. The H<sub>2</sub> production capability of isolated bacteria was performed by cultured in synthetic medium (M solution) [8]. Serum flasks were flushed with nitrogen gas to eliminate oxygen in headspace and to generate the anaerobic condition then incubated at room temperature. After 24 h, the total gas volume was measured by releasing the pressure in the flasks using wetted glass syringe.

### H<sub>2</sub> Production from Lactic Acid Rich Medium by Isolated Strain

Isolated colonies indicated H<sub>2</sub> production capacity obtained from 2.2 were cultured in synthetic medium (M solution) [8]. H<sub>2</sub> production ability of all isolated strains were conducted in the same size of serum flasks with a liquid volume of 70 mL and 50 mL of head space volume. The H<sub>2</sub> production capability of isolated bacteria was accomplished by cultured in lactic acid rich medium (M solution contained sodium acetate, 1.5 g/L sodium lactate and 1 g/L sucrose as carbon sources). The 10% (v/v) inoculum was inoculated into 120 mL serum flasks then incubated at room temperature and activated in an orbital shaker with a rotation speed of 120 rpm. The biogas volume was continuously measured and collected by gas tight syringe for biogas composition analysis.

### H<sub>2</sub> Production from Cassava Starch Wastewater by Isolated Bacteria

Isolated strains showed the high H<sub>2</sub> production capacity were enriched in lactic acid rich medium for 48 h under anaerobic condition before used as seed inoculums. The cassava starch wastewater used as sole substrate for H<sub>2</sub> production consisted of 2.78 g/L starch, 4.59 g/L volatile fatty acid i.e. 0.89 g/L acetic acid, 1.33 g/L lactic acid, 1.09 g/L propionic acid and 1.28 g/L butyric acid. The variation inoculums size of 10, 20, 30 and 40 % (v/v) was adjusted then the effect of incubation temperature at 35, 45 and 55 °C on H<sub>2</sub> production from cassava starch wastewater by isolated bacteria was investigated. The difference inoculums size was inoculated into cassava starch wastewater in 25 mL serum flasks with a liquid volume of 70 mL under adjusted initial pH of 5.5. Serum flasks were flushed with N<sub>2</sub> to remove O<sub>2</sub> in

headspace and to create the anaerobic condition. The bottles were incubated at room temperature and operated in an orbital shaker with a rotation speed of 120 rpm to provide better contact among substrates. After 24 h, the total gas volume was measured by releasing the pressure in the bottles using wetted glass syringe. The 3 mL of biogas produced were collected into another serum bottle then measured the H<sub>2</sub> concentration by gas chromatography analysis.

### Analytical Method and Kinetics Model

H<sub>2</sub> content was measured using a gas chromatograph under the same analytical condition as [9]. Helium was used as the carrier gas at a flow rate of 25 mL/min. H<sub>2</sub> production was calculated from the headspace measurement of gas composition and the total volume of H<sub>2</sub> produced, at each time interval, using the mass balance equation [9].

$$V_{H,i} = V_{H,i-1} + C_{H,i}(V_{G,i} - V_{G,i-1}) + V_{H,0}(C_{H,i} - C_{H,i-1})$$

Where  $V_{H,i}$  and  $V_{H,i-1}$  are the cumulative hydrogen gas volumes at the current ( $i$ ) and previous time interval ( $i - 1$ ), respectively;  $V_{G,i}$  and  $V_{G,i-1}$  are total biogas volume at the current and previous time interval;  $C_{H,i}$  and  $C_{H,i-1}$  are the fraction of hydrogen gas in the headspace at the current and previous time interval;  $V_H$  is the volume of headspace of serum bottles. A modified Gompertz equation was used to adequate the H<sub>2</sub> production profiles [9]. Total sugar, volatile fatty acid (VFAs) and dry cell weight (DW) are measured according to the procedures described in standard methods [10].

$$H = P \exp \left\{ - \exp \left[ \frac{R_m e}{P} (\lambda - t) + 1 \right] \right\}$$

Where,  $H$  represents the cumulative volume of hydrogen produced (mL),  $P_s$  the hydrogen production potential (mL),  $R_m$  the maximum production rate (mL/h),  $\lambda$  the lag-phase time (h),  $t$  the incubation time (h), and  $e$  is 2.718281828. Parameters ( $P_s$ ,  $R_m$  and  $\lambda$ ) were estimated using the solver function in Microsoft Excel version 5.0 (Microsoft, Inc.).

ANOVA was used for selecting forecasting H<sub>2</sub> producing strain isolate based on comparison of means between forecasting results; that is for testing a significant difference between group means [11]. When differences between groups exist, a post hoc test then conducted to identify which group that differs from the others. In this paper, Duncan multiple range test was used.

### 16S rDNA Sequencing

#### PCR amplification of 16S rDNA

DNA templates for PCR amplification were prepared by using "Genomic DNA mini kit (Blood/culture cell)" (Geneaid Biotech Ltd., Taiwan). DNA coding for 16S rRNA regions was amplified by means of PCR with Taq polymerase, as described by

[12-13]. A PCR product for sequencing 16S rDNA regions was prepared by using the following two primers, 20F (5'-GAG TTT GAT CCT GGC TCA G-3', positions 9-27 on 16S rDNA by the *E. coli* numbering system and 1500R (5'-GTT ACC TTG TTA CGA CTT-3', position 1509-1492 on 16S rDNA by the *E. coli* numbering system [14]. The PCR amplification was carried out with DNA Engine Dyad® Thermal Cycler (Bio-Rad Laboratories). One hundred  $\mu$ l of a reaction mixture contained 15-20 ng of template DNA, 2.0  $\mu$ moles each of the two primers, 2.5 units of Taq polymerase, 2.0 mM  $MgCl_2$ , 0.2 mM dNTP and 10  $\mu$ l of 10xTaq buffer, pH 8.8, containing  $(NH_4)_2SO_4$ , which was comprised of 750 mM Tris-HCl, 200 mM  $(NH_4)_2SO_4$  and 0.1% Tween 20. The PCR amplification was programmed to carry out an initial denaturation step at 94 °C for 3 min, 25 cycles of denaturation at 94 °C for 1 min, annealing at 50 °C for 1 min and elongation at 72 °C for 2 min, followed by a final amplification step at 72 °C for 3 min. The PCR product was analyzed by 0.8% (w/v) agarose gel electrophoresis and purified with a GenepHlow™ Gel/PCR Kit (Geneaid Biotech Ltd., Taiwan). The purified PCR product was stored at -20 °C for further step.

#### Direct sequencing of 16S rDNA

Direct sequencing of the single-banded and purified PCR products (ca. 1500 bases, on 16S rDNA by the *E. coli* numbering system [14] was carried out. Then, sequencing of the purified PCR products was performed on an ABI Prism® 3730XL DNA Sequence (Applied Biosystems, Foster City, California, USA) by sequencing service provider. The two primers 27F (5'-AGA GTT TGA TCM TGG CTC AG-3') or 800R (5'-TAC CAG GGT ATC TAA TCC-3') and 518F (5'-CCA GCA GCC GCG GTA ATA CG-3') or 1492R (5'-TAC GGY TAC CTT GTT ACG ACT T-3') for single strand 16S rDNA sequencing, and 4 primers of 27F, 518F, 800R and 1492R for double strands 16S rDNA sequencing were used 3 sequence analyses. The nucleotide sequences obtained from all primers were assembled using Cap contig assembly program, an accessory application in BioEdit (Biological sequence alignment editor) Program. The identification of phylogenetic neighbors was initially carried out by the BLASTN [15] program against the database containing type strains with validly published prokaryotic names [16]. The top thirty sequences with the highest scores were then selected for the calculation of pairwise sequence similarity using global alignment algorithm, which was implemented at the EzTaxon-e server [16-17]. The DNA sequences determined and obtained from databases were aligned with a program CLUSTAL X (version 1.8) [18] in BioEdit Program [19]. Alignment gaps and unidentified bases were eliminated. The evolutionary distances were computed using the Maximum Composite Likelihood

method [20]. Phylogenetic trees were constructed by the neighbor-joining method [21]. The robustness for individual branches was appraised by 100 replications bootstrapping [22] with the program MEGA Version 6.0 [23].

## RESULTS AND DISCUSSION

### H<sub>2</sub> Production from Lactic Acid Rich Medium by Isolated Strains

The 6 colonies isolated from heat-treated sludge (isolation code MK01-MK06) were selected as the H<sub>2</sub> producing bacteria depend on H<sub>2</sub> production capability obtained. They were subsequently characterized by gram-staining, optical microscopy and the colony shape. Results showed the negative gram, circular form and smooth surface of colonies with the different of colonies edge and cell size. Based on the microscopic observation, each colony was characterized with rod shape and endospore formation. The H<sub>2</sub> fermentation of isolated strains was performed in batch experiment under anaerobic condition and analyzed the H<sub>2</sub> production by the gas chromatography. The cumulative H<sub>2</sub> profile of isolated strains was shown in Fig. 1. It was found that each isolate obtained showed the H<sub>2</sub> production capacities when cultured under an adjusted condition. H<sub>2</sub> production from lactic acid rich medium by isolated strain was performed in batch fermentation. The inoculum was cultivated in the serum bottle and transferred anaerobically during the late-exponential phase by a sterile hypodermic disposable syringe into another serum bottle containing with a lactic acid rich medium. The lactic acid rich medium using 1.5 g/L sodium acetate, 1.5 g/L sodium lactate and 1 g/L sucrose as carbon sources was prepared for H<sub>2</sub> production test for each isolate.

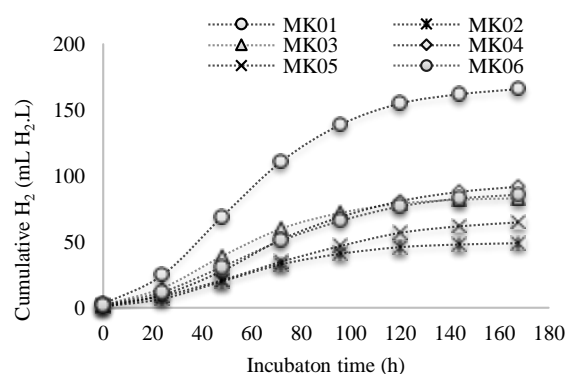


Fig. 1 Cumulative H<sub>2</sub> profile of all isolated strains.

Table 1 showed that all the isolates produced the amounts of H<sub>2</sub> until 120 h of incubation time. The highest amounts of the H<sub>2</sub> production potential and H<sub>2</sub> yield (170.18 mL/L and 3.98 mL/g DW/L) obtained from MK01. The summarizes the batch fermentation results and volatile fatty acids produced with the new isolates when 1.5 g/L sodium acetate, 1.5 g/L sodium lactate and 1 g/L sucrose were used as carbon sources

(Table 2).

Table 1 H<sub>2</sub> production from lactic acid rich medium by isolated strains.

| Isolation code | H <sub>2</sub> production   |                               |                    | H <sub>2</sub> yield* (mL/g DW.L) |
|----------------|-----------------------------|-------------------------------|--------------------|-----------------------------------|
|                | <i>P<sub>s</sub></i> (mL/L) | <i>R<sub>m</sub></i> (mL/L.h) | $\lambda$ (h)      |                                   |
| MK01           | 170.18 <sup>a</sup>         | 0.44 <sup>d</sup>             | 21.78 <sup>a</sup> | 3.98 <sup>a</sup>                 |
| MK02           | 50.58 <sup>f</sup>          | 0.58 <sup>c</sup>             | 12.96 <sup>c</sup> | 0.92 <sup>c</sup>                 |
| MK03           | 84.95 <sup>d</sup>          | 1.05 <sup>a</sup>             | 10.72 <sup>d</sup> | 1.95 <sup>bc</sup>                |
| MK04           | 96.99 <sup>b</sup>          | 0.94 <sup>b</sup>             | 16.31 <sup>b</sup> | 2.27 <sup>b</sup>                 |
| MK05           | 70.98 <sup>e</sup>          | 0.51 <sup>c</sup>             | 16.02 <sup>b</sup> | 1.63 <sup>bc</sup>                |
| MK06           | 90.90 <sup>c</sup>          | 0.85 <sup>b</sup>             | 11.55 <sup>c</sup> | 2.09 <sup>b</sup>                 |

\*H<sub>2</sub> yield (milliliter H<sub>2</sub> per gram of cell dry weight per liter of medium)

A high lactate and acetate of 1.5 g/L and a relatively low glucose concentration of 5 g/L were employed in this experiment because the medium was

performed as lactic acid rich medium. The increasing in total volatile fatty acid produced was obtained from almost isolated strain.

#### Factors Affecting on H<sub>2</sub> Production from Cassava Starch Wastewater by Isolated Strains

The study of effects of inoculums size on H<sub>2</sub> production from cassava starch wastewater by isolated bacteria was performed in batch experiment using 25 mL serum bottles. Three isolated strains i.e. MK01, MK04 and MK06 were preferred to use as seed inoculums depend on high H<sub>2</sub> production capacity (Table 2). The H<sub>2</sub> production capability of isolated bacteria was performed by adjusted initial pH of 5.5. The initial concentration of starch in cassava starch wastewater was 4.63 g/L and total volatile fatty acids including acetic acid, lactic acid, propionic acid and butyric acid were also used as carbon source to produce H<sub>2</sub>.

Table 2 Summarizes of the batch fermentation results of H<sub>2</sub> production from lactic acid rich medium by isolated strains.

| Isolation code | Dry cell weight (g/L) |       | TVFAs* (g/L) |       | Volatile fatty acid composition (g/L) |       |             |       |                |       |              |       |
|----------------|-----------------------|-------|--------------|-------|---------------------------------------|-------|-------------|-------|----------------|-------|--------------|-------|
|                |                       |       |              |       | Acetic acid                           |       | Lactic acid |       | Propionic acid |       | Butyric acid |       |
|                | Init.                 | final | Init.        | final | Init.                                 | final | Init.       | final | Init.          | final | Init.        | final |
| MK01           | 13.3                  | 11.9  | 5.0          | 11.2  | 1.0                                   | 2.2   | 1.4         | 3.2   | 1.2            | 2.7   | 1.4          | 3.2   |
| MK02           | 14.8                  | 14.7  | 5.0          | 14.3  | 1.0                                   | 2.8   | 1.4         | 4.1   | 1.2            | 3.4   | 1.4          | 4.0   |
| MK03           | 13.6                  | 12.8  | 6.5          | 15.9  | 1.2                                   | 3.1   | 1.9         | 4.6   | 1.6            | 3.8   | 1.8          | 4.5   |
| MK04           | 12.6                  | 10.7  | 5.0          | 14.3  | 1.0                                   | 2.8   | 1.4         | 4.1   | 1.2            | 3.4   | 1.4          | 4.0   |
| MK05           | 13.3                  | 11.9  | 6.5          | 12.8  | 1.2                                   | 2.5   | 1.9         | 3.7   | 1.6            | 3.0   | 1.8          | 3.6   |
| MK06           | 13.4                  | 10.8  | 11.2         | 14.3  | 2.1                                   | 2.8   | 3.2         | 4.1   | 2.7            | 3.4   | 3.2          | 4.0   |

\*TVFAs is total volatile fatty acids; Init. is in the initial of fermentation; Final is in the final of fermentation.

Table 3 indicated that increasing in inoculums size of MK01 was improved biogas and H<sub>2</sub> production including content, *P<sub>s</sub>* and yield. The maximum *P<sub>s</sub>* and H<sub>2</sub> yield of MK01 were 836.8 mL/L and 255.9 mL H<sub>2</sub>/g substrate consumed obtained from 40% (v/v) of inoculums size. On the other hand, biogas and H<sub>2</sub> production was suppressed by the increasing in inoculums size of MK04. The maximum *P<sub>s</sub>* and H<sub>2</sub> yield of MK04 were 804.2 mL/L and 175.2 mL H<sub>2</sub>/g substrate consumed obtained from 10% (v/v) of inoculums size. However, the optimum of inoculums size in this experiment was 30% (v/v) of MK06 caused the highest *P<sub>s</sub>* and H<sub>2</sub> yield of 1033.3 mL/L and 467.5 mL H<sub>2</sub>/g substrate consumed. Results suggested that *P<sub>s</sub>* obtained from MK06 was 5 and 6.6 folds greater than MK01 and MK04, respectively. In addition, optimum H<sub>2</sub> yield of MK06 obtained caused 1.3 and 2.7 folds greater than MK01 and MK04, respectively (Table 3).

Results suggested that MK01 has higher ranging of starch consumed than MK04 and MK06. The optimum condition for substrate consumption was under 30% (v/v) inoculums size of MK01 that illustrated 99.54% substrate consumption efficiency. Results also noteworthy that the low substrate consumption efficiency of MK04 and MK06 might be indicated the different of H<sub>2</sub> producing bacteria and starch might adversely affect the biodegradability.

Table 3 Effects of inoculums size on H<sub>2</sub> production from cassava starch wastewater.

| Isolation code | inoculums size (% v/v) | H <sub>2</sub> Production |                             |   |
|----------------|------------------------|---------------------------|-----------------------------|---|
|                |                        | Content (% v/v)           | <i>P<sub>s</sub></i> (mL/L) | Yield (mL H <sub>2</sub> /g substrate consumed) |
| MK01           | 10                     | 2.71 <sup>d</sup>         | 207.86 <sup>d</sup>         | 70.94 <sup>d</sup>                              |
|                | 20                     | 0.30 <sup>fg</sup>        | 15.66 <sup>i</sup>          | 3.38 <sup>gh</sup>                              |
|                | 30                     | 0.32 <sup>fg</sup>        | 18.25 <sup>i</sup>          | 4.25 <sup>fg</sup>                              |
|                | 40                     | 10.50 <sup>b</sup>        | 836.85 <sup>b</sup>         | 255.92 <sup>b</sup>                             |
| MK04           | 10                     | 9.88 <sup>c</sup>         | 804.23 <sup>c</sup>         | 175.21 <sup>c</sup>                             |
|                | 20                     | 0.70 <sup>ef</sup>        | 44.94 <sup>f</sup>          | 12.15 <sup>e</sup>                              |
|                | 30                     | 0.89 <sup>e</sup>         | 48.41 <sup>e</sup>          | 13.45 <sup>e</sup>                              |
|                | 40                     | 0.55 <sup>ef</sup>        | 27.55 <sup>g</sup>          | 11.34 <sup>e</sup>                              |
| MK06           | 10                     | 0.37 <sup>efg</sup>       | 20.57 <sup>h</sup>          | 7.27 <sup>f</sup>                               |
|                | 20                     | -                         | -                           | -   |
|                | 30                     | 11.38 <sup>a</sup>        | 1033.30 <sup>a</sup>        | 467.56 <sup>a</sup>                             |
|                | 40                     | -                         | -                           | -   |

Kapdan and Kargi [24] reported that many agricultural and food industry wastes contain starch may adversely affect the biodegradability. Starch containing solid wastes is easier to process for carbohydrate and H<sub>2</sub> formation. Starch can be hydrolyzed to glucose and maltose by acid or enzymatic hydrolysis followed by conversion of carbohydrates to organic acids and then to H<sub>2</sub> [24]. However, others organic components in cassava

starch wastewater could be used as the substrates to produce  $H_2$  by isolated  $H_2$  producing bacteria in this study.

The effect of incubation temperature on  $H_2$  production from cassava starch wastewater by isolated bacteria was investigated after the optimum inoculum size obtained. Table 3 indicated the optimum of inoculum size was 30% (v/v) of MK06.  $H_2$  producing bacteria strain MK06 was used as seed inoculum at the inoculum size of 30% (v/v) for  $H_2$  production from cassava starch wastewater under various incubation temperatures of 35, 45 and 55 °C. Table 4 showed effect of incubation temperature on  $H_2$  production from cassava starch wastewater by  $H_2$  producing bacteria strain MK06 at the optimum inoculum size (30% v/v). Results illustrated that the maximum cumulative  $H_2$ , yield and production rate of 4.20 L  $H_2$ /L medium, 1.47 L  $H_2$ /g substrate consumed, and 14.00 mL  $H_2$ /L/h were obtained under incubation temperature of 35 °C.

Table 4 Effects of incubation temperatures on  $H_2$  production from cassava starch wastewater by MK06.

| Incubation temperatures | H <sub>2</sub> Production by MK06 at 10% (v/v) of inoculum size |  |   |
|-------------------------|---|--|---|
|                         | $P_s$ (L H <sub>2</sub> /L medium)                              | Yield (L H <sub>2</sub> /g substrate consumed) | H <sub>2</sub> production rate (mL H <sub>2</sub> /L.h) |
| 35°C                    | 4.20 <sup>a</sup>   | 1.47 <sup>a</sup>                              | 14.00 <sup>a</sup>                                      |
| 45°C                    | 2.89 <sup>c</sup>   | 0.99 <sup>c</sup>                              | 9.30 <sup>b</sup>                                       |
| 55°C                    | 3.78 <sup>b</sup>   | 1.26 <sup>b</sup>                              | 12.70 <sup>a</sup>                                      |

### 16S rDNA and phylogenetic analysis of isolated $H_2$ producing bacteria

Isolation of new  $H_2$  producing bacteria with high capacity or unique properties in  $H_2$  production was investigated using 16S rRNA gene sequence analysis.  $H_2$  producing bacteria strain MK06 was preferred for identification of the new isolates via sequencing of the full 16S rDNA followed by phylogenetic analysis. Results showed the 100% similarity of 16S rDNA compare with closely related species was indicated *Klebsiella pneumoniae* subsp. *pneumonia* DSM 30104(T) reported by Schroeter (1886) and Trevisan (1887). In order to better understand the process, the microbial identification was investigated and linked to the  $H_2$  production performance. The used method for microbial characterization in  $H_2$  production is 16S rRNA based DGGE combined with sequencing and similarity-based phylogenetic analysis [25]. The DNA sequences determined and obtained from databases were aligned with a program CLUSTAL X (version 1.8) [18] in BioEdit Program [19]. Alignment gaps and unidentified bases were eliminated. The evolutionary distances were computed using the Maximum Composite Likelihood method [20]. Phylogenetic trees of 16S rRNA genes

were constructed by the neighbor-joining method of [21] which shown in Fig. 2. The percentage of replicate trees in which the associated taxa clustered together in the bootstrap test (1000 replicates) are shown next to the branches [19]. The tree is drawn to scale, with branch lengths in the same units as those of the evolutionary distances used to infer the phylogenetic tree. The evolutionary distances were computed using the maximum composite likelihood method [21] and are in the units of the number of base substitutions per site. The analysis involved 11 nucleotide sequences. All positions containing gaps and missing data were eliminated. There were a total of 1246 positions in the final dataset. Evolutionary analyses were conducted in MEGA6 [20].

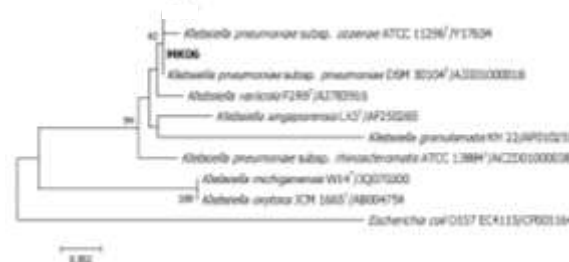


Fig. 2 The phylogenetic relationships based on 16S rDNA.

### CONCLUSIONS

The 6 isolated strains i.e. isolation code of MK01-06 indicated the  $H_2$  production capability when cultured in lactic acid rich medium. MK01, MK04 and MK06 were selected to use as seed inoculum for  $H_2$  production from cassava starch wastewater which consisted of starch and volatile fatty acid i.e. lactic acid and acetic acid in composition. The optimal condition of  $H_2$  production from cassava starch wastewater was 30% (v/v) of MK06 as inoculum under 35 °C which obtained the maximum  $P_s$ ,  $H_2$  yield and  $H_2$  production rate of 4.20 L  $H_2$ /L medium, 1.47 L  $H_2$ /g substrate consumed, and 14.00 mL  $H_2$ /L/h, respectively. Identification and characterization of MK06 indicated that 100% similarity of 16S rDNA compare with closely related species was indicated *Klebsiella pneumoniae* subsp. *pneumonia* DSM 30104(T).

### ACKNOWLEDGMENTS

This research work was financially granted by the Thailand Research Fund and Rajabhat Maha Sarakham University under the TRF Research Scholar Grant No. MRG5580247. The author would like to thank Prof. Dr. Alissara Reungsang for her suggestion and supporting for the research.

### REFERENCES

- [1] Baghchehsaraee B., Nakhla G., Karamanev D., and Margaritis A., Effect of extrinsic lactic acid on fermentative hydrogen production, International

- Journal of Hydrogen Energy, Vol. 34, Issue 6, 2009, pp. 2573-2579.
- [2] Matsumoto M., and Nishimura Y., Hydrogen production by fermentation using acetic acid and lactic acid, Journal of Bioscience and Bioengineering, Vol. 103, Issue 3, 2007, pp. 236-241.
  - [3] Avancini S.R.P., Faccin G.L., Vieira M.A., Rovaris A.A., Rossana Podestá, Ricardo Tramonte, de Souza N.M.A., and Amante Edna R., Cassava starch fermentation wastewater: Characterization and preliminary toxicological studies, Food and Chemical Toxicology, Vol. 45, Issue 11, 2007, pp. 2273-2278.
  - [4] Pereira J.M., Sena Aquino A.C.M., Oliveira D.C., Francisco G.R.A., Barreto P.L.M., and Amante E.R., Ciencia Rural, Vol. 46, Issue 4, 2016, pp. 732-738.
  - [5] Saraphirom P., and Reungsang A., Biological hydrogen production from sweet sorghum syrup by mixed cultures using an anaerobic sequencing batch reactor (ASBR), International Journal of Hydrogen Energy, Vol. 36, Issue 14, 2011, pp. 8765 – 8773.
  - [6] Baghchehsaraee B., Nakhla G., Karamanev D., Margaritis A., and Reid G., The effect of heat pretreatment temperature on fermentative hydrogen production using mixed cultures, International Journal of Hydrogen Energy, Vol. 33, Issue 15, 2008, pp. 4064-4073.
  - [6] Noike T., Takabatake H., Mizuno O., and Ohba M., Inhibition of hydrogen fermentation of organic wastes by lactic acid bacteria, International Journal of Hydrogen Energy, Vol. 27, Issue 11-12, 2002, pp. 1367-1371.
  - [7] Nishio N., and Nakashimada Y., High rate production of hydrogen/methane from various substrates and wastes, Advances in Biochemical Engineering/Biotechnology, Vol. 90, 2004, pp. 63-87.
  - [8] Shiratori H., Sasaya K., Ohiwa H., Ikeno H., Ayame S., Kataoka N., Miya N., Beppu T., and Ueda K., *Clostridium clariflavum* sp. nov. and *Clostridium caenicola* sp. nov., moderately thermophilic, cellulose/cellobiose-digesting bacteria isolated from methanogenic sludge, International Journal of Systematic and Evolutionary Microbiology, Vol. 59, Issue 7, 2009, pp. 1764-1770.
  - [9] Saraphirom P., and Reungsang A., Optimization of biohydrogen production from sweet sorghum syrup using statistical methods, International Journal of Hydrogen Energy, Vol. 35, Issue 24, 2010, pp. 13435-13444.
  - [10] A.P.H.A., Stand Methods for the Examination of Water and Wastewater, 19th ed. Washington DC: American Public Health Association, 1995, pp.1-541.
  - [11] Permanasari A.E., Awang Rambli D.R. and Dhanapal Durai Dominic P., Forecasting method selection using ANOVA and duncan multiple range tests on time series dataset, Conference proceedings, in Proc. 2010 International Symposium on Information Technology, 2010, 10.1109/ITSIM.2010.5561535.
  - [12] Yamada Y., Katsura K., Kawasaki H., Widyastuti Y., Saono S., Seki T., Uchimura T., and Komagata K., *Asaia bogorensis* gen. nov., sp. nov., an unusual acetic acid bacterium in the  $\alpha$ -Proteobacteria, International Journal of Systematic and Evolutionary Microbiology, Vol. 50, 2000, pp. 823-829.
  - [13] Katsura K., Kawasaki H., Potacharoen W., Saono S., Seki T., Yamada Y., Uchimura T., and Komagata K., *Asaia siamensis* sp. nov., an acetic acid bacterium in the  $\alpha$ -Proteobacteria, International Journal of Systematic and Evolutionary Microbiology, Vol. 51, 2000, pp. 559-563.
  - [14] Klappenbach J.A., Saxman P.R., Cole J.R., and Schmidt T.M., rrndb: Ribosomal RNA operon copy number database. Nucleic Acids Research, Vol. 29, Issue 1, 2001, pp. 181-184.
  - [15] Jones D.T., and Swindells M.B., Getting the most from PSI-BLAST. TRENDS in Biochemical Sciences, Vol. 27, Issue 3, 2002, pp. 161-164.
  - [16] Kim O.S., Cho Y.J., Lee K., Yoon S.H., Kim M., Na H., Park S.C., Jeon Y.S., Lee J.H., Yi H., Won S., and Chun J.S., Introducing EzTaxon-e: a prokaryotic 16S rRNA gene sequence database with phylotypes that represent uncultured species. International Journal of Systematic and Evolutionary Microbiology, Vol. 25, 2012, pp. 716-721.
  - [17] <http://eztaxon-e.ezbiocloud.net>
  - [18] Larkin M.A., Blackshields G., Brown N.P., Chenna R., McGettigan P.A., McWilliam H., Valentin F., Wallace I.M., Wilm I.A., Lopez R., Thompson J.D., Gibson T.J. and Higgins D.G., Sequence analysis Clustal W and Clustal X version 2.0. Bioinformatic Application Note, Vol. 23, Issue 21, 2007, pp. 2947-2948.
  - [19] Hall T., BioEdit: An important software for molecular biology, GEF Bulletin of Biosciences, Vol. 2, Issue 1, 2011, pp. 60-61.
  - [20] Tamura K., Nei M., and Kumar S., Prospects for inferring very large phylogenies by using the neighbor-joining method, Proceedings of the National Academy of Sciences (USA), 2004, pp. 11030-11035.
  - [21] Segata N., Börnigen D., Morgan X. C., and Huttenhower C., PhyloPhlAn is a new method for improved phylogenetic and taxonomic placement of microbes. Nature Communication, 2013, DOI: 10.1038/ncomms3304.
  - [22] Shimodaira H., and Hasegawa M., CONSEL: for assessing the confidence of phylogenetic tree selection. Bioinformatic Application Note, Vol. 17, Issue 12, 2001, pp. 1246-1247.
  - [23] Tamura K., Stecher G., Peterson D., Filipinski A., and Kumar S., MEGA6: Molecular Evolutionary Genetics Analysis Version 6.0, Molecular Biology and Evolution, Vol. 30, Issue 12, 2013, pp. 2725-2729.
  - [24] Kapdan I.K., and Kargi F., Review Bio-hydrogen production from waste materials. Enzyme and Microbial Technology, Vol. 38, Issue 5, 2006, pp. 569-582.
  - [25] Guo X.M., Trably E., Latrille E., Carrère H., and Steyer J.P., Hydrogen production from agricultural waste by dark fermentation: a review. International Journal of Hydrogen Energy, Vol. 35, Issue 19, 2010, pp. 106.



## OPTIMIZATION OF PARAQUAT DEGRADATION WITH MICROBIAL CONSORTIUM FROM CONTAMINATED SOIL USING STATISTIC METHOD

Mullika Teerakun<sup>1</sup> Alissara Reungsang<sup>2</sup> Monrodee Chaowarat<sup>3</sup> and Piyawadee Saraphirom<sup>4\*</sup>

<sup>1</sup>Faculty of Agricultural Technology, Kalasin University, Thailand; <sup>2</sup>Faculty of Technology, Khon Kaen University, Thailand; <sup>3</sup>Faculty of Technology, Mahasarakham University, Thailand; <sup>4</sup>Faculty of Science and Technology, Rajabhat Mahasarakham University, Thailand

### ABSTRACT

Paraquat is one of non-selective herbicides, widely used in Thailand and other countries that can be used to prevent and mitigate problems with weeds that have become resistant. It has broad spectrum to weed knockdown herbicide which can be easily distributed in an aquatic environment due to its high solubility in water. The aim of research is to study the optimization condition for biodegradation of paraquat by microbial consortium using an orthogonal array design in culture media. Microbial consortium which can degrade paraquat were isolated from cassava rhizosphere soil with a history area of using paraquat in Kalasin, Thailand. Analysis of the 16S rDNA gene sequences compared with the database in Gen Bank demonstrated that microbial consortium showed the similarity with *Sphingomicrobium marinum* (97%), *Ferrovibrio xuzhouensis* (93%), *Azospirillum lipoferum* (93%), *Altererythrobacter xinjiangensis* (94%), *Xanthobacter autotrophicus* (92%) and *Azospirillum amazonense* (99%). To achieve the biodegradation experiments, orthogonal arrays design was investigated, with the three independent variables: glucose concentration (1-20 g/L), paraquat concentration (10-100 mg/L) and inoculum concentration (1-10%). The biodegradation consortium was done triplicate in 250 mL Erlenmeyer flask at 30°C 150 rpm for 35 days. Paraquat biodegradation was reported as biodegradation percentage. The results demonstrated that the optimum concentrations of glucose, paraquat and inoculum for paraquat biodegradation were 1 g/L, 10 mg/L and 5%, respectively. The paraquat removal efficiency of 95.69% was achieved under the optimal condition.

**Keywords:** Paraquat, Biodegradation, Orthogonal arrays design, Microbial consortium

### INTRODUCTION

Nowadays, chemicals substances are widely used for agriculture in Thailand. One group of these chemical substance is pesticides. Pesticides have been an important part of agriculture to protect crops and increase an agriculture yield [1]. The group of pesticide that commonly used for eliminating weed is paraquat. Paraquat (1,1-dimethyl-4,4-bipyridyl dichloride) is non-selective contact herbicide, quick-acting and killing green plant tissue on contact. It is classified as non-moving herbicides due to strong adsorption on soil particles. However, repeated use of paraquat over the years or the used in large quantities caused an accumulation of paraquat in environment by adsorption to the soil. The interrill erosion and run-off water can cause the leaching of paraquat and spreading to the river bed [2], [3]. In Thailand, it had been reported that paraquat is the main pesticide disseminated to the aquatic environment, for example, in the Chao Phraya River (0.28 and 0.40 µg/L), Pa Sak River (0.22 and 3.23 µg/L), Tha Chin River (0.01-0.79 µg/L), Namphong River (0.02-26.8 ng/L) and Chanthaburi River (0.50-15.00 µg/L) which paraquat in the sample water from those rivers was found to have a higher residue content than other

group of pesticide. [4]-[8]. Paraquat is classified as a moderately toxic chemical for lethal toxicity, with a relatively low potential to bio-accumulate in the aquatic environment [9]. Therefore, the removal of paraquat from contaminated environment is necessary.

Bioremediation is biological processes or activity of the organisms to transform contaminants into less toxic compound. This method is presently the inexpensive and has greater efficiency in the removal of contaminants than conventional physicochemical methods [10]. Previous researches revealed the efficient pesticide removal by microorganisms. *Brevibacterium frigoritolerans*, *Bacillus aerophilus* and *Pseudomonas fulva* were isolated from aged phorate contaminated soil and could degrade phorate with the percentage of removal ranged between 97.65 and 98.31% [11]. Kafilzadeh et al. [12] isolated bacteria from sediments and water samples from high agricultural activity areas. They belong to genus i.e. *Klebsiella*, *Acinetobacter*, *Alcaligenes*, *Flavobacterium*, and *Bacillus*. *Bacillus* sp., *Micrococcus* sp., *Klebsiella* sp., *Pseudomonas* sp., *Listeria* sp., *Proteus* sp., *Streptococcus* sp., and *Staphylococcus* sp. were found as the bacteria capable of utilizing the herbicide (paraquat dichloride) [13].

Design of Experiments techniques was widely used to optimize experimental parameters and enabled to determine simultaneously the individual and interactive effects of many factors that could affect the output results in experiment [14]-[15]. A full factorial experiment tests all possible combinations of the factor levels and can therefore find the overall optimum setting. However, this process became excessive as the number of design parameters or levels increases [16]. An orthogonal array led to the reduction of variability in the process, compliance that is close to the desired result and a decrease of operating costs [17]. This technique has two major requirements consisting of the levels of any factor must occur with the same frequency and two factors, which each possible combination of levels must occur with the same frequency. If all factors have  $q$  levels, an orthogonal array is typically expressed as  $L_M(q^m)$ , where  $m$  is the number of factors and  $M$  represents the number of rows in the array [16].

The aim of this research was to isolate the bacterial consortium capable of paraquat degradation. The paraquat removal efficiency of the isolated bacterial consortium were also examined in the batch experiment with statistical experimental design. In addition, the optimal conditions for paraquat removal by isolated consortium were determined in order to achieve the highest paraquat removal efficiency.

## MATERIALS AND MEHODS

### Soil Sampling

Cassava rhizosphere soil sample was collected from the field, with a history of paraquat application, in Kalasin province, Thailand and used as a source for paraquat degrading bacteria isolation. It was preserved in plastic bag and kept at 4°C for maintain the activity of microorganisms until the usage.

### Isolation of Bacterial Consortium Capable of Degrading Paraquat

Isolation of microbial consortium capable of degrading paraquat from rhizosphere soil was carried out by enrichment culture technique. Soil samples (10 g) were put into 250 mL Erlenmeyer flasks containing 90 mL of the mineral salt medium [18] supplemented with 10 mg/L paraquat. Flasks were incubated at 30°C with shaking at 150 rpm. After 7 days, 10 mL of broth from flask was inoculated to fresh mineral salt medium containing 10 g/L of paraquat. This process was repeated until the paraquat removal at day 7 was less than 50% of the initial value. Isolated consortium was then harvested using method

previously described by Teerakun et al. [19]. The isolated consortium was used in the further experiment. Bacterial community in the isolated consortium was analyzed by Denaturing gradient gel electrophoresis (DGGE) technique.

### Analysis on Community Structure of Bacterial Consortium by DGGE Technique

The genomic DNA of isolated consortium was extracted by using TIANamp Soil DNA Kit (TIANGEN Biotech (Beijing) Co., Ltd.). The 16S rRNA was amplified by the first polymerase chain reaction (PCR) with universal primer 1525r (5' AAGGAGGTGWTCCARCC 3') and 27f (5' GAGTTTGATCCTT GGCTCAG 3'). In the second PCR, primer 518r (5'GTATTACCGCGGCTGCTGG3') and 357f (5'CTCCTACGGGAGGCAGCAG3') with CG clamp (CGCCCGCCGCGCGGCGGGCGG GCGGGGGGCACGGGG GG) were used to amplify the fragment of V3 region of 16S rDNA product from first PCR. PCR products were stored at 4°C and analyzed on 1.0% agarose before DGGE analysis. The DGGE analysis of the PCR products was performed by electrophoresis (DGGE unit, V20-HCDC, Scie-Plas Limited, UK) according to the method previously described by Kongjan et al. [20]. The closest matches for partial 16S rRNA gene sequences were identify base on the sequence data of ribosomal database project (<http://rdp.cme.msu.edu/>). The Seq Match program and basic local alignment search tool (BLAST) with nucleotide database in the National Center for Biotechnology Information were employed [21].

### Determination of Optimal Conditions for Degradation of Paraquat in Culture Media using Orthogonal Arrays Design

Degradation of paraquat by isolated consortium was investigated in 250 mL Erlenmeyer flask with the working volume of 150 mL. The experimental conditions were designed by orthogonal arrays design, with the three independent variables: glucose concentration (A; 1, 10 and 20 g/L), paraquat concentration (B: 10, 50 and 100 mg/L) and inoculum isolated concentration (C: 1, 5 and 10%) on paraquat biodegradation. All experimental runs were conducted in triplicate. The  $L_9$  ( $3^4$ ) orthogonal test parameters was showed in Table 1. The blank factor was a dummy and was used for error assessment.

Table 1. The  $L_9$  ( $3^4$ ) orthogonal design for the paraquat biodegradation.

| Experimental run | A: glucose (g/L) | B: praquat (mg/L) | Blank | C: inoculum (%) |
|------------------|------------------|-------------------|-------|-----------------|
| 1                | 20               | 100               | 2     | 1               |

|   |    |     |   |    |
|---|----|-----|---|----|
| 2 | 20 | 50  | 1 | 10 |
| 3 | 20 | 10  | 3 | 5  |
| 4 | 10 | 50  | 3 | 1  |
| 5 | 1  | 50  | 2 | 5  |
| 6 | 1  | 100 | 3 | 10 |
| 7 | 1  | 10  | 1 | 1  |
| 8 | 10 | 10  | 2 | 10 |
| 9 | 10 | 100 | 1 | 5  |

### Analysis of Paraquat Residue in Culture Media

The culture media was taken at the interval time and centrifuged for 15 min at 4,000 rpm. One milliliter of supernatant was filled in the glass tube with 1 mL of 2% Na<sub>2</sub>S<sub>2</sub>O<sub>4</sub> in 0.3 M NaOH. Paraquat concentration was examined by Spectrophotometer UV-1800 (SHIMADZU, Japan) at 600 nm [22]. The paraquat recovery efficiency of this method was 93%.

## RESULTS AND DISCUSSION

### The Community Structure of a Bacterial Consortium Capable of Degrading Paraquat by DGGE

The community structure of a bacterial consortium capable of degrading Paraquat was analyzed by DGGE. The fingerprints obtained from the bacterial community of isolated consortium demonstrated 6 differently visible bands as shown in Fig. 1. The sequences of the bands were identified base on 16S rRNA gene and exhibited a greater than 92% identity to the sequences deposited in the databases (Table 2) which were closet matched to 6 genera i.e., *Sphingomicrobium marinum*, *Ferrovibrio xuzhouensis*, *Azospirillum lipoferum*, *Altererythrobacter xinjiangensis*, *Xanthobacter autotrophicus* and *Azospirillum amazonense*. *Sphingomicrobium* sp. is members of genus *Sphingomonas* which are often reported as the bacteria capable of degrading recalcitrant natural, anthropogenic compounds and different herbicides and pesticides [23]. Song et al. [24] reported cyhalothrin, synthetic pyrethroid pesticide, degradation by *F. xuzhouensis*. It was isolated from a cyhalothrin contaminated wastewater. *Azospirillum* is of the genera that able to degrade organic and inorganic contaminants in soil [25]-[26] and were capable of biodegradation ethion in minimal salt media [27]. Romeh and Hendawi [28] found that *A. lipoferum* has capability of utilizing organophosphorus insecticides, chlorpyrifos, chlorpyrifos-methyl, cyanophos and malathion in mineral salts media as carbon and phosphorus source. *Azospirillum* sp. could tolerate to pesticides such as monocrotophos and chlorpyrifos at low concentrations. However, the higher concentrations of these pesticides could cause antagonistic effects on

*Azospirillum* sp. and decrease the ammonification process [29]. *X. autotrophicus* could degraded 2-chloroethanol (2-CE) that are metabolite of Tris (2-chloroethyl) phosphate into glycolic acid [30] and growing cells of of *X. autotrophicus* strain GJ10 completely degraded 180 µM of 2-CE within 24 h [31].

Table 2 Identification of dominant fragments in DGGE patterns in paraquat biodegradation isolation consortium

| Bands | Closet Identify Relative                |               |            |
|-------|---|---------------|------------|
|       | Bacterial species                       | Accession No. | % Identity |
| 1     | <i>Sphingomicrobium marinum</i>         | NR_135708.1   | 97%        |
| 2     | <i>Ferrovibrio xuzhouensis</i>          | NR_145543.1   | 93%        |
| 3     | <i>Azospirillum lipoferum</i>           | NR_116846.1   | 93%        |
| 4     | <i>Altererythrobacter xinjiangensis</i> | NR_108901.1   | 94%        |
| 5     | <i>Xanthobacter autotrophicus</i>       | NR_074255.1   | 92%        |
| 6     | <i>Azospirillum amazonense</i>          | NR_104981.1   | 99%        |

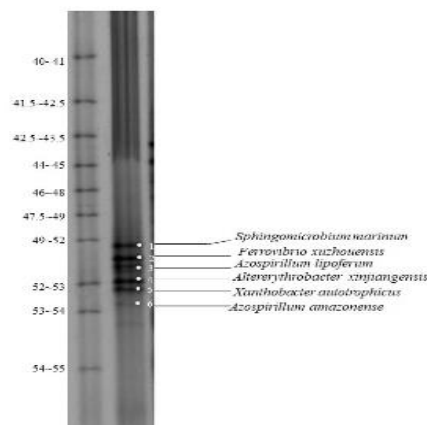


Fig. 1 DGGE fingerprint of 16S rDNA fragments of paraquat biodegradation isolation consortium. Sequence of bands was searched in the GenBank with the BLAST program to determine the closest known relatives of the partial 16S rDNA sequences obtained (Table 2).

### The Orthogonal Experiment Results of Paraquat Biodegradation

Batch paraquat biodegradation (the experimental runs 1 to 9) was examined. The results of orthogonal experiment of paraquat biodegradation

at day 35 were showed in Table 3. The paraquat removal on the orthogonal experiments ranged from 70.02 to 97.87% (Table 3). Range analysis was applied to clarify the important sequence of glucose concentration (factor A), paraquat concentration (factor B) and inoculum concentration (factor C) in the orthogonal experiments (Table 4). The highest range value (R) of 13.63 was found for factor B, while the lowest range value of 7.79 was found for factor A. The bigger R value of a factor represents a greater effect on the paraquat removal. According to the range, the order of influence on the paraquat removal was paraquat concentration > inoculum concentration > glucose concentration. Thus, the optimum condition for improving paraquat removal was determined as A1B1C2 corresponding to glucose concentration, 1 g/L; paraquat concentration, 10 mg/L and inoculum, 5%.

In order to verify the reliability of the results in flasks, an additional experiment with the corresponding parameters under the optimum nutrient condition A1B1C2 was performed in flask 250 mL (data not show). Under the optimum condition, the observed paraquat removal of 95.69% was obtained. This indicated that the statistical experimental design i.e. orthogonal experiment design, is a useful tool for optimizing paraquat removal conditions.

Addition of glucose could lead to higher degradation of pesticide [32]. This is in accordance with a study by Hashemi et al. [33] who reported that paraquat biodegradation increased in the presence of glucose by *Achromobacter xylosoxidans* and *Streptomyces* sp. Kanissery and Sims [34] reported that the addition of glucose was enhanced the extent of mineralization herbicide at a low herbicide concentration.

Paraquat was used as nitrogen source by microorganism [19], [35]-[36]. However, the paraquat concentration was impact affected on growth of the organisms. According to report of Andy et al. [37] found that the cell mass yield of the microbes decreased with increased concentration of the paraquat. Paraquat had toxic effect on the microorganisms leading to the higher counts obtained from the lowest concentration of 25 mg/kg and the lowest counts from the highest concentration of 100 mg/kg [38].

Microbial population density is an important determinant in the biodegradation rate [39]. When the inoculum size is small and viable cell fraction is low, there may be a pseudo-lag phase, which is not a result of adaptation but of the small inoculums size [40]. In addition, higher inoculum sizes would contain a larger population of microorganism that would consume more oxygen. The optimal condition,

especially in terms of specific degradation rate of substrate, did not occur at initial optical density (OD) of 3 [41].

Table 3 Orthogonal experiment results of paraquat biodegradation at the remediation time of 35 days.

| Experimental run | A: glucose (g/L) | B: paraquat (mg/L) | C: inoculum (%) | Paraquat removal (%) |
|------------------|------------------|--------------------|-----------------|----------------------|
| 1                | 20               | 100                | 1               | 70.02                |
| 2                | 20               | 50                 | 10              | 91.28                |
| 3                | 20               | 10                 | 5               | 95.15                |
| 4                | 10               | 50                 | 1               | 87.88                |
| 5                | 1                | 50                 | 5               | 97.87                |
| 6                | 1                | 100                | 10              | 86.72                |
| 7                | 1                | 10                 | 1               | 95.23                |
| 8                | 10               | 10                 | 10              | 93.96                |
| 9                | 10               | 100                | 5               | 86.70                |

Table 4 The range analysis of L<sub>9</sub> (3<sup>4</sup>) orthogonal experiment for paraquat biodegradation.

|    | A: glucose (g/L) | B: paraquat (mg/L) | Blank  | C: inoculum (%) |
|----|------------------|--------------------|--------|-----------------|
| K1 | 279.82           | 284.34             | 273.21 | 253.13          |
| K2 | 268.54           | 277.03             | 261.85 | 279.72          |
| K3 | 256.45           | 243.44             | 269.75 | 271.97          |
| k1 | 93.27            | 94.78              | 91.07  | 84.38           |
| k2 | 89.51            | 92.34              | 87.28  | 93.24           |
| k3 | 85.48            | 81.15              | 89.92  | 90.66           |
| R  | 7.79             | 13.63              | 3.79   | 8.86            |
| Q  | A1               | B1                 |        | C2              |

## CONCLUSIONS

Microbial consortium capable of degrading paraquat were isolated from cassava rhizosphere soil. The microbial analysis using the PCR-DGGE technique demonstrated 6 differently visible bands identified as *S. marinum*, *F. xuzhouensis*, *A. lipoferum*, *Al. xinjiangensis*, *X. autotrophicus* and *A. amazonense*. The orthogonal arrays design results indicate that the optimum conditions for paraquat removal was 1 g/L glucose concentration, 10 mg/L paraquat concentration and 5% inoculum concentration possessing paraquat removal efficiency of 95.69%.

## ACKNOWLEDGMENTS

This project was partially supported by Research Centre for Environmental and Hazardous Substance Management, Khon Kaen University. The authors are grateful to the Research Group for Development of Microbial Hydrogen Production Process from Biomass, Khon Kaen University and Department of Biotechnology, Kalasin University for providing the

necessary laboratory facilities. We would like to thank Dr. Pensri Plangklang and Dr. Khakhanang Ratanikom for providing the comment.

## REFERENCES

- [1] Özkara A., Akyil D. and Konuk M., Pesticides, Environmental Pollution, and Health, Environmental Health Risk - Hazardous Factors to Living Species, Larramendy M.L. and Soloneski S., Ed. Intech Open, 2016, pp. 3-27.
- [2] Kajitvichyanukul P., Complete report of research plan on integrated research to strengthen local authorities in managing and preventing toxic contamination on Nan watershed, National Research Council of Thailand, Bangkok, 2012. [in Thai]
- [3] Yimpoolsap S., Hungspreug N. and Anurugsa B., The Effects of Paraquat Used in Upland Rice and Maize Fields on Biomass of Attached Algae, Thammasat International Journal of Science and Technology, Vol. 19, No. 1, 2014, pp. 32-38.
- [4] Wetchayanon M., Kungsakulniti N., Charoenca N. and Tangbanluekan C., Health risk assessment of contaminated pesticides in the main rivers of Thailand, in The National and International Graduate Research Conference, 2017, pp. 880-890.
- [5] Komarova T., Iwai C.B., Somparn A., Tokhun N., Mueller J., Kennedy I. and Noller B., Pesticide distribution in the Namphong river NE Thailand arising from land use and other practices, International Journal of Environmental and Rural Development, Vol. 6, No. 1, 2015, pp. 175-180.
- [6] Pataranawatab P., Kitkaewab D. and Suppaudomab K., Paraquat contaminations in the Chantaburi River and vicinity area, Chantaburi province, Thailand, Journal of Science, Technology, and Humanities, Vol. 10, No. 1, 2012, pp. 17-24.
- [7] Leadprathom N., Parkpain P., Satayavivad J., Delaune R.D. and Jugsujinda A., Transport and deposition of organochlorine pesticides from farmland to estuary under tropical regime and their potential risk to aquatic biota, J. of Environmental Science and Health Part B, Vol 44, No. 3, 2009, pp. 249-261.
- [8] Leadprathom N., Toxicity of paraquat to aquatic animal, King Mongkut's Agricultural Journal, Vol. 31, No. 2, 2013, pp. 95-101.
- [9] Sawasdee B., Phuthonghin P. and Kunapratom S., Acute Toxicity of Paraquat and Glyphosate on embryonic development of Climbing Perch (*Anabas testudineus*), Prawarun Agricultural Journal, Vol. 13, No. 1, 2016, pp. 70-78.
- [10] Letti L.A.J., Vítola F.M.D., de Melo Pereira G.V., Karp S.G., Medeiros A.B.P., da Costa E.S.F., Bissoqui L. and Soccol C.R., Solid-state fermentation for the production of mushrooms, In Current Developments in Biotechnology and Bioengineering, Pandey A., Larroche C. and Soccol C.R., Ed. Elsevier, 2018, pp. 285-318.
- [11] Jariyal M., Jindal V., Mandal K., Gupta V.K. and Singh B., Bioremediation of organophosphorus pesticide phorate in soil by microbial consortia, Ecotoxicol. Environ. Saf., Vol. 159, 2018, pp.310-316.
- [12] Kafilzadeh F., Ebrahimnezhad M. and Tahery Y., Isolation and identification of endosulfan-degrading bacteria and evaluation of their bioremediation in Kor River, Iran, Osong. Public. Health. Res. Perspect., Vol. 6, No. 1, 2015, pp. 39-46
- [13] Ozoude T.O., Etok C.A., Eleanya E.U. and Agwa O.K., Monitoring the bio-utilization of herbicide (paraquat dichloride) by some bacterial species isolated from soil in Calabar, Cross-River State, Nigeria, Journal of Applied Life Sciences International, Vol. 16, No. 1, 2018, pp. 1-6.
- [14] Wang T.Y. and Huang C.Y., Improving forecasting performance by employing the Taguchi method, European Journal of Operational Research, Vol. 176, No. 2, 2007, pp. 1052-1065.
- [15] de Freitas A.P.B.R., de Freitas L.V., Loures C.C.A., dos Santos M.A.R., Ricardo G.D., Marins F.A.S., dos Santos M.S.A. and Silva M.B., Taguchi Method Applied to Environmental Engineering, Design of Experiments – Applications, Silva M.B., Ed. Intech Open, 2013, pp. 79-92.
- [16] Lee C.T. and Kuo H.C., A Novel algorithm with orthogonal arrays for the global optimization of design of experiments, Appl. Math. Inf. Sci., Vol. 7, No. 3, 2013, pp. 1151-1156.
- [17] de Freitas A.P.B.R., de Freitas L.V., Loures C.C.A., Gonçalves L.G. and Silva M.B., Response surface method and Taguchi Orthogonal Array applied to phenolic wastewater by advanced oxidation process (AOP), American Journal of Theoretical and Applied Statistics, Vol. 3, Issue 6-1, 2014, 35-41.
- [18] Ansari S.M., Dehghani M. and Samaei M.R., Isolation of atrazine degrading bacteria in semi-salinity medium, Journal of Health Sciences and Surveillance System, Vol. 4, No. 3, 2016, pp. 121-128.
- [19] Teerakun M., Saraphirom P. and Reungsang A., Optimization of paraquat degradation by microbial consortium from rhizosphere soil, EAU Heritage Journal Science and Technology, Vol. 11, No. 2, 2017, pp. 90-99.
- [20] Kongjan P., O-Thong S., Kotay M., Min B. and Angelidaki I., Biohydrogen production from wheat straw hydrolysate by dark fermentation using extreme thermophilic mixed culture, Biotechnology and Bioengineering, Vol. 105, No.

- 5, 2010, pp. 899–908.
- [21] Suksong W., Jehlee A., Singkhala A., Kongjan P., Prasertsan P., Imai T. and O-Thong, S., Thermophilic solid-state anaerobic digestion of solid waste residues from palm oil mill industry for biogas production, *Industrial Crops and Products*, Vol. 95, 2017, pp. 502–511.
- [22] Lima T.L., Nicoletti M.A., Munhoz C., De Abreu G.R., Magalhães J.Z., Ricci E.L., Waziry P.A.F., Alves da Costa J.N., Antônio A.C.N. and Fukushima A.R., Determination of paraquat in several commercially available types of rice, *Food and Nutrition Sciences*, Vol. 09, No.12, 2018, pp. 1368-1375.
- [23] Stolz A., Molecular characteristics of xenobiotic-degrading Sphingomonads, *Appl Microbiol Biotechnol.*, Vol. 81, No. 5, 2009, pp. 793-811.
- [24] Song M., Zhang L., Sun B., Zhang H., Ding H., Li Q., Guo S. and Huang X., *Ferrovibrio xuzhouensis* sp. nov., a cyhalothrin-degrading bacterium isolated from cyhalothrin contaminated wastewater, *Antonie van Leeuwenhoek*, Vol. 108, No. 2, 2015, pp. 377–382.
- [25] Zhuang X., Chen J., Shim H. and Bai Z., New advances in plant growth-promoting rhizobacteria for bioremediation, *Environ. Int.*, Vol. 33, No. 3, 2007, pp. 406-413.
- [26] Hong S.H., Ryu H., Kim J. and Cho K.S., Rhizoremediation of diesel-contaminated soil using the plant growth-promoting rhizobacterium *Gordonia* sp. S2RP-17, *Biodegradation*, Vol. 22, No. 3, 2011, pp. 593–601.
- [27] Foster L.J., Kwan B.H. and Vancov T., Microbial degradation of the organophosphate pesticide, Ethion, *FEMS Microbiol Lett.*, Vol. 240, No. 1, 2004, pp. 49-53.
- [28] Romeh A.A. and Hendawi M.Y., Bioremediation of Certain Organophosphorus Pesticides by Two Biofertilizers, *Paenibacillus (Bacillus) polymyxa* (Prazmowski) and *Azospirillum lipoferum* (Beijerinck), *J. Agr. Sci. Tech.*, Vol. 16, 2014, pp. 265-276.
- [29] Venieraki I., Kefalogianni I., Pergalis P., Chatzipavlidis I., Dimou M. and Katinakis P., Isolation of *Azospirillum* and *Pseudomonas diazotrophs* from wheat rhizosphere in Greece, *Proc. Natl. Acad. Sci.*, Vol. 105, No. 21, 2008, pp. 7564-7569.
- [30] Takahashi S., Miura K., Abe K. and Kera Y., Complete detoxification of tris (2-chloroethyl) phosphate by two bacterial strains: *Sphingobium* sp. strain TCM1 and *Xanthobacter autotrophicus* strain GJ10, *J. Biosci. Bioeng.*, Vol. 114, No. 3, 2012, pp. 306-311.
- [31] Takahashi S., Abe K. and Kera Y., Microbial degradation of persistent organophosphorus flame retardants, *Environmental Biotechnology - New Approaches and Prospective Applications*, Petre M., Ed. Intech Open, 2013, pp. 91-122.
- [32] Hindumathy C.K. and Gayathri V., Effect of pesticide (chlorpyrifos) on soil microbial flora and pesticide degradation by strains isolated from contaminated soil, *Journal of Bioremediation and Biodegradation*, Vol. 4, No. 2, 2013, pp. 1-6.
- [33] Hashemi S.S., Aliasgharzad N., Khakvar R. and Oustan S., Isolation and identification of paraquat degrading bacteria from Tabriz soil, *Journal of Soil Biology*, Vol. 3, No. 2, 2015, 117-127.
- [34] Kanissery R.G. and Sims G.K., Biostimulation for the enhanced degradation of herbicides in soil, *Applied and Environmental Soil Science*, Vol. 2011, Article ID 843450, 2011, pp. 1-10.
- [35] Gondar D., López R., Antelo J., Fiol S. and Arce F., Adsorption of paraquat on soil organic matter: Effect of exchangeable cations and dissolved organic carbon, *J. Hazard. Mater.*, Vol. 235-236, 2012, 218–223.
- [36] Devashree Y., Dutta B.K., Paul S.B. and Choudhury S., The effect of paraquat and fipronil on the soil and rhizosphere microflora of tea (*Camellia sinensis* (L) O. kuntze), *International Journal of Innovation and Applied Studies*, Vol. 7, No. 4, 2014, 1534–1543.
- [37] Andy I.E., Edu G.S., Bassey I.U., Markson A.A., Umana E.I. and Udo S.E., Biodegradation of paraquat, *Journal of Biopesticides and Environment*, Vol. 1, 2015, pp. 80-85.
- [38] Obuotor T.M., Yahaya P.B., Akinloye O.A. and Sakariyau A.O., Biodegradation of paraquat dichloride-contaminated soil with fermented corn steep, *Uniosun Journal of Sciences*, Vol. 1, Issue 1, 2016, pp. 67-73.
- [39] Das N. and Chandran P., Microbial degradation of petroleum hydrocarbon contaminants: an overview, *Biotechnology Research International*, Vol. 2011, Article ID 941810, 2011, pp. 1-13.
- [40] Ukpaka C.P., Application of polynomial, exponential techniques to monitor and predict the biokinetics of aromatic hydrocarbon degradation using *Pseudomonas* sp., *SWISS J. Appl. Sci.*, Vol. 2, 2013, pp. 10-30.
- [41] Dong S., Li J. and Shim H., Bioremoval of trichloroethylene/toluene mixture by *Burkholderia vietnamiensis* G4 from Water, *Research Journal of Chemistry and Environment*, Vol. 17, Issue 9, 2013, 32-37.



## CRAFTING A THEORETICAL FRAMEWORK ON WASTE MANAGEMENT: A CASE FOR SUSTAINABLE CITIES

Jennie Lagman-Bautista<sup>1</sup>

<sup>1</sup>Faculty, Holy Angel University, Philippines; PhD Candidate, University of Santo Tomas, Philippines

### ABSTRACT

Theory formulation is crucial in search of a genuine panacea on Solid Waste Management Disposal. Wastes disposal turned out to be a global phenomenon. Urban transformation amidst economic development poses environmental degradation. Stagnation proliferates when this condition exhibited longer than necessary and cities turned into an ecological sacrificial zone. To mitigate, the formulation of policy and implementation instruments are vital tools to reinvent Waste Management Theory. The inner desire to preserve the future's generation can be taken as a staggering investment in transforming urban ecology to sustainable cities. Environmental Sustainability is entrenched on pro-active policy-making theory, delivered through practical eco-innovations, beautifully wrapped into a well-developed waste management program and effectively measured using the triple-bottom lines.

**Keywords:** *Waste management theory, urbanism, Policy making, Eco-innovations, Sustainability*

### INTRODUCTION

Solid Waste Management Disposal is a prevalent global concern, not solely in terms of waste-related diseases affecting living conditions, but more so from an environmental, societal, and economic aspect [1]. The world can no longer afford the time or the resources to produce and insatiably consume endless novelty and needless change [2]. There is a need to deal with multiple problems at the same time, mindfully and synergistically. UNEP lamented that one of the central tenets of Inclusive Green Growth Programs is that environmentally friendly development can become a driver of job creation, investments and economic development and these are not economically inferior to “dirtier” sustainable progress [3]. Hence we should start the journey in reinforcing the theories behind waste management.

#### Theory of Urban Ecology

Antrop illustrates urbanization in denoting the transformation process of a rural living condition into an urban-like lifestyle [4]. It involves a move from old-fashioned cultural environments, including informal economic and political institutions, creating relative anonymity leading to formalized societies of urban settings [4]. In contrast, Kelbaugh recognized the “Theory of Urbanism” as a controlling but neglected strategy to mitigate ecological footprint and global climate change [2]. The author claimed, cities become an ecological sacrifice zone that even the greenest of cities inflict local environmental wounds that nature must heal, they leave wounds in pursuit of economic development. Nevertheless, in the arena of revenue realization, Cities are generally more

productive and creative per capita than rural communities [2].

Drakakis-Smith reiterated the principle of sustainable development requires a triangular relationship between economic, environmental and social agents in a particular community [4]. Further, Urban sustainability compels effective policy and planning, good governance, as well as the participation of local enterprises and residents [5]. We should not wait longer than necessary on said cities that are highly industrialized to transform its focus on widespread economic advancement with expensive environmental costs and detrimental impacts to mankind, to effect restoration phase before final sustainability transformation occurs where and when irreparable costs have already been inflicted [5].

#### Policy Making Theory

Citizens and communities tend to resist existing policy frameworks that require to “include” them in the implementation process, not unless direct benefits can be derived. They oppose being “stuck” into pre-arranged programs that would limit their participation to a menu of equally unacceptable options. As alternative methods and practices evolve, this is a “fitting moment to heed to socio-environmental methods and innovations forged not out of a social accord, but out of social dissensus” [6]. It is then through disruptions and practices of dissent by the people, that can possibly serve as living indicators of what immediately requires to be addressed and where[6].

The government can proactively recognize stages of urban transformation, promote economic growth, establish attainable goals, assign responsibilities and facilitate strategy implementation [5]. In order to

achieve sustainable development, the government must establish environmental regulations and programmes for supporting financial systems and fostering eco-markets [7]. Policies once formed are implemented by means of policy instruments [7]. Vedung classified these instruments as “set of techniques used by governmental authorities to wield their power in order to ensure adherence and support” [7]. Government plays a crucial role as enforcer of policies.

The main principle of policies on waste programs is to protect both human health and environmental condition by imposing normative behavioral consumption changes [8]. Public perceptions can pose a threat to the acceptability and compliance rate on the legal frameworks. Implementing government agencies need to positively side-track public pulse [9]. Public involvement prior to approval and implementation on said regulations can be seen as a strategy to influence perception, drive public effort, and produce legitimacy for a specific regulatory proposal [9].

### Theory of Waste Management

The traditional waste management view is centered on assurance compliance, risks management, health and environmental protection that are short term tactical [10]. The same authors reshaped traditional waste management view into new value creation that can raise productivity, enhance relations, support eco-innovations, and enable growth for long term endeavors. But the focal point of practical waste management lies on three vital objectives; (1) waste quantification (2) waste characterization and (3) waste management methods or practices [10]. And the three waste management practices classification include: (1) prevention practices comprising strategies on waste minimization, (2) end-of-pipe strategies involves recovering the economic value on waste through waste separation, recycling, proper landfilling, incineration and (3) environmental restoration practices, aimed at repairing leakages and damages to the environment [11].

Cooper correspondingly classified improving resident's awareness and legislation as preventive practices [10]. Hence, purportedly instrumental in the attainment of environmental and societal wellbeing as part of the two pillars of the triple bottom line. In the same context, end-of-pipe strategies cover waste segregation methods that are either origin-separated collection or destination-separated collection [12]. These end-of-pipe strategies are classified as eco-innovations. And shredding their shadows on the light of economic boundaries, the prevention practices are less costly but offer the highest effectiveness rate, while environmental restorations are the most expensive yet yield the least effectiveness [10].

### Eco-innovation

The initial scope of eco-innovation includes in part the productions and processes, then on the improvement of the management system, the creation of new markets, material flows and social eco-innovation [7]. Eco-innovation is well-defined as “all measures of relevant actors which develop new behavior, new ideas, process and products, to apply or introduce them in the attainment of ecologically specified sustainability targets that contributes to lessen environmental burdens” [13]-[7]. Simply stated, eco-innovation is innovation in “any form”, which is beneficial to the environment [14]. Eco-Sustainability innovation includes also a social aspect that emphasizes one of the elements in TBL which extends its scope to include institutions, markets and social actors [7].

Innovations include but not limited to the use of renewable energy technologies, green products, and pollution prevention schemes [7]. Cross-disciplinary technological trials related to eco-innovations are the furthestmost precarious and problematic issues when a city or organization moves toward sustainability [13]. Effective eco-innovations lead the way towards sustainable development based on the triple bottom line sustainability [7]-[13].

The benefits of eco-innovation other than complying environmental regulations will also improve economic aspect, the competitiveness of companies and countries by supporting the creation of a new market for green growth products and processes, corresponding employment effects and so on [7]. Hence, the execution of multidisciplinary systems and technologies concerning eco-innovation is the road toward sustainability [14].

### Triple Bottom-Line Concept

The triple bottom line (TBL) term was coined in the 1990s by business consultant John Elkington to describe the economic, environmental, and social value of an investment that may accrue outside a firm's financial bottom line [15]. TBL or sustainable economic development was defined as activities, programs or policies designed to provide or retain jobs and wealth in ways that contribute to economic, social, and environmental well-being over time [16]. It is distinct from economic growth or development, which may or may not contribute to overall well-being including fiscal health, quality of life, resource stewardship, and resilience [16]. This line of thinking suggests that economic systems exist to serve human well-being, that human and economic well-being is inextricably linked to environmental well-being, and thus, that human, environmental, and economic well-

being must be considered in the design and evaluation of economic development efforts [16].

By considering social, environmental, and economic factors, TBL, or sustainable economic development, provides a more meaningful, productive framework for achieving and measuring economic development [16]. Specific programs with regard to training, incentives, assessment, and research that can advance theory and practice are central to the success of the TBL approach.

### Sustainability

Moving towards sustainability is also a social challenge that entails international and national law, urban planning, local and individual lifestyles, and ethical consumerism. The science of sustainability has emerged in the past 30 years and at its core is a holistic approach to generate “solution-oriented discipline that studies the complex relationship between nature and humankind” [17]. Lin further emphasize the need for Ecological Footprint to track down the occurrences of biocapacity deficiency, the anthropogenic impact on ecosystem and biodiversity in order to measure sustainability. According to Hawken like biocapacity, sustainability occurs when the demand placed by the people and industries upon the environment can be met without plummeting the capacity of the environment to sustain even the needs of future generations [18].

A favorable result occurs when a National Footprint is lesser than the ability of the environment and natural resources to regenerate there is what we call biocapacity reserve [19]. The presence of biocapacity reservation does not necessarily imply sustainability but as explained by Bastianoni and Kitzes, it is essentially the minimum condition for sustainability [19]. Consistent with Daly’s two principles of sustainability, “harvest rates should not exceed regeneration rates, and that waste emission rates should not exceed the natural assimilative capacities of the ecosystems into which the wastes are emitted” [19].

A sustainable environment is the end product of sustainable consumption. Ajzen’s theory of planned behavior was the foremost that considers end user’s behavior in purchasing [13]. Rationality dictates the consumer’s intention by considering these aspects: social norms observed behavioral control and a person’s attitude. Much of the environmental glitches are due to human behavior when put into actions are called anthropogenic. Therefore, changing consumers’ behavior toward sustainable consumption is a necessity for a business or successful community modeling [20]. Research studies have enunciated that a significant reduction in environmental damage is possible if users’ behavioral purchases conform to environmental protection [13]. In this context, pro-environmental behavior causes minimal or no harm to

the environment [13]. Businesses must innovate to respond to environmental needs while creating a product’s value in ever-changing consumer’s demand and lifestyle toward environmental sustainability [13]-[14].

Urbanism once embraced does not necessarily imply placing environmental sustainability at arm’s length. Sustainable cities may seek ways to use the capabilities of disruptive technologies toward making proper changes in human behavior, disruptive technologies that change consumer behavior toward pro-environmental behavior. Cities require innovative, cross-industry solutions to facilitate the collection and disposal of solid waste. The solutions should be replicable, adaptable, and scalable [21]. The term ‘Throw Away society’ denotes a society with an exceptionally lofty consumption pattern and depletion of resources generates huge volumes of refuse [22]. The waste volumes did not only expand with a growing population but also evolved in characteristics.



Fig. 1 Theoretical Framework on Waste Management

### FRAMEWORK ANALYSIS AND VALIDATION

Progress is inevitable, hence urban transformation occurs. The upward pressure from economic development creates downward pressure on environmental degradation. This condition when exhibited longer than necessary, stagnation proliferates and cities turned into an ecological sacrificial zone. To mitigate, formulation of policy

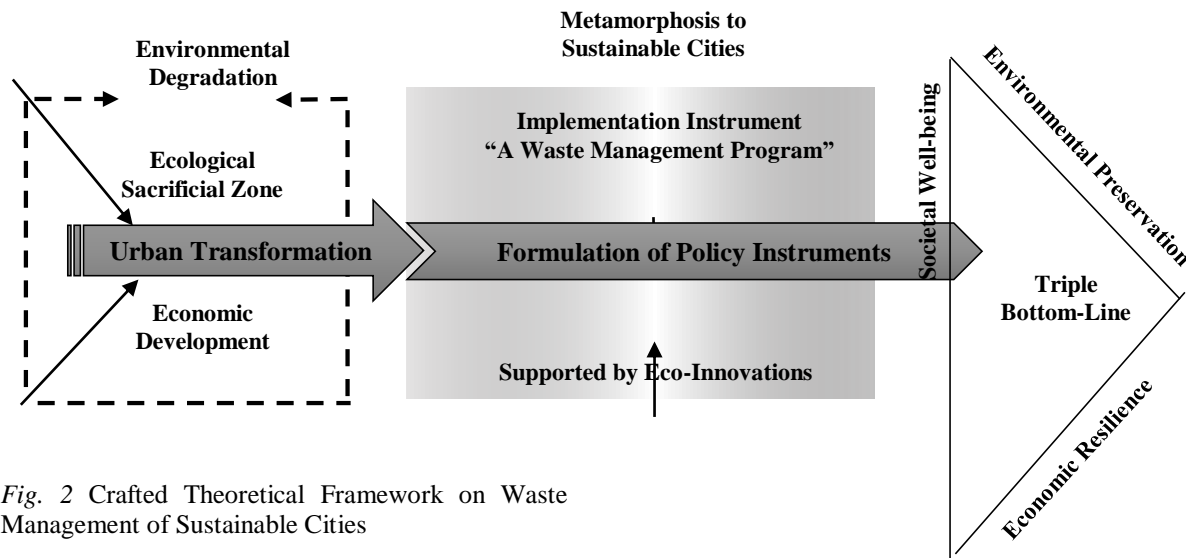


Fig. 2 Crafted Theoretical Framework on Waste Management of Sustainable Cities

instruments as government sticks must transpire. And at the end of the spectrum, regulations and policies embodied in the implementation instruments based on Waste Management Theory must be supported by eco-innovations. These innovations inclusive of new ideas, new behavior, processes, and products in sync in a Waste Management Program measured through environmental preservation/restoration, economic resilience, and social wellbeing commonly called as the “Triple bottom-line”. Thereafter, the metamorphosis of cities from the ecological sacrifice zone into sustainable cities will transpire.

## CONCLUSION

City competitiveness is an important part of the national economy. A competitive city generates wider sources of investments and employment, not only for the benefit of the current generation but more so in securing the future of our grandchildren. Economic growth will not lead to environmental degradation in the presence of strong responsible consumption, rather it can cultivate environmental consciousness. The inner desire to preserve the future’s generation can be taken as a staggering investment in transforming urban ecology to sustainable cities. Environmental Sustainability is entrenched on proactive policy-making theory, delivered through eco-innovations and beautifully wrapped into an effective waste management program that is satisfactorily measured by the triple-bottom lines.

## REFERENCES

- [1]Cervantes D., Martinez A., Hernandez M., & Cortazar A., Using indicators as a tool to evaluate municipal solid waste management: A critical review. *Waste Management*. 2018.
- [2]Kelbaugh, D., The Environmental Paradox of the City, Landscape Urbanism, and New Urbanism. *Consilience*, (13), 2015, 1-15. Retrieved from <http://www.jstor.org/stable/26427272>
- [3]UNEP IGG retrieved from file:///C:/Users/poi/Desktop/Measuring\_Inclusive\_Green\_Growth\_at\_the\_Country\_Level.pdf
- [4]Zhang X., “Sustainable urbanization: a bi-dimensional matrix model”. *Journal of Cleaner Production* 134, 2016, pp 425-433.
- [5]Li Y., Beeton R., Sigler T., Halog A., (2016). Modelling the transition toward urban sustainability: a case study of the industrial city of Jinchang, China. *Journal of Cleaner Production* 134, 2016, pp. 22-30.
- [6]Kaika, Maria. (2017). “Don’t Call Me Resilient Again!’: The New Urban Agenda as Immunology...or... What Happens When Communities Refuse to be Vaccinated With ‘Smart Cities’ and Indicators.” *Environment & Urbanization* Vol. 29, Issue 1, 2017, pp. 89–102.
- [7]Jang E., Park M., Roh T., Han K., JO J., and Kim S., Research Gate /World Sustainability Forum 2014 – Conference Proceedings Paper/ Eco-Innovation Policies Toward Sustainability in Asian Countries, 2014, DOI: 10.3390/wsf-4-a007.
- [8]Greene K., Tonjes D., Quantitative assessment of municipal waste management

- systems: Using different indicators to compare and rank programs in New York State. *Waste Management*. Vol. 34. Issue 4, 2014, pp. 825-836.
- [9]Rolf Lidskog (2016). Public at Risk—Public as Risk: Regulating Nature by Managing People, *Society & Natural Resources*, 29:3, 284-298, DOI: 10.1080/08941920.2015.1054570
- [10]Esmaeilian B., Wang B., Lewis K., Duarte F., Ratti, C., Behdad, S., 2018. The future of waste management in smart and sustainable cities: A review and concept paper. *Waste Management* 81, 2018, pp177-195
- [11] Zaman A., Identification of key assessment indicators of the zero waste management systems. *Ecological Indicators*. 36, 2014, pp. 682-693.
- [12]Sukholthaman, Pitchayanin, Sharp, Alice. A system dynamics model to evaluate effects of source separation of municipal solid waste management: a case of Bangkok, Thailand, *Waste Manage.* (Oxford) 52, 2016, pp. 50-61.
- [13]Kuo T., & Smith, S., A systematic review of technologies involving eco-innovation for enterprises moving towards sustainability. *Journal of Cleaner Production* 192, 2018, pp. 207-220.
- [14]Bossle, M.B., Dutra de Barcellos, M., Vieira, L.M., & Sauv\_ee, L., The drivers for adoption of eco-innovation. *J. Clean. Prod.* 113, 2016, pp. 861-872.
- [15]Elkington, J., Enter the Triple Bottom Line. 2004, <http://www.johnelkington.com/archive/TBL-elkington-chapter.pdf>
- [16]Hammer & Pivo, The Triple Bottom Line and Sustainable Economic Development Theory and Practice. 2016.
- [17]Lin D., Hanscom L., Murthy A., Galli A., Evans M, Neill E.,... Wackernagel M., 2018. Ecological Footprint Accounting for countries: Updates and results of the National Footprint Accounts, 2012-2018. *Resources* p7-58.
- [18]Jerzy A Filar, Jacek B Krawczyk & Manju R Agrawal, Sustainability screw: role of relative production and abatement time scales, *Journal of the Operational Research Society*, Vol. 66, Issue 8, 2015, pp. 1259-1269, DOI: 10.1057/jors.2014.39
- [19]Galli, A., “On the Rationale and Policy Usefulness of Ecological Footprint Accounting (The Case of Morocco)”. *Environmental Science and Policy* 48, 2015, pp. 210-224.
- [20]Pialot, O., Millet, D., Bisiaux, J. “Upgradable PSS”. Clarifying a new concept of sustainable consumption/production based on upgradability. *J. Clean. Prod.* 2017, 141, 538-550. [Google Scholar][Cross Ref]
- [21] Patil, Shivani, Zavare, Shradda, Parashare, Rashmi, Rathod, Pooja, Babanne, Vanita, Smart city waste management. *Int. J. Eng. Sci.* 2017, p. 3990.
- [22]Makarichia L., Jutidamrongphan, W., Techato, K., “The evolution of waste-to-energy incineration: A review”. *Renewable and Sustainable Energy Reviews* 91, 2018, pp.812–821.

## HUMAN BEHAVIOUR AND WORKPLACE SAFETY OF READY-MADE GARMENT FACTORIES IN DHAKA DURING FIRE: A CURRENT SCENARIO

A S M Fahad Hossain<sup>1</sup>, Ishraq Tasnim Hossain<sup>2</sup> and Prof. Dr. Mehedi Ahmed Ansary<sup>3</sup>

<sup>1</sup>Faculty of Civil Engineering, Ahsanullah University of Science and Technology, Bangladesh; <sup>2</sup>Faculty of Civil Engineering, World University of Bangladesh, Bangladesh and <sup>3</sup>Faculty of Civil Engineering, Bangladesh University of Engineering and Technology, Bangladesh.

### ABSTRACT

Safety in a Ready-Made Garments (RMG) factory is the most salient issue especially during fire. The precautions that should be taken by the authorities is a well-studied phenomenon but how the workers working there are prepared to face and perform against fire during an incident is still not evaluated. Metropolitan Fire and Emergency Services Board (MFB) in Melbourne, U.S. Fire Administration's National Fire Incident Reporting System, National Fire Protection Association, Fire and Security Association of India and other organisations has their regular investigation in their country about workplace safety where we have a small amount of survey in Bangladesh though fire incidents have become very frequent now a days which are costing lives. These shows despite of less facilities in factories most of the fatal injuries will not occur if they have proper knowledge of evacuation and training of facing incidents which directs improvement of system and workers behavior. A pre-determined series of questions were asked from different reputed RMG factory workers from top to bottom level and the data was analysed to the condition of facility and psychology of workers.

*Keywords: Human Behaviour, Workplace Fire Safety, Ready-Made Garments.*

### INTRODUCTION

The Ready-Made Garments (RMG) industry occupies a unique position in the economy of Bangladesh. It is the largest exporting industry, which experienced phenomenal growth during the last 25 years. It attained a high profile in terms of foreign exchange earnings, exports, industrialization and contribution to GDP of Bangladesh within a short span of time. The industry plays a key role in employment generation and in the provision of income to the poor. In this study an attempt has been made to describe the overall scenario of Bangladesh Ready Made Garments industry. Despite the phenomenal success of the RMG industry in remittance earning and employment potential, in the last two decades, this sector has experienced some worst industrial accidents in the history the fire.

All factories including those in the RMG sector in Bangladesh, have to obtain certification from Bangladesh Fire Service and Civil Defense Authority (BFSCDA) for their compliance with fire regulations. Purpose-built factories that constructed after 1993 have to comply with Bangladesh National Building Code of 1993 (BNBC-93) and have to obtain the certification of local authorities assigned from the Ministry of Housing and Public Works,

Government of the People's Republic of Bangladesh. Factories operating in old buildings (buildings those were built before the code was formulated but was in practice), have to collect another fitness certificate from the BFSCDA, which allows them to get a second certificate from the Ministry of Housing and Public Works. According to BFSCDA regulations, garment factories have to take an operational certificate at the very beginning of operation from them and this certificate have to be renewed in every month by the respective zone officials. BFSCDA officials check a total of 61 parameters of which 41 parameters are structural or 'hard' in nature. It was defined as 'hard' factors as those whose conditions cannot be changed very quickly. Since the buildings are expected to have been built following the building code, our initial expectation is that the 'hard' parameters would be in a better condition as compared to the 'soft' parameters, the performance in which can change from day-to-day due to management practices.

Two international groups of stakeholders - Alliance for Bangladesh Worker Safety (Alliance) and Accord on Fire and Building Safety in Bangladesh (Accord) - are currently conducting regulatory checks and suggesting remedies for every RMG factory of Bangladesh. Although the focus is wider



safety environment, fire safety forms a part of their monitoring process as well.

## METHODOLOGY

The survey work was done in two phases. One analysis the human behavior during fire and the other phase analyse the workplace safety for fire hazard. In the first phase team randomly selects four garments factory in Bangladesh for survey work. After that the team randomly selects some workers from the garments and asked them some pre determined questions. Then SPSS (Statistical Package for the Social Sciences) tool is used to analyse the survey data collected from the garments factory. In the second phase the team collected some information from the garments factory relevant to fire safety. The information was about factory structure, emergency exit system arrangements for firefighting and workers training facilities.

Data was collected by questionnaire survey from four factories in Dhaka named Pearl Garments Company Ltd., MBM Garments Ltd., Cutting Edge Garments Factory Ltd. and Cosmopolitan Industries Pvt. Ltd- CIPL-Epic group. Data was collected using real interaction with people in the site from officers to workers without informing them earlier so that company cannot give any training to the worker to manipulate their opinion. There were variations in their answers. Questions were asked to both male & female of different ages about their preparation, attitude, training, expected time for leaving the danger place, behavior to others while evacuating & their willing if they would help to overcome the danger situation. Some of them were previously experienced with fire in their workplace. Some were new comer who didn't take training yet.

| Company name | Collected data (person) |
|--------------|-------------------------|
| CIPL         | 701                     |
| MBM          | 364                     |
| CUTTING EDGE | 414                     |
| PGCL         | 291                     |

Collected survey data was then processed in two stages. First, from the survey data an excel file was created for each garments factory. Then the excel file was converted to a data dictionary. Secondly, the data dictionary was converted to SPSS file for analysis.

## ANALYSIS AND RESULT

**Evacuation Behavior:** Workers were asked about their evacuation plan and they were provided with the options like shelter in place, evacuate. If they fail to make choice, then it was considered the

as “undecided”. Any other answer was considered in other category.

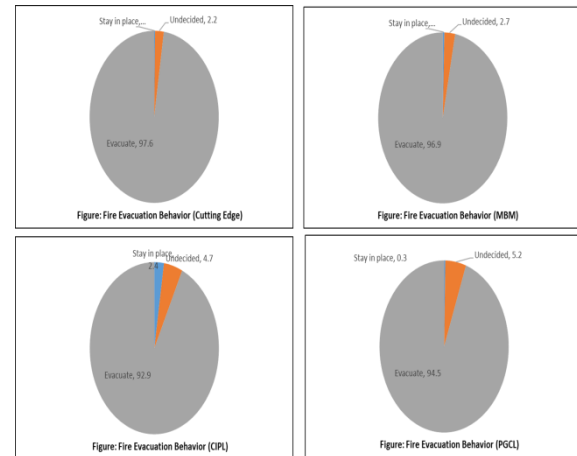


Figure1: Fire evacuation behavior in different factories workers.

These pie charts show us that in the event of fire in the garments factories the workers behavior regarding evacuating that place. In all the factories, more than 95% which is the majority of worker will evacuate that place as early as possible. Other 5% workers have mix opinion about staying in the place, wait for rescue and some have no idea about what they will do in the case of fire hazard in their factory. These indecisions are mostly from newly joined people who did not get any fire training yet and a few are because of age.

### Fire Evacuation Timing Based on Gender:

Following tables show the cross tabulation between gender and time to stop the work and leave if there is any effect or not.

Table 1: Fire Evacuation Timing on Gender (Cutting Edge)

| In case of emergency, how much time would it take to stop your work and leave |            | what is your gender |        | Total  |
|---|------------|---------------------|--------|--------|
|   |            | Male                | Female |        |
| Less than 5 minuets   | Count      | 196                 | 217    | 413    |
|   | % of Total | 47.3%               | 52.4%  | 99.8%  |
| More than 5 minutes   | Count      | 1                   | 0      | 1      |
|   | % of Total | 0.2%                | 0.0%   | 0.2%   |
| Total   | Count      | 197                 | 217    | 414    |
|   | % of Total | 47.6%               | 52.4%  | 100.0% |

Table 2: Fire Evacuation Timing on Gender (MBM)

| In case of emergency, how much time would it take to stop your work and leave |            | what is your gender |        | Total  |
|---|------------|---------------------|--------|--------|
|   |            | Male                | Female |        |
| Less than 5 minutes   | Count      | 191                 | 170    | 361    |
|   | % of Total | 52.5%               | 46.7%  | 99.2%  |
| More than 5 minutes   | Count      | 0                   | 3      | 3      |
|   | % of Total | 0.0%                | 0.8%   | 0.8%   |
| Total   | Count      | 191                 | 173    | 364    |
|   | % of Total | 52.5%               | 47.5%  | 100.0% |

Table 3: Fire Evacuation Timing on Gender (CIPL)

| In case of emergency, how much time would it take to stop your work and leave |            | what is your gender |        | Total  |
|---|------------|---------------------|--------|--------|
|   |            | Male                | Female |        |
| Less than 5 minutes   | Count      | 305                 | 384    | 689    |
|   | % of Total | 43.5%               | 54.8%  | 98.3%  |
| More than 5 minutes   | Count      | 5                   | 7      | 12     |
|   | % of Total | 0.7%                | 1.0%   | 1.7%   |
| Total   | Count      | 310                 | 391    | 701    |
|   | % of Total | 44.2%               | 55.8%  | 100.0% |

Table 4: Fire Evacuation Timing on Gender (PGCL)

| In case of emergency, how much time would it take to stop your work and leave |            | what is your gender |        | Total  |
|---|------------|---------------------|--------|--------|
|   |            | Male                | Female |        |
| Less than 5 minutes   | Count      | 85                  | 197    | 282    |
|   | % of Total | 29.2%               | 67.7%  | 96.9%  |
| More than 5 minutes   | Count      | 0                   | 9      | 9      |
|   | % of Total | 0.0%                | 3.1%   | 3.1%   |
|   | Count      | 85                  | 206    | 291    |
|   | % of Total | 29.2%               | 70.8%  | 100.0% |

From the data chart it is seen that from 1770 workers almost all the workers believe that they can stop what they will be doing and leave the incident place within five minutes. Only 24 workers that they will take more than five minutes where 19 of them are female. This is because they are may be concern about their children staying in day care centre

situated inside the factory. But this quantity is very low as most of the female workers are unmarried.

**Fire Evacuation Timing Based on Age:** Following bar chart summarized the cross tabulation between escape time and age. It was asked that if the people think they will be able to stop the work what they are doing, stop the machine and can leave the compound in less than 5 minutes. The age of the workers is divided into many groups for convenience.

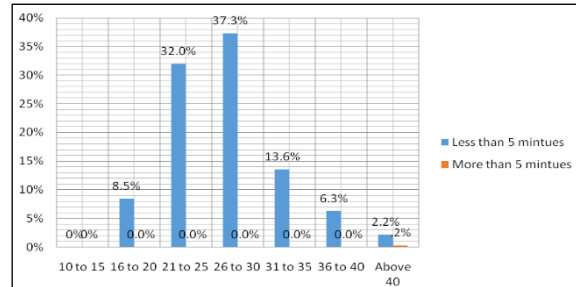


Figure: Cross Tabulation between Escape Time and Age (Cutting Edge)

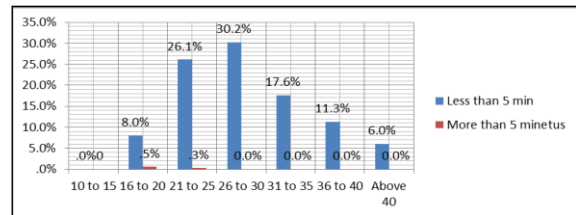


Figure: Cross Tabulation between Escape Time and Age (MBM)

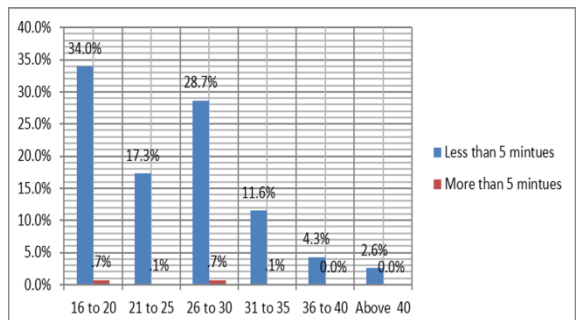


Figure: Cross Tabulation between Escape Time and Age (CIPL)

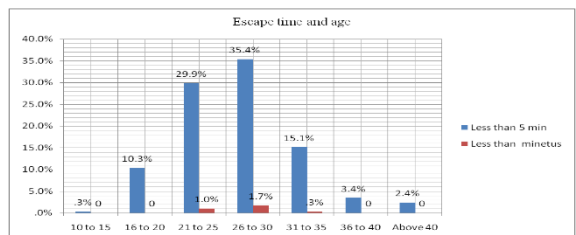


Figure: Cross Tabulation between Escape Time and Age (PGCL)

From the bar chart it is seen that most of the workers are from 21 to 30 years old except one factory named CIPL where they have around 34% workers are 19 to 20 years old. In Cutting Edge factory, among 414 workers 412 of them said that they will be able to move less than 5 minutes. Only 2 out of 414 workers said that they may take more than 5 minutes. This is due to position working place, and age as those people are around or above 40 years old. In other factories, the bar chart illustrates that no matter what the age group is majority of the people think they will be able to stop the work what they are doing, stop the machine and can leave the compound in less than 5 minutes. Only a few workers gave voice that 5 minutes is an inadequate time for leaving. This might be due to their position working place, and some of them are willing to help in stopping fire and in some case the machine on which they are working with is complicated to stop.

**Capacity to Protect Against Injury:** The following pie charts show the result of the question “Do you have necessary preparation to protect yourself from possible injury?” The answer was limited to yes and no.

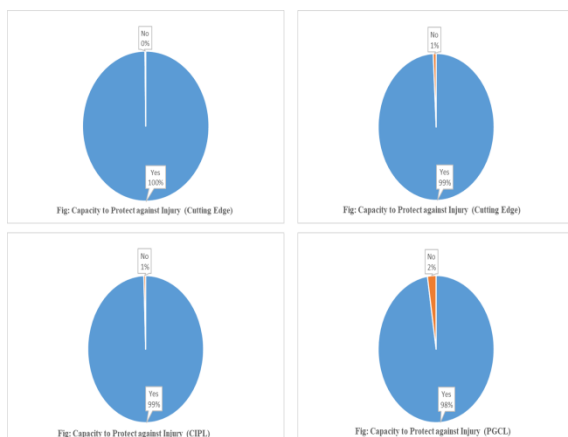


Figure: Capacity to protect against injury in different factories workers.

From the pie charts it is clear that majority of the people think they can protect themselves in the case of injury during fire. This is a great turnover in the mentality of workers as they get regular training from the company authority. In the COSMOPOLITAN INDUSTRY PRIVET LIMITED (CIPL) all the 701 workers are confident about there protection against injury. Only a few workers from other garments do not have the necessary knowledge about how to protect themselves in the event where injury can occur. This is because they are new and yet to receive training from the company.

**Regular Fire Drill:** Total 1770 people were questioned from four garments factory that if they have regular fire drill in their factory. It is a very

positive result that all the workers conduct regular fire drill. Authority also learnt from previous fatal accidents and they are more aware about there workers safety now. Some garments have committee to find out the lackings of fire sare safety and to conduct regular fire drill. Almost all the factories have warning system in each floor which is reachable to all part of the floor.

**Evacuation Plan:** The next pie charts below illustrate the opinion of the workers about how they prefer to evacuate in case of fire incident. They have options like evacuate themselves alone or along with their colleagues.

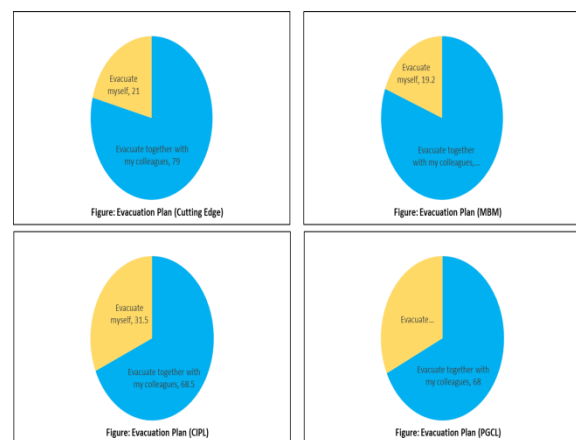


Figure: Evacuation plan in different factories workers.

From the pie charts it is seen that in all of the four garments around 70% of the workers want to evacuate with their colleagues where rest people think they will evacuate themselves alone as early as possible. This is because they are going through regular training and fire drill from company. But still most of the elder people aged above 35 who have family do not want to take risk in case of fire as they have seen some fatal incidents earlier. In total, it is a positive motivation among most of the workers.

**Education and Evacuation Plan:** The following charts represent changes in evacuation plan with the level of education of different level of employees. Most of the workers have studied from Primary School Certificate (PSC) to maximum Higher Secondary Certificate (HSC). Only manger and top-level employees are graduated from university. Some of them has masters but they were considered in University group as well. Security guards and other staffs who are not directly related to production have no educational qualification in some case and they are introduced by ‘None’.

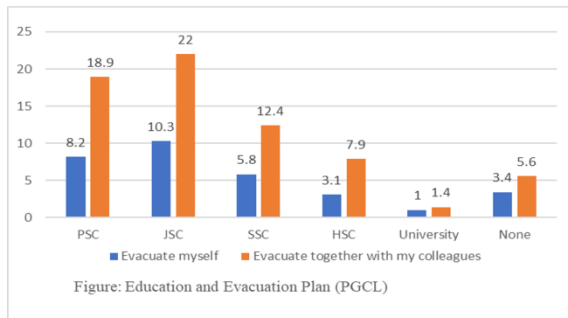
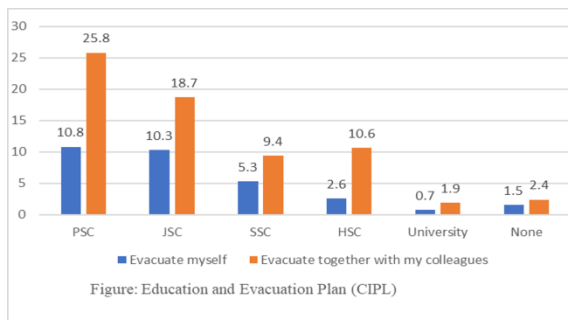
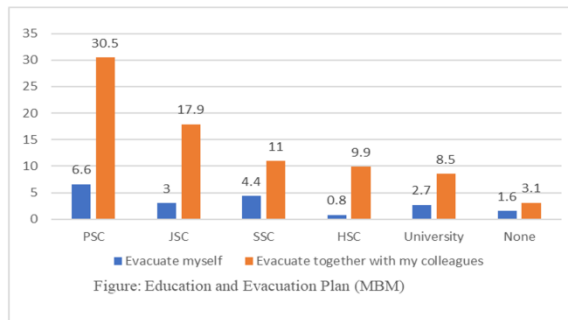
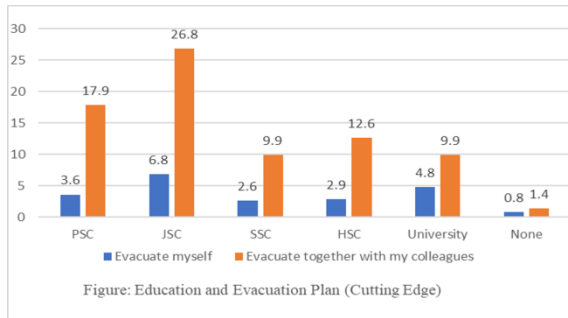


Figure: Education and Evacuation plan in different factories workers.

These charts show the relation between escape plan and highest level of education. It shows that no matter what the level of education is majority of the people will always try to evacuate with their colleagues.

**Help Stopping Fire:** The following bar chart shows the outcome of the question “In case of fire, will you help stopping the fire or evacuate?”. Option was ‘I will help stopping fire’ and ‘I will evacuate’.

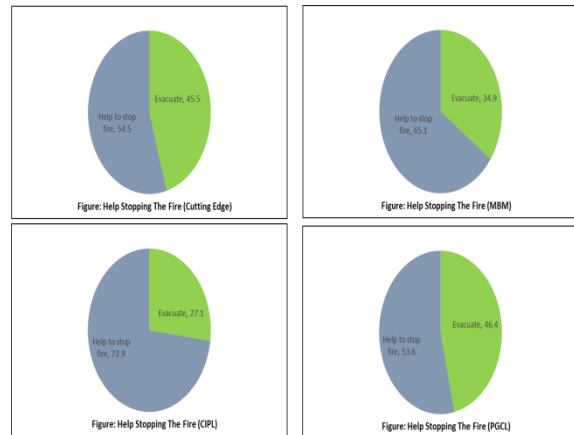


Figure: Willingness to stop fire in case of fire incident in different garments workers.

The bar charts show that more than half workers from all the garments are willing to help stopping fire during a fire emergency. Among them more than 70% of CIPL workers have positive thinking about it where PGCL have 53.6%. This is because they have less worker and CIPL has 2.5 times more worker than PGCL and most of them are young and energetic. This is a positive scenario in RMG factories. It is happening because authority and workers both are conscious about their safety and rules during an incident. And the dramatic changes in mentality and behavior of workers are the results of regular training and fire drill in working place.

## CONCLUSION

This paper explored the current behavior of workers in different RMG factories from manager to operator during a fire incidence. The response is very positive specially their willingness to evacuate with colleagues and help stopping fire. These are because of regular training and fire drill arranged from the authority. This positive behavior will not only save lives but also it will save a lot of goods and reduce a lot of property damage. This is a significant movement in RMG sector of Bangladesh for workers as well as authority after some big fatal incident and bad reputation regarding workplace safety. This observation gives an insight to the turnover in workers behavior during fire incident and allows the investors a second thought before leaving this sector. By conducting this type of behavior analysis will help to avoid accident related injury or death it will also provide perception about strength and weakness of that company to face fire hazard.

## ACKNOWLEDGMENTS

Authors like to give special thanks to Ahsanullah University of Science and Technology (AUST), Dhaka, Bangladesh for giving the opportunity to conduct the survey. Authors also like to give special

thanks to S. M. Tanveer Anjum, Jenath Sultana Joya and Afsana Zaman Pranty for helping in the survey and collecting data.

## REFERENCES

- [1] Wadud Z., Huda F.Y., "Fire Safety in the Readymade Garment Sector in Bangladesh: Structural Inadequacy vs. Management Deficiency", May, 2016.
- [2] Mannan M.S. (PE, CSP, DHC), "The Journey to Safety Excellence in the Garment Industry in Bangladesh: Past, Present and Future", May, 2016.
- [3] Campbell R., "Home Fire Involving Clothes Dryers and Washing Machines", NFPA research, March, 2017.
- [4] Campbell R., "Fires in Structures under Construction, Undergoing Major Renovation or Being Demolished", NFPA research, April 2017.
- [5] Ahrens M., "Fires by Occupancy or Property Type 2010-2014", NFPA research, March 2017.
- [6] Anjum S.M.T., Sultana J. Zaman A. "Human Behaviour and Workplace Safety of Readymade Garment Factories in Dhaka During Fire." June, 2017.
- [7] Colpas E., Zulueta J.D., Pappas D., "An Analysis of Hoarding Fire Incidents and MFB Organizational Response", WPI (Worcester Polytechnic Institute), May, 2012.

# ULTRAFINE PARTICLE FILTER DESIGN FOR MOTORCYCLE EMISSION EXHAUST SYSTEM: A HIGH VOLTAGE ELECTROSTATIC-BASED SYSTEM

Arinto Y. P. Wardoyo<sup>1</sup>, Hari A. Dharmawan<sup>1</sup>, Muhammad Nurhuda<sup>1</sup>, and Arif Budianto<sup>1</sup>  
<sup>1</sup>Mathematics and Natural Sciences Faculty, University of Brawijaya, Indonesia

## ABSTRACT

A large number of motor vehicles in the world have been linked to the increase of the emissions, such as particulate matters and gases. These pollutants, especially for the particulate matters with the diameter less than 0.1 micrometer or ultrafine particles, become detrimental thing to the natural environment and human health. There is a need to develop a better method to decrease the particles. Thus, one step ahead of the technological improvement in the transportation sector is the development of an emission filter applied in a motor vehicle exhaust system. According to this background, we developed an ultrafine particle filtering system based on an electrostatic principle using a direct current - high voltage. The filter is based on a electrostatic principle by using uses aluminum as the anode and cathode. This filter was tested under the different DC voltage of 100, 200, 300, and 400 Volt. The efficiency of the filter was tested by measuring the motor cycle ultrafine particles before and after applying the electrostatic filter. The particle concentrations were measured by using a TSI P-Trak Ultrafine Particle Counter model 8525. The result shows that the designed filter works well in reducing the ultrafine particles., with the efficiency of 7% to 46%. The filter efficiency depends on the applied voltage.

*Keywords: Electrostatic filter, Motorcycle emission, Ultrafine particles, Efficiency*

## INTRODUCTION

The transportation sector has been growing from year to year. It is not only the developing technology, but also the motor vehicle usage in the world is increasing, as expected in Asian countries [1,2]. As the impact of this growing usage, the activity of transportation mode, especially for the motorcycle, exceeds the other kinds of motor vehicles. This phenomenon can be found in many big cities in the world, such as Hanoi, Jakarta, and Macao [3,4].

Besides, due to transportation sector activities using a motor vehicle, a large number of emissions accumulate and spread around ambient air. As confirmed in emission modeling, the emission is strongly related to vehicle number [5]. Furthermore, these emissions can be found as gaseous and PM (particulate matter) pollutants. For example, PM<sub>10</sub> (particulate matter with a diameter less than 10  $\mu\text{m}$ ) with a high concentration of heavy metals (such as Ba, Fe, and Cu) can be identified in the area with a high traffic intensity [6]. Transportation sector also contributes to CO<sub>2</sub> (gaseous emissions), as the result of a combustion process [7]. As confirmed in the previous study of International Energy Agency (IEA), 23% of the total carbon dioxide emissions in the world was contributed by the transportation sector, including automobiles, light trucks, freight trucks, and buses [8]. A heavy duty vehicle such as bus can emit nitrogen oxides and PM<sub>0.1</sub> (particulate

matter with a diameter less than 0.1  $\mu\text{m}$ ) with the emission factors up to 5 g/ km for nitrogen oxides and 0.001 g/ km for PM<sub>0.1</sub> [9]. A recent study also shows that vehicular traffic becomes a contributor to air pollution. It shows a high amount of CO<sub>2</sub>, CO, NO, SO<sub>2</sub>, and PM in which dominantly emitted by four-wheeler gasoline vehicles [10].

A proper approach to dealing with the motor vehicle emissions must be integrated with efforts to decrease the emissions. For an example, improving or mitigating motor vehicle emissions only in existing and future vehicles and traffic by improving engine efficiency and traffic management is not quite adequate to decrease the emissions in the ambient air. Selecting different fuels, or developing more efficient vehicle technologies or fuel additive also need more systems. Another proper approach is urgently needed.

One step of technological improvement in the transportation sector is the development of an emission filter applied in a motor vehicle exhaust system. This particulate matter filtration system can be found as an electrostatic filter, a radiation filter, and a porosity filter. The electrostatic principle is an electricity-based filtration system for reducing particulate matter, *i.e.*, a DPS (electrostatic diesel particulate matter filtration system) technology for a diesel heavy-duty vehicle exhaust system [11]. This kind of filtration technology had also been studied with a combination of a diesel oxidation catalyst and had been applied in non-road diesel machines [12].



In a motorcycle exhaust system, a porosity-based filter has been developed to reduce PM<sub>2.5</sub> emission with the efficiency of 35 – 64% [13]. Another study shows a significant performance (up to 24%) of a heat radiation-based filter when applied in a motorcycle exhaust system [14].

It is true that emission filter technology is a need to reduce air pollutant in ambient air, especially for the contaminant emitted by the motor vehicle. However, different sides must be taken into account when developing an exhaust emission filtration system. As an alternative approach, electrostatic principle has a high potential for the real application in decreasing motor vehicle exhaust emissions. This principle somehow needs less energy and budget. Moreover, the performance and application of electrostatic filtration system are relatively better than the other methods.

## MATERIALS AND METHODS

### Motorcycle Samples

A standard motorcycle (in good condition, no modification) was used as the ultrafine particles source. This motorcycle sample had an automatic transmission with the engine cubication of 125 cm<sup>3</sup>. It used CDI (Capacitor Discharge Ignition) for the electronic ignition system (fuel type: gasoline, research octane number 90) and carburetor for the fuel supply system.

### Filter Fabrication

The electrostatic filter (Fig.1) was made of aluminum plates that were consisted of anodes and cathodes. These electrodes were 1.4 mm apart (*d*). This filter gap was chosen due to the dimension of the motorcycle exhaust system. The filter probes were connected to the high voltage source with a direct current (DC). This voltage was obtained by amplifying the standard accumulator voltage, 12 Volt DC, with a signal conditioning circuit (Fig.2). As the result, there were four different voltages to generate an electric field (*E*), with the variations of *V*<sub>1</sub> (100 Volt), *V*<sub>2</sub> (200 Volt), *V*<sub>3</sub> (300 Volt), and *V*<sub>4</sub> (400 Volt). Each voltage variation was applied to each filter to investigate the best efficiency.

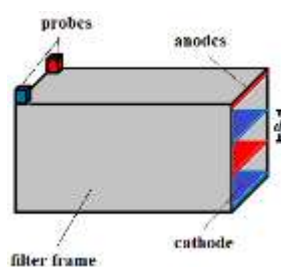


Fig. 1 The schematic of the filter.

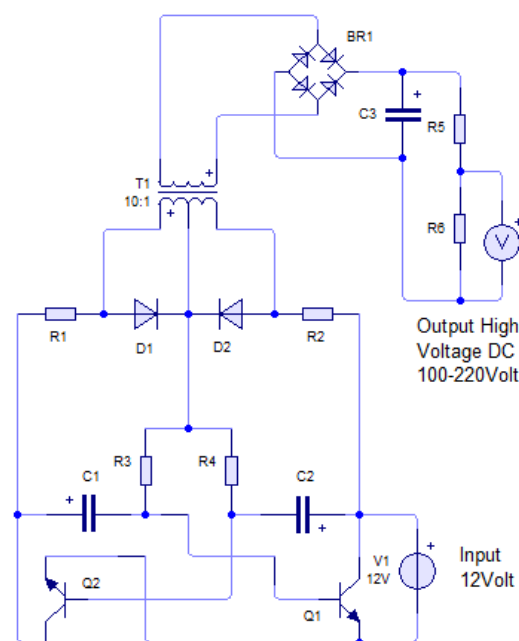


Fig. 2 The schematic of the signal conditioning circuit.

The signal conditioning circuit consists of a variable resistor to generate different voltage. A center tap transformer (T1) and 2N3055 transistors (Q1 and Q2) are used to amplify the input voltage (12 Volt) to 220 Volt AC (alternating current). Then, this resulted voltage is inverted using a diode bridge circuit (BR1). The output signal is filtered using an electrolytic capacitor (C2).

### Filter Performance Test

Figure 3 shows the set-up of the filter performance test. Each filter was tested to investigate the filter performance related to filter efficiency (*E<sub>f</sub>*) in reducing ultrafine particles concentration. This test was applied in the 125 cm<sup>3</sup> motorcycle sample for 60 minutes per voltage variation (with the interval time of five minutes) [13]. Ultrafine particle concentrations before (*C<sub>in</sub>*) and after (*C<sub>out</sub>*) applying the electrostatic filter were measured using a TSI P-Trak Ultrafine Particle Counter, model 8525. The input and output emission temperatures (*T<sub>in</sub>* and *T<sub>out</sub>*) were measured using digital thermometers (with thermocouple type-K sensors). The flow-rate of the emission (*v<sub>out</sub>*) was measured using a Kanomax Anemomaster, model A-031. The filter efficiency was calculated using Eq. (1) below [13].

$$Ef = \frac{C_{in} - C_{out}}{C_{in}} \times 100\% \quad (1)$$

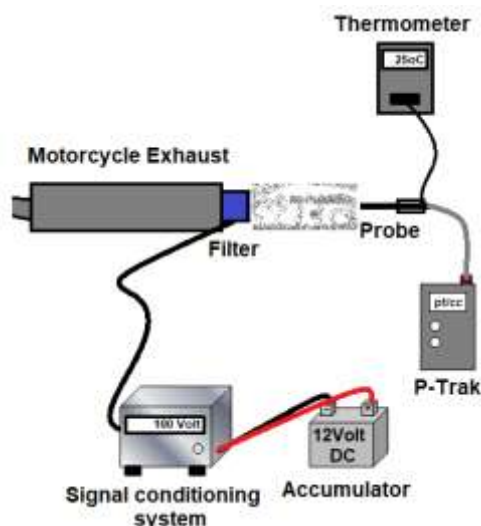


Fig. 3 The set-up of the filtration test using motorcycle sample.

### Statistical Analysis

All recorded values were expressed as mean  $\pm$  SEM (standard of means). The difference between filter performance was analyzed using an ANOVA (analysis of variance) test, in which  $p < 0.05$  was considered statistically different. The correlation between applied voltage and filter performance was approached using a 2<sup>nd</sup> order of polynomial regression model, in which  $R^2 < 0.70$  was considered correlated [15]. All statistical analysis was performed using Microsoft Excel 2016.

## RESULTS AND DISCUSSION

### Ultrafine Particles Concentration

The filters were installed on the motorcycle exhaust system in order to measure the ultrafine particle concentrations. These measurements were repeated three times for each voltage variation, V1, V2, V3, and V4. These measurements were done for 60 minutes for each measurement, with the interval time of five minutes. All results were shown in Table 1-2 below.

According to the results, the filters were tested under different voltage variation in order to investigate the influence of the high voltage level in the filtration system. On each measurement result, the ultrafine particle concentrations without filters had a similar trend, where the highest concentrations were obtained at the first minute (minute 5). Meanwhile, these concentrations decreased significantly in the last measurement time. Interestingly, the installed filters, with the used of voltage variations generated lower concentrations, compared to  $C_{in}$  (as seen in Table 2).

Table 1 Ultrafine particle concentrations before passing through the filters,  $C_{in}$ , from three times measurements (1<sup>st</sup> - 3<sup>rd</sup>)

| Times<br>(minutes) | Ultrafine Particles<br>( $\times 10^3$ particles/ $\text{cm}^3$ ) |                 |                 |
|--------------------|---|-----------------|-----------------|
|                    | 1 <sup>st</sup>   | 2 <sup>nd</sup> | 3 <sup>rd</sup> |
| 5                  | 18.5  | 18.2            | 18.2            |
| 10                 | 18.5  | 18.4            | 18.5            |
| 15                 | 18.4  | 18.1            | 18.4            |
| 20                 | 18.4  | 19.3            | 18.2            |
| 25                 | 17.5  | 20.2            | 17.7            |
| 30                 | 17.8  | 19.5            | 17.6            |
| 35                 | 17.7  | 18.2            | 17.8            |
| 40                 | 17.6  | 16.9            | 17.4            |
| 45                 | 17.4  | 16.7            | 17.2            |
| 50                 | 17.1  | 17.2            | 17.4            |
| 55                 | 16.8  | 16.7            | 17.3            |
| 60                 | 16.1  | 15.7            | 17.1            |

Table 2 Ultrafine particle concentrations of the tested filter after passing through the filter,  $C_{out}$  (mean  $\pm$  SD)

| $t$<br>(min) | Ultrafine Particles ( $\times 10^3$ particles/ $\text{cm}^3$ ) |                |                |                |
|--------------|--|----------------|----------------|----------------|
|              | V1   | V2             | V3             | V4             |
| 5            | 17.1 $\pm$ 0.5   | 16.5 $\pm$ 0.1 | 15.0 $\pm$ 0.5 | 12.6 $\pm$ 0.8 |
| 10           | 16.8 $\pm$ 0.3   | 16.1 $\pm$ 1.1 | 14.6 $\pm$ 1.2 | 11.1 $\pm$ 1.1 |
| 15           | 16.5 $\pm$ 0.7   | 15.6 $\pm$ 1.3 | 14.5 $\pm$ 1.3 | 11.2 $\pm$ 0.6 |
| 20           | 16.8 $\pm$ 0.9   | 15.4 $\pm$ 1.9 | 14.4 $\pm$ 1.9 | 11.4 $\pm$ 0.1 |
| 25           | 16.4 $\pm$ 1.3   | 15.3 $\pm$ 2.1 | 13.9 $\pm$ 2.1 | 10.4 $\pm$ 0.6 |
| 30           | 16.1 $\pm$ 0.9   | 15.2 $\pm$ 1.9 | 13.3 $\pm$ 1.9 | 10.4 $\pm$ 0.8 |
| 35           | 15.8 $\pm$ 1.1   | 15.2 $\pm$ 1.9 | 13.2 $\pm$ 1.9 | 10.0 $\pm$ 0.7 |
| 40           | 15.8 $\pm$ 1.4   | 14.8 $\pm$ 2.2 | 12.8 $\pm$ 2.2 | 10.0 $\pm$ 0.2 |
| 45           | 15.2 $\pm$ 2.0   | 14.9 $\pm$ 2.0 | 12.7 $\pm$ 2.0 | 10.0 $\pm$ 0.5 |
| 50           | 15.5 $\pm$ 1.3   | 14.9 $\pm$ 1.6 | 13.0 $\pm$ 1.6 | 0.9 $\pm$ 0.9  |
| 55           | 15.5 $\pm$ 1.3   | 14.6 $\pm$ 1.7 | 12.4 $\pm$ 1.7 | 0.9 $\pm$ 0.3  |
| 60           | 15.2 $\pm$ 0.8   | 14.6 $\pm$ 1.9 | 12.4 $\pm$ 1.9 | 0.9 $\pm$ 0.3  |

After using the filters, the ultrafine particle concentrations decreased significantly, compared to  $C_{in}$  ( $p < 0.05$ ). These results were consistent for all voltage samples. According to Table 2, V4 yields the lowest ultrafine particle concentrations. On each sampling time, V4 emitted least ultrafine particle concentrations compared to V3, V2, and V1. The highest concentration in V4 is  $12.6 \pm 0.8$  particles/cm<sup>3</sup>, in which this value is obtained from three repeated measurements. Meanwhile, the lowest concentration in V4 is referred to minute 60 (last minute). These values are significantly different with the results yielded by V1, as the lowest applied voltage.

V1 has more ultrafine particle concentrations, compared to V4. The lowest ultrafine particle concentrations in V1 is up to  $15.2 \pm 0.8$  particles/cm<sup>3</sup>. When we compare the values, the highest concentrations of V4 is only 74% of the highest concentration obtained in V1. These results indicate that the applied high voltage influences the reduction of ultrafine particle concentrations emitted by motorcycle sample.

### Filter Efficiencies

Having measured the ultrafine particle concentration, we compared the filter performance from the first minute (minute 5) to the last minute (minute 60). Statistically, there is a significant difference in filter efficiency, since  $p < 0.05$  (illustrated in Fig.4). V1, as the lowest voltage, generates 7% to 12% of filter efficiency, in which the highest efficiency is obtained from the 30<sup>th</sup> minute. This result indicates that V1 has a saturated trend in a half time of the measurement, indicating the saturated zone of the filtration performance.

The similar trend can be found in V2 and V3. In V2, the efficiency is 9% in the first five minutes. This value increases until 17% in minute 30. After that, the performance was drop to 11% in the last minute after passing the saturated point. Compared to V2, V3 has better efficiency. V3 has 17% to 27%, 10% higher than V2 and 15% higher than V1.

Meanwhile, the largest voltage V4 has the best filter performance with the highest filter efficiency, 46% on the last minute (60<sup>th</sup> minute). From the graphic below (Fig.4), a different trendline can be identified, since the saturated point is not pointing the half-time (30<sup>th</sup> minute) of the measurement anymore. Statistically, the difference between each sampling time is shown by the  $p$ -value ( $p$ -value is less than 0.5). It shows that the filter performances are time-dependent and voltage-dependent.

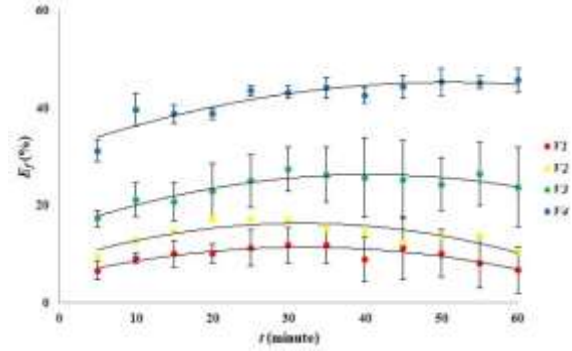


Fig. 4 The association of applied voltages and filter efficiencies (mean $\pm$ SD).

According to the measurement results, there is a little difference between emission velocity before and after passing through the filter. This value is not significant, since  $p < 0.05$ . However, a little change of emission velocity may indicate that there is no emission feedback to the engine due to the filter construction (filter blocking effect).

The filter performance is mostly influenced by the electrostatic force  $F$  and electric field  $E$ . In the electrostatic theory, voltage ( $V$ ) is linearly correlated with the electric field,  $E$  (Eq. (2-4)). According to this theory, a higher electric field is caused by a higher voltage given.

$$E = \frac{V}{d} \quad (2)$$

so:

$$V = E d \quad (3)$$

and:

$$E = \frac{F}{q} \quad (4)$$

As the impact, V4, as the highest voltage, has the highest  $E$ . Meanwhile, the lowest voltage V1, has the lowest  $E$ . According to Eq. (4),  $E$  is linearly correlated with force  $F$ . That is why, by using a constant filter gap ( $d = 1.4$  cm), the value of  $F$  is only influenced by the used  $V$ . As expected, we found that the correlation between the applied voltage and filter efficiency was positive linear, as the usage of a constant filter gap ( $R^2 > 0.89$ ). Based on the calculation, the electric field of the filters is in the range of  $7.14 \times 10^3$  N/C to  $28.57 \times 10^3$  N/C. The highest electric field is referred to 400 Volt, V4, while the lowest one is referred to the lowest voltage used, 100 Volt (V1) Fig.5.

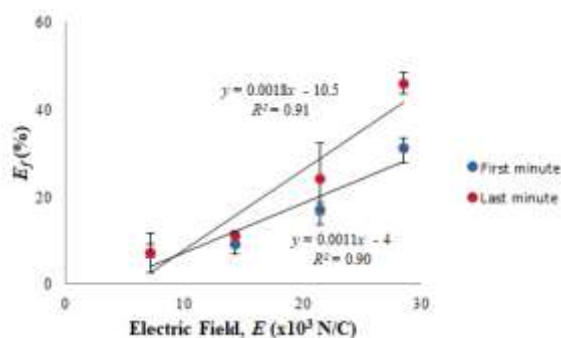


Fig. 5 The association of electric field and filter efficiencies (mean $\pm$ SD).

In the case of time-dependent and the influent of engine temperature ( $T_{eng}$ ), a longer time means that more fuels ( $m$ ) are used to produce energy. As a fundamental law, energy is neither created nor destroyed, and it only changes its form. As a consequent, many formulas of energy exist. Thus, this energy can be found as thermal energy ( $Q$ ) and other forms of energies, where:

$$Q = m c \Delta T \quad (5)$$

Based on Eq. (5) above, it is shown that  $Q$  depends on fuel consumption in the quantity of mass,  $m$ , with a constant  $c$  (specific heat). A higher heat  $Q$  means that the change of temperature ( $\Delta T$ ) is also higher. According to the previous studies, the time of motorcycle warming up process may influence the engine temperature  $T_{eng}$ . In an idling and static position (1000 RPM, cold start of warming up), we found that a longer time ( $t$ ) generated a higher engine temperature [16,17]. This term may impact the increase of output emission temperature, since the emission flows are laminar inside the system. This increase is linearly correlated with the increase of time and engine temperature.

## CONCLUSIONS

This paper integrates high voltage DC electricity with electrostatic principle to decrease the ultrafine particle concentrations of motorcycle emissions. An electrostatic-based filtration system is adapted to capture the particulate matters with the diameter less than  $0.1 \mu\text{m}$  emitted by the motorcycle exhaust system. The high voltage variations, 100 Volts to 400 Volts DC, enable to estimate emissions decreasing due to the applied voltage. According to the results, a higher voltage generates a higher filtration performance. The highest efficiency, 46%, is obtained from 400 Volts DC. Meanwhile, the lowest voltage, 100 Volts DC, generates the lowest filter efficiency, 7%.

## ACKNOWLEDGMENTS

All authors wish to acknowledge the role of the Indonesian Ministry of Research, Technology, and Higher Education as the funding source. The author's team also acknowledge all members of Laboratory of Air Quality Research and Astro Imaging, Physics Department, Brawijaya University: Eko Teguh P. Adi, Buyung Wisma, Agung, Nia, Alma, Vio, Lisa, and Hamid, for their excellent hands and efforts during the experiment.

## REFERENCES

- [1] Senbil M., Zhang J., and Fujiwara A., Motorization in Asia - 14 countries and three metropolitan areas, *Int. Assoc. Traffic Saf. Sci. Res.*, Vol. 31, 2007, pp. 46–58.
- [2] Berri A., A cross-country comparison of household car ownership, *Int. Assoc. Traffic Saf. Sci. Res.*, Vol. 33, 2009, pp. 21–38.
- [3] Wong K. I., An analysis of car and motorcycle ownership in Macao, *Int. J. Sustain. Transp.*, Vol. 7, 2013, pp. 204–225.
- [4] Lan T. T. N. and Minh P. A., BTEX pollution caused by motorcycles in the megacity of HoChiMinh, *J. Environ. Sci.*, Vol. 25, 2013, pp. 348–356.
- [5] Borrego C., Tchepel O., Salmim L., Amorim J. H., Costa A. M., and Janko J., Integrated modeling of road traffic emissions: application to Lisbon Air Quality Management, *Cybern. Syst. An Int. J.*, Vol. 35, 2004, pp. 535–548.
- [6] Elhadi R. E., Abdullah A. M., Abdullah, A. H., Ash'aari Z. H., Kura N. U., G. D. Y., and Adamu A., Source identification of heavy metals in particulate matter (PM10) in a Malaysian traffic area using multivariate techniques, *Polish J. Environ. Stud.*, Vol. 26, 2017, pp. 2523–2532.
- [7] Jovanovic M. M., Belgrade's urban transport CO<sub>2</sub> emissions from an international perspective, *Polish J. Environ. Stud.*, Vol. 25, 2016, pp. 635–646.
- [8] Schipper L., Fabian H., and Leather J., Working Paper, Transport and carbon dioxide emissions: Forecasts, options analysis, and evaluation, December 2019 No. 9, Metro Manila, Asian Development Bank, 2009, pp. 1–56.
- [9] Liu D., Lou D., Liu J., Fang L., and Huang W., Evaluating nitrogen oxides and ultrafine particulate matter emission features of urban bus based on real-world driving conditions in the Yangtze river delta area, China, *Sustainability*, Vol. 10, 2018, pp. 2051.
- [10] Rasool S., Qadri H., and Bhat F. A., Assessment of traffic-generated gaseous and particulate matter emissions of Hirpora

- Wildlife Sanctuary (Shopian), Jammu and Kashmir, *J. Earth Sci. Clim. Change*, Vol. 8, 2017, pp. 421.
- [11] Kim H. J., Han B., Hong W. S., Shin W. H., Cho G. B., Lee Y. K., and Kim Y. J., Development of electrostatic diesel particulate matter filtration systems combined with a metallic flow-through filter and electrostatic methods, *Int. J. Automot. Technol.*, Vol. 11, 2010, pp. 447–453.
- [12] Dou D., Application of diesel oxidation catalyst and diesel particulate filter for diesel engine powered non-road machines, *Platin. Met. Rev.*, Vol. 56, 2012, pp. 144–154.
- [13] Hajar U., Wardoyo A. Y. P., and Masruroh, Developing and characterization of an ultrafine filter made of banana leaf and water hyacinth to reduce motorcycle emission, *Applied Ecology and Environmental Research*, Vol. 17, 2019, pp. 1959–1965.
- [14] Wardoyo A. Y. P. and Dharmawan H. A., Developing reheated motorcycle exhaust for PM<sub>2.5</sub> emission, *International Journal of GEOMATE*, Vol. 16, 2019, pp.109–116.
- [15] Wardoyo A. Y. P., Budianto A., and Abdurrouf, Filtration of submicron particles from motorcycle emission using a DC low electrostatic filter, *International Journal of Applied Engineering Research*, Vol. 12, 2017, pp. 1725–1728.
- [16] Bokde K. K. and Waghmare A. V., Cold start performance enhancement of motorcycle catalytic convertor by latent heat storage system, *Int. J. Innov. Res. Sci. Eng. Technol.*, Vol. 2, 2013, pp. 372–377.
- [17] Iodice P. and Senatore A., Exhaust emissions of new high-performance motorcycles in hot and cold conditions, *International Journal of Environmental Science and Technology*, Vol. 12, 2015, pp. 3133–3144.

## EXPERIMENTAL STUDY ON SOIL IMPROVEMENT OF COHESIVE SOIL FOR CONSTRUCTION FIELD

Shoji Kamao  
Department of Civil Engineering, Nihon University, Japan

### ABSTRACT

Treatment and disposal of construction waste soil and sludge is one of major problem in Japan. The author tries to make effective use of construction waste soil and sludge, in particular, aim to improve the soil properties of cohesive soil and to make it a resource for backfill materials and something like that. Many recycling technologies for construction waste soil and sludge has been proposed so far. The purposes of this study were to understand the change characteristics of water permeability and water retention by adding soil improvement materials (stabilizer) to cohesive soil, and to understand the effect of additive rate of stabilizer and initial water content of cohesive soil. Permeability test and water retention test were conducted with the change of both conditions, as the parameters in this study.

*Keywords: Construction waste soil, Permeability test, Water retention test, Laboratory experiments, cohesive soil,*

### INTRODUCTION

Treatment and disposal of construction waste cohesive soil is one of the major problem in Japan. Until recently, both construction waste cohesive soil which has low water content, and construction sludge which has high water content, were disposed to the reclamation. However, the environmental impact by the reclamation with waste cohesive soil and construction sludge became serious problem, "the recycling and the re-use" has been required instead of reclamation.

The method of dehydrating the water from the construction sludge and adding soil stabilizer such as cement is one of the major recycling methods. Tsuchida *et-al* [1] have been carried out a series of laboratory experiments to propose the prediction method of the unconfined compressive strength of cement treated soil. However, chemical and environmental effects on soil due to cement cannot be ignored, various methods have been proposed by many researchers (for example, Tran *et-al* [2]).

In this study, the author has been investigated the usefulness of the soil stabilizer which are newly developed by Environmental Health Laboratory CO., LTD. [3] for agricultural purpose, to the construction field. This stabilizer is featured by the low impact on the environment because it is made of shelly fossil and gluten. Moreover, it has been recognized that it has the effect of improving the soil and keeping the solidification state for a long time when even a small amount is added. We conducted a laboratory permeability tests and water retention tests to study the changing properties of the soil by adding the stabilizer to soft clay.

In this paper, the author carried out a series of

laboratory water permeability test and water retention test in order to make clear the effects of the additive rate of stabilizer and initial water content of cohesive soil, which was marine clay sampled in Tokyo.

As the experimental results, it was found that a high stabilized effects can be obtained by using this stabilizer, and this treated soil has the possibility of applying to construction materials.

### USED SOIL AND THE SOIL STABILIZER

The soil used for this study were the cohesive soil (marine clay) sampled in the Tokyo metropolitan area. The typical properties of used soil are shown in Table-1.

Table 1 Typical profiles of cohesive soil (clay)

|                       |                            |      |
|-----------------------|----------------------------|------|
| Soil particle density | $\rho_s$ g/cm <sup>3</sup> | 2.51 |
| Liquid limit          | $w_L$ %                    | 55.0 |
| Plastic limit         | $w_P$ %                    | 33.0 |
| Plastisity index      | $I_p$ —                    | 22.0 |
| Ignition loss         | $L_{ig}$ %                 | 5.8  |

The soil stabilizer is produced in the following process: the shell fossil is heated up to 400 to 800°C; it is broken into particles with 0.1 to 10<sup>-9</sup> mm diameter; and the particles are mixed with gluten heated to 50 to 95°C. The main improvement effect of the soil stabilizer is to aggregate the soil particles,



which enlarges the voids to make the soil specimens more water retainable and air permeable. High workability is also the improvement effect due to rapid solidification.

## PERFORMED TESTS

### Permeability Test

The falling head permeability test method was as follows [4]:

The specimen for the permeability test was made by adjusting the improved soil to a specified density and filling it in molds with 6.0 cm diameter and 2.0 cm height. Fig. 1 shows the permeability test apparatus using oedometer device. Porous stones were placed at the top and bottom of the specimens, and they were permeated from the bottom surface through a standpipe for certain period of time. Coefficient of permeability of the specimen is calculated using Eq. (1).

$$k = \frac{2.30aL}{A(t_2 - t_1)} \log_{10} \frac{h_1}{h_2} \quad (1)$$

where  $a$  is cross sectional area of standpipe,  $A$  is cross sectional area of soil specimen,  $L$  is height of soil specimen,  $t$  is time and  $h$  is head of water, respectively.

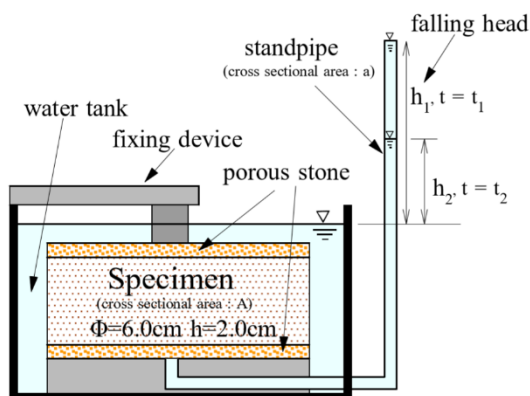


Fig. 1 The permeability test apparatus (oedometer device)

### Water Retention Test

The water retention test method was as follows: The improved soil was put into plastic molds with 5.0 cm diameter and 10.0 cm height, and water was poured to 1 to 2 cm above the soil surface to prevent dryness from the specimen after saturation. Fig-2

shows the water retention test apparatus. While leaving them for 24 hours (1 day), the amount of water coming out from the bottom of the specimens was measured. In this study, the water retention was defined from the amount of water coming out of the saturated specimens due to gravity, which corresponds to a pF value of 1.8. [5]

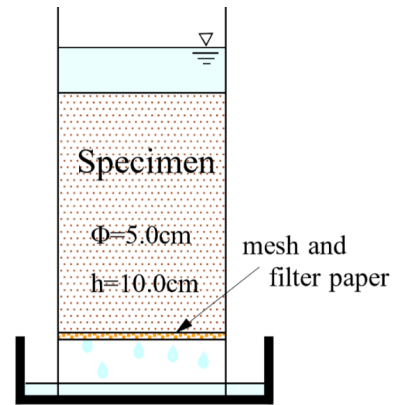


Fig. 2 the water retention test apparatus

### Improvement Method of Cohesive Soil

Improvement method for cohesive soil in these tests, a predetermined of soil stabilizer was added to the dried cohesive soil whose initial water content was adjusted to be 30 to 85% and mixed thoroughly. The additive rate of the stabilizer was varied from 0 to 30 % of dry soil weight in Eq. (2).

$$a_w = c / m_s * 100(\%) \quad (2)$$

where  $c$  is weight of the added stabilizer and  $m_s$  is weight of dry soil.

When the initial water content was a high value exceeding 50%, 3% of bentonite was added to make the soil viscous.

## EXPERIMENTAL RESULTS

### Relationship between the additive rate of soil stabilizer and coefficient of permeability

Addition of the soil stabilizer to the cohesive soil with a 40% water content aggregates the particles of the cohesive soil, which increases permeability of the cohesive soil. Fig. 3 is the graph showing the coefficient of permeability and additive rate of soil stabilizer from the results of the water permeability tests for the improved soil. The vertical axis of the graph represents the coefficient of permeability and the horizontal axis, additive rate of stabilizer. The

tests were conducted at the 0 to 30% stabilizer additive rate, where the 0% stabilizer additive rate means only the cohesive soil. It should be noted that the additive rate is defined as the weight ratio of the stabilizer to the dry soil in Eq. (2).

A change in the coefficient of permeability of the cohesive soil by solidification tends to be proportional to the stabilizer additive rate. The results indicated the coefficient of permeability at the 30% stabilizer additive rate was higher by approximately 3 orders than that at the 0% additive rate.

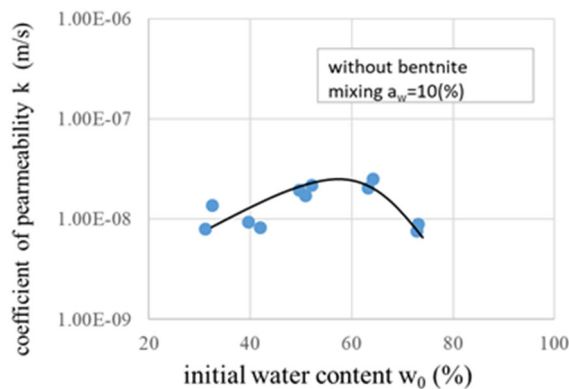


Fig.3 Relationship between coefficient of permeability  $k$  and additive rate  $a_w$

### Results of the water retention tests

Fig. 4 shows the relationship between elapsed time and the amount of dehydration (water coming out) of the improved and saturated soil specimens, for each stabilizer additive rate. No significant difference was observed between 10% and 20% additive rate; however, the dewatering amount tended to decrease with an increase in the stabilizer additive rate. It was confirmed that addition of the stabilizer improved water retainability of the particle surface of the solidified improved soil.

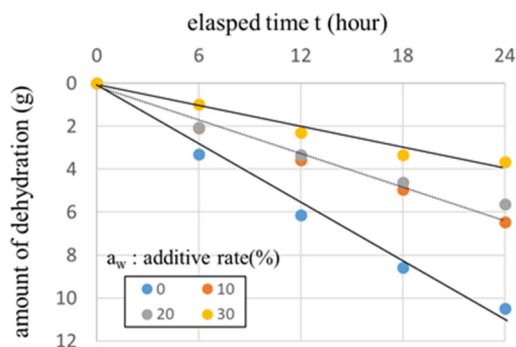


Fig. 4 Relationship between elapsed time and amount of dehydration

### Results of the tests with various initial water content

After the cohesive soil before improvement was adjusted to achieve the various water content (initial water content) ranging from 30 to 80%, the soil stabilizer was added to it and mixed to improve the soil. The water permeability tests were conducted for this improved soil. The stabilizer additive rate was set to a fixed value of 10%.

Fig. 5 shows the relationship between the water permeability coefficient and initial water content obtained from the water permeability tests. The coefficient of permeability tended to slightly increase up to about 60% of the initial water content, but it tended to slightly decrease more than that. This may have been caused by inhibition of solidification by excessive water. Thus, we conducted the similar water permeability tests for the improvement soil with 3% of bentonite added to reduce the amount of water in the soil, and to increase viscosity of the soil.

As shown in Fig. 6, the coefficient of permeability rose with a rise in the initial water content when bentonite was added. It can be thought that the coefficient of permeability rose because bentonite absorbed water in the soil, which avoided inhabitation of solidification. The results demonstrated the possibility in which the solidification effect of the soil stabilizer for the specimens with high water content such as construction sludge could be obtained by adjusting the water content. Figure 7 is an overlapping drawings of Fig. 5 and Fig. 6.

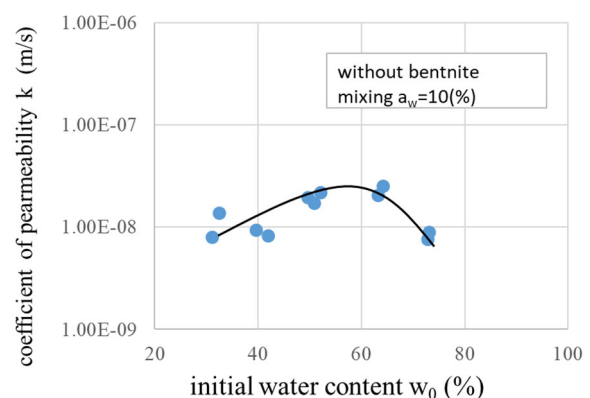


Fig. 5 Relationship between coefficient of permeability  $k$  and initial water content  $w_0$  ( $30 < w_0 < 70\%$ , without bentonite)

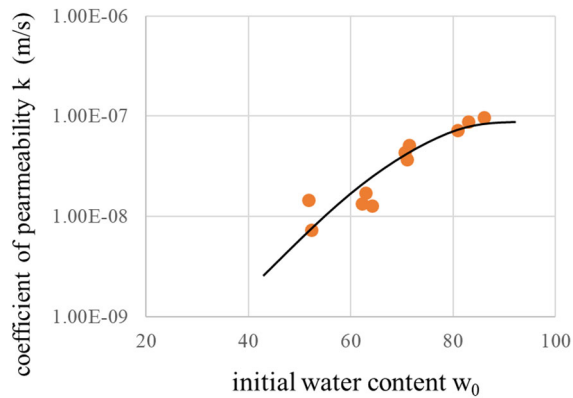


Fig. 6 Relationship between coefficient of permeability  $k$  and initial water content  $w_0$  ( $50 < w_0 < 90\%$ , with bentonite)

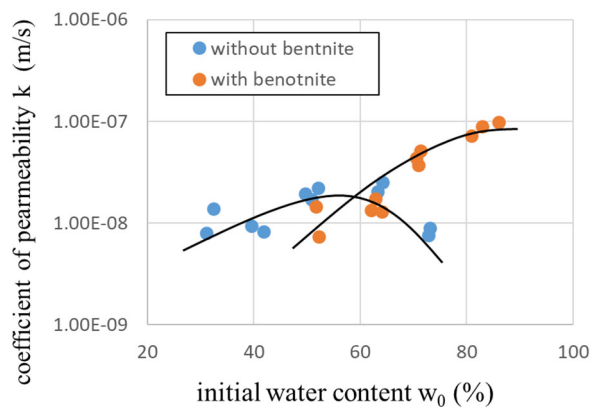


Fig. 7 Relationship between coefficient of permeability  $k$  and initial water content  $w_0$  ( $30 < w_0 < 90\%$ )

## SUMMARY

The summary of this study is as follows:

A change in the coefficient of permeability of the cohesive soil by solidification tends to be

proportional to the stabilizer additive rate. Coefficient of permeability at the 30% stabilizer additive rate was higher by approximately 3 orders than that at the 0% additive rate.

The dewatering amount tended to decrease with an increase in the stabilizer additive rate. It was confirmed that addition of the stabilizer improved water retainability of the particle surface of the solidified improved soil.

The initial water content will affect the solidification. However, it was found that the effect can be reduced by increasing the viscosity.

## ACKNOWLEDGMENTS

All laboratory experiments were done by the student member of Environmental Geotechnics Laboratory, College of Science & Technology, Nihon University. I would like to express the deepest appreciation to them.

## REFERENCES

- [1] Tuchida, and Tang: Estimation of compressive strength of cement-treated marine clays with different initial water contents, soils and Foundation, pp359-374, Vol.55, No.2, 2015.
- [2] Tran, Satomi and Takahashi: Study on strength behavior of cement stabilized sludge reinforced with waste cornsilk fiber, International Journal of GEOMATE, Nov., Vol.13, Issue 39, pp.140-147, 2017.
- [3] Environmental Health Laboratory CO., LTD: <http://www.kankyo-eisei.co.jp/index.html>, (In Japanese only)
- [4] JIS (Japanese Industrial standard) A 1218: Test methods for permeability of saturated soils.
- [5] Water retention test (DOBOKUKANRI SOGO SHIKENJYO), <http://www.dksiken.co.jp/wordpress/uploads/2015/06/tuthinohosui.pdf>, (In Japanese only)

## ANALYSIS OF HABITAT AREA FOR ENDANGERED SPECIES USING MAXENT BY ROAD CONSTRUCTION AND HOUSING LAND DEVELOPMENT IN CHIBA, JAPAN

Hideyuki Ito<sup>1</sup>, Koji Hayakawa<sup>2</sup>, Makoto Ooba<sup>3</sup> and Takahiro Fujii<sup>4</sup>

<sup>1,4</sup>College of Science and Technology, Nihon University, Japan; <sup>2</sup>Chiba Prefecture, Japan;

<sup>3</sup>National Institute for Environmental Studies, Japan

### ABSTRACT

Chiba prefecture in Japan is abound with rich nature and surrounded by many rivers and sea. But, the number of endangered species in Chiba has been increasing after the World War II because various habitat have been destroyed by rapid urbanization. However, there are few researches that analyzed the time-series change of amount of green area and habitat area for endangered species taking adverse impacts by constructing roads and residential land development into consideration in Chiba, Japan. Thus, in this research, we estimated the change of green area and habitat area for some endangered species using MaxEnt (Maximum Entropy Modeling) software for modeling species niches and distributions. As the result, it was shown that the green space area and water environment including rivers, lakes, ponds and coastal area has decreased while the buildup area has increased from 1976 to 2009. Also, it was concluded that total habitat possibility area of the ruddy crane, red fox, Japanese skink and Tokyo salamander have decreased by 3.6%, 6.0%, 1.6% and 0.7%, respectively.

*Keywords: MaxEnt, GIS, Endangered Species, Green Area*

### INTRODUCTION

Chiba Prefecture is blessed with water and green nature, because it is surrounded by the sea and rivers on all sides. On one hand, with the rapid development of transportation infrastructure such as the opening of railways, Narita Airport, and Aqua line, urbanization has progressed, resulting in a decrease in the habitats of organisms such as forests and wetlands, and endangered species tend to be increasing.

For the changes in land used, many of the previous studies have analyzed the area and green coverage depending on the land use classification. For example, Iwasaki et al. [1] discussed the habitat of Japanese monkeys based on the analysis of the temporal changes in land use. Gon et al. [2], Ikemi et al. [3] and Ohara et al. [4] have developed methods to comparatively analyze previously documented data and electronic data using GIS (Geographic Information System). However, the land use classification must be reorganized to compare fairly, because it changes depending on the publication year of the maps. Miyamoto [5] evaluated suitable habitat areas using MaxEnt (Maximum Entropy Modeling), which can estimate the habitat probability of animals. MaxEnt is an open source for modeling tool in which the habitat area is estimated by modeling the existence probability of species and various environmental factors using the appearance data of organisms whose existence has been confirmed and various environmental data from the whole target area.

MaxEnt estimates the parameters of the appearance characteristic function by applying the principle of maximum entropy algorithm (Phillips et al. [6]). In this MaxEnt, the following three analyses are possible; 1) quantification (visualization) of suitable habitat area, 2) calculation of contribution rate for respective environmental factors, 3) comparison of before and after time series by model construction.

For example, MaxEnt is utilized to estimate the suitable habitat area of Chinese Alligator that is a critically endangered crocodilian and predicted its distribution in Anhui Province, China (Pan et al. [7]). West et al. [8] developed a presence-only model of invasive cheat grass (*Bromus tectorum*) distribution in Rocky Mountain National Park, Colorado, USA in from 2007 through 2013 fit with limited data to compare with the result of GLM (Generalized Linear Model). Remya et al. [9] showed current and future habitat suitability distribution of *Myristica dactyloides Gaertn.*, a medicinally and ecologically important tree species by using a MaxEnt species distribution model in order to implement sustainable conservation or adaptation strategy. Matyukhina et al. [10] constructed the model of the geographic distribution of Amur tigers required based on the MaxEnt algorithm using a dataset of 1,027 tiger track records and a set of environmental variables, such as distance to rivers, elevation and habitat type, and anthropogenic variables, such as distance to forest and main roads, distance to settlements and vegetation cover change in the Russian Far East.

Moreno et al. [11] identified potential habitats for two endemic birds of high ecological value, the Black throated Huet-Huet (*Pteroptochos tarnii*), and the Ochre-flanked Tapaculo (*Eugralla paradoxa*) and then showed most important variables that explain the presence of each species. Pratumcharta et al. [12] predicted the distribution of *B. s. goniomphalos* in Thailand on the basis of environmental and climatic factors and also indicated that altitude, land cover, normalized difference vegetation index (NDVI), precipitation in the driest month, land surface temperature and soil pH affected its distribution. Khadka and James [13] made the distribution map of current and future climatic niche of endangered *Himalayan musk deer*, a species endemic to Asia. Mohammadi et al. [14] analyzed the current potential distribution of the *Blanford's Jerboa Jaculus blanfordi* and the *Arabian Jerboa Jaculus loftusi* in Iran and predicted the impact of climate change on their future potential distributions using two different modelling software packages: Maxent and SDM (Species distribution model).

In existing researches concerning MaxEnt, the distribution and suitability habitat of various endangered animals and plants are predicted and then represent the environmental factors that affects them in the world.

However, there have been few studies that have quantitatively analyzed the changes in the habitat area of many endangered species especially in Japan for taking the improvement of transportation infrastructure and urbanization into account. Therefore, the purpose of this research is to quantitatively evaluate the effect of endangered species on the habitat due to the improvement of transportation infrastructure, focusing on the changes in land use in Chiba Prefecture, Japan.

## METHOD

As environmental variables used in MaxEnt, the following seven kinds of data in Chiba Prefecture were used; 1) land use data from 1976, 1987, 1991, 1997, 2006 and 2009, 2) average rainfall amount over 30 years, 3) annual average temperature over 30 years, 4) annual total daylight hours over 30 years, 5) annual average global solar radiation over 30 years, 6) data of average altitudes in 2009 and 7) data of average slope angles in 2009 (Table 2).

Data from 1976 was selected because that was the oldest available GIS data on land used in Chiba Prefecture. The land use data from 2009 and the above data were input into MaxEnt. The change over the years was analyzed by inputting the land use data from the other years using the obtained models and parameters from the analysis result of MaxEnt. Since the land use classification differs depending on the fiscal year of the land use preparation, it was arranged based on the newly unified land use. The definition of

the respective land use was investigated, and the land use was arranged according to the following nine categories; paddy fields, the other agricultural land, forest, wasteland, buildup area, main transportation sites, rivers, lakes and ponds, and coastal area, the other sites.

For selecting the target species, as endangered species with high conservation priority, the following eleven species were chosen and analyzed from the list of red data book in Chiba Prefecture as the target species; quail, ruddy crane, marsh grass bird, Japanese large-footed bat, red fox, Japanese pond turtle, Japanese skink, Japanese mamushi, Tokyo salamander, Japanese fire belly newt, and wrinkled frog. To estimate the existence probability of these species in Chiba Prefecture, it is required to have plot data wherein the existence in the area has been confirmed. Therefore, the suitable habitat area of endangered species was analyzed using MaxEnt based on the habitat spot data written in the red data book of the Chiba Prefecture. In this research, we especially focused on the results for the ruddy crane (*Porzana fusca*), red fox (*Vulpes vulpes*), Japanese skink (*Plestiodon japonicus*), and Tokyo salamander (*Hynobius tokyoensis*) as representative species of birds, mammals, reptiles, and amphibians, respectively (Fig. 1).

Table 2 Data set for inputting into MaxEnt

| Data                                     | Mesh size | Year | Source                                    |
|--|-----------|------|---|
| Land use                                 | 100m      | 2009 | Geospatial Information Authority of Japan |
|  |           | 2006 |   |
|  |           | 1997 |   |
|  |           | 1991 |   |
|  |           | 1987 |   |
|  |           | 1976 |   |
| Average rainfall amount                  | 1km       | 2012 | Japan Meteorological Agency               |
| Annual average temperature               |           |      |   |
| Annual total daylight hours              |           |      |   |
| Average annual amount of solar radiation |           |      |   |
| Average altitudes                        | 250m      | 2009 | Geospatial Information Authority of Japan |
| Average slope angles                     |           |      |   |



Fig. 1 Targeted species



## RESULTS

### Result of comparative analysis of land use area

Table 1 shows the land use area for each year in Chiba Prefecture. It was shown that the green space that consists of rice paddy, forest and other agricultural land and water environment including rivers, lakes, ponds and coastal area have decreased while the buildup area has increased. From these results, it was demonstrated that there is a possibility that the habitat area for species has been also decreasing due to the expansion of the city area.

According to the statistical yearbook of Chiba Prefecture, total road length has been increasing every year. But, it was shown the decrease of “Area of main roads” in Table 1. This is because maximum area of “buildup area” that occupy in 100m mesh of land use has been increasing instead of “Area of main roads” by progress of urbanization.

### Result of suitable habitat area predicted by MaxEnt

The suitable habitat area of 4 endangered species by MaxEnt in 1976 and 2009 is shown in Fig. 2. In these figures, the habitat possibility is represented in colors according to 0–1 values per each mesh (100 m × 100 m) based on the plot data that the habitat was confirmed and the environmental variables.

Ruddy crane lives in common reed, Manchurian wild rice (*Zizania latifolia*) and the grass near wetland such as lake, river and paddy field. It is reported that a lot of Ruddy crane are found in the north of Chiba [15]. As shown in Fig.2, the high habitat possibility area is concentrated in north coastal area and riverside. Comparing between north and south area in Chiba, north area is higher habitat possibility than south one.

Red fox prefers the area mixed with forest, grassland and agricultural land, and riverside and grassland are usually used as resting place [15]. Since there are many rivers, lake and ponds in north of

Table 1 Comparison result of area of each land use

| Land Use                | 1976  | 1987  | 1991  | 1997  | 2006  | 2009  | Comparison between 1976 and 2009 |
|-------------------------|-------|-------|-------|-------|-------|-------|----------------------------------|
| Rice Paddy              | 127.3 | 121.3 | 121.4 | 119.1 | 112.1 | 108.9 | -14.4%                           |
| Other Agricultural Land | 80.8  | 75.6  | 75.5  | 72.5  | 69.2  | 68.1  | -15.7%                           |
| Forest                  | 187.9 | 179.4 | 174.9 | 167.6 | 161.3 | 170.8 | -9.1%                            |
| Waste Land              | 8.0   | 15.0  | 13.8  | 10.6  | 12.3  | 8.9   | +11.0%                           |
| Buildup Area            | 53.6  | 71.5  | 73.1  | 86.4  | 95.3  | 111.2 | +107.4%                          |
| Area of Main Roads      | 1.7   | 2.9   | 3.2   | 4.0   | 5.7   | 1.3   | -22.9%                           |
| Rivers, Lakes and Ponds | 16.2  | 16.0  | 14.7  | 14.8  | 14.8  | 12.6  | -22.7%                           |
| Coastal Area            | 3.9   | 2.3   | 2.3   | 2.3   | 2.0   | 1.7   | -57.9%                           |
| Others                  | 35.4  | 31.0  | 36.0  | 37.6  | 42.2  | 31.5  | -11.1%                           |

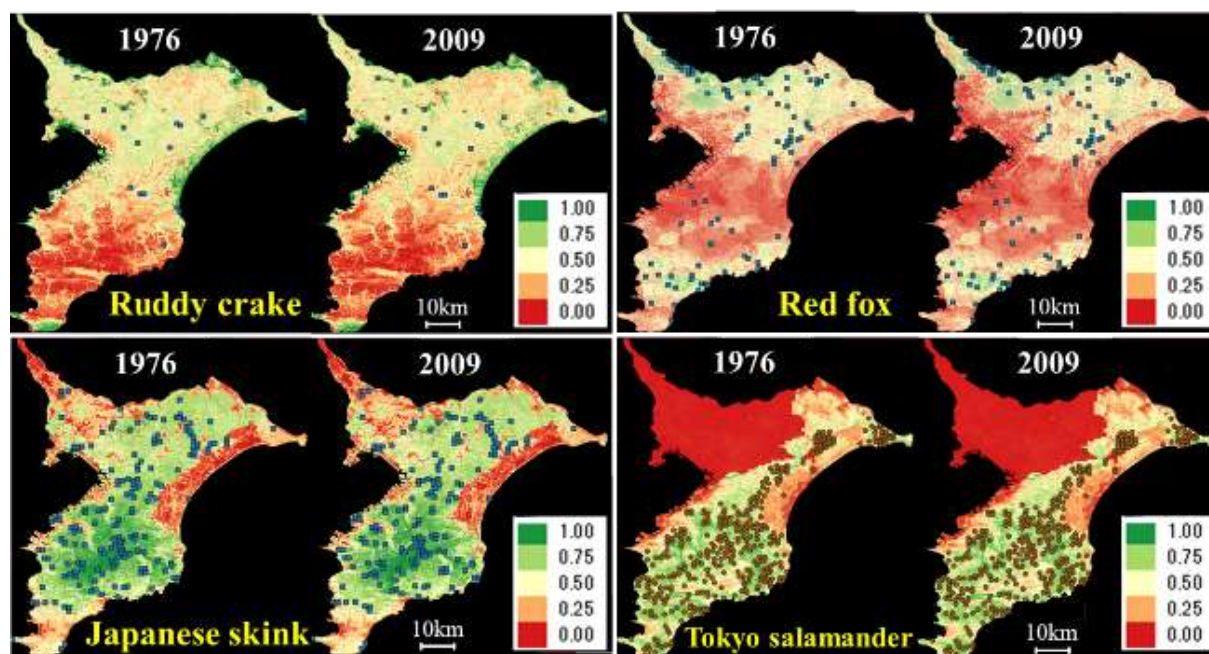


Fig. 2 Result of suitable habitat area of each endangered species by MaxEnt



Chiba in particular, the habitat possibility area covers mainly north area and part of south area as shown in Fig.2. However, it is revealed that the low habitat possibility area expanded slightly from 1976 to 2009.

Japanese skink usually lives in grassland and slope of mountainous area that has good exposure to sunlight. The suitable habitat area of Japanese skink predicted by MaxEnt is concentrated in the south area that the Kazusa-hills expand, whereas Japanese skink does not prefer the east coastal area and west urban area.

Tokyo salamander generally inhabits broad-leaved forests and artificial forest covered by planted Japanese cedar and cypress in hilly area and low mountains. The aquatic environment is also necessary to spawn near forest. The suitable habitat area predicted by MaxEnt is seen in south and east area that expands forest area including hilly area.

### Result of AUC and contribution rate

Table 2 shows the AUC (Area under the receiver operator curve [6]) and contribution rate of respective

environmental factors. AUC is the expectation value that means the ratio between the area identified the existence of targeted species and predicted habitat area by MaxEnt, it is indicated from 0 to 1. Since the results of AUC for all species were over 0.7, all predicted models by MaxEnt were assessed good fit models.

Contribution rate is the rate that each environmental variable affects the habitat probability. From this table, it was observed that the “annual total daylight hours” and “land use” considerably affect the habitat probability of the red fox, while the “average rainfall amount” influences that of the Tokyo salamander because this species prefers a water environment. It was also demonstrated that many of the Japanese skinks were confirmed in the south area where the slope angle is large, while many ruddy crakes were confirmed in the north area with a small slope angle. These results showed that the contribution rate of the slope angle is high for these species. Thus, it was found that there were difference of preference on habitat among targeted species.

Fig. 3 represents the result of response curve on

Table 2 Result of AUC and contribution rate of respective environmental factors

|                  | AUC   | Land use (%) | Average rainfall amount (%) | Annual average temperature (%) | Annual total daylight hours (%) | Average annual amount of solar radiation (%) | Average altitudes (%) | Average slope angles (%) |
|------------------|-------|--------------|-----------------------------|--------------------------------|---------------------------------|--|-----------------------|--------------------------|
| Ruddy crake      | 0.789 | 16.5         | 0.4                         | 6.1                            | 18.7                            | 0.0  | 17.7                  | 40.6                     |
| Red fox          | 0.797 | 28.7         | 16.7                        | 16.4                           | 29.1                            | 1.2  | 5.8                   | 2.0                      |
| Japanese skink   | 0.713 | 6.4          | 12.1                        | 1.0                            | 16.9                            | 2.8  | 12.2                  | 48.5                     |
| Tokyo salamander | 0.789 | 1.5          | 61.8                        | 5.1                            | 1.1                             | 0.0  | 6.1                   | 24.5                     |



Fig. 3 Result of response curve on each land use

each land use. This response curve estimated by MaxEnt was able to reproduce the characteristics of habitat on each species. “Rivers, lakes and ponds” and “Paddy fields” had commonly an influence on almost all species in particular because they prefer freshwater environment near their habitat. “Other agricultural land” and “Forest” are also affected as suitable habitat for many species.

#### Result of time-series change of potential suitable habitat area

The area of potential suitable habitat considering the existence probability was estimated by multiplying the suitable habitat area rate 0–1, obtained by MaxEnt, by the area of each mesh (Fig. 4 and Table 3).

As a result, it was shown that when comparing the results in 1976 with those in 2009, total habitat possibility area of the ruddy crane, red fox, Japanese skink and Tokyo salamander have decreased by 3.6%, 6.0%, 1.6% and 0.7%, respectively. As reasons for this, since the residential land area and road length has increased by 74.5% and 13.6% respectively in this period, the suitable habitat area of each species is considered to have decreased with the expansion of the city area. Especially, the habitat for red fox resulted in significant decrease for 33 years because their habitat is near area that is progressing housing land development. Also, in the northwestern area of Chiba, it has been found total potential suitable habitat area for all species have decreased remarkably in particular.

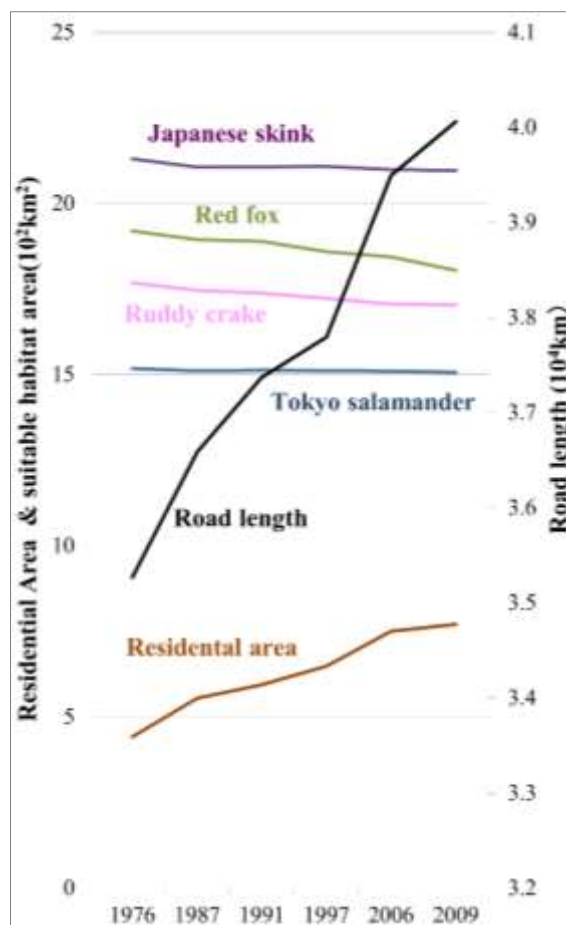


Fig. 4 Relationship between potential suitable habitat area, residential area and road length

Table 3 Result of detailed potential suitable habitat area between 1976 and 2009

|   |              | 1976   | 1987 | 1991 | 1997 | 2006 | 2009 | Comparison between 1976 and 2009 |
|---|--------------|--|------|------|------|------|------|----------------------------------|
| Road length( $10^4$ km)                 |              | 3.5  | 3.7  | 3.7  | 3.8  | 3.9  | 4.0  | 13.6%                            |
| Buildup area ( $10^2$ km <sup>2</sup> ) |              | 4.4  | 5.5  | 5.9  | 6.5  | 7.5  | 7.7  | 74.5%                            |
| Species                                 | Area         | Potential suitable habitat area ( $10^2$ km <sup>2</sup> ) |      |      |      |      |      |                                  |
| Ruddy crane                             | Whole area   | 17.7   | 17.5 | 17.4 | 17.2 | 17.1 | 17.0 | -3.6%                            |
|   | Northwestern | 7.8  | 7.7  | 7.6  | 7.5  | 7.4  | 7.4  | -4.8%                            |
|   | Northeastern | 6.1  | 6.1  | 6.1  | 6.0  | 5.9  | 6.0  | -3.0%                            |
|   | South        | 3.7  | 3.7  | 3.7  | 3.7  | 3.7  | 3.7  | -2.3%                            |
| Red fox                                 | Whole area   | 19.2   | 18.9 | 18.9 | 18.6 | 18.4 | 18.0 | -6.0%                            |
|   | Northwestern | 7.8  | 7.6  | 7.6  | 7.4  | 7.3  | 7.0  | -9.8%                            |
|   | Northeastern | 5.6  | 5.5  | 5.5  | 5.4  | 5.4  | 5.3  | -4.4%                            |
|   | South        | 5.8  | 5.8  | 5.8  | 5.8  | 5.8  | 5.7  | -2.4%                            |
| Japanese skink                          | Whole area   | 21.3   | 21.1 | 21.1 | 21.1 | 21.0 | 21.0 | -1.6%                            |
|   | Northwestern | 7.8  | 7.6  | 7.6  | 7.7  | 7.6  | 7.6  | -2.2%                            |
|   | Northeastern | 5.3  | 5.3  | 5.3  | 5.3  | 5.2  | 5.2  | -1.3%                            |
|   | South        | 8.2  | 8.1  | 8.2  | 8.2  | 8.1  | 8.1  | -1.2%                            |
| Tokyo salamander                        | Whole area   | 15.2   | 15.1 | 15.1 | 15.1 | 15.1 | 15.1 | -0.7%                            |
|   | Northwestern | 2.3  | 2.3  | 2.3  | 2.3  | 2.3  | 2.3  | -1.3%                            |
|   | Northeastern | 4.5  | 4.5  | 4.5  | 4.5  | 4.5  | 4.5  | -0.6%                            |
|   | South        | 8.3  | 8.2  | 8.3  | 8.3  | 8.2  | 8.2  | -0.7%                            |

## CONCLUSIONS

In the research, we analyzed the environmental factors that affected the habitat probability and estimated the possible habitat area for endangered species using MaxEnt in Chiba Prefecture, Japan.

In Japan, it is not required to conduct compensatory mitigation for all developers by law in the pre-process of environmental impact assessment. Thus, the number of endangered species has been increasing every year due to destruction of the natural environment including their valuable habitat. For solving this problem, it is necessary to consider how to avoid, minimize and compensate the adverse impact to their habitat at the planning phase of development based on the potential habitat area predicted by MaxEnt in this research. Since surveying existence of all animal and plant on whole area is impossible, potential habitat area estimated by MaxEnt is valuable information to consider environment conservation countermeasures.

Further research is needed to improve the accuracy of the plot data for habitat places by collecting more data and improve the accuracy by the estimation of the contribution rate including other environmental variables for MaxEnt.

## REFERENCES

- [1] N. Iwasaki and S. David, A study of the land use history in the Japanese macaque habitat expansion area of the Boso Peninsula, Japan. Journal of Rural Planning Association. Vol.24, Special issue, 2005, pp.S1-S6.
- [2] J. Kwon and M. Miyawaki, A STUDY ABOUT THE STABILITY OF LANDSCAPE BASED ON LAND-USE BY GIS, Journal of architecture, planning and environmental engineering, Vol.75, No.658, 2010, pp.2863-2872.
- [3] H. Ikemi, T. Esaki, Y. Mitani and T. Tran, Spatial Distribution of Human Impacts on Terrain Based On Landuse Change Analysis Development and GIS Analysis of Landuse Maps since 1900 in the Fukuoka Prefecture Area, Journal of the Japan Society of Engineering Geology, Vol.52, No.3, 2011, pp.97-108.
- [4] Y. Ohara and A. Yamashita, Mesh Data Analysis on Land Use Change and Its Correlation with Topographic Condition in Sapporo, Tokyo and Osaka Metropolitan Areas, Geographical Studies, No.86, No.1, 2011, pp.55-71.
- [5] M. Miyamoto, Attempts to estimate habitat of cold-water corals, Aquabiology, Vol.36(5), 2014, pp.461-468.
- [6] Steven J. Phillips, Robert P. Anderson, Robert E. Schapire, Maximum entropy modeling of species geographic distributions, Ecological Modelling 190, 2006, pp.231-259.
- [7] T. Pan, H. Wang, S. Duan, I. Ali, P. Yan, R. Cai, M. Wang, J. Zhang, H. Zhang, B. Zhang and X. Wu, Historical population decline and habitat loss in a critically endangered species, the Chinese alligator (*Alligator sinensis*), Global Ecology and Conservation, Vol.20, 2019, e00692.
- [8] A. M. West, S. Kumar, C. S. Brown, T. J. Stohlgren and J. Bromberg, Field validation of an invasive species MaxEnt model, Ecological Informatics, Vol.36, 2016, pp.126-134.
- [9] K. Remya, A. Ramachandran and S. Jayakumar, Predicting the current and future suitable habitat distribution of *Myristica dactyloides* Gaertn using MaxEnt model in the Eastern Ghats, India, Ecological Engineering, Vol.82, 2015, pp.184-188.
- [10] D.S. Matyukhina, D. G. Miquelle, A. A. Murzin, D. G. Pikunov, P. V. Fomenko, V. V. Aramilev, M. N. Litvinov, G. P. Salkina, I. V. Seryodkin, I. G. Nikolaev, A. V. Kostyria, V. V. Gaponov, V. G. Yudin, Y. M. Dunishenko, E. N. Smirnov, V. G. Korkishko, J. Marino, Assessing the Influence of Environmental Parameters on Amur Tiger Distribution in the Russian Far East Using a MaxEnt Modeling Approach, Achievements in the Life Sciences, Vol.8, Issue 2, 2014, pp.95-100.
- [11] R. Moreno, R. Zamora, J. R. Molina, A. Vasquez, M. Á. Herrera, Predictive modeling of microhabitats for endemic birds in South Chilean temperate forests using Maximum entropy (MaxEnt), Ecological Informatics, Vol.6, Issue 6, 2011, pp.364-370.
- [12] K. Pratumcharta, K. Suwannatrai, C. Sereewong, K. Thinkhamrop, J. Chaayos, T. Boonmars and A. T. Suwannatrai, Ecological Niche Model based on Maximum Entropy for mapping distribution of *Bithynia siamensis goniomphalos*, first intermediate host snail of *Opisthorchis viverrini* in Thailand, Acta Tropica, Vol.193, 2019, pp.183-191.
- [13] K. K. Khadka and D. A. James, Modeling and mapping the current and future climatic-niche of endangered Himalayan musk deer, Ecological Informatics, Vol.40, 2017, PP.1-7.
- [14] S. Mohammadi, E. Ebrahimi, M. S. Shahriari, L. Bosso, Modelling current and future potential distributions of two desert jerboas under climate change in Iran, Ecological Informatics, Vol.52, 2019, pp.7-13.
- [15] Chiba Prefecture, Natural History of Chiba Prefecture, Vol.6, No.45, 2002, pp.989.

# SOLID WASTE GENERATION IN THE PHILIPPINES: A CORRELATIONAL ANALYSIS ON ECONOMIC AND SOCIAL METRICS

Jennie Lagman-Bautista<sup>1</sup>

<sup>1</sup>Faculty, Holy Angel University, Philippines; Ph.D. Candidate, University of Santo Tomas, Philippines

## ABSTRACT

The Philippines' waste generation continues to rise from  $37 \cdot 10^3 \text{ kg} \cdot \text{a}^{-1}$  in 2012 to  $40 \cdot 10^3 \text{ kg} \cdot \text{a}^{-1}$  in 2016, with a daily waste generation per capita oscillating from 300 to 700 grams for both rural and urban areas, respectively. The study depicted a five-year correlational analysis on waste generation per capita as against Philippine Economic and Social Metrics for: (1) Average Family Income (2) Average Family Expenditure (3) Population Density and (4) Human Development Index. Both national and regional secondary panel data were analyzed that lead to identifying Average Family Expenditure as an ecological footprint indicator with a direct and highest correlation on waste generation per capita (WgC). On the National Level Analysis, for the five-year observation, all independent variables exhibited a probability value lower than the significant threshold error value of 0.05. Hence, changes in waste generation per capita for the five year sample size is also recurring prior and beyond the sampling period of 2012 to 2016. Based on Regional Level Analysis, the Equation Model was generated in order to predict the degree of changes per unit, stated in gram of WgC (with coefficient = 0.319) in relation to the three EFA Indicators with the exclusion of HDI. As depicted in the Equation Model, for every person increase in population density expressed in per  $\text{km}^2$ , it will generate a positive increases on WgC by 0.0000714; while for every peso (Philippine monetary denomination) increases in family expenditure, has a decreasing effect on WgC by 0.0000009479; and that for every one peso increases in family income, WgC will generate an increase by 0.0000008573.

*Keywords: National footprint accounting, Ecological Footprint Indicators, Waste generation per capita, Multi Regression Analysis*

## INTRODUCTION

The Philippines is at a precarious juncture in its urbanization process and posited for having the second highest average urban density in East Asia and Pacific Region [1]. Like any other developing economy, solid waste management remains a major challenge [2]. The Philippines' waste generation continues to rise from  $37 \cdot 10^3 \text{ kg} \cdot \text{a}^{-1}$  in 2012 to  $40 \cdot 10^3 \text{ kg} \cdot \text{a}^{-1}$  in 2016, with a daily waste generation per capita oscillating from 300 to 700 grams for both rural and urban areas [3]. Unlike developed worlds who's into waste-energy conversion, Philippine regions must efficiently utilize landfill, promote wastes avoidance, reduction, re-use, rethink waste recycling and periodically assess waste generation per capita. The result of the waste assessment per region is vital in relation to Republic Act 9003, known as the Ecological Solid Waste Management Act of 2000.

The Philippines has commendable enacted environmental regulatory policy frameworks [4]. But Sta. Romana lamented that policy implementation in the Philippine government agencies, however, remains a challenge [4]. There is an apparent

substantial disparity between rhetoric statutes enacted by legislators and real outcomes on Solid Waste Management. There is a need to understand and predict the impact of indicators on national economy's improvement as against final waste generation, a globally considered as chaotic human ecological footprint.

## Ecological Footprint Accounting Indicators

The study proposed a scientific method to ascertain the degree of significant changes in the four ecological footprint indicators [5] on (a) level of consumption using average family expenditures (b) quality of population quality using Human Development Index (c) Level of Income or average family income and (d) quality of habitat using population density.

The ecological footprint is used to gauge the exerted degree of consumption of human beings on its ecological environment. According to Galli, It can be applied at scales from global to local and gives insight on the ecosystem services to human requirements to sustain changing lifestyle [6]. To quantify sustainable development amidst the

escalating environmental degradation is to utilize a resource accounting tool called Ecological Footprint (EFA) [7]. It measures human demand on natural resources and services [8]. Based on Millennium Ecosystem Assessment, EFA can track past human pressure on ecosystem, it requires an analysis of historical data in order to predict [9]. A favorable result occurs when a National Footprint is lesser than the ability of the environment and natural resources to regenerate, favorably, there is what we call biocapacity reservation [9].

Four indicators of Ecological Footprints [5] were applied in the study. The major source of Ecological Footprint is explained by the European Environment Agency as anthropogenic effects, these are processes, objects, materials or those that are derived from human activities as opposed to those occurring in natural environments without human influences [10]. Tools such as Ecological indicators can be used as early warning signal and can quantify anthropogenic effects on the ecosystem brought by the growing level of human and global metabolism [11]. The National Footprint Accounting (NFA) are prevalently used since 1961 [12]. To synthesize further, EFA for Municipal Solid Waste (MSW) provides policy-makers with new insights on how to mitigate territorial footprints and just as important as the policy development and implementation [9].

### **Average Family Income**

Auci and Vignani explained the increase in economy's income at a certain high level has a domino effect, people started to be environmental and may demand imposition of regulatory policies to halt pollution impacts on social and economic activities [4]. In the study the average family income was used as economic metrics. When a systems approach is used for technology evaluation, the economic dimension of the system life cycle cannot be omitted. The purpose of economic metrics is to provide the quantitative information needed to make a judgment or a decision on the deployment of a new technology in selecting an alternative option [13].

### **Population Density**

Population density is the number of individuals that live in a unit area in a specified time [14]. It is computed by dividing the total population by its land area. When there are a larger number of people living in a smaller amount of space, the area is densely populated while the reversed is called sparsely populated [15]. The effects of population rate on economic development stem on the type of industry classified either as labor intensive or not, human resources is a principal replacement for diminished input in service oriented industries [16]. Eventually,

workers or consumers are bound to product consumption of scarce resources and later subject for disposal [16]. The Central Asia, Middle East and Asia-Pacific regions experienced an escalating Ecological Footprint due to population growth of 154% and 465% from 1961 to 2014 generating per capita Footprint equivalent to 126% and 146% respectively [12]. Provinces that have larger urban population and higher economic activities generate greater volume of solid waste [3].

### **Human Development Index (HDI)**

In the study, National progress concerning sustainable development dwelled on comparing the NFA results and explored the degree of relationship of WgC as against the Philippine HDI, as published by United Nation Development Programme (UNDP). HDI is the aggregate of education, longevity, and income into a single metric [12]. The same authors in the study entitled "Ecological Footprint Accounting for Countries: Updates and Results of the National Footprint Accounts, 2012-2018" used HDI as a major indicator of Ecological Footprint. Further, the UNDP defines 0.70 HDI as the threshold for a highly developed economy. As stated previously, bio capacity deficiency on the planet earth is gauged at 1.7 gha per capita in 2014. And they reasonably concluded said deficiency combined with HDI measures globally sustainable development of mankind as a minimum condition set. HDI is a social metrics that measures social sustainability. Social sustainability was defined by Western Australia Council of Social Services as "Social sustainability occurs when the formal and informal processes; systems; structures; and relationships actively support the capacity of current and future generations to create healthy and liveable communities. In addition, socially sustainable communities are equitable, diversely connected, and generally provides a good quality of life [13].

### **Average Family Expenditure**

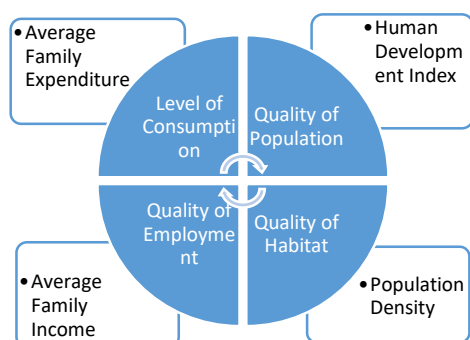
Average Family Expenditure is another economic metrics as a basis for consumption per capita. Philippine Statistics Authority (PSA) [17] showed that the current average annual family income of Filipino families was approximately 267 thousand pesos in 2015. In comparison, the average annual family expenditure for the same year was 215 thousand pesos. Hence, Filipino families have an annual average savings of 52 thousand pesos.

## **METHODOLOGY AND MATERIALS**

Waste assessment is a vital phase of Solid Waste Management and preferably enclosed by macro and/or micro level analysis. Consequently, an

assessment called National Footprint Accounting on wastes will be analyzed using multivariate regression analysis for both level of consumption, level of income, quality of population and quality of habitat in terms of population density. These indicators were introduced by Guo et al. (2018) and adapted in the study to establish empirical data that will provide deeper linkages on economic and social metrics as depicted in Figure 1. The result of the study is vital for the program planning of National Solid Waste Management Commission (NSWMC) to forecast the waste generation per Philippine Region based on the foreseeable economic growth, human development and population growth. The Commission shall oversee the implementation of solid waste management plans and prescribe policies to achieve the objectives of the law on “Ecological Solid Waste Management Act of 2000”.

Fig. 1 Conceptual Framework of NFA



The term regression is credited to Francis Galton [18]. Regression analysis allows researchers to quantify how the average of one variable systematically varies according to the levels of another variable. The former variable is often called a dependent variable or outcome variable and the latter an independent variable, predictor variable, or explanatory variable [18]. Regression analysis is a form of predictive modelling technique which investigates the relationship between a dependent (target) and independent variables (predictors). This technique is used for forecasting, time series modelling and finding the causal effect relationship between the variables [19]. It also indicates the strength of impact of multiple independent variables on a dependent variable.

In the study, secondary national waste assessment panel data from the PSA and UNDP, covering the periods from 2012 to 2016 was utilized. Subsequently, the Correlational Analysis generated 85 observations from the total 17 Philippine Regions over the five-year period. National Ecological Footprint Accounting Data, known as waste generation per capita were processed together with the four EFA indicators using SPSS for Multi Regression Analysis. The dependent variable

(presented in ratio scale for a parametric test) pertains to the waste generation per capita per region. The three independent variables (classified as interval scale) will also be on a per region basis as follows: (1) Average Family Expenditure per Region (2) Average Family Income per Region (3) Population Density was computed based on regional area per square kilometer divided by population per region. While the last indicator or the quality of Population was presented based on parametric variables (ratio scale) on Human Development Index a secondary data. The adjusted  $R^2$  determined the causal effect relationship between the dependent and independent variables. Further the p-value higher than 0.05 was excluded as an independent variable in generating a Regression Model and to be interpreted that no significant relationship exist with the dependent variable representing the waste generation per capita. One of the purpose of the statistical analysis is to generate a Regression Equation Model by transmutation of coefficient values of each independent variables based on the line-intercept.

#### Regression Equation Model (Regional Level)

$$WgC = 0.319 + B1*(0.0000714) + B2*(-0.0000009479) + B3*(0.0000008573) \quad (1)$$

**Research Hypothesis:** There is a significant relationship between Waste generation per capita (WgC) and:

- (B1) Population Density
- (B2) Average Family Expenditure
- (B3) Average Family Income
- (B4) Human Development Index

#### RESULTS AND DISCUSSION

Table 1 presents the panel data for the four independent variables and the dependent variable, waste generation per capita based on the national level.

Table 1 Panel Data for National Level

| Year | WgC    | **<br>HDI | *Ave.<br>Family<br>Income | *Ave.<br>Family<br>Exp. | *Pop<br>ulation<br>Dens<br>ity |
|------|--------|-----------|---------------------------|-------------------------|--------------------------------|
| 2012 | 0.3878 | 0.677     | 182294                    | 168471                  | 301                            |
| 2013 | 0.3879 | 0.685     | 206765                    | 173588                  | 306                            |
| 2014 | 0.3880 | 0.689     | 216824                    | 179706                  | 311                            |
| 2015 | 0.3904 | 0.693     | 227118                    | 187294                  | 315                            |
| 2016 | 0.3912 | 0.696     | 238059                    | 195353                  | 319                            |

Philippine Statistics Authority\*  
United Nations\*\*



The average waste generation per capita between 2012 to 2016 on a nationwide basis is at 389 grams per day which is lesser than the global average of 740 grams per day in 2016 [21]. The HDI Mean is 0.688, a bit lower in comparison to 0.70 as the threshold for a highly developed economy [22]. The five year (2012 to 2016) average annual family income was approximately 214 thousand pesos with average annual family expenditure of 181 thousand pesos, giving Filipino families an annual savings of 60 thousand pesos. While the average five-year national population density is at 310 km<sup>2</sup> using total Philippine land area of 300 000 km<sup>2</sup> (refer to Table 2).

**Table 2 Descriptive Statistics (National Level)**

|                         | Mean    |
|-------------------------|---------|
| WgC                     | 0.38906 |
| HDI                     | 0.68800 |
| Ave. Family Income      | 214 212 |
| Ave. Family Expenditure | 180 882 |
| Population Density      | 310     |

Table 3 shows that 88% of the variation in waste generation per capita is explained by the variation in Average Family expenditure.

**Table 3 Regression Statistics**

|                                      |              |
|--------------------------------------|--------------|
| Pearson's Coefficient of Correlation | 0.0000001414 |
| R Square Change                      | 0.88         |
| Sig. F Change                        | 0.018        |
| Observations                         | 5            |

Waste generation per Capita has significant positive correlation with the following independent variables: (a) Average Family Expenditure ( $r = 0.938$ ,  $p = 0.009$ ), yield the highest and direct correlation with waste generation per capita which means an increase in family expenditure will increase wastes generation; (b) followed by Population Density ( $r = 0.888$ ,  $p = 0.022$ ) also directly predicting that the larger the number of people in a given land area will escalate waste generation; (c) the same is true with HDI ( $r = 0.837$ ,  $p = 0.04$ ) to be interpreted that the greater the human development liken to an economic development, poses greater ecological footprint on wastes; (d) and that positive increases on Average Family Income ( $r = 0.831$ ,  $p = 0.041$ ) has also strong and direct impact on waste generation per capita. All independent variables exhibited a probability value of lower than the significant threshold error value of 0.05. Hence, changes in waste generation per capita for the five year sample size is also recurring prior and beyond the period of study (2012 to 2016).

**Table 4 Correlations**

|                     | WgC | HDI  | Ave. Family Income | Ave. Family Exp. | Population Density |
|---------------------|-----|------|--------------------|------------------|--------------------|
| Pearson Correlation | 1   | 0.84 | 0.831              | 0.938            | 0.888              |
| Sig. (1-tailed)     | 0   | 0.04 | 0.041              | 0.009            | 0.022              |
| N                   | 5   | 5    | 5                  | 5                | 5                  |

Table 5 shows the statistical analysis for the four independent variables in relation to waste generation per capita for each of the 17 regions in the Philippines. It shows that there is a strong positive correlation ( $R = 0.933684$ ) between waste generation per capita and the 4 independent variables namely: Ave. Family Income, Ave. Family Expenditure, Population Density and HDI and 87.1765% of the variation or changes in waste generation per capita is explained by the changes in the 4 independent variables.

**Table 5 Regression Statistics (Regional)**

|              |          |
|--------------|----------|
| Multiple R   | 0.933684 |
| R Square     | 0.871765 |
| Observations | 85       |

The regional weighted waste generation per capita between the periods of 2012 and 2016 is at 368 grams per day which is a bit lower than the national average of 389 grams. HDI per region is not available hence, a reflection of the same five-year national average HDI of 0.688. The regional average annual family income was approximately higher by 13 thousand in comparison per Table 2 (228 less 214 thousand pesos) but with the same average annual family expenditure of 181 thousand pesos. While the average five-year regional population density is at 1 481 km<sup>2</sup> for a total Philippine land area of 300 000 km<sup>2</sup> (refer to Table 6).

**Table 6 Descriptive Statistics (Regional Level)**

|                         | Mean    |
|-------------------------|---------|
| WgC                     | 0.3680  |
| HDI                     | .6880   |
| Ave. Family Income      | 227 553 |
| Ave. Family Expenditure | 180 882 |
| Population Density      | 1 481   |

Table 7 based on regional panel data and in coming up with a Regression Equation Model, HDI was excluded among the indicators, generating ( $r = 0.20$ ,  $p$

= 0.429) which is above the p-value of 0.05, therefore not significant factor of waste generation per capita. But the result of the causal relationship on the regional level is attributable to lack of regional data for Human Development Index, see previously presented Eq. (1).

**Table 7 Correlations**

|                         | <i>Coefficients</i> | <i>Standard Error</i> | <i>t Stat</i> | <i>Sig.</i> |
|-------------------------|---------------------|-----------------------|---------------|-------------|
| Intercept               | 0.319               | 0.00                  | 1.525         | 0.131       |
| Population Density Ave. | 1.714 E-05          | 0.000                 | 13.935        | 0.000       |
| Family Expenditure Ave. | 9.479 E-07          | 0.004                 | 3.070         | 0.003       |
| Family Income           | 8.573 E-07          | 0.001                 | 3.458         | 0.001       |

After HDI removal having a p-value (greater than the alpha ( $p > 0.05$ )), That every unit of change on a per gram of waste generation per capita is attributable to the three remaining independent variables classified as fit for the regression equation model; (a) population density (b) average family expenditure and (c) average family income per Table 7.

## CONCLUSIONS

The study depicted a five-year correlational analysis on WgC for the four ecological footprint indicator on: (1) Average Family Income (2) Average Family Expenditure (3) Population Density and (4) HDI. Both national and regional secondary panel data were analyzed that lead to identifying Average Family Expenditure as an EFA indicator with a direct and highest correlation on WgC. On the National Level Analysis, for the five-year observation, all independent variables exhibited a p-value lower than the significant threshold error value of 0.05. Hence, changes in waste generation per capita for the five year sample size is also recurring prior and beyond the sampling period of 2012 to 2016.

Based on Regional Level Analysis, the Equation Model was generated in order to predict the degree of changes per unit, stated in gram of WgC (with coefficient = 0.319) in relation to three Ecological Footprint Accounting Indicators, excluding HDI. As depicted in the Equational Model, for every person increase in population density expressed in per km<sup>2</sup>, it will generate a positive increases on WgC by 0.0000714; while for every peso (Philippine monetary denomination) increases in family expenditure, has a decreasing effect on WgC by 0.000009479; and for every one peso increases in

family income, WgC will generate an increase by 0.0000008573.

## REFERENCES

- [1] World Bank. Population growth (annual%), 2017. <http://data.worldbank.org/indicator>
- [2] Moriguchi, Y., Hashimoto, S., Material flow analysis and waste management. In: Clift, R., Druckman, A. (Eds.), Taking Stock of Industrial Ecology, [https://doi.org/10.1007/978-3-319-20571-7\\_12](https://doi.org/10.1007/978-3-319-20571-7_12), 2016.
- [3] National Solid Waste Management Commission, National Solid Waste Management Strategy 2012-2016. Retrieved from <https://nswmc.emb.gov.ph/wp-content/uploads/2016/NSWM-Strategy-2012-2016.pdf>, 2016.
- [4] Martinico-Pereza, Schandla H., Tanikawaa H., Sustainability indicators from resource flow trends in the Philippines Marianne Faith G. Graduate School of Environmental Studies, Nagoya University, Japan Commonwealth Scientific and Industrial Research Organisation (CSIRO), Australia. Resources, Conservation and Recycling, 2018.
- [5] Guo, Y., Xia, D., Sun, B., Wang, X., Zhang, D., & Li, J., "Ecological footprints and development trends in Hefei, China". *Management of Environmental Quality: An International Journal* Vol. 29, Issue 1, 2018, pp. 2-14.
- [6] Mancini, Kamaruddin, Hafiz, Suffian & Alrozi. An overview of municipal solid waste management and landfill leachate treatment: Malaysia and Asian perspective. *Environmental Science and Pollution Research* Vol. 77, 2017, pp.123-128.
- [7] Zhang L., Dzakpasu M, Chen R., Wang X., Validity and utility of ecological footprint accounting: A state-of-the-art review. *Sustainable Cities and Society*. Vol. 32, 2017, pp. 411-416.
- [8] Isman M., Archambault M., Racette P., Konga C., Llaque R., Lin David., Iha K., Quellet-Plamondon, Ecological Footprint Assessment for targeting climate change mitigation in cities: A case study of 15 Canadian cities according to census metropolitan areas. *Journal of Cleaner Production*. Vol. 171, 2017, pp. 1032-1043.
- [9] Galli, A., "On the Rationale and Policy Usefulness of Ecological Footprint Accounting (The Case of Morocco)". *Environmental Science and Policy* Vol.48, 2015, pp. 210-224.
- [10] EEA-European Environment Agency, Waste Generation (WWW Document). URL <http://www.eea.europa.eu/data-and-maps/indicators/waste-generation-1/assessment>, 2015.

- [11]Weinzettel, Steen-Olsen, Hertwich, Borucke & Galli 2014. Ecological footprint of nations: Comparison of process analysis, and standard and hybrid multiregional input-output analysis. Ecological Economics Vol. 101, pp.115-126.
- [12]Lin D., Hanscom L., Murthy A., Galli A., Evans M, Neill E.,... Wackernagel M., Ecological Footprint Accounting for countries: Updates and results of the National Footprint Accounts, 2012-2018, Resources, 2018, pp.7-58
- [13]Department of Energy and Mineral Engineering, Technologies for Sustainable System. <https://www.e-education.psu.edu/eme807/node/584> by John and Willie Leone Family date retrieved April 26, 2019.
- [14]Lakna, PEDIAA. <https://pediaa.com/difference-between-population-density-and-population-distribution/> 2018, retrieved on April 26, 2019.
- [15]REFERENCE.<https://www.reference.com/world-view/population-density-9fcc8f4fbc8beada>
- [16]Bretschger L., Climate policy and economic growth. Resource and Energy Economics Vol. 49, 2017, pp. 1-15.
- [17]PSA. Philippine Statistics Authority. Angeles city population index. Retrieved from [https://psa.gov.ph/sites/default/files/03\\_Angeles%20City.pdf](https://psa.gov.ph/sites/default/files/03_Angeles%20City.pdf)
- [18]Gordon, R., Regression analysis for the social sciences, Second edition. Published by Routledge 711 Third Avenue, New York, NY 10017, 2015, pp. 4-6.
- [19]Sunil R., Analytics Vidhya. <https://www.analyticsvidhya.com/blog/2015/08/comprehensive-guide-regression/>, 2015.
- [20]World Bank. Solid Waste Management 2018. Retrieved from <http://www.worldbank.org/en/topic/urbandevelopment/brief/solid-waste-management>, 2018
- [21]UNEP.[http://www.ph.undp.org/content/philippines/en/home/library/human\\_development/2016HumanDevelopmentReport.html](http://www.ph.undp.org/content/philippines/en/home/library/human_development/2016HumanDevelopmentReport.html)

#### Appendix A: Regional Secondary Panel Data

| Year | Region | Population |      | Average Family |             |      |
|------|--------|------------|------|----------------|-------------|------|
|      |        | Density    | HDI  | Income         | Expenditure | WgC  |
| 2012 | 1      | 376.56     | 0.68 | 204000         | 159000      | 0.35 |
| 2012 | 2      | 118.43     | 0.68 | 195000         | 140000      | 0.33 |
| 2012 | 3      | 482.72     | 0.68 | 259000         | 211000      | 0.34 |
| 2012 | 4      | 797.71     | 0.68 | 284000         | 243000      | 0.31 |
| 2012 | 5      | 96.45      | 0.68 | 179000         | 138000      | 0.32 |
| 2012 | 6      | 309.6      | 0.68 | 162000         | 144000      | 0.33 |
| 2012 | 7      | 353.37     | 0.68 | 202000         | 163000      | 0.37 |
| 2012 | 8      | 458.3      | 0.68 | 209000         | 164000      | 0.37 |
| 2012 | 9      | 182.23     | 0.68 | 166000         | 132000      | 0.35 |
| 2012 | 10     | 208.3      | 0.68 | 162000         | 162000      | 0.39 |
| 2012 | 11     | 219.41     | 0.68 | 190000         | 143000      | 0.38 |
| 2012 | 12     | 229.35     | 0.68 | 194000         | 156000      | 0.39 |
| 2012 | 13     | 192.55     | 0.68 | 163000         | 140000      | 0.31 |
| 2012 | 14     | 117.37     | 0.68 | 180000         | 142000      | 0.35 |
| 2012 | 15     | 269.63     | 0.68 | 130000         | 114000      | 0.27 |
| 2012 | 16     | 19981.6    | 0.68 | 379000         | 325000      | 0.69 |
| 2012 | 17     | 92.08      | 0.68 | 257000         | 188000      | 0.37 |
| 2013 | 1      | 380.86     | 0.69 | 215000         | 165000      | 0.35 |
| 2013 | 2      | 119.98     | 0.69 | 208000         | 146000      | 0.33 |
| 2013 | 3      | 491.76     | 0.69 | 272000         | 219000      | 0.34 |
| 2013 | 4      | 819.46     | 0.69 | 293000         | 251000      | 0.31 |
| 2013 | 5      | 97.97      | 0.69 | 193000         | 144000      | 0.32 |
| 2013 | 6      | 313.89     | 0.69 | 170000         | 149000      | 0.34 |
| 2013 | 7      | 357.79     | 0.69 | 210000         | 167000      | 0.37 |
| 2013 | 8      | 465.98     | 0.69 | 218000         | 172000      | 0.37 |
| 2013 | 9      | 184.42     | 0.69 | 176000         | 138000      | 0.35 |
| 2013 | 10     | 211.71     | 0.69 | 171000         | 155000      | 0.39 |
| 2013 | 11     | 223.36     | 0.69 | 200000         | 148000      | 0.38 |
| 2013 | 12     | 233.28     | 0.69 | 211000         | 165000      | 0.39 |
| 2013 | 13     | 196.73     | 0.69 | 171000         | 146000      | 0.31 |
| 2013 | 14     | 119        | 0.69 | 186000         | 147000      | 0.35 |
| 2013 | 15     | 273.46     | 0.69 | 133000         | 113000      | 0.27 |
| 2013 | 16     | 20320.54   | 0.69 | 394000         | 332000      | 0.7  |
| 2013 | 17     | 93.61      | 0.69 | 265000         | 194000      | 0.37 |
| 2014 | 1      | 385.09     | 0.69 | 226000         | 173000      | 0.35 |
| 2014 | 2      | 121.51     | 0.69 | 222000         | 153000      | 0.33 |
| 2014 | 3      | 500.85     | 0.69 | 285000         | 228000      | 0.34 |
| 2014 | 4      | 841.57     | 0.69 | 302000         | 259000      | 0.3  |
| 2014 | 5      | 99.46      | 0.69 | 208000         | 152000      | 0.32 |
| 2014 | 6      | 318.08     | 0.69 | 178000         | 154000      | 0.34 |
| 2014 | 7      | 362.22     | 0.69 | 218000         | 171000      | 0.37 |
| 2014 | 8      | 473.67     | 0.69 | 228000         | 181000      | 0.37 |
| 2014 | 9      | 186.53     | 0.69 | 186000         | 146000      | 0.35 |

| Year | Region | Population |      | Average Family |             |      |
|------|--------|------------|------|----------------|-------------|------|
|      |        | Density    | HDI  | Income         | Expenditure | WgC  |
| 2014 | 10     | 215.05     | 0.69 | 180000         | 149000      | 0.39 |
| 2014 | 11     | 227.31     | 0.69 | 210000         | 154000      | 0.38 |
| 2014 | 12     | 237.26     | 0.69 | 229000         | 176000      | 0.39 |
| 2014 | 13     | 200.95     | 0.69 | 179000         | 153000      | 0.31 |
| 2014 | 14     | 120.63     | 0.69 | 192000         | 152000      | 0.35 |
| 2014 | 15     | 277.29     | 0.69 | 136000         | 112000      | 0.27 |
| 2014 | 16     | 20657.88   | 0.69 | 409000         | 340000      | 0.7  |
| 2014 | 17     | 95.08      | 0.69 | 273000         | 202000      | 0.37 |
| 2015 | 1      | 386.24     | 0.69 | 238000         | 182000      | 0.36 |
| 2015 | 2      | 122.25     | 0.69 | 237000         | 162000      | 0.34 |
| 2015 | 3      | 509.57     | 0.69 | 299000         | 239000      | 0.34 |
| 2015 | 4      | 854.31     | 0.69 | 312000         | 269000      | 0.3  |
| 2015 | 5      | 100.03     | 0.69 | 222000         | 161000      | 0.32 |
| 2015 | 6      | 319.29     | 0.69 | 187000         | 160000      | 0.34 |
| 2015 | 7      | 427.76     | 0.69 | 226000         | 176000      | 0.38 |
| 2015 | 8      | 390.12     | 0.69 | 239000         | 193000      | 0.37 |
| 2015 | 9      | 190.96     | 0.69 | 197000         | 156000      | 0.35 |
| 2015 | 10     | 212.82     | 0.69 | 190000         | 144000      | 0.4  |
| 2015 | 11     | 228.78     | 0.69 | 221000         | 161000      | 0.38 |
| 2015 | 12     | 240.35     | 0.69 | 247000         | 190000      | 0.39 |
| 2015 | 13     | 201.88     | 0.69 | 188000         | 162000      | 0.31 |
| 2015 | 14     | 120.91     | 0.69 | 198000         | 159000      | 0.36 |
| 2015 | 15     | 301.62     | 0.69 | 139000         | 111000      | 0.25 |
| 2015 | 16     | 20783.77   | 0.69 | 425000         | 349000      | 0.7  |
| 2015 | 17     | 94.1       | 0.69 | 282000         | 210000      | 0.38 |
| 2016 | 1      | 387.39     | 0.7  | 250000         | 192000      | 0.36 |
| 2016 | 2      | 122.99     | 0.7  | 252000         | 171000      | 0.34 |
| 2016 | 3      | 518.43     | 0.7  | 313000         | 251000      | 0.34 |
| 2016 | 4      | 867.23     | 0.7  | 322000         | 279000      | 0.3  |
| 2016 | 5      | 100.6      | 0.7  | 236000         | 171000      | 0.33 |
| 2016 | 6      | 320.5      | 0.7  | 196000         | 166000      | 0.35 |
| 2016 | 7      | 499.18     | 0.7  | 234000         | 181000      | 0.37 |
| 2016 | 8      | 321.29     | 0.7  | 250000         | 205000      | 0.37 |
| 2016 | 9      | 195.47     | 0.7  | 208000         | 167000      | 0.35 |
| 2016 | 10     | 210.59     | 0.7  | 200000         | 138000      | 0.42 |
| 2016 | 11     | 230.24     | 0.7  | 232000         | 169000      | 0.38 |
| 2016 | 12     | 243.5      | 0.7  | 265000         | 205000      | 0.39 |
| 2016 | 13     | 202.81     | 0.7  | 197000         | 171000      | 0.32 |
| 2016 | 14     | 121.19     | 0.7  | 204000         | 166000      | 0.36 |
| 2016 | 15     | 328.02     | 0.7  | 142000         | 110000      | 0.24 |
| 2016 | 16     | 20909.66   | 0.7  | 441000         | 359000      | 0.71 |
| 2016 | 17     | 93.11      | 0.7  | 291000         | 220000      | 0.39 |

## **ANALYSIS ON SPATIAL USE AND LAND USE IN NORTH JAKARTA ADMINISTRATIVE CITY**

Galih Jati Utomo<sup>1</sup>, Hafid Setiadi<sup>2</sup>, Rudy P. Tambunan<sup>3</sup> and Komara Djaja<sup>4</sup>  
<sup>1,2,3,4</sup> School of Strategic and Global, University of Indonesia, Indonesia

### **ABSTRACT**

North Jakarta City as part of the Special Capital Region of Jakarta Province has a typical regional characteristic of coastal areas with varied land use functions. Urban development that occurs along with population growth and development activities increases the demand for land. In fact, this city is designed in a planological manner according to the type of allocation and land use that has been determined. This resulted in the occurrence of land use non conformity with the North Jakarta City Regional Spatial Planning (RTRW). This study aims to determine the pattern of changes in land use and utilization (spatial and temporal), the amount of non conformity and to know the implications of the spatial use non conformity and approaches to overcome those problems. The method used in this study was map analysis with overlay using Geographic Information System, qualitative data collection, and quantitative descriptive analysis by identifying and conducting field survey observations.

The results showed a change in the pattern and the amount of spatial use in 2008 to 2018 for some types of land use. Based on the analysis results, the land use in 2018 that complied with the Spatial Plan was 51.05%, supported the Spatial Plan of 12.48%, not complied with the Spatial Plan of 29.48% and the plan that had not been approved was 6.96%. The impact of land use non conformity was the emergence of urban problems such as irregular housing, traffic congestion, natural vulnerability such as floods, damage to environmental quality, reduced public space and the inability to implement government development programs. And approach to overcome these problems is by reviewing spatial plans, increasing the role of the government in monitoring and controlling spatial use, and making priority programs and areas with a tight control system.

**Keywords:** Spatial Analysis, Spatial Violation, Spatial Planning, Spatial Use, Land Use

### **INTRODUCTION**

A common problem faced by big cities in Indonesia is the high growth of urban population. This is due to natural population growth and urbanization factors. These two factors ultimately have an impact on the emergence of various problems in urban areas such as the lack of space for the needs of housing, offices, trade and services. Current urban development has an impact on increasing the need for space in urban areas and the high demand for land. Therefore spatial planning is needed to regulate utilization patterns based on activities, types of activities, location functions, space quality and environmental aesthetics [1]

Based on the DKI Jakarta 2030 Spatial Planning (RTRW), in order to control the development of activities so as not to exceed the carrying capacity and accommodative capacity of the environment, one strategy is to prioritize the development of cities to the east, west and north and limit development to southward [2]. This is also in line with the vision of the North Jakarta Administrative City, namely to realize the North Jakarta Administrative City as a modern coastal city that is neatly organized, advanced, comfortable and prosperous and has a cultured society and a government-oriented public service. As a coastal city, North Jakarta has a strategic

value in controlling space utilization in the DKI Jakarta Province.

Problems in the City of Jakarta related to the control of spatial use are land use and spatial use that are not comply with applicable laws and regulations. This is a factor that triggers the non conformity of urban space utilization. This problem also occurred in the North Jakarta Administrative City, limited land and the high price of land in Jakarta and North Jakarta in particular caused an increase in the intensity of land use in each ownership.

This study is very important considering the great benefits obtained when the land use and spatial use can be identified. Through this study, it is expected to be known to what extent the conditions, dynamics and the extent of non conformity that occurred in spatial planning in the North Jakarta Administrative City. Thus, evaluations can be carried out in the context of proposed changes or providing input on the revision of the Regional Spatial Plan (RTRW) through approaches that are in line with environmental conditions and problems. Based on the facts described above, the authors are interested to conduct a study entitled "Analysis on Spatial Use and Land Use in North Jakarta Administrative City".

### **LITERATURE REVIEW**

## Human and Spatial Planning

According to Kivell [3] the main urban activities that plays an important role in the development of the city are: (a) trading activities; (b) industrial activities; and (c) settlement activities. Land is permanent and limited, as a result a land will be contested for various types of activities which have criteria located in accordance with the land. Even though the city is designed in a planological manner according to the type of allocation and land use that has been determined in the Regional Spatial Planning.

## Spatial Planning, Spatial and Land Use

According to Law No. 26 of 2007 concerning spatial planning, space is a place which includes land space, sea space, and air space, including space within the earth as a unitary area, where humans and other creatures live, carry out activities, and maintain their survival. Spatial planning is a form of spatial structure and spatial pattern. Spatial structure is the arrangement of residential centers and network systems of infrastructure and facilities that function as supporters of socio-economic activities of communities that have a functional relationship hierarchically. [4]

Hamid Shirvani [5] in the book entitled Urban Design Process states that every city design must pay attention to the existing design elements so that later the city will have clear characteristics. There are 8 (eight) elements that form a city (especially the city center) namely land use, building and mass building, open space, parking and circulation, signages, pedestrian ways, supportive activities and preservation. Land use must pay attention to or adjust to problems in how to develop the city. In this book it is also mentioned that zoning ordinance is a practical and useful control mechanism in urban design. The main emphasis lies in the three-dimensional problem, namely the relationship of harmony between buildings and environmental quality. This is the basis of a city spatial planning.

Hamid Shirvani [5] also mentions that zoning ordinance is intended so that the plan runs according to what has been determined, including in the mechanism of permits (building permits) and special provisions that govern it. In addition, zoning ordinance can encourage the creation of public facilities and a humanized city environment, especially in creating a pedestrian atmosphere on street level and providing space for activity support.

Furthermore, Kivell [3] states that land use planning and zoning are instruments in spatial planning. These two instruments are generally detailed in the structure plan or in more detail in the area plan that shows where development can be permitted and in what form of building. The objectives of the area plan are:

- Limit the use of permitted space;
- Guarantee the balance of land use for all activities in all strategic areas; and
- Avoid non-strategic land use.

## Changes in Land Use and Land Use Conformity

The theory of changes in an area and its surroundings as part of a wider urban area according to Gallion and Eisner [6] in the book entitled The Urban Pattern, may cause distortions in land use changes. Based on Chapin and Kaiser's theory [7] urban development will always be associated with urban land use where there are three key systems that influence. The three systems include (a) the city activity system; (b) environmental system; and (c) land development system.

Meanwhile, land conformity is the level of conformity of a plot of land for a particular use. The conformity of the land can be assessed for current conditions (actual land conformity) or after improvements have been made (potential land conformity) [8].

## Land Use Classification

Based on the 2011-2030 DKI Jakarta Spatial Planning, the types of land use classification are as follows:

1. Protected Green Area
2. Cultural Green Area
3. Housing Area
4. Park Housing Area
5. Office, Trade and Service Areas
6. Office, Trade and park Service Areas
7. Blue Open Space
8. Industrial and Warehousing Areas.

Based on those theories and conditions, the study questions are to determine the pattern of changes in land use and utilization (spatial and temporal) in 2008 and 2018, the amount of spatial use non conformity in North Jakarta Administrative City with the DKI Jakarta Regional Spatial Planning (RTRW), to know the implications of spatial use non conformity and approaches to overcome it.

## METHODOLOGY

This study uses a mix-method approach with a stepwise method, namely map analysis, quantitative and qualitative descriptive analysis by conducting in-depth interview with key informant. Changes in land use in the North Jakarta Administrative City area were obtained by analyzing digital maps by overlaying 2008 land use map and 2018 land use map as the secondary data from local government agencies. The results of the overlay produced a map of land use changes at the specified year spacing.

Then to obtain the amount of land use non conformity, it was obtained by classifying the forms of land use or classifications of space allocation on the RTRW which were determined based on the classification standards of the themes listed in the 2011-2030 RTRW Jakarta Spatial Pattern Map. The map used was a comparison of Detailed Spatial Planning map with land use map in 2018.

The amount of space utilization and the non conformity to spatial planning were obtained from visual interpretation using Geographic Information Systems (GIS). Geographic Information System (GIS) is a computer-based system of work that has the ability to enter, manage, analyze and reactivate data that have spatial references for various purposes related to mapping and planning. The final result (output) in the form of geographical display is very useful for decision making [9]

## Land Use Conformity

As a benchmark for conducting an overlay analysis, the matrix was first set as a tool for the land use conformity assessment. The matrix in this study was used to compare two factors, in which the column section was the Spatial Planning zoning and the row section was the classification of land use. The column and row show the strength of the relationship between items or non-linear relationship.

The 2018 land use conformity matrix for Detailed Spatial Planning in North Jakarta City can be seen in table 2. Matrix analysis referred to the approach adapted to Minister of Public Works Regulation No. 20 of 2011 concerning Guidelines for Preparation of Detailed Spatial Planning and District/City Zoning Regulation [10]. The author limited the determination that did not refer to zoning regulation where activities were conditional and limited to the ITBX table Regional Regulation No.1 of 2014 concerning Detailed Spatial Planning and Zoning Regulation in DKI Jakarta Province [11] however the determination of land use conformity was close to that.

Especially for reclamation islands in this study were included in the classification of other land allocation with a study matrix in the form of "plans that have not been approved". This is because the reclamation islands do not yet have zoning and regulations that are set as the legal basis in the management of coastal areas and small islands located in Jakarta Bay (Regional Regulation on the Management Zoning of Small Coastal Areas and Islands (RZWP3K)).

In calculating the conformity amount, this study used the Minister of Agrarian and Spatial Planning (ATR)/Head of National Land Agency (BPN) Regulation No. 6 of 2017 concerning Procedures for Reviewing the Regional Spatial Planning to calculate the percentage of the area of each planned area [12].

$$\frac{A}{X} \mathbf{x} 100\% = a\% \quad (1)$$

a = Land Use Conformity Value

A = Existing Physical Shape

V = Area According to Spatial Plan

## RESULTS AND DISCUSSION

### Changes in Land Use in 2008 and 2018

Based on the analysis of changes in land use, Figure 1 shows the land use patterns in 2008 and Figure 2 shows the land use patterns in 2018 in North Jakarta City. Spatially, subdistricts that have access to or directly adjacent to ports and infrastructure in the form of accessibility to activity centers and adequate road networks had a high level of change.

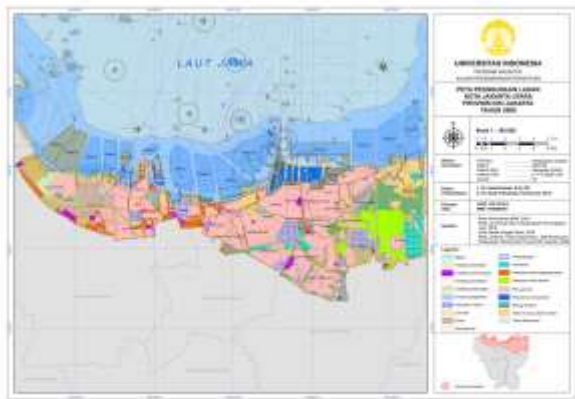


Fig.1 Map of Land Use in North Jakarta Administrative City in 2008.

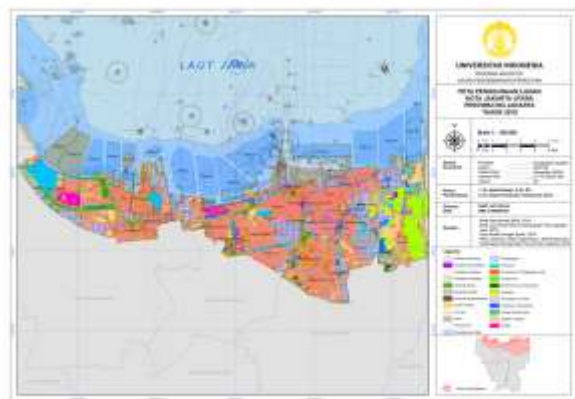


Fig. 2 Map of Land Use in North Jakarta Administrative City in 2018.



Table 1 land Use in North Jakarta Administrative City in 2008 and 2018

| Subdistrict Region | Land Use (in hectare)       |        |                    |        |                            |        |                           |        |   |        |        |        |
|--------------------|-----------------------------|--------|--------------------|--------|----------------------------|--------|---------------------------|--------|---|--------|--------|--------|
|                    | Facility and Infrastructure |        | Occupation/Housing |        | Industrial and Warehousing |        | Office, Trade and Service |        | Open Space, Cemetery, Plantation, Agriculture, and Empty Land |        | Others |        |
|                    | 2008                        | 2018   | 2008               | 2018   | 2008                       | 2018   | 2008                      | 2018   | 2008  | 2018   | 2008   | 2018   |
| Penjaringan        | 132.18                      | 140.77 | 1497.5             | 993.8  | 173.28                     | 463.74 | 252.84                    | 177.11 | 420.18  | 591.94 | 435.49 | 584.51 |
| Pademangan         | 105.34                      | 137.44 | 532.17             | 300.24 | 136.18                     | 149.44 | 150.3                     | 110.65 | 138.12  | 177.82 | 11.097 | 150.3  |
| Tanjung Priok      | 186.08                      | 131.87 | 1327               | 871.11 | 282.26                     | 518.69 | 17.129                    | 154.41 | 98.309  | 169.97 | 111.25 | 83.637 |
| Koja               | 152.99                      | 117.95 | 723.83             | 533.59 | 75.397                     | 215.09 | 21.688                    | 67.257 | 67.759  | 90.127 | 4.356  | 24.856 |
| Kelapa Gading      | 134.73                      | 132.43 | 843.99             | 646.35 | 203.58                     | 144.71 | 9.7427                    | 171.87 | 122.91  | 225.77 | 129.01 | 21.858 |
| Cilincing          | 37.052                      | 344.37 | 784.09             | 876.21 | 474.04                     | 956.29 | 9.2821                    | 54.328 | 1814.3  | 1365.1 | 581.55 | 175.44 |
| Total              | 748.37                      | 1004.8 | 5708.6             | 4221.3 | 1344.7                     | 2448   | 460.99                    | 735.62 | 2661.6  | 2620.7 | 1272.8 | 1040.6 |
| (%)                | 6.13                        | 8.32   | 46.80              | 34.97  | 11.02                      | 20.28  | 3.78                      | 6.09   | 21.82   | 21.71  | 10.43  | 8.62   |

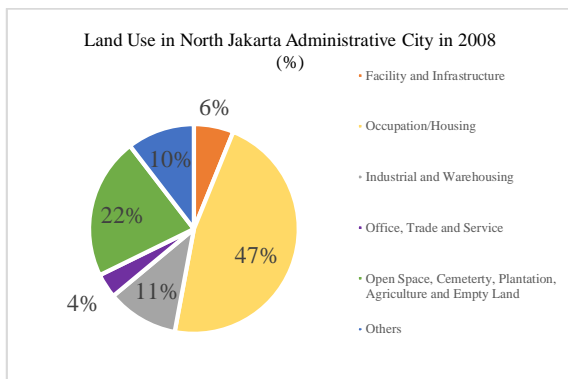


Fig. 3 Land Use in North Jakarta Administrative City in 2008.

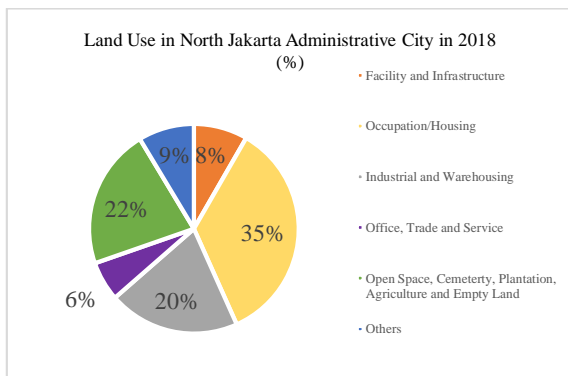


Fig. 4 Land Use in North Jakarta Administrative City in 2018.

The results of the analysis showed that the use of residential land experienced a significant decline in the period of 2008 to 2018. This is in accordance with cases of land use in urban areas, where housing is currently directed as vertical housing. In accordance with the DKI Jakarta Spatial Planning which states that to achieve good density condition for Jakarta can

be done through increasing land carrying capacity and intensifying land use through vertical development.

As a coastal area and to facilitate the need for space, plans to develop industrial estates and warehouses are indeed part of the Spatial Pattern Plan in North Jakarta City. In addition, in the spatial pattern plan referred to in the cultivation area plan, a plan to develop industrial estates and warehouses was established to support the activities of Tanjung Priok Port. This can be seen from the increased use of space in the form of processing industries and warehousing services. Based on the results of the analysis, there was an increase of 9.26% (from 11.02% to 20.28%) for industrial and warehousing use.

### Impact and Carrying Capacity of the Environment on Land Use in North Jakarta

Changes in land use influenced spatial patterns and also had environmental impacts. The occurrence of changes in land use either due to spatial plans or unmet environmental requirements can have a negative impact on land quality. Things that might occur include decreased capacity of ground water, reduced water absorption (infiltration) so that surface run off may increase and impacts on erosion and sedimentation and increases flood potential.

The classic problems faced by North Jakarta City are flood and tidal flood. Artificial landscapes through the Regional Spatial Planning from year to year have changed the ability of land to infiltrate. As a downstream part of the 13 (thirteen) rivers, North Jakarta City is the estuary where the rivers flow. The flood in North Jakarta is also caused by the increase in sea level, so that water cannot be directly flowed into the sea, especially in the north coast area of DKI Jakarta. With land surface lower than sea level, the number of buildings that continue to grow and the loss of coastal areas make this region vulnerable to submergence. Flood is also related to land subsidence

and spring tide due to development in coastal areas and groundwater extraction. Flood phenomena related to this cause are clearly seen in North Jakarta such as Pademangan, Muara Baru, part of Gunung Sahari in the north and Tanjung Priok. Often the flood that occurs in this area is not directly related to the high intensity of rainfall.

Referring to the City Master Plan of 1965-1985 in land use planning, North Jakarta was not planned as an 'available land' area because the topography is not

possible. Environmental engineering through efforts to prevent flood and tidal flood in North Jakarta has been carried out by the Regional Government, including through the normalization of river water flow, making *sodetan*, boundary embankments, sheet pile installation and so on. But the threat still exists, considering that the North Jakarta area is basically a basin area. The delay in the construction of polders and reservoirs, the development of residential areas around the watershed (DAS) and the lack on the use

Table 2 Analysis Matrix of Land Use Conformity with the Regional Spatial Planning of North Jakarta City

| Detailed Spatial Planning (RDTR)    | Mixed Zone | Recreational Zone | Industrial and Warehousing Zone | Road Zone | Green Zone | Protected Zone | Public Service and Social Zone | Regional Government Zone | National Government Zone | Office, Trade and Service Zone | Office, Trade and Service Zone Low Building Basic Coefficient | Village Housing Zone | Housing Zone Low Building Basic Coefficient | Housing Zone Moderate-High Building Basic Coefficient | Vertical Housing Zone | Vertical Housing Zone Low Building Basic Coefficient | Cemetery Zone | Reclamation Zone | City Park Zone Environment | Blue Open Zone |
|-------------------------------------|------------|-------------------|---------------------------------|-----------|------------|----------------|--------------------------------|--------------------------|--------------------------|--------------------------------|---|----------------------|---|---|-----------------------|--|---------------|------------------|----------------------------|----------------|
| <b>Facility and Infrastructure</b>  |            |                   |                                 |           |            |                |                                |                          |                          |                                |   |                      |   |   |                       |  |               |                  |                            |                |
| 1. Health Facility                  | M          | TS                | TS                              | TS        | TS         | TS             | S                              | S                        | S                        | S                              | S   | M                    | M   | M   | M                     | M  | TS            | TS               | TS                         | TS             |
| 2. Government Facility              | S          | TS                | S                               | TS        | TS         | TS             | S                              | S                        | S                        | M                              | M   | TS                   | TS  | TS  | TS                    | TS   | TS            | TS               | TS                         | TS             |
| 3. Education Facility               | S          | TS                | TS                              | TS        | TS         | TS             | S                              | S                        | S                        | M                              | M   | M                    | M   | M   | M                     | M  | TS            | TS               | TS                         | TS             |
| 4. Religious Facility               | M          | TS                | M                               | TS        | TS         | TS             | S                              | M                        | M                        | M                              | M   | M                    | M   | M   | M                     | M  | TS            | TS               | TS                         | TS             |
| 5. Telecommunication Facility       | M          | TS                | M                               | TS        | TS         | TS             | S                              | M                        | M                        | M                              | M   | M                    | M   | M   | M                     | M  | TS            | TS               | TS                         | TS             |
| 6. Art and Culture Facility         | M          | TS                | TS                              | TS        | TS         | TS             | S                              | M                        | M                        | M                              | M   | M                    | M   | M   | M                     | M  | TS            | TS               | TS                         | TS             |
| 7. Market                           | M          | TS                | TS                              | TS        | TS         | TS             | S                              | S                        | S                        | S                              | S   | TS                   | TS  | TS  | TS                    | TS   | TS            | TS               | TS                         | TS             |
| 8. Public Service                   | M          | TS                | M                               | TS        | TS         | TS             | S                              | M                        | M                        | M                              | M   | M                    | M   | M   | M                     | M  | TS            | TS               | TS                         | TS             |
| 9. Study and Research               | M          | TS                | TS                              | TS        | TS         | TS             | S                              | M                        | M                        | M                              | M   | TS                   | TS  | TS  | TS                    | TS   | TS            | TS               | TS                         | TS             |
| <b>Residential/Housing</b>          |            |                   |                                 |           |            |                |                                |                          |                          |                                |   |                      |   |   |                       |  |               |                  |                            |                |
| 1. Residential, Housing, Settlement | S          | TS                | TS                              | TS        | TS         | TS             | M                              | TS                       | TS                       | M                              | M   | S                    | S   | S   | S                     | S  | TS            | TS               | TS                         | TS             |
| <b>Industrial and Warehousing</b>   |            |                   |                                 |           |            |                |                                |                          |                          |                                |   |                      |   |   |                       |  |               |                  |                            |                |
| 1. Industrial                       | TS         | TS                | S                               | TS        | TS         | TS             | TS                             | TS                       | TS                       | M                              | M   | TS                   | TS  | TS  | TS                    | TS   | TS            | TS               | TS                         | TS             |
| 2. Warehousing                      | TS         | TS                | S                               | TS        | TS         | TS             | TS                             | TS                       | TS                       | M                              | M   | TS                   | TS  | TS  | TS                    | TS   | TS            | TS               | TS                         | TS             |
| <b>Office, Trade and Service</b>    |            |                   |                                 |           |            |                |                                |                          |                          |                                |   |                      |   |   |                       |  |               |                  |                            |                |
| 1. Office, Trade and Service        | S          | TS                | M                               | TS        | TS         | TS             | TS                             | TS                       | TS                       | S                              | S   | TS                   | TS  | TS  | TS                    | TS   | TS            | TS               | TS                         | TS             |
| <b>Open Space</b>                   |            |                   |                                 |           |            |                |                                |                          |                          |                                |   |                      |   |   |                       |  |               |                  |                            |                |
| Forest Area                         | M          | S                 | M                               | TS        | S          | S              | M                              | M                        | M                        | M                              | M   | M                    | M   | M   | M                     | M  | M             | TS               | S                          | TS             |
| 1. Empty Land                       | M          | M                 | TS                              | TS        | M          | M              | M                              | M                        | M                        | M                              | M   | M                    | M   | M   | M                     | M  | M             | TS               | S                          | TS             |
| 2. Cemetery                         | TS         | TS                | TS                              | TS        | TS         | TS             | TS                             | TS                       | TS                       | TS                             | TS  | TS                   | TS  | TS  | TS                    | TS   | TS            | TS               | M                          | TS             |
| 3. Plantation                       | TS         | M                 | TS                              | TS        | TS         | TS             | TS                             | TS                       | TS                       | TS                             | TS  | TS                   | TS  | TS  | TS                    | TS   | TS            | TS               | S                          | TS             |
| 4. Agriculture                      | TS         | TS                | TS                              | TS        | TS         | TS             | TS                             | TS                       | TS                       | TS                             | TS  | TS                   | TS  | TS  | TS                    | TS   | TS            | TS               | S                          | TS             |
| 5. Open Space                       | M          | S                 | M                               | TS        | S          | M              | M                              | M                        | M                        | M                              | M   | M                    | M   | M   | M                     | M  | M             | TS               | S                          | TS             |
| 6. Agricultural Field               | TS         | TS                | M                               | TS        | S          | M              | M                              | M                        | M                        | M                              | M   | M                    | M   | M   | M                     | M  | M             | TS               | S                          | TS             |
| <b>Other Allocation</b>             |            |                   |                                 |           |            |                |                                |                          |                          |                                |   |                      |   |   |                       |  |               |                  |                            |                |
| 1. Waters                           | TS         | TS                | TS                              | TS        | TS         | S              | TS                             | TS                       | TS                       | TS                             | TS  | TS                   | TS  | TS  | TS                    | TS   | TS            | TS               | M                          | S              |
| 2. Fishery                          | TS         | TS                | TS                              | TS        | TS         | TS             | TS                             | TS                       | TS                       | M                              | M   | TS                   | TS  | TS  | TS                    | TS   | TS            | TS               | TS                         | S              |
| 3. Defense and Security             | TS         | TS                | S                               | TS        | TS         | TS             | S                              | S                        | S                        | TS                             | TS  | TS                   | TS  | TS  | TS                    | TS   | TS            | TS               | TS                         | TS             |
| 4. Transportation                   | TS         | TS                | M                               | S         | TS         | TS             | S                              | TS                       | TS                       | TS                             | TS  | TS                   | TS  | TS  | TS                    | TS   | TS            | TS               | TS                         | TS             |
| 5. Tourism                          | TS         | S                 | TS                              | TS        | TS         | TS             | M                              | TS                       | TS                       | M                              | M   | TS                   | TS  | TS  | TS                    | TS   | TS            | TS               | S                          | TS             |
| 6. Others                           | TS         | TS                | TS                              | S         | S          | TS             | TS                             | TS                       | TS                       | TS                             | TS  | TS                   | TS  | TS  | TS                    | TS   | TS            | BS               | M                          | S              |
| <b>Information</b>                  |            |                   |                                 |           |            |                |                                |                          |                          |                                |   |                      |   |   |                       |  |               |                  |                            |                |
| S                                   | :          | Appropriate       |                                 |           |            |                |                                |                          |                          |                                |   |                      |   |   |                       |  |               |                  |                            |                |
| M                                   | :          | Supportive        |                                 |           |            |                |                                |                          |                          |                                |   |                      |   |   |                       |  |               |                  |                            |                |
| TS                                  | :          | Inappropriate     |                                 |           |            |                |                                |                          |                          |                                |   |                      |   |   |                       |  |               |                  |                            |                |
| BS                                  | :          | Not Approved      |                                 |           |            |                |                                |                          |                          |                                |   |                      |   |   |                       |  |               |                  |                            |                |

of land as a green open space (RTH), still make this area vulnerable to floods.

## Land Use Non Conformity in North Jakarta City

Inconsistencies between spatial planning and the use can be identified from existing activity and existing land use. The consistency assessment process was carried out by qualitative analysis of the conformity between spatial planning and spatial use identified with existing land use data. The Regional Spatial Planning was considered consistent if there was conformity between the two.

From the results of the overlapping analysis using 2018 land use map with spatial planning, it can be seen that there were 'inappropriate' land use with 'supportive' land use to the North Jakarta Administrative City plan. In conducting the analysis, the authors calculated the appropriate, not appropriate and supportive land area. Conformity between the types of land use for the functions planned in the Spatial Planning in the North Jakarta Administrative City was based on four criteria as follows:

1. **Appropriate (S)**, if land use has been fully was in accordance with regional functions in the Detailed Spatial Planning (RDTR).
2. **Inappropriate (TS)**, if land use was not in

accordance with regional functions in the Detailed Spatial Planning (RDTR).

3. **Supportive (M)**, if land use was not in accordance with regional functions but its existence could be maintained or adjusted as long as it did not interfere and could contribute to the realization of regional functions as stipulated in the Detailed Spatial Planning (RDTR).
4. **Not Approved Yet (BS)**, if the land allocation conditions had not been established or had not been approved in the Detailed Spatial Planning (RDTR).

The results of the conformity overlay between spatial pattern plan contained in the Regional Spatial Planning and Detailed Spatial Planning with the Land Use Map in 2018 can be seen in Figure 6 for the entire North Jakarta City and Figure 7 shows the results based on Subdistrict. The Conformity map is presented in Figure 5.

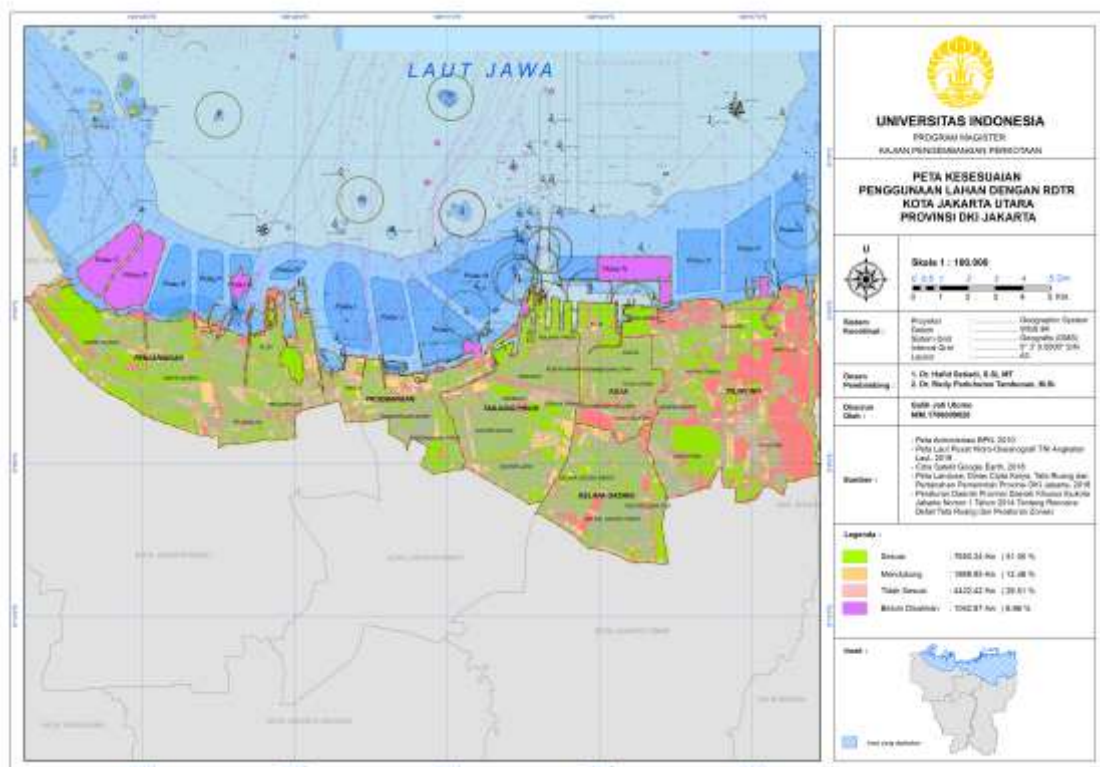


Fig. 5 Map of Land Use Conformity in 2018 with North Jakarta City Detailed Spatial Planning, North Jakarta City

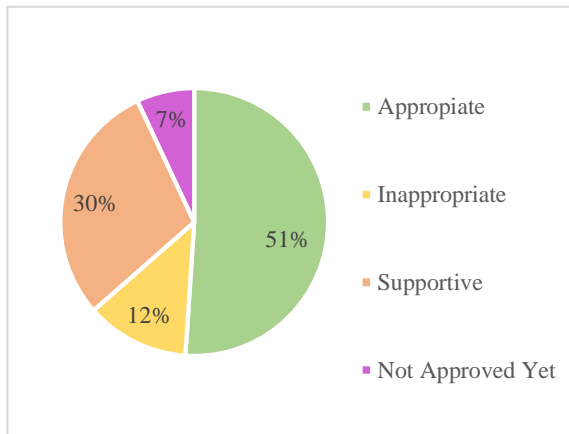


Fig. 6 Percentage of Land Use Conformity in 2018 with North Jakarta City Detailed Spatial Planning

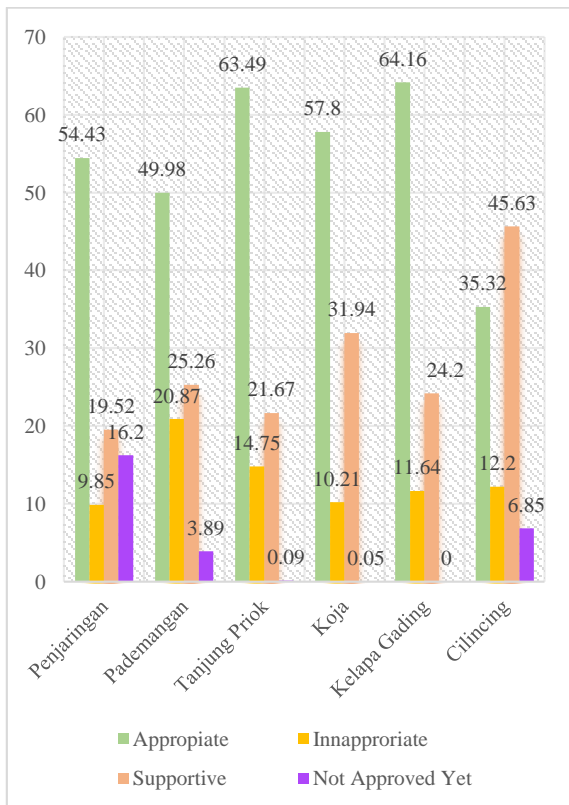


Fig. 7 Percentage of Land Use Conformity in 2018 with North Jakarta City Detailed Spatial Planning Based on Subdistrict

Table 3 Amount of Land Use in 2018 Based on North Jakarta City Detailed Spatial Planning with the Category of Appropriate

| Subdistrict | Appropriate    |            |
|-------------|----------------|------------|
|             | Area (hectare) | Percentage |
| Penjaringan | 2303.32        | 54.43      |
| Pademangan  | 666.40         | 49.98      |

|               |                |              |
|---------------|----------------|--------------|
| Tanjung Priok | 1423.24        | 63.49        |
| Koja          | 661.04         | 57.80        |
| Kelapa Gading | 1033.90        | 64.16        |
| Cilincing     | 1562.34        | 35.32        |
| <b>Total</b>  | <b>7650.24</b> | <b>51.05</b> |

Table 4 Amount of Land Use in 2018 Based on North Jakarta City Detailed Spatial Planning with the Supportive Category

| Subdistrict   | Supportive     |              |
|---------------|----------------|--------------|
|               | Area (hectare) | Percentage   |
| Penjaringan   | 416.77         | 9.85         |
| Pademangan    | 278.25         | 20.87        |
| Tanjung Priok | 330.60         | 14.75        |
| Koja          | 116.77         | 10.21        |
| Kelapa Gading | 187.57         | 11.64        |
| Cilincing     | 539.89         | 12.20        |
| <b>Total</b>  | <b>1869.85</b> | <b>12.48</b> |

Table 5 Amount of Land Use in 2018 Based on North Jakarta City Detailed Spatial Planning with the Category of Inappropriate

| Subdistrict   | Inappropriate  |              |
|---------------|----------------|--------------|
|               | Area (hectare) | Percentage   |
| Penjaringan   | 826.04         | 19.52        |
| Pademangan    | 336.86         | 25.26        |
| Tanjung Priok | 485.73         | 21.67        |
| Koja          | 365.20         | 31.94        |
| Kelapa Gading | 389.91         | 24.20        |
| Cilincing     | 2118.68        | 45.63        |
| <b>Total</b>  | <b>4422.42</b> | <b>29.51</b> |

Table 6 Amount of Land Use in 2018 Based on North Jakarta City Detailed Spatial Planning with the Category of The Plan Had Not Approved Yet

| Subdistrict   | The Plan Had Not Approved Yet |             |
|---------------|-------------------------------|-------------|
|               | Area (hectare)                | Percentage  |
| Penjaringan   | 685.28                        | 16.20       |
| Pademangan    | 51.88                         | 3.89        |
| Tanjung Priok | 2.12                          | 0.09        |
| Koja          | 0.57                          | 0.05        |
| Kelapa Gading | 0.00                          | 0.00        |
| Cilincing     | 303.02                        | 6.85        |
| <b>Total</b>  | <b>1042.87</b>                | <b>6.96</b> |

The percentage of conformity between spatial pattern plan contained in the Regional Spatial Planning and Detailed Spatial Planning with land use in 2018 can be seen in Figure 6 while the conformity

map is presented in Figure 5 as the result of overlaying the two. Based on figure 5, 6, and 7 it was known that 7650.24 ha of land use in 2018 or 51.05% of the total area of North Jakarta City were appropriate based on the Spatial Pattern Plan. Whereas 1869.85 ha (12.48%) were Supportive Spatial Pattern Plan, 4422.42 ha (29.51%) were not appropriate and 1042.87 ha (6.96%) of the plans had not yet been approved yet. The region with the highest conformity value was Kelapa Gading District of 64.16% and the lowest was Cilincing District of 35.32%.

Then based on the Minister of Agrarian Affairs and Spatial Planning (ATR)/Head of National Land Agency (BPN) No. 6 of 2017 concerning Procedures for Reviewing Regional Spatial Planning, calculation of utilization conformity (space pattern) could be taken as follows:

$$\frac{7650,24 \text{ hectare}}{14985,38 \text{ hectare}} \times 100\% = 51,05 \% \quad (1)$$

With a conformity value of 51.05% and viewed from the aspect of realization of the type and amount of spatial utilization implementation, North Jakarta City could be said to had a moderate category. This was due to the realization value of the space utilization implementation was between 51.05% up to 62.53% if the support category was also included in the calculation value.

### Factors That Affected Land Use Non Conformity

According to Lee [13] in Yunus [14], there were 6 (six) determinant factors that could influence changes in land use, including: (1) facilities and public utilities factors; (2) accessibility factor; (3) fiscal characteristic factor; (4) characteristics of landowners and land ownership pattern; (5) spatial regulation factor; and (6) initiative of the developer factor.

Whereas according to Kikuchi [15], the factors that influenced changes in land use could be divided into 2 (two) factors, namely direct and indirect factors. Direct factors consisted of population, economic activities, regional policies, physical resources and social systems. Meanwhile, indirect factors consisted of innovation in technology, value systems, lifestyle and national policies. Broadly speaking, deviations were also influenced by 3 (three) actors, including (1) the community; (2) government; and (3) market or private power. These three factors did not stand alone, but affected each other.

Based on the result of interview conducted with key informant namely the Head of Cipta Karya Office, Spatial Planning and Land Administration of North Jakarta City and field observations, the factors that

allegedly influenced the occurrence of land use non conformity in North Jakarta City included:

1. Land/Space Ownership System  
Regarding land planning, the government plans to use land in legal individual or corporation ownership status. The Indonesian state does not adhere to state ownership of land or development right, but adheres to a property right system. This results in difficult planning and determination of spatial patterns. Land rights such as Property Rights Certificates (SHM) are the basis of the highest ownership rights in Indonesia.
2. Economic Benefits  
Changes in land use were caused by the high economic benefits of land in North Jakarta City. Urban development has led to an increase in economic activity, especially in service activities in the form of industry and warehousing. The need for spatial use related to houses and business places encouraged changes in the spatial use, whereas land has a limited nature. This encouraged land owners in North Jakarta to change the functions, open new land or to consume and utilize their land not in accordance with the applicable spatial planning regulations.
3. Neighborhood Unit  
The theory about Neighborhood Unit is one of the factors mentioned which could influence the changes in the use of land functions. This theory was first created by Clarence Arthur Perry in 1929. This idea was later adapted into ideal settlement planning along with the development or birth of new cities. Register [16] mentioned the concept of the Neighborhood Unit to bring up 'Integral Neighborhood Area', which was the integration of neighborhood areas regarding locations and functions. In the North Jakarta City area, the Neighborhood Unit factor influenced the occurrence of non compliance with the city plan due to the strategic value of the region which is currently dominated by types of business activities.

### Implications and Approaches in Resolving Problems as Directions for Preparation of New Spatial Planning and Evaluation

Coastal areas have a vulnerability to higher land change and development. The implication as a consequence of land use non conformity towards spatial planning may cause threats to the carrying capacity and sustainability of life in the future. Problems that arise as a result of the spatial utilization non conformity that coincide with the unavailability of environmental infrastructure in North Jakarta City resulted in the emergence of irregular housing, traffic congestion, natural vulnerabilities (floods), damage to environmental quality, reduced public space and inability to implement government development

programs and so on.

For this reason, an evaluation of the spatial planning is needed by conducting a review in the Regional Spatial Planning document. This is done on the location of existing land that are still possible to be corrected and in accordance with applicable regulations. The approach in future planning is that utilization and management of space must be harmonious in order to support the development process. For this reason, every planning must refer to the nature of sustainable development with an eco-region approach in accordance with the character of North Jakarta City which is a coastal area.

The direction for the preparation of spatial planning based on existing land use conditions and deviations by considering North Jakarta City as an urban area is to encourage the process of designing a spatial planning that is not top-down, but balanced with a bottom-up process (participatory planning process).

## CONCLUSIONS

Changes in land use utilization in the North Jakarta Administrative City occurred in several land uses. Land with increased utilization in North Jakarta between 2008 and 2018 were industrial and warehousing of 9.26%. Meanwhile, the land with the most decreased utilization was residential/housing of 11.83%. The increase in changes in land use is in accordance with the direction of the DKI Jakarta Spatial Plan, which states that the spatial pattern of North Jakarta City is to provide warehousing and industrial facilities to support trade activities and services to support the activities of Tanjung Priok Port

Compliance between existing land use in 2018 with Detailed Spatial Planning in North Jakarta Administrative City showed a value of 51.05% up to 62.53% which was included in support category. This figure was categorized in moderate level in the evaluation of spatial use conformity based on Minister of Agrarian Affairs and Spatial Planning (ATR)/Head of National Land Agency (BPN) No. 6 of 2017 concerning Procedures for Reviewing Regional Spatial Planning. Based on the results of interviews, the factor that allegedly influenced the occurrence of spatial use non conformity in North Jakarta City was economic (economic determinant).

The implications of land use non conformity in North Jakarta City included the emergence of irregular housing, traffic congestion, natural vulnerabilities such as floods, damage to environmental quality, reduced public space and inability to implement government development programs and so on. And approach to overcome these problems is by reviewing spatial plans, increasing the role of the government in monitoring and controlling spatial use, and making priority programs and areas

with a tight control system.

## ACKNOWLEDGMENTS

This study is part of the Master's Indexed International Publication STUDY (PITMA) of the University of Indonesia with the theme of "Practices of Planning and Conflict of Spatial Use in Urban Development".

## REFERENCES

- [1] Sugandhy, Aca. 1994. Operationalization of Spatial Planning and Development Trilogy. In the PRISMA Economic and Social Study Magazine, No. February 2, 1994.
- [2] Special Capital Region of Jakarta Province, 2012. Regional Regulation Number 1 of 2012 concerning Regional Spatial Planning in 2010-2030
- [3] Kivell, Philips. 1993. Land and The City: Pattern and Process of Urban Changes, London: Routledge
- [4] Republic of Indonesia, 2007. Law No. 26 of 2007 concerning Spatial Planning
- [5] Shirvani, Hamid. 1985. The Urban Design Process, New York: Van Nostrand Reinhold Company, Inc
- [6] Gallion, Arthur B and Simon Eisner. 1986. *The Urban Pattern: City Planning and Design*. New York: Van Nostrand.
- [7] Chapin, F.S and J. Kaiser. 1979. Urban Land Use Planning, Chicago : University of Chicago Press.
- [8] Sitorus, S. R. 1998. Evaluation of Land Resources. Third Edition. TARSITO Publisher Bandung.
- [9] Muta'ali, Lutfi. 2013. Regional and City Spatial Organization (Normative-Technical Review). Yogyakarta: Publisher Agency of Faculty of Geography (BPFG), Gajah Mada University
- [10] Republic of Indonesia, 2011. The Minister of Public Works Regulation No. 20/PRT/M/2011 concerning Guidelines for Preparation of Detailed Spatial Planning (RDTR) and District/City Zoning Regulation
- [11] Special Capital Region of Jakarta Province, 2014. Regional Regulation Number 1 of 2014 concerning Detailed Spatial Planning and Zoning Regulation
- [12] Republic of Indonesia, 2017. The Minister of Agrarian Affairs and Spatial Planning/Head of National Land Agency (BPN) Regulation No. 6 of 2017 concerning Procedures for Reviewing Regional Spatial Planning
- [13] Lee, L. 1979. Factors Affecting Land Use Change at the Rural Urban Fringe. Growth and Change : A journal of Regional Development. Vol. X, Oktober 1979.
- [14] Yunus, H.S. 2005. City Management; Spatial Perspective. Yogyakarta: Pustaka Pelajar.



- [15] Kikuchi, T. 1999. Analysis of LUCC And Forecast With Map Method: A Case of Beijing Metropolitan Area, China. Proceeding of 1999 NIES Workshop on Information Bases and Modelling for Land Use and Land Cover Change Studies in East Asia. Centre for Global Environment Research, Tokyo.
- [16] Register, Richard. 1987. Ecocity Berkeley: Building Cities for Healthy Future. North Atlantic Books, California.

# THE PATHWAY TO THE ORGANIZATION SUSTAINABILITY THROUGH THE LAND FOOTPRINT METHOD

Karin Kandananond

Faculty of Industrial Technology, Valaya Alongkorn Rajabhat University, Thailand

## ABSTRACT

Any supply chains depend on the land use in order to produce the output products or services since all activities of the supply chain occurs on the land. Since the availability of the land is a critical global problem, especially, in the developing countries. The capability to assess the actual amount of land used by an organization or to produce a product is important to understand how effective the organization has utilized the limited amount of land. This pilot study was conducted on the land use of an organization which provides the integrated services to the community. At the first phase, the service outcome of the organization is clearly defined. Afterwards, the land use of the organization is measured in order to determine the relationship between the amount of land use and the outcome. The latter phase is to create the roadmap leading to the sustainability of the land use for the organization.

*Keywords: hectare per student, Land footprint, Organization*

## INTRODUCTION

Ecological footprint is the consumption-based indicator which is used to quantify the amount of resources needed to produce a product. Another aspect is of the ecological footprint is the indicator on the impact of a product produced on the environment. The examples of the environmental footprints are water and Carbon footprint. Since land use is also important to the production, there is another indicator which was applied to quantify the amount of land which was used by an organization or to produce a product. University is an organization which is in charge of educating the tertiary-level students including undergraduate and graduate students. The land is needed by a University in order to carry out the activities regarding the education of students. As a result, if the amount of real land is correctly quantified, it will be used to indicate the effect of the organizational operation on the environment.

## LITERATURE REVIEW

Weinzettel et al. [1] Studied the use of land and ocean area through the whole process of supply chain from the production to the final consumption. The focusing area is the production of agriculture products, food, and forestry products. For the institutional footprint, Klein-Banai and Theis [2] conducted the ecological footprint analysis for a public University with many campuses. The footprint was calculated in the unit of global hectares per total faculty, staff, and students. Bruckner et al. [3] investigated the evaluation of the model for calculating land footprints of the supply chains and studied the contribution of the footprint on the environment. For the agricultural

section, Ruiter et al. [4] studied the agricultural land footprint of the United Kingdom (UK), and the results showed that the meat and dairy production mainly contributed to the large amount of footprint. Ferng [5] utilized the land multiplier to estimate the land footprint based on the production activities.

## METHODOLOGY

The land footprint is the measurement standard of biologically productive land where an individual uses. Therefore, the method used in this study is based on the global hectare (gha) which is a unit for measuring the biological production for human use (biocapacity) per hectare of land. The standard hectare is equivalent to 10,000 square metres. Biocapacity (BC) is the amount of land, and it is weighted by the productivity of the land. The biocapacity is calculated by:

$$BC = YF * EQF * A$$

,where BC is the biocapacity,

YF is the yield factors,

EQF is the equivalence factors, and

A is the amount of available area or land.

The concept of biocapacity depends on the amount of equivalent amount of land area used for five different categories:

- Cropland
- Fisheries
- Forestry
- Grazing ground
- Built-up land.

The measuring unit is hectare per unit per year.

## ORGANIZATION AREA

The study on land footprint of an organization was conducted on a public University, Valaya Alongkorn Rajabhat University, Thailand. The University offers several degrees in both undergraduate and graduate levels. The main campus is located in Prathumthani province (Fig. 1). The aerial view of the University campus is shown in Fig. 2 and 3 respectively.



Fig. 1 University campus



Fig. 2 Satellite map of the campus



Fig. 3 Campus map

## Overall area

The land area of the University campus is divided into many zones, namely education, residential, sport, commercial, self-learning center, recreation area, and agricultural demonstration. Each area with the amount of land is listed in the following table 1.

Table 1 Land for each zone

| Zone                 | Amount of land (rai) |
|----------------------|----------------------|
| Education            | 140                  |
| Residential          | 40                   |
| Commercial           | 62                   |
| Self-learning center | 18                   |
| Sport                | 50                   |
| Recreation           | 66                   |
| Agricultural         | 5                    |

The total area is 381 rai or 60.96 hectare. The amount of land in each zone is represented in a pie-chart (Fig. 4).

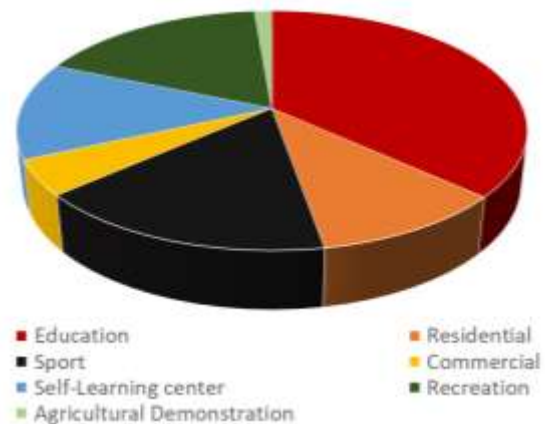


Fig. 4 Amount of land in each zone

## Number of students

The number of undergraduate and graduate students from academic year 2014-2019 is shown in Table 2.

Table 2 Number of students

| Academic year | Number of students |
|---------------|--------------------|
| 2014          | 11,734             |
| 2015          | 11,144             |
| 2016          | 10,970             |
| 2017          | 10,365             |
| 2018          | 10,412             |
| 2019          | 10,313             |

### Agriculture area

Since the University has the agricultural demonstration farm and the crops mainly grown are rice and banana, the biocapacity of these two crops are calculated.



Fig. 5 Agricultural area

#### Rice

Since the approximate amount of land used to grow paddy rice is 1 rai or 0.16 hectare, and the rice yield is 980 kg or 0.98 ton. The rice was grown and harvested in a yearly basis. As a result, the biocapacity of the paddy rice is 6.125 ton per hectare per year.



Fig.6 Paddy rice field

#### Banana

Another crop grow on the campus is banana (Namwa), and the crop yield is while the land is 1 rai. The number of banana trees grown is about 100, and the average yield per tree is 20 kg. Therefore, the biocapacity of banana is about 12.5 ton per hectare per year.



Fig. 7 Banana plantation area

### RESULTS

Since all the land is fully utilized to accomplish the University mission, the yield factor and equivalent factor were set at 1. Therefore, the global hectare from academic year 2013 to 2018 is shown in the following table 3.

Table 3 Hectare per student

| Academic year | hectare per student |
|---------------|---------------------|
| 2013          | 192.49              |
| 2014          | 182.81              |
| 2015          | 179.95              |
| 2016          | 170.03              |
| 2017          | 170.80              |
| 2018          | 169.18              |

According to table 3, the hectare per student gradually decreases. The simple reason is that the amount of productive land remains constant, but the number of students keep dropping from academic year 2013 to 2018.

For the agricultural farm, two crops, rice and banana, were grown, and the biocapacity due to these crops were also calculated. The biocapacity of the paddy rice is 6.125 ton per hectare per year, while that of the banana is 12.5 ton per hectare per year

### CONCLUSIONS

It is interesting to note that the University has several duties, so different areas of the campus were also utilized to fulfil the goal of University. As a result, the whole area of land is fully utilized. The results indicate that the hectare gradually decreases every year, since the number of students slightly drop.

Therefore, it is difficult to increase the efficiency of land use in this aspect. Alternative option to the sustainability through the land use is the agricultural area in the University. Since there is the agricultural demonstration farm on the campus, it is possible to increase the biocapacity by increasing the yield per an area unit. This can be done by the productivity improvement in the farm.

## REFERENCES

- [1] Weinzettel J., Hertwich E.G., Peters G.P., Steen-Olsen K., and Galli A., Affluence drives the global displacement of land use, *Global Environmental Change*, Vol. 23, Issue 2, 2013, pp. 433-438.
- [2] Klein-Banai C, and Theis T.L., An urban university's ecological footprint and the effect of climate change, *Ecological Indicators*, Vol. 11, Issue 3, 2011, pp. 857-860.
- [3] Bruckner M., Fischer G., and Giljun S., Measuring telecouplings in the global land system: a review and comparative evaluation of land footprint accounting methods, *Ecological Economics*, Vol. 114, 2015, pp. 11-21.
- [4] De Ruiter H., Macdiarmid J.I., Mathew R.B., Kastner T., Lynd L.R., and Smith P., Total global agricultural land footprint associated with UK food supply 1986–2011, *Global Environmental Change*, Vol. 43, 2017, pp. 72-81.
- [5] Ferng J.-J., Using composition of land multiplier to estimate ecological footprints associated with production activity, *Ecological Economics*, Vol. 37, Issue 2, 2001, pp. 159-172.

## DESIGN AND ASSESSMENT OF A BATTERY OPERATED ROTARY TYPE LOW COST WEEDER FOR NON-CHEMICAL UP-LAND CROP MANAGEMENT

Mohammad Ashrafuzzaman Gulandaz<sup>1</sup>, Dr. Md. Israil Hossain<sup>2</sup>, Dr. Md. Ayub Hossain<sup>3</sup>  
<sup>1,2&</sup>Bangladesh Agricultural Research Institute

### ABSTRACT

The overall goal of this experiment was to reduce the production cost and drudgery of labor in weeding purpose and use of renewable energy for upland crop production. Adverse effects on environment and cost of chemical weeding are making farmers to consider mechanical methods of weed control. Manual weeding is common practices in Bangladesh but it is labor intensive. The mechanical weeder is to reduce drudgery and cost which ensure a comfortable posture of the farmer during weeding. Weeder is designed and fabricated considering methodological steps. For performance evaluation of weeder, field trials are done among battery operated weeder, BARI push and pull weeder and manual weeding. The performance of battery operated weeder is quite acceptable for wide row crop. We made fields trial on maize at different locations of Bangladesh such as Breeding and Irrigation field of Bangladesh Agricultural Research Institute and Bogra sadar upazila, Debiganj upazila. Weeding index of battery operated weeder for maize is 92.52 % which is very close to manual weeding. Again effective field capacity of weeder for maize is 0.046ha/hr and area coverage of weeder is 12 decimals per hr. Plant damage ratio is very few at low height and low canopy crop. A linear relationship is found between weed density and effective field efficiency. Cost of weeding by battery operated weeder is almost one third compare to BARI weeder and almost one fourth compare to manual weeding. But there is no significant difference in yield is found among these three methods.

*Keyword: Weeder, Battery Operated, Weed Management, Environment friendly, Cost effective*

### Introduction

A weed considers any plant growing in the wrong place at the wrong time and doing more harm than good [8]. Weeds are plant that competes with crops for water, nutrients and light. Crop production can be reduced significantly due to excessive weeds. Weeding and hoeing is generally done 15 to 20 days after sowing. The weed should be controlled and eliminated at their early stage. Depending upon the weed density, 20 to 30 percent loss in grain yield is quite usual which might increase up to 80 per cent if adequate crop management practice is not observed [7]. Weeds waste excessive proportions of farmers' time, thereby acting as a brake on development [5]. Weed control is one of the most difficult tasks in agriculture that accounts for a considerable share of the cost involved in agricultural production [6]. Farmers commonly expressed their concern for effective weed control measures to seize the growth and propagation of weeds.

Weeds pose major problem during warm and humid climate especially affecting Kharif crops. The high cost of weeding can be understood from a comparative study of the losses in the farm due to various causes. Under plant protection, weed control plays an important role for increasing the yield [10]. According to International Rice Research Institute (IRRI), the yield loss in

transplanted and direct seeded rice due to weeds alone was assessed as 34 percent and 45 percent respectively. The research result of Bangladesh Agricultural Research Institute (BARI) showed that weeds affect 80 percent for eggplant production, 43 percent for potato production, and 22 percent for Maize production. Reduction of yield goes more severe when a weed act as harbor of insects. The losses caused by weeds exceed the losses caused by any other category of agricultural pests.

The weeder is to reduce drudgery and ensure a comfortable posture of the farmer or operator during weeding and increase production [6]. Mechanical weeding also keeps the soil surface loose ensuring soil aeration and water intake capacity. Rotary operation will always produce the best result [12]. The Rotary weeder can be made to operate various working depths, widths and soil conditions [12]. The rotating blades chop and mix the residues evenly throughout the working depth, outperforming any other mechanism [3].

Chemical method of weed control i.e. Herbicide technologies can contribute to reduced production losses. However, through negative effects on crop, environment and human health, incorrect herbicide use may unintentionally counteract efforts to increase food security [11]. Excessive use of herbicides over a long time make leads herbicide resistant weeds. There are



some factors including shifting ability of weed population, increase in environmental concerns and increase in cost of management, all these factors made farmers difficult to control resistant weeds within their limited resources [1]. All these adverse effects are making farmers to consider and accept mechanical methods of weed control. Manual weeding is common in Bangladeshi agriculture. It is the most widely used weed control method but it is labor intensive. Agriculture labor is becoming scarce day by day in Bangladesh. The costs associated with mechanical weeding such as operating cost can be lowered; as such mechanical weeding can represent a viable and cost effective option to majority of medium and small scale farmers in developing countries like Bangladesh.

The main objective is to develop a battery operated rotary type weeder which can be used in different crops, plant spacing systems, various plant intra-row distances

## Materials and Methods:

### Assumptions:

The assumptions made in the design of the rotary weeder are presented in terms of field conditions, machine capacity and energy requirement required to power it. The machine is to be powered by a 48 volt 750-watt motor which is operated by 48-volt rechargeable dry cell battery. Belt and sprocket arrangement shall be employed for transmission of power. Motor speed is 700 rpm, Number of teeth on Sprocket = 15, Number of teeth on Sprocket of rotary shaft =  $15 \times 2 = 30$ , Rotary shaft speed = 350 rpm, maximum soil resistance value =  $1.05 \text{ kgf/cm}^2$ , coefficient of friction = 0.1, efficiency of transmission system = 90%. Transmission of power is shown in figure-1.

and growth stages. The need for non-chemical weed control techniques has steadily increased in the last few years, as a consequence of the environmental pollution originated by the intensive application of pesticides in agriculture. Use of rechargeable dry cell battery is also ensuring the sustainable energy use in weeding purpose. The overall goal of the research is to evaluate the performance of a DC motor operated rotary type weeder intended for fossil fuel operated mechanical weeding in upland crop production. The specific objective of this weeder is to remove weeds by using battery power rather than manual operated weeder to reduce time, save money and increase work effort of labor. Therefore, this research was undertaken with the following objectives:

- To design and develop of a DC motor operated dry land weeder.
- To test and evaluate performances of weeder by adaptive trail.

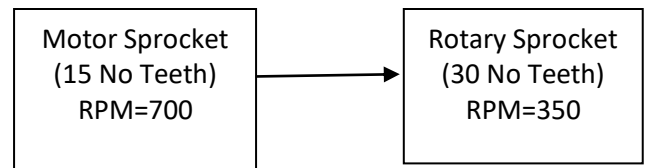


Figure-1: Power transmission system

### Design Process:

In the design process, calculation of power requirement, motor selection, chain and sprocket selection and design and arrangement of tines are needed to be considered. There is no power in the wheel; so, weeder should be pushed manually but continuous pushing of tines makes weeder to go forward easily. The power supply on rotary shaft should be taken into consideration. There are two parts of the weeder, one is body and another is handle. Body part consists of motor, battery, wheel and rotary shaft but handle consists of auto switch and converter. Figure-2 represents the drawing of weeder with dimension. And figure-3 represents the 3D drawing of weeder.

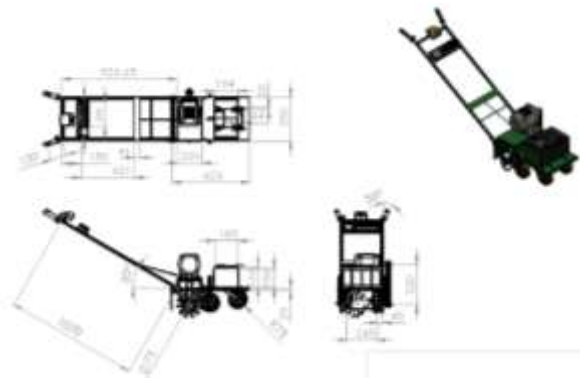


Figure.2: Battery operated dry land rotary weeder with dimension

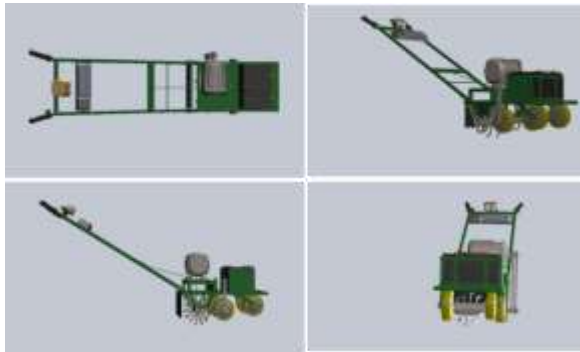


Figure.3: Top, isometric, side and front view Battery operated dry land rotary weeder

#### a. Power requirement:

The power requirement was calculated using the following equations [4]:

$$P_d = \frac{S_r \times d \times w \times v}{75} (h_p) \text{ ----- (1)}$$

Where,

$S_r$  = soil resistance, kgf/cm<sup>2</sup>;

$d$  = depth of cut = 2.5 cm;

$w$  = effective width of cut = 26 cm;

$v$  = linear velocity of the tine at the point of contact with the soil = 1 cm;

Hence, power requirement is estimated as

$$P_d = \frac{S_r \times d \times w \times v}{75} = \frac{1.05 \times 2.5 \times 26 \times 1}{75} = 0.91$$

**Total power required:**

The total power required is estimated as 1.89 hp as follows

$$P_t = \frac{P_d}{\eta} = 1.01 = 1 \text{ hp}$$

Where,

$P_d$  = Power required to dig the soil

$\eta$  = Transmission efficiency (0.90).

Thus, a prime mover of 1.0 hp was required for this weeder.

#### b. Chain and sprocket selection:

Chain and sprocket arrangement was adopted for transmission of power. The chain, sprocket and shaft selection was based on Agricultural Machinery Management Data. The size of chain is 60B and number of teeth of sprocket is 14. Chain and sprocket and shaft is shown in figure-4.



Figure.4: Chain and sprocket for dry land power weeder

#### c. Weeding Tines and Tines arrangement:

A j-shaped tine is designed on the shaft which is shown in figure-4. Length and width of the tine is 80mm, curve angle of tine is 120° and 18mm respectively (Fig.5). Dimension of the shaft is 245 mm and 73 mm respectively. The shaft consists tines of equal lengths and arranged in spiral shaped determined as follows (Fig.6).

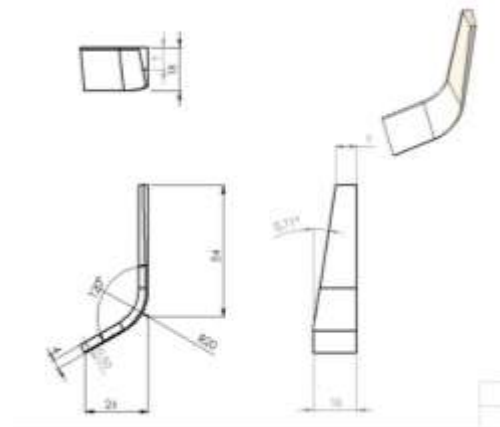


Figure.5: J-shaped tine for dry land power weeder

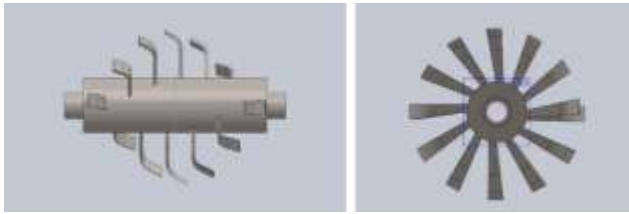


Figure.6: Spiral Arrangement of J-shaped tine for dry land power weeder

#### Machine Description:

The powers to the rotary hoe are supplied from the motor through chain and sprocket. The various components of the machine were constructed while other standard components, such as prime mover and transmission elements were sourced locally and the parts were assembled at the fabrication workshop of the Farm Machinery and Post-harvest Process Engineering Division, Bangladesh Agricultural Research Institute (BARI). The pictorial view of the rotary weeder was

Table.1. Specification of weeder

| Sl no | Items                        |         | Measurement                           |
|-------|------------------------------|---------|---------------------------------------|
| 1     | Power                        | Motor   | 1 hp (750watt)                        |
|       |                              | Battery | 48 volt Dry cell Rechargeable Battery |
| 2     | Dimension (with Rotary tine) |         | 1560 mm x 350 mm                      |
| 3     | Weeder Forward Speed         |         | 2 km/hr                               |
| 4     | Rated Motor Speed            |         | 700 rpm                               |
| 5     | Rated rotary Speed           |         | 350 rpm                               |
| 6     | Rotary                       | Length  | 245 mm                                |

#### Performance Test and evaluation:

##### a. Laboratory Test:

The laboratory test result is summarized in Table.2.

| Parameter                        | Average Value |
|----------------------------------|---------------|
| Rated motor Speed, rpm           | 700           |
| Rotary blade speed, rpm          | 350           |
| Theoretical field capacity, ha/h | 0.10          |

shown as Figures 7. The specification of weeder is shown in table-1.



Figure.7: Pictorial view of Battery operated dry land rotary weeder

|    |                   |                   |             |
|----|-------------------|-------------------|-------------|
|    | Shaft             | Diameter of Shaft | 73 mm       |
| 7  | Tine              | Number of Tine    | 14          |
|    |                   | Type of Tine      | J-shaped    |
|    |                   | Tine Arrangement  | Spiral      |
|    |                   | Width of tine     | 18 mm       |
|    |                   | Length of tine    | 75 mm       |
| 8  | Diameter of wheel |                   | 160mm       |
| 9  | Starting System   |                   | Auto switch |
| 10 | Net Weight        |                   | 27 kg       |

##### b. Site and experimental condition:

The experiment was conducted at Plant breeding research farm of Bangladesh Agricultural Research Institute (BARI), Irrigation and water management research farm of Bangladesh Agricultural Research Institute (BARI) Gazipur and Debiganj upazila under Panchagar district during kharif season 2017-18. The soil was clay loam and soil penetration was recorded before each treatment imposed. The experiment plot was well pulverized and leveled with a tractor.

### c. Crop and weeds

BARI Hybrid Maize 5 (BHM 5) was planted manually in the experimental plot (6 x 4 m each) with 60 cm row to row spacing. Each plot accommodated 6 rows. The planting date was 6 th December, 2017. Density of weed was recorded before and after treatment imposed. The weed sampling was done randomly in middle three rows in 1 x 1 m quadrants. Width of cut is 28 cm, so double pass is done to cover 60 cm width. Number of plant damage is recorded and weeds partially damaged but not up rooted were counted as uncontrolled. Inter row weeds were not removed by mechanical method but all weeds are removed by manual method. The common species of weeds were recorded. The following weeds are significantly present in the testing plots which are shown in table 3.

Table.3. Weeds available in the testing plot

| Local Name      | Specifications              | Comments                  |
|-----------------|-----------------------------|---------------------------|
| Chapra          | <i>Eleusine indica</i> L.   | First three were dominant |
| Durba           | <i>Cynodon dactylon</i> L.  |                           |
| Chapra          | <i>Elusine indica</i>       |                           |
| Mutha           | <i>Cyperus rotundus</i>     |                           |
| Helencha        | <i>Enhydra fluctuans</i> L. |                           |
| Paddy seedlings | <i>Oryza sativa</i>         |                           |

### d. Fertilizer, Irrigation and earthing up:

Fertilizer and irrigation was applied as BARI recommended dose. And earthing up is done manually at 45 days after sawing.

### e. Experimental Design:

The study included three treatments replicated four. The experiment was designed in Randomized Complete Block. The treatments were:

T<sub>1</sub> - Weeding by Battery Operated weeder at 25-45 DAS

T<sub>2</sub> - Weeding by BARI push and pull weeder at 25-45 DAS

T<sub>3</sub> - Manual Weeding at 25-45 DAS

### f. Test Procedure:

Performance indicators used for this experiment includes the following:

#### 1. Weeding Index

Weeding index is a ratio between the number of weeds removed by a weeder and the number present in a unit area and is expressed as a percentage [9].

Six plots of 6m x 4m each were marked out of the main plot for sampling. Weeds in each plot were counted before and after weeding using the constructed battery operated rotary weeder. The time taken to perform this operation was noted. Equation 1 was used to calculate weeding index.

$$\text{Weeding Index, } I_w = \frac{w_1 - w_2}{w_1} \times 100 \quad (1)$$

Where,

W1 = weeds before weeding

W2 = weeds after weeding

#### 2. Plant Damage:

Plant damage was observed in mechanical method and recorded. Plants damaged completely or uprooted were counted as 'damaged' and expressed as percent of each plot the plant damage percent was evaluated by using equation 2.

$$\text{Plant Damage percent, } \Sigma = \frac{w_1 - w_2}{w_1} \times 100 \quad (2)$$

Where,

W1 = number of Plant before weeding,

W2 = number of damaged plant after weeding,

Σ = Plant Damage percent

#### 3. Field Capacity

The weeding tools were tested on the same plots to determine the field capacity of each of them. Field capacity is the amount of area that a weeding tool can cover per unit time as shown in equation 3 (Hunt, 1983).

$$\text{Field Capacity (ha/h)} = \frac{60}{t} \times \frac{A}{10000} \quad (3)$$

Where,

A = Area covered (m<sup>2</sup>),

t = Time taken in hour

### Statistical Analysis

All statistical analyses in this experiment were carried out using statistical package "R 3.4.4" for Windows Version 2010. Analysis of variance (ANOVA), Coefficient of variance (CV) and least significant difference (LSD) between mean values were calculated at 5% significance level.

### Results and Discussion:

**Experimental Factors:**

Experimental factors used in the field evaluation of rotary power weeder were approximately same speed in three blocks. The weeding performance will compare with the BARI manual weeder and traditional weeding method. Weeding is only done in maize field.

The performance evaluations were done to investigate the effect of weed density on performance of three weeding methods such as battery operated weeder ( $T_1$ ), BARI push and pull weeder ( $T_2$ ), and manual weeding by spade ( $T_3$ ). Prior to each weeding schedule, weed density in each experimental unit was determined by laying-out a squared grid (1 m x 1 m) in the plot and weeds in the grid were counted. Four such determinations were made for each experimental unit.

Table. 4. Field performance of different weeding methods in maize fields

| Treatment              | Field capacity (ha/h) | Weeding index (%) | Time of weeding (hr/ha) | Plant damage ratio (%) | Yield of maize grain (t/ha) |
|------------------------|-----------------------|-------------------|-------------------------|------------------------|-----------------------------|
| $T_1$ (Battery weeder) | 0.04643 a             | 92.52 b           | 21.61 b                 | 0.50                   | 8.90                        |
| $T_2$ (BARI weeder)    | 0.01370 c             | 86.19 c           | 73.53 a                 | 0.75                   | 8.42                        |
| $T_3$ (Manual weeding) | 0.01413 c             | 93.48 b           | 70.84 a                 | 0.50                   | 8.42                        |
| CV                     | 3.8087                | 1.92              | 9.27                    | 37.82                  | 10.89                       |
| LSD                    | 0.0033                | 3.57              | 8.86                    | 0.33                   | 1.83                        |

damage of battery operated weeder (0.50%) and manual weeding (0.50%) is found insignificant but little plant damage was found for BARI push and pull weeder (0.75%). Time of weeding was found insignificant between battery weeder (21.61 hr/ha), however battery operated weeder was performed better compare to other practices. Also inconsequential relation was found between BARI push and pull weeder (73.53 hr/ha) and manual weeding (70.84 hr/ha). There were no significant differences in grain yields among the treatments. But battery operated weeder shown better performance among the treatments for weeding in maize field.

Field capacity and field efficiency of weeding in maize were 0.046 ha/h, 92% respectively for battery operated weeder but for BARI push and pull weeder were 0.021 ha/h, 47% respectively. Plant damage ratio was very low which less than 1% for battery operated weeder, Cutting width was 200 mm and depth of cut was 49.3 mm of battery operated weeder. Weeding cost per ha of battery operated weeder was (1843 tk/ha) lower than

that

Field capacity, weeding index, plant damage, time of weeding and grain yield in weeding by battery operated weeder, BARI push and pull weeder and Manual weeding by spade in maize fields and their coefficient of variance (CV) as well as least significant difference (LSD) values are shown in Table 4. Significantly the highest field capacity was found in battery operated weeder (0.04643 ha/h) followed but field capacity of BARI push and pull weeder and manual weeding are scored lowest. Almost similar weeding index was found between battery operated weeder and manual weeding method but the lowest weeding index was found for BARI push and pull weeder. These results indicated that more than 90% weeds were removed by battery operated weeder and manual weeding method and there was no significant difference between them. Plant

of BARI push and pull weeder (4818 tk/ha) and manual weeding (7500 tk/ha). Cost of battery weeder was found half compare to BARI push and pull weeding and one third compare to manual weeding. The performance data of battery weeder for maize is shown in Table 5.

Table 5. The performance of battery operated rotary type weeder for maize, compare to other weeding practices

| Items  | Battery weeder | BARI weeder | Manual weeding |
|--|----------------|-------------|----------------|
| Row to row distance (cm)                     | 60             | 60          | 60             |
| Number of turns per row                      | 3              | 4           | N/A            |
| Average Weeding depth (cm)                   | 4.93           | 1.5         | N/A            |
| Cutting width (mm)                           | 200            | 150         | 180            |
| Average Soil penetration, psi (10 cm height) | 94             | 94          | 94             |
| Forward speed (km/h)                         | 2.5            | 2           | 1.5            |
| Theoretical field capacity (ha/h)            | 0.050          | 0.030       | 0.027          |
| Field efficiency, (%)                        | 92.82          | 45.67       | 52.32          |
| Average Plant height (mm)                    | 153            | 145.67      | 146.67         |

A linear relationship is found between weed density and effective field efficiency which is shown in figure-7. Here, lower weed density indicates higher weeding efficiency

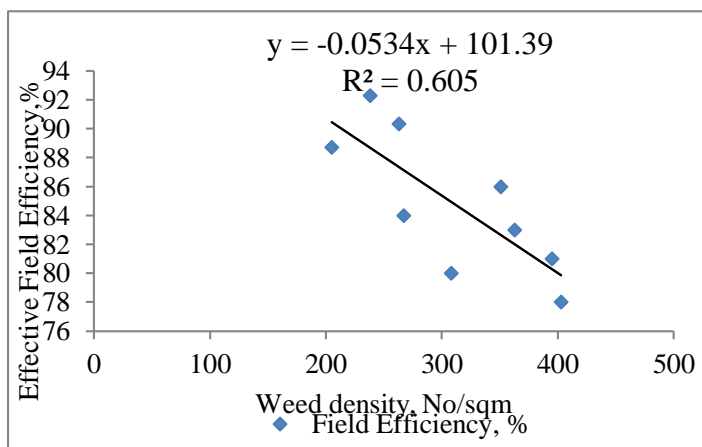


Figure.8. Relationship between weed density and effective field efficiency

### Economic analysis:

For economic analysis, we need to consider that weeder is used for business purpose that is rental farming. Table.8 illustrates the economic analysis of Battery operated weeder.

Table.8. Economic analysis of Battery operated weeder

|   | Battery Operated Weeder | BARI Push and Pull Weeder | Manual weeding |
|---|-------------------------|---------------------------|----------------|
| <b>Cost</b>   |                         |                           |                |
| Purchase Price of weeder                                      | 25000                   | 3000                      |                |
| Salvage Value (5% of Purchase Price of weeder)                | 1250                    | 150                       |                |
| Machine Life  | 5                       | 5                         |                |
| Depreciation cost per year                                    | 4750                    | 570                       |                |
| Days of operation   | 30                      | 30                        |                |
| Depreciation cost per day                                     | 158                     | 19                        |                |
| Operator required for Machine Operation                       | 1                       | 1                         | 25             |
| Cost of Operator  | 800                     | 800                       | 7500           |
| Total weeding cost for weeder per day                         | 958                     | 819                       |                |
| Area covered per ha per day                                   | 0.52                    | 0.17                      | N/A            |
| Number of Weeder  | 1                       | 1                         | N/A            |
| Total weeding cost for weeder per ha                          | 1843                    | 4818                      | 7500           |
| <b>Return</b>   |                         |                           |                |
| Weeding, Decimal/hr   | 17                      | 5                         |                |
| Average Area (decimal) of weeding covered per day (8 hr /day) | 130                     | 42                        |                |
| Rent per  | 20                      | 20                        |                |



|                              |              |               |
|------------------------------|--------------|---------------|
| decimal                      |              |               |
| Income per day               | 2600         | 835           |
| Net income per day           | 1642         | 16            |
| Net income per year          | 49250        | 486           |
| <b>BCR</b>                   | <b>2</b>     | <b>0.16</b>   |
| <b>Payback period in day</b> | <b>15.23</b> | <b>185.19</b> |

The net benefit cost ratio (BCR) of Battery operated low cost weeder is 2 which is greater than 1, so it is justified or acceptable. On the other hand, payback period of Battery operated low cost weeder is 15 that mean by using 15 days, farmer can get their investment.

## REFERENCE

- [1] Asad M, Zahid M, Muhammad M, Adnan A, Muhammad U R, Wajiha A., Bio-economic assessment of non-chemical weed management strategies in minor crops: A review on Weed research issues, challenges, and opportunities in Pakistan. *Journal of Research in Weed Science*, 2019, 2(2), 127-140.
- [2] Bainer, R., Barger, E. L. and Kepner, R. A. 'Principles of Farm Machinery.' Avi publication Co. Inc. Westport, Connecticut. 3rd Edition, 1978.
- [3] Gavali M., Kulkarni S.' Development of rotary weeder blades by Finite Element Method' *International Journal of Scientific Research Engineering & Technology (IJSRET)*, Vol. 3, 2014, pp-941-945
- [4] Hunt, D. 'Farm Power and Machinery Management.' 8th Edition. Iowa State University Press. AMES. Iowa USA, 1983.
- [5] Lavabre, E. M. Weed Control. Macmillan Education Ltd., London, 1991.
- [6] Olaoye J. O., Samuel O. D., and T. A. Adekanye. 'Performance Evaluation of an Indigenous Rotary Power Weeder.', *Energy and Environmental Engineering Journal*, Vol.1(2), 2012, pp-94-97
- [7] Oni, K. C. Performance Analysis of a Ridge Profile Weeder. *Proceeding of Nigerian Society of Agricultural Engineers*. Vol.3, 1990, pp189-199.
- [8] Parish S. 'A review of non-chemical weed control techniques'. *Biological Agriculture and Horticulture*, Vol. 7, 1990, pp-117-137.

## CONCLUSION

The performance of battery operated rotary type low cost weeder is found quite satisfactory and it is an excellent weeding technology for farmers. Weeding index of battery operated weeder is very close to manual weeding. Effective field capacity and plant damage ratio is acceptable. Cost of weeding by battery operated weeder is very low compare to other two weeding method. Though inter plant weed removal is not possible but it has no significant effect on yield. But multipurpose use of battery can ensure the sustainability of weeder.

- [9] Rangasamy, K., Balasubramanian, M. and Swaminathan, K. R. 'Evaluation of Power Weeder Performance.' *AMA*. vol.24 (4), 1993, pp-16-18.
- [10] Rathod r.k., Munde P.A. and Nadre. R. G. 'Development of tractor drawn inter-row rotary weeder'. *International Journal of Agricultural Engineering*, Vol. 3 No. 1, April, 2010, pp- 105-109
- [11] Rodenburg, J., Johnson, JM., Dieng, I. et al. *Food Sec.* (2019) 11: 69. <https://doi.org/10.1007/s12571-018-0878-0>
- [12] Subrata Kr. Mandal, Basudeb Bhattacharyya, Somenath Mukherjee, and Priyabrata Chattopadhyay Design & Development of Rotavator blade: Interrogation of CAD Method, ISSN: 2322-4541; ©2013 ijsrpub

## **SHEAR STRENGTH AND PERMEABILITY ANALYSIS OF GEOTEXTILE FROM PINEAPPLE LEAVES AND LUFFA**

INZ Baharuddin<sup>1</sup>, Hairin Taha<sup>2</sup>, RC Omar<sup>3</sup>, R.Roslan<sup>4</sup> and S.Nadirah<sup>5</sup>

<sup>1,2,3,4</sup> Institute of Energy Infrastructure,

<sup>5</sup> College of Engineering, Universiti Tenaga Nasional, Malaysia.

### **ABSTRACT**

Geotextiles are commonly utilized in many geotechnical and civil engineering applications for soil reinforcement, erosion control, drainage, filtration and separation. The market trend for geotextiles nowadays dominates more on synthetic materials such as polyethylene and polyamide. However, synthetic geotextiles can be costly when the application involves major construction and larger area. In term of environmental concern, geosynthetic materials may contain chemical additives that could leak into the surroundings. Geotextile products from natural fiber such as jute and coir are commonly available especially in India but the market for natural geotextiles is very competitive against polymeric geotextiles. In view of that, this study was aimed to design natural geotextile from local plants. Pineapple leaves were used as the main fibre for the fabrication of geotextile together with luffa and coconut flakes. Four types of designs were developed based on the seam type and number of rows of stitching. The strength and permeability of the geotextiles were tested using direct shear box test and falling head method. Results showed that the geotextile design with J seam and two rows of stitches has the higher strength and lower permeability. This study demonstrated the beneficial use of agricultural waste from pineapple leaves that can be recycled into sustainable product.

*Keywords: geotextile; pineapple leaves; luffa; shear strength; permeability*

### **INTRODUCTION**

Geotextile is mainly used for soil reservation especially in soil reinforcement, erosion control and reducing surface run-off. Other applications of geotextile include separation and filtration between different type of materials, drainage and containment [1]. Geotextile can be defined as permeable textile used together with soil, rock, earth, foundation or geo-engineering materials. Some of the typical materials used to produce geotextile include polypropylene, polyethylene, polyamides or polyester [2].

There are two categories of geotextile; woven and non-woven. The woven geotextiles are manufactured on a loom through the process of weaving or knitting textiles which has two sets of parallel threads [3]. This type of geotextile has excellent tensile strength. Most geosynthetics are woven type. The non-woven geotextiles are made from the process of mechanical or chemical interlocking or thermal bonding of non-woven fabric. The materials are pressed together using adhesive or heat treatment. However, this type has lower tensile strength compared to that of the woven type.

Several factors need to be considered when designing geotextile such as the type of geotextile, seam and stitch type, thread type, numbers of rows of stitching and sewing equipment [4]. The strength of geotextile was mainly influenced by the seam strength and this can be tested using cross machine

direction based on ASTM D4595 "Standard Test Method for Tensile Properties of Geotextiles by the wide width strip method". Another test based on ASTM D4884 can also be done to test the seam strength [5].

In general, there are two types of seam commonly used to produce geotextile, the superimposed seam (S seam) or prayer seam, and J seam. The S seam is made by stitching two fabrics together with one or more row of stitching. This is the easiest type of seam. The J seam is more difficult to make. It is done by superimposing two fabrics and folded to produce a thickness of four plies which contributes to higher seam strength [6]. This type of seam has more strength compared to other type of seam. For fabric geotextile, the seam is sewn 1 to 1.5 inches from the edge and folded to create a double plies thickness. The thread type also affects the strength of the geotextile. It should have similar or higher durability. Numbers of rows of stitching serve as the seam type colleague.

Geotextile should have higher mechanical strength due to the applied load of soil which is directly transferred to it. The occurrence of soil erosion and landslide is mostly caused by the weakening soil that has losses its strength [7]. Several factors that affect soil failure include rainfall, erosion, construction activities and external loading. Soil cannot resist tension but can withstand compression. The shear strength of soil will decrease when there is excessive water content in the soil.

When the water overflow, the soil structure will become loose and this results in soil erosion or landslide. Natural geotextile from plant fiber can help reinforce and fertilize the soil at the same time, unlike geosynthetics [8-9].

In this study, pineapple leaves waste and luffas were used to produce the natural geotextiles for soil reinforcement [10]. The concept was to utilize plant fibers which are acquired from local resources such as the local farms and markets. Malaysia produces more than one million tonnes of agricultural waste annually [11]. Instead of burning the agro waste that highly contribute to greenhouse gas emission, the agro waste could be recycled into sustainable products or converted into biomass as renewable energy.

Pineapple (*Ananas comosus* L.Merr) or known locally as 'Nenas' is a tropical plant native to South East Asia and planted as commodity crop in Malaysia. Pineapple industry contributes significantly to the country's economy and the fiber from the leaves can be developed into commercial products [12]. Pineapple leaf is rich in cellulose and biodegradable. A study on pineapple leaf fiber showed that they are suitable for building and construction materials due to its highest cellulosic content [13-14]. The fibers of pineapple leaves also have the potential as alternative raw materials in paper industries due to its good mechanical properties and high cellulose contents [15]. In recent development, pineapple leaves were also found to be suitable alternative natural acoustic material for sound absorption due to the characteristics of its fiber [16].

*Luffa acutangula* is extensively used throughout the world as materials for hybrid biodegradable geopolymer composites and sound absorbing [17-18]. Luffa fiber has high cellulose content, low cost, biodegradable and absorbs water easily. It has a thick texture that prevents the water to pass through easily [19]. For this research, pineapple leaves waste were obtained from a pineapple plantation in Johor, Malaysia and Luffa fibers were obtained from Sarawak, Malaysia.

The objective of this research was to design natural geotextile from local plant fibers, and evaluate the strength of the geotextile through permeability and direct shear box test. The chosen design based on seam type and number of rows of stitching will be used to develop the natural geotextiles and tested on site to observe the effectiveness of the geotextiles against erosion.

## 2. EXPERIMENTAL

### 2.1 Design of Natural Geotextile

The natural geotextile was designed from natural fibre consist of pineapple leaves and luffa (Fig. 1).

Four samples of geotextile designs arranged in three layers were developed based on seam type and rows of stitching (Fig.2). First, the pineapple leaves and luffa were dried outside for 72 hours until the leaves and the luffa turned brown in color and completely dried. This is important to ensure that there was no water contained in the leaves. When the fiber is fully dried, the mechanical strength of the fiber will also increase. Dried coconut flakes were then added as moisture absorber. Jute thread (5.0 mm thick) was used to stitch the geotextiles. Table 1 shows the types of geotextile design according to seam type and number of rows of stitching which will be tested.

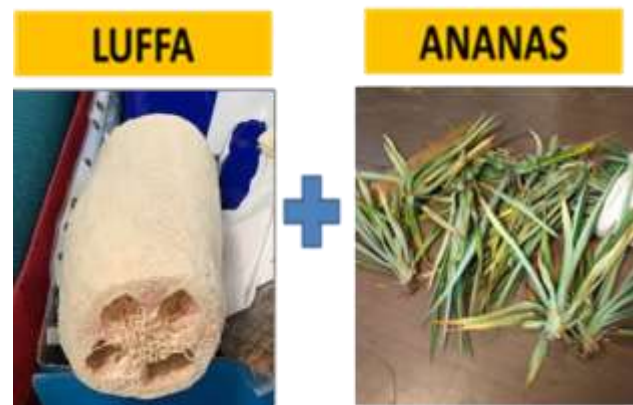


Fig.1 Natural geotextile from luffa and pineapple leaves



Fig. 2 Three layers of geotextile

Table 1. Designs of geotextile

| Samples | Seam Type | Number of rows of stitching |
|---------|-----------|-----------------------------|
|---------|-----------|-----------------------------|

|   |   |   |
|---|---|---|
| A | J | 2 |
| B | J | 1 |
| C | S | 2 |
| D | S | 1 |

## 2.2 Direct shear box test

Laboratory testing was carried out to determine the most appropriate design of geotextile for soil reinforcement. The strength of the geotextile sample was tested using direct shear box test following ASTM D5321 guidelines. The test equipment consists of a metal box (100 mm x 100 mm) in which the soil specimen and the geotextile will be placed. The geotextile sample was placed on the top and below the soil specimen. The strength between the original soil and soil together with geotextile sample was compared. The direct shear box test was done using different weights (5.0, 10.0 and 15.0 kg). The type of soil used was sandy SILT with intermediate plasticity.

## 2.3 Permeability test

The permeability of the geotextile was determined through permeability test of falling head method (ASTM D4491) as described in previous study [16]. The test consists of flow of water passing through soil sample connected to a standpipe that provides the water head and measures the volume of passing water through the sample. The standpipe diameter is governed by the permeability of the tested soil specimen. Water was allowed to flow through the sample until it reached the lower limit and the time was recorded when the water in the standpipe dropped from the upper to the lower level.

## 2.4 Experimental application

The geotextile was tested at the selected area. The soil at the experimental site was classified as sandy SILT with intermediate plasticity. The geotextile (20 cm x 20 cm) was arranged on the eroded surface inside a grid measured 600 mm x 800 mm. Prior to that, the subsurface was cleared first to remove foreign objects. The geotextiles was properly arranged on the surface. The sites with geotextiles were observed for 35 days to monitor the progress.

## 3. RESULTS AND DISCUSSION

### 3.1 Shear Box Test

The shear strength of the geotextile was influenced by the seam type and the number of row of stitching. The results of shear stress at failure against normal stress for Samples A, B, C and D are shown in Table 2. Observation showed that the value of cohesion has decreased, while the friction angles had similar values but for Sample A, the cohesion value was 0.00043 and the value for friction angle was 36.9°. This showed that Sample A has the higher shear strength compared to that of other samples.

Table 2. Cohesion and friction angle values

| Sample | Cohesion | Friction angle |
|--------|----------|----------------|
| A      | 0.0043   | 36.9           |
| B      | 0.0025   | 29.5           |
| C      | 0.0022   | 28.6           |
| D      | 0.002    | 28.4           |

The results of the direct shear box test showed sample A has higher strength compared to other samples, which were 25.83 N/m<sup>2</sup>, 47.5 N/m<sup>2</sup> and 69.44 N/m<sup>2</sup> for 5.0, 10.0 and 15.0 kg weight respectively (See Figure 3-5). The shear strength has decreased from sample A to D. The shear strength of the geotextile was influenced by the number of rows of stitching for sample A and C because the stitches were stronger to hold the fabric together from shearing.

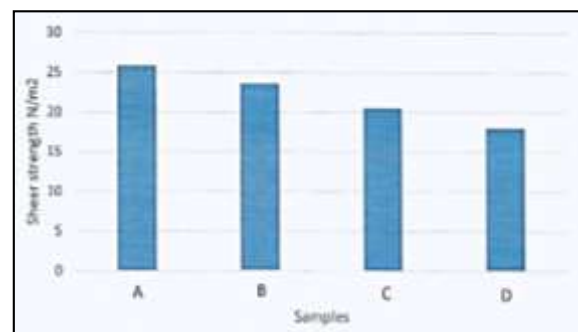


Fig. 3 Shear strength using 5.0 kg weight

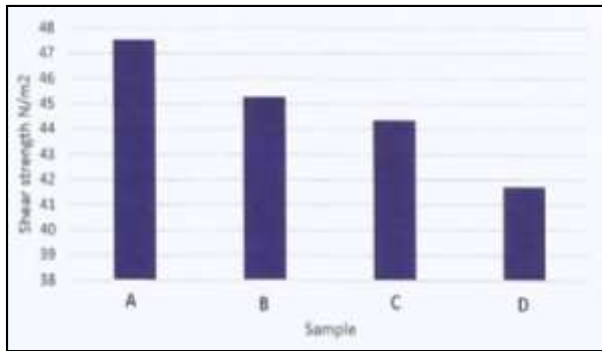


Fig. 4: Shear strength using 10.0 kg weight

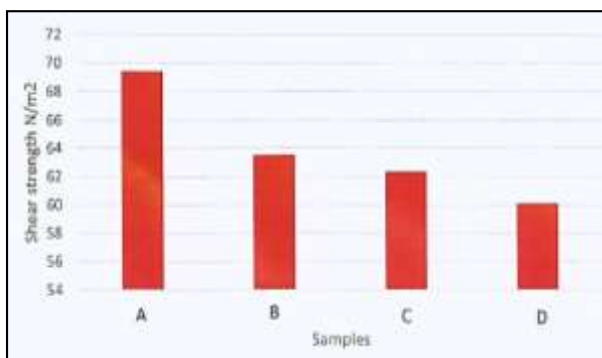


Fig. 5 Shear strength using 15.0 kg weight

### 3.2 Permeability Test

The results of permeability test showed that Sample A has low permeability due to the J seam type design. Sample A has four plies with two rows of stitching compared to S seam type which only has two plies. The test demonstrated that the soil specimen with geotextile was more impermeable. The value of coefficient of permeability,  $k$ , has increased when the geotextile samples were applied (Table 3). This showed that the presence of geotextile has decreased the permeability of the soil specimen. The flow of water through the geotextile took longer time to pass through compared to that of original soil.

Table 3. Percentage of permeability increment

| Sample        | Seam type | Coefficient of permeability (k) | Increment (%) |
|---------------|-----------|---------------------------------|---------------|
| Original soil |           | $7.2 \times 10^{-4}$            | -             |
| A             | J         | $2.16 \times 10^{-7}$           | 98.98         |
| B             | J         | $2.26 \times 10^{-7}$           | 99.87         |
| C             | S         | $2.33 \times 10^{-7}$           | 99.85         |
| D             | S         | $2.36 \times 10^{-7}$           | 99.8          |

### 3.3 Geotextile Application

The results of permeability and shear box test showed that the design of Sample A geotextile based on J seam and two rows of stitching has higher strength compared to other designs. Based on these criteria, the natural geotextile was assembled for experimental site test against soil erosion. The geotextiles were arranged on the eroded surface and observed for 35 days. The observation was documented on day 7, 14, 28 and 35 as shown in Figure 6-9. After 35 days of geotextile application, new batch of grass has grown through the natural geotextile, and the geotextile has integrated with the soil. The eroded surface has been covered with vegetation. This study has demonstrated that the geotextile from pineapple and luffa has performed as protective cover for the exposed area.



Fig. 6: Geotextile application on Day 7





Fig 7: Geotextile application on Day 14



Fig. 8: Geotextile application on Day 28



Fig 9: Geotextile application on Day 35

#### 4. CONCLUSION

In this work, natural geotextile was designed and developed using pineapple leaves waste and luffa for soil reinforcement. The geotextile was tested based on the strength and permeability using shear box test and falling head method. From the results, it was demonstrated that the geotextile design with J seam and two rows of stitching had the higher shear strength to encounter the application of

friction force. The fiber from pineapple and luffa also has lower permeability, thus, suitable for soil reinforcement.

This study demonstrated the capability of pineapple leaves and luffa as renewable resource for natural geotextile. Thus, this innovative method is cost-effective and can be developed as commercial product that would contribute to the economy. On top of that, natural geotextile from pineapple leaves and luffa can provide green solution for sustainable soil reinforcement and slope stabilization. The design of geotextile from pineapple leaves and luffa can encourage the recycling and processing of agricultural materials into sustainable products. Hence, the newly developed natural geotextile from pineapple leaves and luffa can be used to control soil erosion.

#### ACKNOWLEDGMENTS

This study was supported by UNITEN grants J510050884 (UNIIG 2018) and 201901001YCU/02.

#### REFERENCES

- [1] Zornberg, JG (2017), Functions and applications of geosynthetics in roadways. *Procedia engineering*, 189, pp.298-306.
- [2] Stepanovic, JM, Trajkovic D, Stojiljkovic D & Djordjic D, (2016), Predicting the behavior of nonwoven geotextile materials made of polyester and polypropylene fibers. *Textile Research Journal*, 86(13), pp.1385-1397.
- [3] Mishra SR, Mohapatra SR, Sudarsanan N, Rajagopal K & Robinson RG (2017), A simple image-based deformation measurement technique in tensile testing of geotextiles. *Geosynthetics International*, 24(3), pp.306-320.
- [4] Mudgal A, Sarkar R & Shrivastava AK (2018), Influence of geotextiles in enhancing the shear strength of Yamuna sand. *International Journal of Applied Engineering Research*, 13(12), pp.10733-10740.
- [5] Allen JM, Ferreira JA and Athanassopoulos C (2017), Laboratory study of geosynthetic clay liner panel shrinkage forces and seam strength. *Geotechnical Frontiers*, pp. 11-21.
- [6] Guo W, Chu J & Zhou B (2015), Method to increase seam efficiency for woven geotextile materials. *Geosynthetics International*, 22(6), pp.404-410. Annnn B., Unpublished Work but Accepted, Vol., Issue, Year.
- [7] Haeri SM, Noorzad R & Oskoorouchi AM (2000), Effect of geotextile reinforcement on



- the mechanical behavior of sand. *Geotextiles and Geomembranes*, 18(6), pp.385-402.
- [8] Kalibová, J, Jačka, L, & Petrů, J. (2016). The effectiveness of jute and coir blankets for erosion control in different field and laboratory conditions. *Solid Earth*, 7(2), pp. 469-479.
- [9] Müller, W. W., & Saathoff, F. (2015). Geosynthetics in geoenvironmental engineering. *Science and technology of advanced materials*, 16(3), pp. 034605.
- [10] Omar RC, H. Taha, R.Roslan & Baharuddin INZ (2019). GEOTEXTILE FROM PINEAPPLE LEAVES AND BIO-GROUT FOR SLOPE STABILIZATION AND EROSION CONTROL. *International Journal*, 17(60), 219-224.
- [11] Saili, R., Muhamad, Z., & Aziz, N. H. (2017). A Preliminary Study on Sustainable Management of Pineapple Waste: Perspective of Smallholders. *International Journal of Academic Research in Business and Social Sciences*, 7(6), pp. 2222-6990.
- [12] Yusof, Y., Yahya, S. A., & Adam, A. (2015). Novel technology for sustainable pineapple leaf fibers productions. *Procedia CIRP*, 26, pp.756-760.
- [13] Laborel-Préneron A, Aubert JE, Magniont C, Tribout C & Bertron A (2016), Plant aggregates and fibers in earth construction materials: A review. *Construction and building materials*, 111, pp.719-734.
- [14] Asim M, Abdan K, Jawaid M, Nasir M, Dashtizadeh Z, Ishak MR & Hoque ME (2015), A review on pineapple leaves fibre and its composites. *International Journal of Polymer Science*.
- [15] Laftah WA & Wan Abdul Rahman, WA (2016), Pulping process and the potential of using non-wood pineapple leaves fiber for pulp and paper production: A review. *Journal of Natural Fibers*, 13(1), pp.85-102.
- [16] Putra, A., Or, K. H., Selamat, M. Z., Nor, M. J. M., Hassan, M. H., & Prasetyo, I. (2018). Sound absorption of extracted pineapple-leaf fibres. *Applied Acoustics*, 136, pp. 9-15.
- [17] Koruk H & Genç G (2015), Investigation of the acoustic properties of bio luffa fiber and composite materials. *Materials Letters*, 157, pp.166-168.
- [18] Alshaaer M, Mallouh SA, Al-Faiyz Y, Fahmy T, Kallel A & Rocha F (2017), Fabrication, microstructural and mechanical characterization of Luffa Cylindrical Fibre-Reinforced geopolymer composite. *Applied Clay Science*, 143, pp. 125-133.
- [19] Chen Y, Su N, Zhang K, Zhu S, Zhu Z, Qin W, Yang Y, Shi Y, Fan S, Wang Z (2018), Effect of fiber surface treatment on structure, moisture absorption and mechanical properties of luffa sponge fiber bundles. *Industrial crops and products*, 123, pp. 341-352.

# **PARTICIPATION IN WASTE MANAGEMENT BY UNDERGRADUATE STUDENTS OF RAJAMANGALA UNIVERSITY OF TECHNOLOGY THANYABURI.**

Korntouch Kosidphokin<sup>1</sup>

<sup>1</sup>Faculty of Liberal Arts, Rajamangala University of Technology Thanyaburi, Thailand

## **ABSTRACT**

The objective of this research was to 1) study participation of waste management in undergraduate of Rajamangala University of Technology Thanyaburi 2) study knowledge attitude and practice on participation of waste management in undergraduate of Rajamangala University of Technology Thanyaburi, 3) study comparison of knowledge attitude and practice with difference grade and gender of undergraduate of Rajamangala University of Technology Thanyaburi. This research was survey research. Populations were 1,280 undergraduates who enrolled in general education course of social science. Samples were sampling on Simple Random Sampling and determined by Taro Yamane table to obtain 300 undergraduates. The research instruments consisted of questionnaire for participation of waste management, knowledge test of waste management, questionnaire for attitude of waste management and questionnaire for practice of waste management. Results were analyzed by percentage, mean, standard deviation, t-test (Independent) and F-test (One-way ANOVA). The research found that: Undergraduates of Rajamangala University of Technology Thanyaburi were medium level on participation of waste management with 2.83 of mean scores and 0.90 of standard deviation, Knowledge score at 87.03percent, good level on attitude of waste management with 3.75 of mean scores and 0.91 of standard deviation and medium level on practice of waste management with 3.23 of mean scores and 0.86 of standard deviation.

*Keywords: Participation , Waste Management, Undergraduate Student and Thailand*

## **INTRODUCTION**

Currently, Thailand has experienced problems from the imbalance in national development resulting various economic problems encountered due to dependence on foreign capital and technology that resulted in enormously use of natural resources for production. Until the destruction of natural resources and ruin culture and local wisdom due decreased depend upon themselves and migration to work in large cities is causing a variety of problems. From above, there is a tendency of more serious and provide more broadly. The solution of this problem therefore requires cooperation from many segments, including the government, private firm, citizen and involved organizations. Regarding the policy to encourage people to realize and aware the importance of the environment Therefore, in order to easily foster the right knowledge and values for the environment,[1] it is necessary start to from the youth group by using the educational system as a medium to aware impact on the environment and cooperate in solving problems and developing the environment. [2]Solid waste affects the environment and people's health directly. The foster consciousness for participation in the community for allow people learn systematically solid waste management to support the increasing garbage problem. Rajamangala University of Technology Thanyaburi is higher education

institution, that has been placed as a tool for solving the problems of the country. Therefore, university has a duty to find solutions for social problem and should develop teaching and learning that conducive to helping solve problems. Solid waste problems is the major problem form environmental pollution and all environmental problems. [3]Solid waste was considered to closest problem to humans, that is, humans are the produce solid waste from daily consumption. One managing approach is allow waste-contributors participate in solid waste management at the start from the real cause that building consciousness in solid waste management for students, which university will be able to support the appropriately solution and allowing students introduce knowledge to families and households that will result in the learning and manage solid waste within households and communities.

## **Method**

- 1 Prepared a research area and prepared a research plan.
  - 2 Meeting of the team of research assistants for data collection
  - 3 Conduct research according to the research plan.
  - 4 Conferences, research conclusions
- The researcher collected data by surveying the participation in waste management of undergraduate

students at Rajamangala University of Technology Thanyaburi. And collecting data by testing knowledge Inquire, attitude and practice in the participatory waste management of Rajamangala University of Technology Thanyaburi

## RESULTS

**Table 1** The participation in waste management from undergraduate students of Rajamangala University of Technology Thanyaburi

| Activity   | $\bar{X}$ | S.D. | Participation level |
|--|-----------|------|---------------------|
| 1. Students aware that university has a waste management system.   | 2.88      | 0.52 | medium              |
| 2. Students participate in finding solution to manage waste.   | 3.00      | 0.93 | medium              |
| 3. Students are participating in thinking about the cause of waste in university.  | 2.60      | 0.78 | medium              |
| 4. Students are participating in design activities or waste management projects in university.                             | 2.80      | 0.82 | medium              |
| 5. Students participate in controlling activities or waste management projects in university.                              | 2.91      | 0.88 | medium              |
| 6. Students make decision on activities or waste management projects in university.  | 2.78      | 0.97 | medium              |
| 7. Students are participating in activities or waste management projects in university.                                    | 2.78      | 0.86 | medium              |
| 8. Students have become conscious to take responsible in activities or waste management projects in university.            | 2.66      | 0.93 | medium              |
| 9. Students are interested in continuing to conduct activities or waste management projects in university every year.      | 2.87      | 0.93 | medium              |
| 10. Students want to participate in evaluating or monitoring the activities or the waste management program in university. | 2.90      | 0.97 | medium              |
| Total  | 2.83      | 0.90 | medium              |

The participation in waste management from undergraduate students of Rajamangala University of Technology Thanyaburi are as follows: It was found that undergraduate students Rajamangala University of Technology Thanyaburi Participate in waste management in the overall at a moderate level where the average participation score is 2.83, the standard deviation is 0.90.

**Table 2** Study results, knowledge, attitudes and practices in waste management from undergraduate students of Rajamangala University of Technology Thanyaburi

| waste management knowledge  | Sample (N) | Correct answer | Percentage |
|---|------------|----------------|------------|
| 1. Which item gives the most meaning of waste?                            | 300        | 259            | 86.33      |
| 2. Which item most suitable for classify waste?                           | 300        | 283            | 94.33      |
| 3. What is 3Rs for waste reduction?                                       | 300        | 283            | 94.33      |
| 4. What kind of waste in Rajamangala University of Technology Thanyaburi? | 300        | 292            | 97.33      |
| 5. How useful waste sorting is?   | 300        | 172            | 57.33      |
| 6. Which kind of waste is used to make fertilizer?                        | 300        | 256            | 85.33      |
| 7. How can students help to manage the waste in university?               | 300        | 248            | 82.67      |
| 8. Which waste disposal method is the most polluting?                     | 300        | 273            | 91.67      |
| 9. What are the benefits of trash?  | 300        | 283            | 94.33      |
| 10. Who is the most waste contributor on university?                      | 300        | 266            | 88.67      |
| Average   | 300        | 261.90         | 87.03      |

Study results, knowledge, attitudes and practices in waste management from undergraduate students of Rajamangala University of Technology Thanyaburi found percentage of knowledge score at 87.03 percent, while most correct answers is knowledge in the subject What kind of waste in Rajamangala University of Technology Thanyaburi Followed by knowledge of Classification of waste, what is 3Rs for waste reduction and What are the benefits of trash respectively.

**Table 3** The attitude analysis of waste management of undergraduate students at Rajamangala University of Technology Thanyaburi

| waste management attitude   | $\bar{X}$ | S.D. | Attitude level |
|---|-----------|------|----------------|
| 1. University waste management activities are useful and creative.  | 3.76      | 0.84 | medium         |
| 2. Waste management is the duty of university.  | 3.21      | 0.96 | medium         |
| 3. The student's duty is help collect waste into the trash.   | 4.07      | 0.84 | good           |
| 4. You want to have waste sorting on university.  | 3.96      | 1.00 | good           |
| 5. You want to join a waste management campaign.  | 3.51      | 1.13 | good           |
| 6. If there is time, you would like to attend a meeting and comment on waste management on university.                      | 3.40      | 0.84 | medium         |
| 7. Will be a good if waste management has operated in university.   | 3.75      | 0.96 | good           |
| 8. Students have respect to university and would like university to be a green university with waste management activities. | 3.97      | 0.82 | good           |
| 9. You are pleased to help reduce the amount of waste in university.  | 4.07      | 0.88 | good           |
| 10. You have the idea to help the university do the waste disposal campaign.  | 3.76      | 0.80 | good           |
| Total   | 3.75      | 0.91 | good           |

The attitude analysis of waste management of undergraduate students at Rajamangala University of Technology Thanyaburi found that the attitude of waste management of undergraduate students overall at a good level with an average of attitude level of 3.75, standard deviation of 0.91

**Table 4** The results of the analysis of waste management practices of undergraduate students at Rajamangala University of Technology Thanyaburi

| Waste practical   | $\bar{X}$ | S.D. | Attitude level |
|---|-----------|------|----------------|
| 1. You dump waste into trash every time   | 3.98      | 0.36 | good           |
| 2. You always sort the waste before leaving   | 3.26      | 0.30 | medium         |
| 3. You do not request plastic bag after buy something   | 3.11      | 0.25 | medium         |
| 4. If you find waste in the university area, you always keep to trash                                     | 3.03      | 0.30 | medium         |
| 5. You always participate in waste disposal activities with university                                    | 2.91      | 0.40 | medium         |
| 6. If you see a friend, throw away the waste, you always guide them                                       | 3.20      | 0.25 | medium         |
| 7. You will sort out food waste from other waste after you have eaten at the cafeteria                    | 3.28      | 0.23 | medium         |
| 8. After study activities, you collect and sort waste before discarding regularly                         | 3.33      | 0.37 | medium         |
| 9. You advise other students to do waste sorting activities in your class                                 | 3.25      | 0.43 | medium         |
| 10. You can help promote waste management activities to help the university when activities were on going | 2.91      | 0.38 | medium         |
| Total   | 3.23      | 0.36 | medium         |

The results of the analysis of waste management practices of undergraduate students at Rajamangala University of Technology Thanyaburi found that practice in waste management of undergraduate students is moderate level with overall average of 3.23, standard deviation equal to 0.86

**Table 5** The comparative study of knowledge, attitude and practical skill in waste sorting management by student's year of Rajamangala University of Technology Thanyaburi

| Source of variance        | df  | SS        | MS       | F                  | p    |
|---------------------------|-----|-----------|----------|--------------------|------|
| Knowledge with Year       |     |           |          |                    |      |
| External group            | 3   | 50.12     | 16.71    | 5.14 <sup>*</sup>  | 0.00 |
| Internal group            | 296 | 861.91    | 2.91     | -                  | -    |
| Total                     | 299 | 912.03    | -        | -                  | -    |
| Attitude and Year         |     |           |          |                    |      |
| External group            | 3   | 891.06    | 297.02   | 7.91 <sup>*</sup>  | 0.00 |
| Internal group            | 296 | 11,121.61 | 37.57    | -                  | -    |
| Total                     | 299 | 12,012.67 | -        | -                  | -    |
| practical skill with Year |     |           |          |                    |      |
| External group            | 3   | 3,349.21  | 1,123.07 | 43.96 <sup>*</sup> | 0.00 |
| Internal group            | 296 | 6,113.04  | 20.65    | -                  | -    |
| Total                     | 299 | 9,462.25  | -        | -                  | -    |

go=0.05, F<sub>0.05,3,296</sub> = 2.40

The results of data analysis, comparative study of knowledge, attitude and practical skill in waste sorting management by student's year of Rajamangala University of Technology Thanyaburi found undergraduate students at the levels of Year 1, 2, 3 and 4 or in different years, there is a different knowledge, attitude and practical skills in waste management.

**Table 6** The comparative study of knowledge, attitude and practical skill in waste sorting management by student's sex of Rajamangala University of Technology Thanyaburi

| Subject         | Gender | n   | $\bar{X}$ | S.D. | t    | p                 |
|-----------------|--------|-----|-----------|------|------|-------------------|
| Knowledge       | Male   | 87  | 8.39      | 1.13 | 0.00 | 0.10              |
|                 | Female | 213 | 8.85      | 1.93 |      |                   |
| Attitude        | Male   | 87  | 39.23     | 7.58 | 7.68 | 0.02 <sup>*</sup> |
|                 | Female | 213 | 36.74     | 5.62 |      |                   |
| practical skill | Male   | 87  | 35.97     | 5.97 | 0.04 | 0.83              |
|                 | Female | 213 | 30.73     | 5.62 |      |                   |

statistical significance at the level 0.05, t<sub>0.05, 300</sub> = 1.96

From Table 6, it was found that male students had a higher attitude towards waste management than females in different average scores with statistical significance at the level of 0.05 and no difference in knowledge and practical skills between male and female students.

## CONCLUSIONS

1. Participation in waste management of undergraduated students at Rajamangala University of Technology Thanyaburi Participate in moderate waste management

2 Knowledge measurement in waste management of undergraduated students at Rajamangala University of Technology Thanyaburi students is 87.03 percent.

3. Measurement of attitude in waste management of undergraduated students Rajamangala University of Technology Thanyaburi Overall at a good level With an average of 3.75

4.Waste management skills of undergraduated students at Rajamangala University of Technology Thanyaburi At a moderate level with an average of 3.23

## Discussion of research results

1. Discuss the results of the participation of students at Rajamangala University of Technology Thanyaburi. Participation in waste management is at a moderate level, consistent with the study of [4] [6] It was found that knowledge about solid waste disposal of people at moderate level and the participation of people in the disposal of solid waste is relatively low. And the relationship between knowledge and public participation in solid waste disposal is related to statistical significance at the level of 0.05

2. Discussion of the study of knowledge in waste management of students at Rajamangala University of Technology Thanyaburi Consistent with the study of [4] That knowledge of solid waste management of the people is related to the participation of people in solid waste disposal with statistical significance at the level of 0.05 and [5] People have a high level of understanding and consciousness in waste management. And knowledge and understanding of the community were significantly related to participation in waste management

3. Discuss the results of the study on the attitude of waste management of Rajamangala University of Technology Thanyaburi students. [5] People have a high level of consciousness in waste management. There is a reason to participate in waste management activities to make the community clean. With beautiful scenery During reducing environmental problems and increasing family income.

4. Discuss the results of the study of practical skills in waste management of Rajamangala University of Technology Thanyaburi students. [5] found that the community can separate garbage And take the waste to a high level There is a high level of proper household waste disposal behavior. The main reason that communities participate in waste management activities is to make the communities clean, clean, with beautiful scenery. During reducing environmental problems and increasing family income.

5. Discuss the results of the study comparing knowledge, attitudes and practical skills in waste management classified by grade level of Rajamangala University of Technology Thanyaburi students. Residence time Sources that receive information and frequency of receiving different information There is a different behavior in participation in solid waste disposal. [7] It was found that gender, age, education were different in participation in different sorting of waste at statistical significance level. 0.05 [5] found that knowledge Community understanding has a significant relationship with participation in waste management.

#### ACKNOWLEDGMENTS

The author would like to express sincere appreciation to my family ,my friends, the Faculty of

Liberal Arts and the Institute of Research and Development, Rajamangala University of Technology Thanyaburi (RMUTT), for their financial support.

#### REFERENCES

- [1] Department of Environmental Quality Promotion.2000.Environmental Knowledge. Bangkok. Environmental Quality Promotion Department, Ministry of Science and Technology
- [2] Pollution Control Department .Thailand State of Pollution Report 2011. Pollution Control Department, Ministry of Science and Technology
- [3] Suchada Chaisawadi , Penprapa Buoy and Anchalee Chimphalee .2007. Recycling waste management within King Mongkut's University of Technology Thonburi.
- [4] Preecha Kulavanich. 2005. The relationship between knowledge about participation in solid waste disposal: a case study of the Saen Phu Dat Subdistrict Administrative Organization Ban Pho District Chachoengsao
- [5] Kapkaew Panyathai. 2011. Participation of community in waste management in Kokha Municipality, Lampang Province. pp 1-105
- [6] Supot Subphadungchan. 2004. People participation behavior in solid waste disposal: a case study of Ban Chang Municipality, Ban Chang District, Rayong Province.
- [7] Chatchai Nuanphen. 2006. Public participation in waste sorting in Roi - Et Municipality.

## **ENVIRONMENTAL MANAGEMENT FOR GREEN UNIVERSITY BASED ON THE UI GREEN METRIC OF UNIVERSITY SUCCEED.**

Korntouch Kosidphokin<sup>1</sup>

<sup>1</sup>Faculty of Liberal Arts, Division of Social Sciences Rajamangala University of Technology Thanyaburi,  
Thailand

### **ABSTRACT**

The aim of this study was to study the environmental strategic of technical university succeed for green university based on the UI Green Metric World. This research was conducted data collection at two technical universities, King Mongkut's University of Technology Thonburi (KMUTT) and King Mongkut's University of Technology North Bangkok (KMUTNB). This research was study by qualitative research surveys. Observation and in-depth interviews with key persons from universities' officer were used as research tool for collecting the concept data. Data were analyses in content analysis with combination analyzing including observation, in-depth interviews, plan and policy, final and meeting report of related to the UI Green Metric World. The result of this study revealed that the two universities have an action plan based on 5 topics in the UI Green Metric World including 1) green position and infrastructure 2) energy management system and climate change 3) waste management 4) water Management and 5) green transportation. Summarize of this research shown that the KMUTT have had five topic of environmental strategic in same direction with the KMUTNB. However, difference of concept and action plan of each environmental strategic were found. Moreover, this research shown that the KMUTT, where have a master plan for becoming green university based on the UI Green Metric World, which have an environmental management systems continuous and modern for support the global trends.

Keywords: Green university, environmental management, Green metric world, University Succeed

### **INTRODUCTION**

Green University means a university that has good management to make use of resources effectively, using energy efficiently with the prevention of pollution or minimizing emissions of the pollution, enhancing the quality of life with a good and safe working environment as well as preserving the environment and integration for sustainability (UI GreenMetric World University Ranking, 2016, QS Worldwide university rankings, 2012). In order to become the Green University, the university must consider the three vital dimensions: social dimension, economic dimension, and environmental dimension. According to the social dimension, the university has an explicit policy to closely build relationships with surrounding communities by developing communities continuously and organizing useful activities in cooperation with the community corporately implementing projects to expand educational opportunities for the surrounding communities and educational institutions in the area. Regarding to economic dimension, the university arranges some parts of their areas for the private sectors to do their business such as restaurants, convenience stores, banks, a post office to provide services for university staffs working in the university and surrounding communities. Regarding to environmental dimension, the university has an accessible development plan for the landscape system and has research and development that is consistent

with the ecological system, taking into account the integration of environmental management (Stitmannathum, 2016; Mahidol University 2014 ).

Assessment criteria to become a green university has risen from the University of Indonesia since 2010 until the present. In order to rank the green universities which was run by the University of Indonesia, the assessment criteria are six aspects: the system of infrastructure, energy management and climate change, waste management, water management, transportation and environmental education (UI GreenMetric World University Ranking, 2016). With reference to universities in Thailand, there are 7 universities that have been ranked, namely, Mahidol University. King Mongkut's University of Technology Thonburi, Chulalongkorn University, Kasetsart University, Mahasarakrm University, King Mongkut's University of Technology North Bangkok and Burapha University (UI GreenMetric World University Ranking, 2016; Mahidol University 2014). (Suwanna Ruangchanaset 2013; Stit mannaithum, 2016). It has been accepted that the management and systems that the universities had developed with an aim to be recognized as a green university at an international level can be used to drive important factors that supports educational institutes at the higher education around the world, especially imposing policies and organizing the environmental management systems within the university to be sustainable and conducive to reduce the impact that causes global warming by considering



energy conservation, good environmental management and increasing green space and promoting the use of renewable energy (Suwanna Ruangchanaset 2013; Stit mannaithum, 2016) (Kunnatham Santitham, 2549; Mahidol University 2014; Stitmannaitum, 2016). However, the implementation of the green university development policy In Thailand is varied in terms of activities. The activities depend on the readiness of personnel, the readiness of areas and budget of the university as well as participation in the development of the university (Kunnatham Santitham, 2006; Mahidol University 2014; Stitmannaitum, 2016). Therefore, this study focuses on gathering strategies, visions, missions, goals and strategies for green university development within the universities that have achieved their goals and complied with the Green University criteria to be used as a guideline for raising the quality of life for people both inside and outside the university, for conserving sustainable environment and also for being a guideline for driving the planning and implementation of environmental management strategies.

## METHODOLOGY

1. Study essential and related contents from documents and websites of King Mongkut's University of Technology Thonburi and King Mongkut's University of Technology North Bangkok.
2. Interview in-depth and observe university staffs of King Mongkut's University of Technology Thonburi and King Mongkut's University of Technology North Bangkok.

Two universities focusing on technology have been selected according to the criteria of the Green University of 2015, namely King Mongkut's University of Technology Thonburi and King Mongkut's University of Technology North Bangkok. Each of the universities was divided into two sample groups: university executive group consisting of the president or vice president of the university, and personnel group who was responsible for environmental management in accordance with the university's green criteria. Two people in each selected university were selected as informants.

The research tool is an unstructured interview to gain in-depth information on the environmental management strategies based on the Green University criteria of King Mongkut's University of Technology Thonburi and King Mongkut's University of Technology North Bangkok. Content analysis model was used to analyze the data obtained from the in-depth interviews and observations in accordance with the policy of the action plans, project of recording meetings, summary reports and other

## FINDINGS

Regarding to the study using unstructured interviews to gain information about the

environmental management strategies according to the green university criteria of King Mongkut's University of Technology Thonburi and King Mongkut's University of Technology North Bangkok, the findings obtained from the document analysis and the opinions of university executive group and personnel group who were responsible for environmental management operations can be divided into six aspects.

### Aspect 1 Location and Infrastructure

King Mongkut's University of Technology Thonburi had a policy to increase green space in the university by implementing projects and activities in the following topics: 1) management of the location and structure whose the responsible division was the Building of Safety, Environment and Occupational Health Center, 2) building standardized green buildings, 3) brainstorming opinions of university personnel for making Master Plan of Green University, 4) creating Green Heart for students to be leaders and practitioners of which would affect the sustainability of the green university, 5) training the housewives in the separation of garbage at least once a year, and 6) using the Academic Affair Division as a key division to organize activities about the Green University starting from the orientation of how to reduce the amount of energy use in the previous year until at the present time and to continue this reduction to the future. This has been implemented by 1) creating a garden, a fence, and a tree plantation at present and 2) establishing a green university's master plan commencing in 2010 to 2020.

King Mongkut's University of Technology North Bangkok had a policy to increase green space in the university by focusing on providing exercise space by implementing the projects and activities in the following topics: 1) designing the Rayong Campus to be a natural university, 2) creating a green environment area on the decks of the multi-purposes buildings at Bangkok Campus focusing on creating green environment to motivate personnel to do exercises, 5) building roof covers between lecture buildings to reduce energy use, 6) improving the landscape of both sides in front of the university entrance at Prachinburi Campus, 7) implementing Rayong Plantation Project to create gardens, signs, fences with grown perennial plants, providing exercise equipment and supplementary environments for exercises such as bicycle paths.

### Aspect 2 Energy Management and Climate Change

King Mongkut's University of Technology Thonburi had a policy to reduce the energy use and reduce pollution within the university by implementing projects and activities as follows: 1) building a control building to perform energy consumption analysis aiming to send information to the Ministry of Energy by reporting annually, 2) having students conduct research on the university's

energy consumption at the faculty level, 3) appointing a working group at the faculty level to be responsible for the energy of the faculty, 4) setting up a working group at the faculty level to control the amount of energy use, 5) supporting the saving of electricity within every faculty, 6) using renewable energy in the Faculty of Industrial and Agricultural Technology, 7) designing the building which is energy-saving and environmentally friendly, 8) promoting cycling within the university, 9) using the electric buses with a golf cart style in the university, 10) arranging electric shuttle buses between the campus. To reduce the energy use, the activities undertaken were as follows: 1) switching off all classrooms' electric lights and air-conditioners 15 minutes before the classes ended, 2) using renewable energy, for example, biogas and solar energy, 3) providing bicycle loan for riding within the university, 4) "Hop-up electric cars service" for travelling around the university, and 5) electric motorcycle loan to ride within the university.

King Mongkut's University of Technology North Bangkok had a policy to reduce the energy consumption of the university staff and the pollution within the university by undertaking projects and activities in the following topics: 1) changing the light bulbs from T5 to LED, 2) turning off electricity at a specific time and turning off the air-conditioners before the end of classes and meetings, 3) arranging transportation within the university, 4) adjusting air-conditioning system as a separate air-conditioning system, 5) cleaning air conditioners carried out by students, 6) using renewable energy in daily life, in industry and agricultural technology, 7) designing energy-saving and environmentally friendly building, 8) building roof covers by using solar roof on campus and guardhouses, 9) building solar farm power station at Rayong Campus. The reduction performance of energy use has been undertaken as follows: 1) changing 30,000 light bulbs within the university, 2) setting the specific time of 15 minutes for turning off electricity and air-conditioners in every classroom before the end of the class, 3) providing electric buses for transportation within the university, 4) gradually changing the air-conditioners to be the ones certified with electricity saving no. 5, while the university also supporting budget for the project of cleaning air-conditioners by students, 6) every building in the university was certified by energy-saving building standards in both good and very good levels, 7) solar roof producing electricity fed into the surrounding buildings, and 8) conducting research study on station generating electricity, solar farm aiming to be a demonstration station and learning center of solar farm for surrounding communities.

#### Aspect 3 Waste Management

King Mongkut's University of Technology Thonburi had a policy to reduce waste, promoting energy production from waste and processing waste

and treatment of wastewater with the projects and activities in the following topics: 1) creating KMUTT's waste management system by using 5 colors-coded bins: green, blue, red, yellow, and gray, 2) treatment of toxic waste which was sent to eliminate once a year, 3) treatment of organic waste, 4) treatment of inorganic waste water, 5) implementing recycle to cycle project, and 6) treatment of waste water in the university. To reduce the energy use, the activities carried out were as follows: 1) There were specialist for toxic waste treatment in the laboratories. Some toxic waste was recycled. 2) Garbage was made into compost and produced as biogas. 3) There was a waste bank establishment for everyone in the university to be a member. 4) Garbage of bottles and cans from waste banks was sold and the money received was spent on buying bicycles for bicycle loan. 5) There were working staff, volunteer students, who were responsible for bicycle loan. Moreover, if they were able to teach how to fix the bicycles, they would earn more scores for their courses when awarding the grade. 6) The process of borrowing and returning the bicycles in the bicycle loan arose from the scores of cans deposited into the waste bank. If the member of the waste bank were not able to exchange the scores in time as specified in the campaign, he could get a cap from the sponsor, Coke Company Limited as a reward instead. 7) Wastewater treatment from the sources was not combined with chemicals which was inspected throughout the process and there was a standard inspection pond prior to the separation of toxic water and dirty water.

King Mongkut's University of Technology North Bangkok had a policy to reduce waste, promoting energy production from waste and processing waste. There were projects and activities in the following topics: 1) waste recycling campaign and waste separation to put into the correct waste bins, 2) organic and inorganic waste treatment, 3) wastewater treatment in each building, 4) waste water treatment before being released into the canal, 5) creating a pollution-free kiln that was eco-friendly, 6) proper waste management of chemicals used in teaching and learning, 7) promoting the use of 3 Rs principles: Reuse Reduce, and Recycle, 8) Integrated waste and waste management project at Rayong Campus. To reduce the energy use, the following activities were undertaken: 1) providing color-coded waste bins to separate the waste in every area under the buildings and along the pathway, 2) the collected garbage sent to garbage trucks of Bangkok by separating garbage types, 3) wastewater treatment in each building, 4) a total wastewater treatment system before being released into the public canal, 5) reduction of paper use, use of electronic files instead, and use of double-sided paper, and 6) separating plastic water bottles from general waste and separating A4 waste paper prior to sale.

#### Part 4 Water Management

King Mongkut's University of Technology Thonburi had a policy to reduce water consumption and reduce waste water. There were projects and activities in the following topics: 1) installation of a water meter connected to a power meter to check the usage, 2) continuously check the quality of wastewater in the reservoir, 3) measuring the progress of achieving the main factors of water management success by using key performance indicators (KPIs) by means of establishing a joint committee consisting of personnel from various faculties in the university, 4) flushing the toilet using recycle water in the buildings starting from the new buildings, 5) using water-saving devices and using water from natural ponds to water trees, and 6) promoting awareness of water management for sustainable water use by granting shirts, certificates and trophy.

King Mongkut's University of Technology North Bangkok had a policy to reduce water consumption and reduce waste water with projects and activities in the following topics: 1) conservation of water use in scientific laboratories, 2) changing of sanitary ware to save water, 3) applying treated water to watering plants at Prachinburi Campus and 4) reusing water at the Rayong Campus. To reduce the energy use, the following projects and activities were undertaken: 1) water circulation in the laboratory which produced no waste water, 2) installing the urinal system for male using automatic system and water-saving toilet, 3) bringing waste water to a connected pipe line for watering the trees around the buildings, and 4) reusing the treated wastewater for watering the trees and cleaning the streets.

#### Aspect 5 Environment-Friendly Transportation (Eco-Friendly Transportation)

King Mongkut's University of Technology Thonburi had a policy to reduce vehicles use and to use vehicles that do not use gasoline-based fuel. The projects and activities to reduce energy use have been carried out as follows: 1) to promote walking and use of bicycles for students, staff and personnel by loaning to use bicycles within the university, and 2) to provide electric golf carts as a service for lecturers and staff by arranging the points for borrowing and returning the bicycles and the points for passengers disembarking the electric golf carts.

King Mongkut's University of Technology North Bangkok had a policy to reduce vehicle use and to use vehicles that did not use gasoline-based fuel. Their projects and activities were as follows: 1) construction of walking paths with roof cover, 2) bike riding campaign, 3) electric golf carts for lecturers and university staff in the university and at Rayong Campus, and 4) 15-seat electric cars. The activities to reduce energy use have been carried out as follows: 1) construction of walking paths with roof cover, 2) scheduling the service of electric golf carts related to the specified time, 3) reducing the amount of using

private cars, 4) providing three 15-seat electric cars using solar power generation at Rayong Campus.

#### Summary and discussion of research results

The findings of the research study can be summarized as follows:

1. Regarding to the criteria for location and infrastructure, it was revealed that King Mongkut's University of Technology Thonburi and King Mongkut's University of Technology North Bangkok had a policy pulled in the same direction, which was to increase the green areas in the university. Their effective policy implementation was creating gardens and signs, building fences and growing perennial plants. These activities had been done to increase the green areas in other universities in Thailand as well. ) Stit mannaithum, 2016; Kunnatham Santitham, 2006; Thannapat Jarernpanit, 2015; Mahidol University. 2014).

However, when considering the concept of creating a green area, it was shown that King Mongkut's University of Technology North Bangkok focused on providing green space for doing exercises. This project had been piloted at Bangkok Campus by providing the exercise equipment and organizing the green environment in the exercise area. On the other hand, King Mongkut's University of Technology Thonburi developed green areas in the university by focusing on increasing the quantity of the green areas and maintaining the sustainability of them simultaneously. This had been implemented by constructing the Green Campus Master Plan which represented their concept of and determination in sustainably eco-friendly management and sustainably environmental conservation in institutions Kunnatham Santitham, (2006).

.2 Regarding to energy management and climate change criteria, it was revealed that King Mongkut's University of Technology Thonburi and King Mongkut's University of Technology North Bangkok had a policy pulled in the same direction in terms of reducing the energy use of the organization and reducing pollution within the university. Both universities had implemented some activities for the reduction of energy use similarly as follows: ( 1 saving electricity by setting the time to turn off the electricity and the air-conditioners, ( 2 use of renewable energy, namely bio-gas and solar energy, (3 changing the use of common electrical appliances to that of energy-saving ones, especially air-conditioners and light bulbs, and (4 management of using a separate air-conditioning system. However, King Mongkut's University of Technology Thonburi had a different policy, that was the provision of electric cars within the university and electric motorcycle loan service within the university.

.3 Regarding waste management criteria, it was found that King Mongkut's University of Technology Thonburi and King Mongkut's University of Technology North Bangkok had a policy pulled in the

same direction in terms of reducing the amount of waste, promoting energy production from waste and processing waste, together with waste water treatment Kunnatham Santitham, (2006).

However, when considering the concept of waste management, it was found that there were different implementations. This means that King Mongkut's University of Technology Thonburi had a variety of activities including 1) reducing waste while promoting energy production from waste and processing waste which were carried out by university staff, 2) transforming garbage into compost and producing as biogas, 3) setting up a waste bank for everyone in the university to be a member, 4) bringing cans from garbage banks to sell and using the money earned to buy bicycles for bicycle loan, 5) recruiting volunteer students to take care of the loan bicycles with extra points earned if repairing the bikes. 6) borrowing and returning the bicycles or bicycle loan depended on the points earned when delivering the garbage cans into the garbage bank. If the member was not able to redeem his points in time, he would receive other thing as a reward from the support of the soft drink company (sponsor). 7) Wastewater treatment from the sources was not combined with chemicals which has been inspected throughout the process and there was a standard inspection pond prior to the separation of toxic water and dirty water Kunnatham Santitham, (2006). Regarding King Mongkut's University of Technology North Bangkok, there were only two activities implemented: placing waste separation bins at every point under the buildings along the pathway and transferring the separated waste to the garbage truck of Bangkok) Kunnatham Santitham, 2006; Thannapat Jarernpanit, 2015).

4. Regarding to water management criteria, it was found that King Mongkut's University of Technology Thonburi and King Mongkut's University of Technology North Bangkok had a policy pulled in the same direction that is to reduce water consumption and waste water. When considering the concept of waste water management, there were different operations. King Mongkut's University of Technology Thonburi implemented projects and activities of 1) installing a water meter connected to a power meter to check the usage, 2) checking the quality of wastewater in the reservoir continuously, 3) measuring the progress of achievement in the main factors of success in water management by using the key performance indicators (KPIs) by means of establishing a joint committee consisting of personnel from various faculties in the university, 4) installing toilets flushing with recycled water in the buildings, starting at newly constructed buildings, 5) using water saving equipment and water from natural ponds for watering plants, and 6) promoting awareness of water management for sustainable water use by

granting shirts, certificates and trophy Kunnatham Santitham, 2006; Thannapat Jarernpanit, 2015).

King Mongkut's University of Technology North Bangkok had fewer implementations which were 1) water circulation in the laboratory without waste water, 2) installing the urinal system for male using automatic system and water-saving toilet, 3) using treated wastewater in the pipe line to water plants around the buildings, and 4) applying treated wastewater to water plants and cleaning the streets.

5) Regarding the criteria of eco-friendly transportation, it was found that King Mongkut's University of Technology Thonburi and King Mongkut's University of Technology North Bangkok had a policy pulled in the same direction in terms of reducing vehicle use and using vehicles that did not use gasoline-based fuel. There was one similar operation that is providing electric golf carts service for teachers and staff as well as promoting walking within the university to reduce energy consumption. However, when considering the concept of eco-friendly transport management, it was found that King Mongkut's University of Technology Thonburi had different ways to promote the reduction of vehicle use by promoting the use of ordinary bicycles and creating a pilot project for using electric motorcycles within the university. This pilot project for using electric motorcycles has never been implemented in Thailand before.

## CONCLUSIONS

This research shows that successful environmental management based on the green university criteria for universities that focus on technology and whose policies, activities, and master plans have already been started for implementation and are work-in-progress at present like King Mongkut's University of Technology Thonburi depends heavily on continuous environmental management with extension and modernization to support the world's future situations

## ACKNOWLEDGMENTS

The author would like to express sincere appreciation to my family ,my friends, the Faculty of Liberal Arts and the Institute of Research and Development, Rajamangala University of Technology Thanyaburi (RMUTT), for their financial support.

## REFERENCES

- [1] Mahidol University. (2014). Mahidol University has been ranked 1st in Thailand and 31st worldwide by UI Green Metric World Universities Ranking 2013 [In Thai]. Retrieved May 1, 2016, from [http://www.mahidol.ac.th/th/latest\\_news57/UI\\_Green.html](http://www.mahidol.ac.th/th/latest_news57/UI_Green.html)

- [2] Stitmannaitum.(2016).Chulalongkorn University Sustainability Report 2013-2014. Chulalongkorn University. 52 P
- [3] QS Worldwide university rankings. (2015). Green Universities. Retrieved on: May 1, 2016. <https://www.topuniversities.com/university-rankings/world-university-rankings/2015>
- [4] UI GreenMetric World University Ranking.(2016). Criteria & Indicator. Retrieved on:May1,2016,from <http://greenmetric.ui.ac.id/page/criteria>
- [5] Kunnatham Santitham, 2006. Guidelines for improvement of site layout and management to clean green university: Thammasat University, Rangsit Campus. Journal of Architectural/Planning Research and Studies 4 (2). 157-185p.
- [6] Thannapat Jarernpanit. 2015. Application of public policy processes in the development of green universities Of Pibulsongkram Rajabhat University Phitsanulok ProvinceJournal of Environmental Management11 (1). 86-97 p
- [7] Chakrapong Phuwichan. **2012**. Report the project results according to the strategic plan Maejo University Fiscal Year 2012: The Green Land Project, Maejo-Phrae University honor. Maejo University - Phrae honor. 13 p.

# INVESTIGATING OZONE LEVELS IN MUSCAT AREA, OMAN BY USING ARTIFICIAL NEURAL NETWORKS

Mahad Baawain<sup>1</sup>, Hasina Al-Hinai<sup>1</sup> and Abdullah Almamun<sup>1</sup>

<sup>1</sup>Department of Civil and Architectural Engineering, Sultan Qaboos University, Oman

## ABSTRACT

The economic, industrial and infrastructural developments in Muscat Governorate (Oman) has increased the emissions of some air pollutants from several sources. These air pollutants may pose adversely affect the public health in city through cardiorespiratory and pulmonary diseases. The effects of air pollution were not limited only to the health effects of the exposed population but also could have detrimental effects on the quality of the ecosystem, buildings and artifacts. This study aims at assessing the quality of ambient air in Muscat Governorate by assessing the ground level ozone (O<sub>3</sub>) concentrations and its primary sources of emission. It also focuses on finding the non-linear relationship between ozone concentrations and other pollutants concentrations (e.g. nitrogen oxides and volatile organic compounds) including meteorological parameters (e.g. temperature, atmospheric pressure, humidity, wind speed and direction). The concentrations of O<sub>3</sub>, NO<sub>2</sub> and VOC and the metrological parameters were measured by mobile monitoring station in six different administrative locations in Muscat Governorate (Al-Amerat, Al-Seeb, Al-Khuwair, Ruwi, Al-Rusayl and Muttrah). In addition, field datasets were modeled and validated with artificial neural networks by using Python software for ozone concentration levels. The results of the study showed that road transportation and industrial activities were the main sources of air pollution in Muscat Governorate. It was also found that cities of Muscat were subjected to a considerable ozone concentrations which exceeded the local standards of 120 µg/m<sup>3</sup> occasionally.

*Keywords: Ambient air quality, Modeling, Ozone, Artificial neural networks*

## INTRODUCTION

Rapid growth of Oman's population and dramatic increase in on-road traffic emissions and industrial activities could lead to a deterioration in the ambient air quality especially in the capital city (Muscat). Air pollution levels require a robust and accurate assessment of air pollutant levels including emission sources in order to address the current air quality level in Muscat. The study focuses on the changes of ambient air quality in general and the changes of ozone (O<sub>3</sub>) concentration in particular. In addition, measured pollutant concentrations will be compared with the international standards such as WHO, European Union and United States Environmental Protection Agency (US EPA) standards.

Transportation is considered as one of the major sources of air pollution [1]. In addition, the production and distribution activities of petroleum fuel emits a large amount of air pollutants that form the O<sub>3</sub> due to accidental releases, loading and offloading of fuel [2]. During combustion processes transportation leads to the emission of CO, NO<sub>x</sub>, and VOC which ultimately forms the secondary air pollutants like O<sub>3</sub> that are associated with human health risks, damage to properties and vegetation [3].

The ground or field based measurement of air pollutants concentrations is still a major problem as it is very laborious and expensive to conduct [4].

Therefore, the applications of models and forecasting techniques for assessing air pollution levels have attracted attention by many air quality experts in recent years. Many developed countries have established air quality standards and guidelines for assessing the public health and ecological system [5].

## METHODOLOGY

The study includes data collection of ozone (O<sub>3</sub>), nitrogen oxides (NO<sub>x</sub>) and volatile organic compounds (VOC) in the ambient air from six locations in Muscat over one year along with metrological conditions. The collected data was used to predict O<sub>3</sub> levels using artificial neural network (ANN).

### Description of the study area

Muscat Governorate is the capital city of Oman which is characterized by high residential population with heavy traffic density, energy intensive industries, and constructional activities. In 2017, the city had a population of about 1,560,330. The city covers an area of approximately 3,500 km<sup>2</sup> (1,400 sq mi). It contains six provinces (AlAmerat, Bawshar, Muscat, Muttrah, Qurayyat and AlSeeb). It is located on 23°35'09.26" N and 58°24'21.32" E. The climate of Muscat is semi-arid and arid. The major seasons are



summer where average temperatures could reach as high as 49°C and winter season with relatively lower temperature (average 21°C). Rainfall occurs mostly between December and April with total amount of 100 mm.

### Field measurements

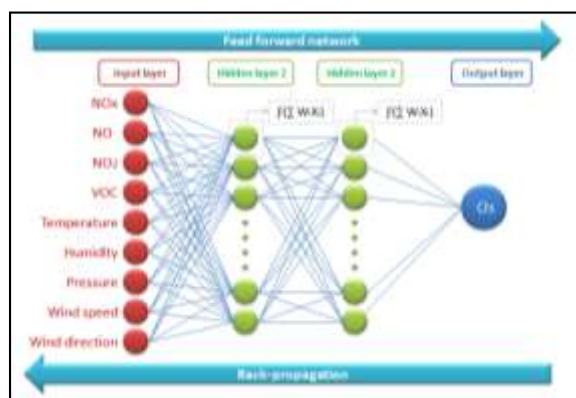
The meteorological parameters (air temperature, ambient pressure, relative humidity, wind direction and wind speed) and air pollutants (NO<sub>x</sub>, NO, NO<sub>2</sub>, VOC and O<sub>3</sub>) concentrations were measured with air pointer instrument. This equipment is designed to satisfy the European Norms and the regulations of the US Environmental Protection Agency. Table 1 shows the locations of the air quality monitoring sites.

Table 1 Air quality monitoring sites

| Location  | Longitude     | Latitude      |
|-----------|---------------|---------------|
| Al Amerat | N 23°28'.102" | E 58°29'.412" |
| AL Khwair | N23° 35'.630" | E58° 26'.527" |
| Muttrah   | N23°36'.915"  | E58° 35'.367" |
| Al Seeb   | N 23°40'.955" | E 58°11'.155" |
| Ruwi      | N 23°35'.645" | E 58°32'.636" |
| Al Rysail | N 23°33'.264" | E 58°12'.749" |

### Artificial neural network (ANN) model

Six ANN models were developed to assess and predict O<sub>3</sub> concentration in six cities of Muscat governorate (AlAmerat, AlSeeb, AlKhuwair, Ruwi, AlRysail and Muttrah). Eight variables were selected as input parameters (NO, NO<sub>2</sub>, VOCs, temperature, pressure, relative humidity, wind direction, and wind speed) while O<sub>3</sub> was selected as an output variable. The architecture of ANN contains an input layer of 8 neurons, two hidden layers of 30 neurons in each one and an output layer of one neuron as shown in Fig. 1.



### ANN Modeling Approach

The collected data were divided into 3 sets: training set (70% of the data), testing test (15%) and validation set (15%) as shown in Table 3. The models consisted of only completed measured data of each hour. Any row containing missing data were entirely deleted. The number of completed recorded data was 6273 for AlAmerat, 12717 for Muttrah, 6588 for Ruwi, 7722 for AlSeeb, 6651 for AlKhwaair and 11456 for AlRysail.

Table 3 The distribution of data to training, testing and validation sets.

| City      | Training | Testing | Validating |
|-----------|----------|---------|------------|
| AlAmerat  | 4391     | 941     | 941        |
| AlKhwaair | 4655     | 998     | 998        |
| Muttrah   | 8903     | 1907    | 1907       |
| AlSeeb    | 5406     | 1158    | 1158       |
| Ruwi      | 4612     | 988     | 988        |
| AlRysail  | 8018     | 1719    | 1719       |

There were close fits between the measured and observed values of  $O_3$  for all cities as shown in the Fig. 2 to Fig. 7 which show the modeling work for all combined sets (training, testing and validation) of each site. The models showed very good matching between simulated and measured  $O_3$  values in all sites. All models have shown  $R^2 > 0.9$  for training set except Al Rysail which got  $R^2 = 0.81$ , while Al Seeb had the highest  $R^2$  of 0.997. The study have shown that the variability of  $O_3$  concentration was greatly influenced by the variables which were used for the models development. After training the models, they were tested by 15% and validated by 15% of measured datasets. The results represented good models performances where  $R^2$  were ranged between 0.70 and 0.88.

In the comparison of upper and lower peaks values, Ruwi had the highest peaks in both predicted and measured  $O_3$  which reached above  $1000 \mu\text{g}/\text{m}^3$ . It is followed by AlRysail with upper peak values of  $419.3 \mu\text{g}/\text{m}^3$  for predicted  $O_3$  and  $364.22 \mu\text{g}/\text{m}^3$  for measured  $O_3$ . AlRysail also shows the highest lower peaks values for both measured and predicted  $O_3$  ( $47.1$  and  $28.83 \mu\text{g}/\text{m}^3$ , respectively). Muttrah had higher  $O_3$  peaks between in February 2018 compared with its  $O_3$  peaks in May 2018. Al Amerat showed  $223.81 \mu\text{g}/\text{m}^3$  as an upper peak for measured and  $217.78 \mu\text{g}/\text{m}^3$  as an upper peak for predicted  $O_3$  which are also considerable peaks values.

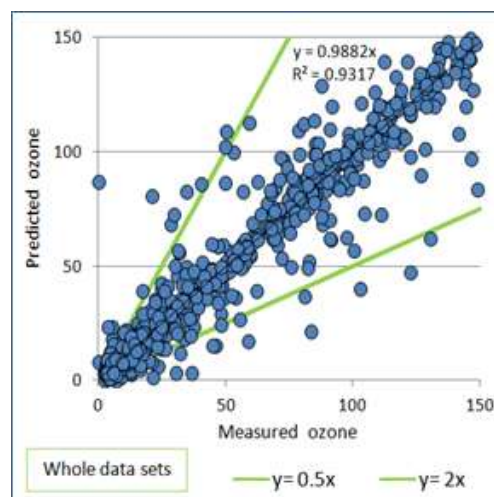


Fig. 2 Al Amerat ANN model.

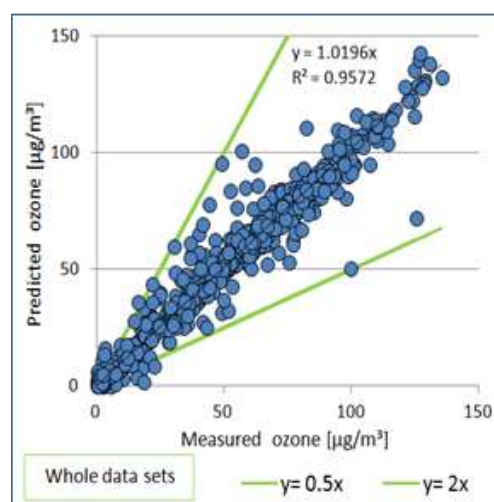


Fig. 3 Al Khuwair ANN model.

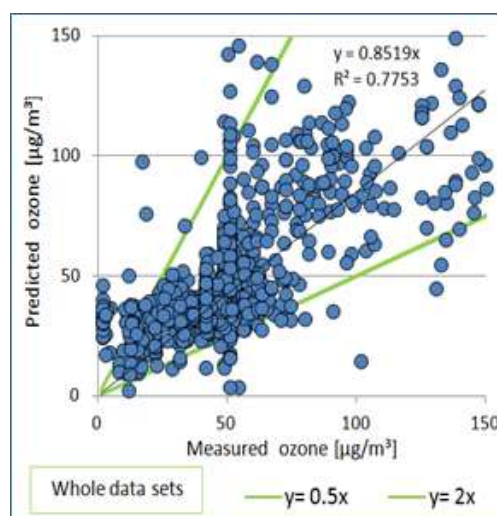


Fig. 4 Al Rysail ANN model.

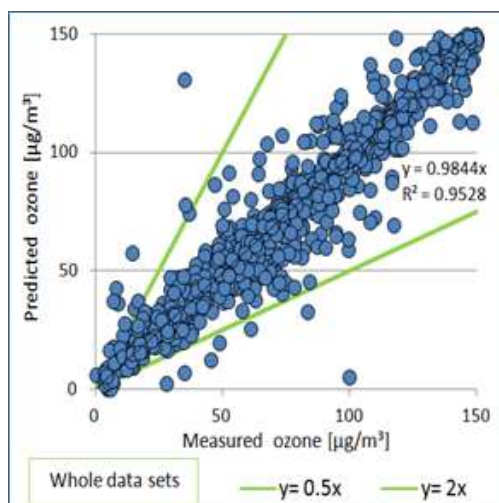


Fig. 5 Mattrah ANN model.

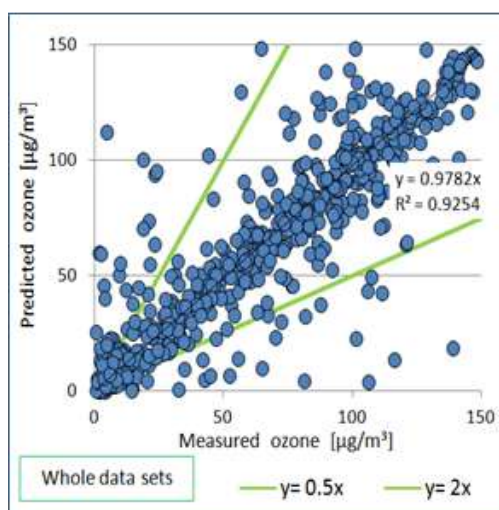


Fig. 6 Al Seeb ANN model.

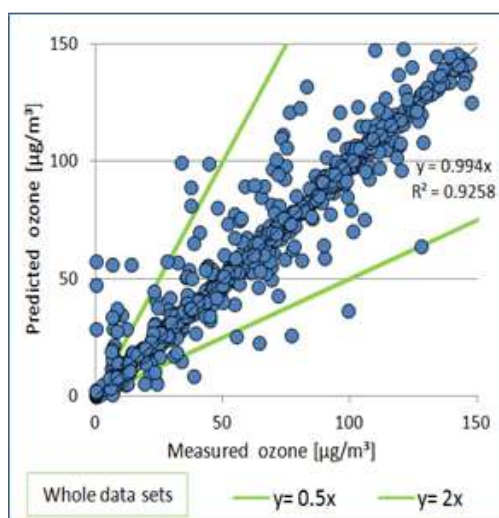


Fig. 7 Ruwi ANN model.

Table 4 illustrates the contribution percentage of metrological factors and air pollutants in the ANN models. The summation of metrological factors contribution percentage ranged between 31% and 63% where Ruwi had the highest percentage. In contrast, the summation of air pollutants (NO, NO<sub>2</sub> and VOC) contribution percentage ranged between 37% and 69% where Al Amerat had the highest percentage.

Table 4 Contribution percentages of input data

| City     | Contribution Percentage (%)                 |                           |
|----------|---|---------------------------|
|          | Air Pollutants<br>(NO,NO <sub>2</sub> ,VOC) | Meteorological<br>Factors |
| AlAmerat | 68.9  | 31.1                      |
| AlKhwait | 45.0  | 55.0                      |
| Muttrah  | 54.0  | 46.0                      |
| AlSeeb   | 44.7  | 55.3                      |
| Ruwi     | 36.8  | 63.2                      |
| AlRysail | 55.7  | 44.3                      |

## CONCLUSIONS

The emission of O<sub>3</sub> from road transportation and industrial sectors has received a serious attention from government and the scientific communities as it may cause considerable effects to the public health and environment. The O<sub>3</sub> levels in Muscat were assessed through application of ANN models in six sites. The O<sub>3</sub> concentration was predicted taking into consideration the metrological parameters and the O<sub>3</sub> precursors (NO<sub>x</sub> and VOCs) concentrations.

The obtained results showed that O<sub>3</sub> levels exceeded the 120 µg/m<sup>3</sup> (maximum level set by Ministry of Environmental and Climate Affairs) in all areas at different times of the days. The most affected area was Ruwi which had O<sub>3</sub> concentration 10 times compared to the recommended standard (1162.27 µg/m<sup>3</sup> as measured O<sub>3</sub> concentration and 1171.6 µg/m<sup>3</sup> as predicted O<sub>3</sub> concentration).

The obtained results showed strong relationship between O<sub>3</sub> and input parameters (NO<sub>x</sub>, VOC and meteorological). There were closed fit between the measured O<sub>3</sub> and the predicted O<sub>3</sub> from these parameters which indicated the dependency of O<sub>3</sub> concentration on these parameter. The negative correlation between O<sub>3</sub> and NO<sub>x</sub> and VOCs have shown that these pollutants are the precursors of O<sub>3</sub>.

It should be noted that the difference among O<sub>3</sub> concentration between cities may be due to their differences in geographical locations, the time periods of O<sub>3</sub> measurements (summer and winter), the presence of industrial areas, the number of vehicles and the presence of green vegetation.

## REFERENCES

- [1] Kinnon M. M., Zhu S., Carreras-Sospedra M., Soukup J.V., Dabdub D., Samuelsen G.S., and Brouwer J., Considering Future Regional Air Quality Impacts of the Transportation Sector. *Energy Policy*, Vol. 124, 2019, pp. 63–80.
- [2] Vijayaraghavan K., Cho S., Morris R., Spink D., Jung J., Pauls R., and Duffett K., Photochemical Model Evaluation of the Ground-Level Ozone Impacts on Ambient Air Quality and Vegetation Health in the Alberta Oil Sands Region: Using Present and Future Emission Scenarios. *Atmos. Environ.*, Vol. 141, 2016, pp. 209–218.
- [3] Alimissis A., Philippopoulos K., Tzanis C.G., and Deligiorgi D., Spatial Estimation of Urban Air Pollution with the use of Artificial Neural Network Models. *Atmos. Environ.*, Vol. 191, 2018, pp. 205–213.
- [4] Bowman K.W., Toward the Next Generation of Air Quality Monitoring: Ozone. *Atmos. Environ.*, Vol. 80, 2013, pp. 571–583.
- [5] Li R., Dong Y., Zhu Z., Li C., and Yang H., A Dynamic Evaluation Framework for Ambient Air Pollution Monitoring. *Appl. Math. Model.*, Vol. 65, 2019, pp. 52–71.

## STUDY ON MUSRENBANG MECHANISM IN INDONESIA TO PROMOTE SANITATION

Eddy Soedjono<sup>1</sup>, Wahyu Wijaya<sup>2</sup> and Nurina Fitriani<sup>3\*</sup>

<sup>1,2</sup>Environmental Engineering Department

Institut Teknologi Sepuluh Nopember, Surabaya, Indonesia

<sup>3</sup>Study Program of Environmental Engineering, Department of Biology, Universitas Airlangga, Surabaya, Indonesia

### ABSTRACT

Development in Indonesia is conducted both ways using top-down and bottom-up approach. A top-down approach is a kind of national development program from the central government to the lowest level of local government like desa or kelurahan. Musrenbangdes is a way to get feedback right from the grassroot for the Central Government. The aim of this research is to study on the musrenbang mechanism for sanitation. This study was conducted in the province of Bali, Jawa Timur (East Java), and Kalimantan Tengah (Central Kalimantan). Bali was selected to represent best sanitation program in Indonesia, while Kalimantan Tengah was selected to represent poor sanitation program. Jawa Timur is a mediocre province which can be easily assessed as ITS is surely in East Java. The selected districts in Bali, Jawa Timur, and Kalimantan Tengah are Karangasem, Bojonegoro, and Katingan. Musrenbang was mostly a male dominated forum. Although in Karangasem, Bali the musrenbang was conducted at day time, but still the participants were dominated by men. The musrenbang alone was conducted at night time during weekend. Women were not considered polite to go out at night to join the Musrenbang. Either it is good or poor it is not because of Musrenbang but it is caused by other mechanisms. However, it may be more formal in Bali, although the involvement of women were not that strong. Musrenbang was conducted at morning time which mean musrenbang is treated as formal as even compared in Kalimantan Tengah and Jawa Timur.

*Keywords: Musrenbang, Sanitation, Women attendance, Wastewater treatment*

### INTRODUCTION

Top-down approach is national development mechanism following the long term development planning or Rencana Pembangunan Jangka Panjang (RPJP) at national level down to the Rencana Pembangunan Jangka Menengah Daerah (RPJMD) or Village Medium Development Plan at village level [1]. Musrenbang (**mus**yarawah **perencanaan** **pembangunan**) or development planning forum is an official development process which implements the principle of bottom-up approach. This type of development approach could be merely used in Indonesia. This annual forum starts in January to approve next year work plan (RKP or Rencana Kerja Pembangunan) for musrenbangdes or musrenbang kelurahan (village musrenbang). Annual RKP is detail of the village five year medium development plan (RPJM Desa or **Rencana Pembangunan Jangka Menengah Desa**). In order to educate any citizen to actively involved in development governance, the Musrenbang was held to facilitate them with participatory and dialogical forum [2]. Some output for musrenbangdes would be list of village development priorities and use of ADD (village

budget allocation or **Anggaran Dana Desa**). Musrenbang mechanism is shown in Figure 1.

Musrenbang functions as a forum to produce agreement between development actors regarding the design of the RKP and the draft RKPD, which focuses on the discussion to synchronize work plans between ministries / institutions / units work of regional apparatus and between the Government, the Government Regions and communities in achieving development goals national and regional [3]. Society always involved in the policy making process produced by the government. This causes every policy produced by the government has big implications for the community [4].

Musrenbang is divided into 3 stages: pre-musrenbang, musrenbang, and post-musrenbang. Musrenbang must prioritize discussion on basic human rights like health, education, sanitation, job opportunities, and feeling secure. On practice, musrenbang is for beyond rich experience nor aspirative forum. It is more to an annual ritual development process with poor content and even is irrelevant for women and poor people. According to Musrenbang Guidance, the gathering must be attended by at least by 30% women and poor communities. Representatives from village must



comprise of at least 1 woman if there are 3 members or 2 women if 5 members. Community participation is influenced by interested parties and have an influence on the program. In this case, for the guidance and provision of information to the public, the role of the government and the private sector is needed [5].

Three provinces were selected to get to know whether Musrenbang was related to sanitation promotion. Bali was selected to represent good

sanitation program while Kalimantan Tengah was selected to represent poor sanitation program. Jawa Timur was also assessed as it was mediocre and located where the ITS was around. Overall, the sanitation condition in Indonesia is as shown in Figure 2a and 2b. The objective of this study is to access the impact of musrenbang mechanism to promote sanitation in order to achieve open defecation free (ODF) target of GOI (Government of Indonesia) universal access by 2019.

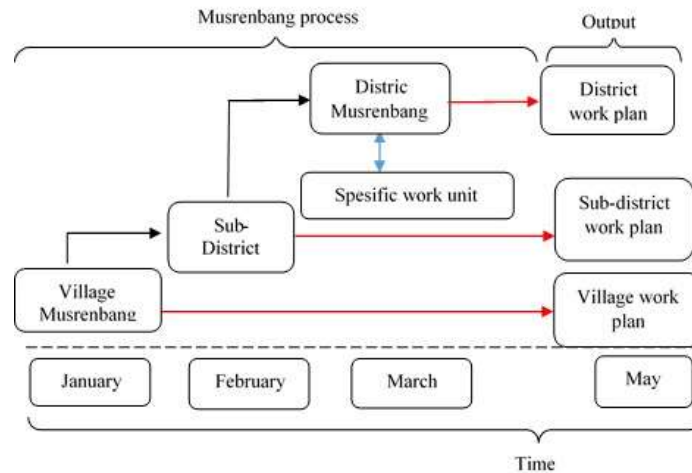


Fig. 1 Musrenbang mechanism

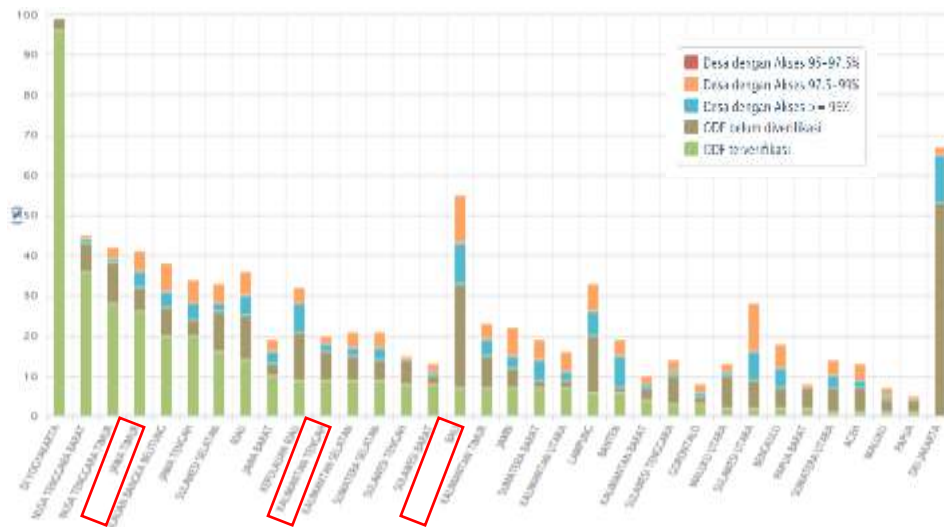


Fig. 2a Sanitation condition based on ODF achievement rank in Indonesia by 2017





Fig. 2b Sanitation condition based on progress in Indonesia by 2017

## MATERIALS AND METHOD

Feed-back for the Musrenbang was conducted through interview and focus group discussion (FGD). The selected districts at Bali, Jawa Timur, dan Kalimantan Tengah were subsequently Karangasem, Bojonegoro, dan Katingan. Interview and FGD were conducted to follow the Musrenbang guidance started from the village level, then to Sub-Distrik, Distrik, than the Provincial level. As Musrenbang Forum was not coincide with the interview and FGD, then Musrenbang Forum could not be attended and the condition during the discussion was asked in the interview or FGD. The interview and FGD was basically around how Musrenbang was conducted in the three selected districts. Important information that was asked were: when the Musrenbang was conducted, was it attended by women, and was sanitation discussed during the Musrenbang.

## RESULTS AND DISCUSSION

Musrenbang visits have been conducted at Karangasem District of Bali Province, Bojonegoro District of Jawa Timur, and Katingan District of Kalimantan Tengah. The musrenbang visits were done from the lowest level of local government or village up to the highest level which were provinces. These results are below.

### Musrenbang at Karangasem District, Bali

The province of Bali consisted of 8 districts and 1 city. Karangasem District as one of the district

consisted of 8 sub-districts. Muntigunung Village as part of Kubu Sub-district was selected as case study area. Karangasem had a lot number of poor people and lacking of decent housing [6]. One problem that was still exist in Karangasem was the availability of clean water in several sub-district areas. From 78 sub-districts in Karangasem district, there are 19 sub-districts that have not been served clean water by the PDAM (Perusahaan Daerah Air Minum) Karangasem district [7]. In the field of sanitation, Karangasem had communal wastewater treatment in some areas. In collaboration with Karangasem BAPPEDA, local government made campaign in all districts in term of sanitation practice. Regular social gathering with latrine as the subject was regularly held by the local community. This agenda belonged to the Community Based Total Sanitation (STBM) which was regulated by Health Ministry. In this case, the local government had a role as facilitator. STBM in Karangasem District was held in 52 villages and resulted of 180 ODF households. The implementation of sanitation program in Karangasem was the result of collaboration between sanitation working group, public health office, and local community. Musrenbang practice in Karangasem was then followed by Kubu and Tianyar Barat as representative of sub-district and village level, respectively.

Beginning with Musrenbang forum at village level, there were many sanitation programs proposed to the sub-district level. This forum was attended by representative of related institutions, local communities, and community leaders. Musrenbangdes was conducted at day time during working hour. Musrenbang was mainly attended by

men where sanitation was hardly ever discussed in the forum. Tianyar Barat was selected as representative of village level in Musrenbang practice. Some households in Tianyar Barat had private latrine in their house. Health Department of Karangasem Regency stated that the use of latrine in Tianyar Barat reached 57,7%. Currently, Tianyar Barat had sanitation committee with the objectives of sanitation planning although they were not optimal yet. Several sanitation programs have been proposed in the Musrenbang forum in Tianyar Barat, such as latrine provision and sanitation counselling. The programs, however, have not been in priority as compared with road construction, house reparation, and water supply. Low level of knowledge of the community caused sanitation was not an urgent issue.

Musrenbang in Kubu Sub-District was held annually in February as continuation of the Musrenbang in Tianyar Barat as lowest level. Kubu Sub-District is divided into 4 villages (Ban, Tianyar, Tianyar Barat, Tianyar Tengah). Musrenbang forum was attended by all village chiefs, community, and related institutions. Musrenbang in sub-district level was a forum to accommodate proposed programs from each village and ranked based on priority scale. Those proposed programs could not be funded by village government would be funded by higher level of government. In arranging scale priority, the meeting was divided into 3 groups to discuss economic, public facility, and environment health and culture. All about this proposals would be discussed in district musrenbang to make bigger priority programs from different sub-district. As the results, each programs would be ranked based on the urgency and budgeting. The feedback from district musrenbang would be given to all sub-districts and villages as confirmation.

#### **Musrenbang at Bojonegoro District, Jawa Timur**

The province of Jawa Timur consisted of 29 districts and another 9 cities. Bojonegoro District consisted of 12 sub-districts. Pagerwesi Village as part of Trucuk Sub-district was selected as case study area. The pre-musrenbang or agencies/SKPD musrenbang was coordinated by Badan Koordinator Wilayah (Bakorwil; a kind of Provincial Office Representative) of Jawa Timur Province. This was based on Provincial Regulation regarding Governance and Responsibility of Bakorwil [8]. Main function of Bakorwil was to arrange technical policy to support the regional administration and development. On this forum, all related SKPD and representatives of each district were to discuss and bargain the proposed programs for priorities.

Musrenbangdes was generally conducted at night time and mostly during weekends. Musrenbang was mainly attended by men which sanitation were almost not discussed in the forum.

Women were not considered polite to attend meeting during night-time. Musrenbangdes was attended by local government, local public figures, religious figure, and the representative of farmer community, fisherman community, woman community, children protection community, environment community and poor people community. There was some triggering practice from the local government and health service (midwife) regarding sanitation. This regularly practice has encouraged sanitation proposed programs. The village government would provide subsidies to latrine installment for poor community; they had to make a statement letter about their willingness to have and use latrines.

Musrenbang in regional level generally was held in April and attended by government, private sector representatives, society, and even students of universities. The forum of regional level would be plenary session I, group session, and plenary session II. Those session aimed to align the needs of each community with the government work plan. In terms of sanitation development plan, the discussion carried out as follows:

- a. Aspirations from the community from periodical discussion held by the related institutions,
- b. Sanitation development plan confirmed by Bupati (head of the district) or Mayors,
- c. Third party involvement in form of Corporate Social Responsibility (CSR) especially in sanitation development,
- d. Collaboration of many institutions in sanitation development plan, such as health agency, public works, environmental agency, and others,

Generally, the group plenary was divided into 4 main fields namely economic (group I), infrastructure and regional development (group II), government, social, statistic and reporting (group III), and Non-Government Financing (group IV). The group plenary would be conducted by chairman and moderator. The group plenary included the exposure of RKPD draft by each chairman in order to get responses and clarification from all of the participant. Then representative of each groups joined the plenary session II. In this session, each representative presented the results of group plenary. The summary of plenary session was included to the agreement of result of Musrenbang. The results of Musrenbang in regional level involved some appropriate programs and financed by Regional APBD.

#### **Musrenbang at Katingan District, Kalimantan Tengah**

The province of Kalimantan Tengah consisted of 13 districts and 1 city. Katingan District as one of the districts consisted of 7 sub-districts. Kalimantan

Tengah Province became representative of worst sanitation case in this research. According to national sanitation index, Kalimantan Tengah placed on rank 24 of 34 provinces in Indonesia. According to the data of latrine and wastewater treatment utilization, the ownership and coverage were very low. It was only 10,7% of ODF had been achieved in 2014. As onsite system for wastewater treatment, about 86,7% of community still used un-standard septic tank; only 2,2% was standard septic tank. The provision of sanitation facilities in Katingan District was still limited. There was no wastewater treatment plants nor fecal sludge processing facility yet. Open defecation still happened particularly for communities who lived along the river. Open defecation became habit of the communities which was coupled with having toilets above the river directly [9]. Most challenge of sanitation development in Katingan was to increase the environmental awareness [10]. Government support in providing proper sanitation system would be recommended.

A different case arose in Kalimantan Tengah Province in term of sanitation development, i.e.: little number of proposed program in sanitation of musrenbangdes. This was to indicate that sanitation was still not an urgent issue. Musrenbang was mainly attended by men which sanitation were almost not discussed in the forum. Most issues mostly involved in the proposed program were road and bridge construction, housing improvement, and water supply. Katingan had already Environmental Health Risk Assessment (EHRA) study and Memorandum Program for Sanitation (MPS) which became the guideline for sanitation development. As the same case with Tianyar Barat, Kalimantan Tengah had also sanitation work group (POKJA Sanitasi) in provincial level although the group was not active yet.

## CONCLUSION

Village musrenbang (musrenbangdes) at Muntigunung Village of Bali was conducted more formal as compared to other villages in Jawa Timur and Kalimantan Tengah. Musrenbang was done during working hours as compared to Jawa Timur which was conducted during night time and even during weekends. The participants of musrenbang, however, it was a male dominated forum in all musrenbangdes. Furthermore, sanitation and water supply as one of basic human rights, were not discussed in the forum. This also concluded that good or poor provincial sanitation condition was not affected by musrenbang.

## REFERENCE

- [1] Undang-Undang Nomor 25 Tahun 2004 tentang Sistem Perencanaan Pembangunan Nasional.
- [2] Soedjono, E.S., Fitriani, N., Rahman, R., Wijaya, I., M., W. 2017. Achieving Water Sensitive City Concept Through Musrenbang Mechanism in Surabaya City, Indonesia. *International Journal of Geomate*, 15 (49), 92-97. DOI: <https://doi.org/10.21660/2018.49.3649>.
- [3] Petunjuk Teknis Penyelenggaraan Musrenbang (PTPM) Tahun 2006.
- [4] Azhar, F. 2015. Partisipasi Masyarakat Dalam Musyawarah Perencanaan Pembangunan (MUSRENBANG) di Kelurahan Pegirian Kecamatan Semampir Kota Surabaya, *Jurnal Kebijakan dan Manajemen Publik* 3(2): ISSN 2303-341X.
- [5] Gedeona, A. B. 2014. Partisipasi Masyarakat Dalam Musyawarah Perencanaan Pembangunan Kecamatan Larantuka Kabupaten Flores Timur, *Jurnal Administrasi Publik dan Birokrasi* 1(3).
- [6] Badan Pusat Statistik Kabupaten Karangasem, 2015, Kabupaten Karangasem Dalam Angka 2015, report.
- [7] Perda Kab. Karangasem No. 9 Thn. 2011. Rencana Pembangunan Jangka Menengah Daerah (RPJMD) Kabupaten Karangasem Tahun 2010-2015. Perda Kab. Karangasem, Karangasem.
- [8] Peraturan Daerah Provinsi Jawa Timur No 12 Tahun 2008 Tentang Organisasi dan Tatakerja Badan Koordinasi Wilayah Pemerintahan dan Pembangunan Jawa Timur.
- [9] Dahal, K. R., Adhikari, B., Tamang, J. 2014. Sanitation Coverage and Impact of Open Defecation Free (ODF) Zone with Special Reference to Nepal. A Review, *International Journal of Engineering Research and Application* 4(8): 118-128.
- [10] Manullang, Z. D. 2014. Evaluasi Dampak Program Sanitasi Berbasis Masyarakat (SANIMAS) Dalam Pemberdayaan Masyarakat (Studi di Kelurahan Bagan Deli Kecamatan Medan Belawan Kota Medan): Master's Thesis, Medan Universitas Sumatera Utara.

## THE IMPACT OF EXPOSURE TO AEROSOL MOSQUITOES REPELLENT RELATED TO FREE RADICALS ON THE ORGANS OF MALE RATS

Unggul P. Juswono<sup>1</sup>, Arinto Y. P. Wardoyo<sup>1</sup>, Chomsin S. Widodo<sup>1</sup>, Johan A. E. Noor<sup>1</sup>, and Didik R. Santoso<sup>1</sup>

<sup>1</sup>Mathematics and Natural Sciences Faculty, University of Brawijaya, Indonesia

### ABSTRACT

From year to year, human activities using chemical substances lead to pollute ambient air and affect human health. This pollutant can pass through the respiratory system and disrupts the organ function, including lung, liver, blood, and kidney. It can be identified by the deformation found in the structure and function change of the related cells in these organs and the existence of free radical. On the other hand, each substance has a different composition and health effect. The possibility of the free radical type that is formed is also different and related to the substance. According to this background, it is a need to determine the presence of free radicals in the rat's organs exposed to one push aerosol mosquito repellents as the substance. This study aimed to investigate the free radicals on the rat's organs due to the exposure to aerosol mosquito repellent and its relation with the organ damage of cell deformation. This study used male rats as the experimental animals that were divided into control and treatment groups. The study included two types of repellents, Type-A (25% of aerosol concentration) and Type-B (21.3% of aerosol concentration). Free radicals were detected using an electron spin resonance device. The results showed that the cell deformation due to the exposure of one push aerosol was different for each organ. The deformation levels were about 36% to 74% that depended on the aerosol concentration. The exposed aerosol generated anion superoxide ( $O_2^-$ ) and singlet oxygen radicals ( $^1O_2$ ) as the free radicals found in the observed organs.

*Keywords: Aerosol; Free radical; Organ damage; Pollutant; Rat.*

### INTRODUCTION

Indonesia is a big country that has a tropical climate, where the tropical climate is very suitable for the breeding process of insects, especially mosquitoes. Mosquitoes themselves can cause various diseases. That is why it needs some efforts to overcome the increasing number of diseases caused by mosquitoes.

Eradication of mosquitoes tends to be carried out using free-selling insecticides. The effort to eradicate mosquitoes by using insecticides is only a temporary thing and has no preventive effects for a longer period. Insecticides that are widely used by the community can have a negative impact on the environment and humans due to the dangerous chemical compounds contained in the insecticide.

One push aerosol mosquito repellent is one of the substances that are often used in Indonesia, especially in daily life due to its practice use compared to another insecticide. However, the usage of this mosquito repellent is growing from time to time. As a consequent, it also contributes to a pollutant in the ambient air. It contains transfluthrin, as an insecticide ingredient.

In the human body, transfluthrin tends to be reactive because it has unpaired electrons [1]. These electrons come from oxygen atoms in transfluthrin in cyclic rings, as a result of their reaction to the

mono oxidase acid (H<sup>+</sup>) enzyme [2]. These unpaired electrons will look for pairs from other parts of the cell [3]. Transfluthrin which enters the body may trigger the formation of free radicals.

Free radicals are atoms, elements, compounds, or molecules that have one or more unpaired electrons in their outer orbitals [4]. These unpaired electrons are very reactive and tend to look for pairs by attacking and binding electrons to stable molecules around them [5–7]. The mechanism or process of free radical formation has several stages. The stages of free radical formation are initiation (initial formation of free radicals), propagation (propagation or new radical formation), and termination (destruction or conversion into stable and unreactive free radicals) [3]. The impact of free radicals on cells is the disruption of cell function or treating abnormal cell function [8]. Disorders of cell function consist of short-age cells characterized by wrinkled skin, premature aging, and degenerative diseases. The body's defense system is reduced so that the body becomes weak and easily injured [9]. Abnormal reactions from cells can grow new cells that trigger tumor cell growth and cancer [10,11].

According to this background, it is urgently required to identify free radicals generation in the body related to the use of one push aerosol mosquito repellent. Thus, the purpose of this study was to identify the types of free radicals in rat's organs that

were exposed to one push aerosol mosquito repellent. This study also investigated the influence of different transfluthrin concentrations on the free radical existence, so that an alternative step can be sought to deal with further organ damage.

## MATERIALS AND METHODS

### Experimental Animals

This study used healthy male Wistar rats with the age of 2-3 months old (with 23-30 grams of BW (body weight)). The rats were treated humanely and feed with food and water *ad libitum* and kept in controlled animal cages (temperature: 24 - 27°C, relative humidity: 75 - 78%) with 12 h dark/ light cycle [12]. All of them ( $n = 21$ ) were acclimatized in an experimental chamber (20 x 20 x 30 cm<sup>3</sup>) for three consecutive days before being divided randomly into two treatment groups (Group-A and Group-B) and one control group (Group-C). The rats in each treatment group received similar treatment related to the transfluthrin concentration ( $n = 7$  per group, Table 1). All procedures were in accordance with the Animal Care and Use Committee of Brawijaya University, Malang, East Java, Indonesia (Ethical Clearance Number: 541-KEP-UB).

Table 1 Scheme of the experimental animals used in the study ( $n = 21$ )

| Groups  | Number of Sprays | Rats | Transfluthrin Type            |
|---------|------------------|------|-------------------------------|
| Group-A | 5 sprays         | 7    | Type-A (25% of transfluthrin) |
| Group-B | 5 sprays         | 7    | Type-B (21.3% transfluthrin)  |
| Group-C | -                | 7    | -                             |

### Transfluthrin Content

This study used two different one push aerosol mosquito repellents. They were Type-A and Type-B mosquito repellents with different transfluthrin concentrations. Type-A and Type-B mosquito repellent had 25% and 21.3% of transfluthrin concentrations, respectively.

### Animal Treatments

According to Table 1, Group A was a group of rats exposed to one push aerosol Type-A mosquito repellent as much as five sprays. Group B was a group of rats which were exposed to one push Type-

B with five times sprays. These treatments were done in a similar time and controlled room temperature. These treatments were conducted for twenty minutes per day within 30 consecutive days.

### Organs Preparation

After exposure procedures, all rats were sacrificed by cervical dislocation. The kidneys, livers, and lungs (organ samples) were cleaned using NaCl (0.9%) and were fixed in buffered formalin (10%) for a week before being dehydrated in upgraded ethanol series. After that, they were processed to the paraffinization and cutting, then colored using hematoxylin and eosin. For the blood samples, the blood smears on the object glass were fixed with methanol solution (70%) and dried. After that, these samples were colored using Giemsa and buffer pro-Giemsa solution. All resulted samples were observed under a microscope (400x of magnification) to investigate the level of cell physical damages (blind counting method) [12–14].

### Free Radicals Investigation

The presence of free radicals in the samples was detected using ESR (Electron Spin Resonance, Fig.1). The sample was placed in a magnetic field and given interference with electromagnetic waves in radio frequency  $f$ . The magnitude of the magnetic field given depending on the amount of electric current  $I$  flowing in the Helmholtz coil and could be calculated using Eq. (1) below.

$$\mu_0 \cdot \left(\frac{4}{5}\right)^{\frac{3}{2}} \cdot \frac{n}{r} \cdot I \quad (1)$$

where,

$$\begin{aligned} \mu_0 &: 1.2566 \times 10^{-6} \text{ (T.m/A)} \\ B &: \text{external magnetic field (T)} \\ I &: \text{current on the Helmholtz coil (A)} \end{aligned}$$

The number of turns of Helmholtz coil was interpreted as  $n$  ( $n = 320$  coils), with the radius ( $r$ ) of 6.8 cm.

The type of the detected free radicals is determined using Lande factor ( $g$  factor) calculation, as expressed in Eq. (2).

$$g = \frac{h \cdot f}{\mu_B \cdot B} \quad (2)$$

where,

$$\begin{aligned} \mu_B &: \text{Bohr magneton } (9.273 \times 10^{-24} \text{ J/T}) \\ h &: \text{Planck constant } (6.625 \times 10^{-34} \text{ Js}) \\ f &: \text{resonance frequency (Hz)} \end{aligned}$$

Table 2 Values of  $g$  factor of singlet oxygen and superoxide free radicals

| Free Radical Name                   | $g$ Factor Value  |
|-------------------------------------|-------------------|
| $^1\text{O}_2$                      | 1.501             |
| $\text{O}_2^-$                      | 1.501 - 1.750     |
| $\text{Fe}^{3+}$                    | 1.77              |
| $\text{MnO}_2$                      | 1.8367            |
| FeS                                 | 1.86              |
| Hydroperoxide                       | 1.9896            |
| $\text{CO}_2^-$                     | 1.996             |
| Cu                                  | 1.997             |
| $\text{SO}_4^-$                     | 1.9976            |
| Hydroxyl                            | 2.00047           |
| $\text{CO}_2$                       | 2.0007            |
| Alkoxy                              | 2.00160 - 2.00197 |
| Helium                              | 2.002             |
| Methanol                            | 2.00205           |
| Alkyl                               | 2.00206           |
| Hydrogen                            | 2.00232           |
| Methyl                              | 2.00255 – 2.00286 |
| DPPH                                | 2.0036            |
| $\text{SO}_3^-$                     | 2.0037            |
| Ethyl                               | 2.0044            |
| C                                   | 2.00505 – 2.00548 |
| Peroxy                              | 2.0155 – 2.0265   |
| $\text{CuO}_x$                      | 2.098             |
| $\text{CuGeO}_3$                    | 2.154             |
| $\text{YBa}_2\text{Cu}_3\text{O}_7$ | 2.24              |
| Cu-HA                               | 2.289             |
| Hg                                  | 4.0 – 4.5         |

According to Eq.(2),  $f$  was determined from the existence of RF wave resonance. This wave resonance was identified by forming a V-shaped curve on the oscilloscope. This curve was a combination of two RF waves with a phase difference of  $135^\circ$  (Lissajous curve).

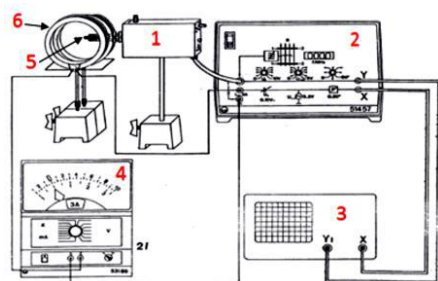


Fig. 1 The set up of Leybold-Heracus ESR devices, where: 1). radio frequency control unit; 2). ESR control unit; 3) oscilloscope; 4). multimeter; 5). sample place; and 6). Helmholtz coil.

## Statistical Analysis

The resulted values were shown as mean  $\pm$  SEM (standard of means). All statistical analysis was performed using Microsoft Excel 2016.

## RESULTS AND DISCUSSION

### ESR Calibration

For a better result, a DPPH calibrator (DPPH radical is a stable free radical) was used to calibrate ESR [15]. The resulted  $g$  factor was compared to the literature. Table 3 below shows the result of the calibration using DPPH. According to the calibration, the resulted calibration factor was 0.9964. The V-shaped curve (RF wave resonance) and a Lissajous curve are shown in Fig.2-Fig.3.

Table 3 Result of ESR calibration using DPPH

| $f$ (MHz) | $I$ (A) | $g$ Factor (literature) | $g$ Factor (calibration) |
|-----------|---------|-------------------------|--------------------------|
| 23.7      | 0.199   | 2.0036                  | 2.0109                   |



Fig. 2 DPPH resonance curve.

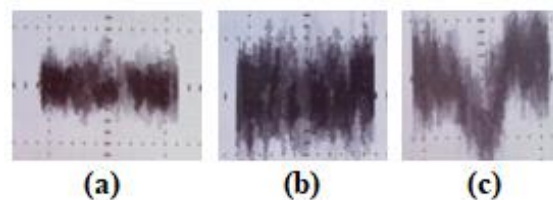


Fig. 3 The Lissajous curves for (a) research tube; (b) control group; and (c) treatment group.

### Formed Free Radicals

The exposure to one push aerosol mosquito repellents (Type-A and Type-B) had a direct impact in rat's organs. According to ESR analysis, the exposure treatments generated some free radicals



with similar  $g$  factor value (Table 4). The presences of  $O_2^-$  (superoxide) and  $^1O_2$  (singlet oxygen) in rat's organs indicate the form of ROS (reactive oxygen species) [9,16,17]. ROS in the rat's organs can be used to predict the presence of oxidative stress in cells, showing the inability of cells in overcoming the excess amount of free radicals.

Based on the results, the level of organ damage varies. The most damage organ is the lung cells (alveolar cells, 74-78%), where Type-B with lesser transfluthrin concentration has 74% of cell physical damage. Liver cells (hepatocytes) has 36% and 40% of cell physical damages, respectively for Type-A and Type-B, having the least impact of transfluthrin exposure. According to these results (see Table 4), we can see that the cell physical damages and free radical generation is directly correlated with the different concentration of the exposed transfluthrin. As an active substance, transfluthrin belongs to the pyrethroid group. According to the previous study, pyrethroids have low toxicity that is safe to use in

humans. Occasionally, the pyrethroid group can be categorized to toxin when the level of deposited pyrethroid exceeds the normal dose. As an impact, if toxin enters the body continuously, it may accumulate and may cause damage to the organ due to the free radicals.

In the human body, free radical is generated during normal cellular metabolism [15]. Besides, the human body has its antioxidant defense mechanisms to equilibrate the free radicals formations [9,17]. However, any disruption in this mechanism may disturb the equilibrium in the body resulting in oxidative stress, including cell deformation or cell physical damage [18].

The mechanism of cell damage due to transfluthrin begins when transfluthrin attaches to the cell membrane. When transfluthrin is inhaled by the respiratory organ, it may follow the bloodstream, passes through the lungs.

Table 4 The detected free radicals in rat's organ exposed to one push aerosol mosquito repellents

| Organs | Type-A     |               |                          | Type-B     |               |                          |
|--------|------------|---------------|--------------------------|------------|---------------|--------------------------|
|        | $g$ Factor | Free Radicals | Cell Physical Damage (%) | $g$ Factor | Free Radicals | Cell Physical Damage (%) |
| Liver  | 1.560      | $O_2^-$       | $40 \pm 3$               | 1.500      | $^1O_2$       | $36 \pm 3$               |
|        | 1.526      | $O_2^-$       |                          | 1.490      | $^1O_2$       |                          |
|        | 1.518      | $O_2^-$       |                          | 1.517      | $O_2^-$       |                          |
|        | 1.492      | $^1O_2$       |                          | 1.593      | $O_2^-$       |                          |
|        | 1.560      | $O_2^-$       |                          | 1.560      | $O_2^-$       |                          |
| Kidney | 1.568      | $O_2^-$       | $47 \pm 3$               | 1.576      | $O_2^-$       | $49 \pm 3$               |
|        | 1.542      | $O_2^-$       |                          | 1.584      | $O_2^-$       |                          |
|        | 1.466      | $^1O_2$       |                          | 1.474      | $^1O_2$       |                          |
|        | 1.483      | $^1O_2$       |                          | 1.483      | $^1O_2$       |                          |
|        | 1.509      | $O_2^-$       |                          | 1.509      | $O_2^-$       |                          |
| Blood  | 1.545      | $O_2^-$       | $71 \pm 3$               | 1.526      | $O_2^-$       | $72 \pm 4$               |
|        | 1.577      | $O_2^-$       |                          | 1.560      | $O_2^-$       |                          |
|        | 1.628      | $O_2^-$       |                          | 1.577      | $O_2^-$       |                          |
|        | 1.550      | $O_2^-$       |                          | 1.507      | $O_2^-$       |                          |
| Lung   | 1.557      | $O_2^-$       | $74 \pm 4$               | 1.517      | $O_2^-$       | $72 \pm 4$               |
|        | 1.535      | $O_2^-$       |                          | 1.508      | $O_2^-$       |                          |
|        | 1.576      | $O_2^-$       |                          | 1.543      | $O_2^-$       |                          |

Besides, the function of normal blood related to the hemoglobin as an oxygen binder may be disrupted. Hemoglobin may tend to bind transfluthrin rather than oxygen to be circulated throughout the body and becomes a toxin in the body. This process then triggers other disruptions, including the bad impacts of nutrients, fats, hormones, and proteins. Moreover, pyrethroid can manifold cypermethrin and fenvalerate, resulting in oxidative stress and changes in antioxidant enzymes [19]. They have a high potential to interfere with nerve activity, membrane depolarization, and synaptic disorders [20]. They then may trigger the

formation of free radical. This free radical formation (singlet oxygen) process occurs during the process of oxidative metabolism where there is an electron leak that can form  $O_2^-$  [3,21]. The entry of transfluthrin as toxins into cells may trigger mitochondria to produce more  $O_2^-$  (Fig.4).

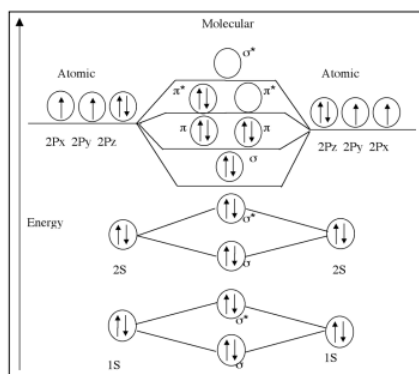


Fig. 4 Singlet oxygen electron configuration [22].

The main formation of ROS (reactive oxygen species) such as superoxide occurs in the mitochondria through the interaction of  $O_2$  with Coenzyme Q (KoQ) [23]. Some electrons moving from NADH and other compounds to  $O_2$  may pass when KoQH interacts with  $O_2$  and form superoxide radicals [24]. Moreover, mitochondria also contain high SOD (superoxide dismutase) and glutathione [25]. Dismutase is determined as the main defense against oxidative stress that occurs in the body, in which it is triggered by chemical enzyme induction or conditions that increase superoxide formation [25].

## CONCLUSIONS

Exposure to transfluthrin contained in one push aerosol mosquito repellents on rats has an influence on the existence of the free radical on the rat's organs. They are detected as superoxide anions (g factor 1.501 - 1.750,  $O_2^-$ ) and singlet oxygen (g factor 1.501,  $^1O_2$ ), in which generating 36% to 74% of cell deformation levels (depending on the transfluthrin concentration and rat's organs). The forming process of free radicals likely takes apart during the oxidative metabolic process where there is an electron leak that can form  $O_2^-$ . The entry of transfluthrin into cells can trigger mitochondria to produce more  $^1O_2$ .

## ACKNOWLEDGMENTS

The author's team acknowledge all members of the Laboratory of Advanced Physics and Biophysics, Physics Department, Brawijaya University (Malang city, East Java province, Indonesia), for their excellent hands and efforts during the experiment.

## REFERENCES

[1] Yoshida T., Biomarkers for monitoring transfluthrin exposure: Urinary excretion

- kinetics of transfluthrin metabolites in rats, *Environ. Toxicol. Pharmacol.*, Vol. 37, 2014, pp. 103–109.
- [2] Pauluhn J. and Ozaki K., Transfluthrin: Comparative efficacy and toxicity of reference and generic versions, *Regul., Toxicol. Pharmacol.*, Vol. 71, 2015, pp. 78–92.
- [3] Halliwell B., Free radicals, antioxidants, and human disease: Curiosity, cause, or consequence?, *Lancet*, Vol. 344, 1994, pp. 721–724.
- [4] Wang G., Jia S., Niu X., Tian H., Liu Y., Chen X., Li L., Zhang Y., and Shi G., Total free radical species and oxidation equivalent in polluted air, *Sci. Total Environ.*, Vol. 609, 2017, pp. 1103–1113.
- [5] Zukowski P., M. Maciejczyk M., and Waszkiel D., Sources of free radicals and oxidative stress in the oral cavity, Vol. 92, 2018, pp. 8–17.
- [6] Wedgwood S., Steinhorn R.H., and Lakshminrusimha S., Optimal oxygenation and role of free radicals in PPHN, *Free Radic. Biol. Med.*, 2019, pp. 1–10.
- [7] Premaratne S., Amaratunga D.T., Mensah F.E., and Mcnamara J.J., Significance of oxygen free radicals in the pathophysiology of hemorrhagic shock – A protocol, *Int. J. Surg. Protoc.* Vol. 9, 2018, pp. 15–19.
- [8] Phaniendra A. and Babu D., Free radicals: Properties, sources, targets, and their implication in various diseases, *Indian J. Clin. Biochem.*, Vol. 30, 2015, pp. 11–26.
- [9] P, S. R., Kalva S., Yerramilli A., and Mamidi S., Free radicals and tissue damage: Role of antioxidants, *Free Radicals Antioxidants*, Vol. 1, 2011.
- [10] Ríos-arrabal S., Artacho-cordón F., León J., Román-marinetto E., Salinas-asensio M. del M., Calvente I., and Núñez M.I., Involvement of free radicals in breast cancer, *Springer Plus*, Vol. 2, 2013, pp. 1–12.
- [11] Pourahmad J., Salimi A., and Seydi E., Role of oxygen free radicals in cancer development and treatment, *IntechOpen*, 2016, pp. 347–362.
- [12] Wardoyo A.Y.P., Juswono U.P., and Noor J.A.E., Association of diesel exhaust particle exposure with erythrocytes deformation of male mice, *Appl. Ecol. Environ. Res.*, Vol. 16, 2018, pp. 5583–5593.
- [13] Wardoyo A.Y.P., Juswono U.P., and Noor J.A.E., A study of the correlation between ultrafine particle emissions in motorcycle smoke and mice erythrocyte damages, *Exp. Toxicol. Pathol.*, Vol. 69, 2017, pp. 649–655.
- [14] Wardoyo A.Y.P., Juswono U.P., and Noor J.A.E., Varied dose exposures to ultrafine particles in the motorcycle smoke cause kidney cell damages in male mice, *Toxicol. Reports.*, Vol. 5, 2018, pp. 383–389.

- [15] Jing Y., Diao Y., and Yu X., Free radical-mediated conjugation of chitosan with tannic acid: Characterization and antioxidant capacity, *React. Funct. Polym.*, Vol. 135, 2019, pp. 16–22.
- [16] Battin E.E. and Brumaghim A.J.L., Antioxidant activity of sulfur and selenium: A review of reactive oxygen species scavenging, glutathione peroxidase, and metal-binding antioxidant mechanisms, *Cell Biochem. Biophys.*, Vol. 55, 2009, pp. 1–23.
- [17] Rahman K., Studies on free radicals, antioxidants, and co-factors, *Clin. Interv. Aging.*, Vol. 2, 2007, pp. 219–236.
- [18] Mason R.P., Imaging free radicals in organelles, cells, tissue, and in vivo with immuno-spin trapping, *Redox Biol.*, Vol. 8, 2016, pp. 422–429.
- [19] Akbar S.M.D., Sharma H.C., Jayalakshmi S.K., and Sreeramulu K., Effect of pyrethroids, permethrin and fenvalerate, on the oxidative stress of *Helicoverpa armigera*, *World J. Sci. Technol.*, Vol. 2, 2012, pp. 1–5.
- [20] Soderlund D.M., Molecular mechanisms of pyrethroid insecticide neurotoxicity, *Arch. Toxicol.*, Vol. 86, 2013, pp. 165–181.
- [21] Takagi D., Takumi S., Hashiguchi M., Sejima T., and Miyake C., Superoxide and singlet oxygen produced within the thylakoid membranes both cause photosystem I photoinhibition, *Plant Physiol.*, Vol. 171, 2016, pp. 1626–1634.
- [22] Min D.B., and Lee H., Chemistry of lipid oxidation, *Flavor Che*, Kluwer Academic/Plenum Publishers, New York, 1999.
- [23] Zabik N.L., Anwar S., Ziu I., and Martic-milne S., Electrochemical reactivity of bulky-phenols with superoxide anion radical, *Electrochim. Acta.*, Vol. 296, 2019, pp. 174–180.
- [24] Min D.B. and Boff J.M., Chemistry and reaction of singlet oxygen in foods, *Compr. Rev. Food Sci. Food Saf.*, Vol. 1, 2002, pp. 58–72.
- [25] Li R., Zhou X., Liu D., and Feng W., Enhancing the activity and stability of Mn-superoxide dismutase by one-by-one ligation to catalase, *Free Radic. Biol. Med.*, Vol. 129, 2018, 138–145.

## VARIATIONS IN WATER QUALITY ALONG ACIDIC RIVERS IN VOLCANIC AREAS OF EASTERN JAPAN

Takeshi Saito<sup>1</sup> and Naoki Watanabe<sup>2</sup>

<sup>1</sup>Graduate School of Science and Engineering, Saitama University, Japan;

<sup>2</sup>Research Institute for Natural Hazards and Disaster Recovery, Niigata University, Japan

### ABSTRACT

There are many acidic rivers in Japan, caused by acidic drainage from mines and hot springs. Low pH values and relatively high concentrations of harmful heavy metals and other toxic elements are often detected in the acidic rivers. In this study, water quality parameters such as pH and concentrations of heavy metals and other elements were investigated in seven representative acidic river basins located in volcanic areas in the Eastern part of Japan. Generally, the lowest pH values were ranged from 1.31 to 5.64. As an example of the positive effects of neutralization treatment, pH values markedly increased and concentrations of As, Pb, Fe, and Al dramatically decreased and reached acceptable values after treatment in the Agatsuma river basin. Opposite in the Nagase river basin, being an example of no specific treatment applied, the pH values gradually increased and concentrations of As, Pb, Fe, and Al steadily decreased along (downstream) the river, mainly due to the dilution effect by the inflow from other rivers. In both acidic river basins, harmful heavy metals such as As and Pb were probably coprecipitated with Fe and Al hydroxides. The sediments deposited in the Nagase river bed may therefore contain much higher concentrations of harmful heavy metals including As and Pb as previously reported in the Shinaki dam of the Agatsuma river basin.

*Keywords: Water quality, pH, Heavy metals, Acidic rivers, Eastern part of Japan*

### INTRODUCTION

Acid mine drainage is one of the most serious environmental issues, resulting in the discharge of the water with low pH values and relatively high concentrations of harmful heavy metals and other toxic elements. The drainage is naturally produced, typically from the oxidation of sulfide minerals such as pyrite reacted with air and water. The mining activities can highly accelerate the amount of the discharge by an increase in possibility for sulfide mineral oxidation [1]-[5].

Especially, in Japan, there are many acidic hot springs associated with volcanic activities. The drainage from acidic hot springs also shows low pH values and relatively high concentrations of harmful heavy metals such as As (arsenic) and Pb (lead). The acidic drainage produced from mines and hot springs discharges into rivers causing the acidic rivers.

For example, the acidic water significantly affects the degradation of infrastructures mainly composed of concrete and iron materials in the rivers. Also, there are possible negative risks for the biosphere in the acidic river basins. In some of acidic rivers in Japan, the neutralization treatment using limestone mainly consisting of calcium carbonate ( $\text{CaCO}_3$ ) is applied to reduce the acidity and concentrations of harmful heavy metals and other toxic elements [6], [7]. The problem applying the neutralization treatment is high cost because the

treatment must be continuously applied [8]. Since the limestone as one of the most common neutralizers is a natural and scarce resource, it is highly important to reduce the usage for achieving the recycle-based society. Therefore, alternative neutralizers which have low cost and highly efficient neutralization capacity are needed to be developed.

In this study, water quality parameters including pH and concentrations of heavy metals and other elements were investigated in seven representative acidic river basins located in volcanic areas in the Eastern part of Japan. The expected outcomes from this study will provide fundamental and important knowledges for developing the alternative neutralizers.

### MATERIALS AND METHOD

Water quality investigation was carried out in seven acidic river basins, Urakawa (Nagano Prefecture), Iougawa (Niigata Prefecture), Nagase (Fukushima Prefecture), Agatsuma (Gunma Prefecture), Sukawa (Yamagata Prefecture), Tamagawa (Akita Prefecture), and Matsukawa (Iwate Prefecture) river basins all in volcanic areas in the Eastern part of Japan (Figs. 1 and 2). In all seven river basins, totally more than 70 water sampling points were selected.



Fig. 1 Study areas of the Urakawa, Iougawa, Nagase, and Agatsuma river basins (orange plots indicate water sampling locations) (the base map was taken from Google LLC).



Fig. 2 Study areas of Sukawa, Tamagawa, and Matsukawa river basins (orange plots mean water sampling locations) (the base map was taken from Google LLC).

Additionally, on-site measurements of water temperature, pH, electric conductivity (EC), and turbidity were performed using portable analyzers (WM-32EP, DKK-TOA CORPORATION, Japan and 2100P Potable Turbidimeter, HACH, USA) calibrated for each measurement. In the laboratory, the sampled river water was filtered using a 0.20  $\mu\text{m}$  membrane filter (DISMIC-25CS, Toyo Roshi Kaisha, Ltd., Japan). Then, major cations and anions ( $\text{Na}^+$ ,  $\text{NH}_4^+$ ,  $\text{K}^+$ ,  $\text{Mg}^{2+}$ ,  $\text{Ca}^{2+}$ ,  $\text{F}^-$ ,  $\text{Cl}^-$ ,  $\text{NO}_3^-$ , and  $\text{SO}_4^{2-}$ ) and heavy metals and other elements (Li, Al, Si, Cr, Mn, Fe, Ni, Cu, Zn, Se, Sr, Cd, and Pb) were analyzed using an ion chromatograph (ICS-1500, Nippon Dionex K.K., Japan) and inductivity coupled plasma (ICP) mass spectrometer (MS) (ICPM-8500, SHIMADZU CORPORATION, Japan).

## RESULTS AND DISCUSSION

### Levels of acidity in seven acidic river basins of the Eastern part of Japan

The pH values were 5.64 (October 2017), 4.32

(August 2018), and 1.93 (May 2019) in the upstream parts of the Urakawa, Iougawa, and Sukawa river basins, respectively. Also, very low pH values of 1.66 (July 2017), 1.82 (June 2017), 1.31 (July 2018), and 3.41 (July 2018) were observed in the Iougawa, Yukawa, Shibukuro, and Akagawa rivers located in the Nagase, Agatsuma, Tamagawa, and Matsukawa river basins, respectively. The neutralization treatment using limestone is applied to the Yukawa, Shibukuro, and Akagawa rivers, while in the Urakawa, Iougawa, Nagase, and Sukawa river basins, there are no specific treatments applied towards increasing river pH values. Especially in the Akagawa river of the Matsukawa river basin, the pH value of 3.41 mentioned above was obtained in the sampling location after the neutralization treatment plant. Therefore, the original pH value was expected to be significantly lower. In the following sections, the results acquired in the Agatsuma river basin as an example of the neutralization treatment applied and Nagase river basin as an example of no specific treatment applied are discussed.

### Variations of water quality along the Agatsuma river basin

In the upstream of the Agatsuma river basin, the Kusatsu hot spring is one of the most famous acidic springs in Japan and closed mines mainly emitting Sulphur are located in the Eastern foot of an active volcano, Mt. Kusatsu-Shirane. Especially, the Yukawa river dominated by the discharged water from the Kusatsu hot spring shows very low pH value, usually less than pH 2.0. Therefore, the neutralization treatment has been applied by the Ministry of Land, Infrastructure, Transport and Tourism (Government of Japan) over 50 years [6], [7]. The resulting compounds from neutralization treatment are continuously produced and finally deposited in an artificial lake named Shinaki dam located approximately 3 km downstream of the neutralization plant (Fig. 3). The water from the Shinaki dam finally discharges to the Tone river (via the mainstream of the Agatsuma river) which is the biggest water resource for the Tokyo Metropolitan area of Japan having a population more than 30 million.

The variation in water quality regarding pH, EC, and concentrations of As, Pb, Fe (iron), and Al (aluminum) from the upstream to downstream along the Agatsuma river basin is illustrated in Fig. 4. The pH value of 1.82 was observed in the Yukawa river before the neutralization treatment plant. After the treatment, the pH value markedly increased to approximately 4.5. Subsequently, the water from the Shinaki dam discharges to the mainstream of the

Agatsuma river where the pH already increased to a neutral value (7.38), while the concentrations of both As and Pb dramatically decreased with applying the neutralization treatment. The Fe and Al concentrations also decreased significantly after the treatment as shown in Fig. 4. These chemical components were almost not detected in the mainstream of the Agatsuma river. The metal hydroxides, especially Fe and Al, are in general easy to precipitate by increasing the pH value in the water. One of the most harmful elements, As, can be simultaneously coprecipitated with metal hydroxides [9], [10]. Therefore, As and Pb were probably coprecipitated with the Fe and Al hydroxides during the neutralization process. The produced compounds deposited in the Shinaki dam contains extremely high concentrations of these harmful chemical components as reported in annual monitoring data by the Ministry of Land, Infrastructure, Transport and Tourism [11].

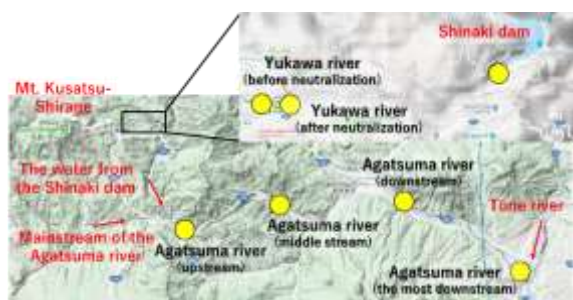


Fig. 3 Study area of the Agatsuma river basin (yellow circles are representative water sampling locations and the acquired data from these locations were illustrated in Fig. 4) (the base map was taken from Google LLC).

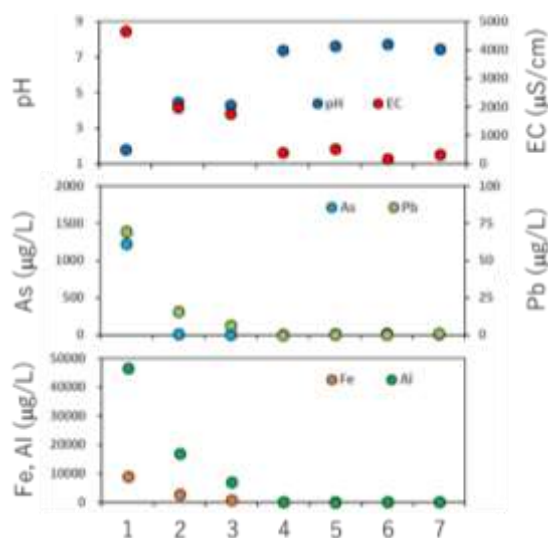


Fig. 4 Variations of water quality for pH, EC, and

the concentration of As, Pb, Fe, and Al from the upstream to downstream along the Agatsuma river basin (1: Yukawa river (before neutralization), 2: Yukawa river (after neutralization), 3: Shinaki dam, 4: Agatsuma river (upstream), 5: Agatsuma river (middle stream), 6: Agatsuma river (downstream), 7: Agatsuma river (the most downstream)).

#### Variations of water quality along the Nagase river basin

In the upstream of the Nagase river basin, acidic hot springs and Sulphur mines already closed are also located in the Western foot of Mt. Adatara that is an active volcano. The Iougawa river which shows the pH value of 1.66 dominated by the hot spring water. The water from the Iougawa river discharges to the lake Inawashiro (via the mainstream of the Nagase river). Then, the water from the lake discharges to Nippashigawa river (Fig. 5) and finally flows into the Agano river which is one of the biggest rivers in Japan.



Fig. 5 Study area of the Nagase river basin (yellow circles are representative water sampling locations and the acquired data from these locations were presented in Fig. 6) (the base map was taken from Google LLC).

The variation in water quality regarding pH, EC, and the concentrations of As, Pb, Fe, and Al from the upstream to downstream along Nagase river basin are also presented in Fig. 6. As described above, the pH value of 1.66 was observed in the Iougawa river due to inflow of the hot spring water. After that, the pH values gradually increased along the river mainly due to the dilution effect by the inflow from other rivers. In the most downstream part of the Nagase river, the pH still showed a low value, around 4.0. It, however, finally became a neutral value in the Nippashigawa river. Also, in the Nagase river basin, the As, Pb, Fe, and Al concentrations gradually decreased. The harmful heavy metals of both As and Pb were probably



coprecipitated with the Fe and Al hydroxides. At least, the Fe hydroxide was clearly deposited in the river bed (Fig. 7). Similarly, in the Nagase river basin, the sediments in the river bed likely contain high concentrations of harmful heavy metals such as As and Pb. The next step of the investigation is to evaluate the chemical stability of these harmful heavy metals in sediments of the river bed in the Nagase river basin and of the Shinaki dam in the Agatsuma river basin.

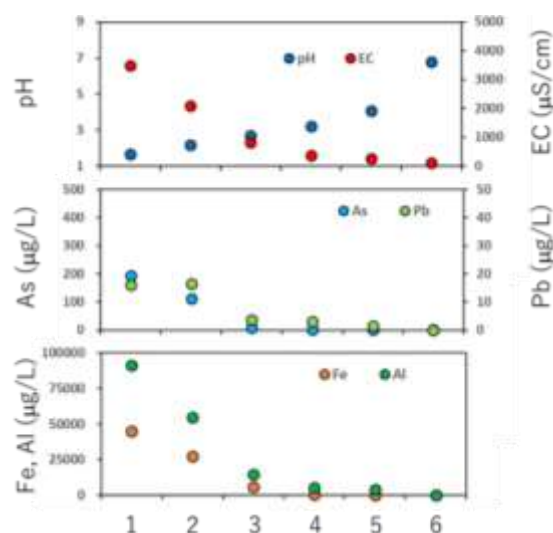


Fig. 6 Variations of water quality for pH, EC, and the concentration of As, Pb, Fe, and Al from the upstream to downstream along the Nagase river basin (1: Iougawa river, 2: Sukawa river (upstream), 3: Sukawa river (downstream), 4: Nagase river, 5: Nagase river (the most downstream), 6: Nippashigawa river).



Fig. 7 The river bed conditions in the Nagase river basin (left: Sukawa river (upstream), right: Nagase river)

## CONCLUSIONS

Water quality parameters such as pH and concentrations of heavy metals and other elements were investigated in seven representative acidic river basins located in volcanic areas in the Eastern part of Japan. Generally, the lowest pH values ranged from 1.31 to 5.64 in each river basin.

In the Agatsuma river basin as an example of the positive effects of neutralization treatment, the pH values markedly increased and concentrations of As, Pb, Fe, and Al dramatically decreased after the treatment. Then, these values reached acceptable levels. On the other hand, in the Nagase river basin, being an example of no specific treatment applied, the pH values gradually increased and concentrations of As, Pb, Fe, and Al steadily decreased along the river, mainly due to the dilution effect by the inflow from other rivers.

In both acidic river basins, harmful heavy metals of As and Pb were probably coprecipitated with the Fe and Al hydroxides. The sediments deposited in the river bed of the Nagase river basin may therefore contain much higher concentrations of harmful heavy metals including As and Pb as previously reported in the Shinaki dam of the Agatsuma river basin. The next step is to evaluate the chemical stability of these harmful components in the sediments.

## ACKNOWLEDGMENTS

This research was supported from a Grant-in Aid for Scientific Research (no. 26889015) by the Japan Society for the Promotion of Science, a research grant by JFE 21st Century Foundation and the Collaborative Research Project (2017-17, 2018-13, and 2019-15) by the Research Institute for Natural Hazards and Disaster Recovery, Niigata University, Japan.

## REFERENCES

- [1] Akcil A., and Koldas S., Acid Mine Drainage (AMD): causes, treatment and case studies. *Journal of Cleaner Production*, Vol. 14, Issue 12-13, 2006, pp.1139-1145.
- [2] Herrera S.P., Uchiyama H., Igarashi T., Asakura K., Ochi Y., Ishizuka F., and Kawada S., Acid mine drainage treatment through a two-step neutralization ferrite-formation process in northern Japan: Physical and chemical characterization of the sludge. *Minerals Engineering*, Vol. 20, Issue 14, 2007, pp.1309-1314.
- [3] Nieto J.M., Sarmiento A.M., Olías M., Canovas C.R., Riba I., Kalman J., and Dlvalls T. A., Acid mine drainage pollution in the Tinto and Odiel rivers (Iberian Pyrite Belt, SW Spain) and bioavailability of the transported metals to the Huelva Estuary. *Environment International*, Vol. 33, Issue 4, 2007, pp.445-455.
- [4] Gaikwad R.W., and Gupta D.V., Review on removal of heavy metals from acid mine drainage. *Applied Ecology and Environmental Research*, Vol. 6, Issue 3, 2008, pp.81-98.
- [5] Lei L., Song C., Xie X., Li Y., and Wang F.,

- Acid mine drainage and heavy metal concentration in groundwater of metal sulfide mine at arid territory (BS mine, Western Australia). *Transactions of Nonferrous Metals Society of China*, Vol. 20, Issue 8, 2010, pp.1488-1493.
- [6] Kikawada Y., Kawai S., Shimada K., and Oi T., Arsenic originating in Kusatsu hot springs, Gunma, Japan, and arsenic pollution status of Kusatsu rivers. *Journal of Disaster Research*, Vol. 3, Issue 4, 2008, pp.261-269.
- [7] Mitsuya D., Hayashi T., Wang Y., Tanaka M., Okai M., Ishida M., and Urano N., Isolation of aquatic yeasts with the ability to neutralize acidic media, from an extremely acidic river near Japan's Kusatsu-Shirane Volcano. *Journal of Bioscience and Bioengineering*, Vol. 123, Issue 1, 2017, pp.43-46.
- [8] Sasaki A., Yoshikawa E., Mizuguchi H., and Endo M., The improvement of water quality in an acidic river environment using waste concrete aggregates. *Journal of Water and Environment Technology*, Vol. 11, Issue 3, 2013, pp.235-247.
- [9] Violante, A., Ricciardella, M., Gaudio, S.D., and Pigna, M., Coprecipitation of arsenate with metal oxides: Nature, mineralogy, and reactivity of aluminum precipitates. *Environmental Science and Technology*, Vol. 40, Issue 16, 2006, pp.4961-4967.
- [10] Jia Y., and Demopoulos G.P., Coprecipitation of arsenate with iron (III) in aqueous sulfate media: Effect of time, lime as base and co-ions on arsenic retention. *Water Research*, Vol. 42, Issue 3, 2008, pp.661-668.
- [11] Ministry of Land, Infrastructure, Transport and Tourism (Government of Japan), Annual monitoring data for sediments in the Shinaki dam, [http://www.ktr.mlit.go.jp/sinaki/sinaki\\_index013.html](http://www.ktr.mlit.go.jp/sinaki/sinaki_index013.html) (accessed on June 5, 2019) (in Japanese).

## WATER FOOTPRINT OF RICE IN MYAUNGMYA TOWNSHIP, MYANMAR

May Myo Han

Faculty of Environment and Resource Studies, Mahidol University, Thailand

### ABSTRACT

Rice is the major crop for Myanmar and water crisis has been one of the challenges in livelihoods and agriculture sectors. This research was conducted to account the Water footprint of Rice in Myaungmya Township, located in delta area and the results are to be used as an indicator for local water resources management. Climate and soil data, cropping patterns and fertilizers consumption are accessed by SEA START, CLIMWAT 2.0 and Myaungmya Agricultural Department. The Green and Blue Water footprints are calculated using the crop evapotranspiration values from CROPWAT Model 8.0. Mainly, rice in the target area is grown in monsoon and summer seasons. Since the target area gets high rainfall, the Green Water Footprint of monsoon 1163 m<sup>3</sup> per ton is higher than the summer, 71 m<sup>3</sup> per ton. And the Blue water footprint for monsoon is assumed as zero meanwhile the summer is 1886 m<sup>3</sup> per ton. According to the practice by the farmers, the fertilizers rate used in summer is relatively higher than monsoon. Therefore, the grey water footprint for monsoon is 252 m<sup>3</sup> per ton and the summer season is 558 m<sup>3</sup> per ton. The total water footprint of rice in monsoon is 1407 m<sup>3</sup> per ton and the summer season is 2515 m<sup>3</sup> per ton, respectively.

*Keywords: Water Footprint, Rice, CROPWAT MODEL 8.0*

### INTRODUCTION

Water crisis has already become one of the most challenges in Myanmar recently. About 700 million of people in 43 countries, especially in China, India and Sub-Saharan Africa, were under the water deficit problems as well (Human Development report, 2006). Agriculture and farming are the main businesses of Myanmar and rice farming depends on water resources. Developing countries including Myanmar account more than 80% for water in agriculture meanwhile the high-income countries account over 40% for agriculture and industries [5].

This research was taken place from January to April during the year of 2017. Myaungmya Township, is located at 16° 35' N and 94° 54' E and has the area of 1146. 2 km<sup>2</sup> (Myanmar Department of population, 2015a). Typically, there are three seasons; rainy season (June to October), summer (March to May) and cold season (November to February). It gets the Tropical monsoon weather and has high temperatures and heavy rainfall [17]. The area gets the precipitation not over 2500 mm per year [1]. The temperature range is 36 °C -15 °C and the humidity 76% in average. Generally, the land is the level plain and lies on the delta region of the 290 km long and 240m wide of Irrawady river basin [10],[15]. Tube pump wells are for drinking water source and the rainfall is mainly for agriculture and there is Myaungmya River nearby [13].

There are two rice cultivating seasons in Myanmar; monsoon and summer. Monsoon rice is

sown in more areas than summer rice because of the water availability. But when comparing the yield, the yield of summer rice is higher than monsoon rice [9]. Natural disasters such as unusual floods in rainy season untimely rain and severe drought become the factor urging the local government to prepare the enough amount of water for rice fields seasonally and in different locations [14].

Water foot print concept could help farmers to use the new practice of rice planting and moreover, local government could be benefit from this research for water resources management. This research aims to give the estimate data to prepare the amount of water that farmers needed for their rice fields in seasonally and also during drought period or for drought prone area in Myanmar.

### METHODOLOGY

Water footprint is the volume of water used in a certain process of producing the goods or products measured by the formulas at a certain point of production [1],[3]. During the plantation of rice to the harvesting time, Total Water Footprint (WF<sub>T</sub>) is calculated on the values of Green Water Footprint (WF<sub>rg</sub>), Blue Water Footprint (WF<sub>rb</sub>) and Grey Water Footprint (WF<sub>rgy</sub>). For Myaungmya rice fields, Total Water Footprint of monsoon rice and summer rice will be the output water footprint according to two planting seasons.

$$WF_T = WF_{rg} + WF_{rb} + WF_{rgy} \quad (1)$$

Green Water Footprint and Blue Water Footprint is based on the calculation of Crop Water Use per production or yield of rice. Crop Water Use values can be computed by the evapotranspiration values exported by CROPWAT 8.0 model to calculate the crop water requirements and irrigation requirements based on the collected input data such as soil, climate and crop data [7].

### Data Collection

This research collected the secondary Data (2013-2016) from Myaungmya Agricultural Department and Myaungmya Research Farm for crop pattern, primary crop and secondary crop data, yearly yield per acre covering the targeted area, fertilizers type used for the plant growth, amount of fertilizer use (especially nitrogen) and soil characteristic of the area. And for climatic data, this study used the secondary climatic Data at least 30 years (1987 - 2016) of Myaungmya Township from SEA START and CLIMWAT 2.0 Climatic Database (1971-2000).

### Green Water Footprint

To get the Total Green Water Footprint ( $m^3 \text{ ton}^{-1}$ ), the climatic parameters and the crop parameters will have to put into CROPWAT 8.0 and it generates the values of the effective rainfall available ( $P_{eff}$ ) and the crop evapotranspiration ( $ET_c$ ) during the rice plantation period as the output in the model. Green water evapotranspiration of rice ( $ET_{rg}$ ) is the minimum value upon the effective rainfall available ( $P_{eff}$ ) and the crop evapotranspiration ( $ET_c$ ) Eq. (2)

Crop Green Water Used ( $CWU_{rg}$ ) is the summation of  $ET_{rg}$  counted from planting day to harvest day multiply with water depth according to Eq. (3). The factor 10 is used to convert water depths in mm into water volumes per land surface in  $m^3/\text{ha}$ . And since the land area unit for Myanmar is used in acre, 0.4 is the value to convert acre to hectare. Lgp means for the length of growing period in days and it started counted from the day of planting (day=1).

When the Crop Green Water Used ( $CWU_{rg}$ ) per acre is divided by the yield of the rice per acre ( $Y$ ), the value of Green Water Footprint is obtained Eq. (4).

$$ET_{rg} = \min(P_{eff}, ET_c) \quad (2)$$

$$CWU_{rg} = 10 \times 0.4 \sum_{d=1}^{Lgp} ET_{rg} \quad (3)$$

$$WF_{rg} = CWU_{rg} \div Y \quad (4)$$

### Blue Water Footprint

For blue water footprint ( $WF_{rb}$ ), the same

calculation has been done as green water footprint ( $WF_{rg}$ ) which the crop water use ( $m^3/\text{acre}$ ) for blue water is divided by the  $Y$  (yield  $\text{ton}/\text{acre}$ ). In this case, crop blue water use ( $CWU_{rb}$ ) is the total irrigation evaporated from the field Eq. (7).

When the crop evapotranspiration ( $ET_c$ ), also known as crop water requirement, is larger than the effective rainfall ( $P_{eff}$ ), irrigation is needed for the crop and it is calculated by taking the difference between ( $ET_c$ ) and ( $P_{eff}$ ). For monsoon season, farmers only depend on the rainfall as Myaungmya receives heavy rainfall. When crop water requirement is smaller than the effective rainfall ( $P_{eff}$ ) in CROPWAT 8.0, blue water evapotranspiration ( $ET_{rb}$ ) will become zero according to Eq. (5). Then we can assume blue Water Footprint as zero especially for this case.

$$ET_{rb} = \max(0, ET_c - P_{eff}) \quad (5)$$

$$CWU_{rb} = 10 \times 0.4 \sum_{d=1}^{Lgp} ET_{rb} \quad (6)$$

$$WF_{rb} = CWU_{rb} \div Y \quad (7)$$

The irrigation is needed when the effective rainfall does not meet the requirement of crop evapotranspiration during a period since the effective rainfall will be decreasing before the harvest time. This gap is also depending on the availability of effective irrigation water supply from the nearest blue water resources. Mostly, the farmers in rain fed agriculture of Myanmar lean on the green water resource and no irrigation system in Myaungmya Township although there are many cases that farmers had to put or pump the blue water to be able to maintain the desired water level.

### Grey Water Footprint

From the Equation (8), the Grey Water Footprint ( $WF_{rgy}$  in  $m^3 \text{ ton}^{-1}$ ) of rice counts on fertilization rate applied (AR in  $\text{kg}/\text{acre}$ ) to the field per acre. Nitrogen is regarded as the representative of the grey water calculation [2]. The leaching of Nitrogen in the paddy will be taken account as 10% of the leaching rate although the leaching run-off varies according to soil texture, amount of precipitation of the region and the irrigation frequencies [2]. The maximum acceptable concentration will be considered as 10 mg nitrate per liter [12].

$$WF_{rgy} = (\alpha \cdot AR) / (c_{max} - c_{nat}) / Y \quad (8)$$

In Equation (8),  $\alpha$  is the leaching-run-off fraction,  $c_{max}$  ( $\text{kg}/m^3$ ) is the maximum acceptable

concentration,  $C_{nat}$  ( $\text{kg/m}^3$ ) is the natural concentration for the pollutant considered in the receiving water body and  $Y$  is the crop yield ( $\text{ton/acre}$ ).

## RESULTS AND DISCUSSION

The results from the research are classified according to two crops seasons. During the period of the 2013 to 2016, the Green Water Footprint for monsoon rice is  $1155 \text{ m}^3$  per ton. From this research, Blue Water Footprint is considered as zero as the cultivation practice is rain-fed system and the total water footprint of monsoon rice  $1407 \text{ m}^3$  per ton is measured over the entire township which owns a 164,493 acre of rice fields. Grey Water Footprint is  $252 \text{ m}^3$  per ton (Table 1).

Planting the monsoon rice is based on the rain fed cultivation system and the farmers started the land preparation according to the weather condition which is suitable and has the enough rain water to puddle. Hence, the blue Water Footprint for the monsoon rice can be considered as zero in this research (Table 1).

Farmers are introduced to use compound fertilizer as for nutrients to rice plants before seeding. The type of fertilizer is 15-15-15 and use one bag (50kg loaded) per acre in a few areas [9]. Although compound fertilizer is famous in recent years since 2010, Urea is widely used because the nitrogen is regarded as the most important nutrients to the plants by farmers. Urea (46%, 50 kg loaded) has been put into the soil in vegetative phase, reproductive phase

and booting stage and the usage of Urea during the period is varied according to farmers' favorite practice. From the following Table 2, the average value of the Urea used ( $\text{ton/acre}$ ) is calculated by dividing the amount of Urea used in monsoon season to the total planted area.

Table 2 Amount of fertilizer uses in Myaungmya Township

| Year | Season | ton/acre |
|------|--------|----------|
| 2013 | Rainy  | 0.10     |
| 2014 | Summer | 0.20     |
| 2014 | Rainy  | 0.16     |
| 2015 | Summer | 0.26     |
| 2015 | Rainy  | 0.70     |
| 2016 | Summer | 0.26     |
| 2016 | Rainy  | 0.10     |

Source: Myaungmya Agricultural Department (2017)

For summer rice, green water footprint is  $71 \text{ m}^3$  per ton and blue water footprint is  $1886 \text{ m}^3$  per ton. As for grey water footprint, the result shows  $558 \text{ m}^3$  per ton which is a bit higher value comparing with the grey water footprint for monsoon rice,  $252 \text{ m}^3$  per ton (Table 1). The application rate of the fertilizer for Monsoon Rice is obviously different as a half of the Summer Rice. Therefore, the Grey Water Footprint of the Summer Rice is three times larger than the Monsoon Rice.

Table 1 Comparison between Water footprints ( $\text{m}^3$  per ton) of Rice fields over Myaungmya Township, Tha Wang Pha district, Thailand, South Korea and water footprint for Myanmar in Hoekstra & Chapagain (2011)

| Period                        | Location                        | Crop                   | $WF_{rg}$   | $WF_{rb}$ | $WF_{rgy}$ | $WF_T$      | Source             |
|-------------------------------|---------------------------------|------------------------|-------------|-----------|------------|-------------|--------------------|
| 2013-2016                     | Myaungmya                       | Monsoon Rice           | 1155        | 0         | 252        | 1407        | From this research |
| 2013-2016                     | Myaungmya                       | Summer Rice            | 71          | 1886      | 558        | 2515        | From this research |
| 2011-2012<br>(July – October) | Tha Wang Pha district, Thailand | <i>Oryza sativa L.</i> | 1470.3<br>3 | 0         | 788.49     | 2258.8<br>2 | [5]                |
| 2004-2009                     | South Korea                     | Wetland Rice           | 294.5       | 501.6     | 48.4       | 844.5       | [16]               |
| 2004-2009                     | Myanmar                         | Rice                   | 846         | 378       | 50         | 1274        | [4]                |

Although the starting date of cultivation of summer rice is different among farmers, the average starting date is set up as the first of January. In Myanmar, rain can be expected in some areas during the earlier stage of the year. Myaungmya is located at the delta region and near to sea. As a result, the Green Water Footprint can be calculated as a small amount of value (Table 1).

The yield in average for the period of 2013 - 2016

for the Summer Rice ( $2.17 \text{ ton per acre}$ ) is also higher than the Monsoon Rice ( $1.8 \text{ ton per acre}$ ). Therefore, it can be assumed as the yield of the paddy directly depends on the fertilizer usage of the farmers to their fields. And the floods and untimely rain which occurs in Monsoon Season due to the climate change cause deficit to the yield (Table 3).

Table 3 Yield in Myaungmya Township

| Year | Season | ton/acre |
|------|--------|----------|
| 2013 | Rainy  | 1.70     |
| 2014 | Summer | 2.12     |
| 2014 | Rainy  | 1.80     |
| 2015 | Summer | 2.20     |
| 2015 | Rainy  | 1.80     |
| 2016 | Summer | 2.20     |
| 2016 | Rainy  | 1.80     |

Source: Myaungmya Agricultural Department (2017)

As a total for two seasons, Total Water Footprint for Summer Rice (2515 m<sup>3</sup> per ton) is higher than the Total Water Footprint for Monsoon Rice (1407 m<sup>3</sup> per ton). In Hoekstra & Chapagain [4], the average value of green water footprint for Myanmar is 846 m<sup>3</sup> per ton, blue water footprint is 378 m<sup>3</sup> per ton and grey water footprint 50 m<sup>3</sup> per ton. Therefore, the results in Myaungmya Township are higher than the average value of the whole country in Myanmar. Moreover, Tha Wang Pha District from Thailand has 1470.33 m<sup>3</sup> per ton of Green Water Footprint and 788.49 m<sup>3</sup> per ton of Grey Water Footprint in 2011-2012 which is less in a number comparing with this research in both Grey Water footprints for two seasons.

The period for 2000-2004 of Hoekstra & Chapagain [4] has a less number in value while comparing with the research. Nonetheless, the global average water footprint in the period 2000 – 2004 for paddy rice was 1325 m<sup>3</sup> per ton. Therefore, the value of this research is higher in value of the global average.

In contrast, the data for the Hoekstra & Chapagain [4] has accessed from the FAO in 2004 - 2009 and this research is accessed from the local data sources in current time. The fact that the key factors for the Green Water Footprint and the Blue Water Footprint, the climatic data which can have some differences as the whole country and the spotted township, has to be considered in this case.

For grey water has the impact to the environment, the appropriate application rate of the paddy fields is important to considered in the near future as the fertilizers usage are increased although it is still less than comparing with the neighboring countries.

This research is based on the heavy precipitation region and extensive water resource (Myaungmya River). Therefore, the results from the research could give the data to build up the policy or the management plan to sustain the existing water resource of the water stress region, especially drought prone area of Myanmar.

### Limitations

The above Water Footprint values are estimated

values as weather data were used from SEA START and CLIMWAT 2.0. The results may not accurate because of long term climate prediction based on the simulation process of scenarios and the datasets of the scenarios based on the 360 calendar year. Based on the location of land area and noises in some grid in some years, the result may not be equally accurate throughout the domain especially for rainfall data. The necessary data like humidity and the sunshine hours could not be accessed from this database.

Myaungmya is not a well-connected Township contrast with another beneficial city which could support the research facilities to get the data of Crop coefficient (Kc), rooting depth (m), Puddling depth (m), nursery area (%), critical depletion (fraction), yield response and crop height (m). CROPWAT 8.0 model provides the essential crop data to calculate the water footprint of the various types of crop. Hence, the crop data for this research is used from the data from FAO which is attached to CROPWAT 8.0.

Although the amount of Urea, potash and T-super used is recorded from the farmers, the amount of 15-15-15 compound could get for some seasons and years. Therefore, Actual Grey Water Footprint will be a little higher in reality than the values in this research. The rate of chemicals applied to the rice field can be accumulated, but it is difficult to measure the fraction of applied chemicals which is not used and reaches the ground and surface water. As a result, the natural nitrogen concentration for the pollutant is considered as zero and the estimated value of the fraction of applied chemicals that enter the water system is used in common.

The calculations of the water footprints of the production of rice are not measured due to the time limit and the difficulties to get the data from the production process of the millers. Besides, the consequences to the environmental pollution due to the grey water footprint and the actual run-off of Nitrogen are hard to measure in the targeted area.

### Recommendation

Based on the data and values of this study, the better accurate values of water footprint of other crops and production of goods and products are encouraged to improve. Further researches on water footprint approach, benefits of using organic fertilizers such as cow manure for the rice plants, rice varieties that used less water footprint are recommended. In past times before the machine are not widely used in farms, cows are used to paddle the ground and manure is stored and preserved with plants to get the fertilizer. This fertilizer could help to reduce the cost of fertilizer and has the benefit for sustainable environment [14].

While comparing with the global average water footprint in the period of 2000 – 2004 (1325 m<sup>3</sup> per ton), both season have higher water footprint (Total



Water Footprint for Summer Rice - 2515 m<sup>3</sup> per ton and the Total Water Footprint for Monsoon Rice - 1407 m<sup>3</sup> per ton). The effective agricultural practice is needed to introduce with the traditional farmers.

## CONCLUSIONS

The role of agriculture perspective in Myanmar plays as an essential business career for the Myanmar people. The whole country depends on the product from the agriculture and the excess products are exported to neighboring countries. The water availability is unbalance as the central Myanmar becomes the drought prone area while the delta areas are faced with unusual flood. And Water scarcity is one of the challenges in central Myanmar and mountainous region. Therefore, the development in the rice practice to reduce Water Footprint and using the amount of water efficiently is important in the future.

## ACKNOWLEDGMENTS

I would like to express my deepest acknowledgement to the “Mahidol-Norway Capacity Building Initiative for ASEAN” from Mahidol University and faculty of Environment and Resource Studies, Mahidol University, Myaungmya Agriculture Department and Myaungmya Agriculture Farm for giving me an opportunity to be able to accomplish this research. With their supports in both financial and supervision, I would be able to finish the master study. And I would like to give my deepest appreciation to Assoc. Professor Nathsuda Pumijumnong, my major advisor for her professional knowledge, wisdom of advices, and support during the study period. I would like to send my honest thanks to my advisors Asst. Professor Achara Ussawarujikulkai and Lecturer Dr. Uthai Chareonwong for their academic interest in my study, excellent academic guidance and honest encouragements throughout the process of my study.

## REFERENCES

- [1] Chapagain, A. K., & Hoekstra, A. Y. (2004). Water Footprints of Nations. Value of Water Research Report Series No. 16. UNESCO-IHE, Delft, the Netherlands.
- [2] Chapagain A.K., Hoekstra, A.Y., Savenije, H.H.G., Gautam, R., 2006. The water footprint of cotton consumption: an assessment of the impact of worldwide consumption of cotton products on the water resources in the cotton producing countries. *Ecological Economics* 60 (1), 186 - 203
- [3] Chapagain, A. K., & Hoekstra, A. Y. (2008). The global component of freshwater demand and supply: An assessment of virtual water flows between nations as a result of trade in agricultural and industrial products. *Water International*, 33(1), 19-2. doi:10.1080/02508060801927812
- [4] Chapagain, A., & Hoekstra, A. Y. (2011). The blue, green and grey water footprint of rice from production and consumption perspectives. *Ecological Economics*, 70(4), 749-758. doi:10.1016/j.ecolecon.2010.11.012
- [5] Chatpanyacharoen, W., Hungspreug, N., Anurugsa, B., & Taweek, S. (2015). Water Footprint Evaluation of *Oryza sativa* L. Tha Wang Pha District, Nan Province. *Thammasat International Journal of Science and Technology*, 20(4), 21-28.
- [6] Hoekstra, A.Y. (2003). Virtual water trade: Proceedings of the International Expert Meeting on Virtual Water Trade, Value of Water Research Report Series No.12, UNESCO-IHE, Delft.
- [7] FAO (2015). Water Management and Development Unit. Food and Agriculture Organization of the United Nations. FAO Water Unit | Water News: water scarcity
- [8] Human development report (2006): Beyond scarcity: Power, poverty and the global water crisis. (2006). Basingstoke: Palgrave Macmillan
- [9] Myaungmya Agriculture Department (2017). Agricultural database of crops and fertilizers
- [10] Mani, M. S. (1974). Biography of the Eastern Borderlands. *Ecology and Biography in India* pp 648-663
- [11] Ministry of Agriculture and Irrigation Union of Myanmar. (2001). Myanmar Agriculture
- [12] Ministry of Agriculture, Livestock and Irrigation (2016). Overview of the Water Environment Standards and Effluent Standards and its Implementation, Myanmar.
- [13] Myanmar family clinic & Garden (MFCG) (2016). Myanmar family clinic & Garden Project Final Report 1 : Improving the health knowledge and social status in Myaungmya Region, Myanmar
- [14] Proximity Designs. (2016). Paddy to Plate. The rice ecosystems in Myanmar: Challenges and opportunities. ISBN: 978-1-939727-05-3
- [15] Simmance, A. (2013). Environmental Flows for the Ayeyarwady (Irrawaddy) River Basin, Myanmar. Unpublished. UNESCO-IHE Online Course on Environmental Flows
- [16] Yoo, S., Choi, J., Lee, S., & Kim, T. (2013). Estimating water footprint of paddy rice in Korea. *Paddy and Water Environment*, 12(1), 43-54. doi:10.1007/s10333-013-0358-2
- [17] Tint, K. K. (2012). Study on “THIN” cultivation in Ayeyawady. *Patheingyi University Research Journal* Vol. 4. 2012

## THE EFFECT OF INSIDE CIRCUMSTANCE OF THE HAZARDOUS WASTE LANDFILL ON THE LEACHING BEHAVIOR OF HARMFUL HEAVY METALS

Yasumasa Tojo<sup>1</sup>, Taira Ikeda<sup>1</sup>, Takayuki Matsuo<sup>1</sup> and Toshihiko Matsuto<sup>1</sup>

<sup>1</sup>Faculty Graduate School of Engineering, Hokkaido University, Japan

### ABSTRACT

Influence of interior condition in the hazardous waste landfill on the leaching behavior of heavy metals were examined from the accelerated weathering experiments for dust which is a kind of wastes to be disposed of at the hazardous waste landfill. Among the main components, a decrease in the leaching amount of Cd, Pb, Mn, and Zn was confirmed in a wet environment where adsorbed water was present on the particle surface. On the other hand, in the dry and CO<sub>2</sub> saturated environment, an increase in leaching amount was observed. The former phenomenon was thought to be the formation of hydroxide through particle surface adsorbed water, and the latter was considered to be the influence of adsorption of gas phase CO<sub>2</sub> to Fe<sub>3</sub>O<sub>4</sub> and ZnO. However, further scientific verification is required for each phenomenon. The findings obtained in this study indicate that the leaching of heavy metals from hazardous wastes disposed of in the hazardous waste landfill may change over time.

*Keywords: Hazardous waste landfill, Dust, Weathering, Heavy metals, Leaching*

### INTRODUCTION

In Japan, solid waste landfill is classified into three types. They are inert waste landfill, non-hazardous waste landfill, and hazardous waste landfill [1]. Among them, in hazardous waste landfill, hazardous waste which exceeds criteria for hazardous heavy metals leaching is disposed of. The hazardous waste landfill is required to be designed and constructed with robust concrete wall and base, and the top is capped. The concept of this landfill is containment of hazardous substance and eliminates the chance of reaction with water and air. In general, in non-hazardous waste landfill, various substances are subjected to many reactions and gradually stabilized. Even for hazardous heavy metals, it is known that their leaching potentials reduce due to the long-term weathering effect. But according to the concept of the hazardous waste landfill, these reactions cannot be expected. This means that the leaching potential of hazardous heavy metals will be kept forever. However, there is no guarantee that the container structure will be permanently maintained because of the impact of natural deterioration of structure or disaster.

In order to prevent sudden emission of hazardous substance due to these occasions in future, some measure must be taken. There are two candidates considered to be able to achieve it. The one is multi-barrier system. To surround the site by various barrier systems such as clay barriers, impact of heavy metal to the surrounding environment can be mitigated. The other is to reduce the leaching potential of hazardous substance itself from solid

waste. For incineration residue, the aging phenomenon is known to be effective for reducing the mobility of heavy metals [2]-[4]. The aging or weathering of the incineration residue is occurred by the contact with rainwater and carbon dioxide in air. As mentioned above, the hazardous waste landfill is surrounded by concrete walls and roof. The waste inside the landfill is isolated from the outside environment. This means that active control of inside circumstance is necessary to create the condition preferable for aging or weathering.

However, it is not clear what kind of on-site management (humidity, gas atmosphere, temperature, etc.) is desirable for insolubilization of heavy metals. Storage of hazardous waste in the containment-type hazardous waste landfill is semi-permanent. That is, an extremely long time can be used. There is room for study whether there can be favorable inside circumstance that can gradually change the heavy metals contained in the hazardous waste into a hardly soluble state within that long time. Controllable parameters may be gas atmosphere, humidity, temperature, etc. These need to be made clear.

In this study, the effect of inside circumstance of the hazardous waste landfill on the leaching behavior of harmful heavy metals was investigated. The electric furnace dust that is designated as hazardous waste was used and it was subjected to the accelerated weathering experiment. The objective of the study is to elucidate suitable condition for reducing heavy metal leaching potential from the waste disposed of in the hazardous waste landfill and to propose the active

control method to achieve it.

## MATERIAL AND METHODS

### Material

According to the statistics of Ministry of Environment, Japan, there are 24 hazardous waste landfills registered [5]. However, among them, the landfill in operation is only one or two. At one hazardous waste landfill, interview was performed regarding kinds of waste accepted at the site. The major waste accepted and disposed of were sludge, cinder, and dust. However, it was difficult to obtain these waste samples at the landfill site due to their contracts. Thus, similar hazardous waste samples were obtained from waste treatment company which generates these wastes. The waste samples were sludge and two dusts. At first, leaching test (Japanese leaching test, JLT-13 [6]) was conducted for each of them. Since one dust sample from electric furnace had high heavy metal leaching potential, it was selected for the experiment in this study.

For the electric furnace dust, elemental composition was analyzed by XRF (Horiba MESA-800) at first, then, mineral composition was analyzed by XRD (Rigaku Rint-2000). Table 1 shows the elemental composition of the dust and Fig.1 shows the diffractogram by XRD analysis. As can be seen Table 1, major component of the dust is Fe and Zn. Besides, from Fig. 1, Fe is contained as Magnetite ( $\text{Fe}_3\text{O}_4$ ) and Zn is contained as Zincite ( $\text{ZnO}$ ). Since both compounds have adsorption capability, they may affect heavy metal leaching characteristics from the dust.

Table 1 Elemental composition of the electric furnace dust analyzed by XRF

| Element | Fe   | Zn   | Cr   | Ca  | Ni  |
|---------|------|------|------|-----|-----|
| %       | 32.6 | 21.0 | 12.0 | 8.6 | 5.8 |
| Element | Si   | Cl   | K    | Mn  | Pb  |
| %       | 5.3  | 3.8  | 3.7  | 3.0 | 2.7 |

Next, for determining of the more accurate content, the contents of Ca, Cd, Cr, Fe, Mn, Ni, Si, Pb, and Zn, which were the main components of the dust by XRF analysis, were measured by

hydrofluoric acid digestion. Also, the leaching amount was measured again by the JLT-13 leaching test of liquid-solid ratio 10. ICP analysis (SHIMADZU ICPE-9000) was used for quantitative analysis in content analysis and leaching test.

Table 2 shows the measurement results of the metal content and the leaching amount. Although the leaching ratio (= leaching amount / content) of main elements such as Fe and Ca is low and it seems to exist in a hardly soluble form, about 43% of the content of cadmium was leached out.

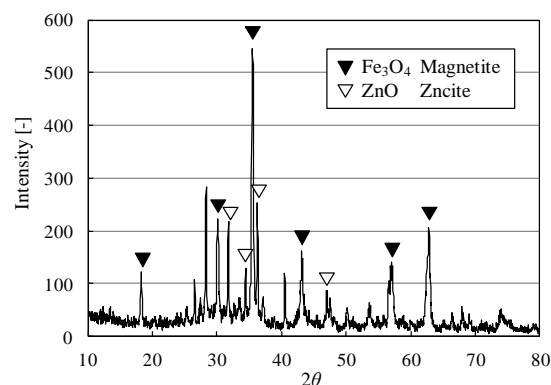


Fig. 1 Diffractogram of the dust sample by XRD

### Accelerated Weathering Experiment

By considering possible circumstance as the inside condition of hazardous waste landfill, a total of 12 series of combinations of gas, humidity, and temperature were set up (Namely, 3 gas conditions, 2 humidity conditions, and 2 temperature conditions ( $3 \times 2 \times 2 = 12$ )). Samples were put in the dish and it was placed in the chamber of which condition was set at each weathering condition. Each condition was set as follows;

Gas: a) Air, b)  $\text{N}_2$  gas, c)  $\text{CO}_2$  gas, the chamber was purged by each gas.

Humidity: a) Dry (hygroscopic silica gel was filled in the bottom of the chamber), b) wet (A metal tray was placed at the bottom of the chamber and filled with distilled water)

Temperature: a) Leave at room temperature (Just leave as it is), b) Freeze and thaw repetition (the sealed chamber was put in the freezer once a day.

Table 2 Content and Leaching amount of metals

| Element          | Ca    | Cd   | Cr    | Fe     | Mn    | Ni    | Pb    | Si    | Zn     |
|------------------|-------|------|-------|--------|-------|-------|-------|-------|--------|
| Content [mg/kg]  | 64139 | 117  | 23045 | 176074 | 12866 | 29301 | 10210 | 29903 | 84528  |
| Leaching [mg/kg] | 63.5  | 50.5 | 0.1   | 0.1    | 110.2 | 47.8  | 6.8   | 49.7  | 1109.5 |
| Ratio [%]        | 0.1   | 43.3 | 0.0   | 0.0    | 0.9   | 0.2   | 0.1   | 0.2   | 1.3    |

Ratio = Leaching amount / Content

After the sample was frozen, leave it in the room and thaw it).

The samples were cured in chambers under each condition. Ten samples were prepared per system, collected one by one weekly, and subjected to the leaching test.

Leaching test was conducted as follows; approximately 2g of a sample taken from each weathering series and then it was weighed. the sample was put into a screw bottle, and 20mL of distilled water was added to make L/S = 10, then it was shaken at 200 rpm for 6 hours with a bench shaker. Thereafter, the supernatant was filtered through a 0.45  $\mu\text{m}$  membrane filter to obtain a test solution, and the concentration of the target metal was analyzed by ICP. The pH was also measured with a HORIBA pH meter.

## RESULTS AND DISCUSSIONS

The influence of the repetition of freezing and thawing on the leaching behavior of heavy metals was not observed. Thus, only the results of standing at room temperature are explained below. Moreover, in the following, drying conditions with  $\text{N}_2$  gas atmosphere is considered as blanks. This is because, under this condition, no change in the leaching was observed for any of the metal elements (this is considered to be the condition that weathering hardly occurs). The results of Cd and Pb are shown in Fig. 2 and Fig. 3. In addition, Fig. 4 shows the Mn results that showed similar behavior to Cd. And Fig. 5 shows the results of Zn that showed a marked change in the leaching behavior especially among the elements with high contents.

Under wet conditions (right in each figure (wet)), the Cd, Pb, Mn, and Zn were confirmed to decrease

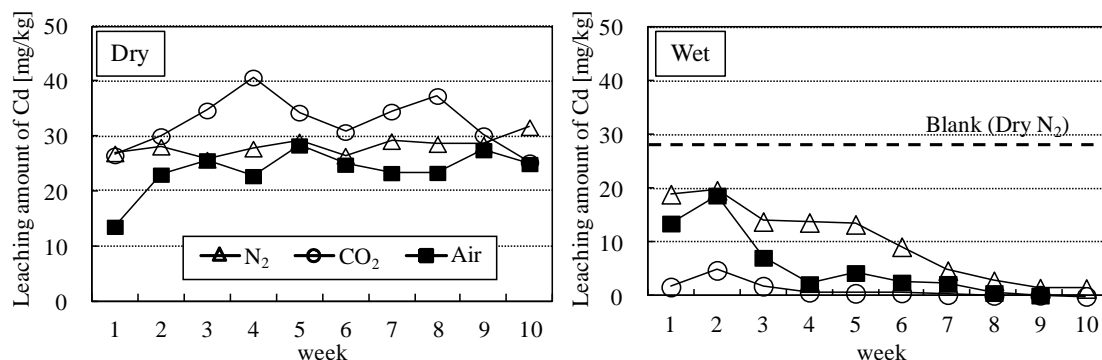


Fig. 2 Change of Cd leaching from dust under each weathering condition

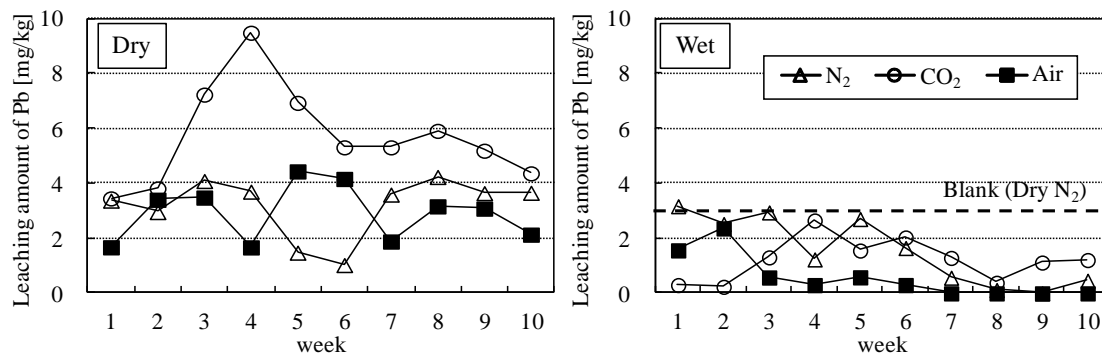


Fig. 3 Change of Pb leaching from dust under each weathering condition

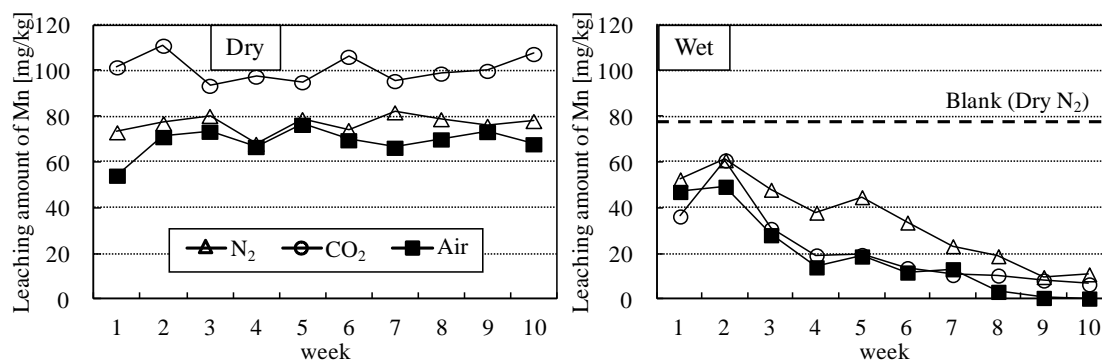


Fig. 4 Change of Mn leaching from dust under each weathering condition

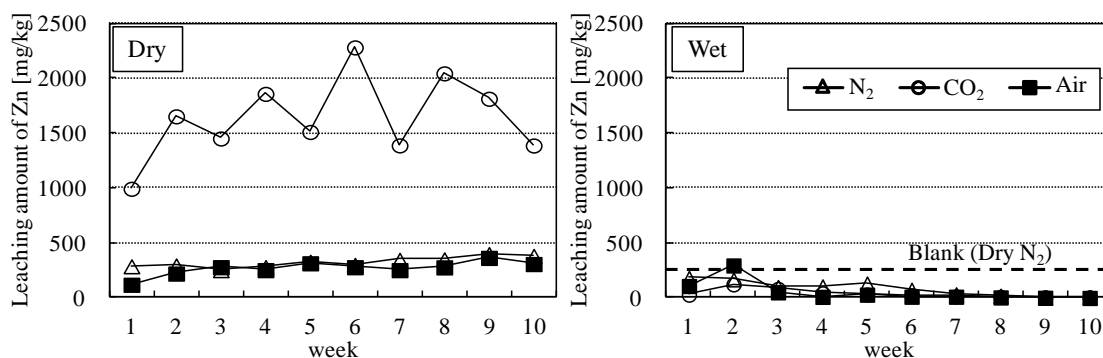


Fig. 4 Change of Zn leaching from dust under each weathering condition

in the amount of leaching regardless of the gas atmosphere, and the results were below the blank line (i.e., the average of the leaching amount under dry/N<sub>2</sub> condition) shown in the figure. Under wet conditions, adsorbed water is present on the particle surface, and a gradual increase in pH is confirmed, so it is considered that the formation of hydroxides of these metals is a factor in the decrease in leaching amount. Cd shows a remarkable decrease in leaching amount under wet/CO<sub>2</sub> conditions. It is considered that CO<sub>2</sub> in the gas phase is dissolved in surface adsorbed water of the particles to form carbonate.

On the other hand, under the drying conditions shown in the left figure, an increase in the leaching amount of Cd, Pb, Mn, and Zn was confirmed under CO<sub>2</sub> exposure conditions, and a significant increase was particularly observed in Zn. Since there is no water in the dry atmosphere, the increase in the leaching amount is likely to be the influence of the reaction between the gas phase CO<sub>2</sub> and the dust sample. It is possible that Fe<sub>3</sub>O<sub>4</sub> and ZnO, which are the predominant components of the sample, both have adsorption capability, and have suppressed the leaching of heavy metals by working as an adsorbent during the leaching test. There is some reports that these oxides adsorb gas phase CO<sub>2</sub> [7]-[8]. As a result of the dust sample being exposed to CO<sub>2</sub> for a long time, the adsorption capacity is lowered due to the occupation of the adsorption site by CO<sub>2</sub>, resulting in the increase of metal leaching amount may have happened.

## CONCLUSIONS

The influence of the inside circumstance in the hazardous waste landfill on the leaching behavior of heavy metals were examined from the accelerated weathering experiment for electric furnace dust which is a kind of hazardous wastes to be disposed at the hazardous waste landfill. Among the main components, a decrease in the leaching amount of Cd, Pb, Mn, and Zn was confirmed in a wet environment where adsorbed water was present on the particle surface. On the other hand, in the dry

and CO<sub>2</sub> saturated environment, an increase in leaching amount was observed. The former phenomenon was thought to be the formation of hydroxide through particle surface adsorbed water and the formation of carbonate for Cd by CO<sub>2</sub> gas dissolution, and the latter was considered to be the influence of adsorption of gas phase CO<sub>2</sub> to Fe<sub>3</sub>O<sub>4</sub> and ZnO, but further scientific verification is required for each of them. The findings obtained in this study indicate that the leaching of heavy metals from hazardous wastes disposed of in a hazardous waste landfill may change over time. And it means that active control of the inside circumstance of containment structure may be effective to reduce the risk of future emission of these hazardous heavy metals.

More specifically, if electric furnace dust is disposed of in a hazardous waste landfill, it is effective to control the humidity to a high level for turning hazardous heavy metals into insoluble state. In particular, if it is desired to suppress Cd leaching, to make the gas atmosphere inside landfill to high CO<sub>2</sub> gas concentration (by using CO<sub>2</sub> gas injection, etc.) is effective for carbonate formation. In this study, the conditions of saturated vapor pressure and CO<sub>2</sub> of 100% were adopted to accelerate weathering. However, since the storage period of waste in the hazardous waste landfill is extremely long, it is deemed to be possible to progress insolubilization of hazardous metals without making these conditions extremely high. Until now, no attention has been paid to the internal condition of hazardous waste landfills, and there has been no particular control. Of course, the conditions under which leaching suppression proceeds depend on the type of waste (dust, sludge, ash, etc.). One pit in hazardous waste landfill sites in Japan is regulated to 250m<sup>3</sup> or less, so the size is small. Therefore, it is possible to accept only a single waste in each pit and control the circumstance. What this research suggests is that leaching suppression of hazardous heavy metals is possible to progress by the control of inside condition because extremely long-term storage is required.

## ACKNOWLEDGMENTS

This research was supported by the Environment Research and Technology Development Fund (3-1802) of the Environmental Restoration and Conservation Agency of Japan.

## REFERENCES

- [1] Ministry of Environment, Japan, Waste disposal and Recycling measures, <https://www.env.go.jp/en/recycle/manage/waste.html>
- [2] Speiser, C., Baumann, T., Niessner, R., Morphological and Chemical Characterization of Calcium-Hydrate Phases Formed in Alteration Processes of Deposited Municipal Solid Waste Incinerator Bottom Ash, *Environmental Science and Technology*, 34, 2000, pp.5030-5037.
- [3] Piantone, P., Bodenan, F., Chatelet-Snidaro, L., Mineralogical study of secondary mineral phases from weathered MSWI bottom ash: implications for the modeling and trapping of heavy metals, *Applied Geochemistry*, 19, 2004, pp.1891–1904.
- [4] Meima, J. A., Comans, R. N. J., The leaching of trace elements from municipal solid waste incinerator bottom ash at different stages of weathering, *Applied Geochemistry*, 14, 1999, pp.159-171.
- [5] Ministry of Environment, Japan, Survey on administrative organization of industrial waste, <https://www.env.go.jp/press/files/jp/108899.pdf>.
- [6] Sakanakura, H. and Miyawaki, K., Role of Japan's Compliance Leaching Test for Landfills and Related Issues, *Material Cycles and Waste Management Research*, 20(6), 2009, pp. 287-291.
- [7] Tang, Q-L. and Luo, Q-H., Adsorption of CO<sub>2</sub> at ZnO: A surface structure effect from DFT+U Calculation, *The Journal of Physical Chemistry*, 117(44), 2013, pp.22954-22966
- [8] Chen, Q. and Bahnemann, W., Reduction of Carbon Dioxide by Magnetite: Implications for the Primordial Synthesis of Organic Molecules, *J. Am. Chem. Soc.* 122, (2000) pp.970-971.



## COSTS AND BENEFITS OF USING PARABOLIC GREENHOUSE SOLAR DRYERS FOR DRIED HERB PRODUCTS IN THAILAND

Samatcha Krungkaew<sup>1</sup>, Kanokwan Kingphadung<sup>1</sup>, Suphaphat Kwonpongsagoon<sup>2</sup>, Busarakorn Mahayothee<sup>1</sup>

<sup>1</sup>Department of Food Technology, Faculty of Engineering and Industrial Technology,  
Silpakorn University, Thailand;

<sup>2</sup>Department of Sanitary Engineering, Faculty of Public Health, Mahidol University, Thailand;  
Center of Excellence on Environmental Health and Toxicology (EHT), Thailand

### ABSTRACT

Parabolic greenhouse solar dryers have been developed to overcome product quality and postharvest loss problems. It uses solar energy, a renewable source of energy. Due to their high investment costs, economic feasibility and the potential of carbon dioxide (CO<sub>2</sub>) mitigation were investigated. Owners and managers of 17 enterprises, producing several varieties of herb products, investing in different sizes of solar dryers and using various traditional drying methods before investing in solar dryers, were interviewed in depth to create a data set. The net present value (NPV), internal rate of return (IRR), payback period and CO<sub>2</sub> mitigation were evaluated. The enterprises with annual production capacities higher than 1,200 kg or the annual revenues higher than solar dryer investment costs tended to have positive NPV indicating that the investments were attractive. Most enterprises showing CO<sub>2</sub> mitigation higher than 130 tCO<sub>2</sub>e over 15 years had positive NPV. The annual production capacity, annual revenue and the amount of CO<sub>2</sub> mitigation could be used to assess investing in greenhouse solar dryers.

*Keywords: Carbon dioxide mitigation, Food loss, Drying selection, Medicinal plants, Renewable energy*

### INTRODUCTION

Drying is an important method used for herb preservation in tropical countries [1]. Traditionally, open sun drying is mostly used due to its simplicity and low cost [2]. Because the process is slow, raw material or product losses can occur. Moreover, it has several limitations that affect the product quality due to dust, wind, pests and insects [3].

In rainy season, open sun drying cannot be conducted. Some enterprises continue the production process using auxiliary heat for which fossil fuel may be used as the heat source. Enterprises endeavoring to avoid raw material losses and product quality problems use other drying methods employing fossil fuel as the major heat source. However, fuel combustion causes greenhouse gas emissions which increase climate change impacts [4].

A solar dryer is a system that uses solar power, a renewable source of energy. It can be used to reduce the cost of energy and decrease carbon dioxide emissions [5]. The parabolic greenhouse solar dryer (Fig.1) has been developed which could support high production capacity and overcome production problems [6]. The systems are W6 × L8.2 m<sup>2</sup>, W8 × L12.4 m<sup>2</sup> and W8 × L20.8 m<sup>2</sup> for small, medium, and large size of solar dryers, respectively. Due to the high price of solar dryers and the different costs of each size, entrepreneurs need to consider the

benefits gained from both economic and environmental aspects to determine their investment. The purpose of this study was to investigate the economic viability and potential CO<sub>2</sub> mitigation in using greenhouse solar drying systems for dried herb production in Thailand.



Fig.1 Large sized parabolic greenhouse solar dryer.

Source: Janjai [6]

### METHODOLOGY

#### Data Collection

A primary data set was obtained from enterprises that invested in various sizes of parabolic greenhouse solar dryers whose main products were dried herbs. The selected enterprises produced the

dried herb products using various traditional drying methods before investing in solar dryers to determine the benefits gained from their investment. The owners or managers of the seventeen enterprises were interviewed in depth after completing tested questionnaires, covering product data, quantity and type of fuel used for drying before investment, annual production capacity, annual revenues, solar dryer size and annual savings gained.

### Economic Analysis

The value of annual total savings per annual revenue ( $V_{s/r}$ ) was determined as:

$$V_{s/r} = \frac{S_T}{R_a} \quad (1)$$

where  $R_a$  represents the annual revenues and  $S_T$  denotes the total savings gained from investing calculated using the following formula:

$$S_T = S_f + S_w + S_l \quad (2)$$

where  $S_f$  is the savings gained from fuel reduction;  $S_w$  denotes the savings gained from food waste or raw material loss reduction, and  $S_l$  is the savings gained from labor cost reduction.

The most commonly used economic indicators, namely, net present value (NPV), internal rate of return (IRR) and payback period (PBP) were investigated in this study. NPV was calculated using the following formula [7]:

$$NPV = C_I + \sum_{t=0}^{t=k} \frac{S_{T,t}}{(1+d)^t} \quad (3)$$

where  $C_I$  denotes the investment cost of the solar dryers which is negative because it represents the expense at the beginning of investing;  $d$  denotes the discount rate;  $t$  denotes the specific year of investing and  $k$  is the total number of years of investing which was 15 years in this study according to the lifespan of the solar dryer [6].

The IRR is one of the economic parameters used to indicate economic feasibility. It is the discount rate that makes NPV equal to zero and was determined using the formula below:

$$NPV = C_I + \sum_{t=0}^{t=k} \frac{S_{T,t}}{(1+IRR)^t} = 0 \quad (4)$$

The PBP is the amount of time required to recover the cost of investing and was calculated using the formula below [8]:

$$PBP = \frac{C_I}{S_T} \quad (5)$$

### Carbon Dioxide Mitigation

Total carbon dioxide mitigation was calculated using the following formula:

$$CM_T = CM_f + CM_w \quad (6)$$

where  $CM_T$  denotes the total carbon dioxide mitigation;  $CM_f$  is the carbon dioxide mitigation from reducing fuel consumption, and  $CM_w$  is the carbon dioxide mitigation from waste reduction.

Carbon dioxide mitigation from fuel use reduction was determined by the following formula:

$$CM_f = CE_{f,b} - CE_{f,a} \quad (7)$$

where  $CE_{f,b}$  and  $CE_{f,a}$  represent the carbon dioxide emissions from fuel consumption before and after investing in the solar dryer, respectively.

Carbon dioxide mitigation from waste reduction was calculated using the following formula:

$$CM_w = CE_{w,b} - CE_{w,a} \quad (8)$$

where  $CE_{w,b}$  and  $CE_{w,a}$  represent carbon dioxide emissions from food waste before and after investing in the solar dryer, respectively.

Carbon dioxide emissions from fuel consumption and food waste can be estimated using the following expressions:

$$CE_{f,b} = Q_{i,b} \times EF_i \quad (9)$$

$$CE_{f,a} = Q_{i,a} \times EF_i \quad (10)$$

$$CE_{w,b} = Q_{j,b} \times EF_j \quad (11)$$

$$CE_{w,a} = Q_{j,a} \times EF_j \quad (12)$$

where  $Q_{i,b}$  and  $Q_{i,a}$  are the quantity of fuel  $i$  used before and after investing in the solar dryer;  $EF_i$  is the carbon dioxide emission factor of fuel  $i$ ;  $Q_{j,b}$  and  $Q_{j,a}$  are the quantity of food waste before and after investing, and  $EF_j$  is the carbon dioxide emission factor of food waste. The study assumed that all the food waste would be disposed of by landfill and the related emission factor was 2.53 kgCO<sub>2</sub>e/kg waste [9].

Carbon dioxide mitigation cost was calculated using the following formula:

$$MC = \frac{C_I}{CM_T} \quad (13)$$

where MC denotes the mitigation cost.

## RESULTS AND DISCUSSION

### Economic Analysis

Nine enterprises had positive NPV indicating that the investment was worthwhile (Table 1). Sixty-seven percent of the enterprises having positive NPV were those that replaced fuel with solar energy. All enterprises in the group using fuel as traditional drying method that invested in small and medium size solar dryers, except enterprise FM3, had positive NPV. Enterprise FM3 gained low savings from fuel reduction. Moreover, enterprise FM3 had incurred expenses using more labor forces to move products from the solar dryer to the drying oven. It showed that lowered savings from one factor and increased expenses from another factor could create a negative NPV.

Only 37.50% of the enterprises using sun drying as a traditional method had a positive NPV.

Enterprise investing in small and medium solar dryers exhibited an annual production capacity more than 1,300 kg and those investing in large solar dryers had 9,600 kg. This indicated that high annual production capacity could generate a positive NPV. The result was similar to the enterprise group using fuel before the solar dryer investment for which 85.71% of these enterprises having a positive NPV exhibited an annual production capacity higher than 1,200 kg. However, some enterprises, having an annual production capacity higher than 1,200 kg, had a negative NPV while some enterprises, having an annual production capacity lower than 1,000 kg, had a positive NPV.

Enterprises FS1 and FS3 invested in small solar dryers and could gain a high amount of savings resulting in the highest IRR and the lowest PBP of 0.69 years for FS1 and 1.11 years for FS3 (Fig.2). Fifty-five percent of the enterprises that had a positive NPV invested in small solar dryers showing that small dryers tended to provide higher economic viability. According to Janjai and Tung [1], another type of solar dryer for drying herbs was investigated and they reported that its payback period of 3.9 years was a feasible investment in Thailand.

Table 1 Summary data of enterprises and calculated NPV.

| No. | Code* | Dried product  | Conventional fuel used | Annual production capacity (kg) | Annual revenues (USD**) | NPV (USD***) |
|-----|-------|--|------------------------|---------------------------------|-------------------------|--------------|
| 1   | SS1   | Moringa leaf, Bamboo grass                                     | -**                    | 1,380                           | 157,500                 | 13,637       |
| 2   | SS2   | Jewel vine, Indian gooseberry, Kariyat, Butterfly pea          | -**                    | 1,445                           | 4,141                   | - 4,239      |
| 3   | SS3   | Bael, Long pepper  | -**                    | 555                             | 1,276                   | - 5,771      |
| 4   | SS4   | Kaffir lime peel, Barbed grass                                 | -**                    | 229                             | 1,653                   | - 6,792      |
| 5   | SM1   | Kariyat, Turmeric  | -**                    | 1,800                           | 61,250                  | 32,100       |
| 6   | SM2   | Cat whiskers plant, Turmeric                                   | -**                    | 758                             | 2,619                   | - 13,014     |
| 7   | SM3   | Pandan leaf  | -**                    | 744                             | 1,976                   | - 17,270     |
| 8   | SL1   | Stevia   | -**                    | 9,600                           | 180,000                 | 75,954       |
| 9   | FS1   | Mixed herbs  | LPG and Wood           | 9,733                           | 1,520,781               | 113,228      |
| 10  | FS2   | Stevia   | Wood                   | 2,850                           | 26,719                  | 2,571        |
| 11  | FS3   | Kariyat, <i>Stephania venosa</i> , <i>Curcuma zanthorrhiza</i> | Electricity            | 2,000                           | 187,500                 | 67,263       |
| 12  | FS4   | Butterfly pea, Sabah snake grass                               | Electricity            | 650                             | 14,219                  | 5,125        |
| 13  | FM1   | Turmeric, Cassumunar ginger                                    | Electricity            | 1,200                           | 25,125                  | 15,077       |
| 14  | FM2   | Turmeric, Pandan leaf  | Electricity            | 1,243                           | 14,129                  | 2,308        |
| 15  | FM3   | Ginger, Galangal   | Electricity            | 1,609                           | 13,134                  | - 14,631     |
| 16  | FL1   | Mixed Tom Yum herbs  | Electricity            | 375                             | 28,125                  | - 30,277     |
| 17  | FL2   | Chilli   | LPG                    | 4,320                           | 16,200                  | - 10,018     |

Note: \*The first code letter represents the traditional drying method (S = sun drying and F = fuel), the second code letter represents solar dryer size (S = small, M = medium and L = large); \*\*The enterprises used open sun drying as a traditional method before investing in solar dryers; \*\*\*1 USD = 32 THB

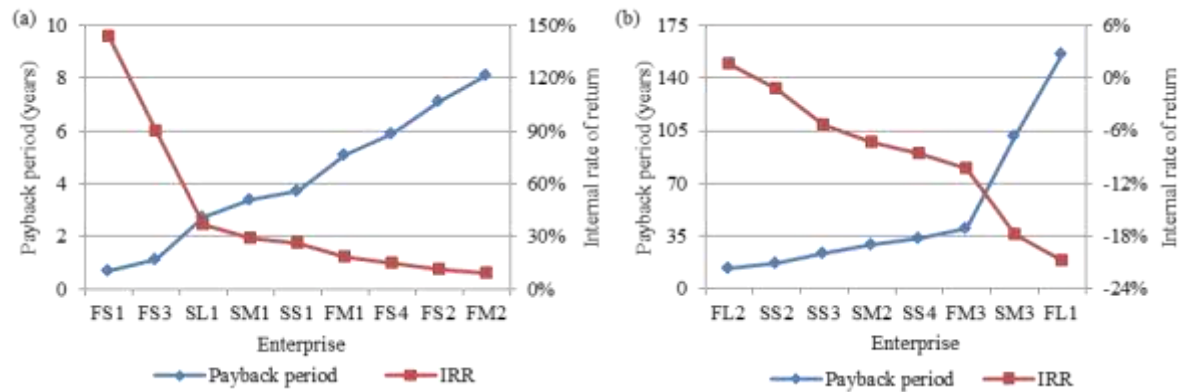


Fig. 2 PBP and IRR of enterprises having positive NPV (a) and negative NPV (b).

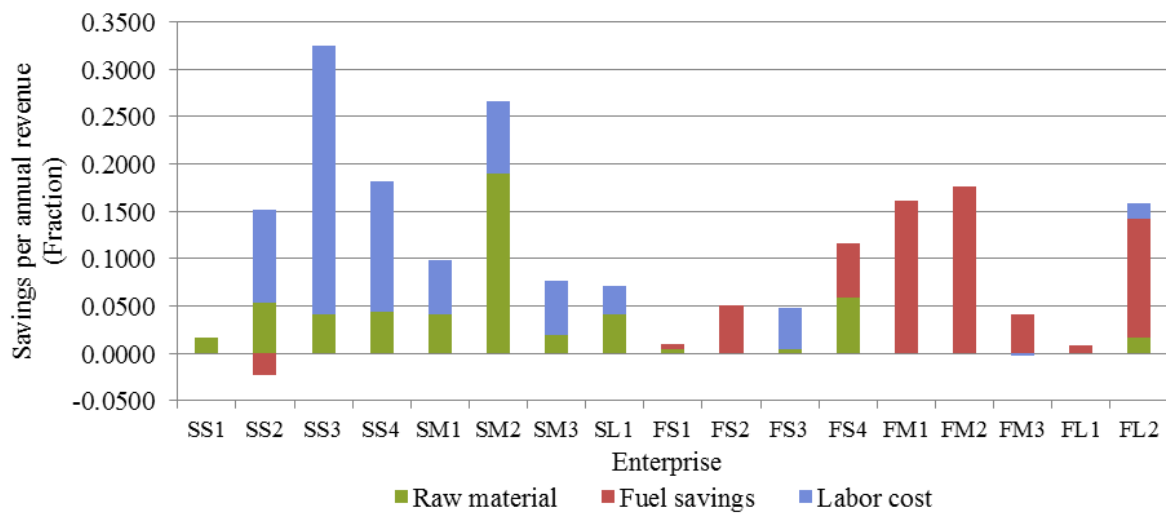


Fig. 3 Total savings per annual product revenue of each enterprise.

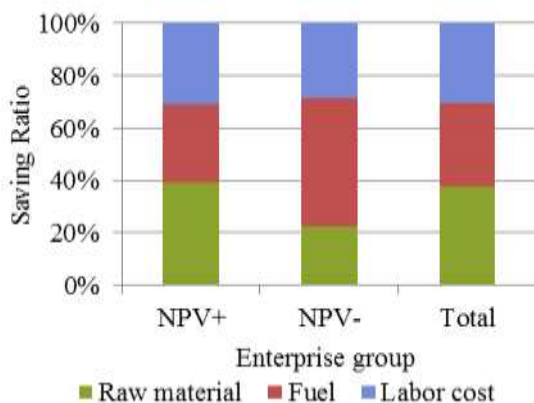


Fig. 4 Savings ratio of the enterprise group that had positive NPV, negative NPV and all enterprises.

All enterprises that had an annual production capacity less than 1,000 kg, except enterprise FS4, had the PBP longer than the lifespan of the dryer. They could hardly breakeven. However, enterprise

FS4 could reduce the use of fuel and invested in a small dryer, so it could achieve a positive NPV.

Figure 3 illustrates small solar dryer enterprises, having low savings per annual revenue including SS1, FS1, FS2 and FS3, had a positive NPV, whereas enterprises having high savings per annual revenue, namely, SS2, SS3 and SS4, had a negative NPV. It reveals that the savings per annual revenue did not indicate economic viability. However, the price of the products affected economic feasibility.

According to the enterprises that had negative NPV, except FL1, the price of their products was low, less than 9 USD/kg. In contrast, the enterprises with positive NPV had product prices higher than 9 USD/kg. Nevertheless, enterprise FL1, with an average product price at 75 USD/kg, had a negative NPV because its annual production capacity was as low as 375 kg. The results showed that the total savings gained per annual revenue did not affect economic viability and enterprises having low priced products or low annual production capacity might not be suitable for the investment.

The group of the enterprises that had a positive NPV gained savings of 30% from reduced fuel, 39% from reduced raw material loss, and 31% from reduced labor cost (Fig.4). Thus, reduced raw material loss played an important role providing benefits to the enterprises.

The investment costs of the solar dryer invested by each enterprise are presented in Fig. 5.

Enterprises with annual revenue higher than the investment costs would have a positive NPV. Entrepreneurs could use annual revenues to decide to invest in a greenhouse solar dryer. However, enterprise FM2, reporting annual revenues less than investment costs, also had a positive NPV. FM2 could gain a positive NPV as a direct result of high savings.

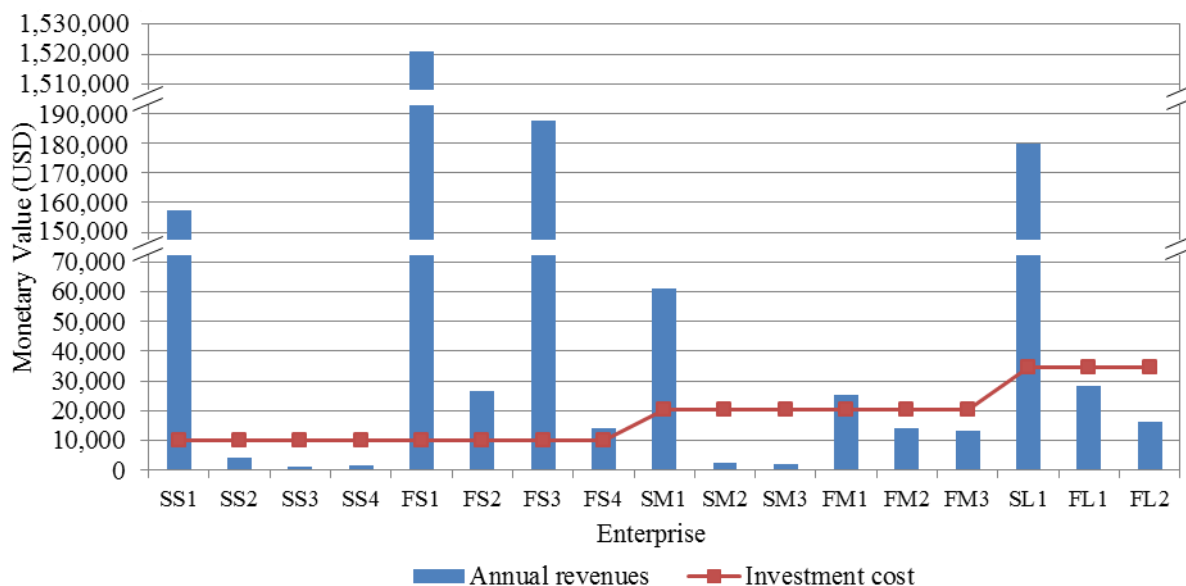


Fig. 5 Annual revenue and the investment cost of each enterprise.

### Carbon Dioxide Mitigation

Seven enterprises could reduce more than 130 tCO<sub>2</sub>e during 15 years of using greenhouse solar dryers (Fig.6). Eighty-six percent had a positive NPV, except FL2. The highest CO<sub>2</sub> mitigation was from enterprise FS1. This enterprise alone could reduce 956 tCO<sub>2</sub>e, with 402 tCO<sub>2</sub>e from reduced fuel and 554 tCO<sub>2</sub>e from reduced waste due to the high amount of fuel replaced and waste reduced. All these seven enterprises could reduce CO<sub>2</sub> up to 1,318 tCO<sub>2</sub>e from reduced fuel and 929 tCO<sub>2</sub>e from reduced waste.

Among nine enterprises using fuel (LPG, wood, and electricity), FS1, FS2 and FL2 could reduce high CO<sub>2</sub> from the use of LPG or wood fuel at the first, the third and the fourth rank, respectively. It showed that enterprises which could reduce the use of LPG or wood fuel tended to have high CO<sub>2</sub> mitigation.

Although enterprise FL2 was in the top seven mitigation rankings, it had a negative NPV. The enterprise invested in the large solar dryer at a high

cost. Its savings gained were low compared with the investment cost; thus, NPV was negative and IRR was low at 2%. Thus, selecting the appropriate size solar dryer is also an important factor to be considered for investing.

When comparing among three different sizes of solar dryers, a lower CO<sub>2</sub> mitigation was related to a higher mitigation cost. For example, enterprise FL1 had almost the same CO<sub>2</sub> mitigation as enterprise FS3, FS4, SS3, and SM2, but its mitigation cost was much higher than the others because of the high investment cost of a large solar dryer. The enterprise FL1 could reduce CO<sub>2</sub> emission to a low amount compared with high investment cost (Fig.5); thus, the mitigation cost was as high as 1,383 USD/tCO<sub>2</sub>e.

From the case of enterprises FL1 and FL2, the size of solar dryer was the factor that entrepreneurs needed to consider because its investment cost could affect either NPV or mitigation cost. When the enterprises invested in smaller solar dryers, which still matched their annual production capacity, at over 1,200 kg, they might achieve a positive NPV or the mitigation cost would be decreased [5].

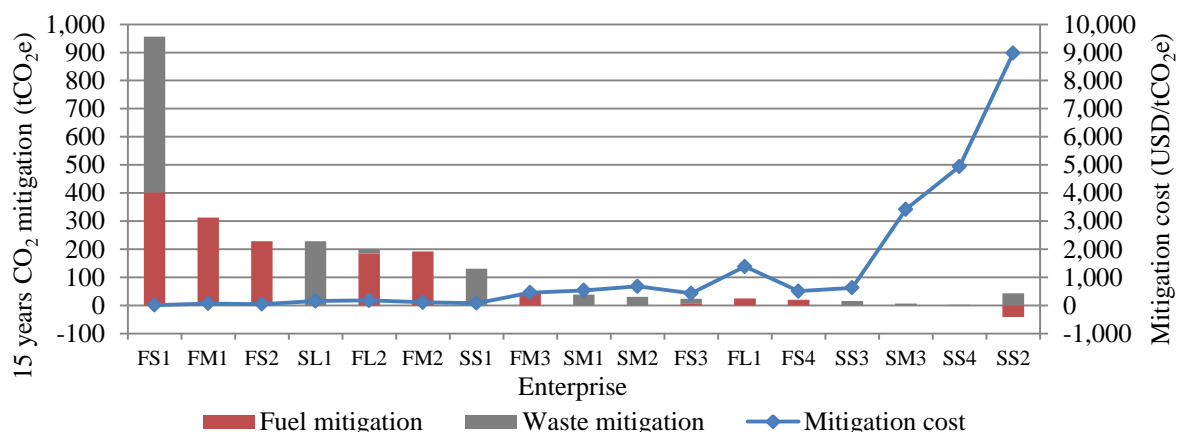


Fig. 6 CO<sub>2</sub> mitigation during 15 years of solar dryer life time.

## CONCLUSIONS

The enterprises with annual revenues higher than their investment costs of solar dryers would have a positive NPV indicating that the investment was attractive. The enterprises that used fuel in the traditional drying method should invest in small or medium sized solar dryers because they tended to obtain a positive NPV. The enterprises with a product price less than 9 USD/kg or annual production capacity less than 1,000 kg should not invest due to the high possibility of obtaining a negative NPV. Enterprises that could substitute the use of fuel by investing in solar dryers would gain more benefits than enterprises using sun drying in the traditional drying method. Most enterprises showing CO<sub>2</sub> mitigation higher than 130 tCO<sub>2</sub>e during 15 years had a positive NPV. To gain the most benefit regarding both economic and environmental aspects in terms of a positive NPV, high IRR and short PBP together with high CO<sub>2</sub> mitigation, entrepreneurs should select the most appropriate size solar dryer for their investments. However, other uncertain parameters, including inflation rate and enterprises' marketing strategies, should be considered in a future study.

## ACKNOWLEDGEMENTS

The authors would like to thank the Department of Alternative Energy Development and Efficiency for inviting and funding Silpakorn University under the solar dryer subsidy program.

## REFERENCES

- [1] Janjai S. and Tung P., Performance of a Solar Dryer Using Hot Air From Roof-integrated Solar Collectors for Drying Herbs and Spices, *Renewable Energy*, Vol. 30, Issue 14, 2005, pp. 2085-2095.
- [2] Chauhan P. S., Kumar A., and Nuntadusit C., Thermo-environmental and Drying Kinetics of Bitter Gourd Flakes Drying under North Wall Insulated Greenhouse dryer, *Solar Energy*, Vol. 162, 2018, pp. 205-216.
- [3] VijayaVenkataRaman S., Iniyan S., and Goic R., A Review of Solar Drying Technologies, *Renewable and Sustainable Energy Reviews*, Vol. 16, Issue 5, 2012, pp. 2652-2670.
- [4] de Gracia A., Barzin R., Fernández C., Farid M. M., and Cabeza L. F., Control Strategies Comparison of a Ventilated Facade with PCM – Energy Savings, Cost Reduction and CO<sub>2</sub> Mitigation, *Energy and Buildings*, Vol. 130, 2016, pp. 821-828.
- [5] El Hage H., Herez A., Ramadan M., Bazzi H., and Khaled M., An Investigation on Solar Drying: A Review With Economic and Environmental Assessment, *Energy*, Vol. 157, 2018, pp. 815-829.
- [6] Janjai S., A Greenhouse Type Solar Dryer for Small-scale Dried Food Industries: Development and Dissemination, *International Journal of Energy and Environment*, Vol. 3, Issue 3, 2012, pp. 383-398.
- [7] Christersson M., Vimpari J., Junnila S., Assessment of Financial Potential of Real Estate Energy Efficiency Investments—A Discounted Cash Flow Approach, *Sustainable Cities and Society*, Vol. 18, 2015, pp. 66-73.
- [8] Saravanan D., Vincent H. W., Kumarasamy S., Life Cycle Cost of Solar Biomass Hybrid Dryer Systems for Cashew Drying of Nuts in India, *Environmental and Climate Technologies*, Vol. 15, Issue 1, 2015, pp. 22-33.
- [9] Thailand Greenhouse Gas Management Organization, "Emission Factor", 2019, [http://thaicarbonlabel.tgo.or.th/products\\_emission/products\\_emission.pnc](http://thaicarbonlabel.tgo.or.th/products_emission/products_emission.pnc), 03 June, 2019. (in Thai)



## AIR POLLUTION CONCENTRATION AND COST FOR THE DIFFERENT ROAD CORRIDORS

LasminiAmbarwati Amelia K. Indriastuti<sup>2</sup>

<sup>1</sup>Faculty of Engineering, Brawijaya University, Malang, East Java, Indonesia

<sup>2</sup>Faculty of Engineering, Diponegoro University, Semarang, Central Java, Indonesia

### ABSTRACT

A lot of disadvantages and disadvantages are caused by the rapid growth of transportation in developing countries. One of advantages is increasing mobility giving negative impact such as decreasing a road performance as well as rising air pollution. Currently, a suitable policy has not formulated to overcome air pollution concentration related to different road corridors. Therefore, traffic demand management (TDM) should be arranged in order to decrease air pollution regards to the different road corridors. This study aims to understand the influence of traffic flow to air pollution concentration and cost in several types of road corridors such as business and residential places in the city of Malang, East Java, Indonesia. This analysis is based on IHCM (Indonesian Highway Capacity Manual) and an approach based on speed in each road corridor. Highway performances of business place have bad service level. On the other hand, road corridor as residential place gives good service level. Based on speed analysis, huge air pollution concentration such as NO and CO<sub>2</sub> give significant negative impact on road corridor as business area. As consequences of the concentration, road corridor as business place give high air pollution cost. The local government should have an effort to reduce air pollution cost by implementing some strategies of TDM such as arrangement of green space, setting up road pricing, minimizing side friction, etc.

*Keywords: Highway performance, Air pollution concentration, Air pollution cost, Road corridor, Travel distance, Speed analysis.*

### INTRODUCTION

Transportation is not the main contributor of air pollutant; however, transportation is the dominant sector that emits 70% air pollutant to the ambient air of urban area [1]. One of the pollutant parameters is CO which is approximately 59.2% emitted from motor-vehicle emission due to traffic congestion. CO emission in human body will react with hemoglobin (Hb) in their blood and further will form CO<sub>2</sub>Hb. In concentration up to 2-5%, this element develops unusual response to five senses and influences the central nerve [2]. CO parameter will decrease air quality causing other impacts such as eye irritation, breath infection, air aesthetic, acid rain, worst visibility that may cause accident, etc. [3].

A strategy was held to reduce air pollution considering on sustainable transport concept. Sustainable transportation refers to transportation with low impact on environment, social and economic aspects. An integrated environment aspect into traffic management becomes a vital necessity in the arrangement of transport policies in order to reduce air pollution and to improve highway capacity [4]. Without a strategic transport system and land use arrangement, the travel demand and emission level of air pollutant will significantly rise [5].

The largest single source of global air pollution comes from the vehicle fleet. Carbon dioxide emissions is exhausted from road traffic, having huge environmental problems with US\$93 billion worth of damage to health and environmental quality each year in the US [6].

Sustainable transport concept should be implemented in big cities, such as Malang City as the recommended study area. This city is the second biggest city in East Java Province - Indonesia, as tourism and education city, and an inter-province connection city. The growth of motor vehicles and trips around Malang and surrounding areas (known as Greater Malang) is significantly increased, thus has the effects on high traffic volume, as recorded 253,904 and 274,664 vehicles in 2006 and 2007 respectively. This condition stimulates the worse air quality as a result of the increasing motor vehicle emission, higher road safety risks and discomfort for people.

Some activities in concentration areas, the impacts deteriorate, since the activities concentration triggers traffic movement. Different land use generates different amount of traffic, thus causes different level of traffic delay and air pollutant.

An insufficient number of studies have considered the air pollution parameters on different road corridors and economic losses due to reduction

of air quality. Therefore, this study has attention on assessment of air emission parameters on different road corridors and air pollution cost imposed on road users.

The study aims to reveal the disadvantage of air pollution caused by transportation using cost analysis of air pollutant. Since different land use produces different level of air pollutant as mentioned before, the analysis is conducted for three areas in Malang City with different combination of land use type and road function. The results of this research are expected to diminish air pollutant in those areas and as a reference in traffic management policies.

This paper is organized as follows: data collection and methodology are elaborated in Section “Methods” consisting of background information on the existing traffic characteristics and highway performance on 3 road sections with different road corridors in the city of Malang. Section “Results” details an analysis of estimating traffic characteristics related to highway performance, measurement of air pollution values as well air pollution cost and concentration. This section discusses the estimation of emission parameters and compares the impacts of each emission parameter as well as air pollution cost for each parameter. Section “Conclusions and recommendations” presents conclusions and recommendations for further research.

## METHODS

### Research Framework

The case study area is Malang City, comprising 5 districts and 57 villages (Fig.1) with the total area of 110 km<sup>2</sup> and population of 861,414 [7]. The average population density in 2017 was estimated approximately 7,826 people per km<sup>2</sup>. High traffic volume loads highway networks serving as gateways to the city center due to expansion of housing development in the suburbs.

This study is focused on some different road corridors with high traffic generation on different road function, in which the areas are around Kyai Tamin, Sulfat, and SP Soedarmo Streets. Those streets are some of major access roads to the city center, as shown in Fig. 1.

Primary data was collected by surveying traffic counting, speed study and road geometry for three road sections with different road corridors as business areas (Kyai Tamin Street), residential areas (Sulfat Street), warehousing areas (SP Darmo Street). Vehicle emission values were determined based on traffic volume and speed. The surveys were carried out on Saturday and Monday during peak and off-peak period (06.00-09.00 am, 11.00-14.00 pm, and 15.00-18.00 pm) in 15 minutes intervals. Secondary

data was collected from the Department of the Environment.



Fig.1 The study area (Malang City), located in East Java Province, Indonesia and location of three road sections

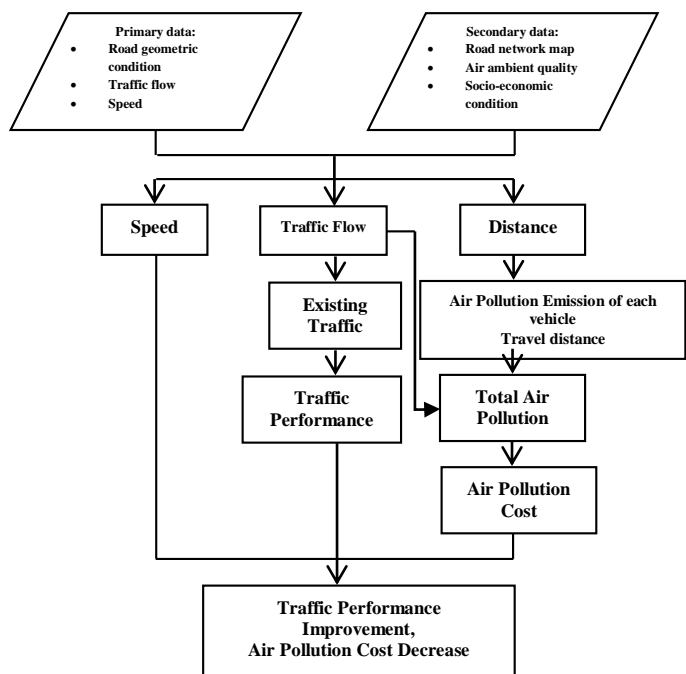


Fig. 2 The research framework

The research framework consists of survey of primary and secondary data in order to assess traffic characteristics, air pollution emission and travel distance. These data are analyzed to estimate traffic performance and concentration and cost for each emission parameter. The result is expected to reduce air pollution emission and to increase the beneficial received from improvement of traffic performance as illustrated in Fig. 2. The result will be recommended the strategies to improve traffic performance and to reduce air pollution cost imposed to the road users.

### Assessment of Highway Performance

Two main parameters determined in this study are traffic performance and air pollution cost. The

traffic performance is analyzed using the Indonesian Highway Capacity Manual [8] and the air pollution cost is calculated based on speed [9].

The traffic performance indicator is the degree of saturation, which is calculated as follow:

$$C = C_o \times FC_w \times FC_{sp} \times FC_{sf} \times FC_{cs} \quad (1)$$

$$DS = Q/C \quad (2)$$

in which  $C$  is the capacity (pcu/hour),  $C_o$  is the basic capacity (pcu/hour),  $FC_w$ ,  $FC_{sp}$ ,  $FC_{sf}$ , and  $FC_{cs}$  are the correction factors due to road width, traffic distribution (directional split), side friction, and city size, respectively,  $DS$  is the degree of saturation, and  $Q$  is the traffic flow (pcu/hour).

The future traffic flow is predicted using the growth of traffic volume.

### Assessment of Emission Load

Air pollutant emissions of each vehicle types are assessed based on traffic speed, whereas the composition of air pollutant is based on traffic volume for each point observation. Thus, the values of pollutant can be calculated based on traffic volume and traffic composition [9], as follows:

*Air pollutant (gr) = traffic flow of each vehicle class (veh) x emission value for each parameter for each type of vehicles (g/veh.mile) x road length mile (3)*

Unit emission loads (g/veh mile) are various for different modes and different speeds. Relevant emission substances are CO, CO<sub>2</sub>, NO<sub>x</sub>, SO, HC and PM. The number of passengers was based on the average vehicle occupancy, i.e. automobiles/private cars, minibuses, medium buses, large buses, trucks and motorcycles accommodate 3 passengers, 8 passengers, 30 passengers, 55 passengers, 2 passengers, and 2 passengers respectively. The standard value of motorized vehicle emissions based on traffic volume and traffic composition is shown in Table 1.

### Calculation of Air Pollution Cost

The air pollution cost is approached by several steps as follows: air pollution cost can be obtained for each gas emission type of each vehicle type. The air pollution cost is determined by the equation 4.

*Air pollution cost (\$) = air pollution cost constant (\$/veh-mile) x peak hour traffic volume (veh) x road length (mile) (4)*

### Evaluation of the results

The results are evaluated to produce two expected recommendations, that is an action to control air pollution impact and, at the same time, to solve the traffic congestion considering the environment and transportation aspects.

Table 1. Emission value for each vehicle (gram/person-mile)

| Mode                                    | Passengers | HC   | CO    | NOx  | SOx  | PM   |
|---|------------|------|-------|------|------|------|
| Motorcycle                              | 2          | 5    | 12    | na   | -    | -    |
| Automobile                              | 3          | 3,15 | 23,57 | 1,91 | 0,07 | 0,01 |
| Diesel Bus (medium or large bus, truck) | 30, 55, 2  | 0,11 | 1,50  | 0,67 | 0,09 | 0,17 |

Source: [9]

The air pollution cost constant is shown in Table 2.

Table 2. Air pollution cost content (\$/veh-mile)

| HC   | CO | NOx         | SOx         | PM        |
|------|----|-------------|-------------|-----------|
| 7.20 | 12 | 0.60 – 8.40 | 0.01 – 0.36 | 0.08-0.13 |

Source: [9].

Note : the value will convert from USD into IDR

## RESULTS

### Vehicle Speed

Speed for each vehicle type (motorcycle, car, and heavy vehicle) on each road is analyzed for 85-percentile and is shown in Table 3. Generally, the lowest speed occurs on SP. Sudarmo Street in the morning and evening time, on the other hand, in the normal time (11.00 am-14.00 pm), all types of vehicles pass on Kyai Tamin Street within lowest speed.

Table 3. The 85-percentile speed data on observed roads

| Time          | Vehicle type | Kyai Tamin |        | SP Sudarmo |        | Sulfat   |        |
|---------------|--------------|------------|--------|------------|--------|----------|--------|
|               |              | Saturday   | Monday | Saturday   | Monday | Saturday | Monday |
| 06.00 - 09.00 | Motor cycle  | 44.4       | 44.6   | 39.0       | 31.5   | 41.0     | 44.0   |
|               | Automobile   | 36.8       | 35.2   | 34.2       | 29.4   | 39.2     | 38.4   |
|               | Diesel       | 37.0       | 33.8   | 28.2       | 24.4   | 37.0     | 37.3   |
| 11.00 - 14.00 | Motor cycle  | 21.4       | 23.6   | 42.0       | 37.4   | 41.6     | 41.0   |
|               | Automobile   | 19.4       | 19.8   | 36.8       | 31.6   | 40.6     | 36.8   |
|               | Diesel       | 18.5       | 17.6   | 32.0       | 26.2   | 37.0     | 35.4   |
| 15.00 - 18.00 | Motor cycle  | 41.0       | 36.8   | 41.6       | 33.0   | 42.0     | 43.2   |
|               | Automobile   | 35.4       | 35.4   | 37.0       | 30.4   | 38.6     | 39.4   |
|               | Diesel       | 31.0       | 30.0   | 31.0       | 24.8   | 32.2     | 34.0   |

### Traffic Performance (Level of Service)

Traffic performance is relied on the road capacity and traffic flow, thus road capacity is depended on road geometry and the presence of the side friction which is related to the activities around the road. The side friction value is affected by the number of pedestrians, stopping vehicles, car parking, and accessing vehicles along the road [8]. The highway performance of each road is as seen in Table 4. Kyai Tamin and Sulfat Street have good service level which is indicated by degree of saturation ( $DS$ )  $\leq$

0.7. On the other hand, the level of service of SP Sudarmo Street approaches traffic jam since huge traffic within heavy vehicles loads this road.

Table 4. The level of service of the observed roads

| Road         | Time          | Capacity (C)<br>(pcu/hour) | Traffic Flow (Q)<br>(pcu/hour) | Road width (m) | Degree of Saturation (DS=Q/C) | Level of Service (LoS) |
|--------------|---------------|----------------------------|--------------------------------|----------------|-------------------------------|------------------------|
| KYAI TAMIN   | Saturday      |                            |                                |                |                               |                        |
|              | 06.00 - 09.00 | 2184.64                    | 1040.60                        | 8.00           | 0.48                          | C                      |
|              | 11.00 - 14.00 | 2210.66                    | 1019.55                        | 8.00           | 0.46                          | C                      |
|              | 15.00 - 18.00 | 2252.09                    | 1005.90                        | 8.00           | 0.45                          | B                      |
|              | Monday        |                            |                                |                |                               |                        |
|              | 06.00 - 09.00 | 2080.38                    | 1335.70                        | 8.00           | 0.64                          | C                      |
|              | 11.00 - 14.00 | 2208.06                    | 1239.30                        | 8.00           | 0.56                          | C                      |
|              | 15.00 - 18.00 | 2354.29                    | 1141.15                        | 8.00           | 0.48                          | C                      |
| S P SOEDARMO | Saturday      |                            |                                |                |                               |                        |
|              | 06.00 - 09.00 | 3476.89                    | 2773.05                        | 10.00          | 0.80                          | D                      |
|              | 11.00 - 14.00 | 3575.98                    | 2308.35                        | 10.00          | 0.65                          | C                      |
|              | 15.00 - 18.00 | 3570.16                    | 2623.70                        | 10.00          | 0.73                          | C                      |
|              | Monday        |                            |                                |                |                               |                        |
|              | 06.00 - 09.00 | 3387.93                    | 3313.75                        | 10.00          | 0.98                          | E                      |
|              | 11.00 - 14.00 | 3426.39                    | 2497.10                        | 10.00          | 0.73                          | C                      |
|              | 15.00 - 18.00 | 3538.68                    | 2889.95                        | 10.00          | 0.82                          | D                      |
| SULFAT       | Saturday      |                            |                                |                |                               |                        |
|              | 06.00 - 09.00 | 3007.56                    | 1722.90                        | 8.00           | 0.57                          | C                      |
|              | 11.00 - 14.00 | 3166.50                    | 1815.20                        | 8.00           | 0.57                          | C                      |
|              | 15.00 - 18.00 | 3002.04                    | 1505.20                        | 8.00           | 0.50                          | C                      |
|              | Monday        |                            |                                |                |                               |                        |
|              | 06.00 - 09.00 | 2868.45                    | 2144.50                        | 8.00           | 0.75                          | C                      |
|              | 11.00 - 14.00 | 3156.68                    | 1517.90                        | 8.00           | 0.48                          | C                      |
|              | 15.00 - 18.00 | 3093.82                    | 1620.30                        | 8.00           | 0.52                          | C                      |

## Emission Parameters for Different Road Corridors

From the analysis, concentration of each emission parameter and cost are determined on different road corridors. The emission concentration is based on vehicle speed investigated. A significant difference in emission concentration and cost is described in Table 5 and Table 6. The value of air pollutant can be analyzed using the Equation (3) and Table 1.

From the analysis, it can be concluded that the amount of CO<sub>2</sub> pollutant is major emission parameter due to predominantly due to increasing numbers of motorcycles and private cars. Current mode choices are private car (30%), motorcycle (66%), and other vehicle types (4%, minibuses, buses and trucks).

Table 5 explains that CO<sub>2</sub> is the major component of the motorized vehicle emission. Thus, motorcycle gives the largest contribution to air pollution, followed by automobile. The amount of air pollution is influenced by the characteristics of the vehicle engine.

The air pollution costs imposed to users on each street can be calculated after the value of air pollutant on Kyai Tamin St. Sunandar P. Sudarmo St. and Sulfat St. were identified, using the Equation (2), and converted into IDR (1 USD = 13,500 IDR). The results of air pollution cost are explained in Table 6.

Table 5. Analysis of air pollutant value for each vehicle unit based on speed measured (gram)

| Street            | Time          | Type of vehicle | HC       | CO        | NO        | CO <sub>2</sub> |
|-------------------|---------------|-----------------|----------|-----------|-----------|-----------------|
| KYAI TAMIN        | Saturday      |                 |          |           |           |                 |
|                   | 06.00 - 09.00 | Motor cycle     | 15,290.6 | 11,762.0  | 13,585.1  | 915,083.6       |
|                   |               | Automobile      | 3,090.6  | 23,634.0  | 2,099.8   | 151,439.4       |
|                   |               | Diesel          | 27.4     | 6.8       | 84.9      | 27,400.0        |
|                   | 11.00 - 14.00 | Motor cycle     | 16,909.0 | 146,240.0 | 8,545.9   | 812,089.0       |
|                   |               | Automobile      | 5,702.4  | 52,272.0  | 2,898.7   | 299,059.2       |
|                   |               | Diesel          | 24.7     | 24.7      | 234.6     | 55,698.5        |
|                   | 15.00 - 18.00 | Motor cycle     | 11,352.0 | 90,816.0  | 9,411.8   | 629,520.0       |
|                   |               | Automobile      | 3,580.2  | 38,610.0  | 3,299.4   | 236,574.0       |
|                   |               | Diesel          | 26.8     | 10.7      | 182.2     | 57,754.0        |
|                   | Monday        |                 |          |           |           |                 |
|                   | 06.00 - 09.00 | Motor cycle     | 17,923.9 | 139,174.2 | 16,166.7  | 1,071,922.5     |
|                   |               | Automobile      | 4,972.8  | 36,960.0  | 3,185.3   | 229,152.0       |
|                   |               | Diesel          | 82.5     | 16.5      | 224.4     | 73,332.6        |
|                   | 11.00 - 14.00 | Motor cycle     | 21,975.0 | 169,940.0 | 11,427.0  | 1,057,730.0     |
|                   |               | Automobile      | 4,989.4  | 44,642.0  | 2,429.1   | 256,691.5       |
|                   |               | Diesel          | 50.5     | 25.2      | 414.1     | 121,452.5       |
|                   | 15.00 - 18.00 | Motor cycle     | 17,061.2 | 130,468.0 | 11,591.5  | 835,998.8       |
|                   |               | Automobile      | 4,998.7  | 37,152.5  | 3,201.8   | 230,345.5       |
|                   |               | Diesel          | 107.1    | 17.8      | 267.7     | 82,288.5        |
| S. PRIYO SOEDARMO | Saturday      |                 |          |           |           |                 |
|                   | 06.00 - 09.00 | Motor cycle     | 39,368.7 | 299,952   | 28,620.42 | 2,018,427       |
|                   |               | Automobile      | 8,062.65 | 82,606.8  | 6,648.15  | 488,002.5       |
|                   |               | Diesel          | 214.75   | 17.18     | 558.35    | 179,101.5       |
|                   | 11.00 - 14.00 | Motor cycle     | 25,665.9 | 202,874.0 | 21,514.1  | 1,401,246.0     |
|                   |               | Automobile      | 11,492.0 | 87,880.0  | 7,807.8   | 563,108.0       |
|                   |               | Diesel          | 92.9     | 27.9      | 659.6     | 195,554.5       |
|                   | 15.00 - 18.00 | Motor cycle     | 29,447.0 | 235,576.0 | 24,414.2  | 1,632,970.0     |
|                   |               | Automobile      | 11,492.0 | 87,880.0  | 7,807.8   | 563,108.0       |
|                   |               | Diesel          | 88.7     | 35.5      | 603.2     | 191,148.5       |
| SULFAT            | Monday        |                 |          |           |           |                 |
|                   | 06.00 - 09.00 | Motor cycle     | 61,659.9 | 443,650.5 | 35,191.3  | 2,684,461.5     |
|                   |               | Automobile      | 11,648.6 | 82,572.0  | 6,723.7   | 517,549.5       |
|                   |               | Diesel          | 179.6    | 10.0      | 748.5     | 195,109.0       |
|                   | 11.00 - 14.00 | Motor cycle     | 27,808.6 | 212,654.0 | 18,893.5  | 1,296,371.5     |
|                   |               | Automobile      | 13,353.7 | 125,394.5 | 7,719.1   | 560,855.4       |
|                   |               | Diesel          | 195.0    | 104       | 936.0     | 263,250.0       |
|                   | 15.00 - 18.00 | Motor cycle     | 43,059.6 | 303,012.0 | 24,666.2  | 1,812,756.0     |
|                   |               | Automobile      | 13,509.0 | 99,864.0  | 7,729.2   | 634,410.0       |
|                   |               | Diesel          | 201.6    | 23.7      | 853.9     | 247,281.0       |
|                   | Saturday      |                 |          |           |           |                 |
|                   | 06.00 - 09.00 | Motor cycle     | 25,171.2 | 207,552.0 | 20,401.9  | 1,435,200.0     |
|                   |               | Automobile      | 5,910.0  | 45,901.0  | 4,550.7   | 306,335.0       |
|                   |               | Diesel          | 40.6     | 10.2      | 125.9     | 40,600.0        |
|                   | 11.00 - 14.00 | Motor cycle     | 20,787.3 | 166,298.0 | 17,234.5  | 1,152,747.5     |
|                   |               | Automobile      | 7,850.9  | 65,424.0  | 6,514.6   | 455,184.0       |
|                   |               | Diesel          | 54.4     | 13.6      | 168.6     | 54,400.0        |
|                   | 15.00 - 18.00 | Motor cycle     | 17,165.9 | 135,686.5 | 14,389.1  | 937,183.5       |
|                   |               | Automobile      | 7,412.1  | 56,905.8  | 5,618.9   | 376,582.5       |
|                   |               | Diesel          | 17.7     | 5.3       | 125.7     | 37,258.5        |
| SULFAT            | Monday        |                 |          |           |           |                 |
|                   | 06.00 - 09.00 | Motor cycle     | 30,109.3 | 229,512.4 | 26,587.1  | 1,778,153.0     |
|                   |               | Automobile      | 8,552.3  | 65,703.0  | 6,570.3   | 437,658.0       |
|                   |               | Diesel          | 35.2     | 3.2       | 99.2      | 31,760.0        |
|                   | 11.00 - 14.00 | Motor cycle     | 22,335.5 | 184,169.5 | 18,103.5  | 1,234,327.5     |

Table 6. Analysis of air pollutant cost for each vehicle unit based on speed measured (IDR)

| Street        | Time                       | cost of emission gas (IDR) |               |              |               | Air pollution cost (IDR) |
|---------------|----------------------------|----------------------------|---------------|--------------|---------------|--------------------------|
|               |                            | HC                         | CO            | NO           | CO2           |                          |
| KYAI TAMIN    | Saturday                   |                            |               |              |               |                          |
|               | 06.00 - 09.00              | 606,909.45                 | 7,762,001.19  | 324,945.44   | 475,861.97    | 9,169,718.05             |
|               | 11.00 - 14.00              | 746,285.05                 | 10,909,194.59 | 240,657.20   | 507,584.15    | 12,403,720.99            |
|               | 15.00 - 18.00              | 493,180.28                 | 7,112,288.89  | 265,676.60   | 401,878.50    | 8,273,024.27             |
|               | Monday                     |                            |               |              |               |                          |
|               | 06.00 - 09.00              | 757,598.30                 | 9,679,128.66  | 403,381.10   | 597,873.96    | 11,437,982.02            |
|               | 11.00 - 14.00              | 890,648.84                 | 11,792,239.17 | 294,043.58   | 624,612.37    | 13,601,543.95            |
|               | 15.00 - 18.00              | 730,819.39                 | 9,211,392.06  | 310,343.56   | 499,661.01    | 10,752,216.01            |
| SP SUDARMO    | Saturday                   |                            |               |              |               |                          |
|               | cost of emission gas (IDR) |                            |               |              |               | Air pollution cost (IDR) |
|               | HC                         | CO                         | NO            | CO2          |               |                          |
|               | 06.00 - 09.00              | 4,712,504.23               | 63,065,354.85 | 2,214,694.80 | 3,504,658.24  | 73,497,212.11            |
|               | 11.00 - 14.00              | 3,684,344.50               | 47,933,646.58 | 1,853,349.54 | 2,818,712.99  | 56,290,053.61            |
|               | 15.00 - 18.00              | 4,057,902.11               | 53,325,629.53 | 2,029,138.98 | 3,115,366.39  | 62,528,037.00            |
|               | Monday                     |                            |               |              |               |                          |
|               | 06.00 - 09.00              | 7,268,442.42               | 86,746,266.93 | 2,637,307.01 | 4,433,292.56  | 101,085,308.93           |
| SULFAT        | 11.00 - 14.00              | 4,090,501.66               | 55,742,410.71 | 1,702,956.80 | 2,767,254.16  | 64,303,123.32            |
|               | 15.00 - 18.00              | 5,614,938.09               | 66,415,601.44 | 2,055,359.06 | 3,516,293.75  | 77,602,192.35            |
|               | Saturday                   |                            |               |              |               |                          |
|               | 06.00 - 09.00              | 2,708,767.78               | 36,768,053.96 | 1,364,232.20 | 2,046,627.36  | 42,887,681.29            |
|               | 11.00 - 14.00              | 2,497,329.87               | 33,616,196.46 | 1,301,088.57 | 1,909,043.44  | 39,323,658.33            |
|               | 15.00 - 18.00              | 2,140,753.23               | 27,938,733.17 | 1,095,238.04 | 1,551,534.37  | 32,726,258.81            |
|               | Monday                     |                            |               |              |               |                          |
|               | 06.00 - 09.00              | 3,368,073.49               | 42,825,213.11 | 1,809,108.73 | 2,581,140.20  | 50,583,535.53            |
| 11.00 - 14.00 | 2,525,611.88               | 34,072,584.08              | 1,240,160.60  | 1,864,470.31 | 39,702,826.86 |                          |
| 15.00 - 18.00 | 2,405,425.96               | 30,851,385.15              | 1,229,131.30  | 1,764,220.95 | 36,250,163.36 |                          |

Tabel 7. The difference of air pollution cost between existing speed and standard speed

| Street        | Time              | Air pollution cost (IDR) |                |                |               |    |            |
|---------------|-------------------|--------------------------|----------------|----------------|---------------|----|------------|
|               |                   | Existing speed (85%)     |                | Standard speed | diference     |    |            |
| KYAI<br>TAMIN | Saturday          |                          |                |                |               |    |            |
|               | 06.00 - 09.00     | Rp                       | 9,169,718.05   | Rp             | 7,632,211.90  | Rp | 1,537,506  |
|               | 11.00 - 14.00     | Rp                       | 12,403,720.99  | Rp             | 5,693,958.58  | Rp | 6,709,762  |
|               | 15.00 - 18.00     | Rp                       | 8,273,024.27   | Rp             | 7,632,211.90  | Rp | 640,812    |
|               | Monday            |                          |                |                |               |    |            |
|               | 06.00 - 09.00     | Rp                       | 11,437,982.02  | Rp             | 9,166,813.48  | Rp | 2,271,168  |
|               | 11.00 - 14.00     | Rp                       | 13,601,543.95  | Rp             | 7,601,303.56  | Rp | 6,000,240  |
|               | 15.00 - 18.00     | Rp                       | 10,752,216.01  | Rp             | 9,166,813.48  | Rp | 1,585,402  |
|               | PRIYO<br>SOEDARMO | Saturday                 |                |                |               |    |            |
| 06.00 - 09.00 |                   | Rp                       | 73,497,212.11  | Rp             | 16,955,760.71 | Rp | 56,541,451 |
| 11.00 - 14.00 |                   | Rp                       | 56,290,053.61  | Rp             | 11,922,180.11 | Rp | 44,367,873 |
| 15.00 - 18.00 |                   | Rp                       | 62,528,037.00  | Rp             | 16,955,760.71 | Rp | 45,572,276 |
| Monday        |                   |                          |                |                |               |    |            |
| 06.00 - 09.00 |                   | Rp                       | 101,085,308.93 | Rp             | 12,286,189.36 | Rp | 88,799,119 |
| 11.00 - 14.00 |                   | Rp                       | 64,303,123.32  | Rp             | 10,950,800.68 | Rp | 53,352,322 |
| 15.00 - 18.00 |                   | Rp                       | 77,602,192.35  | Rp             | 12,286,189.36 | Rp | 65,316,002 |
| SULFAT        |                   | Saturday                 |                |                |               |    |            |
|               | 06.00 - 09.00     | Rp                       | 42,887,681.29  | Rp             | 12,163,560.36 | Rp | 30,724,120 |
|               | 11.00 - 14.00     | Rp                       | 39,323,658.33  | Rp             | 10,329,857.96 | Rp | 28,993,800 |
|               | 15.00 - 18.00     | Rp                       | 32,726,258.81  | Rp             | 12,163,560.36 | Rp | 20,562,697 |
|               | Monday            |                          |                |                |               |    |            |
|               | 06.00 - 09.00     | Rp                       | 50,583,535.53  | Rp             | 24,285,784.53 | Rp | 26,297,751 |
|               | 11.00 - 14.00     | Rp                       | 39,702,826.86  | Rp             | 9,311,157.75  | Rp | 30,391,669 |
|               | 15.00 - 18.00     | Rp                       | 36,250,163.36  | Rp             | 24,285,784.53 | Rp | 11,964,378 |

From Table 6, the highest air pollution cost occurs on Priyo Sudarmo Street on Monday at 06.00-09.00 a.m. (approximately 101,085,308.93 IDR). Using comparison analysis of the standard speed (40 km/hour) and the existing speed, the difference of air pollution cost is 88,799,119.57 IDR, as seen in Table 7. Briefly, the disadvantage cost of those three roads is about 89 million IDR at peak hour. It means that this cost will be charged to neighboring communities and road users. Consequently, it is necessary to improve traffic performance in order to decrease the air pollution cost.

An action program of traffic performance improvement that can simply occupied is to minimize side friction on road section, particularly from the stopping public transit and car parking on the road, since the highest values of side friction is occurred at most roads at certain time (normal and peak hour condition). Side friction contributes in reducing highway performance in terms of road capacity.

The strategies to improve highway performance are considered by equipping a lay-by-lay bus stop for paratransit access, for passenger boarding and alighting. The strategies aim to prevent the traffic flow blocked. Parking lots should be prepared at all building or office in order to decrease on-street parking in around the areas. Finally, conducting 40 km/hour as vehicle speed limit will support this program.

## CONCLUSIONS

Kyai Tamin and Sulfat Streets have a slightly good road performance (C service level) service level. This level means that those roads have stable flow and speed, as well the movements are limited by traffic volume. On the other hand, Priyo Sudarmo Street has worse performance (E service level) at peak hour meaning that traffic volume is approaching value of road capacity and in unstable condition, rarely traffic jam occurred. The highest traffic volume occurs at 07.15-08.15 in Monday (3,313 pcu/hour), due to a lot of activities done in the morning in the road corridors.

The highest air pollutant occurs on Priyo Sudarmo Street at 06.00-09.00 a.m. consisting of 73,588.1 kg HC, 526,232.5 kg CO, 42,663.5 kg NOx and 3,397,120 kg CO<sub>2</sub>. Furthermore, the maximum air pollution cost imposed to road users is approximately Rp 101,085,309.93 at speed investigated, whilst Rp. 12,286,189.00 at normal speed (40 km/hour).

Traffic management in order to improve traffic performance is the program with minimizing side friction from car parking and stop of public transits. These efforts can decline negative impact as well air pollution cost declined.

## ACKNOWLEDGMENTS

This research is supported grant from Directorate of General Higher Education of Indonesia (DGHE). We would like to express deep thank to DGHE and Department of Research, Brawijaya University.

We also want to thank to Dr. B.H. Setiadji, the Associate Professor in Department of Civil Engineering, Diponegoro University for his review to the content of this paper and to M. Nuzulul Anwar in assisting to collect and process data.

## REFERENCES

- [1] Thomas, L. and Cousins, W., The compact city: successful, desirable and achievable? In Jenks, M., Burton, E. & Williams, K. (eds.) the Compact City: A Sustainable Urban Form? Oxford: Oxford Brookes University, 1996.
- [2] Yoky ES., The impact and influences of NOx to the human health, 2009. (in Indonesian) <[http://www.chem-is-try.org/artikel\\_kimia/kimia\\_lingkungan/dampak-pencemaran-nitrogen-oksidasi-nox-dan-pengaruhnya-terhadap-kesehatan/](http://www.chem-is-try.org/artikel_kimia/kimia_lingkungan/dampak-pencemaran-nitrogen-oksidasi-nox-dan-pengaruhnya-terhadap-kesehatan/)> Accessed 3 August 2009.
- [3] Stoker, H. S. and Seager S.L., Environmental Chemistry: Air and Water Pollution. London : Scott, Foresman and Co., 1972.

- [4] Armijaya, H., Application of Environmental Capacity in Measurement Highway Capacity in Indonesia), Proceeding FSTPT III, Yogyakarta, 2000. (in Indonesian)
- [5] Lubis, H., Environment Effect to Transportation and Urban Land Use, Proceeding FSTPT III, Yogyakarta, 2000. (in Indonesian)
- [6] Carley, M., & Christie, I., Managing sustainable development. Routledge, 2017.
- [7] Statistic Bureau of Malang City, the Figures of Malang City in 2017 (in Indonesian).
- [8] Department of Public Works, Republic of Indonesia, Indonesia Highway Capacity Manual (IHCM), Indonesia, 1997.
- [9] Litman, T., Transportation Cost Analysis. Victoria, 1995.



## MICROBIOLOGICAL AND CHEMICAL PROPERTIES OF THE CHI RIVER, MAHA SARAKHAM PROVINCE, THAILAND

Yuwadee Insumran<sup>1</sup>, Jackaphan Sriwongsa<sup>1</sup>, Panuwat Ruenruangrit<sup>2</sup> and Supattra Chinakool<sup>1</sup>

<sup>1</sup> Faculty of Science and Technology, Rajabhat Maha Sarakham University, Maha Sarakham

<sup>2</sup> Faculty of Engineering, Rajabhat Maha Sarakham University, Maha Sarakham, Thailand

### ABSTRACT

Contamination of water, particularly microbiological aspect has been emerging and influencing human health. The aim of this research was to assess the pathogenic contamination of Chi River in Maha Sarakham Province, Thailand. Surface water samples were collected from six stations along the river bimonthly from January to December 2016. Coliforms and fecal coliform bacteria, pathogenic index bacteria, were enumerated by using multiple-tube fermentation approach which was estimated the concentration as MPN index/100 ml. Results indicated that the level of total coliform and fecal coliform bacteria were in the range of less than  $4 \times 10^2$  to  $9 \times 10^3$  MPN index/100 ml. Of 72 collected samples, 67 sample possessed the level of total coliform and fecal coliform exceeding the water quality according to Thai Industrial Standard No.257-2549. Furthermore, chemical qualities of the water samples were determined and results found differently; water temperature = 21.20 -34.17, pH = 6.84-10.00, DO=2.51-9.82 mg/l, BOD = 1.10- 6.07 mg/l, NO<sub>3</sub>-N = 0.30-1.13 mg/l, PO<sub>4</sub><sup>3-</sup>-P = 0.08-0.47 mg/l). In conclusion, these findings demonstrated the Chi River in Maha Sarakham had been contaminated and must be managed and improved intensively for the purpose of human consumption.

**Keywords:** *Coliform Bacteria, Fecal Coliform, the Chi River, Surface Water Quality*

### INTRODUCTION

Chi River is one of the main rivers of the northeastern Thailand. Its total length of 765 km is recognised the longest river in the country. Origination starts from the Phetchabun Mountains, flows through Chaiyaphum, Nakhon Ratchasima, Khon Kaen, Maha Sarakham, Kalasin, Roi Et, Yasothon, Ubon Ratchathani and Sri Sa Ket Provinces of Thailand. However, the river having a length of 60 km occurs in Maha Sarakham Province across Muang, Kosum Phisai and Kantharawichai districts. At least 6 irrigation projects have been located along the river in Maha Sarakham and function as the water sources of domestic, agricultural and industrial utilities. Interestingly, the main consumption and drinking water in Muang and Kosum Phisai depend on water of this river [1].

Coliform bacteria are a large group of various bacteria species including both fecal coliform bacteria and non-fecal coliform bacteria. The fecal coliforms found naturally in the intestines of warm-blooded animals, consisting pathogenic and a non-pathogenic species. Coliforms are frequently used as hygiene indicators, and there are regulatory levels for the presence of coliforms in water for consumption, consequently determination of coliforms plays an important role in the quality control of water [2].

The presence of fecal coliform bacteria indicates contamination of the water body by human and/or

animal fecal material [3-4]. The presence of *E.coli* in water indicates recent fecal contamination it may show the possible presence of disease causing Pathogens such as bacteria, Virus and Parasites. [5]. Indicating the presence of coliform bacteria in the waters of Chi river in Maha Sarakham. Most of the people cause the diseases due to the unavailability of fresh water for drinking purpose This crisis is due to the unplanned urbanization and rapid growth of population in Thailand. Finally, this leads to major water pollution and water crisis by generating many sources of contamination in water in our nation. This research aims to evaluate the microbiological and chemical quality of the water from Chi river in Maha Sarakham, Thailand.

### MATERIALS AND METHODS

#### Sample Collection

Water samples at littoral and limnetic zones of six stations along the Chi river Maha Sarakham Province, (Fig. 1) were separately collected bimonthly during January-December 2016. Locations and geographical positions of the sampling stations are shown in Table 1. One liter of each sample was taken at the depth of 50 cm by using a water sampler, transferred to a sterile water bottle which was kept in a cooling box and then transported to a laboratory at Faculty of

Science and Technology, Rajabhat Maha Sarakham University. The samples were stored at 4°C and

analyzed within 24 hr.

Fig. 1 Sampling sites stations at the Chi river Maha Sarakham Province [6]

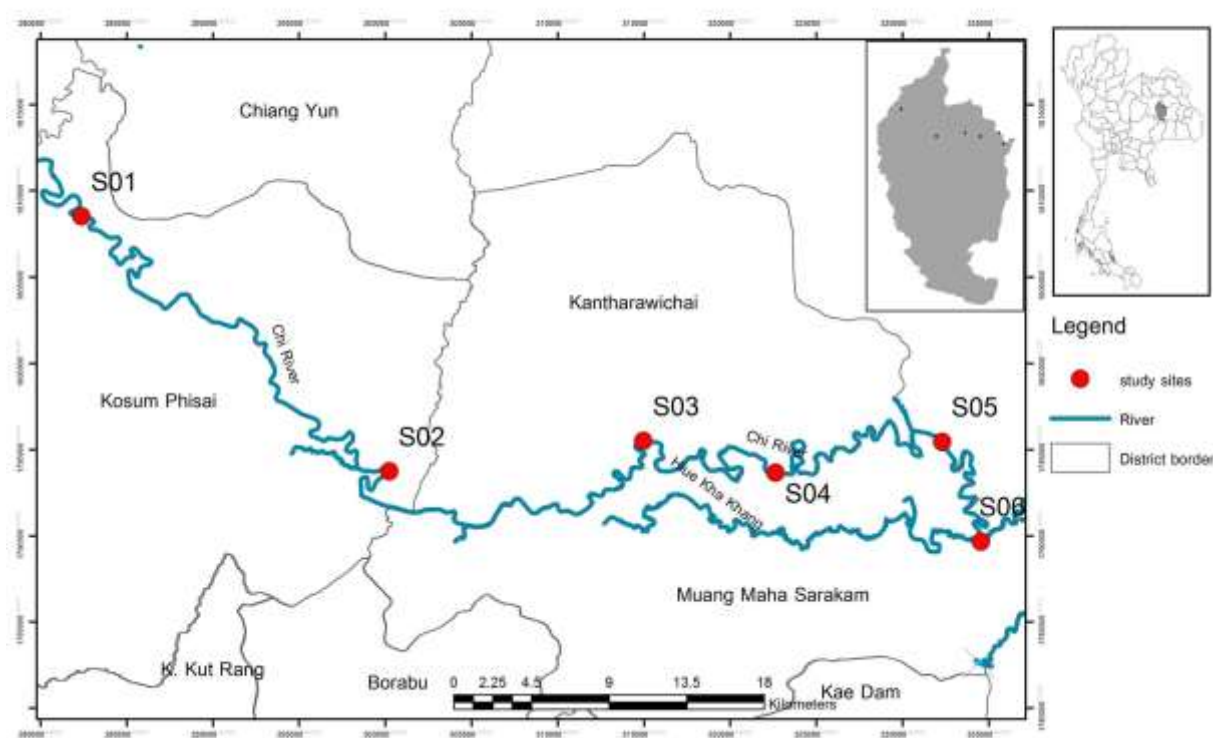


Table 1 List of sampling locations at the Chi river Maha Sarakham Province

| Stations | Locations                     | Geographic positions        |
|----------|-------------------------------|-----------------------------|
| S01      | Kok, Kosum Phisai             | 16°20.869" N 102°57.770" E  |
| S02      | Loeng Tai, Kosum Phisai       | 16°12.941" N 103°07.864" E  |
| S03      | Tha Khon Yang, Kantharawichai | 16°13.965" N 103°16.124" E  |
| S04      | Koeng, Muang Maha Sarakham    | 16°13.003" N 103°20.438" E  |
| S05      | Muang, Muang Maha Sarakham    | 16°14.017" N 103°25.846" E  |
| S06      | Tha Tum, Muang Maha Sarakham  | 16°10.888" N 103° 27.131" E |

### Microbiological Analysis

Microbiological analysis was focused on a hygiene indicator by counting of coliform bacteria in water samples. Most probable number approach was used for total and fecal coliforms enumeration. The number of positive tubes was compared to a standard Most Probable Number chart that expressed in the term MPN/100ml.

### Chemical Analysis

Chemical properties of water samples, including temperature, pH were measured directly at the

sampling stations by using portable electronic meters. On the other hand, concentrations of  $\text{NO}_3\text{-N}$ ,  $\text{PO}_4^{3-}\text{-P}$ , as well as total organic carbon were analyzed according to the method of [7] FAO (2009) at the laboratory.

Dissolved oxygen analysis was carried out by using a DO meter. Two bottles of each water sample were set, one bottle was for DO analysis at day 0 and another bottle was incubated at 20°C for 5 days.

## RESULTS

### Microbiological Analysis

### Chemical Analysis

Total of 72 water samples collected from the Chi river located in Maha Sarakham Province were analyzed for total coliform and fecal coliform. Results are presented in Table 2 and Table 3. Total coliform concentration over a period of year ranged from  $1.20 \times 10^3$  to  $6.25 \times 10^3$  MPN/100 ml, respectively. Fecal coliform concentration ranged from  $4 \times 10^2$  and  $9 \times 10^3$  MPN/100 ml, respectively. Of the total water samples, 93.05% possessed the total coliform and fecal coliform concentrations exceeding the water quality according to Thai Industrial Standard No.257-2549. It demonstrates that water contaminated human and animal faeces.

Chemical analysis of the water samples resulted in Table 4. The water temperature ranged from 21.20 to 34.17 °C, while the water pH values were from 6.84 to 10.00. The suitable range of pH for potable water is between 6.5 to 8.5 [8], however the pH valued could be extended to 9.5. For dissolved oxygen analysis, DO values were between 2.51 and 9.82 mg/l and BOD determination ranged from 1.10 to 6.07 mg/l. The concentrations of nitrate were ranged between 0.30 to 1.13 mg/l, while  $\text{PO}_4^{3-}\text{P}$  value were from 0.08 to 0.47 mg/l.

Table 2 Total coliform of water sample collected from the Chi river Maha Sarakham Province

| Sampling site |               | Total coliform (MPN/100ml) |                    |                    |                    |                    |                    |
|---------------|---------------|----------------------------|--------------------|--------------------|--------------------|--------------------|--------------------|
|               |               | Jan                        | Mar                | May                | July               | Sept               | Nov                |
| S01           | Littoral zone | $6.10 \times 10^3$         | $5.98 \times 10^3$ | $5.70 \times 10^3$ | $5.69 \times 10^3$ | $5.64 \times 10^3$ | $5.50 \times 10^3$ |
|               | Limnetic zone | $6.24 \times 10^3$         | $6.04 \times 10^3$ | $5.64 \times 10^3$ | $5.74 \times 10^3$ | $5.50 \times 10^3$ | $5.64 \times 10^3$ |
| S02           | Littoral zone | $4.24 \times 10^3$         | $4.10 \times 10^3$ | $4.20 \times 10^3$ | $3.76 \times 10^3$ | $4.38 \times 10^3$ | $4.25 \times 10^3$ |
|               | Limnetic zone | $4.19 \times 10^3$         | $4.14 \times 10^3$ | $4.56 \times 10^3$ | $3.43 \times 10^3$ | $4.50 \times 10^3$ | $4.56 \times 10^3$ |
| S03           | Littoral zone | $5.40 \times 10^3$         | $5.30 \times 10^3$ | $5.40 \times 10^3$ | $3.23 \times 10^3$ | $3.78 \times 10^3$ | $6.10 \times 10^3$ |
|               | Limnetic zone | $5.24 \times 10^3$         | $5.36 \times 10^3$ | $5.35 \times 10^3$ | $3.20 \times 10^3$ | $3.70 \times 10^3$ | $6.25 \times 10^3$ |
| S04           | Littoral zone | $3.04 \times 10^3$         | $3.82 \times 10^3$ | $3.30 \times 10^3$ | $2.78 \times 10^3$ | $2.90 \times 10^3$ | $3.76 \times 10^3$ |
|               | Limnetic zone | $3.19 \times 10^3$         | $3.79 \times 10^3$ | $3.24 \times 10^3$ | $2.60 \times 10^3$ | $2.82 \times 10^3$ | $3.50 \times 10^3$ |
| S05           | Littoral zone | $2.84 \times 10^3$         | $2.94 \times 10^3$ | $2.40 \times 10^3$ | $2.20 \times 10^3$ | $1.90 \times 10^3$ | $2.78 \times 10^3$ |
|               | Limnetic zone | $2.70 \times 10^3$         | $2.89 \times 10^3$ | $2.35 \times 10^3$ | $2.00 \times 10^3$ | $1.60 \times 10^3$ | $2.54 \times 10^3$ |
| S06           | Littoral zone | $2.01 \times 10^3$         | $2.50 \times 10^3$ | $2.10 \times 10^3$ | $1.50 \times 10^3$ | $1.20 \times 10^3$ | $2.50 \times 10^3$ |
|               | Limnetic zone | $2.39 \times 10^3$         | $2.00 \times 10^3$ | $1.98 \times 10^3$ | $1.28 \times 10^3$ | $1.24 \times 10^3$ | $2.24 \times 10^3$ |

Table 3 Fecal coliform of water sample collected from the Chi river Maha Sarakham Province

| Sampling site |               | Fecal coliform (MPN/100ml) |                    |                    |                    |                    |                    |
|---------------|---------------|----------------------------|--------------------|--------------------|--------------------|--------------------|--------------------|
|               |               | Jan                        | Mar                | May                | July               | Sept               | Nov                |
| S01           | Littoral zone | $4.90 \times 10^3$         | $4.30 \times 10^3$ | $4.60 \times 10^3$ | $4.60 \times 10^3$ | $3.70 \times 10^3$ | $3.10 \times 10^3$ |
|               | Limnetic zone | $4.6 \times 10^3$          | $3.10 \times 10^3$ | $4.30 \times 10^3$ | $4.30 \times 10^3$ | $3.30 \times 10^3$ | $2.56 \times 10^3$ |
| S02           | Littoral zone | $3.30 \times 10^3$         | $2.70 \times 10^3$ | $2.66 \times 10^3$ | $2.20 \times 10^3$ | $2.20 \times 10^3$ | $2.13 \times 10^3$ |
|               | Limnetic zone | $3.10 \times 10^3$         | $2.60 \times 10^3$ | $2.20 \times 10^3$ | $1.70 \times 10^3$ | $1.83 \times 10^3$ | $1.70 \times 10^3$ |
| S03           | Littoral zone | $3.10 \times 10^3$         | $2.60 \times 10^3$ | $2.56 \times 10^3$ | $1.30 \times 10^3$ | $1.70 \times 10^3$ | $3.30 \times 10^3$ |
|               | Limnetic zone | $2.30 \times 10^3$         | $2.20 \times 10^3$ | $2.10 \times 10^3$ | $1.10 \times 10^3$ | $1.30 \times 10^3$ | $3.10 \times 10^3$ |
| S04           | Littoral zone | $2.96 \times 10^3$         | $1.70 \times 10^3$ | $2.60 \times 10^3$ | $1.50 \times 10^3$ | $1.70 \times 10^3$ | $2.35 \times 10^3$ |
|               | Limnetic zone | $2.90 \times 10^3$         | $1.30 \times 10^3$ | $1.70 \times 10^3$ | $1.70 \times 10^3$ | $1.30 \times 10^3$ | $2.10 \times 10^3$ |
| S05           | Littoral zone | $1.70 \times 10^3$         | $1.90 \times 10^3$ | $1.60 \times 10^3$ | $1.20 \times 10^3$ | $9.0 \times 10^2$  | $1.20 \times 10^3$ |
|               | Limnetic zone | $1.30 \times 10^3$         | $1.60 \times 10^3$ | $6.0 \times 10^2$  | $9.0 \times 10^2$  | $7.0 \times 10^2$  | $1.70 \times 10^3$ |
| S06           | Littoral zone | $1.10 \times 10^3$         | $1.40 \times 10^3$ | $8.0 \times 10^2$  | $6.0 \times 10^2$  | $4.0 \times 10^2$  | $1.30 \times 10^3$ |
|               | Limnetic zone | $1.10 \times 10^3$         | $1.40 \times 10^3$ | $7.0 \times 10^2$  | $5.0 \times 10^2$  | $4.0 \times 10^2$  | $1.10 \times 10^3$ |

Table 4 Chemical properties of water sample collected from the Chi river Maha Sarakham Province

| Sampling site |               | Parameter                   | Month |       |       |       |       |       |
|---------------|---------------|-----------------------------|-------|-------|-------|-------|-------|-------|
|               |               |                             | Jan   | Mar   | May   | July  | Sept  | Nov   |
| S01           | Littoral zone | T (°C)                      | 24.00 | 28.90 | 30.53 | 25.00 | 21.00 | 27.50 |
|               |               | pH                          | 8.22  | 9.28  | 7.53  | 7.03  | 6.84  | 7.26  |
|               |               | DO (mg/l)                   | 2.51  | 2.76  | 4.06  | 7.78  | 6.84  | 4.10  |
|               |               | BOD (mg/l)                  | 3.67  | 5.90  | 4.27  | 3.60  | 2.75  | 3.90  |
|               |               | NO <sub>3</sub> -N (mg/l)   | 0.65  | 0.63  | 1.10  | 0.70  | 0.71  | 0.77  |
|               |               | PO4 <sup>-3</sup> -P (mg/l) | 0.23  | 0.25  | 0.26  | 0.26  | 0.38  | 0.26  |
|               | Limnetic zone | T (°C)                      | 24.00 | 29.43 | 30.57 | 25.00 | 21.20 | 27.50 |
|               |               | pH                          | 8.40  | 9.38  | 7.43  | 7.03  | 6.84  | 7.24  |
|               |               | DO (mg/l)                   | 2.88  | 2.00  | 3.80  | 7.79  | 6.84  | 4.20  |
|               |               | BOD (mg/l)                  | 3.37  | 5.40  | 4.45  | 3.80  | 2.15  | 3.80  |
|               |               | NO <sub>3</sub> -N (mg/l)   | 0.60  | 0.53  | 1.13  | 0.60  | 0.68  | 0.73  |
|               |               | PO4 <sup>-3</sup> -P (mg/l) | 0.37  | 0.27  | 0.23  | 0.35  | 0.30  | 0.38  |
| S02           | Littoral zone | T (°C)                      | 25.33 | 30.00 | 31.97 | 25.00 | 22.10 | 27.00 |
|               |               | pH                          | 8.61  | 9.76  | 7.67  | 6.93  | 7.01  | 7.30  |
|               |               | DO (mg/l)                   | 6.48  | 3.62  | 4.03  | 8.08  | 7.01  | 4.45  |
|               |               | BOD (mg/l)                  | 2.47  | 6.03  | 4.07  | 3.63  | 2.55  | 3.25  |
|               |               | NO <sub>3</sub> -N (mg/l)   | 0.60  | 0.70  | 0.97  | 0.63  | 0.77  | 0.77  |
|               |               | PO4 <sup>-3</sup> -P (mg/l) | 0.23  | 0.14  | 0.25  | 0.08  | 0.28  | 0.34  |
|               | Limnetic zone | T (°C)                      | 25.76 | 30.00 | 32.00 | 25.00 | 22.10 | 27.50 |
|               |               | pH                          | 9.13  | 9.34  | 7.80  | 6.90  | 7.02  | 7.30  |
|               |               | DO (mg/l)                   | 6.29  | 3.75  | 4.13  | 8.08  | 7.02  | 4.50  |
|               |               | BOD (mg/l)                  | 2.57  | 6.07  | 4.27  | 3.15  | 2.85  | 3.20  |
|               |               | NO <sub>3</sub> -N (mg/l)   | 0.50  | 0.77  | 1.05  | 0.53  | 0.75  | 0.73  |
|               |               | PO4 <sup>-3</sup> -P (mg/l) | 0.26  | 0.14  | 0.26  | 0.10  | 0.28  | 0.37  |
| S03           | Littoral zone | T (°C)                      | 26.00 | 30.00 | 34.00 | 26.00 | 22.40 | 27.50 |
|               |               | pH                          | 9.12  | 9.65  | 7.57  | 7.23  | 6.89  | 7.30  |
|               |               | DO (mg/l)                   | 6.03  | 6.60  | 5.54  | 7.61  | 6.89  | 3.90  |
|               |               | BOD (mg/l)                  | 1.93  | 4.57  | 2.88  | 2.55  | 2.50  | 3.30  |
|               |               | NO <sub>3</sub> -N (mg/l)   | 0.60  | 0.67  | 0.70  | 0.70  | 0.87  | 0.93  |
|               |               | PO4 <sup>-3</sup> -P (mg/l) | 0.12  | 0.19  | 0.12  | 0.21  | 0.33  | 0.47  |
|               | Limnetic zone | T (°C)                      | 26.00 | 30.00 | 33.00 | 26.00 | 22.40 | 27.50 |
|               |               | pH                          | 9.24  | 9.40  | 7.77  | 7.21  | 6.89  | 7.30  |
|               |               | DO (mg/l)                   | 5.99  | 6.60  | 6.14  | 7.60  | 6.89  | 4.00  |
|               |               | BOD (mg/l)                  | 2.73  | 3.88  | 2.43  | 2.55  | 2.50  | 3.25  |
|               |               | NO <sub>3</sub> -N (mg/l)   | 0.50  | 0.77  | 0.83  | 0.57  | 0.93  | 0.83  |
|               |               | PO4 <sup>-3</sup> -P (mg/l) | 0.20  | 0.17  | 0.12  | 0.20  | 0.30  | 0.45  |
| S04           | Littoral zone | T (°C)                      | 27.20 | 27.00 | 34.00 | 27.00 | 27.80 | 27.00 |
|               |               | pH                          | 9.50  | 9.41  | 8.03  | 7.67  | 7.06  | 7.36  |
|               |               | DO (mg/l)                   | 6.36  | 7.13  | 5.76  | 7.92  | 7.06  | 4.20  |
|               |               | BOD (mg/l)                  | 2.50  | 3.53  | 3.08  | 3.55  | 2.55  | 3.90  |
|               |               | NO <sub>3</sub> -N (mg/l)   | 0.45  | 0.60  | 0.60  | 0.67  | 0.94  | 0.80  |
|               |               | PO4 <sup>-3</sup> -P (mg/l) | 0.11  | 0.112 | 0.07  | 0.11  | 0.25  | 0.45  |
|               | Limnetic zone | T (°C)                      | 26.83 | 27.67 | 34.00 | 27.00 | 27.80 | 27.00 |
|               |               | pH                          | 9.63  | 9.60  | 8.00  | 7.67  | 7.05  | 7.36  |

| Sampling site | Parameter   | Month |       |       |       |       |       |
|---------------|---|-------|-------|-------|-------|-------|-------|
|               |   | Jan   | Mar   | May   | July  | Sept  | Nov   |
| S05           | DO (mg/l)   | 6.37  | 7.33  | 6.15  | 7.90  | 7.05  | 4.25  |
|               | BOD (mg/l)  | 2.90  | 3.73  | 3.53  | 3.65  | 2.45  | 3.95  |
|               | NO <sub>3</sub> -N (mg/l)                             | 0.45  | 0.57  | 0.67  | 0.40  | 0.95  | 0.80  |
|               | PO <sub>4</sub> <sup>-3</sup> -P (mg/l)               | 0.19  | 0.13  | 0.08  | 0.19  | 0.24  | 0.45  |
|               | Littoral zone T (°C)                                  | 27.07 | 29.47 | 33.67 | 27.00 | 25.90 | 27.00 |
|               | Littoral zone pH                                      | 9.72  | 9.90  | 8.03  | 7.54  | 7.24  | 7.50  |
|               | Littoral zone DO (mg/l)                               | 7.41  | 7.42  | 5.92  | 7.30  | 7.24  | 4.30  |
|               | Littoral zone BOD (mg/l)                              | 1.93  | 2.88  | 3.43  | 3.00  | 1.90  | 3.10  |
|               | Littoral zone NO <sub>3</sub> -N (mg/l)               | 0.40  | 0.43  | 0.60  | 0.50  | 0.87  | 0.63  |
|               | Littoral zone PO <sub>4</sub> <sup>-3</sup> -P (mg/l) | 0.13  | 0.31  | 0.15  | 0.08  | 0.18  | 0.37  |
|               | Limnetic zone T (°C)                                  | 26.00 | 28.53 | 34.00 | 27.00 | 25.90 | 27.00 |
|               | Limnetic zone pH                                      | 9.75  | 9.78  | 8.03  | 7.53  | 7.24  | 7.45  |
|               | Limnetic zone DO (mg/l)                               | 7.48  | 7.45  | 6.27  | 7.30  | 7.24  | 4.30  |
|               | Limnetic zone BOD (mg/l)                              | 1.10  | 3.07  | 3.30  | 3.25  | 1.40  | 3.00  |
|               | Limnetic zone NO <sub>3</sub> -N (mg/l)               | 0.40  | 0.43  | 0.60  | 0.40  | 0.71  | 0.67  |
|               | Limnetic zone PO <sub>4</sub> <sup>-3</sup> -P (mg/l) | 0.12  | 0.23  | 0.16  | 0.12  | 0.16  | 0.39  |
|               | S06 Littoral zone T (°C)                              | 26.00 | 29.17 | 34.17 | 28.00 | 27.10 | 27.00 |
| S06           | Littoral zone pH                                      | 9.62  | 10.03 | 7.73  | 7.43  | 7.21  | 7.45  |
|               | Littoral zone DO (mg/l)                               | 7.23  | 7.45  | 5.32  | 9.82  | 7.21  | 6.20  |
|               | Littoral zone BOD (mg/l)                              | 2.03  | 3.63  | 2.57  | 2.45  | 1.26  | 2.80  |
|               | Littoral zone NO <sub>3</sub> -N (mg/l)               | 0.40  | 0.57  | 0.50  | 0.40  | 0.48  | 0.53  |
|               | Littoral zone PO <sub>4</sub> <sup>-3</sup> -P (mg/l) | 0.16  | 0.40  | 0.14  | 0.15  | 0.13  | 0.23  |
|               | Limnetic zone T (°C)                                  | 26.00 | 29.00 | 34.00 | 28.00 | 27.10 | 27.00 |
|               | Limnetic zone pH                                      | 9.81  | 10.00 | 7.80  | 7.42  | 7.20  | 7.45  |
|               | Limnetic zone DO (mg/l)                               | 7.41  | 7.43  | 5.01  | 9.80  | 7.20  | 6.25  |
|               | Limnetic zone BOD (mg/l)                              | 1.00  | 3.63  | 2.53  | 2.20  | 1.20  | 2.90  |
|               | Limnetic zone NO <sub>3</sub> -N (mg/l)               | 0.30  | 0.53  | 0.50  | 0.40  | 0.48  | 0.57  |
|               | Limnetic zone PO <sub>4</sub> <sup>-3</sup> -P (mg/l) | 0.15  | 0.40  | 0.15  | 0.21  | 0.14  | 0.26  |

## CONCLUSIONS

The microbiological and chemical analyses of water samples from the Chi river located in Maha Sarakham Province demonstrated that the water is not suitable for drinking. According to the Thai Industrial Standard No.257-2549, water sample did not comply the microbiological parameters. In conclusion, these findings demonstrated the Chi River in Maha Sarakham had been contaminated and must be managed and improved intensively for the purpose of human consumption.

## ACKNOWLEDGMENTS

This research was supported by National Research Council of Thailand, grant number 2556 NRCT531148. Authors would like to thank our colleagues from Faculty of Science and Technology for their suggestions.

## EFFECTS OF CLIMATE CHANGE ON MILK YIELD AND MILK COMPOSITION IN THAI CROSSBRED HOLSTEIN COWS

Doungnapa Promket<sup>1\*</sup>, Wootichai Kenchaiwong<sup>2</sup>, and Khanitta Ruangwittayanusorn<sup>1</sup>

<sup>1</sup>Lecture of Animal science, Department of Agricultural Technology, Faculty of Technology, Mahasarakham University, Thailand

<sup>2</sup>Lecture of Veterinary Sciences, Faculty of Veterinary Sciences, Mahasarakham University, Thailand

### ABSTRACT

The purpose of this research was to study the effects of climate changes on milk yield and milk composition of Holstein crossbred in Thailand. This study uses milk yield and milk composition data (from 2013–2017) of each farm from a dairy cooperative member in Mahasarakham Province, Northeast of Thailand. This study used data recording total milk production per farm each day and milk composition data: fat percentage (% Fat), protein percentage (% Pro), solid not fat percentage (% SNF) and total solid percentage (% TS) from 79 dairy farmers in Mahasarakham Province. The temperature and relative humidity data for the period 2013–2017 were obtained from the records of the meteorological center closest to each dairy farm. Using temperature and relative humidity for calculate the temperature humidity index (THI). The effects of THI on milk yield and milk composition in Thai crossbred Holstein cows were assessed by the procedure REG using SAS. The study indicated that, the weather was hot and humid. The temperature ranged from 20.88 – 33.01 ° C. and average humidity was 72.59%. The highest temperature in April (30.85°C) and the lowest temperature in December (23.57 °C). Daily temperature and humidity data from provincial weather station were used to calculate the temperature humidity index (THI). The highest THI (82.07) was in May. The relationship between THI and milk yield was negatively related. The slope value was -0.099, it meaning that when the THI value increased by 1 unit the milk yield decreased by 0.099 kg / cow / day. The THI group for effect of THI on milk yield and milk composition was set to 4 groups (THI 1 = THI ≤70, THI 2 = 74 ≤THI <70, THI 3 = 78 ≤THI <74, THI 4 = THI > 78). The highest THI values (THI 4) effect on low milk yield. In contrast, low THI value (THI 1 and THI 2) effect on high milk yields. Effect of climate changes on Thai Holstein crossbred increase greatly with THI > 78 (THI 4). The climate change, the temperature and humidity increase effects on milk production of dairy cows to decrease.

*Keywords: Climate Change, Milk Yield, Milk Composition*

### INTRODUCTION

Thailand, has a tropical climate with high ambient temperatures and relative humidity. Average temperature is 35.0–39.9 °C and average relative humidity is 72–74 % [1]. Dairy cows that have experienced high temperature and humidity for a long time will reduce milk production and milk quality. Heat stress could be significant reason reduced dairy production in many countries. The exposure of lactating dairy cows to high ambient temperatures, high relative humidity and solar radiation for extended periods decreases their ability to disperse heat. Under heat stress conditions, lactating dairy cows exhibit several physiological responses including a voluntary reduction of feed intake, an increase in maintenance requirements, decrease in milk yield, and milk composition [2]. In addition, heat stress also effects the health of dairy cows because they are at high temperature and humidity and will not be able to maintain balance of the body due to heat stress.

The Temperature Humidity Index (THI) is widely used in hot areas all over the world to assess the impact of heat stress on dairy cows [3]. According to [4] the effect of heat stress on Thai Holstein crossbreds increased greatly with parity and was especially large after a THI of 80 for cows with a high percentage of Holstein genetics (HS ≥ 93.7%). Moreover, [5] showed that heat stress conditions indicated by mean daily values of THI >72 were determined during spring and summer season. The daily THI at which milk production started to decline for milk yield and milk composition ranged from 65 to 76 [6]. When THI reaches 72, milk production as well as feed intake begins to decrease. Milk production during the summer season will be lower than in the winter season by about 10-40% [5].

In addition, heat stress could also cause changes in milk composition, milk somatic cell counts (SCC) and mastitis frequencies. A study comparing milk protein fractions in milk collected from cows in spring and summer, found that the α-casein and β-



casein in serum decreased in the summer season [7].

Some studies have estimated the genetic components for both milk yield and reproduction traits under heat stress. The results showed an unfavorable genetic relationship between THI and productive and reproductive traits. Those findings indicate that the intensive selection (especially for milk production traits) applied to dairy cows might have led to higher heat stress susceptibility in these animals [8]. Therefore, the objective of this research was to study the effects of climate changes on milk yield and milk composition of Thai crossbred Holstein cows in Thailand.

## MATERIALS AND METHODS

### Data and Data Preparation

This study uses data to record total milk production per farm each day and milk composition data: fat percentage (% Fat), protein percentage (% Pro), solid not fat percentage (% SNF) and total solid percentage (% TS) from farms of the Khok Kao Dairy Cooperative Limited (79 farms) in Mahasarakham Province. Data was collected from January 2013 until December 2017. All the dairy farms were managed and maintained in the same way and all dairy cows were raised in an open house. The diet was mixed and fed as TMR. The ratio of concentrate to forage was 4:6 based on DM content. Cows were milked 2 times per day at 06.00 a.m and 17.00 p.m using a milking machine.

The temperature and relative humidity data (from January 2013 – December 2017) obtained from the records of the meteorological center closest to each dairy farm based on postal code. The weather information included daily temperature and relative humidity recorded every 3 h, which were used to calculate the temperature humidity index (THI) by using the equation bellow [9].

$$THI = (0.8 \cdot Ta) + (RH/100) \cdot (Ta - 14.4) + 46.4$$

Where Ta is temperature in °C and RH is relative humidity as a percentage.

The THI values were divided into 4 groups as follows:- THI 1 is  $THI \leq 70$ , THI 2 is  $74 \leq THI < 70$ , THI 3 is  $78 \leq THI < 74$  and THI 4 is  $THI > 78$ . These THI groups (group 1–4) were used for estimating the effects of THI on milk production and milk composition in dairy cattle.

### Statistical Analysis

The means of milk yield and milk composition were analyzed by PROC MEANS using SAS 1998. [13]

The relationships between THI and milk yield and milk composition assessed by the procedure REG in SAS version 8.02 [10].

## RESULTS AND DISCUSSION

### Climatic Condition in Mahasarakham Province of Thailand

Climatic conditions in Mahasarakham Province, Thailand could be characterized as hot and humid with temperature between 23.57 – 33.85 °C and mean relative humidity of 72.59 % (Table 1). The highest temperatures occurred between April– May (30.85 – 30.44°C) and lowest in December (23.57°C). The THI was highest in May (82.07), associated with the summer season and was lowest in December (71.66) in the winter season (Fig 1).

The average of milk/day was 12.69 kg. The milk composition had average values of %fat, %protein, %SNF, and %TS of 3.47% 2.90% 8.33% and 11.79%, respectively. The research of [11] reported % fat and %protein from their study as 3.91% and 3.10% which is higher than this study. Milk production from this study was lower because it was the milk yield from small dairy farms and of poor farm management. Moreover, THI from this study corresponded with values of 72 - 80 reported [12] from Mahasarakham province, with an average higher than the critical point at THI 75. [4] reported that, for third parity, test-day milk yield started to decline above a THI of 74 for cows with  $\geq 87.5\%$  Holstein genetics and declined more rapidly above a THI of 82.

Table 1 Data structure of milk production and milk composition in Thai x Holstein crossbreeds

| Variable | N    | Mean  | SD.  | Min   | Max   |
|----------|------|-------|------|-------|-------|
| Milk/day |      |       |      |       |       |
| (kg)     | 3438 | 12.69 | 5.03 | 5.27  | 37.07 |
| Fat (%)  | 2610 | 3.47  | 0.59 | 1.65  | 10.72 |
| Pro (%)  | 2682 | 2.90  | 0.45 | 2.13  | 22.87 |
| SNF (%)  | 2621 | 8.33  | 0.85 | 2.69  | 13.82 |
| TS (%)   | 2609 | 11.79 | 1.10 | 3.92  | 18.77 |
| Ta (°C)  | 3746 | 27.79 | 2.45 | 23.57 | 30.85 |
| RH (%)   | 3746 | 72.59 | 6.97 | 63.21 | 82.73 |
| THI      | 3746 | 78.34 | 3.70 | 71.66 | 82.07 |

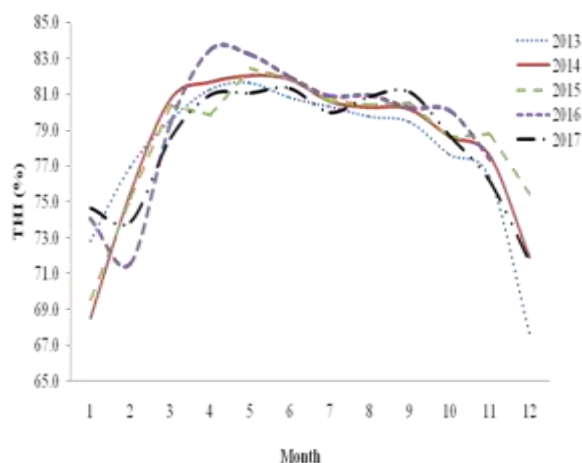


Fig. 1 The average THI in each month of the Northeast of Thailand.

#### The relationship between THI and Milk and Milk composition

Fig. 2 shows the relationship between THI and milk yield and milk compositions in Thai crossbred Holstein cows. The negative slope of the regression line indicates that milk yield decreases as THI increases. The equation for predicting milk is Milk production (kg/cow/day) =  $-0.795(X) + 81.82$  ( $R^2 = 0.361$ ). However, when the THI value is increased, the % fat value increases (Fig. 2). This may be because the % fat value has a negative genetic correlation with the milk yield (data not showed). Season, especially the high-temperature season, significantly affected milk production and milk composition. The Wood equation was appropriate for a quantitative description of seasonal variation in milk composition in individual cows or herds. The changing patterns of milk composition and related indices in different months provide scientific evidence to reasonably improve the feeding management and nutritional supplementation of Chinese Holstein cows [11].

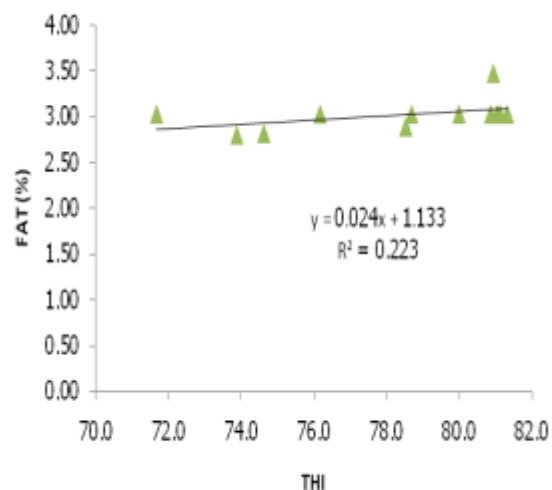
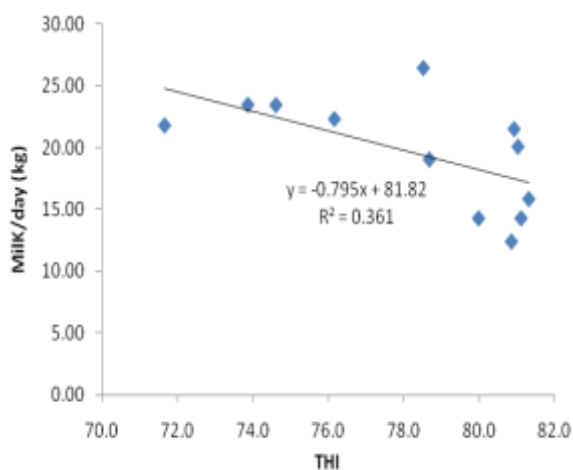


Fig.2 The relationship between THI and milk/day yield, % fat in Thai crossbred Holstein cows

#### Rate of decline of milk and milk composition

The Slope (Fig.2) is rate of decline on milk yield and milk compositions. This regression indicates that, in general, for each point increase in the THI value, there was a decrease in milk yield of 0.099 kg/ cow/ day (slope -0.099). A large part of the variation in milk yield could therefore be attributed to heat stress. Hot weather conditions are associated with reductions in dairy cow feed intake and milk yield [13]. In addition, it can be seen that when the THI value is increased, the % protein value will be reduced 0.004%. The results of this study show that dairy cows suffer from heat stress (higher THI), resulting in reduced milk yield. However, the increased THI values effected an increase in % fat, % SNF and % TS values but did not affect % protein (Table 2). Because of the genetic correlation between the milk yield and milk composition value in milk (%fat, %SNF and %TS) is negative genetic correlation. Approximated genetic correlations between fat and milk production traits in first parity of Canadian Holsteins [14]. The results showed that average daily genetic correlations were negative for the fatty acid groups with milk production ( $-0.62$  to  $-0.59$ ) and with protein yield ( $-0.32$  to  $-0.25$ ). The research of [3] calculated correlations indicated that milk yield was negatively genetic correlated to THI ( $r = -0.75$ ). Moreover, the THI values one, two and three days prior had a greater effect on milk yield than the same day measure. The respective correlation values between milk yield and THI were  $-0.83$ ,  $-0.87$ ,  $-0.89$ .

Table 2 The relationship of THI on Milk yield and Milk composition in dairy cattle

| traits        | N    | Slope  | SE    | P-value |
|---------------|------|--------|-------|---------|
| Milk/day (kg) | 3437 | -0.099 | 0.03  | <0.001  |
| Fat (%)       | 2610 | 0.016  | 0.002 | <0.001  |
| Pro (%)       | 2628 | -0.004 | 0.005 | 0.164   |
| SNF (%)       | 2621 | 0.022  | 0.006 | <0.001  |
| TS (%)        | 2609 | 0.038  | 0.003 | <0.001  |

### The effect of THI on Milk and Milk composition

The results in Table 3 show a significant relationship ( $P < 0.01$ ) between THI groups on milk/day, %fat, %SNF and %TS. The milk/day of the THI 4 group ( $\text{THI} > 78$ ) was lower than the THI 1 THI 2 and THI 3, with an average of 12.50, 14.04, 13.50 and 12.68 kg, respectively ( $P < 0.01$ ).

The %Fat, %SNF and %TS values were highest in the THI 4 range ( $\text{THI} > 78$ ). The % fat in THI 3 is the highest. However, there is non-significant with THI 4, which is 3.49% and 3.48%, respectively. The %fat in THI 1 is the lowest (2.89%). Additionally, the %SNF and %TS values in THI 4 were the highest, 8.38 % and 11.86 %, respectively. The %SNF values in THI1, THI2 and THI3 were 8.09%, 8.22% and 8.13%, respectively ( $P > 0.05$ ). The reason is that when the THI value is higher, the value of milk composition (%Fat, %SNF and %TS) will increase as well; milk composition

values in milk having a negative correlation with the milk production. Therefore THI 1 ( $\text{THI} \leq 70$ ) results in the highest values of milk/day thus, resulting in low %Fat %SNF and %TS values in milk.

The research report that the third parity, test-day milk yield started to decline after a THI of 74 for cows with  $\geq 87.5\%$  Holstein genetics and declined more rapidly after a THI of 82 [4]. Another report in three climactic regions (East, Mediterranean and central) Croatia. Found that heat stress conditions indicated by mean daily values of  $\text{THI} > 72$  were present during spring and summer season in all regions [5]. Moreover, high THI conditions were negatively associated with milking frequency and milk yield in pasture-based automatic milking systems and that research into management and infrastructure (cow cooling) in these systems is warranted to reduce production losses [15]. Dry matter intake and milk yield declined linearly with respective increases in air temperature or THI during the hot period and milk temperature increased linearly with increasing air temperature. Dry matter intake and milk yield both exhibited a curvilinear relationship with milk temperature [16]. Heat stress had negative effects on milk production traits and SCS. The heat stress resulted in decreasing milk yield, fat, and protein percentages, and increasing SCS [17].

Table 3 The effect of THI on Milk and Milk composition

| parameter     | THI 1<br>LSM       | SE   | THI 2<br>LSM       | SE   | THI 3<br>LSM       | SE   | THI 4<br>LSM       | SE   | p-value |
|---------------|--------------------|------|--------------------|------|--------------------|------|--------------------|------|---------|
| Milk/Day (kg) | 14.04 <sup>a</sup> | 0.38 | 13.50 <sup>a</sup> | 0.30 | 12.68 <sup>b</sup> | 0.21 | 12.50 <sup>c</sup> | 0.10 | **      |
| Fat (%)       | 2.89 <sup>a</sup>  | 0.02 | 3.39 <sup>b</sup>  | 0.04 | 3.49 <sup>bc</sup> | 0.03 | 3.48 <sup>c</sup>  | 0.01 | **      |
| Pro (%)       | 2.96               | 0.07 | 2.92               | 0.03 | 2.87               | 0.02 | 2.90               | 0.01 | ns      |
| SNF (%)       | 8.09 <sup>a</sup>  | 0.13 | 8.22 <sup>a</sup>  | 0.06 | 8.13 <sup>a</sup>  | 0.04 | 8.38 <sup>b</sup>  | 0.02 | **      |
| TS (%)        | 10.98 <sup>a</sup> | 0.16 | 11.61 <sup>b</sup> | 0.08 | 11.59 <sup>b</sup> | 0.05 | 11.86 <sup>c</sup> | 0.02 | **      |

Note: THI 1 = ( $\text{THI} \leq 70$ ), THI 2 =  $74 \leq \text{THI} < 70$ , THI 3 =  $78 \leq \text{THI} < 74$ , THI 4 =  $\text{THI} > 78$

\*\* The effect was significance at  $P < 0.01$

<sup>a,b,c</sup> Value within the column with different superscripts are significantly different ( $P < 0.01$ )

### CONCLUSIONS

This study found that Mahasarakham province has temperature between 20.88 - 33.01 ° C and the average humidity is 72.59%. Temperature Humidity Index (THI) is the highest in May (82.07). There was negative relationship between THI and milk

yield with a slope value of -0.099. The slope value explains that when the THI value increased by 1 unit, the milk yield decreased by 0.099 kg / body / day. Dividing the THI group into 4 groups (THI 1 =  $\text{THI} \leq 70$ , THI 2 =  $74 \leq \text{THI} < 70$ , THI 3 =  $78 \leq \text{THI} < 74$ , THI 4 =  $\text{THI} > 78$ ), the result showed that when the highest THI (THI 4) effect on milk yield is the

lowest, while THI1 and THI2 was effect on high milk yield. Temperature and humidity increases will cause a in decrease milk production of dairy cows.

## ACKNOWLEDGMENTS

The research team would like to thank Khok- Koen Dairy Farm Cooperative Limited and dairy farmers, Mahasarakham Province, Thailand for milk yield and milk composition data. Thank you to the Meteorological Department Kosum Phisai District Mahasarakham province, Thailand for temperature and humidity data. Thank you to Faculty of Technology, Mahasarakham University Mahasarakham province.

## REFERENCES

- [1] Meteorological Department, Thai Weather, 2018, Available From [https://www.tmd.go.th/info/climate\\_of\\_thailand-2524-2553.pdf](https://www.tmd.go.th/info/climate_of_thailand-2524-2553.pdf).
- [2] Cowley F. C., Barber D. C., Houlihan A. V., and Poppi D. P., Immediate and Residual Effects of Heat Stress and Restricted Intake on Milk Protein and Casein Composition and Energy Metabolism. *Journal Dairy Science*, Vol. 98, 2015, pp. 2356–2368.
- [3] Bouraoui R., Lahmar M., Majdoub A., Djemali M., Belyea R., The Relationship of Temperature-Humidity Index with Milk Production of Dairy Cows in a Mediterranean Climate. *Journal Animal. Res*, Vol. 51, 2002, pp. 479–491.
- [4] Boonkum W., Misztal I., Duangjinda M., Pattarajinda V., Tumwasorn S., and Sanpote J., Genetic Effects of Heat Stress on Milk Yield of Thai Holstein Crossbreds. *Journal Dairy Science*, Vol. 94, 2011, pp. 487–492.
- [5] Gantner V., Mijic P., Kuterovac K., Solic D., and Gantner R., Temperature-Humidity Index Values and Their Significance on the Daily Production of Dairy Cattle. *Journal Dairy production of dairy cattle*, Vol. 61 (1), 2011, pp. 56-63.
- [6] Bernabucci S., Biffani L., Buggiotti A., Lacetera N., and Nardone A., The Effects of Heat stress in Italian Holstein Dairy Cattle, *Journal Dairy Science*, Vol. 97, 2014, pp. 471–486.
- [7] Bernabucci U., and Calamai L., Effects of Heat Stress on Bovine Milk Yield and Composition, *Journal of Zoot Nutrition Animal*, Vol.24, 1998, pp. 247-257.
- [8] Aguilar I., Misztal I., and Tsuruta S., Genetic Components of Heat Stress in Dairy Cattle with Multiple Lactations, *Journal Dairy Science*, Vol. 92, 2009, pp. 5702–5711.
- [9] Mader T. L., Davis M. S., and Brown-Brandl T., Environmental Factors Influencing Heat Stress in Feedlot Cattle, *Journal of Animal Science*, Vol. 84, 2006, pp. 712–719.
- [10] SAS, User's Guide: Statistics, V.6.12, 1998, SAS Institute Inc., Cary. NC.
- [11] Yang, L., Yang Q., Yi M., Pang Z. H., and Xiong B. H., Effects of seasonal change and parity on raw milk composition and related indices in Chinese Holstein cows in northern China, *Journal Dairy Science*, Vol. 96, 2013, pp. 6863-6869.
- [12] Winai K., Effects of Heat Stress and  $\beta$ -Carotene Supplementation on Postpartum Reproductive Performance in Dairy Cows. Chulalongkorn University, 2011, Bangkok, Thailand.
- [13] Garner, J. B., Douglas M., Williams S. R. O., Wales W. J., Maret L. C., DiGiacomo K., Leury B. J., and Hayes B. J., Responses of dairy cows to short-term heat stress in controlled-climate chambers. *Journal of Animal Production Science*, Vol. 57, 2017, pp.1233–1241.
- [14] Fleming A., Schenkel F. S., Malchiodi F., Ali R. A., Mallard B., Sargolzaei M., Jamrozik J., Johnston J., and Miglior F., Genetic correlations of mid-infrared-predicted milk fatty acid groups with milk production traits, *Journal Dairy Science*, Vol. 101, 2018, pp. 4295-4306.
- [15] Ashleigh M. W., Thomson P. C., Garcia S. C., John A. J., Jongman E. C., Clark C. E. F., and Kerrisk K. L., Short communication: The effect of temperature-humidity index on milk yield and milking frequency of dairy cows in pasture-based automatic milking systems, *Journal Dairy Science*, Vol. 101, 2018, pp. 4479-4482.
- [16] West J. W., Mullinix B. G., and Bernard J. K., Effects of Hot, Humid Weather on Milk Temperature, Dry Matter Intake, and Milk Yield of Lactating Dairy Cows, *Journal Dairy Science*, Vol. 86, 2003, pp. 232–242.
- [17] Lambertz C., Sanker C., and Gauly M., Climatic effects on milk production traits and somatic cell score in lactating Holstein-Friesian cows in different housing systems, *Journal Dairy Science*, Vol. 97, 2014, pp. 319–329.

## STEADY STATE GROUNDWATER FLOW MODEL OF WADI SAMAIL CATCHMENT

Sharifa AL-Hashmi <sup>1</sup>, Luminda Hewawasam <sup>2</sup>, Ahmed Sana <sup>3</sup> and Mahad Baawain <sup>4</sup>

<sup>1</sup> College of Engineering, Sultan Qaboos University, Oman

<sup>2</sup> College of Engineering Sultan Qaboos University, Oman

<sup>3</sup> College of Engineering, Sultan Qaboos University, Oman

<sup>4</sup> College of Engineering, Sultan Qaboos University, Oman

### ABSTRACT

Climate in most of Gulf Cooperation Council (GCC) countries are considered arid with limited water resources. Proper management of scarce water resources is therefore necessary for sustainable water supply while meeting the growing water demands. A three dimensional finite difference groundwater flow model of Wadi Samail Catchment was developed to simulate groundwater flow and to evaluate the sensitivity of model to the varying of input parameters. The model contained historical information of the aquifer and real data of water levels, rainfall, borehole and hydraulic conductivity. The aquifer was divided into 4 layers. The steady state calibration was carried out using data in 14 monitoring wells in July 2016. The hydraulic conductivity (K) and recharge values were calibrated with the estimated root mean squared error (RMSE) of 0.8m. The estimated parameters were verified with groundwater levels in October 2016. The RMSE between observed and simulated water levels was 0.81m. The calibrated model was then used to assess the sensitivity of the model results to the changes in pumping rate, hydraulic conductivity (k) and recharge. Results showed that the water levels were most sensitive to hydraulic conductivity of first layer. While pumping rates and recharge were less sensitive compare to the hydraulic conductivity. In conclusion, the sensitivity analysis results can be used as a management tool for sustainable water resource.

**Keywords:** Numerical groundwater model; Calibration; Sensitivity analysis; Wadi Samail catchment

### INTRODUCTION

Groundwater is a precious, very limited resource and shared without having any fixed boundaries. It is exposed to many risks and great pressure as a result of the rapid increase in population, along with social, agricultural, and industrial development. All these factors have resulted in substantial increase in water demands, placing great pressures on the limited water resources. The main threats to water resources are population growth, urbanization and climate change [1].

Most of Gulf Cooperation Council (GCC) countries are considered as arid region with limited water resources and dependency on groundwater and desalination to meet water demand. The annual rainfall is less than 100 mm/yr and the evaporation rates more than 3000 mm/yr [2]. The limitation in water resources especially in arid regions Like Oman has led to improve the level of water management and conservation for continuous water supply for population growth and development demands [3]. Also, it is necessary to find a way to increase artificial recharge especially in arid regions [4].

For management purpose, the aquifer properties should be examined adequately in order to understand

the groundwater condition and contaminant transport [5]. Therefore, the numerical groundwater model has been used as solution to handle the real world systems [6]. Also for management and protection of water resources by predicting the future status under current circumstances.

The aim of the study is to simulate groundwater level through steady state groundwater model simulation of July 2016. Also to assess the sensitivity of model to the change in pumping rates, hydraulic conductivity (k) and recharge from the calibrate values.

### STUDY AREA

The Sultanate of Oman is picturesquely located in the south-east of the Arabian Peninsula [3]. It has a total area of 309,500 km<sup>2</sup> and a coastline of almost 3,165 km. It is located in an arid region of the world and characterised by limited water resources. Mean annual rainfall throughout most of Oman is relatively low, less than 100 mm and sporadic but in mountain areas rainfall is greater up to 350 mm [7]. Wadi Samail catchment has a total area of 1720 km<sup>2</sup> and it is

triangular in shape as shown in Fig.1. The catchment divided to two part upper and lower which are connected by narrow gorge at AlKhod town[8].



Fig. 1 Study area

creating the conceptual model and 3-D cross section, they were mapped to MODFLOW to simulate the groundwater water level. The steady state groundwater model was run for period of July 2016.



Fig. 2 Study area boundaries

## DATA AND METHOD

### Data:

1. Borehole data: the Ministry of Regional Municipality and Water Resources (MRMWR) provides data of 47 borehole cover the whole catchment area.
2. Groundwater level: the data of groundwater level was provided from MRMWR database of observation wells.
3. Wells: pumping well data for water supply from Public Authority of Water (PAW) and irrigation wells data from National Well Inventory(NWI) from MRMWR
4. Recharge: rainfall station data from MRMWR database
5. Hydraulic conductivity: based on borehole data which classify type of material and previous studies

### Method:

MODFLOW2000: using modular three dimensional finite difference groundwater flow model which use governing equation to simulate the flow [9].

## METHODOLOGY

The conceptual model was created from obtained data of observation wells, pumping wells and borehole. The boundaries of the study area were set as shown in Fig.2. The aquifer was divided to 4 layer: upper gravel, clayey gravel, cemented gravel and ophiolites. Based on borehole data, 3-D cross section was built in order to identify the properties and thickness of layers for 3-D grid construction. After

## RESULTS AND DISCUSSION

The calibration of steady state groundwater model was conducted by using the water level of 14 observation wells that cover the whole catchment. Two methods of calibration were used for calibration: the automated parameter estimation (PEST) and manual trial and error method. The manual trial and error method showed reasonable results than the other method if we compared with the initial values of aquifer parameters such as hydraulic conductivity and recharge. Since the geology of the aquifer is very complex so the automated parameter estimation (PEST) cannot handle it properly. The results of manual calibration are shown in Table 1. We can see that the residual head was less than 2m. The root mean squared error (RMSE) for the steady state simulation was calculated and the result found to be 0.8m.

Once the aquifer parameters estimated, another simulation was run using groundwater levels of October 2016 in order to verify the accuracy of the calibrated parameters. Table 2 displays the computed heads from the simulation and the residual heads. The mean residual head was 0.35m and the RMSE is 0.81m.

Table 1 Calibration result

| Observation well ID | Observed head | Computed head | Residual head |
|---------------------|---------------|---------------|---------------|
| PZ-7                | 569.26        | 569.95        | -0.69         |
| SMA-11B             | 404.54        | 404.33        | 0.21          |
| SLU2B               | 307.31        | 307.26        | 0.05          |
| SJA-2B              | 253.99        | 253.33        | 0.66          |
| SNA-3B              | 242.63        | 241.66        | 0.97          |
| SMN-1B              | 69.91         | 70.52         | -0.61         |
| WRD-10              | 3.32          | 2.7           | 0.62          |



|         |      |      |       |
|---------|------|------|-------|
| WRD-02  | 3.14 | 4.77 | -1.63 |
| WRD-12  | 1.84 | 2.57 | -0.73 |
| 21-6D   | 7.19 | 6.7  | 0.49  |
| 21-6S   | 7.7  | 7.2  | 0.5   |
| RGS-5HS | 0.47 | 1.4  | -0.93 |
| RGS-5F  | 1.47 | 2.05 | -0.58 |
| 21-7S   | 9.62 | 8.47 | 1.15  |

Table 2 Validation results

| Observation well ID | Observed head | Computed head | Residual head |
|---------------------|---------------|---------------|---------------|
| PZ-7                | 564.43        | 564.75        | -0.32         |
| SMA-11B             | 404.19        | 402.82        | 1.37          |
| SLU2B               | 307.22        | 306.41        | 0.81          |
| SJA-2B              | 254           | 252.6         | 1.4           |
| SNA-3B              | 241.74        | 240.95        | 0.79          |
| SMN-1B              | 69.94         | 69.71         | 0.23          |
| WRD-4               | 1.08          | 1.55          | -0.47         |
| WRD-10              | 0.68          | -0.28         | 0.96          |
| WRD-3               | 1.09          | 1.42          | -0.33         |
| WRD-02              | 0.86          | 1.98          | -1.12         |
| WRD-12              | 0.92          | -0.2          | 1.12          |
| WRD-24              | -0.73         | -0.46         | -0.27         |
| 21-6D               | 5.03          | 4.48          | 0.55          |
| 21-6S               | 6.01          | 5             | 1.01          |
| RGS-5HS             | -0.57         | -0.24         | -0.33         |
| RGS-5F              | 0.4           | 0.16          | 0.24          |

## SENSITIVITY ANALYSIS

Sensitivity analysis was conducted using the calibrated groundwater flow model by varying the pumping rates, hydraulic conductivity and recharge from the calibrated values. The parameters were analysed their sensitivity to the change from calibrated values. Each of the former parameters were increased consistently by 10%, 20% to 100% above the calibrated values and decreased on the same pattern. The sensitivity of groundwater level was valued by root mean squared error (RMSE) and mean error (ME). Figures 3 to Fig.7 show the sensitivity of pumping, hydraulic conductivity and recharge.

For the case sensitivity of pumping (Fig.3), as we increased the pumping rates the mean error increased in positive values. For example for the 70% increase from the calibrated value the ME was 2.81 and this means the observed water level was higher than the computed water level. While for 70% decrease from the calibrated value the ME was -2.7 and this indicates that the computed water level was higher than the observed water level. While the RMSE showed that as the pumping increased the residual error increased and the same pattern occurred for reduction in pumping rates.

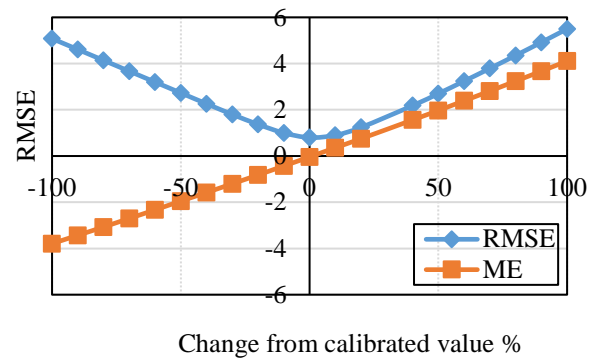


Fig. 3 Sensitivity of pumping parameter

It was notable that the hydraulic conductivity of layer 1 was the most sensitive to the change compare to other layers as shown in Fig. 4 and 5. The value of RMSE reached 83 in zone 2 this can be explained due to the absence of pumping wells so by decreasing the  $k$  values the water level increased and the residual error increased. In Fig.5 the calibrated value of hydraulic conductivity in zone 1 layer 1 is 40.9. As the hydraulic conductivity decreased the RMSE increased to reach 19 while increasing the hydraulic conductivity reduced the RMSE and this means the computed water level match the observed water level with minimum residual error. The remaining layers were less sensitive to the change from the calibrated values as it was remarkable in Fig.6.

For the recharge zone 2 was more sensitive compare to other zones as shown in Fig.7.

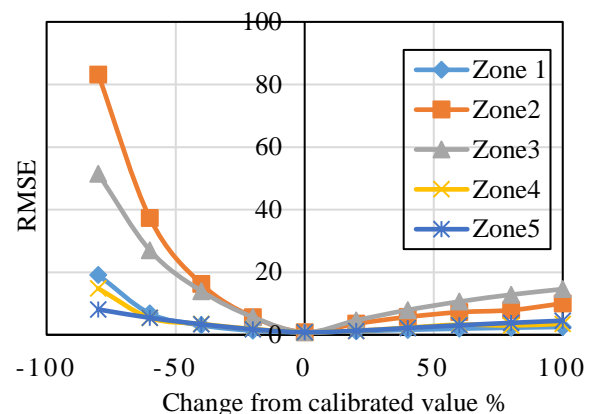


Fig. 4 Sensitivity of hydraulic conductivity of layer 1

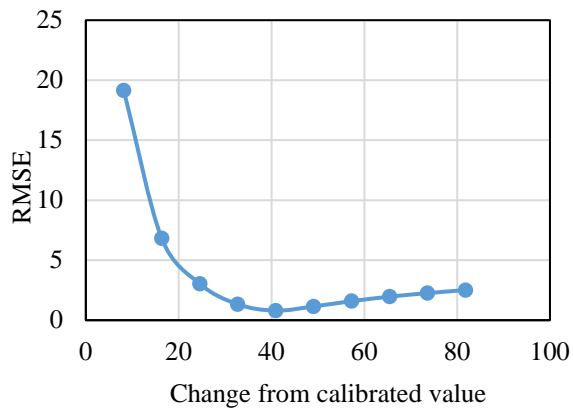


Fig. 5 Sensitivity of hydraulic conductivity of zone1 at layer1

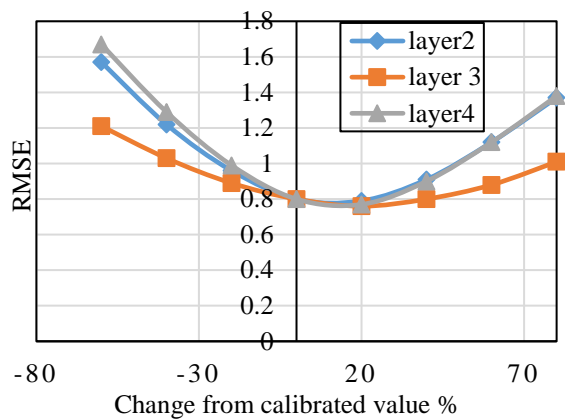


Fig. 6 Sensitivity of hydraulic conductivity

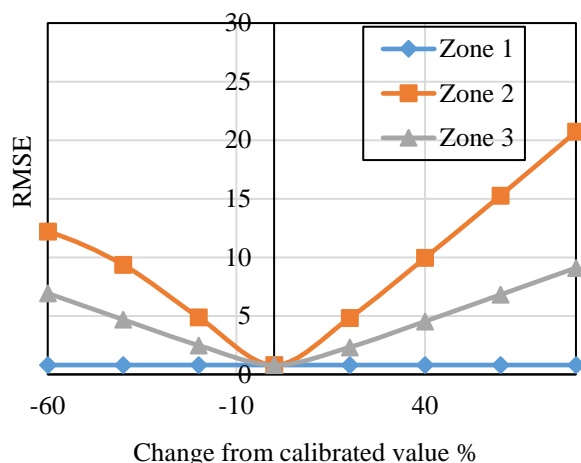


Fig.7 Sensitivity of recharge

## CONCLUSION

The numerical groundwater model has been created to simulate the groundwater level. The model consists of four computational layers which are classified based on borehole data. From the model simulation results we can conclude that the calibrated parameters were matching the initial values since the computed water levels were matching the observed water levels with minimum residual error. This conclusion was supported by the calculated RMSE value which was 0.8m. From sensitivity analysis we noticed that hydraulic conductivity of layer 1 was the most sensitive to the change from calibrated values. Also, pumping and recharge were sensitive to the change from calibrated value but less compared to sensitivity of hydraulic conductivity. For water resource management purpose the groundwater levels should be regularly monitored and the effect of pumping should also be evaluated.

## REFERENCES

- [1] Akbarpour.S., and Niksokhan.M., Investigating effects of climate change, urbanization, and sea level changes on groundwater resources in a coastal aquifer. an integrated assessment. *Environ Monit Assess*, (2018) 190: 579.
- [2] AL-ZUBARI.W.K., *Alternative Water Policies for the Gulf Cooperation Council Countries*. Elsevier Science 2003. p. 155-167.
- [3] MRMWR, *Water Resources in Oman*. 2008.
- [4] Dragoni. W., and Sukhija. B.S., *Climate change and groundwater: a short review*. Geological Society, London, Special Publications, 2008. 288(1): p. 1-12.
- [5] Di Maio. R., Fabbrocino.S. Forte. G. and Piegari.E., A three-dimensional hydrogeological-geophysical model of a multi-layered aquifer in the coastal alluvial plain of Sarno River (southern Italy). *Hydrogeology Journal* (2014) 22: 691-703.
- [6] Rabbani. M.G., and Warner.J.W., A finite-element linked model for analysis of solute transport in 3-D space of multilayer subsurface systems. *Journal of Hydrology*. 199 (1997) 163-182.
- [7] MRMWR, *Water Resources in Oman*. 2012. 3rd.
- [8] Abdalla.O.A.E., and Al-Rawahi.A.S., Groundwater recharge dams in arid areas as tools for aquifer replenishment and mitigating seawater intrusion: example of AlKhod, Oman. *Environmental Earth Sciences*, (2013) 69:1951-1962.
- [9] McDonald. M.G., and Harbaugh. A.W., *A modular three-dimensional finite-difference ground-water flow model*. U.S. Geological Survey report, 1984. 83-875.

# SEE-Kyoto 2020

The Sixth International Conference on

**Science, Engineering & Environment**

**18-20 November 2020**

**Kyoto, Japan**

- The "International Journal of GEOMATE" is a Scientific Journal of the GEOMATE International Society that encompasses a broad area in Geotechnique, Construction Materials and Environment.
- The key objective of this journal is to promote interdisciplinary research from various regions of the globe.
- The editorial board of the journal is comprised of extensively qualified researchers, academicians, scientists from Japan and other countries of the world.
- It is peer-reviewed Journal that is published quarterly till 2015 and now monthly. All articles published in this journal are available on line.
- Contributors may download the manuscript preparation template for submitting paper or contact to the Editors-in-Chief

[[editor@geomatejournal.com](mailto:editor@geomatejournal.com)].

ISSN: 2186-2982 (Print) 2186-2990 (Online)



Scopus

EBSCO

CENGAGE Learning

GIF<sub>4</sub>  
GLOBAL IMPACT FACTOR



VOLUME 00  
Issue 00  
Month, Year

## International Journal of GEOMATE

(Geotechnique, Construction Materials and Environment)



THE GEOMATE INTERNATIONAL SOCIETY

<http://www.geomatejournal.com/>

Tsu, Japan